OXFORD



The Mechanisms of Atmospheric Oxidation of the Oxygenates

Jack G. Calvert,
Abdelwahid Mellouki,
John J. orlando

THE MECHANISMS OF ATMOSPHERIC OXIDATION OF THE OXYGENATES

This page intentionally left blank

THE MECHANISMS OF ATMOSPHERIC OXIDATION OF THE OXYGENATES

JACK G. CALVERT, ABDELWAHID MELLOUKI,
JOHN J. ORLANDO, MICHAEL J. PILLING,
AND TIMOTHY J. WALLINGTON

OXFORD
UNIVERSITY PRESS

OXFORD
UNIVERSITY PRESS

Oxford University Press, Inc., publishes works that further
Oxford University's objective of excellence
in research, scholarship, and education.

Oxford New York
Auckland Cape Town Dar es Salaam Hong Kong Karachi
Kuala Lumpur Madrid Melbourne Mexico City Nairobi
New Delhi Shanghai Taipei Toronto

With offices in
Argentina Austria Brazil Chile Czech Republic France Greece
Guatemala Hungary Italy Japan Poland Portugal Singapore
South Korea Switzerland Thailand Turkey Ukraine Vietnam

Copyright © 2011 by by J.G. Calvert, A. Mellouki, J.J. Orlando,
M.J. Pilling, and T.J. Wallington

Published by Oxford University Press, Inc.
198 Madison Avenue, New York, New York 10016
www.oup.com

Oxford is a registered trademark of Oxford University Press

All rights reserved. No part of this publication may be reproduced,
stored in a retrieval system, or transmitted, in any form or by any means,
electronic, mechanical, photocopying, recording, or otherwise,
without the prior permission of Oxford University Press.

Library of Congress Cataloging-in-Publication Data

The mechanisms of atmospheric oxidation of the oxygenates / by J.G. Calvert . . . [et al.].
p. cm.
Includes bibliographical references.
ISBN 978-0-19-976707-6
1. Atmospheric chemistry. 2. Oxidizing agents—Environmental aspects. 3. Photochemical oxidants—Environmental aspects. 4. Oxidation—Environmental aspects.
I. Calvert, Jack G. (Jack George), 1923–
QC879.9.073M43 2011
551.51'1—dc22 20100022483

---

1 3 5 7 9 8 6 4 2

Printed in the United States of America
on acid-free paper

Contents

Acknowledgments viii
About the Authors xi

I THE OXYGENATES: THEIR PROPERTIES, SOURCES, AND USE AS ALTERNATIVE FUELS 3
- I-A Roles of Oxygenates in Atmospheric Chemistry 3
- I-B Physical Properties of the Oxygenates 6
- I-C Sources of Oxygenates in the Troposphere 19
- I-D Ambient Concentrations of the Oxygenates in the Lower Troposphere 74
- I-E Use of Oxygenates as Fuels or Fuel Additives 96
- I-F Treatment of Kinetic Data and Estimation of Atmospheric Lifetimes of Oxygenates 111

II RATE COEFFICIENTS AND MECHANISMS FOR THE ATMOSPHERIC OXIDATION OF THE ALCOHOLS 116
- II-A Introduction 116
- II-B Acyclic Alcohols 117
- II-C Diols 183
- II-D Unsaturated Alcohols 185
- II-E Aromatic Alcohols 236
- II-F Halogen-Substituted Alcohols 256
- II-G Hydroperoxides and Peroxides 279

III RATE COEFFICIENTS AND MECHANISMS FOR THE ATMOSPHERIC OXIDATION OF THE ETHERS 289
- III-A Introduction 289
- III-B Acyclic Ethers 290
- III-C Multi-Functional Ethers 340
- III-D Unsaturated Ethers 372
- III-E Cyclic Ethers 382
- III-F Aromatic Ethers 420
- III-G Halogen-Substituted Ethers 434
- III-H Rate Coefficient Correlations and Structure–Activity Relationships (SARs) 523

IV RATE COEFFICIENTS AND MECHANISMS FOR THE ATMOSPHERIC OXIDATION OF THE ALDEHYDES 539
- IV-A Introduction 539
- IV-B Acyclic Aldehydes 540
- IV-C Hydroxyaldehydes 585
- IV-E Unsaturated Aldehydes 598
- IV-F Derived from Atmospheric Oxidation of the Aromatic and Biogenic Hydrocarbons 618
- IV-G Halogen-Substituted Aldehydes 634

V RATE COEFFICIENTS AND MECHANISMS FOR THE ATMOSPHERIC OXIDATION OF THE KETONES 651
- V-A Introduction 651
- V-B Alkanones 652
- V-C Hydroxyketones 691
- V-D Diketones 700
- V-E Unsaturated Ketones 706
- V-F Cyclic Ketones 726
- V-G Ketones Derived from Biogenic Hydrocarbons 731
- V-H Halogen-Substituted Ketones 741

VI RATE COEFFICIENTS AND MECHANISMS FOR THE ATMOSPHERIC OXIDATION OF THE ORGANIC ACIDS 747
- VI-A Introduction 747
- VI-B Acyclic Organic Acids 748
- VI-C Dibasic Organic Acids 762
- VI-D Unsaturated Organic Acids 763
- VI-E Keto-Acids 766
- VI-F Organic Acids Derived from Aromatic Compounds and from Terpenes 768
- VI-G Halogen-Substituted Organic Acids 769
- VI-H Acid Anhydrides 772

VII RATE COEFFICIENTS AND MECHANISMS OF ATMOSPHERIC OXIDATION OF THE ESTERS 774
- VII-A Introduction 774
- VII-B Acyclic, Saturated Monofunctional Esters 775
- VII-C Difunctional Esters 841
- VII-D Cyclic Esters (Lactones) 846
- VII-E Unsaturated Esters 848
- VII-F Aromatic Esters 866
- VII-G Carbonates 868
- VII-H Lactates 870
- VII-I Halogen-Substituted Esters 871

VIII RATE COEFFICIENTS AND MECHANISMS FOR THE ATMOSPHERIC OXIDATION OF THE N-ATOM-CONTAINING OXYGENATES 886
- VIII-A Introduction 886
- VIII-B Amides 887
- VIII-C Amino Alcohols 902
- VIII-D Alkyl Nitrates 904
- VIII-E Saturated Dinitrates 924
- VIII-F Unsaturated Dinitrates 928
- VIII-G Hydroxyalkyl Nitrates 929
- VIII-H Carbonyl Nitrates 932
- VIII-I Alkyl Nitrites 934
- VIII-J Nitroalkanes 943
- VIII-K Nitroalkenes 955
- VIII-L Nitroaromatics and Nitroarenes 956
- VIII-M Peroxyacyl Nitrates 962
- VIII-N *N*,*N*-Dimethylnitrosamine and *N*,*N*-Dimethylnitramine 970

IX MECHANISMS OF PHOTODECOMPOSITION OF THE SUNLIGHT-ABSORBING OXYGENATES 974
- IX-A Introduction 974
- IX-B Mechanisms of Photodecomposition of the Acyclic Aldehydes 983
- IX-C Photodecomposition of Aldehydes Containing Additional Functional Groups 1024
- IX-D Photodecomposition of Acyclic Ketones 1089
- IX-E Photodecomposition of Cyclic Ketones 1143
- IX-F Photodecomposition of Ketones Containing Additional Functional Groups 1175
- IX-G Photodecomposition of the Acyl Halides and Carbonyl Halides 1223
- IX-H Photodecomposition of Nitrous Acid, Alkyl Nitrites, Nitroalkanes, and the Nitroso-Compounds 1233
- IX-I Photodecomposition of Nitric Acid, Peroxynitric Acid, and the Alkyl Nitrates 1276
- IX-J Photodecomposition of the Peroxyacyl Nitrates 1298
- IX-K Photodecomposition of Hydrogen Peroxide and the Alkyl Hydroperoxides 1306
- IX-L Photodecomposition of Some Aromatic Oxygenates 1311
- IX-M Summary of Photochemical Processes 1349

X THE INFLUENCE OF OXYGENATES ON THE ATMOSPHERIC CHEMISTRY OF URBAN, RURAL, AND GLOBAL ENVIRONMENTS 1358
- X-A Importance of Oxygenates in Atmospheric Chemistry 1358
- X-B Representation of Oxygenates in Chemical Mechanisms and Models 1359
- X-C Role of Oxygenates in Secondary Organic Aerosol Formation 1372
- X-D Role of Oxygenates in the Upper Troposphere 1377

X-E Role of Oxygenates in Transport of Pollutants (e.g., PAN) 1383
X-F Role of Oxygenates as Proxies for VOC Emissions 1384

References 1391

APPENDIX STRUCTURES OF THE OXYGENATES 1480
App-I Alcohols 1480
App-II Ethers 1490
App-III Aldehydes 1508
App-IV Acyl Halides and Carbonyl Halides 1515
App-V Ketones 1516
App-VI Organic Acids 1523
App-VII Organic Acid Anhydrides 1525
App-VIII Esters 1526
App-IX Nitrogen-Containing Oxygenates 1532

Author Index 1543

Subject Index 1595

Compound Index 1598

Acknowledgments

The authors thank several agencies and their members for support of this research effort: Brent K. Bailey, Executive Director of the Coordinating Research Council (3650 Mansell Road, Suite 140, Alpharetta, GA 30022), and the members of the Coordinating Research Council's Atmospheric Impacts Committee who gave the authors their support and monitored this study: Rory S. MacArthur, Chevron Energy Tech. Co., Richmond, CA; James C. Ball, Ford Motor Co. (Retired), Dearborn, MI; Daniel C. Baker, Shell Global Solutions (U.S.), Houston, TX; Robert Cassidy, Nissan Technical Center North America, Irvine, CA: David P. Chock, Ford Research and Advanced Engineering, Dearborn, MI; Alan M. Dunker, General Motors R&D Center, Warren, MI; Alan J. Krol, BP America, Naperville, IL; Mani Natarajan, Marathon Petroleum Co., LLC, Findlay, OH; David Patterson, Mitsubishi Motors R&D of North America, Cypress, CA; Charles H. Schleyer, Exxon Mobil Research and Engineering, Paulsboro, NJ; Ken Wright, ConocoPhillips Petroleum Co., Bartlesville, OK. Special thanks are extended to Steven Japar and Alan Dunker for their thorough reviews of chapters I through IX and chapter X, respectively. We acknowledge the significant help of Lois Mott (CRC) for her careful editing of the manuscript.

The authors acknowledge their research organizations and educational institutions for the support of their participation in this research: Institut de Combustion Aérothermique Réactivité et Environnement (ICARE) of the Centre National de la Recherche Scientifique (CNRS), Orleans, France; National Center for Atmospheric Research (NCAR), Atmospheric Chemistry Division, Boulder, CO; Ford Motor Company, Physical and Environmental Sciences Department of the Scientific Research Laboratories, Dearborn, MI; Oak Ridge National Laboratories, Environmental Sciences Division, Oak Ridge, TN; and The School of Chemistry, University of Leeds, Leeds, U.K.

NCAR is operated by the University Corporation for Atmospheric Research, under the sponsorship of the U.S. National Science Foundation.

The authors thank their many coworkers who provided them with important new information and other assistance: Geert Moortgat and Hannelore Keller-Rudek, Max-Planck Institute, Mainz, Germany, for providing reprints and spectral data from the files of Mainz Spectral Atlas; James Burkholder (Aeronomy Laboratory, National Oceanic and Atmospheric Administration, Boulder, CO) for providing original spectral data. The authors acknowledge the help of several library staffs in obtaining many of the reprints of the published data that were reviewed and referenced in this study: National Center for Atmospheric Research, Boulder, CO; Institut de Combustion, Aérothermique, Réactivité et Environnement (ICARE) and the Centre National de la Recherche Scientifique (CRNS), Orleans, France; the Oak Ridge National Laboratories, Oak Ridge, TN (especially Larkee Moore, Mary Jacqueline, and William Meyers); The Ohio State University, Columbus, OH (Dr. Belinda L. Hurley, Jose Biaz); Pennsylvania State University, College Station, PA; and Case Western Reserve University, Cleveland, OH. Jack Calvert thanks the Department of Energy, Office of Science, Biological and Environmental Research Program for his Visiting Scientist appointment in the Environmental Sciences Division, Oak Ridge National Laboratories, Oak Ridge, TN, and Gary K. Jacobs for hosting this appointment. Tim Wallington thanks James Anderson, Leandro Benvenutti, and Sherry Mueller (Ford Motor Company) for helpful discussions.

This page intentionally left blank

About the Authors



Jack G. Calvert studied at the University of California, Los Angeles where he received his B.S. (Chemistry) in 1944 and his Ph.D. in 1949 with Professor F. E. Blacet. He continued postdoctoral studies in photochemistry with Dr. E. W. R. Steacie of the National Research Council, Ottawa, Canada (1949–1950). He joined the faculty of The Ohio State University in 1950 and served as Kimberly Professor of Chemistry until1981. He studied with Drs. R.A. Cox and S.A. Penkett at the Harwell Laboratory of the United Kingdom's Atomic Energy Research Establishment (1978). He was appointed Senior Scientist at the National Center for Atmospheric Research (Boulder, CO) in 1981 where he led the Atmospheric Kinetics and Photochemistry Group of the Atmospheric Chemistry Division until his retirement when he was appointed Emeritus Senior Scientist at NCAR (1993–present). Since 2002 he has been a Visiting Scientist in the Environmental Sciences Division of the Oak Ridge National Laboratory. Professor Calvert has authored or coauthored approximately 300 publications in the scientific literature that relate to various aspects of photochemistry, reaction kinetics, and atmospheric chemistry. His honors include: The Distinguished Research Award, The Ohio State University (1981); Simon Guggenheim Memorial Fellowship (1978); American Chemical Society, Columbus Section Award (1981); American Chemical Society Award for Creative Advances in Environmental Science and Technology (1982); Chambers Award of the Air Pollution Control Association (1986). He has been a member and chair of many national and international scientific committees organized to solve recognized problems in atmospheric chemistry. He is co-author of the three preceding books in this series published by Oxford University Press devoted to the mechanisms of atmospheric oxidation of the alkenes, the aromatic hydrocarbons, and the alkanes.



Abdelwahid Mellouki was born in Berkane, Morocco. His undergraduate and graduate studies were conducted in the Universities of Tours, Orleans and Paris 7 (France). He then spent two years as a post-doctoral fellow at the National Oceanic and Atmospheric Administration's Aeronomy Laboratory (Boulder, CO) under the supervision of Dr. A R. Ravishankara. Dr. Mellouki joined the scientific staff at CNRS in 1992, where he is currently a Research Director at the "Institut de Combustion, Aérothermique, Réactivité, et Environnement" (ICARE) in Orleans (France). His research over the years has focused on many aspects of atmospheric chemistry, including studies of the atmospheric oxidation mechanisms of anthropogenic and biogenic carbon-containing species and halogen chemistry. Dr. Mellouki has been involved in a number of EU programs related to atmospheric chemistry and air pollution. He is author or co-author of over 100 scientific publications related to atmospheric chemistry. He has been awarded the title of Professor of Honor of the Research Center for Eco-Environmental Sciences (RCEES)—Chinese Academy of Sciences (CAS) in 2007.



John J. Orlando was born in Timmins, Ontario, Canada in 1960. He received both his B.Sc. (1982) and Ph.D. degrees (1987) in Chemistry from McMaster University in Hamilton, Ontario, Canada with Professors D. R. Smith and J. Reid. He then spent two years as a post-doctoral fellow at the National Oceanic and Atmospheric Administration's Aeronomy Laboratory under the supervision of Drs. C. J. Howard and A. R. Ravishankara, where he worked on problems related to the effects of halogens on stratospheric ozone. Dr. Orlando is presently a Senior Scientist in the Atmospheric Chemistry Division of the National Center for Atmospheric Research (NCAR) where he has been employed since 1989 as an active member of the laboratory kinetics group. His research at NCAR has focused largely on the determination of the mechanisms of the atmospheric oxidation of carbon-containing species, on halogen chemistry of relevance to the stratosphere and troposphere, and on the atmospheric chemistry of nitrogen oxide species. He is author or co-author of over 100 scientific publications related to atmospheric chemistry. Dr. Orlando was the recipient of the American Meteorological Society Special Award (2001), the Velux Foundation Visiting Professor Fellowship at the University of Copenhagen (2002), and the NCAR Special Achievement Award in 2003. Dr. Orlando was co-editor and co-author of the books, *Atmospheric Chemistry and Global Change* published by Oxford University Press in 1998 and *Mechanisms of Atmospheric Oxidation of the Alkanes* published by Oxford University Press in 2008.



Michael J. Pilling was born in Lancashire, England in 1942. His undergraduate and graduate studies were conducted at Churchill College, Cambridge; he obtained a B.A. in Natural Science (Chemistry) in 1964 and a Ph.D. in Physical Chemistry, with Dr. A. B. Callear, in 1967. He continued as a Junior Research Fellow at Churchill College until 1970, during which time he spent a year at National Bureau of Standards (now National Institute of Science and Technology) in Gaithersburg, MD, where he worked on flash photolysis with Dr. W. Braun. He was appointed as a lecturer in Physical Chemistry at Oxford University and a Tutorial Fellow in Jesus College, Oxford in 1970. In 1989, he was appointed Professor of Physical Chemistry at the University of Leeds. His research is centered on reaction kinetics and includes measurements and modeling of elementary radical reactions and the kinetics of complex reactions, including mechanism construction and reduction. He is author and coauthor of over 270 publications, including five books. His honors include: Awards for Reaction Kinetics (1992) and Combustion and Hydrocarbon Oxidation Chemistry (2000), the Polanyi Medal (1994), the John Jeyes Lectureship (2001), and the Distinguished Guest Lectureship in Environmental Chemistry (2006), all from the Royal Society of Chemistry. He has an Honorary Doctorate in Natural Science from the Eotvos Lorand University, Budapest, Hungary. Professor Pilling was the Director of Composition Research at the National Centre for Atmospheric Science from 2002 to 2007, Chair of the Air Quality Expert Group over the same period, and President of the Faraday Division of the Royal Society of Chemistry from 2003 to 2006. Professor Pilling was appointed CBE in the 2008 Birthday Honours List of the Queen of England in recognition of his services to chemistry (2008).



Timothy J. Wallington was born and educated in England. He received B.A. (1981), M.A. (1982), D.Phil (1983), and D.Sc. (2007) degrees from Corpus Christi College, Oxford University where he studied with Professor R. P. Wayne and Dr. R. A. Cox. He has carried out extensive research on various aspects of atmospheric chemistry and the kinetics and mechanisms of many different transient atmospheric species. He carried out postgraduate research studies at the University of California, Los Angeles (1984–1986) with Professor J. N. Pitts and Dr. R. Atkinson. He was Guest Scientist at the U.S. National Bureau of Standards (1986–1987) with Dr. M. J. Kurylo. He joined the research staff at the Ford Motor Company in 1987 where he is currently a Technical Leader in the Systems Analytics and Environmental Sciences Department.

Dr. Wallington has studied the atmospheric chemistry of vehicle and manufacturing emissions and their contribution to local, regional, and global air pollution and global climate change. He is co-author of over 350 peer-reviewed scientific publications dealing with various aspects of air pollution chemistry. He is the recipient of 14 Ford Research Publication Awards (1991–2009), the Ford Motor Company Technical Achievement Award (1995), the Henry Ford Technology Award (1996), a Humboldt Research Fellowship, Universität Wuppertal (1998–1999) with Professor K. H. Becker, and the American Chemical Society Award in Industrial Chemistry in 2008. He has an Honorary Doctorate in Science from Copenhagen University (2006) Dr. Wallington was a co-author of the three previous books on the mechanisms of atmospheric oxidation of the alkenes, the aromatic hydrocarbons, and alkanes, published by Oxford University Press.

THE MECHANISMS OF ATMOSPHERIC OXIDATION OF THE OXYGENATES

This page intentionally left blank

1

The Oxygenates: Their Properties, Sources, and Use as Alternative Fuels

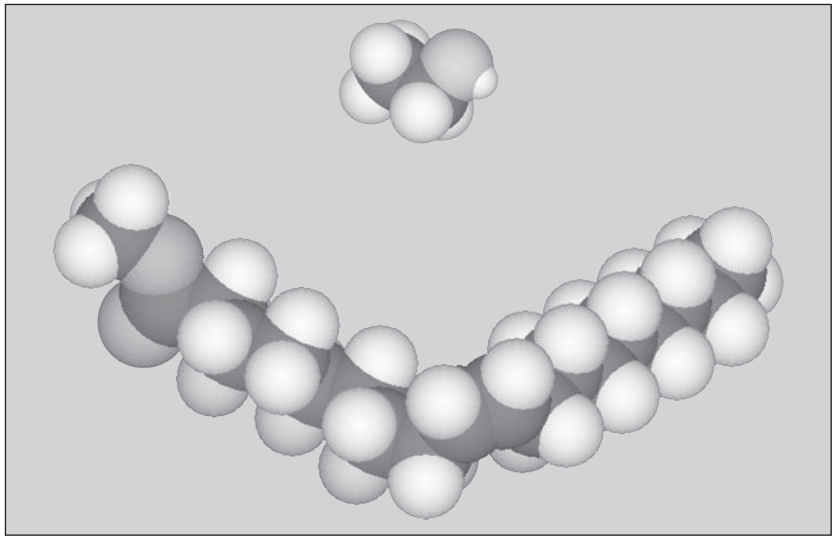

1-A. Roles of Oxygenates in Atmospheric Chemistry

Partially oxidized organic compounds, i.e., those containing carbon, hydrogen, and oxygen atoms, and optionally other heteroatoms, are often referred to as "oxygenates" because they contain O-atoms as well as a C-atom skeleton. These enter the atmosphere as emissions from various industrial and transportation-related operations, evaporation and release from home usage of certain products, and release from vegetation. They are also formed in the atmosphere as oxidation products of all hydrocarbon emissions that enter the atmosphere from mobile and stationary sources as well as natural emissions from plants and animals. The common oxygenates consist of the alcohols (ROH), ethers (ROR), aldehydes (RCHO), ketones [RC(O)R], esters [RC(O)OR], and acids [RC(O)OH] together with N-atom-containing oxygenates and other less abundant classes of oxygen-containing organic compounds. The use of alternative fuels is increasing and is anticipated to continue to grow in the future. Many of these alternative fuels are oxygenates: methanol, ethanol, butanol, fatty acid methyl esters, and other biofuels. Thus, the scientific community is interested in identifying the important sources and sinks for these compounds.

As with the hydrocarbons, the oxygenates serve as fuel for the reactions that generate ozone and other air pollutants within the troposphere. In illustration, consider the influence of the very common and important oxygenate, formaldehyde (CH_2O). The attack of the OH radical in reaction (1) leads to the formation of an important reactive intermediate, the HO_2 radical in reaction (2):

$$CH_2O + OH \rightarrow H_2O + HCO \tag{1}$$

$$HCO + O_2 \rightarrow HO_2 + CO \tag{2}$$

As for the other oxygenates that absorb sunlight, formaldehyde is photodecomposed as well and in this case, additional HO_2, CO, and H-atoms are formed in reactions (3) and (4):

$$CH_2O + h\nu \rightarrow HCO + H \tag{3}$$

$$\rightarrow H_2 + CO \tag{4}$$

The transient species HCO and H formed in these reactions, rapidly generate additional HO_2 radicals in reactions (2) and (5):

$$H + O_2(+N_2, O_2) \rightarrow HO_2(+N_2, O_2) \tag{5}$$

Ultimately, the carbon monoxide molecules formed in reactions (2) and (4) also generate HO_2 radicals through their reactions with HO:

$$CO + OH(+O_2) \rightarrow HO_2 + CO_2 \tag{6}$$

The HO_2 radical product of these reactions is one of the important transients that drives NO to NO_2 conversion leading to ozone formation through the reaction sequences (7), (8), and (9):

$$HO_2 + NO \rightarrow HO + NO_2 \tag{7}$$

$$NO_2 + h\nu \rightarrow O(^3P) + NO \tag{8}$$

$$O(^3P) + O_2(+N_2, O_2) \rightarrow O_3(+N_2, O_2) \tag{9}$$

The larger oxygenates behave in a similar fashion and react with OH in the atmosphere to generate peroxy alkyl radicals (CH_3O_2, $C_2H_5O_2$, … RO_2) and the peroxy acyl radicals [$CH_3C(O)O_2$, $CH_3CH_2C(O)O_2$, … $RC(O)O_2$] that are also important reactants that drive NO to NO_2,

$$RO_2 + NO \rightarrow RO + NO_2 \tag{10}$$

$$RC(O)O_2 + NO \rightarrow RCO_2 + NO_2 \tag{11}$$

and lead to O_3 in reactions (8) and (9). The RO radicals formed in (10) react to form additional HO_2 radicals. Thus for $R = C_2H_5$, reaction (12) occurs:

$$CH_3CH_2O + O_2 \rightarrow CH_3CHO + HO_2 \tag{12}$$

The RCO_2 radical formed in (11) rapidly generates a free radical (R) that reacts quickly to form another RO_2 radical:

$$RCO_2 \rightarrow R + CO_2 \tag{13}$$

$$R + O_2 \rightarrow RO_2 \tag{14}$$

Thus, both the RO_2 and HO_2 radicals formed from the larger oxygenates are important precursors of ozone formation.

All of the oxygenates contribute to the many reactions that lead ultimately to their further oxidation and the enhancement of ozone generation. Some are oxidized rapidly and are very important in ozone development in local urban areas. Others react more slowly and carry their ozone formation potential and other effects to more distant areas through long-range transport. In fact, each of the oxygenates has a unique rate of reaction with OH and other transient molecules [e.g., Cl, NO_3, O_3, $O(^3P)$] and unique rates of light absorption and fragmentation patterns that control their participation in atmospheric chemistry. The major purpose of this book is to review the extensive literature that relates to this chemistry and to help define the important rate coefficients and the mechanisms by which the oxygenates react in the troposphere.

Participation in ozone formation is not the only important role that the oxygenates play in the troposphere. Some are potential health hazards that encourage an accounting of their lifetimes and their ultimate fates. A few are strong infrared light absorbers that can influence climate change by altering the Earth's radiation balance. Others are important sources of aerosols that are potential health hazards, or that can alter the Earth's radiation balance (and thus the climate), or contribute to diminished visibility. In the various chapters of this book, these and other important issues related to the atmospheric chemistry of the oxygenates will be described.

In this chapter we will review the physical properties of the various classes of oxygenates, the major sources, and their use as alterative fuels. The atmospheric oxidation of hydrocarbons forms alcohols, aldehydes, and ketones as primary products. Alcohols are oxidized further to give aldhydes and ketones. Esters are formed from the oxidation of ethers. Organic acids result following the oxidation of carbonyl-containing oxygenates (aldehydes, ketones, esters). This progression is the order of discussion in this book of the various compounds and their reactions. In chapters II, III, IV, V, VI, VII, and VIII, respectively, we discuss the atmospheric chemistry induced by the reaction of OH and other reactive transients with the alcohols, ethers, aldehydes, ketones, organic acids, esters, and the N-atom containing carbon compounds. In chapter IX the reactions promoted by sunlight absorption by the oxygenates are reviewed. Finally, in chapter X we discuss the potential influences of increasing use of oxygenates on the atmospheric chemistry of the urban, rural, and global environments.

I-B. Physical Properties of the Oxygenates

The use of the oxygenates as alternative fuels and the ultimate fates of these compounds in the atmosphere relate in part to their physical properties: their vapor pressure, boiling point, melting point, heats of combustion, Henry's law constants, etc. In this section we review these properties and compare them with the analogous properties of the hydrocarbons.

I-B-1. Vapor Pressures of the Oxygenates

The vapor pressure of a compound is one of the important properties that define its usefulness as a solvent, a fuel, or in other applications. It is also one of the factors that determine whether an oxidation product appears in the gas phase or in the aerosol phase in the atmosphere. The lower the vapor pressure of a compound, the greater is the chance that it will reach its saturation concentration in the atmosphere and condense onto existing particles to form secondary organic aerosol. It is instructive to compare the vapor pressures of the liquid *n*-alkanes as a function of temperature (figure I-B-1) with those of alcohols (figure I-B-2), ethers (figure I-B-3), aldehydes (figure I-B-4), ketones (figure I-B-5), esters (figure I-B-6), organic acids (figure I-B-7), and certain N-atom containing oxygenates (figures I-B-10 and I-B-11, below). For the higher members of a family of compounds, the data may extend below the freezing point of the compounds, and in these cases the vapor pressures reflect those of the supercooled liquid, a state of matter not unusual for atmospheric aerosols. These figures were prepared using vapor pressure data obtained from compilations given by Lide (2001–2002).

Note that in each family of compounds, the slopes of the lines in the semilog plots of vapor pressure versus reciprocal temperature increase regularly as one progresses

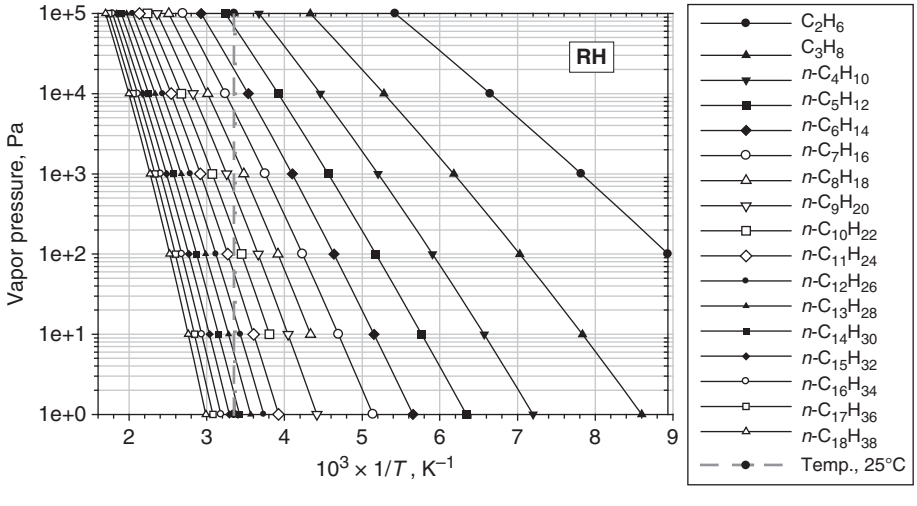

Figure I-B-1. Semilog plot of the vapor pressures of the *n*-alkanes from C_2H_6 to n-$C_{18}H_{38}$ versus the reciprocal temperature.

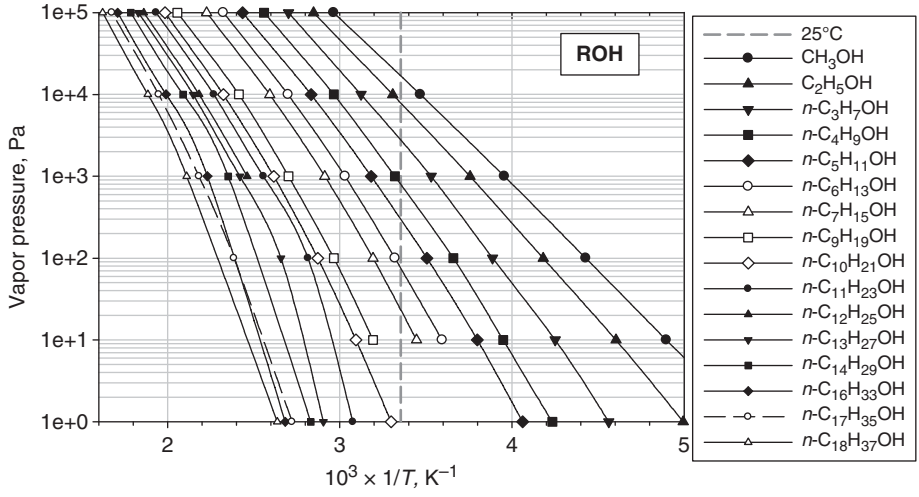

Figure I-B-2. Semilog plot of the vapor pressures of a series of straight chain alcohols from CH_3OH to n-$C_{18}H_{37}OH$ versus the reciprocal temperature.

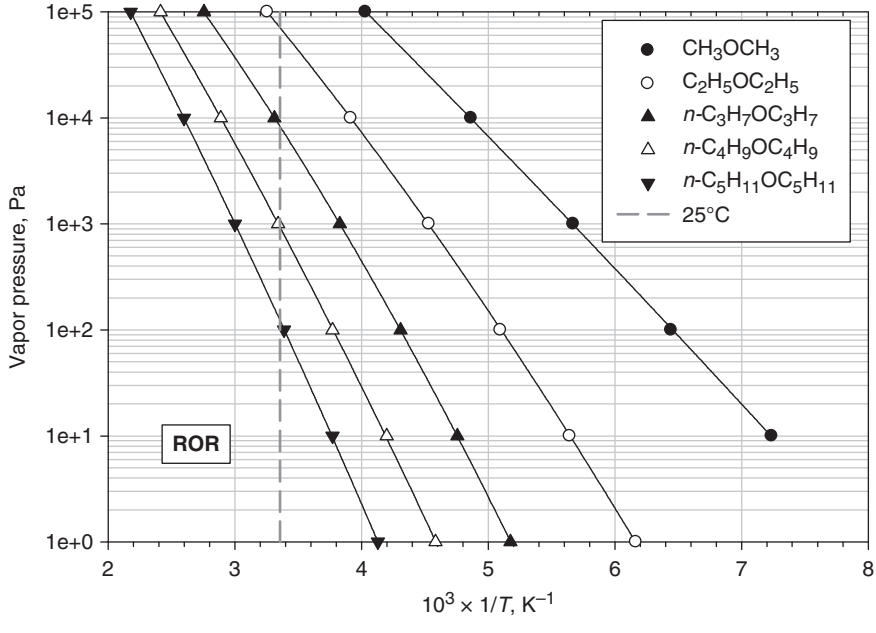

Figure I-B-3. Semilog plot of the vapor pressures of a series of ethers from dimethyl ether to di-n-pentyl ether versus the reciprocal temperature.

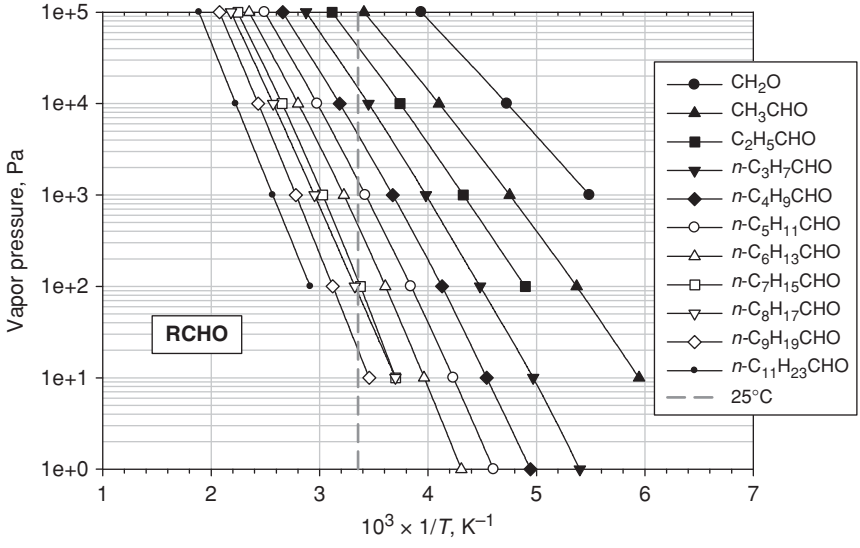

Figure I-B-4. Semilog plot of the vapor pressures of a series of aldehydes from CH_2O to n-$C_{11}H_{23}CHO$ versus the reciprocal temperature.

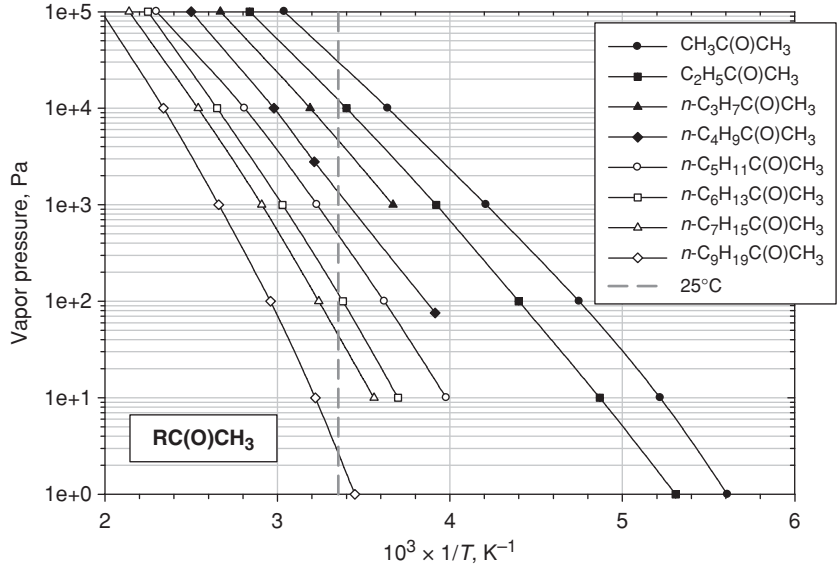

Figure I-B-5. Semilog plot of the vapor pressures of a series of methyl ketones from acetone to 2-undecanone versus the reciprocal temperature.

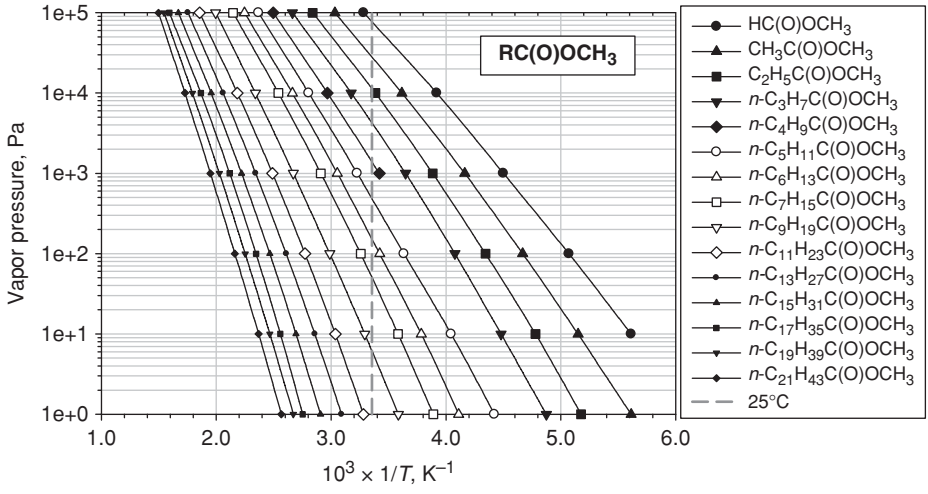

Figure I-B-6. Semilog plot of the vapor pressure of a series of methyl esters from $HC(O)OCH_3$ to n-$C_{21}H_{43}C(O)OCH_3$ versus the reciprocal temperature.

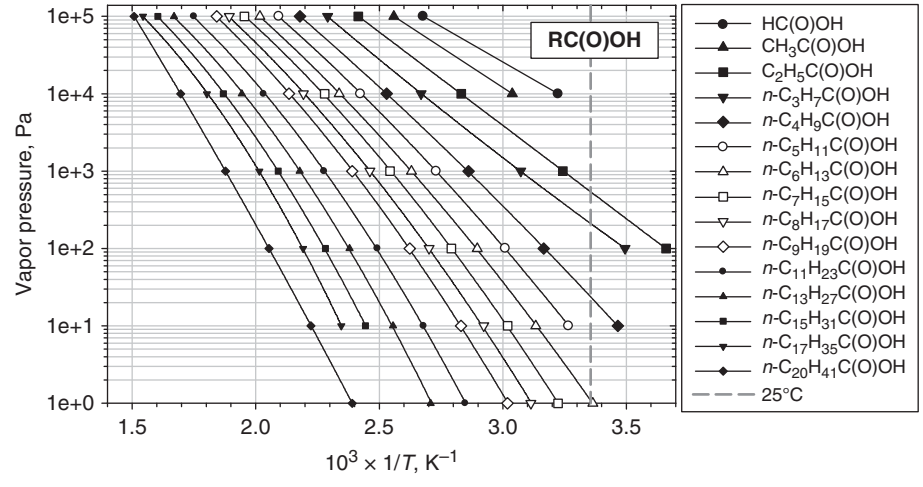

Figure I-B-7. Semilog plot of the vapor pressures of a series of organic acids from HC(O)OH to n-$C_{20}H_{41}C(O)OH$ versus the reciprocal temperature.

to larger molecules in the family, reflecting the increasing enthalpy of vaporization (ΔH_{vap}) with increasing size of the molecule. The slopes of the plots are related to the enthalpy of vaporization by the expression: $d(\ln p)/d(1/T) = -\Delta H_{vap}/R$, where R is the gas constant.

In figure I-B-8, the vapor pressures at 25°C of the various families of oxygenates are compared. It can be seen that for a given carbon number, the vapor pressure of the alkanes is always the highest. In general, as the extent of oxidation increases from ethers, to aldehydes, to esters, the vapor pressure drops from that of the parent

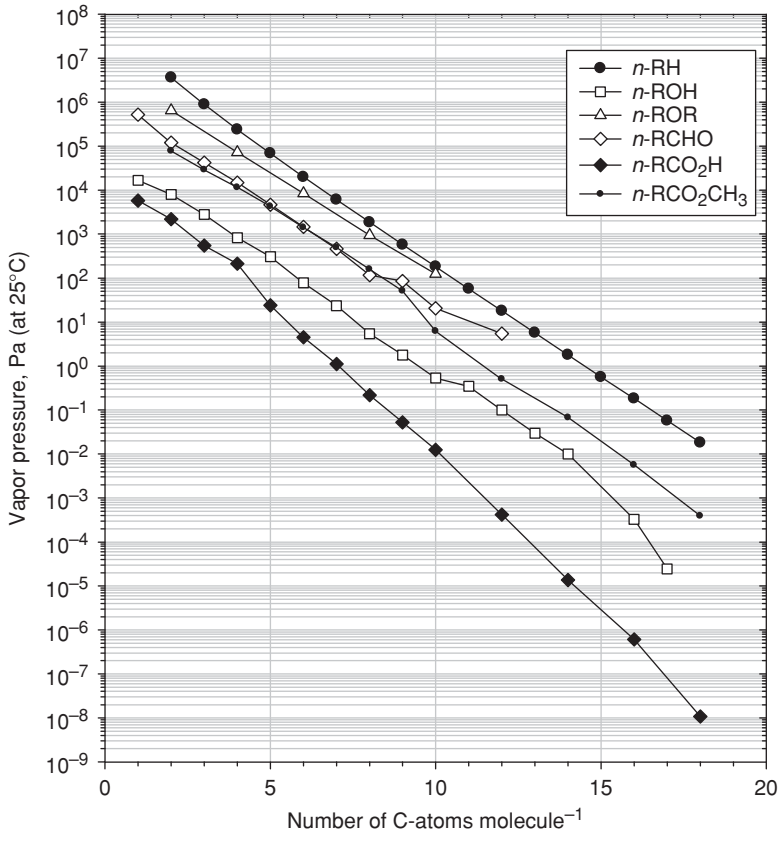

Figure I-B-8. Semilog plot of the vapor pressure at 25°C versus the number of C-atoms in the chain for a series of *n*-alkanes, alcohols, ethers, aldehydes, ketones, acids, and esters.

hydrocarbon, reflecting the more polar nature of the oxygenates. The alcohols have vapor pressures that are significantly lower than those of the ethers, aldehydes or esters with the same number of carbon atoms. This results largely from the presence of the —OH bonds in the alcohols and their ability to form strong hydrogen bonds between molecules in the liquid state. The organic acids show the lowest vapor pressures of all the families of compounds shown here, reflecting their very polar character and ability to form hydrogen bonds.

As the extent of oxidation of an oxygenate is increased by introduction of several functional groups [—C(=O)H, —C(=O)OH, —C(=O)R, or other], as one might expect, the vapor pressure is reduced further. This is seen in the data presented in figure I-B-9 (based on a figure from Calvert et al., 2002), where a series of C_4-compounds of varied extent of oxidation are compared. As one progresses from butane (upper curve in figure I-B-9) to the highly oxidized tartaric acid, HO(O)CCH(OH)CH(OH)C(O)OH (lowest curve in figure I-B-9), the vapor pressure decreases by about 15 orders of magnitude. The data shown for the lowest vapor pressure compounds are approximate

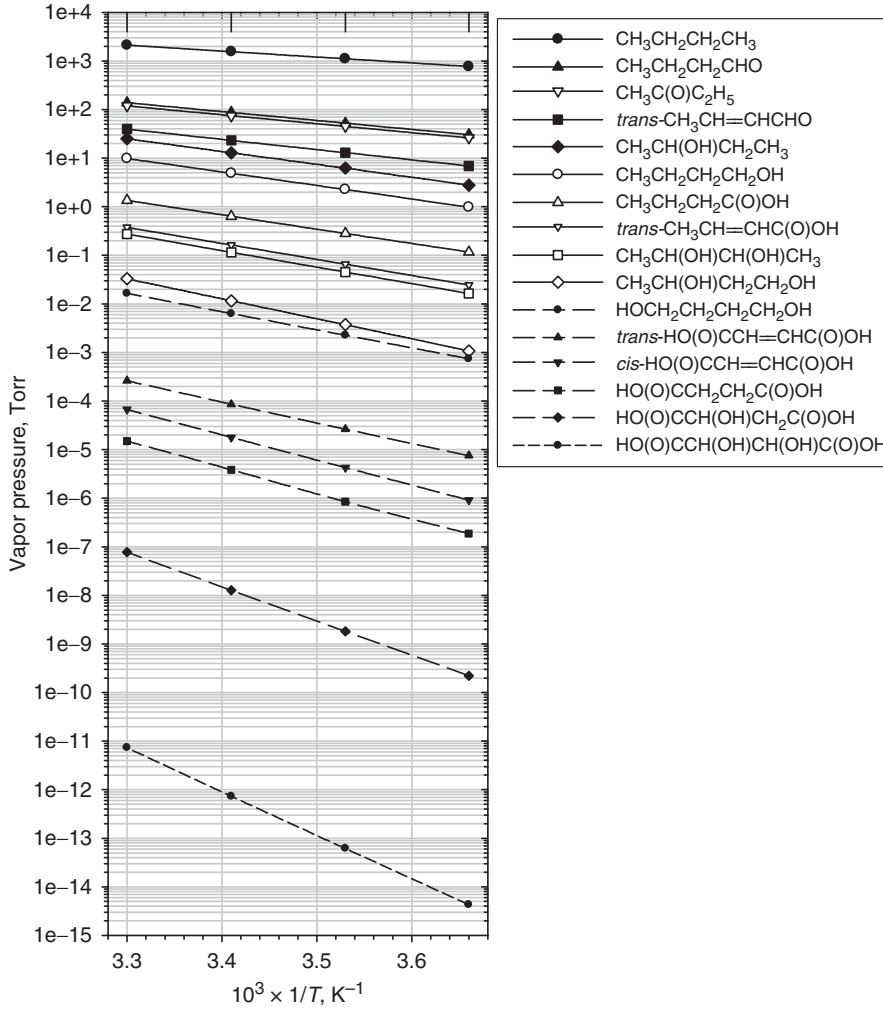

Figure I-B-9. Semilog plot of vapor pressure versus reciprocal temperature for some C_4 compounds with increasing extent of oxidation. Vapor pressure data were calculated from the equations for the compounds in the liquid state as given by Yaws et al. (1999); the data for the compounds of lowest vapor pressure are very approximate since they were obtained by extrapolation of measurements made at much higher temperatures. The figure is from Calvert et al. (2002).

since the existing data were extrapolated to 0°C, 10°C, 20°C, and 30°C from the much higher temperatures at which measurements were made.

The vapor pressures of some of the nitrogen-atom-containing oxygenates that are discussed in this book are given in figures I-B-10 (the amides) and I-B-11 (alkyl nitrites, nitroalkanes, and the alkyl nitrates). Figure I-B-10 shows that the vapor pressures of the formamides (black symbols and lines) at a given temperature fall in the order $HC(O)N(CH_3)_2 > HC(O)NHCH_3 > HC(O)NH_2$, inverse to the order of increase of

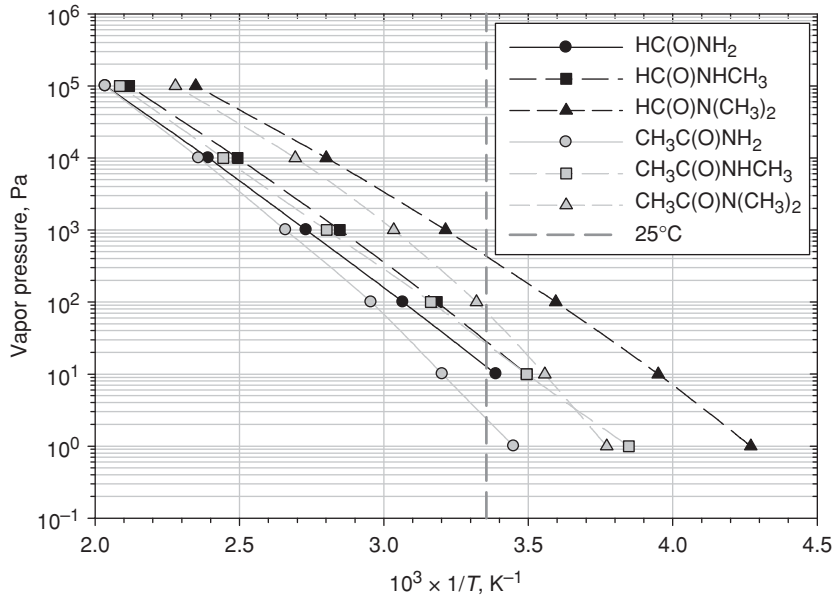

Figure I-B-10. Semilog plot of the vapor pressures as a function of $1/T$ for a series of formamides and acetamides.

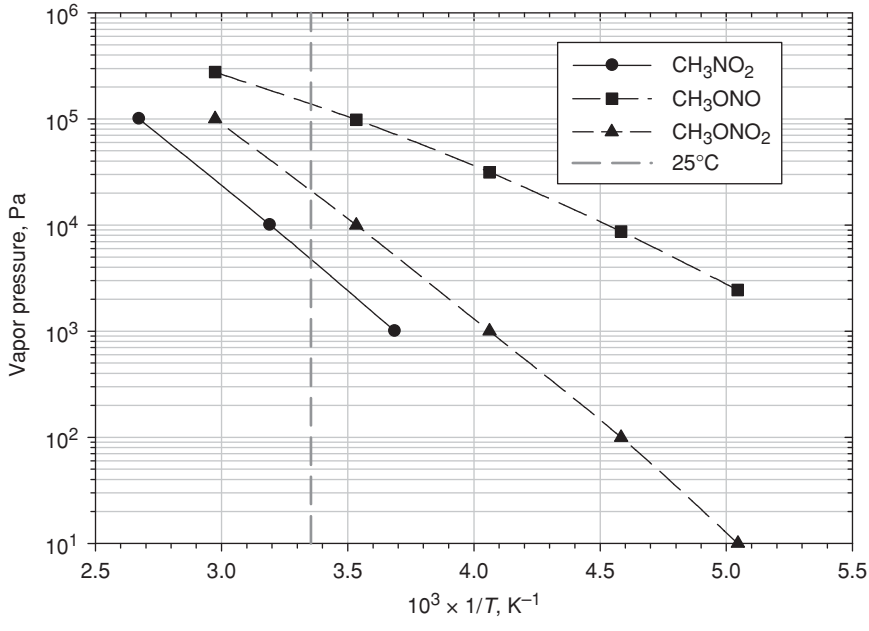

Figure I-B-11. Semilog plot of the vapor pressures of CH_3NO_2, CH_3ONO, and CH_3ONO_2 as a function of $1/T$.

the molecular weight. The observed trend in vapor pressures in the sequence shown is that expected, as the more —N—H bonds are present, the more hydrogen bonding can occur, resulting in stronger intermolecular attraction. As expected with this reasoning, the same trend is seen with the acetamides (grey symbols and lines) where the vapor pressures at a given temperature fall in the order: $CH_3C(O)N(CH_3)_2 > CH_3C(O)NHCH_3 > CH_3C(O)NH_2$.

Figure I-B-11 shows plots of the vapor pressures of methyl nitrite, nitromethane, and methyl nitrate as a function of reciprocal temperature. It is seen that at a given temperature the vapor pressures decrease in the order $CH_3ONO > CH_3ONO_2 > CH_3NO_2$. This is the order of decreasing polarity of the molecules as measured by the calculated dipole moments (μ): $\mu_{CH_3NO_2}$ (3.4 D) $\mu_{CH_3ONO_2}$ (2.9 D) > μ_{CH_3ONO} (2.2 D), and it seems likely that dipole–dipole interactions are important in determining the volatility of these compounds.

I-B-2. Melting and Boiling Points of the Oxygenates

The melting points and normal boiling points of the various classes of oxygenates are compared in figures I-B-12 and I-B-13. In figure I-B-12, for all those compounds for which the data lie above the dashed grey line (20°C), the stable phase is the solid at ambient temperatures ≤ 20°C: *n*-alkanes, > C_{17}; straight-chain esters, > C_{13}; straight-chain aldehydes, > C_{14}; straight-chain ketones, > C_{11}; straight-chain alcohols, > C_{11};

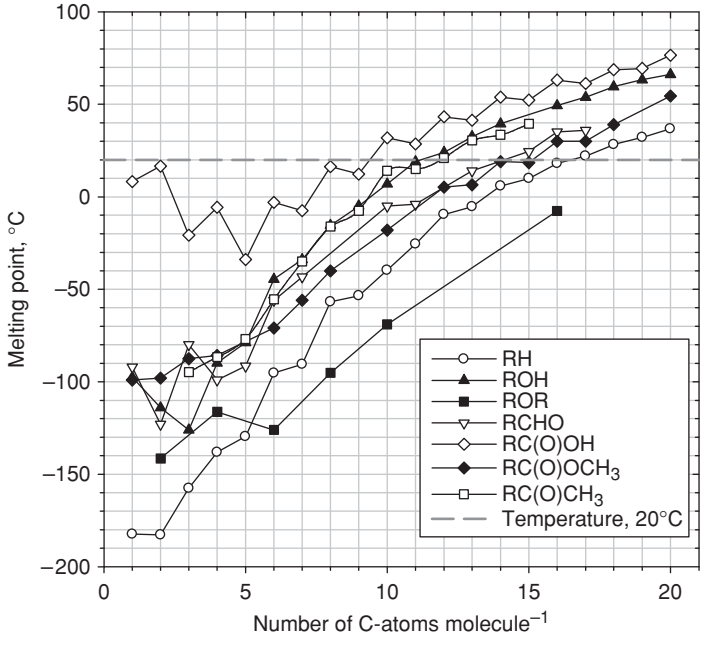

Figure I-B-12. Melting points of the families of oxygenates versus C-number. The solid phase is the stable phase at ambient temperature for all of those compounds whose melting points lie above the grey dashed line.

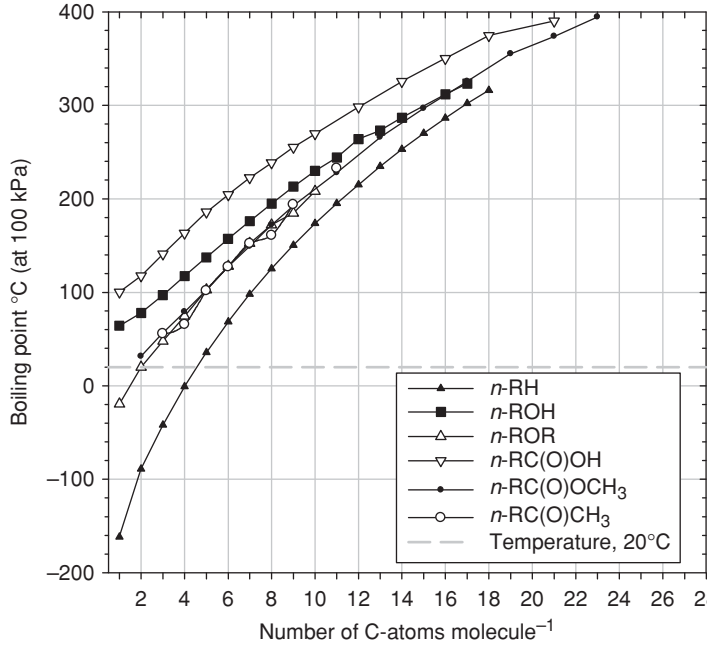

Figure I-B-13. Boiling points of the various families of oxygenates versus the C-number. At equilibrium, the gaseous state is the stable phase at temperatures > 20°C and 1 atm. pressure of the liquid for those compounds whose data lie below the dashed grey line.

straight-chain acids, > C_9. The data showing the normal boiling points of the series of oxygenates (figure I-B-13) reflect the vapor pressure data given in previous plots. It is clear from figure I-B-13 that with the exception of dimethyl ether, all alcohols, ethers, aldehydes, ketones, and esters are either liquids or solids at one atmosphere pressure and 20°C.

I-B-3. Heats of Combustion of the Oxygenates

In the consideration of the oxygenates as fuels, the heats of combustion are of special interest. These are shown for the various families of oxygenates in figure I-B-14. The data show clearly that the heats of combustion are highest for alkanes (circles in figure I-B-14), while those for the alcohols and ethers are somewhat less for a given carbon number, the aldehydes and ketones yet somewhat smaller, and the esters and acids have the lowest heats of combustion. As expected, in progressing from parent alkane to oxygenated analogs, the heat of combustion decreases with increasing oxygen content of the molecule. Note the slopes of the plots of the heats of combustion versus C-number are indistinguishable, reflecting the extra heat provided by each new CH_2 group added in the given sequence: The lines through the data are least squares fits with slopes (kJ mol^{-1} for each CH_2 group added) as follows: *n*-alkanes, 654; straight-chain

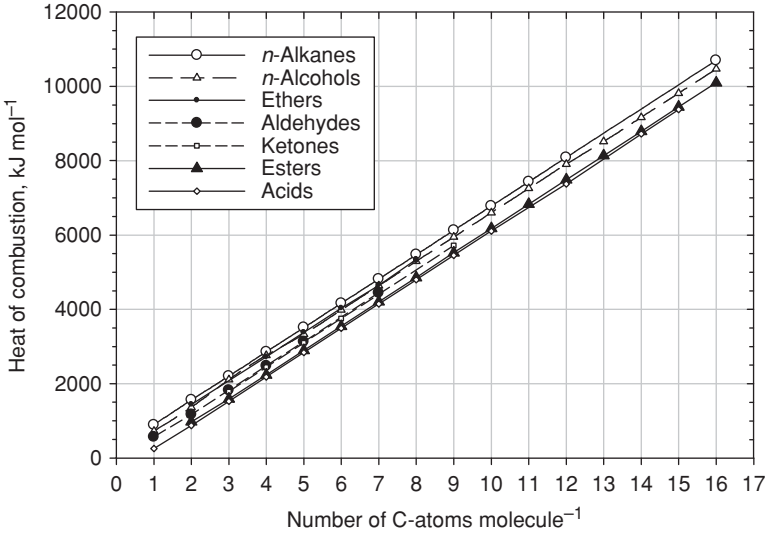

Figure I-B-14. Heats of combustion versus number of carbon atoms in the compound for the various families of oxygenates. The similar slopes of the plots reflect the near equal source of heat provided by each new CH_2 group added to the structure.

alcohols, 648; straight-chain ethers, 647; straight-chain aldehydes, 648; straight-chain ketones, 655; straight-chain esters, 654; straight-chain acids, 653.

A different perspective on the change in heats of combustion with increasing carbon number is obtained from the data presented in figure I-B-15. Here the heat of combustion per C-atom is plotted versus carbon number for the different families of oxygenates. One can see clearly the very large heats of combustion of methane and ethane and the slow decline in heat of combustion per C-atom as one progresses to the higher members of the *n*-alkanes. The ethers and alcohols show the same trend, although the heats are less than those of the alkanes of same C-number. The opposite trend is seen with the acids. Here the small acids that are already highly oxidized provide much less energy per C-atom and show an increase in the heat per C-atom as each energy rich CH_2 group is added. Although less pronounced, the trends for the esters, aldehydes, and ketones are similar to that of the acids with increasing carbon number. As the number of C-atoms is increased, the heats of combustion per mole of C-atoms for all classes of compounds are seen to approach the limiting value of the alkanes, since the effects of added oxygen atoms in the oxygenates are overshadowed by the increasing number of CH_2 groups in the molecules.

Another interesting feature that bears upon the use of the oxygenates as fuels is given in figure I-B-16. Here we compare the heats of combustion per liter of the liquid: $\Delta H_{\text{comb}} \times \rho \times 1{,}000/M$; where ΔH_{comb} is the heat of combustion (kJ mol^{-1}), ρ is the density of the liquid (g cm^{-3}), and M is the molecular weight (g mol^{-1}). In this scenario, for a given carbon number, the alcohols rank above or near equal to the alkanes in providing energy per volume of the liquid. The ketones and aldehydes lie

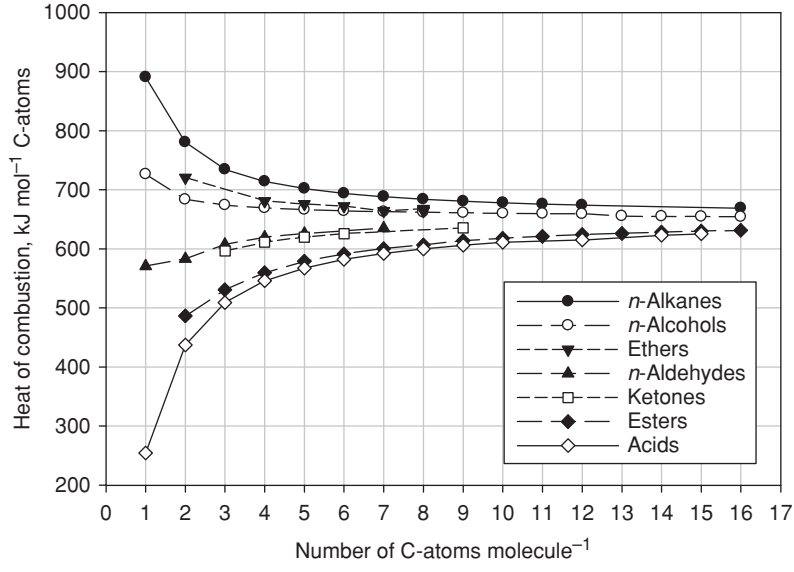

Figure I-B-15. Plot of the heats of combustion per C-atom versus carbon number for some families of oxygenates.

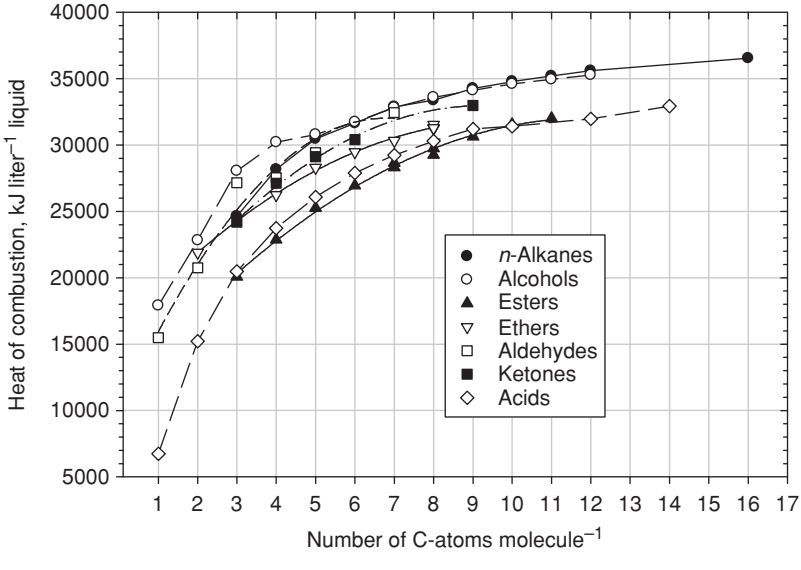

Figure I-B-16. Plot of the heat of combustion in kJ liter^{-1} of the liquid oxygenate.

somewhat below the alkanes, as is the case for the ethers with three or more carbon atoms per molecule. The esters and acids provide the lowest energy per volume of the liquids of those compared in the figure.

I-B-4. Henry's Law Constants of the Oxygenates

Oxygenated compounds are polar and can be solvated by water molecules which form hydrogen bonds with the oxygen atoms. As a result, oxygenates are much more water soluble than the hydrocarbons from which they are derived, and their removal from the atmosphere by wet deposition needs to be considered. The solubility of a gas X in water can be represented by the equilibrium:

$$X(\text{g}) \leftrightarrow X(\text{aq})$$

The equilibrium constant $[X(\text{aq})]/p_X$ is called the Henry's law constant where p_X is the partial pressure (atm.) of the compound X in the gas phase. As defined here, it has units of M (moles liter^{-1}) atm.$^{-1}$ and is directly proportional to the solubility of a gas in water. Very soluble gases such as H_2O_2 have Henry's law constants of the order of 10^5-10^6 M atm.$^{-1}$. Very insoluble gases such as methane and 2,2,4-trimethyl pentane (*iso*-octane) have Henry's law constants of the order of 10^{-3}–10^{-4} M atm.$^{-1}$. As seen from table I-B-1, the oxygenates typically have Henry's law constants that fall between these two extremes. Notable exceptions are the polyols, ethylene glycol (CH_2OHCH_2OH) and 1,3-propane diol ($CH_2OHCH_2CH_2OH$), and glyoxal (HC(O)C(O)H) which have Henry's law constants of the order of 10^5–10^6 M atm.$^{-1}$.

Table I-B-1. Henry's law constants (H) for selected oxygenates (Sander, 1999)

Compound	H, M atm.$^{-1}$ (298 K)[a]	Compound	H, M atm.$^{-1}$ (298 K)[a]
Methanol	2.0×10^2	Benzaldehyde	3.8×10^1
Ethanol	1.8×10^2	Glyoxal	3.6×10^5
n-Propanol	1.4×10^2	Acetone	2.7×10^1
i-Propanol	1.3×10^2	Butanone	1.4×10^1
n-Butanol	1.1×10^2	2-Pentanone	1.2×10^1
n-Pentanol	7.9×10^1	3-Pentanone	2.0×10^1
Ethylene glycol	4.0×10^6	Methyl formate	4.3
1,3-propane diol	9.2×10^5	Methyl acetate	9.2
Methyl hydroperoxide	3.1×10^2	Methyl propanoate	6.0
Ethyl hydroperoxide	3.4×10^2	Methyl hexadecanoate	0.3
Dimethyl ether	1.0	Ethyl acetate	6.7
Diethyl ether	1.0	*n*-Propyl acetate	4.7
Methyl *t*-butyl ether	1.7	Formic acid	5.3×10^3
Formaldehyde	5.7×10^3	Acetic acid	6.2×10^3
Acetaldehyde	1.3×10^1	Propionic acid	4.1×10^3
Propionaldehyde	9.4	Methyl nitrate	2.0
Butryaldehyde	7.9	Ethyl nitrate	1.6

[a]Averages of values tabulated by Sander (1999), outliers not included.

Carbonyl compounds, particularly low-molecular-weight aldehydes such as HCHO and dicarbonyls such as HC(O)C(O)H, are hydrated in water. Approximately 99% of HCHO and 50% of CH_3CHO exists in the diol form in water (Zhou and Mopper, 1990). For such compounds the values in table 1-B-1 are effective Henry's law constants given by $H_{\text{eff}} = (\{[R_1R_2CO\ (aq)] + [R_1R_2C(OH)_2\ (aq)]\}/p_{R_1R_2CO})$. After dissolving in water, the carboxylic acids dissociate to give H^+ and $RC(O)O^-$ ions. The dissociation increases the solubility of the carboxylic acids above that for physical solubility alone. The values given in table I-B-1 for the carboxylic acids are effective Henry's law constants (H_{eff}) and are related to the Henry's law constant (H) by the relation: $H_{\text{eff}} = H(1 + K_a/[H^+])$ where K_a is the acid dissociation constant of the acid ($K_a = [H^+][RC(O)O^-]/[RC(O)OH]$) (Brasseur et al., 1999).

In evaluating the importance of incorporation into water as an atmospheric removal mechanism for oxygenates, we need to consider the rate of this physical removal mechanism with the rates of competing chemical removal mechanisms (principally reaction with OH radicals). Even for the most water-soluble gases (e.g., H_2O_2, HCl), the global average timescale for removal by wet deposition is limited by rain events and is approximately 1 week (Brasseur et al., 1999). Seinfeld and Pandis (1998) have suggested that as a rough guide, species with Henry's law constants below approximately 1,000 M atm.$^{-1}$ will partition strongly into the atmospheric gas phase, and wet/dry deposition will probably not be of major importance. As seen from table I-B-1, most oxygenates have Henry's law constants which are substantially lower than 1,000 M atm.$^{-1}$.

As seen from table I-B-1, within a given family the solubility of the oxygenates decreases with increasing molecular size. This reflects the hydrophobic nature of the CH_2 groups added with increasing size (e.g., CH_3OH, C_2H_5OH, C_3H_7OH, etc.). Methanol is the most soluble alcohol and the least reactive towards OH radicals. Using a global atmospheric model, von Kuhlmann et al. (2003) have estimated that in the atmosphere 63% of methanol loss is via reaction with OH radicals, 30% is through dry deposition, and 7% through wet deposition. It should be noted that the terms "dry" and "wet" deposition refer only to the mechanism by which the methanol reaches the surface and "dry" deposition includes uptake of methanol vapor by surface waters (Finlayson-Pitts and Pitts, 2000). Compared to methanol, ethanol has a slightly lower solubility and is approximately 3.3 times more reactive with OH radicals. Reaction with OH radicals will probably account for approximately 85% of ethanol loss with the remaining 15% occurring via wet and dry deposition. Wet and dry deposition will account for $<10\%$ of the loss of the larger alcohols. The polyols are extremely water soluble, and wet and dry deposition will be important for these species. The hydroperoxides are rather reactive toward OH radicals, and it is expected that wet and dry deposition will not play a major role in their atmospheric chemistry. The ethers, ketones, esters, and nitrates are relatively insoluble and incorporation into water will generally not be of importance. Highly fluorinated ketones and esters can be an exception, as these compounds tend to react slowly with OH radicals and have been shown to form hydrates (Andersen et al., 2006) and undergo hydrolysis (Kutsuna et al., 2005).

Although HCHO is soluble, its lifetime with respect to photolysis and reaction with OH radicals is sufficiently short that incorporation into water is not a major loss for this species. Using a global atmospheric model, von Kuhlmann et al. (2003) have

estimated that approximately 6% of the total removal of HCHO occurs via wet and dry deposition. CH_3CHO and higher aldehydes are reactive towards OH radicals, undergo photolysis, are not particularly soluble, and will not be lost to any substantial degree via wet and dry deposition. In contrast, photolysis is of negligible importance for carboxylic acids and reaction with OH proceeds slowly for the smaller members of the series. For their reactions with OH, formic, acetic, and propanoic acids have lifetimes of approximately 1 month, 2 weeks, and 10 days, respectively. Wet and dry deposition will be an important loss mechanism for the smaller carboxylic acids in the troposphere.

I-C. Sources of Oxygenates in the Troposphere

Oxygenates can enter the atmosphere by several routes: 1) evaporation of oxygenated solvents or fuels used in industrial processes, commercial operations, or consumer products; 2) emissions from hydrocarbon-fueled mobile or stationary sources from incomplete fuel combustion; 3) emissions from biological sources such as growing plants and plant debris; or 4) atmospheric oxidation of hydrocarbons present in the atmosphere. A realistic budget for the sources of the oxygenates in the atmosphere is difficult to prepare and extensive speciation of the many different oxygenates present in the troposphere can never be determined at all sites for all times. However, various control agencies throughout the world must prepare inventories as a necessary part of planning pollution-control strategies. In this section, we review some of the inventories of emission sources of the oxygenates and their measured tropospheric concentrations.

I-C-1. Emissions of Oxygenates from Anthropogenic Sources

The oxygenates, sometimes designated as oxygenated volatile organic compounds, (OVOCs), make up part of the emissions that are classified as volatile organic compounds (VOCs), which also includes the many hydrocarbons. The entire VOC class of compounds is of interest in regard to OVOCs in the troposphere, since VOCs in the atmosphere are oxidized fairly rapidly into oxygenates. For example, the atmospheric lifetimes for the typical hydrocarbons, *n*-butane, 2-butene, and toluene with respect to reaction with OH radials are: 4.7 days, 4.3 h, and 2.1 days, respectively. All the hydrocarbons that enter the atmosphere are eventually converted into oxygenates. Hence, one should consider the entire class of VOCs either as existing or potential oxygenates. VOC inventories provide a useful guide to the many sources of the oxygenates in the atmosphere. The VOC inventory, prepared by the U.S. Environmental Protection Agency (2005) for the year 2001, is shown in table I-C-1 for anthropogenic sources. Figure I-C-1 summarizes graphically the distribution of the major sources of the VOC emissions listed in table I-C-1.

The major anthropogenic sources of VOCs in the U.S. that enter the troposphere and that ultimately form the oxygenates are emissions from the incomplete combustion of fossil fuels: vehicular emissions (28.9%); off-highway sources (15.3%); and emissions from solvent use (29.2%). Incomplete fuel combustion by institutional, residential, commercial, and industrial sources each add additional input of the VOC emissions.

Table I-C-1. Emissions of volatile organic compounds, VOCs (tons year^{-1}) by category in the U.S. for the year 2001 (U.S. Environmental Protection Agency, 2005)

		VOC Emissions (tons year^{-1})		Total in All Categories (tons year^{-1})		
Source	Category	Area Sources	Point Sources	Area Sources	Point Sources	Area and Point
Fuel Combustion Electric Utility	Coal	0	31,039			
	Oil	0	5,847			
	Gas	835	12,357			
	Other	0	1,494			
	Internal combustion	0	8,945	**835**	**59,682**	**60,517**
Fuel Combustion Industrial	Coal	2,447	7,384			
	Oil	2,878	3,737			
	Gas	7,964	56,298			
	Other	2,626	26,237			
	Internal combustion	1,653	64,315	**17,568**	**157,971**	**175,539**
Fuel Combustion Other	Combustion/Institutional coal	692	569			
	Combustion/Institutional oil	2,623	889			
	Combustion/Institutional gas	7,038	9,660			
	Misc. (nonresidential)	884	5,441			
	Residential wood	894,782	0			
	Residential other	27,280	0	**933,299**	**16,559**	**949,858**
Chemical and Allied Product Manufacturing	Organic chemical manufacturing	29,625	48,614			
	Inorganic chemical manufacturing	1,418	2,329			
	Polymer and resin manufacturing	53,563	50,710			
	Agricultural chemical manufacturing	0	7,877			
	Paint, varnish, lacquer, enamel manufacturing	0	8,002			
	Pharmaceutical manufacturing	4,122	4,025			
	Other chemical manufacturing	0	51,583	**88,728**	**173,140**	**261,868**

Metal Processing	Nonferrous metals	122	26,432			
	Ferrous metals	0.28	39,440			
	Metal processing (NEC)[c]	181	5,103	**303**	**70,975**	**71,278**
Petroleum and Related Industry	Oil and gas production	264,577	56,294			
	Petroleum refineries and related industries	60,516	49,805			
	Asphalt manufacturing	2,831	6,815	**327,924**	**112,914**	**440,838**
Other Industry Processes	Agricultural, food and kindred products	59,753	73,027			
	Textiles, leather and apparel products	0	8,150			
	Wood, pulp, paper and publishing products	654	124,010			
	Rubber and misc. plastic products	2,407	58,918			
	Mineral products	663	35,880			
	Machinery products	5.7	15,213			
	Electronic equipment	0	1,301			
	Transportation equipment	0	4,332			
	Construction	0	58.2			
	Misc. industrial processes	8,621	33,629	**72,104**	**354,518**	**426,622**
Solvent Utilization	Degreasing	392,578	20,280			
	Graphic arts	200,639	68,110			
	Dry cleaning	149,595	2,769			
	Surface coating	1,677,793	380,507			
	Other industrial	71,434	41,566			
	Nonindustrial	1,950,268	20.4			
	Solvent utilization (NEC)[c]	56,538	125	**4,498,845**	**513,377**	**5,012,222**

(*continued*)

Table I-C-1. (*continued*)

Source	Category	VOC Emissions (tons year^{-1})		Total in All Categories (tons year^{-1})		
		Area Sources	Point Sources	Area Sources	Point Sources	Area and Point
Storage and Transport	Bulk terminals and plants	152,983	23,862			
	Petroleum and petroleum products storage	38,794	27,788			
	Petroleum, petroleum product, transport	46,189	17,673			
	Service stations: stage I	333,816	2,199			
	Service stations: stage II	459,999	11,613			
	Service stations, breathing and emptying of tanks	47,021	5.6			
	Organic chemical storage	2,765	21,883			
	Organic chemical transport	2,007	1,591			
	Inorganic chemical storage	0	570			
	Inorganic chemical transport	0	2.53			
	Bulk materials storage	0.85	1,430			
	Bulk materials transport	0	122	**1,083,575**	**108,739**	**1,192,314**
Waste Disposal and Recycling	Incineration	19,016	2,522			
	Open burning	248,248	171			
	POTW[a]	36,135	2,057			
	Industrial waste water	20,094	7,058			
	TSDF[b]	28,828	63.8			
	Landfills	15,194	9,784			
	Other	25,397	5,034	**392,912**	**26,690**	**419,602**
Highway Vehicles	Light-duty gas vehicles and motorcycles	2,680,620	0			
	Light-duty gas trucks	1,803,830	0			
	Heavy-duty gas vehicles	249,962	0			
	Diesels	217,682	0	**4,952,094**	**0**	**4,952,094**

Off-Highway	Nonroad gasoline	2,336,182	5.22			
	Nonroad diesel	193,662	5.74			
	Aircraft	21,153	5.78			
	Marine vessels	31,668	0			
	Railroads	38,960	0			
	Other	766	0	**2,622,391**	**17**	**2,622,408**
Miscellaneous	Other combustion	525,637	1.56			
	Catastrophic/accidental releases	3,851	0			
	Repair shops	1,825	0			
	Health services	68	166			
	Cooling towers	0	871			
	Other fugitive dust	0	69.3			
	Other	0	54.7	**531,381**	**1,163**	**532,544**
Grand Total (All Categories)				**15,521,959**	**1,595,742**	**17,117,701**

[a]POTW = Publicly owned treatment works.
[b]TSDF = Treatment, storage and disposal facility.
[c]NEC = Not elsewhere classified.

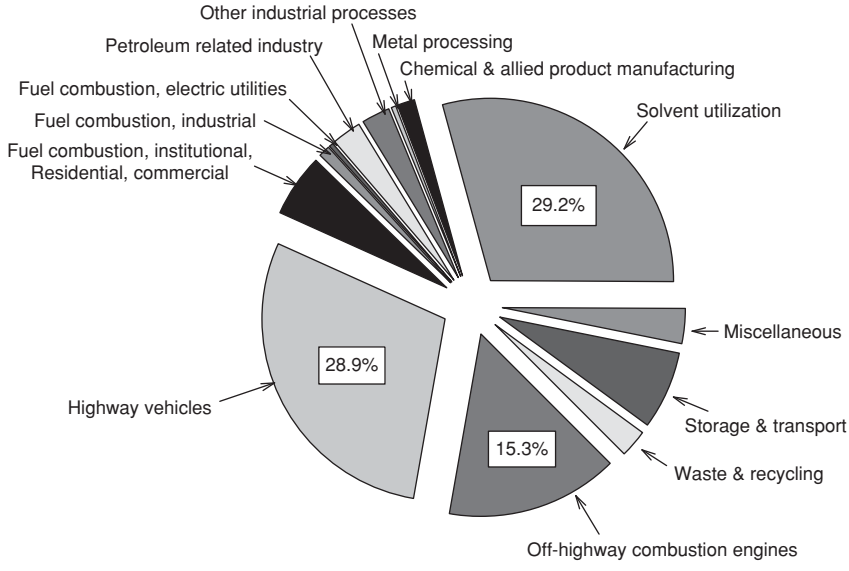

Figure I-C-1. Summary pie chart showing the distribution of components of VOC emissions in the U.S., as reported in 2005 by the U.S. Environmental Protection Agency for the year 2001.

Another perspective is gained by comparison of the emissions inventory and detailed speciation of the VOCs as prepared for the U.K.; see table I-C-2. Shown are the total emissions for each compound in tonnes (metric tons = 10^6 grams or 1.1 short tons) year^{-1} and the fraction of the emissions that each species gives to the total. The compounds are shown in decreasing order of their mass emissions. Of the 612 VOCs listed in table I-C-2, half of the mass of the nonmethane, anthropogenic VOC emissions in the U.K. is accounted for by the first 13 compounds listed; 75% by the first 33; 90% by the first 82; and 95% by the first 133 compounds. It should be emphasized that mass emissions do not necessarily reflect the reactivity or other important parameters that affect the chemistry of the atmosphere, so the entire list of compounds should be considered in the process of selecting those compounds that are expected to be significant contributors to the particular process that is being modeled. The relatively small emissions of many of the oxygenates given in table I-C-2 (e.g., glyoxal and methylglyoxal) points to the fact that the largest part of the ambient concentration of many of the oxygenates observed in the troposphere is not from direct emission but is derived from the oxidation of the hydrocarbons that are emitted into the troposphere.

In table I-C-3, the various emission source categories that are assigned to the U.K. VOC emissions inventory are shown. The compounds are listed in decreasing order of abundance. The numbers shown preceding each category in table I-C-3 are used to identify the specific compounds present in the emissions and to designate the sources of the various OVOC emissions listed in table I-C-4.

Table I-C-2. Inventory and speciation of the nonmethane, volatile organic compounds emitted from anthropogenic sources in the U.K. as calculated from data derived for the year 2000 (Dore et al., 2008)

Species of VOC	Total Emissions, Metric Tons year^{-1}	Fraction of the Total Emissions
Butane	1.22E+02	8.93E−02
Ethanol	1.01E+02	7.39E−02
Ethane	6.81E+01	4.99E−02
Propane	5.27E+01	3.86E−02
Toluene	4.95E+01	3.62E−02
Unspeciated	4.85E+01	3.55E−02
Pentane	4.81E+01	3.52E−02
2-Methylbutane	4.44E+01	3.25E−02
Ethylene	3.86E+01	2.83E−02
Hexane	3.56E+01	2.61E−02
Methanol	2.75E+01	2.01E−02
m-Xylene	2.75E+01	2.01E−02
Trichloroethene	2.67E+01	1.95E−02
2-Methylpropane	2.60E+01	1.90E−02
Formaldehyde	2.31E+01	1.69E−02
C_{13} + Aromatic hydrocarbons	2.25E+01	1.65E−02
Acetone	2.23E+01	1.63E−02
Unspeciated alkanes	2.12E+01	1.55E−02
Heptane	1.99E+01	1.46E−02
Ethylbenzene	1.73E+01	1.27E−02
Propylene	1.67E+01	1.22E−02
Octane	1.58E+01	1.16E−02
C_{13} + alkanes	1.56E+01	1.14E−02
Benzene	1.50E+01	1.10E−02
2-Butanone	1.45E+01	1.06E−02
o-Xylene	1.39E+01	1.02E−02
1,2,4-Trimethylbenzene	1.36E+01	9.96E−03
Dichloromethane	1.30E+01	9.52E−03
Butyl acetate	1.30E+01	9.52E−03
Acetylene	1.27E+01	9.30E−03
p-Xylene	1.19E+01	8.71E−03
2-Propanol	1.14E+01	8.35E−03
2-Methylpropene	1.05E+01	7.69E−03
Ethyl acetate	1.04E+01	7.61E−03
Decane	1.04E+01	7.61E−03
C_7 Alkanes	9.85E+00	7.21E−03
C_9 Aromatic hydrocarbons	9.78E+00	7.16E−03
C_8 Alkanes	8.56E+00	6.27E−03
Tetrachloroethene	6.98E+00	5.11E−03
4-Methyl-2-pentanone	6.55E+00	4.80E−03
2-Butene	6.15E+00	4.50E−03
1-Butanol	6.09E+00	4.46E−03
Nonane	5.68E+00	4.16E−03

(*continued*)

Table I-C-2. (*continued*)

Species of VOC	Total Emissions, Metric Tons year^{-1}	Fraction of the Total Emissions
2-Butoxyethanol	5.35E+00	3.92E−03
C_{10} Alkanes	5.35E+00	3.92E−03
1,3,5-Trimethylbenzene	5.07E+00	3.71E−03
Acetaldehyde	5.06E+00	3.70E−03
1,3-Butadiene	4.89E+00	3.58E−03
2-Methylpentane	4.85E+00	3.55E−03
Methyl acetate	4.82E+00	3.53E−03
Undecane	4.72E+00	3.46E−03
2-Pentene	4.38E+00	3.21E−03
C_{11} Alkanes	4.23E+00	3.10E−03
1-Propanol	3.95E+00	2.89E−03
C_{13} Alkanes	3.92E+00	2.87E−03
1-Methoxy-2-propanol	3.86E+00	2.83E−03
1,2,3-Trimethylbenzene	3.84E+00	2.81E−03
C_9 Alkanes	3.80E+00	2.78E−03
Methylethylbenzene	3.64E+00	2.66E−03
2-Methylhexane	3.53E+00	2.58E−03
Unspeciated aromatic hydrocarbons	3.12E+00	2.28E−03
3-Methylpentane	3.12E+00	2.28E−03
1-Methoxy-2-propyl acetate	3.01E+00	2.20E−03
1-Butene	2.96E+00	2.17E−03
Dipentene	2.81E+00	2.06E−03
3-Methylhexane	2.78E+00	2.04E−03
Unspeciated cycloalkanes	2.74E+00	2.01E−03
C_{12} Alkanes	2.72E+00	1.99E−03
Unspeciated alkenes	2.63E+00	1.93E−03
Dimethyl ether	2.63E+00	1.93E−03
4-Methyldecane	2.59E+00	1.90E−03
Styrene	2.34E+00	1.71E−03
Ethyldimethylbenzene	2.25E+00	1.65E−03
3-Methylnonane	2.14E+00	1.57E−03
2-(2-Butoxyethoxy)ethanol	2.14E+00	1.57E−03
C_{10} Aromatic hydrocarbons	2.11E+00	1.54E−03
3-Ethyl-2-methylheptane	2.09E+00	1.53E−03
1-Pentene	2.06E+00	1.51E−03
Naphthalene	1.97E+00	1.44E−03
Furfural	1.97E+00	1.44E−03
2-Methylnonane	1.86E+00	1.36E−03
Benzaldehyde	1.86E+00	1.36E−03
Cyclohexane	1.84E+00	1.35E−03
Propylcyclohexane	1.78E+00	1.30E−03
2,6-Dimethyloctane	1.73E+00	1.27E−03
2-(2-Ethoxyethoxy)ethanol	1.68E+00	1.23E−03
Acrolein	1.63E+00	1.19E−03
C_{10} Cycloalkanes	1.61E+00	1.18E−03
2-Methyl-1-propanol	1.59E+00	1.16E−03
Methylcyclohexane	1.56E+00	1.14E−03
1-Propanal	1.56E+00	1.14E−03

(*continued*)

Table I-C-2. (*continued*)

Species of VOC	Total Emissions, Metric Tons year^{-1}	Fraction of the Total Emissions
3-Methyldecane	1.55E+00	1.13E−03
2-Propyl acetate	1.54E+00	1.13E−03
3-Methylheptane	1.50E+00	1.10E−03
4-Methyl-4-hydroxy-2-pentanone	1.49E+00	1.09E−03
Unspeciated hydrocarbons	1.49E+00	1.09E−03
Acetonitrile	1.49E+00	1.09E−03
(1-Methylpropyl)cyclohexane	1.48E+00	1.08E−03
4-Methylnonane	1.47E+00	1.08E−03
Acrylonitrile	1.46E+00	1.07E−03
1,2-Dichloroethane	1.46E+00	1.07E−03
Chloroethane	1.43E+00	1.05E−03
1-Methyl-4-isopropylcyclohexane	1.43E+00	1.05E−03
Hexamethylenediamine	1.42E+00	1.04E−03
Propionitrile	1.41E+00	1.03E−03
Adiponitrile	1.41E+00	1.03E−03
Bis-hexamethylenetriamine	1.41E+00	1.03E−03
Propylbenzene	1.38E+00	1.01E−03
2-Methyldecane	1.38E+00	1.01E−03
C_6 Alkenes	1.36E+00	9.96E−04
Butylcyclohexane	1.36E+00	9.96E−04
1-Methyl-4-isopropylbenzene	1.34E+00	9.81E−04
1,2-Propanediol	1.31E+00	9.59E−04
Tetradecane	1.27E+00	9.30E−04
Propyne	1.26E+00	9.22E−04
1-Ethyl-3-methylcyclohexane	1.25E+00	9.15E−04
3-Ethyltoluene	1.24E+00	9.08E−04
1,1-Dichloroethene	1.20E+00	8.78E−04
Ethylene glycol	1.10E+00	8.05E−04
Benzyl alcohol	1.06E+00	7.76E−04
1-(2-Butoxy-1-methyl-ethoxy)-2-propanol	1.05E+00	7.69E−04
2,2,4-Trimethyl-1,3-pentanediol monoisobutyrate	1.04E+00	7.61E−04
Tri-*n*-butyl phosphate	1.04E+00	7.61E−04
1,1,1-Trichloroethane	9.96E−01	7.29E−04
3-Methyl benzaldehyde	9.92E−01	7.26E−04
Propyl acetate	9.91E−01	7.25E−04
Methylpropylbenzene	9.77E−01	7.15E−04
1,4-Dichlorobenzene	9.73E−01	7.12E−04
2-(2-Butoxyethoxy)ethyl acetate	9.48E−01	6.94E−04
1,2,3,5-Tetramethylbenzene	9.45E−01	6.92E−04
2,3-Dimethylbutane	9.32E−01	6.82E−04
1,3-Hexadiene	9.21E−01	6.74E−04
2-Methylheptane	9.17E−01	6.71E−04
Crotonaldehyde	8.57E−01	6.27E−04
Acrylamide	8.29E−01	6.07E−04
(1-Methylethyl)cyclohexane	8.24E−01	6.03E−04
(2-Methylpropyl)cyclohexane	8.05E−01	5.89E−04
2-Methyloctane	7.98E−01	5.84E−04

(*continued*)

Table I-C-2. (*continued*)

Species of VOC	Total Emissions, Metric Tons year^{-1}	Fraction of the Total Emissions
4-Methyloctane	7.86E−01	5.75E−04
Cyclohexanone	7.84E−01	5.74E−04
1-Methyl-3-propylbenzene	7.83E−01	5.73E−04
2-Methoxyethanol	7.60E−01	5.56E−04
Dodecane	7.50E−01	5.49E−04
2-Methyl benzaldehyde	7.42E−01	5.43E−04
3-Methyloctane	7.38E−01	5.40E−04
Pentanal	7.26E−01	5.31E−04
Chloroethene	7.12E−01	5.21E−04
1,2,3-Trimethylcyclohexane	7.00E−01	5.12E−04
5-Methyldecane	6.97E−01	5.10E−04
2-Ethoxyethyl acetate	6.93E−01	5.07E−04
Dimethylformamide	6.92E−01	5.07E−04
1-Hexanal	6.87E−01	5.03E−04
C_7 Cycloalkanes	6.71E−01	4.91E−04
1,2,4,5-Tetramethylbenzene	6.52E−01	4.77E−04
1-Ethoxy-2-propanol	6.50E−01	4.76E−04
C_7 Alkenes	6.12E−01	4.48E−04
Ethylcyclohexane	6.07E−01	4.44E−04
Methylcyclopentane	6.05E−01	4.43E−04
2,2-Dimethylbutane	6.02E−01	4.41E−04
Tetrahydrofuran	5.96E−01	4.36E−04
2,5-Dimethyloctane	5.85E−01	4.28E−04
3,4-Dimethylheptane	5.82E−01	4.26E−04
Diisopropyl ether	5.76E−01	4.22E−04
Butanal	5.70E−01	4.17E−04
C_{11} Aromatic hydrocarbons	5.69E−01	4.17E−04
2-Ethoxyethanol	5.62E−01	4.11E−04
2,2,3,3-Tetramethylhexane	5.43E−01	3.98E−04
1-Ethyl-4-methylcyclohexane	5.41E−01	3.96E−04
Chloromethane	5.39E−01	3.95E−04
Acetic acid	5.38E−01	3.94E−04
Methanethiol	5.31E−01	3.89E−04
2-Methylpropenal	5.08E−01	3.72E−04
4-Ethyltoluene	5.04E−01	3.69E−04
2-Methylfurfural	4.92E−01	3.60E−04
Pine oil	4.91E−01	3.59E−04
3,3-Dimethyloctane	4.89E−01	3.58E−04
1,2,3,4-Tetramethylbenzene	4.88E−01	3.57E−04
2-Methylpropanal	4.86E−01	3.56E−04
3-Ethylheptane	4.82E−01	3.53E−04
Phenol	4.82E−01	3.53E−04
2-Methyl-5-ethyloctane	4.80E−01	3.51E−04
3,7-Dimethylnonane	4.80E−01	3.51E−04
2,3-Dimethylheptane	4.71E−01	3.45E−04
Decalin	4.71E−01	3.45E−04
1-Ethoxy-2-propyl acetate	4.66E−01	3.41E−04
C_8 Alkenes	4.65E−01	3.40E−04

(*continued*)

Table I-C-2. (*continued*)

Species of VOC	Total Emissions, Metric Tons year^{-1}	Fraction of the Total Emissions
1,4-Dimethylcyclohexane	4.64E−01	3.40E−04
1-(2-Methoxy-1-methyl-ethoxy)-2-propanol	4.63E−01	3.39E−04
1-(2-Ethoxy-1-methyl-ethoxy)-2-propanol	4.62E−01	3.38E−04
1,1,3-Trimethylcyclohexane	4.34E−01	3.18E−04
2-Ethyl-1,3-dimethylbenzene	4.28E−01	3.13E−04
Indan	4.28E−01	3.13E−04
2-(Methoxyethoxy)ethanol	4.27E−01	3.13E−04
3,6-Dimethyloctane	4.25E−01	3.11E−04
1-Ethyl-2,2,6-trimethylcyclohexane	4.16E−01	3.05E−04
Isopropylbenzene	4.10E−01	3.00E−04
2,5-Dimethylheptane	4.04E−01	2.96E−04
2-Butoxyethyl acetate	4.04E−01	2.96E−04
Butylbenzene	3.97E−01	2.91E−04
1-Methyl-3-isopropylbenzene	3.97E−01	2.91E−04
1-Methyl-2-propylbenzene	3.95E−01	2.89E−04
2-[2-(2-Ethoxy-ethoxy)-ethoxy]ethanol	3.88E−01	2.84E−04
2-(2-Ethoxyethoxy)ethyl acetate	3.84E−01	2.81E−04
2-Isopropoxyethanol	3.83E−01	2.80E−04
2-Methoxyethyl acetate	3.82E−01	2.80E−04
4-Methyl benzaldehyde	3.73E−01	2.73E−04
1,2,3,5-Tetramethylcyclohexane	3.71E−01	2.72E−04
1-Ethyl-3,5-dimethylbenzene	3.69E−01	2.70E−04
3-Ethyloctane	3.62E−01	2.65E−04
2-Methyl-2-butene	3.57E−01	2.61E−04
Ethylene oxide	3.47E−01	2.54E−04
2,3-Dimethylnonane	3.44E−01	2.52E−04
2,7-Dimethyloctane	3.44E−01	2.52E−04
Diethylbenzene	3.43E−01	2.51E−04
1,1,2-Trimethylcyclohexane	3.38E−01	2.47E−04
1-Methyl-2-isopropylbenzene	3.36E−01	2.46E−04
1,4-Diethylbenzene	3.35E−01	2.45E−04
2-Methyldecalin	3.35E−01	2.45E−04
4,5-Dimethylnonane	3.35E−01	2.45E−04
Pentylcyclohexane	3.35E−01	2.45E−04
1-Ethyl-2,4-dimethylbenzene	3.33E−01	2.44E−04
1,3-Diethylbenzene	3.33E−01	2.44E−04
Hexamethylcyclotrisiloxane	3.19E−01	2.34E−04
2-Butanol	3.02E−01	2.21E−04
Methyl formate	3.01E−01	2.20E−04
1,3-Dimethylcyclohexane	2.97E−01	2.17E−04
4-Ethyl-1,2-dimethylbenzene	2.89E−01	2.12E−04
3,3-Dimethylheptane	2.81E−01	2.06E−04
1-Ethyl-2,3-dimethylbenzene	2.77E−01	2.03E−04
5-Methyl-2-hexanone	2.70E−01	1.98E−04
Isophorone	2.67E−01	1.95E−04
3-Methyl-1-butene	2.66E−01	1.95E−04
1,2-Dimethylcyclohexane	2.66E−01	1.95E−04

(*continued*)

Table I-C-2. (*continued*)

Species of VOC	Total Emissions, Metric Tons year^{-1}	Fraction of the Total Emissions
2,4-Dimethyl-1-(1-methylethyl)benzene	2.63E−01	1.93E−04
3-Methylundecane	2.62E−01	1.92E−04
Tetramethylcyclohexane	2.62E−01	1.92E−04
2-Methyl-2,4-pentanediol	2.54E−01	1.86E−04
C_8 Cycloalkanes	2.49E−01	1.82E−04
2,3-Dimethylpentane	2.47E−01	1.81E−04
N-Methyl pyrrolidone	2.47E−01	1.81E−04
2,4-Dimethylpentane	2.46E−01	1.80E−04
Octahydroindene	2.45E−01	1.79E−04
1,2,4-Trimethylcyclohexane	2.43E−01	1.78E−04
1,1,4,4-Tetramethylcyclohexane	2.35E−01	1.72E−04
2,6-Dimethylheptane	2.35E−01	1.72E−04
Methylindane	2.32E−01	1.70E−04
Trichloromethane	2.32E−01	1.70E−04
Unspeciated ketones	2.28E−01	1.67E−04
2,6-Dimethyldecane	2.26E−01	1.65E−04
2-Methylundecane	2.26E−01	1.65E−04
1-Methyl-4-tertbutylbenzene	2.24E−01	1.64E−04
1-Methylbutylbenzene	2.17E−01	1.59E−04
5-Methylundecane	2.17E−01	1.59E−04
C_{12} Alkenes	2.17E−01	1.59E−04
Methyl methacrylate	2.14E−01	1.57E−04
2-Methyl-1-butene	2.14E−01	1.57E−04
1-Methyl-1-propylcyclopentane	2.08E−01	1.52E−04
1-Butyne	2.04E−01	1.49E−04
1-Hexene	2.01E−01	1.47E−04
Propylcyclopentane	2.01E−01	1.47E−04
2,2-Dimethylpropane	1.98E−01	1.45E−04
4-Methylheptane	1.95E−01	1.43E−04
Unspeciated alcohols	1.90E−01	1.39E−04
1-Ethyl-2,3-dimethylcyclohexane	1.90E−01	1.39E−04
1,3-Dimethylcyclopentane	1.87E−01	1.37E−04
Cyclopentane	1.86E−01	1.36E−04
2,5-Dimethyldecane	1.81E−01	1.33E−04
Dimethylnonane	1.81E−01	1.33E−04
2,4-Dimethylheptane	1.76E−01	1.29E−04
1-Ethyl-2-propylcyclohexane	1.72E−01	1.26E−04
6-Methylundecane	1.72E−01	1.26E−04
1,2-Dimethylcyclopentane	1.70E−01	1.24E−04
Unspeciated aliphatic hydrocarbons	1.69E−01	1.24E−04
1-Ethyl-1,4-dimethylcyclohexane	1.63E−01	1.19E−04
4-Ethyloctane	1.63E−01	1.19E−04
Ethyl butanoate	1.56E−01	1.14E−04
3,5-Dimethyloctane	1.54E−01	1.13E−04
2,3-Dimethyloctane	1.45E−01	1.06E−04
Terpenes	1.45E−01	1.06E−04
1,2,3,4-Tetrahydronaphthalene	1.42E−01	1.04E−04
Limonene	1.40E−01	1.02E−04

(*continued*)

Table I-C-2. (*continued*)

Species of VOC	Total Emissions, Metric Tons year^{-1}	Fraction of the Total Emissions
2,2-Dimethylpentane	1.39E−01	1.02E−04
1,2-Dichloroethene	1.34E−01	9.81E−05
2,4-Dimethylhexane	1.32E−01	9.66E−05
tert-Pentylbenzene	1.32E−01	9.66E−05
Ethylamine	1.31E−01	9.59E−05
α-Pinene	1.30E−01	9.52E−05
m-Cresol	1.29E−01	9.44E−05
o-Cresol	1.29E−01	9.44E−05
p-Cresol	1.29E−01	9.44E−05
2,6-Dimethyl-4-heptanone	1.28E−01	9.37E−05
1,2-Dimethyl-3-isopropylcyclopentane	1.27E−01	9.30E−05
4-Methyl-1-pentene	1.25E−01	9.15E−05
Acrylic acid	1.24E−01	9.08E−05
Phthalic anhydride	1.21E−01	8.86E−05
2,5-Dimethylhexane	1.12E−01	8.20E−05
(2-Methylbutyl)cyclohexane	1.09E−01	7.98E−05
C_{11} Cycloalkanes	1.09E−01	7.98E−05
C_{10} Alkenes	1.06E−01	7.76E−05
1,1-Dimethylcyclopentane	1.06E−01	7.76E−05
Octamethylcyclotetrasiloxane	1.03E−01	7.54E−05
1-Methylindan	1.01E−01	7.39E−05
2,2-Dimethylhexane	1.00E−01	7.32E−05
Bromomethane	9.90E−02	7.25E−05
1-Ethylpropylbenzene	9.87E−02	7.23E−05
2,5-Xylenol	9.63E−02	7.05E−05
3,5-Xylenol	9.63E−02	7.05E−05
3-Ethylhexane	9.46E−02	6.93E−05
2,3-Dimethylhexane	9.44E−02	6.91E−05
Dimethyl adipate	9.34E−02	6.84E−05
Dimethyl glutarate	9.34E−02	6.84E−05
Dimethyl succinate	9.34E−02	6.84E−05
Propylene oxide	9.25E−02	6.77E−05
3,3-Dimethylpentane	9.23E−02	6.76E−05
C_9 Cycloalkanes	9.05E−02	6.63E−05
Glyoxal	9.05E−02	6.63E−05
Propyl propionate	8.90E−02	6.52E−05
Dimethylhexene	8.86E−02	6.49E−05
1-Ethyl-2-propylbenzene	8.55E−02	6.26E−05
β-Pinene	8.49E−02	6.22E−05
Trifluoromethane	8.41E−02	6.16E−05
2,3-Dimethylundecane	8.15E−02	5.97E−05
6-Ethyl-2-methyloctane	8.15E−02	5.97E−05
1-Methyl-1-phenylcyclopropane	7.44E−02	5.45E−05
C_{12} Aromatic hydrocarbons	7.29E−02	5.34E−05
Methyl glyoxal	7.27E−02	5.32E−05
Methylcyclodecane	7.24E−02	5.30E−05
1-Heptene	7.11E−02	5.20E−05

(*continued*)

Table I-C-2. (*continued*)

Species of VOC	Total Emissions, Metric Tons year^{-1}	Fraction of the Total Emissions
Acenaphthylene	7.07E−02	5.18E−05
1,1-Dimethylcyclohexane	6.91E−02	5.06E−05
Cyclohexanamine	6.54E−02	4.79E−05
2,3,5-Trimethylphenol	6.42E−02	4.70E−05
2,3-Xylenol	6.42E−02	4.70E−05
2,4-Dimethylpyridine	6.42E−02	4.70E−05
2,4-Xylenol	6.42E−02	4.70E−05
2,6-Xylenol	6.42E−02	4.70E−05
3,4-Xylenol	6.42E−02	4.70E−05
Benzo[*b*]thiophene	6.42E−02	4.70E−05
1,2,4,4-Tetramethylcyclopentane	6.34E−02	4.64E−05
2,2,5-Trimethylhexane	6.24E−02	4.57E−05
1-Pentanol	6.23E−02	4.56E−05
Ethyl propionate	6.05E−02	4.43E−05
1,1-Dichloroethane	5.78E−02	4.23E−05
Naphthol	5.67E−02	4.15E−05
2,2,3-Trimethylhexane	5.58E−02	4.08E−05
3-Ethylpentane	5.57E−02	4.08E−05
2,2,3-Trimethylbutane	5.47E−02	4.00E−05
2,6-Dimethylundecane	5.39E−02	3.95E−05
3-Methylbutanal	5.30E−02	3.88E−05
1,4-Dimethyl-2-isopropylbenzene	5.26E−02	3.85E−05
Isopentylbenzene	5.26E−02	3.85E−05
Methyl acrylate	5.24E−02	3.84E−05
C_9 Alkenes	5.23E−02	3.83E−05
Formic acid	5.14E−02	3.76E−05
1,2,4-Trimethylcyclopentane	4.91E−02	3.59E−05
Dipropyl ether	4.89E−02	3.58E−05
Diethyl ether	4.85E−02	3.55E−05
3,3,5-Trimethylheptane	4.52E−02	3.31E−05
C_{12} Cycloalkanes	4.52E−02	3.31E−05
Propyl butanoate	4.45E−02	3.26E−05
Ethyl-3-ethoxypropionate	4.42E−02	3.24E−05
Vinyl acetate	4.42E−02	3.24E−05
3-Methylbutanol	4.30E−02	3.15E−05
3,3-Dimethylhexane	4.29E−02	3.14E−05
C_{11} Alkenes	4.26E−02	3.12E−05
Dichlorofluoromethane	4.14E−02	3.03E−05
1,3-Dimethyl-5-propylbenzene	3.95E−02	2.89E−05
1-Decene	3.79E−02	2.77E−05
Ethylcyclopentane	3.74E−02	2.74E−05
2,3,4-Trimethylhexane	3.62E−02	2.65E−05
3-Ethyl-2-methylhexane	3.62E−02	2.65E−05
Carbon tetrachloride	3.61E−02	2.64E−05
2,2,4-Trimethylpentane	3.55E−02	2.60E−05
2-Methyl-1,3-dioxolane	3.52E−02	2.58E−05
3,4-Dimethylhexane	3.47E−02	2.54E−05
4,6-Dimethylindan	3.38E−02	2.47E−05

(*continued*)

Table I-C-2. (*continued*)

Species of VOC	Total Emissions, Metric Tons year^{-1}	Fraction of the Total Emissions
Tetrafluoroethene	3.34E−02	2.45E−05
Bis(2-hydroxyethyl)ether	3.28E−02	2.40E−05
1-Nonene	3.21E−02	2.35E−05
Aniline	3.21E−02	2.35E−05
Pyrrole	3.21E−02	2.35E−05
Pyrrolidine	3.21E−02	2.35E−05
1,1,1-Trichlorotrifluoroethane	3.11E−02	2.28E−05
1,2,3-Trimethylcyclopentane	3.04E−02	2.23E−05
Propadiene	2.95E−02	2.16E−05
Dimethyl disulfide	2.91E−02	2.13E−05
4-Ethyl morpholine	2.84E−02	2.08E−05
2,3,5-Trimethylhexane	2.78E−02	2.04E−05
Ethyl acrylate	2.73E−02	2.00E−05
1,2-Ethylmethylcyclopentane	2.72E−02	1.99E−05
4-Propylheptane	2.72E−02	1.99E−05
6-Ethyl-2-methyldecane	2.72E−02	1.99E−05
Dimethyl sulfide	2.67E−02	1.95E−05
2-Methyl-1-butylbenzene	2.63E−02	1.93E−05
(2-Methyl-1-propyl)acetate	2.54E−02	1.86E−05
1-Octene	2.52E−02	1.84E−05
Tridecane	2.50E−02	1.83E−05
C_5 Alkenes	2.50E−02	1.83E−05
1,3-Ethylmethylcyclopentane	2.46E−02	1.80E−05
4-Ethylheptane	2.38E−02	1.74E−05
Isoprene	2.36E−02	1.73E−05
Triethylamine	2.31E−02	1.69E−05
Cycloheptane	2.29E−02	1.68E−05
3,5-Dimethylheptane	2.21E−02	1.62E−05
Phenanthrene	2.20E−02	1.61E−05
Cyclohexanol	2.19E−02	1.60E−05
8-Methyl-1-nonanol	2.19E−02	1.60E−05
Dimethylcyclopentane	2.15E−02	1.57E−05
Dichlorodifluoromethane	2.14E−02	1.57E−05
Methyltetralin	2.03E−02	1.49E−05
Pentylbenzene	2.03E−02	1.49E−05
Dimethylbutene	1.98E−02	1.45E−05
δ-Limonene	1.97E−02	1.44E−05
3-Pentanone	1.92E−02	1.41E−05
Methyl naphthalenes	1.81E−02	1.33E−05
4,4-Dimethylheptane	1.81E−02	1.33E−05
tert-Butylbenzene	1.74E−02	1.27E−05
2-(2-Hydroxy-propoxy)-1-propanol	1.72E−02	1.26E−05
2,3,4-Trimethylpentane	1.69E−02	1.24E−05
Isobutylbenzene	1.60E−02	1.17E−05
sec-Butylbenzene	1.60E−02	1.17E−05
1-Ethyl-2-methylcyclohexane	1.54E−02	1.13E−05
2-Methoxy-2-methylpropane	1.41E−02	1.03E−05

(*continued*)

Table I-C-2. (*continued*)

Species of VOC	Total Emissions, Metric Tons year^{-1}	Fraction of the Total Emissions
1,2-Ethanediol diacetate	1.37E−02	1.00E−05
4,7-Dimethylindan	1.35E−02	9.88E−06
Ethylisopropylbenzene	1.32E−02	9.66E−06
3-Ethyl-2-Methylpentane	1.29E−02	9.44E−06
Menthene	1.29E−02	9.44E−06
Bromoethene	1.29E−02	9.44E−06
2-Butanone oxime	1.29E−02	9.44E−06
1,1,2-Trimethylcyclopentane	1.25E−02	9.15E−06
Propanoic acid	1.23E−02	9.00E−06
2-Ethyltoluene	1.23E−02	9.00E−06
2-Aminoethanol	1.21E−02	8.86E−06
Ethyl pentanoate	1.20E−02	8.78E−06
1,2-Ethanedioldiacetate	1.20E−02	8.78E−06
Ethyl lactate	1.20E−02	8.78E−06
2-Methyl-2-hexene	1.15E−02	8.42E−06
2,3,6-Trimethylheptane	1.15E−02	8.42E−06
Isopropylcyclohexane	1.08E−02	7.91E−06
2,3,3,4-Tetramethylpentane	1.06E−02	7.76E−06
Aniline	1.06E−02	7.76E−06
Polyisobutene	1.05E−02	7.69E−06
Phenoxyacetic acid (phenoxy acid)	1.04E−02	7.61E−06
1,1,2,2-Tetrachloroethane	1.01E−02	7.39E−06
Methyl pentanoate	9.79E−03	7.17E−06
5-Methylnonane	9.74E−03	7.13E−06
Pentadecane	9.52E−03	6.97E−06
Chlorobenzene	9.27E−03	6.79E−06
1-Methyl-3-isopropylcyclopentane	9.05E−03	6.63E−06
1-Methylindene	9.05E−03	6.63E−06
3,3,4-Trimethylhexane	9.05E−03	6.63E−06
Hexylcyclohexane	9.05E−03	6.63E−06
tert-Butylcyclopropane	9.05E−03	6.63E−06
Chlorobutane	8.98E−03	6.57E−06
1,4-Dimethylpiperazine	8.91E−03	6.52E−06
Trichlorofluoromethane	8.90E−03	6.52E−06
polyvinyl chloride	8.62E−03	6.31E−06
2-Ethyl hexanol	8.42E−03	6.16E−06
1,2-Dichlorobenzene	8.37E−03	6.13E−06
Methylamine	8.24E−03	6.03E−06
3-Methoxy-1-butyl acetate	8.06E−03	5.90E−06
Butyl glycolate	8.06E−03	5.90E−06
Butyl lactate	8.06E−03	5.90E−06
Methylcycloheptane	7.68E−03	5.62E−06
3,3-Diethylpentane	7.60E−03	5.56E−06
1,4-Dioxane	7.47E−03	5.47E−06
Fluorene	7.47E−03	5.47E−06
Chlorodifluoromethane	7.12E−03	5.21E−06
C_{14} Alkanes	7.03E−03	5.15E−06
Maleic anhydride	6.99E−03	5.12E−06

(*continued*)

Table I-C-2. (*continued*)

Species of VOC	Total Emissions, Metric Tons year^{-1}	Fraction of the Total Emissions
Methoxy-2-propoxy-2-propanol	6.80E−03	4.98E−06
Methyl butanoate	6.67E−03	4.88E−06
Methyl styrene	6.67E−03	4.88E−06
Glycerol	6.53E−03	4.78E−06
Nitropentane	6.53E−03	4.78E−06
Unspeciated amines	6.53E−03	4.78E−06
2-Methoxypropane	6.51E−03	4.77E−06
C_{15} Alkanes	6.29E−03	4.60E−06
2,2,4-Trimethylhexane	5.85E−03	4.28E−06
Anthracene	5.85E−03	4.28E−06
Camphor/fenchone	5.78E−03	4.23E−06
1-Methyl-2-propylcyclopentane	5.72E−03	4.19E−06
2-Acetoxy-propyl acetate	5.72E−03	4.19E−06
2-Hexoxyethanol	5.72E−03	4.19E−06
2-Hexene	5.55E−03	4.06E−06
Palmitic acid	5.26E−03	3.85E−06
C_{16} Alkanes	5.26E−03	3.85E−06
tert-Butylamine	5.10E−03	3.73E−06
Butyl acrylate	4.77E−03	3.49E−06
Myrcene	4.61E−03	3.37E−06
Benzyl chloride	4.53E−03	3.32E−06
2-Methyl-1-pentene	4.50E−03	3.29E−06
1,2-Dichlorotetrafluoroethane	4.45E−03	3.26E−06
Chlorofluoromethane	4.45E−03	3.26E−06
2-Heptanone	4.42E−03	3.24E−06
Hexadecane	4.39E−03	3.21E−06
β-Phellandrene	4.16E−03	3.05E−06
Dimethoxymethane	3.97E−03	2.91E−06
Isopropylcyclopentane	3.93E−03	2.88E−06
3-Ethyl-2,3-dimethylpentane	3.72E−03	2.72E−06
Butylcyclopentane	3.51E−03	2.57E−06
Biphenyl	3.43E−03	2.51E−06
4-Methyl-2-pentanol	3.24E−03	2.37E−06
1,1,3,3-Tetramethylcyclopentane	3.22E−03	2.36E−06
2,4-Dimethyloctane	3.22E−03	2.36E−06
Camphene	3.13E−03	2.29E−06
1,3,5-Trimethylcyclohexane	3.00E−03	2.20E−06
Isobutylcyclohexane	2.91E−03	2.13E−06
Dimethyl esters	2.81E−03	2.06E−06
Acenaphthene	2.79E−03	2.04E−06
2,3,3-Trimethylheptane	2.63E−03	1.93E−06
2,4,4-Trimethylhexane	2.51E−03	1.84E−06
3-Hexene	2.48E−03	1.82E−06
3-Ethyl-3-methylpentane	2.41E−03	1.76E−06
4-4′-Methylenediphenyl diisocyanate	2.39E−03	1.75E−06
Trifluoroethene	2.38E−03	1.74E−06
1,3-Dichlorobenzene	2.37E−03	1.73E−06

(*continued*)

Table I-C-2. (*continued*)

Species of VOC	Total Emissions, Metric Tons year^{-1}	Fraction of the Total Emissions
2,5,5-Trimethylheptane	2.34E−03	1.71E−06
1,3-Dioxolane	2.26E−03	1.65E−06
Cyclopentene	2.08E−03	1.52E−06
2-Pentanone	1.87E−03	1.37E−06
1,3,4,5,6-Pentahydroxy-2-hexanone	1.80E−03	1.32E−06
2,3-Dimethylfuran	1.78E−03	1.30E−06
2,4-Dimethylfuran	1.78E−03	1.30E−06
2,5-Dimethylfuran	1.78E−03	1.30E−06
1-Chloro-2,3-epoxypropane	1.76E−03	1.29E−06
Butyrolactone	1.73E−03	1.27E−06
2,4,5-Trimethylheptane	1.67E−03	1.22E−06
Trichlorotoluene	1.63E−03	1.19E−06
1-Methyl-2-propylcyclohexane	1.53E−03	1.12E−06
Pentafluoroethane	1.46E−03	1.07E−06
Toluene-2,4-diisocyanate	1.34E−03	9.81E−07
Toluene-2,6-diisocyanate	1.34E−03	9.81E−07
Diisopropylbenzene	1.29E−03	9.44E−07
sec-Butylcyclohexane	1.07E−03	7.83E−07
Butanethiols	1.07E−03	7.83E−07
Carbon disulfide	8.90E−04	6.52E−07
1,4-Butyrolactone	7.67E−04	5.61E−07
Methacrylic acid	7.06E−04	5.17E−07
Pyridine	6.92E−04	5.07E−07
Nitrobenzene	6.19E−04	4.53E−07
Difluoromethane	5.88E−04	4.30E−07
Pentanethiols	5.34E−04	3.91E−07
Acetic anhydride	4.94E−04	3.62E−07
4-Methyl-1,3-dioxol-2-one	4.69E−04	3.43E−07
Dihydroxyacetone	4.64E−04	3.40E−07
Ethanethiol	4.51E−04	3.30E−07
Nitropropane	4.48E−04	3.28E−07
1,1-Dichlorotetrafluoroethane	4.45E−04	3.26E−07
Bromoethane	4.45E−04	3.26E−07
Carbonyl sulfide	4.45E−04	3.26E−07
Dichlorobutenes	4.45E−04	3.26E−07
Methyl ethyl ether	4.45E−04	3.26E−07
tert-Butylcyclohexane	4.45E−04	3.26E−07
Unspeciated carboxylic acids	4.45E−04	3.26E−07
1-Chloro-4-nitrobenzene	4.05E−04	2.96E−07
Iodomethane	3.82E−04	2.80E−07
Heptadecane	3.66E−04	2.68E−07
Diethyl disulfide	2.67E−04	1.95E−07
1-Butoxy-2-propanol	2.63E−04	1.93E−07
2-Chlorotoluene	2.59E−04	1.90E−07
Sodium phenylacetate	2.49E−04	1.82E−07
1-Chloropropane	2.22E−04	1.63E−07
2-Chloropropane	2.22E−04	1.63E−07
Diacetoneketogulonic acid	1.80E−04	1.32E−07

(*continued*)

Table I-C-2. (*continued*)

Species of VOC	Total Emissions, Metric Tons year^{-1}	Fraction of the Total Emissions
2-Methylfuran	1.78E−04	1.30E−07
3-Methylfuran	1.78E−04	1.30E−07
2-Phenoxy ethanol	1.63E−04	1.19E−07
3-Chloro-4-fluoropicoline	1.41E−04	1.03E−07
Hexachloroethane	1.35E−04	9.88E−08
3-Chloropyridine	1.30E−04	9.52E−08
Propanetriol	1.25E−04	9.15E−08
Formanilide	1.17E−04	8.57E−08
Dimethylamine	1.15E−04	8.42E−08
Sodium acetate	1.04E−04	7.61E−08
Octylamine	8.52E−05	6.24E−08
1-(Butoxyethoxy)-2-propanol	8.49E−05	6.22E−08
11-Methyl-1-dodecanol	8.38E−05	6.13E−08
2-Methylpropyl acetate	8.21E−05	6.01E−08
4-Chlorotoluene	7.01E−05	5.13E−08
Potassium phenylacetate	6.86E−05	5.02E−08
1,2-Dibromoethane	6.46E−05	4.73E−08
3A,4,7,7A-Tetrahydro-4,7-methanoindene	5.73E−05	4.19E−08
Trialkyl phosphate	5.32E−05	3.89E−08
Benzo(a)pyrene	4.78E−05	3.50E−08
2,2′-Iminodi(ethylamine)	4.66E−05	3.41E−08
Styrene acrylate	4.53E−05	3.32E−08
Triethanolamine	4.22E−05	3.09E−08
Polyethylene glycol	3.65E−05	2.67E−08
2-Phenylpropene	3.52E−05	2.58E−08
1-Methoxy-2-butanol	2.79E−05	2.04E−08
3-(2-Hydroxy-propoxy)-1-propanol	2.32E−05	1.70E−08
Phenylacetic acid	2.23E−05	1.63E−08
4-Bromophenyl acetate	2.12E−05	1.55E−08
Hexafluoropropene	2.12E−05	1.55E−08
Ethyl chloroformate	8.36E−06	6.12E−09
Propylamine	7.85E−06	5.75E−09
Tetrahydrofuryl alcohol	7.55E−06	5.53E−09
Ethofumesate	6.17E−06	4.52E−09
2,4,6-Trichloro-1,3,5-triazine	2.74E−06	2.01E−09
Hexamethyldisiloxane	2.34E−06	1.71E−09
2-(2-Hydroxy-ethoxy)ethanol	1.55E−06	1.13E−09
p-Benzoquinone	1.20E−06	8.78E−10
Bis(chloromethyl)ether	1.75E−07	1.28E−10
Trimethylamine	1.03E−07	7.54E−11
Sulfanilamide	4.13E−08	3.02E−11
Diazinon	3.34E−08	2.45E−11
2,2′-Iminodiethanol	2.06E−08	1.51E−11
Permethrin	1.03E−08	7.54E−12
Malathion	1.28E−09	9.37E−13
4,4′-Methylenedianiline	7.23E−11	5.29E−14

Table I-C-3. Estimated emissions in source catagories for the U.K. during years 2000 and 2006 (Dore et al., 2008); the numbers preceding each emission category are used to reference the source of each OVOC in table I-C-4. More detailed emission categories were added in reporting the 2006 year data for vehicles shown here and for other categories that are not shown for year 2000

	Emissions, Metric ktons Year^{-1}	
Emission Category	Year 2000	Year 2006
Aerosols		
1) car care products	2.00E+01	1.69E+01
2) cosmetics and toiletries	2.57E+02	2.47E+01
3) household products	8.00E+00	9.01E+00
Agriculture		
4) coal	3.50E−04	2.50E−04
5) fuel oil	1.22E−03	1.40E−03
6) gas, oil	1.55E−02	
7) natural gas	1.97E−02	1.60E−02
8) power units, gas, oil	3.38E+00	
9) power units, petrol	3.31E−01	
10) straw	1.71E+00	1.81E+00
Agrochemicals, use (11)	3.50E+00	3.86E+00
Aircraft		
12) domestic, aviation turbine fuel	7.39E−01	7.05E−01
13) military, aviation turbine fuel	6.27E−01	7.05E−01
14) support, gas, oil	8.52E−02	
15) international aviation turbine	1.95E+00	5.41E+00
Ammonia combustion, natural gas (16)	4.04E−02	1.83E−02
Animal carcase incineration (17)	2.00E+00	2.00E+00
Autogenerators,		
18) coal	4.31E−02	4.55E−02
19) natural gas	6.69E−01	2.52E−01
Blast furnaces(20)	1.31E+00	1.28E+00
21) blast furnace gas	1.00E−01	8.66E−02
22) coke oven gas	7.52E−02	1.59E−02
23) natural gas	9.23E−03	4.86E−03
Bread baking (24)	2.87E+00	2.65E+00
Brewing		
25) barley malting	3.32E+00	3.23E+00
26) distillers' malting		2.74E+00
27) fermentation	1.11E−01	1.08E−01
28) wort boiling	2.65E−02	2.58E−02
Coal, tar and bitumen processes (29)	4.09E−02	1.84E−02
Cement, nondecarbonizing (30)	1.38E+00	6.98E−01
Chemical industry (31)	7.33E+01	3.07E+01
Chemical waste, incineration (32)	2.49E−01	1.04E+00
Cider manufacture (33)	1.20E−02	1.50E−02
Clinical waste, incineration (34)	4.56E−03	1.20E−03
Coastal shipping		
35) fuel oil	9.08E−02	1.76E+00
36) gas, oil	1.69E+00	4.15E+00

(*continued*)

Table I-C-3. (*continued*)

Emission Category	Emissions, Metric ktons Year^{-1} Year 2000	Year 2006
Coating manufacture		
37) glue	8.83E−01	1.01E+00
38) ink	1.48E+00	1.66E+00
39) paint	5.72E+00	4.14E+00
Coke, blast furnace gas (40)	1.14E−02	1.08E−02
Coke production (41)	1.96E−01	6.71E−02
42) Coke oven gas	3.50E−01	7.56E−03
43) Production, natural gas	2.28E−04	0.00E+00
Collieries		
44) Coal	6.00E−04	1.88E−04
45) Methane	4.77E−03	5.64E−03
46) natural gas	7.60E−05	0.00E+00
Crematoria (47)	5.69E−03	5.41E−03
Decorative paint		
48) retail decorative	2.28E+01	3.40E+01
49) trade decorative	2.47E+01	2.35E+01
Domestic adhesives (50)	6.76E−01	7.73E−01
Domestic combustion		
51) anthracite	1.56E+00	3.61E−01
52) burning oil	3.27E−01	1.18E−01
53) burning oil, premium	3.19E−03	
54) coal	1.39E+01	4.69E+00
55) coke	7.11E−01	1.57E−01
56) fuel oil	3.38E−04	0.00E+00
57) gas, oil	1.91E−02	8.29E−03
58) LPG	2.54E−02	2.42E−02
59) natural gas	8.39E+00	2.90E+00
60) SSF	2.43E+00	1.26E+00
61) Wood	4.87E+00	1.45E+01
Dry cleaning (62)	4.76E+00	4.34E+00
Film coating (63)	5.32E+00	2.26E+00
Fishing vessel, gas, oil (64)	2.41E−01	
Fletton brick manufacture (65)	1.71E+00	2.81E+00
Forests (66)	1.78E+02	
Gas leakage (67)	6.35E+01	4.06E+01
Gas production		
68) LPG	3.61E−03	1.04E−03
69) natural gas	1.01E−01	4.00E−01
Gas separation plant		
70) LPG	1.04E−04	1.04E−03
71) OPG	3.12E−02	2.01E−02
Gasification processes (72)	1.19E−01	1.86E−01
Glass		
73) continuous filament glass fiber	5.44E−02	2.63E−02
74) glass wool	1.35E−01	2.18E−01
House and garden machinery		
75) DERV	1.21E−01	2.62E−02
76) petrol	2.92E+01	1.12E+01

(*continued*)

Table I-C-3. (*continued*)

Emission Category	Emissions, Metric ktons Year^{-1}	
	Year 2000	Year 2006
Industrial adhesives	2.49E+01	3.46E+01
77) pressure sensitive tapes	1.37E+00	3.42E−01
Industrial coatings		
78) agricultural and contruction	2.31E+00	1.59E+00
79) aircraft	8.84E−01	1.62E+00
80) automotive	8.89E+00	4.14E+00
81) coil	3.43E−01	2.96E−01
82) commercial vehicles	4.54E+00	2.82E+00
83) drum	8.67E−01	4.54E−01
84) high performance	7.25E+00	5.54E+00
85) marine	2.37E+00	2.56E+00
86) metal and plastic	2.22E+01	2.49E+01
87) metal packaging	6.42E+00	3.20E+00
88) vehicle refinishing	6.81E+00	4.23E+00
89) wood	1.16E+01	8.74E+00
Iron and steel		
90) blast furnace gas	2.06E−01	2.05E−01
91) electric arc furnaces	3.17E−01	2.45E−01
92) flaring, blast furnace gas	3.21E−02	3.18E−02
93) flaring, coke oven gas	2.05E−02	
94) industry, coal	1.33E−04	
95) industry, coke	9.50E−05	
96) industry, coke oven gas	3.76E−01	
97) industry, fuel oil	3.42E−02	
98) industry, gas oil	1.54E−02	
99) industry, LPG	2.19E−03	
100) industry, natural gas	2.94E−01	
Landfill (101)	5.52E+00	9.24E+00
Leather		
102) coating	3.62E−01	2.28E−01
103) degreasing	1.40E−01	6.77E−02
Lime production		
104) coal	2.12E−03	2.03E−03
105) coke	2.62E−04	2.48E−04
106) natural gas	2.86E−02	7.18E−03
Miscellaneous		
107) burning oil	1.04E−03	
108) coal	7.50E−04	
109) fuel oil	7.55E−03	
110) gas oil	4.50E−02	
111) landfill gas	2.70E−02	
112) MSW	5.25E−03	
113) natural gas	9.17E−01	
Nonaerosol		
114) automotive products	2.68E+01	3.07E+01
115) cosmetics and toiletries	1.28E+01	1.54E+01
116) household products	1.16E+01	1.21E+01

(*continued*)

Table I-C-3. (*continued*)

Emission Category	Emissions, Metric ktons Year^{-1}	
	Year 2000	Year 2006
Offshore		
117) flaring	1.20E+01	1.07E+01
118) loading of crude oil	5.10E+01	3.08E+01
119) oil and gas industry	1.50E+01	
120) natural gas	4.95E−01	4.00E−01
121) venting	1.09E+01	8.89E+00
122) well testing	8.72E−01	6.11E−01
Oil terminal storage (123)	1.10E+01	
Onshore loading of crude oil (124)	6.96E+01	1.34E+01
Other food		
125) animal feed manufacturers	9.89E+00	1.04E+01
126) cakes, biscuits and cereals	1.93E+00	1.84E+00
127) coffee roasting	6.00E−02	6.30E−02
128) malting	1.74E+00	9.55E−01
129) margarine and other solid fats	5.23E+00	5.08E+00
130) meat, fish and poultry	1.08E+00	1.15E+00
131) sugar production	3.26E−02	2.94E−02
Other rubber products (132)	2.00E+00	1.84E+00
Other industrial combustion		
133) burning oil	1.13E−01	
134) coal	5.13E−02	5.59E−02
135) coke	1.14E−02	3.25E−03
136) coke-oven gas	2.15E−02	4.01E−03
137) colliery methane	1.55E−03	4.38E−04
138) combustion, wood		2.03E−01
139) fuel oil	5.59E−02	2.49E−02
140) gas oil	1.36E−01	5.74E−03
141) LPG	6.73E−02	8.87E−02
142) lubricants	2.77E−02	2.96E−02
143) natural gas	2.05E+00	1.13E+00
144) OPG	2.48E−02	5.20E−03
145) SSF	1.80E−03	0.00E+00
146) wood	5.94E−01	2.03E−01
Other industrial		
147) off-road, gas, oil	7.30E+00	1.59E+01
148) off-road, petrol	1.48E+01	6.36E+00
Other solvent use (149)	4.60E+01	4.60E+01
Paint thinners (150)	1.20E+01	1.24E+01
Paper coating (151)	3.03E+00	5.91E−01
Petroleum processes (152)	9.08E+00	2.68E+00
Petrol stations		
153) delivery of leaded petrol	4.41E−01	1.53E−03
154) delivery of unleaded petrol	5.91E+00	1.38E+00
155) spillages of leaded petrol	1.68E−01	2.21E−03
156) spillages of unleaded petrol	2.26E+00	2.00E+00
157) storage tanks, leaded petrol	2.53E−01	3.31E−03
158) storage tanks, unleaded petrol	3.39E+00	3.01E+00
159) vehicle refueling, leaded petrol	2.76E+00	2.63E−02
160) vehicle refueling, unleaded petrol	3.70E+01	2.39E+01

(*continued*)

Table I-C-3. (*continued*)

Emission Category	Emissions, Metric ktons Year^{-1}	
	Year 2000	Year 2006
Petrol terminal storage		
161) leaded petrol	2.50E−01	1.88E−03
162) unleaded petrol	3.46E+00	1.81E+00
163) tanker loading, leaded petrol	7.03E−02	2.39E−04
164) tanker loading, unleaded petrol	9.43E−01	8.10E−01
Power stations		
165) coal	1.14E+00	1.40E+00
166) fuel oil	2.09E−02	1.69E−02
167) gas oil	1.27E−02	2.83E+00
168) MSW	7.37E−02	1.39E−02
169) landfill gases	1.42E+00	1.31E−01
170) natural gas	5.54E+00	2.71E+00
171) poultry litter	2.08E−02	9.56E−03
172) sewage gas	2.38E−01	9.18E−03
173) sour gas	2.07E−02	9.60E−03
Printing		
174) flexible packaging	1.62E+01	6.73E+00
175) heatset web offset	7.07E−01	1.51E+00
176) metal decorating	9.17E−02	6.43E−02
177) newspapers	8.15E+00	4.36E−01
178) other flexography	1.00E+00	1.09E+00
179) other inks	3.01E−01	2.44E−01
180) other offset	2.26E−01	3.99E−01
181) overprint varnishes	8.37E+00	4.29E+00
182) print chemicals	1.13E+00	8.03E−01
183) publication gravure	7.80E−01	8.98E−01
184) screen printing	2.15E+00	6.25E−01
Public services		
185) burning oil	1.04E−03	5.81E−04
186) coal	1.39E−02	6.95E−03
187) fuel oil	2.13E−02	6.45E−03
188) gas, oil	7.61E−02	1.25E−03
189) natural gas	6.80E−01	4.23E−01
190) sewage gas	9.57E−02	9.18E−03
Railways		
191) freight, gas, oil	4.11E−01	1.26E+00
192) intercity, gas, oil	1.05E+00	1.23E+00
193) regional, gas, oil	4.47E−02	1.18E+00
194) stationary sources, burning oil	1.04E−03	5.81E−04
195) stationary sources, natural gas	2.85E−02	1.91E−04
Refineries		
196) drainage	1.13E+01	7.78E+00
197) flares	2.04E+00	1.51E+00
198) fuel oil	1.79E−01	3.45E−02
199) gas oil	6.30E−03	1.20E−03
200) LPG	3.55E−03	6.00E−03
201) miscellaneous		0.00E+00
202) naphtha	1.83E−03	0.00E+00

(*continued*)

Table I-C-3. (*continued*)

Emission Category	Emissions, Metric ktons Year^{-1}	
	Year 2000	Year 2006
Refineries (*continued*)		
203) natural gas	2.32E−03	3.02E−02
204) OPG	4.72E−02	1.84E−01
205) petroleum coke	8.34E−01	7.29E−02
206) process fugitives	6.94E−02	1.89E+01
207) road/rail loading of leaded petrol	2.85E+01	7.28E−04
208) road/rail loading of unleaded petrol	7.91E−02	6.28E−01
209) tankage	1.05E+00	5.03E+00
Road	5.45E+00	
210) construction	7.80E+00	
211) transport cars DERV	2.92E+00	
212) transport LGVs DERV	6.93E+00	
213) transport cars with catalysts petrol	7.19E+01	
214) transport cars without catalysts	1.57E+02	
215) transport, articulated HGVs, DERV	1.48E+01	
216) transport, rigid HGVs, DERV	1.38E+01	
217) transport, LGVs with catalysts, petrol	8.93E−01	
218) transport, LGVs without catalysts, petrol	1.26E+01	
Road transport		
219) 2-stroke motorcycles >50 cc, petrol	3.96E+00	
220) 4-stroke motorcycles >50 cc, petrol	5.28E+00	
221) 2-stroke motorcycles <50 cc, petrol	3.86E+00	
222) Buses, DERV	4.52E+00	
223) Coaches, DERV	1.31E+00	
Categories for mobile sources, 2006 inventory		
cars—motorway driving		2.27E−01
cars noncatalyst—motorway driving		8.80E−01
cars with catalysts—motorway driving		1.97E+00
cars—rural driving		7.69E−01
cars noncatalyst—rural driving		2.38E+00
cars with catalysts—rural driving		4.04E+00
cars—cold start		6.66E−01
cars—urban driving		1.67E+00
cars noncatalyst—cold start		1.76E+00
cars noncatalyst—urban driving		3.59E+00
cars with catalysts—cold start		2.81E+01
cars with catalysts—urban driving		4.50E+00
LGVs—motorway driving		7.91E−01
LGVs noncatalyst—motorway driving		4.96E−02
LGVs with catalysts—motorway driving		1.43E−02
LGVs—rural driving		2.16E+00
LGVs noncatalyst—rural driving		1.22E−01
LGVs with catalysts—rural driving		4.19E−02
LGVs—cold start		1.31E+00
LGVs—urban driving		2.29E+00
LGVs noncatalyst—cold start		9.22E−02
LGVs noncatalyst—urban driving		1.87E−01

(*continued*)

Table I-C-3. (*continued*)

Emission Category	Emissions, Metric ktons Year^{-1}	
	Year 2000	Year 2006
Categories for mobile sources, 2006 inventory (*continued*)		
LGVs with catalysts—cold start		2.81E−01
LGVs with catalysts—urban driving		3.07E−02
buses and coaches—motorway driving		1.21E−01
HGV articulated—motorway driving		6.18E+00
HGV rigid—motorway driving		1.40E+00
buses and coaches—rural driving		3.62E−01
HGV articulated—rural driving		4.23E+00
HGV rigid—rural driving		2.80E+00
buses and coaches—urban driving		1.71E+00
HGV articulated—urban driving		9.48E−01
HGV rigid—urban driving		1.86E+00
mopeds (<50 cc 2-stroke)— urban driving		1.59E+00
motorcycle (>50 cc 4-stroke)—motorway driving		2.51E−01
motorcycle (>50 cc 2-stroke)—rural driving		1.17E+00
motorcycle (>50 cc 4-stroke)—rural driving		1.09E+00
motorcycle (>50 cc 2-stroke)—urban driving		1.54E+00
motorcycle (>50 cc 4-stroke)—urban driving		1.94E+00
cars—evaporative		1.66E+01
LGVs—evaporative		3.57E−01
Rolling mills		
224) cold rolling		
225) hot rolling	9.57E−02	7.05E−02
Seed oil extraction (226)	8.82E−03	7.26E−03
Sewage sludge, incineration (227)	2.34E+00	2.09E+00
Ship purging (228)	1.69E−01	1.55E−01
Shipping, naval, gas oil (229)	1.90E+00	1.90E+00
Sinter plant, coke (230)	6.15E−01	7.98E−01
Solvent and oil recovery (231)	2.60E−01	3.08E−01
Spirit manufacture	3.52E−01	1.74E−01
232) barley malting	2.10E+00	3.23E+00
233) casking	1.38E−01	1.76E−01
234) distillation	3.32E−01	3.92E−01
235) fermentation	6.64E−01	7.84E−01
236) maturation	4.64E+01	4.57E+01
237) spent grain drying	7.28E−01	8.56E−01
SSF production, coke (238)	1.85E−03	
SSF production (239)	9.67E−03	4.64E−03
Surface cleaning		
240) dichloromethane	7.79E−01	7.10E−01
241) hydrocarbons		
242) other	3.06E+00	1.41E+01
243) tetrachloroethylene	1.33E+00	3.02E+00
244) trichloroethylene	2.04E+01	1.05E+00
Textile coating (245)	2.49E+00	6.10E+00
Tire manufacture (246)	1.74E+00	1.38E+00

(*continued*)

Table I-C-3. (*continued*)

Emission Category	Emissions, Metric ktons Year^{-1}	
	Year 2000	Year 2006
Wine manufacture (247)	6.66E−02	1.08E+00
Wood impregnation	2.46E−01	2.36E−01
248) Creosote	2.50E+00	1.48E+00
249) LOSP	9.26E+00	3.54E+00
Wood products manufacture (250)	2.46E−01	2.36E−01

HGV = heavy goods vehicle, LGV = light goods vehicle, LPG = liquified petroleum gas, MSW = municipal solid waste, DERV = diesel engine road vehicle, LOSP = light organic solvent preservative, OPG = other petroleum gas, SSF = solid smokeless fuel.

Table I-C-4. Inventory and speciation of the oxygenates emitted from all anthropogenic sources in the U.K. for the year 2000 (AEA Energy & Environment, 2009)

Species of Oxygenate	Total Emissions Metric ktons Year^{-1}	Fraction of the Total Emissions	Sources of Emissions as Listed in Table I-C-3 (Decreasing Order of Importance)
Ethanol	1.01E+02	3.24E−01	115,2,174,116,3,24,126,84
Methanol	2.75E+01	8.81E−02	114,31,63,25,128,151,101
Formaldehyde	2.31E+01	7.39E−02	170,117,214,59,215,216
Acetone	2.23E+01	7.15E−02	149,31,77,242,89,249,63
2-Butanone	1.45E+01	4.64E−02	115,86,149,77,181,63,242
Butyl acetate	1.30E+01	4.15E−02	89,80,86,83,149,82,77
2-Propanol	1.14E+01	3.64E−02	2,181,1,182,89,31,116,174
Ethyl acetate	1.04E+01	3.34E−02	33,174,149,114,77,80,88
4-Methyl-2-pentanone	6.55E+00	2.10E−02	149,77,89,86,249,63,39
1-Butanol	6.09E+00	1.95E−02	115,86,249,87,80,89,84,88
2-Butoxyethanol	5.35E+00	1.71E−02	87,183,116,86,80,149,249
Acetaldehyde	5.06E+00	1.62E−02	111,214,215,216,212,213
Methyl acetate	4.82E+00	1.54E−02	31,25,232,128,237
1-Propanol	3.95E+00	1.26E−02	242,174,2,77,1,3,11,178
1-Methoxy-2-propanol	3.86E+00	1.24E−02	86,84,80,181,149,87,174
1-Methoxy-2-propyl acetate	3.01E+00	9.64E−03	86,80,149,181,88,174,249
Dimethyl ether	2.63E+00	8.42E−03	31,2,1,3,115,114,101,116
2-(2-Butoxyethoxy)ethanol	2.14E+00	6.85E−03	49,48,80,149,86,78,81,11
Furfural	1.97E+00	6.30E−03	25,232,128,237
Benzaldehyde	1.86E+00	5.94E−03	214,215,216,213,147,148
2-(2-Ethoxyethoxy)ethanol	1.68E+00	5.39E−03	49,48,149,86,78,39,181
Acrolein	1.63E+00	5.23E−03	215,216,212,214,147,213
2-Methyl-1-propanol	1.59E+00	5.08E−03	89,299,85,88,86,82,80,39
1-Propanal	1.56E+00	5.00E−03	25,215,216,214,232,212
2-Propyl acetate	1.54E+00	4.92E−03	174,249,31,38,178,39,151
4-Methyl-4-hydroxy-2-pentanone	1.49E+00	4.77E−03	87,89,86,80,39,249,88,82
1,2-Propanediol	1.31E+00	4.18E−03	49,48,86,78,245,39,116

(*continued*)

Table I-C-4. (*continued*)

Species of Oxygenate	Total Emissions Metric ktons Year^{-1}	Fraction of the Total Emissions	Sources of Emissions as Listed in Table I-C-3 (Decreasing Order of Importance)
Ethylene glycol	1.10E+00	3.53E−03	114,116,31,151,245
Benzyl alcohol	1.06E+00	3.38E−03	115,49,48,39,79,63
1-(2-Butoxy-1-methyl-ethoxy)-2-propanol	1.05E+00	3.35E−03	49,48,39
2,2,4-Trimethyl-1,3-pentanediol monoisobutyrate	1.04E+00	3.34E−03	49,48,39
Tri-*n*-butyl phosphate	1.04E+00	3.33E−03	49,48
3-Methyl benzaldehyde	9.92E−01	3.17E−03	214,215,216,213,148,147
Propyl acetate	9.91E−01	3.17E−03	174,38,39,178,101,151,63
2-(2-Butoxyethoxy)ethyl acetate	9.48E−01	3.03E−03	80,149,87,88,82,181,174
Crotonaldehyde	8.57E−01	2.74E−03	215,216,147,212,222,8,211
Acrylamide	8.29E−01	2.65E−03	31
Cyclohexanone	7.84E−01	2.51E−03	86,31,184,39,88,78,82,38
2-Methoxyethanol	7.60E−01	2.43E−03	114,149,181,174,249,184
2-Methyl benzaldehyde	7.42E−01	2.37E−03	214,215,216,147,213,222
1-Pentanal	7.26E−01	2.32E−03	25,232,128,215,216,237
2-Ethoxyethyl acetate	6.93E−01	2.22E−03	149,86,39,245,78,181,85
Dimethylformamide	6.92E−01	2.21E−03	31,245,63,39,231
1-Hexanal	6.87E−01	2.20E−03	215,216,147,222,8,223,192
1-Ethoxy-2-propanol	6.50E−01	2.08E−03	149,89,181,178,63,174,184
Tetrahydrofuran	5.96E−01	1.91E−03	31,63,101
Diisopropyl ether	5.76E−01	1.84E−03	31,101
Butanal	5.70E−01	1.82E−03	97,98,147,212,222,213,15
2-Ethoxyethanol	5.62E−01	1.80E−03	149,102,88,82,39,63,181
Acetic acid	5.38E−01	1.72E−03	31,116,245,114,231
2-Methylpropenal	5.08E−01	1.63E−03	215,216,147,212,222,213,8
2-Methylfurfural	4.92E−01	1.58E−03	25,232,128,237
2-Methylpropanal	4.86E−01	1.55E−03	212,215,216,211,147,8,192
Phenol	4.82E−01	1.54E−03	248,31,74,39,15,12,13,29
1-Ethoxy-2-propyl acetate	4.66E−01	1.49E−03	149,181,174,184,249,77,11
1-(2-Methoxy-1-methyl-ethoxy)-2-propanol	4.63E−01	1.48E−03	149,181,249,184,77,11,37
1-(2-Ethoxy-1-methyl-ethoxy)-2-propanol	4.62E−01	1.48E−03	149,181,249,184,77,11,37
2-(Methoxyethoxy)ethanol	4.27E−01	1.37E−03	149,116,181,171,249,184
2-Butoxyethyl acetate	4.04E−01	1.29E−03	149,39,181,174,249,184,77
2-[2-(2-Ethoxy-ethoxy)-ethoxy]ethanol	3.88E−01	1.24E−03	149,181,174,24,249,39,184
2-(2-Ethoxyethoxy)ethyl acetate	3.84E−01	1.23E−03	149,181,174,249,184,77,39
2-Isopropoxyethanol	3.83E−01	1.22E−03	149,181,174,249,184,77,11
2-Methoxyethyl acetate	3.82E−01	1.22E−03	149,181,174,249,184,77,11
4-Methyl benzaldehyde	3.73E−01	1.19E−03	214,213,148,212,218,211
Ethylene oxide	3.47E−01	1.11E−03	31,116
Hexamethylcyclotrisiloxane	3.19E−01	1.02E−03	15,12,13
2-Butanol	3.02E−01	9.66E−04	39,31,101,63,245
Methyl formate	3.01E−01	9.63E−04	31
5-Methyl-2-hexanone	2.70E−01	8.65E−04	86,78,39,79,116
Isophorone	2.67E−01	8.56E−04	86,78,39
2-Methyl-2,4-pentanediol	2.54E−01	8.13E−04	86,78,39,245
N-Methyl pyrrolidone	2.47E−01	7.89E−04	86,78,31,39,245
Unspeciated ketones	2.28E−01	7.29E−04	149,52,57,53,56
Methyl methacrylate	2.14E−01	6.86E−04	31

(*continued*)

Table I-C-4. (*continued*)

Species of Oxygenate	Total Emissions Metric ktons Year^{-1}	Fraction of the Total Emissions	Sources of Emissions as Listed in Table I-C-3 (Decreasing Order of Importance)
Unspeciated alcohols	1.90E−01	6.08E−04	24,52,53,56,57,126
Ethyl butanoate	1.56E−01	4.98E−04	101
m-Cresol	1.29E−01	4.13E−04	248,31
o-Cresol	1.29E−01	4.13E−04	248,31
p-Cresol	1.29E−01	4.13E−04	248,31
2,6-Dimethyl-4-heptanone	1.28E−01	4.11E−04	87
Acrylic acid	1.24E−01	3.95E−04	31
Phthalic anhydride	1.21E−01	3.88E−04	31
Octamethylcyclotetrasiloxane	1.03E−01	3.30E−04	15,12,13
2,5-Xylenol	9.63E−02	3.08E−04	248
3,5-Xylenol	9.63E−02	3.08E−04	248
Dimethyl adipate	9.34E−02	2.99E−04	87,81,83
Dimethyl glutarate	9.34E−02	2.99E−04	87,81,83
Dimethyl succinate	9.34E−02	2.99E−04	87,81,83
Propylene oxide	9.25E−02	2.96E−04	31,39
Glyoxal	9.05E−02	2.90E−04	15,12,13
Propyl propionate	8.90E−02	2.85E−04	101
Methyl glyoxal	7.27E−02	2.33E−04	15,12,13
2,3,5-Trimethylphenol	6.42E−02	2.05E−04	248
2,3-Xylenol	6.42E−02	2.05E−04	248
2,4-Xylenol	6.42E−02	2.05E−04	248
2,6-Xylenol	6.42E−02	2.05E−04	248
3,4-Xylenol	6.42E−02	2.05E−04	248
1-Pentanol	6.23E−02	2.00E−04	31
Ethyl propionate	6.05E−02	1.94E−04	101
Naphthol	5.67E−02	1.81E−04	101,116
3-Methylbutanal	5.30E−02	1.70E−04	215,216,212,147,224,211,8
Methyl acrylate	5.24E−02	1.68E−04	31
Formic acid	5.14E−02	1.64E−04	31,63,245
Dipropyl ether	4.89E−02	1.57E−04	101
Diethyl ether	4.85E−02	1.55E−04	63,31,101
Propyl butanoate	4.45E−02	1.42E−04	101
Ethyl-3-ethoxypropionate	4.42E−02	1.41E−04	79
Vinyl acetate	4.42E−02	1.41E−04	31,151
3-Methylbutanol	4.30E−02	1.38E−04	236,235,234,233,27,246,33
2-Methyl-1,3-dioxolane	3.52E−02	1.13E−04	31
Bis(2-hydroxyethyl)ether	3.28E−02	1.05E−04	245,116,39,114
4-Ethyl morpholine	2.84E−02	9.08E−05	31
Ethyl acrylate	2.73E−02	8.75E−05	31
(2-Methyl-1-propyl)acetate	2.54E−02	8.13E−05	39
Cyclohexanol	2.19E−02	7.02E−05	39,245
8-Methyl-1-nonanol	2.19E−02	7.00E−05	39
3-Pentanone	1.92E−02	6.13E−05	39
2-(2-Hydroxy-propoxy)-1-propanol	1.72E−02	5.50E−05	245
2-Methoxy-2-methylpropane	1.41E−02	4.50E−05	31
1,2-Ethanediol diacetate	1.37E−02	4.39E−05	81

(*continued*)

Table I-C-4. (*continued*)

Species of Oxygenate	Total Emissions Metric ktons Year^{-1}	Fraction of the Total Emissions	Sources of Emissions as Listed in Table I-C-3 (Decreasing Order of Importance)
2-Butanone oxime	1.29E−02	4.11E−05	39
Propanoic acid	1.23E−02	3.93E−05	31
2-Aminoethanol	1.21E−02	3.86E−05	116,115,31
Ethyl pentanoate	1.20E−02	3.84E−05	101
1,2-Ethanedioldiacetate	1.20E−02	3.83E−05	39
Ethyl lactate	1.20E−02	3.83E−05	39
Phenoxyacetic acid (phenoxy acid)	1.04E−02	3.31E−05	31
Methyl pentanoate	9.79E−03	3.13E−05	101
2-Ethyl hexanol	8.42E−03	2.70E−05	245
3-Methoxy-1-butyl acetate	8.06E−03	2.58E−05	39
Butyl glycolate	8.06E−03	2.58E−05	39
Butyl lactate	8.06E−03	2.58E−05	39
1,4-Dioxane	7.47E−03	2.39E−05	31
Maleic anhydride	6.99E−03	2.24E−05	31
Methoxy-2-propoxy-2-propanol	6.80E−03	2.18E−05	151
Methyl butanoate	6.67E−03	2.14E−05	101
Glycerol	6.53E−03	2.09E−05	245
Nitropentane	6.53E−03	2.09E−05	39
2-Methoxypropane	6.51E−03	2.08E−05	31
Camphor/fenchone	5.78E−03	1.85E−05	101
2-Acetoxy-propyl acetate	5.72E−03	1.83E−05	39
2-Hexoxyethanol	5.72E−03	1.83E−05	39
Palmitic acid	5.26E−03	1.68E−05	31
Butyl acrylate	4.77E−03	1.53E−05	245,31
Benzyl chloride	4.53E−03	1.45E−05	31
2-Heptanone	4.42E−03	1.41E−05	79
Dimethoxymethane	3.97E−03	1.27E−05	31
4-Methyl-2-pentanol	3.24E−03	1.04E−05	39,114
Dimethyl esters	2.81E−03	9.00E−06	39
1,3-Dioxolane	2.26E−03	7.22E−06	101,63
2-Pentanone	1.87E−03	5.98E−06	101
1,3,4,5,6-Pentahydroxy-2-hexanone	1.80E−03	5.75E−06	31
2,3-Dimethylfuran	1.78E−03	5.69E−06	101
2,4-Dimethylfuran	1.78E−03	5.69E−06	101
2,5-Dimethylfuran	1.78E−03	5.69E−06	101
1-Chloro-2,3-epoxypropane	1.76E−03	5.62E−06	31
Butyrolactone	1.73E−03	5.52E−06	39
1,4-Butyrolactone	7.67E−04	2.45E−06	63
Methacrylic acid	7.06E−04	2.26E−06	31
Nitrobenzene	6.19E−04	1.98E−06	31
Acetic anhydride	4.94E−04	1.58E−06	31
4-Methyl-1,3-dioxol-2-one	4.69E−04	1.50E−06	39
Dihydroxyacetone	4.64E−04	1.49E−06	115
Ethanethiol	4.51E−04	1.44E−06	101,152,72
Nitropropane	4.48E−04	1.43E−06	116
Methyl ethyl ether	4.45E−04	1.42E−06	101

(*continued*)

Table I-C-4. (*continued*)

Species of Oxygenate	Total Emissions Metric ktons Year^{-1}	Fraction of the Total Emissions	Sources of Emissions as Listed in Table I-C-3 (Decreasing Order of Importance)
Unspeciated carboxylic acids	4.45E−04	1.42E−06	101
1-Chloro-4-nitrobenzene	4.05E−04	1.29E−06	31
1-Butoxy-2-propanol	2.63E−04	8.41E−07	116,114,63
Diacetoneketogulonic acid	1.80E−04	5.75E−07	31
2-Methylfuran	1.78E−04	5.69E−07	101
3-Methylfuran	1.78E−04	5.69E−07	101
2-Phenoxy ethanol	1.63E−04	5.22E−07	245
Propanetriol	1.25E−04	4.01E−07	245
Formanilide	1.17E−04	3.73E−07	31
1-(Butoxyethoxy)-2-propanol	8.49E−05	2.72E−07	116
11-Methyl-1-dodecanol	8.38E−05	2.68E−07	245
2-Methylpropyl acetate	8.21E−05	2.63E−07	114
Styrene acrylate	4.53E−05	1.45E−07	151
Triethanolamine	4.22E−05	1.35E−07	245
Polyethylene glycol	3.65E−05	1.17E−07	245
1-Methoxy-2-butanol	2.79E−05	8.93E−08	151
3-(2-Hydroxy-propoxy)-1-propanol	2.32E−05	7.43E−08	63
Phenylacetic acid	2.23E−05	7.12E−08	31
4-Bromophenyl acetate	2.12E−05	6.80E−08	31
Ethyl chloroformate	8.36E−06	2.68E−08	31
Tetrahydrofuryl alcohol	7.55E−06	2.42E−08	63
Ethofumesate	6.17E−06	1.98E−08	31
Hexamethyldisiloxane	2.34E−06	7.48E−09	231
2-(2-Hydroxy-ethoxy)ethanol	1.55E−06	4.95E−09	31
p-Benzoquinone	1.20E−06	3.83E−09	31
Bis(chloromethyl)ether	1.75E−07	5.62E−10	31
Diazinon	3.34E−08	1.07E−10	31
2,2′-Iminodiethanol	2.06E−08	6.61E−11	31
Malathion	1.28E−09	4.11E−12	31
Total of all oxygenates	**312.51 metric ktons year^{-1}**		

The order of the compounds determined by the magnitude of the mass emissions is not intended to reflect the relative influence of these compounds on atmospheric chemistry, greenhouse effect, or other atmospheric phenomena. To illustrate this point, compare in table I-C-5 the orders of importance of the top 31 species in mass emissions in table I-C-2 as estimated from a consideration of criteria other than mass emissions. We list the normalized relative values for molecular emissions (proportional to mass emissions/molecular weight), relative rate of attack by OH radicals (proportional to molecular emissions $\times k_{OH}$), the relative rate of ozone generation as estimated for a polluted urban atmosphere (proportional to mass emissions $\times$ MIR, the maximum incremental reactivity factor; Carter, 1998), and the relative number of CO_2 molecules that atmospheric oxidation of this species will ultimately generate (proportional to molecular emissions $\times$ number of C-atoms molecule^{-1}). The latter comparison

Table I-C-5. The different orders of significance of first 31 VOCs listed in Table I-C-2 when classified by various methods

Relative Mass Emissions[b]		Relative Molecular Emissions[c]		Relative Rate of Attack by OH Radicals[d]		Relative Rate of Ozone Generation[e]		Relative Number of Molecules of CO_2 Formed Ultimately[f]	
Butane	11.7	Ethane	31.0	Ethylene	4.80E4	Ethylene	986	Butane	54.9
Ethanol	9.71	Ethanol	30.0	Propylene	4.17E4	*m*-Xylene	780	Ethane	29.6
Ethane	6.55	Butane	28.7	2-Methylpropene	3.95E4	Formaldehyde	540	Ethanol	28.6
Propane	5.06	Ethylene	18.7	Ethanol	2.97E4	Propylene	5.32	Toluene	24.6
Toluene	4.76	Propane	16.4	Formaldehyde	2.91E4	Toluene	531	Propane	23.4
Pentane	4.63	Methanol	11.8	*m*-Xylene	2.45E4	Ethanol	497	Pentane	21.8
2-Methylbutane	4.27	Formaldehyde	10.5	Butane	2.03E4	Butane	450	2-Methylbutane	20.1
Ethylene	3.71	Pentane	9.11	1,2,4-TMB[a]	1.50E4	*o*-Xylene	279	Ethylene	17.9
Hexane	3.42	2-Methylbutane	8.41	Toluene	1.24E4	1,2,4-TMB[a]	261	Hexane	16.2
Methanol	2.64	Toluene	7.35	Pentane	1.08E4	2-Methylbutane	219	*m*-Xylene	13.5
m-Xylene	2.64	Acetylene	6.68	2-Methylbutane	9.46E3	Pentane	214	2-Methylpropane	11.7
Trichloroethene	2.56	2-Methylpropene	6.12	Hexane	8.93E3	2-Methylpropene	183	Heptane	9.08
2-Methylpropene	2.50	Hexane	5.65	*o*-Xylene	7.30E3	Hexane	154	Ethylbenzene	8.51
Formaldehyde	2.22	Propylene	5.42	*p*-Xylene	6.57E3	*p*-Xylene	135	Propylene	7.77
Acetone	2.14	Acetone	5.25	Propane	5.39E3	Ethylbenzene	131	Benzene	7.52
Heptane	1.91	*m*-Xylene	3.54	Heptane	5.29E3	2-Methylpropane	104	Acetone	7.52
Ethylbenzene	1.66	Trichloroethene	2.78	Ethylbenzene	4.68E3	Propane	86.5	Octane	7.23
Propylene	1.61	2-Butanone	2.75	Octane	4.43E3	Heptane	72.9	*o*-Xylene	6.84
Octane	1.52	Heptane	2.71	2-Propanol	4.12E3	Methanol	69.8	1,2,4-TMB[a]	6.65

Benzene	1.44	Benzene	2.62	2-Methylpropane	3.89E3	Trichloroethene	66.4	Acetylene	6.38
2-Butanone	1.39	2-Propanol	2.59	Methanol	3.31E3	Ethane	61.1	*p*-Xylene	5.86
o-Xylene	1.34	2-Methylpropene	2.56	Decane	3.30E3	Octane	50.2	Methanol	5.61
1,2,4-TMB[a]	1.31	Ethylbenzene	2.23	Ethane	2.30E3	2-Butanone	49.1	2-Butanone	5.25
Dichloromethane	1.25	Dichloromethane	2.09	Butyl acetate	1.93E3	Acetylene	40.1	Formaldehyde	5.03
Butyl acetate	1.25	Octane	1.89	Acetylene	1.80E3	Benzene	38.5	2-Methylpropene	4.89
Acetylene	1.22	*o*-Xylene	1.79	Benzene	1.10E3	Butyl acetate	38.0	Decane	4.77
p-Xylene	1.14	Ethyl acetate	1.61	2-Butanone	9.89E2	Acetone	27.4	Butyl acetate	4.28
2-Propanol	1.09	1,2,4-TMB[a]	1.55	Ethyl acetate	7.75E2	Decane	24.8	2-Propanol	3.71
2-Methylpropene	1.01	*p*-Xylene	1.53	Acetone	3.46E2	2-Propanol	23.7	Ethyl acetate	3.08
Ethyl acetate	1.00	Butyl acetate	1.53	Dichloromethane	6.4.7E1	Ethyl acetate	21.3	Trichloroethene	2.65
Decane	1.00	Decane	1.00	Trichloroethene	1.00	Dichloromethane	1.00	Dichloromethane	1.00

[a] 1,2,4-TMB = 1,2,4-Trimethylbenzene.
[b] Relative mass emissions (table I-C-2).
[c] Relative mass emissions/molecular weight.
[d] Relative molecular emissions × k(OH).
[e] Relative mass emissions × MIR.
[f] Relative molecular emissions × number of C-atoms molecule^{-1}.

relates to the relative greenhouse effect expected. To illustrate the changes in order that occur, note how the position of formaldehyde, highlighted by darkly framed boxes, and trichloroethene, highlighted by lightly framed boxes and grey background, changes in the columns, depending on the nature of the classification chosen. Formaldehyde emissions lie mid-range when ranked by mass, but the ranking climbs when placed on the basis of relative molecular emissions, relative rates of OH-radical attack, or relative rates of ozone generation in a polluted urban atmosphere. The formaldehyde position falls dramatically as one proceeds to the last column that lists the relative number of CO_2 molecules that each species will create ultimately by reactions in the troposphere. However, the impact of the conversion of all of the impurity VOCs present in the atmosphere to CO_2 causes only a very small increase in the the total CO_2 present in the atmosphere.

Trichloroethene mass emissions rank just above mid-column, but the ranking falls when emissions are placed on a molecular basis, falls further when scaled by relative rates of attack by OH, climbs somewhat on the basis of ozone comparison, but falls again when comparing CO_2 formation. The reporting of emission inventories has been expressed historically as mass emissions that are an important part of atmospheric pollution control and modeling. However, it is clear that the relative magnitude of these is not intended to reflect the relative impact of the emissions of a given compound on the chemistry of the atmosphere.

Detailed speciations of VOCs emitted from a variety of anthropogenic emission sources have been reported by Cass and colleagues (Schauer et al., 1999a, b, 2001, 2002a, b). Table I-C-6 lists the tailpipe emissions for C_1 through C_{32} organic compounds from catalyst- and noncatalyst-equipped gasoline-powered light-duty (or light goods) vehicles (<8,500 lb) The values given in table I-C-6 were derived from measurements of nine catalyst-equipped vehicles (Honda Civic, Ford Taurus, Toyota pickup truck, Chevrolet Astrovan, Toyota Celica, GMC pickup truck, Chrysler Reliant, Toyota Tercell, and Honda Accord) from model years 1981–1994 and two noncatalyst-equipped vehicles (1970 Volkswagen Vancamper and 1969 Chevrolet Camaro). These can be compared with the data in table I-C-7, where exhaust emissions for C_1–C_{30} organic compounds derived from a study of two medium-duty diesel trucks (1995 Isuzu 3.8-L turbo diesel and GMC Vandura 6.5-L diesel) are shown. It should be noted that the hydrocarbon emissions on a g km^{-1} basis from vehicles manufactured in 2008 are expected to be approximately a factor of 5 lower that those from the vehicles tested by Schauer et al. (1999b, 2002b), reflecting continuing improvements in emission control technology; see figure 3 in Wallington et al. (2006c) and table 2 in Wallington et al. (2008c).

There are several interesting features that can be seen from the data in table I-C-6. As expected, the total mass (g) of hydrocarbons emitted per km driven by the 1981–1994 model year catalyst-equipped vehicles, is substantially less (by approximately a factor of 100) than for the 1969 and 1970 model year noncatalyst-equipped vehicles. The difference reflects both improvements in engine design which reduce the level of hydrocarbons in the exhaust exiting the engine and the ∼95–99% efficiency of the catalyst system (Wallington et al., 2006c). The mass of the oxygenates emitted by the noncatalyst-equipped vehicles tested by Schauer et al. (2002b, 1999b) is 638 times

Table I-C-6. Exhaust emissions from gasoline-powered, light-duty vehicles (Schauer et al., 2002b)

	Tailpipe Emissions, μg km^{-1}				Gasoline Composition μg g^{-1}
	Catalyst-Equipped Vehicle		Noncatalyst Vehicle		
	Gas Phase	Particle Phase	Gas Phase	Particle Phase	
Hydrocarbons					
n-Alkanes					
Methane	38,000		330,000		
Ethane	7,770		36,900		
Propane	650		9300		100
n-Butane	1,620		191,000		7,620
n-Pentane	4,290		536,000		27,600
n-Hexane	2,900		410,000		
n-Heptane	1,820		268,000		9,700
n-Octane	1,070		131,000		6,380
n-Nonane	430		45,300		2,080
n-Decane	3,090		42,600		1,120
n-Undecane	Nd[a]		Nd		Nd
n-Dodecane	83.9		1,770		136
n-Tridecane	48.2		1,280		96.4
n-Tetradecane	18.4		212		13.8
n-Pentadecane	6.2		112		14.2
n-Hexadecane	6.4	0.2	92		8.3
n-Heptadecane	4.4		130		5.6
n-Octadecane	2	2.2	150	13	7.8
n-Nonadecane	2		92	75	4.7
n-Eicosane	1.8	0.8	100	190	2.5
n-Heneicosane	1.8	0.1	32	214	1.9
n-Docosane		0.8	29.8	228	1.5
n-Tricosane	0.5	1.9	11.9	191	2.2
n-Tetracosane		0.9	8.9	503	1.7
n-Pentacosane		2.7	14.3	489	1.7
n-Hexacosane		0.8	9.6	764	1
n-Heptacosane		0.6	2.4	391	
n-Octacosane			3	119	
n-Nonacosane			2.8	95	
Branched Alkanes					
Isobutane	130				1,040
2,2-Dimethylpropane					110
Isopentane	11,300		1,720,000		79,200
2,2-Dimethylbutane	800		195,000		5,720
2,3-Dimethylbutane	2,140		298,000		12,900
2-Methylpentane	6,310		827,000		36,900
3-Methylpentane	3,760		512,000		22,700
2,4-Dimethylpentane	2,920		354,000		15,700

(*continued*)

Table I-C-6. (*continued*)

	Tailpipe Emissions, μg km^{-1}				Gasoline Composition μg g^{-1}
	Catalyst-Equipped Vehicle		Noncatalyst Vehicle		
	Gas Phase	Particle Phase	Gas Phase	Particle Phase	
Branched Alkanes (*continued*)					
2-Methylhexane	2,880		372,000		15,300
2,3-Dimethylpentane	5,340		714,000		29,400
3-Methylhexane	2,950		415,000		16,200
2,2,4-Trimethylpentane	8,200		1,080,000		34,600
2,5-Dimethylhexane	1,500		205,000		5,070
2,4-Dimethylhexane	1,650		219,000		6,460
2,3,4-Trimethylpentane	2,510		412,000		13,000
2,3-Dimethylhexane	1,040		148,000		5,600
2-Methylheptane	1,340		159,000		6,260
3-Ethylhexane	1,640		205,000		810
2,2,4-Trimethylhexane					190
Norfarnesane	65.5		638		106
Farnesane	18.8		332		22
2,6,10-Trimethyltridecane	8.8		80		15.5
Norpristane	4.6		188		4.3
Pristane	7.8		225		12.1
Phytane	3.2		252		6.9
n-Alkenes					
Ethene	29,200		716,000		
Propene	14,900		436,000		10
1-Butene					170
trans-2-Butene	2,190		69,300		630
cis-2-Butene	900		36,100		720
1-Pentene	400		51,800		1,480
trans-2-Pentene	710		77,400		4,120
cis-2-Pentene	440		42,300		2,290
1-Hexene	430		18,400		770
trans-2-Hexene	300		31,600		1,860
cis-2-Hexene	170		17,300		1,050
Branched Alkenes					
Isobutene	15,600		427,000		170
3-Methyl-1-butene	350		22,500		380
2-Methyl-1-butene	1,120		84,600		2,690
2-Methyl-2-butene	2,270		126,000		6,360
4-Methyl-1-pentene					300
2-Methyl-1-pentene	230		26,600		1,250
2-Methyl-2-pentene	480		50,400		2,700
Alkynes					
Ethyne	12,800		865,000		
Cycloalkanes					
Cyclopentane	780		85,400		4,110
Methylcyclopentane	4,320		604,000		26,200

(*continued*)

Table I-C-6. (*continued*)

	Tailpipe Emissions, μg km^{-1}				Gasoline Composition μg g^{-1}
	Catalyst-Equipped Vehicle		Noncatalyst Vehicle		
	Gas Phase	Particle Phase	Gas Phase	Particle Phase	
Cycloalkanes (*continued*)					
Cyclohexane	1,440		238,000		8,900
Methylcyclohexane	1,860		274,000		7,870
Ethylcyclohexane					930
Nonylcyclohexane			17		7.8
Decylcyclohexane	1.2		14		12.9
Undecylcyclohexane	0.84		16.7		
Dodecylcyclohexane	1.4		15.9		
Tridecylcyclohexane	0.91		22.4	21.5	
Tetadecylcyclohexane	0.67		21.3	66.1	
Pentadecylcyclohexane	1.3		20.4	162	
Hexadecylcyclohexane				206	
Heptadecylcyclohexane				362	
Octadecylcyclohexane				265	
Nonadecylcyclohexane				241	
Eicosylcyclohexane				144	
Heneicoscylcyclohexane				75	
Cycloalkenes					
Cyclopentene	480		31,700		1,120
Aromatic Hydrocarbons					
Benzene	11,900		473,000		7,530
Toluene	21,300		2,360,000		59,500
Ethylbenzene	4,180		434,000		12,800
m- and *p*-Xylene	14,300		1,720,000		50,500
o-Xylene	5,410		562,000		19,700
Isopropylbenzene					830
n-Propylbenzene	830		97,900		3,500
p-Ethyltoluene	4,040		385,000		6,080
m-Ethyltoluene	1,750		175,000		14,200
1,3,5-Trimethylbenzene	1,980		210,000		7,450
o-Ethyltoluene	1,610		142,000		4,800
1,2,4-Trimethylbenzene	5,720		602,000		24,600
Naphthalene	1,000		50,000		1,040
2-Methylnaphthalene	1,000		50,000		1,330
1-Methylnaphthalene	500		30,000		800
C_2-Naphthalenes	183		28,500		624
C_3-Naphthalenes	62.5		5,860		135
C_4-Naphthalenes	25.3		950		55.7
Acenaphthylene	37		2,180		
Acenaphthene	6.55		177		
Fluorene	9.72		358	20.1	4.35
C_1-Fluorene	6.34		398	388	10
C_2-Fluorene	10.5		490	384	17.1

(*continued*)

Table I-C-6. (*continued*)

	Tailpipe Emissions, μg km^{-1}				Gasoline Composition μg g^{-1}
	Catalyst-Equipped Vehicle		Noncatalyst Vehicle		
	Gas Phase	Particle Phase	Gas Phase	Particle Phase	
Aromatic Hydrocarbons (*continued*)					
Phenanthrene	21.7		622	434	9.24
Anthracene	3.69		148	106	4.35
3-Methylphenanthrene	2.92		236	181	6.01
2-Methylphenanthrene	3.35		291	195	9.64
2-Methylanthracene	1.14		94.1	66.7	5.54
9-Methylphenanthrene	2.47		131	107	4.49
1-Methylphenanthrene	1.63		122	65.1	3.91
C_2-MW 178 PAH	8.07		464	575	24.93
C_3-MW 178 PAH	1.51		176	216	10.76
Fluoranthene	4.25	0.069	160	152	1.15
Acephenanthrylene	0.58	0.012	50.8	57.8	0.04
Pyrene	4.28	0.077	160	217	3.38
C_1 MW-202 PAH	2.06		96.5	233	5.27
Benzo[*ghi*]fluoranthene	0.276	0.063	10.7	46.8	
Cyclopenta[*cd*]]pyrene		0.031	5	55.6	
Benz[*a*]anthracene	0.181	0.097	4.8	51.9	
Chrysene and Triphenylene	0.451	0.206	5.07	52.1	
C_1 MW 226 PAH		0.116			
C_1 MW 228 PAH		0.242	4.13	103	
Benzo[*k*]fluoranthene		0.083		32.7	0.28
Benzo[*b*]fluoranthene				37.3	
Benzo[*j*]fluoranthene		0.009		1.52	
Benzo[*e*]pyrene		0.15		38.2	6.79
Benzo[*a*]pyrene		0.021		41	
Perylene		0.031			2.79
Indeno[1,2,3-*cd*]fluoranthene		0.05		28.5	
Indeno[1,2,3-*cd*]pyrene		0.436		92	
Coronene				101	
Tricyclic Terpanes					
8β,13α-Dimethyl-14β-*n*-Butylpodocarpane	1.13	0.2	46.9	119	
8β,13α-Dimethyl-14β-[3′-Methylbutyl]podocarpane	0.46	0.14	20.2	76	
Diasteranes					
20S-13β(*H*),17α(*H*)-Diacholestane				73.6	
20R-13β(*H*),17α(*H*)-Diacholestane				45.2	
Hopanes					
22,29,30-Trisnorneohopane		0.038		125	
17α(*H*)-22,29,30-Trisnorhopane				69	
17-α(*H*),21β(*H*),29-Norhopane		0.019		282	

(*continued*)

Table I-C-6. (*continued*)

	Tailpipe Emissions, μg km^{-1}				Gasoline Composition μg g^{-1}
	Catalyst-Equipped Vehicle		Noncatalyst Vehicle		
	Gas Phase	Particle Phase	Gas Phase	Particle Phase	
Hopanes (*continued*)					
17α(*H*),21β(*H*)-Hopane		0.033		321	
22Rand S,17α(*H*),21β(*H*)-30-Homohopane				259	
22Rand S,17α(*H*),21β(*H*)-30-Bishomohopane				196	
Steranes					
20R-5α(*H*),14β(*H*)-Cholestane				109	
20S-5α(*H*),14β(*H*)-Cholestane				61	
20R-5α(H),14α(*H*),17α(*H*)-Cholestane				119	
20R and S-5α(H),14β(*H*),17β(H)-Ergostane				139	
20R and S-5α(H),14β(*H*),17β(H)-Sitostane				136	
Oxygenates					
Ethers					
Methyl *tert*-butyl ether (MTBE)	5,700		1,620,000		109,000
Ethyl *tert*-butyl ether (ETBE)	200		34,600		
tert-Amyl methyl ether (TAME)	Nd		Nd		550
Aliphatic Aldehydes					
Formaldehyde	8,690		884,000		Nd
Acetaldehyde	3,940		301,000		Nd
Propanal	640		60,000		Nd
Butanal and Isobutanal	370		31,000		Nd
Pentanal	490		27,000		Nd
Isopentanal	250		22,080		Nd
Hexanal	300		19,000		Nd
Heptanal	120		7,300		Nd
Octanal	190		2,600		Nd
Nonanal	30		2,300		Nd
Decanal	50		2,200		Nd
Undecanal	40		2,500		Nd
Dodecanal			870		Nd
Tridecanal			5,800		Nd
Unsaturated Aldehydes					
Crotonaldehyde	1,760		114,000		
Acrolein	60		3,800		
Methylacrolein	300		23,000		

(*continued*)

Table I-C-6. (*continued*)

	Tailpipe Emissions, μg km^{-1}				Gasoline Composition μg g^{-1}
	Catalyst-Equipped Vehicle		Noncatalyst Vehicle		
	Gas Phase	Particle Phase	Gas Phase	Particle Phase	
Aliphatic Ketones					
Acetone	1,190		42,000		
2-Butanone	470		32,000		
Aromatic Aldehydes					
Benzaldehyde	1,270		159,000		
o-Tolualdehyde	390		45,000		
m- and *p*-Tolualdehyde	1,340		145,000		
2,5-Dimethylbenzaldehyde	240		35,000		
Naphalenecarboxaldehydes	5.3				
Aromatic Ketones					
Indanone	30.6		908		
Fluorenone	15.7				
Xanthone	2		30.8		
9,10-Anthracenedione	0.849		25.4		
Dicarbonyls					
Glyoxal	170		28,000		
Methylglyoxal	50		10,000		
Biacetyl	40		1,800		
Other Carbonyls					
2-Furaldehyde			1,700		
n-Alkanoic Acids					
Octanoic acid	12.2		86		
Nonanoic acid	27.9		80.6		
Decanoic acid	9.3		54.7		
Undecanoic acid			75.6		
Heptadecanoic acid		0.26		90.6	
Octadecanoic acid		4.32		147	
Nonadecanoic acid				9.3	
Eicosanioic acid		0.16		14	
Alkanedioic Acids					
Octadecanedioic acid		4.1		42.4	
Nonadecanedioic acid		21.5		177	
Aromatic Acids					
Benzoic acid	124				
Methylbenzoic acids		0.74		55.4	
Other Compounds					
Benzofuran			200	29.2	
Dibenzofuran	5.6	3.43	42.2	4	
Dibenzothiophene	0.32		25.6		
Dibenzothiazole	12.3	0.4			

[a]Nd: Not determined

Table I-C-7. Exhaust emissions from diesel-fueled, medium-duty trucks (Schauer et al., 1999b)

Compound	Emissions, μg km^{-1}		Diesel Fuel Composition, μg g^{-1}
	Gas Phase	Particle Phase	
n-Alkanes			
n-Butane	3,830.0		Nd[a]
n-Pentane	1,860.0		Nd
n-Hexane	470.0		Nd
n-Heptane	260.0		Nd
n-Octane	160.0		Nd
n-Nonane	Nd		Nd
n-Undecane	503.0		15,500
n-Tridecane	477.0		15,700
n-Tetradecane	629.0		13,500
n-Pentadecane	398.0	2.1	10,500
n-Hexadecane	711.0	8.6	10,100
n-Heptadecane	614.0	5.9	5,700
n-Octadecane	601.0	2.8	9,212
n-Nonadecane	411.0	3.8	7,020
n-Eicosane	206.0	95.7	6,530
n-Heneicosane	65.8	40.5	5,220
n-Docosane		52.0	4,340
n-Tricosane		45.5	2,670
n-Tetracosane		40.7	1,680
n-Pentacosane		26.1	730
n-Hexacosane		34.9	290
n-Heptcosane		25.7	180
n-Octcosane		19.7	36
n-Nonacosane		6.1	
Branched Alkanes			
Isopentane	2,740.0		Nd
2,2-Dimethylbutane	310.0		Nd
2,3-Dimethylbutane	570.0		Nd
2-Methylpentane	930.0		Nd
3-Methylpentane	670.0		Nd
2,4-Dimethylpentane	410.0		Nd
2-Methylhexane	570.0		Nd
2,4-Dimethylhexane	720.0		Nd
3-Methylhexane	310.0		Nd
2,2,4-Trimethylpentane	1,240.0		Nd
2,5-Dimethylhexane	50.0		Nd
2,4-Dimethylhexane	50.0		Nd
2,3,4-Trimethylpentane	310.0		Nd
2,3-Dimethylhexane	160.0		Nd
2-Methylheptane	100.0		Nd
3-Ethylhexane	210.0		Nd
Norfarnesane	360.0		16,300
Farnesane	434.0	4.1	9,220
2,6,10-Trimethyltridecane	367.0	1.2	8,830
Norpristane	566.0	4.9	8,670
Pristane	443.0		5,840
Phytane	439.0		5,770

(*continued*)

Table I-C-7. (*continued*)

Compound	Emissions, μg km^{-1}		Diesel Fuel Composition, μg g^{-1}
	Gas Phase	Particle Phase	
n-Alkenes			
Ethene	8,560.0		Nd
Propene	780.0		Nd
trans-2-Butene	520.0		Nd
cis-2-Butene	260.0		Nd
Isobutene	1,140.0		Nd
3-Methyl-1-butene	160.0		Nd
trans-2-Pentene	50.0		Nd
trans-2-Hexene	160.0		Nd
cis-2-Hexene	100.0		Nd
Branched Alkenes			
2-Methyl-1-butene	260.0		Nd
2-Methyl-2-pentene	210.0		Nd
Diolefins			
1-3-Butadiene	310.0		Nd
Alkynes			
Ethyne	4,600.0		Nd
Cycloalkanes			
Cyclopentane	410.0		Nd
Methylcyclopentane	620.0		Nd
Cyclohexane	210.0		Nd
Methylcyclohexane	520.0		Nd
Pentylcyclohexane	83.9		
Hexylcyclohexane	14.9		830
Heptylcyclohexane	20.0		730
Octylcyclohexane	26.2		500
Nonylcyclohexane	24.7		490
Decylcyclohexane	38.2		420
Undecylcyclohexane	23.9		430
Dodecylcyclohexane	16.8		200
Tridecylcyclohexane	16.5		170
Tetradecylcyclohexane	15.9		160
Pentadecylcyclohexane	12.8		150
Hexadecylcyclohexane			
Heptadecylcyclohexane			
Octadecylcyclohexane			
Nonadecylcyclohexane			
Cycloalk enes			
Cyclopentene	210.0		Nd
Aromatic hydrocarbons			
Benzene	2,740.0		Nd
Toluene	3,960.0		Nd
Ethylbenzene	470.0		Nd
m- and *p*-Xylene	2,330.0		Nd
o-Xylene	830.0		Nd
n-Propylbenzene	100.0		Nd

(*continued*)

Table I-C-7. (*continued*)

Compound	Emissions, μg km^{-1}		Diesel Fuel Composition, μg g^{-1}
	Gas Phase	Particle Phase	
Aromatic hydrocarbons (*continued*)			
p-Ethyltoluene	520.0		Nd
m-Ethyltoluene	210.0		Nd
1,3,5-Trimethylbenzene	260.0		Nd
1,2,4-Trimethylbenzene	880.0		Nd
Naphthalene	617.0		600
2-Methylnaphthalene	611.0		980
1-Methylnaphthalene	378.0		580
C_2-Naphthalenes	542.0		2,050
C_3-Naphthalenes	240.0	130.0	1,360
C_4-Naphthalenes	97.3	98.6	760
Acenaphthylene	70.1		
Acenaphthene	19.3		
Fluorene	34.6	9.5	52
C_1-Fluorene	65.2	83.0	190
Phenanthrene	93.1	47.0	57
Anthracene	12.5	10.9	5
3-Methylphenanthrene	30.3	29.4	51
2-Methylphenanthrene	42.0	35.6	45
2-Methylanthracene	10.4	10.4	6
9-Methylphenanthrene	22.9	22.0	35
1-Methylphenanthrene	17.0	17.8	28
C_2 MW 178 PAH	196.0	57.2	2,080
C_3 MW 178 PAH	97.4	97.5	120
Fluoranthene	53.0	56.6	
Acephenanthrylene	12.0	16.2	
Pyrene	71.9	88.5	64
C_1 MW 202 PAH	39.0	81.0	290
Benzo[*ghi*]fluoranthene	5.8	19.8	
Cyclopenta[*cd*]pyrene	2.1	3.5	
Benz[*a*]anthracene	3.0	7.8	
Chrysene and Triphenylene	3.4	15.6	
C_1 MW 228 PAH		6.5	
Tricyclic Terpanes			
8β,13α-dimethyl-14β-*n*-butylpodocarpane	44.0	10.6	2.1
8β,13α-dimethyl-14β-[3′-methylbutyl]-Podocarpane	13.8	4.5	0.6
Diasteranes			
20S-13β(*H*)-17α(*H*)-Diacholestane	1.4		

(*continued*)

Table I-C-7. (*continued*)

Compound	Emissions, μg km^{-1}		Diesel Fuel Composition, μg g^{-1}
	Gas Phase	Particle Phase	
Hopanes			
18α(*H*)-22,29,30-Trisnomeohopane	2.7		
17α(*H*)-22,29,30-Trisnorhopane	1.0		
17α(*H*),21β(*H*)-29-Norhopane	11.3		
17α(*H*),21β(*H*)-hopane	11.4		
Steranes			
20R,5α(*H*),14β(*H*)-17β(*H*)-cholestane	0.8		
20R,5α(*H*),14α(*H*)-17α(*H*)-cholestane	1.2		
20R and S,5α(*H*),14β(*H*)-17β(*H*)-ergostane	3.2		
20R and S,5α(*H*),14β(*H*)-17β(*H*)-sitostane	2.6		
Oxygenates			
Aliphatic Aldehydes			
Formaldehyde	22,300.0		Nd
Acetaldehyde	41,800.0		Nd
Propanal	14,000.0		Nd
Butanal	1,300.0		Nd
Hexanal	2,200.0		Nd
Heptanal	3,200.0		Nd
Octanal	3,100.0		Nd
Nonanal	4,400.0		Nd
Decanal	2,800.0		Nd
Undecanal	2,600.0		Nd
Dodecanal	1,200.0		Nd
Tridecanal	2,000.0		Nd
Olefinic Aldehydes			
Crotonaldehyde	13,400.0		Nd
Acrolein	3,400.0		Nd
Methacrolein	4,000.0		Nd
Aliphatic Ketones			
Acetone	22,000.0		Nd
Butanone	7,500.0		Nd
Aromatic Aldehydes			
Benzaldehyde	3,800.0		Nd
Acetophenone	5,100.0		Nd
2,5-dimethylbenzaldehyde	4,100.0		Nd

(*continued*)

Table I-C-7. (*continued*)

Compound	Emissions, μg km^{-1}		Diesel Fuel Composition, μg g^{-1}
	Gas Phase	Particle Phase	
Aromatic Ketones			
Indanone	69.5		
Fluorenone	34.6	9.8	
Xanthone	12.4	12.4	
Dicarbonyls			
Glyoxal	2,100.0		Nd
Methylglyoxal	1,700.0		Nd
Biacetyl	900.0		Nd
n-Alkanoic Acids			
Octanoic acid	125.0		Nd
Nonanoic acid	240.0		Nd
Decanoic acid	72.9		Nd
Undecanoic acid	206.0		Nd
Dodecanoic acid	58.5		Nd
Tridecanoic acid	13.1		Nd
Tetradecanoic acid	5.3		Nd
Heptadecanoic acid			Nd
Octadecanoic acid			Nd
Nonadecanoic acid			Nd
Eicosanoic acid			Nd
Alkanedioic Acids			
Octanedioic acid		138.0	
Nonanedioic acid		176.0	
Aromatic Acids			
Benzoic acid	1,260.0		Nd
Methylbenzoic acids	772.0	26.7	Nd
Other Compounds			
Benzofuran	53.2		
Dibenzofuran	28.7	6.0	29.0
Dibenzothiophene	2.0		
Dibenzothiazole	251.0		
Unresolved complex mixture	53,800	41,400	Nd

[a]Nd: Not determined.

greater than for the catalyst-equipped vehicles. For the catalyst-equipped vehicles the ratio of OVOC/HC emissions is 0.032. For the noncatalyst-equipped vehicles, the ratio of OVOC/HC emissions is 0.16. The lower OVOC/HC emission ratio for the catalyst-equipped vehicles reflects the fact that, in general, oxygenated compounds are more reactive than the hydrocarbons from which they are derived, and catalyst systems are more efficient for more reactive compounds. The fractions of the total products that appear in the particle phase compared to those that appear in the gas phase are relatively small for both types of gasoline-fueled vehicles: i.e., 3.7×10^{-4} and 3.3×10^{-4} for the catalyst-equipped vehicle and the vehicle with no catalyst, respectively.

From their roadside measurements of carbon monoxide and nitric oxide using spectroscopic measurements of vehicle emission, Bishop and Stedman (1989, 1990) concluded that between 7 and 10% of the 60,000 vehicles monitored were responsible for approximately 50% of the carbon monoxide emissions. Probably a major portion of the observed increased CO from the high-emitting vehicles resulted from deficient or inoperative catalytic converters. Obviously, uncontrolled exhaust emissions from vehicles can be major sources of oxygenates and other pollutants. Recent on-road measurements of emissions in Chicago, Illinois; Denver, Colorado; Los Angeles, California, and Phoenix, Arizona show large fuel-specific tailpipe emissions reductions have occurred during the period 1997–2007 (Bishop and Stedman, 2008); CO emissions decreased between 56% (Denver) and 71% (Chicago); hydrocarbon emissions decreased between 27% (Phoenix) and 63% (Denver); and NO emissions dropped between 48% (West Los Angeles) and 68% (Chicago). These reductions are the result of continued improvement in function and durability of vehicle emission control systems.

There are several interesting features of table I-C-7 related to the emission of the diesel-fueled, medium-duty trucks. Aldehydes are the dominant class of organic compounds identified and represent approximately 38% of the total mass of organic compounds. Acetaldehyde, acetone, and formaldehyde are the three most prominent individual compounds that together comprise 27% of the total mass. Ketones, alkanes, alkenes, and aromatic and carboxylic acids identified in the exhaust account for 9.1, 6.4, 5.3, 5.2, and 0.9% of the total mass, respectively. Finally, unresolved compounds account for 29.5% of the mass. One might expect from the vapor pressure and molecular polarity considerations that the organic acid products would appear largely in the particle fraction; however, the analysis for these compounds in the particle fraction was not determined. As expected, the dicarboxylic acids appear in the particle phase. Recent estimates of emission factors of carbonyl compounds from diesel vehicles from measurement in air in a road tunnel in Hong Kong are broadly consistent with the emissions listed in table I-C-7 (Ho et al., 2007a, 2007b).

I-C-2. Generation of the Oxygenates through Atmospheric Oxidation of Hydrocarbons in the Troposphere

Hydrocarbons emitted into the atmosphere react with OH and other transient oxidants (NO_3 radicals, O_3, Cl-atoms) to form oxygenates. Hydrocarbons have a wide variety of atmospheric lifetimes. Methane is the least reactive hydrocarbon and has an atmospheric lifetime with respect to OH radicals of about 10 years. The lifetimes (days) of ethane, propane, *n*-butane, and *n*-decane are about 47, 11, 4.9, and 1, respectively. Alkenes are more reactive than alkanes of the same carbon number and are transformed into oxygenates much more quickly by reactions with OH and O_3. For example, the lifetimes for reaction with OH for ethene, propene, and *trans*-2-butene are about 1.3 days, 10 h, 4.3 h, respectively. In addition, the alkenes react rapidly with ozone to form oxygenates. In the presence of 60 ppb of O_3, the lifetimes of ethene, propene, and *trans*-2-butene with repect to reaction with ozone are ~4.9 days, 18 h, and 1.0 h, respectively. Of course, the nature of the products formed by reactions of the hydrocarbons with

OH and O_3 are a function of the hydrocarbon reacting (for examples, see Calvert et al., 2000, 2002, 2008).

Oxidation of a given hydrocarbon passes through a variety of oxygenates as it progresses toward the final products of CO_2 and H_2O. In illustration of this, consider the atmospheric oxidation of the simple hydrocarbon, *n*-butane, outlined in figures I-C-2a, b, c, d, e, f. In figure I-C-2a, the first steps in the atmospheric oxidation are shown with the formation of 2-butanone, butanal, ethanal, 4-hydroxybutanal, and the subsequent atmospheric oxidation of the butanal product. The intermediate products of the reaction pathways are shown in enlarged, bold type in each of the figures. For simplification, the NO_2 product of the $RO_2 + NO$ reactions is not shown in these figures. Further steps in the atmospheric oxidation of the products of butane are shown in the subsequent panels: figure I-C-2b, 4-hydroxybutanal and 3-hydroxypropanal; figure I-C-2c, butanedial and propanedial; figure I-C-2d, 2-butanone and biacetyl; figure I-C-2e, 2-hydoxyethanal and propanal; figure I-C-2f, glyoxal, acetaldehyde, formaldehyde, and carbon monoxide. Note that even with one of the smallest hydrocarbons, butane, its atmospheric oxidation leads to 14 different carbonyl species. In addition to these products, and not shown in the figures I-C-2, several other oxygenates are formed. Each of the 11 alkyl peroxy radicals involved in this oxidation will react in part to form alcohols in one of the channels of the disproportionation reactions with CH_3O_2, $RO_2 + CH_3O_2 \rightarrow CH_2O + ROH + O_2$. In addition, each RO_2 will react in part with HO_2 radicals to generate alkyl hydroperoxides: $RO_2 + HO_2 \rightarrow RO_2H + O_2$, and with NO to form alkyl nitrates, $RO_2 + NO \rightarrow RONO_2$. Thus, in the atmospheric oxidation of butane, especially in remote regions of low NO_x, we expect the formation of the following alcohols: $CH_3CH_2CH_2CH_2OH$, $CH_3CH(OH)CH_2CH_3$, $HOCH_2CH_2CH_2CH_2OH$, $CH_3C(O)C(O)CH_2OH$, $CH_3CH_2CH_2OH$, $HOCH_2CH_2CH_2OH$, $CH(O)CH_2CH_2OH$, CH_3CH_2OH, $HOCH_2CH_2OH$, $HC(O)CH_2OH$, CH_3OH. In addition to the alcohol products, aldehydes are expected to form in one channel of the CH_3O_2–RO_2 reactions: CH_2O, CH_3CHO, $HOCH_2CHO$, $HC(O)C(O)H$, CH_3CH_2CHO, $HOCH_2CH_2CHO$, $CH_2CH_2CH_2CHO$, $HC(O)CH_2CHO$, $HOCH_2CH_2CH_2CHO$, and $CH_3C(O)C(O)CHO$. Through the reaction of the peroxy alkyl radicals with NO, we expect formation of the following nitrates, especially in the NO_x-rich regions of the troposphere: $CH_3CH_2CH_2CH_2ONO_2$, $CH_3CH(ONO_2)CH_2CH_3$, $HOCH_2CH_2CH_2CH_2ONO_2$, $CH_3C(O)C(O)CH_2ONO_2$, $CH_3CH_2CH_2ONO_2$, $HOCH_2CH_2CH_2ONO_2$, $CH(O)CH_2CH_2ONO_2$, $CH_3CH_2ONO_2$, $HOCH_2CH_2ONO_2$, $HC(O)CH_2ONO_2$, CH_3ONO_2; for examples, see Atkinson et al. (1982c, 1984a). The alcohol and aldehyde products will undergo further oxidation through attack by OH radicals at rapid rates during sunlight hours (see chapter II). However, the alkyl nitrates are rather longer lived in the atmosphere and act as a temporary storage for NO_x. They eventually return alkoxy radicals and NO_2 to the pool of radical transient products (see chapters VIII and IX).

The peroxyacyl radicals $CH_3C(O)O_2$, $HC(O)C(O)O_2$, $C_2H_5C(O)O_2$, $HC(O)CH_2C(O)O_2$, $HOCH_2CH_2C(O)O_2$, $CH_3CH_2CH_2C(O)O_2$, $HOCH_2CH_2CH_2C(O)O_2$, $HC(O)CH_2CH_2C(O)O_2$, $HC(O)CH_2C(O)O_2$ formed from OH attack on the aldehydes will react not only with NO as shown in the reaction sequences given in figures I-C-2, but they react with NO_2 as well to form

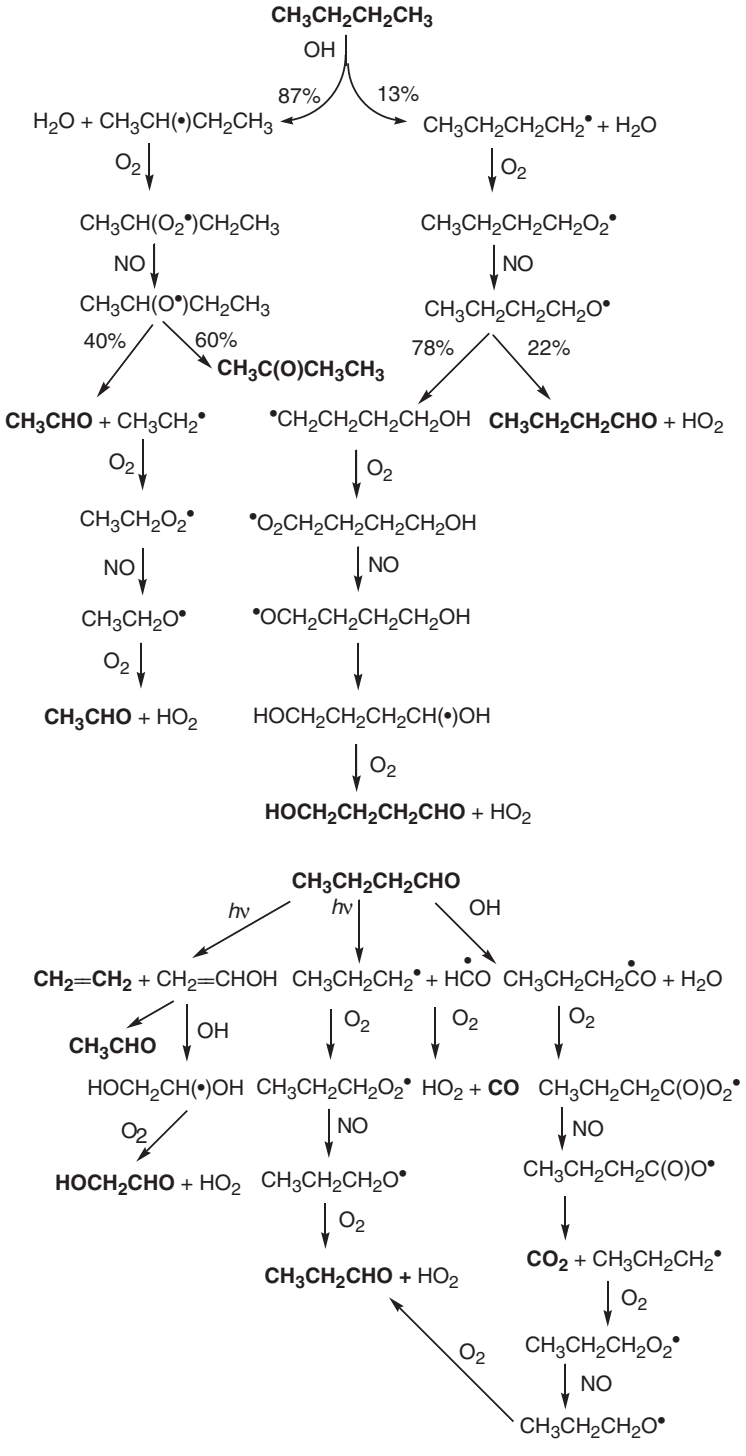

Figure I-C-2a. The mechanisms of formation of oxygenate products in the atmospheric oxidation of *n*-butane. Shown here are the initial steps in the oxidation of *n*-butane that leads to the oxygenates highlighted in larger, bold type. Subsequent steps in the degradation of the butanal product are shown in the lower portion of this figure.

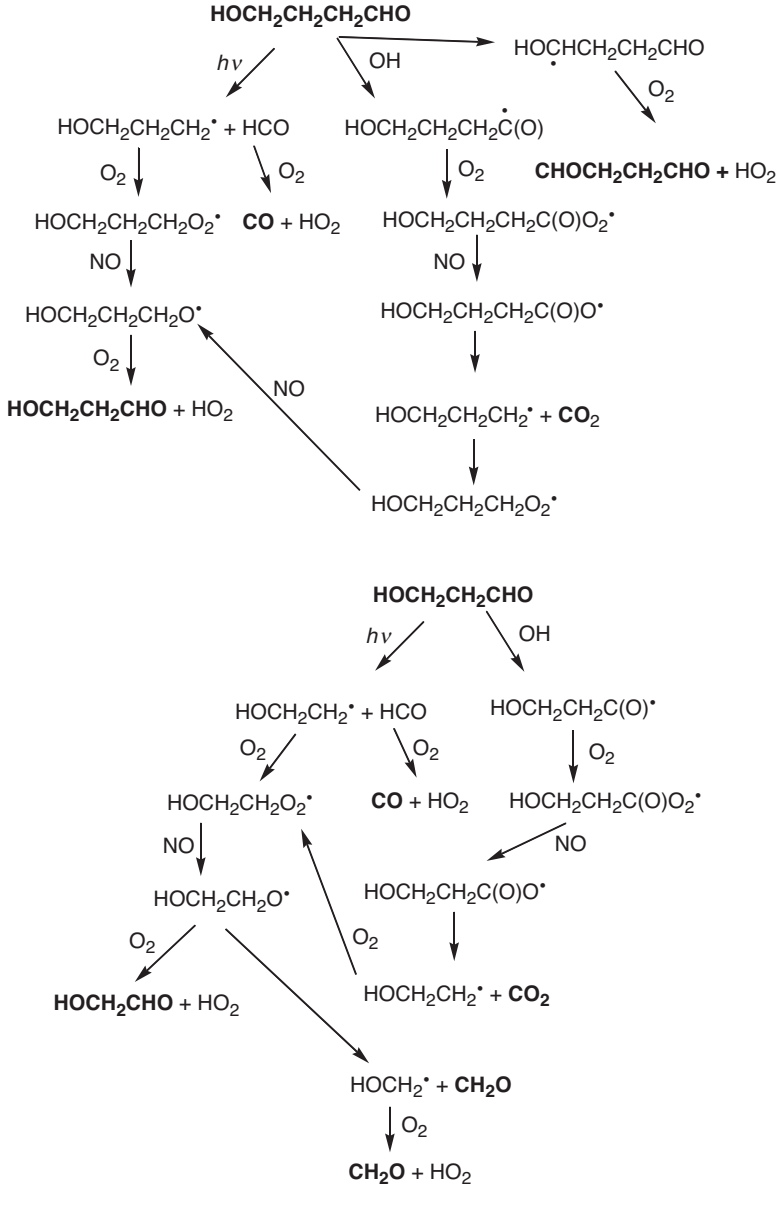

Figure I-C-2b. Steps in the continued atmospheric oxidation of products of *n*-butane: shown here are the reaction pathways in the atmospheric oxidation of $HOCH_2CH_2CH_2CHO$, and $HOCH_2CH_2CHO$.

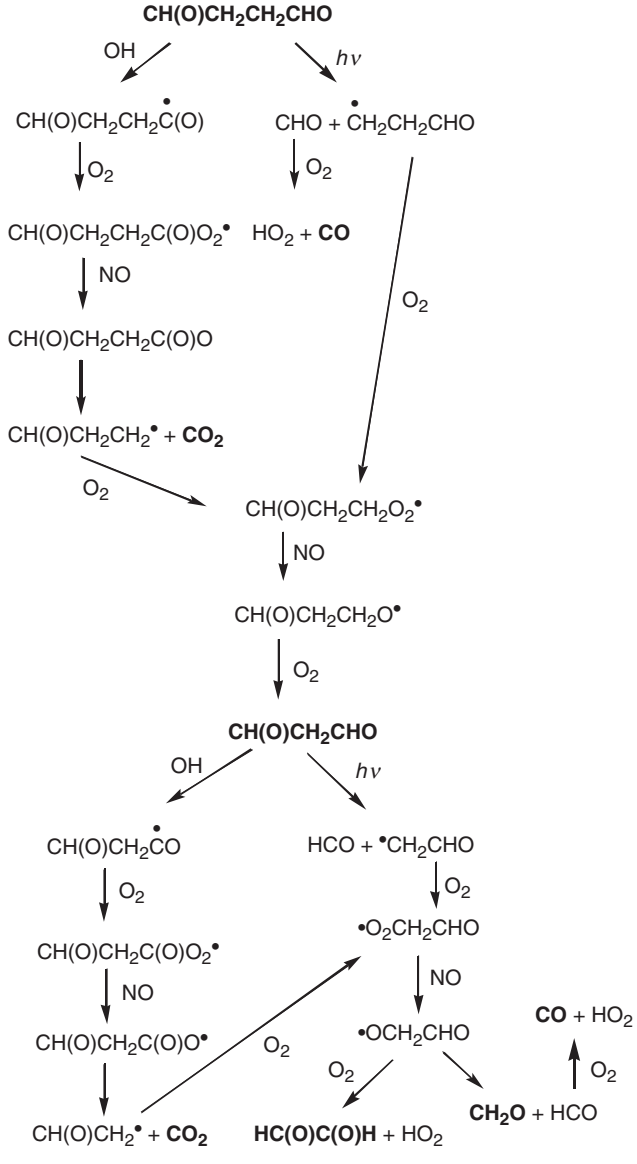

Figure I-C-2c. Steps in the continued atmospheric oxidation of products of *n*-butane: shown here are the reaction pathways in the atmospheric oxidation of $HC(O)CH_2CH_2CHO$ and $CH(O)CH_2CHO$.

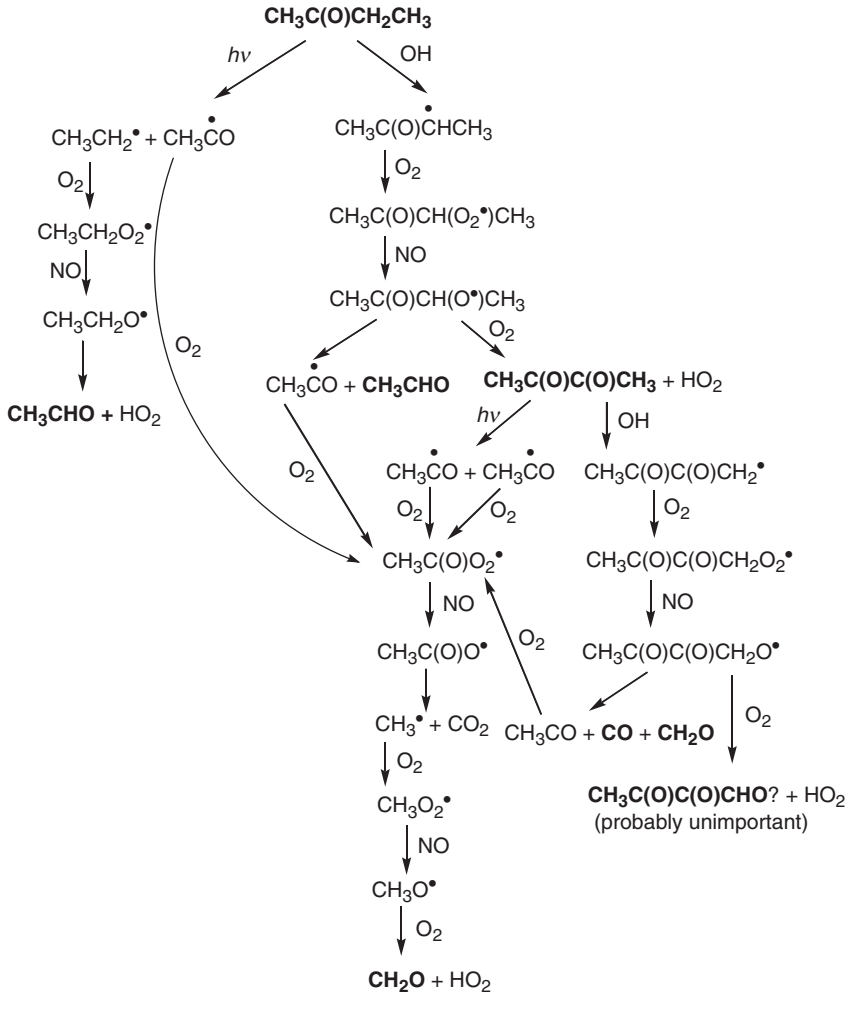

Figure I-C-2d. Steps in the continued atmospheric oxidation of products of *n*-butane. Shown here are the pathways in the atmospheric oxidation of $CH_3C(O)CH_2CH_3$ and $CH_3C(O)C(O)CH_3$.

the peroxyacyl nitrates, $CH_3C(O)O_2NO_2$, $HC(O)C(O)O_2NO_2$, $HOCH_2C(O)O_2NO_2$, $CH_3CH_2C(O)O_2NO_2$, $HC(O)CH_2C(O)O_2NO_2$, $HOCH_2CH_2C(O)O_2NO_2$, $CH_3CH_2CH_2C(O)O_2NO_2$, $HOCH_2CH_2CH_2C(O)O_2NO_2$, and $HC(O)CH_2CH_2C(O)O_2NO_2$. These compounds are also temporary sinks for NO_x in the atmosphere. They are thermally less stable than the organic nitrates, and in the lower atmosphere they eventually return NO_2 and $RC(O)O_2$ radicals to the radical pool.

The peroxyacyl radicals involved in the atmospheric oxidation of butane, particularly in atmospheric regions that are low in NO_x, will lead in part to the generation of organic acids and peroxy acids through two channels of the disproportionation reaction with HO_2: $RC(O)O_2 + HO_2 \rightarrow RC(O)OH + O_3$; $RC(O)O_2 + HO_2 \rightarrow RC(O)OOH + O_2$. The atmospheric oxidation of butane is expected to give the following

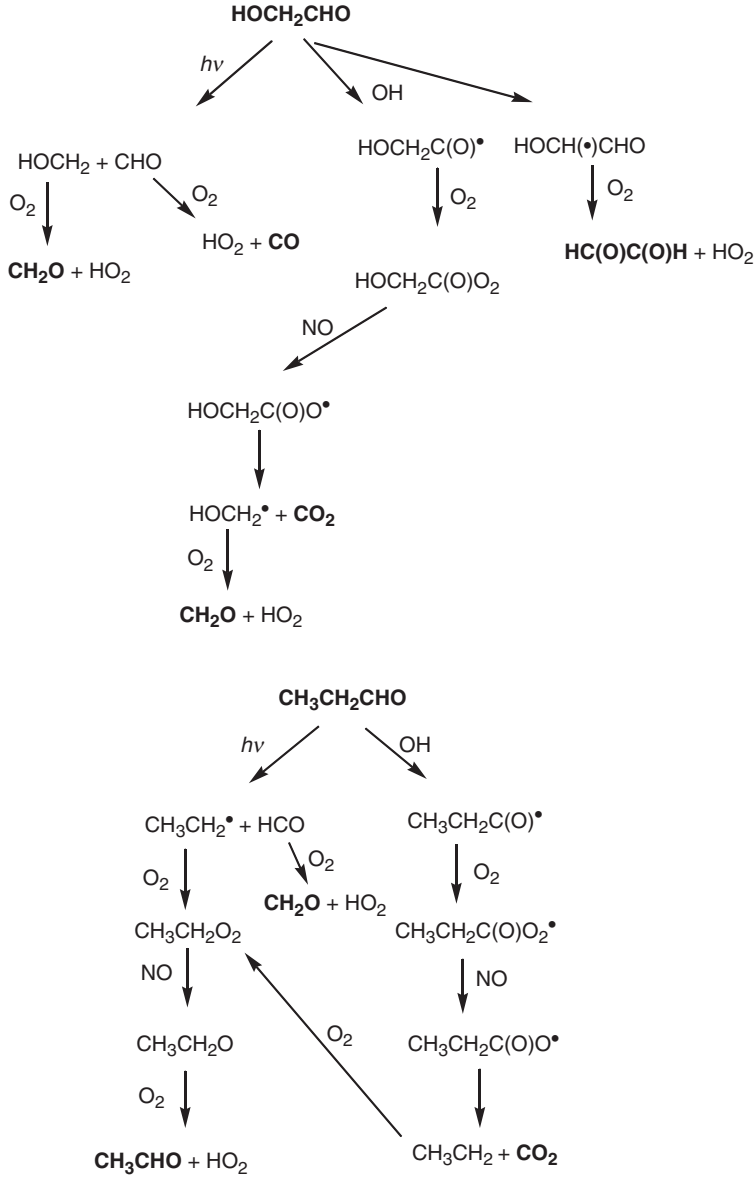

Figure I-C-2e. Steps in the continued atmospheric oxidation of products of *n*-butane. Shown here are the pathways in the atmospheric oxidation of $HOCH_2CHO$ and CH_3CH_2CHO.

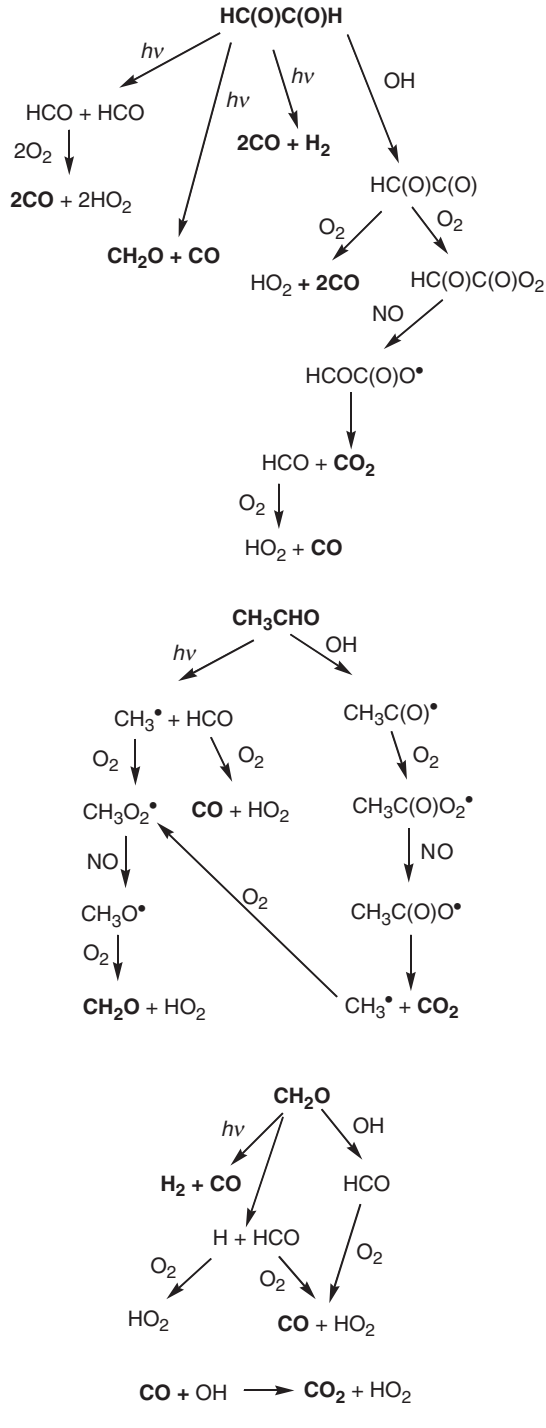

Figure I-C-2f. Steps in the continued atmospheric oxidation of products of *n*-butane. Shown here are the pathways in the atmospheric oxidation of HC(O)C(O)H, CH_3CHO, CH_2O, and CO.

organic acids and peroxy acids: $CH_3CH_2CH_2C(O)OH$, $HOCH_2CH_2CH_2C(O)OH$, $HC(O)CH_2CH_2C(O)OH$, $CH_3CH_2C(O)OH$, $HOCH_2CH_2C(O)OH$, $CH_3C(O)OH$, $HOCH_2C(O)OH$, $HC(O)CH_2CO_2H$, $HC(O)C(O)OH$, $CH_3CH_2CH_2C(O)O_2H$, $HOCH_2CH_2CH_2C(O)O_2H$, $HC(O)CH_2CH_2C(O)O_2H$, $CH_3CH_2C(O)O_2H$, $HOCH_2CH_2C(O)O_2H$, $HC(O)CH_2C(O)O_2H$, $CH_3C(O)O_2H$, $HOCH_2C(O)O_2H$, $HC(O)C(O)O_2H$. Addition of HO_2 to a formaldehyde product will lead in part to the formation of $HC(O)OH$ and HO_2CH_2OH (Su et al., 1979a, 1979b).

The smaller acids react slowly with OH in the atmosphere (see chapter VI). The larger acids have relatively low vapor pressures (see figure I-B-7), and important atmospheric loss mechanisms of organic acids from the gas phase include incorporation into atmospheric aerosols, rainout, and deposition on land or bodies of water.

Starting with the simple hydrocarbon, *n*-butane, we have seen that more than 65 different oxygenates are expected to be formed as its atmospheric oxidation proceeds. The atmospheric oxidation of the larger hydrocarbons leads to very much higher numbers of different oxygenates. The complex array of oxygenates that has been identified in the atmosphere represents only a small fraction of the actual number that are expected to be formed. It is clear that the atmospheric oxidation of the hydrocarbons is a major source of a vast array of oxygenates that have been found or are expected to be formed in the troposphere.

I-C-3. Biogenic Sources of Oxygenates

Vegetation releases many different hydrocarbons into the atmosphere; for example, isoprene, α-pinene, β-pinene, camphene, *p*-cymene, limonene, myrcene, etc. (e.g., see Guenther et al., 1995) as well as oxygenates including alcohols, aldehydes, ketones, ethers, and esters (e.g., see Winer et al., 1992; Atkinson and Arey, 2003b; Atkinson et al., 2008a). In the U.S. in 1992, the emissions of VOCs from global vegetation were estimated to be about 830 Tg year^{-1} (Tg = 10^{12} g), which exceeded that from anthropogenic sources, estimated to be about 19 Tg year^{-1} (see Fehsenfeld et al., 1992).

The Guenther et al. (1995) global model has been used to estimate emissions of natural volatile organic compounds (NVOCs) from terrestrial and ocean sources. The authors grouped these into four categories: isoprene, monoterpenes (e.g., α-pinene), other reactive volatile organic compounds (e.g., 2-methyl-3-buten-2-ol), and other volatile organic compounds (e.g., methanol). They estimated that the annual global VOC flux was 1150 Tg C, composed of 44% isoprene, 11% monoterpenes, 22.5% other reactive VOCs, and 22.5% other VOCs. They indicated that tropical woodlands (rain forest, seasonal, drought-deciduous, and savanna) contribute about half of all global natural VOC emissions. Table I-C-8, based on data given by Guenther et al. (1995), gives a comparison of emission rates that were predicted by global and regional models. As seen from table I-C-8, the estimates of isoprene emissions from the various models differ substantially. However, even the most modest of estimates of the natural organic compound emissions indicate that on global and regional scales, natural emissions are probably greater than those of anthropogenic origin. Guenther et al. (1995) point out that emissions of methanol, formaldehyde, acetaldehyde, and formic, acetic, and

Table I-C-8. A comparison of natural VOC emission rates predicted by the global model of Guenther et al. (1995) and various regional models. Estimates are given in units of 10^9g C year^{-1}

Country	Compounds	Global	Regional	References
Australia	Isoprene	19,600	25,000	Ayers and Gillett (1988)
Germany	Isoprene	370	40–149	Simpson et al. (1995)
	RVOC[a]	1,030	349	Luebkert and Schoepp (1989)
	RVOC	1,030	970	Adryukov and Timofeev (1989)
Hungary	Isoprene	120	25–113	Simpson et al. (1995)
	RVOC	260	22	Luebkert and Schoepp (1989)
	RVOC	260	70	Adryukov and Timofeev (1989)
	RVOC	260	156	Molnar (1990)
Spain	Isoprene	820	138–371	Simpson et al. (1995)
	RVOC	1,580	1,132	Luebkert and Schoepp (1989)
	RVOC	1,580	6,600	Adryukov and Timopfeev (1989)
Sweden	Isoprene	370	25–108	Simpson et al. (1995)
	Monoterpenes	370	370	Janson (1992)
	RVOC	1,040	930	Luebkert and Schoepp (1989)
	RVOC	1,040	600	Adryukov and Timofeev (1989)
United Kindom	Isoprene	110	2–55	Simpson et al. (1995)
	Terpenoids	145	167	Anastasi et al. (1991)
	RVOC	320	38	Luebkert and Schoepp (1989)
	RVOC	320	50	Adrykov and Timofeev (1989)
	RVOC	320	211	Anastasi et al. (1991)
United States	Isoprene	24,000	3,000–14,700	Lamb et al. (1993)
	Isoprene	24,000	4,900	Lamb et al. (1987)
	Isoprene	24,000	15,000	Zimmerman (1979)
	Monoterpenes	8,000	50,000	Zimmerman (1979)
	Monoterpenes	8,000	83,00–33,300	Lamb et al. (1993)
	RVOC	45,000	22,800–80,100	Lamb et al. (1993)
	RVOC	45,000	30,700	Lamb et al. (1987)

[a]RVOC includes isoprene, monoterpenes and other VOCs with a lifetime of less than 1 day (e.g., 2-methyl-3-buten-2-ol but not methanol).

pyruvic acids, may contribute significantly to the observed atmospheric concentrations of these compounds. For example, the measurements of MacDonald and Fall (1993) showed an average methanol flux of 5.4 μg C g^{-1} h^{-1} from leaves of diverse plant species. As noted by Guenther et al. (1995), if these measurements are representative, global emissions of methanol alone could account for more than 100 Tg C. The best estimate of the global source of methanol obtained by Jacob et al. (2005) is 240 Tg year^{-1}.

The 1996 MEGAN model of isoprene emissions (Guenther et al., 2006) predicted an annual global isoprene emission between 500 and 750 Tg isoprene, depending on the choice of driving variables, which include temperature, solar radiation, leaf area index, and plant functional type. Approximately 600 Tg year^{-1} were estimated using standard driving variables. Using temperature distributions simulated by global climate modes for the year 2100 and the MEGAN model, the authors estimated that isoprene emission could increase by more than a factor of 2 by the year 2100 (assuming no changes in the biosphere).

Simpson et al. (1999) have estimated and compared the nonmethane, volatile organic compound emissions (NMVOC) from biogenic and anthropogenic sources in Europe in the 1990s. They estimate that the biogenic emissions exceed those for man-made emissions in Albania, Bulgaria, Finland, Hungary, Latvia, Russia, Sweden, Ukraine, Croatia, Macedonia, and Serbia Montenegro. In the other countries of Europe, the estimated man-made emissions of NMVOCs somewhat exceed those from biogenic sources. The estimated totals for NMVOC emissions (Tg $year^{-1}$) for Europe are: biogenic, 13.5; man-made, 19.3.

In summary, measurements and modeling predictions of the extent of VOC emissions indicate the significance of natural sources in the atmospheric budget. On the global scale, these greatly exceed the anthropogenic input. The emissions of isoprene dominate those of other biogenic hydrocarbons. Methyl vinyl ketone and methacrolein are major primary products of the O_3 and OH radical initiated oxidation of isoprene. The primary products undergo further oxidation to give formaldehyde and other secondary products. The reactions of these compounds with OH and other transient species are reviewed in chapters IV and V, and their photodecomposition is reviewed in chapter IX.

I-D. Ambient Concentrations of the Oxygenates in the Lower Troposphere

Aldehydes and ketones are the dominant oxygenates found within the lower troposphere. As discussed in chapters IV, V, and IX, aldehydes and ketones are reactive towards OH radicals and readily undergo photodecomposition in sunlight. Table I-D-1 lists representative measurements of the ambient concentrations of several oxygenates. Data are shown for regions classified as Urban, Rural, and Remote.

I-D-1. The Urban Atmosphere

Aldehydes are the most important class of oxygenates in facilitating the generation of ozone. They react rapidly with OH radicals, and they photolyze readily. As seen in table I-D-1, the urban concentrations of formaldehyde and acetaldehyde are often quite high, especially in areas with limited or no pollution controls. Obviously, the rates of generation of aldehydes must be large to sustain the observed concentrations in the face of rapid removal reactions. Even the larger aldehydes are detectable in many urban atmospheres.

The ketones are also present in readily detectable amounts, with acetone concentrations usually dominating those of the other ketones. Several alcohols have been observed in urban atmospheres; methanol and ethanol are present at the highest concentrations. Methyl *tert*-butyl ether (MTBE) is observed in urban atmospheres where this compound is used as a gasoline additive. Esters are observed in urban atmospheres, especially near sources of solvent manufacture or heavy use. The smaller organic acids are usually observed in urban areas. Although their sources are not strong, their removal rates by reaction are small, as loss occurs largely by deposition on terrestrial or water surfaces, or by accumulation in aerosols. A number of dicarboxylic acids (C_2–C_{12})

Table I-D-1. Representative concentrations (ppbv) of some oxygenates in the lower troposphere

Urban	Rural	Remote	Range	Location	Reference
1) Aldehydes					
Formaldehyde					
11.3 ± 4.5			18.7 (max)	St. Louis, Missouri	Salas and Singh (1986)
12.3 ± 5.9			28.7 (max)	Denver, Colorado	Salas and Singh (1986)
19.0 ± 7.6			41 (max)	Riverside, California	Salas and Singh (1986)
14.3 ± 9.1			45.9 (max)	Staten Island, New York	Salas and Singh (1986)
18.5 ± 6.7			28.5 (max)	Pittsburgh, Pennsylvania	Salas and Singh (1986)
11.3 ± 3.8			15.6 (max)	Chicago, Illinois	Salas and Singh (1986)
15.5 ± 11.9			67.7 (max)	Downey, California	Salas and Singh (1986)
3.8 ± 8.3			22.5 (max)	Houston, Texas	Salas and Singh (1986)
	1–21			Sonchamp, France	Kalabokas et al. (1988)
	1–20			Montagny, France	Kalabokas et al. (1988)
2–33				Paris, France	Kalabokas et al. (1988)
24.4			58.7 (max)	Mexico City, Mexico (Morning Average)	Báez et al. (1989)
18.5			32.5 (max)	Mexico City, Mexico (Afternoon Average)	Báez et al. (1989)
	1.3 ± 0.5			Egbert, Ontario, Canada	Shepson et al. (1991)
	1.6 ± 1.0			Dorset, Ontario, Canada	Shepson et al. (1991)
			0–2.4	Venezuela, tropical savannah	Trapp and deServes (1995)
	3		6.1 (max)	Park, Candler Co., Georgia (1991)	Lee et al. (1995)
	2.1		4.8 (max)	Park, Candler Co., Georgia (1992)	Lee et al. (1995)
5.3 ± 2.4				Los Angeles, California	Grosjean et al. (1996a)
17				Rome, Italy	Possanzini et al. (1996)
		1.0	0.4–2.3	Schauinsland, Germany	Slemr et al. (1996)
3.92				Denver, Colorado (Winter)	Anderson et al. (1996)
2.3				Denver, Colorado (Spring)	Anderson et al. (1996)

(*continued*)

Table I-D-1. (*continued*)

Urban	Rural	Remote	Range	Location	Reference
Formaldehyde (*continued*)					
2.71				Denver, Colorado (Summer)	Anderson et al. (1996)
		0.154	0–0.586	Mauna Loa, Hawaii (Fall, 1991)	Heikes et al. (1996)
		0.143	0–0.410	Mauna Loa, Hawaii (Winter, 1992)	Heikes et al. (1996)
		0.193	0–0.326	Mauna Loa, Hawaii (Spring, 1992)	Heikes et al. (1996)
		0.1	0–0.320	Mauna Loa, Hawaii (Summer, 1992)	Heikes et al. (1996)
	1.02 ± 0.82		0.22–1.53	Chebogue Point, Nova Scotia	Tanner et al. (1996)
		0.28–2.2		Idaho Hill, Colorado	Fried et al. (1997)
2.6 ± 0.7				Copenhagen, Denmark	Granby et al. (1997a)
	0.9 ± 0.5			Copenhagen, Denmark	Granby et al. (1997a)
13.9				Albuquerque, New Mexico (1993)	Gaffney et al. (1997)
16.8				Albuquerque, New Mexico (1994)	Gaffney et al. (1997)
3.2				Albuquerque, New Mexico (1995)	Gaffney et al. (1997)
2.29 ± 0.74			1.13–4.5	Boulder, Colorado (NCAR)	Gilpin et al. (1997)
	1.8 ± 1.0			Mechlenburg-Vorpommern, Germany	Benning and Wahner (1998)
		0.462 ± 0.206		Flight, 40–50°N, 0.2–2 km	Fried et al. (2003)
		0.311 ± 0.262		Flight, 40–50°N, 2–4 km	Fried et al. (2003)
		0.110 ± 0.119		Flight, 40–50°N, 4–6 km	Fried et al. (2003)
		0.069 ± 0.082		Flight, 40–50°N, 6–8 km	Fried et al. (2003)
		0.220 ± 0.147		Flight, 50–57°N, 0.2–2 km	Fried et al. (2003)
		0.118 ± 0.137		Flight, 50–57°N, 2–4 km	Fried et al. (2003)
		0.075 ± 0.074		Flight, 50–57°N, 4–6 km	Fried et al. (2003)
		0.061 ± 0.084		Flight, 50–57°N, 6–8 km	Fried et al. (2003)
		0.120 ± 0.138		Flight, >57°N, 0.2–2 km	Fried et al. (2003)
		0.090 ± 0.110		Flight, >57°N, 2–4 km	Fried et al. (2003)
		0.059 ± 0.080		Flight, >57°N, 4–6 km	Fried et al. (2003)
		0.072 ± 0.089		Flight, >57°N, 6–8 km	Fried et al. (2003)
	0.0–7			Pabstthum, Germany	Grossman et al. (2003)
	0.39		0.18–0.64	Hyytiälä, Finland	Hellén et al. (2004)

0.24, 1.06				Helsinki, Finland	Hellén et al. (2004)
0.7–2.2				Birmingham, England	Harrison et al. (2006)
18.3 ± 5.6				Hong Kong, outside entrance to tunnel	Ho et al. (2007b)
2.35			1.56–2.76[a]	Zürich (Summer, 2005)	Legreid et al. (2007)
		0.47 ± 0.52		Mid-Atlantic (aircraft)	Lewis et al. (2007)
		0.79		Aircraft over N. America	Snow et al. (2007)
		0.48		Aircraft over N. America	Snow et al. (2007)
		4.2 ± 1.9		Qinghai-Tibetan Plateau, China	Mu et al. (2007)
		2.7 ± 1.4		0–0.5 km over N. America	Fried et al. (2008)
		2.7 ± 1.3		0.5–1 km over N. America	Fried et al. (2008)
		1.9 ± 1.1		1–2 km over N. America	Fried et al. (2008)
		0.66 ± 0.42		2–4 km over N. America	Fried et al. (2008)
		0.16 ± 0.16		10–12 km over N. America	Fried et al. (2008)
2.5 ± 1.3				Tokyo, Japan, Urban site (2003)	Hoshi et al. (2008)
4.1 ± 1.1				Tokyo, Japan, Roadside site (2003)	Hoshi et al. (2008)
Acetaldehyde					
1.4 ± 0.8			2.6 (max)	Pittsburgh, Pennsylvania	Salas and Singh (1986)
2.1 ± 0.9			3.4 (max)	Chicago, Illinois	Salas and Singh (1986)
8.5 ± 6.3			28.4 (max)	Downey, California	Salas and Singh (1986)
2.2 ± 1.7			6.7 (max)	Houston, Texas	Salas and Singh (1986)
1.0 ± 0.5			2.1 (max)	Denver, Colorado	Salas and Singh (1986)
	1–8			Sonchamp, France	Kalabokas et al. (1988)
	1–20			Montagny, France	Kalabokas et al. (1988)
	1–10			Paris, France	Kalabokas et al. (1988)
	0.57 ± 0.28			Egbert, Ontario, Canada	Shepson et al. (1991)
	0.46 ± 0.32			Dorset, Ontario, Canada	Shepson et al. (1991)
	0.85 (Day)			Kinterbish, Alabama	Goldan et al. (1995)
	1.3 (Night)			Kinterbish, Alabama	Goldan et al. (1995)
	0.56		3.8 (max)	Park, Candler Co., Georgia (1991)	Lee et al. (1995)
	0.74		2.4 (max)	Park, Candler Co., Georgia (1992)	Lee et al. (1995)
			0.05–1.34	Chebogue Point, Nova Scotia	Tanner et al. (1996)
		0.7		Schauinsland, Germany	Slemr et al. (1996)

(*continued*)

Table I-D-1. (*continued*)

Urban	Rural	Remote	Range	Location	Reference
Acetaldehyde (*continued*)					
1.64				Denver, Colorado (Winter)	Anderson et al. (1996)
0.88				Denver, Colorado (Spring)	Anderson et al. (1996)
1.43				Denver, Colorado (Summer)	Anderson et al. (1996)
4.0 ± 2.3				Los Angeles, California	Grosjean et al. (1996a)
9.3				Rome, Italy	Possanzini et al. (1996)
		0.77 ± 0.33		Mt. Wank, Garmisch-Partenkirchen, Germany	Leibrock and Slemr (1997)
1.0 ± 0.7				Copenhagen, Denmark	Granby et al. (1997a)
	0.7 ± 0.4			Copenhagen, Denmark	Granby et al. (1997a)
6.6				Albuquerque, New Mexico (1993)	Gaffney et al. (1997)
7.3				Albuquerque, New Mexico (1994)	Gaffney et al. (1997)
1.4				Albuquerque, New Mexico (1995)	Gaffney et al. (1997)
	1.4 ± 1.3			Mechlenburg-Vorpommern, Germany	Benning and Wahner (1998)
	0.919		0.214–1.955	Kinterbish, Alabama	Frost et al. (1998)
	1.56 (Day)			32 km SE Nashville, Tennessee	Riemer et al. (1998)
	1.69 (Night)			32 km SE Nashville, Tennessee	Riemer et al. (1998)
	0.09–0.56			Pabstthum, Germany	Grossman et al. (2003)
	0.20		0.10–0.30	Hyytiälä, Finland	Hellén et al. (2004)
0.07, 0.27				Helsinki, Finland	Hellén et al. (2004)
		1.7 ± 1.5		Mid-Atlantic (aircraft)	Lewis et al. (2007)
		4.3 ± 3.3		Qinghai-Tibetan Plateau, China	Mu et al. (2007)
3.8 ± 1.4				Hong Kong, entrance to tunnel	Ho et al. (2007b)
0.8			0.44–1.10[a]	Zürich (Summer, 2005)	Legreid et al. (2007)
1.8 ± 0.7				Tokyo, Japan, Urban site (2003)	Hoshi et al. (2008)
2.3 ± 0.72				Tokyo, Japan, Roadside site (2003)	Hoshi et al. (2008)

Propanal					
1.8				Rome, Italy	Possanzini et al. (1996)
0.79 ± 0.54				Los Angeles, California	Grosjean et al. (1996a)
0.7				Albuquerque, New Mexico (1993)	Gaffney et al. (1997)
< 0.5				Albuquerque, New Mexico (1994)	Gaffney et al. (1997)
1.4				Porto Alegre, Brazil	Grosjean et al. (1998b)
	0.05–0.30			Pabstthum, Germany	Grossman et al. (2003)
	0.034		0.017–0.063	Hyytiälä, Finland	Hellén et al. (2004)
0.026, 0.035				Helsinki, Finland	Hellén et al. (2004)
1.4				Porto Alegre, Brazil	Grosjean et al. (1998b)
1.4				Porto Alegre, Brazil	Grosjean et al. (1998b)
		1.7 ± 1.5		Mid-Atlantic (aircraft)	Lewis et al. (2007)
		4.3 ± 3.3		Qinghai-Tibetan Plateau, China	Mu et al. (2007)
3.8 ± 1.4				Hong Kong, entrance to tunnel	Ho et al. (2007b)
Butanal					
0.71 ± 0.32				Los Angeles, California	Grosjean et al. (1996a)
		0.037	0.030–0.043[a]	Mauna Loa, Hawaii	Greenberg et al. (1996)
		0.18 ± 0.12		Mt. Wank, Garmisch-Partenkirchen, Germany	Leibrock and Slemr (1997)
	0.055 (Day)			32 km SE Nashville, Tennessee	Riemer et al. (1998)
	0.053 (Night)			32 km SE Nashville, Tennessee	Riemer et al. (1998)
	0.05–0.10			Pabstthum, Germany	Grossman et al. (2003)
	0.019		0.008–0.028	Hyytiälä, Finland	Hellén et al. (2004)
0.019, 0.023				Helsinki, Finland	Hellén et al. (2004)
0.20 ± 0.17				Hong Kong, entrance to tunnel	Ho et al. (2007b)
0.05			0.03–0.06	Zürich (Summer, 2005)	Legreid et al. (2007)
2-Methylpropanal					
	0.01–0.06			Pabstthum, Germany	Grossman et al. (2003)

(*continued*)

Table I-D-1. (*continued*)

Urban	Rural	Remote	Range	Location	Reference
Pentanal					
0.41± 0.32				Los Angeles, California	Grosjean et al. (1996a)
		0.025	0.023–0.036	Mauna Loa, Hawaii	Greenberg et al. (1996)
		0.11 ± 0.12		Mt. Wank, Garmisch-Partenkirchen, Germany	Leibrock and Slemr (1997)
	0.02–0.13			Pabstthum, Germany	Grossman et al. (2003)
	0.014		<0.003–0.027	Hyytiälä, Finland	Hellén et al. (2004)
0.016, 0.020				Helsinki, Finland	Hellén et al. (2004)
0.11 ± 0.14				Hong Kong, entrance to tunnel	Ho et al. (2007b)
0.03			0.02–0.04	Zürich (Summer, 2005)	Legreid et al. (2007)
3-Methylbutanal					
0.34 ± 0.2				Hong Kong, outside entrance to tunnel	Ho et al. (2007b)
Hexanal					
0.42 ± 0.29				Los Angeles, California	Grosjean et al. (1996a)
		0.029	0.023–0.036[a]	Mauna Loa, Hawaii	Greenberg et al. (1996)
	0.06–0.24			Pabstthum, Germany	Grossman et al. (2003)
	0.012		0.007–0.023	Hyytiälä, Finland	Hellén et al. (2004)
0.009, 0.016				Helsinki, Finland	Hellén et al. (2004)
0.07 ± 0.07				Hong Kong, outside entrance to tunnel	Ho et al. (2007b)
0.06			0.04–0.07	Zürich (Summer, 2005)	Legreid et al. (2007)
Heptanal					
0.64 ± 0.28				Los Angeles, California	Grosjean et al. (1996a)
		0.022	0.017–0.028[a]	Mauna Loa, Hawaii	Greenberg et al. (1996)
	0.06–0.24			Pabstthum, Germany	Grossman et al. (2003)
	< 0.006		<0.006–0.011	Hyytiälä, Finland	Hellén et al. (2004)
0.005, 0.010				Helsinki, Finland	Hellén et al. (2004)

Octanal					
0.53 ± 0.39				Los Angeles, California	Grosjean et al. (1996a)
		0.023	0.018–0.034[a]	Mauna Loa, Hawaii	Greenberg et al. (1996)
	0.03–0.05			Pabstthum, Germany	Grossman et al. (2003)
	0.018		<0.007–0.036	Hyytiälä, Finland	Hellén et al. (2004)
0.009, 0.057				Helsinki, Finland	Hellén et al. (2004)
	0.012		0.007–0.023	Hyytiälä, Finland	Hellén et al. (2004)
0.009, 0.016				Helsinki, Finland	Hellén et al. (2004)
Nonanal					
1.09 ± 0.86				Los Angeles, California	Grosjean et al. (1996a)
		28	0.021–0.046[a]	Mauna Loa, Hawaii	Greenberg et al. (1996)
	0.05–0.16			Pabstthum, Germany	Grossman et al. (2003)
	< 0.023			Hyytiälä, Finland	Hellén et al. (2004)
0.021, 0.035				Helsinki, Finland	Hellén et al. (2004)
Decanal					
0.53 ± 0.10				Los Angeles, California	Grosjean et al. (1996a)
		0.023	0.015–0.038[a]	Mauna Loa, Hawaii	Greenberg et al. (1996)
	0.04–0.10			Pabstthum, Germany	Grossman et al. (2003)
	0.014		0.004–0.034	Hyytiälä, Finland	Hellén et al. (2004)
0.021, 0.047				Helsinki, Finland	Hellén et al. (2004)
Undecanal					
0.29 ± 0.08				Los Angeles, California	Grosjean et al. (1996a)
	< 0.001		<0.001–0.001	Hyytiälä, Finland	Hellén et al. (2004)
0.002, 0.003				Helsinki, Finland	Hellén et al. (2004)
Dodecanal					
0.33 ± 0.02				Los Angeles, California	Grosjean et al. (1996a)
Tridecanal					
0.34 ± 0.04				Los Angeles, California	Grosjean et al. (1996a)

(*continued*)

Table I-D-1. (*continued*)

Urban	Rural	Remote	Range	Location	Reference
Tetradecanal					
0.58				Los Angeles, California	Grosjean et al. (1996a)
Acrolein					
0.7				Rome, Italy	Possanzini et al. (1996)
< 0.04				Los Angeles, California	Grosjean et al. (1996a)
		0.60 ± 0.41		Mt. Wank, Garmisch-Partenkirchen, Germany	Leibrock and Slemr (1997)
	0.02–0.07			Pabstthum, Germany	Grossman et al. (2003)
	< 0.004			Hyytiälä, Finland	Hellén et al. (2004)
< 0.004				Helsinki, Finland	Hellén et al. (2004)
0.13 ± 0.13				Hong Kong, outside entrance to tunnel	Ho et al. (2007b)
0.06			0.03–0.07	Zürich (Summer, 2005)	Legreid et al. (2007)
Methacrolein					
	0.66		0.027–2.6	Kinterbish, Alabama	Montzka et al. (1993)
		0.04 ± 0.08		Mt. Wank, Garmisch-Partenkirchen, Germany	Leibrock and Slemr (1997)
< 0.7				Albuquerque, New Mexico (1993)	Gaffney et al. (1997)
< 0.7				Albuquerque, New Mexico (1994)	Gaffney et al. (1997)
0.08				Albuquerque, New Mexico (1995)	Gaffney et al. (1997)
	0.665		0.049–1.747	Kinterbish, Alabama	Frost et al. (1998)
	0.22 (Day)			32 km SE Nashville, Tennessee	Riemer et al. (1998)
	0.30 (Night)			32 km SE Nashville, Tennessee	Riemer et al. (1998)
0.01–0.04				Pabstthum, Germany	Grossman et al. (2003)
	< 0.002			Hyytiälä, Finland	Hellén et al. (2004)
	0.22 (Day)			32 km SE Nashville, Tennessee	Riemer et al. (1998)
	0.30 (Night)			32 km SE Nashville, Tennessee	Riemer et al. (1998)
		0.07 ± 0.01		Pellston, Michigan	Apel et al. (2002)
0.006, 0.007				Helsinki, Finland	Hellén et al. (2004)
0.04			0.02–0.05	Zürich (Summer, 2005)	Legreid et al. (2007)

Crotonaldehyde				
0.30 ± 0.10			Los Angeles, California	Grosjean et al. (1996a)
2.6 ± 1.2			Hong Kong, outside entrance to tunnel	Ho et al. (2007b)
2-Butenal				
	1.9 ± 1.6		Qinghai-Tibetan Plateau, China	Mu et al. (2007)
	< 0.002		Hyytiälä, Finland	Hellén et al. (2004)
< 0.002			Helsinki, Finland	Hellén et al. (2004)
trans-2-Hexenal				
	< 0.001		Hyytiälä, Finland	Hellén et al. (2004)
< 0.001			Helsinki, Finland	Hellén et al. (2004)
Hydroxy-Acetaldehyde				
	0.76		Kinterbish, Alabama	Frost et al. (1998)
Glycolaldehyde				
	0.13	0.67 (max)	Park, Candler Co., Georgia (1991)	Lee et al. (1995)
	0.2	1.91 (max)	Park, Candler Co., Georgia (1992)	Lee et al. (1995)
	0.01–0.20		Pabstthum, Germany	Grossman et al. (2003)
Glyoxal				
	0.031	0.16 (max)	Park, Candler Co., Georgia (1991)	Lee et al. (1995)
	0.088	0.26 (max)	Park, Candler Co., Georgia (1992)	Lee et al. (1995)
1.04 ± 0.61			Los Angeles, California	Grosjean et al. (1996a)
	0.2	0.02–0.55	Kinterbish, Alabama	Frost et al. (1998)
	0.03–0.19		Pabstthum, Germany	Grossman et al. (2003)
0.040–0.14			Cambridge, MA	Sinreich et al. (2007)
<0.1–0.92		0.92 (max)	Mexico City, Mexico	Volkamer et al. (2007)
Methylglyoxal				
	0.031	0.16 (max)	Park, Candler Co., Georgia (1991)	Lee et al. (1995)
	0.088	0.26 (max)	Park, Candler Co., Georgia (1992)	Lee et al. (1995)
1.04 ± 0.61			Los Angeles, California	Grosjean et al. (1996a)
	0.2	0.02–0.55	Kinterbish, Alabama	Frost et al. (1998)
	0.03–0.19		Pabstthum, Germany	Grossman et al. (2003)

(*continued*)

Table I-D-1. (*continued*)

Urban	Rural	Remote	Range	Location	Reference
Benzaldehyde					
0.7				Rome, Italy	Possanzini et al. (1996)
0.22 ± 0.11				Los Angeles, California	Grosjean et al. (1996a)
4.8				Porto Alegre, Brazil	Grosjean et al. (1998b)
	0.021–0.060			Pabstthum, Germany	Grossman et al. (2003)
	0.005		0.003–0.009	Hyytiälä, Finland	Hellén et al. (2004)
0.006, 0.016				Helsinki, Finland	Hellén et al. (2004)
0.35 ± 0.16				Hong Kong, outside entrance to tunnel	Ho et al. (2007b)
m-,p-Tolualdehyde					
0.24 ± 0.10				Los Angeles, California	Grosjean et al. (1996a)
0.02 ± 0.04				Hong Kong, outside entrance to tunnel	Ho et al. (2007b)
	<0.003–0.001			Hyytiälä, Finland	Hellén et al. (2004)
< 0.003				Helsinki, Finland	Hellén et al. (2004)
Pinonaldehyde					
	0–0.17			Pabstthum, Germany	Grossman et al. (2003)
2) Ketones					
Acetone	1.6 ± 0.7			Egbert, Ontario, Canada	Shepson et al. (1991)
	1.8 ± 1.1			Dorset, Ontario, Canada	Shepson et al. (1991)
		1.14 ± 0.43	0.36–2.32	Eastern Canada, 0–6 km	Singh et al. (1994)
	4.4		0.8–8	Kinterbish, Alabama	Goldan et al. (1995)
	1.8		6.7 (max)	Park, Candler Co., Georgia (1991)	Lee et al. (1995)
	1.7		4.5 (max)	Park, Candler Co., Georgia (1992)	Lee et al. (1995)
		37		Schauinsland, Germany	Slemr et al. (1996)
1.6 ± 1.5				Los Angeles, California	Grosjean et al. (1996a)
6.8				Rome, Italy	Possanzini et al. (1996)
		0.703	0.611–0.848[a]	Mauna Loa, Hawaii	Greenberg et al. (1996)
0.9 ± 0.4				Copenhagen, Denmark	Granby et al. (1997a)
	0.9 ± 0.4			Copenhagen, Denmark	Granby et al. (1997a)
	4.4		0.8–8	Kinterbish, Alabama	Goldan et al. (1995)

Acetone (*continued*)					
1.0 ± 0.5				Copenhagen, Denmark	Granby et al. (1997a)
4.3				Albuquerque, New Mexico (1993)	Gaffney et al. (1997)
0.3				Albuquerque, New Mexico (1994)	Gaffney et al. (1997)
1.8				Albuquerque, New Mexico (1995)	Gaffney et al. (1997)
12.6				Porto Alegre, Brazil	Grosjean et al. (1998b)
	3.83		1.03–6.57	Kinterbish, Alabama	Frost et al. (1998)
	3.83 (Day)			32 km SE Nashville, Tennessee	Riemer et al. (1998)
	3.55 (Night)			32 km SE Nashville, Tennessee	Riemer et al. (1998)
	0.56		0.29–0.88	Hyytiälä, Finland	Hellén et al. (2004)
0.36, 0.66				Helsinki, Finland	Hellén et al. (2004)
1.8–4.6				Birmingham, England	Harrison et al. (2006)
		1.2 ± 490		Mid-Atlantic (aircraft)	Lewis et al. (2007)
		2.0 ± 0.9		Qinghai-Tibetan Plateau, China	Mu et al. (2007)
1.0 ± 0.8				Hong Kong, outside entrance to tunnel	Ho et al. (2007b)
2.12			1.40–2.55[a]	Zürich (Summer, 2005)	Legreid et al. (2007)
1.80 ± 3.29			0.07–1.80[a]	Wuppertal, Germany	Niedojadlo et al. (2007)
Hydroxyacetone					
	0.02–0.16			Pabstthum, Germany	Grossman et al. (2003)
2-Butanone					
	0.31		0.08–0.8	Kinterbish, Alabama	Goldan et al. (1995)
1.2 ± 1.7				Los Angeles, California	Grosjean et al. (1996a)
		0.021	0.017–0.028[a]	Mauna Loa, Hawaii	Greenberg et al. (1996)
		0.19 ± 0.06		Mt. Wank, Garmisch-Partenkirchen, Germany	Leibrock and Slemr (1997)
< 0.7				Mt. Wank, Garmisch-Partenkirchen, Germany	Gaffney et al. (1997)
0.9				Albuquerque, New Mexico (1994)	Gaffney et al. (1997)
2.1				Porto Alegre, Brazil	Grosjean et al. (1998b)
	0.456		0.044–1.086	Kinterbish, Alabama	Frost et al. (1998)
	0.39 (Day)			32 km SE Nashville, Tennessee	Riemer et al. (1998)
	0.34 (Night)			32 km SE Nashville, Tennessee	Riemer et al. (1998)
	0.073		<0.046–0.15	Hyytiälä, Finland	Hellén et al. (2004)

(*continued*)

Table I-D-1. (*continued*)

Urban	Rural	Remote	Range	Location	Reference
2-Butanone (*continued*)					
0.017				Helsinki, Finland	Hellén et al. (2004)
0.31 ± 0.27				Hong Kong, outside entrance to tunnel	Ho et al. (2007b)
0.2			0.11–0.25	Zürich (Summer, 2005)	Legreid et al. (2007)
0.05 ± 0.08			0.01–0.42[a]	Wuppertal, Germany	Niedojadlo et al. (2007)
4-Methyl-2-pentanone					
0.01 ± 0.03			0.01–0.18[a]	Wuppertal, Germany	Niedojadlo et al. (2007)
2-Hexanone					
0.01 ± 0.03			0.01–0.1	Wuppertal, Germany	Niedojadlo et al. (2007)
Cyclohexanone					
0.20 ± 0.09				Los Angeles, California	Grosjean et al. (1996a)
0.02 ± 0.03					
4-Acetyl-1-methyl-cyclo-hexane					
0.12 ± 0.09				Los Angeles, California	Grosjean et al. (1996a)
	0.39 (Day)			32 km SE Nashville, Tennessee	Riemer et al. (1998)
Methyl vinyl ketone					
	0.98		0–3.4	Kinterbish, Alabama	Montzka et al. (1993)
< 0.08				Los Angeles, California	Grosjean et al. (1996a)
		0.18 ± 0.08		Mt. Wank, Garmisch-Partenkirchen, Germany	Leibrock and Slemr (1997)
	0.30 (Day)			32 km SE Nashville, Tennessee	Riemer et al. (1998)
	0.34 (Night)			32 km SE Nashville, Tennessee	Riemer et al. (1998)
		0.14 ± 0.04		Pellston, Michigan	Apel et al. (2002)
	0.02–0.09			Pabstthum, Germany	Grossman et al. (2003)
0.08			0.04–0.09a	Zürich (Summer, 2005)	Legreid et al. (2007)
6-Methyl-5-hepten-2-one					
	0.004		<0.004–0.007	Hyytiälä, Finland	Hellén et al. (2004)
0.002, 0.003				Helsinki, Finland	Hellén et al. (2004)

Biacetyl					
	0.02–0.05			Pabstthum, Germany	Grossman et al. (2003)
Nopinone					
0.34 ± 0.29				Los Angeles, California	Grosjean et al. (1996a)
	0.002		<0.001–0.005	Hyytiälä, Finland	Hellén et al. (2004)
0.003				Helsinki, Finland	Hellén et al. (2004)
3) Alcohols					
Methanol					
		12.1		Kinterbish, Alabama	Goldan et al. (1995)
		2.26 ± 0.45		Mt. Wank, Garmisch-Partenkirchen, Germany	Leibrock and Slemr (1997)
	8.262		1.125–16.081	Kinterbish, Alabama	Frost et al. (1998)
	11.35 (Day)			32 km SE Nashville, Tennessee	Riemer et al. (1998)
	7.79 (Night)			32 km SE Nashville, Tennessee	Riemer et al. (1998)
		0.830 ± 610		Mid-Atlantic (aircraft)	Lewis et al. (2007)
3.18			2.15–3.97	Zürich (Summer, 2005)	Legreid et al. (2007)
0.17 ± 0.26			0.01–1.0	Wuppertal, Germany	Niedojadlo et al. (2007)
Ethanol					
		1.7		Kinterbish, Alabama	Goldan et al. (1995)
		0.24 ± 0.15		Mt. Wank, Garmisch-Partenkirchen, Germany	Leibrock and Slemr (1997)
12.1 ± 13.3			0.4–68.2	Porto Alegre, Brazil	Grosjean et al. (1998a)
	0.38 (Day)			32 km SE Nashville, Tennessee	Riemer et al. (1998)
	0.45 (Night)			32 km SE Nashville, Tennessee	Riemer et al. (1998)
1-Propanol					
0.03			0.01–0.04	Zürich (Summer, 2005)	Legreid et al. (2007)
0.06 ± 0.29			0.01–1.55	Wuppertal, Germany	Niedojadlo et al. (2007)
2-Propanol					
0.51			0.23–0.65	Zürich (Summer, 2005)	Legreid et al. (2007)
0.15 ± 0.19			0.01–0.84	Wuppertal, Germany	Niedojadlo et al. (2007)

(*continued*)

Table I-D-1. (*continued*)

Urban	Rural	Remote	Range	Location	Reference
1-Butanol					
	0.052 (Day)			32 km SE Nashville, Tennessee	Riemer et al. (1998)
	0.066 (Night)			32 km SE Nashville, Tennessee	Riemer et al. (1998)
0.07			0.01–0.04	Zürich (Summer, 2005)	Legreid et al. (2007)
0.13 ± 0.43			0.01–2.31	Wuppertal, Germany	Niedojadlo et al. (2007)
2-Methylpropanol					
0.62 ± 1.6			0.01–6.79	Wuppertal, Germany	Niedojadlo et al. (2007)
2-Methyl-3-buten-2-ol					
		0.05–3.0		Niwot Ridge, Colorado	Goldan et al. (1993)
Linalool					
	1.5–2.5			Orange grove, Riverside, Califonia	Arey et al. (1991)
4) Hydroperoxides					
Methyl hydroperoxide					
		0.34 ± 0.08		Mauna Loa, Hawaii (3.4 km)	Staffelbach et al. (1996)
		0.24 ± 0.07		Mauna Loa, Hawaii (3.4 km)	Staffelbach et al. (1996)
		0.44		Aircraft over N. America	Snow et al. (2007)
		0.18		Aircraft over N. America	Snow et al. (2007)
		0.05		Aircraft over N. America	Snow et al. (2007)
Hydroxymethyl-hydroperoxide					
		0.05–0.98		Cool day, State Park, Georgia	Lee et al. (1993)
		2.6–5.3		Hot day, State Park, Georgia	Lee et al. (1993)
5) Ethers					
Methyl tert-butyl ether					
6.6 ± 4.3			0.2–17.1	Porto Alegre, Brazil	Grosjean et al. (1998a)
0.18			0.09–0.22	Zürich (Summer, 2005)	Legreid et al. (2007)

3-Methylfuran				
	0.046 (Day)		32 km SE Nashville, Tennessee	Riemer et al. (1998)
	0.052 (Night)		32 km SE Nashville, Tennessee	Riemer et al. (1998)
6) Esters				
Methyl acetate				
0.05		0.03–0.06[a]	Zürich (Summer, 2005)	Legreid et al. (2007)
0.05 ± 0.08		0.01–0.39	Wuppertal, Germany	Niedojadlo et al. (2007)
Ethyl acetate				
0.19		0.08–0.23[a]	Zürich (Summer, 2005)	Legreid et al. (2007)
0.17 ± 0.26		0.01–1.0[a]	Wuppertal, Germany	Niedojadlo et al. (2007)
iso-Propyl acetate				
0.03 ± 0.09		0.01–0.50[a]	Wuppertal, Germany	Niedojadlo et al. (2007)
n-Propyl acetate				
0.06 ± 0.10		0.01–0.49[a]	Wuppertal, Germany	Niedojadlo et al. (2007)
Butyl acetate				
0.06		0.02–0.08[a]	Zürich (Summer, 2005)	Legreid et al. (2007)
iso-Butyl acetate				
0.02 ± 0.05		0.01–0.28	Wuppertal, Germany	Niedojadlo et al. (2007)
7) Organic Acids				
Formic Acid				
1.5–10			Glendora, California	Grojean et al. (1990)
0.7 ± 0.3			Copenhagen, Denmark	Granby et al. (1997a)
	0.6 ± 0.3		Copenhagen, Denmark	Granby et al. (1997a)
8.6			Albuquerque, New Mexico (1993)	Gaffney et al. (1997)
6.1			Albuquerque, New Mexico (1994)	Gaffney et al. (1997)
4.1			Albuquerque, New Mexico (1995)	Gaffney et al. (1997)
	0.8 ± 0.5	0.4–2.7	Lille Valby, Denmark	Granby et al. (1997a)
		0.8–3.2	Pabstthum, Germany	Grossman et al. (2003)

(*continued*)

Table I-D-1. (*continued*)

Urban	Rural	Remote	Range	Location	Reference
Acetic Acid					
0.7 ± 0.3				Copenhagen, Denmark	Granby et al. (1997b)
	0.6 ± 0.3			Copenhagen, Denmark	Granby et al. (1997b)
8.6				Albuquerque, New Mexico (1993)	Gaffney et al. (1997)
6.1				Albuquerque, New Mexico (1994)	Gaffney et al. (1997)
4.1				Albuquerque, New Mexico (1995)	Gaffney et al. (1997)
	0.8 ± 0.5		0.4–2.7	Lille Valby, Denmark	Granby et al. (1997b)
			0.8–3.2	Pabstthum, Germany	Grossman et al. (2003)
Propanoic Acid					
0.6				Albuquerque, New Mexico (1993)	Gaffney et al. (1997)
0.6				Albuquerque, New Mexico (1994)	Gaffney et al. (1997)
< 1				Albuquerque, New Mexico (1995)	Gaffney et al. (1997)
			0.1–0.3	Pabstthum, Germany	Grossman et al. (2003)
Butanoic Acid					
			0.021–0.098	Pabstthum, Germany	Grossman et al. (2003)
Pentanoic Acid					
			0.015–0.067	Pabstthum, Germany	Grossman et al. (2003)
Hexanoic Acid					
			0.009–0.035	Pabstthum, Germany	Grossman et al. (2003)
Heptanoic Acid					
			0.002–0.096	Pabstthum, Germany	Grossman et al. (2003)
Octanoic Acid					
			0.001–0.017	Pabstthum, Germany	Grossman et al. (2003)
Nonanoic Acid					
			0–0.078	Pabstthum, Germany	Grossman et al. (2003)

Pyruvic Acid					
0.4				Albuquerque, New Mexico (1993)	Gaffney et al. (1997)
2.1				Albuquerque, New Mexico (1994)	Gaffney et al. (1997)
< 1				Albuquerque, New Mexico (1995)	Gaffney et al. (1997)
	0.052		0.35	Park, Candler Co., Georgia (1992)	Lee et al. (1995)
Glyoxylic Acid					
	0.41		3.53 (max)	Park, Candler Co., Georgia (1992)	Lee et al. (1995)
8) Organic Nitrates					
Methyl nitrate					
0.109				Jülich, Germany	Flocke et al. (1991)
	0.010			Schauinsland, Germany	Flocke et al. (1991)
		0.0030 ± 0.0011		Flight over NE Colorado	Stroud et al. (2001)
		0.0040 ± 0.0010		Greenland, Summit (June)	Swanson et al. (2003)
		0.0021 ± 0.0005		Flight (7–12 km) over North America	Singh et al. (2007)
		0.00173 ± 0.00007		North Atlantic, 22,000 ft	Reeves et al. (2007)
		0.00149 ± 0.00003		North Atlantic, 12,000 ft	Reeves et al. (2007)
		0.00153 ± 0.00004		North Atlantic, 1,000 ft	Reeves et al. (2007)
		0.0035		Flight (1–6 km altitude; 40–80°N lat.; 21–27 Feb.)	Blake et al. (2003a)
		0.0022		Flight (1–6 km alttitude; 40–85°N lat.; 15–23 May)	Blake et al. (2003a)
		0.0034 ± 0.0005		Flight Pacific Ocean; Lat. > 10°N; 0–2 km alt.	Blake et al. (2003b)
		0.0283 ± 0.0113		Flight Pacific Ocean; Lat.10°N–5°S; 0–2 km alt.	Blake et al. (2003b)
		0.0092 ± 0.0051		Flight Pacific Ocean; Lat. > 10°S; 0–2 km alt.	Blake et al. (2003b)

(*continued*)

Table I-D-1. (*continued*)

Urban	Rural	Remote	Range	Location	Reference
Ethyl nitrate					
0.048				Jülich, Germany	Flocke et al. (1991)
	0.0095			Schauinsland, Germany	Flocke et al. (1991)
		0.0028 ± 0.0017		Flight over NE Colorado	Stroud et al. (2001)
		0.0033 ± 0.0011		Flight Pacific Ocean; Lat. > 10°N; 0–2 km alt.	Blake et al. (2003b)
		0.0094 ± 0.0038		Flight Pacific Ocean; Lat.10°N–5°S; 0–2 km alt.	Blake et al. (2003b)
		0.0027 ± 0.0018		Flight Pacific Ocean; Lat. > 10°S; 0–2 km alt.	Blake et al. (2003b)
		0.0036± 0.0009		Greenland, Summit (June)	Swanson et al. (2003)
		0.0017 ± 0.0007		Flight (7–12 km) over North America	Singh et al. (2007)
		0.00125 ± 0.00008		North Atlantic, 22,000 ft	Reeves et al. (2007)
		0.00076 ± 0.00003		North Atlantic, 12,000 ft	Reeves et al. (2007)
		0.00079 ± 0.00002		North Atlantic, 1,000 ft	Reeves et al. (2007)
1-Propyl nitrate					
0.0084				Jülich, Germany	Flocke et al. (1991)
	0.0032			Schauinsland, Germany	Flocke et al. (1991)
		0.00064 ± 0.00019		Greenland, Summit (June)	Swanson et al. (2003)
		0.00025 ± 0.00002		North Atlantic, 22,000 ft	Reeves et al. (2007)
		0.00009 ± 0.00002		North Atlantic, 12,000 ft	Reeves et al. (2007)
		0.00008 ± 0.00002		North Atlantic, 1,000 ft	Reeves et al. (2007)
		0.00097 ± 0.00053		Flight Pacific Ocean; Lat. >10°N; 0–2 km alt.	Blake et al. (2003b)
		0.00056 ± 0.00023		Flight Pacific Ocean; Lat.10°N– 5°S; 0–2 km alt.	Blake et al. (2003a)
		0.00014 ± 0.00010		Flight Pacific Ocean; Lat. >10°S; 0–2 km alt.	Blake et al. (2003a)

2-Propyl nitrate				
0.0274			Jülich, Germany	Flocke et al. (1991)
	0.0197		Schauinsland, Germany	Flocke et al. (1991)
		0.0052 ± 0.0058	Flight over NE Colorado	Stroud et al. (2001)
		0.0024 ± 0.0008	Greenland, Summit (June)	Swanson et al. (2003)
		0.0037 ± 0.0030	Flight (7–12 km) over North America	Singh et al. (2007)
		0.00240 ± 0.00034	North Atlantic, 22,000 ft	Reeves et al. (2007)
		0.00079 ± 0.00005	North Atlantic, 12,000 ft	Reeves et al. (2007)
		0.00070 ± 0.00006	North Atlantic, 1,000 ft	Reeves et al. (2007)
		0.00482 ± 0.00260	Flight Pacific Ocean; Lat. >10°N; 0–2 km alt.	Blake et al. (2003b)
		0.00321 ± 0.00120	Flight Pacific Ocean; Lat.10°N– 5°S; 0–2 km alt.	Blake et al. (2003b)
		0.00078 ± 0.00061	Flight Pacific Ocean; Lat. >10°S; 0–2 km alt.	Blake et al. (2003b)
2-Butyl nitrate				
		0.0048 ± 0.0075	Flight over NE Colorado	Stroud et al. (2001)
		0.0018 ± 0.0012	Greenland, Summit (June)	Swanson et al. (2003)
		0.0015 ± 0.0021	Flight (7–12 km) over North America	Singh et al. (2007)
		0.00401 ± 0.00315	Flight Pacific Ocean; Lat. >10°N; 0–2 km alt.	Blake et al. (2003b)
		0.00062 ± 0.00025	Flight Pacific Ocean; Lat.10°N– 5°S; 0–2 km alt.	Blake et al. (2003b)
		0.00014 ± 0.00010	Flight Pacific Ocean; Lat. >10°S; 0–2 km alt.	Blake et al. (2003b)
		0.0085	Flight (1–6 km altitude; 40–80°N lat.; 21–27 Feb.)	Blake et al. (2003a)
		0.001	Flight (1–6 km alttitude; 40–85°N lat.; 15–23 May)	Blake et al. (2003a)
		0.00096 ± 0.00012	Flight Pacific Ocean; Lat. > 10°N; 2–8 km alt.	Blake et al. (2003b)
		0.00021 ± 0.00012	Flight Pacific Ocean; Lat.10°N– 5°S; 2–8 km alt.	Blake et al. (2003b)
		0.0008 ± 0.0006	Flight Pacific Ocean; Lat. > 10°S; 2–8 km alt.	Blake et al. (2003b)

(*continued*)

Table I-D-1. (*continued*)

Urban	Rural	Remote	Range	Location	Reference
iso-Butyl nitrate					
		0.00157 ± 0.00014		North Atlantic, 22,000 ft	Reeves et al. (2007)
		0.00026 ± 0.00002		North Atlantic, 12,000 ft	Reeves et al. (2007)
		0.00026 ± 0.00002		North Atlantic, 1,000 ft	Reeves et al. (2007)
2- and 3-Pentyl nitrate					
		0.00046 ± 0.00012		North Atlantic, 22,000 ft	Reeves et al. (2007)
		0.00010 ± 0.00006		North Atlantic, 12,000 ft	Reeves et al. (2007)
		0.00011 ± 0.00007		North Atlantic, 1,000 ft	Reeves et al. (2007)
9) Peroxyacyl nitrates					
Peroxyacetyl nitrate					
0.1–6.9			high value, 20.5	Paris (Creteil), France	Tsalkani et al. (1991)
0.27 (January)			High value, 2.2	Munich, Germany	Rappenglück et al. (1993)
1.06 (September)			high value, 5.6	Munich, Germany	Rappenglück et al. (1993)
2.49 ± 1.65			high value, 5.52	Long Beach, California	Grosjean et al. (1996b)
0.94 ± 0.45			high value, 6.86	Los Angeles, California	Grosjean et al. (1996b)
1.82 ± 0.55			high value, 2.96	Azusa, California	Grosjean et al. (1996b)
3.20 ± 1.76			high value, 9.88	Claremont	Grosjean et al. (1996b)
		0.049	0.02–0.325	Chebogue Pt. Nova Scotia	Roberts et al. (1996)
	0.4		0.035–2.14	LaVergne, Tennessee	Nouaime et al. (1998)
	0.285		0.021–0.285	Pellston, Michigan	Pippin et al. (2001)
0.677			0.011–2.51	Nashville, Tennessee	Roberts et al. (2003)
0.48			0.015–6.50	LaPorte, Texas	Roberts et al. (2003)
		0.36	0.07–2.79	Gulf of Maine, USA	Roberts et al. (2007)
	0.319		0–3.20	Harvard Forest, Massachusetts	Munger (Roberts et al., 2007)

Peroxy propionyl nitrate				
	0.009		Chebogue Pt. Nova Scotia	Roberts et al. (1996)
0.24 ± 0.08		high value, 0.86	Long Beach, California	Grosjean et al. (1996b)
0.22 ± 0.07		high value, 1.04	Los Angeles, California	Grosjean et al. (1996b)
0.46 ± 0.16		high value, 1.46	Azusa, California	Grosjean et al. (1996b)
0.32 ± 0.16		high value, 1.20	Claremont	Grosjean et al. (1996b)
0.05		0.005–0.320	LaVergne, Tennessee	Nouaime et al. (1998)
0.03		0.004–0.150	LaVergne, Tennessee	Nouaime et al. (1998)
0.06		<0.007–0.233	Pellston, Michigan	Pippin et al. (2001)
0.049		<0.010–0.187	Pellston, Michigan	Pippin et al. (2001)
0.091		<0.005–0.43	Nashville, Tennessee	Roberts et al. (2003)
0.074		<0.005–1.36	LaPorte, Texas	Roberts et al. (2003)
	0.05	<4–0.387	Gulf of Maine, USA	Roberts et al. (2007)
0.0077		<0.004–0.371	Gulf of Maine, USA	Roberts et al. (2007)
Peroxyisobutryl nitrate				
0.015		<0.005–0.077	Nashville, Tennessee	Roberts et al. (2003)
< 0.005		<0.005–0.266	LaPorte, Texas	Roberts et al. (2003)
Peroxy-n-butyl nitrate				
0.04–0.51		2.3 (max)	Southern California (mountain forest)	Grosjean et al. (1993e)

[a] Interquartile range.

were found in $PM_{2.5}$ aerosols in studies from 14 cities in China (Ho et al., 2007a). The organic nitrates are expected and reported in urban atmospheres rich in NO_x since a significant fraction of the reaction of the larger alkyl peroxy radicals (RO_2) with NO occurs by the channel, $RO_2 + NO \rightarrow RONO_2$ that competes successfully with the chain-carrying alternate channel, $RO_2 + NO \rightarrow RO + NO_2$. Concentrations of the C_1–C_5 nitrates measured in the city of Jülich, Germany (Flocke et al., 1991) were in the range between 1 and 230 ppt. The peroxyacyl nitrates, especially the smallest member of the family, peroxyacetyl nitrate (PAN), are common in urban atmospheres. They have been observed at concentrations that are at times high enough to induce eye irritation.

I-D-2. The Rural Atmosphere

Rural areas are removed from large urban sources of VOCs and OVOCs and, as expected, show attenuated levels of most oxygenates and other pollutants. For example, the concentrations of the alkyl nitrates measured in the Black Forest were usually one-fifth to one-tenth of those seen at Jülich (Flocke et al., 1991). However, in some rural agricultural areas, the concentrations of reactive oxygenates like PAN can be present at levels that are harmful to some sensitive crops.

I-D-3. The Remote Atmosphere

Transport of polluted urban air is effective in limiting the number of truly remote sites available on the Earth today. Thus, the alkyl nitrates are observed in aged air masses throughout the troposphere. For example, the summation of the average concentration of all alkyl nitrates measured in flights over North America (0–2 km altitude) averaged 191 ± 204 ppt. Note in table I-D-1 that many VOCs are seen at remote sites such as Mauna Loa, Hawaii, and in flights over the North Atlantic Ocean. Although attenuation of urban pollution levels occurs via dilution with cleaner air and via physical and chemical losses during transport, the lifetimes of many species are sufficiently long to allow retention in the atmosphere for weeks or months, and they can be transported to remote locations. For example, organic nitrates are relatively long-lived in the lower troposphere; and, like acetone, the importance of such species relative to other VOCs increases as the air mass ages.

I-E. Use of Oxygenates as Fuels or Fuel Additives

The use of oxygenates in blends with gasoline serves four main purposes. First, oxygenates such as methyl *tert*-butyl ether (MTBE), *tert*-amyl methyl ether (TAME), ethyl *tert*-butyl ether (ETBE), and ethanol improve the antiknock quality of fuel by resisting autoignition as measured by high octane numbers (see table 1-E-1). Following the removal of tetraethyl lead from gasoline in the late 1970s, oxygenates found widespread use as blending components to boost the octane number of gasoline. Second, by providing extra oxygen during combustion, the presence of oxygenates reduces the emission of carbon monoxide from older vehicles. This benefit is not realized to the same degree

Table I-E-1. Octane numbers for selected compounds (Chevron, 2009)

Compound	Formula	Oxygen Content (% by Mass)	Research Octane Number
n-Hexane	n-C_6H_{14}	–	25
1-Hexene	$CH_2CH(CH_2)_3CH_3$	–	76
Cyclohexane	C_6H_{12}	–	83
2,2,4-trimethylpentane	$CH_3C(CH_3)_2CH_2CH(CH_3)_2$	–	100
Benzene	C_6H_6	–	123
m-Xylene	$C_6H_4(CH_3)_2$	–	118
Methanol	CH_3OH	50	125[a]
Ethanol	C_2H_5OH	35	129[b]
Methyl *tert*-butyl ether	$CH_3OC(CH_3)_3$	18	118[b]
Ethyl *tert*-butyl ether	$C_2H_5OC(CH_3)_3$	16	119[b]
tert-Amyl methyl ether	$CH_3CH_2C(CH_3)_2OCH_3$	16	119[b]

[a]European Fuel Oxygenates Asssociation (2008).
[b]Blending research octane number.

in modern engines equipped with oxygen sensors that measure $[O_2]$ in the exhaust thereby allowing adjustment of fuel and air mixture to ensure appropriate amounts of oxygen during combustion. Third, by physically displacing or diluting some of the fuel components (e.g., aromatics), the presence of oxygenates helps to reduce certain harmful tailpipe emissions. Fourth, oxygenates derived from renewable sources, such as ethanol from corn, sugar cane, and cellulose and fatty acid methyl esters from animal fats and vegetable oils, displace petroleum and can improve energy security and reduce greenhouse gas emissions.

The U.S. Clean Air Act Amendments of 1990 require the use of oxygenated gasoline in areas considered to have unhealthy levels of air pollution (U.S. Environmental Protection Agency, 2008). There are two oxygenated gasoline programs in the U.S. The Winter Oxyfuel Program requires gasoline containing 2.7% oxygen by weight during the cold months in cities with elevated levels of carbon monoxide. The Year-Round Reformulated Gasoline Program requires reformulated gasoline with at least 2% oxygen by weight in cities with significant ground-level ozone pollution. In October 2001, the U.S. cities participating in the Winter Oxyfuel Program included El Paso, Denver, Boulder, Las Vegas, Phoenix, Los Angeles, Reno, Fairbanks, Anchorage, and Tucson (U.S. Environmental Protection Agency, 2008). In November 2008, approximately 30% of the gasoline sold in the U.S. was reformulated gasoline. As shown in figure I-E-1, MTBE was the dominant oxygenate in use in the U.S. in the 1990s but has been phased out and replaced largely by ethanol following concerns over ground water contamination.

Interest in addressing climate change (IPCC, 2001) and energy security issues has led to research to develop alternative fuels that can supplement, or even replace, conventional hydrocarbon fuels. Many alternative fuels are oxygenated compounds. The most prominent are biofuels, ethanol derived from corn and sugar cane, and fatty acid methyl esters from the transesterification of vegetable oils. The U.S. Energy Independence and Security Act of 2007 established a Renewable Fuel Standard (RFS) requiring the use

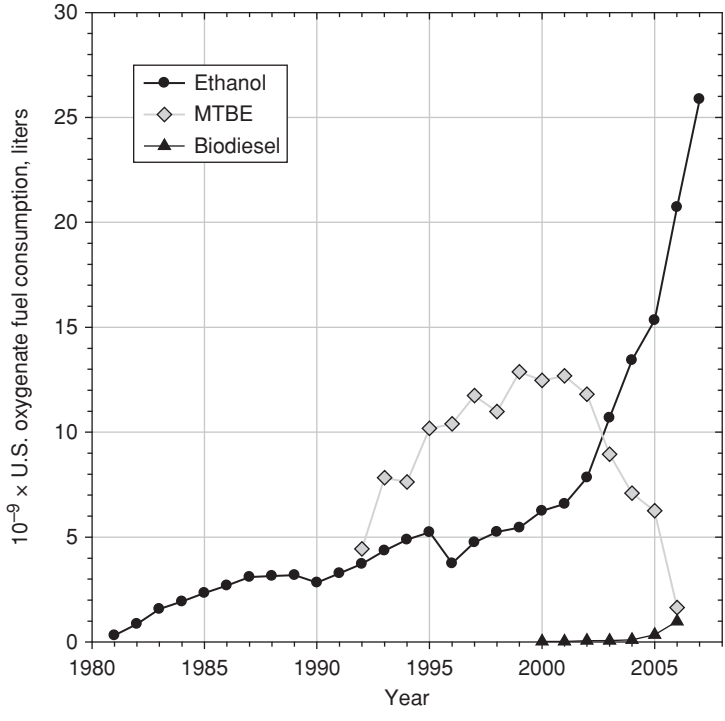

Figure I-E-1. U.S. Consumption of oxygenate fuels (Energy Information Administration, 2008).

of 9×10^9 gallons (34×10^9 liters) of renewable fuel in 2008 that increases to 36×10^9 gallons (136×10^9 liters) in 2022. Oxygenates (principally, ethanol and fatty acid methyl esters) are the major renewable fuels currently in use, and likely to be used in the future, to satisfy the RFS. There is also interest in the European Union (E.U.) in renewable fuels. In contrast to the situation in the U.S., fatty acid methyl ester biodiesel is the dominant biofuel in the E.U. In 2007 the production of ethanol and biodiesel in the U.S. was 26.5×10^9 and 1.7×10^9 liters, respectively. In the E.U. 2.3×10^9 liters of ethanol and 6.1×10^9 liters of biodiesel were produced (OECD, 2008). Brazil produced 22×10^9 liters of ethanol in the 2007 crop year representing approximately 22% of its total road-fuel transportation energy requirement. As illustrated in figure I-E-2, the conversion of biomass into biofuel can be achieved via biotic (e.g., fermentation) or abiotic (e.g., transesterification or gasification) routes leading to a variety of possible fuels. As shown in figure I-E-2, many, but not all, biofuels are oxygenated compounds.

Several studies have been carried out outlining the virtues and potential problems associated with the adoption of alternative fuels (e.g., see Chang et al., 1991; Dunker et al., 1996; Bailey and Colucci, 1997; Good and Francisco, 2003; Energy Information Administration, 2004; Yacobucci, 2005). Many factors determine the suitability of compounds for use as fuels including: volatility, heat of combustion, cetane (hexadecane) number (a measure of the autoignition quality), octane number (a measure

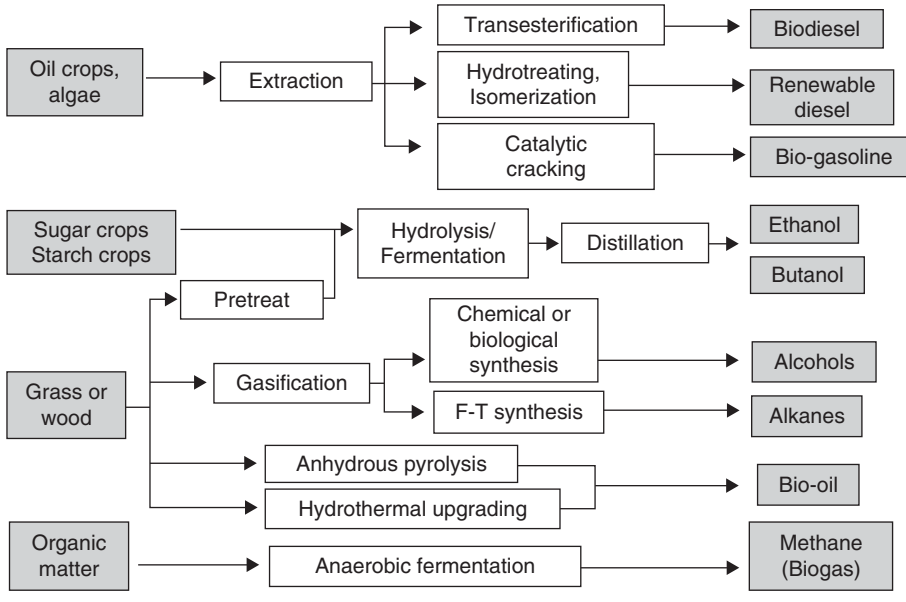

Figure I-E-2. Pathways from biomass to biofuels.

of antiknock quality), flammability, corrosiveness, toxicity, lifecycle greenhouse gas emissions, and cost of production and distribution. In this section, a brief discussion is given of the current use of oxygenates as alternative fuels.

I-E-1. Methanol

Methanol is a volatile liquid (see figure I-B-2) that has been used as a fuel for some race cars for many years. The properties of methanol which make it suitable as a racing fuel are its high latent heat of vaporization and resistance to autoignition (high octane number), which enable engine operation at a high compression ratio (approximately 16:1 compared to 10:1 for a typical gasoline engine); high H:C ratio, which results in a large volume of combustion products for a given amount of air introduced into the engine; and high flame speed. The fact that methanol burns with little, or no, visible flame creates a hazard; therefore, it is commonly used in blends containing 85% methanol and 15% conventional gasoline, often designated as M85. The presence of gasoline containing 15% methanol also improves the cold start performance. Methanol is not well suited for use in diesel engines since it has a low cetane number. However, it has good antiknock qualities and is suitable for use in spark ignition engines. The consumption of methanol as a fuel increased markedly in the 2000s (see figure I-E-3) reaching 5.7×10^9 liters in 2008. It should be noted that direct use as a fuel accounted for only approximately 10% of the total global methanol consumption in 2008 (Methanol Institute, 2008).

Methanol can be made by passing synthesis gas (a mixture of CO and H_2, syn gas) over a suitable catalyst. Synthesis gas can be made by gasification of coal or by

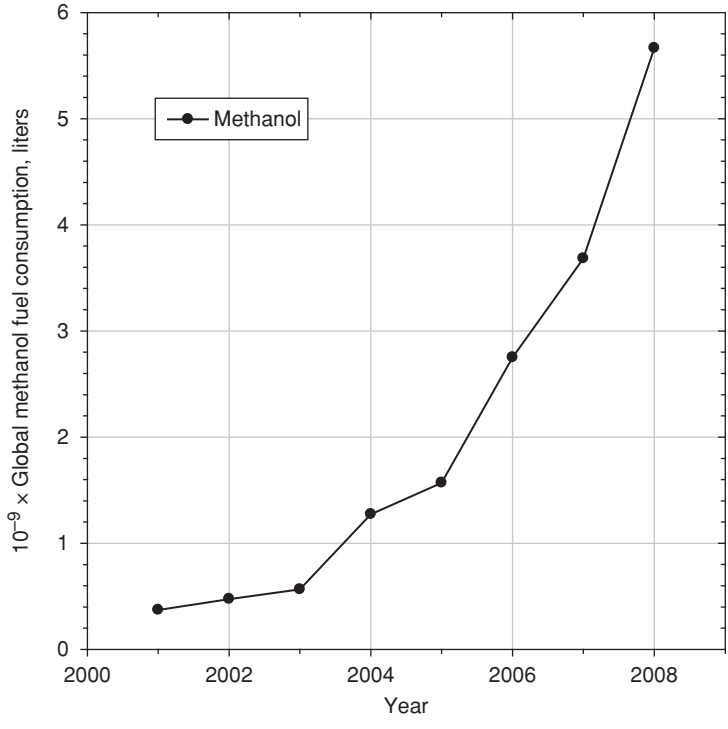

Figure I-E-3. Global methanol fuel consumption (Methanol Institute, 2008).

steam reforming of natural gas (CH_4). This has led to interest in methanol in locations with large coal but limited oil reserves (e.g., China) or in locations with "stranded natural gas" (large reserves far from markets, e.g., Siberia, the Middle East). Olah et al. (2006) have argued that a methanol-based economy could displace the existing hydrocarbon economy. Disadvantages of methanol as a fuel include its low volumetric energy density (approximately a factor of 2 lower than gasoline, see figure I-B-16), toxicity, and solubility in water, which make spills problematic, and the fact that when generated from coal, the life cycle (well-to-wheels) CO_2 emissions are substantially greater (approximately 80%) than those from gasoline. The greenhouse gas and gasoline displacement benefits of methanol derived from a variety of different feedstocks are given in table I-E.2.

I-E-2. Ethanol

Ethanol is of special interest for use as an automotive fuel and in fuel blends. Ethanol is readily obtained by the fermentation of sugars by yeast in a process that has been used for millennia and can be represented by the overall equation:

$$C_6H_{12}O_6 \rightarrow 2C_2H_5OH + 2CO_2$$

Table I-E-2. Petroleum and greenhouse gas impacts of using M85 and E85 blends to replace conventional gasoline evaluated using GREET model (Wang, 2005)

Fuel Blend	Impact on Petroleum Use	Impact on Life Cycle Greenhouse Gas Emissions
Gasoline	none (by definition)	none (by definition)
M85 (biomass gasification)	69% decrease	80% decrease
M85 (natural gas)	69% decrease	3% INCREASE
M85 (coal gasification)	71% decrease	79% INCREASE
E85 (corn fermentation)	67% decrease	16% decrease
E85 (cellulosic biomass fermentation)	63% decrease	57% decrease

Ethanol is nontoxic and biodegradable. Interest in ethanol as a motor fuel can be traced back to 1826 when Samuel Morey invented the internal combustion engine which ran on ethanol or turpentine (Morey, 1826). Over the past century, ethanol has fallen in and out of favor several times. In 1908, Henry Ford developed the first flexible-fuel Model T which could be run on gasoline, ethanol, or gasoline/ethanol blends (U.S. Environmental Protection Agency, 2008). In the 1920s, gasoline became the motor fuel of choice with 6–12% of ethanol added as an anti-knock agent. In 1921, Thomas Midgely developed tetraethyl lead as an anti-knock additive which led to the demise of ethanol blends. In the 1930s, Henry Ford promoted "farm chemurgy" a campaign for industrial uses of farm crops (including the production of fuel ethanol) to boost the U.S. economy. However, in the 1940s, low-priced Middle-East petroleum entered the market and the ethanol fuel industry shut down. The sharp increase in the price of oil in the mid–late 1970s sparked renewed interest in fuel ethanol. Following the 1973 oil crisis in the U.S., the Energy Tax Act established a government subsidy for ethanol–gasoline blends, and the Brazilian government embarked on the "Programa Nacional do Alcool" to reduce its dependence on imported oil. With the phase out of MTBE in the U.S. that began in 1999, ethanol was considered to be the primary replacement satisfying the fuel blend oxygenate requirements and providing the necessary octane benefit. The U.S. Renewable Fuel Standard of 2007 mandated an aggressive schedule of renewable fuel use in the U.S. culminating with the use of 36×10^9 gallons of renewable fuel (including 16×10^9 gallons of cellulosic ethanol) in 2022.

The global production of ethanol in 2007 was 52×10^9 liters (OECD, 2008). Using conversion factors of 3.78 liters = 1 U.S. gallon, 42 U.S. gallons = 1 barrel, volumetric energy content of ethanol = two thirds that of gasoline, and recognizing the fact that approximately 15% of the energy content of petroleum is consumed in transport and refining into gasoline, the global annual production of ethanol provides the same transportation energy as the production of approximately 260 million barrels of oil and represents 1–2% of global road transportation energy demand.

Currently ethanol is produced from food crops (corn in the U.S., sugar cane in Brazil, and sugar beets in the E.U.). As shown in figure I-E-4, the production of ethanol in Brazil and the U.S. has increased substantially over the past few years. It is hoped that cellulosic materials (grasses, wood, municipal solid waste) will provide

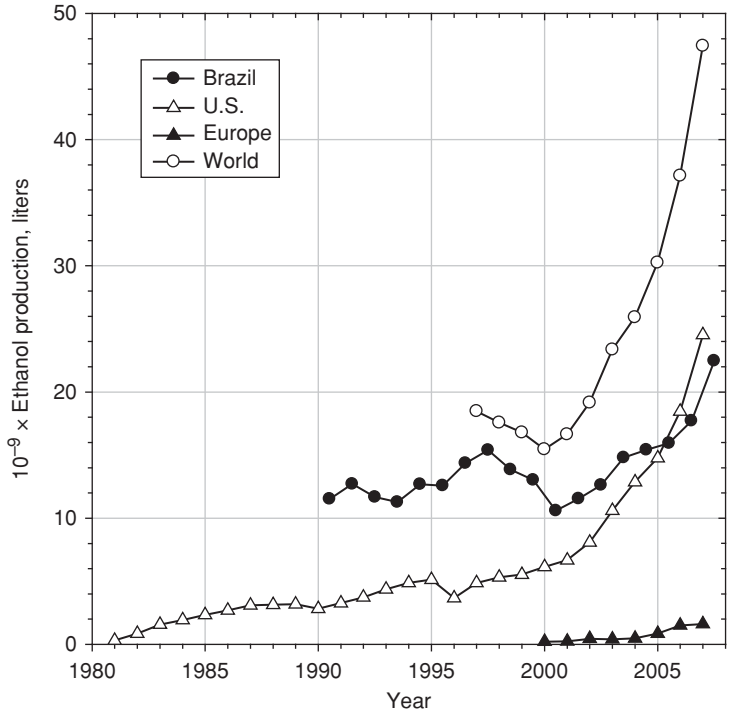

Figure I-E-4. Ethanol production in Brazil (UNICA, 2008), the U.S. (Energy Information Agency, 2008), Europe (British Petroleum, 2008), and globally (British Petroleum, 2008).

the feedstock for a future larger fuel ethanol industry. The development of cellulosic feedstocks could provide the scale, greenhouse gas benefits, and mitigation of the food versus fuel issue required for ethanol to play a greater role in providing transportation energy. Using the GREET model developed by Argonne National Laboratory (Wang, 2005), it has been estimated that powering vehicles with ethanol derived from corn and cellulose in the U.S. results in life-cycle greenhouse gas emissions that are lower than those for gasoline-powered vehicles by approximately 20–30% and 86%, respectively (Wang et al., 2007a). The International Energy Agency (IEA, 2004) has estimated that displacing gasoline with ethanol has life-cycle greenhouse gas emission benefits of approximately 20–40% when using grain in U.S. or E.U., 30–50% using sugar beets in the EU, 85–90% using sugar cane in Brazil, and 50–100% using cellulosic feedstock (IEA, 2004). The greenhouse gas emissions and gasoline displacement benefits of ethanol derived from a variety of corn and cellulose feedstocks are given in table I-E-2. The fuel blends considered in this table contain gasoline; hence, the greenhouse gas benefits are lower than those for pure ethanol fuel given above.

The volume fraction of ethanol in motor fuel is designated by a numerical value. E10 is a blend of 10% ethanol and 90% gasoline, E85 is 85% ethanol and 15% gasoline, E100 is pure ethanol. All on-road gasoline-powered vehicles can utilize ethanol blends

up to E10. Ethanol blends are more corrosive to the fuel delivery sysem than gasoline blends. To enable use of E10–E25, the Brazilian Automotive Industry Association (ANFAVEA) lists possible vehicle modifications including: use of stainless steel fuel injectors, new calibration of air–fuel ratio control, and new Lambda Sensor working range, replacement of polyamide 6.6 (Nylon®) components in the fuel system, protection of the internal surface of the fuel filter, use of ethanol blend compatible adhesives, new calibration of the ignition system, protection of the fuel tank, increased air flow for the purge of the evaporative emission canister, and adjustment of the type and loading of precious metals in the catalytic exhaust treatment system. Moving beyond E25 to E85, could require additional modifications such as the use of new materials for engine valves, and a new intake manifold to facilitate greater air flows may be necessary (ANFAVEA, 2008). All fuel sold for personal light-duty vehicles in Brazil contains at least 20% ethanol. Consumers have a choice of either E20–E25 (the exact blend is regulated by government and is updated periodically), or hydrous ethanol (approximately 95% ethanol and 5% water reflecting the ethanol–water azeotrope). Vehicles in Brazil are designed to operate either solely on E20–E25 (Gasolina), or to be flexible and operate on E20–E25, hydrous ethanol (Alcool), or any mixture of the two. To aid starting in cold weather, the flexible fuel vehicles running on hydrous ethanol in Brazil are equipped with a small additional fuel tank which contains E20–E25. The gasoline in the E20–E25 blend provides the volatility needed to start the engine in cold weather. In 2007 flexible-fuel vehicles accounted for 85.6% of the cars and light-duty commercial vehicles sold in Brazil; in 2008 this fraction increased to 91.8% (ANFAVEA, 2008). In the U.S. vehicle manufacturers supply flexible-fuel vehicles (FFVs) that are capable of running on gasoline, E85, or any mixture of the two. Of the 200 million on-road light-duty vehicle fleet in the U.S. in 2008, more than 6 million were FFVs (U.S. Environmental Protection Agency, 2008). In the U.S. the availability of E85 is limited and pricing of E85 is generally unattractive when compared to gasoline (on an energy content basis) and so currently most FFVs in the U.S. are not fueled with E85.

Limitations on the use of ethanol as a fuel or fuel component include: (i) The water-induced phase separation of ethanol–gasoline mixtures (see figure I-E-5 and Mueller et al., 2009), which makes distribution problematic; (ii) its relatively low energy density (lower heating value of 21 MJ liter^{-1} compared to 32 MJ liter^{-1} for gasoline), which reduces the vehicle range for a given size fuel tank; (iii) vehicle modifications necessary for >E10 blends; (iv) the increased vapor pressure of ethanol–gasoline blends (Caffrey and Machiele, 1994), which makes it more difficult to control evaporative emissions; (v) the limited amount of biomass that can be grown for ethanol production (OECD, 2007); (vi) the cost of ethanol production (IEA, 2004); and (vii) concerns over the competition for food crops and biodiversity (IEA, 2004; OECD, 2007).

There have been relatively few reported measurements of ethanol concentrations in ambient air. Cavanagh et al. (1969) sampled air near Point Barrow, Alaska in 1967 using analysis by gas chromatography. Methanol and ethanol eluted together formed one peak and were observed sporadically at a combined level of approximately 1 ppb. As seen in table I-D-1, measurements in Kinterbush, Alabama by Goldan et al. (1995) and near Garmisch-Partenkirchen, Germany by Leibrock and Slemr (1997) also showed ethanol levels in remote locations of the order of 1 ± 1 ppb. Grosjean et al. (1998a)

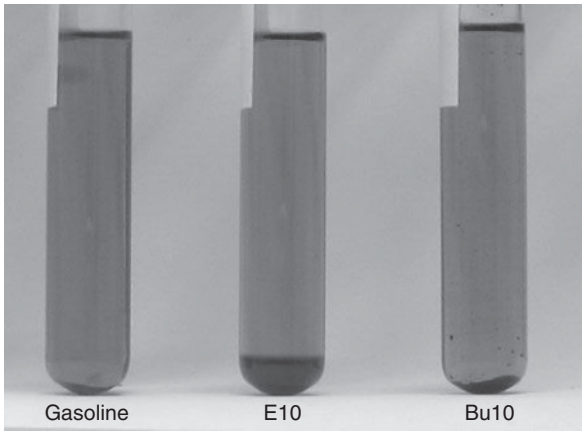

Figure I-E-5. Identical volumes of water added to gasoline, gasoline with 10% ethanol (E10), and gasoline with 10% *n*-butanol (Bu10), illustrating water-induced phase separation of ethanol–gasoline blends taken from Mueller et al. (2009). Dye has been added to make the aqueous phase at the bottom and the hydrocarbon phase (above) more visible. The white areas at top left are labels on the test tubes.

conducted measurements in downtown Porto Alegre, Brazil and reported ethanol levels of 0.4–68.2 ppb with an average value of 12.1 ± 13.1 ppb over an approximately one year period (March 20, 1996–April 16, 1997). Nguyen et al. (2001) observed 8.2 ± 4.6 ppb of ethanol in ambient air in Osaka in May–December, 1997 and 173.3 ± 38.1 ppb in Sao Paulo from 3 to 9 February 1998. Legreid et al. (2007) conducted measurement campaigns in the center of Zürich in 2005 and reported mean ethanol levels of 6.87 ppb (March 18, 2005–April 18, 2005), 3.94 ppb (July 1, 2005–August 1, 2005), 7.61 ppb (November 10, 2005–November 30, 2005), and 7.53 ppb (December 19, 2005–February 1, 2006). The elevated levels of ethanol observed in Porto Alegre and Sao Paulo, Brazil reflect emissions associated with the predominant use ethanol in vehicles.

I-E-3. Butanol

Butanol is under consideration for gasoline blending and, like ethanol, can be produced from bio-based feedstocks (sugars, starches, cellulose) via fermentation. Butanol has two main advantages over ethanol. First, butanol–gasoline blends are less susceptible to phase separation in the presence of water than ethanol–gasoline blends due to the lower water solubility of butanol. When butanol–gasoline blends contact water, two layers form just as when gasoline contacts water; but, as illustrated in figure I-E-5, unlike ethanol–gasoline blends, very little of the butanol partitions into the aqueous layer (Mueller et al., 2009). As a result, butanol–gasoline blends can be transported using the existing distribution infrastructure. Second, as seen in figure 1-B-15, butanol has a volumetric energy density which is similar to that of octane; hence, the use of butanol in fuel blends has little impact on the vehicle range. Commercialization of

butanol as a motor fuel is being explored in a collaboration between BP and DuPont (British Petroleum, 2008).

I-E-4. Dimethyl Ether

Dimethyl ether (DME) is produced by the dehydration of methanol decribed by the overall reaction:

$$2CH_3OH \rightarrow CH_3OCH_3 + H_2O$$

DME has been proposed as an alternative diesel fuel (Sehested et al., 1996; Semelsberger et al., 2006) because it has several desirable fuel properties. First, DME has a high cetane (i.e., low octane) number. Second, when used in diesel engines, DME reduces combustion noise and emissions of particles. Third, the trade-off between NO_x and soot emissions using conventional diesel fuel is eliminated in DME-fueled engines because the combustion is soot free. Hence, a DME-fueled engine can be tuned to give reduced NO_x emissions. Fourth, DME can be produced from hydrocarbons via a relatively inexpensive synthesis (Sehested et al., 1996). Engine tests have shown that DME-fueled diesel engines have low emission levels (Fleisch et al., 1997). Ethers like MTBE (methyl *tert*-butyl ether), ETBE (ethyl *tert*-butyl ether), and TAME (*tert*-amyl methyl ether) have high octane (i.e., low cetane) numbers and are used to boost the octane number of gasoline. It is interesting that DME, which is structurally similar to MTBE, ETBE, and TAME, has a high cetane number and hence is a good diesel fuel, while MTBE, ETBE, and TAME have low cetane numbers (high octane numbers) and would make poor diesel fuels. Sehested et al. (1996) suggested that a possible explanation for this difference is the facile reaction of CH_3OCH_2 radicals with O_2 to give a chemically activated CH_3OCH_2OO radical which undergoes intramolecular rearrangement and decomposition to generate an OH radical and two molecules of formaldehyde (such intramolecular hydrogen abstraction reactions, proceeding through what is known in the combustion literature as a QOOH radical, are important in combustion in diesel engines). It is germane to note that unlike conventional diesel fuel, DME is a gas at ambient temperature (boiling point $-24.8°C$). Hence, any widespread use of DME would require significant investment in new infrastructure associated with fuel distribution and delivery and additional cost for fuel storage on vehicles. DME is currently used as an aerosol spray propellant and in blends with liquified petroleum gas (propane/butane) for home heating and cooking. As shown in figure I-E-6, the global production of DME increased markedly in the 2000s.

I-E-5. Methyl *tert*-Butyl Ether (MTBE)

After the passage of the U.S. Clean Air Act Amendments of 1990 requiring substantial oxygen content in fuels, MTBE use as a fuel blending component increased and dominated the oxygenate market in U.S. in the late 1990s and early 2000s (see figure I-E-1). MTBE is made by addition of methanol to isobutene (over a catalyst) as given by the

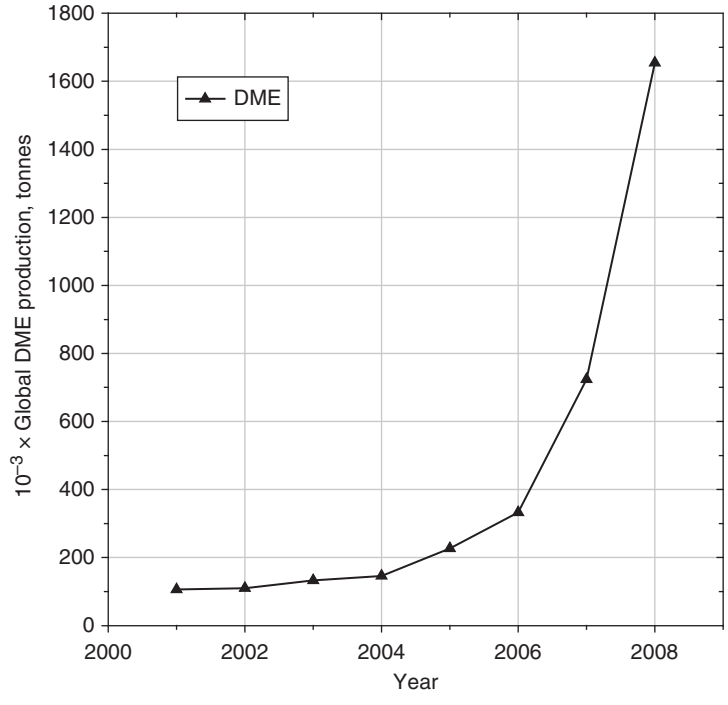

Figure I-E-6. Global dimethyl ether production (Methanol Institute, 2008).

overall reaction:

$$CH_3OH + (CH_3)_2C{=}CH_2 \rightarrow CH_3OC(CH_3)_3$$

As discussed above, methanol is produced from natural gas and is an inexpensive feedstock. MTBE has a high octane number (blending octane number of 118, see table I-E-1), is miscible with gasoline in all proportions, can be distributed in pipelines in blends with gasoline (MTBE–gasoline blends do not undergo water-induced phase separation), and decreases the atmospheric reactivity of vehicle emissions (Dunker et al., 1996). In the late 1990s, it was not unusual for gasoline in the U.S. to contain 10–15% (v/v) MTBE. The solubility of MTBE in water is substantially higher than for other components of gasoline (e.g., at 25°C, approximately 50 g liter^{-1} for MTBE, 1.8 g liter^{-1} for benzene, and 0.5 g liter^{-1} for toluene (Squillace et al., 1997). A study conducted in 1993–1994 found that 27% of 210 wells and springs sampled in eight urban areas in the U.S. were contaminated (>0.2 μg liter^{-1}) with MTBE (Squillace et al., 1996).

The toxicity of MTBE is low. Interestingly, it is injected into patients as part of a medical treatment to dissolve gallstones (van Sonnenberg et al., 1988). However, it gives water an unpleasant turpentine-like taste at concentrations as low as 2 μg liter^{-1} (Chisala et al., 2007). While concern over ground water contamination led to

the phase-out of the use of MTBE in several U.S. states (notably, California and New York), use of MTBE as a fuel additive continues elsewhere in the world.

Levels of MTBE measured in ambient air in Porto Alegre, Brazil in 1996–1997 by Grosjean et al. (1998a) averaged 6.6 ± 4.3 ppb. Carbon monoxide and acetylene in Porto Alegre arise largely from vehicle emissions (∼99%). Scatter plots of MTBE versus CO and MTBE versus acetylene gave near linear relationships with near zero intercepts, suggesting that all three of these compounds arise largely from vehicular emissions. Grosjean et al. (1998a) pointed out that measurements of much higher concentrations of MTBE (as high as 310 ppb) were reported in Sao Paulo, Brazil in 1990 and in Cerqueiro Cesar, Brazil (2,260 ppb). MTBE is no longer used in fuels in Brazil and is not expected to be present in urban air in Brazil. Ambient concentrations of MTBE measured by Zielinska et al. (1997) in various cities in California during 1993–1996 showed averages that ranged from 0.6 ± 0.2 ppb in Santa Monica to 7.2 ± 0.6 ppb in Burbank, California Grosjean et al. (1998a) compare measurements of MTBE in the several locations in the U.S. during the 1994–1996 time period. As expected, in nonurban areas, low concentrations of MTBE (<1 ppb) are usually reported. Since the use of methyl *tert*-butyl ether as an additive to gasoline has been phased out, or reduced, in many parts of the U.S., its current ambient concentrations are expected to be substantially lower than measured in the 1990s.

I-E-6. Ethyl *tert*-Butyl Ether (ETBE)

ETBE is made by reacting ethanol with isobutene over a catalyst by the overall reaction:

$$C_2H_5OH + (CH_3)_2C{=}CH_2 \rightarrow C_2H_5OC(CH_3)_3$$

ETBE has chemical and physical properties which are similar to those of MTBE. It has a high octane number (blending octane number of 119, see table I-E-1), is miscible with gasoline in all proportions, and can be distributed via pipelines in blends with gasoline. Its atmospheric reactivity is higher than that of MTBE and atmospheric model calculations indicate that addition of ETBE to gasoline leads to a slight increase in ozone formation (Dunker et al., 1996). ETBE has a solubility of about 12 g liter^{-1}, which is approximately a factor of 3 less than that of MTBE (EFOA, 2008). ETBE made using bioethanol contains one-third nonfossil carbon atoms. Conversion of ethanol into ETBE provides a method of integrating ethanol into fuel without compromising vehicle range or compatibility of the fuel with the existing fuel and vehicle infrastructure (Tanaka et al., 2006). However, conversion of ethanol into ETBE does add cost. A large fraction (>75% according to the European Fuel Oxygenates Association) of bioethanol in Europe is converted into ETBE before being used in gasoline (EFOA, 2008).

I-E-7. *tert*-Amyl Methyl Ether ($CH_3CH_2C(CH_3)_2OCH_3$)

tert-Amyl methyl ether (TAME) is made by reacting methanol with 2-methyl-2-butene over a catalyst by the overall reaction:

$$CH_3OH + (CH_3)_2C{=}CHCH_3 \rightarrow CH_3CH_2C(CH_3)_2OCH_3$$

TAME has chemical and physical properties that are similar to those of MTBE and ETBE. As expected from its molecular structure, the properties of TAME are closer to gasoline than those of MTBE and ETBE. TAME is miscible with gasoline in all proportions, TAME–gasoline blends are water tolerant (the addition of water does not induce phase separation as with ethanol–gasoline blends; Mueller et al., 2009) and can be distributed via pipelines in blends with gasoline, has a high octane number (blending octane number of 112, see table I-E-1), and solubility in water of 11 g liter^{-1}.

I-E-8. Biodiesel, Fatty Acid Methyl Esters

The transesterification of triglycerides in vegetable oils and animal fats produces a mixture of esters commonly referred to as "biodiesel". Vegetable oils and animal fats are made up of triglycerides, which are esters formed from glycerol [1,2,3-propanetriol, $CH_2OHCH(OH)CH_2OH$] and long-chain fatty acids such as palmitic acid [*n*-$C_{15}H_{31}C(O)OH$], stearic acid [*n*-$C_{17}H_{35}C(O)OH$], and oleic acid [$CH_3(CH_2)_7CH{=}CH(CH_2)_7C(O)OH$]. Fatty acids are often referred to as C*x*:*y* where *x* is the number of carbon atoms and *y* is the number of double bonds in the molecule. Palmitic acid is C16:0, stearic acid is C18:0, and oleic acid is C18:1. The fatty acid profiles of some common vegetable oils are given in table I-E-3. The molecular structures of common fatty acid methyl esters (FAMEs) are shown in figure I-E-7. Methanol is the typical alcohol used in the process producing FAMEs. Higher alcohols such as ethanol, propanol, butanol, etc., can be used to give the corresponding ethyl-, propyl-, and butyl- esters (FAEEs, FAPEs, FABEs, etc.). The transesterification is catalyzed by addition of base (e.g., KOH or NaOH) and can be represented by the following overall reaction equilibrium:

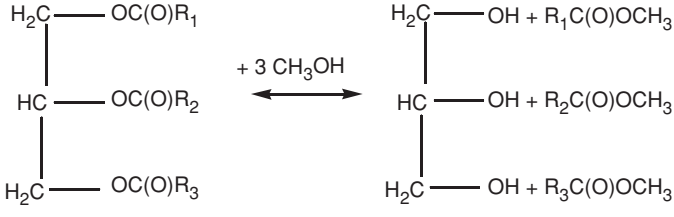

This equilibrium is driven to the right using excess alcohol.

Biodiesel is typically used in blends with fossil diesel fuel with the volume fraction specified by a numerical value (e.g., B2, B5, and B10 contain 2%, 5%, and 10% biodiesel). Most vehicle manufacturers warranty their diesel-powered vehicles to operate on blends up to B5 assuming the fuel meets existing fuel-quality specifications. Research and development is underway to develop vehicles and fuel infrastructures compatible with higher biodiesel blends (e.g., B20).

Advantages of biodiesel over conventional fossil diesel include: (i) very low sulfur and aromatic hydrocarbon content, (ii) lower particle emissions, (iii) displacement of petroleum and improved energy security, and (iv) approximately 40–60% lower greenhouse gas emissions for 100% biodiesel (International Energy Admistration, 2004).

Table I-E-3. Fatty acid profiles (%) of common vegetable oils

	Red Palm[a]	Palm Kernel[a]	Coconut[a]	Soybean[a]	Groundnut[a]	Sunflower[a]	Olive[b]	Jatropha[c]
Caproic 6:0		0.2	0.5					
Caprylic 8:0		3.3	8.0					10.5
Capric 10:0		3.5	6.4					
Lauric 12:0	0.2	47.8	48.5					
Myristic 14:0	1.1	16.3	17.6	0.1	0.1	0.8		2.6
Palmitic 16:0	44.0	8.5	8.4	11.0	11.6	6.5	10.9	20.9
Stearic 18:0	4.5	2.4	2.5	4.0	3.1	4.5		15.7
Oleic 18:1	39.2	15.4	6.5	23.4	48.5	21.1	70.1	31.4
Linoleic 18:2	10.1	2.4	1.5	53.2	31.4	66.2	16.5	5.2
Linolenic 18:3	0.4			7.8			0.6	
Arachidic 20:0	0.1	0.1			1.5	0.3		4.5
Saturates	49.9	82.1	91.9	15.1	16.3	11.3	10.9	56.8
Monounsaturates	39.2	15.4	6.5	23.4	48.5	21.1	71.7	34.6
Polyunsaturates	10.5	2.4	1.5	61.0	31.4	66.2	17.1	5.3

[a]Edem (2002).
[b]Ayorinde et al. (2000).
[c]Ogbobe and Akano (1993), Okieimen (2002).

Challenges faced by biodiesel include: (i) cost, (ii) cold flow performance, (iii) oil dilution by fuel (with the lower volatility of biodiesel the fuel is more prone to be entrained into oil on the cylinder wall and find its way into the engine oil), (iv) oxidative stability (particularly for polyunsaturated FAMEs) leading to a shorter storage life than conventional diesel, and (v) competition with food crops.

Table I-E-4 shows physical and chemical properties for No. 1 diesel fuel, No. 2 diesel fuel, and a typical biodiesel made from soy oil (Canakci, 2005). The fatty acid composition (%) for the soybean oil used was: C16:0, 10.5; C17:0, 0.11; C18:0, 4.76; C18:1, 22.52; C18:2, 52.34; C18:3, 8.19, C20:0, 0.36; unknown components, 0.48; % saturation, 16.3. The composition of the biodiesel methyl esters prepared from the soybean oil is similar: C16:0, 10.56; C17:0, 0.11, C18:0, 4.74; C18:1, 22.51; C18:2, 52.39; C18:3, 8.22; C20:0, 0.44; unknown components, 0.44; % saturation, 16.3. As seen from table I-E-4, the biodiesel has similar properties to fossil diesel. Biodiesel has a greater viscosity and tendency to gel than conventional diesel fuel, which restricts its use at low ambient temperature unless sufficient heating of the fuel and engine components is provided.

Comparison of the performance of biodiesel and diesel fuels in diesel engines (e.g., see Peterson et al., 1999; Canakci, 2005; Canakci et al., 2006) suggests that emissions from biodiesel-blend-powered engines are similar to those from fossil-diesel-fuel engines, with somewhat lower emissions of CO but higher NO_x. In 2005, a small fraction of the diesel engines used biodiesel in the U.S.; about 3.7×10^7 gallons of biodiesel were used compared to 3.9×10^{10} gallons of conventional diesel (Davis and Diegel, 2007). According to the National Biodiesel Board (NBB), production of biodiesel increased from 5×10^5 gallons in 1999 to 4.5×10^8 gallons in 2007. Production of biodiesel was expected to reach 6.0×10^8 gallons in 2008. The U.S. Renewable

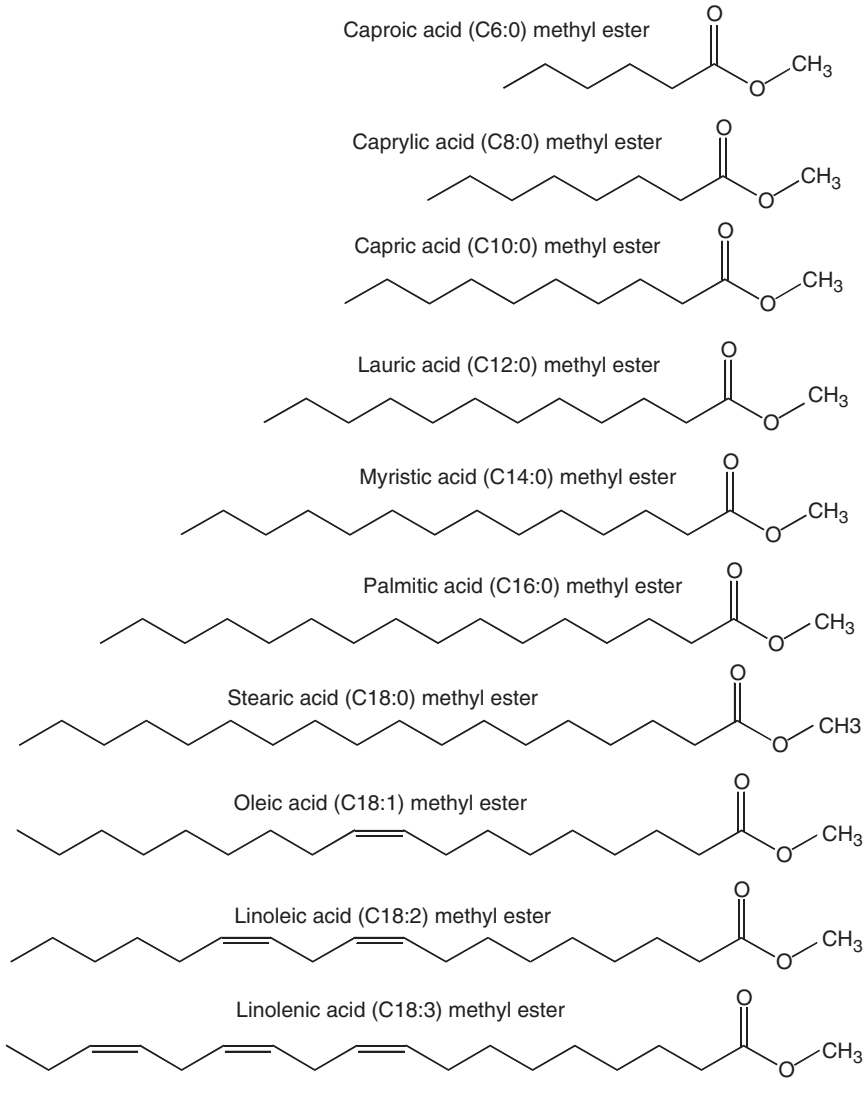

Figure I-E-7. Common fatty acid methyl esters (FAMEs) present in biodiesel.

Fuel Standard (2008) requires 5.0×10^8 gallons of biodiesel (or biomass-derived diesel, e.g., hydrotreated plant oils) in the domestic diesel pool in 2009 and 1×10^9 gallons by 2012 (Tullo, 2008).

I-E-9. Other Oxygenates of Potential Use as Fuels

Abiotic chemical synthetic routes are being developed to convert biomass into furanic compounds such as 2-5-dimethyl furan, 5-(ethoxymethyl) furfural, and

Table I-E-4. Comparison of the physical and chemical properties of No. 1 and No. 2 diesel fuels with those of the biofuel, methyl esters prepared from soy oil (from Canakci, 2005)

Test Property	No. 1 Diesel Fuel	No. 2 Diesel Fuel	Methyl Esters Prepared from Soy Oil
Carbon, % mass	86.83	86.70	77.10
Hydrogen, % mass	12.72	12.71	11.81
Oxygen % mass	–	–	10.97
C/H ratio	6.83	6.82	6.53
Hydrocarbon type, FIA (ASTM D1329)			
Saturates, % volume	77.2	63.0	–
Olefins, % volume	1.3	1.3	–
Aromatics, % volume	21.6	35.7	–
Sulfur, % mass	0.045	0.041	<0.005
Typical formula	$C_{12.38}H_{21.77}$	$C_{14.09}H_{24.78}$	$C_{18.74}H_{34.43}O_2$
Average molecular weight	170.40	193.89	291.62
Cetane No. (ASTM D613)	45.3	42.6	51.5
Gross heat of combustion, kJ kg^{-1}	45.834	45.339	39.871
Net heat of combustion, kJ kg^{-1}	43.133	42.640	37.388
Specific gravity, g cm^{-3} (21°C)	0.8181	0.8537	0.8814
Kinematic viscosity, mm^2 s^{-1}	1.76	2.8271	4.2691
Total glycerin, %	–	–	0.028
Free glycerin, %	–	–	0.000

γ-valerolactone, which may find use as fuel blending components (Román-Leshkov et al., 2007; Mascal and Nikitin, 2008).

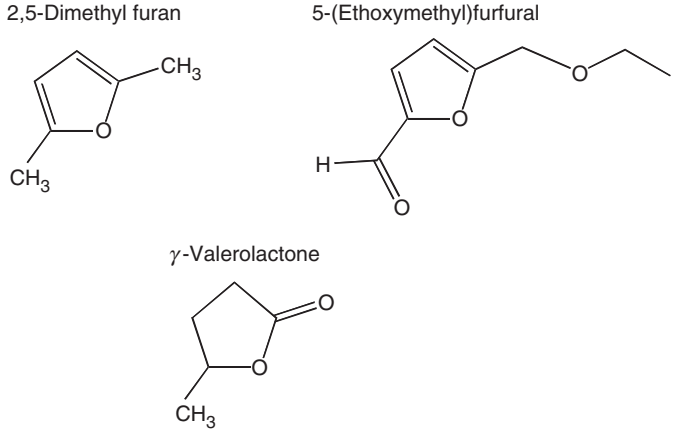

I-F. Treatment of Kinetic Data and Estimation of Atmospheric Lifetimes of Oxygenates

I-F-1. Treatment of Kinetic Data

In the following chapters, we review the available literature for the kinetics of the reactions of OH radicals, NO_3 radicals, chlorine atoms, $O(^3P)$ atoms, and ozone with

oxygenated organic compounds. The compounds are grouped by class in the following order: alcohols, ethers, aldehydes, ketones, esters, acids, and nitrogen-containing oxygenated species. For internal consistency, the data from relative rate studies have been reevaluated using a consistent set of reference rate coefficients taken mainly from Calvert et al. (2000, 2002, 2008), and the IUPAC Subcommittee on Gas Kinetic Data Evaluation (Atkinson et al., 2006, 2008b; IUPAC, 2008). A notable exception was the value of $k(\mathrm{Cl} + \mathrm{C_2H_4}) = 9.52 \times 10^{-11}$ cm^3 molecule^{-1} s^{-1}, which was based upon an average of relative rate data obtained at 700–760 Torr and ambient temperature by Atkinson and Aschmann (1985), Wallington et al. (1990b), Stutz et al. (1998), and Glowacki et al. (2007) with reference rate coefficients taken from IUPAC (2008). Tables I-F-1 and I-F-2 provide selected OH radical and chlorine atom reference rate coefficients that were used. Arrhenius parameters for relative rate studies given in the tables of kinetic data were obtained by fitting the Arrhenius expression to the reevaluated kinetic data. Uncertainties quoted for relative rate studies reflect uncertainties (where given) in the published rate constant ratios and do not include uncertainties in the reference rate coefficients. In all other cases, quoted uncertainties in the rate coefficient tables are those published in the individual studies.

In many cases, within the experimental uncertainties, the simple Arrhenius expression $k = A\exp(-B/T)$ cm^3 molecule^{-1} s^{-1}, provides a reasonable description of the available kinetic data.

Where data are available over a wide temperature range, significant curvature of Arrhenius plots is often observed. In such cases, a modified version of the Arrhenius expression, $k = A\,T^2\exp(-B/T)$ cm^3 molecule^{-1} s^{-1} has been fit to the data. In some cases, the curvature cannot be adequately captured by the modified Arrhenius expression, and we have opted to fit an expression consisting of two Arrhenius expressions

Table I-F-1. Reference rate coefficients for selected OH radical reactions

Compound	k (cm^3 molecule^{-1} s^{-1})	Reference
Methane (CH_4)	$1.85 \times 10^{-12}\exp(-1{,}690/T)$	Calvert et al. (2008)
Acetylene (C_2H_2)	7.8×10^{-13} (298 K, 1 atm.)	Atkinson et al. (2006)
Ethene (C_2H_4)	7.9×10^{-12} (298 K, 1 atm.)	Atkinson et al. (2006)
Ethane (C_2H_6)	$8.6 \times 10^{-12}\exp(-1{,}047/T)$	Calvert et al. (2008)
Propene (C_3H_6)	2.9×10^{-11} (298 K, 1 atm.)	Atkinson et al. (2006)
Propane (C_3H_8)	1.1×10^{-12} (298 K)	Atkinson et al. (2006)
Isobutene (C_4H_8)	5.20×10^{-11} (298 K, 1 atm.)	Calvert et al. (2000)
1,3-Butadiene (C_4H_6)	6.70×10^{-11} (298 K, 1 atm.)	Calvert et al. (2000)
n-Butane (C_4H_{10})	$1.40 \times 10^{-11}\exp(-520/T)$	Calvert et al. (2008)
n-Pentane (C_5H_{12})	$1.81 \times 10^{-11}\exp(-452/T)$	Calvert et al. (2008)
Cyclohexane (C_6H_{12})	$3.26 \times 10^{-17}\,T^2\exp(262/T)$	Calvert et al. (2008)
n-Hexane (C_6H_{14})	$1.98 \times 10^{-11}\exp(-394/T)$	Calvert et al. (2008)
Toluene ($C_6H_5CH_3$)	5.63×10^{-12} (298 K)	Calvert et al. (2002)
m-Xylene ($C_6H_4(CH_3)_2$)	2.31×10^{-11} (298 K)	Calvert et al. (2002)
p-Xylene ($C_6H_4(CH_3)_2$)	1.43×10^{-11} (298 K)	Calvert et al. (2002)
n-Heptane (C_7H_{16})	6.50×10^{-12} (298 K)	Calvert et al. (2008)
n-Octane (C_8H_{18})	7.81×10^{-12} (298 K)	Calvert et al. (2008)

Table I-F-2. Reference rate coefficients for selected chlorine atom reactions

Compound	k (cm^3 $molecule^{-1}$ s^{-1})	Reference
Methane (CH_4)	6.6×10^{-12} exp(−1,240/T)	Atkinson et al. (2006)
Methyl chloride (CH_3Cl)	4.8×10^{-13} (298 K)	Atkinson et al. (2008b)
Acetylene (C_2H_2)	5.2×10^{-11} (298 K, 1 atm.)	Atkinson et al. (2006)
Ethene (C_2H_4)	9.52×10^{-11} (298 K, 1 atm.)	See text
Ethane (C_2H_6)	8.3×10^{-11} exp(−100/T)	Atkinson et al. (2006)
Ethyl chloride (C_2H_5Cl)	7.8×10^{-12} (298 K)	Wine and Semmes (1983) Bryukov et al. (2003)
Methyl formate (CH_3OCHO)	1.40×10^{-12} (298 K)	This work
Propene (C_3H_6)	2.3×10^{-10} (298 K, 1 atm.)	IUPAC (2008)
Propane (C_3H_8)	1.4×10^{-10} (298 K)	Atkinson et al. (2006)
n-Butane (C_4H_{10})	2.05×10^{-10} (298 K)	Atkinson et al. (2006)
n-Pentane (C_5H_{12})	2.70×10^{-10} (298 K)	Calvert et al. (2008)
Cyclohexane (C_6H_{12})	3.3×10^{-10} (298 K)	Calvert et al. (2008)

to the data, $k = A\exp(-B/T) + C\exp(-D/T)$ cm^3 $molecule^{-1}$ s^{-1}. No physical significance is ascribed to the parameters from the modified and double Arrhenius fits. Caution should be exercized in extrapolating beyond the temperature range over which experimental data are available. In the fitting procedure, a nonlinear least squares regression was used with each data point given a weight of $1/k^2$. This procedure is mathematically equivalent to a least squares fit in which the sum of the squares of the ratio $(k_{\text{measured}} - k_{\text{fit}})/k_{\text{fit}}$ is minimized, thereby providing a fit that minimizes relative error. Values at 298 K derived from the Arrhenius expressions are given with an estimate of the uncertainty associated with k at 298 K.

Modern absolute kinetic techniques are capable of measuring rate coefficients with an accuracy of approximately 10–20%. Relative rate methods can typically determine rate coefficients *ratios* with an accuracy of 5–10%. When assessing the accuracy of rate coefficients derived from relative rate studies, the uncertainties in the reference rate coefficients need to be considered. Where only one measurement of a rate coefficient has been reported, we typically assign a conservative uncertainty of ±25 or ±30%. When several studies have been reported and the results are in good agreement, we typically assign an uncertainty of ±10 or ±15% (depending on our assessment of the likely uncertainty). For reactions where different studies give significantly different results and there is no obvious reason to prefer a subset of the reported results, we typically assign uncertainties >15% (the exact value reflecting our judgment of the likely uncertainty). In the tables associated with each reaction, the abbreviations defined in table I-F-3 are used to describe the experimental techniques employed.

I-F-2. Estimation of Atmospheric Lifetimes

Photolysis is an important atmospheric loss mechanism for aldehydes and ketones. The lifetimes with respect to photolysis of oxygenated compounds are estimated in chapter IX. The atmospheric lifetimes of the alcohols, hydroperoxides, ethers, esters,

Table I-F-3. Abbreviations for the experimental techniques used in the text and tables

Abbreviation	Experimental Technique
API	Atmospheric pressure ionization
CEAS	Cavity enhanced absorption spectroscopy
CIMS	Chemical ionization mass spectroscopy
CL	Chemiluminescence detection
DF	Discharge flow tube
DF abs.	Discharge flow tube, absorption spectroscopy
ECD	Electron capture detection
EPR	Electron paramagnetic resonance spectroscopy
FID	Flame ionization detection
FP	Flash photolysis
FTIR	Fourier transform infrared
GC	Gas chromatography
HPLC	High pressure liquid chromatography
IR abs.	Infrared absorption
IR em.	Infrared emission
LIF	Laser-induced fluorescence
MM abs.	Molecular modulation absorption
MMS	Molecular modulation spectroscopy
MS	Mass spectrometry
O_3CL	Ozone chemiluminescence
PLP	Pulsed laser photolysis
PR	Pulse radiolysis
PTR	Proton transfer reaction
RF	Resonance fluorescence
RR	Relative rate measurement
SF	Stopped flow reactor
SC	Smog chamber
SPME	Solid phase microextraction fiber technique
UV abs.	Ultraviolet absorption
VLPR	Very low pressure reactor
VUV abs.	Vacuum ultraviolet absorption

and nitrates are controlled mostly by reaction with OH and have been estimated as follows. For compounds whose lifetime is < 1 day, an average daytime [OH] of 2.5×10^6 molecule cm^{-3} is used in conjunction with the rate coefficient for reaction with OH, evaluated at 298 K. For species with lifetimes between about 1 day and 1 year, a diurnally averaged [OH] of 1.0×10^6 molecule cm^{-3} is used, again in conjunction with the OH rate coefficient at 298 K. For species with lifetimes >1 year, mixing throughout the troposphere is assumed, and for these cases the OH rate coefficient at 272 K is used, with an assumed tropospheric average [OH] $\approx 10^6$ molecule cm^{-3}. Reactions with O_3 and NO_3 are of limited significance; reaction with O_3 is only of potential importance for unsaturated species, while the NO_3 reactions may be of somewhat more general importance. In cases where these reactions may be significant, lifetimes have been estimated using [O_3] $\approx 10^{12}$ molecule cm^{-3} (diurnally averaged) and [NO_3] $\approx 3 \times 10^9$ molecule cm^{-3} (nighttime value for a polluted urban

region, Calvert et al., 2000). Penkett et al. (2007) have argued that similar NO_3 levels (several hundred ppt, 200 ppt $\approx 5 \times 10^9$ molecule cm^{-3}) are widespread across continental areas at night. However, observations by Aldener et al. (2006), for example, indicate lower NO_3 levels of approximately 10–50 ppt downwind of polluted urban areas. Lifetimes with respect to Cl-atom reaction are generally not discussed, as the Cl-atom concentration in the troposphere is not well-established and is quite variable. As a general rule, in the background troposphere [Cl] $\leq 10^3$ molecule cm^{-3}, and Cl-atom chemistry is not expected to play a significant role (Rudolph et al., 1996). However, some contribution may occur in regions of elevated concentrations ([Cl] $\approx 10^4$ molecule cm^{-3} or more), such as the marine boundary layer (Jobson et al., 1994; Wingenter et al., 1996, 2005), in coastal areas (Spicer et al., 1998) and/or in some urban regions (Tanaka et al., 2003).

II

Rate Coefficients and Mechanisms for the Atmospheric Oxidation of the Alcohols

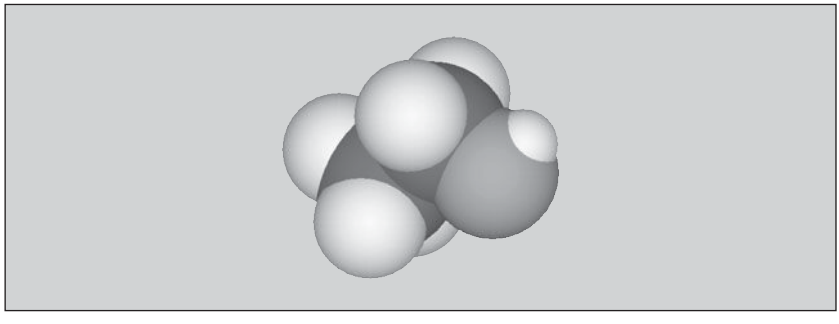

II-A. Introduction

The presence of alcohols in the atmosphere is attributable to natural and anthropogenic sources (e.g., Graedel, 1978). They are released into the atmosphere as a result of their use as fuels (e.g., methanol, ethanol), fuel additives (e.g., ethanol), solvents (e.g., ethanol, propanol) and as starting materials or intermediates for organic synthesis in a large number of industries (e.g., isobutanol, isopentanol, hexylene glycol). Vegetation also provides a significant source of alcohols to the atmosphere (Kesselmeier and Straudt, 1999; Fall, 2003). A number of saturated and unsaturated alcohols have been identified to be biogenically emitted (e.g., methanol, ethanol, methylbutenol, linalool, *Z*-hex-3-en-1-ol "leaf alcohol"). High ambient concentrations of certain alcohols have been measured in some areas, up to 68 ppb for ethanol in Porto Alegre, Brazil (Grosjean et al., 1998a) and up to 3 ppb for 2-methyl-3-buten-2-ol in the Colorado mountains (Goldan et al., 1993). A more complete description of the emission sources and ambient concentrations of alcohols is given in chapter I.

Reaction with OH radicals is the dominant atmospheric loss process for the saturated alcohols while reactions with NO_3, O_3, and photolysis are negligible. The OH-initiated reaction proceeds by H-atom abstraction from the various C—H bonds of the CH_3, —CH_2, and $\rangle$CH groups in the alkyl chain, and to a much lesser extent from the O—H bond. The available mechanistic data for the OH reaction with saturated alcohols show that H-atom abstraction from the α-carbon atom is an important reaction channel, with abstraction from the other positions also making a significant contribution to the

reaction products. The atmospheric degradation of unsaturated alcohols is controlled mainly by reaction with OH, NO_3, and O_3, while the photolysis remains of negligible importance. The primary reaction path is OH, NO_3, or O_3 addition to the double bond to form an adduct for OH and NO_3 and an ozonide for the reactions with O_3. The subsequent reaction mechanisms and end products depend on the molecular structure of the unsaturated alcohol.

This chapter contains kinetic and mechanistic information on the reactions of OH, NO_3, O_3, and Cl with saturated-, unsaturated-, halogenated-, and aromatic-alcohols, and alkyl hydroperoxides. The reactions of OH radicals with saturated alcohols presented here are based on the recent review by Calvert et al. (2008) with relevant updates. Rate coefficients are combined with the tropospheric concentrations of OH, NO_3, and O_3 to estimate atmospheric lifetimes of these compounds.

II-B. Acyclic Alcohols

II-B-1. Methanol (Methyl Alcohol, CH_3OH)

II-B-1.1. OH Reaction Kinetics

The reaction of OH with methanol has been investigated by a large number of groups using both absolute and relative methods. Table II-B-1 summarizes the available data reported in the temperature range relevant to atmospheric chemistry. The data are also plotted in figure II-B-1. Measurements have also been conducted at high temperature (e.g., Bott and Cohen, 1991). The rate coefficients near 298 K are in good agreement, and the recommended value at 298 K is $k = (9.0 \pm 1.0) \times 10^{-13}\,\mathrm{cm^3}$ $\mathrm{molecule^{-1}\,s^{-1}}$ with an estimated uncertainty of $\pm 15\%$ (Atkinson et al., 2006). The temperature dependence of the reaction of OH with methanol has been the subject of a number of studies as seen in table II-B-1. The preferred temperature dependence parameters are obtained from fitting the modified Arrhenius expression $k = CT^2 \exp(-D/T)$ to the rate coefficients of Wallington and Kurylo (1987b), Hess and Tully (1989), Jiménez et al. (2003) and Dillon et al. (2005) over the temperature range 210–866 K to give $k = 6.38 \times 10^{-18} T^2 \exp(144/T)\,\mathrm{cm^3}$ $\mathrm{molecule^{-1}\,s^{-1}}$. For atmospheric purposes, in the temperature range 210–300 K, the simple Arrhenius expression $k = 2.85 \times 10^{-12} \exp(-345/T)\,\mathrm{cm^3}$ $\mathrm{molecule^{-1}\,s^{-1}}$ is recommended (Atkinson et al., 2006).

Oh and Andino (2001) reported an increase of the rate coefficient by ~30% in the presence of ammonium sulfate aerosols. However, Sørensen et al. (2002) conducted experiments which showed that the presence of 500–8,000 $\mu\mathrm{g\,m^{-3}}$ of NaCl or NH_4NO_3 aerosols (levels which far exceed those found in the atmosphere) does not affect the reactivity of OH with methanol. Furthermore, Sørensen et al. (2002) showed that the effect reported by Oh and Andino (2001) is inconsistent with gas kinetic theory and hence is erroneous.

The reaction of OH with CD_3OH was studied by Greenhill and O'Grady (1986) and McCaulley et al. (1989) at 298 K, and by Hess and Tully (1989) between 293 and 862 K. Greenhill and O'Grady and Hess and Tully reported a kinetic isotope effect

Table II-B-1. Rate coefficients (k, cm^3 molecule^{-1} s^{-1}) for reaction of OH with methanol (CH_3OH)

$10^{12} \times A$	B (K)	$10^{12} \times k$	T (K)	Technique[a]	Reference	Temperature Range (K)
		0.95 ± 0.10	292	RR (n-C_4H_{10})[b]	Campbell et al. (1976)	
		1.06 ± 0.10	296 ± 2	FP–RA	Overend and Paraskevopoulos (1978)	
		1.0 ± 0.1	298	FP–RF	Ravishankara and Davis (1978)	
		1.0	300	RR (C_2H_4)[c]	Barnes et al. (1982a)	
		0.9 ± 0.07	300 ± 3	RR (CH_3OCH_3)[d]	Tuazon et al. (1983)	
12 ± 3	810 ± 50	0.79 ± 0.20	298	PLP–RF	Hägele et al. (1983)	295–420
11 ± 3	798 ± 45	0.77	300	DF–LIF	Meier et al. (1985a)	300–1010
		1.1	300	RR (toluene)[e]	Klöpffer et al. (1986)	
8.0 ± 1.9	664 ± 88	0.54 ± 0.04	260	FP–RA	Greenhill and O'Grady (1986)	260–803
		0.76 ± 0.04	292			
		0.75 ± 0.08	300			
		1.13 ± 0.05	331			
		1.44 ± 0.06	362			
		1.44 ± 0.09	453			
		1.35 ± 0.08	465			
		2.06 ± 0.17	570			
		2.67 ± 0.24	597.5			
		2.79 ± 0.25	669			
		5.76 ± 0.59	803			
4.8 ± 1.2	480 ± 70	0.657 ± 0.046	240	FP–RF	Wallington and Kurylo (1987b)	240–440
		0.861 ± 0.047	296			
		1.25 ± 0.08	350			
		1.41 ± 0.12	400			
		1.62 ± 0.14	440			
		0.88 ± 0.18	298	PR–UV abs.	Pagsberg et al. (1988)	
		1.01 ± 0.10	298 ± 2	DF–LIF	McCaulley et al. (1989)	
$k(T)$[f]		0.934 ± 0.041	294	PLP–LIF	Hess and Tully (1989)	294–866
		1.09 ± 0.05	332			
		1.33 ± 0.06	380			
		1.69 ± 0.07	441			
		2.10 ± 0.09	505			
		2.31 ± 0.10	528			
		3.01 ± 0.13	626			
		3.96 ± 0.20	709			
		5.05 ± 0.24	787			
		6.18 ± 0.32	866			

(*continued*)

Table II-B-1. (*continued*)

$10^{12} \times A$	B (K)	$10^{12} \times k$	T (K)	Technique[a]	Reference	Temperature Range (K)
		0.90 ± 0.09	298 ± 2	PR–UV abs.	Nelson et al. (1990a)	
		0.95 ± 0.21		RR (c-C_6H_{12})[g]		
		0.90 ± 0.08	298 ± 4	RR (n-C_5H_{12})[h]	Picquet et al. (1998)	
		0.83 ± 0.07	298 ± 2	RR (*cyclo*-C_6H_{12})[g]	Oh and Andino	
		0.96 ± 0.10	298 ± 2	RR (C_2H_5OH)[i]	(2001)	
		0.761 ± 0.048	296	RR (C_2H_4)[c]	Sørensen et al.	
		0.788 ± 0.047	296	RR (C_2H_2)[j]	(2002)	
3.6 ± 0.8	415 ± 70	0.63 ± 0.15	235	PLP–LIF	Jiménez et al. (2003)	235–360
		0.673 ± 0.005	244			
		0.729 ± 0.033	251			
		0.698 ± 0.059	259			
		0.670 ± 0.049	260 ± 1			
		0.759 ± 0.025	273			
		0.866 ± 0.036	285			
		0.93 ± 0.11	298			
		0.953 ± 0.014	315			
		1.03 ± 0.027	330			
		1.13 ± 0.054	345			
		1.29 ± 0.12	360			
$k(T)$[k]		0.599 ± 0.020	210	PLP–LIF	Dillon et al. (2005)	210–351
		0.523 ± 0.015	214			
		0.634 ± 0.012	218			
		0.642 ± 0.037	219			
		0.620 ± 0.009	223			
		0.630 ± 0.009	226			
		0.653 ± 0.027	228			
		0.663 ± 0.006	231			
		0.632 ± 0.010	232			
		0.706 ± 0.012	240			
		0.675 ± 0.019	241			
		0.766 ± 0.021	253			
		0.780 ± 0.011	263			
		0.808 ± 0.008	273			
		0.93 ± 0.07	298			
		1.10 ± 0.01	322			
		1.12 ± 0.02	328			
		1.22 ± 0.02	351			

[a]Abbreviations used for the techniques are defined in table I-F-3.
[b]Placed on an absolute basis using $k(OH + n\text{-}C_4H_{10}) = 2.35 \times 10^{-12}$ cm^3 molecule^{-1} s^{-1} (IUPAC, 2008).
[c]Placed on an absolute basis using $k(OH + C_2H_4) = 7.9 \times 10^{-12}$ cm^3 molecule^{-1} s^{-1} at 1 bar and 298 K (Atkinson et al., 2006).
[d]Placed on an absolute basis using $k(OH + CH_3OCH_3) = 2.86 \times 10^{-12}$ cm^3 molecule^{-1} s^{-1} (IUPAC, 2008; this book, section V-B-1.1).
[e]Placed on an absolute basis using $k(OH + \text{toluene}) = 5.6 \times 10^{-12}$ cm^3 molecule^{-1} s^{-1} (Calvert et al. 2002).
[f]$k(T) = 5.89 \times 10^{-20} T^{2.65} \exp(833/T)$.
[g]Placed on an absolute basis using $k(OH + \textit{cyclo}\text{-}C_6H_{12}) = 6.97 \times 10^{-12}$ cm^3 molecule^{-1} s^{-1} (Calvert et al., 2008).
[h]Placed on an absolute basis using $k(OH + n\text{-}C_5H_{12}) = 3.96 \times 10^{-12}$ cm^3 molecule^{-1} s^{-1} (Calvert et al., 2008).
[i]Placed on an absolute basis using $k(OH + C_2H_5OH) = 3.2 \times 10^{-12}$ cm^3 molecule^{-1} s^{-1} (Atkinson et al., 2006).
[j]Placed on an absolute basis using $k(OH + C_2H_2) = 7.8 \times 10^{-13}$ cm^3 molecule^{-1} s^{-1} at 1 bar and 298 K (Atkinson et al., 2006).
[k]$k(T) = 6.67 \times 10^{-18} T^2 \exp(140/T)$.

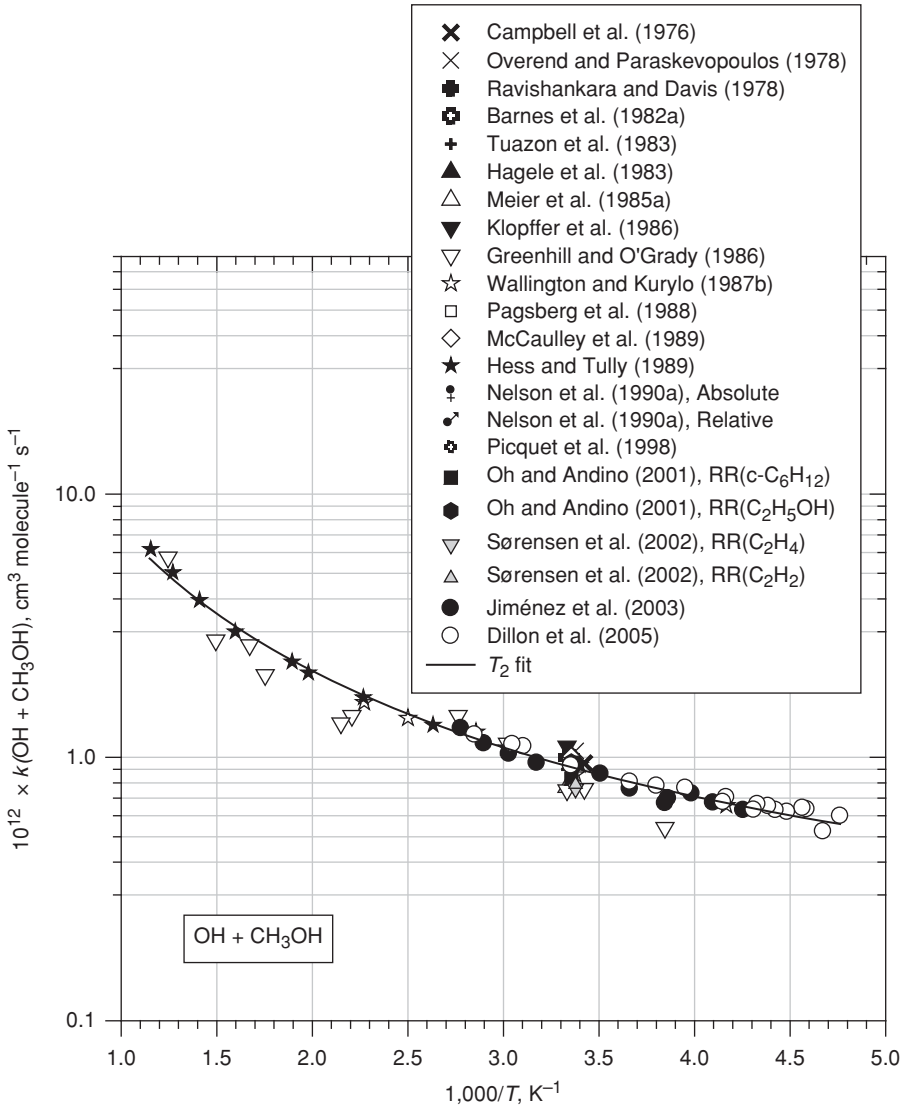

Figure II-B-1. Arrhenius plot of the rate coefficient for the reaction of OH with methanol.

(k_{CH3OH}/k_{CD3OH}) of approximately a factor of 2, while McCaulley et al. observed an effect greater than a factor of 5.

II-B-1.2. NO_3 Reaction Kinetics

The rate coefficient for the reaction of NO_3 with CH_3OH has been measured by Wallington et al. (1987), Canosa-Mas et al. (1989), and Langer and Ljungström (1995); see table II-B-2. The upper limit for the rate coefficient near room temperature reported by Wallington et al. is consistent with the measurements of Canosa-Mas et al. and Langer and Ljungström. As shown in figure II-B-2, the data of Langer and Ljungström

Table II-B-2. Rate coefficients (k, cm^3 molecule^{-1} s^{-1}) for reaction of NO_3 with methanol (CH_3OH)

$10^{12} \times A$	B (K)	$10^{16} \times k$	T (K)	Technique[a]	Reference	Temperature Range (K)
		≤ 6	298 ± 2	FP-A	Wallington et al. (1987)	
1.25	2562 ± 241	2.1 ± 1.1	294	DF–A	Canosa-Mas et al. (1989)	294–473
		4.61 ± 0.92	323			
		6.8 ± 2.7	348			
		12.9 ± 4.9	373			
		31.1 ± 8.4	423			
		25.1 ± 4.5	428			
		63.2 ± 13.5	473			
0.936[b]	2652 ± 312	0.21 ± 0.10	258	DF–A	Langer and Ljunström (1995)	258–367
		0.87 ± 0.55	273			
		1.32 ± 0.24	295			
		2.72 ± 0.50	324			
		4.24 ± 0.70	348			
		6.21 ± 0.32	367			

[a]Abbreviations used for the techniques are defined in table I-F-3.
[b]Obtained from a unweighted least-squares analysis (Atkinson et al., 2006).

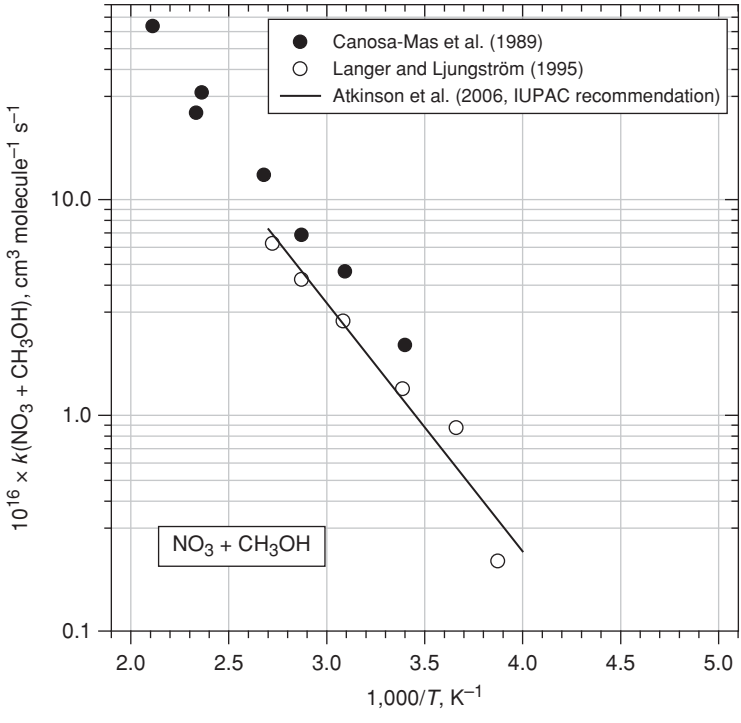

Figure II-B-2. Arrhenius plot of the rate coefficient for the reaction of NO_3 with methanol.

are systematically lower (by a factor of approximately 2) than those from Canosa-Mas et al. The IUPAC Panel preferred Arrhenius expression is based on the work of Langer and Ljungström, $k = 9.4 \times 10^{-13} \exp(-2{,}650/T)$ over the range 250–370 K and $k = 1.3 \times 10^{-16}$ cm^3 molecule^{-1} s^{-1} at 298 K with an uncertainty of ~50%. However, it is possible that these values are high because of potential errors due to secondary loss of NO_3 radicals (Atkinson et al., 2006).

II-B-1.3. Cl-Atom Reaction Kinetics

The reaction of Cl-atoms with CH_3OH has been studied by several groups. The available rate coefficients are summarized in table II-B-3. The values reported by different authors near 298 K are in good agreement leading to the recommended value of $k = 5.5 \times 10^{-11}$ cm^3 molecule^{-1} s^{-1} at 298 K with an uncertainty of ±10%. As shown in figure II-B-3, while Michael et al. (1979a) did not observe any temperature dependence of k over the range 200–500 K, Garzón et al. (2006) reported a significant temperature dependence over the range 266–380K: $k(\mathrm{Cl+CH_3OH}) = (3.55 \pm 0.22) \times 10^{-10} \exp[(533 \pm 77)/T]$ cm^3 molecule^{-1} s^{-1}. Payne et al. (1988)

Table II-B-3. Rate coefficients (k, cm^3 molecule^{-1} s^{-1}) for reaction of Cl with methanol (CH_3OH)

$10^{10} \times A$	B (K)	$10^{11} \times k$	T (K)	Technique[a]	Reference	Temperature Range (K)
		6.33 ± 0.70	200–500	FP–RF	Michael et al. (1979)	200–500
		4.73 ± 0.42	295 ± 2	RR (C_2H_6)[b]	Wallington et al. (1988g)	
		5.08 ± 0.38	298 ± 2	RR (*c*-C_6H_{12})[c]	Nelson et al. (1990a)	
		6.14 ± 0.67	298 ± 2	DF–EPR	Dobé et al. (1993)	
		5.1 ± 0.4	298 ± 2	PLP–RF	Tyndall et al. (1999)	
		5.6 ± 0.6	295 ± 2	RR (C_2H_6)[b]		
		6.0 ± 0.3	295 ± 2	RR (C_2H_4)[d]		
		5.6 ± 0.2	295	PLP–IR	Smith et al. (2002b)	
		5.83 ± 0.77	298	PLP–IR[e]	Seakins et al. (2004)	
		5.38 ± 0.25	298	PLP–IR[f]		
		5.08 ± 0.84	243	PLP–IR		
		5.35 ± 0.24	295 ± 2	FP–LIF	Taketani et al. (2005)	
3.55 ± 0.22	559 ± 40	4.40 ± 0.38	266	FP–RF	Garzón et al. (2006)	266–380
		4.78 ± 0.46	282			
		5.44 ± 0.34	298			
		5.85 ± 0.40	312			
		6.57 ± 0.50	330			
		6.94 ± 0.38	343			
		7.29 ± 0.54	354			
		8.08 ± 0.48	380			

[a] Abbreviations used for the techniques are defined in table I-F-3.
[b] Placed on an absolute basis using $k(\mathrm{Cl} + \mathrm{C_2H_6}) = 5.9 \times 10^{-11}$ cm^3 molecule^{-1} s^{-1} (Atkinson et al., 2006).
[c] Placed on an absolute basis using $k(\mathrm{Cl} + \textit{cyclo}\text{-}\mathrm{C_6H_{12}}) = 3.3 \times 10^{-10}$ cm^3 molecule^{-1} s^{-1} (Calvert et al., 2008).
[d] Placed on an absolute basis using $k(\mathrm{Cl} + \mathrm{C_2H_4}) = 9.5 \times 10^{-11}$ cm^3 molecule^{-1} s^{-1} at 1 bar of air at 298 K (see section I-F-1).
[e] Kinetic data obtained by monitoring the HCl product by tunable infrared diode laser absorption.
[f] Kinetic data obtained by monitoring the HCl product by IR emission spectroscopy.

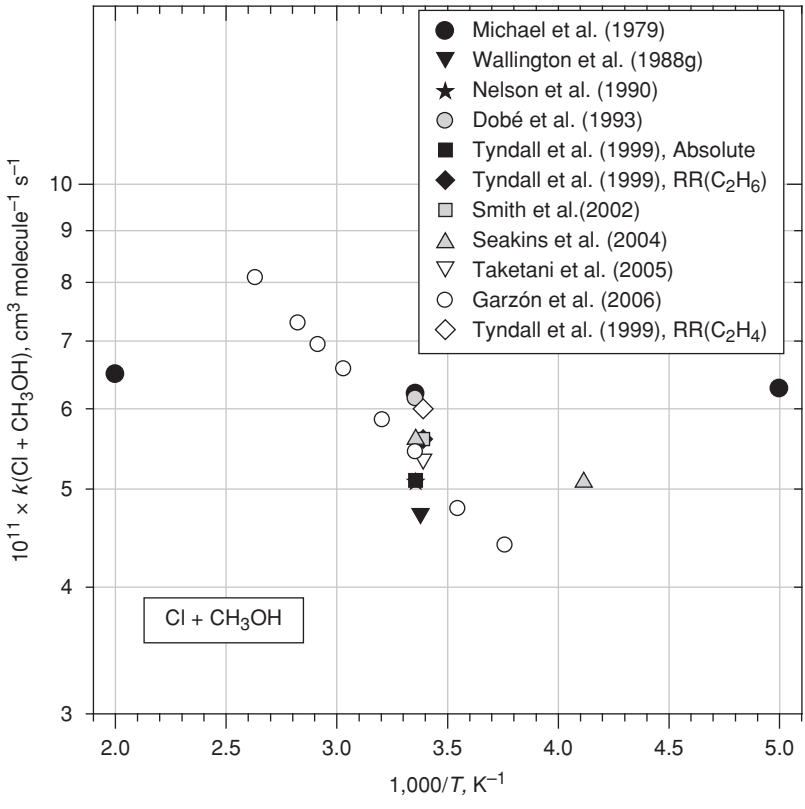

Figure II-B-3. Arrhenius plot of the rate coefficient for reaction of Cl with methanol.

studied the reaction of Cl with CH_3OD using a discharge flow system and reported $k(\mathrm{Cl}+\mathrm{CH_3OD}) = (5.1 \pm 1.0) \times 10^{-11}$ cm^3 $molecule^{-1}$ s^{-1} at 298 K.

II-B-1.4. Summary of the Atmospheric Fate of Methanol

Using the rate coefficient reported in this section, the tropospheric lifetime of methanol with respect to reaction with OH radicals is calculated to be about two weeks. The reaction of OH radicals with methanol proceeds by H-atom abstraction from the CH_3 and —OH groups.

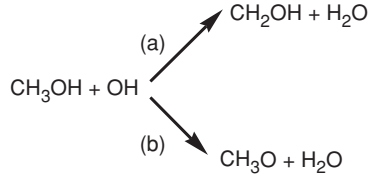

Studies of the reaction of OH radicals with methanol isotopologs by Greenhill and O'Grady (1986), Payne et al. (1988), Hess and Tully (1989), and McCaulley et al.

(1989) suggest that the abstraction occurs largely at the CH_3 group. This is consistent with the studies of Hägele et al. (1983) who found CH_3O yields of 11% at 298 K and 22% at 393 K, Meier et al. (1984, 1985a) who found yields of CH_3O of 17% by mass spectrometry and 25% by laser-induced fluorescence, and by Pagsberg et al. (1988) who found a CH_2OH yield of 83% using the UV absorption technique. Hence, it appears that >75% of the reaction occurs at the methyl group at room temperature and below. The contribution of abstraction from the hydroxyl site (channel b) increases with increasing temperature (Hess and Tully, 1989). The CH_2OH radical formed in channel (a) reacts with O_2 to form CH_2O and HO_2. As discussed by Jiménez et al. (2003) and Dillon et al. (2005), methanol oxidation can be an important source of formaldehyde in the upper troposphere.

The reaction of NO_3 radicals with CH_3OH proceeds via hydrogen abstraction from the CH_3 or the —OH group. The O—H bond is stronger than the alkyl C—H bond by ≈8 kcal mol^{-1} and the abstraction from the —OH group is endothermic; hence, abstraction from the methyl group is favoured at atmospheric temperatures giving CH_2OH radicals, which react with O_2 to give CH_2O (Canosa-Mas et al., 1989; Langer and Ljungström, 1995).

The reaction of Cl-atoms with methanol occurs predominantly (>95%) via hydrogen abstraction from the methyl group forming the CH_2OH radical at room temperature (e.g., Payne et al., 1988; Jadkowski et al., 1998; Rudic et al., 2002; Bechtel et al., 2004; Garzón et al., 2006). The theoretical calculation of Rudic et al. (2002) revealed that H-atom abstraction from CH_3 has no intrinsic barrier, while H-atom abstraction from the —OH group has an energy barrier of 8.27 kcal mol^{-1}.

The reaction of Cl with CH_3OH in the presence of O_2 has been used widely as a source for HO_2 radicals in laboratory studies.

$$Cl + CH_3OH \rightarrow HCl + CH_2OH$$

$$CH_2OH + O_2 \rightarrow HO_2 + CH_2O$$

This system is useful as HCl, CH_2O, and HO_2 are generated in 1:1:1 ratio allowing determination of HO_2 concentrations from measurements of stable compounds (HCl and/or CH_2O).

With a Henry's law constant of 220 M $atm.^{-1}$ (Meylan and Howard, 1991), methanol is not expected to be lost significantly from the atmosphere via wet deposition from the atmosphere. In their global atmospheric model, von Kuhlmann et al. (2003) have estimated that the overall atmospheric loss of methanol is mostly due to reaction with OH (63%), with the remainder due to dry (30%) and wet deposition (7%).

II-B-2. Ethanol (Ethyl Alcohol, C_2H_5OH)

II-B-2.1. OH Reaction Kinetics

The reaction of hydroxy radicals with ethanol has been investigated by a large number of groups using different experimental techniques. The studies were conducted over a

Table II-B-4. Rate coefficients (k, cm^3 molecule^{-1}s^{-1}) for reaction of OH with ethanol (C_2H_5OH)

$10^{12} \times A$	B (K)	$10^{12} \times k$	T (K)	Technique[a]	Reference	Temperature Range (K)
		3.0 ± 0.3	292	RR (n-C_4H_{10})[b]	Campbell et al. (1976)	
		3.74 ± 0.36	296 ± 2	FP–RA	Overend and Paraskevopoulos (1978)	
		2.62 ± 0.36	298	FP–RF	Ravishankara and Davis (1978)	
4.4 ± 1.0	274 ± 90	2.1	300	DF–LIF	Meier et al. (1985a)	300–1000
12.5 ± 2.4	360 ± 52	2.84 ± 0.15	255	FP–RA	Greenhill and O'Grady (1986)	255–459
		3.40 ± 0.14	273			
		3.80 ± 0.24	289			
		3.40 ± 0.17	293			
		4.26 ± 0.19	331			
		4.26 ± 0.18	360			
		5.21 ± 0.36	369			
		5.63 ± 0.48	459			
		3.5 ± 0.4	303 ± 2	RR (C_2H_4)[c]	Kerr and Stocker (1986a)	
7.4 ± 3.2	240 ± 110	2.75 ± 0.14	240	FP–RF	Wallington and Kurylo (1987b)	240–440
		3.33 ± 0.23	296			
		3.25 ± 0.39	350			
		4.07 ± 0.40	400			
		4.58 ± 0.29	440			
		3.26 ± 0.14	293	PLP–LIF	Hess and Tully (1988)	293–750
		3.32 ± 0.16[d]	295			
		3.33 ± 0.14	326.5			
		3.63 ± 0.15	380			
		3.94 ± 0.16	441			
		5.47 ± 0.34[d]	599			
		3.04 ± 0.25	298 ± 2	PR–UV abs.	Nelson et al. (1990a)	
		3.22 ± 0.48		RR ($cyclo$-C_6H_{12})[e]		
		3.83 ± 0.11	298 ± 4	RR (n-C_6H_{14})[f]	Picquet et al. (1998)	
		2.8 ± 0.3	298 ± 2	RR (c-C_6H_{12})[e]	Oh and Andino (2001)	
		2.7 ± 0.2		RR (p-xylene)[g]		
		3.08 ± 0.32	296	RR (C_2H_4)[c]	Sørensen et al. (2002)	
		3.39 ± 0.23	296	RR (C_2H_2)[h]		
		3.46 ± 0.25	295 ± 2	RR (C_3H_8)[i]	Wu et al. (2003)	
4.3 ± 0.7	85 ± 35	2.80 ± 0.23	227	PLP–LIF	Jiménez et al. (2003)	227–360
		3.11 ± 0.10	243			
		3.20 ± 0.11	260			
		3.24 ± 0.08	273			
		3.20 ± 0.10	285			
		3.10 ± 0.40	298			
		3.15 ± 0.04	300			
		3.27 ± 0.10	315			
		3.20 ± 0.25	330			
		3.37 ± 0.22	345			
		3.60 ± 0.11	360			

(*continued*)

Table II-B-4. (*continued*)

$10^{12} \times A$	B (K)	$10^{12} \times k$	T (K)	Technique[a]	Reference	Temperature Range (K)
4.0	42 ± 14	3.38 ± 0.14	216	PLP–LIF	Dillon et al. (2005)	216–368
		3.45 ± 0.08	223			
		3.35 ± 0.13	226			
		3.40 ± 0.09	238			
		3.36 ± 0.07	239			
		3.48 ± 0.09	243			
		3.25 ± 0.13	247			
		3.40 ± 0.06	252			
		3.38 ± 0.11	258			
		3.46 ± 0.07	263			
		3.33 ± 0.10	270			
		3.35 ± 0.07	273			
		3.23 ± 0.12	279			
		3.46 ± 0.09	284			
		3.35 ± 0.17	298 ± 2			
		3.61 ± 0.09	319			
		3.72 ± 0.09	339			
		3.57 ± 0.07	353			
		3.47 ± 0.13	358			
		3.67 ± 0.24	363			
		3.83 ± 0.08	368			
		3.26 ± 0.08	298	PLP–LIF	Rajakumar et al. (2005)	

[a]Abbreviations used for the techniques are defined in table I-F-3.
[b]Placed on an absolute basis using $k(\mathrm{OH} + n\text{-}\mathrm{C_4H_{10}}) = 2.35 \times 10^{-12}\,\mathrm{cm^3\ molecule^{-1}\ s^{-1}}$ (IUPAC, 2008).
[c]Placed on an absolute basis using $k(\mathrm{OH} + \mathrm{C_2H_4}) = 7.9 \times 10^{-12}\,\mathrm{cm^3\ molecule^{-1}\ s^{-1}}$ (Atkinson et al., 2006).
[d]Rate coefficient for $^{18}\mathrm{OH} + \mathrm{C_2H_5OH}$.
[e]Placed on an absolute basis using $k(\mathrm{OH} + \textit{cyclo}\text{-}\mathrm{C_6H_{12}}) = 6.97 \times 10^{-12}\,\mathrm{cm^3\ molecule^{-1}\ s^{-1}}$ (Calvert et al., 2008).
[f]Placed on an absolute basis using $k(\mathrm{OH} + n\text{-}\mathrm{C_6H_{14}}) = 5.48 \times 10^{-12}\,\mathrm{cm^3\ molecule^{-1}\ s^{-1}}$ (Calvert et al., 2008).
[g]Placed on an absolute basis using $k(\mathrm{OH} + p\text{-xylene}) = 1.43 \times 10^{-11}\,\mathrm{cm^3\ molecule^{-1}\ s^{-1}}$ (Calvert et al., 2002).
[h]Placed on an absolute basis using $k(\mathrm{OH}{+}\mathrm{C_2H_2}) = 7.9 \times 10^{-13}\,\mathrm{cm^3\ molecule^{-1}\ s^{-1}}$ (Atkinson et al., 2006).
[i]Placed on an absolute basis using $k(\mathrm{OH} + \mathrm{C_3H_8}) = 1.1 \times 10^{-12}\,\mathrm{cm^3\ molecule^{-1}\ s^{-1}}$ (Atkinson et al., 2006).

wide temperature range. As shown in table II-B-4 and figure II-B-4, there is substantial scatter in the rate coefficient values near 298 K. The data of Hess and Tully (1988) above 500 K are not included since these authors showed that the thermal decomposition of the CH_2CH_2OH radical formed by H-atom abstraction from the CH_3 group regenerates OH radicals leading to an underestimation of the k values above 500 K. Hess and Tully (1988) used isotopically labeled ^{18}OH to determine the rate coefficient at 599 K. The IUPAC Panel preferred rate coefficient value was derived by fitting the modified Arrhenius expression $k = CT^2 \exp(-D/T)$ to the data of Wallington and Kurylo (1987b), Hess and Tully (1988) (using only the data below 500 K and that obtained at 599 K for ^{18}OH), Jiménez et al. (2003), and Dillon et al. (2005). The fit gives $k(\mathrm{OH} + \mathrm{C_2H_5OH}) = 6.7 \times 10^{-18} T^2 \exp(511/T)\,\mathrm{cm^3\ molecule^{-1}\ s^{-1}}$ over the temperature range 216–599 K.

For the atmospheric temperature regime of 210–300 K, the preferred Arrhenius expression is $k = 3.0 \times 10^{-12} \exp(20/T)\,\mathrm{cm^3\ molecule^{-1}\ s^{-1}}$ (Atkinson et al., 2006).

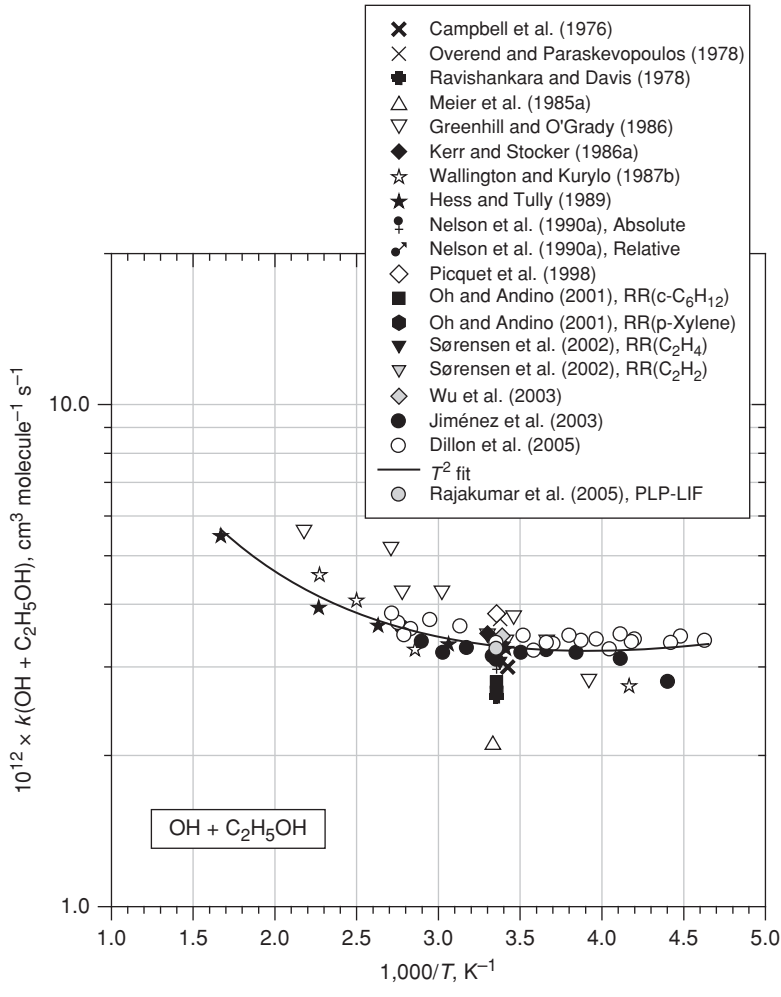

Figure II-B-4. Arrhenius plot of the rate coefficient for the reaction of OH with ethanol.

Note that this expression should be used only over the temperature range 210–300K. For temperatures up to 600 K the expression $k = 6.7 \times 10^{-18} T^2 \exp(511/T)\,\mathrm{cm}^3$ molecule^{-1} s^{-1} should be used (Atkinson et al., 2006). The preferred value at 298 K is $k(\mathrm{OH} + \mathrm{C_2H_5OH}) = 3.2 \times 10^{-12}\,\mathrm{cm}^3$ molecule^{-1} s^{-1} (Atkinson et al., 2006) with an uncertainty estimated to be ~10%.

Oh and Andino (2001) reported about a 30% increase in $k(\mathrm{OH} + \mathrm{C_2H_5OH})$ in the presence of ammonium sulfate aerosols. However, Sørensen et al. (2002) conducted experiments which showed that the presence of 500–8,000 μg m^{-3} of NaCl, $(NH_4)_2SO_4$, or NH_4NO_3 aerosols does not affect the reactivity of OH with ethanol. Furthermore, Sørensen et al. (2002) showed that the effect reported by Oh and Andino (2001) is inconsistent with basic gas kinetic theory and, hence, is erroneous.

II-B-2.2. NO_3 Reaction Kinetics

Langer and Ljungström (1995) measured the rate coefficients of the NO_3-ethanol reaction at temperatures between 273 and 367 K; see table II-B-5 and figure II-B-5. The rate coefficient measured by Langer and Ljungström (1995) near 298 K is larger than the upper limit determined by Wallington et al. (1988g). The larger values of Langer and Ljungström (1995) may reflect the occurrence of secondary reactions in their study. The preferred value, $k < 2 \times 10^{-15}$ cm^3 molecule^{-1} s^{-1} at 298 K, is based on the upper limit of Wallington et al. (1988g) (Atkinson et al., 2006). No recommendation is made for the temperature dependence.

II-B-2.3. Cl-Atom Reaction Kinetics

The reaction of Cl-atoms with ethanol has been studied by several groups using relative and absolute methods. The data are presented in table II-B-6 and plotted in figure II-B-6. We adopt the IUPAC panel recommended value at 298 K of $k = 1.0 \times 10^{-10}$ cm^3 molecule^{-1} s^{-1} (IUPAC, 2008) with an uncertainty we estimate to be ±10%. Taatjes et al. (1999) observed a slight temperature dependence of the rate coefficient over the range 295–600 K. The results reported by Garzón et al. (2006) at 266–382 K suggest a more pronounced negative temperature dependence. The IUPAC Panel preferred value is $k = 6.0 \times 10^{-11}$ exp(155/T) cm^3 molecule^{-1} s^{-1} over the temperature range 260–400 K (IUPAC, 2008). This substantial negative temperature dependence reported by Garzón et al. is suprising, as the reaction is expected to proceed predominantly via hydrogen abstraction from the —CH_2 group with little or no temperature dependence.

Rate coefficients have been also reported for the reactions of Cl-atoms with a series of deuterated ethanols. Taatjes et al. (1999) measured the temperature dependence of the rate coefficients for the reactions of Cl with CD_3CH_2OH and CH_3CD_2OH to be $k_{CD_3CH_2OH} = 6.6 \times 10^{-11}$ exp[(90 ± 40)/T] and $k_{CH_3CD_2OH} = 6.9 \times 10^{-11}$ exp[–(76 ± 40)/T] cm^3 molecule^{-1} s^{-1} over 295–500 K and 295–600 K, respectively; these give: $k_{CD_3CH_2OH} = (9.0 \pm 0.9) \times 10^{-11}$ and $k_{CH_3CD_2OH} = (5.4 \pm 0.4) \times 10^{-11}$ cm^3 molecule^{-1} s^{-1} at 295 K. Crawford et al. (2004) determined the rate coefficient for the reaction of Cl with C_2H_5OD to be $k_{CH_3CH_2OD} = (1.18 \pm 0.22) \times 10^{-10}$ cm^3 molecule^{-1} s^{-1}. These data confirm that abstraction of the hydroxyl hydrogen is negligible.

Table II-B-5. Rate coefficients (k, cm^3 molecule^{-1} s^{-1}) for the reaction of NO_3 with ethanol (CH_3CH_2OH)

$10^{13} \times A$	B (K)	$10^{16} \times k$	T (K)	Technique[a]	Reference	Temperature Range (K)
		≤9	298 ± 2	FP–A	Wallington et al. (1988g)	
6.99	1,815 ± 419	8.4 ± 2.3	273	DF–A	Langer and Ljunström (1995)	273–367
		13.7 ± 1.0	295			
		18.1 ± 2.6	297			
		28.0 ± 3.4	323			
		34.8 ± 8.7	349			
		49.3 ± 9.8	367			

[a]Abbreviations used for the techniques are defined in table I-F-3.

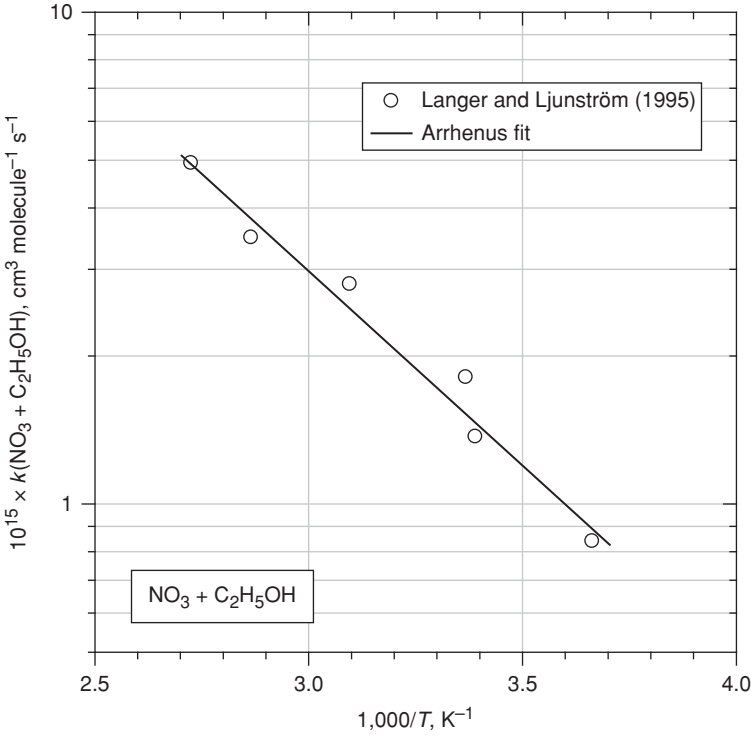

Figure II-B-5. Arrhenius plot of the rate coefficient for the reaction of NO_3 with ethanol.

II-B-2.4. Summary of the Atmospheric Fate of Ethanol

The most important gas-phase loss process of ethanol is reaction with the OH radical. Combining the rate coefficient at 298 K with an average OH concentration of 1×10^6 molecule cm^{-3}, the lifetime of ethanol is estimated to be ~4 days.

The reaction of OH with ethanol proceeds through three possible pathways,

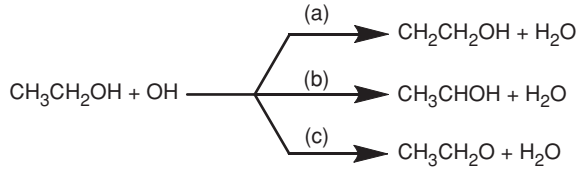

The OH reaction mechanism has been investigated by Meier et al. (1985a, b) who detected CH_3CHOH radicals and determined that the branching ratio for abstraction at the —CH_2 group (channel b) at 298 K is 0.75±0.15. The weak temperature dependence of the overall rate coefficient is also consistent with the majority of the reaction occurring at the more weakly bonded methylene hydrogen atoms. Assuming that H-atom abstraction from the —OH group in ethanol has a similar rate coefficient to the analogous channel in methanol (1.5×10^{-13} cm^3 $molecule^{-1}$ s^{-1}, Atkinson et al., 2006),

Table II-B-6. Rate coefficients (k, cm^3 molecule^{-1} s^{-1}) for reaction of Cl with ethanol (CH_3CH_2OH)

$10^{11} \times A$	B (K)	$10^{11} \times k$	T (K)	Technique[a]	Reference	Temperature Range (K)
		8.75 ± 0.95	295 ± 2	RR (C_2H_6)[b]	Wallington et al. (1988g)	
		10.6 ± 0.6	298 ± 2	RR (*cyclo*-C_6H_{12})[c]	Nelson et al. (1990a)	
		8.3 ± 1.8	295	RR (C_2H_6)[b]	Edelbüttel-Einhaus et al. (1992)	
		9.4 ± 0.8	298	RR (C_2H_6)[b]	Taatjes et al. (1999)	295–600
9.4 ± 1.4	$-(45 \pm 32)$	10.9 ± 0.9	295	LP–IR		
		10.3 ± 0.9	400			
		9.8 ± 0.8	450			
		10.8 ± 0.9	500			
		10.3 ± 0.9	600			
		11.0 ± 0.4	295	RR (C_3H_8)[d]	Wu et al. (2003)	
		10.3 ± 0.8	295	RR (*cyclo*-C_6H_{12})[c]		
		12.0 ± 0.7	298 ± 2	RR (*cyclo*-C_6H_{12})[c]	Crawford et al. (2004)	
		10.2 ± 0.19	298	LP–IR[e]	Seakins et al. (2004)	
		9.50 ± 0.85	295 ± 2	FP–LIF	Taketani et al. (2005)	
5.25 ± 0.52	$-(190 \pm 68)$	10.6 ± 0.8	266	FP–RF	Garzón et al. (2006)	266–382
		11.6 ± 0.8	282			
		9.93 ± 0.98	298			
		9.29 ± 0.68	312			
		9.20 ± 0.66	330			
		9.09 ± 0.72	343			
		8.77 ± 0.22	353			
		8.79 ± 0.22	382			

[a]Abbreviations used for the techniques are defined in table I-F-3.
[b]Placed on an absolute basis using $k(Cl + C_2H_6) = 5.9 \times 10^{-11}$ cm^3 molecule^{-1} s^{-1} (Atkinson et al., 2006).
[c]Placed on an absolute basis using $k(Cl + cyclo\text{-}C_6H_{12}) = 3.3 \times 10^{-10}$ cm^3 molecule^{-1} s^{-1} (Calvert et al., 2008).
[d]Placed on an absolute basis using $k(Cl + C_3H_8) = 1.4 \times 10^{-10}$ cm^3 molecule^{-1} s^{-1} (Atkinson et al., 2006).
[e]Kinetic data obtained by monitoring the HCl product by IR emission spectroscopy.

the contribution of channel (c) is ~5% at 298 K. The kinetic studies of the reactions of OH and ^{18}OH with ethanol indicate that H abstraction from the CH_3 group (channel a) accounts for ~15% of the overall reaction at 600K (Hess and Tully, 1988). Thus, the main pathway for the reaction of OH radical with CH_3CH_2OH at 298 K is H-atom abstraction from the methylene group (channel b) accounting for ~90%, while the other two channels (a and c) account for ~5% each (Atkinson et al., 2006). The CH_3CHOH radical formed in channel (b) reacts with O_2 to give CH_3CHO and HO_2. Recent studies indicate that ethanol can be an important source of acetaldehyde in the upper troposphere (Jiménez et al., 2003; Dillon et al., 2005).

The nitrate radical is expected to react almost exclusively with ethanol through H-atom abstraction from the methylene group to form CH_3CHOH radicals (Langer and Ljungström, 1995).

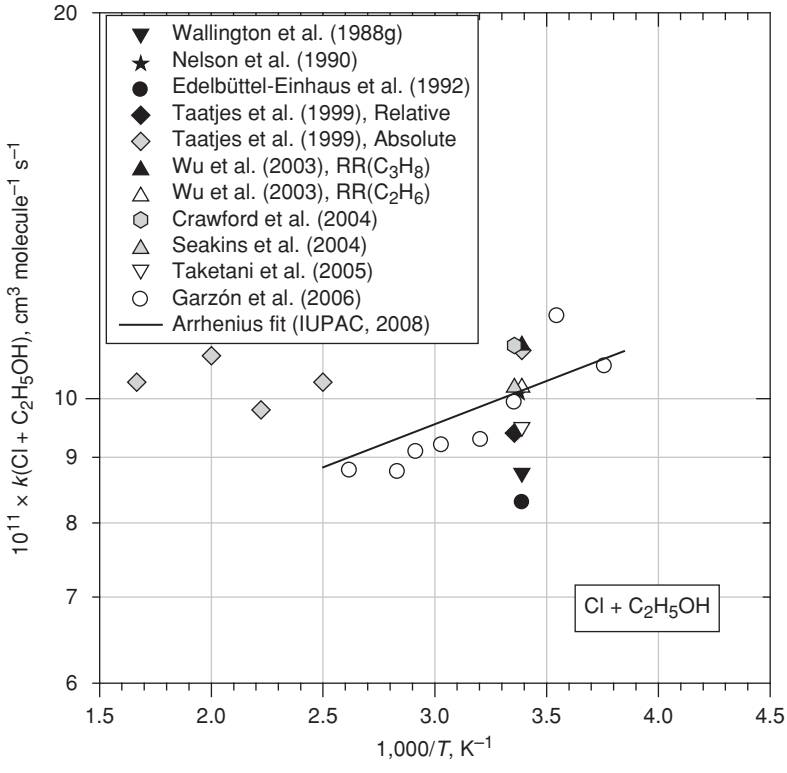

Figure II-B-6. Arrhenius plot of the rate coefficient for the reaction of Cl with ethanol.

The reaction of chlorine atoms with ethanol proceeds almost exclusively (~90%) at the —CH_2 group, hydrogen abstraction from the methyl group contributes approximately 8% and abstraction from the hydroxyl group contributes less than 5% to the overall reaction near room temperature (Meier et al., 1984; Grotheer et al., 1988; Taatjes et al., 1999; Crawford et al., 2004). Taatjes et al. (1999) have shown that the abstraction from —CH_2 group dominates over a large temperature range (295–600 K). The fraction of abstraction of CH_3 group increases only slightly with temperature with an Arrhenius fit to the k_{CH3}/k_{CH2} ratio yielding: $k_{CH3}/k_{CH2} = (0.28 \pm 0.12) \exp[-(350 \pm 160)/T]$.

With a Henry's law constant of approximately 200 M atm.$^{-1}$ (Meylan and Howard, 1991), ethanol is not expected to be lost significantly from the atmosphere through wet deposition.

II-B-3. 1-Propanol (*n*-Propyl Alcohol, $CH_3CH_2CH_2OH$)

II-B-3.1. OH Reaction Kinetics

Rate coefficients have been determined by a number of groups using both absolute and relative methods. The measurements are given in table II-B-7 and plotted in

Table II-B-7. Rate coefficients (k, cm^3 molecule^{-1} s^{-1}) for reaction of OH with 1-propanol ($CH_3CH_2CH_2OH$)

$10^{12} \times A$	B (K)	$10^{12} \times k$	T (K)	Technique[a]	Reference	Temperature Range (K)
		3.9 ± 0.7	292	RR (n-C_4H_{10})[b]	Campbell et al. (1976)	
		5.33 ± 0.54	296 ± 2	FP–RA	Overend and Paraskevopoulos (1978)	
		5.34 ± 0.29	296	FP–RF	Wallington and Kurylo (1987b)	
		5.64 ± 0.48	298 ± 2	PR–UV abs.	Nelson et al. (1990a)	
		5.12 ± 0.41		RR ($cyclo$-C_6H_{12})[c]		
		4.48 ± 0.26	298 ± 2	RR (n-C_6H_{14})[c]	Oh and Andino (2000)	
		6.44 ± 0.43		RR (p-xylene)[d]		
4.68 ± 0.64	-68 ± 41	6.13 ± 0.34	263	PLP–LIF	Mu and Mellouki (2001)	263–372
		6.12 ± 0.17	273			
		5.83 ± 0.18	298			
		5.66 ± 0.18	323			
		5.64 ± 0.13	348			
		5.79 ± 0.26	372			
		5.35 ± 0.20	273	RR (2,3-dimethylbutane)[e]	Cheema et al. (2002)	273–343
		5.84 ± 0.18	298			
		6.10 ± 0.35	313			
		6.53 ± 0.18	343			
		5.41 ± 0.40	295 ± 2	RR (C_3H_8)[f]	Wu et al. (2003)	

[a]Abbreviations used for the techniques are defined in table I-F-3.
[b]Placed on an absolute basis using $k(OH + n\text{-}C_4H_{10}) = 2.35 \times 10^{-12}$ cm^3 molecule^{-1} s^{-1} (IUPAC, 2008).
[c]Placed on an absolute basis using $k(OH + n\text{-}C_6H_{14}) = 5.27 \times 10^{-12}$ cm^3 molecule^{-1} s^{-1} (Calvert et al., 2008).
[d]Placed on an absolute basis using $k(OH + p\text{-xylene}) = 1.43 \times 10^{-11}$ cm^3 molecule^{-1} s^{-1} (Calvert et al., 2002).
[e]Placed on an absolute basis using $k(OH + 2,3\text{-dimethylbutane}) = 1.25 \times 10^{-11} \exp(-212/T)$ cm^3 molecule^{-1} s^{-1} (Calvert et al., 2008).
[f]Placed on an absolute basis using $k(OH + C_3H_8) = 1.1 \times 10^{-12}$ cm^3 molecule^{-1} s^{-1} (Atkinson et al., 2006).

figure II-B-7. There is a general agreement between the different determinations, with the exception of the values of Campbell et al. (1976) and Oh and Andino (2000) with n-hexane as the reference compounds which appear to be anomalously low. The temperature-dependent rate coefficients of Cheema et al. (2002), determined relative to 2,3-dimethylbutane, indicate a slight positive temperature dependence with $E/R = 260$ K, while those of Mu and Mellouki (2001) show a weak negative dependence ($E/R = -68$ K). The preferred Arrhenius expression is obtained from the data presented in table II-B-7 with the exception of the values of Campbell et al. and Oh and Andino with n-hexane as the reference compound, $k = 6.3 \times 10^{-12} \exp(-30/T)$ cm^3 molecule^{-1} s^{-1} in the temperature range 260–380 with $k = 5.7 \times 10^{-12}$ cm^3 molecule^{-1} s^{-1} and an uncertainty of $\pm 15\%$ at 298 K.

Oh and Andino (2000, 2001, 2002) reported a small but statistically significant increase in values of $k(OH + 1\text{-}C_3H_7OH)$ in relative rate experiments in the presence of $(NH_4)_2SO_4$, NH_4NO_3, and NH_4Cl aerosols. Oh and Andino (2000, 2001, 2002) claimed that the presence of aerosols enhanced the OH-radical-initiated oxidation of

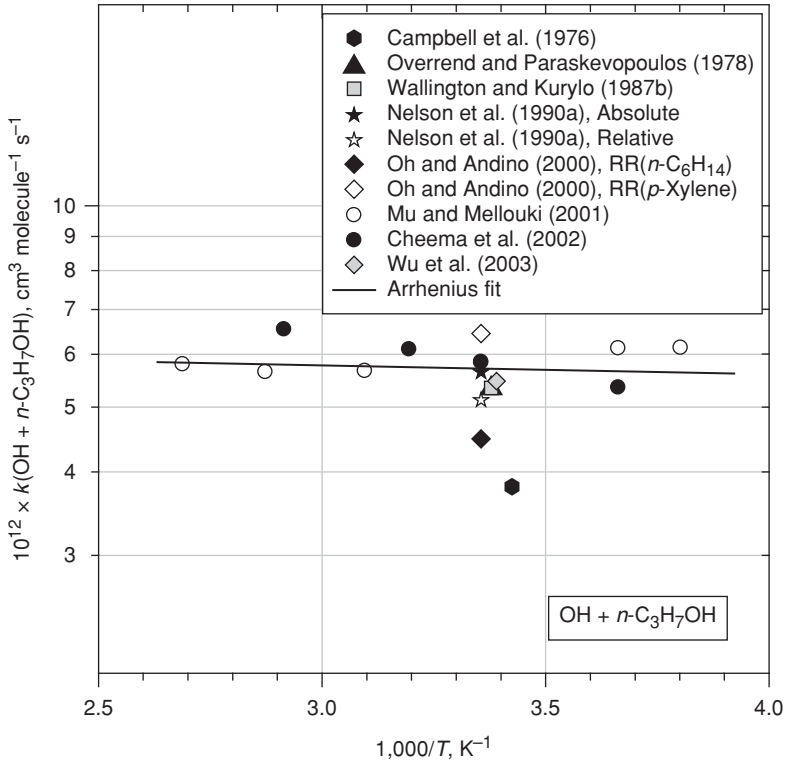

Figure II-B-7. Arrhenius plot of the rate coefficient for the reaction of OH with 1-propanol.

alcohols such as 1-C_3H_7OH. However, as indicated in previous sections, subsequent work by Sørensen et al. (2002) showed that the presence of 500–8,000 μg m^{-3} of NaCl, $(NH_4)_2SO_4$, or NH_4NO_3 aerosols does not affect the reactivity of OH with methanol, ethanol, or phenol. Furthermore, Sørensen et al. (2002) showed that the effect claimed by Oh and Andino is not consistent with basic gas kinetic theory and is hence erroneous.

II-B-3.2. NO_3 Reaction Kinetics

Chew et al. (1998) studied the reaction of NO_3 with 1-propanol using a relative rate method. Chew et al. (1998) recognized the possible complications associated with loss of 1-propanol via heterogeneous reaction with N_2O_5 in their experimental system and chose to quote their measured rate coefficient as an upper limit $\leq (2.1 \pm 0.8) \times 10^{-15}$ cm^3 $molecule^{-1}$ s^{-1} at 298 K; see table II-B-8.

II-B-3.3. Cl-Atom Reaction Kinetics

The reaction of Cl with 1-propanol has been investigated by several groups using both absolute and relative techniques. The available data are presented in table II-B-9, and

Table II-B-8. Rate coefficient (k, cm^3 molecule^{-1} s^{-1}) for the reaction of NO_3 with 1-propanol (n-C_3H_7OH)

$10^{15} \times k$	T (K)	Technique[a]	Reference
$\leq 2.1 \pm 0.8$	298 ± 2	RR (methacrolein)[b]	Chew et al. (1998)

[a]Abbreviations used for the techniques are defined in table I-F-3.
[b]Placed on an absolute basis using $k(NO_3 + \text{methacrolein}) = 3.4 \times 10^{-15}$ cm^3 molecule^{-1} s^{-1} (Atkinson et al., 2006).

Table II-B-9. Rate coefficients (k, cm^3 molecule^{-1} s^{-1}) for reaction of Cl with 1-propanol (n-C_3H_7OH)

$10^{11} \times A$	B (K)	$10^{10} \times k$	T (K)	Technique[a]	Reference	Temperature Range (K)
		1.49 ± 0.12	295 ± 2	RR (C_2H_6)[b]	Wallington et al. (1988g)	
		1.53 ± 0.07	298 ± 2	RR (*cyclo*-C_6H_{12})[c]	Nelson et al. (1990a)	
26.8 ± 2.0	(128 ± 20)	1.65 ± 0.18	273	RR (C_2H_6)[d]	Cheema et al. (2002)	273–342
		1.69 ± 0.19	298			
		1.75 ± 0.21	314			
		1.78 ± 0.20	323			
		1.79 ± 0.20	332			
		1.81 ± 0.21	342			
		1.64 ± 0.14	295 ± 2	RR (C_3H_8)[e]	Wu et al. (2003)	
		1.58 ± 0.12	295 ± 2	RR (*cyclo*-C_6H_{12})[c]		
		1.71 ± 0.11	295 ± 2	PFP–LIF	Taketani et al. (2005)	
2.63 ± 0.21	$-(525 \pm 51)$	1.91 ± 0.12	266	PLP–RF	Garzón et al. (2006)	266–381
		1.70 ± 0.18	282			
		1.53 ± 0.12	298			
		1.45 ± 0.08	312			
		1.25 ± 0.14	330			
		1.24 ± 0.06	343			
		1.13 ± 0.04	354			
		1.05 ± 0.04	381			
		1.52 ± 0.09	296 ± 2	RR (C_3H_6)[f]	Yamanaka et al. (2008)	
		1.75 ± 0.12	296 ± 2	RR (C_2H_4)[g]		

[a]Abbreviations used for the techniques are defined in table I-F-3.
[b]Placed on an absolute basis using $k(Cl + C_2H_6) = 5.9 \times 10^{-11}$ cm^3 molecule^{-1} s^{-1} (Atkinson et al., 2006).
[c]Placed on an absolute basis using $k(Cl + \textit{cyclo}\text{-}C_6H_{12}) = 3.3 \times 10^{-10}$ cm^3 molecule^{-1} s^{-1} (Calvert et al., 2008).
[d]Placed on an absolute basis using $k(Cl + C_2H_6) = 8.3 \times 10^{-11} \exp(-100/T)$ cm^3 molecule^{-1} s^{-1} (Atkinson et al., 2006).
[e]Placed on an absolute basis using $k(Cl + C_3H_8) = 1.4 \times 10^{-10}$ cm^3 molecule^{-1} s^{-1} (Atkinson et al., 2006).
[f]Placed on an absolute basis using $k(Cl + C_2H_4) = 9.5 \times 10^{-11}$ cm^3 molecule^{-1} s^{-1} (see section I-F-1).

displayed in figure II-B-8. While there is excellent agreement between different studies near 298 K, as seen from figure II-B-8, there is significant disagreement in the reported temperature dependencies of $k(Cl + 1\text{-}C_3H_7OH)$. Cheema et al. (2002) reported a slight positive temperature dependence in the range 273–342 K with a value of $E/R = (128 \pm 20)$ K while Garzón et al. (2006) reported a substantial negative temperature dependence in the range 266–381 K with $E/R = -(525 \pm 51)$ K. The preferred 298 K

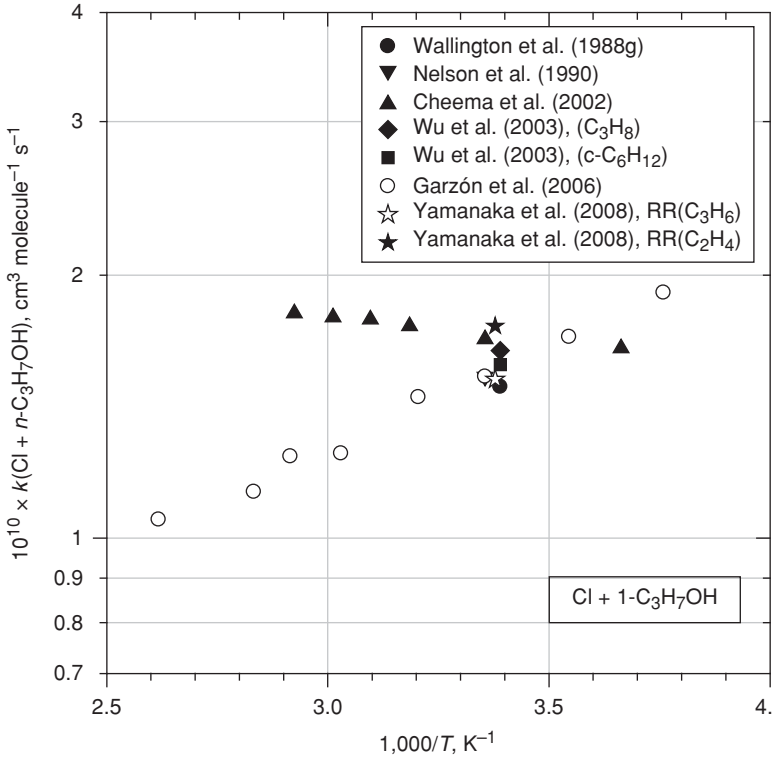

Figure II-B-8. Arrhenius plot of the rate coefficient for the reaction of Cl with 1-propanol.

rate coefficient value is an unweighted average of all values available which gives $k(\mathrm{Cl} + \text{1-}\mathrm{C_3H_7OH}) = 1.7 \times 10^{-10}\,\mathrm{cm^3\ molecule^{-1}\ s^{-1}}$ with an uncertainty estimated to be ±15%. The substantial negative temperature dependence reported by Garzón et al. is surprising as the reaction is expected to proceed predominantly via hydrogen abstraction from the —CH_2 groups with little or no temperature dependence. Further studies are needed and no recommendation is made for the temperature dependence.

II-B-3.4. Summary of the Atmospheric Fate of 1-Propanol

The calculated atmospheric lifetime of 1-propanol with respect to its reaction with OH radicals is about two days. Assuming the reactivity of the —OH group is the same as in methanol [$1.35 \times 10^{-13}\,\mathrm{cm^3\ molecule^{-1}\ s^{-1}}$ (IUPAC, 2008)], reaction of OH radicals with the —OH group in 1-propanol accounts for approximately 2% of the overall reaction. SAR methods can be used to predict that approximately 3% of the reaction occurs via attack at the CH_3 group (Bethel et al., 2001b). Azad and Andino (1999) measured product yields for propanal (72 ± 6%) and acetaldehyde (18 ± 3%) confirming that reaction occurs predominantly via hydrogen abstraction from the α-CH_2 groups (∼72%) and β-CH_2 groups (∼18%). Figure II-B-9 shows the degradation

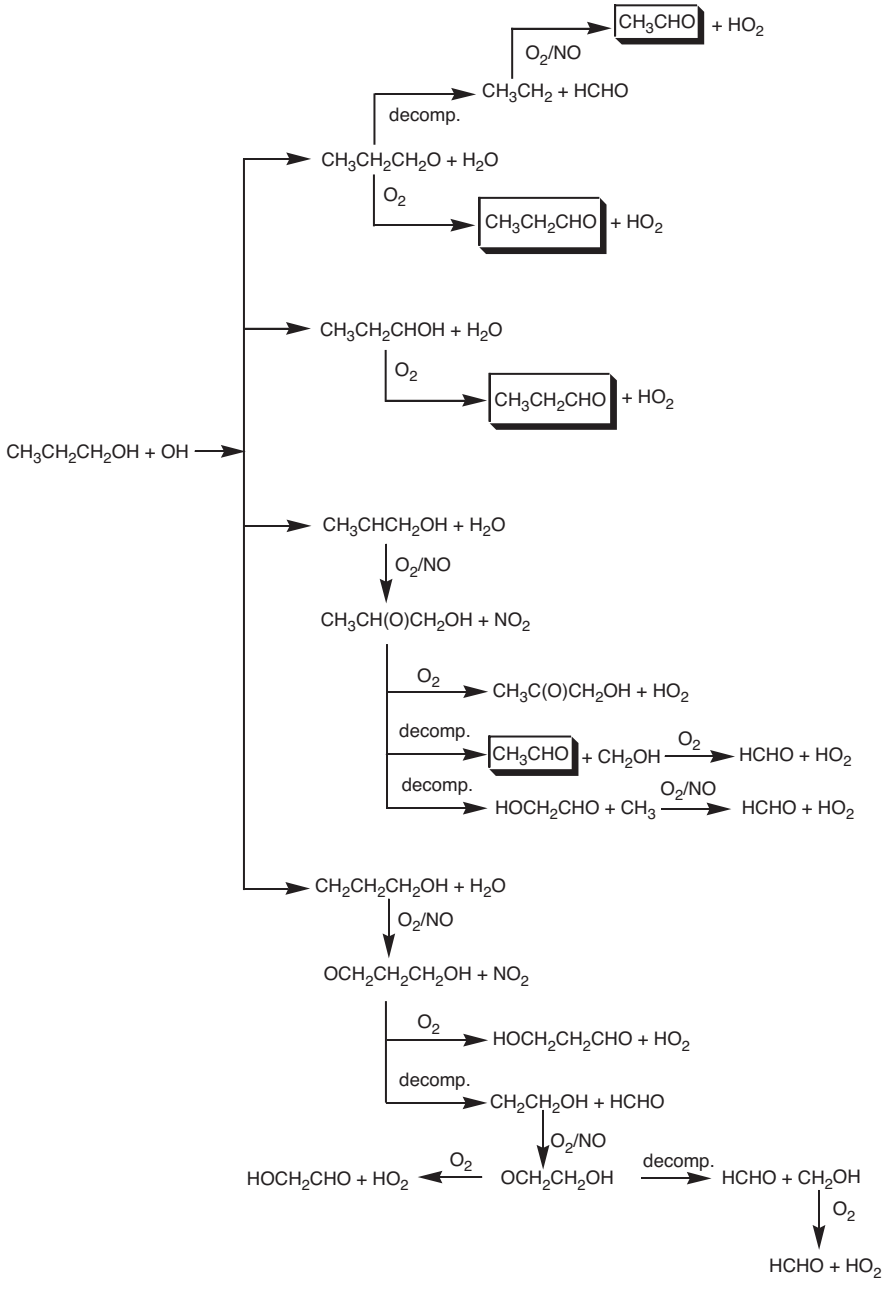

Figure II-B-9. OH-initiated degradation scheme of 1-propanol.

mechanism for 1-propanol. Products highlighted by boxes have been positively identified.

The reaction of 1-propanol with NO_3 has been shown to form propanal with a molar yield >55%, and possibly approaching unity after correction for reaction of propanal with NO_3 (Chew et al., 1998). This suggests that the reaction proceeds essentially exclusively through H-atom abstraction from the CH_2 group attached to the hydroxy group (α-position).

Cheema et al. (2002) have shown that the Cl-initiated oxidation of 1-propanol leads to propanal, acetaldehyde, and formaldehyde as the major reaction products. These products are formed following H-atom abstraction from α, β, and γ positions in $CH_3CH_2CH_2OH$. Abstraction from the OH group is considered to make a negligible contribution to the overall reaction.

$$Cl + CH_3CH_2CH_2OH \rightarrow CH_3CH_2CHOH + HCl \quad \text{(I)}$$

$$Cl + CH_3CH_2CH_2OH \rightarrow CH_3CHCH_2OH + HCl \quad \text{(II)}$$

$$Cl + CH_3CH_2CH_2OH \rightarrow CH_2CH_2CH_2OH + HCl \quad \text{(III)}$$

The branching ratios of the reaction at 298 K are 56%, 30%, and 14% for channels (I), (II), and (III), respectively (Cheema et al., 1999). These results have been confirmed by the more direct study of Yamanaka et al. (2008) who reported 60 ± 5, 25 ± 8, and 15 ± 3% for channels (I), (II), and (III), respectively.

II-B-4. 2-Propanol [Isopropyl Alcohol, $(CH_3)_2CHOH$]

II-B-4.1. OH Reaction Kinetics

Rate coefficients for reaction of OH with 2-propanol, measured over the range 240–502 K, are given in table II-B-10 and are plotted in figure II-B-10. The data of Dunlop and Tully (1993) and Mu and Mellouki (2001) are in excellent agreement over their region of overlap and show a clear upturn above 400 K. The data of Wallington and Kurylo (1987b), while not showing such a clear trend with temperature, agree to better than 15% with the two other temperature-dependent studies. The value reported by Lloyd et al. (1976) is larger than all other measurements. For atmospheric purposes, an Arrhenius expression derived from a fit to the 250–350 K data of Dunlop and Tully (1993) and Mu and Mellouki (2001) of $k = 2.7 \times 10^{-12} \exp(190/T)$ cm^3 molecule^{-1} s^{-1} is recommended. The value of the rate coefficient at 298 K is $k = 5.1 \times 10^{-12}$ cm^3 molecule^{-1} s^{-1} with an uncertainty estimated to be ±10%.

II-B-4.2. NO_3 Reaction Kinetics

As shown in table II-B-11, three investigations of the reaction of NO_3 with 2-propanol have been reported. Using absolute methods, Wallington et al. (1987) determined an upper limit of $k \leq 2.3 \times 10^{-15}$ at 298 K while Langer and Ljungström (1995) reported the Arrhenius expression $k = 1.54 \times 10^{-12} \exp[-(1{,}743 \pm 1{,}009)/T]$ cm^3 molecule^{-1} s^{-1} at 273–364 K with $k = 3.13 \times 10^{-15}$ cm^3 molecule^{-1} s^{-1} at 298 K.

Table II-B-10. Rate coefficients ($k = A \times e^{-B/T}$, cm^3 $molecule^{-1}$ s^{-1}) for reaction of OH with 2-propanol [$CH_3CH(OH)CH_3$]

$10^{12} \times A$	B (K)	$10^{12} \times k$	T (K)	Technique[a]	Reference	Temperature Range (K)
		7.2 ± 2.2	305 ± 2	RR ($CH_2{=}C(CH_3)_2$)[b]	Lloyd et al. (1976)	
		5.48 ± 0.55	296 ± 2	FP–RA	Overend and Paraskevopoulos (1978)	
		4.7	300	RR (toluene)[c]	Klöpffer et al. (1986)	
5.8 ± 1.9	30 ± 90	5.12 ± 0.31	240	FP–RF	Wallington and Kurylo (1987b)	240–440
		5.81 ± 0.34	296			
		5.27 ± 0.38	350			
		5.16 ± 0.44	400			
		5.75 ± 0.55	440			
		5.69 ± 1.09	298 ± 2	PR–UV abs.	Nelson et al. (1990a)	
		5.38 ± 0.70		RR (*cyclo*-C_6H_{12})[d]		
$k(T)$[f]		5.10 ± 0.21	293	PLP–LIF	Dunlop and Tully (1993)	293–502
		4.89 ± 0.20	326			
		4.68 ± 0.20	378			
		4.73 ± 0.22	438			
		4.86 ± 0.24	502			
2.80 ± 0.39	-184 ± 40	5.58 ± 0.20	253	PLP–LIF	Mu and Mellouki (2001)	253–372
		5.74 ± 0.25	263			
		5.51 ± 0.14	273			
		5.30 ± 0.17	283			
		5.17 ± 0.23	298			
		4.83 ± 0.12	323			
		4.66 ± 0.16	348			
		4.71 ± 0.12	372			
		5.46 ± 0.40	295 ± 2	RR (C_3H_8)[e]	Wu et al. (2003)	

[a]Abbreviations used for the techniques are defined in table I-F-3.
[b]Placed on an absolute basis using $k(OH + 2\text{-methylpropene}) = 5.14 \times 10^{-11}$ cm^3 $molecule^{-1}$ s^{-1} (Calvert et al., 2000).
[c]Placed on an absolute basis using $k(OH + \text{toluene}) = 5.6 \times 10^{-12}$ cm^3 $molecule^{-1}$ s^{-1} (Calvert et al., 2002).
[d]Placed on an absolute basis using $k(OH + \textit{cyclo}\text{-}C_6H_{12}) = 6.97 \times 10^{-12}$ cm^3 $molecule^{-1}$ s^{-1} (Calvert et al., 2008).
[e]Placed on an absolute basis using $k(OH + C_3H_8) = 1.1 \times 10^{-12}$ cm^3 $molecule^{-1}$ s^{-1} (Atkinson et al., 2006).
[f]$k(T) = 1.044 \times 10^{-17} T^{1.86} \exp(736/T)$ cm^3 $molecule^{-1}$ s^{-1} over the temperature range 293–745 K.

The larger value reported by Langer and Ljungström (1995) may reflect additional loss of NO_3 radicals via secondary chemistry which was unaccounted for. Chew et al. (1998) used a relative technique and reported an upper limit of $k \leq 1.7 \times 10^{-15}$ cm^3 $molecule^{-1}$ s^{-1} at 298 K. It has been suggested (IUPAC, 2008) that the rate coefficient can be calculated from the acetone yield observed in the experiments by Chew et al. (1998). Using the acetone yield reported by Chew et al. of 0.76 ± 0.09, and assuming an actual yield of unity, a rate coefficient of $k = 1.4 \times 10^{-15}$ cm^3 $molecule^{-1}$ s^{-1} has been recommended at 298 K with an estimated uncertainty of $\pm 30\%$. No recommendation is given for the temperature dependence since the only available temperature dependence study (Langer and Ljungström, 1995) might be affected by secondary chemistry.

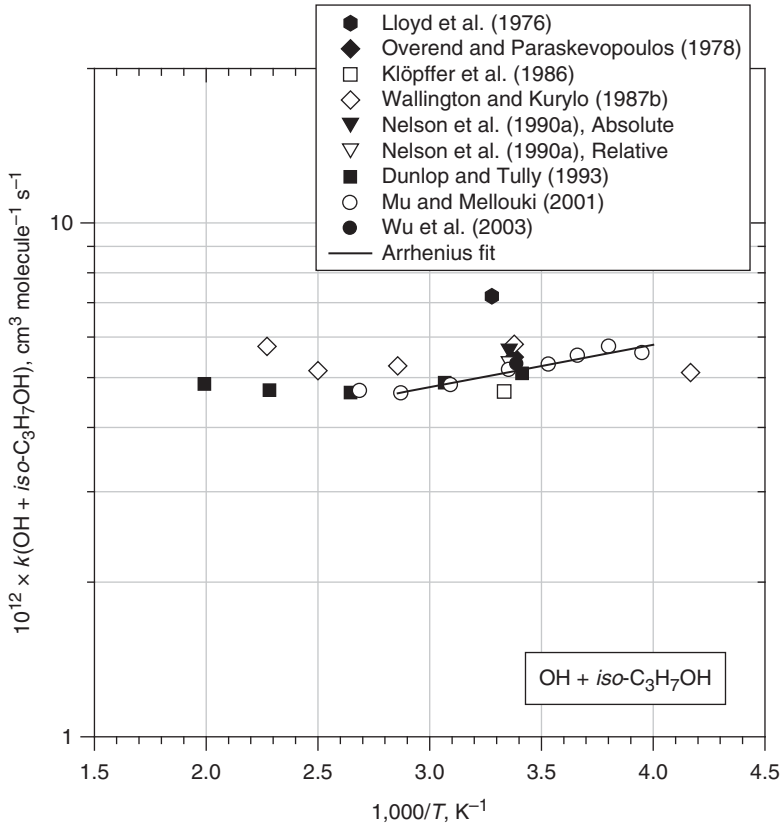

Figure II-B-10. Arrhenius plot of the rate coefficient for the reaction of OH with 2-propanol.

II-B-4.3. Cl-Atom Reaction Kinetics

The reaction of Cl-atoms with 2-propanol has been studied by Nelson et al. (1990a), Wu et al. (2003), Taketani et al. (2005), and Yamanaka et al. (2007); see table II-B-12. The rate coefficients obtained in these different studies are in good agreement, and the preferred value is an unweighted average of these measurements, $k = 8.8 \times 10^{-11}$ cm^3 molecule^{-1} s^{-1} at 298 K with an estimated uncertainty of 10%.

II-B-4.4. Summary of the Atmospheric Fate of 2-Propanol

Combining k(OH + 2-propanol) $= 5.1 \times 10^{-12}$ cm^3 molecule^{-1} s^{-1} with [OH] $= 10^6$ molecule cm^{-3} provides an estimate of the atmospheric lifetime with respect to removal through reaction with OH of 2 days.

In addition to $(CH_3)_2CHOH$, Dunlop and Tully (1993) investigated the kinetics of the reactions of OH radicals with $(CD_3)_2CHOH$, $(CH_3)_2CDOH$, $(CD_3)_2CDOD$, and $(CH_3)_2CHOD$. By combining the results for the various isotopologs, Dunlop and Tully (1993) derived branching ratios for attack at the various sites as a function of temperature. Dunlop and Tully (1993) found that abstraction from the methyl groups accounts

Table II-B-11. Rate coefficients (k, cm^3 molecule^{-1} s^{-1}) for reaction of NO_3 with 2-propanol [$(CH_3)_2CHOH$]

$10^{12} \times A$	B (K)	$10^{15} \times k$	T (K)	Technique[a]	Reference	Temperature Range (K)
		≤ 2.3	298 ± 2	FP–A	Wallington et al. (1987)	
1.54	1,743 ± 1,009	3.28 ± 0.62	273	DF–A	Langer and Ljunström (1995)	273–364
		3.13 ± 0.64	295			
		6.38 ± 0.77	324			
		10.33 ± 3.37	344			
		14.23 ± 2.30	364			
		$\leq 1.8 \pm 0.2$	298 ± 2	RR (methacrolein)[b]	Chew et al. (1998)	

[a]Abbreviations used for the techniques are defined in table I-F-3.
[b]Placed on an absolute basis using $k(NO_3 + \text{methacrolein}) = 3.4 \times 10^{-15}$ cm^3 molecule^{-1} s^{-1} (Atkinson et al., 2006).

Table II-B-12. Rate coefficients (k, cm^3 molecule^{-1} s^{-1}) for reaction of Cl with 2-propanol [$CH_3CH(OH)CH_3$]

$10^{11} \times k$	T (K)	Technique[a]	Reference
8.80 ± 0.35	298 ± 2	RR (*cyclo*-C_6H_{12})[b]	Nelson et al. (1990a)
7.85 ± 0.39	295 ± 2	RR (C_3H_8)[c]	Wu et al. (2003)
8.89 ± 0.80	295 ± 2	RR (*cyclo*-C_6H_{12})[b]	
9.11 ± 0.60	295 ± 2	FP–VUV/LIF	Taketani et al. (2005)
8.32 ± 0.52	296 ± 2	RR (C_2H_2)[d]	Yamanaka et al. (2007)
8.64 ± 0.69	296 ± 2	RR (C_2H_4)[e]	

[a]Abbreviations used for the techniques are defined in table I-F-3.
[b]Placed on an absolute basis using $k(Cl + \textit{cyclo}\text{-}C_6H_{12}) = 3.3 \times 10^{-10}$ cm^3 molecule^{-1} s^{-1} (Calvert et al., 2008).
[c]Placed on an absolute basis using $k(Cl + C_3H_8) = 1.4 \times 10^{-10}$ cm^3 molecule^{-1} s^{-1} (Atkinson et al., 2006).
[d]Placed on an absolute basis using $k(Cl + C_2H_2) = 5.2 \times 10^{-11}$ cm^3 molecule^{-1} s^{-1} (Atkinson et al., 2006).
[e]Placed on an absolute basis using $k(Cl + C_2H_4) = 9.5 \times 10^{-11}$ cm^3 molecule^{-1} s^{-1} (section I-F-1).

for 12% of the reaction at 293 K (and probably less at lower temperatures). Assuming the reactivity of the —OH group is the same as in methanol (1.35×10^{-13} cm^3 molecule^{-1} s^{-1}, IUPAC, 2008), reaction of OH radicals with the —OH group in 2-propanol accounts for approximately 3% of the overall reaction. Reaction at the tertiary C—H bond is expected to dominate and lead to the formation of acetone as the major product:

$$OH + CH_3CH(OH)CH_3 \rightarrow H_2O + CH_3C(OH)CH_3$$
$$CH_3C(OH)CH_3 + O_2 \rightarrow HO_2 + CH_3C(O)CH_3$$

As with OH radicals, the reaction of NO_3 with 2-propanol occurs predominantly via H-atom abstraction from the tertiary C—H group leading to acetone as product (Chew et al., 1998):

$$NO_3 + CH_3CH(OH)CH_3 \rightarrow HNO_3 + CH_3C(OH)CH_3$$
$$CH_3C(OH)CH_3 + O_2 \rightarrow HO_2 + CH_3C(O)CH_3$$

Chew et al. reported formation of acetone with a yield of 0.76 ± 0.09 but mentioned that a fraction of 2-propanol was lost via secondary chemistry. 2-Propanol could have been consumed through reaction with N_2O_5 (gas phase or heterogeneous) to form nitrates in the experimental system (Langer and Ljungström, 1995; Chew et al., 1998).

In their study of the Cl-initiated oxidation of 2-propanol, Ohta et al. (1982) suggested that 85% of the Cl attack occurs at the α-position and 15% at the β-methyl groups at 298 K. These results have been confirmed by the more direct study of Yamanaka et al. (2007) who reported branching ratios of 85 ± 7 and $15 \pm 7\%$ for attack at the α- and β-positions, respectively.

II-B-5. 1-Butanol (*n*-Butyl Alcohol, $CH_3CH_2CH_2CH_2OH$)

II-B-5.1. OH Reaction Kinetics

The kinetics of the reaction of OH with 1-butanol has been the subject of eight studies near 298 K and one study over the range 263–372 K. The measurements are presented in table II-B-13 and displayed in figure II-B-11. The absolute rate coefficient values near 298 K of Wallington and Kurylo (1987b), Nelson et al. (1990a), and Mu and Mellouki

Table II-B-13. Rate coefficients (k, cm^3 molecule^{-1} s^{-1}) for the reaction of OH with 1-butanol (n-C_4H_9OH)

$10^{12} \times A$	B (K)	$10^{12} \times k$	T (K)	Technique[a]	Reference	Temperature Range (K)
		7.0 ± 1.3	292	RR (n-C_4H_{10})[b]	Campbell et al. (1976)	
		8.31 ± 0.63	296	FP–RF	Wallington and Kurylo (1987b)	
		7.80 ± 0.20	298 ± 2	PR–UV abs.	Nelson et al.	
		7.97 ± 0.66		RR (*cyclo*-C_6H_{12})[c]	(1990a)	
		8.8 ± 0.3	298 ± 2	RR (*cyclo*-C_6H_{12})[c]	Oh and Andino	
		10.3 ± 0.4		RR (p-Xylene)[d]	(2001)	
5.30 ± 1.62	-146 ± 92	9.51 ± 0.44	263	PLP–LIF	Mu and Mellouki	263–372
		9.36 ± 0.27	273		(2001)	
		8.47 ± 0.34	298			
		8.11 ± 0.20	323			
		8.24 ± 0.24	348			
		8.09 ± 0.14	372			
		7.67 ± 0.14	298 ± 2	RR (*cyclo*-C_6H_{12})[c]	Cavalli et al. (2002)	
		8.82 ± 0.68	295 ± 2	RR (C_3H_8)[e]	Wu et al. (2003)	
		8.19 ± 0.78	296 ± 2	RR (C_2H_2)[f]	Hurley et al.	
		8.22 ± 0.79	296 ± 2	RR (C_2H_4)[g]	(2009)	

[a]Abbreviations used for the techniques are defined in table I-F-3.
[b]Placed on an absolute basis using $k(OH + n\text{-}C_4H_{10}) = 2.35 \times 10^{-12}$ cm^3 molecule^{-1} s^{-1} (Calvert et al., 2008).
[c]Placed on an absolute basis using $k(OH + cyclo\text{-}C_6H_{12}) = 6.97 \times 10^{-12}$ cm^3 molecule^{-1} s^{-1} (Calvert et al., 2008).
[d]Placed on an absolute basis using $k(OH + p\text{-xylene}) = 1.43 \times 10^{-11}$ cm^3 molecule^{-1} s^{-1} (Calvert et al., 2002).
[e]Placed on an absolute basis using $k(OH + C_3H_8) = 1.1 \times 10^{-12}$ cm^3 molecule^{-1} s^{-1} (Atkinson et al., 2006).
[f]Placed on an absolute basis using $k(OH + C_2H_2) = 7.8 \times 10^{-13}$ cm^3 molecule^{-1} s^{-1} (Atkinson et al., 2006).
[g]Placed on an absolute basis using $k(OH + C_2H_4) = 7.9 \times 10^{-12}$ cm^3 molecule^{-1} s^{-1} (Atkinson et al., 2006).

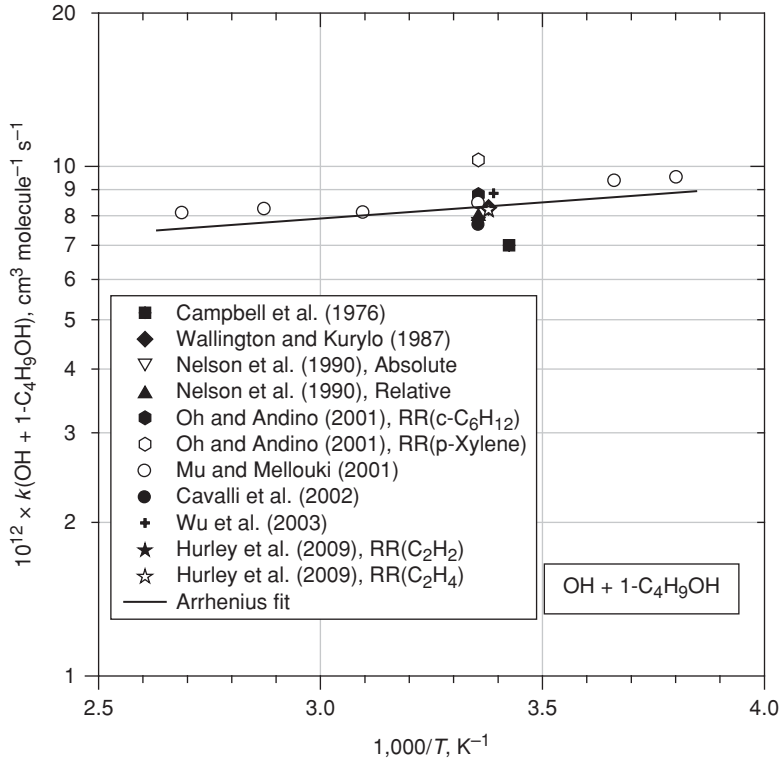

Figure II-B-11. Arrhenius plot of the rate coefficient for the reaction of OH with 1-butanol.

(2001) are in good agreement with the measurements of Nelson et al. (1990a), Oh and Andino (2001) (relative to cyclohexane), Cavalli et al. (2002), Wu et al. (2003), and Hurley et al. (2009). The rate coefficient derived by Oh and Andino (2001) using *p*-xylene as the reference is, for reasons that are unclear, ~20% higher than the results from most other studies. The rate coefficient reported in the early work by Campbell et al. (1976) lies approximately 10–20% below, but is consistent within the experimental uncertainties with those of the other studies. The mean of the measurements reported near 298 K is used to derive the preferred value $k = 8.2 \times 10^{-12}$ cm^3 molecule^{-1} s^{-1} with an estimated uncertainty of ±15% at 298 K. The data of Mu and Mellouki (2001) show a weak negative temperature dependence and were used in combination with the recommended value at 298 K to calculate the preexponential factor for the recommended Arrhenius expression, $k = 5.1 \times 10^{-12} \exp(146/T)$ cm^3 molecule^{-1} s^{-1} over the atmospheric temperature range 260–380 K.

II-B-5.2. NO_3 Reaction Kinetics

The only study of the reaction of NO_3 with 1-butanol is that conducted by Chew et al. (1998) using the relative rate method. Recognizing possible interferences caused

Table II-B-14. Rate coefficient (k, cm^3 molecule^{-1} s^{-1}) for the reaction of NO_3 with 1-butanol (n-C_4H_9OH)

$10^{15} \times k$	T (K)	Technique[a]	Reference
$\leq 2.8 \pm 1.0$	298 ± 2	RR (methacrolein)[b]	Chew et al. (1998)

[a]Abbreviations used for the techniques are defined in table I-F-3.
[b]Placed on an absolute basis using $k(NO_3 + \text{methacrolein}) = 3.4 \times 10^{-15}$ cm^3 molecule^{-1} s^{-1} (Atkinson et al., 2006).

by reaction of 1-butanol with N_2O_5, Chew et al. reported an upper limit, $k(NO_3 +$ 1-butanol$) \leq (2.8 \pm 1.0) \times 10^{-15}$ cm^3 molecule^{-1} s^{-1} at 298 K; see table II-B-14.

II-B-5.3. Cl-Atom Reaction Kinetics

The kinetics of the reaction of chlorine atoms with 1-butanol have been studied by Nelson et al. (1990a), Wu et al. (2003), and Hurley et al. (2009) using relative rate methods and by Garzón et al. (2006) using an absolute method (table II-B-15 and figure II-B-12). The results reported near 298 K are in agreement and an unweighted mean gives our recommended value of $k = 2.2 \times 10^{-10}$ cm^3 molecule^{-1} s^{-1} at 298 K with an estimated uncertainty of ~20%. The only temperature dependence study of this reaction is that conducted by Garzón et al. (2006) who reported $k = 3.12 \times 10^{-11}$ exp[$(548 \pm 65)/T$] cm^3 molecule^{-1} s^{-1} over the range 266–382 K. This expression requires confirmatory measurements.

Table II-B-15. Rate coefficients (k, cm^3 molecule^{-1} s^{-1}) for the reaction of Cl with 1-butanol (n-C_4H_9OH)

$10^{11} \times A$	B (K)	$10^{10} \times k$	T (K)	Technique[a]	Reference	Temperature Range (K)
		2.14± 0.15	298 ± 2	RR (*cyclo*-C_6H_{12})[b]	Nelson et al. (1990a)	
		2.25 ± 0.12	295 ± 2	RR (C_3H_8)[c]	Wu et al. (2003)	
		2.40 ± 0.11	295 ± 2	RR (*cyclo*-C_6H_{12})[b]		
3.12 ± 0.31	−548 ± 65	2.41 ± 0.18	266	PLP–RF	Garzón et al. (2006)	264–382
		2.30 ± 0.26	283			
		1.96 ± 0.19	298			
		1.80 ± 0.12	311			
		1.60 ± 0.08	330			
		1.49 ± 0.06	343			
		1.47 ± 0.04	354			
		1.30 ± 0.10	382			
		2.14 ± 0.21	296	RR (C_2H_2)[d]	Hurley et al. (2009)	
		2.24 ± 0.32	296	RR (C_2H_4)[e]		
		2.05 ± 0.21	296	RR (C_3H_6)[f]		

[a]Abbreviations used for the techniques are defined in table I-F-3.
[b]Placed on an absolute basis using $k(Cl + \textit{cyclo}\text{-}C_6H_{12}) = 3.3 \times 10^{-10}$ cm^3 molecule^{-1} s^{-1}(Calvert et al., 2008).
[c]Placed on an absolute basis using $k(Cl + C_3H_8) = 1.4 \times 10^{-10}$ cm^3 molecule^{-1} s^{-1}(Atkinson et al., 2006).
[d]Placed on an absolute basis using $k(Cl + C_2H_2) = 5.2 \times 10^{-11}$ cm^3 molecule^{-1} s^{-1}(Atkinson et al., 2006).
[e]Placed on an absolute basis using $k(Cl + C_2H_4) = 9.5 \times 10^{-11}$ cm^3 molecule^{-1} s^{-1}(section I-F-1).
[f]Placed on an absolute basis using $k(Cl + C_3H_6) = 2.3 \times 10^{-10}$ cm^3 molecule^{-1} s^{-1} (IUPAC, 2008).

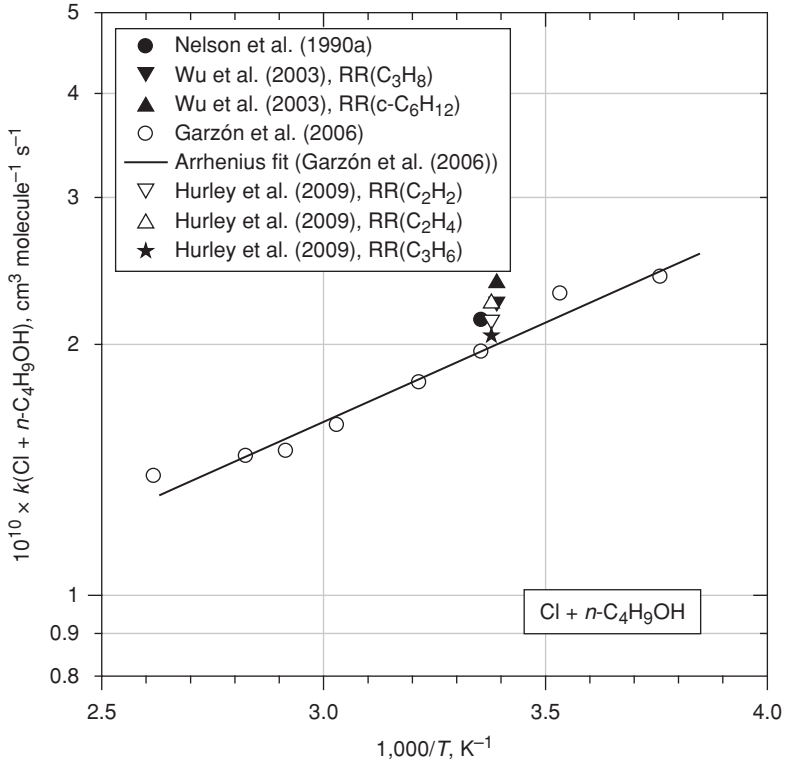

Figure II-B-12. Arrhenius plot of the rate coefficient for the reaction of Cl with 1-butanol.

II-B-5.4. Summary of the Atmospheric Fate of 1-butanol

The rate coefficient values given in this section indicate that the reaction with OH radicals will constitute the most important loss process of this species under atmospheric conditions, leading to a lifetime less than 2 days.

The reaction of OH with 1-butanol proceeds by H-atom abstraction from the various CH_3, —CH_2, and —OH groups.

$$OH + CH_3CH_2CH_2CH_2OH \rightarrow H_2O + CH_3CH_2CH_2CH_2O \quad (1)$$

$$OH + CH_3CH_2CH_2CH_2OH \rightarrow H_2O + CH_3CH_2CH_2CHOH \quad (2)$$

$$OH + CH_3CH_2CH_2CH_2OH \rightarrow H_2O + CH_3CH_2CHCH_2OH \quad (3)$$

$$OH + CH_3CH_2CH_2CH_2OH \rightarrow H_2O + CH_3CHCH_2CH_2OH \quad (4)$$

$$OH + CH_3CH_2CH_2CH_2OH \rightarrow H_2O + CH_2CH_2CH_2CH_2OH \quad (5)$$

Assuming the reactivity of the —OH group is the same as in methanol (1.35×10^{-13} cm^3 $molecule^{-1}$ s^{-1} (IUPAC, 2008), reaction of OH radicals with the —OH group in

1-butanol accounts for approximately 2% of the overall reaction. The most important reaction channels are H abstraction from the —CH_2 groups at the α-position (channel 2), followed by H-atom abstraction from the —CH_2 groups in the β- and γ-positions (channels 3 and 4, respectively) with a lower contribution from channel (5) to the overall reaction.

The products of the OH-initiated oxidation of 1-butanol in the presence of NO_x have been investigated by Cavalli et al. (2002) and Hurley et al. (2009). Cavalli et al. (2002) observed the following products (in molar yields): butanal (51.8 ± 7.1%), propanal (23.4 ± 3.5%), acetaldehyde (12.7 ± 2.2%) and formaldehyde (43.4 ± 2.4%). Hurley et al. (2009) observed butanal (44 ± 2%), propanal (19 ± 2 %), and acetaldehyde (12 ± 2%). The results from Cavalli et al. (2002) and Hurley et al. (2009) are in good agreement. The sole atmospheric fate of α-hydroxy alkyl radicals is reaction with O_2 to give the corresponding aldehyde. Thus, the yield of butanal corresponds to the contribution of channel (2). The main fate of $CH_3CH_2CH(O)CH_2OH$ radicals is decomposition to give propanal and CH_2OH radicals. The yield of propanal provides an indication for the contribution of channel (3). The alkoxy radical formed from channel (4) can also react with O_2 to form 4-hydroxy-2-butanone, but this is probably less important than decomposition to acetaldehyde and two molecules of formaldehyde.

$$CH_3CH(O)CH_2CH_2OH \rightarrow CH_3CHO + CH_2CH_2OH$$

$$CH_2CH_2OH + O_2 + NO \rightarrow 2CH_2O$$

$$CH_3CH(O)CH_2CH_2OH + O_2 \rightarrow CH_3C(O)CH_2CH_2OH$$

Hurley et al. (2009) have suggested that chemical activation plays an important role in the fate of $CH_3CH_2CH(O)CH_2OH$ and $CH_3CH(O)CH_2CH_2OH$ alkoxy radicals. Further experiments are needed to test this suggestion.

The reaction of NO_3 with 1-butanol was found to produce butanal with a yield higher than (22 ± 4)% (Chew et al., 1998). This yield corresponds to H-atom abstraction from the —CH_2 group α- to the hydroxyl group.

$$NO_3 + CH_3CH_2CH_2CH_2OH \rightarrow HNO_3 + CH_3CH_2CH_2CHOH$$

$$CH_3CH_2CH_2CHOH + O_2 \rightarrow CH_3CH_2CH_2CHO + HO_2$$

The occurrence of secondary reactions involving the aldehyde with NO_3 and possible side reaction of 1-butanol with N_2O_5 made it difficult for Chew et al. to report precise product yields for this reaction.

II-B-6. 2-Butanol [*sec*-Butyl Alcohol, $CH_3CH(OH)CH_2CH_3$]

II-B-6.1. OH Reaction Kinetics

This reaction has been the subject of three different studies. Chew and Atkinson (1996) and Baxley and Wells (1998) used relative rate methods while Jiménez et al. (2005b)

used a pulsed-laser photolysis, laser-induced fluorescence technique. The results presented in table II-B-16 and figure II-B-13 show that the different measurements near 298 K are in good agreement. A fit to the data yields the Arrhenius expression $k = 2.7 \times 10^{-12} \exp(329/T)\,\mathrm{cm^3\ molecule^{-1}\ s^{-1}}$ over the temperature range 260–360 K. The rate coefficient derived at 298 K is $k = 8.3 \times 10^{-12}\,\mathrm{cm^3\ molecule^{-1}\ s^{-1}}$ with an estimated uncertainty of ±15 %.

II-B-6.2. NO_3 Reaction Kinetics

Using the relative rate method, Chew et al. (1998) have determined an upper limit of the rate coefficient for the NO_3 reaction with 2-butanol, $k \leq (2.6 \pm 0.8) \times 10^{-15}\,\mathrm{cm^3\ molecule^{-1}\ s^{-1}}$ at 298 K (table II-B-17). The measurement was possibly affected by reaction of 2-butanol with N_2O_5 (gas-phase or heterogeneous) to form nitrates as observed by Langer and Ljungström (1995). The preferred value recommended by IUPAC (2008) is determined from a combination of the rate coefficient and product yield of 2-butanone measured by Chew et al. (1998), assuming that the reaction occurs almost exclusively by H-atom abstraction from the tertiary C—H bond. This procedure leads to $k = 2.0 \times 10^{-15}\,\mathrm{cm^3\ molecule^{-1}\ s^{-1}}$ at 298 K.

II-B-6.3. Cl-Atom Reaction Kinetics

Ballesteros et al. (2007) have used relative and absolute techniques to study the Cl reaction with 2-butanol. The data obtained over the temperature range 267–384 K

Table II-B-16. Rate coefficients ($k = A\ \mathrm{e}^{-B/T}, \mathrm{cm^3\ molecule^{-1}\ s^{-1}}$) for the reaction of OH with 2-butanol [$CH_3CH(OH)CH_2CH_3$]

$10^{12} \times A$	B (K)	$10^{12} \times k$	T (K)	Technique[a]	Reference	Temperature Range (K)
		8.64 ± 0.49	296 ± 2	RR (*cyclo*-C_6H_{12})[b]	Chew and Atkinson (1996)	
		8.85 ± 0.13	297 ± 3	RR (*n*-C_9H_{20})[c]	Baxley and Wells (1998)	
		7.80 ± 0.45		RR (*n*-$C_{12}H_{26}$)[d]		
2.76 ± 1.20	−328 ± 124	9.98 ± 0.30	263	PLP–LIF	Jiménez et al. (2005b)	263–354
		9.77 ± 1.46	268			
		9.34 ± 0.40	273			
		8.40 ± 0.40	278			
		8.07 ± 0.40	283			
		7.90 ± 0.50	288			
		8.77 ± 1.46	298			
		8.51 ± 2.80	303			
		8.32 ± 1.10	321			
		7.93 ± 0.40	327			
		6.99 ± 0.48	338			
		6.64 ± 0.46	354			

[a]Abbreviations used for the techniques are defined in table I-F-3.
[b]Placed on an absolute basis using $k(\mathrm{OH} + \textit{cyclo}\text{-}C_6H_{12}) = 6.97 \times 10^{-12}\,\mathrm{cm^3\ molecule^{-1}\ s^{-1}}$ (Calvert et al., 2008).
[c]Placed on an absolute basis using $k(\mathrm{OH} + n\text{-}C_9H_{20}) = 9.75 \times 10^{-12}\,\mathrm{cm^3\ molecule^{-1}\ s^{-1}}$ (Calvert et al., 2008).
[d]Placed on an absolute basis using $k(\mathrm{OH} + n\text{-}C_{12}H_{26}) = 1.36 \times 10^{-11}\,\mathrm{cm^3\ molecule^{-1}\ s^{-1}}$ (Calvert et al., 2008).

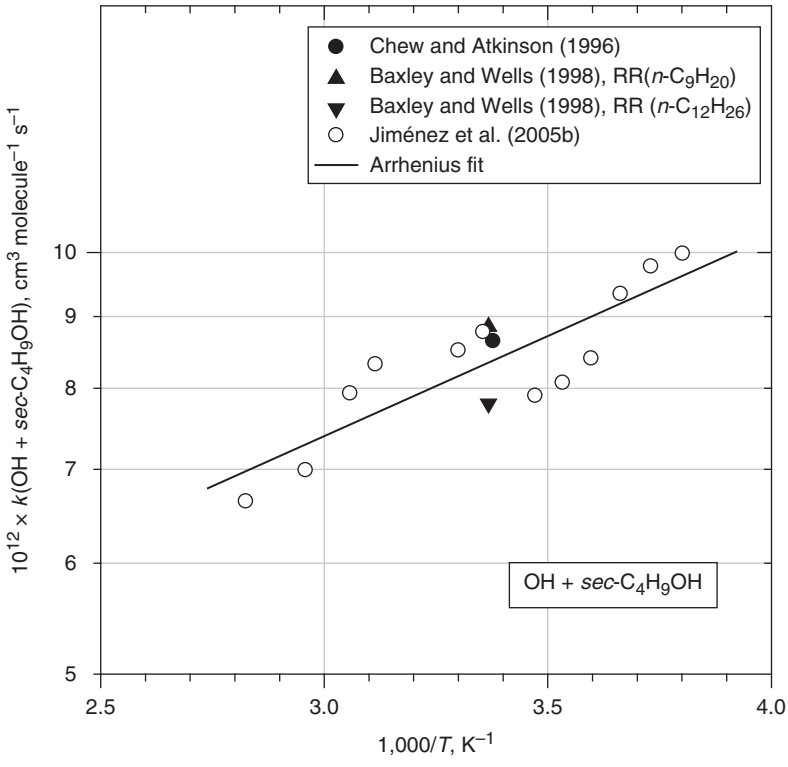

Figure II-B-13. Arrhenius plot of the rate coefficient for the reaction of OH with 2-butanol.

Table II-B-17. Rate coefficient (k, cm^3 molecule^{-1} s^{-1}) for the reaction of NO_3 with 2-butanol [$CH_3CH(OH)CH_2CH_3$]

$10^{15} \times k$	T (K)	Technique[a]	Reference
$\leq 2.6 \pm 0.8$	298 ± 2	RR (methacrolein)[b]	Chew et al. (1998)

[a]Abbreviations used for the techniques are defined in table I-F-3.
[b]Placed on an absolute basis using $k(NO_3 + \text{methacrolein}) = 3.4 \times 10^{-15}$ cm^3 molecule^{-1} s^{-1} (Atkinson et al., 2006).

are summarized in table II-B-18 and shown in figure II-B-14. Fitting the Arrhenius expression to the combined dataset gives $k(\text{Cl} + \text{2-butanol}) = 6.1 \times 10^{-11} \exp(179/T)$ with $k = 1.1 \times 10^{-10}$ cm^3 molecule^{-1} s^{-1} at 298 K. An uncertainty of $\pm 15\%$ is assigned to the 298 K value.

II-B-6.4. Summary of the Atmospheric Fate of 2-Butanol

Combining $k(\text{OH} + \text{2-butanol}) = 8.3 \times 10^{-12}$ cm^3 molecule^{-1} s^{-1} with [OH] = 10^6 molecule cm^{-3} provides an estimate of the atmospheric lifetime with respect to removal through reaction with OH radicals of 1.4 days.

Table II-B-18. Rate coefficients (k, cm^3 molecule^{-1} s^{-1}) for reaction of Cl with 2-butanol [$CH_3CH(OH)CH_2CH_3$]

$10^{11} \times A$	B (K)	$10^{10} \times k$	T (K)	Technique[a]	Reference	Temperature Range (K)
		1.20 ± 0.20	298 ± 2	RR (1,3-butadiene)[b]	Ballesteros et al.	
		1.35 ± 0.10		RR (*cyclo*-C_6H_{12})[c]	(2007)	
6.16 ± 0.58	-174 ± 58	1.20 ± 0.08	267	PLP-RF	Ballesteros et al.	267–384
		1.10 ± 0.15	280		(2007)	
		1.15 ± 0.12	287			
		1.05 ± 0.09	298			
		1.13 ± 0.08	298			
		1.14 ± 0.13	299			
		1.07 ± 0.07	301			
		1.02 ± 0.15	312			
		1.07 ± 0.11	335			
		0.995 ± 0.120	336			
		0.974 ± 0.100	350			
		0.968 ± 0.070	364			
		0.996 ± 0.110	384			
		1.03 ± 0.11	384			

[a]Abbreviations used for the techniques are defined in table I-F-3.
[b]Placed on an absolute basis using $k(Cl + 1,3\text{-butadiene}) = 2.51 \times 10^{-10}$ cm^3 molecule^{-1} s^{-1} (Stutz et al., 1998).
[c]Placed on an absolute basis using $k(Cl + cyclo\text{-}C_6H_{12}) = 3.3 \times 10^{-10}$ cm^3 molecule^{-1} s^{-1} (Calvert et al., 2008).

OH reacts with 2-butanol by H-atom abstraction from the various CH_3, —CH_2, $\rangle$CH, and —OH groups.

$$OH + CH_3CH(OH)CH_2CH_3 \rightarrow H_2O + CH_3CH(O)CH_2CH_3 \quad (1)$$

$$OH + CH_3CH(OH)CH_2CH_3 \rightarrow H_2O + CH_3C(OH)CH_2CH_3 \quad (2)$$

$$OH + CH_3CH(OH)CH_2CH_3 \rightarrow H_2O + CH_2CH(OH)CH_2CH_3 \quad (3)$$

$$OH + CH_3CH(OH)CH_2CH_3 \rightarrow H_2O + CH_3CH(OH)CHCH_3 \quad (4)$$

$$OH + CH_3CH(OH)CH_2CH_3 \rightarrow H_2O + CH_3CH(OH)CH_2CH_2 \quad (5)$$

Assuming the reactivity of the —OH group is the same as in methanol (1.35×10^{-13} cm^3 molecule^{-1} s^{-1}; IUPAC, 2008), reaction of OH radicals with the —OH group in 2-butanol accounts for approximately 2% of the overall reaction. The product studies conducted by Chew and Atkinson (1996) and Baxley and Wells (1998) show that the reaction of OH radicals with 2-butanol proceeds mainly by H-atom abstraction from the tertiary C—H bond (channel 2). The sole fate of the α-hydroxy alkyl radical $CH_3C(OH)CH_2CH_3$ is reaction with O_2 to give 2-butanone in 100% yield:

$$CH_3C(OH)CH_2CH_3 + O_2 \rightarrow HO_2 + CH_3C(O)CH_2CH_3$$

Chew and Atkinson (1996) and Baxley and Wells (1998) investigated the reaction mechanism of OH + 2-butanol and reported, respectively, (70 ± 7)% and (60 ± 2)%

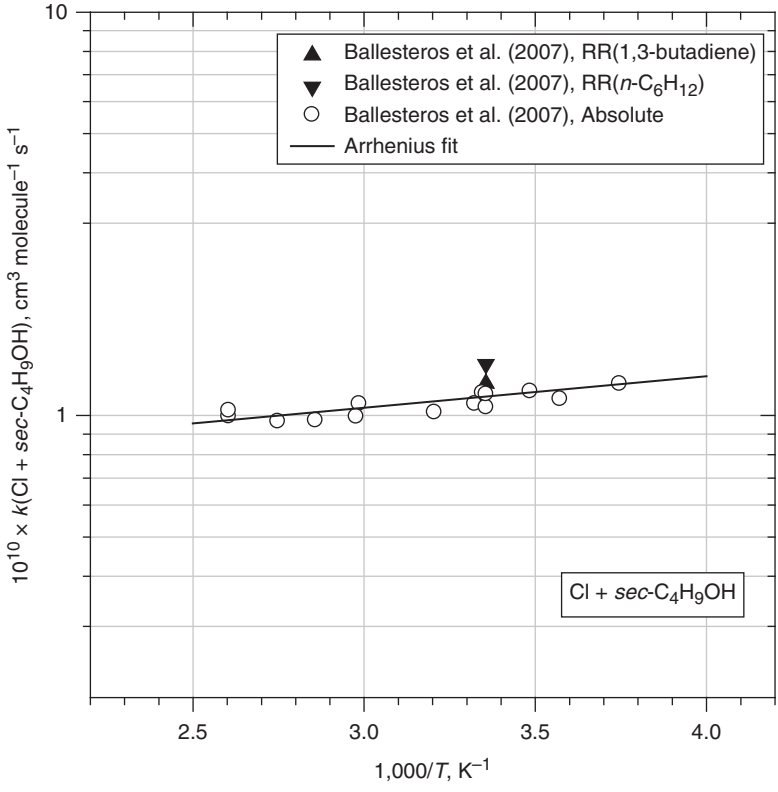

Figure II-B-14. Arrhenius plot of the rate coefficient for the reaction of Cl with 2-butanol.

yield of 2-butanone. These yields provide a measure of the importance of channel (2). Reaction is also expected to proceed via channel (4) which involves H-atom abstraction from the —CH_2 and leads to the formation of two molecules of acetaldehyde. Baxley and Wells reported an acetaldehyde yield of (29 ± 4)%.

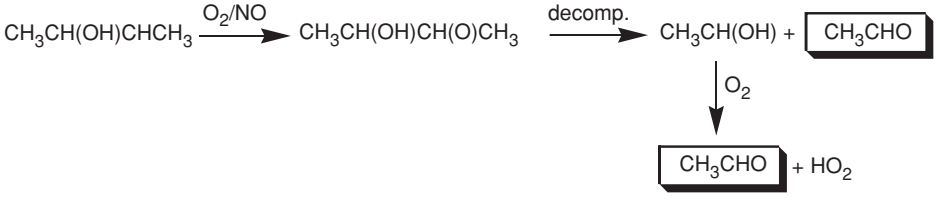

Chew et al. (1998) observed 2-butanone in a yield of (79 ± 9%) following the NO_3-radical-initiated oxidation of 2-butanol.

$$NO_3 + CH_3CH_2CH(OH)CH_3 \rightarrow HNO_3 + CH_3CH_2C(OH)CH_3$$

$$CH_3CH_2C(OH)CH_3 + O_2 \rightarrow HO_2 + CH_3CH_2C(O)CH_3$$

II-B-7. 2-Methyl-1-Propanol [Isobutyl Alcohol, $(CH_3)_2CHCH_2OH$]

II-B-7.1. OH Reaction Kinetics

Measurements of the rate coefficient for this reaction are summarized in table II-B-19 and shown in figure II-B-15. The reaction has been studied using relative and absolute techniques by Wu et al. (2003) and Mellouki et al. (2004). The rate coefficient values at 298 K are in very good agreement. Mellouki et al. (2004) determined the temperature dependence of the rate coefficient in the range 241–370 K and obtained $k = 3.1 \times 10^{-12} \exp(352/T)\,\mathrm{cm^3\ molecule^{-1}\ s^{-1}}$. A fit to the combined data set including the relative determinations gives $k = 2.75 \times 10^{-12} \exp(371/T)\,\mathrm{cm^3\ molecule^{-1}\ s^{-1}}$. This expression gives $k(\mathrm{OH} + \text{2-methyl-1-propanol}) = 9.6 \times 10^{-12}\,\mathrm{cm^3\ molecule^{-1}\ s^{-1}}$ at 298 K with an uncertainty estimated to be ±15%.

II-B-7.2. Cl-Atom Reaction Kinetics

Wu et al. (2003) employed relative rate methods with two reference compounds (propane and cyclohexane) to study the reaction of Cl with 3-methyl-1-propanol. The rate coefficient values obtained with the two different references are in good agreement (see table II-B-20) leading to an average value of $k = 2.0 \times 10^{-10}\,\mathrm{cm^3\ molecule^{-1}\ s^{-1}}$ at 298 K.

II-B-7.3. Summary of the Atmospheric Fate of 2-Methyl-1-propanol

The atmospheric lifetime of 2-methyl-1-propanol with respect to reaction with OH radicals is estimated to be around 1 day. Assuming the reactivity of the —OH group is

Table II-B-19. Rate coefficients (k, $\mathrm{cm^3\ molecule^{-1}\ s^{-1}}$) for reaction of OH with 2-methyl-1-propanol [$(CH_3)_2CHCH_2OH$]

$10^{12} \times A$	B (K)	$10^{12} \times k$	T (K)	Technique[a]	Reference	Temperature Range (K)
		8.8 ± 0.3	295 ± 2	RR (C_3H_8)[b]	Wu et al. (2003)	
		9.3 ± 0.4		RR (*cyclo*-C_6H_{12})[c]		
		8.3 ± 0.1	298 ± 2	RR (1-butanol)[d]	Mellouki et al.	
		8.8 ± 0.1		RR (1,3-dixolane)[e]	(2004)	
3.1 ± 0.9	−352 ± 82	13.8 ± 0.2	241	PLP–LIF	Mellouki et al.	241–370
		12.3 ± 0.5	253		(2004)	
		12.4 ± 0.4	260			
		10.6 ± 0.1	271			
		10.5 ± 0.4	296			
		9.2 ± 0.4	298			
		8.7 ± 0.2	323			
		8.7 ± 0.2	348			
		8.3 ± 0.2	370			

[a]Abbreviations used for the techniques are defined in table I-F-3.
[b]Placed on an absolute basis using $k(\mathrm{OH} + C_3H_8) = 1.05 \times 10^{-12}\,\mathrm{cm^3\ molecule^{-1}\ s^{-1}}$ (Atkinson et al., 2006).
[c]Placed on an absolute basis using $k(\mathrm{OH} + \textit{cyclo}\text{-}C_6H_{12}) = 6.97 \times 10^{-12}\,\mathrm{cm^3\ molecule^{-1}\ s^{-1}}$ (Calvert et al., 2008).
[d]Placed on an absolute basis using $k(\mathrm{OH} + \text{1-butanol}) = 8.5 \times 10^{-12}\,\mathrm{cm^3\ molecule^{-1}\ s^{-1}}$ (this book, section II-B-5.1; Atkinson et al., 2006).
[e]Placed on an absolute basis using $k(\mathrm{OH} + \text{1, 3-dioxolane}) = 1.0 \times 10^{-11}\,\mathrm{cm^3\ molecule^{-1}\ s^{-1}}$ (this book, section III-E-9.1).

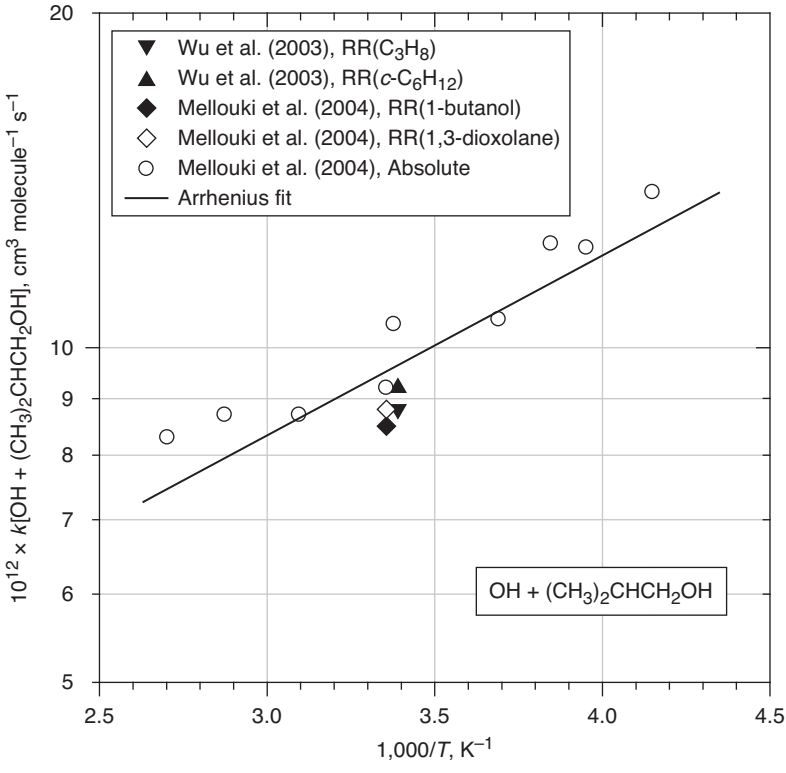

Figure II-B-15. Arrhenius plot of the rate coefficient for the reaction of OH with 2-methyl-1-propanol.

Table II-B-20. Rate coefficients (k, cm^3 $molecule^{-1}$ s^{-1}) for reaction of Cl with 2-methyl-1-propanol [$(CH_3)_2CHCH_2OH$]

$10^{10} \times k$	T (K)	Technique[a]	Reference
1.94 ± 0.04	295 ± 2	RR (C_3H_8)[b]	Wu et al. (2003)
2.11 ± 0.12	295 ± 2	RR (*cyclo*-C_6H_{12})[c]	

[a]Abbreviations used for the techniques are defined in table I-F-3.
[b]Placed on an absolute basis using $k(Cl + C_3H_8) = 1.4 \times 10^{-10}$ cm^3 $molecule^{-1}$ s^{-1} (Atkinson et al., 2006).
[c]Placed on an absolute basis using $k(Cl + cyclo\text{-}C_6H_{12}) = 3.3 \times 10^{-10}$ cm^3 $molecule^{-1}$ s^{-1} (Calvert et al., 2008).

the same as in methanol (1.35×10^{-13} cm^3 $molecule^{-1}$ s^{-1}; IUPAC, 2008), reaction of OH radicals with the —OH group in 2-methyl-1-propanol accounts for approximately 1.4% of the overall reaction. The reaction of OH with 2-methyl-1-propanol is expected to occur largely via H-atom abstraction from the —CH_2 and >CH groups with a lower contribution from the CH_3 groups.

$$OH + (CH_3)_2CHCH_2OH \rightarrow H_2O + (CH_3)_2CHCH_2O \quad (1)$$

$$OH + (CH_3)_2CHCH_2OH \rightarrow H_2O + (CH_3)_2CHCHOH \quad (2)$$

$$OH + (CH_3)_2CHCH_2OH \rightarrow H_2O + (CH_3)_2CCH_2OH \quad (3)$$

$$OH + (CH_3)_2CHCH_2OH \rightarrow H_2O + CH_2CH(CH_3)CH_2OH \quad (4)$$

The α-hydroxy alkyl radical formed by H-atom abstraction from —CH_2 group (channel 2) reacts with O_2 to form 2-methyl propanal, $(CH_3)_2CHCHO$. The hydroxyl alkyl radicals formed in channels 3 and 4 will add O_2 then react with NO to give the alkoxy radicals $(CH_3)_2C(O)CH_2OH$ and $OCH_2CH(CH_3)CH_2OH$. $(CH_3)_2C(O)CH_2OH$ radicals decompose to give acetone and formaldehyde. $OCH_2CH(CH_3)CH_2OH$ radicals react with O_2 to give $HC(O)CH(CH_3)CH_2OH$ and decompose to give $2CH_2O + CH_3CHO$.

II-B-8. 2-Methyl-2-Propanol [*tert*-Butyl Alcohol, $(CH_3)_3COH$]

II-B-8.1. OH Reaction Kinetics

The reaction of OH with 2-methyl-2-propanol has been studied by Wallington et al. (1988c), Saunders et al. (1994), Téton et al. (1996), and Wu et al. (2003). The measurements are given in table II-B-21 and shown in figure II-B-16. The temperature dependence of the reaction was measured by Wallington et al. (1988c) from 240 to 400 K and by Téton et al. (1996) from 253 to 372 K. There is evidence for curvature

Table II-B-21. Rate coefficients ($k = A\ e^{-B/T}$, cm^3 $molecule^{-1}$ s^{-1}) for reaction of OH with 2-methyl-2-propanol [$(CH_3)_3COH$]

$10^{12} \times A$	B (K)	$10^{12} \times k$	T (K)	Technique[a]	Reference	Temperature Range (K)
3.3 ± 1.6	310 ± 150	1.00 ± 0.06	240	FP–RF	Wallington et al. (1988c)	240–440
		1.07 ± 0.08	298			
		1.23 ± 0.08	350			
		1.63 ± 0.07	400			
		1.77 ± 0.17	440			
		0.81 ± 0.17	298	DF–LIF	Saunders et al. (1994)	
2.66 ± 0.48	270 ± 130	1.00 ± 0.08	253	PLP–LIF	Téton et al. (1996)	253–372
		1.00 ± 0.06	262			
		1.00 ± 0.06	273			
		1.02 ± 0.10	282			
		1.16 ± 0.10	294			
		1.08 ± 0.10	298 ± 1			
		1.08 ± 0.08	314			
		1.12 ± 0.06	322			
		1.14 ± 0.05	330			
		1.25 ± 0.06	345			
		1.28 ± 0.06	360			
		1.40 ± 0.08	372			
		1.08 ± 0.07	295 ± 2	RR (C_3H_8)[b]	Wu et al. (2003)	

[a]Abbreviations used for the techniques are defined in table I-F-3.
[b]Placed on an absolute basis using $k(OH + C_3H_8) = 1.05 \times 10^{-12}$ cm^3 $molecule^{-1}$ s^{-1} (Atkinson et al., 2006).

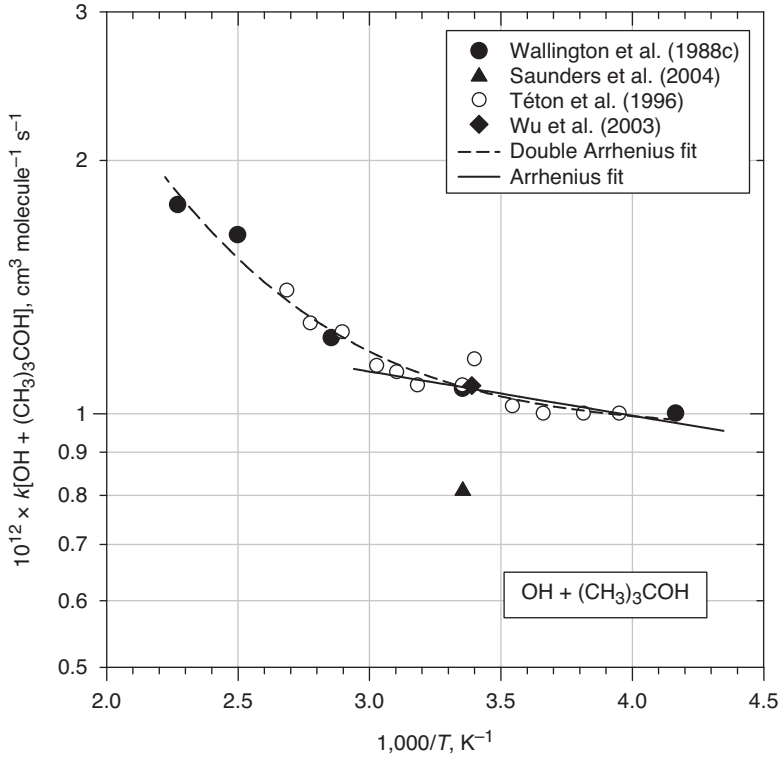

Figure II-B-16. Arrhenius plot of the rate coefficient for the reaction of OH with 2-methyl-2-propanol.

in both data sets. The data of Saunders et al. are somewhat lower than the other measurements which are otherwise in excellent agreement. A fit to the data of Wallington et al., Téton et al., and Wu et al. yields $k = 1.6 \times 10^{-12} \exp(-124/T)$ for temperatures below 314 K, giving $k = 1.1 \times 10^{-12}$ cm^3 molecule^{-1} s^{-1} at 298 K with an uncertainty estimated to be ±15%. In the temperature range 240–440 K, the best fit to the data is described by the expression:

$$k = 9.57 \times 10^{-13} + 5.65 \times 10^{-11} \times \exp(-1,836/T) \text{cm}^3 \text{ molecule}^{-1}\text{s}^{-1}$$

II-B-8.2. Cl-Atom Reaction Kinetics

The rate coefficient for the reaction of Cl with 2-methyl-2-propanol has been determined by Wallington et al. (1988g), Wallington and Hurley (1992), and Wu et al. (2003) using relative rate methods (see table II-B-22). The determinations are in excellent agreement. On the basis of these three studies, a value of $k[\text{Cl} + (\text{CH}_3)_3\text{COH}] = 3.5 \times 10^{-11}$ cm^3 molecule^{-1} s^{-1} is recommended at 298 K with an estimated uncertainty of ±15%.

Table II-B-22. Rate coefficients (k, cm^3 molecule^{-1} s^{-1}) for reaction of Cl with 2-methyl-2-propanol [$(CH_3)_3COH$]

$10^{11} \times k$	T (K)	Technique[a]	Reference
3.37 ± 0.20	295 ± 2	RR (C_2H_6)[b]	Wallington et al. (1988g)
3.67 ± 0.12	295 ± 2	RR (C_2H_6)[b]	Wallington and Hurley (1992)
3.61 ± 0.37			
3.37 ± 0.26	295 ± 2	RR (C_3H_8)[c]	Wu et al. (2003)
3.66 ± 0.28	295 ± 2	RR (*cyclo*-C_6H_{12})[d]	

[a]Abbreviations used for the techniques are defined in table I-F-3.
[b]Placed on an absolute basis using $k(Cl + C_2H_6) = 5.9 \times 10^{-11}$ cm^3 molecule^{-1} s^{-1} (Atkinson et al., 2006).
[c]Placed on an absolute basis using $k(Cl + C_3H_8) = 1.4 \times 10^{-10}$ cm^3 molecule^{-1} s^{-1} (Atkinson et al., 2006).
[d]Placed on an absolute basis using $k(Cl +$ *cyclo*-$C_6H_{12}) = 3.3 \times 10^{-10}$ cm^3 molecule^{-1} s^{-1} (Calvert et al., 2008).

II-B-8.3. Summary of the Atmospheric Fate of 2-Methyl-2-propanol

Combining k(OH + 2-methyl-2-propanol) = 1.1×10^{-12} cm^3 molecule^{-1} s^{-1} with [OH] = 1×10^6 molecule cm^{-3} gives an estimate of 11 days for the atmospheric lifetime of 2-methyl-2-propanol with respect to reaction with OH radicals. Japar et al. (1990) have studied the oxidation of 2-methyl-2-propanol. Since the OH and Cl reactions proceed by the same H-atom abstraction pathway, Japar et al. used the Cl-initiated reaction to study the degradation of 2-methyl-2-propanol. Japar et al. (1990) reported that the consumption of one molecule of the alcohol resulted in the formation of one molecule each of formaldehyde and acetone following the mechanism shown in figure II-B-17.

Japar et al. (1990) proposed that the atmospheric degradation of 2-methyl-2-propanol can be represented by the overall equation:

$$(CH_3)_3COH + OH + NO \rightarrow H_2CO + CH_3C(O)CH_3 + HO_2 + NO_2$$

II-B-9. 2,2-Dimethyl-1-Propanol [Neopentyl Alcohol, $(CH_3)_3CCH_2OH$]

II-B-9.1. OH Reaction Kinetics

The kinetics of the reaction of OH with 2,2-dimethyl-1-propanol has only been investigated by Tully (1990) at the time of this writing. The measurements are summarized in table II-B-23 and shown in figure II-B-18. The reaction has been studied using the laser photolysis–laser induced fluorescence at 750 Torr of helium pressure over the temperature range 293–764 K. As seen from figure II-B-18, there is pronounced curvature in the Arrhenius plot. A fit of the double Arrhenius expression to the entire data set gives $k = 3.10 \times 10^{-10} \exp(-2,930/T) + 4.80 \times 10^{-12} \exp(39/T)$ cm^3 molecule^{-1} s^{-1}. A fit of the Arrhenius expression to the data set below 377 K gives $k = 5.0 \times 10^{-12} \exp(28/T)$ cm^3 molecule^{-1} s^{-1}. This expression gives k(OH + 2, 2-dimethyl-1-propanol) = 5.5×10^{-12} cm^3 molecule^{-1} s^{-1} at 298 K with an estimated uncertainty of ±20%.

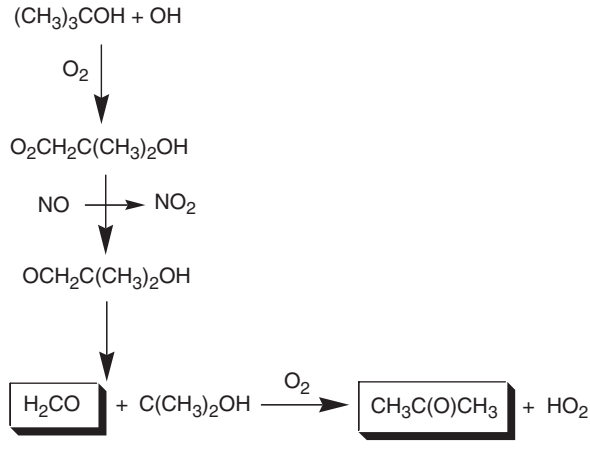

Figure II-B-17. OH-initiated oxidation of 2-methyl-2-propanol.

Table II-B-23. Rate coefficients (k, cm^3 $molecule^{-1}$ s^{-1}) for reaction of OH with 2,2-dimethyl-1-propanol [$(CH_3)_3CCH_2OH$]

$10^{12} \times k$	T (K)	Technique[a]	Reference	Temperature Range (K)
5.53 ± 0.24	293	PLP–LIF	Tully (1990)	293–764
5.41 ±0.24	327			
5.41 ± 0.25	377.5			
5.66 ± 0.35[b]	437.5			
5.78 ± 0.37[b]	456			
6.11 ± 0.38[b]	478			
6.08 ± 0.38[b]	501			
6.25 ± 0.40[b]	521.5			
6.42 ± 0.40[b]	546			
6.89 ± 0.73[b]	572			
7.42 ± 0.41	596			
7.47 ± 0.42	601			
7.83 ± 0.48	619.5			
8.82 ± 0.58	645			
9.08 ± 0.57	673			
10.4 ± 0.67	715.5			
11.6 ± 0.75	763.5			

[a]Abbreviations used for the techniques are defined in table I-F-3.
[b]*T*he decay of OH was nonexponential, data derived from the first 6 ms.

II-B-9.2. Summary of the Atmospheric Fate of 2,2-Dimethyl-1-propanol

Combining the rate coefficient k(OH + 2,2-dimethyl-1-propanol) = 5.5×10^{-12} cm^3 $molecule^{-1}$ s^{-1} at 298 K with [OH] = 10^6 molecule cm^{-3} provides an estimate of the atmospheric lifetime with respect to reaction with OH radicals of about 2 days.

Tully (1990) found that the reaction of OH with $(CH_3)_3CCH_2OH$ proceeds approximately 90% through H-atom abstraction from the —CH_2 group leading to $(CH_3)_3CCHO$ as the main product under atmospheric conditions.

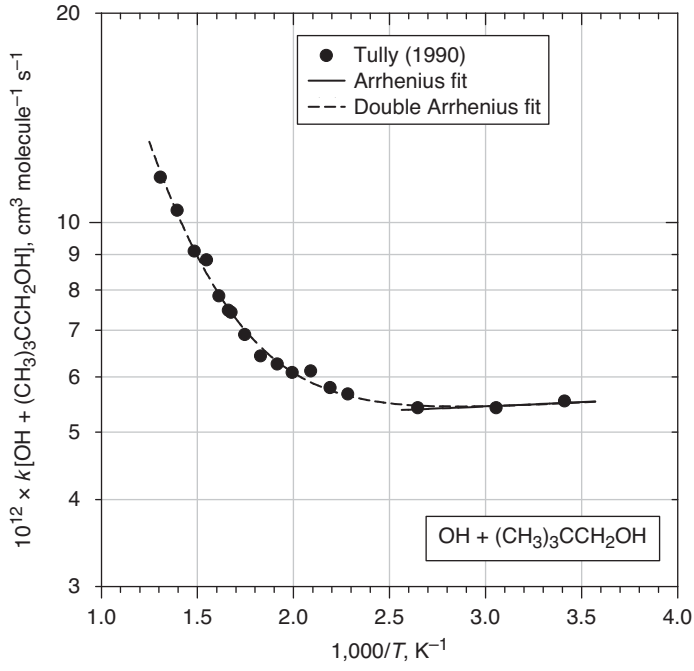

Figure II-B-18. Arrhenius plot of the rate coefficient for the reaction of OH with 2,2-dimethyl-1-propanol.

II-B-10. 1-Pentanol (*n*-Pentyl Alcohol, $CH_3CH_2CH_2CH_2CH_2OH$)

II-B-10.1. OH Reaction Kinetics

Measurements of the rate coefficient for the reaction of OH with 1-pentanol are given in table II-B-24. The studies have been conducted at room temperature using absolute and relative techniques. The values obtained by different authors are in good agreement, and an unweighted mean to these data provides our recommendation of $k(\mathrm{OH} + n\text{-}\mathrm{C_5H_{11}OH}) = 1.1 \times 10^{-11}$ cm^3 molecule^{-1} s^{-1} with an estimated uncertainty of $\pm 15\%$ at 298 K.

II-B-10.2. Cl-Atom Reaction Kinetics

The reaction of Cl with 1-pentanol has been studied by three groups. The rate coefficients values obtained by relative and absolute techniques are presented in table II-B-25 and shown in figure II-B-19. The values near room temperature are in very good agreement. The only study of the temperature dependence is that by Garzón et al. (2006) over the range 264–381 K. A fit to the combined data presented in table II-B-25 gives $k(\mathrm{Cl} + n\text{-}\mathrm{C_5H_{11}OH}) = 3.7 \times 10^{-11} \exp(563/T)$ cm^3 molecule^{-1} s^{-1} in the range 264–381 K. This expression gives $k(\mathrm{Cl} + n\text{-}\mathrm{C_5H_{11}OH}) = 2.4 \times 10^{-10}$ cm^3 molecule^{-1} s^{-1} at 298 K with an uncertainty estimated to be $\pm 15\%$.

Table II-B-24. Rate coefficients (k, cm^3 molecule^{-1} s^{-1}) for reaction of OH with 1-pentanol (n-$C_5H_{11}OH$)

$10^{12} \times k$	T (K)	Technique[a]	Reference
10.8 ± 1.1	296	FP–RF	Wallington and Kurylo (1987b)
12.0 ± 1.6	298 ± 2	PR–UV abs.	Nelson et al. (1990a)
9.8 ± 1.2		RR (*cyclo*-C_6H_{12})[b]	
10.3 ± 1.1	298	RR (*cyclo*-C_6H_{12})[b]	Cavalli et al. (2000a)
11.6 ± 0.6	298 ± 2	RR (*cyclo*-C_6H_{12})	Oh and Andino (2001)
14.0 ± 0.7		RR (*p*-xylene)[c]	
12.4 ± 1.0	295 ± 2	RR (C_3H_8)[d]	Wu et al. (2003)
12.0 ± 0.5		RR (*cyclo*-C_6H_{12})[b]	

[a]Abbreviations used for the techniques are defined in table I-F-3.
[b]Placed on an absolute basis using $k(\text{OH} + \textit{cyclo}\text{-}C_6H_{12}) = 6.97 \times 10^{-12}$ cm^3 molecule^{-1} s^{-1} (Calvert et al., 2008).
[c]Placed on an absolute basis using $k(\text{OH} + p\text{-xylene}) = 1.43 \times 10^{-11}$ cm^3 molecule^{-1} s^{-1} (Calvert et al., 2002).
[d]Placed on an absolute basis using $k(\text{OH} + C_3H_8) = 1.1 \times 10^{-12}$ cm^3 molecule^{-1} s^{-1} (Atkinson et al., 2006).

Table II-B-25. Rate coefficients ($k = A\ e^{-B/T}$, cm^3 molecule^{-1} s^{-1}) for reaction of Cl with 1-pentanol (n-$C_5H_{11}OH$)

$10^{11} \times A$	B (K)	$10^{10} \times k$	T (K)	Technique[a]	Reference	Temperature Range (K)
		2.63 ± 0.14	298 ± 2	RR (*cyclo*-C_6H_{12})[b]	Nelson et al. (1990a)	
		2.75 ± 0.27	295 ± 2	RR (C_3H_8)[c]	Wu et al. (2003)	
		2.77 ± 0.13	295 ± 2	RR (*cyclo*-C_6H_{12})[b]		
3.97 ± 0.48	−(533 ± 77)	3.01 ± 0.22	264	PLP–RF	Garzón et al. (2006)	264–381
		2.59 ± 0.10	282			
		2.37 ± 0.29	298			
		2.20 ± 0.08	311			
		2.19 ± 0.36	329			
		1.80 ± 0.06	343			
		1.72 ± 0.06	353			
		1.70 ± 0.06	381			

[a]Abbreviations used for the techniques are defined in table I-F-3.
[b]Placed on an absolute basis using $k(\text{Cl} + \textit{cyclo}\text{-}C_6H_{12}) = 3.3 \times 10^{-10}$ cm^3 molecule^{-1} s^{-1} (Calvert et al., 2008).
[c]Placed on an absolute basis using $k(\text{Cl} + C_3H_8) = 1.4 \times 10^{-10}$ cm^3 molecule^{-1} s^{-1} (Atkinson et al., 2006).

II-B-10.3. Summary of the Atmospheric Fate of 1-Pentanol

The atmospheric lifetime with respect to reaction with OH radicals is calculated to be about 10 h by combining the rate coefficient $k(\text{OH} + n\text{-}C_5H_{11}OH) = (1.1 \pm 0.2) \times 10^{-11}$ cm^3 molecule^{-1} s^{-1} with [OH] = 2.5×10^6 molecule cm^{-3}. The OH-initiated oxidation of 1-pentanol has been investigated by Cavalli et al. (2000a). The main products reported were pentanal (40.5 ± 8.2%), butanal (16.1 ± 3.7%), propanal (8.1 ± 1.9%), acetaldehyde (18.1 ± 4.2%), and formaldehyde (25.1 ± 1.3%). Pentanal, butanal, and propanal are formed following H-atom abstraction from —CH_2 groups, α, β, and γ to the alcohol group, respectively. H-atom abstraction from the —CH_2 group δ to the alcohol group leads to the formation of the $CH_3CH(O)CH_2CH_2CH_2OH$

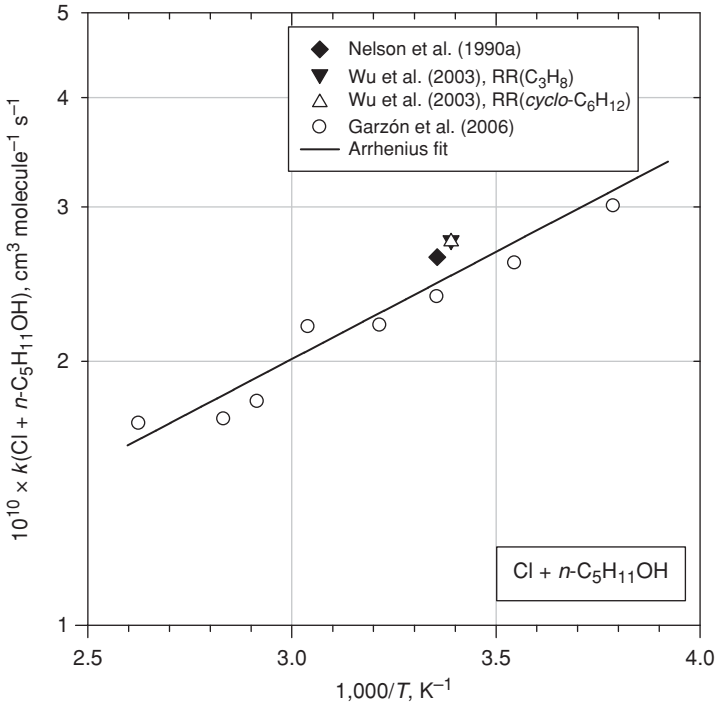

Figure II-B-19. Arrhenius plot of the rate coefficient for the reaction of Cl with *n*-pentanol.

alkoxy radical. This radical is expected to undergo isomerization via a 1,5 hydrogen shift to give the α-hydroxyl alkyl radical $CH_3CH(OH)CH_2CH_2CHOH$ which will react with O_2 to give 4-hydroxypentanal. Cavalli et al. (2000a) did not identify 4-hydroxypentanal as a product in their study. Small amounts of 1-hydroxy-3-pentanone and 3-hydroxypropanal are expected from the H-atom abstraction from the γ- position. On the basis of their experimental results, Cavalli et al. recommended the following expression to represent the atmospheric oxidation of 1-pentanol for the purpose of modelling urban air masses:

$$CH_3CH_2CH_2CH_2CH_2OH + OH \xrightarrow{0.78\ NO}$$

$$0.44\ CH_3CH_2CH_2CH_2C(O)H + 0.16\ CH_3CH_2CH_2C(O)H + 0.02\ HOCH_2CH_2CH_2C(O)CH_2OH +$$
$$0.09\ CH_3CH_2C(O)H + 0.02\ HOCH_2C(O)H + 0.18\ HOCH_2CH_2C(O)H +$$
$$0.05\ CH_3C(O)CH_2CH_2CH_2OH +$$
$$0.18\ CH_3C(O)H + 0.3\ HCHO + 0.87\ HO_2 + 0.72\ NO_2 + 0.06\ RONO_2$$

II-B-11. 2-Pentanol [$CH_3CH(OH)CH_2CH_2CH_3$]

II-B-11.1. OH Reaction Kinetics

The rate coefficient for reaction of OH with 2-pentanol has been measured by Wallington et al. (1988d) using the flash photolysis–resonance fluorescence technique, and by Baxley and Wells (1998) using a relative rate method with two reference compounds (see table II-B-26). The measurement of Baxley and Wells relative to dodecane agrees very well with the absolute measurement of Wallington et al. (1988d), while that relative to heptane is some 20% lower. On the basis of these measurements, an average value is recommended, $k = 1.1 \times 10^{-11}$ cm^3 molecule^{-1} s^{-1} at 298 K with an estimated uncertainty of ±20%.

II-B-11.2. Cl-Atom Reaction Kinetics

The rate coefficient for reaction of Cl with 2-pentanol has been measured by Ballesteros et al. (2007) using a relative rate method at atmospheric pressure. The value obtained at 298 K relative to the reaction of Cl with 1,3-butadiene [k(Cl + 1,3-butadiene) = 2.51×10^{-10}] is k(Cl + 2-pentanol) = 2.2×10^{-10} cm^3 molecule^{-1} s^{-1} with an uncertainty estimated to be ± 25%.

II-B-11.3. Summary of the Atmospheric Fate of 2-Pentanol

Combining the rate coefficient $k = 1.1 \times 10^{-11}$cm^3 molecule^{-1} s^{-1} with an average concentration of [OH] = 2.5×10^6 molecule cm^{-3} provides an estimate of approximately 10 h for the atmospheric lifetime of 2-pentanol with respect to reaction with OH radicals.

Baxley and Wells (1998) conducted a study of the OH-initiated oxidation of 2-pentanol. The main products observed were 2-pentanone (41 ± 4%), propanal (14 ± 2%), and acetaldehyde (40 ± 4%). 2-Pentanone is produced following H-atom abstraction from the —CH group in the α-position, while propanal and acetaldehyde can be formed as co-products following the H-atom abstraction from —CH_2 group in the β-position. Acetaldehyde may be also a product arising from the attack of the —CH_2 group in the γ-position. 4-Hydroxy-2-pentanone, $CH_3C(O)CH_2CH(OH)CH_3$, could also be formed from the H-atom abstraction from γ-position. Isomerization of the $CH_3C(O)CH_2CH(OH)CH_3$ radical is not excluded. H-atom abstraction from the two

Table II-B-26. Rate coefficient (k, cm^3 molecule^{-1} s^{-1}) for reaction of OH with 2-pentanol [$CH_3CH(OH)CH_2CH_2CH_3$]

$10^{12} \times k$	T (K)	Technique[a]	Reference
11.8 ± 0.8	298	FP–RF	Wallington et al. (1988d)
9.4 ± 1.1	297 ± 3	RR (n-C_7H_{16})[b]	Baxley and Wells (1998)
11.9 ± 0.8		RR (n-$C_{12}H_{26}$)[c]	

[a]Abbreviations used for the techniques are defined in table I-F-3.
[b]Placed on an absolute basis using k(OH + n-C_7H_{16}) = 6.50×10^{-12} cm^3 molecule^{-1} s^{-1} (Calvert et al., 2008).
[c]Placed on an absolute basis using k(OH + n-$C_{12}H_{26}$) = 1.36×10^{-11} cm^3 molecule^{-1} s^{-1} (Calvert et al., 2008).

different CH_3 groups, which are expected to be minor processes, leads to other carbonyls via the decomposition of the intermediate alkoxy radicals and/or their reaction with O_2.

II-B-12. 3-Pentanol [$CH_3CH_2CH(OH)CH_2CH_3$]

II-B-12.1. OH Reaction Kinetics

The reaction of OH with 3-pentanol has been investigated by Wallington et al. (1988d) using the flash photolysis–resonance fluorescence technique and Hurley et al. (2008) using a relativerate method. As shown in table II-B-27, the data obtained are in very good agreement. The average value from these measurements is a recommended value of $k = 1.3 \times 10^{-11}$ cm^3 molecule^{-1} s^{-1} with an uncertainty of ±15% at 298 K.

II-B-12.2. Cl-Atom Reaction Kinetics

The reaction of Cl with 3-pentanol has been studied by Hurley et al. (2008) using a relative rate method at 700 Torr of air and 296 K. As shown in table II-B-28, the data obtained with two references are in agreement leading to a recommended rate coefficient value of $k = 2.0 \times 10^{-10}$ cm^3 molecule^{-1} s^{-1} with an uncertainty of ±25% at 298 K.

II-B-12.3. Summary of the Atmospheric Fate of 3-Pentanol

Using $k = 1.3 \times 10^{-11}$ cm^3 molecule^{-1} s^{-1} and [OH] = 2.5×10^6 molecule cm^{-3} the atmospheric lifetime of 3-pentanol with respect to reaction with OH radicals is

Table II-B-27. Rate coefficients (k, cm^3 molecule^{-1} s^{-1}) for the reaction of OH with 3-pentanol [$CH_3CH_2CH(OH)CH_2CH_3$]

$10^{11} \times k$	T (K)	Technique[a]	Reference
1.22 ± 0.07	298	FP–RF	Wallington et al. (1988d)
1.27 ± 0.12	296 ± 2	RR (C_2H_4)[b]	Hurley et al. (2008)
1.36 ± 0.15	296 ± 2	RR (C_2H_2)[c]	

[a]Abbreviations used for the techniques are defined in table I-F-3.
[b]Placed on an absolute basis using $k(OH + C_2H_4) = 7.9 \times 10^{-12}$ cm^3 molecule^{-1} s^{-1} (Atkinson et al., 2006).
[c]Placed on an absolute basis using $k(OH + C_3H_6) = 2.9 \times 10^{-11}$ cm^3 molecule^{-1} s^{-1} (Atkinson et al., 2006).

Table II-B-28. Rate coefficients (k, cm^3 molecule^{-1} s^{-1}) for the reaction of Cl with 3-pentanol [$CH_3CH_2CH(OH)CH_2CH_3$]

$10^{10} \times k$	T (K)	Technique[a]	Reference
2.1 ± 0.2	296 ± 2	RR (C_2H_4)[b]	Hurley et al. (2008)
1.8 ± 0.2	296 ± 2	RR (C_3H_6)[c]	

[a]Abbreviations used for the techniques are defined in table I-F-3.
[b]Placed on an absolute basis using $k(Cl + C_2H_4) = 9.5 \times 10^{-11}$ cm^3 molecule^{-1} s^{-1} (this book, section I-F-1.).
[c]Placed on an absolute basis using $k(Cl + C_3H_6) = 2.3 \times 10^{-10}$ cm^3 molecule^{-1} s^{-1} (IUPAC, 2008).

calculated to be about 9 h. The OH-initiated oxidation of 3-pentanol in the presence of NO_x has been investigated by Hurley et al. (2008). The primary products were found to be (with molar yields): 3-pentanone (58 ± 3%), propanal (28 ± 2%), and acetaldehyde (37 ± 2%). These product yields were found to be independent of oxygen concentration over the partial pressure range 10–700 Torr.

As discussed by Hurley et al. (2008), the reaction of OH radicals with 3-pentanol proceeds via three channels:

$$OH + CH_3CH_2CH(OH)CH_2CH_3 \rightarrow H_2O + CH_3CH_2C(OH)CH_2CH_3 \quad (a)$$

$$OH + CH_3CH_2CH(OH)CH_2CH_3 \rightarrow H_2O + CH_3CHCH(OH)CH_2CH_3 \quad (b)$$

$$OH + CH_3CH_2CH(OH)CH_2CH_3 \rightarrow H_2O + CH_2CH_2CH(OH)CH_2CH_3 \quad (c)$$

By analogy to the behavior of other hydroxyalkyl radicals, the α-hydroxyalkyl radical formed via channel (a) is expected to react exclusively with O_2 to form 3-pentanone

$$CH_3CH_2C(OH)CH_2CH_3 + O_2 \rightarrow CH_3CH_2C(O)CH_2CH_3 + HO_2$$

Hence, channel (a) represents (58 ± 3%) of the reaction of OH with 3-pentanol. The only source of acetaldehyde as a primary product is decomposition of the $CH_3CH(O)CH(OH)CH_2CH_3$ formed through the reaction of $CH_3CHCH(OH)CH_2CH_3$ (from channel b) with O_2/NO. The decomposition of $CH_3CH(O)CH(OH)CH_2CH_3$ is expected to lead to equal amounts of acetaldehyde and propionaldehyde suggesting that channel (b) represents at least (28 ± 2%) of the OH reaction with 3-pentanol (Hurley et al., 2008).

Hurley et al. (2008) have also reported the products of the reaction of the chlorine-atom-initiated oxidation of 3-pentanol in the presence and absence of NO_x. The main products observed in the absence of NO_x were: 3-pentanone (26 ± 2%), propionaldehyde (12 ± 2%), acetaldehyde (13 ± 2%), and formaldehyde (2 ± 1%). The primary products observed in the presence of NO_x were 3-pentanone (51 ± 4%), propionaldehyde (39 ± 2%), acetaldehyde (44 ± 4%), and formaldehyde (4 ± 1%).

II-B-13. 3-Methyl-1-Butanol [Isopentyl Alcohol, $CH_3CH(CH_3)CH_2CH_2OH$]

II-B-13.1. OH Reaction Kinetics

Measurements of the rate coefficient for reaction of OH with 3-methyl-1-butanol are given in table II-B-29 and shown in figure II-B-20. This reaction has been investigated by Saunders et al. (1994) using the discharge flow technique, Wu et al. (2003) using a relative rate method, and Mellouki et al. (2004) using both relative rate and pulsed laser photolysis–laser induced fluorescence methods. The measurements near 298 K are in agreement within the reported uncertainties. There is some evidence for slight curvature in the temperature data set. For atmospheric purposes, a fit of the Arrhenius expression to the combined data set at room temperature and those from Mellouki

Table II-B-29. Rate coefficients (cm^3 $molecule^{-1}$ s^{-1}) for the reaction of OH with 3-methyl-1-butanol [$(CH_3)_2CHCH_2CH_2OH$]

$10^{12} \times A$	B (K)	$10^{12} \times k$	T (K)	Technique[a]	Reference	Temperature Range (K)
		13.1 ± 2.6	298	DF–LIF	Saunders et al. (1994)	
		14.1 ± 0.5	295 ± 2	RR (C_3H_8)[b]	Wu et al. (2003)	
		12.7 ± 1.1		RR (*cyclo*-C_6H_{12})[c]		
		12.5 ± 1.3	298 ± 2	RR (1-butanol)[d]	Mellouki et al. (2004)	
		13.6 ± 1.4		RR (1,3-dioxolane)[e]		
		14.1 ± 1.6		RR (isobutyl alcohol)[f]		
2.8 ± 0.9	-503 ± 98	19.1 ± 0.9	263	PLP–LIF	Mellouki et al. (2004)	263–368
		17.7 ± 0.2	272			
		15.0 ± 1.0	297 ± 1			
		12.8 ± 0.3	322			
		11.6 ± 0.3	353			
		11.3 ± 0.4	368			

[a]Abbreviations used for the techniques are defined in table I-F-3.
[b]Placed on an absolute basis using $k(OH + C_3H_8) = 1.1 \times 10^{-12}$ cm^3 $molecule^{-1}$ s^{-1} (Calvert et al., 2008).
[c]Placed on an absolute basis using $k(OH + cyclo\text{-}C_6H_{12}) = 6.97 \times 10^{-12}$ cm^3 $molecule^{-1}$ s^{-1} (Calvert et al., 2008).
[d]Placed on an absolute basis using $k(OH + 1\text{-butanol}) = 8.2 \times 10^{-12}$ cm^3 $molecule^{-1}$ s^{-1} (this book, section II-B-5.1).
[e]Placed on an absolute basis using $k(OH + 1, 3\text{-dioxolane}) = 1.0 \times 10^{-11}$ cm^3 $molecule^{-1}$ s^{-1} (this book, section III-E-9.1).
[f]Placed on an absolute basis using $k(OH + isobutyl\ alcohol) = 9.6 \times 10^{-12}$ cm^3 $molecule^{-1}$ s^{-1} (this book, section II-B-7.1).

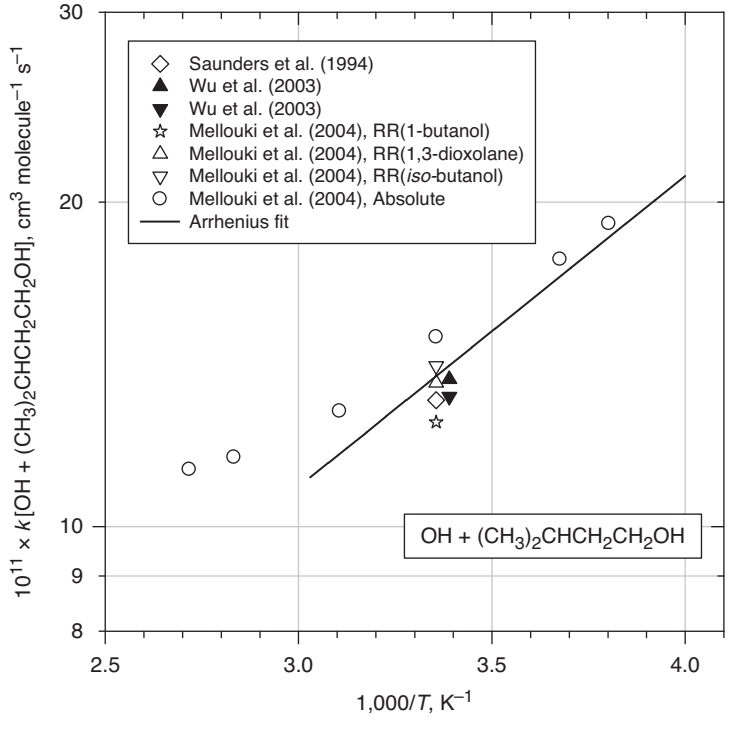

Figure II-B-20. Arrhenius plot of the rate coefficient for the reaction of OH with 3-methyl-1-butanol.

et al. below 322 K gives $k(\text{OH} + \text{3-methyl-1-butanol}) = 1.5 \times 10^{-12} \exp(664/T)\,\text{cm}^3$ molecule^{-1} s^{-1}. This expression gives $k = 1.4 \times 10^{-11}\,\text{cm}^3$ molecule^{-1} s^{-1} at 298 K with an uncertainty estimated to be ±15%.

II-B-13.2. Cl-Atom Reaction Kinetics

Wu et al. (2003) conducted a relative rate study of $k(\text{Cl} + \text{3-methyl-1-butanol})$ using propane and cyclohexane as reference compounds. As seen in table II-B-30, the results obtained using the two different references are in good agreement. We recommend a value of $k = 2.5 \times 10^{-11}\text{cm}^3$ molecule^{-1} s^{-1} at 298 K with an uncertainty of ± 20%.

II-B-13.3. Summary of the Atmospheric Fate of 3-Methyl-1-butanol

The atmospheric lifetime with respect to reaction with OH radicals is about 8 h. As with all saturated alcohols, the reaction of OH with 3-methyl-1-butanol proceeds mainly by H-atom abstraction from CH_3, —CH_2 and $\rangle$CH groups. Using the SAR method with parameters from Bethel et al. (2001b), [F(—CH_2—) = F($\rangle$CH—) = F($\rangle$C$\langle$) = 1.23, F(—OH) = 2.9, and F(—CH_2OH) = F($\rangle$CHOH) = F($\rangle$C(OH)— = 2.6], values of 36%, 32%, and 26% can be estimated for the fraction of reaction of OH radicals with 3-methyl-1-butanol that proceeds via H-atom abstraction from the α-, β-, and γ-positions, respectively. H-atom abstraction from CH_3 and OH groups is estimated to contribute less than 6% to the overall reaction. Hence, the main products expected from the reaction of OH with 3-methyl-1-butanol are $(CH_3)_2CHCH_2CHO$, $(CH_3)_2CHCHO$, and $CH_3C(O)CH_3$. Formaldehyde will also be a major co-product of both $(CH_3)_2CHCHO$ and $CH_3C(O)CH_3$.

II-B-14. 2-Methyl-2-Butanol [*tert*-Amyl Alcohol, $(CH_3)_2C(OH)CH_2CH_3$]

II-B-14.1. OH Reaction Kinetics

Jiménez at al. (2005b) measured rate coefficients as a function of temperature at 263–354 K using pulsed laser photolysis combined with pulsed laser induced fluorescence. The results from Jiménez at al. (2005b) are presented in table II-B-31 and shown in figure II-B-21. An Arrhenius fit to the data gives $k = 2.0 \times 10^{-12}\exp(160/T)\,\text{cm}^3$ molecule^{-1} s^{-1}. This expression gives $k = 3.4 \times 10^{-12}\,\text{cm}^3$ molecule^{-1} s^{-1} at 298 K with an uncertainty estimated to be ±30%.

Table II-B-30. Rate coefficients (cm^3 molecule^{-1} s^{-1}) for reaction of Cl with 3-methyl-1-butanol [$(CH_3)_2CHCH_2CH_2OH$]

$10^{10} \times k$	T (K)	Technique[a]	Reference
2.53 ± 0.07	295 ± 2	RR (C_3H_8)[b]	Wu et al. (2003)
2.53 ± 0.10	295 ± 2	RR (*cyclo*-C_6H_{12})[c]	

[a]Abbreviations used for the techniques are defined in table I-F-3.
[b]Placed on an absolute basis using $k(\text{Cl} + C_3H_8) = 1.4 \times 10^{-10}\,\text{cm}^3$ molecule^{-1} s^{-1} (Atkinson et al., 2006).
[c]Placed on an absolute basis using $k(\text{Cl} + \textit{cyclo}\text{-}C_6H_{12}) = 3.3 \times 10^{-10}\,\text{cm}^3$ molecule^{-1} s^{-1} (Calvert et al., 2008).

Table II-B-31. Rate coefficients (k, cm^3 molecule^{-1} s^{-1}) for reaction of OH with 2-methyl-2-butanol [$(CH_3)_2C(OH)CH_2CH_3$]

$10^{12} \times A$	B (K)	$10^{12} \times k$	T (K)	Technique[a]	Reference	Temperature Range (K)
2.37 ± 1.70	−115 ± 210	3.91 ± 0.98	263	PLP–LIF	Jiménez et al. (2005b)	263–354
		3.58 ± 0.34	266			
		3.39 ± 0.80	268			
		3.89 ± 1.10	278			
		3.85 ± 0.80	283			
		3.15 ± 0.80	288			
		3.64 ± 0.60	298			
		3.00 ± 0.60	303			
		3.94 ± 0.32	313			
		2.84 ± 0.98	321			
		3.67 ± 0.24	334			
		2.78 ± 0.06	343			
		3.78 ± 0.52	354			

[a]Abbreviations used for the techniques are defined in table I-F-3.

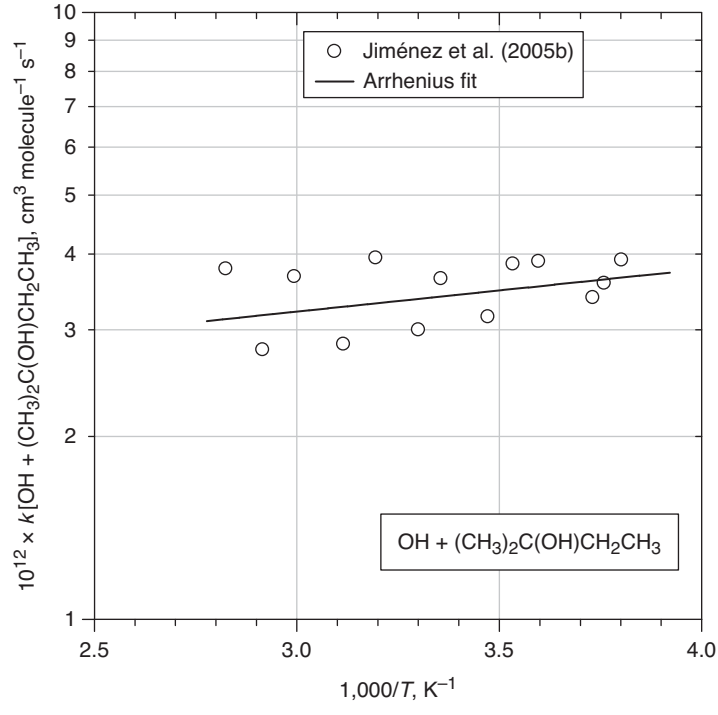

Figure II-B-21. Arrhenius plot of the rate coefficient for the reaction of OH with 2-methyl-2-butanol.

II-B-14.2. Cl-Atom Reaction Kinetics

The reaction of Cl with 2-methyl-2-butanol has been investigated by Ballesteros et al. (2007) using both relative and absolute techniques. Data obtained at 269–352 K are summarized in table II-B-32 and displayed in figure II-B-22. Fitting the Arrhenius expression to the combined data set gives $k(\mathrm{Cl} + \text{2-methyl-2-butanol}) = 2.4 \times 10^{-11} \times \exp(331/T)$, with $k = 7.3 \times 10^{-11}\,\mathrm{cm^3\ molecule^{-1}\ s^{-1}}$ at 298 K. An uncertainty of ±25% is assigned to the 298 K value.

II-B-14.3. Summary of the Atmospheric Fate of 2-Methyl-2-butanol

Combining $k(\mathrm{OH} + \text{2-methyl-2-butanol}) = 3.4 \times 10^{-12}\,\mathrm{cm^3\ molecule^{-1}\ s^{-1}}$ with a diurnal average $[\mathrm{OH}] = 10^6\ \mathrm{molecule\,cm^{-3}}$ provides an estimate of 3 days for the atmospheric lifetime of 2-methyl-2-butanol with respect to reaction with OH. An SAR calculation using the parameters from Kwok and Atkinson (1995) and Bethel et al. (2001b), indicates that the reaction of OH with $(CH_3)_2C(OH)CH_2CH_3$ proceeds via H-atom abstraction: ∼70% at the —CH_2 site, ∼20% at the α-CH_3 groups, ∼5% at the β-CH_3 group and ∼5% at the —OH group. Abstraction from the —CH_2 site probably leads to the formation of $CH_3C(O)CH_3$ and CH_3CHO as main products. Abstraction from the α-CH_3 groups may produce $CH_3C(O)CH_2CH_3$. Finally, hydrogen abstraction from the alcohol functionality will lead mostly to $CH_3C(O)CH_3$ and CH_3CHO.

Table II-B-32. Rate coefficients ($k = A\ \mathrm{e}^{-B/T}, \mathrm{cm^3\ molecule^{-1}\ s^{-1}}$) for reaction of Cl with 2-methyl-2-butanol [$(CH_3)_2C(OH)CH_2CH_3$]

$10^{11} \times A$	B (K)	$10^{11} \times k$	T (K)	Technique[a]	Reference	Temperature Range (K)
		7.0 ± 2.2	298 ± 2	RR [$(CH_3)_3CCl$][b]	Ballesteros et al. (2007)	
2.48 ± 0.17	−328 ± 42	7.92 ± 0.72	269	PLP–RF	Ballesteros et al. (2007)	269–352
		8.20 ± 0.89	269			
		8.65 ± 1.14	269			
		8.04 ± 0.89	280			
		8.13 ± 0.76	280			
		7.63 ± 0.69	290			
		7.50 ± 1.69	290			
		7.55 ± 0.92	298			
		7.66 ± 1.20	298			
		7.47 ± 0.60	299			
		7.28 ± 0.80	300			
		6.82 ± 0.36	323			
		6.81 ± 0.38	323			
		6.28 ± 0.86	352			
		6.12 ± 0.66	352			

[a]Abbreviations used for the techniques are defined in table I-F-3.
[b]Placed on an absolute basis using $k[\mathrm{Cl} + (CH_3)_3CCl] = 1.3 \times 10^{-11}\,\mathrm{cm^3\ molecule^{-1}\ s^{-1}}$ (Donaghy et al., 1993).

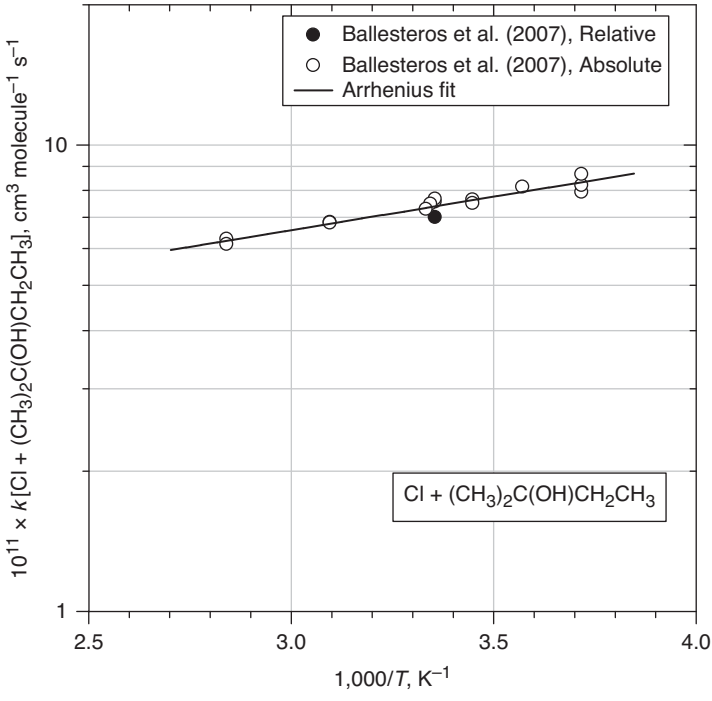

Figure II-B-22. Arrhenius plot of the rate coefficient for the reaction of Cl with 2-methyl-2-butanol.

II-B-15. 3-Methyl-2-Butanol [$CH_3CH(OH)CH(CH_3)_2$]

II-B-15.1. OH Reaction Kinetics

The reaction of OH with 3-methyl-2-butanol has been studied at 298 K by Wallington et al. (1988d) and Mellouki et al. (2004) using relative and absolute rate methods. The measurements, which are in excellent agreement, are given in table II-B-33, and shown in figure II-B-23. A fit to the combined data set gives k(OH + 3-methyl-2-butanol) = 2.5×10^{-12} exp(464/T) cm^3 molecule^{-1} s^{-1}. This expression gives k(OH + 3-methyl-2-butanol) = 1.2×10^{-11} cm^3 molecule^{-1} s^{-1} at 298 K with an uncertainty estimated to be ±15%.

II-B-15.2. Cl-Atom Reaction Kinetics

The reaction of Cl with 3-methyl-2-butanol has been studied by Ballesteros et al. (2007) using both the absolute and relative methods. The data obtained in the temperature range 269–385 K are summarized in table II-B-34 and shown in figure II-B-24. Fitting the Arrhenius expression to the combined data set yields k(Cl + 3-methyl-2-butanol) = 6.6×10^{-11} exp(177/T) with $k = 1.2 \times 10^{-11}$ cm^3 molecule^{-1} s^{-1} at 298 K. An uncertainty of ±25% is assigned to the 298 K value.

Table II-B-33. Rate coefficients ($k = A\ e^{-B/T}$, cm^3 $molecule^{-1}$ s^{-1}) for the reaction of OH with 3-methyl-2-butanol [$CH_3CH(OH)CH(CH_3)_2$]

$10^{12} \times A$	B (K)	$10^{12} \times k$	T (K)	Technique[a]	Reference	Temperature Range (K)
		12.4 ± 0.7	298	FP–RF	Wallington et al. (1988d)	
		11.8 ± 1.4	298	RR (1-butanol)[b]	Mellouki et al. (2004)	
		11.6 ± 1.1		RR (1,3-dioxolane)[c]		
2.6 ± 0.6	-456 ± 65	15.2 ± 0.8	254	PLP–LIF	Mellouki et al. (2004)	254–373
		14.2 ± 1.2	263			
		14.1 ± 0.6	273			
		12.6 ± 0.5	283			
		11.9 ± 0.6	298			
		10.6 ± 0.4	326			
		9.5 ± 0.4	352			
		9.5 ± 0.5	366			
		7.9 ± 0.8	373			

[a]Abbreviations used for the techniques are defined in table I-F-3.
[b]Placed on an absolute basis using $k(OH + 1\text{-butanol}) = 8.5 \times 10^{-12}$ cm^3 $molecule^{-1}$ s^{-1} (this book, section II-B-5.1).
[c]Placed on an absolute basis using $k(OH + 1, 3\text{-dioxolane}) = 1.0 \times 10^{-10}$ cm^3 $molecule^{-1}$ s^{-1} (this book, section III-E-9.1).

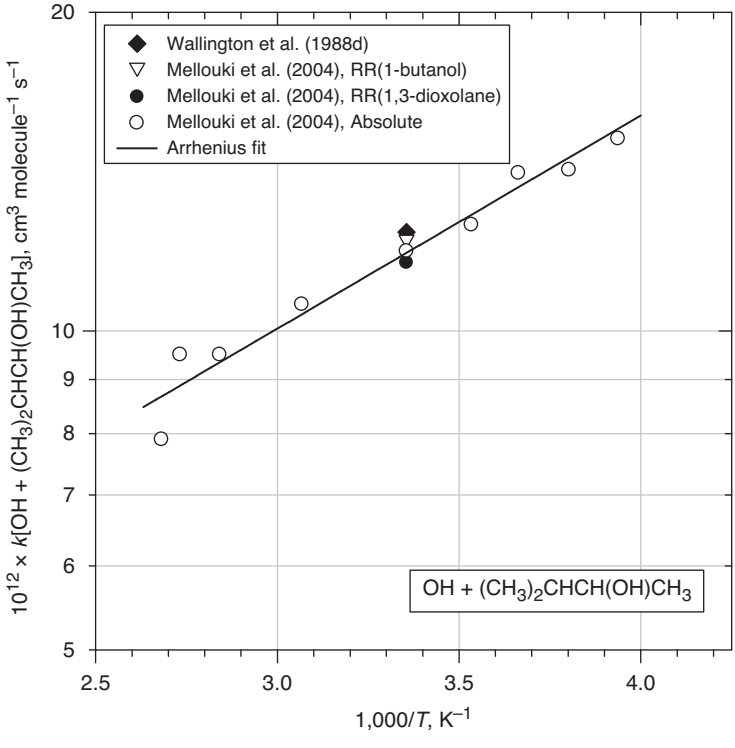

Figure II-B-23. Arrhenius plot of the rate coefficient for the reaction of OH with 3-methyl-2-butanol.

Table II-B-34. Rate coefficients (k, cm^3 molecule^{-1} s^{-1}) for the reaction of Cl with 3-methyl-2-butanol [$CH_3CH(OH)CH(CH_3)_2$]

$10^{11} \times A$	B (K)	$10^{10} \times k$	T (K)	Technique[a]	Reference	Temperature Range (K)
		1.41 ± 0.24	298 ± 2	RR (1,3-butadiene)[b]	Ballesteros et al. (2007)	
		1.70 ± 0.07	298 ± 2	RR (C_3H_6)[c]		
6.29 ± 0.57	-192 ± 56	1.22 ± 0.16	269	PLP–RF	Ballesteros et al. (2007)	269–385
		1.22 ± 0.16	271			
		1.30 ± 0.14	283			
		1.19 ± 0.12	283			
		1.29 ± 0.06	283			
		1.25 ± 0.35	283			
		1.14 ± 0.25	298			
		1.13 ± 0.11	299			
		1.14 ± 0.18	301			
		1.11 ± 0.11	301			
		1.14 ± 0.17	318			
		1.09 ± 0.18	318			
		1.05 ± 0.08	337			
		1.08 ± 0.11	337			
		1.11 ± 0.08	358			
		1.10 ± 0.23	358			
		1.04 ± 0.07	385			
		1.07 ± 0.13	385			

[a]Abbreviations used for the techniques are defined in table I-F-3.
[b]Placed on an absolute basis using $k(\text{Cl} + \text{1,3-butadiene}) = 2.51 \times 10^{-10}$ cm^3 molecule^{-1} s^{-1} (Stutz et al., 1998).
[c]Placed on an absolute basis using $k(\text{Cl} + C_3H_6) = 2.3 \times 10^{-10}$ cm^3 molecule^{-1} s^{-1} (IUPAC, 2008).

II-B-15.3. Summary of the Atmospheric Fate of 3-Methyl-2-butanol

An atmospheric lifetime of 3-methyl-2-butanol with respect to reaction with OH radicals of about 9 h is calculated using [OH] $= 2.5 \times 10^6$ molecule cm^{-3} and $k(\text{OH} + \text{3-methyl-2-butanol}) = 1.2 \times 10^{-11}$ cm^3 molecule^{-1} s^{-1}.

An SAR calculation using parameters from Kwok and Atkinson (1995) and Bethel et al. (2001b) indicates the majority of the reaction with OH radicals proceeds via hydrogen abstraction from the tertiary C—H bonds (~54% from the α-CH group and ~39% from the β-CH group) with most of the remaining (~6%) reaction occurring at the CH_3 groups. Attack at the α-CH_2 site will give $CH_3C(O)CH(CH_3)_2$. Attack at the β-CH site will give mainly $CH_3C(O)CH_3 + CH_3CHO$, with $CH_3CH(OH)C(O)CH_3 + CH_2O$ as possible minor products.

II-B-16. 1-Hexanol [*n*-Hexyl Alcohol, $CH_3CH_2CH_2CH_2CH_2CH_2OH$]

II-B-16.1. OH Reaction Kinetics

The available measurements of the rate coefficient for reaction of OH with 1-hexanol are given in table II-B-35. The results of Aschmann and Atkinson (1998b) and Oh and Andino (2001) are somewhat larger than those obtained by Wallington et al. (1988d)

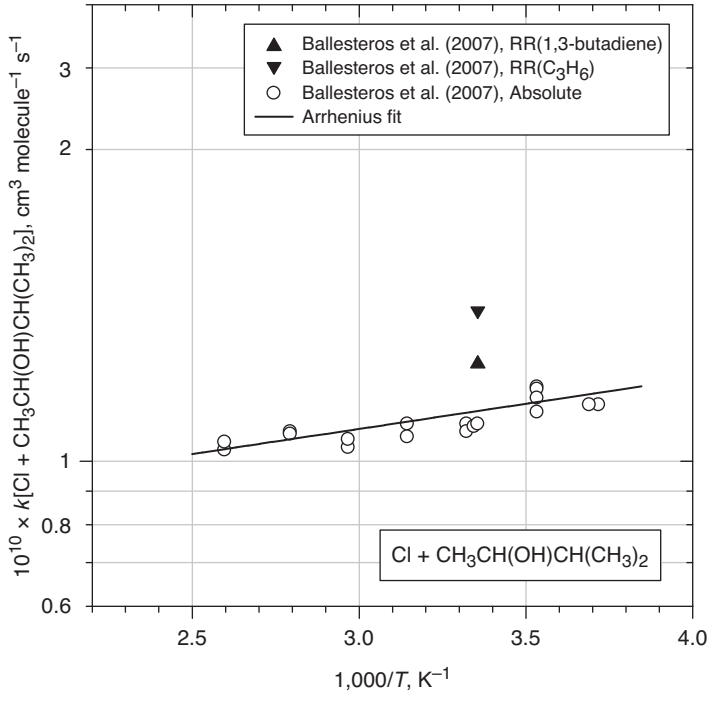

Figure II-B-24. Arrhenius plot of the rate coefficient for the reaction of Cl with 3-methyl-2-butanol.

and Nelson et al. (1990a). As for 1-butanol and 1-pentanol, Oh and Andino's rate coefficient measured relative to *p*-xylene is approximately 25% higher than the other determinations. The unweighted mean of the available data set except that of Oh and Andino (relative to *p*-xylene) leads to $k = 1.3 \times 10^{-11}$ cm^3 $molecule^{-1}$ s^{-1} at 298 K with an uncertainty estimated to be ±25%.

II-B-16.2. Cl-Atom Reaction Kinetics

The reaction of Cl with 1-hexanol has been studied by Nelson et al. (1990a) using a relative method. The rate coefficient value was placed on an absolute basis using $k(cyclo\text{-}C_6H_{12}) = 3.3 \times 10^{-10}$ cm^3 $molecule^{-1}$ s^{-1} (Calvert et al., 2008). Based on this single determination, a value of $k = 3.1 \times 10^{-10}$ cm^3 $molecule^{-1}$ s^{-1} is recommended at 298 K with an estimated uncertainty of ±25%; see table II-B-36.

II-B-16.3. Summary of the Atmospheric Fate of 1-Hexanol

Combining k(OH + 1-hexanol) $= 1.3 \times 10^{-11}$ cm^3 $molecule^{-1}$ s^{-1} with a diurnal average [OH] $= 2.5 \times 10^6$ molecule cm^{-3} provides an estimate of about 9 h for the atmospheric lifetime of 1-hexanol with respect to reaction with OH. According to the SAR method, the reaction of OH with 1-hexanol will proceed by H-atom abstraction

Table II-B-35. Rate coefficients (k, cm^3 molecule^{-1} s^{-1}) for reaction of OH with larger alcohols

Molecule	$10^{12} \times K$	T (K)	Technique[a]	Reference	Temperature Range (K)
1-Hexanol (n-$C_6H_{13}OH$)	12.4 ± 0.7	298	FP–RF	Wallington et al. (1988d)	
	12.2 ± 2.4	298 ± 2	PR–UV abs.	Nelson et al. (1990a)	
	12.0 ± 1.1	298 ± 2	RR (c-C_6H_{12})[b]		
	15.3 ± 1.6	296 ± 2	RR (c-C_6H_{12})[b]	Aschmann and Atkinson (1998b)	
	13.8 ± 0.7	298 ± 2	RR (c-C_6H_{12})[b]	Oh and Andino (2001)	
	17.6 ± 1.1		RR (p-xylene)[c]		
2-Hexanol ($CH_3CH(OH)C_4H_9$)	12.1 ± 0.7	298	FP–RF	Wallington et al. (1988d)	
2-Methyl-2-Pentanol [$CH_3C(CH_3)(OH)CH_2CH_2CH_3$]	7.1 ± 0.5	298 ± 2	RR (n-octane)[d]	Bethel et al. (2003)	
4-Methyl-2-Pentanol [$(CH_3)_2C(OH)CH_2CH_2CH_3$]	17.1 ± 0.9	298 ± 2	RR (n-octane)[d]	Bethel et al. (2003)	
2,3-Dimethyl-2-Butanol [$(CH_3)_2C(OH)CH(CH_3)_2$]	12.3 ± 1.42	268	PLP–LIF	Jiménez et al. (2005b)[e]	268–354
	11.4 ± 0.22	273			
	10.9 ± 0.66	278			
	9.65 ± 0.76	288			
	9.01 ± 0.90	292			
	9.08 ± 1.00	298			
	8.39 ± 1.74	303			
	8.30 ± 0.70	321			
	7.34 ± 1.20	338			
	7.51 ± 0.90	354			

1-Heptanol (n-$C_7H_{15}OH$)	13.6 ± 1.3	298	FP–RF	Wallington et al. (1988d)
	12.7 ± 1.3	298 ± 2	RR ($cyclo$-C_6H_{12})[b]	Nelson et al. (1990a)
2,4-Dimethyl-2-Pentanol [$(CH_3)_2C(OH)CH_2CH(CH_3)_2$]	11.2 ± 3.0	296 ± 2	RR (n-C_6H_{12})[e]	Atkinson and Aschmann (1995)
1-Octanol (n-$C_8H_{17}OH$)	13.4 ± 1.4	298 ± 2	RR ($cyclo$-C_6H_{12})[b]	Nelson et al. (1990a)
3,5-Dimethyl-3-Hexanol [$CH_3CH_2C(CH_3)(OH)CH_2CH(CH_3)_2$]	13.4 ± 3.5	296 ± 2	RR (n-C_6H_{12})[f]	Atkinson and Aschmann (1995)
Cyclopentanol ($cyclo$-C_5H_9OH)	10.7 ± 0.7	298	FP–RF	Wallington et al. (1988d)
Cyclohexanol ($cyclo$-$C_6H_{11}OH$)	19.4 ± 0.8	297 ± 3	RR (decane)[g]	Bradley et al. (2001)
	18.2 ± 0.8		RR (tridecane)[h]	
	14.9 ± 0.3		RR (pentanal)[i]	

[a]Abbreviations used for the techniques are defined in table I-F-3.
[b]Placed on an absolute basis using $k(OH + cyclo\text{-}C_6H_{12}) = 6.97 \times 10^{-12}$ cm^3 molecule^{-1} s^{-1} (Calvert et al., 2008).
[c]Placed on an absolute basis using $k(OH + p\text{-xylene}) = 1.43 \times 10^{-11}$ cm^3 molecule^{-1} s^{-1} (Calvert et al., 2002).
[d]Placed on an absolute basis using $k(OH + n\text{-octane}) = 7.81 \times 10^{-12}$ cm^3 molecule^{-1} s^{-1} (Calvert et al., 2008).
[e]$k = 5.60 \times 10^{-12} + 1.52 \times 10^{-14} e^{(1620/T)}$.
[f]Placed on an absolute basis using $k(OH + n\text{-}C_6H_{12}) = 5.48 \times 10^{-12}$ cm^3 molecule^{-1} s^{-1} (Calvert et al., 2008).
[g]Placed on an absolute basis using $k(OH + \text{decane}) = 1.1 \times 10^{-11}$ cm^3 molecule^{-1} s^{-1} (Calvert et al., 2008).
[h]Placed on an absolute basis using $k(OH + \text{tridecane}) = 1.6 \times 10^{-11}$ cm^3 molecule^{-1} s^{-1} (Calvert et al., 2008).
[i]Placed on an absolute basis using $k(OH + \text{pentanal}) = 2.7 \times 10^{-11}$ cm^3 molecule^{-1} s^{-1} (this book, section IV-B-6.1).

Table II-B-36. Rate coefficients (k, cm^3 molecule^{-1} s^{-1}) for reaction of Cl with larger alcohols

Molecule	$10^{11} \times A$	B (K)	$10^{10} \times k$	T (K)	Technique[a]	Reference	Temperature Range (K)
1-Hexanol (n-$C_6H_{13}OH$)			3.13 ± 0.10	298 ± 2	RR (c*yclo*-C_6H_{12})[b]	Nelson et al. (1990a)	
2,3-Dimethyl-2-butanol			1.05 ± 0.21	298 ± 2	RR (1,3-utadiene)[c]	Ballesteros et al. (2007)	
$[(CH_3)_2C(OH)CH(CH_3)_2]$			0.97 ± 0.30	298 ± 2	RR $[(CH_3)_3CCl]$[d]		
	4.80 ± 0.43	-221 ± 56	1.14 ± 0.10	269	PLP–RF	Ballesteros et al. (2007)	269–384
			1.11 ± 0.05	269			
			1.03 ± 0.14	284			
			1.06 ± 0.13	284			
			0.942 ± 0.08	298			
			0.992 ± 0.13	298			
			0.97 ± 0.07	300			
			1.02 ± 0.09	300			
			0.904 ± 0.050	318			
			0.901 ± 0.050	337			
			0.904 ± 0.080	337			
			0.935 ± 0.090	358			
			0.908 ± 0.080	358			
			0.887 ± 0.090	384			
			0.90 ± 0.07	384			
1-Heptanol (n-$C_7H_{15}OH$)			3.70 ± 0.20	298 ± 2	RR (*cyclo*-C_6H_{12})[b]	Nelson et al. (1990a)	
1-Octanol (n-$C_8H_{17}OH$)			4.18 ± 0.17	298 ± 2	RR (*cyclo*-C_6H_{12})[b]	Nelson et al. (1990a)	

[a]Abbreviations used for the techniques are defined in table I-F-3.
[b]Placed on an absolute basis using $k(Cl + cyclo\text{-}C_6H_{12}) = 3.3 \times 10^{-10}$ cm^3 molecule^{-1} s^{-1} (Calvert et al., 2008).
[c]Placed on an absolute basis using $k(Cl + 1,3\text{-butadiene}) = 2.51 \times 10^{-10}$ cm^3 molecule^{-1} s^{-1} (Stutz et al., 1998).
[d]Placed on an absolute basis using $k[Cl + (CH_3)_3CCl] = 1.3 \times 10^{-11}$ cm^3 molecule^{-1} s^{-1} (Donaghy et al., 1993).

from —CH_2 groups mainly from the α- and β-positions (~30% each) with a non-negligible contribution from the other —CH_2 groups. The products expected from the reaction are the corresponding carbonyls such as hexanal and pentanal. Isomerization may also occur leading to long chain hydroxycarbonyls. The oxidation mechanism will be similar to that of *n*-hexane described by Calvert et al. (2008).

II-B-17. 2-Hexanol [$CH_3CH(OH)CH_2CH_2CH_2CH_3$]

II-B-17.1. OH Reaction Kinetics

The only study performed to date on the reaction of OH with 2-hexanol is that of Wallington et al. (1988d) at 298 K using the flash photolysis–resonance fluorescence technique; see table II-B-35. On the basis of this single investigation, the rate coefficient value recommended for this reaction is $k(\text{OH} + \text{2-hexanol}) = 1.2 \times 10^{-11}$ cm^3 molecule^{-1} s^{-1} at 298 K with an estimated uncertainty of ±25%.

II-B-17.2. Summary of the Atmospheric Fate of 2-Hexanol

The atmospheric lifetime of 2-hexanol with respect to reaction with OH radicals is estimated to be approximately 9 h using a rate coefficient of $(1.2 \pm 0.3) \times 10^{-11}$ cm^3 molecule^{-1} s^{-1} and an average daytime [OH] = 2.5×10^6 molecule cm^{-3}. From the SAR calculations, the reaction of OH with 2-hexanol is expected to occur approximately 53% via H-atom abstraction from the >CH group and 23% from the —CH_2 group in the β-position. The resulting main products are expected to be 2-hexanone, butanal, and acetaldehyde.

II-B-18. 2-Methyl-2-pentanol [$CH_3C(CH_3)(OH)CH_2CH_2CH_3$]

II-B-18.1. OH Reaction Kinetics

The rate coefficient for the reaction of OH with 2-methyl-2-pentanol has been measured by Bethel et al. (2003) using a relative rate method with *n*-octane as the reference; see table II-B-35. Using $k(n\text{-octane}) = 7.81 \times 10^{-12}$ (Calvert et al., 2008) to place the rate coefficient ratio on an absolute basis gives $k(\text{OH} + \text{2-methyl-2-pentanol}) = 7.1 \times 10^{-12}$ cm^3 molecule^{-1} s^{-1} at 298 K with an uncertainty of 20%.

II-B-18.2. Summary of the Atmospheric Fate of 2-Methyl-2-pentanol

Combining $k(\text{OH} + \text{2-methyl-2-pentanol}) = 7.1 \times 10^{-12}$ cm^3 molecule^{-1} s^{-1} with a diurnal average [OH] = 10^6 molecule cm^{-3} provides an estimate of approximately 2 days for the atmospheric lifetime of 2-methyl-2-pentanol with respect to reaction with OH. Bethel et al. (2003) studied the products of the OH-initiated oxidation of 2-methyl-2-pentanol in the presence of NO using GC–FID, GC–MS and API–MS analytical techniques. The identified products were acetaldehyde (22 ± 3%), propanal (35 ± 4%), acetone (56 ± 6%), and 2-pentanone (5 ± 1%). The sum of the hydroxynitrate and dihydroxynitrate yields was ~8%. Acetone is a co-product of both acetaldehyde and

propanal, and its observed yield was indistinguishable from the sum of acetaldehyde and propanal. The results indicate that more than 35% of the reaction of hydroxyl radicals with 2-methyl-2-pentanol occurs at the 3-position and more than 22% occurs at the 4-position. The general degradation mechanisms following the formation of different hydroxyalkoxy radicals as suggested by Bethel et al. (2003) are shown in figure II-B-25.

II-B-19. 4-Methyl-2-Pentanol [$CH_3CH(OH)CH_2CH(CH_3)_2$]

II-B-19.1. OH Reaction Kinetics

Bethel et al. (2003) studied the OH reaction with 4-methyl-2-pentanol using a relative rate method with *n*-octane as reference; see table II-B-35. The rate coefficient $k(n\text{-octane}) = 7.81 \times 10^{-12}$ from Calvert et al. (2008) was used to place the measured rate coefficient ratio on an absolute basis giving $k(\text{OH} + \text{4-methyl-2-pentanol}) = 1.7 \times 10^{-11}\,\text{cm}^3\,\text{molecule}^{-1}\,\text{s}^{-1}$ at 298 K with an uncertainty estimated to be ±20%.

II-B-19.2. Summary of the Atmospheric Fate of 4-Methyl-2-pentanol

The atmospheric lifetime of 4-methyl-2-pentanol with respect to reaction with OH radicals is estimated to be approximately 7 h using $[\text{OH}] = 2.5 \times 10^6$ and $k(\text{OH} + \text{4-methyl-2-pentanol}) = 1.7 \times 10^{-11}\,\text{cm}^3\,\text{molecule}^{-1}\,\text{s}^{-1}\}$. The only product study of the OH-initiated oxidation of 4-methyl-2-pentanol is that by Bethel et al. (2003) conducted using the same approach as for 2-methyl-2-pentanol. The products identified were acetaldehyde (37 ± 6%), acetone (26 ± 3%), 2-methylpropanal (11.1 ± 1.2%), and 4-methyl-2-pentanone (25 ± 2%). The sum of the hydroxynitrates and dihydroxynitrates yields was ~7%. The 4-methyl-2-pentanone should arise exclusively from attack at the 2-position. Acetaldehyde is a co-product of both acetone and 2-methylpropanal, and its yield equals the sum of those molecules. The results appear to be consistent with 25% attack at the 2-position, 11% attack at the 3-position, and more than 25% at the 4-position. The alkoxy radical formed following attack at the 4-position is expected to isomerize, in addition to decomposing to give acetone, acetaldehyde, and formaldehyde. The observed products indicate more than twice as much abstraction at the 4-position than is predicted by the SAR relationship, indicating an activation effect of the —OH group extending at least three carbon atoms down the chain (Bethel et al., 2001b, 2003).

II-B-20. 2,3-Dimethyl-2-Butanol [$(CH_3)_2C(OH)CH(CH_3)_2$]

II-B-20.1. OH Reaction Kinetics

The reaction of OH with 2,3-dimethyl-2-butanol has been studied by Jiménez at al. (2005b) who measured the rate coefficient as a function of temperature (268–354 K) using pulsed laser photolysis with a pulsed laser–induced fluorescence technique. The data are presented in table II-B-35 and shown in figure II-B-26. Jiménez at al. (2005b) fitted a three parameter expression to their data to give $k = (5.6 \pm 0.6) \times 10^{-12} + (1.52 \pm 0.21) \times 10^{-14} \exp[(1{,}620 \pm 268)/T]\,\text{cm}^3$ moleclule$^{-1}\,\text{s}^{-1}$. However, as shown in figure II-B-26, a fit using the simple Arrhenius expression with

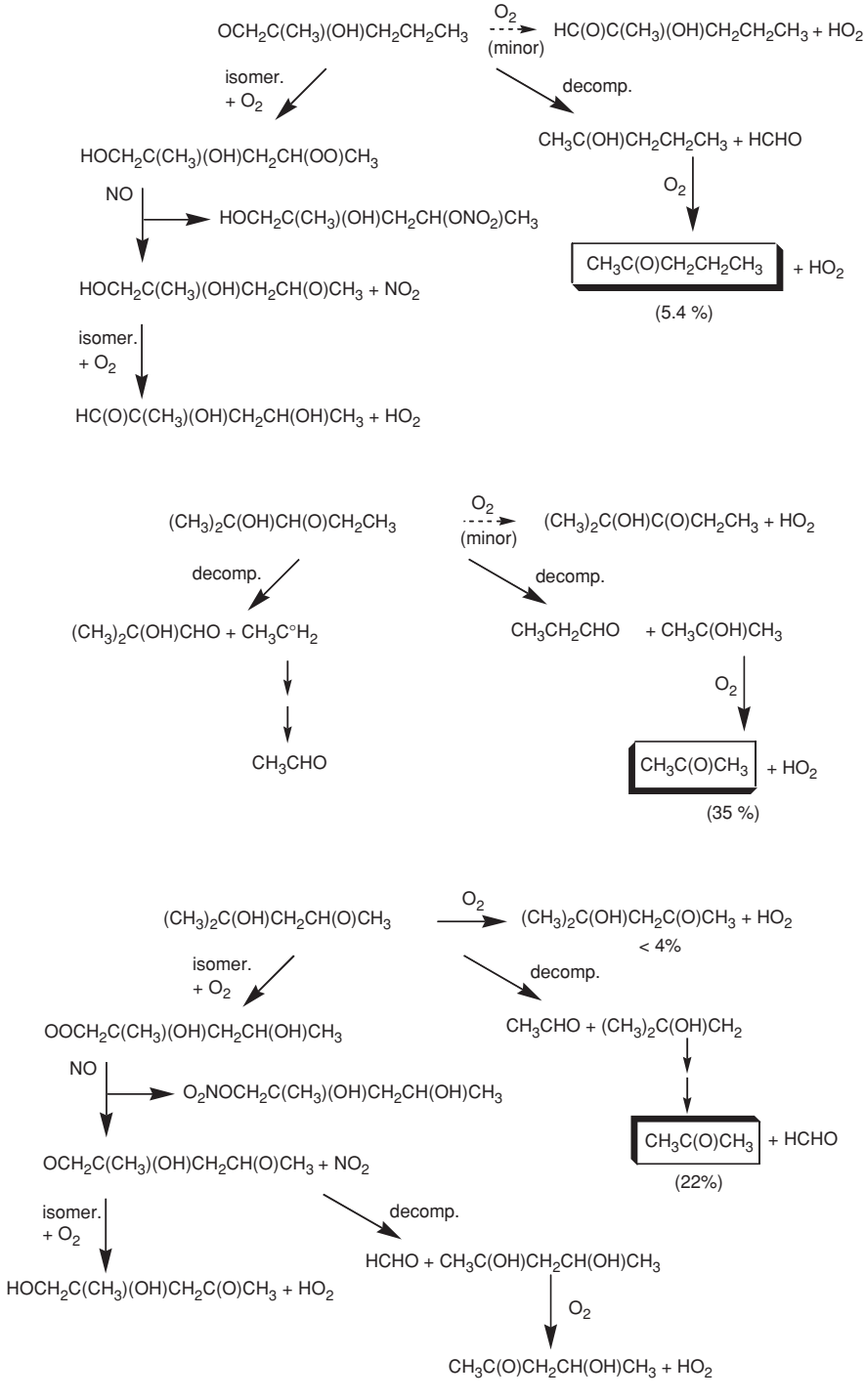

Figure II-B-25. OH-initiated degradation scheme of 2-methyl-2-pentanol (Bethel et al., 2003).

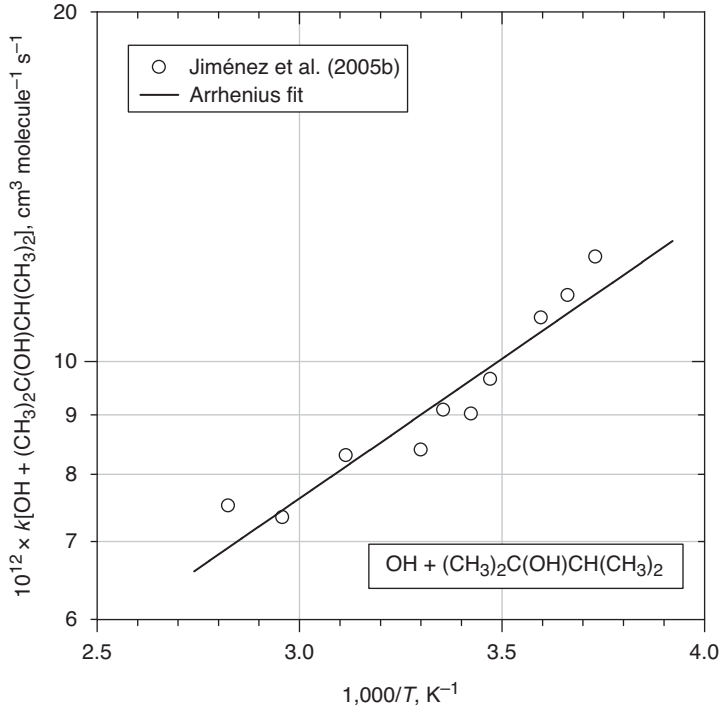

Figure II-B-26. Arrhenius plot of the rate coefficient for the reaction of OH with 2,3-dimethyl-2-butanol.

$k = 1.45 \times 10^{-12} \exp(554/T)\,\mathrm{cm^3\ molecule^{-1}\,s^{-1}}$ gives a reasonable description of the data. This expression gives k(OH + 2, 3-dimethyl-2-butanol) $= 9.3 \times 10^{-12}\,\mathrm{cm^3\ molecule^{-1}\,s^{-1}}$ at 298 K with an uncertainty estimated to be ± 20%.

II-B-20.2. Cl-Atom Reaction Kinetics

The reaction of Cl with 2,3-dimethyl-2-butanol has been studied by Ballesteros et al. (2007) using both absolute and relative methods. The data obtained in the temperature range 269–384 K are summarized in table II-B-36 and plotted in figure II-B-27. Fitting the Arrhenius expression to the combined data set yields k(Cl + 2, 3-dimethyl-2-butanol) $= 5.2 \times 10^{-11} \exp(195/T)\,\mathrm{cm^3\ molecule^{-1}\,s^{-1}}$. This expression gives $k = 1.0 \times 10^{-11}\,\mathrm{cm^3\ molecule^{-1}\,s^{-1}}$ at 298 K with an uncertainty estimated to be ±25%.

II-B-20.3. Summary of the Atmospheric Fate of 2,3-Dimethyl-2-butanol

The atmospheric lifetime of 2,3-dimethyl-2-butanol with respect to reaction with OH radicals is about 1 day, using [OH] $= 10^6\ \mathrm{molecule\,cm^{-3}}$ and k(OH + 2, 3-dimethyl-2-butanol) $= 9.3 \times 10^{-12}\,\mathrm{cm^3\ molecule^{-1}\,s^{-1}}$.

According to the SAR estimates, the reaction of OH with 2,3-dimethyl-2-butanol occurs mainly through H-atom abstraction from the >CH— group in the β-position to

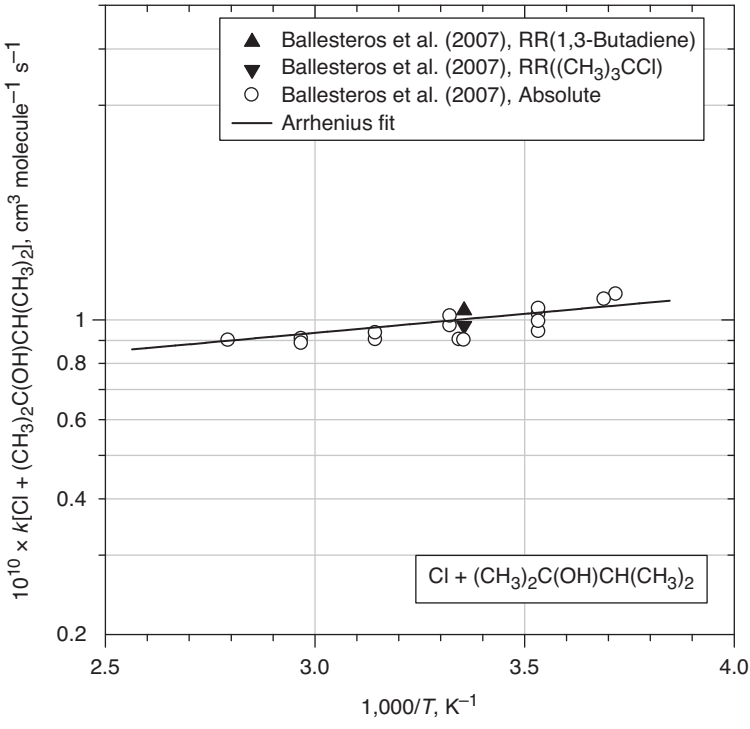

Figure II-B-27. Arrhenius plot of the rate coefficient for the reaction of Cl with 2,3-dimethyl-2-butanol.

the hydroxyl group with a yield of ~83%. Two molecules of acetone are expected to be formed via this pathway.

II-B-21. 1-Heptanol (*n*-Heptyl Alcohol, *n*-$C_7H_{15}OH$)

II-B-21.1. OH Reaction Kinetics

The reaction of OH with 1-heptanol has been studied by Wallington et al. (1988d) and Nelson et al. (1990a) using absolute and relative methods, respectively. The rate coefficient values obtained in these two studies are in good agreement (see table II-B-35). The mean of the two determinations gives our recommendation of $k(\mathrm{OH} + \text{1-}C_7H_{15}OH) = 1.3 \times 10^{-11}$ cm^3 molecule^{-1} s^{-1} at 298 K with an estimated uncertainty of ±15%.

II-B-21.2. Cl-Atom Reaction Kinetics

The rate coefficient of the reaction of Cl with 1-heptanol has been determined by Nelson et al. (1990a) using a relative rate method; see table II-B-36. The rate coefficient ratio was placed on an absolute basis using $k(cyclo\text{-}C_6H_{12}) = 3.3 \times 10^{-10}$

(Calvert et al., 2008) giving $k(\mathrm{Cl} + n\text{-}\mathrm{C_7H_{15}OH}) = 3.7 \times 10^{-10}\,\mathrm{cm^3\ molecule^{-1}\ s^{-1}}$ at 298 K. We estimate the uncertainty to be ±20%.

II-B-21.3. Summary of the Atmospheric Fate of 1-Heptanol

Combining $k(\mathrm{OH} + 1\text{-}\mathrm{C_7H_{15}OH}) = 1.3 \times 10^{-11}\,\mathrm{cm^3\ molecule^{-1}\ s^{-1}}$ and [OH] = $2.5 \times 10^6\,\mathrm{molecule\,cm^{-3}}$ provides the atmospheric lifetime of 1-heptanol with respect to reaction with OH radicals of about 9 h. According to the SAR method, the reaction of OH with 1-heptanol will proceed by H-atom abstraction from —CH_2 groups mainly from the α- and β-positions (∼30% each). The —CH_2 groups in the γ- and δ- positions may also have a nonnegligeable contribution to the total reaction. The products expected from the reaction are the corresponding carbonyls such as heptanal and hexanal as well as hydroxycarbonyls from isomerization.

II-B-22. 4-Heptanol ($CH_3CH_2CH_2CH(OH)CH_2CH_2CH_3$)

II-B-22.1. NO_3 Reaction Kinetics

The only available experimental data concerning the atmospheric chemistry of 4-heptanol come from the relative rate study by Chew et al. (1998) of the kinetics of the reaction with NO_3 radicals at 298 K. Methacrolein was used as the reference compound with $(NO_3 + \text{methacrolein}) = 3.4 \times 10^{-15}\,\mathrm{cm^3\ molecule^{-1}\ s^{-1}}$ (Atkinson et al., 2006). Recognizing possible interferences associated with reaction of 4-heptanol with N_2O_5 (gas-phase or heterogeneous) to form nitrates, gives an upper limit of $k(NO_3 + \text{4-heptanol}) \leq (6.2 \pm 2.1) \times 10^{-15}\,\mathrm{cm^3\ molecule^{-1}\ s^{-1}}$. See table II-B-37.

II-B-22.2. Summary of the Atmospheric Fate of 4-Heptanol

Using SAR, the rate coefficient for a reaction of OH with 4-heptanol of $k = 1.7 \times 10^{-11}\,\mathrm{cm^3\ molecule^{-1}\ s^{-1}}$ can be estimated. Combining this estimate with an average daytime [OH] = $2.5 \times 10^6\,\mathrm{molecule\,cm^{-3}}$ gives an atmospheric lifetime of approximately 6 h. This reaction is expected to occur by H-atom abstraction from the >CH group (∼50%) giving 4-heptanone, and from the —CH_2 groups in the β-position (∼35%) giving butanal and propanal.

Chew et al. (1998) showed that 4-heptanone is formed in a yield of 75 ± 12% following the NO_3-radical-initiated oxidation of 4-heptanol. This indicates that the reaction proceeds mainly by H-atom abstraction from the CH group attached to the

Table II-B-37. Rate coefficient (k, $\mathrm{cm^3\ molecule^{-1}\ s^{-1}}$) for the reaction of NO_3 with 4-heptanol [$CH_3CH_2CH_2CH(OH)CH_2CH_2CH_3$]

$10^{15} \times k$	T (K)	Technique[a]	Reference
$\leq 6.2 \pm 2.1$	298 ± 2	RR (methacrolein)[b]	Chew et al. (1998)

[a]Abbreviations used for the techniques are defined in table I-F-3.
[b]Placed on an absolute basis using $k(NO_3 + \text{methacrolein}) = 3.4 \times 10^{-15}\,\mathrm{cm^3\ molecule^{-1}\ s^{-1}}$ (Atkinson et al., 2006).

hydroxyl group.

$$NO_3 + CH_3CH_2CH_2CH(OH)CH_2CH_2CH_3 \rightarrow HNO_3 + CH_3CH_2CH_2C(OH)CH_2CH_2CH_3$$

$$CH_3CH_2CH_2C(OH)CH_2CH_2CH_3 + O_2 \rightarrow CH_3CH_2CH_2C(O)CH_2CH_2CH_3 + HO_2$$

II-B-23. 2,4-Dimethyl-2-Pentanol [$(CH_3)_2C(OH)CH_2CH(CH_3)_2$]

II-B-23.1. OH Reaction Kinetics

The reaction of OH with 2,4-dimethyl-2-pentanol has been investigated by Atkinson and Aschmann (1995) using a relative rate method with *n*-hexane as reference compound at 740 Torr total pressure of purified air; see table II-B-35. The results were placed on an absolute basis using $k(n\text{-hexane}) = 5.48 \times 10^{-12}$ from Calvert et al. (2008) to give $k(2, 4\text{-dimethyl-2-pentanol}) = 1.1 \times 10^{-11}\,cm^3\ molecule^{-1}\ s^{-1}$ at 298 K with an estimated uncertainty of ±30%.

II-B-23.2. Summary of the Atmospheric Fate of 2,4-Dimethyl-2-pentanol

The atmospheric lifetime of 2,4-dimethyl-2-pentanol with respect to reaction with OH radicals is estimated to be 10 h using $[OH] = 2.5 \times 10^6$ molecule cm^{-3} and the rate coefficient presented in this section. The product study conducted by Atkinson and Aschmann (1995) using GC–FID and GC–MS showed that the reaction of OH with 2,4-dimethyl-2-pentanol gives the following products (molar yields): Acetone (92 ± 15%), 2-methylpropanal (21 ± 22%), 4-methyl-2-pentanone (5 ± 1%), and 4-hydroxy-4-methyl-2-pentanone (12 ± 2%). In addition, the yield of a tertiary nitrate was estimated to be ∼4 ± 1%.

Assuming the reactivity of the —OH group is the same as in methanol ($1.35 \times 10^{-13}\,cm^3\ molecule^{-1}\ s^{-1}$; IUPAC, 2008), reaction of OH radicals with the —OH group in 2,4-dimethyl-2-pentanol accounts for approximately 1% of the overall reaction. As for other long chain alcohols, the reaction with OH occurs through H-atom abstraction from different groups (CH_3, —CH_2, and $\rangle$CH). The major expected degradation mechanisms proposed by Atkinson and Aschmann (1995) are shown in figure II-B-28; only the main routes are presented and the sequences leading to products not observed are omitted. The carbonyl and hydroxycarbonyl products observed by Atkinson and Aschmann (1995) account for 73 ± 9% of the overall reaction with a further 4 ± 1% ascribed to a nitrate compound. The observation of 4-hydroxy-4-methyl-2-pentanone provides conclusive evidence for the importance of isomerization of the alkoxy radical $(CH_3)_2C(OH)CH_2C(O)(CH_3)_2$ [see pathway (C) in figure II-B-28].



Figure II-B-28. Degradation scheme of alkoxy radicals generated during the oxidation of 2,4-dimethyl-2-pentanol (Atkinson and Aschmann, 1995).

II-B-24. 1-Octanol (n-$C_8H_{17}OH$)

II-B-24.1. OH Reaction Kinetics

The rate coefficient of the reaction of OH radicals with 1-octanol has been studied by Nelson et al. (1990a) using a relative rate method with cyclohexane as the reference; see table II-B-35. Using $k(cyclo\text{-}C_6H_{12}) = 6.97 \times 10^{-12}$ (Calvert et al., 2008) gives $k(n\text{-}C_8H_{17}OH) = 1.3 \times 10^{-11}$ cm^3 molecule^{-1} s^{-1} at 298 K. The uncertainty is estimated to be ±30%.

II-B-24.2. Cl-Atom Reaction Kinetics

The rate coefficient of the reaction of Cl with 1-octanol has been determined by Nelson et al. (1990a) using a relative rate method; see table II-B-36. The rate coefficient ratio was placed on an absolute basis using $k(cyclo\text{-}C_6H_{12}) = 3.3 \times 10^{-10}$ (Calvert et al., 2008) to give $k(n\text{-}C_8H_{17}OH) = 4.2 \times 10^{-10}$ cm^3 molecule^{-1} s^{-1} at 298 K. This result is recommended with an uncertainty estimated to be ±30%.

II-B-24.3. Summary of the Atmospheric Fate of 1-Octanol

Combining the rate coefficient presented above with a daytime average OH concentration of 2.5×10^6 molecule cm^{-3} gives an estimate of about 9 h for the atmospheric lifetime of 1-octanol with respect to reaction with OH radicals. According to SAR estimates, the reaction of OH with 1-octanol will proceed by H-atom abstraction from —CH_2 groups mainly at the α- and β-positions (~30% each). Reaction at the CH_2 groups in the γ- and δ- positions will also contribute. The products expected from the reaction are the corresponding carbonyls, such as octanal and heptanal, as well as hydroxycarbonyls from isomerization.

II-B-25. 3,5-Dimethyl-3-Hexanol [$CH_3CH_2C(CH_3)(OH)CH_2CH(CH_3)_2$]

II-B-25.1. OH Reaction Kinetics

The rate coefficient for the reaction of OH radicals with 3,5-dimethyl-3-hexanol has been studied by Atkinson and Aschmann (1995) using a relative rate method with n-hexane as the reference compound at 740 Torr total pressure of purified air; see table II-B-35. The measured ratio, placed on an absolute basis using $k(n\text{-hexane}) = 5.48 \times 10^{-12}$ cm^3 molecule^{-1} s^{-1} from Calvert et al. (2008), gives $k(\text{OH} + 3,5\text{-dimethyl-3-hexanol}) = 1.3 \times 10^{-11}$ cm^3 molecule^{-1} s^{-1} at 298 K with an estimated uncertainty of ±30%.

II-B-25.2. Summary of the Atmospheric Fate of 3,5-Dimethyl-3-hexanol

The atmospheric lifetime of 3,5-dimethyl-3-hexanol with respect to reaction with OH radicals is about 9 h. The OH-initiated oxidation of 3,5-dimethyl-3-hexanol has been investigated by Atkinson and Aschmann (1995). The products (molar yields)

observed were: Acetone (12 ± 3%), 2-butanone (28 ± 2%), 2-methylpropanal (17 ± 2%), 4-methyl-2-pentanone (16 ± 1%), 4-hydroxy-4-methyl-2-pentanone (25 ± 2%), and a tertiary nitrate (~4 ± 1%). The proposed oxidation mechanisms are similar to those for 2,4-dimethyl-2-pentanol. The observation of 4-hydroxy-4-methyl-2-pentanone provides conclusive evidence for the isomerization of the alkoxy radical $CH_3CH_2C(CH_3)(OH)CH_2C(O)(CH_3)_2$. The carbonyl and hydroxycarbonyl products observed by Atkinson and Aschmann (1995) account for 69 ± 5% of the overall reaction with a further ~4 ± 1% ascribed to the formation of a nitrate.

II-B-26. Cyclopentanol (*cyclo*-C_5H_9OH)

II-B-26.1. OH Reaction Kinetics

The rate coefficient for the reaction of OH with cyclopentanol has been measured by Wallington et al. (1988d) using a flash photolysis–resonance fluorescence technique; see table II-B-35. A rate coefficient of $k(\text{OH} + \text{cyclopentanol}) = 1.1 \times 10^{-11}$ cm^3 molecule^{-1} s^{-1} is recommended at 298 K with an uncertainty estimated of ± 20%.

II-B-26.2. Summary of the Atmospheric Fate of Cyclopentanol

The atmospheric lifetime of cyclopentanol with respect to reaction with OH radicals is calculated to be about 10 h using $k(\text{OH} + \text{cyclopentanol}) = 1.1 \times 10^{-11}$ cm^3 molecule^{-1} s^{-1} and $[\text{OH}] = 2.5 \times 10^6$ molecule cm^{-3}.

The reaction of OH with cyclopentanol is expected to occur predominately via the H-atom abstraction from the α-position leading to cyclopentanone. H-atom abstraction from the β- and γ- positions will also contribute to the total reaction.

II-B-27. Cyclohexanol (*cyclo*-$C_6H_{11}OH$)

II-B-27.1. OH Reaction Kinetics

The rate coefficient for the reaction of OH with cyclohexanol has been measured by Bradley et al. (2001) using a relative method at atmospheric pressure in air with three reference compounds; see table II-B-35. The combined data leads to the average value of $k(\text{OH} + \text{cyclohexanol}) = 1.7 \times 10^{-11}$ cm^3 molecule^{-1} s^{-1} with an estimated uncertainty of ±30% at 298 K.

II-B-27.2. Summary of the Atmospheric Fate of Cyclohexanol

Combining the rate coefficient presented in this section with $[\text{OH}] = 2.5 \times 10^6$ molecule cm^{-3} provides an estimate of the atmospheric lifetime of cyclohexanol with respect to reaction with OH radicals of about 7 h. The OH-initiated oxidation of cyclohexanol in the presence of NO_x has been investigated by Bradley et al. (2001). The observed products (and molar yields) were: Cyclohexanone (55 ± 6%), hexanedial (32 ± 15%), 3-hydroxycyclohexanone (31 ± 14%), and 4-hydroxycyclohexanone (8 ± 4%). The formation yield of cyclohexanone corresponds to the H-atom abstraction

from the α-position, ~55% of the total reaction. The observed products account for 126 ± 39% of the cyclohexanol loss. Reaction at the 3- and 4-positions leads to ring retaining products while reaction at the 2-position leads to ring cleavage. Note that abstraction from the 2-position produces a β-hydroxy-alkoxy radical, the same species formed following OH radical addition to alkenes, and that facile C—C bond scission is a common feature in the chemistry of these species. The ring structure precludes isomerization of the alkoxy radicals formed in the oxidation of cyclohexanol.

II-B-28. Trends in the Reactivity of Alcohols

The increase in reactivity shown for H-atom abstraction by OH for alcohols compared to the corresponding alkanes has been, at least in part, rationalized in terms of the lowering of the C—H bond strength. The available kinetic data show that the rate coefficients values at 298 K of the reaction of OH with linear straight-chain alcohols increase almost linearly with the alkyl chain length up to six carbon atoms. This likely indicates that the activation effect of the —OH group extends to at least the —CH_2 group located in the β-position relative to the —OH group, and possibly as far as the γ-position. For further increases in the chain length, the reactivity of the —CH_2 groups is similar to that found in the unsubstituted alkanes. This possible long-range activating effect of the hydroxyl group cannot be explained in terms of bond energy or inductive effects alone, and indicates an alternative reaction pathway to the direct concerted H-atom abstraction process as is the case for alkanes (Wallington et al., 1988d; Nelson et al., 1990a; Mellouki et al., 2003). The formation of an intermediate adduct, where the OH radical is weakly bound to the oxygen atom of the alcohol functional group via a hydrogen bond, could explain both the long-range activation effects and the negative temperature dependence observed for reaction of OH radicals with alcohols (e.g., see figures II-B-13, II-B-15, and II-B-19). The less pronounced increase in the reactivity for secondary and tertiary H-atoms on an α carbon atom relative to the corresponding alkane has been attributed, at least partly, to the smaller decrease in bond dissociation energies (Nelson et al., 1990a). Correlations between OH, Cl, and NO_3 rate coefficients with saturated alkanes, alcohols and ethers, and structure activity relationships (SARs) are presented in chapter III.

II-C. Diols

II-C-1. OH Reaction Kinetics

Table II-C-1 gives the available rate coefficients for reactions of OH radicals with diols. All measurements were conducted using relative rate methods in one atmosphere of air at room temperature. The reactivity of 2-methyl-2,4-pentanediol has been investigated by two different groups (Bethel et al., 2001b; Magneron et al., 2003). Magneron et al. (2003) reported a rate coefficient that is almost a factor of 2 lower than that reported by Bethel et al. (2001b). The origin of this discrepancy is unclear. As seen from table II-C-1, all other diols that have been studied have only been the subject of one investigation.

Table II-C-1. Rate coefficients (k, cm^3 molecule^{-1} s^{-1}) for reaction of OH with diols

Molecule	$10^{11} \times K$	T (K)	Technique[a]	Reference
1,2-Ethanediol ($HOCH_2CH_2OH$)	1.37 ± 0.13	296 ± 2	RR (*cyclo*-C_6H_{12})[b]	Aschmann and Atkinson (1998b)
	1.54 ± 0.14		RR (*m*-xylene)[c]	
1,2-Propanediol	2.18 ± 0.12	296 ± 2	RR (*m*-xylene)[c]	Aschmann and Atkinson (1998b)
[$HOCH_2CH(OH)CH_3$]	2.02 ± 0.14		RR (methyl vinyl ketone)[d]	
1,2-Butanediol [$HOCH_2CH(OH)CH_2CH_3$]	2.43 ± 0.50	296 ± 2	RR (*n*-octane)[e]	Bethel et al. (2001b)
1,3-Butanediol [$HOCH_2CH_2CH(OH)CH_3$]	2.99 ± 0.61	296 ± 2	RR (*n*-octane)[e]	Bethel et al. (2001b)
2,3-Butanediol [$CH_3CH(OH)CH(OH)CH_3$]	2.12 ± 0.57	296 ± 2	RR (*n*-octane)[e]	Bethel et al. (2001b)
2-Methyl-2,4-pentanediol [$(CH_3)_2C(OH)CH_2CH(OH)CH_3$]	2.50 ± 0.55	296 ± 2	RR (*n*-octane)[e]	Bethel et al. (2001b)
	1.22 ± 0.25	298 ± 3	RR (1,3-dioxolane)[f]	Magneron et al. (2003)
	1.68 ± 0.18		RR (CH_3CHO)[g]	
	1.05 ± 0.14		RR (*n*-C_6H_{14})[h]	
	1.48 ± 0.18		RR (*n-octane*)[e]	

[a]Abbreviations used for the techniques are defined in table I-F-3.
[b]Placed on an absolute basis using $k(OH + cyclo\text{-}C_6H_{12}) = 6.97 \times 10^{-12}$ cm^3 molecule^{-1} s^{-1} (Calvert et al., 2008).
[c]Placed on an absolute basis using $k(OH + m\text{-xylene}) = 2.31 \times 10^{-11}$ cm^3 molecule^{-1} s^{-1} (Calvert et al., 2002).
[d]Placed on an absolute basis using k(OH + methyl vinyl ketone) $= 2.0 \times 10^{-11}$ cm^3 molecule^{-1} s^{-1} (this book, section V-E-1.1).
[e]Placed on an absolute basis using $k(OH + n\text{-octane}) = 7.81 \times 10^{-12}$ cm^3 molecule^{-1} s^{-1} (Calvert et al., 2008).
[f]Placed on an absolute basis using k(OH + 1, 3-dioxolane) $= 1.0 \times 10^{-11}$ cm^3 molecule^{-1} s^{-1} (this book, section III-E-9.1).
[g]Placed on an absolute basis using $k(OH + CH_3CHO) = 1.5 \times 10^{-11}$ cm^3 molecule^{-1} s^{-1} (Atkinson et al., 2006).
[h]Placed on an absolute basis using $k(OH + n\text{-}C_6H_{14}) = 5.27 \times 10^{-12}$ cm^3 molecule^{-1} s^{-1} (Calvert et al., 2008).

II-C-2. Summary of the Atmospheric Fate of Diols

Using the rate coefficients in table II-C-1 and a daytime average OH concentration of 2.5×10^6 molecule cm^{-3} gives estimates for the lifetimes of diols with respect to reaction with OH radicals of less than 12 h.

The product studies of the OH reaction with diols conducted by Bethel et al. (2001b) and Magneron et al. (2003) show that these reactions proceed mainly by H-atom abstraction from the $\rangle$CH(OH) or —CH_2OH group leading to formation of hydroxyketones as shown below for 1,2-butanediol.

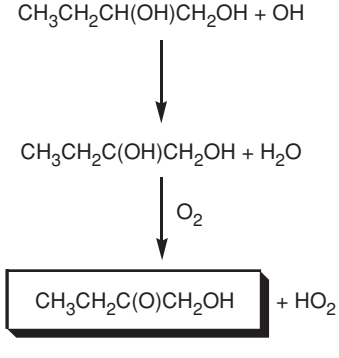

Table II-C-2. Yields of selected hydroxyketones following reaction of OH with diols

Diol	Hydroxyketone product	Molar Yield (%)	Reference
$HOCH_2CH(OH)CH_2CH_3$	$HOCH_2C(O)CH_2CH_3$	66 ± 11	Bethel et al. (2001b)
$HOCH_2CH_2CH(OH)CH_3$	$HOCH_2CH_2C(O)CH_3$	50 ± 9	Bethel et al. (2001b)
$CH_3CH(OH)CH(OH)CH_3$	$CH_3CH(OH)C(O)CH_3$	89 ± 9	Bethel et al. (2001b)
$(CH_3)_2C(OH)CH_2CH(OH)CH_3$	$(CH_3)_2CH(OH)CH_2C(O)CH_3$	47 ± 9	Bethel et al. (2001b)
		47 ± 4	Magneron et al. (2003)

Magneron et al. (2003) observed acetone and peroxyacetyl nitrate as products following the reaction of OH radicals with $(CH_3)_2C(OH)CH_2CH(OH)CH_3$, which enabled them to derive a branching ratio for H-atom abstraction from the $\rangle CH$ group of (47 ± 4)% and a lower limit of (33 ± 7)% for abstraction from the $—CH_2$ group. Table II-C-2 summarizes the formation yields of selected hydroxyketones from the reaction of OH with diols.

II-C-3. Trends in the Reactivity of Diols

The rate coefficients for reaction of OH radicals with diols are significantly higher than those with monoalcohols, indicating an activating effect of the second OH group. It appears that abstraction of a hydrogen atom from a carbon atom attached to the hydroxyl group is enhanced by the presence of a second hydroxyl group at the β- or γ-position. This possible long-range effect is supported by the higher experimental rate coefficient values compared to those calculated using the updated SAR parameters of Bethel et al. (2001b). For example, the experimental values are a factor of 2 larger than the calculated ones for 1,3-butanediol and 2-methyl-2,4-pentanediol (Bethel et al., 2001b).

II-D. Unsaturated Alcohols

II-D-1. 2-Propen-1-ol (Allyl Alcohol, $CH_2=CHCH_2OH$)

II-D-1.1. OH Reaction Kinetics

The reaction of OH with 2-propen-1-ol has been the subject of five kinetic studies (Papagni et al., 2001; Orlando et al., 2001; Upadhyaya et al., 2001; Holloway et al., 2005; Le Person et al., 2009). The only temperature-dependence investigation is that conducted by Le Person et al. over the range 231–373 K. Data are summarized in table II-D-1 and plotted in figure II-D-1. The rate coefficient reported by Upadhyaya et al. obtained at a total pressure of 10–20 Torr is lower than the measurements obtained at higher pressures in the other studies. Upadhyaya et al. (2001) speculated that the difference between their result and those obtained in the other studies reflects a pressure dependence associated with addition of OH to the $\rangle C=C\langle$ double bond. However, Le Person et al. (2009) did not observe any pressure dependence over the range 33–760 Torr. By analogy to the behavior of propene, it would be expected that for total pressures >25 Torr the reaction of OH radicals with 2-propen-1-ol would be independent of

Table II-D-1. Rate coefficients ($k = A\ e^{-B/T}$, cm^3 $molecule^{-1}$ s^{-1}) for reaction of OH with 2-propen-1-ol [$CH_2{=}CHCH_2OH$]

$10^{12} \times A$	B (K)	$10^{11} \times k$	T (K)	Technique[a]	Reference	Temperature Range (K)
		5.5 ± 0.2	296 ± 2	RR (1,3,5-trimethylbenzene)[b]	Papagni et al. (2001)	
		5.0 ± 0.7	298	RR (propene)[c]	Orlando et al. (2001)	
		3.7 ± 0.5	298	PLP–LIF	Upadhyaya et al. (2001)	
		4.60 ± 0.19	298 ± 2	PLP–LIF	Holloway et al. (2005)	
		5.3 ± 0.9	298	RR (butyl vinyl ether)[d]	Le Person et al. (2009)	
		5.4 ± 0.9	298	RR (isopropenyl acetate)[e]		
5.69 ± 0.18	-650 ± 52	9.5 ± 0.4	231	PLP–LIF	Le Person et al. (2009)	231–373
		8.9 ± 0.4	235			
		8.2 ± 0.4	241			
		6.9 ± 0.4	253			
		6.3 ± 0.2	273			
		5.3 ± 0.1	295			
		5.3 ± 0.1	296			
		5.0 ± 0.1	298			
		5.1 ± 0.8	300			
		5.0 ± 0.1	300			
		4.5 ± 0.4	325			
		4.0 ± 0.6	349			
		3.3 ± 0.1	363			
		3.3 ± 0.1	364			
		2.9 ± 0.2	373			

[a]Abbreviations used for the techniques are defined in table I-F-3.

[b]Placed on an absolute basis using $k(OH + 1,3,5\text{-trimethylbenzene}) = 5.7 \times 10^{-11}$ cm^3 $molecule^{-1}$ s^{-1} (Calvert et al., 2002).

[c]Placed on an absolute basis using $k(OH + \text{propene}) = 2.9 \times 10^{-11}$ cm^3 $molecule^{-1}$ s^{-1} (Atkinson et al., 2006).

[d]Placed on an absolute basis using $k(OH + \text{butyl vinyl ether}) = 1.1 \times 10^{-10}$ cm^3 $molecule^{-1}$ s^{-1} (this book, section III-D-4.1).

[e]Placed on an absolute basis using $k(OH + \text{isopropenyl acetate}) = 6.96 \times 10^{-11}$ cm^3 $molecule^{-1}$ s^{-1} (Le Calvé et al., 2000).

pressure (Calvert et al., 2000). A least-squares fit of the simple Arrhenius expression to the data from Papagni et al. (2001), Orlando et al. (2001), Holloway et al. (2005), and Le Person et al. (2009) gives $k(OH + \text{2-propen-1-ol}) = 5.7 \times 10^{-12} \exp(650/T)$ cm^3 $molecule^{-1}$ s^{-1}. This expression gives $k(OH + \text{2-propen-1-ol}) = 5.0 \times 10^{-11}$ cm^3 $molecule^{-1}$ s^{-1} at 298 K, with an uncertainty estimated to be ±15%.

II-D-1.2. O_3 Reaction Kinetics

There have been two studies of the kinetics of the reaction of O_3 with 2-propen-1-ol. The rate coefficients reported by Grosjean et al. (1993a) and Le Person et al. (2009) are in reasonable agreement, see table II-D-2. An average from the two studies gives

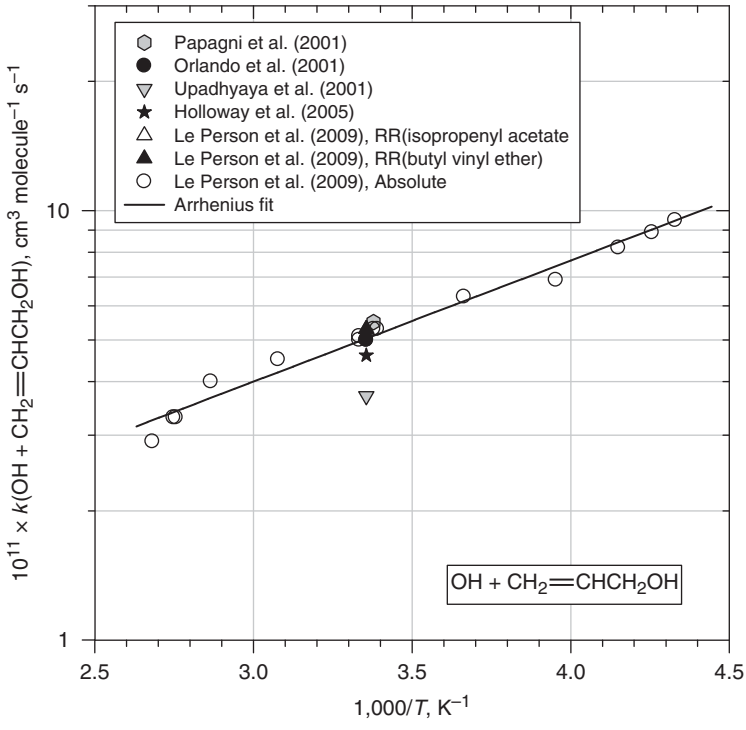

Figure II-D-1. Arrhenius plot of the rate coefficient for the reaction of OH with 2-propen-1-ol.

Table II-D-2. Rate coefficients (k, cm^3 molecule^{-1} s^{-1}) for reaction of O_3 with 2-propen-1-ol [CH_2=$CHCH_2OH$]

$10^{17} \times k$	T (K)	Technique	Reference
1.44 ± 0.20	287 ± 1	Excess of 2-propen-1-ol[a]	Grosjean et al. (1993a)
1.8 ± 0.2	298 ± 3	Excess of 2-propen-1-ol[a]	Le Person et al. (2009)

[a]Pseudo first-order conditions, using excess of 2-propen-1-ol; O_3 measured by absorption spectroscopy.

$k(O_3 + \text{2-propen-1-ol}) = 1.6 \times 10^{-17}$ cm^3 molecule^{-1} s^{-1} at 298 K with an estimated uncertainty of ±20%.

II-D-1.3. NO_3 Reaction Kinetics

Hallquist et al. (1996) and Noda et al. (2002) have reported rate coefficients for the reaction of NO_3 with 2-propen-1-ol. The results are given in table II-D-3 and shown in figure II-D-2. Hallquist et al. (1996) used relative rate and absolute (discharge flow) methods. The discharge flow measurements of Hallquist et al. were performed over the temperature range 273–363 K. As seen from figure II-D-2, there is reasonable

Table II-D-3. Rate coefficients ($k = A\ e^{-B/T}$, cm^3 $molecule^{-1}$ s^{-1}) for reaction of NO_3 with 2-propen-1-ol ($CH_2{=}CHCH_2OH$)

$10^{14} \times A$	B (K)	$10^{14} \times k$	T (K)	Technique[a]	Reference	Temperature Range (K)
4.4	340 ± 300	1.3 ± 0.4	273	DF–AS	Hallquist et al. (1996)	273–363
		1.3 ± 0.2	294			
		1.6 ± 0.3	323			
		1.5 ± 0.3	342			
		1.8 ± 0.4	363			
		1.6 ± 0.4	294	RR (Propene)[b]	Hallquist et al. (1996)	
		1.1 ± 0.3	297 ± 2	RR (Propene)[b]	Noda et al. (2002)	

[a]Abbreviations used for the techniques are defined in table I-F-3.
[b]Placed on an absolute basis using $k(NO_3 + \text{propene}) = 9.5 \times 10^{-15}$ cm^3 $molecule^{-1}$ s^{-1} (Atkinson et al., 2006).

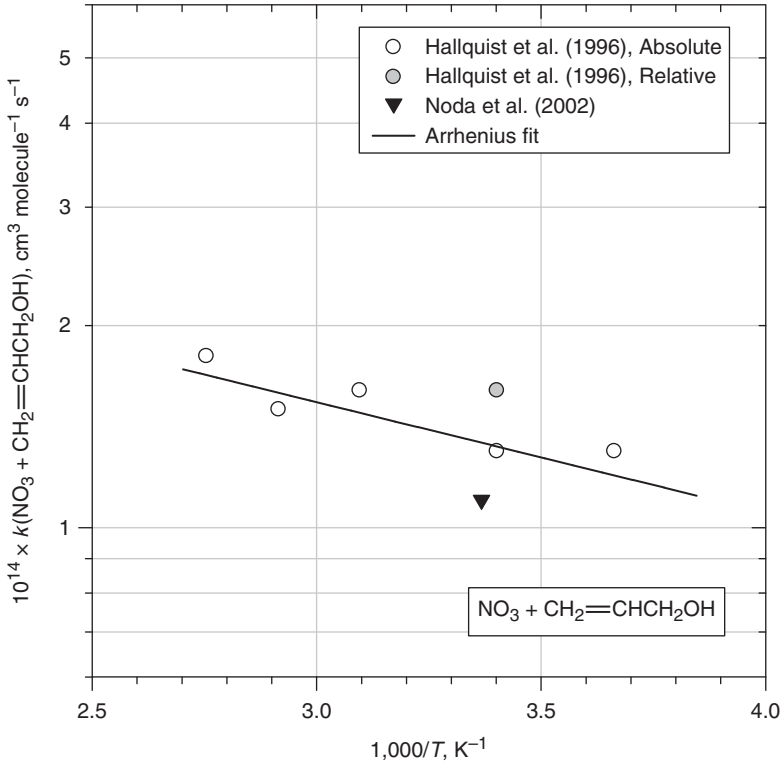

Figure II-D-2. Arrhenius plot of the rate coefficient for the reaction of NO_3 with 2-propen-1-ol.

agreement between the rate coefficients reported near 298 K in the two studies. A least-squares fit of the Arrhenius expression to the combined data set in figure II-D-2 gives $k(OH + \text{2-propen-1-ol}) = 4.8 \times 10^{-14} \exp(-378/T)\,cm^3$ $molecule^{-1}$ s^{-1}. This expression gives $k(OH + \text{2-propen-1-ol}) = 1.3 \times 10^{-14}\,cm^3$ $molecule^{-1}$ s^{-1} at 298 K with an uncertainty estimated to be ±30%.

II-D-1.4. Cl-Atom Reaction Kinetics

The only measurement of the rate coefficient for reaction of Cl with 2-propen-1-ol at the time of this writing is that of Aranda et al. (2003b) using discharge flow–mass spectrometry at low pressure (0.5–3 Torr) over the temperature range 260–333 K. The rate coefficients obtained are given in table II-D-4. Aranda et al. (2003b) reported a slight pressure dependence of the rate coefficient within the range investigated. A least-squares fit of the Arrhenius expression to the reported data gives $k(\mathrm{Cl}+\text{2-propen-1-ol}) = 1.1 \times 10^{-11} \exp(465/T)\,\mathrm{cm^3\ molecule^{-1}\ s^{-1}}$ at 1 Torr total pressure. At 298 K, this expression gives $k(\mathrm{Cl} + \text{2-propen-1-ol}) = 5.2 \times 10^{-11}\,\mathrm{cm^3\ molecule^{-1}\ s^{-1}}$ at low pressures with an uncertainty estimated to be ±25%.

II-D-1.5. Summary of the Atmospheric Fate of 2-Propen-1-ol

The atmospheric degradation of 2-propen-1-ol will be controlled via reaction with OH, O_3, and NO_3. Using $[\mathrm{OH}] = 2.5 \times 10^6$, $[\mathrm{O_3}] = 10^{12}$, and $[\mathrm{NO_3}] = 3 \times 10^9$ molecule $\mathrm{cm^{-3}}$ lifetime estimates of 2, 17, and 7 h are obtained for 2-propen-1-ol with respect to reaction with OH, O_3, and NO_3, respectively.

The products of reaction of OH with 2-propen-1-ol in the presence of NO_x have been investigated by Orlando et al. (2001). The major products observed are formaldehyde and glycolaldehyde ($HOCH_2CHO$) with molar yields of (98 ± 12)% and (90 ± 12)%, respectively. Acrolein ($CH_2{=}CHCHO$) was also identified as a reaction product and its yield was estimated to be (5 ± 2)%. As shown in the OH-initiated mechanism presented in figure II-D-3, glycolaldehyde and formaldehyde are the expected products following OH addition to either end of the double bond. The formation of acrolein ($CH_2{=}CHCHO$) provides evidence for a minor H-atom abstraction channel.

The ozonolysis of 2-propen-1-ol was investigated by Grosjean and Grosjean (1995) and Le Person et al. (2009); see figure II-D-4. In both studies, the major products observed are formaldehyde and glycolaldehyde with approximately the same yields (∼50% each).

Table II-D-4. Rate coefficients (k, $\mathrm{cm^3\ molecule^{-1}\ s^{-1}}$) for reaction of Cl with 2-propen-1-ol ($CH_2{=}CHCH_2OH$)

$10^{11} \times A$	B (K)	$10^{11} \times k$	T (K)	Technique[a]	Reference	Temperature Range (K)
1.1	−470 ± 135	6.9 ± 0.9[b]	260	DF–MS	Aranda et al. (2003b)	260–333
		5.6 ± 0.4[b]	288			
		5.1 ± 1.2[b]	298			
		4.7 ± 0.6[b]	333			
		4.7 ± 0.6[c]	298			
		6.3 ± 0.5[d]	298			
		6.5 ± 0.6[e]	298			

[a]Abbreviations used for the techniques are defined in table I-F-3.
[b]At 1 Torr.
[c]At 0.5 Torr.
[d]At 2 Torr.
[e]At 3 Torr.

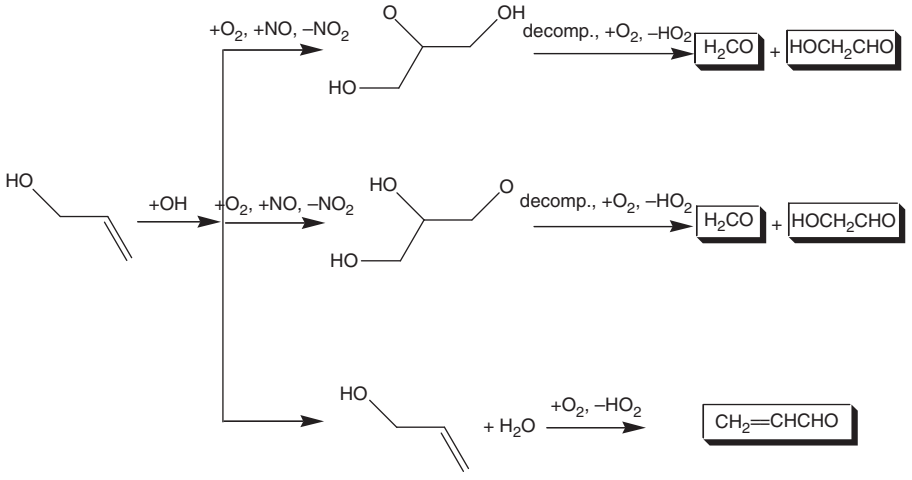

Figure II-D-3. OH-initiated oxidation of 2-propen-1-ol (Orlando et al., 2001).

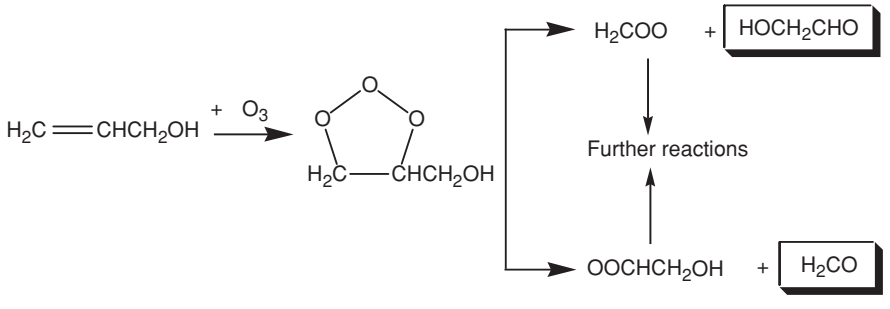

Figure II-D-4. O_3-initiated oxidation of 2-propen-1-ol (Grosjean and Grojean, 1995; Le Person et al., 2009).

The reaction of ozone with allyl alcohol is expected to involve, as for other unsaturated alcohols and olefins, electrophilic addition at the carbon–carbon double bond leading to the formation of a trioxide followed by its unimolecular decomposition into two carbonyls and two biradicals (Criegee intermediates):

Biradicals may form other carbonyl compounds through the following sequences:

$$HOCH_2CHOO \rightarrow CO_2 + H + H_2COH$$

$$H_2COH + O_2 \rightarrow H_2CO + HO_2$$

$$HOCH_2CHOO \rightarrow O + HOCH_2CHO$$

$$HOCH_2CHOO \rightarrow OH + HOCH_2CO$$

H_2COO may decompose leading mainly to OH, HO_2, CO, CO_2 (e.g., see Calvert et al., 2000). The reaction of NO_3 with 2-propen-1-ol has been investigated by Noda et al.

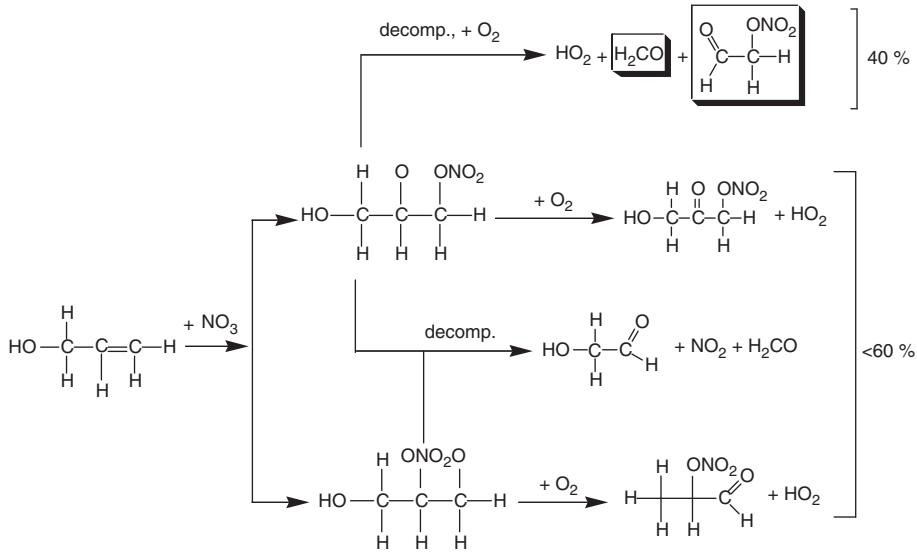

Figure II-D-5. NO_3-initiated oxidation of 2-propen-1-ol (Noda et al., 2000).

(2000). The possible mechanistic degradation mechanism of allyl alcohol initiated by reaction with NO_3 proposed by these authors is shown in figure II-D-5. The reaction proceeds by NO_3 addition to the double bond to form a radical which adds O_2 to form a nitrooxy–alkylperoxy radical. This radical may react at least in part with other species such as NO, NO_2, HO_2 or other peroxy radicals leading to the corresponding alkoxy radicals (via reaction with NO or a peroxy radical), an alcohol, and a carbonyl compound (via reaction with a peroxy radical), or a hydroperoxide (via reaction with HO_2). The degradation mechanism presented in figure II-D-5 summarizes the reaction sequences following the formation of the alkoxy radicals.

Noda et al. (2000) reported CH_2O (37 ± 1)%, $HC(O)CH_2ONO_2$ (41 ± 7)%, and organic nitrates [including $HC(O)CH_2ONO_2$ and an unidentified organic nitrate] (53 ± 10)% as the main reaction products. As shown in figure II-D-5, H_2CO can be formed via two different pathways. However, since no glycolaldehyde was observed, the authors concluded that the formaldehyde was formed as co-product of $HC(O)CH_2ONO_2$ through decomposition and reaction with O_2. The balance of the products was assumed to be hydroperoxides and other multi-functional compounds.

II-D-2. 2-Buten-1-ol (Crotyl Alcohol, $CH_3CH{=}CHCH_2OH$)

II-D-2.1. OH Reaction Kinetics

The reaction of OH radicals with 2-buten-1-ol has been studied by Cometto et al. (2008) using pulsed laser photolysis, laser-induced fluorescence, and relative rate techniques. The data given in table II-D-5 and displayed in figure II-D-6 have been reported in the temperature range 263–370 K. The rate coefficients obtained near 298 K by the two methods are in agreement. Fitting the Arrhenius expression to the data gives

Table II-D-5. Rate coefficients ($k = A\ e^{-B/T}$, cm^3 $molecule^{-1}$ s^{-1}) for reaction of OH with 2-buten-1-ol ($CH_3CH{=}CHCH_2OH$)

$10^{12} \times A$	B (K)	$10^{11} \times k$	T (K)	Technique[a]	Reference	Temperature Range (K)
		8.1 ± 1.5	298	RR[b] (propene)	Cometto et al. (2008)	
		8.8 ± 0.9	298	RR[c] (3-buten-2-ol)		
		10.9 ± 1.0	298	RR[c] (3-buten-2-ol)		
		11 ± 1	298	RR[d] (2-propen-1-ol)		
		10 ± 1	298	RR[e] (propyl vinyl ether)		
6.9 ± 0.9	−744 ± 40	12.02 ± 0.70	263	PLP–LIF	Cometto et al. (2008)	26–370
		10.69 ± 0.29	273			
		11.14 ± 0.70	273			
		9.15 ± 0.44	282			
		8.03 ± 0.48	298			
		8.56 ± 0.28	298			
		7.81 ± 0.40	298			
		7.63 ± 0.30	313			
		6.31 ± 0.23	329			
		6.16 ± 0.40	346			
		5.24 ± 0.24	369			
		5.70 ± 0.40	370			

[a]Abbreviations used for the techniques are defined in table I-F-3.
[b]Placed on an absolute basis using $k(OH + propene) = 2.9 \times 10^{-11}$ cm^3 $molecule^{-1}$ s^{-1} (Atkinson et al., 2006).
[c]Placed on an absolute basis using $k(OH + 3\text{-buten-2-ol}) = 5.9 \times 10^{-11}$ cm^3 $molecule^{-1}$ s^{-1} (this book, section II-D-4.1).
[d]Placed on an absolute basis using $k(OH + 2\text{-propen-1-ol}) = 5.0 \times 10^{-11}$ cm^3 $molecule^{-1}$ s^{-1} (this book, II-D-1.1).
[e]Placed on an absolute basis using $k(OH + propyl\ vinyl\ ether) = 1.0 \times 10^{-10}$ cm^3 $molecule^{-1}$ s^{-1} (this book, III-D-3.1).

$k(OH + 2\text{-buten-1-ol}) = 7.4 \times 10^{-12} \exp(734/T)$ cm^3 $molecule^{-1}$ s^{-1}. This expression gives $k(OH + 2\text{-buten-1-ol}) = 8.7 \times 10^{-11}$ cm^3 $molecule^{-1}$ s^{-1} at 298 K with an uncertainty estimated to be ±20%.

II-D-2.2. O_3 Reaction Kinetics

The rate coefficient for the reaction of O_3 with 2-buten-1-ol has been measured by Grosjean and Grosjean (1994). The value obtained at 287 K is $k = (2.51 \pm 0.47) \times 10^{-16}$ cm^3 $molecule^{-1}$ s^{-1}; see table II-D-6 and figure II-D-7.

II-D-2.3. NO_3 Reaction Kinetics

Noda et al. (2002) have measured the rate coefficient of the reaction of NO_3 with 2-buten-1-ol using a relative rate method. The value obtained at 297 K is $k = (3.9 \pm 0.4) \times 10^{-13}$ cm^3 $molecule^{-1}$ s^{-1}; see table II-D-7.

II-D-2.4. Cl-Atom Reaction Kinetics

The kinetics of the reaction of chlorine atoms with 2-buten-1-ol have been studied using a relative rate technique by Rodriguez et al. (2008). The rate coefficient values obtained are presented in table II-D-8. The authors have reported an Arrhenius expression of

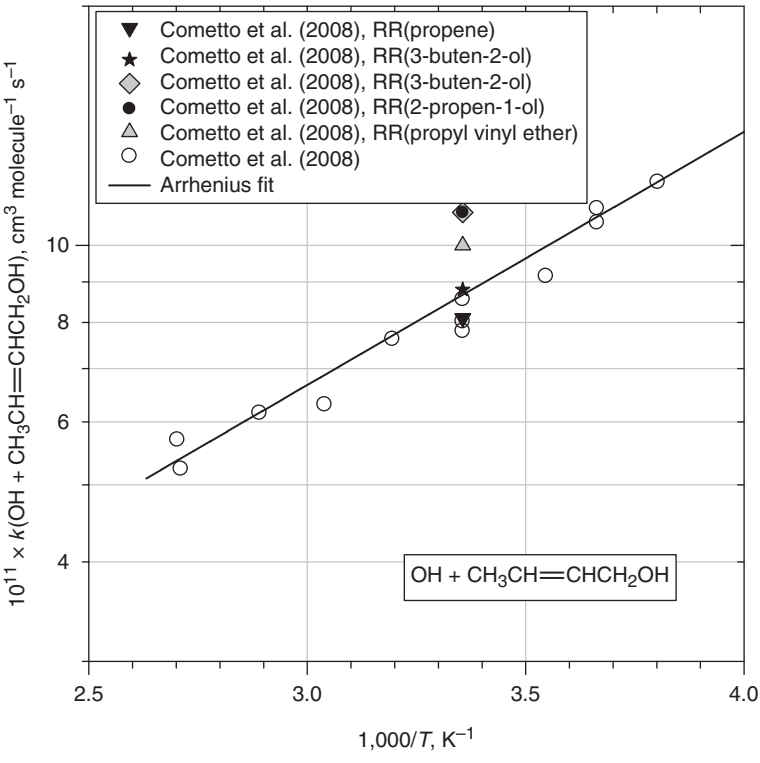

Figure II-D-6. Arrhenius plot of the rate coefficient for the reaction of OH with 2-buten-1-ol.

Table II-D-6. Rate coefficient (k, cm^3 $molecule^{-1}$ s^{-1}) for reaction of O_3 with 2-buten-1-ol ($CH_3CH{=}CHCH_2OH$)

$10^{16} \times k$	T (K)	Technique	Reference
2.51 ± 0.47	287 ± 1	Excess of 2-buten-1-ol[a]	Grosjean and Grosjean (1994)

[a]Pseudo first-order conditions, excess of 2-buten-1-ol, with O_3 measured by absorption spectroscopy.

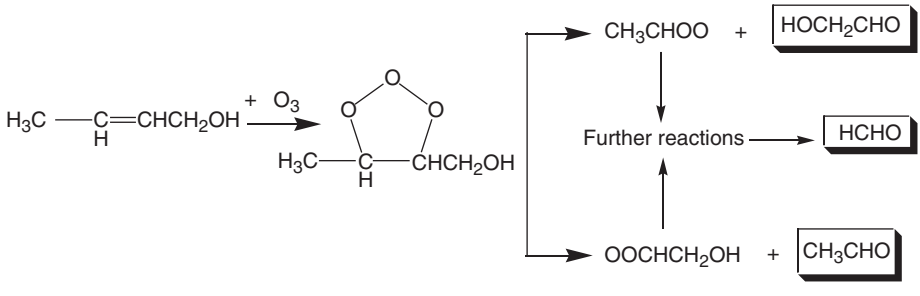

Figure II-D-7. O_3-initiated oxidation of 2-buten-1-ol (Grosjean and Grojean, 1995).

Table II-D-7. Rate coefficient (k, cm^3 molecule^{-1} s^{-1}) for the reaction of NO_3 with 2-buten-1-ol ($CH_3CH{=}CHCH_2OH$)

$10^{13} \times k$	T (K)	Technique[a]	Reference
3.9 ± 0.4	297 ± 2	RR (*trans*-2-butene)[b]	Noda et al. (2002)

[a]Abbreviations used for the techniques are defined in table I-F-3.
[b]Placed on an absolute basis using $k(NO_3 + trans\text{-2-butene}) = 3.9 \times 10^{-13}$ cm^3 molecule^{-1} s^{-1} (Atkinson and Arey, 2003a).

Table II-D-8. Rate coefficients (k, cm^3 molecule^{-1} s^{-1}) for the reaction of Cl with 2-buten-1-ol ($CH_3CH{=}CHCH_2OH$)

$10^{21} \times A$	B (K)	$10^{10} \times k$	T (K)	Technique[a]	Reference	Temperature Range (K)
8.85 ± 0.46	−7,240 ± 1,455	2.87 ± 0.36	298	RR[b] (Octane)	Rodriguez et al. (2008)	256–298
		2.97 ± 0.76	298	RR[c] (1-Butene)		
		196 ± 61	256	RR[d] (Cyclohexane)		
		70.9 ± 18.6	262			
		50.2 ± 13.9	274			
		13.9 ± 4.6	283			
		3.45 ± 0.73	297			

[a]Abbreviations used for the techniques are defined in table I-F-3.
[b]Placed on an absolute basis using $k(Cl + octane) = 3.22 \times 10^{-10}$ cm^3 molecule^{-1} s^{-1} (Li and Pirasteh, 2006).
[c]Placed on an absolute basis using $k(Cl + 1\text{-butene}) = 2.9 \times 10^{-10}$ cm^3 molecule^{-1} s^{-1} (Orlando et al., 2003).
[d]Placed on an absolute basis using $k(Cl + cyclohexane) = 3.3 \times 10^{-10}$ cm^3 molecule^{-1} s^{-1} (Calvert et al., 2008).

$k(Cl{+}2\text{-buten-1-ol}) = 8.85 \times 10^{-21} \exp(7{,}240/T)$ cm^3 molecule^{-1} s^{-1}. The rate coefficient measured at 298 K seems plausible. However, the rate coefficients obtained at low temperature, e.g., $k(256\text{ K}) = 2 \times 10^{-8}$ cm^3 molecule^{-1} s^{-1}, are about 100 times larger than expected from simple collision theory and are not physically plausible (Wallington and Mellouki, 2009). These data are not recommended.

II-D-2.5. Summary of the Atmospheric Fate of 2-Buten-1-ol

Combining the rate coefficients reported in this section with typical atmospheric concentrations of OH, O_3, and NO_3, ($[OH] = 2.5 \times 10^6$, $[O_3] = 1 \times 10^{12}$, and $[NO_3] = 3 \times 10^9$ molecule cm^{-3}), the lifetimes with respect to reactions with OH and O_3 are calculated to be ∼1 h and that with respect to reaction with NO_3 is found to be ∼15 min.

The expected major products of the reaction of OH with 2-buten-1-ol in the presence of NO_x are acetaldehyde (CH_3CHO) and glycolaldehyde ($HOCH_2CHO$) formed following OH-addition to the double bond through the following mechanism:

$$OH + CH_3CH_2{=}CHCH_2OH(+O_2, +NO, -NO_2) \rightarrow CH_3CH(OH)\text{-}CH(O\bullet)CH_2OH$$

$$CH_3CH(OH)\text{-}CH(O\bullet)CH_2OH(\text{decomp.}, +O_2, -HO_2) \rightarrow CH_3CHO + HOCH_2CHO$$

$$OH + CH_3CH_2{=}CHCH_2OH(+O_2, +NO, -NO_2) \rightarrow CH_3CH(O\bullet)CH(OH)CH_2OH$$

$$CH_3CH(O\bullet)CH(OH)CH_2OH(\text{decomp.}, +O_2, -HO_2) \rightarrow CH_3CHO + HOCH_2CHO$$

The overall mechanisms for reaction of O_3 and NO_3 with 2-buten-1-ol are similar to those with 2-propen-1-ol described previously. O_3 will add to the C=C bond resulting in formation of a trioxide which decomposes to form two carbonyl compounds and two biradicals. Grosjean and Grosjean (1995) reported acetaldehyde and glycolaldehyde as major products from the ozonolysis of 2-buten-1-ol with formation yields of (64 ± 6)% and (79 ± 18)%, respectively. Formaldehyde was also observed as a product (23 ± 7)%, its formation involves the reactions of biradicals (CH_3CHOO and $HOCH_2COO$).

Noda et al. (2000) investigated the NO_3-initiated oxidation of 2-buten-1-ol. Only ~20% of the reacted alcohol was identified as gas-phase products. The main observed products were formaldehyde (10 ± 3)%, acetaldehyde (12 ± 2)%, and glycolaldehyde (7 ± 2)%. The remaining 80% was attributed to the formation of nitrooxy and multifunctional compounds.

II-D-3. 3-Buten-1-ol (CH_2=$CHCH_2CH_2OH$)

II-D-3.1. OH Reaction Kinetics

The reaction of OH with 3-buten-1-ol has been studied by Papagni et al. (2001) and Cometto et al. (2008). The values reported at room temperature by these two groups are in good agreement. The only temperature dependence study is that conducted by Cometto et al. in the range 263–371 K. The data are summarized in table II-D-9 and plotted in figure II-D-8. A least-squares fit of the Arrhenius expression to the combined data set from Papagni et al. (2001) and Cometto et al. (2008) gives

Table II-D-9. Rate coefficients ($k = A\ e^{-B/T}$, cm^3 $molecule^{-1}$ s^{-1}) for reaction of OH with 3-buten-1-ol (CH_2=$CHCH_2CH_2OH$)

$10^{12} \times A$	B (K)	$10^{11} \times k$	T (K)	Technique[a]	Reference	Temperature Range (K)
		5.5 ± 0.2	296 ± 2	RR[b](1,3,5-trimethylbenzene)	Papagni et al. (2001)	
		5.7 ± 0.9	298 ± 2	RR[c] (propene)	Cometto	
		5.9 ± 0.2	298 ± 2	RR[d] (cyclohexene)	et al. (2008)	
4.0 ± 0.4	−783 ± 32	7.42 ± 0.24	263	PLP–LIF	Cometto	263–371
		7.00 ± 0.43	273		et al. (2008)	
		6.21 ± 0.20	282			
		6.37 ± 0.25	283			
		5.60 ± 0.23	298			
		5.83 ± 0.36	298			
		4.99 ± 0.28	313			
		4.59 ± 0.15	328			
		4.03 ± 0.22	343			
		3.73 ± 0.16	347			
		3.08 ± 0.16	370			
		3.18 ± 0.15	371			

[a]Abbreviations used for the techniques are defined in table I-F-3.

[b]Placed on an absolute basis using $k(OH + 1,3,5\text{-trimethylbenzene}) = 5.7 \times 10^{-11}$ cm^3 $molecule^{-1}$ s^{-1} (Calvert et al., 2002).

[c]Placed on an absolute basis using $k(OH + propene) = 2.9 \times 10^{-11}$ cm^3 $molecule^{-1}$ s^{-1} (Atkinson et al., 2006).

[d]Placed on an absolute basis using $k(OH + cyclohexene) = 6.77 \times 10^{-11}$ cm^3 $molecule^{-1}$ s^{-1} (Calvert et al., 2000).

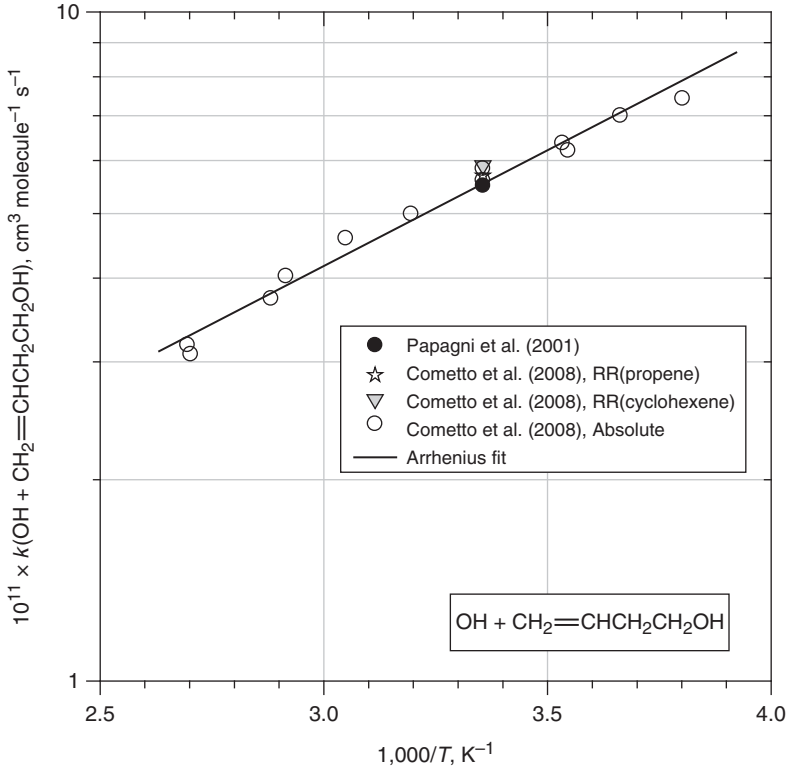

Figure II-D-8. Arrhenius plot of the rate coefficient for reaction of OH with 3-buten-1-ol.

$k(\text{OH} + \text{3-buten-1-ol}) = 3.8 \times 10^{-12} \exp(797/T)\,\text{cm}^3\,\text{molecule}^{-1}\,\text{s}^{-1}$. This expression gives $k(\text{OH} + \text{3-buten-1-ol}) = 5.5 \times 10^{-11}\,\text{cm}^3\,\text{molecule}^{-1}\,\text{s}^{-1}$ at 298 K with an estimated uncertainty of ±15%.

II-D-3.2. O_3 Reaction Kinetics

The reaction of O_3 with 3-buten-1-ol has been studied by Grosjean et al. (1993a). The rate coefficient reported at 287 K is $k = (4.9 \pm 0.4) \times 10^{-18}\,\text{cm}^3\,\text{molecule}^{-1}\,\text{s}^{-1}$; see table II-D-10.

II-D-3.3. Summary of the Atmospheric Fate of 3-Buten-1-ol

Using $k(\text{OH}+\text{3-buten-1-ol}) = 5.5\times10^{-11}$ and $k(\text{O}_3+\text{3-buten-1-ol}) = 4.9\times10^{-18}\,\text{cm}^3$ $\text{molecule}^{-1}\,\text{s}^{-1}$ with $[\text{OH}] = 2.5 \times 10^6$ and $[\text{O}_3] = 10^{12}\,\text{molecule}\,\text{cm}^{-3}$, the atmospheric lifetimes of 3-buten-1-ol with respect to reactions with OH and O_3 are estimated to be 2 h and 2 days, respectively.

The expected major products of the reaction of OH with 3-buten-1-ol in the presence of NO_x are CH_2O, $HOCH_2CH_2CHO$, and $HOCH_2CHO$ following OH addition to either end of the double bond through the mechanism shown in figure II-D-9.

Table II-D-10. Rate coefficient (k, cm^3 $molecule^{-1}$ s^{-1}) for reaction of O_3 with 3-buten-1-ol (CH_2=$CHCH_2CH_2OH$)

$10^{18} \times k$	T (K)	Technique	Reference
4.9 ± 0.4	295 ± 1	Excess of 3-buten-1-ol[a]	Grosjean et al. (1993a)

[a]Pseudo first-order conditions, using an excess of 3-buten-1-ol; O_3 measured by absorption spectroscopy.

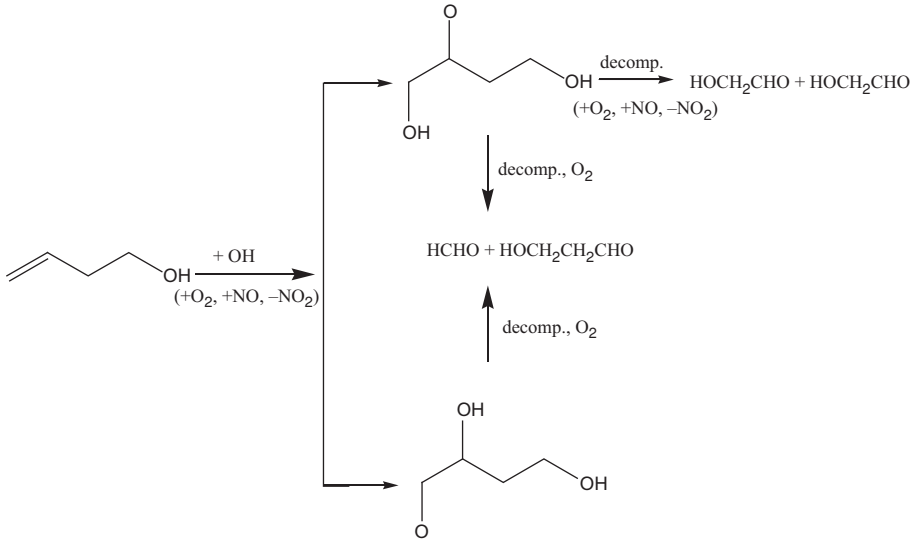

Figure II-D-9. Simplified mechanism for the OH-initiated oxidation of 3-buten-1-ol.

The main products of the O_3 reaction with 3-buten-1-ol reported by Grosjean et al. (1993b) are formaldehyde (37 ± 19)% and glycolaldehyde (12 ± 5)% and/or glyoxal (5 ± 2)%, along with small yields of three unidentified carbonyls. The reactions involved are (Grosjean et al., 1993b):

$$CH_2{=}CHCH_2CH_2OH + O_3 \rightarrow CH_2O + HOCH_2CH_2CHOO + H_2COO + HC(O)CH_2CH_2OH$$

Followed by the reactions of hydroxyethyl-substituted Criegee biradical:

$$HOCH_2CH_2CHOO \rightarrow HOCH_2CH_2C(O)OH$$
$$\rightarrow OH + HOCH_2CH_2CO$$
$$\rightarrow O + HOCH_2CH_2CHO$$
$$\rightarrow HOCH_2CH{=}C(H)OOH$$

As discussed by Grosjean et al. (1993b) and Grosjean and Grosjean (1995), the stability of $HOCH_2CH{=}C(H)OOH$ is unclear.

II-D-4. 3-Buten-2-ol ($CH_2{=}CHCH(OH)CH_3$)

II-D-4.1. OH Reaction Kinetics

The reaction of OH with 3-buten-2-ol has been studied by Papagni et al. (2001) at 296 K and atmospheric pressure using a relative rate method. Papagni et al. (2001) report a rate coefficient of $k = 5.9 \times 10^{-11}$ cm^3 molecule^{-1} s^{-1}. This value is recommended with an estimated uncertainty of ±15%; see table II-D-11.

II-D-4.2. O_3 Reaction Kinetics

This reaction was investigated by Grosjean and Grosjean (1994). The reaction rate coefficient obtained under pseudo first-order conditions is $k(O_3 + CH_2{=}CHCH(OH)CH_3) = (1.62 \pm 0.07) \times 10^{-17}$ cm^3 molecule^{-1} s^{-1} at 290 K; see table II-D-12.

II-D-4.3. NO_3 Reaction Kinetics

The reaction of NO_3 radicals with 3-buten-2-ol has been studied by Hallquist et al. (1996) and Noda et al. (2002). While Hallquist et al. (1996) used both relative and absolute (discharge flow) rate methods, Noda et al. (2002) used a relative rate method. The reaction rate coefficients obtained in these two studies are in very good agreement. An average of the determinations given in table II-D-13 gives $k(NO_3 + 3\text{-buten-2-ol}) = 1.2 \times 10^{-14}$ cm^3 molecule^{-1} s^{-1} with an estimated uncertainty of ±30% at 298 K; see table II-D-13.

Table II-D-11. Rate coefficient (k, cm^3 molecule^{-1} s^{-1}) for reaction of OH with 3-buten-2-ol ($CH_2{=}CHCH(OH)CH_3$)

$10^{11} \times k$	T (K)	Technique[a]	Reference
5.93 ± 0.23	296 ± 2	RR[b] (1,3,5-trimethylbenzene)	Papagni et al. (2001)

[a]Abbreviations used for the techniques are defined in table I-F-3.
[b]Placed on an absolute basis using k(OH + 1, 3, 5-trimethylbenzene) = 5.7×10^{-11} cm^3 molecule^{-1} s^{-1} (Calvert et al., 2002).

Table II-D-12. Rate coefficients (k, cm^3 molecule^{-1} s^{-1}) for reaction of O_3 with 3-buten-2-ol ($CH_2{=}CHCH(OH)CH_3$)

$10^{17} \times k$	T (K)	Technique	Reference
1.62 ± 0.07	290 ± 1	Excess of 3-buten-2-ol[a]	Grosjean and Grosjean (1994)

[a]Pseudo first-order conditions using excess of 3-buten-2-ol; O_3 measured by absorption spectroscopy.

Table II-D-13. Rate coefficients (k, cm^3 $molecule^{-1}$ s^{-1}) for reaction of NO_3 with 3-buten-2-ol (CH_2=$CHCH(OH)CH_3$)

$10^{14} \times k$	T (K)	Technique[a]	Reference
1.2 ± 0.3	294 ± 2	DF abs.	Hallquist et al. (1996)
1.3 ± 0.4	294 ± 2	RR (propene)[b]	Hallquist et al. (1996)
1.2 ± 0.2	297 ± 2	RR (propene)[b]	Noda et al. (2002)

[a]Abbreviations used for the techniques are defined in table I-F-3.
[b]Placed on an absolute basis using $k(NO_3 + \text{propene}) = 4.6 \times 10^{-15} \exp(-1{,}155/T)\,cm^3$ $molecule^{-1}$ s^{-1} (Atkinson et al., 2006).

II-D-4.4. Summary of the Atmospheric Fate of 3-Buten-2-ol

The rate coefficients for reaction of OH, O_3, and NO_3 have been used to estimate the atmospheric lifetimes of 3-buten-2-ol. The derived lifetimes are 2, 17, and 8 h for reaction with OH, O_3 and NO_3, respectively. These three reactants are of importance in the assessment of the atmospheric degradation of 3-buten-2-ol. The expected major products of the reaction of OH with 3-buten-2-ol in the presence of NO_x are CH_2O, CH_3CHO, $HOCH_2CHO$, and $CH_3CH(OH)CHO$ following the addition of OH radicals to C=C double bond.

The ozonolysis of 3-buten-2-ol leads mainly to formaldehyde (44 ± 5)%, 2-hydroxypropanal (30 ± 3)% and acetaldehyde (19 ± 2)% as reported by Grosjean and Grosjean (1995). Acetone and glyoxal were observed as minor products in yields of (2 ± 1)% and (3 ± 1)%, respectively. The proposed mechanism is similar to that for the ozonolysis of other olefins with the initial formation of a trioxide which decomposes to stable carbonyls and biradicals.

The NO_3-initiated oxidation of 3-buten-2-ol was investigated by Noda et al. (2000). Based on the observed products, the authors have suggested the possible degradation mechanism presented in figure II-D-10. The main observed products are acetaldehyde (27 ± 7)% and nitrooxy-acetaldehyde (32 ± 6)% as co-products, which led the authors to conclude that this pathway accounts for about 30% of the reacted alcohol.

II-D-5. *cis*-2-Penten-1-ol (CH_3CH_2CH=$CHCH_2OH$)

II-D-5.1. OH Reaction Kinetics

The rate coefficient for reaction of OH radicals with *cis*-2-penten-1-ol has been measured by Orlando et al. (2001) using a relative rate method. The rate coefficient value obtained by these authors is recommended, $k(OH + C_2H_5CH{=}CHCH_2OH) = 1.17 \times 10^{-10}\,cm^3$ $molecule^{-1}$ s^{-1} at 298 K with an estimated uncertainty of ±15%; see table II-D-14.

II-D-5.2. O_3 Reaction Kinetics

Grosjean and Grosjean (1994) have measured the rate coefficient for reaction of O_3 with *cis*-2-penten-1-ol at atmospheric pressure in air. The value obtained is

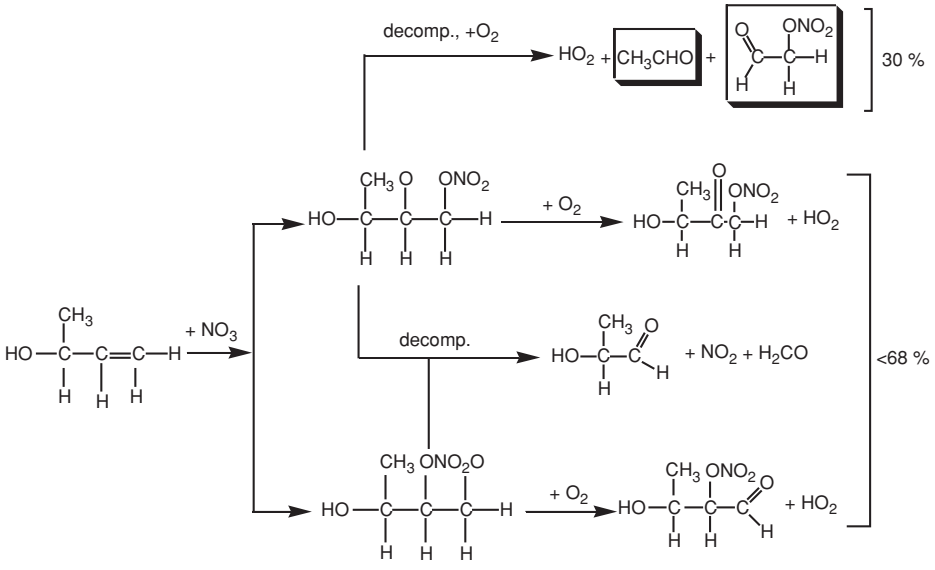

Figure II-D-10. NO_3-initiated oxidation of 3-buten-2-ol (Noda et al., 2000).

Table II-D-14. Rate coefficient (k, cm^3 molecule^{-1} s^{-1}) for reaction of OH with *cis*-2-penten-1-ol ($CH_3CH_2CH{=}CHCH_2OH$)

$10^{10} \times k$	T (K)	Technique[a]	Reference
1.17 ± 0.16	298	RR (propene)[b]	Orlando et al. (2001)

[a]Abbreviations used for the techniques are defined in table I-F-3.
[b]Placed on an absolute basis using k(OH + propene) = 2.9×10^{-11} cm^3 molecule^{-1} s^{-1} (Atkinson et al., 2006).

$k(O_3 + cis\text{-2-penten-1-ol}) = (1.69 \pm 0.25) \times 10^{-16}$ cm^3 molecule^{-1} s^{-1} at 290 K; see table II-D-15.

II-D-5.3. NO_3 Reaction Kinetics

Pfrang et al. (2007) studied the reaction of NO_3 with *cis*-2-penten-1-ol using a discharge flow technique and reported $k(NO_3 + cis\text{-}2\text{-}penten\text{-}1\text{-}ol) = (1.56 \pm 0.24) \times 10^{-13}$ cm^3 molecule^{-1} s^{-1} at 298 K; see table II-D-16.

II-D-5.4. Summary of the Atmospheric Fate of cis-2-Penten-1-ol

The estimated atmospheric lifetimes of *cis*-2-penten-1-ol with respect to removal through reaction with OH, O_3, and NO_3 are of the order of 1 h for the three reactions. Hence, the atmospheric degradation of *cis*-2-penten-1-ol will involve all three processes. The products obtained in the OH-initiated oxidation of *cis*-2-penten-1-ol are glycolaldehyde (87 ± 11)%, propanal (91 ± 13)%, and formaldehyde (11 ± 2)%, accounting for 100 ± 14 % of the reacted carbon (Orlando et al., 2001).

Table II-D-15. Rate coefficient (k, cm^3 molecule^{-1} s^{-1}) for reaction of O_3 with *cis*-2-penten-1-ol ($CH_3CH_2CH{=}CHCH_2OH$)

$10^{16} \times k$	T (K)	Technique[a]	Reference
1.69 ± 0.25	290 ± 1	Excess of *cis*-2-penten-1-ol[b]	Grosjean and Grosjean (1994)

[a]Abbreviations used for the techniques are defined in table I-F-3.
[b]Pseudo first-order conditions (excess of cis-2-penten-1-ol, O_3 measured by absorption).

Table II-D-16. Rate coefficient (k, cm^3 molecule^{-1} s^{-1}) for the reaction of NO_3 with *cis*-2-penten-1-ol ($CH_3CH_2CH{=}CHCH_2OH$)

$10^{13} \times k$	T (K)	Technique[a]	Reference
1.56 ± 0.24[b]	298 ± 3	DF abs.	Pfrang et al. (2007)

[a]Abbreviations used for the techniques are defined in table I-F-3.
[b]Placed on an absolute basis using $k(NO_3 + \text{propene}) = 9.5 \times 10^{-15}$ cm^3 molecule^{-1} s^{-1} (Atkinson et al., 2006).

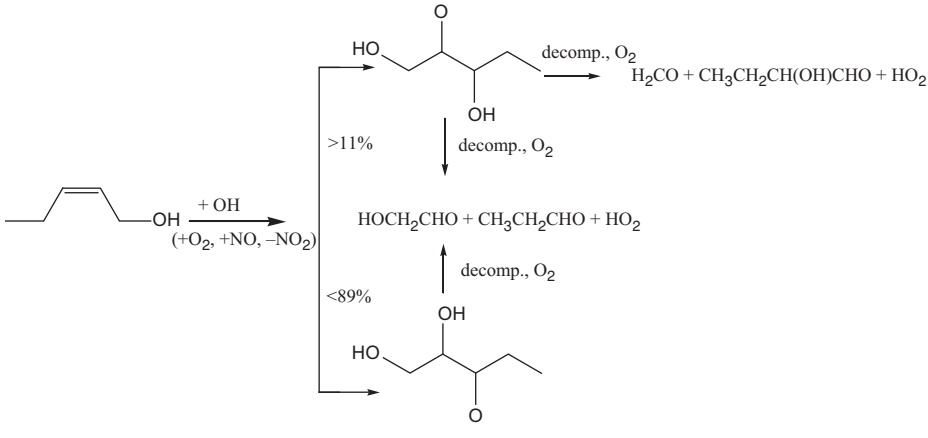

Figure II-D-11. OH-initiated oxidation of *cis*-2-penten-1-ol (Orlando et al., 2001).

Minor contribution from H abstraction at the —CH_2OH site, leading to 2-pentenal is a possibility. The suggested oxidation mechanism following addition to the $\rangle C{=}C\langle$ double bond is presented in figure II-D-11.

According to the mechanistic study of Grosjean and Grosjean (1995), the major products arising from the O_3-initiated degradation of *cis*-2-penten-1-ol are propanal (51 ± 2)% and hydroxyacetaldehyde (53 ± 4)%, while formaldehyde, acetaldehyde, and methylglyoxal were observed as minor reaction products with yields of (7 ± 2)%, (8 ± 1)%, and (4 ± 1)%, respectively.

The reaction of NO_3 with *cis*-2-penten-1-ol may lead to the formation of a series of aldehydes, such as formaldehyde, acetaldehyde, propanal, and glycolaldehyde. The reaction may also produce nitrooxy-aldehydes similarly to that observed for other unsaturated alcohols (Noda et al., 2000).

II-D-6. 1-Penten-3-ol (CH_2=CHCH(OH)CH_2CH_3)

II-D-6.1. OH Reaction Kinetics

The reaction of OH with 1-penten-3-ol has been investigated by Orlando et al. (2001) using a relative method. A rate coefficient value of $k = 7.4 \times 10^{-11}$ cm^3 molecule^{-1} s^{-1} at 298 K was obtained and is recommended here with an uncertainty of ±20%; see table II-D-17.

II-D-6.2. O_3 Reaction Kinetics

The rate coefficient of this reaction has been measured by Grosjean and Grosjean (1994) by monitoring the loss of 1-penten-3-ol in an excess of O_3 in one atmosphere of air. The value obtained was $k(O_3 + \text{1-penten-3-ol}) = (1.79 \pm 0.18) \times 10^{-17}$ cm^3 molecule^{-1} s^{-1} at 289 K; see table II-D-18.

II-D-6.3. NO_3 Reaction Kinetics

The rate coefficient of the reaction of NO_3 with 1-penten-3-ol has been reported by Pfrang et al. (2007). These authors used the discharge flow technique to conduct their investigation and reported $k(NO_3 + \text{1-penten-3-ol}) = (1.42 \pm 0.19) \times 10^{-14}$ cm^3 molecule^{-1} s^{-1} at 298 K; see table II-D-19.

Table II-D-17. Rate coefficient (k, cm^3 molecule^{-1} s^{-1}) for the reaction of OH with 1-penten-3-ol (CH_2=CHCH(OH)CH_2CH_3)

$10^{11} \times k$	T (K)	Technique[a]	Reference
7.4 ± 1.0	298	RR (propene)[b]	Orlando et al. (2001)

[a]Abbreviations used for the techniques are defined in table I-F-3.
[b]Placed on an absolute basis using $k(\text{OH} + \text{propene}) = 2.9 \times 10^{-11}$ cm^3 molecule^{-1} s^{-1} (Atkinson et al., 2006).

Table II-D-18. Rate coefficient (k, cm^3 molecule^{-1} s^{-1}) for the reaction of O_3 with 1-penten-3-ol (CH_2=CHCH(OH)CH_2CH_3)

$10^{17} \times k$	T (K)	Technique	Reference
1.79 ± 0.18	289 ± 1	Excess of 1-penten-3-ol[a]	Grosjean and Grosjean (1994)

[a]Pseudo first-order conditions using an excess of 1-penten-3-ol; O_3 measured by absorption spectroscopy.

Table II-D-19. Rate coefficient (k, cm^3 molecule^{-1} s^{-1}) for the reaction of NO_3 with 1-penten-3-ol (CH_2=CHCH(OH)CH_2CH_3)

$10^{14} \times k$	T (K)	Technique[a]	Reference
1.42 ± 0.19	298 ± 3	DF abs.	Pfang et al. (2007)

[a]Abbreviations used for the techniques are defined in table I-F-3.
[b]Placed on an absolute basis using $k(\text{NO}_3 + \text{propene}) = 9.3 \times 10^{-15}$ cm^3 molecule^{-1} s^{-1} (Atkinson et al., 2006).

II-D-6.4. Summary of the Atmospheric Fate of 1-Penten-3-ol

The estimated atmospheric lifetimes of 1-penten-3-ol with respect to the reactions with OH, O_3, and NO_3 are of the order of 1 h, 15 h, and 7h, respectively. Orlando et al. (2001) reported glycolaldehyde (47 ± 6)% and formaldehyde (35 ± 4)% as the major products following the OH-initiated oxidation of 1-penten-3-ol. The oxidation mechanism proposed by Orlando et al. presented in figure II-D-12 shows that propanal is an expected co-product of glycolaldehyde, and 2-hydroxybutanal is an expected co-product of formaldehyde. Orlando et al. (2001) detected propanal but could not quantify it. The observed products account for 82 ± 8% of the reacted alcohol. These authors suggested that isomerization of the 2,3-dihydroxy-1-pentoxy radical leading to 2,3,4-trihydroxypentanal and/or 2,3-dihydroxypropanal (see figure II-D-12) may be of significance. A small contribution from H abstraction at the 3-position to produce ethyl vinyl ketone is also a possibility.

Grosjean and Grosjean (1995) studied the products of the reaction of O_3 with 1-penten-3-ol and reported formaldehyde (34 ± 4)%, 2-hydroxybutanal (30 ± 5)%, and propanal (12 ± 1)% as the major products.

NO_3 is expected to add to the C=C bond of 1-penten-3-ol leading to formaldehyde, propanal, and nitrooxy-compounds (Noda et al., 2000).

II-D-7. 2-Methyl-2-propen-1-ol [CH_2=$C(CH_3)CH_2OH$]

II-D-7.1. OH Reaction Kinetics

The rate coefficient of the reaction of OH with 2-methyl-2-propen-1-ol has been determined by Cometto et al. (2008) using absolute and relative methods; see table II-D-20.

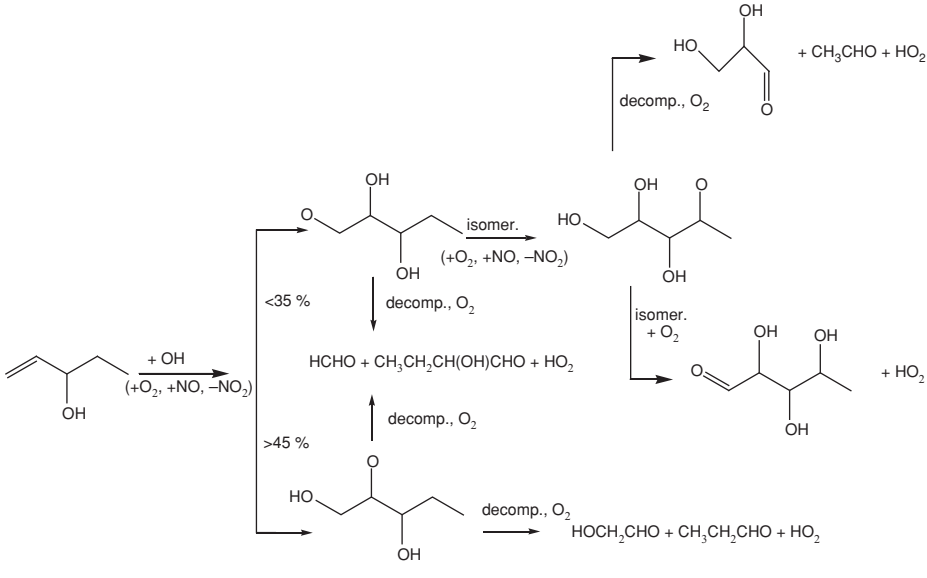

Figure II-D-12. OH-initiated oxidation of 1-penten-3-ol (Orlando et al., 2001).

A fit of the Arrhenius expression to the data gives $k(OH + CH_2{=}C(CH_3)CH_2OH) = 8.1 \times 10^{-12} \exp(716/T)\,cm^3$ molecule^{-1} s^{-1} in the temperature range 263–370 K. This expression gives $k(OH + CH_2{=}C(CH_3)CH_2OH) = 9.0 \times 10^{-11}\,cm^3$ molecule^{-1} s^{-1} at 298 K with an uncertainty estimated to be ± 15%; see table II-D-20 and figure II-D-13.

II-D-7.2. Cl-Atom Reaction Kinetics

The kinetics of the reaction of chlorine atoms with 2-methyl-2-propen-1-ol have been studied using a relative rate technique by Rodriguez et al. (2008). The rate coefficient values obtained are presented in table II-D-21. The authors have reported $k(Cl + 2\text{-methyl-2-propen-1-ol}) = 3.05 \times 10^{-23} \exp(8{,}760/T)\,cm^3$ molecule^{-1} s^{-1} over the temperature range 256–298 K. The rate coefficients obtained at low temperatures (e.g., k(256 K) $\approx 2 \times 10^{-8}\,cm^3$ molecule^{-1} s^{-1}) are approximately 100 times larger than expected from simple collision theory and are not physically plausible (Wallington and Mellouki, 2009). These data are not recommended.

II-D-7.3. Summary of the Atmospheric Fate of 2-Methyl-2-propen-1-ol

The estimated atmospheric lifetime of 2-methyl-2-propen-1-ol with respect to reaction with OH is about 1 h. The expected major products of the reaction of OH with 2-methyl-2-propen-1-ol in the presence of NO_x are CH_2O and $HOCH_2C(O)CH_3$ as co-products following OH-addition to either end of the double bond in the alcohol; the suggested mechanism is given in figure II-D-14.

Table II-D-20. Rate coefficients ($k = A\ e^{-B/T}$, cm^3 molecule^{-1} s^{-1}) for reaction of OH with 2-methyl-2-propen-1-ol ($CH_2{=}C(CH_3)CH_2OH$)

$10^{11} \times A$	B (K)	$10^{11} \times k$	T (K)	Technique[a]	Reference	Temperature Range (K)
		8.9 ± 1.3	298 ± 2	RR[b] (propene)	Cometto et al.	
		9.1 ± 0.5	298 ± 2	RR[c] (3-buten-2-ol)	(2008)	
1.0 ± 0.1	−652 ± 27	12.17 ± 0.27	263	PLP–LIF	Cometto et al.	263–370
		10.81 ± 0.54	273		(2008)	
		11.00 ± 0.38	273			
		9.12 ± 0.41	283			
		9.57 ± 0.48	298			
		9.28 ± 0.58	298			
		7.74 ± 0.20	314			
		7.59 ± 0.31	329			
		6.29 ± 0.46	348			
		5.56 ± 0.38	369			
		5.52 ± 0.30	370			

[a]Abbreviations used for the techniques are defined in table I-F-3.
[b]Placed on an absolute basis using $k(OH + \text{propene}) = 2.9 \times 10^{-11}$ cm^3 molecule^{-1} s^{-1} (Atkinson et al., 2006).
[c]Placed on an absolute basis using $k(OH + \text{3-buten-2-ol}) = 5.9 \times 10^{-11}$ cm^3 molecule^{-1} s^{-1} (this book, section II-D-4.1).

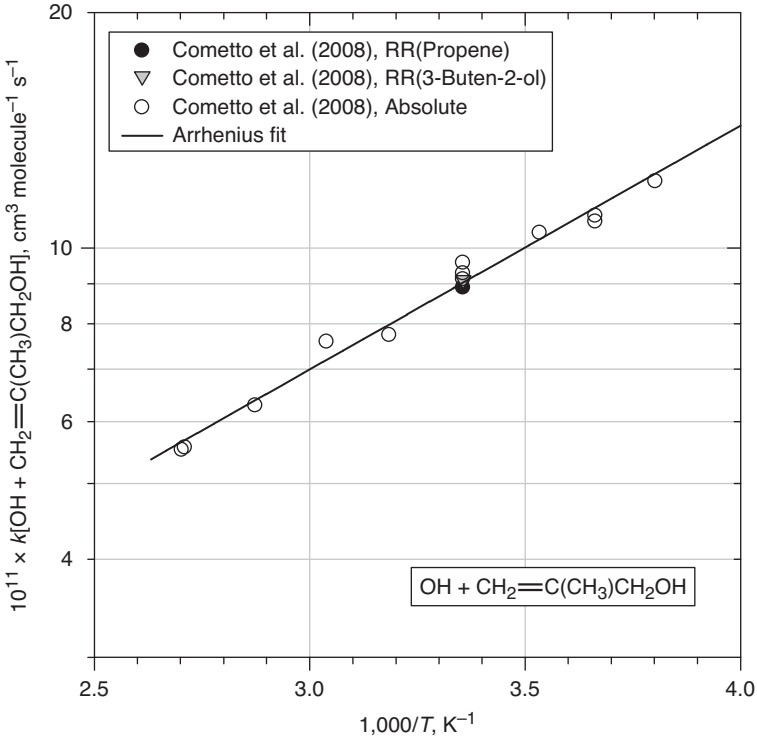

Figure II-D-13. Arrhenius plot of the rate coefficient for the reaction of OH with 2-methyl-2-propen-1-ol.

Table II-D-21. Rate coefficients (k, cm^3 molecule^{-1} s^{-1}) for reaction of Cl with 2-methyl-2-propen-1-ol [CH_2=$C(CH_3)CH_2OH$]

$10^{23} \times A$	B (K)	$10^{10} \times k$	T (K)	Technique[a]	Reference	Temperature Range (K)
3.05 ± 1.40	8,760 ± 1,279	2.18 ± 0.38	298	RR[b] (octane)	Rodriguez et al. (2008)	256–298
		1.85 ± 0.45	298	RR[c] (1-butene)		
		206 ± 93	256	RR[d] (cyclohexane)		
		85.8 ± 13.8	265			
		43 ± 14	274			
		6.9 ± 1.0	285			
		2.5 ± 0.5	298			

[a]Abbreviations used for the techniques are defined in table I-F-3.
[b]Placed on an absolute basis using $k(\mathrm{Cl} + \mathrm{octane}) = 3.22 \times 10^{-10}$ cm^3 molecule^{-1} s^{-1} (Li and Pirasteh, 2006).
[c]Placed on an absolute basis using $k(\mathrm{Cl} + \text{1-butene}) = 2.9 \times 10^{-10}$ cm^3 molecule^{-1} s^{-1} (Orlando et al., 2003).
[d]Placed on an absolute basis using $k(\mathrm{Cl} + \mathrm{cyclohexane}) = 3.3 \times 10^{-10}$ cm^3 molecule^{-1} s^{-1} (Calvert et al., 2008).

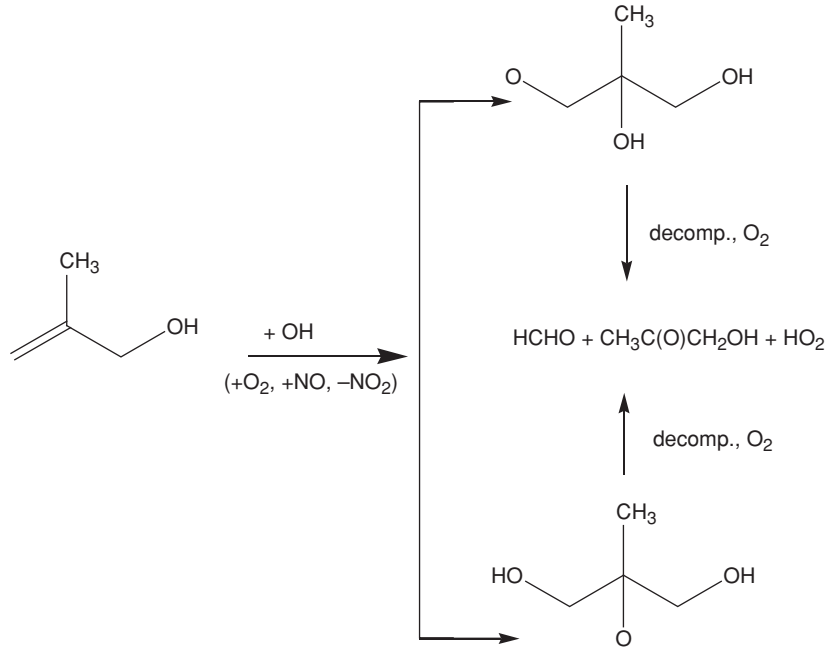

Figure II-D-14. Mechanism of the OH-initiated oxidation of 2-methyl-2-propen-1-ol.

Table II-D-22. Rate coefficients (k, cm^3 $molecule^{-1}$ s^{-1}) for reaction of OH with 3-methyl-2-buten-1-ol [$(CH_3)_2C{=}CHCH_2OH$]

$10^{10} \times k$	T (K)	Technique[a]	Reference
1.40 ± 0.16	298 ± 2	RR (di-*n*-butyl ether)[b]	Imamura et al. (2004)
1.7 ± 0.2	298 ± 2	RR (propene)[c]	

[a]Abbreviations used for the techniques are defined in table I-F-3.
[b]Placed on an absolute basis using k(OH + di-n-butyl ether) $= 2.8 \times 10^{-11}$ cm^3 $molecule^{-1}$ s^{-1} (this book, section III-B-12.1).
[c]Placed on an absolute basis using k(OH + propene) $= 2.9 \times 10^{-11}$ cm^3 $molecule^{-1}$ s^{-1} (Atkinson et al., 2006).

II-D-8. 3-Methyl-2-buten-1-ol [$(CH_3)_2C{=}CHCH_2OH$]

II-D-8.1. OH Reaction Kinetics

Imamura et al. (2004) have measured the rate coefficient for the reaction of OH with 3-methyl-2-buten-1-ol using a relative rate method; see table II-D-22. The rate coefficient values obtained with two reference compounds (di-*n*-butyl ether and propene) were in agreement. The preferred value at 298 K is based on the average of the obtained rate coefficients, $k = 1.6 \times 10^{-10}$ cm^3 $molecule^{-1}$ s^{-1} with an estimated uncertainty of $\pm$ 25 %.

II-D-8.2. NO_3 Reaction Kinetics

The rate coefficient for the reaction of NO_3 with 3-methyl-2-buten-1-ol has been determined by Noda et al. (2002) using a relative rate method. The results obtained using two different analytical techniques (FTIR and SPME–GC) were similar. The rate constant value is $k = 9.6 \times 10^{-13}$ cm^3 molecule^{-1} s^{-1}; see table II-D-23.

II-D-8.3. Cl-Atom Reaction Kinetics

The kinetics of the reaction of chlorine atoms with 3-methyl-2-buten-1-ol have been studied using a relative rate technique by Rodriguez et al. (2008). The rate coefficient values obtained are presented in table II-D-24. The authors have reported an Arrhenius expression of $k(\text{Cl} + \text{3-methyl-2-buten-1-ol}) = 7.55 \times 10^{-21} \exp(7{,}361/T)$ cm^3 molecule^{-1} s^{-1} in the temperature range 257–299 K. As mentioned for the reactions of Cl with 2-buten-1-ol and 2-methyl-2-propene, there is clearly a problem with this study. The rate coefficient obtained at low temperatures are unexpectedly high, $k(257\text{ K}) \approx 3 \times 10^{-8}$ cm^3 molecule^{-1} s^{-1}, about two orders of magnitude larger than that expected from simple collision theory, and they are not physically plausible (Wallington and Mellouki, 2009). In absence of other investigations, no recommendation is made here.

Table II-D-23. Rate coefficient (k, cm^3 molecule^{-1} s^{-1}) for reaction of NO_3 with 3-methyl-2-buten-1-ol [$(CH_3)_2C{=}CHCH_2OH$]

$10^{12} \times k$	T (K)	Technique[a]	Reference
0.96 ± 0.10	298 ± 2	RR (*trans*-2-butene)[b]	Noda et al. (2002)

[a]Abbreviations used for the techniques are defined in table I-F-3.
[b]Placed on an absolute basis using $k(NO_3 + \textit{trans}\text{-2-butene}) = 3.9 \times 10^{-13}$ cm^3 molecule^{-1} s^{-1} (Atkinson and Arey, 2003a).

Table II-D-24. Rate coefficients ($k = A\ e^{-B/T}$, cm^3 molecule^{-1} s^{-1}) for the reaction of Cl with 3-methyl-2-buten-1-ol [$(CH_3)_2C{=}CHCH_2OH$]

$10^{21} \times A$	B (K)	$10^{10} \times k$	T (K)	Technique[a]	Reference	Temperature Range (K)
7.55 ± 0.20	7,361 ± 735	4.02 ± 0.46	298	RR[b] (octane)	Rodriguez et al. (2008)	257–299
		3.39 ± 0.65	298	RR[c] (1-butene)		
		271 ± 47	257	RR[d] (cyclohexane)		
		91.7 ± 31.3	263			
		29.4 ± 12.8	273			
		9.5 ± 5.1	285			
		4.6 ± 0.7	299			

[a]Abbreviations used for the techniques are defined in table I-F-3.
[b]Placed on an absolute basis using $k(\text{Cl} + \text{octane}) = 3.22 \times 10^{-10}$ cm^3 molecule^{-1} s^{-1} (Li and Pirasteh, 2006).
[c]Placed on an absolute basis using $k(\text{Cl} + \text{1-butene}) = 2.9 \times 10^{-10}$ cm^3 molecule^{-1} s^{-1} (Orlando et al., 2003).
[d]Placed on an absolute basis using $k(\text{Cl} + \text{cyclohexane}) = 3.3 \times 10^{-10}$ cm^3 molecule^{-1} s^{-1} (Calvert et al., 2008).

II-D-8.4. Summary of the Atmospheric Fate of 3-Methyl-2-buten-1-ol

Using the rate coefficients measured by Imamura et al. (2004) and Noda et al. (2002), the calculated atmospheric lifetimes with respect to removal via reactions with OH and NO_3 are approximately 1 h and 6 min., respectively. The expected major products of the reaction of OH with 3-methyl-2-buten-1-ol in the presence of NO_x are acetone and glycolaldehyde as co-products following OH addition to either end of the double bond in the alcohol.

Noda et al. (2000) studied the NO_3-radical-initiated oxidation of 3-methyl-2-buten-1-ol in air and reported the formation of acetone (21 ± 6)%, glycolaldehyde (29 ± 10)%, and formaldehyde (11 ± 3)%. Approximately 64% of the alcohol that reacted was unaccounted for, indicating that a number of products were not detected. Noda et al. (2000) observed aerosol formation in their experiments which accounts for part of the oxidation products. The formation of nitrooxy compounds such as 3-nitrooxy-3-methyl-2-butanon-1-ol also probably contributes. Figure II-D-15 shows the mechanism of NO_3-radical-initiated degradation of 3-methyl-2-buten-1-ol proposed by Noda et al. (2000).

II-D-9. 3-Methyl-3-buten-1-ol (CH_2=$C(CH_3)CH_2CH_2OH$)

II-D-9.1. OH Reaction Kinetics

The rate coefficient for the reaction of OH with 3-methyl-3-buten-1-ol has been determined by Imamura et al. (2004) and Cometto et al. (2008). Imamura et al. used a relative method, while Cometto et al. used both absolute and relative methods. The rate

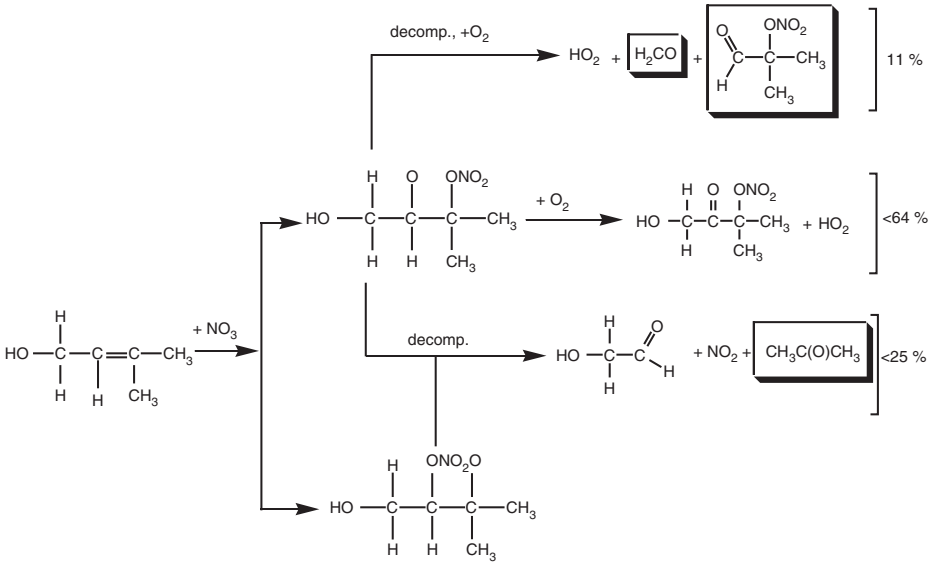

Figure II-D-15. NO_3-radical-initiated oxidation of 3-methyl-2-buten-1-ol (Noda et al., 2000).

coefficient values obtained at 298 K in these two investigations are in good agreement as shown in table II-D-25 and figure II-D-16. Cometto et al. measured the temperature dependence of the rate coefficient over the range 263–369 K. A least-squares fit of the Arrhenius expression to the combined data set from Imamura et al. (2004) and Cometto et al. (2008) gives $k(OH + CH_2{=}C(CH_3)CH_2CH_2OH) = 6.1 \times 10^{-12} \exp(814/T)\,cm^3$ molecule^{-1} s^{-1}. This expression gives $k = 9.4 \times 10^{-11}$ cm^3 molecule^{-1} s^{-1} at 298 K with an uncertainty estimated to be ±15%.

II-D-9.2. NO_3 Reaction Kinetics

The rate coefficient value for the reaction of NO_3 with 3-methyl-3-buten-1-ol has been measured by Noda et al. (2002) using a relative rate method. The value reported at 298 K is $k(NO_3 + CH_2{=}C(CH_3)CH_2CH_2OH) = 2.6 \times 10^{-13}$ cm^3 molecule^{-1} s^{-1} with an estimated uncertainty of ±25%; see table II-D-26.

II-D-9.3. Summary of the Atmospheric Fate of 3-Methyl-3-buten-1-ol

The atmospheric lifetimes of 3-methyl-3-buten-1-ol with respect to reactions with OH and NO_3 are approximately of 1 h and 20 min., respectively. The OH-radical-initiated oxidation of 3-methyl-3-buten-1-ol is expected to give CH_2O, $HOCH_2CH_2C(O)CH_3$, $HOCH_2C(O)CH_3$, and $HOCH_2CHO$ as main products while the NO_3-radical-initiated oxidation will give CH_2O, $HOCH_2CHO$, $HOCH_2CH_2C(O)CH_3$, and nitrooxy-compounds.

Table II-D-25. Rate coefficients ($k = A\ e^{-B/T}$, cm^3 molecule^{-1} s^{-1}) for reaction of OH with 3-methyl-3-buten-1-ol [$CH_2{=}C(CH_3)CH_2CH_2OH$]

$10^{12} \times A$	B (K)	$10^{11} \times k$	T (K)	Technique[a]	Reference	Temperature Range (K)
		9.54 ± 1.05		RR (di-*n*-butyl ether)[b]	Imamura et al. (2004)	
		10.1 ± 1.1		RR[c] (propene)		
		9.3 ± 1.7	298 ± 2	RR (propene)[c]	Cometto et al. (2008)	
		9.7 ± 0.8	298 ± 2	RR (3-buten-2-ol)[d]		
5.5 ± 1.0	−836 ± 54	13.40 ± 0.80	263	PLP–LIF	Cometto et al. (2008)	263–369
		11.80 ± 0.80	272			
		9.05 ± 0.84	294			
		9.72 ± 0.68	298			
		9.09 ± 0.10	298			
		7.60 ± 0.26	312			
		7.17 ± 0.29	327			
		6.37 ± 0.46	347			
		5.54 ± 0.60	369			

[a]Abbreviations used for the techniques are defined in table I-F-3.

[b]Placed on an absolute basis using k(OH + di-*n*-butyl ether) = 2.8×10^{-11} cm^3 molecule^{-1} s^{-1} (this book, section III-B-12.1).

[c]Placed on an absolute basis using k(OH + propene) = 2.9×10^{-11} cm^3 molecule^{-1} s^{-1} (Atkinson et al., 2006).

[d]Placed on an absolute basis using k(OH + 3-buten-2-ol) = 5.9×10^{-11} cm^3 molecule^{-1} s^{-1} (this book, section II-D-4.1).

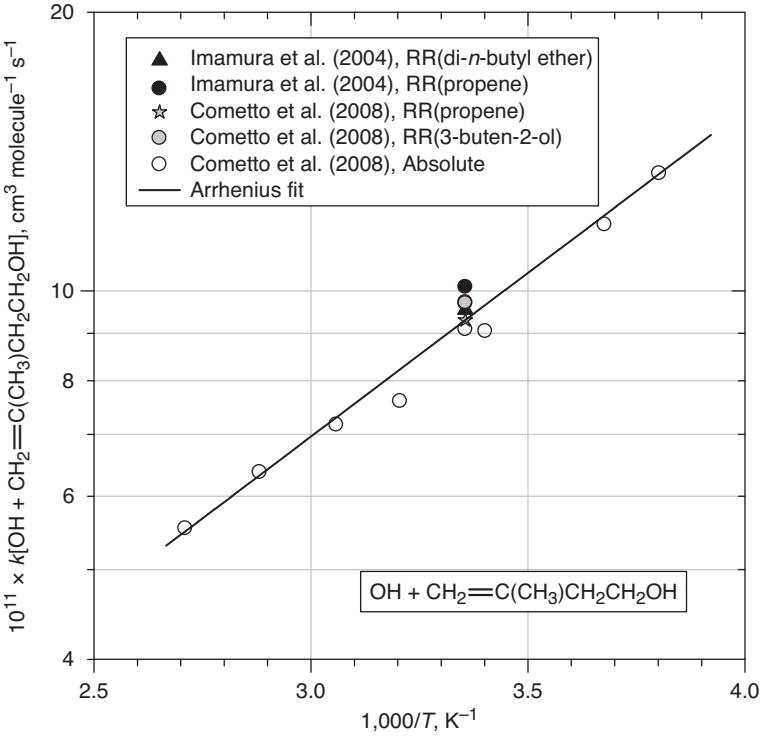

Figure II-D-16. Arrhenius plot of the rate coefficient for the reaction of OH with 3-methyl-3-buten-1-ol.

Table II-D-26. Rate coefficients (k, cm^3 molecule^{-1} s^{-1}) for reaction of NO_3 with 3-methyl-3-buten-1-ol [CH_2=$C(CH_3)CH_2CH_2OH$]

$10^{13} \times k$	T (K)	Technique[a]	Reference
2.6 ± 0.2	298 ± 2	RR (*trans*-2-butene)[b]	Noda et al. (2002)

[a]Abbreviations used for the techniques are defined in table I-F-3.
[b]Placed on an absolute basis using $k(NO_3 + trans\text{-}2\text{-butene}) = 3.9 \times 10^{-13}$ cm^3 molecule^{-1} s^{-1} (Atkinson and Arey, 2003a).

II-D-10. 2-Methyl-3-buten-2-ol [MBO, CH_2=$CHC(OH)(CH_3)_2$]

II-D-10.1. OH Reaction Kinetics

The kinetics of the reaction of OH radicals with 2-methyl-3-buten-2-ol has been the subject of seven studies using absolute and relative methods with results shown in table II-D-27. The room temperature rate coefficients of Rudich et al. (1995), Ferronato et al. (1998), Papagni et al. (2001), Imamura et al. (2004), Baasandorj and Stevens (2007), and Carrasco et al. (2007a) are in reasonable agreement. As seen from figure II-D-17, the results from Fantechi et al. (1998a) are significantly lower than

Table II-D-27. Rate coefficients ($k = A\ e^{-B/T}$, cm^3 $molecule^{-1}$ s^{-1}) for reaction of OH with 2-methyl-3-buten-2-ol [CH_2=CHC(OH)$(CH_3)_2$, MBO]

$10^{12} \times A$	B (K)	$10^{11} \times k$	T (K)	Technique[a]	Reference	Temperature Range (K)
8.2 ± 1.2	−610 ± 50	11.6 ± 1.3	231	PLP–LIF[b]	Rudich et al. (1995)	235–360
		9.0 ± 1.0	255			
		8.7 ± 0.9	264			
		8.3 ± 0.9	268			
		5.9 ± 0.6	301			
		6.2 ± 0.6	301			
		5.3 ± 0.5	319			
		4.2 ± 0.5	353			
		3.5 ± 0.6	373			
		3.9 ± 0.4	373			
		3.0 ± 0.3	408			
7.26	−610 ± 56	7.9 ± 0.8	254	PLP–LIF[c]	Rudich et al. (1995)	254–320
		7.2 ± 0.7	267			
		6.9 ± 0.6	269			
		5.7 ± 0.5	291			
		5.4 ± 0.4	299			
		5.0 ± 0.5	300			
		5.0 ± 0.4	315			
		4.9 ± 0.4	318			
		4.6 ± 0.4	334			
		4.4 ± 0.4	348			
		4.3 ± 0.4	354			
		4.2 ± 0.4	363			
		3.7 ± 0.4	366			
		4.0 ± 0.4	372			
		3.4 ± 0.3	388			
		2.7 ± 0.3	401			
		2.9 ± 0.3	410			
		4.7 ± 2.0	298 ± 2	RR (propene)[d]	Fantechi et al. (1998a, 1998b)	
		3.85 ± 0.80	298 ± 2	RR (isoprene)[e]		
		6.72	295 ± 1	RR (ethene)[f]	Ferronato et al. (1998)	
		6.96	295 ± 1	RR (propene)[d]		
		5.67 ± 0.13	296 ± 2	RR (1,3,5-trimethylbenzene)[g]	Papagni et al. (2001)	
		6.48 ± 0.71	298 ± 2	RR (Di-*n*-butyl ether)[h]	Imamura et al. (2004)	
		7.1 ± 0.8	298 ± 2	RR (propene)[b]		

(*Continued*)

Table II-D-27. (*Continued*)

$10^{12} \times A$	B (K)	$10^{11} \times k$	T (K)	Technique[a]	Reference	Temperature Range (K)
	$k(T)$[i]	6.32 ± 0.27	300	DF–LIF	Baasandorj and Stevens. (2007)	300–415
		5.6 ± 0.6	298 ± 2	RR (isoprene)[e]	Carrasco et al. (2007)	

[a]Abbreviations used for the techniques are defined in table I-F-3.
[b]Results obtained in the presence of O_2.
[c]Results obtained in the absence of O_2.
[d]Placed on an absolute basis using and $k(OH + C_3H_6) = 2.9 \times 10^{-11}$ cm^3 molecule^{-1} s^{-1} (Atkinson et al., 2006).
[e]Placed on an absolute basis using $k(OH + \text{isoprene}) = 1.0 \times 10^{-10}$ cm^3 molecule^{-1} s^{-1} (Atkinson et al., 2006).
[f]Placed on an absolute basis using $k(OH + \text{ethene}) = 7.9 \times 10^{-12}$ cm^3 molecule^{-1} s^{-1} (Atkinson et al., 2006).
[g]Placed on an absolute basis using $k(OH + 1, 3, 5\text{-trimethylbenzene}) = 5.7 \times 10^{-11}$ cm^3 molecule^{-1} s^{-1} (Calvert et al., 2002).
[h]Placed on an absolute basis using $k(OH + \text{di-}n\text{-butyl ether}) = 2.8 \times 10^{-11}$ cm^3 molecule^{-1} s^{-1} (this book section III-B-12.1).
[i]Measurements conducted between 2 and 5 Torr. The rate coefficient begins to show a pressure dependence at temperatures above 335 K. An Arrhenius expression of $k_0 = (2.5 \pm 7.4) \times 10^{-32}$ exp[(4,150 ± 1,150)/T] cm^6 molecule^{-2} s^{-1} was obtained for the low pressure-limiting rate constant. The value quoted for 300 K was obtained in 5 Torr total pressure of helium diluent containing 5–15% O_2.

those from the other studies , which has been explained by the presence of systematic error in this study. Rudich et al. (1995) measured the rate coefficient in the absence and presence of oxygen. In absence of O_2, it was found that 15–20% of the adducts formed following addition of the OH radical to the alcohol C=C bond eliminate the alcohol–OH group. It was also found that O_2 scavenges the adduct before it decomposes at temperatures below 300 K. Rudich et al. (1995) confirmed this mechanism by conducting experiments with isotopically labelled hydroxyl radicals (OD and ^{18}OH) and determining the rate coefficient in the presence of 7–13 Torr of O_2 and in SF_6 buffer gas. Baasandorj and Stevens (2007) studied the kinetics of the reactions of OH and OD with 2-methyl-3-buten-2-ol and showed that the rate coefficient at 300 K was pressure independent in the range 2–5 Torr in the presence of O_2 but becomes pressure dependent at $T \geq 335$ K indicating that the reaction is in the fall-off regime. Only the value at 300 K, applicable to atmospheric conditions, is given in table II-D-27.

The IUPAC panel recommended 298 K rate coefficient is the average of the absolute and relative rate coefficients of Rudich et al. (1995), Ferronato et al. (1998), Papagni et al. (2001), Imamura et al. (2004), and Carrasco et al. (2007a). The preferred temperature dependence is that reported by Rudich et al. (1995), $k = 8.1 \times 10^{-12} \exp(610/T)$ cm^3 molecule^{-1} s^{-1}, with $k = 6.3 \times 10^{-11}$ cm^3 molecule^{-1} s^{-1} at 298 K (Atkinson et al., 2006).

II-D-10.2. O_3 Reaction Kinetics

The rate coefficients for the reaction of O_3 with 2-methyl-3-buten-2-ol reported by Grosjean and Grosjean (1994), Fantechi et al. (1998a), and Klawatsch-Carrasco et al. (2004) are given in table II-D-28. The values measured by Fantechi et al. (1998a) using 2-methyl propene as reference and that of Klawatsch-Carrasco et al. (2004) are about 20% lower than those of Grosjean and Grosjean (1994) and Fantechi et al. (1998a)

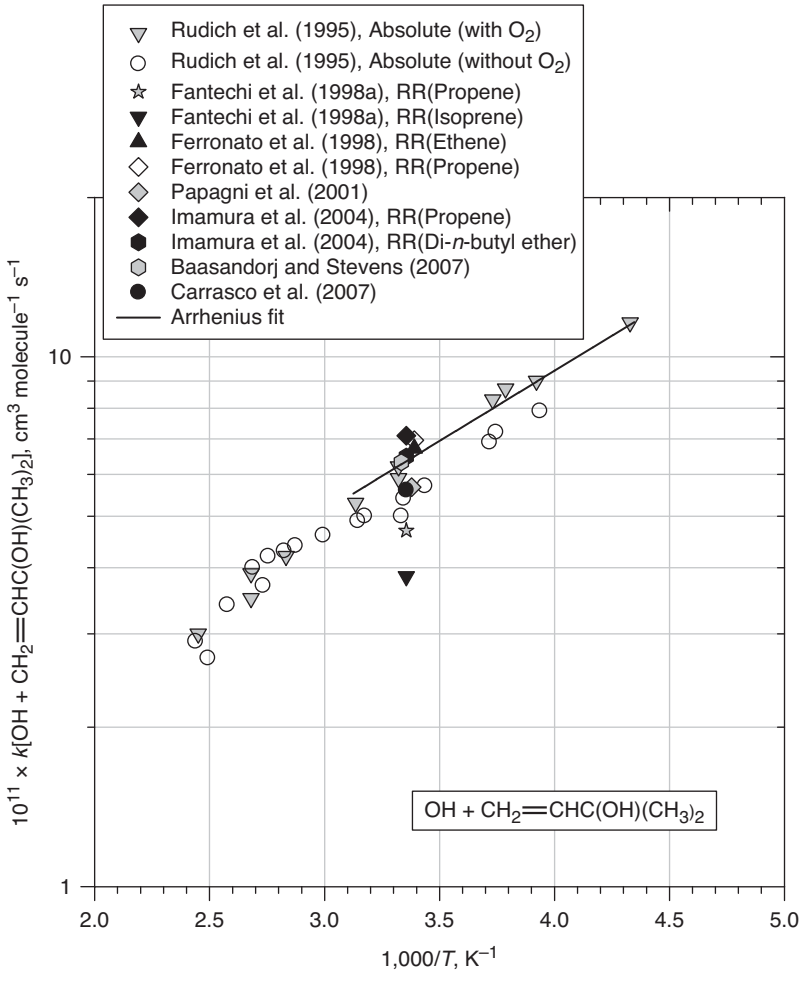

Figure II-D-17. Arrhenius plot of the rate coefficient for the reaction of OH with 2-methyl-3-buten-2-ol.

obtained with propene as a reference. Taking an average of the measurements from the three studies gives our recommended value at 298 K of $k(O_3+2\text{-methyl-3-buten-2-ol}) = 9.0 \times 10^{-18}$ cm^3 $molecule^{-1}$ s^{-1} with an estimated uncertainty of ±25%.

II-D-10.3. NO_3 Reaction Kinetics

The rate coefficient of the NO_3 reaction with 2-methyl-3-buten-2-ol has been measured by Rudich et al. (1996), Hallquist et al. (1996), Fantechi et al. (1998), and Noda et al. (2002) using absolute and relative methods; see table II-D-29 and figure II-D-18. The absolute determination of Hallquist et al. is approximately a factor of 1.7 times larger than the absolute rate determination of Rudich et al. (1996) and the relative rate

Table II-D-28. Rate coefficients (k, cm^3 molecule^{-1} s^{-1}) for reaction of O_3 with 2-methyl-3-buten-2-ol [CH_2=CH(OH)(CH_3)$_2$, MBO]

$10^{17} \times k$	T (K)	Technique[a]	Reference
1.0 ± 0.03	291 ± 2	Excess of MBO[b]	Grosjean and Grosjean (1994)
0.96 ± 0.18	298 ± 2	RR (propene)[c]	Fantechi et al. (1998a)
0.8 ± 0.03	298 ± 2	RR (2-methyl propene)[d]	Fantechi et al. (1998a)
0.83 ± 0.10	293 ± 2	FTIR[e]	Klawatsch-Carrasco et al (2004)

[a]Abbreviations used for the techniques are defined in table I-F-3.
[b]Pseudo first-order conditions (excess of 2-methyl-3-buten-2-ol, O_3 measured by absorption).
[c]Placed on an absolute basis using $k(O_3 + \text{propene}) = 1.0 \times 10^{-17}$ cm^3 molecule^{-1} s^{-1} (Atkinson et al., 2006).
[d]Placed on an absolute basis using $k(O_3 + \text{2-methyl propene}) = 1.13 \times 10^{-17}$ cm^3 molecule^{-1} s^{-1} (Atkinson and Arey, 2003a).
[e]MBO and ozone measured by FTIR.

Table II-D-29. Rate coefficients ($k = A\ e^{-B/T}$, cm^3 molecule^{-1} s^{-1}) for the reaction of NO_3 with 2-methyl-3-buten-2-ol [CH_2=CHC(OH)(CH_3)$_2$, MBO]

$10^{14} \times A$	B (K)	$10^{14} \times k$	T (K)	Technique[a]	Reference	Temperature Range (K)
4.6	400 ± 35	0.95 ± 0.08	267	DF–DLS	Rudich et al. (1996)	267–400
		1.09 ± 0.09	280			
		1.2 ± 0.09	295			
		1.14 ± 0.09	296			
		1.14 ± 0.09	296			
		1.30 ± 0.09	296			
		1.23 ± 0.09	297			
		1.26 ± 0.09	297			
		1.23 ± 0.09	297			
		1.29 ± 0.10	313			
		1.27 ± 0.10	313			
		1.27 ± 0.10	314			
		1.22 ± 0.10	314			
		1.44 ± 0.12	333			
		1.35 ± 0.12	346			
		1.58 ± 0.13	351			
		1.42 ± 0.13	353			
		1.44 ± 0.13	365			
		1.52 ± 0.14	373			
		1.52 ± 0.14	373			
		1.76 ± 0.18	400			
		1.76 ± 0.18	400			
		1.6 ± 0.6	294	RR (propene)[b]	Hallquist et al. (1996)	
		2.1 ± 0.3	294	DF–AS[c]		
		0.87 ± 0.29	298 ± 2	RR (propene)[b]	Fantechi et al. (1998a)	
		1.1 ± 0.1	297 ± 2	RR (butanal)[d]	Noda et al. (2002)	
		1.0 ± 0.2	297 ± 2	RR (propene)[b]		

[a]Abbreviations used for the techniques are defined in table I-F-3.
[b]Placed on an absolute basis using $k(NO_3 + \text{propene}) = 9.5 \times 10^{-15}$ cm^3 molecule^{-1} s^{-1} (Atkinson et al., 2006).
[c]Placed on an absolute basis using $k(NO_3 + C_3H_6) = 9.4 \times 10^{-15}$ cm^3 molecule^{-1} s^{-1} (Atkinson et al., 2006).
[d]Placed on an absolute basis using $k(NO_3 + \text{butanal}) = 1.14 \times 10^{-14}$ cm^3 molecule^{-1} s^{-1} (this book section IV-B-4.2).

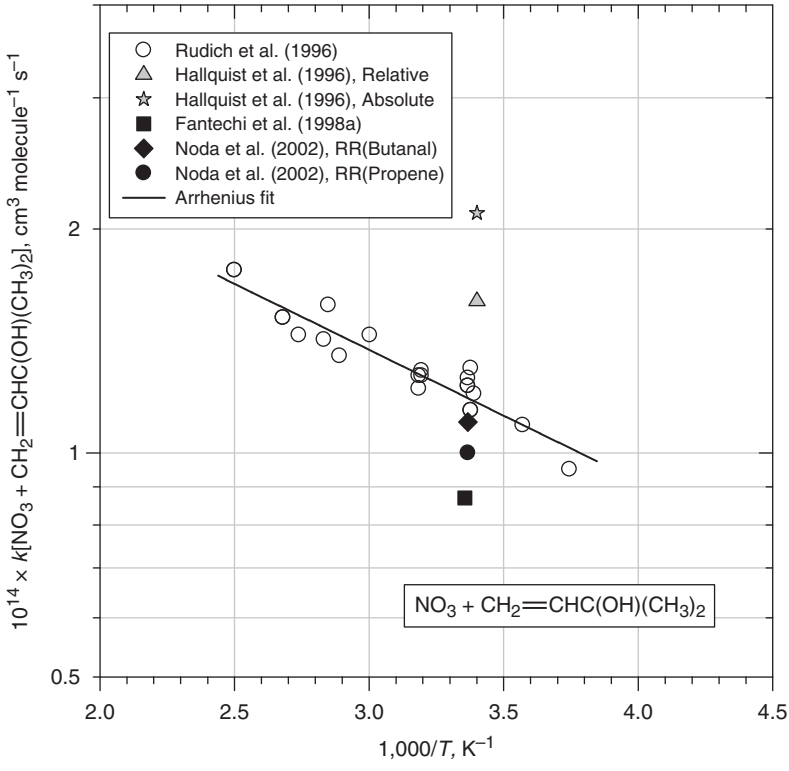

Figure II-D-18. Arrhenius plot of the rate coefficient for the reaction of NO_3 with 2-methyl-3-buten-2-ol.

measurements of Fantechi et al. (1998a) and Noda et al. (2002). However, within the considerable experimental uncertainty, the relative rate coefficient reported by Hallquist et al. (1996) is consistent with the results from Rudich et al. (1996), Fantechi et al. (1998a), and Noda et al. (2002). The recommended rate coefficient at 298K and the temperature dependence parameters in the range 267–400 K are based on the data of Rudich et al.: $k(NO_3 + \text{2-methyl-3-buten-2-ol}) = 4.6 \times 10^{-14} \exp(-400/T)$ cm^3 molecule^{-1} s^{-1}, with $k = 1.2 \times 10^{-14}$ cm^3 molecule^{-1} s^{-1} at 298 K and an estimated uncertainty of ±30%.

II-D-10.4. Cl-Atom Reaction Kinetics

The rate coefficient value reported by Fantechi et al. (1998a) is approximately 50% larger than that determined by Ferronato et al. (1998). Both measurements were conducted using the relative rate method. See table II-D-30.

II-D-10.5. Summary of the Atmospheric Fate of 2-Methyl-3-buten-2-ol

The estimated atmospheric lifetimes of 2-methyl-3-buten-2-ol with respect to reaction with OH, O_3, NO_3, and Cl are approximately 2 h, 1.5 days, 8 h, and 4 days, respectively.

Table II-D-30. Rate coefficients (k, cm^3 $molecule^{-1}$ s^{-1}) for reaction of Cl with 2-methyl-3-buten-2-ol [CH_2=$CH(OH)(CH_3)_2$, MBO]

$10^{10} \times k$	T (K)	Technique[a]	Reference
4.8 ± 1.0	298 ± 2	RR (ethene)[b]	Fantechi et al. (1998a)
3.2 ± 0.4	295 ± 1	RR (ethane)[c]	Ferronato et al. (1998)
3.6 ± 0.4		RR (ethene)[b]	
2.9 ± 0.4		RR (cyclohexane)[d]	

[a]Abbreviations used for the techniques are defined in table I-F-3.
[b]Placed on an absolute basis using $k(Cl + ethene) = 1.1 \times 10^{-10}$ cm^3 $molecule^{-1}$ s^{-1} (this book, section I-F-1.
[c]Placed on an absolute basis using $k(Cl + ethane) = 5.9 \times 10^{-11}$ cm^3 $molecule^{-1}$ s^{-1} (Atkinson et al., 2006).
[d]Placed on an absolute basis using $k(Cl + cyclohexane) = 3.3 \times 10^{-10}$ cm^3 $molecule^{-1}$ s^{-1} (Calvert et al., 2008).

The main atmospheric removal processes of 2-methyl-3-buten-2-ol are reactions with OH and NO_3 radicals with a nonnegligible contribution from the reaction with O_3. The reaction of OH radicals with 2-methyl-3-buten-2-ol proceeds predominately via addition to the C=C bond. The products of this reaction have been investigated by Fantechi et al. (1998b), Ferronato et al. (1998), Alvarado et al. (1999), Spaulding et al. (2002), Reisen et al. (2003), and Carrasco et al. (2007a). The observed products in the presence of NO_x and the corresponding yields obtained in different studies are given in table II-D-31. The proposed mechanism showing the main channels is given in figure II-D-19 (Alvarado et al., 1999). In addition to the compounds reported in table II-D-31, dihydroxynitrates, presumed to be $(CH_3)_2C(OH)CH(OH)CH_2ONO_2$ and $(CH_3)_2C(OH)CH(ONO_2)CH_2OH$, were observed with molar yields of 5 ± 2% (Alvarado et al., 1999). Fantechi et al. (1998b) and Carrasco et al. (2007a) investigated the products of OH-radical-initiated oxidation of 2-methyl-3-buten-2-ol in the absence of NO. In the presence and absence of NO_x, the same reaction products (formaldehyde, acetone, glycolaldehyde, and 2-hydroxy-2-methylpropanal) were observed, but in different yields. Acetone is a major oxidation product of 2-methyl-3-buten-2-ol.

Table II-D-31. OH-initiated oxidation of 2-methyl-3-buten-2-ol showing the observed products in the presence of NO_x and the corresponding molar yields obtained in different studies

Product	Yield	Reference
Acetone	0.52 ± 0.05	Ferronato et al. (1998)
[$CH_3C(O)CH_3$]	0.58 ± 0.04	Alvarado et al. (1999)
	0.67 ± 0.05	Carrasco et al. (2007a)
Formaldehyde	0.35 ± 0.04	Ferronato et al. (1998)
(HCHO)	0.29 ± 0.03	Alvarado et al. (1999)
	0.33 ± 0.08	Carrasco et al. (2007a)
Glycolaldehyde	0.50 ± 0.05	Ferronato et al. (1998)
($HOCH_2CHO$)	0.61 ± 0.09	Alvarado et al. (1999)
	0.67 ± 0.11	Reisen et al. (2003)
	0.78 ± 0.20	Carrasco et al. (2007a)
2-Hydroxy-2-methylpropanal	0.19 ± 0.07	Alvarado et al. (1999)
[$(CH_3)_2C(OH)CHO$]	0.31 ± 0.04	Reisen et al. (2003)
	0.31 ± 0.11	Carrasco et al. (2007a)

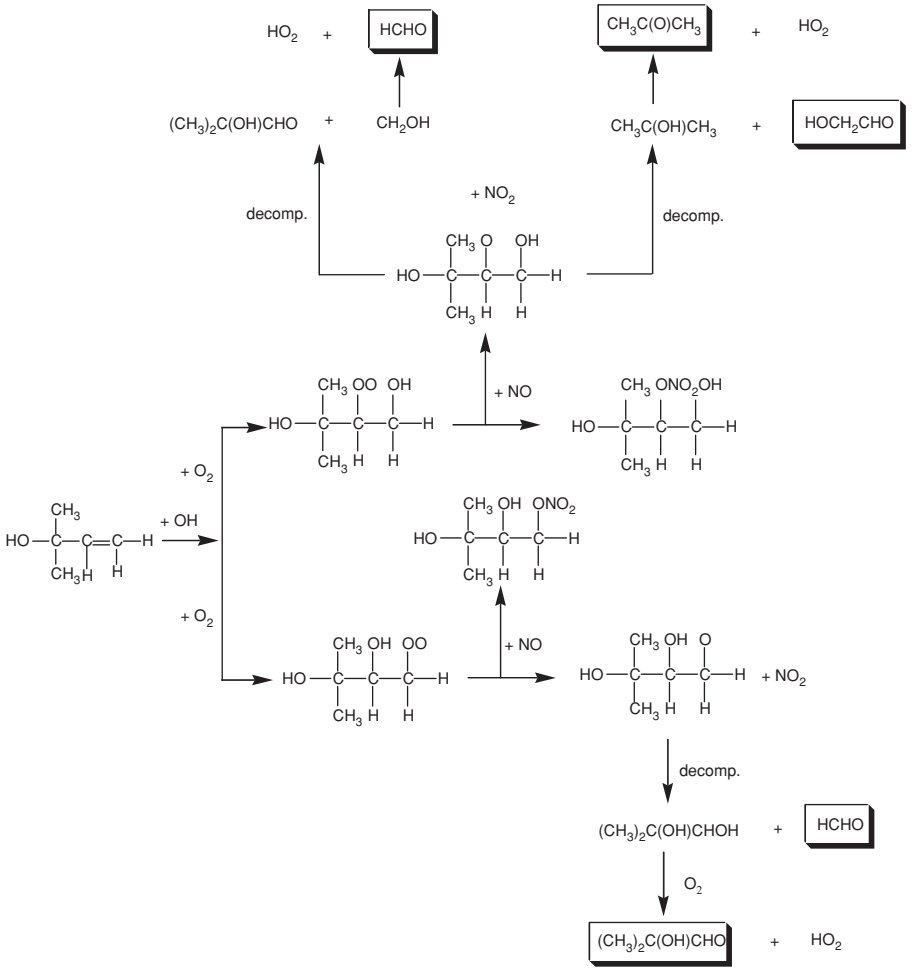

Figure II-D-19. Mechanism of the OH-initiated oxidation of 2-methyl-3-buten-2-ol.

The formation of acetone is of significance because photolysis of acetone is an important source of HO_x in the free troposphere (see chapters V and IX).

Product studies of the reaction of O_3 with 2-methyl-3-buten-2-ol have been carried out by Grosjean and Grosjean (1995), Fantechi et al. (1998b), Alvarado et al. (1999), and Carrasco et al. (2007a). The main observed products are formaldehyde, 2-hydroxy-2-methylpropanal, acetone, formic acid, formic anhydride, and OH radicals. There are significant discrepancies in the measured yields of formaldehyde, 2-hydroxy-2-methylpropanal and acetone between the different studies. Carrasco et al. (2007a) have shown that the yields of acetone and 2-hydroxy-2-methylpropanal depend on the water vapor concentration. Alvarado et al. (1999) reported that at ~5% relative humidity at 298 ± 2 K, the molar formation yields were: CH_2O, 29 ± 3%; $(CH_3)_2C(OH)CHO$, ~47%; $CH_3C(O)CH_3$, initially ~15% and apparently increasing with the extent of

reaction; and OH radicals, 19^{+10}_{-7}%. A simplified reaction mechanism mechanism is presented in figure II-D-20. The reaction proceeds by addition of O_3 across the C=C bond to form a "primary ozonide" which decomposes rapidly to $(CH_3)_2C(OH)CHO$ + $[CH_2OO]^*$ or CH_2O + $[(CH_3)_2C(OH)CHOO]^*$. It has been suggested that acetone could be formed from the $[(CH_3)_2C(OH)CHOO]^*$ Criegee intermediate which may account for the variable yields reported (Grosjean and Grosjean, 1995; Fantechi et al., 1998b; Alvarado et al., 1999) and for the observation by Alvarado et al. (1999) of an increasing acetone yield with extent of reaction. Carrasco et al. (2007a) synthesized a sample of 2-hydroxy-2-methylpropanal and carried out experiments under dry conditions and at 20% and 30% relative humidity at 298 ± 2 K. In dry air, the CH_2O,

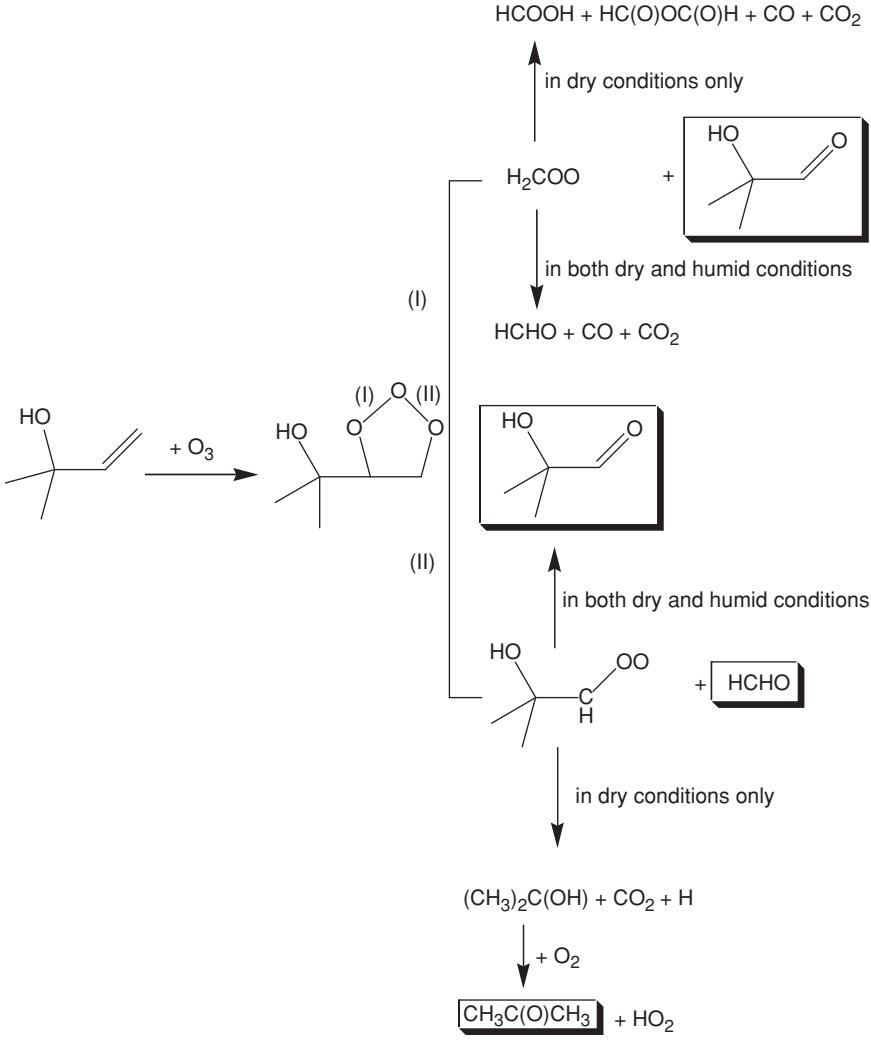

Figure II-D-20. O_3-initiated oxidation of 2-methyl-3-buten-2-ol.

$(CH_3)_2C(OH)CHO$ and $CH_3CO)CH_3$ yields were 44 ± 5%, 43 ± 12%, and 39 ± 22%, respectively, while at 20–30% relative humidity the respective formation yields were 55 ± 3%, 84 ± 8%, and acetone was not detected (Carrasco et al., 2007). The product data indicate that the $[(CH_3)_2C(OH)CHOO]^*$ Criegee intermediate is the source of acetone under dry conditions (or at low water vapor concentrations), while at higher water vapor concentrations $[(CH_3)_2C(OH)CHOO]^*$ reacts with water vapor to form $(CH_3)_2C(OH)CHO$ (Carrasco et al., 2007a).

While there are still some unresolved differences between the various studies, it appears that the reaction initially forms $(CH_3)_2C(OH)CHO$ + $[CH_2OO]^*$ and CH_2O + $[(CH_3)_2C(OH)CHOO]^*$ in approximately equal amounts, with the $[(CH_3)_2C(OH)CHOO]^*$ Criegee intermediate reacting to form at least part of the OH radicals observed (Alvarado et al., 1999) and also reacting with water vapor (when present) to form additional $(CH_3)_2C(OH)CHO$.

A simplified mechanism for the NO_3-radical-initiated oxidation of 2-methyl-3-buten-2-ol is presented in figure II-D-21 (Fantechi et al., 1998b; Noda et al., 2000). The observed products are acetone and 2-nitrooxyacetaldehyde (O_2NOCH_2CHO), with molar yields of 68.7 ± 7.1% (Fantechi et al., 1998b) and 63 ± 6% (Noda et al., 2000) for acetone, and 67 ± 8% for 2-nitrooxyacetaldehyde (Noda et al., 2000). The reaction proceeds by addition of NO_3 to the C=C bond (favoring the most substituted radical) followed by addition of O_2 to give two peroxy radicals $(CH_3)_2C(OH)CH(ONO_2)CH_2OO$ and $(CH_3)_2C(OH)CH(OO)CH_2ONO_2$. These peroxy radicals will react further with other species such as HO_2 radicals, organic peroxy radicals, NO, NO_2, and NO_3 radicals. For the laboratory conditions, the proposed mechanism is given in figure II-D-21.

The mechanism of the Cl-atom-initiated oxidation of 2-methyl-3-buten-2-ol was investigated by Ferronato et al. (1998) and Fantechi et al. (1998c) in absence of NO_x,

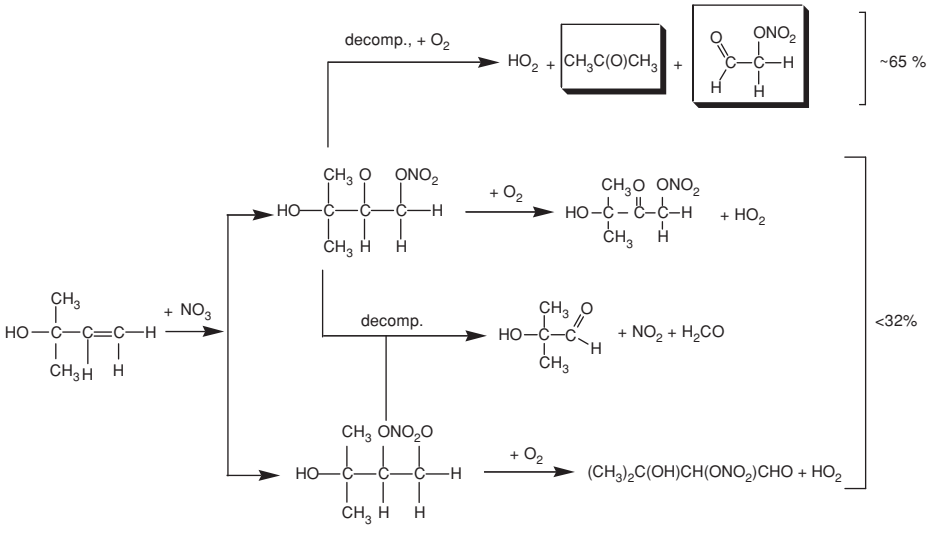

Figure II-D-21. NO_3-initiated oxidation of 2-methyl-3-buten-2-ol.

or with very low concentration of NO_x. The main products observed by Ferronato et al. were acetone (47 ± 5)%, chloroacetaldehyde (53 ± 5)%, formyl chloride (≤11%), and formaldehyde (6 ± 2)%. Fantechi et al. also reported yields for acetone and formyl chloride but with high uncertainties, (38.5 ± 20.6)% and (6.8 ± 5.9)%, respectively. The overall carbon mass balance based on the product yields reported by Ferronato et al. is only 50–55%. This indicates the occurrence of different reactions channels leading to products which could not be detected and identified (such as organic hydroperoxide species).

The majority of the reaction of chlorine atoms with 2-methyl-3-buten-2-ol proceeds via addition to the $\rangle C{=}C\langle$ double bond forming $(CH_3)_2C(OH)CCH_2Cl$ and $(CH_3)_2C(OH)CClCH_2$ radicals which then add O_2 to give the corresponding peroxy radicals. The formation of $(CH_3)_2C(OH)CCH_2Cl$ radicals is likely the most favorable channel and leads to the formation of acetone and chloroacetaldehyde (Ferronato et al., 1998). The importance of this channel is suggested by the fact that the yields of acetone and chloroacetaldehyde are substantial and indistinguishable. The formation of $(CH_3)_2C(OH)CClCH_2$ may lead to the formation of CH_2O, formyl chloride, acetone and 2-hydroxy-2-methylpropanal, and other species. H-atom abstraction from the methyl groups is also a possibility; however, the fact that methyl vinylketone was not observed but expected through this reaction, is an indication that this pathway is minor (Ferronato et al., 1998).

II-D-11. Hexenols

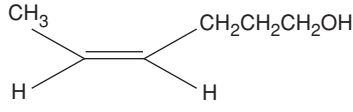

cis-4-hexen-l-ol
[(*Z*)-hex-4-en-l-ol]

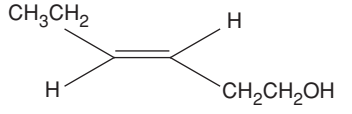

trans-3-hexen-l-ol
[(*E*)-hex-3-en-l-ol]

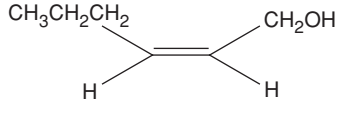

cis-2-hexen-l-ol
[(*Z*)-hex-2-en-l-ol]

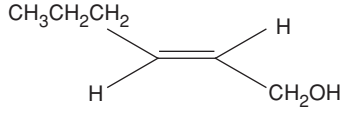

trans-2-hexen-l-ol
[(*E*)-hex-2-en-l-ol]

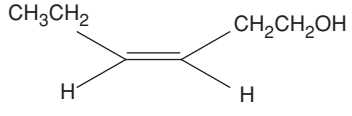

cis-3-hexen-l-ol
[(*Z*)-hex-3-en-l-ol]

The data base concerning the atmospheric chemistry of hexenols is very limited.

II-D-11.1. OH Reaction Kinetics

The only study reported for the reactions of hexenols with OH at the time of this writing is that with *cis*-3-hexen-1-ol by Atkinson et al. (1995) using a relative rate method; see table II-D-32. A value of $k(\text{OH} + \textit{cis-3-hexen-1-ol}) = (1.07 \pm 0.22) \times 10^{-10}$ cm^3 molecule^{-1} s^{-1} was determined. The rate coefficient values of OH reaction with the other hexenols are expected to be of the same order of magnitude $k \approx 1 \times 10^{-10}$ cm^3 molecule^{-1} s^{-1}.

II-D-11.2. O_3 Reaction Kinetics

The rate coefficient for the reaction of O_3 with *cis*-3-hexen-1-ol was measured by Grosjean et al. (1993a) and Atkinson et al. (1995) (table II-D-33). The study of Grosjean et al. was conducted by monitoring the pseudo first-order loss of ozone in the presence of a large excess of the alcohol while the study of Atkinson et al. (1995) was conducted using a relative rate method. The rate coefficient Atkinson et al. obtained is approximately 40% lower than that determined by Grosjean et al. We choose to recommend an average of these two measurements; $k(\text{O}_3 + \textit{cis}\text{-3-hexen-1-ol}) = 8.6 \times 10^{-17}$ cm^3 molecule^{-1} s^{-1}, with an estimated uncertainty of 50%.

II-D-11.3. NO_3 Reaction Kinetics

The reactions of NO_3 with hexenols have been studied by Atkinson et al. (1995) and Pfrang et al. (2006a) (table II-D-34). The rate coefficient values reported for *cis*-3-hexen-1-ol are in good agreement with an average value of $k = 2.7 \times 10^{-13}$ cm^3

Table II-D-32. Rate coefficient (k, cm^3 molecule^{-1} s^{-1}) for the reaction of OH with *cis*-3-hexen-1-ol ($CH_3CH_2CH{=}CHCH_2CH_2OH$)

$10^{10} \times k$	T (K)	Technique[a]	Reference
1.07 ± 0.22	296 ± 2	RR[b] (*trans*-2-butene)	Atkinson et al.. (1995)

[a]Abbreviations used for the techniques are defined in table I-F-3.
[b]Placed on an absolute basis using $k(\text{OH} + \textit{trans}\text{-2-butene}) = 6.4 \times 10^{-11}$ cm^3 molecule^{-1} s^{-1} (Atkinson and Arey, 2003a).

Table II-D-33. Rate coefficients (k, cm^3 molecule^{-1} s^{-1}) for reaction of O_3 with *cis*-3-hexen-1-ol ($CH_3CH_2CH{=}CHCH_2CH_2OH$)

$10^{17} \times k$	T (K)	Technique[a]	Reference
10.5 ± 0.7	285 ± 1	Excess of *cis*-3-hexen-1-ol[b]	Grosjean et al. (1993a)
6.6 ± 1.7	296 ± 2	RR (*cis*-2-butene)[c]	Atkinson et al. (1995)

[a]Abbreviations used for the techniques are defined in table I-F-3.
[b]Pseudo first-order conditions (excess of *cis*-3-hexen-1-ol, O_3 measured by absorption).
[c]Placed on an absolute basis using $k(\text{O}_3 + \textit{cis}\text{-2-butene}) = 1.25 \times 10^{-16}$ cm^3 molecule^{-1} s^{-1} (Atkinson and Arey, 2003a).

Table II-D-34. Rate coefficients (k, cm^3 molecule^{-1} s^{-1}) for reaction of NO_3 with hexenols

Hexen-1-ol	$10^{13} \times k$	T(K)	Technique[a]	Reference
cis-4-Hexen-1-ol	2.93 ± 0.58	298 ± 2	DF abs.	Pfrang et al. (2006a)
trans-3-Hexen-1-ol	4.43 ± 0.91	298 ± 2	DF abs.	Pfrang et al. (2006a)
cis-3-Hexen-1-ol	2.73 ± 0.83	296 ± 2	RR[b] (*trans*-2-butene)	Atkinson et al. (1995)
cis-3-Hexen-1-ol	2.67 ± 0.42	298 ± 2	DF abs.	Pfrang et al. (2006a)
cis-2-Hexen-1-ol	1.56 ± 0.24	298 ± 2	DF abs.	Pfrang et al. (2006a)
trans-2-Hexen-1-ol	1.30 ± 0.24	298 ± 2	DF abs.	Pfrang et al. (2006a)

[a]Abbreviations used for the techniques are defined in table I-F-3.
[b]Placed on an absolute basis using $k(NO_3 + trans\text{-2-butene}) = 3.9 \times 10^{-13}$ cm^3 molecule^{-1} s^{-1} (Atkinson and Arey, 2003a).

molecule^{-1} s^{-1} and an estimated uncertainty of 30% as indicated by Atkinson et al. (1995). The rate coefficients for reactions of NO_3 radicals with *trans*-2-hexen-1-ol, *cis*-2-hexen-1-ol, *trans*-3-hexen-1-ol, and *cis*-4-hexen-1-ol have been measured by Pfrang et al. (2006a) at 298 K in 5–10 Torr of helium diluent. The measurements were conducted using the discharge flow technique with continuous-wave cavity enhanced absorption spectroscopy (CEAS) used to monitor the decay of NO_3 radicals in the presence of hexenols.

II-D-11.4. Summary of the Atmospheric Fate of Hexenols

The rate coefficients for reactions of OH radicals, O_3, and NO_3 radicals were used to calculate the atmospheric lifetimes of *cis*-3-hexen-1-ol with respect to these reactions; the values obtained are 1h, 3h, and 20 min., respectively. The other four hexenols are expected to have lifetimes with respect to reaction with OH radicals which are similar to that of *cis*-3-hexen-1-ol. The OH-initiated oxidation of hexenols is expected to proceed mainly by initial addition of OH to the C=C bond to form two β-hydroxyalkyl radicals. The reaction of OH radicals with *cis*-3-hexen-1-ol gives $CH_3CH_2CH\bullet CH(OH)CH_2CH_2OH$ and $CH_3CH_2CH(OH)CH\bullet CH_2CH_2OH$. These radicals add O_2 and then react with NO to give the corresponding β-hydroxyalkoxy radicals ($CH_3CH_2CH(O^{\cdot})CH(OH)CH_2CH_2OH$ and $CH_3CH_2CH(OH)CH(O^{\cdot})CH_2CH_2OH$) and β-hydroxynitrates. As with other alkoxy radicals, the fate of β-hydroxyalkoxy radicals is decomposition, isomerization, and reaction with O_2.

The products of the OH-radical-initiated oxidation of *cis*-3-hexen-1-ol in air have been determined by Aschmann et al. (1997) and Reisen et al. (2003). Using different analytical techniques, both groups found that 3-hydroxypropanal is a major reaction product. 3-Hydroxypropanal is the co-product of propanal and therefore formed in identical yield (~75%). This indicates that the decomposition pathway of both β-hydroxyalkoxy radicals dominates. The production of dihydroxycarbonyl ($CH_3CH_2CH(OH)CH(OH)CH_2CHO$) arising from the isomerization channel and dihydroxynitrates was experimentally confirmed; these products may account for 25 ± 7% of the reaction (Reisen et al., 2003).

The reaction of O_3 with cis-3-hexen-1-ol proceeds by initial addition of ozone to the C=C bond leading to an ozonide which decomposes:

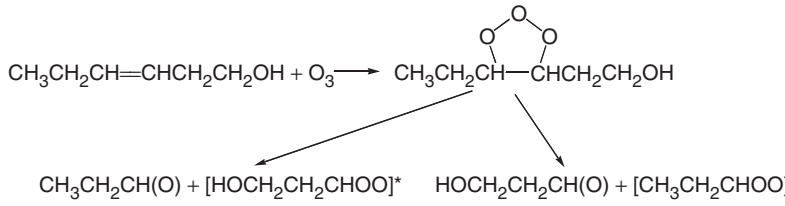

The mechanism of this reaction was studied by Grosjean et al. (1993b) and Aschmann et al. (1997). Both studies reported propanal as major reaction product with a yield of (58.7 ± 12.0%) and (49.3 ± 7.5%), respectively. While Aschmann et al. have observed 3-hydroxypropanal with formation yield of $(33^{+33}_{-16}\%)$, it could not be positively identified by Grosjean et al. (1993b). In their study, Grosjean et al. have also observed methyl glyoxal (17 ± 5%), acetaldehyde (13 ± 2%), and glyoxal and/or hydroxyacetaldehyde (2 ± 1%). These latter compounds are formed through reactions involving the biradicals ($HOCH_2CH_2CHOO$ and CH_3CH_2CHOO). Formation of OH radicals (∼ 26%) was also reported by Atkinson et al. (1995).

Following the general oxidation mechanism, the reaction of NO_3 with hexenols may lead mainly to CH_3CHO, CH_3CH_2CHO, $HOCH_2CHO$, $HOCH_2CH_2CHO$, $HOCH_2CH_2CH(ONO_2)CHO$, and $CH_3CH_2CH(ONO_2)CHO$ for both *cis*- and *trans*-3-hexen-1-ol; to CH_2O, CH_3CH_2CHO, $CH_3CH_2CH_2CHO$, $HOCH_2CHO$, $HOCH_2CH(ONO_2)CHO$, $CH_3CH_2CH_2CH(ONO_2)CHO$ for both *cis*- and *trans*-2-hexen-1-ol, and to CH_2O, CH_3CHO, $HOCH_2CH_2CH_2CHO$, $HOCH_2CH_2CH_2CH(ONO_2)CHO$, and $CH_3CH(ONO_2)CHO$ for *cis*-4-hexen-1-ol.

II-D-12. 2,6-Dimethyl-7-octen-2-ol (Dihydromyrcenol)

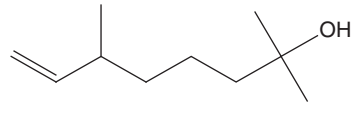

II-D-12.1. OH Reaction Kinetics

Forester et al. (2006) investigated the reaction of OH radicals with dihydromyrcenol using a relative rate method and three references. The rate coefficient obtained is $k = 3.8 \times 10^{-11}$ cm^3 molecule^{-1} s^{-1} at 297 ± 3 K. This value is recommended with an estimated uncertainty of ±30%; see table II-D-35.

II-D-12.2. O_3 Reaction Kinetics

Forester et al. (2006) monitored the decay of O_3 in an excess of dihydromyrcenol and derived an upper limit of $k(O_3 + \text{dihydromycenol}) < 2 \times 10^{-18}$ cm^3 molecule^{-1} s^{-1}, at 297 ± 3 K.

Table II-D-35. Rate coefficient (k, cm^3 molecule^{-1} s^{-1}) for the reaction of OH with 2,6-dimethyl-7-octen-2-ol (dihydromyrcenol): $CH_2{=}CHCH(CH_3)CH_2CH_2CH_2C(OH)(CH_3)_2$

$10^{11} \times k$	T (K)	Technique[a]	Reference
3.8 ± 0.9	297 ± 3	RR (3 reference gases)[b]	Forester et al. (2006)

[a]Abbreviations used for the techniques are defined in table I-F-3.
[b]Placed on an absolute basis using $k(\text{OH} + n\text{-decane}) = 1.1 \times 10^{-11}$, $k(\text{OH} + 2,5\text{-dimethyl furan}) = 1.32 \times 10^{-10}$ and $k(\text{OH} + 2\text{-butanol}) = 8.65 \times 10^{-12}$ cm^3 molecule^{-1} s^{-1}.

II-D-12.3. Summary of the Atmospheric Fate of Dihydromyrcenol

The atmospheric lifetime of dihydromyrcenol calculated using the rate coefficient for the OH reaction in combination with diurnal average OH concentration of 2.5×10^6 molecule cm^{-3} is approximately 3 h. The reaction of OH with dihydromyrcenol occurs mainly through OH addition to the carbon–carbon double bond. The main reaction products reported by Forester et al. (2006) in one atmosphere of air diluent in the presence of NO_x were acetone, 2-methylpropanal [$(CH_3)_2CHCHO$], 2-methylbutanal [$CH_3CH_2CH(CH_3)CHO$], glyoxal [CH(O)CHO], and methyl glyoxal [$CH_3C(O)CHO$].

II-D-13. 3,7-Dimethyl-1,6-octadien-3-ol (Linalool)

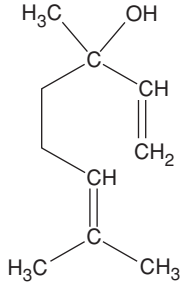

II-D-13.1. OH Reaction Kinetics

The rate coefficient for the reaction of OH with linalool has been measured by Atkinson et al. (1995) and Bernhard and Simonich (2000) using relative rate methods; see table II-D-36. The value obtained by Bernhard and Simonich (2000) is about 30% higher than that of Atkinson et al. (1995). The recommended rate coefficient value is the average of these two determination, $k = 1.9 \times 10^{-10}$ cm^3 molecule^{-1} s^{-1}, with an estimated uncertainty of ±50%.

II-D-13.2. O_3 Reaction Kinetics

Atkinson et al. (1995) and Grosjean and Grosjean (1998) have studied the reaction of O_3 with linalool. The rate coefficient values obtained in these two studies are reported in table II-D-37. The lower limit reported by Grosjean and Grosjean is consistent with the

Table II-D-36. Rate coefficients (k, cm^3 molecule^{-1} s^{-1}) for the reaction of OH with 3,7-dimethyl-1,6-octadien-3-ol [$(CH_3)_2C{=}CHCH_2CH_2C(CH_3)(OH)CH{=}CH_2$ linalool]

$10^{10} \times k$	T (K)	Technique[a]	Reference
1.57 ± 0.40	296 ± 2	RR[b] (isoprene)	Atkinson et al. (1995)
2.14 ± 0.28	295 ± 3	RR[c] (styrene)	Bernhard and Simonich (2000)

[a]Abbreviations used for the techniques are defined in table I-F-3.
[b]Placed on an absolute basis using $k(\text{OH} + \text{isoprene}) = 1.0 \times 10^{-10}$ cm^3 molecule^{-1} s^{-1} (Atkinson et al., 2006).
[c]Placed on an absolute basis using $k(\text{OH} + \text{styrene}) = 5.8 \times 10^{-11}$ cm^3 molecule^{-1} s^{-1} (Calvert et al., 2002).

Table II-D-37. Rate coefficients (k, cm^3 molecule^{-1} s^{-1}) for the reaction of O_3 with 3,7-dimethyl-1,6-octadien-3-ol [$(CH_3)_2C{=}CHCH_2CH_2C(CH_3)(OH)CH{=}CH_2$ linalool]

$10^{16} \times k$	T (K)	Technique[a]	Reference
4.4 ± 1.6	296 ± 2	RR (2-methyl-2-butene)[b]	Atkinson et al. (1995)
≥ 3.15 ± 0.23	290 ± 4	Excess of linalool[c]	Grosjean and Grosjean (1998)

[a]Abbreviations used for the techniques are defined in table I-F-3.
[b]Placed on an absolute basis using $k(O_3 + \text{2-methyl-2-butene}) = 4.03 \times 10^{-16}$ cm^3 molecule^{-1} s^{-1} (Atkinson and Arey, 2003).
[c]Excess of linalool, O_3 measured by absorption spectroscopy.

Table II-D-38. Rate coefficient (k, cm^3 molecule^{-1} s^{-1}) for the reaction of NO_3 with 3,7-dimethyl-1,6-octadien-3-ol [$(CH_3)_2C{=}CHCH_2CH_2C(CH_3)(OH)CH{=}CH_2$ linalool]

$10^{11} \times k$	T (K)	Technique[a]	Reference
1.12 ± 0.40	296 ± 2	RR[b] (2-methyl-2-butene)	Atkinson et al. (1995)

[a]Abbreviations used for the techniques are defined in table I-F-3.
[b]Placed on an absolute basis using $k(NO_3 + \text{2-methyl-2-butene}) = 9.37 \times 10^{-12}$ cm^3 molecule^{-1} s^{-1} (Calvert et al., 2000).

value measured by Atkinson et al. (1995). We recommend the value of Atkinson et al. (1995) determined using the relative rate method, $k(O_3 + \text{linalool}) = 4.4 \times 10^{-16}$ cm^3 molecule^{-1} s^{-1}, with an estimated uncertainty of ±50%.

II-D-13.3. NO_3 Reaction Kinetics

The only study of the reaction of NO_3 with linalool is that of Atkinson et al. (1995) using a relative rate method at atmospheric pressure; see table II-D-38. The recommended value for the rate coefficient is based on this single measurement, $k = 1.1 \times 10^{-11}$ cm^3 molecule^{-1} s^{-1} at 298 K with an estimated uncertainty of ±50%.

II-D-13.4. Summary of the Atmospheric Fate of Linalool

Linalool is very reactive towards atmospheric oxidants; the rate coefficients for reactions with OH, O_3, and NO_3 were used to calculate its atmospheric

lifetime to be less than 1 h with respect to reaction with OH, O_3, and NO_3. The reaction of OH with linalool proceeds mainly by initial addition of OH to the C=C bonds. It is expected that addition to the $(CH_3)_2C{=}CH$ group dominates over that to the $CH_2{=}CH$ group. The major products observed in one atmosphere of air in the presence of NO_x by Shu et al. (1997) were acetone (50.5 ± 4.7%), 6-methyl-5-hepten-2-one (6.8 ± 0.6%), and 4-hydroxy-4-methyl-5-hexen-1-al and/or its cyclized form 2-ethenyl-2-methyl-5-hydroxytetrahydrofuran (46 ± 11%). The suggested reaction mechanism is presented in figure II-D-22. $(CH_3)_2C{=}CHCH_2CH_2C(CH_3)(OH)CH(O)CH_2OH$ radicals formed following OH radical addition to the terminal C=C bond are expected to decompose leading mainly to $HOCH_2CHO$ and $(CH_3)_2C{=}CHCH_2CH_2C(O)CH_3$ as end products (Shu et al., 1997). Addition of OH radicals to the

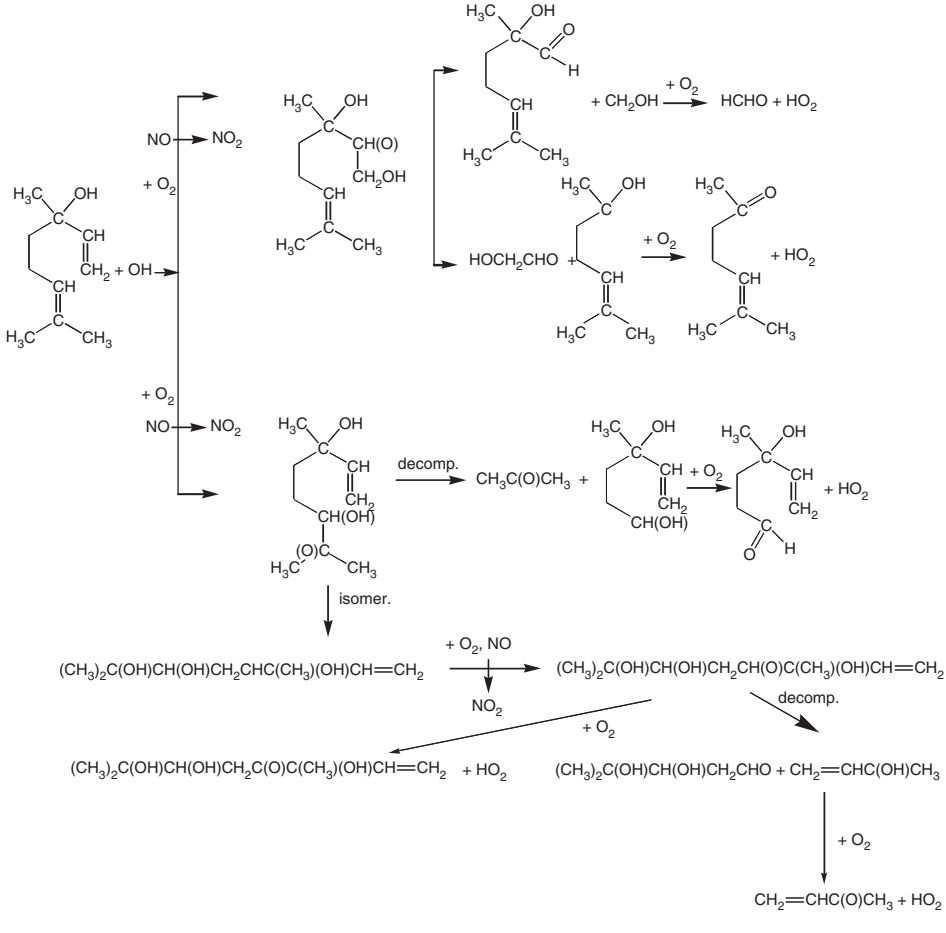

Figure II-D-22. Major pathways in the OH-initiated oxidation of linalool.

$(CH_3)_2C{=}CH{-}$ double bond leads to the formation of two β-hydroxyalkoxy radicals; $(CH_3)_2C(OH)CH(O)CH_2CH_2C(CH_3)(OH)CH{=}CH_2$ and $(CH_3)_2C(O)CH(OH)CH_2CH_2C(CH_3)(OH)CH{=}CH_2$. Shu et al. (1997) have discussed the fate of these radicals. The first β-hydroxyalkoxy radical can react with O_2 or decompose, but cannot isomerize by a 1,5-H shift via a six-member transition state. The decomposition pathway leading to acetone and 4-hydroxy-4-methyl-5-hexen-1-al dominates reaction with O_2 by a factor of 7×10^3. The second β-hydroxyalkoxy radical cannot react with O_2 because it lacks a hydrogen atom in the α-position, but it can isomerize and/or decompose. The observation of a substantial yield of acetone and 4-hydroxy-4-methyl-5-hexen-1-al, and the lack of any detectable methyl vinyl ketone, shows that decomposition dominates (see figure II-D-22). Shu et al. reported that 4-hydroxy-4-methyl-5-hexen-1-al undergoes cyclization to form the thermodynamically favored isomeric compound 2-ethenyl-2-methyl-5-hydroxytetrahydrofuran:

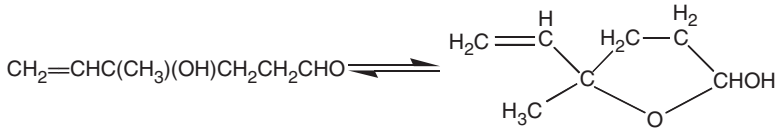

The measured similar formation yields of acetone and 4-hydroxy-4-methyl-5-hexen-1-al (50.5 ± 4.7% and 46 ± 11%, respectively) and 6-methyl-5-hepten-2-one (6.8 ± 0.6%) account for 53 ± 8% of the loss of linalool. Clearly other unidentified products including dihydroxynitrates such as $(CH_3)_2C(OH)CH(ONO_2)CH_2CH_2C(CH_3)(OH)CH{=}CH_2$ and $(CH_3)_2C(ONO_2)CH(OH)CH_2CH_2C(CH_3)(OH)CH{=}CH_2$ are formed in a significant yield.

The reaction of ozone with linalool occurs predominately (~97%) at the more reactive trisubsituted $>C{=}CH{-}$ bond leading to formation of the products: $CH_3C(O)CH_3$ + $[CH_2{=}CHC(CH_3)(OH)CH_2CH_2CH{\bullet}OO{\bullet}]^*$ and $[(CH_3)_2C{\bullet}OO{\bullet}]^*$ + $CH_2{=}CHC(CH_3)(OH)CH_2CH_2CHO$ (Atkinson et al., 1995; Shu et al., 1997; Grosjean and Grosjean, 1997). The main products observed by Shu et al. (1997) were acetone (21.1 ± 2.4%), 4-hydroxy-4-methyl-5-hexen-1-al and/or its cyclized form 2-ethenyl-2-methyl-5-hydroxytetrahydrofuran (85 ± 14%), 5-ethenyldihydro-5-methyl-2(3H)-furanone (12.6 ± 2.5%), and formaldehyde (36 ± 6%). While Grosjean and Grosjean observed acetone in a yield of 28 ± 1% and formaldehyde in a yield of 1.4 ± 1.2%, Lee et al. (2006) confirmed the formation yields of acetone (16 ± 1%) and formaldehyde (34 ± 3%) reported by Shu et al. Secondary reactions of the biradicals $[CH_2{=}CHC(CH_3)(OH)CH_2CH_2CHOO]^*$ and $[(CH_3)_2COO]^*$ lead to the formation of additional products. CH_2O is expected to arise mainly from the reactions of $[(CH_3)_2COO]^*$. Atkinson et al. (1995) have measured an OH radical formation yield of 72% from the reaction of O_3 with linalool which could be attributed mainly to the secondary reactions of $[(CH_3)_2COO]^*$.

Shu et al. have attributed the formation of 5-ethenyldihydro-5-methyl-2(3H)-furanone to the cyclization of $[CH_2{=}CHC(CH_3)(OH)CH_2CH_2CHOO]^*$ with

elimination of H_2O via the following reaction mechanism:

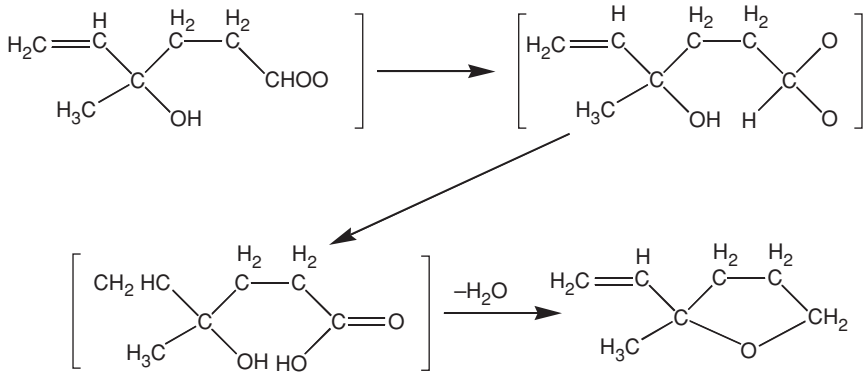

The observed reaction products reported by Shu et al. (1997) account for 78 ± 10% of the consumed linalool. Based on the measured product yields, Shu et al. estimated the importance of the different initial reaction pathways:

$$O_3 + \text{linalool} \rightarrow CH_3C(O)CH_3 + [CH_2{=}CHC(CH_3)(OH)CH_2CH_2CHOO]^* \qquad 15{-}20\%$$

$$O_3 + \text{linalool} \rightarrow [(CH_3)_2COO]^* + CH_2{=}CHC(CH_3)(OH)CH_2CH_2CHO \qquad 80{-}85\%$$

The reaction of NO_3 with linalool is expected to occur via NO_3 addition to the more substituted C=C bond (Shu et al., 1997); this leads under atmospheric conditions to the formation of two β-nitrooxyalkyl peroxy radicals, $(CH_3)_2C(OO)CH(ONO_2)CH_2CH_2C(CH_3)(OH)CH{=}CH_2$ and $(CH_3)_2C(ONO_2)CH(OO)CH_2CH_2C(CH_3)(OH)CH{=}CH_2$, which react with NO to give the corresponding β-nitrooxyalky alkoxy radicals $(CH_3)_2C(O)CH(ONO_2)CH_2CH_2C(CH_3)(OH)CH{=}CH_2$ (which can isomerize or decompose) and $(CH_3)_2C(ONO_2)CH(O)CH_2CH_2C(CH_3)(OH)CH{=}CH_2$ (which can react with O_2 or decompose). Shu et al. observed acetone (22.5 ± 5.2%), 4-hydroxy-4-methyl-5-hexen-1-al (19.1 ± 5.1%) and tentatively identified the nitrooxycarbonyl $[(CH_3)_2C(ONO_2)C(O)CH_2CH_2C(CH_3)(OH)CH{=}CH_2]$ as products. Shu et al. (1997) suggested that for their experimental conditions, the nitrooxycarbonyl could be the major product of the gas-phase reaction of NO_3 with linalool. The reaction products quantified by Shu et al. (1997) account for only 20 ± 4% of the loss of linalool.

II-D-14. 2,6-Dimethyl-2,6-octadien-8-ol (Geraniol)

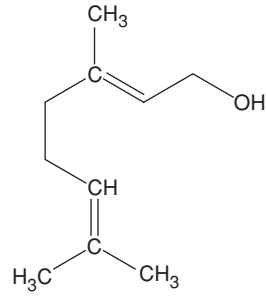

II-D-14.1. OH Reaction Kinetics

Forester et al. (2007) measured the rate coefficient for the reaction of OH with geraniol; see table II-D-39. The average value obtained using a relative rate method with two reference compounds (limonene and myrcene) is $k(\text{OH} + \text{geraniol}) = 2.3 \times 10^{-10}$ cm^3 molecule^{-1} s^{-1} (at 297 ± 3 K). This rate coefficient value is recommended with an estimated uncertainty of ±50%.

II-D-14.2. O_3 Reaction Kinetics

Forester et al. (2007) used a relative rate method to measure $k(\text{O}_3 + \text{geraniol}) = (9.3 \pm 2.3) \times 10^{-16}$ cm^3 molecule^{-1} s^{-1} at 297 ± 3 K; see table II-D-40.

Table II-D-39. Rate coefficient (k, cm^3 molecule^{-1} s^{-1}) for reaction of OH with 2,6-dimethyl-2,6-octadien-8-ol [geraniol, $(CH_3)_2C{=}CHCH_2CH_2C(CH_3){=}CHCH_2OH$]

$10^{10} \times k$	T (K)	Technique[a]	Reference
2.31 ± 0.58	297 ± 3	RR (limonene and myrcene)[b]	Forester et al. (2007)

[a]Abbreviations used for the techniques are defined in table I-F-3.
[b]Placed on an absolute basis using $k(\text{OH} + \text{limonene}) = 1.64 \times 10^{-10}$ and $k(\text{OH} + \text{myrcene}) = 2.15 \times 10^{-10}$ cm^3 molecule^{-1} s^{-1}.

Table II-D-40. Rate coefficient (k, cm^3 molecule^{-1} s^{-1}) for reaction of O_3 with 2,6-dimethyl-2,6-octadien-8-ol [geraniol, $(CH_3)_2C{=}CHCH_2CH_2C(CH_3){=}CHCH_2OH$]

$10^{16} \times k$	T (K)	Technique[a]	Reference
9.3 ± 2.3	297 ± 3	RR (*cis*-cyclooctene and myrcene)[b]	Forester et al. (2007)

[a]Abbreviations used for the techniques are defined in table I-F-3.
[b]Placed on an absolute basis using $k(\text{O}_3 + \textit{cis-cyclooctene}) = 3.8 \times 10^{-16}$ and $k(\text{O}_3 + \text{myrcene}) = 4.7 \times 10^{-16}$ cm^3 molecule^{-1} s^{-1}.

II-D-14.3. Summary of the Atmospheric Fate of Geraniol

Geraniol is very reactive towards atmospheric oxidants. The atmospheric lifetime of geraniol is estimated to be less than 1 h with respect to reaction with either O_3 or OH radicals. The OH-initiated oxidation of geraniol in one atmosphere of air in the presence of NO_x has been investigated by Forester et al. (2007). The reaction proceeds mainly via OH addition to the C=C bonds. Forester et al. (2007) reported acetone [$CH_3C(O)CH_3$], glycolaldehyde ($HOCH_2CHO$), glyoxal [CH(O)CHO], and methylglyoxal ($CH_3C(O)CHO$) as the main reaction products. In addition, 4-oxopentanal [$CH_3C(O)CH_2CH_2CHO$] was suggested as a potential major reaction product (figure II-D-23).

The mechanism of the reaction of O_3 with geraniol has been studied by Nunes et al. (2005) and Forester et al. (2007). In both studies, the main oxidation products reported were acetone [$CH_3C(O)CH_3$], glycolaldehyde ($HOCH_2CHO$), glyoxal [CH(O)CHO], and methylglyoxal [$CH_3C(O)CHO$]. Cyclohexanone was observed and was attributed to the reaction of OH radicals (produced in the ozonolysis of geraniol) with cyclohexane (used as an OH scavenger). 4-Oxopentanal [$CH_3C(O)CH_2CH_2CHO$] was detected in the study of Forester et al. but not by Nunes et al. The reaction mechanism suggested by Nunes et al. and Forester et al. is presented in figure II-D-24.

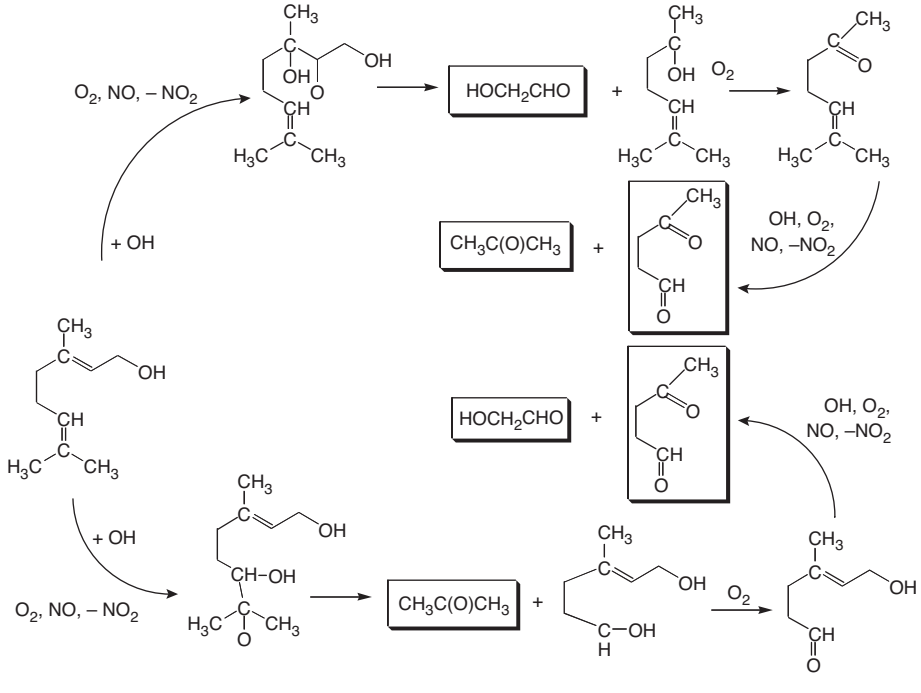

Figure II-D-23. Proposed reaction mechanism for the reaction of OH with geraniol showing formation of acetone, glycolaldehyde, and 4-oxopentanal (Forester et al., 2007).

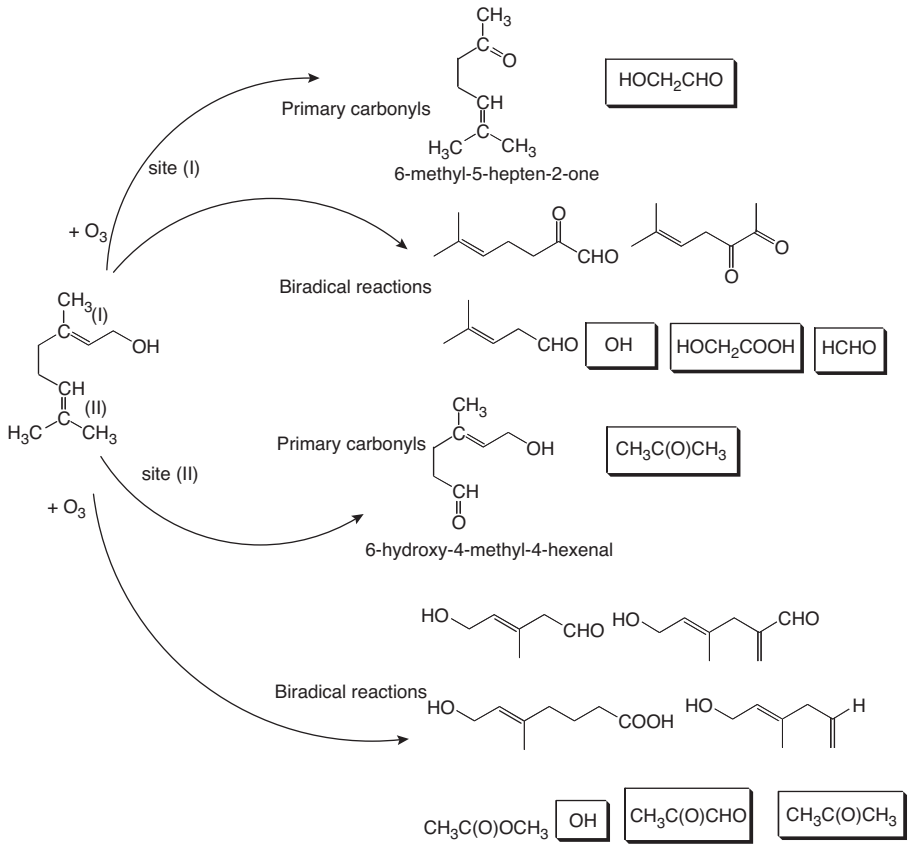

Figure II-D-24. The reaction mechanism for the reaction of O_3 with geraniol (Nunes et al., 2005; Forester et al., 2007).

II-D-15. 3,7-Dimethyl-6-octen-1-ol (Citronellol)

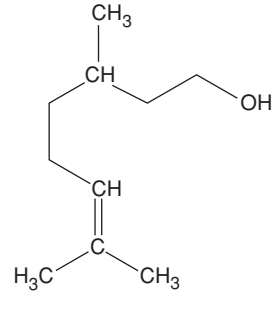

II-D-15.1. OH Reaction Kinetics

The kinetics of the reaction of OH radicals with citronellol have been investigated by Ham et al. (2006) using a relative rate method at atmospheric pressure; see table II-D-41. The average value obtained with two reference compounds (limonene and 3-carene) is $k(\text{OH} + \text{citronellol}) = 1.7 \times 10^{-10}\,\text{cm}^3\ \text{molecule}^{-1}\,\text{s}^{-1}$ at 297 ± 3 K. This rate coefficient value is recommended with an estimated uncertainty of 50%.

II-D-15.2. O_3 Reaction Kinetics

The rate coefficient for reaction of O_3 with citronellol was measured by Ham et al. (2006) by monitoring the decrease in ozone concentration in an excess of citronellol; see table II-D-42. The value obtained is $k(O_3 + \text{citronellol}) = 2.4 \times 10^{-16}\,\text{cm}^3\ \text{molecule}^{-1}\,\text{s}^{-1}$ at 297 ± 3 K. This rate coefficient value is recommended with an estimated uncertainty of ±50%.

II-D-15.3. Summary of the Atmospheric Fate of Citronellol

Citronellol is very reactive towards atmospheric oxidants; its atmospheric lifetime is estimated to be around 1 h with respect to reaction with either O_3 or OH radicals. The reaction of OH with citronellol proceeds mainly by OH addition to the C=C double bond. Ham et al. (2006) reported acetone and 6-hydroxy-4-methylhexanal as major products of the reaction following the mechanism presented in figure II-D-25. These authors also observed glyoxal [HC(O)C(O)H] and methyl glyoxal [CH_3C(O)C(O)H] as products. The same products have been also observed for the reaction of O_3 with citronellol.

Table II-D-41. Rate coefficient (k, $\text{cm}^3\ \text{molecule}^{-1}\ \text{s}^{-1}$) for the reaction of OH with 3,7-dimethyl-6-octen-1-ol [citronellol, $(CH_3)_2C{=}CHCH_2CH_2CH(CH_3)CH_2CH_2OH$]

$10^{10} \times k$	T (K)	Technique[a]	Reference
1.74 ± 0.43	297 ± 3	RR (limonene and 3-carene)[b]	Ham et al. (2006)

[a]Abbreviations used for the techniques are defined in table I-F-3.
[b]Placed on an absolute basis using $k(\text{OH} + \text{limonene}) = 1.64 \times 10^{-10}$ and $k(\text{OH} + \text{3-carene}) = 8.8 \times 10^{-11}\,\text{cm}^3\ \text{molecule}^{-1}\,\text{s}^{-1}$ (Atkinson and Arey, 2003b).

Table II-D-42. Rate coefficient (k, $\text{cm}^3\ \text{molecule}^{-1}\ \text{s}^{-1}$) for the reaction of O_3 with 3,7-dimethyl-6-octen-1-ol [citronellol, $(CH_3)_2C{=}CHCH_2CH_2CH(CH_3)CH_2CH_2OH$]

$10^{16} \times k$	T (K)	Technique[a]	Reference
2.4 ± 0.1	297 ± 3	Excess of citronellol[a]	Ham et al. (2006)

[a]Pseudo first-order conditions using excess of citronellol; O_3 was measured by UV photometric analyzer.

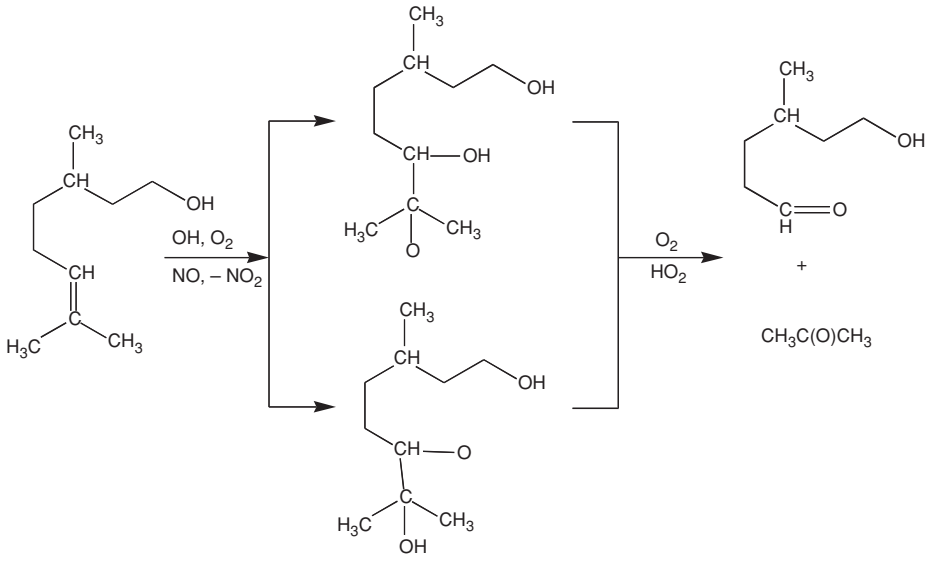

Figure II-D-25. Proposed reaction mechanism for the reaction of OH with citronellol showing formation of acetone and 6-hydroxy-4-methylhexanal (Ham et al., 2006).

II-D-16. 2-(4-Methylcyclohex-3-en-1-yl)propan-2-ol (α-Terpineol) and 1-Methyl 4-isopropenyl-6-cyclohexen-2-ol [(-)Carveol]

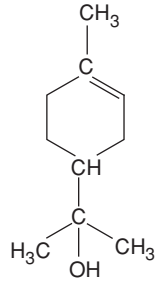

2-(4-methylcyclohex-3-en-1-yl)propan-2-ol
(α-terpineol)

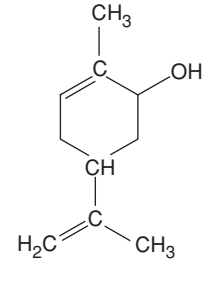

1-methyl-4-isopropenyl-6-cyclohexen-2-ol
[(-)carveol]

II-D-16.1. OH Reaction Kinetics

The kinetics of the reaction of OH radicals with α-terpineol have been investigated by Wells (2005) using a relative rate method at atmospheric pressure; see table II-D-43. The average value obtained with two reference compounds (isoprene and 2,5-dimethyl furan) is $k(\text{OH} + \alpha\text{-terpineol}) = 1.9 \times 10^{-10}\,\text{cm}^3$ molecule^{-1} s^{-1}

Table II-D-43. Rate coefficient (k, cm^3 molecule^{-1} s^{-1}) for reaction of OH with 1-methyl-4-isopropyl-1-cyclohexen-8-ol (α-terpineol)

$10^{10} \times k$	T (K)	Technique[a]	Reference
1.9 ± 0.5	297 ± 3	RR (isoprene and 2,5-dimethylfuran)[b]	Wells (2005)

[a]Abbreviations used for the techniques are defined in table I-F-3.
[b]Placed on an absolute basis using k(OH + isoprene) = 1.0×10^{-10} (Atkinson et al., 2006) and k(OH + 2, 5-dimethyl furan) = 1.3×10^{-10} cm^3 molecule^{-1} s^{-1} (Bierbach et al., 1992).

Table II-D-44. Rate coefficient (k, cm^3 molecule^{-1} s^{-1}) for reaction of O_3 with1-methyl-4-isopropyl-1-cyclohexen-8-ol (α-terpineol)

$10^{16} \times k$	T (K)	Technique[a]	Reference
3.0 ± 0.2	297 ± 3	Excess of α-terpineol[a]	Forester et al. (2007)

[a]Pseudo first-order conditions (excess of α-terpineol, O_3 measured by UV photometric analyzer).

(at 297 ± 3 K). This rate coefficient value is recommended with an estimated uncertainty of ±50%.

II-D-16.2. O_3 Reaction Kinetics

The rate coefficient for reaction of O_3 with α-terpineol was measured by Wells (2005) by monitoring the decrease in ozone concentration in an excess of α-terpineol; see table II-D-44. The value obtained is $k(O_3 + \alpha\text{-terpineol}) = 3 \times 10^{-16}$ cm^3 molecule^{-1} s^{-1} at 297 ± 3 K. This rate coefficient value is recommended with an estimated uncertainty of ±50%.

II-D-16.3. Summary of the Atmospheric Fate of α-Terpineol and (-)-Carveol

α-Terpineol is very reactive towards atmospheric oxidants; its atmospheric lifetime is estimated to be less than 1 h with respect to reactions with either O_3 or OH radicals. The reaction of OH with α-terpineol proceeds mainly by OH addition to the C=C double bond. Wells (2005) identified acetone, glyoxal, and methyl glyoxal as major reaction products. Other reaction products such as butanedial ($HC(O)CH_2CH_2C(O)H$) and 4-oxopentanal ($HC(O)CH_2CH_2C(O)CH_3$) have been suggested using mass spectrometry techniques (Wells, 2005). Methyl glyoxal was positively identified as product of the reaction of ozone with α-terpineol.

(-)-Carveol is also expected to be very reactive towards OH, O_3, and NO_3, probably at a rate at least as great as the compounds with similar structure such as limonene (Calvert et al., 2000). Therefore, its atmospheric lifetime is estimated to be less than 1 h. The only product observed by Nunes et al. (2005) in their study of the ozonolysis of carveol is formaldehyde with a production yield of 19 ± 0.8%.

II-D-17. 2-Propyn-1-ol ($HC{\equiv}CCH_2OH$, Propargyl Alcohol) and 3,5-Dimethyl-1-hexyn-3-ol [$HC{\equiv}CC(OH)(CH_3)CH_2CH(CH_3)_2$]

II-D-17.1. OH Reaction Kinetics

The rate coefficient for reaction of OH radicals with 2-propyn-1-ol has been determined by Upadhyaya et al. (2001); see table II-D-45. The measurement was carried out using a laser photolysis-laser induced fluorescence technique and a value of $k(OH + HC{\equiv}CCH_2OH) = (9.2 \pm 1.4) \times 10^{-12}\,cm^3$ molecule^{-1} s^{-1} was reported. As with their study of k(OH + allyl alcohol), Upadhyaya et al. (2001) measured $k(OH + HC{\equiv}CCH_2OH)$ in 10–20 Torr of argon diluent and reported a value of k(OH + allyl alcohol) which was lower than measured in other studies conducted under atmospheric pressure. This was tentatively ascribed to a pressure dependence of the reaction. Hence, it is possible that the value for $k(OH + HC{\equiv}CCH_2OH)$ measured in 10–20 Torr of argon is not applicable to atmospheric conditions. Further work is needed to clarify the pressure dependence of the rate coefficient of this reaction.

The kinetics of the reaction of OH radicals with 3,5-dimethyl-1-hexyn-3-ol have been investigated by Wells (2004) using a relative rate method. The value reported at 297 ± 3 K is $k = (2.9 \pm 0.9) \times 10^{-11}\,cm^3$ molecule^{-1} s^{-1}.

II-D-17.2. Summary of the Atmospheric Fate of 2-Propyn-1-ol and 3,5-Dimethyl-1 hexyn-3-ol

The atmospheric lifetimes of 2-propyn-1-ol and 3,5-dimethyl-1-hexyn-3-ol with respect to reaction with OH radicals are estimated to be approximately 1 day and 4 h, respectively. The oxidation mechanism of 2-propyn-1-ol has not been investigated experimentally. It is expected that this reaction proceeds mainly through OH addition to the C≡C bond.

Wells (2004) investigated the OH-initiated degradation of 3,5-dimethyl-1-hexyn-3-ol in one atmosphere of air in the presence of NO_x and identified acetone, 3-butyne-2-one [$HC{\equiv}CC(O)CH_3$], 2-methyl-propanal [$(CH_3)_2CHCHO$], 4-methyl-2-pentanone [$(CH_3)_2CHCH_2C(O)CH_3$], glyoxal [CH(O)CHO], methyl glyoxal [$CH_3C(O)CHO$], and 2,3-butanedione [$CH_3C(O)C(O)CH_3$] as the main products. The reported yields of 3-butyne-2-one and 4-methyl-2-pentanone were (8.4 ± 0.3)% and (26 ± 2)%, respectively. A number of other products were detected but could not be positively identified and quantified. These products arise from the OH addition and/or H-atom

Table II-D-45. Rate coefficients (k, cm^3 molecule^{-1} s^{-1}) for reaction of OH with 2-propyn-1-ol ($HC{\equiv}CCH_2OH$) and 3,5-dimethyl-1-hexyn-3-ol [$(CH_3)_2CHCH_2C(OH)(CH_3)C{\equiv}CH$]

Compound	$10^{11} \times k$	T (K)	Technique[a]	Reference
2-Propyn-1-ol	0.92 ± 0.14	298	PLP–LIF	Upadhyaya et al. (2001).
3,5-Dimethyl-1-hexyn-3-ol	2.9 ± 0.9	297 ± 3	RR[b] (two references)	Wells (2004)

[a]Abbreviations used for the techniques are defined in table I-F-3.
[b]Placed on an absolute basis using k(OH+decane) = 1.1×10^{-11} and k(OH+pentanal) = 2.85×10^{-11} cm^3 molecule^{-1} s^{-1}.

abstraction from different sites of the molecule as shown below:

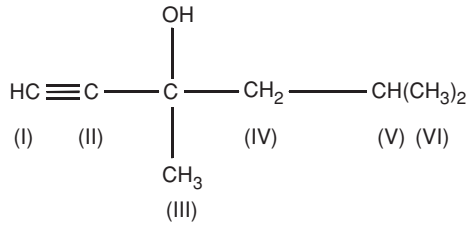

Wells (2004) suggested that approximately 64% of the reaction proceeds via addition to site (II), 16% via H abstraction from site (IV), and 14% via H abstraction from site (V). Reactions at (I), (III), and (VI) are of minor importance.

II-E. Aromatic Alcohols

II-E-1. Phenol

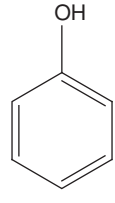

II-E-1.1. OH Reaction Kinetics

There have been four kinetic studies of the reaction of OH with phenol using both absolute and relative methods. No data are available below 296 K but measurements have been conducted at high temperature (e.g., at 1032 K by He et al., 1988). The data reported by different groups above 296 K are given in table II-E-1 and displayed in figure II-E-1. The measurements of Rinke and Zetzsch (1984) were performed over the pressure range 5–733 mbar (3.7–550 Torr) while those from Knispel et al. (1990) were obtained at a total pressure of 133 mbar of argon and those of Semadeni et al. (1995) and Sørensen et al. (2002) were obtained in 730 Torr and 750 Torr of air, respectively. The investigation of Rinke and Zetzsch showed that the rate coefficient is pressure independent above 30–50 mbar of argon. The reported rate coefficient values by different groups near 298 K are in good agreement. A fit of the Arrhenius expression to the data from Rinke and Zetzsch, Knispel et al., Semadeni et al., and Sørensen et al. gives $k = 4.5 \times 10^{-13} \exp(1{,}229/T)\,\mathrm{cm^3\ molecule^{-1}\ s^{-1}}$ over the temperature range 290–350 K. This expression gives $k = 2.8 \times 10^{-11}\,\mathrm{cm^3\ molecule^{-1}\ s^{-1}}$ at 298 K with an uncertainty estimated to be ±20%.

Sørensen et al. (2002) conducted experiments that showed that the presence of 500–8,000 μg $\mathrm{m^{-3}}$ NaCl or NH_4NO_3 aerosols (levels which far exceed those found in the atmosphere) does not affect the reactivity of OH with phenol.

Table II-E-1. Rate coefficients ($k = A\ e^{-B/T}$, cm^3 $molecule^{-1}$ s^{-1}) for reaction of OH with phenol (C_6H_5OH)

$10^{13} \times A$	B (K)	$10^{11} \times k$	T (K)	Technique[a]	Reference	Temperature Range (K)
		2.83 ± 0.57	296 ± 2	FP–RF	Rinke and Zetzsch (1984)	
		2.9 ± 0.31	300	FP–RF	Knispel et al. (1990)	300–374
		2.6 ± 0.31	308			
		2.24 ± 0.21	323			
		1.86 ± 0.21	339			
		1.76 ± 0.21	354			
		1.71 ± 0.21	374			
3.7[f]	−(1,267 ± 233)[f]	2.56 ± 0.27	301	RR (1,3-butadiene)[b]	Semadeni et al. (1995)	301–373
		2.17 ± 0.25	319	RR (1,3-butadiene)[b]		
		1.70 ± 0.40	334	RR (1,3-butadiene)[b]		
		1.50 ± 0.17	348	RR (1,3-butadiene)[b]		
		1.18 ± 0.16	360	RR (1,3-butadiene)[b]		
		1.08 ± 0.15	373	RR (1,3-butadiene)[b]		
		2.38 ± 0.20	301	RR (*o*-cresol)[c]		
		2.05 ± 0.17	314	RR (*o*-cresol)[c]		
		3.1 ± 0.2	296 ± 2	RR (C_2H_4)[d]	Sørensen et al. (2002)	
		3.06 ± 0.21	296 ± 2	RR (*p*-xylene)[e]	Sørensen et al. (2002)	

[a]Abbreviations used for the techniques are defined in table I-F-3.
[b]Placed on an absolute basis using $k(OH + 1, 3\text{-butadiene}) = 1.48 \times 10^{-12} \exp(448/T)\ cm^3\ molecule^{-1}\ s^{-1}$ (Atkinson and Arey, 2003a).
[c]Placed on an absolute basis using $k(OH + o\text{-cresol}) = 1.5 \times 10^{-12} \exp(986/T)\ cm^3\ molecule^{-1}\ s^{-1}$ (this book, section II-E-2.1).
[d]Placed on an absolute basis using $k(OH + C_2H_4) = 7.9 \times 10^{-12}\ cm^3\ molecule^{-1}\ s^{-1}$ (Atkinson et al., 2006).
[e]Placed on an absolute basis using $k(OH + p\text{-xylene}) = 1.43 \times 10^{-11}\ cm^3\ molecule^{-1}\ s^{-1}$ (Calvert et al., 2002).
[f]As stated by the authors (Semadeni et al., 1995).

Berndt and Böge (2003) investigated the products of the reaction of OH with phenol in flow tube experiments (at 100 mbar in presence and absence of O_2 and different concentrations of NO_x) at temperatures in the range 266–364 K. Catechol was found to be the main product under all experimental conditions; its molar yield increased from 0.37 ± 0.06 at 266 K to 0.87 ± 0.04 at 364 K. Other products observed were *p*-benzoquinone, *o*-nitrophenol, 3-nitrocatechol, and *p*-nitrophenol. For NO_2 concentrations $< (3 - 4) \times 10^{13}$ molecule cm^{-3} and room temperature, the molar yields of catechol found , 0.73–0.78, were in good agreement with the chamber results of Olariu et al. (2002), who reported 0.804 ± 0.121 obtained using a smog chamber study.

II-E-1.2. NO_3 Reaction Kinetics

The kinetics of the reaction of NO_3 with phenol have been studied by Carter et al. (1981), Atkinson et al. (1984b, 1992a), and Bolzacchini et al. (2001). Table II-E-2 summarizes the reported data. The measurements from Carter et al. (1981) and that of Atkinson et al. (1984b) using the equilibrium constant of $NO_2 + NO_3 \leftrightarrow N_2O_5$ seem

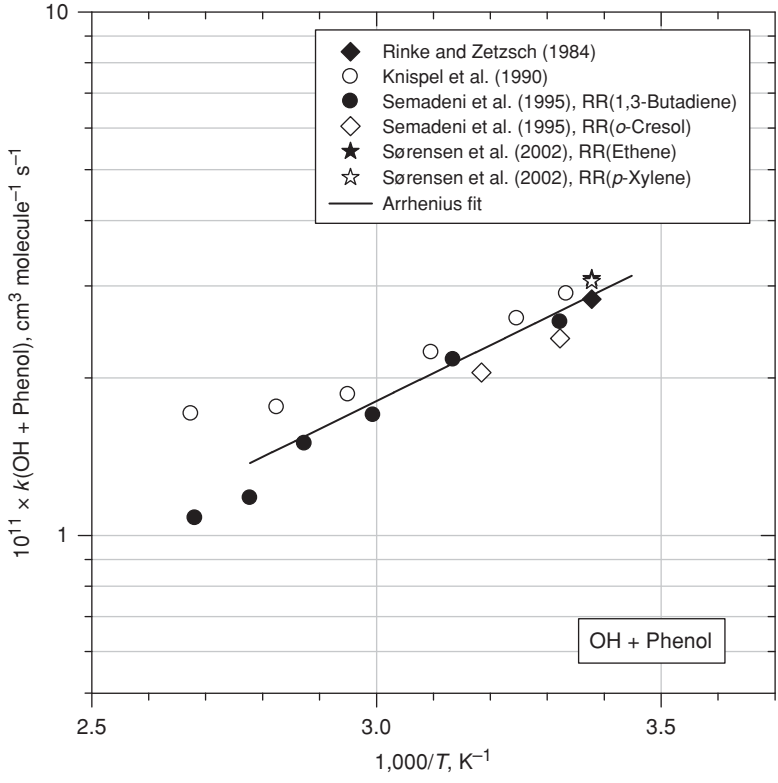

Figure II-E-1. Arrhenius plot of the rate coefficients for the OH + phenol reaction.

Table II-E-2. Rate coefficients (k, cm^3 molecule^{-1} s^{-1}) for reaction of NO_3 with phenol (C_6H_5OH)

$10^{12} \times k$	T (K)	Technique[a]	Reference
2.61 ± 0.53	300 ± 1	RR (*cis*-2-butene)[b]	Carter et al. (1981)
3.64 ± 0.14	298 ± 1	RR (2-methyl-2-butene)[c]	Atkinson et al. (1984b)
4.78 ± 0.52	298 ± 1	RR (NO_2+NO_3 ↔ N_2O_5)[d]	Atkinson et al. (1984b)
3.92 ± 0.25	296 ± 2	RR (2-methyl-2-butene)[c]	Atkinson et al. (1992b)
5.81 ± 1.13	295 ± 2	RR (2-methyl-2-butene)[c]	Bolzacchini et al. (2001)

[a]Abbreviations used for the techniques are defined in table I-F-3.

[b]Placed on an absolute basis using $k(NO_3 + cis\text{-2-butene}) = 3.52 \times 10^{-12}$ cm^3 molecule^{-1} s^{-1} (Atkinson and Arey, 2003a).

[c]Placed on an absolute basis using $k(NO_3 + 2\text{-methyl-2-butene}) = 9.37 \times 10^{-12}$ cm^3 molecule^{-1} s^{-1} (Atkinson and Arey, 2003a).

[d]Placed on an absolute basis using $K(NO_2 + NO_3 \leftrightarrow N_2O_5) = 2.75 \times 10^{-11}$ cm^3 molecule^{-1} s^{-1} (IUPAC, 2008).

to be subject to large uncertainties (IUPAC, 2008). Hence, the preferred value is based on the average of the data from Atkinson et al. (1984b, 1992b) and Bolzacchini et al. (2001), $k = 4.5 \times 10^{-12}\,\mathrm{cm^3\ molecule^{-1}\ s^{-1}}$ at 298 K with an estimated uncertainty of ±30%.

II-E-1.3. Summary of the Atmospheric Fate of Phenol

The lifetime of phenol with respect to the reaction of OH and NO_3 is less than 4 h. The reaction of OH with phenol may proceed through three different pathways:

$$OH + C_6H_5OH \rightarrow H_2O + C_6H_5O \quad (1)$$

$$OH + C_6H_5OH \rightarrow H_2O + C_6H_4OH \quad (2)$$

$$OH + C_6H_5OH \rightarrow HOC_6H_5OH \quad (3)$$

The relative importance of these channels depends on the temperature. The available kinetic and mechanistic data indicate that for the atmospherically relevant temperature range, the reactions proceed essentially through channels (1) and (3). H-atom abstraction from the —OH group (channel 1) accounts for about 12% of the reaction at 298 K and less at lower temperatures. It has been reported that the reaction of OH with phenol leads to 2-nitrophenol (~6%) in the presence of NO_x at 298 K (Atkinson et al., 1992b; Platz et al., 1998; Olariu et al., 2002). The observed yield of 2-nitrophenol shows that at least 6% of the reaction goes through H-atom abstraction from the —OH group.

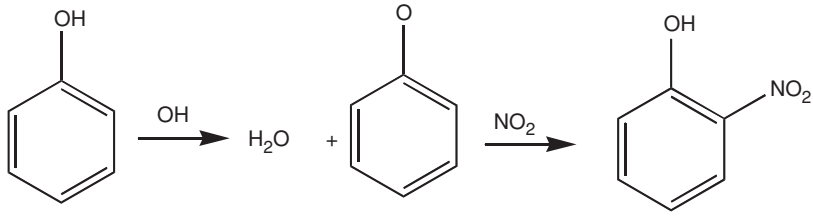

Olariu et al. have reported 1,2-dihydroxybenzene (80.4 ± 12.1)%, 1,4-benzoquinone (3.7 ± 1.2)%, and 2-nitrophenol (5.8 ± 1.0)% as the main OH-initiated oxidation of phenol. 1,2-Dihydroxybenzene is formed through the addition channel as shown in the figure II-E-2. Since they have not observed the formation of 1,4-benzoquinone when phenoxy radicals were produced by reaction of Cl-atoms, they have concluded that 1,4-benzoquinone formation in the OH reaction with phenol must be occurring via the OH addition channel not the abstraction channel. The complete reaction mechanism leading to 1,4-benzoquinone is still not clear.

Regarding the reaction of NO_3 with phenol, Atkinson et al. (1992b) and Bolzacchini et al. (2001) reported 2-nitrophenol as the main product of the reaction. Atkinson et al. (1992b) measured a 2-nitrophenol yield of (25.1 ± 5.1)%, suggesting that the H-atom

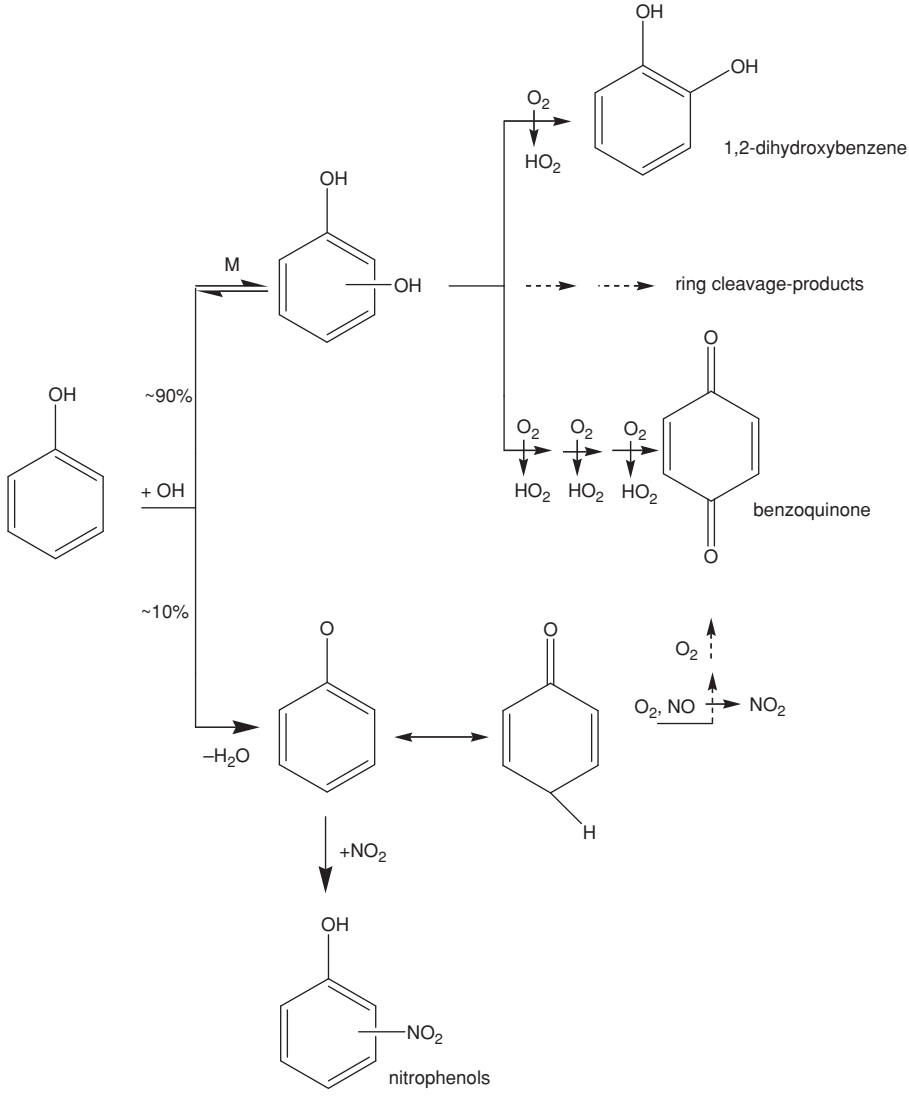

Figure II-E-2. Simplified mechanism of the OH-initiated oxidation of phenol (Olariu et al., 2002).

abstraction channel from —OH accounts for at least 25 ± 5% of the reaction through the following mechanism:

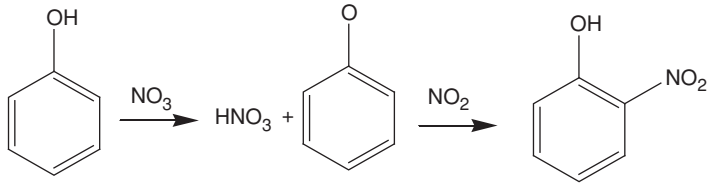

II-E-2. o-Cresol

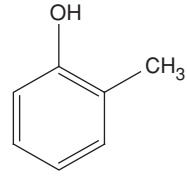

II-E-2.1. OH Reaction Kinetics

The kinetics of the reaction of OH with *o*-cresol have been studied by different groups using both absolute and relative methods. Table II-E-3 summarizes the available kinetic data, and these are plotted in figure II-E-3. The rate coefficient value near 298 K reported by Perry et al. (1977a), using an absolute technique at ∼100 Torr of argon diluent, is lower than those from the other groups derived from the relative rate method and near atmospheric pressure of air. The measurement of Atkinson and Aschmann (1990) is judged to supersede that of Atkinson et al. (1978a). Since the difference between the value of Perry et al. and the other measurements could be due to the pressure dependence of the rate coefficient, only the data obtained at atmospheric pressure were used to derive the temperature dependence and the recommended value at 298 K. Therefore, combining the data of Atkinson and Aschmann (1990), Semadeni et al. (1995), and Coeur-Tourneur et al. (2006) gives $k = 1.6 \times 10^{-12} \exp(999/T)\,\mathrm{cm^3\ molecule^{-1}\ s^{-1}}$ in the temperature range 290–350 K with $k = 4.6 \times 10^{-11}\,\mathrm{cm^3\ molecule^{-1}\ s^{-1}}$ at 298 K and an estimated uncertainty of ±30%. The measurements of Perry et al. in the temperature range 400–423 K give the contribution of the H-atom abstraction channels.

II-E-2.2. O_3 Reaction Kinetics

The rate coefficients obtained by Atkinson et al. (1978a, 1982c) are presented in table II-E-4. The determination of Atkinson et al. (1978a) is considered to be an upper limit to the rate coefficient for this reaction because of the possible occurrence of other reactions consuming *o*-cresol or ozone in their study. The recommended value is based on the study of Atkinson et al. (1982d), $k = 2.6 \times 10^{-19}\,\mathrm{cm^3\ molecule^{-1}\ s^{-1}}$ at 298 K with an estimated uncertainty of ±30%.

Table II-E-3. Rate coefficients ($k = A\ e^{-B/T}$, cm^3 $molecule^{-1}$ s^{-1}) for the reaction of OH with *o*-cresol (*o*-$CH_3C_6H_4OH$)

$10^{12} \times A$	B (K)	$10^{11} \times k$	T (K)	Technique[a]	Reference	Temperature Range (K)
1.6	906 ± 1,007	3.41 ± 0.68	299.4	FP–RF	Perry et al. (1977a)	299–335
		2.93 ± 0.59	310.6			
		2.98 ± 0.60	322			
		2.68 ± 0.54	330.7			
		2.55 ± 0.51	335.4			
50	−(906 ± 1,007)	0.56 ± 0.11	400.6			400–423
		0.54 ± 0.11	407.8			
		0.62 ± 0.12	423.1			
		3.85 ± 0.33	300 ± 1	RR (k(*n*-butane)-k(2,2-dimethylpropane))[b]	Atkinson et al. (1978a)	
		4.64 ± 0.74	296 ± 2	RR (propene)[c]	Atkinson and Aschmann (1990)	
0.98[f]	−(1,166 ± 248)[f]	4.66 ± 0.40	301	RR (1,3-butadiene)[d]	Semadeni et al. (1995)	301–373
		3.98 ± 0.31	319			
		3.11 ± 0.29	334			
		2.63 ± 0.22	348			
		2.57 ± 0.26	360			
		2.26 ± 0.25	373			
		4.25 ± 0.51	294 ± 2	RR (1,3,5-TMB)[e]	Coeur-Tourneur et al. (2006)	

[a]Abbreviations used for the techniques are defined in table I-F-3.
[b]Placed on an absolute basis using $k(OH + n\text{-butane}) - k(OH + 2, 2\text{-dimethylpropane}) = 1.54 \times 10^{-12}$ cm^3 $molecule^{-1}$ s^{-1} (IUPAC, 2008).
[c]Placed on an absolute basis using $k(OH + \text{propene}) = 2.9 \times 10^{-11}$ cm^3 $molecule^{-1}$ s^{-1} (Atkinson et al., 2006).
[d]Placed on an absolute basis using $k(OH + 1,3\text{-butadiene}) = 1.48 \times 10^{-12} \exp(448/T)$ cm^3 $molecule^{-1}$ s^{-1} (Atkinson and Arey, 2003a).
[e]Placed on an absolute basis using $k(OH + 1, 3, 5\text{-trimethylbenzene}) = 5.67 \times 10^{-11}$ cm^3 $molecule^{-1}$ s^{-1} (Calvert et al., 2002).
[f]As stated by the authors (Semadeni et al., 1995).

II-E-2.3. NO_3 Reaction Kinetics

The kinetics of the reaction of NO_3 with *o*-cresol have been investigated by Carter et al. (1981) and Atkinson et al. (1984b, 1992b). The data are given in table II-E-5. The average value of the three measurements $k = 1.4 \times 10^{-11}$ cm^3 $molecule^{-1}$ s^{-1} is recommended at 298 K with an estimated uncertainty of ±50%.

II-E-2.4. Summary of the Atmospheric Fate of o-Cresol

The atmospheric lifetime of *o*-cresol with respect to the gas-phase reactions with OH and NO_3 is of the order of 3 h. The reaction of OH with *o*-cresol proceeds through three channels:

$$OH + CH_3C_6H_4OH \rightarrow H_2O + CH_3C_6H_4O \quad (1)$$

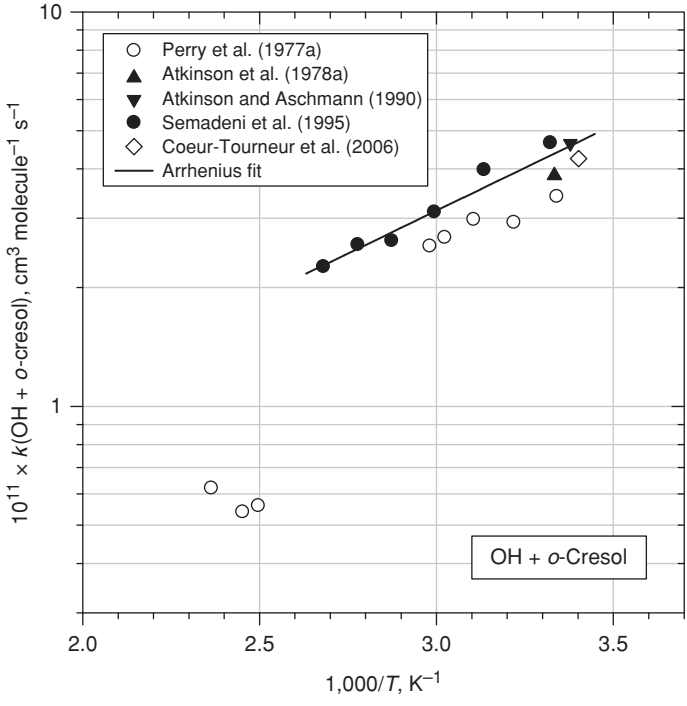

Figure II-E-3. Arrhenius plot of the rate coefficients for the OH + *o*-cresol reaction.

Table II-E-4. Rate coefficients (k, cm^3 molecule^{-1} s^{-1}) for reaction of O_3 with *o*-cresol (*o*-$CH_3C_6H_4OH$)

$10^{19} \times k$	T (K)	Technique[a]	Reference
~ 6	300 ± 1	SC–UV/GC	Atkinson et al. (1978a)
2.55 ± 0.39	296 ± 2	SC–CL	Atkinson et al. (1982d)

[a]Abbreviations used for the techniques are defined in table I-F-3.

Table II-E-5. Rate coefficients (k, cm^3 molecule^{-1} s^{-1}) for the reaction of NO_3 with *o*-cresol (*o*-$CH_3C_6H_4OH$)

$10^{11} \times k$	T (K)	Technique[a]	Reference
1.39 ± 0.24	300 ± 1	RR (2-methyl-2-butene)[b]	Carter et al. (1981)
1.43 ± 0.16	298 ± 1	RR (*m*-cresol)[c]	Atkinson et al. (1984b)
1.37 ± 0.09	296 ± 2	RR (2-methyl-2-butene)[b]	Atkinson et al. (1992b)

[a]Abbreviations used for the techniques are defined in table I-F-3.
[b]Placed on an absolute basis using $k(NO_3 + 2\text{-methyl-2-butene}) = 9.37 \times 10^{-12}$ cm^3 molecule^{-1} s^{-1} (Atkinson and Arey, 2003a).
[c]Placed on an absolute basis using $k(NO_3 + m\text{-cresol}) = 1.1 \times 10^{-11}$ cm^3 molecule^{-1} s^{-1} (this book, section II-E-3.3).

$$OH + CH_3C_6H_4OH \rightarrow H_2O + CH_2C_6H_4OH \quad (2)$$

$$OH + CH_3C_6H_4OH \rightarrow CH_3C_6H_4(OH)_2 \quad (3)$$

The relative importance of these channels varies with temperature. At temperatures relevant to the atmosphere, essentially all of the reaction proceeds through channels (1) and (3). In the presence of NO_x, 6-methyl-2-nitrophenol has been observed as reaction products with a yield of ~5% at ~296 K (Atkinson et al., 1992b; Olariu et al., 2002; Coeur-Tourneur et al., 2006). Since 6-methyl-2-nitrophenol is formed via NO_2 reaction with 2-methylphenoxy radicals, it is believed that at ~296 K, channel (1) represents at least 5% of the overall reaction of OH radicals with *o*-cresol. Olariu et al. have observed 3-methyl-1,2-dihydroxybenzene (73.4 ± 14.6)%, methyl-1,4-benzoquinone (6.8 ± 1.0)%, and 6-methyl-2-nitrophenol (6.8 ± 1.5)% in their investigation of the OH-initiated oxidation of *o*-cresol.

At elevated temperatures (>400–450 K), the adduct formed in channel (3) rapidly decomposes back to the reactants and the *o*-cresol is lost through channels (1) and (2). In the range ~325–400 K, the decomposition of the adduct is still important while at $T < 325 - 350$ K the formed adduct is stable against decomposition, and channel (3) is dominant (IUPAC, 2008). The similar kinetic data of the OH reactions with *o*-cresol and phenol in the temperature range 350–400 K indicate that the H-atom abstraction from the —OH group dominates over that from the CH_3 group and the CH group in the ring.

6-Methyl-2-nitrophenol has also been observed as a product of the reaction of NO_3 radicals with *o*-cresol with a yield of ~13% which indicates that the channel proceeding by an H-atom abstraction from the —OH group accounts for at least 13% of the reaction (Atkinson et al., 1992b).

II-E-3. *m*-Cresol

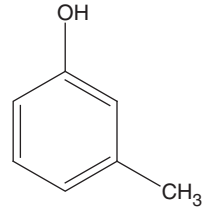

II-E-3.1. OH Reaction Kinetics

The reaction of OH radicals with *m*-cresol has been studied by Atkinson et al. (1978a, 1990), Semadeni et al. (1995), and Coeur-Tourneur et al. (2006) using relative rate methods in one atmosphere of air. The data obtained by these groups are given in table II-E-6 and shown in figure II-E-4. Semadeni et al. (1995) measured the temperature dependence of the reaction using *o*-cresol as the reference compound. Fitting the Arrhenius expression to the data given in table II-E-6 yields $k = 2.4 \times 10^{-12} \exp(969/T)$ over the temperature range 280–380 K, with $k(298) = 6.2 \times 10^{-11}$ cm^3 molecule^{-1} s^{-1} and an estimated uncertainty of ±30%.

Table II-E-6. Rate coefficients ($k = A\ e^{-B/T}$, cm^3 $molecule^{-1}$ s^{-1}) for the reaction of OH with *m*-cresol (*m*-$CH_3C_6H_4OH$)

$10^{12} \times A$	B (K)	$10^{11} \times k$	T (K)	Technique[a]	Reference	Temperature Range (K)
		6.0 ± 0.3	300 ± 1	RR (*o*-cresol)[b]	Atkinson et al. (1978a)	
		7.4 ± 1.2	296 ± 2	RR (propene)[c]	Atkinson and Aschmann (1990)	
5.17[e]	$-(686 \pm 231$[e])	5.97 ± 0.59	299	RR (*o*-cresol)[b]	Semadeni et al. (1995)	299–373
		5.67 ± 0.28	309			
		4.50 ± 0.35	324			
		4.03 ± 0.15	339			
		4.10 ± 0.12	343			
		3.38 ± 0.10	353			
		3.22 ± 0.09	363			
		3.42 ± 0.13	373			
		5.78 ± 0.91	294 ± 2	RR (1,3,5-TMB)[d]	Coeur-Tourneur et al. (2006)	

[a]Abbreviations used for the techniques are defined in table I-F-3.
[b]Placed on an absolute basis using $k(OH + o\text{-cresol}) = 1.6 \times 10^{-12} \exp(999/T)\ cm^3\ molecule^{-1}\ s^{-1}$ (this book, section II-E-2.1).
[c]Placed on an absolute basis using $k(OH + \text{propene}) = 2.9 \times 10^{-11}\ cm^3\ molecule^{-1}\ s^{-1}$ (Atkinson et al., 2006).
[d]Placed on an absolute basis using $k(OH + 1, 3, 5\text{-trimethylbenzene}) = 5.67 \times 10^{-11}\ cm^3\ molecule^{-1}\ s^{-1}$ (Calvert et al., 2002).
[e]As stated by the authors, determined relative to $k(OH + o\text{-cresol}) = 2.1 \times 10^{-12} \exp[(881 \pm 356)/T\ cm^3\ molecule^{-1}\ s^{-1}$ (Semadeni et al., 1995).

II-E-3.2. O_3 Reaction Kinetics

The rate coefficients for the O_3-*m*-cresol reaction were obtained by Atkinson et al. (1978a, 1982d) and are presented in table II-E-7. The determination of Atkinson et al. (1978a) is considered to be an upper limit for the reason mentioned for the reaction of O_3 with *o*-cresol. The recommended value is based on the study of Atkinson et al. (1982d), $k = 1.9 \times 10^{-19}\ cm^3\ molecule^{-1}\ s^{-1}$ at 298 K with an estimated uncertainty of ±30%.

II-E-3.3. NO_3 Reaction Kinetics

The kinetics of the reaction of NO_3 with *m*-cresol have been investigated by Carter et al. (1981) and Atkinson et al. (1984c, 1992b). The data are given in table II-E-8. The IUPAC panel recommended rate coefficient value is based on the measurement of Atkinson et al. (1992b), $k = 1.0 \times 10^{-11}\ cm^3\ molecule^{-1}\ s^{-1}$ at 298 K with an estimated uncertainty of ±40% (IUPAC, 2008).

II-E-3.4. Summary of the Atmospheric Fate of m-Cresol

The atmospheric lifetime of *m*-cresol with respect to the gas-phase reactions with OH and NO_3 is of the order of 2 h. As with *o*-cresol, it is expected that over the

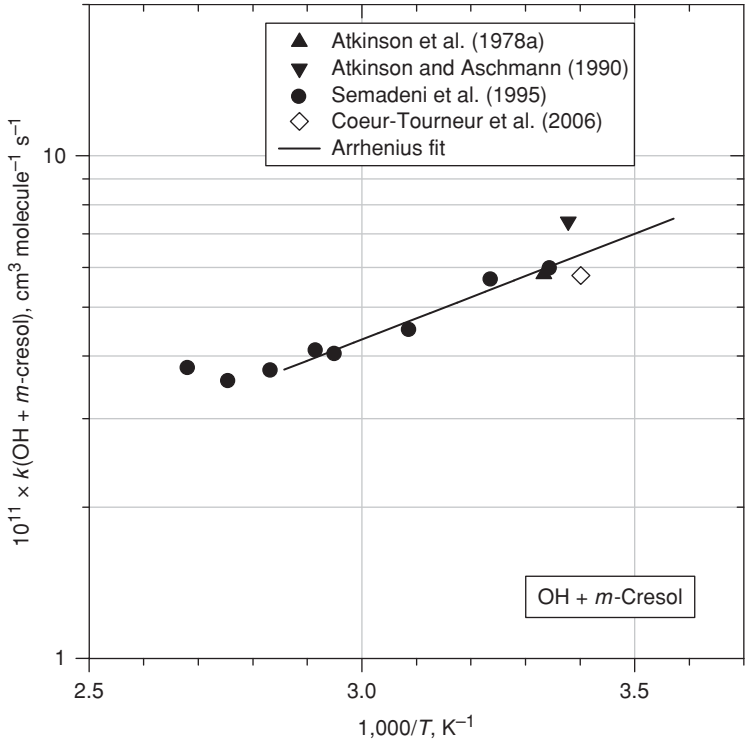

Figure II-E-4. Arrhenius plot of the rate coefficients for the OH + *m*-cresol reaction.

Table II-E-7. Rate coefficients (k, cm^3 molecule^{-1} s^{-1}) for reaction of O_3 with *m*-cresol (*m*-$CH_3C_6H_4OH$)

$10^{19} \times k$	T (K)	Technique[a]	Reference
~ 6	300 ± 1	SC–UV/GC	Atkinson et al. (1978a)
1.94 ± 0.35	296 ± 2	SC–CL	Atkinson et al. (1982d)

[a]Abbreviations used for the techniques are defined in table I-F-3.

Table II-E-8. Rate coefficients (k, cm^3 molecule^{-1} s^{-1}) for the reaction of NO_3 with *m*-cresol (*m*-$CH_3C_6H_4OH$)

$10^{11} \times k$	T (K)	Technique[a]	Reference
0.810 ± 0.116	300 ± 1	RR (2-methyl-2-butene)[b]	Carter et al. (1981)
1.96 ± 0.21	298 ± 1	RR (phenol)[c]	Atkinson et al. (1984c)
≈ 1.33	298 ± 1	RR (NO_3+$NO_2 \leftrightarrow N_2O_5$)[d]	Atkinson et al. (1984c)
0.974 ± 0.047	296 ± 2	RR (2-methyl-2-butene)[b]	Atkinson et al. (1992b)

[a]Abbreviations used for the techniques are defined in table I-F-3.
[b]Placed on an absolute basis using $k(NO_3 + 2\text{-methyl-2-butene}) = 9.37 \times 10^{-12}$ cm^3 molecule^{-1} s^{-1} (Atkinson and Arey, 2003).
[c]Placed on an absolute basis using $k(NO_3 + \text{phenol}) = 4.5 \times 10^{-12}$ cm^3 molecule^{-1} s^{-1} (this book, section II-E-1.2).
[d]Placed on an absolute basis using $K(NO_3 + NO_2 \leftrightarrow N_2O_5) = 2.75 \times 10^{-11}$ cm^3 molecule^{-1} s^{-1} (IUPAC, 2008).

atmospherically relevant temperature range, the reaction of OH with *m*-cresol proceeds mainly via addition to the aromatic ring with H-atom abstraction making a minor contribution. Laboratory experiments conducted in the presence of NO_x have shown that the reaction of OH with *m*-cresol produces 5-methyl-2-nitrophenol and 3-methyl-2-nitrophenol with a total yield of ∼3% at 296 K (Atkinson et al., 1992b; Olariu et al., 2002; Coeur-Tourneur et al., 2006). This indicates that abstraction of the H-atom from the —OH group accounts for ∼3% of the total reaction. In their investigation of the OH-initiated oxidation of *m*-cresol, Olariu et al. (2002) have observed 3-methyl-1,2-dihydroxybenzene (68.6 ± 13.4%), 4-methyl-1,2-dihydroxybenzene (9.7 ± 2.7)%, methyl-1,4-benzoquinone (11.3 ± 2.5)%, 5-methyl-2-nitrophenol (4.4 ± 1.5)%, and 3-methyl-2-nitrophenol (4.3 ± 1.6)%. 5-Methyl-2-nitrophenol and 3-methyl-2-nitrophenol have been observed by Atkinson et al. (1992b) as products of the reaction of NO_3 with *m*-cresol with yields of ∼16.8% and ∼19.6%, respectively. These product yields indicate that abstraction channel from the —OH group accounts for at least 36% of the total reaction.

II-E-4. *p*-Cresol

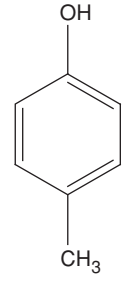

II-E-4.1. OH Reaction Kinetics

The kinetics of the reaction of OH with *p*-cresol have been studied by Atkinson et al. (1978a), Atkinson and Aschmann (1990), Semadeni et al. (1995), and Coeur-Tourneur et al. (2006) using a relative rate method at atmospheric pressure of air. The data obtained by these groups are given in table II-E-9 and shown in figure II-E-5. Fitting the Arrhenius expression to the combined data of Semadeni et al. below 350 K and the other measurements near 298 K yields $k = 4.5 \times 10^{-12} \exp(720/T)\,\mathrm{cm^3\ molecule^{-1}\ s^{-1}}$. At 298 K, this expression yields $k = 5.0 \times 10^{-11}\,\mathrm{cm^3\ molecule^{-1}\ s^{-1}}$ with an uncertainty estimated to be ±30%

II-E-4.2. O_3 Reaction Kinetics

The rate coefficients obtained by Atkinson et al. (1978a, 1982c) are presented in table II-E-10. The determination of Atkinson et al. (1978a) is considered to be an upper limit as discussed for the reaction of O_3 with *o*-cresol. The recommended value

Table II-E-9. Rate coefficients ($k = A\ e^{-B/T}$, cm^3 $molecule^{-1}$ s^{-1}) for reaction of OH with *p*-cresol (*p*-$CH_3C_6H_4OH$)

$10^{12} \times A$	B (K)	$10^{11} \times k$	T (K)	Technique[a]	Reference	Temperature Range (K)
		4.41 ± 0.20	300 ± 1	RR (*o*-cresol)[b]	Atkinson et al. (1978a)	
		5.28 ± 0.97	296 ± 2	RR (propene)[c]	Atkinson and Aschmann (1990)	
2.21[f]	$-(943 \pm 449)$[f]	5.25 ± 0.53	301	RR (1,3-butadiene)[d]	Semadeni et al. (1995)	301–373
		5.25 ± 0.49	319			
		3.96 ± 0.46	334			
		3.22 ± 0.33	348			
		2.93 ± 0.36	360			
		2.71 ± 0.25	373			
		4.82 ± 0.75	301	RR (*o*-cresol)[b]	Semadeni et al. (1995)	301–314
		4.97 ± 0.42	314			
		4.88 ± 0.74	294 ± 2	RR (1,3,5-TMB)[e]	Coeur-Tourneur et al. (2006)	

[a] Abbreviations used for the techniques are defined in table I-F-3.

[b] Placed on an absolute basis using $k(OH + o\text{-cresol}) = 1.6 \times 10^{-12} \exp(999/T)\ cm^3\ molecule^{-1}\ s^{-1}$ (this book, section II-E-2.1).

[c] Placed on an absolute basis using $k(OH + \text{propene}) = 2.9 \times 10^{-11}\ cm^3\ molecule^{-1}\ s^{-1}$ (Atkinson et al., 2006).

[d] Placed on an absolute basis using $k(OH + 1, 3\text{-butadiene}) = 1.48 \times 10^{-12} \exp(448/T)\ cm^3\ molecule^{-1}\ s^{-1}$ (Atkinson and Arey, 2003).

[e] Placed on an absolute basis using $k(OH + 1, 3, 5\text{-trimethylbenzene}) = 5.67 \times 10^{-11}\ cm^3\ molecule^{-1}\ s^{-1}$ (Calvert et al., 2002).

[f] As stated by the authors (Semadeni et al., 1995).

is based on the study of Atkinson et al. (1982d), $k = 4.7 \times 10^{-19}\ cm^3\ molecule^{-1}\ s^{-1}$ at 298 K with an estimated uncertainty of ±30%.

II-E-4.3. NO_3 Reaction Kinetics

The kinetics of the reaction of NO_3 with *p*-cresol have been investigated by Carter et al. (1981) and Atkinson et al. (1984b, 1992b). The data are given in table II-E-11. The recommended rate coefficient is based on the measurement of Atkinson et al. (1992a), $k = 1.1 \times 10^{-11}\ cm^3\ molecule^{-1}\ s^{-1}$ at 298 K with an estimated uncertainty of ±15%.

II-E-4.4. Summary of the Atmospheric Fate of p-Cresol

The atmospheric lifetime of *p*-cresol with respect to the reactions with OH and NO_3 radicals is estimated to be of the order of 2 h. By analogy to the reaction of OH with *o*-cresol, it is expected that the reaction of OH with *p*-cresol proceeds mainly by OH-addition to the aromatic ring at temperatures relevant to the atmosphere. Abstraction of hydrogen from the —OH group is expected to be of minor importance. Atkinson et al. (1992b), Olariu et al. (2002), and Coeur-Tourneur et al. (2006)

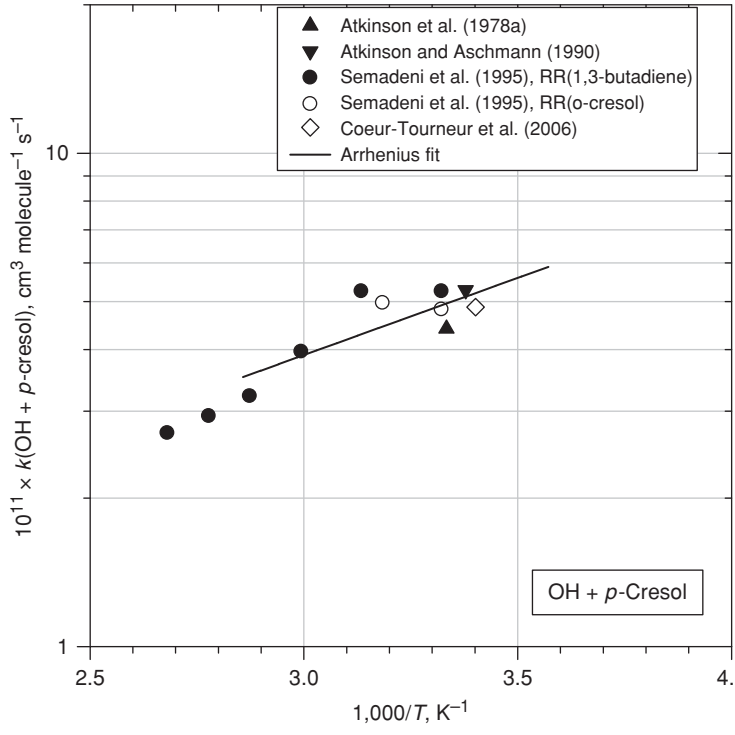

Figure II-E-5. Arrhenius plot of the rate coefficients for the OH + *p*-cresol reaction.

Table II-E-10. Rate coefficients (k, cm^3 molecule^{-1} s^{-1}) for reaction of O_3 with *p*-cresol (*p*-$CH_3C_6H_4OH$)

$10^{19} \times k$	T (K)	Technique[a]	Reference
~ 6	300 ± 1	SC–UV/GC	Atkinson et al. (1978a)
4.71 ± 0.66	296 ± 2	SC–CL	Atkinson et al. (1982d)

[a]Abbreviations used for the techniques are defined in table I-F-3.

have reported 4-methyl-2-nitrophenol (7-17% at ~296 K) as a product of the reaction in presence of NO_x. This observation shows that the abstraction channel from the —OH group occurs to at least this extent at the temperatures used in these studies. Olariu et al. (2002) reported 4-methyl-1,2-dihydroxybenzene (64.1 ± 11.3)% and 4-methyl-2-nitrophenol (7.6 ± 2.2)% in their investigation of the OH-initiated oxidation of *p*-cresol.

The mechanistic study of Atkinson et al. (1992b) showed that the reaction of NO_3 with *p*-cresol leads to 4-methyl-2-nitrophenol as the major product (74 ± 16)%. This indicates that hydrogen abstraction from the —OH group comprises at least (74 ± 16)% of the total reaction.

Table II-E-11. Rate coefficients (k, cm^3 molecule^{-1} s^{-1}) for reaction of NO_3 with p-cresol (p-$CH_3C_6H_4OH$)

$10^{11} \times k$	T (K)	Technique[a]	Reference
1.50 ± 0.24	300 ± 1	RR (2-methyl-2-butene)[b]	Carter et al. (1981)
1.38 ± 0.15	298 ± 1	RR (m-cresol)[c]	Atkinson et al. (1984b)
1.07 ± 0.10	296 ± 2	RR (2-methyl-2-butene)[b]	Atkinson et al. (1992b)

[a]Abbreviations used for the techniques are defined in table I-F-3.
[b]Placed on an absolute basis using $k(NO_3 + 2\text{-methyl-2-butene}) = 9.37 \times 10^{-12}$ cm^3 molecule^{-1} s^{-1} (Atkinson and Arey, 2003).
[c]Placed on an absolute basis using $k(NO_3 + m\text{-cresol}) = 1.0 \times 10^{-11}$ cm^3 molecule^{-1} s^{-1} (this book, section II-E-4.3).

II-E-5. Benzyl Alcohol

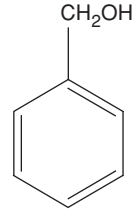

II-E-5.1. OH Reaction Kinetics

The kinetics of the reaction of OH with benzyl alcohol has been investigated by Harrison and Wells (2009) using a relative rate method at atmospheric pressure of air. The rate coefficient values obtained are presented in table II-E-12. The preferred value is an average of the relative rate coefficients reported by these authors obtained with two reference compounds: $k = 2.7 \times 10^{-11}$ cm^3 molecule^{-1} s^{-1} with an uncertainty estimated to be $\pm 20\%$.

II-E-5.2. O_3 Reaction Kinetics

Harrison and Wells (2009) have determined an upper limit to the reaction of ozone with benzyl alcohol of $k \leq 6 \times 10^{-19}$ cm^3 molecule^{-1} s^{-1}.

Table II-E-12. Rate coefficients (k, cm^3 molecule^{-1} s^{-1}) for reaction of OH with benzyl alcohol ($C_6H_5CH_2OH$)

$10^{11} \times k$	T (K)	Technique[a]	Reference
2.75 ± 0.66	297 ± 3	RR (decane)[b]	Harrison and Wells (2009)
2.59 ± 0.58	297 ± 3	RR (hexanal)[c]	Harrison and Wells (2009)

[a]Abbreviations used for the techniques are defined in table I-F-3.
[b]Placed on an absolute basis using $k(OH + \text{decane}) = 1.1 \times 10^{-11}$ cm^3 molecule^{-1} s^{-1} (Calvert et al., 2008).
[c]Placed on an absolute basis using $k(OH + \text{hexanal}) = 2.88 \times 10^{-11}$ cm^3 molecule^{-1} s^{-1} (this book, section IV-B-10.1).

II-E-5.3. Summary of the Atmospheric Fate of Benzyl Alcohol

The atmospheric lifetime of benzyl alcohol with respect to reaction with OH radicals is estimated to be of the order of 4 h. In their mechanistic study of the OH-initiated oxidation of benzyl alcohol, Harrison and Wells (2009) observed benzaldehyde, glyoxal, and 4-oxo-pentanal as products of the reaction. These products indicate that the reaction occurs via abstraction from the —CH_2OH group as well via addition to the aromatic ring.

II-E-6. Dimethylphenols

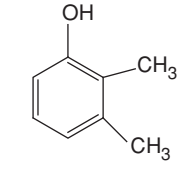

2,3-dimethylphenol

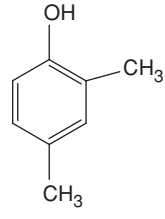

2,4-dimethylphenol

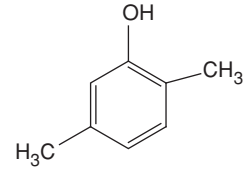

2,5-dimethylphenol

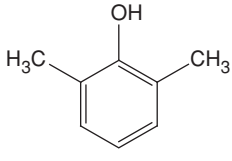

2,6-dimethylphenol

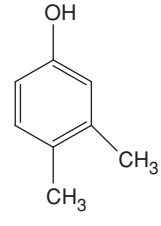

3,4-dimethylphenol

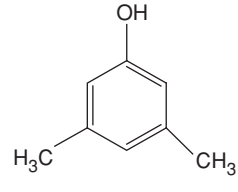

3,5-dimethylphenol

II-E-6.1. OH Reaction Kinetics

The reactions of OH radicals with dimethylphenols have been studied by Atkinson and Aschmann (1990) and Thüner et al. (2004a) using relative rate methods. As seen in table II-E-13, the data reported in these two studies are in excellent agreement.

II-E-6.2. NO_3 Reaction Kinetics

The kinetics of the reaction of NO_3 with dimethylphenols have been investigated by Thüner et al. (2004a) using a relative rate method at atmospheric pressure and 295 K. The data obtained are summarized in table II-E-14.

II-E-6.3. Summary of the Atmospheric Fate of Dimethylphenols

The gas-phase reactions of OH and NO_3 radicals with dimethylphenols are rapid as described in this section and are expected to be the major atmospheric removal processes. The estimated atmospheric lifetimes with respect to reactions with OH and NO_3 are approximately 1 h.

Table II-E-13. Rate coefficients (k, cm^3 molecule^{-1} s^{-1}) for reaction of OH with dimethylphenols

Molecule	$10^{11} \times K$	T (K)	Technique[a]	Reference
2,3-Dimethylphenol	8.02 ± 2.03	296 ± 2	RR (isoprene)[b]	Atkinson and Aschmann (1990)
	8.45 ± 1.13	295 ± 2	RR (1,3,5-TMB)[c]	Thüner et al. (2004a)
2,4-Dimethylphenol	7.15 ± 1.84	296 ± 2	RR (isoprene)[b]	Atkinson and Aschmann (1990)
	7.48 ± 0.76	295 ± 2	RR (1,3,5-TMB)[c]	Thüner et al. (2004a)
2,5-Dimethylphenol	8.00 ± 2.29	296 ± 2	RR (isoprene)[b]	Atkinson and Aschmann (1990)
	8.96 ± 1.17	295 ± 2	RR (1,3,5-TMB)[c]	Thüner et al. (2004a)
2,6-Dimethylphenol	6.59 ± 1.73	296 ± 2	RR (isoprene)[b]	Atkinson and Aschmann (1990)
	6.75 ± 0.92	295 ± 2	RR (1,3,5-TMB)[c]	Thüner et al. (2004a)
3,4-Dimethylphenol	8.14 ± 2.12	296 ± 2	RR (isoprene)[b]	Atkinson and Aschmann (1990)
	8.39 ± 0.94	295 ± 2	RR (1,3,5-TMB)[c]	Thüner et al. (2004a)
3,5-Dimethylphenol	11.3 ± 3.0	296 ± 2	RR (isoprene)[b]	Atkinson and Aschmann (1990)
	11.57 ± 1.39	295 ± 2	RR (1,3,5-TMB)[c]	Thüner et al. (2004a)

[a]Abbreviations used for the techniques are defined in table I-F-3.
[b]Placed on an absolute basis using $k(\text{OH} + \text{isoprene}) = 1.0 \times 10^{-10}$ cm^3 molecule^{-1} s^{-1} (Atkinson et al., 2006).
[c]Placed on an absolute basis using $k(\text{OH} + 1, 3, 5\text{-trimethylbenzene}) = 5.67 \times 10^{-11}$ cm^3 molecule^{-1} s^{-1} (Calvert et al., 2002).

Table II-E-14. Rate coefficients (k, cm^3 molecule^{-1} s^{-1}) for reaction of NO_3 with dimethylphenols

Molecule	$10^{11} \times K$	T (K)	Technique[a]	Reference
2,3-Dimethylphenol	2.97 ± 0.26	295 ± 2	RR (*o*-cresol)[b]	Thüner et al. (2004a)
2,4-Dimethylphenol	3.12 ± 0.32	295 ± 2	RR (*o*-cresol)[b]	Thüner et al. (2004a)
2,5-Dimethylphenol	3.07 ± 0.36	295 ± 2	RR (*o*-cresol)[b]	Thüner et al. (2004a)
2,6-Dimethylphenol	5.01 ± 0.55	295 ± 2	RR (*o*-cresol)[b]	Thüner et al. (2004a)
3,4-Dimethylphenol	2.55 ± 0.23	295 ± 2	RR (*o*-cresol)[b]	Thüner et al. (2004a)
3,5-Dimethylphenol	1.13 ± 0.10	295 ± 2	RR (*o*-cresol)[b]	Thüner et al. (2004a)

[a]Abbreviations used for the techniques are defined in table I-F-3.
[b]Placed on an absolute basis using $k(NO_3 + o\text{-cresol}) = 1.4 \times 10^{-11}$ cm^3 molecule^{-1} s^{-1} (this book, section II-E-2.3).

As for the reactions of OH with phenol and cresols, it is expected that the reaction of OH with dimethylphenols proceeds predominantly by OH addition to the aromatic ring at the temperatures relevant to the atmosphere.

II-E-7. Trimethylphenols

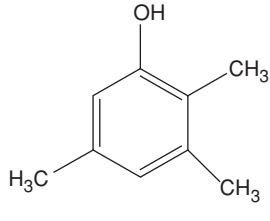

2,3,5-trimethylphenol

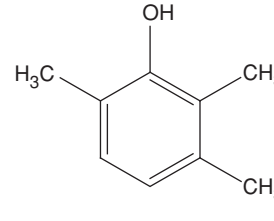

2,3,6-trimethylphenol

II-E-7.1. OH Reaction Kinetics

Tse et al. (1997) have determined the rate coefficients for the reactions of OH with 2,3,5-trimethylphenol and 2,3,6-trimethylphenol using a relative rate method at atmospheric pressure of air. The data obtained are given in table II-E-15.

II-E-7.2. Summary of the Atmospheric Fate of Trimethylphenols

The calculated tropospheric lifetime of the two trimethylphenols with respect to reaction with OH radicals is approximately 1 h. With such short atmospheric lifetimes, these compounds will be removed near their emission sources.

II-E-8. Dihydroxyarenes

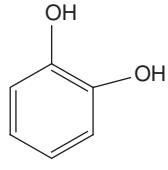

1,2-dihydroxybenzene

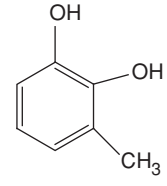

1,2-dihydroxy-3-methylbenzene

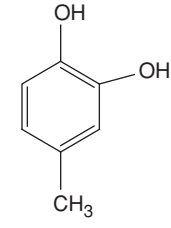

1,2-dihydroxy-4-methylbenzene

II-E-8.1. OH Reaction Kinetics

Olariu et al. (2000) used a relative rate method in one atmosphere of air at 300 K to determine the rate coefficients listed in table II-E-16. The rate coefficients obtained with three different reference compounds are in very good agreement.

II-E-8.2. O_3 Reaction Kinetics

The rate coefficient values measured by Tomas et al. (2003) are shown in table II-E-17. The data obtained using a relative rate method, and those determined under pseudo first-order conditions are in agreement.

Table II-E-15. Rate coefficients (k, cm^3 molecule^{-1} s^{-1}) for reaction of OH with trimethylphenols

Molecule	$10^{10} \times K$	T (K)	Technique[a]	Reference
2,3,5-Trimethylphenol	1.25 ± 0.19	299 ± 2	RR (1,2,4-trimethylbenzene)[b]	Tse et al. (1997)
2,3,6-Trimethylphenol	1.18 ± 0.18	298 ± 2	RR (1,2,4-trimethylbenzene)[b]	Tse et al. (1997)

[a]Abbreviations used for the techniques are defined in table I-F-3.
[b]Placed on an absolute basis using k(OH + 1, 2, 4-trimethylbenzene) = 3.25×10^{-11} cm^3 molecule^{-1} s^{-1} (Calvert et al., 2002).

Table II-E-16. Rate coefficients (k, cm^3 molecule^{-1} s^{-1}) for reaction of OH with 1,2-benzenediol and methyl-substituted 1,2-benzenediols

Molecule	$10^{10} \times K$	T (K)	Technique[a]	Reference
1,2-Benzenediol	1.02 ± 0.21	300 ± 5	RR (isoprene)[b]	Olariu et al. (2000)
	1.07 ± 0.22	300 ± 5	RR (1,3-butadiene)[c]	
	1.03 ± 0.21	300 ± 5	RR (*E*-2-butene)[d]	
3-Methyl-1,2-benzenediol	1.92 ± 0.43	300 ± 5	RR (isoprene)[b]	Olariu et al. (2000)
	2.01 ± 0.42	300 ± 5	RR (1,3-butadiene)[c]	
	2.02 ± 0.45	300 ± 5	RR (*E*-2-butene)[d]	
4-Methyl-1,2-benzenediol	1.61 ± 0.32	300 ± 5	RR (isoprene)[b]	Olariu et al. (2000)
	1.54 ± 0.31	300 ± 5	RR (1, 3-butadiene)[c]	
	1.52 ± 0.30	300 ± 5	RR (*E*-2-butene)[d]	

[a]Abbreviations used for the techniques are defined in table I-F-3.
[b]Placed on an absolute basis using $k(\text{OH} + \text{isoprene}) = 1.0 \times 10^{-10}$ cm^3 molecule^{-1} s^{-1} (Atkinson et al., 2006).
[c]Placed on an absolute basis using $k(\text{OH} + 1,3\text{-butadiene}) = 6.66 \times 10^{-11}$ cm^3 molecule^{-1} s^{-1} (Atkinson and Arey, 2003a).
[d]Placed on an absolute basis using $k(\text{OH} + E\text{-2-butene}) = 6.4 \times 10^{-11}$ cm^3 molecule^{-1} s^{-1} (Atkinson and Arey, 2003a).

Table II-E-17. Rate coefficients (k, cm^3 molecule^{-1} s^{-1}) for reaction of O_3 with 1,2-benzenediol and methyl-substituted 1,2-benzenediols

Molecule	$10^{17} \times K$	T (K)	Technique[a]	Reference
1,2-Benzenediol	0.85 ± 0.80	298 ± 3	RR (propene)[b]	Tomas et al. (2003)
	1.07 ± 0.14	298 ± 3	RR (1,3-butadiene)[c]	
	0.859	298 ± 3	Pseudofirst-order conditions[d]	
3-Methyl-1,2-benzenediol	2.70 ± 0.33	298 ± 3	RR (propene)[b]	Tomas et al. (2003)
	2.90 ± 0.14	298 ± 3	RR (1,3-butadiene)[c]	
	2.78 ± 0.30	298 ± 3	Pseudo first-order conditions[d]	
3-Methyl-1,2-benzenediol	2.51 ± 0.24	298 ± 3	RR (propene)[b]	Tomas et al. (2003)
	2.95 ± 0.35	298 ± 3	RR (1,3-butadiene)[c]	
	2.39 ± 0.41	298 ± 3	Pseudo first-order conditions[d]	

[a]Abbreviations used for the techniques are defined in table I-F-3.
[b]Placed on an absolute basis using $k(\text{O}_3 + \text{propene}) = 1.0 \times 10^{-17}$ cm^3 molecule^{-1} s^{-1} (Atkinson et al., 2006).
[c]Placed on an absolute basis using $k(\text{O}_3 + 1,3\text{-butadiene}) = 6.3 \times 10^{-18}$ cm^3 molecule^{-1} s^{-1} (Atkinson and Arey, 2003a).
[d]Pseudo first-order conditions using an excess of O_3 over dihydrobenzenes.

II-E-8.3. NO_3 Reaction Kinetics

Olariu et al. (2004) determined rate coefficients for reactions of NO_3 with three benzenediols using a relative method in one atmosphere of air. The data are presented in table II-E-18.

II-E-8.4. Summary of the Atmospheric Fate of Dihydroxybenzenes

Using the kinetic data given in this section, the atmospheric lifetimes are estimated to be less than 1 h for dihydrobenzenes with respect to the reaction with OH and NO_3. Thus, both processes are important in the removal of dihydrobenzenes from the atmosphere. Over the temperature range relevant to the atmosphere, the reaction of OH with dimethylphenols is expected to proceed predominantly through the OH addition to the aromatic ring. The reaction with NO_3 may proceed via an overall H-atom

Table II-E-18. Rate coefficients (k, cm^3 molecule^{-1} s^{-1}) for reaction of NO_3 with 1,2-benzenediol and methyl-substituted 1,2-benzenediols

Molecule	$10^{11} \times K$	T (K)	Technique[a]	Reference
1,2-Benzenediol	9.8 ± 5.0	298 ± 2	RR (2,3-dimethyl-2-butene)[b]	Olariu et al. (2004)
3-Methyl-1,2-benzenediol	17.2 ± 5.6	298 ± 2	RR (2,3-dimethyl-2-butene)[b]	Olariu et al. (2004)
3-Methyl-1,2-benzenediol	14.7 ± 6.5	298 ± 2	RR (2,3-dimethyl-2-butene)[b]	Olariu et al. (2004)

[a]Abbreviations used for the techniques are defined in table I-F-3.
[b]Placed on an absolute basis using $k(NO_3 + 2, 3\text{-dimethyl-2-butene}) = 5.72 \times 10^{-11}$ cm^3 molecule^{-1} s^{-1} (Atkinson and Arey, 2003a).

abstraction mechanism. Both OH and NO_3 reactions may produce nitro-containing aromatic compounds.

Dihydrobenzenes are polar with high Henry's law constants at 298 K, and they can be efficiently scavenged from the gas phase by fog droplets and rain (Mackay et al., 1995).

II-E-9. Reactivity Trends in OH-Containing Aromatic Compounds

As discussed by a number of authors (e.g., Calvert et al., 2002; Olariu et al., 2002; Thüner et al., 2004a) the number and position of the OH and CH_3 groups substituents greatly affect the reactivity of aromatic compounds towards OH and NO_3 radicals. For example, at room temperature and atmospheric pressure, dimethylphenols show larger reactivity towards OH and NO_3 than the cresols but they are less reactive than trimethylphenols. Reactions of OH radicals with phenol and cresols proceed mainly (>90%) by electrophilic OH addition to the aromatic ring, and this is also expected to be the case for the dimethylphenols and trimethylphenols at room temperature and atmospheric pressure. Both OH and CH_3 groups donate electron density to the aromatic ring and activate the *ortho*- and *para*-positions towards electophilic addition. This results in an increase of the reactivity towards OH radicals with an increase in the number of OH and CH_3 groups on the aromatic ring [k(OH + trimethylphenols) > k(OH + dimethylphenols) > k(OH+cresols) > k(OH+phenol)]. For aromatic compounds containing the same number of hydroxyl or methyl groups, it seems that the OH-donating electron density via resonance effect is more efficient than the CH_3 inductive effect in determining the reactivity towards OH radicals (Thüner et al., 2004a).

The reaction of NO_3 with phenolic compounds is believed to proceed via an overall H-atom abstraction mechanism preceded by electrophilic addition of NO_3 to the aromatic ring (Calvert et al., 2002). The presence of the electron density donating CH_3 groups has an important effect on the reactivity. For example, the increase in the reactivity observed for the methylated 1,2-dihydroxybenzenes compared to nonmethylated 1,2-dihydroxybenzenes has been attributed to the positive inductive effect of the methyl group (e.g., Calvert et al., 2002; Olariu et al., 2002; Thüner et al., 2004a).

II-F. Halogen-Substituted Alcohols

II-F-1. α-Halogen-Substituted Alcohols [CF_3OH, CH_2ClOH, $CHCl_2OH$, CCl_3OH, $CH_3CHClOH$, $CH_3CH_2CHClOH$, $CH_3CCl(OH)CH_3$]

The α-halogen-substituted alcohols that have been prepared in environmental chamber systems to date (CF_3OH, CH_2ClOH, $CHCl_2OH$, CCl_3OH, $CH_3CHClOH$, $CH_3CH_2CHClOH$, $CH_3CCl(OH)CH_3$) have been observed to undergo decomposition via elimination of HF or HCl to give the corresponding carbonyl compound on a timescale of minutes to hours (Sehested et al. 1993; Tyndall et al. 1993; Taatjes et al. 1999; Wallington et al. 2000; Yamanaka et al. 2007, 2008). Conditioning effects have been reported in which the rate of decomposition decreases after the chamber system is exposed to the alcohol (Sehested et al. 1993), indicating that a significant fraction of the reaction occurs via a heterogeneous mechanism.

Huey et al. (1995) investigated the gas-phase homogeneous decomposition of CF_3OH at elevated temperature (700–1,000 K) and reported an activation energy for HF elimination of 163 kJ mol^{-1}. Extrapolating their results to ambient temperature, Huey et al. (1995) derived a lower limit of 10^4 years for the lifetime of CF_3OH with respect to homogeneous gas-phase decomposition. Computational studies of CF_3OH by Francisco (1994), Schneider et al. (1996), and Nguyen et al. (2008) have shown that the activation barrier for homogeneous elimination of HF is substantial (approximately 188 kJ mol^{-1}) and that homogeneous decomposition occurs at a negligibly slow rate (rate $\sim 10^{-17}$ s^{-1}, lifetime $\sim 10^9$ years). The activation barriers for homogeneous gas-phase HF elimination from CH_2FOH and CHF_2OH, and HCl elimination from CCl_3OH, $CH_3CCl(OH)CH_3$, and $CH_3CH_2CHClOH$ has been calculated to be 179 and 180 kJ mol^{-1} (Nguyen et al., 2008), and >130, 134, and 138 kJ mol^{-1}, respectively (Wallington et al., 2000; Yamanaka et al., 2007, 2008). The lifetime of these chloro-alcohols with respect to homogeneous gas-phase decomposition is of the order of 100 years. The available data show that the homogeneous gas-phase decomposition of α-fluoro and α-chloro substituted alcohols is negligible.

Lovejoy et al. (1995) observed the rapid loss of gas-phase CF_3OH on exposure to bulk water, sulfuric acid surfaces, and sulfuric acid aerosol, and estimated a tropospheric lifetime of a few days with respect to cloud or aerosol mediated decomposition. Computational studies have shown that CF_3OH, and by analogy probably other α-halogen-substituted alcohols, form adducts with H_2O (Schneider et al., 1996) and HF (Nguyen et al., 2008) and that the presence of H_2O and HF reduces the activation barrier for CF_3OH decomposition. However, as discussed by Schneider et al. (1996), while the presence of H_2O in the $CF_3OH{\bullet}H_2O$ adduct has a large impact on the activation barrier and lowers the lifetime with respect to decomposition from 10^9 to approximately 2 years, homogeneous gas-phase decomposition is still probably a minor loss mechanism when compared with heterogeneous decomposition. Young and Donaldson (2007) conducted a computational study of the $CF_3OH{\bullet}H_2O$ and $C_2F_5OH{\bullet}H_2O$ adducts and estimated that in the troposphere a few percent of perfluoroalcohols exist as $C_xF_{2x+2}OH{\bullet}H_2O$ adducts. Young and Donaldson (2007) noted that absorption of

near IR solar radiation and excitation to low-lying O-H vibrational overtone levels of $C_xF_{2x+2}OH{\bullet}H_2O$ adducts (e.g., $4\nu_{OH}$ in $CF_3OH{\bullet}H_2O$ = 877 nm) will increase the rate of decomposition. As discussed by Young and Donaldson (2007), while overtone-induced dissociation of $C_xF_{2x+2}OH$ in $C_xF_{2x+2}OH{\bullet}H_2O$ adducts may occur in the atmosphere, the rate of this process is probably not competitive with heterogeneous decomposition when $C_xF_{2x+2}OH$ molecules encounter aerosols or clouds, which occurs on a timescale of a few days (Lelieveld and Crutzen, 1990; Wallington et al., 1994b; Brasseur et al., 1999).

There are very few available data concerning the chemistry of α-bromo and α-iodo-substituted alcohols. In a computational study of CH_2BrOH, Papayannis et al. (2002) concluded that decomposition via elimination of HBr was the most important decomposition channel. By analogy to the behavior of α-fluoro and α-chloro-substituted alcohols discussed previously, it seems likely that the atmospheric fate of α-bromo and α-iodo-substituted alcohols is heterogeneous decomposition to give the corresponding carbonyl compound.

II-F-2. Halogenated Alcohols

With the exception of α-haloalcohols, the atmospheric lifetime of halogen substituted saturated alcohols is determined by their reaction with hydroxyl radicals. In laboratory experiments to simulate the atmospheric oxidation of halogen substituted alcohols, it is often convenient to use chlorine atoms, rather than OH radicals to initiate the oxidation. To aid in the design and interpretation of such experiments, a knowledge of the kinetics of reactions with chlorine atoms is desirable. Rate constants for the reactions of organic compounds with chlorine atoms are also useful because they can be used to estimate the rate constants of reactions with OH radicals.

The available kinetic data for the reaction of OH radicals and chlorine atoms with halogenated alcohols are listed in tables II-F-1 and II-F-2. There are no available data for reactions of halogen substituted alcohols with either NO_3 radicals or ozone, although for saturated organic molecules the rates of reaction are generally slow and not of atmospheric significance. As seen from tables II-F-1 and II-F-2, the database for reactions of halogen substituted alcohols with OH radicals and chlorine atoms is rather limited and dominated by data for fluorinated alcohols. The prevalence of fluorinated alcohols in the database reflects the significant industrial use of such compounds and consequent interest in their environmental impacts. In particular, there is interest in the possibility that the atmospheric oxidation of fluorinated alcohols produces significant amounts of perfluorocarboxylic acids. This topic is the subject of active discussion in the scientific literature.

Ellis et al. (2004) and Wallington et al. (2006b) have suggested that the oxidation of fluorotelomer alcohols (n-$C_xF_{2x+1}CH_2CH_2OH$, where $x = 2, 4, 6, 8, \ldots$) is a likely source of the perfluorocarboxylic acid pollution observed in remote locations (Martin et al. 2004). Prevedouros et al. (2006) and Wania (2007) estimate that oceanic transport is the dominant mechanism by which perfluorocarboxylic acids get to the Arctic Ocean. Yarwood et al. (2007) presented the results of a modelling study which suggest that the atmospheric oxidation of fluorotelomer alcohols contributes only 1–2% of

Table II-F-1. Rate coefficients ($k = A\ e^{-B/T}\ cm^3\ molecule^{-1}\ s^{-1}$) for reaction of OH with halogen substituted alcohols

Molecule	$10^{12} \times A$	B (K)	$10^{12} \times k$	T (K)	Technique[a]	Reference	Temperature Range (K)
CH_2FCH_2OH			1.49 ± 0.05[b]	298	RR (C_2H_6)[c]	Sellevåg et al. (2004b)	
	5.15 ± 0.88	330 ± 45	1.37	238	PLP–LIF	Rajakumar et al. (2005)	238–355
			1.41	249			
			1.41	253			
			1.45	262			
			1.42	270			
			1.53	273			
			1.60	295			
			1.65	295			
			1.63	297			
			1.66	295			
			1.76	322			
			1.92	322			
			1.87	336			
			2.03	355			
			2.03	355			
			2.15	355			
			2.14	355			
CHF_2CH_2OH			0.487 ± 0.004[b]	298	RR (C_2H_6)[c]	Sellevåg et al. (2004b)	

CF_3CH_2OH			0.0955 ± 0.0071	298	FP–RF	Wallington et al. (1988a)	
	2.00 ± 0.37	890 ± 60	0.0566 ± 0.0022	250	LP–LIF	Tokuhashi et al. (1999a)	250–430
			0.0601 ± 0.0023	250	FP–LIF		
			0.0730 ± 0.038	273	LP–LIF		
			0.107 ± 0.005	298	DF–LIF		
			0.0986 ± 0.0041	298	LP–LIF		
			0.0968 ± 0.0023	298	FP–LIF		
			0.140 ± 0.005	331	DF–LIF		
			0.124 ± 0.004	331	FP–LIF		
			0.178 ± 0.005	375	LP–LIF		
			0.267 ± 0.008	430	DF–LIF		
			0.244 ± 0.010	430	LP–LIF		
			0.261 ± 0.007	430	FP–LIF		
			0.140 ± 0.005[b]	298	RR (C_2H_6)[c]	Sellevåg et al. (2004b)	
			0.094 ± 0.008	296	RR (C_2H_2)[d]	Hurley et al. (2004c)	
			0.106 ± 0.030	300	FP–RF	Kovacs et al. (2005)	
$CF_3CH_2CH_2OH$			0.89 ± 0.03	298	LP–LIF	Kelly et al. (2005)	
			1.06 ± 0.04	298	RR [$HC(O)O(CH_2)_3CH_3$][e]	Kelly et al. (2005)	
			1.05 ± 0.05	298	RR (n-C_6H_{12})[f]	Kelly et al. (2005)	
			1.48 ± 0.03	298	RR (CH_2FCH_2OH)[g]	Kelly et al. (2005)	
			0.679 ± 0.070	298	RR (C_2H_2)[d]	Hurley et al. (2005)	
			0.703 ± 0.079		RR (C_2H_4)[h]		
$C_2F_5CH_2OH$	1.40 ± 0.27	780 ± 60	0.0642 ± 0.0027	250	LP–LIF	Tokuhashi et al. (1999a)	250–430
			0.0631 ± 0.0021	250	FP–LIF		
			0.0801 ± 0.027	273	LP–LIF		
			0.105 ± 0.05	298	DF–LIF		
			0.0978 ± 0.0037	298	LP–LIF		
			0.0974 ± 0.0035	298	FP–LIF		
			0.121 ± 0.004	331	FP–LIF		
			0.176 ± 0.007	375	LP–LIF		
			0.234 ± 0.009	430	LP–LIF		
			0.236 ± 0.007	430	FP–LIF		
			0.094 ± 0.008	296	RR (C_2H_2)[d]	Hurley et al. (2004c)	

(*continued*)

Table II-F-1. (*continued*)

Molecule	$10^{12} \times A$	B (K)	$10^{12} \times k$	T (K)	Technique[a]	Reference	Temperature Range (K)
$CF_3CH(OH)CF_3$	0.699 ± 0.156	990 ± 70	0.0140 ± 0.0007	250	LP–LIF	Tokuhashi et al. (1999a)	250–430
			0.0143 ± 0.0005	250	FP–LIF		
			0.0179 ± 0.011	273	LP–LIF		
			0.0258 ± 0.012	298	DF–LIF		
			0.0265 ± 0.020	298	LP–LIF		
			0.0234 ± 0.012	298	FP–LIF		
			0.0345 ± 0.014	331	DF–LIF		
			0.0309 ± 0.014	331	FP–LIF		
			0.0483 ± 0.021	375	LP–LIF		
			0.0754 ± 0.029	430	DF–LIF		
			0.0711 ± 0.030	430	LP–LIF		
			0.0723 ± 0.024	430	FP–LIF		
$CF_3CHFCF_2CH_2OH$	2.49 ± 0.30	880 ± 40	0.0784 ± 0.0069	250	PFP–LIF	Chen et al. (2003)	250–430
			0.0790 ± 0.0058	250	LP–LIF		
			0.0982 ± 0.0077	273	FP–LIF		
			0.127 ± 0.008	298	FP–LIF		
			0.133 ± 0.007	298	LP–LIF		
			0.169 ± 0.009	331	FP–LIF		
			0.236 ± 0.009	375	FP–LIF		
			0.315 ± 0.012	430	FP–LIF		
			0.329 ± 0.015	430	LP–LIF		
	0.660	527	0.0666 ± 0.026	230	RR (CH_2Cl_2)[i]	Chen et al. (2003)	230–308
			0.0792 ± 0.017	248			
			0.0991 ± 0.0050	278			
			0.106 ± 0.0047	288			
			0.108 ± 0.0041	298			
			0.123 ± 0.0034	308			
	1.50	752	0.0561 ± 0.0049	230	RR ($CHCl_3$)[j]	Chen et al. (2003)	
			0.0737 ± 0.0049	248			
			0.0987 ± 0.0060	278			
			0.110 ± 0.0026	288			
			0.117 ± 0.0028	298			
			0.132 ± 0.0064	308			

n-$C_3F_7CH_2OH$	0.094 ± 0.008	296	RR (C_2H_2)[d]	Hurley et al. (2004c)
n-$C_4F_9CH_2OH$	0.094 ± 0.008	296	RR (C_2H_2)[d]	Hurley et al. (2004c)
n-$C_4F_9CH_2CH_2OH$	0.920 ± 0.117	296	RR (C_2H_2)[d]	Ellis et al. (2003)
	1.03 ± 0.142	296	RR (C_2H_4)[h]	
$C_6F_{13}CH_2CH_2OH$	0.920 ± 0.117	296	RR (C_2H_2)[d]	Ellis et al. (2003)
	0.779 ± 0.035	298	RR ($HC(O)O(CH_2)_3CH_3$)[e]	Kelly et al. (2005)
	0.791 ± 0.052	298	RR (n-C_6H_{14})[f]	
$C_8F_{17}CH_2CH_2OH$	0.920 ± 0.117	296	RR (C_2H_2)[d]	Ellis et al. (2003)
CH_2ClCH_2OH	1.28 ± 0.09	298	FP–RF	Wallington et al. (1988a)
CCl_3CH_2OH	0.245 ± 0.024	298	FP–RF	Wallington et al. (1988a)
Diols				
$CF_3CH(OH)_2$	0.114 ± 0.012	296	RR (C_2H_2)[d]	Andersen et al. (2006)
	0.118 ± 0.011		RR (C_2H_4)[h]	

[a]Abbreviations used for the techniques are defined in table I-F-3.
[b]Different values are given in the abstract and text; this value was taken from text.
[c]Placed on an absolute basis using $k(OH + C_2H_6) = 2.56 \times 10^{-13}$ cm^3 molecule^{-1} s^{-1} (Calvert et al., 2008).
[d]Placed on an absolute basis using $k(OH + C_2H_2) = 7.8 \times 10^{-13}$ cm^3 molecule^{-1} s^{-1} at 1 bar (Atkinson et al., 2006).
[e]Placed on an absolute basis using $k(OH + HC(O)O(CH_2)_3CH_3) = 3.54 \times 10^{-12}$ cm^3 molecule^{-1} s^{-1} (Le Calvé et al. 1997).
[f]Placed on an absolute basis using $k(OH + n\text{-}C_6H_{14}) = 5.28 \times 10^{-12}$ cm^3 molecule^{-1} s^{-1} (Calvert et al., 2008).
[g]Placed on an absolute basis using $k(OH + CH_2FCH_2OH) = 1.56 \times 10^{-12}$ cm^3 molecule^{-1} s^{-1} (this evaluation).
[h]Placed on an absolute basis using $k(OH + C_2H_4) = 7.9 \times 10^{-12}$ cm^3 molecule^{-1} s^{-1} at 1 bar (Atkinson et al., 2006).
[i]Placed on an absolute basis using $k(OH + CH_2Cl_2) = 1.97 \times 10^{-12}\exp(-877/T)$ cm^3 molecule^{-1} s^{-1} (Calvert et al., 2008).
[j]Placed on an absolute basis using $k(OH + CHCl_3) = 2.86 \times 10^{-12}\exp(-1,011/T)$ cm^3 molecule^{-1} s^{-1} (Calvert et al., 2008).

Table II-F-2. Rate coefficients (k, cm^3 molecule^{-1} s^{-1}) for reaction of chlorine atoms with halogen substituted alcohols

Molecule	$10^{11} \times A$	B (K)	$10^{11} \times k$	T (K)	Technique[a]	Reference	Temperature Range (K)
CH_2FCH_2OH	7.57 ± 0.98	408 ± 40	1.71 ± 0.31	273	DF–MS	Papadimitriou et al. (2003)	273–363
			1.96 ± 0.29	303			
			2.24 ± 0.61	333			
			2.47 ± 0.64	363			
			2.68 ± 0.02	298	RR (C_2H_6)[b]	Sellevåg et al. (2004b)	
CHF_2CH_2OH	2.61 ± 0.49	662 ± 60	0.231 ± 0.038	273	DF–MS	Papadimitriou et al. (2003)	273–363
			0.295 ± 0.039	303			
			0.361 ± 0.041	333			
			0.424 ± 0.069	363			
			0.329 ± 0.004	298	RR (CH_3COCH_3)[c]	Sellevåg et al. (2004b)	
CF_3CH_2OH	0.85 ± 0.19	792 ± 74	0.046 ± 0.007	273	DF–MS	Papadimitriou et al. (2003)	273–363
			0.063 ± 0.009	303			
			0.078 ± 0.009	333			
			0.096 ± 0.009	363			
			0.0769 ± 0.0019	298	RR (CH_2ClCH_2Cl)[d]	Sellevåg et al. (2004b)	
			0.0751 ± 0.0017	298	RR (CH_3COCH_3)[c]		
			0.0624 ± 0.0024	296	RR (CH_3Cl)[e] RR	Hurley et al. (2004c)	
			0.0673 ± 0.0028	296	[$CH_3OC(O)H$][f]		
$CF_3CH_2CH_2OH$			1.72 ± 0.03	298	RR (C_2H_5OCHO)[g]	Kelly et al. (2005)	
			1.53 ± 0.12	296	RR (C_2H_5Cl)[h]	Hurley et al. (2005)	
			1.62 ± 0.17	296	RR (CH_3OH)[i]		
	4.42 ± 0.48	255 ± 20	1.74 ± 0.04	273	VLPR	Papadimitriou et al. (2007)	273–363
			1.68 ± 0.15	273			
			1.69 ± 0.09	273			
			1.90 ± 0.03	303			
			1.85 ± 0.10	303			
			1.97 ± 0.07	303			
			2.04 ± 0.07	333			
			2.13 ± 0.10	333			
			2.07 ± 0.12	333			
			2.20 ± 0.08	363			
			2.31 ± 0.15	363			
			2.12 ± 0.09	363			

$C_2F_5CH_2OH$			0.0624 ± 0.0024	296	RR (CH_3Cl)[e]	Hurley et al. (2004c)	
			0.0673 ± 0.0028	296	RR (CH_3OCHO)[f]		
	2.23 ± 0.31	$1{,}065 \pm 106$	0.0440 ± 0.0009	273	VLPR	Papadimitriou et al. (2007)	273–363
			0.0422 ± 0.0009	273			
			0.0434 ± 0.0009	273			
			0.0678 ± 0.0014	303			
			0.0686 ± 0.0023	303			
			0.0668 ± 0.0020	303			
			0.0932 ± 0.0028	333			
			0.0892 ± 0.0051	333			
			0.0922 ± 0.0042	333			
			0.1150 ± 0.0045	363			
			0.1159 ± 0.0060	363			
			0.1135 ± 0.0063	363			
$CHF_2CF_2CH_2OH$	0.85 ± 0.06	681 ± 72	0.0700 ± 0.0025	273	VLPR	Papadimitriou et al. (2007)	273–363
			0.0716 ± 0.0034	273			
			0.0684 ± 0.0029	273			
			0.0900 ± 0.0009	303			
			0.0918 ± 0.0040	303			
			0.0892 ± 0.0034	303			
			0.110 ± 0.0030	333			
			0.106 ± 0.0050	333			
			0.112 ± 0.0044	333			
			0.1300 ± 0.0040	363			
			0.1321 ± 0.0063	363			
			0.1273 ± 0.0069	363			

(*continued*)

Table II-F-2. (*continued*)

Molecule	$10^{11} \times A$	B (K)	$10^{11} \times k$	T (K)	Technique[a]	Reference	Temperature Range (K)
n-$C_3F_7CH_2OH$			0.0624 ± 0.0024	296	RR (CH_3Cl)[e]	Hurley et al. (2004c)	
			0.0673 ± 0.0028	296	RR (CH_3OCHO)[f]		
$CF_3CHFCF_2CH_2OH$	0.62 ± 0.08	736 ± 42	0.0420 ± 0.0012	273	VLPR	Papadimitriou et al. (2007)	273–363
			0.0418 ± 0.0012	273			
			0.0422 ± 0.0029	273			
			0.0536 ± 0.0010	303			
			0.0563 ± 0.0014	303			
			0.0542 ± 0.0034	303			
			0.0672 ± 0.0015	333			
			0.0644 ± 0.0030	333			
			0.0690 ± 0.0045	333			
			0.0820 ± 0.0036	363			
			0.0868 ± 0.0035	363			
			0.0833 ± 0.0069	363			
n-$C_4F_9CH_2OH$			0.0624 ± 0.0024	296	RR (CH_3Cl)[e]	Hurley et al. (2004c)	
			0.0673 ± 0.0028	296	RR (CH_3OCHO)[f]		
n-$C_4F_9CH_2CH_2OH$			1.84 ± 0.31	296	RR (C_2H_4)[j]	Ellis et al. (2003)	
			1.39 ± 0.16	296	RR (C_2H_5Cl)[h]		
n-$C_6F_{13}CH_2OH$			0.065 ± 0.005	298	RR (CH_3Cl)[e]	Solignac et al. (2006)	
n-$C_6F_{13}CH_2CH_2OH$			1.84 ± 0.31	296	RR (C_2H_4)[j]	Ellis et al. (2003)	
			1.39 ± 0.16	296	RR (C_2H_5Cl)[h]		
n-$C_8F_{17}CH_2CH_2OH$			1.84 ± 0.31	296	RR (C_2H_4)[j]	Ellis et al. (2003)	
			1.39 ± 0.16	296	RR (C_2H_5Cl)[h]		
CH_2ClCH_2OH			3.12 ± 0.22	298	RR (C_2H_6)[b]	Wallington et al. (1990b)	
CCl_3CH_2OH			0.297 ± 0.024	296	RR (C_2H_5Cl)[h]	Platz et al. (1995)	

Diols				
$C_xF_{2x+1}CH(OH)_2$	0.0553 ± 0.0059	296	RR (CH_4)[k]	Andersen et al. (2006)
x = 1, 3, 4	0.0614 ± 0.0062		RR (CH_3Cl)[e]	
Hydroperoxides				
CH_2FOOH	0.016 ± 0.004	296	RR (CH_3F)[l]	Wallington et al. (1994a)
CH_2ClOOH	0.057 ± 0.005	296	RR (CH_3Cl)[e]	Wallington et al. (1996c)

[a]Abbreviations used for the techniques are defined in table I-F-3.
[b]Placed on an absolute basis using $k(Cl + C_2H_6) = 5.9 \times 10^{-11}$ cm^3 molecule^{-1} s^{-1} (Atkinson et al., 2006).
[c]Placed on an absolute basis using $k(Cl + CH_3COCH_3) = 2.1 \times 10^{-12}$ cm^3 molecule^{-1} s^{-1} (Atkinson et al., 2006).
[d]Placed on an absolute basis using $k(Cl + CH_2ClCH_2Cl) = 1.3 \times 10^{-12}$ cm^3 molecule^{-1} s^{-1} (Wallington et al., 1996b).
[e]Placed on an absolute basis using $k(Cl + CH_3Cl) = 4.8 \times 10^{-13}$ cm^3 molecule^{-1} s^{-1} (Atkinson et al., 2008).
[f]Placed on an absolute basis using $k(Cl + CH_3OCHO) = 1.4 \times 10^{-12}$ cm^3 molecule^{-1} s^{-1} (Wallington et al., 1993b)
[g]Placed on an absolute basis using $k(Cl + C_2H_5OCHO) = 1.03 \times 10^{-11}$ cm^3 molecule^{-1} s^{-1} (average from Wallington et al., 2006a, and Sellevåg and Nielsen, 2003).
[h]Placed on an absolute basis using $k(Cl + C_2H_5Cl) = 7.8 \times 10^{-12}$ cm^3 molecule^{-1} s^{-1} (Wine and Semmes, 1983; Bryukov et al., 2003).
[i]Placed on an absolute basis using $k(Cl + CH_3OH) = 5.5 \times 10^{-11}$ cm^3 molecule^{-1} s^{-1} (Atkinson et al., 2006).
[j]Placed on an absolute basis using $k(Cl + C_2H_4) = 9.52 \times 10^{-11}$ cm^3 molecule^{-1} s^{-1} (see section I-F-1).
[k]Placed on an absolute basis using $k(Cl + CH_4) = 1.0 \times 10^{-13}$ cm^3 molecule^{-1} s^{-1} (Atkinson et al., 2006).
[l]Placed on an absolute basis using $k(Cl + CH_3F) = 3.4 \times 10^{-13}$ cm^3 molecule^{-1} s^{-1} (Atkinson et al., 2008).

the perfluorocarboxylic acids (PFCAs) observed in North American rainfall. However, field measurements of fluorotelomer alcohols (FTOHs) in air and PFCAs in water by Lowen et al. (2008) in mountain lakes in Western Canada supports atmospheric FTOH degradation as the source of PFCAs. The relative importance of the atmospheric source, local pollution, and oceanic transport depends on location and the perfluorocarboxylic acid in question. Further work is needed to clarify our understanding of the sources and fates of perfluorocarboxylic acids in the environment.

Inspection of tables II-F-1 and II-F-2 reveals the fact that for many of the compounds kinetic data are available from just one laboratory. However, where comparison is possible, there is generally reasonable agreement between results from different laboratories. Comparison with the data for the corresponding nonfluorinated alcohols reveals that the halogen substitution causes a substantial decrease in the reactivity of the molecule. This behavior is observed in most organic compounds and is attributable to a general trend of increased C—H bond strengths as molecules become more fluorinated.

II-F-3. CH_2FCH_2OH

II-F-3.1. OH Reaction Kinetics

The rate coefficients for reaction with OH radicals with CH_2FCH_2OH measured by Sellevåg et al. (2004b) and Rajakumar et al. (2005) are given in table II-F-1 and plotted in figure II-F-1. The value of $k(OH+CH_2FCH_2OH)$ reported in the abstract differs from that reported in the body of the paper by Sellevåg et al. (2004b). The value in the body of the paper is consistent with the experimental data reported by Sellevåg et al. (2004b) and is given in table II-F-1. As seen from figure II-F-1, the data from Sellevåg et al. (2004b) and Rajakumar et al. (2005) are in good agreement. Taking an average of the data near 298 K from the two studies together with the temperature dependence from Rajakumar et al. (2005) gives $k(OH+CH_2FCH_2OH) = 4.72\times10^{-12}\exp(-330/T)\,cm^3$ molecule^{-1} s^{-1}. This expression gives $k(OH + CH_2FCH_2OH) = 1.56 \times 10^{-12}\,cm^3$ molecule^{-1} s^{-1} at 298 K with an estimated uncertainty of ±20%.

II-F-3.2. Cl-Atom Reaction Kinetics

The rate coefficients for reaction with chlorine atoms measured by Papadimitriou et al. (2003) and Sellevåg et al. (2004b) are given in table II-F-2 and plotted in figure II-F-2. Within the likely combined experimental uncertainties the results from Papadimitriou et al. (2003) and Sellevåg et al. (2004b) are consistent. A fit to the combined data set gives $k(Cl + CH_2FCH_2OH) = 6.59 \times 10^{-11}\exp(-351/T)\,cm^3$ molecule^{-1} s^{-1}. This expression yields $k(Cl + CF_3CH_2OH) = 2.03 \times 10^{-11}\,cm^3$ molecule^{-1} s^{-1} at 298 K. The uncertainty in $k(Cl + CF_3CH_2OH)$ at 298 K is estimated to be ±25%.

II-F-3.3. Summary of the Atmospheric Fate of CH_2FCH_2OH

Combining $k(OH + CH_2FCH_2OH) = 1.56 \times 10^{-12}\,cm^3$ molecule^{-1} s^{-1} at 298 K with a diurnal average of [OH] = 10^6 molecule cm^{-3} gives an estimate of 7 days

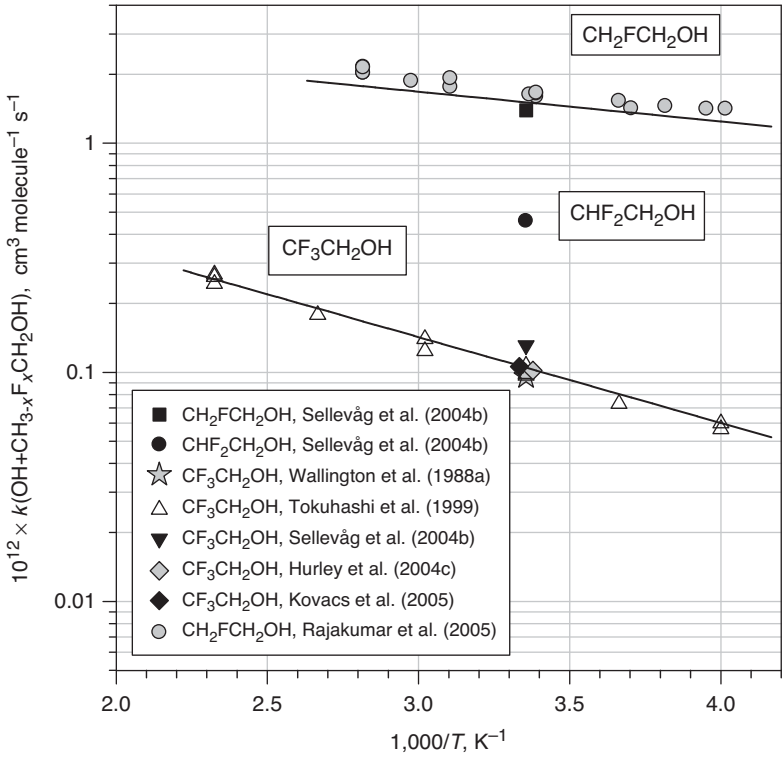

Figure II-F-1. Measurements of the rate coefficients for reaction of OH radicals with selected C_2-fluorinated alcohols. The lines are fits to the data, see text for details.

for the atmospheric lifetime of CH_2FCH_2OH with respect to reaction with OH radicals. Papadimitriou et al. (2003) and Sellevåg et al. (2004b) have shown that the chlorine-atom-initiated oxidation of CH_2FCH_2OH leads to the formation of the aldehyde CH_2FCHO. Papadimitriou et al. (2003) conducted their experiments using the very low pressure reactor (VLPR) with an added 0.3–3.0 mTorr of O_2. Papadimitriou et al. (2003) did not specify the temperature at which the product experiments were performed, but it seems reasonable to assume it was near 298 K. Sellevåg et al. (2004b) conducted their experiments in 1013 mbar (760 Torr) of air at 298 K. The atmospheric oxidation of CH_2FCH_2OH is initiated by reaction with OH radicals which leads to the formation of CH_2FCHO.

$$CH_2FCH_2OH + OH \rightarrow CH_2FCHOH + H_2O$$

$$CH_2FCHOH + O_2 \rightarrow CH_2FCHO + HO_2$$

The atmospheric oxidation of CH_2FCHO gives HC(O)F, CO and CO_2 as major products and $CH_2FC(O)OH$ and $CH_2FC(O)OOH$ as minor products.

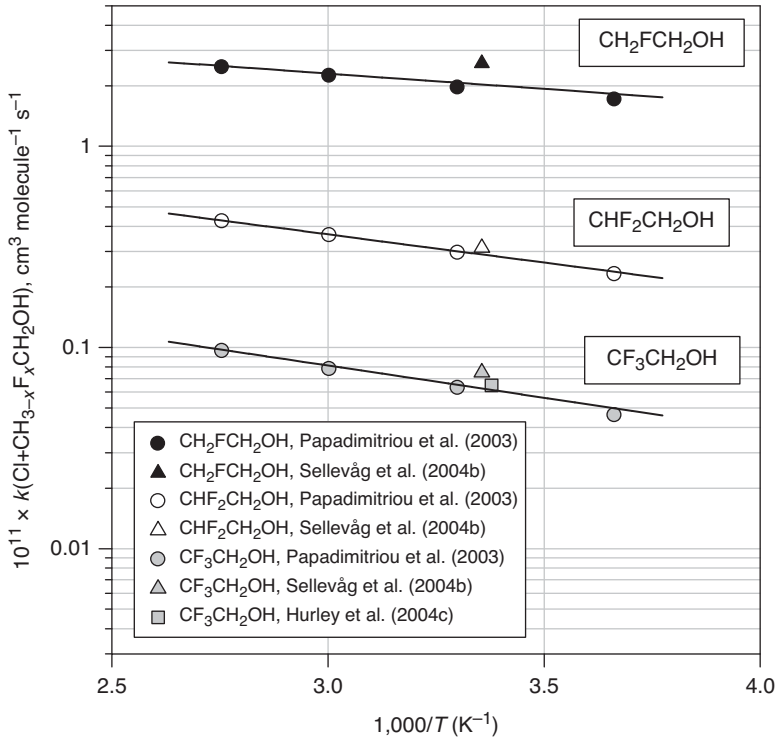

Figure II-F-2. Measurements of the rate coefficients for reaction of chlorine atoms with selected C_2-fluorinated alcohols.

II-F-4. CHF_2CH_2OH

II-F-4.1. OH Reaction Kinetics

The rate coefficient for reaction with OH radicals measured by Sellevåg et al. (2004b) at 298 K is given in table II-F-1 and plotted in figure II-F-1. The value of $k(\mathrm{OH} + \mathrm{CHF_2CH_2OH})$ reported in the abstract differs from that reported in the body of the paper by Sellevåg et al. (2004b). The value in the body of the paper is consistent with the experimental data reported by Sellevåg et al. (2004b) and is given in table II-F-1.

II-F-4.2. Cl-Atom Reaction Kinetics

The rate coefficients for reaction with chlorine atoms measured by Papadimitriou et al. (2003) and Sellevåg et al. (2004b) are given in table II-F-2 and plotted in figure II-F-2. As seen from figure II-F-2, the results from Papadimitriou et al. (2003) and Sellevåg et al. (2004b) are in good agreement. A fit to the combined data set gives $k(\mathrm{Cl} + \mathrm{CH_2FCH_2OH}) = 2.53 \times 10^{-11} \exp(-646/T)\ \mathrm{cm^3\ molecule^{-1}\ s^{-1}}$. This expression yields $k(\mathrm{Cl} + \mathrm{CF_3CH_2OH}) = 2.90 \times 10^{-12}\ \mathrm{cm^3\ molecule^{-1}\ s^{-1}}$ at 298 K. The uncertainty in $k(\mathrm{Cl} + \mathrm{CF_3CH_2OH})$ at 298 K is estimated to be $\pm 20\%$.

II-F-4.3. Summary of the Atmospheric Fate of CHF_2CH_2OH

Combining $k(OH + CHF_2CH_2OH) = 4.87 \times 10^{-13}\,cm^3$ molecule^{-1} s^{-1} at 298 K (Sellevåg et al., 2004b) with a diurnal average of [OH] = 10^6 molecule cm^{-3} gives an estimate of 24 days for the atmospheric lifetime of CHF_2CH_2OH with respect to reaction with OH radicals. Papadimitriou et al. (2003) and Sellevåg et al. (2004b) have shown that the chlorine-atom-initiated oxidation of CHF_2CH_2OH leads to the formation of the aldehyde CHF_2CHO. Papadimitriou et al. (2003) conducted their experiments using the very low pressure reactor with an added 0.3–3.0 mTorr of O_2. Papadimitriou et al. (2003) did not specify the temperature at which the product experiments were performed, but it seems reasonable to assume it was near 298 K. Sellevåg et al. (2004b) conducted their experiments in 1013 mbar (760 Torr) of air at 298 K. The atmospheric oxidation of CHF_2CH_2OH is initiated by reaction with OH radicals which leads to the formation of CHF_2CHO.

$$CHF_2CH_2OH + OH \rightarrow CHF_2CHOH + H_2O$$

$$CHF_2CHOH + O_2 \rightarrow CHF_2CHO + HO_2$$

The atmospheric oxidation of CHF_2CHO gives COF_2, CO, and CO_2 as major products and $CHF_2C(O)OH$ and $CHF_2C(O)OOH$ as minor products.

II-F-5. CF_3CH_2OH

II-F-5.1. OH Reaction Kinetics

The kinetics of the reaction of OH radicals with CF_3CH_2OH have been studied by Wallington et al. (1988a), Tokuhashi et al. (1999a), Sellevåg et al. (2004b), Hurley et al. (2004c), and Kovacs et al. (2005). Rate constants reported by these workers are listed in table II-F-1 and plotted in figure II-F-1. As seen from figure II-F-1, there is good agreement between the results from these studies. A fit to the combined data set gives $k(OH + CF_3CH_2OH) = 1.90 \times 10^{-12} \exp(-863/T)\,cm^3$ molecule^{-1} s^{-1}. This expression yields $k(OH + CF_3CH_2OH) = 1.05 \times 10^{-13}\,cm^3$ molecule^{-1} s^{-1} at 298 K. The uncertainty in $k(OH + CF_3CH_2OH)$ at 298 K is estimated to be ±15%.

II-F-5.2. Cl-Atom Reaction Kinetics

The rate coefficients for reaction with chlorine atoms measured by Papadimitriou et al. (2003), Sellevåg et al. (2004b), and Hurley et al. (2004c) are given in table II-F-2 and plotted in figure II-F-2. As seen from figure II-F-2, the results from Papadimitriou et al. (2003), Sellevåg et al. (2004b), and Hurley et al. (2004c) are in good agreement. A fit to the combined data set gives $k(Cl + CF_3CH_2OH) = 7.47 \times 10^{-12} \exp(-739/T)\,cm^3$ molecule^{-1} s^{-1}. This expression yields $k(Cl + CF_3CH_2OH) = 6.26 \times 10^{-13}\,cm^3$ molecule^{-1} s^{-1} at 298 K. The uncertainty in $k(Cl + CF_3CH_2OH)$ at 298 K is estimated to be ±20%.

II-F-5.3. Summary of the Atmospheric Fate of CF_3CH_2OH

Combining $k(OH + CF_3CH_2OH) = 1.05 \times 10^{-13}$ cm^3 molecule^{-1} s^{-1} with a diurnal average of [OH] = 10^6 molecule cm^{-3} gives an estimate of 4 months for the atmospheric lifetime of CHF_2CH_2OH with respect to reaction with OH radicals. Hurley et al. (2004c) have reported the formation of CF_3CHO in a yield of 97 ± 3% following the chlorine-atom-initiated oxidation of CF_3CH_2OH in 700 Torr of air diluent. The atmospheric oxidation of CF_3CH_2OH is initiated by reaction with OH radicals and is expected to proceed via the same mechanism as that initiated by chlorine atoms. Hence the atmospheric oxidation of CF_3CH_2OH leads to essentially quantitative conversion into CF_3CHO as the primary product. The atmospheric oxidation of CF_3CHO gives COF_2 and CO as major products and $CF_3C(O)OH$ and $CF_3C(O)OOH$ as minor products.

II-F-6. $CF_3CH_2CH_2OH$, *n*-$C_4F_9CH_2CH_2OH$, *n*-$C_6F_{13}CH_2CH_2OH$, and *n*-$C_8F_{17}CH_2CH_2OH$

II-F-6.1. OH Reaction Kinetics

The kinetics of the reaction of OH radicals with $CF_3CH_2CH_2OH$, *n*-$C_4F_9CH_2CH_2OH$, *n*-$C_6F_{13}CH_2CH_2OH$, and *n*-$C_8F_{17}CH_2CH_2OH$ have been studied by Ellis et al. (2003), Kelly et al. (2005), and Hurley et al. (2005) at ambient temperatures. Rate coefficients reported by these workers are listed in table II-F-1 and plotted in figure II-F-3. As seen from figure II-F-3, there is no discernable trend in the reactivity of the $C_xF_{2x+1}CH_2CH_2OH$ molecule towards OH radicals with size of the C_xF_{2x+1} group. Accordingly, we average the rate data in table II-E-1 to provide a value of $k(OH + C_xF_{2x+1}CH_2CH_2OH) = 9.35 \times 10^{-13}$ cm^3 molecule^{-1} s^{-1} at 298 K with an estimated uncertainty of ±15%.

II-F-6.2. Cl-Atom Reaction Kinetics

The kinetics of the reaction of chlorine atoms with $CF_3CH_2CH_2OH$, *n*-$C_4F_9CH_2CH_2OH$, *n*-$C_6F_{13}CH_2CH_2OH$, and *n*-$C_8F_{17}CH_2CH_2OH$ have been studied by Ellis et al. (2003), Kelly et al. (2005), Hurley et al. (2005), and Papadimitriou et al. (2007). Rate coefficients reported by these workers are listed in table II-F-2 and plotted in figure II-F-4. As seen from figure II-F-4, there is no discernable trend in the reactivity of the $C_xF_{2x+1}CH_2CH_2OH$ molecule with size of the C_xF_{2x+1} group. A fit to the combined data set gives $k(Cl+C_xF_{2x+1}CH_2CH_2OH) = 6.67\times10^{-11}\exp(-403/T)$ cm^3 molecule^{-1} s^{-1}. This expression yields $k(Cl + C_xF_{2x+1}CH_2CH_2OH) = 1.73 \times 10^{-11}$ cm^3 molecule^{-1} s^{-1} at 298 K. The uncertainty in $k(Cl + C_xF_{2x+1}CH_2CH_2OH)$ at 298 K is estimated to be ±20%.

II-F-6.3. Summary of the Atmospheric Fate of $CF_3CH_2CH_2OH$, n-$C_4F_9CH_2CH_2OH$, n-$C_6F_{13}CH_2CH_2OH$, and n-$C_8F_{17}CH_2CH_2OH$

Combining $k(OH + C_xF_{2x+1}CH_2CH_2OH) = 9.35 \times 10^{-13}$ cm^3 molecule^{-1} s^{-1} with a diurnal average of [OH] = 10^6 molecule cm^{-3} gives an estimate of 2 weeks for the

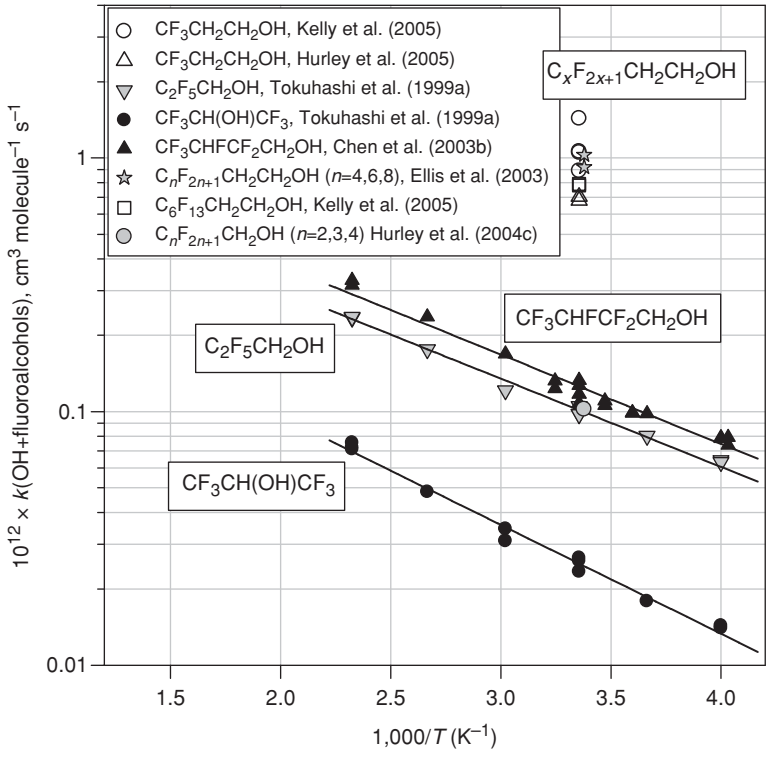

Figure II-F-3. Measurements of the rate coefficients for reaction of OH radicals with selected larger fluorinated alcohols. The lines through the data are (in order from top) fits to: (i) the $CF_3CHFCF_2CH_2OH$ data from Chen et al. (2003b), (ii) the combined data set for $C_2F_5CH_2OH$ from Tokuhashi et al. (1999a) and Hurley et al. (2004c), and (iii) the $CF_3CH(OH)CF_3$ data from Tokuhashi et al. (1999a).

atmospheric lifetime of $C_xF_{2x+1}CH_2CH_2OH$ with respect to reaction with OH radicals. It is well established that C_xF_{2x+1} groups deactivate and —OH groups activate neighboring —CH_2 groups with respect to reaction with OH radicals. The reactivity of $C_xF_{2x+1}CH_2OH$ molecules then provides an upper limit to the rate of reaction of OH radicals with the —CH_2 group attached to the fluorinated alkyl chain in $C_xF_{2x+1}CH_2CH_2OH$. From table II-F-1 it can be seen that OH radicals are approximately an order of magnitude less reactive towards $C_xF_{2x+1}CH_2OH$ than towards $C_xF_{2x+1}CH_2CH_2OH$. Hence, it follows that the majority (>90%) of reaction of OH with $C_xF_{2x+1}CH_2CH_2OH$ is expected to proceed via attack on the terminal carbon atom. As with other α-hydroxy alkyl radicals, the atmospheric fate of $C_xF_{2x+1}CH_2CHOH$ radicals will be reaction with O_2 to give the corresponding aldehyde.

$$C_xF_{2x+1}CH_2CH_2OH + OH \rightarrow C_xF_{2x+1}CH_2CHOH + H_2O$$

$$C_xF_{2x+1}CH_2CHOH + O_2 \rightarrow C_xF_{2x+1}CH_2CHO + HO_2$$

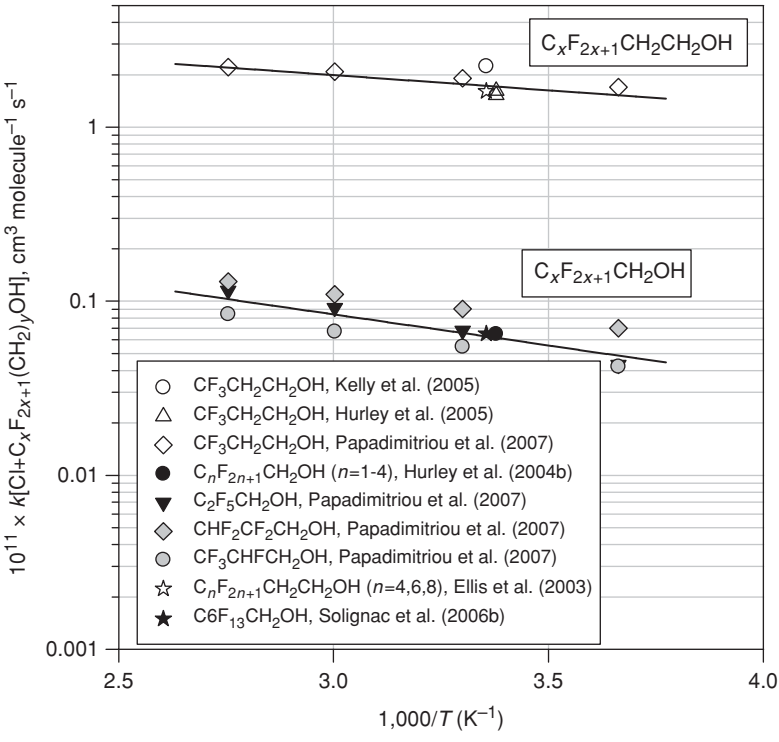

Figure II-F-4. Measurements of the rate coefficients for reaction of chlorine atoms with selected fluorinated alcohols. The data from Papadimitriou are averages of the values reported at each temperature. By analogy to the data base for hydrofluorocarbons, the reaction of chlorine atoms with $CHF_2CF_2CH_2OH$ and CF_3CHFCH_2OH are expected to proceed via attack on the —CH_2 group. Hence these compounds are included in the $C_xF_{2x+1}CH_2OH$ group.

Product studies of the chlorine-atom-initiated oxidation of $CF_3CH_2CH_2OH$, n-$C_4F_9CH_2CH_2OH$, n-$C_6F_{13}CH_2CH_2OH$, and n-$C_8F_{17}CH_2CH_2OH$ in 700 Torr of air at 296 K by Hurley et al. (2004c, 2005), Andersen et al. (2005a), Kelly et al. (2005), and Chiappero et al. (2008) have shown that $C_xF_{2x+1}CH_2CH_2OH$ is oxidized to give $C_xF_{2x+1}CH_2CHO$ in a yield which is indistinguishable from 100%. The atmospheric oxidation of $C_xF_{2x+1}CH_2CH_2OH$ gives $C_xF_{2x+1}CH_2CHO$ as the primary product. As discussed in Chapter IV, the oxidation of $C_xF_{2x+1}CH_2CHO$ gives $C_xF_{2x+1}CH_2C(O)OH$, $C_xF_{2x+1}CH_2C(O)OOH$, and $C_xF_{2x+1}CHO$ as secondary products. Further oxidation of these secondary products gives COF_2 as the major product and a series of perfluorocarboxylic acids $C_nF_{2n+1}C(O)OH$ (where $n = 1, 2, 3, \ldots x$) as minor products (Ellis et al., 2005). There are three mechanisms which convert $C_xF_{2x+1}CHO$ into perfluorocarboxylic acids. First, reaction of $C_xF_{2x+1}CHO$ with OH radicals, leading to the formation of $C_xF_{2x+1}C(O)O_2$ radicals which then react with HO_2 radicals to give, in part, $C_xF_{2x+1}C(O)OH$. Second, hydration of $C_xF_{2x+1}CHO$ to give $C_xF_{2x+1}C(OH)_2H$ which react with OH radicals leading to the formation of $C_xF_{2x+1}C(O)OH$. Third, oxidation of $C_xF_{2x+1}CHO$ giving $C_xF_{2x+1}O_2$

radicals which react with CH_3O_2 radicals to give either $C_xF_{2x+1}O$ alkoxy radicals, or the alcohol $C_xF_{2x+1}OH$. As discussed in section II-F-1, the atmospheric fate of the alcohol $C_xF_{2x+1}OH$ is decomposition via HF elimination to give an acyl fluoride, $C_{x-1}F_{2x-1}C(O)F$, which then hydrolyses to give $C_{x-1}F_{2x-1}C(O)OH$. The atmospheric fate of $C_xF_{2x+1}O$ alkoxy radicals is elimination of COF_2 and formation of a perfluoro alkyl peroxy radical with one less carbon atom ($C_{x-1}F_{2x-1}O_2$) which can repeat the process. The first and second mechanisms convert $C_xF_{2x+1}CHO$ into $C_xF_{2x+1}C(O)OH$. The third mechanism converts $C_xF_{2x+1}CHO$ into a series of acids $C_nF_{2n+1}C(O)OH$ ($n = 1, 2, 3, \ldots [x-1]$). In total the three mechanisms lead to the formation of a range of acids $C_nF_{2n+1}C(O)OH$ ($n = 1, 2, 3, \ldots x$) from $C_xF_{2x+1}CHO$. The relative and absolute importance of the three mechanisms is uncertain and more research is needed to reduce the uncertainties in assessments of the formation of perfluorocarboxylic acids from fluorinated alcohols.

II-F-7. $C_2F_5CH_2OH$, n-$C_3F_7CH_2OH$, n-$C_4F_9CH_2OH$, and n-$C_6F_{13}CH_2OH$

II-F-7.1. OH Reaction Kinetics

The kinetics of the reaction of OH radicals with $C_2F_5CH_2OH$ have been studied by Tokuhashi et al. (1999a) and Hurley et al. (2004c). Rate coefficients reported by these workers are listed in table II-F-1 and plotted in figure II-F-3. As seen from figure II-F-3, the rate coefficient measured at 296 K by Hurley et al. (2004c) is in good agreement with the results from Tokuhashi et al. (1999a). A fit to the combined data set gives $k(OH + C_2F_5CH_2OH) = 1.49 \times 10^{-12} \exp(-800/T)\,cm^3$ molecule^{-1} s^{-1} (1.02×10^{-13} at 298 K). The uncertainty in $k(OH + C_2F_5CH_2OH)$ at 298 K is estimated to be ±20%. As seen from table II-F-1, the reactivities of CF_3CH_2OH and $C_2F_5CH_2OH$ towards OH radicals measured by Tokuhashi et al. (1999a) over the temperature range 250–430 K are indistinguishable. Hurley et al. (2004c) also reported that at 296 K the reactivities of n-$C_xF_{2x+1}CH_2OH$ ($x = 1 - 4$) are indistinguishable within the experimental uncertainties. We have fitted the Arrhenius expression to the combined data set of CF_3CH_2OH, $C_2F_5CH_2OH$, n-$C_3F_7CH_2OH$, and n-$C_4F_9CH_2OH$ to give $k(OH + C_xF_{2x+1}CH_2OH) = 1.68 \times 10^{-12} \exp(-835/T)\,cm^3$ molecule^{-1} s^{-1}. This expression yields $k(OH + C_xF_{2x+1}CH_2OH) = 1.02 \times 10^{-13}\,cm^3$ molecule^{-1} s^{-1} at 298 K [exactly the same as $k(OH + C_2F_5CH_2OH)$].

II-F-7.2. Cl-Atom Reaction Kinetics

The kinetics of the reaction of chlorine atoms with $CF_3CF_2CH_2OH$, n-$C_3F_7CH_2OH$, n-$C_4F_9CH_2OH$, and n-$C_6F_{13}CH_2OH$ have been studied by Tokuhashi et al. (1999a), Ellis et al. (2003), Hurley et al. (2004c), and Solignac et al. (2006b). Rate coefficients reported by these workers are listed in table II-F-2 and plotted in figure II-F-4. As seen from figure II-F-4, there is no discernable trend in the reactivity of the $C_xF_{2x+1}CH_2OH$ molecule with size of the C_xF_{2x+1} group. A fit to the combined data set (including $CF_3CHFCF_2CH_2OH$ and $CHF_2CF_2CH_2OH$, see below) gives $k(Cl + C_xF_{2x+1}CH_2OH) = 9.92 \times 10^{-12} \exp(-823/T)\,cm^3$ molecule^{-1} s^{-1}.

This expression yields $k(\mathrm{Cl} + \mathrm{C}_x\mathrm{F}_{2x+1}\mathrm{CH}_2\mathrm{OH}) = 6.27 \times 10^{-13}\,\mathrm{cm}^3\,\mathrm{molecule}^{-1}\,\mathrm{s}^{-1}$ at 298 K. The uncertainty in $k(\mathrm{Cl} + \mathrm{C}_x\mathrm{F}_{2x+1}\mathrm{CH}_2\mathrm{OH})$ at 298 K is estimated to be ±20%.

II-F-7.3. Summary of the Atmospheric Fate of $C_2F_5CH_2OH$, n-$C_3F_7CH_2OH$, n-$C_4F_9CH_2OH$, and n-$C_6F_{13}CH_2OH$

Combining $k(\mathrm{OH} + \mathrm{C}_x\mathrm{F}_{2x+1}\mathrm{CH}_2\mathrm{OH}) = 1.02 \times 10^{-13}\,\mathrm{cm}^3\,\mathrm{molecule}^{-1}\,\mathrm{s}^{-1}$ with a diurnal average of $[\mathrm{OH}] = 10^6\,\mathrm{molecule\,cm}^{-3}$ gives an estimate of 4 months for the atmospheric lifetime of $\mathrm{C}_x\mathrm{F}_{2x+1}\mathrm{CH}_2\mathrm{OH}$ with respect to reaction with OH radicals. Hurley et al. (2004a) have reported the formation of n-$\mathrm{C}_x\mathrm{F}_{2x+1}\mathrm{CHO}$ ($x = 2, 3, 4$) in yields indistinguishable from 100% following the chlorine-atom-initiated oxidation of n-$\mathrm{C}_x\mathrm{F}_{2x+1}\mathrm{CH}_2\mathrm{OH}$ ($x = 2, 3, 4$) in 700 Torr of air diluent. The atmospheric oxidation of n-$\mathrm{C}_x\mathrm{F}_{2x+1}\mathrm{CH}_2\mathrm{OH}$ is initiated by reaction with OH radicals and is expected to proceed via the same mechanism as that initiated by chlorine atoms. Hence the atmospheric oxidation of n-$\mathrm{C}_x\mathrm{F}_{2x+1}\mathrm{CH}_2\mathrm{OH}$ leads to essentially quantitative conversion into n-$\mathrm{C}_x\mathrm{F}_{2x+1}\mathrm{CHO}$ as the primary product. As discussed in Chapter IV, the atmospheric oxidation of n-$\mathrm{C}_x\mathrm{F}_{2x+1}\mathrm{CHO}$ gives COF_2 and CO as major products and a series of perfluorocarboxylic acids n-$\mathrm{C}_x\mathrm{F}_{2x+1}\mathrm{C(O)OH}$ ($n = 1, 2, \ldots x$) as minor products.

II-F-8. $CF_3CH(OH)CF_3$

II-F-8.1. OH Reaction Kinetics

The kinetics of the reaction of OH radicals with $\mathrm{CF_3CH(OH)CF_3}$ have been studied by Tokuhashi et al. (1999a). Rate coefficients reported by Tokuhashi et al. (1999a) are listed in table II-F-1 and plotted in figure II-F-3. A fit to these data gives $k(\mathrm{OH} + \mathrm{CF_3CH(OH)CF_3}) = 6.90 \times 10^{-13}\exp(-987/T)\,\mathrm{cm}^3\,\mathrm{molecule}^{-1}\,\mathrm{s}^{-1}$. This expression yields $k(\mathrm{OH} + \mathrm{CF_3CH(OH)CF_3}) = 2.51 \times 10^{-14}\,\mathrm{cm}^3\,\mathrm{molecule}^{-1}\,\mathrm{s}^{-1}$ at 298 K. The uncertainty in $k(\mathrm{OH} + \mathrm{CF_3CH(OH)CF_3})$ at 298 K is estimated to be ±25%.

II-F-8.2. Summary of the Atmospheric Fate of $CF_3CH(OH)CF_3$

Combining $k(\mathrm{OH} + \mathrm{CF_3CH(OH)CF_3}) = 2.51 \times 10^{-14}\,\mathrm{cm}^3\,\mathrm{molecule}^{-1}\,\mathrm{s}^{-1}$ with a diurnal average of $[\mathrm{OH}] = 10^6\,\mathrm{molecule\,cm}^{-3}$ gives an estimate of 1.3 years for the atmospheric lifetime of $\mathrm{CF_3CH(OH)CF_3}$ with respect to reaction with OH radicals. The oxidation of $\mathrm{CF_3CH(OH)CF_3}$ will give $\mathrm{CF_3C(O)CF_3}$.

$$\mathrm{OH} + \mathrm{CF_3CH(OH)CF_3} \rightarrow \mathrm{CF_3C(OH)CF_3} + \mathrm{H_2O}$$

$$\mathrm{CF_3C(OH)CF_3} + \mathrm{O_2} \rightarrow \mathrm{CF_3C(O)CF_3} + \mathrm{HO_2}$$

II-F-9. $CF_3CHFCF_2CH_2OH$

II-F-9.1. OH Reaction Kinetics

The kinetics of the reaction of OH radicals with $\mathrm{CF_3CHFCF_2CH_2OH}$ have been studied by Chen et al. (2003b). Rate coefficients reported by Chen et al. (2003b) are listed in

table II-F-1 and plotted in figure II-F-3. A fit to the data from Chen et al. (2003b) gives $k(\mathrm{OH} + \mathrm{CF_3CHFCF_2CH_2OH}) = 1.91 \times 10^{-12} \exp(-811/T)\,\mathrm{cm^3\ molecule^{-1}\ s^{-1}}$. This expression yields $k(\mathrm{OH} + \mathrm{CF_3CHFCF_2CH_2OH}) = 1.26 \times 10^{-13}\,\mathrm{cm^3\ molecule^{-1}\ s^{-1}}$ at 298 K. The uncertainty in $k(\mathrm{OH} + \mathrm{CF_3CHFCF_2CH_2OH})$ at 298 K is estimated to be ±25%.

II-F-9.2. Cl-Atom Reaction Kinetics

The kinetics of the reaction of chlorine atoms with $\mathrm{CF_3CHFCF_2CH_2OH}$ have been studied by Papadimitriou et al. (2007). Rate coefficients are listed in table II-F-2 and plotted in figure II-F-4. By comparison with $k(\mathrm{Cl} + \mathrm{CF_3CHFCF_3}) = (4.5 \pm 1.2) \times 10^{-17}\,\mathrm{cm^3\ molecule^{-1}\ s^{-1}}$ (Møgelberg et al., 1996) it is expected that the —CHF group does not contribute significantly to the overall reactivity of the molecule. Consistent with this expectation, it can be seen from figure II-F-4 that the reactivity of $\mathrm{CF_3CHFCF_2CH_2OH}$ is indistinguishable, within the experimental uncertainties, from that of $\mathrm{C}_x\mathrm{F}_{2x+1}\mathrm{CH_2OH}$ molecules. Accordingly, $\mathrm{CF_3CHFCF_2CH_2OH}$ was included in the combined data set (see figure II-F-4) that was fit to give $k(\mathrm{Cl} + \mathrm{C}_x\mathrm{F}_{2x+1}\mathrm{CH_2OH}) = 9.92 \times 10^{-12} \exp(-823/T)\,\mathrm{cm^3\ molecule^{-1}\ s^{-1}}$. This expression is recommended for $k(\mathrm{Cl} + \mathrm{CF_3CHFCF_2CH_2OH})$.

II-F-9.3. Summary of the Atmospheric Fate of $CF_3CHFCF_2CH_2OH$

Combining $k(\mathrm{OH} + \mathrm{CF_3CHFCF_2CH_2OH}) = 1.29 \times 10^{-13}\,\mathrm{cm^3\ molecule^{-1}\ s^{-1}}$ with a diurnal average of $[\mathrm{OH}] = 10^6\,\mathrm{molecule\,cm^{-3}}$ gives an estimate of 3 months for the atmospheric lifetime of $\mathrm{CF_3CHFCF_2CH_2OH}$ with respect to reaction with OH radicals. From the kinetics data base for reactions of OH radicals with hydrofluorocarbons [e.g., $k(\mathrm{OH} + \mathrm{CF_3CHFCF_3}) = (1.51 \pm 0.30) \times 10^{-15}\,\mathrm{cm^3\ molecule^{-1}\ s^{-1}}$] the reactivity of the —CHF group in $\mathrm{CF_3CHFCF_2CH_2OH}$ would be expected to contribute a rate coefficient of the order of $10^{-15}\,\mathrm{cm^3\ molecule^{-1}\ s^{-1}}$ at 298 K (Calvert et al., 2008). The reaction of OH radicals with $\mathrm{CF_3CHFCF_2CH_2OH}$ will proceed via attack at the —$\mathrm{CH_2OH}$ leading to the formation of the aldehyde $\mathrm{CF_3CHFCF_2CHO}$. Further oxidation of the aldehyde will lead to the formation of $\mathrm{COF_2}$ and the $\mathrm{CF_3CHF}$ radical. The $\mathrm{CF_3CHF}$ radical is also formed during the atmospheric oxidation of $\mathrm{CF_3CFH_2}$ (HFC-134a). It is well established that the atmospheric fate of the $\mathrm{CF_3CHFO}$ alkoxy radical derived from HFC-134a is C—C bond scission leading to $\mathrm{COF_2}$ and HC(O)F, and reaction with $\mathrm{O_2}$ giving $\mathrm{CF_3C(O)F}$ (Calvert et al, 2008).

$$\mathrm{OH} + \mathrm{CF_3CHFCF_2CH_2OH} \rightarrow \mathrm{CF_3CHFCF_2CHOH} + \mathrm{H_2O}$$

$$\mathrm{CF_3CHFCF_2CHOH} + \mathrm{O_2} \rightarrow \mathrm{CF_3CHFCF_2CHO} + \mathrm{HO_2}$$

II-F-10. $\mathrm{CHF_2CF_2CH_2OH}$

II-F-10.1. OH Reaction Kinetics

There have been no studies of the kinetics of the reaction of OH radicals with $\mathrm{CHF_2CF_2CH_2OH}$. The reactivity of the —$\mathrm{CH_2OH}$ group is expected to be similar to

that in $C_xF_{2x+1}CH_2OH$; $k(OH + C_xF_{2x+1}CH_2OH) = 1.02 \times 10^{-13}$ cm^3 molecule^{-1} s^{-1} at 298 K. The reactivity of the CHF_2 group is expected to be similar to that in $CHF_2(CF_2)_4CF_3$; $k(OH + CHF_2(CF_2)_4CF_3) = (1.85 \pm 0.36) \times 10^{-15}$ cm^3 molecule^{-1} s^{-1} at 298 K (Calvert et al., 2008). The reactivity of the —CH_2OH group will dominate the overall reactivity of the $CHF_2CF_2CH_2OH$ molecule. We recommend the use of $k(OH + CHF_2CF_2CH_2OH) = k(OH + C_xF_{2x+1}CH_2OH) = 1.68 \times 10^{-12} \exp(-835/T)$ cm^3 molecule^{-1} s^{-1}. At 298 K, this expression gives $k(OH + CHF_2CF_2CH_2OH) = 1.02 \times 10^{-13}$ cm^3 molecule^{-1} s^{-1}.

II-F-10.2. Cl-Atom Reaction Kinetics

The kinetics of the reaction of chlorine atoms with $CHF_2CF_2CH_2OH$ have been studied by Papadimitriou et al. (2007). Rate coefficients are listed in table II-F-2 and plotted in figure II-F-4. By comparison of $k(Cl + CHF_2CF_2CH_2OH) = 9.03 \times 10^{-13}$ (Papadimitriou et al., 2007) with $k(Cl + CHF_2CF_2CF_3) = (3.4 \pm 0.6) \times 10^{-16}$ cm^3 molecule^{-1} s^{-1} (Giessing et al., 1996), it is expected that the CHF_2 group does not contribute significantly to the overall reactivity of the $CHF_2CF_2CH_2OH$ molecule. Consistent with this expectation it can be seen from figure II-F-4 that the reactivity of $CHF_2CF_2CH_2OH$ is indistinguishable, within the experimental uncertainties, from that of $C_xF_{2x+1}CH_2OH$. Accordingly, $CHF_2CF_2CH_2OH$ was included in the combined data set (see figure II-F-4) that was fit to give $k(Cl + C_xF_{2x+1}CH_2OH) = 9.92 \times 10^{-12} \exp(-823/T)$ cm^3 molecule^{-1} s^{-1}. This expression is recommended for $k(Cl + CHF_2CF_2CH_2OH)$.

II-F-10.3. Summary of the Atmospheric Fate of $CHF_2CF_2CH_2OH$

Combining $k(OH + CHF_2CF_2CH_2OH) = 1.02 \times 10^{-13}$ cm^3 molecule^{-1} s^{-1} with a diurnal average of [OH] = 10^6 molecule cm^{-3} gives an estimate of 4 months for the atmospheric lifetime of $CHF_2CF_2CH_2OH$ with respect to reaction with OH radicals. Atmospheric oxidation of $CHF_2CF_2CH_2OH$ will be initiated by reaction with OH radicals giving an α-hydroxy-alkyl radical which will react with O_2 to give the corresponding aldehyde, CHF_2CF_2CHO. Subsequent oxidation of the aldehyde (via photolysis and reaction with OH radicals) will lead to the formation of COF_2, CO, and CO_2 as major secondary products with small amounts of the C_3 acid and peracid [$CHF_2CF_2C(O)OH$ and $CHF_2CF_2C(O)OOH$], and small amounts of the C_2 acid $CHF_2C(O)OH$.

II-F-11. CH_2ClCH_2OH

II-F-11.1. OH Reaction Kinetics

A value of $k(OH + CH_2ClCH_2OH) = (1.28 \pm 0.09) \times 10^{-12}$ cm^3 molecule^{-1} s^{-1} at 298 K has been reported by Wallington et al. (1988a) using a FP–RF technique.

II-F-11.2. Cl-Atom Reaction Kinetics

The kinetics of the reaction of chlorine atoms with CH_2ClCH_2OH have been studied using a relative rate technique by Wallington et al. (1988a). As shown in table II-F-2,

when placed upon an absolute basis, the data give $k(Cl + CH_2ClCH_2OH) = (3.12 \pm 0.22) \times 10^{-11}$ cm^3 molecule^{-1} s^{-1} at 298 K.

II-F-11.3. Summary of the Atmospheric Fate of CH_2ClCH_2OH

Combining $k(OH + CH_2ClCH_2OH) = (1.28 \pm 0.09) \times 10^{-12}$ cm^3 molecule^{-1} s^{-1} with a diurnal average of [OH] = 10^6 molecule cm^{-3} gives an estimate of 9 days for the atmospheric lifetime of CH_2ClCH_2OH with respect to reaction with OH radicals. Comparing $k(OH + CH_2ClCH_2OH) = (1.28 \pm 0.09) \times 10^{-12}$ with $k(OH + CH_2ClCH_2Cl) = 2.42 \times 10^{-13}$ cm^3 molecule^{-1} s^{-1} at 298 K (Calvert et al., 2008) suggests that the majority of the reaction of OH radicals with CH_2ClCH_2OH proceeds via attack at the —CH_2OH group which will then lead to the formation of CH_2ClCHO.

$$OH + CH_2ClCH_2OH \rightarrow CH_2ClCHOH + H_2O$$

$$CH_2ClCHOH + O_2 \rightarrow CH_2ClCHO + HO_2$$

II-F-12. CCl_3CH_2OH

II-F-12.1. OH Reaction Kinetics

A value of $k(OH + CCl_3CH_2OH) = (2.45 \pm 0.24) \times 10^{-13}$ cm^3 molecule^{-1} s^{-1} at 298 K has been measured by Wallington et al. (1988a) using a FP–RF technique.

II-F-12.2. Cl-Atom Reaction Kinetics

The kinetics of the reaction of chlorine atoms with CCl_3CH_2OH have been studied using a relative rate technique by Platz et al. (1995). As shown in table II-F-2, when placed upon an absolute basis the data give $k(Cl + CCl_3CH_2OH) = (2.97 \pm 0.24) \times 10^{-12}$ cm^3 molecule^{-1} s^{-1} at 298 K.

II-F-12.3. Summary of the Atmospheric Fate of CCl_3CH_2OH

Combining $k(OH + CCl_3CH_2OH) = (2.45 \pm 0.24) \times 10^{-13}$ cm^3 molecule^{-1} s^{-1} with a diurnal average of [OH] = 10^6 molecule cm^{-3} gives an estimate of 1.5 months for the atmospheric lifetime of CCl_3CH_2OH with respect to reaction with OH radicals. Platz et al. (1995) have shown that chloral, CCl_3CHO, is the major atmospheric oxidation product of CCl_3CH_2OH.

$$OH + CCl_3CH_2OH \rightarrow CCl_3CHOH + H_2O$$

$$CCl_3CHOH + O_2 \rightarrow CCl_3CHO + HO_2$$

II-F-13. $C_xF_{2x+1}CH(OH)_2$ (x = 1, 3, 4)

II-F-13.1. OH Reaction Kinetics

The kinetics of the reaction of OH with the diol $CF_3CH(OH)_2$ has been studied by Andersen et al. (2006) at 296 K. Rate coefficients reported by Andersen et al. (2006) are listed in table II-F-1. An average of the determinations by Andersen et al. (2006) gives $k(OH + CF_3CH(OH)_2) = 1.16 \times 10^{-13}$ cm^3 molecule^{-1} s^{-1}.

II-F-13.2. Cl-atom Reaction Kinetics

The kinetics of the reaction of chlorine atoms with the diols $C_xF_{2x+1}CH(OH)_2$ ($x = 1, 3, 4$) have been studied by Andersen et al. (2006) at 296 K. Rate coefficients reported by Andersen et al. (2006) are listed in table II-F-2. There was no observable dependence of the reactivity of $C_xF_{2x+1}CH(OH)_2$ with the length of the n-C_xF_{2x+1} chain. An average of the determinations by Andersen et al. (2006) gives $k(Cl + C_xF_{2x+1}CH(OH)_2) = 5.84 \times 10^{-13}$ cm^3 molecule^{-1} s^{-1} at 296 K.

II-F-13.3. Summary of the Atmospheric Fate of $C_xF_{2x+1}CH(OH)_2$

Combining $k(OH + C_xF_{2x+1}CH(OH)_2) = 1.16 \times 10^{-13}$ cm^3 molecule^{-1} s^{-1} with [OH] = 10^6 provides an estimate of approximately 3 months for the atmospheric lifetime of $C_xF_{2x+1}CH(OH)_2$ with respect to reaction with OH radicals. For saturated compounds such as $C_xF_{2x+1}CH(OH)_2$, reaction with NO_3 radicals and O_3 are typically too slow to be of importance. Reaction with Cl-atoms will not be an important atmospheric loss mechanism for $C_xF_{2x+1}CH(OH)_2$ since the average concentration of Cl-atoms in the troposphere is several orders of magnitude less than that of OH radicals, and Andersen et al. (2006) report that Cl-atoms are approximately 5 times more reactive than OH radicals towards $C_xF_{2x+1}CH(OH)_2$. Alcohols do not absorb at UV wavelengths >200 nm and fluorination causes a further shift to shorter wavelengths (Schneider et al., 1995). It is likely that gem-diols express similar properties, and thus, photolysis of $C_xF_{2x+1}CH(OH)_2$ will not be important in the troposphere.

Estimation of the significance of wet and dry deposition for $C_xF_{2x+1}CH(OH)_2$ is complicated by the lack of physico-chemically relevant parameters for perfluorinated aldehyde hydrates. Given the water solubility of $C_xF_{2x+1}CH(OH)_2$, it seems likely that incorporation into rain, cloud, and sea water will be a significant atmospheric removal mechanism for the short chain hydrates. However, the work of Andersen et al. (2006) suggests that partitioning of the hydrates back into the gas phase will be significant where their fate will be dictated by gas-phase OH chemistry. This process is expected to increase in importance for the more environmentally relevant long chain hydrates such as $C_8F_{17}CH(OH)_2$, which possess long hydrophobic fluorinated tails that are less soluble than the hydrophillic —$CH(OH)_2$ ends, and they will likely reside at the gas–water interface, which can enhance their evaporation into the gas phase readily. It is difficult to estimate the rate of wet deposition for these long chain hydrates.

Andersen et al. (2006) showed that reaction of Cl-atoms with $C_xF_{2x+1}CH(OH)_2$ proceeds via H-atom abstraction to give $C_xF_{2x+1}C(OH)_2$ radicals. The sole atmospheric fate of $C_xF_{2x+1}C(OH)_2$ radicals is reaction with O_2 to give HO_2 radicals and the perfluorinated carboxylic acid, $C_xF_{2x+1}C(O)OH$. For saturated compounds with only one type of reactive C—H bond such as $C_xF_{2x+1}CH(OH)_2$, the products of reaction with OH radicals are expected to be the same as those for reaction with Cl-atoms. Hence, OH-radical-initiated oxidation of $C_xF_{2x+1}CH(OH)_2$ gives the corresponding perfluorinated carboxylic acid. Atmospheric oxidation of $C_xF_{2x+1}CH(OH)_2$ hydrates could be a source of perfluorinated carboxylic acids in the environment. However, it is difficult to provide a quantitative assessment of the environmental relevance of this source of perfluorinated carboxylic acids given the absence of information concerning: (i) the equilibrium between $C_xF_{2x+1}CHO$ and $C_xF_{2x+1}CH(OH)_2$ under environmentally relevant conditions, and (ii) the rate of wet deposition of $C_xF_{2x+1}CH(OH)_2$. Further work in this area is needed.

II-G. Hydroperoxides and Peroxides

II-G-1. Hydrogen Peroxide (H_2O_2)

II-G-1.1. OH Reaction Kinetics

The reaction of OH radicals with hydrogen peroxide has been the subject of a number of kinetic studies. Table II-G-1 summarizes the available data reported in the temperature range relevant to the atmospheric conditions. The data are also shown in figure II-G-1. Measurements conducted at temperatures above 800 K (e.g., Hippler et al., 1995) show a strong increase of the rate coefficient with increase in temperature. The rate coefficients near 298 K are in good agreement and the recommended value at 298 K is $k = 1.8 \times 10^{-12}$ cm^3 molecule^{-1} s^{-1} at 298 K with an estimated uncertainty of ±15%. The measurements of Lamb et al. (1983) and Vaghjiani and Ravishankara (1989c) below room temperature show an increase of the rate coefficient with decreasing temperature; these are slightly higher than the other measurements. Vakhtin et al. (2003) reported a significant increase in the rate coefficient in the temperature range 96–165 K. A fit of the modified Arrhenius expression to the combined data set over the range 245–460 K gives $k = 2.6 \times 10^{-18} T^2 \exp(607/T)$ cm^3 molecule^{-1} s^{-1}.

II-G-1.2. O_3 Reaction Kinetics

Wallington et al. (1998c) have reported an upper limit of 4×10^{-20} cm^3 molecule^{-1} s^{-1} for the reaction of O_3 with H_2O_2 at 296 K.

II-G-1.3. NO_3 Reaction Kinetics

The upper limit for the reaction of NO_3 with H_2O_2 reported by Burrows et al. (1985) is 2×10^{-15} cm^3 molecule^{-1} s^{-1} at 296 K.

Table II-G-1. Rate coefficients ($k = A\ e^{-B/T}$, cm^3 $molecule^{-1}$ s^{-1}) for reaction of OH with hydrogen peroxide (H_2O_2)

$10^{12} \times A$	B (K)	$10^{12} \times k$	T (K)	Technique[a]	Reference	Temperature Range (K)
2.51 ± 0.6	126 ± 76	1.92 ± 0.08	423	DF–RF	Keyser (1980)	245–423
		1.76 ± 0.14	371			
		1.63 ± 0.05	335			
		1.64 ± 0.32	298			
		1.71 ± 0.10	273			
		1.45 ± 0.07	245			
2.96 ± 0.50	164 ± 52	2.24 ± 0.33	459	DF–LIF	Sridharan et al. (1980)	250–459
		2.13 ± 0.32	454			
		2.02 ± 0.36	422			
		1.93 ± 0.17	394			
		1.85 ± 0.21	340			
		1.72 ± 0.11	312			
		1.69 ± 0.06	295			
		1.64 ± 0.17	250			
		1.61 ± 0.45	250			
3.7 ± 0.6	260 ± 50	1.98 ± 0.15	410	LP–RF	Wine et al. (1981)	273–410
		1.93 ± 0.17	371			
		1.72 ± 0.12	332			
		1.53 ± 0.13	300			
		1.56 ± 0.17	299			
		1.59 ± 0.08	297			
		1.50 ± 0.16	273			
		1.81 ± 0.24	298	LP–RF	Marinelli and Johnston (1982)	
2.93 ± 0.49	158 ± 52	1.90 ± 0.28	370	FP–RF	Kurylo et al. (1982)	250–370
		1.77 ± 0.25	323			
		1.79 ± 0.14	296			
		1.64 ± 0.25	278			
		1.56 ± 0.21	250			
		1.67 ± 0.33	296	DF–LMR	Temps and Wagner (1982)	
1.47 ± 0.20	−70 ± 41	1.84 ± 0.21	413	FP–RF	Lamb et al. (1983)	241–413
		1.78 ± 0.14	365			
		1.72 ± 0.07	333			
		1.80 ± 0.06	294			
		1.92 ± 0.05	251			
		2.07 ± 0.10	241			
2.76 ± 0.80	110 ± 60	2.14 ± 0.40	410	LP–LIF	Vaghjiani et al. (1989c)	273–410
		2.01 ± 0.20	348			
		1.86 ± 0.18	298			
		1.90 ± 0.12	273			
		1.93 ± 0.11	299	LP–LIF	Lovejoy et al. (1990)	249–299
		1.99 ± 0.04	249			
		1.53 ± 0.40	298 ± 3	LP–RF	Turnipseed et al. (1991)	
		1.75 ± 0.20	298	LP–LIF	Mellouki et al. (1994)	

(*continued*)

Table II-G-1. (*continued*)

$10^{12} \times A$	B (K)	$10^{12} \times k$	T (K)	Technique[a]	Reference	Temperature Range (K)
0.68 ± 0.10	-285 ± 27	1.78 ± 0.19	296 ± 2	LP–LIF	Vakhtin et al. (2003)	96–296
		3.4 ± 1.4	165 ± 14			
		10.1 ± 2.8	110 ± 7			
		12.3 ± 4.5	96 ± 4			
2.9 ± 1.8	110 ± 150	2.21 ± 0.38	356	LP–LIF	Jiménez et al. (2004)	273–356
		2.10 ± 0.26	335			
		2.51 ± 0.10	315			
		2.00 ± 0.08	298			
		1.99 ± 0.10	273			
		1.86 ± 0.10	266			
		2.16 ± 0.48	254			

[a]Abbreviations used for the techniques are defined in table I-F-3.

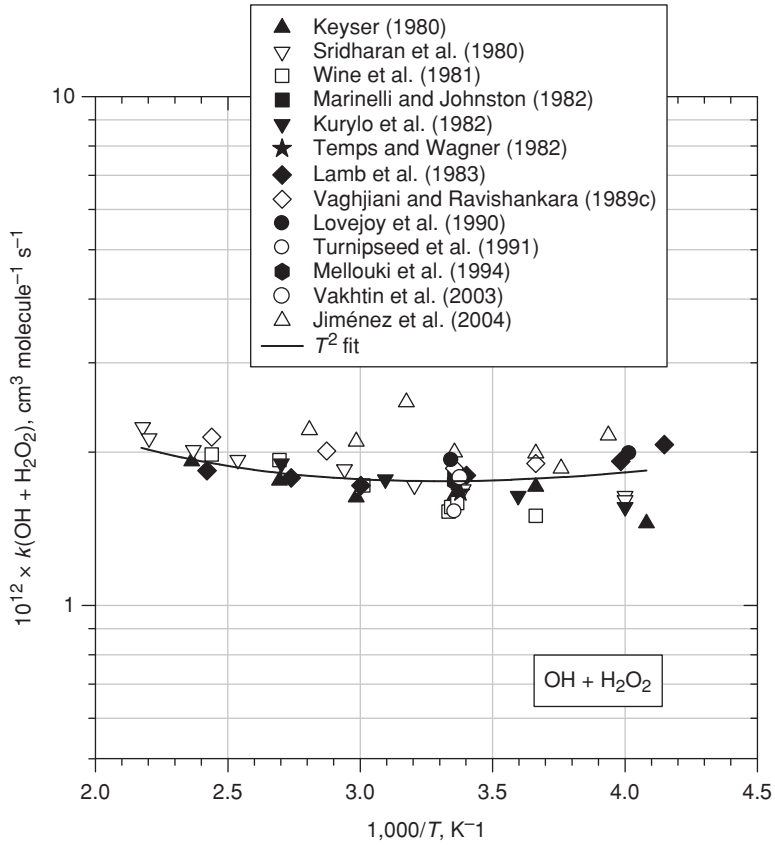

Figure II-G-1. Arrhenius plot of the rate coefficients for the OH + hydrogen peroxide reaction.

II-G-1.4. Cl-Atom Reaction Kinetics

The kinetics of the reaction of Cl with H_2O_2 have been measured by different groups using absolute techniques (Watson et al., 1976; Leu and De More, 1976; Michael et al., 1977; Poulet et al., 1978; Keyser et al., 1980). The available data are summarized in table II-G-2 and plotted in figure II-G-2. Near 298 K, the rate coefficient values reported lie in the range $(3.6-6.2) \times 10^{-13}$ cm^3 molecule^{-1} s^{-1}. Above room temperature, the results from Michael et al. (1977) lie below those of Keyser et al. (1980). The measurements of Poulet et al. (1978) and Keyser (1980) are considered to be the most reliable, and the preferred Arrhenius expression is that of Keyser, $k = 1.1 \times 10^{-11} \exp(-980/T)$ over the temperature range 298–430 K with $k = 4.1 \times 10^{-13}$ cm^3 molecule^{-1} s^{-1} and an uncertainty of $\pm 30\%$ at 298 K.

Using mass spectrometry, Heneghan and Benson (1983) confirmed that this reaction proceeds only by H-atom abstraction.

II-G-1.5. Summary of the Atmospheric Fate of Hydrogen Peroxide

Hydrogen peroxide is formed in the atmosphere via the $HO_2 + HO_2$ reaction and in the H-atom abstraction processes involving reaction of HO_2 with alkoxy, HCO, and other radicals. Once formed, H_2O_2 may be lost via different atmospheric processes (rainout, uptake onto condensed matter, photolysis, and reaction with atmospheric radicals). In the lower stratosphere and upper troposphere, the dominant loss processes of H_2O_2 are photolysis and reaction with OH, while in the mid- and lower-troposphere the removal of H_2O_2 is controlled by the rainout and uptake processes. H_2O_2 is very soluble in water. The reactions involving aqueous H_2O_2 are very important in the context of the chemistry of the atmosphere. H_2O_2 is one of the most effective oxidants of SO_2 to H_2SO_4 in clouds and fogs.

Combining the rate coefficient for the reaction of OH with a diurnal average [OH] = 10^6 molecule cm^{-3}, a tropospheric lifetime of 6 days is estimated for H_2O_2 with respect to reaction with OH radicals in the gas phase. Using a global model, von Kuhlmann

Table II-G-2. Rate coefficients (k, cm^3 molecule^{-1} s^{-1}) for the reaction of Cl with hydrogen peroxide (H_2O_2)

$10^{12} \times A$	B (K)	$10^{13} \times k$	T (K)	Technique[a]	Reference	Temperature Range (K)
		~ 5.8	298	FP–RF	Watson et al. (1976)	
		6.2 ± 1.5	295	DF–MS	Leu and De More (1976)	
1.24 ± 0.74	384 ± 168	4.94 ± 1.08	400	FP–RF	Michael et al. (1977)	265–400
		3.89 ± 0.72	359			
		3.64 ± 0.52	299			
		2.83 ± 0.60	265			
		4.0 ± 0.4	298	DF–MS	Poulet et al. (1978)	
10.5 ± 3.1	982 ± 102	11.0 ± 1.6	424	DF–RF	Keyser (1980)	298–524
		7.19 ± 0.14	374			
		5.58 ± 0.10	340			
		4.08 ± 0.09	298			

[a]Abbreviations used for the techniques are defined in table I-F-3.

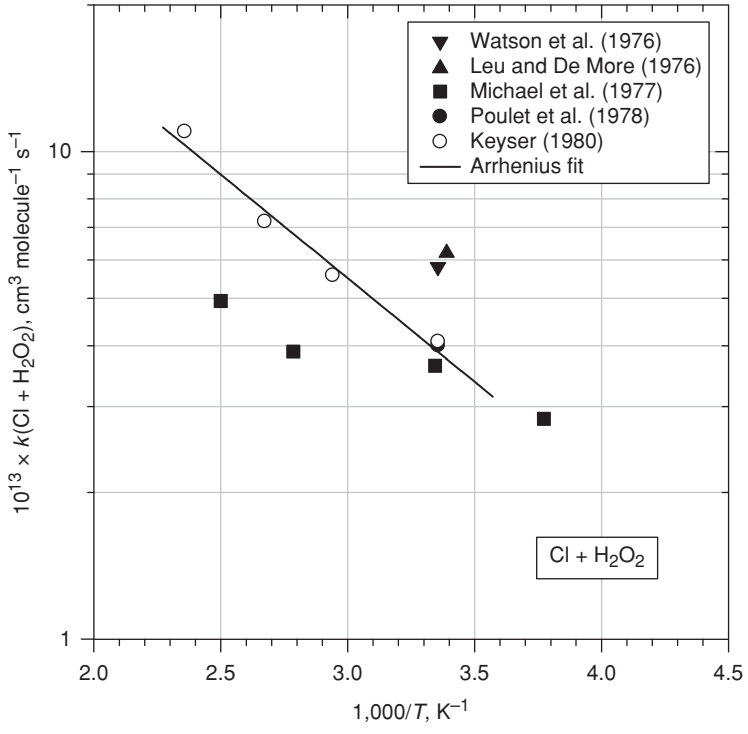

Figure II-G-2. Arrhenius plot of the rate coefficients for the Cl + hydrogen peroxide reaction.

et al. (2003) have estimated the importance of different loss processes of H_2O_2 from the atmosphere to be: wet deposition, 23%; dry deposition, 16%; photolysis, 31%; and reaction with OH radicals, 30%. The temperature dependence kinetic studies suggest that the reaction mechanism changes from direct abstraction at high temperature to a mechanism involving formation of a hydrogen-bonded complex at low temperature. At around room temperature, Vaghjiani et al. (1989c) have shown that the reaction of OH with H_2O_2 is likely to be a simple H-atom abstraction.

II-G-2. Methyl Hydroperoxide (CH_3OOH)

II-G-2.1. OH Reaction Kinetics

The kinetics of the reaction of OH with methyl hydroperoxide have been investigated by Niki et al. (1983), Vaghjiani and Ravishankara (1989a), and Blitz et al. (2005). The measurements are summarized in table II-G-3 and figure II-G-3. Niki et al. measured the overall rate coefficient, and performed product studies to determine the branching ratio for the reaction.

$$OH + CH_3OOH \rightarrow H_2O + CH_3O_2 \quad \text{(a)}$$

$$OH + CH_3OOH \rightarrow H_2O + (CH_2OOH) \rightarrow H_2O + CH_2O + OH \quad \text{(b)}$$

Table II-G-3. Rate coefficients ($k = A\ e^{-B/T}$, cm^3 $molecule^{-1}$ s^{-1}) for the reaction of OH with methyl hydroperoxide (CH_3OOH)

$10^{12} \times A$	B (K)	$10^{12} \times k$	T (K)	Technique[a]	Reference	Temperature Range (K)
Overall reaction[c]						
		9.3	298	RR (C_2H_4)[b]	Niki et al. (1983)	
2.93 ± 0.30	−190 ± 14	6.93 ± 0.26	223	PLP–LIF	Vaghjiani and Ravishankara (1989a)	223–348
		6.45 ± 0.20	244			
		6.29 ± 0.23	249			
		5.38 ± 0.20	298			
		4.97 ± 0.48	348			
		5.06 ± 0.14	373			
		4.61 ± 0.41	423			
Reaction (a)[c]						
		5.3 ± 1.1	298	FTIR	Niki et al. (1983)	
1.78 ± 0.25	−220 ± 21	5.13 ± 0.19	203	PLP–LIF	Vaghjiani and Ravishankara (1989a)	203–348
		5.00 ± 0.29	223			
		4.33 ± 0.54	244			
		3.85 ± 0.23	298			
		3.29 ± 0.32	348			
		9.0 ± 0.2	295	PLP–LIF	Blitz et al. (2005)	

[a]Abbreviations used for the techniques are defined in table I-F-3.
[b]Placed on an absolute basis using $k(OH + C_2H_4) = 7.9 \times 10^{-12}$ cm^3 $molecule^{-1}$ s^{-1} at 1 bar and 298 K (Atkinson et al., 2006).
[c]$OH + CH_3OOH \rightarrow H_2O + CH_3O_2$(a); $OH + CH_3OOH \rightarrow H_2O + (CH_2OOH) \rightarrow H_2O + CH_2O + OH$ (b)

Niki et al. (1983) found an overall rate coefficient of 9.3×10^{-12} cm^3 $molecule^{-1}$ s^{-1} using the relative rate technique, and a branching ratio $k_a/k_b = 1.30 \pm 0.25$. Vaghjiani and Ravishankara (1989a) followed the loss of OH directly. Using isotopically substituted OH, Vaghjiani and Ravishankara determined the overall rate coefficient ($k_a + k_b$) and the rate coefficient for the channel which does not lead to regeneration of OH (k_a). Their expression for the overall rate coefficient, $k = (2.93 \pm 0.30) \times 10^{-12}$ $\exp[(190 \pm 14)/T]$ gives $k = 5.54 \times 10^{-12}$ cm^3 $molecule^{-1}$ s^{-1} at 298 K. Their branching ratio at room temperature calculated from the individual rate coefficients is $k_a/k_b = 2.2 \pm 0.4$. Thus, both the overall rate coefficient and the individual channels are in some disagreement with the work of Niki et al. Blitz et al. (2005) reported $k_a = (9.0 \pm 0.2) \times 10^{-12}$ cm^3 $molecule^{-1}$ s^{-1} at 295 K, which is more than a factor of 2 larger than that of Vaghjiani and Ravishankara. Clearly, the rate coefficient for this reaction has not yet been fully defined, and further work is required.

II-G-2.2. O_3 Reaction Kinetics

The reaction of ozone with CH_3OOH has been studied by Chen and Wang (2006). The rate coefficient was obtained at 293 ± 2 K and in air at atmospheric pressure, with an excess of O_3 over CH_3OOH: $k = (7.3 \pm 0.1) \times 10^{-21}$ cm^3 $molecule^{-1}$ s^{-1}.

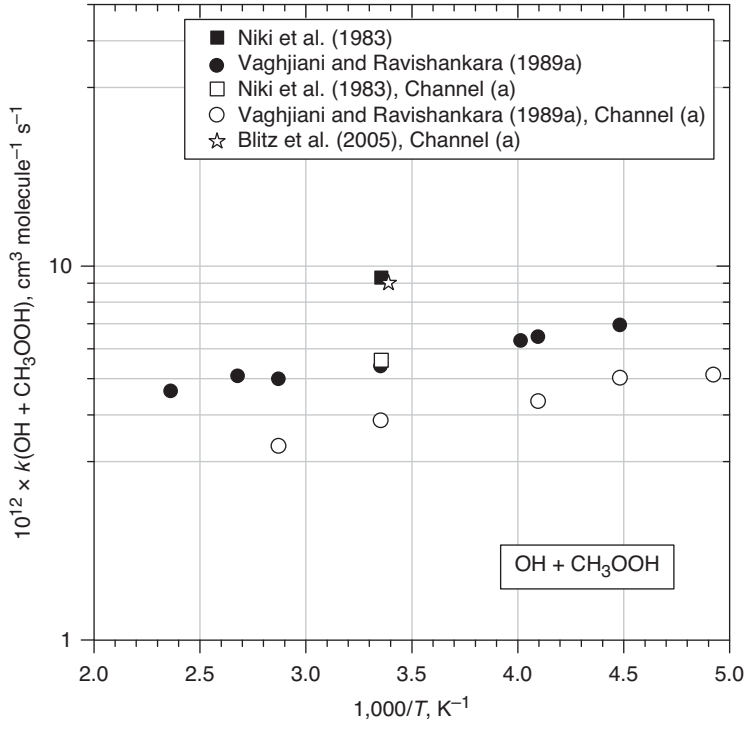

Figure II-G-3. Arrhenius plot of the rate coefficients for the OH + methyl hydroperoxide reaction.

II-G-2.3. Cl-Atom Reaction Kinetics

The reaction of chlorine atoms with CH_3OOH has been studied by Wallington et al. (1990a) using a relative rate technique in 700 Torr of N_2 diluent at 295 K; see table II-G-4. Using ethane as the reference compound with $k(Cl+C_2H_6) = 5.9\times10^{-11}$, the rate coefficient ratio reported by these authors at 295 K gives $k(Cl + CH_3OOH) = (5.9 \pm 0.24) \times 10^{-11}$ cm^3 molecule^{-1} s^{-1}. A value of $k(Cl + CH_3OOH) = 5.9 \times 10^{-11}$ cm^3 molecule^{-1} s^{-1} is recommended at 298 K with an uncertainty estimated to be $\pm$ 20%.

Table II-G-4. Rate coefficients (k, cm^3 molecule^{-1} s^{-1}) for the reaction of chlorine atoms with methyl hydroperoxide (CH_3OOH) and ethyl hydroperoxide (C_2H_5OOH)

Compound	$10^{11} \times k$	T (K)	Technique[a]	Reference
Methyl hydroperoxide (CH_3OOH)	5.90 ± 0.24	295	RR (C_2H_6)[b]	Wallington et al. (1990a)
Ethyl hydroperoxide (C_2H_5OOH)	11.1 ± 0.8	295	RR (C_2H_6)[b]	Wallington et al. (1989b)

[a]Abbreviations used for the techniques are defined in table I-F-3.

[b]Placed on an absolute basis using $k(Cl + C_2H_6) = 5.9 \times 10^{-11}$ cm^3 molecule^{-1} s^{-1} (Atkinson et al., 2006).

II-G-2.4. Summary of the Atmospheric Fate of Methyl Hydroperoxide

Methyl hydroperoxide is about 1/100th as soluble in water as hydrogen peroxide and ~3 times more reactive toward OH. Therfore, the atmospheric degradation of methyl hydroperoxide involves mainly reaction with OH radicals and photolysis. The reported rate coefficients for reaction of OH radicals with CH_3OOH lie in the range $(0.3-1.0) \times 10^{-11}$ cm^3 molecule^{-1} s^{-1}. Combining this range with a diurnal average [OH] = 10^6 molecule cm-^{3} gives an atmospheric lifetime for CH_3OOH of approximately 1–4 days with respect to reaction with OH radicals. This can be compared to a diurnal average lifetime at 40° N latitude with respect to photolysis for CH_3OOH which is estimated to be 6–23 days depending on season (see table IX-M-1). Reaction with OH is probably the dominant atmospheric loss of CH_3OOH. von Kuhlmann et al. (2003) have estimated from a global model that 80% of the atmospheric removal of CH_3OOH is through reaction with OH, and 16% is due to photolysis; wet and dry depositions constitute minor loss processes (1% and 3%, respectively).

The reaction of OH with CH_3OOH proceeds via hydrogen abstraction from the CH_3 and —OH groups. Reaction at the CH_3 group gives the CH_2OOH radical which will decompose to give H_2CO and an OH radical. Reaction at the —OH group gives a methyl peroxy radical which can further react with NO to give a methoxy radical; CH_3O in turn will react with O_2 to give H_2CO, or it will react with other peroxy radicals. The latter process is the dominant pathway in clean air and leads to formation of peroxides. Peroxides are considered to be indicators of chemical processing in the troposphere, they also act as both sources and sinks of OH radicals. The photolysis of CH_3OOH is a potential source of OH and HO_2 radicals, while its reaction with OH and rainout or dry deposition may act as sinks that remove free radicals.

II-G-3. Ethyl Hydroperoxide (C_2H_5OOH)

II-G-3.1. OH Reaction Kinetics

The rate coefficient for reaction of OH radicals with ethyl hydroperoxide has been measured at 293 K by Wang and Chen (2008) using relative rate methods. Experiments were performed in 760 Torr of air with cyclohexane, *m*-xylene, and 1,3,5-trimethyl-benzene as reference compounds. The results are listed in table II-G-5. An unweighted average of the determinations gives $k(OH + C_2H_5OOH) = 6.0 \times 10^{-12}$ cm^3 molecule^{-1} s^{-1}.

$$OH + C_2H_5OOH \rightarrow H_2O + C_2H_5O_2(a)$$

$$OH + C_2H_5OOH \rightarrow H_2O + CH_3CHOOH(b)$$

$$OH + C_2H_5OOH \rightarrow H_2O + CH_2CH_2OOH(c)$$

There is no experimental information available concerning the relative importance of channels (a–c). Since the study of Wang and Chen (2008) was conducted in an atmosphere of air, the oxidation of C_2H_5OOH and the reference compounds is expected to produce HO_2 radicals which will react with $C_2H_5O_2$ radicals formed in channel (a) to reform C_2H_5OOH (Spittler et al., 2000). It is difficult to assess the magnitude of such

Table II-G-5. Rate coefficients (k, cm^3 molecule^{-1} s^{-1}) for the reaction of OH with ethyl hydroperoxide (C_2H_5OOH)

$10^{12} \times k$	T (K)	Technique[a]	Reference
5.99 ± 0.17	293	RR (*cyclo*-C_6H_{12})[b]	Wang and Chen (2008)
6.10 ± 0.30		RR (*m*-xylene)[c]	
6.01 ± 0.51		RR (1,3,5-trimethylbenzene)[d]	

[a]Abbreviations used for the techniques are defined in table I-F-3.
[b]Placed on an absolute basis using $k(OH + cyclohexane) = 6.84 \times 10^{-12}$ cm^3 molecule^{-1} s^{-1} (Calvert et al., 2008).
[c]Placed on an absolute basis using $k(OH + m\text{-xylene}) = 2.31 \times 10^{-11}$ cm^3 molecule^{-1} s^{-1} (Calvert et al., 2002).
[d]Placed on an absolute basis using $k(OH + 1, 3, 5\text{-trimethybenzene}) = 5.67 \times 10^{-11}$ cm^3 molecule^{-1} s^{-1} (Calvert et al., 2002).

C_2H_5OOH formation and hence the potential underestimation of $k(OH + C_2H_5OOH)$ by Wang and Chen (2008). No recommendation is made for $k(OH + C_2H_5OOH)$.

II-G-3.2. Cl-Atom Reaction Kinetics

The reaction of chlorine atoms with C_2H_5OOH has been studied by Wallington et al. (1989b) using a relative rate technique in 700 Torr of N_2 diluent at 295 K (table II-G-4). Based upon this single study, a value of $k(Cl + C_2H_5OOH) = 1.1 \times 10^{-10}$ cm^3 molecule^{-1} s^{-1} is recommended at 298 K with an uncertainty estimated to be ±20%.

II-G-3.3. Summary of the Atmospheric Fate of Ethyl Hydroperoxide

The atmospheric fate of ethyl hydroperoxide is expected to be photolysis and reaction with OH radicals. While the UV spectrum of C_2H_5OOH has not been reported, it is expected to be similar to that of CH_3OOH but extending to somewhat longer wavelengths.Thus, it seems likely that photolysis of C_2H_5OOH will occur at a rate greater than $(4-6) \times 10^{-6}$ s^{-1} for solar zenith angles from 45° to 0° and that photodecomposition will proceed via O—O bond scission.

$$C_2H_5OOH + h\nu \rightarrow C_2H_5O + OH$$

While no recommendation is made for $k(OH + C_2H_5OOH)$, the reported rate coefficients for reactions of OH radicals with CH_3OOH and C_2H_5OOH (see preceding discussion) lie in the range $(0.5-1.0) \times 10^{-11}$ cm^3 molecule^{-1} s^{-1}. Combining this range with a diurnal average [OH] = 10^6 molecule cm^{-3} gives an atmospheric lifetime of C_2H_5OOH of approximately 1–2 days with respect to reaction with OH radicals. This can be compared to an estimated diurnal average lifetime at 40° N latitude with respect to photolysis for CH_3OOH of 6–23 days depending on season (see table IX-M-1). Reaction with OH is probably the dominant atmospheric loss of C_2H_5OOH.

Comparing the reactivity of C_2H_5OOH with C_2H_5OH (see section II-B-2), it seems likely that the bulk of the reaction of OH with C_2H_5OOH proceeds via hydrogen abstraction from the the —CH_2 and —OH groups. Reaction at the —CH_2 group gives the CH_3CHOOH radical which will decompose to give CH_3CHO and an OH radical. Reaction at the —OH group gives an ethyl peroxy radical which can react with NO to give an ethoxy radical; this in turn will react with O_2 to give CH_3CHO.

Table II-G-6. Rate coefficients (k, cm^3 molecule^{-1} s^{-1}) for reaction of OH radicals with *tert*-butyl hydroperoxide [$(CH_3)_3COOH$]

$10^{12} \times k$	T (K)	Technique[a]	Reference
3.0 ± 0.8	298	FP–RA	Anastasi et al. (1978)
78 ± 25	86	LP–LIF	Taylor et al. (2008)

[a]Abbreviations used for the techniques are defined in table I-F-3.

II-G-4. *tert*-Butyl Hydroperoxide [$(CH_3)_3COOH$]

II-G-4.1. OH Reaction Kinetics

The reaction of OH radicals with $(CH_3)_3COOH$ has been studied by Anastasi et al. (1978) and Taylor et al. (2008) at 298 K and 86 K, respectively. The results are given in table II-G-6. The measurement of Anastasi et al. at 298 K is recommended: $k = 3.0 \times 10^{-12}$ cm^3 molecule^{-1} s^{-1} with an uncertainty of $\pm 50\%$. The effect of temperature on the reaction of OH with *tert*-butyl hydroperoxide may be similar to that reported for the reaction of OH with H_2O_2.

II-G-4.2. Summary of the Atmospheric Fate of tert-Butyl Hydroperoxide

The atmospheric lifetime of *tert*-butyl hydroperoxide with respect to reaction with OH radicals is of the order of few days. Similar to other hydroperoxides, photolysis could also have an important contribution to the atmospheric removal of *tert*-butyl hydroperoxide. The reaction of OH with *tert*-butyl hydroperoxide is expected to proceed through H-atom abstraction from the —OOH group to give $(CH_3)_3CO_2$ radicals which will react with NO, other peroxy radicals, and ozone as suggested in the previous sections for methyl and ethyl peroxy radicals.

III

Rate Coefficients and Mechanisms for the Atmospheric Oxidation of the Ethers

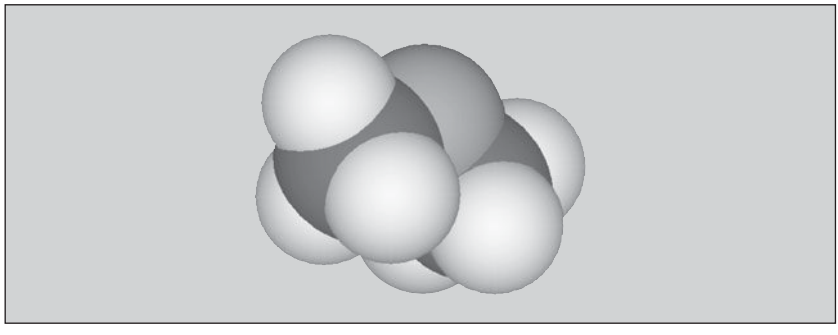

III-A. Introduction

The presence of ethers in the atmosphere is almost entirely the result of direct emissions from anthropogenic sources (e.g., Arif et al., 1997; Intergovernmental Panel on Climate Change, 2001; Johnson and Andino, 2001; http://en.wikipedia.org/wiki/Ethers; and references therein). These sources can be quite varied and species dependent; for example, many ethers are commonly used as industrial solvents; many are formed as combustion intermediates and in the burning of biomass; various branched ethers (e.g., methyl *tert*-butyl ether) are (or have been) used as fuel additives to increase octane number and reduce CO emissions; dimethyl ether has being proposed as an alternative diesel fuel; many fluorinated species have been manufactured, evaluated and used as possible chlorofluorocarbon (CFC) and hydrochlorofluorocarbon (HCFC) replacement compounds; some halogenated species are used as inhalation anaesthetics or as chlorofluorocarbon replacements; and polybrominated diphenyl ethers (PBDEs) are used as flame retardants. There are no major routes to ether formation in the atmosphere itself.

The atmospheric behavior of the simple aliphatic ethers, to a first approximation, mirrors that of the alkanes. Reaction with OH is the dominant removal pathway, and occurs via abstraction of an H-atom. In general, however, the ethers are more reactive than the alkanes, as the ether linkage leads to a weakening of the neighboring C—H bonds, and thus imparts an "activation effect" on the OH reaction. The major oxidation steps occurring subsequent to abstraction are also similar to those occurring in atmospheric alkane chemistry, involving the formation of a peroxy radical and an alkoxy

radical prior to end product formation; e.g.,

$$OH + CH_3CH_2OCH_2CH_3 \rightarrow CH_3CH_2OC\bullet HCH_3 + H_2O$$

$$CH_3CH_2OC\bullet HCH_3 + O_2 \rightarrow CH_3CH_2OCH(OO\bullet)CH_3$$

$$CH_3CH_2OCH(OO\bullet)CH_3 + NO \rightarrow CH_3CH_2OCH(O\bullet)CH_3 + NO_2$$

$$CH_3CH_2OCH(O\bullet)CH_3 + O_2 \rightarrow CH_3CH_2OC(=O)CH_3 + HO_2$$

$$CH_3CH_2OCH(O\bullet)CH_3 \rightarrow CH_3CH_2OCH(=O) + CH_3$$

However, less is know about the quantitative details of these processes than is the case for the alkanes. In general, unimolecular decomposition of the alkoxy radicals [e.g., $CH_3CH_2OCH(O\bullet)CH_3$ in the above reaction sequence] is more rapid than for an alkane-derived radical of similar structure. The major end product of ether oxidation is quite often an ester, the analog to the carbonyl compounds (aldehydes and ketones) generated from alkane oxidation.

Data regarding the atmospheric behavior of individual ether species are presented in the following sections, including kinetic data for their reaction with OH, O_3, NO_3, Cl, and $O(^3P)$, when available, and an assessment of the ether's atmospheric lifetime and fate. The discussion includes unsubstituted acyclic ethers, multifunctional ethers, unsaturated ethers, cyclic ethers, aromatic ethers, and halogen-substituted ethers. Following the discussion of the atmospheric behavior of the individual ethers, general trends in reactivity are presented, including structure–activity relationships (SARs) for calculation of OH rate coefficients with various classes of ethers, correlations between OH, Cl, and NO_3 rate coefficient data, and general comparisons of the reactivity of the ethers with that of the alkanes and the alcohols.

III-B. Acyclic Ethers

III-B-1. Dimethyl Ether (CH_3OCH_3)

III-B-1.1. OH Reaction Kinetics

The reaction of OH with dimethyl ether (DME) has been measured extensively (Perry et al., 1977b; Tully and Droege, 1987; Wallington et al., 1988e; Wallington et al., 1989a; Nelson et al., 1990a; Mellouki et al., 1995; Arif et al., 1997; DeMore and Bayes, 1999; Tranter and Walker, 2001; Bonard et al., 2002), over a large range of temperatures (230–753 K) and using a variety of techniques. As seen in figure III-B-1 and table III-B-1, the data are in reasonable accord, although some minor discrepancies are apparent. For example, the data of Perry et al. (1977b) are about 25% higher than the mean of the remaining datasets, while the values of Wallington et al. (1988e) are about 15–20% lower.

A fit of an equation of the form $k = A \times T^2 \times \exp(-B/T)$ to the entire data set yields the following expression, $k = 1.16 \times 10^{-17} T^2 \exp(300/T)$ cm^3 molecule^{-1} s^{-1}. This is essentially identical to the expression obtained from a consideration of only the data

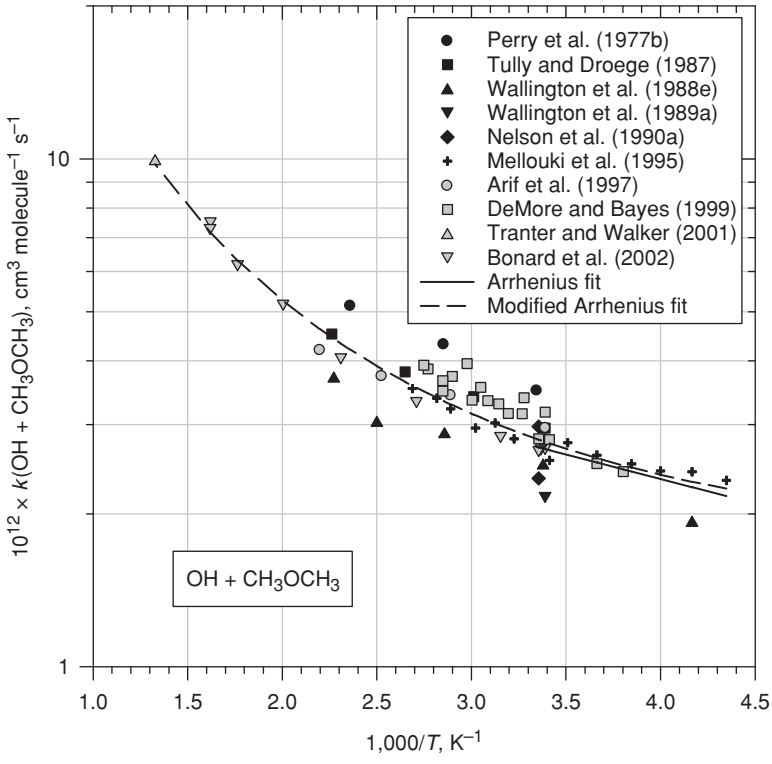

Figure III-B-1. Arrhenius plot of the rate coefficient for the reaction of OH with dimethyl ether.

Table III-B-1. Rate coefficients ($k = A \times T^n \times e^{-B/T}$, cm^3 $molecule^{-1}$ s^{-1}) for reaction of OH with dimethyl ether (CH_3OCH_3)

$10^{12} \times A$	n	B (K)	$10^{12} \times k$	T (K)	Technique[a]	Reference	Temperature Range (K)
12.9	0	388 ± 151	3.50 ± 0.35	298.9	FP–RF	Perry et al. (1977b)	299–424
			4.31 ± 0.43	350.5			
			5.13 ± 0.51	423.9			
10.4 ± 1.0	0	372 ± 34	2.95 ± 0.12	295	PLP–LIF	Tully and Droege (1987)	295–442
			3.40 ± 0.14	332			
			3.81 ± 0.16	377.5			
			4.52 ± 0.19	442			
6.7 ± 1.5	0	300 ± 70	1.92 ± 0.22	240	FP–RF	Wallington et al. (1988e)	240–440
			2.49 ± 0.22	296			
			2.87 ± 0.40	350			
			3.02 ± 0.22	400			
			3.69 ± 0.35	440			
			2.17 ± 0.22	295	RR[b] (n-C_4H_{10})	Wallington et al. (1989a)	

(*continued*)

Table III-B-1. (*continued*)

$10^{12} \times A$	n	B (K)	$10^{12} \times k$	T (K)	Technique[a]	Reference	Temperature Range (K)
			2.35 ± 0.24	298	PR–UV	Nelson et al.	
			2.97 ± 0.65	298	RR[c] ($cyclo$-C_6H_{12})	(1990a)	
6.3 ± 0.1	0	234 ± 34	2.33 ± 0.04	230	PLP–LIF	Mellouki et al. (1995)	230–372
			2.42 ± 0.04	240			
			2.43 ± 0.04	250			
			2.51 ± 0.06	260			
			2.61 ± 0.04	273			
			2.76 ± 0.08	285			
			2.55 ± 0.12	293			
			2.80 ± 0.05	294			
			2.82 ± 0.07	295			
			2.81 ± 0.07	310			
			3.02 ± 0.07	320			
			2.95 ± 0.09	331			
			3.22 ± 0.12	346			
			3.38 ± 0.06	355			
			3.53 ± 0.18	372			
$(1.05 \pm 0.1) \times 10^{-5}$	2.0	-328 ± 32	2.95 ± 0.21	295	PLP–LIF	Arif et al. (1997)	295–650
			3.42 ± 0.18	346			
			3.73 ± 0.20	396			
			4.20 ± 0.11	455			
			4.62 ± 0.25	490			
			6.27 ± 0.31	549			
			7.12 ± 0.47	601			
			8.19 ± 0.39	650			
15.1 ± 1.5	0	496 ± 31	2.42	263	RR[d] (n-C_4H_{10})	DeMore and Bayes (1999)	263–361
			2.51	273			
			2.80	293			
			2.81	298			
			3.16	313			
			3.35	333			
			3.49	351			
			3.17	295	RR[e] (n-C_5H_{12})		
			3.39	305			
			3.29	318			
			3.55	328			
			3.95	336			
			3.73	345			
			3.92	364			
			3.15	306	RR[f] ($cyclo$-C_6H_{12})		
			3.34	324			
			3.66	351			
			3.86	361			
			9.89 ± 1.38	753	RR[g] (H_2)	Tranter and Walker (2001)	
$(3.02 \pm 0.1) \times 10^{-8}$	2.85	-618 ± 13	2.70 ± 0.08	295	PLP–LIF	Bonard et al. (2002)	295–618
			2.69 ± 0.07	297			
			2.67 ± 0.07	298			

(*continued*)

Table III-B-1. (*continued*)

$10^{12} \times A$	n	B (K)	$10^{12} \times k$	T (K)	Technique[a]	Reference	Temperature Range (K)
			2.85 ± 0.06	317		Bonard et al.	
			3.34 ± 0.11	369		(2002)	
			4.07 ± 0.11	433		(*continued*)	
			5.19 ± 0.14	499			
			6.21 ± 0.12	567			
			7.54 ± 0.20	617			
			7.31 ± 0.24	618			

[a]Abbreviations used for the techniques are defined in table I-F-3.
[b]Placed on an absolute basis using $k(\text{OH+ } n\text{-}C_4H_{10}) = 2.36 \times 10^{-1-12}$ cm^3 molecule^{-1-1} s^{-1} (Calvert et al., 2008).
[c]Placed on an absolute basis using $k(\text{OH+ } cyclo\text{-}C_6H_{12}) = 6.97 \times 10^{-12}$ cm^3 molecule^{-1} s^{-1} (Calvert et al., 2008).
[d]Placed on an absolute basis using $k(\text{OH+ } n\text{-}C_4H_{10}) = 1.40 \times 10^{-11} \exp(-520/T)$ cm^3 molecule^{-1} s^{-1} (Calvert et al., 2008).
[e]Placed on an absolute basis using $k(\text{OH+ } n\text{-}C_5H_{12}) = 1.81 \times 10^{-11} \exp(-452/T)$ cm^3 molecule^{-1} s^{-1} (Calvert et al., 2008).
[f]Placed on an absolute basis using $k(\text{OH+ } cyclo\text{-}C_6H_{12}) = 3.0 \times 10^{-11} \exp(-440/T)$ cm^3 molecule^{-1} s^{-1} (Calvert et al., 2008).
[g]Placed on an absolute basis using $k(\text{OH+H}_2) = 7.86 \times 10^{-13}$ cm^3 molecule^{-1} s^{-1} at 753 K (Tully and Ravishankara, 1980).

of Tully and Droege (1987), Nelson et al. (1990a), Mellouki et al. (1995), Arif et al. (1997), DeMore and Bayes (1999), Tranter and Walker (2001), Bonard et al. (2002), or to that obtained by the IUPAC data panel (Atkinson et al., 2006) from a consideration of an even more limited data set (those of Tully and Droege, 1987; Mellouki et al., 1995; Arif et al.,1997; Bonard et al., 2002). For atmospheric purposes (230 K < T < 300 K), the simple Arrhenius expression: $k = 5.7 \times 10^{-12} \exp(-222/T)$ cm^3 molecule^{-1} s^{-1}, is obtained from a fit to all data below 300 K, yielding $k(298\text{ K}) = 2.7 \times 10^{-12}$ cm^3 molecule^{-1} s^{-1}, with an estimated uncertainty of ±15%. This expression is very similar to that recommended by the IUPAC panel, $k = 5.7 \times 10^{-12} \exp(-215/T)$ cm^3 molecule^{-1} s^{-1}; retrieved rate coefficients from the two expressions agree to better than 3%.

III-B-1.2. NO_3 Reaction Kinetics

The reaction of NO_3 with DME has been the subject of two studies (Wallington et al., 1986; Langer and Ljungström, 1994a). Data are summarized in table III-B-2 and figure III-B-2. Langer and Ljungström employed both a relative rate technique and a discharge flow–visible absorption technique. The reasonable consistency between the two techniques was used as evidence for the lack of significant complications from secondary chemistry in the discharge flow studies. A least squares fit of the Arrhenius expression to the entire Langer and Ljungström (1994a) dataset leads to $k = 2.3 \times 10^{-12} \exp(-2{,}714/T)$ cm^3 molecule^{-1} s^{-1}, with $k(298\text{K}) = 2.3 \times 10^{-16}$ cm^3 molecule^{-1} s^{-1}. The data are consistent with the upper limit reported by Wallington et al. (1986) using a flash photolysis–visible absorption system, $k < 3 \times 10^{-15}$ cm^3 molecule^{-1} s^{-1} at 298 K. Given the small rate coefficient, the lack of an extensive

Table III-B-2. Rate coefficients ($k = A \times e^{-B/T}$, cm^3 $molecule^{-1}$ s^{-1}) for reaction of NO_3 with dimethyl ether

$10^{15} \times A$	B (K)	$10^{15} \times k$	T (K)	Technique[a]	Reference	Temperature Range (K)
		< 3	298 ± 2	FP vis. abs.	Wallington et al. (1986)	
		0.19 ± 0.06	295	RR (n-C_6H_{14})	Langer and Ljungström (1994a)	258–373
1,400 ± 420	2,525 ± 600	0.15 ± 0.03	273	DF vis. abs.		
		0.26 ± 0.11	295			
		0.47 ± 0.07	323			
		0.96 ± 0.38	348			
		1.85 ± 0.62	373			

[a]Abbreviations used for the techniques are defined in table I-F-3.
[b]Placed on an absolute basis using $k(NO_3 + n\text{-}C_6H_{14}) = 1.1 \times 10^{-16}$ cm^3 $molecule^{-1}$ s^{-1} (Calvert et al., 2008).

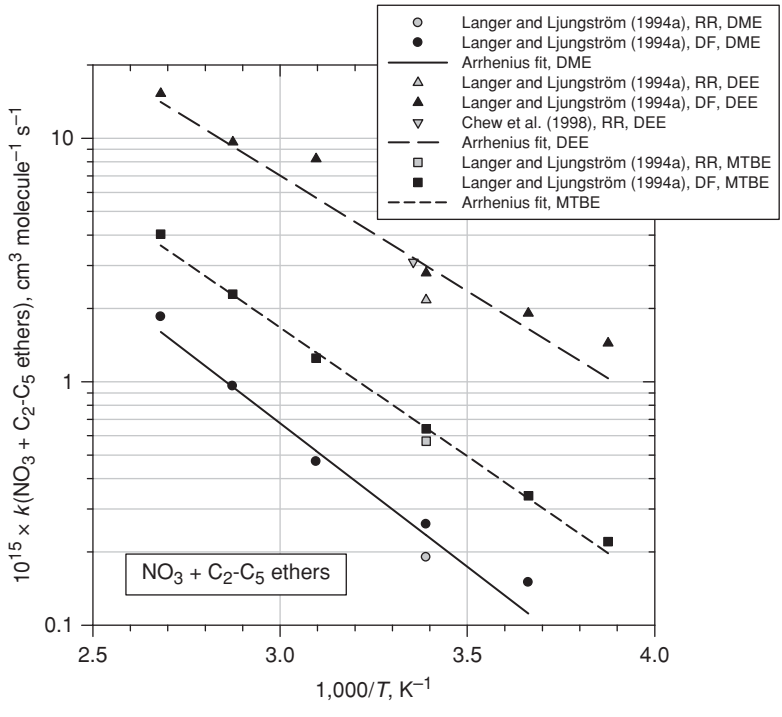

Figure III-B-2. Arrhenius plot of the rate coefficient for the reaction of NO_3 with dimethyl ether (DME), diethyl ether (DEE), and methyl *tert*-butyl ether (MTBE). RR = relative rate; DF = discharge flow.

dataset, and the possibility of some contribution of secondary chemistry in the discharge flow work, an overall uncertainty of ±50% is recommended.

III-B-1.3. Cl-Atom Reaction Kinetics

The many studies of the reaction of Cl with DME are summarized in table III-B-3 (Michael et al., 1979a; Park et al., 1983; Wallington et al., 1988g; Nelson et al., 1990a; Jenkin et al., 1993b; Langer et al., 1996; Notario et al., 2000b). The data are in good agreement, with the exception of the data point from Notario et al., which is about 25% lower than the average of the other data. An average of the data [excluding the Notario et al. (2000b) data point] gives the recommended value, $k = (1.8 \pm 0.3) \times 10^{-10}$ cm^3 molecule^{-1} s^{-1}. The rate coefficient is independent of temperature ($200 < T < 500$ K, Michael et al., 1979a), and has an assumed uncertainty of ±15%.

III-B-1.4. O(^{3}P) Reaction Kinetics

The most recent study of the reaction of O(^{3}P) atoms with DME is that of Liu et al. (1990a), using a flash photolysis–resonance fluorescence technique ($200 < T < 400$ K). They report $k = (5.39 \pm 1.94) \times 10^{-12} \exp[(-1{,}320 \pm 120)/T]$ cm^3 molecule^{-1} s^{-1}, with a measured $k(298\text{K}) = (5.7 \pm 0.3) \times 10^{-14}$ cm^3 molecule^{-1} s^{-1}.

III-B-1.5. Summary of the Atmospheric Fate of Dimethyl Ether, and the End Products of Its Oxidation

The major route for the removal of dimethyl ether from the atmosphere is via its reaction with OH. With an average atmospheric [OH] = 1×10^6 molecule cm^{-3}, a lifetime of about 4 days is derived. Nighttime removal via reaction with NO_3 may also make a minor contribution in polluted urban and rural regions (a lifetime of 17

Table III-B-3. Rate coefficients ($k = A \times e^{-B/T}$, cm^3 molecule^{-1} s^{-1}) for reaction of Cl with dimethyl ether

$10^{10} \times A$	B (K)	$10^{15} \times k$	T (K)	Technique[a]	Reference	Temperature Range (K)
1.76 ± 0.15	0	1.86 ± 0.21	200	FP–RF	Michael et al. (1979a)	200–500
		1.80 ± 0.09	300			
		1.61 ± 0.14	500			
		1.70 ± 0.06	298	DF–PIMS	Park et al. (1983)	
		1.87 ± 0.07	295	RR[b] (n-C_4H_{10})	Wallington et al. (1988g)	
		1.60 ± 0.08	298	RR[c] ($cyclo$-C_6H_{12})	Nelson et al. (1990a)	
		1.93 ± 0.06	295	RR[d] (C_2H_4)	Jenkin et al. (1993b)	
		1.9 ± 0.1	295	RR[d] (C_2H_4)	Langer et al. (1996)	
		1.3 ± 0.2	298	PLP–RF	Notario et al. (2000b)	

[a]Abbreviations used for the techniques are defined in table I-F-3.
[b]Placed on an absolute basis using $k(\text{Cl}+n\text{-}C_4H_{10}) = 2.05 \times 10^{-10}$ cm^3 molecule^{-1} s^{-1} (Calvert et al., 2008).
[c]Placed on an absolute basis using $k(\text{Cl}+cyclo\text{-}C_6H_{12}) = 3.3 \times 10^{-10}$ cm^3 molecule^{-1} s^{-1} (Calvert et al., 2008).
[d]Placed on an absolute basis using $k(\text{Cl}+C_2H_4) = 0.95 \times 10^{-10}$ cm^3 molecule^{-1} s^{-1} (this book, table I-F-2).

days is estimated for polluted conditions, [NO_3] $\approx 3 \times 10^9$ molecule cm^{-3}), and reaction with Cl atoms cannot be ruled out as a competing removal process in some circumstances (for example, in coastal urban locations, particular in the early morning, where Cl-atom levels may be elevated relative to OH).

The OH, NO_3, and Cl-atom reactions with DME all proceed via abstraction, and thus the subsequent chemistry will be indentical for all three cases, e.g.,

$$OH + CH_3OCH_3 \rightarrow CH_3OCH_2\bullet + H_2O$$

The alkyl radical, $CH_3OCH_2\bullet$, reacts exclusively in the atmosphere with O_2, although via a complex mechanism (e.g., Jenkin et al., 1993b; Sehested et al., 1996, 1997; Maricq et al., 1997b; Rosado-Reyes et al., 2005; Andersen and Carter, 2006). The initially created ("activated") peroxy radical, [$CH_3OCH_2OO\bullet$]*, can rearrange and decompose to generate formaldehyde and OH, or it can be collisionally stabilized:

$$CH_3OCH_2\bullet + O_2 \rightarrow [CH_3OCH_2OO\bullet]^* \rightarrow [\bullet CH_2OCH_2OOH]^* \rightarrow 2CH_2O + OH$$

$$+ M \searrow$$

$$CH_3OCH_2OO\bullet$$

Under atmospheric conditions (i.e., reasonably high pressure), collisional stabilization dominates and the peroxy radical yield exceeds 90% throughout the troposphere (Jenkin et al., 1993b). The peroxy radical will mainly react with NO (Langer et al., 1995), HO_2 (Wallington et al., 1993b), and CH_3O_2 (Shallcross et al., 2005), as follows, with stable products highlighted in bold:

$$CH_3OCH_2OO\bullet + NO \rightarrow CH_3OCH_2O\bullet + NO_2$$

$$CH_3OCH_2OO\bullet + HO_2 \rightarrow \mathbf{CH_3OCH_2OOH} \quad (\approx 57\%, \text{Wallington et al., 1993b})$$

$$\rightarrow \mathbf{CH_3OCHO} + H_2O \quad (\approx 43\%, \text{Wallington et al., 1993b})$$

$$CH_3OCH_2OO\bullet + CH_3O_2 \rightarrow CH_3OCH_2O\bullet + CH_3O\bullet + O_2$$

$$\rightarrow \mathbf{CH_3OCHO} + CH_3OH + O_2$$

$$\rightarrow \mathbf{CH_3OCH_2OH} + CH_2O + O_2$$

Finally, the oxy radical, $CH_3OCH_2O\bullet$, generates methyl formate exclusively via two competing pathways, reaction with O_2 and direct H-atom elimination:

$$CH_3OCH_2O\bullet + O_2 \rightarrow \mathbf{CH_3OCHO} + HO_2$$

$$CH_3OCH_2O\bullet + M \rightarrow \mathbf{CH_3OCHO} + H + M$$

Thus, the major product of the oxidation is methyl formate, CH_3OCHO, with minor yields of CH_3OCH_2OH and CH_3OCH_2OOH likely formed as well. Selected rate coefficient data for the radical processes just described are summarized in table III-B-4.

Table III-B-4. Selected rate coefficient data (k, cm^3 molecule^{-1} s^{-1}) for reactions involved in the atmospheric oxidation of dimethyl ether

$10^{12} \times k$	T (K)	Pressure (Torr)	Technique[a]	Reference
$CH_3OCH_2 + O_2$				
10.9 ± 0.3	296	750	PR–UV abs.	Sehested et al. (1997)
10.7 ± 0.4	296	150		
9.5 ± 0.4	296	75		
12.9 ± 1.7	220	111	PLP–UV/IR abs.	Maricq et al. (1997b)
12.4 ± 2.0	229	118		
13.1 ± 1.8	252	108		
10.2 ± 1.2	270	120		
9.3 ± 1.2	295	120		
10.0 ± 1.3	295	206		
10.8 ± 1.3	295	442		
11.6 ± 1.8	295	480		
11.8 ± 1.2	295	690		
$CH_3OCH_2O_2 + NO$				
9.1 ± 1.0	296		PR–UV abs.	Langer et al. (1995)
$CH_3OCH_2O_2 + CH_3O_2$				
1.1	298		Estimated	Shallcross et al. (2005)

[a]Abbreviations used for the techniques are defined in table I-F-3.

III-B-2. Methyl Ethyl Ether ($CH_3OCH_2CH_3$)

III-B-2.1. OH Reaction Kinetics

The reaction of OH with methyl ethyl ether has been the subject of two relative rate studies, one covering the range 276–345 K (Starkey et al., 1997) and the other one conducted at 753 K (Tranter and Walker, 2001). Data are summarized in table III-B-5. The data of Starkey et al. (1997) suggest very little temperature dependence to the rate coefficient near room temperature, although the rate coefficient clearly increases at higher temperatures. A rate coefficient of 6.3×10^{-12} cm^3 molecule^{-1} s^{-1} (the average of the Starkey et al. data points) is recommended at 298 K, with an uncertainty of $\pm 50\%$. Further studies are required before lower temperature recommendations can be made.

III-B-2.2. NO_3 Reaction Kinetics

No data are available for this reaction. On the basis of data for reaction of dimethyl and diethyl ether with NO_3, a rate coefficient of about 1×10^{-15} cm^3 molecule^{-1} s^{-1} is estimated near 298 K, with an uncertainty of about a factor of 2.5.

III-B-2.3. Cl-Atom Reaction Kinetics

The only available data are from the relative rate study of Starkey et al. (1997), using ethane as the reference compound, see table III-B-6. There are, however, two reasons to question the accuracy of these data. Firstly, although the authors suggest that their

Table III-B-5. Rate coefficients (k, cm^3 molecule^{-1} s^{-1}) for reaction of OH with methyl ethyl ether ($CH_3OCH_2CH_3$)

$10^{12} \times k$	T (K)	Technique[a]	Reference	Temperature Range (K)
$6.60\ ^{+3.94}_{-2.49}$	276	RR[b] ($C_2H_5OC_2H_5$)	Starkey et al. (1997)	276–345
$6.27\ ^{+3.51}_{-2.27}$	301			
$6.16\ ^{+3.38}_{-2.20}$	315			
$6.2\ ^{+3.38}_{-2.22}$	325			
$6.28\ ^{+3.34}_{-2.21}$	335			
$6.25\ ^{+3.25}_{-2.17}$	345			
15.4 ± 2.5	753	RR[c] (H_2)	Tranter and Walker (2001)	

[a]Abbreviations used for the techniques are defined in table I-F-3.
[b]Placed on an absolute basis using $k(\mathrm{OH}+\mathrm{C_2H_5OC_2H_5}) = 1.15 \times 10^{-17} T^2 \exp(743/T)$ cm^3 molecule^{-1} s^{-1} (this book, see section III-B-3.1).
[c]Placed on an absolute basis using $k(\mathrm{OH}+\mathrm{H_2}) = 7.86 \times 10^{-13}$ cm^3 molecule^{-1} s^{-1} at 753 K (Tully and Ravishankara, 1980).

Table III-B-6. Rate coefficients (k, cm^3 molecule^{-1} s^{-1}) for reaction of Cl with methyl ethyl ether

$10^{10} \times k$	T (K)	Technique[a]	Reference	Temperature Range (K)
3.03 ± 0.34	274	RR[b] (C_2H_6)	Starkey et al. (1997)	274–344
3.27 ± 0.35	303			
3.56 ± 0.38	314			
3.77 ± 0.41	324			
3.92 ± 0.41	334			
3.81 ± 0.40	344			

[a]Abbreviations used for the techniques are defined in table I-F-3.
[b]Placed on an absolute basis using $k(\mathrm{Cl}+\mathrm{C_2H_6}) = 8.3 \times 10^{-11} \exp(-100/T)$ cm^3 molecule^{-1} s^{-1} (Calvert et al., 2008).

rate coefficient data show little dependence on temperature, a clear (and unexpected) positive temperature dependence is evident. Secondly, the reported values are larger than those obtained for reaction of Cl with diethyl ether (see section III-B-3.3), contrary to expectations. In light of these apparent inconsistencies, the data of Starkey et al. (1997) should be treated with caution, and no recommendation is made. On the basis of the more thoroughly studied reactions of Cl with dimethyl and diethyl ether, a rate coefficient of roughly $k = (2.0\text{–}2.8) \times 10^{-10}$ cm^3 molecule^{-1} s^{-1}, independent of temperature, seems likely.

III-B-2.4. O(^{3}P) Reaction Kinetics

No data are available for this reaction. On the basis of the available data for dimethyl and diethyl ethers, a rate coefficient of $\approx 2 \times 10^{-13}$ cm^3 molecule^{-1} s^{-1} can be estimated near room temperature.

III-B-2.5. Summary of the Atmospheric Fate of Methyl Ethyl Ether, and the End Products of Its Oxidation

Removal of methyl ethyl ether from the atmosphere will be controlled mainly by its reaction with OH. A lifetime of about 2 days is derived, assuming an average atmospheric [OH] = 1×10^6 molecule cm^{-3}. Reaction with NO_3 and with Cl-atoms may be significant in some circumstances. A lifetime of about 4 days with respect to reaction with NO_3 is estimated, for polluted conditions ([NO_3] = 3×10^9 molecule cm^{-3}).

No detailed studies of the end products of the atmospheric oxidation of methyl ethyl ether have been carried out. From structure–activity relationships (Kwok and Atkinson, 1995), the major site of attack is expected to be at the CH_2 group:

$$OH + CH_3OCH_2CH_3 \rightarrow CH_3OCH\bullet CH_3 + H_2O$$

The major end product (formed via the subsequent production and loss of a peroxy and oxy species) is then expected to be methyl formate, with small yields of methyl acetate:

$$CH_3OCH\bullet CH_3 + O_2 + M \rightarrow CH_3OCH(OO\bullet)CH_3 + M$$

$$CH_3OCH(OO\bullet)CH_3 + NO \rightarrow CH_3OCH(O\bullet)CH_3 + NO_2$$

$$CH_3OCH(O\bullet)CH_3 + M \rightarrow \mathbf{CH_3OCHO} + \bullet CH_3 + M$$

$$CH_3OCH(O\bullet)CH_3 + M \rightarrow \mathbf{CH_3OC(O)CH_3} + H + M$$

$$CH_3OCH(O\bullet)CH_3 + O_2 \rightarrow \mathbf{CH_3OC(O)CH_3} + HO_2$$

The structure–activity calculations (Kwok and Atkinson, 1995) suggest that about 10% of the OH reaction will occur via abstraction from the CH_3O group, which would result mainly in the production of ethyl formate, CH_3CH_2OCHO.

III-B-3. Diethyl Ether ($CH_3CH_2OCH_2CH_3$)

III-B-3.1. OH Reaction Kinetics

The reaction of OH with diethyl ether (DEE) has been studied over a range of temperatures (230–753 K) by a variety of direct (Tully and Droege, 1987; Wallington et al., 1988e; Nelson et al., 1990a; Mellouki et al., 1995) and relative rate techniques (Lloyd et al., 1976; Bennett and Kerr, 1989, 1990; Nelson et al., 1990a; Semadeni et al., 1993; Tranter and Walker, 2001). The data, summarized in table III-B-7 and displayed in figure III-B-3, are in reasonable accord and suggest a weak negative temperature dependence to the rate coefficient near 298 K.

Table III-B-7. Rate coefficients ($k = A \times T^n \times e^{-B/T}$, cm^3 $molecule^{-1}$ s^{-1}) for reaction of OH with diethyl ether ($CH_3CH_2OCH_2CH_3$)

$10^{12} \times A$	n	B (K)	$10^{12} \times k$	T (K)	Technique[a]	Reference	Temperature Range (K)
			9.6 ± 1.9	305	RR[b] (isobutene)	Lloyd et al. (1976)	
9.13 ± 0.35	0	-115 ± 14	13.4 ± 0.6	295	PLP–LIF	Tully and Droege (1987)	295–442
			12.9 ± 0.5	332			
			12.4 ± 0.5	377.5			
			11.8 ± 0.5	442			
5.6 ± 1.7	0	-270 ± 100	17.7 ± 1.5	240	FP–RF	Wallington et al. (1988e)	240–440
			13.6 ± 0.9	296			
			11.4 ± 1.2	350			
			11.5 ± 1.2	400			
			11.4 ± 1.7	440			
			11.9 ± 1.1	294	RR[b] (isobutene)	Bennett and Kerr (1989)	
7.1 [c]	0	−121[c]	11.6	242	RR[d] (2,3-dimethyl butane)	Bennett and Kerr (1990)	242–325
			11.3	263			
			11.4	273			
			10.4	289			
			10.6	304			
			10.6	317			
			10.2	325			
			11.3 ± 0.1	298	PR–UV	Nelson et al. (1990a)	
			11.9 ± 0.6	298	RR[e] (*cyclo*-C_6H_{12})		
10.4 [c]		−50[c]	12.0	250	RR[d] (2,3-dimethyl butane)	Semadeni et al. (1993)	250–373
			12.8	263			
			12.5	273			
			13.2	283			
			12.9	298			
			12.3	308			
			11.5	323			
			12.0	338			
			12.4	353			
			11.6	373			
$(1.02 \pm 0.08) \times 10^{-5}$	2	-797 ± 24	17.5 ± 0.4	230	PLP–LIF	Mellouki et al. (1995)	230–371
			15.6 ± 0.4	240			
			15.3 ± 0.4	253			
			14.2 ± 0.5	263			
			14.3 ± 0.2	273			
			13.6 ± 0.4	293			
			11.6 ± 0.6	297			
			12.3 ± 0.6	321			
			12.6 ± 0.2	328			
			13.2 ± 0.6	347			
			11.4 ± 0.3	347			

(*continued*)

Table III-B-7. (*continued*)

$10^{12} \times A$	n	B (K)	$10^{12} \times k$	T (K)	Technique[a]	Reference	Temperature Range (K)
			12.2 ± 0.2	358			
			12.0 ± 0.3	371			
			21.3 ± 3.9	753	RR[f] (H_2)	Tranter and Walker (2001)	753

[a]Abbreviations used for the techniques are defined in table I-F-3.
[b]Placed on an absolute basis using $k(\text{OH+isobutene}) = 5.2 \times 10^{-11}$ cm^3 molecule^{-1} s^{-1} (Calvert et al., 2000).
[c]Values obtained from least-squares fit of data obtained using updated reference rate coefficients, and thus differ from those originally reported.
[d]Placed on an absolute basis using $k(\text{OH+2,3-dimethylbutane}) = 1.25 \times 10^{-11} \exp(-212/T)$ cm^3 molecule^{-1} s^{-1} (Calvert et al., 2008).
[e]Placed on an absolute basis using $k(\text{OH+}cyclo\text{-}C_6H_{12}) = 6.97 \times 10^{-12}$ cm^3 molecule^{-1} s^{-1} (Calvert et al., 2008).
[f]Placed on an absolute basis using $k(\text{OH+}H_2) = 7.86 \times 10^{-13}$ cm^3 molecule^{-1} s^{-1} at 753 K (Tully and Ravishankara, 1980).

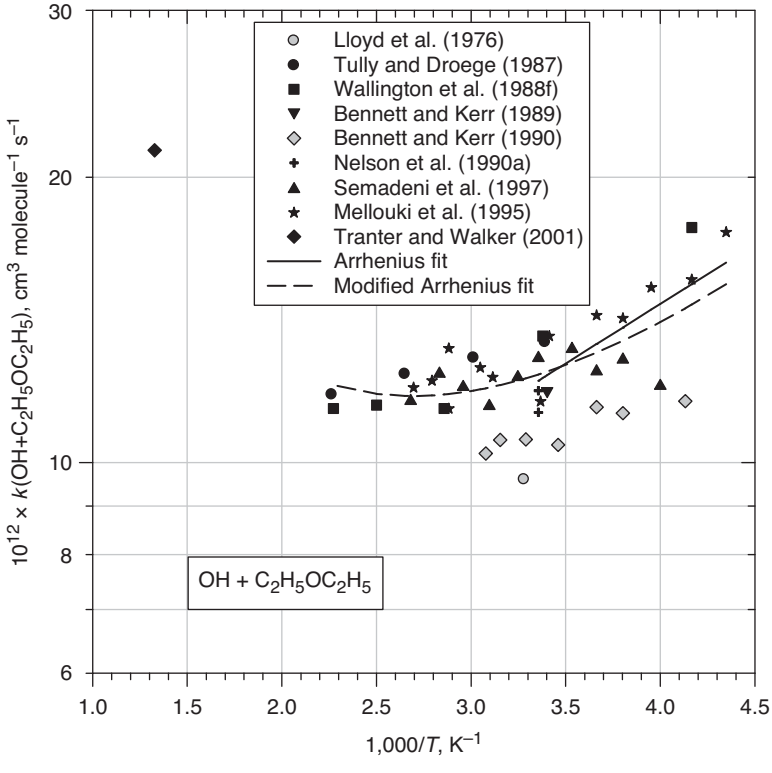

Figure III-B-3. Arrhenius plot of the rate coefficient for the reaction of OH with diethyl ether.

Data fits were carried out with the combined dataset, excluding the data from Lloyd et al. (1976) and Bennett and Kerr (1990), which are somewhat lower than the remaining data, and the high temperature data point of Tranter and Walker (2001). A fit of the Arrhenius expression to the remaining data measured at $T < 300$ K yields $k(\text{OH} + \text{DEE}) = 4.62 \times 10^{-12} \exp(289/T)$ cm^3 molecule^{-1} s^{-1} with $k = 1.22 \times 10^{-11}$ cm^3 molecule^{-1} s^{-1} at 298 K. The estimate uncertainty at 298 K is ±15%. For $230 < T < 440$ K, the modified Arrhenius expression, $k(\text{OH} + \text{DEE}) = 1.15 \times 10^{-17} T^2 \exp(743/T)$ cm^3 molecule^{-1} s^{-1}, is obtained from a consideration of all data except those of Lloyd et al. (1976), Bennett and Kerr (1990) and Tranter and Walker (2001). The data point of Tranter and Walker suggests an obvious increase in the rate coefficient at higher temperature.

III-B-3.2. NO_3 Reaction Kinetics

The reaction of NO_3 with diethyl ether has been the subject of two studies, a combined absolute and relative rate study by Langer and Ljungström (1994a) and a relative rate study by Chew et al. (1998). Data are summarized in table III-B-8 and figure III-B-2. A fit of the simple Arrhenius expression to the combined dataset yields $k(\text{NO}_3 + \text{DEE}) = 4.95 \times 10^{-12} \exp(-2{,}186/T)$ cm^3 molecule^{-1} s^{-1} with $k = 3.2 \times 10^{-15}$ cm^3 molecule^{-1} s^{-1} at 298 K. An uncertainty of ±35% is recommended.

III-B-3.3. Cl-Atom Reaction Kinetics

The four measurements of the rate coefficient for reaction of Cl-atoms with DEE (Wallington et al., 1988g; Nelson et al., 1990a; McLoughlin et al., 1993; Notario et al., 2000b), all conducted near 298 K, are in reasonable agreement; see table III-B-9. The average of the four determinations, $k = 2.8 \times 10^{-10}$ cm^3 molecule^{-1} s^{-1}, is recommended with an uncertainty of ±20%.

Table III-B-8. Rate coefficients (k, cm^3 molecule^{-1} s^{-1}) for reaction of NO_3 with diethyl ether

$10^{15} \times A$	B (K)	$10^{15} \times k$	T (K)	Technique[a]	Reference	Temperature Range (K)
		2.17 ± 0.72	295	RR[b](CH_3CHO)	Langer and Ljungström (1994a)	258–373
3,880 ± 1120	2,065 ± 480	1.44 ± 0.09	258	DF vis. abs.		
		1.91 ± 0.18	273			
		2.80 ± 0.23	295			
		8.22 ± 1.31	323			
		9.65 ± 1.02	348			
		15.25 ± 1.31	373			
		3.1 ± 0.1	298	RR[c] (methacrolein)	Chew et al. (1998)	

[a]Abbreviations used for the techniques are defined in table I-F-3.
[b]Placed on an absolute basis using $k(\text{NO}_3 + \text{CH}_3\text{CHO}) = 2.3 \times 10^{-15}$ cm^3 molecule^{-1} s^{-1} at 295 K (Calvert et al., 2008).
[c]Placed on an absolute basis using $k(\text{NO}_3 + \text{methacrolein}) = 3.3 \times 10^{-15}$ cm^3 molecule^{-1} s^{-1} (Chew et al., 1998).

Table III-B-9. Rate coefficients (k, cm^3 molecule^{-1} s^{-1}) for reaction of Cl with diethyl ether

$10^{10} \times k$	T (K)	Technique[a]	Reference
3.24 ± 0.25	298	RR[b] (n-C_4H_{10})	Wallington et al. (1988g)
2.70 ± 0.18	298	RR[c] (*cyclo*-C_6H_{12})	Nelson et al. (1990a)
2.60 ± 0.44	298	RR[d] (C_2H_6)	McLoughlin et al. (1993)
2.5 ± 0.3	298	PLP–RF	Notario et al. (2000b)

[a]Abbreviations used for the techniques are defined in table I-F-3.
[b]Placed on an absolute basis using $k(\text{Cl}+n\text{-}C_4H_{10}) = 2.05 \times 10^{-10}$ cm^3 molecule^{-1} s^{-1} (Calvert et al., 2008).
[c]Placed on an absolute basis using $k(\text{Cl}+cyclo\text{-}C_6H_{12}) = 3.3 \times 10^{-10}$ cm^3 molecule^{-1} s^{-1} (Calvert et al., 2008).
[d]Placed on an absolute basis using $k(\text{Cl}+C_2H_6) = 5.9 \times 10^{-11}$ cm^3 molecule^{-1} s^{-1} (Calvert et al., 2008).

III-B-3.4. O(^{3}P) Reaction Kinetics

The most recent measurement of the rate coefficient for reaction of O(^{3}P) with diethyl ether is that of Buchta et al. (1991), who report: $k = 2.66 \times 10^{-11} \exp(-1{,}530/T)$ cm^3 molecule^{-1} s^{-1} for $298 < T < 873$ K, with $k = 1.6 \times 10^{-13}$ cm^3 molecule^{-1} s^{-1} at 298 K. These data are considerably lower than those reported by Liu et al. (1990a), $k = 1.42 \times 10^{-11} \exp(-1{,}070/T)$ cm^3 molecule^{-1} s^{-1} for $240 < T < 440$ K, with $k = 3.9 \times 10^{-13}$ cm^3 molecule^{-1} s^{-1} at 298 K. No recommendation is made.

III-B-3.5. Summary of the Atmospheric Fate of Diethyl Ether, and the End Products of Its Oxidation

The atmospheric destruction of DEE will be controlled mainly via its reaction with OH, with an estimated lifetime of about 8 h (for daytime [OH] $\approx 2.5 \times 10^6$ molecule cm^{-3}). Reaction with NO_3 and Cl-atoms may also play a role in specific circumstances (e.g., reaction with NO_3 at night, and reaction with Cl in certain urban locations, particularly in the early morning). For example, a lifetime of about 1 day is estimated for reaction with NO_3 for highly polluted conditions, $[NO_3] = 3 \times 10^9$ molecule cm^{-3}.

The products of the oxidation of DEE have been studied in detail by Wallington and Japar (1991), Eberhard et al. (1993), Cheema et al. (1999), and Orlando (2007), both in the presence and absence of NO_x, over a range of temperatures and using either Cl or OH to initiate the chemistry. The major products identified in these studies are ethyl formate, ethyl acetate, formaldehyde and acetaldehyde, with ethyl formate being the dominant product under most experimental conditions.

Reaction of OH with DEE occurs predominantly at the CH_2 groups, and all observed products result from subsequent chemistry of the resulting peroxy radical:

$$\text{OH} + \text{C}_2\text{H}_5\text{OCH}_2\text{CH}_3(+\text{O}_2) \rightarrow \text{C}_2\text{H}_5\text{OCH(OO•)CH}_3$$

Orlando (2007) showed that reaction of the peroxy with NO results in the formation, in part, of chemically activated alkoxy radicals,

$$\text{C}_2\text{H}_5\text{OCH(OO•)CH}_3 + \text{NO} \rightarrow [\text{C}_2\text{H}_5\text{OCH(O•)CH}_3]^* + \text{NO}_2$$

which eliminate CH_3 (with a yield of $\approx 40\%$) and H-atoms (with a yield of $\approx 10-15\%$).

$$[C_2H_5OCH(O\bullet)CH_3]^* \rightarrow CH_3CH_2OCH(=O) + \bullet CH_3$$

$$[C_2H_5OCH(O\bullet)CH_3]^* \rightarrow CH_3CH_2OC(=O)CH_3 + H\bullet$$

$$\bullet CH_3 \rightarrow\rightarrow\rightarrow CH_2O$$

The remainder of the product alkoxy radicals are thermalized by collisions and then either decompose via $\bullet CH_3$ elimination, or react with O_2:

$$CH_3CH_2OCH(O\bullet)CH_3 \rightarrow CH_3CH_2OCH(=O) + \bullet CH_3 \quad (1)$$

$$CH_3CH_2OCH(O\bullet)CH_3 + O_2 \rightarrow CH_3CH_2OC(=O)CH_3 + HO_2 \quad (2)$$

with $k_1/k_2 = 6.9 \times 10^{24} \exp(-3{,}130/T)$ molecule cm^{-3}. Data from Eberhard et al. (1993) and Cheema et al. (1999) indicate a minor occurrence of C—O bond rupture as well (yield $\approx$ 5–10%), resulting in acetaldehyde formation:

$$CH_3CH_2OCH(O\bullet)CH_3 \rightarrow CH_3CH_2O\bullet + CH_3CHO$$

$$CH_3CH_2O\bullet + O_2 \rightarrow CH_3CHO + HO_2$$

In summary, at 298 K in an urban environment (i.e., in the presence of NO_x), product yields from the OH-initiated oxidation of DEE are as follows: ethyl formate and formaldehyde, $\sim$80%; ethyl acetate, $10 - 15\%$; acetaldehyde, $\sim$15%. Yields of ethyl acetate will increase at the expense of the other products as temperature is decreased.

III-B-4. Methyl *n*-Butyl Ether ($CH_3OCH_2CH_2CH_2CH_3$)

III-B-4.1. OH Reaction Kinetics

The reaction of OH with methyl *n*-butyl ether has been the subject of three studies (Wallington et al., 1988c; Wallington et al., 1989a; Semadeni et al., 1993); data are summarized in table III-B-10 and in figure III-B-4. The data are in reasonable agreement, with each room temperature measurement falling within 20% of the mean. A fit of the entire dataset to the Arrhenius expression yields $k = 1.01 \times 10^{-11} \exp(107/T)$ cm^3 molecule^{-1} s^{-1} with $k = 1.4 \times 10^{-11}$ cm^3 molecule^{-1} s^{-1} at 298 K. An uncertainty of $\pm$25% is assigned at 298 K.

III-B-4.2. NO_3 Reaction Kinetics

The reaction of NO_3 with methyl *n*-butyl ether has not been studied. On the basis of structure–activity relationships developed later in this chapter (section III-H), a rate coefficient of $k \approx 2.5 \times 10^{-15}$ cm^3 molecule^{-1} s^{-1} is estimated at 298 K.

Table III-B-10. Rate coefficients ($k = A \times e^{-B/T}$, cm^3 molecule^{-1} s^{-1}) for reaction of OH with methyl *n*-butyl ether [$CH_3O(CH_2)_3CH_3$]

$10^{12} \times A$	B (K)	$10^{11} \times k$	T (K)	Technique[a]	Reference	Temperature Range (K)
		1.64 ± 0.06	298	FP–RF	Wallington et al. (1988d)	
		1.19 ± 0.03	295	RR[b] ($C_2H_5OC_2H_5$)	Wallington et al. (1989a)	
10.7[c]	−100[c]	1.60	247	RR[c] (2,3-dimethylbutane)	Semadeni et al. (1993)	247–353
		1.54	263			
		1.59	298			
		1.47	313			
		1.39	353			

[a]Abbreviations used for the techniques are defined in table I-F-3.
[b]Placed on an absolute basis using $k(OH+C_2H_5OC_2H_5) = 1.24 \times 10^{-12}$ cm^3 molecule^{-1} s^{-1} (this book, section III-B-3.1).
[c]Values obtained from least-squares fit of data obtained using updated reference rate coefficients, and thus differ from those originally reported.
[d]Placed on an absolute basis using $k(OH+2,3\text{-dimethylbutane}) = 1.25 \times 10^{-11} \exp(-212/T)$ cm^3 molecule^{-1} s^{-1} (Calvert et al., 2008).

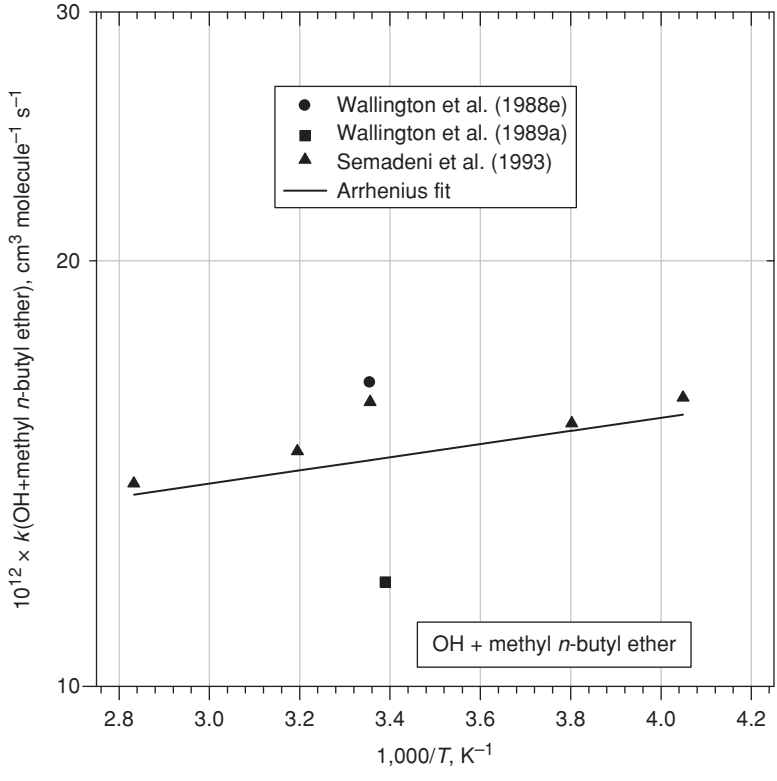

Figure III-B-4. Arrhenius plot of the rate coefficient for the reaction of OH with methyl *n*-butyl ether.

III-B-4.3. Summary of the Atmospheric Fate of Methyl n-Butyl Ether, and the End Products of Its Oxidation

The atmospheric destruction of methyl *n*-butyl ether will occur primarily via reaction with OH, with NO_3 and Cl-atoms potentially playing a role. The lifetime against OH attack is estimated to be about 8 h, for a daytime [OH] $\approx 2.5 \times 10^6$ molecule cm^{-3}.

The OH-initiated oxidation of methyl *n*-butyl ether has been studied in detail by Aschmann and Atkinson (1999a). Observed products, with molar yields in parentheses, were as follows: methyl formate (51 ± 11%), propanal (43 ± 6%), butanal (4.5 ± 1%), methyl butyrate (∼1.6%), and $CH_3C(O)CH_2CH_2OCH_3$ and/or $CH_3CH_2C(O)CH_2OCH_3$ (19 ± 4%). Products with molecular weights of 118, 149, and 165, corresponding to five-carbon hydroxycarbonyls, nitrates, and hydroxynitrates, were also identified.

The major site of attack is at the —CH_2O— group, leading to the formation of the $CH_3CH_2CH_2CH(O\bullet)OCH_3$ radical, whose subsequent decomposition yields methyl formate and propanal, the two major products identified. The minor product, methyl butyrate [$CH_3CH_2CH_2C(O)OCH_3$], also results from reaction at this site, possibly via reaction of the $CH_3CH_2CH_2CH(O\bullet)OCH_3$ radical with O_2, but more likely via elimination of a hydrogen atom from the chemically activated alkoxy radical. The 19 ± 4% combined yield of $CH_3C(O)CH_2CH_2OCH_3$ and/or $CH_3CH_2C(O)CH_2OCH_3$ is consistent with attack of OH at the other —CH_2— groups on the *n*-butyl chain, followed by reaction of the relevant alkoxy radical with O_2. However, the theoretical studies of Ferenac et al. (2003) point to the likelihood of isomerization as an important fate for the $CH_3CH_2CH(O\bullet)CH_2OCH_3$ radical, a process that would likely generate a hydroxycarbonyl species of MW 118, $HOCH_2OCH_2C(O)CH_2CH_3$. Reaction of OH at the —OCH_3 group in methyl *n*-butyl ether will lead predominantly to *n*-butyl formate, although this species was not observed in the Aschmann and Atkinson (1999a) study.

III-B-5. Methyl *tert*-Butyl Ether [$CH_3OC(CH_3)_3$]

III-B-5.1. OH Reaction Kinetics

The reaction of OH with methyl *tert*-butyl ether (MTBE) has been studied over the temperature range 230–753 K using both direct and relative rate methods (Cox and Goldstone, 1982; Wallington et al., 1988c; Wallington et al., 1989a; Bennett and Kerr, 1990; Smith et al., 1991b; Téton et al., 1996; Arif et al., 1997; Picquet et al., 1998; Tranter and Walker, 2001; Bonard et al., 2002).

As summarized in table III-B-11 and in figure III-B-5, there is general accord between all measurements. The rate coefficient shows a weak positive temperature dependence at atmospheric temperatures, with significant curvature evident in the Arrhenius plot at higher temperatures. A fit of all data obtained at temperatures below 320 K yields the simple Arrhenius expression $k = 4.0 \times 10^{-12} \exp(-80/T)$ cm^3 $molecule^{-1}$ s^{-1}. Elimination of the Cox and Goldstone (1982) data, which are lower than the other data, leads to no significant change in the fitted rate coefficients. The modified Arrhenius expression, $k = 1.22 \times 10^{-17} T^2 \exp(309/T)$ cm^3 $molecule^{-1}$ s^{-1}, obtained using all available data, provides a reasonable fit over the entire temperature

Table III-B-11. Rate coefficients ($k = A \times T^n \times e^{-B/T}$, cm^3 molecule^{-1} s^{-1}) for reaction of OH with methyl *tert*-butyl ether [$CH_3OC(CH_3)_3$]

$10^{12} \times A$	n	B (K)	$10^{12} \times k$	T (K)	Technique[a]	Reference	Temperature Range (K)
			2.6 ± 0.5	295	RR[b] (C_2H_4)	Cox and Goldstone (1982)	
			2.4 ± 0.4	295	RR[c] (n-C_6H_{14})		
5.1 ± 1.6	0	155 ± 100	2.74 ± 0.19	240		Wallington et al. (1988c)	240–440
			3.09 ± 0.15	298			
			3.20 ± 0.26	350			
			3.21 ± 0.25	400			
			3.97 ± 0.36	440			
			3.02 ± 0.07	298	RR[d] (n-C_4H_{10})	Wallington et al. (1989a)	
			(2.52)[e]	298	RR[f] ($C_2H_5OC_2H_5$)		
			2.72	246	RR[f] ($C_2H_5OC_2H_5$)	Bennett and Kerr (1990)	246–314
			2.77	251			
			2.90	275			
			3.16	284			
			3.19	306			
			3.48	314			
			2.78 ± 0.11	298	RR[d] (n-C_4H_{10})	Smith et al. (1991)	
5.03 ± 0.27	0	133 ± 30	2.96 ± 0.14	231	PLP–LIF	Téton et al. (1996)	231–372
			2.95 ± 0.09	240			
			2.98 ± 0.07	250			
$(7.92 \pm 0.40) \times 10^{-5}$	2	-447 ± 32	2.96 ± 0.10	260			
			2.98 ± 0.10	273			
			3.09 ± 0.08	293			
			3.17 ± 0.20	293			
			3.18 ± 0.08	293			
			3.11 ± 0.03	293			
			3.32 ± 0.07	297			
			3.25 ± 0.07	320			
			3.45 ± 0.08	340			
			3.54 ± 0.06	354			
			3.56 ± 0.12	372			
$(1.11 \pm 3.18) \times 10^{-5}$	2.04 ± 0.4	-266 ± 177	2.98 ± 0.11	293	PLP–LIF	Arif et al. (1997)	293–750
			3.65 ± 0.22	330			
			3.92 ± 0.30	350			
			4.30 ± 0.49	380			
			$4.91 \pm .37$	400			
			6.15 ± 0.52	430			
			6.86 ± 0.30	480			
			8.03 ± 0.25	550			
			9.45 ± 0.47	600			
			11.1 ± 0.90	650			
			12.7 ± 0.51	700			
			2.97 ± 0.06	298	RR[g] (n-C_5H_{12})	Picquet et al. (1998)	
			15.4	753	RR[h] (H_2)	Tranter and Walker (2001)	

(*continued*)

Table III-B-11. (*continued*)

$10^{12} \times A$	n	B (K)	$10^{12} \times k$	T (K)	Technique[a]	Reference	Temperature Range (K)
			3.15 ± 0.04	297	PLP–LIF	Bonard et al. (2002)	297–616
			3.01 ± 0.09	297			
			3.08 ± 0.09	297			
			2.96 ± 0.04	298			
			3.13 ± 0.05	316			
			3.71 ± 0.07	367			
			4.47 ± 0.10	433			
			5.26 ± 0.18	498			
			6.40 ± 0.14	566			
			7.27 ± 0.27	616			
			7.34 ± 0.23	616			
			7.42 ± 0.22	616			

[a]Abbreviations used for the techniques are defined in table I-F-3.
[b]Placed on an absolute basis using $k(\mathrm{OH}+\mathrm{C_2H_4}) = 7.9 \times 10^{-12}$ cm^3 molecule^{-1} s^{-1} (Atkinson et al., 2006).
[c]Placed on an absolute basis using $k(\mathrm{OH}+n\text{-}\mathrm{C_6H_{14}}) = 5.48 \times 10^{-12}$ cm^3 molecule^{-1} s^{-1} (Calvert et al., 2008).
[d]Placed on an absolute basis using $k(\mathrm{OH}+n\text{-}\mathrm{C_4H_{10}}) = 2.36 \times 10^{-12}$ cm^3 molecule^{-1} s^{-1} (Calvert et al., 2008).
[e]Value considered less accurate by authors than that measured versus *n*-butane, so not used in analysis.
[f]Placed on an absolute basis using $k(\mathrm{OH}+\mathrm{C_2H_5OC_2H_5}) = 1.15 \times 10^{-17} T^2 \exp(743/T)$ cm^3 molecule^{-1} s^{-1} (this book, section III-B-3.1).
[g]Placed on an absolute basis using $k(\mathrm{OH}+n\text{-}\mathrm{C_5H_{12}}) = 3.92 \times 10^{-12}$ cm^3 molecule^{-1} s^{-1} (Calvert et al., 2008).
[h]Placed on an absolute basis using $k(\mathrm{OH}+\mathrm{H_2}) = 7.86 \times 10^{-13}$ cm^3 molecule^{-1} s^{-1} at 753 K (Tully and Ravishankara, 1980).

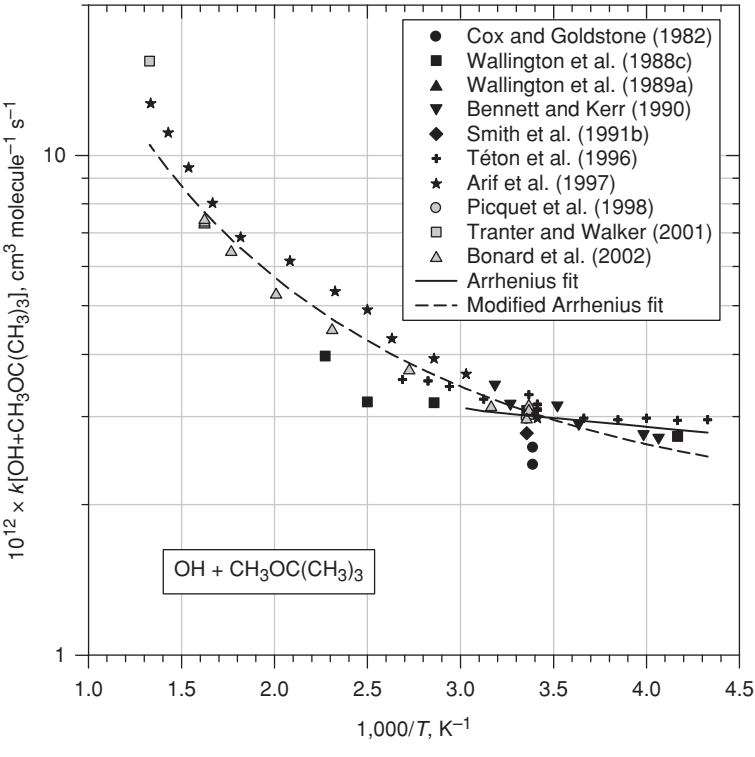

Figure III-B-5. Arrhenius plot of the rate coefficient for the reaction of OH with methyl *tert*-butyl ether.

range studied. For purposes of representing methyl *tert*-buyl ether chemistry in atmospheric models, we recommend the simple Arrhenius expression, $k = 4.0 \times 10^{-12} \exp(-80/T)$ cm^3 molecule^{-1} s^{-1}, which provides a better fit to the data at atmospherically relevant temperatures. This expression gives $k = 3.0 \times 10^{-12}$ cm^3 molecule^{-1} s^{-1} at 298 K with an estimated uncertainty of ±15%.

III-B-5.2. NO_3 Reaction Kinetics

The reaction of NO_3 with MTBE has been studied by Langer and Ljungström (1994a), using both discharge flow–visible absorption, and relative rate approaches. Data are summarized in table III-B-12 and in figure III-B-2. A fit of the simple Arrhenius expression to the combined dataset yields $k(NO_3 + MTBE) = 2.5 \times 10^{-12} \exp(-2{,}435/T)$ cm^3 molecule^{-1} s^{-1} with $k = 7.0 \times 10^{-16}$ cm^3 molecule^{-1} s^{-1} at 298 K. Given the lack of confirming studies, an uncertainty of ±50% is recommended.

III-B-5.3. Cl-Atom Reaction Kinetics

The three measurements of the rate coefficient for reaction of Cl-atoms with MTBE (Wallington et al., 1988g; Langer et al., 1996; Notario et al., 2000b) are in good agreement, see table III-B-13. The average of these three data points, $k = 1.5 \times 10^{-10}$ cm^3 molecule^{-1} s^{-1}, is recommended with an uncertainty of ±15%.

III-B-5.4. Summary of the Atmospheric Fate of Methyl tert-Butyl Ether, and the End Products of Its Oxidation

Loss of MTBE in the atmosphere will occur mainly via its reaction with OH (lifetime of about 4 days, for average [OH] = 10^6 molecule cm^{-3}), while reaction with NO_3 and Cl-atoms will play lesser roles. For example, under polluted nighttime conditions ([NO_3] = 3×10^9 molecule cm^{-3}), a lifetime of about 5.5 days can be estimated.

The products of the OH-initiated oxidation of MTBE have been studied extensively (Cox and Goldstone, 1981; Smith et al., 1991b; Tuazon et al., 1991). Major products,

Table III-B-12. Rate coefficients ($k = A \times e^{-B/T}$, cm^3 molecule^{-1} s^{-1}) for reaction of NO_3 with methyl *tert*-butyl ether

$10^{15} \times A$	B (K)	$10^{15} \times k$	T (K)	Technique[a]	Reference	Temperature Range (K)
		0.57 ± 0.36	295	RR[b](CH_3CHO)	Langer and Ljungström (1994a)	
2,400 ± 290	2,415 ± 199	0.22 ± 0.03	258	DF vis. abs.		258–373
		0.34 ± 0.08	273			
		0.64 ± 0.06	295			
		1.25 ± 0.11	323			
		2.29 ± 0.38	348			
		4.03 ± 0.91	373			

[a]Abbreviations used for the techniques are defined in table I-F-3.
[b]Placed on an absolute basis using $k(NO_3 + CH_3CHO) = 2.3 \times 10^{-15}$ cm^3 molecule^{-1} s^{-1} at 295 K (Calvert et al., 2008).

Table III-B-13. Rate coefficients (k, cm^3 molecule^{-1} s^{-1}) for reaction of Cl with methyl *tert*-butyl ether

$10^{10} \times k$	T (K)	Technique[a]	Reference
1.51 ± 0.11	298	RR[b] (n-C_4H_{10})	Wallington et al. (1988g)
1.5 ± 0.2	295	RR[c] (C_2H_4)	Langer et al. (1996)
1.4 ± 0.2	298	PLP–RF	Notario et al. (2000b)

[a]Abbreviations used for the techniques are defined in table I-F-3.
[b]Placed on an absolute basis using $k(Cl+n\text{-}C_4H_{10}) = 2.05 \times 10^{-10}$ cm^3 molecule^{-1} s^{-1} (Calvert et al., 2008).
[c]Placed on an absolute basis using $k(Cl+C_2H_4) = 0.95 \times 10^{-10}$ cm^3 molecule^{-1} s^{-1} (this book, table I-F-3).

with molar yields in parentheses (average of Smith et al., 1991b and Tuazon et al., 1991), were as follows: *tert*-butyl formate (72 ± 10%), formaldehyde (43 ± 10%), methyl acetate (16 ± 4%), and acetone (∼2–3%). Reaction of OH at the CH_3O-site clearly dominates (∼75% of the reaction), and is the origin of the *tert*-butyl formate product:

$$OH + CH_3OC(CH_3)_3(+O_2) \rightarrow \bullet OOCH_2OC(CH_3)_3$$

$$\bullet OOCH_2OC(CH_3)_3 + NO \rightarrow \bullet OCH_2OC(CH_3)_3 + NO_2$$

$$\bullet OCH_2OC(CH_3)_3 + O_2 \rightarrow O{=}CHOC(CH_3)_3 + HO_2$$

Reaction at the *tert*-butyl sites accounts for the remainder of the OH reaction, and leads predominantly to methyl acetate and two molecules of formaldehyde (see Tuazon et al., 1991, for example).

III-B-6. Di-*n*-Propyl Ether [$(CH_3CH_2CH_2)_2O$]

III-B-6.1. OH Reaction Kinetics

The reaction of OH with di-*n*-propyl ether (DnPE) has been studied between 230 and 440 K, using both direct and relative rate methods (Lloyd et al., 1976; Wallington et al., 1988e; Wallington et al., 1989a; Bennett and Kerr, 1989, 1990; Nelson et al., 1990a; Mellouki et al., 1995; Harry et al., 1999). The data are summarized in table III-B-14 and figure III-B-6, and are in reasonable accord. A fit of the Arrhenius equation to all the data yields $k = 1.03 \times 10^{-11} \times \exp(197/T)$ cm^3 molecule^{-1} s^{-1}, which gives $k = 2.0 \times 10^{-11}$ cm^3 molecule^{-1} s^{-1} at 298 K with an estimated uncertainty of ±15%.

III-B-6.2. NO_3 Reaction Kinetics

The reaction of NO_3 with DnPE has been studied by Langer and Ljungström (1994a) and by Chew et al. (1998). Data are summarized in table III-B-15 and are plotted in figure III-B-7. A fit of the simple Arrhenius expression to the combined dataset yields $k(NO_3 + DnPE) = 3.2 \times 10^{-12} \times \exp(-1{,}868/T)$ cm^3 molecule^{-1} s^{-1} with $k = 6.0 \times 10^{-15}$ cm^3 molecule^{-1} s^{-1} at 298 K. An uncertainty of ±25% is recommended.

Table III-B-14. Rate coefficients ($k = A \times T^n \times e^{-B/T}$, cm^3 molecule^{-1} s^{-1}) for reaction of OH with di-*n*-propyl ether [$(CH_3CH_2CH_2)_2O$]

$10^{12} \times A$	n	B (K)	$10^{12} \times k$	T (K)	Technique[a]	Reference	Temperature Range (K)
			17.7 ± 3.6	305	RR[b](isobutene)	Lloyd et al. (1976)	
11 ± 3	0	−150 ± 80	21.8 ± 2.4	240		Wallington et al. (1988e)	240–440
			18.0 ± 2.2	296			
			16.3 ± 1.8	350			
			15.9 ± 1.0	400			
			16.4 ± 2.0	440			
			18.1 ± 0.7	298	RR ($C_2H_5OC_2H_5$)[c]	Wallington et al. (1989a)	
			15.1 ± 1.6	294	RR[b](isobutene)	Bennett and Kerr (1989)	
			21.3	242	RR ($C_2H_5OC_2H_5$)[c]	Bennett and Kerr (1990)	246–314
			20.1	264			
			20.3	273			
			21.0	283			
			20.8	300			
			21.3	323			
			19.9 ± 1.7	298	PR–UV	Nelson et al. (1990a)	
			18.9 ± 1.7	298	RR[d] (*cyclo*-C_6H_{12})		
(1.84 ± 0.23) × 10^{-5}	2	−767 ± 34	28.0 ± 1.0	230	PLP–LIF	Mellouki et al. (1995)	230–372
			25.8 ± 0.6	240			
			24.7 ± 0.3	249			
			23.1 ± 0.6	262			
			22.3 ± 0.7	273			
			21.8 ± 0.4	298			
			21.3 ± 0.3	298			
			22.0 ± 0.5	299			
			21.6 ± 0.9	314			
			21.2 ± 0.6	325			
			20.8 ± 0.8	345			
			18.6 ± 0.8	359			
			18.2 ± 1.0	372			
			21.8 ± 1.7	296	RR[e] (methyl vinyl ketone)	Harry et al. (1999)	

[a]Abbreviations used for the techniques are defined in table I-F-3.
[b]Placed on an absolute basis using k(OH+isobutene) = 5.2×10^{-11} cm^3 molecule^{-1} s^{-1} (Calvert et al., 2000).
[c]Placed on an absolute basis using k(OH+$C_2H_5OC_2H_5$) = $1.15 \times 10^{-17} T^2 \exp(743/T)$ cm^3 molecule^{-1} s^{-1} (this book, section III-B-3.1).
[d]Placed on an absolute basis using k(OH+*cyclo*-C_6H_{12}) = 6.97×10^{-12} cm^3 molecule^{-1} s^{-1} (Calvert et al., 2008).
[e]Placed on an absolute basis using k(OH+methyl vinyl ketone) = 2.06×10^{-11} cm^3 molecule^{-1} s^{-1} (this book, section V-E-1.1).

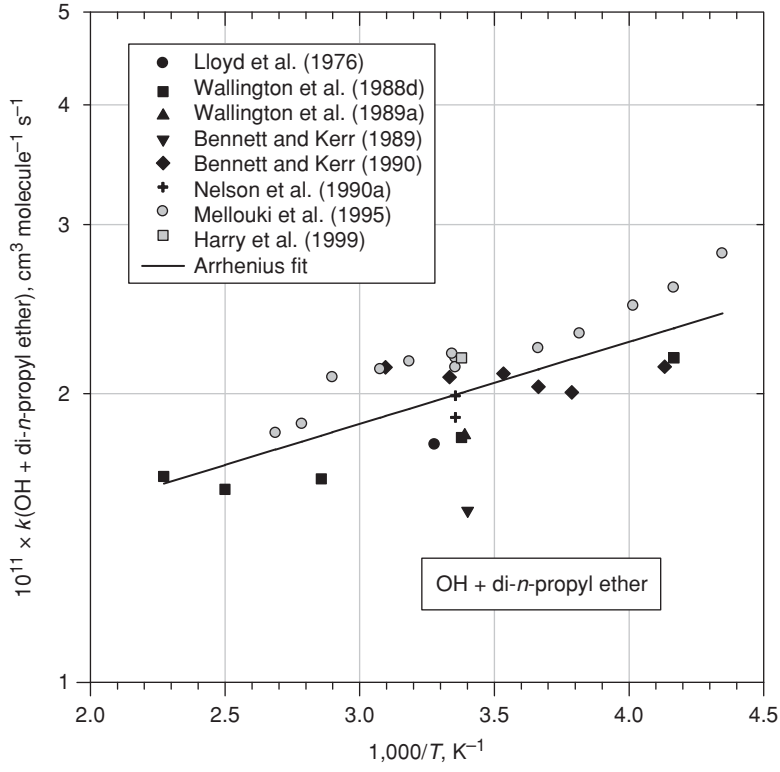

Figure III-B-6. Arrhenius plot of the rate coefficient for the reaction of OH with di-*n*-propyl ether [$(CH_3CH_2CH_2)_2O$].

Table III-B-15. Rate coefficients ($k = A \times e^{-B/T}$ cm^3 molecule^{-1} s^{-1}) for reaction of NO_3 with di-*n*-propyl ether

$10^{15} \times A$	B (K)	$10^{15} \times k$	T (K)	Technique[a]	Reference	Temperature Range (K)
		6.62 ± 2.86	295	RR[b] (1-chloro-2-butene)	Langer and Ljungström (1994a)	258–373
3,300 ± 510	1,870 ± 250	2.39 ± 0.50	258	DF vis. abs.		
		3.41 ± 0.49	273			
		6.49 ± 0.65	295			
		9.59 ± 0.61	323			
		13.86 ± 0.65	348			
		24.37 ± 1.81	373			
		4.9	298	RR[c] (methacrolein)	Chew et al. (1998)	
		5.2	298	RR[d] (diethyl ether)		

[a]Abbreviations used for the techniques are defined in table I-F-3.
[b]Placed on an absolute basis using $k(NO_3$+1-chloro-2-butene$) = 21 \times 10^{-15}$ cm^3 molecule^{-1} s^{-1} (Aird et al., 1992).
[c]Placed on an absolute basis using $k(NO_3$+methacrolein$) = 3.3 \times 10^{-15}$ cm^3 molecule^{-1} s^{-1} (Chew et al., 1998).
[d]Placed on an absolute basis using $k(NO_3$+diethyl ether$) = 3.2 \times 10^{-15}$ cm^3 molecule^{-1} s^{-1} (this book, section III-B-3.2).

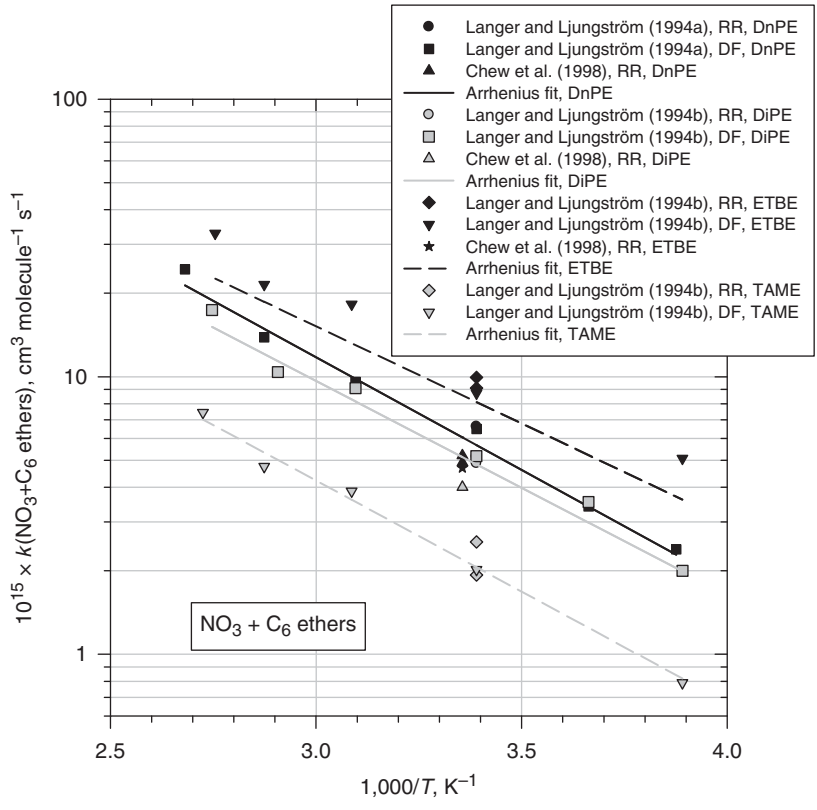

Figure III-B-7. Arrhenius plot of the rate coefficient for the reaction of NO_3 with C_6 ethers (di-*n*-propyl ether, DnPE; di-isopropyl ether, DiPE; ethyl *tert*-butyl ether, ETBE; and *tert*-amyl methyl ether, TAME).

III-B-6.3. Cl-Atom Reaction Kinetics

There are three studies of the reaction of Cl with DnPE available in the literature, all conducted near 298 K (Nelson et al., 1990a; Harry et al., 1999; Notario et al., 2000b). The data are in excellent agreement, see table III-B-16. An unweighted average of the three determinations is recommended: $k = 3.7 \times 10^{-10}$ cm^3 molecule^{-1} s^{-1}, with an uncertainty of $\pm 15\%$.

III-B-6.4. O(^3P) Reaction Kinetics

The reaction has been studied by both Liu et al. (1990a) and Buchta et al. (1991). As was the case with diethyl ether, the data of Buchta et al., $k = 3.32 \times 10^{-11} \exp(-1{,}530/T)$ cm^3 molecule^{-1} s^{-1} for $298 < T < 873$ K, fall considerably below those of Liu et al., $k = 1.41 \times 10^{-11} \exp(-960/T)$ cm^3 molecule^{-1} s^{-1} for $240 < T < 440$ K. No recommendation is made.

Table III-B-16. Rate coefficients (k, cm^3 molecule^{-1} s^{-1}) for reaction of Cl with di-*n*-propyl ether

$10^{10} \times k$	T (K)	Technique[a]	Reference
3.84 ± 0.15	298	RR (*cyclo*-C_6H_{12})[b]	Nelson et al. (1990a)
3.66 ± 0.05	296	RR (*n*-C_8H_{18})[c]	Harry et al. (1999)
3.6 ± 0.4	298	PLP–RF	Notario et al. (2000b)

[a]Abbreviations used for the techniques are defined in table I-F-3.
[b]Placed on an absolute basis using k(Cl+*cyclo*-C_6H_{12}) = 3.3 × 10^{-10} cm^3 molecule^{-1} s^{-1} (Calvert et al., 2008).
[c]Placed on an absolute basis using k(Cl+*n*-C_8H_{18}) = 4.4 × 10^{-10} cm^3 molecule^{-1} s^{-1} (Calvert et al., 2008).

III-B-6.5. Summary of the Atmospheric Fate of Di-n-Propyl Ether, and the End Products of Its Oxidation

Reaction with OH will be the major atmospheric loss process for DnPE. With an assumed daytime [OH] ≈ 2.5 × 10^6 molecule cm^{-3}, the DnPE lifetime will be approximately 6 h. Nighttime loss via reaction with NO_3 could also play a role in DnPE destruction; for nighttime [NO_3] ≈ 3 × 10^9 molecule cm^{-3}, typical of a polluted urban setting, a lifetime of 15 h is estimated. Reaction with Cl-atoms may also be important under certain circumstances.

The mechanism and end products of the reaction of OH with DnPE have been studied by Sempeles and Andino (2000). Reported products, with molar yields in parentheses, were as follows: propyl formate (61±4%), acetaldehyde (60±6%), propanal (15±6%), and propyl propionate (4.3 ± 1.5%). Reaction of OH with DnPE is predicted to occur predominantly (~85–90%) at the CH_2 group adjacent to the O-atom of the ether, and all observed products arise from the ensuing chemistry (Sempeles and Andino, 2000). Decomposition of the resultant alkoxy radical, $CH_3CH_2CH(O\bullet)OC_3H_7$, via C—C bond cleavage yields the major products, propyl formate and acetaldehyde:

$$OH + CH_3CH_2CH_2OC_3H_7(+O_2) \rightarrow CH_3CH_2CH(OO\bullet)OC_3H_7$$

$$CH_3CH_2CH(OO\bullet)OC_3H_{7+}NO \rightarrow CH_3CH_2CH(O\bullet)OC_3H_7 + NO_2$$

$$CH_3CH_2CH(O\bullet)OC_3H_7 \rightarrow CH_3CH_2\bullet + HC(=O)OC_3H_7$$

$$CH_3CH_2\bullet \rightarrow\rightarrow\rightarrow CH_3CHO$$

By analogy to the chemistry of diethyl ether (Orlando, 2007), the minor yield of propyl propionate likely results from H-atom elimination from chemically activated $CH_3CH_2CH(O\bullet)OC_3H_7$ radicals. Formation of two molecules of propanal could result from C—O bond cleavage in $CH_3CH_2CH(O\bullet)OC_3H_7$, although this pathway is not thermodynamically favored.

$$CH_3CH_2CH(O\bullet)OC_3H_7 \rightarrow CH_3CH_2CHO + C_3H_7O\bullet$$

$$C_3H_7O\bullet + O_2 \rightarrow CH_3CH_2CHO + HO_2$$

Sempeles and Andino (2000) suggested that propanal could be a secondary product, resulting from the formation and subsequent oxidation of an organic nitrate, $CH_3CH_2CH(ONO_2)OCH_2CH_2CH_3$:

$$OH + CH_3CH_2CH(ONO_2)OCH_2CH_2CH_3 \rightarrow CH_3CH_2CH(ONO_2)OCH\bullet CH_2CH_3$$

$$CH_3CH_2CH(ONO_2)OCH\bullet CH_2CH_3 \rightarrow NO_2 + 2CH_3CH_2CHO$$

Another possible route to propanal formation is via the isomerization of the $CH_3CH_2CH(OO\bullet)OC_3H_7$ peroxy radical (see Collins et al., 2005, Orlando, 2007), and the discussion below on di-isopropyl ether oxidation]:

$$CH_3CH_2CH(OO\bullet)OC_3H_7 \rightarrow CH_3CH_2CH(OOH)OCH\bullet CH_2CH_3$$

$$\rightarrow OH + 2CH_3CH_2CHO$$

Reaction of OH at the CH_2 group located beta to the ether linkage is likely to result in either $CH_3CH(OH)CH_2OCHO$ or $CH_3C(=O)CH_2OCH(OH)CH_2CH_3$ formation, following the isomerization of the $CH_3CH(O\bullet)CH_2OCH_2CH_2CH_3$ radical (Ferenac et al., 2003).

III-B-7. Di-isopropyl Ether $[(CH_3)_2CH)_2O]$

III-B-7.1. OH Reaction Kinetics

There have been four studies of the reaction of OH with di-isopropyl ether (DiPE), covering the range 230–400 K (Nelson et al., 1990a; McLoughlin et al., 1993; Wallington et al., 1993a; Mellouki et al., 1995). The data are summarized in table III-B-17 and displayed in figure III-B-8.

Although there is general agreement on the magnitude and temperature dependence of the rate coefficient, there is a minor quantitative (≈20–25%) disagreement between the high temperature data of Wallington et al. (1993a) and those of Mellouki et al. (1995). As there is no obvious reason to prefer one dataset over the other, and the differences are rather small, fits were conducted using the combined dataset. Least-squares fitting using a simple Arrhenius expression yields $k(OH + DiPE) = 2.97 \times 10^{-12} \exp(361/T)$ cm^3 molecule^{-1} s^{-1}, with $k = 10.0 \times 10^{-12}$ cm^3 molecule^{-1} s^{-1} at 298 K. An uncertainty of ±15% is assigned to the 298 K value.

III-B-7.2. NO_3 Reaction Kinetics

Langer and Ljungström (1994b) and Chew et al. (1998) have both reported rate coefficients for the reaction of NO_3 with DiPE. As summarized in table III-B-18 and shown in figure III-B-7, there is reasonable agreement between the two datasets. Fitting the simple Arrhenius expression to the combined dataset yields $k(NO_3 + DiPE) = 1.97 \times 10^{-12} \exp(-1{,}772/T)$ cm^3 molecule^{-1} s^{-1}, and $k = 5.1 \times 10^{-15}$ cm^3 molecule^{-1} s^{-1} at 298 K. An uncertainty of ±25% is recommended.

Table III-B-17. Rate coefficients ($k = A \times e^{-B/T}$, cm^3 molecule^{-1} s^{-1}) for reaction of OH with di-isopropyl ether $[(CH_3)_2CH]_2O$

$10^{12} \times A$	B (K)	$10^{12} \times k$	T (K)	Technique[a]	Reference	Temperature Range (K)
		10.7 ± 2.0	298	PR–UV	Nelson et al.	
		10.5 ± 0.7	298	RR[b] (*cyclo*-C_6H_{12})	(1990a)	
		10.0 ± 2.1	300	RR[c] ($C_2H_5OC_2H_5$)	McLoughlin et al. (1993)	
$2.2^{+1.4}_{-0.8}$	−445 ± 115	9.2 ± 0.2	295	RR[b] (*cyclo*-C_6H_{12})	Wallington et al. (1993a)	
		12.9 ± 1.4	240	FP–RF		240–400
		12.4 ± 0.7	270			
		10.6 ± 0.9	296			
		8.67 ± 1.16	330			
		6.51 ± 1.02	365			
		6.98 ± 1.38	400			
4.13 ± 0.10	−274 ± 26	13.5 ± 0.4	230	PLP–LIF	Mellouki et al. (1995)	230–372
		12.8 ± 0.5	240			
		12.6 ± 0.5	253			
		11.5 ± 0.5	263			
		11.6 ± 0.4	273			
		10.4 ± 0.3	293			
		10.2 ± 0.5	298			
		9.4 ± 0.3	320			
		9.0 ± 0.3	340			
		8.9 ± 0.2	360			
		8.8 ± 0.2	372			

[a]Abbreviations used for the techniques are defined in table I-F-3.
[b]Placed on an absolute basis using $k(OH+cyclo\text{-}C_6H_{12}) = 6.97 \times 10^{-12}$ cm^3 molecule^{-1} s^{-1} (Calvert et al., 2008).
[c]Placed on an absolute basis using $k(OH+C_2H_5OC_2H_5) = 1.15 \times 10^{-17} T^2 \exp(743/T)$ cm^3 molecule^{-1} s^{-1} (this book, section III-B-3.1).

III-B-7.3. Cl-Atom Reaction Kinetics

There have been three studies of the reaction of Cl with DiPE, all conducted near 298 K (Nelson et al., 1990a; McLoughlin et al., 1993; Notario et al., 2000b); see table III-B-19. The average from the three studies, $k = 1.66 \times 10^{-10}$ cm^3 molecule^{-1} s^{-1}, is recommended with an estimated uncertainty of ±15%.

III-B-7.4. Summary of the Atmospheric Fate of Di-isopropyl Ether, and the End Products of Its Oxidation

Atmospheric destruction of DiPE will occur mainly via its reaction with OH, with lesser contributions from NO_3 (at night) and Cl-atoms (in certain urban locations, particularly in the morning). With daytime [OH] = 2.5×10^6 molecule cm^{-3}, the DiPE lifetime against OH reaction will be about one-half of a day. The lifetime against nighttime NO_3 reaction will be comparable in polluted urban regions, about 18 h for $[NO_3] \approx 3 \times 10^9$ molecule cm^{-3}.

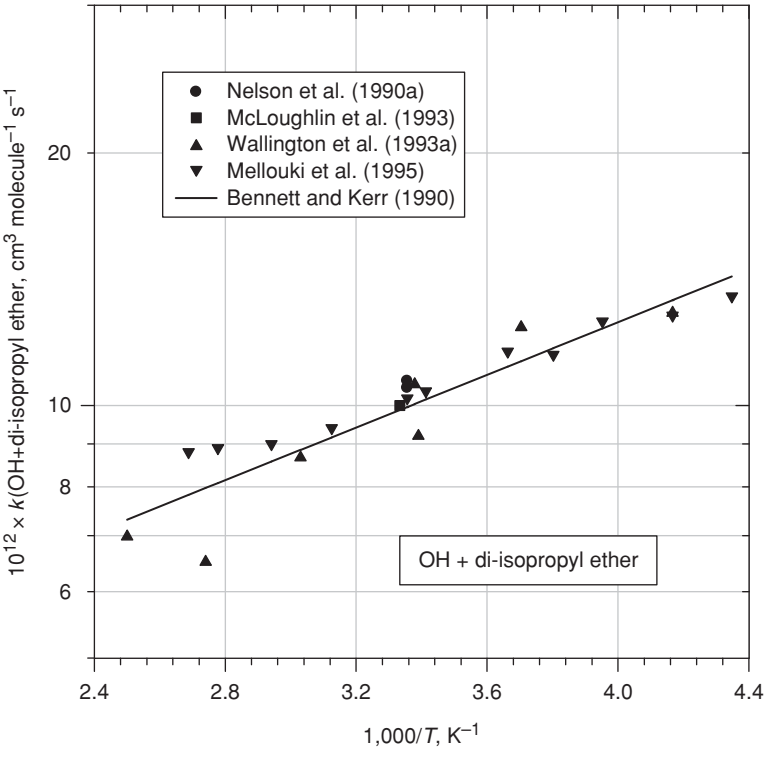

Figure III-B-8. Arrhenius plot of the rate coefficient for the reaction of OH with di-isopropyl ether $[(CH_3)_2CH]_2O$.

Table III-B-18. Rate coefficients ($k = A \times e^{-B/T}$, cm^3 molecule^{-1} s^{-1}) for reaction of NO_3 with di-isopropyl ether

$10^{15} \times A$	B (K)	$10^{15} \times k$	T (K)	Technique[a]	Reference	Temperature Range (K)
		5.15 ± 1.81	295	RR[b] (3-chloro-1-butene)	Langer and Ljungström (1994b)	257–364
		4.88 ± 1.22	295	RR[c] (propene)		
2,020 ± 350	1,759 ± 301	2.00 ± 0.65	257	DF vis. abs.		
		3.54 ± 1.66	273			
		5.18 ± 0.98	295			
		9.10 ± 2.68	323			
		10.41 ± 3.35	344			
		17.39 ± 6.31	364			
		4.0	298	RR[d] (methacrolein)	Chew et al. (1998)	

[a]Abbreviations used for the techniques are defined in table I-F-3.
[b]Placed on an absolute basis using $k(NO_3 + 3\text{-chloro-1-butene}) = 2.8 \times 10^{-15}$ cm^3 molecule^{-1} s^{-1} (Aird et al., 1992).
[c]Placed on an absolute basis using $k(NO_3 + CH_3CH{=}CH_2) = 9.2 \times 10^{-15}$ cm^3 molecule^{-1} s^{-1} at 295 K (Atkinson et al., 2006).
[d]Placed on an absolute basis using $k(NO_3 + \text{methacrolein}) = 3.3 \times 10^{-15}$ cm^3 molecule^{-1} s^{-1} (Chew et al., 1998).

Table III-B-19. Rate coefficients (k, cm^3 molecule^{-1} s^{-1}) for reaction of Cl with di-isopropyl ether

$10^{10} \times k$	T (K)	Technique[a]	Reference
1.60 ± 0.07	298	RR[b] (*cyclo*-C_6H_{12})	Nelson et al. (1990a)
1.79 ± 0.58	300	RR[c] ($C_2H_5OC_2H_5$)	McLoughlin et al. (1993)
1.6 ± 0.2	298	PLP–RF	Notario et al. (2000b)

[a]Abbreviations used for the techniques are defined in table I-F-3.
[b]Placed on an absolute basis using $k(\text{Cl}+\textit{cyclo}\text{-}C_6H_{12}) = 3.3 \times 10^{-10}$ cm^3 molecule^{-1} s^{-1} (Calvert et al., 2008).
[c]Placed on an absolute basis using $k(\text{Cl}+C_2H_5OC_2H_5) = 2.8 \times 10^{-10}$ cm^3 molecule^{-1} s^{-1} (this book, section III-B-3.3).

The products of the reaction of OH with DiPE have been investigated by Wallington et al. (1993a) and by Collins et al. (2005). In the presence of NO_x, Wallington et al. (1993a) observed essentially unity yields of both isopropyl acetate and the sum of formaldehyde, methyl nitrite, and methyl nitrate. Reaction of OH with DiPE is expected to occur mainly at the tertiary >CH—O— sites. For example, Wallington et al. estimate 80% of the reaction occurs at the tertiary site on the basis of kinetic data for related species such as MTBE, while the Kwok and Atkinson estimation method predicts > 98% of the reaction will occur at the tertiary site. As first described by Wallington et al., reaction at the tertiary site can clearly lead to the observed products:

$$\text{OH} + (\textit{iso}\text{-}C_3H_7)_2O(+O_2) \rightarrow \textit{iso}\text{-}C_3H_7OC(OO\bullet)(CH_3)_2 + H_2O$$

$$\textit{iso}\text{-}C_3H_7OC(OO\bullet)(CH_3)_2 + \text{NO} \rightarrow \textit{iso}\text{-}C_3H_7OC(O\bullet)(CH_3)_2 + NO_2$$

$$\textit{iso}\text{-}C_3H_7OC(O\bullet)(CH_3)_2 \rightarrow \textit{iso}\text{-}C_3H_7OC(=O)CH_3 + CH_3\bullet$$

$$CH_3\bullet \rightarrow\rightarrow \text{HCHO}, CH_3ONO, CH_3ONO_2$$

Wallington et al. also noted the possibility of the formation of isopropyl acetate and HCHO from reaction at the tertiary groups, via the following set of reactions:

$$\text{OH} + (\textit{iso}\text{-}C_3H_7)_2O(+O_2) \rightarrow \textit{iso}\text{-}C_3H_7OCH(CH_3)CH_2OO\bullet + H_2O$$

$$\textit{iso}\text{-}C_3H_7OCH(CH_3)CH_2OO\bullet + \text{NO} \rightarrow \textit{iso}\text{-}C_3H_7OCH(CH_3)CH_2O\bullet + NO_2$$

$$\textit{iso}\text{-}C_3H_7OCH(CH_3)CH_2O\bullet(+O_2) \rightarrow \textit{iso}\text{-}C_3H_7OCH(OO\bullet)CH_3 + CH_2O$$

$$\textit{iso}\text{-}C_3H_7OCH(OO\bullet)CH_3 + \text{NO} \rightarrow \textit{iso}\text{-}C_3H_7OCH(O\bullet)CH_3 + NO_2$$

$$\textit{iso}\text{-}C_3H_7OCH(O\bullet)CH_3 + O_2 \rightarrow \textit{iso}\text{-}C_3H_7OC(=O)CH_3 + HO_2$$

However, on the basis of the chemistry of diethyl ether and ethyl *tert*-butyl ether, for example, decomposition of the $\textit{iso}\text{-}C_3H_7OCH(O\bullet)CH_3$ radical will likely dominate over its reaction with O_2, generating isopropyl formate rather than isopropyl acetate:

$$\textit{iso}\text{-}C_3H_7OCH(O\bullet)CH_3 \rightarrow \textit{iso}\text{-}C_3H_7OCH(=O) + CH_3\bullet$$

Thus, it seems likely that the vast majority of the reaction of OH with DiPE occurs at the tertiary sites.

Collins et al. (2005) studied the end products of OH-initiated DiPE oxidation in "traditional" high-NO_x conditions, as well as in low-NO_x and no-NO_x environments. An interesting change in mechanism was noted, characterized by reduced yields of isopropyl acetate and increased yields of acetone and acetic acid in situations where NO_x was absent or very low. They proposed isomerization of thermalized *iso*-$C_3H_7OC(O\bullet)(CH_3)_2$ radicals via a 1,4-H shift as a source of acetone and acetic acid,

$$\textit{iso}\text{-}C_3H_7OC(OO\bullet)(CH_3)_2 + RO_2 \rightarrow \textit{iso}\text{-}C_3H_7OC(O\bullet)(CH_3)_2 + RO\bullet + O_2$$

$$\textit{iso}\text{-}C_3H_7OC(O\bullet)(CH_3)_2 \rightarrow (CH_3)_2C\bullet OC(OH)(CH_3)_2$$

$$(CH_3)_2C\bullet OC(OH)(CH_3)_2 \rightarrow\rightarrow (CH_3)_2C(O\bullet)OC(OH)(CH_3)_2$$

$$(CH_3)_2C(O\bullet)OC(OH)(CH_3)_2 \rightarrow (CH_3)_2C(=O) + CH_3COOH + CH_3$$

$$CH_3 + O_2 \rightarrow\rightarrow CH_2O$$

and decomposition of the hydroperoxide, *iso*-$C_3H_7OC(OOH)(CH_3)_2$ as a source of acetone in the absence of NO_x. Orlando (2007), on the basis of studies of diethyl ether at slightly elevated temperatures, proposed an alternative explanation for the formation of acetone, involving the isomerization of the *iso*-$C_3H_7OC(OO\bullet)(CH_3)_2$ peroxy radical, whose lifetime is considerably longer in the absence of NO_x than in its presence:

$$\textit{iso}\text{-}C_3H_7OC(OO\bullet)(CH_3)_2 \rightarrow (CH_3)_2C\bullet OC(OOH)(CH_3)_2$$

$$(CH_3)_2C\bullet OC(OOH)(CH_3)_2 \rightarrow 2CH_3C(=O)CH_3 + OH$$

Clearly, further study of this system and other branched ethers over a range of conditions of temperature and NO_x concentration are warranted to examine this interesting change in mechanism.

Interestingly, Langer and Ljungström (1994b) have conducted product studies of the NO_3-initiated oxidation of DiPE, and report large yields of both acetone (107%) and isopropyl acetate (31%). The formation of acetone, again in the absence of NO, may offer support for the occurrence of the isomerization of the *iso*-$C_3H_7OC(OO\bullet)(CH_3)_2$ peroxy radical.

III-B-8. Ethyl *n*-Butyl Ether ($CH_3CH_2OCH_2CH_2CH_2CH_3$)

III-B-8.1. OH Reaction Kinetics

There have been seven studies of the reaction of ethyl *n*-butyl ether (EnBE) with OH, covering the range 243–371 K (Wallington et al., 1988d, 1989a; Bennett and Kerr, 1989, 1990; Nelson et al., 1990a; Semadeni et al., 1993; Téton et al., 1996). Data are summarized in table III-B-20, and plotted in figure III-B-9. There are significant quantitative discrepancies evident in this dataset. Measurements near 296 K

Table III-B-20. Rate coefficients ($k = A \times T^n \times e^{-B/T}$, cm^3 molecule^{-1} s^{-1}) for reaction of OH with ethyl *n*-butyl ether [$CH_3CH_2O(CH_2)_3CH_3$]

$10^{12} \times A$	n	B (K)	$10^{12} \times k$	T (K)	Technique[a]	Reference	Temperature Range (K)
			22.8 ± 0.9	298	FP–RF	Wallington et al. (1988d)	
			20.8 ± 0.8	295	RR[b] ($C_2H_5OC_2H_5$)	Wallington et al. (1989a)	
			13.3 ± 0.4	294	RR[c] (isobutene)	Bennett and Kerr (1989)	
			16.9	253	RR[b] ($C_2H_5OC_2H_5$)	Bennett and Kerr (1990)	253–315
			17.0	263			
			16.6	278			
			16.7	294			
			16.9	300			
			17.0	315			
			18.7 ± 0.7	298	PR–UV	Nelson et al. (1990a)	
			22.8	248	RR[d] (2,3-dimethyl butane)	Semadeni et al. (1993)	248–353
			24.2	251			
			25.4	261			
			23.5	273			
			21.8	298			
			20.7	323			
			21.4	353			
6.59 ± 0.66	0	−362 ± 60	30.9 ± 2.2	243	PLP–LIF	Téton et al. (1996)	243–371
			28.5 ± 1.4	253			
			26.7 ± 1.8	262			
(9.01 ± 1.80) $\times 10^{-6}$	2	−994 ± 38	27.2 ± 1.2	268			
			23.2 ± 1.5	271			
			24.1 ± 1.2	283			
			24.8 ± 0.9	283			
			25.4 ± 0.7	283			
			20.8 ± 1.3	294			
			20.7 ± 0.8	311			
			19.4 ± 1.2	326			
			19.3 ± 0.4	341			
			18.9 ± 1.2	357			
			18.1 ± 1.0	371			

[a]Abbreviations used for the techniques are defined in table I-F-3.
[b]Placed on an absolute basis using $k(OH+C_2H_5OC_2H_5) = 1.15 \times 10^{-17} T^2 \exp(743/T)$ cm^3 molecule^{-1} s^{-1} (this book, section III-B-3.1).
[c]Placed on an absolute basis using k(OH+isobutene) $= 5.2 \times 10^{-11}$ cm^3 molecule^{-1} s^{-1} (Calvert et al., 2000).
[d]Placed on an absolute basis using k(OH+2,3-dimethylbutane) $= 1.25 \times 10^{-11} \exp(-212/T)$ cm^3 molecule^{-1} s^{-1} (Calvert et al., 2008).

vary over the range $(1.3 - 2.3) \times 10^{-11}$ cm^3 molecule^{-1} s^{-1}, and similar discrepancies are evident at reduced temperature. Data from Kerr and co-workers (Bennett and Kerr, 1990; Semadeni et al., 1993), updated to reflect current recommendations for the reference rate coefficients (2,3-dimethylbutane and diethyl ether), indicate no significant temperature dependence to k(OH + EnBE) while the direct measurements of Téton et al. (1996) indicate a negative temperature dependence. Note however, that

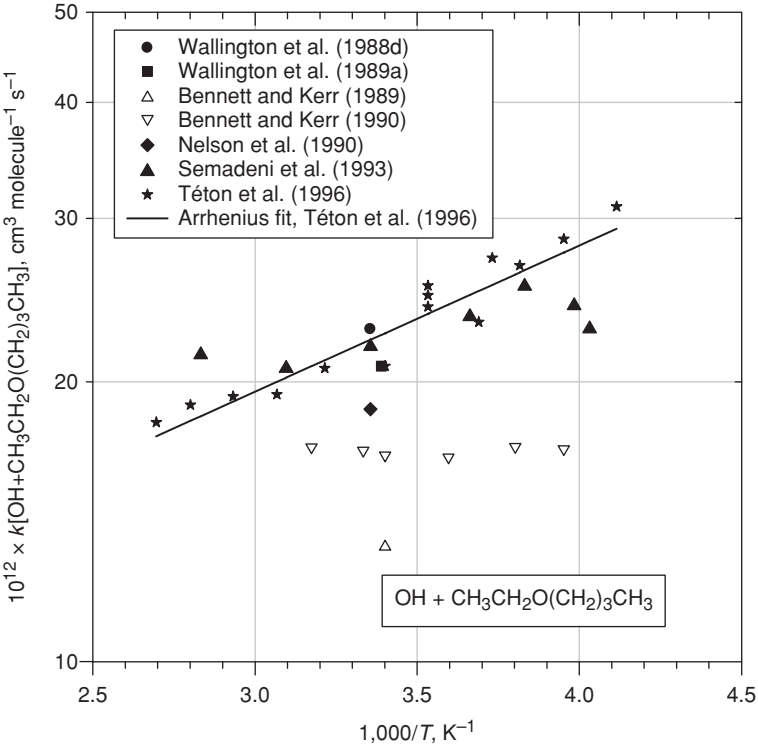

Figure III-B-9. Arrhenius plot of the rate coefficient for the reaction of OH with ethyl *n*-butyl ether.

both Bennett and Kerr (1990) and Semadeni et al. (1993) report negative temperature dependences to k(OH + EnBE), using reference rate coefficient data relevant to the early 1990's.

For atmospheric purposes, the Arrhenius expression derived by Téton et al. (1995) is recommended, $k(\text{OH} + \text{EnBE}) = 6.6 \times 10^{-12} \exp(362/T)$ cm^3 molecule^{-1} s^{-1}, giving $k = 2.2 \times 10^{-11}$ cm^3 molecule^{-1} s^{-1} at 298 K with an estimated uncertainty of ±15%. A fit of the data of Téton et al. (1996), Semadeni et al. (1993), Wallington et al. (1988d, 1989a), and Nelson et al. (1990a) to the simple Arrhenius expression gives $k = 8.6 \times 10^{-12} \exp(279/T)$ cm^3 molecule^{-1} s^{-1}, which yields slightly lower rate coefficients at low temperature (e.g., 8% lower near 240 K).

III-B-8.2. NO_3 Reaction Kinetics

No studies of the reaction of NO_3 with EnBE have been conducted. On the basis of structure–activity estimates provided at the end of this chapter, a value of 4×10^{-15} cm^3 molecule^{-1} s^{-1} can be estimated.

III-B-8.3. Summary of the Atmospheric Fate of Ethyl n-Butyl Ether, and the End Products of Its Oxidation

Atmospheric destruction of ethyl *n*-butyl ether will occur mostly via its reaction with OH, although reaction with NO_3 will also contribute at nighttime, and reaction with Cl-atoms may play an additional role in certain circumstances. For daytime [OH] = 2.5×10^6 molecule cm^{-3}, a lifetime of only about 5 h is estimated. Similarly, combining the estimated NO_3 rate coefficient with nighttime polluted [NO_3] $\approx 3 \times 10^9$ molecule cm^{-3}, a lifetime of 30 h is obtained.

Products of the OH-initiated oxidation of EnBE in the presence of NO_x have been studied by Johnson and Andino (2001). The observed products, with their molar yields in parentheses, were: butyl formate (24.1 ± 0.9%), ethyl formate (21.9 ± 3.3%), acetaldehyde (17.3 ± 1.2%), butanal (7.6 ± 0.4%), butyl acetate (3.2 ± 0.1%), and ethyl butyrate (0.44 ± 0.06%). Note that these products account for only about 45% of the EnBE consumed.

Reaction of OH with EnBE is expected to occur predominantly at the CH_2 groups located adjacent (alpha) to the ether linkage, leading to the production of the corresponding alkoxy radicals, $CH_3CH_2CH_2CH(O\bullet)$—O—CH_2CH_3 and $CH_3CH_2CH_2CH_2OCH(O\bullet)CH_3$ (Johnson and Andino, 2001). The major observed products, butyl and ethyl formate, are produced from C—C bond cleavage in these alkoxy species (Johnson and Andino, 2001):

$$CH_3CH_2CH_2CH(O\bullet)OCH_2CH_3 \rightarrow CH_3CH_2CH_2\bullet + HC(O)OCH_2CH_3$$

$$CH_3(CH_2)_3OCH(O\bullet)CH_3 \rightarrow CH_3(CH_2)_3OCHO + CH_3\bullet$$

Surprisingly, propanal, the expected end product of $CH_3CH_2CH_2\bullet$ radical oxidation and hence the expected co-product of ethyl formate, was not observed. Formaldehyde, the expected co-product of the butyl formate, is not likely detected by the GC–MS method employed by Johnson and Andino, and is also formed in the OH source chemistry.

Butanal and acetaldehyde, both observed in significant quantity, could be obtained from C—O bond cleavage in the same two alkoxy radicals (Johnson and Andino, 2001):

$$CH_3CH_2CH_2CH(O\bullet)—O—CH_2CH_3 \rightarrow CH_3CH_2CH_2CHO + \bullet OCH_2CH_3$$

$$CH_3(CH_2)_3—O—CH(O\bullet)CH_3 \rightarrow CH_3(CH_2)_3O\bullet + CH_3CHO$$

with subsequent chemistry of ethoxy and *n*-butoxy radical leading to additional acetaldehyde and butanal. However, C—O bond rupture is not thermodynamically favored relative to C—C rupture, and the large yields of these aldehydes via this pathway is somewhat surprising. The small yields of butyl acetate and ethyl butyrate result either from reaction of the two alkoxy species with O_2 (Johnson and Andino, 2001), or from direct elimination of an H-atom. Johnson and Andino also suggest that isomerization of the two alkoxy species (via 1,5-H-atom transfers) could be operative, although these pathways would not seem capable of competing with the rapid C—C bond cleavage pathway. Additional multi-functional species would also be expected via reaction of OH at the CH_2 groups located β- and γ- to the ether linkage.

III-B-9. Ethyl *tert*-Butyl Ether [$CH_3CH_2OC(CH_3)_3$]

III-B-9.1. OH Reaction Kinetics

The reaction of OH with ethyl *tert*-butyl ether (ETBE) has been the subject of seven kinetic studies (Wallington et al., 1988d, 1989a; Bennett and Kerr, 1989, 1990; Smith et al., 1992; Téton et al., 1996; Tranter and Walker, 2001). The temperature range covered, 234–372 K, is defined by the study of Téton et al. and the single data point of Tranter and Walker at 753 K. Data are summarized in table III-B-21 and are plotted in figure III-B-10. As was the case for diethyl ether and ethyl *n*-butyl ether, clearly the data of Bennett and Kerr (1989, 1990) fall significantly below the remainder of the dataset. For atmospheric purposes, a least-squares fit of the remaining data obtained at $T < 320$ K to the simple Arrhenius expression yields $k(\mathrm{OH} + \mathrm{ETBE}) = 3.4 \times 10^{-12} \exp(280/T)$ cm^3 molecule^{-1} s^{-1}, giving $k = 8.7 \times 10^{-12}$ cm^3 molecule^{-1} s^{-1} at 298 K with an uncertainty estimated to be ±20%. The modified Arrhenius expression given by Téton et al. (1996), $k(\mathrm{OH} + \mathrm{ETBE}) = 6.7 \times 10^{-18} T^2 \exp(800/T)$ cm^3 molecule^{-1} s^{-1}, provides an excellent fit to the available data for $230 < T < 400$ K. Corroborative studies of the temperature dependence of this rate coefficient are warranted.

III-B-9.2. NO_3 Reaction Kinetics

Langer and Ljungström (1994b) and Chew et al. (1998) have both reported rate coefficients for the reaction of NO_3 with ETBE, see table III-B-22. Data from Langer and Ljungström (1994b), using both a relative rate method and a discharge flow tube method, yield rate coefficients near 298 K that are approximately a factor of 2 higher than the relative rate measurement of Chew et al. (1998). This discrepancy is rather surprising, given the generally good agreement between these two groups on other reactions of ethers with NO_3. As there is no obvious reason to prefer either study, an average value of $k = 8.1 \times 10^{-15}$ cm^3 molecule^{-1} s^{-1} is adopted at 295 K. Combining this value with the activation energy determined in the discharge flow study by Langer and Ljungström yields: $k(\mathrm{NO_3} + \mathrm{ETBE}) = 1.92 \times 10^{-12} \exp(-1{,}613/T)$ cm^3 molecule^{-1} s^{-1}. Given the discrepancies noted above, an uncertainty of ±60% is recommended at 295 K.

III-B-9.3. Cl-Atom Reaction Kinetics

The only measurement of the rate coefficient for reaction of Cl with ETBE is that of Notario et al. (2000b), obtained via pulsed laser photolysis–resonance fluorescence, see table III-B-23. Their value of $k = 1.5 \times 10^{-10}$ cm^3 molecule^{-1} s^{-1}, is recommended, with an estimated uncertainty of ±20%.

III-B-9.4. $O(^3P)$ Reaction Kinetics

Liu et al. (1990a) have studied this reaction at 298 K using the flash photolysis–resonance fluorescence technique, and reported $k = 3.7 \times 10^{-13}$ cm^3 molecule^{-1} s^{-1}.

Table III-B-21. Rate coefficients ($k = A \times T^n \times e^{-B/T}$, cm^3 molecule^{-1} s^{-1}) for reaction of OH with ethyl *tert*-butyl ether [$CH_3CH_2OC(CH_3)_3$]

$10^{12} \times A$	n	B (K)	$10^{12} \times k$	T (K)	Technique[a]	Reference	Temperature Range (K)
			8.12 ± 0.32	298	FP–RF	Wallington et al. (1988d)	
			8.11± 0.24	295	RR[b] ($C_2H_5OC_2H_5$)	Wallington et al. (1989a)	
			5.5 ± 0.5	294	RR[c] (isobutene)	Bennett and Kerr (1989)	
			5.61	253	RR[b]	Bennett and	253–325
			5.47	273	($C_2H_5OC_2H_5$)	Kerr (1990)	
			5.41	293			
			5.53	302			
			5.74	325			
			9.56 ± 0.32		RR[d] (n-C_6H_{14})	Smith et al. (1992)	
4.40 ± 0.24	0	−210 ± 37	11.4 ± 0.6	234	PLP–LIF	Téton et al.	234–372
			10.4 ± 1.1	242		(1996)	
(6.70 ± 0.10)	2	−800 ± 44	10.5 ± 0.4	249			
$\times 10^{-6}$			10.0 ± 0.6	256			
			9.7 ± 0.5	263			
			9.6 ± 0.3	272			
			9.1 ± 0.3	283			
			8.6 ± 0.4	291			
			9.0 ± 0.6	291			
			8.8 ± 0.2	292			
			8.8 ± 0.6	292			
			8.6 ± 0.4	304			
			8.4 ± 0.1	313			
			8.3 ± 0.2	323			
			8.3 ± 0.2	333			
			8.3 ± 0.3	343			
			8.2 ± 0.3	363			
			8.0 ± 0.3	372			
			22.4 ± 4.0	753	RR (H_2)	Tranter and Walker (2001)	

[a]Abbreviations used for the techniques are defined in table I-F-3.
[b]Placed on an absolute basis using $k(\text{OH}+C_2H_5OC_2H_5) = 1.15 \times 10^{-17} T^2 \exp(743/T)$ cm^3 molecule^{-1} s^{-1} (this book, section III-B-3.1).
[c]Placed on an absolute basis using $k(\text{OH}+\text{isobutene}) = 5.2 \times 10^{-11}$ cm^3 molecule^{-1} s^{-1} (Calvert et al., 2000).
[d]Placed on an absolute basis using $k(\text{OH}+n\text{-}C_6H_{14}) = 5.48 \times 10^{-12}$ cm^3 molecule^{-1} s^{-1} (Calvert et al., 2008).
[e]Placed on an absolute basis using $k(\text{OH}+H_2) = 7.86 \times 10^{-13}$ cm^3 molecule^{-1} s^{-1} at 753 K (Tully and Ravishankara, 1980).

III-B-9.5. Summary of the Atmospheric Fate of Ethyl tert-Butyl Ether, and the End Products of Its Oxidation

Atmospheric destruction of ETBE will be controlled during the daytime via its reaction with OH. For [OH] $\approx 2.5 \times 10^6$ molecule cm^{-3}, a lifetime of 12 h is obtained. A similar lifetime against reaction with NO_3 is obtained for an estimated [NO_3] $= 3 \times 10^9$ molecule cm^{-3}, typical of polluted urban settings.

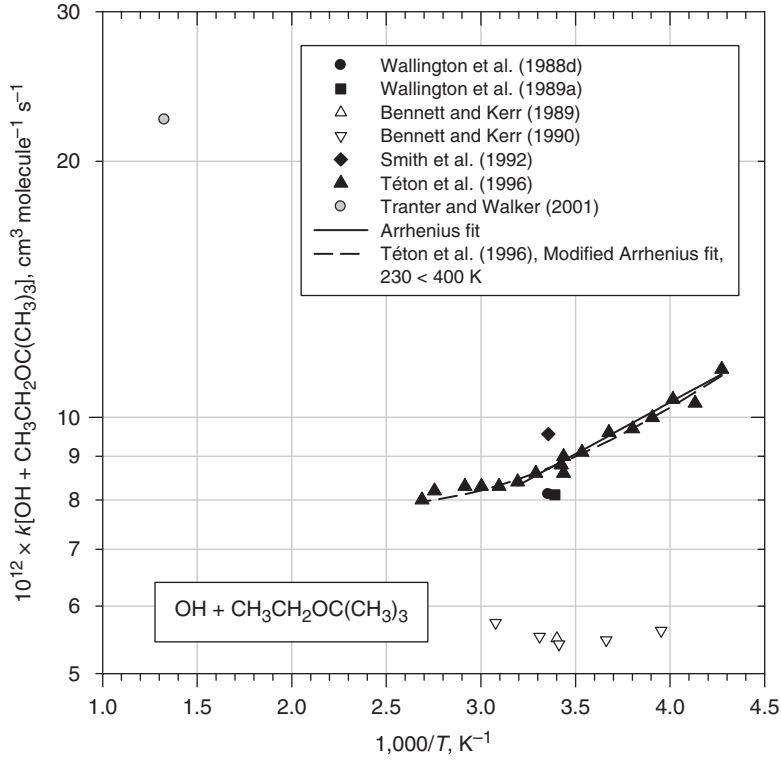

Figure III-B-10. Arrhenius plot of the rate coefficient for the reaction of OH with ethyl *tert*-butyl ether.

Table III-B-22. Rate coefficients ($k = A \times e^{-B/T}$, cm^3 $molecule^{-1}$ s^{-1}) for reaction of NO_3 with ethyl *tert*-butyl ether

$10^{15} \times A$	B (K)	$10^{15} \times k$	T (K)	Technique[a]	Reference	Temperature Range (K)
		9.94 ± 3.27	295	RR[b] (3-chloro-1-butene)	Langer and Ljungström (1994)	
		9.11 ± 2.54	295	RR[c] (propene)		
2,020 ± 350	1,759 ± 301	5.08 ± 2.82	257	DF vis. abs.		257–363
		8.71 ± 2.26	295			
		18.24 ± 2.26	324			
		21.50 ± 6.57	348			
		32.87 ± 3.11	363			
		4.7 ± 1.5	298	RR[d] ($C_2H_5OC_2H_5$)	Chew et al. (1998)	

[a]Abbreviations used for the techniques are defined in table I-F-3.
[b]Placed on an absolute basis using $k(NO_3 + 3\text{-chloro-1-butene}) = 2.8 \times 10^{-15}$ cm^3 $molecule^{-1}$ s^{-1} (Aird et al., 1992).
[c]Placed on an absolute basis using $k(NO_3 + CH_3CH{=}CH_2) = 9.2 \times 10^{-15}$ cm^3 $molecule^{-1}$ s^{-1} at 295 K (Atkinson et al., 2006).
[d]Placed on an absolute basis using $k(NO_3 + C_2H_5OC_2H_5) = 3.2 \times 10^{-15}$ cm^3 $molecule^{-1}$ s^{-1} (this book, section III-B-3.2).

Table III-B-23. Rate coefficients (k, cm^3 molecule^{-1} s^{-1}) for reaction of Cl with ethyl *tert*-butyl ether

$10^{10} \times k$	T (K)	Technique[a]	Reference
1.5 ± 0.2	298	PLP–RF	Notario et al. (2000b)

[a]Abbreviations used for the techniques are defined in table I-F-3.

The products of the reaction of OH with ETBE in the presence of NO_x have been investigated by Wallington and Japar (1991) and Smith et al. (1992). The major product observed in both studies was *tert*-butyl formate, with yields of 76 ± 6% and 64 ± 3% reported, respectively. Smith et al. (1992) also observed formaldehyde (molar yield 53 ± 4%), *tert*-butyl acetate (13 ± 1%), ethyl acetate (4.3 ± 0.3%), acetaldehyde (16 ± 1%), and acetone (1.9 ± 0.2%).

Production of *tert*-butyl formate occurs via decomposition of the alkoxy radical, *tert*-$C_4H_9OCH(O\bullet)CH_3$, formed following OH attack at the CH_2 group in ETBE, while *tert*-butyl acetate is obtained from reaction of this radical with O_2, and acetaldehyde can be formed from its decomposition via C—O bond cleavage:

$$OH + \textit{tert}\text{-}C_4H_9OCH_2CH_3(+O_2) \rightarrow \textit{tert}\text{-}C_4H_9OCH(OO\bullet)CH_3 + H_2O$$

$$\textit{tert}\text{-}C_4H_9OCH(OO\bullet)CH_3 + NO \rightarrow \textit{tert}\text{-}C_4H_9OCH(O\bullet)CH_3 + NO_2$$

$$\textit{tert}\text{-}C_4H_9OCH(O\bullet)CH_3 \rightarrow \textit{tert}\text{-}C_4H_9OCH{=}O + CH_3$$

$$\textit{tert}\text{-}C_4H_9OCH(O\bullet)CH_3 + O_2 \rightarrow \textit{tert}\text{-}C_4H_9OC(=O)CH_3 + HO_2$$

$$\textit{tert}\text{-}C_4H_9OCH(O\bullet)CH_3 \rightarrow \textit{tert}\text{-}C_4H_9O\bullet + CH_3CHO$$

The occurrence of C—O bond cleavage is not generally thermodynamically favorable, however, and alternative routes to acetaldehyde may exist. Ethyl acetate is an expected product of the chemistry occurring pursuant to OH abstraction from the *tert*-butyl group (Smith et al., 1992).

Langer and Ljungström (1994b) showed that the vast majority of the reaction of NO_3 with ETBE occurs at the CH_2 group, leading to large yields of *tert*-butyl formate (71%) and *tert*-butyl acetate (25%). Reactions involved are entirely analogous to those seen in the OH-initiated oxidation.

III-B-10. Methyl *tert*-Amyl Ether [$CH_3OC(CH_3)_2CH_2CH_3$]

III-B-10.1. OH Reaction Kinetics

The reaction of OH with methyl *tert*-amyl ether (TAME) has been the subject of four studies (Wallington et al., 1988d, 1993c; Smith et al., 1995; Téton et al,. 1996), see table III-B-24 and figure III-B-11. The original measurement by Wallington et al. (1988d) is higher than the remainder of the data, likely due to a reactive impurity in the sample used (Wallington et al., 1993c), and is not considered in the analyses

Table III-B-24. Rate coefficients ($k = A \times T^n \times e^{-B/T}$, cm^3 molecule^{-1} s^{-1}) for reaction of OH with methyl *tert*-amyl ether [$CH_3OC(CH_3)_2CH_2CH_3$]

$10^{12} \times A$	n	B (K)	$10^{12} \times k$	T (K)	Technique[a]	Reference	Temperature Range (K)
			7.91 ± 0.42	298	FP–RF	Wallington et al. (1988d)	
			5.5 ± 0.3	295	RR[b](ETBE)	Wallington et al. (1993c)	240–400
			5.0 ± 0.2	295	RR[c] (*cyclo*-C_6H_{12})		
			5.2 ± 0.4	295	RR[d] (DIPE)		
			5.12 ± 0.48	240	FP–RF		
			5.76 ± 0.43	270			
			5.68 ± 0.36	296			
			5.66 ± 0.38	330			
			5.45 ± 0.48	365			
			5.85 ± 0.62	400			
			5.49 ± 0.07	298	RR[e] (*n*-C_6H_{14})	Smith et al. (1995)	
			4.86 ± 0.05	298	RR[f] (*n*-C_7H_{16})		
			5.03 ± 0.09	298	RR[b] (ETBE)		
4.7 ± 0.7	0	-82 ± 85	7.31 ± 0.32	231	PLP–LIF	Téton et al. (1996)	231–372
			6.86 ± 0.32	240			
$(7.56 \pm 0.56) \times 10^{-6}$	2	-656 ± 44	6.53 ± 0.24	253			
			6.19 ± 0.42	262			
			6.05 ± 0.14	272			
			5.99 ± 0.22	297			
			5.89 ± 0.26	297			
			6.28 ± 0.14	298			
			6.10 ± 0.34	298			
			5.78 ± 0.42	298			
			5.51 ± 0.24	312			
			5.61 ± 0.18	328			
			6.21 ± 0.20	343			
			6.20 ± 0.32	359			
			6.43 ± 0.22	372			

[a]Abbreviations used for the techniques are defined in table I-F-3.
[b]Placed on an absolute basis using k[OH+$C_2H_5OC(CH_3)_3$, ETBE] = 8.8×10^{-12} cm^3 molecule^{-1} s^{-1} (this book, section III-B-9.1).
[c]Placed on an absolute basis using k(OH+*cyclo*-C_6H_{12}) = 6.97×10^{-12} cm^3 molecule^{-1} s^{-1} (Calvert et al., 2008).
[d]Placed on an absolute basis using k[OH+$(CH_3)_2CHOCH(CH_3)_2$, DIPE] = 1.00×10^{-11} cm^3 molecule^{-1} s^{-1} (this book, section III-B-7.1).
[e]Placed on an absolute basis using k(OH+*n*-C_6H_{14}) = 5.48×10^{-12} cm^3 molecule^{-1} s^{-1} (Calvert et al., 2008).
[f]Placed on an absolute basis using k(OH+*n*-C_7H_{16}) = 6.5×10^{-12} cm^3 molecule^{-1} s^{-1} (Calvert et al., 2008).

discussed below. The remainder of the data is in reasonable accord, although the measurements of Wallington et al. (1993c) and Téton et al. (1996) diverge at low temperature, with those of Wallington et al. showing a positive temperature dependence and those of Téton et al. a negative temperature dependence. An unweighted average of the data obtained between 295 and 298 K gives $k = 5.6 \times 10^{-12}$ cm^3 molecule^{-1} s^{-1}, a value which is adopted here with an estimated uncertainty of ±15%. A fit to all data obtained below 300 K gives $k = 3.07 \times 10^{-12} \exp(172/T)$ cm^3 molecule^{-1} s^{-1}. Further studies of this rate coefficient, particularly below 298 K, are required.

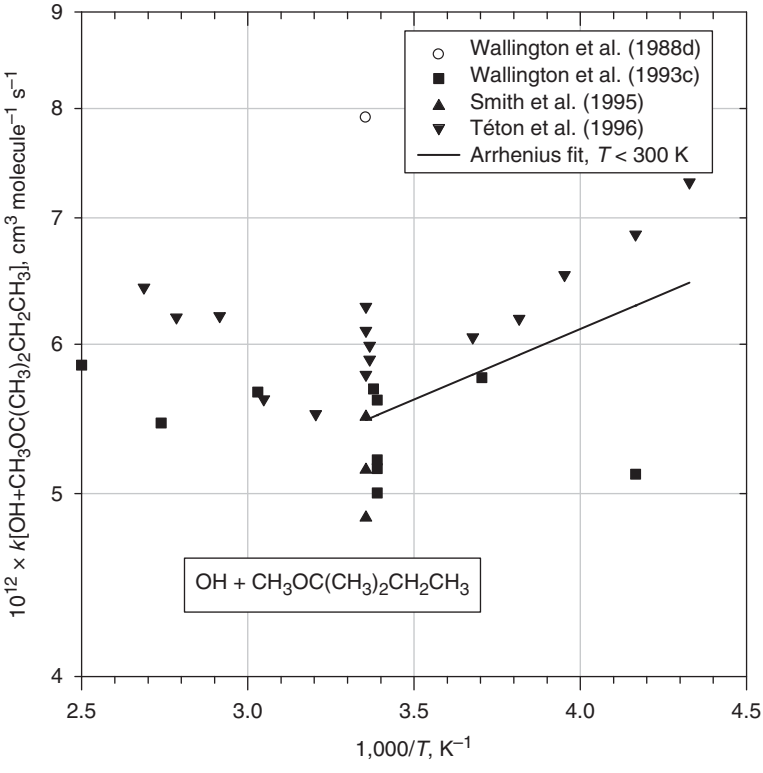

Figure III-B-11. Arrhenius plot of the rate coefficient for the reaction of OH with *tert*-amyl methyl ether.

III-B-10.2. NO_3 Reaction Kinetics

Langer and Ljungström (1994b) have studied this reaction using both relative rate and discharge flow methodologies. A fit to all of their data gives $k(NO_3 + \text{TAME}) = 1.06 \times 10^{-12} \exp(-1{,}843/T)$ cm^3 molecule^{-1} s^{-1}, with $k = 2.2 \times 10^{-15}$ cm^3 molecule^{-1} s^{-1} at 298 K. The data are summarized in table III-B-25.

III-B-10.3. $O(^3P)$ Reaction Kinetics

Liu et al. (1990a) obtained a value of 5.7×10^{-13} cm^3 molecule^{-1} s^{-1} for this rate coefficient at 298 K, using a flash photolysis–resonance fluorescence technique.

III-B-10.4. Summary of the Atmospheric Fate of Methyl tert-Amyl Ether, and the End Products of Its Oxidation

Reaction with OH will represent the major atmospheric loss process for TAME, with contributions from reaction with NO_3 and Cl-atoms also expected under certain circumstances. The lifetime against OH reaction is estimated to be 20 h for typical daytime

Table III-B-25. Rate coefficients ($k = A \times e^{-B/T}$, cm^3 molecule^{-1} s^{-1}) for reaction of NO_3 with methyl *tert*-amyl ether

$10^{15} \times A$	B (K)	$10^{15} \times k$	T (K)	Technique[a]	Reference	Temperature Range (K)
		2.54 ± 1.03	295	RR[b] (3-chloro-1-butene)	Langer and Ljungström (1994b)	257–367
		1.93 ± 0.52	295	RR[c] (propene)		
1,210 ± 220	1,874 ± 304	0.79 ± 0.27	257	DF vis. abs.		257–367
		2.02 ± 0.49	295			
		3.87 ± 1.08	324			
		4.74 ± 1.44	348			
		7.43 ± 2.16	367			

[a]Abbreviations used for the techniques are defined in table I-F-3.
[b]Placed on an absolute basis using $k(NO_3 + 3\text{-chloro-1-butene}) = 2.8 \times 10^{-15}$ cm^3 molecule^{-1} s^{-1} (Aird et al., 1992).
[c]Placed on an absolute basis using $k(NO_3 + CH_3CH{=}CH_2) = 9.2 \times 10^{-15}$ cm^3 molecule^{-1} s^{-1} (Calvert et al., 2000).

[OH] $\approx 2.5 \times 10^6$ molecule cm^{-3}. For an estimated nighttime [NO_3] $\approx 3 \times 10^9$ molecule cm^{-3}, typical of polluted urban settings, a 40 h lifetime is obtained.

The products of the OH-initiated oxidation of TAME in the presence of NO_x have been measured by Smith et al. (1995). The products observed, with their molar yields in parentheses, are as follows: *tert*-amyl formate (36.6 ± 4.9%), methyl acetate (34.9 ± 3.3%), acetaldehyde (43 ± 4.3%), formaldehyde (54.9 ± 7.6%), acetone (3.6 ± 0.2%), 3-methoxy-3-methyl-butanal (4.4±0.5%), *tert*-amyl alcohol (2.6±0.2%), *tert*-amyloxy methyl nitrate (2.9 ± 0.3%), 3-methoxy-3-methyl-2-butyl nitrate (1.0 ± 0.1%), and 2-methoxy-2-methyl-1-butyl nitrate (0.4 ± 0.3%).

As detailed by Smith et al. (1995), *tert*-amyl formate is the major expected product from attack at the CH_3 group adjacent to the ether linkage,

$$OH + CH_3OC(CH_3)_2CH_2CH_3(+O_2) \rightarrow (\bullet OO)CH_2OC(CH_3)_2CH_2CH_3 + H_2O$$

$$(\bullet OO)CH_2OC(CH_3)_2CH_2CH_3 + NO \rightarrow (\bullet O)CH_2OC(CH_3)_2CH_2CH_3 + NO_2$$

$$(\bullet O)CH_2OC(CH_3)_2CH_2CH_3 + O_2 \rightarrow HC(=O)OC(CH_3)_2CH_2CH_3 + HO_2$$

while methyl acetate, acetaldehyde, and formaldehyde (all highlighted in bold below) are the major expected products from attack at the CH_2 group,

$$OH + CH_3OC(CH_3)_2CH_2CH_3(+O_2) \rightarrow CH_3OC(CH_3)_2CH(OO\bullet)CH_3 + H_2O$$

$$CH_3OC(CH_3)_2CH(\bullet OO)CH_3 + NO \rightarrow CH_3OC(CH_3)_2CH(O\bullet)CH_3 + NO_2$$

$$CH_3OC(CH_3)_2CH(O\bullet)CH_3(+O_2) \rightarrow CH_3OC(CH_3)_2(OO\bullet) + \mathbf{CH_3CHO}$$

$$CH_3OC(CH_3)_2(OO\bullet) + NO \rightarrow CH_3OC(CH_3)_2(O\bullet) + NO_2$$

$$CH_3OC(CH_3)_2(O\bullet) \rightarrow \mathbf{CH_3OC(=O)CH_3} + CH_3$$

$$CH_3 + O_2 \rightarrow\rightarrow\rightarrow \mathbf{CH_2O}$$

OH attack at the two equivalent methyl groups on the α-carbon would lead to the same set of products, while attack at the terminal CH_3 on the *tert*-amyl fragment provides the source of the minor product, 3-methoxy-3-methyl-butanal.

Langer and Ljungström (1994b) have shown that the NO_3-initiated oxidation of TAME proceeds mainly via abstraction from the CH_3O group, leading to the main product *tert*-amyl formate, observed in 80% yield.

III-B-11. Isopropyl Isobutyl Ether [$(CH_3)_2CH—O—CH_2CH(CH_3)_2$]

III-B-11.1. OH Reaction Kinetics

The reaction of OH with isopropyl isobutyl ether has been studied at 298 K by Stemmler et al. (1997a), using a relative rate technique. A value of 2.1×10^{-11} cm^3 $molecule^{-1}$ s^{-1} is obtained, as detailed in table III-B-26. Given the lack of corroborative data, an uncertainty of $\pm 35\%$ is assigned.

III-B-11.2. NO_3 Reaction Kinetics

There are no measurements available for this rate coefficient. On the basis of the structure–activity relationship presented in section III-H, a rate coefficient of 1×10^{-14} cm^3 $molecule^{-1}$ s^{-1} can be estimated for temperatures near 298 K.

III-B-11.3. Summary of the Atmospheric Fate of Isopropyl Isobutyl Ether, and the End Products of Its Oxidation

Reaction with OH will represent the major atmospheric loss process for this species, with contributions from reaction with NO_3 and Cl-atoms also expected under specific circumstances. The lifetime against OH reaction is estimated to be 5 h for typical daytime [OH] $\approx 2.5 \times 10^6$ molecule cm^{-3}. A nighttime lifetime of 10 h is estimated for the NO_3 reaction, for urban polluted conditions ([NO_3] $= 3 \times 10^9$ molecule cm^{-3}).

The mechanism of the OH-initiated oxidation of isopropyl isobutyl ether has been studied in the presence of NO_x by Stemmler et al. (1997a). The major products observed, with their molar yields in parentheses, were acetone ($56 \pm 4\%$), isopropyl formate ($48 \pm 3\%$), isobutyl acetate ($28 \pm 2\%$), and 2-hydroxy-2-methylpropyl acetate ($25 \pm 10\%$). Smaller yields ($< 10\%$) of isobutanal, isopropyl nitrate, 1,1,4-trimethyl-3-oxapentyl nitrate, isopropyl isobutyrate, and isobutyl formate were also observed.

Table III-B-26. Rate coefficients (k, cm^3 $molecule^{-1}$ s^{-1}) for reaction of OH with isobutyl isopropyl ether

$10^{11} \times k$	T (K)	Technique[a]	Reference
2.10 ± 0.04	298	RR (di-*n*-propyl ether)[b]	Stemmler et al. (1997a)

[a]Abbreviations used for the techniques are defined in table I-F-3.

[b]Placed on an absolute basis using k(OH+di-*n*-propyl ether) $= 2.0 \times 10^{-11}$ cm^3 $molecule^{-1}$ s^{-1} (this book, section III-B-6.1).

Acetone and isopropyl formate are co-products of the attack of OH at the CH_2 group, and account for about one-half of the oxidation:

$$OH + (CH_3)_2CHOCH_2CH(CH_3)_2(+O_2) \rightarrow (CH_3)_2CHOCH(OO\bullet)CH(CH_3)_2$$

$$(CH_3)_2CHOCH(OO\bullet)CH(CH_3)_2 + NO \rightarrow (CH_3)_2CHOCH(O\bullet)CH(CH_3)_2 + NO_2$$

$$(CH_3)_2CHOCH(O\bullet)CH(CH_3)_2 \rightarrow \mathbf{(CH_3)_2CHOCH{=}O} + CH(CH_3)_2$$

$$CH(CH_3)_2 + O_2 \rightarrow\rightarrow \mathbf{CH_3C(=O)CH_3}$$

Isobutyl acetate (and its undetected co-product, formaldehyde) is formed following OH attack at the isopropyl CH group, and accounts for another 25–30% of the chemistry,

$$OH + (CH_3)_2CHOCH_2CH(CH_3)_2(+O_2) \rightarrow (CH_3)_2C(OO\bullet)OCH_2CH(CH_3)_2$$

$$(CH_3)_2C(OO\bullet)OCH_2CH(CH_3)_2 + NO \rightarrow (CH_3)_2C(O\bullet)OCH_2CH(CH_3)_2 + NO_2$$

$$(CH_3)_2C(O\bullet)OCH_2CH(CH_3)_2 \rightarrow \mathbf{CH_3C(=O)OCH_2CH(CH_3)_2} + CH_3$$

$$CH_3 + O_2 \rightarrow\rightarrow \mathbf{HCHO}$$

Much of the remaining chemistry involves attack at the isobutyl CH group leading, via alkoxy radical isomerization, to 2-hydroxy-2-methylpropyl acetate:

$$OH + (CH_3)_2CHOCH_2CH(CH_3)_2(+O_2) \rightarrow (CH_3)_2CHOCH_2C(OO\bullet)(CH_3)_2$$

$$(CH_3)_2CHOCH_2C(OO\bullet)(CH_3)_2 + NO \rightarrow (CH_3)_2CHOCH_2C(O\bullet)(CH_3)_2 + NO_2$$

$$(CH_3)_2CHOCH_2C(O\bullet)(CH_3)_2 \rightarrow (CH_3)_2C\bullet OCH_2C(OH)(CH_3)_2$$

$$(CH_3)_2C\bullet OCH_2C(OH)(CH_3)_2 \rightarrow\rightarrow\rightarrow CH_3C(=O)OCH_2C(OH)(CH_3)_2$$

III-B-12. Di-*n*-Butyl Ether [$CH_3(CH_2)_3O(CH_2)_3CH_3$]

III-B-12.1. OH Reaction Kinetics

The reaction of OH with di-*n*-butyl ether (DnBE) has been studied using direct and relative rate techniques (Wallington et al., 1988d, 1989a; Bennett and Kerr, 1989; Nelson et al., 1990a; Semadeni et al., 1993; Mellouki et al., 1995; Kramp and Paulson, 1998; Harry et al., 1999; Aschmann et al., 2005, 2006). With the exception of the single relative rate measurement of Bennett and Kerr (1989), the data are in substantive agreement, as shown in table III-B-27 and figure III-B-12. Least-squares fitting of the data to the simple Arrhenius expression gives $k = 4.5 \times 10^{-12} \exp(550/T)$ cm^3 molecule^{-1} s^{-1}, with $k = 2.8 \times 10^{-11}$ cm^3 molecule^{-1} s^{-1} at 298 K. An uncertainty of ±15% is estimated at 298 K.

Table III-B-27. Rate coefficients ($k = A \times T^n \times e^{-B/T}$, cm^3 $molecule^{-1}$ s^{-1}) for reaction of OH with di-*n*-butyl ether [$CH_3(CH_2)_3O(CH_2)_3CH_3$]

$10^{12} \times A$	n	B (K)	$10^{12} \times k$	T (K)	Technique[a]	Reference	Temperature Range (K)
			27.8 ± 3.6	296	FP–RF	Wallington et al. (1988d)	
			25.2 ± 2.9	295	RR[b] ($C_2H_5OC_2H_5$)	Wallington et al. (1989a)	
			16.9 ± 0.9	294	RR[c] (isobutene)	Bennett and Kerr (1989)	
			27.2 ± 0.2	298	PR–UV	Nelson et al. (1990a)	
			26.8 ± 1.1	298	RR[d] (*c*-C_6H_{12})		
4.68[e]		−539[e]	37.5	251	RR[f] (2,3-dimethylbutane)	Semadeni et al. (1993)	248–353
			35.6	258			
			34.9	265			
			31.9	273			
			30.9	298			
			27.6	323			
			27.9	353			
			41.7	248	RR[b] ($C_2H_5OC_2H_5$)		
			41.4	251			
			40.0	254			
			35.8	260			
			37.7	263			
			36.2	266			
			37.4	268			
			35.2	273			
			35.2	273			
			35.9	275			
			29.3	286			
			26.1	297			
			30.4	298			
			27.3	301			
			24.8	317			
			26.7	328			
			23.7	343			
3.78 ± 0.28	0	-599 ± 80	52.3 ± 1.3	230	PLP–LIF	Mellouki et al. (1995)	230–372
			47.9 ± 3.0	240			
$(6.29 \pm 0.74) \times 10^{-6}$	2	-1164 ± 34	50.1 ± 1.8	242			
			39.3 ± 2.0	252			
			36.7 ± 2.2	263			
			31.5 ± 1.4	273			
			26.9 ± 0.8	296			
			25.7 ± 1.1	313			
			21.1 ± 1.1	323			
			22.3 ± 0.8	324			
			21.4 ± 0.9	343			
			21.8 ± 0.7	363			
			21.0 ± 0.6	372			

(*continued*)

Table III-B-27. (*continued*)

$10^{12} \times A$	n	B (K)	$10^{12} \times k$	T (K)	Technique[a]	Reference	Temperature Range (K)
			27.5 ± 0.2	296	RR[g] (n-C_9H_{20})	Kramp and	
			28.5 ± 0.3	296	RR[h] (c-$C_6H_{11}CH_3$)	Paulson	
			27.1 ± 0.3	296	RR[i] (1,3-butadiene)	(1998)	
			33.0 ± 2.5	296	RR[j] (MVK)	Harry et al. (1999)	
			30.6 ± 0.8	296	RR[k] (α-pinene)	Aschmann et al. (2005)	
			29.6 ± 0.9	278	RR[k] (α-pinene)	Aschmann et al. (2006)	278–348
			27.3 ± 0.7	298			
			28.1 ± 0.4	303			
			22.4 ± 0.6	343			
			22.0 ± 0.6	348			
			29.9 ± 0.9	297	RR[l] (n-decane)		

[a]Abbreviations used for the techniques are defined in table I-F-3.

[b]Placed on an absolute basis using $k(\text{OH}+\text{C}_2\text{H}_5\text{OC}_2\text{H}_5) = 1.15 \times 10^{-17} T^2 \exp(743/T)$ cm^3 molecule^{-1} s^{-1} (this book, section III-B-3.1).

[c]Placed on an absolute basis using $k(\text{OH}+\text{isobutene}) = 5.2 \times 10^{-11}$ cm^3 molecule^{-1} s^{-1} (Calvert et al., 2000).

[d]Placed on an absolute basis using $k(\text{OH}+cyclo\text{-}\text{C}_6\text{H}_{12}) = 6.97 \times 10^{-12}$ cm^3 molecule^{-1} s^{-1} (Calvert et al., 2008).

[d]Values obtained from least-squares fit of data obtained using updated reference rate coefficients, and thus differ from those originally reported.

[f]Placed on an absolute basis using $k(\text{OH}+2,3\text{-dimethylbutane}) = 1.25 \times 10^{-11} \exp(-212/T)$ cm^3 molecule^{-1} s^{-1} (Calvert et al., 2008).

[g]Placed on an absolute basis using $k(\text{OH}+n\text{-}\text{C}_9\text{H}_{20}) = 9.8 \times 10^{-12}$ cm^3 molecule^{-1} s^{-1} (Calvert et al., 2008).

[h]Placed on an absolute basis using k(OH+methylcyclohexane) $= 9.6 \times 10^{-12}$ cm^3 molecule^{-1} s^{-1} (Calvert et al., 2008).

[i]Placed on an absolute basis using $k(\text{OH}+1,3\text{-butadiene}) = 6.7 \times 10^{-11}$ cm^3 molecule^{-1} s^{-1} (Calvert et al., 2000).

[j]Placed on an absolute basis using k(OH+methyl vinyl ketone) $= 2.06 \times 10^{-11}$ cm^3 molecule^{-1} s^{-1} (this book, chapter V-E-1).

[k]Placed on an absolute basis using $k(\text{OH}+\alpha\text{-pinene}) = 1.2 \times 10^{-11} \exp(440/T)$ cm^3 molecule^{-1} s^{-1} (Atkinson et al., 2006).

[l]Placed on an absolute basis using $k(\text{OH}+n\text{-}\text{C}_{10}\text{H}_{22}) = 11.0 \times 10^{-12}$ cm^3 molecule^{-1} s^{-1} (Calvert et al., 2008).

III-B-12.2. NO_3 Reaction Kinetics

There are no measurements available for this rate coefficient. On the basis of the structure–activity relationship presented in section III-H, a rate coefficient of 5×10^{-15} cm^3 molecule^{-1} s^{-1} can be estimated for temperatures near 298 K.

III-B-12.3. Cl-Atom Reaction Kinetics

The three measurements (Nelson et al., 1990a; Harry et al., 1999; Notario et al., 2000b) of the rate coefficient for reaction of Cl with DnBE are in good agreement; see table III-B-28. The unweighted average of the three determinations, $k = 4.7 \times 10^{-10}$ cm^3 molecule^{-1} s^{-1}, is recommended, with an estimated uncertainty of ±15%.

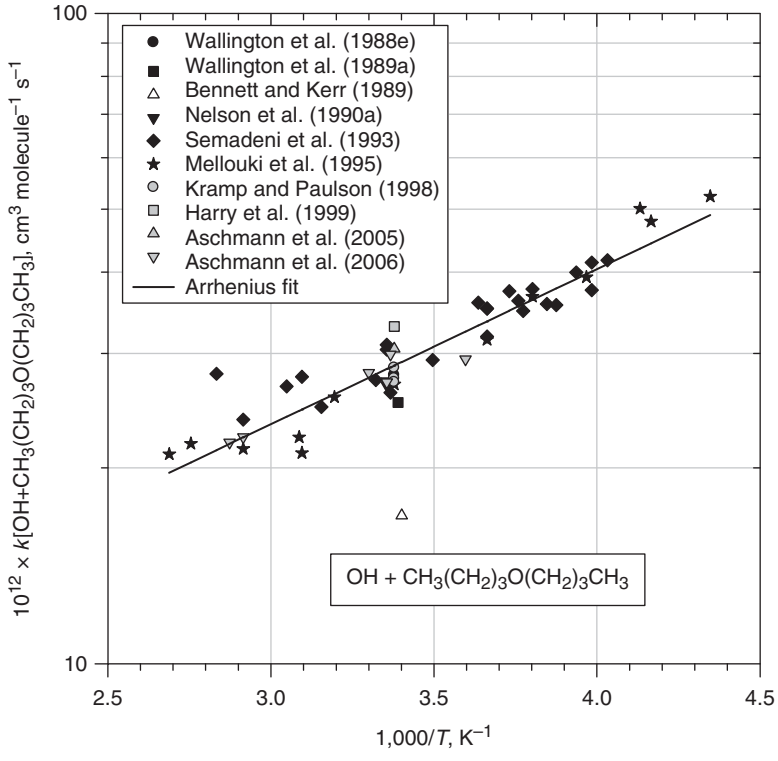

Figure III-B-12. Arrhenius plot of the rate coefficient for the reaction of OH with di-*n*-butyl ether.

Table III-B-28. Rate coefficients (k, cm^3 molecule^{-1} s^{-1}) for reaction of Cl with di-*n*-butyl ether

$10^{10} \times k$	T (K)	Technique[a]	Reference
4.68 ± 0.42	298	RR[b] (*cyclo*-C_6H_{12})	Nelson et al. (1990a)
4.93 ± 0.05	300	RR[c] (*n*-C_8H_{18})	Harry et al. (1999)
4.5 ± 0.5	298	PLP–RF	Notario et al. (2000b)

[a]Abbreviations used for the techniques are defined in table I-F-3.
[b]Placed on an absolute basis using k(Cl+*cyclo*-C_6H_{12}) = 3.3×10^{-10} cm^3 molecule^{-1} s^{-1} (Calvert et al., 2008).
[c]Placed on an absolute basis using k(Cl+*n*-C_8H_{18}) = 4.4×10^{-10} cm^3 molecule^{-1} s^{-1} (Calvert et al., 2008).

III-B-12.4. O(^{3}P) Reaction Kinetics

Liu et al. (1990a), using a flash photolysis–resonance fluorescence technique, report $k = 1.37 \times 10^{-11} \exp(-880/T)$ cm^3 molecule^{-1} s^{-1} for reaction of O(^{3}P) with di-*n*-butyl ether.

III-B-12.5. Summary of the Atmospheric Fate of Di-n-Butyl Ether, and the End Products of Its Oxidation

The major atmospheric loss process for DnBE will be via reaction with OH, with minor contributions expected from its reaction with NO_3 and Cl-atoms. For typical daytime

[OH] $\approx 2.5 \times 10^6$ molecule cm^{-3}, the lifetime against OH reaction is estimated to be about 4 h.

Johnson and Andino (2001) conducted a detailed study of the products obtained from the OH-initiated oxidation of DnBE in the presence of NO_x. Major products identified, with their molar yields in parentheses, were butyl formate ($41.0 \pm 0.9\%$), propanal ($37.9 \pm 2.2\%$), butanal ($11.9 \pm 0.3\%$), and butyl butyrate ($1.9 \pm 0.1\%$).

Reaction of OH with DnBE should occur mostly at the CH_2 group adjacent to the ether linkage, and all products listed above can be obtained from the resultant alkoxy radical, $CH_3(CH_2)_3OCH(O\bullet)(CH_2)_2CH_3$, via C—C bond rupture, C—O bond rupture, and C—H bond rupture and/or O_2 reaction:

$$CH_3(CH_2)_3OCH(O\bullet)(CH_2)_2CH_3 \rightarrow \mathbf{CH_3(CH_2)_3OCHO} + \bullet CH_2CH_2CH_3$$

$$CH_3(CH_2)_3OCH(O\bullet)(CH_2)_2CH_3 \rightarrow CH_3CH_2CH_2CH_2O\bullet + \mathbf{CH_3CH_2CH_2CHO}$$

$$CH_3(CH_2)_3OCH(O\bullet)(CH_2)_2CH_3 \rightarrow \mathbf{CH_3(CH_2)_3OC(=O)(CH_2)_2CH_3} + H$$

$$CH_3(CH_2)_3OCH(O\bullet)(CH_2)_2CH_3 + O_2 \rightarrow \mathbf{CH_3(CH_2)_3OC(=O)(CH_2)_2CH_3} + HO_2$$

Johnson and Andino suggest isomerization as an alternative pathway for the $CH_3(CH_2)_3OCH(O\bullet)(CH_2)_2CH_3$ radical, but the subsequent theoretical study of Ferenac et al. (2003) would argue against the significant occurrence of this process. The products observed by Johnson and Andino account for about 50% of the reacted DnBE. Multi-functional species obtained from reaction of OH further down the *n*-butyl chains likely make up much of the remaining product distribution.

III-B-13. Di-isobutyl Ether [$(CH_3)_2CHCH_2OCH_2CH(CH_3)_2$]

The only information available regarding the atmospheric chemistry of di-isobutyl ether is a relative rate measurement of the rate coefficient for its reaction with OH (Bennett and Kerr, 1989), $k = 2.6 \times 10^{-11}$ cm^3 molecule^{-1} s^{-1}; see table III-B-29. However, we note that the majority of other OH+ ether rate coefficients reported by Bennett and Kerr (1989) have subsequently been found to be significantly low. Thus, no recommendation for the rate coefficient for reaction of OH with di-isobutyl ether can be made at this time. Despite these quantitative limitations, it seems likely that the atmospheric lifetime of this species will be quite short, about 4 h for [OH] $= 2.5 \times 10^6$ molecule cm^{-3}. An important site for OH reaction will likely be at the CH_2 groups adjacent to the ether linkage; major expected products from reaction at this site are acetone and isobutyl formate:

$$OH + (CH_3)_2CHCH_2OCH_2CH(CH_3)_2 + O_2 \rightarrow (CH_3)_2CHCH_2OCH(OO\bullet)CH(CH_3)_2$$

$$(CH_3)_2CHCH_2OCH(OO\bullet)CH(CH_3)_2 + NO \rightarrow (CH_3)_2CHCH_2OCH(O\bullet)CH(CH_3)_2 + NO_2$$

$$(CH_3)_2CHCH_2OCH(O\bullet)CH(CH_3)_2 \rightarrow \mathbf{(CH_3)_2CHCH_2OCHO} + CH(CH_3)_2$$

$$CH(CH_3)_2 \rightarrow\rightarrow\rightarrow \mathbf{(CH_3)_2C{=}O}$$

Table III-B-29. Rate coefficients (k, cm^3 molecule^{-1} s^{-1}) for reaction of OH with di-*iso*-butyl ether [$(CH_3)_2CHCH_2OCH_2CH(CH_3)_2$]

$10^{12}\times k$	T (K)	Technique[a]	Reference
16.9 ± 0.9	294	RR[b] (isobutene)	Bennett and Kerr (1989)

[a]Abbreviations used for the techniques are defined in table I-F-3.
[b]Placed on an absolute basis using k(OH+isobutene) = 5.2×10^{-11} cm^3 molecule^{-1} s^{-1} (Calvert et al., 2000).

III-B-14. Di-*tert*-Butyl Ether [$(CH_3)_3COC(CH_3)_3$]

III-B-14.1. OH Reaction Kinetics

The reaction of OH with di-*tert*-butyl ether has been studied near 296 K by Nielsen et al. (1995) and Langer et al. (1996). The two determinations are in reasonable agreement (see table III-B-30) and an unweighted average of the two measurements, $k = 3.7 \times 10^{-12}$ cm^3 molecule^{-1} s^{-1}, is recommended. An uncertainty of ±25% is estimated. The rate coefficient likely possesses a positive temperature dependence.

III-B-14.2. NO_3 Reaction Kinetics

Langer et al. (1996) report a rate coefficient $k = 2.9 \times 10^{-16}$ cm^3 molecule^{-1} s^{-1} for reaction of NO_3 with di-*tert*-butyl ether at 295 K, see table III-B-31. In the absence of corroborative data, an uncertainty of ±50% is assigned.

III-B-14.3. Cl-Atom Reaction Kinetics

The rate coefficient for reaction of Cl with di-*tert*-butyl ether has been measured at 295 K by Langer et al. (1996) using a relative rate technique, see table III-B-32. The average of their two measurements, $k = 1.4 \times 10^{-10}$ cm^3 molecule^{-1} s^{-1}, is recommended with an uncertainty of ±20%.

Table III-B-30. Rate coefficients (k, cm^3 molecule^{-1} s^{-1}) for reaction of OH with di-*tert*-butyl ether [$(CH_3)_3COC(CH_3)_3$]

$10^{12}\times k$	T (K)	Technique[a]	Reference
4.0 ± 0.9	296	PR–UV abs.	Nielsen et al. (1995)
3.4 ± 0.6	295	RR[b] (C_2H_4)	Langer et al. (1996)

[a]Abbreviations used for the techniques are defined in table I-F-3.
[b]Placed on an absolute basis using k(OH+C_2H_4) = 7.9×10^{-11} cm^3 molecule^{-1} s^{-1} (Atkinson et al., 2006).

Table III-B-31. Rate coefficients (k, cm^3 molecule^{-1} s^{-1}) for reaction of NO_3 with di-*tert*-butyl ether

$10^{16}\times k$	T (K)	Technique[a]	Reference
2.9 ± 0.9	295	RR[b] (C_2H_4)	Langer et al. (1996)

[a]Abbreviations used for the techniques are defined in table I-F-3.
[b]Placed on an absolute basis using k(NO_3+C_2H_4) = 1.9×10^{-16} cm^3 molecule^{-1} s^{-1} (Atkinson et al., 2006).

Table III-B-32. Rate coefficients (k, cm^3 molecule^{-1} s^{-1}) for reaction of Cl with di-*tert*-butyl ether

$10^{10} \times k$	T (K)	Technique[a]	Reference
1.4 ± 0.2	295	RR[b] (C_2H_4)	Langer et al. (1996)
1.4 ± 0.2	295	RR[b] (C_2H_4)	

[a]Abbreviations used for the techniques are defined in table I-F-3.
[b]Placed on an absolute basis using $k(Cl+C_2H_4) = 0.95 \times 10^{-10}$ cm^3 molecule^{-1} s^{-1} (this book, table I-F-2).

III-B-14.4. Summary of the Atmospheric Fate of Di-tert-Butyl Ether, and the End Products of Its Oxidation

The atmospheric destruction of di-*tert*-butyl ether will occur predominantly via reaction with OH, with contributions from NO_3 (at night) and Cl-atoms also being possible. For diurnally averaged [OH] $\approx 1.0 \times 10^6$ molecule cm^{-3}, a lifetime of about 3 days is predicted. End products of the OH-initiated oxidation of di-*tert*-butyl ether in the presence of NO_x have been quantified by Langer et al. (1996). Products observed included *tert*-butyl acetate (yield 85 ± 15%), and HCHO, CH_3ONO, and CH_3ONO_2 (combined yield 1.88 ± 0.11). The following reaction sequence leads quantitatively to the observed products (see figure 5 of Langer et al., 1996):

$$OH + (CH_3)_3COC(CH_3)_3(+O_2) \rightarrow (CH_3)_3COC(CH_3)_2CH_2OO\bullet$$

$$(CH_3)_3COC(CH_3)_2CH_2OO\bullet + NO \rightarrow (CH_3)_3COC(CH_3)_2CH_2O\bullet + NO_2$$

$$(CH_3)_3COC(CH_3)_2CH_2O\bullet(+O_2) \rightarrow (CH_3)_3COC(CH_3)_2OO\bullet + \mathbf{HCHO}$$

$$(CH_3)_3COC(CH_3)_2OO\bullet + NO \rightarrow (CH_3)_3COC(CH_3)_2O\bullet + NO_2$$

$$(CH_3)_3COC(CH_3)_2O\bullet \rightarrow \mathbf{(CH_3)_3COC(=O)CH_3} + CH_3$$

$$CH_3 \rightarrow\rightarrow\rightarrow \mathbf{CH_3ONO, CH_3ONO_2, HCHO}$$

III-B-15. Di-*n*-Pentyl Ether [$CH_3(CH_2)_4O(CH_2)_4CH_3$]

III-B-15.1. OH Reaction Kinetics

The reaction of OH with di-*n*-pentyl ether has been studied by both direct and relative rate techniques (Wallington et al., 1988e, 1989a; Nelson et al., 1990a; Semadeni et al., 1993). The only study of the temperature dependence is from Semadeni et al. (1993) which covered the range 263 to 373 K. The data are summarized in table III-B-33 and figure III-B-13, and are seen to be in reasonable accord. Fitting to the simple Arrhenius expression yields: $k = 7.7 \times 10^{-12} \times \exp(429/T)$ cm^3 molecule^{-1} s^{-1}, with $k = 3.3 \times 10^{-11}$ cm^3 molecule^{-1} s^{-1} at 298 K. An uncertainty of ±15% is estimated at 298 K.

Table III-B-33. Rate coefficients ($k = A \times e^{-B/T}$, cm^3 $molecule^{-1}$ s^{-1}) for reaction of OH with di-*n*-pentyl ether [$CH_3(CH_2)_4O(CH_2)_4CH_3$]

$10^{12} \times A$	B (K)	$10^{12} \times k$	T (K)	Technique[a]	Reference	Temperature Range (K)
		34.7 ± 2.0	296	FP–RF	Wallington et al. (1988e)	
		28.4 ± 2.4	295	RR[b] ($C_2H_5OC_2H_5$)	Wallington et al. (1989a)	
		31.6 ± 1.4	298	RR[c] (*cyclo*-C_6H_{12})	Nelson et al. (1990a)	
7.33 [d]	−454[d]	41.1	263	RR[e] (di-*n*-butyl ether)	Semadeni et al. (1993)	263–373
		38.9	275			
		33.6	298			
		30.8	313			
		28.4	333			
		25.2	373			

[a]Abbreviations used for the techniques are defined in table I-F-3.
[b]Placed on an absolute basis using $k(OH+C_2H_5OC_2H_5) = 1.15 \times 10^{-17} T^2 \exp(743/T)$ cm^3 $molecule^{-1}$ s^{-1} (this book, section III-B-3.1).
[c]Placed on an absolute basis using $k(OH+cyclo\text{-}C_6H_{12}) = 6.97 \times 10^{-12}$ cm^3 $molecule^{-1}$ s^{-1} (Calvert et al., 2008).
[d]Values obtained from least-squares fit of data obtained using updated reference rate coefficients, and thus differ from those originally reported.
[e]Placed on an absolute basis using $k(OH+di\text{-}n\text{-butyl ether}) = 4.5 \times 10^{-12} \exp(550/T)$ cm^3 $molecule^{-1}$ s^{-1} (this book, section III-B-12.1).

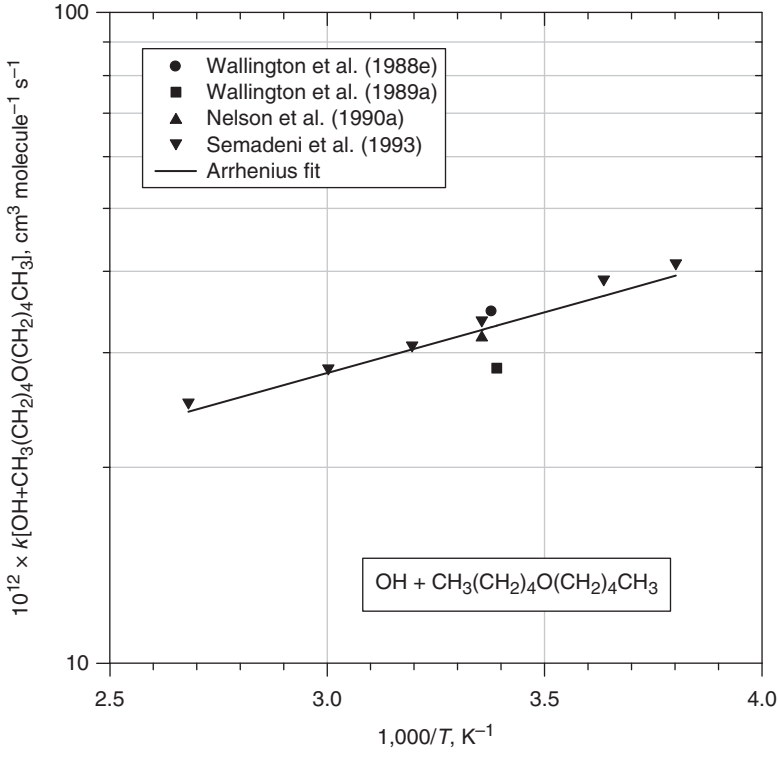

Figure III-B-13. Arrhenius plot of the rate coefficient for the reaction of OH with di-*n*-pentyl ether.

Table III-B-34. Rate coefficients (k, cm^3 molecule^{-1} s^{-1}) for reaction of Cl with di-*n*-pentyl ether

$10^{10} \times k$	T (K)	Technique[a]	Reference
5.27 ± 0.24	298	RR[b] (*cyclo*-C_6H_{12})	Nelson et al. (1990a)

[a]Abbreviations used for the techniques are defined in table I-F-3.
[b]Placed on an absolute basis using k(Cl+*cyclo*-C_6H_{12}) = 3.3×10^{-10} cm^3 molecule^{-1} s^{-1} (Calvert et al., 2008).

III-B-15.2. NO_3 Reaction Kinetics

There are no data available for this reaction. However, on the basis of structure–activity relationships developed in section III-H, an estimate of $k = 5 \times 10^{-15}$ cm^3 molecule^{-1} s^{-1} can be made for 298 K.

III-B-15.3. Cl-Atom Reaction Kinetics

The relative rate study of Nelson et al. (1990a) gives $k = 5.3 \times 10^{-10}$ cm^3 molecule^{-1} s^{-1}, see table III-B-34, with an estimated uncertainty of ±15%.

III-B-15.4. O(^{3}P) Reaction Kinetics

Liu et al. (1990a) studied the reaction of O(^{3}P) with di-*n*-pentyl ether over the temperature range 240–400 K, using a flash photolysis–resonance fluorescence technique. They report $k = 1.26 \times 10^{-11} \exp(-780/T)$ cm^3 molecule^{-1} s^{-1}.

III-B-15.5. Summary of the Atmospheric Fate of Di-n-Pentyl Ether, and the End Products of Its Oxidation

Atmospheric destruction of di-*n*-pentyl ether will be quite rapid, with loss occurring mainly via reaction with OH. Reactions with NO_3 and Cl-atoms may also play a minor role. For daytime [OH] ≈ 2.5×10^6 molecule cm^{-3}, a lifetime of 3 h is determined. The main site for OH reaction will be at the CH_2 groups located adjacent to the ether linkage; expected products include *n*-pentyl formate and $HOCH_2CH_2CH_2CHO$ (the end product of 1-butyl radical oxidation):

$$OH + C_5H_{12}OCH_2(CH_2)_3CH_3(+O_2) \rightarrow C_5H_{12}OCH(OO\bullet)(CH_2)_3CH_3 + H_2O$$

$$C_5H_{12}OCH(OO\bullet)(CH_2)_3CH_3 + NO \rightarrow C_5H_{12}OCH(O\bullet)(CH_2)_3CH_3 + NO_2$$

$$C_5H_{12}OCH(O\bullet)(CH_2)_3CH_3 \rightarrow C_5H_{12}OCHO + \bullet(CH_2)_3CH_3$$

$$\bullet(CH_2)_3CH_3 + O_2 \rightarrow\rightarrow\rightarrow HOCH_2CH_2CH_2CHO, \text{ butanal, other products}$$

III-C. Multi-Functional Ethers

III-C-1. Dimethoxymethane ($CH_3OCH_2OCH_3$)

III-C-1.1. OH Reaction Kinetics

The reaction of OH with dimethoxymethane has been studied by Porter et al. (1997), Wallington et al. (1997a), Thüner et al. (1999), and Vovelle et al. (2001). As shown in table III-C-1 and figure III-C-1, the data are in good agreement. For atmospheric purposes, fitting of all data obtained at $T < 300$ K leads to: $k = 2.7 \times 10^{-18} T^2 \exp(879/T)$ cm^3 molecule^{-1} s^{-1} (valid for $230 < T < 300$ K), with $k = 4.5 \times 10^{-12}$ cm^3 molecule^{-1} s^{-1} at 298 K. The expression derived by Vovelle et al. (2001), $k = 6.05 \times 10^{-26} T^{4.69} \exp(1{,}555/T)$ cm^3 molecule^{-1} s^{-1} provides an excellent

Table III-C-1. Rate coefficients ($k = A \times T^n \times e^{-B/T}$, cm^3 molecule^{-1} s^{-1}) for reaction of OH with dimethoxymethane ($CH_3OCH_2OCH_3$)

$10^{18} \times A$	n	B (K)	$10^{12} \times k$	T (K)	Technique[a]	Reference	Temperature Range (K)
			4.9 ± 0.8	298	RR[b]	Porter et al. (1997)	
4.0 ± 1.0	2	−780 ± 70	6.62 ± 0.15	231	PLP–LIF		231–372
			5.50 ± 0.11	249			
			4.94 ± 0.11	273			
			4.61 ± 0.05	298			
			4.60 ± 0.20	323			
			4.57 ± 0.17	348			
			4.72 ± 0.10	372			
			4.6 ± 1.6	346	PR–UV	Wallington et al.	
			4.7 ± 0.4	296	RR[c] (C_2H_4)	(1997a)	
			5.2 ± 0.6	296	RR[d] (*cyclo*-C_6H_{12})		
			4.5 ± 0.2	298	RR[d] (*cyclo*-C_6H_{12})	Thüner et al. (1999)	
6.05×10^{-8}	4.69	−1,555	4.43 ± 0.10	293	PLP–LIF	Vovelle et al. (2001)	293–617
			4.48 ± 0.14	294			
			4.40 ± 0.06	296			
			4.30 ± 0.08	297			
			4.50 ± 0.11	317			
			4.62 ± 0.14	368			
			5.38 ± 0.22	433			
			6.05 ± 0.20	499			
			7.67 ± 0.29	566			
			9.07 ± 0.24	616			
			9.14 ± 0.24	617			
			9.37 ± 0.47	617			

[a]Abbreviations used for the techniques are defined in table I-F-3.
[b]Reference compound used not specified. Study involved use of a number of alkyl ethers and ethanol as reference compounds, reference rate coefficients quoted are within 10% of those recommended in the various sections of this book and in Calvert et al. (2008).
[c]Placed on an absolute basis using $k(OH+C_2H_4) = 7.9 \times 10^{-12}$ cm^3 molecule^{-1} s^{-1} (Atkinson et al., 2006).
[d]Placed on an absolute basis using $k(OH+cyclo\text{-}C_6H_{12}) = 6.97 \times 10^{-12}$ cm^3 molecule^{-1} s^{-1} (Calvert et al., 2008).

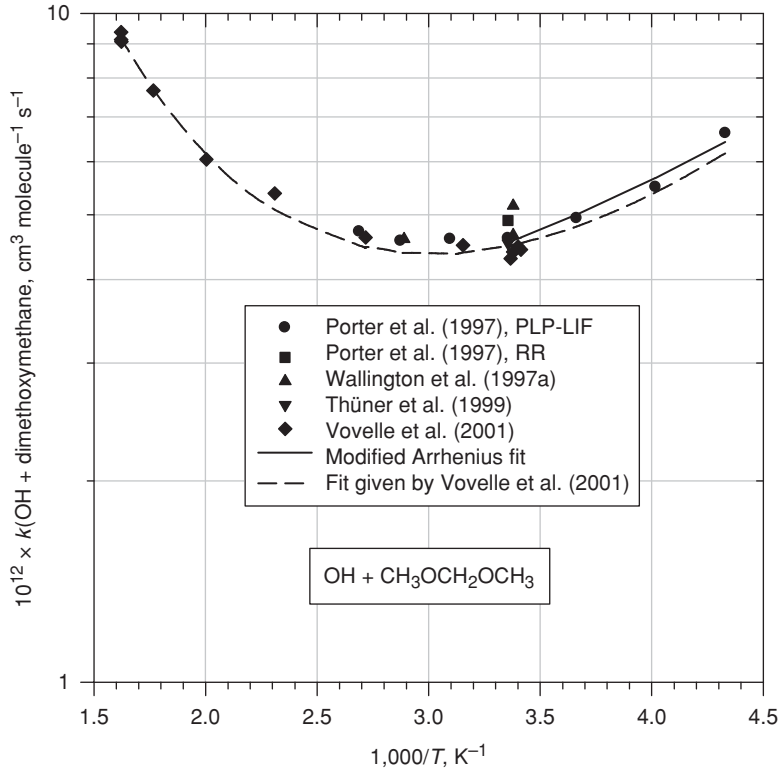

Figure III-C-1. Arrhenius plot of the rate coefficient for the reaction of OH with dimethoxymethane ($CH_3OCH_2OCH_3$).

representation of the entire dataset. The uncertainty in the 298 K value is estimated at ±15%.

III-C-1.2. Cl-Atom Reaction Kinetics

The rate coefficient for reaction of Cl-atoms with dimethoxymethane has been determined by Wallington et al. (1997a) using a relative rate technique, $k = 1.4 \times 10^{-10}$ cm^3 molecule^{-1} s^{-1} at 296 K. The uncertainty on this value is estimated to be ±25%. See table III-C-2 for details.

III-C-1.3. Summary of the Atmospheric Fate of Dimethoxymethane, and the End Products of Its Oxidation

The atmospheric lifetime of dimethoxymethane is determined by its reaction with OH. With an assumed diurnally averaged [OH] ≈ 10^6 molecule cm^{-3}, the lifetime will be about 2.5 days. The oxidation of dimethoxymethane, initiated by OH and/or Cl-atoms, has been reported by Wallington et al. (1997a), Geiger and Becker (1999), and Wenger et al. (1999).

Table III-C-2. Rate coefficients (k, cm^3 molecule^{-1} s^{-1}) for reaction of Cl with dimethoxymethane

$10^{10} \times k$	T (K)	Technique[a]	Reference
1.3 ± 0.1	298	RR[b] (C_2H_4)	Wallington et al. (1997a)
1.4 ± 0.1		RR[c] (n-C_4H_{10})	

[a]Abbreviations used for the techniques are defined in table I-F-3.
[b]Placed on an absolute basis using $k(\mathrm{Cl}+\mathrm{C_2H_4}) = 0.95 \times 10^{-10}$ cm^3 molecule^{-1} s^{-1} (this book, table I-F-2).
[c]Placed on an absolute basis using $k(\mathrm{Cl}+n\text{-}\mathrm{C_4H_{10}}) = 2.05 \times 10^{-10}$ cm^3 molecule^{-1} s^{-1} (Calvert et al., 2008).

Reaction of OH with dimethoxymethane occurs mostly (~70–75%) via abstraction from the terminal CH_3 groups. The main end product is methoxymethyl formate, CH_3OCH_2OCHO, formed from either reaction of the resultant $CH_3OCH_2OCH_2O\bullet$ radical with O_2, or via H-atom elimination from this radical. The remainder of the reaction occurs via abstraction at the CH_2 site in dimethoxymethane, leading mainly to the formation of dimethyl carbonate, $CH_3OC(=O)OCH_3$, via reaction of the $CH_3OCH(O\bullet)OCH_3$ radical with O_2, or from H-atom elimination from this radical.

III-C-2. 2-Methoxyethanol ($CH_3OCH_2CH_2OH$)

III-C-2.1. OH Reaction Kinetics

The reaction of OH with 2-methoxyethanol, $CH_3OCH_2CH_2OH$, has been studied by both relative rate and flash photolysis techniques (Dagaut et al., 1989b; Stemmler et al., 1996a; Porter et al., 1997), see table III-C-3 and figure III-C-2. There are signs of curvature in the Arrhenius plot of the Dagaut et al. data (240–440 K), thus a modified T^2 fit was used. Fitting of the modified Arrhenius expression to the combined dataset

Table III-C-3. Rate coefficients ($k = A \times e^{-B/T}$, cm^3 molecule^{-1} s^{-1}) for reaction of OH with 2-methoxyethanol ($CH_3OCH_2CH_2OH$)

$10^{12} \times A$	B (K)	$10^{11} \times k$	T (K)	Technique[a]	Reference	Temperature Range (K)
4.5 ± 1.4	−325 ± 100	1.88 ± 0.13	240	FP–RF	Dagaut et al. (1989b)	240–440
		1.25 ± 0.07	298			
		1.10 ± 0.06	350			
		1.04 ± 0.08	400			
		1.01 ± 0.06	440			
		1.41 ± 0.28	298	RR[b]	Porter et al. (1997)	
		1.14 ± 0.1	298	PLP–LIF		
		1.12 ± 0.11	297	RR[c] (1-hexanol)	Stemmler et al. (1996a)	

[a]Abbreviations used for the techniques are defined in table I-F-3.
[b]Reference compound used not specified. Study involved use of a number of alkyl ethers and ethanol as reference compounds; reference rate coefficients quoted are within 10% of those recommended in the various sections of this book and in Calvert et al. (2008).
[c]Placed on an absolute basis using $k(\mathrm{OH}+1\text{-}\mathrm{C_6H_{13}OH}) = 1.30 \times 10^{-11}$ cm^3 molecule^{-1} s^{-1} (Calvert et al., 2008).

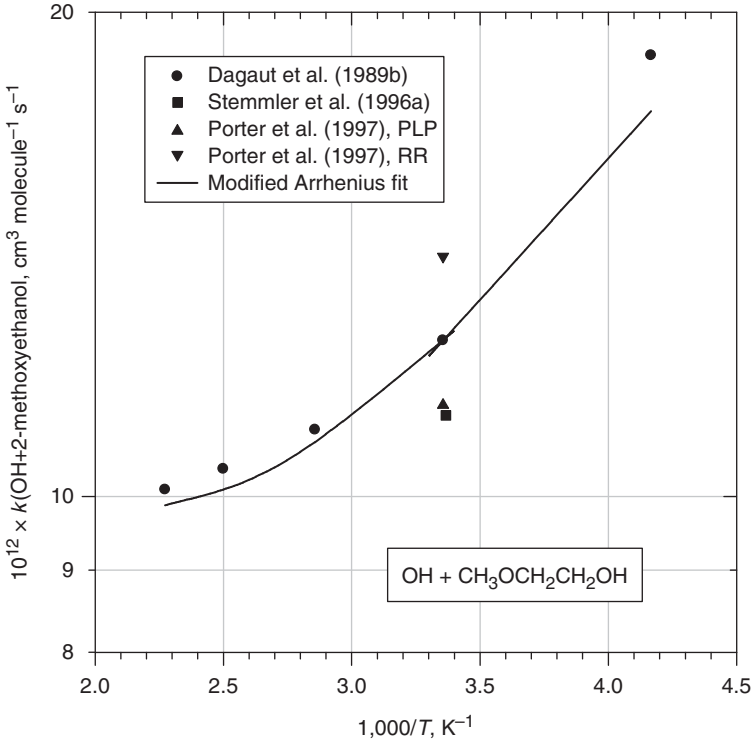

Figure III-C-2. Arrhenius plot of the rate coefficient for the reaction of OH with 2-methoxyethanol ($CH_3OCH_2CH_2OH$).

yields $k = 6.0 \times 10^{-18} T^2 \exp(938/T)$ cm^3 molecule^{-1}s^{-1}, giving $k = 1.3 \times 10^{-11}$ cm^3 molecule^{-1} s^{-1} at 298 K with an estimated uncertainty of ±20%.

III-C-2.2. Summary of the Atmospheric Fate of 2-Methoxyethanol, and the End Products of its Oxidation

The atmospheric lifetime of 2-methoxyethanol, determined by its reaction with OH, will be about 9 h for daytime [OH] = 2.5×10^6 molecule cm^{-3}. End products of the OH-initiated oxidation have not been determined. However, some reasonable predictions can be made on the basis of structure–activity considerations and product data on related species. The major site for OH attack is predicted to be at the CH_2 group adjacent to the ether linkage (Kwok and Atkinson, 1995), leading to methyl formate and HCHO via C—C bond rupture in the resulting alkoxy radical, $CH_3OCH(O\bullet)CH_2OH$. A significant amount of reaction (about 1/3) should also occur at the CH_2 group adjacent to the alcohol functionality, likely leading to 2-methoxyacetaldehyde ($CH_3OCH_2CH{=}O$).

III-C-3. 1,2-Dimethoxyethane ($CH_3OCH_2CH_2OCH_3$)

III-C-3.1. OH Reaction Kinetics

The only study of this reaction is a combined relative rate and pulsed laser photolysis study of Porter et al. (1997), see table III-C-4 and figure III-C-3. They report $k = 5.3 \times 10^{-18} T^2 \times \exp(1{,}220/T)$ cm^3 molecule^{-1} s^{-1}, with $k = 2.8 \times 10^{-11}$ cm^3 molecule^{-1} s^{-1} at 298 K. An uncertainty of ±20% is assigned at 298 K.

III-C-3.2. Summary of the Atmospheric Fate of 1,2-Dimethoxyethane, and the End Products of Its Oxidation

Reaction with OH will be the major atmospheric loss process for 1,2-dimethoxyethane. Its lifetime will be about 4 h for daytime [OH] = 2.5×10^6 molecule cm^{-3}.

End products of the Cl-initiated oxidation for this species have been reported by Wenger et al. (1999), while results of an OH-initiated oxidation study were reported by Geiger and Becker (1999). In both studies, the major reaction pathway (~75% in the case of Cl, ~90% in the case of OH) involves abstraction from the CH_2 groups, leading predominantly to the formation of two molecules of methyl formate.

$$OH + CH_3OCH_2CH_2OCH_3(+O_2) \rightarrow CH_3OCH_2CH(OO\bullet)OCH_3$$

$$CH_3OCH_2CH(OO\bullet)OCH_3 + NO \rightarrow CH_3OCH_2CH(O\bullet)OCH_3 + NO_2$$

$$CH_3OCH_2CH(O\bullet)OCH_3(+O_2) \rightarrow CH_3OCH_2OO\bullet + CH_3OCH{=}O$$

$$CH_3OCH_2OO\bullet + NO \rightarrow CH_3OCH_2O\bullet + NO_2$$

$$CH_3OCH_2O\bullet + O_2 \rightarrow CH_3OCH{=}O + HO_2$$

Abstraction from the CH_3 groups is a minor channel, and leads mainly to the formation of methoxyethyl formate ($CH_3OCH_2CH_2OCH{=}O$).

Table III-C-4. Rate coefficients ($k = A \times T^n \times e^{-B/T}$, cm^3 molecule^{-1} s^{-1}) for reaction of OH with 1,2-dimethoxyethane ($CH_3OCH_2CH_2OCH_3$)

$10^{18} \times A$	n	B (K)	$10^{12} \times k$	T (K)	Technique[a]	Reference	Temperature Range (K)
			28.1 ± 1.0	298	RR[b]	Porter et al. (1997)	
5.3 ± 0.5	2	−1,220 ± 20	52.0 ± 0.9	234	PLP–LIF		234–372
			42.0 ± 1.4	252			
			34.1 ± 2.0	273			
			26.7 ± 3.1	298			
			21.2 ± 1.4	348			
			19.2 ± 0.7	372			

[a] Abbreviations used for the techniques are defined in table I-F-3.

[b] Reference compound used not specified. Study involved use of a number of alkyl ethers and ethanol as reference compounds; reference rate coefficients quoted are within 10% of those recommended in the various secdions of this book and in Calvert et al. (2008).

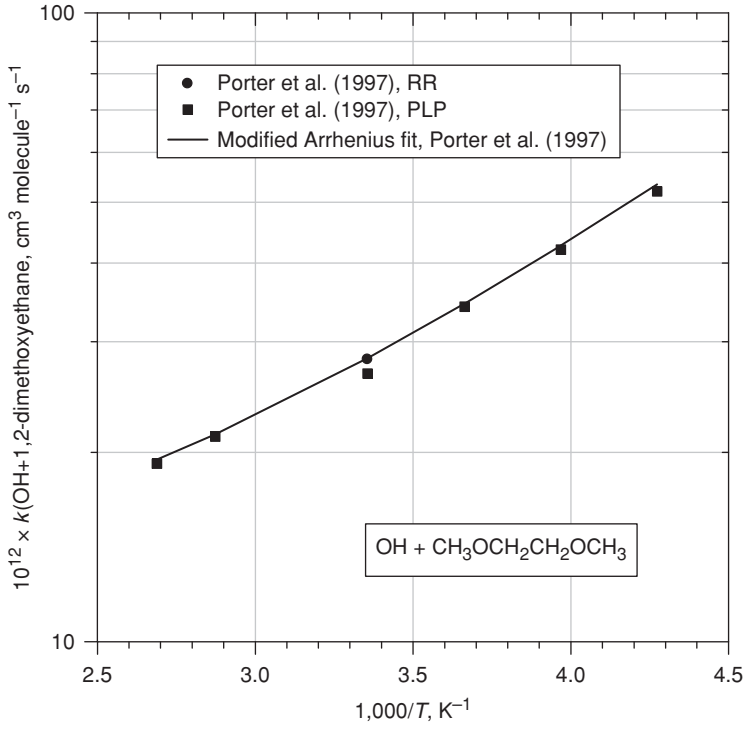

Figure III-C-3. Arrhenius plot of the rate coefficient for the reaction of OH with 1,2-dimethoxyethane ($CH_3OCH_2CH_2OCH_3$).

III-C-4. 2-Ethoxyethanol ($CH_3CH_2OCH_2CH_2OH$)

III-C-4.1. OH Reaction Kinetics

Rate coefficients for reaction of OH with 2-ethoxyethanol, $CH_3CH_2OCH_2CH_2OH$, have been reported near 298 K by Hartmann et al. (1987), Dagaut et al. (1989b), Stemmler et al. (1996a), and Porter et al. (1997), and at 485 K by Hartmann et al. (1987), see table III-C-5. The 298 K data point from Hartmann et al. (1987) is about 30% lower than the mean of the other values, and is thus not considered in deriving the final value, $k = 1.9 \times 10^{-11}$ cm^3 molecule^{-1} s^{-1}, with an estimated uncertainty of $\pm 25\%$. Insufficient data are available to make any recommendation on the temperature dependence of the reaction.

III-C-4.2. Summary of the Atmospheric Fate of 2-Ethoxyethanol, and the End Products of its Oxidation

Reaction with OH will be the major atmospheric loss process for 2-ethoxyethanol, with a lifetime of about 6 h for daytime [OH] $= 2.5 \times 10^6$ molecule cm^{-3}. Stemmler et al. (1996b) determined the end products of OH-initiated oxidation of this species in the presence of NO_x. Major products observed included ethylene

Table III-C-5. Rate coefficients (k, cm^3 molecule^{-1} s^{-1}) for reaction of OH with 2-ethoxyethanol ($CH_3CH_2OCH_2CH_2OH$)

$10^{11} \times k$	T (K)	Technique[a]	Reference
1.2 ± 0.3	298	PLP–RF	Hartmann et al. (1987)
1.4 ± 0.3	485		
1.87 ± 0.2	298	FP–RF	Dagaut et al. (1989b)
1.51 ± 0.04	298	RR[b] (1-$C_6H_{13}OH$)	Stemmler et al. (1996)
1.74 ± 0.31	298	RR[c]	Porter et al. (1997)
2.12 ± 0.07	298	PLP–LIF	

[a]Abbreviations used for the techniques are defined in table I-F-3.
[b]Placed on an absolute basis using k(OH+1-$C_6H_{13}OH$) = 1.3×10^{-11} cm^3 molecule^{-1} s^{-1} (Calvert et al., 2008).
[c]Reference compound used not specified. Study involved use of a number of alkyl ethers and ethanol as reference compounds; reference rate coefficients quoted are within 10% of those recommended in the various sections of this book and in Calvert et al. (2008).

glycol monoformate [$HC(O)OCH_2CH_2OH$, molar yield 36 ± 7%], ethyl formate [$HC(O)OCH_2CH_3$, 34 ± 10%], ethoxyacetaldehyde [$CH_3CH_2OCH_2CHO$, 24 ± 13%], and ethylene glycol monoacetate [$CH_3C(O)OCH_2CH_2OH$, 7.8 ± 2.4%]. The origin of these products has been presented in detail by Stemmler et al. (1996b). The ethylene glycol monoformate, with co-product HCHO, results from C—C bond cleavage in the $CH_3CH(O\bullet)OCH_2CH_2OH$ radical. Ethylene glycol monoacetate originates from either H-atom elimination from this same alkoxy species, or via its reaction with O_2. Ethyl formate is obtained (also with formaldehyde as a co-product) from C—C bond cleavage in the $CH_3CH_2OCH(O\bullet)CH_2OH$ radical, while ethoxyacetaldehyde is obtained from oxidation of the —CH_2OH functionality. Interestingly, the cyclic species 2-methyl-1, 3-dioxolane was observed in small (~3%) yield; Stemmler et al. postulate that it results from the cyclization of the $CH_3CH(\bullet)OCH_2CH_2OH$ radical, which presumably occurs in competition with its reaction with O_2. The large combined yield of the ethylene glycol monoesters, coupled with the excellent mass balance achieved in the Stemmler et al. experiments, argues against the significant occurrence of isomerization of the $CH_3CH(O\bullet)OCH_2CH_2OH$ radical via a 1,5-H-atom shift. This is in keeping with the theoretical work of Ferenac et al. (2003), who showed that isomerizations of this type (i.e., with an ether oxygen located adjacent to the alkoxy radical site) are not favorable.

III-C-5. 1-Methoxy-2-propanol ($CH_3OCH_2CH(OH)CH_3$)

III-C-5.1. OH Reaction Kinetics

Rate coefficients for reaction of OH with 1-methoxy-2-propanol have been determined near 298 K by Porter et al. (1997) and by Aschmann and Atkinson (1998b), see table III-C-6. The unweighted average of the measurements, $k = 2.0 \times 10^{-11}$ cm^3 molecule^{-1} s^{-1}, is recommended with an estimated uncertainty of ±20%.

Table III-C-6. Rate coefficients (k, cm^3 molecule^{-1} s^{-1}) for reaction of OH with 1-methoxy-2-propanol [$CH_3OCH_2CH(OH)CH_3$]

$10^{11} \times k$	T (K)	Technique[a]	Reference
1.79 ± 0.16	298	RR[b]	Porter et al. (1997)
1.92 ± 0.09	298	PLP–LIF	
2.34 ± 0.16	296	RR[c] (propene)	Aschmann and Atkinson (1998b)
1.90 ± 0.06	296	RR[d] (MVK)	

[a]Abbreviations used for the techniques are defined in table I-F-3.
[b]Reference compound used not specified. Study involved use of a number of alkyl ethers and ethanol as reference compounds; reference rate coefficients quoted are within 10% of those recommended in the various sections of this book and in Calvert et al. (2008).
[c]Placed on an absolute basis using $k(OH+C_3H_6) = 2.9 \times 10^{-11}$ cm^3 molecule^{-1} s^{-1} (Atkinson et al., 2006).
[d]Placed on an absolute basis using $k(OH+MVK) = 2.0 \times 10^{-11}$ cm^3 molecule^{-1} s^{-1} (this book, section V-E-1.1).

III-C-5.2. O_3 Reaction Kinetics

Aschmann and Atkinson (1998b) reported an upper limit for this rate coefficient, $k(O_3) < 1.1 \times 10^{-19}$ cm^3 molecule^{-1} s^{-1}. The reaction is too slow to be of atmospheric significance. The data are summarized in table III-C-7.

III-C-5.3. NO_3 Reaction Kinetics

The reaction of NO_3 with 1-methoxy-2-propanol has been studied by Chew et al. (1998) and Aschmann and Atkinson (1998b). The data are in good agreement (see table III-C-8), and an average value of $k(NO_3) = 1.6 \times 10^{-15}$ cm^3 molecule^{-1} s^{-1} is recommended with an estimated uncertainty of ±30%.

Table III-C-7. Rate coefficients (k, cm^3 molecule^{-1} s^{-1}) for reaction of O_3 with 1-methoxy-2-propanol [$CH_3OCH_2CH(OH)CH_3$]

$10^{19} \times k$	T (K)	Technique[a]	Reference
< 1.1	296	GC–FID	Aschmann and Atkinson (1998b)

[a]Abbreviations used for the techniques are defined in table I-F-3.

Table III-C-8. Rate coefficients (k, cm^3 molecule^{-1} s^{-1}) for reaction of NO_3 with 1-methoxy-2-propanol [$CH_3OCH_2CH(OH)CH_3$]

$10^{15} \times k$	T (K)	Technique[a]	Reference
1.7 ± 0.7	296	RR[b] (propene)	Aschmann and Atkinson (1998b)
1.5 ± 0.5	298	RR[c] (methacrolein)	Chew et al. (1998)

[a]Abbreviations used for the techniques are defined in table I-F-3.
[b]Placed on an absolute basis using $k(NO_3+C_3H_6) = 9.3 \times 10^{-15}$ cm^3 molecule^{-1} s^{-1} (Atkinson et al., 2006).
[c]Placed on an absolute basis using $k(NO_3+methacrolein) = 3.3 \times 10^{-15}$ cm^3 molecule^{-1} s^{-1} (Chew et al., 1998). Rate coefficient reported as an upper limit, due to possible contribution from reaction with N_2O_5.

III-C-5.4. Summary of the Atmospheric Fate of 1-Methoxy-2-propanol, and the End Products of its Oxidation

Reaction with OH will control the atmospheric lifetime of 1-methoxy-2-propanol. For daytime [OH] = 2.5×10^6 molecule cm^{-3}, a lifetime of about 5.5 h is estimated. Tuazon et al. (1998a) have studied the products formed in the OH-initiated oxidation of 1-methoxy-2-propanol. The major products were methyl formate (molar yield $59 \pm 5\%$) and acetaldehyde ($56 \pm 7\%$). These species are formed following abstraction from the CH_2 group, via C—C bond cleavage in the resulting $CH_3OCH(O\bullet)CH(OH)CH_3$ alkoxy radical. Methoxyacetone [$CH_3OCH_2C(=O)CH_3$] was also an important product ($39 \pm 4\%$); it is formed via abstraction at the CH group followed by reaction of the resultant $CH_3OCH_2C\bullet(OH)CH_3$ radical with O_2 (Tuazon et al., 1998a). Chew et al. (1988) report a yield of methoxyacetone of $52 \pm 8\%$ from the NO_3-initiated oxidation of 1-methoxy-2-propanol, indicating that about one-half of the NO_3 reaction occurs via abstraction from the CH group in the parent molecule.

III-C-6. 1,1-Dimethoxyethane [$CH_3CH(OCH_3)_2$]

III-C-6.1. OH Reaction Kinetics

The only study of the reaction of OH with 1,1-dimethoxyethane is that of Dagaut et al. (1989a), $k = 8.9 \times 10^{-12}$ cm^3 $molecule^{-1}$ s^{-1} at 298 K. See table III-C-9 for details. Given the lack of corroborative data, an uncertainty of $\pm35\%$ is assigned.

III-C-6.2. Summary of the Atmospheric Fate of 1,1-Dimethoxyethane, and the End Products of Its Oxidation

For daytime [OH] = 2.5×10^6 molecule cm^{-3}, an atmospheric lifetime of 12 h is estimated for 1,1-dimethoxyethane. Possible products of its oxidation include dimethylcarbonate and HCHO from C—C bond cleavage in the $CH_3C(O\bullet)(OCH_3)_2$ radical, or $HC(=O)OCH(OCH_3)CH_3$ from oxidation of the —OCH_3 groups.

III-C-7. 2-Propoxyethanol ($CH_3CH_2CH_2OCH_2CH_2OH$)

III-C-7.1. OH Reaction Kinetics

The rate coefficient for reaction of OH with 2-propoxyethanol has been determined at 297 K via relative rate methods (Stemmler et al., 1996a; Markgraf et al., 1999). Markgraf et al. used two reference compounds to make their determination

Table III-C-9. Rate coefficients (k, cm^3 $molecule^{-1}$ s^{-1}) for reaction of OH with 1,1-dimethoxyethane [$CH_3CH(OCH_3)_2$]

$10^{12}\times k$	T (K)	Technique[a]	Reference
8.9 ± 1.0	298	FP–RF	Dagaut et al. (1989a)

[a]Abbreviations used for the techniques are defined in table I-F-3.

Table III-C-10. Rate coefficients (k, cm^3 molecule^{-1} s^{-1}) for reaction of OH with 2-propoxyethanol [$CH_3CH_2CH_2OCH_2CH_2OH$]

$10^{12} \times k$	T (K)	Technique[a]	Reference
17.1 ± 0.7	297	RR[b] (1-hexanol)	Stemmler et al. (1996a)
17.5 ± 1.0	297	RR[c,d] (2-pentanone; *n*-octane)	Markgraf et al. (1999)

[a]Abbreviations used for the techniques are defined in table I-F-3.
[b]Placed on an absolute basis using $k(OH+1\text{-}C_6H_{13}OH) = 1.3 \times 10^{-11}$ cm^3 molecule^{-1} s^{-1} (Calvert et al., 2008).
[c]Placed on an absolute basis using $k(OH+2\text{-pentanone}) = 3.6 \times 10^{-12}$ cm^3 molecule^{-1} s^{-1} (Calvert et al., 2008).
[d]Placed on an absolute basis using $k(OH+n\text{-octane}) = 7.8 \times 10^{-12}$ cm^3 molecule^{-1} s^{-1} (Calvert et al., 2008).

(2-pentanone and *n*-octane), but do not give the relative rates measured against the individual compounds. To re-normalize their data to currently recommended reference rate coefficients, an average downward correction of 18% has been applied to their determination. As seen in table III-C-10, the updated data of Stemmler et al. and Markgraf et al. are in excellent agreement; the unweighted average, $k = 1.73 \times 10^{-11}$ cm^3 molecule^{-1} s^{-1}, is recommended with an estimated uncertainty of ±20%.

III-C-7.2. Summary of the Atmospheric Fate of 2-Propoxyethanol, and the End Products of Its Oxidation

For daytime [OH] = 2.5×10^6 molecule cm^{-3}, an atmospheric lifetime of about 6.5 h is estimated for 2-propoxyethanol. Products of its OH-initiated oxidation have been determined by Markgraf et al. (1999). Major products observed (molar yields in parentheses) were propyl formate (47 ± 2%), 2-propoxyacetaldehyde ($CH_3CH_2CH_2OCH_2CH{=}O$ (15 ± 1%) and 2-ethyl-1,3-dioxolane (5.4 ± 0.4%). As described by Markgraf et al. (1999), OH reaction occurs predominantly at the CH_2 groups located adjacent to O-atoms. Propyl formate (with formaldehyde as a co-product) is obtained from C—C bond scission of the $CH_3CH_2CH_2OCH(O\bullet)CH_2OH$ alkoxy radical, while 2-propoxyacetaldehyde is the expected product of the oxidation of the —CH_2OH moiety. The cyclic species, 2-ethyl-1,3-dioxolane, is likely obtained from cyclization of the $CH_3CH_2C\bullet HOCH_2CH_2OH$ alkyl species. Other products may evolve from this alkyl radical as well (Markgraf et al., 1999), including $CH_3CH_2CH(OH)OCH_2CH{=}O$ from isomerization of the $CH_3CH_2CH(O\bullet)OCH_2CH_2OH$ alkoxy species.

III-C-8. Diethoxymethane ($CH_3CH_2OCH_2OCH_2CH_3$)

III-C-8.1. OH Reaction Kinetics

The rate coefficient for reaction of OH with diethoxymethane has been determined by Dagaut et al. (1989a), Porter et al. (1997), Thüner et al. (1999), and Vovelle et al. (2001). The temperature range covered extends from 252 to 619 K. The data at 297 ± 1 K are in good agreement, see table III-C-11 and figure III-C-4. Fitting of the data below 400 K yields $k = 3.8 \times 10^{-18} T^2 \exp(1{,}212/T)$ cm^3 molecule^{-1} s^{-1}, with $k = 1.96 \times 10^{-11}$ cm^3 molecule^{-1} s^{-1} at 298 K. The uncertainty at 298 K is estimated to be ±15%. As suggested by Vovelle et al. (2001) and Becker et al. (1999a),

Table III-C-11. Rate coefficients ($k = A \times T^n \times e^{-B/T}$, cm^3 molecule^{-1} s^{-1}) for reaction of OH with diethoxymethane [$CH_3CH_2OCH_2OCH_2CH_3$]

$10^{18} \times A$	n	B (K)	$10^{12} \times k$	T (K)	Technique[a]	Reference	Temperature Range (K)
			16.8 ± 1.6	298	FP–RF	Dagaut et al. (1989a)	
			20.4 ± 1.4	298	RR[b]	Porter et al. (1997)	252–372
4.2 ± 0.5	2	−1,200 ± 40	31.5 ± 0.5	252	PLP–LIF		
			26.0 ± 1.0	273			
			20.6 ± 0.8	298			
			17.3 ± 1.0	323			
			15.9 ± 0.3	348			
			14.8 ± 0.2	372			
			18.9 ± 1.4	298	RR[c] (1-hexene)	Thüner et al. (1999)	
			19.7 ± 1.0		RR[d] (propene)		
			19.0 ± 0.6	296	PLP–LIF	Vovelle et al. (2001)	296–619
			19.1 ± 1.1	297			
			19.5 ± 0.4	297			
			19.9 ± 1.0	298			
			16.9 ± 0.2	317			
			13.4 ± 0.2	368			
			12.2 ± 0.5	433			
			11.6 ± 0.3	498			
			12.7 ± 0.3	567			
			15.9 ± 0.7	617			
			15.8 ± 0.4	618			
			15.2 ± 0.8	619			

[a]Abbreviations used for the techniques are defined in table I-F-3.
[b]Reference compound used not specified. Study involved use of a number of alkyl ethers and ethanol as reference compounds; reference rate coefficients quoted are within 10% of those recommended in the various sectioins of this book and in Calvert et al. (2008).
[c]Placed on an absolute basis using k(OH+1-hexene) = 3.7×10^{-11} cm^3 molecule^{-1} s^{-1} (Calvert et al., 2000).
[d]Placed on an absolute basis using k(OH+propene) = 2.9×10^{-11} cm^3 molecule^{-1} s^{-1} (Atkinson et al., 2006).

representation of the rate coefficient over the entire temperature range studied is best accomplished using the sum of two Arrhenius expressions. Fitting of the complete dataset to a function of this form gives: $k = 2.1 \times 10^{-12} \exp(662/T) + 3.0 \times 10^{-10} \times \exp(-2{,}158/T)$ cm^3 molecule^{-1} s^{-1}.

III-C-8.2. O(^{3}P) Reaction Kinetics

The reaction of O(^{3}P) with diethoxymethane has been studied by Liu et al. (1990a), who report $k = 4.0 \times 10^{-13}$ cm^3 molecule^{-1} s^{-1} at 298 K.

III-C-8.3. Summary of the Atmospheric Fate of Diethoxymethane, and the End Products of Its Oxidation

The lifetime of diethoxymethane will be controlled by its reaction with OH. A lifetime of about 6 h is estimated, assuming daytime [OH] = 2.5×10^6 molecule cm^{-3}. Reaction products from its OH-initiated oxidation have not been determined. Reaction

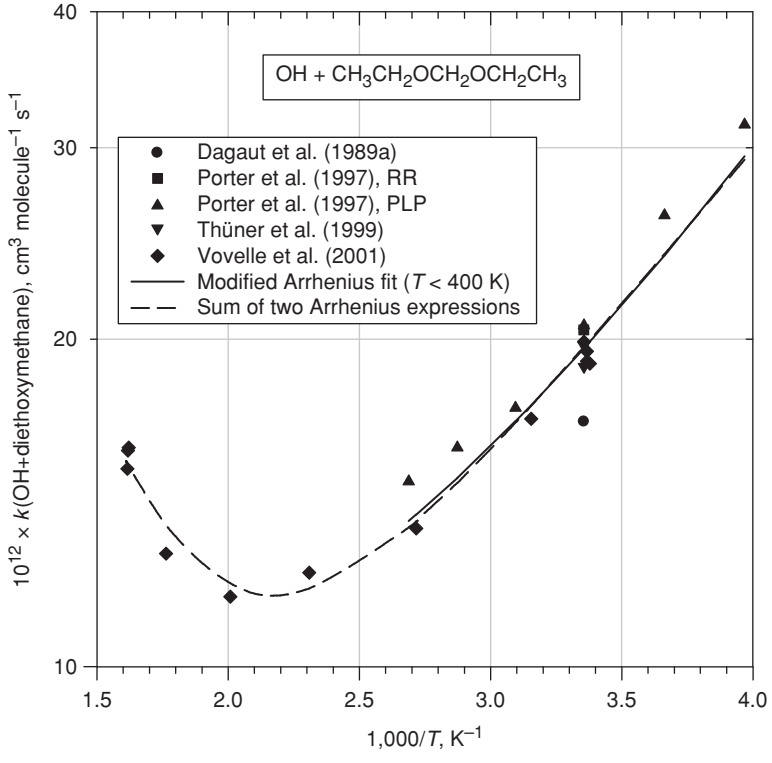

Figure III-C-4. Arrhenius plot of the rate coefficient for the reaction of OH with diethoxymethane ($CH_3CH_2OCH_2OCH_2CH_3$).

at the central CH_2 group would likely lead to production of diethyl carbonate, $CH_3CH_2OC(=O)OCH_2CH_3$ while reaction at the ethoxy-CH_2 groups would most likely lead to the formation of ethoxymethyl formate, $CH_3CH_2OCH_2OCH(=O)$, and co-product formaldehyde via C—C bond cleavage in the relevant alkoxy radical, $CH_3CH_2OCH_2OCH(O\bullet)CH_3$.

III-C-9. 1,2-Dimethoxypropane [$CH_3OCH_2CH(OCH_3)CH_3$]

III-C-9.1. OH Reaction Kinetics

The reaction of OH with 1,2-dimethoxypropane, $CH_3OCH_2CH(OCH_3)CH_3$, has been studied by Dagaut et al. (1989a), and by Porter et al. (1997). As is evident from table III-C-12, significant discrepancies exist between the two groups, a surprising finding given their agreement on other species and general consistency with other measurement groups. While there is no obvious reason to exclude either measurement, it seems likely that the rate coefficient for reaction of OH with 1,2-dimethoxypropane will be similar to (or larger than) that for 1,2-dimethoxyethane, $k(CH_3OCH_2CH_2OCH_3) = 2.8 \times 10^{-11}$ cm^3 molecule^{-1} s^{-1} (see section III-C-3), thus favoring the Porter et al. (1997) data. Further work on this reaction is required.

Table III-C-12. Rate coefficients (k, cm^3 molecule^{-1} s^{-1}) for reaction of OH with 1,2-dimethoxypropane [$CH_3OCH_2CH(OCH_3)CH_3$]

$10^{12} \times k$	T (K)	Technique[a]	Reference
14.3 ± 1.5	298	FP–RF	Dagaut et al. (1989a)
34.0 ± 0.8	298	RR[b]	Porter et al. (1997)
28.4 ± 1.8	298	PLP–LIF	

[a]Abbreviations used for the techniques are defined in table I-F-3.

[b]Reference compound used not specified. Study involved use of a number of alkyl ethers and ethanol as reference compounds; reference rate coefficients quoted are within 10% of those recommended in the various sections of this book and in Calvert et al. (2008).

III-C-9.2. Summary of the Atmospheric Fate of 1,2-Dimethoxypropane, and the End Products of Its Oxidation

If it is assumed that the data of Porter et al. (1997) provide a reasonable estimate of the OH reactivity of 1,2-dimethoxypropane, its lifetime (assuming daytime [OH] = 2.5×10^6 molecule cm^{-3}) would be about 3.5 h. Reaction products from its OH-initiated oxidation have not been determined. Major sites of OH attack are predicted to be at the CH and CH_2 groups (Kwok and Atkinson, 1995). Attack at the CH group will likely lead to both methyl acetate and methyl formate, via C—C bond cleavage in the resultant $CH_3OCH_2C(O\bullet)(OCH_3)CH_3$ alkoxy radical. Attack at the CH_2 group will produce the $CH_3OCH(O\bullet)CH(OCH_3)CH_3$ alkoxy radical. Carbon—carbon bond cleavage in this species will likely produce two molecules of methyl formate, with formaldehyde as a co-product:

$$CH_3OCH(O\bullet)CH(OCH_3)CH_3(+O_2) \rightarrow CH_3OCH(=O) + (\bullet OO)CH(OCH_3)CH_3$$

$$(\bullet OO)CH(OCH_3)CH_3 + NO \rightarrow (\bullet O)CH(OCH_3)CH_3 + NO_2$$

$$(\bullet O)CH(OCH_3)CH_3 \rightarrow HC(=O)OCH_3 + \bullet CH_3$$

$$\bullet CH_{3+}O_2 \rightarrow\rightarrow\rightarrow CH_2O$$

III-C-10. 2,2-Dimethoxypropane [$(CH_3)_2C(OCH_3)_2$]

III-C-10.1. OH Reaction Kinetics

Rate coefficients for reaction of OH with 2,2-dimethoxypropane, $(CH_3O)_2C(CH_3)_2$, have been reported by Dagaut et al. (1989a) as a function of temperature and by Porter et al. (1997) at 298 K. Although some scatter is evident, reasonable agreement exists between the two groups at 298 K, see table III-C-13. The recommended value is obtained from the unweighted average of the 298 K determinations, $k = 4.1 \times 10^{-12}$ cm^3 molecule^{-1} s^{-1}. An uncertainty of ±25% is estimated. The study of Dagaut et al. (1989a) shows the rate coefficient to be essentially independent of temperature over the range studied (240–440 K); they report $k = 3.55 \times 10^{-12} \exp(30/T)$ cm^3 molecule^{-1} s^{-1}.

Table III-C-13. Rate coefficients ($k = A \times e^{-B/T}$, cm^3 $molecule^{-1}$ s^{-1}) for reaction of OH with 2,2-dimethoxypropane [$CH_3C(OCH_3)_2CH_3$]

$10^{12} \times A$	B (K)	$10^{12} \times k$	T (K)	Technique[a]	Reference	Temperature Range (K)
3.55 ± 0.39	-30 ± 35	4.09 ± 0.89	240	FP–RF	Dagaut et al. (1989a)	240–440
		3.93 ± 0.17	298			
		3.75 ± 0.18	350			
		3.80 ± 0.51	400			
		3.93 ± 0.35	440			
		3.6 ± 0.6	298	RR[b]	Porter et al. (1997)	
		4.7 ± 0.2	298	PLP–LIF		

[a]Abbreviations used for the techniques are defined in table I-F-3.
[b]Reference compound used not specified. Study involved use of a number of alkyl ethers and ethanol as reference compounds; reference rate coefficients quoted are within 10% of those recommended in the various sections of this book and in Calvert et al. (2008).

III-C-10.2. Summary of the Atmospheric Fate of 2,2-Dimethoxypropane, and the End Products of Its Oxidation

With a diurnally averaged [OH] $\approx 10^6$ molecule cm^{-3}, the estimated lifetime for 2,2-dimethoxypropane is about 3 days. The most reactive sites in the molecule are predicted to be the —OCH_3 groups. Oxidation at these sites likely leads to the formation of the corresponding formate ester, $(CH_3)_2C(OCH_3)OCH{=}O$.

III-C-11. 2-Isopropoxyethanol [$(CH_3)_2CHOCH_2CH_2OH$]

III-C-11.1. OH Reaction Kinetics

The rate coefficient for reaction of OH with 2-isopropoxyethanol has been measured by Porter et al. (1997), using both a relative rate and pulsed laser photolysis–laser-induced fluorescence technique. An average value of 2.1×10^{-11} cm^3 $molecule^{-1}$ s^{-1} was reported at 298 K; see table III-C-14. In the absence of corroborative measurements, an uncertainty of $\pm 25\%$ is estimated.

Table III-C-14. Rate coefficients (k, cm^3 $molecule^{-1}$ s^{-1}) for reaction of OH with 2-isopropoxyethanol [$(CH_3)_2CHOCH_2CH_2OH$]

$10^{12} \times k$	T (K)	Technique[a]	Reference
22.6 ± 1.8	298	RR[b]	Porter et al. (1997)
18.5 ± 0.7	298	PLP–LIF	

[a]Abbreviations used for the techniques are defined in table I-F-3.
[b]Reference compound used not specified. Study involved use of a number of alkyl ethers and ethanol as reference compounds; reference rate coefficients quoted are within 10% of those recommended in the various sections of this book and in Calvert et al. (2008).

III-C-11.2. Summary of the Atmospheric Fate of 2-Isopropoxyethanol, and the End Products of its Oxidation

The estimated lifetime of 2-isopropoxyethanol is 4 h, for a daytime [OH] $\approx 2.5 \times 10^6$ molecule cm^{-3}. Aschmann and Atkinson (1999a) conducted a detailed study of the products obtained from the OH-initiated oxidation of this species in the presence of NO_x. Products observed were isopropyl formate (molar yield 57 ± 5%) and 2-hydroxyethyl acetate (44 ± 5%). As outlined by Aschmann and Atkinson (1999a), isopropyl formate (with co-product formaldehyde) is formed from OH attack at the CH_2 group adjacent to the ether oxygen, via C—C bond cleavage in the $(CH_3)_2CHOCH(O•)CH_2OH$ radical. The 2-hydroxyethyl acetate product is obtained in analogous fashion from OH reaction at the CH group adjacent to the ether linkage, from decomposition of the $(CH_3)_2C(O•)OCH_2CH_2OH$ radical.

III-C-12. Other Five-Carbon Multifunctional Ethers

There are five additional five-carbon multifunctional ethers that have been the subject of a single study of their OH reactivity. These include 1-ethoxy-2-methoxyethane (Dagaut et al., 1989a), 3-methoxy-1-butanol (Dagaut et al., 1989b), 3-ethoxy-1-propanol (Dagaut et al., 1989b), 2-isopropoxyethanol (Porter et al., 1997), and 1,3-dimethoxypropane (Moriarty et al., 2003). For the 1,3-dimethoxypropane relative rate study of Moriarty et al. (2003), the rate coefficient data of Porter et al. (1997) have been used for the reference reaction (OH + 2-ethoxy ethyl ether, see section III-C-14 for details). Data are summarized in table III-C-15. In the absence of corroborative measurements, uncertainties of ±35% are estimated for these rate coefficients.

Table III-C-15. Rate coefficients, k, for reaction of OH with a series of five-carbon multifunctional ethers

$10^{12} \times k$	T (K)	Technique[a]	Reference
OH + 1-Ethoxy-2-methoxyethane ($CH_3CH_2OCH_2CH_2OCH_3$)			
17.5 ± 1.1	298	FP–RF	Dagaut et al. (1989a)
OH + 3-Methoxy-1-butanol ($CH_3CH(OCH_3)CH_2CH_2OH$)			
23.6 ± 1.6	298	FP–RF	Dagaut et al. (1989b)
OH + 3-Ethoxy-1-propanol ($CH_3CH_2OCH_2CH_2CH_2OH$)			
22.0 ± 1.3	298	FP–RF	Dagaut et al. (1989b)
OH + 2-Isopropoxy-ethanol [$(CH_3)_2CHOCH_2CH_2OH$]			
22.6 ± 1.8	298	RR[b]	Porter et al. (1997)
18.5 ± 0.7	298	PLP–LIF	
OH + 1,3-Dimethoxypropane ($CH_3OCH_2CH_2CH_2OCH_3$)			
51.0 ± 5.2	298	RR[c]	Moriarty et al. (2003)
47.5±1.3	298	PLP–LIF	

[a]Abbreviations used for the techniques are defined in table I-F-3.

[b]Reference compound used not specified. Study involved use of a number of alkyl ethers and ethanol as reference compounds; reference rate coefficients quoted are within 10% of those recommended in the various sections of this book and in Calvert et al. (2008).

[c]Placed on an absolute basis using $k(OH+C_2H_5OCH_2CH_2OC_2H_5) = 5.79 \times 10^{-11}$ cm^3 $molecule^{-1}$ s^{-1}.

Table III-C-16. Rate coefficients (k, cm^3 molecule^{-1} s^{-1}) for reaction of OH with 2-butoxyethanol ($CH_3CH_2CH_2CH_2OCH_2CH_2OH$)

$10^{12} \times k$	T (K)	Technique[a]	Reference
14 ± 3	298	PLP–RF	Hartmann et al. (1987)
14 ± 3	505		
23.1 ± 0.9	298	FP–RF	Dagaut et al. (1989b)
20.2 ± 2.1	298	RR[b] (1-hexanol)	Stemmler et al. (1997b)
32.8 ± 2.4	296	RR[c] (propene)	Aschmann and Atkinson (1998b)
27.2 ± 1.1	296	RR[d] (MVK)	

[a]Abbreviations used for the techniques are defined in table I-F-3.
[b]Placed on an absolute basis using $k(OH+1\text{-}C_6H_{13}OH) = 1.3 \times 10^{-11}$ cm^3 molecule^{-1} s^{-1} (Calvert et al., 2008).
[c]Placed on an absolute basis using $k(OH+C_3H_6) = 2.9 \times 10^{-11}$ cm^3 molecule^{-1} s^{-1} (Atkinson et al., 2006).
[d]Placed on an absolute basis using $k(OH+MVK) = 2.0 \times 10^{-11}$ cm^3 molecule^{-1} s^{-1} (this book, chapter V-E-1.1).

III-C-13. 2-*n*-Butoxyethanol ($CH_3CH_2CH_2CH_2OCH_2CH_2OH$)

III-C-13.1. OH Reaction Kinetics

The reaction of OH with 2-butoxyethanol has been studied by Hartmann et al. (1987), Dagaut et al. (1989b), Stemmler et al. (1996a), and Aschmann and Atkinson (1998b). As seen from the summary in table III-C-16, considerable scatter exists in the dataset, with values near 298 K ranging from (14–33) $\times 10^{-12}$ cm^3 molecule^{-1} s^{-1}. Aschmann and Atkinson (1998b) suggest that wall adsorption/desorption problems might have contributed to some of the lower values reported. A rate coefficient, $k = 3 \times 10^{-11}$ cm^3 molecule^{-1} s^{-1}, is tentatively assigned for this species, but further study is clearly required.

III-C-13.2. O_3 Reaction Kinetics

Aschmann and Atkinson (1998b) determined an upper limit for the rate coefficient for reaction of O_3 with 2-butoxyethanol, $k < 1.1 \times 10^{-19}$ cm^3 molecule^{-1} s^{-1}, see table III-C-17. The reaction is too slow to be of atmospheric importance.

III-C-13.3. NO_3 Reaction Kinetics

The reaction of NO_3 with 2-butoxyethanol has been studied by Atkinson and co-workers (Aschmann and Atkinson, 1998b; Chew et al., 1998), see table III-C-18 for a summary. A rate coefficient of $k = 3.1 \times 10^{-15}$ cm^3 molecule^{-1} s^{-1} has been obtained in

Table III-C-17. Rate coefficients (k, cm^3 molecule^{-1} s^{-1}) for reaction of O_3 with 2-butoxyethanol ($CH_3CH_2CH_2CH_2OCH_2CH_2OH$)

$10^{19} \times k$	T (K)	Technique[a]	Reference
< 1.1	296	GC–FID	Aschmann and Atkinson (1998b)

[a]Abbreviations used for the techniques are defined in table I-F-3.

Table III-C-18. Rate coefficients (k, cm^3 molecule^{-1} s^{-1}) for reaction of NO_3 with 2-butoxyethanol ($CH_3CH_2CH_2CH_2OCH_2CH_2OH$)

$10^{15} \times k$	T (K)	Technique[a]	Reference
3.1 ± 1.2	296	RR[b] (propene)	Aschmann and Atkinson (1998b)
3.1 ± 1.1	298	RR[c] (methacrolein)	Chew et al. (1998)

[a]Abbreviations used for the techniques are defined in table I-F-3.
[b]Placed on an absolute basis using $k(NO_3+C_3H_6) = 9.3 \times 10^{-15}$ cm^3 molecule^{-1} s^{-1}.
[c]Placed on an absolute basis using $k(NO_3+\text{methacrolein}) = 3.3 \times 10^{-15}$ cm^3 molecule^{-1} s^{-1} (Chew et al., 1998). Rate coefficient reported as an upper limit, due to possible contribution from reaction with N_2O_5.

both studies; this value is recommended with an estimated uncertainty of ±25%. The reaction will likely only make a minor contribution to the atmospheric chemistry of 2-butoxyethanol.

III-C-13.4. Summary of the Atmospheric Fate of 2-Butoxyethanol, and the End Products of Its Oxidation

For daytime [OH] $\approx 2.5 \times 10^6$ molecule cm^{-3}, the estimated lifetime for 2-butoxyethanol is about 4 h. Products of the OH-initiated oxidation of 2-butoxyethanol in the presence of NO_x have been determined by Stemmler et al. (1997b) and Tuazon et al. (1998a). Although quantitative discrepancies are evident (see summary in Tuazon et al., 1998a), the major products identified in both studies were butyl formate, 2-hydroxyethyl formate ($HOCH_2CH_2OCH{=}O$), propanal, and 3-hydroxybutyl formate [$HC(=O)OCH_2CH_2CH(OH)CH_3$]. Butoxyacetaldehyde ($n$-$C_4H_9OCH_2CHO$) was also reported in significant yield (12 ± 9%) by Stemmler et al. Routes to the major products have been described by Stemmler et al. and Tuazon et al. Butyl formate (with expected co-product formaldehyde) is obtained following OH-attack at the carbon labeled "2" in the structure below. Attack at the 1-position leads to butoxyacetaldehyde, attack at the 3-position yields hydroxybutyl formate and propanal, and attack at the 5-position is the proposed source of the 3-hydroxybutyl formate.

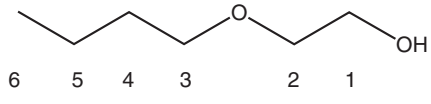

III-C-14. 1,2-Diethoxyethane ($CH_3CH_2OCH_2CH_2OCH_2CH_3$)

III-C-14.1. OH Reaction Kinetics

The reaction of OH with 1,2-diethoxyethane has been studied by Dagaut et al. (1989a) and Porter et al. (1997), see table III-C-19. There is significant disagreement between the measurements at 298 K; the Dagaut et al. (1989a) measurement is about a factor of 2 lower than both the relative rate and flash photolysis–laser-induced fluorescence measurements of Porter et al. (1997). Loss of the parent compound in the Dagaut et al. (1989a) experimental system is a possible explanation for the low value. Thus, the data of Porter et al. (1997) are recommended, with $k = 5.8 \times 10^{-18} T^2 \exp(1{,}400/T)$ and

Table III-C-19. Rate coefficients ($k = A \times T^n \times e^{-B/T}$, cm^3 molecule^{-1} s^{-1}) for reaction of OH with 1,2-diethoxyethane [$CH_3CH_2OCH_2CH_2OCH_2CH_3$]

$10^{18} \times A$	n	B (K)	$10^{12} \times k$	T (K)	Technique[a]	Reference	Temperature Range (K)
			26.8 ± 2.4	298	FP–RF	Dagaut et al. (1989a)	
			57.9 ± 5.3	298	RR[b]	Porter et al. (1997)	298–372
5.8 ± 1.1	2	$-1{,}400 \pm 50$	81.3 ± 2.5	262	PLP–LIF		
			73.6 ± 3.0	273			
			57.9 ± 2.4	294			
			47.4 ± 0.7	322			
			39.8 ± 1.1	348			
			33.6 ± 1.4	372			

[a]Abbreviations used for the techniques are defined in table I-F-3.

[b]Reference compound used not specified. Study involved use of a number of alkyl ethers and ethanol as reference compounds, reference rate coefficients quoted are within 10% of those recommended in the various sections of this book and in Calvert et al. (2008).

$k = 5.8 \times 10^{-11}$ cm^3 molecule^{-1} s^{-1} at 298 K. The uncertainty on the 298 K value is estimated to be ±25%.

III-C-14.2. Summary of the Atmospheric Fate of 1,2-Diethoxyethane, and the End Products of Its Oxidation

The lifetime of 1,2-diethoxyethane will be governed predominantly by its reaction with OH and is about 2 h for daytime $\approx 2.5 \times 10^6$ molecule cm^{-3}. No end product studies have been conducted. However, OH attack will likely occur at either of the two unique CH_2 sites in the molecule. Attack at the central sites could lead to two molecules of ethyl formate, via C—C bond rupture in the resultant alkoxy radical, $CH_3CH_2OCH(O)CH_2OCH_2CH_3$. However, isomerization via a 1,5-H-atom shift could also occur, resulting in a more complex product distribution. OH attack on the ethoxy fragment likely will lead to formaldehyde and $HC(O)OCH_2CH_2OCH_2CH_3$ via C—C bond rupture in the relevant alkoxy species, $CH_3CH(O\bullet)OCH_2CH_2OCH_2CH_3$.

III-C-15. 1,4-Dimethoxybutane ($CH_3OCH_2CH_2CH_2CH_2OCH_3$)

III-C-15.1. OH Reaction Kinetics

The only study of the reaction of OH with 1,4-dimethoxybutane is that of Moriarty et al. (2003), see table III-C-20 for a summary. Their relative rate and flash photolysis data, both measured at 298 K, are in good agreement. The average of these two determinations, $k = 3.0 \times 10^{-11}$ cm^3 molecule^{-1} s^{-1}, is recommended with an estimated uncertainty of ±20%.

III-C-15.2. Summary of the Atmospheric Fate of 1,4-Dimethoxybutane, and the End Products of Its Oxidation

The lifetime of 1,4-dimethoxybutane is about 4 h for daytime [OH] $= 2.5 \times 10^6$ molecule cm^{-3}. No end product studies have been conducted. However, the main site

Table III-C-20. Rate coefficients (k, cm^3 molecule^{-1} s^{-1}) for reaction of OH with 1,4-dimethoxybutane ($CH_3OCH_2CH_2CH_2CH_2OCH_3$)

$10^{12} \times k$	T (K)	Technique[a]	Reference
28.3 ± 1.2	298	RR[b] (di-*n*-butyl ether)	Moriarty et al. (2003)
30.7 ± 0.8	298	PLP–LIF	

[a]Abbreviations used for the techniques are defined in table I-F-3.
[b]Placed on an absolute basis using $k[OH+(n\text{-}C_4H_9)_2O] = 2.8 \times 10^{-11}$ cm^3 molecule^{-1} s^{-1} (this book, section III-B-12.1).

for OH reaction is likely at the CH_2 groups adjacent to the ether linkages, leading to the formation of the $CH_3OCH(O\bullet)CH_2CH_2CH_2OCH_3$ alkoxy species. Decomposition via C—C bond cleavage and isomerization are potentially important fates of this radical in the lower troposphere. Decomposition would yield mostly methyl formate and $HC(=O)CH_2CH_2OCH_3$, while isomerization would likely lead to the multi-functional species, $CH_3OC(=O)CH_2CH(OH)OCH_3$.

III-C-16. Di-*n*-propoxymethane [$CH_3CH_2CH_2OCH_2OCH_2CH_2CH_3$]

III-C-16.1. OH Reaction Kinetics

The reaction of OH with di-*n*-propoxy methane has been studied between 263 and 616 K (Thüner et al., 1999; Vovelle et al., 2001; Le Calvé et al., 2002), see table III-C-21 and figure III-C-5. The data provide a consistent picture for this reaction, which possesses a negative temperature dependence between 260 and 500 K, and a positive temperature dependence at $T > 500$ K. A fit of all data below 400 K to the Arrhenius equation yields $k = 4.3 \times 10^{-12} \exp(546/T)$ cm^3 molecule^{-1} s^{-1}, with $k = 2.7 \times 10^{-11}$ cm^3 molecule^{-1} s^{-1} at 298 K. An uncertainty of ±15% is estimated at 298 K. The entire dataset is well represented by the sum of two Arrhenius expressions (Vovelle et al., 2001): $k = 2.10 \times 10^{-12} \exp(745/T) + 1.29 \times 10^{-10} \exp(-1{,}368/T)$ cm^3 molecule^{-1} s^{-1}.

III-C-16.2. Summary of the Atmospheric Fate of Di-n-propoxymethane, and the End Products of Its Oxidation

The lifetime of di-*n*-propoxymethane in the lower atmosphere will be controlled by its reaction with OH. For daytime [OH] $\approx 2.5 \times 10^6$ molecule cm^{-3}, the lifetime is about 4 h. Possible end products include di-*n*-propyl carbonate, following OH attack at the central CH_2 group, or $CH_3CH_2CH_2OCH_2OCH{=}O$ and acetaldehyde, following OH attack at the two equivalent CH_2 groups adjacent to the ether site.

III-C-17. 2,2-Diethoxypropane [$(CH_3)_2C(OCH_2CH_3)_2$]

III-C-17.1. OH Reaction Kinetics

Dagaut et al. (1989a) have studied the reaction of OH with 2,2-diethoxypropane as a function of temperature (240–440 K). As summarized in table III-C-22, the rate

Table III-C-21. Rate coefficients ($k = A \times e^{-B/T}$, cm^3 molecule^{-1} s^{-1}) for reaction of OH with di-*n*-propoxymethane [$CH_3CH_2CH_2OCH_2OCH_2CH_2CH_3$]

$10^{12} \times A$	B (K)	$10^{11} \times k$	T (K)	Technique[a]	Reference	Temperature Range (K)
		3.07 ± 0.03	298	RR[b] (*m*-xylene)	Thüner et al. (1999)	
		2.43 ± 0.22	298	RR[c] (*cyclo*-C_6H_{12})		
		2.23 ± 0.22	298	RR[d] (toluene)		
		2.53 ± 0.08	296	PLP–LIF	Vovelle et al. (2001)	296–616
		2.63 ± 0.06	297			
		2.58 ± 0.06	297			
		2.65 ± 0.07	297			
		2.27 ± 0.04	316			
		1.86 ± 0.03	368			
		1.78 ± 0.05	433			
		1.62 ± 0.06	500			
		1.85 ± 0.05	566			
		2.09 ± 0.05	616			
		2.16 ± 0.05	616			
		2.25 ± 0.10	616			
4.39 ± 1.06	−563 ± 74	3.88 ± 0.26	263	PLP–LIF	Le Calvé et al. (2002)	263–372
		3.55 ± 0.23	273			
		3.51 ± 0.25	273			
		3.21 ± 0.29	283			
		2.84 ± 0.19	298			
		2.68 ± 0.22	298			
		2.86 ± 0.22	298			
		2.65 ± 0.23	298			
		2.37 ± 0.20	323			
		2.45 ± 0.29	323			
		2.23 ± 0.16	348			
		2.12 ± 0.15	372			
		1.98 ± 0.19	372			

[a]Abbreviations used for the techniques are defined in table I-F-3.
[b]Placed on an absolute basis using k(OH+*m*-xylene) = 2.31×10^{-11} cm^3 molecule^{-1} s^{-1} (Calvert et al., 2002).
[c]Placed on an absolute basis using k(OH+*cyclo*-C_6H_{12}) = 6.97×10^{-12} cm^3 molecule^{-1} s^{-1} (Calvert et al., 2008).
[d]Placed on an absolute basis using k(OH+toluene) = 5.6×10^{-12} cm^3 molecule^{-1} s^{-1} (Calvert et al., 2002).

coefficient was found to be essentially independent of temperature over the range studied with $k = 10.6 \times 10^{-12} \exp(15/T)$ cm^3 molecule^{-1} s^{-1}, which gives $k = 1.11 \times 10^{-11}$ cm^3 molecule^{-1} s^{-1} at 298 K. Given the lack of corroborative measurements, an uncertainty of ±25% is estimated at 298 K.

III-C-17.2. Summary of the Atmospheric Fate of 2,2-Diethoxypropane, and the End Products of Its Oxidation

The lifetime of 2,2-diethoxypropane will be determined by its reaction with OH. A lifetime of 10 h is estimated, for daytime [OH] $\approx 2.5 \times 10^6$ molecule cm^{-3}. Reaction with OH will likely occur predominantly at the —OCH_2 groups, likely leading to $CH_3CH_2OC(CH_3)_2OCHO$ as a major end product.

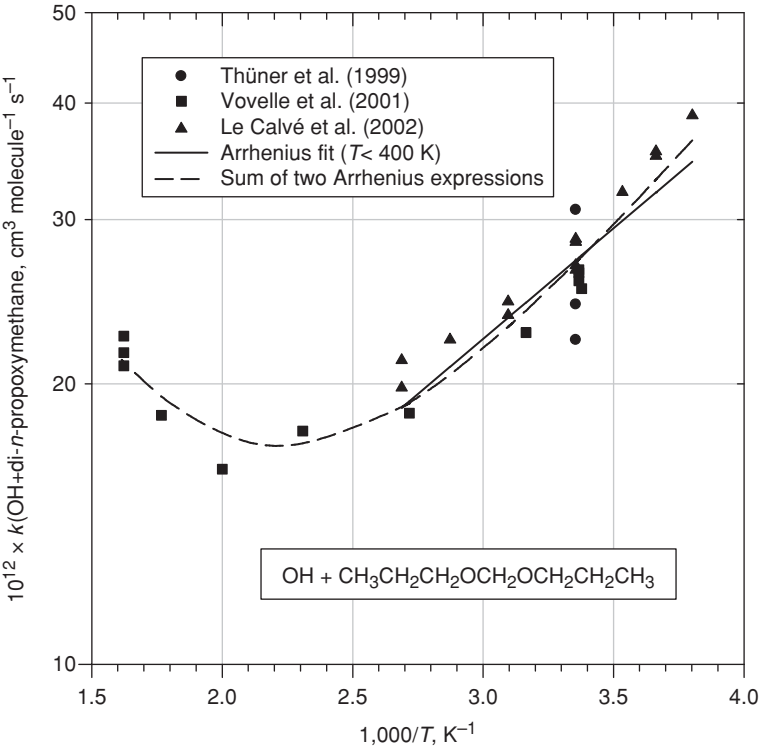

Figure III-C-5. Arrhenius plot of the rate coefficient for the reaction of OH with di-*n*-propoxymethane ($CH_3CH_2CH_2OCH_2OCH_2CH_2CH_3$).

Table III-C-22. Rate coefficients ($k = A \times e^{-B/T}$, cm^3 $molecule^{-1}$ s^{-1}) for reaction of OH with 2,2-diethoxypropane [$(CH_3CH_2O)_2C(CH_3)_2$]

$10^{12} \times A$	B (K)	$10^{12} \times k$	T (K)	Technique[a]	Reference	Temperature Range (K)
10.6 ± 2.5	−15 ± 75	11.1 ± 1.7	240	FP–RF	Dagaut et al. (1989a)	240–440
		11.7 ± 1.3	298			
		10.5 ± 1.0	350			
		11.7 ± 1.0	400			
		10.6 ± 0.7	440			

[a]Abbreviations used for the techniques are defined in table I-F-3.

III-C-18. Di-isopropoxymethane [$(CH_3)_2CHOCH_2OCH(CH_3)_2$]

III-C-18.1. OH Reaction Kinetics

Rate coefficients for the reaction of OH with di-isopropoxymethane have been reported by Thüner et al. (1999), Becker et al. (1999a), and Freitas Dinis et al. (2001). Data are summarized in table III-C-23 and figure III-C-6. The rate coefficient shows a minimum

Table III-C-23. Rate coefficients (k, cm^3 molecule^{-1} s^{-1}) for reaction of OH with di-isopropoxymethane [$(CH_3)_2CHOCH_2OCH(CH_3)_2$]

$10^{11} \times k$	T (K)	Technique[a]	Reference	Temperature Range (K)
3.88 ± 0.06	298	RR[b] (*m*-xylene)	Thüner et al. (1999)	
3.86 ± 0.24	298	RR[c] (*cyclo*-C_6H_{12})		
3.47 ± 0.20	296	PLP–LIF	Becker et al. (1999b)	296–697
2.81 ± 0.12	350			
2.22 ± 0.10	410			
2.32 ± 0.20	503			
3.17 ± 0.33	602			
3.43 ± 0.08	697			
5.52 ± 1.7	250	PLP–LIF	Freitas Dinis et al. (2001)	250–270
5.55 ± 2.0	270			

[a]Abbreviations used for the techniques are defined in table I-F-3.
[b]Placed on an absolute basis using k(OH+*m*-xylene) = 2.31 × 10^{-11} cm^3 molecule^{-1} s^{-1} (Calvert et al., 2002).
[c]Placed on an absolute basis using k(OH+*cyclo*-C_6H_{12}) = 6.97 × 10^{-12} cm^3 molecule^{-1} s^{-1} (Calvert et al., 2008).

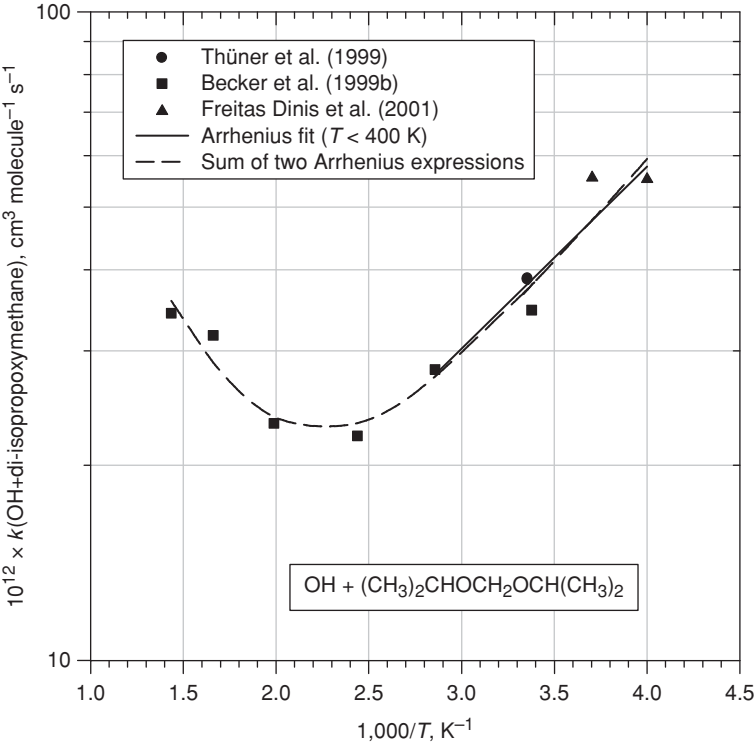

Figure III-C-6. Arrhenius plot of the rate coefficient for the reaction of OH with di-isopropoxymethane [$(CH_3)_2CHOCH_2OCH(CH_3)_2$].

near 400 K, a positive temperature dependence above this temperature, and a negative temperature dependence below it. A fit of all data obtained at $T < 400$ K to the Arrhenius equation yields: $k = 4.4 \times 10^{-12} \times \exp(646/T)$ cm^3 molecule^{-1} s^{-1}, with $k = 3.8 \times 10^{-11}$ cm^3 molecule^{-1} s^{-1} at 298 K. An uncertainty of ±15% is estimated at 298 K. The full dataset ($250 < T < 700$ K) is well represented by the sum of two Arrhenius expressions; best fit is obtained with: $k = 2.9 \times 10^{-12} \exp(756/T) + 3.0 \times 10^{-10} \times \exp(-1{,}673/T)$ cm^3 molecule^{-1} s^{-1}.

III-C-18.2. Summary of the Atmospheric Fate of Di-isopropoxymethane, and the End Products of Its Oxidation

Reaction of di-isopropoxymethane with OH is quite rapid; with daytime [OH] = 2.5×10^6 molecule cm^{-3}, a lifetime of 3 h is estimated. Products of the OH-initiated oxidation of this species have not been determined. However, reaction of OH at the isopropyl CH groups is probably the major site of attack and likely leads to the formation of the acetate ester, $CH_3C(O\bullet)OCH_2OCH(CH_3)_2$. Attack at the central CH_2 group is also likely to be important, possibly leading to the formation of the carbonate species, $(CH_3)_2CHOC(=O)OCH(CH_3)_2$.

III-C-19. 1-Butoxy-2-propanol [$CH_3CH_2CH_2CH_2OCH_2CH(OH)CH_3$]

III-C-19.1. OH Reaction Kinetics

Aschmann et al. (2001b) used a relative rate method to obtain a rate coefficient, $k = 3.8 \times 10^{-11}$ cm^3 molecule^{-1} s^{-1}, for the reaction of OH with 1-butoxy-2-propanol. Their measurements are summarized in table III-C-24. Given the lack of corroborative measurements, an uncertainty of ±25% is estimated at 298 K.

III-C-19.2. Summary of the Atmospheric Fate of 1-Butoxy-2-propanol, and the End Products of its Oxidation

Given its rapid reaction with OH, the atmospheric lifetime of 1-butoxy-2-propanol will be quite short, about 3 h for daytime [OH] ≈ 2.5×10^6 molecule cm^{-3}. Products of the OH-initiated oxidation in the presence of NO_x have been quantified by Aschmann et al. (2001b), using a combination of GC, FTIR, and

Table III-C-24. Rate coefficient (k, cm^3 molecule^{-1} s^{-1}) for reaction of OH with 1-butoxy-2-propanol [n-$C_4H_9OCH_2CH(OH)CH_3$].

$10^{11} \times k$	T (K)	Technique[a]	Reference
3.76 ± 0.39	296	RR[b] (2-methyl-propene)	Aschmann et al. (2001b)

[a]Abbreviations used for the techniques are defined in table I-F-3.
[b]Placed on an absolute basis using k(OH+2-methyl-propene) = 5.2×10^{-11} cm^3 molecule^{-1} s^{-1} (Calvert et al. 2000).

mass spectroscopy techniques. Products observed (molar yields) included acetaldehyde (49 ± 6%), *n*-butyl formate (44 ± 4%), propanal (23 ± 3%), and *n*-$C_4H_9OCH_2C(=O)CH_3$ (or isomers, 22 ± 4%), and total organic nitrate (~8%). Products of molecular weight 118 [possibly $CH_3CH_2CH(OH)CH_2OCHO$] and 146 [possibly $CH_3C(O)CH_2CH_2OCH_2CH(OH)CH_3$] were also identified, but not quantified. As detailed by Aschmann et al. (2001b), there are likely three main sites for OH reaction on 1-butoxy-propanol: the two CH_2 groups adjacent to the ether oxygen, and the CH group adjacent to the alcohol functionality. The two main products, acetaldehyde and *n*-butyl formate, are formed in concert from attack at the CH_2 group on the propane portion of the molecule, from C—C bond rupture in the *n*-$C_4H_9OCH(O•)CH(OH)CH_3$ radical. OH attack at the CH_2 site on the *n*-butoxy side of the ether linkage, leads to both propanal and $CH_3CH(OH)CH_2OCHO$ via C—C bond rupture in the $CH_3CH_2CH_2CH(O•)OCH_2CH(OH)CH_3$ alkoxy species. Lastly, the *n*-$C_4H_9OCH_2C(=O)CH_3$ product is obtained from oxidation at the —CH(OH) site.

III-C-20. Di-*n*-butoxymethane ($CH_3CH_2CH_2CH_2OCH_2OCH_2CH_2CH_2CH_3$)

III-C-20.1. OH Reaction Kinetics

Rate coefficient for the reaction of OH with di-*n*-butoxy-methane have been reported by Thüner et al. (1999), Becker et al. (1999b), Freitas Dinis et al. (2001), and Le Calvé et al. (2002). The data cover the range 260–710 K, see table III-C-25 and figure III-C-7. The rate coefficient possesses a minimum in the 350–500 K range, while higher values are found above and below these temperatures. Fitting all data measured below 400 K to the Arrhenius equation yields: $k = 5.2 \times 10^{-12} \exp(580/T)$ cm^3 molecule^{-1} s^{-1}, with $k = 3.6 \times 10^{-11}$ cm^3 molecule^{-1} s^{-1} at 298 K. An uncertainty of ±15% is estimated at 298 K. Data over the entire temperature range studied can be represented as the sum of two Arrhenius expressions: $k = 1.4 \times 10^{-12} \exp(917/T) + 8.9 \times 10^{-11} \exp(-818/T)$ cm^3 molecule^{-1} s^{-1}.

III-C-20.2. Summary of the Atmospheric Fate of Di-n-butoxymethane, and the End Products of Its Oxidation

The lifetime of di-*n*-butoxymethane in the lower atmosphere, as determined by its reaction with OH, will be about 3 h for daytime [OH] ≈ 2.5×10^6 molecule cm^{-3}. The products of the OH-initiated oxidation have been studied in the presence of NO_x by Maurer et al. (2000). The major products observed are *n*-butoxy methyl formate [$HC(O)OCH_2OC_4H_9$] and propanal, both of which are produced from OH-attack at the 4-position on the parent species, following decomposition of the resultant $CH_3CH_2CH_2CH(O•)OC_4H_9$ radical. On the basis of the observed yields of *n*-butoxy methyl formate, these species likely account for about 80% of the product distribution. Di-*n*-butyl carbonate [*n*-$C_4H_9OC(=O)OC_4H_9$, the product of OH attack at the central CH_2 group] was found in small yield (< 10%).

Table III-C-25. Rate coefficients ($k = A \times e^{-B/T}$, cm^3 $molecule^{-1}$ s^{-1}) for reaction of OH with di-*n*-butoxymethane [$CH_3CH_2CH_2CH_2OCH_2OCH_2CH_2CH_2CH_3$]

$10^{12} \times A$	B (K)	$10^{11} \times k$	T (K)	Technique[a]	Reference	Temperature Range (K)
		3.18 ± 0.23	298	RR[b] (1-hexene)	Thüner et al. (1999)	
		3.86 ± 0.13	298	RR[c] (*m*-xylene)		
		3.42 ± 0.07	298	RR[d] (1,3,5-trimethylbenzene)		
		3.39 ± 0.46	298	PLP–LIF	Becker et al. (1999b)	298–710
		2.57 ± 0.30	400			
		2.94 ± 0.62	600			
		3.31 ± 0.69	710			
		4.95 ± 0.27	260	PLP–LIF	Freitas Dinis et al. (2001)	260–500
		4.56 ± 0.18	270			
		4.06 ± 0.30	280			
		2.58 ± 0.14	500			
5.15 ± 0.66	−590 ± 38	4.90 ± 0.57	263	PLP–LIF	Le Calvé et al. (2002)	263–372
		4.59 ± 0.64	273			
		4.55 ± 0.62	273			
		3.99 ± 0.55	283			
		3.62 ± 0.59	298			
		3.78 ± 0.46	298			
		3.65 ± 0.49	298			
		3.77 ± 0.71	298			
		3.23 ± 0.52	323			
		2.75 ± 0.35	348			
		2.58 ± 0.41	372			
		2.56 ± 0.33	372			

[a]Abbreviations used for the techniques are defined in table I-F-3.
[b]Placed on an absolute basis using k(OH+1-hexene) = 3.7×10^{-11} cm^3 $molecule^{-1}$ s^{-1} (Calvert et al., 2000).
[c]Placed on an absolute basis using k(OH+*m*-xylene) = 2.31×10^{-11} cm^3 $molecule^{-1}$ s^{-1} (Calvert et al., 2002).
[d]Placed on an absolute basis using k(OH+1,3,5-trimethylbenzene) = 5.7×10^{-11} cm^3 $molecule^{-1}$ s^{-1} (Calvert et al., 2002).

III-C-21. Di-*sec*-butoxymethane [$CH_3CH_2CH(CH_3)OCH_2OCH(CH_3)CH_2CH_3$]

III-C-21.1. OH Reaction Kinetics

The reaction of OH with di-*sec*-butoxymethane has been studied between 260 and 700 K by Thüner et al. (1999), Becker et al. (1999a), and Freitas Dinis et al. (2001), see table III-C-26 and figure III-C-8. As for a number of other structurally similar species (di-*n*-propoxy-, di-isopropoxy-, and di-*n*-butoxy-methane, see discussion in previous sections), the rate coefficient displays a complex temperature dependence, with a minimum value observed near 500 K. Fitting of the Arrhenius equation to all the data measured at 401 K and below yields: $k = 8.7 \times 10^{-12} \times \exp(477/T)$ cm^3 $molecule^{-1}$ s^{-1}, which gives $k = 4.3 \times 10^{-11}$ cm^3 $molecule^{-1}$ s^{-1} at 298 K. An uncertainty of ±15% is assigned at 298 K. For a wider temperature range (260–700 K), the expression: $k = 7.2 \times 10^{-12} \exp(530/T) + 7.8 \times 10^{-11} \exp(-2{,}907/T)$ cm^3 $molecule^{-1}$ s^{-1} provides an excellent fit to the data.

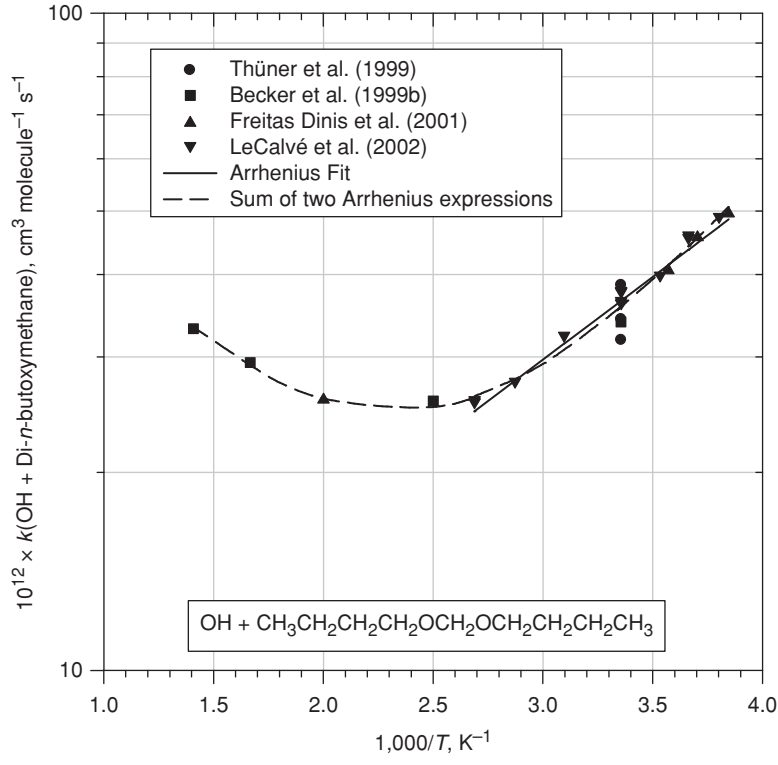

Figure III-C-7. Arrhenius plot of the rate coefficient for the reaction of OH with di-*n*-butoxymethane ($CH_3CH_2CH_2CH_2OCH_2OCH_2CH_2CH_2CH_3$).

Table III-C-26. Rate coefficients (k, cm^3 molecule^{-1} s^{-1}) for reaction of OH with di-*sec*-butoxymethane [$CH_3CH_2CH(CH_3)OCH_2OCH(CH_3)CH_2CH_3$]

$10^{11} \times k$	T (K)	Technique[a]	Reference	Temperature Range (K)
4.92 ± 0.05	298	RR[b] (*m*-xylene)	Thüner et al. (1999)	
4.25 ± 0.13	295	PLP–LIF	Becker et al. (1999b)	295–700
2.82 ± 0.24	401			
2.15 ± 0.38	501			
2.56 ± 0.22	602			
2.70 ± 0.43	700			
5.50 ± 0.17	261	PLP–LIF	Freitas Dinis et al. (2001)	261–270
4.85 ± 0.15	270			

[a]Abbreviations used for the techniques are defined in table I-F-3.
[b]Placed on an absolute basis using k(OH+*m*-xylene) = 2.31×10^{-11} cm^3 molecule^{-1} s^{-1} (Calvert et al., 2002).

III-C-21.2. Summary of the Atmospheric Fate of Di-sec-butoxymethane, and the End Products of Its Oxidation

The reaction of OH with di-*sec*-butoxymethane is rapid and thus its lifetime is quite short, about 2.5 h, assuming daytime [OH] $\approx 2.5 \times 10^6$

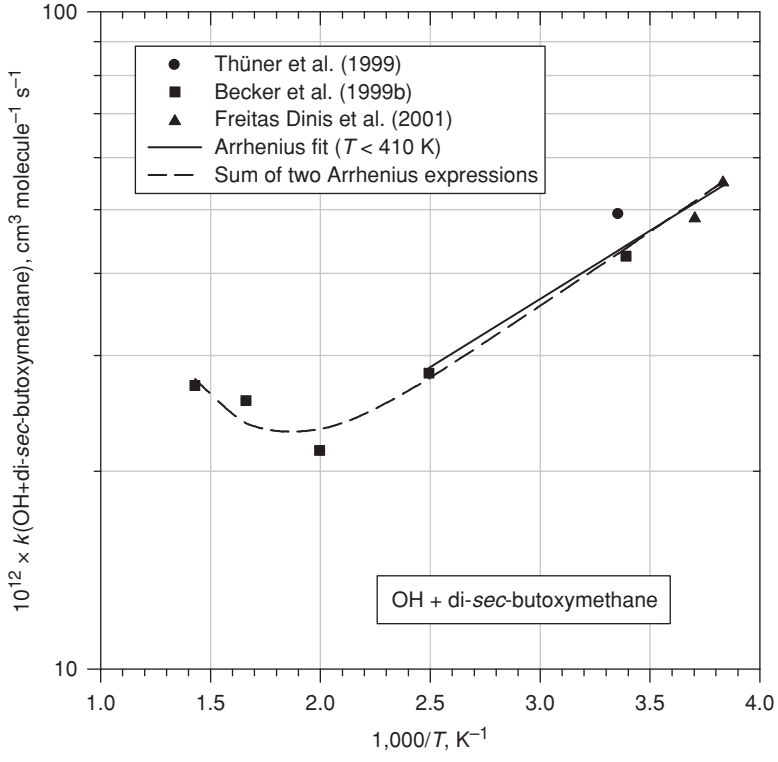

Figure III-C-8. Arrhenius plot of the rate coefficient for the reaction of OH with di-*sec*-butoxymethane [$CH_3CH_2CH(CH_3)OCH_2OCH(CH_3)CH_2CH_3$].

molecule cm^{-3}. No data are available regarding the products of the OH-initiated oxidation of this species. However, reaction of OH with di-*sec*-butoxymethane will likely occur mainly at the two equivalent CH groups located alpha to the ether linkages. This will likely result in the formation of acetaldehyde and *sec*-butoxymethyl acetate [$CH_3CH_2CH(CH_3)OCH_2OC(O)CH_3$], via decomposition of the $CH_3CH_2CH(CH_3)OCH_2OC(O\bullet)(CH_3)CH_2CH_3$ radical. OH reaction at the central CH_2 group will likely lead to the di-*sec*-butoxycarbonate species, $CH_3CH_2(CH_3)CHOC(=O)OCH(CH_3)CH_2CH_3$.

III-C-22. Di-isobutoxymethane [$(CH_3)_2CHCH_2OCH_2OCH_2CH(CH_3)_2$]

III-C-22.1. OH Reaction Kinetics

The only study of the reaction of OH with di-isobutoxymethane is the 298 K relative rate study of Thüner et al. (1999). The average of their three determinations gives $k = 3.6 \times 10^{-11}$ cm^3 $molecule^{-1}$ s^{-1}, see table III-C-27 for a summary. Given the lack of corroborative measurements, an uncertainty of ±25% is assigned to this value.

Table III-C-27. Rate coefficients (k, cm^3 molecule^{-1} s^{-1}) for reaction of OH with di-isobutoxymethane [$(CH_3)_2CHCH_2OCH_2OCH_2CH(CH_3)_2$]

$10^{11} \times k$	T (K)	Technique[a]	Reference
4.00 ± 0.14	298	RR[b] (*m*-xylene)	Thüner et al. (1999)
3.74 ± 0.17	298	RR[c] (cyclohexane)	
3.19 ± 0.10	298	RR[d] (1,3,5-trimethylbenzene)	

[a]Abbreviations used for the techniques are defined in table I-F-3.
[b]Placed on an absolute basis using k(OH+*m*-xylene) = 2.31×10^{-11} cm^3 molecule^{-1} s^{-1} (Calvert et al., 2002).
[c]Placed on an absolute basis using k(OH+cyclohexane) = 6.97×10^{-12} cm^3 molecule^{-1} s^{-1} (Calvert et al., 2008).
[d]Placed on an absolute basis using k(OH+1,3,5-trimethylbenzene) = 5.7×10^{-11} cm^3 molecule^{-1} s^{-1} (Calvert et al., 2002).

III-C-22.2. Summary of the Atmospheric Fate of Di-isobutoxymethane, and the End Products of Its Oxidation

For daytime [OH] $\approx 2.5 \times 10^6$ molecule cm^{-3}, the lifetime of di-isobutoxymethane will be about 4 h. No studies of the products of the OH-initiated oxidation of this species have been carried out. However, the major site for OH attack is likely at the two equivalent CH_2 groups on the isobutoxy groups, located alpha to the ether oxygens. Attack at these sites will likely generate *sec*-butoxymethyl formate and acetone as major products. The formation of di-isobutoxycarbonate from OH attack at the central CH groups also seems plausible.

III-C-23. Tri-functional Ethers

There have only been a few studies related to the atmospheric behavior of trifunctional ethers. Compounds studied include 1,1,3-trimethoxypropane [$(CH_3O)_2CHCH_2CH_2OCH_3$, Dagaut et al., 1989a], trimethoxymethane [$(CH_3O)_3CH$, Platz et al., 1999], diethylene glycol ethyl ether ($CH_3CH_2OCH_2CH_2OCH_2CH_2OH$), and diethylene glycol *n*-butyl ether (n-$C_4H_9OCH_2CH_2OCH_2CH_2OH$), both the latter compounds studied by Aschmann et al. (2001b). The available data are summarized below.

III-C-23.1. OH Reaction Kinetics

There exists a single room-temperature determination of the rate coefficient for reaction of OH with each of the four compounds listed above (Dagaut et al., 1989a; Platz et al., 1999; Aschmann et al., 2001b). The data are summarized in table III-C-28. Given the lack of corroborative studies, these rate coefficients are recommended with uncertainties of $\pm 35\%$.

III-C-23.2. Cl-Atom Reaction Kinetics

The reaction of Cl-atoms with trimethoxymethane was studied by Platz et al. (1999), using a relative rate technique. They report a rate coefficient, $k = 1.56 \times 10^{-10}$ cm^3 molecule^{-1} s^{-1}, near 298 K. Data are summarized in table III-C-29.

Table III-C-28. Rate coefficients (k, cm^3 molecule^{-1} s^{-1}) for reaction of OH with some tri-functional ether species

$10^{12}\times k$	T (K)	Technique[a]	Reference	Lifetime, h
OH + 1,1,3-Trimethoxypropane, $(CH_3O)_2CHCH_2CH_2OCH_3$				
16.7 ± 1.0	298	FP–RF	Dagaut et al. (1989a)	7[b]
OH + Trimethoxymethane, $(CH_3O)_3CH$				
6.0 ± 0.5	295	PR–UV abs.	Platz et al. (1999)	46[c]
OH + Diethylene glycol ethyl ether, $CH_3CH_2OCH_2CH_2OCH_2CH_2OH$				
57.2 ± 6.3	296	RR[d] (2-methyl-propene)	Aschmann et al. (2001b)	2[b]
OH + Diethylene glycol *n*-butyl ether, $CH_3CH_2CH_2CH_2OCH_2CH_2OCH_2CH_2OH$				
74.4 ± 5.8	296	RR[d] (2-methyl-propene)	Aschmann et al. (2001b)	1.5[b]

[a]Abbreviations used for the techniques are defined in table I-F-3.
[b]Assuming daytime [OH] $\approx 2.5 \times 10^6$ molecule cm^{-3}.
[c]Assuming diurnally averaged [OH] $\approx 1 \times 10^6$ molecule cm^{-3}.
[d]Placed on an absolute basis using k(OH+2-methyl-propene) $= 5.2 \times 10^{-11}$ cm^3 molecule^{-1} s^{-1} (Calvert et al., 2000).

Table III-C-29. Rate coefficients (k, cm^3 molecule^{-1} s^{-1}) for reaction of Cl with trimethoxymethane [$(CH_3O)_3CH$]

$10^{10}\times k$	T (K)	Technique[a]	Reference
1.54 ± 0.10	296	RR[b] (ethene)	Platz et al. (1999)
1.58 ± 0.15	296	RR[c] (1,3,5-trioxane)	

[a]Abbreviations used for the techniques are defined in table I-F-3.
[b]Placed on an absolute basis using k(Cl+ethene) $= 9.5 \times 10^{-11}$ cm^3 molecule^{-1} s^{-1} (this book, table I-F-2).
[c]Placed on an absolute basis using k(Cl+1,3,5-trioxane) $= 10.5 \times 10^{-11}$ cm^3 molecule^{-1} s^{-1} (this book, section III-E-12.2).

III-C-23.3. Summary of the Atmospheric Fate of Various Tri-functional Ether Species, and the End Products of Their Oxidation

Estimated lifetimes for the four tri-functional species under consideration here are presented in table III-C-28.

The mechanism of OH-initiated oxidation of trimethoxymethane was studied by Platz et al. (1999). The only product observed was dimethyl carbonate [DMC, $CH_3OC(=O)OCH_3$], with a yield of 81 ± 10%. Platz et al. reasoned that the major site for OH attack would be on the methoxy groups, leading to the formation of the $(CH_3O)_2CHOCH_2O\bullet$ radical. DMC then results from C—O bond rupture in this radical:

$$(CH_3O)_2CHOCH_2O\bullet \rightarrow (CH_3O)_2CH(O\bullet) + CH_2O$$

$$(CH_3O)_2CH(O\bullet) + O_2 \rightarrow (CH_3O)_2C{=}O(\text{DMC}) + HO_2$$

However, as pointed out by Platz et al., DMC is also the expected product of OH attack at the CH moiety in trimethyoxymethane:

$$OH + (CH_3O)_3CH(+O_2) \rightarrow (CH_3O)_3C(OO\bullet)$$

$$(CH_3O)_3C(OO\bullet) + NO \rightarrow (CH_3O)_3C(O\bullet) + NO_2$$

$$(CH_3O)_3C(O\bullet) \rightarrow (CH_3O)_2C(=O) + CH_3O\bullet$$

$$CH_3O\bullet + O_2 \rightarrow CH_2O + HO_2$$

Aschmann et al. (2001b) reported on the products of the OH-initiated oxidation of the two ethers of diethylene glycol, $ROCH_2CH_2OCH_2CH_2OH$, where R is C_2H_5 or n-C_4H_9. Products were identified and quantified using a combination of gas chromatographic, infrared absorption, and mass spectral techniques. For the ethyl ether, major products identified were formaldehyde (39 ± 3% yield), 2-hydroxyethyl formate [$HC(=O)OCH_2CH_2OH$, 38 ± 8% yield], ethyl formate (38 ± 7% yield), $CH_3CH_2OCH_2CH_2CH=O$ (26 ± 4% yield), and $HOCH_2CH_2OCH_2CH_2OCH=O$ (17±4% yield). Pathways to these species are given in reaction mechanism III-C-23.3.1 (only the relevant alkoxy radical intermediates are shown).

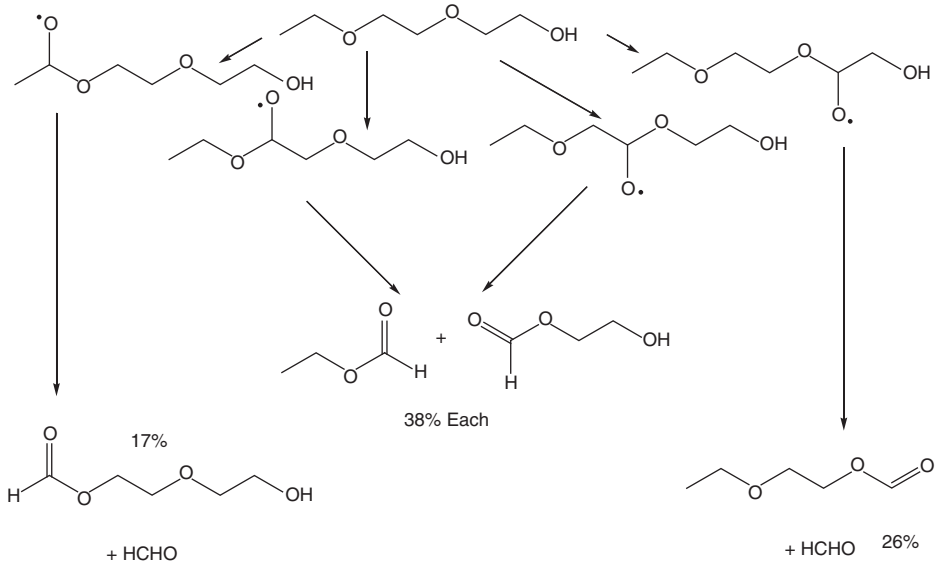

Reaction mechanism III-C-23.3.1

For the larger n-butyl ether, analogous products were observed, and analogous reaction pathways were assumed to be operative (with product yields of 20%, 34%, and 16% in the case of the n-butyl ether, compared to the 17%, 38%, and 26% shown above for the ethyl case).

III-C-24. Alkoxy Esters [$RC(O)O(CH_2)_nOR'$, R = H, CH_3; n = 1,2; R′ = CH_3, C_2H_5]

The rate coefficients for reactions of OH with a series of eight alkoxy esters [general formula $RC(O)O(CH_2)_nOR'$, with R = H, CH_3; n = 1 or 2; R′ = CH_3 or C_2H_5] have been determined by O'Donnell et al. (2004) using a combination of

relative and absolute techniques. Additional data are available for the OH reaction rate coefficient with one of these eight species, $CH_3C(O)OCH_2CH_2OCH_2CH_3$ (Hartmann et al., 1987; Williams et al., 1993) as well as for two additional species, $(CH_3)_2CHCH_2C(O)OCH_2CH_2OCH_2CH_3$ (Williams et al., 1993) and $CH_3CH_2OCH_2CH_2C(O)OCH_2CH_3$ (Baxley et al., 1997). The OH rate coefficient data for these 10 alkoxy esters are summarized in table III-C-30 and are used to estimate their atmospheric lifetimes.

III-C-24.1. OH Reaction Kinetics

As noted above, O'Donnell et al. (2004) studied the reaction of a series of alkoxy esters with OH, using both pulsed laser photolysis–laser-induced fluorescence (263–372 K) and a relative rate method (298 K only). Agreement between the relative and absolute rate data at 298 K is generally very good, around 10% on average and always better than 20%. The compounds possess 298 K rate coefficients that range from about 1.7×10^{-12} for the simplest species, $HC(O)OCH_2OCH_3$, to about 13×10^{-12} cm^3 molecule^{-1} s^{-1} for the most complex, $CH_3C(O)OCH_2CH_2OCH_2CH_3$. Rate coefficients for all compounds display negative temperature dependences. Additional 298 K data for the $CH_3C(O)OCH_2CH_2OCH_2CH_3$ species (Hartmann et al., 1987; Williams et al., 1993) are in excellent agreement with the O'Donnell et al. (2004) study. Rate coefficients have also been determined at 298 K for two other alkoxy ester species. The data of Williams et al. (1993) yield $k = 15 \times 10^{-12}$ cm^3 molecule^{-1} s^{-1} for the rate coefficient for reaction of OH with 2-ethoxyethyl isobutyrate, $(CH_3)_2CHC(O)OCH_2CH_2OCH_2CH_3$, while those of Baxley et al. (1997) give $k = 22 \times 10^{-12}$ cm^3 molecule^{-1} s^{-1} for reaction of OH with ethyl 3-ethoxypropionate, $CH_3CH_2OCH_2CH_2C(O)OCH_2CH_3$.

III-C-24.2. Summary of the Atmospheric Fate of the Alkoxy Ester Species, and the End Products of Their Oxidation

Assuming globally averaged [OH] $\approx 10^6$ molecule cm^{-3}, lifetimes for the 10 alkoxy esters discussed above range from 7 days ($HC(O)OCH_2OCH_3$) to as little as 0.5 days ($CH_3CH_2OCH_2CH_2C(O)OCH_2CH_3$).

Product studies on the alkoxy ester species are limited to only a pair of studies. Wells et al. (1996) studied the OH-initiated oxidation of 2-ethoxyethyl acetate [$CH_3C(O)OCH_2CH_2OCH_2CH_3$], and observed the formation of two major products: $CH_3C(O)OCH_2CH_2OCHO$ ($37 \pm 3\%$ yield, obtained via oxidation of the CH_2 group in —OCH_2CH_3), and ethyl formate ($33 \pm 2\%$, obtained via oxidation of the CH_2 group adjacent to the ether linkage). Expected co-products of the ethyl formate (CO, acetic acid, and formic acetic anhydride) were either not quantified or not observed.

Baxley et al. (1997) quantified the products of the OH-initiated oxidation of ethyl 3-ethoxypropionate, $CH_3CH_2OCH_2CH_2C(O)OCH_2CH_3$. Major products identified (molar yields) were: ethyl formate ($37 \pm 1\%$) and ethyl glyoxylate ($25 \pm 1\%$), both obtained from oxidation of the CH_2 group attached to the ethoxy fragment; and $HC(O)OCH_2CH_2C(O)OCH_2CH_3$ ($30 \pm 1\%$), obtained via oxidation at the ethoxy

Table III-C-30. Rate coefficients ($k = A \times e^{-B/T}$, cm^3 $molecule^{-1}$ s^{-1}) for reaction of OH with ten alkoxy ester species

$10^{12} \times A$	B (K)	$10^{12} \times k$	T (K)	Technique[a]	Reference	Temperature Range (K)
OH + $HC(O)OCH_2OCH_3$						
		1.80 ± 0.17	298	RR[b] (n-C_3H_7OH)	O'Donnell et al. (2004)	
1.4 ± 0.4	−(56 ± 97)	1.82 ± 0.07	263	PLP–LIF	O'Donnell et al. (2004)	263–372
		1.77 ± 0.08	273			
		1.62 ± 0.10	298			
		1.61 ± 0.10	323			
		1.67 ± 0.13	348			
		1.73 ± 0.10	372			
OH + $CH_3C(O)OCH_2OCH_3$						
		2.78 ± 0.17	298	RR[b] (n-C_3H_7OH)	O'Donnell et al. (2004)	
1.8 ± 0.4	−(134 ± 75)	3.08 ± 0.07	263	PLP–LIF	O'Donnell et al. (2004)	263–372
		3.06 ± 0.06	273			
		2.70 ± 0.07	298			
		2.77 ± 0.10	323			
		2.78 ± 0.08	348			
		2.61 ± 0.10	372			
OH + $HC(O)OCH_2OCH_2CH_3$						
		3.65 ± 0.22	298	RR[b] (n-C_3H_7OH)	O'Donnell et al. (2004)	
1.6 ± 0.3	−(317 ± 64)	5.51 ± 0.16	263	PLP–LIF	O'Donnell et al. (2004)	263–372
		5.09 ± 0.20	273			
		4.54 ± 0.19	298			
		4.14 ± 0.21	323			
		3.94 ± 0.19	348			
		3.90 ± 0.21	372			
OH + $CH_3C(O)OCH_2OCH_2CH_3$						
		6.21 ± 0.28	298	RR[b] (n-C_3H_7OH)	O'Donnell et al. (2004)	
1.9 ± 0.8	−(380 ± 144)	7.79 ± 0.28	263	PLP–LIF	O'Donnell et al. (2004)	263–372
		8.40 ± 0.37	273			
		6.39 ± 0.43	298			
		5.79 ± 0.22	323			
		5.61 ± 0.16	348			
		5.53 ± 0.30	372			
OH + $HC(O)OCH_2CH_2OCH_3$						
		6.10 ± 0.33	298	RR[b] (n-C_3H_7OH)	O'Donnell et al. (2004)	
2.2 ± 1.0	−(324 ± 142)	7.49 ± 0.47	273	PLP–LIF	O'Donnell et al. (2004)	263–372
		6.60 ± 0.14	298			
		5.75 ± 0.23	323			
		5.57 ± 0.24	368			
OH + $CH_3C(O)OCH_2CH_2OCH_3$						
		8.72 ± 0.76	298	RR[b] (n-C_3H_7OH)	O'Donnell et al. (2004)	

(*continued*)

Table III-C-30. (*continued*)

$10^{12} \times A$	B (K)	$10^{12} \times k$	T (K)	Technique[a]	Reference	Temperature Range (K)
2.9 ± 1.5	−(309 ± 162)	8.95 ± 0.78	273	PLP–LIF	O'Donnell et al. (2004)	263–372
		7.83 ± 0.31	298			
		7.79 ± 0.29	333			
		6.38 ± 0.30	372			
OH + $HC(O)OCH_2CH_2OCH_2CH_3$						
		10.71 ± 0.68	298	RR[c] (n-C_4H_9OH)	O'Donnell et al. (2004)	
2.9 ± 1.2	−(405 ± 132)	14.30 ± 0.54	263	PLP–LIF	O'Donnell et al. (2004)	263–372
		12.07 ± 0.70	273			
		11.38 ± 0.45	298			
		9.28 ± 0.38	333			
		9.09 ± 0.27	368			
OH + $CH_3C(O)OCH_2CH_2OCH_2CH_3$						
		13 ± 2	298	PLP–RF	Hartmann et al. (1987)	
		11.64 ± 1.44	298	RR[d] ($CH_3CH{=}CH_2$)	Williams et al. (1993)	
		13.94 ± 0.64	298	RR[c] (n-C_4H_9OH)	O'Donnell et al. (2004)	
1.4 ± 0.6	−(642 ± 148)	15.53 ± 0.68	273	PLP–LIF	O'Donnell et al. (2004)	263–372
		12.10 ± 0.29	298			
		9.37 ± 0.61	333			
		8.55 ± 0.43	368			
OH + $(CH_3)_2CHC(O)OCH_2CH_2OCH_2CH_3$, 2-ethoxyethyl isobutyrate						
		14.8 ± 2.5	298	RR[d] ($CH_3CH{=}CH_2$)	Williams et al. (1993)	
OH + $CH_3CH_2OCH_2CH_2C(O)OCH_2CH_3$, ethyl 3-ethoxypropionate						
		22 ± 7	298	RR[e] (n-nonane and n-dodecane)	Baxley et al. (1997)	

[a]Abbreviations used for the techniques are defined in table I-F-3.
[b]Placed on an absolute basis using $k(OH+n\text{-}C_3H_7OH) = 5.45 \times 10^{-12}$ cm^3 molecule^{-1} s^{-1} (Calvert et al., 2008).
[c]Placed on an absolute basis using $k(OH+n\text{-}C_4H_9OH) = 8.3 \times 10^{-12}$ cm^3 molecule^{-1} s^{-1} (Calvert et al., 2008).
[d]Placed on an absolute basis using $k(OH+CH_3CH{=}CH_2) = 2.9 \times 10^{-11}$ cm^3 molecule^{-1} s^{-1} (Atkinson et al., 2006).
[e]Placed on an absolute basis using $k(OH+n\text{-nonane}) = 1.0 \times 10^{-11}$ cm^3 molecule^{-1} s^{-1} and $k(OH+n\text{-dodecane}) = 1.3 \times 10^{-11}$ cm^3 molecule^{-1} s^{-1} (Calvert et al., 2008).

CH_2 group. Acetaldehyde and $HC(O)CH_2C(O)OCH_2CH_3$ were both observed in approximately 5% yields, and also likely originate from OH attack at this site.

III-D. Unsaturated Ethers

III-D-1. Methyl Vinyl Ether ($CH_3OCH{=}CH_2$)

III-D-1.1. OH Reaction Kinetics

The only available data regarding the reaction of OH with methyl vinyl ether (MVE) were obtained by Perry et al. (1977b) using a flash photolysis–resonance fluorescence technique (table III-D-1). They found: $k = 6.1 \times 10^{-12} \exp(511/T)$ cm^3

Table III-D-1. Rate coefficients ($k = A \times e^{-B/T}$, cm^3 $molecule^{-1}$ s^{-1}) for reaction of OH with methyl vinyl ether

$10^{12} \times A$	B (K)	$10^{12} \times k$	T (K)	Technique[a]	Reference	Temperature Range (K)
6.10	-511 ± 151	33.5 ± 3.4	299.1	FP–LIF	Perry et al. (1977b)	299–427
		26.0 ± 2.6	352.4			
		20.1 ± 2.0	427.0			

[a]Abbreviations used for the techniques are defined in table I-F-3.

molecule^{-1} s^{-1}, which yields k(298 K) = 3.4×10^{-11} cm^3 molecule^{-1} s^{-1}. In the absence of corroborative data, an uncertainty of ±25% is assigned at 298 K.

III-D-1.2. O_3 Reaction Kinetics

No data are available for this reaction. However, on the basis of the data on other vinyl ethers, a rate coefficient of about 10^{-16} cm^3 molecule^{-1} s^{-1} can be estimated for temperatures near 298 K.

III-D-1.3. NO_3 Reaction Kinetics

The relative rate study of Scarfogliero et al. (2006) gives $k = 7.2 \times 10^{-13}$ cm^3 molecule^{-1} s^{-1} for this reaction at 293 K, see table III-D-2.

III-D-1.4. $O(^3P)$ Reaction Kinetics

Atkinson and Pitts (1977) report $k[O(^3P) + MVE] = 6.32 \times 10^{-12} \exp(38/T)$ cm^3 molecule^{-1} s^{-1}, with $k(298) = 7.1 \times 10^{-12}$ cm^3 molecule^{-1} s^{-1}.

III-D-1.5. Summary of the Atmospheric Fate of Methyl Vinyl Ether, and the End Products of Its Oxidation

The tropospheric lifetime of methyl vinyl ether is likely very short, as reaction with OH, O_3, and NO_3 could all contribute to its atmospheric removal. Lifetimes against removal via OH, O_3, and NO_3 are estimated to be approximately 3 h, 2 h, and 8 min., respectively, assuming daytime [OH] = 2.5×10^6 molecule cm^{-3}, [O_3] = 1.5×10^{12}

Table III-D-2. Rate coefficient (k, cm^3 molecule^{-1} s^{-1}) for reaction of NO_3 with methyl vinyl ether

$10^{10} \times k$	T (K)	Technique[a]	Reference
7.2 ± 1.5	293	RR[b] (isoprene)	Scarfogliero et al. (2006)

[a]Abbreviations used for the techniques are defined in table I-F-3.
[b]Placed on an absolute basis using $k(NO_3 + \text{isoprene}) = 7.0 \times 10^{-13}$ cm^3 molecule^{-1} s^{-1} (Atkinson et al., 2006).

molecule cm^{-3}, and nighttime polluted $[NO_3] = 3 \times 10^9$ molecule cm^{-3}. The main products formed from each of the three oxidants are methyl formate and formaldehyde. Molar yields for these species are as follows: from NO_3-initiated oxidation, about 50% for both methyl formate and CH_2O (Scarfogliero et al., 2006; Klotz et al., 2004); from O_3, 73.5% for methyl formate, 28% for CH_2O (Klotz et al., 2004); from OH, in the presence of NO_x, about 80% for both products (Klotz et al., 2004); from OH, in the absence of NO_x, about 50–60% for both products (Klotz et al., 2004). The origin of these two product species form the OH-initiated oxidation in the presence of NO_x is illustrated below:

$$OH + CH_3OCH{=}CH_2(+O_2) \rightarrow CH_3OCH(OO\bullet)CH_2OH$$

$$CH_3OCH(OO\bullet)CH_2OH + NO \rightarrow CH_3OCH(O\bullet)CH_2OH + NO_2$$

$$CH_3OCH(O\bullet)CH_2OH \rightarrow CH_3OCHO + CH_2OH$$

$$CH_2OH + O_2 \rightarrow CH_2O + HO_2$$

III-D-2. Ethyl Vinyl Ether ($CH_3CH_2OCH{=}CH_2$)

III-D-2.1. OH Reaction Kinetics

Thiault et al. (2002b) and Zhou et al. (2006a) have both obtained data for the reaction of OH with ethyl vinyl ether (EVE). The data, as summarized in table III-D-3, are in good agreement. Averaging the data obtained at 298 K leads to $k = 7.3 \times 10^{-11}$ cm^3 $molecule^{-1}$ s^{-1}, with an estimated uncertainty of ±15%. Combining this value with the temperature dependence determined by Thiault et al., gives $k = 1.64 \times 10^{-11} \exp(445/T)$ cm^3 $molecule^{-1}$ s^{-1}.

III-D-2.2. O_3 Reaction Kinetics

The data of Grosjean and Grosjean (1996c), Thiault et al. (2002b), and Zhou et al. (2006a) for reaction of O_3 with EVE are in reasonable agreement, see table III-D-4. A simple average of the data yields $k = 1.9 \times 10^{-16}$ cm^3 $molecule^{-1}$ s^{-1} near 295 K, with an estimated uncertainty of ±20%.

III-D-2.3. NO_3 Reaction Kinetics

The relative rate studies of Scarfogliero et al. (2006), Pfrang et al. (2006b), and Zhou et al. (2006a) are in good agreement, and give $k = 1.5 \times 10^{-12}$ cm^3 $molecule^{-1}$ s^{-1} for this reaction at 298 K, with an estimated uncertainty of ±25%. The data are summarized in table III-D-5.

III-D-2.4. Summary of the Atmospheric Fate of Ethyl Vinyl Ether, and the End Products of Its Oxidation

Reaction of ethyl vinyl ether with OH, O_3, and NO_3 are all of potential importance, and limit the lifetime of this species to less than 1 h under most tropospheric conditions.

Table III-D-3. Rate coefficients ($k = A \times e^{-B/T}$, cm^3 $molecule^{-1}$ s^{-1}) for reaction of OH with ethyl vinyl ether

$10^{12} \times A$	B (K)	$10^{11} \times k$	T (K)	Technique[a]	Reference	Temperature Range (K)
15.5 ± 2.5	−455 ± 13	10.97 ± 0.19	230	PLP–LIF	Thiault et al. (2002b)	230–372
		10.78 ± 0.24	233			
		9.68 ± 0.25	240			
		8.61 ± 0.37	252			
		9.06 ± 0.34	252			
		7.64 ± 0.51	272			
		8.03 ± 0.21	272			
		7.77 ± 0.26	272			
		8.49 ± 0.23	272			
		6.84 ± 0.37	298			
		6.53 ± 0.45	298			
		6.66 ± 0.25	298			
		7.14 ± 0.49	298			
		6.98 ± 0.15	298			
		7.13 ± 0.23	298			
		6.88 ± 0.26	298			
		6.23 ± 0.17	323			
		5.73 ± 0.13	348			
		5.06 ± 0.31	372			
		5.05 ± 0.29	372			
		6.92	298	RR[b] (isoprene)		
		7.05	298			
		7.20	298	RR[c]		
		7.56	298	(2,3-dimethyl-1,3-butadiene)		
		7.91 ± 1.60	298	RR[d] (isobutene)	Zhou et al.	
		7.66 ± 1.58	298	RR[b] (isoprene)	(2006a)	

[a]Abbreviations used for the techniques are defined in table I-F-3.
[b]Placed on an absolute basis using k(OH+isoprene) = 10.1×10^{-11} cm^3 $molecule^{-1}$ s^{-1} (Atkinson et al., 2006).
[c]Placed on an absolute basis using k(OH+2,3-dimethyl-1,3-butadiene) = 1.2×10^{-10} cm^3 $molecule^{-1}$ s^{-1} (Calvert et al., 2000).
[d]Placed on an absolute basis using k(OH+isobutene) = 5.14×10^{-11} cm^3 $molecule^{-1}$ s^{-1} (Calvert et al., 2000).

Table III-D-4. Rate coefficients (k, cm^3 $molecule^{-1}$ s^{-1}) for reaction of O_3 with ethyl vinyl ether

$10^{18} \times k$	T (K)	Technique[a]	Reference
150 ± 16	290	UV abs.	Grosjean and Grosjean (1998)
169 ± 17	293		
136 ± 11	296		
162 ± 14	291		
200 ± 20	298	IR–UV abs.	Thiault et al. (2002b)
206 ± 42	298	RR[b] (c-C_6H_{10})	Zhou et al. (2006a)

[a]Abbreviations used for the techniques are defined in table I-F-3.
[b]Placed on an absolute basis using k(O_3+cyclohexene) = 8.1×10^{-17} cm^3 $molecule^{-1}$ s^{-1} (Calvert et al., 2000).

Table III-D-5. Rate coefficients (k, cm^3 molecule^{-1} s^{-1}) for reaction of NO_3 with ethyl vinyl ether

$10^{13} \times k$	T (K)	Technique[a]	Reference
13.1 ± 2.7	293	RR[b] (isoprene)	Scarfogliero et al. (2006)
18 ± 14	300	RR[c] (*trans*-2-butene)	Pfrang et al. (2006b)
13.9 ± 2.9	298	RR[b] (isoprene)	Zhou et al. (2006a)
15.9 ± 3.3	298	RR[d] (2,3-dimethyl-1,3-butadiene)	

[a]Abbreviations used for the techniques are defined in table I-F-3.
[b]Placed on an absolute basis using $k(NO_3+\text{isoprene}) = 7.0 \times 10^{-13}$ cm^3 molecule^{-1} s^{-1} (Atkinson et al., 2006).
[c]Placed on an absolute basis using $k(NO_3+\textit{trans}\text{-2-butene}) = 3.9 \times 10^{-13}$ cm^3 molecule^{-1} s^{-1} (Calvert et al., 2000).
[d]Placed on an absolute basis using $k(NO_3+\text{2,3-dimethyl-1,3-butadiene}) = 23 \times 10^{-13}$ cm^3 molecule^{-1} s^{-1} (Calvert et al., 2000).

The reaction with NO_3 is of particular importance in polluted nighttime atmospheres (lifetime $\approx$ 4 min. for $[NO_3] = 3 \times 10^9$ molecule cm^{-3}), and this reaction will clearly play a role under more moderately polluted conditions as well. Ethyl formate and formaldehyde are the main oxidation products obtained following reaction with OH, O_3, and NO_3. Approximate yields are as follows: from NO_3-initiated oxidation, 53% for ethyl formate and 44% for CH_2O (Scarfogliero et al., 2006); from O_3, 87% for ethyl formate and 20% for CH_2O (Thiault et al., 2002b); from O_3, > 39% for ethyl formate and 49% for formaldehyde (Grosjean and Grosjean, 1999); from OH, both in the presence and absence of NO_x, > 80% for both products (Thiault et al., 2002b).

III-D-3. *n*-Propyl Vinyl Ether ($CH_3CH_2CH_2OCH{=}CH_2$)

III-D-3.1. OH Reaction Kinetics

The rate coefficient for reaction of OH with *n*-propyl vinyl ether (PVE) has been studied by Thiault and Mellouki (2006) using both relative and absolute techniques and by Zhou et al. (2006a) via relative rate methods. There is good agreement between the two datasets near 298 K (see table III-D-6). A simple average of the determinations gives k (298 K) $= 10.0 \times 10^{-11}$ cm^3 molecule^{-1} s^{-1}, with an estimated uncertainty of ±15%. Combining the temperature dependence determined by Thiault and Mellouki with the 298 K value leads to $k = 9.3 \times 10^{-12} \exp(708/T)$ cm^3 molecule^{-1} s^{-1}.

III-D-3.2. O_3 Reaction Kinetics

The only study of the reaction of O_3 with PVE is that of Zhou et al. (2006a), who obtained $k = 2.3 \times 10^{-16}$ cm^3 molecule^{-1} s^{-1} at 298 K using a relative rate technique. The study is summarized in table III-D-7.

III-D-3.3. NO_3 Reaction Kinetics

There is reasonable agreement between the relative rate data of Scarfogliero et al. (2006) and Zhou et al. (2006a) for the reaction of NO_3 with PVE. A simple average of the determinations gives$k = 1.7 \times 10^{-12}$ cm^3 molecule^{-1} s^{-1} at 298 K, with an estimated uncertainty of ±30%. The data are summarized in table III-D-8.

Table III-D-6. Rate coefficients ($k = A \times e^{-B/T}$, cm^3 molecule^{-1} s^{-1}) for reaction of OH with *n*-propyl vinyl ether

$10^{12} \times A$	B (K)	$10^{11} \times k$	T (K)	Technique[a]	Reference	Temperature Range (K)
9.3 ± 0.6	−708 ± 20	18.97 ± 0.62	233	PLP–LIF	Thiault and Mellouki (2006)	233–373
		18.55 ± 0.66	235			
		15.59 ± 0.28	253			
		16.01 ± 0.68	253			
		12.30 ± 0.74	273			
		12.44 ± 0.37	273			
		10.18 ± 0.34	298			
		9.92 ± 0.29	298			
		10.09 ± 0.34	298			
		9.75 ± 0.15	298			
		10.05 ± 0.28	298			
		10.06 ± 0.44	298			
		9.55 ± 0.32	298			
		8.99 ± 0.21	313			
		8.18 ± 0.14	325			
		7.74 ± 0.22	333			
		6.84 ± 0.20	353			
		6.15 ± 0.21	373			
		6.31 ± 0.16	373			
		10.9 ± 1.4	298	RR[b] (isoprene)		
		10.0 ± 0.6	298	RR[c] (2,3-dimethyl-1,3-butadiene)		
		9.71 ± 1.96	298	RR[d] (isobutene)	Zhou et al. (2006a)	
		9.75 ± 1.00	298	RR[b] (isoprene)		

[a]Abbreviations used for the techniques are defined in table I-F-3.
[b]Placed on an absolute basis using k(OH+isoprene) = 10.1×10^{-11} cm^3 molecule^{-1} s^{-1} (Atkinson et al., 2006).
[c]Placed on an absolute basis using k(OH+2,3-dimethyl-1,3-butadiene) = 1.2×10^{-10} cm^3 molecule^{-1} s^{-1} (Calvert et al., 2000).
[d]Placed on an absolute basis using k(OH+isobutene) = 5.14×10^{-11} cm^3 molecule^{-1} s^{-1} (Calvert et al., 2000).

Table III-D-7. Rate coefficient (k, cm^3 molecule^{-1} s^{-1}) for reaction of O_3 with *n*-propyl vinyl ether

$10^{18} \times k$	T (K)	Technique[a]	Reference
234 ± 48	298	RR[b] (*cyclo*-C_6H_{10})	Zhou et al. (2006a)

[a]Abbreviations used for the techniques are defined in table I-F-3.
[b]Placed on an absolute basis using k(O_3+cyclohexene) = 8.1×10^{-17} cm^3 molecule^{-1} s^{-1} (Calvert et al., 2000).

III-D-3.4. Summary of the Atmospheric Fate of Propyl Vinyl Ether, and the End Products of Its Oxidation

As was the case for the smaller members of the series of vinyl ethers, atmospheric loss of propyl vinyl ether will occur on a relatively short timescale (< 1 h under most conditions), with reaction with OH, O_3, and NO_3 all playing a role. The reaction with NO_3 is again of particular importance (lifetime ≈ 3 min. for highly polluted conditions, [NO_3] = 3×10^9 molecule cm^{-3}). In keeping with the smaller vinyl ethers, reaction

Table III-D-8. Rate coefficients (k, cm^3 molecule^{-1} s^{-1}) for reaction of NO_3 with n-propyl vinyl ether

$10^{13} \times k$	T (K)	Technique[a]	Reference
13.3 ± 3.0	293	RR[b] (isoprene)	Scarfogliero et al. (2006)
17.8 ± 3.6	298	RR[b] (isoprene)	Zhou et al. (2006a)
21.6 ± 4.4	298	RR[c] (2,3-dimethyl-1,3-butadiene)	

[a]Abbreviations used for the techniques are defined in table I-F-3.
[b]Placed on an absolute basis using $k(NO_3+\text{isoprene}) = 7.0 \times 10^{-13}$ cm^3 molecule^{-1} s^{-1} (Atkinson et al., 2006).
[c]Placed on an absolute basis using $k(NO_3+\textit{trans}\text{-2-butene}) = 3.9 \times 10^{-13}$ cm^3 molecule^{-1} s^{-1} (Calvert et al., 2000).
[d]Placed on an absolute basis using $k(NO_3+\text{2,3-dimethyl-1,3-butadiene}) = 23 \times 10^{-13}$ cm^3 molecule^{-1} s^{-1} (Calvert et al., 2000).

with OH, O_3, and NO_3 leads to an alkyl formate (in this case, propyl formate) and formaldehyde as the main oxidation products. Zhou et al. (2006b) obtained a yield of 75–80% for each of these products from the OH-initiated oxidation of PVE in the presence of NO_x, and a 60–65% yield of each product in the absence of NO_x. Yields from the NO_3-initiated oxidation are ~50–55% for both products (Scarfogliero et al., 2006; Zhou et al., 2006b), while ozonolysis generates about an 89% yield of propyl formate and a 20% yield for CH_2O (Zhou et al., 2006b).

III-D-4. n-Butyl Vinyl Ether ($CH_3CH_2CH_2CH_2OCH{=}CH_2$)

III-D-4.1. OH Reaction Kinetics

There is good agreement between the data of Thiault and Mellouki (2006) and Zhou et al. (2006a) for reaction of OH with n-butyl vinyl ether (nBVE) near 298 K, see table III-D-9. Averaging the available data gives k (298 K) = 10.9×10^{-11} cm^3 molecule^{-1} s^{-1} at 298 K, with an estimated uncertainty of ±15%. Combining this result with the temperature dependence determined by Thiault and Mellouki leads to $k = 1.6 \times 10^{-11} \exp(572/T)$ cm^3 molecule^{-1} s^{-1}.

III-D-4.2. O_3 Reaction Kinetics

Zhou et al. (2006a) report $k = 2.6 \times 10^{-16}$ cm^3 molecule^{-1} s^{-1} for the reaction of O_3 with nBVE at 298 K. The study is summarized in table III-D-10.

III-D-4.3. NO_3 Reaction Kinetics

Scarfogliero et al. (2006) and Zhou et al. (2006a) have used relative rate techniques to determine the rate coefficient for reaction of NO_3 with nBVE; see table III-D-11. The data are in fair agreement, and lead to $k = 2.0 \times 10^{-12}$ cm^3 molecule^{-1} s^{-1} at 298 K, with an estimated uncertainty of ±40%.

III-D-4.4. Summary of the Atmospheric Fate of n-Butyl Vinyl Ether, and the End Products of Its Oxidation

n-Butyl vinyl ether will be rapidly destroyed in the troposphere, with a lifetime of < 1 h under most conditions. Reaction with OH, O_3, and NO_3 are likely all of some

Table III-D-9. Rate coefficients ($k = A \times e^{-B/T}$, cm^3 $molecule^{-1}$ s^{-1}) for reaction of OH with *n*-butyl vinyl ether

$10^{12} \times A$	B (K)	$10^{11} \times k$	T (K)	Technique[a]	Reference	Temperature Range (K)
15 ± 2	−572 ± 42	16.39 ± 0.71	232	PLP–LIF	Thiault and Mellouki (2006)	232–373
		15.98 ± 0.41	234			
		14.89 ± 0.31	253			
		12.50 ± 0.44	273			
		12.28 ± 0.72	273			
		10.18 ± 0.31	298			
		10.56 ± 0.35	298			
		10.09 ± 0.44	298			
		10.70 ± 0.39	298			
		10.46 ± 0.58	298			
		9.99 ± 0.30	298			
		10.48 ± 0.25	298			
		9.17 ± 0.19	313			
		8.08 ± 0.22	335			
		7.47 ± 0.41	353			
		6.56 ± 0.24	373			
		6.48 ± 0.20	373			
		11.0 ± 1.4	298	RR[b] (isoprene)		
		11.1 ± 0.7	298	RR[c] (2,3-dimethyl-1,3-butadiene)		
		11.2 ± 1.1	298	RR[d] (propyl vinyl ether)		
		10.9 ± 2.2	298	RR[e] (isobutene)	Zhou et al. (2006a)	
		11.5 ± 2.4	298	RR[b] (isoprene)		

[a]Abbreviations used for the techniques are defined in table I-F-3.
[b]Placed on an absolute basis using k(OH+isoprene) = 10.1×10^{-11} cm^3 $molecule^{-1}$ s^{-1} (Atkinson et al., 2006).
[c]Placed on an absolute basis using k(OH+2,3-dimethyl-1,3-butadiene) = 1.2×10^{-10} cm^3 $molecule^{-1}$ s^{-1} (Calvert et al., 2000).
[d]Placed on an absolute basis using k(OH+propyl vinyl ether) = 10.0×10^{-11} cm^3 $molecule^{-1}$ s^{-1} (this book, section III-D-3).
[e]Placed on an absolute basis using k(OH+isobutene) = 5.14×10^{-11} cm^3 $molecule^{-1}$ s^{-1} (Calvert et al., 2000).

Table III-D-10. Rate coefficient (k, cm^3 $molecule^{-1}$ s^{-1}) for reaction of O_3 with butyl vinyl ether

$10^{18} \times k$	T (K)	Technique[a]	Reference
259 ± 52	298	RR[b] (*cyclo*-C_6H_{10})	Zhou et al. (2006a)

[a]Abbreviations used for the techniques are defined in table I-F-3.
[b]Placed on an absolute basis using k(O_3+cyclohexene) = 8.1×10^{-17} cm^3 $molecule^{-1}$ s^{-1} (Calvert et al., 2000).

importance, with nighttime destruction via reaction with NO_3 likely the most important loss process (lifetime ≈ 3 min. for highly polluted conditions, $[NO_3] = 3 \times 10^9$ molecule cm^{-3}). Scarfogliero et al. (2006) demonstrated that *n*-butyl formate and CH_2O were the main products of the NO_3-initiated oxidation (molar yields of both

Table III-D-11. Rate coefficients (k, cm^3 molecule^{-1} s^{-1}) for reaction of NO_3 with propyl vinyl ether

$10^{13} \times k$	T (K)	Technique[a]	Reference
13.3 ± 3.0	293	RR[b] (isoprene)	Scarfogliero et al. (2006)
20.6 ± 4.1	298	RR[c] (*trans*-2-butene)	Zhou et al. (2006a)
24.2 ± 4.8	298	RR[d] (2,3-dimethyl-1,3-butadiene)	

[a]Abbreviations used for the techniques are defined in table I-F-3.
[b]Placed on an absolute basis using $k(NO_3+\text{isoprene}) = 7.0 \times 10^{-13}$ cm^3 molecule^{-1} s^{-1} (Atkinson et al., 2006).
[c]Placed on an absolute basis using $k(NO_3+\textit{trans}\text{-2-butene}) = 3.9 \times 10^{-13}$ cm^3 molecule^{-1} s^{-1} (Calvert et al., 2000).
[d]Placed on an absolute basis using $k(NO_3+\text{2,3-dimethyl-1,3-butadiene}) = 23 \times 10^{-13}$ cm^3 molecule^{-1} s^{-1} (Calvert et al., 2000).

species ≈ 45%). On the basis of these data and data for the smaller vinyl ethers, butyl formate and formaldehyde are also likely the dominant products of the OH-initiated oxidation, while butyl formate is expected in high yield from the ozonolysis.

III-D-5. Isobutyl and *tert*-Butyl Vinyl Ethers

III-D-5.1. OH Reaction Kinetics

Thiault and Mellouki (2006) have measured the rate coefficient for reaction of OH with these two species using both absolute and relative rate techniques, see table III-D-12. Rate coefficients for both species are found to be 1.1×10^{-10} cm^3 molecule^{-1} s^{-1} at 298 K, consistent with the data shown in the previous sections for other vinyl ethers. The pulsed laser photolysis–LIF data from Thiault and Mellouki lead to $k = 1.6 \times 10^{-11} \exp(567/T)$ cm^3 molecule^{-1} s^{-1} and $k = 1.7 \times 10^{-11} \times \exp(549/T)$ cm^3 molecule^{-1} s^{-1}, respectively, for isobutyl and *tert*-butyl vinyl ethers, respectively. The uncertainty on the 298 K rate coefficient is estimated to be ±15%.

III-D-5.2. Summary of the Atmospheric Fate of Isobutyl and tert-Butyl Vinyl Ethers, and the End Products of Their Oxidation

On the basis of the data of Thiault and Mellouki (2006) for the OH reaction, and data presented earlier for other vinyl ethers, the tropospheric lifetimes of isobutyl and *tert*-butyl vinyl ethers will likely be quite short (< 1 h under most conditions), and will be controlled by reaction with NO_3, OH, and O_3. Major end products of the OH-, O_3-, and NO_3-initiated oxidation will be CH_2O and either isobutyl or *tert*-butyl formate.

III-D-6. Ethyl 1-Propenyl Ether, (cis / trans $CH_3CH_2OCH{=}CHCH_3$)

III-D-6.1. O_3 Reaction Kinetics, and Summary of Atmospheric Fate

Grosjean and Grosjean (1999) determined a lower limit for the reaction of cis/trans-ethyl 1-propenyl ether, $k > 5 \times 10^{-16}$ cm^3 molecule^{-1} s^{-1}. The study is summarized in table III-D-13. Because of the greater substitution at the C=C double bond, this

Table III-D-12. Rate coefficients ($k = A \times e^{-B/T}$, cm^3 molecule^{-1} s^{-1}) for reaction of OH with isobutyl and *tert*-butyl vinyl ethers

$10^{12} \times A$	B (K)	$10^{11} \times k$	T (K)	Technique[a]	Reference	Temperature Range (K)
OH + Isobutyl vinyl ether						
16 ± 1	−567 ± 20	17.86 ± 0.38	233	PLP–LIF	Thiault and Mellouki (2006)	233–373
		17.55 ± 0.51	234			
		14.65 ± 0.22	253			
		12.97 ± 0.36	273			
		12.74 ± 0.30	273			
		10.23 ± 0.35	298			
		10.60 ± 0.32	298			
		10.34 ± 0.18	298			
		10.66 ± 0.38	298			
		10.33 ± 0.32	298			
		10.62 ± 0.52	298			
		10.81 ± 0.18	298			
		9.60 ± 0.23	313			
		8.50 ± 0.24	333			
		7.63 ± 0.23	353			
		7.29 ± 0.24	373			
		7.18 ± 0.16	373			
		11.5 ± 1.3	298	RR[b] (isoprene)		
		10.7 ± 0.7	298	RR[c] (2,3-dimethyl-1,3-butadiene)		
		10.8 ± 1.2	298	RR[d] (propyl vinyl ether)		
OH + *tert*- Butyl vinyl ether						
17 ± 2	−549 ± 25	17.60 ± 0.60	233	PLP–LIF	Thiault and Mellouki (2006)	233–372
		17.86 ± 0.76	234			
		14.89 ± 0.39	253			
		12.80 ± 0.44	273			
		13.03 ± 0.34	273			
		10.78 ± 0.35	298			
		10.89 ± 0.37	298			
		10.30 ± 0.44	298			
		11.09 ± 0.44	298			
		10.80 ± 0.27	298			
		11.25 ± 0.59	298			
		10.91 ± 0.18	298			
		9.74 ± 0.26	312			
		8.77 ± 0.23	334			
		7.87 ± 0.30	353			
		7.57 ± 0.46	372			
		7.31 ± 0.23	372			
		11.4 ± 1.3	298	RR[b] (isoprene)		
		11.1 ± 0.7	298	RR[c] (2,3-dimethyl-1,3-butadiene)		
		11.3 ± 1.1	298	RR[d] (propyl vinyl ether)		

[a]Abbreviations used for the techniques are defined in table I-F-3.

[b]Placed on an absolute basis using k(OH+isoprene) = 10.1 × 10^{-11} cm^3 molecule^{-1} s^{-1} (Atkinson et al., 2006).

[c]Placed on an absolute basis using k(OH+2,3-dimethyl-1,3-butadiene) = 1.2 × 10^{-10} cm^3 molecule^{-1} s^{-1} (Calvert et al., 2000).

[d]Placed on an absolute basis using k(OH+propyl vinyl ether) = 10.0 × 10^{-11} cm^3 molecule^{-1} s^{-1} (this book, section III-D-3).

Table III-D-13. Rate coefficients (k, cm^3 molecule^{-1} s^{-1}) for reaction of O_3 with *cis*/*trans* ethyl 1-propenyl ether

$10^{18} \times k$	T (K)	Technique[a]	Reference
$\geq 550 \pm 58$	288	UV abs.	Grosjean and Grosjean (1999)
$\geq 580 \pm 86$	289		
$\geq 625 \pm 96$	287		

[a]Abbreviations used for the techniques are defined in table I-F-3.

species is expected to be more reactive than the vinyl ethers discussed in sections III-D-1 through III-D-5. The major end products of the ozonolysis were determined (molar yields) by Grosjean and Grosjean (1999) to be acetaldehyde (35.3±1.4%) and ethyl formate (> 43.4%). These are the expected major end products from OH- and NO_3-initiated oxidation as well.

III-D-7. Ethylene Glycol Vinyl Ethers

Using relative rate techniques, Zhou et al. (2009) have determined rate coefficients for reaction of OH, O_3, and NO_3 with three ethylene glycol vinyl ethers: ethylene glycol monovinyl ether (EGMVE, $HOCH_2CH_2OCH{=}CH_2$), ethylene glycol divinyl ether (EGDVE, $CH_2{=}CHOCH_2CH_2OCH{=}CH_2$) and diethylene glycol divinyl ether (DEGDVE, $CH_2{=}CHOCH_2CH_2OCH_2CH_2OCH{=}CH_2$). The data are summarized in table III-D-14. Given the lack of corroborative data, uncertainties are estimated at ±30% for all data.

From the data of table III-D-14, is clear that these EGVE species are very reactive with all three atmospheric oxidants. Atmospheric lifetimes of these species are estimated to be less than 1 h in daytime and nighttime conditions, with both OH and O_3 reactions making a significant contribution in the daytime, and NO_3 and O_3 both contributing at night.

III-E. Cyclic Ethers

III-E-1. Ethylene Oxide (Epoxyethane, Oxirane, Dimethylene Oxide)

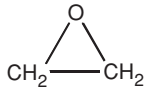

III-E-1.1. OH Reaction Kinetics

The reaction of OH radicals with ethylene oxide has been studied at temperatures of 296 K and above (Zetzsch et al., 1980; Fritz et al., 1982; Lorenz and Zellner, 1984; Baldwin et al., 1984; Wallington et al., 1988e). The room temperature values from Wallington et al. and from Zellner and co-workers (Fritz et al., 1982; Lorenz and

Table III-D-14. Rate coefficients (k, cm^3 molecule^{-1} s^{-1}) for reaction of OH, O_3, and NO_3 with three ethylene glycol vinyl ethers: ethylene glycol monovinyl ether (EGMVE, $HOCH_2CH_2OCH{=}CH_2$), ethylene glycol divinyl ether (EGDVE, $CH_2{=}CHOCH_2CH_2OCH{=}CH_2$), and diethylene glycol divinyl ether (DEGDVE, $CH_2{=}CHOCH_2CH_2OCH_2CH_2OCH{=}CH_2$)

Compound	$10^{13} \times k$	T (K)	Technique[a]	Reference
OH + EGVEs				
EGMVE	1,040 ± 220	298	RR[b] (1,3,5-trimethylbenzene)	Zhou et al. (2009)
EGDVE	1,290 ± 270	298	RR[b] (1,3,5-trimethylbenzene)	
	1,250 ± 260	298	RR[c] (isoprene)	
	1,270	**298**	**AVERAGE**	
DEGDVE	1,450 ± 290	298	RR[d] (isobutene)	
	1,420 ± 290	298	RR[c] (isoprene)	
	1,440	**298**	**AVERAGE**	
O_3 + EGVEs				
EGMVE	0.00202 ± 0.00041	298	RR[e] (cyclohexene)	Zhou et al. (2009)
EGDVE	0.00163 ± 0.00033	298	RR[e] (cyclohexene)	
	0.00175 ± 0.00035	298	RR[f] (*trans*-2-butene)	
	0.00169	**298**	**AVERAGE**	
DEGDVE	0.00270 ± 0.00056	298	RR[f] (*trans*-2-butene)	
NO_3 + EGVEs				
EGMVE	24.4 ± 5.0	298	RR[g] (2,3-dimethyl-1,3-butadiene)	Zhou et al. (2009)
EGDVE	19.1 ± 3.9	298	RR[h] (isoprene)	
	22.5 ± 4.5	298	RR[g] (2,3-dimethyl-1,3-butadiene)	
	20.8	**298**	**AVERAGE**	
DEGDVE	66.5 ± 13.6	298	RR[g] (2,3-dimethyl-1,3-butadiene)	
	62.1 ± 13.1	298	RR[i] (1,3-cycloheptadiene)	
	64.3	**298**	**AVERAGE**	

[a]Abbreviations used for the techniques are defined in table I-F-3.
[b]Placed on an absolute basis using k(OH+1,3,5-trimethylbenzene) = 5.67×10^{-11} cm^3 molecule^{-1} s^{-1} (Calvert et al., 2002).
[c]Placed on an absolute basis using k(OH+isoprene) = 10.1×10^{-11} cm^3 molecule^{-1} s^{-1} (Atkinson et al., 2006).
[d]Placed on an absolute basis using k(OH+isobutene) = 5.2×10^{-11} cm^3 molecule^{-1} s^{-1} (Calvert et al., 2000).
[e]Placed on an absolute basis using k(O_3+cyclohexene) = 8.1×10^{-17} cm^3 molecule^{-1} s^{-1} (Calvert et al., 2000).
[f]Placed on an absolute basis using k(O_3+*trans*-2-butene) = 1.9×10^{-16} cm^3 molecule^{-1} s^{-1} (Calvert et al., 2000).
[g]Placed on an absolute basis using k(NO_3+2,3-dimethyl-1,3-butadiene) = 2.3×10^{-12} cm^3 molecule^{-1} s^{-1} (Calvert et al., 2000).
[h]Placed on an absolute basis using k(NO_3+isoprene) = 7.0×10^{-13} cm^3 molecule^{-1} s^{-1} (Atkinson et al., 2006).
[i]Placed on an absolute basis using k(NO_3+1,3-cycloheptadiene) = 6.5×10^{-12} cm^3 molecule^{-1} s^{-1} (Calvert et al., 2000).

Zellner, 1984) are in good agreement, but are nearly a factor of 2 higher than the value reported by Zetzsch et al. See figure III-E-1 and table III-E-1. The average of the values of Lorenz and Zellner (1984) and Wallington et al. (1988e), $k = 8.8 \times 10^{-14}$ cm^3 molecule^{-1} s^{-1}, is recommended at 296 K, with an estimated uncertainty of ±25%. Fitting of the limited data from Zellner and co-workers, Baldwin et al., and Wallington et al. yields $k = 1.5 \times 10^{-17} T^2 \exp(-856/T)$ cm^3 molecule^{-1} s^{-1}, an expression that provides an adequate representation of the high-temperature data. Further studies at room temperature and below would be useful.

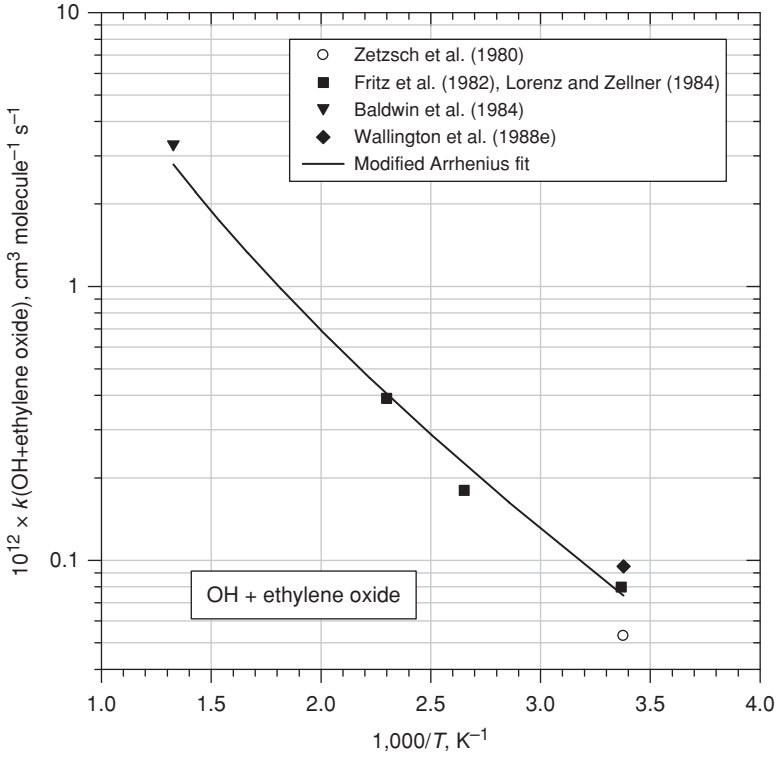

Figure III-E-1. Arrhenius plot of the rate coefficient for the reaction of OH with ethylene oxide.

Table III-E-1. Rate coefficients (k, cm^3 molecule^{-1} s^{-1}) for reaction of OH with ethylene oxide (*cyclo*-C_2H_4O-)

$10^{13} \times A$	T (K)	Technique[a]	Reference	Temperature Range (K)
0.53 ± 0.1	296	FP–RF	Zetzsch et al. (1980)	
0.80 ± 0.16	297	PLP–RF	Fritz et al. (1982),	297–435
(1.8)[b]	377		Lorenz and Zellner (1984)	
(3.9)[b]	435			
33.3 ± 2.1	753	RR[c] (H_2)	Baldwin et al. (1984)	
0.95 ± 0.05	296	FP–RF	Wallington et al. (1988e)	

[a]Abbreviations used for the techniques are defined in table I-F-3.
[b]Values estimated from graphical presentation of the data in the original references.
[c]Placed on an absolute basis using $k(OH+H_2) = 7.86 \times 10^{-13}$ cm^3 molecule^{-1} s^{-1} at 753 K (Tully and Ravishankara, 1980).

III-E-1.2. Cl-Atom Reaction Kinetics

It can be seen in table III-E-2 that the relative rate study of Ponomarev et al. (2002) yielded rate coefficients for the reaction of Cl-atoms with ethylene oxide that are considerably smaller than the value reported by Bartels et al. (1989). Ponomarev et al. (2002)

Table III-E-2. Rate coefficients (k, cm^3 molecule^{-1} s^{-1}) for reaction of Cl with ethylene oxide

$10^{12} \times k$	T (K)	Technique[a]	Reference
2.89 ± 0.24	298	RR[b] (C_2H_6)	Bartels et al. (1989)
4.6 ± 0.6	295	RR[c] (C_2H_5Cl)	Ponomarev et al. (2002)
5.2 ± 0.6	295	RR[d](CH_3OCHO)	

[a]Abbreviations used for the techniques are defined in table I-F-3.
[b]Placed on an absolute basis using $k(Cl+C_2H_6) = 5.9 \times 10^{-11}$ cm^3 molecule^{-1} s^{-1} (Atkinson et al., 2006).
[c]Placed on an absolute basis using $k(Cl+C_2H_5Cl) = 7.8 \times 10^{-12}$ cm^3 molecule^{-1} s^{-1} (this book, table I-F-2).
[d]Placed on an absolute basis using $k(Cl+CH_3OCHO) = 1.4 \times 10^{-12}$ cm^3 molecule^{-1} s^{-1} (Wallington et al., 1993b).

suggest the possibility of interference in the Bartels et al. study from a heterogeneous reaction of ethylene oxide with Cl_2. The average of the Ponomarev et al.'s measurements (using multiple reference reactions), $k = 4.9 \times 10^{-12}$ cm^3 molecule^{-1} s^{-1}, is recommended.

III-E-1.3. O(^{3}P) Reaction Kinetics

Herron (1988) recommends $k(O^3P + \text{ethylene oxide}) = 7 \times 10^{-17}$ cm^3 molecule^{-1} s^{-1} near 298 K. The reaction is too slow to be of atmospheric significance.

III-E-1.4. Summary of the Atmospheric Fate of Ethylene Oxide, and the End Products of Its Oxidation

The lifetime of ethylene oxide with respect to gas-phase oxidation processes is quite long, about 230 days for [OH] = 1×10^6 molecule cm^{-3} and an average tropospheric temperature of 270 K. The mechanism of the Cl-atom-initiated oxidation of ethylene oxide, which should mimic the atmospheric OH-initiated process, has been studied in the absence of NO_x by Chen et al. (1995). Major products observed in air were formic acid anhydride [HC(O)OCHO, molar yield = 61 ± 4%], CO (33 ± 3%) and formic acid (18 ± 4%). Minor products (yields of 10% or less) included CO_2, HCHO, and hydroxymethyl formate, $HOCH_2OCHO$. As discussed by Chen et al. (1995), and as shown in figure III-E-2, the reaction of OH, like that of Cl with ethylene oxide, proceeds via abstraction, leading to the formation of a cyclic peroxy, and then a cyclic alkoxy radical. Decomposition of the alkoxy radical via C—C bond rupture leads to $\bullet CH_2OC(=O)H$, a radical also formed in methyl formate oxidation. That formic acid anhydride, formic acid, and CO are major products obtained from methyl formate oxidation as well as ethylene oxide oxidation, is then consistent with the formation of $\bullet CH_2OC(=O)H$ in both systems. Note that, at the time of the writing of the Chen et al. (1995) paper, the so-called "α-ester rearrangement" (Tuazon et al., 1998b; Wallington et al., 2001a) had yet to be discovered; this process can now be identified as the likely source of formic acid. Finally, a measurable yield of CH_2O (about 10% after accounting for secondary loss), a species not likely formed from $\bullet CH_2OC(=O)H$, was observed by Chen et al. The possibility of a minor channel to its formation directly from decomposition of the cyclic alkoxy radical is thus proposed.

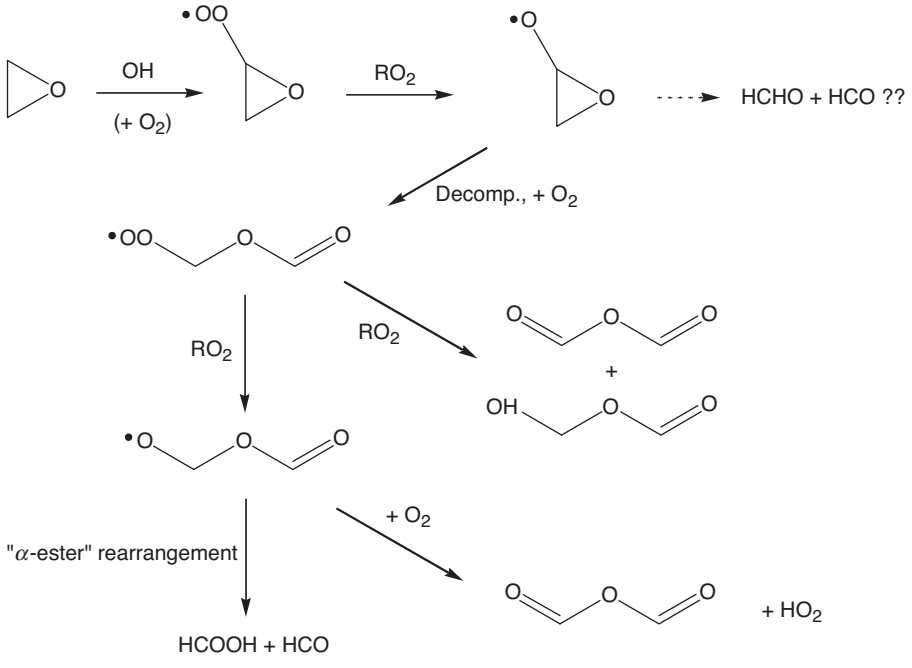

Figure III-E-2. Major reactions occurring in the atmospheric oxidation of ethylene oxide (adapted from Chen et al., 1995).

III-E-2. Methyl Oxirane (Propylene Oxide), and Other Methyl-Substituted Oxiranes

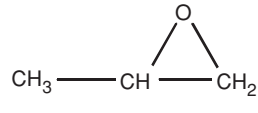

III-E-2.1. OH Reaction Kinetics

There have been four studies of the reaction of OH radicals with methyl oxirane near 298 K (Winer et al., 1978; Zetzsch et al., 1980; Edney et al., 1986; Wallington et al., 1988e). See table III-E-3. The data are not in good agreement; two measurements (Zetzsch et al., 1980; Wallington et al., 1988e) fall near 5.0×10^{-13} cm^3 molecule^{-1} s^{-1}, while the other two are about a factor of 2 higher. While no recommendation is made for this rate coefficient, we note that the two high values have large uncertainties associated with them. Further studies of this reaction are clearly warranted.

III-E-2.2. NO_3 Reaction Kinetics

The reactions of NO_3 with *cis*-2,3-dimethyloxirane and tetramethyl oxirane have been studied by Kind et al. (1996a), using a relative rate method. Upper limits of 5×10^{-15} cm^3 molecule^{-1} s^{-1} are reported for both species.

Table III-E-3. Rate coefficients (k, cm^3 molecule^{-1} s^{-1}) for reaction of OH with methyl oxirane (CH_3-*cyclo*-C_2H_3O-)

$10^{13} \times k$	T (K)	Technique[a]	Reference
12 ± 7	296	RR[b]	Winer et al. (1978)
5.2 ± 1	296	FP–RF	Zetzsch et al. (1980)
10.4 ± 7.0	296	RR[c] (n-C_4H_{10})	Edney et al. (1986)
4.95 ± 0.52	296	FP–RF	Wallington et al. (1988e)

[a]Abbreviations used for the techniques are defined in table I-F-3.
[b]As quoted in Wallington et al. (1988e); reference compound not specified.
[c]Placed on an absolute basis using $k(OH+n\text{-}C_4H_{10}) = 2.36 \times 10^{-12}$ cm^3 molecule^{-1} s^{-1} (Calvert et al., 2008).

III-E-2.3. Summary of the Atmospheric Fate of Methyl Oxirane, and the End Products of Its Oxidation

The lifetime of methyl oxirane with respect to reaction with OH will be about 25 days, assuming that the lower rate coefficients noted above are correct. No studies of the mechanism of the oxidation have been conducted. By analogy to chemistry of oxirane presented in section III-E-1.4, OH attack at the CH group (likely the dominant site) will result in the formation of acetic acid and CO, via α-ester rearrangement of the $CH_3C(O)OCH_2O\bullet$ radical, and formic acetic anhydride [$CH_3C(O)OC(O)H$] via reaction of this radical with O_2.

III-E-3. Ethyl Oxirane (1,2-Butylene Oxide)

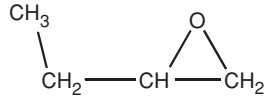

III-E-3.1. OH Reaction Kinetics

The only study relevant to the atmospheric behavior of this species is a measure of the rate coefficient for its reaction with OH (Wallington et al., 1988a), $k = 1.9 \times 10^{-12}$ cm^3 molecule^{-1} s^{-1}. See table III-E-4. In the absence of corroborative data, an uncertainty of ±35% is assigned.

Table III-E-4. Rate coefficient (k, cm^3 molecule^{-1} s^{-1}) for reaction of OH with ethyl oxirane (C_2H_5-*cyclo*-C_2H_3O-)

$10^{12} \times k$	T (K)	Technique[a]	Reference
1.91 ± 0.08	296	FP–RF	Wallington et al. (1988a)

[a]Abbreviations used for the techniques are defined in table I-F-3.

III-E-3.2. Summary of the Atmospheric Fate of Ethyl Oxirane, and the End Products of Its Oxidation

The lifetime of ethyl oxirane with respect to reaction with OH will be about 6 days, assuming a global average [OH] = 10^6 molecule cm^{-3}. No studies of the mechanism of the oxidation have been conducted. By analogy to the chemistry of oxirane presented in section III-E-2, OH attack at the CH group on the oxirane ring (likely the dominant site) will result in the formation of propanoic acid and CO, via α-ester rearrangement of the $CH_3CH_2C(O)OCH_2O\bullet$ radical, and propanoic formic anhydride [$CH_3CH_2C(O)OC(O)H$] via reaction of this radical with O_2.

III-E-4. Oxetane (trimethylene oxide)

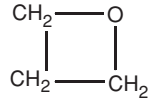

III-E-4.1. OH Reaction Kinetics

The only study relevant to the atmospheric behavior of this species is a measure of the rate coefficient for its reaction with OH (Dagaut et al., 1990), $k = 10.3 \times 10^{-12}$ cm^3 molecule^{-1} s^{-1}. The study is summarized in table III-E-5. In the absence of corroborative data, an uncertainty of ±25% is assigned.

III-E-4.2. Summary of the Atmospheric Fate of Oxetane, and the End Products of Its Oxidation

For daytime [OH] $\approx 2.5 \times 10^6$ molecule cm^{-3}, the lifetime of oxetane will be about 11 h. No studies of the mechanism of the oxidation have been conducted.

III-E-5. Tetrahydrofuran (Tetramethylene Oxide)

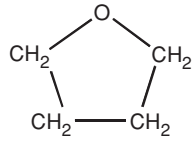

Table III-E-5. Rate coefficient (k, cm^3 molecule^{-1} s^{-1}) for reaction of OH with oxetane (*cyclo*-C_3H_6O-)

$10^{12} \times k$	T (K)	Technique[a]	Reference
10.3 ± 0.6	296	FP–RF	Dagaut et al. (1988a)

[a]Abbreviations used for the techniques are defined in table I-F-3.

Table III-E-6. Rate coefficients ($k = A \times e^{-B/T}$, cm^3 molecule^{-1} s^{-1}) for reaction of OH with tetrahydrofuran (*cyclo*-C_4H_8O-)

$10^{12} \times A$	B (K)	$10^{12} \times k$	T (K)	Technique[a]	Reference	Temperature Range (K)
		15.0 ± 3.1	305	RR[b] (isobutene)	Winer et al. (1977)	
		16.3 ± 1.6	298	FP–RF	Ravishankara and	
		15.9 ± 3.9	298		Davis (1978)	
		17.8 ± 1.6	296	FP–RF	Wallington et al. (1988e)	
		19.4 ± 0.8	298	RR[c] ($CH_3CHOHCH_2OCH_3$)	Moriarty et al. (2003)	
9.7 ± 3.2	-177 ± 67	19.2 ± 1.0	263	PLP–LIF		263–372
		19.1 ± 1.0	273			
		16.7 ± 0.7	298			
		16.9 ± 0.8	323			
		16.1 ± 0.6	348			
		15.8 ± 0.7	372			

[a]Abbreviations used for the techniques are defined in table I-F-3.
[b]Placed on an absolute basis using k(OH+isobutene) $= 5.2 \times 10^{-11}$ cm^3 molecule^{-1} s^{-1} (Calvert et al., 2000).
[c]Placed on an absolute basis using k(OH+$CH_3CHOHCH_2OCH_3$) $= 2.0 \times 10^{-11}$ cm^3 molecule^{-1} s^{-1} (this book, section III-C-5-1).

III-E-5.1. OH Reaction Kinetics

Rate coefficients for reaction of OH with tetrahydrofuran have been reported near 300 K by Winer et al. (1977), Ravishankara and Davis (1978), Wallington et al. (1988e), and over a range of temperatures by Moriarty et al. (2003), see table III-E-6 and figure III-E-3 for a summary. Values near 300 K lie in the range $(15 - 19) \times 10^{-12}$ cm^3 molecule^{-1} s^{-1}, with an unweighted average of 17.0×10^{-12} cm^3 molecule^{-1} s^{-1}. Combining this value with the activation energy reported by Moriarty et al. (2003) yields: $k = 9.4 \times 10^{-12} \exp(177/T)$ cm^3 molecule^{-1} s^{-1}. An uncertainty of $\pm 15\%$ is estimated near 300 K.

III-E-5.2. NO_3 Reaction Kinetics

The reaction has been studied by Atkinson et al. (1988) and Cabañas et al. (2004), see table III-E-7 and figure III-E-4 for a summary. Fitting of the combined dataset yields $k = 1.3 \times 10^{-9} \exp(-3{,}710/T)$ cm^3 molecule^{-1} s^{-1}, with $k = 4.7 \times 10^{-15}$ cm^3 molecule^{-1} s^{-1} at 296 K, and an assumed uncertainty of $\pm 25\%$ at 296 K.

III-E-5.3. O(^{3}P) Reaction Kinetics

Liu et al. (1990a), using a flash photolysis–resonance fluorescence technique, obtained $k = 3.75 \times 10^{-13}$ cm^3 molecule^{-1} s^{-1} for reaction of O(^{3}P) with tetrahydrofuran.

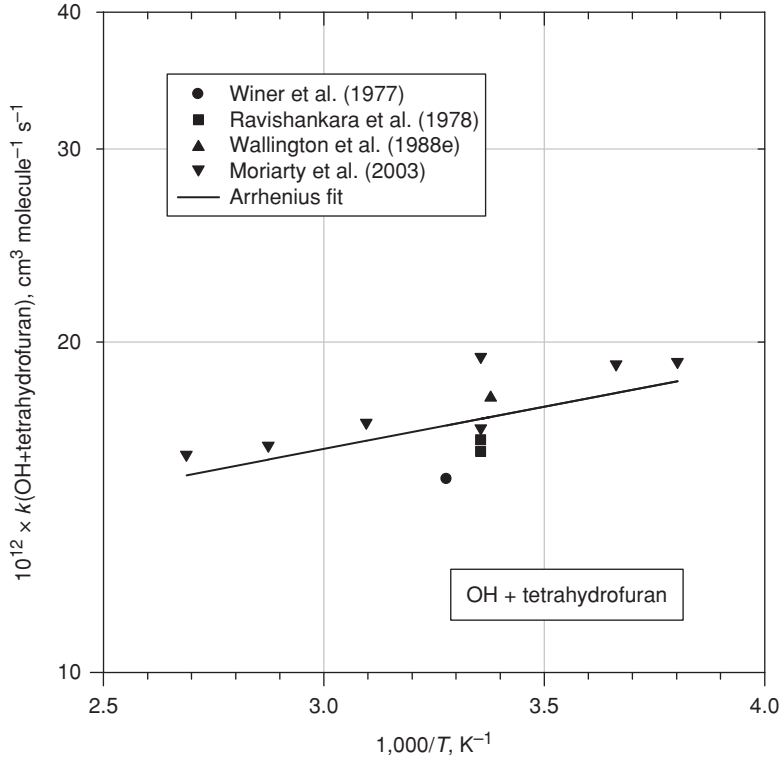

Figure III-E-3. Arrhenius plot of the rate coefficient for the reaction of OH with tetrahydrofuran.

Table III-E-7. Rate coefficients (k, cm^3 molecule^{-1} s^{-1}) for reaction of NO_3 with tetrahydrofuran (*cyclo*-C_4H_8O)

$10^{10} \times A$	B (K)	$10^{15} \times k$	T (K)	Technique[a]	Reference	Temperature Range (K)
		4.84 ± 0.63	296	RR[b] (C_3H_6)	Atkinson et al. (1988)	
20 ± 20	$3{,}800 \pm 400$	3.17 ± 0.43	287	DF–LIF	Cabañas et al. (2004)	287–340
		5.1 ± 0.2	298			
		9 ± 1	315			
		16 ± 1	325			
		20 ± 2	335			
		24 ± 2	340			

[a]Abbreviations used for the techniques are defined in table I-F-3.
[b]Placed on an absolute basis using $k(NO_3+C_3H_6) = 9.3 \times 10^{-15}$ cm^3 molecule^{-1} s^{-1} (Atkinson et al., 2006).

III-E-5.4. Summary of the Atmospheric Fate of Tetrahydrofuran, and the End Products of Its Oxidation

For daytime [OH] $\approx 2.5 \times 10^6$ molecule cm^{-3}, a tetrahydrofuran lifetime of about 7 h is estimated.

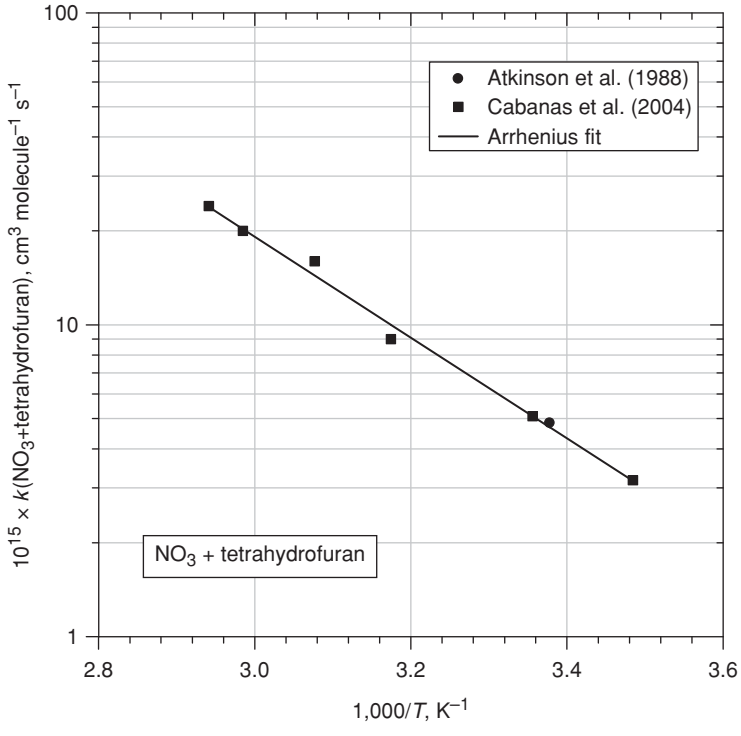

Figure III-E-4. Arrhenius plot of the rate coefficient for the reaction of NO_3 with tetrahydrofuran.

No studies of the mechanism of the oxidation have been conducted. The main site for OH attack will likely be at the CH_2 groups adjacent (alpha) to the oxygen atom. However, attack at either the alpha or beta CH_2 groups likely leads to the formation of a multi-functional species, $HC(O)OCH_2CH_2CH{=}O$, in large yield.

III-E-6. 2-Methyl-tetrahydrofuran

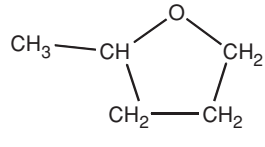

III-E-6.1. OH Reaction Kinetics

Rate coefficients for reaction of OH with 2-methyl-tetrahydrofuran have been reported over a range of temperatures by Wallington et al. (1990e), see table III-E-8 and figure III-E-5. Fitting of their combined relative rate and flash photolysis data gives $k = 2.20 \times 10^{-12} \exp(690/T)$ cm^3 molecule^{-1} s^{-1}, with $k = 2.27 \times 10^{-11}$ cm^3 molecule^{-1} s^{-1} at 298 K. An uncertainty of $\pm 20\%$ is estimated at 298 K.

Table III-E-8. Rate coefficients ($k = A \times e^{-B/T}$, cm^3 $molecule^{-1}$ s^{-1}) for reaction of OH with 2-methyl-tetrahydrofuran (CH_3-*cyclo*-C_4H_7O-)

$10^{12} \times A$	B (K)	$10^{12} \times k$	T (K)	Technique[a]	Reference	Temperature Range (K)
		24.4 ± 2.0	295	RR[b] ($C_2H_5OC_2H_5$)	Wallington	
		24.2 ± 1.8	295	RR[c] [(n-C_4H_{10})$_2$O]	et al. (1990e)	
2.52 ± 0.74	−(650 ± 80)	37.7 ± 4.7	240	FP–RF		240–400
		25.8 ± 2.2	273			
		22.7 ± 1.7	298			
		18.3 ± 2.5	330			
		15.0 ± 3.0	360			
		11.6 ± 2.3	400			

[a]Abbreviations used for the techniques are defined in table I-F-3.
[b]Placed on an absolute basis using $k(OH + C_2H_5OC_2H_5) = 1.24 \times 10^{-11}$ cm^3 $molecule^{-1}$ s^{-1}.
[c]Placed on an absolute basis using $k[OH + (n\text{-}C_4H_{10})_2O] = 2.8 \times 10^{-11}$ cm^3 $molecule^{-1}$ s^{-1}.

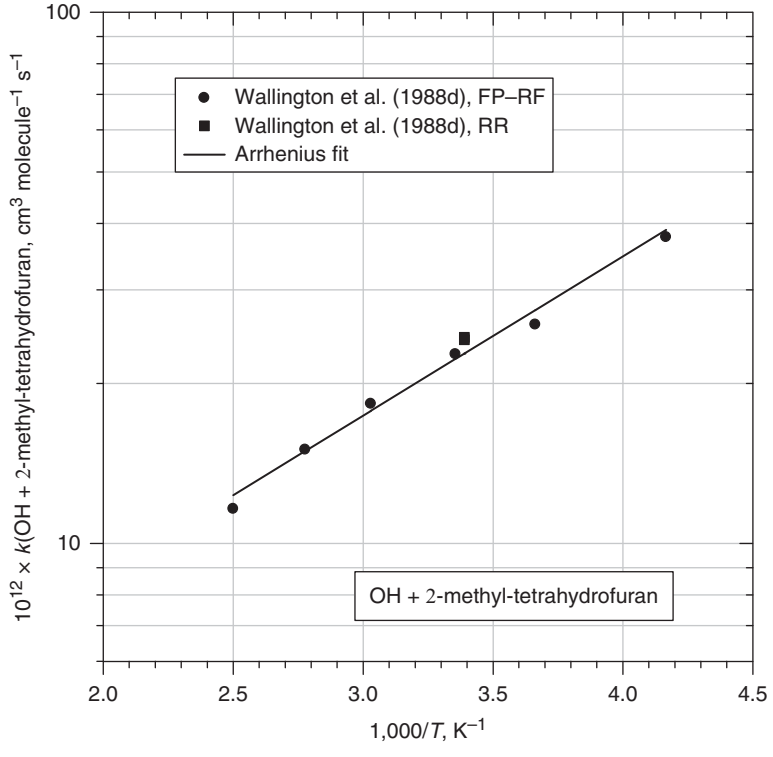

Figure III-E-5. Arrhenius plot of the rate coefficient for the reaction of OH with 2-methyl-tetrahydrofuran.

III-E-6.2. Summary of the Atmospheric Fate of 2-Methyl-tetrahydrofuran and the End Products of Its Oxidation

The lifetime of this species against reaction with OH is estimated to be about 5 h, assuming daytime [OH] $\approx 2.5 \times 10^6$ molecule cm^{-3}. No studies of the mechanism of the oxidation have been conducted. The main site for OH attack will likely be at the CH group adjacent to the cyclic oxygen. A likely important end product is thus the multi-functional species, $CH_3C(O)OCH_2CH_2CH{=}O$.

III-E-7. Tetrahydropyran

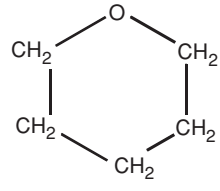

III-E-7.1. OH Reaction Kinetics

The reaction of OH with tetrahydropyran has been studied by Dagaut et al. (1990) and Moriarty et al. (2003), see table III-E-9 and figure III-E-6. Fitting of the combined data set gives $k = 7.8 \times 10^{-12} \exp(136/T)$ cm^3 molecule^{-1} s^{-1}, with $k = 1.2 \times 10^{-11}$ cm^3 molecule^{-1} s^{-1} at 298 K. An uncertainty of $\pm 20\%$ is estimated at 298 K.

Table III-E-9. Rate coefficients ($k = A \times e^{-B/T}$, cm^3 molecule^{-1} s^{-1}) for reaction of OH with tetrahydropyran (*cyclo*-$C_5H_{10}O$-)

$10^{12} \times A$	B (K)	$10^{12} \times k$	T (K)	Technique[a]	Reference	Temperature Range (K)
		13.8 ± 0.7	298	FP–RF	Dagaut et al. (1990)	
		12.4 ± 0.7	298	RR[b] ($CH_3CHOHCH_2OCH_3$)	Moriarty et al.(2003)	
7.8 ± 1.0	-130 ± 44	13.0 ± 0.4	263	PLP–LIF		263–372
		12.2 ± 0.3	273			
		12.3 ± 0.4	298			
		11.5 ± 0.5	323			
		11.3 ± 0.2	348			
		11.2 ± 0.3	372			

[a]Abbreviations used for the techniques are defined in table I-F-3.

[b]Placed on an absolute basis using $k(OH+CH_3CHOHCH_2OCH_3) = 2.0 \times 10^{-11}$ cm^3 molecule^{-1} s^{-1} (this book, section III-C-5-1).

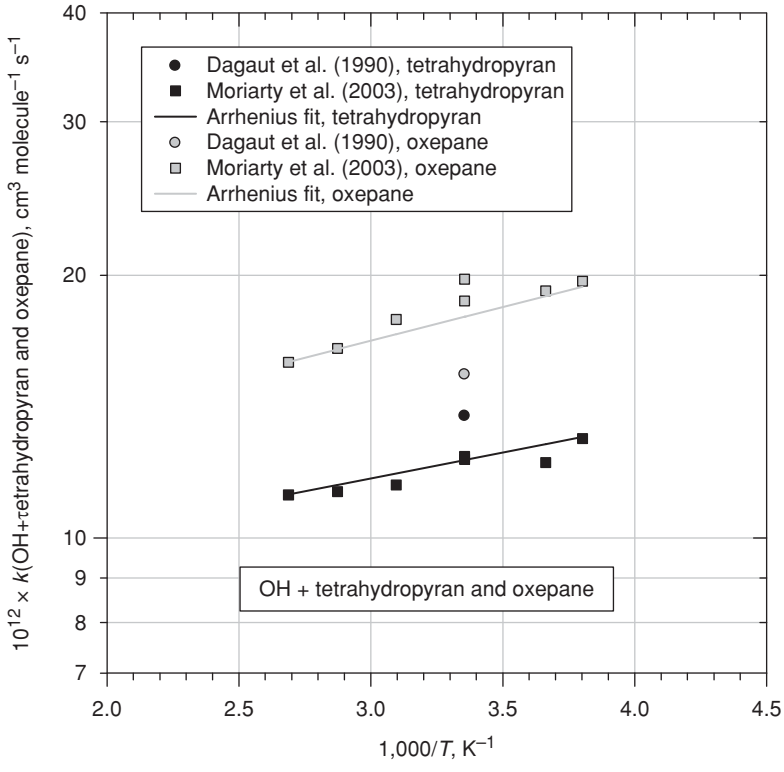

Figure III-E-6. Arrhenius plot of the rate coefficient for the reaction of OH with tetrahydropyran and oxepane.

III-E-7.2. Summary of the Atmospheric Fate of Tetrahydropyran, and the End Productsof Its Oxidation

The lifetime of tetrahydropyran against reaction with OH is about 10 h for daytime [OH] $\approx 2.5 \times 10^6$ molecule cm^{-3}. No studies of the mechanism of the oxidation have been conducted. The main site for OH attack will likely be at the CH_2 groups adjacent to the oxygen; a possible abundant end product is the multi-functional species $HC(O)OCH(OH)CH_2CH_2CHO$ as shown in figure III-E-7.

III-E-8. Oxepane

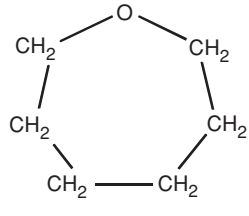

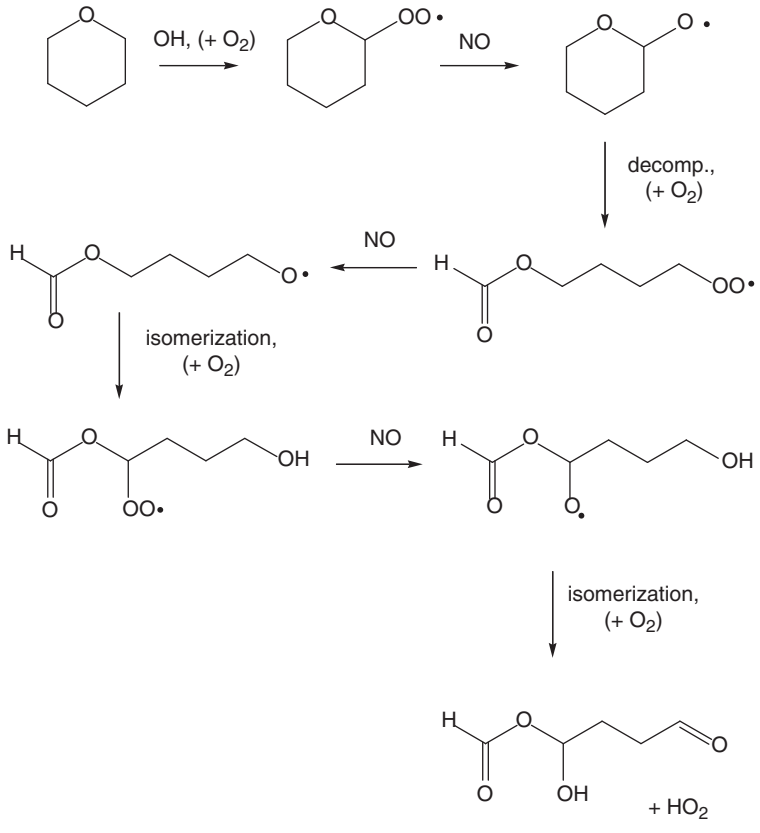

Figure III-E-7. Possible pathway for OH-initiated oxidation of tetrahydropyran. Only major expected pathways are shown.

III-E-8.1. OH Reaction Kinetics

Dagaut et al. (1990) and Moriarty et al. (2003) have both studied the reaction of OH with oxepane, see table III-E-10 and figure III-E-6. Their data near 298 K fall within about 20% of each other. Fitting of the combined data set gives: $k = 9.8 \times 10^{-12} \exp(179/T)$ cm^3 molecule^{-1} s^{-1}, with $k = 1.8 \times 10^{-11}$ cm^3 molecule^{-1} s^{-1} at 298 K. An uncertainty of $\pm 25\%$ is estimated at 298 K.

III-E-8.2. Summary of the Atmospheric Fate of Oxepane, and the End Products of Its Oxidation

The lifetime of oxepane against reaction with OH is about 6 h, assuming daytime [OH] $\approx 2.5 \times 10^6$ molecule cm^{-3}. No studies of the mechanism of the oxidation have been conducted. The main site of OH attack should be at the CH_2 groups adjacent to the oxygen atom. By analogy to the mechanism presented above for tetrahydropyran, the multi-functional species $HC(O)OCH_2CH(OH)CH_2CH_2CH{=}O$ is a likely end product.

Table III-E-10. Rate coefficients ($k = A \times e^{-B/T}$, cm^3 molecule^{-1} s^{-1}) for reaction of OH with oxepane (*cyclo*-$C_6H_{12}O$-)

$10^{12} \times A$	B (K)	$10^{12} \times k$	T (K)	Technique[a]	Reference	Temperature Range (K)
		15.4 ± 1.3	298	FP–RF	Dagaut et al. (1990)	
		19.8 ± 1.5	298	RR[b] [$CH_3CHOHCH_2OCH_3$]	Moriarty et al. (2003)	
9.9 ± 1.3	−184 ± 39	19.7 ± 0.2	263	PLP–LIF		263–372
		19.2 ± 0.9	273			
		18.7 ± 0.2	298			
		17.8 ± 0.4	323			
		16.5 ± 0.8	348			
		15.9 ± 1.1	372			

[a]Abbreviations used for the techniques are defined in table I-F-3.
[b]Placed on an absolute basis using $k(OH+CH_3CHOHCH_2OCH_3) = 2.0 \times 10^{-11}$ cm^3 molecule^{-1} s^{-1} (this book, section III-C-5-1).

III-E-9. 1,3-Dioxolane

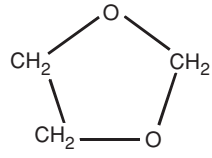

III-E-9.1. OH Reaction Kinetics

Measured rate coefficients for the reaction of OH radicals with 1,3-dioxolane (Sauer et al., 1999; Freitas Dinis et al., 2001; Le Calvé et al., 2002; Moriarty et al., 2003) are summarized in table III-E-11 and these data are plotted in figure III-E-8. The agreement near 296 K is not very good, with values in the range $(7.9 - 12.4) \times 10^{-12}$ cm^3 molecule^{-1} s^{-1}. An average of the available data near 298 K gives $k = 1.0 \times 10^{-11}$ cm^3 molecule^{-1} s^{-1}. However, given the observed scatter and the potential for systematic error in one or more of the datasets, an uncertainty of ±35% is assigned. There is also considerable disagreement regarding the temperature dependence of the rate coefficient, as Le Calvé et al. find a significant negative temperature dependence, and Freitas Dinis et al. find the rate coefficient to be insensitive to temperature. Given these discrepancies, no recommendation is made for the temperature dependence of this rate coefficient.

III-E-9.2. Cl-Atom Reaction Kinetics

This rate coefficient has been studied near 298 K by Sauer et al. (1999), using a relative rate technique. The average of their three measurements, $k = 1.65 \times 10^{-10}$

Table III-E-11. Rate coefficients ($k = A \times e^{-B/T}$, cm^3 $molecule^{-1}$ s^{-1}) for reaction of OH with 1,3-dioxolane

$10^{12} \times A$	B (K)	$10^{12} \times k$	T (K)	Technique[a]	Reference	Temperature Range (K)
		8.8 ± 0.9	295	PR–UV abs.	Sauer et al. (1999)	
		9.34 ± 0.75	300	RR[b] (n-C_4H_{10})		
		10.5 ± 0.6	300	RR[c] ($cyclo$-C_6H_{12})		
8.2 ± 1.3		7.9 ± 0.4	250	PLP–LIF	Freitas Dinis et al. (2001)	
		7.9 ± 0.1	270			
		8.7 ± 0.3	280			
		7.9 ± 0.4	296			
		7.8 ± 0.2	350			
		7.7 ± 0.3	400			
		8.7 ± 0.4	498			
		9.5 ± 0.2	550			
6.70 ± 0.86	-154 ± 36	12.6 ± 1.1	243	PLP–LIF	Le Calvé et al. (2002)	243–372
		12.4 ± 1.0	253			
		12.6 ± 0.9	253			
		11.7 ± 1.1	273			
		11.1 ± 0.8	298			
		11.1 ± 0.9	298			
		11.1 ± 0.8	298			
		10.5 ± 0.8	323			
		10.2 ± 0.7	348			
		10.2 ± 0.7	372			
		11.0 ± 1.1	372			
		12.4 ± 0.5	298	RR[d] (tetrahydrofuran)	Moriarty et al. (2003)	

[a]Abbreviations used for the techniques are defined in table I-F-3.
[b]Placed on an absolute basis using $k(OH+n\text{-}C_4H_{10}) = 2.36 \times 10^{-12}$ cm^3 $molecule^{-1}$ s^{-1} (Calvert et al., 2008).
[c]Placed on an absolute basis using $k(OH+cyclo\text{-}C_6H_{12}) = 6.97 \times 10^{-12}$ cm^3 $molecule^{-1}$ s^{-1} (Calvert et al., 2008).
[c]Placed on an absolute basis using k(OH+tetrahydrofuran) $= 1.70 \times 10^{-11}$ cm^3 $molecule^{-1}$ s^{-1} (this book, section III-E-5.1).

cm^3 $molecule^{-1}$ s^{-1} (see table III-E-12), is recommended with an estimated uncertainty of $\pm 15\%$.

III-E-9.3. Summary of the Atmospheric Fate of 1,3-Dioxolane, and the End Products of Its Oxidation

The lifetime of 1,3-dioxolane with respect to oxidation by OH is about 10 h for daytime [OH] $= 2.5 \times 10^6$ molecule cm^{-3}. Sauer et al. (1999) have examined the OH- and Cl-initiated oxidation of 1,3-dioxolane in the presence of NO_x. Major products of the OH-initiated process were ethylene carbonate (molar yield $48 \pm 7\%$), and methylene glycol diformate ($50 \pm 14\%$). As shown in figure III-E-9, the cyclic species ethylene carbonate is the end product of OH abstraction from the lone CH_2 group located between the two O-atoms, while methylene glycol diformate is the end product of OH abstraction from the two equivalent CH_2 groups in the parent molecule.

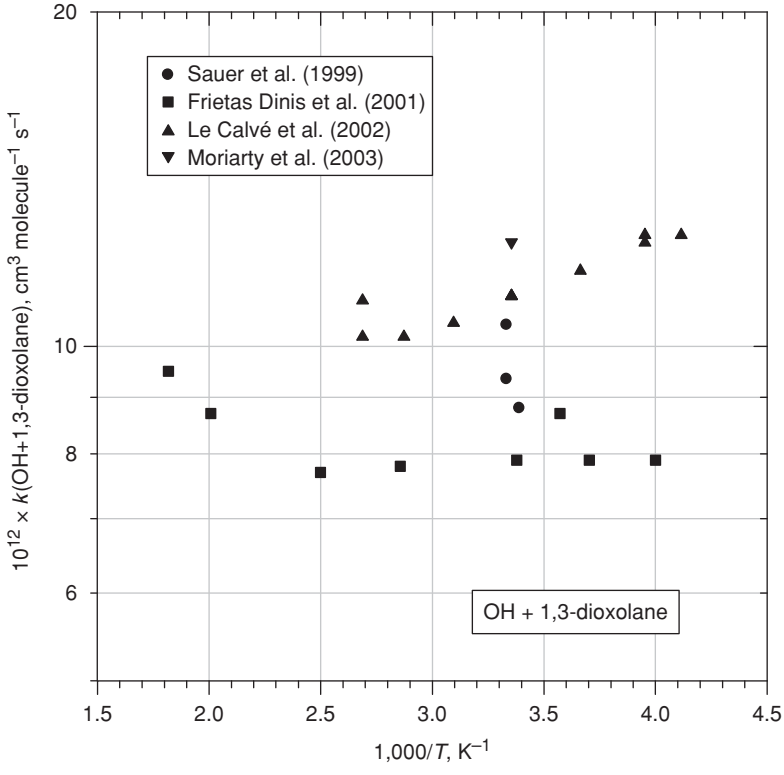

Figure III-E-8. Arrhenius plot of the rate coefficient for the reaction of OH with 1,3-dioxolane.

III-E-10. 1,4-Dioxane

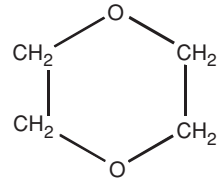

III-E-10.1. OH Reaction Kinetics

Rate coefficients for the reaction of OH with 1,4-dioxane have been reported by Dagaut et al. (1990), Porter et al. (1997), Maurer et al. (1999), and Moriarty et al. (2003), and are summarized in table III-E-13 and in figure III-E-10. Agreement between the various datasets is satisfactory, although data near 298 K range from $(9.7 - 13.6) \times 10^{-12}$ cm^3 molecule^{-1} s^{-1}, and the data of Moriarty et al. show a greater (negative) temperature dependence than do the data of Dagaut et al. As there is no obvious reason to eliminate any of the measurements, fits were conducted using the entire dataset. The following

Table III-E-12. Rate coefficients (k, cm^3 molecule^{-1} s^{-1}) for reaction of Cl with 1,3-dioxolane

$10^{10} \times k$	T (K)	Technique[a]	Reference
1.57 ± 0.09	296	RR[b] (C_2H_6)	Sauer et al. (1999)
1.69 ± 0.09	296	RR[c] (C_3H_8)	
1.69 ± 0.08	296	RR[d] (C_2H_4)	

[a]Abbreviations used for the techniques are defined in table I-F-3.
[b]Placed on an absolute basis using $k(\mathrm{Cl}+\mathrm{C_2H_6}) = 5.9 \times 10^{-11}$ cm^3 molecule^{-1} s^{-1} (Calvert et al., 2008).
[c]Placed on an absolute basis using $k(\mathrm{Cl}+\mathrm{C_3H_8}) = 1.4 \times 10^{-10}$ cm^3 molecule^{-1} s^{-1} (Calvert et al., 2008).
[d]Placed on an absolute basis using $k(\mathrm{Cl}+\mathrm{C_2H_4}) = 0.95 \times 10^{-10}$ cm^3 molecule^{-1} s^{-1} (this book, table I-F-2).

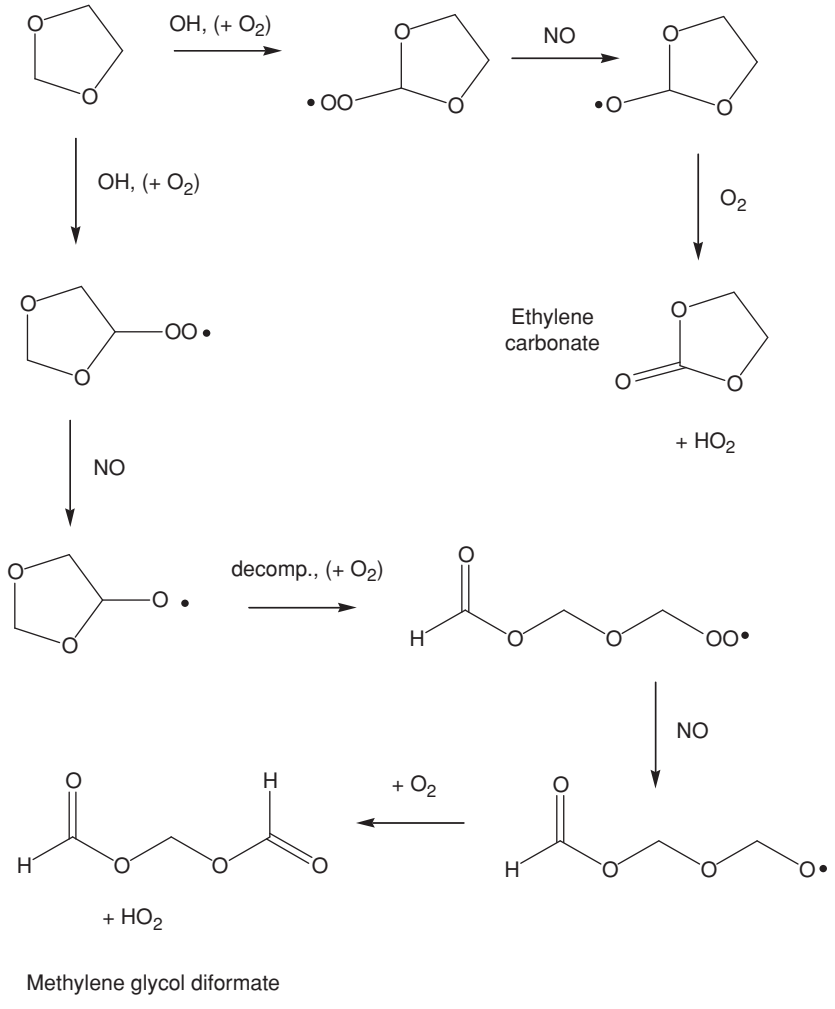

Figure III-E-9. Major reactions occurring in the atmospheric oxidation of 1,3-dioxolane (adapted from Sauer et al., 1999).

Table III-E-13. Rate coefficients ($k = A \times e^{-B/T}$, cm^3 molecule^{-1} s^{-1}) for reaction of OH with 1,4-dioxane

$10^{12} \times A$	B (K)	$10^{12} \times k$	T (K)	Technique[a]	Reference	Temperature Range (K)
8.3 ± 2.2	−80 ± 90	11.8 ± 0.8	240	FP–RF	Dagaut et al. (1990)	240–440
		10.9 ± 0.5	298			
		9.55 ± 0.58	350			
		9.68 ± 0.83	400			
		10.4 ± 0.9	440			
		9.7 ± 0.7	298	RR[b]	Porter et al. (1997)	
		12.6 ± 0.3	298	PLP–LIF		
		13.6 ± 0.4	298	RR[c] (C_3H_6)	Maurer et al. (1999)	
		10.8 ± 0.9	298	RR[d] ($CH_3OCH_2CH_2OH$)	Moriarty et al. (2003)	
4.5 ± 2.5	−(332 ± 109)	15.2 ± 0.7	263	PLP–LIF		
		14.4 ± 0.6	273			
		12.2 ± 0.4	298			
		11.4 ± 0.5	323			
		11.1 ± 0.6	348			
		10.8 ± 0.4	372			

[a]Abbreviations used for the techniques are defined in table I-F-3.

[b]Reference compound used not specified. Study involved use of a number of alkyl ethers and ethanol as reference compounds; reference rate coefficients quoted are within 10% of those recommended in the various sections of this book and in Calvert et al. (2008).

[c]Placed on an absolute basis using $k(OH+C_3H_6) = 2.9 \times 10^{-11}$ cm^3 molecule^{-1} s^{-1} (Atkinson et al., 2006).

[d]Placed on an absolute basis using $k(OH+CH_3OCH_2CH_2OH) = 1.3 \times 10^{-11}$ cm^3 molecule^{-1} s^{-1} (this book, section III-C-2.1).

Arrhenius expression is obtained, $k = 6.8 \times 10^{-12} \exp(159/T)$ cm^3 molecule^{-1} s^{-1}, with $k = 11.5 \times 10^{-12}$ cm^3 molecule^{-1} s^{-1} at 298 K. An uncertainty of ±20% is assigned near 298 K. Note, however, that the uncertainty is considerably larger at lower temperatures; the Dagaut et al. (1990) and Moriarty et al. (2003) data differ by about 50% at 250 K. Further studies at low temperature are recommended.

III-E-10.2. Cl-Atom Reaction Kinetics

The rate coefficient for reaction of Cl-atoms with 1,4-dioxane has been studied using relative rate techniques, at 296 K by Platz et al. (1997) and between 240 and 340 K by Li and Pirasteh (2006). See table III-E-14. The rate coefficient displays no obvious dependence on temperature, and the average of all reported values is recommended, $k = 1.85 \times 10^{-10}$ cm^3 molecule^{-1} s^{-1}.

III-E-10.3. O(^{3}P) Reaction Kinetics

Liu et al. (1990a) report a rate coefficient $k = 6.8 \times 10^{-14}$ cm^3 molecule^{-1} s^{-1} at 298 K, using a flash photolysis–resonance fluorescence technique.

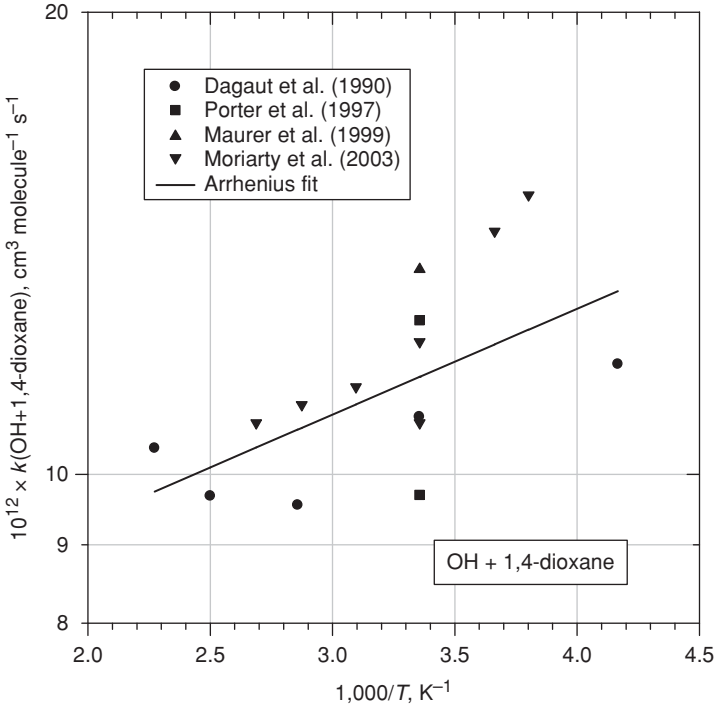

Figure III-E-10. Arrhenius plot of the rate coefficient for the reaction of OH with 1,4-dioxane.

Table III-E-14. Rate coefficients (k, cm^3 molecule^{-1} s^{-1}) for reaction of Cl with 1,4-dioxane

$10^{10} \times k$	T (K)	Technique[a]	Reference	Temperature Range (K)
2.0 ± 0.1	296	RR[b] (C_2H_4)	Platz et al. (1997)	
1.9 ± 0.2	296	RR[c] (CH_3OCH_3)		
1.83 ± 0.20	240	RR[c] (CH_3OCH_3)	Li and Pirasteh (2006)	240–340
1.85 ± 0.20	260			
1.85 ± 0.20	277			
1.82 ± 0.19	298			
1.80 ± 0.19	320			
1.78 ± 0.20	340			

[a]Abbreviations used for the techniques are defined in table I-F-3.
[b]Placed on an absolute basis using $k(Cl+C_2H_4) = 0.95 \times 10^{-10}$ cm^3 molecule^{-1} s^{-1} (this book, table I-F-2).
[c]Placed on an absolute basis using $k(Cl+CH_3OCH_3) = 1.8 \times 10^{-10}$ cm^3 molecule^{-1} s^{-1}, independent of T (this book, section III-B-1.3).

III-E-10.4. Summary of the Atmospheric Fate of 1,4-Dioxane, and the End Products of Its Oxidation

The atmospheric lifetime of 1,4-dioxane will be controlled mainly by its reaction with OH. For daytime [OH] $= 2.5 \times 10^6$ molecule cm^{-3}, a lifetime of about 10 h is obtained.

Products of the OH-initiated oxidation of 1,4-dioxane have been reported by Platz et al. (1997), Geiger et al. (1999), and Maurer et al. (1999). The predominant product obtained in the presence of NO_x in all studies is ethylene glycol diformate, $HC(=O)OCH_2CH_2OCH=O$, which results from ring-opening of the cyclic alkoxy radical, *cyclo*(-$OCH_2CH_2OCH_2CHO$•-) . The analysis of Geiger et al. (1999) suggest the likelihood of the formation of organic nitrates, *cyclo*(-$OCH_2CH_2OCH_2CH$-)ONO_2, in small yield.

III-E-11. 1,3-Dioxane

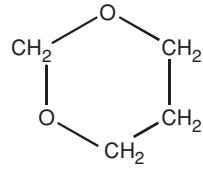

III-E-11.1. OH Reaction Kinetics

Dagaut et al. (1990) and Moriarty et al. (2003) have studied the reaction of OH with 1,3-dioxane as a function of temperature, see table III-E-15 and in figure III-E-11. The data are in substantive agreement. Fitting of the combined dataset gives: $k = 8.6 \times 10^{-12} \exp(45/T)$ cm^3 molecule^{-1} s^{-1}, with $k = 10.0 \times 10^{-12}$ cm^3 molecule^{-1} s^{-1} at 298 K. An uncertainty of ±15% is assigned near 298 K.

Table III-E-15. Rate coefficients ($k = A \times e^{-B/T}$, cm^3 molecule^{-1} s^{-1}) for reaction of OH with 1,3-dioxane

$10^{12} \times A$	B (K)	$10^{12} \times k$	T (K)	Technique[a]	Reference	Temperature Range (K)
9.4 ± 0.2	−10 ± 60	10.0 ± 0.5	240	FP–RF	Dagaut et al. (1990)	240–440
		9.15 ± 0.43	298			
		10.6 ± 0.2	350			
		9.65 ± 0.31	400			
		9.72 ± 1.18	440			
		12.1 ± 0.5	298	RR[b] (tetrahydrofuran)	Moriarty et al. (2003)	253–372
6.7 ± 1.2	−121 ± 46	10.6 ± 0.2	253	PLP–LIF		
		10.5 ± 0.4	273			
		10.3 ± 0.4	298			
		9.03 ± 0.2	333			
		9.44 ± 0.2	372			

[a]Abbreviations used for the techniques are defined in table I-F-3.

[b]Placed on an absolute basis using k(OH+tetrahydrofuran) = 1.70×10^{-11} cm^3 molecule^{-1} s^{-1} (this book, section III-E-5.1).

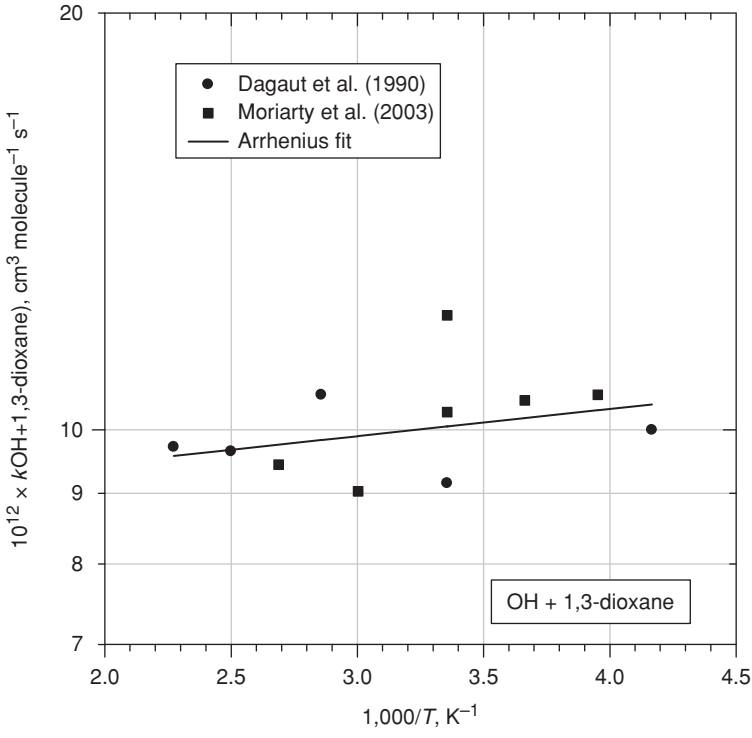

Figure III-E-11. Arrhenius plot of the rate coefficient for the reaction of OH with 1,3-dioxane.

III-E-11.2. Summary of the Atmospheric Fate of 1,3-Dioxane, and the End Products of Its Oxidation

The atmospheric lifetime of 1,3-dioxane is about 11 h, assuming a daytime [OH] = 2.5×10^6 molecule cm^{-3}.

No data are available regarding the products of the OH-initiated oxidation of this species. Unlike the symmetric 1,4-dioxane species, there are three unique sites for OH attack on 1,3-dioxane. Reaction at the 2-position will, by analogy to the chemistry of 1,3-dioxolane (figure III-E-8), likely lead to the formation of 1,3-dioxan-2-one. Decomposition of the alkoxy radical formed following OH attack at the identical 4- or 6-positions in 1,3-dioxane will lead to the $HC(O)OCH_2OCH_2CH_2O\bullet$ radical, which may decompose and/or isomerize as outlined below:

$$HC(O)OCH_2OCH_2CH_2O\bullet(+O_2) \rightarrow HC(O)OCH_2OCH_2OO\bullet + CH_2O \text{ (decomposition)}$$

$$HC(O)OCH_2OCH_2OO\bullet + NO \rightarrow HC(O)OCH_2OCH_2O\bullet + NO_2$$

$$HC(O)OCH_2OCH_2O\bullet + O_2 \rightarrow HC(O)OCH_2OCHO + HO_2$$

$$HC(O)OCH_2OCH_2CH_2O\bullet(+O_2) \rightarrow HC(O)OCH(OO\bullet)OCH_2CH_2OH \text{ (isomerization)}$$

$$HC(O)OCH(OO\bullet)OCH_2CH_2OH + NO \rightarrow HC(O)OCH(O\bullet)OCH_2CH_2OH + NO_2$$

$$HC(O)OCH(O\bullet)OCH_2CH_2OH\,(+O_2) \rightarrow HC(O)OCH(OH)OCH_2CHO(+HO_2)$$

$$HC(O)OCH(O\bullet)OCH_2CH_2OH + O_2 \rightarrow HC(O)OC(O)OCH_2CH_2OH + HO_2$$

$$HC(O)OCH(O\bullet)OCH_2CH_2OH\,(+O_2) \rightarrow$$

$$HC(O)OH + \bullet O_2C(=O)OCH_2CH_2OH\,(+HO_2)$$

$$\bullet O_2C(=O)OCH_2CH_2OH \rightarrow\rightarrow CO_2, HCHO, HOCH_2CHO$$

III-E-12. 4-Methyl-1,3-Dioxane

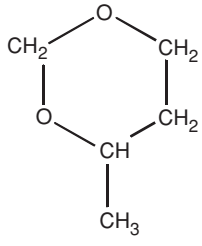

III-E-12.1. OH Reaction Kinetics

The only study of this reaction is from Dagaut et al. (1990). A value of $k = 1.13 \times 10^{-11}$ cm^3 $molecule^{-1}$ s^{-1} was obtained at 298 K, see table III-E-16. In the absence of corroborative data, an uncertainty of ±25% is assigned.

III-E-12.2. Summary of the Atmospheric Fate of 4-Methyl-1,3-Dioxane, and the End Products of Its Oxidation

The atmospheric lifetime of 4-methyl-1,3-dioxane is about 10 h, assuming a daytime [OH] = 2.5×10^6 molecule cm^{-3}. No data are available regarding the products of the OH-initiated oxidation of this species.

Table III-E-16. Rate coefficient (k, cm^3 $molecule^{-1}$ s^{-1}) for reaction of OH with 4-methyl-1,3-dioxane

$10^{12} \times k$	T (K)	Technique[a]	Reference
11.3 ± 0.6	298	FP–RF	Dagaut et al. (1990)

[a]Abbreviations used for the techniques are defined in table I-F-3.

III-E-13. 1,3-Dioxepane

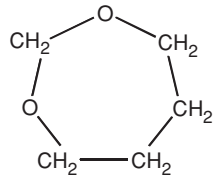

III-E-13.1. OH Reaction Kinetics

The reaction of OH with 1,3-dioxepane has been studied from 263 to 372 K by Moriarty et al. (2003), see table III-E-17 and figure III-E-12. Their data give $k = 6.0 \times 10^{-12} \exp(250/T)$ cm^3 molecule^{-1} s^{-1}, with $k = 1.4 \times 10^{-11}$ cm^3 molecule^{-1} s^{-1} at 298 K. In the absence of corroborative data, an uncertainty of $\pm 25\%$ is assigned at 298 K.

III-E-13.2. Summary of the Atmospheric Fate of 1,3-Dioxepane, and the End Productsof Its Oxidation

The atmospheric lifetime of 1,3-dioxepane is about 8 h, assuming a daytime [OH] = 2.5×10^6 molecule cm^{-3}. No data are available regarding the products of its oxidation.

III-E-14. 1,3,5-Trioxane

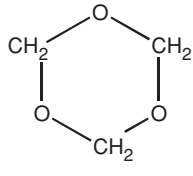

Table III-E-17. Rate coefficients ($k = A \times e^{-B/T}$, cm^3 molecule^{-1} s^{-1}) for reaction of OH with 1,3-dioxepane

$10^{12} \times A$	B (K)	$10^{12} \times k$	T (K)	Technique[a]	Reference	Temperature Range (K)
		12.2 ± 0.9	298	RR[b] $[(CH_3)_2CHOCH_2CH_2OH]$	Moriarty et al. (2003)	
5.9 ± 1.1	-269 ± 94	17.1 ± 0.9	263	PLP–LIF		263–372
		15.4 ± 0.5	273			
		13.9 ± 0.4	298			
		12.9 ± 0.6	323			
		12.4 ± 0.6	348			
		12.7 ± 0.4	372			

[a]Abbreviations used for the techniques are defined in table I-F-3.

[b]Placed on an absolute basis using $k(\text{OH}+(\text{CH}_3)_2\text{CHOCH}_2\text{CH}_2\text{OH}) = 2.1 \times 10^{-11}$ cm^3 molecule^{-1} s^{-1} (Porter et al., 1997).

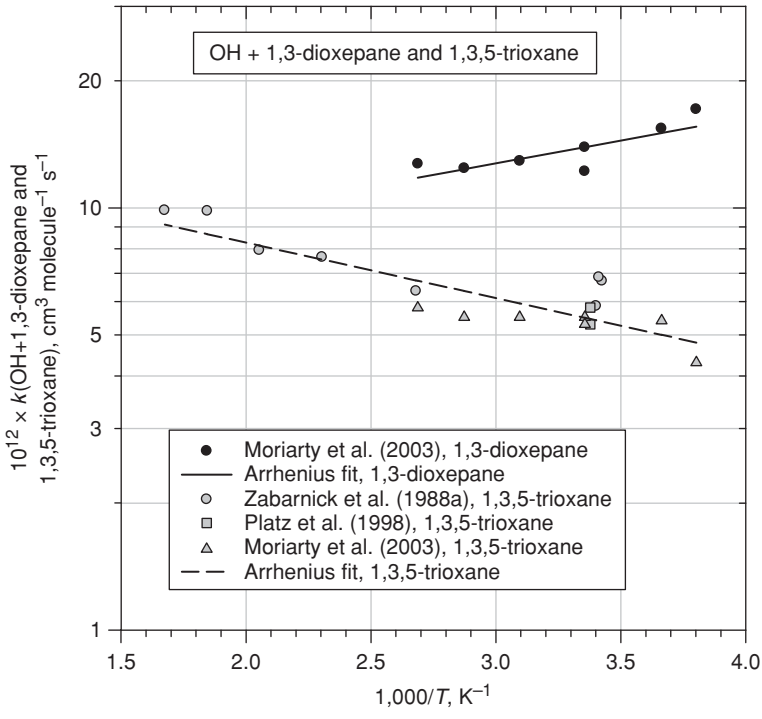

Figure III-E-12. Arrhenius plot of the rate coefficient for the reaction of OH with 1,3-dioxepane and 1,3,5-trioxane.

III-E-14.1. OH Reaction Kinetics

Rate coefficients for the reaction of OH with 1,3,5-trioxane have been reported by Zabarnick et al. (1988a), Platz et al. (1998), and Moriarty et al. (2003), see table III-E-18 and figure III-E-12. The data are in good agreement. Fitting of the Arrhenius expression to the entire dataset gives: $k = 1.5 \times 10^{-11} \exp(-302/T)$ cm^3 molecule^{-1} s^{-1}, with $k = 5.5 \times 10^{-12}$ cm^3 molecule^{-1} s^{-1} at 298 K. An uncertainty of $\pm 15\%$ is assigned at 298 K.

III-E-14.2. Cl-Atom Reaction Kinetics

The rate coefficient for reaction of Cl with 1,3,5-trioxane has been studied near 296 K by Platz et al. (1998), using a relative rate technique. See table III-E-19. The average of their three determinations is recommended: $k = 10.2 \times 10^{-11}$ cm^3 molecule^{-1} s^{-1}, with an estimated uncertainty of $\pm 15\%$.

III-E-14.3. Summary of the Atmospheric Fate of 1,3,5-Trioxane, and the End Products of Its Oxidation

The atmospheric lifetime of 1,3,5-trioxane is about 2 days, assuming a diurnally averaged [OH] = 10^6 molecule cm^{-3}. End products of the OH-initiated oxidation of

Table III-E-18. Rate coefficients ($k = A \times e^{-B/T}$, cm^3 molecule^{-1} s^{-1}) for reaction of OH with 1,3,5-trioxane

$10^{12} \times A$	B (K)	$10^{12} \times k$	T (K)	Technique[a]	Reference	Temperature Range (K)
13.6 ± 2.0	232 ± 50	6.71 ± 0.21	292	PLP–LIF	Zabarnick	292–597
		6.85 ± 0.18	293		et al. (1988)	
		5.85 ± 0.15	294			
		6.35 ± 0.17	373			
		7.64 ± 0.17	473			
		7.94 ± 0.37	487			
		9.82 ± 0.14	542			
		9.86 ± 0.15	597			
		5.3 ± 0.4	296	RR[b] (C_2H_4)	Platz et al.	
		5.8 ± 0.3	296	RR[c] (*cyclo*-C_6H_{12})	(1998)	
		5.5 ± 0.7	298	RR[d] (*n*-butanol)	Moriarty	
9.6 ± 1.5	184 ± 39	4.3 ± 0.4	263	PLP–LIF	et al. (2003)	263–372
		5.4 ± 0.2	273			
		5.3 ±0.2	298			
		5.5 ± 0.2	323			
		5.5 ± 0.2	348			
		5.8 ± 0.2	372			

[a]Abbreviations used for the techniques are defined in table I-F-3.
[b]Placed on an absolute basis using $k(OH+C_2H_4) = 7.9 \times 10^{-12}$ cm^3 molecule^{-1} s^{-1} (Atkinson et al., 2006).
[c]Placed on an absolute basis using $k(OH+cyclo\text{-}C_6H_{12}) = 6.97 \times 10^{-12}$ cm^3 molecule^{-1} s^{-1} (Calvert et al., 2008).
[d]Placed on an absolute basis using $k(OH+n\text{-butanol}) = 8.3 \times 10^{-12}$ cm^3 molecule^{-1} s^{-1} (Calvert et al., 2008).

Table III-E-19. Rate coefficients (k, cm^3 molecule^{-1} s^{-1}) for reaction of Cl with 1,3,5-trioxane

$10^{10} \times k$	T (K)	Technique[a]	Reference
1.03 ± 0.06	296	RR[b] (C_2H_6)	Platz et al. (1998)
1.06 ± 0.06	296	RR[c] (CH_3OCH_3)	
0.97 ± 0.05	296	RR[d] (CH_3OH)	

[a]Abbreviations used for the techniques are defined in table I-F-3.
[b]Placed on an absolute basis using $k(Cl+C_2H_4) = 0.95 \times 10^{-10}$ cm^3 molecule^{-1} s^{-1} (this book, table I-F-2)
[c]Placed on an absolute basis using $k(Cl+CH_3OCH_3) = 1.8 \times 10^{-10}$ cm^3 molecule^{-1} s^{-1} (this book, section III-B-1.3).
[d]Placed on an absolute basis using $k(Cl+CH_3OH) = 5.5 \times 10^{-11}$ cm^3 molecule^{-1} s^{-1} (Atkinson et al., 2006).

1,3,5-trioxane have been studied in the presence of NO_x by Platz et al. (1998). The major product identified was methylene glycol diformate, HC(=O)OCH_2OCH(=O). The chemistry proceeds via the formation of the (*cyclo*-$C_3H_5O_3$)O• radical, whose predominant fate is decomposition via C—O bond rupture, leading to the formation of the acyclic HC(O)OCH_2OCH_2O• radical. Platz al. (1998) showed that methylene glycol diformate was then formed via H-atom elimination from this alkoxy species, or via its reaction with O_2. As pointed out by Platz et al. (1998), the C—O bond rupture process observed for the (*cyclo*-$C_3H_5O_3$)O• radical is unusual, and may be driven by ring-strain associated with the trioxane structure.

Table III-E-20. Rate coefficients (k, cm^3 molecule^{-1} s^{-1}) for reaction of OH with glycidaldehyde

$10^{12} \times k$	T (K)	Technique[a]	Reference
15.7 ± 0.4	298	RR[b] (ethene)	Ma et al. (1998)

[a]Abbreviations used for the techniques are defined in table I-F-3.
[b]Placed on an absolute basis using k(OH+ethene) = 7.9×10^{-12} cm^3 molecule^{-1} s^{-1} (Atkinson et al., 2006).

III-E-15. Glycidaldehyde

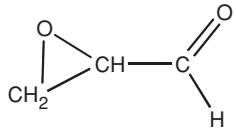

III-E-15.1. OH Reaction Kinetics

The rate coefficient for reaction of OH with glycidaldehyde was determined via the relative rate technique (Ma et al., 1998), $k = 1.6 \times 10^{-11}$ cm^3 molecule^{-1} s^{-1}. See table III-E-20. In the absence of corroborative studies, an uncertainty of ±35% is estimated at 298 K.

III-E-15.2. Summary of the Atmospheric Fate of Glycidaldehyde and the End Products of Its Oxidation

The lifetime of glycidaldehyde against reaction with OH is estimated to be about 7 h for daytime [OH] $\approx 2.5 \times 10^6$ molecule cm^{-3}. Ma et al. (1998) also showed that photolysis is likely an important loss process, with an estimated lifetime of 4 h for a noontime, mid-latitude summer day; see section IX-C-2 and table IX-M-1. These workers also studied the OH-initiated oxidation of glycidaldehyde in the absence of NO_x, and identified initial yields of formic acid anhydride (∼45%), formic acid (∼20%), formaldehyde (∼25%), and CO_2 (∼20%), as the major products. The main channel for OH reaction is likely via abstraction of the aldehydic H-atom, which would be expected to lead (in part) to formation of CO_2 and the oxiranoxy radical, whose chemistry is outlined in figure III-E-2.

III-E-16. Vinyl Oxirane (3,4-Epoxy-1-Butene) and Its Methyl-Substituted Derivatives

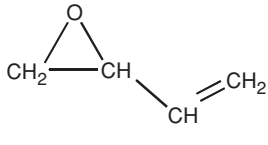

Table III-E-21. Rate coefficient (k, cm^3 molecule^{-1} s^{-1}) for reaction of O_3 with vinyl oxirane

$10^{18} \times k$	T (K)	Technique[a]	Reference
1.6 ± 0.4	296	UV abs.	Kramp and Paulson (2000)

[a]Abbreviations used for the techniques are defined in table I-F-3.

Table III-E-22. Rate coefficients (k, cm^3 molecule^{-1} s^{-1}) for reaction of NO_3 with vinyl oxirane and its methyl-substituted derivatives

Species	$10^{15} \times k$	T (K)	Technique[a]	Reference
Vinyl oxirane	6.4 ± 2.1	295	RR[b] (1-butene)	Kind et al. (1996a)
2-Methyl-2-vinyl oxirane	9.8 ± 2.7	295	RR[b] (1-butene)	Kind et al. (1996a)
2-Methyl-2-(2-propenyl) oxirane	160 ± 30	295	RR[c] (isobutene)	Kind et al. (1996a)
2,2-Dimethyl-3-(2,2-dimethylvinyl) oxirane	(4.7 ± 0.6) × 10^3	295	RR[d] (2-methyl-2-butene)	Kind et al. (1996a)

[a]Abbreviations used for the techniques are defined in table I-F-3.
[b]Placed on an absolute basis using $k(NO_3+1\text{-butene}) = 1.3 \times 10^{-14}$ cm^3 molecule^{-1} s^{-1} (Calvert et al., 2000).
[c]Placed on an absolute basis using $k(NO_3+\text{isobutene}) = 3.4 \times 10^{-13}$ cm^3 molecule^{-1} s^{-1} (Calvert et al., 2000).
[d]Placed on an absolute basis using $k(NO_3+2\text{-methyl-2-butene}) = 9.4 \times 10^{-12}$ cm^3 molecule^{-1} s^{-1} (Calvert et al., 2000).

Limited data are available regarding the atmospheric behavior of vinyl oxirane and some of its methylated analogs. The kinetic data for the reactions with O_3 and with NO_3 radical are summarized in the tables III-E-21 and III-E-22, respectively.

III-E-17. Furan

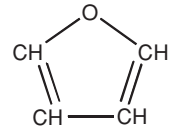

III-E-17.1. OH Reaction Kinetics

The reaction of OH with furan has been studied as a function of temperature by Wine and Thompson (1984), and near 298 K by Lee and Tang (1982), Atkinson et al. (1983a), Tuazon et al. (1984a), and Bierbach et al. (1992). The data, summarized in table III-E-23, have also been reviewed by Calvert et al. (2002). As pointed out in that review, the data are in good agreement with the exception of the measurement of Lee and Tang. Averaging the remaining data gives $k = 4.1 \times 10^{-11}$ cm^3 molecule^{-1} s^{-1} at 298 K, with an estimated uncertainty of ±20%. Combining this with the temperature dependence reported by Wine and Thompson (1984) gives $k = 1.3 \times 10^{-11} \exp(333/T)$ cm^3 molecule^{-1} s^{-1}.

Table III-E-23. Rate coefficients ($k = A \times e^{-B/T}$, cm^3 molecule^{-1} s^{-1}) for reaction of OH with furan

$10^{12} \times A$	B (K)	$10^{12} \times k$	T (K)	Technique[a]	Reference	Temperature Range (K)
		105 ± 8	295	DF–RF	Lee and Tang (1982)	
		38.6 ± 2.8	298	RR[b] (*n*-hexane)	Atkinson et al. (1983a)	
13.2 ± 2.9	−333 ± 67	49.6 ± 3.3	254	FP–RF	Wine and Thompson (1984)	254–424
		40.8 ± 1.8	297			
		43.1 ± 1.2	297			
		38.7 ± 2.2	299			
		41.6 ± 3.5	299			
		38.3 ± 4.5	300			
		31.9 ± 1.6	365			
		29.9 ± 2.0	424			
		42.3 ± 3.2	295	RR[c] (isoprene)	Tuazon et al. (1984a)	
		45.1 ± 2.3	300	RR[d] (propene)	Bierbach et al. (1992)	

[a]Abbreviations used for the techniques are defined in table I-F-3.
[b]Placed on an absolute basis using k(OH+*n*-hexane) = 5.48×10^{-12} cm^3 molecule^{-1} s^{-1} (Calvert et al., 2008).
[c]Placed on an absolute basis using k(OH+isoprene) = 1.02×10^{-10} cm^3 molecule^{-1} s^{-1} (Atkinson et al., 2006).
[d]Placed on an absolute basis using k(OH+propene) = 2.6×10^{-11} cm^3 molecule^{-1} s^{-1} (Atkinson et al., 2006).

III-E-17.2. O_3 Reaction Kinetics

The only study of this reaction is that of Atkinson et al. (1983a), who report $k = 2.4 \times 10^{-18}$ cm^3 molecule^{-1} s^{-1}. In the absence of corroborating data, an uncertainty of ±35% is assigned. The study is summarized in table III-E-24.

III-E-17.3. NO_3 Reaction Kinetics

The rate coefficient for reaction of NO_3 with furan has been studied as a function of temperature by Cabañas et al. (2004) and at 295 K by Atkinson et al. (1985) and Kind et al. (1996b). Averaging the three determinations near 298 K gives $k = 1.2 \times 10^{-12}$ cm^3 molecule^{-1} s^{-1}, with an estimated uncertainty of ±35%. Using this value with the temperature dependence from Cabañas et al. leads to $k = 1.15 \times 10^{-13} \exp(700/T)$ cm^3 molecule^{-1} s^{-1}. The data are summarized in table III-E-25.

Table III-E-24. Rate coefficients (k, cm^3 molecule^{-1} s^{-1}) for reaction of O_3 with furan and 3-methylfuran

$10^{18} \times k$	T (K)	Technique[a]	Reference
O_3 + Furan			
2.42 ± 0.28	298	O_3CL	Atkinson et al. (1983a)
O_3 + 3-Methylfuran			
20.3 ± 0.8	296	RR[b] (propene)	Alvarado et al. (1996)

[a]Abbreviations used for the techniques are defined in table I-F-3.
[b]Placed on an absolute basis using k(O_3+propene) = 9.6×10^{-18} cm^3 molecule^{-1} s^{-1} (Atkinson et al., 2006).

Table III-E-25. Rate coefficients (k, cm^3 molecule^{-1} s^{-1}) for reaction of NO_3 with furan

$10^{13} \times A$	B (K)	$10^{13} \times k$	T (K)	Technique[a]	Reference	Temperature Range (K)
		14.4 ± 0.2	295	RR[b] (*trans*-2-butene)	Atkinson et al. (1985)	
		9.93 ± 0.62	295	RR[b] (*trans*-2-butene)	Kind et al. (1996b)	
1.3 ± 0.8	-700 ± 200	17.5 ± 0.8	263	DF–LIF	Cabañas et al. (2004)	263–335
		15 ± 1	277			
		14.0 ± 0.8	287			
		13 ± 2	298			
		12 ± 1	306			
		11 ± 1	315			
		10.2 ± 0.9	325			
		10.1 ± 0.7	335			

[a]Abbreviations used for the techniques are defined in table I-F-3.
[b]Placed on an absolute basis using $k(NO_3 + trans\text{-2-butene}) = 3.9 \times 10^{-13}$ cm^3 molecule^{-1} s^{-1} (Calvert et al., 2000).

III-E-17.4. Cl-Atom Reaction Kinetics

A rate coefficient $k = 2.0 \times 10^{-10}$ cm^3 molecule^{-1} s^{-1} for reaction of Cl with furan can be derived from the relative rate study of Cabañas et al. (2005). Given the excellent agreement obtained with multiple reference compounds, an uncertainty of $\pm 20\%$ is assigned. The study is summarized in table III-E-26.

III-E-17.5. Summary of the Atmospheric Fate of Furan, and the End Products of Its Oxidation

The atmospheric lifetime of furan will be controlled by reaction with NO_3 at night (lifetime $\leq$ 0.5 h, even for moderately polluted conditions) and by reaction with OH

Table III-E-26. Rate coefficients (k, cm^3 molecule^{-1} s^{-1}) for reaction of Cl with furan and methyl-substituted furans

Species	$10^{10} \times k$	T (K)	Technique[a]	Reference
Furan	2.0 ± 0.4	298	RR[b] (propane)	Cabañas et al. (2005)
	2.0 ± 0.3	298	RR[c] (1-butene)	Cabañas et al. (2005)
	1.9 ± 0.2	298	RR[d] (nonane)	Cabañas et al. (2005)
	2.0 ± 0.3	298	RR[e] (*E*-2-butene)	Cabañas et al. (2005)
2-Methylfuran	3.9 ± 0.2	298	RR[d] (nonane)	Cabañas et al. (2005)
2-Ethylfuran	4.4 ± 0.3	298	RR[d] (nonane)	Cabañas et al. (2005)
3-Methylfuran	4.0 ± 0.3	298	RR[d] (nonane)	Cabañas et al. (2005)
2,5-Dimethylfuran	5.4 ± 0.3	298	RR[d] (nonane)	Cabañas et al. (2005)

[a]Abbreviations used for the techniques are defined in table I-F-3.
[b]Placed on an absolute basis using $k(Cl + propane) = 1.4 \times 10^{-11}$ cm^3 molecule^{-1} s^{-1} (Calvert et al., 2008).
[c]Placed on an absolute basis using $k(Cl + 1\text{-butene}) = 3.0 \times 10^{-10}$ cm^3 molecule^{-1} s^{-1} (Orlando et al., 2003).
[d]Placed on an absolute basis using $k(Cl + E\text{-2-butene}) = 3.3 \times 10^{-10}$ cm^3 molecule^{-1} s^{-1} (average of values reported by Orlando et al., 2003; Kaiser et al., 2007; and Ezell et al., 2002).
[e]Placed on an absolute basis using $k(Cl + nonane) = 4.6 \times 10^{-10}$ cm^3 molecule^{-1} s^{-1} (Calvert et al., 2008).

during the day (lifetime ≈ 3 h). End product studies have been conducted for oxidation initiated by OH (Bierbach et al., 1995), NO_3 (Berndt et al., 1997), and Cl-atoms (Villaneuva et al., 2007). *E*-butenedial is a major product of the NO_3-initiated oxidation process (molar yield 77%), while *E*- and *Z*-butenedial are formed in large yield (> 70%) from the OH-initiated oxidation. 3*H*-Furandione is also formed following reaction with NO_3 (yield ≈ 19%). Mechanisms proposed by the authors (Berndt et al., 1997; Bierbach et al., 1995) are shown in mechanism III-E-17.5.1.

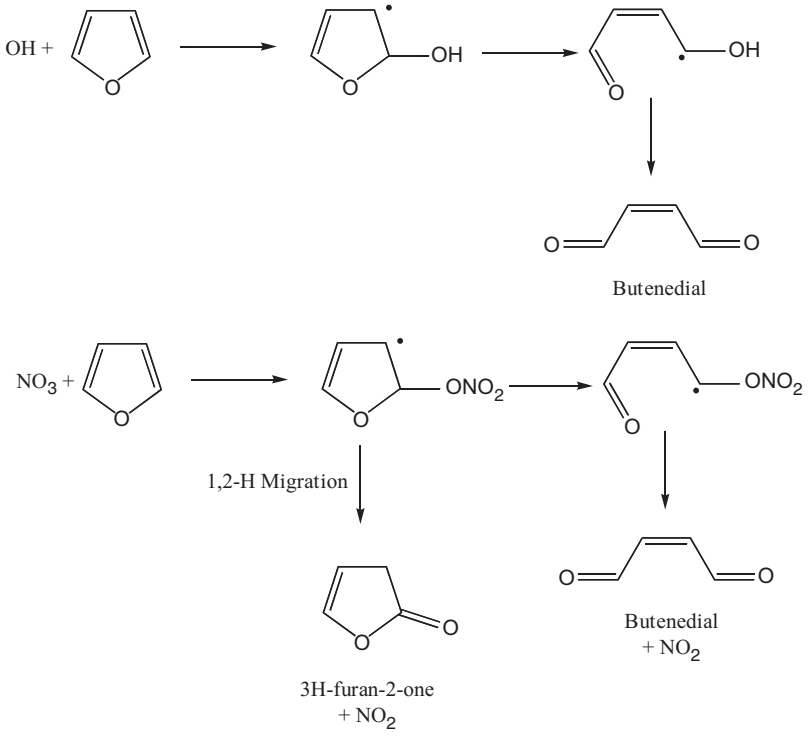

Reaction mechanism III-E-17.5.1

III-E-18. Alkyl Substituted Furans: 2-Methylfuran, 2-Ethylfuran, 3-Methylfuran, 2,5-Dimethylfuran, 2,4-Dimethylfuran, 2,3-Dimethylfuran, and Tetramethylfuran

III-E-18.1. OH Reaction Kinetics

The reaction of OH with 2-methylfuran (Bierbach et al., 1992), 2-ethylfuran (Bierbach et al., 1992), 3-methylfuran (Atkinson et al., 1989c), and 2,5-dimethylfuran (Bierbach et al., 1992) have each been the subject of one relative rate study, see table III-E-27. Values found near 298 K are as follows: k(OH + 2-methylfuran) = 6.7×10^{-11} cm^3 molecule^{-1} s^{-1}, k(OH + 2-ethylfuran) = 12.0×10^{-11} cm^3 molecule^{-1} s^{-1}, k(OH + 3-methylfuran) = 9.3×10^{-11} cm^3 molecule^{-1} s^{-1} and k(OH + 2,5-dimethylfuran)

Table III-E-27. Rate coefficients (k, cm^3 molecule^{-1} s^{-1}) for reaction of OH with methyl-substituted furans

Species	$10^{12} \times k$	T (K)	Technique[a]	Reference
2-Methylfuran	66.7 ± 3.4	300	RR[b] (propene)	Bierbach et al. (1992)
2-Ethylfuran	116 ± 24	300	RR[b] (propene)	Bierbach et al. (1992)
3-Methylfuran	92.6 ± 2.4	296	RR[c] (2,3-dimethyl-2-butene)	Atkinson et al. (1989c)
2,5-Dimethylfuran	132 ± 10	300	RR[b] (*trans*-2-butene)	Bierbach et al. (1992)

[a]Abbreviations used for the techniques are defined in table I-F-3.
[b]Placed on an absolute basis using k(OH+propene) = 2.6×10^{-11} cm^3 molecule^{-1} s^{-1} (Atkinson et al., 2006).
[c]Placed on an absolute basis using k(OH+2,3-dimethyl-2-butene) = 1.1×10^{-10} cm^3 molecule^{-1} s^{-1} (Calvert et al., 2000).
[d]Placed on an absolute basis using k(OH+*trans*-2-butene) = 6.3×10^{-11} cm^3 molecule^{-1} s^{-1} (Calvert et al., 2000).

= 13.2×10^{-11} cm^3 molecule^{-1} s^{-1}. In the absence of corroborative measurements, uncertainties of ±35% are assigned.

III-E-18.2. O_3 Reaction Kinetics

Alvarado et al. (1996) used a relative rate technique to obtain $k = 2.0 \times 10^{-17}$ cm^3 molecule^{-1} s^{-1} for reaction of O_3 with 3-methylfuran. In the absence of corroborating data, an uncertainty of ±35% is assigned. The study is summarized in table III-E-24.

III-E-18.3. NO_3 Reaction Kinetics

There is poor agreement between the two relative rate studies of the reaction of 3-methylfuran with NO_3 (Kind et al., 1996b; Alvarado et al., 1996), see table III-E-28. An average value of $k = 2.0 \times 10^{-12}$ cm^3 molecule^{-1} s^{-1} is recommended, with an estimated uncertainty of ±70%. Single determinations of the rate coefficient for reaction of NO_3 with other substituted furans have been carried out by Kind et al. (1996b). Rate coefficients obtained, in units of 10^{-12} cm^3 molecule^{-1} s^{-1}, are as follows: 2-methylfuran, 2.6; 2,5-dimethylfuran, 5.8; 2,4-dimethylfuran, 5.7; 2,3-dimethylfuran, 5.8; and tetramethylfuran, 11.8. These data are also summarized in table III-E-28. Given the disagreement just noted regarding the NO_3 + 3-methylfuran reaction, uncertainties of ±70% are assigned.

III-E-18.4. Cl-Atom Reaction Kinetics

The relative rate study of Cabañas et al. (2005) leads to the following rate coefficient data: k(Cl + 2-methylfuran) = 3.9×10^{-10} cm^3 molecule^{-1} s^{-1}, k(Cl + 2-ethylfuran) = 4.4×10^{-10} cm^3 molecule^{-1} s^{-1}, k(Cl + 3-methylfuran) = 4.0×10^{-10} cm^3 molecule^{-1} s^{-1} and$k$(Cl + 2,5-dimethylfuran) = 5.4×10^{-10} cm^3 molecule^{-1} s^{-1}, see table III-E-26. An uncertainty of ±25% is assigned to these data.

Table III-E-28. Rate coefficients (k, cm^3 molecule^{-1} s^{-1}) for reaction of NO_3 with methyl-substituted furans

Species	$10^{12} \times k$	T (K)	Technique[a]	Reference
2-Methylfuran	2.57 ± 0.18	295	RR[b] (2,3-dimethyl-2-butene)	Kind et al. (1996b)
3-Methylfuran	2.86 ± 0.06	295	RR[b] (2,3-dimethyl-2-butene)	Kind et al. (1996b)
	1.23 ± 0.02	296	RR[c] (2-methyl-2-butene)	Alvarado et al. (1996)
2,5-Dimethylfuran	5.78 ± 0.35	295	RR[b] (2,3-dimethyl-2-butene)	Kind et al. (1996b)
2,3-Dimethylfuran	5.83 ± 0.46	295	RR[b] (2,3-dimethyl-2-butene)	Kind et al. (1996b)
2,4-Dimethylfuran	5.76 ± 0.46	295	RR[b] (2,3-dimethyl-2-butene)	Kind et al. (1996b)
Tetramethylfuran	11.8 ± 1.6	295	RR[b] (2,3-dimethyl-2-butene)	Kind et al. (1996b)

[a]Abbreviations used for the techniques are defined in table I-F-3.
[b]Placed on an absolute basis using $k(NO_3+2,3\text{-dimethyl-2-butene}) = 5.7 \times 10^{-11}$ cm^3 molecule^{-1} s^{-1} (Calvert et al., 2000).
[c]Placed on an absolute basis using $k(NO_3+2\text{-methyl-2-butene}) = 8.8 \times 10^{-12}$ cm^3 molecule^{-1} s^{-1} (Calvert et al., 2000).

III-E-18.5. Summary of the Atmospheric Fate of the Alkyl-substituted Furans, and the End Products of Their Oxidation

Reaction of these substituted species with NO_3 will provide an important nighttime removal process (lifetime only a few minutes for heavily polluted conditions, and ≤ 0.5 h for more moderately polluted conditions). Reaction with OH will be the major daytime removal process, occurring on a timescale of $\approx 1 - 2$ h, while reaction with O_3 will be a minor loss throughout the day and night.

End product studies for these substituted furan species are quite limited, but indications are that the substituted analogs to butenedial are formed in large yield from both the OH- and NO_3-initiated oxidation. Berndt et al. (1997) tentatively identified *cis*-3,4-dimethylhex-3-en-2,5-dione, $CH_3C(=O)C(CH_3)=C(CH_3)C(=O)CH_3$, as a major product following reaction of NO_3 with tetramethylfuran, while Bierbach et al. (1995) observed 4-oxo-2-pentenal, $CH_3C(=O)CH=CHCH=O$, in about 70% yield from reaction of OH with 2-methylfuran.

III-E-19. Furfurals: 2-Furancarboxaldehyde (2-Furfural), 3-Furancarboxaldehyde (3-Furfural), and 5-Methyl-2-Furfural

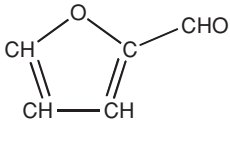

2-Furfural

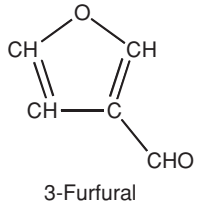

3-Furfural

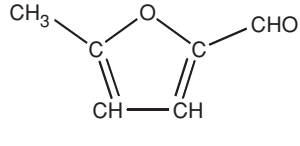

5-Methyl-2-furfural

III-E-19.1. OH Reaction Kinetics

The reactions of OH with 2-furfural, 3-furfural, and 5-methyl-2-furfural have been studied by Bierbach et al. (1995) using a relative rate technique, see table III-E-29.

Table III-E-29. Rate coefficients (k, cm^3 molecule^{-1} s^{-1}) for reaction of OH with furfurals

Species	$10^{12} \times k$	T (K)	Technique[a]	Reference
OH Reactions				
2-Furancarboxaldehyde	35.1 ± 1.1	300	RR[b] (*trans*-2-butene)	Bierbach et al. (1995)
3-Furancarboxaldehyde	48.5 ± 1.6	300	RR[b] (*trans*-2-butene)	Bierbach et al. (1995)
5-Methyl-2-furancarboxaldehyde	51.0 ± 2.1	300	RR[b] (*trans*-2-butene)	Bierbach et al. (1995)
Cl-Atom Reactions				
2-Furancarboxaldehyde	244 ± 16	298	RR[c] (nonane)	Cabañas et al. (2008)
	260 ± 22		RR[d] (2-ethylfuran)	
3-Furancarboxaldehyde	304 ± 15	298	RR[c] (nonane)	Cabañas et al. (2008)
	295 ± 23		RR[d] (2-ethylfuran)	
5-Methyl-2-furancarboxaldehyde	345 ± 35	298	RR[c] (nonane)	Cabañas et al. (2008)
	405 ± 32		RR[d] (2-ethylfuran)	

[a]Abbreviations used for the techniques are defined in table I-F-3.
[b]Placed on an absolute basis using k(OH+*trans*-2-butene) = 6.3×10^{-11} cm^3 molecule^{-1} s^{-1} (Calvert et al., 2000).
[c]Placed on an absolute basis using k(Cl+nonane) = 4.6×10^{-10} cm^3 molecule^{-1} s^{-1} (Calvert et al., 2008).
[d]Placed on an absolute basis using k(Cl+2-ethylfuran) = 4.4×10^{-10} cm^3 molecule^{-1} s^{-1} (this book, section III-E-18.4).

Values found near 298 K are as follows: k(OH + 2-furfural) = 3.5×10^{-11} cm^3 molecule^{-1} s^{-1}, k(OH + 3-furfural) = 4.9×10^{-11} cm^3 molecule^{-1} s^{-1} and k(OH + 5-methyl-2-furfural) = 5.1×10^{-11} cm^3 molecule^{-1} s^{-1}. Uncertainties of ±30% are assigned.

III-E-19.2. Cl-Atom Reaction Kinetics

The reactions of 2-furfural, 3-furfural, and 5-methyl-2-furfural with Cl-atoms have been studied by Cabañas et al. (2008) using a relative rate method. The values obtained are as follows: k(Cl + 2-furfural) = 2.5×10^{-10} cm^3 molecule^{-1} s^{-1}, k(Cl + 3-furfural) = 3.0×10^{-10} cm^3 molecule^{-1} s^{-1}, and k(OH + 5-methyl-2-furfural) = 3.7×10^{-10} cm^3 molecule^{-1} s^{-1}. Uncertainties are estimated at ±25%. The study is summarized in table III-E-29.

III-E-19.3. Summary of the Atmospheric Fate of the Alkyl-substituted Furans, and the End Products of Their Oxidation

Reaction of the furfurals with OH is quite rapid, and will limit their lifetime to about 2–3 h for typical daytime OH levels of 2.5×10^6 molecule cm^{-3}. By analogy to the furans, reaction with NO_3 will also likely be rapid, and will provide an important nighttime removal process. No end product studies have been carried out. While reaction (with OH and NO_3) may be expected to occur via both addition to the ring and via abstraction of the aldehydic H-atom, we note that the reactivity of the furfurals with OH are quite similar to that of the parent furan.

III-E-20. Unsaturated Dihydrofurans and Tetrahydrofurans

There are limited data available regarding the atmospheric behavior of three unsaturated furan derivatives, 2,5-dihydrofuran (Adeniji et al., 1981), 5-methyl-2,3-dihydrofuran (Martin et al., 2002), and 5-methyl-5-vinyl-tetrahydrofuran-2-ol (Calogirou et al., 1999):

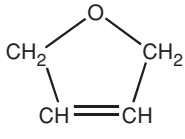

2,5-Dihydrofuran

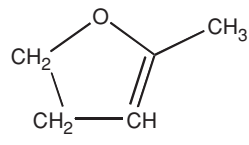

2,3-Dihydro-5-methylfuran
(4,5-Dihydro-2-methylfuran)

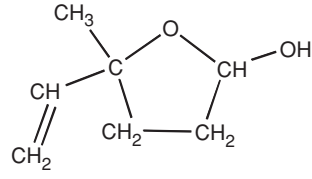

5-Methyl-5-vinyl-
tetrahydrofuran-2-ol

The 2,3-dihydro-5-methylfuran species is formed in the atmosphere at low humidity via the cyclization and subsequent dehydration of 5-hydroxy-2-pentanone, itself an important product in the oxidation of pentane (Martin et al., 2002). Similar species are expected to be formed in the oxidation of other alkanes (C_4 and larger), when isomerization of the initially formed alkoxy radical is of importance. Similarly, the species 5-methyl-5-vinyl-tetrahydrofuran-2-ol is a by-product of linalool oxidation, formed via the cyclization of an initially formed unsaturated hydroxycarbonyl species (Calogirou et al., 1999). The available data are summarized in table III-E-30.

As discussed by Martin et al. (2002), the species 2,3-dihydro-5-methylfuran will exist in equilibrium with the hydrated, acyclic 5-hydroxy-2-pentanone, the relative distribution of the two species depending on humidity. Should the cyclized compound be formed, the data of Martin et al. (2002) clearly demonstrate that its atmospheric lifetime is very short, probably no more than a few minutes for most conditions. Reaction with O_3 will be important throughout the day and night (lifetime $\approx$ 3 min. for $[O_3] = 1.5 \times 10^{12}$ molecule cm^{-3}). NO_3 reaction will dominate in the nighttime for even moderately polluted conditions (lifetime $\approx$ a few seconds), and OH reaction will play a minor daytime role. Products of the OH-, O_3-, and NO_3-initiated oxidation of 2,3-dihydro-5-methylfuran were also determined by Martin et al. (2002). The ester species, $CH_3C(O)OCH_2CH_2CHO$, was identified as a major product of the OH-initiated oxidation (molar yield $\approx$ 74%) and a minor product of the O_3- (23%) and NO_3-initiated chemistry ($\sim$5–12%). Additional products in the ozonolysis were the relatively simple species, CH_2O (28%), CH_3OH (9.5%), $CH_2{=}CH_2$ (6.6%), CO (20%) and CO_2 (47%).

For 5-methyl-5-vinyl-tetrahydrofuran-2-ol, the data of Calogirou et al. (1999) suggest that reaction with OH will dominate the daytime loss (lifetime $\approx$ 1.5 h). The reaction with NO_3 will play a role at night in heavily polluted conditions (lifetime $\approx$ 5 h for $[NO_3] = 3 \times 10^9$ molecule cm^{-3}). The major product of the OH-initiated oxidation is 4-oxopentanal. Calogirou et al. (1999) postulate that this species is formed following OH addition to the acyclic isomer of 5-methyl-5-vinyl-tetrahydrofuran-2-ol, namely, 4-methyl-4-hydroxy-hex-5-enal, with glycolaldehyde as a likely co-product.

Table III-E-30. Rate coefficients (k, cm^3 molecule^{-1} s^{-1}) for reaction of OH, O_3, and NO_3 with some unsaturated dihydro- and tetrahydrofurans

$10^{12} \times k$	T (K)	Technique[a]	Reference
O_3 + 2,5-Dihydrofuran			
1.61×10^{-5}	294	O_3 Chemiluminescence	Adeniji et al. (1981)
OH + 4,5-Dihydro-2-methylfuran			
218 ± 22	298	RR[b] (cyclohexene)	Martin et al. (2002)
217 ± 12	298	RR[c] (2-methylpropene)	
O_3 + 4,5-Dihydro-2-methylfuran			
$(3.49 \pm 0.24) \times 10^{-3}$	298	RR[d] (2,3-dimethyl-2-butene)	Martin et al. (2002)
NO_3 + 4,5-Dihydro-2-methylfuran			
168 ± 12	298	RR[e] (2,3-dimethyl-2-butene)	Martin et al. (2002)
OH + 5-Methyl-5-vinyl-tetrahydrofuran-2-ol			
74 ± 9	298	RR[c] (2-methylpropene)	Calogirou et al. (1999)
O_3 + 5-Methyl-5-vinyl-tetrahydrofuran-2-ol			
$(3.5 \pm 0.7) \times 10^{-6}$	298	RR[f] (2-methylrpropene)	Calogirou et al. (1999)
NO_3 + 5-Methyl-5-vinyl-tetrahydrofuran-2-ol			
$(17 \pm 8) \times 10^{-3}$	298	RR[g] (1-butene)	Calogirou et al. (1999)

[a]Abbreviations used for the techniques are defined in table I-F-3.
[b]Placed on an absolute basis using k(OH+cyclohexene) = 6.77×10^{-11} cm^3 molecule^{-1} s^{-1} (Calvert et al., 2000)
[c]Placed on an absolute basis using k(OH+2-methyl-propene) = 5.14×10^{-11} cm^3 molecule^{-1} s^{-1} (Calvert et al., 2000).
[d]Placed on an absolute basis using k(O_3+2,3-dimethyl-2-butene) = 1.13×10^{-15} cm^3 molecule^{-1} s^{-1} (Calvert et al., 2000).
[e]Placed on an absolute basis using k(NO_3+2,3-dimethyl-2-butene) = 5.72×10^{-11} cm^3 molecule^{-1} s^{-1} (Calvert et al., 2000).
[f]Placed on an absolute basis using k(O_3+2-methyl-2-propene) = 1.13×10^{-17} cm^3 molecule^{-1} s^{-1} (Calvert et al., 2000).
[g]Placed on an absolute basis using k(NO_3+1-butene) = 1.35×10^{-14} cm^3 molecule^{-1} s^{-1} (Calvert et al., 2000).

III-E-21. Benzene Oxide (Oxepin) and Toluene-1,2-Oxide (2-Methyl Oxepin)

The species benzene oxide and toluene-1,2-oxide have been proposed as intermediates in the oxidation of benzene and toluene, respectively. Note that these epoxides exist in equilibrium with an oxepin form, with the equilibrium likely favoring the oxepin in the gas-phase (see Klotz et al., 1997, 2000, and references therein).

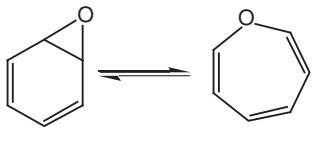

Benzene Oxide / Oxepin

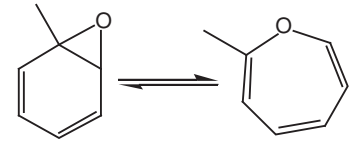

Toluene-1,2-Oxide / 2-Methyl Oxepin

The kinetic data for the reactions of these species with OH and NO_3 are summarized in table III-E-31. The work of Klotz et al. (1997) suggests that photolysis and reaction with OH are rapid loss processes for benzene oxide/oxepin, with the photolysis estimated to occur on a timescale of about 40 min. (overhead Sun, table IX-M-1) and the

Table III-E-31. Rate coefficients ($k = A \times e^{-B/T}$, cm^3 molecule^{-1} s^{-1}) for reaction of OH and NO_3 with benzene oxide, toluene oxide, and 3,4-epoxy-cyclohexene

$10^{12} \times k$	T (K)	Technique[a]	Reference
OH + Benzene oxide			
100 ± 4	298	RR[b] (*trans*-2-butene)	Klotz et al. (1997)
NO_3 + Benzene oxide			
9.3 ± 0.3	298	RR[c] (2-methyl-2-butene)	Klotz et al. (1997)
OH + Toluene oxide			
210 ± 10	295	RR[d] (isoprene)	Klotz et al. (2000)
NO_3 + Toluene oxide			
12.7 ± 1.0	295	RR[c] (2-methyl-2-butene)	Klotz et al. (2000)
NO_3 + 3,4-Epoxy-cyclohexene			
0.30 ± 0.02	295	RR[e] (cyclohexene)	Kind et al. (1996a)

[a]Abbreviations used for the techniques are defined in table I-F-3.
[b]Placed on an absolute basis using k(OH+*trans*-2-butene) = 6.4×10^{-11} cm^3 molecule^{-1} s^{-1} (Calvert et al., 2000).
[c]Placed on an absolute basis using k(NO_3+2-methyl-2-butene) = 9.4×10^{-12} cm^3 molecule^{-1} s^{-1} (Calvert et al., 2000).
[d]Placed on an absolute basis using k(OH+isoprene) = 1.01×10^{-10} cm^3 molecule^{-1} s^{-1} (Atkinson et al., 2006).
[e]Placed on an absolute basis using k(NO_3+cyclohexene) = 5.9×10^{-13} cm^3 molecule^{-1} s^{-1} (Calvert et al., 2000).

OH reaction on a timescale of about 1 h (assuming peak daytime [OH] = 2.5×10^6 molecule cm^{-3}). Major products of the OH-initiated oxidation (Klotz et al., 1997) were the *E*, *E*- and *E*, *Z*-isomers of 2,4-hexadienedial, while phenol is a major product of the photolysis in the near UV. The rapid reaction with NO_3 suggests a very rapid nighttime loss for benzene oxide/oxepin, although it is unlikely to be formed at night and its rapid daytime removal suggests little build-up of its concentration at night (Klotz et al., 1997).

For toluene-1,2-oxide/2-methyl oxepin, photolysis and OH reaction are again competing daytime losses (Klotz et al., 2000). The OH reaction is calculated to occur on a timescale of about 0.5 h, while the photolysis lifetime is about 40 min. with overhead Sun. Products of the OH-initiated oxidation are the *E*, *E*- and *E*, *Z*- isomers of 6-oxohepta-2,4-dienal, analogous to the 2,4-hexadiendial products of the benzene oxide/oxepin case. The main photolysis product identified was o-cresol, albeit only in about 10% yield. The reaction with NO_3 is also very rapid, and should this species be present at nighttime, its removal via reaction with NO_3 would be expected to occur in less than 1 min. in heavily polluted conditions.

III-E-22. 3,4-Epoxy-Cyclohexene
(7-Oxabicyclo[4.1.0]hept-2-ene)

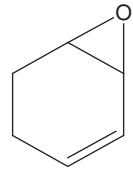

Kind et al. (1996a), as part of a study of NO_3/oxirane reactivity, measured $k(NO_3 +$ 3,4-epoxy-cyclohexene$) = 3.0 \times 10^{-13}$ cm^3 molecule^{-1} s^{-1} at 298 K. The measurement is summarized in table III-E-31.

III-E-23. 1,8-Cineole (1,3,3-Trimethyl-2-oxabicyclo[2.2.2]octane)

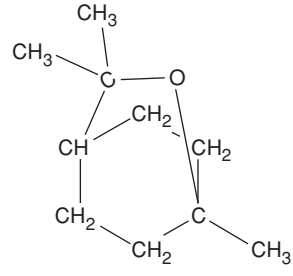

III-E-23.1. OH Reaction Kinetics

The rate coefficient for reaction of OH with 1,8-cineole has been determined by Corchnoy and Atkinson (1990) using a relative rate technique. Their value, $k = 10.4 \times 10^{-12}$ cm^3 molecule^{-1} s^{-1} at 298 K, is recommended; in the absence of corroborative data, an uncertainty of ±35% is assigned; see table III-E-32.

III-E-23.2. NO_3 Reaction Kinetics

Corchnoy and Atkinson (1990) obtained $k = 1.7 \times 10^{-16}$ cm^3 molecule^{-1} s^{-1} for reaction of NO_3 with 1,8-cineole using a relative rate method; see table III-E-32. The value is recommended with an estimated uncertainty of ±35%.

Table III-E-32. Rate coefficients ($k = A \times e^{-B/T}$, cm^3 molecule^{-1} s^{-1}) for reaction of OH and NO_3 with 1,8-cineole

$10^{14} \times k$	T (K)	Technique[a]	Reference
OH + 1,8-cineole			
1,040 ± 280	295	RR[b] (*cyclo*-C_6H_{12})	Corchnoy and Atkinson (1990)
NO_3 + 1,8-cineole			
0.017 ± 0.011	295	RR[c] (2,3-dimethylbutane)	Corchnoy and Atkinson (1990)

[a]Abbreviations used for the techniques are defined in table I-F-3.
[b]Placed on an absolute basis using k(OH+cyclohexane) $= 6.97 \times 10^{-12}$ cm^3 molecule^{-1} s^{-1} (Calvert et al., 2008).
[c]Placed on an absolute basis using $k(NO_3$+2,3-dimethylbutane$) = 4.06 \times 10^{-16}$ cm^3 molecule^{-1} s^{-1} (Calvert et al., 2008).

III-E-23.3. Summary of the Atmospheric Fate of 1,8-cineole, and the End Products of Its Oxidation

The atmospheric lifetime of 1,8-cineole will be controlled mainly by its reaction with OH. For daytime [OH] = 2.5×10^6 molecule cm^{-3}, a lifetime of 11 h is obtained. Products of the OH-initiated oxidation have not been determined.

III-F. Aromatic Ethers

III-F-1. Methoxybenzene (Anisole, $CH_3OC_6H_5$)

III-F-1.1. OH Reaction Kinetics

The rate coefficient for reaction of OH with methoxybenzene has been studied over a range of temperatures by Perry et al. (1977b), and near 298 K by Ohta and Ohyama (1985). Data are summarized in table III-F-1, and plotted in figure III-F-1. The data of Perry et al. (1977b) point to a complex reaction mechanism. At $T < 330$ K, the dominant reaction channel is "irreversible" formation of an OH/methoxybenzene adduct (adduct lifetime $\geq$ 10 ms or so). At higher temperatures ($T > 390$ K), adduct decomposition is rapid on the timescale of the flash photolysis system and OH loss is dominated by a slower abstraction process (occurring at the methyl group). At intermediate temperatures, the OH temporal behavior is nonexponential as equilibration of the OH/methoxybenzene adduct occurs on the timescale of the flash photolysis experiment.

Table III-F-1. Rate coefficients (k, cm^3 molecule^{-1} s^{-1}) for reaction of OH with methoxybenzene (anisole, $CH_3OC_6H_5$)

$10^{12} \times k$	T (K)	Technique[a]	Reference	Temperature Range (K)
19.6 ± 2.4	299.9	FP–RF	Perry et al. (1977b)	299.9–435.3
17.3 ± 2.6	309			
17.5 ± 2.6	309.7			
17.5 ± 2.6	318.5			
17.8 ± 2.7	321.7			
12.7[b]	329.5			
6.7[b]	357.4			
3.0[b]	370.4			
3.33 ± 0.50	385.5			
3.25 ± 0.50	392.3			
3.31 ± 0.50	404.1			
3.90 ± 0.56	413.2			
2.85 ± 0.43	417.9			
3.30 ± 0.40	422			
2.76 ± 0.41	428.7			
2.72 ± 0.41	435.3			
13.8 ± 0.5	298	RR[c] (n-C_6H_{14})	Ohta and Ohyama (1985)	

[a]Abbreviations used for the techniques are defined in table I-F-3.
[b]Observed decays were nonexponential. Rate coefficient determined from initial rate of OH decay.
[c]Placed on an absolute basis using $k(OH+n\text{-}C_6H_{14}) = 5.48 \times 10^{-12}$ cm^3 molecule^{-1} s^{-1} (Calvert et al., 2008).

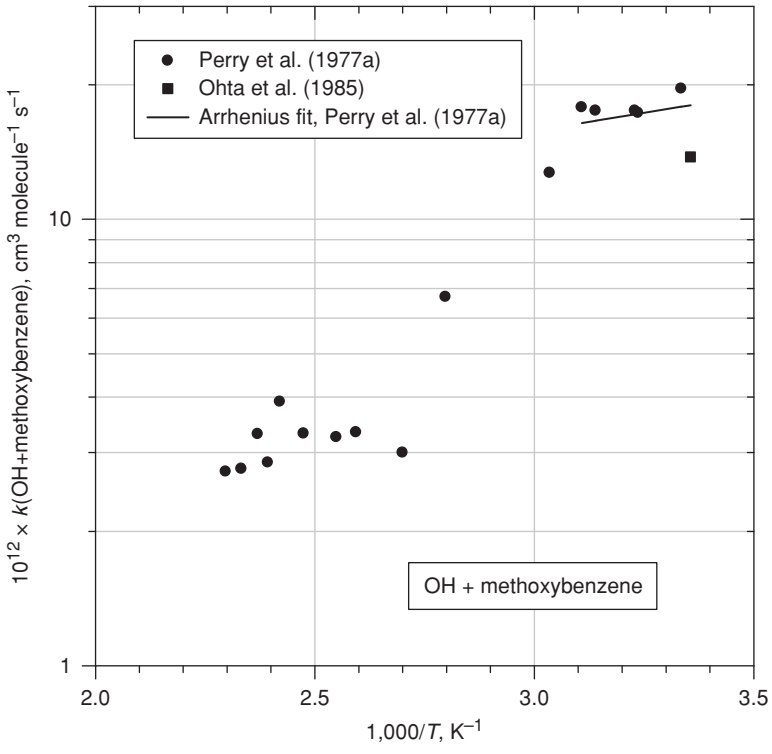

Figure III-F-1. Arrhenius plot of the rate coefficient for the reaction of OH with methoxybenzene ($CH_3OC_6H_5$, anisole). The fit shown is only to the data in the low temperature regime ($T <$ 325 K), where OH-anisole adduct formation is irreversible on the timescale of a flash photolysis experiment.

For atmospheric purposes, the analysis of Perry et al. (1977b) is adopted, with $k_{adduct} = 3.7 \times 10^{-12} \exp(402/T)$ cm^3 molecule^{-1} s^{-1} and $k_{abstraction} = 1.7 \times 10^{-12} \exp(252/T)$ cm^3 molecule^{-1} s^{-1}, giving $k_{total} = 5.2 \times 10^{-12} \exp(370/T)$ cm^3 molecule^{-1} s^{-1}. Note, however, that no measurements have been made below 298 K, and caution should be used when extrapolating to lower temperatures. Further work at reduced temperature is clearly warranted.

III-F-1.2. NO_3 Reaction Kinetics

The reaction of NO_3 with methoxybenzene has been studied near 298 K using relative rate methods (Carter et al., 1981; Atkinson et al., 1984b; Kwok et al., 1994b). The measurements of Atkinson et al. (1984b) fall in the range ($\sim$1–2) $\times 10^{-16}$ cm^3 molecule^{-1} s^{-1}, and thus an intermediate value of 1.5×10^{-16} cm^3 molecule^{-1} s^{-1} is recommended near 298 K, with an uncertainty of $\pm$50%; see table III-F-2. The reaction is too slow to be of atmospheric significance.

Table III-F-2. Rate coefficients (k, cm^3 molecule^{-1} s^{-1}) for reaction of NO_3 with methoxybenzene (anisole, $CH_3OC_6H_5$)

$10^{16} \times k$	T (K)	Technique[a]	Reference
< 50	300	RR[b] (propene)	Carter et al. (1981)
0.9 ± 0.5	296	RR[b] (propene)	Atkinson et al. (1984b)
2.1 ± 1.0	296	RR[c] (*n*-heptane)	
< 14	297	RR[d] (1-butene)	Kwok et al. (1994b)

[a]Abbreviations used for the techniques are defined in table I-F-3.
[b]Placed on an absolute basis using $k(NO_3+C_3H_6) = 4.6 \times 10^{-13} \exp(-1{,}155/T)$ cm^3 molecule^{-1} s^{-1} (Atkinson et al., 2006).
[c]Placed on an absolute basis using $k(NO_3 + n\text{-}C_7H_{16}) = 1.4 \times 10^{-16}$ cm^3 molecule^{-1} s^{-1} (Calvert et al., 2008).
[d]Placed on an absolute basis using $k(NO_3+1\text{-butene}) = 1.4 \times 10^{-14}$ cm^3 molecule^{-1} s^{-1} (Calvert et al., 2000).

III-F-1.3. O(^{3}P) Reaction Kinetics

The reaction of O(^{3}P) with methoxybenzene has been investigated most recently by Frerichs et al. (1990), who report $k = 2.2 \times 10^{-11} \exp(-1{,}400/T)$ cm^3 molecule^{-1} s^{-1}, with $k = 2.0 \times 10^{-13}$ cm^3 molecule^{-1} s^{-1} near 298 K.

III-F-1.4. Summary of the Atmospheric Fate of Methoxybenzene, and the End Products of Its Oxidation

The lifetime of methoxybenzene against OH reaction will be reasonably short, about 6 h for daytime [OH] $= 2.5 \times 10^6$ molecule cm^{-3}. There are no product studies of the OH-initiated oxidation of methoxybenzene. However, the kinetic analysis of Perry et al. (1977b) suggests that the majority of the reaction occurs via OH addition to the aromatic ring. By analogy to other aromatics, hydroxyl-substituted methoxybenzene species, and multi-functional ring-opened products are likely.

III-F-2. 1,2-Dimethoxybenzene; 1,3-Dimethoxybenzene; 1,4-Dimethoxybenzene; [$(CH_3O)_2C_6H_4$]

III-F-2.1. OH Reaction Kinetics

The rate coefficient for reaction of OH with 1,2-dimethoxybenzene has been studied at 297 K by Kwok et al. (1995) using a relative rate technique. As summarized in table III-F-3, their two determinations are in good agreement with each other, and an average value of 3.6×10^{-11} cm^3 molecule^{-1} s^{-1} is adopted. In the absence of corroborative studies, an uncertainty of $\pm 30\%$ is assigned. Rate coefficients have not been determined for the 1,3- or 1,4-isomers.

III-F-2.2. NO_3 Reaction Kinetics

The reaction of NO_3 with 1,2-, 1,3-, and 1,4-dimethoxybenzene has been studied near 298 K by Kwok et al. (1994b) using a relative rate method. As described by Kwok et al., the reactions are complex, involving both an abstraction and a (reversible)

Table III-F-3. Rate coefficients (k, cm^3 molecule^{-1} s^{-1}) for reaction of OH with 1,2-dimethoxybenzene

$10^{12} \times k$	T (K)	Technique[a]	Reference
40.0 ± 6.0	297	RR[b] (propene)	Kwok et al. (1995)
32.0 ± 8.2	297	RR[c] (isoprene)	

[a]Abbreviations used for the techniques are defined in table I-F-3.
[b]Placed on an absolute basis using $k(\mathrm{OH}+\mathrm{C_3H_6}) = 2.9 \times 10^{-11}$ cm^3 molecule^{-1} s^{-1} (Atkinson et al., 2008).
[c]Placed on an absolute basis using $k(\mathrm{OH}+\mathrm{isoprene}) = 10.0 \times 10^{-11}$ cm^3 molecule^{-1} s^{-1} (Atkinson et al., 2008).

addition channel. Information on the kinetics of these two channels is obtained from studies of the dependence of the observed rate coefficient on the concentration of added NO_2, as NO_2 acts as a scavenger for the adduct (reaction mechanism III-F-2.2.1).

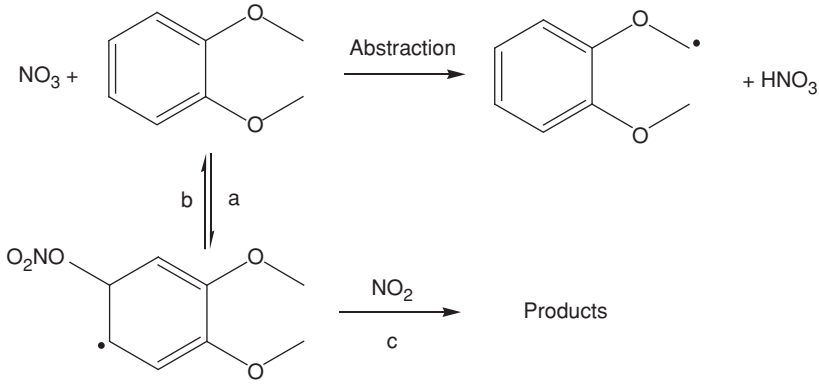

Reaction mechanism III-F-2.2.1

Thus, the rate coefficient for the abstraction channel is determined at low [NO_2], and information on the adduct-forming channel (i.e., $k_a k_c / k_b$) is obtained from the rate of increase of the observed rate coefficient with NO_2 addition.

Data for the abstraction and adduct formation channels in the reaction of NO_3 with 1,2-, 1,3-, and 1,4-dimethoxybenzene, from the analysis of Kwok et al. (1994b), are summarized in table III-F-4. Rate coefficients for NO_3 abstraction from 1,2-, 1,3-, and 1,4-dimethoxybenzene are all similar and quite large, $\sim 10^{-14}$ cm^3 molecule^{-1} s^{-1}. Atmospheric levels of NO_2 would have to be quite high (1 ppm or more) for reaction of the adduct with NO_2 to contribute.

III-F-2.3. Summary of the Atmospheric Fate of the Dimethoxybenzenes, and the End Products of Their Oxidation

The lifetime of 1,2-methoxybenzene against OH reaction will be only about 3 h, assuming daytime [OH] = 2.5×10^6 molecule cm^{-3}. Similar rate coefficients for OH reaction with the 1,3- and 1,4-isomers (and thus similar lifetimes for these species)

Table III-F-4. Rate coefficients (k, cm^3 molecule^{-1} s^{-1}) for reaction of NO_3 with 1,2-, 1,3-, and 1,4-dimethoxybenzene

$10^{14} \times k_{abs}$	$10^{28} \times k_a k_b / k_c$	T (K)	Technique[a]	Reference
1,2-Dimethoxybenzene				
1.15 ± 0.67	1.2 ± 0.5	297	RR[b] (1-butene)	Kwok et al. (1994b)
1,3-Dimethoxybenzene				
1.20 ± 0.55	0.39 ± 0.14	297	RR[b] (1-butene)	Kwok et al. (1994b)
1,4-Dimethoxybenzene				
1.04 ± 0.33	1.5 ± 0.5	297	RR[b] (1-butene)	Kwok et al. (1994b)

[a]Abbreviations used for the techniques are defined in table I-F-3.
[b]Placed on an absolute basis using k(NO_3+1-butene) = 1.4×10^{-14} cm^3 molecule^{-1} s^{-1} (Calvert et al., 2000).

seem likely. Nighttime loss of these species via reaction with NO_3 will likely also occur (lifetime $\approx$ 9 h for $k(NO_3) \approx 10^{-14}$ cm^3 molecule^{-1} s^{-1} and $[NO_3] = 3 \times 10^9$ molecule cm^{-3}).

There are no product studies of the OH-initiated oxidation of 1,2-, 1,3-, or 1,4-dimethoxybenzene. Kwok et al. (1994b) have observed the formation of nitrodimethoxybenzenes from the reaction of NO_3 with dimethoxybenzene species in the presence of NO_2, indicating that these nitrodimethoxybenzene species are obtained from NO_3 addition to the parent species [pathway (a), followed by pathway (c) in the reaction mechanism in section III-F-2.2].

III-F-3. 4-Methoxytoluene and 4-Ethoxytoluene

III-F-3.1. OH Reaction Kinetics

The rate coefficients for reaction of OH with these (or other) alkoxytoluenes have not been studied. However, a rate coefficient of $\approx 3 \times 10^{-11}$ cm^3 molecule^{-1} s^{-1} or larger is expected on the basis of data presented above for anisole and 1,2-dimethoxybenzene.

III-F-3.2. NO_3 Reaction Kinetics

Bolzacchini et al. (1999) used a relative rate technique to determine the rate coefficients for reaction of NO_3 with 4-methoxytoluene and 4-ethoxytoluene at 298 K: k(4-methoxytoluene) = 3.3×10^{-15} cm^3 molecule^{-1} s^{-1} and k(4-ethoxytoluene) = 2.7×10^{-15} cm^3 molecule^{-1} s^{-1}. It should be noted, however, that the relative rate experiments were conducted in the presence of a few ppm NO_2, and it seems likely that reaction of an NO_3-aromatic adduct with NO_2 is contributing to the loss (see section III-F-2.2 and discussion of products in section III-F-3.3). Thus, the rate coefficients measured are likely upper limits to those that will pertain under atmospheric conditions (i.e., lower NO_2 mixing ratios). The results are summarized in table III-F-5.

Table III-F-5. Rate coefficients (k, cm^3 molecule^{-1} s^{-1}) for reaction of NO_3 with 4-methoxytoluene and 4-ethoxytoluene

$10^{15} \times k$	T (K)	Technique[a]	Reference
NO_3 + 4-Methoxytoluene			
3.27 ± 0.59	298	RR[b] (1,3,5-trimethylbenzene)	Bolzacchini et al. (1999)
NO_3 + 4-Ethoxytoluene			
2.70 ± 0.54	298	RR[b] (1,3,5-trimethylbenzene)	Bolzacchini et al. (1999)

[a]Abbreviations used for the techniques are defined in table I-F-3.
[b]Placed on an absolute basis using $k(NO_3+1,3,5\text{-trimethylbenzene}) = 8.0 \times 10^{-16}$ cm^3 molecule^{-1} s^{-1} (Calvert et al., 2002).

III-F-3.3. Summary of the Atmospheric Fate of the Alkoxytoluenes, and the End Products of Their Oxidation

Reaction with OH is likely the major loss process for 4-methoxytoluene and 4-ethoxytoluene; lifetimes of about 4 h can be estimated for these processes. Reaction with NO_3 may play a minor role at night, although the lifetime for this process will exceed 30 h even in very highly polluted conditions. Products of the NO_3-initiated oxidation (Bolzacchini et al., 1999) include alkoxybenzaldehydes, which are obtained following abstraction from the CH_3 group bonded directly to the aromatic ring, and nitrophenols and nitrocresols (with co-product CH_3OH or CH_3CH_2OH) which are obtained via an O-dealkylation mechanism that involves NO_2 reaction with the adduct.

III-F-4. Diphenyl Ether [$(C_6H_5)_2O$]

III-F-4.1. OH Reaction Kinetics

The rate coefficient for reaction of OH with diphenyl ether has been studied at 297 K by Kwok et al. (1995) and over a range of temperatures by Raff and Hites (2006), using relative rate techniques. Data are summarized in table III-F-6. A rate coefficient of 8.2×10^{-12} cm^3 molecule^{-1} s^{-1} is obtained near 298 K from the average of the Kwok et al. (1995) and Raff and Hites (2006) data. Although there is reasonable agreement between the two measurements, it should be noted that significant disagreements between the measurements of these two groups and those of Taylor et al. (2005) exist for the related dibenzo-*p*-dioxin compound and its chlorinated derivatives. Further studies, particularly of the temperature dependence of this reaction, are thus warranted, and no recommendation is made.

III-F-4.2. Summary of the Atmospheric Fate of Diphenyl Ether, and the End Products of Its Oxidation

The lifetime of diphenyl ether against reaction with OH is about 1.4 days, assuming a diurnally averaged [OH] $\approx 10^6$ molecule cm^{-3}. As noted above, however, there is the

Table III-F-6. Rate coefficients (k, cm^3 molecule^{-1} s^{-1}) for reaction of OH with diphenyl ether

$10^{12} \times k$	T (K)	Technique[a]	Reference	Temperature Range (K)
9.0 ± 2.4	297	RR[b] (*cyclo*-C_6H_{12})	Kwok et al. (1995)	
7.38 ± 1.27	326	RR[c] (biphenyl)	Raff and Hites (2006)	326–367
7.31 ± 0.27	326	RR[c] (biphenyl)		
7.51 ± 1.37	326	RR[d] (C_3F_6)		
7.10 ± 1.37	326	RR[d] (C_3F_6)		
7.38 ± 0.60	331	RR[c] (biphenyl)		
7.81 ± 0.90	336	RR[d] (C_3F_6)		
7.18 ± 0.70	336	RR[d] (C_3F_6)		
7.67 ± 0.14	339	RR[c] (biphenyl)		
7.53 ± 0.05	342	RR[c] (biphenyl)		
7.46 ± 1.09	342	RR[c] (biphenyl)		
7.60 ± 0.25	346	RR[c] (biphenyl)		
7.81 ± 0.57	346	RR[c] (biphenyl)		
7.19 ± 0.19	346	RR[d] (C_3F_6)		
7.46 ± 0.48	352	RR[c] (biphenyl)		
7.95 ± 0.25	357	RR[c] (biphenyl)		
7.14 ± 0.31	367	RR[d] (C_3F_6)		

[a]Abbreviations used for the techniques are defined in table I-F-3.
[b]Placed on an absolute basis using $k(\text{OH}+\textit{cyclo}\text{-}C_6H_{12}) = 6.97 \times 10^{-12}$ cm^3 molecule^{-1} s^{-1} (Calvert et al., 2008).
[c]Placed on an absolute basis using $k(\text{OH}+\text{biphenyl}) = 7.1 \times 10^{-12}$ cm^3 molecule^{-1} s^{-1} (Calvert et al., 2002).
[b]Placed on an absolute basis using $k(\text{OH}+CF_3CF{=}CF_2) = 8.74 \times 10^{-13} \exp(260/T)$ cm^3 molecule^{-1} (Tokuhashi et al., 2000a).

possibility of significant systematic error in the measured OH rate coefficient. There are no product studies of the OH-initiated oxidation.

III-F-5. 2,3-Dihydrobenzofuran

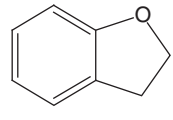

III-F-5.1. OH Reaction Kinetics

The reaction of OH with 2,3-dihydrobenzofuran has been determined by Atkinson et al. (1992a), using a relative rate technique. The value obtained is $k = 4.0 \times 10^{-11}$ cm^3 molecule^{-1} s^{-1}, with an estimated uncertainty of ±30%. The study is summarized in table III-F-7.

III-F-5.2. O_3 Reaction Kinetics

An upper limit, $k < 10^{-19}$ cm^3 molecule^{-1} s^{-1}, has been reported for this reaction at 298 K (Atkinson et al., 1992a), see table III-F-7.

Table III-F-7. Rate coefficients (k, cm^3 molecule^{-1} s^{-1}) for reaction of OH, O_3 and NO_3 with 2,3-dihydrobenzofuran

$10^{12} \times k$	T (K)	Technique[a]	Reference
OH + 2,3-Dihydrobenzofuran			
40.3 ± 6.2	298	RR[b] (propene)	Atkinson et al. (1992a)
O_3 + 2,3-Dihydrobenzofuran			
$< 1 \times 10^{-7}$	298	O_3 CL	Atkinson et al. (1992a)
NO_3 + 2,3-Dihydrobenzofuran			
(0.11 ± 0.03)	298	RR[c] (*trans*-2-butene)	Atkinson et al. (1987b)

[a]Abbreviations used for the techniques are defined in table I-F-3.
[b]Placed on an absolute basis using $k(OH+C_3H_6) = 2.9 \times 10^{-11}$ cm^3 molecule^{-1} s^{-1} (Atkinson et al., 2006).
[c]Placed on an absolute basis using $k(NO_3+$*trans*-2-butene$) = 3.9 \times 10^{-13}$ cm^3 molecule^{-1} s^{-1} (Calvert et al., 2000).

III-F-5.3. NO_3 Reaction Kinetics

The rate coefficient for reaction of NO_3 with 2,3-dihydrobenzofuran has been determined by Atkinson et al. (1987b) using a relative rate technique, see table III-F-7. The value obtained is $k = 1.1 \times 10^{-13}$ cm^3 molecule^{-1} s^{-1}, with an estimated uncertainty of $\pm 50\%$.

III-F-5.4. Summary of the Atmospheric Fate of 2,3-Dihydrobenzofuran, and the End Products of Its Oxidation

The atmospheric lifetime of 2,3-dihydrobenzofuran is quite short. Reaction with OH will occur with a lifetime of about 3 h for daytime [OH] $= 2.5 \times 10^6$ molecule cm^{-3}. Reaction with NO_3 will also be an important nighttime loss under highly polluted conditions; lifetime $\approx$ 1 h for $[NO_3] = 3 \times 10^9$ molecule cm^{-3}. Reaction of both OH and NO_3 likely occur mainly via abstraction from the O-containing ring, although the identity and yield of these products are unknown (Atkinson et al., 1987b, 1992a).

III-F-6. 2,3-Benzofuran (C_8H_6O)

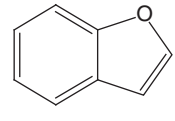

III-F-6.1. OH Reaction Kinetics

Using a relative rate technique, Atkinson et al. (1992a) determined $k = 4.1 \times 10^{-11}$ cm^3 molecule^{-1} s^{-1} for reaction of OH with 2,3-benzofuran. In the absence of corroborating data, an uncertainty of $\pm 30\%$ is assigned. The study is summarized in table III-F-8.

Table III-F-8. Rate coefficients (k, cm^3 molecule^{-1} s^{-1}) for reaction of OH and O_3 with 2,3-benzofuran

$10^{12} \times k$	T (K)	Technique[a]	Reference
OH + 2,3-Benzofuran			
41 ± 8	298	RR[b] (propene)	Atkinson et al. (1992a)
O_3 + 2,3-Benzofuran			
1.83×10^{-6}	298	O_3CL	Atkinson et al. (1992a)

[a]Abbreviations used for the techniques are defined in table I-F-3.
[b]Placed on an absolute basis using $k(\mathrm{OH}+\mathrm{C_3H_6}) = 2.9 \times 10^{-11}$ cm^3 molecule^{-1} s^{-1} (Atkinson et al., 2006).

III-F-6.2. O_3 Reaction Kinetics

Atkinson et al. (1992a) report $k = 1.8 \times 10^{-18}$ cm^3 molecule^{-1} s^{-1} for reaction of O_3 with 2,3-benzofuran at 298 K. An uncertainty of ±35% is assigned. The study is summarized in table III-F-8.

III-F-6.3. Summary of the Atmospheric Fate of 2,3-Benzofuran, and the End Products of Its Oxidation

Reaction with OH will represent an important daytime loss for 2,3-benzofuran with a lifetime ≈ 3 h for [OH] = 2.5×10^6 molecule cm^{-3}. The only product quantified in both the ozonolysis and OH-initiated oxidation of 2,3-benzofuran was 2-hydroxybenzaldehyde (salicylaldehyde) (Atkinson et al., 1992a). Observed yields were $13 \pm 7\%$ from the ozonolysis and $26 \pm 5\%$ from the OH reaction in the presence of NO_x. This product is likely obtained from attack of O_3 or OH on the nonaromatic ring. Atkinson et al. (1992a) suggest that the OH reaction may proceed roughly 30% via addition to the nonaromatic double bond (leading to salicylaldehyde), and 70% via addition to the aromatic ring (products unknown).

III-F-7. 1,4-Benzodioxan ($C_8H_8O_2$)

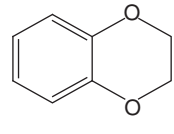

III-F-7.1. OH Reaction Kinetics

Atkinson et al. (1992a) used a relative rate technique to determine $k = 2.8 \times 10^{-11}$ cm^3 molecule^{-1} s^{-1} for reaction of 1,4-benzodioxan with OH at 298 K; see table III-F-9. Given the lack of corroborative studies, an uncertainty of ±30% is assigned.

Table III-F-9. Rate coefficients (k, cm^3 molecule^{-1} s^{-1}) for reaction of OH, O_3 and NO_3 with 1,4-benzodioxan

$10^{12} \times k$	T (K)	Technique[a]	Reference
OH + 1,4-Benzodioxan			
27.8 ± 4.2	298	RR[b] (propene)	Atkinson et al. (1992a)
O_3 + 1,4-Benzodioxan			
$< 1.2 \times 10^{-8}$	298	O_3 CL	Atkinson et al. (1992a)
NO_3 + 1,4-Benzodioxan			
$(6 \pm 3) \times 10^{-4}$	298	RR[c] (propene)	Atkinson et al. (1987b)

[a]Abbreviations used for the techniques are defined in table I-F-3.
[b]Placed on an absolute basis using $k(OH+C_3H_6) = 2.9 \times 10^{-11}$ cm^3 molecule^{-1} s^{-1} (Atkinson et al., 2006).
[c]Placed on an absolute basis using $k(NO_3+C_3H_6) = 9.5 \times 10^{-15}$ cm^3 molecule^{-1} s^{-1} (Atkinson et al., 2006).

III-F-7.2. O_3 Reaction Kinetics

Atkinson et al. (1992a) report an upper limit for reaction of O_3 with 1,4-benzodioxan, $k < 1.2 \times 10^{-20}$ cm^3 molecule^{-1} s^{-1} at 298 K; see table III-F-9.

III-F-7.3. NO_3 Reaction Kinetics

Atkinson et al. (1987b) determined $k = 6.0 \times 10^{-16}$ cm^3 molecule^{-1} s^{-1} for reaction of NO_3 with 1,4-benzodioxan at 298 K, using a relative rate technique. See table III-F-9. The uncertainty assigned to this value is estimated at ±50%.

III-F-7.4. Summary of the Atmospheric Fate of 1,4-Benzodioxan, and the End Products of Its Oxidation

The major atmospheric loss process for 1,4-benzodioxan will be via reaction with OH; a lifetime of about 4 h is estimated for daytime [OH] = 2.5×10^6 molecule cm^{-3}. Atkinson et al. (1992a) suggest that the reaction proceeds via OH addition to the aromatic ring and via abstraction from the CH_2 groups at roughly equal rates.

III-F-8. Isochroman (3,4-Dihydro-1H-2-benzopyran, $C_9H_{10}O$) and 1,3,4,6,7,8-Hexahydro-4,6,6,7,8,8-hexamethycyclopenta-[γ]-2-benzopyran ($C_{18}H_{26}O$, HHCB)

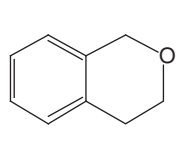

Isochroman

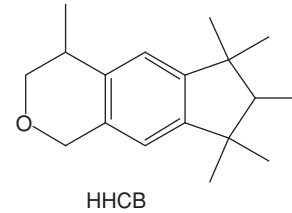

HHCB

The compound HHCB (1,3,4,6,7,8-hexahydro-4,6,6,7,8,8-hexamethycyclopenta-[γ]-2-benzopyran) is an important semi-volatile fragrance material, while isochroman

Table III-F-10. Rate coefficients (k, cm^3 molecule^{-1} s^{-1}) for reaction of OH with isochroman and HHCB

$10^{12} \times k$	T (K)	Technique[a]	Reference
OH + isochroman			
37 ± 6	298	RR[b] (methyl vinyl ketone)	Aschmann et al. (2001a)
OH + HHCB			
26 ± 6	298	RR[b] (methyl vinyl ketone)	Aschmann et al. (2001a)

[a]Abbreviations used for the techniques are defined in table I-F-3.
[b]Placed on an absolute basis using k(OH+MVK) = 2.06×10^{-11} cm^3 molecule^{-1} s^{-1} (this book, section V-D-1.1).

is a simpler, more volatile, and thus a more easily studied structural analog. The rate coefficient for reaction of OH with both species was determined by Aschmann et al. (2001a) using a relative rate technique. Values found were k(isochroman) = 3.7×10^{-11} cm^3 molecule^{-1} s^{-1} and k(HHCB) = 2.6×10^{-11} cm^3 molecule^{-1} s^{-1} at 296 K, see table III-F-10. Given the lack of corroborative data, the uncertainty is estimated at ±35%.

III-F-9. Dibenzofuran ($C_{12}H_8O$)

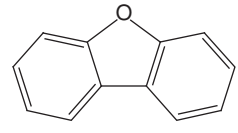

III-F-9.1. OH Reaction Kinetics

Rate coefficients for the reaction of OH with dibenzofuran have been reported by Kwok et al. (1994a) and by Brubaker and Hites (1998) using relative rate techniques. The data are summarized in table III-F-11. Fitting of the combined data yields $k = 1.35 \times 10^{-11} \exp(-374/T)$ cm^3 molecule^{-1} s^{-1}, with $k = 3.8 \times 10^{-12}$ cm^3 molecule^{-1} s^{-1} at 298 K. However, it must be noted that data obtained by these workers on dibenzo-*p*-dioxin and its chlorinated analogs are in disagreement with the recent direct measurements of Taylor et al. (2005). Thus, no recommendation for the rate coefficients for reaction of OH with dibenzofuran is made at this time; further studies should be conducted.

III-F-9.2. O_3 Reaction Kinetics

Kwok et al. (1994a) report an upper limit of $k < 8 \times 10^{-20}$ cm^3 molecule^{-1} s^{-1}. The reaction is too slow to be of atmospheric significance.

III-F-9.3. NO_3 Reaction Kinetics

The relative rate study of Kwok et al. (1994a) shows that the reaction of NO_3 with dibenzofuran is rather slow, $k < 1.8 \times 10^{-15}$ cm^3 molecule^{-1} s^{-1}. The study is summarized in table III-F-12.

Table III-F-11. Rate coefficients ($k = A \times e^{-B/T}$, cm^3 molecule^{-1} s^{-1}) for reaction of OH with dibenzofuran

$10^{12} \times A$	B (K)	$10^{12} \times k$	T (K)	Technique[a]	Reference
		4.23 ± 0.89	297	RR[b] (propene)	Kwok et al. (1994a)
		3.78 ± 1.24	297	RR[c] (*cyclo*-C_6H_{12})	
26[d]	619 ± 148[d]	4.1 ± 1.0	345	RR[c] (*cyclo*-C_6H_{12})	Brubaker and Hites (1998)
		4.2 ± 1.1	345		
		4.6 ± 1.2	345		
		4.7 ± 1.2	345		
		4.7 ± 1.2	366		
		5.0 ± 1.3	366		
		4.7 ± 1.2	366		
		4.8 ± 1.2	366		
		4.9 ± 1.2	385		
		5.6 ± 1.4	386		
		5.2 ± 1.3	386		
		5.8 ± 1.5	386		

[a]Abbreviations used for the techniques are defined in table I-F-3.
[b]Placed on an absolute basis using $k(OH+C_3H_6) = 2.9 \times 10^{-11}$ cm^3 molecule^{-1} s^{-1} (Atkinson et al., 2008).
[c]Placed on an absolute basis using $k(OH+c\text{-}C_6H_{12}) = 3.26 \times 10^{-17} T^2 \exp(262/T)$ cm^3 molecule^{-1} s^{-1} (Calvert et al., 2008).
[d]Values obtained from least-squares fit of data obtained using updated reference rate coefficients, and thus differ from those originally reported.

Table III-F-12. Rate coefficients (k, cm^3 molecule^{-1} s^{-1}) for reaction of NO_3 with dibenzofuran

$10^{14} \times k_{abs}$	$10^{28} \times k_a k_b / k_c$	T (K)	Technique[a]	Reference
< 0.18	< 0.08	297	RR[b] (1-butene)	Kwok et al. (1994a)

[a]Abbreviations used for the techniques are defined in table I-F-3.
[b]Placed on an absolute basis using $k(NO_3+1\text{-butene}) = 1.4 \times 10^{-14}$ cm^3 molecule^{-1} s^{-1} (Calvert et al., 2000).

III-F-9.4. Summary of the Atmospheric Fate of Dibenzofuran, and the End Products of Its Oxidation

Assuming the data on the OH reaction with dibenzofuran to be reasonably accurate, a lifetime of 3 h is estimated, for daytime [OH] = 2.5×10^6 molecule cm^{-3}. Kwok et al. (1994a) observed low yields (about 2%) of nitrodibenzofurans from the OH-initiated oxidation of this species.

III-F-10. Dibenzo-*p*-dioxin ($C_{12}H_8O_2$)

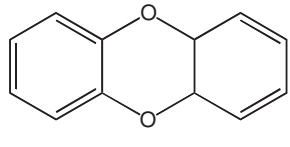

III-F-10.1. OH Reaction Kinetics

Data for the reaction of OH with dibenzo-*p*-dioxin have been obtained by Kwok et al. (1994a), Brubaker and Hites (1998), and Taylor et al. (2005). The data are not in agreement, see table III-F-13 and figure III-F-2. Data from Taylor et al. (2005) on a series of chlorinated dibenzo-*p*-dioxins appear to provide a consistent picture of the temperature dependence for these reactions and trends in reactivity from species to species. Thus, their Arrhenius expression, $k(\text{OH} + \text{dibenzo-}p\text{-dioxin}) = 1.7 \times 10^{-12} \exp(979/T)$ cm^3 molecule^{-1} s^{-1}, is preferred; extrapolation to 298 K gives $k(\text{OH} + \text{dibenzo-}p\text{-dioxin}) = 4.5 \times 10^{-11}$ cm^3 molecule^{-1} s^{-1}.

III-F-10.2. O_3 Reaction Kinetics

Kwok et al. (1994a) report an upper limit of $k < 5 \times 10^{-20}$ cm^3 molecule^{-1} s^{-1}. The reaction is too slow to be of atmospheric significance.

III-F-10.3. NO_3 Reaction Kinetics

Kwok et al. (1994a) have studied the reaction of NO_3 with dibenzo-*p*-dioxin near 298 K using a relative rate method. As described above for the dimethoxybenzene species (section III-F-2), the observed rate coefficient displays a dependence on NO_2 concentration due to scavenging of an NO_3/dibenzo-*p*-dioxin complex by NO_2. For dibenzo-*p*-dioxin, no abstraction reaction is observed ($k < 10^{-14}$ cm^3 molecule^{-1} s^{-1}),

Table III-F-13. Rate coefficients ($k = A \times e^{-B/T}$, cm^3 molecule^{-1} s^{-1}) for reaction of OH with dibenzo-*p*-dioxin

$10^{12} \times A$	B (K)	$10^{12} \times k$	T (K)	Technique[a]	Reference	Temperature Range (K)
		13.2 ± 4.1	297	RR[b] (propene)	Kwok et al. (1994a)	
		16.5 ± 3.1	297	RR[c] (*cyclo*-C_6H_{12})		
13.6	48 ± 81	12 ± 3	345	RR[c] (*cyclo*-C_6H_{12})	Brubaker and Hites (1998)	
		12 ± 3	345			
		12 ± 3	345			
		12 ± 3	345			
		11 ± 3	365			
		12 ± 3	365			
		12 ± 3	365			
		12 ± 3	385			
		12 ± 3	385			
		12 ± 3	385			
		12 ± 3	385			
1.70 ± 0.22	−979 ± 55			PLP–LIF	Taylor et al. (2005)[d]	326–907

[a]Abbreviations used for the techniques are defined in table I-F-3.
[b]Placed on an absolute basis using $k(\text{OH}+C_3H_6) = 2.9 \times 10^{-11}$ cm^3 molecule^{-1} s^{-1} (Atkinson et al., 2008).
[c]Placed on an absolute basis using $k(\text{OH}+\textit{cyclo}\text{-}C_6H_{12}) = 3.26 \times 10^{-17} T^2 \exp(262/T)$ cm^3 molecule^{-1} s^{-1} (Calvert et al., 2008).
[d]Taylor et al. (2005) did not report actual measured data; the table gives their final Arrhenius parameters.

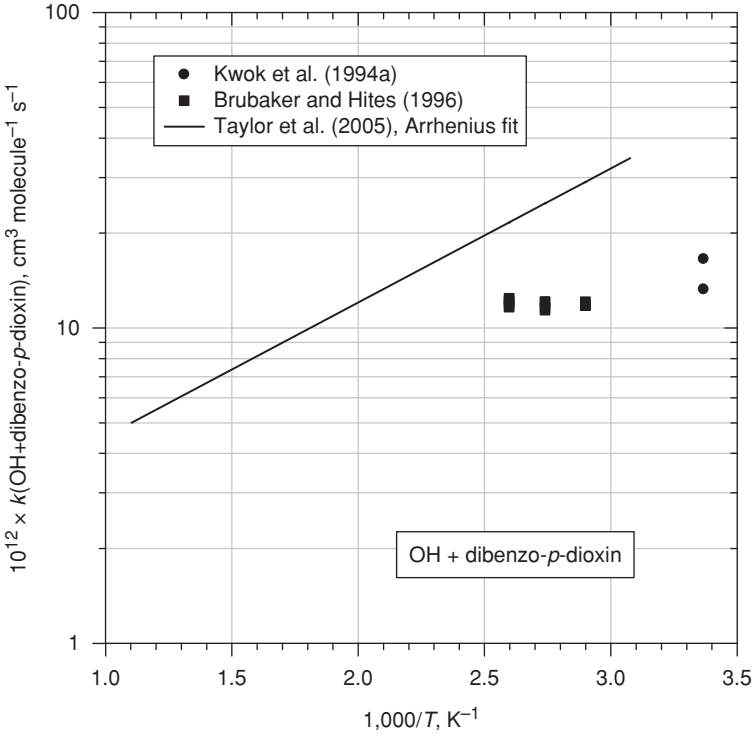

Figure III-F-2. Arrhenius plot of the rate coefficient for the reaction of OH with dibenzo-*p*-dioxin. The lines is the Arrhenius expression reported by Taylor et al. (2005), while the data points are those of Kwok et al. (1994a), circles, and Brubaker and Hites (1996), squares.

Table III-F-14. Rate coefficients ($k = A \times e^{-B/T}$, cm^3 molecule^{-1} s^{-1}) for reaction of NO_3 with dibenzo-*p*-dioxin

$10^{14} \times k_{abs}$	$10^{28} \times k_a k_b / k_c$	T (K)	Technique[a]	Reference
< 0.9	46	297	RR[b] (1-butene)	Kwok et al. (1994a)

[a]Abbreviations used for the techniques are defined in table I-F-3.
[b]Placed on an absolute basis using $k(NO_3 + 1\text{-butene}) = 1.4 \times 10^{-14}$ cm^3 molecule^{-1} s^{-1} (Calvert et al., 2000).

but adduct formation followed by adduct reaction with NO_2 may be significant (for 100 ppb of NO_2 or more). Data are summarized in table III-F-14.

III-F-10.4. Summary of the Atmospheric Fate of Dibenzo-p-dioxin, and the End Products of Its Oxidation

The lifetime of dibenzo-*p*-dioxin against OH reaction will be only about 2.5 h, assuming daytime [OH] $= 2.5 \times 10^6$ molecule cm^{-3}. Nighttime reaction with NO_3 may play a role in polluted (i.e., high NO_x) urban regions. Kwok et al. (1994a) observed minor

yields (< 1%) of nitrodibenzo-*p*-dioxins from the OH-initiated oxidation of the parent dibenzo-*p*-dioxin.

III-G. Halogen-Substituted Ethers

III-G-1. Difluoro(methoxy)methane (Difluoromethyl Methyl Ether, CH_3OCHF_2, HFE-152a)

III-G-1.1. OH Reaction Kinetics

The only study of the reaction of OH with CH_3OCHF_2 is that of Orkin et al. (1994), see table III-G-1. Their data were obtained from a combination of flash photolysis–resonance fluorescence and discharge flow–EPR techniques, and covered the range 253–460 K. They report $k = 6.0 \times 10^{-12} \exp[-(1{,}530 \pm 150)/T]$ cm^3 molecule^{-1} s^{-1}, with $k = (3.5 \pm 0.6) \times 10^{-14}$ cm^3 molecule^{-1} s^{-1} at 298 K. Corroborative measurements would be useful, and an uncertainty of ±25% is assigned at 298 K.

III-G-1.2. Summary of the Atmospheric Fate of CH_3OCHF_2, and the End Products of Its Oxidation

Assuming OH as the major loss mechanism for CH_3OCHF_2, its atmospheric lifetime is estimated at 1.5 years (for a tropospheric average temperature of 272 K, and global [OH] ≈ 10^6 molecule cm^{-3}). Product studies have not been conducted. However, the major site for OH attack is likely to be at the CH_3 group, with $CHF_2OCH{=}O$ the likely end product:

$$OH + CH_3OCHF_2(+O_2) \rightarrow \bullet OOCH_2OCHF_2$$

$$\bullet OOCH_2OCHF_2 + NO \rightarrow \bullet OCH_2OCHF_2 + NO_2$$

$$\bullet OCH_2OCHF_2 + O_2 \rightarrow HC(O)OCHF_2 + HO_2$$

III-G-2. Fluoro(fluoromethoxy)methane [bis(Fluoromethyl) Ether, CH_2FOCH_2F, HFE-152)

III-G-2.1. OH Reaction Kinetics

While there have been no measurements of the rate coefficient for this reaction, an estimate can be obtained using the Cl-atom rate coefficient for this species and estimation

Table III-G-1. Rate coefficients ($k = A \times e^{-B/T}$, cm^3 molecule^{-1} s^{-1}) for reaction of OH with CH_3OCHF_2 (HFE-152a)

$10^{12} \times k$	T (K)	Technique[a]	Reference	Temperature Range (K)
6.0	1530 ± 150	DF–EPR FP–RF	Orkin et al. (1994)	253–460

[a]Abbreviations used for the techniques are defined in table I-F-3.

method of Andersen et al. (2005b) and Wallington et al. (2008a). Using the empirical relationship $\log[k(\text{OH})] = 0.416 \times \log[k(\text{Cl})] - 8.16$, and $k(\text{Cl} + \text{CH}_2\text{FOCH}_2\text{F}) = 4.6 \times 10^{-13}$ cm^3 molecule^{-1} s^{-1} (see the following section, III-G-2.2), gives $k(\text{OH} + \text{CH}_2\text{FOCH}_2\text{F}) = 6 \times 10^{-14}$ cm^3 molecule^{-1} s^{-1} at 298 K with an uncertainty of a factor of 2.

III-G-2.2. Cl-Atom Reaction Kinetics

The reaction of Cl-atoms with $\text{CH}_2\text{FOCH}_2\text{F}$ has been studied by Goto et al. (2002b) using a relative rate technique, see table III-G-2. They report $k = 4.6 \times 10^{-13}$ cm^3 molecule^{-1} s^{-1}, with an assigned uncertainty of $\pm 30\%$.

III-G-2.3. Summary of the Atmospheric Fate of CH_2FOCH_2F, and the End Products of Its Oxidation

Combining the estimated value for the OH rate coefficient with a diurnally averaged [OH] = 10^6 molecule cm^{-3}, gives an atmospheric lifetime for $\text{CH}_2\text{FOCH}_2\text{F}$ of approximately 7 months.

Products of the Cl-atom-initiated oxidation of $\text{CH}_2\text{FOCH}_2\text{F}$, which should mimic those of the OH-initiated process in the atmosphere, have been reported by Goto et al. (2002b). Two products were identified, HC(O)F and $\text{CH}_2\text{FOC(O)F}$, that result from chemistry of the alkoxy radical, $\text{CH}_2\text{FOCHFO}\bullet$. When produced from the reaction of the corresponding peroxy radical ($\text{CH}_2\text{FOCHFOO}\bullet$) with NO, the alkoxy species is formed in an "activated" state, and decomposes via both H-atom elimination ($55 \pm 4\%$) and C—O bond cleavage ($45 \pm 4\%$):

$$\text{CH}_2\text{FOCHFO}\bullet \rightarrow \text{CH}_2\text{FO}\bullet + \text{HC(O)F}$$

$$\text{CH}_2\text{FO}\bullet + \text{O}_2 \rightarrow \text{HC(O)F} + \text{HO}_2$$

$$\text{CH}_2\text{FOCHFO}\bullet \rightarrow \text{CH}_2\text{FOCF=O} + \text{H}\bullet$$

In the absence of NO, the alkoxy CH_2FOCHFO is formed from peroxy radical–peroxy radical reactions and is not activated. In this case, an additional process was identified,

Table III-G-2. Rate coefficients (k, cm^3 molecule^{-1} s^{-1}) for reaction of Cl with $\text{CH}_2\text{FOCH}_2\text{F}$ (HFE-152)

$10^{13} \times k$	T (K)	Technique[a]	Reference
4.55 ± 0.42	296	RR[b] (CH_4)	Goto et al. (2002b)
4.56 ± 0.47	296	RR[c] (CH_3Cl)	

[a]Abbreviations used for the techniques are defined in table I-F-3.
[b]Placed on an absolute basis using $k(\text{Cl}+\text{CH}_4) = 1.00 \times 10^{-13}$ cm^3 molecule^{-1} s^{-1} (Atkinson et al., 2008).
[c]Placed on an absolute basis using $k(\text{Cl}+\text{CH}_3\text{Cl}) = 4.7 \times 10^{-13}$ cm^3 molecule^{-1} s^{-1} (Atkinson et al., 2008).

reaction with O_2, also producing $CH_2FOCF{=}O$.

$$CH_2FOCHFO\bullet + O_2 \rightarrow CH_2FOCF{=}O + HO_2\bullet$$

In air (and in the absence of NO), the O_2 reaction contributes $21 \pm 4\%$ to the alkoxy chemistry, while H-atom elimination contributes $31 \pm 4\%$ and C—O bond cleavage contributes $48 \pm 3\%$.

III-G-3. Trifluoro(methoxy)methane (Methyl Trifluoromethyl Ether, CH_3OCF_3, HFE-143a)

III-G-3.1. OH Reaction Kinetics

Rate coefficients for reaction of OH with CH_3OCF_3 have been reported by Zhang et al. (1992), Orkin et al. (1994), Hsu and DeMore (1995), and Chen et al. (2001), see table III-G-3 and figure III-G-1. The 298 K data point of Zhang et al. (1992) is significantly higher than the remainder of the data, and is not considered further. The remaining data are in reasonable agreement, although the relative rate data from Hsu and DeMore (1995) and Chen et al. (2001) fall about 10% below the absolute data from Orkin et al. (1994). The recommended Arrhenius expression: $k = 2.1 \times 10^{-12} \exp(-1{,}540/T)$ cm^3 molecule^{-1} s^{-1}, is obtained from an average of the determinations at 298 K ($k = 1.2 \times 10^{-14}$ cm^3 molecule^{-1} s^{-1}) coupled with the average of the activation energies reported by Orkin et al. (1994), Hsu and DeMore (1995), and Chen et al. (2001). Estimated uncertainty at 298 K is $\pm 15\%$.

III-G-3.2. Cl-Atom Reaction Kinetics

Christensen et al. (1999), using a relative rate technique, reported $k(Cl + CH_3OCF_3) = 1.3 \times 10^{-12}$ cm^3 molecule^{-1} s^{-1}. An uncertainty of $\pm 30\%$ is assigned to this value. Details are provided in table III-G-4.

III-G-3.3. Summary of the Atmospheric Fate of CH_3OCF_3, and the End Products of Its Oxidation

The atmospheric lifetime of CH_3OCF_3 is estimated to be 4.3 years, assuming an average tropospheric temperature of 272 K and [OH] $\approx 10^6$ molecule cm^{-3}. Product studies (using Cl-atoms to initiate the oxidation) have been carried out by Christensen et al. (1999), Good et al. (1999), and Chen et al. (2001); the sole primary product observed is $CF_3OCH{=}O$, which derives from the reaction of the alkoxy radical $CF_3OCH_2O\bullet$ with O_2, or possibly via H-atom elimination from this same radical:

$$CF_3OCH_2O\bullet + O_2 \rightarrow CF_3OCH{=}O + HO_2$$

$$CF_3OCH_2O\bullet \rightarrow CF_3OCH{=}O + H$$

Table III-G-3. Rate coefficients ($k = A \times e^{-B/T}$, cm^3 $molecule^{-1}$ s^{-1}) for reaction of OH with CH_3OCF_3 (HFE-143a)

$10^{12} \times A$	B (K)	$10^{14} \times k$	T (K)	Technique[a]	Reference	Temperature Range (K)
		21.4 ± 1.5	296	FP–RF	Zhang et al. (1992)	
1.13	$1{,}330 \pm 23$			DF–EPR FP–RF	Orkin et al. (1994)	
1.9	1,555	1.18	298	RR[b] (HFC-152a)	Hsu and DeMore (1995)	298–381
		1.62	318			
		1.85	333			
		2.25	348			
		2.53	363			
		2.95	381			
		1.13	301	RR[c] (CH_2F_2)		
		1.54	321			
		2.98	370			
4.22 ± 0.84	$1{,}750 \pm 350$	0.77 ± 0.10	278	RR[d] (CH_4)	Chen et al. (2001)	278–308
		1.08 ± 0.09	288			
		1.22 ± 0.08	298			
		1.57 ± 0.22	308			
		0.61 ± 0.07	268	RR[e] (CH_3CCl_3)		
		0.91 ± 0.05	281			
		1.15 ± 0.22	290			
		1.20 ± 0.08	298			
		1.34 ± 0.07	308			

[a]Abbreviations used for the techniques are defined in table I-F-3.
[b]Placed on an absolute basis using $k(OH+CH_3CHF_2) = 1.21 \times 10^{-12} \exp(-1{,}055/T)$ cm^3 $molecule^{-1}$ s^{-1} (Calvert et al., 2008).
[c]Placed on an absolute basis using $k(OH+CH_2F_2) = 1.33 \times 10^{-12} \exp(-1{,}432/T)$ cm^3 $molecule^{-1}$ s^{-1} (Calvert et al., 2008).
[d]Placed on an absolute basis using $k(OH+CH_4) = 1.85 \times 10^{-20} T^{2.82} \exp(-987/T)$ cm^3 $molecule^{-1}$ s^{-1} (Calvert et al., 2008).
[e]Placed on an absolute basis using $k(OH+CH_3CCl_3) = 1.81 \times 10^{-12} \exp(-1{,}543/T)$ cm^3 $molecule^{-1}$ s^{-1} (Calvert et al., 2008).

III-G-4. (Difluoromethoxy)difluoromethane (*bis*-Difluoromethyl Ether, CHF_2OCHF_2, HFE-134)

III-G-4.1. OH Reaction Kinetics

Rate coefficients for reaction of OH with CHF_2OCHF_2 have been reported by Zhang et al. (1992), Garland et al. (1993), Hsu and DeMore (1995), Orkin et al. (1999), and Wilson et al. (2001). The data are summarized in table III-G-5, and displayed in figure III-G-2. The 298 K data of Zhang et al. (1992) are an order of magnitude above the remaining data, likely the result of reactive impurities in the samples used; these data are not considered further. There is reasonable agreement among the remaining data, although the absolute measurements of Garland et al. (1993) and of Orkin et al. (1999) tend to fall above the relative rate data of Hsu and DeMore (1995) and Wilson et al. (2001), particularly at low temperature. This behavior is again consistent with the

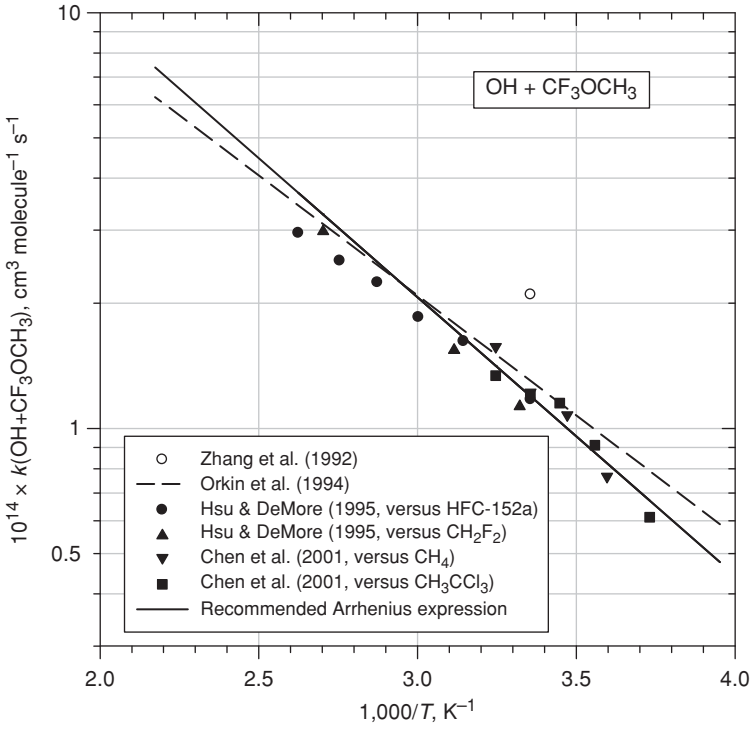

Figure III-G-1. Arrhenius plot of the rate coefficient for the reaction of OH with CH_3OCF_3.

Table III-G-4. Rate coefficients (k, cm^3 molecule^{-1} s^{-1}) for reaction of Cl with CH_3OCF_3 (HFE-143a)

$10^{12} \times k$	T (K)	Technique[a]	Reference
1.35 ± 0.10	295	RR[b] (CH_4)	Christensen et al. (1999)
1.33 ± 0.07	295	RR[c] (CH_3Cl)	

[a]Abbreviations used for the techniques are defined in table I-F-3.
[b]Placed on an absolute basis using $k(Cl+CH_4) = 0.99 \times 10^{-13}$ cm^3 molecule^{-1} s^{-1}.
[c]Placed on an absolute basis using $k(Cl+CH_3Cl) = 4.7 \times 10^{-13}$ cm^3 molecule^{-1} s^{-1}.

contribution of reactive impurities to the data obtained via absolute methods. Thus, our recommendation is based solely on the relative rate studies of Hsu and DeMore (1995) and Wilson et al. (2001), $k = 1.17 \times 10^{-12} \exp(-1{,}855/T)$ cm^3 molecule^{-1} s^{-1}. This expression gives $k = 2.3 \times 10^{-15}$ cm^3 molecule^{-1} s^{-1} at 298 K, with an estimated uncertainty of ±20%. The recommendation is consistent with the Orkin et al. (1999) data at $T > 298$ K.

III-G-4.2. Cl-Atom Reaction Kinetics

The reaction of Cl-atoms has been studied as a function of temperature (273–363 K) by Kambanis et al. (1998), using the Very Low Pressure Reactor technique. As summarized

Table III-G-5. Rate coefficients ($k = A \times e^{-B/T}$, cm^3 molecule^{-1} s^{-1}) for reaction of OH with CHF_2OCHF_2 (HFE-134)

$10^{12} \times A$	B (K)	$10^{15} \times k$	T (K)	Technique[a]	Reference	Temperature Range (K)
		25 ± 2	296	FP–RF	Zhang et al. (1992)	
0.54 ± 0.35	1,560 ± 200	1.5 ± 0.1	269	PLP–LIF	Garland et al. (1993)	269–312
		1.9 ± 0.2	279			
		2.5 ± 0.2	294			
		3.0 ± 0.7	295			
		3.4 ± 0.4	311			
		3.3 ± 0.3	312			
1.9	2,006	2.41	298	RR[b] (CH_3CCl_3)	Hsu and DeMore (1995)	298–368
		2.37	298			
		2.64	307			
		3.35	315			
		4.61	333			
		6.24	350			
		8.50	368			
$0.63^{+0.20}_{-0.16}$	1,646 ± 76	1.70 ± 0.15	277	FP–RF	Orkin et al. (1999)	
		2.47 ± 0.12	298			
		3.77 ± 0.35	323			
		5.67 ± 0.52	349			
		7.48 ± 0.45	370			
1.29 ± 0.50	1,895 ± 100	1.29	273.0	RR[c] (CF_3CHF_2)	Wilson et al. (2001)	273–464.5
		2.24	298.7			
		3.68	322.5			
		5.73	348.9			
		7.78	370.1			
		11.36	400.8			
		14.95	427.2			
		18.22	447.7			
		21.13	464.5			

[a]Abbreviations used for the techniques are defined in table I-F-3.
[b]Placed on an absolute basis using $k(OH+CH_3CCl_3) = 1.81 \times 10^{-12} \exp(-1{,}543/T)$ cm^3 molecule^{-1} s^{-1} (Calvert et al., 2008).
[c]Placed on an absolute basis using $k(OH+CF_3CHF_2) = 5.10 \times 10^{-13} \exp(-1{,}666/T)$ cm^3 molecule^{-1} s^{-1} (Calvert et al., 2008).

in table III-G-6, they report $k = 1.03 \times 10^{-12} \exp(-867/T)$ cm^3 molecule^{-1} s^{-1}, which yields $k = 5.6 \times 10^{-14}$ cm^3 molecule^{-1} s^{-1} at 298 K. However, as seen in the following sections, measurements made by Kambanis et al. (1998) for other species do not agree favorably with data obtained by other methods. Thus, no recommendation is made for this rate coefficient, and further study is recommended.

III-G-4.3. Summary of the Atmospheric Fate of CHF_2OCHF_2, and the End Products of Its Oxidation

The atmospheric lifetime of CHF_2OCHF_2 is estimated to be 26 years, assuming an average tropospheric temperature of 272 K and [OH] $\approx 10^6$ molecule cm^{-3}. The Cl-atom-initiated oxidation of CHF_2OCHF_2 has been studied by Good et al. (1999).

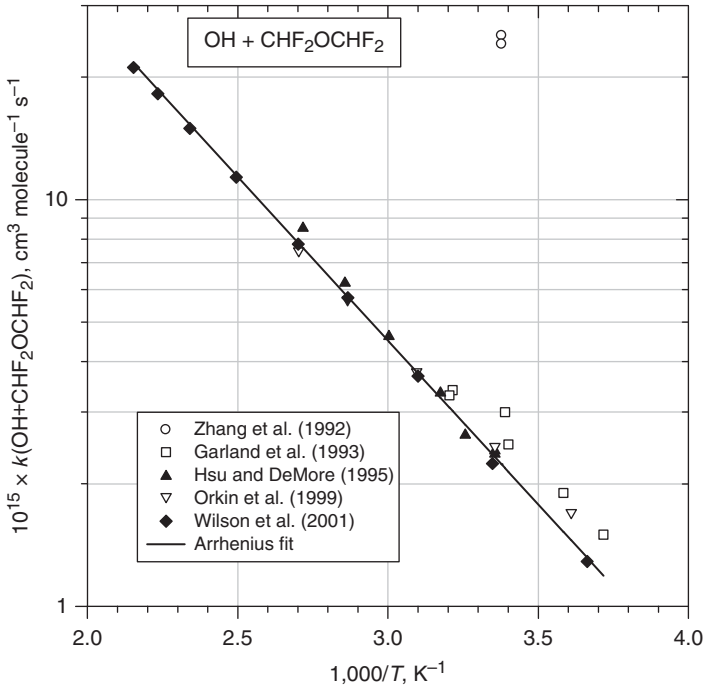

Figure III-G-2. Arrhenius plot of the rate coefficient for the reaction of OH with CHF_2OCHF_2.

Table III-G-6. Rate coefficients ($k = A \times e^{-B/T}$, cm^3 $molecule^{-1}$ s^{-1}) for reaction of Cl with CHF_2OCHF_2 (HFE-134)

$10^{12} \times A$	B (K)	$10^{14} \times k$	T (K)	Technique[a]	Reference
1.03 ± 0.19	867 ± 106	4.35 ± 0.24	273	VLPR	Kambanis et al. (1998)
		5.73 ± 0.30	303		
		7.72 ± 0.26	333		
		9.38 ± 0.50	363		

[a]Abbreviations used for the techniques are defined in table I-F-3.

COF_2, with a yield of 200±12%, was the only observed end product, and the following mechanism was proposed to describe the atmospheric behavior of CHF_2OCHF_2:

$$OH + CHF_2OCHF_2(+O_2) \rightarrow CHF_2OCF_2OO\bullet + H_2O$$

$$CHF_2OCF_2OO\bullet + NO \rightarrow CHF_2OCF_2O\bullet + NO_2$$

$$CHF_2OCF_2O\bullet \rightarrow CHF_2O\bullet + COF_2$$

$$CHF_2O\bullet + O_2 \rightarrow COF_2 + HO_2$$

III-G-5. (Difluoromethoxy)trifluoromethane (Trifluoromethyl Difluoromethyl Ether, CF_3OCHF_2, HFE-125)

III-G-5.1. OH Reaction Kinetics

The reaction of OH with CF_3OCHF_2 has been studied by Zhang et al. (1992), Orkin et al. (1994), and Hsu and DeMore (1995), see summary in table III-G-7 and figure III-G-3. As with other compounds, the data from Zhang et al. (1992) fall well above the remainder of the dataset, likely due to the presence of reactive impurities in the samples used. There is excellent agreement between the absolute data of Orkin et al. (1994) and the relative rate data from Hsu and DeMore (1995). Both groups derive $k = 4.7 \times 10^{-13} \exp(-2{,}100/T)$ cm^3 molecule^{-1} s^{-1}, a recommendation that is adopted here. This expression gives $k = 4.1 \times 10^{-16}$ cm^3 molecule^{-1} s^{-1} at 298 K, with an estimated uncertainty of ±20%.

III-G-5.2. Cl-Atom Reaction Kinetics

The rate coefficient for the reaction of Cl-atoms with CF_3OCHF_2 has been determined at 295 K by Inoue et al. (2001), using a relative rate technique. A value of $k = 1.9 \times 10^{-17}$ cm^3 molecule^{-1} s^{-1} is reported, and is assigned an uncertainty of ±25%. Details are provided in table III-G-8.

Table III-G-7. Rate coefficients ($k = A \times e^{-B/T}$, cm^3 molecule^{-1} s^{-1}) for reaction of OH with CF_3OCHF_2 (HFE-125)

$10^{12} \times A$	B (K)	$10^{16} \times k$	T (K)	Technique[a]	Reference	Temperature Range (K)
		35 ± 5	296	FP–RF	Zhang et al. (1992)	
0.47	2,100 ± 300			DF–EPR FP–RF	Orkin et al. (1994)	253–460
0.47	2,095	4.67	298	RR[b] (CH_4)	Hsu and DeMore (1995)	298–368
		6.89	313			
		11.54	345			
		17.15	377			
		5.14	298	RR[c] (CHF_3)		
		7.37	317			
		9.46	333			
		15.82	360			
		21.8	385			
		25.1	393			
		6.03	318	RR[d] (CF_3CHF_2)		

[a]Abbreviations used for the techniques are defined in table I-F-3.

[b]Placed on an absolute basis using $k(OH+CH_4) = 1.85 \times 10^{-20} T^{2.82} \exp(-987/T)$ cm^3 molecule^{-1} s^{-1} (Calvert et al., 2008). These data were not used in obtaining final value; see Hsu and DeMore (1995) for details.

[c]Placed on an absolute basis using $k(OH+CHF_3) = 4.89 \times 10^{-13} \exp(-2{,}200/T)$ cm^3 molecule^{-1} s^{-1} (Calvert et al., 2008).

[d]Placed on an absolute basis using $k(OH+CF_3CHF_2) = 5.1 \times 10^{-13} \exp(-1{,}666/T)$ cm^3 molecule^{-1} s^{-1} (Calvert et al., 2008).

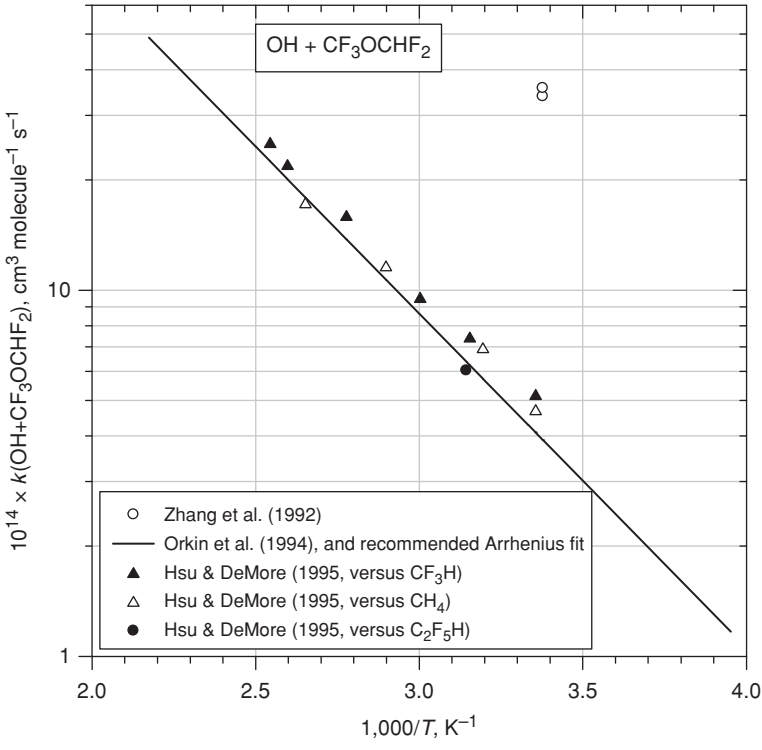

Figure III-G-3. Arrhenius plot of the rate coefficient for the reaction of OH with CF_3OCHF_2.

Table III-G-8. Rate coefficients (k, cm^3 molecule^{-1} s^{-1}) for reaction of Cl with CF_3OCHF_2 (HFE-125)

$10^{17} \times k$	T (K)	Technique[a]	Reference
2.1 ± 0.1	295	RR[b] (CH_3CF_2Cl)	Inoue et al. (2001)
1.8 ± 0.1	295	RR[c] (CH_3CF_3)	

[a]Abbreviations used for the techniques are defined in table I-F-3.
[b]Placed on an absolute basis using $k(Cl+CH_3CF_2Cl) = 3.8 \times 10^{-16}$ cm^3 molecule^{-1} s^{-1} at 295 K (Atkinson et al., 2008).
[c]Placed on an absolute basis using $k(Cl+CH_3CF_3) = 2.8 \times 10^{-17}$ cm^3 molecule^{-1} s^{-1} at 295 K (IUPAC, 2008).
[d]Note that there is a typographical error in the Inoue et al. (2001) paper; the uncertainties are a factor of 10 larger than reported.

III-G-5.3. Summary of the Atmospheric Fate of CF_3OCHF_2, and the End Products of Its Oxidation

The atmospheric lifetime of CF_3OCHF_2 is long, about 150 years for [OH] $\approx 10^6$ molecule cm^{-3} and an average tropospheric temperature of 272 K. Good et al. (1999) and Inoue et al. (2001) reported COF_2 as the major product (152 ± 13% and 132 ± 15% yield, respectively) in the Cl-atom-initiated oxidation of this species in the presence of O_2. The mechanism is expected to proceed via the formation and subsequent

decomposition of the CF_3OCF_2O radical,

$$Cl + CF_3OCHF_2 \rightarrow CF_3OCF_2OO\bullet$$

$$CF_3OCF_2OO\bullet + ROO\bullet \rightarrow CF_3OCF_2O\bullet + RO\bullet + O_2$$

$$CF_3OCF_2O\bullet \rightarrow CF_3O\bullet + CF_2O$$

In these laboratory experiments (in the absence of NO), $CF_3O\bullet$ can react with another CF_3O radical to form the peroxide, CF_3OOCF_3, or with $CF_3OCF_2OO\bullet$ to form the trioxide ($CF_3OOOCF_2OCF_3$). However, in the atmosphere, such reactions are not important and conversion of $CF_3O\bullet$ to COF_2 via reaction with NO or CH_4 is efficient. The overall atmospheric fate of CF_3OCHF_2 is thus conversion into two molecules of COF_2.

III-G-6. (Trifluoromethoxy)ethane (Trifluoromethyl Ethyl Ether, $CH_3CH_2OCF_3$)

III-G-6.1. OH Reaction Kinetics

A rate coefficient for reaction of OH with $CH_3CH_2OCF_3$, $k = 1.5 \times 10^{-13}$ cm^3 molecule^{-1} s^{-1} at 298 K, has been obtained by Oyaro et al. (2005) using a relative rate technique. Details are given in table III-G-9. Given the lack of corroborative data, an uncertainty of ±30% is assigned.

III-G-6.2. Cl-Atom Reaction Kinetics

Oyaro et al. (2005) studied this reaction at 298 K using a relative rate technique. As is shown in table III-G-10, agreement between the values obtained using two different reference reactions is not good: $k = 1.9 \times 10^{-12}$ cm^3 molecule^{-1} s^{-1} and $k = 3.0 \times 10^{-12}$ cm^3 molecule^{-1} s^{-1}. In the absence of additional data for this reaction, an average value of $k = 2.4 \times 10^{-12}$ cm^3 molecule^{-1} s^{-1} is recommended, with an uncertainty of ±60%.

III-G-6.3. Summary of the Atmospheric Fate of $CH_3CH_2OCF_3$, and the End Products of Its Oxidation

On the basis of the rate coefficient for its reaction with OH, the atmospheric lifetime of $CH_3CH_2OCF_3$ is estimated to be about 80 days. The mechanism for the atmospheric

Table III-G-9. Rate coefficients (k, cm^3 molecule^{-1} s^{-1}) for reaction of OH with $CH_3CH_2OCF_3$

$10^{13} \times k$	T (K)	Technique[a]	Reference
1.49 ± 0.24	298	RR[b] ($CHCl_3$)	Oyaro et al. (2005)

[a]Abbreviations used for the techniques are defined in table I-F-3.
[b]Placed on an absolute basis using $k(OH+CHCl_3) = 9.6 \times 10^{-14}$ cm^3 molecule^{-1} s^{-1} (Calvert et al., 2008).

Table III-G-10. Rate coefficient (k, cm^3 molecule^{-1} s^{-1}) for reaction of Cl with $CH_3CH_2OCF_3$

$10^{12} \times k$	T (K)	Technique[a]	Reference
1.9 ± 1.0	298	RR[b] (CH_2ClCH_2Cl)	Oyaro et al. (2005)
3.0 ± 1.5	298	RR[c] (CH_3CH_2Cl)	

[a]Abbreviations used for the techniques are defined in table I-F-3.
[b]Placed on an absolute basis using $k(Cl+CH_2ClCH_2Cl) = 1.3 \times 10^{-12}$ cm^3 molecule^{-1} s^{-1} at 298 K (Wallington et al., 1996b).
[c]Placed on an absolute basis using $k(Cl+CH_3CH_2Cl) = 7.8 \times 10^{-12}$ cm^3 molecule^{-1} s^{-1} at 298 K (this book, table I-F-2).

oxidation of this species has not been determined. However, likely end products include either $CH_3C(O)OCF_3$ or HCHO and $HC(O)OCF_3$, resulting from OH attack at the CH_2-group.

III-G-7. 1,1,1-Trifluoro-2-methoxyethane (2,2,2-Trifluoroethyl Methyl Ether, $CF_3CH_2OCH_3$)

III-G-7.1. OH Reaction Kinetics

Rate coefficients have been reported near 298 K for the reaction of OH with $CF_3CH_2OCH_3$ by Zhang et al. (1992), Nolan et al. (1999), and Oyaro et al. (2005). As can be seen from table III-G-11, all data are in reasonable agreement, and an average value of $k = 5.9 \times 10^{-13}$ cm^3 molecule^{-1} s^{-1} is recommended with an estimated uncertainty of ±20% for temperatures near 298K.

III-G-7.2. Cl-Atom Reaction Kinetics

The reaction of Cl with $CF_3CH_2OCH_3$ has been studied as a function of temperature by Kambanis et al. (1998) and near 298 K by Oyaro et al. (2005), see table III-G-12. Kambanis et al. (1998) find no temperature dependence to the reaction rate coefficient. As a note of caution, it should be pointed out that the data of Kambanis et al. (1998) for reaction of Cl with $CF_3CH_2OCHF_2$ are considerably higher than other measurements of this reaction. Also, the reference reaction used by Oyaro et al. (2005) has been the

Table III-G-11. Rate coefficients (k, cm^3 molecule^{-1} s^{-1}) for reaction of OH with $CF_3CH_2OCH_3$

$10^{13} \times k$	T (K)	Technique[a]	Reference
6.24 ± 0.67	296	FP–RF	Zhang et al. (1992)
6.4 ± 0.5	298	RR[b]	Nolan et al. (1999)
5.7 ± 0.9	298	RR[c] ($CHCl_3$)	Oyaro et al. (2005)
5.2 ± 0.4		RR[d] (acetone)	

[a]Abbreviations used for the techniques are defined in table I-F-3.
[b]Reference compound not specified.
[c]Placed on an absolute basis using $k(OH+CHCl_3) = 9.6 \times 10^{-14}$ cm^3 molecule^{-1} s^{-1} (Calvert et al., 2008).
[d]Placed on an absolute basis using $k(OH+CH_3C(O)CH_3) = 1.8 \times 10^{-13}$ cm^3 molecule^{-1} s^{-1} (Calvert et al., 2008).

subject of only one study. An average value of 2.1×10^{-11} cm^3 molecule^{-1} s^{-1} is recommended, with an estimated uncertainty of ±50%.

III-G-7.3. Summary of the Atmospheric Fate of $CF_3CH_2OCH_3$, and the End Products of Its Oxidation

The atmospheric lifetime of $CF_3CH_2OCH_3$ is estimated to be 20 days, assuming an average [OH] $\approx 10^6$ molecule cm^{-3}. The Cl-atom-initiated oxidation of $CF_3CH_2OCH_3$ has been studied by Nolan et al. (1999); products observed are CF_3CH_2OCHO (∼ 90% yield) and CF_2O (∼10% yield). The high yield of CF_3CH_2OCHO indicates that the majority of the Cl-atom attack is at the CH_3 group; a similar result is expected from the OH-initiated oxidation.

III-G-8. 1,1,2,2-Tetrafluoro-1-methoxyethane (1,1,2,2-Tetrafluoroethyl Methyl Ether, $CH_3OCF_2CHF_2$)

III-G-8.1. OH Reaction Kinetics

Data for the reaction of OH with $CH_3OCF_2CHF_2$ have been reported by Heathfield et al. (1998), Nolan et al. (1999), and Tokuhashi et al. (2000b), see table III-G-13 and figure III-G-4. The 298 K datapoint from Heathfield et al. (1998) is an order of magnitude higher than the Tokuhashi et al. data, likely due to the presence of reactive impurities in their samples, while the Nolan et al. data point is about 25% higher. Tokuhashi et al. took great care in purifying their samples (to greater than 99.99% purity), and showed that even a 0.1% impurity in the original samples led to a ≈ 30% increase in the apparent rate coefficient. Thus, the final data of Tokuhashi et al. (2000b) are recommended, $k = 2.6 \times 10^{-12} \exp(-1{,}420/T)$ cm^3 molecule^{-1} s^{-1}. This expression gives $k = 2.24 \times 10^{-14}$ cm^3 molecule^{-1} s^{-1} at 298 K, with an estimated uncertainty of ±20%.

Table III-G-12. Rate coefficients ($k = A \times e^{-B/T}$, cm^3 molecule^{-1} s^{-1}) for reaction of Cl with $CF_3CH_2OCH_3$

$10^{12} \times A$	B (K)	$10^{12} \times k$	T (K)	Technique[a]	Reference	Temperature Range (K)
22.6 ± 2.0	0	22.8 ± 1.3	273	VLPR	Kambanis et al. (1998)	273–363
		23.1 ± 1.0	303			
		22.7 ± 0 .8	333			
		21.6 ± 0.77	363			
		15 ± 8	298	RR[b] (n-$C_4F_9OC_2H_5$)	Oyaro et al. (2005)	

[a]Abbreviations used for the techniques are defined in table I-F-3.

[b]Placed on an absolute basis using k(Cl+n-$C_4F_9OC_2H_5$) = 2.3×10^{-12} cm^3 molecule^{-1} s^{-1} at 298 K (this book, section III-G-43.2).

Table III-G-13. Rate coefficients ($k = A \times e^{-B/T}$, cm^3 $molecule^{-1}$ s^{-1}) for reaction of OH with $CH_3OCF_2CHF_2$

$10^{12} \times A$	B (K)	$10^{14} \times k$	T (K)	Technique[a]	Reference	Temperature Range (K)
		20.4 ± 3.3	296	PR–UV abs.	Heathfield et al. (1998)	
		2.6 ± 0.16	298	RR[b]	Nolan et al. (1999)	
2.60	1,420 ± 170	0.966 ± 0.115	250	FP or PLP–LIF	Tokuhashi et al. (2000b)	250–430
		0.998 ± 0.107	250			
		1.35 ± 0.15	273			
		1.48 ± 0.16	273			
		2.10 ± 0.25	298			
		2.25 ± 0.26	298			
		3.23 ± 0.36	331			
		5.66 ± 0.60	375			
		10.1 ± 1.1	430			
		10.5 ± 1.1	430			
		2.27 ± 0.25	298	DF–LIF		

[a]Abbreviations used for the techniques are defined in table I-F-3.
[b]Reference compound not specified.

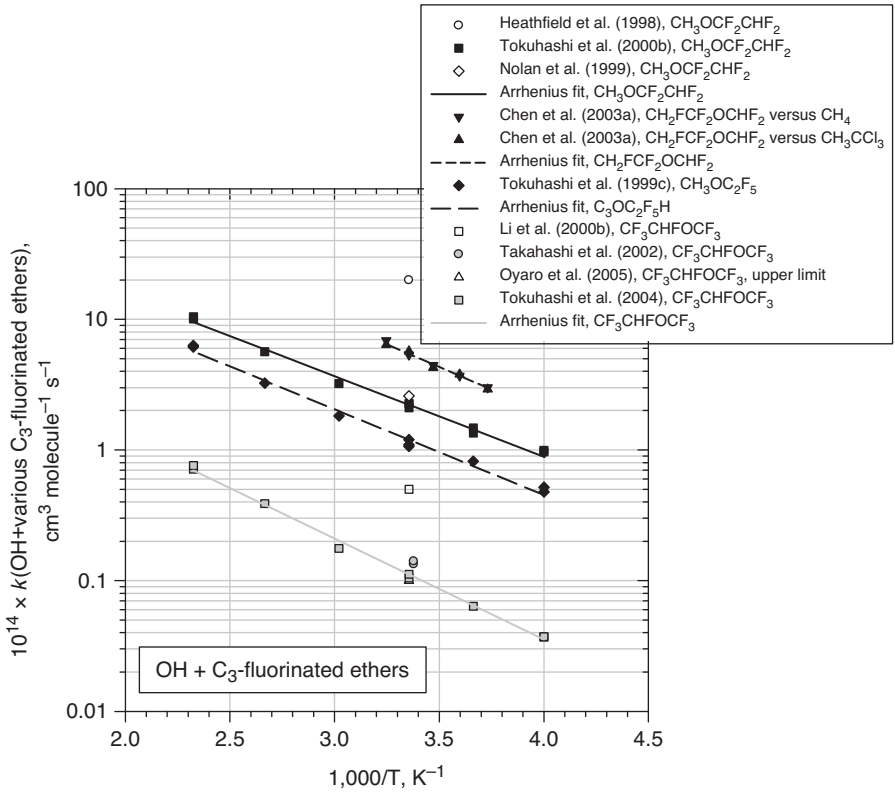

Figure III-G-4. Arrhenius plot of the rate coefficient for the reaction of OH with various three-carbon fluorinated ethers.

Table III-G-14. Rate coefficients ($k = A \times e^{-B/T}$, cm^3 $molecule^{-1}$ s^{-1}) for reaction of Cl with $CH_3OCF_2CHF_2$

$10^{12} \times A$	B (K)	$10^{14} \times k$	T (K)	Technique[a]	Reference
5.49 ± 1.51	928 ± 155	18.5 ± 2.0	273	VLPR	Papadimitriou et al. (2004)
		23.6 ± 4.9	303		
		34.4 ± 2.8	333		
		42.1 ± 5.2	363		

[a]Abbreviations used for the techniques are defined in table I-F-3.

III-G-8.2. Cl-Atom Reaction Kinetics

The reaction of Cl with $CH_3OCF_2CHF_2$ has been studied as a function of temperature by Papadimitriou et al. (2004) using the very-low-pressure reactor technique. Their data (table III-G-14) give $k = 5.49 \times 10^{-12} \exp(-928/T)$ cm^3 $molecule^{-1}$ s^{-1}, with $k = 2.4 \times 10^{-13}$ cm^3 $molecule^{-1}$ s^{-1} at 298 K.

III-G-8.3. Summary of the Atmospheric Fate of $CH_3OCF_2CHF_2$, and the End Products of Its Oxidation

The atmospheric lifetime of $CH_3OCF_2CHF_2$ is estimated to be 2.3 years, assuming an average [OH] $\approx 10^6$ molecule cm^{-3} and an average tropospheric temperature of 272 K. The mechanism of the OH-initiated oxidation of this species has not been studied. However, the Cl-atom-initiated oxidation has been studied by Nolan et al. (1999), who showed formation of the formate ester, $HC(O)OCF_2CHF_2$, which is obtained from the reaction of the alkoxy radical, $\bullet OCH_2OCF_2CHF_2$ with O_2.

III-G-9. 1,1,1,2-Tetrafluoro-2-methoxyethane (Methyl 1,2,2,2-tetrafluoroethyl Ether, $CF_3CHFOCH_3$)

III-G-9.1. OH Reaction Kinetics

The reaction of OH with $CF_3CHFOCH_3$ has been studied by Chen et al. (2006) between 253 and 328 K using a relative rate method. Fitting of their data, following scaling to currently recommended reference rate coefficient data, gives $k = 2.0 \times 10^{-12} \exp(-738/T)$ cm^3 $molecule^{-1}$ s^{-1} with $k = 1.6 \times 10^{-13}$ cm^3 $molecule^{-1}$ s^{-1} at 298 K. In the absence of corroborative measurements, an uncertainty of ±25% is assigned. Details are provided in table III-G-15.

III-G-9.2. Summary of the Atmospheric Fate of $CF_3CHFOCH_3$, and the End Products of Its Oxidation

The atmospheric lifetime of $CF_3CHFOCH_3$ is estimated to be 72 days, for [OH] $\approx 10^6$ molecule cm^{-3}. Products of the OH-initiated oxidation have been determined by Chen et al. (2006). The majority of the reaction (about 80%) occurs via abstraction from

Table III-G-15. Rate coefficients ($k = A \times e^{-B/T}$, cm^3 $molecule^{-1}$ s^{-1}) for reaction of OH with $CF_3CHFOCH_3$

$10^{12} \times A$	B (K)	$10^{14} \times k$	T (K)	Technique[a]	Reference	Temperature Range (K)
2.0 ± 0.8	738 ± 112	10.5 ± 0.4	253	RR[b] (C_2H_6)	Chen et al. (2006)	253–328
		11.9 ± 0.4	268			
		13.9 ± 0.2	283			
		16.2 ± 1.2	298			
		18.2 ± 1.4	313			
		19.4 ± 0.8	328			
		10.7 ± 0.9	253	RR[c] (CH_3CHF_2)		
		13.1 ± 1.2	268			
		14.7 ± 2.6	283			
		17.1 ± 1.2	298			
		19.4 ±1.3	313			
		21.5 ± 3.0	328			

[a]Abbreviations used for the techniques are defined in table I-F-3.
[b]Placed on an absolute basis using $k(OH+C_2H_6) = 8.61 \times 10^{-12} \exp(-1{,}047/T)$ cm^3 $molecule^{-1}$ s^{-1} (Calvert et al., 2008).
[c]Placed on an absolute basis using $k(OH+CH_3CHF_2) = 1.21 \times 10^{-12} \exp(-1{,}055/T)$ cm^3 $molecule^{-1}$ s^{-1} (Calvert et al., 2008).

the CH_3 group, leading to the formation of $HC(O)OCHFCF_3$. The remainder of the reaction occurs via abstraction of an H atom at the CHF group, leading to $FC(O)OCH_3$ and COF_2 formation.

III-G-10. 2-(Difluoromethoxy)-1,1,1-trifluoroethane (Difluoromethyl 2,2,2- trifluoroethyl Ether, $CF_3CH_2OCHF_2$)

III-G-10.1. OH Reaction Kinetics

The reaction of OH with $CF_3CH_2OCHF_2$ has been studied by Zhang et al. (1992), Orkin et al. (1994), Nolan et al. (1999), Beach et al. (2001), and Oyaro et al. (2005). Data are summarized in table III-G-16 and are displayed in figure III-G-5. There is general consensus among the various measurements, with the exception of the data from Beach et al. (2001), which lie significantly higher than the other data; thus, the Beach et al. (2001) data are not considered further in the analysis. An unweighted average of the remaining 298 K data yields $k = 1.1 \times 10^{-14}$ cm^3 $molecule^{-1}$ s^{-1}, with an estimated uncertainty of ±25%. Combining this value with the temperature dependence measured by Orkin et al. (1994) yields $k = 2.5 \times 10^{-12} \exp(-1{,}610/T)$ cm^3 $molecule^{-1}$ s^{-1}.

III-G-10.2. Cl-Atom Reaction Kinetics

Six different studies of the rate coefficient for reaction of Cl with $CF_3CH_2OCHF_2$ can be found in the literature (Kambanis et al., 1998; Beach et al., 2001; Hickson and Smith, 2001; Wallington et al., 2002; Oyaro et al., 2005; Dalmasso et al., 2006a).

Table III-G-16. Rate coefficients ($k = A \times e^{-B/T}$, cm^3 $molecule^{-1}$ s^{-1}) for reaction of OH with $CF_3CH_2OCHF_2$

$10^{12} \times A$	B (K)	$10^{15} \times k$	T (K)	Technique[a]	Reference	Temperature Range (K)
		12.5 ± 0.9	296	FP–RF	Zhang et al. (1992)	
		12.0 ± 1.6	296			
2.6	1,610 ± 34			DF–EPR	Orkin et al. (1994)	253–460
				FP–RF		
		11.0 ± 0.3	298	RR[b]	Nolan et al. (1999)	
20 ± 8	2,110 ± 150	21 ± 3	292	DF–RF	Beach et al. (2001)	292–402
		17 ± 1	298			
		42 ± 3	347			
		109 ± 12	402			
		9.5 ± 1.4	298	RR[c] (CH_3CCl_3)	Oyaro et al. (2005)	
		8.5 ± 1.7	298	RR[d] (CHF_2CH_2F)		

[a]Abbreviations used for the techniques are defined in table I-F-3.
[b]Reference compound not specified.
[c]Placed on an absolute basis using $k(OH+CH_3CCl_3) = 1.02 \times 10^{-14}$ cm^3 $molecule^{-1}$ s^{-1} (Calvert et al., 2008).
[d]Placed on an absolute basis using $k(OH+CHF_2CH_2F) = 1.63 \times 10^{-14}$ cm^3 $molecule^{-1}$ s^{-1} (Calvert et al., 2008).

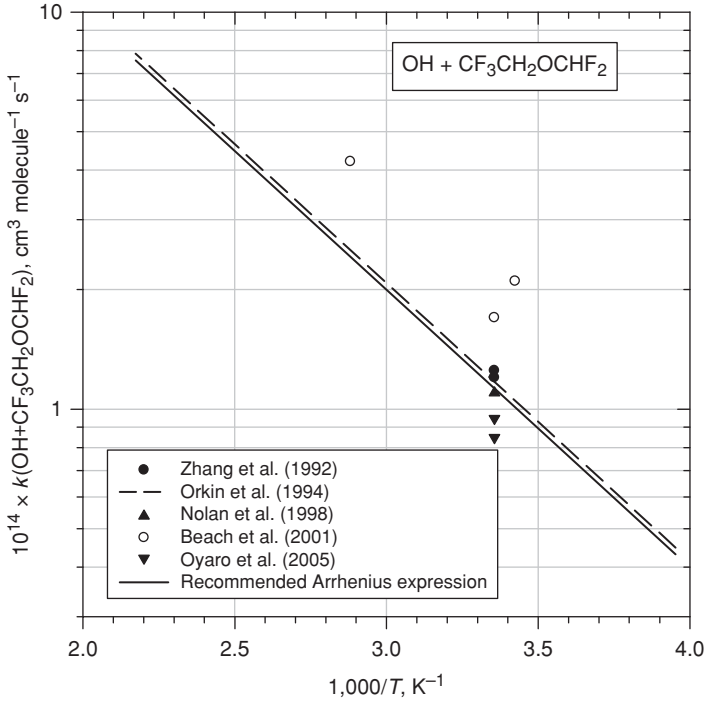

Figure III-G-5. Arrhenius plot of the rate coefficient for the reaction of OH with $CF_3CH_2OCHF_2$.

Table III-G-17. Rate coefficients ($k = A \times e^{-B/T}$, cm^3 molecule^{-1} s^{-1}) for reaction of Cl with $CF_3CH_2OCHF_2$

$10^{12} \times A$	B (K)	$10^{15} \times k$	T (K)	Technique[a]	Reference	Temperature Range (K)
3.84 ± 1.00	1,451 ± 147	19.4 ± 1.1	273	VLPR	Kambanis et al. (1998)	
		31.1 ± 1.4	303			
		48.7 ± 1.7	333			
		72.4 ± 3.9	363			
6.1 ± 1.4	1,830 ± 90	11 ± 1	294	DF–RF	Beach et al. (2001)	294–398
		38 ± 2	362			
		63 ± 2	398			
5.1 ± 0.7	1,830 ± 410	11 ± 2	295	RR[b] (CD_4)	Hickson et al. (2001)	295–363
		14 ± 2	323			
		31 ± 7	363			
		11.9 ± 1.0	295	RR[c] (CH_4)	Wallington et al. (2002)	
		11.8 ± 0.6	295	RR[b] (CD_4)		
		17 ± 5	298	RR[d] ($CHCl_3$)	Oyaro et al. (2005)	
		22 ± 66	298	RR[e] (CHF_2CH_2F)		
		9.5 ± 2.3	296	RR[f] (CH_3CCl_3)	Dalmasso et al. (2006a)	

[a]Abbreviations used for the techniques are defined in table I-F-3.
[b]Placed on an absolute basis using $k(Cl+CD_4) = 8.3 \times 10^{-12} \exp(-2{,}124/T)$ cm^3 molecule^{-1} s^{-1} (Hickson et al., 2001, scaled to 298 K value recommended in Calvert et al., 2008).
[c]Placed on an absolute basis using $k(Cl+CH_4) = 0.99 \times 10^{-13}$ cm^3 molecule^{-1} s^{-1} at 295 K (Atkinson et al., 2006).
[d]Placed on an absolute basis using $k(Cl+CHCl_3) = 1.13 \times 10^{-13}$ cm^3 molecule^{-1} s^{-1} (Atkinson et al., 2008).
[e]Placed on an absolute basis using $k(Cl+CHF_2CH_2F) = 5.0 \times 10^{-14}$ cm^3 molecule^{-1} s^{-1} (Atkinson et al., 2008).
[f]Placed on an absolute basis using $k(Cl+CH_3CCl_3) = 8.3 \times 10^{-15}$ cm^3 molecule^{-1} s^{-1} at 296 K (IUPAC, 2008).

As can be seen in table III-G-17 and figure III-G-6, the data of Kambanis et al. (1998) and Oyaro et al. (2005) fall above the remainder of the dataset. Analysis of the remaining data yields $k = 6.3 \times 10^{-12} \exp(-1{,}897/T)$ cm^3 molecule^{-1} s^{-1}. This expression gives $k = 1.1 \times 10^{-14}$ cm^3 molecule^{-1} s^{-1} at 298 K, with an estimated uncertainty of ±20%.

III-G-10.3. Summary of the Atmospheric Fate of $CF_3CH_2OCHF_2$, and the End Products of Its Oxidation

The atmospheric lifetime of $CF_3CH_2OCHF_2$ is 4.7 years, assuming an average [OH] ≈ 10^6 molecule cm^{-3} and an average tropospheric temperature of 272 K. Wallington et al. (2002) have studied the Cl-atom-initiated oxidation of this species, which should be very similar to the OH-initiated process. Abstraction at the CH_2 group dominates, leading to the eventual formation of $CF_3CH(O•)OCHF_2$ alkoxy radicals. When formed from the exothermic reaction of $CF_3CH(OO•)OCHF_2$ radicals with NO, the sole fate of $CF_3CH(O•)OCHF_2$ is decomposition via C—C bond cleavage to yield CF_3 radicals and the formate ester, $HC(O)OCHF_2$. When formed from the near-thermoneutral peroxy radical–peroxy radical reaction, a minor (10%) channel involving reaction of $CF_3CH(O•)OCHF_2$ with O_2, is also observed:

$$CF_3CH(O•)OCHF_2 + O_2 \rightarrow CF_3C(O)OCHF_2 + HO_2$$

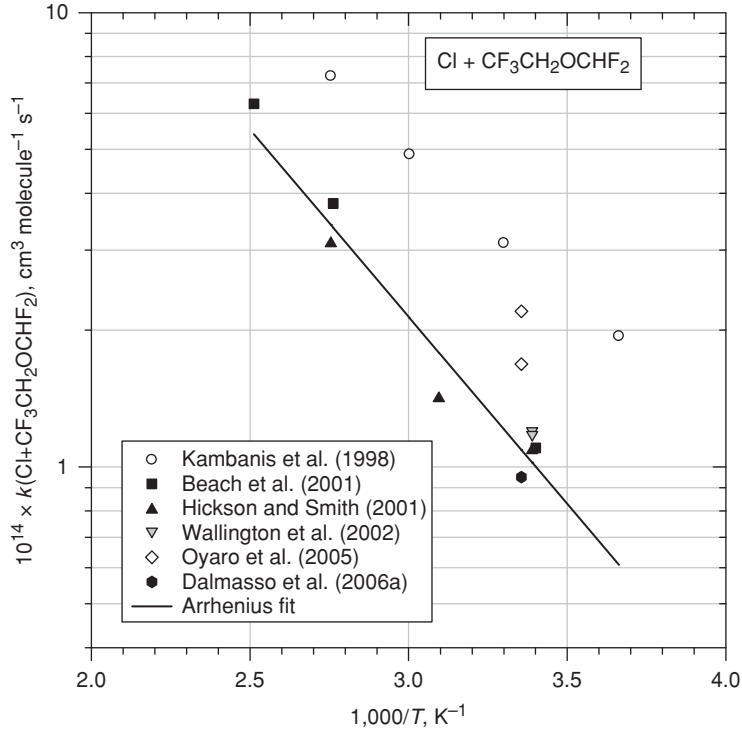

Figure III-G-6. Arrhenius plot of the rate coefficient for the reaction of Cl with $CF_3CH_2OCHF_2$.

III-G-11. 1-(Difluoromethoxy)-1,1,2-trifluoroethane (1,1,2-Trifluoroethyl Difluoromethyl Ether, $CH_2FCF_2OCHF_2$)

III-G-11.1. OH Reaction Kinetics

The reaction of OH with $CH_2FCF_2OCHF_2$ has been studied as a function of temperature by Chen et al. (2003a), using a relative rate method. The data are summarized in table III-G-18 and in figure III-G-4. Two well-studied reference compounds were used, CH_4 and CH_3CCl_3, and the data obtained using these two references were consistent. An Arrhenius fit to the Chen et al. data yields $k = 1.11 \times 10^{-12} \exp(-1{,}588/T)$ cm^3 molecule^{-1} s^{-1}, with $k = 5.4 \times 10^{-15}$ cm^3 molecule^{-1} s^{-1} at 298 K. The uncertainty at 298 K is estimated to be $\pm 20\%$.

III-G-11.2. Summary of the Atmospheric Fate of $CH_2FCF_2OCHF_2$, and the End Products of Its Oxidation

Assuming an average [OH] $\approx 10^6$ molecule cm^{-3} and an average tropospheric temperature of 272 K, the lifetime of $CH_2FCF_2OCHF_2$ in the atmosphere is 10 years. The mechanism of the OH-initiated oxidation of this species has not been studied. However, attack at the CHF_2 group is likely important and would likely lead to two molecules of COF_2 and one molecule of HC(O)F.

Table III-G-18. Rate coefficients ($k = A \times e^{-B/T}$, cm^3 molecule^{-1} s^{-1}) for reaction of OH with $CH_2FCF_2OCHF_2$

$10^{12} \times A$	B (K)	$10^{16} \times k$	T (K)	Technique[a]	Reference	Temperature Range (K)
$1.68^{+1.07}_{-0.65}$	1710 ± 140	30 ± 2	268	RR[b] (CH_4)	Chen et al. (2003a)	268–308
		37 ± 3	278			
		44 ± 3	288			
		54 ± 3	298			
		69 ± 4	308			
		29 ± 2	268	RR[c] (CH_3CCl_3)		
		38 ± 5	278			
		43 ± 2	288			
		57 ± 4	298			
		64 ± 3	308			

[a]Abbreviations used for the techniques are defined in table I-F-3.
[b]Placed on an absolute basis using $k(OH+CH_4) = 1.85 \times 10^{-12} \exp(-1{,}690/T)$ cm^3 molecule^{-1} s^{-1} (Calvert et al., 2008).
[c]Placed on an absolute basis using $k(OH+CH_3CCl_3) = 1.81 \times 10^{-12} \exp(-1{,}543/T)$ cm^3 molecule^{-1} s^{-1} (Calvert et al., 2008).

Table III-G-19. Rate coefficients ($k = A \times e^{-B/T}$, cm^3 molecule^{-1} s^{-1}) for reaction of OH with $CH_3OCF_2CF_3$

$10^{12} \times A$	B (K)	$10^{15} \times k$	T (K)	Technique[a]	Reference	Temperature Range (K)
$1.90^{+0.90}_{-0.61}$	1,510 ± 120	4.78 ± 0.16	250	FP or PLP–LIF	Tokuhashi et al. (1999c)	250–430
		5.19 ± 0.26	250			
		8.19 ± 0.25	273			
		11.0 ± 0.5	298			
		12.0 ± 0.6	298			
		18.2 ± 0.8	331			
		32.5 ± 1.3	375			
		62.9 ± 2.7	430			
		61.5 ± 2.1	430			
		10.7 ± 1.0	298	DF–LIF		

[a]Abbreviations used for the techniques are defined in table I-F-3.

III-G-12. 1,1,1,2,2-Pentafluoro-2-methoxyethane (1,1,2,2,2-Pentafluoroethyl Methyl Ether, $CH_3OCF_2CF_3$)

III-G-12.1. OH Reaction Kinetics

Rate coefficients for the reaction of OH with $CH_3OCF_2CF_3$ have been obtained as a function of temperature by Tokuhashi et al. (1999c), see table III-G-19 and figure III-G-4. These workers report: $k = 1.90 \times 10^{-12} \exp(-1{,}510/T)$ cm^3 molecule^{-1} s^{-1}. This expression gives $k = 1.20 \times 10^{-14}$ cm^3 molecule^{-1} s^{-1} at 298 K, with an estimated uncertainty of ±20%.

Table III-G-20. Rate coefficient (k, cm^3 molecule^{-1} s^{-1}) for reaction of Cl with $CH_3OCF_2CF_3$

$10^{14} \times k$	T (K)	Technique[a]	Reference
10.9 ± 1.4	295	RR[b] (CH_4)	Nohara et al. (2001)

[a]Abbreviations used for the techniques are defined in table I-F-3.
[b]Placed on an absolute basis using $k(Cl + CH_4) = 0.99 \times 10^{-13}$ cm^3 molecule^{-1} s^{-1} (Atkinson et al., 2008).

III-G-12.2. Cl-Atom Reaction Kinetics

Nohara et al. (2001) report $k = 1.1 \times 10^{-13}$ cm^3 molecule^{-1} s^{-1} for the Cl-atom reaction rate coefficient at 295 K. See table III-G-20 for a summary.

III-G-12.3. Summary of the Atmospheric Fate of $CH_3OCF_2CF_3$, and the End Products of Its Oxidation

The atmospheric lifetime for $CH_3OCF_2CF_3$ is 4.3 years, assuming an average [OH] $\approx 10^6$ molecule cm^{-3} and an average tropospheric temperature of 272 K. The data of Nohara et al. (2001) suggest that the formate ester $HC(O)OCF_2CF_3$ is the dominant primary end product.

III-G-13. 1-(Trifluoromethoxy)-1,2,2-trifluoroethane (1,2,2-Trifluoroethyl Trifluoromethyl Ether ($CHF_2CHFOCF_3$)

III-G-13.1. OH Reaction Kinetics

The only data regarding the reaction of OH with $CHF_2CHFOCF_3$ are from Oyaro et al. (2005), who used a relative rate technique. As seen in table III-G-21, there is scatter in their data obtained with multiple reference compounds. Taking the unweighted average of the three determinations gives $k = 6.7 \times 10^{-15}$ cm^3 molecule^{-1} s^{-1} at 298 K. An uncertainty of ±50% is assigned to this value.

Table III-G-21. Rate coefficients (k, cm^3 molecule^{-1} s^{-1}) for reaction of OH with $CHF_2CHFOCF_3$

$10^{15} \times k$	T (K)	Technique[a]	Reference
7.0 ± 1.3	298	RR[b] (CH_3CCl_3)	Oyaro et al. (2005)
5.0 ± 2.5	298	RR[c] (CH_3CN)	
7.9 ± 3.4	298	RR[d] (CHF_2CH_2F)	

[a]Abbreviations used for the techniques are defined in table I-F-3.
[b]Placed on an absolute basis using $k(OH + CH_3CCl_3) = 1.02 \times 10^{-14}$ cm^3 molecule^{-1} s^{-1} (Calvert et al., 2008).
[c]Placed on an absolute basis using $k(OH + CH_3CN) = 2.2 \times 10^{-14}$ cm^3 molecule^{-1} s^{-1} (Atkinson et al., 2006).
[d]Placed on an absolute basis using $k(OH + CHF_2CH_2F) = 1.63 \times 10^{-14}$ cm^3 molecule^{-1} s^{-1} (Calvert et al., 2008).

Table III-G-22. Rate coefficients ($k = A \times e^{-B/T}$, cm^3 $molecule^{-1}$ s^{-1}) for reaction of Cl with $CHF_2CHFOCF_3$

$10^{15} \times k$	T (K)	Technique[a]	Reference
1.3 ± 2.5	298	RR[b] (CH_3CCl_3)	Oyaro et al. (2005)
2 ± 7	298	RR[c] (CHF_2CH_2F)	

[a]Abbreviations used for the techniques are defined in table I-F-3.
[b]Placed on an absolute basis using $k(Cl+CH_3CCl_3) = 8.5 \times 10^{-15}$ cm^3 $molecule^{-1}$ s^{-1} at 298 K (IUPAC, 2008).
[c]Placed on an absolute basis using $k(Cl+ CHF_2CH_2F) = 5.0 \times 10^{-14}$ cm^3 $molecule^{-1}$ s^{-1} at 298 K (Atkinson et al., 2008).

III-G-13.2. Cl-Atom Reaction Kinetics

The only study of this reaction is the relative rate study of Oyaro et al. (2005), conducted at 298 K with two reference compounds. As is shown in table III-G-22, agreement between the two reported values is poor. As the rate coefficient for reaction of Cl with CHF_2CH_2F is not well established and is considerably different than that for $CHF_2CHFOCF_3$, this measurement is deemed less reliable than the measurement made using CH_3CCl_3 as the reference. Thus, the value obtained against CH_3CCl_3, $k = 1.3 \times 10^{-15}$ cm^3 $molecule^{-1}$ s^{-1} is recommended, with an estimated uncertainty of a factor of 2. Further studies of this reaction are warranted.

III-G-13.3. Summary of the Atmospheric Fate of $CHF_2CHFOCF_3$, and the End Products of Its Oxidation

On the basis of the rate coefficient for its reaction with OH at 298 K, $k = 6.7 \times 10^{-15}$ cm^3 $molecule^{-1}$ s^{-1}, the atmospheric lifetime of $CHF_2CHFOCF_3$ is estimated to be ≥ 5 years. The mechanism for the atmospheric oxidation of this species has not been determined. However, abstraction of either of the available H-atoms will likely lead to the same main end products, COF_2 and $FC(O)OCF_3$.

III-G-14. 2-(Difluoromethoxy)-1,1,1,2-tetrafluoroethane [1,2,2,2-Tetrafluoroethyl Difluoromethyl Ether ($CF_3CHFOCHF_2$, Desflurane)]

III-G-14.1. OH Reaction Kinetics

The reaction of OH with $CF_3CHFOCHF_2$ (Desflurane, an inhalational anaesthetic) has been studied at 298 K by Langbein et al. (1999) and Oyaro et al. (2005), see table III-G-23. Agreement between the three data points is fair. An unweighted average value of $k = 5.7 \times 10^{-15}$ cm^3 $molecule^{-1}$ s^{-1} is recommended at 298 K, with an estimated uncertainty of $\pm 50\%$. Further data, particularly at reduced temperature, are required for an accurate assessment of the atmospheric lifetime of this species.

Table III-G-23. Rate coefficients (k, cm^3 molecule^{-1} s^{-1}) for reaction of OH with $CF_3CHFOCHF_2$

$10^{15} \times k$	T (K)	Technique[a]	Reference
4.4 ± 0.8	298	PLP–UV abs.	Langbein et al. (1999)
6.8 ± 1.0	298	R R[b] (CH_3CCl_3)	Oyaro et al. (2005)
5.9 ± 1.4	298	RR[c] (CHF_2CH_2F)	

[a]Abbreviations used for the techniques are defined in table I-F-3.
[b]Placed on an absolute basis using $k(OH+CH_3CCl_3) = 1.02 \times 10^{-14}$ cm^3 molecule^{-1} s^{-1} (Calvert et al., 2008).
[c]Placed on an absolute basis using $k(OH+CHF_2CH_2F) = 1.63 \times 10^{-14}$ cm^3 molecule^{-1} s^{-1} (Calvert et al., 2008).

Table III-G-24. Rate coefficients (k, cm^3 molecule^{-1} s^{-1}) for reaction of Cl with $CF_3CHFOCHF_2$

$10^{15} \times k$	T (K)	Technique[a]	Reference
1.2 ± 2.3	298	RR[b] (CH_3CCl_3)	Oyaro et al. (2005)
2 ± 7	298	RR[c] (CHF_2CH_2F)	
1.12 ± 0.11	296	RR[d] (CF_3CH_2F)	Dalmasso et al. (2006a)

[a]Abbreviations used for the techniques are defined in table I-F-3.
[b]Placed on an absolute basis using $k(Cl+CH_3CCl_3) = 8.5 \times 10^{-15}$cm^3 molecule^{-1} s^{-1} at 298 K (IUPAC, 2008).
[c]Placed on an absolute basis using $k(Cl+ CHF_2CH_2F) = 5.0 \times 10^{-14}$ cm^3 molecule^{-1} s^{-1} at 298 K (Atkinson et al., 2008).
[d]Placed on an absolute basis using $k(Cl+CF_3CH_2F) = 1.4 \times 10^{-15}$ cm^3 molecule^{-1} s^{-1} (Atkinson et al., 2008).

III-G-14.2. Cl-Atom Reaction Kinetics

This reaction has been studied by Oyaro et al. (2005) and Dalmasso et al. (2006a) using relative rate techniques, see table III-G-24. For reasons discussed in section III-G-13.4, the Oyara et al. value obtained with CH_3CCl_3 as the reference species is preferred over their other determination. Combining this measurement with that of Dalmasso et al. gives $k = 1.2 \times 10^{-15}$ cm^3 molecule^{-1} s^{-1} near 298 K, with an estimated uncertainty of ±30%.

III-G-14.3. Summary of the Atmospheric Fate of $CF_3CHFOCHF_2$, and the End Products of Its Oxidation

On the basis of the rate coefficient for its reaction with OH at 298 K, the atmospheric lifetime of $CF_3CHFOCHF_2$ exceeds 5 years. No studies of the atmospheric oxidation mechanism of this species have been conducted.

III-G-15. 1-(Difluoromethoxy)-1,1,2,2-tetrafluoroethane (1,1,2,2-Tetrafluoroethyl Difluoromethyl Ether, $CHF_2OCF_2CHF_2$)

III-G-15.1. OH Reaction Kinetics

The reaction of OH with $CHF_2OCF_2CHF_2$ has been the subject of two relative rate studies (Chen et al., 2005a; Wilson et al., 2007), both conducted as a function

Table III-G-25. Rate coefficients ($k = A \times e^{-B/T}$, cm^3 $molecule^{-1}$ s^{-1}) for reaction of OH with $CHF_2OCF_2CHF_2$

$10^{13} \times A$	B (K)	$10^{15} \times k$	T (K)	Technique[a]	Reference	Temperature Range (K)
7.58 ± 3.30	1,720 ± 130	0.744 ± 0.041	253	RR[b] ($C_2F_5OCH_3$)	Chen et al. (2005a)	253–328
		1.28 ± 0.19	268			
		1.66 ± 0.05	283			
		2.24 ± 0.20	298			
		2.99 ± 0.04	313			
		3.96 ± 0.29	328			
		0.924 ± 0.099	253	RR[c] (n-$C_3F_7OCH_3$)		
		1.35 ± 0.12	268			
		1.67 ± 0.06	283			
		2.42 ± 0.08	298			
		3.12 ± 0.20	313			
		4.07 ± 0.22	328			
7.74[d]	1,652[d]	1.58	266	RR[e] (CF_3CH_2F, HFC-134a)	Wilson et al. (2007)	
		1.92	276			
		2.20	281			
		2.73	293			
		3.12	299			
		3.95	314			
		4.55	321			
		5.42	335			
		6.28	342			
		7.91	361			
		8.90	369			
		11.64	394			
		13.44	406			
7.41[d]	1,634[d]	2.48	287	RR[f] (CH_3CF_3, HFC-143a)		
		3.63	306			
		4.93	327			
		6.72	348			
		10.58	383			
		13.3	407			

[a] Abbreviations used for the techniques are defined in table I-F-3.

[b] Placed on an absolute basis using $k(OH+C_2F_5OCH_3) = 1.90 \times 10^{-12} \exp(-1{,}510/T)$ cm^3 $molecule^{-1}$ s^{-1} (Tokuhashi et al., 1999c).

[c] Placed on an absolute basis using $k(OH+n\text{-}C_3F_7OCH_3) = 2.06 \times 10^{-12} \exp(-1{,}540/T)$ cm^3 $molecule^{-1}$ s^{-1} (Tokuhashi et al., 1999c).

[d] Values obtained from least-squares fit of data obtained using updated reference rate coefficients, and thus differ from those originally reported.

[e] Placed on an absolute basis using $k(OH+CF_3CH_2F) = 1.01 \times 10^{-12} \exp(-1{,}640/T)$ cm^3 $molecule^{-1}$ s^{-1} (Calvert et al., 2008).

[f] Placed on an absolute basis using $k(OH+CF_3CH_3) = 1.06 \times 10^{-12} \exp(-1{,}998/T)$ cm^3 $molecule^{-1}$ s^{-1} (Calvert et al., 2008).

of temperature. See table III-G-25. The data from the two studies, both using multiple reference compounds, are in substantive agreement. Fitting of the combined dataset gives: $k = 1.2 \times 10^{-12} \exp(-1{,}837/T)$ cm^3 $molecule^{-1}$ s^{-1}, yielding $k = 2.6 \times 10^{-15}$ cm^3 $molecule^{-1}$ s^{-1} at 298 K. An uncertainty of ±20% is recommended near 298 K. Data are summarized in table III-G-25 and displayed in figure III-G-7.

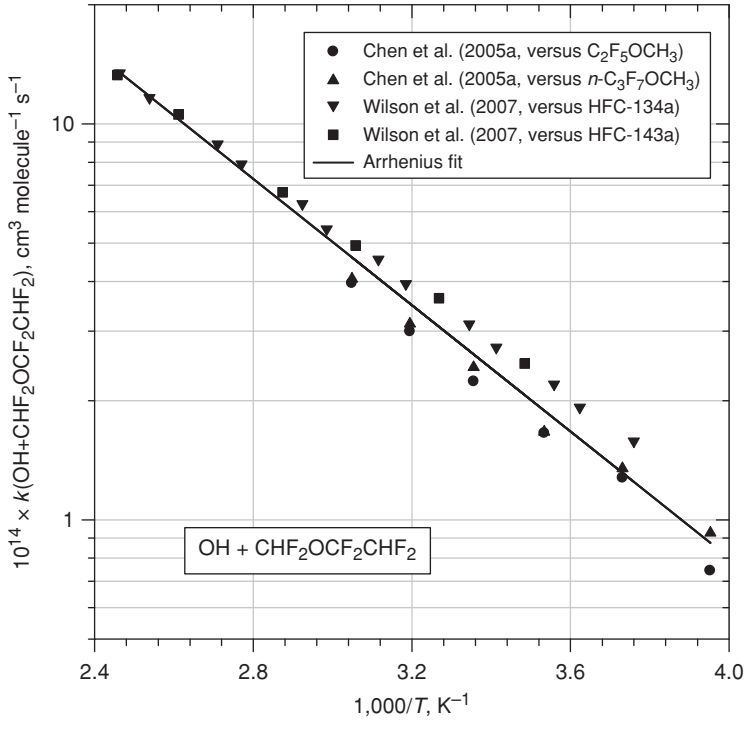

Figure III-G-7. Arrhenius plot of the rate coefficient for the reaction of OH with $CHF_2OCF_2CHF_2$.

III-G-15.2. Summary of the Atmospheric Fate of $CHF_2OCF_2CHF_2$, and the End Products of Its Oxidation

The lifetime of $CHF_2OCF_2CHF_2$ is estimated to be 21 years, assuming tropospheric [OH] $\approx 10^6$ molecule cm^{-3} and an average tropospheric temperature of 272 K. No product studies have been conducted for this species.

III-G-16. 1,1,1,2-Tetrafluoro-2-(trifluoromethoxy)ethane (1,2,2,2-Tetrafluoroethyl Trifluoromethyl Ether, $CF_3CHFOCF_3$, HFE-227ea)

III-G-16.1. OH Reaction Kinetics

Rate coefficients for the reaction of OH with $CF_3CHFOCF_3$ have been obtained by Li et al. (2000b), Takahashi et al. (2002), Tokuhashi et al. (2004), and Oyaro et al. (2005), see table III-G-26 and figure III-G-4. There is satisfactory agreement among the various measurements, with the exception of the data point from Li et al. (2000b), which is significantly higher than the remaining data. The Arrhenius expression from Tokuhashi et al. (2004) is recommended: $k = 4.39 \times 10^{-13} \exp(-1{,}780/T)$ cm^3 $molecule^{-1}$ s^{-1}, with $k = 1.2 \times 10^{-15}$ cm^3 $molecule^{-1}$ s^{-1} at 298 K. The uncertainty at 298 K is estimated to be $\pm 30\%$.

Table III-G-26. Rate coefficients ($k = A \times e^{-B/T}$, cm^3 molecule^{-1} s^{-1}) for reaction of OH with $CF_3CHFOCF_3$

$10^{13} \times A$	B (K)	$10^{16} \times k$	T (K)	Technique[a]	Reference	Temperature Range (K)
		49.8 ± 16.4	298	DF–RF	Li et al. (2000b)	
		13.4 ± 1.1	295	RR[b] (C_2H_4)	Takahashi et al. (2002)	
		14.0 ± 1.6	295	RR[c] (C_2H_2)		
4.39 ± 1.38	1,780 ± 100	3.70 ± 0.31	250	FP or PLP–LIF	Tokuhashi et al. (2004)	250–430
		3.72 ± 0.39	250			
		6.36 ± 0.37	273			
		10.5 ± 0.7	298			
		11.2 ± 0.8	298			
		17.7 ± 1.0	331			
		38.0 ± 2.4	375			
		71.5 ± 5.2	430			
		76.1 ± 4.1	430			
		< 10	298	RR[d] (CHF_2CH_2F)	Oyaro et al. (2005)	

[a]Abbreviations used for the techniques are defined in table I-F-3.
[b]Placed on an absolute basis using $k(OH+C_2H_4) = 7.9 \times 10^{-12}$ cm^3 molecule^{-1} s^{-1} (Atkinson et al., 2006).
[c]Placed on an absolute basis using $k(OH+C_2H_2) = 7.8 \times 10^{-13}$ cm^3 molecule^{-1} s^{-1} (Atkinson et al., 2006).
[d]Placed on an absolute basis using $k(OH+CHF_2CH_2F) = 1.63 \times 10^{-14}$ cm^3 molecule^{-1} s^{-1} (Calvert et al., 2008).

Table III-G-27. Rate coefficients (k, cm^3 molecule^{-1} s^{-1}) for reaction of Cl with $CF_3CHFOCF_3$

$10^{16} \times k$	T (K)	Technique[a]	Reference
300 ± 200	298	RR[b,c] (CH_3F, CH_2F_2)	Li et al. (2000b)
0.46 ± 0.03	295	RR[d] (CF_3CH_3)	Takahashi et al. (2002)
0.60 ± 0.02		RR[e] (CF_2ClCH_3)	
< 30	298	RR[f] (CHF_2CH_2F)	Oyaro et al. (2005)

[a]Abbreviations used for the techniques are defined in table I-F-3.
[b]Placed on an absolute basis using $k(Cl+CH_3F) = 3.5 \times 10^{-13}$ cm^3 molecule^{-1} s^{-1} (Atkinson et al., 2008).
[c]Placed on an absolute basis using $k(Cl+CH_2F_2) = 3.2 \times 10^{-14}$ cm^3 molecule^{-1} s^{-1} (IUPAC, 2008).
[d]Placed on an absolute basis using $k(Cl+CF_3CH_3) = 2.8 \times 10^{-17}$ cm^3 molecule^{-1} s^{-1} (IUPAC, 2008).
[e]Placed on an absolute basis using $k(Cl+CF_2ClCH_3) = 3.8 \times 10^{-16}$ cm^3 molecule^{-1} s^{-1} (Atkinson et al., 2008).
[f]Placed on an absolute basis using $k(Cl+CHF_2CH_2F) = 5.0 \times 10^{-14}$ cm^3 molecule^{-1} s^{-1} (Atkinson et al., 2008).

III-G-16.2. Cl-Atom Reaction Kinetics

The reaction of Cl-atoms with $CF_3CHFOCF_3$ is very slow. Takahashi et al. (2002) obtained $k = 5 \times 10^{-17}$ cm^3 molecule^{-1} s^{-1}, a value that is recommended here. This measurement is consistent with the upper limit reported by Oyaro et al. (2005), $k < 3 \times 10^{-15}$ cm^3 molecule^{-1} s^{-1} at 298 K. The measurement of Li et al. (2000b) is inconsistent with the recommendation. Data are summarized in table III-G-27.

III-G-16.3. Summary of the Atmospheric Fate of $CF_3CHFOCF_3$, and the End Products of Its Oxidation

The atmospheric lifetime of $CF_3CHFOCF_3$ will be very long. Assuming a global average [OH] $\approx 10^6$ molecule cm^{-3} and an average tropospheric temperature of 272 K, a lifetime of 50 years is obtained. Reaction of OH with this species must occur at the CHF site, which will lead to the $CF_3CF(O\bullet)OCF_3$ alkoxy species. The predominant fate of this radical in the atmosphere is decomposition via C—C bond cleavage (Takahashi et al., 2002):

$$CF_3CF(O\bullet)OCF_3 \rightarrow CF_3 + FC(O)OCF_3$$

III-G-17. 1,1,2,2-Tetrafluoro-1-(trifluoromethoxy)ethane (1,1,2,2-Tetrafluoroethyl Trifluoromethyl Ether, $CF_3OCF_2CF_2H$)

III-G-17.1. OH Reaction Kinetics

The reaction of OH with $CF_3OCF_2CF_2H$ has been the subject of two relative rate studies, one at 295 K (Andersen et al., 2005b) and one over the range 269–403 K (Wilson et al., 2007). There is good agreement between the two measurement groups. Fitting of the combined dataset yields: $k = 5.3 \times 10^{-13} \exp(-1{,}655/T)$ cm^3 molecule^{-1} s^{-1}, with $k = 2.1 \times 10^{-15}$ cm^3 molecule^{-1} s^{-1} at 298 K. The uncertainty of the 298 K value is estimated to be ±20%. Details of the measurements are provided in table III-G-28.

III-G-17.2. Cl-Atom Reaction Kinetics

The reaction of Cl-atoms with $CF_3OCF_2CF_2H$ was studied by Andersen et al. (2005b), using a relative rate technique. The average of their two determinations is recommended, $k = 2.5 \times 10^{-16}$ cm^3 molecule^{-1} s^{-1}, with an estimated uncertainty of ±30%. See table III-G-29 for details.

III-G-17.3. Summary of the Atmospheric Fate of $CF_3OCF_2CF_2H$, and the End Products of Its Oxidation

The atmospheric lifetime of $CF_3CF_2OCF_2H$ has been estimated by Andersen et al. (2005b) to be 27 years. This value was obtained by using an estimated activation energy for the OH reaction (obtained from a structure–activity calculation) to extrapolate the OH rate coefficient to 272 K (the tropospheric average temperature). As detailed by Andersen et al. (2005b), the OH-initiated oxidation of $CF_3CF_2OCF_2H$ will proceed via abstraction of the only available H-atom, leading under atmospheric conditions to the formation of three molecules of COF_2 via decomposition of the resultant $CF_3CF_2OCF_2O\bullet$ radical:

$$CF_3CF_2OCF_2O\bullet \rightarrow CF_3CF_2O\bullet + COF_2$$

$$CF_3CF_2O\bullet \rightarrow CF_{3+}COF_2$$

$$CF_3 \rightarrow\rightarrow COF_2$$

Table III-G-28. Rate coefficients ($k = A \times e^{-B/T}$, cm^3 molecule^{-1} s^{-1}) for reaction of OH with $CF_3OCF_2CF_2H$

$10^{13} \times A$	B (K)	$10^{16} \times k$	T (K)	Technique[a]	Reference	Temperature Range (K)
		20.6 ± 1.5	295	RR[b] (C_2H_4)	Andersen et al. (2005b)	
		20.7 ± 1.6	295	RR[c] (C_2H_2)		
5.24 ± 0.29	1,648 ± 18	11.8	269	RR[d] (CF_3CHF_2, HFC-125)	Wilson et al. (2007)	269–406
		13.7	276			
		17.7	288			
		20.9	298			
		25.3	309			
		30.9	322			
		36.3	332			
		42.3	343			
		51.3	358			
		59.6	370			
		71.0	386			
		87.8	406			
		11.2	273	RR[e] (CF_3CHFCF_3, HFC-227ea)		
		17.9	294			
		27.4	316			
		39.8	338			
		58.6	365			
		86.8	397			

[a]Abbreviations used for the techniques are defined in table I-F-3.
[b]Placed on an absolute basis using $k(OH+C_2H_4) = 7.9 \times 10^{-12}$ cm^3 molecule^{-1} s^{-1} (Atkinson et al., 2008).
[c]Placed on an absolute basis using $k(OH+C_2H_2) = 7.8 \times 10^{-13}$ cm^3 molecule^{-1} s^{-1} (Atkinson et al., 2008).
[d]Placed on an absolute basis using $k(OH+HFC\text{-}125) = 5.1 \times 10^{-13} \exp(-1{,}666/T)$ cm^3 molecule^{-1} s^{-1} (Calvert et al., 2008).
[e]Placed on an absolute basis using $k(OH+HFC\text{-}227ea) = 6.55 \times 10^{-13} \exp(-1{,}809/T)$ cm^3 molecule^{-1} s^{-1} (Calvert et al., 2008).

Table III-G-29. Rate coefficients (k, cm^3 molecule^{-1} s^{-1}) for reaction of Cl with $CF_3OCF_2CF_2H$

$10^{16} \times k$	T (K)	Technique[a]	Reference
2.53 ± 0.30	296	RR[b] (C_2F_5H)	Andersen et al. (2005b)
2.52 ± 0.32	296	RR[c] ($CHClF_2$)	

[a]Abbreviations used for the techniques are defined in table I-F-3.
[b]Placed on an absolute basis using $k(Cl+C_2F_5H) = 2.5 \times 10^{-16}$ cm^3 molecule^{-1} s^{-1} (Atkinson et al., 2008).
[c]Placed on an absolute basis using $k(Cl+CHClF_2) = 1.6 \times 10^{-15}$ cm^3 molecule^{-1} s^{-1} (Atkinson et al., 2008).

In the chamber studies (Andersen et al., 2005b), where elevated levels of NO were present, some production of $CF_3C(O)F$ was observed (at the expense of COF_2):

$$CF_3CF_2O\bullet + NO \rightarrow CF_3C(O)F + FNO$$

III-G-18. 2,2,3,4,4-Pentafluorooxetane and Perfluorooxetane

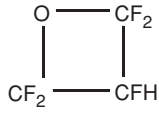

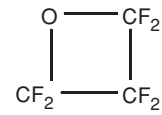

III-G-18.1. OH Reaction Kinetics

Rate coefficients for reaction of OH with *cyclo*-(-CF_2CHFCF_2O-) and *cyclo* (-$CF_2CF_2CF_2O$-) have been reported by Zhang et al. (1992), see table III-G-30. Their value for *cyclo*(-CF_2CHFCF_2O-), $k = 2.5 \times 10^{-15}$ cm^3 molecule^{-1} s^{-1} at 296 K, should be treated as an upper limit, given that rate coefficients reported by Zhang et al. for other compounds were considerably higher than later measurements. An upper limit was reported for *cyclo*(-$CF_2CF_2CF_2O$-), $k < 2 \times 10^{-16}$ cm^3 molecule^{-1} s^{-1} at 296 K (Zhang et al., 1992).

III-G-18.2. Summary of the Atmospheric Fate cyclo(-CF_2CHFCF_2O-) and cyclo(-$CF_2CF_2CF_2O$-), and the End Products of Their Oxidation

The atmospheric lifetimes for *cyclo*(-CF_2CHFCF_2O-) and *cyclo*(-$CF_2CF_2CF_2O$-) are greater than 12 years and greater than 150 years, respectively. No end product studies have been conducted for these species.

III-G-19. 1-Ethoxy-1,1,2,2-tetrafluoroethane
(1,1,2,2-Tetrafluoroethyl Ethyl Ether, $CH_3CH_2OCF_2CF_2H$)

III-G-19.1. OH Reaction Kinetics

Tokuhashi et al. (1999b) conducted a careful study of the reaction of OH with $CH_3CH_2OCF_2CF_2H$. Their data are recommended: $k = 2.57 \times 10^{-12} \exp(-730/T)$ cm^3 molecule^{-1} s^{-1}, with $k = 2.2 \times 10^{-13}$ cm^3 molecule^{-1} s^{-1} at 298 K and an estimated uncertainty at 298 K of ±20%. As with other compounds, the 298 K value of Heathfield et al. (1998) is considerably larger, likely due to the presence of reactive

Table III-G-30. Rate coefficients (k, cm^3 molecule^{-1} s^{-1}) for reaction of OH with *cyclo*(-CF_2CHFCF_2O-) and *cyclo*(-C_3F_6O-)

$10^{16} \times k$	T (K)	Technique[a]	Reference
OH + *cyclo*(-CF_2CHFCF_2O-)			
25.1 ± 3.5	296	FP–RF	Zhang et al. (2002)
24.0 ± 3.0	296		
OH + *cyclo*(-$CF_2CF_2CF_2O$-)			
< 2	296	FP–RF	Zhang et al. (2002)

[a]Abbreviations used for the techniques are defined in table I-F-3.

Table III-G-31. Rate coefficients ($k = A \times e^{-B/T}$, cm^3 $molecule^{-1}$ s^{-1}) for reaction of OH with $CH_3CH_2OCF_2CF_2H$

$10^{12} \times A$	B (K)	$10^{13} \times k$	T (K)	Technique[a]	Reference	Temperature Range (K)
		4.33 ± 0.69	298	PR–UV abs.	Heathfield et al. (1998)	
2.57 ± 0.44	730 ± 50	1.46 ± 0.03	250	FP or PLP–LIF	Tokuhashi et al. (1999b)	250–430
		1.45 ± 0.04	250			
		1.77 ± 0.05	273			
		2.19 ± 0.05	298			
		2.11 ± 0.08	298			
		2.69 ± 0.11	331			
		3.65 ± 0.12	375			
		4.96 ± 0.16	430			
		4.88 ± 0.13	430			
		2.23 ± 0.12	298	DF–LIF		

[a]Abbreviations used for the techniques are defined in table I-F-3.

impurities in their samples. The available data are summarized in table III-G-31, and are plotted in figure III-G-8.

III-G-19.2. Cl-Atom Reaction Kinetics

The reaction of Cl-atoms with $CH_3CH_2OCF_2CF_2H$ has been studied by Papadimitriou et al. (2004), see table III-G-32. Their data are consistent with a temperature-independent value of $k = 1.8 \times 10^{-12}$ cm^3 $molecule^{-1}$ s^{-1}.

III-G-19.3. Summary of the Atmospheric Fate of $CH_3CH_2OCF_2CF_2H$, and the End Products of Its Oxidation

The atmospheric lifetime of $CH_3CH_2OCF_2CF_2H$ is about 2 months, for [OH] $\approx 10^6$ molecule cm^{-3}. End products of its atmospheric oxidation have not been determined. However, the dominant site for OH attack will likely be at the CH_2 group, which will probably lead to formation of the formate ester, $HC(O)OCF_2CF_2H$ (with formaldehyde as a co-product) and/or the acetate ester, $CH_3C(O)OCF_2CF_2H$.

III-G-20. 1,1,2,2-Tetrafluoro-3-methoxypropane (2,2,3,3-Tetrafluoro-*n*-propyl Methyl Ether, $CHF_2CF_2CH_2OCH_3$)

III-G-20.1. OH Reaction Kinetics

The data of Oyaro et al. (2004), obtained via a relative rate method, lead to $k = 9.3 \times 10^{-13}$ cm^3 $molecule^{-1}$ s^{-1} for the rate coefficient for reaction of OH

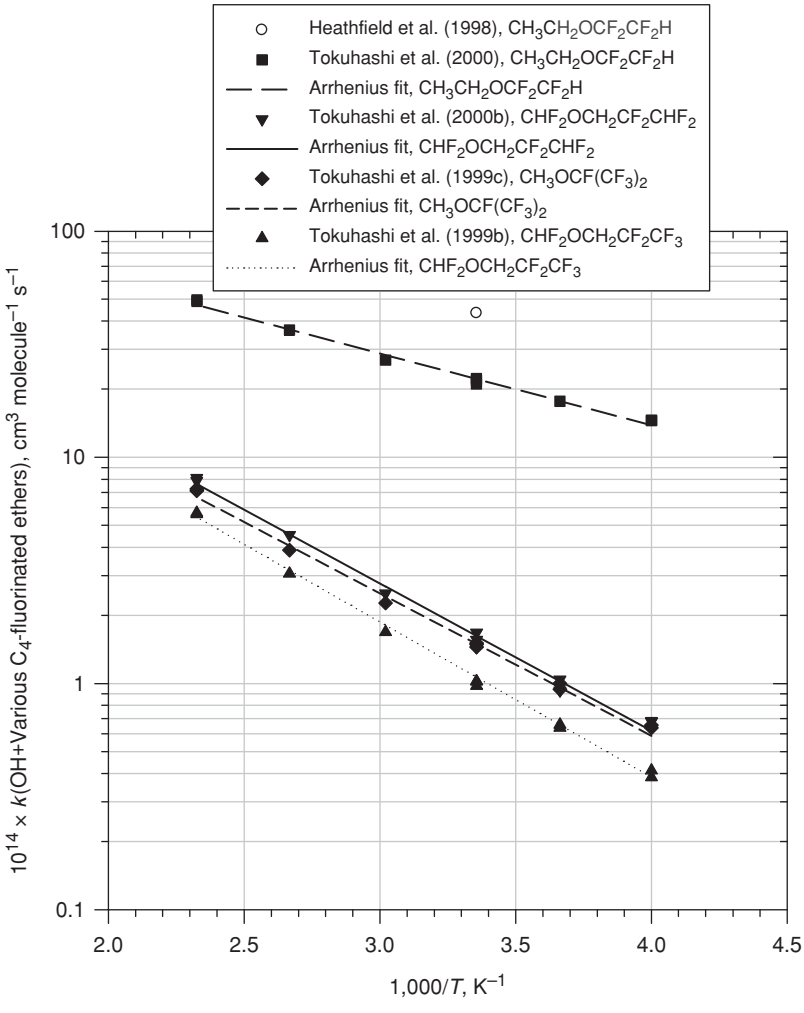

Figure III-G-8. Arrhenius plot of the rate coefficient for the reaction of OH with various four-carbon fluorinated ethers.

Table III-G-32. Rate coefficients ($k = A \times e^{-B/T}$, cm^3 $molecule^{-1}$ s^{-1}) for reaction of Cl with $CH_3CH_2OCF_2CF_2H$

$10^{12} \times A$	B (K)	$10^{12} \times k$	T (K)	Technique[a]	Reference	Temperature Range (K)
1.99 ± 0.12	36 ± 33	1.75 ± 0.22	273	VLPR	Papadimitriou et al. (2004)	273–363
		1.75 ± 0.21	303			
		1.80 ± 0.22	333			
		1.80 ± 0.15	363			

[a]Abbreviations used for the techniques are defined in table I-F-3.

Table III-G-33. Rate coefficients (k, cm^3 molecule^{-1} s^{-1}) for reaction of OH with $CHF_2CF_2CH_2OCH_3$

$10^{13} \times k$	T (K)	Technique[a]	Reference
9.1 ± 0.5	298	RR[b] ($CF_3CH_2OCH_3$)	Oyaro et al. (2004)
9.4 ± 1.6	298	RR[c] ($CHCl_3$)	

[a]Abbreviations used for the techniques are defined in table I-F-3.
[b]Placed on an absolute basis using $k(OH+CF_3CH_2OCH_3) = 5.9 \times 10^{-13}$ cm^3 molecule^{-1} s^{-1} (this book, section III-G-7.1).
[c]Placed on an absolute basis using $k(OH+CHCl_3) = 9.6 \times 10^{-14}$ cm^3 molecule^{-1} s^{-1} (Calvert et al., 2008).

Table III-G-34. Rate coefficients (k, cm^3 molecule^{-1} s^{-1}) for reaction of Cl with $CHF_2CF_2CH_2OCH_3$

$10^{11} \times k$	T (K)	Technique[a]	Reference
2.41 ± 0.15	298	RR[b] ($CF_3CH_2OCH_3$)	Oyaro et al. (2004)

[a]Abbreviations used for the techniques are defined in table I-F-3.
[b]Placed on an absolute basis using $k(Cl+CF_3CH_2OCH_3) = 2.1 \times 10^{-11}$ cm^3 molecule^{-1} s^{-1} at 298 K (this book, section III-G-7.2).

with $CHF_2CF_2CH_2OCH_3$ at 298 K. Given the lack of corroborative measurements, an uncertainty of ±35% is assigned. Details of the measurements are provided in table III-G-33.

III-G-20.2. Cl-Atom Reaction Kinetics

The relative rate study of Oyaro et al. (2004) leads to $k = 2.4 \times 10^{-11}$ cm^3 molecule^{-1} s^{-1}, see table III-G-34. Given the lack of corroborative measurements, an uncertainty of ±50% is assigned.

III-G-20.3. Summary of the Atmospheric Fate of $CHF_2CF_2CH_2OCH_3$, and the End Products of Its Oxidation

The atmospheric lifetime of $CHF_2CF_2CH_2OCH_3$ is about 2 weeks. Oyaro et al. (2004) identified two products in the Cl-atom-initiated oxidation of this species, $CHF_2CF_2C(O)OCH_3$ (major) and $CHF_2CF_2CH_2OCHO$ (minor). These species are formed from the abstraction at the CH_2 group and CH_3 group, respectively, followed by reaction of the resulting alkoxy radicals with O_2.

III-G-21. 1,1,1,2,2-Pentafluoro-3-methoxypropane (Methyl 2,2,3,3,3-pentafluoro-*n*-propyl Ether, $CF_3CF_2CH_2OCH_3$)

III-G-21.1. OH Reaction Kinetics

A 298 K rate coefficient, $k = 6.8 \times 10^{-13}$ cm^3 molecule^{-1} s^{-1}, for the reaction of OH with $CF_3CF_2CH_2OCH_3$ is derived from the relative rate study of Oyaro et al. (2004).

Table III-G-35. Rate coefficient (k, cm^3 molecule^{-1} s^{-1}) for reaction of OH with $CF_3CF_2CH_2OCH_3$

$10^{13} \times k$	T (K)	Technique[a]	Reference
6.83 ± 0.35	298	RR[b] ($CF_3CH_2OCH_3$)	Oyaro et al. (2004)

[a]Abbreviations used for the techniques are defined in table I-F-3.
[b]Placed on an absolute basis using $k(OH+CF_3CH_2OCH_3) = 5.9\times10^{-13}$ cm^3 molecule^{-1} s^{-1} (this book, section III-G-7.1).

Table III-G-36. Rate coefficient (k, cm^3 molecule^{-1} s^{-1}) for reaction of Cl with $CF_3CF_2CH_2OCH_3$

$10^{11} \times k$	T (K)	Technique[a]	Reference
4.2 ± 0.8	298	RR[b] (CH_3CH_2OH)	Oyaro et al. (2004)

[a]Abbreviations used for the techniques are defined in table I-F-3.
[b]Placed on an absolute basis using $k(Cl+CH_3CH_2OH) = 10.0 \times 10^{-11}$ cm^3 molecule^{-1} s^{-1} at 298 K (Atkinson et al., 2006).

Given the lack of corroborative measurements, an uncertainty of ±35% is assigned. Details are provided in table III-G-35.

III-G-21.2. Cl-Atom Reaction Kinetics

The relative rate study of Oyaro et al. (2004) leads to $k = 4.2 \times 10^{-11}$ cm^3 molecule^{-1} s^{-1}, see table III-G-36.

III-G-21.3. Summary of the Atmospheric Fate of $CF_3CF_2CH_2OCH_3$, and the End Products of Its Oxidation

The atmospheric lifetime for $CF_3CF_2CH_2OCH_3$ is estimated to be about 17 days. As for $CF_2HCF_2CH_2OCH_3$, Oyaro et al. (2004) observed the formation of two esters in the Cl-atom-initiated oxidation of this species. The major product, $CF_3CF_2C(O)OCH_3$ is obtained following Cl-atom attack at the CH_2 group, while the minor product $CF_3CF_2CH_2OCHO$ is obtained following attack at the CH_3 group.

III-G-22. 1,1,1,3,3,3-Hexafluoro-2-methoxypropane (Methyl 1,1,1,3,3,3-hexafluoro-2-propyl Ether, $CH_3OCH(CF_3)_2$)

III-G-22.1. OH Reaction Kinetics

The rate coefficient for reaction of OH with $CH_3OCH(CF_3)_2$ has been the subject of two relative rate studies (Oyaro et al., 2004; Chen et al., 2005). As seen in table III-G-37, the studies differ by a factor of 2 near 298 K, despite the fact that a common reference reaction was used. Thus, no recommendation can be made at this time.

Table III-G-37. Rate coefficients ($k = A \times e^{-B/T}$, cm^3 molecule^{-1} s^{-1}) for reaction of OH with $CH_3OCH(CF_3)_2$

$10^{12} \times A$	B (K)	$10^{14} \times k$	T (K)	Technique[a]	Reference	Temperature Range (K)
		8.2 ± 1.0	298	RR[b] (n-$C_4F_9OCH_2CH_3$)	Oyaro et al. (2004)	
		12.8 ± 2.0	298	RR[c] (CH_2Cl_2)		
1.46[d]	544[d]	18.1 ± 1.7	253	RR[e] (C_2H_6)	Chen et al. (2005b)	253–328
		19.0 ± 1.1	268			
		21.7 ± 0.6	283			
		24.1 ± 0.9	298			
		25.0 ± 0.4	313			
		27.8 ± 2.0	328			
		16.5 ± 1.4	253	RR[c] (CH_2Cl_2)		
		17.9 ± 1.3	268			
		21.3 ± 0.7	283			
		23.9 ± 1.3	298			
		25.0 ± 0.4	313			
		28 ± 0.7	328			

[a]Abbreviations used for the techniques are defined in table I-F-3.
[b]Placed on an absolute basis using $k(OH+n\text{-}C_4F_9OCH_2CH_3) = 0.65 \times 10^{-13}$ cm^3 molecule^{-1} s^{-1} (this book, section III-G-43.1).
[c]Placed on an absolute basis using $k(OH+CH_2Cl_2) = 1.97 \times 10^{-12} \exp(-877/T)$ cm^3 molecule^{-1} s^{-1} (Calvert et al., 2008).
[d]Values obtained from least-squares fit of data obtained using updated reference rate coefficients, and thus differ from those originally reported.
[e]Placed on an absolute basis using $k(OH+C_2H_6) = 8.6 \times 10^{-12} \exp(-1{,}047/T)$ cm^3 molecule^{-1} s^{-1} (Calvert et al., 2008).

Table III-G-38. Rate coefficients ($k = A \times e^{-B/T}$, cm^3 molecule^{-1} s^{-1}) for reaction of Cl with $CH_3OCH(CF_3)_2$

$10^{12} \times k$	T (K)	Technique[a]	Reference
8.3 ± 1.8	298	RR[b] (CH_3OH)	Oyaro et al. (2004)
8.9 ± 2.0	298	RR[c] (CH_3CH_2OH)	

[a]Abbreviations used for the techniques are defined in table I-F-3.
[b]Placed on an absolute basis using $k(Cl+CH_3OH) = 5.5 \times 10^{-11}$ cm^3 molecule^{-1} s^{-1} at 298 K (Atkinson et al., 2006).
[c]Placed on an absolute basis using $k(Cl+CH_3CH_2OH) = 10.0 \times 10^{-11}$ cm^3 molecule^{-1} s^{-1} at 298 K (Atkinson et al., 2006).

III-G-22.2. Cl-Atom Reaction Kinetics

Oyaro et al. (2004) report a value of $k = 8.6 \times 10^{-12}$ cm^3 molecule^{-1} s^{-1} for the rate coefficient for reaction of Cl-atoms with $CH_3OCH(CF_3)_2$, see table III-G-38.

III-G-22.3. Summary of the Atmospheric Fate of $CH_3OCH(CF_3)_2$, and the End Products of Its Oxidation

The atmospheric lifetime for this species is not well established, given the discrepancy in the OH rate coefficient data noted above, but likely is on the order of 1–2 months. Chen et al. (2005b) studied the OH-initiated oxidation of $CH_3OCH(CF_3)_2$,

and found three major primary products, $HC(O)OCH(CF_3)_2$ ($66 \pm 11\%$ molar yield), $CF_3C(O)OCH_3$ ($33 \pm 2\%$), and COF_2 ($22 \pm 2\%$). The formate ester $HC(O)OCH(CF_3)_2$ is the logical end product obtained from OH abstraction at the CH_3 group, while $CF_3C(O)OCH_3$ and COF_2 are co-products of OH attack at the CH group in the parent species. Oyaro et al. (2004) carried out a brief study of the Cl-atom-initiated oxidation of $CH_3OCH(CF_3)_2$ and identified the presence of the two ester products, $CF_3C(O)OCH_3$ and $HC(O)OCH(CF_3)_2$. They report $CF_3C(O)OCH_3$ as the major product, but this is based on uncalibrated mass spectrometer signals.

III-G-23. 1,1,1,2,3,3-Hexafluoro-3-methoxypropane (Methyl 1,1,2,3,3,3-hexafluoro-*n*-propyl Ether, $CF_3CHFCF_2OCH_3$)

III-G-23.1. OH Reaction Kinetics

The only study of the reaction of OH with $CF_3CHFCF_2OCH_3$ is a relative rate study by Nolan et al. (1999), $k = 2.1 \times 10^{-14}$ cm^3 molecule^{-1} s^{-1}. Note, however, that these data appear in a Eurotrac Report, and the reference compound(s) and reference rate coefficients used were not specified. However, we also note that other data published by Nolan et al. in this report agree favorably with literature data. Furthermore, we note that methyl perfluoroalkyl ethers (e.g., CF_3OCH_3, $C_2F_5OCH_3$, $C_3F_7OCH_3$) react with OH with rate coefficients of approximately 1.2×10^{-14} cm^3 molecule^{-1} s^{-1} at 298 K. Given the additional CHF reaction site in $CF_3CHFCF_2OCH_3$, and that the CF_3CHFCF_2 is likely less deactivating than a perfluoroalkyl group, the value obtained by Nolan et al. (i.e., similar to, but somewhat greater than methyl perfluoroalkyl ethers), is reasonable. Given the paucity of data, and the lack of detail presented in the Nolan et al. report, an uncertainty of a factor of 2 is assigned to their value.

III-G-23.2. Cl-Atom Reaction Kinetics

The reaction of Cl with $CF_3CHFCF_2OCH_3$ has been studied by Papadimitriou et al. (2004). They report: $k = 8.7 \times 10^{-12} \exp(-1{,}112/T)$ cm^3 molecule^{-1} s^{-1}, with $k = 2.1 \times 10^{-13}$ cm^3 molecule^{-1} s^{-1} at 298 K. The data are summarized in table III-G-39.

III-G-23.3. Summary of the Atmospheric Fate of $CF_3CHFCF_2OCH_3$, and the End Products of Its Oxidation

Using the 298 K OH rate coefficient estimated by Nolan et al. (1999), an assumed temperature dependence similar to that for $CH_3OCF_2CF_3$ ($E/R = 1{,}510$ K), an average tropospheric temperature of 272 K, and a diurnally average [OH] = 10^6 molecule cm^{-3}, a qualitative estimate of 2.4 years can be obtained for the tropospheric lifetime of $CF_3CHFCF_2OCH_3$.

End products of its oxidation by OH have not been determined in the laboratory. However, OH reaction will likely occur predominantly at the CH_3 group, leading to the formate ester, $HC(O)OCF_2CHFCF_3$.

Table III-G-39. Rate coefficients ($k = A \times e^{-B/T}$, cm^3 $molecule^{-1}$ s^{-1}) for reaction of OH and Cl with $CF_3CHFCF_2OCH_3$

$10^{12} \times A$	B (K)	$10^{13} \times k$	T (K)	Technique[a]	Reference	Temperature Range (K)
OH + $CF_3CHFCF_2OCH_3$						
		0.21 ± .013	298	RR[b]	Nolan et al. (1999)	
Cl + $CF_3CHFCF_2OCH_3$						
8.72 ± 2.93	1,112 ± 186	1.46 ± 0.18	273	VLPR	Papadimitriou et al. (2004)	273–363
		2.31 ± 0.41	303			
		3.23 ± 0.52	333			
		3.91 ± 0.62	363			

[a]Abbreviations used for the techniques are defined in table I-F-3.
[b]Reference compound not specified.

III-G-24. 1,1,1-Trifluoro-2-(2,2,2-trifluoroethoxy)ethane [bis(2,2,2-Ttrifluoroethyl)ether, $CF_3CH_2OCH_2CF_3$]

III-G-24.1. OH Reaction Kinetics

There are four studies of the rate coefficient for reaction of OH radicals with $CF_3CH_2OCH_2CF_3$ (O'Sullivan et al., 1997; Orkin et al., 1999; Oyaro et al., 2004; Wilson et al., 2007); see table III-G-40 for a summary of the available data. The results from the relative rate study of O'Sullivan falls significantly below the remaining measurements, and are not considered further. Fitting of the remaining data yields: $k = 1.7 \times 10^{-12} \exp(-751/T)$ cm^3 $molecule^{-1}$ s^{-1}, with $k = 1.35 \times 10^{-13}$ cm^3 $molecule^{-1}$ s^{-1} at 298 K. The uncertainty at 298 K is estimated to be ±20%.

III-G-24.2. Cl-Atom Reaction Kinetics

The measurements of Kambanis et al. (1998) fall significantly below the data from both Wallington et al. (1998b) and Oyaro et al. (2004). Given discrepancies with other data from the VLPR technique of Kambanis et al. (1998), the data from these latter two studies are preferred, and a rate coefficient of $k = 7.0 \times 10^{-13}$ cm^3 $molecule^{-1}$ s^{-1} is recommended at 298 K. The available data are summarized in table III-G-41.

III-G-24.3. Summary of the Atmospheric Fate of $CF_3CH_2OCH_2CF_3$, and the End Products of Its Oxidation

The atmospheric lifetime for $CF_3CH_2OCH_2CF_3$ is estimated to be about 90 days, for average tropospheric [OH] $\approx 10^6$ molecule cm^{-3}. The Cl-atom-initiated oxidation of this species has been studied by Wallington et al. (1998b), O'Sullivan et al. (2001), and Oyaro et al. (2004). The major product (yield > 85%) is the formate ester, $HC(O)OCH_2CF_3$ while $CF_3C(O)OCH_2CF_3$ was reported by O'Sullivan et al. and Oyaro et al. as a minor product. Reaction must occur via abstraction at the identical CH_2 groups, leading to the $CF_3CH(O\bullet)OCH_2CF_3$ alkoxy species. The dominant fate of this alkoxy radical is thus decomposition via C—C bond rupture (leading to the formate ester), while its reaction with O_2 is of minor significance.

Table III-G-40. Rate coefficients ($k = A \times e^{-B/T}$, cm^3 molecule^{-1} s^{-1}) for reaction of OH with $CF_3CH_2OCH_2CF_3$

$10^{12} \times A$	B (K)	$10^{14} \times k$	T (K)	Technique[a]	Reference	Temperature Range (K)
		10.1 ± 1.5		RR[b]	O'Sullivan et al. (1997)	
$2.32^{+0.46}_{-0.41}$	790 ± 47	13.5 ± 0.9	277	FP–RF	Orkin et al. (1999)	277–370
		16.3 ± 0.3	298			
		19.3 ± 1.7	323			
		23.8 ± 1.9	349			
		27.7 ± 1.2	370			
		14.5 ± 2.3	298	RR[c] ($CHCl_3$)	Oyaro et al. (2004)	
1.67[d]	759[d]	10.4	268	RR[e] (CH_3CHF_2, HFC-152a)	Wilson et al. (2007)	268–409
		10.5	279			
		12.5	289			
		12.7	299			
		14.3	312			
		15.7	324			
		18.8	339			
		19.7	354			
		22.1	369			
		24.7	399			
		25.9	409			
1.70[d]	774[d]	10.0	275	RR[f] (C_2H_5F, HFC-161)		
		11.0	283			
		13.6	307			
		18.8	347			
		22.4	383			
		24.9	407			

[a] Abbreviations used for the techniques are defined in table I-F-3.
[b] Value quoted in Orkin et al. (1999); reference reaction not reported.
[c] Placed on an absolute basis using $k(OH+CHCl_3) = 9.6 \times 10^{-14}$ cm^3 molecule^{-1} s^{-1} (Calvert et al., 2008).
[d] Values obtained from least-squares fit of data obtained using updated reference rate coefficients, and thus differ from those originally reported.
[e] Placed on an absolute basis using $k(OH+HFC\text{-}152a) = 1.21 \times 10^{-12} \exp(-1{,}055/T)$ cm^3 molecule^{-1} s^{-1} (Calvert et al., 2008).
[f] Placed on an absolute basis using $k(OH+HFC\text{-}161) = 2.62 \times 10^{-12} \exp(-738/T)$ cm^3 molecule^{-1} s^{-1} (Calvert et al., 2008).

III-G-25. 3-(Difluoromethoxy)-1,1,2,2-tetrafluoropropane (2,2,3,3-Tetrafluoro-*n*-propyl Difluoromethyl Ether, $CHF_2OCH_2CF_2CHF_2$)

III-G-25.1. OH Reaction Kinetics

The rate coefficient for reaction of OH with $CHF_2OCH_2CF_2CHF_2$ has been studied by Tokuhashi et al. (2000b), using a combination of flash photolysis and discharge flow techniques. Great care was taken in sample purification. The measurements are summarized in table III-G-42 and displayed in figure III-G-8, and yield: $k = 2.49 \times 10^{-12} \exp(-1{,}500/T)$ cm^3 molecule^{-1} s^{-1}. This expression gives $k = 1.62 \times 10^{-14}$ cm^3 molecule^{-1} s^{-1} at 298 K, with an estimated uncertainty of $\pm 20\%$.

Table III-G-41. Rate coefficients ($k = A \times e^{-B/T}$, cm^3 $molecule^{-1}$ s^{-1}) for reaction of Cl with $CF_3CH_2OCH_2CF_3$

$10^{12} \times A$	B (K)	$10^{14} \times k$	T (K)	Technique[a]	Reference	Temperature Range (K)
4.03 ± 0.87	680 ± 121	33.2 ± 2.3	273	VLPR	Kambanis et al. (1998)	273–363
		44.0 ± 3.5	303			
		51.2 ± 2.5	333			
		62.9 ± 4.2	363			
		67 ± 8	295	RR[b] (CH_3Cl)	Wallington et al. (1998b)	
		72 ± 8	295	RR[c] (CH_3OCHO)		
		76 ± 23	298	RR[d] ($CHCl_3$)	Oyaro et al. (2004)	
		64 ± 32	298	RR[e] (CH_2Cl_2)		

[a]Abbreviations used for the techniques are defined in table I-F-3.
[b]Placed on an absolute basis using $k(Cl+CH_3Cl) = 4.9 \times 10^{-13}$ cm^3 $molecule^{-1}$ s^{-1} (Atkinson et al., 2008).
[c]Placed on an absolute basis using $k(Cl+CH_3OCHO) = 1.4 \times 10^{-12}$ cm^3 $molecule^{-1}$ s^{-1} (Wallington et al., 1993b).
[d]Placed on an absolute basis using $k(Cl+CHCl_3) = 1.1 \times 10^{-13}$ cm^3 $molecule^{-1}$ s^{-1} (Atkinson et al., 2008).
[e]Placed on an absolute basis using $k(Cl+CH_2Cl_2) = 3.4 \times 10^{-13}$ cm^3 $molecule^{-1}$ s^{-1} (Atkinson et al., 2008).

Table III-G-42. Rate coefficients ($k = A \times e^{-B/T}$, cm^3 $molecule^{-1}$ s^{-1}) for reaction of OH with $CHF_2OCH_2CF_2CHF_2$

$10^{12} \times A$	B (K)	$10^{15} \times k$	T (K)	Technique[a]	Reference	Temperature Range (K)
2.49	1,500 ± 170	6.82 ± 0.75	250	FP or PLP–LIF	Tokuhashi et al. (2000b)	250–430
		6.77 ± 0.72	250			
		9.32 ± 1.1	273			
		10.4 ± 1.1	273			
		14.5 ± 1.6	298			
		15.6 ± 1.7	298			
		25.0 ± 2.6	331			
		45.3 ± 4.8	375			
		81.1 ± 8.4	430			
		78.7 ± 8.1	430			
		16.8 ± 2.2	298	DF–LIF		

[a]Abbreviations used for the techniques are defined in table I-F-3.

III-G-25.2. Summary of the Atmospheric Fate of $CHF_2OCH_2CF_2CHF_2$, and the End Products of Its Oxidation

On the basis of the OH rate coefficient measurement from Tokuhashi et al. (2000b), the atmospheric lifetime for $CHF_2OCH_2CF_2CHF_2$ is estimated to be 3.2 years. No studies of the OH-initiated oxidation mechanism have been carried out. However, OH attack at the CH_2 group is likely important, leading to the formation of the $CHF_2OCH(O\bullet)CF_2CHF_2$ alkoxy radical. Possible end products include $CHF_2OC(=O)CF_2CHF_2$ (from reaction of the alkoxy with O_2) and $CHF_2OCH=O$ (from decomposition of the alkoxy by C—C bond rupture). The CF_2CHF_2 fragment

formed in the bond rupture process will likely generate two molecules of COF_2, as co-products of the $CHF_2OCH{=}O$.

III-G-26. 1,1,1,3,3,3-Hexafluoro-2-(fluoromethoxy)propane [1,1,1,3,3,3-Hexafluoro-2-propyl Fluoromethyl Ether, $CH_2FOCH(CF_3)_2$, Sevoflurane]

III-G-26.1. OH Reaction Kinetics

The species $CH_2FOCH(CF_3)_2$, commonly referred to as Sevoflurane, is a widely used inhalational anaesthetic. The two measurements of the rate coefficient for its reaction with OH (Brown et al., 1989a, 1990; Langbein et al., 1999) are in poor agreement, see table III-G-43. Given that the measurements of Brown et al. (1989a, 1990) for some other species tend to be high, the measurement of Langbein et al. is preferred: $k = 2.7 \times 10^{-14}$ cm^3 molecule^{-1} s^{-1} at 298 K. An uncertainty of $\pm 50\%$ is assigned, and corroborative measurements are required.

III-G-26.2. Summary of the Atmospheric Fate of $CH_2FOCH(CF_3)_2$, and the End Products of Its Oxidation

The data of Langbein et al. (1999) for the OH rate coefficient imply an atmospheric lifetime for $CH_2FOCH(CF_3)_2$ of at least 1.1 years. Further measurements of the OH rate coefficient, particularly at reduced temperature are required. No studies of the OH-initiated oxidation mechanism have been carried out.

III-G-27. 1,1,2,2-Tetrafluoro-1-(2,2,2-trifluoroethoxy)ethane (1,1,2,2-Tetrafluoroethyl 2,2,2-Trifluoroethyl Ether, $CF_3CH_2OCF_2CF_2H$)

III-G-27.1. OH Reaction Kinetics

The data of Tokuhashi et al. (2000b), Chen et al. (2003a), and Wilson et al. (2007) for the rate coefficient for reaction of OH radicals with $CF_3CH_2OCF_2CF_2H$ are in excellent agreement, see table III-G-44 and figure III-G-9 for a summary. Fitting of the combined dataset to the simple Arrhenius equation yields: $k = 1.0 \times 10^{-12} \exp(-1{,}394/T)$ cm^3 molecule^{-1} s^{-1}. This expression gives $k = 9.4 \times 10^{-15}$ cm^3 molecule^{-1} s^{-1} at 298 K, with an estimated uncertainty of $\pm 15\%$. The data point of Heathfield et al. (1998) is considerably higher than the more recent data, and is not included in the analysis.

Table III-G-43. Rate coefficients (k, cm^3 molecule^{-1} s^{-1}) for reaction of OH with $CH_2FOCH(CF_3)_2$

$10^{14} \times k$	T (K)	Technique[a]	Reference
7.3 ± 2.2	299	DF–RF	Brown et al. (1989a; 1990)
17.7 ± 1.4	422		
2.7 ± 0.5	298	PLP–UV abs.	Langbein et al. (1999)

[a]Abbreviations used for the techniques are defined in table I-F-3.

Table III-G-44. Rate coefficients ($k = A \times e^{-B/T}$, cm^3 $molecule^{-1}$ s^{-1}) for reaction of OH with $CF_3CH_2OCF_2CF_2H$

$10^{12} \times A$	B (K)	$10^{15} \times k$	T (K)	Technique[a]	Reference	Temperature Range (K)
		93.5 ± 2.2		PR–UV abs.	Heathfield et al. (1998)	
2.49	1,500 ± 170	3.40 ± 0.42	250	FP or PLP–LIF	Tokuhashi et al. (2000b)	
		3.62 ± 0.43	250			
		5.91 ± 0.67	273			
		8.54 ± 1.01	298			
		9.21 ± 1.07	298			
		13.9 ± 1.5	331			
		24.7 ± 2.7	375			
		46.3 ± 4.8	430			
		46.3 ± 4.9	430			
		9.26 ± 1.17	298	DF–LIF		
		6.0 ± 0.3	268	RR[b] (CH_3CCl_3)	Chen et al. (2003a)	268–308
		7.2 ± 0.5	278			
		8.5 ± 0.2	288			
		9.7 ± 0.4	298			
		11.7 ± 0.4	308			
		5.5 ± 0.3	268	RR[c] (CHF_2Cl)		
		7.0 ± 0.3	278			
		8.6 ± 0.3	288			
		10.3 ± 0.4	298			
		12.2 ± 0.3	308			
0.74[d]	1,293[d]	6.13	270	RR[e] (CH_3CHF_2, HFC-152a)	Wilson et al. (2007)	270–407
		6.53	272			
		8.93	289			
		8.72	293			
		11.3	312			
		12.6	322			
		17.3	341			
		18.6	352			
		21.6	363			
		21.7	371			
		27.5	389			
		31.2	407			
0.75[d]	1,306[d]	6.18	273	RR[f] (CH_2F_2, HFC-32)		
		7.34	279			
		8.28	291			
		9.64	303			
		14.2	331			
		23.2	380			
		24.2	382			
		29.9	399			
		13.1	322	RR[g] (C_2H_5F, HFC-161)		

(*continued*)

Table III-G-44. (*continued*)

$10^{12} \times A$	B (K)	$10^{15} \times k$	T (K)	Technique[a]	Reference	Temperature Range (K)
		39.0	407	RR[h] (CF_3CHFCF_3, HFC-227ea)		

[a]Abbreviations used for the techniques are defined in table I-F-3.
[b]Placed on an absolute basis using $k(OH+CH_3CCl_3) = 1.81 \times 10^{-12} \exp(-1{,}543/T)$ cm^3 molecule^{-1} s^{-1} (Calvert et al., 2008).
[c]Placed on an absolute basis using $k(OH+CHF_2Cl) = 1.48 \times 10^{-12} \exp(-1{,}710/T)$ cm^3 molecule^{-1} s^{-1} (Calvert et al., 2008).
[d]Values obtained from least-squares fit of data obtained using updated reference rate coefficients, and thus differ from those originally reported.
[e]Placed on an absolute basis using $k(OH+HFC\text{-}152a) = 1.21 \times 10^{-12} \exp(-1{,}055/T)$ cm^3 molecule^{-1} s^{-1} (Calvert et al., 2008).
[f]Placed on an absolute basis using $k(OH+HFC\text{-}32) = 1.33 \times 10^{-12} \exp(-1{,}432/T)$ cm^3 molecule^{-1} s^{-1} (Calvert et al., 2008).
[g]Placed on an absolute basis using $k(OH+HFC\text{-}161) = 2.62 \times 10^{-12} \exp(-738/T)$ cm^3 molecule^{-1} s^{-1} (Calvert et al., 2008).
[h]Placed on an absolute basis using $k(OH+HFC\text{-}227ea) = 6.55 \times 10^{-13} \exp(-1{,}809/T)$ cm^3 molecule^{-1} s^{-1} (Calvert et al., 2008).

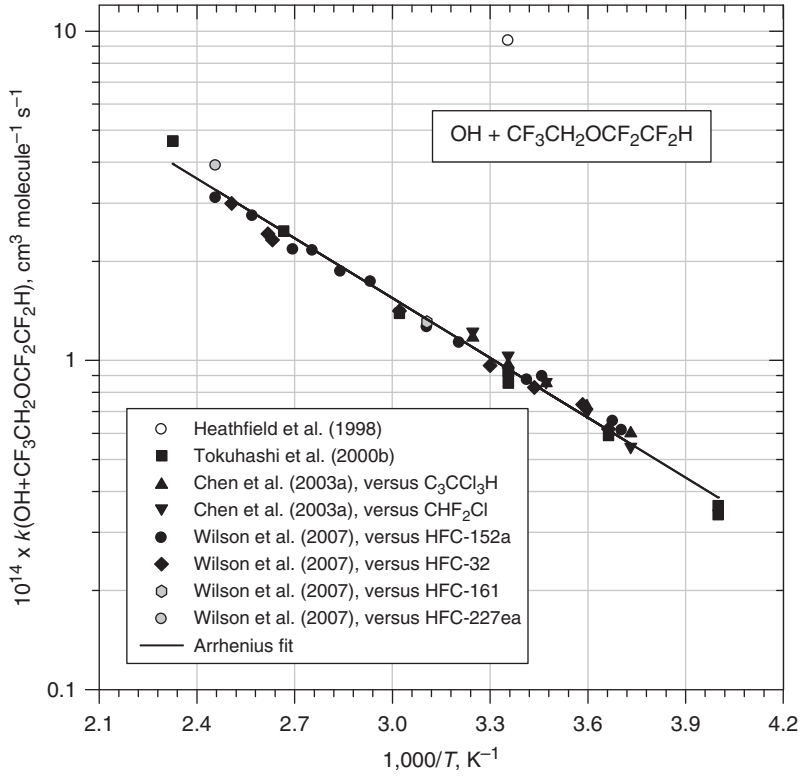

Figure III-G-9. Arrhenius plot of the rate coefficient for the reaction of OH with $CF_3CH_2OCF_2CF_2H$.

Table III-G-45. Rate coefficients ($k = A \times e^{-B/T}$, cm^3 molecule^{-1} s^{-1}) for reaction of Cl with $CF_3CH_2OCF_2CF_2H$

$10^{12} \times A$	B (K)	$10^{16} \times k$	T (K)	Technique[a]	Reference	Temperature Range (K)
1.95 ± 0.72	1,616 ± 202	52.8 ± 5.2	273	VLPR	Papadimitriou et al. (2004)	273–363
		91.1 ± 10.3	303			
		163 ± 23	333			
		222 ± 30	363			

[a]Abbreviations used for the techniques are defined in table I-F-3.

III-G-27.2. Cl-Atom Reaction Kinetics

The only data are those of Papadimitriou et al. (2004), $k = 1.95 \times 10^{-12} \exp(-1{,}616/T)$ cm^3 molecule^{-1} s^{-1}, with $k = 8.6 \times 10^{-15}$ cm^3 molecule^{-1} s^{-1} at 298 K. The data are summarized in table III-G-45.

III-G-27.3. Summary of the Atmospheric Fate of $CF_3CH_2OCF_2CF_2H$, and the End Products of Its Oxidation

The atmospheric lifetime for $CF_3CH_2OCF_2CF_2H$ is estimated to be 5.4 years. No product studies have been carried out. However, OH reaction at the CH_2 site in the molecule is likely dominant. Likely end products following OH abstraction at this site are the formate ester, $HC(O)OCF_2CF_2H$ and COF_2, following C—C bond rupture in the $CF_3CH(O\bullet)OCF_2CF_2H$ radical.

III-G-28. 1,1,1,2,3,3,3-Heptafluoro-2-methoxypropane [Methyl Perfluoro-*iso*-propyl Ether, $CH_3OCF(CF_3)_2$]

III-G-28.1. OH Reaction Kinetics

Tokuhashi et al. (1999c) have made the only measurements of the rate coefficient for reaction of OH with $CH_3OCF(CF_3)_2$. Their measurements, characterized by careful sample purification and involving a combination of flash photolysis and discharge flow techniques, yield $k = 1.94 \times 10^{-12} \exp(-1{,}450/T)$ cm^3 molecule^{-1} s^{-1}, with $k = 1.5 \times 10^{-14}$ cm^3 molecule^{-1} s^{-1} at 298 K and an estimated uncertainty of ±20%. The data are summarized in table III-G-46, and displayed in figure III-G-8.

III-G-28.2. Summary of the Atmospheric Fate of $CH_3OCF(CF_3)_2$, and the End Products of Its Oxidation

The OH rate coefficient data from Tokuhashi et al. (1999c) can be used to estimate an atmospheric lifetime for $CH_3OCF(CF_3)_2$ of 3.4 years. No studies of the OH-initiated oxidation mechanism have been carried out. However, reaction with OH must occur at the CH_3 group, a process that should lead to the production of the formate ester, $HC(O)OCF(CF_3)_2$.

Table III-G-46. Rate coefficients ($k = A \times e^{-B/T}$, cm^3 $molecule^{-1}$ s^{-1}) for reaction of OH with $CH_3OCF(CF_3)_2$

$10^{12} \times A$	B (K)	$10^{15} \times k$	T (K)	Technique[a]	Reference	Temperature Range (K)
$1.94^{+0.48}_{-0.38}$	1,450 ± 70	6.55 ± 0.37	250	FP or PLP–LIF	Tokuhashi et al. (1999c)	250–430
		6.36 ± 0.22	250			
		9.44 ± 0.44	273			
		10.0 ± 0.3	273			
		14.5 ± 0.6	298			
		14.9 ± 0.7	298			
		22.7 ± 0.9	331			
		38.8 ± 1.1	375			
		71.1 ± 1.8	430			
		72.4 ± 2.3	430			
		15.1 ± 0.7	298	DF–LIF		

[a]Abbreviations used for the techniques are defined in table I-F-3.

III-G-29. 1,1,1,2,2,3,3-Heptafluoro-3-methoxypropane (Methyl Perfluoro-*n*-propyl Ether, $CH_3OCF_2CF_2CF_3$)

III-G-29.1. OH Reaction Kinetics

The rate coefficient for reaction of OH with $CH_3OCF_2CF_2CF_3$ has been studied by Tokuhashi et al. (1999c) and Ninomiya et al. (2000). The data are summarized in table III-G-47. The analysis of Tokuhashi et al. (1999c) is recommended, $k = 2.06 \times 10^{-12} \exp(-1{,}540/T)$ cm^3 $molecule^{-1}$ s^{-1} with $k = 11.7 \times 10^{-15}$ cm^3 $molecule^{-1}$ s^{-1} at 298 K. The 298 K value is in excellent agreement with the measurement of Ninomiya et al. (2000). The uncertainty is estimated at ±20% at 298 K.

III-G-29.2. Cl-Atom Reaction Kinetics

The relative rate studies of Ninomiya et al. (2000) and Nohara et al. (2001) are in reasonable agreement, and yield $k(Cl + CH_3OCF_2CF_2CF_3) = 9.8 \times 10^{-14}$ cm^3 $molecule^{-1}$ s^{-1} at 298 K. The uncertainty is estimated at ±25% at 298 K. Data are summarized in table III-G-48.

III-G-29.3. Summary of the Atmospheric Fate of $CH_3OCF_2CF_2CF_3$, and the End Products of Its Oxidation

The atmospheric lifetime for $CH_3OCF_2CF_2CF_3$ is estimated to be 4.4 years, assuming an average tropospheric temperature of 272 K and [OH] ≈ 10^6 molecule cm^{-3}. The major, perhaps exclusive, end product of its oxidation is the formate ester, $HC(O)OCF_2CF_2CF_3$ (Ninomiya et al., 2000; Nohara et al., 2001), formed following OH abstraction from the CH_3 group and reaction of the resultant alkoxy radical with O_2.

Table III-G-47. Rate coefficients ($k = A \times e^{-B/T}$, cm^3 molecule^{-1} s^{-1}) for reaction of OH with $CH_3OCF_2CF_2CF_3$

$10^{12} \times A$	B (K)	$10^{15} \times k$	T (K)	Technique[a]	Reference	Temperature Range (K)
$2.06^{+0.58}_{-0.45}$	1,540 ± 80	4.73 ± 0.17	250	FP or PLP–LIF	Tokuhashi et al. (1999c)	250–430
		4.77 ± 0.24	250			
		7.41 ± 0.23	273			
		10.6 ± 0.3	298			
		11.8 ± 0.6	298			
		18.6 ± 0.6	331			
		33.3 ± 2.4	375			
		61.1 ± 2.1	430			
		60.1 ± 2.4	430			
		11.5 ± 1.1	298	DF–LIF		
		10.1 ± 1.1	295	RR[b] (CH_4)	Ninomiya et al. (2000)	
		13.0 ± 1.1	295	RR[c] (CH_3Cl)		

[a]Abbreviations used for the techniques are defined in table I-F-3.
[b]Placed on an absolute basis using $k(OH+CH_4) = 6.0 \times 10^{-15}$ cm^3 molecule^{-1} s^{-1} at 295 K (Calvert et al., 2008).
[c]Placed on an absolute basis using $k(OH+CH_3Cl) = 3.7 \times 10^{-14}$ cm^3 molecule^{-1} s^{-1} at 295 K (Calvert et al., 2008).

Table III-G-48. Rate coefficients (k, cm^3 molecule^{-1} s^{-1}) for reaction of Cl with $CH_3OCF_2CF_2CF_3$

$10^{14} \times k$	T (K)	Technique[a]	Reference
9.2 ± 0.5	295	RR[b] (CH_4)	Ninomiya et al. (2000)
8.5 ± 0.3	295	RR[c] (CH_3Cl)	
11.8 ± 1.4	298	RR[b] (CH_4)	Nohara et al. (2001)

[a]Abbreviations used for the techniques are defined in table I-F-3.
[b]Placed on an absolute basis using $k(Cl+CH_4) = 0.99 \times 10^{-13}$ cm^3 molecule^{-1} s^{-1} at 295 K, 1.0×10^{-13} cm^3 molecule^{-1} s^{-1} at 298 K (Atkinson et al., 2006).
[c]Placed on an absolute basis using $k(Cl+CH_3Cl) = 4.7 \times 10^{-13}$ cm^3 molecule^{-1} s^{-1} (Atkinson et al., 2008).

III-G-30. 3-(Difluoromethoxy)-1,1,1,2,2-pentafluoropropane (Difluoromethyl 2,2,3,3,3-Pentafluoro-*n*-propyl Ether, $CHF_2OCH_2CF_2CF_3$)

III-G-30.1. OH Reaction Kinetics

The only data available regarding the rate coefficient for reaction of OH with $CHF_2OCH_2CF_2CF_3$ are those of Tokuhashi et al. (2000b). The data are summarized in table III-G-49 and displayed in figure III-G-8, and yield: $k = 2.14 \times 10^{-12} \exp(-1{,}580/T)$ cm^3 molecule^{-1} s^{-1} with $k = 1.1 \times 10^{-14}$ cm^3 molecule^{-1} s^{-1} at 298 K. An uncertainty of ±20% is assigned at 298 K.

Table III-G-49. Rate coefficients ($k = A \times e^{-B/T}$, cm^3 $molecule^{-1}$ s^{-1}) for reaction of OH with $CHF_2OCH_2CF_2CF_3$

$10^{12} \times A$	B (K)	$10^{15} \times k$	T (K)	Technique[a]	Reference	Temperature Range (K)
$2.06^{+0.58}_{-0.45}$	1540 ± 80	3.85 ± 0.42	250	FP or PLP–LIF	Tokuhashi et al. (2000b)	250–430
		4.13 ± 0.45	250			
		6.36 ± 0.73	273			
		6.59 ± 0.71	273			
		9.75 ± 1.03	298			
		10.2 ± 1.3	298			
		16.9 ± 1.8	331			
		30.6 ± 3.3	375			
		56.8 ± 5.8	430			
		56.1 ± 6.2	430			
		10.2 ± 1.1	298	DF–LIF		

[a]Abbreviations used for the techniques are defined in table I-F-3.

III-G-30.2. Summary of the Atmospheric Fate of $CHF_2OCH_2CF_2CF_3$, and the End Products of Its Oxidation

Assuming an average tropospheric temperature of 272 K and [OH] $\approx 10^6$ molecule cm^{-3}, the atmospheric lifetime for $CHF_2OCH_2CF_2CF_3$ is estimated to be 5 years. OH attack at the CH_2 group seems likely to be important, with the expected end products then being $HC(O)OCHF_2$ (with two molecules of COF_2 as co-product) and/or $CF_3CF_2C(O)OCHF_2$.

III-G-31. 1,1,1,2-Tetrafluoro-2-(1,1,2,2-tetrafluoroethoxy)ethane (1,1,2,2-Tetrafluoroethyl 1,2,2,2-tetrafluoroethyl Ether, $CHF_2CF_2OCHFCF_3$)

III-G-31.1. OH Reaction Kinetics

The rate coefficient for reaction of OH with $CHF_2CF_2OCHFCF_3$ has recently been studied as a function of temperature by Wilson et al. (2007), using a relative rate technique. The data are summarized in table III-G-50. Fitting of all the Wilson et al. data, except the single datapoint obtained using C_2H_5F (HFC-161) as the reference, leads to $k = 5.5 \times 10^{-13} \exp(-1{,}462/T)$ cm^3 $molecule^{-1}$ s^{-1} with $k = 4.0 \times 10^{-15}$ cm^3 $molecule^{-1}$ s^{-1} at 298 K. An uncertainty of ±25% is assigned at 298 K.

III-G-31.2. Summary of the Atmospheric Fate of $CHF_2CF_2OCHFCF_3$, and the End Products of Its Oxidation

Assuming an average tropospheric temperature of 272 K and [OH] $\approx 10^6$ molecule cm^{-3}, the atmospheric lifetime for $CHF_2CF_2OCHFCF_3$ is estimated to be 13 years. The mechanism of oxidation of this species has not been studied.

Table III-G-50. Rate coefficients ($k = A \times e^{-B/T}$, cm^3 $molecule^{-1}$ s^{-1}) for reaction of OH with $CHF_2CF_2OCHFCF_3$

$10^{12} \times A$	B (K)	$10^{14} \times k$	T (K)	Technique[a]	Reference	Temperature Range (K)
0.52[b]	1,456[b]	0.224	267	RR[c] (CH_2F_2 HFC-32)	Wilson et al. (2007)	267–407
		0.272	277			
		0.306	284			
		0.345	290			
		0.387	299			
		0.471	312			
		0.583	324			
		0.749	347			
		0.939	363			
		1.11	380			
		1.34	399			
		1.49	407			
0.53[b]	1,430[b]	0.297	274	RR[d] (C_2F_5H, HFC-125)		
		0.414	294			
		0.491	306			
		0.741	333			
		0.944	354			
		1.26	381			
		1.61	403			
		0.800	347	RR[e] (CH_2FCH_2F, HFC-152)		
		1.10	398	RR[f] (C_2H_5F, HFC-161)		

[a]Abbreviations used for the techniques are defined in table I-F-3.
[b]Values obtained from least-squares fit of data obtained using updated reference rate coefficients, and thus differ from those originally reported.
[c]Placed on an absolute basis using $k(\text{OH+HFC-32}) = 1.33 \times 10^{-12} \exp(-1{,}432/T)$ cm^3 $molecule^{-1}$ s^{-1} (Calvert et al., 2008).
[d]Placed on an absolute basis using $k(\text{OH+HFC-125}) = 5.1 \times 10^{-13} \exp(-1{,}666/T)$ cm^3 $molecule^{-1}$ s^{-1} (Calvert et al., 2008).
[e]Placed on an absolute basis using $k(\text{OH+HFC-152}) = 2.84 \times 10^{-18} T^2 \exp(-277/T)$ cm^3 $molecule^{-1}$ s^{-1} (Calvert et al., 2008).
[f]Placed on an absolute basis using $k(\text{OH+HFC-161}) = 2.62 \times 10^{-12} \exp(-738/T)$ cm^3 $molecule^{-1}$ s^{-1} (Calvert et al., 2008).

III-G-32. 1-(Difluoromethoxy)-1,1,2,3,3,3-hexafluoropropane (Difluoromethyl 1,1,2,3,3,3-Hexafluoro-*n*-propyl Ether, $CF_3CFHCF_2OCF_2H$)

III-G-32.1. OH Reaction Kinetics

As summarized in table III-G-51, the data regarding reaction of OH with $CF_3CFHCF_2OCF_2H$ from Wallington et al. (2004) and Oyaro et al. (2005), both obtained via relative rate methods, differ by over an order of magnitude. It seems reasonable to assume that the reaction of OH with $CF_3CFHCF_2OCF_2H$ will be considerably slower than that with $CHF_2OCH_2CF_2CF_3$ (section III-G-28), and thus the

Table III-G-51. Rate coefficients (k, cm^3 molecule^{-1} s^{-1}) for reaction of OH with $CF_3CFHCF_2OCF_2H$

$10^{15} \times k$	T (K)	Technique[a]	Reference
1.62 ± 0.25	295	RR[b] (C_2H_4)	Wallington et al. (2004)
1.65 ± 0.31	295	RR[c] (C_2H_2)	
20 ± 10	298	RR[d] (CH_3CN)	Oyaro et al. (2005)
13.2 ± 4.5	298	RR[e] (n-$C_4F_9OCH_3$)	

[a]Abbreviations used for the techniques are defined in table I-F-3.
[b]Placed on an absolute basis using $k(OH+C_2H_4) = 7.9 \times 10^{-12}$ cm^3 molecule^{-1} s^{-1} (Atkinson et al., 2006).
[c]Placed on an absolute basis using $k(OH+C_2H_2) = 7.8 \times 10^{-13}$ cm^3 molecule^{-1} s^{-1} (Atkinson et al., 2006).
[d]Placed on an absolute basis using $k(OH+CH_3CN) = 2.2 \times 10^{-14}$ cm^3 molecule^{-1} s^{-1} (Atkinson et al., 2006).
[e]Placed on an absolute basis using $k(OH+n\text{-}C_4F_9OCH_3) = 12 \times 10^{-15}$ cm^3 molecule^{-1} s^{-1} (this book, section III-G-37.1).

Table III-G-52. Rate coefficients (k, cm^3 molecule^{-1} s^{-1}) for reaction of Cl with $CF_3CFHCF_2OCF_2H$

$10^{17} \times k$	T (K)	Technique[a]	Reference
6.33 ± 0.59	296	RR[b] (C_2F_5H)	Wallington et al. (2004)
6.00 ± 0.65	296	RR[c] (CF_3CH_3)	
< 60	298	RR[d] (CH_3CN)	Oyaro et al. (2005)

[a]Abbreviations used for the techniques are defined in table I-F-3.
[b]Placed on an absolute basis using $k(Cl+C_2F_5H) = 2.5 \times 10^{-16}$cm^3 molecule^{-1} s^{-1} (Atkinson et al., 2008).
[c]Placed on an absolute basis using $k(Cl+CF_3CH_3) = 2.9 \times 10^{-17}$ cm^3 molecule^{-1} s^{-1} (IUPAC, 2008).
[d]Placed on an absolute basis using $k(Cl+CH_3CN) = 1.2 \times 10^{-14}$ cm^3 molecule^{-1} s^{-1} (Atkinson et al., 2006).

data of Wallington et al. (2004) are preferred, $k = 1.6 \times 10^{-15}$ cm^3 molecule^{-1} s^{-1} at 296 K. Corroborative measurements are required.

III-G-32.2. Cl-Atom Reaction Kinetics

Relative rate studies of the reaction of Cl with $CF_3CFHCF_2OCF_2H$ have been carried out by Wallington et al. (2004) and Oyaro et al. (2005), see table III-G-52. The data of Wallington et al., $k = 6.3 \times 10^{-17}$ cm^3 molecule^{-1} s^{-1} at 296 K, are consistent with the upper limit obtained by Oyaro et al., $k < 6 \times 10^{-16}$ cm^3 molecule^{-1} s^{-1} at 298 K.

III-G-32.3. Summary of the Atmospheric Fate of $CF_3CFHCF_2OCF_2H$, and the End Products of Its Oxidation

Assuming the OH rate coefficient of Wallington et al. (2004) to be correct, the atmospheric lifetime for $CF_3CFHCF_2OCF_2H$ is estimated to exceed 18 years. The Cl-atom-initiated oxidation of this species has been studied by Wallington et al. (2004), and leads to the formation of $CF_3C(O)F$ and two molecules of COF_2. As detailed by Wallington et al., the products are obtained from initial attack at the CFH group,

followed by the decomposition of the resultant alkoxy radical, $CF_3CF(O\bullet)CF_2OCF_2H$:

$$CF_3CF(O\bullet)CF_2OCF_2H(+O_2) \rightarrow CF_3C(O)F + \bullet OOCF_2OCF_2H$$

$$2\ \bullet OOCF_2OCF_2H \rightarrow 2\ \bullet OCF_2OCF_2H$$

$$\bullet OCF_2OCF_2H \rightarrow COF_2 + CF_2HO\bullet$$

$$\bullet OCF_2H + O_2 \rightarrow COF_2 + HOO\bullet$$

Note that Wallington et al. (2004) conducted similar Cl-atom kinetic and mechanistic studies on the related species, $CF_3CHFCF_2OCF_3$. Although most of the reaction appears to occur at the CHF group in both molecules, the Cl-atom reaction is considerably (∼50%) faster with $CF_3CHFCF_2OCF_2H$ than with $CF_3CHFCF_2OCF_3$.

III-G-33. 2-(Difluoromethoxy)-1,1,1,3,3,3-hexafluoropropane [Difluoromethyl 1,1,1,3,3,3-Hexafluoro-2-propyl Ether, $(CF_3)_2CHOCHF_2$]

III-G-33.1. OH Reaction Kinetics

The reaction of OH with $(CF_3)_2CHOCHF_2$ has been the subject of a relative rate study (Wilson et al., 2007), see table III-G-53. Analysis of their dataset provides the following Arrhenius expression: $k = 9.6 \times 10^{-13} \exp(-1{,}738/T)$ cm^3 molecule^{-1} s^{-1} with $k = 2.8 \times 10^{-15}$ cm^3 molecule^{-1} s^{-1} at 298 K. An uncertainty of ±25% is assigned at 298 K.

III-G-33.2. Summary of the Atmospheric Fate of $(CF_3)_2CHOCHF_2$, and the End Products of Its Oxidation

The atmospheric lifetime for $(CF_3)_2CHOCHF_2$ is estimated to be about 20 years, assuming an average tropospheric temperature of 272 K and an average tropospheric [OH] ≈ 10^6 molecule cm^{-3}. The mechanism of oxidation of this species has not been studied.

III-G-34. 1,1,1,2,3,3-Hexafluoro-3-(trifluoromethoxy)propane (1,1,2,3,3,3-Hexafluoro-*n*-propyl Trifluoromethyl Ether, $CF_3CFHCF_2OCF_3$)

III-G-34.1. OH Reaction Kinetics

The reaction of OH with $CF_3CFHCF_2OCF_3$ has been the subject of two relative rate studies (Wallington et al., 2004, at 296 K; Wilson et al., 2007, from 270 to 406 K), see table III-G-54. The data near 296 K are in reasonable agreement, those of Wallington et al. (2004) giving $k = 1.3 \times 10^{-15}$ cm^3 molecule^{-1} s^{-1} and those of Wilson et al. (2007) giving $k = (1.6 - 1.7) \times 10^{-15}$ cm^3 molecule^{-1} s^{-1}. To arrive at the recommended Arrhenius expression, the activation energy obtained from a fit

Table III-G-53. Rate coefficients ($k = A \times e^{-B/T}$, cm^3 $molecule^{-1}$ s^{-1}) for reaction of OH with $(CF_3)_2CHOCHF_2$

$10^{12} \times A$	B (K)	$10^{14} \times k$	T (K)	Technique[a]	Reference	Temperature Range (K)
1.37[b]	1,878[b]	0.333	312	RR[c] (CF_3CH_2F, HFC-134a)	Wilson et al. (2007)	284–398
		0.821	367			
		0.846	369			
0.96[b]	1,735[b]	0.209	284	RR[d] (CF_3CH_3, HFC-143a)		
		0.240	289			
		0.276	296			
		0.329	307			
		0.351	309			
		0.423	317			
		0.508	332			
		0.605	341			
		0.636	347			
		0.779	360			
		0.969	379			
		1.17	393			
		1.23	398			

[a]Abbreviations used for the techniques are defined in table I-F-3.

[b]Values obtained from least-squares fit of data obtained using updated reference rate coefficients, and thus differ from those originally reported.

[c]Placed on an absolute basis using $k(\text{OH+HFC-134a}) = 1.01 \times 10^{-12} \exp(-1{,}640/T)$ cm^3 $molecule^{-1}$ s^{-1} (Calvert et al., 2008).

[d]Placed on an absolute basis using $k(\text{OH+HFC-143a}) = 1.06 \times 10^{-12} \exp(-1{,}998/T)$ cm^3 $molecule^{-1}$ s^{-1} (Calvert et al., 2008).

to the Wilson et al. data is combined with the average of the 296 K determinations ($k = 1.5 \times 10^{-15}$ cm^3 $molecule^{-1}$ s^{-1}) to give: $k = 4.1 \times 10^{-13} \exp(-1{,}662/T)$ cm^3 $molecule^{-1}$ s^{-1}. This expression returns $k = 1.55 \times 10^{-15}$ cm^3 $molecule^{-1}$ s^{-1} at 298 K, with an estimated uncertainty of ±25%.

III-G-34.2. Summary of the Atmospheric Fate of $CF_3CFHCF_2OCF_3$, and the End Products of Its Oxidation

The atmospheric lifetime for $CF_3CFHCF_2OCF_3$ is estimated to be 35 years, for a tropospheric average temperature of 272 K and [OH] $\approx 10^6$ molecule cm^{-3}. The Cl-atom-initiated oxidation of this species has been studied by Wallington et al. (2004). Major products identified were $CF_3C(O)F$ (82 ± 5% molar yield) and COF_2. The data are consistent with Cl-atom attack occurring at the CFH group, leading to formation of the $CF_3CF(O\bullet)CF_2OCF_3$ alkoxy species. The subsequent decomposition of this radical leads to $CF_3C(O)F$, COF_2 and a $CF_3O\bullet$ radical.

$$CF_3CF(O\bullet)CF_2OCF_3(+O_2) \rightarrow CF_3C(O)F + \bullet OOCF_2OCF_3$$

$$2\ \bullet OOCF_2OCF_3 \rightarrow \bullet OCF_2OCF_3$$

$$\bullet OCF_2OCF_3 \rightarrow COF_2 + CF_3O\bullet$$

Table III-G-54. Rate coefficients ($k = A \times e^{-B/T}$, cm^3 $molecule^{-1}$ s^{-1}) for reaction of OH with $CF_3CFHCF_2OCF_3$

$10^{12} \times A$	B (K)	$10^{14} \times k$	T (K)	Technique[a]	Reference	Temperature Range (K)
		0.130 ± 0.025	295	RR[b] (C_2H_4)	Wallington et al. (2004)	
		0.130 ± 0.024	295	RR[c] (C_2H_2)		
0.33[d]	1,559[d]	0.104	270	RR[e] (C_2F_5H, HFC-125)	Wilson et al. (2007)	270–404
		0.182	299			
		0.293	329			
		0.457	363			
		0.584	385			
		0.703	404			
0.59[d]	1,743[d]	0.128	284	RR[f] (CF_3CHFCF_3, HFC-227ea)		284–406
		0.139	288			
		0.158	294			
		0.162	296			
		0.212	310			
		0.237	315			
		0.271	324			
		0.325	334			
		0.362	354			
		0.423	353			
		0.537	371			
		0.764	402			
		0.821	406			

[a] Abbreviations used for the techniques are defined in table I-F-3.
[b] Placed on an absolute basis using $k(OH+C_2H_4) = 7.9 \times 10^{-12}$ cm^3 $molecule^{-1}$ s^{-1} (Atkinson et al., 2006).
[c] Placed on an absolute basis using $k(OH+C_2H_2) = 7.8 \times 10^{-13}$ cm^3 $molecule^{-1}$ s^{-1} (Atkinson et al., 2006).
[d] Values obtained from least-squares fit of data obtained using updated reference rate coefficients, and thus differ from those originally reported.
[e] Placed on an absolute basis using $k(OH+HFC\text{-}125) = 5.1 \times 10^{-12} \exp(-1{,}666/T)$ cm^3 $molecule^{-1}$ s^{-1} (Calvert et al., 2008).
[f] Placed on an absolute basis using $k(OH+HFC\text{-}227ea) = 6.55 \times 10^{-13} \exp(-1{,}809/T)$ cm^3 $molecule^{-1}$ s^{-1} (Calvert et al., 2008).

The atmospheric fate of $CF_3O\bullet$ is reaction with NO to produce COF_2. Thus, the atmospheric degradation of $CF_3CFHCF_2OCF_3$ likely produces $CF_3C(O)F$ and two molecules of COF_2 [see Wallington et al. (2004) for details].

III-G-35. 1,1,1,3,3,3-Hexafluoro-2-(trifluoromethoxy)propane [Trifluoromethyl 1,1,1,3,3,3-Hexafluoro-2-propyl Ether, $CF_3OCH(CF_3)_2$]

III-G-35.1. OH Reaction Kinetics

The relative rate study of Andersen et al. (2005b) gives $k = 3.0 \times 10^{-16}$ cm^3 $molecule^{-1}$ s^{-1} for the reaction of OH with $CF_3OCH(CF_3)_2$ at 296 K. In the absence of corroborating data, an uncertainty of ±30% is assigned. The data are summarized in table III-G-55.

Table III-G-55. Rate coefficient (k, cm^3 molecule^{-1} s^{-1}) for reaction of OH with $CF_3OCH(CF_3)_2$

$10^{16} \times k$	T (K)	Technique[a]	Reference
3.00 ± 0.88	295	RR[b] (C_2H_2)	Andersen et al. (2005b)

[a]Abbreviations used for the techniques are defined in table I-F-3.
[b]Placed on an absolute basis using $k(OH+C_2H_2) = 7.8 \times 10^{-13}$ cm^3 molecule^{-1} s^{-1} (Atkinson et al., 2006).

Table III-G-56. Rate coefficient (k, cm^3 molecule^{-1} s^{-1}) for reaction of Cl with $CF_3OCH(CF_3)_2$

$10^{18} \times k$	T (K)	Technique[a]	Reference
1.27 ± 0.22	296	RR[b] (CF_3CH_3)	Andersen et al. (2005b)

[a]Abbreviations used for the techniques are defined in table I-F-3.
[b]Placed on an absolute basis using $k(Cl+CF_3CH_3) = 2.9 \times 10^{-17}$ cm^3 molecule^{-1} s^{-1} (IUPAC, 2008).

III-G-35.2. Cl-Atom Reaction Kinetics

Andersen et al. (2005b) conducted a relative rate study of the reaction of Cl with $CF_3OCH(CF_3)_2$, from which a rate coefficient $k = 1.3 \times 10^{-18}$ cm^3 molecule^{-1} s^{-1} is obtained at 296 K. An uncertainty of ±50% is assigned. The data are summarized in table III-G-56.

III-G-35.3. Summary of the Atmospheric Fate of $CF_3OCH(CF_3)_2$, and the End Products of Its Oxidation

The atmospheric lifetime of $CF_3OCH(CF_3)_2$is estimated to exceed 105 years. Andersen et al. showed that $CF_3OC(O)CF_3$ and COF_2 are formed in unity yield in the Cl-atominitiated oxidation of this species. These products result from initial attack at the only available C—H bond, followed by C—C bond rupture in the resulting alkoxy radical $CF_3OC(O\bullet)(CF_3)_2$,

$$CF_3OC(O\bullet)(CF_3)_2 \rightarrow CF_3OC(O)CF_3 + \bullet CF_3$$

$$\bullet CF_3 + O_2 \rightarrow\rightarrow\rightarrow COF_2$$

III-G-36. 1-Ethoxy-1,1,2,3,3,3-hexafluoropropane (1,1,2,3,3,3-Hexafluoro-*n*-propyl Ethyl Ether, $CF_3CHFCF_2OCH_2CH_3$)

III-G-36.1. OH Reaction Kinetics

Rate coefficients for reaction of OH radicals with $CF_3CHFCF_2OCH_2CH_3$ have been obtained by Oyaro et al. (2005) using a relative rate technique. There is some

Table III-G-57. Rate coefficients (k, cm^3 molecule^{-1} s^{-1}) for reaction of OH with $CF_3CHFCF_2OCH_2CH_3$

$10^{14} \times k$	T (K)	Technique[a]	Reference
16.2 ± 2.7	298	RR[b] ($CHCl_3$)	Oyaro et al. (2005)
11.0 ± 1.2	298	RR[b] (n-$C_4F_9OC_2H_5$)	

[a]Abbreviations used for the techniques are defined in table I-F-3.
[b]Placed on an absolute basis using $k(OH+CHCl_3) = 9.6 \times 10^{-14}$ cm^3 molecule^{-1} s^{-1} (Calvert et al., 2008).
[c]Placed on an absolute basis using $k(OH+n\text{-}C_4F_9OC_2H_5) = 6.5 \times 10^{-14}$ cm^3 molecule^{-1} s^{-1} (this book, section III-G-37.1)

Table III-G-58. Rate coefficients (k, cm^3 molecule^{-1} s^{-1}) for reaction of Cl with $CF_3CHFCF_2OCH_2CH_3$

$10^{13} \times k$	T (K)	Technique[a]	Reference
34 ± 17	298	RR[b] (CH_2ClCH_2Cl)	Oyaro et al. (2005)
30 ± 15	298	RR[c] (CH_2Cl_2)	

[a]Abbreviations used for the techniques are defined in table I-F-3.
[b]Placed on an absolute basis using $k(Cl+CH_2ClCH_2Cl) = 1.3 \times 10^{-12}$ cm^3 molecule^{-1} s^{-1} at 298 K (Wallington et al., 1996a).
[c]Placed on an absolute basis using $k(Cl+CH_2Cl_2) = 3.4 \times 10^{-13}$ cm^3 molecule^{-1} s^{-1} (Atkinson et al., 2008).

disagreement between their two measurements, and likely considerable uncertainty associated with one of the reference reactions (reaction of OH with n-$C_4F_9OCH_2CH_3$). The average of the two determinations of Oyaro et al., $k = 1.4 \times 10^{-13}$ cm^3 molecule^{-1} s^{-1}, is recommended at 298 K with an uncertainty of ±40%. The data are summarized in table III-G-57.

III-G-36.2. Cl-Atom Reaction Kinetics

The relative rate study of Oyaro et al. (2005) leads to $k(Cl + CF_3CHFCF_2OCH_2CH_3) = 3.2 \times 10^{-12}$ cm^3 molecule^{-1} s^{-1} at 298 K. The data are summarized in table III-G-58.

III-G-36.3. Summary of the Atmospheric Fate of $CF_3CHFCF_2OCH_2CH_3$, and the End Products of Its Oxidation

The atmospheric lifetime for $CF_3CHFCF_2OCH_2CH_3$ is estimated to be 2.4 months for a globally averaged [OH] $\approx 10^6$ molecule cm^{-3}. Likely products of the OH-initiated oxidation include $HC(O)OCF_2CHFCF_3$ (with co-product HCHO) and/or $CH_3C(O)OCF_2CHFCF_3$, which could result from OH attack at the CH_2 group.

III-G-37. 1,1,1,2,2,3,3,4,4-Nonafluoro-4-methoxybutane (Methyl Perfluoro-*n*-butyl Ether, *n*-$C_4F_9OCH_3$, *n*-HFE-7100); and 1,1,1,2,3,3-Hexafluoro-2-(trifluoromethyl)-3-methoxypropane (Methyl Perfluoro-*iso*-butyl Ether, $(CF_3)_2CFCF_2OCH_3$, *i*-HFE-7100]

III-G-37.1. OH Reaction Kinetics

Relative rate techniques have been employed by Wallington et al. (1997b), Cavalli et al. (1998), and Nolan et al. (1999) to study the rate coefficient for reaction of OH with *n*-$C_4F_9OCH_3$and *iso*-$C_4F_9OCH_3$, also known as HFE-7100 and i-HFE-7100, respecrtively. Wallington et al. (1997b) and Cavalli et al. (1998) carried out their studies on mixtures containing differing amounts of two isomers (*n*-C_4F_9 and *iso*-C_4F_9 methyl ethers). In the Wallington et al. (1997b) study, the mixture used was predominantly *n*-$C_4F_9OCH_3$ (95%), with a small (5%) contribution from *iso*-$C_4F_9OCH_3$. In the Cavalli et al. (1998) study, the mixture contained more of the *iso*-$C_4F_9OCH_3$ isomer (75%) than the *n*-$C_4F_9OCH_3$ (25%) isomer. Given the fact that the mixtures used by Wallington et al. and Cavalli et al. were different, and given the substantial uncertainties quoted (particularly in the Wallington et al. study), the agreement between the two measurements is reasonable. Although the value of Cavalli et al., $k = 6.9 \times 10^{-15}$ cm^3 $molecule^{-1}$ s^{-1}, is more precise, the values of Wallington et al. (1997b) are more consistent with those reported for other methyl perfluoroalkyl ethers (e.g, see the previous discussions of CF_3OCH_3, $CF_3CF_2OCH_3$, and $C_3F_7OCH_3$). Thus, we recommend $k \approx 1.2 \times 10^{-14}$ cm^3 $molecule^{-1}$ s^{-1}, with an estimated uncertainty of ±35%. The Nolan et al. data are in agreement with this recommendation, although it should be noted that this study was presented in a Eurotrac report, with no information on the sample make-up or the reference compound(s) used. The data are summarized in table III-G-59.

Table III-G-59. Rate coefficients (k, cm^3 $molecule^{-1}$ s^{-1}) for reaction of OH with mixtures of *n*-$C_4F_9OCH_3$ and *iso*-$C_4F_9OCH_3$

$10^{15} \times k$	T (K)	Technique[a]	Reference
OH + *n*-$C_4F_9OCH_3$ (95%), *iso*-$C_4F_9OCH_3$ (5%)			
~ 12	295	RR[b] (CH_3Cl)	Wallington et al. (1997b)
~ 15	295	RR[d] (CH_4)	
OH + *n*-$C_4F_9OCH_3$ (25%), *i*-$C_4F_9OCH_3$ (75%)			
6.9 ± 1.5	295	RR[b] (CH_4)	Cavalli et al. (1998)
OH + $C_4F_9OCH_3$			
13 ± 0.9	298	RR[c,e]	Nolan et al. (1999)

[a]Abbreviations used for the techniques are defined in table I-F-3.
[b]Placed on an absolute basis using $k(OH+CH_3Cl) = 3.7 \times 10^{-14}$ cm^3 $molecule^{-1}$ s^{-1} at 295 K (Calvert et al., 2008).
[c]Value deemed less accurate by the authors, and not used in the final analysis.
[d]Placed on an absolute basis using $k(OH+CH_4) = 6.0 \times 10^{-15}$ cm^3 $molecule^{-1}$ s^{-1} at 295 K (Calvert et al., 2008).
[e]Reference compound not specified.

III-G-37.2. Cl-Atom Reaction Kinetics

Wallington et al. (1997b), using a relative rate technique, report $k(\text{Cl} + \text{HFE-7100}) = 9.6 \times 10^{-14}$ cm^3 molecule^{-1} s^{-1} at 295 K. The sample used consisted of 65% *iso*-$C_4F_9OCH_3$ and 35% *n*-$C_4F_9OCH_3$, but the authors report no significant difference in the reactivity of the two isomers. Aranda et al. (2006) studied the temperature dependence of the rate coefficient (234–315 K), again using a sample consisting of about 2:1 *iso*-$C_4F_9OCH_3$ to *n*-$C_4F_9OCH_3$. The data are in reasonable agreement, with the Wallington et al. data point falling about 15% lower than a fit to the Aranda et al. data. Fitting the simple Arrhenius expression to the combined dataset yields $k = 1.1\times10^{-10}\exp(-2{,}069/T)$ cm^3 molecule^{-1} s^{-1}, which gives $k = 1.1\times10^{-13}$ cm^3 molecule^{-1} s^{-1} at 298 K with an estimated uncertainty of ±25%. The measurements are summarized in table III-G-60.

III-G-37.3. Summary of the Atmospheric Fate of $C_4F_9OCH_3$, and the End Products of Its Oxidation

The atmospheric lifetimes of the two isomers of $C_4F_9OCH_3$ are both likely similar to those for other methyl perfluoroalkyl ethers, approximately 4.5 years. Wallington et al. (1997b) have examined the end products of the Cl-atom-initiated oxidation of both *n*-$C_4F_9OCH_3$ and *iso*-$C_4F_9OCH_3$; they conclude that the major end products of the oxidation are the corresponding perfluorobutyl formates, *n*- and *iso*-C_4F_9OCHO. The results of Nolan et al. (1999) agree with this assessment; they report an approximate 100% yield of perfluorobutyl formate end product. The same products are expected from the more atmospherically relevant OH-initiated oxidation process.

Table III-G-60. Rate coefficients ($k = A\times e^{-B/T}$, cm^3 molecule^{-1} s^{-1}) for reaction of Cl with a mixture of *n*-$C_4F_9OCH_3$ and *iso*-$C_4F_9OCH_3$

$10^{10}\times A$	B (K)	$10^{14}\times k$	T (K)	Technique[a]	Reference	Temperature Range (K)
		9.9 ± 0.5	295	RR[b] (CH_4)	Wallington et al. (1997b)	
		8.9 ± 0.5	295	RR[c] (CH_3Cl)		
2.3 ± 1.4	2,254 ± 177	1.7 ± 0.7	234	DF–MS	Aranda et al. (2006)	234–315
		4.6 ± 1.1	263			
		5.5 ± 0.9	273			
		7.3 ± 1.5	285			
		14.3 ± 2.8	298			
		17.6 ± 2.0	315			

[a]Abbreviations used for the techniques are defined in table I-F-3.
[b]Placed on an absolute basis using $k(\text{Cl+CH}_4) = 0.99 \times 10^{-13}$ cm^3 molecule^{-1} s^{-1} at 295 K (Atkinson et al., 2006).
[c]Placed on an absolute basis using $k(\text{Cl+CH}_3\text{Cl}) = 4.7 \times 10^{-13}$ cm^3 molecule^{-1} s^{-1} (Atkinson et al., 2008).

III-G-38. 1,1,1,2,3,3-Hexafluoro-3-(2,2,2-trifluoroethoxy) propane (2,2,2-Trifluoroethyl 1,1,2,3,3,3-hexafluoro-*n*-propyl Ether, $CF_3CHFCF_2OCH_2CF_3$)

III-G-38.1. OH Reaction Kinetics

The rate coefficient for reaction of OH with $CF_3CHFCF_2OCH_2CF_3$ has been determined by Chen et al. (2003a) and by Wilson et al. (2007) as a function of temperature using relative rate techniques, see table III-G-61. Data obtained by the two groups are in good agreement. Fitting of the combined data to a simple Arrhenius expression yields $k = 1.2 \times 10^{-12} \exp(-1{,}469/T)$ cm^3 molecule^{-1} s^{-1}, with $k = 8.8 \times 10^{-15}$ cm^3 molecule^{-1} s^{-1} at 298 K. An uncertainty of $\pm 15\%$ is estimated at 298 K.

III-G-38.2. Summary of the Atmospheric Fate of $CF_3CHFCF_2OCH_2CF_3$, and the End Products of Its Oxidation

The atmospheric lifetime for $CF_3CHFCF_2OCH_2CF_3$ is estimated to be 6 years, for a globally averaged [OH] $\approx 10^6$ molecule cm^{-3} and a tropospheric average temperature of 272 K. No products studies have been conducted for this species.

III-G-39. 1,1,1,2,2,3,3-Heptafluoro-3-(1,2,2,2-tetrafluoroethoxy) propane ([1,2,2,2-Tetrafluoroethyl Perfluoro-*n*-propyl Ether, $CF_3CF_2CF_2OCHFCF_3$)

III-G-39.1. OH Reaction Kinetics

Oyaro et al. (2005) have reported an upper limit for the rate coefficient for reaction of OH radicals with $CF_3CF_2CF_2OCHFCF_3$, $k < 1 \times 10^{-15}$ cm^3 molecule^{-1} s^{-1} at 298 K. The data are summarized in table III-G-62.

III-G-39.2. Cl-Atom Reaction Kinetics

An upper limit to the rate coefficient for reaction of Cl-atoms with $CF_3CF_2CF_2OCHFCF_3$ has been reported by Oyaro et al. (2005), $k < 3 \times 10^{-15}$ cm^3 molecule^{-1} s^{-1} at 298 K. The data are summarized in table III-G-62.

III-G-39.3. Summary of the Atmospheric Fate of $CF_3CF_2CF_2OCHFCF_3$, and the End Products of Its Oxidation

On the basis of the upper limit for its rate coefficient with OH (Oyaro et al., 2005), the atmospheric lifetime for $CF_3CF_2CF_2OCHFCF_3$ will be in excess of 30 years. Likely products of the OH-initiated oxidation, which must occur via abstraction at the CHF group, are $FC(O)OCF_2CF_2CF_3$ (with COF_2 as co-product), or $CF_3CF_2CF_2OC(=O)CF_3$.

Table III-G-61. Rate coefficients ($k = A \times e^{-B/T}$, cm^3 $molecule^{-1}$ s^{-1}) for reaction of OH with $CF_3CHFCF_2OCH_2CF_3$

$10^{13} \times A$	B (K)	$10^{15} \times k$	T (K)	Technique[a]	Reference	Temperature Range (K)
21[b]	1,624[b]	4.7 ± 0.6	268	RR[c] (CH_3CCl_3)	Chen et al. (2003a)	268–308
		5.9 ± 0.4	278			
		7.1 ± 0.3	288			
		8.5 ± 0.3	298			
		9.7 ± 0.4	308			
		4.8 ± 0.3	268	RR[d] (CHF_2Cl)		
		6.1 ± 0.4	278			
		7.8 ± 0.3	288			
		9.2 ± 0.3	298			
		10.5 ± 0.3	308			
9.8[b]	1,400[b]	5.74	272	RR[e] (CF_3CH_2F,	Wilson et al. (2007)	272–407
		6.17	276	HFC-134a)		
		7.48	287			
		8.43	292			
		10.7	313			
		12.6	324			
		14.6	332			
		14.3	338			
		18.2	352			
		21.3	363			
		27.7	391			
		27.7	391			
		31.3	407			
16.5[b]	1,564[b]	5.28	270	RR[f] (CF_3CHFCF_3,		270–404
		5.63	275	HFC-227ea)		
		8.44	298			
		12.5	323			
		18.2	348			
		25.6	374			
		35.6	404			

[a]Abbreviations used for the techniques are defined in table I-F-3.
[b]Values obtained from least-squares fit of data obtained using updated reference rate coefficients, and thus differ from those originally reported.
[c]Placed on an absolute basis using $k(OH+CH_3CCl_3) = 1.81 \times 10^{-12} \exp(-1{,}543/T)$ cm^3 $molecule^{-1}$ s^{-1} (Calvert et al., 2008).
[d]Placed on an absolute basis using $k(OH+CHF_2Cl) = 1.48 \times 10^{-12} \exp(-1{,}710/T)$ cm^3 $molecule^{-1}$ s^{-1} (Calvert et al., 2008).
[e]Placed on an absolute basis using $k(OH+HFC\text{-}134a) = 1.01 \times 10^{-12} \exp(-1{,}640/T)$ cm^3 $molecule^{-1}$ s^{-1} (Calvert et al., 2008).
[f]Placed on an absolute basis using $k(OH+HFC\text{-}227ea) = 6.55 \times 10^{-13} \exp(-1{,}809/T)$ cm^3 $molecule^{-1}$ s^{-1} (Calvert et al., 2008).

III-G-40. 1,1,1,2,2,3,3,4,4,5,5-Undecafluoro-5-methoxypentane (Methyl Perfluoro-*n*-pentyl Ether, $CH_3OCF_2CF_2CF_2CF_2CF_3$)

III-G-40.1. OH Reaction Kinetics

There are no data available regarding the reaction of OH with $CH_3OCF_2CF_2CF_2CF_2CF_3$. However, on the basis of data for the reaction of OH with other methyl perfluoroalkyl ethers, a value of $k = 1.2 \times 10^{-14}$ cm^3 $molecule^{-1}$ s^{-1} can be estimated near 298 K.

Table III-G-62. Rate coefficients (k, cm^3 molecule^{-1} s^{-1}) for reaction of OH and Cl with $CF_3CF_2CF_2OCHFCF_3$

$10^{15} \times k$	T (K)	Technique[a]	Reference
OH + $CF_3CF_2CF_2OCHFCF_3$			
< 1	298	RR[b] (CHF_2CH_2F)	Oyaro et al. (2005)
Cl + $CF_3CF_2CF_2OCHFCF_3$			
< 3	298	RR[c] (CHF_2CH_2F)	Oyaro et al. (2005)

[a]Abbreviations used for the techniques are defined in table I-F-3.
[b]Placed on an absolute basis using $k(OH+CHF_2CH_2F) = 1.6 \times 10^{-14}$ cm^3 molecule^{-1} s^{-1} (Calvert et al., 2008).
[c]Placed on an absolute basis using $k(Cl + CHF_2CH_2F) = 5.0 \times 10^{-14}$ cm^3 molecule^{-1} s^{-1} (Atkinson et al., 2008).

Table III-G-63. Rate coefficients (k, cm^3 molecule^{-1} s^{-1}) for reaction of Cl with $CH_3OCF_2CF_2CF_3$

$10^{14} \times k$	T (K)	Technique[a]	Reference
10.2 ± 1.4	295	RR[b] (CH_4)	Nohara et al. (2001)

[a]Abbreviations used for the techniques are defined in table I-F-3.
[b]Placed on an absolute basis using $k(Cl+CH_4) = 0.99 \times 10^{-13}$ cm^3 molecule^{-1} s^{-1} (Atkinson et al., 2006).

III-G-40.2. Cl-Atom Reaction Kinetics

Nohara et al. (2001) have determined $k(Cl + CH_3OCF_2CF_2CF_3) = 10.2 \times 10^{-14}$ cm^3 molecule^{-1} s^{-1} at 298 K, using a relative rate technique, see table III-G-63.

III-G-40.3. Summary of the Atmospheric Fate of $CH_3OCF_2CF_2CF_2CF_2CF_3$, and the End Products of Its Oxidation

The atmospheric lifetime for $CH_3OCF_2CF_2CF_2CF_2CF_3$ can be estimated roughly to be 3–5 years, on the basis of data for other methyl perfluoroalkyl ethers. Nohara et al. (2001) show that the formate ester, $HC(O)OCF_2CF_2CF_2CF_2CF_3$, is the dominant primary product in the Cl-atom-initiated oxidation; this product will be formed in high yield from the OH-initiated oxidation as well.

III-G-41. 1,1,1,2,3,3-Hexafluoro-3-(2,2,3,3,3-pentafluoropropoxy)propane (1,1,2,3,3,3-Hexafluoropropyl 2,2,3,3,3-pentafluoropropyl Ether, $CF_3CHFCF_2OCH_2CF_2CF_3$)

III-G-41.1. OH Reaction Kinetics

The reaction of $CF_3CHFCF_2OCH_2CF_2CF_3$ with OH has been studied as a function of temperature by Chen et al. (2005a), using a relative rate technique. The data are summarized in table III-G-64 and are displayed in figure III-G-10. The Arrhenius expression of Chen et al. (2005a) is recommended, $k = 8.46 \times 10^{-13} \exp(-1{,}460/T)$

Table III-G-64. Rate coefficients ($k = A \times e^{-B/T}$, cm^3 $molecule^{-1}$ s^{-1}) for reaction of OH with $CF_3CHFCF_2OCH_2CF_2CF_3$

$10^{13} \times A$	B (K)	$10^{15} \times k$	T (K)	Technique[a]	Reference	Temperature Range (K)
8.46 ± 1.83	1,460 ± 60	2.72 ± 0.11	253	RR[b] ($C_2F_5OCH_3$)	Chen et al. (2005a)	253–328
		3.58 ± 0.44	268			
		4.77 ± 0.32	283			
		6.27 ± 0.47	298			
		7.78 ± 0.47	313			
		10.5 ± 0.7	328			
		2.60 ± 0.06	253	RR[c] (n-$C_3F_7OCH_3$)		
		3.69 ± 0.26	268			
		4.54 ± 0.20	283			
		6.19 ± 0.27	298			
		7.85 ± 0.99	313			
		9.75 ± 0.70	328			

[a]Abbreviations used for the techniques are defined in table I-F-3.
[b]Placed on an absolute basis using $k(OH+C_2F_5OCH_3) = 1.90 \times 10^{-12} \exp(-1{,}510/T)$ cm^3 $molecule^{-1}$ s^{-1} (Tokuhashi et al., 1999b, and this book, section III-G-12.1).
[c]Placed on an absolute basis using $k(OH+n\text{-}C_3F_7OCH_3) = 2.06 \times 10^{-12} \exp(-1{,}540/T)$ cm^3 $molecule^{-1}$ s^{-1} (Tokuhashi et al., 1999b, and this book, section III-G-29.1).

cm^3 $molecule^{-1}$ s^{-1}, with k (298 K) $= 6.3 \times 10^{-15}$ cm^3 $molecule^{-1}$ s^{-1}. An uncertainty of ±25% is assigned to the 298 K value.

III-G-41.2. Summary of the Atmospheric Fate of $CF_3CHFCF_2OCH_2CF_2CF_3$, and the End Products of Its Oxidation

The lifetime of $CF_3CHFCF_2OCH_2CF_2CF_3$ is estimated to be about 8 years, for [OH] ≈ 10^6 molecule cm^{-3} and an average tropospheric temperature of 272 K. Products of the oxidation of this species have not been studied. However, the majority of the reaction of OH with $CF_3CHFCF_2OCH_2CF_2CF_3$ is expected to occur at the CH_2 group. The likely end products are the formate ester, $CF_3CHFCF_2OC(O)H$ (with two molecules of COF_2 as co-product), or the propionate ester, $CF_3CHFCF_2OC(O)CF_2CF_3$.

III-G-42. 1,1,1,2,3,3-Hexafluoro-3-(2,2,3,3-tetrafluoropropoxy)propane (1,1,2,3,3,3-Hexafluoro-*n*-propyl 2,2,3,3-tetrafluoro-*n*-propyl Ether ($CF_3CHFCF_2OCH_2CF_2CHF_2$)

III-G-42.1. OH Reaction Kinetics

Chen et al. (2003a) used a relative rate technique to obtain rate coefficients for reaction of OH with $CF_3CHFCF_2OCH_2CF_2CHF_2$ as a function of temperature. As summarized in table III-G-65, their data using two different reference reactions are internally consistent. Fitting a simple Arrhenius expression to the dataset yields: $k = 2.44 \times 10^{-12} \exp(-1{,}563/T)$ cm^3 $molecule^{-1}$ s^{-1}, with $k = 1.28 \times 10^{-14}$ cm^3 $molecule^{-1}$ s^{-1} at 298 K. The uncertainty at 298 K is estimated to be ±25%.

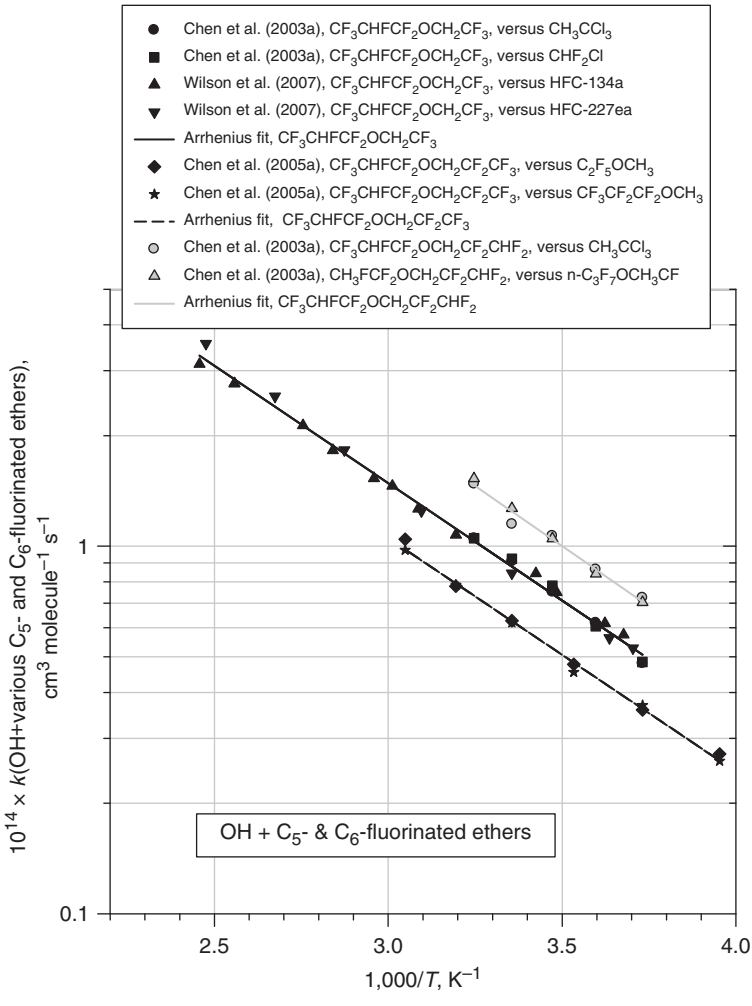

Figure III-G-10. Arrhenius plot of the rate coefficient for the reaction of OH with various five- and six-carbon fluorinated ethers.

III-G-42.2. Summary of the Atmospheric Fate of $CF_3CHFCF_2OCH_2CF_2CHF_2$, and the End Products of Its Oxidation

The atmospheric lifetime for $CF_3CHFCF_2OCH_2CF_2CHF_2$ can be estimated from the OH rate coefficient of Chen et al. (2003a). Assuming a global average [OH] $\approx 10^6$ molecule cm^{-3} and a tropospheric average temperature of 272 K, a lifetime of 4.1 years is estimated.

Products of the OH-initiated oxidation have not been determined. However, the majority of the reaction is likely to occur at the CH_2 group, resulting in the production of the formate ester, $CF_3CHFCF_2OC(O)H$ (with two molecules of COF_2 as co-product), or the propionate ester, $CF_3CHFCF_2OC(O)CF_2CHF_2$.

Table III-G-65. Rate coefficients ($k = A \times e^{-B/T}$, cm^3 molecule^{-1} s^{-1}) for reaction of OH with $CF_3CHFCF_2OCH_2CF_2CHF_2$

$10^{12} \times A$	B (K)	$10^{15} \times k$	T (K)	Technique[a]	Reference	Temperature Range (K)
2.44[b]	1,563[b]	7.4 ± 0.5	268	RR[c] (CH_3CCl_3)	Chen et al. (2003a)	268–308
		9.0 ± 0.6	278			
		11.3 ± 0.3	288			
		12.3 ± 0.6	298			
		15.9 ± 0.8	308			
		7.0 ± 0.3	268	RR[d] ($CH_3OCF_2CF_2CF_3$)		
		8.4 ± 0.5	278			
		10.5 ± 0.3	288			
		12.7 ± 0.5	298			
		15.3 ± 0.7	308			

[a]Abbreviations used for the techniques are defined in table I-F-3.

[b]Values obtained from least-squares fit of data obtained using updated reference rate coefficients, and thus differ from those originally reported.

[c]Placed on an absolute basis using $k(OH+CH_3CCl_3) = 1.41 \times 10^{-12} \exp(-1{,}543/T)$ cm^3 molecule^{-1} s^{-1} (Calvert et al., 2008).

[d]Placed on an absolute basis using $k(OH+CH_3OCF_2CF_2CF_3) = 2.06 \times 10^{-12} \exp(-1{,}540/T)$ cm^3 molecule^{-1} s^{-1} (Calvert et al., 2008).

III-G-43. 1-Ethoxy-1,1,2,2,3,3,4,4,4-nonafluorobutane (Ethyl Perfluoro-*n*-butyl Ether, *n*-$C_4F_9OCH_2CH_3$, *n*-HFE-7200) and 1-Ethoxy-1,1,2,3,3,3-hexafluoro-2-(trifluoromethyl)propane (Ethyl Perfluoro-*iso*-butyl Ether, *iso*-$C_4F_9OCH_2CH_3$, *i*-HFE-7200)

III-G-43.1. OH Reaction Kinetics

The reactions of OH with the two isomers of $C_4F_9OCH_2CH_3$ have been studied by Christensen et al. (1998a), using a relative rate technique.The reactivities of the two species near 295 K are measurably different, $k(OH + n\text{-}C_4F_9OCH_2CH_3) = 6.5 \times 10^{-14}$ cm^3 molecule^{-1} s^{-1} and $k(OH + iso\text{-}C_4F_9OCH_2CH_3) = 7.9 \times 10^{-14}$ cm^3 molecule^{-1} s^{-1}. The measurements are summarized in table III-G-66.

III-G-43.2. Cl-Atom Reaction Kinetics

The relative rate study of Christensen et al. (1998a) demonstrated that the rate coefficients for reaction of Cl with *n*-$C_4F_9OCH_2CH_3$ and *iso*-$C_4F_9OCH_2CH_3$ are indistinguishable, $k = 2.7 \times 10^{-12}$ cm^3 molecule^{-1} s^{-1} near 296 K. Aranda et al. (2006) studied an unspecified mixture of *n*- and *iso*-$C_4F_9OCH_2CH_3$ over a range of temperatures, using a discharge flow–mass spectrometric technique. Their data near 298 K are in reasonable agreement with those of Christensen et al. The recommended Arrhenius expression: $k = 4.1 \times 10^{-11} \exp(-852/T)$ cm^3 molecule^{-1} s^{-1}, is obtained by combining an average of the two determinations near 295 K, $k = 2.4 \times 10^{-12}$ cm^3 molecule^{-1} s^{-1}, with the temperature dependence of Aranda et al. An uncertainty of ±25% is estimated at 295 K. The data are summarized in table III-G-67.

Table III-G-66. Rate coefficients (k, cm^3 molecule^{-1} s^{-1}) for reaction of OH with n-$C_4F_9OCH_2CH_3$ and iso-$C_4F_9OCH_2CH_3$

$10^{14} \times k$	T (K)	Technique[a]	Reference
OH + *n*-$C_4F_9OCH_2CH_3$			
6.5 ± 0.7	295	RR[b] (CH_3Cl)	Christensen et al. (1998a)
5.0 ± 1.0[c]	295	RR[d] (CH_4)	
OH + *iso*-$C_4F_9OCH_2CH_3$			
7.9 ± 0.8	295	RR[b] (CH_3Cl)	Christensen et al. (1998a)

[a]Abbreviations used for the techniques are defined in table I-F-3.
[b]Placed on an absolute basis using $k(OH+CH_3Cl) = 3.7 \times 10^{-14}$ cm^3 molecule^{-1} s^{-1} at 295 K (Calvert et al., 2008).
[c]Value deemed less accurate by the authors, and not used in the final analysis.
[d]Placed on an absolute basis using $k(OH+CH_4) = 6.0 \times 10^{-15}$ cm^3 molecule^{-1} s^{-1} at 295 K (Calvert et al., 2008).

Table III-G-67. Rate coefficients ($k = A \times e^{-B/T}$, cm^3 molecule^{-1} s^{-1}) for reaction of Cl with a mixture of n-$C_4F_9OCH_2CH_3$ and iso-$C_4F_9OCH_2CH_3$

$10^{11} \times A$	B (K)	$10^{12} \times k$	T (K)	Technique[a]	Reference	Temperature Range (K)
		2.96 ± 0.16	295	RR[b] (C_2H_5Cl)	Christensen et al. (1998a)	
		2.68 ± 0.18	295	RR[c] (CH_3Cl)		
		2.38 ± 0.08	295	RR[d] (CH_3OCHO)		
3.7 ± 0.5	852 ± 38	1.0 ± 0.1	234	DF–MS	Aranda et al. (2006)	234–333
		1.5 ± 0.1	266			
		2.1 ± 0.1	298			
		2.5 ± 0.2	315			
		3.1 ± 0.4	333			

[a]Abbreviations used for the techniques are defined in table I-F-3.
[b]Placed on an absolute basis using $k(Cl+C_2H_5Cl) = 7.8 \times 10^{-12}$ cm^3 molecule^{-1} s^{-1} (this book, table I-F-2).
[c]Placed on an absolute basis using $k(Cl+CH_3Cl) = 4.7 \times 10^{-13}$ cm^3 molecule^{-1} s^{-1} (Atkinson et al., 2008).
[d]Placed on an absolute basis using $k(Cl+CH_3OCHO) = 1.4 \times 10^{-12}$ cm^3 molecule^{-1} s^{-1} (Wallington et al., 1993b).

III-G-43.3. Summary of the Atmospheric Fate of n- and iso-$C_4F_9OCH_2CH_3$, and the End Products of Its Oxidation

The atmospheric lifetime for n- and iso-$C_4F_9OCH_2CH_3$ can be estimated from the OH rate coefficient data of Christensen et al. (1998a), 0.5 and 0.4 years, respectively. The Cl-atom-initiated oxidation of iso-$C_4F_9OCH_2CH_3$ was studied by Christensen et al. (1998a). Their data show that the main site for Cl-atom attack is at the CH_2 group, which leads to two products, the acetate ester, $CH_3C(O)OCF(CF_3)CF_2CF_3$ ($\sim$ 70% molar yield in air), and the formate ester, $HC(O)OCF(CF_3)CF_2CF_3$ ($\sim$ 25%). The two products result from competing pathways in the chemistry of the alkoxy radical, iso-$C_4F_9OCH(O\bullet)CH_3$, reaction with O_2 and C—C bond rupture:

$$iso\text{-}C_4F_9OCH(O\bullet)CH_3 + O_2 \rightarrow iso\text{-}C_4F_9OC(=O)CH_3 + HO_2$$

$$iso\text{-}C_4F_9OCH(O\bullet)CH_3 \rightarrow iso\text{-}C_4F_9OC(=O)H + \bullet CH_3$$

III-G-44. Chloro(methoxy)methane (Methyl Chloromethyl Ether, CH_3OCH_2Cl)

III-G-44.1. OH Reaction Kinetics

No experimental data are available for this reaction.

III-G-44.2. Cl-Atom Reaction Kinetics

As part of a study of the atmospheric chemistry of dimethyl ether, Jenkin et al. (1993b) conducted a relative rate study of the reaction of Cl-atoms with CH_3OCH_2Cl. Their study leads to $k = 2.8 \times 10^{-11}$ cm^3 molecule^{-1} s^{-1} at 295 K, with an estimated uncertainty of ±35%. The data are summarized in table III-G-68.

III-G-44.3. Summary of the Atmospheric Fate of CH_3OCH_2Cl, and the End Products of Its Oxidation

The atmospheric lifetime of CH_3OCH_2Cl is unknown. Potential end products of its OH-initiated oxidation are $HC(O)OCH_2Cl$, $CH_3OC(O)Cl$, and CH_3OCHO.

III-G-45. Dichloro(methoxy)methane (Methyl Dichloromethyl Ether, CH_3OCHCl_2)

III-G-45.1. OH Reaction Kinetics

No data are available for this reaction.

III-G-45.2. Cl-Atom Reaction Kinetics

Dalmasso et al. (2005, 2008) determined the rate coefficient for reaction of Cl-atoms with CH_3OCHCl_2 using a relative rate technique, see table III-G-68. Their data lead

Table III-G-68. Rate coefficients (k, cm^3 molecule^{-1} s^{-1}) for reaction of Cl with CH_3OCH_2Cl and CH_3OCHCl_2

$10^{12} \times k$	T (K)	Technique[a]	Reference
Cl + CH_3OCH_2Cl			
29.5	295	RR[b] (C_2H_4)	Jenkin et al. (1993b)
26.5	295	RR[c] (CH_3OCH_3)	
Cl + CH_3OCHCl_2			
1.04 ± 0.20	298	RR[d] (CH_2ClCH_2Cl)	Dalmasso et al. (2005; 2008)
0.90 ± 0.26	298	RR[e] ($CH_3C(O)CH_3$)	
1.03 ± 0.11	296	RR[d] (CH_2ClCH_2Cl)	

[a]Abbreviations used for the techniques are defined in table I-F-3.
[b]Placed on an absolute basis using $k(Cl+C_2H_4) = 9.5 \times 10^{-11}$ cm^3 molecule^{-1} s^{-1} (this book, table I-F-2).
[c]Placed on an absolute basis using $k(Cl+CH_3OCH_3) = 18 \times 10^{-11}$ cm^3 molecule^{-1} s^{-1} (this book, section III-B-1.3).
[d]Placed on an absolute basis using $k(Cl+CH_2ClCH_2Cl) = 1.3 \times 10^{-12}$ cm^3 molecule^{-1} s^{-1} (Wallington et al., 1996b).
[e]Placed on an absolute basis using $k(Cl+CH_3C(O)CH_3) = 2.1 \times 10^{-12}$ cm^3 molecule^{-1} s^{-1} (Atkinson et al., 2006).

to $k = 9.9 \times 10^{-13}$ cm^3 molecule^{-1} s^{-1} at 298 K, with an estimated uncertainty of ±25%.

III-G-45.3. Summary of the Atmospheric Fate of CH_3OCHCl_2, and the End Products of Its Oxidation

The atmospheric lifetime of CH_3OCHCl_2 is not known. Potential end products of its OH-initiated oxidation include $HC(O)OCHCl_2$ and $CH_3OC(O)Cl$.

III-G-46. 1-Chloro-2-methoxyethane (2-Chloroethyl Methyl Ether, $CH_3OCH_2CH_2Cl$)

III-G-46.1. OH Reaction Kinetics

McLoughlin et al. (1993) have conducted a relative rate study of the reaction of OH with $CH_3OCH_2CH_2Cl$; their data, summarized in table III-G-69, lead to a rate coefficient $k = 4.3 \times 10^{-12}$ cm^3 molecule^{-1} s^{-1} at 300 K. An uncertainty of ±35% is assigned, in the absence of corroborative data.

III-G-46.2. Cl-Atom Reaction Kinetics

There are three relative rate determinations of the rate coefficient for reaction of Cl-atoms with $CH_3OCH_2CH_2Cl$ in the literature (McLoughlin et al., 1993; Dalmasso et al., 2005, 2008). The three values are in reasonable agreement, see table III-G-70, and an average value, $k = 1.3 \times 10^{-10}$ cm^3 molecule^{-1} s^{-1}, is recommended near 298 K.

III-G-46.3. Summary of the Atmospheric Fate of $CH_3OCH_2CH_2Cl$, and the End Products of Its Oxidation

The atmospheric lifetime for $CH_3OCH_2CH_2Cl$ will be about 3 days, assuming a diurnally averaged [OH] $\approx 10^6$ molecule cm^{-3}. End products of the atmospheric oxidation process are not known. However, OH attack at the CH_3 and CH_2 sites adjacent to the ether oxygen seems likely, leading to $HC(O)OCH_2CH_2Cl$ and either $CH_3OC(O)CH_2Cl$ or CH_3COCHO and HC(O)Cl, respectively.

Table III-G-69. Rate coefficient (k, cm^3 molecule^{-1} s^{-1}) for reaction of OH with $CH_3OCH_2CH_2Cl$

$10^{12} \times k$	T (K)	Technique[a]	Reference
4.30 ± 0.95	300	RR[b] ($C_2H_5OC_2H_5$)	McLoughlin et al. (1993)

[a]Abbreviations used for the techniques are defined in table I-F-3.
[b]Placed on an absolute basis using $k(OH+C_2H_5OC_2H_5) = 1.2 \times 10^{-11}$ cm^3 molecule^{-1} s^{-1} (this book, section III-B-3.1).

Table III-G-70. Rate coefficients (k, cm^3 molecule^{-1} s^{-1}) for reaction of Cl with $CH_3OCH_2CH_2Cl$

$10^{11} \times k$	T (K)	Technique[a]	Reference
15.7 ± 5.5	300	RR[b] ($C_2H_5OC_2H_5$)	McLoughlin et al. (1993)
11.1 ± 2.0	298	RR[c] (C_2H_6)	Dalmasso et al. (2005, 2008)
12.2 ± 1.1	296	RR[d] (n-C_5H_{12})	

[a]Abbreviations used for the techniques are defined in table I-F-3.
[b]Placed on an absolute basis using $k(Cl+C_2H_5OC_2H_5) = 2.8 \times 10^{-10}$ cm^3 molecule^{-1} s^{-1} (this book, section III-B-3.3).
[c]Placed on an absolute basis using $k(Cl+C_2H_6) = 5.9 \times 10^{-11}$ cm^3 molecule^{-1} s^{-1} (Calvert et al., 2008; Atkinson et al., 2006).
[d]Placed on an absolute basis using $k(Cl+n\text{-}C_5H_{12}) = 2.7 \times 10^{-10}$ cm^3 molecule^{-1} s^{-1} (Calvert et al., 2008).

III-G-47. 1,1-Dichloro-2-methoxyethane (2,2-Dichloroethyl Methyl Ether, $CH_3OCH_2CHCl_2$)

III-G-47.1. OH Reaction Kinetics

A relative rate study of the reaction of OH with $CH_3OCH_2CHCl_2$ (McLoughlin et al., 1993) leads to a rate coefficient $k = 2.1 \times 10^{-12}$ cm^3 molecule^{-1} s^{-1} at 300 K, see table III-G-71. An uncertainty of ±35% is assigned.

III-G-47.2. Cl-Atom Reaction Kinetics

The relative rate study of McLoughlin et al. (1993) for reaction of Cl-atoms with $CH_3OCH_2CHCl_2$ leads to a rate coefficient, $k = 4.8 \times 10^{-11}$ cm^3 molecule^{-1} s^{-1} at 300 K. The data are summarized in table III-G-72.

Table III-G-71. Rate coefficient (k, cm^3 molecule^{-1} s^{-1}) for reaction of OH with $CH_3OCH_2CHCl_2$

$10^{12} \times k$	T (K)	Technique[a]	Reference
2.14 ± 0.45	300	RR[b] ($C_2H_5OC_2H_5$)	McLoughlin et al. (1993)

[a]Abbreviations used for the techniques are defined in table I-F-3.
[b]Placed on an absolute basis using $k(OH+C_2H_5OC_2H_5) = 1.24 \times 10^{-11}$ cm^3 molecule^{-1} s^{-1} (this book, section III-B-3.1).

Table III-G-72. Rate coefficient (k, cm^3 molecule^{-1} s^{-1}) for reaction of Cl with $CH_3OCH_2CH_2Cl$

$10^{11} \times k$	T (K)	Technique[a]	Reference
4.8 ± 1.8	300	RR[b] ($C_2H_5OC_2H_5$)	McLoughlin et al. (1993)

[a]Abbreviations used for the techniques are defined in table I-F-3.
[b]Placed on an absolute basis using $k(Cl+C_2H_5OC_2H_5) = 2.8 \times 10^{-10}$ cm^3 molecule^{-1} s^{-1} (this book, section III-B-3.3).

III-G-47.3. Summary of the Atmospheric Fate of $CH_3OCH_2CHCl_2$, and the End Products of Its Oxidation

On the basis of the OH rate coefficient measurement of McLouglin et al. (1993) and an assumed average [OH] $\approx 10^6$ molecule cm^{-3}, the atmospheric lifetime for $CH_3OCH_2CHCl_2$ is 5.5 days. Expected end products of the OH-initiated oxidation in the atmosphere include $HC(O)OCH_2CHCl_2$ (following OH attack at the CH_3 group), and either $CH_3OC(O)CHCl_2$ or CH_3OCHO and $COCl_2$ (following OH attack at the CH_2 group).

III-G-48. Bromo(methoxy)methane (Bromomethyl Methyl Ether, CH_3OCH_2Br)

III-G-48.1. OH Reaction Kinetics

No data are available for this reaction.

III-G-48.2. Cl-Atom Reaction Kinetics

Kambanis et al. (1995) report a temperature-independent value for the rate coefficient for reaction of Cl-atoms with CH_3OCH_2Br, $k = 2.6 \times 10^{-11}$ cm^3 $molecule^{-1}$ s^{-1} for $273 < T < 363$ K. Their data are summarized in table III-G-73.

III-G-48.3. Summary of the Atmospheric Fate of CH_3OCH_2Br, and the End Products of Its Oxidation

The atmospheric lifetime of CH_3OCH_2Br is not known. Potential end products of its OH-initiated oxidation include $HC(O)OCH_2Br$ and CH_3OCHO.

Table III-G-73. Rate coefficients ($k = A \times e^{-B/T}$, cm^3 $molecule^{-1}$ s^{-1}) for reaction of Cl with CH_3OCH_2Br

$10^{11} \times A$	B (K)	$10^{11} \times k$	T (K)	Technique[a]	Reference	Temperature Range (K)
2.61 ± 0.46	0	2.90 ± 0.45	273	VLPR–MS	Kambanis et al. (1995)	273–363
		2.67 ± 0.65	273			
		2.37 ± 0.18	273			
		2.78 ± 0.21	303			
		2.80 ± 0.24	303			
		2.53 ± 0.17	303			
		2.60 ± 0.52	333			
		2.58 ± 0.18	333			
		2.98 ± 0.13	333			
		2.40 ± 0.56	363			
		2.50 ± 0.22	363			
		2.22 ± 0.52	363			

[a]Abbreviations used for the techniques are defined in table I-F-3.

III-G-49. 1-Bromo-2-methoxyethane (2-Bromoethyl Methyl Ether, $CH_3OCH_2CH_2Br$)

III-G-49.1. OH Reaction Kinetics

The reaction of OH with $CH_3OCH_2CH_2Br$ has been studied by McLoughlin et al. (1993), using a relative rate technique. Their data lead to a rate coefficient $k = 6.3 \times 10^{-12}$ cm^3 molecule^{-1} s^{-1} at 300 K, see table III-G-74. An uncertainty of ±30% is assigned in the absence of corroborative data.

III-G-49.2. Cl-Atom Reaction Kinetics

McLoughlin et al. (1993) report $k = 17.9 \times 10^{-11}$ cm^3 molecule^{-1} s^{-1} for the rate coefficient for reaction of Cl with $CH_3OCH_2CH_2Br$ at 300 K. The data are summarized in table III-G-75.

III-G-49.3. Summary of the Atmospheric Fate of $CH_3OCH_2CH_2Br$, and the End Products of Its Oxidation

For daytime [OH] $\approx 2.5 \times 10^6$ molecule cm^{-3}, the atmospheric lifetime for $CH_3OCH_2CH_2Br$ is estimated to be 0.8 days. Alternatively, for a diurnally average [OH] $\approx 10^6$ molecule cm^{-3}, an estimated lifetime of 1.9 days is obtained. Among the expected end products of the atmospheric oxidation of this species are $HC(O)OCH_2CH_2Br$ (following OH attack at the CH_3 group), and either $CH_3OC(O)CH_2Br$ or CH_3OCHO and formaldehyde (following OH attack at the CH_2 group adjacent to the ether).

Table III-G-74. Rate coefficient (k, cm^3 molecule^{-1} s^{-1}) for reaction of OH with $CH_3OCH_2CH_2Br$

$10^{12} \times k$	T (K)	Technique[a]	Reference
6.29 ± 1.25	300	RR[b] ($C_2H_5OC_2H_5$)	McLoughlin et al. (1993)

[a]Abbreviations used for the techniques are defined in table I-F-3.
[b]Placed on an absolute basis using $k(OH+C_2H_5OC_2H_5) = 1.24 \times 10^{-11}$ cm^3 molecule^{-1} s^{-1} (this book, section III-B-3.1).

Table III-G-75. Rate coefficient (k, cm^3 molecule^{-1} s^{-1}) for reaction of Cl with $CH_3OCH_2CH_2Br$

$10^{11} \times k$	T (K)	Technique[a]	Reference
17.9 ± 5.9	300	RR[b] ($C_2H_5OC_2H_5$)	McLoughlin et al. (1993)

[a]Abbreviations used for the techniques are defined in table I-F-3.
[b]Placed on an absolute basis using $k(Cl+C_2H_5OC_2H_5) = 2.8 \times 10^{-10}$ cm^3 molecule^{-1} s^{-1} (this book, section III-B-3.3).

III-G-50. Iodo(methoxy)methane (Iodomethyl Methyl Ether, CH_3OCH_2I)

III-G-50.1. OH Reaction Kinetics

No data are available for this reaction.

III-G-50.2. Cl-Atom Reaction Kinetics

The reaction of Cl with CH_3OCH_2I has been studied as a function of temperature by Kambanis et al. (1996). They report: $k = 1.53 \times 10^{-12} \exp(750/T)$ cm^3 molecule^{-1} s^{-1}, with $k = 1.9 \times 10^{-11}$ cm^3 molecule^{-1} s^{-1} at 298 K. The negative temperature-dependence suggests the formation of a Cl—ICH_2OCH_3 complex in the reaction (Kambanis et al., 1996), and further kinetic and mechanistic studies would be interesting. Their data are summarized in table III-G-76.

III-G-50.3. Summary of the Atmospheric Fate of CH_3OCH_2I, and the End Products of Its Oxidation

The atmospheric lifetime of this species is not known. End products of its OH-initiated oxidation are likely two formate esters, $HC(O)OCH_3$ following OH attack at the CH_2I site, and $HC(O)OCH_2I$ following OH attack at the CH_3 site. Given the presence of a CH_2—I bond in the molecule, photolysis could also be an important atmospheric loss process.

III-G-51. 2-Chloro-1,1,2-trifluoro-1-methoxyethane (2-Chloro-1,1,2- trifluorethyl Methyl Ether, CH_3OCF_2CHFCl)

III-G-51.1. OH Reaction Kinetics

The reaction of OH with CH_3OCF_2CHFCl has been studied as a function of temperature by Tokuhashi et al. (1999b). As with all studies by this group, multiple techniques were used and care was taken in sample purification. Their data, $k = 2.59 \times 10^{-12} \exp(-1{,}260/T)$ cm^3 molecule^{-1} s^{-1} with $k = 3.8 \times 10^{-14}$ cm^3 molecule^{-1} s^{-1} at 298 K, are recommended. The estimated uncertainty at 298 K is ±20%. The 298 K data point from Heathfield et al. (1998) is considerably higher than

Table III-G-76. Rate coefficients ($k = A \times e^{-B/T}$, cm^3 molecule^{-1} s^{-1}) for reaction of Cl with CH_3OCH_2I

$10^{12} \times A$	B (K)	$10^{11} \times k$	T (K)	Technique[a]	Reference	Temperature Range (K)
1.53 ± 0.82	−(750 ± 300)	2.22 ± 0.37	273	VLPR–MS	Kambanis et al. (1996)	273–363
		1.83 ± 0.08	303			
		1.64 ± 0.25	333			
		1.17 ± 0.10	363			

[a]Abbreviations used for the techniques are defined in table I-F-3.

this recommendation, likely due to reactive impurities in the samples used. The data are summarized in table III-G-77 and figure III-G-11.

III-G-51.2. Cl-Atom Reaction Kinetics

The relative rate study of Dalmasso et al. (2006b) for the reaction of Cl-atoms with CH_3OCF_2CHFCl gives $k = 3.1 \times 10^{-13}$ cm^3 molecule^{-1} s^{-1} at 298 K. An uncertainty of ±35% is assigned to this value. The study is summarized in table III-G-78.

III-G-51.3. Summary of the Atmospheric Fate of CH_3OCF_2CHFCl, and the End Products of Its Oxidation

An atmospheric lifetime of 1.3 years is derived for CH_3OCF_2CHFCl, assuming an average tropospheric temperature of 272 K and [OH] $\approx 10^6$ molecule cm^{-3}. Reaction with OH will occur mainly at the CH_3 group, with the formate ester, $HC(O)OCF_2CHFCl$, a likely end product.

III-G-52. 2-Chloro-1,1,2-trifluoro-1-(difluoromethoxy)ethane ([Difluoromethyl 2-Chloro-1,1,2-trifluoroethyl Ether, CHF_2OCF_2CHFCl, Enflurane) and 1-Chloro-2,2,2-trifluoroethyl Difluoromethyl Ether ($CHF_2OCHClCF_3$, Isoflurane)

III-G-52.1. OH Reaction Kinetics

The two structurally similar compounds, CHF_2OCF_2CHFCl (Enflurane) and $CHF_2OCHClCF_3$ (Isoflurane), have found use as inhalational anesthetics. This usage, coupled with their potential effects on stratospheric ozone (due to the presence of Cl), has led to numerous studies of their atmospheric behavior. As summarized in table III-G-79 and figure III-G-12, rate coefficients for reaction of OH with both species

Table III-G-77. Rate coefficients ($k = A \times e^{-B/T}$, cm^3 molecule^{-1} s^{-1}) for reaction of OH with CH_3OCF_2CHFCl

$10^{12} \times A$	B (K)	$10^{14} \times k$	T (K)	Technique[a]	Reference	Temperature Range (K)
		16.5 ± 3.2	298	PR–UV abs.	Heathfield et al. (1998)	
2.59 ± 0.51	1,260 ± 60	1.71 ± 0.07	250	FP or PLP–LIF	Tokuhashi et al. (1999b)	250–430
		1.75 ± 0.07	250			
		2.67 ± 0.12	273			
		3.55 ± 0.13	298			
		3.61 ± 0.14	298			
		5.55 ± 0.26	331			
		8.93 ± 0.23	375			
		14.1 ± 0.4	430			
		14.4 ± 0.4	430			
		3.57 ± 0.15	298	DF–LIF		

[a]Abbreviations used for the techniques are defined in table I-F-3.

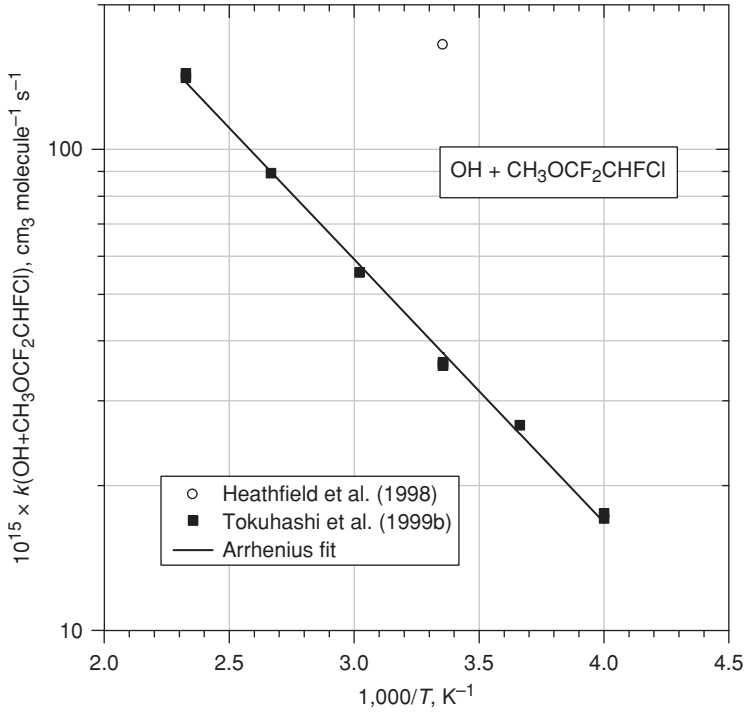

Figure III-G-11. Arrhenius plot of the rate coefficient for the reaction of OH with CH_3OCF_2CHFCl.

Table III-G-78. Rate coefficients (k, cm^3 molecule^{-1} s^{-1}) for reaction of Cl with CH_3OCF_2CHFCl

$10^{14} \times k$	T (K)	Technique[a]	Reference
30.3 ± 2.5	298	RR[b] (CH_2Cl_2)	Dalmasso et al. (2006b)
30.6 ± 2.3	298	RR[b] (CH_2Cl_2)	
32.5 ± 4.7	298	RR[c] (CH_2ClCH_2Cl)	

[a]Abbreviations used for the techniques are defined in table I-F-3.
[b]Placed on an absolute basis using $k(Cl+CH_2Cl_2) = 3.4 \times 10^{-13}$ cm^3 molecule^{-1} s^{-1} (Atkinson et al., 2008).
[c]Placed on an absolute basis using $k(Cl+CH_2ClCH_2Cl) = 1.3 \times 10^{-12}$ cm^3 molecule^{-1} s^{-1} at 298 K (Wallington et al., 1996b).

have been reported by Tokuhashi et al. (1999b) over the temperature range 250–430 K. As with all studies from this group, multiple techniques were used and care was taken in sample purification. Their data for these two reactions are recommended, k[OH + Enflurane (CHF_2OCF_2CHFCl)] = $7.46 \times 10^{-13} \exp(-1{,}230/T)$ cm^3 molecule^{-1} s^{-1} and k[OH + Isoflurane ($CHF_2OCHClCF_3$)] = $1.12 \times 10^{-12} \exp(-1{,}280/T)$ cm^3 molecule^{-1} s^{-1}. For 298 K, these expressions give values of 1.2×10^{-14} and 1.5×10^{-14} cm^3 molecule^{-1} s^{-1}, respectively, for the two compounds and are recommended with uncertainties of ±20%. For Enflurane, the 298 K measurement of

Table III-G-79. Rate coefficients ($k = A \times e^{-B/T}$, cm^3 $molecule^{-1}$ s^{-1}) for reaction of OH with CHF_2OCF_2CHFCl and $CHF_2OCHClCF_3$

$10^{12} \times A$	B (K)	$10^{15} \times k$	T (K)	Technique[a]	Reference	Temperature Range (K)
OH + CHF_2OCF_2CHFCl (Enflurane)						
		17 ± 5	302	DF–RF	Brown et al.	302–422
		47 ± 7	422		(1989a, 1990)	
		< 300	300	RR[b] ($C_2H_5OC_2H_5$)	McLoughlin et al. (1993)	
		12 ± 2	298	PLP–UV abs.	Langbein et al. (1999)	
0.746 ± 0.185	1,230 ± 80	5.05 ± 0.25	250	FP or PLP–LIF	Tokuhashi et al.	250–430
		5.91 ± 0.34	250		(1999b)	
		8.32 ± 0.55	273			
		11.4 ± 0.9	298			
		11.7 ± 0.7	298			
		17.0 ± 1.0	331			
		27.5 ± 1.0	375			
		44.4 ± 1.9	430			
		42.4 ± 2.3	430			
		12.4 ± 0.9	298	DF–LIF		
OH + $CHF_2OCHClCF_3$ (Isoflurane)						
		21 ± 7	298	DF–RF	Brown et al. (1989a, 1990)	
		< 300	300	RR[b] ($C_2H_5OC_2H_5$)	McLoughlin et al. (1993)	
		23 ± 1.9	298	RR[c]	Nolan et al. (1999)	
		17 ± 3	298	PLP–UV abs.	Langbein et al. (1999)	
1.12 ± 0.18	1,280 ± 50	6.58 ± 0.30	250	FP or PLP–LIF	Tokuhashi et al.	250–430
		6.93 ± 0.30	250		(1999b)	
		9.91 ± 0.56	273			
		10.4 ± 0.4	273			
		14.8 ± 0.6	298			
		14.8 ± 0.7	298			
		22.3 ± 0.9	331			
		35.1 ± 1.3	375			
		58.9 ± 2.1	430			
		57.0 ± 2.3	430			
		16.3 ± 0.8	298	DF–LIF		
0.45 ± 0.13	940 ± 100	19 ± 2	293	DF–RF	Beach et al.	293–393
		31 ± 3	360		(2001)	
		43 ± 4	393			

[a]Abbreviations used for the techniques are defined in table I-F-3.
[b]Placed on an absolute basis using $k(OH+C_2H_5OC_2H_5) = 1.24 \times 10^{-11}$ cm^3 $molecule^{-1}$ s^{-1} (this book, section III-B-3.1).
[c]Reference compound not specified.

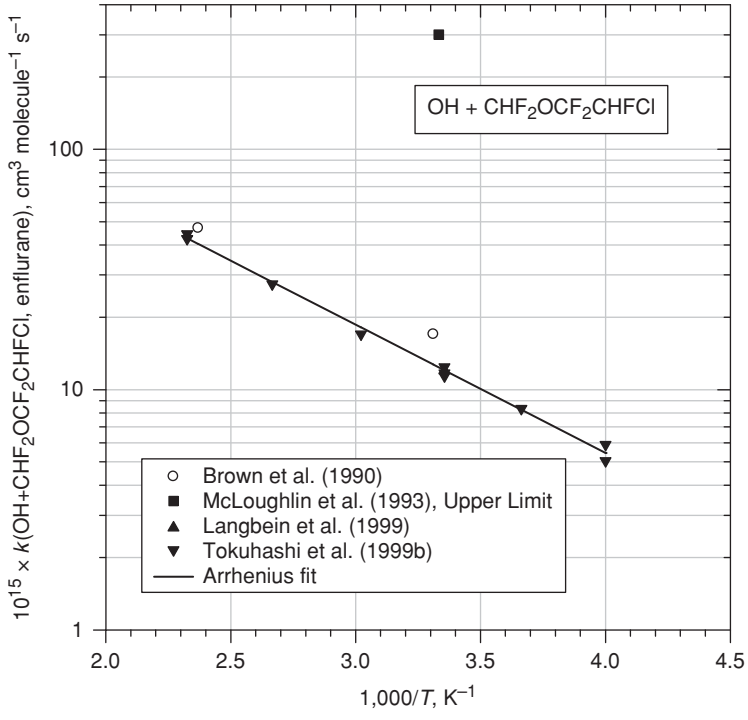

Figure III-G-12. Arrhenius plot of the rate coefficient for the reaction of OH with CHF_2OCF_2CHFCl (Enflurane).

Langbein et al. (1999) is in excellent agreement with the recommendation, as is the upper limit reported by McLoughlin et al. (1993). The 422 K data point of Brown et al. (1989a, 1990) also agrees well with the recommendation, while their 302 K data point is about 35% high (possibly due to the presence of reactive impurities). For Isoflurane, the upper limit of McLoughlin et al. (1993), the 298 K data point from Langbein et al. (1999), and the high temperature data from Beach et al. (2001) are all in agreement with the recommendation, while the 298 K data from Brown et al. (1989a, 1990), Nolan et al. (1999), and Beach et al. (2001) are somewhat high; see figure III-G-13.

III-G-52.2. Cl-Atom Reaction Kinetics

Dalmasso et al. (2006b) determined k[Cl + Enflurane (CHF_2OCF_2CHFCl)] = 3.2×10^{-15} cm^3 molecule^{-1} s^{-1} at 298 K, using a relative rate technique. The upper limit of McLoughlin et al. (1993), $k < 10^{-13}$ cm^3 molecule^{-1} s^{-1}, is consistent with this measurement. The four studies of the rate coefficient for reaction of Cl with Isoflurane (McLoughlin et al., 1993; Hickson and Smith., 2001; Beach et al., 2001; Wallington et al., 2002) are in reasonable agreement. Fitting of the Arrhenius expression to the combined dataset (except the upper limit of McLoughlin et al.) yields k[Cl + Isoflurane

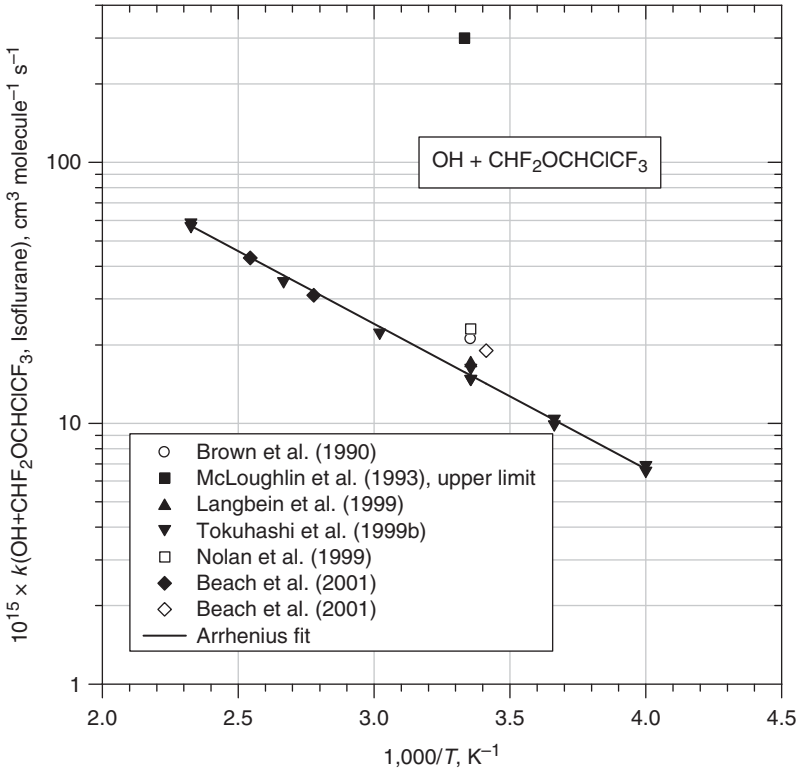

Figure III-G-13. Arrhenius plot of the rate coefficient for the reaction of OH with Isoflurane ($CHF_2OCHClCF_3$).

$(CHF_2OCHClCF_3)] = 1.6 \times 10^{-11} \exp(-2{,}450/T)$ cm^3 molecule^{-1} s^{-1}, exactly as reported by Hickson and Smith (2001). This expression returns a value of 4.3×10^{-15} cm^3 molecule^{-1} s^{-1} at 298 K, which is recommended with an uncertainty of ±40%. Data for both species are summarized in table III-G-80.

III-G-52.3. Summary of the Atmospheric Fate of CHF_2OCF_2CHFCl and $CHF_2OCHClCF_3$, and the End Products of Their Oxidation

Atmospheric lifetimes of 3.9 and 3.2 years are derived for CHF_2OCF_2CHFCl and $CHF_2OCHClCF_3$, respectively, assuming an average tropospheric temperature of 272 K and [OH] ≈ 10^6 molecule cm^{-3}. End products of the OH- and Cl-atom-initiated oxidation of isoflurane ($CHF_2OCHClCF_3$) have been determined by Wallington et al. (2002). The chemistry occurs predominantly (about 95% in the OH case) at the CHCl site, leading to the formation of $CF_3C(O)OCHF_2$ via Cl-atom elimination from the $CF_3CCl(O•)OCHF_2$ alkoxy radical.

Table III-G-80. Rate coefficients ($k = A \times e^{-B/T}$, cm^3 molecule^{-1} s^{-1}) for reaction of Cl with CHF_2OCF_2CHFCl and $CHF_2OCHClCF_3$

$10^{12} \times A$	B (K)	$10^{15} \times k$	T (K)	Technique[a]	Reference	Temperature Range (K)
Cl + CHF_2OCF_2CHFCl (Enflurane)						
		< 1,000	300	RR[b] ($C_2H_5OC_2H_5$)	McLoughlin et al. (1993)	
		3.17 ± 0.30	298	RR[c] (CF_3CH_2F)	Dalmasso et al. (2006b)	
		3.22 ± 0.32	298			
Cl + $CHF_2OCHClCF_3$ (Isoflurane)						
		< 1, 000	300	RR[b] ($C_2H_5OC_2H_5$)	McLoughlin et al. (1993)	
78 ± 26	2,980 ± 130	5.9 ± 0.5	318	FP–UV abs.	Beach et al. (2001)	318–399
		22 ± 2	362			
		44 ± 4	399			
16 ± 2	2,450 ± 250	3.9 ± 0.6	295	RR[d] (CD_4)	Hickson et al. (2001)	295–363
		6.7 ± 1.1	323			
		17 ± 4	363			
		5.9 ± 1.0	295	RR[e] (CH_4)	Wallington et al. (2002)	
		5.0 ± 0.5	295	RR[d] (CD_4)		

[a]Abbreviations used for the techniques are defined in table I-F-3.
[b]Placed on an absolute basis using $k(Cl+C_2H_5OC_2H_5) = 2.8 \times 10^{-10}$ cm^3 molecule^{-1} s^{-1} (this book, section III-B-3.3).
[c]Placed on an absolute basis using $k(Cl+CF_3CH_2F) = 1.5 \times 10^{-15}$ cm^3 molecule^{-1} s^{-1} (Atkinson et al., 2008).
[d]Placed on an absolute basis using $k(Cl+CD_4) = 8.3 \times 10^{-12} \exp(-2{,}124/T)$ cm^3 molecule^{-1} s^{-1} (Hickson et al., 2001, scaled to 298 K value recommended in Calvert et al., 2008).
[e]Placed on an absolute basis using $k(Cl+CH_4) = 0.99 \times 10^{-13}$ cm^3 molecule^{-1} s^{-1} (Calvert et al., 2008).

III-G-53. 2-[Chloro(difluoro)methoxy]-1,1,1-trifluoroethane (Chlorodifluoromethyl 2,2,2-Trifluoroethyl Ether, $CF_3CH_2OCClF_2$)

III-G-53.1. OH Reaction Kinetics

The only study of the reaction of OH with $CF_3CH_2OCClF_2$ is that of Beach et al. (2001), who report $k = 1.6 \times 10^{-12} \exp(-1{,}100/T)$ cm^3 molecule^{-1} s^{-1}, with $k = 4.0 \times 10^{-14}$ cm^3 molecule^{-1} s^{-1} at 298 K. The data are summarized in table III-G-81. In the absence of corroborative measurements, an uncertainty of ±30% is assigned.

III-G-53.2. Cl-Atom Reaction Kinetics

The data of Beach et al. (2001) and of Hickson and Smith (2001) for the reaction of Cl-atoms with $CF_3CH_2OCClF_2$ are in good agreement. Fitting of the combined dataset to a simple Arrhenius expression leads to: $k = 1.26 \times 10^{-11} \exp(-2{,}515/T)$ cm^3 molecule^{-1} s^{-1}, with $k = 2.7 \times 10^{-15}$ cm^3 molecule^{-1} s^{-1} at 298 K. The data are summarized in table III-G-82.

Table III-G-81. Rate coefficients ($k = A \times e^{-B/T}$, cm^3 molecule^{-1} s^{-1}) for reaction of OH with $CF_3CH_2OCClF_2$

$10^{12} \times A$	B (K)	$10^{14} \times k$	T (K)	Technique[a]	Reference	Temperature Range (K)
1.6 ± 0.6	1,100 ± 125	3.9 ± 0.9	293	DF–RF	Beach et al. (2001)	293–410
		3.6 ± 0.2	298			
		8.5 ± 0.9	378			
		10.2 ± 0.5	410			

[a]Abbreviations used for the techniques are defined in table I-F-3.

Table III-G-82. Rate coefficients ($k = A \times e^{-B/T}$, cm^3 molecule^{-1} s^{-1}) for reaction of Cl with $CF_3CH_2OCClF_2$

$10^{12} \times A$	B (K)	$10^{15} \times k$	T (K)	Technique[a]	Reference	Temperature Range (K)
22 ± 2	2,700 ± 40	5.0 ± 0.3	323	DF–RF	Beach et al. (2001)	323–402
		12 ± 1	359			
		27 ± 2	402			
		2.60 ± 0.41	295	RR[b] (CD_4)	Hickson and Smith (2001)	295–363
		5.6 ± 0.9	323			
		11 ± 3	363			

[a]Abbreviations used for the techniques are defined in table I-F-3.
[b]Placed on an absolute basis using $k(Cl+CD_4) = 8.3 \times 10^{-12} \exp(-2{,}124/T)$ cm^3 molecule^{-1} s^{-1} (Hickson et al., 2001, scaled to 298 K value recommended in Calvert et al., 2008).

III-G-53.3. Summary of the Atmospheric Fate of $CF_3CH_2OCClF_2$, and the End Products of Its Oxidation

The OH rate coefficient data of Beach et al. (2001) can be used to derive an atmospheric lifetime of 1.1 years for $CF_3CH_2OCClF_2$. Reaction with OH must occur via abstraction at the CH_2 group; expected end products of the oxidation process are $HC(O)OCClF_2$ (with COF_2 as a co-product) and/or $CF_3C(O)OCClF_2$.

III-G-54. 2-Chloro-2-ethoxy-1,1,1-trifluoroethane (1-Chloro-2,2,2-trifluoroethyl Ethyl Ether, $CF_3CHClOCH_2CH_3$)

III-G-54.1. OH Reaction Kinetics

McLoughlin et al. (1993) report an upper limit for the reaction of OH with $CF_3CHClOCH_2CH_3$, $k < 3 \times 10^{-13}$ cm^3 molecule^{-1} s^{-1} at 300 K, see table III-G-83.

III-G-54.2. Cl-Atom Reaction Kinetics

McLoughlin et al. (1993) used a relative rate technique to determine $k = 3 \times 10^{-12}$ cm^3 molecule^{-1} s^{-1} for the rate coefficient for reaction of Cl with $CF_3CHClOCH_2CH_3$ at 300 K, see table III-G-83.

Table III-G-83. Rate coefficients (k, cm^3 molecule^{-1} s^{-1}) for reaction of OH with $CF_3CHClOCH_2CH_3$

$10^{12}\times k$	T (K)	Technique[a]	Reference
OH + $CF_3CHClOCH_2CH_3$			
< 0.3	300	RR[b] ($C_2H_5OC_2H_5$)	McLoughlin et al. (1993)
Cl + $CF_3CHClOCH_2CH_3$			
3 ± 1	300	RR[c] (C_2H_6)	McLoughlin et al. (1993)

[a]Abbreviations used for the techniques are defined in table I-F-3.
[b]Placed on an absolute basis using $k(OH+C_2H_5OC_2H_5) = 1.2 \times 10^{-11}$ cm^3 molecule^{-1} s^{-1} (this book, section III-B-3.1).
[c]Placed on an absolute basis using $k(Cl+C_2H_6) = 5.9 \times 10^{-11}$ cm^3 molecule^{-1} s^{-1} (Calvert et al., 2008).

III-G-54.3. Summary of the Atmospheric Fate of $CF_3CHClOCH_2CH_3$, and the End Products of Its Oxidation

The atmospheric lifetime of $CF_3CHClOCH_2CH_3$ will be greater than 40 days. Among the expected end products of the atmospheric oxidation of this species are $HC(O)OCHClCF_3$ (with CH_2O as a co-product), and/or $CH_3C(O)OCHClCF_3$, following OH attack at the CH_2 group.

III-G-55. 1,1,1,2,3,4,4,5,5,6,6,6-Dodecafluoro-2-(trifluoromethyl)hexan-3-yl Ethyl Ether $CF_3CF_2CF_2CF(OCH_2CH_3)CF(CF_3)_2$, HFE-7500]

III-G-55.1. OH Reaction Kinetics

The reaction of OH radicals with HFE-7500, n-$C_3F_7CF(OCH_2CH_3)CF(CF_3)_2$ has been studied by Goto et al. (2002a), using a relative rate technique. Their study leads to $k[OH + n\text{-}C_3F_7CF(OCH_2CH_3)CF(CF_3)_2] = 2.2 \times 10^{-14}$ cm^3 molecule^{-1} s^{-1}, with an estimated uncertainty of $\pm 35\%$. The measurements are summarized in table III-G-84.

Table III-G-84. Rate coefficients (k, cm^3 molecule^{-1} s^{-1}) for reaction of OH with n-$C_3F_7CF(OCH_2CH_3)CF(CF_3)_2$

$10^{14}\times k$	T (K)	Technique[a]	Reference
2.70 ± 0.58	295	RR[b] (CH_3Cl)	Goto et al. (2002a)
1.77 ± 0.28[c]	295	RR[d] (CH_4)	

[a]Abbreviations used for the techniques are defined in table I-F-3.
[b]Placed on an absolute basis using $k(OH+CH_3Cl) = 3.7 \times 10^{-14}$ cm^3 molecule^{-1} s^{-1} at 295 K (Calvert et al., 2008).
[c]Value deemed less accurate by the authors, and not used in the final analysis.
[d]Placed on an absolute basis using $k(OH+CH_4) = 6.0 \times 10^{-15}$ cm^3 molecule^{-1} s^{-1} at 295 K (Calvert et al., 2008).

Table III-G-85. Rate coefficients (k, cm^3 molecule^{-1} s^{-1}) for reaction of Cl with n-$C_3F_7CF(OCH_2CH_3)CF(CF_3)_2$

$10^{12} \times k$	T (K)	Technique[a]	Reference
2.5 ± 0.3	295	RR[b] (CH_3CH_2Cl)	Goto et al. (2002a)
2.0 ± 0.3	295	RR[c] (CH_3OCHO)	

[a]Abbreviations used for the techniques are defined in table I-F-3.
[b]Placed on an absolute basis using $k(Cl+CH_3CH_2Cl) = 7.8 \times 10^{-12}$ cm^3 molecule^{-1} s^{-1} (this book, table I-F-2).
[c]Placed on an absolute basis using $k(Cl+CH_3OCHO) = 1.4 \times 10^{-12}$ cm^3 molecule^{-1} s^{-1} (Wallington et al., 1993b).

III-G-55.2. Cl-Atom Reaction Kinetics

Goto et al. (2002a) also studied the reaction of Cl-atoms with n-$C_3F_7CF(OCH_2CH_3)CF(CF_3)_2$, using a standard relative rate method. The rate coefficient obtained from their data is $k = 2.3 \times 10^{-12}$ cm^3 molecule^{-1} s^{-1} near 295 K, with an estimated uncertainty of ±25%, see table III-G-85.

III-G-55.3. Summary of the Atmospheric Fate of HFE-7500, n-$C_3F_7CF(OCH_2CH_3)CF(CF_3)_2$ and the End Products of Its Oxidation

Goto et al. (2002a) use their 295 K OH rate coefficient measurement, and a scaling procedure involving methyl chloroform (atmospheric lifetime ≈ 5.7 years), to estimate an atmospheric lifetime of 2.2 years for HFE-7500. The Cl-atom-initiated oxidation of HFE-7500 generates two major products, identified by Goto et al. (2002a) as the acetate and formate esters, n-$C_3F_7CF(OC(=O)CH_3)CF(CF_3)_2$ and n-$C_3F_7CF(OCH=O)CF(CF_3)_2$, respectively. These species are both formed following Cl-atom abstraction at the CH_2 group in the parent species, which accounts for about 80% of the reaction {in the following reactions R = (n-C_3F_7)C•F[$CF(CF_3)_2$]}:

$$Cl + ROCH_2CH_3(+O_2) \rightarrow ROCH(OO\bullet)CH_3 + HCl$$

$$ROCH(OO\bullet)CH_3 + RO_2 \rightarrow ROCH(O\bullet)CH_3 + RO + O_2$$

$$ROCH(O\bullet)CH_3 + O_2 \rightarrow ROC(=O)CH_3 + HO_2$$

$$ROCH(O\bullet)CH_3 \rightarrow ROC(=O)H + CH_3$$

In 1 atm. air at 295 K, the reaction of $ROCH(O\bullet)CH_3$ with O_2 to generate the acetate is about twice as rapid as the decomposition to produce the formate. About 20% of the Cl-atom reaction with HFE-7500 appears to occur at the CH_3 group, which leads to additional formate production, presumably via formation and subsequent oxidation of the aldehydic species, $ROCH_2CH=O$.

III-G-56. Species of General Formula, $CHF_2O(CF_2CF_2O)_m(CF_2O)_nCHF_2$: $CHF_2OCF_2OCHF_2$(bis(difluoromethoxy)(difluoro)methane), $CHF_2OCF_2CF_2OCHF_2$(1,2-bis(difluoromethoxy)-1,1,2,2-tetrafluoroethane), and $CHF_2OCF_2CF_2OCF_2OCHF_2$ (1-(difluoromethoxy)-2-[(difluoromethoxy)(difluoro)methoxy]-1,1,2,2-tetrafluoroethane)

Partially fluorinated polyethers with the general formula: $CHF_2O(CF_2CF_2O)_m(CF_2O)_nCHF_2$ ($m = 0 - 7$, $n = 0 - 5$) have been proposed (Tuazon, 1997; Cavalli et al., 1998) as replacements for the longer-lived perfluorinated ethers, as well as for CFCs. Atmospheric studies of some of the smaller members of the series have been performed, as summarized in this section.

III-G-56.1. OH Reaction Kinetics

Cavalli et al. (1998), using a relative rate technique, have provided the only measurement of the rate coefficient for reaction of OH with $CHF_2OCF_2OCHF_2$, $CHF_2OCF_2CF_2OCHF_2$, and $CHF_2OCF_2CF_2OCF_2OCHF_2$. Their study yields $k = 2.3 \times 10^{-15}$ cm^3 molecule^{-1} s^{-1}, 4.5×10^{-15} cm^3 molecule^{-1} s^{-1}, and 4.4×10^{-15} cm^3 molecule^{-1} s^{-1}, respectively, at 295 K for the three species, with estimated uncertainties of ±50%. The data are summarized in table III-G-86.

III-G-56.2. Cl-Atom Reaction Kinetics

Relative rate studies have been conducted by Tuazon (1997) and Wallington et al. (2008a). Tuazon (1997) reported rate coefficients of $k = 5.2 \times 10^{-17}$ cm^3 molecule^{-1} s^{-1}, 4.7×10^{-17} cm^3 molecule^{-1} s^{-1}, and 3.8×10^{-17} cm^3 molecule^{-1} s^{-1} for the rate coefficients for reaction of Cl-atoms with $CHF_2OCF_2OCHF_2$, $CHF_2OCF_2CF_2OCHF_2$, and $CHF_2OCF_2CF_2OCF_2OCHF_2$, respectively. Wallington et al. (2008a) studied the reaction of Cl-atoms with $CHF_2OCF_2CF_2OCF_2OCHF_2$

Table III-G-86. Rate coefficients (k, cm^3 molecule^{-1} s^{-1}) for reaction of OH with $CHF_2OCF_2OCHF_2$, $CHF_2OCF_2CF_2OCHF_2$, and $CHF_2OCF_2CF_2OCF_2OCHF_2$

$10^{15} \times k$	T (K)	Technique[a]	Reference
OH + $CHF_2OCF_2OCHF_2$			
2.3 ± 0.7	295	RR[b] (CH_4)	Cavalli et al. (1998)
OH + $CHF_2OCF_2CF_2OCHF_2$			
4.5 ± 1.5	295	RR[b] (CH_4)	Cavalli et al. (1998)
OH + $CHF_2OCF_2CF_2OCF_2OCHF_2$			
4.4 ± 1.5	295	RR[b] (CH_4)	Cavalli et al. (1998)

[a]Abbreviations used for the techniques are defined in table I-F-3.
[b]Placed on an absolute basis using $k(OH+CH_4) = 6.0 \times 10^{-15}$ cm^3 molecule^{-1} s^{-1} at 295 K (Calvert et al., 2008).

and with a sample consisting of a mixture of compounds with the general formula $CHF_2O(CF_2CF_2O)_m(CF_2O)_nCHF_2$ ($m = 0 - 7$, $n = 0 - 5$) and an average molecular weight of 572. There was no discernable difference between the reactivity of the $CHF_2OCF_2CF_2OCF_2OCHF_2$ and the $CHF_2O(CF_2CF_2O)_m(CF_2O)_nCHF_2$ mixture. Analysis of the composite data set gave $k(Cl) = 5.0 \times 10^{-17}$ cm^3 molecule^{-1} s^{-1}. On the basis of the results of Tuazon (1997) and Wallington et al. (2008a), we recommend $k(Cl + CHF_2O(CF_2CF_2O)_m(CF_2O)_nCHF_2) = 5.0 \times 10^{-17}$ cm^3 molecule^{-1} s^{-1} at 298 K with an uncertainty of ±35%. The data are summarized in table III-G-87.

III-G-56.3. Summary of the Atmospheric Fate of $CHF_2OCF_2OCHF_2$, $CHF_2OCF_2CF_2OCHF_2$, and $CHF_2OCF_2CF_2OCF_2OCHF_2$, and the End Products of Their Oxidation

Lower limits of 14, 7, and 7 years for the atmospheric lifetimes of $CHF_2OCF_2OCHF_2$, $CHF_2OCF_2CF_2OCHF_2$, and $CHF_2OCF_2CF_2OCF_2OCHF_2$, respectively, can be obtained from the 295 K OH rate coefficient of Cavalli et al. (1998), and a globally averaged [OH] ≈ 10^6 molecule cm^{-3}. Given that these rate coefficients will possess positive temperature dependences, and that these polyethers will be well mixed throughout the troposphere, the actual atmospheric lifetime is likely even longer. The Cl-atom-initiated oxidation of $CHF_2O(CF_2CF_2O)_m(CF_2O)_nCHF_2$ has been studied by Tuazon (1997), Cavalli et al. (1998), and Wallington et al. (2008a). The studies show that COF_2 is the only detectible end product, and that COF_2 formation typically accounts for 90–95% of the reacted carbon. The mechanism proceeds via abstraction of the terminal H-atoms, followed by "unzipping" of the resultant oxy radical to produce multiple COF_2 molecules.

Table III-G-87. Rate coefficients (k, cm^3 molecule^{-1} s^{-1}) for reaction of Cl with $CHF_2OCF_2OCHF_2$, $CHF_2OCF_2CF_2OCHF_2$, and $CHF_2OCF_2CF_2OCF_2OCHF_2$

$10^{17} \times k$	T (K)	Technique[a]	Reference
Cl + $CHF_2OCF_2OCHF_2$			
5.2 ± 1.1	298	RR[b] (CF_3CF_2H)	Tuazon (1997)
Cl + $CHF_2OCF_2CF_2OCHF_2$			
4.7 ± 1.0	298	RR[b] (CF_3CF_2H)	Tuazon (1997)
Cl + $CHF_2OCF_2CF_2OCF_2OCHF_2$			
3.8 ± 0.8	298	RR[b] (CF_3CF_2H)	Tuazon (1997)
Cl + $CHF_2O(CF_2CF_2)_mO(CF_2)_nOCHF_2$ (see text)			
5.1 ± 1.3	296	RR[b] (CF_3CF_2H)	Wallington et al.(2008a)
5.2 ± 0.9	296	RR[c] (CH_3CF_2Cl)	

[a]Abbreviations used for the techniques are defined in table I-F-3.

[b]Placed on an absolute basis using $k(Cl+CF_3CF_2H) = 2.5 \times 10^{-16}$ cm^3 molecule^{-1} s^{-1} at 298 K (Atkinson et al., 2008).

[c]Placed on an absolute basis using $k(Cl+CH_3CF_2Cl) = 4.16 \times 10^{-16}$ cm^3 molecule^{-1} s^{-1} at 298 K (Atkinson et al., 2008).

III-G-57. Species of General Formula $CH_3O(CF_2CF_2O)_m(CF_2O)_nCH_3$

Another set of partially fluorinated polyethers that have been proposed as CFC replacements are the species with general formula $CH_3O(CF_2CF_2O)_m(CF_2O)_nCH_3$ (Andersen et al., 2004a, and references therein). The atmospheric behavior of a subset of these species ($n = 0$; $m = 1, 2$, and 3) has been studied by Andersen et al. (2004a), as summarized below.

III-G-57.1. OH Reaction Kinetics

Rate coefficients for the reaction of OH with $CH_3O(CF_2CF_2O)_mCH_3$ ($m = 1, 2, 3$) have been obtained by Andersen et al. (2004a), using a relative rate technique. Data for the three compounds were indistinguishable, within the experimental uncertainties, and a value of $k = 2.7 \times 10^{-14}$ cm^3 molecule^{-1} s^{-1} is obtained at 296 K. The estimated uncertainty is ±25%. The data are summarized in table III-G-88. The reactivity of $CH_3O(CF_2CF_2O)_mCH_3$ molecules are indistinguishable from twice the recommended reactivity of the methyl perfluoroalkyl ethers $C_xF_{2x+1}OCH_3$ ($x = 1 - 4$). As expected, the reactivities of the CH_3 groups in $CH_3O(CF_2CF_2O)_mCH_3$ are independent and additive.

III-G-57.2. Cl-Atom Reaction Kinetics

The reaction of Cl-atoms with $CH_3O(CF_2CF_2O)_mCH_3$ ($m = 1, 2, 3$) has been studied by Andersen et al. (2004a), using a relative rate technique. No measurable dependence of the rate coefficient on the chain-length (i.e., on the value of m) was noted; thus, $k = 3.7 \times 10^{-13}$ cm^3 molecule^{-1} s^{-1} for all three species, with an estimated uncertainty of ±30%. The measurements are summarized in table III-G-89.

III-G-57.3. Summary of the Atmospheric Fate of $CH_3O(CF_2CF_2O)_mCH_3$ ($m = 1, 2, 3$),and the End Products of Their Oxidation

Andersen et al. (2004a) estimate an atmospheric lifetime of 2 years for the three species, $CH_3O(CF_2CF_2O)_mCH_3$ ($m = 1, 2, 3$). This value was obtained by scaling to the known

Table III-G-88. Rate coefficients (k, cm^3 molecule^{-1} s^{-1}) for reaction of OH with $CH_3O(CF_2CF_2O)_mCH_3$ ($m = 1, 2, 3$)

$10^{14} \times k$	T (K)	Technique[a]	Reference
2.76 ± 0.32	296	RR[b] (C_2H_4)	Andersen et al. (2004a)
2.53 ± 0.24	296	RR[c] (C_2H_2)	

[a]Abbreviations used for the techniques are defined in table I-F-3.

[b]Placed on an absolute basis using $k(OH+C_2H_4) = 7.9 \times 10^{-12}$ cm^3 molecule^{-1} s^{-1} (Atkinson et al., 2006). From a combined study of the three species ($m = 1, 2, 3$).

[c]Placed on an absolute basis using $k(OH+C_2H_2) = 7.8 \times 10^{-13}$ cm^3 molecule^{-1} s^{-1} (Atkinson et al., 2006). From the study of $CH_3O(CF_2CF_2O)_2CH_3$ only.

Table III-G-89. Rate coefficients (k, cm^3 molecule^{-1} s^{-1}) for reaction of Cl with $CH_3O(CF_2CF_2O)_mCH_3$ ($m = 1, 2, 3$)

$10^{13} \times k$	T (K)	Technique[a]	Reference
3.36 ± 0.32	296	RR[b] (CH_4)	Andersen et al. (2004a)
3.95 ± 0.40	296	RR[c] (CH_3Cl)	

[a]Abbreviations used for the techniques are defined in table I-F-3.
[b]Placed on an absolute basis using $k(Cl+CH_4) = 1.0 \times 10^{-13}$ cm^3 molecule^{-1} s^{-1} (Calvert et al., 2008).
[c]Placed on an absolute basis using $k(Cl+CH_3Cl) = 4.7 \times 10^{-13}$ cm^3 molecule^{-1} s^{-1} (Atkinson et al., 2008).

CH_4 lifetime and known rate coefficient for reaction of OH with CH_4, assuming the two rate coefficients have similar temperature dependences. Studies of the Cl-atom-initiated oxidation of these species (Andersen et al., 2004a) show that the dominant product formed under atmospheric conditions is the formate species, $HC(O)O(CF_2CF_2O)_mCH_3$, which results from OH abstraction at the terminal CH_3 groups, followed by reaction of the resultant alkoxy radical, $\bullet OCH_2O(CF_2CF_2O)_mCH_3$, with O_2.

III-G-58. Perfluoropolymethylisopropyl Ethers

Perfluorinated polyethers are a group of very long-lived compounds that have found application as replacements for CFCs (Young et al., 2006). Young et al. (2006) have studied the atmospheric chemistry of a representative class of perfluorinated polyethers; namely, the perfluoropolymethylisopropyl ethers (PFPMIEs), general formula $CF_3[OCF(CF_3)CF_2]_m(OCF_2)_nOCF_3$. More specifically, the study was carried out on a mixture containing mostly $CF_3OCF(CF_3)CF_2OCF_2OCF_3$, although smaller amounts of longer chain species were also present. The data obtained are summarized in this section.

III-G-58.1. OH Reaction Kinetics

Young et al. (2006), using a relative rate technique, report an upper limit to the rate coefficient for reaction of OH with the PFPMIE mixture discussed above, $k < 6.3 \times 10^{-16}$ cm^3 molecule^{-1} s^{-1} at 296 K. The data are summarized in table III-G-90.

Table III-G-90. Rate coefficient (k, cm^3 molecule^{-1} s^{-1}) for reaction of OH with a mixture of PFPMIEs [mostly $CF_3OCF(CF_3)CF_2OCF_2OCF_3$]

$10^{16} \times k$	T (K)	Technique[a]	Reference
< 6.3	296	RR[b] (C_2H_2)	Young et al. (2006)

[a]Abbreviations used for the techniques are defined in table I-F-3.
[c]Placed on an absolute basis using $k(OH+C_2H_2) = 7.8 \times 10^{-13}$ cm^3 molecule^{-1} s^{-1} (Atkinson et al., 2008).

Table III-G-91. Rate coefficient (k, cm^3 molecule^{-1} s^{-1}) for reaction of Cl with a mixture of PFPMIEs [mostly $CF_3OCF(CF_3)CF_2OCF_2OCF_3$]

$10^{16} \times k$	T (K)	Technique[a]	Reference
< 2	296	RR[b] (CF_2HCl)	Young et al. (2006)

[a]Abbreviations used for the techniques are defined in table I-F-3.
[b]Placed on an absolute basis using $k(Cl+CF_2HCl) = 1.5 \times 10^{-15}$ cm^3 molecule^{-1} s^{-1} (IUPAC, 2008).

III-G-58.2. Cl-Atom Reaction Kinetics

Young et al. (2006) also report an upper limit to the rate coefficient for reaction of Cl-atoms with the PFPMIE mixture, $k < 2 \times 10^{-17}$ cm^3 molecule^{-1} s^{-1} at 296 K. The data are summarized in table III-G-91.

III-G-58.3. Summary of the Atmospheric Fate of Perfluoropolymethylisopropyl Ethers

On the basis of their measured upper limit to OH reaction rate coefficient, Young et al. (2006) estimate a lifetime for the PFPMIE mixture studied of > 48 years. However, Young et al. point out that the atmospheric lifetime (like that of other perfluorinated species) could be considerably longer. They propose upper atmospheric photolysis by Lyman-αgadiation (at 121.6 nm) as a potential loss mechanism for these perfluorinated polyethers, which implies atmospheric lifetimes in excess of 800 years.

III-G-59. 1,1,1,2,2,3,3,4,4-Nonafluoro-4-[3-(nonafluorobutoxy)propoxy]butane [n-$C_4F_9O(CH_2)_3O$-n-C_4F_9] and 1,1,1,2,3,3-Hexafluoro-3-[3-(1,1,2,3,3,3-hexafluoropropoxy)propoxy]propane [$CF_3CFHCF_2O(CH_2)_3OCF_2CFHCF_3$]

III-G-59.1. OH Reaction Kinetics

The rate coefficient for reaction of OH with n-$C_4F_9O(CH_2)_3O$-n-C_4F_9 and $CF_3CFHCF_2O(CH_2)_3OCF_2CFHCF_3$ have been studied by Toft et al. (2006). The rate coefficients for these two species are $k = 1.3 \times 10^{-13}$ cm^3 molecule^{-1} s^{-1} and 2.3×10^{-13} cm^3 molecule^{-1} s^{-1}, respectively, at 296 K. Their data are summarized in table III-G-92. In the absence of corroborative information, an uncertainty of $\pm 35\%$ is assumed.

III-G-59.2. Cl-Atom Reaction Kinetics

Toft et al. (2006) also report Cl-atom rate coefficients for both n-$C_4F_9O(CH_2)_3O$-n-C_4F_9 and $CF_3CFHCF_2O(CH_2)_3OCF_2CFHCF_3$. Their relative rate study leads to $k = 1.4 \times 10^{-12}$ cm^3 molecule^{-1} s^{-1} and $k = 2.9 \times 10^{-12}$ cm^3 molecule^{-1} s^{-1} at 296 K for the two species, respectively. The data are summarized in table III-G-93.

Table III-G-92. Rate coefficients (k, cm^3 molecule^{-1} s^{-1}) for reaction of OH with n-$C_4F_9O(CH_2)_3O$-n-C_4F_9 and $CF_3CFHCF_2O(CH_2)_3OCF_2CFHCF_3$

$10^{13}\times k$	T (K)	Technique[a]	Reference
OH + *n*-$C_4F_9O(CH_2)_3O$-*n*-C_4F_9			
1.33 ± 0.09	296	RR[b] (C_2H_2)	Toft et al. (2006)
OH + $CF_3CFHCF_2O(CH_2)_3OCF_2CFHCF_3$			
2.26 ± 0.13	296	RR[b] (C_2H_2)	Toft et al. (2006)

[a]Abbreviations used for the techniques are defined in table I-F-3.
[b]Placed on an absolute basis using $k(OH+C_2H_2) = 7.8 \times 10^{-13}$ cm^3 molecule^{-1} s^{-1} (Atkinson et al., 2006).

Table III-G-93. Rate coefficients (k, cm^3 molecule^{-1} s^{-1}) for reaction of Cl with n-$C_4F_9O(CH_2)_3O$-n-C_4F_9 and $CF_3CFHCF_2O(CH_2)_3OCF_2CFHCF_3$

$10^{12}\times k$	T (K)	Technique[a]	Reference
Cl + *n*-$C_4F_9O(CH_2)_3O$-*n*-C_4F_9			
1.36 ± 0.11	296	RR[b] (CH_3Cl)	Toft et al. (2006)
1.46 ± 0.11	296	RR[c] (CH_3CH_2Cl)	
Cl + $CF_3CFHCF_2O(CH_2)_3OCF_2CFHCF_3$			
2.91 ± 0.15	296	RR[b] (CH_3Cl)	Toft et al. (2006)
2.89 ± 0.16	296	RR[c] (CH_3CH_2Cl)	

[a]Abbreviations used for the techniques are defined in table I-F-3.
[b]Placed on an absolute basis using $k(Cl+CH_3Cl) = 4.7 \times 10^{-13}$ cm^3 molecule^{-1} s^{-1} (Atkinson et al., 2008).
[c]Placed on an absolute basis using $k(Cl+CH_3CH_2Cl) = 7.8 \times 10^{-12}$ cm^3 molecule^{-1} s^{-1} (this book, table I-F-2).

III-G-59.3. Summary of the Atmospheric Fate of n-$C_4F_9O(CH_2)_3O$-n-C_4F_9 and $CF_3CFHCF_2O(CH_2)_3OCF_2CFHCF_3$

The OH rate coefficient measurements of Toft et al. (2006) can be used to estimate lifetimes of about 80 and 45 days for n-$C_4F_9O(CH_2)_3O$-n-C_4F_9 and $CF_3CFHCF_2O(CH_2)_3OCF_2CFHCF_3$, respectively. Toft et al. also report on the products of the Cl-atom-initiated oxidation of these species. Products identified were ROCH=O, $ROCH_2CH$=O, and either $ROC(O)CH_2CH_2OR$ and/or $ROCH_2C(O)CH_2OR$, R = n-C_4F_9 or CF_3CFHCF_2. Reaction occurs predominantly at either of the two unique —O—CH_2 sites in the molecule. Although the products could not be quantified due to the unavailability of standard samples, product yields were shown to be dependent on O_2 partial pressure, reflecting competition between decomposition of the alkoxy radical(s) and their reaction with O_2; e.g.:

$$OH + RO(CH_2)_3OR(+O_2) \rightarrow ROCH(OO\bullet)CH_2CH_2OR$$

$$ROCH(OO\bullet)CH_2CH_2OR + NO \rightarrow ROCH(O\bullet)CH_2CH_2OR + NO_2$$

$$ROCH(O\bullet)CH_2CH_2OR \rightarrow \mathbf{ROCH{=}O} + ROCH_2CH_2$$

$$ROCH_2CH_2\bullet + O_2\bullet \rightarrow\rightarrow\rightarrow ROCH_2CH{=}O$$

$$ROCH(O\bullet)CH_2CH_2OR + O_2 \rightarrow \mathbf{ROC(O)CH_2CH_2OR} + HO_2$$

Reaction at the central —CH_2 group would provide the source of $ROCH_2C(O)CH_2OR$, if it is formed. Further details are provided by Toft et al. (2006).

III-G-60. 2-Ethoxy-3,3,4,4,5-pentafluorotetrahydro-2,5-*bis*[1,2,2,2-tetrafluoro-1-(trifluoromethyl)ethyl]-furan

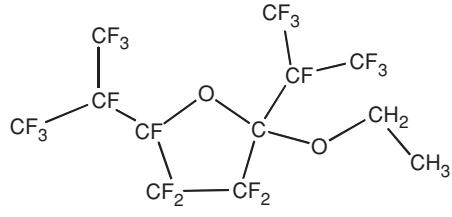

III-G-60.1. OH Reaction Kinetics

The rate coefficient for reaction of OH with this species has been studied by Javadi et al. (2007). A rate coefficient of $k = 5.5 \times 10^{-14}$ cm^3 molecule^{-1} s^{-1} was reported at 294 K. The data are summarized in table III-G-94. In the absence of corroborative information, an uncertainty of ±30% is assumed.

III-G-60.2. Cl-Atom Reaction Kinetics

Javadi et al. (2007) also report the Cl-atom rate coefficients for the highly substituted furan shown above. Their relative rate study leads to $k = 2.7 \times 10^{-12}$ cm^3 molecule^{-1} s^{-1} at 294 K. The data are summarized in table III-G-95.

Table III-G-94. Rate coefficient (k, cm^3 molecule^{-1} s^{-1}) for reaction of OH with 2-ethoxy-3,3,4,4,5-pentafluorotetrahydro-2,5-bis[1,2,2,2-tetrafluoro-1-(trifluoromethyl)ethyl]-furan

$10^{14} \times k$	T (K)	Technique[a]	Reference
5.48 ± 0.60	296	RR[b] (C_2H_2)	Javadi et al. (2007)

[a]Abbreviations used for the techniques are defined in table I-F-3.
[b]Placed on an absolute basis using $k(OH+C_2H_2) = 7.8 \times 10^{-13}$ cm^3 molecule^{-1} s^{-1} (Atkinson et al., 2006).

Table III-G-95. Rate coefficients (k, cm^3 molecule^{-1} s^{-1}) for reaction of Cl with 2-ethoxy-3,3,4,4,5-pentafluorotetrahydro-2,5-bis[1,2,2,2-tetrafluoro-1-(trifluoromethyl)ethyl]-furan

$10^{12} \times k$	T (K)	Technique[a]	Reference
2.60 ± 0.21	296	RR[b] (CH_3OCHO)	Javadi et al. (2007)
2.81 ± 0.24	296	RR[c](CH_3CH_2Cl)	

[a]Abbreviations used for the techniques are defined in table I-F-3.
[b]Placed on an absolute basis using $k(Cl+CH_3OCHO) = 1.4 \times 10^{-12}$ cm^3 molecule^{-1} s^{-1} (Wallington et al., 1993b).
[c]Placed on an absolute basis using $k(Cl+CH_3CH_2Cl) = 7.8 \times 10^{-12}$ cm^3 molecule^{-1} s^{-1} (this book, table I-F-2).

III-G-60.3. Summary of the Atmospheric Fate of 2-Ethoxy-3,3,4,4,5-pentafluorotetrahydro-2,5-bis[1,2,2,2-tetrafluoro-1-(trifluoromethyl)ethyl]-furan

The OH rate coefficient measurements of Javadi et al. (2007) can be combined with a diurnally averaged [OH] of 1.0×10^6 molecule cm^{-3} to give an estimated atmospheric lifetime of about 6 months. Javadi et al. (2007) also reported the results of a study of the Cl-atom-initiated oxidation of this species in 700 Torr of N_2/O_2 diluent. Oxidation of proceeds at the $—OC_2H_5$ group leading to the formation of corresponding formate and acetate esters.

III-G-61. 1,1,2-Trifluoro-2-(trifluoromethoxy)ethene ($CF_3OCF{=}CF_2$)

III-G-61.1. OH Reaction Kinetics

There are three studies of the reaction of OH with $CF_3OCF{=}CF_2$, two using absolute techniques as a function of temperature (Li et al., 2000c; Tokuhashi et al., 2000a) and one using a relative rate technique at 295 K (Mashino et al., 2000); see table III-G-96. Although there is rough agreement on the rate coefficient near 298 K, there is poor agreement on the temperature dependence; Li et al. (2000c) derived a positive temperature dependence and Tokuhashi et al. (2000a) showed a negative temperature dependence. Although there is no obvious reason to discount either study, OH addition reactions typically show negative temperature dependences and thus the Tokuhashi et al. (2000a) data seem more reasonable. No recommendation is made, however, and further studies are required.

III-G-61.2. Cl-Atom Reaction Kinetics

Mashino et al. (2000) derive $k = 3.0 \times 10^{-11}$ cm^3 $molecule^{-1}$ s^{-1} near 295 K, using the relative rate technique. The data are summarized in table III-G-97.

III-G-61.3. Summary of the Atmospheric Fate of $CF_3OCF{=}CF_2$, and the End Products of Its Oxidation

On the basis of the available data, the rate coefficient for reaction of OH with $CF_3OCF{=}CF_2$ is likely near 3×10^{-12} cm^3 $molecule^{-1}$ s^{-1} at 298 K. This implies an atmospheric lifetime of about 4 h, assuming a peak daytime [OH] $= 2.5 \times 10^6$ molecule cm^{-3}. Mashino et al. (2000) have reported that the OH-initiated oxidation of $CF_3OCF{=}CF_2$ in 700 Torr of air at 295 K gives COF_2, $CF_3OC(O)F$, and $FC(O)C(O)F$ in molar yields of 90, 53, and 40%, respectively.

III-G-62. Polychlorinated Dibenzodioxins (PCDDs) and Polychlorinated Dibenzofurans (PCDFs)

The polychlorinated dibenzodioxins (PCDDs) and polychlorinated dibenzofurans (PCDFs) are important classes of semi-volatile, persistent organic pollutants, formed

Table III-G-96. Rate coefficients ($k = A \times e^{-B/T}$, cm^3 $molecule^{-1}$ s^{-1}) for reaction of OH with $CF_3OCF{=}CF_2$

$10^{13} \times A$	B (K)	$10^{12} \times k$	T (K)	Technique[a]	Reference	Temperature Range (K)
		2.25 ± 0.29	295	RR[b] (C_2H_2)	Mashino et al. (2000)	
		2.29 ± 0.28	295	RR[c] (C_2H_4)		
641 ± 82	868 ± 40	2.07 ± 0.24	253	DF–RF	Li et al. (2000c)	253–348
		2.76 ± 0.39	277			
		3.58 ± 0.42	298			
		4.36 ± 0.90	323			
		5.26 ± 0.90	348			
10.1 ± 0.4	-320 ± 10	3.68 ± 0.09	250	FP or PLP–LIF	Tokuhashi et al. (2000a)	250–430
		3.73 ± 0.10	250			
		3.79 ± 0.12	250			
		3.73 ± 0.13	250			
		3.25 ± 0.09	273			
		3.31 ± 0.12	273			
		2.96 ± 0.04	298			
		2.92 ± 0.06	298			
		2.93 ± 0.06	298			
		2.88 ± 0.07	298			
		2.67 ± 0.07	331			
		2.67 ± 0.08	331			
		2.41 ± 0.05	375			
		2.38 ± 0.08	375			
		2.17 ± 0.07	430			
		2.13 ± 0.06	430			
		2.14 ± 0.07	430			
		2.18 ± 0.05	430			

[a]Abbreviations used for the techniques are defined in table I-F-3.
[c]Placed on an absolute basis using $k(OH{+}C_2H_2) = 7.8 \times 10^{-13}$ cm^3 $molecule^{-1}$ s^{-1} (Atkinson et al., 2006).
[c]Placed on an absolute basis using $k(OH{+}C_2H_4) = 7.9 \times 10^{-12}$ cm^3 $molecule^{-1}$ s^{-1} (Atkinson et al., 2006).

Table III-G-97. Rate coefficients (k, cm^3 $molecule^{-1}$ s^{-1}) for reaction of Cl with $CF_3OCF{=}CF_2$

$10^{11} \times k$	T (K)	Technique[a]	Reference
3.04 ± 0.19	295	RR[b] (C_2H_4)	Mashino et al. (2000)
2.89 ± 0.19	295	RR[c] (CH_3CH_2Cl)	

[a]Abbreviations used for the techniques are defined in table I-F-3.
[b]Placed on an absolute basis using $k(Cl{+}C_2H_4) = 9.5 \times 10^{-11}$ cm^3 $molecule^{-1}$ s^{-1} (this book, table I-F-2).
[c]Placed on an absolute basis using $k(Cl{+}CH_3CH_2Cl) = 7.6 \times 10^{-12}$ cm^3 $molecule^{-1}$ s^{-1} (this book, table I-F-2).

as by-products in the combustion of chlorine-containing organic compounds. These species, which are known carcinogens (e.g., see: http://www.oehha.ca.gov/prop65/prop65_list/files/P65single062708.pdf), are now ubiquitously found in all compartments of the environment (air, water, soil) as well as in living entities (including humans). The basic dibenzodioxin and dibenzofuran skeletons are shown below, along

with the numbering scheme used to identify the position of chlorine substituents.

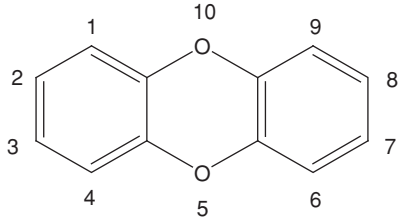

Dibenzo-*p*-dioxin

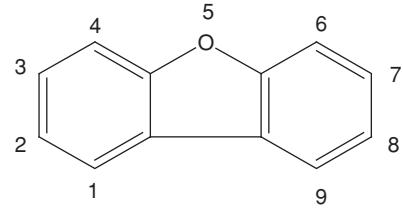

Dibenzofuran

Altogether, there are 75 different PCDDs and 135 different PCDFs (so-called "congeners") that result from substitution of one to eight chlorines onto the basic dibenzodioxin or dibenzofuran skeleton. The vapor pressures of these species are quite low, ranging from about 10^{-2} Torr to as little as 8×10^{-9} Torr, depending on the degree of chlorination (Brubaker and Hites, 1997). Thus, the study of the gas-phase chemistry of these species is exceedingly difficult, and is often limited to temperatures above 300 K. The available information regarding the gas-phase chemistry of the PCDDs and PCDFs is summarized in this section.

III-G-62.1. OH Reaction Kinetics

There are rate coefficient data available for the reaction of six PCDD congeners with OH in the gas-phase (Kwok et al., 1995; Brubaker and Hites, 1997, 1998; Taylor et al., 2005). As with the parent dibenzodioxin (section III-F-4), agreement is semi-quantitative at best when multiple measurements are available for a single congener. The data set of Taylor et al. (2005) appears to provide a consistent picture for the reactivity of different congeners, and these data are thus recommended with estimated uncertainties of about a factor of 2 near 298 K. Clearly, further studies to confirm the data of Taylor et al. and to extend the database to a larger number of congeners are needed. Nonetheless, some general statements can be made regarding the reactivity of the PCDDs as a function of chlorine-substitution (Taylor et al., 2005). Firstly, the OH rate coefficients measured by Taylor et al. in most cases exhibit a negative temperature dependence, consistent with the reaction occurring via addition of OH to the aromatic rings. The lone exception is for the fully chlorinated octachlorodibenzo-*p*-dioxin, for which an OH addition/Cl-atom elimination mechanism has been suggested (Taylor et al., 2005). This addition/elimination process could occur for other highly chlorinated congeners as well. There is also a general trend towards a decreasing rate coefficient with increasing chlorine substitution; the rate coefficients at 298 K are about 40×10^{-12} cm^3 molecule^{-1} s^{-1} for the unsubstituted dibenzo-*p*-dioxin, $(18 - 40) \times 10^{-12}$ cm^3 molecule^{-1} s^{-1} when Cl-atoms are present on one ring, and $(3 - 7) \times 10^{-12}$ cm^3 molecule^{-1} s^{-1} when Cl-atoms are present on both rings. The available data (Kwok et al., 1995; Brubaker and Hites, 1997, 1998; Taylor et al., 2005) are summarized in table III-G-98. The Taylor et al. rate coefficient data are also shown in figure III-G-14.

Table III-G-98. Rate coefficients ($k = A \times e^{-B/T}$, cm^3 molecule^{-1} s^{-1}) for reaction of OH with chlorinated dibenzo-*p*-dioxins (PCDDs; DD = dibenzo-*p*-dioxin)

$10^{12} \times A$	B (K)	$10^{12} \times k$	T (K)	Technique[a]	Reference	Temperature Range (K)
OH + 1-Chloro-DD						
		4.4 ± 1.5	297	RR[b] (c-C_6H_{12})	Kwok et al. (1995)	
OH + 2-Chloro-DD						
2.79 ± 0.27	−784 ± 54			PLP–LIF	Taylor et al. (2005)	346–905
OH + 2,3-Dichloro-DD						
1.83 ± 0.19	−742 ± 67			PLP–LIF	Taylor et al. (2005)	400–927
OH + 2,7-Dichloro-DD						
1.10 ± 0.27	−569 ± 53			PLP–LIF	Taylor et al. (2005)	390–769
81[b]	892[b]	6.6 ± 1.7	355	RR[c] (c-C_6H_{12})	Brubaker and Hites (1998)	355–395
		7.4 ± 1.9	365			
		7.6 ± 1.9	365			
		6.7 ± 1.7	365			
		6.8 ± 1.7	375			
		7.7 ± 1.9	375			
		7.8 ± 2.0	375			
		7.6 ± 1.9	375			
		9.2 ± 2.3	395			
		8.2 ± 2.1	395			
		8.5 ± 2.1	395			
OH + 2,8-Dichloro-DD						
1.02 ± 0.10	−580 ± 68			PLP–LIF	Taylor et al. (2005)	379–931
OH + 1,2,3,4-Tetrachloro-DD						
1.66 ± 0.38	−713 ± 114			PLP–LIF	Taylor et al. (2005)	409–936
194[b]	1,586[b]	3.0 ± 0.9	373	RR[d] (C_6F_6)	Brubaker and Hites (1997)	355–395
		2.7 ± 0.8	373			
		2.6 ± 0.8	373			
		3.5 ± 1.0	393			
		3.4 ± 1.0	393			
		5.0 ± 1.5	403			
		2.9 ± 0.8	403			
		5.1 ± 1.0	424	RR[e] (PCB-116)		
		4.9 ± 1.0	430			
		4.8 ± 1.0	431			
		4.7 ± 0.9	431			
		4.9 ± 1.0	432			
OH + Octachloro-DD						
31.8 ± 5.4	667 ± 115			PLP–LIF	Taylor et al. (2005)	514–928

[a] Abbreviations used for the techniques are defined in table I-F-3.

[b] Values obtained from least-squares fit of data obtained using updated reference rate coefficients, and thus differ from those originally reported.

[c] Placed on an absolute basis using k(OH+*cyclo*-C_6H_{12}) = $3.26 \times 10^{-17} T^2 \exp(262/T)$ cm^3 molecule^{-1} s^{-1} (Calvert et al., 2008).

[d] Placed on an absolute basis using k(OH+hexafluorobenzene) = $4.8 \times 10^{-12} \exp(-1{,}000/T)$ cm^3 molecule^{-1} s^{-1} (McIlroy and Tully, 1993).

[e] Placed on an absolute basis using k(OH+PCB-116, 2,3,4,5,6-pentachlorbiphenyl) = $1.1 \times 10^{-10} \exp(-1{,}440/T)$ cm^{3}molecule^{-1} s^{-1} (Anderson and Hites, 1996).

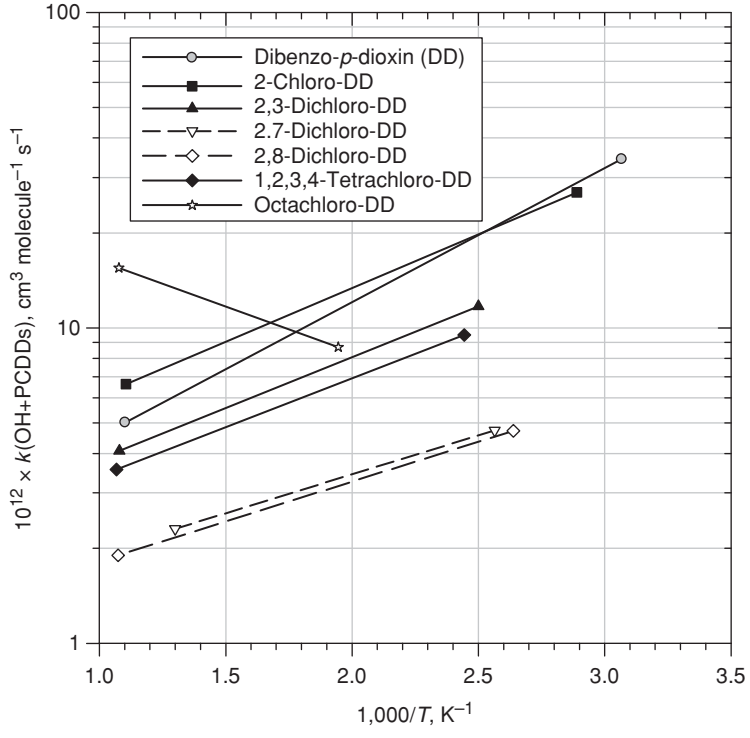

Figure III-G-14. Arrhenius plot of the rate coefficient for the reaction of OH with PCDDs. All data are from Taylor et al. (2005). Note that individual data points were not provided by the authors; the figure shows the reported Arrhenius expressions for each compound, extending over the range of temperatures studied. Filled symbols and solid lines are shown for Cl-atoms present on only one aromatic ring; open symbols and broken lines are shown for Cl-atoms present on both rings.

Data regarding the reaction of OH with PCDFs are very sparse. In fact, the only study is that of Brubaker and Hites (1998), who studied the 2,8-dichloro-dibenzofuran congener using a relative rate technique (table III-G-99). The study was conducted over the 355–405 K range, and the reported rate coefficients increase from about 3×10^{-12} to 4×10^{-12} cm^3 $molecule^{-1}$ s^{-1} over this temperature range. Given the lack of confirming data, and the discrepancies just noted in the database for OH reactions with the PCDDs, no recommendations are made at this time.

III-G-62.2. O_3 Reaction Kinetics

Kwok et al. (1995) measured an upper limit for the reaction of O_3 with 1-chloro-dibenzo-p-dioxin, $k < 7 \times 10^{-20}$ cm^3 $molecule^{-1}$ s^{-1}, see table III-G-100.

III-G-62.3. NO_3 Reaction Kinetics

Kwok et al. (1995) also studied the reaction of NO_3 with 1-chloro-dibenzo-*p*-dioxin. They demonstrated that the reaction proceeds almost exclusively via reversible addition

Table III-G-99. Rate coefficients (k, cm^3 molecule^{-1} s^{-1}) for reaction of OH with 2,8-dichloro-dibenzofuran

$10^{12} \times A$	B (K)	$10^{12} \times k$	T (K)	Technique[a]	Reference	Temperature Range (K)
22[b]	711[b]	2.9 ± 0.7	355	RR[c] (*cyclo*-C_6H_{12})	Brubaker and Hites (1998)	355–405
		3.0 ± 0.8	355			
		2.8 ± 0.7	355			
		3.2 ± 0.8	365			
		3.1 ± 0.8	365			
		3.3 ± 0.8	365			
		3.2 ± 0.8	365			
		3.6 ± 0.9	376			
		3.5 ± 0.9	376			
		3.6 ± 0.9	376			
		3.6 ± 0.9	376			
		3.6 ± 0.9	376			
		3.6 ± 0.9	376			
		3.7 ± 0.9	395			
		3.9 ± 1.0	395			
		3.7 ± 0.9	395			
		3.5 ± 0.9	395			
		3.3 ± 0.8	395			
		3.9 ± 1.0	405			
		4.0 ± 1.0	405			

[a]Abbreviations used for the techniques are defined in table I-F-3.
[b]Values obtained from least-squares fit of data obtained using updated reference rate coefficients, and thus differ from those originally reported.
[c]Placed on an absolute basis using $k(\text{OH}+\textit{cyclo}\text{-}C_6H_{12}) = 3.26 \times 10^{-17} T^2 \exp(262/T)$ cm^3 molecule^{-1} s^{-1} (Calvert et al., 2008).

Table III-G-100. Rate coefficients (k, cm^3 molecule^{-1} s^{-1}) for reaction of O_3 with 1-chloro-dibenzo-*p*-dioxin

$10^{20} \times k$	T (K)	Technique[a]	Reference
< 7	297	GC–FID	Kwok et al. (1995)

[a]Abbreviations used for the techniques are defined in table I-F-3.

of the NO_3 to the aromatic rings of the PCDD, with reaction of the adduct with NO_2 competing with its decomposition back to reactants. The results of the study are summarized in table III-G-101.

III-G-62.4. Summary of the Atmospheric Fate of PCDDs/PCDFs, and the End Products of Their Oxidation

On the basis of the data of Taylor et al. (2005), the lifetime of PCDDs against reaction with OH will vary with molecular structure but will typically fall in the range $\approx 0.1 - 3$ days in the lower troposphere (the longer lifetime applying to the more

Table III-G-101. Rate coefficients (k, cm^3 molecule^{-1} s^{-1}) for reaction of NO_3 with 1-chloro-dibenzo-*p*-dioxin

$10^{28} \times k_a k_b / k_c$	T (K)	Technique[a]	Reference
3.5 ± 1.7	297	RR[b] (1-butene)	Kwok et al. (1995)

[a]Abbreviations used for the techniques are defined in table I-F-3.
[b]Placed on an absolute basis using $k(NO_3+1\text{-butene}) = 1.4 \times 10^{-14}$ cm^3 molecule^{-1} s^{-1} (Calvert et al., 2000). Rate coefficients k_a, k_b, k_c are as defined in section III-F-2.2.

heavily chlorinated congeners). The limited data on the reactivity of the PCDFs suggests similar gas-phase removal rates. However, given the semi-volatile nature of these species (especially the more chlorinated congeners), their atmospheric behavior will be quite complex, involving partitioning between the gas and particulate phase, and removal via wet and dry deposition (from both the gas and particle phase). For example, the modeling study of Lohmann et al. (2006) suggests that degradation via OH reaction is only a minor loss process for heavily chlorinated PCDDs/PCDFs (those containing six or more Cl-atoms), as particulate deposition to soils and oceans will dominate the loss. However, degradation via reaction with OH will play a greater role for the less-chlorinated congeners, with gas-phase removal via reaction with OH roughly competitive with heterogeneous losses for congeners containing about four Cl-atoms. Presumably, loss via reaction with OH in the gas phase will play an important role for the less chlorinated congeners as well.

III-G-63. Polybrominated Diphenyl Ethers (PBDEs)

The polybrominated diphenyl ethers (PBDEs) are an important class of semi-volatile, persistent organic pollutants. These species are of anthropogenic origin, and are used as flame retardants in electronics, fabrics, and furniture. Theoretically, there are 209 different PBDE congeners that result from the presence of 1–10 bromine atoms on the basic diphenyl ether structure:

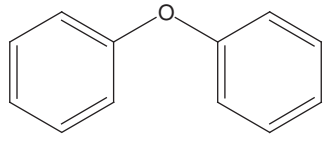

Like the PCDD/PCDFs discussed previously, the environmental persistence of these species is controlled not only by their gas-phase chemistry, but also by processes occurring in the particle phase, on surfaces, and in the aqueous phase. The vapor pressures of these species, especially the multiply brominated congeners, are quite low, and so gas-phase studies are difficult and usually limited to temperatures above 300 K. The limited knowledge of the atmospheric chemistry of the PBDEs is summarized below.

III-G-63.1. OH Reaction Kinetics

The only study of the gas-phase reaction of OH with the PBDEs is the relative rate study of Raff and Hites (2006), in which seven congeners were studied in addition to the parent diphenyl ether. As summarized in table III-G-102, rate coefficients were determined from about 325–380 K. In general, rate coefficients for reaction of OH with the PBDEs show a positive temperature dependence (with one exception) and are seen to decrease with increasing Br-substitution, with $k = 8 \times 10^{-12}$, $(4.5 - 6) \times 10^{-12}$, and $(1 - 5) \times 10^{-12}$ cm^3 molecule^{-1} s^{-1} for the parent diphenyl ether, monobrominated diphenyl ethers, and dibrominated diphenyl ethers, respectively.

III-G-63.2. Summary of the Atmospheric Fate of PBDEs, and the End Products of Their Oxidation

For the species studied by Raff and Hites (2006), the atmospheric lifetime against OH reaction ranges from about 2 to 9 days. However, in a very detailed study of the environmental fate of PBDEs, Raff and Hites (2007) point out that reaction with OH is only one of many potential loss mechanisms for the PBDEs, and indeed may only represent a minor loss process for many PBDE congeners. Their work shows that the overall atmospheric lifetime for all PBDEs is at most a couple of days and in many cases less than one day, with loss controlled by a combination of gas-phase reaction with OH, gas-phase photolysis, and depositional processes involving both the gas- and condensed-phase. While the overall system is quite complex and still subject to many unknowns and uncertainties, some general points of summary (taken from the Raff and Hites study) can be made. Firstly, the more heavily brominated the PBDE, the lower its vapor pressure and thus the more likely the species is to be found in the condensed phase. For example, PBDEs with nine or ten bromines are found almost exclusively in the condensed phase. Thus, the atmospheric lifetime of these high-bromine congeners is quite short ($<$ 1 day) and is controlled almost entirely by wet depositional processes from the condensed phase. Conversely, the lighter congeners (roughly speaking, those species with one to four bromines) are found predominantly in the gas-phase, and thus are lost mostly via gas-phase photolysis or reaction with OH. In general, the higher the bromine content, the faster the photolysis rate and the slower the OH reaction. Thus for mono-brominated congeners, the OH reaction is the major loss mechanism (lifetime $\approx$ 2 days), while for the those congeners containing four to five bromines, gas-phase photolysis dominates and lifetimes are shorter, generally on the order of 5–10 h.

III-H. Rate Coefficient Correlations and Structure–Activity Relationships (SARs)

In this section, trends in reactivity of the ethers, comparisons of their reactivity with other compound classes, correlations of their reactivity with various oxidants, and structure–activity relationships for their reaction with various oxidants will be discussed. Many of the comparisons and relationships discussed build upon previously

Table III-G-102. Rate coefficients ($k = A \times e^{-B/T}$, cm^3 $molecule^{-1}$ s^{-1}) for reaction of OH with polybrominated diphenyl ethers (PBDEs)

$10^{11} \times A$	B (K)	$10^{12} \times k$	T (K)	Technique[a]	Reference	Temperature Range (K)
OH + 2-Bromodiphenyl ether						
$2.81^{+0.89}_{-0.68}$	533 ± 96	5.38 ± 0.55	326	RR[b] (biphenyl)	Raff and Hites (2006)	326–367
		5.63 ± 0.08	331			
		6.09 ± 0.27	336			
		5.59 ± 0.18	336			
		5.74 ± 0.31	346			
		6.09 ± 0.27	357			
		6.32 ± 0.14	367			
		6.74 ± 0.15	367			
		6.25 ± 0.86	346	RR[c] (fluorene)		
		6.52 ± 0.55	356			
		6.68 ± 0.59	367			
OH + 3-Bromodiphenyl ether						
$8.35^{+4.29}_{-3.83}$	863 ± 142	5.67 ± 0.14	326	RR[b] (biphenyl)	Raff and Hites (2006)	326–367
		6.15 ± 0.21	336			
		6.11 ± 0.45	341			
		7.62 ± 0.88	346			
		7.02 ± 0.19	346			
		6.85 ± 0.43	351			
		7.93 ± 0.39	356			
		7.73 ± 0.52	361			
		8.19 ± 0.50	367			
		6.75 ± 0.18	326	RR[d] (3-chloro-biphenyl)		
		5.62 ± 0.16	326			
		6.03 ± 0.64	331			
		6.62 ± 0.79	336			
		6.43 ± 0.37	346			
		6.97 ± 0.66	354			
		7.65 ± 0.25	367			
OH + 4-Bromodiphenyl ether						
$0.830^{+0.171}_{-0.142}$	109 ± 65	6.14 ± 0.19	326	RR[b] (biphenyl)	Raff and Hites (2006)	326–368
		6.11 ± 0.40	326			
		5.66 ± 0.57	326			
		6.09 ± 0.24	334			
		5.76 ± 0.18	337			
		6.17 ± 0.75	347			
		6.09 ± 0.46	347			
		5.90 ± 0.28	357			
		5.97 ± 0.32	357			
		6.28 ± 0.37	368			
		6.28 ± 0.29	368			
		6.17 ± 0.40	368			
OH + 2,2′-Dibromodiphenyl ether						
$19.8^{+1.0}_{-0.7}$	1,492 ± 152	2.57 ± 0.15	346	RR[b] (biphenyl)	Raff and Hites (2006)	346–378
		2.56 ± 0.09	346			
		3.02 ± 0.51	357			

(*continued*)

Table III-G-102. (*continued*)

$10^{11} \times A$	B (K)	$10^{12} \times k$	T (K)	Technique[a]	Reference	Temperature Range (K)
		3.31 ± 0.42	367			
		3.28 ± 0.20	367			
		3.98 ± 0.46	378			
		4.03 ± 0.64	378			
		2.79 ± 0.03	346	RR[d] (3-chloro-		
		3.26 ± 0.50	357	biphenyl)		
		3.41 ± 0.66	367			
		3.58 ± 0.38	378			
OH + 2,4-Dibromodiphenyl ether						
$2.09^{+1.03}_{-0.69}$	501 ± 145	4.84 ± 0.26	347	RR[b] (biphenyl)	Raff and	347–379
		4.98 ± 0.65	347		Hites (2006)	
		5.39 ± 0.49	358			
		5.71 ± 0.32	369			
		5.12 ± 0.84	379			
		5.91 ± 0.49	379			
		5.53 ± 0.21	379			
		4.82 ± 0.40	347	RR[d] (3-chloro-		
		4.93 ± 0.54	358	biphenyl)		
		5.44 ± 0.33	369			
		5.39 ± 0.78	379			
OH + 3,3′-Dibromodiphenyl ether						
$8.09^{+3.92}_{-2.64}$	960 ± 142	5.12 ± 0.45	346	RR[b] (biphenyl)	Raff and	346–378
		5.27 ± 0.16	357		Hites (2006)	
		6.21 ± 0.13	367			
		6.44 ± 0.24	378			
		5.04 ± 0.17	346			
		5.29 ± 0.11	346	RR[d] (3-chloro-		
		5.14 ± 0.36	357	biphenyl)		
		5.85 ± 0.31	367			
		6.43 ± 0.40	378			
OH + 4,4′-Dibromodiphenyl ether						
$0.0919^{+.034}_{-0.0248}$	-501 ± 145	3.80 ± 0.10	357	RR[e]	Raff and	357–388
		3.78 ± 0.22	357	($CF_3CF{=}CF_2$)	Hites (2006)	
		3.77 ± 0.12	357			
		4.06 ± 0.16	357			
		3.75 ± 0.16	367			
		3.78 ± 0.14	367			
		3.61 ± 0.21	378			
		3.57 ± 0.24	378			
		3.43 ± 0.08	386			
		3.27 ± 0.09	386			
		3.63 ± 0.18	388			

[a]Abbreviations used for the techniques are defined in table I-F-3.

[b]Placed on an absolute basis using k(OH+biphenyl) = 7.1×10^{-12} cm^3 molecule^{-1} s^{-1} (Calvert et al., 2002).

[c]Placed on an absolute basis using k(OH+fluorene) = 1.4×10^{-11} cm^3 molecule^{-1} s^{-1}, independent of temperature (Calvert et al., 2002).

[d]Placed on an absolute basis using k(OH+3-chloro-biphenyl) = $9.7 \times 10^{-12} \exp(-200/T)$ cm^3 molecule^{-1} s^{-1} (Anderson and Hites, 1996).

[e]Placed on an absolute basis using k(OH+$CF_3CF{=}CF_2$) = $8.74 \times 10^{-13} \exp(260/T)$ cm^3 molecule^{-1} s^{-1} (Tokuhashi et al., 2000).

published work (e.g., Bennett and Kerr, 1989; Wayne et al., 1991; Langer and Ljungstrom, 1994a; Kwok and Atkinson, 1995; Porter et al., 1997; Notario et al., 2000b; Bethel et al., 2001b; Le Calvé et al., 2002) and represent updates to relationships presented in those earlier works.

III-H-1. Influence of Ether Functionality on Reactivity

It is well established that the "insertion" of an ether linkage into an aliphatic alkane leads to a weakening of the C—H bonds adjacent to the ether site, and a concomitant enhancement in reactivity. For example, the $CH_3CH_2CH(CH_3)$—H bond strength in *n*-butane is about 410 kJ mole^{-1} (IUPAC, 2008), while the analogous $CH_3CH_2OCH(CH_3)$—H bond in diethyl ether is only 384 kJ mole^{-1} (Kondo and Benson, 1984). This bond weakening effect and enhanced reactivity is similar to that seen upon "insertion" of an —OH functionality into the parent alkane.

The enhancement in reactivity of a given aliphatic ether with OH, Cl, and NO_3 compared to its "parent" alkane is readily apparent from the data presented in table III-H-1. Enhancements are on the order of a factor of 4 for the OH reactions, 10–70 for the NO_3 reactions (note that only limited data are available for these reactions), and 1.5 for the Cl-atom reactions. Whether the enhancement in reactivity is restricted to the C—H bonds located near the ether linkage, or whether the enhancement extends further down the molecule, is difficult to ascertain given the data currently available and is open to interpretation. This point will be discussed further in section III-H-3.

The influence of the addition of an ether functionality to the reactivity of a halogenated alkane is less clear. As can be seen from table III-H-2, rate coefficients for reaction of OH with some saturated, halogenated ethers are larger than those for the corresponding halogenated alkane, while others are smaller. This result likely reflects conflicting effects of the activating ether function and the deactivating fluorine atoms.

Table III-H-1. Rate coefficients (298 K) for reaction of OH, NO_3 and Cl with various aliphatic ethers and their corresponding alkane (k, cm^3 molecule^{-1} s^{-1})

Ether	$10^{12}\times$ k(OH)	$10^{15}\times$ k(NO_3)	$10^{11}\times$ k(Cl)	Analogous Alkane	$10^{12}\times$ k(OH)	$10^{15}\times$ k(NO_3)	$10^{11}\times$ k(Cl)
CH_3OCH_3	2.7	0.23	18	C_2H_6	0.25		5.9
$CH_3CH_2OCH_2CH_3$	12	3.2	28	*n*-C_4H_{10}	2.4	0.046	21
$CH_3OCH_2CH_2CH_2CH_3$	14			*n*-C_5H_{12}	3.9	0.083	27
$CH_3OC(CH_3)_3$	3	0.7	16	$C(CH_3)_4$	0.82		11
$(CH_3CH_2CH_2)_2O$	20	6.0	37	*n*-C_6H_{14}	5.5	0.11	33
$[(CH_3)_2CH]_2O$	10	5.1	17	$(CH_3)_2CHCH(CH_3)_2$	6.1	0.41	
$CH_3CH_2OCH_2CH_2CH_2CH_3$	22			*n*-C_6H_{14}	5.5	0.11	33
$CH_3CH_2OC(CH_3)_3$	8.7	8.1	15	$CH_3CH_2C(CH_3)_3$	2.2		
$CH_3OC(CH_3)_2CH_2CH_3$	5.6	2.2		$CH_3CH_2C(CH_3)_3$	2.2		
$(CH_3)_2CHOCH_2CH(CH_3)_2$	21			$(CH_3)_2CHCH_2CH(CH_3)_2$	5.7	0.15	
$(CH_3CH_2CH_2CH_2)_2O$	28		47	*n*-C_8H_{18}	7.8	0.19	44
$(CH_3)_3COC(CH_3)_3$	3.7		15	$(CH_3)_3CC(CH_3)_3$	0.97		
$(CH_3CH_2CH_2CH_2CH_2)_2O$	33		53	*n*-$C_{10}H_{22}$	11	0.26	53

Table III-H-2. Rate coefficients (298 K) for reaction of OH with various halogenated aliphatic ethers and their corresponding alkane (k, cm^3 molecule^{-1} s^{-1})

Ether	$10^{14} \times k$(OH)	Analogous Alkane	$10^{14} \times k$(OH)
CH_3OCF_3	1.2	CH_3CF_3	0.13
CHF_2OCHF_2	0.23	CHF_2CHF_2	0.60
CF_3OCHF_2	0.041	CF_3CHF_2	0.19
$CH_3CH_2OCF_3$	15	$CH_3CH_2CF_3$	5.5
$CF_3CH_2OCH_3$	59	$CF_3CH_2CH_3$	5.5
$CF_3OCH_2CHF_2$	1.1	$CF_3CH_2CHF_2$	0.71
$CHF_2CHFOCF_3$	0.67	CHF_2CHFCF_3	0.51
$CF_3CHFOCHF_2$	0.60	$CF_3CHFCHF_2$	0.51
$CF_3CHFOCF_3$	0.12	CF_3CHFCF_3	0.15
$CF_3CH_2OCH_2CF_3$	13	$CF_3CH_2CH_2CF_3$	0.84
$CH_3OCH_2CH_2Cl$	430	$CH_3CH_2CH_2Cl$	86
$CH_3OCH_2CH_2Br$	610	$CH_3CH_2CH_2Br$	110

In general, it can be seen from the table that molecules showing the largest enhancement from the presence of the ether function are those in which fluorine-free alkyl groups are positioned adjacent to the ether oxygen.

Although the data are quite limited, the insertion of an ether moiety into an unsaturated compound appears to also enhance the observed reactivity over that observed in the parent alkene. As can been seen from table III-H-3, the magnitude of the enhancement is about a factor of 2.5 for OH addition reactions, a factor of 100 for NO_3 reactions (based on only two rate coefficient pairs), and a factor of 20 for O_3 reactions (based on only three reaction pairs). This enhancement factor for the OH addition reactions is larger than the value of 1.3 given by Kwok and Atkinson (1995); however, we note that the nature of the alkyl group in the —OR group appears to play a role in determining the degree of enhancement observed; see the first three entries in table III-H-3. The enhanced reactivity induced by the —OR moiety is similar to that seen for inclusion of an —OH substituent, see chapter II.

Table III-H-3. Rate coefficients (298 K) for reaction of OH, NO_3 and O_3 with various unsaturated ethers and with their corresponding alkene: k(OH), k(NO_3), k(O_3), units are cm^3 molecule^{-1} s^{-1}

Ether	$10^{11} \times k$(OH)	$10^{13} \times k$(NO_3)	$10^{17} \times k$(O_3)	Analogous Alkane	$10^{11} \times k$(OH)	$10^{13} \times k$(NO_3)	$10^{17} \times k$(O_3)
$CH_3OCH{=}CH_2$	3.4	7.2		C_3H_6	2.9	0.095	1
$CH_3CH_2OCH{=}CH_2$	7.3	15	19	1-C_4H_8	3.2	0.135	0.96
$CH_3CH_2CH_2OCH{=}CH_2$	10	17	23	1-C_5H_{10}	3.2		1.1
$CH_3CH_2CH_2CH_2OCH{=}CH_2$	10.9	20	26	1-C_6H_{12}	3.7		1.1
$(CH_3)_3COCH{=}CH_2$	11			$(CH_3)_3CCH{=}CH_2$	2.9		

III-H-2. Correlations between OH, Cl and NO_3 Rate Coefficients with Saturated Alkanes, Alcohols, and Ethers

The reactions of OH, Cl, and NO_3 with saturated ethers all involve net abstractions, e.g.,

$$\{OH, Cl, NO_3\} + CH_3OCH_3 \rightarrow CH_3OCH_2 + \{H_2O, HCl, HONO_2\}$$

Thus, it seems likely that correlations would exist between the rate coefficients for reaction of the ethers with these oxidants (see, for example, Wayne et al., 1991; Langer and Ljungström, 1995). Further, given the structural similarity between the ethers and the alcohols, it seems likely that similar correlations may apply to both sets of species.

Figure III-H-1 shows a log–log plot of the rate coefficients for reaction of Cl with the saturated, nonhalogenated alcohols and ethers (treated collectively) versus those for reaction of OH with the same set of compounds. A clear correlation is observed ($R^2 = 0.72$), which is described by the following relationship: $\log_{10}[k(\text{Cl} + \text{ether/alcohol})] = 0.634 \times \log_{10}[k(\text{OH} + \text{ether/alcohol})] - 2.71$, with the rate coefficients (k) in cm^3 $molecule^{-1}$ s^{-1}. Also shown in figure III-H-1 for comparison is a log–log plot comparing the reactivity of the alkanes with Cl-atoms versus their reactivity with

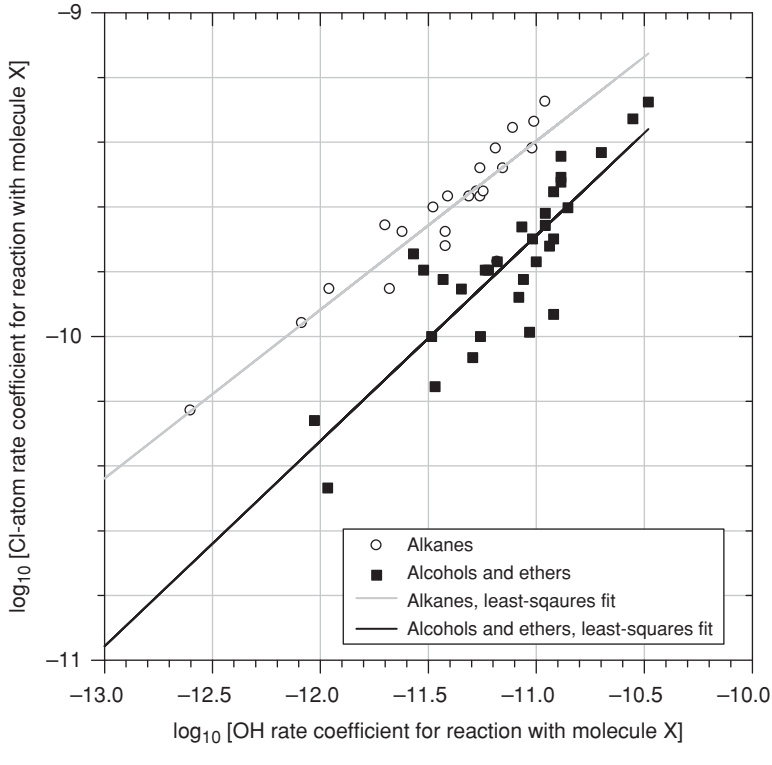

Figure III-H-1. Plots of the logarithm (base 10) of the rate coefficients (cm^3 $molecule^{-1}$ s^{-1}) for reaction of Cl-atoms versus those for reaction of OH with the alkanes (open circles) and with the alcohols and ethers (treated collectively, filled squares). Solid lines are unweighted least-squares fits to the data.

OH. This plot, an update to the one provided in Calvert et al. (2008), gives $\log_{10}[k(\text{Cl} + \text{alkane})] = 0.521 \times \log_{10}[k(\text{OH} + \text{alkane})] - 3.67$, with $R^2 = 0.85$. Thus, while the reactivities of the ethers/alcohols with Cl-atoms and with OH are clearly correlated, the correlation is significantly different to the one observed for reaction of the alkanes with the same two oxidants. As examples, nonane, 2-methyl- 1-propanol and di-isopropyl ether (DIPE) react with OH at nearly identical rates [$k(\text{OH} + \text{nonane}) = 9.8 \times 10^{-12}$ cm^3 molecule^{-1} s^{-1} (Calvert et al., 2008); $k(\text{OH} + \text{2-methyl-1-propanol}) = 9.6 \times 10^{-12}$ cm^3 molecule^{-1} s^{-1} (this book, section II-B); $k(\text{OH} + \text{DIPE}) = 10 \times 10^{-12}$ cm^3 molecule^{-1} s^{-1} (this book; section III-B)]. However, the rate coefficients for reaction of Cl with the two oxygenates {$k(\text{Cl} + \text{2-methyl-1-propanol}) = 2.0 \times 10^{-10}$ cm^3 molecule^{-1} s^{-1} (this book, section II-B), $k(\text{OH} + \text{DIPE}) = 1.7 \times 10^{-10}$ cm^3 molecule^{-1} s^{-1} (this book, section III-B)] are about 2.5 times lower than that for nonane [$k(\text{Cl} + \text{nonane}) = 4.6 \times 10^{-10}$ cm^3 molecule^{-1} s^{-1} (Calvert et al., 2008)]. Correlations of this sort clearly provide predictive power. For example, estimates for the rate coefficients for reaction of Cl with methyl *n*-butyl ether and ethyl *n*-butyl ether, for which no measurements have been made, can be obtained: $k(\text{Cl} + \text{methyl } n\text{-butyl ether}) = 2.6 \times 10^{-10}$ cm^3 molecule^{-1} s^{-1} and $k(\text{Cl} + \text{ethyl } n\text{-butyl}) = 3.4 \times 10^{-10}$ cm^3 molecule^{-1} s^{-1}.

Similar analyses for rate coefficients for reaction of NO_3 with the alcohols and ethers versus those for reaction of OH with the same compounds are shown in figure III-H-2. Again, a correlation is evident ($R^2 = 0.66$), and is described by the following relationship: $\log_{10}[k(\text{NO}_3 + \text{ether/alcohol})] = 1.11 \times \log_{10}[k(\text{OH} + \text{ether/alcohol})] - 2.42$. This can be compared with the relationship obtained for the alkanes (an update of that given in Calvert et al., 2008), also shown in figure III-H-2: $\log_{10}[k(\text{NO}_3 + \text{alkane})] = 0.805 \times \log_{10}[k(\text{OH} + \text{alkane})] - 6.73$; $R^2 = 0.76$. In this case, for a given reactivity toward OH, the oxygenated species tend to be more reactive toward NO_3 than do the alkanes; compare, for example, nonane [$k(\text{OH} + \text{nonane}) = 9.8 \times 10^{-12}$ cm^3 molecule^{-1} s^{-1}, $k(\text{NO}_3 + \text{nonane}) = 2.2 \times 10^{-16}$ cm^3 molecule^{-1} s^{-1}, Calvert et al., 2008] and DIPE [$k(\text{OH} + \text{DIPE}) = 10 \times 10^{-12}$ cm^3 molecule^{-1} s^{-1}, $k(\text{NO}_3 + \text{DIPE}) = 51 \times 10^{-16}$ cm^3 molecule^{-1} s^{-1}, this book, section III-B]. The relationship shown in figure III-H-2 can be used to provide estimates for the unknown rate coefficients of NO_3 with, for example, methyl *n*-butyl ether, $k = 3.4 \times 10^{-15}$ cm^3 molecule^{-1} s^{-1} and ethyl *n*-butyl ether, $k = 5.6 \times 10^{-15}$ cm^3 molecule^{-1} s^{-1}.

Lastly, we note that Andersen et al. (2005b) and Wallington et al. (2008a) have presented a correlation between the reactivity of Cl-atoms and OH with halogenated alkanes and ethers. The correlation they report is $\log[k(\text{OH})] = 0.416 \times \log[k(\text{Cl})] - 8.16$, which can be rearranged to give $\log[k(\text{Cl})] = 2.427 \times \log[k(\text{OH})] + 19.806$.

III-H-3. Structure–Activity Relationships (SARs) for Reaction of OH, Cl and NO_3 with Saturated Alkanes, Alcohols, and Ethers

The use of so-called structure–activity relationships (e.g., Kwok and Atkinson, 1995 and references therein) has proven very valuable for the prediction of rate coefficients, not only for reactions involving the OH radical, but also for Cl-atom (e.g., Tyndall et al., 1997a) and NO_3 reactions (e.g., Aschmann and Atkinson, 1995). The concept of these relationships is that, for a given oxidant, the rate coefficient at a primary,

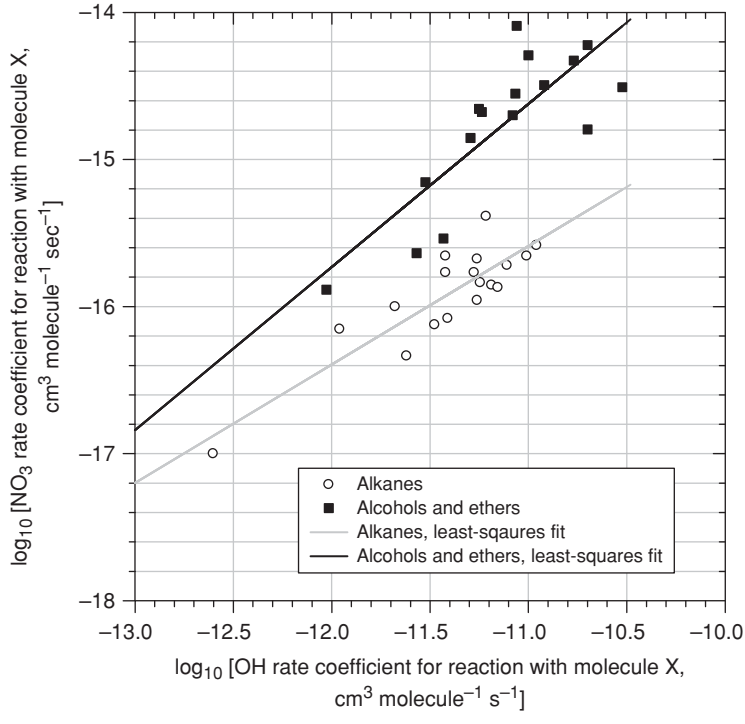

Figure III-H-2. Plots of the logarithm (base 10) of the rate coefficients (cm^3 $molecule^{-1}$ s^{-1}) for reaction of NO_3 versus those for reaction of OH with the alkanes (open circles) and with the alcohols and ethers (treated collectively, filled squares). Solid lines are unweighted least-squares fits to the data.

secondary and tertiary site on an organic species are given rate coefficients, k_{prim}, k_{sec}, and k_{tert}, and these group rate coefficients are then modified by "substituent factors," $F(X)$, that account for the activating or deactivating effects of neighboring groups. Thus, for the CH_2 groups in diethyl ether, $CH_3CH_2OCH_2CH_3$, the rate coefficient would be calculated as $k_{sec} \times F(—CH_3) \times F(—OR)$, where $F(—CH_3)$ is the substituent factor for the methyl group bonded to the $—CH_2$ and $F(—OR)$ is the substituent factor for the —OR group. In the sections that follow, structure–activity relationships are developed or updated for the reaction of OH, Cl, and NO_3 with the alcohols and ethers, using parameters derived for the alkanes as foundations.

III-H-3.1. Structure–Activity Relationships (SARs) for reaction of OH with Alcohols, Ethers, and Alkanes

Existing structure–activity relationships for reaction of OH with organics (e.g., Kwok and Atkinson, 1995; Bethel et al., 2001b) already include substituent factors for alcohol and ether functional groups, and thus what is given below represents an update to these previous studies. The procedure used is as follows. The group rate coefficients and substituent factors of Kwok and Atkinson (1995) that are specific to the alkanes are

used as fixed input, $k_{prim} = 1.36 \times 10^{-13}$, $k_{sec} = 9.34 \times 10^{-13}$, and $k_{tert} = 1.94 \times 10^{-12}$ cm^3 molecule^{-1} s^{-1}, $F(\text{—}CH_3) = 1.0$ and $F(\text{—}CH_2\text{—}, >CH\text{—}) = 1.23$, while the three substituent factors needed to quantify the presence of an ether or alcoholic functionality, F(—OH), F(—OR), and $F(\text{—}CR_2OR)$, are treated as fit parameters [note that for $F(\text{—}CR_2OR)$, R = H or any alkyl group]. The compounds considered include all the acyclic, saturated, nonhalogenated alcohols (chapter II-B), diols (chapter II-C), ethers (chapter III-B), and multifunctional ethers (chapter III-C). It has been noted (Becker et al., 1999b; Le Calvé et al., 2002) that for multi-functional species, e.g., $CH_3OCH_2OCH_3$, the effects of multiple ether linkages attached to the same group are not cumulative. Thus, for these cases, the group rate coefficient is modified only once; i.e., in the above example, the reactivity of the CH_2 group would be given by $k_{sec} \times F(\text{—OR})$, not $k_{sec} \times F(\text{—OR})^2$.

Calculated rate coefficient data, obtained from a least-squares fitting procedure, are compared with measured rate coefficient data in table III-H-4 and figure III-H-3. Values obtained for the three substituent factors are as follows: $F(\text{—OH}) = 2.35$, $F(\text{—OR}) = 4.13$ and $F(\text{—}CR_2OR) = 2.84$. The values for F(—OH) and $F(\text{—}CR_2OR)$ are similar to those derived by Bethel et al. (2001b), but the value for F(—OR) is about half that given by Kwok and Atkinson (1995). The choice of parameters represents something of a compromise; the larger Bethel et al. value for F(—OR) gives a better fit for smaller, monofunctional ethers (e.g., diethyl ether), but overestimates the rate coefficient for more complex, multifunctional species (e.g., $CH_3CH_2OCH_2CH_2OCH_3$). More complex representations of the substituent factors for these multifunctional species, although beyond the scope of this book, would obviously lead to improvements in the overall fit.

Lastly, we note that there has been considerable discussion in the literature regarding the possible long-range effects of —OH and —OR moieties on reactivity (e.g., see Wallington et al., 1988e; Mellouki et al., 1995). The basis of the argument for the existence of long-range effects is the roughly linear increase with chain length in the rate coefficient for reaction OH with the symmetrical, straight-chain 1-alcohols and the symmetrical di-*n*-alkyl ethers, implying equal and enhanced reactivity of each CH_2 group in the chain. Recommended rate coefficients for the 1-alcohols and the di-*n*-alkyl ethers do indeed show a linear increase for chain lengths of 1–5 carbons, with slopes that exceed that expected for a $\text{—}CH_2$ group in a long chain alkane. However, we note that the structure–activity relationship used here, which assumes only an influence on the carbons located α and β to the alcohol–ether function, also predicts an increase in reactivity with chain length greater than expected for chain lengths of five or less. Clearly, more accurate data on the longer-chain *n*-alcohols and di-*n*-alkyl ethers will be required to determine the exact extent of the enhancement of the alcohol or ether moiety.

III-H-3.2. Structure–Activity Relationships (SARs) for reaction of Cl-Atoms with Alcohols, Ethers, and Alkanes

In this section, a structure–activity relationship is developed that applies to reactions of Cl-atoms with acyclic, saturated, monofunctional alcohols and ethers. The relationship

Table III-H-4. Measured and estimated rate coefficients (298 K) for reaction of OH with alcohols and ethers (in units of 10^{-12} cm^3 $molecule^{-1}$ s^{-1}). Estimated values are from the structure–activity parameters discussed in the text

Ether/Alcohol	k(OH) Measured	k(OH) Estimated
CH_3OCH_3	2.7	1.1
$CH_3CH_2OCH_3$	6.3	4.8
$CH_3CH_2OCH_2CH_3$	12	8.5
$CH_3OCH_2CH_2CH_2CH_3$	14	9.9
$CH_3OC(CH_3)_3$	3	2.1
$(CH_3CH_2CH_2)_2O$	20	15.1
$[(CH_3)_2CH]_2O$	10	17.6
$CH_3CH_2OCH_2CH_2CH_2CH_3$	22	13.4
$CH_3CH_2OC(CH_3)_3$	8.7	5.4
$CH_3OC(CH_3)_2CH_2CH_3$	5.6	4.2
$(CH_3)_2CHOCH_2CH(CH_3)_2$	21	19.4
$(CH_3CH_2CH_2CH_2)_2O$	28	18.7
$(CH_3)_3COC(CH_3)_3$	3.7	2.3
$(CH_3CH_2CH_2CH_2CH_2)_2O$	33	21.5
$CH_3OCH_2OCH_3$	4.5	5.0
$CH_3OCH_2CH_2OH$	13	17.9
$CH_3OCH_2CH_2OCH_3$	28	23.1
$CH_3CH_2OCH_2CH_2OH$	19	21.6
$CH_3OCH_2CH(OH)CH_3$	20	24.9
$CH_3CH(OCH_3)_2$	8.9	9.5
$CH_3CH_2CH_2OCH_2CH_2OH$	17	24.8
$CH_3CH_2OCH_2OCH_2CH_3$	20	12.3
$CH_3OCH_2CH(OCH_3)CH_3$	28	35.3
$CH_3C(OCH_3)_2CH_3$	4.1	1.90
$(CH_3)_2CHOCH_2CH_2OH$	21	26.1
$CH_3CH_2OCH_2CH_2OCH_3$	17.5	26.7
$CH_3CH(OCH_3)CH_2CH_2OH$	23.6	21.2
$CH_3CH_2OCH_2CH_2CH_2OH$	22	19.4
$CH_3OCH_2CH_2CH_2OCH_3$	49.3	18.2
$CH_3CH_2CH_2CH_2OCH_2CH_2OH$	30	26.5
$CH_3CH_2OCH_2CH_2OCH_2CH_3$	58	30.4
$CH_3OCH_2CH_2CH_2CH_2OCH_3$	30	17.1
$CH_3CH_2CH_2OCH_2OCH_2CH_2CH_3$	27	19.0
$CH_3C(OCH_2CH_3)_2CH_3$	11	9.3
$(CH_3)_2CHOCH_2OCH(CH_3)_2$	38	21.4
$CH_3CH_2CH_2CH_2OCH_2CH(OH)CH_3$	38	33.8
$CH_3CH_2CH_2CH_2OCH_2OCH_2CH_2CH_2CH_3$	36	17.8
$CH_3CH_2CH(CH_3)OCH_2OCH(CH_3)CH_2CH_3$	43	30.0
$(CH_3)_2CHCH_2OCH_2OCH_2CH(CH_3)_2$	36	25.0
$(CH_3O)_2CHCH_2CH_2OCH_3$	16.7	23.8
$(CH_3O)_3CH$	6	9.9
$CH_3CH_2OCH_2CH_2OCH_2CH_2OH$	57.2	43.5
$CH_3CH_2CH_2CH_2OCH_2CH_2OCH_2CH_2OH$	74.4	48.6
CH_3OH	0.9	0.46
CH_3CH_2OH	3.2	2.7
$CH_3CH_2CH_2OH$	5.8	5.7
$CH_3CH(OH)CH_3$	5.1	5.5

(*continued*)

Table III-H-4. (*continued*)

Ether/Alcohol	k(OH) Measured	k(OH) Estimated
$CH_3CH_2CH_2CH_2OH$	8.5	7.4
$CH_3CH(OH)CH_2CH_3$	8.3	9.0
$(CH_3)_3COH$	1.1	1.3
$(CH_3)_2CHCH_2OH$	9.6	13.1
$(CH_3)_3CCH_2OH$	5.53	3.3
$CH_3CH_2CH_2CH_2CH_2OH$	11	8.8
$CH_3CH(OH)CH_2CH_2CH_3$	11	10.7
$CH_3CH_2CH(OH)CH_2CH_3$	12	12.7
$CH_3CH(CH_3)CH_2CH_2OH$	14	8.8
$CH_3CH_2C(OH)(CH_3)_2$	3.4	3.7
$(CH_3)_2CHCH(OH)CH_3$	12	12.0
$CH_3CH_2CH_2CH_2CH_2CH_2OH$	13	10.3
$CH_3CH_2CH_2CH_2CH(OH)CH_3$	12	13.3
$(CH_3)_2C(OH)CH_2CH_2CH_3$	7.1	5.5
$CH_3CH(OH)CH_2CH(CH_3)_2$	17	10.9
$(CH_3)_2C(OH)CH(CH_3)_2$	9.3	6.8
$CH_3CH_2CH_2CH_2CH_2CH_2CH_2OH$	13	11.7
$(CH_3)_2C(OH)CH_2CH(CH_3)_2$	11	6.9
$CH_3CH_2CH_2CH_2CH_2CH_2CH_2CH_2OH$	13	13.1
$CH_3CH_2C(CH_3)(OH)CH_2CH(CH_3)_2$	13	9.3
$HOCH_2CH_2OH$	14.5	12.8
$CH_3CH(OH)CH_2OH$	21	19.9
$CH_3CH_2CH(OH)CH_2OH$	24.3	25.3
$CH_3CH(OH)CH_2CH_2OH$	29.9	20.1
$CH_3CH(OH)CH(OH)CH_3$	21.2	27.0

builds upon parameters obtained for the reaction of Cl-atoms with alkanes (Calvert et al., 2008), which are fixed in the present calculations: $k(\text{—}CH_3) = 2.84 \times 10^{-11}$ cm^3 molecule^{-1} s^{-1}; $k(\text{—}CH_2\text{—}) = 8.95 \times 10^{-11}$ cm^3 molecule^{-1} s^{-1}; $k(\text{>}CH\text{—}) = 6.48 \times 10^{-11}$ cm^3 molecule^{-1} s^{-1}; $F(\text{—}CH_3) = 1.0$; $F(\text{—}CH_2\text{—}, \text{>}CH\text{—}) = 0.80$. To incorporate the alcohols and ethers into the calculation, three substituent factors, F(—OH), F(—OR), and $F(\text{—}CR_2OR$, R = H, R), were added as fit parameters. Note that for reaction at CH_3 groups, $k(\text{—}CH_3)$ was modified only by F(—OH), F(—OR), or $F(\text{—}CR_2OR)$, but not by $F(\text{—}CH_2\text{—}, \text{>}CH\text{—})$ (Tyndall et al., 1997a; Calvert et al., 2008).

The measured rate coefficient data used as input, and the data retrieved from the fit are given in table III-H-5. Retrieved substituent factors are F(—OH) = 1.18, F(—OR) = 1.45, and $F(\text{—}CR_2OR) = 0.40$. The value obtained for F(—OR) is somewhat higher than that determined by Notario et al. (2000b), F(—OR) = 1.18. That the values of F(—OH) and F(—OR) exceed unity is consistent with the expectation that the presence of an ether or alcohol functionality enhances the reactivity. The calculated and experimental rate coefficient data are plotted against one another in figure III-H-4. It is evident that the data for the alkanes are very well reproduced, each predicted rate coefficient falls within 6% of the measured value. Predictions are also quite good for the alcohols, with all predicted values but one (methanol, 40%) falling within 20%

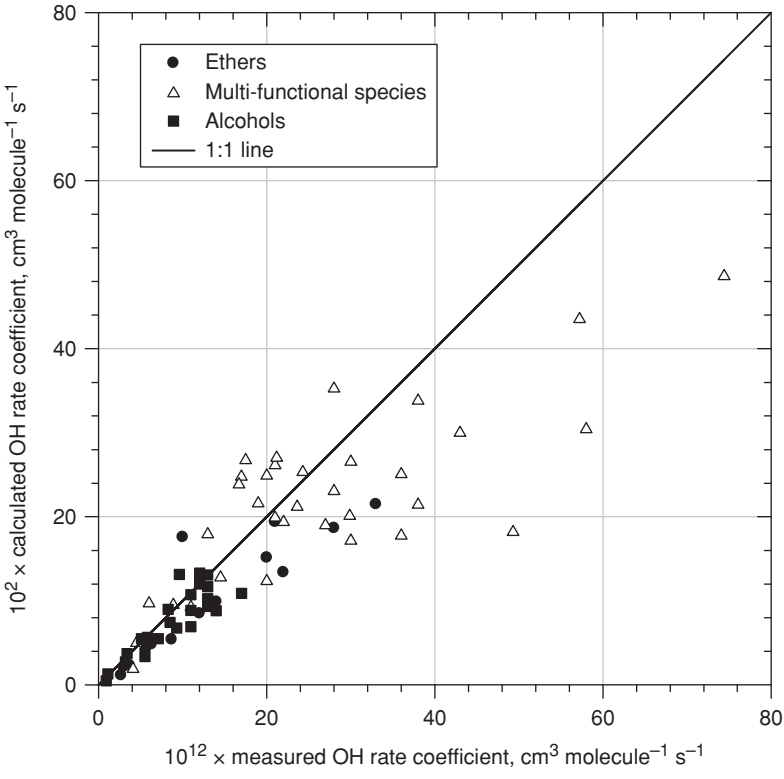

Figure III-H-3. Estimated versus measured rate coefficients for reaction of OH with alcohols, ethers, and multi-functional species containing —OH and/or —OR linkages. Estimates are from the structure–activity relationship presented in the text.

of the measured values. Predictions are not as good for the ethers, particularly those with branched structures. For example, predicted values for methyl *tert*-butyl ether and di-*tert*-butyl ether are about a factor of 2 lower than measured values, although predictions for straight-chain species (e.g., diethyl ether through di-*n*-pentyl ether) generally fall within 10% of measured values.

III-H-3.3. Structure–Activity Relationships (SARs) for reaction of NO_3 with Alcohols, Ethers, and Alkanes

A structure–reactivity relationship for reaction of NO_3 with alkanes was presented in Calvert et al. (2008). In that work, which was essentially an update of the treatment of Aschmann and Atkinson (1995), the following rate coefficients and substituent factors were determined:

$$k_{\text{primary}}(298\ \text{K}) = 7 \times 10^{-19}\text{cm}^3\ \text{molecule}^{-1}\ \text{s}^{-1}$$

Table III-H-5. Measured and estimated rate coefficients (298 K) for reaction of Cl-atoms with alcohols and ethers (in units of 10^{-11} cm^3 molecule^{-1} s^{-1}). Estimated values are from the structure–activity parameters discussed in the text

Ether/Alcohol	k(Cl) Measured	k(Cl) Estimated
CH_3OH	5.5	3.35
CH_3CH_2OH	10	11.7
$CH_3CH_2CH_2OH$	16	14.9
$CH_3CH(OH)CH_3$	8.6	9.95
$CH_3CH_2CH_2CH_2OH$	21.8	21.3
$CH_3CH(OH)CH_2CH_3$	13.2	13.7
$(CH_3)_3COH$	3.4	3.42
$(CH_3)_2CHCH_2OH$	20	16.7
$CH_3CH_2CH_2CH_2CH_2OH$	24	27.1
$CH_3CH(OH)CH_2CH_2CH_3$	22	20.1
$CH_3CH_2CH(OH)CH_2CH_3$	20	17.8
$(CH_3)_2CHCH_2CH_2OH$	25	22.2
$(CH_3)_2C(OH)CH_2CH_3$	7	8.7
$(CH_3)_3CCH_2OH$		17.0
$CH_3CH_2CH_2CH_2CH_2CH_2OH$	30	32.8
$CH_3CH(CH_3)C(OH)C(CH_3)_2$	10.3	10.6
$CH_3CH_2(CH_2)_3CH_2CH_2OH$	36	38.5
$CH_3CH_2(CH_2)_4CH_2CH_2OH$	41	44.2
CH_3OCH_3	18	8.25
$CH_3CH_2OCH_3$	24	18.3
$CH_3CH_2OCH_2CH_3$	28	28.3
$CH_3OC(CH_3)_3$	16	7.55
$(CH_3CH_2CH_2)_2O$	37	33.7
$[(CH_3)_2CH]_2O$	17	23.4
$CH_3CH_2OC(CH_3)_3$	15	17.6
$(CH_3CH_2CH_2CH_2)_2O$	47	46.5
$(CH_3)_3COC(CH_3)_3$	15	6.85
$(CH_3CH_2CH_2CH_2CH_2)_2O$	53	58.0

$$k_{\text{secondary}}(298\text{ K}) = 1.74 \times 10^{-17}\text{cm}^3\text{ molecule}^{-1}\text{ s}^{-1}$$

$$k_{\text{tertiary}}(298\text{ K}) = 11.7 \times 10^{-17}\text{cm}^3\text{ molecule}^{-1}\text{ s}^{-1}$$

with F (—CH_3) = 1.00 by definition, and F(—CH_2—) = F(>C—) = F(>C<) = 1.33.

These parameters were used as input for the basis for the more general structure–activity relationship (applicable to alcohols and ethers) developed below.

It is clear from table III-H-1 and from the data and discussion presented in chapter II that the aliphatic ethers and alcohols are considerably more reactive with the NO_3 radical than are the corresponding alkanes. Further examination of the available data suggests that the degree of enhancement on the groups located adjacent (α) to the —OH or —OR functionality is dependent on whether that group is tertiary (>CH), secondary (—CH_2) or primary (CH_3), with the degree of enhancement smallest for a tertiary group and largest for a primary one. Thus, it appears necessary to include in this case three

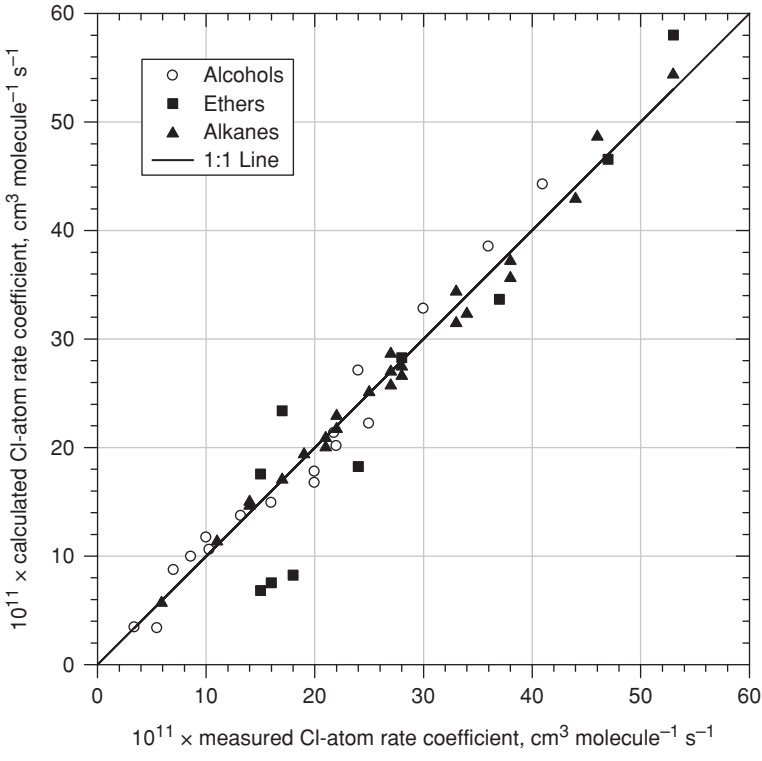

Figure III-H-4. Estimated versus measured rate coefficients for reaction of Cl-atoms with alkanes, alcohols, and ethers. Estimates are from the structure–activity relationship presented in the text.

Table III-H-6. Measured and estimated rate coefficients (298 K) for reaction of NO_3 with alcohols and ethers (in units of 10^{-16} cm^3 molecule^{-1} s^{-1}). Estimated values are from the structure–activity parameters discussed in the text

Ether/Alcohol	$k(NO_3)$ Measured	$k(NO_3)$ Estimated
$CH_3CH_2CH_2OH$	21	27.8
$CH_3CH(OH)CH_3$	14	13.4
$CH_3CH_2CH_2CH_2OH$	28	31.6
$CH_3CH(OH)CH_2CH_3$	21	28.2
CH_3OCH_3	2.3	2.58
$CH_3CH_2OCH_2CH_3$	32	25.3
$CH_3OC(CH_3)_3$	7	2.69
$(CH_3CH_2CH_2)_2O$	60	55.6
$((CH_3)_2CH)_2O$	51	26.8
$CH_3CH_2OC(CH_3)_3$	81	14.0
$CH_3OC(CH_3)_2CH_2CH_3$	22	13.9
$(CH_3)_3COC(CH_3)_3$	2.9	2.8

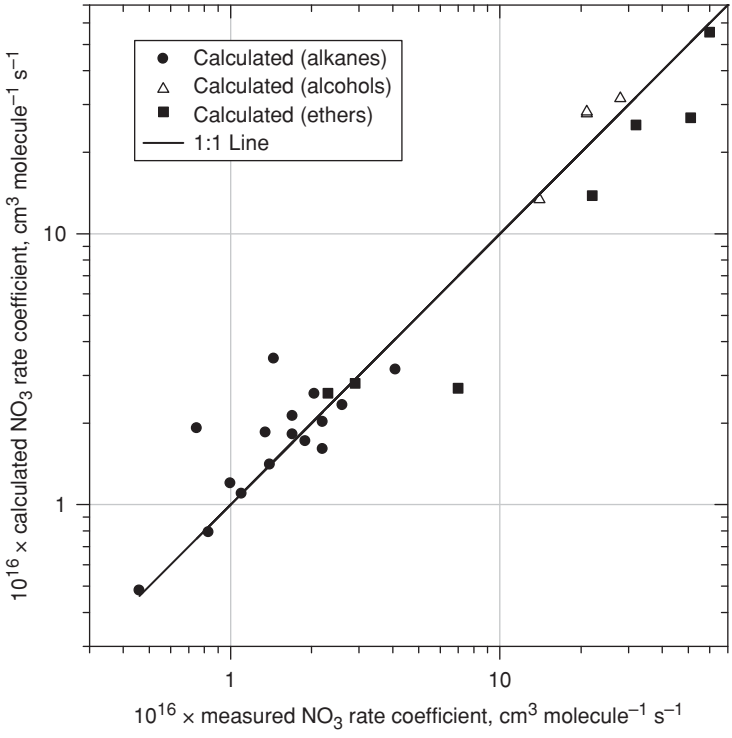

Figure III-H-5. Estimated versus measured rate coefficients for reaction of NO_3 with alkanes, alcohols, and ethers. Estimates are from the structure–activity relationship presented in the text.

substituent factors for the *F*(—OH) or *F*(—OR) functionality, one each for adjacent primary [designated *F*(—OR)/primary], secondary [*F*(—OR)/secondary], or tertiary groups [*F*(—OR)/tertiary]. Thus, in dimethyl ether, the rate coefficient estimate would be obtained from the following expression, $k_{est} = 2 \times k_{prim} \times$ [*F*(—OR)/primary], while reaction at the tertiary groups in di-isopropyl ether would be estimated as: $k_{est} = 2 \times k_{tert} \times$ [*F*(—OR)/tertiary]. We also note that the reaction of NO_3 with di-*tert*-butyl ether ($k = 2.9 \times 10^{-16}$ cm^3 $molecule^{-1}$ s^{-1}, Langer et al. (1996) is considerably more rapid than for a similarly structured alkane, $k(NO_3 + 2,2,3,3\text{-tetramethylbutane}) < 5 \times 10^{-17}$ cm^3 $molecule^{-1}$ s^{-1}, Aschmann and Atkinson (1995), implying that the activating effect of the ether function is operative at least as far as the β-position. Thus, an additional substituent factor, *F*(—CR_2OR), was included (where R can be an H-atom or any alkyl group). Least-squares fitting, varying the four fit parameters: *F*(—OR)/primary, *F*(—OR)/secondary, *F*(—OR)/tertiary, and *F*(—CR_2OR), led to the calculated rate coefficients given in table III-H-6 and plotted in figure III-H-5. The large activation effect is evident from the magnitude of the retrieved substituent factors, *F*(—OR)/primary = 184, *F*(—OR)/secondary = 70, *F*(—OR)/tertiary = 10.6, and *F*(—CR_2OR) = 67. While the set of parameters derived here does a reasonable job of

retrieving the measured rate coefficients for most species (except for a few branched species), it should be noted that the database for reaction of NO_3 with the alcohols and ethers is very limited, and extrapolation to molecules substantially different in structure from those used to derive the fit should be carried out with caution.

IV

Rate Coefficients and Mechanisms for the Atmospheric Oxidation of the Aldehydes

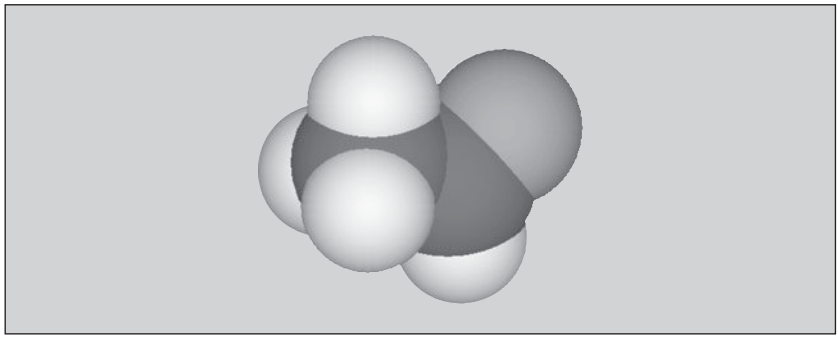

IV-A. Introduction

Aldehydes are emitted from a variety of anthropogenic sources associated with natural gas and petroleum combustion (for examples, see tables I-C-2 and I-C-3). Winer et al. (1992) have discussed direct emissions of aldehydes from biogenic sources. They are also important intermediates in the oxidation of directly emitted organic compounds. For example, formaldehyde, CH_2O formed in the reaction of CH_3O with O_2

$$CH_3O + O_2 \rightarrow CH_2O + HO_2$$

CH_3O is formed in the oxidation of methane, and a number of other compounds. There are also many other sources of CH_2O; for example, the Leeds University's Master Chemical Mechanism (MCM) lists a total of ~140 CH_2O precursors: http://mcm.leeds.ac.uk/MCM/.

Aldehydes with saturated hydrocarbon chains (termed *alkanals* or *acyclic aldehydes*) react mainly with OH during the day and with NO_3 at night. The aldehydic C—H bond is weaker than those in the hydrocarbon chain; and, certainly for the shorter carbon chain species, abstraction by both OH and NO_3 occurs primarily at the aldehydic center to form an acyl radical which reacts rapidly with O_2 to form an acylperoxy radical, e.g.,

$$CH_3CHO + OH \rightarrow CH_3CO + H_2O$$

$$CH_3CO + O_2 \rightarrow CH_3C(O)O_2$$

An important reaction of the acylperoxy radical is with NO_2 to form an acylperoxy nitrate. In the example shown, the oxidation of acetaldehyde gives acetyl peroxy radicals which can react with NO_2 to form peroxyacetyl nitrate, $CH_3C(O)O_2NO_2$, generally known as PAN:

$$CH_3C(O)O_2 + NO_2 \rightarrow CH_3C(O)O_2NO_2$$

Peroxyacyl nitrates dissociate quite quickly at 298 K, to regenerate peroxyacyl radicals. For example, PAN has a lifetime of about 50 min. The lifetime increases rapidly at the lower temperatures experienced at higher altitudes and is several months at the temperatures (~250 K) of the upper troposphere. This long lifetime provides a mechanism for the transport of NO_x from polluted areas to less polluted areas, by transfer of peroxyacyl nitrates from the boundary layer to the free troposphere; subsequent subsidence can return them to the boundary layer where they dissociate at the higher temperatures encountered there. The atmospheric reactions of the nitrates are discussed in detail in chapters VIII and IX.

For aldehydes with unsaturated side chains as in acrolein (2-propenal, CH_2=CHCHO), reaction with OH radicals can take place by addition at the multiple bond, and this can compete with abstraction at the —CHO group.

Photolysis of aldehydes competes with reaction with OH and is discussed in chapter IX.

In this chapter we examine the thermal reactions of the several classes of the aldehydes in the atmosphere: aldehydes with saturated hydrocarbon chains (alkanals), hydroxyaldehydes, dialdehydes (with saturated and unsaturated hydrocarbon chains), unsaturated aldehydes, aldehydes derived from aromatic and biogenic hydrocarbons and halogen substituted aldehydes. The rate coefficients and mechanisms of atmospheric oxidation of the alkanals are reviewed in the following section (IV-B), which draws on the analysis provided by Calvert et al. (2008) for reactions of alkanals with OH and NO_3 with an update of information where it is available.

IV-B. Acyclic Aldehydes

IV-B-1. Formaldehyde (Methanal, CH_2O)

IV-B-1.1. OH Reaction Kinetics

The reaction between OH and CH_2O has been the subject of a number of studies which cover a wide range of temperatures (202–576 K). The rate coefficients for this reaction are given in table IV-B-1. The direct studies of Atkinson and Pitts (1978), Stief et al. (1980), Temps and Wagner (1984), Yetter et al. (1989), and Sivakumaran et al. (2003b) all agree to within ±10%. The relative rate measurement by Niki et al. (1984) also agrees with the above measurements. The unweighted mean of these determinations gives a rate coefficient of 8.5×10^{-12} cm^3 molecule^{-1} s^{-1} at 298 K, with an uncertainty of ±15%.

The rate coefficients determined by Sivakumaran et al. (2003b) show a nonlinear Arrhenius temperature dependence, with a minimum rate coefficient at around 315 K.

Table IV-B-1. Rate coefficients ($k = A\ e^{-B/T}$, cm^3 $molecule^{-1}$ s^{-1}) for reaction of OH with formaldehyde (CH_2O)

$10^{12} \times A$	B (K)	$10^{12} \times k$	T (K)	Technique[a]	Reference	Temperature Range (K)
		14.0 ± 3.5	298	DF–MS	Morris and Niki (1971a)	
		15 ± 3	298	DF–RR (C_3H_6)[b]	Morris and Niki (1971b)	
		14 ± 2	298	RR (C_2D_4/C_2H_4)[c]	Niki et al. (1978a)	
12.5	88 ± 151	9.4 ± 1.0	299	FP–RF	Atkinson and Pitts (1978)	299–426
		9.4 ± 1.0	356			
		10.3 ± 1.1	426			
65 ± 15	720 ± 240	6.0 ± 0.7	268	DF–MS (relative to OH + OH)[d]	Smith (1978)	268–334
		6.5 ± 1.5	298			
		9.6 ± 1.2	334			
10.5 ± 1.1	0 ± 100	11.2 ± 1.0	228	FP–RF	Stief et al. (1980)	228–362
		10.3 ± 0.9	257			
		9.9 ± 1.1	298			
		10.5 ± 1.5	362			
		8.1 ± 1.7	296	DF–LMR	Temps and Wagner (1984)	
		7.8 ± 1.1	299 ± 2	RR (C_2H_4)[c]	Niki et al. (1984)	
16.6	86 ± 40	12.5 ± 0.11	298	PLP–LIF	Zabarnick et al. (1988a)	296–576
		13.9 ± 0.4	378			
		13.3 ± 0.3	473			
		14.5 ± 2.0	572			
		8.0 ± 1.2	298	DF–RF	Yetter et al. (1989)	
$9.52 \times 10^{-6} \times T^{2.03}$	636	10.8 ± 0.05	202	PLP–LIF	Sivakumaran et al. (2003)	202–399
		9.49 ± 0.07	212			
		9.89 ± 0.06	222			
		9.69 ± 0.05	233			
		9.28 ± 0.06	243			
		9.31 ± 0.06	253			
		8.72 ± 0.07	263			
		8.81 ± 0.09	273			
		8.37 ± 0.18	276			
		8.46 ± 0.07	284			
		8.06 ± 0.17	288			
		8.46 ± 0.40	298			
		8.56 ± 0.09	308			
		8.60 ± 0.09	312			
		8.20 ± 0.11	323			
		8.88 ± 0.07	334			
		8.51 ± 0.14	336			
		8.67 ± 0.08	366			
		9.28 ± 0.14	399			

[a]Abbreviations used for the techniques are defined in table I-F-3.

[b]Placed on an absolute basis using $k(OH + C_3H_6) = 1.7 \times 10^{-11}$ cm^3 $molecule^{-1}$ s^{-1} in 1 Torr He (Atkinson et al., 2008) give a value of 1.8×10^{-11} cm^3 $molecule^{-1}$ s^{-1} in 1 Torr N_2. The value in He will be slightly smaller.

[c]Placed on an absolute basis using $k(OH + C_2H_4) = 7.9 \times 10^{-12}$ cm^3 $molecule^{-1}$ s^{-1} at 1 bar and 298 K (Atkinson et al., 2006).

[d]Based on $k(OH + OH) = 2.24 \times 10^{-12}$ cm^3 $molecule^{-1}$ s^{-1} at 298 K and $E_a = 4$ kJ mol^{-1}.

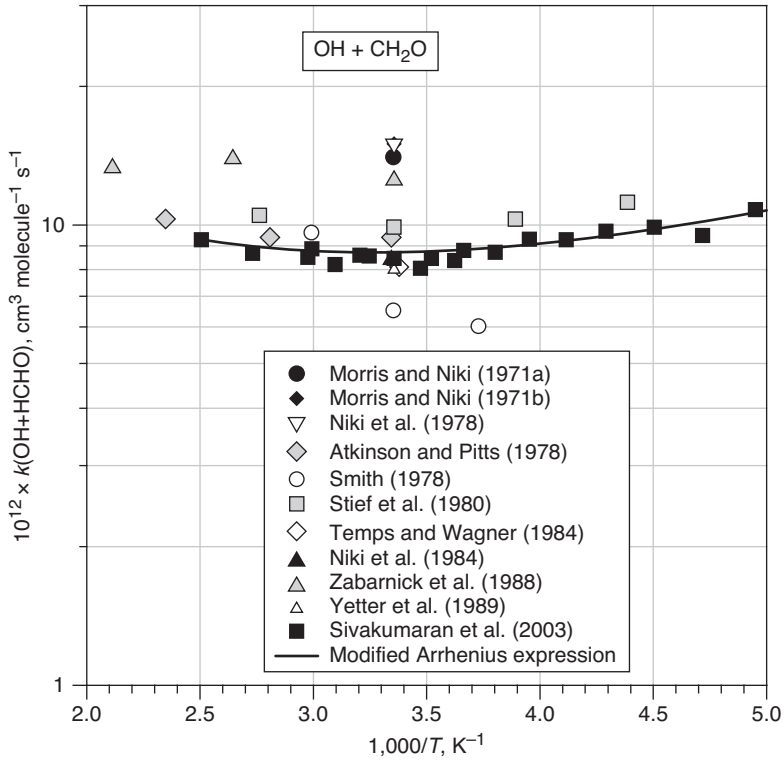

Figure IV-B-1. Arrhenius plot for the rate coefficients for the OH + CH_2O reaction.

Figure IV-B-1 shows the available measurements, along with a nonlinear fit to the data of Atkinson and Pitts (1978), Stief et al. (1980), Temps and Wagner (1984), Niki et al. (1984), Yetter et al. (1989), and Sivakumaran et al. (2003b). We recommend the use of the rate coefficient defined by the equation: $k = 1.26 \times 10^{-17} T^2 \exp(613/T)$ over the range 200–400 K which gives $k(298) = 8.8 \times 10^{-12}$ cm^3 molecule^{-1}; this expression is almost identical to that given in the 2006 IUPAC evaluation (Atkinson et al., 2006).

Xu et al. (2006) carried out a study of the CH_2O–OH reaction using variational transition state theory based on electronic structure calculations. The calculations show a van der Waals complex with a binding energy of ~5 kJ mol^{-1} that is located before the transition state that in turn lies ~4 kJ mol^{-1} below the reactant energies. Such a transition state is termed *submerged.* Over the temperature range 200–400 K, Xu et al. (2006) obtained a rate coefficient for the abstraction reaction of $2.45 \times 10^{-21} T^{2.98} \exp(1{,}750/T)$, that lies well above the experimental values. For example, at 298 K, the expression of Xu et al. gives $k = 2.1 \times 10^{-11}$ cm^3 molecule^{-1} s^{-1}, a factor of 2.4 times that measured experimentally.

The time resolved studies of Temps and Wagner (1984) and Sivakumaran et al. (2003b) indicate that the major products are the formyl radical and water, rather than formic acid and hydrogen atoms; the latter products account for less than 4% of the

reaction. Furthermore, chamber studies by Morrison and Heicklen (1980), Niki et al. (1984), and D'Anna et al. (2003) all indicate that the yield of formic acid is no more than a few percent.

$$OH + CH_2O \rightarrow H_2O + HCO$$

$$OH + CH_2O \rightarrow [HOCH_2O\cdot]^{\dagger} \rightarrow H + HCOOH$$

The latter pathway could be envisaged as proceeding by addition of the OH to the carbonyl group. However, calculations show that the barrier to addition is too high for such a rapid reaction to occur (Soto and Page, 1990; Alvárez-Idaboy et al., 2001b; D'Anna et al., 2003). The calculations of Xu et al. (2006) show that the formation of the hydroxymethoxy adduct makes a negligible contribution to the rate coefficient at atmospheric temperatures.

D'Anna et al. (2003) and Feilberg et al. (2004) have measured the isotope effects for reaction of a number of isotopomers of formaldehyde with OH at the temperature of 298 K. Expressed relative to normal CH_2O, the two studies can be combined to give the following rate coefficient ratios: $k(OH + CH_2O)/k(OH + CD_2O) = 1.65 \pm 0.03$; $k(OH + CH_2O)/k(OH + CDHO) = 1.28 \pm 0.02$; $k(OH + CH_2O)/k(OH + {}^{13}CH_2O) = 0.96 \pm 0.02$; $k(OH + CH_2O)/k(OH + CH_2{}^{18}O) = 0.97 \pm 0.02$, with our estimate of the three standard deviations uncertainty.

IV-B-1.2. NO_3 Reaction Kinetics

All of the measurements on the reaction of NO_3 with CH_2O have been made at room temperature using environmental chambers. Cantrell et al. (1985) and Doussin et al. (2003) used in situ optical detection of NO_3 and FTIR detection of stable species, coupled with computer simulation of a complex reaction mechanism. Atkinson et al. (1984c) and Hjorth et al. (1988) did not use direct measurement of NO_3, but measured N_2O_5 and relied on knowledge of the equilibrium constant, K, for the equilibrium:

$$NO_2 + NO_3 \rightleftharpoons N_2O_5$$

The values for these two determinations have been rescaled using the values of K recently measured by Osthoff et al. (2007), $K = 5.1 \times 10^{-27} \exp(10{,}871/T)$ over the temperature range 278–323 K; $K = 3.55 \times 10^{-11}$ cm^3 molecule^{-1} at 298 K and 5.13×10^{-11} cm^3 molecule^{-1} at 295 K. For comparison, the current IUPAC recommendation gives $K = 2.75 \times 10^{-11}$ cm^3 molecule^{-1} at 298 K and 4.01×10^{-11} cm^3 molecule^{-1} at 295 K. As can be seen from table IV-B-2, even after correction to a common expression for the equilibrium constant, the data are scattered. The strong dependence of K on T over the uncertainty range of the experimental temperature, casts doubt on the accuracy of the measurements based on N_2O_5 detection to determine $[NO_3]$. In addition, Cantrell et al. (1985), in a detailed analysis of the validity of the N_2O_5 technique, point out that, under the conditions used by Atkinson et al., there is a significant loss of NO_3 by

Table IV-B-2. Rate coefficients (k, cm^3 molecule^{-1} s^{-1}) for reaction of NO_3 with formaldehyde (CH_2O)

$10^{16} \times k$	T (K)	Technique[a]	Reference
6.2 ± 0.4	298 ± 1	N_2O_5 decay[b]	Atkinson et al. (1984c)
6.4 ± 0.4	300 ± 1	NO_3 abs.	Cantrell et al. (1985)
9.3 ± 1.1	298 ± 2	N_2O_5 decay–FTIR[b]	
14.7 ± 2.4	295 ± 2	N_2O_5 decay–FTIR[b]	Hjorth et al. (1988)
5.2 ± 0.9	298 ± 2	NO_3 abs.–FTIR	Doussin et al. (2003)

[a]Abbreviations used for the techniques are defined in table I-F-3.
[b]The rate coefficients have been rescaled to a common K for N_2O_5 dissociation (see section IV-B-1.2).

reaction with HO_2, which should lead to a large increase in the apparent rate coefficient for $NO_3 + CH_2O$. The direct determinations of Cantrell et al. (1985) and of Doussin et al. (2003) are in good agreement, and an average of their values is the basis of our recommendation of $k(298) = 5.8 \times 10^{-16}$ cm^3 molecule^{-1} s^{-1} with an estimated uncertainty of ±30%.

D'Anna et al. (2003) showed that the NO_3 reaction with CH_2O proceeds by H-atom abstraction so that the sole products of this reaction are $HNO_3 + HCO$. Mora-Diez and Boyd (2002) examined the mechanism of the reactions between NO_3 and formaldehyde and acetaldehyde theoretically; comparisons with experiment are consistent with a direct abstraction mechanism. Alvárez-Idaboy et al. (2001a) reached a similar conclusion for NO_3 reaction with formaldehyde, acetaldehyde, propanal, *n*-butanal, and 2-methylpropanal. Their calculations showed that all reactions proceed via abstraction of the α-carbonyl H-atom; the dependence of the rate constant on molecular size was shown to be attributable to the increase in the internal rotational partition function with the size of the aldehyde.

Measurements of rate coefficients for NO_3 with isotopically substituted formaldehydes have been made by D'Anna et al. (2003) and Feilberg et al. (2004). The measurements were made relative to unsubstituted CH_2O using FTIR analysis. The ratios obtained are: $k(NO_3 + CH_2O)/k(NO_3 + CDHO) = 1.78 \pm 0.09$ (Feilberg et al.); $k(NO_3 + CH_2O)/k(NO_3 + CD_2O) = 3.00 \pm 0.15$ (average from both studies); $k(NO_3 + CH_2O)/k(NO_3 + {}^{13}CH_2O) = 0.96 \pm 0.05$ (average from both studies); $k(NO_3 + CH_2O)/k(NO_3 + CH_2{}^{18}O) = 0.98 \pm 0.05$ (Feilberg et al.) where the uncertainties in the ratios have been widened to 5%. The results show a strong primary kinetic isotope effect that is derived from the abstraction of H by NO_3, but also nonnegligible secondary isotope effects.

IV-B-1.3. Cl-Atom Reaction Kinetics

Good agreement is shown at 298 K by all six determinations of the $Cl + CH_2O$ reaction (Niki et al., 1978a; Michael et al., 1979b; Anderson and Kurylo, 1979; Poulet et al., 1981; Fasano and Nogar, 1981; Seakins et al., 2004; see table IV-B-3) giving an unweighted average value for k(298 K) of 7.0×10^{-11} cm^3 molecule^{-1}s^{-1}. Fitting the temperature dependence to the data of Michael et al. (1979b) and Anderson and Kurylo (1979) gives $k = 8.2 \times 10^{-11} \exp(46/T)$ cm^3 molecule^{-1} s^{-1} (figure IV-B-2),

Table IV-B-3. Rate coefficients ($k = A\ e^{-B/T}$, cm^3 $molecule^{-1}$ s^{-1}) for reaction of Cl with formaldehyde (CH_2O)

$10^{12} \times A$	B (K)	$10^{12} \times k$	T (K)	Technique[a]	Reference	Temperature Range (K)
		76 ± 6.0	298	RR[b] (ethane)	Niki et al. (1978a)	
75.8 ± 5.8	0	75.2 ± 5.9	200	PLP–RF	Michael et al. (1979b)	200–500
		74.6 ± 4.3	298			
		74.5 ± 4.8	500			
109	131 ± 98	59.8 ± 9.6	223	PLP–RF	Anderson and Kurylo (1979)	223–323
		65.0 ± 9.2	250			
		67.6 ± 9.8	273			
		71.8 ± 6.1	293			
		70.7 ± 7.4	323			
		68 ± 14	295	DF–MS–RR[b] (ethane)	Poulet et al. (1981)	
		74 ± 7	298	PLP–CL	Fasano and Nogar (1981)	
		69.8 ± 6.8	298	PLP–IR emission	Seakins et al. (2004)	

[a]Abbreviations used for the techniques are defined in table I-F-3.
[b]Placed on an absolute basis using $k(Cl + C_2H_6) = 5.9 \times 10^{-11}$ cm^3 $molecule^{-1}$ s^{-1} (Atkinson et al., 2006).

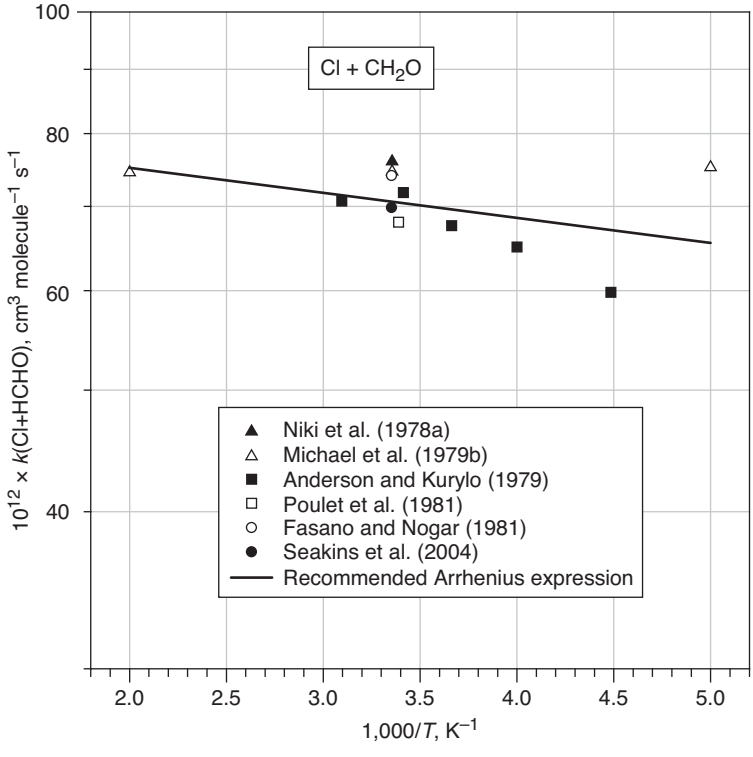

Figure IV-B-2. Arrhenius plot for the rate coefficients for the Cl + CH_2O reaction.

in agreement with the IUPAC recommendation (Atkinson et al., 2005). The reaction proceeds exclusively by H abstraction:

$$Cl + CH_2O \rightarrow HCl + HCO$$

IV-B-1.4. $O(^3P)$ Reaction Kinetics

A recent NASA recommendation (Sander et al., 2006) gives $k[O(^3P) + CH_2O] = 1.6 \times 10^{-11}$ cm^3 molecule^{-1}s^{-1} at 298 K, with an uncertainty of ± 25%, and $k(T) = 3.4 \times 10^{-11} \exp(-1{,}600/T)$ cm^3 molecule^{-1} s^{-1}, based on the temperature dependent measurements of Klemm et al. (1980) over the temperature range 250–750 K and Chang and Barker (1979) over the range 296–436 K.

IV-B-1.5. Summary of the Atmospheric Fate of Formaldehyde and the End Products of Its Oxidation

During the day, the destruction of CH_2O is controlled primarily by photolysis and reaction with OH. The photolysis lifetime of CH_2O in the lower troposphere with an overhead Sun is about 3 h; its dependence on latitude and time is discussed in chapter IX. For [OH] $\approx 2.5 \times 10^6$ molecule cm^{-3}, a lifetime with respect to reaction with OH is 13 h. The lifetime for removal by NO_3, with [NO_3] $\approx 3 \times 10^9$ molecule cm^{-3} is about 3.5 days. Both bimolecular processes occur by H abstraction to give HCO, which, under atmospheric conditions, reacts with O_2 to form CO and HO_2.

IV-B-2. Acetaldehyde (Ethanal, CH_3CHO)

IV-B-2.1. OH Reaction Kinetics

The reaction of OH with acetaldehyde has been well characterized over the temperature range 200–400 K. The rate coefficients are given in table IV-B-4. There is good agreement between the room temperature measurements of Morris and Niki (1974), Morris et al. (1971), Niki et al. (1978a), Michael et al. (1985), Scollard et al. (1993), Tyndall et al. (1995), D'Anna et al. (2001a), Wang et al. (2003), Sivakumaran and Crowley (2003), Taylor et al. (2006), Vöhringer-Martinez et al. (2007), and Zhu et al. (2008). An unweighted average gives $k(298) = 1.53 \times 10^{-11}$ cm^3 molecule^{-1}s^{-1} with an estimated uncertainty of ±15%. The temperature dependence has been extensively studied by Michael et al. (1985), Sivakumaran and Crowley (2003), Taylor et al. (2006), and Zhu et al. (2008). The reaction has a negative temperature dependence with no obvious signs of curvature in the Arrhenius plot at atmospheric temperatures; this is in contrast to the behavior of formaldehyde. Figure IV-B-3 shows the available measurements, along with an Arrhenius fit to the data of Morris and Niki (1974), Morris et al. (1971), Niki et al. (1978b), Michael et al. (1985), Scollard et al. (1993), Tyndall et al. (1995), D'Anna et al. (2001a), Wang et al. (2003), Sivakumaran and Crowley (2003), Taylor et al. (2006), Vöhringer-Martinez et al. (2007), and Zhu et al. (2008), over the temperature range 200–500 K; we recommend a rate coefficient $k = 5.2 \times 10^{-12} \exp(322/T)$ cm^3 molecule^{-1} s^{-1} over this range which gives $k(298) = 1.53 \times 10^{-11}$ cm^3 molecule^{-1}s^{-1}. The IUPAC data evaluation panel (Atkinson et al., 2006) recommends

Table IV-B-4. Rate coefficients ($k = A\ \mathrm{e}^{-B/T}$, cm^3 $\mathrm{molecule}^{-1}$ s^{-1}) for the reaction of OH with acetaldehyde (CH_3CHO)

$10^{12} \times A$	B (K)	$10^{12} \times k$	T (K)	Technique[a]	Reference	Temperature Range (K)
		15 ± 4	300	DF–MS	Morris et al. (1971)	
		15 ± 3	298	DF–RR (C_3H_6)[b]	Morris and Niki (1971b)	
		15 ± 2	298 ± 2	RR (C_2H_4)[c]	Niki et al. (1978b)	
6.87	-257 ± 150	16.0 ± 1.6	299	FP–RF	Atkinson and Pitts (1978)	299–426
		14.4 ± 1.5	355			
		12.4 ± 1.3	426			
		11.9 ± 4.3	298 ± 4	RR (C_2H_4)[c]	Kerr and Sheppard (1981)	
7.1 ± 0.2	-165 ± 91	14.0 ± 3.1	253	FP–RF	Semmes et al. (1985)	253–424
		12.2 ± 2.7	298			
		10.7 ± 2.3	356			
		11.0 ± 2.3	424			
5.52 ± 0.80	-307 ± 52	19.8 ± 1.2	244	DF–RF	Michael et al. (1985)	244–528
		18.4 ± 1.9	259			
		17.3 ± 1.6	273			
		14.7 ± 2.8	298			
		13.0 ± 1.2	333			
		14.0 ± 0.8	355			
		13.0 ± 0.4	367			
		15.0 ± 1.0	373			
		11.6 ± 0.6	393			
		11.7 ± 0.8	420			
		10.6 ± 0.6	424			
		11.0 ± 0.6	433			
		11.5 ± 0.8	466			
		10.4 ± 0.4	468			
		10.4 ± 0.4	492			
		9.2 ± 1.4	499			
		9.9 ± 0.4	528			
8.6 ± 1.8	-200 ± 60	16.9 ± 3.3	298	DF–RF/LIF	Dóbé et al. (1989)	297–517
		15.1 ± 3.2	390			
		13.8 ± 2.7	423			
		13.4 ± 2.7	467			
		17 ± 3	298	PLP–RF	Balestra-Garcia et al. (1992)	
		15.0 ± 1.0	298 ± 2	RR (C_2H_4)[c]	Scollard et al. (1993)	
		14.4 ± 2.5	298	DF–LIF	Tyndall et al. (1995)	
		14.4 ± 0.7	298	RR (1-C_4H_8)[d]	D'Anna et al. (2001a)	
		16.7	296	PLP–IR abs.	Wang et al. (2003)	

(*continued*)

Table IV-B-4. (*continued*)

$10^{12} \times A$	B (K)	$10^{12} \times k$	T (K)	Technique[a]	Reference	Temperature Range (K)
4.4	-366 ± 30	26.9 ± 2.0	202(He)	PLP–LIF	Sivakumaran and Crowley (2003)	202–348
		24.9 ± 0.6	211			
		22.7 ± 0.2	224			
		21.4 ± 0.2	234			
		19.0 ± 0.2	244			
		18.2 ± 0.2	253			
		17.3 ± 0.3	263			
		17.3 ± 0.2	273			
		15.9 ± 0.3	283			
		15.5 ± 0.5	296 ± 2			
		16.7 ± 0.3	273(Ar)			
		16.6 ± 0.2	278			
		16.1 ± 0.2	284			
		15.3 ± 0.3	289			
		15.1 ± 0.2	292			
		15.2 ± 0.3	296			
		14.4 ± 0.2	304			
		14.1 ± 0.2	314			
		13.8 ± 0.3	319			
		13.6 ± 0.3	324			
		13.0 ± 0.2	333			
		12.5 ± 0.2	342			
		12.6 ± 0.2	348			
83.6 ± 0.55[e]	2,410.3[e]	16.2 ± 2.0	297	PLP–LIF	Taylor et al. (2006)	297–860
4.34 ± 0.55[e]	368.9[e]	10.8 ± 1.3	383			
		15	295	PLP–LIF	Vöhringer-Martinez et al. (2007)	
5.32 ± 0.55	-315 ± 40	25.6 ± 0.6	204	PLP–LIF	Zhu et al. (2008)	204–373
		23.6 ± 0.4	212			
		21.9 ± 0.4	220			
		21.3 ± 0.3	225			
		20.4 ± 0.2	233			
		19.7 ± 0.3	240			
		18.8 ± 0.4	248			
		17.8 ± 0.6	255			
		17.4 ± 0.3	264			
		16.5 ± 0.3	273			
		15.7 ± 0.3	288			
		15.0 ± 0.5	296			
		14.4 ± 0.2	313			
		14.0 ± 0.2	328			
		13.3 ± 0.2	344			
		13.1 ± 0.3	358			
		12.5 ± 0.2	373			

[a]Abbreviations used for the techniques are defined in table I-F-3.

[b]Placed on an absolute basis using $k(\mathrm{OH} + \mathrm{C_3H_6}) = 1.7 \times 10^{-11}$ cm^3 molecule^{-1} s^{-1} in 1 Torr He: Atkinson et al. (2008) give a value of 1.8×10^{-11} cm^3 molecule^{-1} s^{-1} in 1 Torr N_2. The value in He will be slightly smaller.

[c]Placed on an absolute basis using $k(\mathrm{OH} + \mathrm{C_2H_4}) = 7.9 \times 10^{-12}$ cm^3 molecule^{-1} s^{-1} at 1 bar, 298 K (Atkinson et al., 2006).

[d]Placed on an absolute basis using $k(\mathrm{OH} + \text{1-}\mathrm{C_4H_8}) = 3.14 \times 10^{-11}$ cm^3 molecule^{-1} s^{-1} at 1 bar, 298 K (Atkinson et al., 2006).

[e]Biexponential fit to the data of Taylor et al. and of Sivakumaran and Crowley over the range 202–860 K.

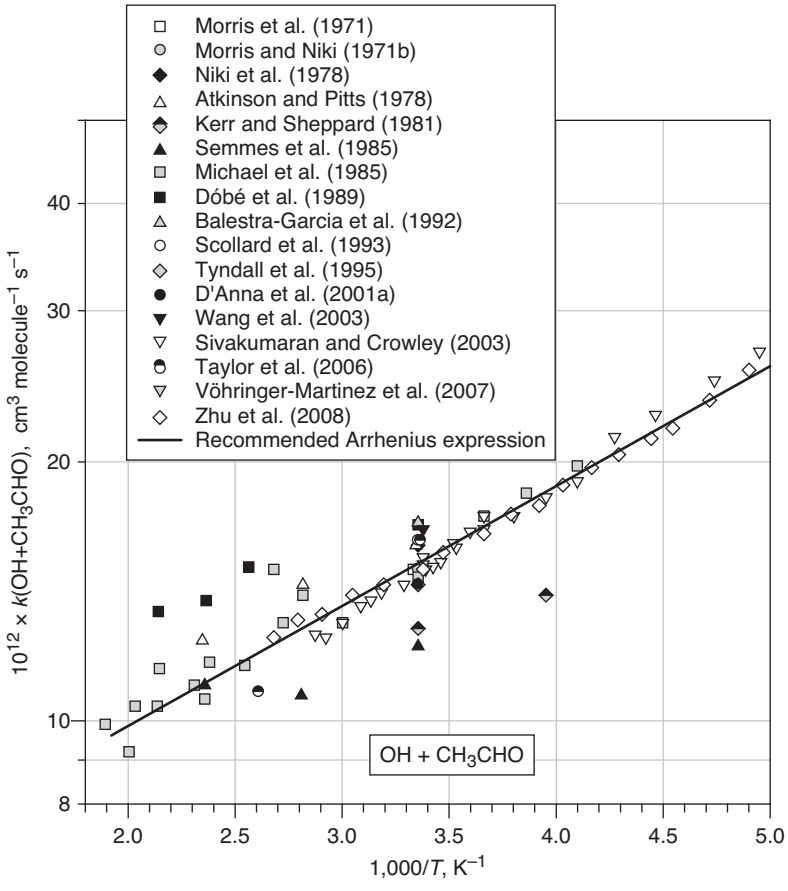

Figure IV-B-3. Arrhenius plot for the rate coefficients for the OH + CH_3CHO reaction.

$k = 4.74 \times 10^{-12}$ exp(345/T), over the range 200–350 K, which gives an identical value for $k(298) = 1.53 \times 10^{-11}$ cm^3 molecule^{-1}s^{-1} with an uncertainty at 298 K of ±20%. The two expressions agree to within 5% over the entire atmospheric range of temperatures. The measurements of Taylor et al. (2006) extend to higher temperatures, and show that the rate coefficient passes though a minimum and increases rapidly above ~600 K.

Vöhringer-Martinez et al. (2007) showed that the overall rate coefficient for OH + CH_3CHO increases at low temperatures in the presence of water. Addition of water vapor (7.8×10^{15} molecule cm^{-3}) had a negligible effect at 295 K, but the rate coefficient increased by a factor of ~2 at 60 K. They ascribed this effect to the formation of a hydrogen-bonded complex CH_3CHO—H_2O, and of a pre-reaction complex CH_3CHO—H_2O—HO, that substantially lowers the intrinsic, submerged barrier for reaction. The results also show that the negative temperature dependence for the rate coefficient persists down to 60 K.

Taylor et al. (2006) made direct measurements of the rates for OH radical reaction with the isotopically substituted acetaldehydes CH_3CDO, CD_3CHO, and CD_3CDO at several temperatures in the 297 to 860 K range. D'Anna et al. (2001b, 2003) measured rate coefficients for OH with the same compounds, using the relative rate method with FTIR detection in experiments at 298 K. The relative rate experiments of D'Anna et al. give a more direct measurement of the kinetic isotope effect and are thus probably more reliable.The rate coefficient ratios obtained at 298 K were: $k(CH_3CHO)/k(CH_3CDO) = 2.39 \pm 0.07$, $k(CH_3CHO)/k(CD_3CHO) = 1.19 \pm 0.11$, and $k(CH_3CHO)/k(CD_3CDO) = 2.51 \pm 0.09$. Both the Taylor et al. and the D'Anna et al. studies show that introduction of a D-atom in the aldehyde group causes a much larger reduction in the rate coefficient than does deuteration of the methyl group, confirming the importance of abstraction of the carbonyl hydrogen. Since the reaction proceeds via a complex, it is not obvious whether the deuterium kinetic isotope effect should be large or small (Smith and Ravishankara, 2002). The quantum chemical calculations of D'Anna et al. agree quite well with their measurements, and it should also be noted that the isotope effect found by D'Anna et al. for CD_3CDO is identical to that for DCDO.

IV-B-2.2. NO_3 Reaction Kinetics

The reaction of NO_3 with acetaldehyde has been studied in chambers at 298 ± 2 K by Morris and Niki (1974), Atkinson et al. (1984c), Cantrell et al. (1986), D'Anna et al. (2001b), and Doussin et al. (2003), and as a function of temperature using absolute methods by Dlugokencky and Howard (1989), D'Anna et al. (2001b), and Cabañas et al. (2001a). Bossmeyer et al. (2006) used a large outdoor simulation chamber (SAPHIR), coupled with measurements of both NO_3 and acetaldehyde. The rate coefficients measured at ambient temperatures agree quite well, with a mean of 2.6×10^{-15} cm^3 molecule^{-1} s^{-1} and an uncertainty of ±20% (table IV-B-5). The measurements by Morris and Niki (1974), Atkinson et al. (1984c), and Cantrell et al. (1986) are all based on measurements of N_2O_5 to infer the concentration of NO_3 and hence on the equilbrium constant for $N_2O_5 \rightleftharpoons NO_2 + NO_3$. As discussed in section IV-B-1.2, the equilibrium constant depends very sensitively on temperature, and its absolute value is subject to significant uncertainty, decreasing the reliability of this method. Therefore, these values have not been used in determining the recommended rate coefficient. While the ambient temperature measurement of Cabañas et al. agrees with the others, the data from experiments above ambient temperatures diverge. It is likely that this study suffered from adverse effects of secondary chemistry at the high [NO_3] used, and the resulting additional loss of NO_3 by the rapid reactions RCO+NO_3 and R+NO_3. The preferred Arrhenius expression (figure IV-B-4) is derived from a fit to the data of Dlugokencky and Howard and D'Anna et al., along with the room temperature values other than those determined via N_2O_5: $k = 1.6 \times 10^{-12} \exp(-1{,}920/T)$ cm^3 molecule^{-1} s^{-1} (see figure IV-B-4). This expression gives a value at 298 K of $k = 2.57 \times 10^{-15}$ cm^3 molecule^{-1} s^{-1} with an estimated uncertainty of ±20%. A recent evaluation (Atkinson et al., 2006) gives $k(T) = 1.4 \times 10^{-12} \times \exp(-1{,}860/T)$ cm^3 molecule^{-1} s^{-1} and $k(298\text{ K}) = 2.7 \times 10^{-15}$ cm^3 molecule^{-1} s^{-1}, in excellent agreement with our recommendation.

Table IV-B-5. Rate coefficients ($k = A\,e^{-B/T}$, cm^3 molecule^{-1} s^{-1}) for the reaction of NO_3 with acetaldehyde (CH_3CHO)

$10^{12} \times A$	B (K)	$10^{15} \times k$	T (K)	Technique[a]	Reference	Temperature Range (K)
		2.7 ± 0.5	300	N_2O_5 decay[b]	Morris and Niki (1974)	
		2.6 ± 0.4	298 ± 1	N_2O_5 decay[c]	Atkinson et al. (1984c)	
		3.4 ± 0.5	299 ± 1	N_2O_5 decay–FTIR[d]	Cantrell et al. (1986)	
1.44 ± 0.18	1,860 ± 300	1.26 ± 0.04	264	DF–LIF	Dlugokencky and Howard (1989)	264–374
		2.74 ± 0.07	298			
		5.27 ± 0.17	332			
		10.0 ± 0.20	374			
62 ± 75	2,830 ± 870	3.2 ± 0.8	298	DF–LIF	Cabañas et al. (2001a)	298–433
		21.1 ± 3.5	345			
		42.0 ± 4.3	389			
		74.4 ± 14.3	433			
		2.71 ± 0.29	298 ± 2	RR (1-butene)[e]	D'Anna et al. (2001b)	
	2,020 ± 160	0.95 ± 0.13	263	DF–LPA	D'Anna et al. (2001b)	263–363
		1.50 ± 0.13	275			
		2.49 ± 0.15	296			
		3.66 ± 0.12	322			
		5.11 ± 0.34	348			
		10.0 ± 0.5	363			
		2.1 ± 0.7	298	NO_3 abs.–FTIR	Doussin et al. (2003)	
		2.6 ± 0.5	300	Outdoor simulation chamber–GC–DOAS	Bossmeyer et al. (2006)	

[a]Abbreviations used for the techniques are defined in table I-F-3.
[b]Based on $K(NO_2 + NO_3 \rightleftharpoons N_2O_5) = 2.79 \times 10^{-11}$ cm^3 molecule^{-1} at 300 K (Osthoff et al., 2007).
[c]Based on $K(NO_2 + NO_3 \rightleftharpoons N_2O_5) = 3.55 \times 10^{-11}$ cm^3 molecule^{-1} at 298 K (Osthoff et al., 2007).
[d]Based on $K(NO_2 + NO_3 \rightleftharpoons N_2O_5) = 3.14 \times 10^{-11}$ cm^3 molecule^{-1} at 299 K (Osthoff et al., 2007).
[e]Placed on an absolute basis using $k(NO_3 + 1\text{-butene}) = 1.40 \times 10^{-14}$ cm^3 molecule^{-1} s^{-1} (Calvert et al., 2000).

IV-B-2.3. Cl-Atom Reaction Kinetics

The rate coefficient has been measured using absolute methods by Bartels et al. (1989), Tyndall et al. (1999), Kegley Owen et al. (1999), Smith et al. (2002b), and Seakins et al. (2004), and using relative methods by Niki et al. (1985b), Wallington et al. (1988g), Scollard et al. (1993), and Tyndall et al. (1999). There is good agreement between the measurements (see table IV-B-6), and an unweighted fit at 298 K gives $k(298\text{ K}) = 8.0 \times 10^{-11}$ cm^3 molecule^{-1} s^{-1}, with an uncertainty of ±15%. The measurements of Payne et al. (1990) show that the rate coefficient is independent of temperature over the range 210–340 K, although confirmatory measurements are needed. The branching ratio was measured by Niki et al. (1985b), using FTIR spectroscopy to determine the product yields. They showed that the yield of H abstraction from the methyl group is less than 1% of the total.

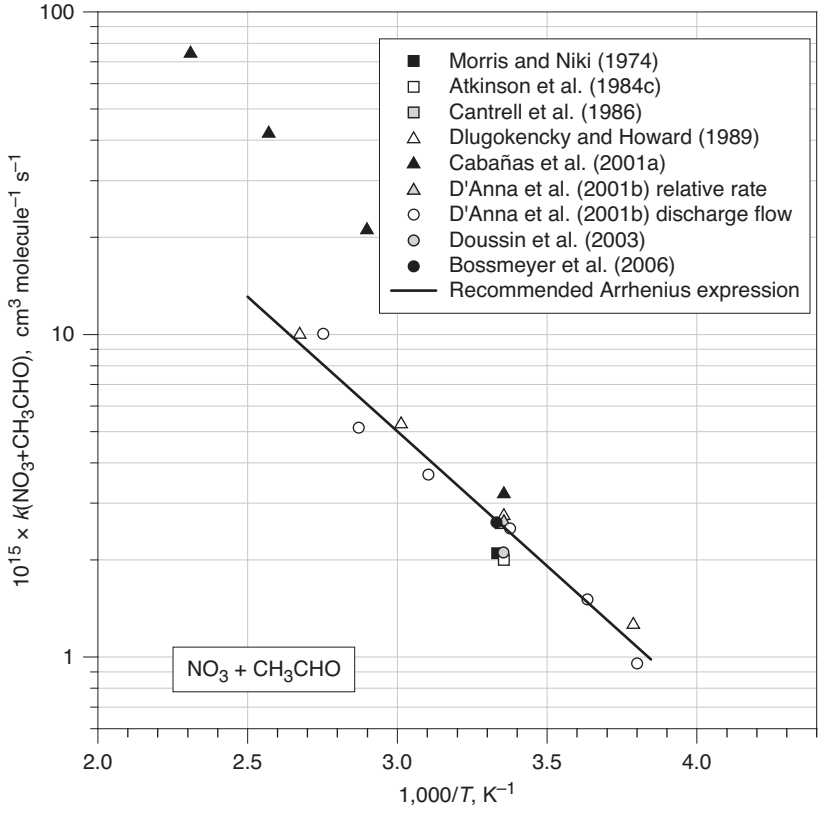

Figure IV-B-4. Arrhenius plot for the rate coefficients for the $NO_3 + CH_3CHO$ reaction.

Table IV-B-6. Rate coefficients ($k = A\ e^{-B/T}$, cm^3 $molecule^{-1}$ s^{-1}) for the reaction of Cl with acetaldehyde (CH_3CHO)

$10^{11} \times A$	B (K)	$10^{12} \times k$	T (K)	Technique[a]	Reference	Temperature Range (K)
		79 ± 12	298	RR[b] (ethane)	Niki et al. (1985b)	
		81 ± 8	295	RR[b] (ethane)	Wallington et al. (1988g)	
		61 ± 5	298	DF–MS–RR[b] (ethane)	Bartels et al. (1989)	
66 ± 14	0	71.0 ± 9.0	210	PLP–RF	Payne et al. (1990)	210–343
		65.2 ± 5.7	298			
		62.2 ± 4.0	343			
		95 ± 6	298	RR[c] (dimethyl ether)	Scollard et al. (1993)	
		79 ± 8	298	PLP–TDLAS	Kegley-Owen et al. (1999)	
		73 ± 7	298	PLP–RF	Tyndall et al. (1999)	
		88 ± 10	298	RR[b] (ethane)		
		86 ± 10	298	RR[d] (ethene)		
		83 ± 10	298	PLP–IR absorption	Smith et al. (2002b)	
		88 ± 15	298	PLP–IR emission	Seakins et al. (2004)	
		77 ± 11	298	PLP–TDLAS		

[a]Abbreviations used for the techniques are defined in table I-F-3.
[b]Placed on an absolute basis using $k(Cl + C_2H_6) = 5.9 \times 10^{-11}$ cm^3 $molecule^{-1}$ s^{-1} (Atkinson et al., 2006).
[c]Placed on an absolute basis using $k(Cl + CH_3OCH_3) = 1.80 \times 10^{-10}$ cm^3 $molecule^{-1}$ s^{-1} (this book, section III-B-1.3).
[d]Placed on an absolute basis using $k(Cl + C_2H_4) = 9.5 \times 10^{-11}$ cm^3 $molecule^{-1}$ s^{-1} (see section I-F-1).

Deuterium kinetic isotope effects were investigated at 298 K by Beukes et al. (2000) who obtained: $k(Cl + CH_3CHO)/k(Cl + CH_3CDO) = 1.34 \pm 0.02$; $k(Cl + CH_3CHO)/k(Cl + CD_3CDO) = 1.32 \pm 0.02$; $k(Cl + CD_3CHO)/k(Cl + CH_3CDO) = 1.35 \pm 0.02$; $k(Cl + CD_3CHO)/k(Cl + CD_3CDO) = 1.39 \pm 0.02$, confirming the prevalence of abstraction of the carbonyl H-atom.

IV-B-2.4. O(^{3}P) Reaction Kinetics

A recent NASA recommendation (Sander et al., 2006) gives $k(298) = 4.5 \times 10^{-13}$ cm^3 molecule^{-1} s^{-1}, with an uncertainty of ±25%, and $k(T) = 1.8 \times 10^{-11} \exp(-1{,}100/T)$ cm^3 molecule^{-1} s^{-1}, based on the temperature-dependent measurements of Cadle and Powers (1967), Singleton et al. (1977), and the room temperature measurement of Mack and Thrush (1974).

IV-B-2.5. Summary of the Atmospheric Fate of Acetaldehyde and the End Products of Its Oxidation

During the day, the destruction of CH_3CHO occurs by photolysis and reaction with OH. The photolysis lifetime is about 1.6 days with an overhead Sun; see table IX-M-1. For [OH] $\approx 2.5 \times 10^6$ molecule cm^{-3}, a lifetime of 7 h is obtained. The lifetime for removal by NO_3, with [NO_3] $\approx 3 \times 10^9$ molecule cm^{-3} is about 3.5 days.

It is well established that the major products of the OH–acetaldehyde reaction are acetyl radical and water, reaction (a). Other possible reaction channels have been proposed:

$$OH + CH_3CHO \rightarrow H_2O + CH_3CO \quad \text{(a)}$$

$$OH + CH_3CHO \rightarrow H_2O + CH_2CHO \quad \text{(b)}$$

$$OH + CH_3CHO \rightarrow [HOCH(CH_3)O]^\dagger \rightarrow H + CH_3C(O)OH \quad \text{(c)}$$

$$OH + CH_3CHO \rightarrow [HOCH(CH_3)O]^\dagger \rightarrow CH_3 + HCOOH \quad \text{(d)}$$

The dominance of channel (a) has been confirmed in recent studies, through experiments designed to quantify both the major and potential minor products. Butkovskaya et al. (2004a) determined that the total yield of H_2O is (97.7 ± 4.7)%, with abstraction from the methyl group accounting for ~ 5.5% of the reaction. Vandenberk and Peeters (2003) measured an H_2O yield of 0.89 ± 0.06, and showed that less than 3% formic acid is produced. Cameron et al. (2002) found a yield of CH_3CO of 0.93 ± 0.18, and showed that the yields of CH_3 and H are less than 0.03 and 0.02, respectively. Wang et al. (2003) gave an upper bound for the yield CH_3 of 0.05; they gave the yield of H as 0.05 ± 0.05. In chamber studies, Tyndall et al. (2002) were unable to detect either HCOOH or $CH_3C(O)OH$, and placed upper limits of 10% on both these species. Hence, we recommend that channel (a) be assigned a branching fraction of (95 ± 5)% and channel (b) (5 ± 5)% for atmospheric purposes.

The absence of addition-displacement products such as H and CH_3 suggest strongly that an intermediate radical $HOCH(O)(CH_3)$ is not formed. As in the case of formaldehyde, the reaction probably proceeds through formation of a hydrogen-bonded complex (Alvárez-Idaboy et al., 2001b; D'Anna et al., 2003; Xu et al., 2006), which accounts for the observed negative temperature dependence.

All evidence points to effectively exclusive abstraction of the aldehydic H by NO_3 and Cl, as well as OH. The acetyl radical so formed reacts rapidly with O_2 to form the acetyl peroxy radical, which in turn gives peroxyacetylnitrate (PAN) on reaction with NO_2 and CH_3 (and hence CH_3O_2 under atmospheric conditions) on reaction with NO:

$$CH_3C(O)O_2 + NO_2 + M \rightleftharpoons CH_3C(O)O_2NO_2 + M$$

$$CH_3C(O)O_2 + NO \rightarrow NO_2 + (CH_3CO_2) \rightarrow CH_3 + CO_2 + NO_2$$

These reactions dominate the chemistry of acetylperoxy under polluted conditions.

IV-B-3. Propanal (Propionaldehyde, C_2H_5CHO)

IV-B-3.1. OH Reaction Kinetics

The rate coefficient for the reaction of OH with propanal has been measured by Morris and Niki (1971b), Niki et al. (1978b), Audley et al. (1981), Kerr and Sheppard (1981), Semmes et al. (1985), Papagni et al. (2000), Thévenet et al. (2000), D'Anna et al. (2001a), and Le Crâne et al. (2005). Both direct and relative methods have been used. The rate coefficients are given in table IV-B-7. The agreement is very good, with most values at 298 ± 3 K ranging from 1.7×10^{-11} to 2.0×10^{-11} cm^3 $molecule^{-1}$ s^{-1}. The measurement by Morris and Niki (1971b) is higher than the consensus, and Semmes et al. noted some difficulties in handling both acetaldehyde and propanal. The unweighted average of the other values is 1.87×10^{-11} cm^3 $molecule^{-1}$ s^{-1} (298 K) with ±15% uncertainty. The only study of the temperature dependence is that of Thévenet et al., who found a temperature coefficient of −405 K between 240 and 372 K. Taking the 298 K value, together with the temperature dependence of Thévenet et al., gives $k(T) = 4.8 \times 10^{-12} \exp(405/T)$ cm^3 $molecule^{-1}$ s^{-1} with $k(298) = 1.87 \times 10^{-11}$ cm^3 $molecule^{-1}$ s^{-1}. A recent evaluation (IUPAC 2007) gives $k = 4.9 \times 10^{-12} \exp(405/T)$ cm^3 $molecule^{-1}$ s^{-1} and $k(298\ K) = 1.9 \times 10^{-11}$ cm^3 $molecule^{-1}$ s^{-1}.

On the basis of the observed trends in aldehyde rate coefficients (see later in this chapter) we expect that abstraction from the aldehyde group accounts for a large fraction of the overall reaction. Vandenberk and Peeters (2003) found that the overall yield of H_2O from the reaction is 100 ± 10%, and that the formation of formic acid in an addition-elimination mechanism accounts for less than 3%.

A number of rate coefficients for OH with aldehydes have been measured by Audley et al. (1981) by using a a dark, heterogeneous source of OH, flowing H_2O_2 and NO_2 over boric-acid- coated glass walls. The characteristics of this source are uncertain, and while some of their rate coefficients agree with the consensus, others differ

Table IV-B-7. Rate coefficients ($k = A\ e^{-B/T}$, cm^3 molecule^{-1} s^{-1}) for the reaction of OH with propanal (C_2H_5CHO)

$10^{12} \times A$	B (K)	$10^{12} \times k$	T (K)	Technique[a]	Reference	Temperature Range (K)
		27 ± 5	298	DF–RR (C_3H_6)[b]	Morris and Niki (1971b)	
		20 ± 2	298 ± 2	RR (C_2H_4)[c]	Niki et al. (1978b)	
		16.7 ± 2.3	298	RR (CH_3CHO)[d]	Audley et al. (1981)	
		18 ± 1	298 ± 4	RR (C_2H_4)[c]	Kerr and Sheppard (1981)	
		17.1 ± 2.4	298	FP–RF	Semmes et al. (1985)	
		20.2 ± 1.4	298	RR (MVK)[e]	Papagni et al. (2000)	
5.3 ± 0.5	−405 ± 30	28.5 ± 2.4	240	PLP–LIF	Thévenet et al. (2000)	240–372
		25.7 ± 1.0	253			
		23.7 ± 0.5	273			
		20 ± 3	298			
		18.6 ± 0.8	323			
		17.3 ± 0.8	348			
		15.5 ± 1.5	372			
		19.0 ± 1.5	298 ± 2	RR (C_3H_6)[f]	D'Anna et al. (2001a)	
		17.2 ± 2.1	295 ± 2	RR (C_2H_4)[b]	Le Crâne et al. (2005)	
		17.8 ± 1.9		RR (C_3H_6)[f]		

[a]Abbreviations used for the techniques are defined in table I-F-3.
[b]Placed on an absolute basis using $k(OH + C_3H_6) = 1.7 \times 10^{-11}$ cm^3 molecule^{-1} s^{-1} in 1 Torr He. Atkinson et al. (2008) give a value of 1.8×10^{-11} cm^3 molecule^{-1} s^{-1} in 1 Torr N_2. The value in He will be slightly smaller.
[c]Placed on an absolute basis using $k(OH + C_2H_4) = 7.9 \times 10^{-12}$ cm^3 molecule^{-1} s^{-1} at 1 bar and 298 K (Atkinson et al., 2006).
[d]Placed on an absolute basis using $k(OH + CH_3CHO) = 1.53 \times 10^{-11}$ cm^3 molecule^{-1} s^{-1} (this book, section IV-B-2.1).
[e]Placed on an absolute basis using k(OH + methyl vinyl ketone) $= 2.0 \times 10^{-11}$ cm^3 molecule^{-1} s^{-1} (this book, section V-E-1.1).
[f]Placed on an absolute basis using $k(OH + C_3H_6) = 2.9 \times 10^{-11}$ cm^3 molecule^{-1} s^{-1} at 1 bar and 298 K (Atkinson et al., 2006).

considerably. Their rate coefficients are included in the tables, but have not been considered further in the derivation of preferred values, because of uncertainties in the methodology.

IV-B-3.2. NO_3 Reaction Kinetics

The reaction of NO_3 with propanal has been measured by D'Anna and Nielsen (1997), D'Anna et al. (2001a), and Papagni et al. (2000), all using relative methods, by Cabañas et al. (2001a) using an absolute technique, and by Bossmeyer et al. (2006) who used a large simulation chamber (SAPHIR) (table IV-B-8). The results are in reasonably good agreement; an unweighted fit gives $k(298\ K) = 6.3 \times 10^{-15}$ cm^3 molecule^{-1} s^{-1} with an uncertainty of ±20%. As in the case of acetaldehyde, the Arrhenius plot of the results of Cabañas et al. show curvature above room temperature, which leads to very large A-factors; their Arrhenius expression overestimates the recommended room temperature value by nearly 50%. At present, no temperature dependence can be recommended.

Table IV-B-8. Rate coefficients ($k = A\ e^{-B/T}$, cm^3 molecule^{-1} s^{-1}) for the reaction of NO_3 with propanal (C_2H_5CHO)

$10^{12} \times A$	B (K)	$10^{15} \times k$	T (K)	Technique[a]	Reference	Temperature Range (K)
		5.80 ± 0.48	298	RR (C_3H_6)[b]	D'Anna and Nielsen (1997)	
		6.18 ± 0.57	298	RR (C_3H_6)[b]	D'Anna et al. (2001a)	
17 ± 10	2,250 ± 190	6.0 ± 0.6	298	DF–LIF	Cabañas et al. (2001a)	298–433
		24 ± 6	345			
		62 ± 8	389			
		92 ± 12	433			
		7.3 ± 0.4	296	RR (MACR)[c]	Papagni et al. (2000)	
		5.8 ± 1.0	300	SC–GC–DOAS	Bossmeyer et al. (2006)	

[a]Abbreviations used for the techniques are defined in table I-F-3.
[b]Placed on an absolute basis using $k(NO_3 + C_3H_6) = 9.5 \times 10^{-15}$ cm^3 molecule^{-1} s^{-1} (Atkinson et al., 2006).
[c]Placed on an absolute basis using $k(NO_3 + \text{methacrolein}) = 3.4 \times 10^{-15}$ cm^3 molecule^{-1} s^{-1} (Atkinson et al., 2006).

Table IV-B-9. Rate coefficients ($k = A\ e^{-B/T}$, cm^3 moleclue^{-1} s^{-1}) for the reaction of Cl with propanal (C_2H_5CHO)

$10^{12} \times A$	B (K)	$10^{12} \times k$	T (K)	Technique[a]	Reference	Temperature Range (K)
		117 ± 10	298	RR[b] (ethane)	Wallington et al. (1988g)	
		145 ± 8	298	RR[b] (ethane)	Thévenet et al. (2000)	
		120 ± 7		RR[c] (propane)		
		125 ± 6		RR[d] (*n*-butane)		
		141 ± 10		RR[e] (*n*-hexane)		
		120 ± 20	297	RR[f] (propene)	Ullerstam et al. (2001)	
		126 ±13	298	RR[b] (ethane)	Le Crâne et al. (2005)	
		131 ± 14		RR[g] (ethene)		
		111 ± 14		RR[c] (propane)		
24.1 ± 2.3	–453 ± 54	139 ± 14	265	PLP–RF	Cuevas et al. (2006)	265–380
		119 ± 5	283			
		112 ± 17	298			
		102 ± 12	311			
		85.7 ± 0.8	330			
		87.5 ± 3.6	356			
		77.7 ± 7.8	380			

IV-B-3.3. Cl-Atom Reaction Kinetics

The reaction has been studied using relative methods by Wallington et al. (1988g), Thévenet et al. (2000), Ullerstam et al. (2001), and Le Crâne et al. (2005). Cuevas et al. (2006) measured the rate coefficient over the temperature range 265–380 K, using pulsed laser photolysis coupled with detection of Cl by resonance fluorescence. See table IV-B-9. An unweighted fit to all the data at 298 K gives $k = 1.25 \times 10^{-10}$ cm^3 molecule^{-1} s^{-1} with an uncertainty of ±20%, in agreement with the IUPAC recommendation (Atkinson et al., 2006). Taking this value and the temperature dependence of Cuevas et al. (2006) gives: $k = 2.8 \times 10^{-11}\ \exp(453\ \text{K}/T)$ cm^3 molecule^{-1} s^{-1}. Confirmatory measurements of the temperature dependence are needed.

IV-B-3.4. O(^{3}P) Reaction Kinetics

The only measurement of the rate coefficient for O(^{3}P) + propanal was made by Singleton et al. (1977), who obtained: $k(T) = 1.29 \times 10^{-11} \exp(-869/T)$ cm^3 molecule^{-1} s^{-1} with $k(298\ \text{K}) = 7.0 \times 10^{-13}$ cm^3 molecule^{-1} s^{-1}.

IV-B-3.5. Summary of the Atmospheric Fate of Propanal and the End Products of Its Oxidation

During the day, the destruction of propanal occurs by photolysis and reaction with OH. The photolysis lifetime in the lower troposphere with an overhead Sun is about 1 day; see table IX-M-1. For [OH] $\approx 2.5 \times 10^6$ molecule cm^{-3}, a lifetime of 5.5 h is obtained for reaction with OH. The lifetime for removal by NO_3, with [NO_3] $\approx 3 \times 10^9$ molecule cm^{-3} is $\approx$ 15 h. The mechanisms for these reactions are discussed at the end of this section. The major product, for all three reactants discussed here, is the propionyl radical, CH_3CH_2CO, which reacts with O_2 to form the peroxypropanoyl radical, which reacts in the atmosphere in a comparable way to peroxyacetyl. Le Crâne et al. (2005), using FTIR and UV detection of products in air and with added NO, showed that (88 $\pm$ 4%) of the reaction of Cl with propanal leads to formation of the acyl radical. In the absence of NO they detected <3% CO, showing that, in air at atmospheric pressure, the acyl radical reacts exclusively with O_2, with negligible decomposition.

Under polluted conditions, peroxypropanoyl reacts with NO_2 to form peroxypropanoyl nitrate ($CH_3CH_2C(O)O_2NO_2$, PPN), which, like PAN, acts as a reservoir for NO_x in its long range transport. The peroxy radical reacts with NO to form the ethyl radical, which in turn reacts with O_2 to form the ethylperoxy radical (Le Crâne et al., 2005):

$$CH_3CH_2COO_2 + NO \rightarrow NO_2 + (CH_3CH_2CO_2) \rightarrow NO_2 + CH_3CH_2 + CO_2$$

$$CH_3CH_2 + O_2 \rightarrow CH_3CH_2O_2$$

IV-B-4. Butanal (*n*-Butyraldehyde, $CH_3CH_2CH_2CHO$)

IV-B-4.1. OH Reaction Kinetics

The rate coefficient for the reaction of OH with butanal has been the subject of six studies (Audley et al., 1981; Semmes et al., 1985; Kerr and Sheppard, 1981; Papagni et al., 2000; D'Anna et al., 2001a; and Albaladejo et al., 2002). The rate coefficients are given in table IV-B-10. The studies are in reasonable agreement, with measurements ranging from 2.1×10^{-11} to 2.9×10^{-11} cm^3 molecule^{-1} s^{-1} ($\sim$298 K). The unweighted mean value (not including the data of Audley et al.) is 2.37×10^{-11} cm^3 molecule^{-1} s^{-1} with an uncertainty of $\pm$20%. The only study of the temperature dependence was that of Semmes et al., who found an activation temperature of -411 K, similar to that for propanal. Using this temperature dependence, coupled with the 298 K mean gives: $k = 6.2 \times 10^{-12} \exp(411/T)$ cm^3 molecule^{-1} s^{-1}. An IUPAC (2008)

Table IV-B-10. Rate coefficients ($k = A\ e^{-B/T}$, cm^3 $molecule^{-1}$ s^{-1}) for reaction of OH with butanal (n-C_3H_7CHO)

$10^{12} \times A$	B (K)	$10^{12} \times k$	T (K)	Technique[a]	Reference	Temperature Range (K)
		25.2 ± 3.2	298	RR (CH_3CHO)[b]	Audley et al. (1981)	
		20.7 ± 0.6	298 ± 4	RR (C_2H_4)[c]	Kerr and Sheppard (1981)	
5.7 ± 0.3	-411 ± 164	30.8 ± 4.2	258	FP–RF	Semmes et al. (1985)	258–422
		20.6 ± 3.0	298			
		18.2 ± 2.6	361			
		15.4 ± 2.3	422			
		24.7 ± 1.5	298	RR (MVK)[d]	Papagni et al. (2000)	
		23.9 ± 1.6	298 ± 2	RR (1-C_4H_8)[e]	D'Anna et al. (2001a)	
		28.8 ± 2.6	298	PLP–LIF	Albaladejo et al. (2002)	

[a]Abbreviations used for the techniques are defined in table I-F-3.
[b]Placed on an absolute basis using $k(OH + CH_3CHO) = 1.5 \times 10^{-11}$ cm^3 $molecule^{-1}$ s^{-1} (section IV-B-2.1).
[c]Placed on an absolute basis using $k(OH + C_2H_4) = 7.9 \times 10^{-12}$ cm^3 $molecule^{-1}$ s^{-1} at 1 bar and 298 K (Atkinson et al., 2006).
[d]Placed on an absolute basis using k(OH + methyl vinyl ketone) $= 2.0 \times 10^{-11}$ cm^3 $molecule^{-1}$ s^{-1} (section V-E-1.1).
[e]Placed on an absolute basis using k(OH + 1-butene) $= 3.14 \times 10^{-11}$ cm^3 $molecule^{-1}$ s^{-1} at 1 bar and 298 K (Calvert et al., 2008).

evaluation adopted a similar approach and gives $k = 6.0 \times 10^{-12}\ \exp(410/T)$ cm^3 $molecule^{-1}$ s^{-1}.

IV-B-4.2. NO_3 Reaction Kinetics

The rate coefficient for the reaction of NO_3 with butanal has been studied by D'Anna and Nielsen (1997), Ullerstam et al. (2000), D'Anna et al. (2001a), Papagni et al. (2000), Cabañas et al. (2001a), and Bossmeyer et al. (2006). Absolute measurements as a function of temperature were made by Ullerstam et al. and Cabañas et al. (table IV-B-11). At 298 K the recommended rate coefficient, based on the unweighted mean of all of these measurements (excluding that of Cabañas et al) is 1.14×10^{-14} cm^3 $molecule^{-1}$ s^{-1} with an uncertainty of $\pm 15\%$. Ullerstam et al. included O_2 in their flow tube experiments to suppress secondary reactions which remove NO_3, and showed that the presence of O_2 led to lower rate coefficients than those they obtained in its absence. The rate coefficients reported in the temperature dependent study by Cabañas et al. are larger than those measured by Ullerstam et al. in the presence of O_2 and show a stronger temperature dependence, possibly as a result of secondary chemistry. Figure IV-B-5 illustrates the effect of the addition of O_2 on the measurements. It can be seen that the results of Cabañas et al. are similar to those measured by Ullerstam et al. in the absence of O_2, except at room temperature. Ullerstam et al. showed that the effect of temperature is independent of the presence or absence of O_2 (see figure IV-B-5). On the basis of the temperature effect reported by Ullerstam et al., and consistent with other rate coefficients for NO_3 reactions with aldehydes, we recommend $k = 1.50 \times 10^{-12}\ \exp(-1{,}500/T)$ cm^3 $molecule^{-1}$ s^{-1}. A similar expression was recommended by the IUPAC panel in their 2008 evaluations: $k = 1.7 \times 10^{-12}$ $\exp(-1{,}500/T)$ cm^3 $molecule^{-1}$ s^{-1} (IUPAC, 2008).

Table IV-B-11. Rate coefficients ($k = A\ e^{-B/T}$, cm^3 molecule^{-1} s^{-1}) for reaction of NO_3 with butanal (n-C_3H_7CHO)

$10^{12} \times A$	B (K)	$10^{15} \times k$	T (K)	Technique[a]	Reference	Temperature Range (K)
		11.3 ± 0.9	298	RR (1-butene)[b]	D'Anna and Nielsen (1997)	
		10.4 ± 1.1	297	RR (C_3H_6)[c]	Ullerstam et al. (2000)	
12 ± 1.0	1,460 ± 270	4.4 ± 0.1	267	DF vis. abs.	Ullerstam et al. (2000)	267–332
		11 ± 1	296			
		13 ± 2	332			
		12.8 ± 1.0	298	RR (1-butene)[b]	D'Anna et al. (2001a)	
		12.2 ± 0.6	296	RR (MACR)[d]	Papagni et al. (2000)	
76 ± 98	2,470 ± 500	14.6 ± 1.6	298	DF–LIF	Cabañas et al. (2001a)	298–433
		72 ± 12	345			
		142 ± 6	389			
		166 ± 2	433			
		11.9 ± 1.4	300	SC–GC–DOAS	Bossmeyer et al. (2006)	

[a]Abbreviations used for the techniques are defined in table I-F-3.
[b]Placed on an absolute basis using $k(NO_3 + 1\text{-butene}) = 1.35 \times 10^{-14}$ cm^3 molecule^{-1} s^{-1} (Calvert et al., 2000).
[c]Placed on an absolute basis using $k(NO_3 + C_3H_6) = 9.5 \times 10^{-15}$ cm^3 molecule^{-1} s^{-1} (Atkinson et al., 2006).
[d]Placed on an absolute basis using $k(NO_3 + \text{methacrolein}) = 3.4 \times 10^{-15}$ cm^3 molecule^{-1} s^{-1} (Atkinson et al., 2006).

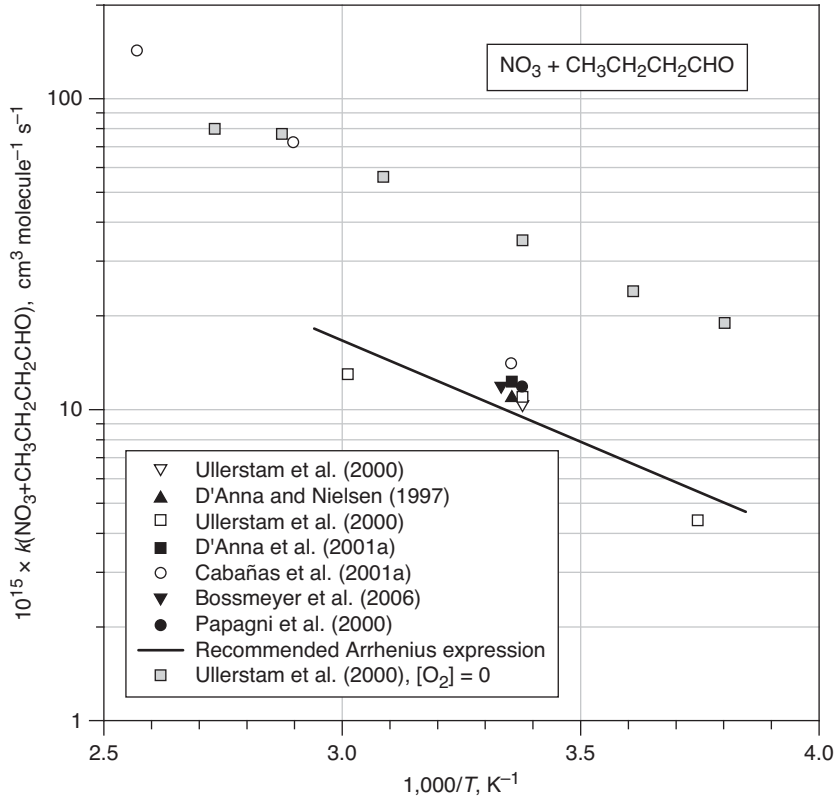

Figure IV-B-5. Arrhenius plot for the rate coefficients for the NO_3 + butanal reaction.

IV-B-4.3. Cl-Atom Reaction Kinetics

Cl + butanal reaction has been studied using pulsed laser photolysis, coupled with resonance fluorescence, over the temperature range 265–380 K by Cuevas et al. (2006), and by relative rate methods at room temperature by Ullerstam et al. (2001), Wu and Mu (2007), and Singh et al. (2009); see table IV-B-12. There is a discrepancy of ~30% between the room temperature measurements; the unweighted mean is 1.66×10^{-10} cm^3 molecule^{-1} s^{-1}, with an uncertainty of ±25%. Using the temperature dependence of Cuevas et al. and this mean value gives: $k = 3.8 \times 10^{-11} \exp(446/T)$ cm^3 molecule^{-1} s^{-1}.

IV-B-4.4. O(^{3}P) Reaction Kinetics

The only measurement of the rate coefficient for O(^{3}P) + butanal was made by Singleton et al. (1977), who obtained: $k(T) = 1.65 \times 10^{-11} \exp(-857/T)$ cm^3 molecule^{-1} s^{-1} with $k(298\ \text{K}) = 9.3 \times 10^{-13}$ cm^3 molecule^{-1} s^{-1}.

IV-B-4.5. Summary of the Atmospheric Fate of Butanal and the End Products of Its Oxidation

During the day, the destruction of butanal is by photolysis and reaction with OH. The photolysis lifetime in the lower troposphere with overhead Sun is about 14 h; see table IX-M-1. For [OH] ≈ 2.5×10^6 molecule cm^{-3}, a lifetime of about 4 h is obtained with respect to reaction with OH. The lifetime for removal by NO_3, with

Table IV-B-12. Rate coefficients ($k = A\ e^{-B/T}$, cm^3 molecule^{-1} s^{-1}) for reaction of Cl with butanal (n-C_3H_7CHO)

$10^{11} \times A$	B (K)	$10^{12} \times k$	T (K)	Technique[a]	Reference	Temperature Range (K)
		150 ± 30	297	RR[b] (propene)	Ullerstam et al. (2001)	
30.9 ± 4.0	−446 ± 77	165 ± 12	265	PLP–RF	Cuevas et al. (2006)	265–380
		159 ± 23	283			
		142 ± 16	298			
		119 ± 15	313			
		128 ± 36	318			
		121 ± 15	330			
		197 ± 12	354			
		102 ± 14	381			
		210 ± 34	298	RR[c] (2-propanol)	Wu and Mu (2007)	
		195 ± 26		RR[d] (propane)		
		144 ± 34	298	RR[c] (2-propanol)	Singh et al. (2009)	
		157 ± 75		RR[e] (ethene)		

[a]Abbreviations used for the techniques are defined in table I-F-3).
[b]Placed on an absolute basis using $k(\text{Cl} + \text{propene}) = 2.3 \times 10^{-10}$ cm^3 molecule^{-1} s^{-1} (Atkinson et al., 2006).
[c]Placed on an absolute basis using $k(\text{Cl} + \text{2-propanol}) = 8.8 \times 10^{-11}$ cm^3 molecule^{-1} s^{-1} (this book, II-B-4.3).
[d]Placed on an absolute basis using $k(\text{Cl} + \text{propane}) = 1.4 \times 10^{-10}$ cm^3 molecule^{-1} s^{-1} (Atkinson et al., 2006).
[e]Placed on an absolute basis using $k(\text{Cl} + \text{ethene}) = 9.5 \times 10^{-11}$ cm^3 molecule^{-1} s^{-1} (section I-F-1).

$[NO_3] \approx 3 \times 10^9$ molecule cm^{-3} is about 8 h. The mechanisms for these reactions and the atmospheric fate of the products are discussed at the in section IV-B-13.

Reaction of butanal with all three reactive species leads primarily to the formation of the butanoyl radical by abstraction of the aldehydic H-atom. Papagni et al. (2000) noted an increase in the rate coefficient of OH with butanal, compared with that with propanal, which is compatible with the sensitization of the C—H bond β to the carbonyl group proposed by Kwok and Atkinson (1995). Application of their structure–activity relations (SARs) gives 17% abstraction at this site with a channel yield of 78% for production of the acyl radical. Reaction of the acylperoxy radical with NO_2 forms peroxybutanoyl nitrate, while reaction with NO forms CO_2 and the *n*-propyl radical, which then reacts with O_2 to form the *n*-propylperoxy radical, whose main atmospheric fate is conversion to propanal.

Using end product analysis, Wu and Mu obtained percentage yields for abstraction by Cl at the carbonyl and at the α, β, and γ positions of $\geq$ 42%, <25%, 21%, and $\leq$12%, respectively. Singh et al. (2009) obtained a yield for abstraction at the carbonyl position of 66%.

IV-B-5. 2-Methylpropanal [Isobutyraldehyde, $(CH_3)_2CHCHO$]

IV-B-5.1. OH Reaction Kinetics

The rate coefficient for this reaction has been studied seven times at room temperature (Audley et al., 1981; Kerr and Sheppard, 1981; Semmes et al., 1985; Dóbé et al., 1989; Stemmler et al., 1997a; Thévenet et al., 2000; D'Anna et al., 2001a). The measurements are given in table IV-B-13 and figure IV-B-6. The value reported by Dóbé et al. at 298 K is roughly 70% larger than the others, and that of Audley et al. (1981) about 40% lower than the others. The remaining data have an unweighted mean of 2.59×10^{-11} cm^3 $molecule^{-1}$ s^{-1}, with an uncertainty of ±20%. The temperature dependence was measured by Semmes et al. (255–423 K) and Thévenet et al. (243–372 K), who found almost identical activation temperatures (E/R) of −393 K and −390 K, respectively. Dóbé et al. found a slightly weaker temperature dependence, although their data could be interpreted as showing curvature at higher temperatures. The Arrhenius expression obtained from the measurements shown in figure IV-B-6, excluding those of Audley et al., Dóbé et al., and Glasius et al. gives $k(T) = 6.7 \times 10^{-12} \exp(400/T)$ cm^3 $molecule^{-1}$ s^{-1} for atmospheric purposes, with $k(298) = 2.56 \times 10^{-11}$ cm^3 $molecule^{-1}$ s^{-1}.

IV-B-5.2. NO_3 Reaction Kinetics

The rate coefficient for the reaction of NO_3 with 2-methylpropanal has been measured at room temperature by D'Anna and Nielsen (1997), Glasius et al. (1997), Ullerstam et al. (2000), D'Anna et al. (2001a), and Cabañas et al. (2001a); see table IV-B-14. The value obtained by Cabañas et al. is higher than the others, possibly because of secondary reactions as discussed in section IV-B-4.2. The unweighted mean of the other measurements at ~298 K gives a rate coefficient of 1.17×10^{-14} cm^3 $molecule^{-1}$ s^{-1} with an uncertainty of ±20%. The temperature dependence has been measured by

Table IV-B-13. Rate coefficients ($k = A\ e^{-B/T}$, cm^3 $molecule^{-1}$ s^{-1}) for reaction of OH with 2-methylpropanal [$(CH_3)_2CHCHO$]

$10^{12} \times A$	B (K)	$10^{12} \times k$	T (K)	Technique[a]	Reference	Temperature Range (K)
		17.4 ± 2.0	298	RR (CH_3CHO)[b]	Audley et al. (1981)	
		27 ± 5	298 ± 4	RR (C_2H_4)[c]	Kerr and Sheppard (1981)	
6.8 ± 0.3	$-(393 \pm 125)$	33.4 ± 4.5	255	FP–RF	Semmes et al. (1985)	255–423
		24.2 ± 3.3	298			
		19.7 ± 2.7	354			
		18.2 ± 2.7	423			
15.8 ± 5.0	$-(313 \pm 145)$	46.3 ± 7.3	298	DF–RF	Dóbé et al. (1989)	298–519
		39.7 ± 6.3	349			
		32.7 ± 7.8	420			
		32.6 ± 6.1	452			
		40.5 ± 6.1	471			
		43.0 ± 6.0	519			
		25.8 ± 0.7	298	RR (dipropyl ether)[d]	Stemmler et al. (1997a)	
7.3 ± 1.9	$-(390 \pm 78)$	38.5 ± 0.9	243	PLP–LIF	Thévenet et al. (2000)	243–372
		34.2 ± 1.3	253			
		29.9 ± 1.1	273			
		26 ± 4	298			
		25.8 ± 0.8	323			
		21.9 ± 1.0	348			
		22.0 ± 1.1	372			
		26.6 ± 2.1	298 ± 2	RR (1-C_4H_8)[e]	D'Anna et al. (2001a)	

[a]Abbreviations used for the techniques are defined in table I-F-3.
[b]Placed on an absolute basis using $k(OH + CH_3CHO) = 1.5 \times 10^{-11}$ cm^3 $molecule^{-1}$ s^{-1} (this book, section IV-B-2.1).
[c]Placed on an absolute basis using $k(OH + C_2H_4) = 7.9 \times 10^{-12}$ cm^3 $molecule^{-1}$ s^{-1} at 1 bar and 298 K (Atkinson et al., 2006).
[d]Placed on an absolute basis using k(OH + dipropyl ether) $= 2.0 \times 10^{-11}$ cm^3 $molecule^{-1}$ s^{-1} (this book, section III-B-6.1).
[e]Placed on an absolute basis using k(OH + 1-butene) $= 3.14 \times 10^{-11}$ cm^3 $molecule^{-1}$ s^{-1} at 1 bar and 298 K (Calvert et al., 2000).

Ullerstam et al. and by Cabañas et al. (figure IV-B-7). Again, the temperature dependence inferred by Ullerstam et al. is preferred, coupled with the 298 K mean value leading to: $k = 3.9 \times 10^{-12} \exp(-1{,}730/T)$ cm^3 $molecule^{-1}$ s^{-1}.

IV-B-5.3. O_3 Reaction Kinetics

Glasius et al. (1997) measured the rate constant for O_3 + 2-methylpropanal, obtaining $k = (3.9 \pm 0.6) \times 10^{-20}$ cm^3 $molecule^{-1}$ s^{-1}. In the absence of any confirmatory measurements, an uncertainty of ±40% is attached to this value.

IV-B-5.4. Cl-Atom Reaction Kinetics

The reaction between Cl and 2-methylpropanal has been studied by relative rate techniques at room temperature by Thévenet et al. (2000), Ullerstam et al. (2001), and

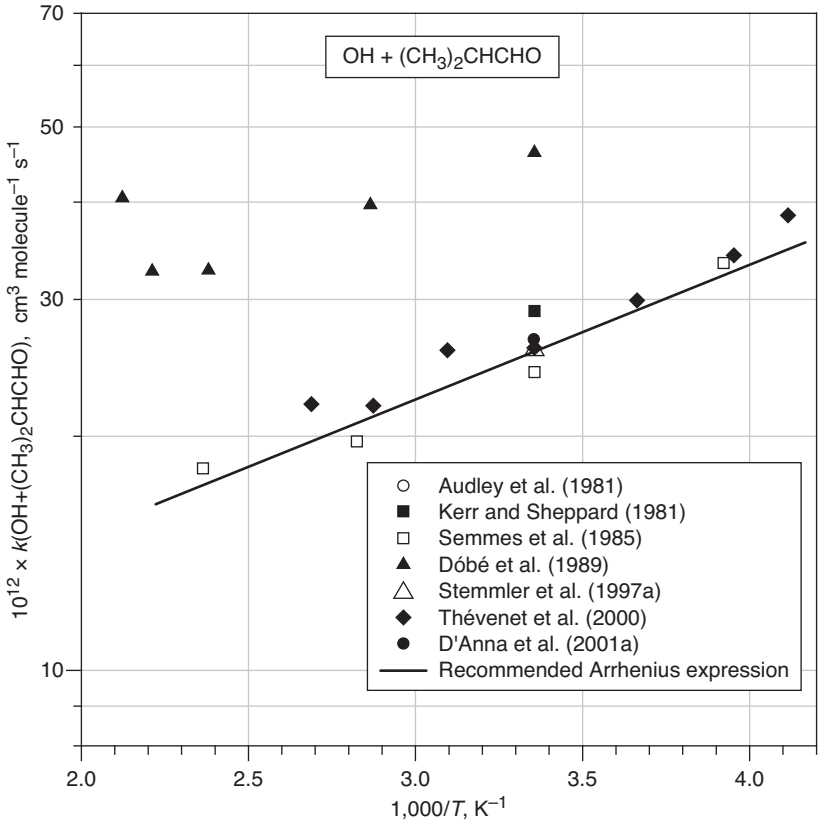

Figure IV-B-6. Arrhenius plot for the rate coefficients for the OH + 2-methylpropanal reaction.

Table IV-B-14. Rate coefficients ($k = A\ e^{-B/T}$, cm^3 $molecule^{-1}$ s^{-1}) for reaction of NO_3 with 2-methylpropanal [$(CH_3)_2CHCHO$]

$10^{12} \times A$	B (K)	$10^{15} \times k$	T (K)	Technique[a]	Reference	Temperature Range (K)
		12.5 ± 0.6	298	RR (1-butene)[b]	D'Anna and Nielsen (1997)	
		12 ± 3	300	RR (1-butene)[b]	Glasius et al. (1997)	
		12 ± 1	297	RR (C_3H_6)[c]	Ullerstam et al. (2000)	
2.9 ± 1.5	1,720 ± 140	4.6 ± 1.0	267	DF vis. abs.	Ullerstam et al. (2000)	267–332
		9 ± 1	296			
		16 ± 3	332			
		13.0 ± 1.4	298	RR (1-butene)[b]	D'Anna et al. (2001a)	
100 ± 50	2,600 ± 380	16.1 ± 1.3	298	DF–LIF	Cabañas et al. (2003)	298–433
		88 ± 12	345			
		140 ± 21	389			
		260 ± 12	433			

[a]Abbreviations used for the techniques are defined in table I-F-3.
[b]Placed on an absolute basis using $k(NO_3 + 1\text{-butene}) = 1.40 \times 10^{-14}$ cm^3 $molecule^{-1}$ s^{-1} (Calvert et al., 2000).
[c]Placed on an absolute basis using $k(NO_3 + C_3H_6) = 9.5 \times 10^{-15}$ cm^3 $molecule^{-1}$ s^{-1} (Atkinson et al., 2006).

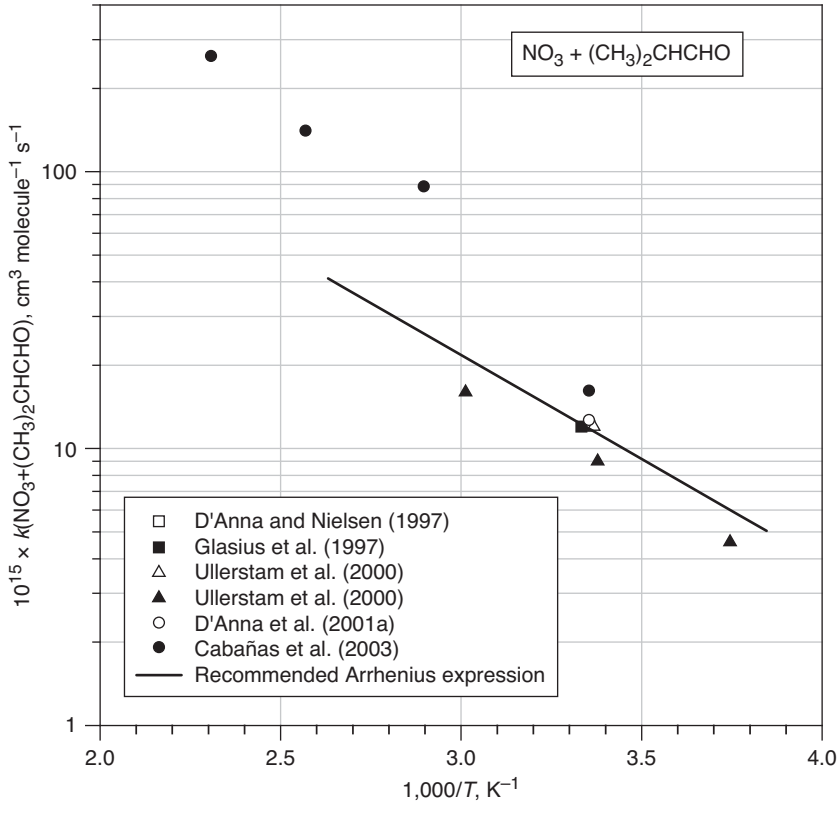

Figure IV-B-7. Arrhenius plot for the rate coefficients for the NO_3 + 2-methylpropanal reaction.

Le Crâne et al. (2004); see table IV-B-15. There is generally good agreement between the measurements and an unweighted mean gives $k = 1.56 \times 10^{-10}$ cm^3 molecule^{-1} s^{-1} with an uncertainty of ±15%. Ullerstam et al. also determined the product channel yields by chamber measurements using FTIR and pulsed laser photolysis coupled with UV absorption. They obtained channel yields for abstraction of the aldehydic H of 0.85 ± 0.10 and 0.85 ± 0.05, respectively, using these techniques. They also measured the rate of dissociation of the 2-methylpropanoyl radical, to form CO + $(CH_3)_2CHCH$, relative to the rate of reaction with Cl_2 and showed that, under atmospheric conditions, reaction with O_2 to form the 2-methylpropanoylperoxy radical dominates, with <0.2% dissociating.

IV-B-5.5. Summary of the Atmospheric Fate of 2-Methylpropanal and the End Products of Its Oxidation

During the day, the destruction of 2-methylpropanal is by photolysis and reaction with OH. The photolysis lifetime in the lower troposphere with overhead Sun is about 5 h; see table IX-M-1. For [OH] ≈ 2.5 × 10^6 molecule cm^{-3}, a lifetime of about 4 h is

Table IV-B-15. Rate coefficients (k, cm^3 molecule^{-1} s^{-1}) for reaction of Cl with 2-methylpropanal [$(CH_3)_2CHCHO$]

$10^{12} \times k$	T (K)	Technique[a]	Reference
178 ± 25	298	RR[b] (ethane)	Thévenet et al. (2000)
173 ± 30		RR[c] (propane)	
170 ± 35		RR[d] (*n*-butane)	
150 ± 30	297	RR[e] (propene)	Ullerstam et al. (2001)
141 ± 14	298	RR[f] (ethene)	Le Crâne et al. (2004)
124 ± 18		RR[g] (cyclohexane)	

[a]Abbreviations used for the techniques are defined in table I-F-3.
[b]Placed on an absolute basis using $k(Cl + C_2H_6) = 5.9 \times 10^{-11}$ cm^{-3} molecule^{-1} s^{-1} (Atkinson et al., 2006).
[c]Placed on an absolute basis using $k(Cl + \text{propane} = 1.4 \times 10^{-10}$ cm^3 molecule^{-1} s^{-1} (Atkinson et al., 2006).
[d]Placed on an absolute basis using $k(Cl + n\text{-butane}) = 2.05 \times 10^{-10}$ cm^{-3} molecule^{-1} s^{-1} (Atkinson et al., 2006).
[e]Placed on an absolute basis using $k(Cl + \text{propene}) = 2.3 \times 10^{-10}$ cm^{-3} molecule^{-1} s^{-1} (IUPAC, 2008).
[f]Placed on an absolute basis using $k(Cl + \text{ethene}) = 9.5 \times 10^{-11}$ cm^{-3} molecule^{-1} s^{-1} (section I-F-1).
[g]Placed on an absolute basis using $k(Cl + \text{cyclohexane}) = 3.3 \times 10^{-10}$ cm^{-3} molecule^{-1} s^{-1} (Calvert et al., 2008).

obtained with respect to reaction with OH. The lifetime for removal by NO_3, with $[NO_3] \approx 3 \times 10^9$ molecule cm^{-3}, is about 8 h. The mechanisms for these reactions and the atmospheric fate of the products are discussed in section IV-B-13.

IV-B-6. Pentanal (Valeraldehyde, n-C_4H_9CHO)

IV-B-6.1. OH Reaction Kinetics

The rate coefficient for the reaction of OH with pentanal has been measured at 298 K by Audley et al. (1981), Kerr and Sheppard (1981), Semmes et al. (1985), Papagni et al. (2000), Thévenet et al. (2000), D'Anna et al. (2001a), and Albaladejo et al. (2002). The results, given in table IV-B-16, are in good agreement. An unweighted average gives $k = 2.66 \times 10^{-11}$ cm^3 molecule^{-1} s^{-1}, with an uncertainty estimated to be ±15%. The temperature dependence was measured by Semmes et al. (253–410 K), who found an activation temperature (E/R) of −451 K, and by Thévenet et al. (243–372 K), who found a somewhat weaker dependence of −306 K. A fit to the combined data set (figure IV-B-8) leads to a recommended expression $k = 8.6 \times 10^{-12} \exp(336/T)$ cm^3 molecule^{-1} s^{-1} for use in atmospheric models.

IV-B-6.2. NO_3 Reaction Kinetics

The rate coefficient for the reaction of NO_3 with pentanal has been measured by D'Anna and Nielsen (1997), D'Anna et al. (2001a), Papagni et al. (2000), and Cabañas et al. (2001a). The latter group performed the only direct study, and the only measurements as a function of temperature (see table IV-B-17). The room temperature values are in fairly good agreement, and a rate coefficient $k = 1.62 \times 10^{-14}$ cm^3 molecule^{-1} s^{-1} is recommended, with an uncertainty of ±20%. In light of the strong curvature in the Arrhenius plot of Cabañas et al., and in the absence of confirmatory observations, no recommendation is made for the temperature dependence.

Table IV-B-16. Rate coefficients ($k = A\ e^{-B/T}$, cm^3 $molecule^{-1}$ s^{-1}) for reaction of OH with pentanal (n-C_4H_9CHO)

$10^{12} \times A$	B (K)	$10^{12} \times k$	T (K)	Technique[a]	Reference	Temperature Range (K)
		13.8 ± 1.7	298	RR (CH_3CHO)[b]	Audley et al. (1981)	
		24 ± 4	298 ± 4	RR (C_2H_4)[c]	Kerr and Sheppard (1981)	
6.3 ± 0.2	-451 ± 108	38.9 ± 5.7	253	FP–RF	Semmes et al. (1985)	253–410
		26.9 ± 3.9	298			
		23.3 ± 3.4	355			
		19.0 ± 2.8	410			
		29.9 ± 1.9	298	RR (MVK)[d]	Papagni et al. (2000)	
9.9 ± 1.9	-306 ± 56	33.4 ± 0.5	243	PLP–LIF	Thévenet et al. (2000)	243–372
		33.3 ± 0.6	253			
		31.8 ± 0.6	263			
		30.3 ± 1.0	273			
		28.2 ± 1.3	298			
		25.1 ± 0.4	313			
		23.9 ± 0.5	333			
		23.5 ± 0.7	353			
		22.3 ± 0.7	372			
		26.1 ± 1.4	298 ± 2	RR (1-C_4H_8)[e]	D'Anna et al. (2001a)	
		24.8 ± 2.4	298	PLP–LIF	Albaladejo et al. (2002)	

[a]Abbreviations used for the techniques are defined in table I-F-3.

[b]Placed on an absolute basis using $k(OH + CH_3CHO) = 1.5 \times 10^{-11}$ cm^3 $molecule^{-1}$ s^{-1} (this book, section IV-B-2.1).

[c]Placed on an absolute basis using $k(OH + C_2H_4) = 7.9 \times 10^{-12}$ cm^3 $molecule^{-1}$ s^{-1} at 1 bar and 298 K (Atkinson et al., 2006).

[d]Placed on an absolute basis using k(OH + methyl vinyl ketone) $= 2.0 \times 10^{-11}$ cm^3 $molecule^{-1}$ s^{-1} (this book, section IV-B-2.1).

[e]Placed on an absolute basis using k(OH + 1-butene) $= 3.14 \times 10^{-11}$ cm^3 $molecule^{-1}$ s^{-1} at 1 bar and 298 K (Calvert et al., 2008).

IV-B-6.3. Cl-Atom Reaction Kinetics

The rate coefficient for Cl + pentanal has been measured at room temperature by Thévenet et al. (2000), Rodriguez et al. (2005), Iwasaki et al. (2008b), and Singh et al. (2009) by relative rate techniques, and by Cuevas et al. (2006) and Iwasaki et al. by absolute methods, using pulsed laser photolysis coupled with resonance fluorescence and laser induced fluorescence, respectively; see table IV-B-18. The unweighted mean gives $k(298) = 2.4 \times 10^{-10}$ cm^3 $molecule^{-1}$ s^{-1}, with an uncertainty of ±15%. The only measurement of the temperature dependence is that by Cuevas et al. (2006); combining this with $k(298)$ gives: $k = 5.3 \times 10^{-12}$ $\exp(450/T)$ cm^3 $molecule^{-1}$ s^{-1}, although this expression requires confirmatory measurements. Iwasaki et al. measured the channel yield for abstraction of the aldehydic H, using FTIR in their chamber experiments, obtaining a value of 0.42 ± 0.03. This determination is supported by the measurements of Singh et al., who obtained a yield for formation of the pentanoyl radical of 0.45 ± 0.04. Iwasaki et al. compared the remaining reactivity with that in pentane and commented that the —CHO group deactivates the rest of the molecule with respect to H abstraction and that this deactivation extends over at least two carbon atoms in the chain.

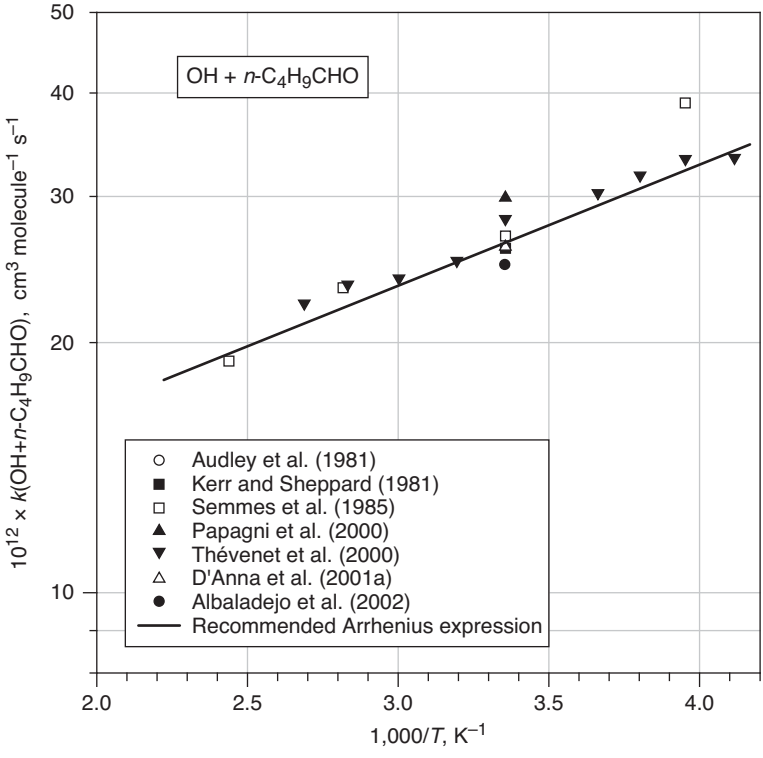

Figure IV-B-8. Arrhenius plot for the rate coefficients for the OH + pentanal reaction.

Table IV-B-17. Rate coefficients ($k = A\ e^{-B/T}$, cm^3 $molecule^{-1}$ s^{-1}) for reaction of NO_3 with pentanal (n-C_4H_9CHO)

$10^{12} \times A$	B (K)	$10^{15} \times k$	T (K)	Technique[a]	Reference	Temperature Range (K)
		15.1 ± 0.9	298	RR (1-butene)[b]	D'Anna and Nielsen (1997)	
		17.7 ± 2.1	298	RR (1-butene)[b]	D'Anna et al. (2001a)	
28 ± 14	2,190 ± 160	17.5 ± 0.6	298	DF–LIF	Cabañas et al. (2001a)	298–433
		54.8 ± 5.2	345			
		98.1 ± 12.6	389			
		133 ± 24	433			
		14.4 ± 1.7	298	RR (MACR)[c]	Papagni et al. (2000)	

[a]Abbreviations used for the techniques are defined in table I-F-3.
[b]Placed on an absolute basis using $k(NO_3 + 1\text{-butene}) = 1.40 \times 10^{-14}$ cm^3 $molecule^{-1}$ s^{-1} (Calvert et al., 2000).
[c]Placed on an absolute basis using $k(NO_3 + \text{methacrolein}) = 3.4 \times 10^{-15}$ cm^3 $molecule^{-1}$ s^{-1} (Calvert et al., 2000).

Table IV-B-18. Rate coefficients ($k = A\ e^{-B/T}$, cm^3 $molecule^{-1}$ s^{-1}) for the reaction of Cl with pentanal (n-C_4H_9CHO)

$10^{12} \times A$	B (K)	$10^{12} \times k$	T (K)	Technique[a]	Reference	Temperature Range (K)
		255 ± 25	298	RR[b] (ethane)	Thévenet et al. (2000)	
		251 ± 35		RR[c] (propane)		
		272 ± 25		RR[d] (n-butane)		
		261 ± 30		RR[b] (ethane)	Rodriguez et al. (2005)	
		237 ± 30		RR[e] (propene)		
		260 ± 30		RR[f] (1-butene)		
41.7 ± 5.4	−450 ± 80	205 ± 20	265	PLP–RF	Cuevas et al. (2006)	265–380
		205 ± 20	283			
		196 ± 20	298			
		178 ± 24	310			
		161 ± 12	329			
		141 ± 17	354			
		142 ± 21	380			
		231 ± 35	295	RR[c] (propane)	Iwasaki et al. (2008b)	
		224 ± 20		PLP–LIF		
		233 ± 55	298	RR[g] (2-propanol)	Singh et al. (2009)	
		207 ± 100		RR[h] (ethene)		

[a]Abbreviations used for the techniques are defined in table I-F-3.
[b]Placed on an absolute basis using $k(Cl + C_2H_6) = 5.9 \times 10^{-11}$ cm^3 $molecule^{-1}$ s^{-1} (Atkinson et al., 2006).
[c]Placed on an absolute basis using $k(Cl + propane) = 1.4 \times 10^{-10}$ cm^3 $molecule^{-1}$ s^{-1} (Atkinson et al., 2006).
[d]Placed on an absolute basis using $k(Cl + n\text{-butane}) = 2.05 \times 10^{-10}$ cm^3 $molecule^{-1}$ s^{-1} (Atkinson et al., 2006).
[e]Placed on an absolute basis using $k(Cl + propene) = 2.3 \times 10^{-10}$ cm^3 $molecule^{-1}$ s^{-1} (IUPAC, 2008).
[f]Placed on an absolute basis using $k(Cl + 1\text{-butene}) = 2.9 \times 10^{-10}$ cm^3 $molecule^{-1}$ s^{-1} (Orlando et al., 2003).
[g]Placed on an absolute basis using $k(Cl + 2\text{-propanol}) = 8,6 \times 10^{-11}$ cm^3 $molecule^{-1}$ s^{-1} (Atkinson et al., 2006).
[h]Placed on an absolute basis using $k(Cl + ethene) = 9.5 \times 10^{-11}$ cm^3 $molecule^{-1}$ s^{-1} (section I-F-1).

IV-B-6.4. Summary of the Atmospheric Fate of Pentanal

During the day the destruction of pentanal is by photolysis and reaction with OH. The photolysis lifetime in the lower troposphere is about 16 h with an overhead Sun; see table IX-M-1. For $[OH] \approx 2.5 \times 10^6$ molecule cm^{-3}, a lifetime for loss by reaction with OH of about 4 h is obtained. The lifetime for removal by NO_3, with $[NO_3] = 3 \times 10^9$ molecule cm^{-3}, and by Cl with $[Cl] \approx 10^4$ molecule cm^{-3} are about 6 h and about 8 days, respectively. The mechanisms for these reactions and the atmospheric fate of the products are discussed in section IV-B-13.

IV-B-7. 2-Methylbutanal [$CH_3CH_2CH(CH_3)CHO$]

IV-B-7.1. OH Reaction Kinetics

This reaction has been studied only by D'Anna et al. (2001a). They obtained a rate coefficient of $(3.33 \pm 0.09) \times 10^{-11}$ cm^3 $molecule^{-1}$ s^{-1} at 298 ± 2 K using a relative rate technique, and placed on an absolute basis using k(1-butene) = 3.19×10^{-11} cm^3 $molecule^{-1}$ s^{-1} at 1 bar and 298 K (Calvert et al., 2000); the estimated uncertainty is ±40%.

Table IV-B-19. Rate coefficients (k, cm^3 molecule^{-1} s^{-1}) for reaction of NO_3 with 2-methylbutanal [$CH_3CH_2CH(CH_3)CHO$]

$10^{12} \times A$	B (K)	$10^{15} \times k$	T (K)	Technique[a]	Reference	Temperature Range (K)
		27.8 ± 1.1	298	RR (1-butene)[b]	D'Anna et al. (2001a)	
55 ± 31	$2{,}300 \pm 550$	25.6 ± 4.9	298	DF–LIF	Cabañas et al. (2003)	298–433
		59.2 ± 5.0	345			
		145 ± 2.4	389			
		224 ± 20	433			

[a]Abbreviations used for the techniques are defined in table I-F-3.
[b]Placed on an absolute basis using $k(NO_3 + \text{1-butene}) = 1.40 \times 10^{-14}$ cm^3 molecule^{-1} s^{-1} (Calvert et al., 2000).

IV-B-7.2. NO_3 Reaction Kinetics

This reaction between NO_3 and 2-methylbutanal has been studied at room temperature by D'Anna et al. (2001a), using a relative rate technique, and by Cabañas et al. (2003), using discharge flow with laser induced fluorescence. The latter also measured the rate coefficient as a function of temperature (see table IV-B-19). The room temperature values agree quite well and give a mean value of $k = 2.67 \times 10^{-14}$ cm^3 molecule^{-1} s^{-1}, with an uncertainty of $\pm 30\%$. A fit to all the data gives $k = 3.0 \times 10^{-11} \exp(-2{,}100/T)$ cm^3 molecule^{-1} s^{-1}, but further measurements of the temperature dependence are needed before a recommendation can be made.

IV-B-7.3. Summary of the Atmospheric Fate of 2-Methylbutanal

During the day, the destruction of 2-methylbutanal is by photolysis and reaction with OH. Data for quantitiative estimation of the lifetime for photodecomposition is lacking, but it is likely that it is in the range of 5–15 h with an overhead Sun. See chapter IX. For [OH] $\approx 2.5 \times 10^6$ molecule cm^{-3}, a lifetime for loss by reaction with OH of about 3.4 h is obtained. The lifetime for removal by NO_3, with [NO_3] $\approx 3 \times 10^9$ molecule cm^{-3} is about 3.6 h. The mechanisms for these reactions and the atmospheric fate of the products are discussed section IV-B-13.

IV-B-8. 3-Methylbutanal [Isovaleraldehyde, $(CH_3)_2CHCH_2CHO$]

IV-B-8.1. OH Reaction Kinetics

This reaction has been studied by Audley et al. (1981), Kerr and Sheppard (1981), Semmes et al. (1985), Glasius et al. (1997), and D'Anna et al. (2001a). All the measurements were made at 298 K. The results are given in table IV-B-20. The measurement of Glasius et al. was made relative to isoprene, and the large difference in rate coefficients may have led to an overestimation. The other values, excluding that of Audley et al., are in quite good agreement, and the unweighted mean value of 2.59×10^{-11} cm^3 molecule^{-1} s^{-1} is recommended for temperatures near 298 K with an uncertainty of $\pm 20\%$.

Table IV-B-20. Rate coefficient (k, cm^3 molecule^{-1} s^{-1}) for reaction of OH with 3-methylbutanal [$(CH_3)_2CHCH_2CHO$]

$10^{12} \times k$	T (K)	Technique[a]	Reference
18.4 ± 2.0	298	RR (CH_3CHO)[b]	Audley et al. (1981)
24 ± 1	298 ± 4	RR (C_2H_4)[c]	Kerr and Sheppard (1981)
25.8 ± 4.0	298	FP–RF	Semmes et al. (1985)
40 ± 0.7	298	RR (isoprene)[d]	Glasius et al. (1997)
27.9 ± 0.7	298 ± 2	RR (1-C_4H_8)[e]	D'Anna et al. (2001a)

[a]Abbreviations used for the techniques are defined in table I-F-3.
[b]Placed on an absolute basis using $k(OH + CH_3CHO) = 1.5 \times 10^{-11}$ cm^3 molecule^{-1} s^{-1} (this book, section IV-B-2.1).
[c]Placed on an absolute basis using $k(OH + C_2H_4) = 7.9 \times 10^{-12}$ cm^3 molecule^{-1} s^{-1} at 1 bar and 298 K (Atkinson et al., 2006).
[d]Placed on an absolute basis using k(OH + isoprene) $= 1.0 \times 10^{-10}$ cm^3 molecule^{-1} s^{-1} (Atkinson et al., 2006).
[e]Placed on an absolute basis using k(OH + 1-butene) $= 3.1 \times 10^{-11}$ cm^3 molecule^{-1} s^{-1} at 1 bar and 298 K (IUPAC, 2008).

Table IV-B-21. Rate coefficients ($k = A\ e^{-B/T}$, cm^3 molecule^{-1} s^{-1}) for reaction of NO_3 with 3-methylbutanal [$(CH_3)_2CHCH_2CHO$]

$10^{12} \times A$	B (K)	$10^{15} \times k$	T (K)	Technique[a]	Reference	Temperature Range (K)
		13.5 ± 3	300	RR (1-butene)[b]	Glasius et al. (1997)	
		19.3 ± 0.8	298	RR (1-butene)[b]	D'Anna et al. (2001a)	
37 ± 14	2,180 ± 230	24.5 ± 2.0	298	DF–LIF	Cabañas et al. (2003)	298–433
		71.7 ± 3.8	345			
		110 ± 9.3	389			
		257 ± 19	433			

[a]Abbreviations used for the techniques are defined in table I-F-3.
[b]Placed on an absolute basis using $k(NO_3$ + 1-butene) $= 1.40 \times 10^{-14}$ cm^3 molecule^{-1} s^{-1} (Calvert et al., 2000).

IV-B-8.2. NO_3 Reaction Kinetics

The reaction of NO_3 with 3-methylbutanal has been measured by Glasius et al. (1997), D'Anna et al. (2001a), and Cabañas et al. (2003). The latter group measured the rate coefficient as a function of temperature. The results are given in table IV-B-21. The ambient temperature measurements vary from 1.3×10^{-14} to 2.5×10^{-14} cm^3 molecule^{-1} s^{-1}, with the measurement of Glasius et al. being the lowest. The unweighted mean of the data of D'Anna et al. and Cabañas et al. gives $k(298) = 2.19 \times 10^{-14}$ cm^3 molecule^{-1} s^{-1} with an uncertainty of ±30%. An Arrhenius fit to their data gives: $k(T) = 4.9 \times 10^{-11}\ \exp(-2{,}300/T)$ cm^3 molecule^{-1} s^{-1}; further measurements are needed before a recommendation can be made for the temperature dependence.

IV-B-8.3. Summary of the Atmospheric Fate of 3-Methylbutanal

During the day the destruction of 3-methylbutanal is by photolysis and reaction with OH. The photolysis lifetime in the lower troposphere with an overhead Sun is in

the range of 15–30 h; see table IX-M-1. For [OH] $\approx 2.5 \times 10^6$ molecule cm^{-3}, a lifetime for loss by reaction with OH of about 4.1 h is obtained. The lifetime for removal by NO_3, with [NO_3] $\approx 3 \times 10^9$ molecule cm^{-3} is about 3.6 h. The mechanisms for these reactions and the atmospheric fate of the products are discussed in section IV-B-13.

IV-B-9. 2,2-Dimethylpropanal [Pivaldehyde, $(CH_3)_3CCHO$]

IV-B-9.1. OH Reaction Kinetics

The reaction of OH with 2,2-dimethylpropanal has been studied by Audley et al. (1981), Kerr and Sheppard (1981), Semmes et al. (1985), Dóbé et al. (1989), Thévenet et al. (2000), D'Anna et al. (2001a), and Ullerstam et al. (2001) (see table IV-B-22). The reported rate coefficients at ambient temperatures range from 8.5×10^{-12} to 5.2×10^{-11} cm^3 molecule^{-1} s^{-1}. An unweighted mean, excluding the data of Audley et al. and Dóbé et al., which are outliers, gives $k(298\ \text{K}) = 2.64 \times 10^{-11}$ cm^3 molecule^{-1} s^{-1} with an uncertainty of ±20%. The temperature dependent data of Semmes et al. (1985) and Thévenet et al. (2000) overlap quite well, and a fit to the data of Semmes et al.

Table IV-B-22. Rate coefficients ($k = A\ e^{-B/T}$, cm^3 molecule^{-1} s^{-1}) for reaction of OH with 2,2-dimethylpropanal [$(CH_3)_3CCHO$]

$10^{12} \times A$	B (K)	$10^{12} \times k$	T (K)	Technique[a]	Reference	Temperature Range (K)
		8.5 ± 0.8	298	RR (CH_3CHO)[b]	Audley et al. (1981)	
		22 ± 6	298 ± 4	RR (C_2H_4)[c]	Kerr and Sheppard (1981)	
6.7 ± 0.3	−423 ± 154	33.9 ± 6.4	254	FP–RF	Semmes et al. (1985)	254–425
		30.6 ± 4.4	298			
		21.8 ± 3.2	354			
		17.6 ± 2.9	425			
13.3 ± 6.7	−409 ± 205	51.7 ± 13.6	300	DF–RF	Dóbé et al. (1989)	300–405
		40.2 ± 15.1	386			
		33.2	405			
9.9 ± 1.9	−306 ± 56	43.9 ± 1.4	243	PLP–LIF	Thévenet et al. (2000)	243–372
		40.9 ± 1.2	253			
		37.8 ± 0.7	263			
		33.5 ± 1.8	273			
		27.4 ± 2.3	298			
		23.8 ± 0.3	323			
		21.5 ± 0.6	348			
		22.9 ± 0.8	358			
		20.4 ± 0.4	372			
		26.8 ± 1.2	298 ± 2	RR (1-C_4H_8)[d]	D'Anna et al. (2001a)	
		27 ± 2	297	RR (C_3H_6)[e]	Ullerstam et al. (2001)	

[a]Abbreviations used for the techniques are defined in table I-F-3.
[b]Placed on an absolute basis using $k(\text{OH} + CH_3CHO) = 1.5 \times 10^{-11}$ cm^3 molecule^{-1} s^{-1} (this book, section IV-B-2.1).
[c]Placed on an absolute basis using $k(\text{OH} + C_2H_4) = 7.9 \times 10^{-12}$ cm^3 molecule^{-1} s^{-1} (Atkinson et al., 2006).
[d]Placed on an absolute basis using $k(\text{OH} + \text{1-butene}) = 3.14 \times 10^{-11}$ cm^3 molecule^{-1} s^{-1} (Calvert et al., 2000).
[e]Placed on an absolute basis using $k(\text{OH} + C_3H_6) = 2.9 \times 10^{-11}$ cm^3 molecule^{-1} s^{-1} (Atkinson et al., 2006).

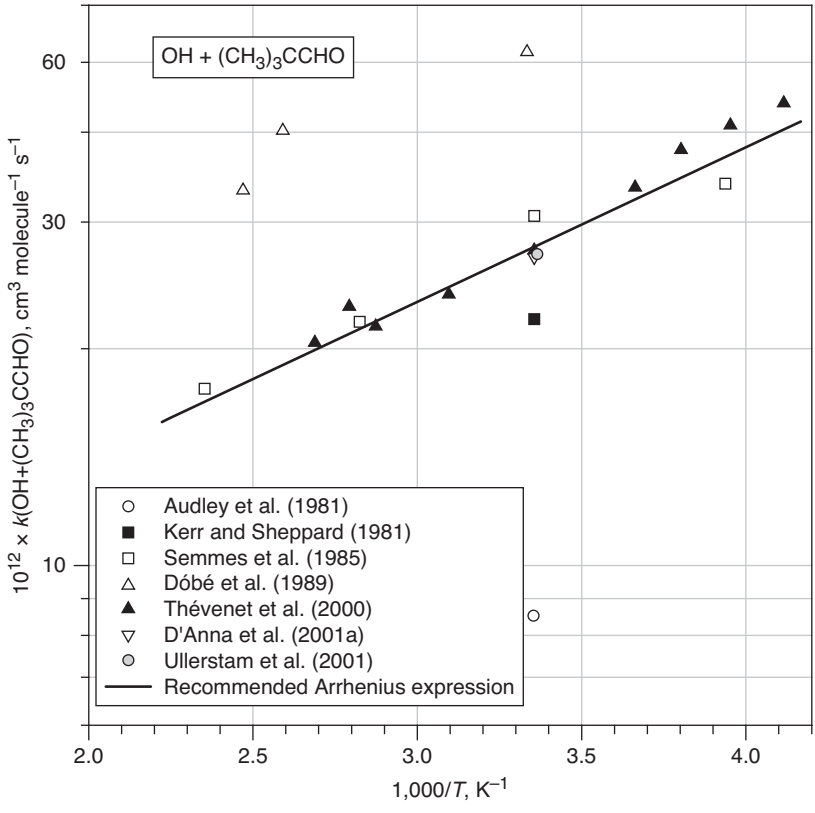

Figure IV-B-9. Arrhenius plot for the rate coefficients for the OH + 2,2-dimethylpropanal reaction.

(1985), Thévenet et al. (2000), and D'Anna et al. (2001a) leads to a recommendation of $k = 5.3 \times 10^{-12} \exp(494/T)\,\mathrm{cm^3\ molecule^{-1}\ s^{-1}}$. The corresponding value at 298 K is $2.8 \times 10^{-11}\mathrm{cm^3\ molecule^{-1}\ s^{-1}}$. The data and fit are shown in figure IV-B-9.

IV-B-9.2. NO_3 Reaction Kinetics

This reaction has been studied on two occasions by D'Anna et al. (1997, 2001a), using a relative rate technique with FTIR detection. They obtained rate coefficients at 298 K of $(2.37 \pm 0.09) \times 10^{-14}\,\mathrm{cm^3\ molecule^{-1}\ s^{-1}}$ and $(2.69 \pm 0.21) \times 10^{-14}\,\mathrm{cm^3\ molecule^{-1}\ s^{-1}}$, respectively, using $k(\mathrm{NO_3} + \text{1-butene}) = 1.40 \times 10^{-14}\,\mathrm{cm^3\ molecule^{-1}\ s^{-1}}$ (Calvert et al., 2000) to place the measurements on an absolute basis. Ullerstam et al. (2001) obtained a rate coefficient at 297 K of $(2.2 \pm 0.3) \times 10^{-14}\,\mathrm{cm^3\ molecule^{-1}\ s^{-1}}$, based on $k(\mathrm{NO_3} + \text{propene}) = 9.4 \times 10^{-15}\,\mathrm{cm^3\ molecule^{-1}\ s^{-1}}$ (Atkinson et al., 2006). The measurements give an unweighted mean of $2.4 \times 10^{-14}\,\mathrm{cm^3\ molecule^{-1}\ s^{-1}}$ with an uncertainty of ±20%.

IV-B-9.3. Cl-Atom Reaction Kinetics

The rate coefficient for Cl + 2,2-dimethylpropanal has been measured by Thévenet et al. (2000), Ullerstam et al. (2001), and Le Crâne et al. (2004) using relative rate techniques; together they used a total of six different reference compounds; see table IV-B-23. The values range from 1.0×10^{-10} to 1.7×10^{-10} cm^3 molecule^{-1} s^{-1}; an unweighted mean gives $k(298) = 1.42 \times 10^{-10}$ cm^3 molecule^{-1} s^{-1} with an uncertainty of ±20%. Le Crâne et al. used FTIR-chamber and UV absorption–pulsed photolysis methods to obtain channel yields for abstraction of the aldehydic H of 0.81 ± 0.08 and 0.88 ± 0.06 respectively; the remainder corresponds to abstraction at a primary H. They also measured the rate coefficient for dissociation of the 2,2-dimethylpropanoyl radical relative to that for its reaction with Cl_2 and obtained a value of 10^5 s^{-1} for the former, showing that the major fate of the radical in the atmosphere is reaction with O_2 to form the peroxy-2,2-dimethylpropanoyl radical.

IV-B-9.4. Summary of the Atmospheric Fate of 2,2-Dimethylpropanal

During the day the destruction of 2,2-dimethylpropanal is by photolysis and reaction with OH. The photolysis lifetime in the lower troposphere with an overhead Sun is probably in the range of 8–19 h; see table IX-M-1. For [OH] ≈ 2.5×10^6 molecule cm^{-3}, a lifetime for loss by reaction with OH of about 4 h is obtained. The lifetime for removal by NO_3(3×10^9 molecule cm^{-3}) is about 4 h. The mechanisms for these reactions and the atmospheric fate of the products are discussed in section IV-B-13.

IV-B-10. Hexanal (n-$C_5H_{11}CHO$)

IV-B-10.1. OH Reaction Kinetics

The reaction of OH with hexanal has been measured at 298 K by Papagni et al. (2000), D'Anna et al. (2001a), and Albaladejo et al. (2002); see table IV-B-24. The first two

Table IV-B-23. Rate coefficients (k, cm^3 molecule^{-1} s^{-1}) for reaction of Cl with 2,2-dimethylpropanal [$(CH_3)_3CCHO$]

$10^{12} \times k$	T (K)	Technique[a]	Reference
165 ± 35	298	RR[b] (ethane)	Thévenet et al. (2000)
158 ± 25		RR[c] (propane)	
157 ± 30		RR[d] (n-butane)	
165 ± 35		RR[e] (n-hexane)	
120 ± 20	297	RR (C_3H_6)[f]	Ullerstam et al. (2001)
130 ± 18	298	RR[g] (ethene)	Le Crâne et al. (2004)
100 ± 12		RR[h] (cyclohexane)	

[a]Abbreviations used for the techniques are defined in table I-F-3.
[b]Placed on an absolute basis using $k(Cl + C_2H_6) = 5.9 \times 10^{-11}$ cm^3 molecule^{-1} s^{-1} (Atkinson et al., 2006).
[c]Placed on an absolute basis using $k(Cl + \text{propane}) = 1.4 \times 10^{-10}$ cm^3 molecule^{-1} s^{-1} (Atkinson et al., 2006).
[d]Placed on an absolute basis using $k(Cl + n\text{-butane}) = 2.05 \times 10^{-10}$ cm^3 molecule^{-1} s^{-1} (Atkinson et al., 2006).
[e]Placed on an absolute basis using $k(Cl + n\text{-hexane}) = 3.3 \times 10^{-10}$ cm^3 molecule^{-1} s^{-1} (Calvert et al., 2008).
[f]Placed on an absolute basis using $k(Cl + \text{propene}) = 2.3 \times 10^{-10}$ cm^3 molecule^{-1} s^{-1} (Atkinson et al., 2006).
[g]Placed on an absolute basis using $k(Cl + \text{ethene}) = 9.5 \times 10^{-11}$ cm^3 molecule^{-1} s^{-1} (section I-F-1).
[h]Placed on an absolute basis using $k(Cl + \text{cyclohexane}) = 3.3 \times 10^{-10}$ cm^3 molecule^{-1} s^{-1} (Calvert et al., 2008).

Table IV-B-24. Rate coefficients ($k = A \times e^{-B/T}$, cm^3 $molecule^{-1}$ s^{-1}) for the reaction of OH with hexanal (n-$C_5H_{11}CHO$)

$10^{12} \times A$	B (K)	$10^{12} \times k$	T (K)	Technique[a]	Reference	Temperature Range (K)
		31.7 ± 1.5	298	RR (MVK)[b]	Papagni et al. (2000)	
		28.6 ± 1.3	298 ± 2	RR (1-C_4H_8)[c]	D'Anna et al. (2001a)	
		26.0 ± 2.1	298	PLP–LIF	Albaladejo et al. (2002)	
4.2 ± 0.8	-565 ± 65	33.0 ± 4.0	263	PLP–LIF	Jimenez et al. (2007)	263–353
		31.9 ± 4.4	268			
		34.6 ± 2.2	273			
		32.2 ± 4.4	278			
		31.8 ± 4.0	286			
		27.8 ± 5.0	298			
		27.8 ± 2.2	307			
		25.5 ± 2.2	321			
		20.9 ± 1.4	336			
		21.0 ± 0.7	353			

[a]Abbreviations used for the techniques are defined in table I-F-3.
[b]Placed on an absolute basis using k(OH + methyl vinyl ketone) = 2.0×10^{-11} cm^3 $molecule^{-1}$ s^{-1} (this book, section V-E-1.1).
[c]Placed on an absolute basis using k(OH + 1-butene) = 3.1×10^{-11} cm^3 $molecule^{-1}$ s^{-1} (IUPAC, 2008).

measurements were made using relative rate techniques while the last was made using flash photolysis with LIF detection of OH. Jimenez et al. (2007) used pulsed laser photolysis to measure the rate coefficient over the temperature range 263–353 K.The measurements are in good agreement, and each individual study shows a 5–10% increase for the rate coefficient of hexanal versus that of pentanal. We recommend a rate coefficient at 298 K of 2.85×10^{-11} cm^3 $molecule^{-1}$ s^{-1} with an uncertainty of ±15%. Combining the temperature dependence determined by Jimenez et al. with this value gives $k = 4.3 \times 10^{-12} \exp(565/T)$ cm^3 $molecule^{-1}$ s^{-1}.

IV-B-10.2. NO_3 Reaction Kinetics

The rate coefficient for reaction of NO_3 with hexanal has been measured at 298 K by D'Anna and Nielsen (1997), Papagni et al. (2000), D'Anna et al. (2001a), and by Noda et al. (2003), all using relative rate techniques; see table IV-B-25. The measurements agree well with an unweighted mean of 1.61×10^{-14} cm^3 $molecule^{-1}$ s^{-1}, and an uncertainty of ±15%.

IV-B-10.3. Cl-Atom Reaction Kinetics

The rate coefficient for Cl + hexanal has been measured at 298 K by Rodriguez et al. (2005), using a relative rate technique with three reference compounds, and by Cuevas et al. (2006) using pulsed laser photolysis coupled with resonance fluorescence, over the temperature range 265–380 K. The 298 K rate coefficients range from 2.5×10^{-10} to 3.1×10^{-10} cm^3 $molecule^{-1}$ s^{-1}; an unweighted mean gives $k(298) = 2.79 \times 10^{-10}$ cm^3 $molecule^{-1}$ s^{-1} with an uncertainty of ±20%; see table IV-B-26. Coupling this rate

Table IV-B-25. Rate coefficients (k, cm^3 molecule^{-1} s^{-1}) for reaction of NO_3 with hexanal (n-$C_5H_{11}CHO$)

$10^{15} \times k$	T (K)	Technique[a]	Reference
17.9 ± 1.8	298	RR (1-C_4H_8)[b]	D'Anna and Nielsen (1997)
15.3 ± 2.1	298	RR (methacrolein)[c]	Papagni et al. (2000)
14.6 ± 1.6		RR (1-C_4H_8)[b]	
15.0 ± 1.9	298 ± 2	RR (1-C_4H_8)[b]	D'Anna et al. (2001a)
17.0 ± 1.0	297 ± 2	RR (butanal)[d]	Noda et al. (2003)
16.6 ± 2.0		RR (1-C_4H_8)[b]	

[a]Abbreviations used for the techniques are defined in table I-F-3.
[b]Placed on an absolute basis using $k(NO_3 + \text{1-butene}) = 1.40 \times 10^{-14}$ cm^3 molecule^{-1} s^{-1} (Atkinson et al., 2006).
[c]Placed on an absolute basis using $k(NO_3 + \text{methacrolein}) = 3.4 \times 10^{-15}$ cm^3 molecule^{-1} s^{-1} (Atkinson et al., 2006).
[d]Placed on an absolute basis using $k(NO_3 + \text{butanal}) = 1.12 \times 10^{-14}$ cm^3 molecule^{-1} s^{-1} (this book, section IV-B-4.2).

Table IV-B-26. Rate coefficients ($k = A \times e^{-B/T}$, cm^3 molecule^{-1} s^{-1}) for reaction of Cl with hexanal (n-$C_5H_{11}CHO$)

$10^{12} \times A$	B (K)	$10^{12} \times k$	T (K)	Technique[a]	Reference	Temperature Range (K)
		272 ± 35	298	RR[b] (ethane)	Rodriguez et al. (2005)	
		279 ± 30	298	RR[c] (propene)		
		314 ± 35	298	RR[d] (1-butene)		
79.1 ± 6.6	−349 ± 51	291 ± 28	264	PLP–RF	Cuevas et al. (2006)	265–380
		279 ± 22	282			
		252 ± 20	298			
		238 ± 20	313			
		229 ± 22	329			
		211 ± 24	343			
		200 ± 28	355			
		205 ± 20	380			

[a]Abbreviations used for the techniques are defined in table I-F-3.
[b]Placed on an absolute basis using $k(Cl + C_2H_6) = 5.9 \times 10^{-11}$ cm^3 molecule^{-1} s^{-1} (Atkinson et al., 2006).
[c]Placed on an absolute basis using $k(Cl + \text{propene}) = 1.4 \times 10^{-10}$ cm^3 molecule^{-1} s^{-1} (Atkinson et al., 2006).
[d]Placed on an absolute basis using $k(Cl + \text{1-butene}) = 2.9 \times 10^{-10}$ cm^3 molecule^{-1} s^{-1} (Orlando et al., 2003).

coefficient with the temperature dependence obtained by Cuevas et al. gives $k = 8.6 \times 10^{-11} \exp(349/T)$ cm^3 molecule^{-1} s^{-1}. However, a temperature dependence cannot be recommended in the absence of further measurements.

IV-B-10.4. Summary of the Atmospheric Fate of Hexanal

During the day, the destruction of hexanal is by photolysis and reaction with OH. The photolysis lifetime in the lower troposphere with an overhead Sun is about 12 h; see table IX-M-1. For [OH] $\approx 2.5 \times 10^6$ molecule cm^{-3}, a lifetime for reaction with OH of about 3.8 h is obtained. The lifetime for removal by NO_3 with $\approx 3 \times 10^9$ molecule cm^{-3} is about 6 h. The mechanisms for these reactions and the atmospheric fate of the products are discussed in section IV-B-13.

IV-B-11. Higher Alkanals

IV-B-11.1. OH Reaction Kinetics

Table IV-B-27 shows measured rate coefficients for some C_6–C_9 aldehydes. All are single determinations and the uncertainty should be increased from the reported statistical uncertainty to one of about ±40%. The atmospheric lifetimes for reaction with OH, with [OH] = 2.5×10^6 molecule cm^{-3}, are also shown in table IV-B-28.

IV-B-11.2. NO_3 Reaction Kinetics

D'Anna et al. (2001a) have measured the rate coefficients for the branched hexanals, 2-methylpentanal, 3-methylpentanal, 4-methylpentanal, 3,3-dimethylbutanal, and 2-ethylbutanal, with NO_3 using relative rate techniques at 298 K with 1-butene as the reference reactant. Noda et al. (2002) have measured rate coefficients for NO_3 + heptanal, octanal, and nonanal. The rate coefficients are shown in table IV-B-28, together with the atmospheric lifetimes for $[NO_3] \approx 3 \times 10^9$ molecule cm^{-3}.

IV-B-11.3. Cl-Atom Reaction Kinetics

Table IV-B-29 shows data for the reaction of Cl with heptanal as a function of temperature as obtained by Rodriguez et al. (2005) by a relative rate technique and by Cuevas et al. (2006) using pulsed laser photolysis with LIF detection. The mean value at 298 K is 3.0×10^{-10} cm^3 $molecule^{-1}$ s^{-1} with an uncertainty of ±20%. The Arrhenius expression of Cuevas et al. gives $k = 1.1 \times 10^{-10} \exp(306/T)$ cm^3 $molecule^{-1}$ s^{-1}.

Table IV-B-27. Rate coefficients (k, cm^3 $molecule^{-1}$ s^{-1}) for the reaction of OH with higher aldehydes

Molecule	$10^{12} \times k$	T (K)	Technique[a]	Reference	Lifetime (h)[b]
2-Methylpentanal	33 ± 2.1	298 ± 2	RR (1-C_4H_8)[c]	D'Anna et al. (2001a)	3.4
3-Methylpentanal	29.1 ± 1.5	298 ± 2	RR (1-C_4H_8)[c]	D'Anna et al. (2001a)	3.9
4-Methylpentanal	26.3 ± 1.1	298 ± 2	RR (1-C_4H_8)[c]	D'Anna et al. (2001a)	4.3
3,3-Dimethylbutanal	21.4 ± 1.4	298 ± 2	RR (1-C_4H_8)[c]	D'Anna et al. (2001a)	5.3
2-Ethylbutanal	40.2 ± 4.0	298 ± 2	RR (1-C_4H_8)[c]	D'Anna et al. (2001a)	2.8
Heptanal	29.6 ± 2.3	298	PLP–LIF	Albaladejo et al. (2002)	3.7
2,3-Dimethylpentanal	42 ± 10	298	RR ($CH_2{=}C(CH_3)_2$)[d]	Tuazon et al. (2003)	2.7
Nonanal	32 ± 5	298	RR (octane)[e]	Bowman et al. (2003)	3.5

[a]Abbreviations used for the techniques are defined in table I-F-3.
[b]For [OH] = 2.5×10^6 molecule cm^{-3}.
[c]Placed on an absolute basis using k(OH + 1-butene) = 3.1×10^{-11} cm^3 $molecule^{-1}$ s^{-1} at 1 bar and 298 K (IUPAC, 2008).
[d]Placed on an absolute basis using k(OH + 2-methylpropene) = 5.14×10^{-11} cm^3 $molecule^{-1}$ s^{-1} at 1 bar and 298 K (Calvert et al., 2000).
[e]Placed on an absolute basis using k(OH + octane) = 7.81×10^{-12} cm^3 $molecule^{-1}$ s^{-1} (Calvert et al., 2008).

Table IV-B-28. Rate coefficients (k, cm^3 molecule^{-1} s^{-1}) for reaction of NO_3 with higher aldehydes

Compound	$10^{15} \times k$	T (K)	Technique[a]	Reference	Lifetime (h)[b]
2-Methylpentanal	27.9 ± 1.1	298	RR (1-C_4H_8)[c]	D'Anna et al. (2001a)	3.4
3-Methylpentanal	25.0 ± 0.8	298	RR (1-C_4H_8)[c]	D'Anna et al. (2001a)	3.8
4-Methylpentanal	17.4 ± 0.9	298	RR (1-C_4H_8)[c]	D'Anna et al. (2001a)	5.4
3,3-Dimethylbutanal	17.7 ± 1.4	298	RR (1-C_4H_8)[c]	D'Anna et al. (2001a)	5.4
2-Ethylbutanal	46.3 ± 2.3	298	RR (1-C_4H_8)[c]	D'Anna et al. (2001a)	2.0
Heptanal	21 ± 3	297	RR (butanal)[d]	Noda et al. (2002)	4.8
	19 ± 2		RR (C_3H_6)[e]		
	19 ± 1		RR (1-C_4H_8)[c]		
	(19.7 ± 5)[f]				
Octanal	15 ± 2	297	RR (butanal)[d]	Noda et al. (2002)	5.1
	20 ± 3		RR (C_3H_6)[e]		
	(18 ± 5)[f]				
Nonanal	18 ± 2	297	RR (butanal)[d]	Noda et al. (2002)	4.6
	22 ± 2		RR (C_3H_6)[e]		
	(20 ± 5)[f]				
Decanal	22 ± 4	297	RR (butanal)[d]	Noda et al. (2002)	4.2

[a]Abbreviations used for the techniques are defined in table I-F-3.
[b]For $[NO_3] = 3 \times 10^9$ molecule cm^{-3}.
[c]Placed on an absolute basis using $k(NO_3 + \text{1-butene}) = 1.35 \times 10^{-14}$ cm^3 molecule^{-1} s^{-1} (Calvert et al., 2000).
[d]Placed on an absolute basis using $k(NO_3 + \text{butanal}) = 1.12 \times 10^{-14}$ cm^3 molecule^{-1} s^{-1} (this book, section IV-B-4.2).
[e]Placed on an absolute basis using $k(NO_3 + \text{propene}) = 9.3 \times 10^{-15}$ cm^3 molecule^{-1} s^{-1} (Atkinson et al., 2006).
[f]Unweighted average.

Table IV-B-29. Rate coefficients ($k = A \times e^{-B/T}$, cm^3 molecule^{-1} s^{-1}) for reaction of Cl with heptanal (n-$C_6H_{13}CHO$)

$10^{12} \times A$	B (K)	$10^{12} \times k$	T (K)	Technique[a]	Reference	Temperature Range (K)
		292 ± 35	[e]	RR[b] (ethane)	Rodriguez et al. (2005)	
		303 ± 30	[e]	RR[c] (propene		
		316 ± 35	[e]	RR[d] (1-butene)		
106 ± 20	-306 ± 115	302 ± 32	265	PLP–RF	Cuevas et al. (2006)	265–380
		303 ± 36	283			
		301 ± 30	298			
		279 ± 25	311			
		259 ± 36	329			
		251 ± 46	341			
		268 ± 40	356			
		222 ± 22	380			

[a]Abbreviations used for the techniques are defined in table I-F-3.
[b]Placed on an absolute basis using $k(Cl + C_2H_6) = 5.9 \times 10^{-11}$ cm^3 molecule^{-1} s^{-1} (Atkinson et al., 2006).
[c]Placed on an absolute basis using $k(Cl + \text{propane}) = 1.4 \times 10^{-10}$ cm^3 molecule^{-1} s^{-1} (Atkinson et al., 2006).
[d]Placed on an absolute basis using $k(Cl + \text{1-butene}) = 3.1 \times 10^{-10}$ cm^3 molecule^{-1} s^{-1} (IUPAC, 2008).
[e]Room temperature.

IV-B-12. Cycloalkylcarbaldehydes

These compounds have an aldehyde group attached to an alkane ring. Their reactions were studied by D'Anna et al. (2005b) in order to understand the reactions of similar compounds formed in the oxidation of biogenic compounds; e.g., norpinonaldehyde, formed in the oxidation of α-pinene. They used chamber experiments, coupled with FTIR and PTRMS to study the products and infer the mechanism, obtaining carbon balances in the range 89–97%.

IV-B-12.1. OH Reaction Kinetics

The rate coefficients for reaction with OH of the cycloalkylcarbaldehydes with 3–6-membered rings are shown in table IV-B-30. These values are recommended with an uncertainty of ±40%.

IV-B-12.2. NO_3 Reaction Kinetics

The rate coefficients for reaction with NO_3 of the cycloalkylcarbaldehydes with 3–6-membered rings are shown in table IV-B-31. These values are recommended with an uncertainty of ±40%.

Table IV-B-30. Rate coefficients (k, cm^3 molecule^{-1} s^{-1}) for reaction of OH with cycloalkylcarbaldehydes

Molecule	$10^{12} \times k$	Technique[a]	Reference	Lifetime (h)[b]
Cyclopropanecarbaldehyde	21.0 ± 0.5	RR (1-butene)[c]	D'Anna et al. (2005b)	5.2
Cyclobutanecarbaldehyde	26.3 ± 0.6	RR (1-butene)[c]		4.2
Cyclopentanecarbaldehyde	32.3 ± 0.7	RR (1-butene)[c]		
	30.2 ± 0.5	RR (propene)[d]		
	31.3 ± 0.5	Mean value		3.5
Cyclohexanecarbaldehyde	37.0 ± 0.5	RR (1-butene)[c]		3.0

[a]Abbreviations used for the techniques are defined in table I-F-3.
[b]Lifetime for reaction with OH, with [OH] = 2.5×10^6 molecule cm^3.
[c]Placed on an absolute basis using $k(\text{OH} + \text{1-C}_4\text{H}_8) = 3.1 \times 10^{-11}$ cm^3 molecule^{-1} s^{-1} (IUPAC, 2008).
[d]Placed on an absolute basis using $k(\text{OH} + \text{C}_3\text{H}_6) = 2.9 \times 10^{-11}$ cm^3 molecule^{-1} s^{-1} (Atkinson et al., 2006).

Table IV-B-31. Rate coefficients (k, cm^3 molecule^{-1} s^{-1}) for reaction of NO_3 with cycloalkylcarbaldehydes

Molecule	$10^{15} \times k$	Technique[a]	Reference	Lifetime (h)[b]
Cyclopropanecarbaldehyde	6.3 ± 0.4	RR (1-butene)[c]	D'Anna et al. (2005b)	15
Cyclobutanecarbaldehyde	20.6 ± 0.6	RR (1-butene)[c]		4.7
Cyclopentanecarbaldehyde	26.4 ± 1.0	RR (1-butene)[c]		3.7
Cyclohexanecarbaldehyde	33.1 ± 1.2	RR (1-butene)[c]		2.9

[a]Abbreviations used for the techniques are defined in table I-F-3.
[b]Lifetime for reaction with NO_3, with [NO_3] = 3×10^9 molecule cm^3.
[c]Placed on an absolute basis using $k(\text{NO}_3 + \text{1-C}_4\text{H}_8) = 1.40 \times 10^{-14}$ cm^3 molecule^{-1} s^{-1} (Calvert et al., 2000).

IV-B-12.3. Summary of the Atmospheric Fate of Cycloalkylcarbaldehydes and the End Products of Their Oxidation

The atmospheric lifetimes for reaction with [OH] = 2.5×10^6 molecule cm^{-3} and with [NO_3] = 3×10^9 molecule cm^{-3} are shown in tables IV-B-30 and IV-B-31.

D'Anna et al. (2005b) showed that the major reaction channel for OH is abstraction of the aldehydic H, although some abstraction of ring hydrogen atoms occurs (e.g., ~11% for cyclobutanecarbaldehyde). The acyl peroxy radical, formed following abstraction from —CHO and subsequent reaction with O_2, can add NO_2 to form a [(nitroperoxy)carbonyl] cycloalkane, [e.g., *cyclo*-$C_3H_5C(O)O_2NO_2$], or a cycloalkyloxy radical by reaction with NO, decaboxylation and further reaction with NO:

$$\textit{cyclo}\text{-}C_3H_5C(O)O_2 + NO \rightarrow \textit{cyclo}\text{-}C_3H_5C(O)O + NO_2$$

$$\textit{cyclo}\text{-}C_3H_5C(O)O + O_2 \rightarrow \textit{cyclo}\text{-}C_3H_5O_2 + CO_2$$

$$\textit{cyclo}\text{-}C_3H_5O_2 + NO \rightarrow \textit{cyclo}\text{-}C_3H_5O + NO_2$$

The oxy radical ring opens to form carbonyl alkoxy radicals, e.g., $HC(O)CH_2CH_2O$, which react with O_2, dissociate or isomerise, depending on the size of the original alkane ring.

IV-B-13. General Observations and Trends in Rate Coefficients for Alkanals

A negative temperature dependence seems to be common to all the reactions of OH with aldehydes. The temperature coefficient ($-E/R$) is in the range 350–450 K except for pivaldehyde (2,2-dimethylpropanal), which is somewhat more negative. Formaldehyde shows a change in behavior around room temperature, switching from a negative temperature coefficient below room temperature to a positive one above. This may be indicative of a change of reaction mechanism, but not necessarily of products. The negative temperature dependence is probably associated with a van der Waals well that precedes the transition state. Greenwald et al. (2005) have made a careful analysis of the temperature dependence of the high pressure limiting rate coefficient for the addition of OH to ethene where the transition state for forming the adduct lies below the energy of the reactants (a so-called submerged transition state) and is preceded by a van der Waals well. They showed that the Arrhenius temperature dependence is negative and becomes more negative at low temperatures, with the rate coefficient tending to the capture value, where every collision leads to reaction, as T approaches 0 K. Similar behavior probably applies to the abstraction reaction of OH with aldehydes. At low temperatures, the rate of reaction is determined by an outer transition state that lies at inter-reactant distances greater than that of the van der Waals complex. At higher temperatures, the inner transition state, leading directly to the abstraction products, determines the rate coefficient. The temperature dependence at these higher T depends on the energy of this inner transition state. If it is submerged, then the dependence is negative, but becomes positive for reactions with barriers close to, or slightly higher

than the reactants. This may explain the change in behavior of OH + CH_2O. Alvarez Idaboy et al. (2001b) discussed the negative temperature dependence in terms of a thermalized pre-reaction complex. Such behaviour is unlikely, because the van der Waals complex is so short-lived that collisional stabilization at normal pressures is unlikely. Greenwald et al. showed that such a model is also unnecessary.

Similar behavior is observed for Cl + aldehydes, where the rate coefficients are even higher and a negative temperature dependence applies. Reactions of NO_3 are significantly slower and have a positive temperature dependence.

Figure IV-B-10 compares the experimental rate coefficients for straight chain C_1–C_{10} alkanes and alkanals for OH, NO_3, and Cl. For OH and especially NO_3, the alkanal values lie significantly above those for the alkanes, reflecting, as discussed below, the lower C—H bond energy in the —CHO group. For OH, the two sets of rate coefficients approach one another as abstraction from the hydrocarbon chain becomes more significant and the partial rate coefficient for abstraction of the carbonyl H-atom makes a smaller fractional contribution. Even for C_9, there is a 2 orders of magnitude difference between the alkanal and alkane rate coefficients for NO_3, reflecting the dominance of —CHO abstraction for this radical. It is difficult though to explain the continuing increase in the rate coefficient up to pentanal on this basis, a point returned to in the discussion of structure–activity relations. The Cl rate coefficients are higher than those for OH, and the abstraction site is less specific. The rate coefficient for

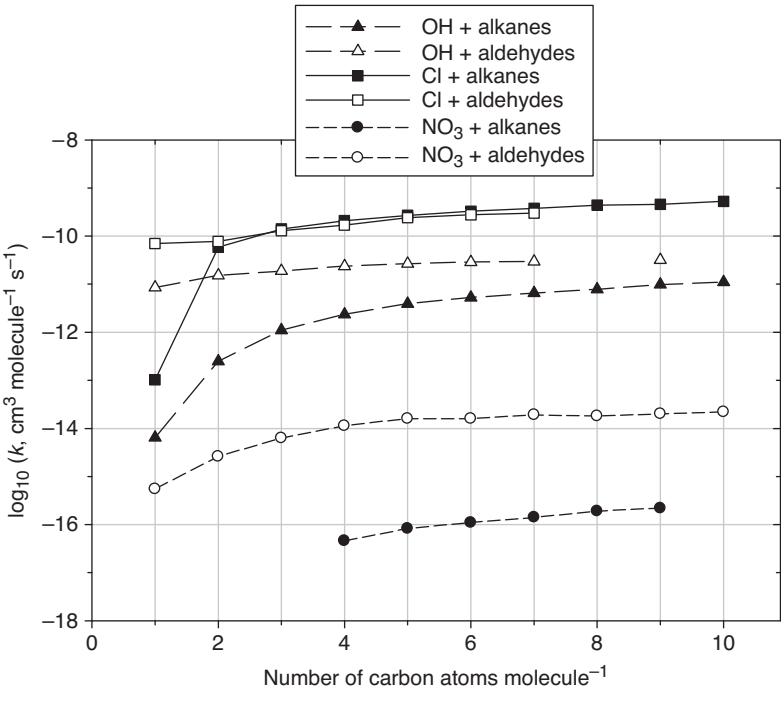

Figure IV-B-10. Comparison of rate coefficients for reactions of OH, NO_3, and Cl with straight chain alkanes and alkanals.

CH_2O is much higher than that for CH_4, but the values for Cl reactions with alkanes and alkanals are quite similar for higher carbon numbers.

Where mechanistic studies have been performed, abstraction from the —CHO group is dominant for all three radical species, with a partial rate coefficient for OH of roughly 1.9×10^{-11} cm^3 molecule^{-1} s^{-1}. As the chain length increases the contribution from the aldehyde group remains approximately constant, and hence the fractional contribution decreases (Bowman et al., 2003).

The behaviour for OH can be rationalized using the structure–activity relation (SAR) developed by Kwok and Atkinson (1995). For example, the SAR gives an overall rate coefficient at 298 K for butanal of 2.5×10^{-11} cm^3 molecule^{-1} s^{-1}, in good agreement with the mean value reported in this work. The rate coefficient is calculated from the SAR by adding together the rate constants for abstraction from the four distinct sites in butanal. These values give percentage channel yields for abstraction at the 1-, 2-, 3-, and 4-positions in butanal of 78%, 2%, 17%, and 1%, respectively. These values can be rationalized on the basis of the C—H bond energies: the C(O)—H bond is weakest, followed by the C—H bond at the 3-position, where the radical formed by abstraction is resonance stabilized. Reaction occurs faster at the secondary carbon located at the 2-position compared with the primary C at the 4-position. As further CH_2-groups are added in a straight chain aldehyde, the SAR predicts that the rate coefficient increases slowly, since the partial rate constant for reaction at such a site is 1.7×10^{-12} cm^3 molecule^{-1} s^{-1}. D'Anna et al. (2001a) measured rate coefficients somewhat larger than those predicted by the SAR for a range of larger aldehydes, suggesting that the parameterization provided by the SAR may be an oversimplification. Figure IV-B-11 compares the experimental rate coefficients (k_{expt}), with those calculated from the SAR (k_{SAR}) for the C_2–C_6 alkanals discussed in this section. Figure IV-B-12 shows the percentage abstraction from the —CHO group as calculated using the SAR for straight chain C_2–C_6 alkanals; this demonstrates the decrease in the fractional abstraction as the chain lengthens.

D'Anna et al. compared their results for NO_3 + aldehydes with the SAR proposed by Atkinson (1991). NO_3 + aldehyde reactions have a significant activation barrier, so that these reactions are much more sensitive to the C—H bond energy than is the case for OH and Cl. It is expected, therefore, that reaction is completely dominated by abstraction of the aldehydic H and the SAR predicts rate coefficients that are fairly constant, at $\sim 5 \times 10^{-15}$ cm^3 molecule^{-1} s^{-1} for aldehydes with more than one carbon atom. The data of D'Anna et al. (2001a) and of Noda et al. (2002) show that the rate coefficients increase significantly for the higher aldehydes, with a value of 4.5×10^{-14} cm^3 molecule^{-1} s^{-1} for 2-ethylbutanal, for example, although it is difficult to discern a pattern. Noda et al. (2002) could find no correlation with bond strength or numbers of different types of C—H bond.

The Cl-atom is less specific in the site of abstraction than OH, as discussed previously. This is reflected in the product studies, for example, on butanal. Wu and Mu (2007) found percentage yields of $\geq$42%, $<$ 25%, 21%, and $\leq$12% for abstraction at the 1-, 2-, 3-, and 4-positions, respectively. Singh et al. (2009) found a yield for abstraction at the 1-position of 66%, but this was reduced to 45% for pentanal, a value supported by Iwasaki et al. (2008b), who obtained a value of 42%.

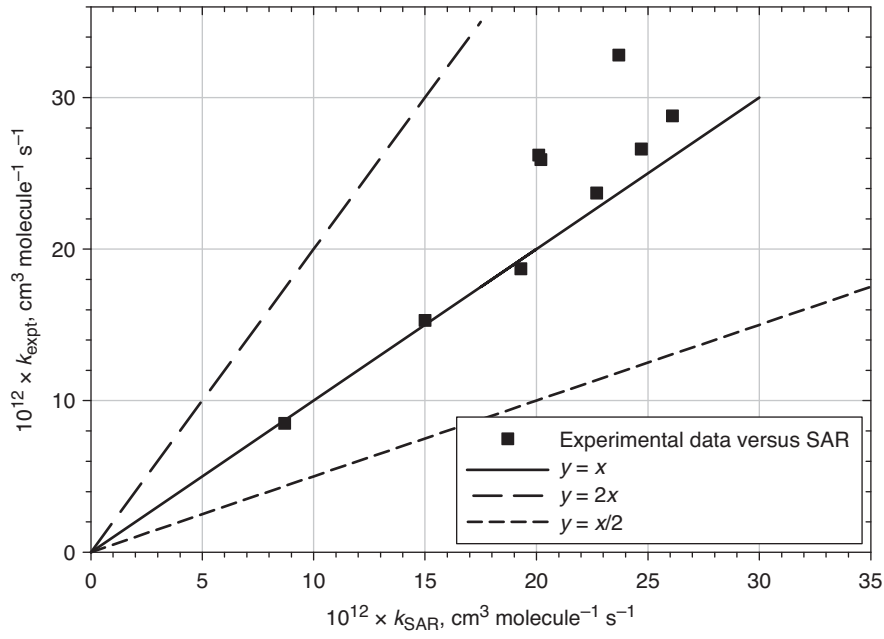

Figure IV-B-11. Comparison of experimental rate coefficients and those calculated using the SAR of Kwok and Atkinson (1995).

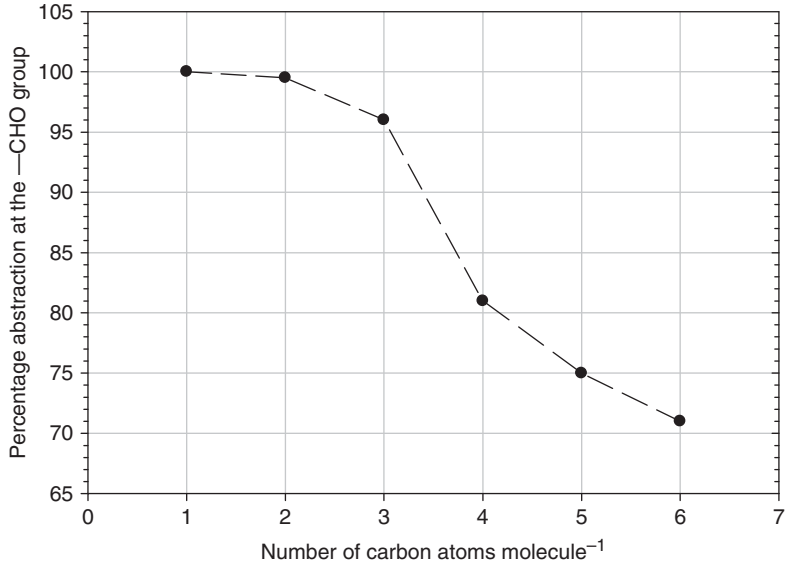

Figure IV-B-12. Percentage abstraction by OH at the —CHO site, according to SAR calculations for straight-chain alkanals.

Figure IV-B-13 shows the mechanism of oxidation of butanal in a polluted atmosphere (high [NO_x], i.e., no peroxy + peroxy radical reactions) following reaction with OH. The minor abstraction reactions at the 2- and 4-positions have been omitted for clarity and the initial channel yields normalized, so that 82% of abstraction occurs at the aldehydic position and 18% at the 2-position.

The peroxybutanoyl radical, formed following abstraction at the 1-position and reaction with O_2, reacts with NO_2 to form peroxybutanoyl nitrate (PBN). At 298 K, the lifetime for dissociation of PBN to regenerate peroxybutanoyl and NO_2 is about 45 min.; even for an NO_2 mixing ratio of only 100 pptv, the ratio of [PBN]:[peroxybutanoyl] is ~80 at equilibrium and the timescale for establishment of the equilibrium is only 30 s. Reaction of PBN with OH to form propanal has a timescale of about 2.5 days for [OH] = 10^6 molecule cm^{-3}, and so is not competitive. The peroxybutanoyl radical also reacts with NO, on a timescale of about 20 s for an NO mixing ratio of 100 pptv and forms the propyl radical and CO_2. After reaction with O_2 and then NO, this reaction channel leads to formation of propanal.

As illustrated on the left of figure IV-B-13, the 3-butanal radical, formed by abstraction at the 3-position, adds O_2 and reacts with NO to give the 3-oxobutanal radical which either dissociates to form acetaldehyde and the CH_2CHO radical, or reacts with O_2 to give $CH_3C(O)CH_2CHO$. The former route dominates under boundary layer conditions, occurring about an order of magnitude faster than the latter. CH_2CHO radicals add O_2 and then react with NO to form an alkoxy radical, which dissociates to give HCHO + CO.

Oxidation mechanisms have been investigated for a number of larger aldehydes, using chamber methods with end product analysis. Tuazon et al. (2003) studied the mechanism of the reaction of OH radicals with 2,3-dimethylpentanal. They found that acetaldehyde and 2-butanone were the main products with a small yield (5.4%) of 3-methyl-2-pentanone. The latter product arises exclusively from abstraction at the 2-position, adjacent to the carbonyl group; the equivalent abstraction is excluded from the butanal mechanism for the sake of clarity.

$$OH + CH_3CH_2CH(CH_3)CH(CH_3)CHO(+O_2) \rightarrow H_2O + CH_3CH_2CH(CH_3)C(O_2)(CH_3)CHO$$

$$CH_3CH_2CH(CH_3)C(O_2)(CH_3)CHO + NO \rightarrow CH_3CH_2CH(CH_3)C(O)(CH_3)CHO + NO_2$$

$$CH_3CH_2CH(CH_3)C(O)(CH_3)CHO \rightarrow HCO + CH_3CH_2CH(CH_3)C(O)(CH_3)$$

OH attack at the aldehyde group should lead either to three acetaldehyde molecules, or to one molecule each of acetaldehyde and 2-butanone via the 2-butoxy radical.

$$OH + CH_3CH_2CH(CH_3)CH(CH_3)CHO(+O_2) \rightarrow H_2O + CH_3CH_2CH(CH_3)CH(CH_3)C(O)O_2$$

$$CH_3CH_2CH(CH_3)CH(CH_3)C(O)O_2 + NO \rightarrow NO_2 + CO_2 + CH_3CH_2CH(CH_3)CH(CH_3)$$

$$CH_3CH_2CH(CH_3)CH(CH_3) + O_2 \rightarrow CH_3CH_2CH(CH_3)CH(O_2)(CH_3)$$

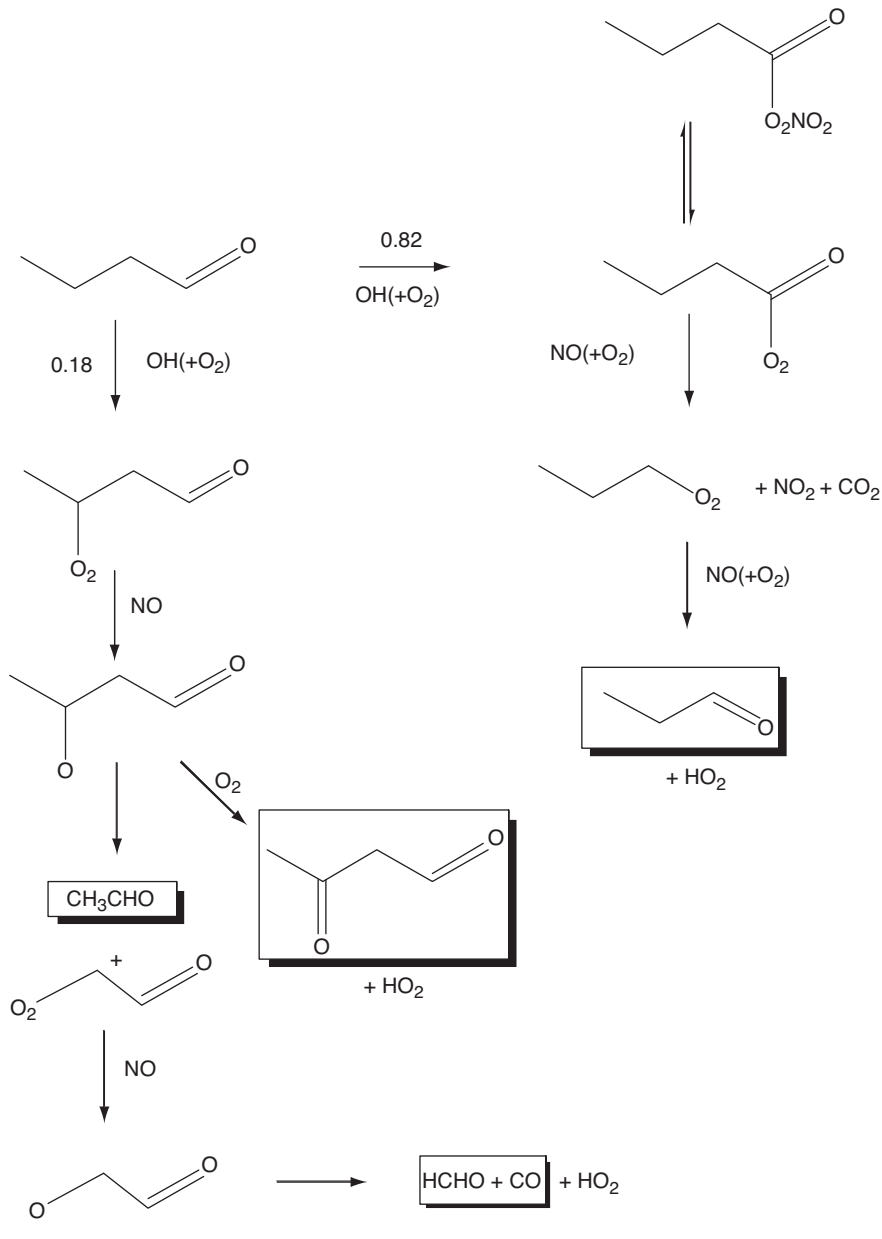

Figure IV-B-13. Major channels in the mechanism for the oxidation of butanal at high NO_x concentrations.

$$CH_3CH_2CH(CH_3)CH(O_2)(CH_3) + NO \rightarrow CH_3CH_2CH(CH_3)CH(O)(CH_3) + NO_2$$

$$CH_3CH_2CH(CH_3)CH(O)(CH_3) \rightarrow CH_3CH_2CH(CH_3) + CH_3CHO$$

$$CH_3CH_2C{\cdot}H(CH_3) + O_2 + NO \rightarrow CH_3CH_2CH(O)(CH_3) + NO_2$$

$$CH_3CH_2CH(O)(CH_3) + O_2 \rightarrow C_2H_5C(O)CH_3 + HO_2$$

$$CH_3CH_2CH(O)(CH_3) \rightarrow CH_3CHO + C_2H_5 \rightarrow\rightarrow 2CH_3CHO$$

Acetaldehyde and 2-butanone are also produced together from abstraction at the 3-position, while attack at the 4-position should lead to three acetaldehyde molecules. These results are broadly consistent with 45–60% abstraction at the aldehyde group, along with a considerable fraction at the 3- and 4-sites (approx 20–30%). The SAR of Atkinson and Kwok (1995) gives results consistent with these conclusions. The overall rate coefficient predicted is 3.0×10^{-11} cm^3 molecule^{-1} s^{-1}, which is lower than, but within the combined uncertainties of that measured by Tuazon et al. (4.2×10^{-11} cm^3 molecule^{-1} s^{-1}). The 3-position is a tertiary carbon and the percentage yield of abstraction at this site calculated from the SAR is 31%, while that at the aldehydic site is 57%.

Similar conclusions can be drawn from measurements on the atmospheric chemistry of nonanal by Bowman et al. (2003). By conducting the oxidation in the presence of excess NO_2 and detecting the PAN-analog formed, they showed that only 50% of the reaction proceeds by abstraction at the aldehydic hydrogen atom.

$$OH + n\text{-}C_8H_{17}CHO \rightarrow H_2O + n\text{-}C_8H_{17}CO$$

$$n\text{-}C_8H_{17}CO + O_2 \rightarrow n\text{-}C_8H_{17}C(O)O_2$$

$$n\text{-}C_8H_{17}C(O)O_2 + NO_2 \rightarrow n\text{-}C_8H_{17}C(O)O_2NO_2$$

Based on the total rate coefficient, this corresponds to a partial rate coefficient for abstraction at the —CHO group of $(1.6–1.7) \times 10^{-11}$ cm^3 molecule^{-1} s^{-1}, which is very similar to the overall rate coefficient for OH + acetaldehyde. This result supports the partial rate coefficient obtained from the SAR of Kwok and Atkinson (1995). The overall rate coefficient calculated from the SAR is 3.0×10^{-11} cm^3 molecule^{-1} s^{-1}, compared with the measured value of 3.2×10^{-11} cm^3 molecule^{-1} s^{-1}. These mechanistic studies confirm the conclusions drawn from the comparison between the experimental and SAR rate coefficients, shown in figure IV-B-11.

IV-C. Hydroxyaldehydes

IV-C-1. Introduction

Hydroxyaldehydes are formed in the atmosphere by the oxidation of multifunctional compounds such as dienes and unsaturated carbonyls. For example, methylvinylketone (MVK) is formed in the oxidation of isoprene. Addition of OH to MVK in the

4-position, followed by addition of O_2 and then reaction with NO generates the oxy radical, which dissociates to form the acetyl radical and hydroxyacetaldehyde:

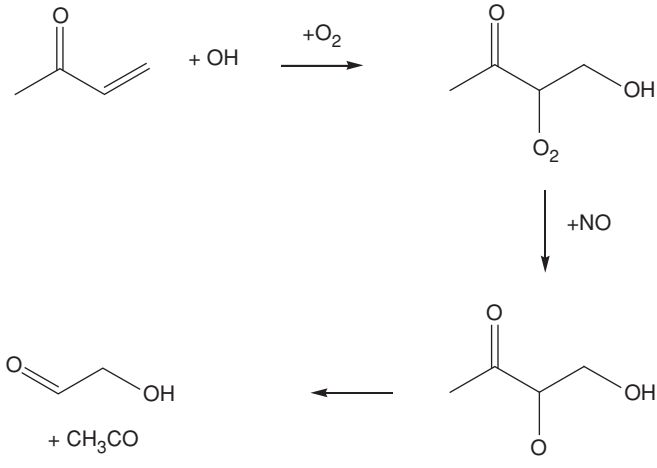

Hydroxyacetaldehyde is also formed as a minor product in the OH-initiated oxidation of ethene via reaction of the 1-oxy-2-hydroxyethyl radical with O_2. For higher alkenes, the equivalent radicals rapidly dissociate to form two aldehydes; e.g., for propene the products are CH_3CHO and CH_2O, and the radicals do not generate hydroxyaldehydes.

IV-C-2. Hydroxyacetaldehyde (Glycolaldehyde, 2-hydroxyethanal, $HOCH_2CHO$)

IV-C-2.1. OH Reaction Kinetics

The experimental data are shown in table IV-C-1. The large number of relative rate determinations by Niki et al. (1987), Bacher et al. (2001), Baker et al. (2004a), and Magneron et al. (2005), range from 7.9×10^{-12} to 13.8×10^{-12} cm^3 molecule^{-1} s^{-1} with a mean value of $k = 11 \times 10^{-12}$ cm^3 molecule^{-1} s^{-1}, while the direct measurements of Butkovskaya et al. (2006a) and Karunanandan et al. (2007) give a mean at 298 K of $k = 8.0 \times 10^{-12}$ cm^3 molecule^{-1} s^{-1}. The measurements of Karunanandan et al. (2007) show that the rate coefficient is independent of temperature over the range 240–362 K. The average of these determinations gives $k = 8.3 \times 10^{-12}$ cm^3 molecule^{-1} s^{-1} with an uncertainty estimated to be ±20% over the temperature range 240–360 K (figure IV-C-1).

IV-C-2.2. Cl-Atom Reaction Kinetics

The relative rate measurements of Niki et al. (1987) and Bacher et al. (2001) are in good agreement, giving an average of $k(298) = 7.3 \times 10^{-11}$ cm^3 molecule^{-1} s^{-1} with an uncertainty of ±20%; see table IV-C-2.

Table IV-C-1. Rate coefficients ($k = A\ e^{-B/T}$, cm^3 $molecule^{-1}$ s^{-1}) for the reaction of OH with hydroxyacetaldehyde ($HOCH_2CHO$)

$10^{12} \times A$	B (K)	$10^{12} \times k$	T (K)	Technique[a]	Reference	Temperature Range (K)
		9.4 ± 0.9	298 ± 2	RR[b] (CH_3CHO)	Niki et al. (1987)	
		11 ± 3	298	RR[c] (propene; CH_3CHO)	Bacher et al. (2001)	
		12.2 ± 2.0	296 ± 2	RR[d] (1,2-butanediol)	Baker et al. (2004)	
		7.9 ± 1.6		RR[e] (2-methyl-3-butenen-2-ol)		
		10.8 ± 0.8	298 ± 3	RR[f] (diisopropyl ether)	Magneron et al. (2005)	
		13.3 ± 1.5		RR[g] (diethyl ether)		
		9.9 ± 0.9		RR[h] (1,3-dioxolane)		
		13.8 ± 1.7		RR[b] (CH_3CHO)		
		8.2 ± 0.4	298	TF–CIMS	Butkovskaya et al. (2006a)	
8.0 ± 0.8	0	8.02 ± 0.19	240	PLP–LIF	Karunanandan et al. (2007)	240–362
		8.06 ± 0.20	243			
		7.80 ± 0.14	245			
		8.40 ± 0.16	248			
		8.01 ± 0.18	250			
		8.12 ± 0.33	253			
		8.02 ± 0.68	254			
		7.89 ± 0.24	255			
		8.28 ± 0.24	258			
		8.14 ± 0.18	263			
		8.26 ± 0.19	268			
		8.15 ± 0.23	274			
		7.59 ± 0.16	275			
		8.89 ± 0.23	278			
		8.04 ± 0.35	280			
		8.80 ± 0.70	280			
		7.86 ± 0.19	289			
		7.54 ± 0.08	296			
		7.94 ± 0.19	296			
		7.91 ± 0.16	297			
		8.84 ± 0.20	297			
		7.89 ± 0.15	297			
		7.20 ± 0.50	298			
		8.40 ± 0.70	299			
		7.74 ± 0.13	298			
		7.58 ± 0.25	300			
		8.17 ± 0.24	304			
		8.08 ± 0.25	311			
		7.69 ± 0.17	316			
		7.92 ± 0.05	324			
		7.59 ± 0.19	324			
		7.69 ± 0.14	332			
		8.68 ± 0.17	337			
		7.74 ± 0.19	338			
		8.46 ± 0.28	338			
		8.40 ± 0.70	338			
		8.32 ± 0.14	339			
		8.03 ± 0.31	343			

(*continued*)

Table IV-C-1. (*continued*)

$10^{12} \times A$	B (K)	$10^{12} \times k$	T (K)	Technique[a]	Reference	Temperature Range (K)
		8.32 ± 0.09	344			
		8.07 ± 0.21	352			
		8.11 ± 0.19	362			

[a]Abbreviations used for the techniques are defined in table I-F-3.

[b]Placed on an absolute basis using $k(\mathrm{OH} + \mathrm{CH_3CHO}) = 1.5 \times 10^{-11}\ \mathrm{cm^3\ molecule^{-1}\ s^{-1}}$ at 298 K (this book, section IV-B-2.1).

[c]A weighted average of measurements: $14.2 \times 10^{-12}\ \mathrm{cm^3\ molecule^{-1}\ s^{-1}}$, placed on an absolute basis using $k(\mathrm{OH} + \mathrm{propene}) = 2.9 \times 10^{-11}\ \mathrm{cm^3\ molecule^{-1}\ s^{-1}}$ at 1 bar and 298 K (Atkinson et al., 2006) and $15.5 \times 10^{-12}\ \mathrm{cm^3\ molecule^{-1}\ s^{-1}}$, placed on an absolute basis using $k(\mathrm{OH} + \mathrm{CH_3CHO}) = 1.5 \times 10^{-11}\ \mathrm{cm^3\ molecule^{-1}\ s^{-1}}$ (298 K); this book, section IV-B-2.1. Final value, given in the table allows for a minor contribution to the loss of glycolaldehyde at the chamber walls.

[d]Placed on an absolute basis using $k(\mathrm{OH} + \text{1,2-butanediol}) = 2.51 \times 10^{-11}\ \mathrm{cm^3\ molecule^{-1}\ s^{-1}}$ at 296 K (this book, table II-C-1).

[e]Placed on an absolute basis using $k(\mathrm{OH} + \text{2-methyl-3-buten-2-ol}) = 6.36 \times 10^{-11}\ \mathrm{cm^3\ molecule^{-1}\ s^{-1}}$ at 296 K (this book, section II-D-10.1).

[f]Placed on an absolute basis using $k(\mathrm{OH} + \text{diisopropyl ether}) = 1.02 \times 10^{-11}\ \mathrm{cm^3\ molecule^{-1}\ s^{-1}}$ at 298 K (this book, section II-B-7.1).

[g]Placed on an absolute basis using $k(\mathrm{OH} + \text{diethyl ether}) = 1.24 \times 10^{-11}\ \mathrm{cm^3\ molecule^{-1}\ s^{-1}}$ at 298 K (this book).

[h]Placed on an absolute basis using $k(\mathrm{OH} + \text{1,3-dioxolane}) = 1.11 \times 10^{-11}\ \mathrm{cm^3\ molecule^{-1}\ s^{-1}}$ at 298 K (this book).

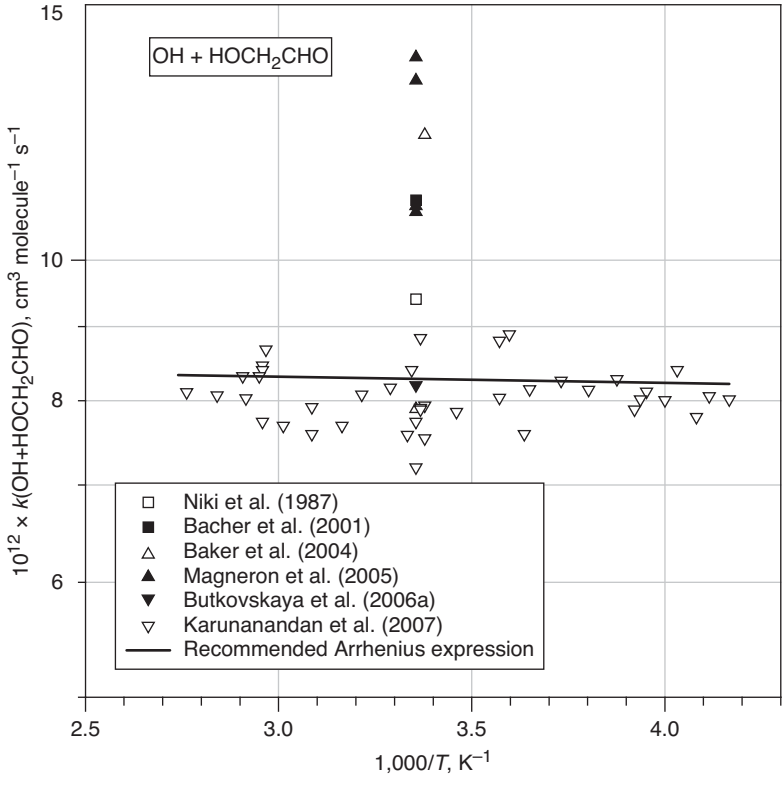

Figure IV-C-1. Arrhenius plot for the rate coefficients for the OH + hydroxyacetaldehyde reaction.

Table IV-C-2. Rate coefficients (k, cm^3 molecule^{-1} s^{-1}) for the reaction of Cl with hydroxyacetaldehyde ($HOCH_2CHO$)

$10^{12} \times k$	T (K)	Technique[a]	Reference
71	298 ± 2	RR[b] (CH_3CHO)	Niki et al. (1987)
76 ± 15	298	RR[c] (CH_3OH)	Bacher et al. (2001)

[a]Abbreviations used for techniques are defined in table I-F-3.

[b]Placed on an absolute basis using $k(Cl + CH_3CHO) = 8.0 \times 10^{-11}$ cm^3 molecule^{-1} s^{-1} at 298 K (this book, section IV-B-2.3).

[c]An average of measurements: 8.0×10^{-11} cm^3 molecule^{-1} s^{-1}, placed on an absolute basis using $k(Cl + CH_3OH) = 5.5 \times 10^{-11}$ cm^3 molecule^{-1} s^{-1} at 298 K (this book, section II-B-1.3) and 7.4×10^{-11} cm^3 molecule^{-1} s^{-1}, placed on an absolute basis using $k(Cl + CH_3CHO) = 8.0 \times 10^{-11}$ cm^3 molecule^{-1} s^{-1} at 298 K (this book, section IV-B-2.3).

IV-C-2.3. Summary of the Atmospheric Fate of Hydroxyacetaldehyde

During the day, the destruction of hydroxyacetaldehyde is by photolysis and reaction with OH. The photolysis lifetime for hydroxyacetaldehyde in the lower troposphere with an overhead Sun is about 19 h; see table IX-M-1. For a diurnal average [OH] of $\approx 1.0 \times 10^6$ molecule cm^{-3}, a lifetime resulting from OH reaction is about 30 h. Bacher et al. (2001) noted that hydroxyacetaldyde is very soluble in water, and that uptake into hydrometers may be an important loss process.

The possible channels for reaction of hydroxyacetaldehyde with OH are:

$$OH + HOCH_2CHO \rightarrow H_2O + HOCH_2CO \quad (1a)$$

$$\rightarrow H_2O + HOCHCHO \quad (1b)$$

$$\rightarrow H_2O + OCH_2CHO \quad (1c)$$

Niki et al. (1987) give fractional yields for channels (1a) and (1b) of 0.80 and 0.20, respectively. Magneron et al. (2005) obtained a yield of 0.22 ± 0.06 for channel (1b). Butkovskaya et al. (2006a) studied the mechanism of the reaction, in the presence of O_2, over the temperature range 233–296 K using a turbulent flow reactor with chemical ionization mass spectrometry. They obtained channel yields for reactions (1a) and (1b) of 0.84 and 0.16, respectively. Abstraction of the hydroxyl H is generally considered negligible. An average yield for channel (1a) is 0.8, with a 20% uncertainty, and the remainder of the reaction occurs via channel (1b). Both Niki et al. (1987) and Bacher et al. (2001) obtained yields of 0.65 and 0.35 for the equivalent of channels (1a) and (1b) in the reaction of Cl with hydroxyacetaldehyde.

The stable intermediates produced in the atmosphere from reactions of the radicals formed in reactions (1a) and (1b) are given in the Master Chemical Mechanism (http://mcm.leeds.ac.uk/MCM/) as formaldehyde and glyoxal, respectively. The system has been studied in detail by Butkovskaya et al. (2006a) at reduced pressure (200 Torr). They observed a yield of 0.18 for formic acid at 296 K, compared with yields of 0.82 for formaldehyde and 0.14 for glyoxal. They found that the yield of formic acid increased as the temperature was reduced, reaching 0.52 at 233 K, where the yields of formaldehyde and glyoxal were 0.50 and 0.041, respectively. They also found strong evidence

for regeneration of OH and formation of HO_2. They interpreted these observations using the following mechanisms for reactions of the radicals formed by abstraction at the 1- and 2-positions:

$$O_2 + HOCH_2CO \rightarrow HO_2 + CH_2O + CO \quad (2a)$$

$$O_2 + HOCH_2CO \rightarrow OH + CH_2O + CO_2 \quad (2b)$$

$$O_2 + HOCH_2CO \rightarrow H + HC(O)OH + CO_2 \quad (2c)$$

where the H-atom formed in channel (2c) reacts with O_2 to form HO_2.

Reaction (2a) occurs by abstraction of H and subsequent dissociation of OCH_2CO. For reactions (2b) and (2c), Butkovskaya et al. proposed the following rearrangements in the *E*- and *Z*-peroxy radicals formed from addition of O_2:

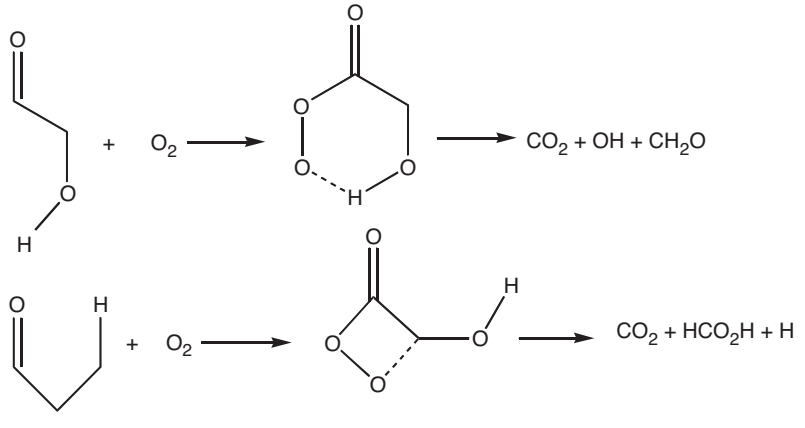

From their product yields, Butkovskaya et al. obtained fractional yields for (2a):(2b):(2c) of 0.58:0.26:0.15 at 296 K.

They proposed that the radical formed in reaction (1b) reacts with O_2 via two channels:

$$HOCHCHO + O_2 \rightarrow HO_2 + (HCO)_2 \quad (3a)$$

$$HOCHCHO + O_2 \rightarrow OH + HC(O)OH + CO \quad (3b)$$

where (3a) occurs via H abstraction and (3b) involves a 5-membered transition state with O_2 bridging across the aldehydic H and the carbon atom at the 2-position. Analysis of the product yields gave the fractional yields (3a):(3b) of 0.81:0.19 at 296 K.

Reactions (2b) and (3b) formally involve H-atom transfer reactions from the —OH and —CHO groups, respectively, to the peroxy group and fragmentation of the hydroperoxide so formed. This type of chemistry is common in reactions of alkyl radicals in hydrocarbon combustion, but at temperatures in the 700–800 K range (Walker and Morley, 1997); this chemistry is responsible for the phenomenon

of autoignition. Its involvement in the chemistry of oxygenated species is becoming recognized increasingly (see, for example, the reactions of the CH_3OCH_2 radical formed from dimethylether). However, it is important to recognize that the relative channel yields of such reactions may depend on pressure and that the experiments of Butkovskaya et al. were performed at 200 Torr N_2, so that the conclusions may not be directly transferrable to atmospheric conditions.

The main fate in the aqueous phase is likely to be oxidation following reaction with radicals, rather than photolysis, because the hydrated form of this compound contains no light-absorbing carbonyl group, $HOCH_2CH(OH)_2$ and is not subject to photolysis within the troposphere. Reaction in the aqueous phase leads to multifunctional compounds, such as glycolic and oxalic acids.

IV-C-3. Other Hydroxyaldehydes

IV-C-3.1. OH Reaction Kinetics

Table IV-C-3 shows rate coefficients obtained by Baker et al. (2004a) for a number of hydroxyaldehydes, using a relative rate technique. The values are in the range (1.4–3.0) $\times 10^{-11}$ cm^3 molecule^{-1} s^{-1}. An uncertainty of $\pm 40\%$ is appropriate since they are all single determinations.

IV-C-3.2. Summary of the Atmospheric Fate of Hydroxyaldehydes

Data from which photolysis lifetimes can be calculated relate only to hydroxyacetaldehyde, but it is anticipated that the larger members of this family will photodecompose on a similar timescale (about 20 h). Their lifetimes with respect to reaction with OH are in the range 4–8 h, for a daytime [OH] of 2.5×10^6 molecule cm^{-3}.

Table IV-C-3. Rate coefficients (k, cm^3 molecule^{-1} s^{-1}) for reaction of OH with 1,2- and 1,3-hydroxycarbonyls at 297 ± 3 K

Molecule	$10^{12} \times k$	Technique[a,b]	Reference
2-Hydroxypropanal	17.0 ± 2.0	RR (2-methyl-3-buten-2-ol)[c]	Baker et al. (2004)
3-Hydroxypropanal	19.9 ± 2.9	RR (*cis*-3-hexen-1-ol)[d]	Baker et al. (2004)
2-Hydroxybutanal	23.7 ± 2.3	RR (1,2-butandiol)[e]	Baker et al. (2004)
3-Hydroxybutanal	29.5 ± 2.4	RR (1,3-butanediol)[f]	Baker et al. (2004)
2-Hydroxy-2-methylpropanal	14.0 ± 2.5	RR (2-methyl-3-buten-2-ol)[g]	Baker et al. (2004)

[a]Abbreviations used for the techniques are defined in table I-F-3.

[b]Analysis involves production and secondary removal of product; rate coefficient does not scale simply with that of the parent compound.

[c]Placed on an absolute basis using k(OH + 2-methyl-3-buten-2-ol) = 6.0×10^{-11} cm^3 molecule^{-1} s^{-1} (this book, section II-D-10.1).

[d]Placed on an absolute basis using k(OH + *cis*-3-hexen-1-ol) = 1.08×10^{-11} cm^3 molecule^{-1} s^{-1} (this book, section II-D-11.1).

[e]Placed on an absolute basis using k(OH + 1,2-butandiol) = 2.51×10^{-11} cm^3 molecule^{-1} s^{-1} (this book, table II-C-1).

[f]Placed on an absolute basis using k(OH + 1,3-butandiol) = 3.09×10^{-11} cm^3 molecule^{-1} s^{-1} (this book, table II-C-1).

[g]Placed on an absolute basis using k(OH + 2-methyl-3-buten-2-ol) = 6.0×10^{-11} cm^3 molecule^{-1} s^{-1} (this book, section II-D-10.1).

IV-D. Dialdehydes

IV-D-1. Introduction

Dialdehydes are important, photochemically reactive intermediates, formed from a wide range of precursors, most importantly isoprene and aromatic hydrocarbons. Glyoxal is formed following reaction of OH with hydroxyacetaldehyde, an intermediate in isoprene oxidation, as discussed previously. Methylglyoxal is formed following reaction of O_3 with both methyl vinyl ketone and methacrolein, major intermediates in isoprene oxidation, and following reaction of methacrolein with OH.

Aromatic oxidation proceeds primarily by addition of OH to the ring to form a hydroxycyclohexadienyl radical (HCHD), which then either reacts with O_2 to form a phenol and HO_2 or adds O_2 to form a peroxy radical. This radical is very short-lived and does not react with NO under normal atmospheric conditions. Instead it isomerizes to form species where the O_2 group bridges the ring and the radical center is on the ring. Subsequent addition of O_2 and reaction with NO leads to ring-opening and dissociation and hence to the formation of coupled pairs of dicarbonyls. For example, in the oxidation of toluene, glyoxal is formed with 4-oxopentenal, while methylglyoxal is formed with butenedial (Bloss et al., 2005).

IV-D-2. Glyoxal [Ethandial, $(HCO)_2$]

IV-D-2.1. OH Reaction Kinetics

The reaction has been studied over the temperature range 210–390 K by Feierabend et al. (2008), using a range of OH sources. Their room temperature value agrees well with the earlier relative rate measurement by Plum et al. (1983), giving an average room temperature value of 9.0×10^{-12} cm^3 molecule^{-1} s^{-1}, with an uncertainty of ±20%; see table IV-D-1. Figure IV-D-1 shows an Arrhenius fit to the data over the temperature range 210–300K, which gives $k(T) = 3.1 \times 10^{-12} \times \exp(318/T)$ cm^3 molecule^{-1} s^{-1}. A fit of the modified Arrhenius expression to the data over the range 210–400 K gives: $k = (6.6 \pm 0.6) \times 10^{-18} T^2 \exp([820 \pm 30]/T)$ cm^3 molecule^{-1} s^{-1}; this is in agreement with Feierabend et al, who showed that the rate coefficients for OD and OH + $(CHO)_2$ are indistinguishable, within experimental error, over the temperature range 293–390 K.

IV-D-2.2. O_3 Reaction Kinetics

Plum et al. (1983) obtained an upper limit of 3×10^{-21} cm^3 molecule^{-1} s^{-1} for the rate coefficient for the reaction of O_3 with glyoxal, using chemiluminescence to monitor the decay of ozone in excess glyoxal.

IV-D-2.3. Cl-Atom Reaction Kinetics

Niki et al. (1985a) measured the rate coefficient for Cl + $(CHO)_2$ using a relative rate method, obtaining a value of 3.6×10^{-11} cm^3 molecule^{-1} s^{-1} at 298 K,

Table IV-D-1. Rate coefficients (k, cm^3 molecule^{-1} s^{-1}) for the reaction of OH with glyoxal [HC(O)C(O)H]

$10^{12} \times A$	B (K)	$10^{12} \times k$	T (K)	Technique[a]	Reference	Temperature Range (K)
		10.6 ± 0.4	298 ± 2	RR[b]	Plum et al. (1983)	
$(6.6 \pm 0.6) \times 10^{-6}T^2$	820 ± 30	12.3 ± 0.29	240	PLP–LIF[c]	Feierabend et al. (2008)	210–390
		11.7 ± 0.29	247			
		9.67 ± 0.30	257			
2.8 ± 0.7	340 ± 50	9.47 ± 0.25	281			
(210–296 K)	(210–296 K)	9.15 ± 0.8	296			
		8.70 ± 0.27	317			
		8.60 ± 0.27	343			
		8.21 ± 0.18	367			
		8.27 ± 0.23	388			
		8.15 ± 0.27	388			
		8.24 ± 0.25	391			
		14.2 ± 0.32	209	PLP–LIF[d]		
		14.0 ± 0.53	211			
		13.5 ± 0.59	221			
		12.1 ± 0.53	231			
		11.7 ± 0.50	241			
		10.0 ± 0.86	255			
		9.39 ± 0.87	268			
		8.88 ± 0.40	296			
		8.47 ± 0.33	323			
		8.08 ± 1.00	388			

[a]Abbreviations used for the techniques are defined in table I-F-3.
[b]Placed on an absolute basis using $k(\text{OH} + \text{cyclohexane}) = 6.97 \times 10^{-12}$ cm^3 molecule^{-1} s^{-1} at 298 K (Calvert et al., 2008).
[c]Using H_2O_2 as the source of OH.
[d]Using N_2O/CH_4 as the source of OH.

They used CH_2O as the reference compound with $k(\text{Cl} + CH_2O) = 7.0 \times 10^{-11}$ cm^3 molecule^{-1} s^{-1} (section IV-B-1.3). Given the absence of confirmatory measurements, we estimate an uncertainty of ±40%.

IV-D-2.4. Summary of the Atmospheric Fate of Glyoxal

Glyoxal mainly reacts by photolysis (1.8–2.2 h for an overhead Sun; see chapter IX). For a diurnal average [OH] $= 1.0 \times 10^6$ molecule cm^{-3}, its lifetime for reaction with OH is about 28 h.

The immediate product of reaction with both OH and Cl is the radical CHOCO. Niki et al. (1985) proposed that, when formed from Cl + $(CHO)_2$, this radical has a lifetime less than 10^{-7} s. Orlando and Tyndall (2001) found that, when formed from reaction of OH with glyoxal under atmospheric conditions, the dissociation of HCOCO competes with reaction with O_2. Assuming a rate coefficient of 10^{-11} cm^3 molecule^{-1} s^{-1} for the latter, they obtained a rate coefficient for dissociation of HC(O)CO of $1.4 \times 10^{12} \exp(-3{,}160/T)$ s^{-1}, corresponding to a lifetime of 4×10^{-8} s

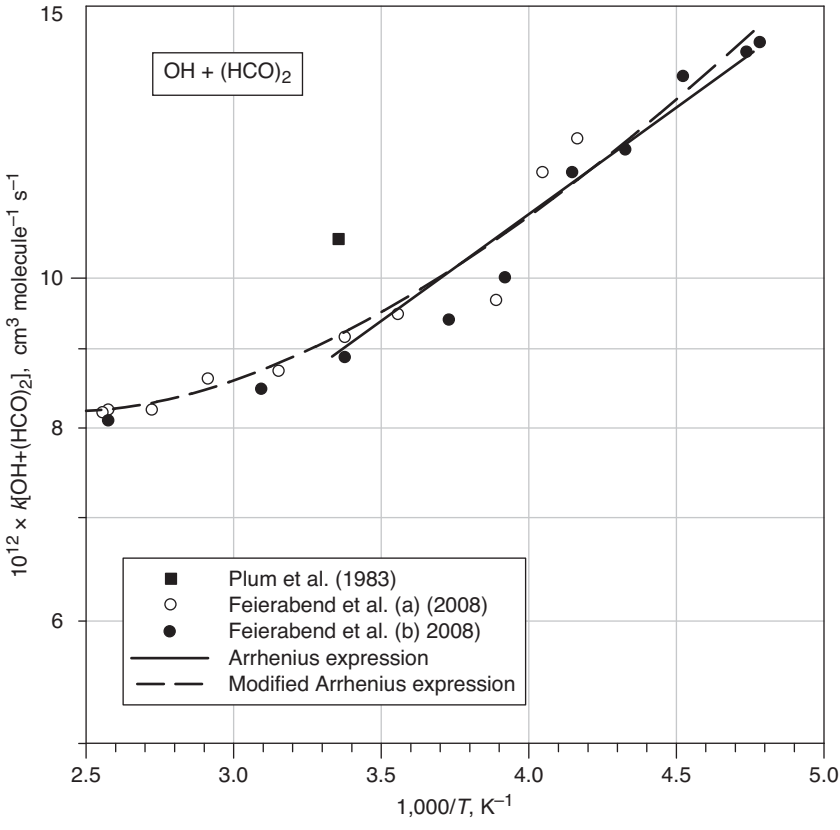

Figure IV-D-1. Arrhenius plot for the rate coefficients for the OH + glyoxal reaction. Feierabend et al. (2008) used two different sources of OH: (a) H_2O_2 photolysis, (b) N_2O photolysis in the presence of CH_4.

at 298 K. Under atmospheric conditions, at the Earth's surface, the two reactions:

$$HC(O)CO + O_2 \rightarrow HC(O)C(O)O_2$$

$$HC(O)CO \rightarrow HCO + CO$$

have comparable rates. It is generally supposed that the peroxy radical reacts with NO to form an oxy radical, which dissociates to form HCO + CO_2. Feierabend et al. (2008) found that, in the presence of O_2, OH was regenerated under their reaction conditions (45–300 Torr He, N_2), which is not consistent with the reaction mechanism for HC(O)CO proposed by Orlando and Tyndall (2001). Such a reaction could occur by formation of the hydroperoxide via a 5-membered transition state with H being transferred from the remaining aldehydic group to the peroxy group. Dissociation of the hydroperoxide would generate OH + CO_2+ CO.

IV-D-3. Methylglyoxal [$CH_3C(O)CHO$]

IV-D-3.1. OH Reaction Kinetics

The rate data for the OH-methylglyoxal reaction by Kleindienst et al. (1982) and of Plum et al. (1983) differ by over a factor of 2. The more recent measurements of Tyndall et al. (1995) by discharge flow and by Baeza-Romero et al. (2007) by pulsed photolysis lie between the earlier determinations and agree well with one another; see table IV-D-2 and figure IV-D-2. The mean of these two measurements at 298 K is 1.30×10^{-11} cm^3 molecule^{-1} s^{-1}, which lies close to the mean of the earlier measurements. The temperature dependent measurements of Tyndall et al. and of Baeza Romero et al. agree well and give an overall expression $k(T) = 1.82 \times 10^{-12} \times \exp(585/T)$ cm^3 molecule^{-1} s^{-1}.

IV-D-3.2. O_3 Reaction Kinetics

Plum et al. (1983) obtained an upper limit of 6×10^{-21} cm^3 molecule^{-1} s^{-1} for the rate coefficient for the reaction of O_3 with methylglyoxal, using chemiluminescence to monitor the decay of ozone in excess methylglyoxal.

IV-D-3.3. Cl-Atom Reaction kinetics

Green et al. (1990) determined the rate coefficient at 298 K, relative to that for ethane. Using $k(Cl+C_2H_6) = 5.9 \times 10^{-11}$ cm^3 molecule^{-1} s^{-1} gives $k(298) = 5.0 \times 10^{-11}$ cm^3 molecule^{-1} s^{-1} with an uncertainty of $\pm 40\%$ since this is the only measurement.

Table IV-D-2. Rate coefficients ($k = A \times e^{-B/T}$, cm^3 molecule^{-1} s^{-1}) for reaction of OH with methylglyoxal [$CH_3C(O)C(O)H$]

$10^{12} \times A$	B (K)	$10^{12} \times k$	T (K)	Technique[a]	Reference	Temperature Range (K)
		7.1 ± 1.6	297	PP–RF	Kleindienst et al. (1982)	
		16.0 ± 1.2	298 ± 2	RR[b]	Plum et al. (1983)	
0.84	830 ± 300	19.6 ± 2.5	260	DF–LIF	Tyndall et al. (1995)	260–333
		18.4 ± 2.5	273			
		13.2 ± 1.5	298			
		10.1 ± 1.5	333			
1.83 ± 0.48	560 ± 70	21.3 ± 2.4	223	PLP–LIF	Baeza-Romero et al. (2007)	233–500
		21.0 ± 1.8	233			
		18.5 ± 0.8	243			
		18.7 ± 7.0	253			
		17.7 ± 3.5	263			
		16.1 ± 3.3	273			
		14.5 ± 2.3	288			
		12.8 ± 2.7	318			
		9.4 ± 0.5	366			
		7.6 ± 1.0	409			
		8.1 ± 0.5	470			
		5.1 ± 1.5	500			

[a]Abbreviations used for the techniques are defined in table I-F-3.
[b]Placed on an absolute basis using $k(\text{OH} + \text{cyclohexane}) = 6.97 \times 10^{-12}$ cm^3 molecule^{-1} s^{-1} (Calvert et al., 2008).

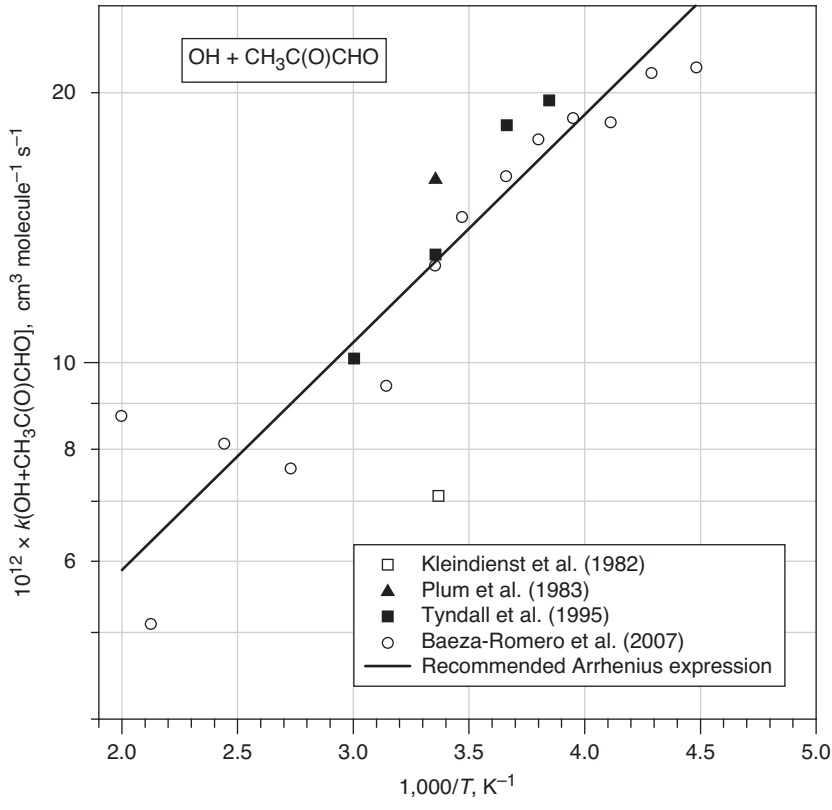

Figure IV-D-2. Arrhenius plot for the rate coefficients for the OH + methylglyoxal reaction.

IV-D-3.4. Summary of the Atmospheric Fate of Methylglyoxal

Photolysis lifetime is estimated to be about 1.9 h with an overhead Sun; see chapter IX. For a diurnal average [OH] = 1.0×10^6 molecule cm^{-3}, its lifetime for reaction with OH is about 25 h.

Reaction occurs exclusively by abstraction of the aldehydic H-atom to form $CH_3C(O)CO$, which has a very short lifetime, dissociating to form $CH_3CO + CO$ (Green et al., 1990). This conclusion is supported by the observation of OH regeneration from the reaction of acetyl + O_2, in the studies of Tyndall et al. (1995) and Baeza-Romero et al. (2007). The reaction forms an energized acetyl peroxy radical that can dissociate to form OH at low pressures (Michael et al., 1985; Tyndall et al., 1995; Blitz et al., 2002). Collisional stabilization of the acetyl peroxy radical leads to a reduction in the OH yield with increasing pressure; Tyndall et al. found no evidence of OH regeneration in chamber experiments at atmospheric pressure.

The results of Baeza-Romero et al. (2007) indicate that regeneration of OH from CH_3CO at low pressures is less than expected; they suggested that the CH_3CO might have enough energy to dissociate further giving $CH_3 + CO$; $CH_3 + O_2$ does not form OH. They supported these conclusions with *ab initio* and energy disposal/

master equation calculations, that showed that, if the energy disposal in the OH + $CH_3C(O)CHO$ and $CH_3C(O)CO$ dissociation reactions is statistical, then about half of the acetyl radicals formed have sufficient energy to dissociate. These conclusions need confirmation. Note that Butkovskaya and Setser (2003) found, from observation of H_2O chemiluminescence, that about half of the energy release in OH + aldehyde reactions is located in H_2O vibrations.

IV-D-4. Unsaturated Dialdehydes

Unsaturated dialdehydes are included in this section, rather than the following one on unsaturated aldehydes, because of their close relationship with glyoxal and methylglyoxal, especially through their roles as co-products in the oxidation of some aromatic compounds. 4-oxo-2-pentenal is included for the same reason (see also section V-E-11).

IV-D-4.1. OH Reaction Kinetics

Table IV-D-3 shows the rate coefficients determined using relative rate techniques for *Z*- and *E*- butenedials and 4-oxo-2-pentenal (*E* and *Z* were not differentiated) by Bierbach et al. (1994) and for two hexadienedials and (*E*-,*E*-) 2-methyl-hexadienedial by Klotz et al. (1995, 1999). The 1995 study was made in a quartz-glass laboratory chamber, while the 1999 study used the EUPHORE large outdoor chamber at Valencia in Spain. An improved method was used in the latter analysis of the overlapping isomer IR spectra and this may account for some differences. The means of the published values, $k(E,E\text{-})$ 2,4-hexadienedial) $= 8.2 \times 10^{-11}$ and $k(Z\text{-},E\text{-})$ 2,4-hexadienedial) $= (9.2 \pm 4) \times 10^{-11}$ cm^3 molecule^{-1} s^{-1}, are recommended with uncertainties of ±40%.

IV-D-4.2. O_3 Reaction Kinetics

Klotz et al. (1995) carried out a preliminary study on the reaction of O_3 with *E*-,*E*-2,4-hexadienedial, relative to ethene and propene. Radical scavengers were not used in the experiments and an upper limit of $k(298\text{ K}) < 10^{-17}$ cm^3 molecule^{-1} s^{-1} was reported.

Table IV-D-3. Rate coefficients (k, cm^3 molecule^{-1} s^{-1}) for the reaction of OH with unsaturated dialdehydes and 4-oxo-2-pentenal

Compound	$10^{12} \times k$	T (K)	Technique[a]	Reference
Z-Butenedial	57 ± 1	296 ± 2	RR[b]	Bierbach et al. (1994)
E-Butenedial	≥ 26 ± 8	296 ± 2	RR[b]	Bierbach et al. (1994)
E-/*Z*-4-Oxo-2-pentenal	61 ± 2	296 ± 2	RR[b]	Bierbach et al. (1994)
E-,*E*-2,4-Hexadienedial	88 ± 3	298 ± 2	RR[c]	Klotz et al. (1995)
E-,*E*-2,4-Hexadienedial	76 ± 8	298 ± 3	RR[c]	Klotz et al. (1999)
E-,*Z*-2,4-Hexadienedial	109 ± 11	298 ± 2	RR[c]	Klotz et al. (1995)
E-,*Z*-2,4-Hexadienedial	74 ± 19	298 ± 3	RR[c]	Klotz et al. (1999)
E-,*E*-2-Methyl 2,4-Hexadienedial	118 ± 2	298 ± 2	RR[c]	Klotz et al. (1995)

[a]Abbreviations used for the techniques are defined in table I-F-3.
[b]Placed on an absolute basis using $k(\text{OH} + \text{propene}) = 2.9 \times 10^{-11}$ cm^3 molecule^{-1} s^{-1} (Atkinson et al., 2006).
[c]Placed on an absolute basis using $k(\text{OH} + \textit{trans}\text{-2-butene}) = 6.4 \times 10^{-11}$ cm^3 molecule^{-1} s^{-1} (IUPAC, 2008).

IV-D-4.3. Summary of the Atmospheric Fate of Unsaturated Dialdehydes

Approximate photolysis lifetimes for the 2,4-hexadienedials with an overhead Sun are in the range of 1–2 h; see section IX-C-10. For a daytime average [OH] of 2.5×10^6 molecule cm^{-3}, the lifetimes with respect to reaction with OH are also in the range of 1–2 h.

There is a good deal of uncertainty over the mechanisms of reaction of these compounds with OH under atmospheric conditions. A major difficulty is the commercial unavailability of the compounds, so that they have to be custom synthesized; impurities and difficulties in determining the stereochemistry, coupled with their high reactivity present additional challenges. The major products found by Bierbach et al. (1992) for butenedial are glyoxal, maleic anhydride, and 3-H-furan-2-one. Glyoxal was expected to be the major product, but it was not possible to quantify its yield because of the presence of impurities. Figure IV-D-3 shows the mechanism from the Master Chemical Mechanism (http://mcm.leeds.ac.uk/MCM/), which accounts for all of these products, except the furanone. The major channel involves abstraction of one of the aldehydic hydrogen atoms followed by reaction with O_2 to form the peroxy radical. There are two dissociation channels open to the oxy radical formed following reaction with NO, leading to two of the major observed products.

The main products observed by Bierbach et al. (1992) following reaction of OH with 4-oxo-2-pentenal under atmospheric conditions were maleic anhydride, 5-methyl-3H-furanone, glyoxal, and methylglyoxal. Quantification was not feasible because of the presence of impurities.

Klotz et al. (1995) showed that *E*-butenedial, glyoxal, CH_2O, and CO are major products of the OH-initiated oxidation of both *E*-,*Z*- 2,4-hexadienedial and *E*-,*E*- 2,4-hexadienedial. A mechanism was proposed involving only addition of OH to the double bonds, followed by fragmentation of the alkoxy radical formed following peroxy radical formation and reaction with NO.

IV-E. Unsaturated Aldehydes

IV-E-1. Introduction

Unsaturated aldehydes are important intermediates in the oxidation of volatile organic compounds. One of the most important is methacrolein, $CH_2{=}C(CH_3)CHO$, which is formed in substantial quantities as a first generation intermediate in the oxidation of isoprene. The mechanism of its formation in the presence of NO_x, involves terminal addition of OH to the nonmethyl-substituted double bond, followed by reaction with O_2 and NO to form the oxy radical, which dissociates to form methacrolein:

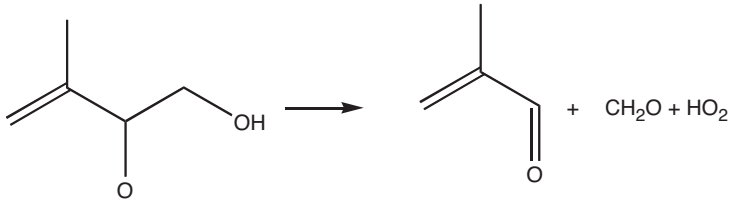

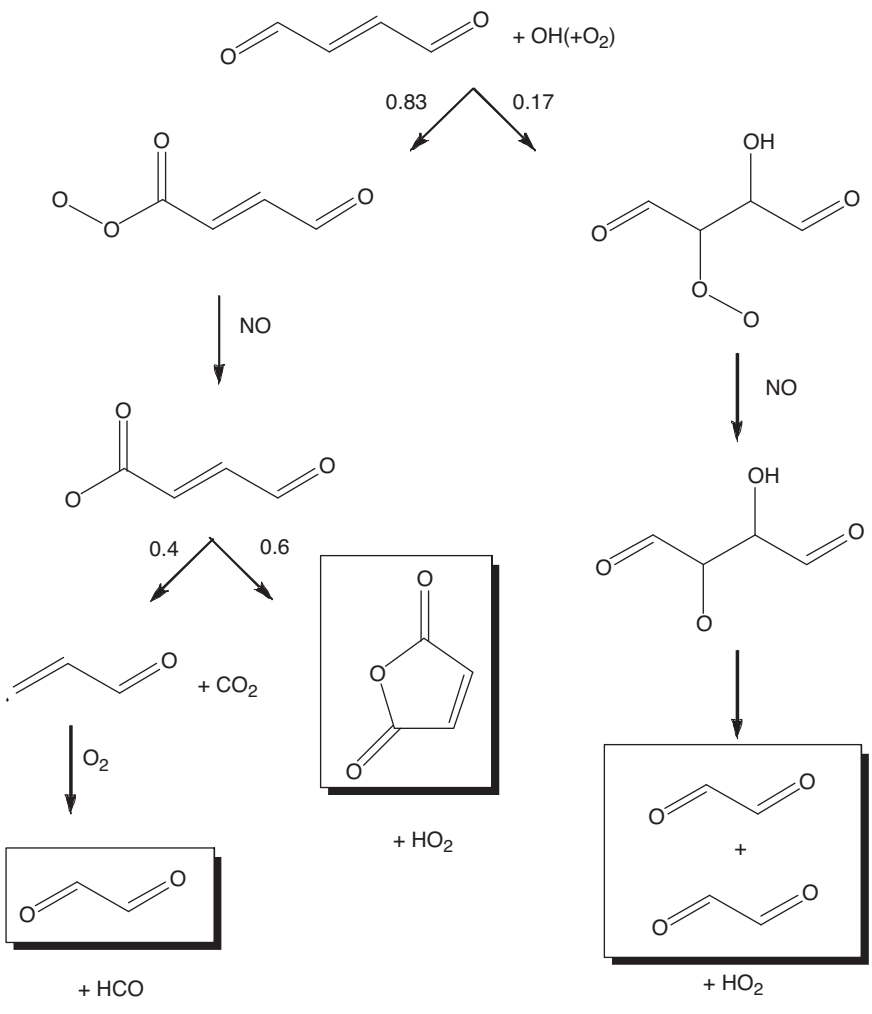

Figure IV-D-3. Postulated mechanism of oxidation of E-butenedial.

A similar mechanism leads to the formation of acrolein, CH_2=CHCHO, from 1,3-butadiene. Unsaturated aldehydes are also directly emitted to the atmosphere, for example crotonaldehyde, CH_3CH=CHCHO, is emitted in substantial quantities from noncatalyst-equipped gasoline and diesel vehicles (see chapter I).

IV-E-2. Acrolein (2-Propenal, CH_2=CHCHO)

IV-E-2.1. OH Reaction Kinetics

The reaction between OH and acrolein has been studied at room temperature by Maldotti et al. (1980), Kerr and Sheppard (1981), Atkinson et al. (1983b), Edney et al. (1986), and Ullerstam et al. (2001) using relative rate techniques, and by Magneron

et al. (2002) using pulsed laser photolysis coupled to laser induced fluorescence; see table IV-E-1. The measurements are in good agreement, giving a mean value at 298 K of 2.16×10^{-11} cm^3 molecule^{-1} s^{-1}, with an uncertainty of ±20%. The only temperature dependent study is that by Magneron et al. (2002), over the temperature range 243–373 K. Using this dependence with the mean 298 K value gives $k(T) = 7.1 \times 10^{-12}$ exp(333/T) cm^3 molecule^{-1} s^{-1}.

IV-E-2.2. O_3 Reaction Kinetics

The kinetics of O_3 + acrolein have been investigated by Atkinson et al. (1981) using chemiluminscence and by Treacy et al. (1992) using UV absorption. The measurements agree well, giving an unweighted mean value at 298 K of 2.9×10^{-19} cm^3 molecule^{-1} s^{-1}, with an uncertainty of ±30%. Grosjean and Grosjean (1993a) also measured the rate coefficient at 286 K, using UV absorption and obtained 2.6×10^{-19} cm^3 molecule^{-1} s^{-1}; see table IV-E-2.

Table IV-E-1. Rate coefficients ($k = A \times e^{-B/T}$, cm^3 molecule^{-1} s^{-1}) for reaction of OH with acrolein (CH_2=CHCHO)

$10^{12} \times A$	B (K)	$10^{10} \times k$	T (K)	Technique[a]	Reference	Temperature Range (K)
		19 ± 2	298	RR[b] (ethene)	Kerr and Sheppard (1981)	
		21 ± 1	299	RR[c] (propene)	Atkinson et al. (1983b)	
		23 ± 3	298	RR[d] (n-C_4H_{10})	Maldotti et al. (1980)	
		22.3 ± 0.1	298	RR[c] (propene)	Edney et al. (1986)	
		24 ± 2	298	RR[c] (propene)	Ullerstam et al. (2001)	
6.55 ± 1.22	−333 ± 54	26.6 ± 0.4	243	PLP–LIF	Magneron et al. (2002)	243–373
		25.3 ± 0.9	253			
		22.6 ± 0.7	273			
		20.1 ± 0.7	298			
		18.4 ± 0.6	323			
		18.0 ± 0.5	348			
		16.8 ± 0.3	372			

[a]Abbreviations used for the techniques are defined in table I-F-3.
[b]Placed on an absolute basis using $k(OH + C_2H_4) = 7.9 \times 10^{-12}$ cm^3 molecule^{-1} s^{-1} (Atkinson et al., 2006).
[c]Placed on an absolute basis using $k(OH + C_3H_6) = 2.9 \times 10^{-11}$ cm^3 molecule^{-1} s^{-1} (Atkinson et al., 2006).
[d]Placed on an absolute basis using $k(OH + n$-butane$) = 2.35 \times 10^{-11}$ cm^3 molecule^{-1} s^{-1} (IUPAC, 2008).

Table IV-E-2. Rate coefficients (k, cm^3 molecule^{-1} s^{-1}) for reaction of O_3 with acrolein (CH_2=CHCHO)

$10^{20} \times k$	T (K)	Technique[a]	Reference
28 ± 5	296	Chemiluminescence	Atkinson et al. (1981)
30 ± 4	298	UV abs.	Treacy et al. (1992)
26 ± 5	286	UV abs.	Grosjean and Grosjean (1993)

[a]Abbreviations used for the techniques are defined in table I-F-3.

IV-E-2.3. NO_3 Reaction Kinetics

Relative rate measurements on the NO_3 + acrolein reaction have been made by Atkinson et al. (1987a), Canosa-Mas et al. (1999a), and Ullerstam et al. (2001). Canosa-Mas et al. (1999a) also measured the rate constant at 298 K, using discharge flow with laser induced fluorescence. Cabañas et al. (2001b) and Salgado et al. (2008) used the same technique to measure the temperature dependence. See table IV-E-3 and figure IV-E-1. There is substantial disagreement in the room temperature measurements. Canosa-Mas et al. (1999a) suggested that there were possible interferences in their discharge flow measurements and that their relative rate method gave a more reliable determination. Taking an unweighted mean of the three relative rate values gives $k(298) = 1.15 \times 10^{-15}$ cm^3 molecule^{-1} s^{-1}, with an uncertainty of ±40%, given the discrepancy from the discharge flow measurements. The temperature dependences obtained by Cabañas et al. (2001b) and Salgado et al. (2008) differ substantially, although their determinations agree quite well at 298 K. The data of Salgado et al. suggest that there is a change of slope of the ln(k) versus 1/T plot above this temperature, possibly indicating a change of mechanism. In view of the difficulties referenced in section IV-B regarding the measurements of Cabañas et al., the discrepancies between the discharge flow and relative rate measurements, and the comments of Canosa-Mas et al., it is not possible to recommend a reliable temperature dependence under atmospheric conditions until further studies have been conducted.

IV-E-2.4. Cl-Atom Reaction Kinetics

Relative rate methods have been used by Thévenet et al. (2000), Ullerstam et al. (2001), Canosa-Mas et al. (2001), and Wang et al. (2002). Canosa-Mas et al. (2001) used a discharge flow–resonance fluorescence method at room temperature, while

Table IV-E-3. Rate coefficients ($k = A \times e^{-B/T}$, cm^3 molecule^{-1} s^{-1}) for reaction of NO_3 with acrolein (CH_2=CHCHO)

$10^{15} \times A$	B (K)	$10^{15} \times k$	T (K)	Technique[a]	Reference	Temperature Range (K)
		1.1 ± 0.6	298	RR[b] (ethene)	Atkinson et al. (1987a)	
		1.25 ± 0.4	296	RR[b] (ethene)	Canosa-Mas et al. (1999a)	
		8.9 ± 2.8	293	DF–LIF	Canosa-Mas et al. (1999a)	
			303			
		1.1 ± 0.2	297	RR[c] (propene)	Ullerstam et al. (2001)	
170 ± 320	3,232 ± 355	2.5 ± 0.4	298	DF–LIF	Cabanas et al. (2001b)	298–433
		15.0 ± 3.2	345			
		48.5 ± 3.7	389			
		83.7 ± 6.6	433			
172 ± 50[d]	1,190 ± 43[d]			DF–LIF	Salgado et al. (2008)	249–330

[a]Abbreviations used for the techniques are defined in table I-F-3.
[b]Placed on an absolute basis using $k(NO_3 + \text{ethene}) = 2.1 \times 10^{-16}$ cm^3 molecule^{-1} s^{-1} (Atkinson et al., 2006).
[c]Placed on an absolute basis using $k(NO_3 + \text{propene}) = 9.5 \times 10^{-15}$ cm^3 molecule^{-1} s^{-1} (Atkinson et al., 2006).
[d]From temperature dependent rate data which were not published.

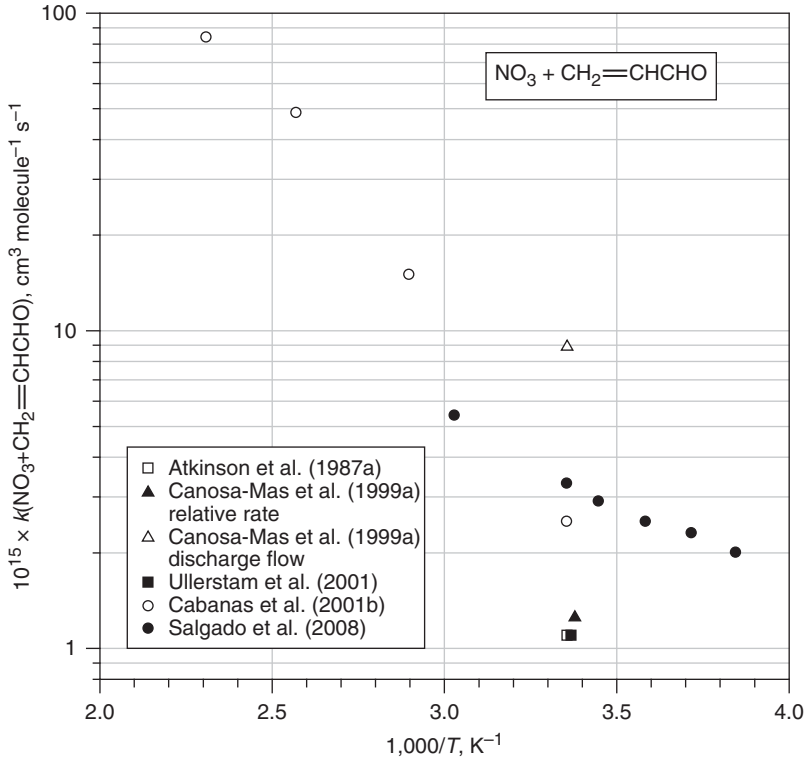

Figure IV-E-1. Arrhenius plot for the rate coefficients for the NO_3 + acrolein reaction.

Aranda et al. (2003a) used discharge flow–mass spectrometry over the temperature range 260–333 K. The discharge flow measurements were conducted at pressures of 1–4.5 Torr; the relative rate measurements were made at atmospheric pressure. Canosa-Mas et al. suggested that there is a significant difference between the high and low pressure experiments, and this is confirmed by inspection of table IV-E-4. Taking only the relative rate measurements gives an unweighted mean value of 2.23×10^{-10} cm^3 molecule^{-1} s^{-1} with an uncertainty of $\pm 15\%$. Aranda et al. (2003a) obtained a branching ratio for abstraction at 1 Torr of 83 $\pm$ 13%, while Canosa-Mas et al. (2001) obtained a value of 22 $\pm$ 13%, at 760 Torr, further confirming that the reaction is pressure dependent with the addition channel dominating under atmospheric conditions. The temperature dependence determined by Aranda et al. does not, therefore, apply under atmospheric conditions, and it is not possible at this stage to give a temperature dependence appropriate to tropospheric oxidation.

IV-E-2.5. O(^{3}P) Reaction Kinetics

Gaffney et al. (1975) studied the reaction between O(^{3}P) and acrolein, using a relative rate technique over the temperature range 296–423 K. They obtained

Table IV-E-4. Rate coefficients ($k = A \times e^{-B/T}$, cm^3 $molecule^{-1}$ s^{-1}) for reaction of Cl with acrolein (CH_2=CHCHO)

$10^{10} \times A$	B (K)	$10^{10} \times k$	T (K)	Technique[a]	Reference	Temperature Range (K)
		2.37	298	RR[b] (ethane)	Thévenet et al. (2000)	
		2.26		RR[c] (propane)		
		2.07		RR[d] (*n*-butane)		
		2.04		RR[e] (*n*-hexane)		
		1.8 ± 0.3	298	RR[f] (propene)	Ullerstam et al. (2001)	
		11 ± 0.2 (1.6 Torr)	298	DF–RF	Canosa-Mas et al. (2001)	
		1.4 ± 0.4 (4.5 Torr)				
		2.2 ± 0.3	298	RR[c] (propane)	Canosa-Mas et al. (2001)	
		2.7 ± 0.6	298	RR[g] (ethyne)	Wang et al. (2002)	
		2.4 ± 0.4	298	RR[d] (*n*-butane)		
0.93 ± 9.7	149 ± 297	0.50 ± 0.06 (1 Torr)	260	DF–MS	Aranda et al. (2003a)	260–333
		0.59 ± 0.06 (1 Torr)	280			
		0.50 ± 0.03 (0.5 Torr)	280			
		0.50 ± 0.09 (1 Torr)	298			
		0.48 ± 0.07 (3 Torr)	298			
		0.59 ± 0.08 (1 Torr)	315			
		0.58 ± 0.09 (1 Torr)	333			

[a]Abbreviations used for the techniques are defined in table I-F-3.
[b]Placed on an absolute basis using $k(Cl + ethane) = 5.9 \times 10^{-11}$ cm^3 $molecule^{-1}$ s^{-1} (Atkinson et al., 2006).
[c]Placed on an absolute basis using $k(Cl + propane) = 1.4 \times 10^{-10}$ cm^3 $molecule^{-1}$ s^{-1} (Atkinson et al., 2006).
[d]Placed on an absolute basis using $k(Cl + n\text{-butane}) = 2.05 \times 10^{-10}$ cm^3 $molecule^{-1}$ s^{-1} (Atkinson et al., 2006).
[e]Placed on an absolute basis using $k(Cl + n\text{-hexane}) = 3.3 \times 10^{-10}$ cm^3 $molecule^{-1}$ s^{-1} (Calvert et al., 2008).
[f]Placed on an absolute basis using $k(Cl + propene) = 2.3 \times 10^{-10}$ cm^3 $molecule^{-1}$ s^{-1} (IUPAC, 2008).
[g]Placed on an absolute basis using $k(Cl + ethyne) = 5.2 \times 10^{-11}$ cm^3 $molecule^{-1}$ s^{-1} (Atkinson et al., 2006).

$k(T) = 2.32 \times 10^{-11} \times \exp(-1{,}210/T)$ cm^3 $molecule^{-1}$ s^{-1} and $k(296\ K) = 3.85 \times 10^{-13}$ cm^3 $molecule^{-1}$ s^{-1}, to which an uncertainty of ±40% should be attached.

IV-E-2.6. Summary of the Atmospheric Fate of Acrolein and the End Products of Its Oxidation

During the day, the destruction of acrolein is controlled primarily by photolysis and reaction with OH. The photolysis lifetime is about 8 days for an overhead Sun; see chapter IX. For $[OH] \approx 2.5 \times 10^6$ molecule cm^{-3}, its lifetime with respect to reaction with OH is about 5 h.

Orlando and Tyndall (2002) carried out an extensive analysis of the products of the OH-initiated oxidation of acrolein in synthetic air, with added NO, at a total pressure of 1 atm. The main products were CO_2, CO, CH_2O, hydroxyacetaldehyde, and the PAN species peroxyacryloyl nitrate. They obtained an excellent carbon balance of 97 ± 7%. On the basis of the product yields, they showed that abstraction (channel 1c) accounts for ∼ 68 ± 8% of the initial reaction of OH with acrolein, while the main addition

channel involves the terminal site (1a):

$$CH_2{=}CHCHO + OH(+O_2) \rightarrow HOCH_2CH(OO)CHO \quad (1a)$$

$$\rightarrow OOCH_2CH(OH)CHO \quad (1b)$$

$$\rightarrow CH_2{=}CHC(O)OO + H_2O \quad (1c)$$

They suggested that the oxy radical formed from the reaction of the $HOCH_2CH(OO)CHO$ with NO dissociates to generate CO, CH_2O, and hydroxyacetaldehyde, while that from the reaction of the peroxy radical from (1b) with NO gives CH_2O and glyoxal. The absence of observable glyoxal allowed them to conclude that $k_{1a} \geq 5k_{1b}$.

The oxy radical formed from reaction of $CH_2{=}CHC(O)OO$ with NO is expected to dissociate to form the vinyl radical and CO_2. While the yields of the products of reaction of the vinyl radical with O_2 under atmospheric condtions are uncertain, it is usually assumed that the main channel involves formation of CH_2O and HCO, although $CH_3 + CO_2$ is a possible alternative channel:

$$CH_2{=}CH + O_2 \rightarrow CH_2O + HCO$$

$$\rightarrow CH_3 + CO_2$$

Under atmospheric, high NO_x conditions, CH_3 generates CH_2O. The other main product of the abstraction channel is the peroxyacyl nitrate, whose yield depends on the NO_2 to NO ratio.

The system was also investigated by Magneron et al. (2002), who reached similar conclusions, except they observed glyoxal as a product; from the hydroxyacetaldehyde and glyoxal yields, they concluded that addition accounts for ~25% of the reaction, in good agreement with the measurements of Orlando and Tyndall (2002). Magneron et al. compared their results with calculations based on structure–activity relations for OH + acrolein, obtaining $k(298\ K) = 2.6 \times 10^{-11}$ cm^3 molecule^{-1} s^{-1}, in good agreement with the mean value given here. The SARs predict that 65% of the reaction proceeds via abstraction and 35% via addition, which is also in good agreement with the observations.

Salgado et al. (2008) measured the products from the reaction of NO_3 + acrolein at atmospheric pressure and obtained yields of 47 ± 3%, 21 ± 2% and 32 ± 2% for the peroxyacyl nitrate, CH_2O and CO, respectively.

As discussed above, Cl reacts mainly by addition at atmospheric pressure. Canosa-Mas et al. (2001) proposed that the main product is chloroacetaldehyde under low NO_x conditions. Orlando and Tyndall (2002) observed the peroxyacyl nitrate under higher NO_x conditions, indicating that some abstraction occurs.

IV-E-3. Crotonaldehyde (2-Butenal, $CH_3CH{=}CHCHO$)

IV-E-3.1. OH Reaction Kinetics

The reaction between OH and crotonaldehyde has been studied by Kerr and Sheppard (1981), Atkinson et al. (1983b), and Ullerstam et al. (2001) using relative rate techniques, and by Magneron et al. (2002) using pulsed laser photolysis; see table IV-E-5. There is good agreement between the four determinations giving a mean value at 298 K of 3.6×10^{-11} cm^3 molecule^{-1} s^{-1}, with an uncertainty of ±20%. Albaladejo et al. (2002) obtained a significantly lower value at 298 K, and this has not been included in the mean value obtained here. Combining this value with the temperature dependence determined by Magneron et al. gives: $k = 6.0 \times 10^{-12} \exp(533/T)$ cm^3 molecule^{-1} s^{-1}.

IV-E-3.2. O_3 Reaction Kinetics

Atkinson et al. (1981) and Grosjean and Grosjean (1998) measured the rate constant by observing the decay of ozone in the presence of excess crotonaldehyde, while Sato et al. (2004) used a relative rate technique; see table IV-E-6. The measurements are quite scattered. An unweighted mean value for the rate coefficient is 1.39×10^{-18} cm^3 molecule^{-1} s^{-1}, with an uncertainty of ±40%.

IV-E-3.3. NO_3 Reaction Kinetics

The rate coefficients for NO_3 + crotonaldehyde have been determined by Atkinson et al. (1987a) and Ullerstam et al. (2001) using relative rate techniques, and by Cabañas et al. (2001b) and Salgado et al. (2008) using discharge flow; see table IV-E-7. The data at room temperature are quite scattered and give an unweighted mean rate coefficient at 298 K of 1.0×10^{-14} cm^3 molecule^{-1} s^{-1} with an uncertainty of ±50%. The two

Table IV-E-5. Rate coefficients ($k = A \times e^{-B/T}$, cm^3 molecule^{-1} s^{-1}) for reaction of OH with crotonaldehyde ($CH_3CH{=}CHCHO$)

$10^{12} \times A$	B (K)	$10^{12} \times k$	T (K)	Technique[a]	Reference	Temperature Range (K)
		32 ± 6	298	RR[b] (ethene)	Kerr and Sheppard (1981)	
		40.2 ± 4.0	299	RR[c] (propene)	Atkinson et al. (1983b)	
		40 ± 3	297	RR[c] (propene)	Ullerstam et al. (2001)	
5.77 ± 1.14	−533 ± 58	53.0 ± 1.1	243	PLP–LIF	Magneron et al. (2002)	243–373
		48.8 ± 1.9	253			
		37.4 ± 1.5	273			
		35.0 ± 1.0	298			
		30.6 ± 1.4	323			
		26.4 ± 0.8	348			
		25.2 ± 1.3	372			
		23.5 ± 3.2	298	PLP–LIF	Albaladejo (2002)	

[a]Abbreviations used for the techniques are defined in table I-F-3.
[b]Placed on an absolute basis using $k(OH + C_2H_4) = 7.9 \times 10^{-12}$ cm^3 molecule^{-1} s^{-1} (Atkinson et al., 2006).
[c]Placed on an absolute basis using $k(OH + C_3H_6) = 2.9 \times 10^{-11}$ cm^3 molecule^{-1} s^{-1} (Atkinson et al., 2006).

Table IV-E-6. Rate coefficients (k, cm^3 molecule^{-1} s^{-1}) for reaction of O_3 with crotonaldehyde ($CH_3CH{=}CHCHO$)

$10^{20} \times k$	T (K)	Technique[a]	Reference
90 ± 18	296	Chemiluminescence	Atkinson et al. (1981)
174 ± 20	290	Uv photometry	Grosjean and Grosjean (1998)
158 ± 23	298	RR[b]	Sato et al. (2004)

[a]Abbreviations used for the techniques are defined in table I-F-3.
[b]Placed on an absolute basis using $k(O_3 + C_3H_6) = 1.0 \times 10^{-17}$ cm^3 molecule^{-1} s^{-1} (Atkinson et al., 2006).

Table IV-E-7. Rate coefficients ($k = A \times e^{-B/T}$, cm^3 molecule^{-1} s^{-1}) for reaction of NO_3 with crotonaldehyde ($CH_3CH{=}CHCHO$)

$10^{13} \times A$	B (K)	$10^{15} \times k$	T (K)	Technique[a]	Reference	Temperature Range (K)
		5.2 ± 1.1	298	RR[b] (propene)	Atkinson et al. (1987a)	
		6.0 ± 0.8	297	RR[c] (propene)	Ullerstam et al. (2001)	
550 ± 80	2,418 ± 60	16.0 ± 1.9	298	DF–LIF	Cabanas et al. (2001b)	298–433
		51.0 ± 6.4	345			
		101.2 ± 24.9	389			
		208.7 ± 23.2	433			
502 ± 70[c]	1,076 ± 47[c]			DF–LIF	Salgado et al. (2008)	249–330

[a]Abbreviations used for the techniques are defined in table I-F-3.
[b]Placed on an absolute basis using $k(NO_3 + \text{propene}) = 9.5 \times 10^{-15}$ cm^3 molecule^{-1} s^{-1} (Atkinson et al., 2006).
[c]Temperature dependent data not published.

meaurements of the temperature dependence by Cabañas et al. (2001b) and Salgado et al. (2008), using the same technique in the same laboratory, agree in the region of overlapping temperatures, but show evidence of a distinct change of slope in the Arrhenius plot. In view of the difficulties in comparing the temperature dependences for NO_3 + aldehydes made by this group and referred to in section IV-B, and the unavailability of the temperature dependent data of Salgado et al. (2008), it is difficult to recommend a temperature dependence for this reaction without further measurements.

IV-E-3.4. Cl-Atom Reaction Kinetics

The rate coefficients for Cl + crotonaldehyde have been determined by Thévenet et al. (2000), Ullerstam et al. (2001), and Wang et al. (2002) using relative rate techniques; see table IV-E-8. The unweighted mean rate coefficient is 2.65×10^{-10} cm^3 molecule^{-1} s^{-1} with an uncertainty of ±20%.

IV-E-3.5. O(^{3}P) Reaction Kinetics

Gaffney et al. (1975) studied the reaction between O(^{3}P) and crotonaldehyde, using a relative rate technique over the temperature range 296–423 K. They obtained $k(T) = 2.49 \times 10^{-11} \times \exp(-996/T)$ cm^3 molecule^{-1} s^{-1} and $k(296\text{ K}) = 8.49 \times 10^{-13}$ cm^3 molecule^{-1} s^{-1}, to which an uncertainty of ±40% should be attached.

Table IV-E-8. Rate coefficients (k, cm^3 molecule^{-1} s^{-1}) for reaction of Cl with crotonaldehyde ($CH_3CH{=}CHCHO$)

$10^{10} \times k$	T (K)	Technique[a]	Reference
2.54	298	RR[b] (propane)	Thévenet et al. (2000)
2.40		RR[c] (*n*-butane)	
2.48		RR[d] (*n*-pentane)	
2.74		RR[e] (*n*-hexane)	
2.2 ± 0.4	297	RR[f] (propene)	Ullerstam et al. (2001)
3.1 ± 0.8	298	RR[g] (ethyne)	Wang et al. (2002)
3.1 ± 0.6		RR[c] (*n*-butane)	

[a]Abbreviations used for the techniques are defined in table I-F-3.
[b]Placed on an absolute basis using $k(\mathrm{Cl} + \text{propane}) = 1.4 \times 10^{-10}$ cm^3 molecule^{-1} s^{-1} (Atkinson et al., 2006).
[c]Placed on an absolute basis using $k(\mathrm{Cl} + n\text{-butane}) = 2.05 \times 10^{-10}$ cm^3 molecule^{-1} s^{-1} (Atkinson et al., 2006).
[d]Placed on an absolute basis using $k(\mathrm{Cl} + n\text{-pentane}) = 2.7 \times 10^{-10}$ cm^3 molecule^{-1} s^{-1} (Atkinson et al., 2006).
[e]Placed on an absolute basis using $k(\mathrm{Cl} + n\text{-hexane}) = 3.3 \times 10^{-10}$ cm^3 molecule^{-1} s^{-1} (Calvert et al., 2008).
[f]Placed on an absolute basis using $k(\mathrm{Cl} + \text{propene}) = 2.3 \times 10^{-10}$ cm^3 molecule^{-1} s^{-1} (IUPAC, 2008).
[g]Placed on an absolute basis using $k(\mathrm{Cl} + C_2H_2) = 5.2 \times 10^{-11}$ cm^3 molecule^{-1} s^{-1} (Atkinson et al., 2006).

IV-E-3.6. Summary of the Atmospheric Fate of Crotonaldehyde and the End Products of Its Oxidation

During the day, the destruction of crotonaldehyde is controlled primarily by reaction with OH. The photolysis lifetime is 1.8 days for an overhead Sun; see chapter IX. For $[\mathrm{OH}] = 2.5 \times 10^6$ molecule cm^{-3}, the lifetime with respect to reaction with OH is about 3 h. The lifetime for nighttime removal by NO_3, with $[NO_3] \approx 3 \times 10^9$ molecule cm^{-3} is about 7 h.

Magneron et al. (2002) investigated the products in a large outdoor chamber. The main species found were glyoxal (16 ± 2)% and acetaldehyde (30 ± 5)%, together with large amounts of CO and smaller yields of CH_2O, HC(O)OH, and PAN type species. Orlando and Tyndall (2002) also investigated the products, obtaining yields for CO (42 ± 45%), CO_2 (41 ± 4%), glyoxal (21 ± 5%), acetaldehyde (51 ± 9%), and a small yield of CH_2O (<12%). They also observed spectral features that they assigned to peroxycrotonoyl nitrate, $CH_3CH{=}CHC(O)O_2NO_2$. Their carbon balance, at 77 ± 12%, was not as good as that which they found for acrolein.

Orlando and Tyndall (2002) discussed the product distribution using a mechanism similar to that discussed above for acrolein, with abstraction from —CHO and addition at the α-and β-sites. They argued that at least part of the missing carbon could be accounted for by 2-hydroxypropanal, formed by addition. The interpretation was more difficult than for acrolein, but a detailed consideration of the mechanism and the observed yields allowed them to speculate that ~50% of reaction occurred by abstraction and a maximum of 56% by addition. On the assumption that all of the missing carbon could be assigned to 2-hydroxypropanal, they were able to ascribe the product yields to specific channels and to conclude that abstraction and addition occur at roughly equal rates.

Magneron et al. (2002) compared their results for OH with calculations based on the Kwok and Atkinson (1995) structure–activity relations, which give

$k(298\ \mathrm{K}) = 3.9 \times 10^{-11}\ \mathrm{cm^3\ molecule^{-1}\ s^{-1}}$, in good agreement with the mean value given previously. The SARs indicate the reaction proceeds 56% via abstraction and 44% via addition, again in good agreement with the conclusions of Orlando and Tyndall (2002).

IV-E-4. Methacrolein (2-Methyl-2-propenal, $CH_2{=}C(CH_3)CHO$)

IV-E-4.1. OH Reaction Kinetics

The reaction between OH and methacrolein has been studied by Edney et al. (1986) and by Atkinson et al. (1983b) by relative rate techniques, by Gierczak et al. (1997) by pulsed laser photolysis, and by Chuong and Stevens (2003) by discharge flow; see table IV-E-9. There is reasonable agreement between the four determinations, giving a mean value at 298 K of $3.2 \times 10^{-11}\ \mathrm{cm^3\ molecule^{-1}\ s^{-1}}$, with an uncertainty of ±30%. Combining this value with the temperature dependence determined by Gierczak et al. gives $k = 9.0 \times 10^{-12} \exp(380/T)\ \mathrm{cm^3\ molecule^{-1}\ s^{-1}}$ over the range 230–380 K.

IV-E-4.2. O_3 Reaction Kinetics

Atkinson et al. (1981), Treacy et al. (1992), Grosjean et al. (1993f), and Grosjean and Grosjean (1998) measured the rate coefficient by observing the decay of ozone in the presence of excess methacrolein. Neeb et al. (1998) measured the decay of methacrolein by FTIR in the presence of excess O_3; see table IV-E-10. There is good agreement between the measurements, which give an unweighted mean value for the

Table IV-E-9. Rate coefficients ($k = A \times e^{-B/T}$, $\mathrm{cm^3\ molecule^{-1}\ s^{-1}}$) for reaction of OH with methacrolein [$CH_2{=}C(CH_3)CHO$]

$10^{12} \times A$	B (K)	$10^{12} \times k$	T (K)	Technique[a]	Reference	Temperature Range (K)
		26.0 ± 2.3	299	RR[b] (propene)	Atkinson et al. (1983b)	
		42.1 ± 3.1	298	RR (propene[b], *trans*-2-butene[c])	Edney et al. (1986)	
7.73 ± 0.65	−379 ± 46	38.6 ± 2.2	232	LFP–LIF	Gierczak et al. (1997)	232–378
		36.5 ± 3.4	235			
		29.7 ± 1.3	253			
		26.5 ± 1.2	272			
		20.3 ± 1.7	298			
		18.0 ± 1.0	323			
		15.1 ± 1.0	351			
		16.0 ± 0.8	354			
		13.3 ± 1.0	378			
		32.2 ±1.0	300	DF–LIF	Chuong and Stevens (2003)	

[a]Abbreviations used for the techniques are defined in table I-F-3.
[b]Placed on an absolute basis using $k(\mathrm{OH} + C_3H_6) = 2.9 \times 10^{-11}\ \mathrm{cm^3\ molecule^{-1}\ s^{-1}}$ (Atkinson et al., 2006).
[c]Placed on an absolute basis using $k(\mathrm{OH} + \textit{trans}\text{-}2\text{-}C_4H_8) = 6.41 \times 10^{-11}\ \mathrm{cm^3\ molecule^{-1}\ s^{-1}}$ (Calvert et al., 2000).

Table IV-E-10. Rate coefficients ($k = A \times e^{-B/T}$, cm^3 molecule^{-1} s^{-1}) for reaction of O_3 with methacrolein [CH_2=C(CH_3)CHO]

$10^{15} \times A$	B (K)	$10^{20} \times k$	T (K)	Technique[a]	Reference	Temperature Range (K)
		112 ± 13	296	Chemiluminescence	Atkinson et al. (1981)	
1.3	2,109	110 ± 20[b]	298	UV photometry	Treacy et al. (1992)	230–324
		102 ± 5	298	UV photometry	Grosjean et al. (1993f)	
		108 ± 20	290	UV photometry	Gosjean and Grosjean (1998)	
		130 ± 14	296	FTIR	Neeb et al. (1998)	

[a]Abbreviations used for the techniques are defined in table I-F-3.
[b]Rate coefficients not published. The value given here is calculated from the published Arrhenius expression.

rate coefficient of 1.12×10^{-18} cm^3 molecule^{-1} s^{-1} with an uncertainty of ±20%. Combining the room temperature rate coefficient with the temperature dependence obtained by Treacy et al. (1992) gives: $k = 1.3 \times 10^{-15} \exp(-2{,}110/T)$ cm^3 molecule^{-1} s^{-1}.

IV-E-4.3. NO_3 Reaction Kinetics

The rate coefficients for NO_3 + methacrolein have been determined by Rudich et al. (1996) by a flow–laser absorption method, using N_2O_5 thermal dissociation as the source of NO_3, and by Kwok et al. (1996a), Chew et al. (1998), and Canosa-Mas et al. (1999a) with relative rate techniques. Canosa-Mas et al. also used discharge flow–absorption spectroscopy; see table IV-E-11. Chew et al. commented that the 1998 determination was preferable to that completed in the same laboratory in 1996 by Kwok et al. and proposed that the 1998 results should be used. The unweighted mean rate constant at (298 ± 2) K, based on the determinations of Chew et al. and Canosa-Mas et al. is 3.4×10^{-15} cm^3 molecule^{-1} s^{-1} with an uncertainty of ± 30%. Canosa-Mas ascribed the higher value obtained in the discharge flow experiments to interferences from secondary chemistry. Rudich et al. were only able to obtain an upper limit, which is compatible with the relative rate measurements.

Table IV-E-11. Rate coefficients ($k = A \times e^{-B/T}$, cm^3 molecule^{-1} s^{-1}) for reaction of NO_3 with methacrolein [CH_2=C(CH_3)CHO]

$10^{15} \times k$	T (K)	Technique[a]	Reference
≤ 8	298	Flow-laser absorption	Rudich et al. (1996)
4.3 ± 1.7	296	RR[b] (propene)	Kwok et al. (1996a)
3.0	298	RR[c] (propene)	Chew et al. (1998)
3.6		RR[d] (1-C_4H_8)	
3.6 ± 1.0	296	RR[b] (propene)	Canosa-Mas et al. (1999a)
9.6 ± 2.0	296	DF abs.	

[a]Abbreviations used for the techniques are defined in table I-F-3.
[b]Placed on an absolute basis using $k(NO_3 + \text{propene}) = 9.3 \times 10^{-15}$ cm^3 molecule^{-1} s^{-1} at 296 K (Atkinson et al., 2006).
[c]Placed on an absolute basis using $k(NO_3 + \text{propene}) = 9.5 \times 10^{-15}$ cm^3 molecule^{-1} s^{-1} at 298 K (Atkinson et al., 2006).
[d]Placed on an absolute basis using $k(NO_3 + 1\text{-}C_4H_8) = 1.40 \times 10^{-14}$ cm^3 molecule^{-1} s^{-1} (Calvert et al., 2000).

Table IV-E-12. Rate coefficients (k, cm^3 molecule^{-1} s^{-1}) for reaction of Cl with methacrolein [CH_2=C(CH_3)CHO]

$10^{10} \times k$	T (K)	Technique[a]	Reference
3.1 ± 0.6	298	DF–RF	Canosa-Mas et al. (2001)
3.1 ± 0.7	298	RR[b] (ethyne)	Wang et al. (2002)
2.4 ± 0.4	298	RR[c] (*n*-butane)	
2.5 ± 0.4	298	RR[d] (propane)	Orlando et al. (2003)
1.9 ± 0.4	298	RR[e] (propene)	

[a]Abbreviations used for the techniques are defined in table I-F-3.
[b]Placed on an absolute basis using k(Cl + ethyne) = 5.2×10^{-11} cm^3 molecule^{-1} s^{-1} (Atkinson et al., 2006).
[c]Placed on an absolute basis using k(Cl + *n*-butane) = 2.05×10^{-10} cm^3 molecule^{-1} s^{-1} (Atkinson et al., 2006).
[d]Placed on an absolute basis using k(Cl + propane) = 1.4×10^{-10} cm^3 molecule^{-1} s^{-1} (Atkinson et al., 2006).
[e]Placed on an absolute basis using k(Cl + propene) = 2.3×10^{-10} cm^3 molecule^{-1} s^{-1} (Atkinson et al., 2006).

IV-E-4.4. Cl-Atom Reaction Kinetics

The rate coefficient for reaction of Cl with methacrolein has been determined by Canosa-Mas et al. (2001) using a discharge flow technique, and by Wang et al. (2002) and Orlando et al. (2003) using relative rate techniques; see table IV-E-12. The determinations agree well and give an unweighted mean rate coefficient of 2.6×10^{-10} cm^3 molecule^{-1} s^{-1} at 298 K, with an estimated uncertainty of ±15%.

IV-E-4.5. Summary of the Atmospheric Fate of Methacrolein and the End Products of Its Oxidation

During the day, the destruction of methacrolein is controlled primarily by photolysis and reaction with OH. The photolysis lifetime with an overhead Sun is estimated to be about 1.8 days; see chapter IX. For [OH] ≈ 2.5×10^6 molecule cm^{-3}, the lifetime with respect to reaction with OH is about 3.7 h. Removal at night by NO_3 is slow; for [NO_3] ≈ 3×10^9 molecule cm^{-3} the lifetime is about 1 day, while that for reaction with O_3 for [O_3] = 2.5×10^{12} molecule cm^{-3} is about 4 days.

Tuazon and Atkinson (1990) and Orlando et al. (1999b) determined the end products in the OH-inititated oxidation of methacrolein; there is generally good agreement with their results. The major products are CO, CO_2, hydroxyacetone, CH_2O, and peroxymethacryloyl nitrate (MPAN). The measurements of Orlando et al. and the deduced mechanism are consistent with 55% of the reaction occurring by addition and 45% by abstraction of the aldehydic H-atom. Tuazon and Atkinson obtained a 50:50 ratio for these two channels. Hydroxyacetone is formed following terminal addition, reaction with O_2 to form the peroxy radical and then with NO to form the oxy radical, which dissociates:

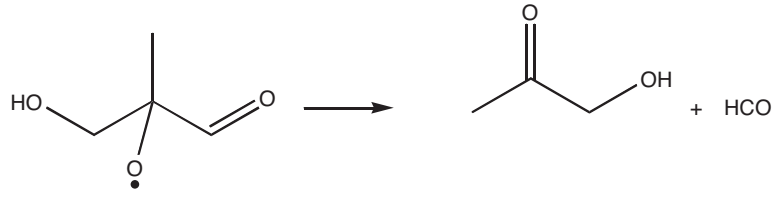

Abstraction followed by reaction with O_2 leads to formation of the peroxymethacryloyl radical ($CH_2C(CH_3)C(O)O_2$), which reacts with NO_2 [$k(298) = 1.2 \times 10^{-11}$ cm^3 molecule^{-1} s^{-1}] to form the peroxynitrate, or with NO [$k(298) = 3 \times 10^{-11}$ cm^3 molecule^{-1} s^{-1}], to form the oxy radical, which dissociates to form methylvinyl + CO_2. A major focus of the work of Orlando et al. was the fate of the methylvinyl radical, which they proposed reacts with O_2 to form acetyl + CH_2O or methyl + $CO + CH_2O$.

Orlando and Tyndall (2002) reviewed the trends in the reactivity of the three unsaturated aldehydes, acrolein, crotonaldehyde, and methacrolein. The percentage addition increases from 32 ± 5% for acrolein to 50 ± 15% for crotonaldehyde and 55 ± 5% for methacrolein. The results demonstrate the deactivating effect of the —CHO group and the activating effect of —CH_3. They suggested a small decrease in the substituent factor for —CHO from the value of 0.34 proposed by Kwok and Atkinson (1995) to 0.27. The site of addition is easier to discern for acrolein and methacrolein, for which the product yields indicate at least 80% of addition occurs at the β-carbon. The results for crotonaldehyde are more uncertain, but they suggested that ~40% of the addition occurs at the α-carbon, compatible with stablization of the hydroxyalkyl radical by the CH_3 group.

Roberts et al. (1998) used MPAN as an indicator of recent ozone production in the oxidation of isoprene in intensive campaigns in Nashville, Tennessee as part of the Southern Oxidant Study. They used peroxypropionyl nitrate (PPN) as a marker for anthropogenic hydrocarbon (AHC) oxidation, MPAN for biogenics (BHC), and PAN (peroxyacetyl nitrate) as a general marker for both AHC and BHC. By examining the ratios of these compounds, they were able to attribute the sources of ozone formation, showing, for example, that 50–60 ppb of ozone could be formed from BHC oxidation in regions where biogenic emissions were impacted with high NO_x plumes from power plants. The contribution to ozone from AHC was of a comparable magnitude.

IV-E-5. The Larger Unsaturated Aldehydes

IV-E-5.1. OH Reaction Kinetics

Rate coefficients for the reaction between OH and *E*-2-pentenal, *E*-2-hexenal and *E*-2-heptenal have been determined by Albaladejo et al. (2002) at room temperature and by Davis et al. (2007a) over the temperature range 244–374 K; all these determinations were made using pulsed laser photolysis. In addition, Atkinson et al. (1995) determined the rate coefficient for *E*-2-hexenal using a relative rate technique; Jimenez et al. (2007) used pulsed laser photolysis coupled with laser induced fluorescence; the latter measurements were made as a function of temperature; see table IV-E-13. While there is good agreement between the results obtained by Atkinson et al., Jimenez et al., and Davis et al. (4.4×10^{-11}, 4.7×10^{-11} and 4.3×10^{-11} cm^3 molecule^{-1} s^{-1} at 298 K, respectively), the measurements of Albaladejo et al. are systematically lower than those of Davis et al.; see figure IV-E-2. The reactivities of *E*-2-pentenal, *E*-2-hexenal and *E*-2-heptenal reported by Albaladejo et al. (2002) are comparable to, or lower than, the well-established reactivity of pentanal discussed above. This is not chemically

Table IV-E-13. Rate coefficients ($k = A \times e^{-B/T}$, cm^3 $molecule^{-1}$ s^{-1}) for reaction of OH with the larger unsaturated aldehydes

$10^{12} \times A$	B (K)	$10^{12} \times k$	T (K)	Technique[a]	Reference	Temperature Range (K)
E-2-Pentenal						
		24 ± 3	298	PLP–LIF	Albaladejo et al. (2002)	
7.9 ± 1.2	−510 ± 20	63 ± 8	243	PLP–LIF	Davis et al. (2007a)	244–374
		51 ± 7	271			
		43 ± 6	297			
		38 ± 6	323			
		34 ± 5	348			
		32 ± 5	374			
E-2-Hexenal						
		44 ± 9	296	RR[b] (*E*-2-butene)	Atkinson et al. (1995)	
		30 ± 5	298	PLP–LIF	Albaladejo et al. (2002)	
7.5 ± 1.1	−520 ± 30	63 ± 8	244	PLP–LIF	Davis et al. (2007a)	244–374
		52 ± 7	267			
		50 ± 7	271			
		39 ± 6	323			
		34 ± 5	329			
		34 ± 5	348			
		31 ± 5	352			
		31 ± 5	374			
4.2 ± 0.8	−565 ± 65	54.4 ± 2.0	263	PLP–LIF	Jimenez et al. (2007)	263–353
		54.0 ± 3.2	268			
		55.0 ± 4.0	273			
		51.7 ± 2.0	278			
		48.3 ± 2.0	286			
		46.8 ± 10	298			
		40.7 ± 11	307			
		39.1 ± 4.1	321			
		38.3 ± 3.4	336			
		35.0 ± 4.4	353			
E-2-Heptenal						
		25 ± 3	298	PLP–LIF	Albaladejo et al. (2002)	
9.7 ± 1.5	−450 ± 30	57 ± 8	255	PLP–LIF	Davis et al. (2007a)	255–374
		51 ± 7	271			
		44 ± 7	297			
		39 ± 6	323			
		35 ± 5	349			
		32 ± 5	374			
3-Z-4-Methylhexa-3,5-dienal						
		161 ± 35	296	RR[c] (2,3-dimethyl-2-butene)	Baker et al. (2004b)	
3-E-4-Methylhexa-3,5-dienal						
		252 ± 65	296	RR[c] (2,3-dimethyl-2-butene)	Baker et al. (2004b)	

[a]Abbreviations used for the techniques are defined in table I-F-3.
[b]Placed on an absolute basis using $k(OH + E\text{-}2\text{-}C_4H_8) = 6.5 \times 10^{-11}$ cm^3 $molecule^{-1}$ s^{-1} (Calvert et al., 2000).
[c]Placed on an absolute basis using $k(OH + 2,3\text{-dimethyl-2-butene}) = 1.10 \times 10^{-10}$ cm^3 $molecule^{-1}$ s^{-1} (Calvert et al., 2000).

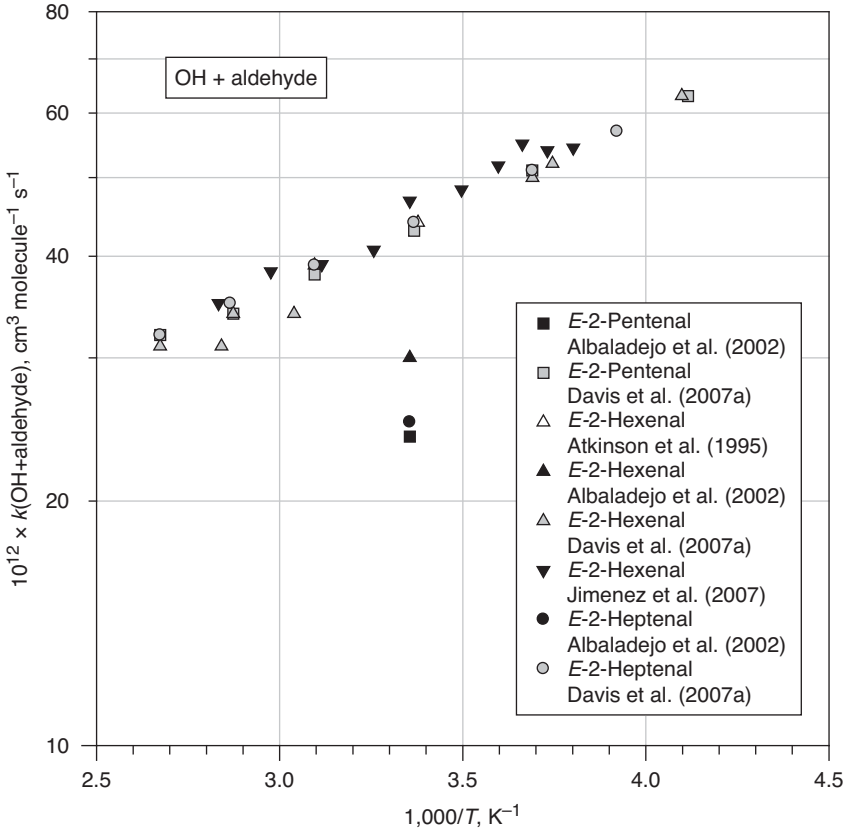

Figure IV-E-2. Arrhenius plot for the OH + 2-pentenal, 2-hexenal, and 2-heptenal reactions.

reasonable, and the results from Albaladejo et al. are not considered further; the values from Davis et al. are recommended:

E-2-pentenal:

$$k = 7.9 \times 10^{-12} \exp(510/T) \text{cm}^3 \text{ molecule}^{-1} \text{ s}^{-1};$$

$$k(298 \text{ K}) = 4.4 \times 10^{-11} \text{cm}^3 \text{ molecule}^{-1} \text{ s}^{-1}$$

E-2-hexenal:

$$k = 7.5 \times 10^{-12} \exp(520/T) \text{ cm}^3 \text{ molecule}^{-1} \text{ s}^{-1};$$

$$k(298 \text{ K}) = 4.3 \times 10^{-11} \text{cm}^3 \text{ molecule}^{-1} \text{ s}^{-1}$$

E-2-heptenal:

$$k = 9.7 \times 10^{-12} \exp(450/T) \text{ cm}^3 \text{ molecule}^{-1} \text{ s}^{-1};$$

$$k(298 \text{ K}) = 4.4 \times 10^{-11} \text{cm}^3 \text{ molecule}^{-1} \text{ s}^{-1}$$

An uncertainty of ±40% is estimated, given the lack of confirmatory measurements for *E*-2-pentenal and *E*-2-heptenal; for *E*-2-hexenal, an uncertainty of ±30% is estimated, given the good agreement with Atkinson et al. and Jimenez et al.

Baker et al. (2004) made relative rate measurements on a series of C_7 dienals (table IV-E-13). The rate coefficients (296 K) are:

$$k(\text{4-methylenehex-5-enal}) = 1.55 \times 10^{-10}\ \text{cm}^3\ \text{molecule}^{-1}\ \text{s}^{-1}$$

$$k(\text{3(}Z\text{-)4-methylhex-3,5-dienal}) = 1.61 \times 10^{-10}\ \text{cm}^3\ \text{molecule}^{-1}\ \text{s}^{-1}$$

$$k(\text{3(}E\text{-)4-methylhex-3,5-dienal}) = 2.52 \times 10^{-10}\ \text{cm}^3\ \text{molecule}^{-1}\ \text{s}^{-1}$$

These are all substantially higher than those for the C_5–C_7 enals just described, indicating that addition is a significant contributor to the reaction mechanism. In the absence of corroborating measurements, an uncertainty of ±40% is estimated.

IV-E-5.2. O_3 Reaction Kinetics

Sato et al. (2004) measured the rate coefficients at 298 K for O_3 + three pentenals using a relative rate method; see table IV-E-14.

$$k(\text{}E\text{-2-pentenal}) = 1.59 \times 10^{-18}\ \text{cm}^3\ \text{molecule}^{-1}\ \text{s}^{-1}$$

$$k(\text{3-methyl-2-butenal}) = 1.82 \times 10^{-18}\ \text{cm}^3\ \text{molecule}^{-1}\ \text{s}^{-1}$$

$$k(\text{}E\text{-2-methyl-2-butenal}) = 5.3 \times 10^{-18}\ \text{cm}^3\ \text{molecule}^{-1}\ \text{s}^{-1}$$

An uncertainty of ±40% should be attached to these measurements. Sato et al. (2004) compared the experimental results for these and other unsaturated aldehydes and ketones with results of conventional transition state theory, based on *ab initio* and density functional electronic structure calculations. They found that the differences in the rate coefficients derived from differences in activation energies, rather than significant changes in the *A* factors.

Atkinson et al. (1995) obtained $k(296) = 2.1 \times 10^{-18}\,\text{cm}^3\ \text{molecule}^{-1}\,\text{s}^{-1}$ for *E*-2-hexenal, while Baker et al. (2004b) obtained the following results for a series of C_7 dienals at 298 K:

$$k(\text{4-methylenehex-5-enal}) = 1.50 \times 10^{-17}\ \text{cm}^3\ \text{molecule}^{-1}\ \text{s}^{-1}$$

$$k(\text{3(}Z\text{)-4-methylhex-3,5-dienal}) = 4.4 \times 10^{-17}\ \text{cm}^3\ \text{molecule}^{-1}\ \text{s}^{-1}$$

$$k(\text{3(}E\text{)-4-methylhex-3,5-dienal}) = 5.7 \times 10^{-17}\ \text{cm}^3\ \text{molecule}^{-1}\ \text{s}^{-1}$$

In the absence of corroborating measurements, an uncertainty of ±40% applies to all of these rate coefficients.

Table IV-E-14. Rate coefficients (k, cm^3 molecule^{-1} s^{-1}) for reaction of O_3 with larger unsaturated aldehydes

Compound	$10^{18} \times k$	T (K)	Technique[a]	Reference
E-2-Pentenal				
	1.59 ± 0.22	298	RR[b] (propene)	Sato et al. (2004)
3-Methyl-2-butenal				
	1.82 ± 0.26	298	RR[b] (propene)	Sato et al. (2004)
E-2-Methyl-2-butenal				
	5.3 ± 0.7	298	RR[b] (propene)	Sato et al. (2004)
E-2-Hexenal				
	3.0 ± 2.1	296	RR[c] (*Z*-2-butene)	Atkinson et al. (1995)
	1.9 ± 0.9		RR[b] (propene)	
	2.1 ± 1.0		Weighted average	
4-Methylenehex-5-enal				
	15.0 ± 1.2	296	RR[d] (isoprene)	Baker et al. (2004b)
3-Z-4-Methylhexa-3,5,dienal				
	43.6 ± 8.1	296	RR[e] (α-pinene)	Baker et al. (2004b)
3-E-4-Methylhexa-3,5,dienal				
	56.6 ± 2.8	296	RR[e] (α-pinene)	Baker et al. (2004b)

[a]Abbreviations used for the techniques are defined in table I-F-3.
[b]Placed on an absolute basis using $k(O_3 + C_3H_6) = 1.0 \times 10^{-17}$ cm^3 molecule^{-1} s^{-1} (Atkinson et al., 2006).
[c]Placed on an absolute basis using $k(O_3 + Z\text{-2-butene}) = 1.22 \times 10^{-16}$ cm^3 molecule^{-1} s^{-1} (Calvert et al., 2000).
[d]Placed on an absolute basis using $k(O_3 + \text{isoprene}) = 1.27 \times 10^{-17}$ cm^3 molecule^{-1} s^{-1} (IUPAC, 2008).
[e]Placed on an absolute basis using $k(O_3 + \alpha\text{-pinene}) = 9.0 \times 10^{-17}$ cm^3 molecule^{-1} s^{-1} (IUPAC, 2008).

IV-E-5.3. NO_3 Reaction Kinetics

Cabañas et al. (2001b) determined the temperature dependence of the rate coefficient for reaction of NO_3 with four C_5–C_7 enals; see table IV-E-15. Their Arrhenius expressions are:

$$k(E\text{-2-pentenal}) = 5.4 \times 10^{-12} \exp(1{,}540/T) \text{ cm}^3 \text{ molecule}^{-1} \text{ s}^{-1}$$

$$k(E\text{-2-hexenal}) = 1.2 \times 10^{-12} \exp(926/T) \text{ cm}^3 \text{ molecule}^{-1} \text{ s}^{-1}$$

$$k(E\text{-2-heptenal}) = 8 \times 10^{-13} \exp(625/T) \text{ cm}^3 \text{ molecule}^{-1} \text{ s}^{-1}$$

$$k(\text{Z-4-heptenal}) = 2 \times 10^{-13} \exp(662/T) \text{ cm}^3 \text{ molecule}^{-1} \text{ s}^{-1}$$

Their room temperature measurement for *E*-2-hexenal (5.5×10^{-14} cm^3 molecule^{-1} s^{-1}) differs by nearly a factor of 5 from that of Atkinson et al. (1995) (1.2×10^{-14} cm^3 molecule^{-1} s^{-1}). These results should be treated with caution, and it is difficult to assign a realistic uncertainty.

Baker et al. (2004b) used relative rate techniques for NO_3 + three C_7 dienals, obtaining the following results:

$$k(\text{4-methylenehex-5-enal}) = 4.8 \times 10^{-13} \text{cm}^3 \text{ molecule}^{-1} \text{ s}^{-1}$$

Table IV-E-15. Rate coefficients ($k = A \times e^{-B/T}$, cm^3 molecule^{-1} s^{-1}) for reaction of NO_3 with the larger unsaturated aldehydes

$10^{12} \times A$	B (K)	$10^{14} \times k$	T (K)	Technique[a]	Reference	Temperature Range (K)
E-2-Pentenal						
5.4 ± 3.0	1,540 ± 205	2.9 ± 0.3	298	DF–LIF	Cabanas et al. (2001b)	298–433
		6.6 ± 0.5	345			
		10.1 ± 0.8	389			
		15.0 ± 1.3	433			
E-2-Hexenal						
		1.24 ± 0.44	296	RR[b] (propene)	Atkinson et al. (1995)	
1.2 ± 0.3	926 ± 205	5.5 ± 1.0	298	DF–LIF	Cabanas et al. (2001b)	298–433
		8.6 ± 0.6	345			
		10.9 ± 1.0	289			
		15.2 ± 1.8	433			
E-2-Heptenal						
0.8 ± 0.2	625 ± 48	9.6 ± 0.2	298	DF–LIF	Cabanas et al. (2001b)	298–433
		11.8 ± 0.1	345			
		14.6 ± 0.2	289			
		18.0 ± 0.2	433			
Z-4-Heptenal						
0.2 ± 0.1	662 ± 12	26.4 ± 0.4	298	DF–LIF	Cabanas et al. (2001b)	298–433
		35.6 ± 0.3	345			
		44.0 ± 0.5	289			
		52.9 ± 0.6	433			
4-Methylenehex-5-enal						
		47.5 ± 3.5	296	RR[c] (*E*-2-butene)	Baker et al. (2004b)	
3-Z-4-Methylhexa-3,5,dienal						
		217 ± 30	296	RR[c] (*E*-2-butene)	Baker et al. (2004b)	
3-E-4-Methylhexa-3,5,dienal						
		175 ± 27	296	RR[c] (*E*-2-butene)	Baker et al. (2004b)	

[a]Abbreviations used for the techniques are defined in table I-F-3.
[b]Placed on an absolute basis using $k(NO_3 + \text{propene}) = 9.5 \times 10^{-15}$ cm^3 molecule^{-1} s^{-1} (Atkinson et al., 2006).
[c]Placed on an absolute basis using $k(NO_3 + E\text{-2-butene}) = 3.89 \times 10^{-13}$ cm^3 molecule^{-1} s^{-1} (Calvert et al., 2000).

$$k(3(Z)\text{-4-methylhex-3,5-dienal}) = 2.2 \times 10^{-12} \text{ cm}^3 \text{ molecule}^{-1} \text{ s}^{-1}$$

$$k(3(E)\text{-4-methylhex-3,5-dienal}) = 1.8 \times 10^{-12} \text{ cm}^3 \text{ molecule}^{-1} \text{ s}^{-1}$$

Since these are the only available measurements, an uncertainty of ±40% should be employed.

IV-E-5.4. Cl-Atom Reaction Kinetics

Rodriguez et al. (2005) measured rate coefficients at 298 K for C_5–C_7 2-enals (see table IV-E-16) obtaining the following results:

$$k(E\text{-2-pentenal}) = 1.3 \times 10^{-10} \text{ cm}^3 \text{ molecule}^{-1} \text{ s}^{-1}$$

Table IV-E-16. Rate coefficients (k, cm^3 molecule^{-1} s^{-1}) for reaction of Cl with larger unsaturated aldehydes

Compound	$10^{10} \times k$	T (K)	Technique[a]	Reference
E-2-Pentenal				
	1.22	298	RR[b] (ethane)	Rodriguez et al. (2005)
	1.38		RR[c] (propene)	
	1.32		RR[d] (1-butene)	
	1.31 ± 0.19		Unweighted mean	
E-2-Hexenal				
	1.89	298	RR[b] (ethane)	Rodriguez et al. (2005)
	1.94		RR[c] (propene)	
	1.94		RR[d] (1-butene)	
	1.92 ± 0.22		Unweighted mean	
E-2-Heptenal				
	2.62	298	RR[b] (ethane)	Rodriguez et al. (2005)
	2.46		RR[c] (propene)	
	2.13		RR[d] (1-butene)	
	2.40 ± 0.29		Unweighted mean	

[a]Abbreviations used for the techniques are defined in table I-F-3.
[b]Placed on an absolute basis using $k(\mathrm{Cl} + \mathrm{C_2H_6}) = 5.9 \times 10^{-11}$ cm^3 molecule^{-1} s^{-1} (Atkinson et al., 2006).
[c]Placed on an absolute basis using $k(\mathrm{Cl} + \mathrm{C_3H_6}) = 2.31 \times 10^{-10}$ cm^3 molecule^{-1} s^{-1} (Atkinson et al., 2006).
[d]Placed on an absolute basis using $k(\mathrm{Cl} + \text{1-}\mathrm{C_4H_8}) = 3.0 \times 10^{-10}$ cm^3 molecule^{-1} s^{-1} (Orlando et al., 2003).

$$k(E\text{-2-hexenal}) = 1.9 \times 10^{-11} \text{ cm}^3 \text{ molecule}^{-1} \text{ s}^{-1}$$

$$k(E\text{-2-heptenal}) = 2.4 \times 10^{-11} \text{ cm}^3 \text{ molecule}^{-1} \text{ s}^{-1}$$

An uncertainty of ±40% is appropriate since they are the only determinations.

IV-E-5.5. Summary of the Atmospheric Fate of the Larger Unsaturated Aldehydes and the End Products of Their Oxidation

Representative lifetimes of the unsaturated aldehydes discussed in this section are shown in table IV-E-17. The lifetimes during the day for the alkenals are about 3 h and are determined by reaction with OH, while removal by ozone is much less significant. At night, provided [NO_3] is sufficiently high, removal by NO_3 is rapid, with lifetimes ranging from about 20 min. to 3 h. The dienals are much more reactive, with lifetimes for removal by OH below 1 h. Ozone removal can also be significant, with lifetimes of 3–12 h. At night, reaction with NO_3 is very rapid with lifetimes of a few minutes for the high [NO_3] concentration considered.

Davis et al. (2007a) discussed the OH oxidation of the larger 2-enals by analogy with the mechanisms discussed above for acrolein, crotonaldehyde, and methacrolein. They argued that the compound RCH=CHCHO reacts by:

1) Abstraction of the aldehydic H-atom to form a peroxynitrate, RCH=CHC(O)O_2NO_2 or an alkyl substituted glyoxal, RC(O)CHO, or aldehyde, RCHO, via reaction of the peroxy radical with NO. The latter sequence was presumed to proceed via a substituted vinoxy radical RCHCHO.

Table IV-E-17. Summary of atmospheric lifetimes τ for unsaturated aldehydes with respect to reaction with OH = 2.5×10^6 molecule cm^{-3}, $O_3 = 1.5 \times 10^{12}$ molecule cm^{-3}, and $NO_3 = 3 \times 10^9$ molecule cm^{-3}. Dashes indicate that rate coefficients are not available

Compound	τ(OH)	$\tau(O_3)$	$\tau(NO_3)$
E-2-Pentenal	2.6 h	4.8 days	3.2 h
3-Methyl-2-butenal	–	4.2 days	–
E-2-Methyl-2-butenal	–	1.4 days	–
E-2-Hexenal	2.6 h	3.6 days	1.7 h
E-2-Heptenal	2.6 h	–	1.0 h
Z-4-Heptenal	–	–	21 min.
4-Methylenehex-5-enal	45 min.	12 h	12 min.
3*Z*-4-Methylhexa-3,5-dienal	41 min.	4.2 h	3 min.
3*E*-4-Methylhexa-3,5-dienal	25 min.	3.3 h	3 min.

2) Addition in the 2-position, producing glyoxal and RCHO and in the 3-position, producing an alkylglycoaldehyde, RC(OH)CHO.

Baker et al. (2004b) compared their measured rate coefficients for reaction of OH with the dienals with those estimated on the basis of the Kwok and Atkinson (1995) SARs. The agreement was generally very good, usually within 20%. The greatest disagreement was found for 3-*Z*-4-methylhex-3,5-dienal, where the SAR gave $k = 1.64 \times 10^{-10}$ cm^3 $molecule^{-1}$ s^{-1} compared with the experimental value of 2.52×10^{-10} cm^3 $molecule^{-1}$ s^{-1}. The SARs were less successful for NO_3, where it was expected that reaction would proceed almost exclusively by addition. The rate coefficients were estimated on the basis of SARs for dienes with the same degree of substitution. Agreement was generally within a factor of 5 with the estimated rate coefficients exceeding the measured values. Estimates for O_3 were based on a range of dienes. Agreement was generally within a factor of 2–3.

IV-F. Derived from Atmospheric Oxidation of the Aromatic and Biogenic Hydrocarbons

IV-F-1. Introduction

Aromatic aldehydes are formed in the atmospheric oxidation of aromatic hydrocarbons. The mechanism of formation involves H abstraction by OH from an alkyl side group, followed by reaction with O_2 and then NO to form the oxy radical. The oxy radical reacts with O_2 to form the aldehyde and HO_2. OH primarily adds to the ring, so the yield of the aldehyde is small, e.g., the yield of benzaldehyde from toluene is 7% (Bloss et al., 2005). Aromatic aldehydes are also emitted directly from vehicle tailpipes; see chapter I.

Carbonyl compounds are key intermediates in the oxidation of biogenic compounds. For example, pinonaldehyde is a first generation intermediate following addition of OH to α-pinene. The oxy radical formed following reaction with O_2 and then NO rapidly

dissociates to form the aldehyde:

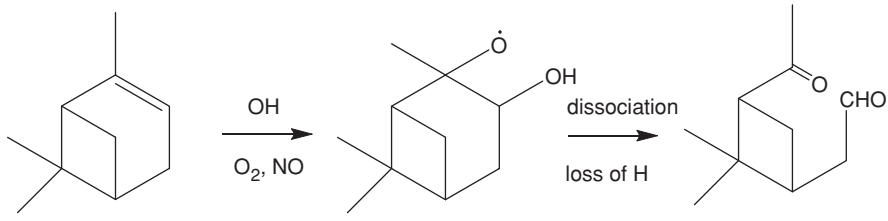

Three such aldehydes are considered in this section, pinonaldehyde, caronaldehyde that is formed from Δ^3 carene, and 3-isopropenyl-6-oxo-heptenal that is formed from limonene. Citronellal, a component of citronella oil, is also discussed.

IV-F-2. The Aromatic Aldehydes

IV-F-2.1. OH Reaction Kinetics

Table IV-F-1 shows the rate data for reaction of OH with aromatic aldehydes. All of the measurements have been made using relative rate techniques. The most extensive measurements were made by Thiault et al. (2002a), Clifford et al. (2005), and Clifford and Wenger (2006). The mean values for the rate coefficients for OH with each of the substituted benzaldehydes are shown in table IV-F-1; all measurements were used to derive the mean values. Methyl substitution in the aromatic ring enhances the rate coefficient by 40–50% over that for benzaldehyde, and this increase is repeated with the substitution of a second methyl group.

Semadeni et al. (1995) measured the temperature dependence of k(OH + benzaldehyde) using a relative rate method in a thermostated flow reactor. Their measurements are shown in table IV-F-2. There is a slight negative temperature dependence, although this was not reflected in the 294 K measurement, which has been excluded from the calculation of the temperature dependence. Using this dependence and the mean value for the rate coefficient at 298 K gives k(OH + benzaldehyde) $= 6.8 \times 10^{-12}$ exp(185/ T) cm^3 molecule^{-1} s^{-1}.

IV-F-2.2. NO_3 Reaction Kinetics

Measurements have been made only for benzaldehyde, using relative rate techniques (table IV-F-3). Carter et al. (1981) were only able to obtain an upper limit of 8×10^{-15} cm^3 molecule^{-1} s^{-1}, but Atkinson et al. (1984b) obtained a rate coefficient of 2.6×10^{-15} cm^3 molecule^{-1} s^{-1}. The reaction has also been studied by Clifford et al. (2005), who obtained a value close to that of Atkinson et al. The unweighted mean is 4.0×10^{-15} cm^3 molecule^{-1} s^{-1}, with an uncertainty of ±30%.

IV-F-2.3. Cl-Atom Reaction Kinetics

Table IV-F-4 shows the measured rate coefficients, all of which relate to the ambient temperature. The most extensive measurements have been made by Mellouki and

Table IV-F-1. Rate coefficients (k, cm^3 molecule^{-1} s^{-1}) for reaction of OH with aromatic aldehydes at $\sim$ 298 K

Compound	$10^{12} \times k$	T (K)	Technique[a]	Reference	Mean ($10^{12} \times k$)
Benzaldehyde	12.0 ± 2.0	298	RR[b] (ethene)	Niki et al. (1978b)	12.6 ± 2.0
	10.0 ± 2.0	298	RR[b] (ethene)	Kerr and Sheppard (1981)	
	11.8 ± 1.5	299	RR[c] (diethylether)	Semadeni et al. 1995)	
	11.4 ± 1.6	298	RR[d] (di-isopropyl ether)	Thiault et al. (2002a)	
	11.9 ± 1.5	298	RR[c] (diethyl ether)	Thiault et al. (2002a)	
	13.2 ± 1.6	298	RR[e] (1,3-dioxolane)	Thiault et al. (2002a)	
	12.6 ± 1.2	295	RR[h] (di-*n*-butyl ether)	Clifford et al. (2005)	
	13.9 ± 0.4	295	RR[k] (tetrahydrofuran)	Clifford et al. (2005)	
	14.6 ± 2.0	295	RR[j] (1,2,4 trimethylbenzene)	Clifford et al. (2005)	
	13.8 ± 0.8	295	RR[c] (diethyl ether)	Clifford et al. (2005)	
	14.4 ± 0.7	295	RR[f] (*n*-hexane)	Clifford et al. (2005)	
o-Tolualdehyde	17.5 ± 1.4	298	RR[c] (diethyl ether)	Thiault et al. (2002a)	18.9 ± 2.0
	17.1 ± 1.3	298	RR[f] (hexane)	Thiault et al. (2002a)	
	19.0 ± 1.5	298	RR[g] (benzaldehyde)	Thiault et al. (2002a)	
	18.8 ± 1.9	298	RR[e] (1,3-dioxolane)	Thiault et al. (2002a)	
	19.8 ± 1.2	295	RR[h] (di-*n*-butyl ether)	Clifford et al. (2005)	
	21.1 ± 1.3	295	RR[j] (1,2,4-trimethylbenzene)	Clifford et al. (2005)	
	20.1 ± 0.8	295	RR[c] (diethyl ether)	Clifford et al. (2005)	
	19.5 ± 2.3	295	RR[f] (*n*-hexane)	Clifford et al. (2005)	
	17.4 ± 1.7	295	RR[g] (benzaldehyde)	Clifford et al. (2005)	
m-Tolualdehyde	15.1 ± 1.6	298	RR[c] (diethyl ether)	Thiault et al. (2002a)	16.8 ± 4.0
	15.8 ± 0.8	298	RR[f] (hexane)	Thiault et al. (2002a)	
	16.4 ± 2.0	298	RR[g] (benzaldehyde)	Thiault et al. (2002a)	
	17.8 ± 1.8	298	RR[e] (1,3-dioxolane)	Thiault et al. (2000a)	
	22.1 ± 1.2	295	RR[h] (di-*n*-butyl ether)	Clifford et al. (2005)	
	21.6 ± 1.0	295	RR[k] (tetrahydrofuran)	Clifford et al. (2005)	
	20.8 ± 0.3	295	RR[j] (1,2,4-trimethylbenzene)	Clifford et al. (2005)	
	18.1 ± 1.1	295	RR[c] (diethyl ether)	Clifford et al. (2005)	
	20.6 ± 2.4	295	RR[f] (*n*-hexane)	Clifford et al. (2005)	
	17.1 ± 0.8	295	RR[g] (benzaldehyde)	Clifford et al. (2005)	
p-Tolualdehyde	12.8 ± 1.5	298	RR[c] (diethyl ether)	Thiault et al. (2002a)	16.8 ± 4.0
	11.6 ± 0.8	298	RR[f] (hexane)	Thiault et al. (2002a)	
	14.0 ± 2.0	298	RR[g] (benzaldehyde)	Thiault et al. (2002a)	
	13.5 ± 1.6	298	RR[e] (1,3-dioxolane)	Thiault et al. (2002a)	
	21.5 ± 0.6	295	RR[h] (di-*n*-butyl ether)	Clifford et al. (2005)	
	21.8 ± 1.6	295	RR[j] (1,2,4-trimethyl benzene)	Clifford et al. (2005)	
	17.1 ± 1.1	295	RR[c] (diethyl ether)	Clifford et al. (2005)	
	23.0 ± 2.2	295	RR[f] (*n*-hexane)	Clifford et al. (2005)	
	15.6 ± 0.8	295	RR[g] (benzaldehyde)	Clifford et al. (2005)	

(*continued*)

Table IV-F-1. (*continued*)

Compound	$10^{12} \times k$	T (K)	Technique[a]	Reference	Mean ($10^{12} \times k$)
2,3-Dimethylbenzaldehyde	24.9 ± 2.5	298	RR[h] (*n*-butyl ether)	Clifford and Wenger (2006)	25.5 ± 5.0
	26.1 ± 2.7	298	RR[i] (*n*-propyl ether)	Clifford and Wenger (2006)	
2,4-Dimethylbenzaldehyde	43.2 ± 6.7	298	RR[j] (1,2,4-trimethylbenzene)	Tse et al. (1997)	31.2 ± 10.0
	26.9 ± 3.6	298	RR[h] (*n*-butyl ether)	Clifford and Wenger (2006)	
	28.1 ± 3.1	298	RR[i] (*n*-propyl ether)	Clifford and Wenger (2006)	
	26.7 ± 4.4	298	RR[j] (1,2,4-trimethylbenzene)	Clifford and Wenger (2006)	
2,5-Dimethylbenzaldehyde	43.7 ± 6.8	298	RR[j] (1,2,4-trimethylbenzene)	Tse et al. (1997)	31.5 ± 10.0
	27.7 ± 2.4	298	RR[h] (*n*-butyl ether)	Clifford and Wenger (2006)	
	28.9 ± 2.7	298	RR[i] (*n*-propyl ether)	Clifford and Wenger (2006)	
	26.3 ± 5.1	298	RR[j] (1,2,4-trimethylbenzene)	Clifford and Wenger (2006)	
2,6-Dimethylbenzaldehyde	29.7 ± 2.7	298	RR[h] (*n*-butyl ether)	Clifford and Wenger (2006)	30.3 ± 8.0
	30.9 ± 3.0	298	RR[i] (*n*-propyl ether)	Clifford and Wenger (2006)	
3,4-Dimethylbenzaldehyde	21.4 ±3.4	298	RR[j] (1,2,4-trimethylbenzene)	Tse et al. (1997)	23.6 ±4.0
	23.3 ± 3.0	298	RR[h] (*n*-butyl ether)	Clifford and Wenger (2006)	
	24.1 ± 2.6	298	RR[i] (*n*-propyl ether)	Clifford and Wenger (2006)	
	25.7 ± 4.0	298	RR[j] (1,2,4-trimethylbenzene)	Clifford and Wenger (2006)	
3,5-Dimethylbenzaldehyde	27.7 ± 2.4	298	RR[h] (di-*n*-butyl ether)	Clifford and Wenger (2006)	27.8 ± 6.0
	27.9 ± 2.5	298	RR[i] (di-*n*-propyl ether)	Clifford and Wenger (2006)	

[a]Abbreviations used for the techniques are defined in table I-F-3.
[b]Placed on an absolute basis using $k(\text{OH} + \text{ethene}) = 7.9 \times 10^{-12}$ cm^3 molecule^{-1} s^{-1} (Atkinson et al., 2006).
[c]Placed on an absolute basis using $k(\text{OH} + \text{diethyl ether}) = 1.22 \times 10^{-11}$ cm^3 molecule^{-1} s^{-1} (this book, section III-B-3.1).
[d]Placed on an absolute basis using $k(\text{OH} + \text{di-isopropyl ether}) = 1.00 \times 10^{-11}$ cm^3 molecule^{-1} s^{-1} (this book, section III-B-7.1).
[e]Placed on an absolute basis using $k(\text{OH} + \text{1,3-dioxolane}) = 1.0 \times 10^{-11}$ cm^3 molecule^{-1} s^{-1} (this book, section III-E-9.1).
[f]Placed on an absolute basis using $k(\text{OH} + \text{hexane}) = 5.48 \times 10^{-12}$ cm^3 molecule^{-1} s^{-1} (Calvert et al., 2008).
[g]Placed on an absolute basis using $k(\text{OH} + \text{benzaldehyde}) = 1.26 \times 10^{-11}$ cm^3 molecule^{-1} s^{-1} (this book, table IV-F-1).
[h]Placed on an absolute basis using $k(\text{OH} + \text{di-}n\text{-butyl ether}) = 2.80 \times 10^{-11}$ cm^3 molecule^{-1} s^{-1} (this book, section III-B-12.1).
[i]Placed on an absolute basis using $k(\text{OH} + \text{di-}n\text{-propyl ether}) = 2.00 \times 10^{-11}$ cm^3 molecule^{-1} s^{-1} (this book, section III-B-6.1).
[j]Placed on an absolute basis using $k(\text{OH} + \text{1,2,4-trimethylbenzene}) = 3.27 \times 10^{-11}$ cm^3 molecule^{-1} s^{-1} (Calvert et al., 2002).
[k]Placed on an absolute basis using $k(\text{OH} + \text{tetrahydrofuran}) = 1.70 \times 10^{-11}$ cm^3 molecule^{-1} s^{-1} (this book, section III-E-5.1).

Table IV-F-2. Rate coefficients ($k = A\ e^{-B/T}$, cm^3 molecule^{-1} s^{-1}) for reaction of OH + benzaldehyde (C_6H_5CHO) as a function of temperature

$10^{12} \times A$	B (K)	$10^{12} \times k$	T (K)	Technique[a]	Reference	Temperature Range (K)
5.6	243 ± 85	9.2[b]	289	RR[c] (diethyl ether)	Semadeni et al. (1995)	289–343 K
		11.3	294			
		11.6	299			
		11.1	307			
		10.9	314			
		10.7	324			
		10.8	334			
		10.4	343			

[a]Abbreviations used for the techniques are defined in table I-F-3.
[b]Not included in the Arrhenius fit.
[c]Placed on an absolute basis using $k(\text{OH} + \text{diethyl ether}) = 1.15 \times 10^{-17} T^2 \exp(585/T)$ cm^3 molecule^{-1} s^{-1} (this book, section III-B-3.1).

Table IV-F-3. Rate coefficients (k, cm^3 molecule^{-1} s^{-1}) for reaction of NO_3 with benzaldehyde (C_6H_5CHO)

$10^{15} \times k$	T (K)	Technique[a]	Reference
< 8	300	RR[b] (propene)	Carter et al. (1981)
2.6 ± 0.6	298	RR[b] (propene)	Atkinson et al. (1984b)
4.00 ± 0.20	295	RR[c] (tetrahydrofuran)	Clifford et al. (2005)
5.52 ± 0.29		RR[d] (di-*n*-propyl ether)	

[a]Abbreviations used for the techniques are defined in table I-F-3.
[b]Placed on an absolute basis using $k(NO_3 + \text{propene}) = 9.5 \times 10^{-15}$ cm^3 molecule^{-1} s^{-1} (Atkinson et al., 2006).
[c]Placed on an absolute basis using $k(NO_3 + \text{tetrahydrofuran}) = 4.7 \times 10^{-15}$ cm^3 molecule^{-1} s^{-1} (this book, section III-E-5.2).
[d]Placed on an absolute basis using k (NO_3+di-*n*-propyl ether) = 6.0×10^{-15} cm^3 molecule^{-1} s^{-1} (this book, section III-B-6.2).

co-workers (Thiault et al., 2002a; El Dib et al., 2008), although measurements of the rate coefficient for benzaldehyde have also been made by Buth et al. (1992) by discharge flow and mass spectrometry and by Nozière et al. (1994) by a relative rate method. There is good agreement between the different determinations, and all of the rate coefficients are in the range 1–2 × 10^{-10} cm^3 molecule^{-1} s^{-1}.

IV-F-2.4. O(^{3}P) Reaction Kinetics

Filby and Guesten (1978) measured the rate coefficient for O(^{3}P) + benzaldehyde using discharge flow with ESR detection. At 6.27 mbar and 298 K, they obtained $k = 4.8 \times 10^{-13}$ cm^3 molecule^{-1} s^{-1}. Assuming that the reaction occurs by H abstraction from the carbonyl group, no pressure dependence is anticipated. An uncertainty of ±40% should be attached, since this is the only measurement.

IV-F-2.5. Summary of the Atmospheric Fate of Aromatic Aldehydes and the End Products of Their Oxidation

During the day, the destruction of aromatic aldehydes is controlled primarily by photolysis and reaction with OH. The limited data related to the photolysis lifetimes are

Table IV-F-4. Rate coefficients (k, cm^3 molecule^{-1} s^{-1}) for reaction of Cl with aromatic aldehydes at $\sim$ 298 K

Compound	$10^{12} \times k$	T (K)	Technique[a]	Reference	Mean ($k \times 10^{10}$)
Benzaldehyde	0.90 ± 0.027		DF–MS	Buth et al. (1992)	0.99 ± 0.2
	0.98 ± 0.04	293 ± 6	RR[b] (ethane, [c]ethene)	Nozière et al. (1994)	
	0.98 ± 0.11	298	RR[b] (ethane)	Thiault et al. (2002a)	
	1.09 ± 0.18	298	RR[d] (propane)	Thiault et al. (2002a)	
	0.99 ± 0.14	298	RR[e] (*n*-pentane)	Thiault et al. (2002a)	
o-Tolualdehyde	1.83 ± 0.15	298	RR[b] (ethane)	Thiault et al. (2002a)	1.86 ± 0.5
	1.88 ± 0.17	298	RR[e] (*n*-pentane)	Thiault et al. (2002a)	
	1.86 ± 0.16	298	RR[f] (benzaldehyde)	Thiault et al. (2002a)	
m-Tolualdehyde	2.90 ± 0.04	298	RR[b] (ethane)	Thiault et al. (2002a)	1.71 ± 0.7
	0.53 ± 0.03	298	RR[e] (*n*-pentane)	Thiault et al. (2002a)	
	1.70 ± 0.02	298	RR[f] (benzaldehyde)	Thiault et al. (2002a)	
p-Tolualdehyde	1.32 ± 0.12	298	RR[b] (ethane)	Thiault et al. (2002a)	1.41 ± 0.3
	1.46 ± 0.20	298	RR[e] (*n*-pentane)	Thiault et al. (2002a)	
	1.45 ± 0.14	298	RR[f] (benzaldehyde)	Thiault et al. (2002a)	
2,4-Dimethylbenzaldehyde	0.76 ± 0.06	298	RR[b] (ethane)	El Dib et al. (2008)	0.87 ± 0.20
	0.94 ± 0.15	298	RR[d] (propane)	El Dib et al. (2008)	
	0.90 ± 0.12	298	RR[e] (*n*-pentane)	El Dib et al. (2008)	
2,5-Dimethylbenzaldehyde	0.93 ± 0.12	298	RR[e] (*n*-pentane)	El Dib et al. (2008)	0.93 ± 0.30
	0.92 ± 0.12	298	RR[g] (*n*-hexane)	El Dib et al. (2008)	
3,5-Dimethylbenzaldehyde	0.93 ± 0.13	298	RR[b] (ethane)	El Dib et al. (2008)	0.93 ± 0.20
	0.99 ± 0.14	298	RR[c] (propane)	El Dib et al. (2008)	
	0.88 ± 0.08	298	RR[e] (*n*-pentane)	El Dib et al. (2008)	

[a] Abbreviations used for the techniques are defined in table I-F-3.
[b] Placed on an absolute basis using $k(\mathrm{Cl} + \mathrm{ethane}) = 5.9 \times 10^{-11}$ cm^3 molecule^{-1} s^{-1} (Atkinson et al., 2006).
[c] Placed on an absolute basis using $k(\mathrm{Cl} + \mathrm{ethene}) = 9.5 \times 10^{-11}$ cm^3 molecule^{-1} s^{-1} (section I-F-1).
[d] Placed on an absolute basis using $k(\mathrm{Cl} + \mathrm{propane}) = 1.4 \times 10^{-10}$ cm^3 molecule^{-1} s^{-1} (Atkinson et al., 2006).
[e] Placed on an absolute basis using $k(\mathrm{Cl} + n\text{-pentane}) = 2.7 \times 10^{-10}$ cm^3 molecule^{-1} s^{-1} (Calvert et al., 2008).
[f] Placed on an absolute basis using $k(\mathrm{Cl} + \mathrm{benzaldehyde}) = 9.9 \times 10^{-11}$ cm^3 molecule^{-1} s^{-1} (this book, table IV-F-4).
[g] Placed on an absolute basis using $k(\mathrm{Cl} + n\text{-hexane}) = 3.3 \times 10^{-10}$ cm^3 molecule^{-1} s^{-1} (Calvert et al., 2008).

discussed in chapter IX. For [OH] $\approx 2.5 \times 10^6$ molecule cm^{-3}, lifetimes with respect to reaction with OH are in the range 4–9 h. The lifetimes for removal by Cl, with [Cl] $\approx 10^4$ molecule cm^{-3} are in the range 6–12 days. Removal of benzaldehyde at night by NO_3 is slow; with [NO_3] $\approx 3 \times 10^9$ molecule cm^{-3} the lifetime is 4 days.

Reactions with OH, NO_3, and Cl with benzaldehyde all occur by abstraction of the aldehydic H to form the benzoyl radical. The following mechanism (figure IV-F-1) and rate coefficient data are taken from the Master Chemical Mechanism (MCMv3.1: http://mcm.leeds.ac.uk/MCM/). Addition of O_2 to benzoyl leads to formation of the benzoyl peroxy radical. Subsequent reaction with NO, followed by O_2 and then decarboxylation, gives the phenyl peroxy radical which reacts with NO to form phenoxy. The main reactions of phenoxy are with O_3 to regenerate phenyl peroxy and with NO_2 to form nitrophenol; the rate coefficents for these two reactions are 3×10^{-13} and 2×10^{-12} cm^3 $molecule^{-1}$ s^{-1}, respectively.

Reaction of benzoyl peroxy with NO_2 generates peroxybenzoyl nitrate, a PAN type species. At 298 K, the equilibrium constant for formation of the nitrate is 5×10^{-8} cm^3 $molecule^{-1}$, so that, for [NO_2] $= 2.5 \times 10^{11}$ molecule cm^{-3} (10 ppb), the equilibrium ratio of the nitrate to the peroxy radical is 10^4 and the equilibrium is established in less than 1 s. The nitrate reacts with OH, with a rate constant of 1×10^{-12} cm^3 $molecule^{-1}$ s^{-1}, corresponding to a lifetime of about 12 days for [OH] $= 1 \times 10^6$ molecule cm^{-3}. The more likely fate at 298 K is dissociation to regenerate the peroxy radical and reaction with NO to form the phenyl peroxy radical, as discussed here. The effective timescale for the process is $(k[NO]/K[NO_2])^{-1}$, where k is the rate coefficient for reaction of the benzoyl peroxy radical with NO ($k = 2 \times 10^{-11}$ cm^3 $molecule^{-1}$ s^{-1}) and K is the equilibrium constant for formation of the peroxybenzoyl nitrate. For [NO] $=$ [NO_2], this timescale is ~30 min. and so, at least at the Earth's surface, reaction with NO clearly determines the fate of the peroxy radical, even though its fractional concentration in the peroxybenzoyl/peroxybenzoyl nitrate equilibrium is small.

Thus, the main, long-lived intermediate formed in the atmospheric oxidation of benzaldehyde is nitrophenol. The oxidation involves two NO to NO_2 conversions, but one of these NO_2 species is then incorporated in the nitrophenol and so the route is inefficient at generating ozone. Furthermore, it leads to scavenging of NO_x in forming the nitrophenol. The net result is that benzaldehyde has a *negative* photochemical ozone creation potential, largely because of the NO_x scavenging effect (Derwent et al., 1998).

IV-F-3. *trans*-Cinnamaldehyde (Phenyl Acrolein, 3-Phenyl-2-propenal, $C_6H_5CH{=}CHCHO$)

IV-F-3.1. Reaction Kinetics

The kinetics and products of the reactions of *trans*-cinnamaldehyde with OH, O_3, and NO_3 were studied by Smith et al. (1996) The motivation for the work was the structural relationship between this compound and commercially unavailable ring-opened C_{10}-dicarbonyls formed in significant yields from the OH-initiated oxidation of naphthalene. The following rate coefficients were obtained at 296 ± 2 K, using relative rate methods: $k(OH) = (4.8 \pm 1.4) \times 10^{-11}$ cm^3 $molecule^{-1}$ s^{-1} (placed on an

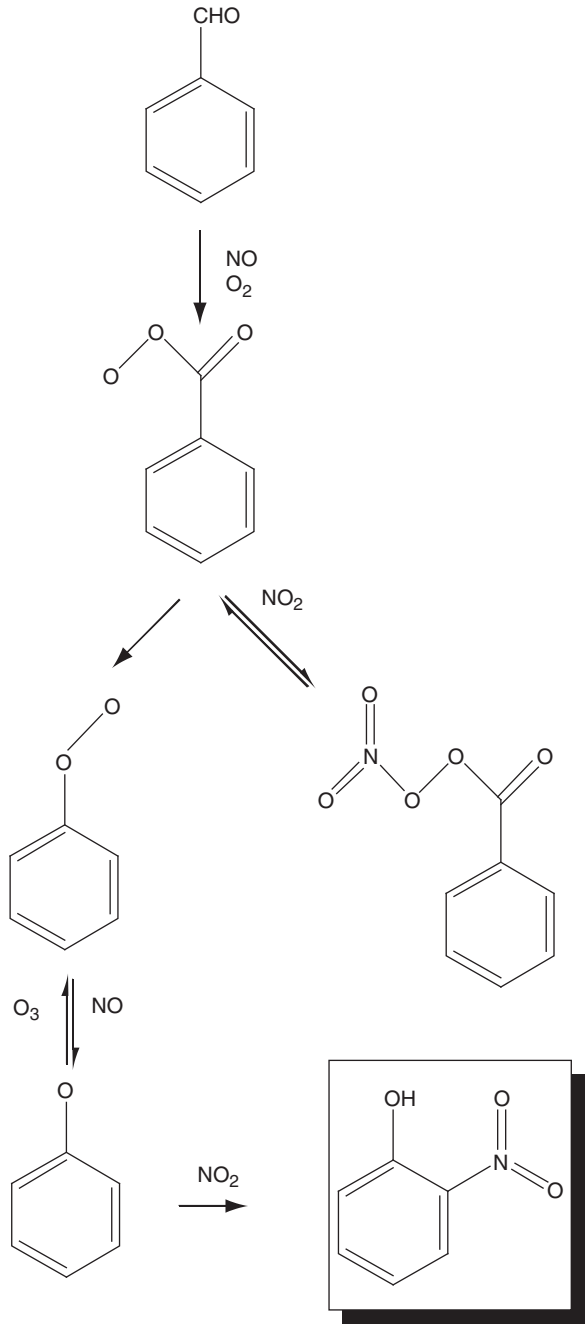

Figure IV-F-1. Mechanism for the atmospheric oxidation of benzaldehyde.

absolute basis using $k(\text{OH} + \textit{trans}\text{-2-butene}) = 6.48 \times 10^{-11}\,\text{cm}^3\ \text{molecule}^{-1}\,\text{s}^{-1}$); $k(\text{O}_3) = (2.3 \pm 0.7) \times 10^{-18}\,\text{cm}^3\ \text{molecule}^{-1}\,\text{s}^{-1}$ [placed on an absolute basis using $k(\text{O}_3 + \text{propene}) = 1.0 \times 10^{-17}\,\text{cm}^3\ \text{molecule}^{-1}\,\text{s}^{-1}$]; $k(\text{NO}_3) = (1.9 \pm 1.4) \times 10^{-14}\,\text{cm}^3\ \text{molecule}^{-1}\,\text{s}^{-1}$ [placed on an absolute basis using $k(\text{NO}_3 + \text{propene}) = 9.24 \times 10^{-15}\,\text{cm}^3\ \text{molecule}^{-1}\,\text{s}^{-1}$].

The rate constant for OH is within 20% of estimates based on structure–activity relations (Kwok and Atkinson, 1995). Those for O_3 and NO_3 are about a factor of 2 larger than estimates based on the reactions of these species with crotonaldehyde. Since all these values result from single determinations, an uncertainty of ±40% is appropriate.

IV-F-3.2. Summary of the Atmospheric Fate of Cinnamaldehyde and the End Products of Its Oxidation

During the day, the destruction of cinnamaldehyde is controlled primarily by its reaction with OH. The possible significance of photodecomposition in the loss of cinnamaldehyde is unclear at the time of writing (Smith et al., 1996), but both isomerization and photodecomposition occur. For $[\text{OH}] \approx 2.5 \times 10^6$ molecule cm^{-3}, the lifetime with respect to reaction with OH is about 2.3 h. Removal of cinnamaldehyde at night by NO_3 is fast; with $[\text{NO}_3] \approx 3 \times 10^9$ molecule cm^{-3} the lifetime is about 5 h.

Smith et al. (1996) investigated the products of the OH-initated oxidation of cinnamaldehyde, generating OH by photolysis of CH_3ONO. The yield of benzaldehyde formed in the presence of NO and air was 0.90 ± 0.39, after corrections were made for photolysis of cinnamaldehyde and for reaction of benzaldehyde with OH. There are two probable channels, involving abstraction of the aldehydic H and addition to the double bond in the substituent group. In the former route, the initially formed acyl radical, $C_6H_5CHCHCO$, reacts with O_2 to form the peroxy radical, and then NO to form benzaldehyde, at least in part. The two β-hydroxy alkyl radicals formed by OH addition to the olefinic double bond react with O_2 followed by NO to form β-hydroxy alkoxy radicals, which will then dissociate to form benzaldehyde + formaldehyde. Thus, the formation of benzaldehyde is compatible with both channels of reaction, but it was not feasible to assign channel yields.

IV-F-4. Aromatic Dicarbonyls: Phthaldialdehyde (2-Formylbenzaldehyde, $C_6H_4(CHO)_2$) and 2-Acetylbenzaldehyde ($C_6H_4(CHO)C(O)CH_3$)

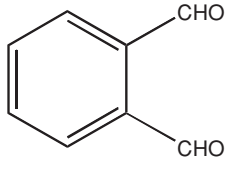

Phthaldialdehyde

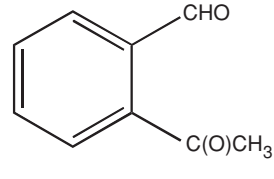

2-Acetylbenzaldehyde

IV-F-4.1. OH Reaction Kinetics

The kinetics of the reaction with OH were studied by Wang et al. (2006) using a relative rate technique and with 1,2,4-trimethyl benzene as the reference compound. At 298 K, they obtained $k(\text{OH} + \text{phthaldialdehyde}) = (2.3 \pm 0.3) \times 10^{-11}\ \text{cm}^3\ \text{molecule}^{-1}\ \text{s}^{-1}$ $k(\text{OH} + \text{2-acetylbenzaldehyde}) = (1.7 \pm 0.3) \times 10^{-11}\ \text{cm}^3\ \text{molecule}^{-1}\ \text{s}^{-1}$. The rate constants were placed on an absolute basis using $k(\text{OH} + \text{1,2,4-trimethyl benzene}) = 3.25 \times 10^{-11}\ \text{cm}^3\ \text{molecule}^{-1}\ \text{s}^{-1}$. The Kwok and Atkinson (1995) rate coefficients from SARs for phthaldialdehyde and 2-acetylbenzaldehyde are $3.3 \times 10^{-11}\ \text{cm}^3$ $\text{molecule}^{-1}\ \text{s}^{-1}$ and $1.7 \times 10^{-11}\ \text{cm}^3\ \text{molecule}^{-1}\ \text{s}^{-1}$.

IV-F-4.2. Summary of the Atmospheric Fate Phthaldialdehyde and 2-Acetylbenzaldehyde, and the End Products of Their Oxidation

During the day, the lifetimes for the destruction of phthaldialdehyde and 2-acetylbenzaldehyde by reaction with OH are 4.8 h and 6.5 h, respectively. Wang et al. (2006) calculated the photolysis lifetimes for both compounds to be ~1.5 h. In chapter IX of this book, we estimate that the lifetimes for photodissociation for phthaldialdehyde and 2-acetylbenzaldehyde are about 20 min. and 19 min., respectively for an overhead Sun and 1.0 h and 0.9 h, repectively, for the diurnal cycle near June 22.

Reaction with OH for both compounds occurs by H abstraction from the —CHO group. Wang et al. observed that phthalic anyhydride is the main product from the OH reaction, and that the yield is independent of the ratio of NO to NO_2. On this basis, they tentatively suggested the mechanism shown in figure IV-F-2.

IV-F-5. Aldehydes Formed in the Oxidation of Biogenic Compounds: Pinonaldeyde

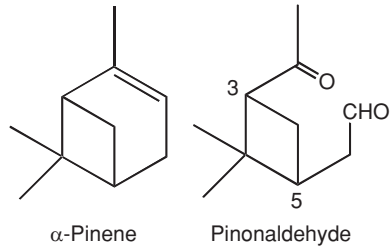

α-Pinene Pinonaldehyde

Pinonaldehyde is formed in the oxidation of α-pinene, following reaction with OH, NO_3, and O_3. Davis et al. (2007b) recently reviewed the literature yields of pinonaldehyde for reaction with each of these species in the presence of O_2 and NO. For OH, yields range from 28 to 87%, for O_3 they are in the range 14–20%, with a possible dependence on relative humidity, while for NO_3 the yield is ~ 60%. Emission of monoterpenes is important at night; provided NO_3 is high enough, this reaction provides a significant source of pinonaldehyde at night.

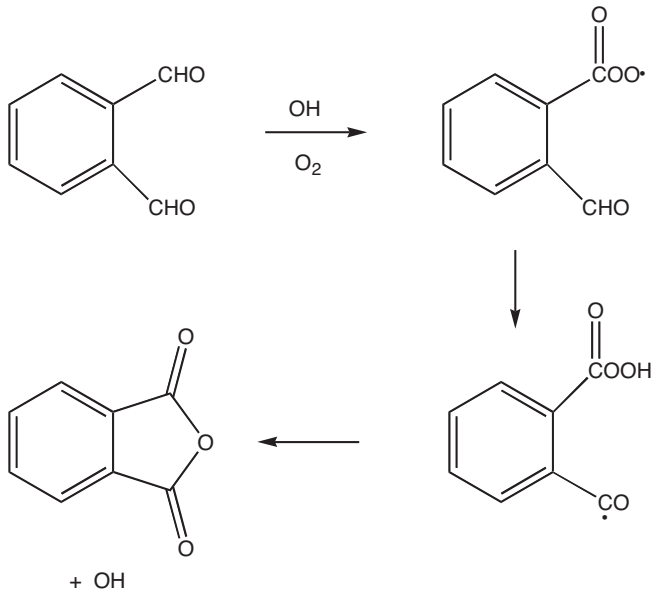

Figure IV-F-2. Mechanism for the formation of phthalic anhydride in the oxidation of phthaldialdehyde.

IV-F-5.1. OH Reaction Kinetics

The results of relative rate studies of k(OH + pinonaldehyde) at room temperature have been reported by Glasius et al. (1997), Hallquist et al. (1997), Alvarado et al. (1998), and Nozière et al. (1999a). In addition, Davis et al. (2007b) used a laser flash photolysis technique over the temperature range 297–374 K; see table IV-F-5. The results of Glasius et al. and Hallquist et al. are significantly higher than the other three room temperature determinations. Alvarado et al. suggested that the difference might arise from the use of high pinonaldehyde concentrations in small reactors, but this explanation seems unlikely to be correct, since Nozière et al. found no evidence for such an effect; they carried out experiments in both a small reactor in Wuppertal and the large outdoor chamber in Valencia, Spain (EUPHORE), obtaining similar results. The measurements of Alvarado et al., Nozière et al., and Davis et al. together give an unweighted mean value at 298 K of 4.2×10^{-11} cm^3 molecule^{-1} s^{-1}, with an uncertainty of ±30%. Coupling these with the temperature dependence of Davis et al. gives: $k = 5.6 \times 10^{-12} \exp(600/T)$ cm^3 molecule^{-1} s^{-1} over the temperature range 290–380 K. These are close to the values recommended by IUPAC ($k = 3.9 \times 10^{-11}$ cm^3 molecule^{-1}s^{-1} at 298 K, $k = 5.2 \times 10^{-12} \exp(600/T)$ cm^3 molecule^{-1}s^{-1}over the temperature range 290–380 K (IUPAC, December, 2007).

IV-F-5.2. NO_3 Reaction Kinetics

The reaction has been studied using relative rate techniques by Glasius et al. (1997), Hallquist et al. (1997), and Alvarado et al. (1998). The measurements of Glasius et al.

Table IV-F-5. Rate coefficients (k, cm^3 molecule^{-1} s^{-1}) for reaction of OH with pinonaldehyde

$10^{12} \times A$	B (K)	$10^{12} \times k$	T (K)	Technique[a]	Reference	Temperature Range (K)
		90 ± 26	300	RR[b] (isoprene)[c]	Glasius et al. (1997)	
		92 ± 13		RR[c] (1,3-C_4H_6)[d]		
		95 ± 11	298	DF–RR (C_3H_6)[d]	Hallquist et al. (1997)	
		49 ± 11	296	RR (C_3H_6)[d]	Alvarado et al. (1998)	
		49 ± 15		RR (1-C_4H_8)[e]		
		54 ± 17		RR (*m*-xylene)[f]		
		30 ± 8	293	RR (isoprene)[b]	Nozière et al. (1999b)	
		43 ± 10		RR (1,3-C_4H_6)[d]		
		32 ± 5		RR (cyclohexane)[g]		
		42 ± 7		RR (cyclohexane)[g*]		
4.5 ± 1.3	600 ± 100	34.6 ± 0.4	297	PLP–LIF	Davis et al. (2007b)	297–374
		26.9 ± 0.6	325			
		25.6 ± 0.4	349			
		23.5 ± 0.4	374			

[a]Abbreviations used for the techniques are defined in table I-F-3.
[b]Placed on an absolute basis using $k(\mathrm{OH} + \mathrm{C_5H_8}) = 1.00 \times 10^{-10}$ cm^3 molecule^{-1} s^{-1} (Atkinson et al., 2006).
[c]Placed on an absolute basis using $k(\mathrm{OH} + \mathrm{C_4H_6}) = 6.7 \times 10^{-11}$ cm^3 molecule^{-1} s^{-1} (Calvert et al., 2000).
[d]Placed on an absolute basis using $k(\mathrm{OH} + \mathrm{C_3H_6}) = 2.9 \times 10^{-11}$ cm^3 molecule^{-1} s^{-1} (Atkinson et al., 2006).
[e]Placed on an absolute basis using $k(\mathrm{OH} + 1\text{-}\mathrm{C_4H_8}) = 3.19 \times 10^{-11}$ cm^3 molecule^{-1} s^{-1} (Calvert et al., 2000).
[f]Placed on an absolute basis using $k(\mathrm{OH} + m\text{-xylene}) = 2.31 \times 10^{-11}$ cm^3 molecule^{-1} s^{-1} (Calvert et al., 2002).
[g]Placed on an absolute basis using $k(\mathrm{OH} + \mathrm{cyclohexane}) = 6.9 \times 10^{-12}$ cm^3 molecule^{-1} s^{-1} (Calvert et al., 2008).
[g*]Obtained at the EUPHORE outdoor chamber in Spain.

Table IV-F-6. Rate coefficients (k, cm^3 molecule^{-1} s^{-1}) for reaction of NO_3 with pinonaldehyde

$10^{15} \times k$	T (K)	Technique[a]	Reference
54 ± 18	300	RR[b] (1-butene)	Glasius et al. (1997)
26 ± 4	298	DF–RR (C_3H_6)[c]	Hallquist et al. (1997)
19 ± 9	296	RR (C_3H_6)[c]	Alvarado et al. (1998)
23 ± 9		RR (1-C_4H_8)[b]	
19 ± 8		RR (thiophene)[d]	

[a]Abbreviations used for the techniques are defined in table I-F-3.
[b]Placed on an absolute basis using $k(\mathrm{NO_3} + 1\text{-}\mathrm{C_4H_8}) = 1.40 \times 10^{-14}$ cm^3 molecule^{-1} s^{-1} (Calvert et al., 2000).
[c]Placed on an absolute basis using $k(\mathrm{NO_3} + \mathrm{C_3H_6}) = 9.5 \times 10^{-15}$ cm^3 molecule^{-1} s^{-1} (Atkinson et al., 2006).
[d]Placed on an absolute basis using $k(\mathrm{NO_3} + \mathrm{thiophene}) = 3.94 \times 10^{-14}$ cm^3 molecule^{-1} s^{-1} (Atkinson, 1991).

are again significantly larger, compared with those of the other two determinations; see table IV-F-6. In view of the difficulties experienced with OH by both Glasius et al. and by Hallquist et al., it is appropriate to follow the recommendation of IUPAC (2008) and use only the determinations of Alvarado et al. to obtain a mean value at 298 K of 2.0×10^{-14} cm^3 molecule^{-1} s^{-1}, with an uncertainty of ±40%.

IV-F-5.3. O_3 Reaction Kinetics

The reaction has been studied at room temperature by Glasius et al. (1997) and by Alvarado et al. (1999) by measuring the loss of pinonaldehyde (table IV-F-7).

Table IV-F-7. Rate coefficients (k, cm^3 $molecule^{-1}$ s^{-1}) for reaction of O_3 with pinonaldehyde

$10^{20} \times k$	T (K)	Technique[a]	Reference
8.9 ± 1.4	300	Reactant decay	Glasius et al. (1997)
< 2	296	Reactant decay	Alvarado et al. (1998)

The difficulties discussed above with the results of Glasius et al. suggest the upper limit of $k < 2 \times 10^{-20}$ cm^3 $molecule^{-1}$ s^{-1} should be used.

IV-F-5.4. Cl-Atom Reaction Kinetics

The reaction of Cl with pinonaldehyde was studied by Nozière et al. (1999b) using a relative rate technique, with cyclohexane ($k = 3.3 \times 10^{-10}$ cm^3 $molecule^{-1}$ s^{-1}) as the reference. They obtained a value of 2.3×10^{-10} cm^3 $molecule^{-1}$ s^{-1} to which an uncertainty of ±40% should be attached.

IV-F-5.5. Summary of the Atmospheric Fate of Pinonaldehyde and the End Products of Its Oxidation

The lifetime for photodissociation of pinonaldehyde is about 20 h with an overhead Sun; see section IX-C-13. For [OH] $\approx 2.5 \times 10^6$ molecule cm^{-3}, the lifetime of pinonaldehyde with respect to reaction with OH is about 2.6 h. The lifetime for removal by O_3 is not significant, given the upper limit obtained by Alvarado et al. (1999), while that for removal by Cl, with [Cl] $= 10^4$ molecule cm^{-3} is about 5 days. Removal of pinonaldehyde at night by NO_3 is fast; with [NO_3] $\approx 3 \times 10^9$ molecule cm^{-3} the lifetime is about 4.6 h. Nozière et al. (1999b) measured product yields following reaction of pinonaldehyde with OH in the presence of NO and air. They obtained yields for acetone and formaldehyde of (14 ± 8)% and (152 ± 56)%, respectively. They also obtained yields of unidentified carbonyl and aldehyde products of (107 ± 54)% and (47 ± 24)%. On the basis of structure–activity relations, they argued that abstraction of the aldehydic H should be the major channel (77%), a conclusion confirmed by earlier measurements based on the detection of the resulting PAN species in excess NO_2, which gave a yield of 81%.

The acetone product derives from the minor abstractions occurring at the 3- and 5-positions (see above), which account for ~14% of the yield according to the structure–activity relations. The co-product of acetone is the same for both channels and contains three keto and one aldehyde groups. Nozière et al. (1999b) found it more difficult to account for the high yield of CH_2O, which suggests that it is formed following abstraction of the aldehydic H. They could not propose a mechanism, however, that led to CH_2O formation. The Master Chemical Mechanism (MCMv3.1) does contain such a mechanism, although it involves a sequence of nine steps via a succession of peroxy and oxy radicals. The coproduct of CH_2O is 3,4 dioxopentanal. Reaction of this compound by photolysis or by reaction with OH yields the oxy radical from biacetyl, $CH_3C(O)C(O)CH_2O$, which dissociates to form CH_2O, CO, and the acetyl radical.

There are a number of competing reactions, however, even at high NO, which promote conversion of RO_2 into RO, such as the formation of nitrates in reaction of peroxy radicals with NO. Acetone is also produced by this route requiring an acetone yield higher than that found experimentally.

Fantechi et al. (2002) have constructed a detailed mechanism for the oxidation of pinonaldehyde using theoretical quantum chemistry methods. Under both atmospheric conditions and under the high NO_x conditions used by Nozière et al. (1999b), they obtained yields for acetone and formaldehyde of 9.9% and 12%, respectively. Their mechanism differs from the MCM in that isomerizations of the oxy radicals by 1,5 and 1,7 H-shifts are found to be important; whereas, the MCM invokes dissociation solely, which leads to a faster breakdown of the molecular structure. The mechanism developed by Fantechi et al. (2002) gives a high yield of organic nitrates. The main stable intermediate in the mechanism is 4-hydroxynorpinonaldehyde with a yield of 38% under atmospheric conditions.

IV-F-6. Caronaldehyde

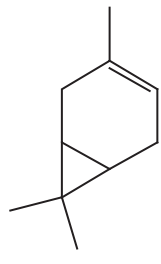

Δ^3-Carene

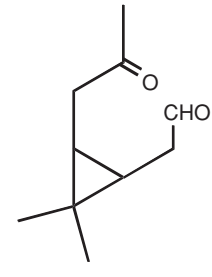

Caronaldehyde

Caronaldehyde is formed in the OH-initiatiated oxidation of Δ^3-carene in yields of 31–34% (Arey et al., 1990a; Hakola et al., 1994). It is also formed in lower yields (8%) in the ozone-initiated oxidation of Δ^3-carene.

IV-F-6.1. OH Reaction Kinetics

The reaction of OH with caronaldehyde has been studied by Hallquist et al. (1997) and by Alvarado et al. (1999) (table IV-F-8). The rate coefficient reported by Hallquist et al. is approximately a factor of 2 greater than that reported by Alvarado et al. Following the arguments advanced for pinonaldehyde, the experiments of Alvarado et al. appear the more reliable and give an unweighted mean rate coefficient at 296 K of 5.0×10^{-11} cm^3 molecule^{-1} s^{-1} with an uncertainty of $\pm 40\%$.

IV-F-6.2. NO_3 Reaction Kinetics

Hallquist et al. (1997) and Alvarado et al. (1998) have used relative rate techniques to study the reaction of NO_3 with caronaldehyde; see table IV-F-9. The results agree

Table IV-F-8. Rate coefficients (k, cm^3 $molecule^{-1}$ s^{-1}) for reaction of OH with caronaldehyde

$10^{12} \times k$	T (K)	Technique[a]	Reference
132 ± 36	298	DF–RR (C_3H_6)[b]	Hallquist et al. (1997)
53 ± 9	296	RR (C_3H_6)[b]	Alvarado et al. (1998)
47 ± 11		RR (1-C_4H_8)[c]	

[a]Abbreviations used for the techniques are defined in table I-F-3.
[b]Placed on an absolute basis using $k(OH + C_3H_6) = 2.9 \times 10^{-11}$ cm^3 $molecule^{-1}$ s^{-1} (Atkinson et al., 2006).
[c]Placed on an absolute basis using $k(OH + C_4H_8) = 3.17 \times 10^{-11}$ cm^3 $molecule^{-1}$ s^{-1} (Calvert et al., 2000).

Table IV-F-9. Rate coefficients (k, cm^3 $molecule^{-1}$ s^{-1}) for reaction of NO_3 with caronaldehyde

$10^{15} \times k$	T (K)	Technique[a]	Reference
28.0 ± 1.5	298	DF–RR (C_3H_6)[b]	Hallquist et al. (1997)
24 ± 12	296	RR (C_3H_6)[b]	Alvarado et al. (1998)
26 ± 12		RR (1-C_4H_8)[c]	
24 ± 11		RR (thiophene)[d]	

[a]Abbreviations used for the techniques are defined in table I-F-3.
[b]Placed on an absolute basis using $k(NO_3 + C_3H_6) = 9.5 \times 10^{-15}$ cm^3 $molecule^{-1}$ s^{-1} (Atkinson et al., 2006).
[c]Placed on an absolute basis using $k(NO_3 + 1\text{-}C_4H_8) = 1.35 \times 10^{-14}$ cm^3 $molecule^{-1}$ s^{-1} (Calvert et al., 2000).
[d]Placed on an absolute basis using $k(NO_3 + \text{thiophene}) = 3.93 \times 10^{-14}$ cm^3 $molecule^{-1}$ s^{-1} (Atkinson et al., 1988).

well, but, as discussed for pinonaldehyde, the data of Alvarado are probably the more reliable and give a mean value at 296 K of 2.5×10^{-14} cm^3 $molecule^{-1}$ s^{-1} with an uncertainty of ±40%.

IV-F-6.3. Summary of the Atmospheric Fate of Caronaldehyde and the End Products of Its Oxidation

Photodissociation lifetimes for caronaldehyde are uncertain, but they are probably similar to those for pinonaldehyde (roughly 20 h); see section IX-C-13. For [OH] $\approx 2.5 \times 10^6$ molecule cm^{-3}, the lifetime of caronaldehyde with respect to reaction with OH is about 2.3 h. Removal of caronaldehyde at night by NO_3 with [NO_3] $\approx 3 \times 10^9$ molecule cm^{-3} gives a lifetime of about 3.7 h.

Information on the products of the oxidation of caronaldehyde is limited. Colville and Griffin (2004) have developed a mechanism for the oxidation of Δ^3-carene using the protocols for the MCM by Jenkin et al. (1997). Their main aim was to provide information to understand the formation of secondary organic aerosol, so that they were interested in the formation of condensable intermediates rather than in the complete degradation pathway. They showed that initial abstraction by OH of the aldehydic H or photolysis, followed by reaction with O_2, both lead to decarboxylation and formation of a peroxy radical similar to that formed in the initial stages of pinonaldehyde oxidation. They did not, however, pursue the mechanism further.

IV-F-7. 3-Isopropenyl-6-oxo-heptanal (IPOH)

A major product of the atmospheric oxidation of the biogenic hydrocarbon, limonene, is 3-isopropenyl-6-oxo-heptanal (IPOH)

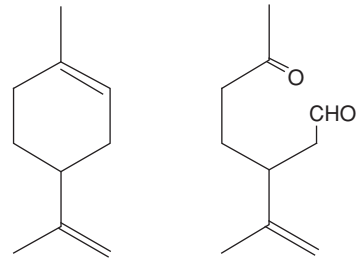

Limonene IPOH

Calogirou et al. (1999) studied the kinetics of the reactions of OH, NO_3, and O_3 with IPOH. They measured all rate coefficients relative to isobutene, using the following isobutene rate coefficients: $k(\text{OH} + \text{isobutene}) = 5.2 \times 10^{-11}\,\text{cm}^3\ \text{molecule}^{-1}\,\text{s}^{-1}$, $k(\text{NO}_3 + \text{isobutene}) = 3.4 \times 10^{-13}\,\text{cm}^3\ \text{molecule}^{-1}\,\text{s}^{-1}$ and $k(\text{O}_3 + \text{isobutene}) = 1.13 \times 10^{-17}\,\text{cm}^3\ \text{molecule}^{-1}\,\text{s}^{-1}$ (Calvert et al., 2000). They obtained:

$$k(\text{OH} + \text{IPOH}) = 1.1 \times 10^{-10}\ \text{cm}^3\ \text{molecule}^{-1}\ \text{s}^{-1}$$

$$k(\text{NO}_3 + \text{IPOH}) = 2.6 \times 10^{-13}\ \text{cm}^3\ \text{molecule}^{-1}\ \text{s}^{-1}$$

$$k(\text{O}_3 + \text{IPOH}) = 7.8 \times 10^{-18}\ \text{cm}^3\ \text{molecule}^{-1}\ \text{s}^{-1}$$

In the absence of confirmatory measurements, an uncertainty of ±40% should be attached to these values.

The atmospheric lifetime of IPOH during the day is primarily determined by its reaction with OH and is about 1 h for $[\text{OH}] = 2.5 \times 10^6$ molecule cm^{-3}. At night, and for $[\text{NO}_3] = 2.5 \times 10^9$ molecule cm^{-3}, it has a lifetime of about 25 min.

The products of its atmospheric oxidation are not known, although Calogirou et al. (1999) observed 2-isopropenyl-5-oxo-hexanal in the OH-initiated oxidation of IPOH in a chamber.

IV-F-8. Citronellal (3,7-dimethyl-6-octen-1-al)

Citronellal is a component of citronella oil that is used as an indoor fragrance and air freshener. Harrison et al. (2007) measured the rate coefficients for reaction of citronellal with OH and O_3 using relative rate techniques. They obtained a rate coefficient at 298 K for OH + citronellal of $(1.51 \pm 0.4) \times 10^{-10}\,\text{cm}^3\ \text{molecule}^{-1}\,\text{s}^{-1}$, using limonene ($k = 1.7 \times 10^{-10}\,\text{cm}^3\ \text{molecule}^{-1}\,\text{s}^{-1}$; Calvert et al., 2000) and 3-carene ($k = 8.0 \times 10^{-11}\,\text{cm}^3\ \text{molecule}^{-1}\ \text{s}^{-1}$; Calvert et al., 2000) as reference compounds. An overall uncertainty of ±30% is estimated. They determined $k(\text{O}_3 + \text{citronellal}) = (3.5 \pm 1.2) \times 10^{-16}\,\text{cm}^3\ \text{molecule}^{-1}\,\text{s}^{-1}$, using limonene

($k = 2.0 \times 10^{-16}$ cm^3 molecule^{-1} s^{-1}; Calvert et al., 2000) and 6-methyl-5-hepten-2-one ($k = 3.9 \times 10^{-16}$ cm^3 molecule^{-1} s^{-1}; section V-E-8.1) as reference compounds. An overall uncertainty of ±30% is estimated.

Harrison et al. (2007) also examined the reaction products using derivatization methods, coupled with mass spectrometry. They found, following initial reaction with both OH and O_3, that 3-methyl-hexanedial is the major product and glyoxal a minor product. The atmospheric lifetime for reaction with OH is about 45 min. with [OH] $= 2.5 \times 10^6$ molecule cm^{-3} and about 30 min. for reaction with [O_3] $= 1.5 \times 10^{12}$ molecule cm^{-3}.

IV-G. Halogen-Substituted Aldehydes

IV-G-1. Formyl Fluoride [HC(O)F]

IV-G-1.1. OH Reaction Kinetics

Wallington and Hurley (1993) studied the rate of reaction of OH radicals with HC(O)F using a relative rate method in 740 Torr of O_2 diluent at 296 K. There was no evidence of reaction and an upper limit of k(OH + HC(O)F) $< 5 \times 10^{-15}$ cm^3 molecule^{-1} s^{-1} at 296 K was reported (see table IV-G-1).

IV-G-1.2. Cl-Atom Reaction Kinetics

Results from a relative rate study of the reaction of chlorine atoms with HC(O)F by Meagher et al. (1997) are given in table IV-G-2. Taking an average of the determinations by Meagher et al. (1997) gives k(Cl + HC(O)F) $= 1.9 \times 10^{-15}$ cm^3 molecule^{-1} s^{-1} at 295 K.

IV-G-1.3. Summary of the Atmospheric Fate of HC(O)F

Combining an estimate of the diurnal average [OH] $= 1 \times 10^6$ molecule cm^{-3} with the upper limit for k(OH + HC(O)F) above gives a lower limit of 6 years for the atmospheric lifetime of HC(O)F with respect to reaction with OH radicals. The removal of HC(O)F from the atmosphere is believed to dominated by hydrolysis on contact with cloud-rain-sea water giving HF and HC(O)OH (Wallington et al., 1994b).

IV-G-2. Difluoroacetaldehyde (CHF_2CHO)

IV-G-2.1. OH Reaction Kinetics

The kinetics of the reaction of OH radicals with CHF_2CHO have been studied by Scollard et al. (1993) and Sellevåg et al. (2005) using relative rate methods. The results are given in table IV-G-1. Within the likely combined experimental uncertainties, the results from the two studies are in good agreement. An average of the results from Scollard et al. (1993) and Sellevåg et al. (2005) gives k(OH + CHF_2CHO) $= 1.5 \times 10^{-12}$ cm^3 molecule^{-1} s^{-1} at 298 K with an uncertainty estimated to be ±25%.

Table IV-G-1. Rate coefficients (k, cm^3 molecule^{-1} s^{-1}) for reaction of OH with halogen substituted aldehydes

Molecule	$10^{12} \times A$	B (K)	$10^{12} \times k$	T (K)	Technique[a]	Reference	Temperature Range (K)
HC(O)F			< 0.005	296	RR (CH_3F)[b]	Wallington and Hurley (1993)	
CHF_2CHO			1.3 ± 0.3	298	RR ($C_6H_5CH_3$)[c]	Scollard et al. (1993)	
			1.7 ± 0.2		PLP–RF		
			1.79 ± 0.05	298	RR (C_3H_8)[d]	Sellevåg et al. (2005)	
CF_3CHO			1.1 ± 0.5	298	DF–RF	Dóbé et al. (1989)	
			0.65 ± 0.05	298	PLP–RF	Scollard et al. (1993)	
			0.44 ± 0.10	298	RR (CH_3COCH_3)[e]		
			0.480 ± 0.031	298	RR (C_2H_6)[f]	Sellevåg et al. (2004a)	
			0.568 ± 0.074	296	RR (C_2H_2)[g]	Andersen et al. (2004b)	
			0.642 ± 0.075		RR (C_2H_4)[h]		
C_2F_5CHO			0.463 ± 0.051	296	RR (C_2H_2)[g]	Andersen et al. (2003)	
			0.510 ± 0.029		RR (C_2H_4)[h]		
C_3F_7CHO			0.568 ± 0.074	296	RR (C_2H_2)[g]	Andersen et al. (2004b)	
			0.642 ± 0.075		RR (C_2H_4)[h]		
	2.0 ± 0.6	369 ± 90	0.49 ± 0.01	252	PLP–LIF	Solignac et al. (2007)	252–373
			0.51 ± 0.02	262			
			0.52 ± 0.03	272			
			0.58 ± 0.05	297			
			0.53 ± 0.01	297			
			0.67 ± 0.03	323			
			0.75 ± 0.02	348			
			0.75 ± 0.03	373			
C_4F_9CHO			0.568 ± 0.074	296	RR (C_2H_2)[g]	Andersen et al. (2004b)	
			0.642 ± 0.075		RR (C_2H_4)[h]		
	2.0 ± 0.5	356 ± 70	0.48 ± 0.02	253	PLP–LIF	Solignac et al. (2007)	252–373
			0.51 ± 0.02	263			
			0.58 ± 0.03	273			
			0.61 ± 0.03	294			
			0.64 ± 0.03	299			
			0.64 ± 0.03	323			
			0.71 ± 0.01	345			
			0.76 ± 0.02	359			
			0.79 ± 0.01	373			

(*continued*)

Table IV-G-1. (*continued*)

Molecule	$10^{12} \times A$	B (K)	$10^{12} \times k$	T (K)	Technique[a]	Reference	Temperature Range (K)
CF_3CH_2CHO			3.87 ± 0.16	298	RR (C_2H_5OH)[i]	Sellevåg et al. (2004a)	
			3.07 ± 0.08		RR [$HC(O)OC_2H_5$][j]		
			2.96 ± 0.04	298	PLP–LIF	Kelly et al. (2005)	
			2.48 ± 0.27	296	RR (C_2H_2)[g]	Hurley et al. (2005)	
			2.65 ± 0.36		RR (C_2H_4)[h]		
$C_8F_{17}CH_2CHO$			1.82 ± 0.32	296	RR (C_2H_4)[h]	Chiappero et al. (2008a)	
HC(O)Cl			< 0.32	298	RR (n-C_4H_{10})[k]	Libuda et al. (1990)	
CH_2ClCHO			3.06	298	RR (n-C_4H_{10})[k,l]	Starcke et al. (1990)	
			3.0 ± 0.6	298	PLP–RF	Balestra-Garcia et al. (1992)	
			3.4 ± 0.2	298	RR ($CH_3COC_2H_5$)[m]	Scollard et al. (1993)	
$CHCl_2CHO$			2.68[l]	298	RR (n-C_4H_{10})[k]	Starcke et al. (1990)	
			2.4 ± 0.5	298	PLP–RF	Balestra-Garcia et al. (1992)	
			2.5 ± 0.1	298	RR ($CH_3COC_2H_5$)[m]	Scollard et al. (1993)	
CCl_3CHO	1.56 ± 0.33	600 ± 100	1.61[q]	298	DF–RF	Dóbé et al. (1989)	298–520
			1.56 ± 0.25	300			
			1.69 ± 0.52	304			
			2.13 ± 0.22	339			
			2.48 ± 0.47	391			
			2.91 ± 0.37	449			
			3.29[q]	483			
			3.94 ± 1.10	520			
			1.15[l]	300	RR (n-C_4H_{10})[k]	Starcke et al. (1990)	
			1.76 ± 0.31	298	RR [$CH_3C(O)OC_2H_5$][n]	Nelson et al. (1990b)	
			0.86 ± 0.17	298	PLP–RF	Balestra-Garcia et al. (1992)	
			1.5 ± 0.2	298	RR ($C_6H_5CH_3$)[d]	Scollard et al. (1993)	
			0.97 ± 0.02	298	RR [$(CH_3)_3CH$][p]	Barry et al. (1994)	
			1.28 ± 0.25		DF–RF		
			0.89 ± 0.15		DF–EPR		

	1.79 ± 0.17	240 ± 66	0.669 ± 0.009	233	PLP–LIF	Talukdar et al. (2001)	233–415
			0.701 ± 0.010	233			
			0.705 ± 0.009	251			
			0.755 ± 0.006	252			
			0.794 ± 0.002	253			
			0.762 ± 0.004	271			
			0.798 ± 0.006	295			
			0.788 ± 0.005	295			
			0.747 ± 0.034	296			
			0.804 ± 0.015	297			
			0.833 ± 0.005	323			
			0.92 ± 0.012	327			
			0.885 ± 0.013	348			
			1.06 ± 0.061	374			
			1.02 ± 0.027	413			
			1.17 ± 0.008	415			
$CHClFCHO$			1.9 ± 0.3	298	RR ($C_6H_5CH_3$)[c]	Scollard et al. (1993)	
			2.2 ± 0.2[o]	298	PLP–RF		
$CFCl_2CHO$			1.0 ± 0.2	298	RR ($C_6H_5CH_3$)[c]	Scollard et al. (1993)	
			1.3 ± 0.1	298	PLP–RF		
CF_2ClCHO			0.69 ± 0.05	298	RR (C_2H_5OH)[i]	Scollard et al. (1993)	
			0.95 ± 0.05	298	PLP–RF		

[a]Abbreviations used for the techniques are defined in table I-F-3.
[b]Placed on an absolute basis using $k(OH + CH_3F) = 2.0 \times 10^{-14}$ cm^3 molecule^{-1} s^{-1} (Calvert et al., 2008).
[c]Placed on an absolute basis using $k(OH + C_6H_5CH_3) = 5.63 \times 10^{-12}$ cm^3 molecule^{-1} s^{-1} (Calvert et al., 2002).
[d]Placed on an absolute basis using $k(OH + C_3H_8) = 1.1 \times 10^{-12}$ cm^3 molecule^{-1} s^{-1} (Atkinson et al., 2006).
[e]Placed on an absolute basis using $k(OH + CH_3COCH_3) = 1.8 \times 10^{-13}$ cm^3 molecule^{-1} s^{-1} (Atkinson et al., 2006).
[f]Placed on an absolute basis using $k(OH + C_2H_6) = 2.4 \times 10^{-13}$ cm^3 molecule^{-1} s^{-1} (Atkinson et al., 2006).
[g]Placed on an absolute basis using $k(OH + C_2H_2) = 7.8 \times 10^{-13}$ cm^3 molecule^{-1} s^{-1} (Atkinson et al., 2006).
[h]Placed on an absolute basis using $k(OH + C_2H_4) = 7.9 \times 10^{-12}$ cm^3 molecule^{-1} s^{-1} (Atkinson et al., 2006).
[i]Placed on an absolute basis using $k(OH + C_2H_5OH) = 3.2 \times 10^{-12}$ cm^3 molecule^{-1} s^{-1} (Atkinson et al., 2006).
[j]Placed on an absolute basis using $k(OH + HC(O)OC_2H_5) = 8.74 \times 10^{-13}$ cm^3 molecule^{-1} s^{-1} (this book, section VII-B-2.1).
[k]Placed on an absolute basis using $k(OH + n\text{-}C_4H_{10}) = 2.45 \times 10^{-12}$ cm^3 molecule^{-1} s^{-1} (Calvert et al., 2008).
[l]Quoted as "preliminary values, probably lower limits" by Starcke et al. (1990).
[m]Placed on an absolute basis using $k(OH + CH_3C(O)C_2H_5) = 1.2 \times 10^{-12}$ cm^3 molecule^{-1} s^{-1} (Atkinson et al., 2006).
[n]Placed on an absolute basis using $k(OH + CH_3C(O)OC_2H_5) = 1.73 \times 10^{-12}$ cm^3 molecule^{-1} s^{-1} (Picquet et al., 1998).
[o]Uncertainty estimated from rate data in figure 4 in Scollard et al. (1993).
[p]Placed on an absolute basis using $k[OH + (CH_3)_3CH] = 2.16 \times 10^{-12}$ cm^3 molecule^{-1} s^{-1} (Calvert et al., 2008).
[q]Single determination.

Table IV-G-2. Rate coefficients (k, cm^3 molecule^{-1} s^{-1}) for reaction of chlorine atoms with halogen substituted aldehydes

Molecule	$10^{11} \times A$	B (K)	$10^{11} \times k$	T (K)	Technique[a]	Reference	Temperature Range (K)
HC(O)F			0.000195 ± 0.000012	295	RR (CD_4)[b]	Meagher et al. (1997)	
			0.000193 ± 0.000004		RR (CH_3CFCl_2)[c]		
			0.000189 ± 0.000012		RR (CH_2ClCF_3)[d]		
			0.000193 ± 0.000008		RR (CH_2FCF_3)[e]		
CHF_2CHO			0.44 ± 0.09	298	RR (CH_3COCH_3)[f]	Scollard et al. (1993)	
CF_3CHO			0.160 ± 0.014	295	RR (CH_3Cl)[g]	Wallington and Hurley (1993)	
			0.184 ± 0.027		RR (C_2H_5Cl)[h]		
			0.240 ± 0.009	298	RR (CH_3COCH_3)[f]	Scollard et al. (1993)	
			0.185 ± 0.026	296	RR (CH_3Cl)[g]	Andersen et al. (2004b)	
			0.179 ± 0.023		RR (C_2H_5Cl)[h]		
			0.183 ± 0.010	296	RR (CF_3CH_2OH)[i]	Hurley et al. (2004c)	
C_2F_5CHO			0.185 ± 0.013	296	RR (CH_3Cl)[g]	Andersen et al. (2003)	
			0.201 ± 0.016		RR (C_2H_5Cl) [h]		
			0.226 ± 0.023	296	RR ($C_2F_5CH_2OH$)[i]	Hurley et al. (2004c)	
CF_3CH_2CHO			1.90 ± 0.03	298	RR [$HC(O)OC_2H_5$][j]	Kelly et al. (2005)	
			1.83 ± 0.16	296	RR (C_2H_5Cl)[h]	Hurley et al. (2005)	
			1.76 ± 0.22		RR (CH_3OH)[l]		
n-C_3F_7CHO			0.247 ± 0.014	296	RR ($C_3F_7CH_2OH$)[i]	Hurley et al. (2004c)	
			0.202 ± 0.021	296	RR (CH_3Cl)[g]	Andersen et al. (2004b)	
			0.197 ± 0.022		RR (C_2H_5Cl)[h]		
n-C_4F_9CHO			0.240 ± 0.011	296	RR ($C_4F_9CH_2OH$)[i]	Hurley et al. (2004b)	
			0.233 ± 0.024	296	RR (CH_3Cl)[g]	Andersen et al. (2004b)	
			0.229 ± 0.023		RR (C_2H_5Cl)[h]		
$C_4F_9CH_2CHO$			1.97 ± 0.09	296	RR ($C_4F_9CH_2CH_2OH$)[k]	Hurley et al. (2004b)	
$C_6F_{13}CHO$			0.257 ± 0.063	298	RR ($C_6F_{19}CH_2OH$)[i]	Solignac et al. (2006b)	
$C_8F_{17}CH_2CHO$			1.72 ± 0.16	296	RR (C_2H_5Cl)[h]	Chiappero et al. (2008)	
			2.04 ± 0.22		RR (CH_3OH)[l]		
HC(O)Cl			0.00619	305	RR (CH_2Cl_2)[m]	Sanhueza and Heicklen (1975)	
			0.0768 ± 0.0096	298	RR (CH_3Cl)[g]	Niki et al. (1980)	

	0.82	703	0.0571	265.8	RR (CH_4)[n]	Libuda et al. (1990)	265.8–321.3
			0.0570	265.8			
			0.0614	265.8			
			0.0685	281.8			
			0.0654	282.0			
			0.0702	282.0			
			0.0822	301.2			
			0.0167	301.8			
			0.0756	303.2			
			0.0958	321.0			
			0.0919	321.2			
			0.0958	321.2			
			0.0871	321.3			
CH_2ClCHO			1.12	298	RR (C_2H_6)[o]	Starcke et al. (1990)	
			1.5 ± 0.3	298	RR ($C_6H_5CH_3$)[p]	Scollard et al. (1993)	
$CHCl_2CHO$			1.31	298	RR (C_2H_6)[o]	Starcke et al. (1990)	
			1.3 ± 0.2	298	RR ($C_6H_5CH_3$)[p]	Scollard et al. (1993)	
CCl_3CHO			0.93	298	RR (C_2H_6)[o]	Starcke et al. (1990)	
			0.74 ± 0.05	298	RR ($C_6H_5CH_3$)[p]	Scollard et al. (1993)	
			0.54 ± 0.07	298	PLP–RF	Talukdar et al. (2001)	
CHClFCHO			1.0 ± 0.2	298	RR ($C_6H_5CH_3$)[p]	Scollard et al. (1993)	
$CFCl_2CHO$			5.9 ± 1.2	298	RR ($C_6H_5CH_3$)[p]	Scollard et al. (1993)	
CF_2ClCHO			0.44 ± 0.03	298	RR (CH_3COCH_3)[f]	Scollard et al. (1993)	

[a]Abbreviations used for the techniques are defined in table I-F-3.
[b]Placed on an absolute basis using $k(Cl + CD_4) = 6.1 \times 10^{-15}$ cm^3 molecule^{-1} s^{-1} (Wallington and Hurley, 1992).
[c]Placed on an absolute basis using $k(Cl + CH_3CFCl_2) = 2.1 \times 10^{-15}$ cm^3 molecule^{-1} s^{-1} (Atkinson et al., 2008).
[d]Placed on an absolute basis using $k(Cl + CF_3CH_2Cl) = 6.5 \times 10^{-15}$ cm^3 molecule^{-1} s^{-1} (Sander et al., 2006).
[e]Placed on an absolute basis using $k(Cl + CF_3CFH_2) = 1.5 \times 10^{-15}$ cm^3 molecule^{-1} s^{-1} (Atkinson et al., 2008).
[f]Placed on an absolute basis using $k(CH_3COCH_3) = 2.1 \times 10^{-12}$ cm^3 molecule^{-1} s^{-1} (Atkinson et al., 2006).
[g]Placed on an absolute basis using $k(Cl + CH_3Cl) = 4.8 \times 10^{-13}$cm^3 molecule^{-1} s^{-1} (Atkinson et al., 2008).
[h]Placed on an absolute basis using $k(Cl + C_2H_5Cl) = 7.8 \times 10^{-12}$ cm^3 molecule^{-1} s^{-1} (section I-F).
[i]Placed on an absolute basis using $k(Cl + C_xF_{2x+1}CH_2OH) = 6.27 \times 10^{-13}$ cm^3 molecule^{-1} s^{-1} (this book, section II-F-7.2).
[j]Placed on an absolute basis using $k(Cl + HC(O)OC_2H_5) = 9.92 \times 10^{-12}$ cm^3 molecule^{-1} s^{-1} (this book, section VII-B-2.3).
[k]Placed on an absolute basis using $k(Cl + C_4F_9CH_2CH_2OH) = 1.73 \times 10^{-11}$ cm^3 molecule^{-1} s^{-1} (this book, table II-F-2).
[l]Placed on an absolute basis using $k(Cl + CH_3OH) = 5.5 \times 10^{-11}$ cm^3 molecule^{-1} s^{-1} (Atkinson et al., 2006).
[m]Placed on an absolute basis using $k(Cl + CH_2Cl_2) = 3.64 \times 10^{-13}$ cm^3 molecule^{-1} s^{-1} at 305 K (Atkinson et al., 2008).
[n]Placed on an absolute basis using $k(Cl + CH_4) = 6.6 \times 10^{-12}$ exp(−1,240/T) cm^3 molecule^{-1} s^{-1} (Atkinson et al., 2006).
[o]Placed on an absolute basis using $k(Cl + C_2H_6) = 5.9 \times 10^{-11}$ cm^3 molecule^{-1} s^{-1} (Atkinson et al., 2006).
[p]Placed on an absolute basis using $k(Cl + C_6H_5CH_3) = 5.79 \times 10^{-11}$ and $k(Cl + C_2H_6) = 5.9 \times 10^{-11}$ cm^3 molecule^{-1} s^{-1} (Wallington et al., 1988f; Atkinson et al., 2006).

IV-G-2.2. Cl-Atom Reaction Kinetics

The kinetics of the reaction of chlorine atoms with CHF_2CHO have been studied by Scollard et al. (1993) using a relative rate method (see table IV-G-2). The result from Scollard et al. (1993) of $k(Cl + CHF_2CHO) = 4.4 \times 10^{-12}\,cm^3$ molecule^{-1} s^{-1} at 298 K is recommended with an uncertainty estimated to be ±30%.

IV-G-2.3. Summary of the Atmospheric Fate of CHF_2CHO

Combining $k(OH + CHF_2CHO) = 1.6 \times 10^{-12}$ cm^3 molecule^{-1} s^{-1} at 298 K with a diurnal average [OH] $= 1.0 \times 10^6$ molecule cm^{-3} provides an estimate of 7 days for the atmospheric lifetime of CHF_2CHO with respect to reaction with OH radicals. As with other aldehydes photolysis is expected to be an important fate of CHF_2CHO with a lifetime for photodissociation of about 6 h; see section IX-C-17. COF_2 is expected to be the main atmospheric oxidation product of CHF_2CHO. It is possible that small amounts of $CHF_2C(O)OH$ are formed in the atmospheric oxidation of CHF_2CHO via formation of the hydrate $CHF_2C(OH)_2H$ and/or via reaction of $CHF_2C(O)O_2$ with HO_2 radicals. Details of the mechanisms for the formation of halogenated carboxylic acids are given in the following sections.

IV-G-3. CF_3CHO, C_2F_5CHO, n-C_3F_7CHO, n-C_4F_9CHO

IV-G-3.1. OH Reaction Kinetics

The kinetics of the reaction of OH radicals with $C_xF_{2x+1}CHO$ ($x = 1, 2, 3, 4$) have been studied by Dóbé et al. (1989), Scollard et al. (1993), Sellevåg et al. (2004a), Andersen et al. (2003, 2004b), and Solignac et al. (2007) using a variety of relative and absolute rate methods. The results are listed in table IV-G-1 and plotted in figure IV-G-1. As seen from figure IV-G-1, within the experimental uncertainties there is no evidence for a dependence of reactivity on the size of the C_xF_{2x+1}-group in $C_xF_{2x+1}CHO$. This finding is consistent with the reaction proceeding via abstraction of the aldehydic hydrogen with the size of the C_xF_{2x+1}-group having little, or no, influence on the reactivity at this site. Excluding the data of Dóbé et al. (1989) which is consistent with, but much less precise than the other studies, a fit to the combined data set in figure IV-G-1 gives $k(OH + C_xF_{2x+1}CHO) = 2.05 \times 10^{-12} \exp(-378/T)\,cm^3$ molecule^{-1} s^{-1}. This expression gives $k(OH + C_xF_{2x+1}CHO) = 5.77 \times 10^{-13}\,cm^3$ molecule^{-1} s^{-1} at 298 K with an uncertainty estimated to be ±15%.

IV-G-3.2. Cl-Atom Reaction Kinetics

The kinetics of the reaction of chlorine atoms with $C_xF_{2x+1}CHO$ ($x = 1, 2, 3, 4, 6$) have been studied by Wallington and Hurley (1993), Scollard et al. (1993), Andersen et al. (2003, 2004b), Hurley et al. (2004c), and Solignac et al. (2006b) using relative rate methods at ambient temperature. The results are listed in table IV-G-2, within the experimental uncertainties there is no evidence for a dependence of the reactivity of $C_xF_{2x+1}CHO$ towards chlorine atoms on the size of the C_xF_{2x+1}-group.

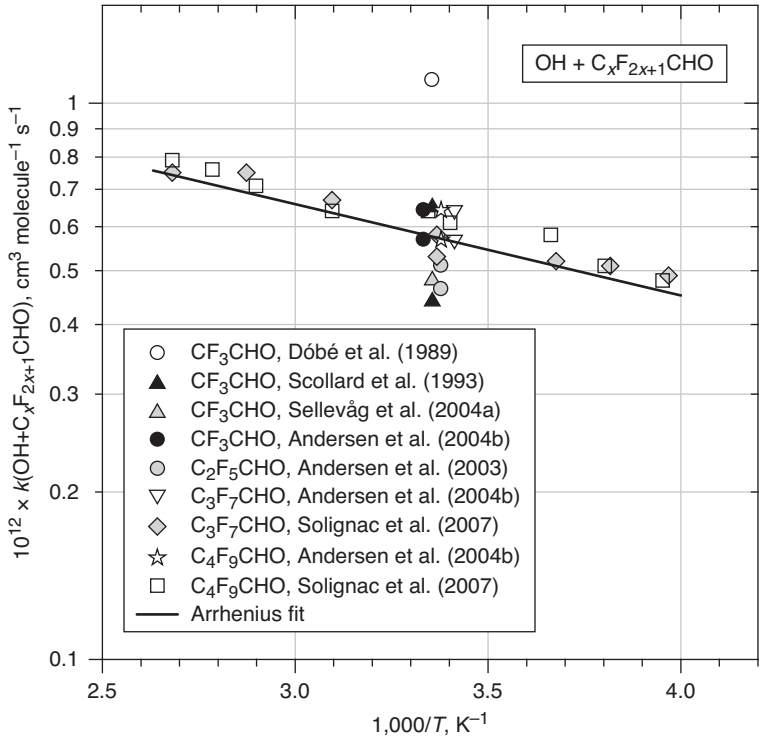

Figure IV-G-1. Measurements of the rate coefficients for reaction of OH radicals with $C_xF_{2x+1}CHO$ ($x = 1, 2, 3, 4$).

An average of the results in table IV-G-2 gives $k(Cl+C_xF_{2x+1}CHO) = 2.1 \times 10^{-12}$ cm^3 molecule^{-1} s^{-1} at 298 K with an uncertainty estimated to be ±20%.

IV-G-3.3. Summary of the Atmospheric Fate of $C_xF_{2x+1}CHO$

Combining $k(OH + C_xF_{2x+1}CHO) = 5.77 \times 10^{-13}$ cm^3 molecule^{-1} s^{-1} at 298 K with a diurnal average [OH] $= 1.0 \times 10^6$ molecule cm^{-3} provides an estimate of 20 days for the atmospheric lifetime of $C_xF_{2x+1}CHO$ with respect to reaction with OH radicals. As discussed by Chiappero et al. (2006) and in chapter IX, photolysis is likely to be approximately an order of magnitude more important than reaction with OH radicals as an atmospheric loss mechanism for $C_xF_{2x+1}CHO$; see section IX-C-18. Andersen et al. (2006) have suggested that contact with liquid water (e.g., in aerosols or clouds) resulting in hydration of $C_xF_{2x+1}CHO$ to give $C_xF_{2x+1}C(OH)_2H$, contributes to atmospheric removal of $C_xF_{2x+1}CHO$.

There is considerable research interest in the potential for the atmospheric oxidation of $C_xF_{2x+1}CHO$ to give toxic bioaccumulative perfluorocarboxylic acids. Figure IV-G-2 shows a simplified atmospheric oxidation mechanism for $C_xF_{2x+1}CHO$ illustrating the three potential formation routes for perfluorocarboxylic acids suggested by Ellis et al. (2004) and Andersen et al. (2006). The majority of atmospheric oxidation

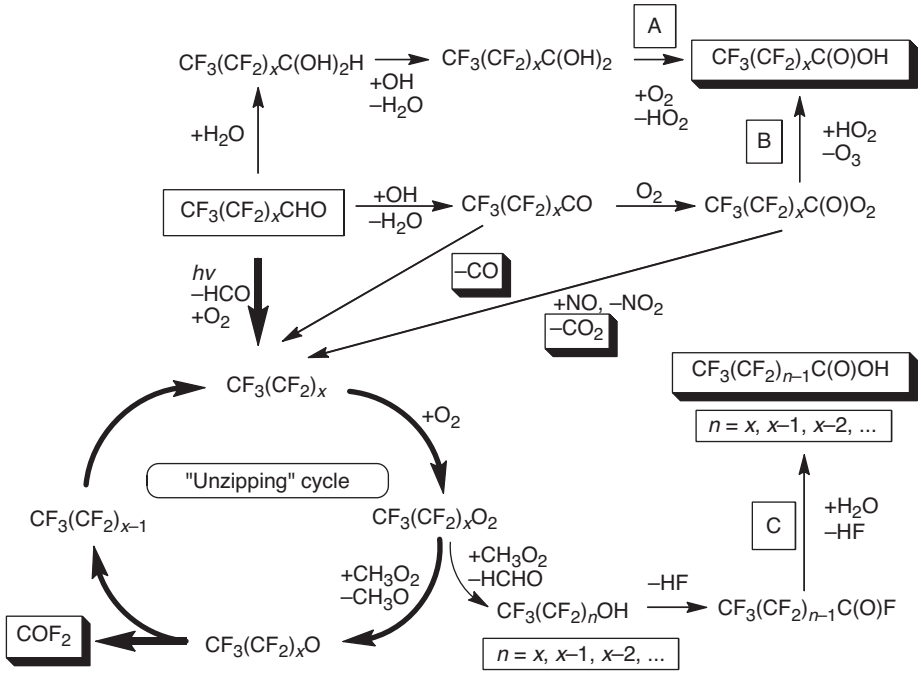

Figure IV-G-2. Simplified oxidation mechanism for $C_xF_{2x+1}CHO$ illustrating the three possible mechanisms for perfluorocarboxylic acid formation: A, reaction of hydrate with OH; B, reaction of perfluoroacylperoxy with HO_2 radicals; and C, reaction of perfluoroalkyl peroxy with α-hydrogen-containing peroxy radicals (e.g., CH_3O_2).

proceeds via photolysis followed by the "unzipping" cycle in which successive COF_2 units are shed. The result of the "unzipping"cycle is conversion of $CF_3(CF_2)_x$ radicals into a CF_3 radical and x molecules of COF_2. The CF_3 radical adds O_2 and reacts with other peroxy radicals or NO to give the CF_3O radical. The atmospheric fate of CF_3O radicals is reaction with NO or CH_4 leading to the formation of another molecule of COF_2.

$$CF_3O + NO \rightarrow COF_2 + FNO$$

$$CF_3O + CH_4 \rightarrow CF_3OH + CH_3$$

$$CF_3OH \rightarrow COF_2 + HF$$

As indicated by the thick arrows in figure IV-G-2, the majority of the oxidation of $C_xF_{2x+1}CHO$ proceeds to give COF_2. In addition to COF_2 formation there are three mechanisms by which $C_xF_{2x+1}CHO$ can be converted into perfluorocarboxylic acids; these mechanisms are labeled A, B, and C in figure IV-G-2. The first mechanism, indicated by route "A" in figure IV-G-2, involves formation of the hydrate $C_xF_{2x+1}C(OH)_2H$. Andersen et al. (2006) showed that the hydrate $C_xF_{2x+1}C(OH)_2H$ reacts with OH radicals leading to formation of the perfluorocarboxylic acid $C_xF_{2x+1}C(O)OH$. The second mechanism consists of reaction of OH

radicals with $C_xF_{2x+1}CHO$ to give fluorinated acyl radicals which add O_2 to give fluorinated acyl peroxy radicals which can react with HO_2 to give the acid via pathway "B" in figure IV-G-2 (Andersen et al., 2004c; Hurley et al., 2006). This mechanism is not likely to be efficient because reaction with OH is a minor loss mechanism for $C_xF_{2x+1}CHO$, and reaction with O_2 is probably a minor fate of $C_xF_{2x+1}CO$ radicals (Hurley et al., 2006; Waterland and Dobbs, 2007; Wallington et al., 2008b). The third mechanism intercepts $C_xF_{2x+1}O_2$ radicals as they pass through the "unzipping" cycle by reaction with α-hydrogen containing peroxy radicals (e.g., CH_3O_2) to give the alcohol $CF_3(CF_2)_nOH$ by the peroxy radical disproportionation mechanism first suggested by Russell (1957). The conversion of $CF_3(CF_2)_nOH$ into $CF_3(CF_2)_{n-1}C(O)OH$ via elimination of HF and hydrolysis (pathway "C" in figure IV-G-2) is expected to be 100% efficient. In a global atmospheric modeling study, Wallington et al. (2006b) reported that in remote areas with low NO_x, approximately 1-10% of the $C_xF_{2x+1}O_2$ radicals were intercepted at each pass through the unzipping cycle leading to the formation of a series of perfluorocarboxylic acids from long chain $C_xF_{2x+1}CHO$ molecules.

IV-G-4. CF_3CH_2CHO, n-$C_4F_9CH_2CHO$, n-$C_8F_{17}CH_2CHO$

IV-G-4.1. OH Reaction Kinetics

The kinetics of the reaction of OH radicals with $C_xF_{2x+1}CH_2CHO$ ($x = 1, 8$) have been studied by Sellevåg et al. (2004a), Kelly et al. (2005), Hurley et al. (2005), and Chiappero et al. (2008) using relative and absolute rate methods at ambient temperature. The results are listed in table IV-G-1. There is considerable scatter in the results reported for $k(OH + CF_3CH_2CHO)$ with the measurement by Hurley et al. (2005) relative to $k(OH + C_2H_2)$ being approximately 40% below that from Sellevåg et al. (2004a) relative to $k(OH + C_2H_5OH)$. The absolute result from Kelly et al. (2005) lies between those from the relative rate studies by Sellevåg et al. (2004a) and Hurley et al. (2005). Finally, the value of $k(OH + n\text{-}C_8F_{17}CH_2CHO)$ reported by Chiappero et al. (2008) lies about 40% below the average of the values of $k(OH + CF_3CH_2CHO)$ reported by Sellevåg et al. (2004a), Kelly et al. (2005), and Hurley et al. (2005). As discussed elsewhere (sections IV-G-3.1, IV-G-3.3, IV-G-4.1), the available data suggests that the reactivity of OH radicals at 298 K towards molecules of the general formula $C_xF_{2x+1}CHO$, $C_xF_{2x+1}CH_2OH$, and $C_xF_{2x+1}CH_2CH_2OH$ is not dependent on the size of the C_xF_{2x+1} group. We would expect the same behavior for molecules in the $C_xF_{2x+1}CH_2CHO$ series. Given this expectation and recognizing the scatter in the data reported for CF_3CH_2CHO listed in table IV-G-2, we recommend an average of the data for CF_3CH_2CHO and n-$C_8F_{17}CH_2CHO$; $k(OH + C_xF_{2x+1}CH_2CHO) = 2.8 \times 10^{-12}$ cm^3 molecule^{-1} s^{-1} with an uncertainty of $\pm 50\%$. Further work is needed to reduce the uncertainties in $k(OH + C_xF_{2x+1}CH_2CHO)$.

IV-G-4.2. Cl-Atom Reaction Kinetics

The kinetics of the reaction of chlorine atoms with $C_xF_{2x+1}CH_2CHO$ ($x = 1, 4, 8$) have been studied by Kelly et al. (2005), Hurley et al. (2004b, 2005), and Chiappero et al. (2008) using relative rate methods at ambient temperature. The results are

listed in table IV-G-2, within the experimental uncertainties there is no evidence for a dependence of the reactivity of $C_xF_{2x+1}CH_2CHO$ on the size of the C_xF_{2x+1} group. An average of the results in table IV-G-2 gives $k(Cl + C_xF_{2x+1}CH_2CHO) = 1.87 \times 10^{-11}\,cm^3$ molecule^{-1} s^{-1} at 298 K with an uncertainty estimated to be ±20%.

IV-G-4.3. Summary of the Atmospheric Fate of $C_xF_{2x+1}CH_2CHO$

Combining $k(OH + C_xF_{2x+1}CH_2CHO) = 2.8 \times 10^{-13}\,cm^3$ molecule^{-1} s^{-1} at 298 K with a diurnal average [OH] $= 1.0 \times 10^6$ molecule cm^{-3} provides an estimate of 4 days for the atmospheric lifetime of $C_xF_{2x+1}CHO$ with respect to reaction with OH radicals. Sellevåg et al., (2004a), Chiappero et al. (2006), and Solignac et al. (2007) have studied the photolysis of CF_3CH_2CHO and n-$C_6F_{13}CH_2CHO$. While significant uncertainties in the photolysis quantum yields for CF_3CH_2CHO and $C_6F_{13}CH_2CHO$ over the wavelength range of atmospheric relevance, it is clear from the work of Chiappero et al. (2006) and Solignac et al. (2007) that photolysis is an important, probably dominant, atmospheric fate of these species; see section IX-C-18. Photolysis of $C_xF_{2x+1}CH_2CHO$ will lead to the formation of $C_xF_{2x+1}CHO$.

$$C_xF_{2x+1}CH_2CHO + h\nu \rightarrow C_xF_{2x+1}CH_2 + HCO$$

$$C_xF_{2x+1}CH_2 + O_2 \rightarrow C_xF_{2x+1}CH_2O_2$$

$$C_xF_{2x+1}CH_2O_2 + NO \rightarrow C_xF_{2x+1}CH_2O$$

$$C_xF_{2x+1}CH_2O + O_2 \rightarrow C_xF_{2x+1}CHO + HO_2$$

In low NO_x environments, the reaction of OH with $C_xF_{2x+1}CH_2CHO$ leads to the formation of $C_xF_{2x+1}CH_2C(O)OH$, $C_xF_{2x+1}CH_2C(O)OOH$, and $C_xF_{2x+1}CHO$ as primary products (Hurley et al., 2004b, 2005, 2006). In high NO_x environments, the reaction of OH with $C_xF_{2x+1}CH_2CHO$ leads to the formation of $C_xF_{2x+1}CH_2C(O)O_2NO_2$ and $C_xF_{2x+1}CHO$ as primary products (Andersen et al., 2005b; Hurley et al., 2005).

IV-G-5. Formyl Chloride [HC(O)Cl]

IV-G-5.1. OH Reaction Kinetics

The kinetics of the reaction of OH radicals with HC(O)Cl have been studied by Libuda et al. (1990) using relative rate methods. An upper limit of $k(OH + HC(O)Cl) < 3.2 \times 10^{-13}$ cm^3 molecule^{-1} s^{-1} at 298 K was established and is recommended.

IV-G-5.2. Cl-Atom Reaction Kinetics

The kinetics of the reaction of chlorine atoms with HC(O)Cl have been studied by Sanhueza and Heicklen (1975), Niki et al. (1980), and Libuda et al. (1990). Rate coefficients are listed in table IV-G-2 and plotted in figure IV-G-3. As seen from figure IV-G-3, the data from Niki et al. (1980) and Libuda et al. (1990) are in excellent

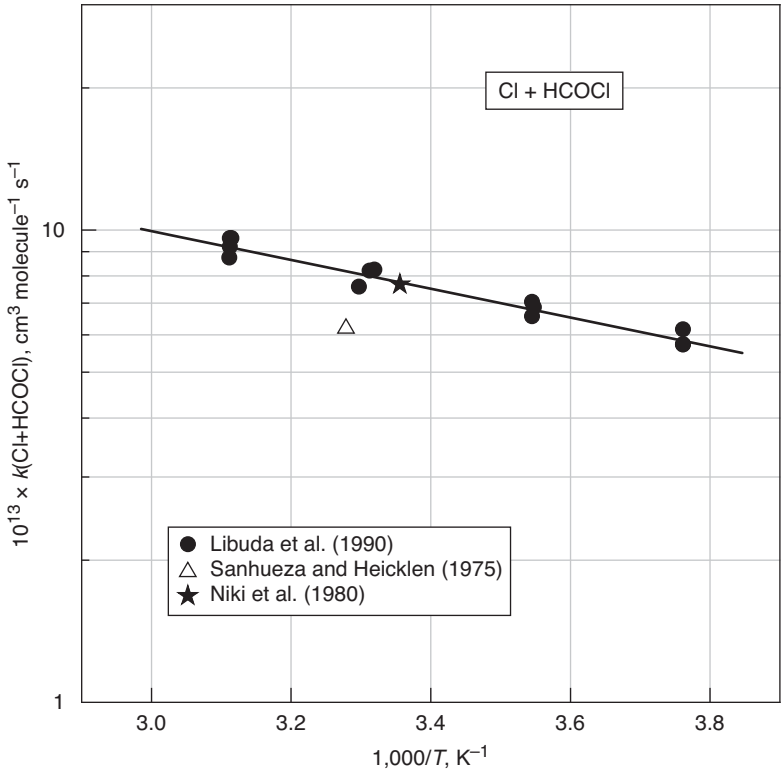

Figure IV-G-3. Measurements of the rate coefficients for reaction of chlorine atoms with HC(O)Cl. The line is a fit to the data from Niki et al. (1980) and Libuda et al. (1990).

agreement. The rate coefficient from Sanhueza and Heicklen (1975) lies approximately 20% below but is in agreement with those from Niki et al. (1980) and Libuda et al. (1990) within the likely experimental uncertainties. A fit to the combined data from Niki et al. (1980), and Libuda et al. (1990) gives $k[\mathrm{Cl} + \mathrm{HC(O)Cl}] = 8.18 \times 10^{-12} \exp(-702/T)\,\mathrm{cm^3\ molecule^{-1}\ s^{-1}}$. This expression yields $k(\mathrm{Cl} + \mathrm{HC(O)Cl}) = 7.76 \times 10^{-13}\,\mathrm{cm^3\ molecule^{-1}\ s^{-1}}$ at 298 K. The uncertainty in k[Cl + HC(O)Cl] at 298 K is estimated to be ±20%.

IV-G-5.3. Summary of the Atmospheric Fate of HC(O)Cl

Combining $k(\mathrm{OH} + \mathrm{HC(O)Cl}) < 3.2 \times 10^{-13}\ \mathrm{cm^3\ molecule^{-1}\ s^{-1}}$ at 298 K with a diurnal average $[\mathrm{OH}] = 1.0 \times 10^6\ \mathrm{molecule\,cm^{-3}}$ provides a lower limit of 40 days for the atmospheric lifetime of HC(O)Cl with respect to reaction with OH radicals. Heterogeneous decomposition of HC(O)Cl into HCl and CO is observed in experimental studies on a timescale of minutes to hours (Libuda et al., 1990; Niki et al., 1980). Computational studies have shown that the activation barrier for homogeneous decomposition of HC(O)Cl is large, approximately 41 kcal mol^{-1} (Francisco and Zhao, 1992; Phillips et al., 2005) and this reaction is not important. Heterogeneous decomposition,

and possibly homogeneous decomposition catalyzed by water trimers and tetramers (Phillips et al., 2005), probably dominates the atmospheric loss of HC(O)Cl.

IV-G-6. 2-Chloroethanal [Chloroacetaldehyde, $CH_2ClC(O)H$]

IV-G-6.1. OH Reaction Kinetics

The kinetics of the reaction of OH radicals with $CH_2ClC(O)H$ have been studied by Starcke et al. (1989), Balestra-Garcia et al. (1992), and Scollard et al. (1993) using absolute and relative rate methods. The results are listed in table IV-G-1. There is good agreement between the three determinations. An average value from the three studies of $k(OH + CH_2ClC(O)H) = 3.15 \times 10^{-12}$ cm^3 molecule^{-1} s^{-1} at 298 K is recommended with an uncertainty of ±20%.

IV-G-6.2. Cl-Atom Reaction Kinetics

Starcke et al. (1990) and Scollard et al. (1993) have studied this reaction using relative rate methods. The results are listed in table IV-G-2 and are in good agreement. An average from the two determinations of $k(Cl + CH_2ClC(O)H) = 1.31 \times 10^{-11}$ cm^3 molecule^{-1} s^{-1} at 298 K is recommended with an uncertainty of ±20%.

IV-G-6.3. Summary of the Atmospheric Fate of $CH_2ClC(O)H$

Combining $k(OH + CH_2ClC(O)H = 3.15 \times 10^{-12}$ cm^3 molecule^{-1} s^{-1} at 298 K with a diurnal average [OH] = 10^6 molecule cm^{-3} provides an estimate of 4 days for the atmospheric lifetime of $CH_2Cl(CO)H$ with respect to reaction with OH radicals. Starcke et al. (1990) measured the UV spectrum of CH_2ClCHO, assumed a photolysis quantum yield of unity and calculated a lifetime of 4.4 h with respect to photolysis at noon for 40° N in July. Clearly, photolysis is likely to be an important loss mechanism for CH_2ClCHO. Reaction with OH and photolysis will lead to conversion of CH_2ClCHO into HC(O)Cl as the main oxidation product. Formation of $CH_2ClC(O)OH$ as a minor product is possible via the hydrate or the $CH_2ClC(O)O_2$ + HO_2 mechanisms (see figure IV-G-2 and $C_xF_{2x+1}CHO$ sections for details).

IV-G-7. 2,2-Dichloroethanal [Dichloroacetaldehyde, $CHCl_2C(O)H$]

IV-G-7.1. OH Reaction Kinetics

The kinetics of the reaction of OH radicals with $CHCl_2C(O)H$ have been studied by Starcke et al. (1990), Balestra-Garcia et al. (1992), and Scollard et al. (1993) using absolute and relative rate methods. The results are listed in table IV-G-1. There is good agreement between the three determinations. An average value from the three studies of $k(OH + CHCl_2C(O)H) = 2.52 \times 10^{-12}$ cm^3 molecule^{-1} s^{-1} at 298 K is recommended with an uncertainty of ±20%.

IV-G-7.2. Cl-Atom Reaction Kinetics

Starcke et al. (1990) and Scollard et al. (1993) have studied this reaction using relative rate methods. The results are listed in table IV-G-2 and are in excellent agreement. An average from the two determinations of $k(\mathrm{Cl} + \mathrm{CHCl_2C(O)H}) = 1.31 \times 10^{-11}$ cm^3 molecule^{-1} s^{-1} at 298 K is recommended with an uncertainty of ±20%.

IV-G-7.3. Summary of the Atmospheric Fate of $CH_2ClC(O)H$

Combining $k(\mathrm{OH} + \mathrm{CHCl_2C(O)H}) = 2.52 \times 10^{-12}$ cm^3 molecule^{-1} s^{-1} at 298 K with a diurnal average [OH] $= 1.0 \times 10^6$ molecule cm^{-3} provides an estimate of 5 days for the atmospheric lifetime of $\mathrm{CHCl_2C(O)H}$ with respect to reaction with OH radicals. Starcke et al. (1990) measured the UV spectrum of $\mathrm{CHCl_2CHO}$, assumed a photolysis quantum yield of unity and calculated a lifetime of 3.9 h with respect to photolysis at noon for 40° N in July. Clearly, photolysis is likely to be an important loss mechanism for $\mathrm{CHCl_2CHO}$. Reaction with OH and photolysis will lead to conversion of $\mathrm{CHCl_2CHO}$ into $\mathrm{COCl_2}$ as the main oxidation product. Formation of $\mathrm{CHCl_2C(O)OH}$ is possible as a minor product via the hydrate or the $\mathrm{CHCl_2C(O)O_2 + HO_2}$ mechanisms (see figure IV-G-2 and $\mathrm{C}_x\mathrm{F}_{2x+1}\mathrm{CHO}$ section IV-G-3 for more details).

IV-G-8. 2,2,2-Trichloroethanal (Trichloroacetaldehyde, Chloral, CCl_3CHO)

IV-G-8.1. OH Reaction Kinetics

The kinetics of the reaction of OH radicals with $\mathrm{CCl_3CHO}$ have been studied by Dóbé et al. (1989), Starcke et al. (1990), Nelson et al. (1990b), Balestra-Garcia et al. (1992), Scollard et al. (1993), Barry et al. (1994), and Talukdar et al. (2001). Rate coefficients are listed in table IV-G.1 and plotted in figure IV-G-4. As seen from figure IV-G-4, there is considerable scatter in the reported rate coefficients. Dóbé et al. (1989), Balestra-Garcia et al. (1992), Barry et al. (1994), and Talukdar et al. (2001) used absolute rate techniques. The results from Balestra-Garcia et al. (1992), Barry et al. (1994), and Talukdar et al. (2001) are in agreement within the combined experimental uncertainties. The results from Dóbé et al. (1989) are approximately a factor of 2 greater than those of Balestra-Garcia et al. (1992), Barry et al. (1994), and Talukdar et al. (2001). The study by Dóbé et al. (1989) included investigations of the rates of reaction of OH radicals with $\mathrm{CF_3CHO}$, $\mathrm{(CH_3)_2CHCHO}$, and $\mathrm{(CH_3)_3CCHO}$. The rate coefficients reported by Dóbé et al. (1989) for these molecules are a factor of 2–3 greater than those of other workers and our recommended values. It appears that there is a systematic error in the work of Dóbé et al. (1989), which led to an overestimation of $k(\mathrm{OH} + \mathrm{CCl_3CHO})$. We will not consider the work of Dóbé et al. (1989) further.

As shown in figure IV-G-4 there is substantial scatter in the results from the relative rate studies by Starcke et al. (1990), Nelson et al. (1990b), Scollard et al. (1993), and Barry et al. (1994). It is well established that the oxidation of $\mathrm{CCl_3CHO}$ leads to the formation of chlorine atoms (Calvert et al., 2008). The formation of chlorine

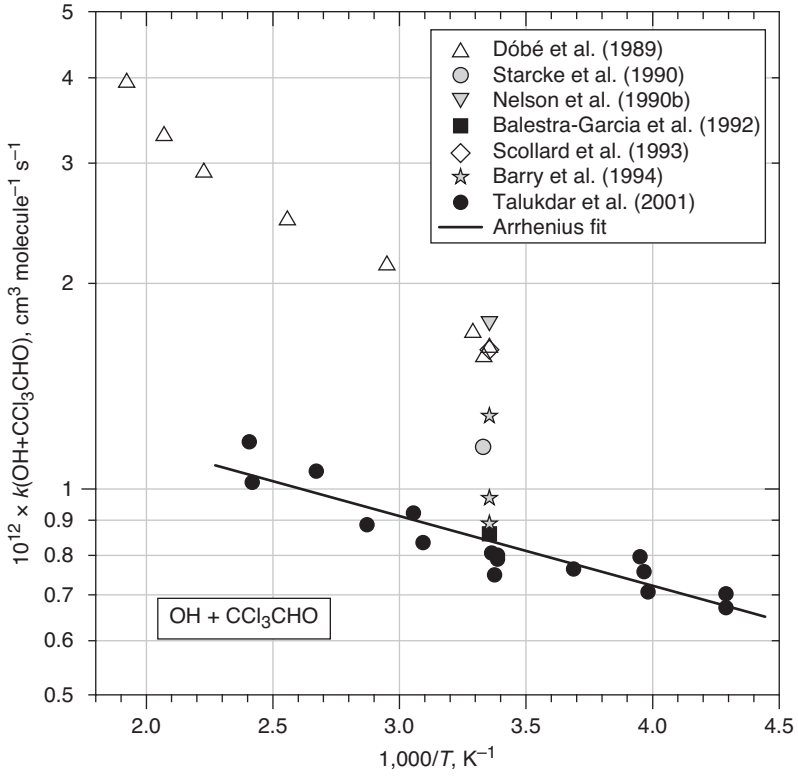

Figure IV-G-4. Measurements of the rate coefficients for reaction of OH radicals with CCl_3CHO. The line is a fit to the data from Balestra-Garcia et al. (1992), Barry et al. (1994), and Talukdar et al. (2001); see text for details.

atoms presents a potentially serious complication in relative rate studies of OH reaction kinetics. As discussed by Talukdar et al. (2001), the reactivity of chlorine atoms towards the reference compounds used in the OH relative rate studies are substantially greater than that towards CCl_3CHO. If secondary reactions involving chlorine atoms were important in the relative rate studies, this would lead to *smaller* values of $k(OH + CCl_3CHO)$ than those from the absolute studies. However, the rate coefficients from the relative rate studies of Nelson et al. (1990b) and Scollard et al. (1993) are *greater* than those from the absolute studies, and so secondary reactions involving chlorine atoms are not responsible for the discrepancy. As discussed by Barry et al. (1994), photolysis can be a significant loss of CCl_3CHO in the relative rate studies and is a possible explanation of the fact that the results from Nelson et al. (1990b) and Scollard et al. (1993) are greater than those from the absolute rate studies of Balestra-Garcia et al. (1992), Barry et al. (1994), and Talukdar et al. (2001). A fit to the data from Balestra-Garcia et al. (1992), Barry et al. (1994), and Talukdar et al. (2001) gives $k(OH + CCl_3CHO) = 1.85 \times 10^{-12} \exp(-235/T)\,cm^3$ molecule^{-1} s^{-1}. This expression yields $k(OH + CCl_3CHO) = 8.41 \times 10^{-13}\,cm^3$

molecule^{-1} s^{-1} at 298 K. The uncertainty in $k(\mathrm{OH} + \mathrm{CCl_3CHO})$ at 298 K is estimated to be ±25%.

IV-G-8.2. Cl-Atom Reaction Kinetics

Starcke et al. (1990), Scollard et al. (1993), and Talukdar et al. (2001) have studied this reaction using relative and absolute rate methods. The results are listed in table IV-G-2. The results from Scollard et al. (1993) and Talukdar et al. (2001) are consistent, within the likely combined experimental uncertainties. The result from Starcke et al. (1990) is, for reasons which are unclear, substantially larger than the measurements by Scollard et al. (1993) and Talukdar et al. (2001). Taking an average of the results from Scollard et al. (1993) and Talukdar et al. (2001) gives our recommended value of $k(\mathrm{Cl} + \mathrm{CCl_3CHO}) = 6.4 \times 10^{-12}$ cm^3 molecule^{-1} s^{-1} at 298 K with an uncertainty estimated to be ±25%.

IV-G-8.3. Summary of the Atmospheric Fate of CCl_3CHO

Combining $k(\mathrm{OH} + \mathrm{CCl_3CHO}) = 8.41 \times 10^{-13}$ cm^3 molecule^{-1} s^{-1} at 298 K with a diurnal average [OH] = 10^6 molecule cm^{-3} provides an estimate of 14 days for the atmospheric lifetime of CCl_3CHO with respect to reaction with OH radicals. As discussed in chapter IX, photolysis of CCl_3CHO occurs on a timescale of approximately 1–2 days. Photolysis will be the dominant loss atmospheric mechanism for CCl_3CHO and will lead to the formation of $COCl_2$ as the main oxidation product. Formation of $CCl_3C(O)OH$ as a minor product is possible via the hydrate, or the $CCl_3C(O)O_2$ + HO_2 mechanisms shown in figure IV-G-2 and discussed in the $C_xF_{2x+1}CHO$ section (IV-G-3) previously.

IV-G-9. $CHClFCHO$, CF_2ClCHO, $CFCl_2CHO$

IV-G-9.1. OH Reaction Kinetics

The kinetics the reaction of OH radicals with $CHClFCHO$, CF_2ClCHO, and $CFCl_2CHO$ have been studied by Scollard et al. (1993) using relative and absolute methods at 298 K. The results are listed in table IV-G-1. There is good agreement between the values of $k(\mathrm{OH})$ reported by Scollard et al. (1993) using absolute and relative techniques. Taking an average of the results from the two different techniques provides our recommendations for $k(\mathrm{OH} + \mathrm{CHClFCHO}) = 2.05 \times 10^{-12}$, $k(\mathrm{OH} + \mathrm{CF_2ClCHO}) = 1.15 \times 10^{-12}$, and $k(\mathrm{OH} + \mathrm{CFCl_2CHO}) = 8.2 \times 10^{-13}$ cm^3 molecule^{-1} s^{-1} at 298 K with uncertainties estimated to be ±25%.

IV-G-9.2. Cl-Atom Reaction Kinetics

Scollard et al. (1993) used a relative rate method to study the reactions of chlorine atoms with $CHClFCHO$, CF_2ClCHO, and $CFCl_2CHO$. The results are given in table IV-G-2 and are recommended with uncertainties estimated to be ±30%.

IV-G-9.3. Summary of the Atmospheric Fate of $CHClFCHO$, CF_2ClCHO, and $CFCl_2CHO$

Combining the recommended $k(OH)$ values at 298 K with a diurnal average $[OH] = 10^6$ molecule cm^{-3} gives estimates of 6, 10, and 14 days, respectively, for the atmospheric lifetimes of $CHClFCHO$, CF_2ClCHO, and $CFCl_2CHO$ with respect to reaction with OH radicals. As discussed above, photolysis of halogenated aldehydes proceeds on a timescale of the order of a few days, or less. Photolysis will probably be the dominant loss atmospheric mechanism for $CHClFCHO$, CF_2ClCHO, and $CFCl_2CHO$, and will lead to the formation of $COFCl$ (from $CHClFCHO$ and $CFCl_2CHO$) and COF_2 (from CF_2ClCHO) as the main oxidation products. Formation of halogenated acetic acids as minor products is possible via the hydrate, or the $RC(O)O_2 + HO_2$ mechanisms shown in figure IV-G-2 and discussed above.

V

Rate Coefficients and Mechanisms for the Atmospheric Oxidation of the Ketones

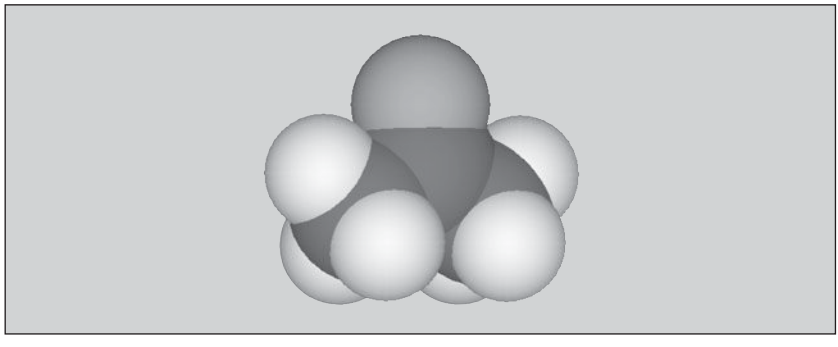

V-A. Introduction

Ketones are emitted directly to the atmosphere, and their sources were discussed in detail in chapter I. In the U.K. acetone and butanone comprise about 7% and 5%, respectively, of the total anthropogenic emissions of oxygenated compounds, and 1.6% and 1.1%, respectively, of the total anthropogenic emissions of nonmethane volatile organic compounds. Ketone emissions from solvents (both industrial and personal) are substantial; emissions from both gasoline- and diesel-fueled vehicles also contribute. Ketones are also formed extensively in the atmosphere in the oxidation of other compounds. Acetone, for example is formed in the OH-initiated oxidation of propane, *iso*-butane, *iso*-pentane, and neopentane and from a number of higher hydrocarbons. It is also formed in the oxidation of terpenes. The distribution, sources, and sinks of acetone in the atmosphere have been analyzed by Simpson et al. (1994). Methyl vinyl ketone is an important first generation product in the OH-initiated oxidation of isoprene.

In this chapter, we discuss the rate coefficients and the mechanisms of oxidation of ketones. The classes covered include alkanones, hydroxyketones, diketones, unsaturated ketones, ketenes, cyclic ketones, ketones derived from biogenic compounds, and halogen-substituted ketones. Photolysis is a major atmospheric process for many ketones, and will be discussed in chapter IX. The major bimolecular reactions removing ketones from the atmosphere are with OH. Although less important than the OH

reactions, reactions with Cl have been studied quite extensively. Other than for unsaturated ketones, reactions with NO_3 and O_3 are unimportant in tropospheric chemistry and have been studied little.

The carbonyl group deactivates the α-position with respect to reaction with OH, but activates the β-position, and possibly more distant sites as well. The net result is that the overall rate coefficient of an alkanone generally exceeds that of the equivalent alkane. The temperature dependences of the rate coefficients can be quite complex, with acetone and possibly butanone showing a minimum in the rate coefficient at ~250 K, while the higher alkanones show negative temperature dependences across the more limited temperature ranges that have been investigated. The most likely explanation of this behavior is the formation of a pre-reaction, hydrogen-bonded complex.

The atmospheric lifetimes of the compounds are assessed with respect to reaction with OH and, where necessary, with NO_3 and O_3. The likely mechanism of reaction is also discussed on the basis of available product studies, although such information is quite limited. At the end of each section, the reactivity of the class of reactants is assessed and, where feasible, the structure–activity relations (SARs) are examined.

Section V-B draws extensively on the analysis provided by Calvert et al. (2008), but has been updated to include more recent studies.

V-B. Alkanones

V-B-1. Acetone [2-propanone, $CH_3C(O)CH_3$]

V-B-1.1. OH Reaction Kinetics

The reaction of OH with acetone has been studied over a wide range of temperatures, and there is now good agreement on the kinetics of this reaction (see table V-B-1). The rate coefficient has a weak positive temperature dependence above room temperature (Wallington and Kurylo, 1987a; Le Calvé et al., 1998), but passes through a minimum near 240 K (Wollenhaupt et al., 2000: Gierczak et al., 2003). The data of Wallington and Kurylo (1987a), Le Calvé et al. (1998), Wollenhaupt et al. (2000), Vasvári et al. (2001), Gierczak et al. (2003), Yamada et al. (2003), Raff et al. (2005), and Davis et al. (2005a) between 200 K and 800 K are shown in figure V-B-1. The data give an unweighted mean rate coefficient at room temperature of 1.8×10^{-13} cm^3 molecule^{-1} s^{-1}, which is the same as that recommended by the IUPAC panel (Atkinson et al., 2006). Over the temperature range 195–440 K, they recommend a sum of two exponentials: $k = 8.8 \times 10^{-12} \exp(-1,320/T) + 1.7 \times 10^{-14} \exp(423/T)$ cm^3 molecule^{-1} s^{-1}. This expression was derived by Wollenhaupt et al. (2000) as a fit to their own data, but it represents most of the cited data to within ±15% over the stated temperature range, as shown in figure V-B-1. There is no evidence for any pressure dependence for reaction of OH with this or any of the ketones, which is of importance in the following discussion on the reaction mechanism.

The products of the reaction have been the subject of some controversy. The positive temperature dependence shown in the earlier studies was interpreted as evidence of a hydrogen abstraction mechanism (Wallington and Kurylo, 1987a; Le Calvé

Table V-B-1. Rate coefficients ($k = A \times e^{-B/T}$, cm^3 molecule^{-1} s^{-1}) for the reaction of OH with acetone [$CH_3C(O)CH_3$]

$10^{12} \times A$	B (K)	$10^{12} \times k$	T (K)	Technique[a]	Reference	Temperature Range (K)
		< 0.5	300	RR (C_2H_4)[b]	Cox et al. (1980b)	
		0.63 ± 0.09	298	RR (n-C_6H_{14})[c]	Chiorboli et al. (1983)	
		0.27 ± 0.08	303	RR (C_2H_4)[d]	Kerr and Stocker (1986a)	
1.7 ± 0.4	600 ± 75	0.145 ± 0.015	240	FP–RF	Wallington and Kurylo (1987a)	240–440
		0.216 ± 0.016	296			
		0.292 ± 0.023	350			
		0.407 ± 0.030	400			
		0.436 ± 0.050	440			
		0.132 ± 0.010	243	PLP–LIF	Le Calvé et al. (1998)	243–372
		0.140 ± 0.007	253			
		0.153 ± 0.010	273			
		0.184 ± 0.015	298			
		0.203 ± 0.017	323			
		0.249 ± 0.023	348			
		0.283 ± 0.010	372			
		0.148 ± 0.005	202	PLP–LIF	Wollenhaupt et al. (2000)	202–355
		0.141 ± 0.004	209			
		0.144 ± 0.003	220 ± 2			
		0.138 ± 0.002	225 ± 1			
		0.138 ± 0.004	228			
		0.129 ± 0.004	236 ± 2			
		0.142 ± 0.002	247			
		0.137 ± 0.003	255 ± 1			
		0.147 ± 0.001	267			
		0.150 ± 0.002	274			
		0.156 ± 0.002	281			
		0.167 ± 0.002	289			
		0.169 ± 0.004	295			
		0.196 ± 0.002	311			
		0.208 ± 0.002	321			
		0.226 ± 0.003	332			
		0.250 ± 0.003	344			
		0.267 ± 0.003	355			
		0.125 ± 0.002	221	PLP–RF		
		0.135 ± 0.015	233			
		0.141 ± 0.008	236			
		0.142 ± 0.015	245 ± 2			
		0.145 ± 0.010	260 ± 2			
		0.177 ± 0.003	298			
		0.209 ± 0.004	318			
		0.274 ± 0.015	361 ± 1			
		0.354 ± 0.003	395			
		0.173 ± 0.005	298	DF–RF	Vasvári et al. (2001)	
		0.136 ± 0.010	199	PLP–LIF	Gierczak et al. (2003)	199–383
		0.146 ± 0.010	208			
		0.151 ± 0.020	213			
		0.139 ± 0.010	224 ± 1			
		0.137 ± 0.008	232			
		0.149 ± 0.008	238			
		0.144 ± 0.004	244			
		0.148 ± 0.006	250			
		0.142 ± 0.002	259			

(*continued*)

Table V-B-1. (*Continued*)

$10^{12} \times A$	B (K)	$10^{12} \times k$	T (K)	Technique[a]	Reference	Temperature Range (K)
		0.155 ± 0.020	271			
		0.177 ± 0.010	296			
		0.207 ± 0.005	323			
		0.246 ± 0.026	333			
		0.277 ± 0.010	355 ± 2			
		0.341 ± 0.014	383			
		0.156 ± 0.008	298	PLP–LIF	Yamada et al. (2003)	298–832
		0.158 ± 0.007	310			
		0.182 ± 0.018	324			
		0.197 ± 0.006	339			
		0.213 ± 0.012	355			
		0.221 ± 0.026	373			
		0.285 ± 0.018	390			
		0.369 ± 0.013	414			
		0.455 ± 0.027	439			
		0.476 ± 0.034	467			
		0.605 ± 0.062	498			
		0.822 ± 0.017	534			
		0.949 ± 0.017	575			
		1.19 ± 0.12	628			
		1.56 ± 0.11	681			
		2.11 ± 0.13	685			
		1.93 ± 0.13	710			
		3.25 ± 0.16	832			
		0.238 ± 0.004	298	RR[e] (CH_2ClCH_2Cl)	Carr et al.(2003)	
		0.149 ± 0.029	253	RR (CH_3CHF_2)[f]	Raff et al. (2005)	253–373
		0.160 ± 0.018	263			
		0.177 ± 0.017	273			
		0.172 ± 0.022	283			
		0.186 ± 0.013	293			
		0.208 ± 0.022	303			
		0.198 ± 0.016	308			
		0.192 ± 0.011	313			
		0.220 ± 0.018	323			
		0.217 ± 0.015	333			
		0.246 ± 0.012	343			
		0.294 ± 0.023	373			
3.92 ± 0.81	938 ± 70	0.152 ± 0.012	271	DF–LIF	Davis et al. (2005a)	271–402
		0.164 ± 0.014	287			
		0.173 ± 0.006	300			
		0.218 ± 0.010	325			
		0.246 ± 0.006	341			
		0.254 ± 0.014	342			
		0.311 ± 0.014	371			
		0.373 ± 0.014	402			

[a]Abbreviations used for the techniques are defined in table I-F-3.
[b]Placed on an absolute basis using $k(OH + C_2H_4) = 7.9 \times 10^{-12}$ cm^3 molecule^{-1} s^{-1} (Atkinson et al., 2006).
[c]Placed on an absolute basis using $k(OH + n\text{-}C_6H_{14}) = 5.48 \times 10^{-12}$ cm^3 molecule^{-1} s^{-1} (Calvert et al., 2008).
[d]Placed on an absolute basis using $k(OH + C_2H_4) = 8.32 \times 10^{-12}$ cm^3 molecule^{-1} s^{-1} at 1 bar and 303 K (Atkinson et al., 2006).
[e]Placed on an absolute basis using $k(OH + CH_2ClCH_2Cl) = 2.42 \times 10^{-13}$ cm^3 molecule^{-1} s^{-1} (Calvert et al., 2008).
[f]Placed on an absolute basis using $k(OH + CH_3CHF_2) = 2.10 \times 10^{-18} T^2 \exp(-503/T)$ cm^3 molecule^{-1} s^{-1} (Calvert et al., 2008).

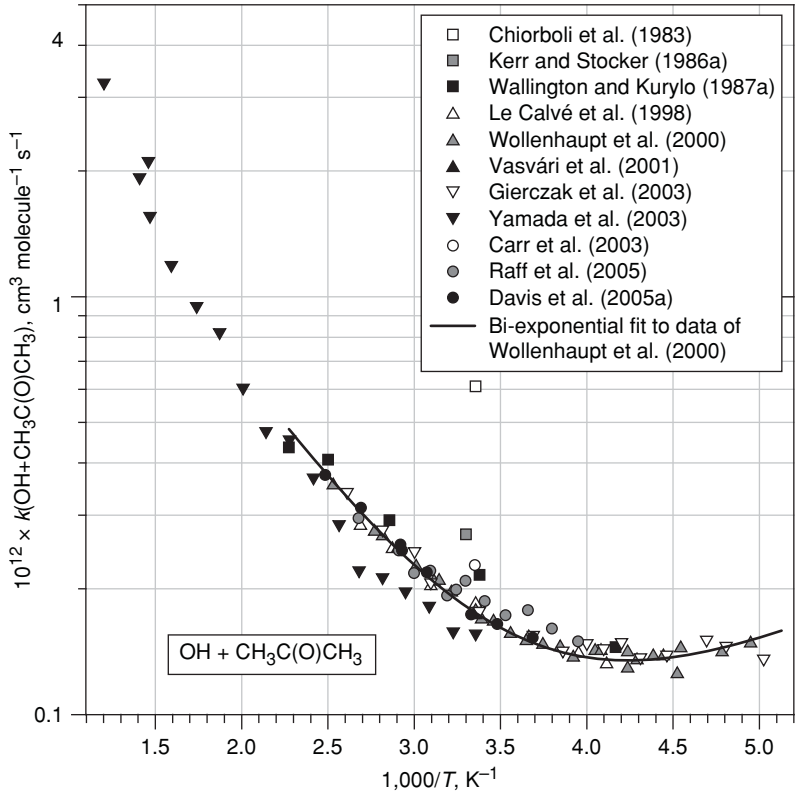

Figure V-B-1. Arrhenius plot for the rate coefficients for the OH + acetone reaction.

et al., 1998). However, Wollenhaupt and Crowley (2000) and Vasvári et al. (2001) both found evidence for up to 50% yield of methyl radicals which they suggested were derived from an addition–elimination pathway.

$$OH + CH_3C(O)CH_3 \rightarrow H_2O + CH_3C(O)CH_2$$

$$OH + CH_3C(O)CH_3 \rightarrow [HOC(CH_3)_2O\bullet]^{\dagger} \rightarrow CH_3 + CH_3C(O)OH$$

The strong curvature in the Arrhenius plot was also taken as evidence for the occurrence of two parallel reaction pathways. Several recent product studies have shown that abstraction of H to give the acetonyl (2-oxo-1-propyl) radical is the major, and possibly the only, pathway under atmospheric conditions. Vandenberk et al. (2002), Tyndall et al. (2002), Talukdar et al. (2003), Raff et al. (2005), and Turpin et al. (2006) all found yields of acetic acid, $CH_3C(O)OH$, of less than 10% at room temperature. Talukdar et al. used the discharge flow technique with detection with chemical ionization mass spectrometry to show that the $CH_3C(O)OH$ yield is less than 1% between 237 and 353 K. Tyndall et al. also showed that the acetic acid yield is less than 10% at 251 K. The results of Raff et al. indicate a slight disagreement with the other studies: they

found a 10% yield of acetic acid at 298 K and a slight negative temperature dependence, with the yield varying between (12 ± 5)% at 273 K and (4.7 ± 0.4)% at 353 K. Their analysis suggested that (60 ± 10)% of the observed acetic acid may have resulted from secondary chemistry involving acetonoxy and HO_x radical chemistry. Interestingly, they observed an enhanced yield of d_3-acetic acid in studies of OH with d_6-acetone (e.g., 20% at 283 K); in this case, they could not ascribe the majority of the yield to secondary chemistry. Turpin et al. (2006) obtained a yield of acetic acid of $< 5\%$, but confirmed the enhanced yield (20% at room temperature) for the deuterium isotopomer. The yield for the major channel (H abstraction) was measured by Talukdar et al. (2003) and by Turpin et al. (2003), both of whom found yields of $CH_3C(O)CH_2$ greater than 85%.

The reaction is thought to proceed by a loose hydrogen-bonded complex, similar to the reactions of OH with the aldehydes, leading to the negative temperature dependence below room temperature. However, Gierczak et al. (2003), Talukdar et al. (2003), Yamada et al. (2003), Davis et al. (2005a), and Raff et al. (2005) found a significant deuterium isotope effect (factors between 5 and 7 at room temperature) indicating that the rate-limiting step involves the breaking of a C—H (C—D) bond. The isotope effect increases to a factor of about 10 near 200 K, consistent with a tunneling contribution. Theoretical calculations on the system indicate that the barrier to addition of OH to the carbonyl group to form $CH_3C(O)(OH)CH_3$, which could be followed by elimination of CH_3, is too high to compete with abstraction (Vandenberk et al., 2002; Yamada et al., 2003). Yamada et al. examined two mechanisms, one involving direct abstraction, the other abstraction via a complex and argued that the former provides the major contribution to reaction at temperatures above ∼500 K, and the latter at temperatures below ∼300 K.

There have been a number of theoretical treatments of the lower temperature mechanism, viz. abstraction via a complex. There are two pre-reactive hydrogen-bonded complexes, with binding energies of about 17 kJ mol^{-1} followed by transition states that lie 6.3–8.4 kJ mol^{-1} above the reactants. This contrasts with the surface for OH + acetaldehyde, where the transition states are "submerged," that is they lie below the reactants; this accounts for the negative activation energy discussed in section IV-B-2. There is also an outer transition state, for which there is no defined maximum, that lies to larger distances than the complex.

Alvarez-Idaboy et al. (2001b) suggested that reaction occurs via equilibration between the complex and the reactants, implying Boltzmann distributions in each and therefore collisional relaxation in the complex. Yamada et al. pointed out that this was unlikely and modeled the system without collisional relaxation, so that their model essentially corresponds to a low pressure limiting value. The most detailed study to date is that by Caralp et al. (2006), who allowed for collisional relaxation using a master equation analysis. They found no pressure dependence, even with quite high collisional energy transfer efficiencies, supporting the model employed by Yamada et al., and in agreement with experiment. Caralp et al. used a standard RRKM approach, but included tunneling, which they showed to be significant. They were able to model the experimental results, and the substantial isotope effect observed with OH + acetone-d_6 (Gierczak et al., 2003; Yamada et al., 2003).

Since abstraction is the major channel, it is of interest to compare the rate coefficient with that for ethane. At 298 K, $k(\mathrm{OH} + \text{ethane}) = 2.4 \times 10^{-13}\,\mathrm{cm^3\ molecule^{-1}\ s^{-1}}$ at 298 K (Atkinson et al., 2006), which is very close to the recommended value for acetone. The ratio of rate coefficients [$k(\text{acetone})/k(\text{ethane}) = 0.75$] shows evidence for a slight deactivation effect of the keto group on the adjacent methyl groups although the effect is within the combined uncertainties. It is reflected in the Kwok and Atkinson (1995) SAR group value, $F(\rangle\mathrm{C{=}O}) = 0.75$. At lower temperatures, acetone becomes the more reactive species, and the rate coefficient ratio is about 5 at 200 K, reflecting the stronger curvature found in the Arrhenius plot for acetone and the role of the H-bonded complex.

V-B-1.2. NO_3+ Acetone Reaction Kinetics

Boyd et al. (1991) used a stopped-flow technique with optical detection of NO_3 and observed the rate coefficient: $k = (1.7 \pm 0.5) \times 10^{-17}\,\mathrm{cm^3\ molecule^{-1}\ s^{-1}}$. Secondary chemistry results in further removal of NO_3, and to accommodate a stoichiometry of two or greater, they reported $k \leq 8.5 \times 10^{-18}\,\mathrm{cm^3\ molecule^{-1}\ s^{-1}}$. Atkinson et al. (2006) gave a more conservative upper limit of $k < 3 \times 10^{-17}\ \mathrm{cm^3\ molecule^{-1}\ s^{-1}}$.

V-B-1.3. Cl-Atom + Acetone Reaction Kinetics

The reaction of Cl + acetone has been studied by Wallington et al. (1990a), Olsson et al. (1997), Orlando et al. (2000), Christensen et al. (2000), Sellevåg and Nielsen (2003), and Carr et al. (2003) using relative rate techniques; by Notario et al. (2000a), Albaladejo et al. (2003b), and Zhao et al. (2008) by pulsed laser photolysis–resonance fluorescence; by Takahashi et al. (2007) using pulsed laser photolysis–laser-induced fluorescence; and by Martinez et al. (2004) using discharge flow–mass spectrometry. See table V-B-2. There is generally good agreement between the determinations, although the values of Notario et al. and Albaladejo et al. are significantly greater than the other ambient temperature measurements. The IUPAC panel (Atkinson et al., 2006) questioned the accuracy of the approach used by Olsson et al. on a number of counts. Excluding these three determinations gives a mean value at room temperature of $2.13 \times 10^{-12}\,\mathrm{cm^3\ molecule^{-1}\ s^{-1}}$ with an uncertainty of ±15%. Orlando et al. and Zhao et al. determined the temperature dependence of the reaction. The IUPAC panel took the *E*/*R* values from these two determinations, together with the average rate coefficient at 298 K and recommended $k(T) = 1.5 \times 10^{-11}\ \exp(-590/T)\,\mathrm{cm^3\ molecule^{-1}\ s^{-1}}$ over the range 215–300 K. This expression underweights the low temperature data of Orlando et al. (see figure V-B-2). An Arrhenius fit to the data, constrained to the average room temperature value gives $k(T) = 2.60 \times 10^{-11}\ \exp(-745/T)\,\mathrm{cm^3\ molecule^{-1}\ s^{-1}}$ over the range 215–440 K. This expression provides a less biased fit to the available data and is the one we recommend. However, the temperature range should be restricted to 215–300 K, since there are more limited measurements above 300 K. At 215 K, the rate coefficients from the two expressions differ by 20%.

The rate coefficient for Cl + ethane at 298 K is $5.9 \times 10^{-11}\,\mathrm{cm^3\ molecule^{-1}\ s^{-1}}$ (Atkinson et al., 2006), significantly greater than that for $CH_3C(O)CH_3$ ($2.1 \times 10^{-12}\,\mathrm{cm^3\ moleclule^{-1}\ s^{-1}}$), indicating a substantial deactivating effect of the keto

Table V-B-2. Rate coefficients ($k = A \times e^{-B/T}$, cm^3 molecule^{-1} s^{-1}) for the reaction of Cl with acetone [$CH_3C(O)CH_3$]

$10^{12} \times A$	B (K)	$10^{12} \times k$	T (K)	Technique[a]	Reference	Temperature Range (K)
		2.3 ± 0.2	295	RR[b] (C_2H_5Cl)	Wallington et al. (1990a)	
		1.7 ± 0.3	294	RR[c] ($ClONO_2$)	Olsson et al. (1997)	
12.8	580 ± 28	2.02	298	RR[d] (CH_2Cl_2)	Orlando et al. (2000)	215–298
		1.42	267			
		1.17	251			
		1.03	240			
		0.81	225			
		0.71	215			
		3.06 ± 0.38	298	PLP–RF	Notario et al. (2000a)	
		2.09 ± 0.25	296	RR[e] (C_2H_5F)	Christensen et al. (2000)	
		2.25 ± 0.24		RR[f] (CH_3Cl)		
		2.15 ± 0.23		RR[g] (CH_3F)		
		2.21 ± 0.27		RR[b] (C_2H_5Cl)		
		2.93 ± 0.29	298	PLP–RF	Albaladejo et al. (2003b)	
		2.00 ± 0.09	298	RR[h] (CH_2ClCH_2Cl)	Sellevåg and Nielsen (2003)	
		2.12 ± 0.05	298	RR[f] (CH_3Cl)	Carr et al. (2003)	
		2.20 ± 0.14	298	DF–MS	Martinez et al. (2004)	
		2.30 ± 0.12	295	PLP–LIF	Takahashi et al. (2007)	
15.3	594 ± 33	0.96	216	PLP–RF	Zhao et al. (2008)	210–440
		1.07	223			
		1.27	235			
		1.66	269			
		2.06	298			
		2.81	355			
		3.17	369			

[a]Abbreviations used for the techniques are defined in table I-F-3.
[b]Placed on an absolute basis using $k(Cl + C_2H_5Cl) = 7.8 \times 10^{-12}$ cm^3 molecule^{-1} s^{-1} (section I-F).
[c]Placed on an absolute basis using $k(Cl + ClONO_2) = 1.0 \times 10^{-11}$ cm^3 molecule^{-1} s^{-1} (Atkinson et al., 2006).
[d]Placed on an absolute basis using $k(Cl + CH_2Cl_2) = 5.9 \times 10^{-12} \exp(-850/T)$ cm^3 molecule^{-1} s^{-1} (Atkinson et al., 2008b).
[e]Placed on an absolute basis using $k(Cl + C_2H_5F) = 7.24 \times 10^{-12}$ cm^3 molecule^{-1} s^{-1} (Atkinson et al., 2008b).
[f]Placed on an absolute basis using $k(Cl + CH_3Cl) = 4.8 \times 10^{-13}$ cm^3 molecule^{-1} s^{-1} (Atkinson et al., 2008b).
[g]Placed on an absolute basis using $k(Cl + CH_3F) = 3.5 \times 10^{-13}$ cm^3 molecule^{-1} s^{-1} (Atkinson et al., 2008b).
[h]Placed on an absolute basis using $k(Cl + CH_2ClCH_2Cl) = 1.3 \times 10^{-12}$ cm^3 molecule^{-1} s^{-1} (Calvert et al., 2008).

group on the adjacent methyl groups with respect to abstraction by Cl. This effect contrasts with that for abstraction by OH, despite the higher activation temperature for the latter reaction ($B = 1,000$ K for OH + ethane and 100 K for Cl + ethane). These issues are discussed in more detail in section V-B-18.

V-B-1.4. O(^{3}P) + Acetone Reaction Kinetics

The kinetics of O(^{3}P) + acetone have been reviewed by Herron (1988). Measurements have been made by Ambidge et al. (1976), using discharge flow–ESR, Lee

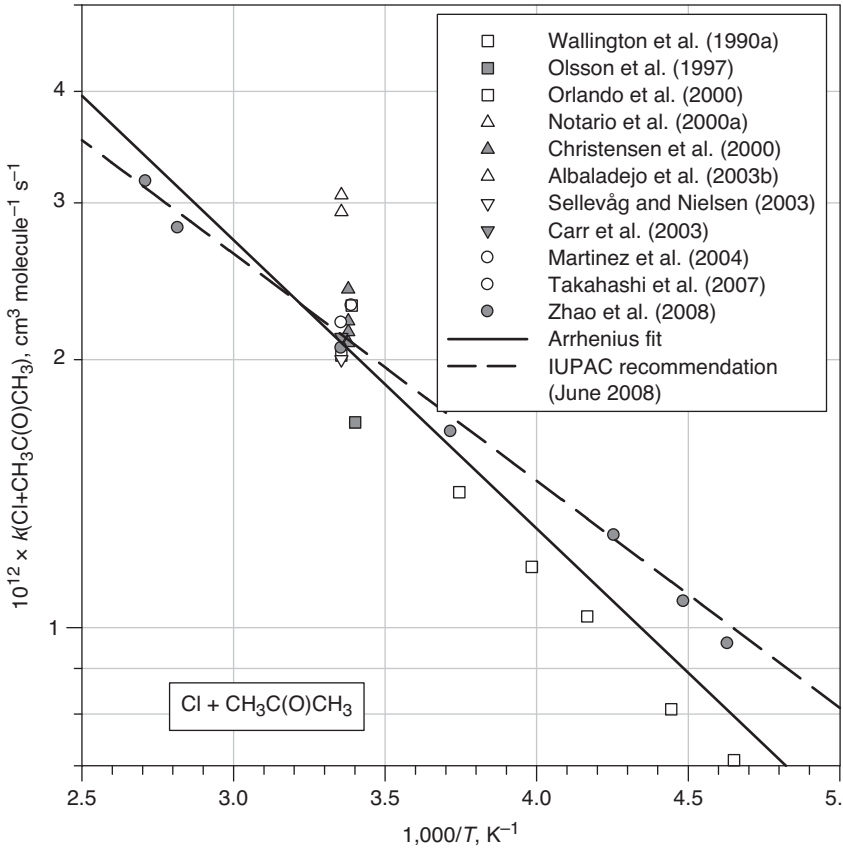

Figure V-B-2. Arrhenius plot for the rate coefficients for the Cl + acetone reaction.

and Timmons (1977), Faubel et al. (1982), and Mix and Wagner (1983) using discharge flow–mass spectrometry and by Roscoe (1986, 1988), using discharge flow–NO chemiluminescence. The data together span the range 298–700 K. The experimental data agree to within a factor of about 2 over their overlapping ranges, but give quite different values of the pre-exponential factor and the activation energy; this is especially the case for the data of Roscoe, which give low values for both parameters. Herron recommended: $k = 1.7 \times 10^{-11} \exp(-3{,}000/T)\,\mathrm{cm^3\ molecule^{-1}\,s^{-1}}$ which gives a rate coefficient at 298 K of $7.2 \times 10^{-16}\,\mathrm{cm^3\ molecule^{-1}\,s^{-1}}$. He suggested that the uncertainty is about a factor of 3. He also estimated $k(298)$ on the basis of a correlation with k_{OH}, obtaining a value about a factor of 2 smaller than that recommended here. Hou et al. (2006) carried out a very detailed theoretical analysis of the reaction, calculating the energetics to a high level and using transition state theory to calculate the rate constant. They showed that tunneling is important, obtaining: $k = 4.66 \times 10^{-23} T^{3.71} \exp(-1{,}289/T)\,\mathrm{cm^3\ molecule^{-1}\,s^{-1}}$ over the temperature range 200–3,000 K, in good agreement with experiment.

V-B-1.5. Summary of the Atmospheric Fate of Acetone and the End Products of Its Oxidation

Acetone is primarily removed from the atmosphere by photolysis and by reaction with OH. Blitz et al. (2004) discussed the competition between these two reactions, showing that reaction with OH is faster at the surface, with photolysis becoming more important at higher altitudes. Here we estimate the lifetime for photodecomposition of acetone in the lower troposphere with an overhead Sun to be about 12 to 16 days (see table IX-M-1). For [OH] = 10^6 molecule cm^{-3}, while the lifetime at the Earth's surface with respect to reaction with OH is about 64 days.

Orlando et al. (2000) have discussed in detail the atmospheric fate of the acetonoxy radical, $CH_3C(O)CH_2O$, which is the major product of OH + acetone, following subsequent reaction with O_2 and then NO. Their experimental results, supported by detailed theory, show that acetonoxy dissociates rapidly:

$$CH_3C(O)CH_2O + M \rightarrow CH_3CO + HCHO$$

and that its reaction with O_2 to form methylglyoxal and HO_2 is uncompetitive. They argued that reaction of acetone with OH, followed by the dissociation of acetonoxy accounts for about 10% of the CH_2O formed in the upper troposphere.

V-B-2. 2-Butanone [Methyl Ethyl Ketone, $CH_3C(O)C_2H_5$]

V-B-2.1. OH + 2-Butanone Reaction Kinetics

The measured rate coefficients for the reaction of OH with 2-butanone are given in table V-B-3. The more recent absolute measurements of Wallington and Kurylo (1987a), Le Calvé et al. (1998), Jiménez et al. (2005a), and Carr et al. (2008) are in good agreement, giving an unweighted average near 298 K of 1.11×10^{-12} cm^3 $molecule^{-1}$ s^{-1} with an uncertainty of ±20%. These four groups also measured the temperature dependence, which is weak at and below ambient temperature, but the higher temperature measurements of Carr et al. show a strong curvature. A nonlinear fit to the data shown in figure V-B-3 over the temperature range 215–400 K gives: $k = 3.23 \times 10^{-18}$ T^2 $\exp(391/T)$ cm^3 $molecule^{-1}$ s^{-1}, which we recommend over this temperature range. The IUPAC recommendations (Atkinson et al., 2006) are: $k(298) = 1.2 \times 10^{-12}$ cm^3 $molecule^{-1}$ s^{-1} at 298 K and $k = 1.3 \times 10^{-12}$ $\exp(-25/T)$ cm^3 $molecule^{-1}$ s^{-1} over the temperature range 240–300 K. They excluded the data of Jiménez et al. from their evaluation, and the data of Carr et al. had not been published at that time. Carr et al. fitted the data to a modified Arrhenius expression with a temperature exponent of 4. Such a plot, with $1/k^2$ weighting, is shown in figure V-B-3, and gives $k = 3.9 \times 10^{-24}$ T^4 $\exp(1{,}039/T)$ cm^3 $molecule^{-1}$ s^1. These rate coefficients and those from the T^2 fit differ by 13%, 6%, and 2% at 215, 298, and 400 K, respectively.

Cox et al. (1981) measured the yield of acetaldehyde from the OH-initiated oxidation of 2-butanone to be 62%. This should represent the yield of abstraction from the CH_2 group, and corresponds to a partial rate coefficient of 6.6×10^{-13} cm^3 $molecule^{-1}$ s^1, which is some 30% smaller than the equivalent rate coefficient in an unsubstituted

Table V-B-3. Rate coefficient ($k = A \times e^{-B/T}$, cm^3 molecule^{-1} s^{-1}) for reaction of OH with 2-butanone [$CH_3C(O)CH_2CH_3$]

$10^{12} \times A$	B (K)	$10^{12} \times k$	T (K)	Technique[a]	Reference	Temperature Range (K)
		3.6 ± 1.0	305	RR (2-methylpropene)	Winer et al. (1976)	
		< 2.5	300	RR (C_2H_4)[c]	Cox et al. (1980b)	
		0.88 ± 0.09	298	RR (C_2H_4)[c]	Cox et al. (1981)	
		0.93 ± 0.17	297	RR (C_3H_8)[d]	Edney et al. (1986)	
2.3 ± 1.1	170 ± 120	1.23 ± 0.10	240	FP–RF	Wallington and Kurylo (1987a)	240–440
		1.15 ± 0.10	296			
		1.41 ± 0.09	350			
		1.55 ± 0.07	400			
		1.65 ± 0.09	440			
1.19 ± 0.18	60 ± 61	1.24 ± 0.08	243	PLP–LIF	Le Calvé et al. (1998)	243–372
		1.20 ± 0.05	253			
		1.19 ± 0.05	263			
		1.21 ± 0.09	273			
		1.19 ± 0.18	298			
		1.12 ± 0.11	313			
		1.24 ± 0.09	333			
		1.19 ± 0.09	353			
		1.38 ± 0.10	372			
1.35 ± 0.35	78 ± 52	0.99 ± 0.04	228	PLP–LIF	Jiménez et al. (2005a)	228–388
		0.80 ± 0.06	238			
		1.00 ± 0.06	248			
		0.91 ± 0.09	253			
		0.98 ± 0.04	273			
		1.04 ± 0.07	298			
		0.93 ± 0.11	313			
		1.10 ± 0.08	318			
		0.98 ± 0.11	343			
		1.20 ± 0.12	363			
		1.09 ± 0.40	388			
(3.84±0.12)T^4	−(1038 ±11)	0.93 ± 0.20	213	PLP–LIF	Carr et al. (2008)	213–598
		0.91 ± 0.04	223			
		0.98 ±0.02	248			
		1.10 ± 0.07	273			
		0.98 ± 0.03	285			
		1.00 ± 0.09	295			
		1.06 ± 0.06	298			
		1.05 ± 0.02	348			
		1.35 ± 0.10	398			
		1.63 ± 0.05	448			
		1.97 ± 0.20	498			
		2.36 ± 0.06	548			
		2.48 ± 0.28	598			

[a]Abbreviations used for the techniques are defined in table I-F-3.
[b]Placed on an absolute basis using $k(OH + 2\text{-methylpropene}) = 5.14 \times 10^{-11}$ cm^3 molecule^{-1} s^{-1} (Calvert et al., 2000).
[c]Placed on an absolute basis using $k(OH + C_2H_4) = 7.9 \times 10^{-12}$ cm^3 molecule^{-1} s^{-1} at 1 bar and 298 K (Atkinson et al., 2008).
[d]Placed on an absolute basis using $k(OH + C_3H_8) = 1.1 \times 10^{-12}$ cm^3 molecule^{-1} s^{-1} (Atkinson et al., 2006).

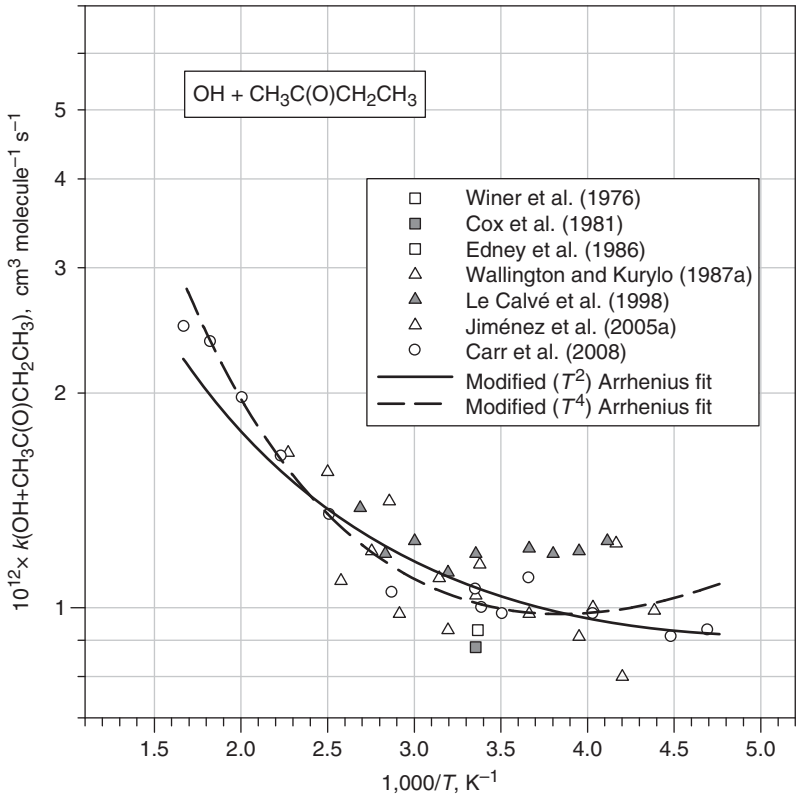

Figure V-B-3. Arrhenius plot for the rate coefficients for OH + 2-butanone.

alkane. This deactivation is reflected in the group value $F(\rangle C{=}O) = 0.75$ (Kwok and Atkinson, 1995). The estimated total rate coefficient at 298 K, based on the SAR, is 1.33×10^{-12} cm^3 molecule^{-1} s^1, with 53% of the abstraction occurring at the CH_2 group.

V-B-2.2. Cl-Atom + 2-Butanone Reaction Kinetics

The rate coefficient for Cl + 2-butanone has been studied by Wallington et al. (1990a), Taketani et al. (2006), Kaiser and Wallington (2007), and Kaiser et al. (2009) using relative rate techniques, by Notario et al. (2000a), Albaladejo et al. (2003b), Cuevas et al. (2004), and Zhao et al. (2008) using pulsed laser photolysis–resonance fluorescence, and by Takahashi et al. (2007) using pulsed laser photolysis–laser-induced fluorescence. See table V-B-4 and figure V-B-4. There is good agreement between the relative rate measurements and the time resolved measurements of Takahashi et al. and Zhao et al. The IUPAC evaluation (Atkinson et al., 2006) questioned the results of the other investigations, suggesting that the consistently low rate coefficients resulted from secondary chemistry that was avoided by Takahashi et al. and Zhao et al. Excluding the three low measurements gives a room temperature

Table V-B-4. Rate coefficient ($k = A \times e^{-B/T}$, cm^3 molecule^{-1} s^{-1}) for reaction of Cl with 2-butanone [$CH_3C(O)CH_2CH_3$]

$10^{12} \times A$	B (K)	$10^{12} \times k$	T (K)	Technique[a]	Reference	Temperature Range (K)
		42.8 ± 5.9	295	RR[b] (C_2H_6)	Wallington et al. (1990a)	
		32.4 ± 3.8	298	PLP–RF	Notario et al. (2000a)	
		33.0 ± 2.0	298	PLP–RF	Albaladejo et al. (2003b)	
73 ± 1.2	239 ± 108	27.8 ± 2.0	270	PLP–RF	Cuevas et al. (2004)	270–380
		29.9 ± 2.8	283			
		32.3 ± 4.2	298			
		34.9 ± 4.2	310			
		35.4 ± 2.2	320			
		36.2 ± 3.6	331			
		36.6 ± 2.6	354			
		37.5 ± 2.8	380			
		38.6 ± 2.8	296	RR[c] (C_2H_5Cl)	Taketani et al. 2006)	
		41.8 ± 2.8		RR[d] (C_2H_4)		
		38 ± 3	296	RR[e] (C_3H_8)	Kaiser and Wallington (2007)	
		40.8 ± 2.1	295	PLP–LIF	Takahashi et al. (2007)	
27.7	76 ± 33	39.8 ± 1.5	214	PLP–RF	Zhao et al. (2008)	210–440
		37.4 ± 1.1	234			
		35.8 ± 1.2	270			
		36.6 ± 1.8	298			
		33.9 ± 1.8	340			
		33.5 ± 1.5	370			
40 ± 3	0	42 ± 2	297	RR[f] (C_2H_6)	Kaiser et al. (2009)	297–475
		41 ± 2	382			
		38 ± 2	474			
		39 ± 2	476			

[a]Abbreviations used for the techniques are defined in table I-F-3.
[b]Placed on an absolute basis using $k(Cl + C_2H_6) = 5.9 \times 10^{-11}$ cm^3 molecule^{-1} s^{-1} (Atkinson et al., 2006).
[c]Placed on an absolute basis using $k(Cl + C_2H_5Cl) = 7.8 \times 10^{-12}$ cm^3 molecule^{-1} s^{-1} (section I-F).
[d]Placed on an absolute basis using $k(Cl + C_2H_4) = 9.5 \times 10^{-11}$ cm^3 molecule^{-1} s^{-1} (section I-F).
[e]Placed on an absolute basis using $k(Cl + C_3H_8) = 1.4 \times 10^{-10}$ cm^3 molecule^{-1} s^{-1} (Atkinson et al., 2006).
[f]Placed on an absolute basis using $k(Cl + C_2H_6) = 8.3 \times 10^{-11} \exp(-100/T)$ cm^3 molecule^{-1} s^{-1} (Atkinson et al., 2006).

rate coefficient of 4.0×10^{-11} cm^3 molecule^{-1} s^{-1}, with an uncertainty of ±15%. The temperature dependence has been investigated by Cuevas et al. (2004), Zhao et al. (2008), and Kaiser et al. (2009). Excluding the first of these measurements, for the reasons discussed previously, gives a weak temperature dependence ($k = 3.8 \times 10^{-11} \exp(16/T)$ cm^3 molecule^{-1} s^{-1}) which differs from a temperature independent mean value of 4.0×10^{-11} cm^3 molecule^{-1} s^{-1} by only 3% at 500 K and 8% at 200 K; we recommend the temperature independent value over the range 200–500 K. IUPAC (Atkinson et al., 2008) recommends $k(T) = 3.05 \times 10^{-11} \exp(80/T)$ cm^3 molecule^{-1} s^{-1} (200–450 K), but the evaluation was completed before publication of the data of Kaiser et al. (2009).

The most thorough analysis of the product yields was made by Kaiser et al. (2009), who measured the relative yields of 1-, 3-, and 4-chlorobutanone. These compounds were formed from the corresponding radical by reaction with Cl_2. The results show

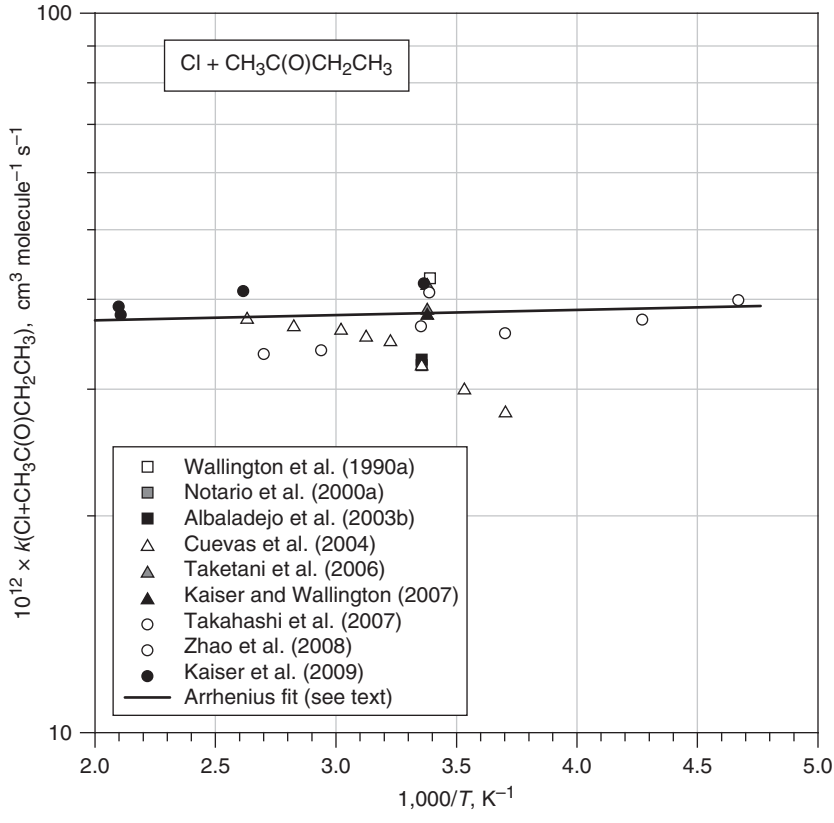

Figure V-B-4. Arrhenius plot for the rate coefficients for Cl + 2-butanone.

that the 3-butanonyl radical dominates, but the fractional yields of the other species increase as the temperature increases. At 298 K, the fractional yields of the 1-, 3-, and 4-butanonyl radicals are, respectively, 0.03, 0.74, and 0.23. The fractional yields of the 1- and 4-butanonyl radicals increase over the temperature range 297–517 K by factors of 3 and 1.2, respectively.

V-B-2.3. $O(^3P)$ + 2-Butanone Reaction Kinetics

The reaction has been studied by Roscoe (1986) using discharge flow–NO chemiluminescence over the temperature range 301–565 K. On the basis of these measurements, Herron (1988) recommended the expression: $k = 8 \times 10^{-13} \exp(-1{,}300/T)\,\mathrm{cm}^3$ molecule^{-1} s^{-1}, which gives $k(298) = 1 \times 10^{-14}\,\mathrm{cm}^3$ molecule^{-1} s^{-1}; this value is about a factor of 2 larger than the value Herron estimated from a correlation with k_{OH}. Overall, he estimated an uncertainty of about a factor of 3 in the rate expression. As discussed for acetone, the Arrhenius parameters obtained from the Roscoe data may be too small, and the expression should not be used outside the experimental range.

V-B-2.4. Summary of the Atmospheric Fate of 2-Butanone and the End Products of Its Oxidation

2-Butanone is primarily removed from the atmosphere by photolysis and by reaction with OH. The lifetime for photodecomposition of 2-butanone in the lower troposphere with an overhead Sun is about 2.5 days; see chapter IX. For [OH] = 10^6 molecule cm^{-3}, the lifetime with respect to reaction with OH is about 3 days.

Kaiser et al. (2009) examined the products formed in the presence of O_2. Under their conditions the reactions were dominated by peroxy–peroxy radical reactions, but the results confirmed the validity of the general outline of the reactions contained in the master chemical mechanism for high NO_x conditions, in which the 3-butanoyl radical reacts to form acetaldehyde and the acetyl radical:

$$CH_3C(O)CHCH_3 + O_2(+NO) \rightarrow CH_3C(O)CH(O)CH_3$$

$$CH_3C(O)CH(O)CH_3 \rightarrow CH_3CHO + CH_3CO$$

The 4-butanonyl radical forms CH_2O, glycolaldehyde, 3-oxobutanal, and a PAN species:

$$CH_3C(O)CH_2CH_2 + O_2(+NO) \rightarrow CH_3C(O)CH_2CH_2O + NO_2$$

$$CH_3C(O)CH_2CH_2O + O_2 \rightarrow CH_3C(O)CH_2CHO + HO_2$$

$$CH_3C(O)CH_2CH_2O(+O_2) \rightarrow CH_2(O_2)C(O)CH_2CH_2OH$$

$$CH_2(O_2)C(O)CH_2CH_2OH + NO \rightarrow CH_2(O)C(O)CH_2CH_2OH + NO_2$$

$$CH_2(O)C(O)CH_2CH_2OH(+O_2) \rightarrow CH_2O + C(O)(O_2)CH_2CH_2OH$$

$$C(O)(O_2)CH_2CH_2OH + NO_2 \rightarrow O_2NC(O)(O_2)CH_2CH_2OH$$

$$C(O)(O_2)CH_2CH_2OH + NO(+O_2) \rightarrow CH_2(O_2)CH_2OH + CO_2$$

$$CH_2(O_2)CH_2OH + NO \rightarrow CH_2(O)CH_2OH + NO_2$$

$$CH_2(O)CH_2OH + O_2 \rightarrow CH(O)CH_2OH + HO_2$$

$$CH_2(O)CH_2OH + (+O_2) \rightarrow 2CH_2O + HO_2$$

The isomerization of the oxy radical, $CH_2(O)C(O)CH_2CH_2OH$, via transfer of a hydrogen atom from the carbon atom in the 4-position to the oxy group, could compete with the dissociation reaction shown above, since the H-atom transferred is activated by the hydroxyl group. Subsequent reaction of the radical so-formed with O_2, followed by elimination of HO_2, would produce the hydroxy dicarbonyl $CH_2(OH)C(O)CH_2CHO$. This sequence of reactions is not included in the Master Chemical Mechanism (http://mcm.leeds.ac.uk/MCM) for 2-butanone, on the basis that the dissociation reaction is significantly faster.

V-B-3. 2-Pentanone [Methyl *n*-Propyl Ketone, n-$C_3H_7C(O)CH_3$]

V-B-3.1. OH + 2-Pentanone Reaction Kinetics

The reaction of OH with 2-pentanone has been studied by Atkinson et al. (1982a), Atkinson and Aschmann (1988), and Atkinson et al. (2000) using relative rate techniques, by Wallington and Kurylo (1987a) using flash photolysis–resonance fluorescence and by Jiménez et al. (2005a) using pulsed laser photolysis–laser-induced fluorescence. The rate coefficients are given in table V-B-5. The agreement among the three relative rate measurements is excellent; all were made relative to cyclohexane, and there is close agreement with Wallington and Kurylo's absolute measurement. The more recent results of Jiménez et al. are somewhat smaller, possibly because of contributions from secondary reactions as discussed above. An unweighted mean of all the data gives a rate coefficient of 4.1×10^{-12} cm^3 molecule^{-1} s^{-1}($\sim$298 K) with an uncertainty of $\pm$30%. Jiménez et al. also measured the rate coefficient between 248 and 388 K. Their measurements indicate some curvature in the Arrhenius plot, superimposed on a negative temperature dependence (similar to acetone). Jiménez et al. reported a 3-parameter fit to the data: $k = 6.74 \times 10^{-19}\ T^2 \exp(1{,}215/T)$ cm^3 molecule^{-1} s^{-1} (figure V-B-5). Over the range of atmospheric temperatures the curvature is small, and we recommend an Arrhenius fit to all the data measured at temperatures up to 323 K, constrained to the

Table V-B-5. Rate coefficients (k, cm^3 molecule^{-1} s^{-1}) for the reaction of OH with 2-pentanone [$CH_3C(O)CH_2CH_2CH_3$]

$10^{12} \times k$	T (K)	Technique[a]	Reference	Temperature Range (K)
4.37 ± 0.13	299	RR (*cyclo*-C_6H_{12})[b]	Atkinson et al. (1982a)	
4.00 ± 0.29	296	FP–RF	Wallington and Kurylo (1987a)	
4.74 ± 0.24	296	RR (*cyclo*-C_6H_{12})[b]	Atkinson and Aschmann (1988)	
4.42 ± 0.29	298	RR (*cyclo*-C_6H_{12})[b]	Atkinson et al. (2000)	
6.14 ± 0.16	248	PLP–LIF	Jiménez et al. (2005a)[c]	248–388
5.94 ± 0.56	253			
4.95 ± 0.18	257			
4.65 ± 0.36	263			
4.64 ± 0.14	268			
4.26 ± 0.32	273			
3.99 ± 0.66	283			
3.59 ± 0.10	288			
3.14 ± 0.40	298			
2.98 ± 0.38	308			
2.90 ± 0.02	323			
2.72 ± 0.01	334			
2.71 ± 0.04	343			
2.49 ± 0.20	354			
2.56 ± 0.08	373			
2.64 ± 0.06	388			

[a]Abbreviations used for the techniques are defined in table I-F-3.
[b]Placed on an absolute basis using k(OH + cyclohexane) = 6.97×10^{-12} cm^3 molecule^{-1} s^{-1} (Calvert et al., 2008).
[c]$k(T) = 2.2 \times 10^{-12} + 1.73 \times 10^{-15} \exp(1{,}917/T)$ cm^3 molecule^{-1} s^{-1}.

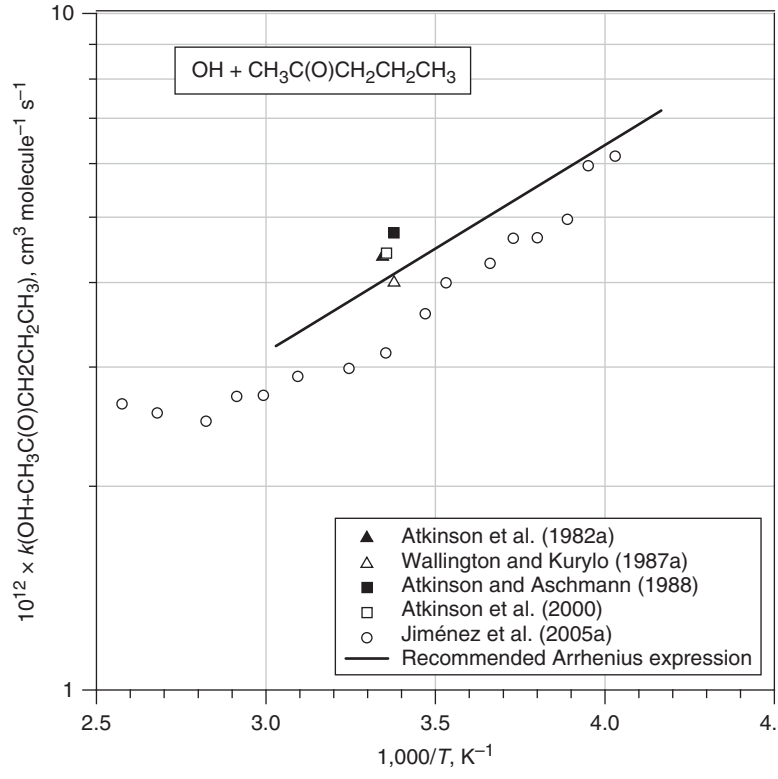

Figure V-B-5. Arrhenius plot for the rate coefficients for OH + 2-pentanone.

average value at 298 K. This leads to the expression: $k = 3.8 \times 10^{-13} \exp(705/T)\,\mathrm{cm}^3$ molecule^{-1} s^{-1}.

Atkinson et al. (2000) studied the mechanism experimentally, and showed that >19% of reaction occurs at the α-CH_2 group, and > 63% at the β-CH_2 group. The activation at the β-carbon will be discussed further at the end of this section.

V-B-3.2. Cl-Atom + 2-Pentanone Reaction Kinetics

The measured rate coefficients for Cl + 2-pentanone are shown in table V-B-6. There is good agreement between the relative rate measurements of Taketani et al. (2006) and the time resolved measurements of Takahashi et al. (2007), but these measurements are more than a factor of two higher than those of Albaladejo et al. (2003b) and Cuevas et al. (2004) at 298 K. Some concern was expressed about possible contributions from secondary chemistry in these earlier measurements in the discussion of 2-butanone. In addition, the data of Cuevas et al. show a very strong negative temperature dependence, which would mark a substantial change from the dependence found for butanone and that found for the alkanes. An unweighted average of the measurements of Taketani et al. and Takahashi et al. is recommended, giving $k(298) = 1.16 \times 10^{-10}\,\mathrm{cm}^3$ molecule^{-1} s^{-1} with an uncertainty of ±30%.

Table V-B-6. Rate coefficients ($k = A \times e^{-B/T}$, cm^3 molecule^{-1} s^{-1}) for the reaction of Cl with 2-pentanone [$CH_3C(O)CH_2CH_2CH_3$]

$10^{12} \times A$	B (K)	$10^{12} \times k$	T (K)	Technique[a]	Reference	Temperature Range (K)
		45.7 ± 2.8	298	PLP–RF	Albaladejo et al. (2003b)	
7.8 ± 2.3	−1,186 ± 178	60.6 ± 1.6	266	PLP–RF	Cuevas et al. (2004)	270–380
		52.0 ± 1.8	283			
		46.1 ± 1.2	298			
		37.6 ± 1.4	310			
		26.8 ± 2.7	331			
		23.5 ± 1.7	354			
		16.1 ± 4.8	380			
		112 ± 8	296	RR[b] (C_2H_2)	Taketani et al. (2006)	
		114 ± 9		RR[c] (C_2H_4)		
		123 ± 13	295	PLP–RF	Takahashi et al. (2007)	

[a]Abbreviations used for the techniques are defined in table I-F-3.
[b]Placed on an absolute basis using $k(Cl + C_2H_2) = 5.2 \times 10^{-11}$ cm^3 molecule^{-1} s^{-1} (Atkinson et al., 2006).
[c]Placed on an absolute basis using $k(Cl + C_2H_4) = 9.5 \times 10^{-11}$ cm^3 molecule^{-1} s^{-1} (section I-F).

V-B-3.3. Summary of the Atmospheric Fate of 2-Pentanone

Both photodecomposition (see chapter IX) and reaction with OH are important for the removal of 2-pentanone in the troposphere. The lifetime with respect to reaction with OH is given in table V-B-19 and the oxidation products of the higher ketones are discussed in section V-B-18.

V-B-4. 3-Pentanone [Diethyl Ketone, $C_2H_5C(O)C_2H_5$]

V-B-4.1. OH + 3-Pentanone Reaction Kinetics

The flash photolysis measurement of Wallington and Kurylo (1987a) lies approximately 30% higher than the two relative rate studies of Atkinson et al. (1982a) and Atkinson and Aschmann (1988); see table V-B-7. The reasons for the discrepancy are not known. It seems unlikely that the rate coefficient for 3-pentanone would be more than twice that for 2-butanone, which contains a single —$C(O)C_2H_5$ group. Hence, we tentatively recommend $k(298\ K) = 2.0 \times 10^{-12}$ cm^3 molecule^{-1} s^{-1} on the basis of the later study from Atkinson's group, but with an increased uncertainty of ±30%. Wallington and Kurylo measured the rate coefficient as a function of temperature, finding a rate coefficient that was essentially independent of temperature over the range 240–440 K. Hence, we recommend that the room temperature value of Atkinson and Aschmann be used over the atmospheric temperature range.

V-B-4.2. Cl-Atom + 3-Pentanone Reaction Kinetics

The measured rate coefficients for Cl + 3-pentanone are shown in table V-B-8. There is good agreement between the relative rate measurements of Taketani et al. (2006) and

Table V-B-7. Rate coefficients ($k = A \times e^{-B/T}$, cm^3 $molecule^{-1}$ s^{-1}) for the reaction of OH with 3-pentanone [$CH_3CH_2C(O)CH_2CH_3$]

$10^{12} \times A$	B (K)	$10^{12} \times k$	T (K)	Technique[a]	Reference	Temperature Range (K)
		1.72 ± 0.31	299	RR (*cyclo*-C_6H_{12})[b]	Atkinson et al. (1982a)	
2.8 ± 0.3	10 ± 35	2.85 ± 0.17	240	FP–RF	Wallington and Kurylo (1987a)	240–440
		2.74 ± 0.13	296			
		2.91 ± 0.17	350			
		2.79 ± 0.32	400			
		2.78 ± 0.40	440			
		1.95 ± 0.13	296	RR (*cyclo*-C_6H_{12})[b]	Atkinson and Aschmann (1988)	

[a]Abbreviations used for the techniques are defined in table I-F-3.
[b]Placed on an absolute basis using $k(OH + cyclohexane) = 6.97 \times 10^{-12}$ cm^3 $molecule^{-1}$ s^{-1} (Calvert et al., 2008).

Table V-B-8. Rate coefficients ($k = A \times e^{-B/T}$, cm^3 $molecule^{-1}$ s^{-1}) for the reaction of Cl with 3-pentanone [$CH_3CH_2C(O)CH_2CH_3$]

$10^{12} \times A$	B (K)	$10^{12} \times k$	T (K)	Technique[a]	Reference	Temperature Range (K)
		45.0 ± 3.2	298	PLP–RF	Albaladejo et al. (2003b)	
150 ± 70	281 ± 138	54 ± 16	260	DF–MS	Aranda et al. (2004)	260–333
		56 ± 9	274			
		55 ± 4	288			
		59 ± 5	298			
		60 ± 4	315			
		66 ± 6	333			
		84.2 ± 5.1	296	RR[b] (C_2H_2)	Taketani et al. (2006)	
		81.5 ± 7.4		RR[c] (C_2H_4)		
		88.7 ± 9.2	295	PLP–RF	Takahashi et al. (2007)	
56.6 ± 4.1	-87 ± 22	83.9 ± 3.3	228	PLP–RF	Zhao et al. (2008)	228–436
		81.4 ± 3.8	265			
		74.7 ± 3.0	299			
		75.4 ± 3.0	300			
		71.1 ± 3.8	362			
		70.3 ± 6.0	436			

[a]Abbreviations used for the techniques are defined in table I-F-3.
[b]Placed on an absolute basis using $k(Cl + C_2H_2) = 5.2 \times 10^{-11}$ cm^3 $molecule^{-1}$ s^{-1} (Atkinson et al., 2006).
[c]Placed on an absolute basis using $k(Cl + C_2H_4) = 9.5 \times 10^{-11}$ cm^3 $molecule^{-1}$ s^{-1} (section I-F).

the time-resolved measurements of Takahashi et al. (2007) and Zhao et al. (2008), but their room temperature measurements are substantially higher than those of Albaladejo et al. (2003b) and Aranda et al. (2004). See figure V-B-6. An Arrhenius fit to the set of higher room temperature measurements and the temperature dependent data of Zhao et al. gives: $k(T) = 5.7 \times 10^{-11} \exp(98/T)$ cm^3 $molecule^{-1}$ s^{-1} over the temperature range 220–440 K. The recommended rate coefficient at 298 K is 7.9×10^{-11} cm^3 $molecule^{-1}$ s^{-1} with an uncertainty of ±25%.

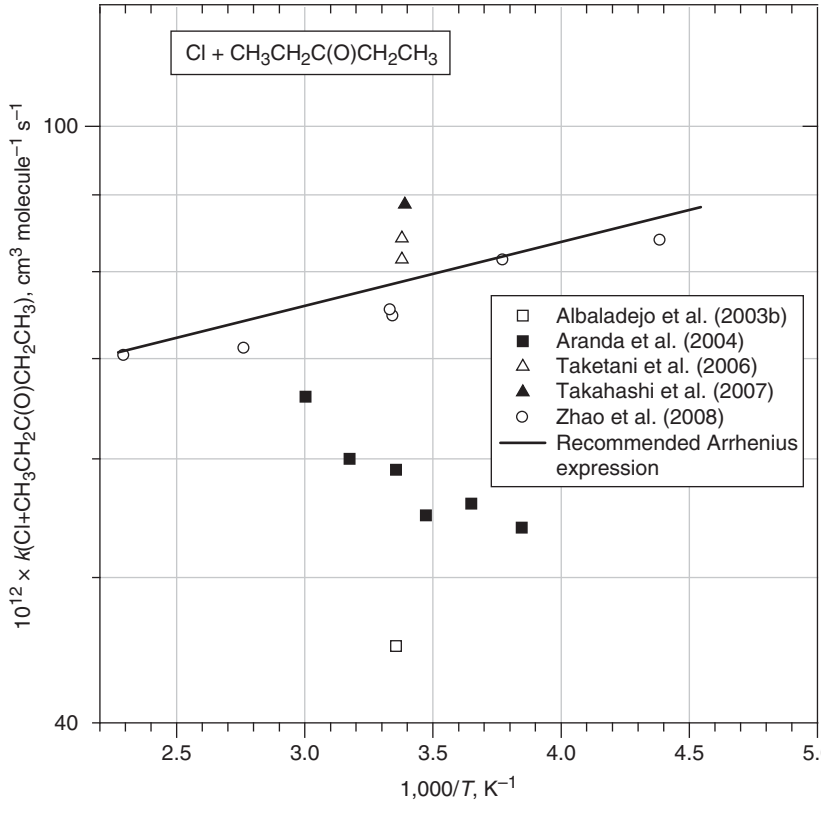

Figure V-B-6. Arrhenius plot for the rate coefficients for the reaction of Cl + 3-pentanone.

V-B-4.3. $O(^3P)$ + 3-Pentanone Reaction Kinetics

The reaction has been studied by Roscoe (1986) using discharge flow–NO chemiluminescence over the temperature range 301–565 K. On the basis of these measurements, Herron (1988) recommended the relation: $k = 5 \times 10^{-13} \exp(-1{,}000/T)\,\mathrm{cm}^3$ molecule^{-1} s^{-1}, which gives $k(298) = 1.7 \times 10^{-14}\,\mathrm{cm}^3$ molecule^{-1} s^{-1}. Herron estimated an uncertainty of a factor of 3. As discussed for acetone, the Arrhenius parameters obtained from the Roscoe data may be too small, and the expression should not be used outside the experimental range.

V-B-4.4. Summary of the Atmospheric Fate of 3-Pentanone

Both photodecomposition (see chapter IX) and reaction with OH are important loss mechanisms for 3-pentanone in the atmosphere. The atmospheric lifetime with respect to reaction with OH is given in table V-B-19 (section V-B-12.3) and the oxidation products of the higher ketones are discussed in section V-B-18.

V-B-5. 3-Methylbutanone [Methyl *iso*-Propyl Ketone, $(CH_3)_2CHC(O)CH_3$]

V-B-5.1. OH + 3-Methylbutanone Reaction Kinetics

The reaction of OH with 3-methyl-butanone has been studied by Le Calvé et al. (1998). The measurements are given in table V-B-9. They used pulsed laser photolysis with LIF detection of OH radicals and found a small negative temperature dependence, with some evidence of curvature in the Arrhenius plot; the rate coefficient was essentially independent of temperature above room temperature. Calvert et al. (2008) fitted the Arrhenius expression to the data from Le Calvé et al. (1998), obtaining the relation: $k = 1.45 \times 10^{-12} \exp(219/T)\,\mathrm{cm^3\ molecule^{-1}\ s^{-1}}$ for use in atmospheric models, with $k(298) = 3.0 \times 10^{-12}\,\mathrm{cm^3\ molecule^{-1}\ s^{-1}}$. In the absence of confirmatory measurements the uncertainty is estimated to be ±40%.

V-B-5.2. O_3+ 3-Methylbutanone Reaction Kinetics

Glasius et al. (1997) measured the rate coefficient using the decay of the ketone in the presence of excess O_3. They obtained: $k = (6.3 \pm 1.3) \times 10^{-21}\,\mathrm{cm^3\ molecule^{-1}\ s^{-1}}$. In the absence of confirmatory measurements, a higher uncertainty of ±40% is recommended.

V-B-5.3. NO_3+ 3-Methylbutanone Reaction Kinetics

Glasius et al. (1997) measured the rate coefficient using a relative rate technique, with 1-butene ($k = 1.4 \times 10^{-14}\,\mathrm{cm^3\ molecule^{-1}\ s^{-1}}$; Calvert et al., 2000) and ethene ($k = 2.0 \times 10^{-16}\,\mathrm{cm^3\ molecule^{-1}\ s^{-1}}$, Atkinson et al., 2006) as reference compounds. They obtained $k < 5 \times 10^{-16}\,\mathrm{cm^3\ molecule^{-1}\ s^{-1}}$.

V-B-5.4. Cl-Atom + 3-Methylbutanone Reaction Kinetics

The rate coefficient has been measured by Notario et al. (2000a) and by Cuevas et al. (2004); the 298 K values differ by about 50%. See table V-B-10. A mean value of $6 \times 10^{-11}\,\mathrm{cm^3\ molecule^{-1}\ s^{-1}}$ with a large uncertainty of ±40% is recommended.

Table V-B-9. Rate coefficients ($k = A \times \mathrm{e}^{-B/T}, \mathrm{cm^3\ molecule^{-1}\ s^{-1}}$) for the reaction of OH with 3-methylbutanone [$CH_3C(O)CH(CH_3)_2$]

$10^{12} \times A$	B (K)	$10^{12} \times k$	T (K)	Technique[a]	Reference	Temperature Range (K)
1.58 ± 0.35	−193 ± 65	3.68 ± 0.15	253	PLP–LIF	Le Calvé et al. (1998)	253–372
		3.26 ± 0.08	263			
		3.26 ± 0.08	273			
		2.84 ± 0.12	298			
		2.78 ± 0.11	323			
		2.74 ± 0.11	348			
		2.75 ± 0.10	372			

[a]Abbreviations used for the techniques are defined in table I-F-3.

Table V-B-10. Rate coefficients ($k = A \times e^{-B/T}$, cm^3 molecule^{-1} s^{-1}) for the reaction of Cl with 3-methylbutanone [$CH_3C(O)CH(CH_3)_2$]

$10^{12} \times A$	B (K)	$10^{12} \times k$	T (K)	Technique[a]	Reference	Temperature Range (K)
		70.2 ± 8.9	298	PLP–RF	Notario et al. (2000a)	
18.6 ± 1.1	−254 ± 36	48.9 ± 4.4	268	PLP–RF	Cuevas et al. (2004)	268–380
		47.0 ± 6.2	283			
		45.0 ± 2.5	298			
		42.1 ± 2.2	310			
		38.8 ± 2.6	331			
		38.0 ± 3.4	354			
		36.9 ± 2.2	380			

[a]Abbreviations used for the techniques are defined in table I-F-3.

V-B-5.5. Summary of the Atmospheric Fate of 3-Methylbutanone

Both photodecomposition (see chapter IX) and reaction with OH are important in the removal of 3-methylbutanone in the troposphere. The atmospheric lifetime with respect to reaction with OH is given in table V-B-19 (section V-B-12.3) and the oxidation products of the higher ketones are discussed in section V-B-18.

V-B-6. 2-Hexanone [Methyl *n*-Butyl Ketone, $CH_3C(O)CH_2CH_2CH_2CH_3$]

V-B-6.1. OH + 2-Hexanone Reaction Kinetics

The measured rate coefficients are given in table V-B-11. The absolute studies of Wallington and Kurylo (1987a) and Jiménez et al. (2005a) are in good agreement, reporting rate coefficients at 298 ± 3 K of $(6.64 \pm 0.56) \times 10^{-12}$ and $(6.37 \pm 1.40) \times 10^{-12}$ cm^3 molecule^{-1} s^{-1}, respectively. However, the relative rate determinations of Atkinson et al. (1982a), $(8.43 \pm 0.56) \times 10^{-12}$, and Atkinson and Aschmann (1988), $(8.51 \pm 0.42) \times 10^{-12}$ cm^3 molecule^{-1} s^{-1}, are about 30% higher. The reasons for this discrepancy are not known. The unweighted mean of these four values gives our recommended rate coefficient, $k(298) = 7.5 \times 10^{-12}$ cm^3 molecule^{-1} s^{-1}, with an uncertainty of ±30%. Jiménez et al. (2005) found a distinct negative temperature dependence for the rate coefficient over the entire range of their measurements (263–405 K), and gave $k = 2.13 \times 10^{-18}\ T^2\ \exp(1{,}038/T)$ cm^3 molecule^{-1} s^{-1}. A linear Arrhenius fit to all the data over the range 263–353 K, constrained to the recommended value at 298 K, gives $k = 8.4 \times 10^{-13}\ \exp(654/T)$ cm^3 molecule^{-1} s^{-1} (figure V-B-7).

V-B-6.2. Cl-Atom + 2-Hexanone Reaction Kinetics

The rate coefficients have been measured by a relative rate technique by Taketani et al. (2006) and by pulsed laser photolysis by Albaladejo et al. (2003b), Cuevas et al. (2004), and Takahashi et al. (2007). See table V-B-12. The two latest measurements exceed the earlier measurements by a factor of about 3. An unweighted mean of these higher

Table V-B-11. Rate coefficients (k, cm^3 molecule^{-1} s^{-1}) for the reaction of OH with 2-hexanone [$CH_3C(O)CH_2CH_2CH_2CH_3$]

$10^{12} \times k$	T (K)	Technique[a]	Reference	Temperature Range (K)
8.43 ± 0.56	299	RR (*cyclo*-C_6H_{12})[b]	Atkinson et al. (1982a)	
6.64 ± 0.56	296	FP–RF	Wallington and Kurylo (1987a)	
8.51 ± 0.42	296	RR (*cyclo*-C_6H_{12})[b]	Atkinson and Aschmann (1988)	
10.2 ± 1.20	263	PLP–LIF	Jiménez et al. (2005a)[c]	263–405
7.84 ± 0.84	273			
7.13 ± 0.87	279			
7.34 ± 0.94	284			
6.41 ± 0.20	286			
6.30 ± 0.42	288			
6.37 ± 1.40	298			
5.97 ± 0.16	313			
5.63 ± 0.10	316			
5.32 ± 0.76	328			
4.62 ± 0.46	349			
4.84 ± 0.52	353			
4.70 ± 0.20	370			
4.61 ± 1.40	380			
5.05 ± 0.26	390			
4.50 ± 0.64	405			

[a]Abbreviations used for the techniques are defined in table I-F-3.
[b]Placed on an absolute basis using $k(\text{OH} + \text{cyclohexane}) = 6.97 \times 10^{-12}$ cm^3 molecule^{-1} s^{-1} (Calvert et al., 2008).
[c]$k(T) = 2.13 \times 10^{-18} T^2 \exp(1{,}038/T)$.

determinations is recommended, $k(298) = 2.0 \times 10^{-10}$ cm^3 molecule^{-1} s^{-1} with an uncertainty of ±40%; this is assigned on the basis of the better agreement with the structure–activity relation as discussed in section V-B-18.

V-B-6.3. Summary of the Atmospheric Fate of 2-Hexanone

Both photodecomposition (see chapter IX) and reaction with OH are important in the removal of 2-hexanone in the troposphere. The atmospheric lifetime with respect to reaction with OH is given in table V-B-19 (section V-B-12.3) and the oxidation products of the higher ketones are discussed in section V-B-18.

V-B-7. 3-Hexanone [Ethyl *n*-Propyl Ketone, $CH_3CH_2C(O)CH_2CH_2CH_3$]

V-B-7.1. OH + 3-Hexanone Reaction Kinetics

This reaction has been studied by Atkinson et al. (1982a) using the relative rate method. They found a rate coefficient ratio, relative to cyclohexane, of 0.919 ± 0.038. Using the value of the rate coefficient for OH + cyclohexane of 6.97×10^{-12} cm^3 molecule^{-1} s^{-1} (Calvert et al., 2008) gives a rate coefficient for OH + 3-hexanone of 6.4×10^{-12} cm^3 molecule^{-1} s^{-1} at 298 ± 3 K, with an uncertainty of ±40%. No recommendation

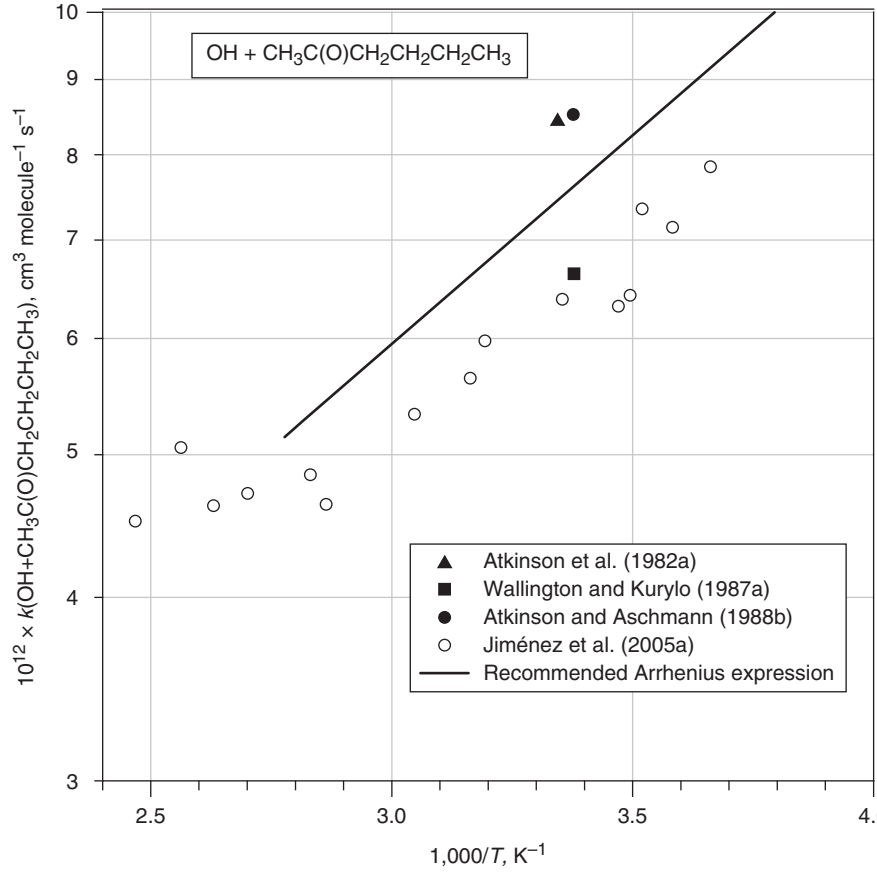

Figure V-B-7. Arrhenius plot for the rate coefficients for OH + 2-hexanone.

Table V-B-12. Rate coefficients ($k = A \times e^{-B/T}$, cm^3 $molecule^{-1}$ s^{-1}) for the reaction of Cl with 2-hexanone [$CH_3C(O)CH_2CH_2CH_2CH_3$]

$10^{12} \times A$	B (K)	$10^{12} \times k$	T (K)	Technique[a]	Reference	Temperature Range (K)
		65.4 ± 5.8	298	PLP–RF	Albaladejo et al. (2003b)	
10.0 ± 1.5	-565 ± 92	78.8 ± 8.6	268	PLP–RF	Cuevas et al.(2004)	268–380
		76.1 ± 7.2	283			
		64.9 ± 3.8	298			
		61.0 ± 1.1	310			
		57.1 ± 4.6	331			
		46.2 ± 6.2	354			
		43.2 ± 5.0	380			
		195 ± 15	296	RR[b] (C_2H_2)	Taketani et al. (2006)	
		189 ± 15		RR[c] (C_2H_4)		
		208 ± 32	295	PLP–RF	Takahashi et al. (2007)	

[a]Abbreviations used for the techniques are defined in table I-F-3.
[b]Placed on an absolute basis using $k(Cl + C_2H_2) = 5.2 \times 10^{-11}$ cm^3 $molecule^{-1}$ s^{-1} (Atkinson et al., 2006).
[c]Placed on an absolute basis using $k(Cl + C_2H_4) = 9.5 \times 10^{-11}$ cm^3 $molecule^{-1}$ s^{-1} (see section I-F).

for the temperature dependence can be made at present, although it is expected to be slightly negative.

V-B-7.2. Cl-Atom + 3-Hexanone Reaction Kinetics

The rate coefficients have been measured by a relative rate technique by Taketani et al. (2006), by pulsed laser photolysis by Albaladejo et al. (2003b) and Takahashi et al. (2007), and by discharge flow–mass spectrometry by Aranda et al. (2004). See table V-B-13. The two latest measurements exceed the earlier measurements by a factor of about 2. An unweighted mean of these two determinations is recommended, giving $k(298) = 1.44 \times 10^{-10}$ cm^3 molecule^{-1} s^{-1}, with an uncertainty of ±40%. The positive temperature dependence obtained by Aranda et al. is very large for a reaction of this type and gives an unrealistically large *A*-factor.

V-B-7.3. Summary of the Atmospheric Fate of 3-Hexanone

Both photodecomposition (see chapter IX) and reaction with OH are important in the removal of 3-hexanone in the troposphere. The atmospheric lifetime with respect to reaction with OH is given in table V-B-19 (section V-B-12.3) and the oxidation products of the higher ketones are discussed in section V-B-18.

V-B-8. 3-Methyl-2-Pentanone [Methyl *sec*-Butyl Ketone, $CH_3C(O)CH(CH_3)CH_2CH_3$]

V-B-8.1. OH + 3-Methyl-2-Pentanone Reaction Kinetics

Tuazon et al. (2003) measured the rate coefficient for the reaction of OH with 3-methyl-2-pentanone relative to that of octane. Using $k(\text{OH} + \text{octane}) = 7.81 \times 10^{-12}$ cm^3 molecule^{-1} s^{-1} (Calvert et al., 2008), and the measured ratio 0.789 ± 0.009, gives

Table V-B-13. Rate coefficients ($k = A \times e^{-B/T}$, cm^3 molecule^{-1} s^{-1}) for the reaction of Cl with 3-hexanone [$CH_3CH_2C(O)CH_2CH_2CH_3$]

$10^{12} \times A$	B (K)	$10^{12} \times k$	T (K)	Technique[a]	Reference	Temperature Range (K)
		66.9 ± 6.2	298	PLP–RF	Albaladejo et al. (2003b)	
1,600 ± 400	884 ± 69	52 ± 17	263	DF–MS	Aranda et al. (2004)	260–330
		66 ± 9	279			
		83 ± 17	298			
		94 ± 10	315			
		109 ± 13	333			
		152 ± 12	296	RR[b] (C_2H_4)	Taketani et al. (2006)	
		138 ± 13		RR[c] (*cyclo*-C_6H_{12})		
		143 ± 19	295	PLP–RF	Takahashi et al. (2007)	

[a]Abbreviations used for the techniques are defined in table I-F-3.
[b]Placed on an absolute basis using $k(\text{Cl} + C_2H_4) = 9.5 \times 10^{-11}$ cm^3 molecule^{-1} s^{-1} (section I-F).
[c]Placed on an absolute basis using $k(\text{Cl} + \text{cyclohexane}) = 3.3 \times 10^{-10}$ cm^3 molecule^{-1} s^{-1} (Calvert et al., 2008).

$k = 6.2 \times 10^{-12}$ cm^3 molecule^{-1} s^{-1} for a temperature of 298 K; an estimated uncertainty of ±40% is recommended.

V-B-8.2. Summary of the Atmospheric Fate of 3-Methyl-2-Pentanone

Both photodecomposition (see chapter IX) and reaction with OH are important in the removal of 3-methyl-2-pentanone in the troposphere. The atmospheric lifetime with respect to reaction with OH is given in table V-B-19 (section V-B-12.3) and the oxidation products of the higher ketones are discussed in section V-B-18.

V-B-9. 4-Methyl-2-Pentanone [Methyl *iso*-Butyl Ketone, $CH_3C(O)CH_2CH(CH_3)_2$]

V-B-9.1. OH + 4-Methyl-2-Pentanone Reaction Kinetics

The reaction of OH with 4-methyl-2-pentanone has been measured by Winer et al. (1976), Cox et al. (1980b, 1981), Atkinson et al. (1982a), and O'rji and Stone (1992) using relative rate methods, and by Le Calvé et al. (1998) using pulsed laser photolysis; see table V-B-14. The results are in good agreement, ranging between 1.2×10^{-11} and 1.5×10^{-11} cm^3 molecule^{-1} s^{-1} at 298 K. Le Calvé et al. also measured the temperature dependence of the reaction, between 253 and 372 K, finding a decrease in the rate coefficient with increasing temperature. Calvert et al. (2008) made an Arrhenius fit to all the data other than the point of Winer et al. giving $k = 8.0 \times 10^{-13} \exp(828/T)$ cm^3 molecule^{-1} s^{-1}, leading to a rate

Table V-B-14. Rate coefficients ($k = A \times e^{-B/T}$, cm^3 molecule^{-1} s^{-1}) for the reaction of OH with 4-methyl-2-pentanone [$CH_3C(O)CH_2CH(CH_3)_2$]

$10^{12} \times A$	B (K)	$10^{12} \times k$	T (K)	Technique[a]	Reference	Temperature Range (K)
		15.0 ± 5.0	305	RR ($CH_2{=}C(CH_3)_2$)[b]	Winer et al. (1976)	
		12.1	300	RR (C_2H_4)[c]	Cox et al. (1980b)	
		12.0 ± 0.3	296	RR (C_2H_4)[c]	Cox et al. (1981)	
		13.3 ± 0.7	299	RR (*cyclo*-C_6H_{12})[d]	Atkinson et al. (1982a)	
		15.4 ± 0.7	297	RR (C_3H_6)[e]	O'rji and Stone (1992)	
0.76 ± 0.13	−834 ± 46	21.3 ± 1.0	253	PLP–LIF	Le Calvé et al. (1998)	253–372
		18.2 ± 0.2	263			
		16.2 ± 0.3	273			
		12.1 ± 0.5	298			
		10.6 ± 0.2	313			
		9.25 ± 0.5	333			
		8.28 ± 0.14	353			
		7.57 ± 0.3	372			

[a]Abbreviations used for the techniques are defined in table I-F-3.
[b]Placed on an absolute basis using $k(OH + 2\text{-methylpropene}) = 5.14 \times 10^{-11}$ cm^3 molecule^{-1} s^{-1} (Calvert et al., 2000).
[c]Placed on an absolute basis using $k(OH + C_2H_4) = 7.9 \times 10^{-12}$ cm^3 molecule^{-1} s^{-1} at 1 bar and 298 K (Atkinson et al., 2006).
[d]Placed on an absolute basis using $k(OH + \text{cyclohexane}) = 6.97 \times 10^{-12}$ cm^3 molecule^{-1} s^{-1} (Calvert et al., 2008).
[e]Placed on an absolute basis using $k(OH + C_3H_6) = 2.9 \times 10^{-11}$ cm^3 molecule^{-1} s^{-1} at 1 bar and 298 K (Atkinson et al., 2006).

coefficient at 298 K of 1.28×10^{-11} cm^3 molecule^{-1} s^{-1}, with an estimated uncertainty of ±20%.

Cox et al. (1981) measured an acetone yield of 90%, suggesting that most of the OH attack occurs at the activated tertiary 4-position. The structure–activity relations discussed in section V-B-18 give a percentage abstraction at this position of ~80%.

V-B-9.2. Cl-Atom + 4-Methyl-2-Pentanone Reaction Kinetics

The rate coefficient has been measured by Notario et al. (2000a) and by Cuevas et al. (2004). The data are given in table V-B-15. An unweighted average at 298 K gives $k(298) = 9.1 \times 10^{-11}$ cm^3 molecule^{-1} s^{-1}, with an uncertainty of ±40%. In view of the difficulties discussed earlier with the measurements of Cuevas et al., a temperature dependence cannot be recommended.

V-B-9.3. Summary of the Atmospheric Fate of 4-Methyl-2-Pentanone

Both photodecomposition (see chapter IX) and reaction with OH are important in the removal of 4-methyl-2-pentanone in the troposphere. The atmospheric lifetime with respect to reaction with OH is given in table V-B-19 (section V-B-12.3), and the oxidation products of the higher ketones are discussed in section V-B-18.

V-B-10. 3,3-Dimethyl-2-Butanone [Methyl *tert*-Butyl Ketone, $(CH_3)_3CC(O)CH_3$]

V-B-10.1. OH + 3,3-Dimethyl-2-Butanone Reaction Kinetics

The reaction of OH with 3,3-dimethyl-2-butanone has been studied by Wallington and Kurylo (1987a), who used flash photolysis with resonance fluorescence detection. They determined a rate coefficient of $(1.21 \pm 0.05) \times 10^{-12}$ cm^3 molecule^{-1} s^{-1} at 298 ± 3 K. In the absence of other measurements, we recommend this rate coefficient, but with an increased uncertainty of ±40%. The reaction probably has a negative temperature dependence similar to that of 4-methyl-2-pentanone. Most of the reaction

Table V-B-15. Rate coefficients ($k = A \times e^{-B/T}$, cm^3 molecule^{-1} s^{-1}) for the reaction of Cl with 4-methyl-2-pentanone [$CH_3C(O)CH_2CH(CH_3)_2$]

$10^{12} \times A$	B (K)	$10^{12} \times k$	T (K)	Technique[a]	Reference	Temperature Range (K)
		97.2 ± 12	298	PLP–RF	Notario et al. (2000a)	
5.26 ± 0.60	−827 ± 68	118 ± 8	267	PLP–RF	Cuevas et al. (2004)	267–380
		99.6 ± 6.2	283			
		85.2 ± 4.0	298			
		75.1 ± 2.0	310			
		63.9 ± 6.8	331			
		55.9 ± 16.0	354			
		48.8 ± 5.6	380			

[a]Abbreviations used for the techniques are defined in table I-F-3.

is expected to occur at the *tert*-butyl group. The SAR gives about 94% of the reaction occurring via abstraction at one of the three methyl groups of the $(CH_3)_3C$-portion of the molecule.

V-B-10.2. Summary of the Atmospheric Fate of 3,3-Dimethyl-2-Butanone

Both photodecomposition (see chapter IX) and reaction with OH are important in the removal of 3,3-dimethyl-2-butanone in the troposphere. The atmospheric lifetime with respect to reaction with OH is given in table V-B-19 (section V-B-12.3) and the oxidation products of the higher ketones are discussed in section V-B-18.

V-B-11. 2-Heptanone [Methyl *n*-Pentyl Ketone, $CH_3C(O)CH_2CH_2CH_2CH_2CH_3$]

V-B-11.1. OH + 2-Heptanone Reaction Kinetics

The reaction of OH with 2-heptanone has been the subject of three studies. The measurements are given in table V-B-16. The relative rate study of Atkinson et al. (2000) gives a value of $k(298) = (1.11 \pm 0.11) \times 10^{-11}$ cm^3 molecule^{-1} s^{-1}. The two absolute studies of Wallington and Kurylo (1987a) and Jiménez et al. (2005a) both give smaller values, $(8.67 \pm 0.84) \times 10^{-12}$ and $(8.22 \pm 1.10) \times 10^{-12}$ cm^3 molecule^{-1} s^{-1}, respectively, at ambient temperatures. The reason for the discrepancy between absolute and relative methods is unknown. An unweighted mean of the three determinations gives our recommended rate coefficient: $k(298) = 9.4 \times 10^{-12}$ cm^3 molecule^{-1} s^{-1}, with an uncertainty of ±30%. Jiménez et al. also measured the rate coefficient between 260 and 405 K, finding a monotonic decrease in k with increasing temperature up to about

Table V-B-16. Rate coefficient (k, cm^3 molecule^{-1} s^{-1}) for the reaction of OH with 2-heptanone [n-$C_5H_{11}C(O)CH_3$]

$10^{12} \times k$	T (K)	Technique[a]	Reference	Temperature Range (K)
8.67 ± 0.84	296	FP–RF	Wallington and Kurylo (1987a)	
11.1 ± 1.10	298	RR (c-C_6H_{12})[b]	Atkinson et al. (2000)	
10.2 ± 0.60	260	PLP–LIF	Jiménez et al. (2005a)[c]	260–405
9.46 ± 0.36	263			
9.25 ± 0.28	267			
8.53 ± 0.76	273			
8.62 ± 0.46	283			
8.20 ± 0.08	287			
8.22 ± 1.10	298			
7.54 ± 0.42	313			
7.55 ± 0.40	323			
7.55 ± 0.26	333			
7.05 ± 0.12	343			
6.97 ± 0.50	354			
7.19 ± 0.44	374			
7.17 ± 0.02	405			

[a]Abbreviations used for the techniques are defined in table I-F-3.
[b]Placed on an absolute basis using $k(\text{OH} + \text{cyclohexane}) = 6.97 \times 10^{-12}$ cm^3 molecule^{-1} s^{-1} (Calvert et al., 2008).
[c]$k(T) = 1.54 \times 10^{-6} T^2 \exp(1{,}144/T)$.

330 K, and a flat minimum value above 330 K. The dashed curve in figure V-B-8 is a nonlinear fit to the data of Jiménez et al., which gives $k = 4.75 \times 10^{-18}\ T^2 \exp(880/T)\ \mathrm{cm^3\ molecule^{-1}\ s^{-1}}$; this expression differs from that given by Jiménez et al. (table V-B-16) because of our use of $1/k^2$ weighting. All the data below 330 K have been fitted to an Arrhenius expression, constrained to the recommended value at 298 K, to give a recommended rate coefficient expression: $k = 2.8 \times 10^{-12} \exp(317/T)\ \mathrm{cm^3\ molecule^{-1}\ s^{-1}}$ over the range 260–330 K (figure V-B-8).

V-B-11.2. Summary of the Atmospheric Fate of 2-Heptanone

Both photodecomposition (see chapter IX) and reaction with OH are important in the removal of 2-heptanone in the troposphere. The atmospheric lifetime with respect to reaction with OH is given in table V-B-19 (section V-B-12.3).

Atkinson et al. (2000) studied the product distribution from the reaction of OH with 2-heptanone, using a combination of detection techniques. In addition to the simple aldehydes, formaldehyde (38% yield), acetaldehyde (15%), propanal (10%), butanal (7%), and pentanal (9%), evidence was found for a number of dicarbonyls and hydroxydicarbonyls, presumably produced following isomerization of the initially

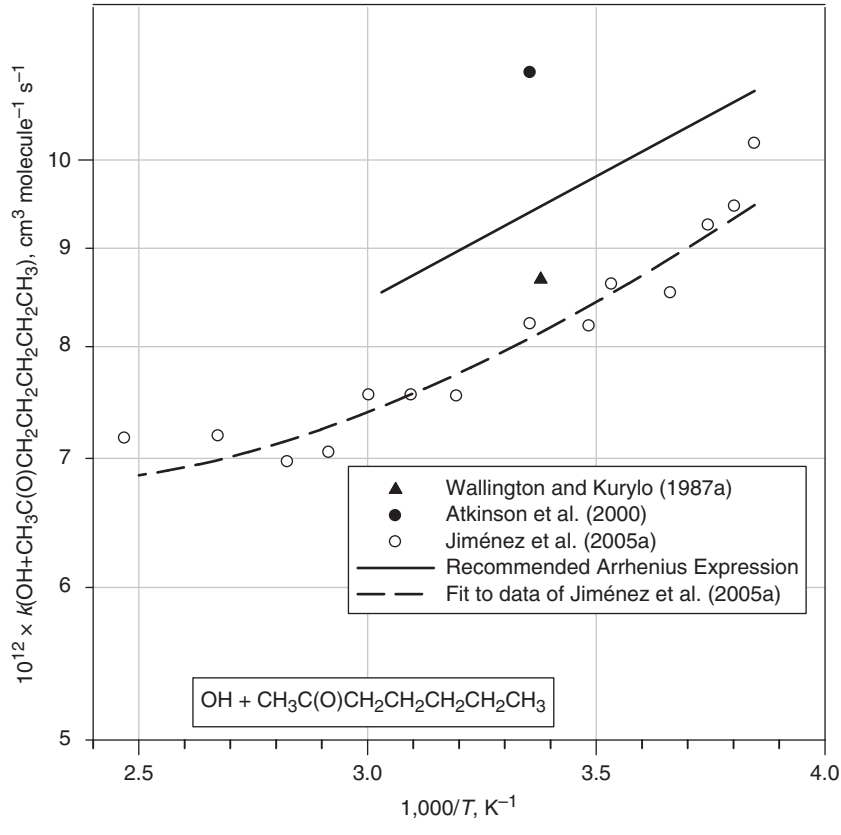

Figure V-B-8. Arrhenius plot for the reaction of OH + 2-heptanone.

formed alkoxy radicals. The yields of the identified products were consistent with the calculated fractions of attack at the various sites as predicted from the SAR of Kwok and Atkinson (1995); however, it was not possible to derive a unique mechanism from the observed products. A general discussion of the oxidation products of the higher ketones is given in section V-B-18.

V-B-12. 5-Methyl-2-Hexanone [Methyl Isopentyl Ketone, $(CH_3)_2CHCH_2CH_2C(O)CH_3$]

V-B-12.1. OH + 5-Methyl-2-Hexanone Reaction Kinetics

This reaction has been studied by Le Calvé et al. (1998) (see table V-B-17 and figure V-B-9) who showed that the rate coefficient decreases monotonically with increasing temperature. An Arrhenius fit to the data gives $k(T) = 1.24 \times 10^{-12} \times \exp(674/T)\,\mathrm{cm^3\ molecule^{-1}\ s^{-1}}$ and $k(298) = 1.20 \times 10^{-11}\,\mathrm{cm^3\ molecule^{-1}\ s^{-1}}$; an uncertainty of ±40% is estimated. The Arrhenius parameters differ from those given by Le Calvé et al. (table V-B-17) because of our use of $1/k^2$ weighting.

V-B-12.2. Cl-Atom + 5-Methyl-2-Hexanone Reaction Kinetics

The rate coefficient has been measured by Notario et al. (2000a) and by Cuevas et al. (2004). See table V-B-18. An unweighted average at 298 K gives $k(298) = 1.3 \times 10^{-10}\,\mathrm{cm^3\ molecule^{-1}\ s^{-1}}$, with an uncertainty of ±40%. In view of the difficulties discussed earlier with the temperature dependent measurements of Cuevas et al., an Arrhenius expression cannot be recommended.

V-B-12.3. Summary of the Atmospheric Fate of 5-Methyl-2-Hexanone

Both photodecomposition (see chapter IX) and reaction with OH are important in the removal of 5-methyl-2-hexanone in the troposphere. The atmospheric lifetime with respect to reaction with OH is given in table V-B-19 (below) and the oxidation products of the higher ketones are discussed in section V-B-18.

Table V-B-17. Rate coefficients ($k = A \times e^{-B/T}, \mathrm{cm^3\ molecule^{-1}\ s^{-1}}$) for the reaction of OH with 5-methyl-2-hexanone [$CH_3C(O)CH_2CH_2CH(CH_3)_2$]

$10^{12} \times A$	B (K)	$10^{12} \times k$	T (K)	Technique[a]	Reference	Temperature Range (K)
1.33 ± 0.63	−649 ± 140	17.0 ± 0.4	263	PLP–LIF	Le Calvé et al. (1998)	263–372
		15.4 ± 0.9	273			
		13.8 ± 0.5	283			
		12.8 ± 0.3	286			
		13.3 ±0.3	291			
		12.2 ± 0.3	293			
		10.3 ± 0.5	298			
		9.77 ± 0.98	323			
		8.90 ± 0.26	348			
		8.00 ± 0.50	372			

[a]Abbreviations used for the techniques are defined in table I-F-3.

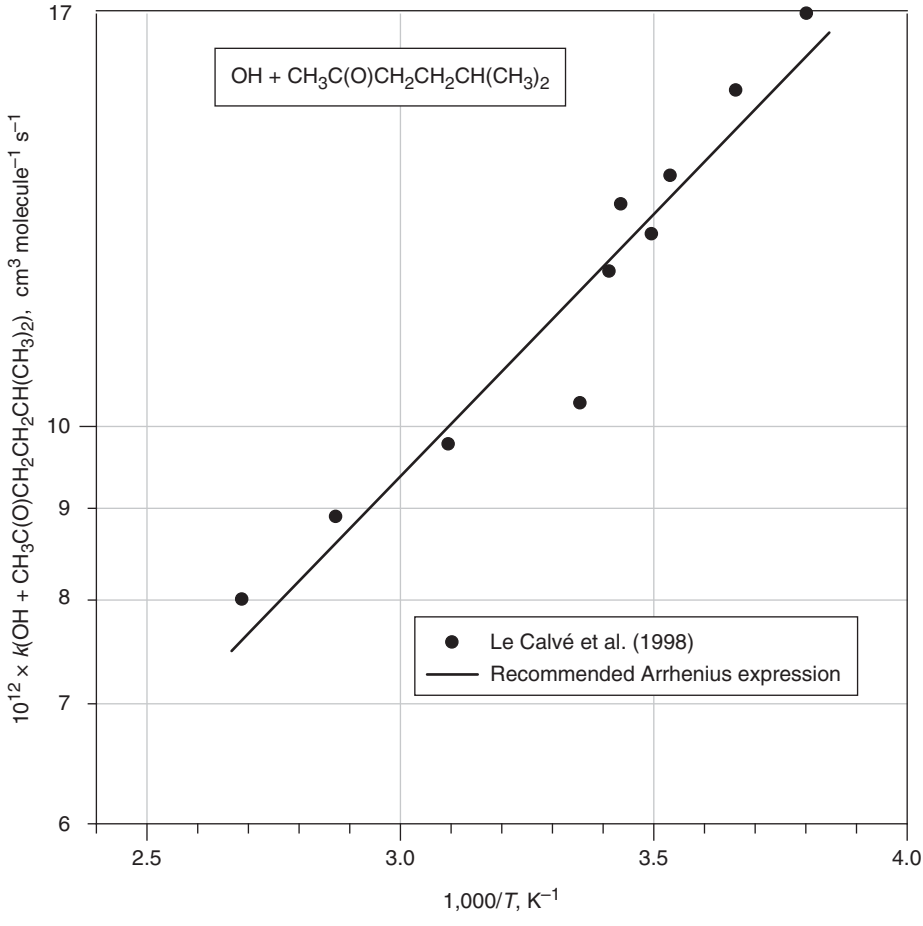

Figure V-B-9. Arrhenius plot for the reaction of OH + 5-methyl-2-hexanone.

Table V-B-18. Rate coefficients ($k = A \times e^{-B/T}$, cm^3 molecule^{-1} s^{-1}) for the reaction of Cl with 5-methyl-2-hexanone [$CH_3C(O)CH_2CH_2CH(CH_3)_2$]

$10^{12} \times A$	B (K)	$10^{12} \times k$	T (K)	Technique[a]	Reference	Temperature Range (K)
		106 ± 14	298	PLP–RF	Notario et al. (2000a)	
8.17 ± 1.06	−877 ± 84	229 ± 9	268	PLP–RF	Cuevas et al. (2004)	267–380
		182 ± 34	284			
		148 ± 10	298			
		128 ± 9	310			
		110 ± 5	331			
		98.7 ± 2.8	354			
		88.3 ± 7.2	380			

[a]Abbreviations used for the techniques are defined in table I-F-3.

Table V-B-19. Lifetimes of alkanones with respect to reaction with [OH] = 10^6 molecule cm^{-3}

Compound	Lifetime, days
Acetone	64
Butanone	10
2-Pentanone	2.8
3-Pentanone	5.8
3-Methylbutanone	3.9
2-Hexanone	1.5
3-Hexanone	1.8
3-Methyl-2-pentanone	1.9
4-Methyl-2-pentanone	0.90
3,3-Dimethyl-2-butanone	9.6
2-Heptanone	1.2
5-Methyl-2-hexanone	1.0
2,4-Dimethyl-2-pentanone	2.4
2-Octanone	1.1
2-Nonanone	0.95
2-Decanone	0.88

V-B-13. 2,4-Dimethyl-3-Pentanone [Di-*iso*-propyl Ketone, $(CH_3)_2CHC(O)CH(CH_3)_2$]

V-B-13.1. OH + 2,4-Dimethyl-3-Pentanone Reaction Kinetics

The reaction of OH with 2,4-dimethyl-3-pentanone has been studied by Atkinson et al. (1982a) at 299 ± 2 K. They used the relative rate technique with cyclohexane as the reference compound. Using $k(\mathrm{OH} + \mathrm{cyclohexane}) = 6.97 \times 10^{-12}$ cm^3 $molecule^{-1}$ s^{-1} (Calvert et al., 2008) gives a rate coefficient of 4.9×10^{-12} cm^3 $molecule^{-1}$ s^{-1} at 298 K; the uncertainty is estimated as ±40% to reflect the lack of confirmatory data.

V-B-14. 2-Octanone [Methyl *n*-Hexyl Ketone, $CH_3C(O)CH_2CH_2CH_2CH_2CH_2CH_3$]

V-B-14.1. OH + 2-Octanone Reaction Kinetics

This reaction was studied at 296 K by Wallington and Kurylo (1987a) using flash photolysis with resonance fluorescence detection of OH. They found a rate coefficient of $(1.10 \pm 0.09) \times 10^{-11}$ cm^3 $molecule^{-1}$ s^{-1}. In the absence of other data, we recommend this value, with an estimated uncertainty of ±40%.

V-B-15. 2-Nonanone [Methyl *n*-Heptyl Ketone, $CH_3C(O)CH_2CH_2CH_2CH_2CH_2CH_2CH_3$]

V-B-15.1. OH + 2-Nonanone Reaction Kinetics

This reaction was studied at 296 K by Wallington and Kurylo (1987a) using flash photolysis with resonance fluorescence detection of OH. They found a rate coefficient of

$(1.22 \pm 0.13) \times 10^{-11}$ cm^3 molecule^{-1} s^{-1}. In the absence of other data, we recommend this value with an estimated uncertainty of ±40%.

V-B-16. 2,6-Dimethyl-4-Heptanone [Di-*iso*-Butyl Ketone, $(CH_3)_2CHCH_2C(O)CH_2CH(CH_3)_2$]

V-B-16.1. OH + 2,6-Dimethyl-4-Heptanone Reaction Kinetics

The reaction of OH with 2,6-dimethyl-4-heptanone has been measured by Winer et al. (1976) and Atkinson et al. (1982a) using the relative rate technique. Winer et al. obtained $k = (2.5 \pm 0.8) \times 10^{-11}$ cm^3 molecule^{-1} s^{-1}, using 2-methyl propene as the reference compound ($k = 5.14 \times 10^{-11}$, Calvert et al., 2000). Atkinson et al. found a rate coefficient of $(2.5 \pm 0.5) \times 10^{-11}$ cm^3 molecule^{-1} s^{-1} using cyclohexane as the reference compound ($k = 6.97 \times 10^{-12}$, Calvert et al., 2008). We estimate an uncertainty of ±30% in the recommended value from these two determinations, $k = 2.5 \times 10^{-11}$ cm^3 molecule^{-1} s^{-1}. The compound has two tertiary C—H bonds, both of which are in the activated position β to the >C=O group, and this rate coefficient is the highest for any alkanone discussed in this section. A comparison with SARs is given in section V-B-18. Most of the abstraction occurs at the tertiary positions, with the Kwok and Atkinson (1995) SAR giving 86% abstraction at these sites.

V-B-17. OH + 2-Decanone [Methyl *n*-Octyl Ketone, n-$C_8H_{17}C(O)CH_3$]

V-B-17.1. OH + 2-Decanone Reaction Kinetics

This reaction was studied at 296 K by Wallington and Kurylo (1987a) using flash photolysis with resonance fluorescence detection of OH. They found a rate coefficient of $(1.32 \pm 0.12) \times 10^{-11}$ cm^3 molecule^{-1} s^{-1} at 296 K. In the absence of other data, we recommend this value with an estimated uncertainty of ±40%.

V-B-18. Summary of the Atmospheric Fate of the Higher Ketones (>C_4) and the End Products of Their Oxidation

The lifetimes of the alkanones with respect to reaction with OH for [OH] = 10^6 molecule cm^{-3} are summarized in table V-B-19. The limited data related to the photodissociation lifetimes of the ketones indicate that these are comparable to the lifetimes shown for reaction with OH in this table. Thus lifetimes for photodissociation in the lower troposphere with an overhead Sun are estimated as follows: acetone, 12 to 16 days; butanone, about 2.5 days; 2-pentanone, 4.3 to 24 days; 1-hexanone, 1.4 to 8.3 days. See chapter IX and table IX-M-1.

The reactions occurring following reaction of butanone with OH were discussed in section V-B-2.4. There have been very few investigations of the products of the oxidation of the higher ketones. The results of Atkinson et al. (2000) for 2-heptanone were discussed in section V-B-11.2, where it was noted that a unique mechanism could not be formulated on the basis of the observations, but that they were compatible with the Kwok and Atkinson (1995) SARs.

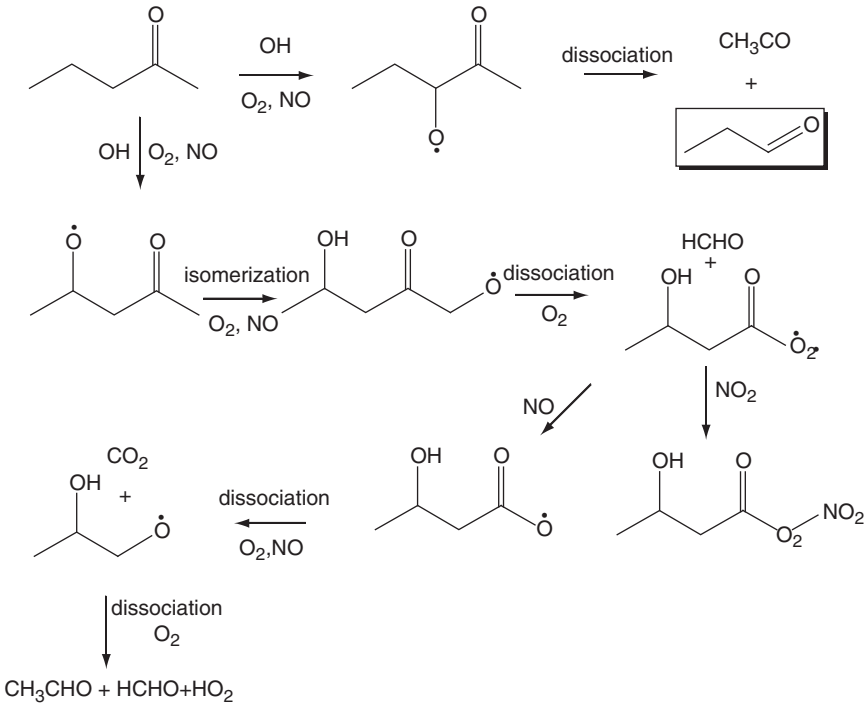

Figure V-B-10. Main routes in the oxidation mechanism of 2-pentanone under high NO_x conditions.

The Master Chemical Mechanism (MCM) contains full mechanisms, constructed on the basis of a set of protocols formulated using known rate data, SARs, and estimated rate data (Jenkin et al., 1997; Saunders et al., 2003). Figure V-B-10 shows the oxidation mechanism for 2-pentanone to illustrate the types of reactions involved under high NO_x conditions, where peroxy–peroxy radical reactions are unimportant. Abstraction occurs mainly at the 3- and 4-positions, with the latter occurring at a higher rate: the MCM gives the relative rates of abstraction at the 4- and 3- carbon atoms as 4.5:1, based on the Kwok and Atkinson SAR (1995). Abstraction at the 3-position follows closely the equivalent reaction in butanone, leading to formation of propanal and the acetyl radical. Abstraction at the 4-position leads, following isomerization of the resulting oxy radical, to the formation of formaldehyde and the 3-hydroxy-butanoyl peroxy radical, which generates 3-hydroxy-butanoyl peroxynitrate on reaction with NO_2 or the oxy radical on reaction with NO. The latter undergoes decarboxylation forming 2-hydroxy-propanoxy, leading to CH_2O and CH_3CHO.

V-B-19. Structure-Activity Relations (SARs) in the Reactions of OH with the Ketones

It has been known for many years (Atkinson et al., 1982a; Le Calvé et al., 1998) that the presence of a carbonyl group deactivates the hydrogen atoms at the adjacent (α-)

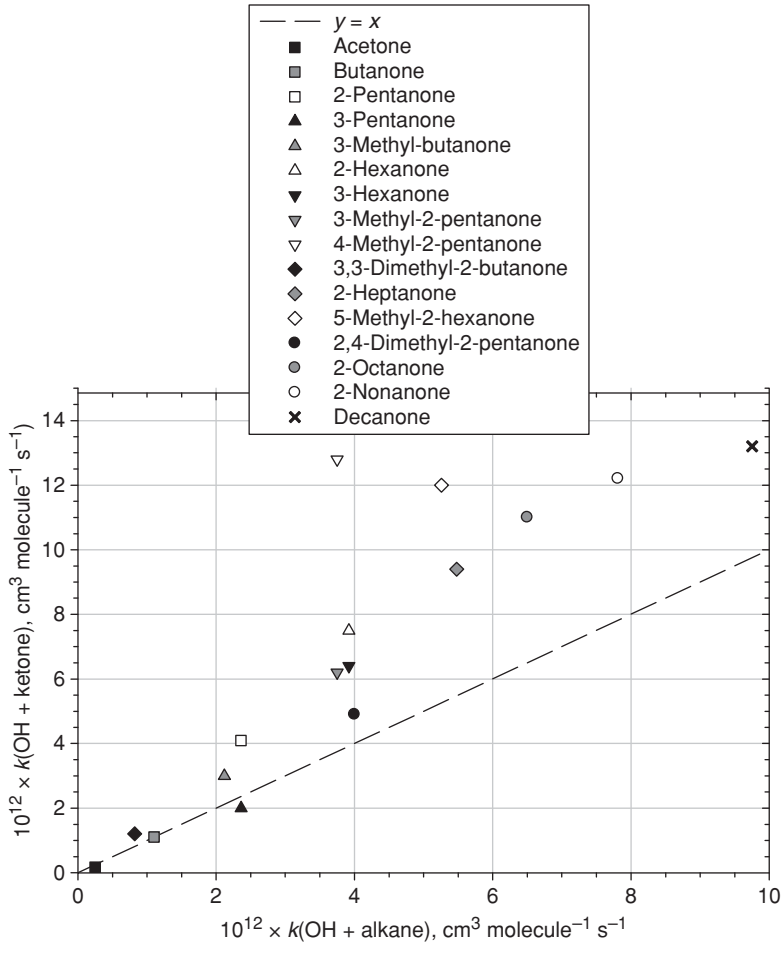

Figure V-B-11. Plot of the rate coefficients for OH + the C_n alkanones versus OH + the equivalent C_{n-1} alkanes.

carbon atom, while activating the hydrogen atoms at the β-carbon atom. The magnitude of the β-activation appears to be roughly a factor of 4. Figure V-B-11 shows a plot of the rate coefficients for the reactions of the C_n alkanones with OH versus the rate coefficients for the equivalent C_{n-1} alkanes. The rate coefficients for the alkanones generally exceed those of the alkanes, reflecting the activation of the β-carbon. The lowest rate coefficients are found for those compounds with no β-carbon (acetone), a primary β-carbon (butanone) or a fully methyl substituted β-carbon (3,3-dimethyl-2-butanone).

The SAR of Atkinson and Kwok (1995) gives the deactivation factor for the α-carbon as 0.75, and the activation factor for the β-carbon as 3.9. Figure V-B-12 shows a plot of the experimental rate coefficients versus those calculated using this SAR. The correlation is good, although the fractional deviations become larger as the alkanones increase in size, suggesting, perhaps, that the activating influence of the carbonyl group extends beyond the β-carbon.

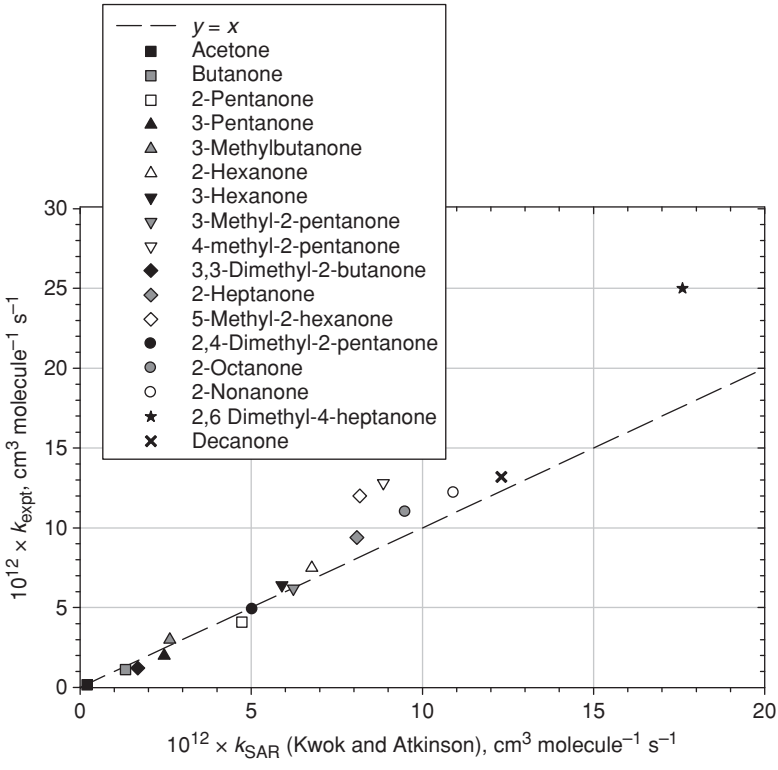

Figure V-B-12. Plot of the rate coefficients for OH + the alkanones versus those calculated using the Kwok and Atkinson SAR (1995).

Mellouki et al. (2003) examined rate coefficients for a number of different types of oxygenates and argued that hydrogen bonding in the transition state provides a mechanism for these longer range interactions, which had been discussed earlier by Smith and Ravishankara (2002). Table V-B-20 shows the group rate coefficients from their analysis for alkanones.

The Mellouki group values are greater than those of Kwok and Atkinson not only for H abstraction at the γ-position, but also for H abstraction from tertiary carbon atoms. Figure V-B-13 shows a plot of the experimental rate coefficients versus the estimated values calculated using the group values of Mellouki et al., while figure V-B-14 shows the ratios $k_{\text{expt}}/k_{\text{SAR}}$ for the two approaches. All of the rate coefficients are predicted within a factor of 2, and for many of the ketones, much better than that. The SARs of Mellouki et al. provide a better estimate of the high rate coefficient observed for 4-methyl-2-pentanone and 2,6-dimethyl-4-heptanone. The χ^2 value for the fractional deviations of the experimental and SAR estimated rate coefficients is better than that for the Kwok and Atkinson estimates. Importantly, the two methods predict different fractional yields for radicals resulting from abstraction from different sites, which has consequences for the formulation of oxidation mechanisms.

Table V-B-20. CH_x group rate coefficients (units are 10^{-12} cm^3 molecule^{-1} s^{-1}) for reaction of OH with alkanones (Mellouki et al., 2003). The figures in brackets show the values from the Kwok and Atkinson (1995) SARs. In the calculation of these values, it is assumed that the secondary and tertiary carbons are adjacent to methyl group(s) when β to >C═O, while when γ or δ to >C═O they have a CH_2 group in the inner position and methyl group(s) in the outer position(s)

CH_x group	α-position	β-position	γ-position	$\geq\delta$-position
—CH_3	0.10 (0.10)	0.37 (0.53)	0.27 (0.17)	0.12 (0.17)
—CH_2—	0.7 (0.7)	3.5 (3.6)	2.4 (1.2)	1.2 (1.2)
>CH—	2.0 (1.3)	12.7 (7.1)	7.8 (2.3)	2.9 (2.3)

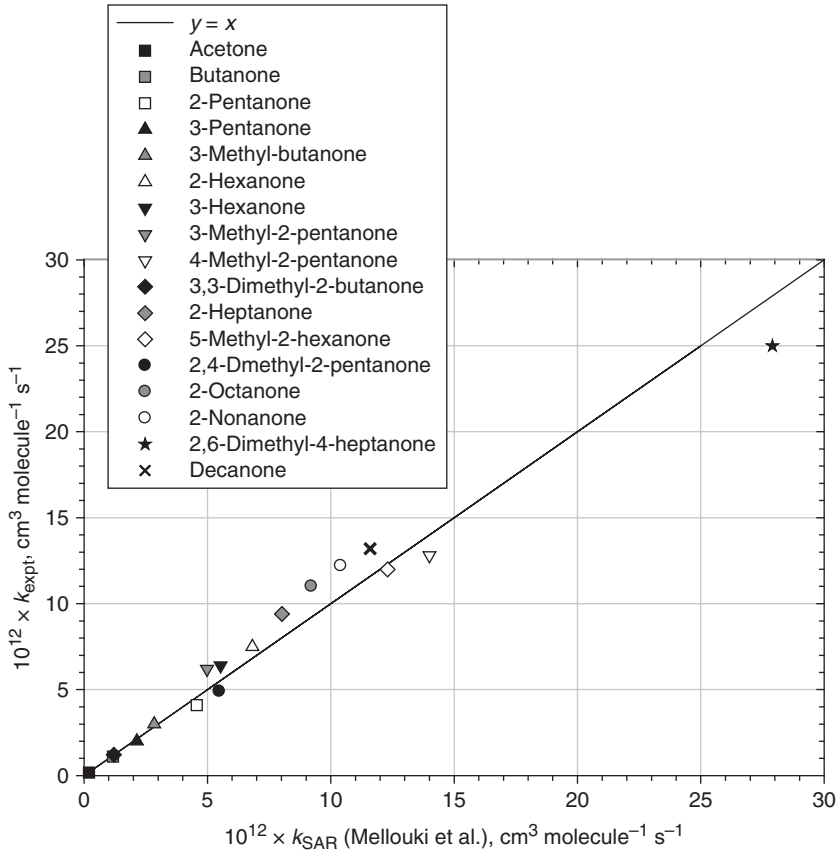

Figure V-B-13. Plot of the rate coefficients for OH + the alkanones versus those calculated using the SARs of Mellouki et al. (2003).

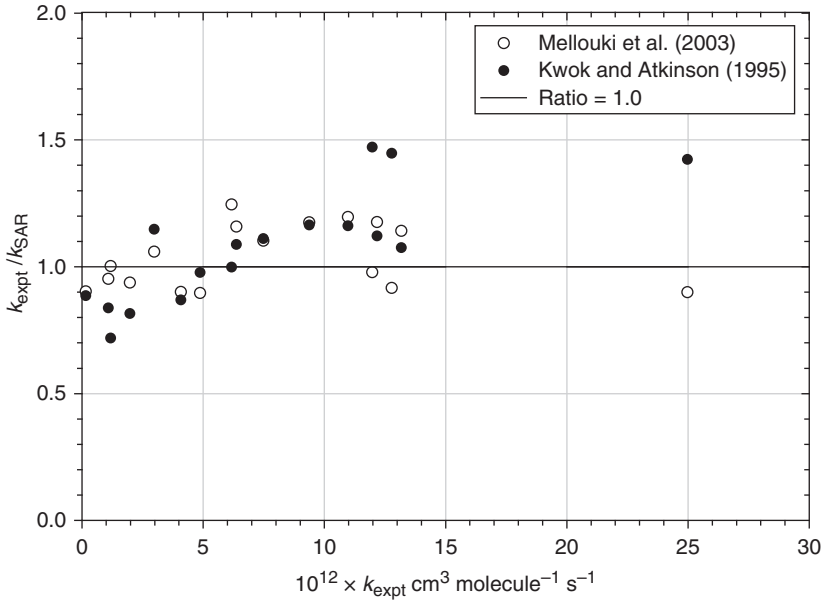

Figure V-B-14. Plot of the ratio of the experimental and estimated rate coefficients versus the experimental values using the SARs of Kwok and Atkinson (1995) and of Mellouki et al. (2003).

The SARs, as discussed above, relate specifically to reactions at ambient temperature. The temperature dependence of the rate coefficients is complex, with acetone and possibly butanone showing evidence of a minimum in the Arrhenius plot, and the higher ketones showing negative temperature dependences over the experimental range. As discussed below, the negative temperature dependences are probably related to the contributions from pre-reaction hydrogen bonded complexes that are significant at low temperatures. The simple abstraction is likely to predominate at higher temperatures, accounting for the positive temperature dependence observed for acetone and butanone. The transition between these different regimes depends on the alkanone in question, so that accurate correlations at a specific temperature are difficult. In the circumstances, the performance of both SARs appears to be satisfactory.

The mechanism of reaction between OH and acetone has been the subject of extensive investigation, as discussed in section V-B-1. It is now accepted that the main product is the acetonyl radical, and that the temperature dependence results for the involvement of a pre-transition state, hydrogen-bonded complex. Frank et al. (1998) used molecular dynamics simulations to study the mechanism of OH + 3-hexanone, varying the initial mean energy of molecular velocities which conformed to a Maxwell–Boltzmann distribution. They found that, at high energies, a direct abstraction mechanism predominated with abstraction mainly from the 2- and 3-positions. At lower energies, they found reaction occurred exclusively from the 5-position; however, given the number of simulations they were able to carry out, they were unable to preclude abstraction from other positions. They found that the mechanism involves an initial hydrogen bond between the hydroxyl H-atom and the O-atom of the keto group,

followed by an interaction between one of the H-atoms on the 5-position and the O-atom of the hydroxyl radical, to form a 7-membered ring:

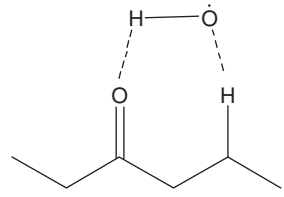

They used density functional theory to provide the potential for the reaction, so that the results cannot be considered quantitative, but they provide an interesting insight into interaction between OH and a large alkanone.

Overall, it is surprising that so few studies of the kinetics and mechanisms of the reactions of OH with simple ketones have been made. Further experiments and theoretical studies on both the temperature dependence and reaction products are clearly required, before temperature dependent predictive rules can be formulated with confidence.

V-B-20. Structure–Activity Relations with the Cl + Alkanone Reactions

The database for Cl + ketones is even more limited than that for OH + ketones, and it is difficult to make quantitative generalizations about the rate coefficients. Comparisons with alkanes show the strong deactivating effect of the carbonyl group. Activation of the β-carbon is limited. Figure V-B-15 shows a comparison between the C_{n-1} alkane and C_n alkanone rate coefficients, and demonstrates the effects of the deactivation by the carbonyl group.

The uncertainty in the experimental rate coefficients for the higher alkanones, and especially the grouping of the measured rate coefficients into high and low values that differ by up to a factor of 3, makes it difficult to optimize SAR parameters across the whole data set. The following analysis is based on an optimization using acetone, butanone and 2- and 3-pentanone, together with the SAR parameters for Cl + alkanes derived by Calvert et al. (2008). The alkane values are:

$$k(\text{primary}) = 2.84 \times 10^{-11}\ \text{cm}^3\ \text{molecule}^{-1}\ \text{s}^{-1}$$

$$k(\text{secondary}) = 8.95 \times 10^{-11}\ \text{cm}^3\ \text{molecule}^{-1}\ \text{s}^{-1}$$

$$k(\text{tertiary}) = 6.48 \times 10^{-11}\ \text{cm}^3\ \text{molecule}^{-1}\ \text{s}^{-1}$$

$$F(\text{—}CH_3) = 1.00$$

$$F(\text{—}CH_2\text{—}) = F(\rangle CH\text{—}) = 0.80$$

Fitting to the acetone rate coefficient gives $F(\text{—CO—}) = 0.037$; using this value and fitting to the butanone and 2- and 3- pentanone rate coefficients gives

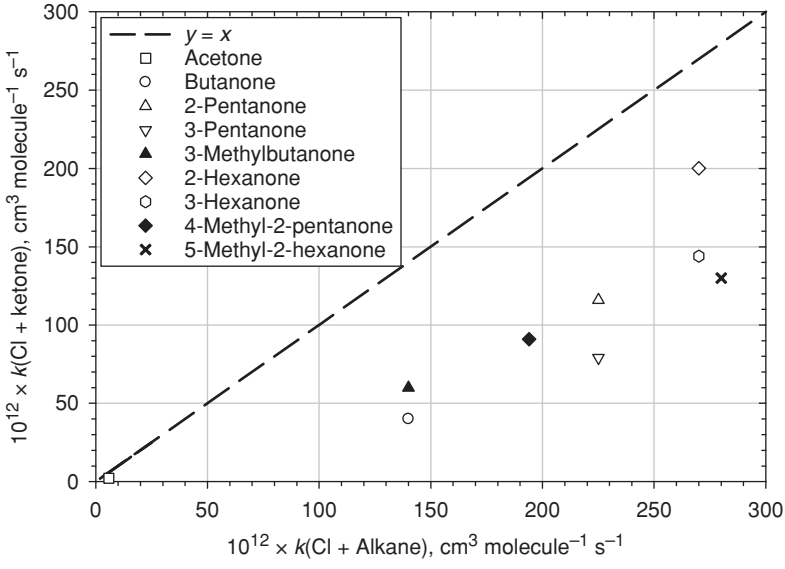

Figure V-B-15. Plot of the rate coefficients for Cl + the C_n alkanones *versus* OH + the equivalent C_{n-1} alkanes.

Table V-B-21. Comparison of experimental and calculated rate coefficients (k, cm^3 molecule^{-1} s^{-1}) for Cl + alkanones

Compound	$10^{11} \times k_{expt}$	$10^{11} \times k_{calc}$	Percentage Difference[a]
Acetone	0.21	0.21	0
Butanone	4.0	3.8	5
2-Pentanone	11.6	13.1	−13
3-Pentanone	7.9	7.3	8
3-Methyl-butanone	6.0	7.0	−17
2-Hexanone	20.0	18.2	9
3-Hexanone	14.4	16.7	−16
4-Methyl-2-pentanone	9.1	12.5	−40
5-Methyl-2-hexanone	13.0	18.5	−42

[a] $100 \times (k_{expt} - k_{calc})/k_{expt}$

$F(\text{—}CH_2CO) = 1.17$. The rate coefficients calculated using these SAR parameters are compared with the experimental values in table V-B-21. The agreement is satisfactory. Generally, the calculated values are slightly larger than the recommended experimental rate coefficients, but the uncertainty in the latter precludes a fuller optimization. The reasonably good agreement for the higher ketones supports the decision to recommend rate coefficients based on the higher values, where two disparate sets of values have been determined. The differences between the calculated and experimental rate coefficients is generally less than or comparable to the uncertainty in the experimental values. The agreement is poorest for the branched alkanones.

V-C. Hydroxyketones

V-C-1. Hydroxyacetone [Acetol, Hydroxypropanone, $HOCH_2C(O)CH_3$]

Hydroxyacetone is formed in the tropospheric oxidation of isoprene. It is a second-generation intermediate, formed from methacrolein, just as methylglyoxal is a second-generation product formed from methyl vinyl ketone.

V-C-1.1. OH + Hydroxyacetone Reaction Kinetics

The rate coefficient for OH + hydroxyacetone has been measured at room temperature by Orlando et al. (1999a) using a relative rate technique, by Dagaut et al. (1989b), Chowdhury et al. (2002a), and Dillon et al. (2006) using pulsed photolysis, and by Butkovskaya et al. (2006b) in a turbulent flow reactor at 200 Torr; see table V-C-1 and figure V-C-1. The measurement by Dillon et al. is about a factor of 2 higher than the other measurements. They ascribed the difference from the other pulsed photolysis measurements to their own use of an absorption cell to measure directly the in situ concentration of hydroxyacetone; they suggested that the concentration of the reactant in the earlier studies might have been lower than that measured using manometric techniques because of the "sticky" nature of the compound. However, Butkovskaya et al. used the same technique. It is difficult to identify any failings in the measurements of Dillon et al. which were carried out very carefully, using three different sources of OH (or OD). The recommended value at 298 K of 4.1×10^{-12} cm^3 $molecule^{-1}$ s^{-1} is based on an unweighted mean of all of the measurements at ambient temperature, treating the three determinations by Dillon et al. (including that for OD) and the two determinations of Orlando et al. (1999a) as independent measurements. A large uncertainty of ±40% is estimated, to accommodate the range of measurements. Dillon et al. also determined the rate coefficient over the temperature range 233–363 K. Adopting their temperature dependence together with the mean value at 298 K gives: $k(T) = 1.5 \times 10^{-12}$ $\exp(305/T)$ cm^3 $molecule^{-1}$ s^{-1} (figure V-C-1). A similar approach was adopted by IUPAC (Atkinson et al., 2006).

V-C-1.2. Cl-Atom + Hydroxyacetone Reaction Kinetics

Orlando et al. (1999a) measured the rate coefficient for Cl + hydroxyacetone at 298 K using a relative rate technique, with CH_3OH as the reference compound. Taking $k(Cl + CH_3OH) = 5.5 \times 10^{-11}$ cm^3 $molecule^{-1}$ s^{-1} (Calvert et al., 2008) gives $k(298) = 5.4 \times 10^{-11}$ cm^3 $molecule^{-1}$ s^{-1}; the uncertainty is estimated as ±40%, since this is a single determination.

V-C-1.3. $O(^3P)$ + Hydroxyacetone Reaction Kinetics

As part of their study on OH + hydroxyacetone, Dillon et al. (2006) also measured the reaction of $O(^3P)$ with hydroxyacetone, using pulsed laser photolysis, coupled with

Table V-C-1. Rate coefficients ($k = A \times e^{-B/T}$, cm^3 $molecule^{-1}$ s^{-1}) for the reaction of OH with hydroxyacetone [$HOCH_2C(O)CH_3$]

$10^{12} \times A$	B (K)	$10^{12} \times k$	T (K)	Technique[a]	Reference	Temperature Range (K)
		3.0 ± 0.3	298	FP–RF	Dagaut et al. (1989b)	
		2.55 ± 0.27	298	RR[b] (methanol)	Orlando et al. (1999a)	
		3.52 ± 0.32		RR[c] (ethanol)		
		2.8 ± 0.2	298	PLP–LIF	Chowdhury et al. (2002a)	
2.15 ± 1.30	305 ± 10	$8.04 \pm 0.80(4)$[d]	233	PLP–LIF	Dillon et al. (2006)	233–363
		7.80 ± 0.70 (2)[e]	237			
		8.00 ± 0.50 (1)[d]	243			
		7.47 ± 0.50 (2)[e]	243			
		7.52 ± 0.46 (2)[e]	252			
		6.73 ± 0.33 (1)[d]	253			
		6.86 ± 0.35 (2)[e]	262			
		6.52 ± 0.26 (1)[d]	268			
		6.57 ± 0.30 (2)[e]	273			
		5.87 ± 0.26 (1)[d]	283			
		6.37 ± 0.21 (1)[e]	288			
		5.83 ± 0.20 (6)[d]	298			
		6.47 ± 0.08 (1)[f]	298			
		6.00 ± 0.15 (9)[e]	298			
		6.01 ± 0.30 (2)[e]	318			
		5.66 ± 0.30 (1)[e]	328			
		5.36 ± 0.13 (2)[e]	338			
		5.32 ± 0.31 (1)[e]	343			
		5.27 ± 0.30 (2)[e]	358			
		4.44 ± 0.30 (1)[d]	363			
		3.0 ± 0.6	298	Turbulent DF–MS (200 Torr)	Butovskaya et al. (2006b)	

[a] Abbreviations used for the techniques are defined in table I-F-3.
[b] Placed on an absolute basis using $k(OH + methanol) = 9.0 \times 10^{-13}$ cm^3 $molecule^{-1}$ s^{-1} (this book, section II-B-1.1).
[c] Placed on an absolute basis using $k(OH + ethanol) = 3.2 \times 10^{-12}$ cm^3 $molecule^{-1}$ s^{-1} (this book, section II-B-2.l).
[d] OH generated by HONO photolysis at 251 nm.
[e] OH generated by O_3 photolysis at 248 nm and reaction of $O(^1D)$ with CH_4.
[f] OD generated by photolysis of D_2O_2 at 248 nm.

resonance fluorescence. They obtained $k(358) = 6.4 \times 10^{-14}$ cm^3 $molecule^{-1}$ s^{-1}; the uncertainty is estimated as ±40%, since it is a single determination.

V-C-1.4. Summary of the Atmospheric Fate of Hydroxyacetone, and the End Products of Its Oxidation

The lifetime of hydroxyacetone in the atmosphere is determined by its reaction with OH, and is 2.8 days for [OH] = 10^6 molecule cm^{-3}. Photodissociation lifetimes for hydroxyacetone in the lower troposphere with an overhead Sun are estimated to be in the range of 5.5 to 11 days; see section IX-F-2.

The recommended rate coefficient is about 22 times larger than that for OH + acetone; abstraction occurs primarily from the —CH_2 group which is activated by

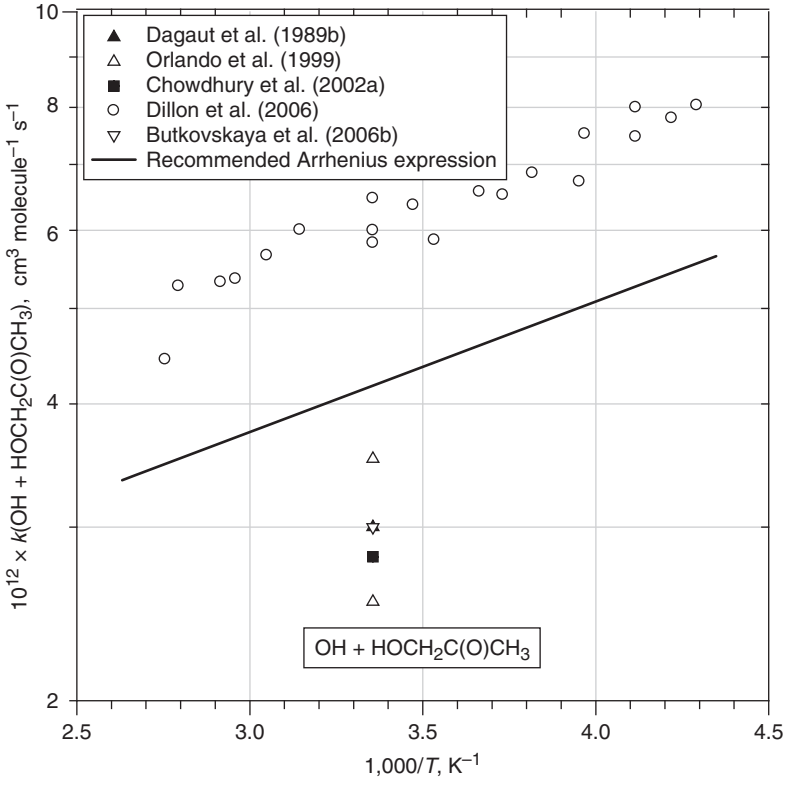

Figure V-C-1. Arrhenius plot for the rate coefficients for OH + hydroxyacetone.

the —OH group. The Kwok and Atkinson SAR gives a value of 2.7×10^{-12} cm^3 molecule^{-1} s^{-1}, with 91% of the reaction occurring at this group. Dillon et al. (2006) used theoretical methods to elucidate the mechanism and showed that reaction occurs via a number of H-bonded complexes with binding energies as large as 24 kJ mol^{-1}, via two transition states with energies close to the reactant energies. They showed that the increase in rate coefficient for hydroxyacetone compared with acetone could be ascribed to a reduction in the transition state energy, coupled with a slight loosening of the transition state which leads to a small increase in the entropy change of activation.

The radical formed following abstraction at the —CH_2 site reacts rapidly with O_2 to form methylglyoxal which is the major product of reaction at 298 K (Orlando et al., 1999):

$$CH(OH)C(O)CH_3 + O_2 \rightarrow CH(O)C(O)CH_3 + HO_2$$

Butkovskaya et al. (2006b) reported a yield of methylglyoxal of 82% at 298 K, in their turbulent flow system, but found that the yield decreased to 49% at 236 K. They observed formic and acetic acids, whose yields increased from about 8% at 298 K to about 20% at 236 K, as well as HO_2 and $CH_3C(O)O_2$. They also observed ~10%

regeneration of OH. They suggested that the following reactions occur, in addition to that forming methylglyoxal:

$$\begin{aligned} CH(OH)C(O)CH_3 + O_2 &\rightarrow CH_2{=}C{=}O + OH + HC(O)OH \\ &\rightarrow CH_3 + CO_2 + HC(O)OH \\ &\rightarrow CH_3C(O)OH + CO + OH \\ &\rightarrow CH_3C(O)OH + CO_2 + H \end{aligned}$$

They suggested that these reactions occur via cyclic $R–O_2$ complexes, and so would be favored over the abstraction reaction at low temperatures. Note that the experiments were conducted at 200 Torr, so that the product distribution may differ from that at atmospheric pressure.

V-C-2. The Larger Hydroxyketones

A number of hydroxyketones are formed in the oxidation of alkanes and alkane diols. Atkinson et al. (2008a) discussed their formation from alkanes in the presence of NO_x. The species formed are predominantly 1,4-hydroxyketones as a result of isomerization reactions. Figure V-C-2 shows the mechanism for the oxidation of pentane, starting from the 2-oxy radical formed by abstraction at the 2-position, followed by reaction with O_2 and NO. The oxy radical can react via three channels: 1) reaction with O_2 which abstracts the remaining H in the 2- position to form a ketone; 2) dissociation to form, in this case, acetaldehyde + the propyl radical; and 3) isomerization, where a 1,5 hydrogen shift gives a hydroxy alkyl radical. Subsequent reactions, including a second isomerization, lead to formation of 5-hydroxy-2-pentanone. The isomerization reaction is sensitive to the size of the ring in the transition state, shown bracketed, and is not sufficiently fast for smaller alkyl chains for this sequence to occur. For the larger normal alkanes, though, 1,4 hydroxyketones are dominant products.

Section V-D discusses the oxidation chemistry of diketones. Keto-enol tautomerism is important for the 2,4-diketones and the enol form, a hydroxyl ketone, can be the dominant tautomer.

For branched alkanes, the alkoxy radical dissociation rate coefficients are higher than for the straight alkanes, and these reactions compete more effectively with isomerization, so that the dominant products become carbonyls. For example, from *n*-hexane, carbonyls constitute 10% of the products and hydroxycarbonyls 57%, while for 2,2,4-trimethylpentane the carbonyls constitute 50–55% of the products and the hydroxycarbonyls 25–30% (Atkinson et al., 2008).

Some 1,3-hydroxyketones are formed if the initial attack is at a tertiary site, in which case the oxy radical formed after the first isomerization cannot itself isomerize. Instead, oxy radical dissociation may occur, leading to a 1,3-hydroxyketone.

Baker et al. (2004a) discussed formation of hydroxycarbonyls from alkanediols; for example, 1-hydroxy-2-butanone is formed in the oxidation of 1,2-butanediol.

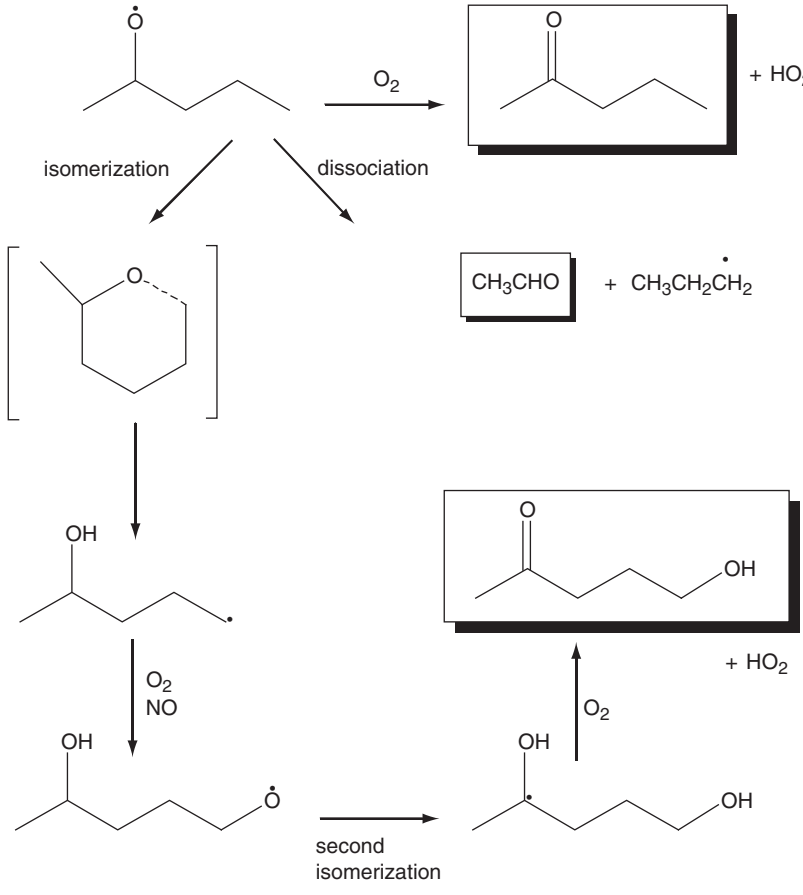

Figure V-C-2. Mechanism of formation of 5-hydroxy-2-pentanone from the 2-oxy radical formed from pentane.

V-C-2.1. Kinetics of the OH + Larger Hydroxyketone Reactions

The published data on higher hydroxycarbonyls are collected in table V-C-2. Many of the rate coefficients have only been determined in single investigations, and an uncertainty of ±40% is estimated for the values given; the 1,4-hydroxyketones studied by Baker et al. (2005) are an exception. In these cases, the uncertainty should be increased relative to the value estimated by Baker et al. as given in table V-C-2. Where more than one determination has been made, the mean values and uncertainties are given in the table.

A number of these rate coefficients were obtained by following the production and secondary loss of the hydroxycarbonyl as a function of the loss of the parent hydrocarbon (Baker et al., 2005). In these cases the hydroxycarbonyl concentration shows a biexponential dependence on $\ln([RH]_o/[RH]_t)$. The rate coefficient ratio can be abstracted from the data, via a nonlinear analysis, but the changes in the measured rate

Table V-C-2. Rate coefficients (k, cm^3 molecule^{-1} s^{-1}) for the reaction of OH with hydroxyketones at 296 ± 2 K

Molecule	$10^{12} \times k$	Technique[a]	Reference	Lifetime (OH reaction) (days)	$10^{12} \times k_{SAR}$ (Bethel et al., 2001b)[m]
1-Hydroxy-2-butanone	6.9 ± 1.5	RR[c] (octane)	Aschmann et al. (2000)	1.5	7.5
	8.2 ± 1.8	RR[d] (1,2-butanediol)[b]	Baker et al. (2004a)		
	7.6 ± 2.0	Mean			
3-Hydroxy-2-butanone	9.3 ± 1.5	RR[c] (octane)	Aschmann et al. (2000)	1.3	5.8
4-Hydroxy-2-butanone	7.3 ± 1.6	RR[c] (octane)	Aschmann et al. (2000)	1.1	12.6
	13.5 ± 2.8	RR[e] (1,3-butanediol)[b]	Baker et al. (2004a)		
	10.4 ± 3.0	Mean			
5-Hydroxy-2-pentanone	15 ± 4	RR[f] (4-methyl-2-pentanone)	Aschmann et al. (2003)	0.7	16.0
	16 ± 8	RR[g] (pentane)[b]	Baker et al. (2005)		
	15.5 ± 4	Mean			
4-Hydroxy-3-methyl-2-butanone	14.6 ± 3.0	RR[c] (octane)	Aschmann et al. (2000)	0.8	15.1
3-Hydroxy-3-methyl-2-butanone	0.85 ± 0.33	RR[c] (octane)	Aschmann et al. (2000)	14	3.0
5-Hydroxy-2-hexanone	22 ± 6	RR[h] (hexane)[b]	Baker et al. (2005)	0.5	17.8
4-Hydroxy-3-hexanone	13.6 ± 2.8	RR[c] (octane)	Aschmann et al. (2000)	0.8	16.4
6-Hydroxy-3-hexanone	17 ± 8	RR[h] (hexane)[b]	Baker et al. (2005)	0.7	15.0
4-Hydroxy-4-methyl-2- pentanone	3.8 ± 1.1	RR[i] (butane)	Atkinson and Aschmann (1995)	3	2.7
	3.8 ± 0.6	RR[j] (three reference compounds)	Magneron et al. (2003)		
	< 4.1	RR[k] (2-methyl-2,4-pentanediol)[b]	Baker et al. (2004a)		
	3.8 ± 0.7	Mean			

5-Hydroxy-2-heptanone	19 ± 7	RR[l] (heptane)[b]	Baker et al. (2005)	0.6	21.7
6-Hydroxy-3-heptanone	16 ± 7	RR[l] (heptane)[b]	Baker et al. (2005)	0.7	19.0
1-Hydroxy-4-heptanone	10 ± 7	RR[l] (heptane)[b]	Baker et al. (2005)	1.2	18.5
5-Hydroxy-2-octanone	23 ± 9	RR[v] (octane)[b]	Baker et al. (2005)	0.5	23.4
6-Hydroxy-3-octanone	15 ± 9	RR[c] (octane)[b]	Baker et al. (2005)	0.8	22.8
7-Hydroxy-4-octanone	19 ± 9	RR[c] (octane)[b]	Baker et al. (2005)	0.6	22.4

[a]Abbreviations used for the techniques are defined in table I-F-3.

[b]Analysis involves production and secondary removal of product (see text); rate coefficient does not scale simply with that of the parent compound which is used as a reference. Over the small ranges used here, the scaling is near linear.

[c]Placed on an absolute basis using $k(\mathrm{OH} + \mathrm{octane}) = 7.81 \times 10^{-12}\ \mathrm{cm^3\ molecule^{-1}\ s^{-1}}$ (Calvert et al., 2008).

[d]Placed on an absolute basis using $k(\mathrm{OH} + 1,2\text{-butanediol}) = 2.43 \times 10^{-11}\ \mathrm{cm^3\ molecule^{-1}\ s^{-1}}$ (this book, section II-C-1).

[e]Placed on an absolute basis using k(OH+1,3-butanediol) $= 2.99 \times 10^{-11}\ \mathrm{cm^3\ molecule^{-1}\ s^{-1}}$ (this book, section II-C-1).

[f]Placed on an absolute basis using k(OH+4-methyl-2-pentanone) = $1.28 \times 10^{-11}\ \mathrm{cm^3\ molecule^{-1}\ s^{-1}}$ (Calvert et al.,2008).

[g]Placed on an absolute basis using $k(\mathrm{OH} + \mathrm{pentane}) = 3.96 \times 10^{-12}\ \mathrm{cm^3\ molecule^{-1}\ s^{-1}}$ (Calvert et al., 2008).

[h]Placed on an absolute basis using $k(\mathrm{OH} + \mathrm{hexane}) = 5.48 \times 10^{-12}\ \mathrm{cm^3\ molecule^{-1}\ s^{-1}}$ (Calvert et al., 2008).

[i]Placed on an absolute basis using $k(\mathrm{OH} + \mathrm{butane}) = 2.35 \times 10^{-12}\ \mathrm{cm^3\ molecule^{-1}\ s^{-1}}$. (Atkinson et al., 2006).

[j]Placed on an absolute basis using $k(\mathrm{OH} + \mathrm{dioxolane}) = 1.11 \times 10^{-11}\ \mathrm{cm^3\ molecule^{-1}\ s^{-1}}$, $k(\mathrm{OH} + n\text{-butyl formate}) = 3.68 \times 10^{-12}\ \mathrm{cm^3\ molecule^{-1}\ s^{-1}}$ (this book, section VII-B-5.1), $k(\mathrm{OH} + \mathrm{hexane}) = 5.48 \times 10^{-12}\ \mathrm{cm^3\ molecule^{-1}\ s^{-1}}$ (Calvert et al., 2008).

[k]Placed on an absolute basis using $k(\mathrm{OH} + 2\text{-methyl-2,4-pentanediol}) = 2.50 \times 10^{-11}\ \mathrm{cm^3\ molecule^{-1}\ s^{-1}}$ (Calvert et al., this book, section II-C-1.

[l]Placed on an absolute basis using $k(\mathrm{heptane}) = 6.5 \times 10^{-12}\ \mathrm{cm^3\ molecule^{-1}\ s^{-1}}$ (Calvert et al., 2008).

[m]*E*stimated rate coefficients using SARs taken from Bethel et al. (2001) and Baker et al. (2005). See text.

coefficient do not scale linearly if the reference rate coefficient changes substantially. In the present case, all the changes needed in the reference rate coefficients are small and simple scaling is valid. Baker et al. suggested that it might be more accurate to use the values estimated on the basis of the SARs of Bethel et al. (2001b); see the following discussion. The agreement between the values is generally good and within the estimated uncertainty (see figure V-C-3). The exception is 1-hydroxy-4-heptanone, where the discrepancy is 85% (based on the experimental value).

V-C-2.2. NO_3 + Hydroxyketone Reaction Kinetics

Table V-C-3 shows the rate coefficients determined for NO_3 with some hydroxyketones by Aschmann et al. (2000), using relative rate techniques. The mean rate coefficients, and estimated uncertainties are given in the table.

V-C-2.3. Summary of the Atmospheric Fate of Hydroxyketones and the End Products of Their Oxidation

Tables V-C-2 and V-C-3 show the atmospheric lifetimes for hydroxyketones with respect to reaction with OH (with [OH] = 10^6 molecule cm^{-3}) and NO_3 (with [NO_3] = 3×10^9 molecule cm^{-3}). The former range from 12 h to 14 days, the latter from 2.4 days to >16 days. The longest-lived species is 3-hydroxy-3-methyl-2-butanone, which has,

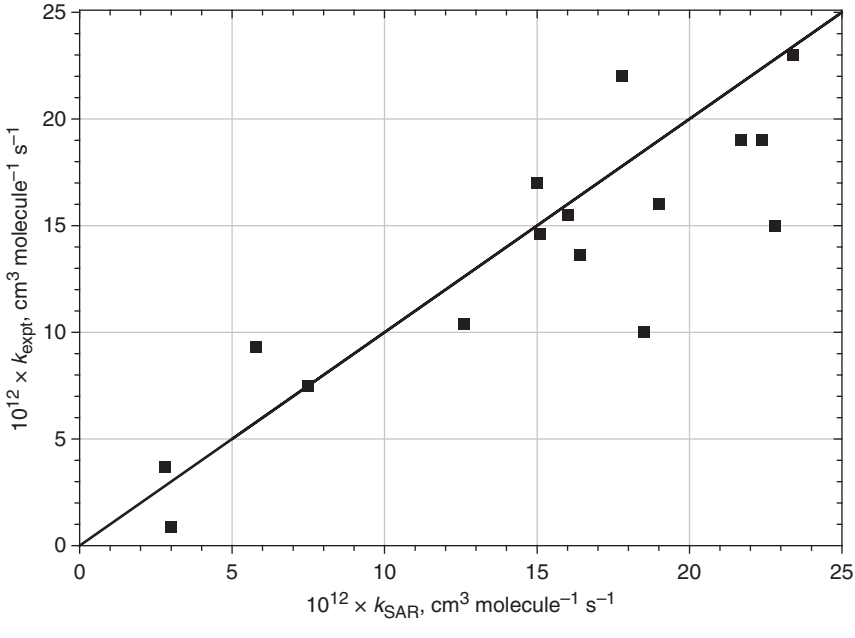

Figure V-C-3. Plot of the experimental rate coefficients for OH + hydroxyketones versus those calculated using the SARs of Kwok and Atkinson (1995), and extended by Bethel et al. (2001b).

Table V-C-3. Rate coefficients (k, cm^3 molecule^{-1} s^{-1}) for the reaction of NO_3 with hydroxyketones at 296 ± 2 K (Aschmann et al. (2000)

Molecule	$10^{16} \times k$	Technique[a]	Mean rate coefficient $10^{16} \times k$	Atmospheric lifetime, reaction with ZNO_3 (days)
1-Hydroxy-2-butanone	≤ 6.6	RR[b] (1-butene)	6.0 ± 2.4	3.9
	6.5 ± 4.6	RR[c] (crotonaldehyde)		
	5.5 ± 2.3	RR[d] (methacrolein)		
3-Hydroxy-2-butanone	6.9 ± 2.0	RR[b] (1-butene)	7.8 ± 2.0	4.9
	6.7 ± 2.1	RR[c] (crotonaldehyde)		
	9.9 ± 1.5	RR[d] (methacrolein)		
4-Hydroxy-2-butanone	≤ 19	RR[b] (1-butene)	16 ± 5	2.4
	16 ± 3	RR[d] (methacrolein)		
4-Hydroxy-3-methyl-2-butanone	≤ 17	RR[b] (1-butene)	16 ± 5	2.4
	16 ± 3	RR[d] (methacrolein)		
3-Hydroxy-3-methyl-2-butanone	< 2.7	RR[b] (1-butene)	< 2.3	> 16
	< 2.3	RR[d] (methacrolein)		
4-Hydroxy-3-hexanone	16 ± 4	RR[b] (1-butene)	14 ± 3	2.7
	12 ± 3	RR[c] (crotonaldehyde)		
	13 ± 3	RR[d] (methacrolein)		

[a]Abbreviations used for the techniques are defined in table I-F-3.
[b]Placed on an absolute basis using $k(NO_3 + 1\text{-butene}) = 1.40 \times 10^{-14}$ cm^3 molecule^{-1} s^{-1} (Calvert et al., 2000).
[c]Placed on an absolute basis using $k(NO_3 + \text{crotonaldehyde}) = 5.2 \times 10^{-15}$ cm^3 molecule^{-1} s^{-1} (this book, section IV-E-3.1.
[d]Placed on an absolute basis using $k(NO_3 + \text{methacrolein}) = 3.0 \times 10^{-15}$ cm^3 molecule^{-1} s^{-1} (this book, section IV-IV-E-4.1).

other than the OH group, only primary hydrogens and no H-atoms at the activated carbon atom β to the carbonyl group. Figure V-C-3 shows a comparison between the SAR predicted rate coefficients, based on the Kwok and Atkinson methodology, extended by Bethel et al. (2001b), and the experimental values. The agreement is generally within a factor of 2. In addition to the F-parameters discussed previously for the alkanones, the following parameters are used: $k_{OH} = 1.4 \times 10^{-13}$ cm^3 molecule^{-1} s^{-1}, $F(\text{—}CH_2OH) = F(\rangle CHOH) = F(\rangle C(OH)\text{—}) = 2.6$, $F(\text{—}OH) = 2.9$.

Reaction occurs principally by abstraction at the —CH(OH)— and —CH_2(OH) positions and at the positions β to the carbonyl group. Aschmann et al. (2000) found high yields of α-dicarbonyls from 3-hydroxy-2-butanone (79%) and 4-hydroxy-3-hexanone (84%), both arising from abstraction at the —CH(OH) sites.

Magneron et al. (2003) determined products for the OH-initiated oxidation of 4-hydroxy-4-methyl-2-pentanone (diacetone alcohol). They obtained molar yields, in the presence of NO, of (94 ± 14)% for acetone and (10 ± 2)% for PAN and an unquantified yield of CH_2O. They had indications of a dicarbonyl compound, derived from the parent structure, with the second carbonyl on the 3-position. Their carbon balance was about 53%, showing that there were many undetermined compounds. They proposed mechanisms for the formation of the observed products based on abstraction at the 1-, 3-, and 5-positions.

Evidence has been obtained that 1,4-hydroxycarbonyls can undergo a cyclization to form a hemiacetal, with subsequent elimination of water to form a dihydrofuran

(Cavalli et al., 2000a; Martin et al., 2002; Holt et al., 2005). It was suggested that the steps are reversible, with the reverse step depending on the concentration of water vapor. The significance of the proposed conversion derives from the high reactivity of the dihydrofurans with OH, NO_3, and O_3 (Martin et al., 2002). It is also possible that the dihydrofurans can lead to the formation or growth of aerosol particles in the atmosphere (Lim and Ziemann, 2005).

Dibble (2007) argued that activation barriers for cyclization and for 1,2 elimination of water are too high for these reactions to occur in the gas phase at ambient temperatures. He supported his argument with electronic structure calculations obtaining, for example, barriers of 146 and 230 kJ mol^{-1} for the two steps involved in conversion of 4-hydroxy-4-methyl-2-pentanone to 4,5-dihydro-2-methylfuran. He suggested that the observed reaction occurs heterogeneously. This mechanism was subsequently investigated experimentally by Atkinson et al. (2008) who confirmed that the reverse reaction occurs heterogeneously at the chamber wall and is probably acid catalyzed.

V-D. Diketones

V-D-1. 2,3-Butanedione [Biacetyl, $CH_3C(O)C(O)CH_3$]

Butanedione is formed in the oxidation of *o*-xylene via a bridged bicyclic peroxy radical, and is a co-product of butenedial and of 2,5(H)-furanone. It is also formed in the oxidation of methyl ethyl ketone under low to moderate NO_x via peroxy–peroxy radical reactions.

V-D-1.1. OH + 2,3-Butanedione Reaction Kinetics

The rate coefficient has been measured by Darnall et al. (1979) at 298 K and by Dagaut et al. (1988a) over the temperature range 240–440 K using flash photolysis coupled with resonance fluorescence. The rate coefficients are given in table V-D-1. There is good agreement between the ambient temperature measurements, and an unweighted mean gives $k(298) = 2.35 \times 10^{-13}\,cm^3$ molecule^{-1} s^{-1} with an estimated uncertainty of ±30%. The Arrhenius expression obtained using this ambient

Table V-D-1. Rate coefficients ($k = A \times e^{-B/T}, cm^3$ molecule^{-1} s^{-1}) for reaction of OH with 2,3-butanedione [$CH_3C(O)C(O)CH_3$]

$10^{12} \times A$	B (K)	$10^{12} \times k$	T (K)	Technique[a]	Reference	Temperature Range (K)
		0.24 ± 0.7	298	FP–RF	Darnall et al. (1979)	
1.12 ± 0.65	450 ± 90	0.19 ± 0.02	240	FP–RF	Dagaut et al. (1988b)	240–440
		0.23 ± 0.02	298			
		0.26 ± 0.02	350			
		0.39 ± 0.02	400			
		0.44 ± 0.03	440			

[a]Abbreviations used for the techniques are given in table I-F-3.

temperature value and the temperature dependence obtained by Dagaut et al. is $k(T) = 1.14 \times 10^{-12} \exp(-450/T)\,\mathrm{cm^3\ molecule^{-1}\,s^{-1}}$. The Kwok and Atkinson (1995) SAR gives $k(298) = 2.0 \times 10^{-13}\,\mathrm{cm^3\ molecule^{-1}\,s^{-1}}$.

V-D-1.2. Cl-Atom + 2,3-Butanedione Reaction Kinetics

The reaction between Cl and 2,3-butanedione has been studied at room temperature by Olsson et al. (1997) and Christensen et al. (1998b) by relative rate methods and by Albaladejo et al. (2003b) by pulsed photolysis. Cuevas et al. (2004) measured the rate coefficient using pulsed photolysis over the temperature range 266–380 K. See table V-D-2. The Olsson rate coefficient is somewhat higher than the others, and the IUPAC panel (2008) have cast some doubt on the validity of the technique that they used. A mean of the other measurements gives $k(298) = 4.5 \times 10^{-13}\,\mathrm{cm^3\ molecule^{-1}\,s^{-1}}$, with an uncertainty of ±20%. If the temperature dependence determined by Cuevas et al. is used with the recommended 298 K value, then this gives $k(T) = 2.2 \times 10^{-11} \times \exp(-1{,}156/T)\,\mathrm{cm^3\ molecule^{-1}\,s^{-1}}$, although this temperature dependence needs corroboration.

V-D-1.3. Summary of the Atmospheric Fate of 2,3-Butanedione and the End Products of Its Oxidation

2,3-Butanedione is removed from the troposphere primarily by photolysis; estimates of the lifetime for photodissociation within the lower troposphere with an overhead Sun are uncertain but estimated to be in the range from 0.8 h to 4 h (see figure IX-F-26 and table IX-M-1). The lifetime with respect to reaction with OH, for $[OH] = 10^6$ molecule $\mathrm{cm^{-3}}$, is about 50 days.

Table V-D-2. Rate coefficients ($k = A \times \mathrm{e}^{-B/T}, \mathrm{cm^3\ molecule^{-1}\,s^{-1}}$) for reaction of Cl with butanedione [$CH_3C(O)C(O)CH_3$]

$10^{12} \times A$	B (K)	$10^{12} \times k$	T (K)	Technique[a]	Reference	Temperature Range (K)
		0.76 ± 0.17	294	RR[b] ($ClONO_2$)	Olsson et al. (1997)	
		0.40 ± 0.03	295	RR[c] (CH_3Cl)	Christensen et al. (1998b)	
		0.40 ± 0.02		RR[d] (CH_4)		
		0.49 ± 0.04	298	PLP–RF	Albaladejo et al. (2003b)	
25.5 ± 4.9	1,156	0.34	268	PLP–RF	Cuevas et al. (2004)	266–380
		0.44	283			
		0.50	298			
		0.72	310			
		0.82	331			
		0.96	354			
		1.17	380			

[a]Abbreviations used for the techniques are given in table I-F-3
[b]Placed on an absolute basis using $k(Cl + ClONO_2) = 1.0 \times 10^{-11}\,\mathrm{cm^3\ molecule^{-1}\,s^{-1}}$ (Atkinson et al., 2007).
[c]Placed on an absolute basis using $k(Cl + CH_3Cl) = 4.8 \times 10^{-13}\,\mathrm{cm^3\ molecule^{-1}\,s^{-1}}$ (Atkinson et al., 2008).
[d]Placed on an absolute basis using $k(Cl + CH_4) = 1.0 \times 10^{-13}\,\mathrm{cm^3\ molecule^{-1}\,s^{-1}}$ (Atkinson et al., 2006).

OH reacts by abstracting a hydrogen from one of the methyl groups. The resulting peroxy radical reacts with NO to form the alkoxy radical, that can then either dissociate or react with O_2.

$$CH_3C(O)C(O)CH_2O \rightarrow CH_3C(O)C(O) + CH_2O \quad (1a)$$

$$CH_3C(O)C(O)CH_2O + O_2 \rightarrow CH_3C(O)C(O)CHO + HO_2 \quad (1b)$$

From experiments with methyl glyoxal, it is known that the radical formed in (1a) rapidly dissociates to form $CH_3CO + CO$ (section IV-D-3.4). Christensen et al. (1998b) demonstrated, using end product analysis, that reaction (1a) occurs exclusively, so that the products of the reaction of OH with butanedione under atmospheric conditions are $CH_3C(O)O_2$, CH_2O, and CO.

Christensen et al. also showed that Cl reacts with butanedione via two channels:

$$Cl + CH_3C(O)C(O)CH_3 \rightarrow CH_3C(O)C(O)CH_2 + HCl \quad (2a)$$

$$\rightarrow CH_3C(O)Cl + CH_3CO. \quad (2b)$$

They showed that $k_{2b}/(k_{2a} + k_{2b}) = 0.23 \pm 0.02$ at room temperature. There is no evidence that a channel equivalent to (2b) occurs for OH.

V-D-2. Larger Diketones

V-D-2.1. Kinetics of the OH + Larger Diketone Reactions

A number of higher diketones have been studied by Dagaut et al. (1988b) using flash photolysis coupled with resonance fluorescence, by Holloway et al. (2003), using both pulsed laser photolysis–laser-induced fluorescence (PLP–LIF) and relative rate techniques, and by Zhou et al. (2008) using a relative rate method.

For 2,4-pentanedione, Dagaut et al. obtained $k(298) = (1.15 \pm 0.15) \times 10^{-12}$ cm^3 molecule^{-1} s^{-1}, while Holloway et al. obtained $k(298) = (8.80 \pm 0.05) \times 10^{-11}$ cm^3 molecule^{-1} s^{-1} by PLP–LIF and $(8.76 \pm 0.57) \times 10^{-11}$ cm^3 molecule^{-1} s^{-1} by a relative rate method. The measured rate coefficients are given in table V-D-3. Holloway et al. pointed out that the compound exists predominantly (>95%) in the enolic form ($CH_3C(O)CH{=}C(OH)CH_3$) in the gas phase, and OH is expected to react by addition to the C=C double bond, presumably with a higher rate coefficient than that observed by Dagaut et al. More recently, Zhou et al. (2008) have measured the rate coefficient as a function of temperature, obtaining very good agreement at 298 K with Holloway et al. Figure V-D-1 shows an Arrhenius fit to the data of Holloway et al. and Zhou et al.; this gives $k(T) = 3.3 \times 10^{-12} \exp(985/T)$ cm^3 molecule^{-1} s^{-1}, with $k(298) = 9.0 \times 10^{-11}$ cm^3 molecule^{-1} s^{-1}, with an uncertainty of ±20%.

Dagaut et al. also measured the rate coefficient for OH + 2,5-hexanedione, which exists purely in the keto form. See table V-D-4. They obtained $k(298) = 7.13 \times 10^{-12}$ cm^3 molecule $^{-1}$ s^{-1}, to which an uncertainty of ±40% should be attached (single determination). The Kwok and Atkinson (1995) SAR gives a rate coefficient

Table V-D-3. Rate coefficients (k, cm^3 molecule^{-1} s^{-1}) for reaction of OH with 2,4-pentanedione [$CH_3C(O)CH_2C(O)CH_3$]

$10^{12} \times A$	B (K)	$10^{12} \times k$	T (K)	Technique[a]	Reference	Temperature Range (K)
		1.15 ± 0.15	298	FP–RF	Dagaut et al. (1988b)	
		87.6 ± 5.7	298	RR[b] (2,3 dimethyl-2-butene)	Holloway et al. (2003)	
		88.0 ± 0.5	298	PLP–LIF		
3.35	-983 ± 130	107 ± 22	285	RR[c] (isobutene)	Zhou et al. (2008)	285–310
		97.0 ± 19.9	290	RR[d] (isoprene)		
		90.5 ± 18.1	298	RR[c] (isobutene)		
		85.5 ± 17.7	304	RR[d] (isoprene)		
		79.8 ± 16.2	310	RR[c] (isobutene)		

[a]Abbreviations used for the techniques are given in table I-F-3

[b]Placed on an absolute basis using $k(\text{OH}+2, 3\text{dimethyl-2-butene}) = 1.1 \times 10^{-10}$ cm^3 molecule^{-1} s^{-1} (Calvert et al., 2000).

[c]Placed on an absolute basis using $k(\text{OH} + \text{isobutene}) = 9.47 \times 10^{-12} \exp(504/T)$ cm^3 molecule^{-1} s^{-1} (Calvert et al., 2000).

[d]Placed on an absolute basis using $k(\text{OH} + \text{isoprene}) = 2.7 \times 10^{-11} \exp(390/T)$ cm^3 molecule^{-1} s^{-1} (Atkinson et al., 2006).

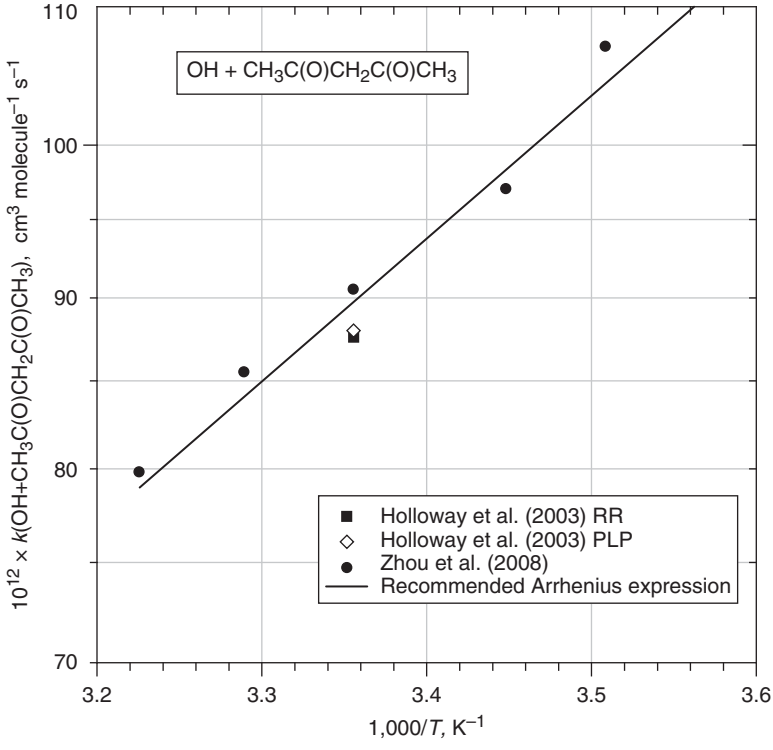

Figure V-D-1. Arrhenius plot for the reaction of OH with 2,4-pentanedione.

Table V-D-4. Rate coefficients (k, cm^3 molecule^{-1} s^{-1}) for reaction of OH with 2,5-hexanedione [$CH_3C(O)CH_2CH_2C(O)CH_3$]

$10^{12} \times A$	B (K)	$10^{12} \times k$	T (K)	Technique[a]	Reference	Temperature Range (K)
1.49 ± 0.3	−450 ± 90	9.4 ± 1.2	240	FP–RF	Dagaut et al. (1988b)	240–440
		7.13 ± 0.34	298			
		5.07 ± 0.47	350			
		4.20 ± 0.38	400			
		4.35 ± 0.53	440			

[a]Abbreviations used for the techniques are given in table I-F-3.

Table V-D-5. Rate coefficients (k, cm^3 molecule^{-1} s^{-1}) for reaction of OH with 3-methyl-2,4-pentanedione [$CH_3C(O)CH(CH_3)C(O)CH_3$]

$10^{12} \times k$	T (K)	Technique[a]	Reference
69.9 ± 3.2 (enol)	298	RR[b](n-decane)	Holloway et al. (2003)
11.6 ± 0.9 ($k$eto)			
28.1 ± 1.6 ($k$eto + enol)	298	PLP–LIF	
51.2 ± 4.4 (enol)[c]			

[a]Abbreviations used for the techniques are given in table I-F-3.
[b]Placed on an absolute basis using $k(\text{OH} + n\text{-decane}) = 1.1 \times 10^{-11}$ cm^3 molecule^{-1} s^{-1} (Calvert et al., 2008).
[c]Based on a value of 1.16×10^{-11} cm^3 molecule^{-1} s^{-1} for the keto tautomer (Holloway et al., 2003).

of 5.7×10^{-12} cm^3 molecule $^{-1}$ s^{-1}; abstraction occurs primarily from the two —CH_2 groups, which are activated because of their positions β to one of the carbonyl groups.

Holloway et al. (2005) measured rate coefficients for 3-methyl-2,4-pentanedione, which exists as both keto (60 ± 5%) and enol tautomers. See table V-D-5. They were able to determine the kinetics of these two forms separately by adding ozone to the system which removed the enol but not the keto form. Re-equilibration took ~10 h and was negligible on the experimental timescale. They obtained k(enol, 298) = $(6.99 \pm 0.32) \times 10^{-11}$ cm^3 molecule $^{-1}$ s^{-1} and k($k$eto) = $(1.16 \pm 0.09) \times 10^{-11}$ cm^3 molecule $^{-1}$ s^{-1} using the relative rate technique. They also measured the overall rate coefficient for the equilibrated system, using PLP–LIF, obtaining $k(298) = (2.81 \pm 0.16) \times 10^{-11}$ cm^3 molecule $^{-1}$ s^{-1}. Using the rate coefficient for the keto form from the relative rate measurements and applying the literature values for the tautomer fractions, they obtained: k(enol, 298) = $(5.12 \pm 0.44) \times 10^{-11}$ cm^3 molecule $^{-1}$ s^{-1}.

The average values give:

$$k(CH_3C(O)C(CH_3)=C(OH)CH_3, 298) = 6.1 \times 10^{-11} \text{ cm}^3 \text{ molecule}^{-1} \text{ s}^{-1}$$

$$k(CH_3C(O)CH(CH_3)C(O)CH_3, 298) = 1.16 \times 10^{-11} \text{ cm}^3 \text{ molecule}^{-1} \text{ s}^{-1}$$

An uncertainty of ±30% should be attached to each value.

V-D-2.2. O_3+ Larger Diketones Reaction Kinetics

Zhou et al. (2008) measured the rate coefficient for O_3+ 2,4-pentanedione using a relative rate technique, with ethene as the reference compound ($k = 1.6 \times 10^{-18}$ cm^3 molecule $^{-1}$ s^{-1}; Atkinson et al., 2006), giving: $k(O_3$+2,4-pentanedione, 298) = 1.03×10^{-18} cm^3 molecule $^{-1}$ s^{-1}. They commented that this is a surprisingly small value for an unsaturated alcohol.

V-D-2.3. Summary of the Atmospheric Fate of the Larger Diketones and the End Products of Their Oxidation

The atmospheric lifetime of the γ-diketone, 2,5 hexanedione with respect to reaction with OH is about 38 h for [OH] = 10^6 molecule cm^{-3}. This ketone exists predominantly in the keto form. That for the β-diketone, 2,4-pentanedione, that exists purely as the enol is about 1.3 h for an average daytime [OH] = 2.5×10^6 molecule cm^{-3}. Removal of the larger diketones by photodecomposition in tropospheric sunlight is expected to compete with loss by OH radicals, but quantification of this assertion is not possible at this writing.

3-Methyl-2,4-pentanedione exists as a 60:40 tautomeric mixture and presents a more complicated case. The lifetime of the keto form, with respect to reaction with OH, is about 10 h, with [OH] = 2.5×10^6 molecule cm^{-3}. That for the enol form is about 1.8 h. Holloway et al. report the equilibration lifetime ($1/e$) as about 14 h, much longer than the lifetime of the enol form, but comparable to that of the keto form. Any enol formed directly would react rapidly without involving the keto form. If the keto-configuration is formed, then there will be a competition between equilibration to form the enol and reaction of the keto form with OH. Which tautomer is formed directly by atmospheric reactions is not clear. The master chemical mechanism (MCM v3.1) only considers the keto form of 3-methyl-2,4-pentanedione. It is formed, for example, in the oxidation of 3-methyl-2-pentanone. Abstraction at the 4-position, followed by reaction with O_2 and NO leads to the formation of the 4-oxy radical, which can dissociate or react with O_2. The latter reaction, which occurs at roughly half the rate of the dissociation at 298 K, leads directly to the keto form of 4-methyl-2,4-pentanedione, according to the MCM. An alternative mechanism can be written for formation of the enol, although this requires a more extended electronic rearrangement. 4-Hydroxy-3-methyl-2-pentanone provides another source of the dione. It reacts with OH predominantly at the 4-position. In the MCM, O_2 abstracts from the OH group, to generate the keto form, but an equally plausible mechanism can be written for H-abstraction at the 3-position to create the enol form; see figure V-D-2.

Zhou et al. (2008) determined products in the OH-initiated oxidation of 2,4-pentanedione. They obtained the following molar yields for the products: methylglyoxal ($20.8 \pm 4.5\%$), acetic acid ($16.9 \pm 3.4\%$) and PAN ($2.0 \pm 0.5\%$). From residual FTIR spectra, they identified 2,3,4-pentanetrione and its hydrated analogue pentan-2,3-dione-4-diol ($CH_3C(O)C(O)C(OH)_2CH_3$), based on assignments of O—H and C=O stretches in the system and an authentic sample of the trione. They proposed a mechanism involving addition to either end of the double bond. The reactions proposed

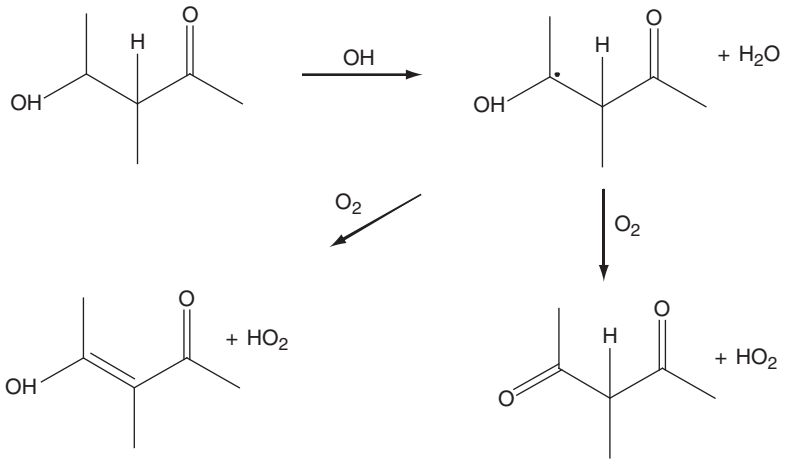

Figure V-D-2. Formation of keto and enol forms of 4-methyl-2,4-pentanedione in the OH-initiated oxidation of 4-hydroxy-3-methyl-2-pentanone.

for the oxy radicals formed following reactions of the two primary radicals with O_2 and then NO are shown in figure V-D-3. The mechanism requires the methylglyoxal yield to be equal to the sum of the acetic acid and PAN yields, which is observed to be the case within experimental error. The channel forming the trione, following 4-addition, is likely to be slow under atmospheric conditions compared with the two dissociation channels. An alternative carrier for the observed spectrum might be 3-hydroxy-2,4-pentanedione, resulting from abstraction by O_2 from the initially formed radical following 3-addition:

$$CH_3C(O)CH(OH)C(OH)CH_3 + O_2 \rightarrow CH_3C(O)CH(OH)C(O)CH_3 + HO_2$$

V-E. Unsaturated Ketones

V-E-1. Methyl Vinyl Ketone (3-Buten-2-one, $CH_3C(O)CH{=}CH_2$)

V-E-1.1. OH + Methyl Vinyl Ketone Reaction Kinetics

The rate coefficient for reaction of OH with methyl vinyl ketone (MVK) has been the subject of numerous relative and absolute measurements, conducted over a range of temperatures and pressures (Cox et al., 1981; Kleindienst et al., 1982; Atkinson et al., 1983b; Gierczak et al., 1997; Aschmann and Atkinson, 1998b; Chuong and Stevens, 2003, 2004; Holloway et al., 2005). The data set is summarized in table V-E-1, and is displayed in figure V-E-1. The measurements made above 5 Torr total pressure are consistent with each other, with the exception of the relative rate measurement of Cox et al. (1981), which falls somewhat below the remainder of the data. The data of Chuong and Stevens (2003) conducted at temperatures $\geq$300 K and at pressures $<$ 5 Torr, show the expected falloff with pressure, particularly at elevated temperature.

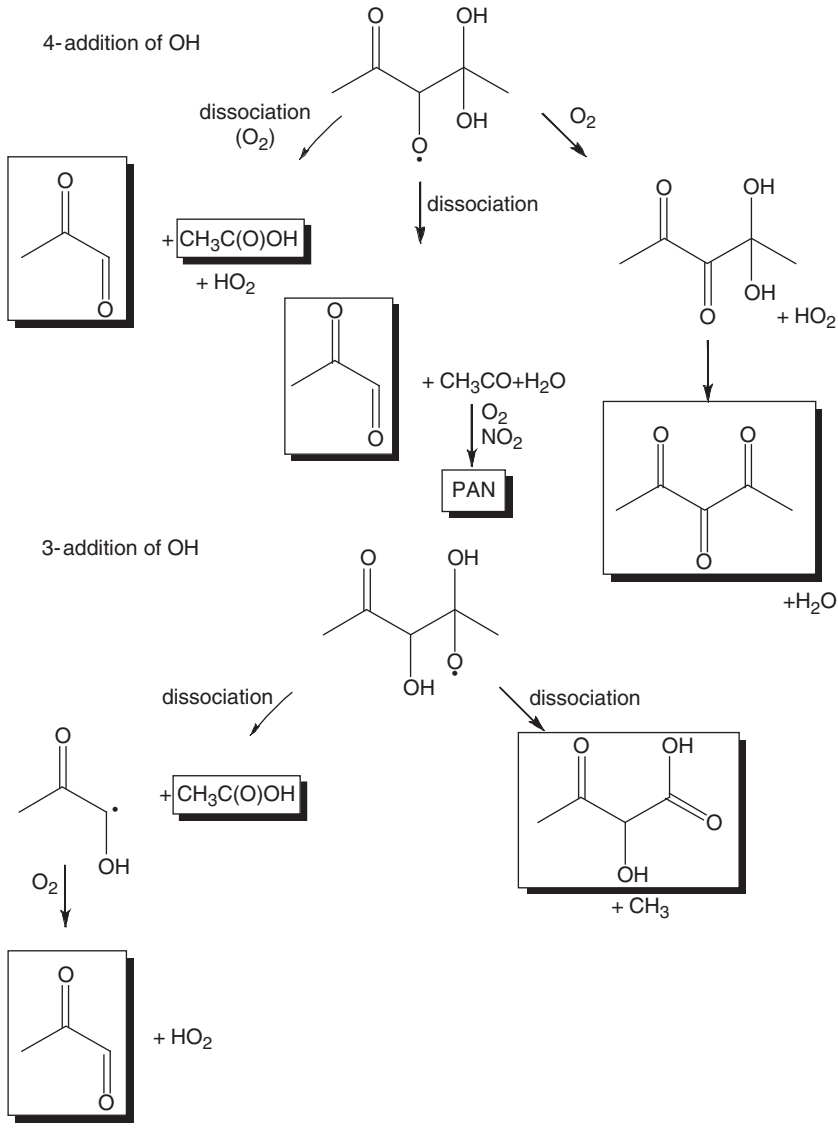

Figure V-D-3. Mechanism proposed by Zhou et al. (2008) for the OH-initiated oxidation of the enol form of 2,4-pentanedione. The mechanisms are given for the oxy radicals formed from addition of OH to the C═C double bond in the enol form in the 3- and 4-positions.

Table V-E-1. Rate coefficients ($k = A \times e^{-B/T}$, cm^3 $molecule^{-1}$ s^{-1}) for reaction of OH with methyl vinyl ketone [$CH_3C(O)CH{=}CH_2$]

$10^{12} \times A$	B (K)	$10^{12} \times k$	T (K)	Technique[a]	Reference	Temperature Range (K)
		14	300	RR[b] (propene)	Cox et al. (1981)	
3.85	−456 ± 73	17.9 ± 2.8	298	FP–RF	Kleindienst et al. (1982)	298–424
		13.5 ± 2.4	350			
		11.4 ± 2.1	424			
		21.7 ± 1.6	299	RR[b] (propene)	Atkinson et al. (1983b)	
2.67± 0.45	−612 ± 130	38.6 ± 2.2	232	FP–LIF	Gierczak et al. (1997)	232–378
		36.5 ± 3.4	235			
		28.3 ± 1.9	253			
		28.0 ± 1.6	253			
		31.6 ± 1.8	253			
		30.8 ± 1.3	253			
		25.7 ± 0.9	272			
		27.6 ± 1.6	272			
		19.6 ± 0.8	298			
		20.2 ± 1.2	298			
		21.8 ± 3.0	298			
		19.9 ± 1.2	298			
		20.1 ± 0.7	298			
		17.3 ± 1.0	323			
		18.6 ± 1.3	323			
		15.5 ± 1.2	351			
		14.6 ± 0.7	351			
		15.2 ± 1.4	351			
		16.4 ± 1.0	354			
		15.1 ± 0.3	354			
		16.6 ± 1.2	354			
		12.8 ± 0.8	378			
		13.6 ± 1.2	378			
		13.5 ± 1.2	378			
		24.1± 1.3	296	RR[b] (propene)	Aschmann and Atkinson (1998b)	
		21.3 ± 0.5	296	RR[c](*m*-xylene)		
	[He] (10^{16} molecule cm^{-3})			DF–LIF/RF	Chuong and Stevens (2003)	
	6.1	16.5 ± 0.8	300			
	9.7	16.3 ± 1.0	300			
	16.1	17.3 ± 0.4	300			
	5.6	7.8 ± 0.8	328			
	9.1	9.0 ± 1.2	328			
	14.1	12.2 ± 0.8	328			
	4.8	5.8 ± 0.4	361			
	8.0	6.8 ± 0.2	361			
	13.4	8.6 ± 0.2	361			
	4.9	4.8 ± 0.4	390			
	7.7	5.9 ± 0.4	390			

(*continued*)

Table V-E-1. (*continued*)

[He] (10^{16} molecule cm^{-3})	$10^{12} \times k$	T (K)	Technique[a]	Reference	Temperature Range (K)
12.4	7.1 ± 0.4	390			
4.3	3.7 ± 0.2	422			
7.1	4.9 ± 0.4	422			
11.0	5.6 ± 0.4	422			
	17.8 ± 0.8	300	DF–LIF	Chuong and Stevens (2004)	
	18.6 ± 1.2	298	PLP–LIF	Holloway et al. (2005)	

[a]Abbreviations used for the techniques are defined in table I-F-3.
[b]Placed on an absolute basis using $k(\text{OH} + \text{propene}) = 2.9 \times 10^{-11}$ cm^3 molecule^{-1} s^{-1} (Atkinson et al., 2006).
[c]Placed on an absolute basis using $k(\text{OH} + m\text{-xylene}) = 2.3 \times 10^{-11}$ cm^3 molecule^{-1} s^{-1} (Calvert et al., 2002).

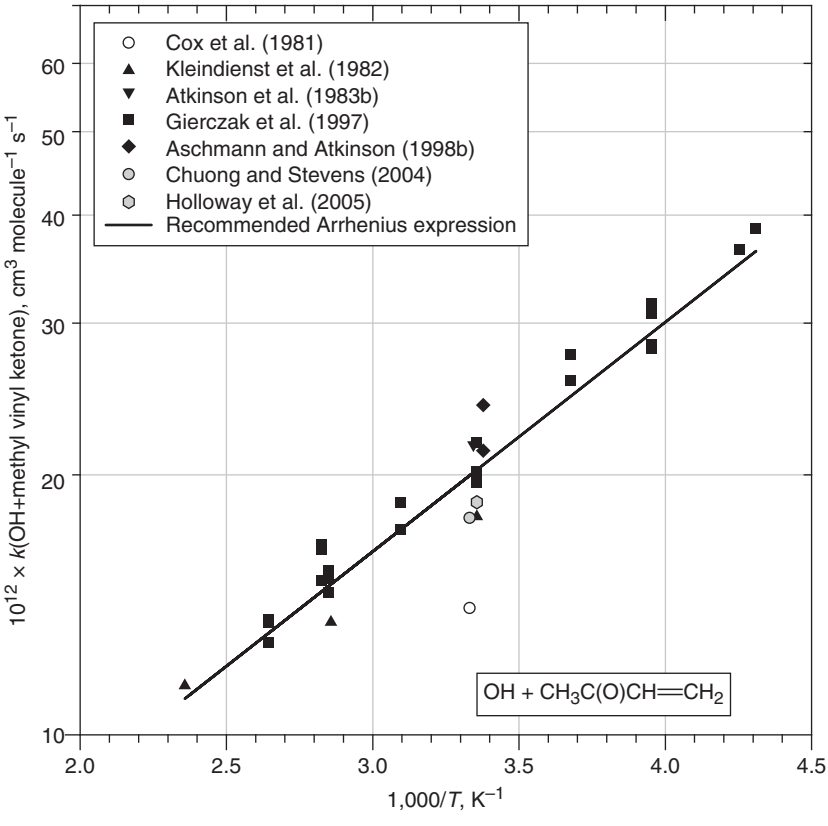

Figure V-E-1. Arrhenius plot of the rate coefficient for the reaction of OH with methyl vinyl ketone.

Excluding the data of Cox et al. (1981) and those of Chuong and Stevens (2003), which were mostly obtained in the falloff region, an average rate coefficient of 2.0×10^{-11} cm^3 molecule^{-1} s^{-1} is obtained at 298 K, with an estimated uncertainty of ±15%. Coupling this value with the temperature dependence determined by Gierczak et al. (1997) leads to $k(\mathrm{OH} + \mathrm{MVK}) = 2.6 \times 10^{-12} \exp(612/T)\,\mathrm{cm}^3$ molecule^{-1} s^{-1}.

V-E-1.2. O_3+ Methyl Vinyl Ketone Reaction Kinetics

The five measurements of the rate coefficient for reaction of O_3 with MVK are in reasonable agreement near 298 K, see table V-E-2 (Atkinson et al., 1981; Treacy et al., 1992; Grosjean et al., 1993a; Grosjean and Grosjean, 1998; Neeb et al., 1998). The simple average of the five reported values, $k = 5.0 \times 10^{-18}$ cm^3 molecule^{-1} s^{-1} near 295 K, is recommended. The uncertainty of this value is estimated to be ±25%. Treacy et al. (1992) report a strong positive temperature dependence to the rate coefficient, $k = 6.9 \times 10^{-16} \exp(-1{,}521/T)\,\mathrm{cm}^3$ molecule^{-1} s^{-1} for 240 K < T < 324 K.

V-E-1.3. NO_3+ Methyl Vinyl Ketone Reaction Kinetics

The reaction of NO_3 with MVK has been the subject of three investigations (Kwok et al., 1996a; Rudich et al., 1996; Canosa-Mas et al., 1999a). As is summarized

Table V-E-2. Rate coefficients ($k = A \times e^{-B/T}$, cm^3 molecule^{-1} s^{-1}) for reaction of O_3 with methyl vinyl ketone [$CH_3C(O)CH{=}CH_2$]

$10^{15} \times A$	B (K)	$10^{18} \times k$	T (K)	Technique[a]	Reference	Temperature Range (K)
		4.77 ± 0.59	296	O_3 CL	Atkinson et al. (1981)	
0.69 ± 0.14	1,521 ± 78	4.2 ± 0.4	298	UV abs.	Treacy et al. (1992)	240–324
		4.72 ± 0.09	291	UV abs.	Grosjean et al. (1993a)	
		5.80	290	UV abs.	Grosjean and Grosjean	
		5.46	291		(1998)	
		6.25	292			
		5.4 ± 0.6	296	FT–IR abs.	Neeb et al. (1998)	

[a]Abbreviations used for the techniques are defined in table I-F-3.

Table V-E-3. Rate coefficients (k, cm^3 molecule^{-1} s^{-1}) for reaction of NO_3 with methyl vinyl ketone [$CH_3C(O)CH{=}CH_2$]

$10^{16} \times k$	T (K)	Technique[a]	Reference
< 6	296	RR[b] (C_3H_6)	Kwok et al. (1996a)
< 1.2	298	vis. abs.	Rudich et al. (1996)
5.31 ± 1.34	298	RR[c] (C_2H_4)	Canosa-Mas et al. (1999a)
3.2 ± 0.6	298	DF	

[a]Abbreviations used for the techniques are defined in table I-F-3.
[b]Placed on an absolute basis using $k(\mathrm{NO_3} + \mathrm{C_3H_6}) = 9.3 \times 10^{-15}$ cm^3 molecule^{-1} s^{-1} (Atkinson et al., 2006).
[c]Placed on an absolute basis using $k(\mathrm{NO_3} + \mathrm{C_2H_4}) = 2.1 \times 10^{-16}$ cm^3 molecule^{-1} s^{-1} (Atkinson et al., 2006).

in table V-E-3, the earlier two studies reported only upper limits for the rate coefficient. The rate coefficients obtained by Canosa-Mas et al. (1999a) using relative ($k = 5.3 \times 10^{-16}$ cm^3 molecule^{-1} s^{-1}) and absolute ($k = 3.2 \times 10^{-16}$ cm^3 molecule^{-1} s^{-1}) methods, are inconsistent with the Rudich et al. upper limit. Conservatively, the relative rate value of Canosa-Mas et al. (1999a) is recommended as an upper limit to this reaction rate coefficient.

V-E-1.4. Cl-Atom + Methyl Vinyl Ketone Reaction Kinetics

There have been four relative rate studies of the rate coefficient for reaction of Cl-atoms with MVK near atmospheric pressure (Canosa-Mas et al., 1999b; Finlayson-Pitts et al., 1999; Wang et al., 2002; Orlando et al., 2003), and an additional direct study carried out at reduced pressure (Canosa-Mas et al., 2001). The rate data are given in table V-E-4. The relative rate studies are all in substantive agreement, and an average value of $k = 2.0 \times 10^{-10}$ cm^3 molecule^{-1} s^{-1} is recommended near 298 K with an uncertainty of ±15%.

V-E-1.5. Summary of the Atmospheric Fate of Methyl Vinyl Ketone, and the End Products of Its Oxidation

The major loss mechanism for methyl vinyl ketone is its reaction with OH. The lifetime is estimated at 5.5 h for a daytime [OH] = 2.5×10^6 molecule cm^{-3}. Lifetimes for photodissociation of methyl vinyl ketone are relatively long, 2.5 days in the lower troposphere for an overhead Sun; see section IX-F-10 and table IX-M-1.

The products of this oxidative process have been determined by Tuazon et al. (1989). The major pathway (accounting for about 72% of the reaction) involves OH addition to the terminal CH_2 group, leading to formation of glycolaldehyde; the co-product acetyl

Table V-E-4. Rate coefficients (k, cm^3 molecule^{-1} s^{-1}) for reaction of Cl with methyl vinyl ketone [$CH_3C(O)CH{=}CH_2$]

$10^{10} \times k$	T (K)	Technique[a]	Reference
2.1 ± 0.5	298	RR[b] (C_3H_8)	Canosa-Mas et al. (1999b)
1.9 ± 0.2	298	RR[c] (*n*-nonane)	Finlayson-Pitts et al. (1999)
0.99 ± 0.20 (1.6 Torr)	298	DF–RF[d]	Canosa-Mas et al. (2001)
1.1 ± 0.3 (4.5 Torr)			
1.91 ± 0.46	298	RR[e] (C_2H_2)	Wang et al. (2002)
1.90 ± 0.26	298	RR[f] (*n*-C_4H_{10})	
2.10 ± 0.31	298	RR[b] (C_3H_8)	Orlando et al. (2003)
1.86 ± 0.25	298	RR[g] (C_3H_6)	

[a]Abbreviations used for the techniques are defined in table I-F-3.
[b]Placed on an absolute basis using $k(Cl + C_3H_8) = 1.4 \times 10^{-10}$ cm^3 molecule^{-1} s^{-1} (Calvert et al., 2008).
[c]Placed on an absolute basis using $k(Cl + n\text{-}C_9H_{20}) = 4.6 \times 10^{-10}$ cm^3 molecule^{-1} s^{-1} (Calvert et al., 2008).
[d]Study conducted in He buffer gas, total pressure in parentheses.
[e]Placed on an absolute basis using $k(Cl + C_2H_2) = 5.2 \times 10^{-11}$ cm^3 molecule^{-1} s^{-1} (Atkinson et al., 2006).
[f]Placed on an absolute basis using $k(Cl + n\text{-}C_4H_{10}) = 2.1 \times 10^{-10}$ cm^3 molecule^{-1} s^{-1} (Calvert et al., 2008).
[g]Placed on an absolute basis using $k(Cl + C_3H_6) = 2.3 \times 10^{-10}$ cm^3 molecule^{-1} s^{-1} (Calvert et al., 2008).

radical generates mostly formaldehyde and CO_2 or PAN:

$$OH + CH_3C(O)CH{=}CH_2(+O_2) \rightarrow CH_3C(O)CH(OO\bullet)CH_2OH$$

$$CH_3C(O)CH(OO\bullet)CH_2OH + NO \rightarrow CH_3C(O)CH(O\bullet)CH_2OH + NO_2$$

$$CH_3C(O)CH(O\bullet)CH_2OH \rightarrow CH_3CO + HC(O)CH_2OH$$

Internal OH addition is the minor pathway (about 28% of the reaction), and leads to formation of formaldehyde and methylglyoxal. Products of the Cl-atom-initiated process have also been studied (Fantechi et al., 1998c; Canosa-Mas et al., 2001; Orlando et al., 2003). Chloroacetaldehyde (with formaldehyde co-product) is seen as a major product, by analogy to glycolaldehyde production in the OH system.

V-E-2. Ethyl Vinyl Ketone [1-Penten-3-one, $CH_2{=}CHC(O)CH_2CH_3$]

V-E-2.1. OH + Ethyl Vinyl Ketone Reaction Kinetics

No studies of the reaction of OH with ethyl vinyl ketone (EVK) are available in the literature. However, structure–reactivity relationships (Kwok and Atkinson, 1995) can be used to estimate $k(OH + EVK) = 2.5 \times 10^{-11}$ cm^3 molecule^{-1} s^{-1} near 298 K.

V-E-2.2. O_3+ Ethyl Vinyl Ketone Reaction Kinetics

The rate coefficient for reaction of O_3 with EVK has been investigated by Grosjean et al. (1993a), who report $k = 6.0 \times 10^{-18}$ cm^3 molecule^{-1} s^{-1} near 290 K. Details are provided in table V-E-5.

V-E-2.3. NO_3+ Ethyl Vinyl Ketone Reaction Kinetics

Pfrang et al. (2006b) used a relative rate technique to determine $k = 9.9 \times 10^{-17}$ cm^3 molecule^{-1} s^{-1} for the reaction of NO_3 with EVK at 300 K. See table V-E-6.

V-E-2.4. Summary of the Atmospheric Fate of Ethyl Vinyl Ketone, and the End Products of its Oxidation

The atmospheric destruction of ethyl vinyl ketone appears to be controlled under most circumstances by its reaction with OH. Assuming an OH rate coefficient similar to that of MVK, a lifetime of about 4 h is estimated for peak daytime

Table V-E-5. Rate coefficients (k, cm^3 molecule^{-1} s^{-1}) for reaction of O_3 with ethyl vinyl ketone [$CH_3CH_2C(O)CH{=}CH_2$]

$10^{15} \times k$	T (K)	Technique[a]	Reference
6.0 ± 0.4	290 ± 5	UV abs.	Grosjean et al. (1993a)

[a]Abbreviations used for the techniques are defined in table I-F-3.

Table V-E-6. Rate coefficients (k, cm^3 molecule^{-1} s^{-1}) for reaction of NO_3 with ethyl vinyl ketone [$CH_3CH_2C(O)CH{=}CH_2$]

$10^{15} \times k$	T (K)	Technique[a]	Reference
9.9 ± 2.8	300	RR[b] (ethene)	Pfrang et al. (2006b)

[a]Abbreviations used for the techniques are defined in table I-F-3.
[b]Placed on an absolute basis using $k(NO_3 + \text{ethene}) = 2.2 \times 10^{-16}$ cm^3 molecule^{-1} s^{-1} (Atkinson et al., 2006).

[OH] = 2.5×10^6 molecule cm^{-3}. By analogy to MVK (section V-E-1), the major products of the OH-initiated oxidation are expected to be glycolaldehyde, CO_2 and propanal. Minor yields of formaldehyde and 2-oxobutanal are also likely. Reaction with ozone would appear to be a minor atmospheric fate of EVK, lifetime about 30 h for [O_3] = 1.5×10^{12} molecule cm^{-3}. The necessary information to calculate lifetimes for photodissociation of ethyl vinyl ketone is not available at this writing, but it is expected to be much longer than reaction with OH, probably about 2–3 days. Major products of the ozonolysis have been quantified by Grosjean et al. (1996c), who report yields of CH_2O and 2-oxobutanal of 54.8 ± 6.9% and 44.4 ± 2.5%, respectively.

V-E-3. 3-Penten-2-one [$CH_3C(O)CH{=}CHCH_3$]

V-E-3.1. OH + 3-Penten-2-one Reaction Kinetics

No data are available regarding the reaction of OH with 3-penten-2-one. However, an estimate for the *E*-isomer of $k = 6 \times 10^{-11}$ cm^3 molecule^{-1} s^{-1} can be obtained at 298 K using structure–reactivity relationships (Kwok and Atkinson, 1995).

V-E-3.2. O_3+ 3-Pentene-2-one Reaction Kinetics

The reaction of 3-penten-2-one with O_3 has been the subject of three separate investigations (Atkinson et al., 1981; Greene and Atkinson, 1994; Sato et al., 2004). The data are summarized in table V-E-7. The sample used in both the Atkinson et al. (1981) and the Sato et al. (2004) studies is mainly the *trans*-isomer, while Greene and Atkinson do not specify the isomeric composition of their sample. As pointed out by Greene and Atkinson (1994), the absolute rate coefficient measurement of Atkinson et al. (1981) is likely low due to the then-unrecognized presence of a relatively unreactive impurity, 4-methyl-3-penten-2-one (see section V-E-6). Thus, the recommended value is obtained from an average of the final values of the relative rate studies of Greene and Atkinson (1994) and Sato et al. (2004), $k = 3.2 \times 10^{-17}$ cm^3 molecule^{-1} s^{-1} near 298 K. The uncertainty assigned to this value is estimated at ±25%.

V-E-3.3. NO_3 + 3-Penten-2-one Reaction Kinetics

Canosa-Mas et al. (2005) obtained a rate coefficient $k = 1.0 \times 10^{-14}$ cm^3 molecule^{-1} s^{-1} for reaction of *E*-3-penten-2-one with NO_3, using a relative rate method. The uncertainty of this value is estimated at ±50%. The study is summarized in table V-E-8.

Table V-E-7. Rate coefficients (k, cm^3 molecule^{-1} s^{-1}) for reaction of O_3 with 3-penten-2-one [$CH_3C(O)CH{=}CHCH_3$]

$10^{18} \times k$	T (K)	Technique[a]	Reference
21.3 ± 3.9	296	O_3 Chemi-luminescence	Atkinson et al. (1981)
34.8 ± 1.5	296	RR[b] (propene)	Greene and Atkinson (1994)
25.5	298	RR[c] (propene)	Sato et al. (2004)
33.0	298		
23.7	298		
31.6	298		

[a]Abbreviations used for the techniques are defined in table I-F-3.
[b]Placed on an absolute basis using $k(O_3 + \text{propene}) = 0.96 \times 10^{-13}$ cm^3 molecule^{-1} s^{-1} at 296 K (Atkinson et al., 2006).
[c]Placed on an absolute basis using $k(O_3 + \text{propene}) = 1.0 \times 10^{-13}$ cm^3 molecule (Atkinson et al., 2006).

Table V-E-8. Rate coefficients (k, cm^3 molecule^{-1} s^{-1}) for reaction of NO_3 with *E*-3-penten-2-one [$CH_3C(O)CH{=}CHCH_3$]

$10^{15} \times k$	T (K)	Technique[a]	Reference
1.03 ± 0.31	298	RR[b] (propene)	Canosa-Mas et al. (2005)

[a]Abbreviations used for the techniques are defined in table I-F-3.
[b]Placed on an absolute basis using $k(NO_3 + \text{propene}) = 9.5 \times 10^{-15}$ cm^3 molecule^{-1} s^{-1} (Atkinson et al., 2006).

V-E-3.4. Summary of the Atmospheric Fate of 3-Penten-2-one, and the End Products of Its Oxidation

The oxidation of 3-penten-2-one is likely to occur via both reaction with OH (lifetime of about 2 h for [OH] = 2.5×10^6 molecule cm^{-3}) and O_3 (lifetime of about 6 h for [O_3] ≈ 1.5×10^{12} molecule cm^{-3}). Reaction of NO_3 may also play a role during polluted nighttime conditions. By analogy with the behavior of acrolein and methacrolein, lifetimes for photodecomposition are probably much greater than those for reaction with OH and O_3.

V-E-4. 3-Methyl-3-buten-2-one [$CH_3C(O)C(CH_3){=}CH_2$]

V-E-4.1. OH + 3-Methyl-3-butene-2-one Reaction Kinetics

There are no studies in the literature regarding the reaction of OH with 3-methyl-3-buten-2-one. However, a value of $k = 5 \times 10^{-11}$ cm^3 molecule^{-1} s^{-1} can be estimated at 298 K using structure–reactivity relationships (Kwok and Atkinson, 1995).

V-E-4.2. NO_3+ 3-Methyl-3-butene-2-one Reaction Kinetics

Canosa-Mas et al. (2005) used a relative rate technique to determine $k = (8.3 \pm 6.4) \times 10^{-15}$ cm^3 molecule^{-1} s^{-1} for the reaction of NO_3 with 3-methyl-3-butene-2-one, see table V-E-9 for details.

Table V-E-9. Rate coefficients (k, cm^3 molecule^{-1} s^{-1}) for reaction of NO_3 with 3-methyl-3-butene-2-one [$CH_3C(O)C(CH_3)=CH_2$]

$10^{15} \times k$	T (K)	Technique[a]	Reference
8.27 ± 6.44	298	RR[b] (propene)	Canosa-Mas et al. (2005)

[a]Abbreviations used for the techniques are defined in table I-F-3.
[b]Placed on an absolute basis using $k(NO_3 + \text{propene}) = 9.5 \times 10^{-15}$ cm^3 molecule^{-1} s^{-1} at 295 K (Atkinson et al., 2006).

V-E-4.3. Summary of the Atmospheric Fate of 3-Methyl-3-buten-2-one, and the End Products of Its Oxidation

The reaction of 3-methyl-3-buten-2-one with OH likely plays an important role in the atmospheric oxidation of this species. A lifetime of about 2 h is predicted, using the rate coefficient estimated in this section. By analogy to the structurally similar methacrolein, hydroxyacetone is anticipated as a major end product, with CO_2 and CH_2O as important co-products. Reaction with NO_3 may also play a minor role in polluted nighttime conditions (lifetime of about 10 h for $[NO_3] \approx 3 \times 10^9$ molecule cm^{-3}). Lifetimes for photodissociation are probably not competive with those for reaction with OH and O_3.

V-E-5. 4-Hexen-3-one [$CH_3CH_2C(O)CH=CHCH_3$]

V-E-5.1. OH + 4-Hexen-3-one Reaction Kinetics

The reaction of OH with 4-hexen-3-one has not been studied. However, structure–reactivity relationships can be used to estimate $k \approx 6 \times 10^{-11}$ cm^3 molecule^{-1} s^{-1} at 298 K (Kwok and Atkinson, 1995).

V-E-5.2. O_3+ 4-Hexene-3-one Reaction Kinetics

The reaction of O_3 with 4-hexen-3-one has been studied by Grosjean and Grosjean (1999), by monitoring O_3 decay in the presence of excess ketone and an OH scavenger. Their data lead to a rate coefficient of $k = 6.4 \times 10^{-17}$ cm^3 molecule^{-1} s^{-1} near 294 K; see table V-E-10 for details.

V-E-5.3. Summary of the Atmospheric Fate of 4-Hexen-3-one, and the End Products of Its Oxidation

The atmospheric destruction of 4-hexen-3-one likely involves a combination of O_3-, OH-, and possibly NO_3-initiated oxidation. The lifetimes against O_3 and OH loss

Table V-E-10. Rate coefficients (k, cm^3 molecule^{-1} s^{-1}) for reaction of O_3 with 4-hexen-3-one [$CH_3CH_2C(O)CH=CHCH_3$]

$10^{18} \times k$	T (K)	Technique[a]	Reference
59.4 ± 6.5	291	UV abs.	Grosjean and Grosjean (1999)
64.4 ± 5.3	293		
67.3 ± 5.3	297		

[a]Abbreviations used for the techniques are defined in table I-F-3.

are both estimated to be about 2–3 h. Lifetimes for photodissociation are not known at this writing, but they are probably not competitive with those of OH and O_3.

Grosjean and Grosjean (1999) reported significant yields of acetaldehyde (molar yield of 50.6 ± 1.2%) and 2-oxobutanal (55.8 ± 1.9%) from the ozonolysis of this species. These same species are likely the main products of the OH-initiated process as well. Smaller yields of glyoxal, formaldehyde, and acetic acid (all 4–9%) were also reported in the ozonolysis experiments (Grosjean and Grosjean, 1999).

V-E-6. 4-Methyl-3-penten-2-one [Mesitylene Oxide, $CH_3C(O)CH{=}C(CH_3)_2$]

V-E-6.1. OH + 4-Methyl-3-pentene-2-one Reaction Kinetics

The reaction of OH with 4-methyl-3-penten-2-one has not been studied. However, structure–reactivity relationships can be used to estimate $k \approx 8 \times 10^{-11}$ cm^3 molecule^{-1} s^{-1} at 298 K.

V-E-6.2. O_3+ 4-Methyl-3-penten-2-one Reaction Kinetics

Sato et al. (2004) have studied the reaction of O_3 with 4-methyl-3-penten-2-one, using a relative rate technique. Their data leads to $k = 8.1 \times 10^{-18}$ cm^3 molecule^{-1} s^{-1} at 298 K. The uncertainty is estimated at ±35%. The study is summarized in table V-E-11.

V-E-6.3. NO_3+ 4-Methyl-3-penten-2-one Reaction Kinetics

The reaction of NO_3 with 4-methyl-3-penten-2-one has been studied by Canosa-Mas et al. (2005) using a relative rate technique; see table V-E-12. They report $k = 1.4 \times 10^{-13}$ cm^3 molecule^{-1} s^{-1} at 298 K. An uncertainty of ±50% is assumed.

V-E-6.4. Summary of the Atmospheric Fate of 4-Methyl-3-penten-2-one, and the End Products of Its Oxidation

Reaction with OH will probably be the main atmospheric loss process for 4-methyl-3-penten-2-one under most circumstances. For daytime [OH] = 2.5×10^6 molecule cm^{-3}, a lifetime of about 1.4 h is estimated. Reaction with O_3 appears to play only a minor role for this species, while reaction with NO_3 will be important at night in highly polluted

Table V-E-11. Rate coefficients (k, cm^3 molecule^{-1} s^{-1}) for reaction of O_3 with 4-methyl-3-penten-2-one [$CH_3C(O)CH{=}C(CH_3)CH_3$]

$10^{18} \times k$	T (K)	Technique[a]	Reference
8.1	298	RR[b] (propene)	Sato et al. (2004)
7.9	298		
8.4	298	RR[c] (isobutene)	

[a]Abbreviations used for the techniques are defined in table I-F-3.
[b]Placed on an absolute basis using $k(O_3 + \text{propene}) = 1.0 \times 10^{-17}$ cm^3 molecule^{-1} s^{-1} (Atkinson et al., 2006).
[c]Placed on an absolute basis using $k(O_3 + \text{isobutene}) = 1.1 \times 10^{-17}$ cm^3 molecule^{-1} s^{-1} (Calvert et al., 2000).

Table V-E-12. Rate coefficients (k, cm^3 molecule^{-1} s^{-1}) for reaction of NO_3 with 4-methyl-3-penten-2-one [$CH_3C(O)CH{=}C(CH_3)CH_3$]

$10^{18} \times k$	T (K)	Technique[a]	Reference
1.44 ± 0.26	298	RR[b] (*E*-2-butene)	Canosa-Mas et al. (2005)

[a]Abbreviations used for the techniques are defined in table I-F-3.
[b]Placed on an absolute basis using $k(NO_3 + E\text{-2-butene}) = 3.9 \times 10^{-13}$ cm^3 molecule^{-1} s^{-1} at 298 K (Calvert et al., 2000).

areas; for example, a lifetime for the NO_3 reaction of less than 1 h is predicted for very polluted nighttime conditions, $[NO_3] \approx 3 \times 10^9$ molecule cm^{-3}. Lifetimes for photodissociation are not known at this writing, but they are probably not competitive with those for OH.

Products of the atmospheric oxidation of this species have not been determined, but high yields of acetone and methylglyoxal are anticipated from the OH-initiated process.

V-E-7. *E*-3-Methyl-3-penten-2-one [$CH_3C(O)C(CH_3){=}CHCH_3$]

V-E-7.1. OH + 3-Methyl-3-penten-2-one Reaction Kinetics

No data are available for this reaction. However, using structure–reactivity relationships (Kwok and Atkinson, 1995), an estimate of $k \approx 8 \times 10^{-11}$ cm^3 molecule^{-1} s^{-1} can be derived at 298 K.

V-E-7.2. NO_3+ 3-Methyl-3-penten-2-one Reaction Kinetics

The reaction of NO_3 with *E*-3-methyl-3-penten-2-one has been studied by Canosa-Mas et al. (2005), using a relative rate technique. They report $k = 1.6 \times 10^{-13}$ cm^3 molecule^{-1} s^{-1} at 298 K. In the absence of corroborative data, the uncertainty is estimated at ±40%. The study is summarized in table V-E-13.

V-E-7.3. Summary of the Atmospheric Fate of E-3-Methyl-3-penten-2-one, and the End Products of Its Oxidation

The atmospheric destruction of *E*-3-methyl-3-penten-2-one is likely controlled by its reaction with OH and O_3, with the NO_3 reaction playing a role in polluted nighttime situations. Using the estimated rate coefficient for OH with the species, a lifetime of

Table V-E-13. Rate coefficients (k, cm^3 molecule^{-1} s^{-1}) for reaction of NO_3 with *E*-3-methyl-3-penten-2-one [$CH_3C(O)C(CH_3){=}CHCH_3$]

$10^{13} \times k$	T (K)	Technique[a]	Reference
1.55 ± 0.20	298	RR[b] (*E*-2-butene)	Canosa-Mas et al. (2005)

[a]Abbreviations used for the techniques are defined in table I-F-3.
[b]Placed on an absolute basis using $k(NO_3 + E\text{-2-butene}) = 3.9 \times 10^{-13}$ cm^3 molecule^{-1} s^{-1} at 298 K (Calvert et al., 2000).

about 1.4 h is obtained. The lifetime against reaction with NO_3 is less than an hour for $[NO_3] = 3 \times 10^9$ molecule cm^{-3}. Destruction by photodissociation is probably not competitive. The end products of the OH-initiated oxidation of this species have not been determined.

V-E-8. 6-Methyl-5-hepten-2-one [$CH_3C(O)CH_2CH_2CH{=}C(CH_3)_2$]

V-E-8.1. OH + 6-Methyl-5-hepten-2-one Reaction Kinetics

The reaction of OH with 6-methyl-5-hepten-2-one has been studied by Smith et al. (1996) using the relative rate method. Their value, 1.57×10^{-10} cm^3 molecule^{-1} s^{-1} at 296 K, is recommended; see table V-E-14. In the absence of corroborative data, an uncertainty of ±35% is assigned to this value.

V-E-8.2. O_3+ 6-Methyl-5-hepten-2-one Reaction Kinetics

Grosjean et al. (1996c) and Smith et al. (1996) have studied the reaction of 6-methyl-5-hepten-2-one with O_3. The two determinations, although obtained at slightly different temperatures, are in excellent agreement, and lead to $k = 3.9 \times 10^{-16}$ cm^3 molecule^{-1} s^{-1} near 290–296 K. The data are summarized in table V-E-14.

V-E-8.3. Summary of the Atmospheric Fate of 6-methyl-5-hepten-2-one, and the End Products of Its Oxidation

The lifetimes of 6-methyl-5-hepten-2-one via reaction with O_3 (for $[O_3] \approx 10^{12}$ molecule cm^{-3}) and via reaction with OH (for $[OH] \approx 2.5 \times 10^6$ molecule cm^{-3})

Table V-E-14. Rate coefficients (k, cm^3 molecule^{-1} s^{-1}) for reaction of OH, O_3, and NO_3 with 6-methyl-5-hepten-2-one [$CH_3C(O)CH_2CH_2CH{=}CH(CH_3)_2$]

$10^{12} \times k$	T (K)	Technique[a]	Reference
OH + 6-methyl-5-hepten-2-one			
157 ± 39	296	RR[b] (trans-2-butene)	Smith et al. (1996)
O_3 + 6-methyl-5-hepten-2-one			
3.36×10^{-4}	287.0	UV abs.	Grosjean et al. (1995c)
4.24×10^{-4}	288.5		
4.03×10^{-4}	291.5		
4.14×10^{-4}	290.1		
$(3.9 \pm 1.5) \times 10^{-4}$	296	RR[c] (2-methyl-2-butene)	Smith et al. (1996)
NO_3 + 6-methyl-5-hepten-2-one			
7.5 ± 3.0	296	RR[c] (2-methyl-2-butene)	Smith et al. (1996)

[a]Abbreviations used for the techniques are defined in table I-F-3.
[b]Placed on an absolute basis using k(OH + *trans*-2-butene) = 6.48×10^{-11} cm^3 molecule^{-1} s^{-1} at 298 K (Calvert et al., 2000).
[c]Placed on an absolute basis using k(O_3 + 2-methyl-2-butene) = 4.0×10^{-16} cm^3 molecule^{-1} s^{-1} at 298 K (Calvert et al., 2000).
[d]Placed on an absolute basis using k(NO_3 + 2-methyl-2-butene) = 4.0×10^{-16} cm^3 molecule^{-1} s^{-1} at 298 K (Calvert et al., 2000).

are both less than 1 h. Reaction with NO_3 will also be very rapid (timescale of about 1 min. for polluted nighttime [NO_3] = 3×10^9 molecule cm^{-3}). Lifetimes for photodecomposition are probably not competitive with those of OH, O_3, and NO_3.

Major products of the OH-initiated oxidation in molar yields (Smith et al., 1996) are acetone (70.6%) and 4-oxopentanal (59%). Products of the ozonolysis of 6-methyl-5-hepten-2-one have been quantified by Grosjean et al. (1996c) and Smith et al. (1996); major products include 4-oxopentanal, methylglyoxal, acetone, and formaldehyde.

V-E-9. *trans*-4-Methoxy-3-buten-2-one [$CH_3C(O)CH{=}CHOCH_3$]

V-E-9.1. OH + trans-4-Methoxy-3-buten-2-one Reaction Kinetics

No data are available for this reaction. However, an estimate of $k \approx 7 \times 10^{-11}$ cm^3 molecule^{-1} s^{-1} can be derived at 298 K using structure–reactivity relationships (Kwok and Atkinson, 1995).

V-E-9.2. O_3+ trans-4-Methoxy-3-buten-2-one Reaction Kinetics

Grosjean and Grosjean (1999) report $k = 1.3 \times 10^{-16}$ cm^3 molecule^{-1} s^{-1} for the reaction of O_3 with *trans*-4-methoxy-3-buten-2-one. The data are summarized in table V-E-15.

V-E-9.3. Summary of the Atmospheric Fate of trans-4-Methoxy-buten-2-one, and the End Products of its Oxidation

The data of Grosjean and Grosjean (1999) indicate that the ozonolysis of *trans*-4-methoxy-3-buten-2-one will be rapid with a lifetime of about 1.4 h for [O_3] = 1.5×10^{12} molecule cm^{-3}. Using the rate coefficient estimated in this section, the OH-initiated oxidation process will also contribute significantly (lifetime about 1.6 h for daytime [OH] = 2.5×10^6 molecule cm^{-3}). Lifetimes for photodecomposition are probably not competitive.

Grosjean and Grosjean (1999) identified two main products from the ozonolysis (molar yields): methylglyoxal (31.2 ± 1.9%) and methyl formate (> 15.7%). These two species are potential products of the OH-initiated oxidation as well, although the formation of $CH_3OCH(OH)CHO$ (with co-products CO_2 and CH_2O) is also possible.

Table V-E-15. Rate coefficients (k, cm^3 molecule^{-1} s^{-1}) for reaction of O_3 with *trans*-4-methoxy-3-buten-2-one [$CH_3C(O)CH{=}CHOCH_3$]

$10^{17} \times k$	T (K)	Technique[a]	Reference
12.6 ± 0.97	294	UV abs.	Grosjean and
12.5 ± 0.98	297		Grosjean (1999)
12.3 ± 0.94	297		

[a]Abbreviations used for the techniques are defined in table I-F-3.

V-E-10. Halogen-Substituted Unsaturated Ketones

V-E-10.1. Chloromethyl Vinyl Ketone [$ClCH_2COCH{=}CH_2$]

The reaction of Cl-atoms with chloromethyl vinyl ketone, a product of the Cl-atom-initiated oxidation of 1,4-butadiene, has been studied by Wang et al. (2002), using the relative rate method. Their data lead to $k = 1.9 \times 10^{-10}$ cm^3 molecule^{-1} s^{-1}. The study is summarized in table V-E-16.

V-E-11. Unsaturated 1,4-Dicarbonyls

The unsaturated 1,4-dicarbonyl compounds, e.g., 3-hexene-2,5-dione [$CH_3C(O)CH{=}CHC(O)CH_3$], are formed in significant yield from the oxidation of aromatic compounds. Their atmospheric behavior is summarized below. Butenedial, which is a co-product of methylglyoxal in the oxidation of toluene, is discussed with other unsaturated 1,4-dials in section IV-D-4.

V-E-11.1. OH + Unsaturated 1,4-Dicarbonyls Reaction Kinetics

OH rate coefficients have been determined for three members of this series: 4-oxo-2-pentenal [$CH_3C(O)CH{=}CHCHO$], 3-hexene-2,5-dione [$CH_3C(O)CH{=}CHC(O)CH_3$], and 3,4-dihydroxy-3-hexen-2,5-dione [$CH_3C(O)C(OH){=}C(OH)C(O)CH_3$]. All data have been obtained using relative rate methods and are summarized in table V-E-17. Bierbach et al. (1994) determined $k = 6.2 \times 10^{-11}$ cm^3 molecule^{-1} s^{-1} for reaction of OH with a mixture of *cis*- and *trans*-4-oxo-2-pentenal, while Wiesen et al. (1995) report $k = 2.7 \times 10^{-10}$ cm^3 molecule^{-1} s^{-1} for reaction of OH with 3,4-dihydroxy-3-hexen-2,5-dione. Data are available for both the *cis*- and *trans*-isomers of 3-hexene-2,5-dione (Tuazon et al., 1985; Bierbach et al., 1994). There is reasonable agreement between the two determinations, and average values of $k = 7.2 \times 10^{-11}$ cm^3 molecule^{-1} s^{-1} and $k = 5.1 \times 10^{-11}$ cm^3 molecule^{-1} s^{-1} are obtained for the *cis*- and *trans*- species, respectively.

V-E-11.2. O_3+ Unsaturated 1,4-Dicarbonyls Reaction Kinetics

Liu et al. (1999) have made the only measurement of the reaction of O_3 with 4-oxo-2-pentenal, $k = 4.8 \times 10^{-18}$ cm^3 molecule^{-1} s^{-1} for a mixture of *cis*- and *trans*-isomers.

Table V-E-16. Rate coefficients (k, cm^3 molecule^{-1} s^{-1}) for reaction of Cl with chloromethyl vinyl ketone, $ClCH_2C(O)CH_3$

$10^{11} \times k$	T (K)	Technique[a]	Reference
19.3 ± 2.1	298	RR[b] (nonane)	Wang et al. (2002)

[a]Abbreviations used for the techniques are defined in table I-F-3.
[b]Placed on an absolute basis using k(Cl + nonane) = 4.6×10^{-10} cm^3 molecule^{-1} s^{-1} at 298 K (Calvert et al., 2008).

Table V-E-17. Rate coefficients (k, cm^3 molecule^{-1} s^{-1}) for reaction of OH with unsaturated 1,4-dicarbonyl species

$10^{11} \times k$	T (K)	Technique[a]	Reference
OH + *cis/trans*-4-oxo-2-pentenal, $CH_3C(O)CH{=}CHCHO$			
6.18 ± 0.23	296	RR[b] (propene)	Bierbach et al. (1994)
OH + *cis*-3-hexene-2,5-dione, $CH_3C(O)CH{=}CHC(O)CH_3$			
7.0 ± 0.7	298	RR[b] (propene)	Tuazon et al. (1985)
7.42 ± 2.30	296	RR[b] (propene)	Bierbach et al. (1994)
OH + *trans*-3-hexene-2,5-dione, $CH_3C(O)CH{=}CHC(O)CH_3$			
5.9 ± 0.6	298	RR[b] (propene)	Tuazon et al. (1985)
4.29 ± 0.43	296	RR[b] (propene)	Bierbach et al. (1994)
OH + 3,4-dihydroxy-3-hexene-2,5-dione, $CH_3C(O)C(OH){=}C(OH)C(O)CH_3$			
25 ± 7	296	RR[b] (propene)	Wiesen et al. (1995)
29 ± 7	296	RR[c] (isoprene)	

[a]Abbreviations used for the techniques are defined in table I-F-3.
[b]Placed on an absolute basis using $k(\text{OH} + \text{propene}) = 2.9 \times 10^{-11}$ cm^3 molecule^{-1} s^{-1} (Ammann et al., 2008).
[c]Placed on an absolute basis using $k(\text{OH} + \text{isoprene}) = 10 \times 10^{-11}$ cm^3 molecule^{-1} s^{-1} (Ammann et al., 2008).

Table V-E-18. Rate coefficients (k, cm^3 molecule^{-1} s^{-1}) for reaction of O_3 with unsaturated 1,4-dicarbonyl species

$10^{18} \times k$	T (K)	Technique[a]	Reference
O_3 + *cis/trans*-4-oxo-2-pentenal, $CH_3C(O)CH{=}CHCHO$			
4.8 ± 0.8	296	O_3 UV abs.	Liu et al. (1999)
O_3+*cis*-3-hexene-2,5-dione, $CH_3C(O)CH{=}CHC(O)CH_3$			
1.8 ± 0.2	298	O_3 Chemi-luminescence	Tuazon et al. (1985)
O_3+*trans*-3-hexene-2,5-dione, $CH_3C(O)CH{=}CHC(O)CH_3$			
8.3 ± 1.2	298	O_3 Chemi-luminescence	Tuazon et al. (1985)
O_3 + 3,4-dihydroxy-3-hexene-2,5-dione, $CH_3C(O)C(OH){=}C(OH)C(O)CH_3$			
3.6 ± 0.3	296	O_3 UV abs.	Liu et al. (1999)

[a]Abbreviations used for the techniques are defined in table I-F-3.

The measurement of Liu et al. (1999) for a mixture of *cis*- and *trans*-3-hexene-2,5-dione, $k = 3.6 \times 10^{-18}$ cm^3 molecule^{-1} s^{-1}, is in reasonable agreement with measurements made by Tuazon et al. (1985) on the individual isomers, $k = 1.8 \times 10^{-18}$ and 8.3×10^{-18} cm^3 molecule^{-1} s^{-1} for the *cis*- and *trans*- species, respectively. The data are summarized in table V-E-18.

V-E-11.3. Summary of the Atmospheric Fate of Unsaturated 1,4-Dicarbonyls, and the End Products of Their Oxidation

The studies of Tuazon and co-workers (Tuazon et al., 1985; Bethel et al., 2001a; Tuazon and Atkinson, 2003), Bierbach et al. (1994), and Liu et al. (1999) lead

to the conclusion that photolysis and reaction with OH likely play a role in the atmospheric destruction of 4-oxo-2-pentenal [$CH_3C(O)CH{=}CHCHO$] and 3-hexene-2,5-dione [$CH_3C(O)CH{=}CHC(O)CH_3$], while reaction with O_3 is of minor importance. Photolysis of the *cis*- and *trans*-isomers of both these species is estimated to occur on timescales of 10–30 min. However, Tuazon et al. (1985) and Bierbach et al. (1994) both noted that interconversion of the *cis*- and *trans*-isomers of 3-hexene-2,5-dione accounted for >80% of the photolytic loss; hence, the actual photolytic destruction rate of the *cis*-/*trans*- pair could be in excess of 3 h, allowing for a significant contribution from OH reaction (lifetime about 2 h for peak daytime [OH] = 2.5×10^6 molecule cm^{-3}). In the case of 4-oxo-2-pentenal, Bierbach et al. noted that cyclization to maleic anhydride and 5-methyl-3H-furanone occurs, with *cis*-/*trans*- isomerization accounting for only about 30% of the photolytic loss. See section IX-C-9.

Product yields from the OH-initiated oxidation of 3-hexene-2,5-dione (in particular, the yield of methylglyoxal) are the subject of some controversy (Tuazon et al., 1985; Bierbach et al., 1994; Liu et al., 1999; Tuazon and Atkinson, 2003); see the discussion in Tuazon and Atkinson (2003). This most recent work demonstrates a negligible yield of methylglyoxal, indicating the likelihood of production of significant yields of $CH_3C(O)CH(OH)CHO$:

$$OH + CH_3C(O)CH{=}CHC(O)CH_3(+O_2) \rightarrow CH_3C(O)CH(OH)CH(OO\bullet)C(O)CH_3$$

$$CH_3C(O)CH(OH)CH(OO\bullet)C(O)CH_3 + NO \rightarrow CH_3C(O)CH(OH)CH(O\bullet)C(O)CH_3 + NO_2$$

$$CH_3C(O)CH(OH)CH(O\bullet)C(O)CH_3 + NO \rightarrow CH_3C(O)CH(OH)CHO + CH_3C\bullet(O)$$

The behavior of the alkoxy radical (decomposition via loss of RCO rather than RCHOH) is consistent with that observed in the chemistry of structurally similar radicals; e.g., that formed following OH addition to methyl vinyl ketone.

The work of Wiesen et al. (1995) suggests that, although photolysis of 3,4-dihydroxy-3-hexene-2,5-dione is rapid (a timescale of 20–25 min. in the summertime lower troposphere), isomerization of the enediol to the keto form (and vice versa) is the predominant outcome, and thus does not represent a permanent loss mechanism:

$$CH_3C(O)C(OH){=}C(OH)C(O)CH_3 \leftrightarrow CH_3C(O)CH(OH)C(O)C(O)CH_3$$

The lifetime of 3,4-dihydroxy-3-hexene-2,5-dione against OH reaction will be quite short, about 0.4 h for a daytime [OH] = 2.5×10^6 molecule cm^{-3}. Wiesen et al. (1995) reasoned that the main product of this chemistry will be 3,3-dihydroxyhexane-2,4,5-trione, $CH_3C(O)C(OH)_2C(O)C(O)CH_3$, which could eliminate water to form the tetraone, $CH_3C(O)C(O)C(O)C(O)CH_3$.

V-E-12. Ketene and Its Derivatives (CH_2=C=O and RR′C=C=O)

V-E-12.1. OH + Ketenes Reaction Kinetics

Available data regarding the rate coefficient for reaction of OH with ketene (Hatakeyama et al., 1985b; Brown et al., 1989b; Oehlers et al., 1992) are summarized in table V-E-19. Considerable scatter exists, with the 298 K data of Brown et al. (1989) falling a factor of 2.8 and 2.1 higher than those of Oehlers et al. (1992) and of Hatakeyama et al. (1985b), respectively. We note that rate coefficient data from Brown et al. in various studies are generally too high, and thus the average of the data of Hatakeyama et al. and Oehlers et al., $k = 1.4 \times 10^{-11}$ cm^3 molecule^{-1} s^{-1}, is recommended with an uncertainty of ±35%.

Hatakeyama et al. (1985b) have also studied the reaction of OH with CH_3-substituted ketenes: CH_3CH=C=O, CH_3CH_2CH=C=O, and $(CH_3)_2C$=C=O. The data show the expected trend of increased reactivity with substitution at the C=C double bond. Their data, summarized in table V-E-19, are recommended with an uncertainty of ±40%.

V-E-12.2. O_3+ Ketenes Reaction Kinetics

Hatakeyama et al. (1985a) have reported upper limits for the reaction of O_3 with ketene and three of its alkyl derivatives, CH_3CH=C=O, CH_3CH_2CH=C=O,

Table V-E-19. Rate coefficients (k, cm^3 molecule^{-1} s^{-1}) for reaction of OH with ketene and its derivatives

$10^{12} \times A$	B (K)	$10^{11} \times k$	T (K)	Technique[a]	Reference	Temperature Range (K)
OH + Ketene (CH_2=C=O)						
		1.6 ± 0.2	299	RR[b] (*cyclo*-C_6H_{12})	Hatakeyama et al. (1985b)	
6.19 ± 9.96	510 ± 420	10.6 ± 2.0	193	DF–RF	Brown et al. (1989b)	193–423
		8.9 ± 2.7	204			
		4.6 ± 1.6	234			
		5.5 ± 1.0	269			
		3.3 ± 0.6	298			
		2.2 ± 0.5	373			
		2.1 ± 0.2	423			
		1.2 ± 0.3	296	DF–LMR	Oehlers et al. (1992)	
OH + Methyl Ketene (CH_3CH=C=O)						
		5.6 ± 1.2	299	RR[b] (*cyclo*-C_6H_{12})	Hatakeyama et al. (1985b)	
		8.7 ± 1.6	299	RR[c] (propene)		
OH + Ethyl Ketene (CH_3CH_2CH=C=O)						
		13 ± 4	299	RR[c] (propene)	Hatakeyama et al. (1985b)	
OH + Dimethyl Ketene, $(CH_3)_2C$=C=O						
		12 ± 4	299	RR[c] (propene)	Hatakeyama et al. (1985b)	

[a]Abbreviations used for the techniques are defined in table I-F-3.
[b]Placed on an absolute basis using k(OH + *cyclo*-C_6H_{12}) = 0.70×10^{-11} cm^3 molecule^{-1} s^{-1} (Calvert et al., 2008).
[c]Placed on an absolute basis using k(OH + propene) = 2.9×10^{-11} cm^3 molecule^{-1} s^{-1} (Atkinson et al., 2006).

$(CH_3)_2C{=}C{=}O$. The data are summarized in table V-E-20. Note that in the case of the three alkyl derivatives, enhanced loss was observed in the presence of ozone, but the rate coefficients derived were considered to be upper limits due to the possibility of secondary losses. No enhancement in the loss rate of ketene was noted upon addition of ozone.

V-E-12.3. NO_3+ Ketenes Reaction Kinetics

The rate coefficient for reaction of NO_3 with ketene has been determined by Seland et al. (1996) using a relative rate method, $k = 1.1 \times 10^{-13}$ cm^3 molecule^{-1} s^{-1}; see table V-E-21. In the absence of corroborative data, an uncertainty of ±50% is assigned. None of the higher analogues have been studied.

V-E-12.4. Cl-Atom + Ketenes Reaction Kinetics

The rate coefficient for reaction of Cl with ketene has been the subject of three investigations (Ebrecht et al., 1990; Wallington et al., 1996a; Maricq et al., 1997a), see table V-E-22. The discharge flow–mass spectrometric study of Ebrecht et al. yielded data that are a factor of 4 lower than the relative rate study of Wallington et al. (1996a) and the flash photolysis–infrared absorption study of Maricq et al. (1997a). Although no obvious reason can be presented for the discrepancy, the good agreement between the Wallington et al. and Maricq et al. studies favors the use of these data. Given the semiquantitative nature of the Maricq et al. study, the value obtained by Wallington et al., $k = 2.8 \times 10^{-10}$ cm^3 molecule^{-1} s^{-1}, is recommended at 298 K. On the basis of the observations of Maricq et al., the rate coefficient is likely independent of temperature.

Table V-E-20. Rate coefficients (k, cm^3 molecule^{-1} s^{-1}) for reaction of O_3 with ketene and various alkyl derivatives

Compound	$10^{19} \times k$	T (K)	Technique[a]	Reference
$CH_2{=}C{=}O$	< 0.01	298	FTIR	Hatakeyama et al. (1985b)
$CH_3CH{=}C{=}O$	< 7	303		
$CH_3CH_2CH{=}C{=}O$	< 10	303		
$(CH_3)_2C{=}C{=}O$	< 400	303		

[a]Abbreviations used for the techniques are defined in table I-F-3.

Table V-E-21. Rate coefficients (k, cm^3 molecule^{-1} s^{-1}) for reaction of NO_3 with ketene ($CH_2{=}C{=}O$)

$10^{13} \times k$	T (K)	Technique[a]	Reference
1.05 ± 0.13	298	RR[b] (*trans*-2-butene)	Seland et al. (1996)

[a]Abbreviations used for the techniques are defined in table I-F-3.
[b]Placed on an absolute basis using $k(NO_3 + trans\text{-}2\text{-butene}) = 3.9 \times 10^{-13}$ cm^3 molecule^{-1} s^{-1} (Calvert et al., 2000).

Table V-E-22. Rate coefficients (k, cm^3 molecule^{-1} s^{-1}) for reaction of Cl with ketene (CH_2═C═O)

$10^{11} \times k$	T (K)	Technique[a]	Reference	Temperature Range (K)
6.8 ± 1.6	294	DF–MS	Ebrecht et al. (1990)	
31 ± 2	295	RR[b] (ethene)	Wallington et al. (1996a)	
25 ± 2	295	RR[c] (*cyclo*-C_6H_{12})		
25 ± 5	235	FP–IR abs.	Maricq et al. (1997a)	235–353
25 ± 5	298			
25 ± 5	353			

[a]Abbreviations used for the techniques are defined in table I-F-3.
[b]Placed on an absolute basis using k(Cl+ethene) = 10.4×10^{-11} cm^3 molecule^{-1} s^{-1} (Atkinson et al., 2006).
[c]Placed on an absolute basis using k(Cl + *cyclo*-C_6H_{12}) = 3.3×10^{-10} cm^3 molecule^{-1} s^{-1} (Calvert et al., 2008).

Table V-E-23. Rate coefficients ($k = A \times e^{-B/T}$, cm^3 molecule^{-1} s^{-1}) for reaction of O(^{3}P) with ketene and its alkyl derivatives

Species	$10^{12} \times A$	B (K)	$10^{12} \times k$ (298 K)	Reference
CH_2═C═O	2.99	683 ± 198	0.3	Cvetanovic (1987)
CH_3CH═C═O	4.82	−251 ± 100	11	Cvetanovic (1987)
CH_3CH_2CH═C═O	5.31	−221 ± 99	11	Cvetanovic (1987)
$(CH_3)_2$C═C═O	5.98	−572 ± 104	40	Cvetanovic (1987)

V-E-12.5. O(^{3}P) + Ketenes Reaction Kinetics

The reactions of O(^{3}P) with ketene and some of its higher analogs has been reviewed by Cvetanović (1987). His recommended rate coefficients are summarized in table V-E-23.

V-E-12.6. Summary of the Atmospheric Fate of Ketene and Its Alkyl-Substituted Derivatives, and the End Products of Their Oxidation

Although uncertainty exists in the rate coefficients of OH with ketene and its derivatives, it is very likely that these reactions will be important atmospheric loss mechanisms. Note that the lifetime will only be about 8 h for ketene itself, using the rate coefficient recommended above and assuming daytime [OH] = 2.5×10^6 molecule cm^{-3}. Reaction with NO_3 is also very rapid, and will likely contribute in polluted nighttime atmospheres; for example, the lifetime of ketene against NO_3 reaction will be less than 1 h for [NO_3] = 3×10^9 molecule cm^{-3}. The lifetime for photodecomposition of ketene in the lower troposphere with an overhead sun is about 1 h, and this will clearly be an important loss process for ketene. See section IX-E-6 for further details.

The work of Hatakeyama et al. (1985b) and of Grussdorf et al. (1994) indicates that the reaction of OH with the ketenes proceeds mainly via addition, with subsequent decomposition of the resulting adduct into CO and a hydroxyalkyl radical:

$$OH + CH_2{=}C{=}O \rightarrow [HOCH_2C{\bullet}{=}O]^* \rightarrow {\bullet}CH_2OH + CO$$

$${\bullet}CH_2OH + O_2 \rightarrow CH_2O + HO_2$$

A similar mechanism, leading to $\bullet CH_2Cl$ and CO, has been proposed for the Cl-atom reaction with ketene (Wallington et al., 1996a).

V-F. Cyclic Ketones

V-F-1. Cyclobutanone [*cyclo*-$CH_2CH_2CH_2C(O)$-]

V-F-1.1. OH + Cyclobutanone Reaction Kinetics

The reaction of OH with cyclobutanone was studied at 298 K by Dagaut et al. (1988a), using the flash photolysis–resonance fluorescence technique. Their measurement, $k = 8.7 \times 10^{-13}\,cm^3$ molecule^{-1} s^{-1}, is recommended. In the absence of corroborative studies, an uncertainty of ±35% is assigned. The study is summarized in table V-F-1.

V-F-1.2. Summary of the Mechanism and End Products of Cyclobutanone Oxidation, and Summary of Its Atmospheric Fate

The atmospheric lifetime of cyclobutanone is estimated to be about 13 days for [OH] = 10^6 molecule cm^{-3}. The lifetime for photodissociation in the lower troposphere with an overhead Sun is about 10 h; see section IX-E-2.3. The atmospheric oxidation products of cyclobutanone have not been determined.

Table V-F-1. Rate coefficients ($k = A \times e^{-B/T}$, cm^3 molecule^{-1} s^{-1}) for reaction of OH with cyclobutanone [*cyclo*-$C_3H_6C(O)$-], cyclopentanone [*cyclo*-$C_4H_8C(O)$-], and cyclohexanone [*cyclo*-$C_5H_{10}C(O)$-]

$10^{13} \times k$	T (K)	Technique[a]	Reference
OH + Cyclobutanone			
8.7 ± 0.6	298	FP–RF	Dagaut et al. (1988a)
OH + Cyclopentanone			
29.4 ± 1.8	298	FP–RF	Dagaut et al. (1988a)
OH + Cyclohexanone			
63.9 ± 5.1	298	FP–RF	Dagaut et al. (1988a)

[a]Abbreviations used for the techniques are defined in table I-F-3.

V-F-2. Cyclopentanone [*cyclo*-$CH_2CH_2CH_2CH_2C(O)$-]

V-F-2.1. OH + Cyclopentanone Reaction Kinetics

Dagaut et al. (1988a) studied the reaction of OH with cyclopentanone at 298 K, using the flash photolysis–resonance fluorescence technique. They report $k = 2.9 \times 10^{-12}$ cm^3 molecule^{-1} s^{-1}; this value is adopted with an assumed uncertainty of ±35%. The study is summarized in table V-F-1.

V-F-2.2. Cl-Atom + Cyclopentanone Reaction Kinetics

The reaction of Cl-atoms with cyclopentanone has been the subject of three investigations, two using the relative rate technique (Olsson et al., 1997; Wallington et al., 1998a) and one using flash photolysis–laser-induced fluorescence (Takahashi et al., 2007). The data are summarized in table V-F-2. The value from Olsson et al. (1997), obtained by measuring NO_3 formation from the reaction of Cl with $ClONO_2$ in the presence and absence of added ketone, is about a factor of 2 lower than the other data. As discussed by Wallington et al. (1998a), the low values reported by Olsson et al. for this rate coefficient (and also the well-studied rate coefficient for Cl with acetone and cyclohexanone) may be due to an inaccurate measurement of the ketone concentration, which was required input for the determination of the rate coefficient. The recommended value for k(Cl+cyclopentanone), 1.2×10^{-10} cm^3 molecule^{-1} s^{-1}, is obtained by averaging the Wallington et al. (1998a) and Takahashi et al. (2007) data. An uncertainty of ±15% is assigned.

V-F-2.3. O(^{3}P) + Cyclopentanone Reaction Kinetics

The review of Herron (1988) recommends a rate coefficient $k = 4.0 \times 10^{-11} \exp(-2{,}300/T)$ cm^3 molecule^{-1} s^{-1} for reaction of O(^{3}P) with cyclopentanone ($300 < T < 600$ K), with an estimated uncertainty of a factor of three.

Table V-F-2. Rate coefficients (k, cm^3 molecule^{-1} s^{-1}) for reaction of Cl with cyclopentanone [*cyclo*-$C_4H_8C(O)$-]

$10^{11} \times k$	T (K)	Technique[a]	Reference
4.76 ± 0.33	298	RR[b] ($ClONO_2$)	Olsson et al. (1997)
12.5 ± 1.0	295	RR[c] (C_2H_4)	Wallington et al. (1998a)
10.4 ± 1.0	295	RR[d] (cyclopentane)	
11.6 ± 1.2	298	FP–LIF	Takahashi et al. (2007)

[a]Abbreviations used for the techniques are defined in table I-F-3.

[b]Placed on an absolute basis using $k(Cl + ClONO_2) = 1.0 \times 10^{-11}$ cm^3 molecule^{-1} s^{-1} (Atkinson et al., 2006).

[c]Placed on an absolute basis using $k(Cl + C_2H_4) = 1.04 \times 10^{-10}$ cm^3 molecule^{-1} s^{-1} (Atkinson et al., 2006).

[d]Placed on an absolute basis using k(Cl + *cyclo*-C_5H_{10}) $= 2.9 \times 10^{-10}$ cm^3 molecule^{-1} s^{-1} (Calvert et al., 2008).

V-F-2.4. Summary of the Mechanism and End Products of Cyclopentanone Oxidation, and Summary of Its Atmospheric Fate

Using the OH rate coefficient measurement of Dagaut et al. (1988b), an atmospheric lifetime of about 4 days is estimated for cyclopentanone. The lifetimes for photodecomposition are probably competitive with those for loss by OH; see section IX-E-4. Atmospheric oxidation products have not been determined.

V-F-3. Cyclohexanone [*cyclo*-$CH_2CH_2CH_2CH_2CH_2C(O)$-]

V-F-3.1. OH + Cyclohexanone Reaction Kinetics

The only available data concerning the reaction of OH with cyclohexanone is from the flash photolysis–resonance fluorescence study of Dagaut et al. (1988a), who report $k = 6.4 \times 10^{-12}$ cm^3 molecule^{-1} s^{-1} at 298 K. In the absence of corroborative data, an uncertainty of ±35% is assigned to this value. The study is summarized in table V-F-1.

V-F-3.2. Cl-Atom + Cyclohexanone Reaction Kinetics

Considerable scatter exists in the multiple measurements of the rate coefficient for reaction of Cl with cyclohexanone (Olsson et al., 1997; Wallington et al., 1998a; Albaladejo et al., 2003b; Martinez et al., 2004; Iwasaki et al., 2007), see table V-F-3. For reasons discussed in detail by Iwasaki et al. (2008a), the higher rate coefficient data [i.e., those of Wallington et al. (1998a) and Iwasaki et al. (2008a) and the relative rate data of Martinez et al. (2004)] are preferred. Averaging of these measurements

Table V-F-3. Rate coefficients ($k = A \times e^{-B/T}$, cm^3 molecule^{-1} s^{-1}) for reaction of Cl with cyclohexanone [*cyclo*-$C_5H_{10}C(O)$-]

$10^{10} \times A$	B (K)	$10^{11} \times k$	T (K)	Technique[a]	Reference	Temperature Range (K)
		7.00 ± 1.15	298	RR[b] ($ClONO_2$)	Olsson et al. (1997)	
		21.6 ± 3.0	295	RR[c] (C_2H_4)	Wallington et al. (1998a)	
		16.2 ± 3.0	295	RR[d] (cyclopentane)		
		6.75 ± 0.52	298	FP–RF	Albaladejo et al. (2003b)	
7.7 ± 4.1	540 ± 169	9.6 ± 1.8	273	DF–MS	Martinez et al. (2004)	273–333
		10 ± 2	283			
		13 ± 2	298			
		14 ± 1	315			
		14 ± 2	333			
		17 ± 3	298	RR[e] (C_3H_6)		
		18.8 ± 3.8	295	FP–LIF	Iwasaki et al. (2008a)	
		16.6 ± 2.6	295	RR[f] (C_3H_8)		

[a]Abbreviations used for the techniques are defined in table I-F-3.
[b]Placed on an absolute basis using $k(Cl + ClONO_2) = 1.0 \times 10^{-11}$ cm^3 molecule^{-1} s^{-1} (Atkinson et al., 2007).
[c]Placed on an absolute basis using $k(Cl + C_2H_4) = 1.04 \times 10^{-10}$ cm^3 molecule^{-1} s^{-1} (Atkinson et al., 2006).
[d]Placed on an absolute basis using $k(Cl + cyclo\text{-}C_5H_{10}) = 2.9 \times 10^{-10}$ cm^3 molecule^{-1} s^{-1} (Calvert et al., 2008).
[e]Placed on an absolute basis using $k(Cl + C_3H_6) = 2.3 \times 10^{-10}$ cm^3 molecule^{-1} s^{-1} (IUPAC, 2008).
[f]Placed on an absolute basis using $k(Cl + C_3H_8) = 1.4 \times 10^{-10}$ cm^3 molecule^{-1} s^{-1} (Calvert et al., 2008).

leads to $k = 1.8 \times 10^{-10}$ cm^3 molecule^{-1} s^{-1} at 298 K, with an estimated uncertainty of ±20%.

V-F-3.3. O(^{3}P) + Cyclohexanone Reaction Kinetics

The review of Herron (1988) provides a value of $k = 5.0 \times 10^{-12}\exp(-2,300/T)$ cm^3 molecule^{-1} s^{-1} ($300 < T < 600$ K) for the rate coefficient for reaction of O(^{3}P) with cyclohexanone.

V-F-3.4. Summary of the Mechanism and End Products of Cyclohexanone Oxidation, and Summary of Its Atmospheric Fate

The atmospheric lifetime of cyclohexanone for OH attack is estimated to be about 1.8 days using the OH rate coefficient determination of Dagaut et al. (1988a) and assuming tropospheric [OH] = 10^6 molecule cm^{-3}. There are insufficient data to estimate quantitatively the lifetime for photodissociation of cyclohexanone (see section IX-E-5), but it is anticipated that the rate of photolysis will be competitive with that of OH-attack.

End products of the atmospheric oxidation of cyclohexanone have not been studied, although Martinez et al. (2004) showed that the reaction with Cl-atoms with cyclohexanone occurred predominantly (if not exclusively) via H-atom abstraction.

V-F-4. Cyclohexenone and Its Derivatives

V-F-4.1. Kinetics of the OH + Cyclohexenone Derivatives Reactions

McQuaid et al. (2002) have studied the rate coefficient for reaction of OH with two methyl-substituted cyclohexenones, 3-methyl-2-cyclohexen-1-one and 3,5,5-trimethyl-2-cyclohexen-1-one, using a relative rate method. Their data give $k = 3.1 \times 10^{-11}$ cm^3 molecule^{-1} s^{-1} for 3-methyl-2-cyclohexen-1-one and $k = 2.4 \times 10^{-11}$ cm^3 molecule^{-1} s^{-1} for 3,5,5-trimethyl-2-cyclohexen-1-one at 298 K; these data are summarized in table V-F-4. In the absence of corroborative data, an uncertainty of ±30% is assigned to these data.

Table V-F-4. Rate coefficients (k, cm^3 molecule^{-1} s^{-1}) for reaction of OH or O_3 with 2-cyclohexen-1-one and its methyl derivatives

$10^{12} \times k$	T (K)	Technique[a]	Reference
O_3 + 2-Cyclohexen-1-one			
$(1.22 \pm 0.26) \times 10^{-6}$	296	CL	Atkinson et al. (1981)
$< 2 \times 10^{-6}$	296	RR[b] (propene)	Greene and Atkinson (1994)
OH + 3-methyl-2-cyclohexen-1-one			
31 ± 10	298	RR[c] (*cyclo*-C_6H_{10})	McQuaid et al. (2002)
OH + 3,3,5-Trimethyl-2-cyclohexen-1-one			
24 ± 7	298	RR[c] (*cyclo*-C_6H_{10})	McQuaid et al. (2002)

[a]Abbreviations used for the techniques are defined in table I-F-3.
[b]Placed on an absolute basis using $k(O_3 + C_3H_6) = 1.0 \times 10^{-17}$ cm^3 molecule^{-1} s^{-1} (Calvert et al., 2000).
[c]Placed on an absolute basis using $k(OH + cyclo\text{-}C_6H_{10}) = 6.77 \times 10^{-11}$ cm^3 molecule^{-1} s^{-1} (Calvert et al., 2000).

V-F-4.2. Kinetics of O_3+ Cyclohexenone Derivatives Reactions

Atkinson et al. (1981) determined $k = 1.2 \times 10^{-18}$ cm^3 molecule^{-1} s^{-1} for reaction of ozone with 2-cyclohexen-1-one at 296 K. Greene and Atkinson (1994) report an upper limit for this same rate coefficient, $k < 2 \times 10^{-18}$ cm^3 molecule^{-1} s^{-1} at 296 K. The data are summarized in table V-F-4.

V-F-4.3. Summary of the Mechanism and End Products of Atmospheric Oxidation of Cyclohexenone and Derivatives and Their Atmospheric Fate

On the basis of the data of McQuaid et al. (2002), the lifetimes of these cyclohexenone species will be quite short, about 3–4 h for daytime [OH] = 2.5 $\times$ 10^6 molecule cm^{-3}. There are insufficient data to estimate the lifetime for photodissociation of these compounds.

V-F-5. 1,4-Naphthoquinone

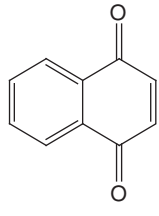

V-F-5.1. OH + 1,4-Naphthoquinone Reaction Kinetics

The reaction of OH with 1,4-naphthoquinone (a by-product of 1-nitronaphthalene photolysis) has been determined by Atkinson et al. (1989b), using the relative rate method. Using an updated value for the reference reaction, they find $k = 2.9 \times 10^{-12}$ cm^3 molecule^{-1} s^{-1}. The study is summarized in table V-F-5.

Table V-F-5. Rate coefficients (k, cm^3 molecule^{-1} s^{-1}) for reaction of OH, O_3, and NO_3 with 1,4-naphthoquinone

$10^{12} \times k$	T (K)	Technique[a]	Reference
OH + 1,4-Naphthoquinone			
2.9 ± 1.1	298	RR[b] (*cyclo*-C_6H_{12})	Atkinson et al. (1989b)
O_3 + 1,4-Naphthoquinone			
$< 2 \times 10^{-7}$	298	GC–FID	Atkinson et al. (1989b)
NO_3 + 1,4-Naphthoquinone			
$< 1 \times 10^{-3}$	298	RR[c] (propene)	Atkinson et al. (1989b)

[a]Abbreviations used for the techniques are defined in table I-F-3.
[b]Placed on an absolute basis using k(OH + *cyclo*-C_6H_{12}) = 7.0 $\times$ 10^{-12} cm^3 molecule^{-1} s^{-1} (Calvert et al., 2008).
[b]Placed on an absolute basis using k(NO_3 + propene) = 9.5 $\times$ 10^{-15} cm^3 molecule^{-1} s^{-1} (Atkinson et al., 2006).

V-F-5.2. O_3+ 1,4-Naphthoquinone Reaction Kinetics

Atkinson et al. (1989b) find an upper limit for this reaction of $k < 2 \times 10^{-19}$ cm^3 molecule^{-1} s^{-1} near 298 K; see table V-F-5.

V-F-5.3. NO_3+ 1,4-Naphthoquinone Reaction Kinetics

An upper limit for reaction of NO_3 with 1,4-naphthoquinone, $k = 1.0 \times 10^{-15}$ cm^3 molecule^{-1} s^{-1}, was determined by Atkinson et al. (1989b), using a relative rate method. The study is summarized in table V-F-5.

V-F-5.4. Summary of the Atmospheric Fate of 1,4-Naphthoquinone, and the End Products of Its Oxidation

Atkinson et al. (1989b) concluded that photolysis will be the dominant atmospheric loss process for this species (lifetime about 2 h), while the reaction with OH will occur at about one-tenth of this rate.

V-G. Ketones Derived from Biogenic Hydrocarbons

V-G-1. Introduction

A number of ketones are formed in the oxidation of biogenic compounds, and especially those terpenes with an exocyclic double bond, as illustrated by the formation of nopinone from β-pinene following reaction with OH:

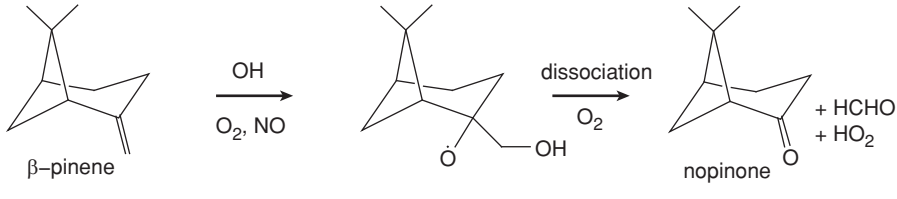

According to the SARs of Kwok and Atkinson (1995), over 80% of the OH addition occurs in the position shown, and the oxy radical reacts rapidly and exclusively by dissociation, so that, under high NO_x conditions, nopinone is the major product of reaction of OH with β-pinene. For example, in a MCMv3.1 simulation of a chamber experiment on the OH-initiated oxidation of β-pinene, Pinho et al. (2007) simulated a 70% yield of nopinone. Experimental determinations of the yield of nopinone in chamber studies using OH initiation have been reviewed by Atkinson and Aschmann (1993); the observed yields are in the range 25–80%, but with a preponderance of measured yields around 25–30%.

Other ketones considered in this section are sabinaketone from sabinene, camphenilone from camphene, and 4-methylcyclohex-3-en-1-one from terpinolene. In addition we will discuss the reactions of camphor, which is emitted directly into the atmosphere from certain trees and grasslands, carvone, a component of, for example, spearmint oil, and a number of fragrance compounds.

V-G-2. Nopinone [6,6-Dimethylbicyclo[3.1.1]heptan-2-one]

As discussed in the introduction to this section, nopinone is an important first-generation intermediate formed on reaction of OH with β-pinene. It is also a first-generation intermediate in the reaction of O_3 with β-pinene (Atkinson and Aschmann, 2003).

V-G-2.1. Reaction Kinetics of Nopinone Atmospheric Reactions

The reaction of OH with nopinone has been studied by Atkinson and Aschmann (1993) and Calogirou et al. (1999) by relative rate techniques (table V-G-1). The rate coefficients agree well and give a mean value of 1.52×10^{-11} cm^3 molecule^{-1} s^{-1}, with an uncertainty of $\pm 20\%$.

Calogirou et al. placed upper limits on the rate coefficients for reaction of nopinone with NO_3 and O_3 of $< 2 \times 10^{-15}$ cm^3 molecule^{-1} s^{-1} and $< 5 \times 10^{-21}$ cm^3 molecule^{-1} s^{-1}, respectively.

V-G-2.2. Summary of the Atmospheric Fate of Nopinone and the End Products of Its Oxidation

For [OH] $= 2.5 \times 10^6$ molecule cm^{-3}, the lifetime of nopinone with respect to reaction with OH is about 7 h. Reactions with NO_3 and O_3 are not atmospherically significant. The lifetime for photodissociation of nopinone is estimated to be about 4 days for an overhead Sun within the lower troposphere; see section IX-F-13. Calogirou et al. identified acetone and a number of multi-functional (hydroxyl and carbonyl) bicyclic products of the oxidation of nopinone. They also made a tentative assignment of methylglyoxal. No yields were determined. Some information can be gained from measurements on β-pinene, but they are difficult to interpret without detailed modeling, because nopinone reacts more slowly than β-pinene, so that there is a substantial time lag between the loss of β-pinene and formation of second- and third-generation intermediates from nopinone. Some of these later-generation intermediates are even longer-lived than nopinone. Application of the master chemical mechanism (MCM v3.1) based on the Kwok and Atkinson SARs, leads to a significant yield of acetone, which is not supported by experiment, where the yields are $\sim$10% (Atkinson and Aschmann); this may possibly be a result of the long timescales involved compared with those used in the experiments.

There has been some discussion of modifying the suggested reaction mechanisms that lead to nopinone from β-pinene. For example, Davis et al. (2005b) monitored OH

Table V-G-1. Rate coefficients (k, cm^3 molecule^{-1} s^{-1}) for reaction of OH with nopinone

$10^{11} \times k$	T (K)	Technique[a]	Reference
1.34 ± 0.35	296	RR[b] (cyclohexane)	Atkinson and Aschmann (1993)
1.7 ± 0.2	298	RR[c] (isobutene)	Calogirou et al. (1999)

[a]Abbreviations used for the techniques are defined in table I-F-3.
[b]Placed on an absolute basis using k(OH + cyclohexane) $= 6.97 \times 10^{-12}$ cm^3 molecule^{-1} s^{-1} (Calvert et al., 2008).
[c]Placed on an absolute basis using k(OH + isobutene) $= 5.2 \times 10^{-11}$ cm^3 molecule^{-1} s^{-1} (Calvert et al., 2000).

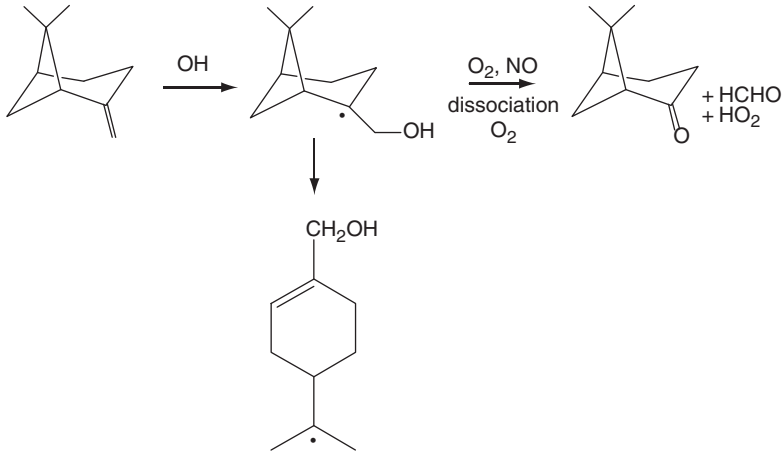

Figure V-G-1. Atmospheric reaction pathways proposed by Vereecken and Peeters (2004), showing the competition between isomerization and reaction with O_2 for the radical formed by terminal addition of OH to the exocyclic double bond in β-pinene. The mechanism significantly reduces the yield of nopinone from that predicted by the earlier mechanisms.

in a discharge flow study of OH + β-pinene, and found evidence of OH regeneration on addition of NO and O_2. Simulations with the MCM reproduced the OH profile better if the alkoxy radicals that only dissociate in the MCM to form nopinone, also underwent a competitive 1,5 H shift isomerization, thus decreasing the yield of nopinone in favour of formation of dihydroxypinanones. Wisthaler et al. (2001) used a proton-transfer-reaction mass spectrometer to study acetone and nopinone formation on a 1 h timescale in the OH-initiated oxidation of β-pinene. They found evidence for formation of acetone as a first generation product and suggested that it is produced by isomerization of the radical formed by the initial addition of OH in the terminal position on the exocyclic double bond to form a single ring radical (figure V-G-1) that reacts with O_2 and NO to form acetone and a substituted cyclohexenyl radical. Vereecken and Peeters (2004) examined the competition between reaction with O_2 and isomerization of the initially formed radical, using theoretical methods, and concluded that as much as 70% of reaction went via isomerization, significantly reducing the yield of nopinone, a result in better agreement with experiment.

Lewis et al. (2005) have carried out a computational study of OH + nopinone, and may provide an alternative explanation of the low acetone yield. The Kwok and Atkinson SAR predicts ~50% abstraction at the 4-position because of the activation of the position β to the carbonyl group.

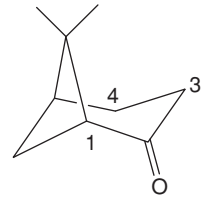

The calculations, on the other hand, show higher channel yields at the 3- (44%) and 1- positions (23%) than at the 4-position (13%). This was ascribed to the influence of hydrogen bonding in the transition state, which leads to a lower transition state energy even at the bridgehead where the C—H bond energy is large. The calculations were performed using density functional theory, and it might be argued that the level of theory is not sufficiently high to give accurate results. The authors were careful to calibrate the functional they used against higher level *ab initio* theory, and they argued that the approach should provide reasonable estimates of the *differences* in the transition state energies for the different abstraction positions. The overall rate coefficient they calculated was 6.9×10^{-12} cm^3 molecule^{-1} s^{-1}, compared with the experimental value of 1.5×10^{-11} cm^3 molecule^{-1} s^{-1}. Pinho et al. (2007) examined the effects of these changes in channel yields on ozone formation in chamber simulations. They found that the simulations were not very sensitive to such changes.

V-G-3. Sabinaketone
[5-(1-Methylethyl)-bicyclo[3.1.0]hexan-2-one]

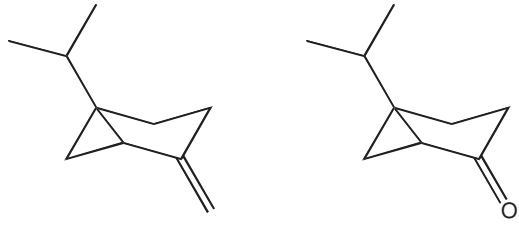

Sabinene Sabinaketone

Sabinene is emitted by a number of tree species, and experiments have demonstrated that sabinaketone is a significant product of its oxidation, initiated by reaction with both OH and O_3.

V-G-3.1. Reaction Kinetics

The reaction of OH with sabinaketone has been studied by Atkinson and Aschmann (1993) and Carrasco et al. (2007b) by relative rate techniques (table V-G-2). The former value is about 30% lower than the latter, a difference ascribed by Carrasco et al. to the generation of sabinaketone from O_3+ sabinene in the work of Atkinson and Aschmann, compared with pre-synthesis in their own work. An unweighted mean gives a rate coefficient of 6.0×10^{-12} cm^3 molecule^{-1} s^{-1}, with an uncertainty of $\pm$30%.

Alvarado et al. (1998) measured the rate coefficient for NO_3+ sabinaketone, relative to methacrolein ($k = 3.4 \times 10^{-15}$ cm^3 molecule^{-1} s^{-1}, section IV-E-4.3) obtaining a value of 3.7×10^{-16} cm^3 molecule^{-1} s^{-1}, with an estimated uncertainty of $\pm$40%.

Table V-G-2. Rate coefficients (k, cm^3 $molecule^{-1}$ s^{-1}) for reaction of OH with sabinaketone

$10^{12} \times k$	T (K)	Technique[a]	Reference
5.0 ± 1.4	296	RR[b] (cyclohexane)	Atkinson and Aschmann (1993)
7.0 ± 0.2	295	RR[c] (isoprene)	Carrasco et al. (2007b)

[a]Abbreviations used for the techniques are defined in table I-F-3.
[b]Placed on an absolute basis using $k(OH + cyclohexane) = 6.97 \times 10^{-12}$ cm^3 $molecule^{-1}$ s^{-1} (Calvert et al., 2008).
[c]Placed on an absolute basis using $k(OH + isoprene) = 1.0 \times 10^{-10}$ cm^3 $molecule^{-1}$ s^{-1} (Atkinson et al., 2006).

V-G-3.2. Summary of the Atmospheric Fate of Sabinaketone and the End Products of Its Oxidation

For [OH] = 1.0×10^6 molecule cm^{-3}, the lifetime of sabinaketone with respect to reaction with OH is about 2 days. The lifetime with respect to removal by NO_3, with [NO_3] = 3×10^9 molecule cm^{-3}, is about 10 days. There are insufficient data to estimate meaningful lifetimes for photodissociation of sabinaketone at this writing.

Carrasco et al. (2007b) determined the yields of formaldehyde and acetone in the OH-initiated oxidation of sabinaketone in the presence of O_2 and NO, obtaining molar yields of 1.19 ± 0.26 and 0.95 ± 0.24, respectively, on a 2 h timescale. Acetone was formed only as a primary (first generation) product, with formaldehyde as a first- and second-generation product. They proposed a mechanism involving initial abstraction from the carbon atom adjacent to the carbonyl group in the nonbridgehead position, followed by opening of the 6-membered ring in the resulting oxy radical. They also considered the SARs using both the approaches of Kwok and Atkinson (1995) and of Neeb (2000). The latter includes an activating effect for carbon atoms adjacent to the carbonyl group, which parallels that investigated by Lewis et al. (2003) and discussed above for nopinone; the former incorporates an attenuation factor for carbon atoms on the 3-membered ring. The combined SAR gives $k = 8.0 \times 10^{-12}$ cm^3 $molecule^{-1}$ s^{-1}, in good agreement with experiment. The modified SAR gives a high yield (~50%) for the channel discussed above involving abstraction from the nonbridgehead carbon adjacent to the carbonyl group.

V-G-4. Camphenilone [3,3-Dimethylbicyclo[2.2.1]heptan-2-one]

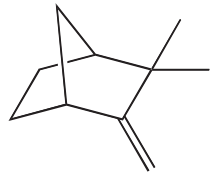

Camphene Camphenilone

Camphenilone is formed by the tropospheric oxidation of camphene, initiated by reaction with O_3. Since reaction with O_3 is a minor loss mechanism for camphene, the yields of camphenoline are low (Atkinson and Aschmann, 2003).

V-G-4.1. Reaction Kinetics of the Atmospheric Oxidation of Camphenilone

The reaction of OH with camphenilone has been studied by Atkinson and Aschmann (1993) relative to OH + cyclohexane ($k = 6.97 \times 10^{-12}$ cm^3 molecule^{-1} s^{-1}, Calvert et al., 2008). They obtained a value of 4.8×10^{-11} cm^3 molecule^{-1} s^{-1}; an uncertainty of $\pm 40\%$ is estimated since this is a single determination.

V-G-4.2. Summary of the Atmospheric Fate of Camphenilone and the End Products of Its Oxidation

For [OH] = 10^6 molecule cm^{-3}, the lifetime of camphenilone with respect to reaction with OH is about 2.5 days. Reactions with NO_3 and O_3 are not atmospherically significant. Photodecomposition may be a significant pathway for reaction in the sunlight irradiated troposphere. There have been no investigations of the products of its oxidation.

V-G-5. 4-Methylcyclohex-3-en-1-one

4-Methylcyclohex-3-en-1-one is formed by the tropospheric oxidation of terpinolene (Baker et al., 2004b).

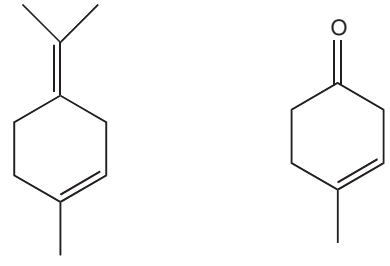

Terpinolene 4-Methylcyclohex-3-en-1-one

V-G-5.1. Reaction Kinetics of the Atmospheric Oxidation of 4-Methylcylohex-3-en-1-one

The reactions of OH, NO_3, and O_3 with methylcyclohex-3-en-1-one have been studied by Baker et al. (2004b) using relative rate techniques. The measurements were made relative to OH+2, 3-dimethyl-2-butene ($k = 1.10 \times 10^{-10}$ cm^3 molecule^{-1} s^{-1}, Calvert et al., 2000), NO_3 + α-pinene ($k = 6.2 \times 10^{-12}$ cm^3 molecule^{-1} s^{-1}, Atkinson et al., 2006) and O_3 + α-pinene (($k = 9.0 \times 10^{-17}$ cm^3 molecule^{-1} s^{-1}, Atkinson et al., 2006). They obtained:

$$k(\text{OH} + \text{methylcyclohex-3-en-1-one}) = 1.10 \times 10^{-10}\ \text{cm}^3\ \text{molecule}^{-1}\ \text{s}^{-1}$$

$$k(NO_3 + \text{methylcyclohex-3-en-1-one}) = 1.81 \times 10^{-12}\,\text{cm}^3\ \text{molecule}^{-1}\,\text{s}^{-1}$$

$$k(O_3 + \text{methylcyclohex-3-en-1-one}) = 7.4 \times 10^{-17}\,\text{cm}^3\ \text{molecule}^{-1}\,\text{s}^{-1}$$

Since these are all single determinations, uncertainties of ±40% are estimated.

V-G-5.2. Summary of the Atmospheric Fate of 4-Methylcyclohex-3-en-1-one and the End Products of Its Oxidation

For $[OH] = 2.5 \times 10^6$ molecule cm^{-3}, the lifetime of methylcyclohex-3-en-1-one with respect to reaction with OH is about 1 h, while those with respect to reaction with NO_3($[NO_3] = 3 \times 10^9$ molecule cm^{-3}) and O_3($[O_3] = 1.0 \times 10^{12}$ molecule cm^{-3}) are about 3 min. and 3.8 h, respectively. There have been investigations of neither the products of the oxidation of 4-methylcyclohex-3-en-1-one nor the photodecomposition lifetimes.

V-G-6. Camphor (1-Methyl-7,7-dimethylbicyclo[2.2.1]heptan-2-one)

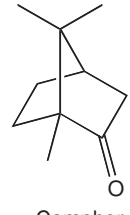

Camphor

Camphor is emitted directly into the atmosphere from a number of tree species (e.g., Black Sage, California Sagebrush, European Fir) and from grassland (Reissell et al. (2001).

V-G-6.1. Reaction Kinetics of the Atmospheric Oxidation of Camphor

The reactions of OH, NO_3, and O_3 with camphor have been studied by Reissell et al. (2001). Using the reference rate coefficients, $k(\text{OH} + \text{octane}) = 7.81 \times 10^{-12}\,\text{cm}^3$ $\text{molecule}^{-1}\,\text{s}^{-1}$ (Calvert et al., 2008) and $k(NO_3 + \text{methacrolein}) = 3.4 \times 10^{-15}\,\text{cm}^3$ $\text{molecule}^{-1}\,\text{s}^{-1}$ (section IV-E-4.3), they obtained:

$$k(\text{OH} + \text{camphor}) = 4.1 \times 10^{-12}\,\text{cm}^3\ \text{molecule}^{-1}\,\text{s}^{-1}$$

$$k(NO_3 + \text{camphor}) \leqslant 3 \times 10^{-16}\,\text{cm}^3\ \text{molecule}^{-1}\,\text{s}^{-1}$$

where uncertainties of ±40% are estimated since these are single determinations. They also obtained an upper limit for the reaction with ozone by measuring directly the rate of loss of camphor by mass spectrometry:

$$k(O_3 + \text{camphor}) \leq 7 \times 10^{-20}\,\text{cm}^3\ \text{molecule}^{-1}\,\text{s}^{-1}$$

V-G-6.2. Summary of the Atmospheric Fate of Camphor and the End Products of Its Oxidation

For [OH] = 10^6 molecule cm^{-3}, the lifetime of camphor with respect to reaction with OH is about 2.5 days. Reactions with NO_3 and O_3 are not atmospherically significant. Photodecomposition within the troposphere is probably significant, but no experimental data are available to define the photochemical processes.

Reissell et al. (2001) measured a first generation yield of 29 ± 4% of acetone in the OH-initiated oxidation of camphor in the presence of NO and air. They ascribed its formation to a mechanism involving abstraction at the tertiary bridgehead carbon, followed by ring-opening of the resulting oxy radical:

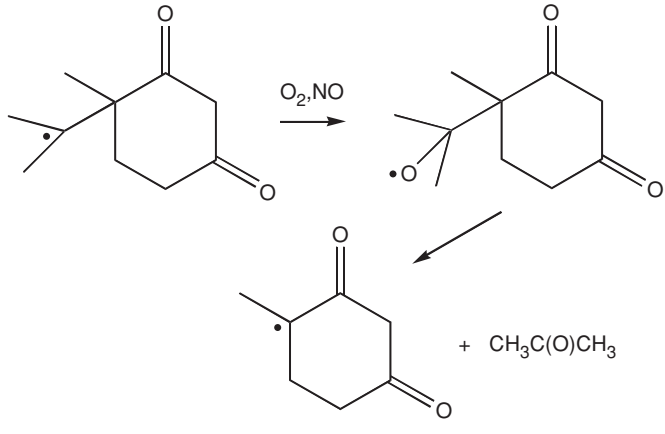

They also detected C_{10}-dicarbonyl and hydroxydicarbonyl compounds, a C_{10}-carbonyl nitrate, and a C_{10}-hydroxycarbonylnitrate. They suggested that these might arise from abstraction at the 6-position (γ to the carbonyl group) followed by a sequence of reactions involving competitive isomerization and reaction with O_2 by the oxy radicals.

V-G-7. Carvone
(2-Methyl-5(-1-methylethenyl)-2-cyclohexen-1-one)

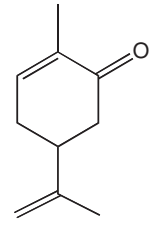

Carvone is an oxygenated monoterpenoid found in spearmint oil, caraway and dill seed oils, mandarin peel, and gingergrass oil (Craveiro et al., 1981). It exists as a

number of enantiomers. Its kinetics have not been studied, but the mechanism of its reaction with O_3 has been investigated by Nunes et al. (2005), in the dark and in the presence of an OH scavenger (cyclohexane). The reactions were unaffected by the configuration of the asymmetric center, and ozonolysis occurred primarily at the terminal double bond, forming CH_2O. Some reaction at the internal double bond occurred, leading to cyclohexanone formation, indicating production of OH; however, the radical yield was low.

V-G-8. Fragrance compounds

Fragrance compounds are widely used, especially in the indoor environment, for air freshening purposes. Many of the compounds used are not biogenic in origin, but are included here because of their structural similarities to naturally occurring compounds.

V-G-8.1. Reaction Kinetics of the Atmospheric Oxidation of β-Ionone [4-(2,6,6-Trimethyl-1-cyclohexen-1-yl)-3-buten-2-one]

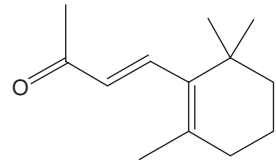

Forester et al. (2007) studied the kinetics of the reactions of OH and O_3 with β-ionone using relative rate methods. For OH they used limonene ($k = 1.7 \times 10^{-10}$ cm^3 molecule^{-1} s^{-1}, Calvert et al., 2000) and 3-carene ($k = 8.8 \times 10^{-11}$ cm^3 molecule^{-1} s^{-1}, Calvert et al., 2000) as reference compounds to obtain two estimates of the rate coefficients: $k(\text{OH} + \beta\text{-ionone}) = (1.18 \pm 0.02) \times 10^{-10}$ cm^3 molecule^{-1} s^{-1} and $(1.23 \pm 0.02) \times 10^{-10}$ cm^3 molecule^{-1} s^{-1}, respectively, at 297 ± 3 K; the uncertainties are statistical and do not include the uncertainties in the rate coefficients for the reference compounds. An unweighted mean gives $k = 1.21 \times 10^{-10}$ cm^3 molecule^{-1} s^{-1}, with an uncertainty of ±30%. They identified glyoxal and methyl glyoxal as products in the presence of NO_x and air at atmospheric pressure. Using derivatization coupled with mass spectrometry, they observed a product that they proposed was 2,6,6-trimethylcyclohex-1-ene-carbaldehyde. They proposed a mechanism involving addition of OH to the external double bond, that leads to additional products resulting from cyclization of the radical adduct. The atmospheric lifetime of β-ionone with respect to reaction with OH for [OH] $= 2.5 \times 10^6$ molecule cm^{-3} is about 1 h.

For determination of the rate coefficient with O_3, they used the reference compounds limonene ($k = 2.0 \times 10^{-16}$ cm^3 molecule^{-1} s^{-1}, Calvert et al., 2000), 3-carene

($k = 3.7 \times 10^{-17}$ cm^3 molecule^{-1} s^{-1}, Calvert et al., 2000), and α-pinene ($k = 9.0 \times 10^{-17}$ cm^3 molecule^{-1} s^{-1}, IUPAC, 2008); they obtained rate coefficients for O_3 + β-ionone at 297 ± 3 K of (2.51 ± 0.08) × 10^{-17} cm^3 molecule^{-1} s^{-1}, (1.82 ± 0.04) × 10^{-17} cm^3 molecule^{-1} s^{-1}, and (2.21 ± 0.06) × 10^{-17} cm^3 molecule^{-1} s^{-1}, respectively; the uncertainties are statistical and do not include the uncertainties in the rate coefficients for the reference compounds. An unweighted mean gives $k(O_3 + \beta\text{-ionone}) = 2.18 \times 10^{-17}$ cm^3 molecule^{-1} s^{-1} with an estimated uncertainty of ±30%. The main product observed was methyl glyoxal, and they also proposed 2,6,6-trimethylcyclohex-1-ene-carbaldehyde as a product on the basis of derivatization and mass spectrometry. Both species can be rationalized as co-products of Criegee biradicals in the dissociation of the ozonide formed from addition across the external double bond. The atmospheric lifetime of β-ionone with respect to reaction with O_3 for $[O_3] = 1.5 \times 10^{12}$ molecule cm^{-3} is about 8 h.

V-G-8.2. Reaction Kinetics of the Atmospheric Oxidation of 1-(1,2,3,4,5,6,7,8-Octahydro-2,3,8,8-tetramethyl-2-naphthalenyl)ethanone (OTNE)

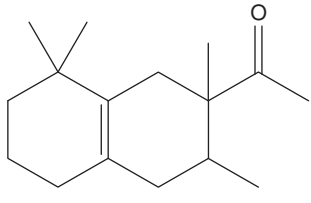

Aschmann et al. (2001a) measured the rate coefficients for reaction of OTNE with OH, O_3, and NO_3 using relative rate techniques. For OH, they used 2,3-dimethyl-2-butene ($k = 1.1 \times 10^{-10}$ cm^3 molecule^{-1} s^{-1}, Calvert et al., 2000) as the reference compound, obtaining $k(OH + OTNE) = 9.9 \times 10^{-11}$ cm^3 molecule^{-1} s^{-1} at 296 ± 2 K; the rate coefficient estimated using the Kwok and Atkinson (1995) SAR is 12.9 × 10^{-11} cm^3 molecule^{-1} s^{-1}. For O_3, they used propene as the reference compound ($k = 1.0 \times 10^{-17}$ cm^3 molecule^{-1} s^{-1}, Atkinson et al., 2006), and obtained $k(O_3 + OTNE) = 2.1 \times 10^{-18}$ cm^3 molecule^{-1} s^{-1} at 296 ± 2 K. For NO_3, they used as the reference compound, 2-methyl-2-butene ($k = 9.37 \times 10^{-12}$ cm^3 molecule^{-1} s^{-1}, Calvert et al., 2000), and obtained $k(NO_3 + OTNE) = 1.71 \times 10^{-11}$ cm^3 molecule^{-1} s^{-1} at 296 ± 2 K. An uncertainty of ±40% is estimated for each of these rate coefficients, since each is a single determination.

The atmospheric lifetime of OTNE is determined primarily by reaction with OH during the day. For $[OH] = 2.5 \times 10^6$, the lifetime is about 1.1 h. At night, for $[NO_3] = 3 \times 10^9$ molecule cm^{-3}, the lifetime is about 20 s. There have been no studies of the products of its oxidation or the photodecomposition lifetimes.

V-G-8.3. Reaction Kinetics of the Atmospheric Oxidation of Acetyl Cedrene [(3R-(3a,3ab,7b,8aa))-1-(2,3,4,7,8,8a-hexahydro-3,6,8,8-tetramethyl-1H-3a,7-methanoazulen-5-yl)ethan-1-one].

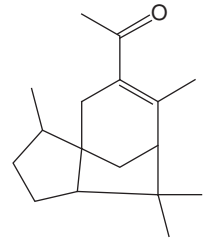

Aschmann et al. (2001a) measured the rate coefficients for reaction of acetyl cedrene with OH, O_3, and NO_3 using relative rate techniques. For the OH reaction, they used 2-methyl-2-butene ($k = 8.8 \times 10^{-11}$ cm^3 molecule^{-1} s^{-1}, Calvert et al., 2000) as the reference compound, obtaining k(OH + acetyl cedrene) $= 7.7 \times 10^{-11}$ cm^3 molecule^{-1} s^{-1} at 296 ± 2 K; the rate coefficient estimated using the Kwok and Atkinson (1995) SAR is 10.9×10^{-11} cm^3 molecule^{-1} s^{-1}. For the O_3 reaction, they used propene ($k = 1.0 \times 10^{-17}$ cm^3 molecule^{-1} s^{-1}, Atkinson et al., 2006) as the reference compound, obtaining: k(O_3-acetyl cedrene) $< 2.2 \times 10^{-18}$ cm^3 molecule^{-1} s^{-1} at 296 ± 2 K. For the NO_3 reaction they used 1-butene ($k = 1.40 \times 10^{-14}$ cm^3 molecule^{-1} s^{-1}, Calvert et al., 2000) as the reference compound, obtaining k(NO_3 + acetyl cedrene) $= 4.3 \times 10^{-15}$ cm^3 molecule^{-1} s^{-1} at 296 ± 2 K. An uncertainty of ±40% is estimated for each of these rate coefficients, since each is a single determination.

The atmospheric lifetime of acetyl cedrene is determined primarily by reaction with OH during the day. For [OH] $= 2.5 \times 10^6$, the lifetime is about 1.4 h. There have been no studies of the products of its oxidation or the photodissociation lifetimes.

V-H. Halogen-Substituted Ketones

V-H-1. 1-Fluoro-2-propanone [Fluoroacetone, $CH_2FC(O)CH_3$]

V-H-1.1. OH + 1-*Fluoro-2-propanone Reaction Kinetics*

The kinetics of the reaction of OH with CH_2FCOCH_3 have been studied by Carr et al. (2003) at 298 K. The rate coefficient reported by Carr et al. (2003) is given in table V-H-1 and is recommended with an uncertainty estimated to be ±25%. CH_2FCOCH_3 has approximately the same reactivity towards OH radicals as CH_3COCH_3.

V-H-1.2. Cl-Atom + 1-*Fluoro-2-propanone Reaction Kinetics*

The kinetics of the reaction of chlorine atoms with CH_2FCOCH_3 have been studied by Carr et al. (2003) at 298 K. The rate coefficient reported by Carr et al. (2003) is given in table V-H-2 and is recommended with an uncertainty estimated to be ±25%.

Table V-H-1. Rate coefficients (k, cm^3 molecule^{-1} s^{-1}) for reaction of OH radicals with halogen-atom-substituted ketones

Molecule	$10^{12} \times K$	T (K)	Technique[a]	Reference
CH_2FCOCH_3	0.215 ± 0.005	298	RR (CH_2ClCH_2Cl)[b]	Carr et al. (2003)
CF_3COCH_3	0.0151 ± 0.0013	298	FP–RF	Wallington et al. (1988a)
	0.0070 ± 0.0011	298	RR (CH_3CN)[c]	Carr et al. (2003)
$CH_2ClCOCH_3$	0.438 ± 0.029	298	RR (CH_2ClCH_2Cl)[b]	Carr et al. (2003)
$CHCl_2COCH_3$	0.402 ± 0.027	298	RR (CH_2ClCH_2Cl)[b]	Carr et al. (2003)
CCl_3COCH_3	0.0154 ± 0.0015	298	RR (CH_3CN)[c]	Carr et al. (2003)

[a]Abbreviations used for the techniques are defined in table I-F-3.
[b]Placed on an absolute basis using $k(OH + CH_2ClCH_2Cl) = 2.43 \times 10^{-13}$ cm^3 molecule^{-1} s^{-1} (Calvert et al., 2008).
[c]Placed on an absolute basis using $k(OH + CH_3CN) = 2.2 \times 10^{-14}$ cm^3 molecule^{-1} s^{-1} (Atkinson et al., 2006).

Table V-H-2. Rate coefficients (k, cm^3 molecule^{-1} s^{-1}) for reaction of chlorine atoms with halogen-substituted ketones

Molecule	$10^{12} \times K$	T (K)	Technique[a]	Reference
CH_2FCOCH_3	0.832 ± 0.013	298	RR (CH_2ClCH_2Cl)[b]	Carr et al. (2003)
CF_3COCH_3	0.00924 ± 0.00044	298	RR ($CHCl_3$)[c]	Carr et al. (2003)
$CH_2ClCOCH_3$	1.91 ± 0.11	298	RR (CH_3COCH_3)[d]	Carr et al. (2003)
$CH_2ClCOCH_2Cl$	0.570 ± 0.050	295	RR (CH_4)[e]	Voicu et al. (2001)
	0.499 ± 0.038		RR (CH_3Cl)[f]	
	0.588 ± 0.070		RR (CH_3OCHO)[g]	
$CHCl_2COCH_3$	0.177 ± 0.014	298	RR (CH_2Cl_2)[h]	Carr et al. (2003)
CCl_3COCH_3	0.0198 ± 0.0022	298	RR ($CHCl_3$)[c]	Carr et al. (2003)

[a]Abbreviations used for the techniques are defined in table I-F-3.
[b]Placed on an absolute basis using $k(Cl + CH_2ClCH_2Cl) = 1.30 \times 10^{-12}$ cm^3 molecule^{-1} s^{-1} (Wallington et al., 1996b).
[c]Placed on an absolute basis using $k(Cl + CHCl_3) = 1.1 \times 10^{-13}$ cm^3 molecule^{-1} s^{-1} (Atkinson et al., 2008).
[d]Placed on an absolute basis using $k(Cl + CH_3COCH_3) = 2.1 \times 10^{-12}$ cm^3 molecule^{-1} s^{-1} (this book, section V-B-1.3).
[e]Placed on an absolute basis using $k(Cl + CH_4) = 1.0 \times 10^{-13}$ cm^3 molecule^{-1} s^{-1} (Atkinson et al., 2006).
[f]Placed on an absolute basis using $k(Cl + CH_3Cl) = 4.8 \times 10^{-13}$ cm^3 molecule^{-1} s^{-1} (Atkinson et al., 2008).
[g]Placed on an absolute basis using $k(Cl + CH_3OCHO) = 1.4 \times 10^{-12}$ cm^3 molecule^{-1} s^{-1} (this book, section VII-B-1).
[h]Placed on an absolute basis using $k(Cl + CH_2Cl_2) = 3.4 \times 10^{-13}$ cm^3 molecule^{-1} s^{-1} (Atkinson et al., 2008).

CH_2FCOCH_3 is a factor of approximately 2.5 less reactive than CH_3COCH_3 towards chlorine atoms.

V-H-1.3. Summary of the Atmospheric Fate of CH_2FCOCH_3

Combining $k(OH + CH_2FCOCH_3) = 2.15 \times 10^{-13}$ cm^3 molecule^{-1} s^{-1} (Carr et al., 2003) with [OH] $= 1 \times 10^6$ cm^{-3} provides an estimate of approximately 2 months for the atmospheric lifetime of CH_2FCOCH_3 with respect to reaction with OH radicals. As discussed in chapter IX, by analogy with CH_3COCH_3, CF_3COCH_3, and CF_3COCF_3 it is expected that CH_2FCOCH_3 will have a lifetime with respect to photolysis of the order of 2 months. Reaction with OH radicals and photolysis will be competing fates for CH_2FCOCH_3; both are expected to lead to the formation of HCOF and CO_2

as major products. HCOF will undergo hydrolysis to give HF and CO_2 (Wallington et al., 1994b).

V-H-2. 1,1,1-Trifluoroacetone [$CF_3C(O)CH_3$]

V-H-2.1. OH + $CF_3C(O)CH_3$ Reaction Kinetics

The kinetics of the reaction of OH with CF_3COCH_3 have been studied by Wallington et al. (1988a) using a flash photolysis-resonance fluorescence technique and Carr et al. (2003) using a relative rate technique. The rate coefficients reported by Wallington et al. (1988a) and Carr et al. (2003) are given in table V-H-1. The value of $k(OH + CF_3COCH_3)$ reported by Wallington et al. (1988a) is approximately a factor of 2 greater than that found by Carr et al. (2003). As noted by Carr et al. (2003), the study of relatively unreactive compounds such as CF_3COCH_3 using the flash photolysis–resonance fluorescence technique can be complicated by the presence of reactive impurities. The presence of reactive impurities in the sample of CF_3COCH_3 used by Wallington et al. (1988a) provides a possible explanation of the discrepancy. In the relative rate study by Carr et al. (2003), the oxidation of CF_3COCH_3 will lead to the formation of CF_3O radicals. CF_3O radicals are reactive and may consume additional CF_3COCH_3 or the reference compound. Preferential consumption of the reference compound (CH_3CN) by reaction with CF_3O radicals provides a possible explanation of the discrepancy. There being no obvious reason to prefer either study, we recommend an average from the two studies of $k(OH + CF_3COCH_3) = 1.11 \times 10^{-14}$ cm^3 molecule^{-1} s^{-1} at 298 K with an uncertainty of ±50%. CF_3COCH_3 is approximately a factor of 20 times less reactive than CH_3COCH_3 towards OH radicals. The presence of the fluorine substituent has a substantial deactivating impact on the molecule.

V-H-2.2. Cl + $CF_3C(O)CH_3$ Reaction Kinetics

The kinetics of the reaction of chlorine atoms with CF_3COCH_3 have been studied by Carr et al. (2003) at 298 K. The rate coefficient reported by Carr et al. (2003) is given in table V-H.2 and is recommended with an uncertainty estimated to be ±25%. CF_3COCH_3 is approximately 1/200th as reactive as CH_3COCH_3 towards chlorine atoms.

V-H-2.3. Summary of the Atmospheric Fate of CF_3COCH_3

Combining $k(OH + CF_3COCH_3) = 1.11 \times 10^{-14}$ cm^3 molecule^{-1} s^{-1} with [OH] = 1×10^6 provides an estimate of approximately 3 years for the atmospheric lifetime of CF_3COCH_3 with respect to reaction with OH radicals. As discussed in chapter IX, CF_3COCH_3 has a lifetime with respect to photolysis of approximately 2 months for a diurnal cycle (March to September). Photolysis is the main atmospheric loss mechanism for CF_3COCH_3 with a photodissociation lifetime of about 11 to 13 days with an overhead Sun; photodissociation leads to the formation of COF_2 and CO_2 as major products. COF_2 will undergo hydrolysis to give HF and CO_2 (Wallington et al., 1994b).

V-H-3. 1-Chloro-2-propanone [Chloroacetone, $CH_2ClC(O)CH_3$]

V-H-3.1. OH + $CH_2ClC(O)CH_3$ Reaction Kinetics

The kinetics of the reaction of OH with $CH_2ClCOCH_3$ have been studied by Carr et al. (2003) at 298 K. The rate coefficient reported by Carr et al. (2003) is given in table V-H-1 and is recommended with an uncertainty estimated to be ±25%. $CH_2ClCOCH_3$ is approximately twice as reactive as CH_3COCH_3 towards OH radicals.

V-H-3.2. Cl-Atom + $CH_2ClC(O)CH_3$ Reaction Kinetics

The kinetics of the reaction of chlorine atoms with $CH_2ClCOCH_3$ have been studied by Carr et al. (2003) at 298 K. The rate coefficient reported by Carr et al. (2003) is given in table V-H-2 and is recommended with an uncertainty estimated to be ±25%. With respect to chlorine atoms, the reactivities of $CH_2ClCOCH_3$ and CH_3COCH_3 are indistinguishable.

V-H-3.3. Summary of the Atmospheric Fate of $CH_2ClCOCH_3$

Combining $k(OH + CH_2ClCOCH_3) = 4.38 \times 10^{-13}$ cm^3 molecule^{-1} s^{-1} with [OH] = 10^6 cm^{-3} provides an estimate of approximately 1 month for the atmospheric lifetime of $CH_2ClCOCH_3$ with respect to reaction with OH radicals. As discussed in chapter IX, $CH_2ClCOCH_3$ has a lifetime with respect to photolysis of from 3 to 6 h with an overhead Sun. Photolysis is the main atmospheric loss mechanism for $CH_2ClCOCH_3$ and leads to the formation of HCOCl and CO_2 as major products. HCOCl will undergo hydrolysis to give HCl and CO_2 (Wallington et al., 1994b) and heterogeneous decomposition to give HCl and CO on a timescale of approximately 5–15 days.

V-H-4. 1,3-Dichloro-2-propanone [$CH_2ClC(O)CH_2Cl$]

V-H-4.1. Cl-Atom + $CH_2ClC(O)CH_2Cl$ Reaction Kinetics

The kinetics of the reaction of chlorine atoms with $CH_2ClCOCH_2Cl$ have been studied by Voicu et al. (2001) at 298 K. See table V-H-2. Taking an average of the three determinations by Voicu et al. (2001) gives our recommendation of $k(Cl + CH_2ClCOCH_2Cl) = 5.52 \times 10^{-13}$ cm^3 molecule^{-1} s^{-1} with an uncertainty estimated to be ±20%. With respect to chlorine atoms, $CH_2ClCOCH_2Cl$ has approximately one-fourth the reactivity of CH_3COCH_3.

V-H-4.2. Summary of the Atmospheric Fate of $CH_2ClC(O)CH_2Cl$

As discussed by Voicu et al. (2001), reaction with OH radicals is not expected to be a significant atmospheric fate of $CH_2ClC(O)CH_2Cl$. By analogy to $CH_2ClCOCH_3$ we would expect photolysis to be the main atmospheric loss mechanism for $CH_2ClC(O)CH_2Cl$ leading to the formation of HC(O)Cl and CO_2 as major products.

HC(O)Cl will undergo hydrolysis to give HCl and CO_2 and heterogeneous decomposition to give HCl and CO on a timescale of approximately 5–15 days (Wallington et al., 1994b).

V-H-5. 1,1-Dichloro-2-propanone [$CHCl_2C(O)CH_3$]

V-H-5.1. OH + $CHCl_2C(O)CH_3$ Reaction Kinetics

The kinetics of the reaction of OH with $CHCl_2COCH_3$ have been studied by Carr et al. (2003) at 298 K. The rate coefficient reported by Carr et al. (2003) is given in table V-H-1 and is recommended with an uncertainty estimated to be ±25%. $CHCl_2COCH_3$ is approximately twice as reactive as CH_3COCH_3 towards OH radicals.

V-H-5.2. Cl-Atom + $CHCl_2C(O)CH_3$ Reaction Kinetics

The kinetics of the reaction of chlorine atoms with $CHCl_2COCH_3$ have been studied by Carr et al. (2003) at 298 K. The rate coefficient reported by Carr et al. (2003) is given in table V-H-2 and is recommended with an uncertainty estimated to be ±25%. With respect to chlorine atoms, $CHCl_2COCH_3$ is approximately an order of magnitude less reactive than CH_3COCH_3.

V-H-5.3. Summary of the Atmospheric Fate of $CHCl_2COCH_3$

Combining $k(OH + CH_2ClCOCH_3) = 4.02 \times 10^{-13}\,cm^3$ molecule^{-1} s^{-1} with [OH] = 10^6 provides an estimate of approximately 1 month for the atmospheric lifetime of $CHCl_2COCH_3$ with respect to reaction with OH radicals. By analogy to $CH_2ClCOCH_3$ we would expect photolysis to be the main atmospheric loss mechanism for $CHCl_2COCH_3$, leading to the formation of $COCl_2$, CO, and CO_2 as major products. The atmospheric fate of $COCl_2$ is hydrolysis to give HCl and CO_2 on a timescale of approximately 5–15 days (Wallington et al., 1994b).

V-H-6. 1,1,1-Trichloro-2-propanone [$CCl_3C(O)CH_3$]

V-H-6.1. OH + $CCl_3C(O)CH_3$ Reaction Kinetics

The kinetics of the reaction of OH with $CCl_3C(O)CH_3$ have been studied by Carr et al. (2003) at 298 K. The rate coefficient reported by Carr et al. (2003) is given in table V-H-1 and is recommended with an uncertainty estimated to be ±25%. $CCl_3C(O)CH_3$ is approximately twice as reactive as $CH_3C(O)CH_3$ towards OH radicals.

V-H-6.2. Cl-Atom + $CCl_3C(O)CH_3$ Reaction Kinetics

The kinetics of the reaction of chlorine atoms with $CCl_3C(O)CH_3$ have been studied by Carr et al. (2003) at 298 K. The rate coefficient reported by Carr et al. (2003) is given in table V-H-2 and is recommended with an uncertainty estimated to be ±25%.

With respect to chlorine atoms, $CCl_3C(O)CH_3$ is approximately an order of magnitude less reactive than CH_3COCH_3.

V-H-6.3. Summary of the Atmospheric Fate of CCl_3COCH_3

Combining $k(OH + CCl_3COCH_3) = 1.54 \times 10^{-14}$ cm^3 molecule^{-1} s^{-1} with [OH] = 10^6 cm^{-3} provides an estimate of approximately 2 years for the atmospheric lifetime of CCl_3COCH_3 with respect to reaction with OH radicals. By analogy to $CH_2ClCOCH_3$ we would expect CCl_3COCH_3 to have a lifetime with respect to photolysis of considerably less than 1 month. Photolysis is probably the main atmospheric loss mechanism for CCl_3COCH_3 and leads to the formation of $COCl_2$, CO, and CO_2 as major products. The atmospheric fate of $COCl_2$ is hydrolysis to give HCl and CO_2 on a timescale of approximately 5–15 days (Wallington et al., 1994b).

VI

Rate Coefficients and Mechanisms for the Atmospheric Oxidation of the Organic Acids

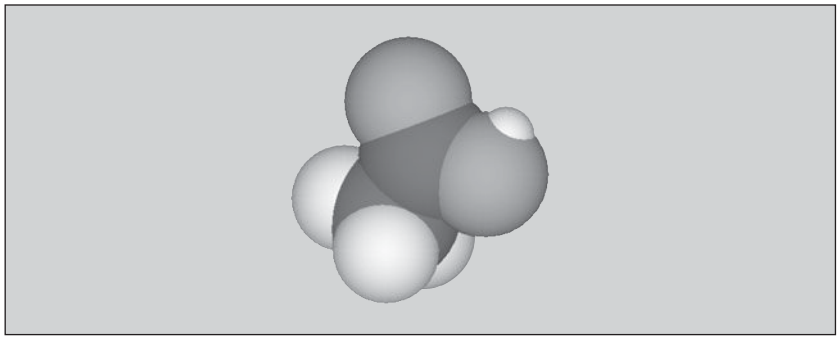

VI-A. Introduction

Organic acids, particularly formic and acetic acid, are ubiquitous components of the troposphere (Chebbi and Carlier, 1996); see table I-D-1. However, the atmospheric budget of these species is at present poorly constrained, and global models often underestimate their abundance (von Kuhlmann et al., 2003).

The presence of organic acids in the atmosphere can be attributed to two distinct mechanisms: direct emission from anthropogenic and natural sources; and in situ production via gas-phase or condensed-phase chemistry. Direct emissions result from biomass burning (e.g., Christian et al., 2007), from motor vehicle use (Kawamura et al., 2000) and other anthropogenic activities (see chapter I), and from biogenic sources (e.g., Seco et al., 2007). Production in the gas phase can occur via the reactions of acylperoxy radicals with HO_2:

$$CH_3C(O)O_2 + HO_2 \rightarrow CH_3C(O)OOH + O_2$$

$$CH_3C(O)O_2 + HO_2 \rightarrow CH_3C(O)O + OH + O_2$$

$$CH_3C(O)O_2 + HO_2 \rightarrow CH_3C(O)OH + O_3$$

or via the ozonolysis of unsaturated species (Orzechowska and Paulson, 2005a, b). Additional in situ acid production (particularly with multi-functional species

and diacids) likely occurs in the condensed phase as well, via the oxidation of carbonyl and other oxygen-containing and multi-functional organics (e.g., Ervens et al., 2004).

In general, the organic acid moiety, —C(O)OH, is rather unreactive in the gas phase. This is in large part due to the strength of the O—H bond, ~460 kJ mole^{-1} versus 400–420 kJ mole^{-1} for typical C—H bonds (Sander et al., 2006). The organic acid moiety also acts to inhibit somewhat the reactivity of neighboring sites (Kwok and Atkinson, 1995), further decreasing the reactivity of small saturated acids. UV spectra for unsubstituted acids are located at relatively short wavelengths, [e.g., $\lambda_{max} <$ 210 nm for acetic acid, Orlando and Tyndall (2003); see figure IX-A-1], so tropospheric photolysis is of negligible importance. Thus, the gas-phase lifetime for small saturated organic acids (e.g., formic and acetic acid) can be quite long, about 1 month. This gas-phase stability, coupled with the high water solubilities for the acids, means that aerosol scavenging and depositional processes often play a key role in their removal from the troposphere.

Unsaturated organic acids (e.g., acrylic acid) represent an exception, however, as the presence of the C=C double bond in these molecules provides a site for reasonably rapid OH addition and thus shorter gas-phase lifetimes. Furthermore, limited data on the ketoacids [e.g., pyruvic acid, $CH_3C(O)C(O)OH$] suggested that these species undergo rapid photolysis; see section IX-F-9.

The available data for the reactions of the organic acids (acyclic species, dicarboxylic acids, unsaturated species, and other multifunctional species) with OH, O_3, NO_3 and Cl-atoms and the atmospheric lifetimes and fates of these species are summarized in this chapter. In general, reactions of saturated species with O_3 and NO_3 have not been studied, but are expected to be exceedingly slow and of no atmospheric significance.

VI-B. Acyclic Organic Acids

VI-B-1. Formic Acid (Methanoic Acid, HC(O)OH)

VI-B-1.1. OH Reaction Kinetics

The reaction of OH with formic acid has been the subject of five direct studies, two over a range of temperatures (Wine et al., 1985; Singleton et al., 1988) and three at ambient temperature only (Zetzsch and Stuhl, 1982; Jolly et al., 1986a; Dagaut et al., 1988b). Data are summarized in table VI-B-1 and figure VI-B-1. All investigators used flash or pulsed laser photolysis to generate OH, while either resonance absorption (Jolly et al., 1986a; Singleton et al., 1988) or resonance fluorescence (Zetzsch and Stuhl, 1982; Wine et al., 1985; Dagaut et al., 1988b) was used for OH detection. All investigators needed to account for the presence of formic acid dimer, either in the preparation of concentrated samples or in the actual reaction mixtures. Procedures used to account for the presence of the dimer appear to be consistent and appropriate throughout all studies. The dimer has been shown to be very unreactive toward OH (Jolly et al., 1986a; Singleton et al., 1988). Agreement between the studies of the rate coefficient

Table VI-B-1. Rate coefficients ($k = A \times e^{-B/T}$, cm^3 $molecule^{-1}$ s^{-1}) for reaction of OH with formic acid (methanoic acid, HC(O)OH)

$10^{13} \times A$	B(K)	$10^{13} \times k$	T(K)	Technique[a]	Reference	Temperature Range (K)
		3.2 ± 1.0	298	FP–RF	Zetzsch and Stuhl	
		3.5 ± 1.0			(1982)	
3.63 ± 0.86	−77 ± 75	4.61 ± 0.51	298	FP–RF	Wine et al. (1985)	298–430
or		4.05 ± 0.47	298			
4.62 ± 1.16	0	5.45 ± 0.12	298			
		4.48 ± 0.32	298			
		4.32 ± 0.65	298			
		4.46 ± 0.11	298			
		4.49 ± 0.26	298			
		4.28 ± 0.49	298			
		4.81 ± 0.59	298			
		4.82 ± 0.42	298			
		5.23 ± 0.30	299			
		4.66 ± 0.07	299			
		4.80 ± 0.75	299			
		4.64 ± 0.37	299			
		4.95 ± 0.81	299			
		4.90 ± 0.94	300			
		5.39 ± 0.76	300			
		4.46 ± 0.33	300			
		4.43 ± 0.53	300			
		4.95 ± 0.50	320			
		4.06 ± 0.24	337			
		4.33 ± 0.37	374			
		5.05 ± 0.02	378			
		4.79 ± 0.68	402			
		4.07 ± 0.34	428			
		4.09 ± 0.51	428			
		4.39 ± 0.72	430			
		4.34 ± 0.53	430			
		4.8 ± 1.0	296	PLP–RA	Jolly et al. (1986a)	
2.91 ± 1.59	−102 ± 194	4.47 ± 0.28	296.9	PLP–RA	Singleton et al.	297–445.2
or		3.65 ± 0.30	326.3		(1988)	
3.65 ± 0.33	0	3.69 ± 0.32	356.2			
		3.67 ± 0.12	396.2			
		3.90 ± 0.28	445.2			
		3.7 ± 0.4	298	FP–RF	Dagaut et al. (1988b)	

[a]Abbreviations used for the techniques are defined in table I-F-3.

for reaction of OH with formic acid is quite good, although the 298 K results of Zetzsch and Stuhl (1982) are about 20–30% below the average of the other data. Both Wine et al. (1985) and Singleton et al. (1988) reported weak, negative temperature dependencies to the data (298–445 K), but both groups also noted consistency with a temperature-independent rate coefficient. No pressure dependence to the rate coefficient has been observed (Zetzsch and Stuhl, 100–200 Torr; Wine et al., 50–300 Torr; Jolly et al.,

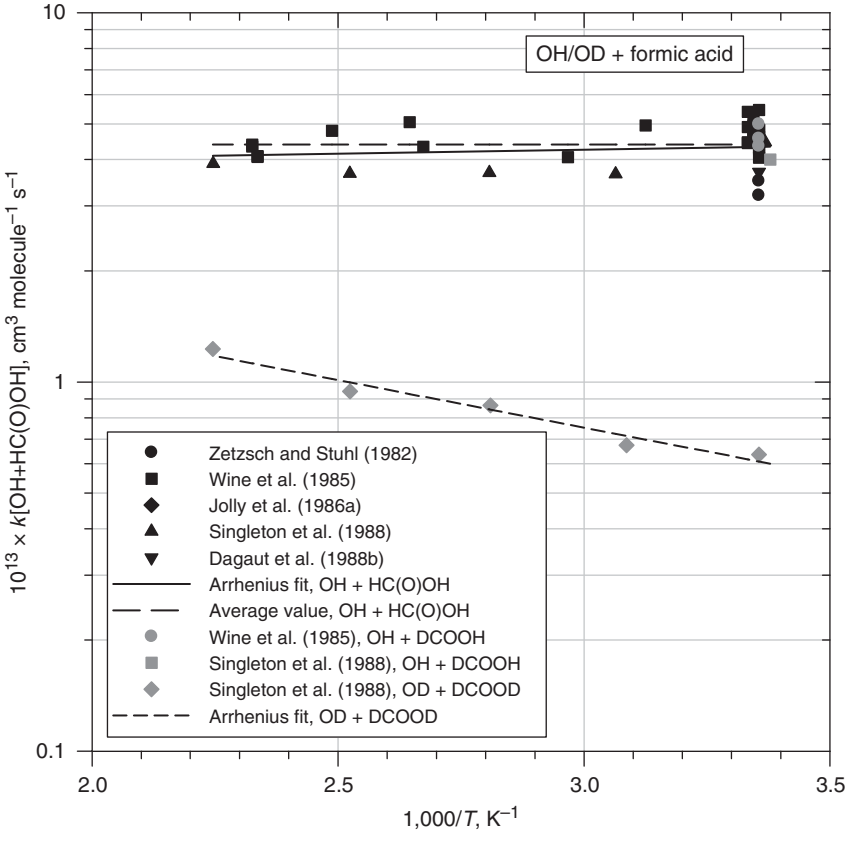

Figure VI-B-1. Arrhenius plot of the rate coefficient for the reaction of OH/OD with formic acid and its deuterated analogs.

0.5–500 Torr). A least-squares fit of all the data to the Arrhenius expression yields $k = 3.66 \times 10^{-13}$ exp $(50/T)$ cm^3 molecule^{-1} s^{-1}. Alternatively, an unweighted average of the data leads to a temperature-independent value of $k = 4.4 \times 10^{-13}$ cm^3 molecule^{-1} s^{-1} (298–445 K). Excluding the Zetzsch and Stuhl (1982) data from the fits leads to differences of $< 5\%$ in the retrieved rate coefficients. This recommendation is very similar to those made by the JPL (Sander et al., 2006) and IUPAC (Atkinson et al., 2006) evaluation panels, $k = 4.0 \times 10^{-13}$ cm^3 molecule^{-1} s^{-1} and $k = 4.5 \times 10^{-13}$ cm^3 molecule^{-1} s^{-1}, respectively, independent of temperature. Uncertainties in the data are estimated at $\pm 20\%$ over the temperature range that has been studied. No data are available below 298 K, i.e., under conditions relevant for the free troposphere; the JPL panel (Sander et al., 2006) recommends uncertainties of $\pm 30\%$ near 250 K and $\pm 40\%$ near 200 K.

Kinetic data for the reaction of OH with DCOOH (Wine et al., 1985; Singleton et al., 1988) and for the reaction of OD with HCOOD and DCOOD (Singleton et al., 1988) have also been reported; see table VI-B-2 and figure VI-B-1. Values for

Table VI-B-2. Rate coefficients ($k = A \times e^{-B/T}$, cm^3 $molecule^{-1}$ s^{-1}) for reaction of OH/OD with isotopic variants of formic acid (DC(O)OH and DC(O)OH)

$10^{13} \times A$	B(K)	$10^{13} \times k$	T(K)	Technique[a]	Reference	Temperature Range (K)
OH + DCOOH						
		4.35 ± 0.38	298	FP–RF	Wine et al. (1985)	298–430
		4.98 ± 0.99	298			
		4.56 ± 0.28	298			
		3.98 ± 0.33	296.0	PLP–RA	Singleton et al. (1988)	
OD + HCOOD						
		≤ 1.5	296	PLP–RA	Singleton et al. (1988)	
OD + DCOOD						
4.47 ± 1.63	594 ± 134	0.636 ± 0.13	298.0	PLP–RA	Singleton et al. (1988)	296–445.3
		0.674 ± 0.052	324.0			
		0.863 ± 0.038	355.9			
		0.943 ± 0.045	396.1			
		1.23 ± 0.055	445.3			

[a]Abbreviations used for the techniques are defined in table I-F-3.

k(OH + DCOOH) were indistinguishable from those for the OH + HCOOH reaction, while k(OD + HCOOD) and k(OD + DCOOD) are considerably smaller than k(OH + HCOOH). The reaction of OD with DCOOD possesses a significant positive temperature dependence. The mechanistic implications of these data are discussed in section VI-B-1.3.

VI-B-1.2. Cl-Atom Reaction Kinetics

The two studies of the Cl-formic acid reaction (Wallington et al., 1990a; Li et al., 2000a), both conducted at ambient temperature, are in excellent agreement; see table VI-B-3. An average of the two determinations yields a value of $k = 1.9 \times 10^{-13}$ cm^3 $molecule^{-1}$ s^{-1}, with an estimated uncertainty of ±15%. Tyndall et al. (1991b) provide evidence that reaction occurs via abstraction at the formyl (C—H) site, rather than at the acidic (O—H) site, in contrast to the OH–formic acid reaction.

VI-B-1.3. Summary of the Mechanism and End Products of Formic Acid Oxidation, and Summary of Its Atmospheric Fate

The only significant gas-phase loss process for formic acid in the troposphere will be via reaction with OH. Even so, the lifetime of formic acid against OH loss is quite long, about 1 month for an assumed global [OH] of 10^6 molecule cm^{-3}.

The kinetic data for deuterated formic acid [DC(O)OH, HC(O)OD, and DC(O)OD] presented here and the lower reactivity of formic acid dimer compared to the monomer, coupled with the theoretical study of Galano et al. (2002), provide strong evidence that

Table VI-B-3. Rate coefficients (k, cm^3 molecule^{-1} s^{-1}) for reaction of Cl-atoms with formic acid [HC(O)OH]

$10^{13} \times k$	T(K)	Technique[a]	Reference
2.00 ± 0.25[b]	295 ± 2	RR (CH_4, CH_3Cl)	Wallington et al. (1990a)
1.83 ± 0.12	ambient	FP–IR abs.	Li et al. (2000a)

[a]Abbreviations used for the techniques are defined in table I-F-3.
[b]Placed on an absolute basis using $k(Cl + CH_4) = 1.0 \times 10^{-13}$ cm^3 molecule^{-1} s^{-1}, $k(Cl + CH_3Cl) = 4.8 \times 10^{-13}$ cm^3 molecule^{-1} s^{-1} (Atkinson et al., 2006, 2008).

the major site of reaction is at the acidic hydrogen rather than the formyl hydrogen, despite the stronger O—H versus C—H bond:

$$OH + HC(O)OH \rightarrow HC(O)O + H_2O$$

Reaction at either site is thought to occur via the formation of a pre-reactive complex, with the "acidic" complex [HC(O)OH•••OH] more stable than the formyl one [HO•••HC(O)OH] (Galano et al., 2002). Tunneling is also thought to play a large role in enhancing the reactivity at the acidic site (Galano et al., 2002). The resultant HC(O)O radical is expected to decompose rapidly to H + CO_2, leading to the net production of H_2O, HO_2 and CO_2 in the OH + HCOOH reaction:

$$HC(O)O \rightarrow H + CO_2$$

$$H + O_2 + M \rightarrow HO_2 + M$$

Note that large yields of H-atoms were observed by Wine et al. (1985) and Jolly et al. (1986a) in their studies of the OH + HCOOH reaction, consistent with the above mechanism.

Given the long gas-phase lifetime for formic acid (1 month), it is clear that heterogeneous processes (wet and dry deposition) also must be considered as sinks for this species, particularly in the lower troposphere. An important parameter in determining the rate of wet deposition (uptake of a gas into a hydrometer, followed by removal via precipitation) is the solubility of the gas in aqueous solution, an equilibrium process described by the Henry's law constant, $H_X = [X]_{aq}/p_X$; see also section I-B-4. Here, H_X is the Henry's law constant for species X, $[X]_{aq}$ is its equilibrium concentration in the aqueous phase, and p_X is its partial pressure of the gas. For the organic acids under consideration here, increased solubility can result from ionization in solution, e.g.:

$$HC(O)OH_{(g)} \leftrightarrow HC(O)OH_{(aq)}$$

$$HC(O)OH_{(aq)} \leftrightarrow HC(O)O^- + H^+$$

and an effective Henry's law constant (H^*) is defined: $H^* = H \times (1 + K_a/[H^+])$, where K_a is the acid dissociation constant (see, for example, Brasseur et al., 1999).

Table VI-B-4. Henry's law coefficients $H(T) = H(298\text{K}) \times \exp(-B/T)$, in units of M atm^{-1}, and pK_a values for various saturated, unsaturated, and keto acids

Acid	$10^{-3} \times H$ at 298 K	B[K]	Reference for Henry's Law Data	pK_a^a
Formic	5.5 ± 0.3		Khan et al. (1995)	3.75
	8.9 ± 1.3	6,100	Johnson et al. (1996)	
Acetic	5.5 ± 0.3		Khan et al. (1995)	4.76
	4.1 ± 0.4	6,300	Johnson et al. (1996)	
Propanoic	5.7 ± 0.3		Khan et al. (1995)	4.86
Butanoic	4.7 ± 0.2		Khan et al. (1995)	4.83
2-Methylpropanoic	1.1 ± 0.1		Khan et al. (1995)	4.88
n-Pentanoic	2.2 ± 0.1	6,583	Khan et al. (1995)	4.84
n-Hexanoic	1.4 ± 0.1	6,304	Khan et al. (1995)	4.85
Acrylic				4.25
Methacrylic	2.6		Khan et al. (1992)	
Pyruvic	311	5,100	Khan et al. (1995)	2.39

[a]Data from http://www.zirchrom.com/organic.htm

Temperature-dependent Henry's law coefficients and pK_a values [p$K_a = -\log_{10}(K_a)$] for a series of organic acids are given in table VI-B-4. For soluble species such as formic acid, effective scavenging into a typical cloud (pH ≈ 5, 270 K, $H^* > 10^5$ M atm^{-1}) would occur, and thus removal via rainout would be anticipated on the timescale of about 1 week in the lower troposphere (Brasseur et al., 1999). The lifetime against heterogeneous loss will be extended in the upper troposphere, however, allowing for a larger contribution from OH reaction in this region.

VI-B-2. Acetic Acid (Ethanoic Acid, $CH_3C(O)OH$)

VI-B-2.1. OH Reaction Kinetics

There are studies of the reaction of OH with acetic acid that span the temperature range, 229–802 K (Zetzsch and Stuhl, 1982; Dagaut et al., 1988b; Singleton et al., 1989; Butkovskaya et al., 2004b; Vimal and Stevens, 2006; Khamaganov et al., 2006; Crunaire et al., 2006; Huang et al., 2009). Data are summarized in table VI-B-5 and figure VI-B-2. Although some scatter is evident, the data of Zetzsch and Stuhl (1982), Singleton et al. (1989), Butkovskaya et al. (2004b), Vimal and Stevens (2006), Khamaganov et al. (2006), Crunaire et al. (2006), and Huang et al. (2009) present a reasonably consistent picture: the rate coefficient decreases with increasing temperature over the range 230–450 K, then increases rapidly above 450 K. The data of Dagaut et al. (1988b) are not consistent with this picture, however, showing a positive temperature dependence between 298 and 440 K. For atmospheric purposes, the data of Zetzsch and Stuhl (1982), Butkovskaya et al. (2004b), Vimal and Stevens (2006), Crunaire et al. (2006), Huang et al. (2009), and those of Singleton et al. (1989) and Khamaganov et al. (2006) at $T < 400$ K are used to derive an Arrhenius expression: $k = 5.3 \times 10^{-14} \exp(767/T)$ cm^3 molecule^{-1} s^{-1}. This expression returns the 298 K value,

Table VI-B-5. Rate coefficients ($k = A \times e^{-B/T}$, cm^3 $molecule^{-1}$ s^{-1}) for reaction of OH with acetic acid [ethanoic acid, $CH_3C(O)OH$]

$10^{14} \times A$	B(K)	$10^{13} \times k$	T(K)	Technique[a]	Reference	Temperature Range (K)
		6.0 ± 0.8	298	FP–RF	Zetzsch and Stuhl	
		7.3 ± 1.0			(1982)	
130 ± 10	170 ± 20	(6.4 ± 0.9)[b]	240	FP–RF	Dagaut et al.	298–440
		7.4 ± 0.6	298		(1988b)	
		8.1 ± 0.9	350			
		8.7 ± 1.4	400			
		8.8 ± 0.8	440			
		8.67 ± 0.65	296.8	PLP–RA	Singleton et al.	296.8–446.2
		5.63 ± 0.43	326.2		(1989)	
		4.88 ± 0.17	356.4			
		4.08 ± 0.13	396.8			
		3.95 ± 0.07	446.2			
2.2 ± 0.2	−1,012 ± 80	18.3 ± 3.7	229	DF–CIMS	Butkovskaya et al.	229–300
		13.1 ± 2.5	247		(2004b)	
		13.6 ± 3.2	251			
		11.2 ± 2.1	253			
		8.9 ± 0.5	269			
		6.6 ± 0.3	300			
2.52 ± 1.22	−1,010 ± 150	9.09 ± 0.12	273	DF–RF	Vimal and	273–373
		7.42 ± 0.12	300		Stevens (2006)	
		4.92 ± 0.31	323			
		4.39 ± 0.28	353			
		4.10 ± 0.77	373			
		9.15 ± 0.11	287	PLP–LIF	Khamaganov	287–802
		8.49 ± 0.12	296		et al. (2006)	
		7.12 ± 0.20	322			
		6.34 ± 0.12	355			
		5.22 ± 0.11	399			
		4.98 ± 0.09	446			
		4.77 ± 0.12	456			
		4.47 ± 0.09	503			
		4.08 ± 0.11	550			
		4.97 ± 0.21	597			
		7.35 ± 0.73	653			
		9.06 ± 0.44	703			
		18.7 ± 0.60	802			
		6.5 ± 0.5	296	RR[c]	Crunaire et al.	
				(CH_3OH)	(2006)	
5.38 ± 0.28	−740 ± 51	9.69 ± 0.32	256	DF–LIF	Huang et al.	255–355
		8.57 ± 0.45	266		(2009)	
		7.79 ± 0.36	275			
		6.91 ± 0.13	286			
		6.77 ± 0.14	295			
		6.26 ± 0.51	307			
		5.86	315			
		5.27 ± 0.12	328			
		4.89 ± 0.09	338			
		4.44 ± 0.13	346			
		3.99 ± 0.14	357			

[a]Abbreviations used for the techniques are defined in table I-F-3.
[b]Value obtained assuming similar reactivity for monomer and dimer.
[c]Placed on an absolute basis using $k(OH + CH_3OH) = 9.0 \times 10^{-13}$ cm^3 $molecule^{-1}$ s^{-1} (Atkinson et al., 2006).

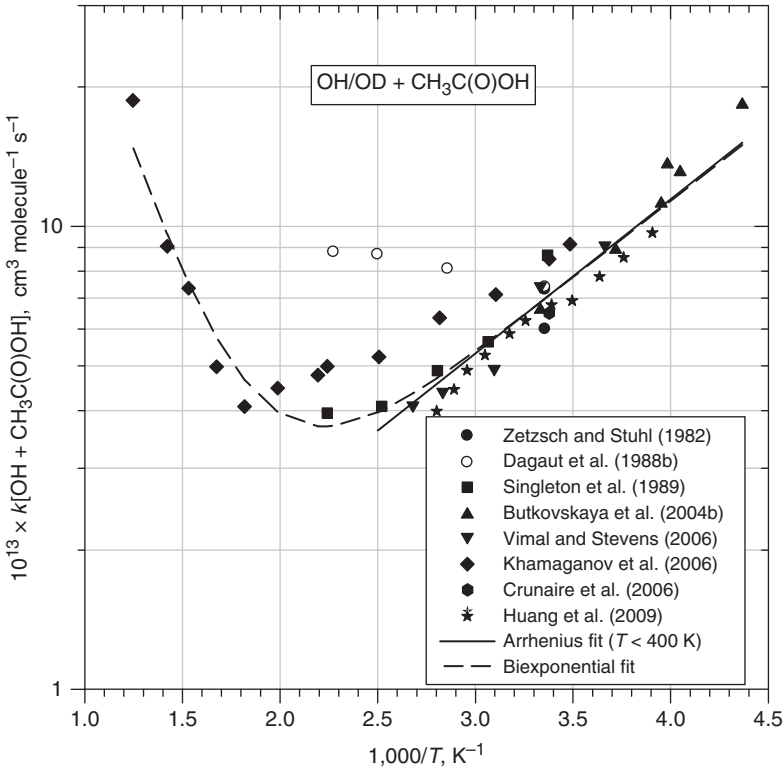

Figure VI-B-2. Arrhenius plot of the rate coefficient for the reaction of OH/OD with acetic acid.

$k = 7.0 \times 10^{-13}$ cm^3 molecule^{-1} s^{-1}. The uncertainty in the 298 K value is estimated to be ±20%. Fitting of a biexponential expression [as is done in Khamaganov et al. (2006)] to all the data except those of Dagaut et al. (1988b) yields the following expression: $k = 5.3 \times 10^{-11}\ \exp(-2,944/T) + 5.4 \times 10^{-14}\ \exp(760/T)$ cm^3 molecule^{-1} s^{-1}.

Kinetic studies of reaction of OH with deuterated variants of acetic acid, $CD_3C(O)OH$ and $CD_3C(O)OD$, have been conducted by Singleton et al. (1989) and Vimal and Stevens (2006), see table VI-B-6 and figure VI-B-3 for a summary. Rate coefficient data for $CD_3C(O)OH$ are essentially identical to those for $CH_3C(O)OH$, and are represented by the expression $k(OH + CD_3C(O)OH) = 5.8 \times 10^{-14}\exp(776/T)$ cm^3 molecule^{-1} s^{-1}. Rate coefficient data for the OH + $CD_3C(O)OD$ reaction, although not in particularly good agreement, are considerably smaller than those for the OH + $CH_3C(O)OH$ or OH + $CD_3C(O)OH$ reactions, pointing to the likelihood that the bulk of the reaction occurs at the acidic end of the molecule. This conclusion is consistent with the finding that the acetic acid dimer is considerably less reactive towards OH than is the monomer (Singleton et al., 1989), and with the product studies discussed further in section VI-B-2.3 (Butkovskaya et al., 2004b; De Smedt et al., 2005; Crunaire et al., 2006).

Table VI-B-6. Rate coefficients ($k = A \times e^{-B/T}$, cm^3 $molecule^{-1}$ s^{-1}) for reaction of OH with isotopic variants of acetic acid

$10^{16} \times A$	B(K)	$10^{13} \times k$	T(K)	Technique[a]	Reference	Temperature Range (K)
OH + $CD_3C(O)OH$						
		8.10 ± 0.37	297.8	PLP–RA	Singleton et al. (1989)	297.8–444.6
		6.48 ± 0.27	326.9			
		4.83 ± 0.15	356.7			
		4.47 ± 0.07	374.2			
		4.13 ± 0.13	396.8			
		3.54 ± 0.08	444.6			
		7.79 ± 0.16	300	DF–RF	Vimal and Stevens (2006)	
OH + $CD_3C(O)OD$						
		2.36 ± 0.17	297.8	PLP–RA	Singleton et al. (1989)	298–445.3
		1.39 ± 0.07	326.5			
		1.13 ± 0.09	357			
		1.07 ± 0.06	397			
		1.14 ± 0.06	444			
4.62 ± 1.33	−1,640 ± 160	2.34 ± 0.29	263	DF–RF	Vimal and Stevens (2006)	263–323
		1.90 ± 0.24	273			
		1.09 ± 0.18	300			
		0.70 ± 0.24	323			

[a]Abbreviations used for the techniques are defined in table I-F-3.

VI-B-2.2. Cl-Atom Reaction Kinetics

The reaction of Cl-atoms with acetic acid has been the subject of two studies at ambient temperatures (Koch and Moortgat, 1990; Crawford et al., 1999), both using the relative rate technique with methane as the reference. Data are in excellent agreement; see table VI-B-7. The average of the two measurements, $k = 2.7 \times 10^{-14}$ cm^3 $molecule^{-1}$ s^{-1}, is recommended with an estimated uncertainty of ±20%. Kinetic isotope studies (Koch and Moortgat, 1990) indicate that the reaction proceeds via abstraction from the CH_3 group, in line with expectations based on the energetics of the competing pathways.

VI-B-2.3. Mechanism and End Products of Gas-Phase Acetic Acid Oxidation, and Summary of Its Atmospheric Fate

Reaction with OH will be the only significant gas-phase loss process for acetic acid. For a global [OH] of 10^6 molecule cm^{-3}, a lifetime of about 2 weeks is determined for this process in the lower troposphere. The significant negative temperature dependence to the reaction for atmospherically relevant temperatures may imply a shorter gas-phase lifetime in the upper troposphere.

There is now a great deal of evidence (kinetic isotope studies, observation of the low reactivity of the acetic acid dimer, theoretical studies, and end product studies) indicating that more than half of the reaction of OH with acetic acid is via abstraction of the acidic hydrogen (Singleton et al., 1989; Butkovskaya et al., 2004b; De Smedt

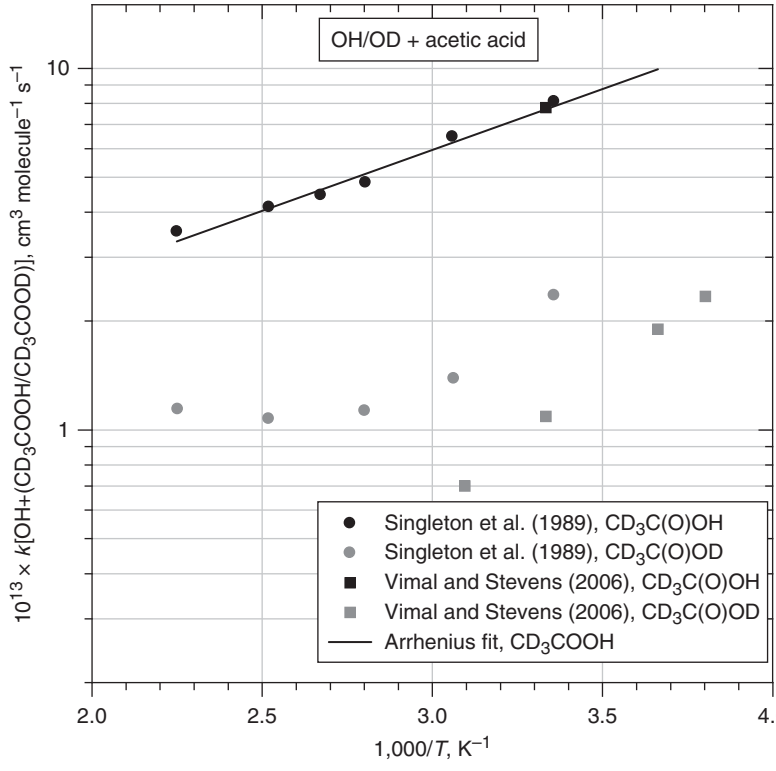

Figure VI-B-3. Arrhenius plot of the rate coefficient for the reaction of OH/OD with deuterated analogs of acetic acid.

Table VI-B-7. Rate coefficients (k, cm^3 $molecule^{-1}$ s^{-1}) for reaction of Cl-atoms with acetic acid [ethanoic acid, $CH_3C(O)OH$]

$10^{14} \times k$	T(K)	Technique[a]	Reference
2.8 ± 0.7	298	RR[b] (CH_4)	Koch and Moortgat (1990)
2.5 ± 0.3	295	RR[b] (CH_4)	Crawford et al. (1999)

[a]Abbreviations used for the techniques are defined in table I-F-3.
[b]Placed on an absolute basis using $k(Cl + CH_4) = 1.0 \times 10^{-13}$ cm^3 $molecule^{-1}$ s^{-1} (Atkinson et al., 2006).

et al., 2005; Vimal and Stevens, 2006; Rosado-Reyes and Francisco, 2006; Crunaire et al., 2006), leading to the net production of CO_2, H_2O, and CH_3O_2 radicals:

$$OH + CH_3C(O)OH \rightarrow CH_3C(O)O + H_2O$$

$$CH_3C(O)O \rightarrow CH_3 + CO_2$$

$$CH_3 + O_2 + M \rightarrow CH_3O_2 + M$$

The most quantitative evidence is obtained from measurements of the CO_2 yield from the reaction; reported values are $64 \pm 17\%$ for $249 < T < 298$ K (Butkovskaya et al., 2004b), $64 \pm 14\%$ for $T = 290$ K (De Smedt et al., 2005), and $78 \pm 13\%$ for $T = 296$ K (Crunaire et al., 2006). A lower CO_2 yield from reaction of OH with $CH_3C(O)OD$, $36 \pm 7\%$ at 296 K (Crunaire et al., 2006), is consistent with the existence of a kinetic isotope effect at the acidic site. The minor channel of attack, at the —CH_3 group, produces glyoxylic acid as the main product (Rosado-Reyes and Francisco, 2006; Crunaire et al., 2006), via reaction of the $\bullet OCH_2C(O)OH$ radical with O_2.

In addition to the gas-phase loss, heterogeneous removal processes (e.g., rainout, with an approximate time constant of 1 week) will also provide an important sink, particularly in the lower troposphere.

VI-B-3. Propanoic Acid (Propionic Acid, $CH_3CH_2C(O)OH$)

VI-B-3.1. OH Reaction Kinetics

The reaction of OH with propanoic acid has been studied by three groups, all using variations of the flash (or pulsed laser) photolysis technique (Zetzsch and Stuhl, 1982; Dagaut et al., 1988b; Singleton et al., 1989). As seen in table VI-B-8 and figure VI-B-4, the data are in reasonable agreement. A temperature-independent value of $k = 1.2 \times 10^{-12}$ cm^3 molecule^{-1} s^{-1}, the average of the available data, is recommended (Sander et al., 2006; Atkinson et al., 2006). Uncertainties are estimated at $\pm 25\%$ near 298 K. The only rate information below 298 K comes from

Table VI-B-8. Rate coefficients ($k = A \times e^{-B/T}$, cm^3 molecule^{-1} s^{-1}) for reaction of OH with propanoic acid [propionic acid, $CH_3CH_2C(O)OH$]

$10^{12} \times A$	B(K)	$10^{12} \times k$	T(K)	Technique[a]	Reference	Temperature Range (K)
		1.6 ± 0.1 (1.2)[b]	298	FP–RF	Zetzsch and Stuhl (1982)	
		(1.22 ± 0.12)[c]	240	FP–RF	Dagaut et al. (1988b)	298–440
		1.22 ± 0.12	298			
		1.28 ± 0.13	350			
		1.36 ± 0.13	400			
		1.37 ± 0.10	440			
1.07 ± 0.05	0	1.02 ± 0.55	298.2	PLP–RA	Singleton et al. (1989)	298.2–444.7
		0.88 ± 0.19	327.1			
		1.14 ± 0.15	356.6			
		1.20 ± 0.06	374.9			
		1.09 ± 0.03	397.1			
		1.04 ± 0.03	444.7			

[a]Abbreviations used for the techniques are defined in table I-F-3.
[b]Obtained using a "static" method, where wall chemistry renders final number unreliable.
[c]Value obtained assuming similar reactivity for monomer and dimer.

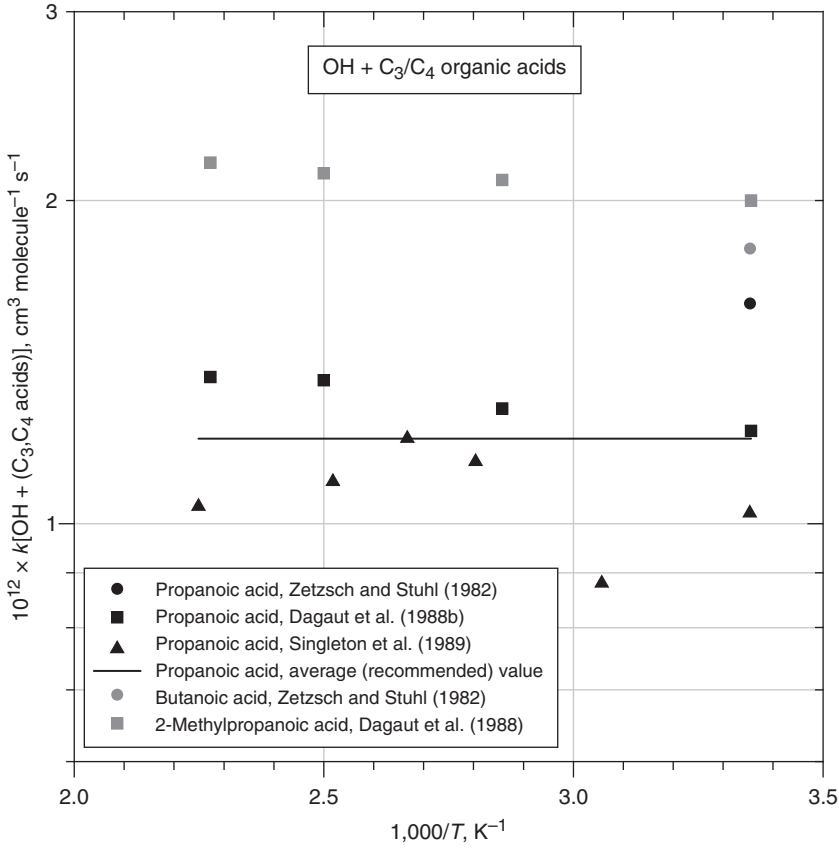

Figure VI-B-4. Arrhenius plot of the rate coefficient for the reaction of OH with propanoic, butanoic, and 2-methylpropanoic acids.

a single data point of Dagaut et al. (1988b), obtained at 240 K under the assumption of equal reactivity of propanoic acid monomer and dimer. Although some reactivity is expected on the alkyl chain and thus the reactivity of the dimer is likely nonnegligible (Singleton et al., 1989), the quantitative validity of this assumption is not known. Hence, more measurements at reduced temperatures are clearly desirable.

VI-B-3.2. Cl-Atom Reaction Kinetics

The relative rate study of Cavalli et al. (2000b) leads to a value of $k = 4.7 \times 10^{-12}$ cm^3 molecule^{-1} s^{-1} for the reaction of Cl-atoms with propanoic acid. Details are provided in table VI-B-9. Given that only one measurement has been made, an uncertainty of $\pm 30\%$ is assigned.

Table VI-B-9. Rate coefficients (k, cm^3 molecule^{-1} s^{-1}) for reaction of Cl with propanoic acid [propionic acid, $CH_3CH_2C(O)OH$]

$10^{12} \times k$	T(K)	Technique[a]	Reference
4.52 ± 0.51	296	RR[b] (C_2H_5Cl)	Cavalli et al. (2000b)
4.79 ± 0.55	296	RR[c] (CH_3OCHO)	

[a]Abbreviations used for the techniques are defined in table I-F-3.
[b]Placed on an absolute basis using $k(Cl + C_2H_5Cl) = 7.8 \times 10^{-12}$ cm^3 molecule^{-1} s^{-1} (section I-F-1).
[c]Placed on an absolute basis using $k(Cl + CH_3OCHO) = 1.4 \times 10^{-12}$ cm^3 molecule^{-1} s^{-1} (this book, section VII-B-1.1).

VI-B-3.3. Mechanism and End-products of Propanoic Acid Oxidation, and Summary of Its Atmospheric Fate

The destruction of propanoic acid in the gas phase will occur mainly via reaction with OH; the atmospheric lifetime for this process is about 10 days, assuming global [OH] = 10^6 molecule cm^{-3}. Although the end products of this reaction have not been examined quantitatively, it is expected that reaction will occur both at the acidic site and at the —CH_2 site (Singleton et al., 1989):

$$OH + CH_3CH_2C(O)OH \rightarrow CH_3CH_2C(O)O + H_2O$$

$$OH + CH_3CH_2C(O)OH \rightarrow CH_3CH\bullet C(O)OH + H_2O$$

The $CH_3CH_2C(O)O$ radical will decompose, leading to the formation of ethylperoxy radicals, the main fate of which will be conversion to acetaldehyde and CO_2:

$$CH_3CH_2C(O)O \rightarrow CH_3CH_2 + CO_2$$

$$CH_3CH_2 + O_2 + M \rightarrow CH_3CH_2O_2 + M$$

The $CH_3CH\bullet C(O)OH$ radical will be converted first to a peroxy radical, $CH_3CH(OO\bullet)C(O)OH$, and then to an alkoxy radical, $CH_3CH(O\bullet)C(O)OH$:

$$CH_3CH\bullet C(O)OH + O_2 + M \rightarrow CH_3CH(OO\bullet)C(O)OH + M$$

$$CH_3CH(OO\bullet)C(O)OH + NO \rightarrow CH_3CH(O\bullet)C(O)OH + NO_2$$

On the basis of the work of Cavalli et al. (2000b) on methyl propionate chemistry, the $CH_3CH(O\bullet)C(O)OH$ radical is expected to react mainly with O_2 to produce pyruvic acid,

$$CH_3CH(O\bullet)C(O)OH + O_2 \rightarrow CH_3C(O)C(O)OH + HO_2$$

but also to decompose to generate acetaldehyde, CO_2 and HO_2:

$$CH_3CH(O\bullet)C(O)OH \rightarrow CH_3CHO + HOCO$$

$$HOCO + O_2 \rightarrow HO_2 + CO_2$$

Removal of propanoic acid via rainout, lifetime of about 1 week, will compete with the gas-phase removal via reaction with OH.

VI-B-4. Butanoic Acid [Butyric Acid, $CH_3CH_2CH_2C(O)OH$] and 2-Methylpropanoic Acid [*iso*-Butyric Acid, $(CH_3)_2CHC(O)OH$]

VI-B-4.1. OH Reaction Kinetics

The reactions of OH with butanoic and 2-methylpropanoic acids have each been the subject of one investigation, see table VI-B-10. Zetzsch and Stuhl (1982) reported an ambient temperature value of 1.8×10^{-12} cm^3 molecule^{-1} s^{-1} for the reaction of OH with butanoic acid. Dagaut et al. (1988b) report $k = 2.6 \times 10^{-12} \exp(-70/T)$ cm^3 molecule^{-1} s^{-1} for the reaction of OH with 2-methylpropanoic acid, although a temperature-independent value of 2.1×10^{-12} cm^3 molecule^{-1} s^{-1} would also adequately represent the data. Given the paucity of available data, uncertainties of ±30% are recommended near 298 K.

VI-B-4.2. Mechanism and End Products of Butanoic and 2-Methylpropanoic Acid Oxidation, and Summary of Their Atmospheric Fate

The gas-phase removal of these two species will be controlled by their reaction with OH, a process having a lifetime of about 1 week, assuming [OH] = 10^6 molecule cm^{-3}. The reaction will likely occur partially at the acidic site and partially on the alkyl chain, with reaction on the alkyl chain contributing to a larger degree than for the shorter-chain acids discussed previously. As with the shorter-chain acids, reaction at the acidic

Table VI-B-10. Rate coefficients ($k = A \times e^{-B/T}$, cm^3 molecule^{-1} s^{-1}) for reaction of OH with butanoic acid [$CH_3CH_2CH_2C(O)OH$] and 2-methylpropanoic acid [$(CH_3)_2CHC(O)OH$]

$10^{12} \times A$	B(K)	$10^{12} \times k$	T(K)	Technique[a]	Reference	Temperature Range (K)
OH + Butanoic acid						
		1.8 ± 0.16	298	FP–RF	Zetzsch and Stuhl (1982)	
OH + 2-Methylpropanoic acid						
2.6 ± 0.2	70 ± 25	(1.86 ± 0.14)[b]	240	FP–RF	Dagaut et al. (1988b)	298–440
		2.00 ± 0.20	298			
		2.09 ± 0.18	350			
		2.12 ± 0.13	400			
		2.17 ± 0.17	440			

[a]Abbreviations used for the techniques are defined in table I-F-3.
[b]Value obtained assuming similar reactivity for monomer and dimer.

site will result in the production of CO_2 and an alkylperoxy radical:

$$OH + RC(O)OH \rightarrow RC(O)O + H_2O$$

$$RC(O)O \rightarrow R + CO_2$$

$$R + O_2 + M \rightarrow RO_2 + M$$

Reaction on the alkyl chain of 2-methypropanoic acid will occur mostly at the tertiary C—H, leading to acetone and CO_2 as major end products, via decomposition of the resultant oxy radical, $(CH_3)_2C(O\bullet)C(O)OH$. The oxy radicals produced via reaction of OH on the alkyl chain of butanoic acid, $CH_3CH(O\bullet)CH_2C(O)OH$ and $CH_3CH_2CH(O\bullet)C(O)OH$, will likely react with O_2 to produce keto-acids and/or decompose via C—C bond cleavage; e.g.,

$$CH_3CH(O\bullet)CH_2C(O)OH + O_2 \rightarrow CH_3C(=O)CH_2C(O)OH + HO_2$$

$$CH_3CH(O\bullet)CH_2C(O)OH \rightarrow CH_3CHO + \bullet CH_2C(O)OH$$

$$\bullet CH_2C(O)OH + O_2 \rightarrow\rightarrow\rightarrow HC(O)C(O)OH$$

Removal by rainout will occur on approximately a 1 week timescale in the lower troposphere, similar to the timescale of the gas-phase removal via OH.

VI-C. Dibasic Organic Acids

VI-C-1. Summary of Atmospheric Behavior of the Dibasic Acids

The dibasic acids (or dicarboxylic acids) include species of general formula $HO(O)C(CH_2)_nC(O)OH$; see table VI-C-1. These species are ubiquitous components of organic aerosol and cloudwater (e.g., Sorooshian et al., 2006, and references therein). In general, it is believed that these species are produced in small yields in the gas

Table VI-C-1. Henry's law coefficients (H^*, M atm^{-1}) and saturation vapor pressures (p^o, Pa) for the C_2–C_6 dicarboxylic acids

Species	Formula	H^* at 298 K[a]	p^o at 298 K
Oxalic acid	$HO(O)CC(O)OH$	5×10^8	
Malonic acid	$HO(O)CCH_2C(O)OH$	4×10^8	6.0×10^{-4}[b]
Succinic acid	$HO(O)C(CH_2)_2C(O)OH$	3×10^8	3.2×10^{-5}[c]
Glutaric acid	$HO(O)C(CH_2)_3C(O)OH$	2×10^8	1.2×10^{-4}[c]
Adipic acid	$HO(O)C(CH_2)_4C(O)OH$	2×10^8	2.6×10^{-6}[c]

[a] H^* data are estimates obtained from Saxena and Hildemann (1996).
[b] p^o data from Bilde et al. (2003).
[c] p^o data from Cappa et al. (2007).

phase, but that they can be generated from the condensed-phase oxidation of multifunctional species; for example, species such as glycolaldehyde [$HOCH_2CHO$], glyoxal [HC(O)CHO], glycolic acid [$HOCH_2C(O)OH$], or glyoxylic acid [HC(O)C(O)OH] can be converted to oxalic acid in aqueous media (e.g., Ervens et al., 2004).

Because of their high solubilities and low saturation vapor pressures, the dicarboxylic acids are present predominantly in the condensed phase in the atmosphere (see table VI-C-1 for a summary). The low vapor pressures render studies of the gas-phase reactivity of these species difficult, and thus no kinetic data have been obtained. The diacids can be further oxidized in the condensed phase (e.g., Herrmann et al., 2005),

$$OH + HO(O)CCH_2C(O)OH \rightarrow\rightarrow HO(O)CC(O)C(O)OH$$

but the removal of the diacids and their condensed phase by-products from the atmosphere is assuredly controlled by heterogeneous processes (rainout, and aerosol wet and dry deposition).

VI-D. Unsaturated Organic Acids

VI-D-1. Summary of Atmospheric Behavior of the Unsaturated Organic Acids

Unsaturated organic acids(e.g., acrylic acid, $CH_2{=}CHC(O)OH$ and its derivatives) are produced as minor products in the ozonolysis of dienes, and from the OH-initiated oxidation of unsaturated aldehydes. The most important examples in the atmosphere involve the formation of methacrylic and acrylic acids from the ozonolysis of isoprene (Orzechowska and Paulson, 2005a) and the formation of methacrylic acid from the oxidation of methacrolein, itself a by-product of isoprene oxidation:

$$O_3 + CH_2{=}C(CH_3)CH{=}CH_2 \rightarrow CH_2{=}C(CH_3)CH{\bullet}OO{\bullet} + CH_2O$$

$$\rightarrow CH_2{=}CH{-}C{\bullet}(CH_3)OO{\bullet} + CH_2O$$

$$CH_2{=}C(CH_3)CH{\bullet}OO{\bullet} \rightarrow \mathbf{CH_2{=}C(CH_3)C(O)OH}$$

$$CH_2{=}CH{-}C{\bullet}(CH_3)OO{\bullet} \rightarrow\rightarrow \mathbf{CH_2{=}CHC(O)OH}$$

$$OH + CH_2{=}C(CH_3)CHO(+O_2) \rightarrow CH_2{=}C(CH_3)C(O)O_2 + H_2O$$

$$CH_2{=}C(CH_3)C(O)O_2 + HO_2 \rightarrow \mathbf{CH_2{=}C(CH_3)C(O)OH} + O_3, \text{ other products}$$

Data regarding the gas-phase atmospheric chemistry of the unsaturated organic acids are rather limited; the only available data concern the reactions of acrylic acid with ozone, OH and Cl, and the reaction of methacrylic acid with ozone and OH. However, given the presence of a C=C double bond in these species, they are expected to be very reactive in the gas-phase. Thus, in the discussion that follows, estimates of the rate data for potentially relevant processes will be provided, via comparison with structurally similar species. The discussion will be limited to the three simplest members of the

series: acrylic acid, $CH_2{=}CHC(O)OH$, abbreviated here as AcA; methacrylic acid, $CH_2{=}C(CH_3)C(O)OH$, MAcA; and crotonic acid, $CH_3CH{=}CHC(O)OH$, CrA.

VI-D-1.1. OH Reaction Kinetics

The only study of the reaction of OH with the unsaturated organic acids is a relative rate study (Teruel et al., 2007) of the OH–acrylic acid reaction; data are summarized in table VI-D-1. A value of $k = 1.7 \times 10^{-11}$ cm^3 molecule^{-1} s^{-1} is obtained, using updated reference rate data. An uncertainty of ±30% is assumed. On the basis of this study, rate coefficients of approximately 2.5×10^{-11} cm^3 molecule^{-1} s^{-1} for reaction of OH with methacrylic and crotonic acid are estimated, with uncertainties of about a factor of 2.

VI-D-1.2. O_3 Reaction Kinetics

The kinetics of the reactions of acrylic acid (AcA) and methacrylic acid (MAcA) with ozone have been studied by Neeb et al. (1998), see table VI-D-2. The studies were carried out in excess ozone, and the pseudo first-order decay of the acids was monitored using FTIR spectroscopy. Final kinetic data were obtained in the presence of added cyclohexane (an OH scavenger) and formic acid (a Criegee radical scavenger). Values reported are as follows: $k(O_3 + AcA) = (0.65 \pm 0.13) \times 10^{-18}$ cm^3 molecule^{-1} s^{-1} and

Table VI-D-1. Rate coefficients (k, cm^3 molecule^{-1} s^{-1}) for reaction of OH with acrylic acid [$CH_2{=}CHC(O)OH$]

$10^{11} \times k$	T(K)	Technique[a]	Reference
1.49 ± 0.17	298 ± 2	RR[b] ($ClCH_2CH{=}CH_2$)	Teruel et al. (2007)
1.67 ± 0.17	298 ± 2	RR[b] ($ClCH_2CH{=}CH_2$)	
1.63 ± 0.23	298 ± 2	RR[c] ($C_2H_5OC_2H_5$)	
1.82 ± 0.42	298 ± 2	RR[c] ($C_2H_5OC_2H_5$)	

[a]Abbreviations used for the techniques are defined in table I-F-3.
[b]Placed on an absolute basis using $k(OH + ClCH_2CH{=}CH_2) = 1.69 \times 10^{-11}$ cm^3 molecule^{-1} s^{-1} (Albaladejo et al., 2003a).
[c]Placed on an absolute basis using $k(OH + C_2H_5OC_2H_5) = 1.22 \times 10^{-11}$ cm^3 molecule^{-1} s^{-1} (this book, section III-B-3).

Table VI-D-2. Rate coefficients (k, cm^3 molecule^{-1} s^{-1}) for reaction of O_3 with acrylic acid [$CH_2{=}CHC(O)OH$] and methacrylic acid [$CH_2{=}C(CH_3)C(O)OH$]

$10^{18} \times k$	T(K)	Technique[a]	Reference
O_3 + Acrylic acid			
0.65 ± 0.13	296	IR abs.	Neeb et al. (1998)
O_3 + Methacrylic acid			
4.1 ± 0.4	296	IR abs.	Neeb et al. (1998)
4.2	296	RR[b] (MVK)	

[a]Abbreviations used for the techniques are defined in table I-F-3.
[b]Placed on an absolute basis using $k(O_3 + MVK) = 5.0 \times 10^{-18}$ cm^3 molecule^{-1} s^{-1} (Atkinson et al., 2006).

$k(O_3 + MAcA) = (4.1 \pm 0.4) \times 10^{-18}$ cm^3 molecule^{-1} s^{-1}. Neeb et al. also carried out a relative rate determination of $k(O_3 + MAcA)$, using MVK as the reference compound. Consistent results were obtained that give $k(O_3 + MAcA) = 4.2 \times 10^{-18}$ cm^3 molecule^{-1} s^{-1}. Given that only one study has been conducted, an uncertainty of $\pm 35\%$ is assigned to the measurements. The rate coefficient for reaction of ozone with crotonic acid (CrA) is likely to be similar to that for methacrylic acid.

VI-D-1.3. NO_3 Reaction Kinetics

On the basis of studies of the kinetics of reaction of NO_3 with the methyl esters of the unsaturated acids (Canosa-Mas et al., 1999a), rate coefficients of k (NO_3 + AcA) $\approx 2 \times 10^{-16}$ cm^3 molecule^{-1} s^{-1} and $k(NO_3 + MAcA, CrA) \approx 2 \times 10^{-15}$ cm^3 molecule^{-1} s^{-1} are estimated, with uncertainties of about a factor of 3.

VI-D-1.4. Cl-Atom Reaction Kinetics

The reaction Cl-atoms with acrylic acid has been studied at atmospheric pressure by Teruel et al. (2007) using a relative rate technique. An average value of 3.7×10^{-10} cm^3 molecule^{-1} s^{-1} is obtained from their study, with an uncertainty of $\pm 20\%$, see table VI-D-3. Lower values for the rate coefficient were obtained by Aranda et al. (2003b) using a discharge flow–mass spectrometric technique at reduced pressure (0.5–3 Torr), as expected for an addition process in the low pressure, fall-off region.

VI-D-1.5. Mechanism and End Products of Gas-Phase Oxidation of the Unsaturated Organic Acids, and Summary of Their Atmospheric Fate

The dominant removal process for the unsaturated organic acids is likely reaction with OH; for daytime [OH] $\approx 2.5 \times 10^6$ molecule cm^{-3}, lifetimes of 6 h for acrylic acid

Table VI-D-3. Rate coefficients (k, cm^3 molecule^{-1} s^{-1}) for reaction of Cl with acrylic acid [CH_2=CHC(O)OH]

Pressure (Torr)	$10^{11} \times k$	T(K)	Technique[a]	Reference	Temperature Range (K)
1	7.8 ± 1.6	260	DF–MS	Aranda et al. (2003b)	260–333
1	4.3 ± 0.4	288			
0.5	2.4 ± 0.4	298			
1	3.1 ± 0.7	298			
2	3.6 ± 0.3	298			
3	4.0 ± 0.3	298			
1	1.9 ± 0.3	333			
760	40.4 ± 7.5	298	RR[b] (n-C_5H_{12})	Teruel et al. (2007)	
760	39.0 ± 8.4	298	RR[b] (n-C_5H_{12})		
760	31.6 ± 4.4	298	RR[c] ($C_2H_5OC_2H_5$)		

[a]Abbreviations used for the techniques are defined in table I-F-3.
[b]Placed on an absolute basis using $k(Cl + n\text{-}C_5H_{12}) = 2.71 \times 10^{-10}$ cm^3 molecule^{-1} s^{-1} (Calvert et al., 2008).
[c]Placed on an absolute basis using $k(Cl + C_2H_5OC_2H_5) = 2.78 \times 10^{-10}$ cm^3 molecule^{-1} s^{-1} (section III-B-3.1).

and about 4 h for methacrylic and crotonic acid are estimated. Clearly, kinetic studies of the reaction of OH with methacrylic and crotonic acid are desirable, however, to improve these estimates. Reaction with O_3 will play a minor but not insignificant role; e.g., methacrylic and crotonic acid lifetimes for removal by O_3 are about 3 days. In urban or rural regions, nighttime removal via reaction with NO_3 may also be of some importance; for $[NO_3] \approx 3 \times 10^9$ molecule cm^{-3}, methacrylic and crotonoic acid lifetimes will be about 2 days.

Products of the reaction of OH with methacrylic acid have been determined by Orlando et al. (2002). Major products (molar yield) were pyruvic acid (80 ± 8%) and CH_2O (83 ± 5%), while CO_2 was observed as a minor product (24 ± 4%). Reactions involved in the formation of these products are as follows:

$$OH + CH_2{=}C(CH_3)C(O)OH(+O_2) \rightarrow HOCH_2C(CH_3)(OO\bullet)C(O)OH$$

$$HOCH_2C(CH_3)(OO\bullet)C(O)OH + NO \rightarrow HOCH_2C(CH_3)(O\bullet)C(O)OH + NO_2$$

$$HOCH_2C(CH_3)(O\bullet)C(O)OH \rightarrow CH_2OH + \mathbf{CH_3C(O)C(O)OH}$$

$$CH_2OH + O_2 \rightarrow \mathbf{CH_2O} + HO_2$$

$$HOCH_2C(CH_3)(O\bullet)C(O)OH \rightarrow HOCH_2C(O)CH_3 + HOCO$$

$$HOCO + O_2 \rightarrow \mathbf{CO_2} + HO_2$$

The likely co-product of CO_2, hydroxyacetone, was not observed (yield ≤ 25%). By analogy, production of a carbonyl compound and an oxo-acid species is likely for the other unsaturated acids under consideration here (e.g., HC(O)COOH and CH_2O from acrylic acid, HC(O)COOH and CH_3CHO from crotonic acid).

VI-E. Keto-Acids

VI-E-1. Pyruvic Acid [2-Oxopropanoic Acid, $CH_3C(O)C(O)OH$]

The only kinetic study regarding the atmospheric destruction of the ketoacids involves the simplest member of the series [pyruvic acid, $CH_3C(O)C(O)OH$], and this is restricted to a single measurement of its reaction with OH.

VI-E-1.1. OH Reaction Kinetics

Mellouki and Mu (2003) measured k(OH + pyruvic acid) over a range of temperatures (273–371 K) using pulsed laser photolysis–laser-induced fluorescence. The data are summarized in table VI-E-1 and figure VI-E-1, and can be described by the simple Arrhenius expression $k = 4.9 \times 10^{-14} \exp(276/T)$ cm^3 $molecule^{-1}$ s^{-1}, with a rate coefficient of 1.2×10^{-13} cm^3 $molecule^{-1}$ s^{-1} at 298 K. Given the fact that only one measurement has been made, an uncertainty of a factor of ±30% is assigned.

Table VI-E-1. Rate coefficients (k, cm^3 molecule^{-1} s^{-1}) for reaction of OH with pyruvic acid, [$CH_3C(O)C(O)OH$]

$10^{13} \times A$	B(K)	$10^{13} \times k$	T(K)	Technique[a]	Reference	Temperature Range (K)
0.49 ± 0.19	−276 ± 123	1.35 ± 0.17	273	PLP–LIF	Mellouki and Mu (2003)	273–371
		1.46 ± 0.10	283			
		1.35 ± 0.13	298			
		1.16 ± 0.13	298			
		0.98 ± 0.08	298			
		1.14 ± 0.08	298			
		1.38 ± 0.09	323			
		1.11 ± 0.16	348			
		1.08 ± 0.08	348			
		0.88 ± 0.05	371			
		1.13 ± 0.17	371			

[a]Abbreviations used for the techniques are defined in table I-F-3.

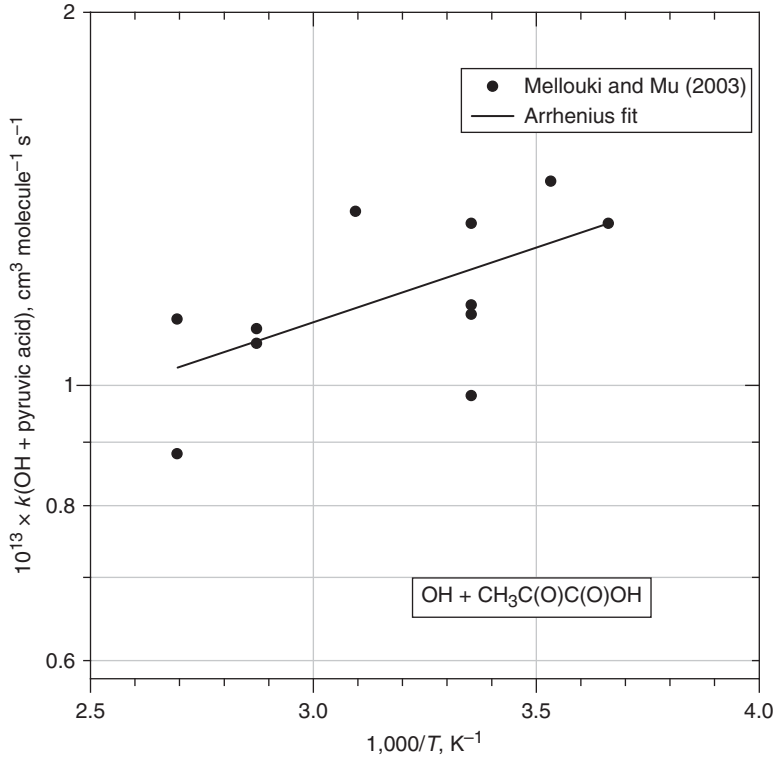

Figure VI-E-1. Arrhenius plot of the rate coefficient for the reaction of OH with pyruvic acid.

VI-E-1.2. Atmospheric Fate of Pyruvic Acid

The atmospheric destruction of pyruvic acid appears to be dominated by its photolysis, a process that is discussed in detail in section IX-F-9. This process is rapid, occurring with a lifetime of a few hours or less and appears to occur via a variety of molecular and radical processes:

$$CH_3C(O)C(O)OH + h\nu \rightarrow CH_3CHO + CO_2$$

$$CH_3C(O)C(O)OH + h\nu \rightarrow CH_3CO + HOCO$$

$$CH_3C(O)C(O)OH + h\nu \rightarrow CH_3C(O)OH + CO$$

$$CH_3C(O)C(O)OH + h\nu \rightarrow CH_3CO + CO + OH$$

Reaction with OH is expected to play only a minor role, as the lifetime against OH reaction is about 100 days (Mellouki and Mu, 2003).

VI-F. Organic Acids Derived from Aromatic Compounds and from Terpenes

VI-F-1. Summary of Atmospheric Behavior of the Organic Acids Obtained from Aromatic Compounds

Acids are minor products of the oxidation of aromatic compounds. For example, benzoic acid is formed in small yield from the oxidation of benzaldehyde, itself a minor product of toluene oxidation, as shown in the following reaction mechanism (mechanism VI-F-1); note that only reactions leading from toluene to benzaldehyde to benzoic acid are shown in mechanism VI-F-1.

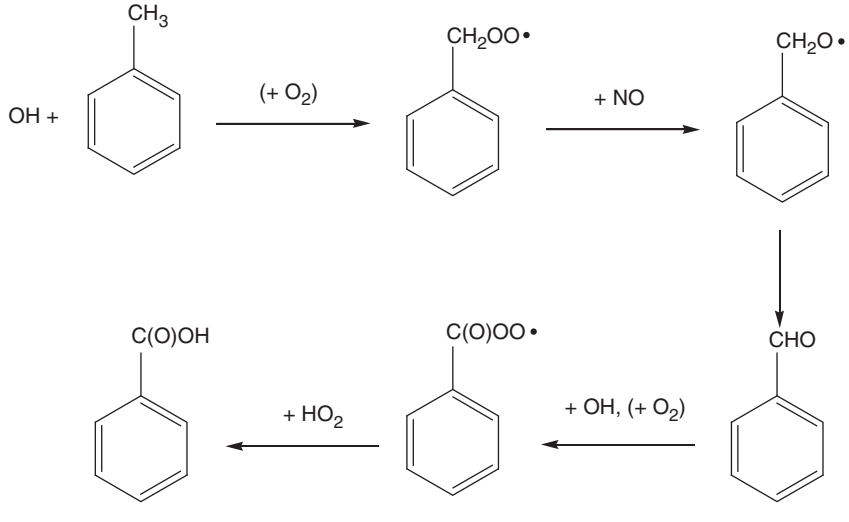

Mechanism VI-F-1

The vapor pressures of benzoic acid and its substituted analogs are quite low, about 1 mTorr for benzoic acid at 298 K, and lower for more highly substituted species (NIST webbook, 2009). Thus, gas-phase studies of these species near ambient temperatures would be quite difficult, and no data concerning their reactions with the common atmospheric oxidants (OH, O_3, or NO_3) are available. Like other organic acids, these species are also very soluble, and efficient scavenging by clouds would be expected. For example, the Henry's law constant for benzoic acid is about 20,000 M atm^{-1} (Sander, 2005), somewhat larger than the simple organic acids.

Gas-phase destruction of these species will likely be dominated by their reaction with OH. The Master Chemical Mechanism (http://mcm.leeds.ac.uk/MCM) assumes a rate coefficient of $k = 1.1 \times 10^{-12}$ cm^3 $molecule^{-1}$ s^{-1} for this process, with reaction occurring via abstraction of the carboxyl group H-atom:

$$OH + C_6H_5C(O)OH \rightarrow C_6H_5C(O)O + H_2O$$

This leads to an estimated gas-phase lifetime of about 10 days. In the lower troposphere, this process would compete with rainout, which typically occurs on about the same timescale.

VI-F-2. Summary of Atmospheric Behavior of Organic Acids Obtained from Terpenes

The ozonolysis of the monoterpenes, biogenic species of molecular formula $C_{10}H_{16}$ (e.g., α- and β-pinene), provides a significant source of secondary organic aerosol. A number of multi-functional organic acids, such as norpinic acid from β-pinene ozonolysis, and pinonic acid and pinic acid from α-pinene ozonolysis, have been conclusively identified as components of the organic aerosol formed (e.g., Presto et al., 2005 and references therein). As summarized in table VI-F-1, these acidic species possess very low vapor pressures (typically $\leq 10^{-4}$ Pa at 298 K, Bilde and Pandis, 2001), and thus have a strong tendency to partition to the condensed phase, where they are removed via depositional processes. The low vapor pressures preclude any studies of their gas-phase kinetics. However, the structure–activity relations (SARs) of Kwok and Atkinson (1995) can be used to estimate rate coefficients of about (1–5) $\times 10^{-12}$ cm^3 $molecule^{-1}$ s^{-1} for the species shown in table VI-F-1, implying gas-phase lifetimes of about 2–12 days.

VI-G. Halogen-Substituted Organic Acids

VI-G-1. Trifluoroacetic Acid [$CF_3C(O)OH$]

VI-G-1.1. OH Reaction Kinetics

The kinetics of the reaction of OH with $CF_3C(O)OH$ have been studied by Møgelberg et al. (1994), Carr et al. (1994), and Hurley et al. (2004a). Rate coefficients are listed in table VI-G-1 and plotted in figure VI-G-1. Absolute rate data for $k(OH + CF_3C(O)OH)$ were obtained using a pulse radiolysis technique at 315 and 348 K and using a relative

Table VI-F-1. Structures and vapor pressures for some acid products of the reaction of ozone with α- and β-pinene (adapted from Bilde and Pandis, 2001; additional data from Presto et al., 2005)

Compound	Structure	Terpene Precursor	Vapor Pressure, Pa (296 K)
cis-Pinonic acid	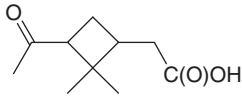	α-pinene	7×10^{-5}
Pinic acid	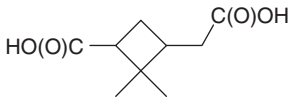	α-pinene	3.2×10^{-5}
Norpinonic acid	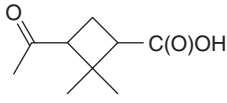	α-pinene	
trans-Norpinic acid	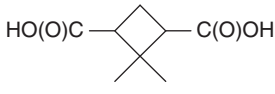	β-pinene	13×10^{-5}
10-Hydroxypinonic acid	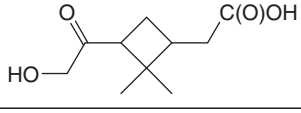	α-pinene	

Table VI-G-1. Rate coefficients (k, cm^3 molecule^{-1} s^{-1}) for reaction of OH radicals with halogen-substituted acids

Molecule	$10^{12} \times A$	B(K)	$10^{13} \times k$	T(K)	Technique[a]	Reference	Temperature Range (K)
CF_3COOH			1.6 ± 0.4	315	PR–UVA	Møgelberg	
			1.5 ± 0.2	348		et al. (1994)	
			1.8 ± 0.5	296	RR (C_2H_6)[b]		
	0.2	146 ± 500	1.14	283	RR (C_2H_6)[b]	Carr et al.	283–323
			1.32	288		(1994)	
			1.14 ± 0.21	298			
			1.05	310			
			1.22	323			
			1.21 ± 0.22	298	RR (C_3H_8)[c]		
			0.803 ± 0.133	296	RR (C_2H_2)[d]	Hurley et al.	
			0.916 ± 0.095		RR (C_2H_4)[e]	(2004a)	
$C_xF_{2x+1}COOH$			1.54 ± 0.17	296	RR (C_2H_2)[d]	Hurley et al.	
$x = 2, 3, 4$			1.56 ± 0.11		RR (C_2H_4)[e]	(2004a)	

[a]Abbreviations used for the techniques are defined in table I-F-3.
[b]Placed on an absolute basis using $k(OH + C_2H_6) = 8.6 \times 10^{-12} \exp(-1{,}047/T)$ cm^3 molecule^{-1} s^{-1} (Calvert et al., 2008).
[c]Placed on an absolute basis using $k(OH + C_3H_8) = 1.1 \times 10^{-12}$ cm^3 molecule^{-1} s^{-1} (Atkinson et al., 2006).
[d]Placed on an absolute basis using $k(OH + C_2H_2) = 7.8 \times 10^{-13}$ cm^3 molecule^{-1} s^{-1} (Atkinson et al., 2006).
[e]Placed on an absolute basis using $k(OH + C_2H_4) = 7.9 \times 10^{-12}$ cm^3 molecule^{-1} s^{-1} (Atkinson et al., 2006).

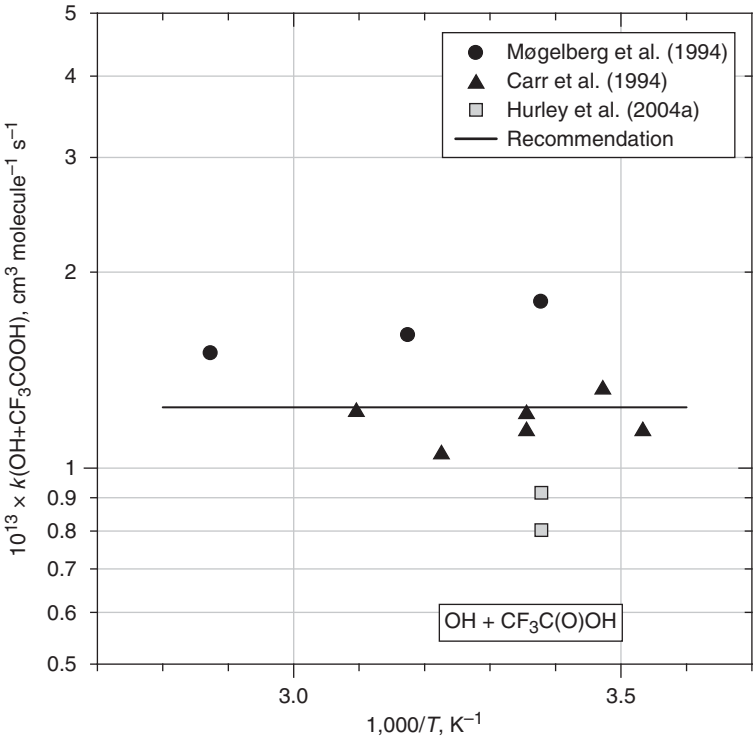

Figure VI-G-1. Measurements of the rate coefficients for reaction of OH radicals with $CF_3C(O)OH$.

rate method at 296 K by Møgelberg et al. (1994). High partial pressures (up to 15 mbar) of $CF_3C(O)OH$ were used with pulsed radiolysis–UV absorption and relative rate experiments, and it was necessary for Møgelberg et al. (1994) to apply substantial corrections (up to 30%) to account for the presence of the dimer $[CF_3C(O)OH]_2$. Carr et al. (1994) and Hurley et al. (2004a) used relative rate methods to study $k(OH + CF_3C(O)OH)$. Two points are evident from inspection of figure VI-G-1. First, there is considerable scatter in the data with reported values of $k(OH + CF_3C(O)OH)$ near 298 K spanning a range of approximately a factor of 2. Second, there is no discernable dependence of $k(OH + CF_3C(O)OH)$ on temperature over the rather limited range studied. Taking an average of the values reported by Møgelberg et al. (1994), Carr et al. (1994), and Hurley et al. (2004a) determined at ambient temperatures gives $k(OH + CF_3C(O)OH) = 1.24 \times 10^{-13}$ cm^3 molecule^{-1} s^{-1} which we recommend over the temperature range 280–350 K with an uncertainty of ±50%.

VI-G-1.2. Cl-Atom Reaction Kinetics

The kinetics of the reaction of chlorine atoms with $CF_3C(O)OH$ have been studied by Wallington and Hurley (1995) and an upper limit of $k(Cl + CF_3C(O)OH) < 1 \times 10^{-17}$ cm^3 molecule^{-1} s^{-1} was reported (see table VI-G-2). The fact that chlorine

Table VI-G-2. Rate coefficients (k, cm^3 molecule^{-1} s^{-1}) for reaction of chlorine atoms with trifluoroacetic acid [$CF_3C(O)OH$]

Molecule	$10^{17} \times k$	T(K)	Technique[a]	Reference
$CF_3C(O)OH$	<1.0	295	RR (CF_2ClH)[b]	Wallington and Hurley (1995)

[a]Abbreviations used for the techniques are defined in table I-F-3.
[b]Placed on an absolute basis using $k(Cl + CF_2ClH) = 1.7 \times 10^{-15}$ cm^3 molecule^{-1} s^{-1} (Atkinson et al., 2008).

atoms are essentially unreactive towards $CF_3C(O)OH$ reflects the fact that the H-atom abstraction reaction is endothermic.

VI-G-1.3. Summary of the Atmospheric Fate of CF_3COOH

Combining $k(OH + CF_3C(O)OH) = 1.24 \times 10^{-13}$ cm^3 molecule^{-1} s^{-1} with a diurnal average of [OH] = 10^6 molecule cm^{-3} gives an estimate of 3 months for the atmospheric lifetime of $CF_3C(O)OH$ with respect to reaction with OH radicals. As discussed by Hurley et al. (2004a), the main atmospheric loss of $CF_3C(O)OH$, and other perfluorocarboxylic acids, is dry and wet (particle mediated) deposition which are estimated to occur on a timescale of the order of 10 days.

VI-G-2. The Fluorine-Atom Substituted Larger Acids: $C_xF_{2x+1}C(O)OH$ ($x = 2, 3, 4$)

VI-G-2.1. OH Reaction Kinetics

The reactions of OH with $C_2F_5C(O)OH$, $C_3F_7C(O)OH$, and $C_4F_9C(O)OH$ have been studied by Hurley et al. (2004a). There was no discernible difference in the reactivity of these acids, and an average of the combined data gives $k[OH + C_xF_{2x+1}C(O)OH] = 1.55 \times 10^{-13}$ cm^3 molecule^{-1} s^{-1} at 296 K (see table VI-G-1) which is recommended with an uncertainty of ±30%. It is puzzling that Hurley et al. (2004a) did not report any effect of C_xF_{2x+1} group size for $x = 2$–4, but did report a substantially lower reactivity for $x = 1$ (see table VI-G-1). Further studies are warranted.

VI-H. Acid Anhydrides

The acid anhydrides, compounds of general formula RC(=O)OC(=O)R, are formed in the atmosphere from the atmospheric degradation of esters; see chapter VII. For example, formic acetic anhydride, $CH_3C(O)OCHO$, is a product of methyl acetate oxidation (Christensen et al., 2000):

$$OH + CH_3C(O)OCH_3(+O_2) \rightarrow CH_3C(O)OCH_2O_2 + H_2O$$

$$CH_3C(O)OCH_2O_2 + NO \rightarrow CH_3C(O)OCH_2O + NO_2$$

$$CH_3C(O)OCH_2O + O_2 \rightarrow \mathbf{CH_3C(O)OCHO} + HO_2$$

$$CH_3C(O)OCH_2O \rightarrow CH_3C(O)OH + HCO$$

Table VI-H-1. Rate coefficients (k, cm^3 molecule^{-1} s^{-1}) for reaction of Cl with acid anhydrides

$10^{13} \times k$	T(K)	Technique[a]	Reference
Cl + Formic acetic anhydride [HC(O)OC(O)CH$_3$]			
1.02 ± 0.13	296	RR[b] (CH$_3$Cl)	Christensen et al. (2000)
1.00 ± 0.12	296	RR[c] (CH$_4$)	
Cl + Formic propanoic anhydride [HC(O)OC(O)CH$_2$CH$_3$]			
28.1 ± 2.9	296	RR[d] (C$_2$H$_5$Cl)	Cavalli et al. (2000b)
29.2 ± 3.0	296	RR[e] (CH$_3$OCHO)	

[a]Abbreviations used for the techniques are defined in table I-F-3.
[b]Placed on an absolute basis using $k(\text{Cl} + \text{CH}_3\text{Cl}) = 4.8 \times 10^{-13}$ cm^3 molecule^{-1} s^{-1} (Atkinson et al., 2008).
[c]Placed on an absolute basis using $k(\text{Cl} + \text{CH}_4) = 1.0 \times 10^{-13}$ cm^3 molecule^{-1} s^{-1} (Atkinson et al., 2006).
[d]Placed on an absolute basis using $k(\text{Cl} + \text{C}_2\text{H}_5\text{Cl}) = 7.8 \times 10^{-12}$ cm^3 molecule^{-1} s^{-1} (section I-F-1).
[e]Placed on an absolute basis using $k(\text{Cl} + \text{CH}_3\text{OCHO}) = 1.4 \times 10^{-12}$ cm^3 molecule^{-1} s^{-1} (section VII-B-1.3).

The database regarding the gas-phase degradation of the acid anhydrides is limited to only a pair of Cl-atom rate coefficient measurements, as is summarized in table VI-H-1. Gas-phase destruction of these species is likely controlled by reaction with OH, for which no data are presently available. However, on the basis of estimates from structure–activity relationships (Kwok and Atkinson, 1995; Kwok et al., 1996b), these rate coefficients are likely quite small. For example, rate coefficients of 12, 6.5, and 0.9 (all in units of 10^{-13} cm^3 molecule^{-1} s^{-1}) can be estimated for formic anhydride [HC(O)OCHO], formic acetic anhydride [HC(O)OC(O)CH$_3$], and acetic anhydride [CH$_3$C(O)OC(O)CH$_3$], respectively, implying lifetimes for reaction of OH of about 10, 18, and 130 days for these species, respectively. Heterogeneous processes (e.g., hydrolysis to acetic acid on aerosol) seem likely to be important in the atmospheric removal of the anhydrides.

VII

Rate Coefficients and Mechanisms of Atmospheric Oxidation of the Esters

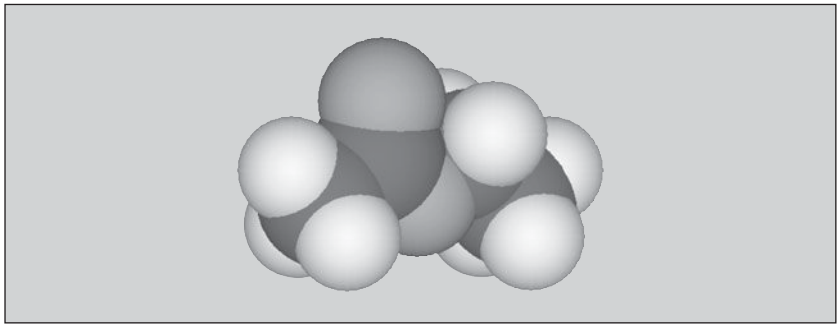

VII-A. Introduction

Esters are emitted directly into the atmosphere from both natural and anthropogenic sources and are produced during the atmospheric oxidation of ethers. Methyl acetate and ethyl acetate have found widespread use as solvents. Vegetable oils and animal fats are esters. Transesterification of vegetable oils and animal fats with methanol gives fatty acid methyl esters (FAMEs) which are used in biodiesel. Many esters have pleasant odors and are present in essential oils, fruits, and pheromones, and are often added to fragrances and consumer products to provide a pleasant odor. Table VII-A-1 provides a list of common esters and their odors.

It is surprising to note that despite their ubiquitous nature, volatility, and fragrance, it is only very recently that quantitative measurements of esters in ambient air have been reported (Niedojadlo et al., 2007; Legreid et al., 2007). The atmospheric oxidation of saturated esters is largely initiated by OH radical attack. Reaction with O_3 and NO_3 radicals contributes to the atmospheric oxidation of unsaturated esters. As discussed in chapter IX, UV absorption by esters is only important for wavelengths below approximately 240 nm and, hence, photolysis is not a significant tropospheric loss mechanism. When compared to the ethers from which they can be derived, the esters are substantially less reactive towards OH radicals. The ester functionality —C(O)O— in $R_1C(O)OR_2$ deactivates the alkyl groups to which it is attached with the deactivation being most pronounced for the R_1 group attached to the carbonyl group. The atmospheric oxidation mechanisms of the esters are reviewed in the present chapter.

Table VII-A-1. Some common esters and their odors

Ester	Formula	Odor
Ethyl formate	$C_2H_5OC(O)H$	Lemon, rum, strawberry
Isobutyl formate	$(CH_3)_2CHCH_2OC(O)H$	Raspberry
Ethyl acetate	$C_2H_5OC(O)CH_3$	Nail polish remover
Propyl acetate	$CH_3(CH_2)_2OC(O)CH_3$	Pear
Isobutyl acetate	$(CH_3)_2CHCH_2OC(O)CH_3$	Cherry, raspberry, strawberry
Isoamyl acetate	$(CH_3)_2CHCH_2CH_2OC(O)CH_3$	Banana
Octyl acetate	$C_8H_{17}OC(O)CH_3$	Orange
Benzyl acetate	$C_6H_5OC(O)CH_3$	Pear, strawberry, jasmine
Ethyl phenylacetate	$C_2H_5OC(O)C_6H_5$	Honey
Ethyl butyrate	$C_2H_5OC(O)(CH_2)_2CH_3$	Banana, pineapple, strawberry
Ethyl pentanoate	$C_2H_5OC(O)(CH_2)_3CH_3$	Apple
Allyl hexanoate	$CH_3(CH_2)_4C(O)OCH_2CH{=}CH_2$	Pineapple
Methyl salicylate	$CH_3OC(O)C_6H_4(OH)$	Wintergreen
Methyl anthranilate	$CH_3OC(O)C_6H_4(NH_2)$	Grape

VII-B. Acyclic, Saturated Monofunctional Esters

VII-B-1. Methyl Formate (CH_3OCHO)

VII-B-1.1. OH Reaction Kinetics

The reaction of OH with methyl formate has been studied by Wallington et al. (1988b) and Le Calvé et al. (1997a) over the temperature range 233–372 K. Data are summarized in table VII-B-1 and are plotted in figure VII-B-1. The room temperature determination

Table VII-B-1. Rate coefficients ($k = A \times e^{-B/T}$, cm^3 $molecule^{-1}$ s^{-1}) for reaction of OH with methyl formate (CH_3OCHO)

$10^{12} \times A$	B (K)	$10^{13} \times k$	T (K)	Technique[a]	Reference	Temperature Range (K)
		2.27 ± 0.34	296	FP–RF	Wallington et al. (1988b)	
0.854 ± 0.198	461 ± 70	1.29 ± 0.06	233	PLP–LIF	Le Calvé et al. (1997a)	233–372
		1.39 ± 0.06	253			
		1.38 ± 0.11	253			
		1.56 ± 0.05	273			
		1.80 ± 0.07	298			
		1.60 ± 0.12	298			
		1.82 ± 0.09	298			
		1.69 ± 0.12	298			
		1.75 ± 0.07	298			
		1.95 ± 0.13	323			
		2.25 ± 0.09	348			
		2.41 ± 0.10	348			
		2.48 ± 0.08	372			
		2.71 ± 0.12	372			

[a]Abbreviations used for the techniques are defined in table I-F-3.

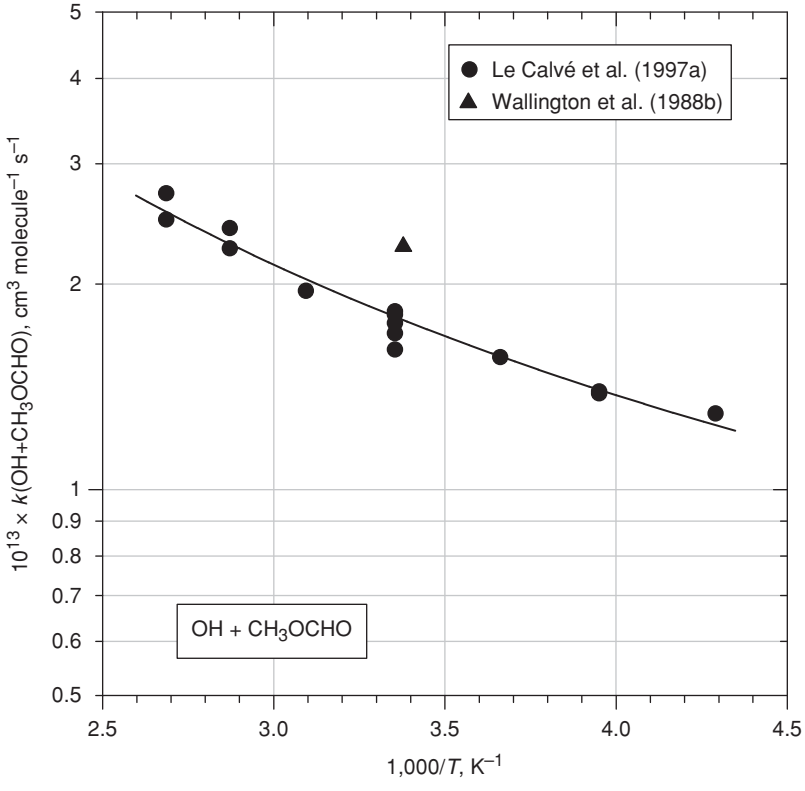

Figure VII-B-1. Measurements of the rate coefficients for reaction of OH radicals with CH_3OCHO. The curve is a fit to the data from Wallington et al. (1988b) and Le Calvé et al. (1997a).

of $k(OH + CH_3OCHO)$ by Wallington et al. is in agreement with that by Le Calvé et al. (1997) within the experimental uncertainties. Significant curvature is evident in the Arrhenius plot in figure VII-B-1. A fit of the modified Arrhenius expression to the data from Wallington et al. (1988b) and Le Calvé et al. (1997a) gives: $k(OH + CH_3OCHO) = 1.28 \times 10^{-18}\ T^2 \exp(136/T)$ cm^3 molecule^{-1} s^{-1}. This expression gives $k(OH + CH_3OCHO) = 1.79 \times 10^{-13}$ cm^3 molecule^{-1} s^{-1} at 298 K with an estimated uncertainty of ±30%. Corroborative studies of the temperature dependence of this rate coefficient are warranted.

VII-B-1.2. NO_3 Reaction Kinetics

Langer et al. (1993) have reported $k(NO_3 + CH_3OCHO) = 3.6 \times 10^{-18}$ cm^3 molecule^{-1} s^{-1} at 296 K using a discharge flow technique in 23–33 mbar of helium diluent. Given the difficulties in studying such a slow reaction using an absolute rate method, an uncertainty of a factor of 2 is estimated at 296 K.

Table VII-B-2. Rate coefficients ($k = A \times e^{-B/T}$, cm^3 $molecule^{-1}$ s^{-1}) for reaction of chlorine atoms with methyl formate (CH_3OCHO)

$10^{12} \times A$	B (K)	$10^{12} \times k$	T (K)	Technique[a]	Reference	Temperature Range (K)
		1.35 ± 0.34	295	RR (CH_3Cl)[b]	Wallington et al. (1993b)	
		1.83 ± 0.21	298	PLP–RF	Notario et al. (1998)	
		1.59 ± 0.07	298	RR (CH_3F)[c]	Good et al. (2000)	
		1.48 ± 0.06		RR (CH_2Cl_2)[d]		
		0.83 ± 0.14		RR (CH_2F_2)[e]		
		1.34 ± 0.09	296	RR (CH_3Cl)[b]	Wallington et al. (2006a)	
		1.22 ± 0.10		RR (C_2H_5Cl)[f]		
17 ± 14	810 ± 250	0.75 ± 0.18	253	DF–MS	Bravo et al. (2009)	253–333
		0.84 ± 0.13	273			
		1.01 ± 0.15	298			
		1.33 ± 0.20	315			
		1.41 ± 0.25	333			

[a]Abbreviations used for the techniques are defined in table I-F-3.
[b]Placed on an absolute basis using $k(Cl + CH_3Cl) = 4.8 \times 10^{-13}$ cm^3 $molecule^{-1}$ s^{-1} (Atkinson et al. 2008).
[c]Placed on an absolute basis using $k(Cl + CH_3F) = 3.5 \times 10^{-13}$ cm^3 $molecule^{-1}$ s^{-1} (Atkinson et al. 2008).
[d]Placed on an absolute basis using $k(Cl + CH_2Cl_2) = 3.4 \times 10^{-13}$ cm^3 $molecule^{-1}$ s^{-1} (Atkinson et al. 2008).
[e]Placed on an absolute basis using $k(Cl + CH_2F_2) = 5.0 \times 10^{-14}$ cm^3 $molecule^{-1}$ s^{-1} (Atkinson et al. 2008).
[f]Placed on an absolute basis using $k(Cl + C_2H_5Cl) = 7.8 \times 10^{-12}$ cm^3 $molecule^{-1}$ s^{-1} (section I-F).

VII-B-1.3. Cl-Atom Reaction Kinetics

Wallington et al. (1993b), Notario et al. (1998), Good et al. (2000), Wallington et al. (2006a), and Bravo et al. (2009) have reported measurements of $k(Cl + CH_3OCHO)$. The results are listed in table VII-B-2 and plotted in figure VII-B-2. The results obtained using CH_2F_2 as reference by Good et al. (2000) were derived from a rate constant ratio which was far from unity, are likely to be subject to considerable uncertainties, and are not considered further. The relative rate measurements at ambient temperature by Wallington et al. (1993b), Good et al. (2000) other than with CH_2F_2 as the reference, and Wallington et al. (2006a) are in good agreement. The value of $k(Cl + CH_3OCHO)$ from the absolute rate study of Notario et al. (1998) is approximately 20% higher than those from the relative rate studies. Where comparisons were possible, the rate data reported by Notario et al. (1998) are systematically 20–30% higher than values from relative rate studies. Wallington et al. (2006a) suggested that the loss of chlorine atoms via reaction with peroxy radicals led to an overestimation of $k(Cl + CH_3OCHO)$ by Notario et al. (1998).

The rate coefficient measured by Bravo et al. (2009) at 298 K is approximately 25% lower than the results from Wallington et al. (1993b), Good et al. (2000), and Wallington et al. (2006a). Regeneration of chlorine atoms via reaction of organic radicals with Cl_2 can be a complication in absolute rate studies. Absolute studies such as that by Bravo et al. (2009) may underestimate $k(Cl + \text{organic})$ where Cl_2 is present and where the timescales for loss of chlorine atoms via the reaction of interest and regeneration via reaction of organic radicals are not sufficiently decoupled. This complication

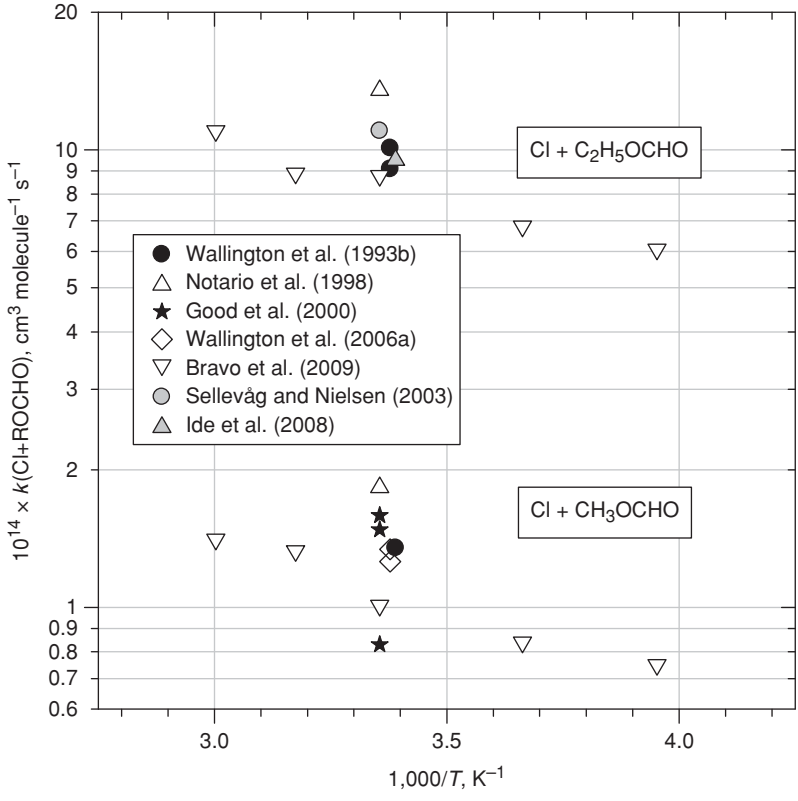

Figure VII-B-2. Measurements of the rate coefficients for reaction of chlorine atoms with CH_3OCHO and C_2H_5OCHO.

will probably be most pronounced in studies of relatively low reactivity compounds such as methyl formate. Bravo et al. (2009) were aware of this complication and ran a control experiment with elevated $[Cl_2]$ and reported "no change" in the value of $k(Cl + CH_3OC(O)H)$. Given the likely experimental uncertainties, it seems possible that a difference of approximately 25% might go undetected in the work of Bravo et al. (2009). The simplest explanation of the discrepancy between the room temperature value of Bravo et al. (2009) and those of Wallington et al. (1993b), Good et al. (2000), and Wallington et al. (2006a) is that regeneration of chlorine atoms was a complication in the study by Bravo et al. (2009).

An average of the results from Wallington et al. (1993b), Good et al. (2000), and Wallington et al. (2006a) gives our recommendation of $k(Cl + CH_3OCHO) = 1.40 \times 10^{-12}$ cm^3 molecule^{-1} s^{-1} at 298 K with an estimated uncertainty of $\pm 25\%$. No recommendation is given for the temperature dependence, and further studies are warranted. Bravo et al. (2009) have reported an HCl yield of $95 \pm 9\%$ consistent with the expectation that the reaction of chlorine atoms with CH_3OCHO proceeds via hydrogen abstraction.

VII-B-1.4. Summary of the Atmospheric Fate of Methyl Formate

Good and Francisco (2000) conducted a computational study of the gas-phase homogeneous reaction of methyl formate with water. Homogeneous gas-phase hydrolysis of methyl formate involves substantial molecular rearrangement and consequently has a high activation barrier of 189 kJ mol^{-1} (Good and Francisco, 2000). Assuming a pre-exponential factor of 5×10^{-12} gives a rate coefficient of the order of $k(H_2O + CH_3OCHO) = 10^{-45}$ cm^3 $molecule^{-1}$ s^{-1} at 298 K. Even in the presence of 20 Torr of water vapor the lifetime of CH_3OCHO with respect to homogeneous hydrolysis will be approximately 10^{20} years! Clearly gas-phase homogeneous reaction of methyl formate with water is not important in the atmosphere.

Kutsuna et al. (2005) determined the Henry's law constant for methyl formate at 298 K to be 4.2 M $atm.^{-1}$ and established an upper limit at 288 K for the rate of hydrolysis of $k_h < 5 \times 10^{-6}$ s^{-1} (estimated from figure 1A, Kutsuna et al., 2005). As described by Seinfeld and Pandis (1998), species with Henry's law constants below 1,000 M $atm.^{-1}$ partition strongly into the gas phase and are considered relatively insoluble. Loss of methyl formate by dissolution into cloud-rain-sea-water will not be of major atmospheric significance. Atmospheric destruction of methyl formate will be controlled via its reaction with OH radicals. Combining $k(OH + CH_3OCHO) = 1.79 \times 10^{-13}$ cm^3 $molecule^{-1}$ s^{-1} at 298 K with a diurnal average of $[OH] \approx 1.0 \times 10^6$ molecule cm^{-3} gives an estimate of 65 days for the atmospheric lifetime with respect to reaction with OH radicals. Le Calvé et al. (1997a) have used structure–activity arguments to estimate that approximately 50% of the reaction occurs via hydrogen abstraction from the CH_3 group with the remaining 50% occurring from the formate —OC(O)H group. Computational results from Good and Francisco (2000) are consistent with this estimation. Tyndall et al. (2004) measured the yields of formic acid, acetic formic anhydride, CO_2, and $CH_3OC(O)O_2NO_2$ following the OH-radical-initiated oxidation of methyl formate in 700 Torr of air at 296 K and concluded that hydrogen abstraction occurs with roughly equal efficiency at each end of the molecule.

$$OH + CH_3OC(O)H \rightarrow CH_2OC(O)H + H_2O \quad (1a)$$

$$OH + CH_3OC(O)H \rightarrow CH_3OCO + H_2O \quad (1b)$$

Wallington et al. (2001a) studied the chlorine-atom-initiated oxidation of methyl formate and reported that the sole atmospheric fate of $CH_2OC(O)H$ and CH_3OCO radicals is addition of O_2 to give the corresponding peroxy radicals [$OOCH_2OC(O)H$ and $CH_3OC(O)OO$]. The peroxy radicals react with NO to give alkoxy radicals [$OCH_2OC(O)H$ and $CH_3OC(O)O$]. The atmospheric fate of $CH_3OC(O)O$ radicals is decomposition to give CH_3O and CO_2 and was unaffected by the method used to generate the $CH_3OC(O)O$ radicals [reaction of $CH_3OC(O)OO$ with either NO or with other peroxy radicals]. CH_3O radicals will react with O_2 to give CH_2O. There are two competing atmospheric loss mechanisms for $OCH_2OC(O)H$ radicals (see figure VII-B-3);

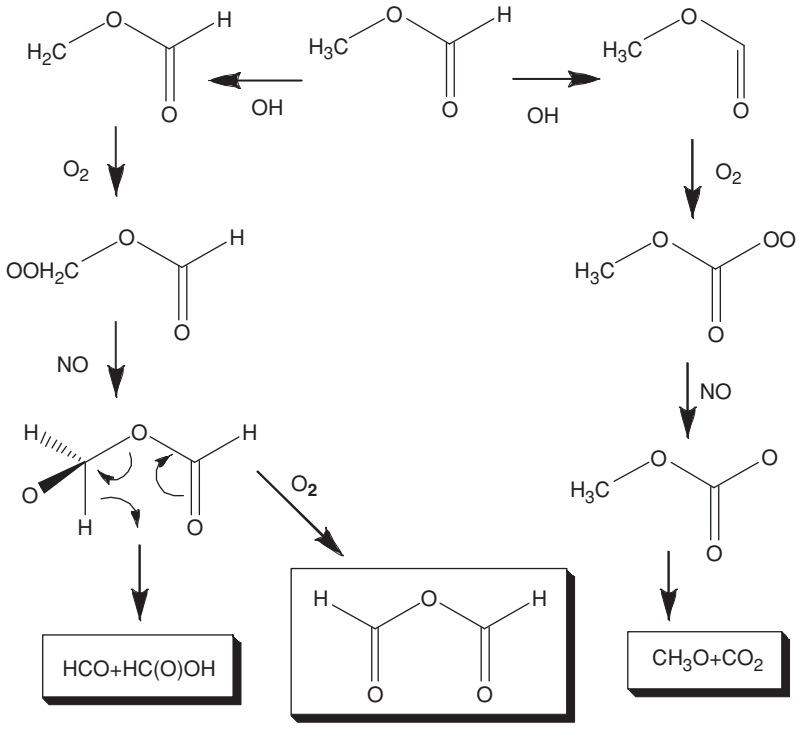

Figure VII-B-3. Simplified oxidation mechanism for methyl formate.

α-ester rearrangement (Tuazon et al., 1998b) to give HC(O)OH and HCO radicals and reaction with O_2 to give HC(O)OC(O)H (formic acid anhydride).

$$OCH_2OC(O)H + M \rightarrow HC(O)OH + HCO \quad (2)$$

$$OCH_2OC(O)H + O_2 \rightarrow HC(O)OC(O)H + HO_2 \quad (3)$$

Wallington et al. (2001a) determined $k_2/k_3 = (1.5 \pm 0.3) \times 10^{18}$ molecule cm^{-3} in 700 Torr of N_2/O_2 diluent at 296 K. Tyndall et al. (2004) measured k_2/k_3 in 700 Torr over the temperature range 273–324 K. As seen from figure VII-B-4, the results from Wallington et al. (2001a) and Tyndall et al. (2004) are in good agreement. A least-squares analysis of the data from Wallington et al. (2001a) and Tyndall et al. (2004) gives $k_2/k_3 = 1.22 \times 10^{25} \exp(-4{,}748/T)$ molecule cm^{-3}. This expression gives $k_2/k_3 = 1.5 \times 10^{18}$ molecule cm^{-3} at 298 K with an estimated uncertainty of $\pm 25\%$. From the Arrhenius expression for k_2/k_3 it can be concluded that the activation barrier for the α-ester rearrangement reaction (2) is 39.5 kJ mole^{-1} greater than for reaction (3). As noted by Tyndall et al. (2004), reactions of alkoxy radicals such as $OCH_2OC(O)H$ with O_2 usually have an activation barrier of 2–5 kJ mol^{-1} and hence the activation barrier for reaction (3) is probably approximately 43 kJ mol^{-1} (10 kcal mole^{-1}).

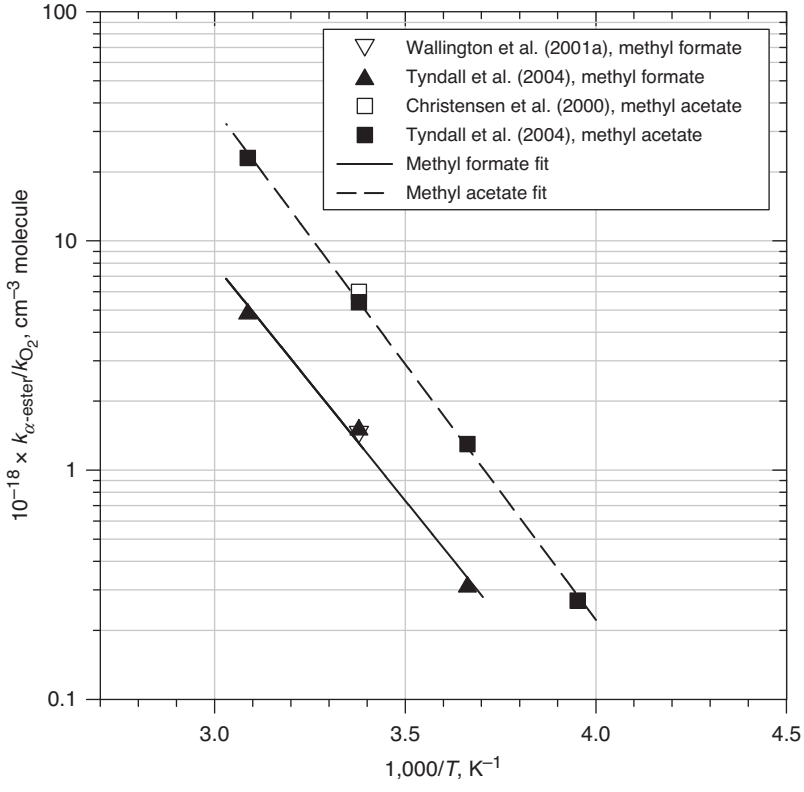

Figure VII-B-4. Arrhenius plots for the rate constant ratio for α-ester rearrangement and reaction with O_2 for $RC(O)OCH_2O$ radicals formed in methyl formate (R = H) and methyl acetate ($R = CH_3$) oxidation.

The exothermicity of reactions of peroxy radicals with NO to give alkoxy radicals and NO_2 is typically approximately 45 kJ mole^{-1}, and a significant fraction of the exothermicity is retained in the RO fragment. The fact that the barrier for decomposition via reaction (3) is comparable to the reaction exothermicity for the formation of $OCH_2OC(O)H$ radicals in the reaction of $OOCH_2OC(O)H$ radicals with NO raises the possibility that chemical activation may be important. Wallington et al. (2001a) found that α-ester rearrangement is more important when $OCH_2OC(O)H$ radicals were produced via the $OOCH_2OC(O)H + NO$ reaction than when they were produced via the peroxy radical–peroxy radical reactions. This observation was ascribed to the formation of chemically activated $OCH_2OC(O)H$ radicals in the $OOCH_2OC(O)H + NO$ reaction. For 1 atm. of air ($[O_2] = 160$ Torr) containing NO at 296 K, it was calculated that $33 \pm 5\%$ of the $OCH_2OC(O)H$ radicals undergo α-ester rearrangement while $67 \pm 12\%$ react with O_2. The OH-radical-initiated oxidation of $CH_3OC(O)H$ gives $HC(O)OC(O)H$, HCOOH, CH_2O, CO, and CO_2 as products. A simplified oxidation mechanism for methyl formate is given in figure VII-B-3.

VII-B-2. Ethyl Formate (C_2H_5OCHO)

VII-B-2.1. OH Reaction Kinetics

The reaction of OH with ethyl formate has been studied by Wallington et al. (1988b) and Le Calvé et al. (1997a) over the temperature range 243–372 K. Data are summarized in table VII-B-3 and are plotted in figure VII-B-5. The room temperature determination of $k(OH + C_2H_5OCHO)$ by Wallington et al. is in agreement with that by Le Calvé et al. (1997a) within the experimental uncertainties. Significant curvature is evident in the Arrhenius plot in figure VII-B-5. A fit of the modified Arrhenius expression to the data from Wallington et al. (1988b) and Le Calvé et al. (1997a) gives: $k(OH + C_2H_5OCHO) = 9.00 \times 10^{-19}\ T^2 \exp(713/T)$ cm^3 molecule^{-1} s^{-1}. This expression gives $k(OH + C_2H_5OCHO) = 8.74 \times 10^{-13}$ cm^3 molecule^{-1} s^{-1} at 298 K with an uncertainty estimated to be ±25%. Corroborative studies of the temperature dependence of this rate coefficient are warranted.

VII-B-2.2. NO_3 Reaction Kinetics

Langer et al. (1993) have reported $k(NO_3 + C_2H_5OCHO) = 1.7 \times 10^{-17}$ cm^3 molecule^{-1} s^{-1} at 296 K using a discharge flow technique in 20–30 mbar of helium diluent. Given the difficulties in studying such a slow reaction using an absolute rate method, an uncertainty of a factor of 2 is estimated at 296 K.

VII-B-2.3. Cl-Atom Reaction Kinetics

Notario et al. (1998), Sellevåg and Nielsen (2003), Wallington et al. (2006a), Ide et al. (2008), and Bravo et al. (2009) have reported measurements of $k(Cl + C_2H_5OCHO)$. The results are listed in table VII-B-4 and shown in figure VII-B-2. The relative

Table VII-B-3. Rate coefficients ($k = A \times e^{-B/T}$, cm^3 molecule^{-1} s^{-1}) for reaction of OH with ethyl formate (C_2H_5OCHO)

$10^{12} \times A$	B (K)	$10^{13} \times k$	T (K)	Technique[a]	Reference	Temperature Range (K)
		10.2 ± 1.4	296	FP–RF	Wallington et al. (1988b)	
0.566 ± 0.110	−134 ± 53	10.26 ± 0.39	243	PLP–LIF	Le Calvé et al. (1997a)	243–372
		9.70 ± 0.11	253			
		9.80 ± 0.25	253			
		9.12 ± 0.33	263			
		8.90 ± 0.42	273			
		8.43 ± 0.32	298			
		8.32 ± 0.27	298			
		8.82 ± 0.32	298			
		8.30 ± 0.32	323			
		8.51 ± 0.53	348			
		8.74 ± 0.36	372			
		8.41 ± 0.58	372			

[a]Abbreviations used for the techniques are defined in table I-F-3.

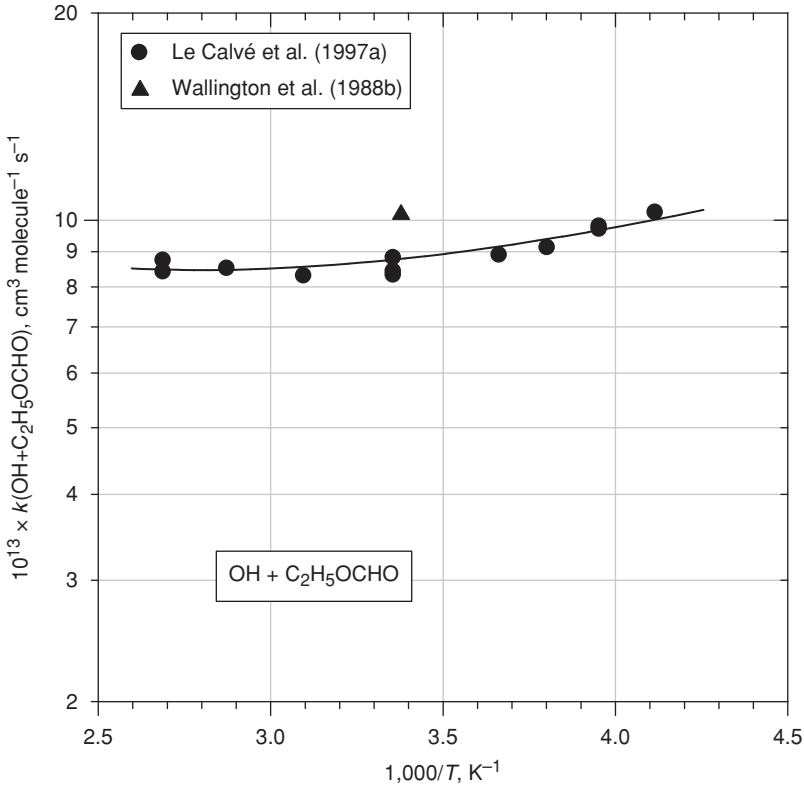

Figure VII-B-5. Measurements of the rate coefficients for reaction of OH radicals with C_2H_5OCHO. The curve is a fit to the data from Wallington et al. (1988b) and Le Calvé et al. (1997a).

Table VII-B-4. Rate coefficients ($k = A \times e^{-B/T}$, cm^3 $molecule^{-1}$ s^{-1}) for reaction of chlorine atoms with ethyl formate (C_2H_5OCHO)

$10^{12} \times A$	B (K)	$10^{11} \times k$	T (K)	Technique[a]	Reference
		1.35 ± 0.15	298	PLP–RF	Notario et al. (1998)
		1.10 ± 0.07	298	RR (C_2H_6)[b]	Sellevåg and Nielsen (2003)
		0.881 ± 0.078	296	RR (C_2H_5Cl)[c]	Wallington et al. (2006a)
		1.03 ± 0.07		RR (C_2H_2)[d]	
		0.95 ± 0.03	295	PLP–LIF	Ide et al. (2008)
55 ± 48	556 ± 268	0.607 ± 0.133	253	DF–MS	Bravo et al. (2009)
		0.681 ± 0.146	273		
		0.878 ± 0.122	298		
		0.889 ± 0.123	315		
		1.10 ± 0.182	333		

[a]Abbreviations used for the techniques are defined in table I-F-3.
[b]Placed on an absolute basis using $k(Cl + C_2H_6) = 5.9 \times 10^{-11}$ cm^3 $molecule^{-1}$ s^{-1} (Atkinson et al., 2006).
[c]Placed on an absolute basis using $k(Cl + C_2H_5Cl) = 7.8 \times 10^{-12}$ cm^3 $molecule^{-1}$ s^{-1} (see section I-F).
[d]Placed on an absolute basis using $k(Cl + C_2H_2) = 5.2 \times 10^{-11}$ cm^3 $molecule^{-1}$ s^{-1} (Atkinson et al., 2006).

rate measurements of Sellevåg and Nielsen (2003) and Wallington et al. (2006a) and the absolute rate study of Ide et al. (2008) are in good agreement. The value of $k(Cl + C_2H_5OCHO)$ from the absolute rate study of Notario et al. (1998) is approximately 25% higher than those from the relative rate studies. Where comparisons were possible, the rate data reported by Notario et al. (1998) are systematically 20–30% higher than values from relative rate studies. As described previously, Wallington et al. (2006a) and Ide et al. (2008) have suggested that the loss of chlorine atoms via reaction with peroxy radicals led to an overestimation of $k(Cl + C_2H_5OCHO)$ by Notario et al. (1998). As seen from figure VII-B-2, the results from the absolute rate study by Bravo et al. (2009) using a discharge flow–mass spectrometer lie slightly (10–20%) below those from Sellevåg and Nielsen (2003), Wallington et al. (2006a), and Ide et al. (2008). As discussed in section VII-B-1.3, regeneration of chlorine atoms leading to an underestimation of $k(Cl + C_2H_5OC(O)H)$ is likely to be a complicating factor in the study by Bravo et al. (2009).

Our recommendation is based upon an average of the values reported by Wallington et al. (2006a), Sellevåg and Nielsen (2003), and Ide et al. (2008); $k(Cl + C_2H_5OCHO) = 9.92 \times 10^{-12}$ cm^3 molecule^{-1} s^{-1} at 298 K with an estimated uncertainty of ±20%. Bravo et al. (2009) have reported an HCl yield of 96 ± 11% consistent with the expectation that the reaction of chlorine atoms with C_2H_5OCHO proceeds via hydrogen abstraction.

VII-B-2.4. Summary of the Atmospheric Fate of Ethyl Formate

Kutsuna et al. (2005) have determined the Henry's law constant for ethyl formate at 298 K to be 3.4 M atm.$^{-1}$ and established an upper limit at 288 K for the rate of hydrolysis of $k_h < 5 \times 10^{-6}$ s^{-1} (estimated from figure 1A, Kutsuna et al., 2005). Species with Henry's law constants below 1,000 M atm.$^{-1}$ partition strongly into the gas phase and are considered relatively insoluble (Seinfeld and Pandis, 1998). Loss of ethyl formate by dissolution into cloud-rain-sea-water will not be of atmospheric significance. Atmospheric destruction of ethyl formate will be controlled via its reaction with OH radicals. Combining $k(OH + CH_3OCHO) = 8.74 \times 10^{-13}$ cm^3 molecule^{-1} s^{-1} at 298 K with a diurnal average of [OH] $\approx 1.0 \times 10^6$ molecule cm^{-3} gives an estimate of 13 days for the atmospheric lifetime with respect to reaction with OH radicals. Reaction with OH radicals dominates the atmospheric fate of ethyl formate.

Using the structure–activity relationships (SARs) outlined by Kwok and Atkinson (1995) together with values of F(—OC(O)H) = 0.6 and k(—OC(O)H) = 0.9×10^{-13} cm^3 molecule^{-1} s^{-1} from Le Calvé et al. (1997a), it can be estimated that attack of OH radicals on ethyl formate occurs 20% at the CH_3 group, 67% at the —CH_2 group, and 11% at the formate group.

$$OH + CH_3CH_2OC(O)H \rightarrow CH_2CH_2OC(O)H + H_2O$$

$$OH + CH_3CH_2OC(O)H \rightarrow CH_3CHOC(O)H + H_2O$$

$$OH + CH_3CH_2OC(O)H \rightarrow CH_3CH_2OCO + H_2O$$

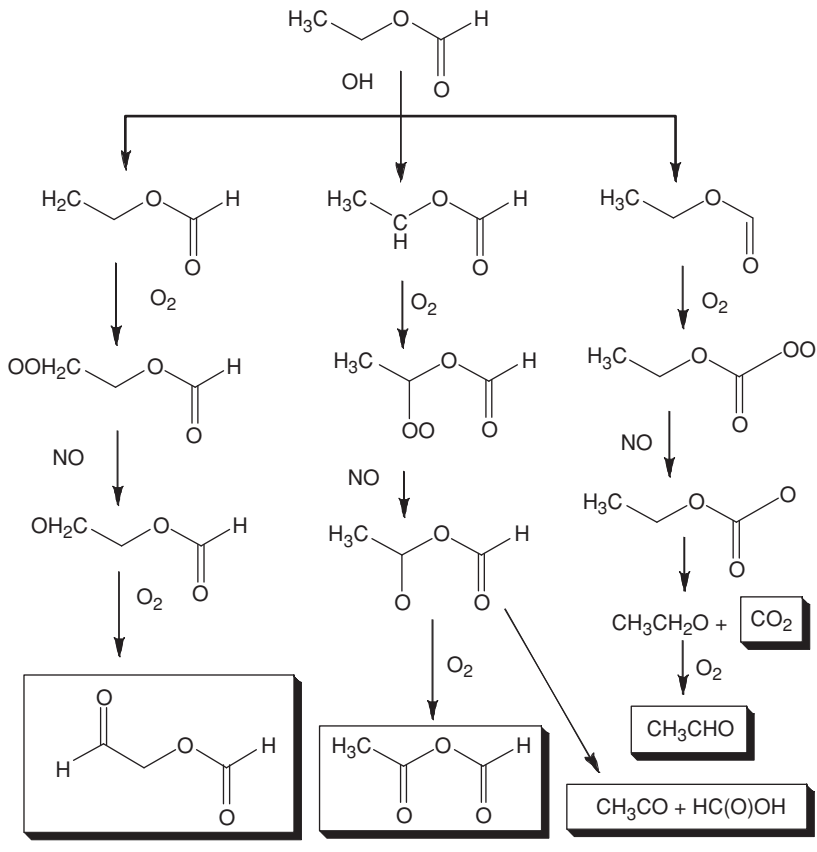

Figure VII-B-6. Simplified oxidation mechanism for ethyl formate.

The $CH_2CH_2OC(O)H$ radical will add O_2 to give a peroxy radical which will be converted into $OCH_2CH_2OC(O)H$, which is expected to react with O_2 to give $HC(O)CH_2OC(O)H$. As illustrated in figure VII-B-6, the fate of the other two alkoxy radicals formed in the oxidation of ethyl formate are expected to be similar to those in the oxidation of methyl formate (see figure VII-B-3). The OH-radical-initiated oxidation of ethyl formate is expected to give $HC(O)CH_2OC(O)H$, $CH_3C(O)OCHO$, CH_2O, HC(O)OH, CO, and CO_2 as primary products. A product study is needed to test this expectation and provide kinetic data for the radical reactions involved.

VII-B-3. *n*-Propyl Formate (n-C_3H_7OCHO)

VII-B-3.1. OH Reaction Kinetics

The reaction of OH with *n*-propyl formate has been studied by Wallington et al. (1988b) and Le Calvé et al. (1997a) over the temperature range 253–372 K. Data are summarized in table VII-B-5 and are plotted in figure VII-B-7. The room temperature determination of $k(OH + n\text{-}C_3H_7OCHO)$ by Wallington et al. is in agreement, within

Table VII-B-5. Rate coefficients ($k = A \times e^{-B/T}$, cm^3 molecule^{-1} s^{-1}) for reaction of OH with *n*-propyl formate (*n*-C_3H_7OCHO)

$10^{12} \times A$	B (K)	$10^{13} \times k$	T (K)	Technique[a]	Reference	Temperature Range (K)
		2.38 ± 0.27	296	FP–RF	Wallington et al. (1988b)	
1.65 ± 0.45	-42 ± 78	1.95 ± 0.06	253	PLP–LIF	Le Calvé et al. (1997a)	253–372
		2.08 ± 0.05	253			
		1.99 ± 0.03	263			
		1.87 ± 0.04	273			
		1.73 ± 0.08	298			
		1.82 ± 0.04	298			
		1.86 ± 0.05	298			
		1.74 ± 0.09	323			
		1.87 ± 0.06	348			
		1.92 ± 0.04	372			
		2.00 ± 0.11	372			

[a]Abbreviations used for the techniques are defined in table I-F-3.

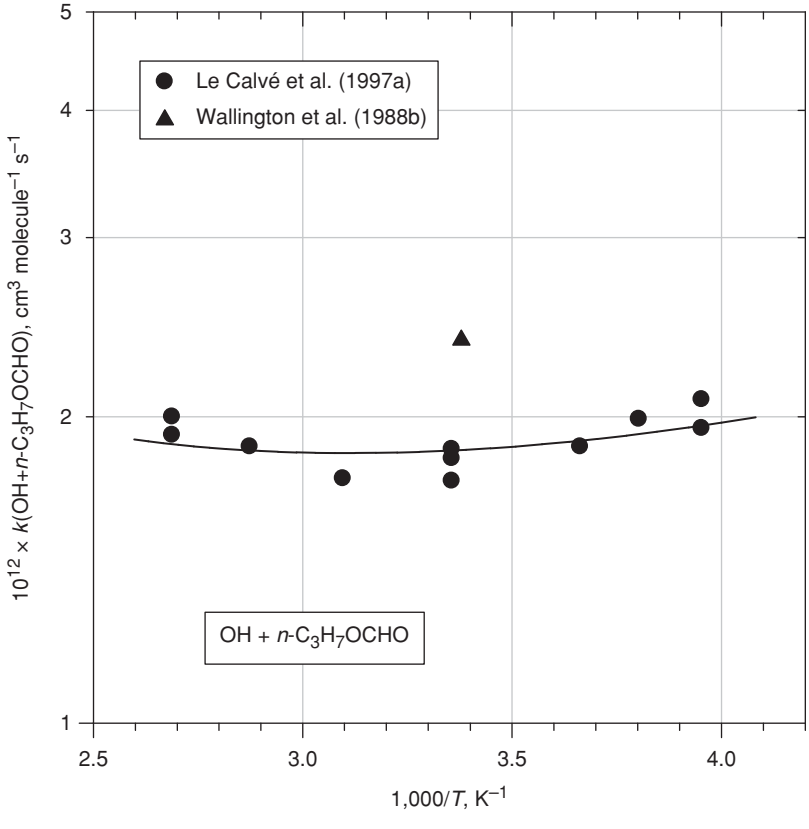

Figure VII-B-7. Measurements of the rate coefficients for reaction of OH radicals with *n*-C_3H_7OCHO. The curve is a fit to the data from Le Calvé et al. (1997a).

the likely combined experimental uncertainties, with that by Le Calvé et al. (1997a). Significant curvature is evident in the Arrhenius plot in figure VII-B-7. A fit of the modified Arrhenius expression to the data from Le Calvé et al. (1997a) gives: $k(\mathrm{OH} + n\text{-}\mathrm{C_3H_7OCHO}) = 2.41 \times 10^{-18}\ T^2 \exp(643/T)$ cm^3 molecule^{-1} s^{-1}. This expression gives $k(\mathrm{OH} + n\text{-}\mathrm{C_3H_7OCHO}) = 1.85 \times 10^{-12}$ cm^3 molecule^{-1} s^{-1} at 298 K with an estimated uncertainty of ±25%. Corroborative studies of this rate coefficient are warranted.

VII-B-3.2. NO_3 Reaction Kinetics

Langer et al. (1993) have reported $k(\mathrm{NO_3} + n\text{-}\mathrm{C_3H_7OCHO}) = 5.4 \times 10^{-17}$ cm^3 molecule^{-1} s^{-1} at 296 K using a discharge flow technique in 21–24 mbar of helium diluent. Given the difficulties in studying such a slow reaction using an absolute rate method, an uncertainty of a factor of two is estimated at 296 K.

VII-B-3.3. Cl-Atom Reaction Kinetics

Notario et al. (1998), Wallington et al. (2006a), and Ide et al. (2008) have reported measurements of $k(\mathrm{Cl} + n\text{-}\mathrm{C_3H_7OCHO})$ at, or near, 298 K. The results are listed in table VII-B-6. The value of $k(\mathrm{Cl} + n\text{-}\mathrm{C_3H_7OCHO})$ from the absolute rate study of Notario et al. (1998) is approximately 25% higher than those from Wallington et al. (2006a) and Ide et al. (2008). Where comparisons are possible, the rate data reported by Notario et al. (1998) are systematically 20–30% higher than values from relative rate studies. As described in previous sections, Wallington et al. (2006a) and Ide et al. (2008) have suggested that the loss of chlorine atoms via reaction with peroxy radicals led to an overestimation of $k(\mathrm{Cl} + n\text{-}\mathrm{C_3H_7OCHO})$ by Notario et al. (1998). Our recommendation is based upon an average of the values reported by Wallington et al. (2006a) and Ide et al. (2008); $k(\mathrm{Cl} + n\text{-}\mathrm{C_3H_7OCHO}) = 4.6 \times 10^{-11}$ cm^3 molecule^{-1}s^{-1} at 298 K with an estimated uncertainty of ±25%.

VII-B-3.4. Summary of the Atmospheric Fate of n-Propyl Formate

Kutsuna et al. (2005) have determined the Henry's law constant for *n*-propyl formate at 298 K to be 2.6 M atm.$^{-1}$ and established an upper limit at 288 K for the rate of

Table VII-B-6. Rate coefficients ($k = A \times e^{-B/T}$, cm^3 molecule^{-1} s^{-1}) for reaction of chlorine atoms with *n*-propyl formate (n-$\mathrm{C_3H_7OCHO}$)

$10^{11} \times k$	T (K)	Technique[a]	Reference
5.63 ± 0.65	298	LP–RF	Notario et al. (1998)
4.36 ± 0.30	296	RR ($\mathrm{C_2H_5Cl}$)[b]	Wallington et al. (2006a)
4.93 ± 0.24		RR ($\mathrm{C_2H_2}$)[c]	
4.5 ± 0.3	295	LP–LIF	Ide et al. (2008)

[a]Abbreviations used for the techniques are defined in table I-F-3.
[b]Placed on an absolute basis using $k(\mathrm{Cl} + \mathrm{C_2H_5Cl}) = 7.8 \times 10^{-12}$ cm^3 molecule^{-1} s^{-1} (section I-F).
[c]Placed on an absolute basis using $k(\mathrm{Cl} + \mathrm{C_2H_2}) = 5.2 \times 10^{-11}$ cm^3 molecule^{-1} s^{-1} (Atkinson et al., 2006).

hydrolysis of $k_h < 5 \times 10^{-6}$ s^{-1} (estimated from figure 1A, Kutsuna et al. 2005). As described by Seinfeld and Pandis (1998), species with Henry's law constants below 1000 M atm.$^{-1}$ partition strongly into the gas phase and are considered relatively insoluble. Loss of *n*-propyl formate by dissolution into cloud-rain-sea-water will not be of atmospheric significance. Combining $k(\text{OH} + n\text{-}C_3H_7OCHO) = 1.85 \times 10^{-12}$ cm^3 molecule^{-1} s^{-1} at 298 K with a diurnal average of [OH] $\approx 1.0 \times 10^6$ molecule cm^{-3} gives an estimate of 6 days for the atmospheric lifetime with respect to reaction with OH radicals. Reaction with OH radicals dominates the atmospheric fate of *n*-propyl formate.

Using the structure–activity relationship method outlined by Kwok and Atkinson (1995) together with values of F(—OC(O)H) = 0.6 and k(—OC(O)H) = 0.9×10^{-13} cm^3 molecule^{-1} s^{-1} from Le Calvé et al. (1997a), it can be estimated that attack of OH radicals on *n*-propyl formate occurs 8% at the CH_3 group, 54% at the CH_2 group β to the ester group, 33% at the CH_2 group α to the ester group, and 5% at the formate group.

$$\text{OH} + CH_3CH_2CH_2OC(O)H \rightarrow CH_2CH_2CH_2OC(O)H + H_2O$$

$$\text{OH} + CH_3CH_2CH_2OC(O)H \rightarrow CH_3CHCH_2OC(O)H + H_2O$$

$$\text{OH} + CH_3CH_2CH_2OC(O)H \rightarrow CH_3CH_2CHOC(O)H + H_2O$$

$$\text{OH} + CH_3CH_2CH_2OC(O)H \rightarrow CH_3CH_2CH_2OCO + H_2O$$

Abstraction of the formate hydrogen atom will lead to the formation of CO_2 and C_2H_5CHO following a mechanism similar to that for methyl and ethyl formate. Abstraction of hydrogen from the CH_2 group α to the ester functionality will lead to the formation of the alkoxy radical $CH_3CH_2C(O)HOC(O)H$ which will react with O_2 and decompose via the α ester rearrangement (see figures VII-B-3 and VII-B-6). Abstraction of hydrogen from the CH_2 group β to the ester functionality will lead to the formation of the alkoxy radical $CH_3CH(O)CH_2OC(O)H$ which is expected to react with O_2 to give $CH_3C(O)CH_2OC(O)H$. Finally, hydrogen abstraction from the CH_3 group will lead to formation of $HC(O)CH_2CH_2OC(O)H$.

VII-B-4. *iso*-Propyl Formate (*iso*-C_3H_7OCHO)

VII-B-4.1. OH Reaction Kinetics

Stemmler et al. (1997a) and Pimentel et al. (2010) have studied the reaction of OH with *iso*-propyl formate using relative rate techniques. As seen from table VII-B-7, the results reported by Stemmler et al. (1997a) and Pimentel et al. (2010) are in excellent agreement. An average gives $k(\text{OH} + iso\text{-}C_3H_7OCHO) = 2.29 \times 10^{-12}$ cm^3 molecule^{-1} s^{-1} which is recommended with an uncertainty of ±20%.

VII-B-4.2. Cl-Atom Reaction Kinetics

Pimentel et al. (2010) used relative rate methods to measure $k(\text{Cl} + iso\text{-}C_3H_7OCHO) = 1.76 \times 10^{-11}$ cm^3 molecule^{-1} s^{-1}; see table VII-B-8 for details.

Table VII-B-7. Rate coefficients (k, cm^3 molecule^{-1} s^{-1}) for reaction of OH with *iso*-propyl formate (*iso*-C_3H_7OCHO)

$10^{12} \times k$	T (K)	Technique[a]	Reference
2.2 ± 0.2	297	RR [(*n*-$C_3H_7)_2O$][b]	Stemmler et al. (1997a)
2.37 ± 0.40	296	RR (C_2H_4)[c]	Pimentel et al. (2010)

[a]Abbreviations used for the techniques are defined in table I-F-3.
[b]Placed on an absolute basis using $k[(OH + n\text{-}C_3H_7)_2O] = 2.0 \times 10^{-11}$ cm^3 molecule^{-1} s^{-1} (this book, section III-B-6.1).
[c]Placed on an absolute basis using $k(OH + C_2H_4) = 7.9 \times 10^{-12}$ cm^3 molecule^{-1} s^{-1} (Atkinson et al., 2006).

Table VII-B-8. Rate coefficients (k, cm^3 molecule^{-1} s^{-1}) for reaction of chlorine atoms with *iso*-propyl formate (*iso*-C_3H_7OCHO)

$10^{12} \times k$	T (K)	Technique[a]	Reference
1.76 ± 0.17	296	RR (CH_3OH)[b]	Pimentel et al. (2010)

[a]Abbreviations used for the techniques are defined in Table I-F-3.
[b]Placed on an absolute basis using $k(Cl+CH_3OH) = 5.5 \times 10^{-11}$ cm^3 molecule^{-1} s^{-1} (Atkinson et al., 2006).

VII-B-4.3. Summary of the Atmospheric Fate of iso-Propyl Formate

Combining $k(OH + iso\text{-}C_3H_7OCHO) = 2.29 \times 10^{-12}$ cm^3 molecule^{-1} s^{-1} at 298 K with a diurnal average of [OH] $\approx 1.0 \times 10^6$ molecule cm^{-3} gives an estimate of 5 days for the atmospheric lifetime of *iso*-propyl formate.

Using the structure–activity relationship (SAR) method outlined by Kwok and Atkinson (1995) together with values of F(—OC(O)H) = 0.6 and k(—OC(O)H) = 0.9×10^{-13} cm^3 molecule^{-1} s^{-1} from Le Calvé et al. (1997a), it can be estimated that attack of OH radicals on *iso*-propyl formate occurs 21% at the CH_3 groups, 72% at the tertiary C—H group, and 7% at the formate group.

$$OH + (CH_3)_2CHOC(O)H \rightarrow CH_2(CH_3)CHOC(O)H + H_2O$$

$$OH + (CH_3)_2CHOC(O)H \rightarrow (CH_3)_2COC(O)H + H_2O$$

$$OH + (CH_3)_2CHOC(O)H \rightarrow (CH_3)_2CHOCO + H_2O$$

Pimentel et al. (2010) studied the OH-radical-initiated oxidation of isopropyl formate in the presence of NO_x and reported the following products (molar yields): acetic formic anhydride (43%), acetone (43%), and HCOOH (15–20%). From the observed formation of CH_2O in the chlorine-atom-initiated oxidation of *iso*-propyl formate, Pimentel et al. (2010) deduced that the fate of $OCH_2(CH_3)CHOC(O)H$ alkoxy radicals is decomposition (rather than reaction with O_2). The resulting alkyl radical $(CH_3)CHOC(O)H$ is converted into the alkoxy radical $O(CH_3)CHOC(O)H$ which then decomposes via

the α-ester rearrangement and reacts with O_2 to give formic acetic anhydride:

$$OCH_2(CH_3)CHOC(O)H \rightarrow HCHO + (CH_3)CHOC(O)H$$

$$(CH_3)CHOC(O)H + O_2 + NO \rightarrow\rightarrow O(CH_3)CHOC(O)H + NO_2$$

$$O(CH_3)CHOC(O)H \rightarrow CH_3CO + HC(O)OH$$

$$O(CH_3)CHOC(O)H + O_2 \rightarrow CH_3C(O)OC(O)H + HO_2$$

Abstraction of the tertiary C—H leads to the formation of the $O(CH_3)_2COC(O)H$ alkoxy radical which decomposes (via elimination of a CH_3 group) and isomerizes:

$$O(CH_3)_2COC(O)H \rightarrow CH_3 + CH_3C(O)OC(O)H$$

$$O(CH_3)_2COC(O)H \rightarrow HO(CH_3)_2COCO$$

$$HO(CH_3)_2COC(O) + O_2 \rightarrow HO(CH_3)_2COC(O)OO$$

$$HO(CH_3)_2COC(O)OO + NO + O_2 \rightarrow\rightarrow CH_3C(O)CH_3 + CO_2 + NO_2 + HO_2$$

Abstraction of the formyl hydrogen leads to the formation of the $(CH_3)_2CHOC(O)O$ radical which eliminates CO_2:

$$(CH_3)_2CHOC(O)O \rightarrow (CH_3)_2CHO + CO_2$$

$$(CH_3)_2CHO + O_2 \rightarrow CH_3C(O)CH_3 + HO_2$$

VII-B-5. *n*-Butyl Formate (*n*-C_4H_9OCHO)

VII-B-5.1. OH Reaction Kinetics

The reaction of OH with *n*-butyl formate has been studied by Wallington et al. (1988b) and Le Calvé et al. (1997a) over the temperature range 253–371 K. Data are summarized in table VII-B-9 and are plotted in figure VII-B-8. The room temperature determination of $k(OH + n\text{-}C_4H_9OCHO)$ by Wallington et al. (1988b) is in agreement with that by Le Calvé et al. (1997a). Significant curvature is evident in the Arrhenius plot in figure VII-B-8. A fit of the modified Arrhenius expression to the data from Wallington et al. (1988b) and Le Calvé et al. (1997a) gives $k(OH + n\text{-}C_4H_9OCHO) = 4.95 \times 10^{-18}\ T^2 \exp(633/T)$ cm^3 molecule^{-1} s^{-1}. This expression gives $k(OH + n\text{-}C_4H_9OCHO) = 3.68 \times 10^{-12}$ cm^3 molecule^{-1} s^{-1} at 298 K with an uncertainty estimated to be $\pm 20\%$. Corroborative studies of the temperature dependence of this rate coefficient are warranted.

Table VII-B-9. Rate coefficients ($k = A\ e^{-B/T}$, cm^3 $molecule^{-1}$ s^{-1}) for reaction of OH with *n*-butyl formate (*n*-C_4H_9OCHO)

$10^{12} \times A$	B (K)	$10^{13} \times k$	T (K)	Technique[a]	Reference	Temperature Range (K)
		3.12 ± 0.33	296	FP–RF	Wallington et al. (1988b)	
3.63 ± 1.08	-15 ± 88	4.30 ± 0.26	253	PLP–LIF	Le Calvé et al. (1997a)	253–371
		3.91 ± 0.32	253			
		3.82 ± 0.34	263			
		4.06 ± 0.22	263			
		4.06 ± 0.39	263			
		4.06 ± 0.14	273			
		3.55 ± 0.32	273			
		3.47 ± 0.28	283			
		3.56 ± 0.34	297			
		3.61 ± 0.23	298			
		3.45 ± 0.18	298			
		3.64 ± 0.32	313			
		3.82 ± 0.22	333			
		3.75 ± 0.18	333			
		3.95 ± 0.28	353			
		4.10 ± 0.16	371			

[a]Abbreviations used for the techniques are defined in table I-F-3.

VII-B-5.2. Cl-Atom Reaction Kinetics

Notario et al. (1998), Wallington et al. (2006a), and Ide et al. (2008) have reported measurements of $k(Cl + n\text{-}C_4H_9OCHO)$ at, or near, 298 K. The results are listed in table VII-B-10. The value of $k(Cl + n\text{-}C_4H_9OCHO)$ from the absolute rate study of Notario et al. (1998) is approximately 25% higher than those from Wallington et al. (2006a) and Ide et al. (2008). As described in previous sections, Wallington et al. (2006a) and Ide et al. (2008) have suggested that the loss of chlorine atoms via reaction with peroxy radicals led to an overestimation of $k(Cl + n\text{-}C_4H_9OCHO)$ by Notario et al. (1998). Our recommendation is based upon an average of the values reported by Wallington et al. (2006a) and Ide et al. (2008) giving $k(Cl + n\text{-}C_4H_9OCHO) = 1.16 \times 10^{-10}$ cm^3 $molecule^{-1}$ s^{-1} at 298 K with an estimated uncertainty of ±25%.

VII-B-5.3. Summary of the Atmospheric Fate of n-Butyl Formate

Combining $k(OH + n\text{-}C_4H_9OCHO) = 3.68 \times 10^{-12}$ cm^3 $molecule^{-1}$ s^{-1} at 298 K with a diurnal average of $[OH] \approx 1.0 \times 10^6$ molecule cm^{-3} gives an estimate of 3 days for the atmospheric lifetime with respect to reaction with OH radicals. Reaction with OH radicals dominates the atmospheric fate of *n*-butyl formate.

Using the structure–activity relationship method outlined by Kwok and Atkinson (1995) together with values of F(—OC(O)H) = 0.6 and k(—OC(O)H) = 0.9×10^{-13} cm^3 $molecule^{-1}$ s^{-1} from Le Calvé et al. (1997a), it can be estimated that attack of OH radicals on *n*-butyl formate occurs 5% at the CH_3 group , 33% at

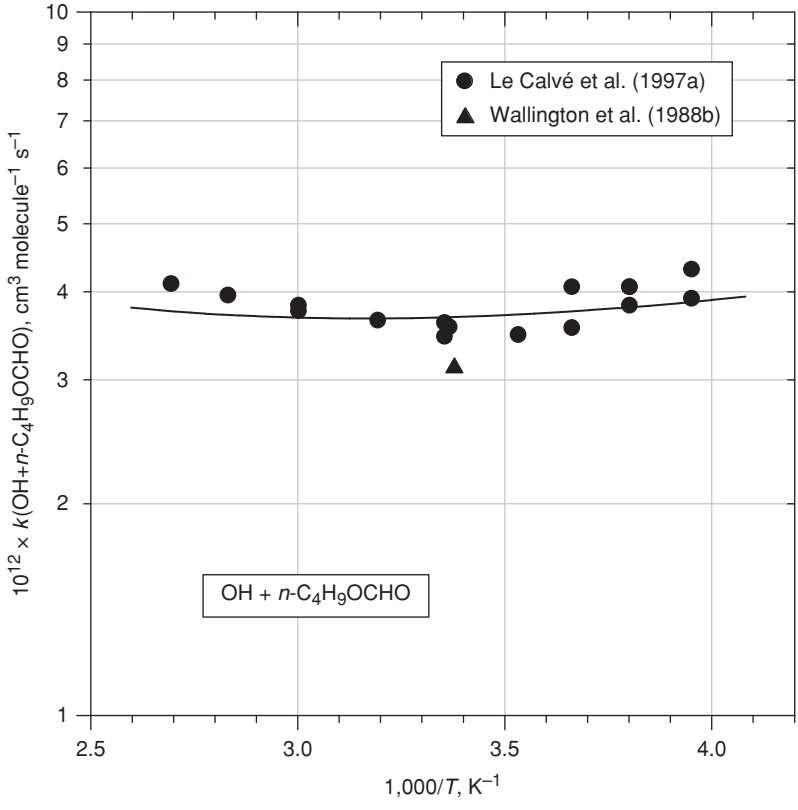

Figure VII-B-8. Measurements of the rate coefficients for reaction of OH radicals with n-C_4H_9OCHO. The curve is a fit to the data of Wallington et al. (1988b) and Le Calvé et al. (1997a).

Table VII-B-10. Rate coefficients (k, cm^3 molecule^{-1} s^{-1}) for reaction of chlorine atoms with n-butyl formate (n-C_4H_9OCHO)

$10^{10} \times k$	T (K)	Technique[a]	Reference
1.41 ± 0.17	298	PLP–RF	Notario et al. (1998)
1.10 ± 0.09	296	RR (C_2H_2)[b]	Wallington et al. (2006a)
1.19 ± 0.07		RR (C_2H_4)[c]	
1.2 ± 0.1	295	PLP–LIF	Ide et al. (2008)

[a]Abbreviations used for the techniques are defined in table I-F-3.
[b]Placed on an absolute basis using $k(Cl + C_2H_2) = 5.2 \times 10^{-11}$ cm^3 molecule^{-1} s^{-1} (Atkinson et al., 2006).
[c]Placed on an absolute basis using $k(Cl+C_2H_4) = 9.52 \times 10^{-11}$ cm^3 molecule^{-1} s^{-1} (section I-F).

the CH_2 group γ to the formate group, 40% at the CH_2 group β to the formate group, 19% at the CH_2 group α to the formate group, and 3% at the formate group.

$$OH + CH_3CH_2CH_2CH_2OC(O)H \rightarrow CH_2CH_2CH_2CH_2OC(O)H + H_2O$$

$$OH + CH_3CH_2CH_2CH_2OC(O)H \rightarrow CH_3CHCH_2CH_2OC(O)H + H_2O$$

$$OH + CH_3CH_2CH_2CH_2OC(O)H \rightarrow CH_3CH_2CHCH_2OC(O)H + H_2O$$

$$OH + CH_3CH_2CH_2CH_2OC(O)H \rightarrow CH_3CH_2CH_2CHOC(O)H + H_2O$$

$$OH + CH_3CH_2CH_2CH_2OC(O)H \rightarrow CH_3CH_2CH_2CH_2OCO + H_2O$$

The subsequent fate of the alkoxy radicals generated following the above reactions is expected to be similar to that described for the alkoxy radicals generated in the oxidation of *n*-propyl formate.

VII-B-6. *tert*-Butyl Formate (*tert*-C_4H_9OCHO)

VII-B-6.1. OH Reaction Kinetics

The reaction of OH with *tert*-butyl formate has been studied by Le Calvé et al. (1997a) over the temperature range 253–372 K. Data are summarized in table VII-B-11 and are plotted in figure VII-B-9. Significant curvature is evident in the Arrhenius plot in figure VII-B-9. A fit of the modified Arrhenius expression to the data from Le Calvé et al. (1997a) gives $k(OH + tert\text{-}C_4H_9OCHO) = 5.41 \times 10^{-18}\, T^2 \exp(145/T)$ cm^3 $molecule^{-1}$ s^{-1}. This expression gives $k(OH + tert\text{-}C_4H_9OCHO) = 7.82 \times 10^{-13}$ cm^3 $molecule^{-1}$ s^{-1} at 298 K with an uncertainty estimated to be ±25%. Corroborative studies of this rate coefficient are warranted.

Table VII-B-11. Rate coefficients ($k = A \times e^{-B/T}$, cm^3 $molecule^{-1}$ s^{-1}) for reaction of OH with *tert*-butyl formate (*tert*-C_4H_9OCHO)

$10^{12} \times A$	B (K)	$10^{13} \times k$	T (K)	Technique[a]	Reference	Temperature Range (K)
3.59 ± 0.98	449 ± 82	6.20 ± 0.24	253	PLP–LIF	Le Calvé et al. (1997a)	253–372
		6.34 ± 0.75	253			
		6.87 ± 0.25	263			
		6.98 ± 0.32	273			
		7.29 ± 0.43	298			
		7.46 ± 0.30	298			
		7.50 ± 0.52	298			
		7.58 ± 0.54	298			
		8.87 ± 0.52	323			
		10.25 ± 0.82	348			
		11.15 ± 0.83	372			
		11.63 ± 0.64	372			

[a]Abbreviations used for the techniques are defined in table I-F-3.

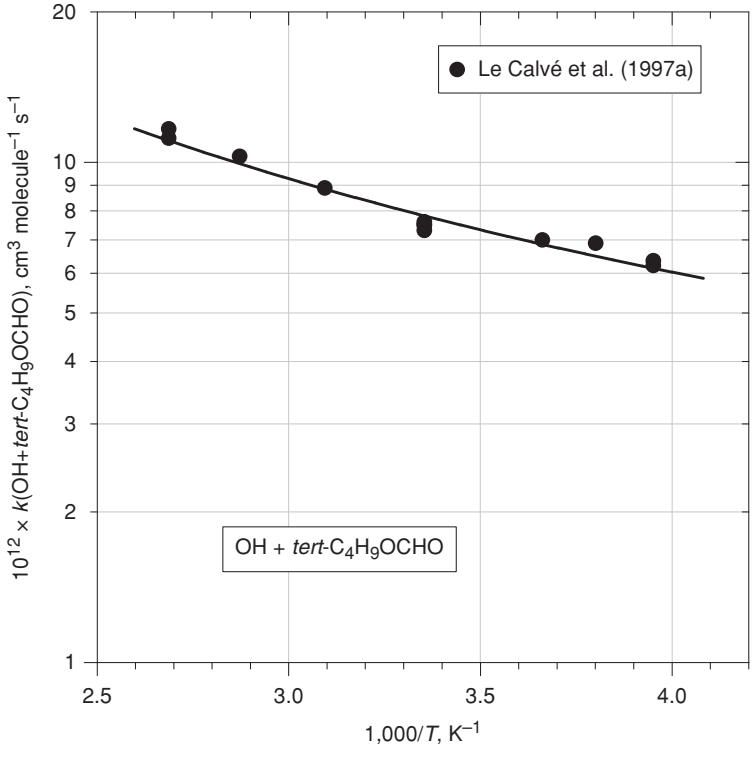

Figure VII-B-9. Measurements of the rate coefficients for reaction of OH radicals with *tert*-C_4H_9OCHO. The curve is a fit to the data.

VII-B-6.2. Cl-Atom Reaction Kinetics

The kinetics of the reaction of chlorine atoms with *tert*-butyl formate have been studied using relative rate methods with three different reference compounds in two different experimental systems by Pimentel et al. (2010). An average of the results listed in table VII-B-12 gives $k(\mathrm{Cl} + \textit{tert}\text{-}\mathrm{C_4H_9OCHO}) = 1.45 \times 10^{-11}$ cm^3 molecule^{-1} s^{-1}.

VII-B-6.3. Summary of the Atmospheric Fate of tert-Butyl Formate

Combining $k(\mathrm{OH} + \textit{tert}\text{-}\mathrm{C_4H_9OCHO}) = 7.82 \times 10^{-12}$ cm^3 molecule^{-1} s^{-1} at 298 K with a diurnal average of [OH] $\approx 1.0 \times 10^6$ molecule cm^{-3} gives an estimate of 15 days for the atmospheric lifetime of *tert*-butyl formate. Using the structure–activity relationship method outlined by Kwok and Atkinson (1995) together with values of F(—OC(O)H) = 0.6 and k(—OC(O)H) = 0.9 $\times 10^{-13}$ cm^3 molecule^{-1} s^{-1} from Le Calvé et al. (1997a) it can be estimated that attack of OH radicals on *tert*-butyl formate occurs 85% at the CH_3 groups and 15% at the —OC(O)H group.

$$\mathrm{OH} + (\mathrm{CH_3})_3\mathrm{COC(O)H} \rightarrow \mathrm{CH_2(CH_3)_2COC(O)H} + \mathrm{H_2O}$$

$$\mathrm{OH} + (\mathrm{CH_3})_3\mathrm{COC(O)H} \rightarrow (\mathrm{CH_3})_3\mathrm{COCO} + \mathrm{H_2O}$$

Table VII-B-12. Rate coefficients (k, cm^3 molecule^{-1} s^{-1}) for reaction of chlorine atoms with *tert*-butyl formate (*tert*-C_4H_9OCHO)

$10^{11} \times k$	T (K)	Technique[a]	Reference
1.38 ± 0.14	296	RR (CH_3COCH_3)[b]	Pimentel et al. (2010)
1.46 ± 0.30		RR (CH_3OH)[c]	
1.50 ± 0.12		RR (C_2H_5Cl)[d]	

[a]Abbreviations used for the techniques are defined in table I-F-3.
[b]Placed on an absolute basis using $k(Cl+C_2H_2) = 2.1 \times 10^{-11}$ cm^3 molecule^{-1} s^{-1} (Atkinson et al., 2006).
[c]Placed on an absolute basis using $k(Cl + CH_3OH) = 5.5 \times 10^{-11}$ cm^3 molecule^{-1} s^{-1} (Atkinson et al., 2006).
[d]Placed on an absolute basis using $k(Cl + C_2H_5Cl) = 7.8 \times 10^{-12}$ cm^3 molecule^{-1} s^{-1} (section I-F).

Pimentel et al. (2010) studied the products of the chlorine-atom- and OH-radical-initiated oxidation of *tert*-butyl formate in 700 Torr of N_2/O_2 diluent with and without NO_x. Photolysis of Cl_2–*tert*-butyl formate–N_2 mixtures with less than 200 m Torr Cl_2 showed no strong evidence for the formation of an acyl chloride, but instead led to large yields of CO_2. The yield of CO_2 at low Cl_2 was found to be 0.50 ± 0.05. Pimentel et al. (2010) assigned this yield to the fraction of attack at the formyl group which is followed by decomposition of the resulting *tert*-butoxycarbonyl radical.

$$Cl + (CH_3)_3COC(O)H \rightarrow HCl + (CH_3)_3COC(O)$$

$$(CH_3)_3COCO \rightarrow CO_2 + (CH_3)_3C$$

It follows that the fraction of attack of chlorine atoms at the $(CH_3)_3C$ group is also 0.50 ± 0.05. In experiments using Cl_2–*tert*-butyl formate–NO–air mixtures, little or no CH_3 radical formation was observed (no evidence for formation of CH_3ONO or CH_3ONO_2), the combined molar yield of CH_2O and CO was 0.45–0.55, and CH_2O was formed as a primary product in a molar yield of at least 0.40. The absence of CH_3 radical formation was ascribed to efficient scavenging of $(CH_3)_3CO$ radicals in the system by NO and NO_2 (leading to formation of *tert*-butyl nitrite and *tert*-butyl nitrate). There are two possible fates for $OCH_2(CH_3)_2COC(O)H$ radicals which would account for their observed yield of CH_2O (∼100%): C—C bond scission, or isomerization followed by decomposition. Decomposition leads to $O(CH_3)_2COC(O)H$ alkoxy radicals. Pimentel et al. (2010) using *iso*-propyl formate showed that $O(CH_3)_2COC(O)H$ alkoxy radicals decompose via eliminating CH_3 radicals. Hence, to explain the formation of CH_2O and absence of CH_3 radicals, Pimentel et al. (2010) concluded that the fate of $OCH_2(CH_3)_2COC(O)H$ radicals is isomerization:

$$OCH_2(CH_3)_2COC(O)H \rightarrow HOCH_2(CH_3)_2COCO$$

$$HOCH_2(CH_3)_2COCO + O_2 + NO \rightarrow\rightarrow HOCH_2(CH_3)_2COC(O)O + NO_2$$

$$HOCH_2(CH_3)_2COC(O)O \rightarrow HOCH_2 + CH_3C(O)CH_3 + CO_2$$

$$HOCH_2 + O_2 \rightarrow HCHO + HO_2$$

Pimentel et al. (2010) identified acetone in a molar yield of approximately 0.40, and $(CH_3)_3CONO$, $(CH_3)_3CONO_2$, and CO_2 as major products of the OH-radical-initiated oxidation of *tert*-butyl formate in air in the presence of NO_x. The combined yields of acetone, $(CH_3)_3CONO$, and $(CH_3)_3CONO_2$ were indistinguishable from that of the CO_2 within the experimental uncertainties. Pimentel et al. (2010) concluded that the reaction of OH radicals with *tert*-butyl formate proceeds with roughly equal abstraction at the two sites. Interestingly, this is a significantly different branching ratio from that predicted from the SAR method. Additional studies are needed.

VII-B-7. Methyl Acetate [$CH_3OC(O)CH_3$]

VII-B-7.1. OH Reaction Kinetics

The reaction of OH with methyl acetate has been studied by Campbell and Parkinson (1978), Wallington et al. (1988b), Smith et al. (1995), and El Boudali et al. (1996) over the temperature range 240–440 K. The results are summarized in table VII-B-13 and are plotted in figure VII-B-10. The early study by Campbell and Parkinson (1978) was the least direct investigation, and the result from this study lies substantially below those from subsequent studies. It seems likely that the study by Campbell and Parkinson

Table VII-B-13. Rate coefficients ($k = A \times e^{-B/T}$, cm^3 $molecule^{-1}$ s^{-1}) for reaction of OH with methyl acetate [$CH_3OC(O)CH_3$]

$10^{12} \times A$	B (K)	$10^{13} \times k$	T (K)	Technique[a]	Reference	Temperature Range (K)
		1.65 ± 0.27	292	RR (n-C_4H_{10})[b]	Campbell and Parkinson (1978)	
0.83 ± 0.35	260 ± 150	4.86 ± 0.37	240	FP–RF	Wallington et al. (1988b)	240–440
($T = 296$–440)	($T = 296$–440)	4.19 ± 0.32	263			
		3.41 ± 0.29	296			
		4.14 ± 0.30	350			
		3.95 ± 0.38	400			
		4.74 ± 0.66	440			
		3.70 ± 0.15	298	RR (C_3H_8)[c]	Smith et al. (1995)	
0.53 ± 0.09	128 ± 102	3.54 ± 0.24	243	PLP–LIF	El Boudali et al. (1996)	243–369
		3.24 ± 0.14	253			
		3.27 ± 0.15	263			
		3.19 ± 0.12	273			
		3.26 ± 0.08	298			
		3.18 ± 0.10	298			
		3.09 ± 0.14	298			
		3.17 ± 0.16	298			
		3.15 ± 0.26	298			
		3.40 ± 0.14	323			
		3.78 ± 0.11	348			
		4.05 ± 0.19	369			

[a]Abbreviations used for the techniques are defined in table I-F-3.
[b]Placed on an absolute basis using $k(OH + n\text{-}C_4H_{10}) = 2.36 \times 10^{-12}$ cm^3 $molecule^{-1}$ s^{-1} (Calvert et al., 2008).
[c]Placed on an absolute basis using $k(OH + C_3H_8) = 1.10 \times 10^{-12}$ cm^3 $molecule^{-1}$ s^{-1} (Calvert et al., 2008).

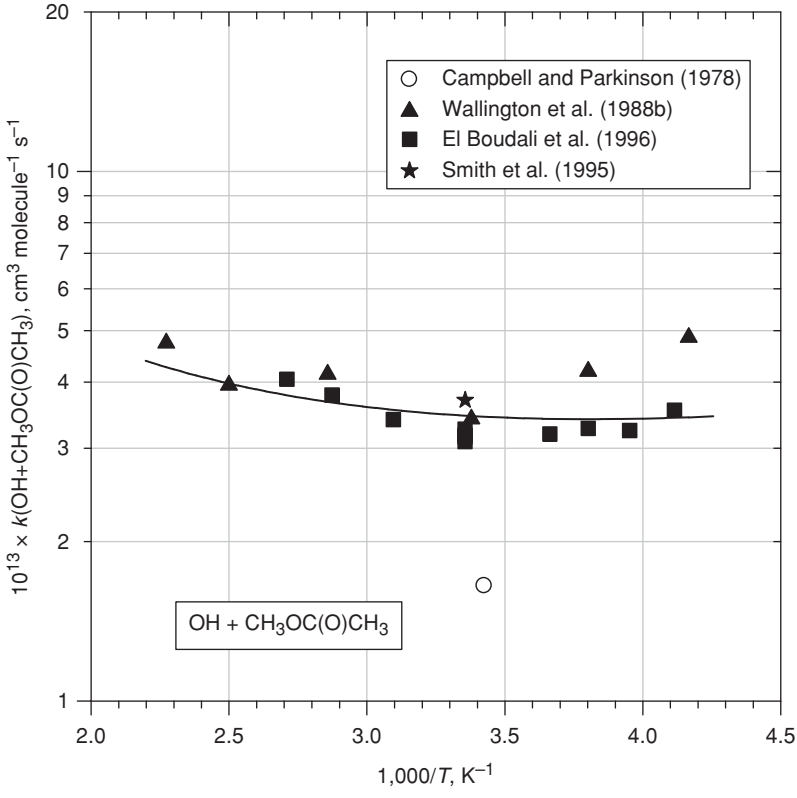

Figure VII-B-10. Measurements of the rate coefficients for reaction of OH radicals with $CH_3OC(O)CH_3$. The curve is a fit to the data of Wallington et al. (1988b), Smith et al. (1995), and El Boudali et al. (1996).

(1978) was subject to substantial systematic error. Significant curvature is evident in the Arrhenius plot in figure VII-B-10. A fit of the modified Arrhenius expression to the data from Wallington et al. (1988b), Smith et al. (1995), and El Boudali et al. (1996) gives: $k(\mathrm{OH} + \mathrm{CH_3OC(O)CH_3}) = 6.69 \times 10^{-19}\, T^2 \exp(525/T)$ cm^3 molecule^{-1} s^{-1}. This expression gives $k(\mathrm{OH} + \mathrm{CH_3OC(O)CH_3}) = 3.46 \times 10^{-13}$ cm^3 molecule^{-1} s^{-1} at 298 K with an estimated uncertainty of $\pm 20\%$.

VII-B-7.2. Cl-Atom Kinetics

The reaction of chlorine atoms with methyl acetate has been the subject of absolute rate studies by Notario et al. (1998) and Cuevas et al. (2005) and a relative rate study by Christensen et al. (2000). The rate coefficient data are summarized in table VII-B-14 and are plotted in figure VII-B-11. The values of $k(\mathrm{Cl} + \mathrm{CH_3OC(O)CH_3})$ measured by Notario et al. (1998) and Cuevas et al. (2005) are approximately 25% higher than those measured by Christensen et al. (2000). As described previously, Wallington et al. (2006a) have argued that there may have been secondary loss of chlorine atoms via

Table VII-B-14. Rate coefficients ($k = A \times e^{-B/T}$, cm^3 $molecule^{-1}$ s^{-1}) for reaction of chlorine atoms with methyl acetate [$CH_3OC(O)CH_3$]

$10^{12} \times A$	B (K)	$10^{12} \times k$	T(K)	Technique[a]	Reference
		2.85 ± 0.35	298	PLP–RF	Notario et al. (1998)
		2.15 ± 0.23	296	RR (C_2H_5F)[b]	Christensen et al. (2000)
		1.96 ± 0.16		RR (CH_3Cl)[c]	
		2.27 ± 0.22		RR (CH_3OCHO)[d]	
9.31 ± 1.02	359 ± 70	2.16 ± 0.27	264.5	PLP–RF	Cuevas et al. (2005)
		2.56 ± 0.12	274.5		
		2.33 ± 0.25	281.5		
		2.73 ± 0.42	298		
		2.79 ± 0.20	298		
		2.72 ± 0.25	298		
		2.92 ± 0.22	298		
		2.95 ± 0.26	310		
		3.23 ± 0.30	331		
		3.46 ± 0.20	354		
		3.49 ± 0.20	380		

[a]Abbreviations used for the techniques are defined in table I-F-3.
[b]Placed on an absolute basis using $k(Cl + C_2H_5F) = 7.24 \times 10^{-12}$ cm^3 $molecule^{-1}$ s^{-1} (Atkinson et al., 2008).
[c]Placed on an absolute basis using $k(Cl + CH_3Cl) = 4.8 \times 10^{-13}$ cm^3 $molecule^{-1}$ s^{-1} (Atkinson et al., 2008).
[d]Placed on an absolute basis using $k(Cl + CH_3OCHO) = 1.4 \times 10^{-12}$ cm^3 $molecule^{-1}$ s^{-1} (this book, section VII-B-1).

reaction with peroxy radicals in the pulsed laser photolyis with resonance fluorescence measurements of Notario et al. (1998) which lead to an overestimate of the value of k(Cl). A similar argument can be made for the experimental conditions employed by Cuevas et al. (2005). In the absence of further information we opt to recommend a value of $k(Cl + CH_3OC(O)CH_3) = 2.55 \times 10^{-12}$ cm^3 $molecule^{-1}$ s^{-1} at 298 K derived from an average of the values reported by Notario et al. (1998), Christensen et al. (2000), and Cuevas et al. (2005) with an estimated uncertainty of ±30%. No recommendation is made for the temperature dependence.

VII-B-7.3. Summary of the Atmospheric Fate of Methyl Acetate

Methyl acetate has a Henry's law constant of approximately 10 M atm^{-1} (Sander, 1999). Loss of methyl acetate by dissolution into cloud-rain-sea-water will not be of atmospheric significance. Combining $k(OH + CH_3OC(O)CH_3) = 3.46 \times 10^{-13}$ cm^3 $molecule^{-1}$ s^{-1} at 298 K with a diurnal average of [OH] $\approx 1.0 \times 10^6$ molecule cm^{-3} gives an estimate of 33 days for the atmospheric lifetime with respect to reaction with OH radicals. Reaction with OH radicals dominates the atmospheric fate of methyl acetate.

Christensen et al. (2000) and Tyndall et al. (2004) have studied the chlorine atom and OH-radical-initiated oxidation of methyl acetate in 700 Torr of N_2/O_2 diluent. The observed products included $CH_3C(O)OH$, $CH_3C(O)OC(O)H$, and CO. Experiments were conducted using a range of [O_2], and it was observed that the yields of $CH_3C(O)OH$ and $CH_3C(O)OC(O)H$ varied with [O_2] reflecting a competition of

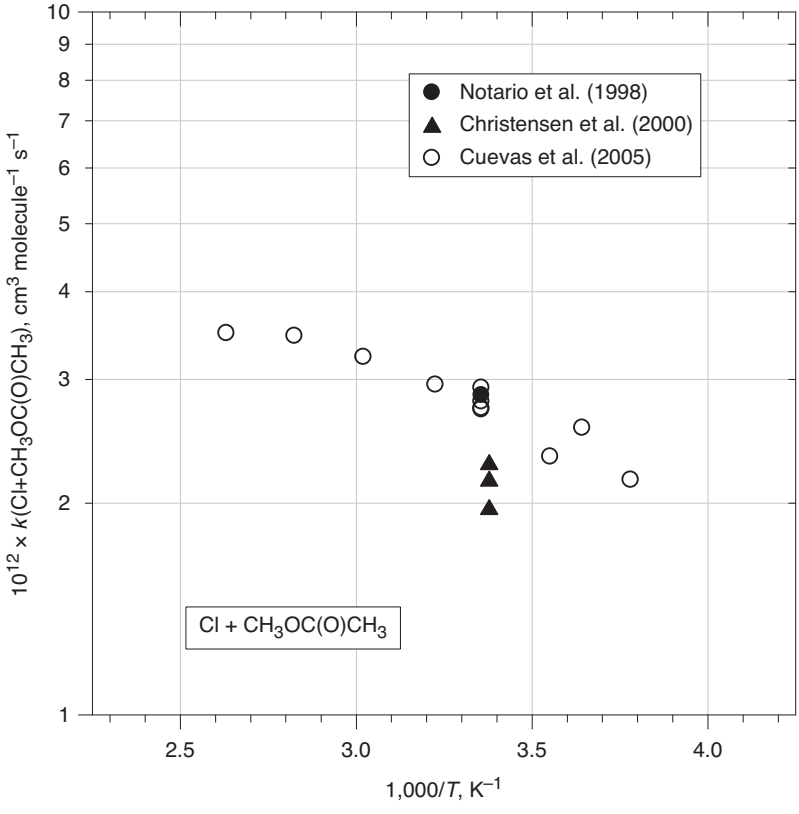

Figure VII-B-11. Measurements of the rate coefficients for reaction of chlorine atoms with $CH_3OC(O)CH_3$.

α-ester rearrangement and reaction with O_2 as losses for $OCH_2OC(O)CH_3$ radicals:

$$OCH_2OC(O)CH_3 \rightarrow HCO + CH_3C(O)OH$$

$$OCH_2OC(O)CH_3 + O_2 \rightarrow HO_2 + CH_3C(O)OC(O)H$$

Tyndall et al. (2004) measured the rate coefficient ratio $k_{\alpha\text{-ester}}/k_{O_2}$ over the temperature range 253–324 K. As seen from figure VII-B-4, the results obtained by Christensen et al. (2000) and Tyndall et al. (2004) are in excellent agreement. A least-squares analysis of the data from Christensen et al. (2000) and Tyndall et al. (2004) gives $k_{\alpha\text{-ester}}/k_{O_2} = 1.87 \times 10^{26} \exp(-5{,}138/T)$ molecule cm^{-3}. Tyndall et al. (2004) observed substantial amounts of CO_2 formed as a secondary product of the OH-radical-initiated oxidation of methyl acetate and ascribed this CO_2 to oxidation of methyl glyoxylate, $CH_3OC(O)C(O)H$, formed by reaction of O_2 with the $CH_3OC(O)CH_2O$ alkoxy radical.

$$CH_3OC(O)CH_2O + O_2 \rightarrow HO_2 + CH_3OC(O)C(O)H$$

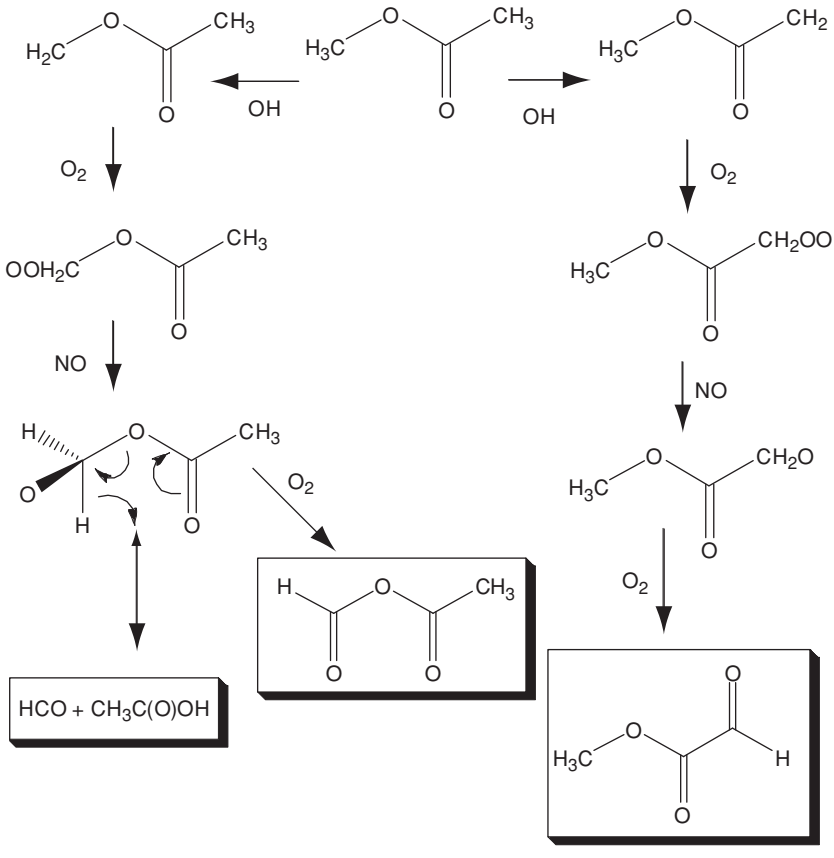

Figure VII-B-12. Simplified oxidation mechanism for methyl acetate.

Using the structure–activity relationship method outlined by Kwok and Atkinson (1995) it can be estimated that attack of OH radicals on methyl acetate occurs 32% at the $CH_3C(O)$ group and 68% at the —OCH_3 group. As discussed previously and illustrated in figure VII-B-12, reaction at the $CH_3C(O)$ group leads to the formation of $CH_3OC(O)C(O)H$ while reaction at the —OCH_3 group leads to $CH_3C(O)OH$ and $CH_3C(O)OCHO$.

VII-B-8. Ethyl Acetate [$C_2H_5OC(O)CH_3$]

VII-B-8.1. OH Reaction Kinetics

The reaction of OH with ethyl acetate has been studied by Campbell and Parkinson (1978), Wallington et al. (1988b), El Boudali et al. (1996), and Picquet et al. (1998) over the temperature range 240–440 K. Data are summarized in table VII-B-15 and are plotted in figure VII-B-13. Two points are evident from inspection of figure VII-B-13. First, the results from the four independent studies are in good agreement. Second, there is significant curvature in the Arrhenius plot. A fit of the modified Arrhenius

Table VII-B-15. Rate coefficients ($k = A \times e^{-B/T}$, cm^3 molecule^{-1} s^{-1}) for reaction of OH with ethyl acetate [$C_2H_5OC(O)CH_3$]

$10^{12} \times A$	B (K)	$10^{13} \times k$	T (K)	Technique[a]	Reference	Temperature Range (K)
		1.76 ± 0.35	292	RR (n-C_4H_{10})[b]	Campbell and Parkinson (1978)	
2.3 ± 0.2	131 ± 28	3.26 ± 0.21	240	FP–RF	Wallington	240–440
(T = 296–440 K)	(T = 296–440 K)	2.40 ± 0.15	263		et al. (1988b)	
		1.51 ± 0.14	296			
		1.57 ± 0.10	350			
		1.72 ± 0.13	400			
		1.73 ± 0.13	440			
0.48 ± 0.09	397 ± 103	2.60 ± 0.14	243	PLP–LIF	El Boudali	243–369
		2.30 ± 0.05	253		et al. (1996)	
		2.05 ± 0.10	273			
		2.26 ± 0.10	273			
		1.81 ± 0.06	283			
		1.74 ± 0.09	298			
		1.60 ± 0.14	298			
		1.71 ± 0.08	298			
		1.76 ± 0.08	298			
		1.66 ± 0.15	323			
		1.55 ± 0.14	348			
		1.52 ± 0.10	369			
		1.66 ± 0.12	298	RR (n-C_5H_{12})[c]	Picquet et al.	
		1.74 ± 0.11	298	RR (n-C_6H_{14})[d]	(1998)	
		1.69 ± 0.16	298	RR (n-C_6H_{14})[d]		
		1.56 ± 0.12	298	RR (CH_3OH)[e]		

[a]Abbreviations used for the techniques are defined in table I-F-3.
[b]Placed on an absolute basis using $k(OH + n\text{-}C_4H_{10}) = 2.36 \times 10^{-12}$ cm^3 molecule^{-1} s^{-1} (Calvert et al., 2008).
[c]Placed on an absolute basis using $k(OH + n\text{-}C_5H_{12}) = 3.96 \times 10^{-12}$ cm^3 molecule^{-1} s^{-1} (Calvert et al., 2008).
[d]Placed on an absolute basis using $k(OH + n\text{-}C_6H_{14}) = 5.27 \times 10^{-12}$ cm^3 molecule^{-1} s^{-1} (Calvert et al., 2008).
[e]Placed on an absolute basis using $k(OH + CH_3OH) = 9.0 \times 10^{-13}$ cm^3 molecule^{-1} s^{-1} (this book, section II-B-1).

expression gives $k(OH + C_2H_5OC(O)CH_3) = 8.90 \times 10^{-19} T^2 \exp(932/T)$ which gives $k(OH + C_2H_5OC(O)CH_3) = 1.80 \times 10^{-12}$ cm^3 molecule^{-1} s^{-1} at 298 K. As seen in figure VII-B-13, the modified Arrhenius expression is not able to capture fully the curvature in the plot and underestimates the rate coefficients measured at the highest and lowest temperatures and overestimates the rate coefficient at room temperature. For the purposes of including the reaction in atmospheric models, we have fitted the Arrhenius expression to the subambient ($T < 300$ K) data to give $k(OH + C_2H_5OC(O)CH_3) = 1.69 \times 10^{-13} \exp(683/T)$ which gives $k(OH + C_2H_5OC(O)CH_3) = 1.67 \times 10^{-12}$ cm^3 molecule^{-1} s^{-1} at 298 K with an estimated uncertainty of ±15%.

VII-B-8.2. Cl-Atom Reaction Kinetics

The rate coefficient for the reaction of chlorine atoms with ethyl acetate has been studied using absolute (Notario et al., 1998; Cuevas et al., 2005; Xing et al., 2009) and relative rate methods (Xing et al., 2009). The results are presented in table VII-B-16

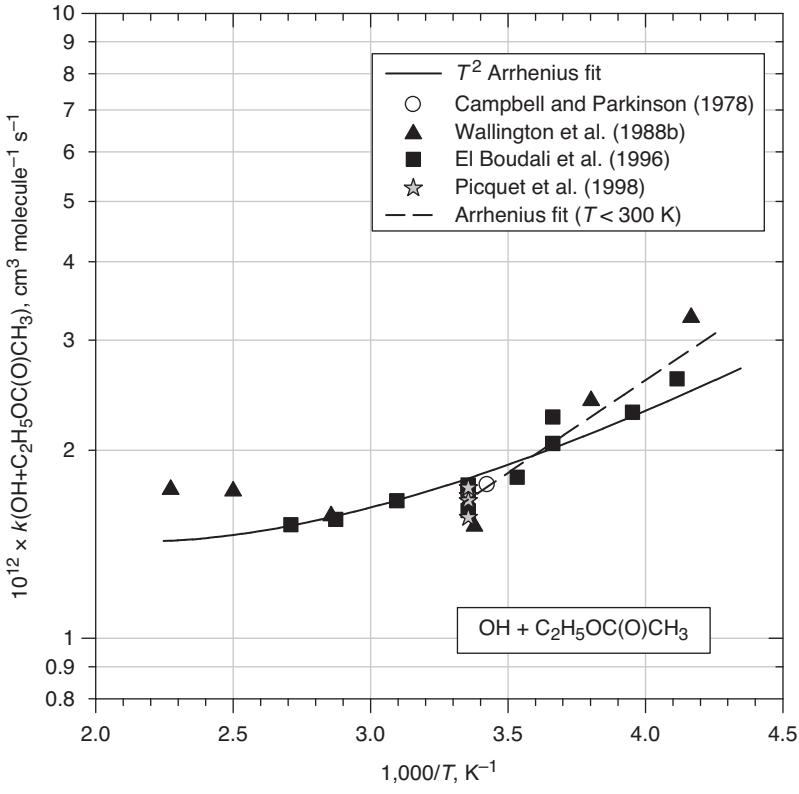

Figure VII-B-13. Measurements of the rate coefficients for reaction of OH radicals with $C_2H_5OC(O)CH_3$. The solid curve is a fit of the modified Arrhenius expression to the entire data set of Campbell and Parkinson (1978), Wallington et al. (1988b), El Boudali et al. (1996), and Picquet et al. (1998). The dashed curve is a fit of the Arrhenius expression to the $T < 300$ K data.

and figure VII-B-14. Notario et al. (1998) and Cuevas et al. (2005) employed very similar experimental techniques, but for reasons which are unclear, there is a substantial disagreement between the results reported at 298 K. We would expect the reaction to proceed via a hydrogen atom abstraction, and the negative temperature dependence reported by Cuevas et al. (2005) is puzzling. Xing et al. (2009) conducted a relative and absolute rate study and reported results at room temperature which are lower than, but consistent with that of Notario et al. (1998) within the experimental uncertainties. An average of the results from Notario et al. (1998) and Xing et al. (2009) gives $k(\mathrm{Cl} + \mathrm{C_2H_5OC(O)CH_3}) = 1.85 \times 10^{-11}$ cm^3 molecule^{-1} s^{-1} at 298 K which we recommend with an uncertainty estimated to be ±20%.

VII-B-8.3. NO_3 Radical Reaction Kinetics

The rate coefficient for the reaction of NO_3 radicals with ethyl acetate has been studied using an absolute rate method by Langer et al. (1993) and a value of $k(\mathrm{NO_3} + \mathrm{C_2H_5OC(O)CH_3}) = 1.3 \times 10^{-17}$ cm^3 molecule^{-1} s^{-1} was reported at 296 K.

Table VII-B-16. Rate coefficients ($k = A \times e^{-B/T}$, cm^3 $molecule^{-1}$ s^{-1}) for reaction of chlorine atoms with ethyl acetate [$C_2H_5OC(O)CH_3$]

$10^{12} \times A$	B (K)	$10^{11} \times k$	T (K)	Technique[a]	Reference	Temperature Range (K)
		2.01 ± 0.25	298	PLP–RF	Notario et al. (1998)	
4.35 ± 0.65	-342 ± 92	1.59 ± 0.21	264.5	PLP–RF	Cuevas et al. (2005)	264.5–380
		1.55 ± 0.22	281.8			
		1.32 ± 0.20	298			
		1.29 ± 0.15	298			
		1.26 ± 0.26	298			
		1.44 ± 0.20	298			
		1.32 ± 0.20	310			
		1.19 ± 0.18	331			
		1.24 ± 0.22	331			
		1.17 ± 0.15	354			
		1.06 ± 0.32	380			
		1.76 ± 0.11	297	PLP–LIF	Xing et al. (2009)	
		1.75 ± 0.21	296	RR (C_2H_2)[b]	Xing et al. (2009)	
		1.87 ± 0.15		RR (C_2H_4)[c]		

[a]Abbreviations used for the techniques are defined in table I-F-3.
[b]Placed on an absolute basis using $k(Cl + C_2H_2) = 5.2 \times 10^{-11}$ cm^3 $molecule^{-1}$ s^{-1} (Atkinson et al., 2006).
[c]Placed on an absolute basis using $k(Cl + C_2H_4) = 9.52 \times 10^{-11}$ cm^3 $molecule^{-1}$ s^{-1} (section I-F).

Given the difficulties in studying such a slow reaction using an absolute rate method, an uncertainty of a factor of 2 is estimated at 296 K.

VII-B-8.4. Summary of the Atmospheric Fate of Ethyl Acetate

Kutsuna et al. (2005) have determined the Henry's law constant for ethyl acetate at 298 K to be 6 M $atm.^{-1}$ and established an upper limit at 288 K for the rate of hydrolysis of $k_h < 5 \times 10^{-6}$ s^{-1} (estimated from figure 1A, Kutsuna et al., 2005). Loss of ethyl acetate by dissolution into cloud-rain-sea-water will not be of atmospheric significance. Combining $k(OH + C_2H_5OC(O)CH_3) = 1.67 \times 10^{-12}$ cm^3 $molecule^{-1}$ s^{-1} at 298 K with a diurnal average of [OH] $\approx 1.0 \times 10^6$ molecule cm^{-3} gives an estimate of 7 days for the atmospheric lifetime with respect to reaction with OH radicals. Reaction with OH radicals dominates the atmospheric fate of ethyl acetate.

Using the structure–activity relationship method outlined by Kwok and Atkinson (1995) with values of F(—OC(O)R) = 1.6 and F(—C(O)OR) = 0.74 it can be estimated that attack of OH radicals on ethyl acetate occurs 94% at the ethyl group and 6% at the acetyl group.

$$OH + CH_3CH_2OC(O)CH_3 \rightarrow CH_2CH_2OC(O)CH_3 + H_2O$$

$$OH + CH_3CH_2OC(O)CH_3 \rightarrow CH_3CHOC(O)CH_3 + H_2O$$

$$OH + CH_3CH_2OC(O)CH_3 \rightarrow CH_3CH_2OC(O)CH_2 + H_2O$$

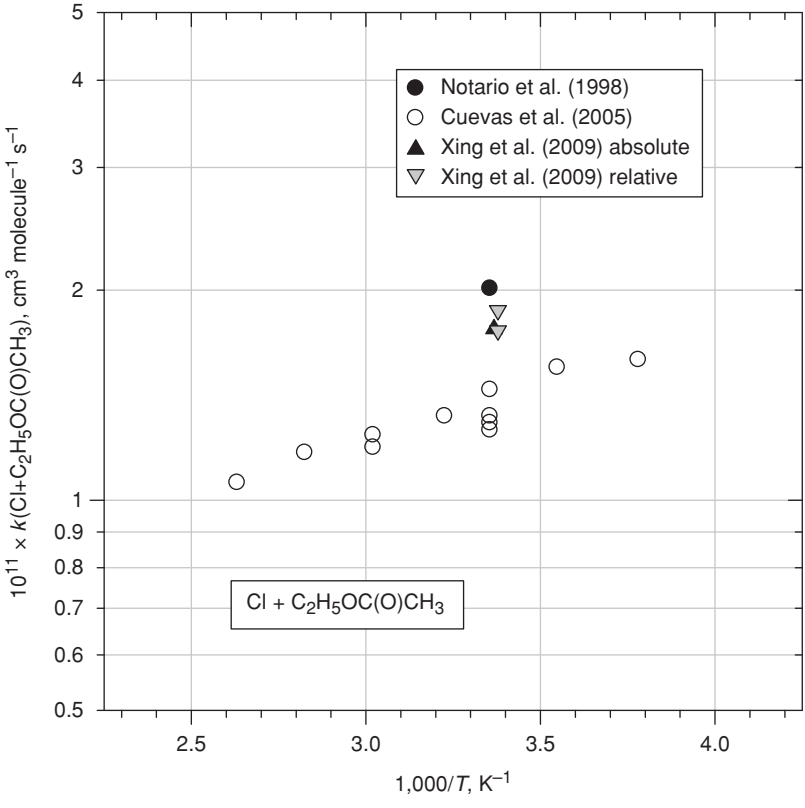

Figure VII-B-14. Measurements of the rate coefficients for reaction of chlorine atoms with $C_2H_5OC(O)CH_3$.

Tuazon et al. (1998b) and Picquet-Varrault et al. (2001) have conducted product studies of the OH-radical-initiated oxidation of ethyl acetate in air in the presence of NO_x. Tuazon et al. (1998b) reported the formation of acetic acid in a molar yield of 0.96 ± 0.08. Picquet-Varrault et al. (2001) reported the following products (molar yields): acetic acid (0.75 ± 0.13), acetoxyacetaldehyde (0.15 ± 0.05), acetic anhydride (0.02 ± 0.01), formic acetic anhydride (0.02 ± 0.01), and peroxyacetyl nitrate, PAN, (0.75 ± 0.20). The observation of essentially unity yield of acetic acid by Tuazon et al. (1998) and 75% yield of acetic acid and PAN by Picquet-Varrault et al. (2001) shows that the majority of the reaction proceeds via H-atom abstraction from the CH_2 group. The resulting alkoxy radical undergoes decomposition by the α-ester rearrangement first proposed by Tuazon et al. (1998b). H-atom abstraction from CH_3 of the ethyl group leads to the formation of acetoxyacetaldehyde. Picquet-Varrault et al. (2001) observed small amounts of acetic anhydride and formic acetic anhydride indicating that reaction with O_2 and decomposition via CH_3 radical elimination compete to a minor extent with the α-ester rearrangement as fates for $CH_3C(O\bullet)HOC(O)CH_3$ radicals. Picquet-Varrault et al. (2001) looked for, but did not find (<0.05 molar yield) products which

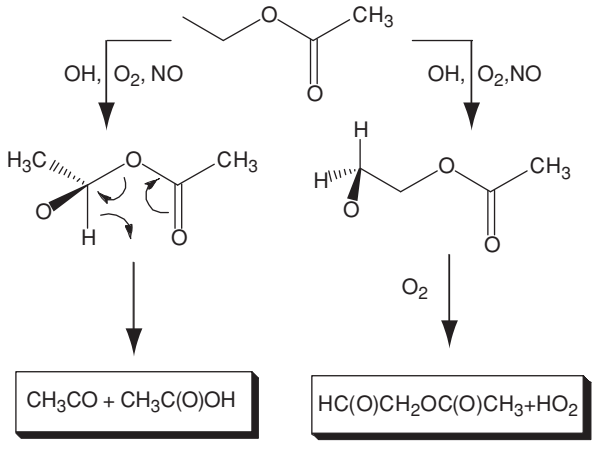

Figure VII-B-15. Simplified oxidation mechanism for ethyl acetate.

might originate from H-atom abstraction from the acetate group. A simplified oxidation mechanism for ethyl acetate is given in figure VII-B-15.

VII-B-9. *n*-Propyl Acetate [n-$C_3H_7OC(O)CH_3$]

VII-B-9.1. OH Reaction Kinetics

The reaction of OH with *n*-propyl acetate has been studied by Winer et al. (1977), Kerr and Stocker (1986b), Wallington et al. (1988b), Williams et al. (1993), El Boudali et al. (1996), and Ferrari et al. (1996) over the temperature range 240–440 K. The results from these studies are summarized in table VII-B-17 and are plotted in figure VII-B-16. As seen from the figure, the results from the absolute rate studies of Wallington et al. (1988b) and El Boudali et al. (1996) are in excellent agreement. In contrast, there is substantial scatter in the results from the relative rate studies by Winer et al. (1977), Kerr and Stocker (1986b), Williams et al. (1993), and Ferrari et al. (1996). The results of Williams et al. (1993) agree with the absolute rate studies, but those from Winer et al. (1977), Kerr and Stocker (1986b), and Ferrari et al. (1996) do not agree. Given the similarity in the techniques used, the spread of data from the relative rate studies is puzzling. A fit of the modified Arrhenius expression to the data from Wallington et al. (1988b), Williams et al. (1993), and El Boudali et al. (1996) gives $k(\mathrm{OH} + n\text{-}\mathrm{C_3H_7OC(O)CH_3}) = 1.46 \times 10^{-18}\, T^2 \times \exp(978/T)$ which gives $k(\mathrm{OH} + n\text{-}\mathrm{C_3H_7OC(O)CH_3}) = 3.45 \times 10^{-12}$ cm^3 molecule^{-1} s^{-1} at 298 K with an uncertainty estimated to be $\pm 25\%$. Corroborative studies of the temperature dependence are needed.

VII-B-9.2. Cl-Atom Reaction Kinetics

The rate coefficient for the reaction of chlorine atoms with *n*-propyl acetate has been studied using PLP–RF techniques by Notario et al. (1998) and Cuevas et al. (2005) and by PLP–LIF and relative rate methods by Xing et al. (2009). Data are listed in

Table VII-B-17. Rate coefficients ($k = A \times e^{-B/T}$, cm^3 molecule^{-1} s^{-1}) for reaction of OH with *n*-propyl acetate [*n*-$C_3H_7OC(O)CH_3$]

$10^{12} \times A$	B (K)	$10^{12} \times k$	T (K)	Technique[a]	Reference	Temperature Range (K)
		4.37	305	RR (isobutene)[b]	Winer et al. (1977)	
		2.56 ± 0.26	303	RR (C_2H_4)[c]	Kerr and Stocker (1986a)	
		3.45 ± 0.34	296	FP–RF	Wallington et al. (1988b)	
		3.42 ± 0.87	298	RR (propene)[d]	Williams et al. (1993)	
		3.32 ± 0.79		RR (*n*-C_4H_{10})[e]		
		1.82 ± 0.22	295	RR (*n*-C_8H_{18})[f]	Ferrari et al. (1996)	
1.03 ± 0.12	−370 ± 69	4.56	258	PLP–LIF	El Boudali et al. (1996)	258–372
		4.37	263			
		4.03	273			
		3.71	283			
		3.43	298			
		3.40	298			
		3.40	298			
		3.2	298			
		3.32	298			
		3.18	313			
		2.99	333			
		2.98	353			
		2.93	372			
		2.91	372			

[a]Abbreviations used for the techniques are defined in table I-F-3.
[b]Placed on an absolute basis using $k(OH + C_2H_4) = 8.52 \times 10^{-12}$ cm^3 molecule^{-1} s^{-1} (Calvert et al., 2000).
[c]Placed on an absolute basis using $k(OH + \text{isobutene}) = 5.14 \times 10^{-11}$ cm^3 molecule^{-1} s^{-1} (Calvert et al., 2000).
[d]Placed on an absolute basis using $k(OH + \text{propene}) = 2.63 \times 10^{-11}$ cm^3 molecule^{-1} s^{-1} (Calvert et al., 2000).
[e]Placed on an absolute basis using $k(OH + n\text{-}C_4H_{10}) = 2.36 \times 10^{-12}$ cm^3 molecule^{-1} s^{-1} (Calvert et al., 2008).
[f]Placed on an absolute basis using $k(OH + n\text{-}C_8H_{18}) = 7.81 \times 10^{-12}$ cm^3 molecule^{-1} s^{-1} (Calvert et al., 2008).

table VII-B-18 and plotted in figure VII-B-17. As seen from figure VII-B-17 the results from Cuevas et al. (2005) lie substantially below those from the other studies. The studies by Notario et al. (1998) and Cuevas et al. (2005) were conducted using very similar experimental techniques and experimental conditions and yet the results are in significant disagreement. Cuevas et al. (2005) noted the disagreement, but did not offer an explanation. An average of the results from Notario et al. (1998) and Xing et al. (2009) gives our recommendation: $k(Cl + n\text{-}C_3H_7OC(O)CH_3) = 7.38 \times 10^{-11}$ cm^3 molecule^{-1} s^{-1} at 298 K with an uncertainty estimated to be ±20%. Further work is needed to establish the temperature dependence of this reaction.

VII-B-9.3. NO_3 Radical Reaction Kinetics

The rate coefficient for the reaction of NO_3 radicals with *n*-propyl acetate has been studied using an absolute rate method by Langer et al. (1993) and a value of $k(NO_3 + n\text{-}C_3H_7OC(O)CH_3) = 5 \times 10^{-17}$ cm^3 molecule^{-1} s^{-1} was reported at 296 K. Given the difficulties in studying such a slow reaction using an absolute rate method, an uncertainty of a factor of 2 is estimated at 296 K.

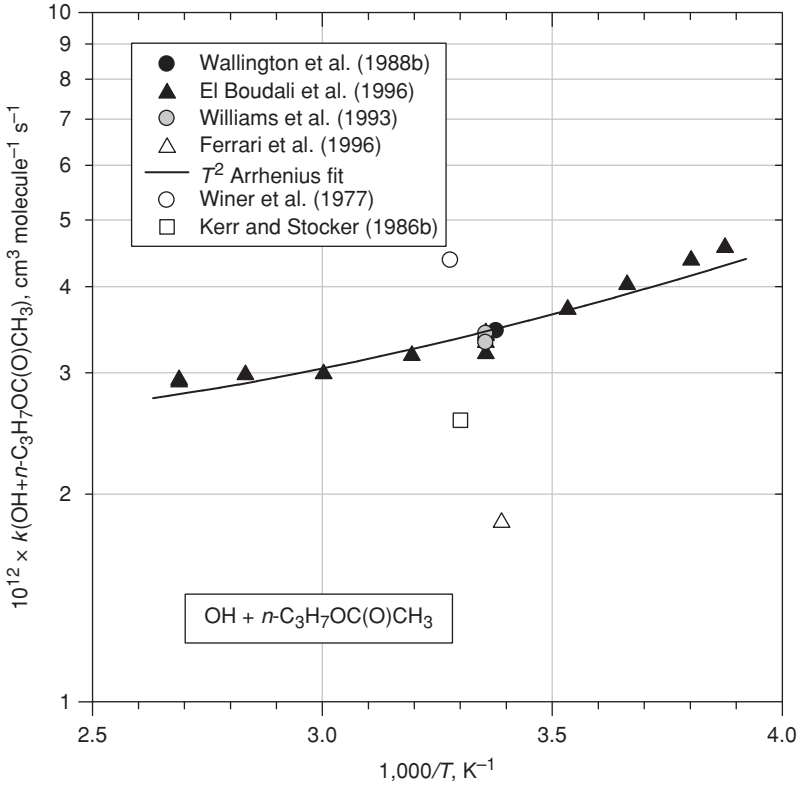

Figure VII-B-16. Measurements of the rate coefficients for reaction of OH radicals with n-$C_3H_7OC(O)CH_3$. The solid curve is a fit of the modified Arrhenius expression to the data from Wallington et al. (1988b), Williams et al. (1993), and El Boudali et al. (1996).

VII-B-9.4. Summary of the Atmospheric Fate of n-Propyl Acetate

The Henry's law constant for *n*-propyl acetate is 5 M atm.$^{-1}$ (Sander, 1999). Aqueous-phase processes will not play an important role in the atmospheric chemistry of *n*-propyl acetate. Combining $k(\text{OH} + n\text{-}C_3H_7OC(O)CH_3) = 3.45 \times 10^{-12}$ cm^3 molecule^{-1} s^{-1} at 298 K with a diurnal average of [OH] $\approx 1.0 \times 10^6$ molecule cm^{-3} gives an estimate of 3 days for the atmospheric lifetime with respect to reaction with OH radicals. Reaction with OH radicals dominates the atmospheric fate of *n*-propyl acetate.

Using the structure–activity relationship method outlined by Kwok and Atkinson (1995) it can be estimated that attack of OH radicals on *n*-propyl acetate occurs 97% at the propyl group and 3% at the acetyl group. Kerr and Stocker (1986b) and Picquet-Varrault et al. (2001) have conducted product studies of the OH-radical-initiated oxidation of *n*-propyl acetate in 1 atm. of air at, or near, 298 K in the presence of NO_x. Kerr and Stocker (1986b) reported the formation of acetaldehyde and propionaldehyde in molar yields of approximately 0.32 and 0.06, respectively, judged from figure 2 in Kerr and Stocker (1986b). Picquet-Varrault et al. (2001) reported the

Table VII-B-18. Rate coefficients ($k = A \times e^{-B/T}$, cm^3 molecule^{-1} s^{-1}) for reaction of chlorine atoms with *n*-propyl acetate [*n*-$C_3H_7OC(O)CH_3$]

$10^{12} \times A$	B (K)	$10^{11} \times k$	T(K)	Technique[a]	Reference
		7.76 ± 0.92	298	PLP–RF	Notario et al. (1998)
2.22 ± 0.20	−217 ± 55	5.22	265.5	PLP–RF	Cuevas et al. (2005)
		6.03	281		
		4.85	282		
		4.61	298		
		4.76	298		
		4.51	298		
		4.51	298		
		4.52	311		
		4.36	331		
		4.27	352		
		3.73	382		
		7.19 ± 0.47	297	PLP–LIF	Xing et al. (2009)
		7.59 ± 1.72	296	RR (C_2H_2)[b]	Xing et al. (2009)
		6.97 ± 0.70		RR (C_2H_4)[c]	

[a]Abbreviations used for the techniques are defined in table I-F-3.
[b]Placed on an absolute basis using $k(Cl + C_2H_2) = 5.2 \times 10^{-11}$ cm^3 molecule^{-1} s^{-1} (Atkinson et al., 2006).
[c]Placed on an absolute basis using $k(Cl + C_2H_4) = 9.52 \times 10^{-11}$ cm^3 molecule^{-1} s^{-1} (section I-F).

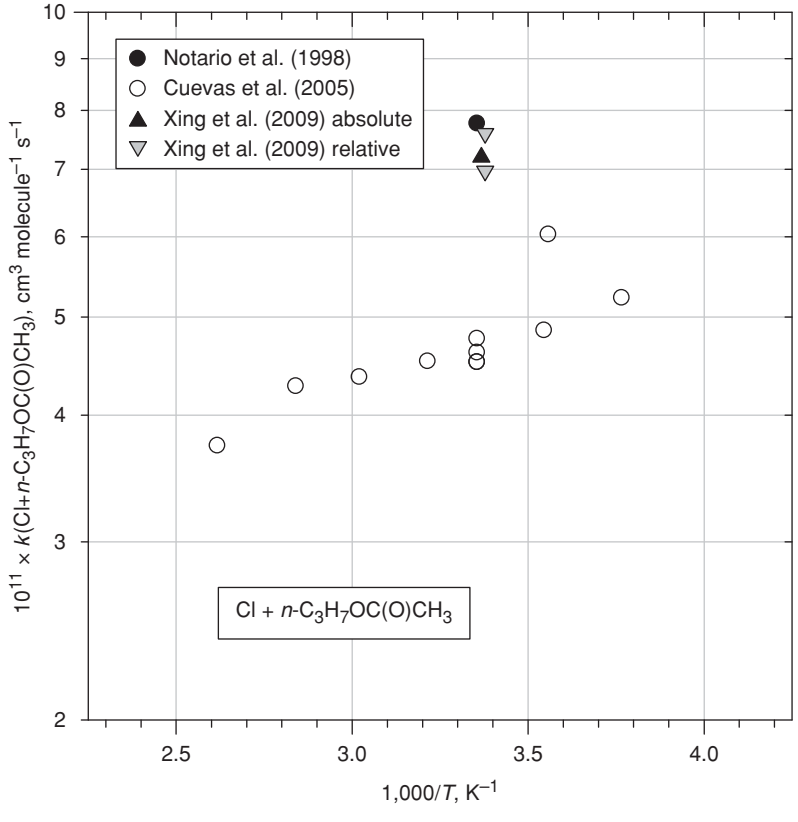

Figure VII-B-17. Measurements of the rate coefficients for reaction of chlorine atoms with *n*-$C_3H_7OC(O)CH_3$.

following products (molar yields): acetoxyacetaldehyde (0.22 ± 0.06), formic acetic anhydride (0.28 ± 0.03), acetic acid (0.15 ± 0.02), acetaldehyde (0.35 ± 0.10), peroxypropionyl nitrate, PPN, $\leq (0.26 \pm 0.10)$, and acetoxypropionaldehyde [probably] (0.30 ± 0.10). Picquet-Varrault et al. (2001) sought evidence in the FTIR spectra for the formation of acetoxyacetone and propionic acetic anhydride but these products were not observed (molar yields <0.01 and <0.03, respectively). The absence of such products shows that the fate of $CH_3CH(O\bullet)CH_2OC(O)CH_3$ and $CH_3CH_2CH(O\bullet)OC(O)CH_3$ alkoxy radicals is decomposition not reaction with O_2. As noted by Picquet-Varrault et al. (2001), this behavior contrasts with the fate of the analogous $CH_3CH(O\bullet)CH_2CH_3$ alkoxy radical derived from *n*-butane whose main (68%) fate in 1 atm. of air at 298 K is reaction with O_2 and minor (32%) fate is decomposition (Calvert et al., 2008). The observation of acetic acid and peroxypropionyl nitrate products probably reflects the importance of the α-ester rearrangement as a significant loss process for $CH_3CH_2CH(O\bullet)OC(O)CH_3$ alkoxy radicals.

VII-B-10. *iso*-Propyl Acetate [*iso*-$C_3H_7OC(O)CH_3$]

VII-B-10.1. OH Reaction Kinetics

The reaction of OH with *iso*-propyl acetate has been studied by Kerr and Stocker (1986b), Wallington et al. (1988b), Ferrari et al. (1996), Le Calvé et al. (1997c), and Picquet et al. (1998) over the temperature range 253–372 K. Data are summarized in table VII-B-19 and are plotted in figure VII-B-18. As seen from the figure, with the exception of the data from Ferrari et al. (1996), there is excellent agreement between the absolute and relative rate studies. Excluding the results from Ferrari et al. (1996), a fit of the modified Arrhenius expression to the combined data set gives: $k(\text{OH} + \textit{iso}\text{-}C_3H_7OC(O)CH_3) = 4.55 \times 10^{-19}\, T^2 \exp(1{,}353/T)$ which gives $k(\text{OH} + \textit{iso}\text{-}C_3H_7OC(O)CH_3) = 3.79 \times 10^{-12}$ cm^3 molecule^{-1} s^{-1} at 298 K with an uncertainty estimated to be $\pm 20\%$.

VII-B-10.2. Cl-Atom Reaction Kinetics

Notario et al. (1998) and Xing et al. (2009) have studied the kinetics of the reaction of chlorine atoms with *iso*-propyl acetate at 298 K using absolute and relative rate techniques (see table VII-B-20). Xing et al. (2009) argued that the result from Notario et al. (1998) may be an overestimate resulting from secondary chemistry in the system. Nevertheless, the results of the two studies are consistent within the combined experimental uncertainties. An average of the results given in table VII-B-20, $k(\text{Cl} + \textit{iso}\text{-}C_3H_7OC(O)CH_3) = 2.44 \times 10^{-11}$ cm^3 molecule^{-1} s^{-1}, is recommended at 298 K with an uncertainty of $\pm 25\%$.

VII-B-10.3. Summary of the Atmospheric Fate of iso-Propyl Acetate

Given the low solubility of *iso*-propyl acetate (Henry's law approximately 3 M atm.$^{-1}$; Sander, 1999), loss via dissolution in rain-cloud-sea-water will not be significant. Combining $k(\text{OH} + \textit{iso}\text{-}C_3H_7OC(O)CH_3) = 3.79 \times 10^{-12}$ cm^3 molecule^{-1} s^{-1} at

Table VII-B-19. Rate coefficients ($k = A \times e^{-B/T}$, cm^3 molecule^{-1} s^{-1}) for reaction of OH with *iso*-propyl acetate [*iso*-$C_3H_7OC(O)CH_3$]

$10^{12} \times A$	B (K)	$10^{12} \times k$	T (K)	Technique[a]	Reference	Temperature Range (K)
		3.15 ± 0.85	303	RR (C_2H_4)[b]	Kerr and Stocker (1986b)	
		3.72 ±0.29	296	FP–RF	Wallington et al. (1988b)	
		2.90 ± 0.27	295	RR (*n*-C_8H_{18})[c]	Ferrari et al. (1996)	
0.30 ± 0.03	−770 ± 52	6.31 ± 0.30	253	PLP–LIF	Le Calvé et al. (1997c)	258–372
		6.46 ± 0.06	253			
		5.56 ± 0.07	263			
		4.77 ± 0.14	273			
		4.34 ± 0.08	283			
		3.74 ± 0.10	298			
		3.80 ± 0.07	298			
		3.85 ± 0.10	298			
		3.75 ± 0.12	298			
		3.79 ± 0.11	298			
		3.42 ± 0.13	313			
		2.92 ± 0.05	333			
		2.64 ± 0.06	353			
		2.49 ± 0.08	372			
		2.53 ± 0.09	372			
		3.74 ± 0.11	298	RR (*n*-C_6H_{14})[d]	Picquet et al. (1998)	
		3.79 ± 0.16	298			

[a]Abbreviations used for the techniques are defined in table I-F-3.
[b]Placed on an absolute basis using $k(OH + C_2H_4) = 8.52 \times 10^{-12}$ cm^3 molecule^{-1} s^{-1} (Calvert et al., 2000).
[c]Placed on an absolute basis using $k(OH + n\text{-}C_8H_{18}) = 7.81 \times 10^{-12}$ cm^3 molecule^{-1} s^{-1} (Calvert et al., 2008).
[d]Placed on an absolute basis using $k(OH + n\text{-}C_6H_{14}) = 5.27 \times 10^{-12}$ cm^3 molecule^{-1} s^{-1} (Calvert et al., 2008).

298 K with a diurnal average of [OH] $\approx 1.0 \times 10^6$ molecule cm^{-3} gives an estimate of 3 days for the atmospheric lifetime with respect to reaction with OH radicals. Reaction with OH radicals dominates the atmospheric fate of *iso*-propyl acetate. Using the structure–activity relationship method outlined by Kwok and Atkinson (1995), it can be estimated that attack of OH radicals on *iso*-propyl acetate occurs 97% at the *iso*-propyl group and 3% at the acetyl group. Kerr and Stocker (1986b), Tuazon et al. (1998b), and Picquet-Varrault et al. (2002) have conducted product studies of the OH-radical-initiated oxidation of *iso*-propyl acetate in 1 atm. of air at, or near, 298 K in the presence of NO_x. Kerr and Stocker (1986b) reported the formation of acetone in a molar yield of approximately 0.10 (judged from figure 4 in Kerr and Stocker, 1986b). Tuazon et al. (1998b) observed the following products (molar yields): acetic anhydride (0.76 ± 0.07), acetone (0.24 ± 0.02), and acetic acid (0.09 ± 0.03). Picquet-Varrault et al. (2002) reported: acetic anhydride (0.72 ± 0.07), acetone (0.26 ± 0.03), acetic acid (0.06 ± 0.03), acetaldehyde (<0.08), and peroxyacetyl nitrate, PAN ($\leq$ 0.09 ± 0.03). The results from Tuazon et al. (1998b) and Picquet-Varrault et al. (2002) are in excellent agreement. The reason for the apparent underestimation for the acetone yield by Kerr and Stocker (1986b) is unknown.

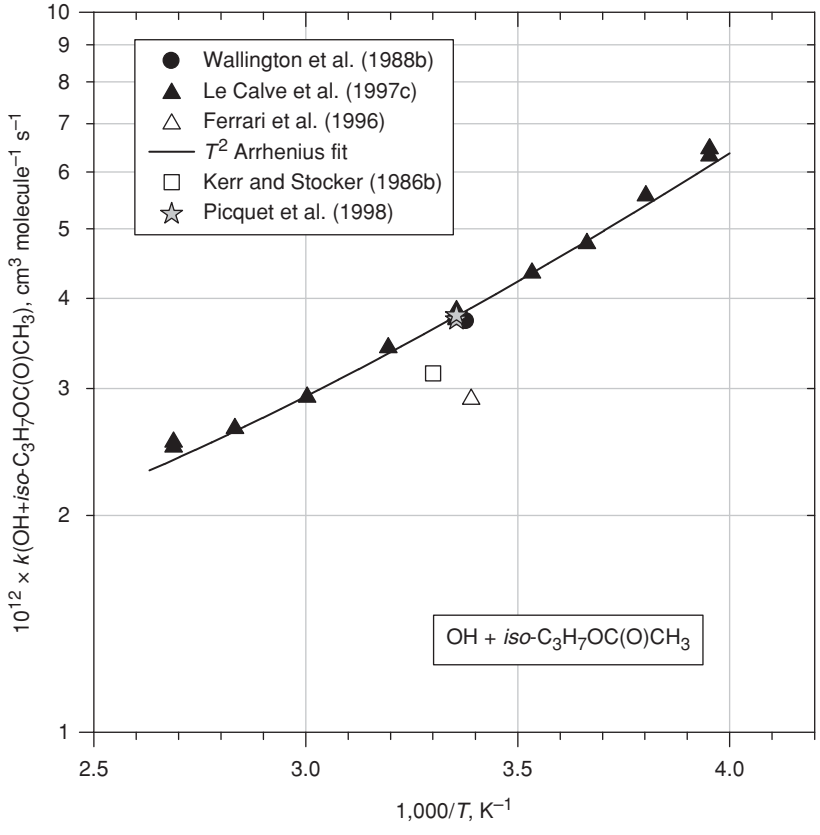

Figure VII-B-18. Measurements of the rate coefficients for reaction of OH radicals with *iso*-$C_3H_7OC(O)CH_3$. The solid curve is a fit of the modified Arrhenius expression to the data from Kerr and Stocker (1986b), Wallington et al. (1988b), Le Calvé et al. (1997c), and Picquet et al. (1998).

Table VII-B-20. Rate coefficients (k, cm^3 molecule^{-1} s^{-1}) for reaction of chlorine atoms with *iso*-propyl acetate [*iso*-$C_3H_7OC(O)CH_3$]

$10^{11} \times k$	T (K)	Technique[a]	Reference
2.68 ± 0.34	298	PLP–RF	Notario et al. (1998)
1.97 ± 0.24	297	PLP–LIF	Xing et al. (2009)
2.59 ± 0.44	296	RR (C_2H_2)[b]	Xing et al. (2009)
2.51 ± 0.23		RR (C_2H_4)[c]	

[a]Abbreviations used for the techniques are defined in table I-F-3.
[b]Placed on an absolute basis using $k(Cl + C_2H_2) = 5.2 \times 10^{-11}$ cm^3 molecule^{-1} s^{-1} (Atkinson et al., 2006).
[c]Placed on an absolute basis using $k(Cl + C_2H_4) = 9.52 \times 10^{-11}$ cm^3 molecule^{-1} s^{-1} (section I-F).

Given the expected relative unreactivity of the acetate group towards OH radicals, the acetic anhydride and acetone products can be attributed to reactions following abstraction of the tertiary hydrogen. While loss of methyl from the $OC(CH_3)_2OC(O)CH_3$ alkoxy radical results in acetic anhydride formation, there are two possible routes for conversion of this radical into acetone; isomerization or decomposition via C—O bond scission. Noting that decomposition routes via C—O bond scission are typically not favored on energetic grounds, and that Pimentel et al. (2009) have presented evidence for the importance of isomerization for $OC(CH_3)_2OC(O)H$ radicals formed from *tert*-butyl formate, we proceed on the assumption that isomerization of $OC(CH_3)_2OC(O)CH_3$ radicals is the main source of acetone. Hydrogen abstraction from a methyl in the *iso*-propyl group leads to the formation of the $OCH_2CH(CH_3)OC(O)CH_3$ alkoxy radical which eliminates CH_2O leading to the formation of the $OCH(CH_3)OC(O)CH_3$ alkoxy radical. The fate of the $OCH(CH_3)OC(O)CH_3$ alkoxy radical is α-ester rearrangement to give acetic acid and an acetyl radical (as discussed for ethyl acetate in section VII-B-8).

VII-B-11. *n*-Butyl Acetate [n-$C_4H_9OC(O)CH_3$]

VII-B-11.1. OH Reaction Kinetics

The reaction of OH with *n*-butyl acetate has been studied by Hartmann et al. (1987), Wallington et al. (1988b), Williams et al. (1993), Veillerot et al. (1996), Ferrari et al. (1996), El Boudali et al. (1996), and Picquet et al. (1998) over the temperature range 263–372 K. The data are summarized in table VII-B-21 and are plotted in figure VII-B-19. As seen from the figure, the results from Williams et al. (1993), El Boudali et al. (1996), and Picquet et al. (1998) are in excellent agreement. The results from Hartmann et al. (1987), Wallington et al. (1988b), and Veillerot et al. (1996) lie approximately 20% below those from Williams et al. (1993), El Boudali et al. (1996), and Picquet et al. (1998) but are probably consistent within the combined experimental uncertainties. Finally, the result from Ferrari et al. (1996) is substantially below the other data; it is below the recommended value for *n*-propyl acetate and is likely erroneous. A fit of the modified Arrhenius expression to the combined data set from Williams et al. (1993), El Boudali et al. (1996), and Picquet et al. (1998) gives: $k(OH + n\text{-}C_4H_9OC(O)CH_3) = 3.03 \times 10^{-18}\, T^2 \exp(908/T)$ which gives $k(OH + n\text{-}C_4H_9OC(O)CH_3) = 5.66 \times 10^{-12}$ cm^3 molecule^{-1} s^{-1} at 298 K with an uncertainty estimated to be $\pm 20\%$.

VII-B-11.2. Cl-Atom Reaction Kinetics

Notario et al. (1998), Cuevas et al. (2005), and Xing et al. (2009) have studied the kinetics of the reaction of chlorine atoms with *n*-butyl acetate. Data are summarized in table VII-B-22 and are plotted in figure VII-B-20. As seen from figure VII-B-20, the data reported by Cuevas et al. (2005), while scattered, suggest a negative temperature dependence which is surprising for a reaction which probably proceeds via hydrogen abstraction. At 298 K we recommend the average of the data from Notario et al. (1998) and Xing et al. (2009) giving $k(Cl + n\text{-}C_4H_9OC(O)CH_3) = 1.53 \times 10^{-10}$

Table VII-B-21. Rate coefficients ($k = A \times e^{-B/T}$, cm^3 molecule^{-1} s^{-1}) for reaction of OH with *n*-butyl acetate [*n*-$C_4H_9OC(O)CH_3$]

$10^{12} \times A$	B (K)	$10^{12} \times k$	T(K)	Technique[a]	Reference	Temperature Range (K)
		4.3 ± 0.8	303	RR (C_2H_4)[b]	Hartmann et al. (1987)	
		4.15 ± 0.30	296	FP–RF	Wallington et al. (1988b)	
		5.71 ± 0.95	297	RR (propene)[c]	Williams et al. (1993)	
		5.15 ± 0.80	297	RR (*n*-C_4H_{10})[d]		
		4.7 ± 0.5	298	RR (*n*-C_8H_{18})[e]	Veillerot et al. (1996)	
		3.05 ± 0.32	295	RR (*n*-C_8H_{18})[e]	Ferrari et al. (1996)	
2.10 ± 0.28	−299 ± 88	6.96 ± 0.23	263	PLP–LIF	El Boudali et al. (1996)	273–372
		7.08 ± 0.18	263			
		6.39 ± 0.23	273			
		6.01 ± 0.20	283			
		5.57 ± 0.16	298			
		5.44 ± 0.09	298			
		5.46 ± 0.10	298			
		5.61 ± 0.23	298			
		5.71 ± 0.21	298			
		5.53 ± 0.22	298			
		6.15 ± 0.15	298			
		5.20 ± 0.18	313			
		5.00 ± 0.14	333			
		5.12 ± 0.09	333			
		5.00 ± 0.11	353			
		5.07 ± 0.35	372			
		5.05 ± 0.18	372			
		5.48 ± 0.14	298	RR (*n*-C_6H_{14})[f]	Picquet et al. (1998)	

[a]Abbreviations used for the techniques are defined in table I-F-3.
[b]Placed on an absolute basis using $k(OH + C_2H_4) = 8.52 \times 10^{-12}$ cm^3 molecule^{-1} s^{-1} (Calvert et al., 2000).
[c]Placed on an absolute basis using $k(OH + \text{propene}) = 2.63 \times 10^{-11}$ cm^3 molecule^{-1} s^{-1} (Calvert et al., 2000).
[d]Placed on an absolute basis using $k(OH + n\text{-}C_4H_{10}) = 2.36 \times 10^{-12}$ cm^3 molecule^{-1} s^{-1} (Calvert et al., 2008).
[e]Placed on an absolute basis using $k(OH + n\text{-}C_8H_{18}) = 7.81 \times 10^{-12}$ cm^3 molecule^{-1} s^{-1} (Calvert et al., 2008).
[f]Placed on an absolute basis using $k(OH + n\text{-}C_6H_{14}) = 5.27 \times 10^{-12}$ cm^3 molecule^{-1} s^{-1} (Calvert et al., 2008).

cm^3 molecule^{-1} s^{-1} with an uncertainty of ±25%. Further studies of the temperature dependence are required.

VII-B-11.3. Summary of the Atmospheric Fate of n-Butyl Acetate

Combining $k(OH + n\text{-}C_4H_9OC(O)CH_3) = 5.63 \times 10^{-12}$ cm^3 molecule^{-1} s^{-1} at 298 K with a diurnal average of [OH] $\approx 1.0 \times 10^6$ molecule cm^{-3} gives an estimate of about 2 days for the atmospheric lifetime with respect to reaction with OH radicals. Reaction with OH radicals dominates the atmospheric fate of *n*-butyl acetate.

Using the structure–activity relationship method outlined by Kwok and Atkinson (1995), it can be estimated that attack of OH radicals on *n*-butyl acetate occurs 98% at the *n*-butyl group and 2% at the acetate group.

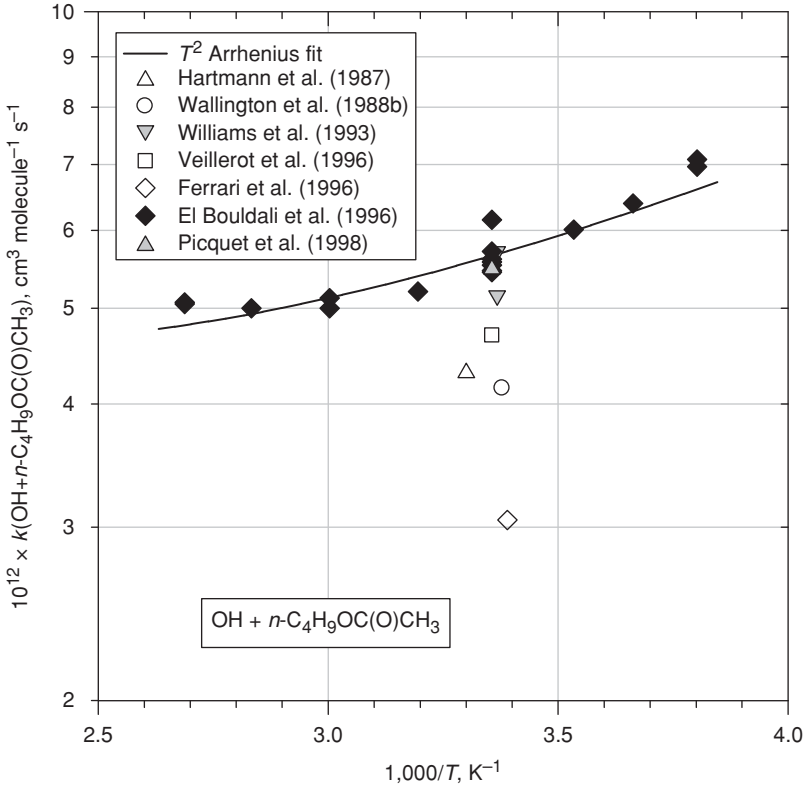

Figure VII-B-19. Measurements of the rate coefficients for reaction of OH radicals with n-$C_4H_9OC(O)CH_3$. The solid line is a fit of the modified Arrhenius expression to the combined data set from Williams et al. (1993), El Boudali et al. (1996), and Picquet et al. (1998).

VII-B-12. *iso*-Butyl Acetate [$(CH_3)_2CHCH_2OC(O)CH_3$]

VII-B-12.1. OH Reaction Kinetics

The reaction of OH with *iso*-butyl acetate has been studied by Le Calvé et al. (1997c), Stemmler et al. (1997a), and Picquet et al. (1998) over the temperature range 263–372 K. Data are summarized in table VII-B-23 and are plotted in figure VII-B-21. As seen from the figure, there is excellent agreement between the absolute rate study by Le Calvé et al. (1997c) and the relative rate studies of Stemmler et al. (1997a) and Picquet et al. (1998). A fit of the modified Arrhenius expression to the combined data set gives: $k(\mathrm{OH} + iso\text{-}C_4H_9OC(O)CH_3) = 1.50 \times 10^{-18}\, T^2 \times \exp(1{,}157/T)$ which gives: $k(\mathrm{OH} + iso\text{-}C_4H_9OC(O)CH_3) = 6.47 \times 10^{-12}$ cm^3 molecule^{-1} s^{-1} at 298 K with an uncertainty estimated to be ±15%.

VII-B-12.2. Cl-Atom Reaction Kinetics

Notario et al. (1998) and Xing et al. (2009) have studied the kinetics of the reaction of chlorine atoms with *iso*-$C_4H_9OC(O)CH_3$ at ambient temperature. The results arte listed

Table VII-B-22. Rate coefficients ($k = A \times e^{-B/T}$, cm^3 molecule^{-1} s^{-1}) for reaction of chlorine atoms with *n*-butyl acetate [*n*-$C_4H_9OC(O)CH_3$]

$10^{11} \times A$	B (K)	$10^{11} \times k$	T(K)	Technique[a]	Reference
		17.4 ± 2.0	298	PLP–RF	Notario et al. (1998)
5.41 ± 1.51	−245 ± 168	15.2 ± 1.6	265	PLP–RF	Cuevas et al. (2005)
		13.7 ± 1.2	283		
		11.3 ± 1.5	298		
		12.5 ± 2.4	298		
		12.2 ± 0.8	298		
		14.6 ± 2.2	298		
		11.4 ± 2.2	298		
		14.0 ± 2.2	298		
		11.2 ± 0.8	298		
		11.7 ± 1.1	310		
		9.71 ± 1.12	311		
		12.2 ± 2.2	331		
		11.4 ± 1.6	343		
		11.4 ± 1.2	354		
		10.8 ± 1.1	383		
		15.8 ± 1.0	297	PLP–LIF	Xing et al. (2009)
		14.1 ± 1.7	296	RR (C_2H_2)[b]	Xing et al. (2009)
		13.9 ± 1.4		RR (C_2H_4)[c]	

[a]Abbreviations used for the techniques are defined in table I-F-3.
[b]Placed on an absolute basis using $k(Cl + C_2H_2) = 5.2 \times 10^{-11}$ cm^3 molecule^{-1} s^{-1} (Atkinson et al., 2006).
[c]Placed on an absolute basis using $k(Cl + C_2H_4) = 9.52 \times 10^{-11}$ cm^3 molecule^{-1} s^{-1} (section I-F).

in table VII-B-24. An average of the results from Notario et al. (1998) and Xing et al. (2009) gives our recommendation of $k(Cl + iso\text{-}C_4H_9OC(O)CH_3) = 1.05 \times 10^{-10}$ cm^3 molecule^{-1} s^{-1} with an estimated uncertainty of ±15%.

VII-B-12.3. Summary of the Atmospheric Fate of iso-Butyl Acetate

Combining $k(OH + iso\text{-}C_4H_9OC(O)CH_3) = 6.47 \times 10^{-12}$ cm^3 molecule^{-1} s^{-1} at 298 K with a diurnal average of [OH] $\approx 1.0 \times 10^6$ molecule cm^{-3} gives an estimate of about 2 days for the atmospheric lifetime with respect to reaction with OH radicals. Reaction with OH radicals dominates the atmospheric fate of *iso*-butyl acetate. Using the structure–activity relationship method outlined by Kwok and Atkinson (1995) it can be estimated that H-atom abstraction by OH radicals occurs 98% at the *iso*-butyl group and 2% at the acetate group.

Picquet-Varrault et al. (2002) have conducted a product study of the OH-radical-initiated oxidation of *iso*-butyl acetate in 1 atm. of air at 298 K in the presence of NO_x. Picquet-Varrault et al. (2002) reported the following products (molar yields): acetone (0.78 ± 0.12), formic acetic anhydride (0.52 ± 0.06), acetoxyacetaldehyde (0.18 ± 0.06), acetic acid (0.08 ± 0.02), acetaldehyde (<0.07), and acetoxyacetone (<0.02). As noted by Picquet-Varrault et al. (2002), because most of the observed products do not provide definite markers for the occurence of a specific reaction pathway, it is difficult to construct a precise oxidation mechanism. For example,

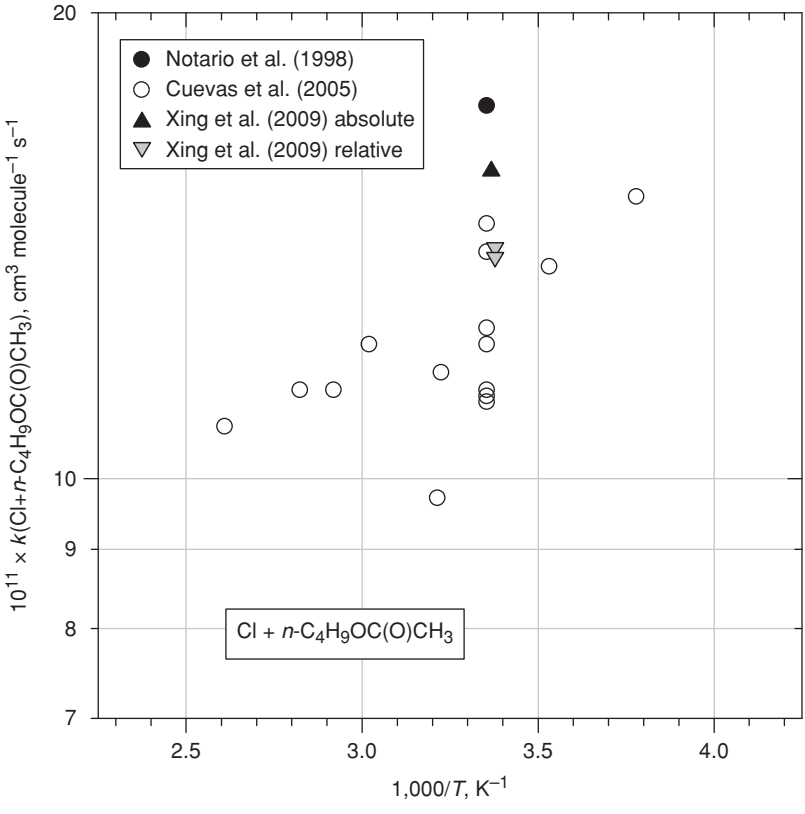

Figure VII-B-20. Measurements of the rate coefficients for reaction of chlorine atoms with n-$C_4H_9OC(O)CH_3$.

acetone can be formed from the decomposition of $(CH_3)_2CHCH(O)OC(O\bullet)CH_3$, or $(CH_3)_2C(O\bullet)CH_2OC(O)CH_3$ radicals, or both. However, Picquet-Varrault et al. (2002) noted that while formic acetic anhydride can be formed from each of the three alkoxy radicals produced following reaction of OH radicals at the *iso*-butyl group, the low yield of acetic acid [a marker for the presence of $CH_3C(O\bullet)OCH_2O$ radicals (see methyl acetate section, VII-B-7)] and the absence of CH_3CHO indicate that the main route of formic acetic anhydride formation is decomposition of $(CH_3)_2CHCH(O\bullet)OC(O)CH_3$ radicals via C—C bond scission. Given the large yield of formic acetic anhydride, it can be concluded that α-ester rearrangement is a minor fate of $(CH_3)_2CHCH(O\bullet)OC(O)CH_3$ radicals. This behavior can be contrasted with the dominance of the α-ester rearrangement as a fate of $CH_3CH(O\bullet)OC(O)CH_3$ radicals (produced in the oxidation of ethyl acetate oxidation). The different behavior of the two alkoxy radicals presumably reflects the fact that the isopropyl radical is a better leaving group than the methyl radical.

Table VII-B-23. Rate coefficients ($k = A \times e^{-B/T}$, cm^3 $molecule^{-1}$ s^{-1}) for reaction of OH with *iso*-butyl acetate [$(CH_3)_2CHCH_2OC(O)CH_3$]

$10^{12} \times A$	B (K)	$10^{12} \times k$	T(K)	Technique[a]	Reference	Temperature Range (K)
1.09 ± 0.14	-534 ± 79	8.91 ± 0.31	263	PLP–LIF	Le Calvé et al. (1997c)	263–372
		8.72 ± 0.22	263			
		8.03 ± 0.24	273			
		7.02 ± 0.24	283			
		6.27 ± 0.20	298			
		6.23 ± 0.11	298			
		6.50 ± 0.19	298			
		6.41 ± 0.26	298			
		6.53 ± 0.20	298			
		6.17 ± 0.25	298			
		5.91 ± 0.10	313			
		5.06 ± 0.19	333			
		5.03 ± 0.11	353			
		5.00 ± 0.19	372			
		4.76 ± 0.12	372			
		6.4 ± 0.6	297	RR $[(C_3H_7)_2O]$[b]	Stemmler et al. (1997a)	
		6.38 ± 0.16	298	RR (n-C_6H_{14})[c]	Picquet et al. (1998)	
		6.38 ± 0.32	298			

[a]Abbreviations used for the techniques are defined in table I-F-3.
[b]Placed on an absolute basis using $k(\text{OH-}C_3H_7)_2O) = 2.0 \times 10^{-11}$ cm^3 $molecule^{-1}$ s^{-1} this book, section III-B-6.1).
[c]Placed on an absolute basis using $k(\text{OH-}n\text{-}C_6H_{14}) = 5.27 \times 10^{-12}$ cm^3 $molecule^{-1}$ s^{-1} (Calvert et al., 2008).

VII-B-13. *sec*-Butyl Acetate [$CH_3CH_2CH(CH_3)OC(O)CH_3$]

VII-B-13.1. OH Reaction Kinetics

The reaction of OH with *sec*-butyl acetate has been studied by Winer et al. (1977), Wallington et al. (1988b), and Le Calvé et al. (1997c) over the temperature range 263–372 K. The data are summarized in table VII-B-25 and are plotted in figure VII-B-22. As seen from the figure, there is excellent agreement in the results from Winer et al. (1977), Wallington et al. (1988b), and Le Calvé et al. (1997c). A fit of the modified Arrhenius expression to the combined data set gives: $k(\text{OH} + sec\text{-}C_4H_9OC(O)CH_3) = 1.07 \times 10^{-18} T^2 \exp(1{,}240/T)$ which gives: $k(\text{OH} + sec\text{-}C_4H_9OC(O)CH_3) = 6.1 \times 10^{-12}$ cm^3 $molecule^{-1}$ s^{-1}at 298 K with an uncertainty estimated to be ±20%.

VII-B-13.2. Cl-Atom Reaction Kinetics

Notario et al. (1998) and Xing et al. (2009) have studied the reaction of chlorine atoms with *sec*-$C_4H_9OC(O)CH_3$. The results are consistent within the experimental uncertainties. The data in table VII-B-26 give $k(\text{Cl} + sec\text{-}C_4H_9OC(O)CH_3) = 9.07 \times 10^{-11}$ cm^3 $molecule^{-1}$ s^{-1} at 298 K which is recommended with an uncertainty estimated to be ±20%.

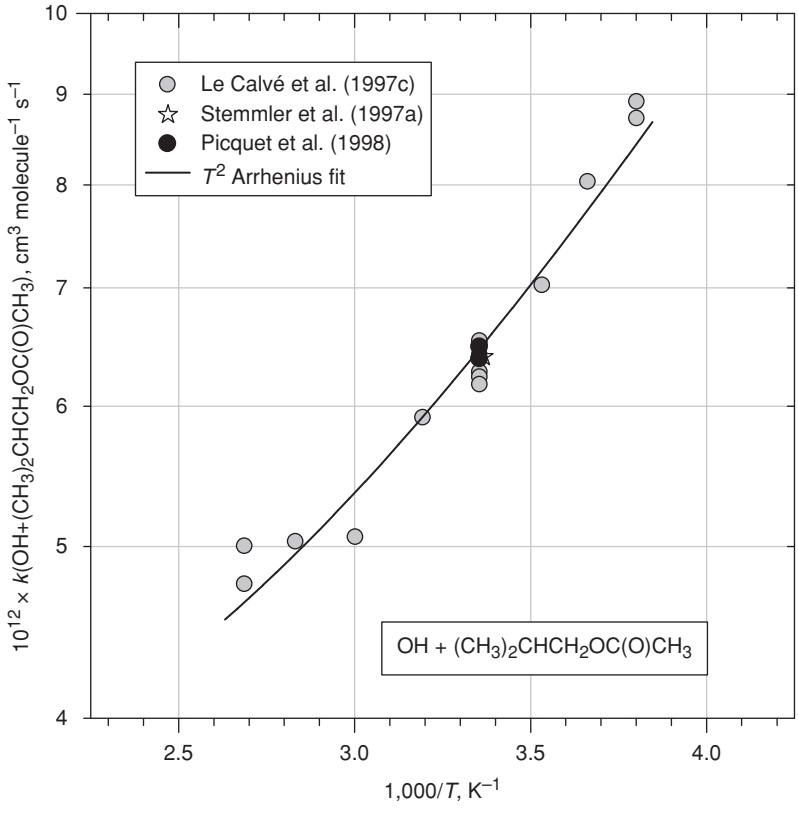

Figure VII-B-21. Measurements of the rate coefficients for reaction of OH radicals with *iso*-$C_4H_9OC(O)CH_3$. The solid curve is a fit of the modified Arrhenius expression to the data.

Table VII-B-24. Rate coefficients (k, cm^3 $molecule^{-1}$ s^{-1}) for reaction of chlorine atoms with *iso*-butyl acetate [$(CH_3)_2CHCH_2OC(O)CH_3$]

$10^{10} \times k$	T (K)	Technique[a]	Reference
1.08 ± 0.13	298	PLP–RF	Notario et al. (1998)
0.997 ± 0.006	297	PLP–LIF	Xing et al. (2009)
1.03 ± 0.08	296	RR (C_2H_2)[b]	Xing et al. (2009)
1.11 ± 0.10		RR (C_2H_4)[c]	

[a]Abbreviations used for the techniques are defined in table I-F-3.
[b]Placed on an absolute basis using $k(Cl + C_2H_2) = 5.2 \times 10^{-11}$ cm^3 $molecule^{-1}$ s^{-1} (Atkinson et al., 2006).
[c]Placed on an absolute basis using $k(Cl + C_2H_4) = 9.52 \times 10^{-11}$ cm^3 $moleclule^{-1}$ s^{-1} (section I-F).

VII-B-13.3. Summary of the Atmospheric Fate of sec-Butyl Acetate

Combining $k(OH + sec\text{-}C_4H_9OC(O)CH_3) = 6.1 \times 10^{-12}$ cm^3 $molecule^{-1}$ s^{-1} at 298 K with a diurnal average of [OH] $\approx$ 1.0×10^6 molecule cm^{-3} gives an estimate of about 2 days for the atmospheric lifetime with respect to reaction with OH radicals.

Table VII-B-25. Rate coefficients ($k = A \times e^{-B/T}$, cm^3 molecule^{-1} s^{-1}) for reaction of OH with *sec*-butyl acetate [$C_2H_5CH(CH_3)OC(O)CH_3$]

$10^{12} \times A$	B (K)	$10^{12} \times k$	T(K)	Technique[a]	Reference	Temperature Range (K)
		5.65	305	RR (isobutene)[b]	Winer et al. (1977)	
		5.65 ± 0.59	296	FP–RF	Wallington et al. (1988b)	
0.73 ± 0.08	−640 ± 62	8.58 ± 0.26	263	PLP–LIF	Le Calvé et al. (1997c)	263–372
		8.58 ± 0.14	263			
		7.83 ± 0.30	273			
		7.17 ± 0.09	283			
		6.12 ± 0.28	298			
		6.02 ± 0.10	298			
		5.99 ± 0.18	298			
		6.27 ± 0.17	298			
		5.97 ± 0.16	298			
		6.01 ± 0.20	298			
		5.46 ± 0.13	313			
		4.94 ± 0.21	333			
		4.56 ± 0.13	353			
		4.34 ± 0.16	372			
		4.27 ± 0.14	372			

[a]Abbreviations used for the techniques are defined in table I-F-3.
[b]Placed on an absolute basis using $k(OH + \text{isobutene}) = 5.14 \times 10^{-11}$ cm^3 molecule^{-1} s^{-1} (Calvert et al., 2000).

Reaction with OH radicals dominates the atmospheric fate of *sec*-butyl acetate. Using the structure–activity relationship method outlined by Kwok and Atkinson (1995), it can be estimated that attack of OH radicals occurs 98% at the *sec*-butyl group and 2% from the acetate group.

VII-B-14. *tert*-Butyl Acetate [$(CH_3)_3COC(O)CH_3$]

VII-B-14.1. OH Reaction Kinetics

The reaction of OH with *tert*-butyl acetate has been studied by Smith et al. (1992), Le Calvé et al. (1997c), and Picquet et al. (1998) over the temperature range 253–372 K. The data are summarized in table VII-B-27 and are plotted in figure VII-B-23. For reasons which are unclear, there is significant scatter in the data reported by Smith et al. (1992). As seen from figure VII-B-23, there is excellent agreement between the results from Le Calvé et al. (1997c) and Picquet et al. (1998). A fit of the modified Arrhenius expression to the combined data set gives: $k(OH + tert\text{-}C_4H_9OC(O)CH_3) = 3.19 \times 10^{-18}\, T^2 \exp(211/T)$ which gives $k(OH + tert\text{-}C_4H_9OC(O)CH_3) = 5.75 \times 10^{-13}$ cm^3 molecule^{-1} s^{-1} at 298 K with an uncertainty estimated to be ±25%.

VII-B-14.2. Cl-Atom Reaction Kinetics

Notario et al. (1998) and Xing et al. (2009) have studied the rate of reaction of chlorine atoms with *tert*-butyl acetate. As seen from table VII-B-28 there is a significant

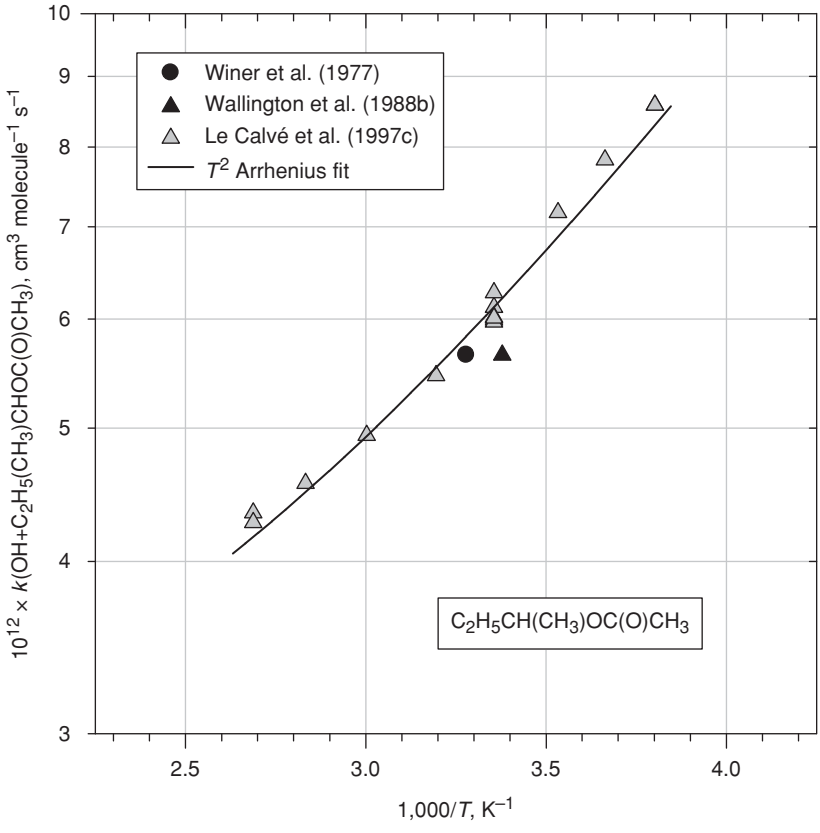

Figure VII-B-22. Measurements of the rate coefficients for reaction of OH radicals with *sec*-$C_4H_9OC(O)CH_3$. The solid curve is a fit of the modified Arrhenius expression to the data.

Table VII-B-26. Rate coefficients (k, cm^3 molecule^{-1} s^{-1}) for reaction of chlorine atoms with *sec*-butyl acetate [$C_2H_5CH(CH_3)OC(O)CH_3$]

$10^{11} \times k$	T (K)	Technique[a]	Reference
9.1 ± 1.0	298	PLP–RF	Notario et al. (1998)
8.01 ± 0.48	297	PLP–LIF	Xing et al. (2009)
9.15 ± 1.09	296	RR (C_2H_2)[b]	Xing et al. (2009)
10.0 ± 1.2		RR (C_2H_4)[c]	

[a]Abbreviations used for the techniques are defined in table I-F-3.
[b]Placed on an absolute basis using $k(Cl + C_2H_2) = 5.2 \times 10^{-11}$ cm^3 molecule^{-1} s^{-1} (Atkinson et al., 2006).
[c]Placed on an absolute basis using $k(Cl + C_2H_4) = 9.52 \times 10^{-11}$ cm^3 molecule^{-1} s^{-1} (section I-F).

discrepancy between the results reported in the two studies. As noted in several earlier sections, Xing et al. (2009) have argued that the result from Notario et al. (1998) is overestimated because of unwanted secondary loss of chlorine atoms. No recommendation is made and further work is needed.

Table VII-B-27. Rate coefficients ($k = A \times e^{-B/T}$, cm^3 molecule^{-1} s^{-1}) for reaction of OH with *tert*-butyl acetate [$(CH_3)_3COC(O)CH_3$]

$10^{12} \times A$	B (K)	$10^{13} \times k$	T(K)	Technique[a]	Reference	Temperature Range (K)
		4.08 ± 0.33	298	RR (n-C_4H_{10})[b]	Smith et al. (1992)	
		3.95 ± 0.50	298	RR (C_3H_8)[c]		
		5.32 ± 0.47	298	RR[$(CH_3)_3COC(O)H$][d]		
2.22 ± 0.34	395 ±92	4.87 ± 0.34	253	PLP–LIF	Le Calvé et al. (1997c)	253–372
		5.07 ± 0.21	253			
		5.00 ± 0.21	263			
		5.26 ± 0.32	273			
		5.66 ± 0.15	283			
		5.84 ± 0.26	298			
		5.39 ± 0.26	298			
		5.83 ± 0.21	298			
		5.41 ± 0.13	298			
		5.84 ± 0.14	298			
		5.35 ± 0.16	298			
		5.57 ± 0.20	298			
		6.18 ± 0.33	313			
		6.44 ± 0.34	333			
		6.65 ± 0.21	333			
		7.71 ± 0.38	353			
		8.29 ± 0.35	372			
		8.11 ± 0.38	372			
		5.42 ± 0.29	298	RR (CH_3OH)[e]	Picquet et al. (1998)	

[a]Abbreviations used for the techniques are defined in table I-F-3.
[b]Placed on an absolute basis using $k(OH + n\text{-}C_4H_{10}) = 2.36 \times 10^{-12}$ cm^3 molecule^{-1} s^{-1} (Calvert et al., 2008).
[c]Placed on an absolute basis using $k(OH + C_3H_8) = 1.1 \times 10^{-12}$ cm^3 molecule^{-1} s^{-1} (Atkinson et al., 2006).
[d]Placed on an absolute basis using $k[OH + (CH_3)_3COC(O)H] = 7.82 \times 10^{-13}$ cm^3 molecule^{-1} s^{-1} (section VII-B-6.1).
[e]Placed on an absolute basis using $k(OH + CH_3OH) = 9.0 \times 10^{-13}$ cm^3 molecule^{-1} s^{-1} (Atkinson et al., 2006).

VII-B-14.3. Summary of the Atmospheric Fate of tert-Butyl Acetate

Combining $k(OH + (CH_3)_3COC(O)CH_3) = 5.75 \times 10^{-13}$ cm^3 molecule^{-1} s^{-1} at 298 K with a diurnal average of [OH] $\approx 1.0 \times 10^6$ molecule cm^{-3} gives an estimate of about 20 days for the atmospheric lifetime with respect to reaction with OH radicals. Reaction with OH radicals dominates the atmospheric fate of *tert*-butyl acetate.

Using the structure–activity relationship method outlined by Kwok and Atkinson (1995), it can be estimated that attack of OH radicals on *tert*-butyl acetate occurs 87% at the *tert*-butyl group and 13% at the acetate group.

Tuazon et al. (1998) and Picquet-Varrault et al. (2002) have conducted product studies of the OH-radical-initiated oxidation of *tert*-butyl acetate in 1 atm. of air at, or near, 298 K in the presence of NO_x. Tuazon et al. (1998) observed acetic anhydride in a molar yield of 0.49 ± 0.05 and acetone in a yield of 0.20 ± 0.02. Picquet-Varrault et al. (2002) observed acetic anhydride in a molar yield of 0.49 ± 0.04 and acetone in a yield of 0.24 ± 0.04. Neither study found any evidence for acetic acid formation (molar yields <0.07 and <0.02, respectively, were reported in the two studies). The results from Tuazon et al. (1998) and Picquet-Varrault et al. (2002) are in excellent agreement.

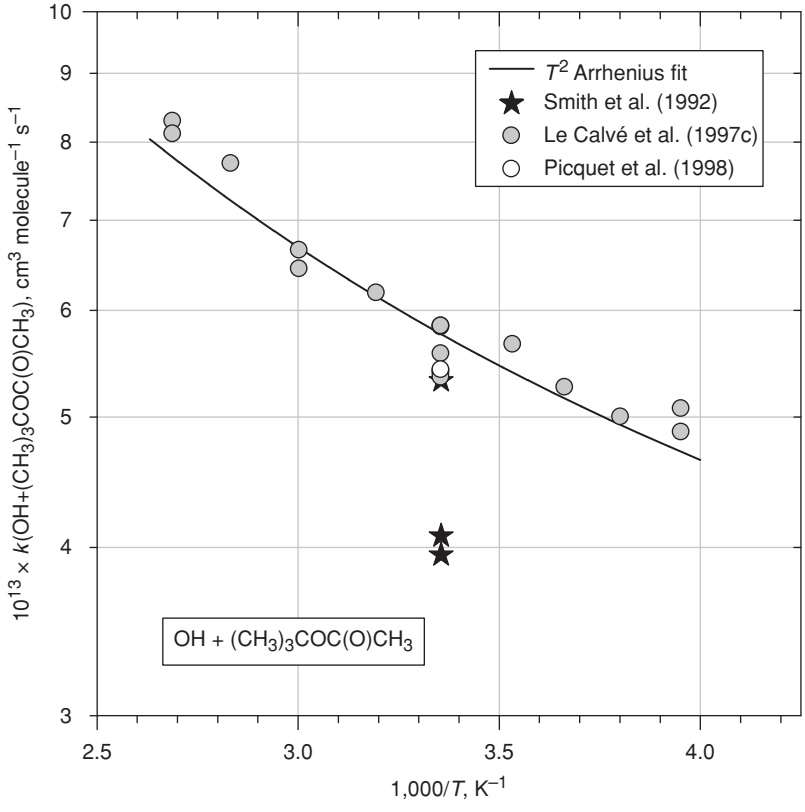

Figure VII-B-23. Measurements of the rate coefficients for reaction of OH radicals with $(CH_3)_3COC(O)CH_3$. The solid line is a fit of the modified Arrhenius expression to the data.

Table VII-B-28. Rate coefficients (k, cm^3 molecule^{-1} s^{-1}) for reaction of chlorine atoms *tert*-butyl acetate [$(CH_3)_3COC(O)CH_3$]

$10^{11} \times k$	T (K)	Technique[a]	Reference
2.42 ± 0.28	298	PLP–RF	Notario et al. (1998)
1.64 ± 0.10	297	PLP–LIF	Xing et al. (2009)
1.53 ± 0.13	296	RR (C_2H_2)[b]	Xing et al. (2009)
1.51 ± 0.12		RR (C_2H_4)[c]	

[a]Abbreviations used for the techniques are defined in table I-F-3.
[b]Placed on an absolute basis using $k(Cl + C_2H_2) = 5.2 \times 10^{-11}$ cm^3 molecule^{-1} s^{-1} (Atkinson et al., 2006).
[c]Placed on an absolute basis using $k(Cl + C_2H_4) = 9.52 \times 10^{-11}$ cm^3 molecule^{-1} s^{-1} (section I-F).

The observation of a large yield of acetic anhydride, $CH_3C(O)OC(O)CH_3$, clearly shows that a significant fraction of the $OCH_2(CH_3)_2COC(O)CH_3$ alkoxy radicals decompose via C—C bond scission:

$$OCH_2(CH_3)_2COC(O)CH_3 \rightarrow CH_2O + C(CH_3)_2OC(O)CH_3$$

$$C(CH_3)_2OC(O)CH_3 + O_2 + NO \rightarrow\rightarrow OC(CH_3)_2OC(O)CH_3 + NO_2$$

$$OC(CH_3)_2OC(O)CH_3 \rightarrow CH_3C(O)OC(O)CH_3 + CH_3$$

Interestingly, the major fate of the analogous alkoxy radical formed in the oxidation of *tert*-butyl formate is isomerization rather than decomposition via C—C bond scission. Isomerization is presumable favored by the six-membered transition state and lower C—H bond strength in the *tert*-butyl formate system. Further work is needed to identify the *tert*-butyl acetate oxidation products required for a 100% carbon balance.

VII-B-15. *n*-Pentyl Acetate [n-$C_5H_{11}OC(O)CH_3$]

VII-B-15.1. OH Reaction Kinetics

The reaction of OH with *n*-pentyl acetate has been studied by El Boudali et al. (1996) over the temperature range 273–372 K. The data are summarized in table VII-B-29 and are plotted in figure VII-B-24. A fit of the modified Arrhenius expression to the combined data set gives $k(OH + n\text{-}C_5H_{11}OC(O)CH_3) = 3.71 \times 10^{-18}\, T^2 \exp(927/T)$ which gives $k(OH + n\text{-}C_5H_{11}OC(O)CH_3) = 7.39 \times 10^{-12}$ cm^3 molecule^{-1} s^{-1} at 298 K with an uncertainty estimated to be ±25%.

VII-B-15.2. Summary of the Atmospheric Fate of n-Pentyl Acetate

Combining $k(OH + n\text{-}C_5H_{11}OC(O)CH_3) = 7.39 \times 10^{-12}$ cm^3 molecule^{-1} s^{-1} at 298 K with a diurnal average of [OH] $\approx 1.0 \times 10^6$ molecule cm^{-3} gives an estimate of about 1.5 days for the atmospheric lifetime with respect to reaction with OH radicals. Reaction with OH radicals dominates the atmospheric fate of *n*-pentyl acetate. Using the structure–activity relationship method outlined by Kwok and Atkinson (1995) with F(—OC(O)H) = 0.6 and k(—OC(O)H) = 0.9×10^{-13} cm^3 molecule^{-1} s^{-1}, it can be estimated that attack of OH radicals on *n*-pentyl acetate occurs 98% at the *n*-pentyl group, and 2% at the acetate group.

VII-B-16. Bornyl Acetate
(1,7,7-Trimethyl-bicyclo[2,2,1]-heptan-2-ol-acetate)

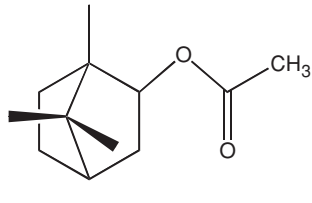

Table VII-B-29. Rate coefficients ($k = A \times e^{-B/T}$, cm^3 $molecule^{-1}$ s^{-1}) for reaction of OH with *n*-pentyl acetate [n-$C_5H_{11}CO(O)CH_3$]

$10^{12} \times A$	B (K)	$10^{13} \times k$	T(K)	Technique[a]	Reference	Temperature Range (K)
2.75 ± 0.46	-302 ± 102	8.92 ± 0.58	273	PLP–LIF	El Boudali et al. (1996)	273–372
		9.01 ± 0.46	273			
		8.19 ± 0.31	283			
		7.00 ± 0.25	298			
		7.26 ± 0.19	298			
		7.77 ± 0.17	298			
		7.13 ± 0.32	298			
		7.55 ± 0.54	298			
		7.10 ± 0.34	298			
		7.07 ± 0.42	298			
		6.89 ± 0.33	298			
		7.07 ± 0.16	313			
		6.76 ± 0.30	333			
		6.67 ± 0.22	333			
		6.13 ± 0.35	333			
		6.29 ± 0.12	353			
		6.35 ± 0.39	372			
		7.08 ± 0.34	372			

[a]Abbreviations used for the techniques are defined in table I-F-3.

VII-B-16.1. OH Reaction Kinetics

The reaction of OH with bornyl acetate has been studied by Coeur et al. (1998) using a relative rate technique with *n*-octane as reference at 298 K. Placing the rate coefficient ratio on an absolute basis using $k(\text{OH} + n\text{-octane}) = 7.81 \times 10^{-12}$ (Calvert et al., 2008) gives $k(\text{OH} + \text{bornyl acetate}) = 1.25 \times 10^{-11}$ cm^3 $molecule^{-1}$ s^{-1}. This value is recommended with an uncertainty of ±30%.

VII-B-16.2. Summary of the Atmospheric Fate of Bornyl Acetate

Combining $k(\text{OH} + \text{bornyl acetate}) = 1.25 \times 10^{-11}$ cm^3 $molecule^{-1}$ s^{-1} at 298 K with a diurnal average of $[\text{OH}] \approx 1.0 \times 10^6$ molecule cm^{-3} gives an estimate of about 1 day for the atmospheric lifetime with respect to reaction with OH radicals. Reaction with OH radicals is expected to dominate the atmospheric fate of *n*-bornyl acetate. Coeur et al. (1999) observed the formation of aerosol following the OH-radical-initiated oxidation in 1 atm. of air in the presence of NO_x. The aerosol yield was approximately 5% and 1,7,7-trimethyl-6-acetyloxy-bicyclo[2.2.1]-heptan-2,3-dione was tentatively identified in the aerosol.

VII-B-17. Methyl Propionate [$CH_3OC(O)C_2H_5$]

VII-B-17.1. OH Reaction Kinetics

The reaction of OH with methyl propionate has been the subject of relative rate studies by Campbell and Parkinson (1978) and Cavalli et al. (2000b) and absolute rate

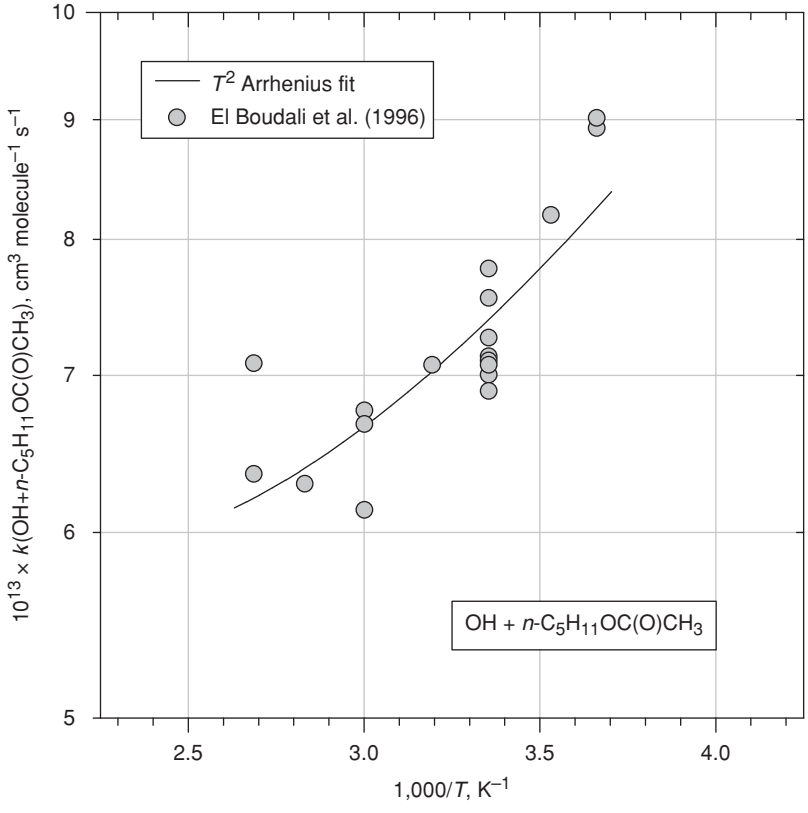

Figure VII-B-24. Measurements of the rate coefficients for reaction of OH radicals with n-$C_5H_{11}CO(O)CH_3$. The solid line is a fit of the modified Arrhenius expression to the data.

studies by Wallington et al. (1988b) and Le Calvé et al. (1997b). The results are listed in table VII-B-30 and plotted in figure VII-B-25. The study by Campbell and Parkinson (1978) is the least direct of any of the studies and gives a result which is approximately a factor of 4 lower than those from the other studies. The result from Wallington et al. (1988b) is approximately 20% above those of Le Calvé et al. (1997b) and Cavalli et al. (2000b), but it is consistent within the likely combined experimental uncertainties. As seen from figure VII-B-25 there is significant curvature in the Arrhenius plot. A fit of the modified Arrhenius expression to the combined data set gives $k(OH + CH_3OC(O)C_2H_5) = 2.00 \times 10^{-18}\, T^2 \exp(475/T)$ which gives $k(OH + CH_3OC(O)C_2H_5) = 8.73 \times 10^{-13}$ cm^3 molecule^{-1} s^{-1} at 298 K with an estimated uncertainty of $\pm 20\%$. Corroborative studies of the temperature dependence of this rate coefficient are warranted.

VII-B-17.2. Cl-Atom Reaction Kinetics

As given in table VII-B-31, Notario et al. (1998) have measured $k(Cl + CH_3OC(O)C_2H_5) = 1.98 \times 10^{-11}$ using an absolute rate method while an average of the results from the relative rate technique employed by Cavalli et al. (2000b) gives

Table VII-B-30. Rate coefficients ($k = A \times e^{-B/T}$, cm^3 $molecule^{-1}$ s^{-1}) for reaction of OH with methyl propionate [$CH_3OC(O)C_2H_5$]

$10^{12} \times A$	B (K)	$10^{13} \times k$	T(K)	Technique[a]	Reference	Temperature Range (K)
		1.65± 0.27	292	RR (n-C_4H_{10})	Campbell and Parkinson (1978)	
		10.3 ± 0.4	296	FP–RF	Wallington et al. (1988b)	
1.45 ± 0.12	148 ± 86	8.71 ± 0.47	253	PFP–LIF	Le Calvé et al. (1997b)	253–372
		8.33 ± 0.31	253			
		8.46 ± 0.24	263			
		8.68 ± 0.32	273			
		8.52 ± 0.45	298			
		8.00 ± 0.29	298			
		8.41 ± 0.29	298			
		8.43 ± 0.50	323			
		9.50 ± 0.42	348			
		10.6 ± 0.4	372			
		10.1 ± 0.3	372			
		9.09 ± 0.36	296	RR (CH_3OH)[c]	Cavalli et al. (2000b)	
		8.96 ± 0.32	296	RR (C_2H_5OH)[d]		

[a]Abbreviations used for the techniques are defined in table I-F-3.
[b]Placed on an absolute basis using $k(OH + n\text{-}C_4H_{10}) = 2.36 \times 10^{-12}$ cm^3 $molecule^{-1}$ s^{-1} (Calvert et al., 2008)).
[c]Placed on an absolute basis using $k(OH + CH_3OH) = 9.0 \times 10^{-13}$ cm^3 $molecule^{-1}$ s^{-1} (Atkinson et al., 2006).
[d]Placed on an absolute basis using $k(OH + C_2H_5OH) = 3.2 \times 10^{-12}$ cm^3 $molecule^{-1}$ s^{-1} (Atkinson et al., 2006).

$k(Cl + CH_3OC(O)C_2H_5) = 1.51 \times 10^{-11}$ cm^3 $molecule^{-1}$ s^{-1} at 298 K. The rate data reported by Notario et al. (1998) are generally approximately 25% higher than those reported in relative rate studies. The simplest explanation for this systematic difference is a slight overestimation by Notario et al. (1998) caused by secondary loss of chlorine atoms via reaction with organic peroxy radicals. A value of $k(Cl + CH_3OC(O)C_2H_5) = 1.51 \times 10^{-11}$ cm^3 $molecule^{-1}$ s^{-1} at 298 K is recommended with an uncertainty of ±30%.

VII-B-17.3. Summary of the Atmospheric Fate of Methyl Propionate

Combining $k(OH + CH_3OC(O)C_2H_5) = 8.73 \times 10^{-13}$ cm^3 $molecule^{-1}$ s^{-1} at 298 K with a diurnal average of [OH] $\approx 1.0 \times 10^6$ molecule cm^{-3} gives an estimate of about 1.3 days for the atmospheric lifetime with respect to reaction with OH radicals. Reaction with OH radicals dominates the atmospheric loss of methyl propionate. Using the structure–activity relationship method outlined by Kwok and Atkinson (1995) with F(—$CH_2C(O)OR$) = 2.2 from Le Calvé et al. (1997b), it can be estimated that attack of OH radicals occurs 18% at the methyl and 82% at the propionate group. Cavalli et al. (2000b) conducted a study of the chlorine-atom-initiated oxidation of methyl propionate in 1 atm. of air in the presence of NO_x and observed the following products (molar yields): propionic formic anhydride, $CH_3CH_2C(O)OC(O)H$ (0.099 ± 0.019); propionic acid, $CH_3CH_2C(O)OH$ (0.139 ± 0.027); carbon monoxide (0.132 ± 0.026);

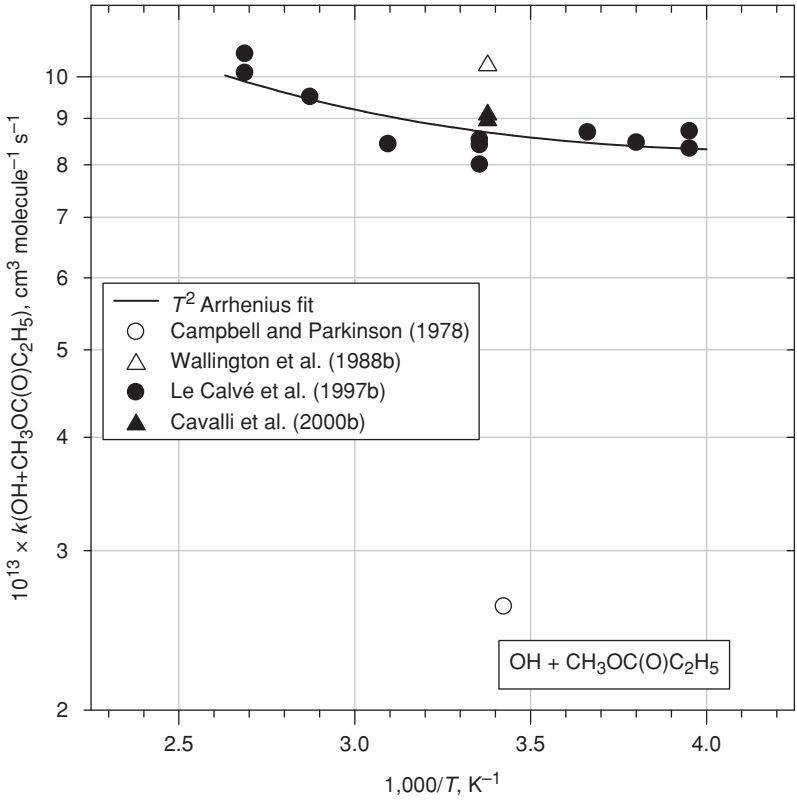

Figure VII-B-25. Measurements of the rate coefficients for reaction of OH radicals with methyl propionate. The solid line is a fit of the modified Arrhenius expression to the data from Le Calvé et al. (1997b).

Table VII-B-31. Rate coefficients (k, cm^3 molecule^{-1} s^{-1}) for reaction of chlorine atoms methyl propionate [$CH_3OC(O)C_2H_5$]

$10^{11} \times k$	T (K)	Technique[a]	Reference
1.98 ± 0.26	298	PLP–RF	Notario et al. (1998)
1.38 ± 0.15	296	RR (C_2H_5Cl)[b]	Cavalli et al. (2000b)
1.59 ± 0.12	296	RR (C_2H_6)[c]	

[a]Abbreviations used for the techniques are defined in table I-F-3.
[b]Placed on an absolute basis using $k(Cl + C_2H_5Cl) = 7.8 \times 10^{-12}$ cm^3 molecule^{-1} s^{-1} (section I-F).
[c]Placed on an absolute basis using $k(Cl + C_2H_6) = 5.9 \times 10^{-11}$ cm^3 molecule^{-1} s^{-1} (Atkinson et al., 2006).

methyl pyruvate, $CH_3C(O)C(O)OCH_3$ (0.289 ± 0.057); acetaldehyde (0.077 ± 0.015); methoxy formylperoxynitrate, $CH_3OC(O)O_2NO_2$ (0.083 ± 0.016); methyl glyoxylate, $H(O)CC(O)OCH_3$ (0.11 ± 0.02); organic nitrates (0.07 ± 0.02); and formaldehyde (observed but not quantitied). The atmospheric fate of the alkoxy radicals derived from methyl propionate is shown in figure VII-B-26. Further work is needed to corroborate

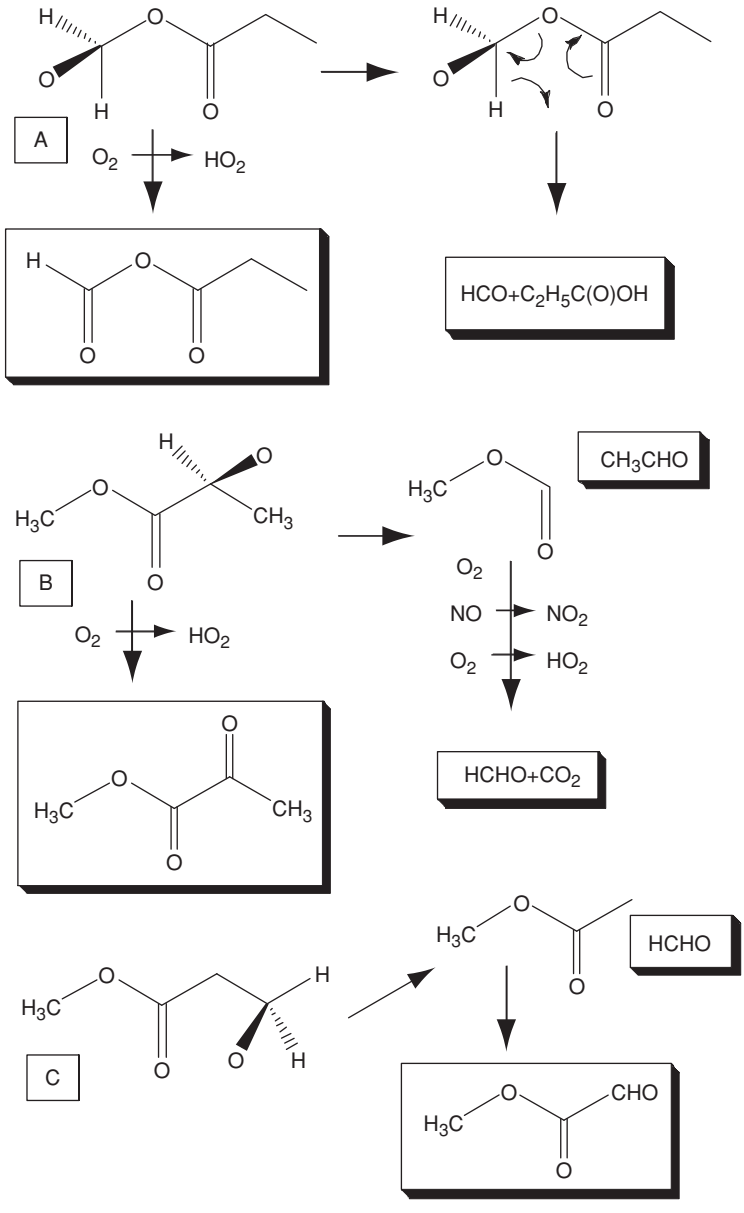

Figure VII-B-26. Atmospheric fate of the alkoxy radicals formed during the atmospheric oxidation of methyl propionate; A = $OCH_2OC(O)C_2H_5$, B = $CH_3OC(O)CHOCH_3$, C = $CH_3OC(O)CH_2CH_2O$ (Cavalli et al., 2000b).

the results from Cavalli et al. (2000b) and to better define the relative importance of the OH reaction at the three possible sites.

VII-B-18. Ethyl Propionate [$C_2H_5OC(O)C_2H_5$]

VII-B-18.1. OH Reaction Kinetics

The reaction of OH with ethyl propionate has been the subject of a relative rate study by Campbell and Parkinson (1978) and an absolute rate study by Wallington et al. (1988b). The results are listed in table VII-B-32. As discussed in previous sections, the results from Campbell and Parkinson (1978) are often lower than those reported from subsequent studies. Based upon the work by Wallington et al. (1988b), we recommend a value of $k(OH + C_2H_5OC(O)C_2H_5) = 2.1 \times 10^{-12}$ cm^3 molecule^{-1} s^{-1} with an estimated uncertainty of $\pm$30%. Corroborative studies of this rate coefficient are warranted.

VII-B-18.2. Summary of the Atmospheric Fate of Ethyl Propionate

Combining $k(OH + C_2H_5OC(O)C_2H_5) = 2.1 \times 10^{-12}$ cm^3 molecule^{-1} s^{-1} at 298 K with a diurnal average of [OH] $\approx 1.0 \times 10^6$ molecule cm^{-3} gives an estimate of about 6 days for the atmospheric lifetime of ethyl propionate. Using the structure–activity relationship method outlined by Kwok and Atkinson (1995) with F(—$CH_2C(O)OR$) = 2.2 from Le Calvé et al. (1997b), it can be estimated that H-atom abstraction from ethyl propionate by OH radicals occurs about 37% at the ethyl group and 63% at the propionate group.

VII-B-19. *n*-Propyl Propionate [*n*-$C_3H_7OC(O)C_2H_5$]

VII-B-19.1. OH Reaction Kinetics

The reaction of OH with *n*-propyl propionate has been the subject of an absolute rate study by Wallington et al. (1988b). The results are listed in table VII-B-33. Based upon the work by Wallington et al. (1988b), we recommend a value of $k(OH + n\text{-}C_3H_7OC(O)C_2H_5) = 4.0 \times 10^{-12}$ cm^3 molecule^{-1} s^{-1} with an estimated uncertainty of $\pm$30%. Corroborative studies of this rate coefficient are warranted.

Table VII-B-32. Rate coefficients (k, cm^3 molecule^{-1} s^{-1}) for reaction of OH with ethyl propionate [$C_2H_5OC(O)C_2H_5$]

$10^{12} \times k$	T (K)	Technique[a]	Reference
1.60± 0.34	292	RR (OH + *n*-C_4H_{10})	Campbell and Parkinson (1978)
2.14 ± 0.30	296	FP–RF	Wallington et al. (1988b)

[a]Abbreviations used for the techniques are defined in table I-F-3.
[b]Placed on an absolute basis using $k(OH + n\text{-}C_4H_{10}) = 2.36 \times 10^{-12}$ cm^3 molecule^{-1} s^{-1} (Calvert et al., 2008).

Table VII-B-33. Rate coefficients (k, cm^3 molecule^{-1} s^{-1}) for reaction of OH with n-propyl propionate [n-$C_3H_7OC(O)C_2H_5$]

$10^{12} \times k$	T (K)	Technique[a]	Reference
4.02 ± 0.32	296	FP–RF	Wallington et al. (1988b)

[a]Abbreviations used for the techniques are defined in table I-F-3.

VII-B-19.2. Summary of the Atmospheric Fate of n-Propyl Propionate

Combining $k(OH + n\text{-}C_3H_7OC(O)C_2H_5) = 4.0 \times 10^{-12}$ cm^3 molecule^{-1} s^{-1} at 298 K with a diurnal average of [OH] $\approx 1.0 \times 10^6$ molecule cm^{-3} gives an estimate of 3 days for the atmospheric lifetime of n-propyl propionate. Using the structure–activity relationship method outlined by Kwok and Atkinson (1995) with F(—$CH_2C(O)OR$) = 2.2 from Le Calvé et al. (1997b), it can be estimated that H-atom abstraction by OH radicals occurs 76% at the n-propyl group and 24% at the propionate group.

VII-B-20. Methyl n-Butyrate [$CH_3OC(O)CH_2CH_2CH_3$]

VII-B-20.1. OH Reaction Kinetics

The reaction of OH with methyl n-butyrate has been the subject of absolute rate studies by Wallington et al. (1988b) and Le Calvé et al. (1997b). The results are listed in table VII-B-34 and plotted in figure VII-B-27. As seen from the figure, there is significant curvature in the Arrhenius plot. A fit of the modified

Table VII-B-34. Rate coefficients ($k = A \times e^{-B/T}$, cm^3 molecule^{-1} s^{-1}) for reaction of OH with methyl n-butyrate [$CH_3OC(O)CH_2CH_2CH_3$]

$10^{12} \times A$	B (K)	$10^{12} \times k$	T(K)	Technique[a]	Reference	Temperature Range (K)
		3.04 ± 0.33	296	FP–RF	Wallington et al. (1988b)	
0.96 ± 0.29	−380 ± 91	4.08 ± 0.16	263	PFP–LIF	Le Calvé et al. (1997b)	263–372
		4.33 ± 0.06	263			
		3.97 ± 0.09	273			
		4.03 ± 0.06	273			
		3.69 ± 0.06	283			
		3.37 ± 0.07	295			
		3.37 ± 0.04	298			
		3.32 ± 0.08	298			
		3.21 ± 0.06	298			
		2.84 ± 0.10	323			
		2.83 ± 0.14	348			
		2.89 ± 0.05	372			
		2.84 ± 0.11	372			

[a]Abbreviations used for the techniques are defined in table I-F-3.

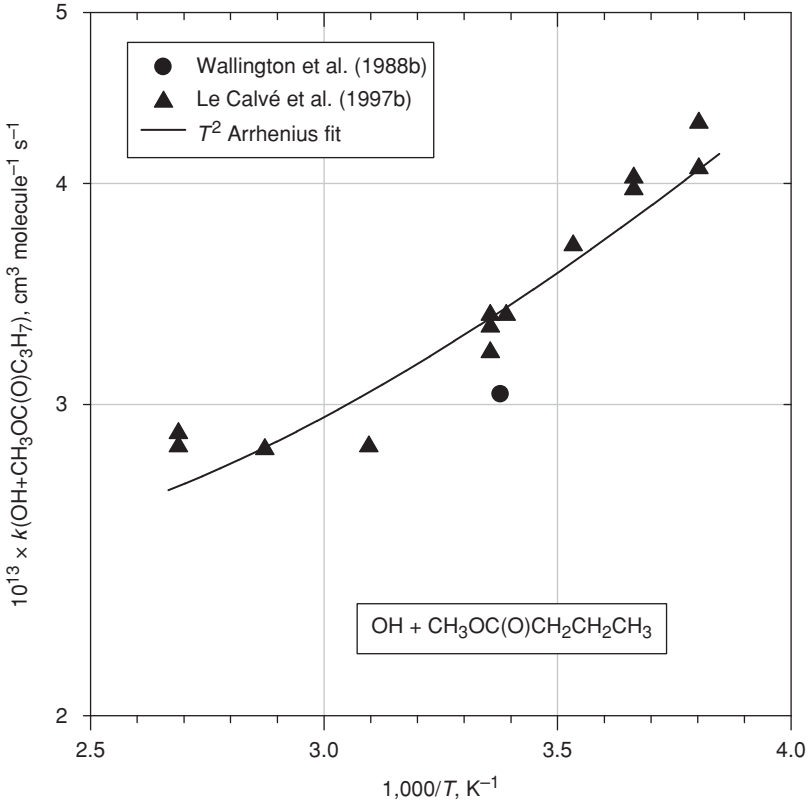

Figure VII-B-27. Measurements of the rate coefficients for reaction of OH radicals with methyl *n*-butyrate. The solid line is a fit of the modified Arrhenius expression to the data from Wallington et al. (1988b) and Le Calvé et al. (1997b).

Arrhenius expression to the combined data set gives $k[OH + CH_3OC(O)(CH_2)_3CH_3] = 1.35 \times 10^{-18} T^2 \exp(993/T)$ cm^3 molecule^{-1} s^{-1}. At 298 K this expression gives $k(OH + CH_3OC(O)(CH_2)_3CH_3) = 3.36 \times 10^{-12}$ cm^3 molecule^{-1} s^{-1} with an uncertainty estimated to be ±20%.

VII-B-20.2. Cl-Atom Reaction Kinetics

Notario et al. (1998) used resonance fluorescence to study the kinetics of the reaction of chlorine atoms with methyl butyrate. The results are given in table VII-B-35 and give $k[Cl + CH_3OC(O)CH_2CH_2CH_3] = (8.6 \pm 0.9) \times 10^{-11}$ cm^3 molecule^{-1} s^{-1} at 298 K. This value is recommended with an uncertainty of ±25%.

VII-B-20.3. Summary of the Atmospheric Fate of Methyl n-Butyrate

Combining $k[OH + CH_3OC(O)CH_2CH_2CH_3] = 3.36 \times 10^{-12}$ cm^3 molecule^{-1} s^{-1} at 298 K with a diurnal average of [OH] $\approx 1.0 \times 10^6$ molecule cm^{-3} gives an estimate of

Table VII-B-35. Rate coefficients (k, cm^3 molecule^{-1} s^{-1}) for reaction of chlorine atoms with methyl n-butyrate [$CH_3OC(O)CH_2CH_2CH_3$]

$10^{11} \times k$	T (K)	Technique[a]	Reference
8.6 ± 0.9	298	PLP–RF	Notario et al. (1998)

[a]Abbreviations used for the techniques are defined in table I-F-3.

3.4 days for the atmospheric lifetime of methyl butyrate. Using the structure–activity relationship method outlined by Kwok and Atkinson (1995) with F(—$CH_2C(O)OR$) = 2.2 from Le Calvé et al. (1997b), it can be estimated that H-atom abstraction by OH radicals occurs 7% at the methyl group and 93% at the butyrate group.

VII-B-21. Ethyl n-Butyrate [$C_2H_5OC(O)CH_2CH_2CH_3$]

VII-B-21.1. OH Reaction Kinetics

The reaction of OH with ethyl butyrate has been the subject of an absolute rate study by Wallington et al. (1988b) and a relative rate study by Ferrari et al. (1996). The results are listed in table VII-B-36. The results from these two studies differ by approximately 20%, which is close to the combined experimental uncertainties. Taking an average of the results from Wallington et al. (1988b) and Ferrari et al. (1996) gives our recommended value of $k(OH + C_2H_5OC(O)CH_2CH_2CH_3] = 4.5 \times 10^{-12}$ cm^3 molecule^{-1} s^{-1} at 298 K with an estimated uncertainty of ±35%. Corroborative studies of this rate coefficient are warranted.

VII-B-21.2. Summary of the Atmospheric Fate of Ethyl n-Butyrate

Combining $k(OH + C_2H_5OC(O)CH_2CH_2CH_3) = 4.5 \times 10^{-12}$ cm^3 molecule^{-1} s^{-1} at 298 K with a diurnal average of [OH] $\approx 1.0 \times 10^6$ molecule cm^{-3} gives an estimate of about 3 days for the atmospheric lifetime of ethyl butyrate.

Using the structure–activity relationship method outlined by Kwok and Atkinson (1995) with F(—$CH_2C(O)OR$) = 2.2 from Le Calvé et al. (1997b), it can be estimated that H-atom abstraction by OH radicals occurs 36% at the ethyl group and 64% at the butyrate group.

Table VII-B-36. Rate coefficients (k, cm^3 molecule^{-1} s^{-1}) for reaction of OH with ethyl butyrate [$C_2H_5OC(OCH_2CH_2CH_3$]

$10^{12} \times k$	T (K)	Technique[a]	Reference
4.94 ± 0.38	296	FP–RF	Wallington et al. (1988b)
4.05 ± 0.38	296	RR (n-C_8H_{18})[b]	Ferrari et al. (1996)

[a]Abbreviations used for the techniques are defined in table I-F-3.
[b]Placed on an absolute basis using $k(OH + n\text{-}C_8H_{18}) = 7.81 \times 10^{-12}$ cm^3 molecule^{-1} s^{-1} (Calvert et al., 2008).

Table VII-B-37. Rate coefficients (k, cm^3 molecule^{-1} s^{-1}) for reaction of OH with n-propyl$n$-butyrate [n-$C_3H_7OC(OCH_2CH_2CH_3$]

$10^{12} \times k$	T (K)	Technique[a]	Reference
4.71 ± 0.32	296	FP–RF	Wallington et al. (1988b)

[a]Abbreviations used for the techniques are defined in table I-F-3.

VII-B-22. n-Propyl n-Butyrate [n-$C_3H_7OC(O)CH_2CH_2CH_3$]

VII-B-22.1. OH Reaction Kinetics

The reaction of OH with n-propyl n-butyrate has been the subject of an absolute rate study by Wallington et al. (1988b). The results are listed in table VII-B-37. Based upon the work by Wallington et al. (1988b), we recommend a value of $k(OH + C_2H_5OC(O)CH_2CH_2CH_3) = 4.71 \times 10^{-12}$ cm^3 molecule^{-1} s^{-1} with an estimated uncertainty of ±30%. Corroborative studies of this rate coefficient are warranted.

VII-B-22.2. Summary of the Atmospheric Fate of n-Propyl n-Butyrate

Combining $k(OH + n\text{-}C_3H_7OC(O)CH_2CH_2CH_3) = 4.7 \times 10^{-12}$ cm^3 molecule^{-1} s^{-1} at 298 K with a diurnal average of [OH] $\approx 1.0 \times 10^6$ molecule cm^{-3} gives an estimate of about 2 days for the atmospheric lifetime of n-propyl butyrate. Using the structure–activity relationship method outlined by Kwok and Atkinson (1995) with F(—$CH_2C(O)OR$) = 2.2 from Le Calvé et al. (1997b), it can be estimated that H-atom abstraction by OH radicals occurs 51% at the n-propyl group and 49% at the n-butyrate group.

VII-B-23. n-Butyl n-Butyrate [n-$C_4H_9OC(O)CH_2CH_2CH_3$]

VII-B-23.1. OH Reaction Kinetics

The reaction of OH with n-butyl n-butyrate has been the subject of an absolute rate study by Wallington et al. (1988b). The results are listed in table VII-B-38. Based upon the work by Wallington et al. (1988b), we recommend a value of $k(OH + n\text{-}C_4H_9OC(O)CH_2CH_2CH_3) = 1.06 \times 10^{-11}$ cm^3 molecule^{-1} s^{-1} with an estimated uncertainty of ±30%. Corroborative studies of this rate coefficient are warranted.

Table VII-B-38. Rate coefficients (k, cm^3 molecule^{-1} s^{-1}) for reaction of OH with n-butyl n-butyrate [n-$C_4H_9OC(O)CH_2CH_2CH_3$]

$10^{11} \times k$	T (K)	Technique[a]	Reference
1.06 ± 0.13	296	FP–RF	Wallington et al. (1988b)

[a]Abbreviations used for the techniques are defined in table I-F-3.

VII-B-23.2. Summary of the Atmospheric Fate of n-Butyl n-Butyrate

Combining $k(\mathrm{OH} + n\text{-}\mathrm{C_4H_9OC(O)CH_2CH_2CH_3}) = 1.06 \times 10^{-11}$ cm^3 molecule^{-1} s^{-1} at 298 K with a diurnal average of [OH] $\approx 1.0 \times 10^6$ molecule cm^{-3} gives an estimate of about 1 day for the atmospheric lifetime of *n*-butyl butyrate. Using the structure–activity relationship method outlined by Kwok and Atkinson (1995) with F(—$\mathrm{CH_2C(O)OR}$) = 2.2 from Le Calvé et al. (1997b) it can be estimated that H-atom abstraction by OH radicals occurs 59% at the *n*-butyl group and 41% at the butyrate group.

VII-B-24. Methyl *iso*-Butyrate [$\mathrm{CH_3OC(O)CH(CH_3)_2}$]

VII-B-24.1. OH Reaction Kinetics

Wyatt et al. (1999) studied the reaction of OH with methyl *iso*-butyrate at 297 K using relative rate methods with 2-butanone, *iso*-octane, and 3-pentanone as reference compounds. The results obtained using the three different references were in good agreement. The rate coefficients ratios were not reported by Wyatt et al. (1999) and they cannot be derived from the data that Wyatt et al. (1999) presented. Hence, rescaling to the latest recommended data for the reference rate coefficients is not possible. The reference rate coefficients used by Wyatt et al. (1999) differ by less than 10% from those recommended here and by Calvert et al. (2008). Wyatt et al. (1999) reported $k(\mathrm{OH} + \mathrm{CH_3OC(O)CH(CH_3)_2}) = (1.7 \pm 0.4) \times 10^{-12}$ cm^3 molecule^{-1} s^{-1}. Corroborative studies of this rate coefficient are warranted.

VII-B-24.2. Summary of the Atmospheric Fate of Methyl iso-Butyrate

Combining $k(\mathrm{OH} + \mathrm{CH_3OC(O)CH(CH_3)_2}) = 1.7 \times 10^{-12}$ cm^3 molecule^{-1} s^{-1} at 298 K with a diurnal average of [OH] $\approx 1.0 \times 10^6$ molecule cm^{-3} gives an estimate of about 7 days for the atmospheric lifetime of methyl *iso*-butyrate. Wyatt et al. (1999) reported the formation of acetone and methyl pyruvate ($\mathrm{CH_3C(O)C(O)OCH_3}$) in molar yields of $97 \pm 1\%$ and $3.3 \pm 0.3\%$, respectively, from the OH-radical-initiated oxidation in 1 atm. of air in the presence of NO_x. The observation of acetone in a molar yield close to unity indicates that the majority of reaction of OH with methyl *iso*-butyrate proceeds via attack at the tertiary C—H bond leading to an alkoxy radical which decomposes via C—C bond scission to give acetone:

$$\mathrm{CH_3OC(O)CH(CH_3)_2 + OH \rightarrow CH_3OC(O)C(CH_3)_2 + H_2O}$$

$$\mathrm{CH_3OC(O)C(CH_3)_2 + O_2 + M \rightarrow CH_3OC(O)C(OO)(CH_3)_2 + M}$$

$$\mathrm{CH_3OC(O)C(OO)(CH_3)_2 + NO \rightarrow CH_3OC(O)C(O)(CH_3)_2 + NO_2}$$

$$\mathrm{CH_3OC(O)C(O)(CH_3)_2 \rightarrow CH_3OC(O) + CH_3C(O)CH_3}$$

Table VII-B-39. Rate coefficients (k, cm^3 molecule^{-1} s^{-1}) for reaction of OH with *iso*-propyl *iso*-butyrate [$(CH_3)_2CHOC(O)CH(CH_3)_2$]

$10^{12} \times k$	T (K)	Technique[a]	Reference
7.0 ± 0.4	297	RR (n-$C_3H_7)_2O$	Stemmler et al. (1997a)

[a]Abbreviations used for the techniques are defined in table I-F-3.
[b]Placed on an absolute basis using $k[(n\text{-}C_3H_7)_2O] = 2.0 \times 10^{-11}$ cm^3 molecule^{-1} s^{-1} (this book, section III-B-6.1).

VII-B-25. *iso*-Propyl *iso*-Butyrate [$(CH_3)_2CHOC(O)CH(CH_3)_2$]

VII-B-25.1. OH Reaction Kinetics

Stemmler et al. (1997a) studied the reaction of OH with *iso*-propyl *iso*-butyrate at 297 K using relative rate methods. The result is given in table VII-B-39 and is recommended with an uncertainty estimated to be ±30%. Corroborative studies of this rate coefficient are warranted.

VII-B-25.2. Summary of the Atmospheric Fate of iso-Propyl iso-Butyrate

Combining $k(OH + (CH_3)_2CHOC(O)CH(CH_3)_2) = 7.0 \times 10^{-12}$ cm^3 molecule^{-1} s^{-1} at 298 K with a diurnal average of [OH] $\approx 1.0 \times 10^6$ molecule cm^{-3} gives an estimate of about 2 days for the atmospheric lifetime of *iso*-propyl *iso*-butyrate.

VII-B-26. Methyl *n*-Pentanoate [Methyl Valerate, $CH_3OC(O)CH_2CH_2CH_2CH_3$]

VII-B-26.1. OH Reaction Kinetics

The reaction of OH with methyl *n*-pentanoate has been the subject of an absolute rate study by Le Calvé et al. (1997b). The results are listed in table VII-B-40 and plotted in figure VII-B-28. Significant curvature is evident in the Arrhenius plot. A fit of the modified Arrhenius expression to the data from Le Calvé et al. (1997b) gives $k(OH + CH_3OC(O)CH_2CH_2CH_2CH_3) = 1.88 \times 10^{-18} T^2 \exp(1{,}028/T)$ cm^3 molecule^{-1} s^{-1}. This expression yields $k(OH + CH_3OC(O)CH_2CH_2CH_2CH_3) = 5.26 \times 10^{-12}$ cm^3 molecule^{-1} s^{-1} at 298 K with an estimated uncertainty of ±25%. Corroborative studies of this rate coefficient are warranted.

VII-B-26.2. Cl-Atom Reaction Kinetics

Notario et al. (1998) used PLP–RF methods (see table VII-B-41) to measure $k(Cl + CH_3OC(O)CH_2CH_2CH_2CH_3) = (1.7 \pm 0.2) \times 10^{-10}$ cm^3 molecule^{-1} s^{-1} at 298 K. This value is recommended with an uncertainty estimated to be ±35%.

Table VII-B-40. Rate coefficients ($k = A \times e^{-B/T}$, cm^3 $molecule^{-1}$ s^{-1}) for reaction of OH with methyl pentanoate [methyl valerate, $CH_3OC(O)CH_2CH_2CH_2CH_3$]

$10^{12} \times A$	B (K)	$10^{12} \times k$	T(K)	Technique[a]	Reference	Temperature Range (K)
0.96 ± 0.29	-380 ± 91	4.08 ± 0.16	263	PLP–LIF	Le Calvé et al. (1997b)	263–372
		4.33 ± 0.06	263			
		3.97 ± 0.09	273			
		4.03 ± 0.06	273			
		3.69 ± 0.06	283			
		3.37 ± 0.07	295			
		3.37 ± 0.04	298			
		3.32 ± 0.08	298			
		3.21 ± 0.06	298			
		2.84 ± 0.10	323			
		2.83 ± 0.14	348			
		2.89 ± 0.05	372			
		2.84 ± 0.11	372			

[a]Abbreviations used for the techniques are defined in table I-F-3.

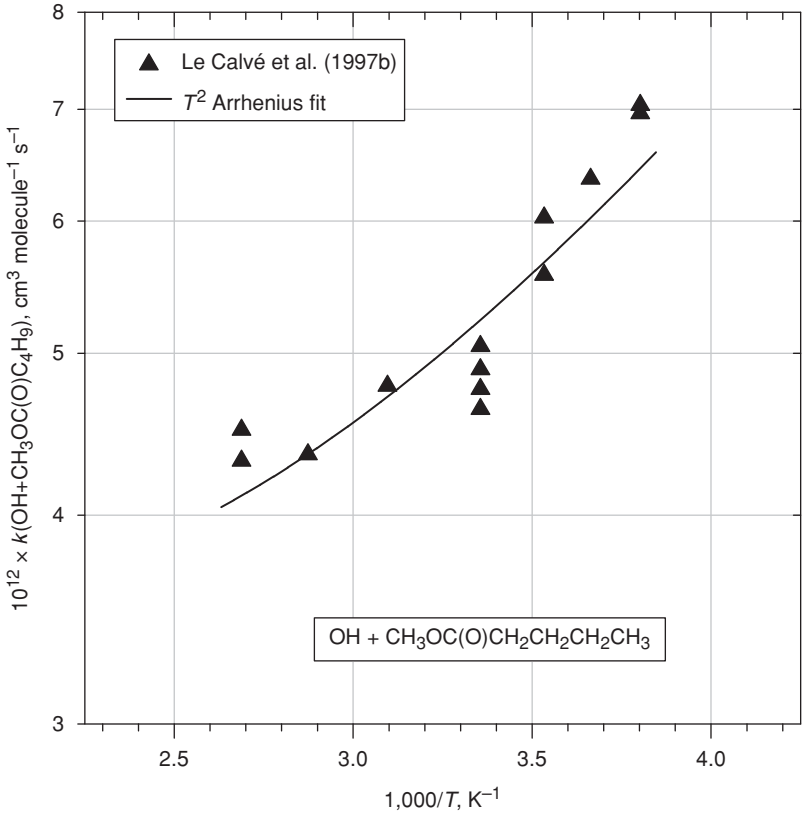

Figure VII-B-28. Measurements of the rate coefficients for reaction of OH radicals with methyl *n*-pentanoate. The solid line is a fit of the modified Arrhenius expression to the data from Le Calvé et al. (1997b).

Table VII-B-41. Rate coefficients (k, cm^3 molecule^{-1} s^{-1}) for reaction of chlorine atoms with methyl pentanoate, methyl valerate [$CH_3OC(O)CH_2CH_2CH_2CH_3$]

$10^{10} \times k$	T (K)	Technique[a]	Reference
1.7 ± 0.2	298	PLP–RF	Notario et al. (1998)

[a]Abbreviations used for the techniques are defined in table I-F-3.

VII-B-26.3. Summary of the Atmospheric Fate of Methyl n-Pentanoate

Combining $k(OH + CH_3OC(O)CH_2CH_2CH_2CH_3) = 5.26 \times 10^{-12}$ cm^3 molecule^{-1} s^{-1} at 298 K with a diurnal average of [OH] $\approx 1.0 \times 10^6$ molecule cm^{-3} gives an estimate of about 2 days for the atmospheric lifetime of methyl *n*-pentanoate. Using the structure–activity relationship method outlined by Kwok and Atkinson (1995) with F(—$CH_2C(O)OR$) = 2.2 from Le Calvé et al. (1997b), it can be estimated that H-atom abstraction by OH radicals occurs 4% at the methyl group and 96% at the pentanoate group.

VII-B-27. Methyl Pivalate [Methyl Ester of 2,2-Dimethylpropanoic Acid, $CH_3OC(O)C(CH_3)_3$]

VII-B-27.1. OH Reaction Kinetics

The reaction of OH with methyl pivalate has been the subject of an absolute rate study by Wallington et al. (2001b). The results are listed in table VII-B-42 and plotted in figure VII-B-29. Significant curvature is evident in the Arrhenius plot. A fit of the modified Arrhenius expression to the data from Wallington et al. (2001b) gives $k[OH + CH_3OC(O)C(CH_3)_3] = 1.86 \times 10^{-18} T^2 \times \exp(604/T)$ cm^3 molecule^{-1} s^{-1}. As seen from figure VII-B-29, the modified Arrhenius expression (solid curve) does not fully capture the curvature in the plot. Representation of the rate coefficient over the entire temperature range studied is best accomplished using the sum of two Arrhenius expressions. Fitting the sum of two Arrhenius expressions to the data gives $k = 3.47 \times 10^{-11} \exp(-1{,}431/T) + 1.68 \times 10^{-13} \exp(503/T)$ cm^3 molecule^{-1} s^{-1}. This expression yields $k(OH + CH_3OC(O)C(CH_3)_3) = 1.19 \times 10^{-12}$ cm^3 molecule^{-1}

Table VII-B-42. Rate coefficients (k, cm^3 molecule^{-1} s^{-1}) for reaction of OH with methyl pivalate [$CH_3OC(O)C(CH_3)_3$]

$10^{12} \times k$	T (K)	Technique[a]	Reference	Temperature Range (K)
1.37 ± 0.03	250	FP–RF	Wallington et al. (2001b)	250–370
1.24 ± 0.02	272			
1.20 ± 0.03	298			
1.22 ± 0.02	330			
1.38 ± 0.03	370			

[a]Abbreviations used for the techniques are defined in table I-F-3.

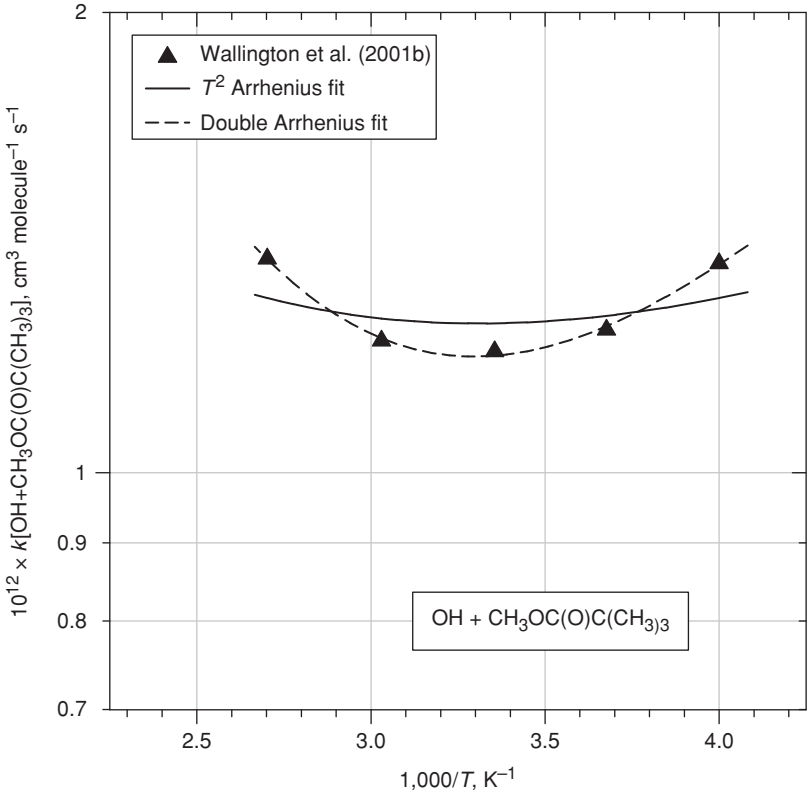

Figure VII-B-29. Measurements of the rate coefficients for reaction of OH radicals with methyl pivalate. The solid and dashed lines are fits of the modified Arrhenius and double Arrhenius expressions to the data from Wallington et al. (2001b).

s^{-1} at 298 K with an estimated uncertainty of ±25%. Corroborative studies of this rate coefficient are warranted.

VII-B-27.2. Cl-Atom Reaction Kinetics

An average from the determinations of Wallington et al. (2001b) listed in table VII-B-43 gives $k[Cl + CH_3OC(O)C(CH_3)_3] = 4.07 \times 10^{-11}$ cm^3 molecule^{-1} s^{-1}. This value is recommended at 298 K with an uncertainty estimated to be ±25%.

VII-B-27.3. Summary of the Atmospheric Fate of Methyl Pivalate

Combining $k[OH + CH_3OC(O)C(CH_3)_3] = 1.19 \times 10^{-12}$ cm^3 molecule^{-1} s^{-1} at 298 K with a diurnal average of [OH] $\approx 1.0 \times 10^6$ molecule cm^{-3} gives an estimate of about 10 days for the atmospheric lifetime of methyl pivalate. Using the structure–activity relationship method outlined by Kwok and Atkinson (1995), it can be estimated that attack of OH radicals on methyl pivalate occurs approximately 30% at the alkoxy

Table VII-B-43. Rate coefficients (k, cm^3 molecule^{-1} s^{-1}) for reaction of chlorine atoms with methyl pivalate [$CH_3OC(O)C(CH_3)_3$]

$10^{11} \times k$	T (K)	Technique[a]	Reference
4.19 ± 0.29	296	RR (C_2H_4)[b]	Wallington et al. (2001b)
3.95 ± 0.47		RR (C_2H_5Cl)[c]	

[a]Abbreviations used for the techniques are defined in table I-F-3.
[b]Placed on an absolute basis using $k(Cl + C_2H_4) = 9.52 \times 10^{-11}$ cm^3 molecule^{-1} s^{-1} (section I-F).
[c]Placed on an absolute basis using $k(Cl + C_2H_5Cl) = 7.8 \times 10^{-12}$ cm^3 molecule^{-1} s^{-1} (section I-F).

CH_3O-group and 70% at the acyl-$C(O)C(CH_3)_3$ group. The products observed in the experimental study conducted by Wallington et al. (2001b) are consistent with this branching ratio.

$$OH + CH_3OC(O)C(CH_3)_3 \rightarrow CH_2OC(O)C(CH_3)_3 + H_2O$$

$$OH + CH_3OC(O)C(CH_3)_3 \rightarrow CH_3OC(O)C(CH_3)_2CH_2 + H_2O$$

The alkyl radicals $CH_2OC(O)C(CH_3)_3$ and $CH_3OC(O)C(CH_3)_2CH_2$ add O_2 to give the corresponding peroxy radicals which in turn react with NO to give alkoxy radicals and organic nitrates. Based upon the observed reduction of the rates of NO oxidation and O_3 formation in smog chamber experiments caused by addition of methyl pivalate, Wallington et al. (2001b) estimated that for both peroxy radicals shown below $k_a/(k_a + k_b) = 0.87$ and $k_b/(k_a + k_b) = 0.13$.

$$OOCH_2OC(O)C(CH_3)_3 + NO \rightarrow OCH_2OC(O)C(CH_3)_3 + NO_2 \quad (a)$$

$$OOCH_2OC(O)C(CH_3)_3 + NO \rightarrow O_2NOCH_2OC(O)C(CH_3)_3 \quad (b)$$

$$CH_3OC(O)C(CH_3)_2CH_2OO + NO \rightarrow CH_3OC(O)C(CH_3)_2CH_2O + NO_2 \quad (a)$$

$$CH_3OC(O)C(CH_3)_2CH_2OO + NO \rightarrow CH_3OC(O)C(CH_3)_2CH_2ONO_2 \quad (b)$$

The main fate of the alkoxy radical $CH_3OC(O)C(CH_3)_2CH_2O$ in 1 atm. of air at 298 K is decomposition via C—C bond scission. The resulting $CH_3OC(O)C(CH_3)_2$ is oxidized further to give acetone. The main fate of the $OCH_2OC(O)C(CH_3)_3$ alkoxy radical is α-ester rearrangement to give pivalic acid [$(CH_3)_3CC(O)OH$] and HCO radicals.

VII-B-28. Methyl *n*-Hexanoate [Methyl Caproate, $CH_3OC(O)CH_2CH_2CH_2CH_2CH_3$]

VII-B-28.1. OH Reaction Kinetics

The reaction of OH with methyl *n*-hexanoate has been the subject of an absolute rate study by Le Calvé et al. (1997b). The results are listed in table VII-B-44 and plotted in figure VII-B-30. Significant curvature is evident in the Arrhenius plot.

Table VII-B-44. Rate coefficients ($k = A \times e^{-B/T}$, cm^3 $molecule^{-1}$ s^{-1}) for reaction of OH with methyl hexanoate, methyl caproate [$CH_3OC(O)CH_2CH_2CH_2CH_2CH_3$]

$10^{12} \times A$	B (K)	$10^{12} \times k$	T(K)	Technique[a]	Reference	Temperature Range (K)
2.46 ± 1.04	−326 ± 130	8.40 ± 0.30	273	PLP–LIF	Le Calvé et al. (1997b)	273–372
		8.67 ± 0.37	273			
		8.02 ± 0.22	283			
		7.03 ± 0.34	295			
		7.25 ± 0.13	298			
		7.72 ± 0.20	298			
		6.53 ± 0.18	298			
		7.00 ± 0.32	323			
		6.11 ± 0.24	348			
		5.91 ± 0.22	372			
		6.38 ± 0.18	372			

[a]Abbreviations used for the techniques are defined in table I-F-3.

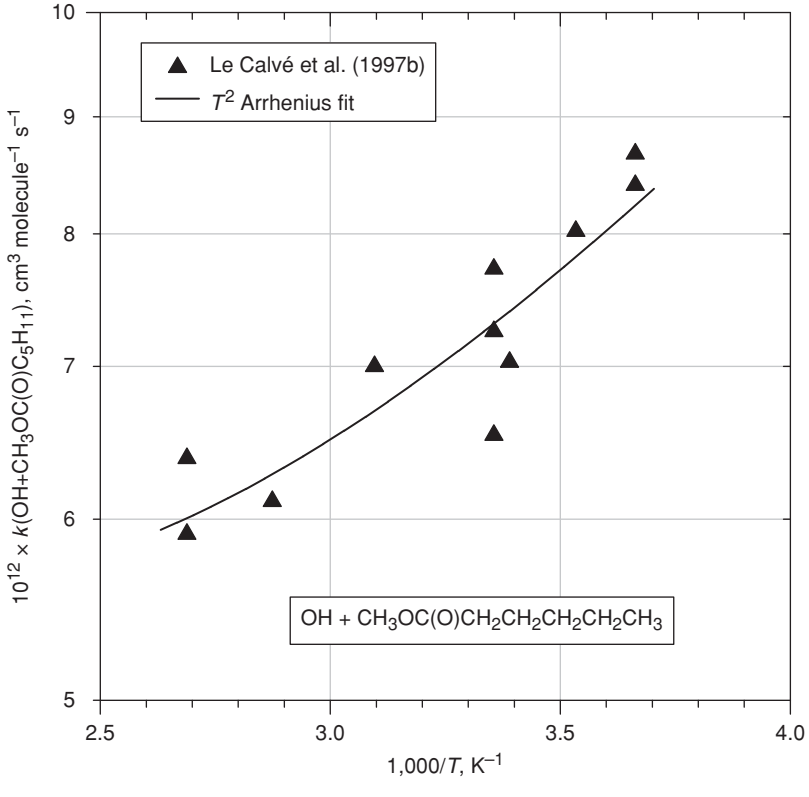

Figure VII-B-30. Measurements of the rate coefficients for reaction of OH radicals with methyl *n*-hexanoate. The solid curve is a fit of the modified Arrhenius expression to the data from Le Calvé et al. (1997b).

A fit of the modified Arrhenius expression to the data from Le Calvé et al. (1997b) gives: $k(OH + CH_3OC(O)CH_2CH_2CH_2CH_2CH_3) = 3.30 \times 10^{-18} T^2 \exp(958/T)$ cm^3 molecule^{-1} s^{-1}. This expression yields $k[OH + CH_3OC(O)CH_2CH_2CH_2CH_2CH_3] = 7.36 \times 10^{-12}$ cm^3 molecule^{-1} s^{-1} at 298 K with an estimated uncertainty of ±25%. Corroborative studies of this rate coefficient are warranted.

VII-B-28.2. Cl-Atom Reaction Kinetics

Notario et al. (1998) have measured $k[Cl + CH_3OC(O)CH_2CH_2CH_2CH_2CH_3] = (2.72 \pm 0.32) \times 10^{-10}$ cm^3 molecule^{-1} s^{-1} using a PLP–RF method at 298 K. This value is recommended with an uncertainty estimated to be ±25%.

VII-B-28.3. Summary of the Atmospheric Fate of Methyl n-Hexanoate

Combining $k[OH + CH_3OC(O)CH_2CH_2CH_2CH_2CH_3] = 7.36 \times 10^{-12}$ cm^3 molecule^{-1} s^{-1} at 298 K with a diurnal average of [OH] $\approx 1.0 \times 10^6$ molecule cm^{-3} gives an estimate of about 1.6 days for the atmospheric lifetime of methyl hexanoate. Using the structure–activity relationship method outlined by Kwok and Atkinson (1995) with F(—$CH_2C(O)OR$) = 2.2 from Le Calvé et al. (1997b), it can be estimated that H-atom abstraction by OH radicals occurs 3% at the methyl group and 97% at the hexanoate group.

VII-C. Difunctional Esters

VII-C-1. Ethylene Glycol Diformate [$HC(O)OCH_2CH_2OC(O)H$]

VII-C-1.1. OH Reaction Kinetics

The reaction of OH with ethylene glycol diformate has been the subject of a relative rate study by Maurer et al. (1999) at 298 K. The results from Maurer et al. (1999) in table VII-C-1 give $k(OH + HC(O)OCH_2CH_2OC(O)H) = 4.84 \times 10^{-13}$ cm^3 molecule^{-1} s^{-1} with an uncertainty estimated to be ±25%. Corroborative studies of this rate coefficient are warranted.

Table VII-C-1. Rate coefficients (k, cm^3 molecule^{-1} s^{-1}) for reaction of OH with ethylene glycol diformate [$HC(O)OCH_2CH_2OC(O)H$]

$10^{13} \times k$	T (K)	Technique[a]	Reference
4.84 ± 0.32	298	RR (C_2H_6)[b]	Maurer et al. (1999)

[a]Abbreviations used for the techniques are defined in table I-F-3.
[b]Placed on an absolute basis using $k(OH + C_2H_6) = 2.56 \times 10^{-13}$ cm^3 molecule^{-1} s^{-1} (Calvert et al., 2008).

Table VII-C-2. Rate coefficients (k, cm^3 molecule^{-1} s^{-1}) for reaction of chlorine atoms with ethylene glycol diformate [HC(O)OCH$_2$CH$_2$OC(O)H]

$10^{12} \times k$	T (K)	Technique[a]	Reference
3.16 ± 0.08	298	RR (C_2H_5Cl)[b]	Maurer et al. (1999)

[a]Abbreviations used for the techniques are defined in table I-F-3.
[b]Placed on an absolute basis using $k(Cl + C_2H_5Cl) = 7.8 \times 10^{-12}$ cm^3 molecule^{-1} s^{-1} (section I-F).

VII-C-1.2. Cl-Atom Reaction Kinetics

The reaction of chlorine atoms with ethylene glycol diformate has been the subject of a relative rate study by Maurer et al. (1999) at 298 K. The results from Maurer et al. (1999) in table VII-C-2 give $k(Cl + HC(O)OCH_2CH_2OC(O)H) = 3.16 \times 10^{-12}$ cm^3 molecule^{-1} s^{-1} with an uncertainty estimated to be ±25%. Corroborative studies of this rate coefficient are warranted.

VII-C-1.3. Summary of the Atmospheric Fate of Ethylene Glycol Diformate

Combining $k(OH + HC(O)OCH_2CH_2OC(O)H) = 4.84 \times 10^{-13}$ cm^3 molecule^{-1} s^{-1} at 298 K with a diurnal average of [OH] $\approx 1.0 \times 10^6$ molecule cm^{-3} gives an estimate of about 24 days for the atmospheric lifetime of ethylene glycol diformate with respect to reaction with OH radicals. Ethylene glycol diformate is soluble in water, and it is likely that rain-out and dry deposition will be significant atmospheric loss mechanisms. Maurer et al. (1999) studied the products of the chlorine-atom-initiated oxidation of ethylene glycol diformate in 1 atm. of air at 298 K in the presence and absence of NO_x. In the absence of NO_x the observed products (molar yields) were: formic acid anhydride (1.44 ± 0.29), formic acid (0.39 ± 0.08), and CO (0.22 ± 0.04). In the presence of NO_x the observed products (molar yields) were: formic acid anhydride (1.73 ± 0.34), formic acid (0.45 ± 0.09), and CO (0.41 ± 0.08). The observation of a large yield of formic acid anhydride shows that the majority of reaction proceeds via H-atom abstraction from the CH_2 groups and that decomposition via C—C bond scission is the main fate of HC(O)OCH(O•)CH$_2$OC(O)H radicals.

$$HC(O)OCH(O\bullet)CH_2OC(O)H \rightarrow HC(O)OC(O)H + CH_2OC(O)H$$

The $CH_2OC(O)H$ radical is the same as that produced in the oxidation of methyl formate, and the observed formic acid yield (formed in the α-ester rearrangement) is consistent with that expected based on the study of methyl formate oxidation by Wallington et al. (2001a) as discussed in section VII-B-1. Maurer et al. (1999) noted the decreased yield of formic acid anhydride and the increase in the HC(O)OH/CO yield ratio observed in experiments conducted in the presence of NO. Maurer et al. (1999) suggested this probably reflects chemical activation of HC(O)OCH(O•)CH$_2$OC(O)H radicals formed in the reaction of the corresponding peroxy radical with NO which may favor loss via C—C bond scission (see figure VII-C-1).

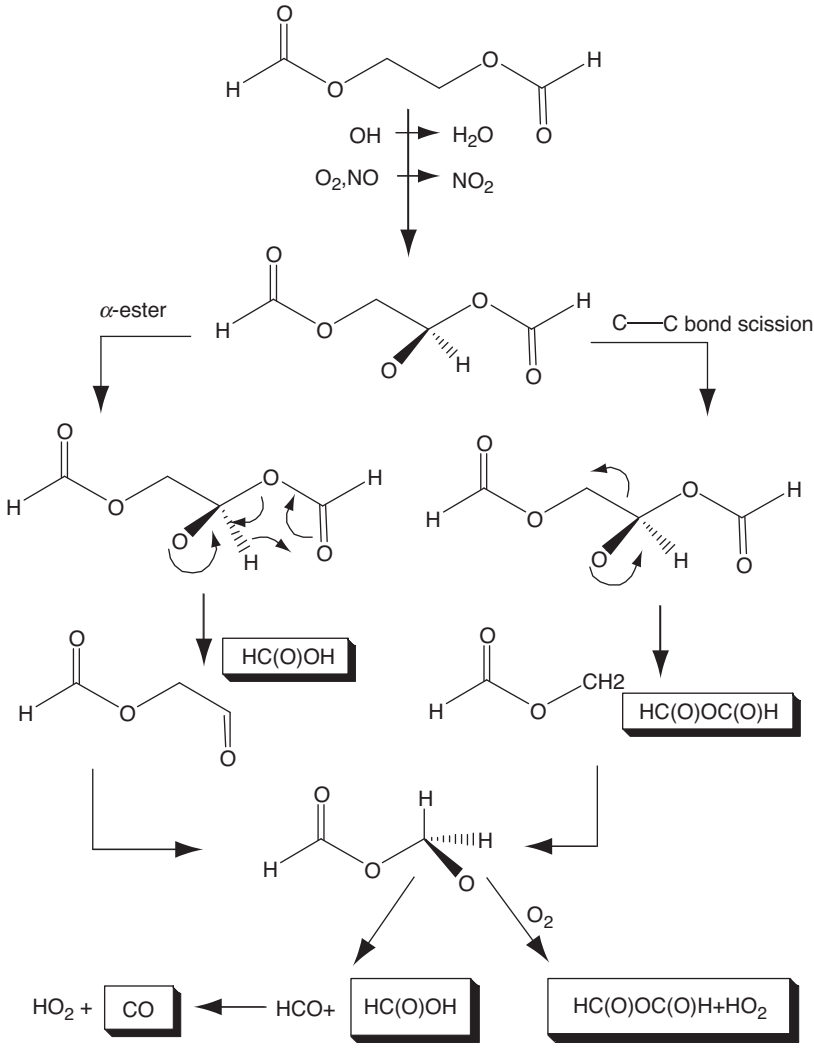

Figure VII-C-1. Simplified oxidation mechanism for ethylene glycol diformate.

VII-C-2. Ethylene Glycol Diacetate [$CH_3C(O)OCH_2CH_2OC(O)CH_3$]

VII-C-2.1. OH Reaction Kinetics

The reaction of OH with ethylene glycol diacetate has been the subject of a relative rate study at 296 K by Hurley et al. (2007), see table VII-C-3. An average of the results from Hurley et al. (2007) gives $k(\mathrm{OH} + \mathrm{CH_3C(O)OCH_2CH_2OC(O)CH_3}) = 2.16 \times 10^{-12}$ $\mathrm{cm^3\ molecule^{-1}\ s^{-1}}$ with an uncertainty estimated to be ±25%. Corroborative studies of this rate coefficient are warranted.

Table VII-C-3. Rate coefficients (k, cm^3 molecule^{-1} s^{-1}) for reaction of OH with ethylene glycol diacetate [$CH_3C(O)OCH_2CH_2OC(O)CH_3$]

$10^{12} \times k$	T (K)	Technique[a]	Reference
2.21 ± 0.24	296	RR (C_2H_4)[b]	Hurley et al. (2007)
2.11 ± 0.23	296	RR (C_2H_2)[c]	

[a]Abbreviations used for the techniques are defined in table I-F-3.
[b]Placed on an absolute basis using k (OH + C_2H_4) = 7.9×10^{-12} cm^3 molecule^{-1} s^{-1} (Atkinson et al., 2006).
[c]Placed on an absolute basis using k (OH + C_2H_2) = 7.8×10^{-12} cm^3 molecule^{-1} s^{-1} (Atkinson et al., 2006).

Table VII-C-4. Rate coefficients (k, cm^3 molecule^{-1} s^{-1}) for reaction of chlorine atoms with ethylene glycol diacetate [$CH_3C(O)OCH_2CH_2OC(O)CH_3$]

$10^{12} \times k$	T (K)	Technique[a]	Reference
5.23 ± 0.53	296	RR (CH_3Cl)[b]	Hurley et al. (2007)
6.19 ± 0.64	296	RR (C_2H_5Cl)[c]	

[a]Abbreviations used for the techniques are defined in table I-F-3.
[b]Placed on an absolute basis using k(Cl + CH_3Cl) = 4.8×10^{-13} cm^3 molecule^{-1} s^{-1} (Atkinson et al., 2008).
[c]Placed on an absolute basis using k(Cl + C_2H_5Cl) = 7.8×10^{-12} cm^3 molecule^{-1} s^{-1} (section I-F).

VII-C-2.2. Cl-Atom Reaction Kinetics

The reaction of chlorine atoms with ethylene glycol diacetate has been the subject of a relative rate study by Hurley et al. (2007) at 296 K. The results are shown in table VII-C-4. An average of the results from Hurley et al. (2007) gives k(Cl + $CH_3C(O)OCH_2CH_2OC(O)CH_3$) = 5.71×10^{-12} cm^3 molecule^{-1} s^{-1} with an uncertainty estimated to be ±25%. Corroborative studies of this rate coefficient are warranted.

VII-C-2.3. Summary of the Atmospheric Fate of Ethylene Glycol Diacetate

Combining k(OH + $CH_3C(O)OCH_2CH_2OC(O)CH_3$) = 2.16×10^{-12} cm^3 molecule^{-1} s^{-1} at 298 K with a diurnal average of [OH] ≈ 1.0×10^6 molecule cm^{-3} gives an estimate of about 5 days for the atmospheric lifetime of ethylene glycol diacetate.

VII-C-3. Dimethyl Succinate [$CH_3OC(O)CH_2CH_2C(O)OCH_3$]

VII-C-3.1. OH Reaction Kinetics

The reaction of OH with dimethyl succinate has been the subject of a relative rate study by Aschmann and Atkinson (1998a). The result of k(OH + $CH_3C(O)OCH_2CH_2OC(O)CH_3$) = 1.36×10^{-12} cm^3 molecule^{-1} s^{-1} from Aschmann and Atkinson (1998a) at 298 K (see table VII-C-5) is recommended with an uncertainty estimated to be ±25%. Corroborative studies of this rate coefficient are warranted.

Table VII-C-5. Rate coefficients (k, cm^3 molecule^{-1} s^{-1}) for reaction of OH with dimethyl succinate [$CH_3OC(O)CH_2CH_2C(O)OCH_3$]

$10^{12} \times k$	T (K)	Technique[a]	Reference
1.36 ± 0.40	298	RR (cyclohexane)[b]	Aschmann and Atkinson (1998a)

[a]Abbreviations used for the techniques are defined in table I-F-3.
[b]Placed on an absolute basis using $k(\text{OH} + \text{cyclohexane}) = 6.97 \times 10^{-12}$ cm^3 molecule^{-1} s^{-1} (Calvert et al., 2008).

Table VII-C-6. Rate coefficients (k, cm^3 molecule^{-1} s^{-1}) for reaction of OH with dimethyl glutarate [$CH_3OC(O)CH_2CH_2CH_2C(O)OCH_3$]

$10^{12} \times k$	T (K)	Technique[a]	Reference
3.23 ± 0.59	298	RR (cyclohexane)[b]	Aschmann and Atkinson (1998a)

[a]Abbreviations used for the techniques are defined in table I-F-3.
[b]Placed on an absolute basis using k (OH + cyclohexane) $= 6.97 \times 10^{-12}$ cm^3 molecule^{-1} s^{-1} (Calvert et al. 2008).

VII-C-4. Dimethyl Glutarate [$CH_3OC(O)CH_2CH_2CH_2C(O)OCH_3$]

VII-C-4.1. OH Reaction Kinetics

The reaction of OH with dimethyl glutarate has been the subject of a relative rate study by Aschmann and Atkinson (1998a). Details are given in table VII-C-6. The result of $k(\text{OH} + CH_3C(O)O(CH_2)_3OC(O)CH_3) = 3.23 \times 10^{-12}$ cm^3 molecule^{-1} s^{-1} from Aschmann and Atkinson (1998a) at 298 K is recommended with an uncertainty estimated to be $\pm 25\%$. Corroborative studies of this rate coefficient are warranted.

VII-C-4.2. Summary of the Atmospheric Fate of Dimethyl Glutarate

Combining the recommended rate coefficient for reaction with OH radicals with a diurnal average [OH] $= 1 \times 10^6$ molecule cm^{-3} gives an estimate of about 3.5 days for the atmospheric lifetime of dimethyl glutarate. Following OH-radical-initiated oxidation of dimethyl glutarate in 1 atm. of air in the presence of NO, Tuazon et al. (1999) have reported the formation of organic nitrates, mono-methylglutarate [$CH_3OC(O)CH_2CH_2CH_2C(O)OH$], and dimethyl 1,3-acetone dicarboxylate [$CH_3OC(O)CH_2C(O)CH_2C(O)OCH_3$] in molar yields of 15 ± 6, 34 ± 16, and $28 \pm 8\%$, respectively.

VII-C-5. Dimethyl Adipate [$CH_3OC(O)CH_2CH_2CH_2CH_2C(O)OCH_3$]

VII-C-5.1. OH Reaction Kinetics

The reaction of OH with dimethyl adipate has been the subject of a relative rate study by Aschmann and Atkinson (1998a), see table VII-C-7. The result of $k(\text{OH} + CH_3C(O)O(CH_2)_4OC(O)CH_3) = 8.15 \times 10^{-12}$ cm^3 molecule^{-1} s^{-1} from

Table VII-C-7. Rate coefficients ($k = A \times e^{-B/T}$, cm^3 $molecule^{-1}$ s^{-1}) for reaction of OH with dimethyl adipate [$CH_3OC(O)CH_2CH_2CH_2CH_2C(O)OCH_3$]

$10^{12} \times k$	T (K)	Technique[a]	Reference
8.15 ± 1.25	298	RR (cyclohexane)[b]	Aschmann and Atkinson (1998a)

[a]Abbreviations used for the techniques are defined in table I-F-3.
[b]Placed on an absolute basis using $k(OH + cyclohexane) = 6.97 \times 10^{-12}$ cm^3 $molecule^{-1}$ s^{-1} (Calvert et al., 2008).

Aschmann and Atkinson (1998a) at 298 K is recommended with an uncertainty estimated to be ±25%. Corroborative studies of this rate coefficient are warranted.

VII-C-5.2. Summary of the Atmospheric Fate of Dimethyl Adipate

Combining the recommended rate coefficient for reaction with OH radicals with a diurnal average [OH] = 1×10^6 molecule cm^{-3} gives an estimate of about 1.5 days for the atmospheric lifetime of dimethyl adipate.

VII-D. Cyclic Esters (Lactones)

VII-D-1. 3H-Furan-2-one

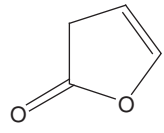

VII-D-1.1. OH Reaction Kinetics

The reaction of OH with 3H-furan-2-one has been the subject of a relative rate study by Bierbach et al. (1994). The result of $k(OH + 3H\text{-furan-2-one}) = 4.42 \times 10^{-11}$ cm^3 $molecule^{-1}$ s^{-1} from Bierbach et al. (1994) is recommended at 298 K with an uncertainty estimated to be ±25%; see table VII-D-1. Corroborative studies of this rate coefficient are warranted.

Table VII-D-1. Rate coefficients (k, cm^3 $molecule^{-1}$ s^{-1}) for reaction of OH with 3H-furan-2-one

$10^{11} \times k$	T (K)	Technique[a]	Reference
4.42 ± 0.26	296	RR (propene)[b]	Bierbach et al. (1994)

[a]Abbreviations used for the techniques are defined in table I-F-3.
[b]Placed on an absolute basis using $k(OH + propene) = 2.63 \times 10^{-11}$ cm^3 $molecule^{-1}$ s^{-1} (Calvert et al., 2002).

Table VII-D-2. Rate coefficients (k, cm^3 molecule^{-1} s^{-1}) for reaction of NO_3 with 3H-furan-2-one

$10^{13} \times k$	T (K)	Technique[a]	Reference
1.76 ± 0.23	298	RR (*trans*-2-butene)[b]	Berndt et al. (1997)

[a]Abbreviations used for the techniques are defined in table I-F-3.
[b]Placed on an absolute basis using $k(NO_3 + trans\text{-2-butene}) = 3.90 \times 10^{-13}$ cm^3 molecule^{-1} s^{-1} (Calvert et al., 2000).

VII-D-1.2. NO_3 Reaction Kinetics

The reaction of NO_3 radicals with 3H-furan-2-one has been the subject of a relative rate study by Berndt et al. (1997); details are given in table VII-D-2. The result of $k(NO_3 + 3H\text{-furan-2-on}) = 1.76 \times 10^{-13}$ cm^3 molecule^{-1} s^{-1} from Berndt et al. (1997) is recommended at 298 K with an uncertainty estimated to be ±25%. Corroborative studies of this rate coefficient are warranted.

VII-D-1.3. Summary of the Atmospheric Fate of 3H-Furan-2-one

Combining the recommended rate coefficient for reaction with OH radicals with an average daytime [OH] of 2.5×10^6 molecule cm^{-3} gives an estimate of about 2.5 h for the daytime lifetime of 3H-furan-2-one.

VII-D-2. 5-Methyl-3H-furan-2-one (4-Hydroxy-3-pentenoic Acid γ-Lactone, α-Angelica Lactone)

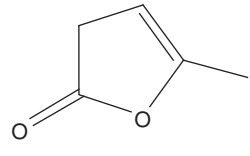

VII-D-2.1. OH Reaction Kinetics

The reaction of OH with 5-methyl-3H-furan-2-one has been the subject of a relative rate study by Bierbach et al. (1994). Details are given in table VII-D-3. The result of $k(OH + 5\text{-methyl-3H-furan-2-one}) = 6.78 \times 10^{-11}$ cm^3 molecule^{-1} s^{-1} from Bierbach et al. (1994) is recommended at 298 K with an uncertainty estimated to be ±25%. Corroborative studies of this rate coefficient are warranted.

VII-D-2.2. Summary of the Atmospheric Fate of 5-Methyl-3H-furan-2-one

Combining the recommended rate coefficient for reaction with OH radicals with an average daytime [OH] of 2.5×10^6 molecule cm^{-3} gives an estimate of about 1.6 h for the daytime lifetime of 5-methyl-3H-furan-2-one.

Table VII-D-3. Rate coefficients (k, cm^3 molecule^{-1} s^{-1}) for reaction of OH with 5-methyl-3H-furan-2-one

$10^{11} \times k$	T (K)	Technique[a]	Reference
6.78 ± 0.45	296	RR (*trans*-2-butene)[b]	Bierbach et al. (1994)

[a]Abbreviations used for the techniques are defined in table I-F-3.
[b]Placed on an absolute basis using k(OH + *trans*-2-butene) = 6.40×10^{-11} cm^3 molecule^{-1} s^{-1} (Calvert et al., 2000).

VII-E. Unsaturated Esters

VII-E-1. Vinyl Acetate [CH_2=CHOC(O)CH_3]

VII-E-1.1. OH Reaction Kinetics

The reaction of OH radicals with vinyl acetate has been studied at 298 K in 1 Torr of helium diluent by Saunders et al. (1994) using a discharge flow method and by Blanco et al. (2009) in 1 atm. at 287–313 K using a relative rate method. The results are given in table VII-E-1 and plotted in figure VII-E-1. As seen from figure VII-E-1, the results from Saunders et al. (1994) and Blanco et al. (2009) are in excellent agreement. A fit to the composite data set gives: k[OH + CH_2=CHOC(O)CH_3] = $4.77 \times 10^{-12} \exp(493/T)$ cm^3 molecule^{-1} s^{-1}. At 298 K this expression gives k(OH + CH_2=CHOC(O)CH_3) = 2.49×10^{-11} cm^3 molecule^{-1} s^{-1} with an uncertainty estimated to be ±20%.

VII-E-1.2. O_3 Reaction Kinetics

The reaction of ozone with vinyl acetate has been studied by Grosjean and Grosjean (1998) by monitoring the rate of decay of vinyl acetate when exposed to a large excess of ozone in 1 atm. of air at 291–292 K. A rate coefficient of k[O_3 + CH_2=CHOC(O)CH_3] = $(3.20 \pm 0.47) \times 10^{-18}$ cm^3 molecule^{-1} s^{-1} was derived.

Table VII-E-1. Rate coefficient ($k = A \times e^{-B/T}$, cm^3 molecule^{-1} s^{-1}) for reaction of OH with vinyl acetate [CH_2=CHOC(O)CH_3]

$10^{12} \times A$	B (K)	$10^{11} \times k$	T(K)	Technique[a]	Reference
		2.5 ± 0.4	298	DF–LIF	Saunders et al. (1994)
0.48	−492	2.60 ± 0.10	287	RR (1-butene)[b]	Blanco et al. (2009)
		2.57 ± 0.13	294	RR (1-butene)[b]	
		2.57 ± 0.05	298	RR (iso-butene)[c]	
		2.48 ± 0.06	298	RR (1-butene)[b]	
		2.42 ± 0.06	303	RR (1-butene)[b]	
		2.27 ± 0.06	313	RR (1-butene)[b]	

[a]Abbreviations used for the techniques are defined in table I-F-3.
[b]Placed on an absolute basis using k(OH + 1-butene) = $6.55 \times 10^{-12} \exp(467/T)$ cm^3 molecule^{-1} s^{-1} (Calvert et al., 2000).
[c]Placed on an absolute basis using k(OH + isobutene) = 5.14×10^{-11} cm^3 molecule^{-1} s^{-1} (Calvert et al., 2000).

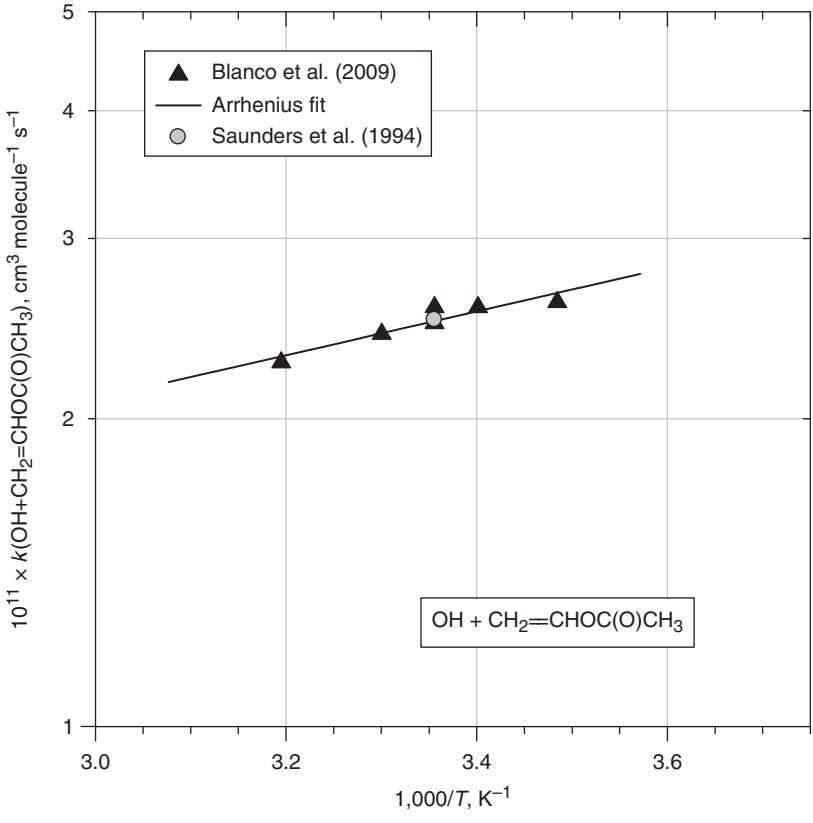

Figure VII-E-1. Measurements of the rate coefficients for reaction of OH radicals with vinyl acetate. The line is a fit of the Arrhenius expression to the composite data set.

VII-E-1.3. Summary of the Atmospheric Fate of Vinyl Acetate

Combining the rate coefficients for reaction with OH radicals and O_3 with a daytime average [OH] = 2.5×10^6 and a diurnal average [O_3] = 10^{12} molecule cm^{-3} gives estimates of about 4 h for the daytime atmospheric lifetime of vinyl acetate with respect to reaction with OH radicals and about 4 days with respect to reaction with O_3. Reaction with OH radicals is an important atmospheric fate of vinyl acetate and is expected to proceed via addition to the $\rangle C{=}C\langle$ double bond leading to the formation of CH_2O and formic acetic anhydride as major products.

VII-E-2. Allyl Acetate (2-Propenyl Acetate, $CH_2{=}CHCH_2OC(O)CH_3$)

VII-E-2.1. OH Reaction Kinetics

The kinetics of the reaction of OH radicals with allyl acetate have been studied by Ferrari et al. (1996) using relative rate methods and Le Calvé et al. (2000)

Table VII-E-2. Rate coefficients ($k = A \times e^{-B/T}$, cm^3 molecule^{-1} s^{-1}) for reaction of OH with allyl acetate [CH_2=$CHCH_2OC(O)CH_3$]

$10^{12} \times A$	B (K)	$10^{11} \times k$	T(K)	Technique[a]	Reference
		2.28 ± 0.22	295	RR (*n*-octane)[b]	Ferrari et al. (1996)
2.33 ± 0.27	−732 ± 34	4.14 ± 0.16	253	PLP–LIF	Le Calvé et al. (2000)
		4.26 ± 0.10	253		
		4.19 ± 0.17	253		
		3.74 ± 0.13	263		
		3.88 ± 0.20	263		
		3.34 ± 0.16	273		
		2.75 ± 0.08	298		
		2.58 ± 0.12	298		
		2.74 ± 0.06	298		
		2.69 ± 0.14	298		
		2.58 ± 0.16	298		
		2.90 ± 0.08	298		
		2.70 ± 0.15	298		
		2.73 ± 0.12	298		
		2.15 ± 0.09	323		
		1.93 ± 0.07	348		
		1.88 ± 0.09	348		
		1.67 ± 0.04	372		
		1.70 ± 0.14	372		

[a]Abbreviations used for the techniques are defined in table I-F-3.
[b]Placed on an absolute basis using $k(OH + n\text{-octane}) = 7.81 \times 10^{-12}$ cm^3 molecule^{-1} s^{-1} (Calvert et al., 2008).

using absolute techniques. The results are given in table VII-E-2 and plotted in figure VII-E-2. A linear least squares fit to the data in figure VII-E-2 gives: $k[OH + CH_2$=$CHCH_2OC(O)CH_3] = 2.29 \times 10^{-12} \exp(731/T)$ cm^3 molecule^{-1} s^{-1}. This expression gives $k[OH + CH_2$=$CHCH_2OC(O)CH_3] = 2.66 \times 10^{-11}$ cm^3 molecule^{-1} s^{-1} at 298 K with an uncertainty estimated to be ±20%.

VII-E-2.2. O_3 Reaction Kinetics

Le Calvé et al. (2000) used relative rate methods to determine the reactivity of allyl acetate relative to methyl vinyl ketone (MVK). Scaling the results from Le Calvé et al. (2000) to our recommended value of $k(O_3 + MVK) = 5.0 \times 10^{-18}$ gives $k(O_3 + \text{allyl acetate}) = (2.5 \pm 0.7) \times 10^{-18}$ cm^3 molecule^{-1} s^{-1} at 298 K.

VII-E-2.3. Summary of the Atmospheric Fate of Allyl Acetate

Combining the recommended rate coefficients for reactions with OH radicals and O_3 with a daytime average [OH] = 2.5×10^6 molecule cm^{-3} and a diurnal average [O_3] ≈ 10^{12} molecule cm^{-3} gives estimates of about 4 h and about 5 days for the atmospheric lifetimes of allyl acetate with respect to reaction with OH radicals and O_3, respectively. Reaction with OH radicals dominates the atmospheric loss of allyl acetate. The reaction is expected to proceed via addition to the $\rangle C{=}C\langle$ double bond leading to the formation of CH_2O and $HC(O)CH_2OC(O)CH_3$ as major products.

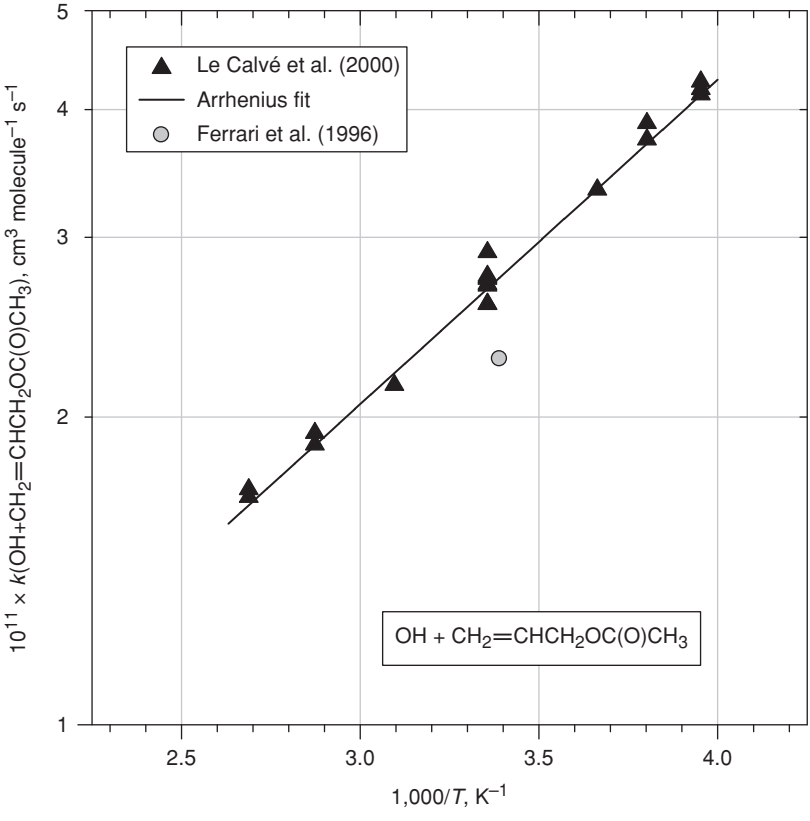

Figure VII-E-2. Measurements of the rate coefficients for reaction of OH radicals with allyl acetate. The line is a fit of the Arrhenius expression to the composite data set.

VII-E-3. *iso*-Propenyl Acetate (CH_2=$C(CH_3)OC(O)CH_3$)

VII-E-3.1. OH Reaction Kinetics

The kinetics of the reaction of OH radicals with *iso*-propenyl acetate have been studied by Ferrari et al. (1996) using relative rate methods and Le Calvé et al. (2000) using absolute techniques. As seen in table VII-E-3 and figure VII-E-3 the results from the two studies are indistinguishable within the likely combined experimental uncertainties. A linear least-squares fit to the data in figure VII-E-3 gives: $k[OH + CH_2{=}(CH_3)OC(O)CH_3] = 4.36 \times 10^{-12} \exp(815/T)$ cm^3 molecule^{-1} s^{-1}. This expression gives $k[OH + CH_2{=}C(CH_3)OC(O)CH_3] = 6.72 \times 10^{-11}$ cm^3 molecule^{-1} s^{-1} at 298 K with an uncertainty estimated to be $\pm$20%.

VII-E-3.2. O_3 Reaction Kinetics

Le Calvé et al. (2000) used relative rate methods to determine the reactivity of *iso*-propenyl acetate relative to methyl vinyl ketone (MVK). Scaling the results from

Table VII-E-3. Rate coefficients ($k = A \times e^{-B/T}$, cm^3 $molecule^{-1}$ s^{-1}) for reaction of OH with *iso*-propenyl acetate [$CH_2{=}C(CH_3)OC(O)CH_3$]

$10^{12} \times A$	B (K)	$10^{11} \times k$	T(K)	Technique[a]	Reference
		5.80 ± 0.12	295	RR (*n*-octane)[b]	Ferrari et al. (1996)
4.52 ± 0.62	−809 ± 39	11.92 ± 0.32	243	PLP–LIF	Le Calvé et al. (2000)
		11.07 ± 0.52	253		
		11.38 ± 0.30	253		
		10.86 ± 0.21	253		
		9.73 ± 0.35	263		
		8.56 ± 0.25	273		
		9.11 ± 0.40	273		
		7.27 ± 0.21	298		
		6.87 ± 0.29	298		
		6.76 ± 0.13	298		
		7.24 ± 0.16	298		
		6.79 ± 0.31	298		
		6.81 ± 0.60	298		
		5.59 ± 0.21	323		
		4.53 ± 0.17	348		
		3.90 ± 0.12	372		
		3.84 ± 0.10	372		

[a]Abbreviations used for the techniques are defined in table I-F-3.
[b]Placed on an absolute basis using $k(OH + n\text{-octane}) = 7.81 \times 10^{-12}$ cm^3 $molecule^{-1}$ s^{-1} (Calvert et al., 2008).

Le Calvé et al. (2000) to our recommended value of $k(O_3 + MVK) = 5.0 \times 10^{-18}$ gives $k(O_3 + iso\text{-propenyl acetate}) = (7 \pm 2) \times 10^{-19}$ cm^3 $molecule^{-1}$ s^{-1} at 298 K.

VII-E-3.3. Summary of the Atmospheric Fate of iso-Propenyl Acetate

Combining the recommended rate coefficient for reaction with OH radicals and O_3 with a daytime average [OH] = 2.5×10^6 molecule cm^{-3} and a diurnal average [O_3] ≈ 10^{12} molecule cm^{-3} gives estimates of about 2 h and about 16 days for the atmospheric lifetimes of *iso*-propenyl acetate with respect to reaction with OH radicals and O_3, respectively. Reaction with OH radicals dominates the atmospheric loss of *iso*-propenyl acetate. The reaction is expected to proceed via addition to the $\rangle C{=}C\langle$ double bond leading to the formation of CH_2O, acetic anhydride, and possibly $CH_3C(O)OC(O)CH_2OH$ as products.

VII-E-4. 4-Pentenyl Acetate [$CH_2{=}CHCH_2CH_2CH_2OC(O)CH_3$]

VII-E-4.1. OH Reaction Kinetics

The kinetics of the reaction of OH radicals with 4-pentenyl acetate have been studied by Williams et al. (1993) using relative rate methods. The results are given in table VII-E-4. An average of the results from Williams et al. (1993) gives $k(OH + CH_2{=}CHCH_2CH_2CH_2OC(O)CH_3) = 4.3 \times 10^{-11}$ cm^3 $molecule^{-1}$ s^{-1}; this is recommended with an uncertainty estimated to be ±25%.

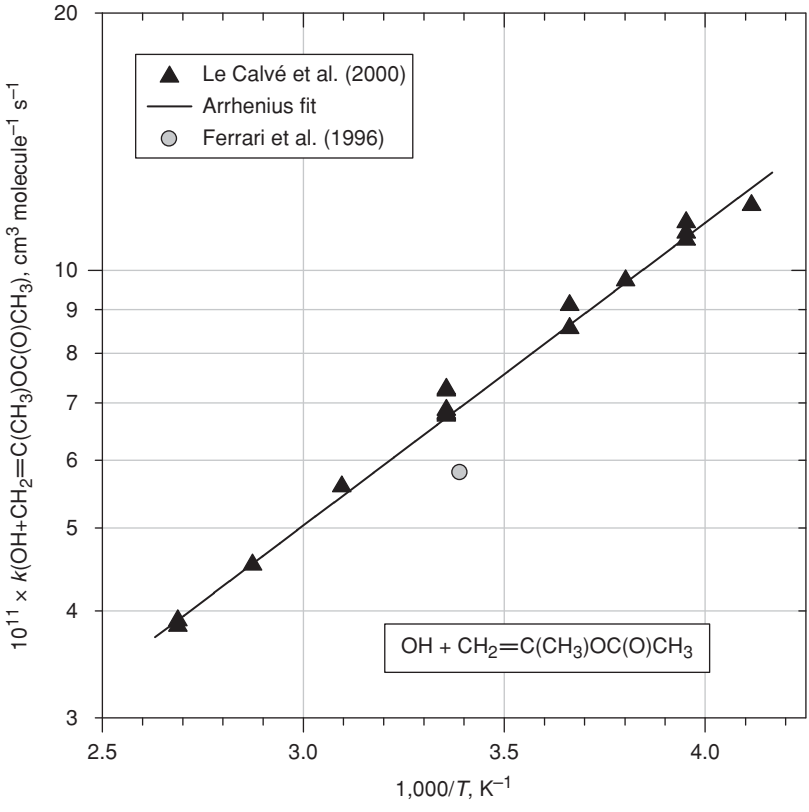

Figure VII-E-3. Measurements of the rate coefficients for reaction of OH radicals with *iso*-propenyl acetate.

Table VII-E-4. Rate coefficients (k, cm^3 molecule^{-1} s^{-1}) for reaction of OH with 4-pentenyl acetate [CH_2=$CHCH_2CH_2CH_2OC(O)CH_3$]

$10^{11} \times k$	T(K)	Technique[a]	Reference
4.33 ± 0.38	297	RR (propene)[b]	Williams et al. (1993)
4.28 ± 0.29		RR (*trans*-2-butene)[c]	

[a]Abbreviations used for the techniques are defined in table I-F-3.
[b]Placed on an absolute basis using k(OH + propene) = 2.63 × 10^{-11} cm^3 molecule^{-1} s^{-1} (Calvert et al., 2002).
[c]Placed on an absolute basis using k(OH + *trans*-2-butene) = 6.4 × 10^{-11} cm^3 molecule^{-1} s^{-1} (Calvert et al., 2002).

VII-E-5. *cis*-3-Hexenyl Acetate [CH_3CH_2CH=$CHCH_2CH_2OC(O)CH_3$]

VII-E-5.1. OH Reaction Kinetics

The kinetics of the reaction of OH radicals with *cis*-3-hexenyl acetate have been studied by Atkinson et al. (1995) using relative rate methods. The result is given in table VII-E-5 and is recommended with an uncertainty estimated to be ±20%.

Table VII-E-5. Rate coefficient (k, cm^3 molecule^{-1} s^{-1}) for reaction of OH with *cis*-3-hexenyl acetate [$CH_3CH_2CH{=}CHCH_2CH_2OC(O)CH_3$]

$10^{11} \times k$	T(K)	Technique[a]	Reference
7.74 ± 0.45	296	RR (*trans*-2-butene)[b]	Atkinson et al. (1995)

[a]Abbreviations used for the techniques are defined in table I-F-3.
[b]Placed on an absolute basis using k(OH + *trans*-2-butene) = 6.4×10^{-11} cm^3 molecule^{-1} s^{-1} (Calvert et al., 2002).

Table VII-E-6. Rate coefficient (k, cm^3 molecule^{-1} s^{-1}) for reaction of NO_3 with *cis*-3-hexenyl acetate [$CH_3CH_2CH{=}CHCH_2CH_2OC(O)CH_3$]

$10^{13} \times k$	T(K)	Technique[a]	Reference
2.46 ± 0.13	296	RR (*trans*-2-butene)[b]	Atkinson et al. (1995)

[a]Abbreviations used for the techniques are defined in table I-F-3.
[b]Placed on an absolute basis using k(NO_3 + *trans*-2-butene) = 3.9×10^{-13} cm^3 molecule^{-1} s^{-1} (Calvert et al., 2002).

VII-E-5.2. NO_3 Reaction Kinetics

The kinetics of the reaction of NO_3 radicals with *cis*-3-hexenyl acetate have been studied by Atkinson et al. (1995) using relative rate methods. The result is given in table VII-E-6 and is recommended with an uncertainty estimated to be ±30%.

VII-E-5.3. O_3 Reaction Kinetics

The reaction of ozone with *cis*-3-hexenyl acetate has been studied by Grosjean and Grosjean (1998) by monitoring the rate of decay of *cis*-3-hexenyl acetate when exposed to a large excess of ozone in 1 atm. of air at 291 K. A rate coefficient of $k(O_3) = (5.90 \pm 0.87) \times 10^{-17}$ cm^3 molecule^{-1} s^{-1} was derived.

VII-E-5.4. Summary of the Atmospheric Fate of cis-3-Hexenyl Acetate

Combining the rate coefficients for reactions with OH and NO_3 radicals and O_3, with daytime average [OH] = 2.5×10^6, nighttime polluted urban area [NO_3] = 3×10^9, and a diurnal average [O_3] = 10^{12} molecule cm^{-3} concentrations gives estimates of 1.4 h, 0.4 h, and 5 h for the lifetimes of *cis*-3-hexenyl acetate with respect to reaction with OH and NO_3 radicals and O_3, respectively. *cis*-3-Hexenyl acetate has a short atmospheric lifetime and will be oxidized close to its emission sources.

VII-E-6. Methyl Acrylate (Methyl Propenoate, $CH_2{=}CHC(O)OCH_3$)

VII-E-6.1. OH Reaction Kinetics

The kinetics of the reaction of OH radicals with methyl acrylate have been studied by Saunders et al. (1994) and Teruel et al. (2006). The results are listed in

Table VII-E-7. Rate coefficients ($k = A \times e^{-B/T}$, cm^3 $molecule^{-1}$ s^{-1}) for reaction of OH with methyl acrylate [CH_2=CHC(O)OCH_3]

$10^{12} \times A$	B (K)	$10^{11} \times k$	T(K)	Technique[a]	Reference
		2.5 ± 0.4	298	DF–LIF	Saunders et al. (1994)
		1.34 ± 0.03	298	RR (cyclohexane)[b]	Teruel et al. (2006)
		1.34 ± 0.12	298	RR (isobutanol)[c]	
2.0 ± 0.8	-553 ± 51	1.7 ± 0.2	253	PLP–LIF	Teruel et al. (2006)
		1.56 ± 0.08	273		
		1.53 ± 0.06	274		
		1.37 ± 0.08	294		
		1.41 ± 0.12	295		
		1.22 ± 0.04	297		
		1.33 ± 0.10	298		
		1.16 ± 0.02	315		
		1.07 ± 0.06	317		
		1.12 ± 0.08	336		
		0.87 ± 0.04	366		

[a]Abbreviations used for the techniques are defined in table I-F-3.
[b]Placed on an absolute basis using $k(OH + cyclohexane) = 6.97 \times 10^{-12}$ cm^3 $molecule^{-1}$ s^{-1} (Calvert et al., 2008).
[c]Placed on an absolute basis using $k(OH + isobutyl\ alcohol) = 9.6 \times 10^{-12}$ cm^3 $molecule^{-1}$ s^{-1} (this book, section II-B-7.1).

table VII-E-7 and plotted in figure VII-E-4. Saunders et al. (1994) used an absolute method in 1 Torr of helium diluent. Teruel et al. (2006) used a relative rate method in 1 atm. of air and an absolute rate method in 100 Torr of helium diluent. The results obtained by Teruel et al. (2006) using two different techniques are in good agreement and show that in 100 Torr of helium, the reaction is at or near its high pressure limit. Fitting the Arrhenius expression to the data from Teruel et al. (2006) gives: $k(OH + CH_2$=$CHC(O)OCH_3) = 2.00 \times 10^{-12} \exp(556/T)$ cm^3 $molecule^{-1}$ s^{-1}. At 298 K this expression gives $k(OH + CH_2$=$CHC(O)OCH_3) = 1.29 \times 10^{-11}$ cm^3 $molecule^{-1}$ s^{-1} with an uncertainty estimated to be ±20%.

VII-E-6.2. NO_3 Radical Reaction Kinetics

The kinetics of the reaction of NO_3 radicals with methyl acrylate have been studied by Canosa-Mas et al. (1999a). Details are given in table VII-E-8. Based upon the result from Canosa-Mas et al. (1999a) we recommend $k(NO_3 + CH_2$=$CHC(O)OCH_3) = 1.1 \times 10^{-16}$ cm^3 $molecule^{-1}$ s^{-1} with an uncertainty estimated to be ±50%.

VII-E-6.3. Ozone Reaction Kinetics

The kinetics of the reaction of ozone with methyl acrylate were studied by Grosjean and Grosjean (1998) by observing the pseudo first-order loss of ozone in the presence of excess methyl acrylate. A value of $k(O_3 + CH_2$=$CHC(O)OCH_3) = (1.05 \pm 0.15) \times 10^{-18}$ cm^3 $molecule^{-1}$ s^{-1} was reported at 291 K.

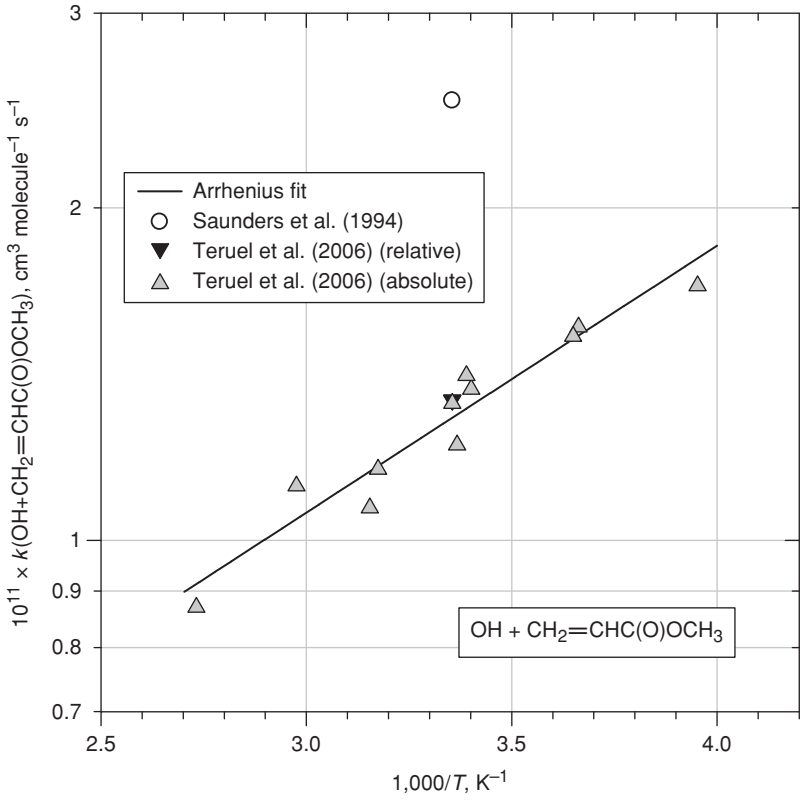

Figure VII-E-4. Measurements of the rate coefficients for reaction of OH radicals with methyl acrylate. The line is a fit of the Arrhenius expression to the data from Teruel et al. (2006).

Table VII-E-8. Rate coefficient (k, cm^3 molecule^{-1} s^{-1}) for reaction of NO_3 radicals with methyl acrylate [CH_2=CHC(O)OCH_3]

$10^{13} \times k$	T(K)	Technique[a]	Reference
1.15 ± 0.51	296	RR (C_2H_4)[b]	Canosa-Mas et al. (1999a)

[a]Abbreviations used for the techniques are defined in table I-F-3.
[b]Placed on an absolute basis using $k(NO_3 + C_2H_4) = 2.05 \times 10^{-16}$ cm^3 molecule^{-1} s^{-1} (Calvert et al., 2000).

VII-E-6.4. Summary of the Atmospheric Fate of Methyl Acrylate

Combining the rate coefficients for reactions with OH, NO_3 radicals, and O_3 with daytime average [OH] $= 2.5 \times 10^6$, nighttime polluted urban area [NO_3] $= 3 \times 10^9$, and a diurnal average [O_3] = 10^{12} molecule cm^{-3} concentrations gives lifetime estimates of 9 h, 35 days, and 11 days for reaction with OH and NO_3 radicals and O_3, respectively. Clearly, reaction with OH dictates the atmospheric lifetime of methyl acrylate. As with alkenes (Calvert et al., 2000) and methacrylates (Blanco et al., 2006), the reaction of OH

with methyl acrylate likely proceeds predominately via addition to the $\rangle C{=}C\langle$ double bond followed by decomposition of the $HOCH_2CH(O)C(O)OCH_3$ alkoxy radical:

$$OH + CH_2{=}CHC(O)OCH_3 \rightarrow HOCH_2CHC(O)OCH_3$$

$$HOCH_2CHC(O)OCH_3 + O_2 \rightarrow HOCH_2CH(OO)C(O)OCH_3$$

$$HOCH_2CH(OO)C(O)OCH_3 + NO \rightarrow HOCH_2CH(O)C(O)OCH_3 + NO_2$$

$$HOCH_2CH(O)C(O)OCH_3 \rightarrow HOCH_2 + HC(O)C(O)OCH_3$$

$$HOCH_2 + O_2 \rightarrow CH_2O + HO_2$$

VII-E-7. Ethyl Acrylate (Ethyl Propenoate, $CH_2{=}CHC(O)OC_2H_5$)

VII-E-7.1. OH Reaction Kinetics

The kinetics of the reaction of OH radicals with ethyl acrylate have been studied using absolute and relative rate methods by Teruel et al. (2006). The results are given in table VII-E-9 and plotted in figure VII-E-5. There is good agreement between the results from the relative rate and absolute rate experiments. A least-squares fit to the combined data set shown in figure VII-E-5 gives: $k(OH + CH_2{=}CHC(O)OC_2H_5) = 2.50 \times 10^{-12} \exp(552/T)$ cm^3 molecule^{-1} s^{-1}. At 298 K this expression gives $k(OH + CH_2{=}CHC(O)OC_2H_5) = 1.59 \times 10^{-11}$ cm^3 molecule^{-1} s^{-1} with an uncertainty estimated to be ±20%.

Table VII-E-9. Rate coefficients ($k = A \times e^{-B/T}$, cm^3 molecule^{-1} s^{-1}) for reaction of OH with ethyl acrylate [$CH_2{=}CHC(O)OC_2H_5$]

$10^{12} \times A$	B (K)	$10^{11} \times k$	T(K)	Technique[a]	Reference
		1.74 ± 0.18	298	RR (cyclohexane)[b]	Teruel et al. (2006)
		1.80 ± 0.17	298	RR (isobutanol)[c]	
2.3 ± 0.8	−580 ± 65	2.10 ± 0.06	255	PLP–LIF	Teruel et al. (2006)
		1.96 ± 0.12	255		
		2.13 ± 0.06	273		
		1.65 ± 0.04	296		
		1.49 ± 0.03	298		
		1.59 ± 0.06	298		
		1.47 ± 0.04	325		
		1.19 ± 0.04	341		
		1.23 ± 0.06	346		
		1.21 ± 0.04	366		
		0.978 ± 0.004	374		

[a]Abbreviations used for the techniques are defined in table I-F-3.
[b]Placed on an absolute basis using $k(OH + \text{cyclohexane}) = 6.97 \times 10^{-12}$ cm^3 molecule^{-1} s^{-1} (Calvert et al., 2008).
[c]Placed on an absolute basis using $k(OH + \text{isobutyl alcohol}) = 9.6 \times 10^{-12}$ cm^3 molecule^{-1} s^{-1} (this book, section II-B-7.1).

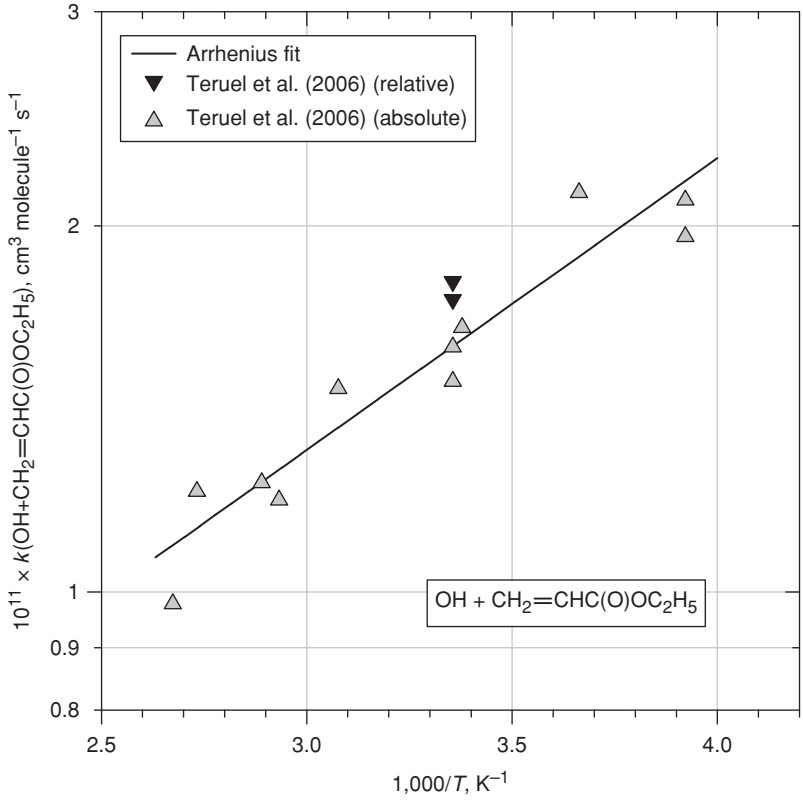

Figure VII-E-5. Measurements of the rate coefficients for reaction of OH radicals with ethyl acrylate. The line is a fit of the Arrhenius expression to the data from Teruel et al. (2006).

VII-E-7.2. Summary of the Atmospheric Fate of Ethyl Acrylate

Combining the recommended rate coefficient for reaction with OH radicals with a daytime average [OH] = 2.5×10^6 molecule cm^{-3} gives an estimate of about 7 h for the daytime atmospheric lifetime of ethyl acrylate. As with alkenes (Calvert et al., 2000) and methacrylates (Blanco et al., 2006), the reaction of OH with ethyl acrylate is believed to proceed via addition to the double bond followed by decomposition of the resulting alkoxy radical. The major oxidation products are CH_2O and $HC(O)C(O)OC_2H_5$ (ethyl glyoxylate).

VII-E-8. *n*-Butyl Acrylate (*n*-Butyl Propenoate [CH_2=$CHC(O)O(CH_2)_3CH_3$]

VII-E-8.1. OH Reaction Kinetics

The kinetics of the reaction of OH radicals with *n*-butyl acrylate have been studied using relative rate methods by Blanco and Teruel (2008) and Blanco et al. (2009). The results are given in table VII-E-10 and plotted in figure VII-E-6. As seen from

Table VII-E-10. Rate coefficients (k, cm^3 molecule^{-1} s^{-1}) for reaction of OH with n-butyl acrylate [CH_2=CHC(O)$OCH_2CH_2CH_2CH_3$]

$10^{12} \times A$	B (K)	$10^{11} \times k$	T(K)	Technique[a]	Reference
		1.60 ± 0.12[b]	298	RR (diethyl ether)[c]	Blanco and Teruel (2008)
		1.78 ± 0.10[b]	298	RR (n-pentane)[d]	
0.44 ± 0.25	1,177 ± 105	2.67 ± 0.07	287	RR (1-butene)[e]	Blanco et al. (2009)
		2.41 ± 0.10	294	RR (1-butene)[e]	
		2.16 ± 0.05	298	RR (iso-butene)[f]	
		2.23 ± 0.09	298	RR (1-butene)[e]	
		2.05 ± 0.06	303	RR (1-butene)[e]	
		1.95 ± 0.06	313	RR (1-butene)[e]	

[a]Abbreviations used for the techniques are defined in table I-F-3.
[b]Values are based on averages of reported rate coefficient ratios with uncertainties which encompass extremes of individual determinations.
[c]Placed on an absolute basis using $k(\mathrm{OH} + \text{diethyl ether}) = 1.2 \times 10^{-11}$ cm^3 molecule^{-1} s^{-1} (this book, section III-B-3.1).
[d]Placed on an absolute basis using $k(\mathrm{OH} + n\text{-pentane}) = 3.96 \times 10^{-12}$ cm^3 molecule^{-1} s^{-1} (Calvert et al., 2008).
[e]Placed on an absolute basis using $k(\mathrm{OH} + \text{1-butene}) = 6.55 \times 10^{-12} \exp(467/T)$ cm^3 molecule^{-1} s^{-1} (Calvert et al., 2000).
[f]Placed on an absolute basis using $k(\mathrm{OH} + iso\text{-butene}) = 5.14 \times 10^{-11}$ cm^3 molecule^{-1} s^{-1} (Calvert et al., 2000).

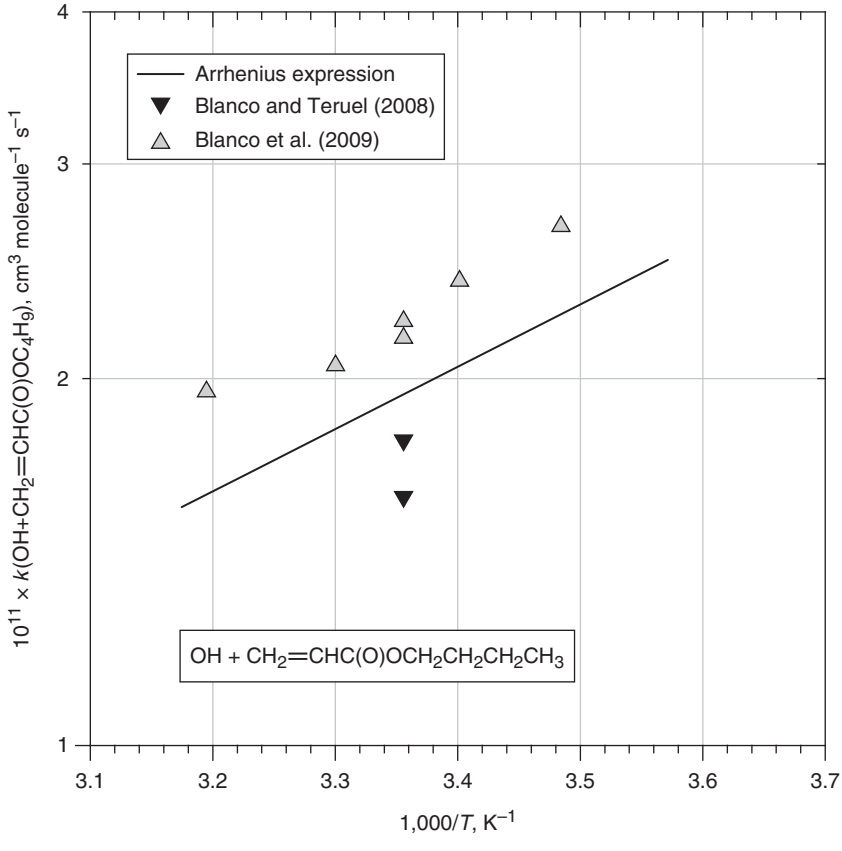

Figure VII-E-6. Measurements of the rate coefficients for reaction of OH radicals with n-butyl acrylate.

figure VII-E-6, the results from Blanco and Teruel (2008) lie approximately 20% below those from Blanco et al. (2009). There being no obvious reason to prefer either dataset, we recommend the average 298 K value from Blanco and Teruel (2006) and Blanco et al. (2009) of $k(OH + CH_2{=}CHC(O)OC_4H_9) = 1.94 \times 10^{-11}$ cm^3 molecule^{-1} s^{-1} with an uncertainty of ±35%. Adopting the temperature dependence from Blanco et al. (2009) gives $k(OH + CH_2{=}CHC(O)OC_4H_9) = 3.74 \times 10^{-13} \exp(1{,}177/T)$ cm^3 molecule^{-1} s^{-1}.

VII-E-8.2. Summary of the Atmospheric Fate of n-Butyl Acrylate

Combining the recommended rate coefficient for reaction with OH radicals with a daytime average [OH] = 2.5×10^6 molecule cm^{-3} gives an estimate of about 7 h for the daytime atmospheric lifetime of *n*-butyl acrylate. Blanco et al. (2006) identified butyl glyoxylate [$HC(O)C(O)OC_4H_9$] as the major oxidation product of the OH-radical-initiated oxidation of butyl acrylate. The oxidation mechanism is similar to those described for methyl- and ethyl-acrylate giving $HC(O)C(O)OC_4H_9$ as the major product.

VII-E-9. Methyl Methacrylate [$CH_2{=}C(CH_3)C(O)OCH_3$]

VII-E-9.1. OH Reaction Kinetics

The kinetics of the reaction of OH radicals with methyl methacrylate have been the subject of absolute rate studies by Saunders et al. (1994) and Teruel et al. (2006) and relative rate studies by Blanco et al. (2006, 2009). The results are given in table VII-E-11 and plotted in figure VII-E-7. The result from Saunders et al. (1994) lies significantly below those reported by Teruel et al. (2006) and Blanco et al. (2006, 2009). This may reflect the lower total pressure (1 Torr helium) used by Saunders et al. (1994) compared to the 100 Torr of helium and 1 atm. of air diluents in the experiments by Teruel et al. (2006) and Blanco et al. (2006, 2009). A fit to the data of Teruel et al. (2006) and Blanco et al. (2006, 2009) gives $k(OH + CH_2{=}C(CH_3)C(O)OCH_3) = 2.68 \times 10^{-12} \exp(811/T)$ cm^3 molecule^{-1} s^{-1}. At 298 K this expression gives $k(OH + CH_2{=}C(CH_3)C(O)OCH_3) = 4.07 \times 10^{-11}$ cm^3 molecule^{-1} s^{-1} with an uncertainty estimated to be ±20%.

VII-E-9.2. NO_3 Radical Reaction Kinetics

The kinetics of the reaction of NO_3 radicals with methyl methacrylate have been studied by Canosa-Mas et al. (1999a). Details are given in table VII-E-12. Based upon the result from Canosa-Mas et al. (1999a) we recommend $k(NO_3 + CH_2{=}C(CH_3)C(O)OCH_3) = 1.1 \times 10^{-16}$ cm^3 molecule^{-1} s^{-1} with an uncertainty estimated to be ±30%.

VII-E-9.3. Summary of the Atmospheric Fate of Methyl Methacrylate

Combining the recommended rate coefficient for reaction with OH radicals with a daytime average [OH] = 2.5×10^6 molecule cm^{-3} gives an estimate of about 3 h for the daytime atmospheric lifetime of methyl methacrylate. Blanco et al. (2006) identified methyl pyruvate ($CH_3C(O)C(O)OCH_3$) as the major oxidation

Table VII-E-11. Rate coefficients ($k = A \times e^{-B/T}$, cm^3 $molecule^{-1}$ s^{-1}) for reaction of OH with methyl methacrylate [$CH_2{=}C(CH_3)C(O)OCH_3$]

$10^{12} \times A$	B (K)	$10^{11} \times k$	T(K)	Technique[a]	Reference
		2.6 ± 0.5	298	DF–LIF	Saunders et al. (1994)
		4.35 ± 0.56	298	RR (isobutanol)[b]	Teruel et al. (2006)
2.5 ± 0.8	-821 ± 55	6.29 ± 0.08	255	PLP–LIF	Teruel et al. (2006)
		4.78 ± 0.22	273		
		4.27 ± 0.12	297		
		4.09 ± 0.08	298		
		3.77 ± 0.12	299		
		3.18 ± 0.10	321		
		2.88 ± 0.14	341		
		2.56 ± 0.10	351		
		4.15 ± 0.32	298	RR (3-chloropropene)[c]	Blanco et al. (2006)
0.25	-848	4.77 ± 0.10	287	RR (1-butene)[d]	Blanco et al. (2009)
		4.49 ± 0.06	294		
		4.30 ± 0.06	298		
		4.04 ± 0.06	303		
		3.76 ± 0.03	313		

[a]Abbreviations used for the techniques are defined in table I-F-3.

[b]Placed on an absolute basis using $k(OH + \text{isobutyl alcohol}) = 9.6 \times 10^{-12}$ cm^3 $molecule^{-1}$ s^{-1} (this book, section II-B-7.1).

[c]Placed on an absolute basis using $k(OH + \text{3-chloropropene}) = 1.69 \times 10^{-11}$ cm^3 $molecule^{-1}$ s^{-1} (Albaladejo et al., 2003).

[d]Placed on an absolute basis using $k(OH + \text{1-butene}) = 6.55 \times 10^{-12} \exp(467/T)$ cm^3 $molecule^{-1}$ s^{-1} (Calvert et al., 2000).

product of the OH-radical-initiated oxidation of methyl methacrylate. As with alkenes (Calvert et al., 2000), the reaction of OH with methyl acrylate proceeds predominately via addition to the $\rangle C{=}C\langle$ double bond with the resulting alkoxy radical $HOCH_2C(O\bullet)(CH_3)C(O)OCH_3$ decomposing via C—C bond scission:

$$OH + CH_2{=}C(CH_3)C(O)OCH_3 \rightarrow HOCH_2C(CH_3)C(O)OCH_3$$

$$HOCH_2C(CH_3)C(O)OCH_3 + O_2 \rightarrow HOCH_2C(OO)(CH_3)C(O)OCH_3$$

$$HOCH_2C(OO)(CH_3)C(O)OCH_3 + NO \rightarrow HOCH_2C(O\bullet)(CH_3)C(O)OCH_3 + NO_2$$

$$HOCH_2C(O\bullet)(CH_3)C(O)OCH_3 \rightarrow HOCH_2 + CH_3C(O)C(O)OCH_3$$

$$HOCH_2 + O_2 \rightarrow CH_2O + HO_2$$

VII-E-10. Ethyl Methacrylate [$CH_2{=}C(CH_3)C(O)OCH_2CH_3$]

VII-E-10.1. OH Reaction Kinetics

The kinetics of the reaction of OH radicals with ethyl methacrylate have been the subject of a relative rate study by Blanco et al. (2006). The results are given in table VII-E-13. Taking an average of the results from Blanco et al. (2006) gives $k(OH + CH_2{=}C(CH_3)C(O)OC_2H_5) = 4.3 \times 10^{-11}$ cm^3 $molecule^{-1}$ s^{-1} with an uncertainty estimated to be ±25%.

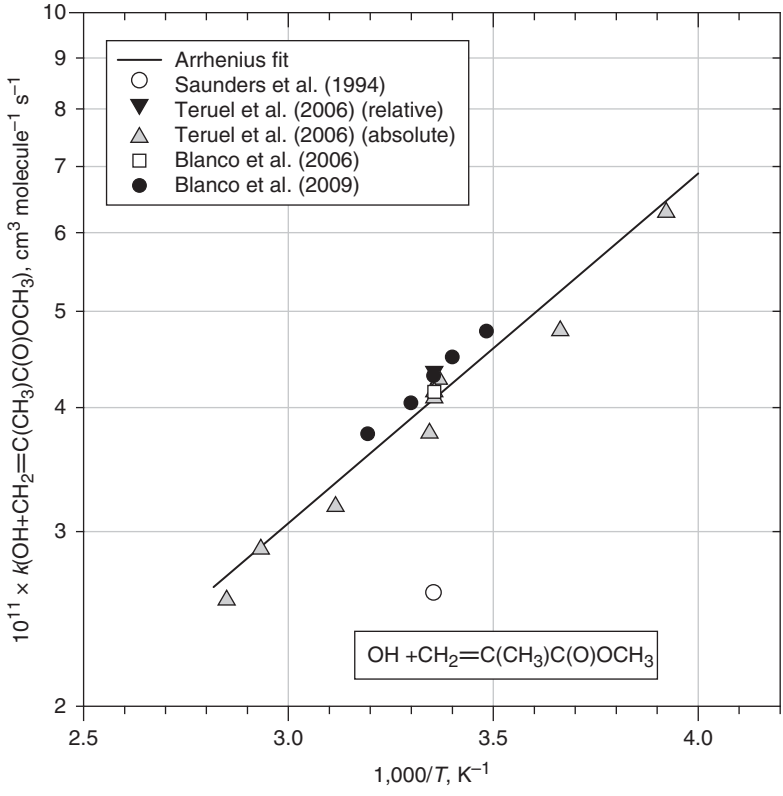

Figure VII-E-7. Measurements of the rate coefficients for reaction of OH radicals with methyl methacrylate. The line is a fit of the Arrhenius expression to the data from Teruel et al. (2006) and Blanco et al. (2006, 2009).

Table VII-E-12. Rate coefficient (k, cm^3 molecule^{-1} s^{-1}) for reaction of NO_3 radicals with methyl methacrylate [CH_2=$C(CH_3)C(O)OCH_3$]

$10^{15} \times k$	T(K)	Technique[a]	Reference
3.70 ± 0.57	296	RR (C_3H_6)[b]	Canosa-Mas et al. (1999a)

[a]Abbreviations used for the techniques are defined in table I-F-3.
[b]Placed on an absolute basis using $k(NO_3 + C_3H_6) = 9.49 \times 10^{-15}$ cm^3 molecule^{-1} s^{-1} (Calvert et al., 2000).

VII-E-10.2. Summary of the Atmospheric Fate of Ethyl Methacrylate

Combining the recommended rate coefficient for reaction with OH radicals with a daytime average [OH] = 2.5×10^6 molecule cm^{-3} gives an estimate of about 3 h for the daytime atmospheric lifetime of ethyl methacrylate. Blanco et al. (2006) identified ethyl pyruvate ($CH_3C(O)C(O)OC_2H_5$) as the major oxidation product of the OH-radical-initiated oxidation of ethyl methacrylate. As with alkenes (Calvert et al., 2000) the reaction of OH with ethyl methacrylate proceeds predominately via addition to the

Table VII-E-13. Rate coefficients (k, cm^3 molecule^{-1} s^{-1}) for reaction of OH with ethyl methacrylate [CH_2=C(CH_3)C(O)OCH_2CH_3]

$10^{11} \times k$	T(K)	Technique[a]	Reference
4.41 ± 0.36	298	RR (3-chloropropene)[b]	Blanco et al. (2006)
4.20 ± 0.18		RR (diethyl ether)[c]	

[a]Abbreviations used for the techniques are defined in table I-F-3.
[b]Placed on an absolute basis using k(OH + 3-chloropropene) = 1.69×10^{-11} cm^3 molecule^{-1} s^{-1} (Albaladejo et al., 2003).
[c]Placed on an absolute basis using k(OH + diethyl ether) = 1.2×10^{-11} cm^3 molecule^{-1} s^{-1} (this book, section III-B-3.1).

>C=C< double bond with the resulting alkoxy radical $HOCH_2C(O\bullet)(CH_3)C(O)OC_2H_5$ decomposing via C—C bond scission to give ethyl pyruvate ($CH_3C(O)C(O)OC_2H_5$) and the $HOCH_2$ radical (which reacts with O_2 to give CH_2O).

VII-E-11. *n*-Butyl Methacrylate (CH_2=C(CH_3)C(O)O$CH_2CH_2CH_2CH_3$)

VII-E-11.1. OH Reaction Kinetics

The kinetics of the reaction of OH radicals with *n*-butyl methacrylate have been studied using relative rate methods by Blanco et al. (2006, 2009). The results are given in table VII-E-14 and plotted in figure VII-E-8. Fitting the Arrhenius expression to the data from Blanco et al. (2006, 2009) gives $k(OH + CH_2{=}C(CH_3)C(O)OC_4H_9) = 2.44 \times 10^{-12} \exp(982/T)$ which gives 6.58×10^{-11} cm^3 molecule^{-1} s^{-1} at 298 K with an uncertainty estimated to be ±20%.

VII-E-11.2. Summary of the Atmospheric Fate of n-Butyl Methacrylate

Combining the recommended rate coefficient for reaction with OH radicals with a daytime average [OH] = 2.5×10^6 molecule cm^{-3} gives an estimate of about 1.7

Table VII-E-14. Rate coefficients ($k = A \times e^{-B/T}$, cm^3 molecule^{-1} s^{-1}) for reaction of OH with *n*-butyl methacrylate [CH_2=C(CH_3)C(O)O$CH_2CH_2CH_2CH_3$]

$10^{12} \times A$	B (K)	$10^{11} \times k$	T(K)	Technique[a]	Reference
		7.11 ± 0.46	298	RR (3-chloropropene)[b]	Blanco et al. (2006)
		6.20 ± 0.29		RR (diethyl ether)[c]	
0.24	−983	7.43 ± 0.13	287	RR (1-butene)[d]	Blanco et al. (2009)
		6.93 ± 0.13	294		
		6.62 ± 0.06	298		
		6.30 ± 0.09	303		
		5.59 ± 0.06	313		

[a]Abbreviations used for the techniques are defined in table I-F-3.
[b]Placed on an absolute basis using k(OH + 3-chloropropene) = 1.69×10^{-11} cm^3 molecule^{-1} s^{-1} (Albaladejo et al., 2003).
[c]Placed on an absolute basis using k(OH + diethyl ether) = 1.2×10^{-11} cm^3 molecule^{-1} s^{-1} (this book, section III-B-3.1).
[d]Placed on an absolute basis using k(OH + 1-butene) = $6.55 \times 10^{-12} \exp(467/T)$ cm^3 molecule^{-1} s^{-1} (Calvert et al., 2000).

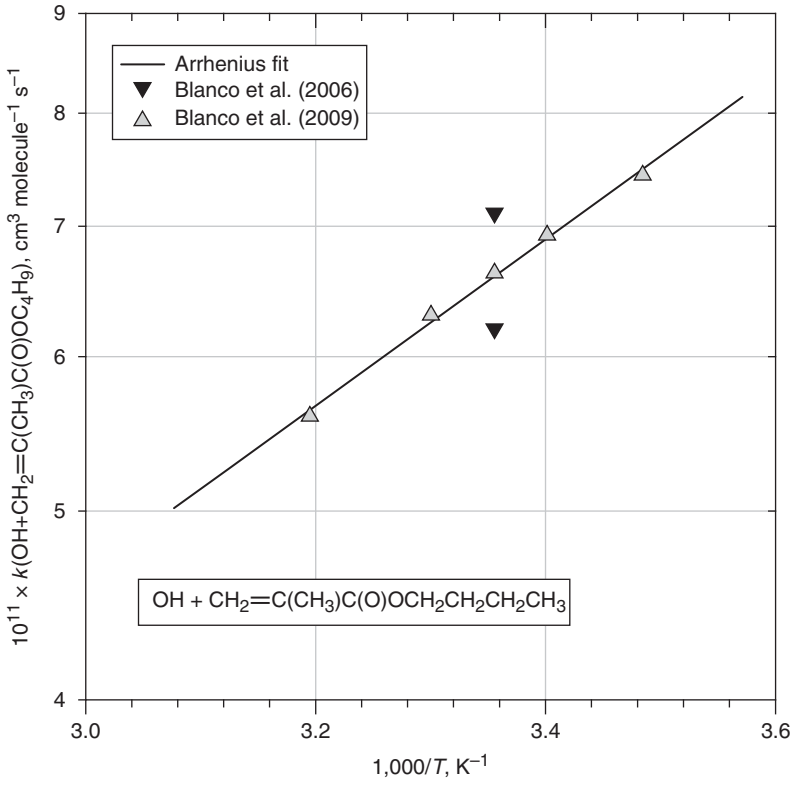

Figure VII-E-8. Measurements of the rate coefficients for reaction of OH radicals with *n*-butyl methacrylate.

h for the daytime atmospheric lifetime of methyl methacrylate. Blanco et al. (2006) identified butyl pyruvate ($CH_3C(O)C(O)OC_4H_9$) as the oxidation product of the OH-radical-initiated oxidation of butyl methacrylate. As with alkenes (Calvert et al., 2000) the reaction of OH with butyl methacrylate proceeds predominately via addition to the $\rangle C{=}C\langle$ double bond with the resulting alkoxy radical $HOCH_2C(O\bullet)(CH_3)C(O)OC_4H_9$ decomposing via C—C bond scission to give butyl pyruvate.

VII-E-12. Methyl *E*-2-Butenoate, Methyl 3-Methyl-2-butenoate and Methyl *E*-2-Methyl-2-butenoate

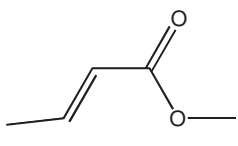

Methyl *E*-2-Butenoate

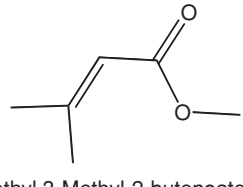

Methyl 3-Methyl-2-butenoate

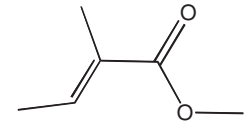

Methyl *E*-2-Methyl-2-butenoate

Table VII-E-15. Rate coefficients (k, cm^3 molecule^{-1} s^{-1}) for reaction of NO_3 radicals with methyl *E*-2-butenoate, methyl 3-methyl-2-butenoate, methyl *E*-2-methyl-2-butenoate

Compound	$10^{15} \times k$	T(K)	Technique[a]	Reference
Methyl *E*-2-butenoate	1.85 ± 0.52	296	RR (C_3H_6)[b]	Canosa-Mas et al. (2005)
Methyl 3-methyl-2-butenoate	14.1 ± 1.7	296	RR (C_3H_6)[b]	Canosa-Mas et al. (2005)
Methyl *E*-2-methyl-2-butenoate	49.2 ± 1.0	296	RR (C_3H_6)[b]	Canosa-Mas et al. (2005)

[a]Abbreviations used for the techniques are defined in table I-F-3.
[b]Placed on an absolute basis using $k(NO_3 + C_3H_6) = 9.49 \times 10^{-15}$ cm^3 molecule^{-1} s^{-1} (Calvert et al., 2000).

VII-E-12.1. NO_3 Radical Reaction Kinetics

The kinetics of the reaction of NO_3 radicals with methyl *E*-2-butenoate, methyl 3-methyl-2-butenoate, and methyl *E*-2-methyl-2-butenoate have been studied by Canosa-Mas et al. (2005). The results are given in table VII-E-15 and are recommended with an uncertainty estimated to be ±25%.

VII-E-12.2. Summary of the Atmospheric Fate of Methyl E-2-Butenoate, Methyl 3-Methyl-2-butenoate, and Methyl E-2-Methyl-2-butenoate

The reactivity of these species towards OH radicals has not been measured, but based on the similarity in molecular structure is expected to be comparable to, or greater than, that of methyl methacrylate (CH_2=$C(CH_3)C(O)OCH_3$). Hence, we can provide an estimate of approximately 3 h for the lifetime of these compounds with respect to reaction of OH radicals in the daytime. Combining the rate coefficients for reaction with NO_3 radicals with $[NO_3] = 3 \times 10^9$ gives lifetimes with respect to reaction with NO_3 in nighttime polluted urban areas of 2 days, 7 h, and 2 h for methyl *E*-2-butenoate, methyl 3-methyl-2-butenoate, and methyl *E*-2-methyl-2-butenoate, respectively. The dominant atmospheric loss mechanism for methyl *E*-2-butenoate is reaction with OH radicals leading to the formation of methyl glyoxylate as the main product. Methyl 3-methyl-2-butenoate and methyl *E*-2-methyl-2-butenoate will be lost via reaction with OH radicals in the daytime and reaction with NO_3 radicals in the nighttime. Reaction with ozone may also contribute.

VII-E-13. Comparison of the Reactivity of Unsaturated Esters and Alkenes

Table VII-E-16 lists the reactivity of OH radicals towards unsaturated esters and the corresponding alkenes in 1 atm. of air at 298 K. As seen from this table, with the exception of methyl-, ethyl-, and *n*-butyl-acrylate, the reactivities of the unsaturated esters are indistinguishable from those of the corresponding alkenes within the approximately ±20% uncertainties in the individual rate coefficients. The acrylates, CH_2=$CHC(O)OR$, are approximately a factor of 2 less reactive than their corresponding alkenes. This lower reactivity of the acrylates presumably reflects the delocalization of the electron density associated with the $\rangle C{=}C\langle$ double bond by the neighboring

Table VII-E-16. Comparison of the rate coefficients recommended with those for the corresponding alkenes at 298 K in 1 atm. of air

Unsaturated ester	k (298 K)	Alkene	k (298 K)[a]
$CH_2{=}CHOC(O)CH_3$	2.5×10^{-11}	$CH_2{=}CHCH_3$	2.63×10^{-11}
$CH_2{=}CHCH_2OC(O)CH_3$	2.66×10^{-11}	$CH_2{=}CHCH_2CH_3$	3.14×10^{-11}
$CH_2{=}C(CH_3)OC(O)CH_3$	6.72×10^{-11}	$CH_2{=}C(CH_3)_2$	5.14×10^{-11}
$CH_2{=}CHCH_2CH_2CH_2OC(O)CH_3$	4.3×10^{-11}	$CH_2{=}CHCH_2CH_2CH_2CH_3$	3.7×10^{-11}
$CH_3CH_2CH{=}CHCH_2CH_2OC(O)CH_3$	7.74×10^{-11}	$CH_3CH_2CH{=}CHCH_2CH_2CH_3$	6.9×10^{-11}[b]
$CH_2{=}CHC(O)OCH_3$	1.29×10^{-11}	$CH_2{=}CHCH_3$	2.63×10^{-11}
$CH_2{=}CHC(O)OC_2H_5$	1.59×10^{-11}	$CH_2{=}CHC_2H_5$	3.14×10^{-11}
$CH_2{=}CHC(O)O(CH_2)_3CH_3$	1.69×10^{-11}	$CH_2{=}CH(CH_2)_3CH_3$	3.7×10^{-11}
$CH_2{=}C(CH_3)C(O)OCH_3$	4.0×10^{-11}	$CH_2{=}C(CH_3)_2$	5.14×10^{-11}
$CH_2{=}C(CH_3)C(O)OC_2H_5$	4.3×10^{-11}	$CH_2{=}C(CH_3)C_2H_5$	6.1×10^{-11}
$CH_2{=}C(CH_3)C(O)OC_4H_9$	6.65×10^{-11}	$CH_2{=}C(CH_3)C_4H_9$	6.1×10^{-11}[c]

[a]Taken from Calvert et al. (2000).
[b]Data for *trans*-4-octene (data for 3-heptene are unavailable).
[c]Data for 2-methyl-1-butene (data for 2-methyl-1-hexene are unavailable).

electron withdrawing carbonyl group. Reduction of electron density associated with the $\rangle C{=}C\langle$ double bond then leads to reduced reactivity towards the electrophilic OH radical.

VII-F. Aromatic Esters

VII-F-1. Methyl Salicylate (Methyl Ester of 2-Hydroxybenzoic Acid)

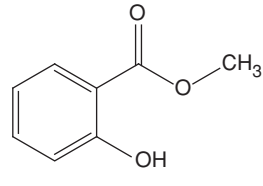

Methyl salicylate is a semi-volatile plant hormone, believed to be produced and released into the atmosphere as the result of plant stress (Karl et al., 2008; Canosa-Mas et al., 2002). As summarized below, limited information is available regarding its atmospheric behavior.

VII-F-1.1. OH Reaction Kinetics

The rate coefficient for reaction of OH with methyl salicylate has not been studied. However, the structure–activity methods of Kwok and Atkinson (1995) can be used to estimate $k = 1.1 \times 10^{-11}$ cm^3 molecule^{-1} s^{-1}.

Table VII-F-1. Rate coefficients (k, cm^3 molecule^{-1} s^{-1}) for reaction of O_3 with methyl salicylate

$10^{21} \times k$	T(K)	Technique[a]	Reference
≈ 4	298	GC	Canosa-Mas et al. (2002)

[a]Abbreviations used for the techniques are defined in table I-F-3.

VII-F-1.2. O_3 Reaction Kinetics

Canosa-Mas et al. (2002) estimate a rate coefficient $k \approx 4 \times 10^{-21}$ cm^3 molecule^{-1} s^{-1} for reaction of O_3 with methyl salicylate. The study is summarized in table VII-F-1.

VII-F-1.3. NO_3 Reaction Kinetics

The reaction of NO_3 with methyl salicylate has not been studied. However, on the basis of the rapid reaction of NO_3 with phenol, $k = 5.8 \times 10^{-12}$ cm^3 molecule^{-1} s^{-1} (Canosa-Mas et al., 2002), it seems reasonable that this reaction could represent an important loss for methyl salicylate.

VII-F-1.4. Cl-Atom Reaction Kinetics

Canosa-Mas et al. (2002) used the relative rate method to determine $k = 2.5 \times 10^{-12}$ cm^3 molecule^{-1} s^{-1} for reaction of Cl-atoms with methyl salicylate, see table VII-F-2 for a summary. The uncertainty is estimated to be $\pm 25\%$.

VII-F-1.5. Summary of the Atmospheric Fate of Methyl Salicylate

Insufficient data are available to assess accurately the atmospheric fate of methyl salicylate. However, the rate coefficient estimates presented in this section indicate that reaction with NO_3 could be an important loss mechanism, limiting the nighttime lifetime of methyl salicylate to as little as a few minutes even under moderately polluted conditions. Canosa-Mas et al. (2002) also report that this species possesses a strong absorption band in the near UV ($\sigma_{max} \approx 1.5 \times 10^{-17}$ cm^2 molecule^{-1} near 315 nm) which, when coupled with the assumption of a unit quantum yield for photodissociation, implies a photolysis lifetime of about 1 min. However, the photolysis quantum yield for methyl salicylate at 308 nm in cyclohexane solution has been reported to be

Table VII-F-2. Rate coefficients (k, cm^3 molecule^{-1} s^{-1}) for reaction of Cl with methyl salicylate

$10^{12} \times k$	T(K)	Technique[a]	Reference
2.5 ± 0.3	298	RR[b] (CH_3COCH_3)	Canosa-Mas et al. (2002)

[a]Abbreviations used for the techniques are defined in table I-F-3.
[b]Placed on an absolute basis using $k(Cl + CH_3COCH_3) = 2.1 \times 10^{-12}$ cm^3 molecule^{-1} s^{-1} (Calvert et al., 2008).

only 1.5×10^{-4} (Catalán et al., 1999), and applying this value in the gas phase at all wavelengths increases the lifetime to a few days, longer than that estimated for reaction with OH (10 h). Clearly, further studies of the kinetics (OH, NO_3) and photochemistry (quantum yields) of methyl salicylate are warranted.

VII-G. Carbonates

VII-G-1. Dimethyl Carbonate [$CH_3OC(O)OCH_3$]

VII-G-1.1. OH Reaction Kinetics

The reaction of OH with dimethyl carbonate has been the subject of a flash photolysis resonance fluorescence study by Bilde et al. (1997), see table VII-G-1 and figure VII-G-1. A fit of the modified Arrhenius expression to the data from Bilde et al. (1997) gives $k(OH + CH_3OC(O)OCH_3) = 6.31 \times 10^{-19} T^2 \exp(525/T)$ cm^3 molecule^{-1} s^{-1}. This expression gives $k(OH + CH_3OC(O)OCH_3) = 3.26 \times 10^{-13}$ cm^3 molecule^{-1} s^{-1} at 298 K with an uncertainty estimated to be ±25%. Corroborative studies of this rate coefficient are warranted.

VII-G-1.2. Cl-Atom Reaction Kinetics

The reaction of chlorine atoms with dimethyl carbonate has been the subject of a relative rate study by Bilde et al. (1997) at 296 K. The results are shown in table VII-G-2. An average of the results from Bilde et al. (1997) gives $k(Cl + CH_3OC(O)OCH_3) = 2.26 \times 10^{-12}$ cm^3 molecule^{-1} s^{-1} with an uncertainty estimated to be ±25%. Corroborative studies of this rate coefficient are warranted.

VII-G-1.3. Summary of the Atmospheric Fate of Dimethyl Carbonate

Combining $k(OH + CH_3OC(O)OCH_3) = 3.26 \times 10^{-13}$ cm^3 molecule^{-1} s^{-1} at 298 K with a diurnal average of [OH] $\approx 1.0 \times 10^6$ molecule cm^{-3} gives an estimate of about 35 days for the atmospheric lifetime of dimethyl carbonate. Bilde et al. (1997)

Table VII-G-1. Rate coefficients (k, cm^3 molecule^{-1} s^{-1}) for reaction of OH with dimethyl carbonate [$CH_3OC(O)OCH_3$]

$10^{12} \times k$	T(K)	Technique[a]	Reference	Temperature Range (K)
3.33 ± 0.29	252	FP–RF	Bilde et al. (1997)	252–370
3.27 ± 0.13	273			
3.14 ± 0.10	277			
3.15 ± 0.07	298			
3.32 ± 0.19	330			
3.35 ± 0.13	349			
3.82 ± 0.09	370			

[a]Abbreviations used for the techniques are defined in table I-F-3.

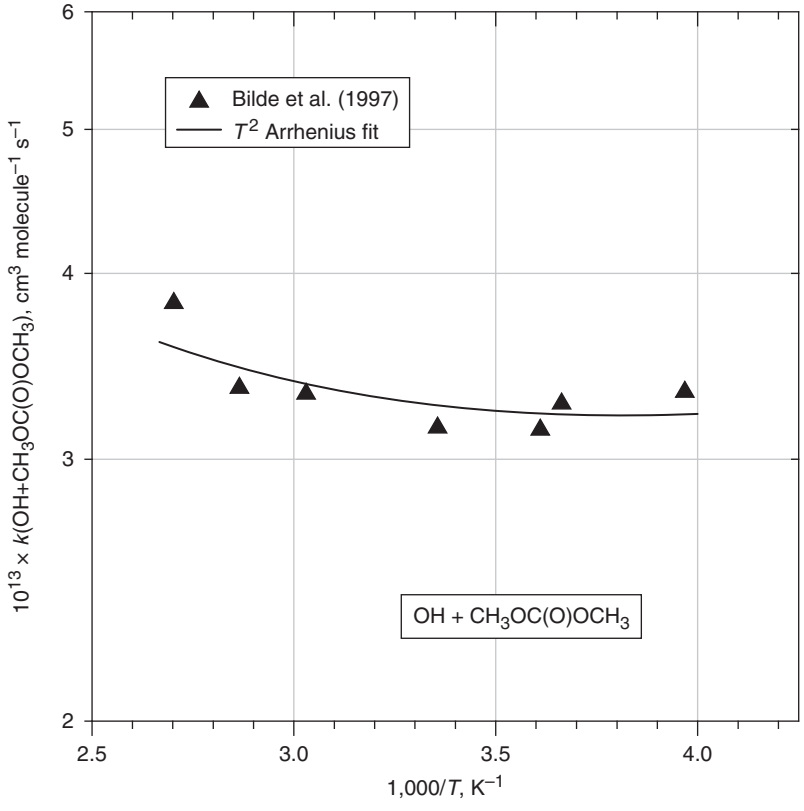

Figure VII-G-1. Measurements of the rate coefficients for reaction of OH radicals with dimethyl carbonate. The line is a fit of the modified Arrhenius expression to the data.

Table VII-G-2. ate coefficients (k, cm^3 $molecule^{-1}$ s^{-1}) for reaction of chlorine atoms with dimethyl carbonate [$CH_3OC(O)OCH_3$]

$10^{12} \times k$	T(K)	Technique[a]	Reference
2.18 ± 0.55	296	RR (C_2H_5Cl)[b]	Bilde et al. (1997)
2.28 ± 0.72	296	RR (CH_3Cl)[c]	
2.33 ± 0.13	296	RR (CH_2ClCH_2Cl)[d]	

[a]Abbreviations used for the techniques are defined in table I-F-3.
[b]Placed on an absolute basis using $k(Cl + C_2H_5Cl) = 7.8 \times 10^{-12}$ cm^3 $molecule^{-1}$ s^{-1} (section I-F).
[c]Placed on an absolute basis using $k(Cl + CH_3Cl) = 4.8 \times 10^{-13}$ cm^3 $molecule^{-1}$ s^{-1} (Atkinson et al., 2008).
[d]Placed on an absolute basis using $k(Cl + CH_2ClCH_2Cl) = 1.3 \times 10^{-12}$ cm^3 $molecule^{-1}$ s^{-1} (Wallington et al., 1996b).

studied the products of the chlorine-initiated oxidation of dimethyl carbonate in 700 Torr of N_2/O_2 diluent at 296 K. IR product features consistent with the formation of $CH_3OC(O)OC(O)H$ were observed. The yield of $CH_3OC(O)OC(O)H$ varied with $[O_2]$ in a manner consistent with competition between three reaction pathways for

the $CH_3OC(O)OCH_2O$ alkoxy radicals:

$$CH_3OC(O)OCH_2O + O_2 \rightarrow CH_3OC(O)OC(O)H + HO_2$$

$$CH_3OC(O)OCH_2O \rightarrow CH_3OC(O)OC(O)H + H$$

$$CH_3OC(O)OCH_2O \rightarrow CH_3OC(O)O + CH_2O$$

Bilde et al. (1997) concluded that in 760 Torr of air at 296 K, reaction with O_2, H-atom elimination, and decomposition via C—C bond scission and/or isomerization account for $42 \pm 15\%$, $14 \pm 2\%$, and $44 \pm 10\%$ of the fate of the alkoxy radicals, respectively. It is highly unusual that three processes are competitive atmospheric loss mechanisms for an alkoxy radical. Corroborative studies are warranted.

VII-H. Lactates

VII-H-1. Methyl Lactate [$CH_3CH(OH)C(O)OCH_3$]

VII-H-1.1. OH Reaction Kinetics

The rate coefficient for reaction of OH with methyl lactate has been studied by Kwok et al. (1996b) using a relative rate method. Scaling the rate coefficient ratio to $k(\text{OH} + \text{cyclohexane}) = 6.97 \times 10^{-12}$ gives $k(\text{OH} + \text{methyl lactate}) = (2.59 \pm 0.19) \times 10^{-12}$ cm^3 molecule^{-1} s^{-1}. See table VII-H-1.

VII-H-1.2. Summary of the Atmospheric Fate of Methyl Lactate

Combining $k(\text{OH} + \text{methyl lactate}) = (2.59 \pm 0.19) \times 10^{-12}$ cm^3 molecule^{-1} s^{-1} with a diurnal average [OH] $= 1 \times 10^6$ molecule cm^{-3} provides an estimate for the atmospheric lifetime of methyl lactate of about 4.5 days. As discussed by Kwok et al. (1996b), 80% of the reaction is expected to occur at the tertiary C—H group. The resulting α-hydroxy alkyl radical will react with O_2 to give methyl pyruvate, $CH_3C(O)C(O)OCH_3$.

VII-H-2. Ethyl Lactate [$CH_3CH(OH)C(O)OC_2H_5$]

VII-H-2.1. OH Reaction Kinetics

The rate coefficient for reaction of OH with ethyl lactate has been studied by Kwok et al. (1996b) using a relative rate method. Scaling the rate coefficient ratio to

Table VII-H-1. Rate coefficients (k, cm^3 molecule^{-1} s^{-1}) for reaction of OH with lactates

Lactate	$10^{12} \times k$	T(K)	Technique[a]	Reference
Methyl lactate	2.59 ± 0.19	296	RR (cyclohexane)[b]	Kwok et al. (1996b)
Ethyl lactate	3.66 ± 0.25	296	RR (cyclohexane)[b]	Kwok et al. (1996b)

[a]Abbreviations used for the techniques are defined in table I-F-3.
[b]Placed on an absolute basis using $k(\text{OH} + \text{cyclohexane}) = 6.97 \times 10^{-12}$ cm^3 molecule^{-1} s^{-1} (Calvert et al., 2008).

$k(\mathrm{OH} + \text{cyclohexane}) = 6.97 \times 10^{-12}$ gives $k(\mathrm{OH} + \text{ethyl lactate}) = (3.66 \pm 0.25) \times 10^{-12}$ cm^3 molecule^{-1} s^{-1}. See table VII-H-1.

VII-H-2.2. Summary of the Atmospheric Fate of Ethyl Lactate

Combining $k(\mathrm{OH} + \text{ethyl lactate}) = (3.66 \pm 0.25) \times 10^{-12}$ cm^3 molecule^{-1} s^{-1} with a diurnal average [OH] $= 1 \times 10^6$ molecule cm^{-3} provides an estimate for the atmospheric lifetime of ethyl lactate of about 3.2 days. As discussed by Kwok et al. (1996b), the dominant reaction pathway (52%) is hydrogen abstraction from the tertiary C—H group. The resulting α-hydroxy alkyl radical will react with O_2 to give ethyl pyruvate, $CH_3C(O)C(O)OCH_2CH_3$ which will hydrolyze in water solution to give acetic and propionic acids.

VII-I. Halogen-Substituted Esters

VII-I-1. Trifluoromethyl Formate [$CF_3OC(O)H$]

VII-I-1.1. OH Reaction Kinetics

The kinetics of the reaction of OH with $CF_3OC(O)H$ have been studied by Chen et al. (2004a) over the temperature range 242–338 K. Rate coefficients are listed in table VII-I-1 and plotted in figure VII-I-1. The line in figure VII-I-1 is a fit to the data which gives $k(\mathrm{OH} + CF_3OC(O)H) = 1.17 \times 10^{-12} \exp(-1{,}274/T)$ which yields $k(\mathrm{OH} + CF_3OC(O)H) = 1.63 \times 10^{-14}$ cm^3 molecule^{-1} s^{-1} at 298 K. The uncertainty in $k(\mathrm{OH} + CF_3OC(O)H)$ at 298 K is estimated to be $\pm 25\%$.

VII-I-1.2. Cl-Atom Kinetics

The kinetics of the reaction of Cl-atoms with $CF_3OC(O)H$ have been studied by Christensen et al. (1999) at 296 K. Rate coefficients are listed in table VII-I-2. Taking an average of the determinations by Christensen et al. (1999) gives $k(\mathrm{Cl} + CF_3OC(O)H) = 9.84 \times 10^{-15}$ cm^3 molecule^{-1} s^{-1}. The uncertainty in $k(\mathrm{Cl} + CF_3OC(O)H)$ at 296 K is estimated to be $\pm 25\%$.

VII-I-1.3. Summary of the Atmospheric Fate of $CF_3OC(O)H$

Combining $k(\mathrm{OH} + CF_3OC(O)H) = 1.08 \times 10^{-14}$ cm^3 molecule^{-1} s^{-1} at 272 K with a diurnal average of [OH] $= 1 \times 10^6$ molecule cm^{-3} gives an estimate of about 3 years for the lifetime of $CF_3OC(O)H$ with respect to reaction with OH radicals. Kutsuna et al. (2004, 2005) have studied the rate of uptake and hydrolysis of fluorinated esters by a column-stripping technique. In contrast to the corresponding nonfluorinated esters, Kutsuna et al. (2004, 2005) showed that uptake into the ocean and hydrolysis can be a significant atmospheric loss mechanism for fluorinated esters. Kutsuna et al. (2004, 2005) estimated that the lifetime of fluorinated esters with respect to loss to the ocean is approximately of the order of 1 year. Dissolution and hydrolysis in the ocean is probably a significant fate of $CF_3OC(O)H$.

Table VII-I-1. Rate coefficients ($k = A \times e^{-B/T}$, cm^3 $molecule^{-1}$ s^{-1}) for reaction of OH with halogen substituted esters

Molecule	$10^{12} \times A$	B (K)	$10^{13} \times k$	T (K)	Technique[a]	Reference	Temperature Range (K)
$CF_3OC(O)H$	1.17	1,274	0.0617	242	RR(CF_3OCH_3)[b]	Chen et al. (2004a)	242–328
			0.0754	253			
			0.100	268			
			0.134	283			
			0.165	298			
			0.197	313			
			0.244	328			
$CF_3CHFOC(O)H$	0.88	1,181	0.085 ± 0.005	253	RR (CH_2F_2)[c]	Chen et al. (2006)	253–328
			0.100 ± 0.004	268			
			0.127 ± 0.005	283			
			0.163 ± 0.003	298			
			0.203 ± 0.008	313			
			0.245 ± 0.008	328			
			0.088 ± 0.002	253	RR (CH_3CHF_2)[d]		
			0.111 ± 0.010	268			
			0.138 ± 0.004	283			
			0.165 ± 0.006	298			
			0.207 ± 0.002	313			
			0.248 ± 0.006	328			
$C_2F_5OC(O)H$	1.91	1,511	0.0486	253	RR($C_2F_5OCH_3$)[e]	Chen et al. (2004b)	253–328
			0.0679	268			
			0.0915	283			
			0.120	298			
			0.153	313			
			0.190	328			
n-$C_3F_7OC(O)H$	1.45	1,274	0.0966	253	RR(n-$C_3F_7OCH_3$)[f]	Chen et al. (2004b)	253–328
			0.120	268			
			0.166	283			
			0.205	298			
			0.252	313			
			0.295	328			

$FC(O)OCH_3$	0.21	631	0.178 ± 0.007	253	RR (CH_2F_2)[c]	Chen et al. (2006)	253–328
			0.189 ± 0.015	268			
			0.214 ± 0.008	283			
			0.249 ± 0.005	298			
			0.277 ± 0.011	313			
			0.319 ± 0.008	328			
			0.187 ± 0.006	253	RR (CH_3CHF_2)[d]		
			0.207 ± 0.010	268			
			0.227 ± 0.003	283			
			0.255 ± 0.009	298			
			0.286 ± 0.003	313			
			0.319 ± 0.019	328			
$CF_2HC(O)OCH_3$			1.22 ± 0.07[i]	296	RR (CH_3Cl)[g]	Blanco and Teruel (2007)	
			1.43 ± 0.11[i]		RR (C_2H_6)[h]		
$CF_3C(O)OCH_3$	0.30 ± 0.07	512 ± 78	0.37 ± 0.03	240	FP–RF	Wallington et al. (1988b)	240–440
			0.52 ± 0.08	296			
			0.64 ± 0.05	350			
			0.83 ± 0.11	400			
			0.99 ± 0.08	440			
			0.419 ± 0.031[i]	296	RR (CH_3Cl)[g]	Blanco and Teruel (2007)	
			0.468 ± 0.036[i]		RR (C_2H_6)[h]		
$CF_3C(O)OC_2H_5$			2.16 ± 0.29[i]	296	RR (CH_3Cl)[g]	Blanco and Teruel (2007)	
			2.56 ± 0.23[i]		RR (C_2H_6)[h]		
$CF_3C(O)OCH_2CF_3$			0.82 ± 0.07[i]	296	RR (CH_3Cl)[g]	Blanco and Teruel (2007)	
			1.06 ± 0.07[i]		RR (C_2H_6)[h]		
$CH_2{=}CHC(O)OCH_2CH_2C_4F_9$			108 ± 8	296	RR (C_2H_4)[j]	Butt et al. (2009)	
			122 ± 9		RR (C_3H_6)[k]		

[a]Abbreviations used for the techniques are defined in table I-F-3.
[b]Placed on an absolute basis using $k(OH + CH_3OCF_3) = 2.1 \times 10^{-12} \exp(-1{,}540/T)$ cm^3 molecule^{-1} s^{-1} (this book, section III-G-3.1).
[c]Placed on an absolute basis using $k(OH + CH_2F_2) = 1.33 \times 10^{-12} \exp(-1{,}432/T)$ cm^3 molecule^{-1} s^{-1} (Calvert et al., 2008).
[d]Placed on an absolute basis using $k(OH + CH_3CHF_2) = 1.21 \times 10^{-12} \exp(-1{,}055/T)$ cm^3 molecule^{-1} s^{-1} (Calvert et al., 2008).
[e]Placed on an absolute basis using $k(OH + CH_3OC_2F_5) = 1.9 \times 10^{-12} \exp(-1{,}510/T)$ cm^3 molecule^{-1} s^{-1} (this book, section III-G-12.1).
[f]Placed on an absolute basis using $k(OH + CH_3OC_3F_7) = 2.06 \times 10^{-12} \exp(-1{,}540/T)$ cm^3 molecule^{-1} s^{-1} (this book, section III-G-29.1).
[g]Placed on an absolute basis using $k(OH + CH_3Cl) = 3.6 \times 10^{-14}$ cm^3 molecule^{-1} s^{-1} (Atkinson et al., 2008).
[h]Placed on an absolute basis using $k(OH + C_2H_6) = 2.4 \times 10^{-13}$ cm^3 molecule^{-1} s^{-1} (Atkinson et al., 2006).
[i]Average from two determinations, uncertainties encompass the extremes of the individual determinations.
[j]Placed on an absolute basis using $k(OH + C_2H_4) = 7.9 \times 10^{-12}$ cm^3 molecule^{-1} s^{-1} (Atkinson et al., 2006).
[k]Placed on an absolute basis using $k(OH + C_3H_6) = 2.9 \times 10^{-11}$ cm^3 molecule^{-1} s^{-1} (Atkinson et al., 2006).

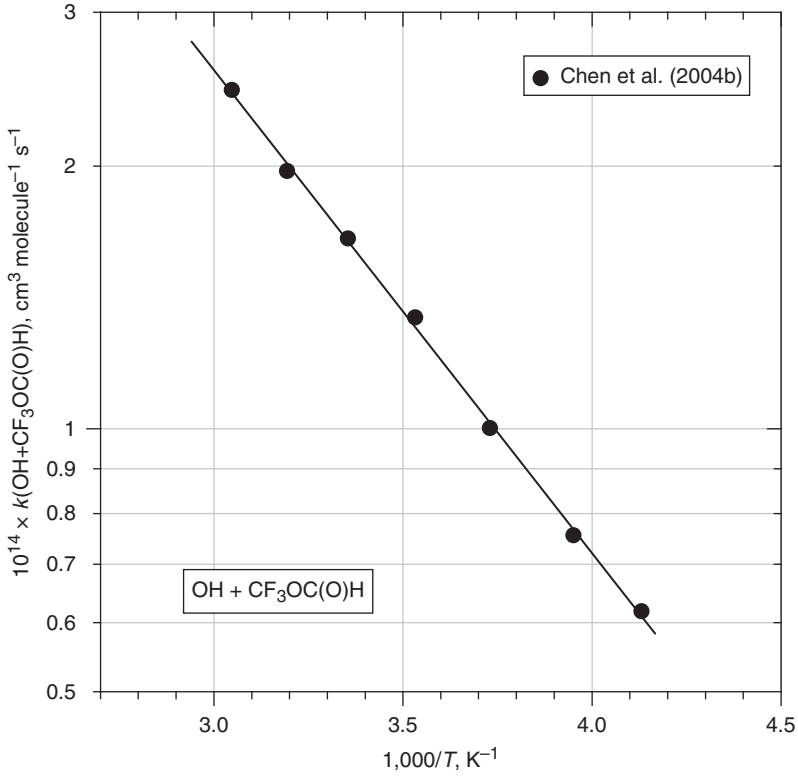

Figure VII-I-1. Measurements of the rate coefficients for reaction of OH radicals with $CF_3OC(O)H$. The line is a fit to the data.

VII-I-2. 1,2,2,2-Tetrafluoroethyl Formate [$CF_3CFHOC(O)H$]

VII-I-2.1. OH Reaction Kinetics

The kinetics of the reaction of OH with $CF_3CFHOC(O)H$ have been studied by Chen et al. (2006) over the temperature range 253–328 K. Rate coefficients are listed in table VII-I-1 and plotted in figure VII-I-2. The line in figure VII-I-2 is a fit to the data that give $k(OH + CF_3CFHOC(O)H) = 8.84 \times 10^{-13} \exp(-1{,}181/T)$, which gives $k(OH + CF_3CFHOC(O)H) = 1.68 \times 10^{-14}$ cm^3 molecule^{-1} s^{-1} at 298 K. The uncertainty in $k(OH + CF_3CFHOC(O)H)$ at 298 K is estimated to be $\pm 25\%$.

VII-I-2.2. Summary of the Atmospheric Fate of $CF_3CFHOC(O)H$

Combining $k(OH + CF_3CFHOC(O)H) = 1.34 \times 10^{-14}$ cm^3 molecule^{-1} s^{-1} at 272 K with a diurnal average of [OH] $= 1 \times 10^6$ molecule cm^{-3} gives an estimate of about 2 years for the lifetime of $CF_3CFHOC(O)H$ with respect to reaction with OH radicals. Kutsuna et al. (2004, 2005) have shown that loss via dissolution into the oceans and hydrolysis probably occurs on a timescale of the order of 1 year and so this process is likely important for $CF_3CFHOC(O)H$.

Table VII-I-2. Rate coefficients (k, cm^3 molecule^{-1} s^{-1}) for reaction of chlorine atoms with halogenated esters

Molecule	$10^{12} \times k$	T (K)	Technique[a]	Reference
$CF_3OC(O)H$	0.00970 ± 0.00012	296	RR (CD_4)[b]	Christensen et al. (1999)
	0.00998 ± 0.00046		RR (CHD_3)[c]	
$CHF_2OC(O)H$	0.0200 ± 0.0017	296	RR ($CF_3CH_2OCHF_2$)[d]	Wallington et al. (2002)
$C_2F_5OC(O)H$	0.013 ± 0.002	298	RR ($C_2F_5OCH_3$)[e]	Nohara et al. (2001)
n-$C_3F_7OC(O)H$	0.0082 ± 0.0002	295	RR (n-$C_3F_7OCH_3$)[f]	Ninomiya et al. (2000)
	0.0091 ± 0.0018	298	RR (n-$C_3F_7OCH_3$)[f]	Nohara et al. (2001)
n-$C_4F_9OC(O)H$	0.0165 ± 0.0068	296	RR (n-$C_4F_9OCH_3$)[g]	Wallington et al. (1997b)
iso-$C_4F_9OC(O)H$	0.0165 ± 0.0068		RR (i-$C_4F_9OCH_3$)[g]	
n-$C_5F_{11}OC(O)H$	0.017 ± 0.006	298	RR (n-$C_5F_{11}OCH_3$)[h]	Nohara et al. (2001)
(n-C_3F_7)($CF(CF_3)_2$)C(F)OC(O)H	0.00964 ± 0.00073	295	RR (CD_4)[b]	Goto et al. (2002a)
	0.00974 ± 0.00093		RR (CHD_3)[c]	
(n-C_3F_7)($CF(CF_3)_2$)C(F)OC(O)CH_3	< 0.00006	295	RR (CD_4)[b]	Goto et al. (2002a)
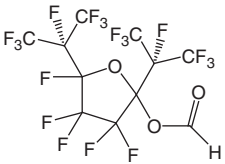 (a)	0.0126 ± 0.0009		RR (CD_4)[b]	Javadi et al. (2007)
	0.0142 ± 0.0012		RR (CHD_3)[c]	
$CF_3C(O)OCH_3$	0.0864 ± 0.0048	298	RR (CH_3Cl)[i]	Blanco et al. (2008)
	0.0900 ± 0.0030		RR (CH_4)[d]	
$CF_3C(O)OC_2H_5$	1.60 ± 0.04	298	RR (CH_3Cl)[i]	Blanco et al. (2008)
	1.89 ± 0.04		RR (CH_3COOCH_3)[j]	
$CHF_2C(O)OCH_3$	0.187 ± 0.005	298	RR (CH_3Cl)[i]	Blanco et al. (2008)
	0.220 ± 0.004		RR (CH_4)[k]	
$CF_3C(O)OCH_2CF_3$	0.000945 ± 0.000063	298	RR (CH_3CFCl_2)[l]	Wallington et al. (1998b)
	0.000952 ± 0.000067		RR (CD_4)[b]	
	0.001170 ± 0.000075	298	RR (CH_2FCF_3)[m]	Blanco et al. (2008)
	0.000952 ± 0.000051		RR (CHF_2Cl)[n]	

(*continued*)

Table VII-I-2. (*continued*)

Molecule	$10^{12} \times k$	T (K)	Technique[a]	Reference
$CHF_2OC(O)CF_3$	< 0.00004	296	RR (CD_4)[b]	Wallington et al. (2002)
CH_2=CHC(O)$OCH_2CH_2C_4F_9$	225 ± 14	296	RR (C_2H_4)[p]	Butt et al. (2009)
	193 ± 12		RR (C_3H_6)[q]	

[a]Abbreviations used for the techniques are defined in table I-F-3.
[b]Placed on an absolute basis using $k(Cl + CD_4) = 6.1 \times 10^{-15}$ cm^3 molecule^{-1} s^{-1} (Wallington and Hurley, 1992).
[c]Placed on an absolute basis using $k(Cl + CHD_3) = 2.32 \times 10^{-14}$ cm^3 molecule^{-1} s^{-1} (Wallington and Hurley, 1992).
[d]Placed on an absolute basis using $k(Cl + CF_3CH_2OCHF_2) = 1.2 \times 10^{-14}$ cm^3 molecule^{-1} s^{-1} (Wallington et al., 2002).
[e]Placed on an absolute basis using $k(Cl + C_2F_5OCH_3) = 9.1 \times 10^{-14}$ cm^3 molecule^{-1} s^{-1} (Nohara et al., 2001).
[f]Placed on an absolute basis using $k(Cl + n\text{-}C_3F_7OCH_3) = 9.1 \times 10^{-14}$ cm^3 molecule^{-1} s^{-1} (this book, section III-G-29.2).
[g]Placed on an absolute basis using $k(Cl + n\text{-}C_4F_9OCH_3) = k(i\text{-}C_4F_9OCH_3) = 9.7 \times 10^{-14}$ cm^3 molecule^{-1} s^{-1} (Wallington et al., 1997b).
[h]Placed on an absolute basis using $k(Cl + n\text{-}C_5F_{11}OCH_3) = 9.1 \times 10^{-14}$ cm^3 molecule^{-1} s^{-1} (Nohara et al., 2001).
[i]Placed on an absolute basis using $k(Cl + CH_3Cl) = 4.8 \times 10^{-13}$ cm^3 molecule^{-1} s^{-1} (Atkinson et al., 2008).
[j]Placed on an absolute basis using $k(Cl + CH_3C(O)OCH_3) = 2.2 \times 10^{-12}$ cm^3 molecule^{-1} s^{-1} (Christensen et al., 2000).
[k]Placed on an absolute basis using $k(Cl + CH_4) = 1.0 \times 10^{-13}$ cm^3 molecule^{-1} s^{-1} (Atkinson et al., 2006).
[l]Placed on an absolute basis using $k(Cl + CH_3CFCl_2) = 1.5 \times 10^{-15}$ cm^3 molecule^{-1} s^{-1} (Atkinson et al., 2008).
[m]Placed on an absolute basis using $k(Cl + CH_2FCF_3) = 1.5 \times 10^{-15}$ cm^3 molecule^{-1} s^{-1} (Atkinson et al., 2008).
[n]Placed on an absolute basis using $k(Cl + CHF_2Cl) = 1.7 \times 10^{-15}$ cm^3 molecule^{-1} s^{-1} (Atkinson et al., 2008).
[o]Placed on an absolute basis using $k(Cl + HC(O)F) = 1.9 \times 10^{-15}$ cm^3 molecule^{-1} s^{-1} (this book, section IV-G-1.2).
[p]Placed on an absolute basis using $k(Cl + C_2H_4) = 9.52 \times 10^{-11}$ cm^3 molecule^{-1} s^{-1} (section I-F-3).
[q]Placed on an absolute basis using $k(Cl + C_3H_6) = 2.3 \times 10^{-10}$ cm^3 molecule^{-1} s^{-1} (Atkinson et al., 2006).

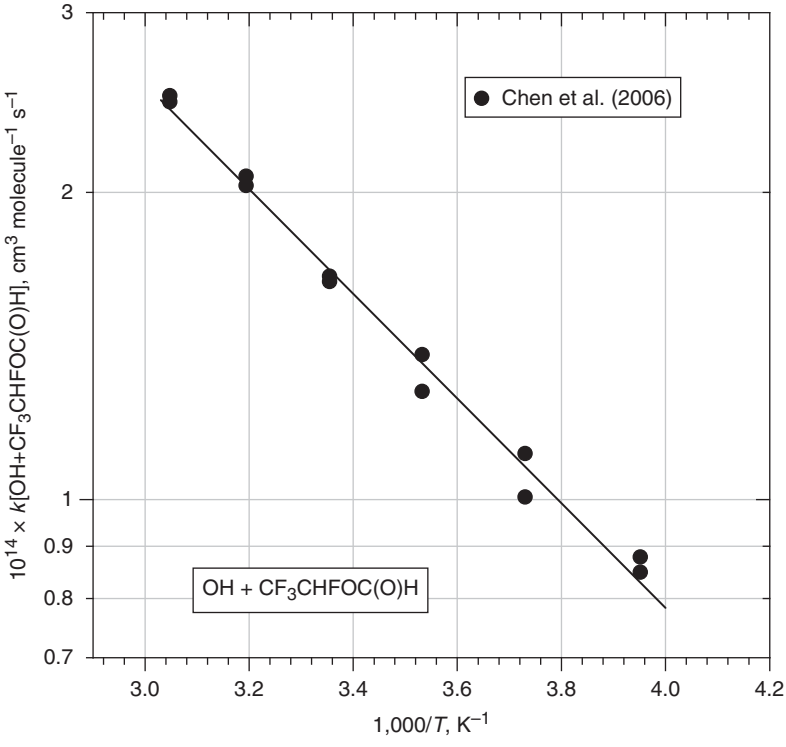

Figure VII-I-2. Measurements of the rate coefficients for reaction of OH radicals with $CF_3CFHOC(O)H$. The line is a fit to the data.

VII-I-3. Perfluoroethyl Formate [1,1,2,2,2-Pentafluoroethyl Formate, $C_2F_5OC(O)H$]

VII-I-3.1. OH Reaction Kinetics

The kinetics of the reaction of OH with $C_2F_5OC(O)H$ have been studied by Chen et al. (2004b) over the temperature range 253–328 K. Rate coefficients are listed in table VII-I-1 and plotted in figure VII-I-3. The line in figure VII-I-3 is a fit to the data, $k(OH + C_2F_5OC(O)H) = 1.91 \times 10^{-12} \exp(-1{,}511/T)$, which gives $k(OH + C_2F_5OC(O)H) = 1.19 \times 10^{-14}$ cm^3 molecule^{-1} s^{-1} at 298 K. The uncertainty in $k(OH + C_2F_5OC(O)H)$ at 298 K is estimated to be ±25%.

VII-I-3.2. Cl-Atom Reaction Kinetics

The kinetics of the reaction of Cl-atoms with $C_2F_5OC(O)H$ have been studied by Nohara et al. (2001) at 298 K. The result is listed in table VII-I-2. The value from Nohara et al. (2001) of $k(Cl + C_2F_5OC(O)H) = 1.3 \times 10^{-14}$ cm^3 molecule^{-1} s^{-1} is recommended with an uncertainty estimated to be ±35%.

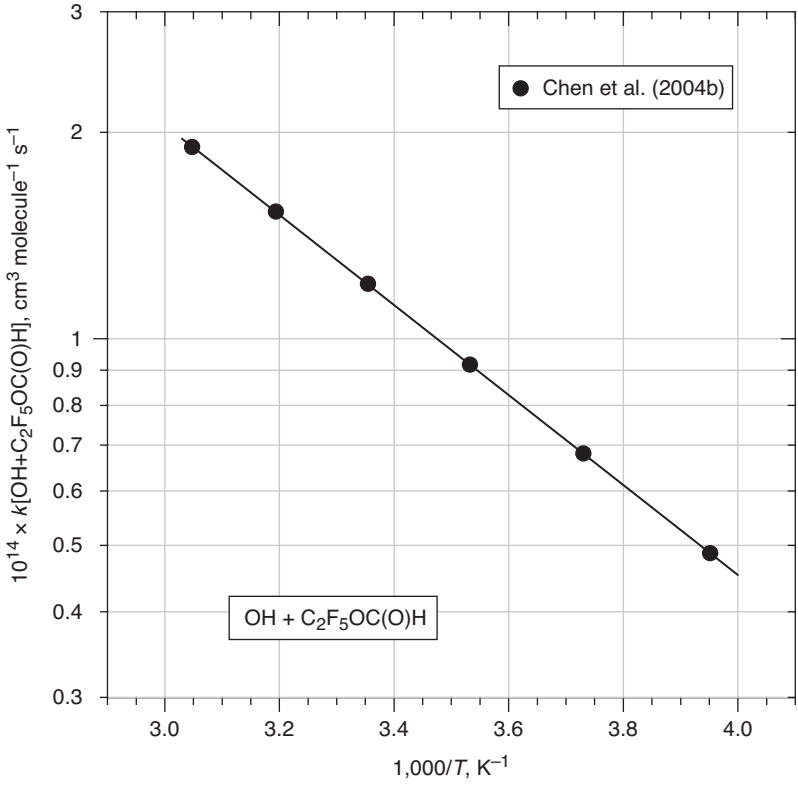

Figure VII-I-3. Measurements of the rate coefficients for reaction of OH radicals with $C_2F_5OC(O)H$. The line is a fit to the data.

VII-I-3.3. Summary of the Atmospheric Fate of $C_2F_5OC(O)H$

Combining $k(OH + C_2F_5OC(O)H) = 1.19 \times 10^{-14}$ cm^3 molecule^{-1} s^{-1} at 298 K with a diurnal average of [OH] $= 1 \times 10^6$ molecule cm^{-3} gives an estimate of about 3 years for the lifetime of $C_2F_5OC(O)H$ with respect to reaction with OH radicals. Kutsuna et al. (2005) have estimated that the atmospheric lifetime of $C_2F_5OC(O)H$ with respect to dissolution into the oceans and hydrolysis lies in the range <4–37 years, assuming Henry's law constants of 0.10–0.01 of that measured for $CF_3CH_2OC(O)H$ (0.55 M atm.$^{-1}$ at 298 K). It seems likely that loss to the oceans is a significant fate of $C_2F_5OC(O)H$.

VII-I-4. Perfluoro-*n*-Propyl Formate [1,1,2,2,3,3,3-Heptafluoropropyl Formate, n-$C_3F_7OC(O)H$]

VII-I-4.1. OH Reaction Kinetics

The kinetics of the reaction of OH with n-$C_3F_7OC(O)H$ have been studied by Chen et al. (2004b) over the temperature range 253–328 K. Rate coefficients are listed

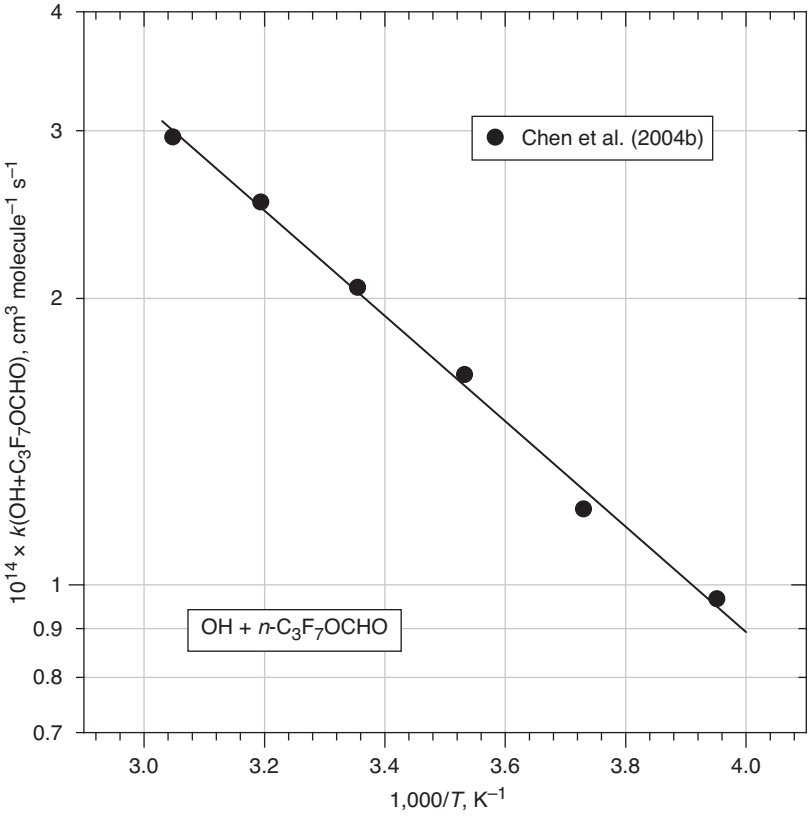

Figure VII-I-4. Measurements of the rate coefficients for reaction of OH radicals with *n*-$C_3F_7OC(O)H$. The line is a fit to the data.

in table VII-I-1 and plotted in figure VII-I-4. The line in figure VII-I-4 is a fit to the data, $k(OH + C_3F_7OC(O)H) = 1.45 \times 10^{-12} \exp(-1{,}274/T)$, which gives $k(OH + C_3F_7OC(O)H) = 2.02 \times 10^{-14}$ cm^3 molecule^{-1} s^{-1} at 298 K. The uncertainty in $k(OH + C_3F_7OC(O)H)$ at 298 K is estimated to be ±25%.

VII-I-4.2. Cl-Atom Reaction Kinetics

The kinetics of the reaction of Cl-atoms with $C_3F_7OC(O)H$ have been studied by Ninomiya et al. (2000) and Nohara et al. (2001) at about 298 K. Rate coefficients are listed in table VII-I-2. While the results from the two studies are in good agreement, as seen from table VII-I-2, the value reported by Ninomiya et al. (2000) is somewhat lower than those measured for other perfluorinated formates. Accordingly, we base our recommendation on the measurement by Nohara et al. (2001); $k(Cl + C_3F_7OC(O)H) = 9.1 \times 10^{-15}$ cm^3 molecule^{-1} s^{-1} with an uncertainty estimated to be ±35%.

VII-I-4.3. Summary of the Atmospheric Fate of n-$C_3F_7OC(O)H$

Combining $k(OH + C_3F_7OC(O)H) = 2.02 \times 10^{-14}$ cm^3 molecule^{-1} s^{-1} at 298 K with a diurnal average of [OH] $= 1 \times 10^6$ molecule cm^{-3} gives an estimate of about 1.6 years for the lifetime of $C_3F_7OC(O)H$ with respect to reaction with OH radicals. As noted in the previous section, Kutsuna et al. (2005) have shown that dissolution into the oceans and hydrolysis is probably an important fate for $C_2F_5OC(O)H$. It seems likely that loss to the oceans is also significant for *n*-$C_3F_7OC(O)H$.

VII-I-5. The Larger Perfluorinated *n*-Alkyl Formates: *n*-$C_4F_9OC(O)H$, *iso*-$C_4F_9OC(O)H$, *n*-$C_5F_{11}OC(O)H$, *n*-$C_7F_{15}OC(O)H$, *n*-$C_{10}F_{19}OC(O)H$ (see table VII-I-2 for structures)

VII-I-5.1. Cl-Atom Reaction Kinetics

The kinetics of the reaction of Cl-atoms with several perfluorinated formates have been studied by Wallington et al. (1997b), Nohara et al. (2001), Goto et al. (2002a), and Javadi et al. (2007). The results are shown in table VII-I-2. Given that the reaction will occur from abstraction of the formate hydrogen atom and that the chemical environment of the formate group in large perfluorinated formates is similar, it would be expected that the reactivity of these species should be similar. Consistent with expectations, the measured reactivities of these species are indistinguishable within the experimental uncertainties. Taking an average of the determinations from table VII-I-2 gives the rate coefficient at 298 K of: $k(Cl + n\text{-}C_xF_{2x+1}OC(O)H) = 1.4 \times 10^{-14}$ cm^3 molecule^{-1} s^{-1} with an uncertainty estimated to be $\pm 35\%$.

VII-I-5.2. Summary of the Atmospheric Fate of n-$C_4F_9OC(O)H$, iso-$C_4F_9OC(O)H$, n-$C_5F_{11}OC(O)H$, n-$C_7F_{15}OC(O)H$, $C_{10}F_{19}OC(O)H$ (compound (a) in table VII-I-2)

There have yet to be any studies of the kinetics of the reaction of OH radicals with these species. However, by analogy to the reactivity of smaller members of the series ($CF_3OC(O)H$, $C_2F_5OC(O)H$, $C_3F_7OC(O)H$) discussed above, it seems likely that the atmospheric lifetime of *n*-$C_4F_9OC(O)H$, *iso*-$C_4F_9OC(O)H$, *n*-$C_5F_{11}OC(O)H$, and *n*-$C_7F_{15}OC(O)H$ with respect to reaction with OH radicals will be approximately 2 years. Kutsuna et al. (2005) have shown that dissolution into the oceans and hydrolysis is probably an important fate for $C_2F_5OC(O)H$. It seems likely that loss to the oceans is also significant for the larger perfluorinated formates.

VII-I-6. Methyl Fluoroformate [Methyl Carbonofluoridate, $FC(O)OCH_3$]

VII-I-6.1. OH Reaction Kinetics

The kinetics of the reaction of OH with $FC(O)OCH_3$ have been studied by Chen et al. (2006) over the temperature range 253–328 K. Rate coefficients are listed in table VII-I-1 and plotted in figure VII-I-5. The line in Figure VII-I-5 is a fit to the

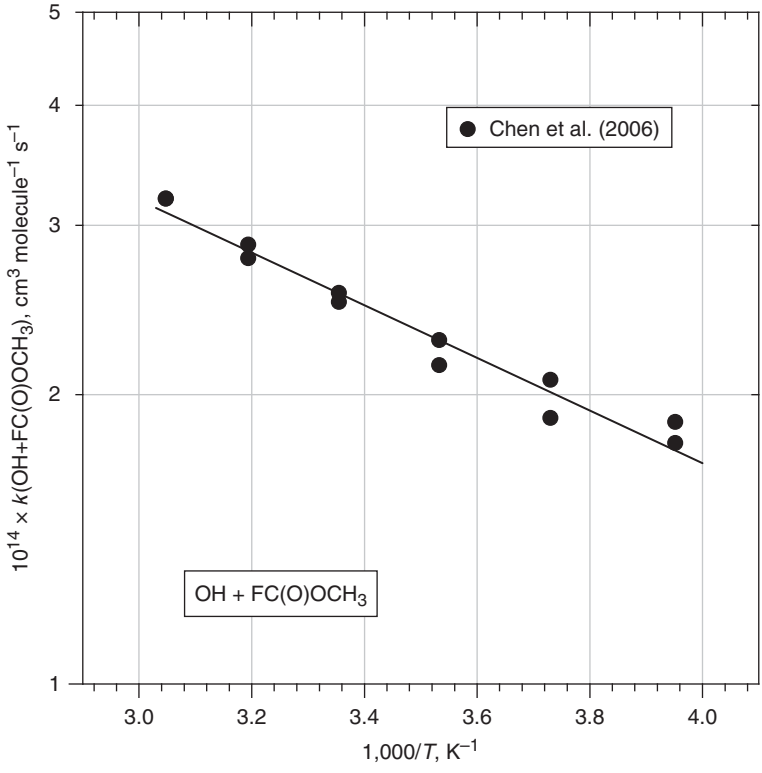

Figure VII-I-5. Measurements of the rate coefficients for reaction of OH radicals with $FC(O)OCH_3$. The line is a fit to the data.

data which gives $k(OH + FC(O)OCH_3) = 2.12 \times 10^{-13} \exp(-631/T)$ which yields $k(OH + FC(O)OCH_3) = 2.55 \times 10^{-14}$ cm^3 molecule^{-1} s^{-1} at 298 K. The uncertainty in $k(OH + FC(O)OCH_3)$ at 298 K is estimated to be ±25%.

VII-I-6.2. Summary of the Atmospheric Fate of FC(O)OCH$_3$

Combining $k(OH + FC(O)OCH_3) = 2.08 \times 10^{-14}$ cm^3 molecule^{-1} s^{-1} at 272 K with a diurnal average of [OH] $= 1 \times 10^6$ molecule cm^{-3} gives an estimate of about 1.5 years for the lifetime of $FC(O)OCH_3$ with respect to reaction with OH radicals. Based upon the work by Kutsuna et al. (2004, 2005) it seems likely that loss to the oceans is a competing atmospheric fate of $FC(O)OCH_3$.

VII-I-7. Methyl 2,2-Di-fluoroacetate [Methyl Difluoroacetate, $CHF_2C(O)OCH_3$]

VII-I-7.1. OH Reaction Kinetics

The kinetics of the reaction of OH with $CHF_2C(O)OCH_3$ have been studied by Blanco and Teruel (2007) using relative rate methods. Rate coefficients are listed

in table VII-I-1. An average of the results from Blanco and Teruel (2007) give $k(OH + CHF_2C(O)OCH_3) = 1.33 \times 10^{-13}$ cm^3 molecule^{-1} s^{-1} at 298 K with an uncertainty is estimated to be ±25%.

VII-I-7.2. Cl-Atom Kinetics

The kinetics of the reaction of Cl-atoms with $CHF_2C(O)OCH_3$ have been studied by Blanco et al. (2008) at 298 K. Rate coefficients are listed in table VII-I-2. Taking an average of the determinations by Blanco et al. (2008) gives $k(Cl + CHF_2C(O)OCH_3) = 2.04 \times 10^{-13}$ cm^3 molecule^{-1} s^{-1} with an uncertainty estimated to be ±25%.

VII-I-7.3. Summary of the Atmospheric Fate of $CHF_2C(O)OCH_3$

Combining $k(OH + CHF_2C(O)OCH_3) = 1.33 \times 10^{-13}$ cm^3 molecule^{-1} s^{-1} at 298 K with a diurnal average of [OH] = 1×10^6 molecule cm^{-3} gives an estimate of about 3 months for the lifetime of $CHF_2C(O)OCH_3$ with respect to reaction with OH radicals. As with other fluorinated esters studied by Kutsuna et al. (2005), it seems likely that uptake into the ocean and hydrolysis will occur on a timescale of the order of 1 year and also contribute to the removal of $CHF_2C(O)OCH_3$ from the atmosphere.

VII-I-8. Methyl Trifluoroacetate [$CF_3C(O)OCH_3$]

VII-I-8.1. OH Reaction Kinetics

The kinetics of the reaction of OH with $CF_3C(O)OCH_3$have been studied by Wallington et al. (1988b) and Blanco and Teruel (2007) over the temperature range 240–440 K. Rate coefficients are listed in table VII-I-1 and plotted in figure VII-I-6. The absolute rate data from Wallington et al. (1988b) and the relative rate data from Blanco and Teruel (2007) are in good agreement. While there is evidence for curvature in the Arrhenius plot shown in figure VII-I-6, the data can also be represented reasonably well using the unmodified Arrhenius expression. The solid and dashed lines in figure VII-I-6 are fits to the data from Wallington et al. (1988b) and Blanco and Teruel (2007), which give $k(OH + CF_3C(O)OCH_3) = 3.23 \times 10^{-13} \exp(-557/T)$ and $k(OH + CF_3C(O)OCH_3) = 3.99 \times 10^{-19} T^2 \exp(95/T)$ cm^3 molecule^{-1} s^{-1}. These expressions give $k(OH + CF_3C(O)OCH_3) = 4.98 \times 10^{-14}$ and 4.87×10^{-14} cm^3 molecule^{-1} s^{-1} at 298 K, respectively. The uncertainty in $k(OH + CF_3C(O)OCH_3)$ at 298 K is estimated to be ±25%.

VII-I-8.2. Cl-Atom Kinetics

The kinetics of the reaction of Cl-atoms with $CF_3C(O)OCH_3$ have been studied by Blanco et al. (2008) at 298 K. Rate coefficients are listed in table VII-I-2. Taking an average of the determinations by Blanco et al. (2008) gives $k(Cl + CF_3C(O)OCH_3) = 8.82 \times 10^{-14}$ cm^3 molecule^{-1} s^{-1}. The uncertainty in $k(Cl + CF_3C(O)OCH_3)$ at 298 K is estimated to be ±25%.

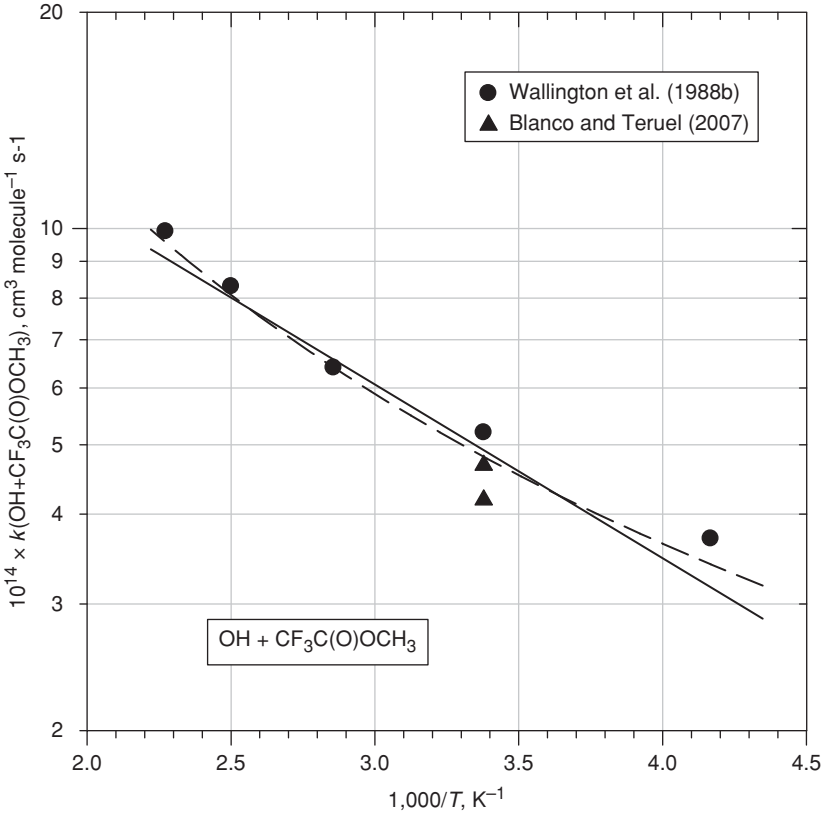

Figure VII-I-6. Measurements of the rate coefficients for reaction of OH radicals with $CF_3C(O)OCH_3$. The solid and dashed lines are fits of normal and modified Arrhenius expressions to the data, see text.

VII-I-8.3. Summary of the Atmospheric Fate of $CF_3C(O)OCH_3$

Combining $k(\mathrm{OH} + \mathrm{CF_3C(O)OCH_3}) = 4.98 \times 10^{-14}$ cm^3 molecule^{-1} s^{-1} at 298 K with a diurnal average of [OH] $= 1 \times 10^6$ molecule cm^{-3} gives an estimate of about 8 months for the lifetime of $CF_3C(O)OCH_3$with respect to reaction with OH radicals. Kutsuna et al. (2005) have studied the uptake of $CF_3C(O)OCH_3$ into water using a column-stripping technique. Kutsuna et al. (2005) estimate lifetimes of 0.48 and 1.3 years for loss of $CF_3C(O)OCH_3$ to the oceans for ocean temperatures of 273 and 288 K, respectively. $CF_3C(O)OCH_3$ will be removed from the atmosphere both by reaction with OH and loss to the oceans. Loss via the two mechanisms appears to occur at comparable rates and the overall atmospheric lifetime of $CF_3C(O)OCH_3$ is probably approximately 4 months.

VII-I-9. Ethyl Trifluoroacetate [$CF_3C(O)OC_2H_5$]

VII-I-9.1. OH Reaction Kinetics

The kinetics of the reaction of OH with $CF_3C(O)OC_2H_5$ have been studied by Blanco and Teruel (2007) using a relative rate method in 1 atm. of air at 298 K. Rate coefficients are listed in table VII-I-1. An average of the results from Blanco and Teruel (2007) give $k(OH + CF_3C(O)OC_2H_5) = 2.36 \times 10^{-13}$ cm^3 molecule^{-1} s^{-1} at 298 K with an uncertainty estimated to be ±25%.

VII-I-9.2. Cl-Atom Kinetics

The kinetics of the reaction of Cl-atoms with $CF_3C(O)OC_2H_5$ have been studied by Blanco et al. (2008) at 298 K. Rate coefficients are listed in table VII-I-2. Taking an average of the determinations by Blanco et al. (2008) gives $k(Cl + CF_3C(O)OC_2H_5) = 1.75 \times 10^{-12}$ cm^3 molecule^{-1} s^{-1} with an uncertainty estimated to be ±25%.

VII-I-9.3. Summary of the Atmospheric Fate of $CF_3C(O)OC_2H_5$

Combining $k(OH + CF_3C(O)OC_2H_5) = 2.36 \times 10^{-12}$ cm^3 molecule^{-1} s^{-1} at 298 K with a diurnal average of [OH] = 1×10^6 molecule cm^{-3} gives an estimate of about 50 days for the lifetime of $CF_3C(O)OC_2H_5$ with respect to reaction with OH radicals. By analogy to $CF_3C(O)OCH_3$ it seems likely that loss of $CF_3C(O)OC_2H_5$ by uptake and hydrolysis in the ocean will occur on a timescale of the order of 1 year. Hence, removal of $CF_3C(O)OC_2H_5$ from the atmosphere will be dominated by reaction with OH, with oceanic uptake making a minor contribution.

VII-I-10. 2,2,2-Trifluoroethyl Trifluoroacetate [$CF_3C(O)OCH_2CF_3$]

VII-I-10.1. OH Reaction Kinetics

The kinetics of the reaction of OH with $CF_3C(O)OCH_2CF_3$ have been studied by Blanco and Teruel (2007) using a relative rate method in 1 atm. of air at 298 K. Rate coefficients are listed in table VII-I-1. An average of the results from Blanco and Teruel (2007) give $k(OH + CF_3C(O)OCH_2CF_3) = 9.4 \times 10^{-14}$ cm^3 molecule^{-1} s^{-1} at 298 K with an uncertainty estimated to be ±25%.

VII-I-10.2. Cl-Atom Kinetics

The kinetics of the reaction of Cl-atoms with $CF_3C(O)OCH_2CF_3$ have been studied by Wallington et al. (1998b) and Blanco et al. (2008) at 298 K. As seen from table VII-I-2, the results from the two studies are in good agreement. Taking an average of the determinations by Wallington et al. (1998b) and Blanco et al. (2008) gives: $k(Cl + CF_3C(O)OCH_2CF_3) = 9.4 \times 10^{-14}$ cm^3 molecule^{-1} s^{-1} with an uncertainty estimated to be ±25%.

VII-I-10.3. Summary of the Atmospheric Fate of $CF_3C(O)OCH_2CF_3$

Combining $k(OH + CF_3C(O)OCH_2CF_3) = 1.0 \times 10^{-15}$ cm^3 molecule^{-1} s^{-1} at 298 K with a diurnal average of [OH] $= 1 \times 10^6$ molecule cm^{-3} gives an estimate of about 4 months for the lifetime of $CF_3C(O)OCH_2CF_3$ with respect to reaction with OH radicals. By analogy to $CF_3C(O)OCH_3$ it seems likely that loss of $CF_3C(O)OC_2H_5$ by uptake and hydrolysis in the ocean will occur on a timescale of the order of 1 year (Kutsuna et al., 2005). Hence, removal of $CF_3C(O)OCH_2CF_3$ from the atmosphere will be dominated by reaction with OH, with oceanic uptake making a contribution.

VII-I-11. CH_2=CHC(O)$OCH_2CH_2CF_2CF_2CF_2CF_3$
(4:2 Fluorotelomer Acrylate, 3,3,4,4,5,5,6,6,6-Nonafluorohexyl Prop-2-enoate]

VII-I-11.1. OH Reaction Kinetics

The kinetics of the reaction of OH with CH_2=CHC(O)$OCH_2CH_2(CF_2)_3CF_3$ have been studied by Butt et al. (2009) using relative rate techniques in 1 atm. of air at 296 K. Rate coefficients are listed in table VII-I-1. An average of the results from Butt et al. (2009) gives $k(OH + CH_2$=CHC(O)$OCH_2CH_2(CF_2)_3CF_3) = 1.15 \times 10^{-11}$ cm^3 molecule^{-1} s^{-1} with an uncertainty estimated to be ±20%.

VII-I-11.2. Cl-Atom Kinetics

The kinetics of the reaction of Cl with CH_2=CHC(O)$OCH_2CH_2(CF_2)_3CF_3$ have been studied by Butt et al. (2009) using relative rate techniques in 1 atm. of air at 296 K. Rate coefficients are listed in table VII-I-2. An average of the results from Butt et al. (2008) gives $k(Cl + CH_2$=CHC(O)$OCH_2CH_2(CF_2)_3CF_3) = 2.07 \times 10^{-10}$ cm^3 molecule^{-1} s^{-1} with an uncertainty estimated to be ±20%.

VII-I-11.3. Summary of the Atmospheric Fate of CH_2=CHC(O)$OCH_2CH_2(CF_2)_3CF_3$

Combining $k(OH + CH_2$=CHC(O)$OCH_2CH_2(CF_2)_3CF_3) = 1.15 \times 10^{-11}$ cm^3 molecule^{-1} s^{-1} at 298 K with a daytime average of [OH] $= 2.5 \times 10^6$ molecule cm^{-3} gives an estimate of about 10 h for the lifetime of CH_2=CHC(O)$OCH_2CH_2(CF_2)_3CF_3$ with respect to reaction with OH radicals.

Butt et al. (2009) reported that the OH-radical-initiated oxidation of CH_2=CHC(O)$OCH_2CH_2(CF_2)_3CF_3$ in 700 Torr of air in the presence of NO gives CH_2O in a molar yield of 102 ± 7%, with $C_4F_9CH_2CH_2OC(O)C(O)H$ (4:2 fluorotelomer glyoxylate) as the expected co-product.

VIII

Rate Coefficients and Mechanisms for the Atmospheric Oxidation of the N-Atom-Containing Oxygenates

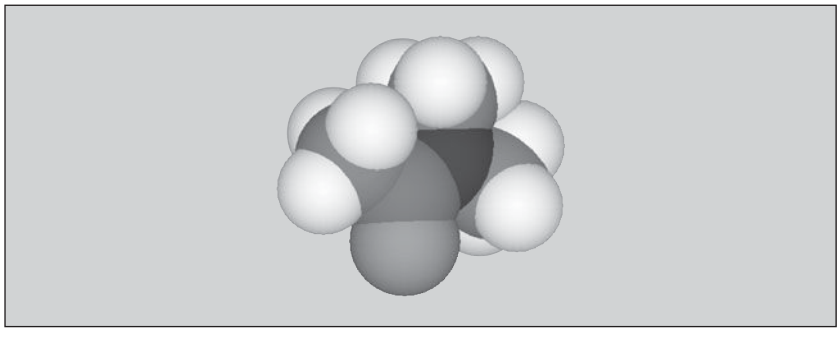

VIII-A. Introduction

The many different nitrogen-containing oxygenated volatile organic compounds that are present in the troposphere play important roles in the chemistry of our atmosphere. They can be emitted directly into the atmosphere, such as in the case of amides that are widely used as organic solvents, starting materials, or intermediates in different industries (e.g., synthetic polymers, manufacture of dyes, and synthesis of pesticides). Amides are formed in situ as intermediate products in the degradation of amines (e.g., see Tuazon et al., 1994; Finlayson-Pitts and Pitts, 2000). Nitrogen-containing oxygenated organic compounds are formed in the atmosphere also via reactions of alkoxy (RO) and alkyl peroxy radicals (RO_2) with NO or NO_2 leading to alkyl nitrates, alkyl nitrites, and peroxy acetyl nitrates. However, primary sources of these organic species have also been suggested such as diesel and other engines and biomass burning (e.g., see Simpson et al., 2002). Alkyl nitrates ($RONO_2$) have been detected in both the urban and the remote troposphere (e.g., see Roberts, 1990; Walega et al., 1992; Atlas et al., 1992; Ridley et al., 1997; and Stroud et al., 2001; see also section I-D). Nitrates are formed as minor products in the reaction of peroxy radicals with NO. The nitrate yield increases with the size of peroxy radicals and can be as high as 20–30% for large ($>C_6$) radicals (Calvert et al., 2008).

Peroxyacyl nitrates ($RC(O)O_2NO_2$) are important constituents of urban air pollution. They have been identified in ambient air (e.g., see Bertman and Roberts, 1991;

Williams et al., 1997, 2000; Nouaime et al., 1998; Hansel and Wisthaler, 2000; also see section I-D). They are formed from photochemical reactions via $RC(O)O_2 + NO_2$. A major role of these compounds is their capacity to act as a reservoir for NO_x that can be transported from polluted urban to remote regions that are poor NO_x regions and where their presence can increase NO_x levels (Roberts, 1990).

As with other volatile organic compounds (VOCs), once released to the atmosphere, nitrogen-containing organic compounds are expected to undergo degradation primarily via reaction with hydroxyl and nitrate radicals, reaction with ozone, and photolysis. Thermal decomposition is an important loss process for the peroxyacyl nitrates. Also, wet and dry deposition can be important atmospheric removal processes for nitrogen-containing species.

In this chapter, the kinetics and mechanisms of the gas-phase reactions of the main tropospheric oxidants (OH, NO_3, O_3, and Cl) with nitrogen-containing oxygenated VOCs are reviewed. When possible, recommendations for the rate coefficients have been made and mechanistic information is given when available. Combining the kinetic parameters with the average atmospheric concentrations of the main oxidants provides estimates of the atmospheric lifetimes of nitrogen-containing oxygenated compounds. The compounds reviewed include amides, aminoalcohols, alkyl nitrates, alkyl nitrites, hydroxyalkyl nitrates, nitroalkanes, nitroaromatics, peroxyacyl nitrates, and nitrosamines.

VIII-B. Amides

Kinetic and mechanistic studies of the gas-phase atmospheric chemistry of amides are limited to a few investigations (Koch et al., 1997; Aschmann and Atkinson, 1999b; Solignac et al., 2005, 2006a; El Dib and Chakir, 2007). The available structure–activity relationships (SARs) used for rate coefficient estimations are based on a very limited kinetic database for amines.

VIII-B-1. *N*-Methylformamide (NMF, $HC(O)NHCH_3$)

VIII-B-1.1. OH Reaction Kinetics

The only study of the reaction of OH with *N*-methylformamide is that conducted by Solignac et al. (2005). The measurements were performed using the relative rate technique in combination with long path Fourier transform infrared spectroscopy (FTIR). An unweighted mean of the values presented in table VIII-B-1 obtained using three reference compounds gives $k = 8.0 \times 10^{-12}$ cm^3 molecule^{-1} s^{-1} at 298 K with an estimated uncertainty of ±35%.

VIII-B-1.2. Cl-Atom Reaction Kinetics

The rate coefficients of Solignac et al. (2005), obtained from a relative rate study at ambient temperature and atmospheric pressure of air are given in table VIII-B-2. This is the only reported study of this reaction. An unweighted mean of the values obtained

Table VIII-B-1. Rate coefficients (k, cm^3 molecule^{-1} s^{-1}) for the reaction of OH with *N*-methylformamide [HC(O)NHCH$_3$]

$10^{12} \times k$	T (K)	Technique[a]	Reference
8.0 ± 0.8	298 ± 2	RR (C_2H_4)[b]	Solignac et al. (2005)
8.4 ± 2.0		RR (C_3H_6)[c]	
7.7 ± 1.3		RR (cy*clo*-C_6H_{12})[d]	

[a]Abbreviations used for the techniques are defined in table I-F-3.
[b]Placed on an absolute basis using $k(\mathrm{OH} + \mathrm{C_2H_4}) = 7.9 \times 10^{-12}$ cm^3 molecule^{-1} s^{-1} (Atkinson et al., 2006).
[c]Placed on an absolute basis using $k(\mathrm{OH} + \mathrm{C_3H_6}) = 2.9 \times 10^{-11}$ cm^3 molecule^{-1} s^{-1} (Atkinson et al., 2006).
[d]Placed on an absolute basis using $k(\mathrm{OH} + \textit{cyclo}\text{-}\mathrm{C_6H_{12}}) = 6.97 \times 10^{-12}$ cm^3 molecule^{-1} s^{-1} (Calvert et al., 2008).

Table VIII-B-2. Rate coefficients (k, cm^3 molecule^{-1} s^{-1}) for the reaction of Cl with *N*-methylformamide [HC(O)NHCH$_3$]

$10^{11} \times k$	T (K)	Technique[a]	Reference
9.8 ± 0.6	298 ± 2	RR (C_2H_4)[b]	Solignac et al. (2005)
7.4 ± 0.5		RR (C_3H_6)[c]	

[a]Abbreviations used for the techniques are defined in table I-F-3.
[b]Placed on an absolute basis using $k(\mathrm{Cl} + \mathrm{C_2H_4}) = 9.5 \times 10^{-11}$ cm^3 molecule^{-1} s^{-1} (section I-F).
[c]Placed on an absolute basis using $k(\mathrm{Cl} + \mathrm{C_3H_6}) = 2.3 \times 10^{-10}$ cm^3 molecule^{-1} s^{-1} (Atkinson et al., 2006).

with the two references gives $k = 8.6 \times 10^{-11}$ cm^3 molecule^{-1} s^{-1} at 298 K with an estimated uncertainty of ±30%.

VIII-B-1.3. Summary of the Atmospheric Fate of N-Methylformamide

Using a daytime average OH concentration of 2.5×10^6 molecule cm^{-3} together with the suggested rate coefficient gives an estimate of approximately 1 h for the lifetime with respect to reaction with OH radicals. The degradation of *N*-methylformamide will occur near its emission sources, and it is expected to impact local air quality.

VIII-B-2. *N,N*-Dimethylformamide [DMF, $(CH_3)_2NCHO$]

VIII-B-2.1. OH Reaction Kinetics

The reaction of OH with *N,N*-dimethylformamide has been studied by Solignac et al. (2005) using a relative rate method in combination with long path Fourier transform infrared spectroscopy (FTIR) and gas chromatography (GC). Six different reference compounds were used to derive the rate coefficient values (table VIII-B-3). An unweighted mean of the six values obtained gives $k = 1.4 \times 10^{-11}$ cm^3 molecule^{-1} s^{-1} at 298 K with an estimated uncertainty of ±30%.

VIII-B-2.2. NO_3 Reaction Kinetics

The rate coefficient of the reaction of NO_3 with *N,N*-dimethylformamide has been determined by El Dib and Chakir (2007) using laser photolysis combined with UV–visible

Table VIII-B-3. Rate coefficients (k, cm^3 molecule^{-1} s^{-1}) for the reaction of OH with *N*,*N*-dimethylformamide [$(CH_3)_2NCHO$]

$10^{11} \times k$	T (K)	Technique[a]	Reference
1.11 ± 0.04	298 ± 2	RR (C_2H_4)[b]	Solignac et al. (2005)
1.28 ± 0.09		RR (C_3H_6)[c]	
1.42 ± 0.13		RR (*cyclo*-C_6H_{12})[d]	
1.31 ± 0.38		RR (1,3-dioxolane)[e]	
1.40 ± 0.40		RR (CH_3CHO)[f]	
1.64 ± 0.33		RR (CH_2CHCO)[g]	

[a]Abbreviations used for the techniques are defined in table I-F-3.
[b]Placed on an absolute basis using $k(OH + C_2H_4) = 7.9 \times 10^{-12}$ cm^3 molecule^{-1} s^{-1} (Atkinson et al., 2006).
[c]Placed on an absolute basis using $k(OH + C_3H_6) = 2.9 \times 10^{-11}$ cm^3 molecule^{-1} s^{-1} (Atkinson et al., 2006).
[d]Placed on an absolute basis using $k(OH + cyclo\text{-}C_6H_{12}) = 6.97 \times 10^{-12}$ cm^3 molecule^{-1} s^{-1} (Calvert et al., 2008).
[e]Placed on an absolute basis using k(OH + 1,3-dioxolane) = 1.0×10^{-11}, cm^3 molecule^{-1} s^{-1} (this book, section III-E-9.1).
[f]Placed on an absolute basis using $k(OH + CH_3CHO) = 1.5 \times 10^{-11}$ cm^3 molecule^{-1} s^{-1} (Atkinson et al., 2006).
[g]Placed on an absolute basis using $k(OH + CH_2CHCHO) = 2.16 \times 10^{-11}$ cm^3 molecule^{-1} s^{-1} (this book, section IV-E-2.1).

Table VIII-B-4. Rate coefficients ($k = A \times e^{-B/T}$), cm^3 molecule^{-1} s^{-1}) for the reaction of NO_3 with *N*,*N*-dimethylformamide [$(CH_3)_2NCHO$]

$10^{11} \times A$	B (K)	$10^{14} \times k$	T (K)	Technique[a]	Reference	Temperature Range (K)
1.06	1,600 ± 300	3.4 ± 0.6	273	PLP–UV abs.	El Dib and Chakir (2007)	273–353
		4.5 ± 1.1	298			
		5.6 ± 0.7	313			
		7.5 ± 0.5	333			
		13.9 ± 2.8	353			

[a]Abbreviations used for the techniques are defined in table I-F-3.

absorption spectroscopy. The measurements were conducted over the temperature range 273–353 K. The data obtained are given in table VIII-B-4 and shown in figure VIII-B-1. An unweighted fit to the data leads to the Arrhenius expression: $k = 8.8 \times 10^{-12} \exp(-1{,}553/T)$ cm^3 molecule^{-1} s^{-1} over the range 273–353 K with $k = 4.8 \times 10^{-14}$ cm^3 molecule^{-1} s^{-1} at 298 K and an estimated uncertainty of ±30%. El Dib and Chakir (2007) reported $k = 1.06 \times 10^{-11} \exp(-1{,}600/T)$ cm^3 molecule^{-1} s^{-1}, which returns rate coefficients within 5% of those obtained from the Arrhenius expression presented above.

VIII-B-2.3. Cl-Atom Reaction Kinetics

The reaction of Cl with *N*,*N*-dimethylformamide has been studied by Solignac et al. (2005) using a relative rate method. An unweighted mean of the measurements obtained with three reference compounds given in table VIII-B-5 leads to $k = 1.7 \times 10^{-10}$ cm^3 molecule^{-1} s^{-1} at 298 K with an estimated uncertainty of ±30%.

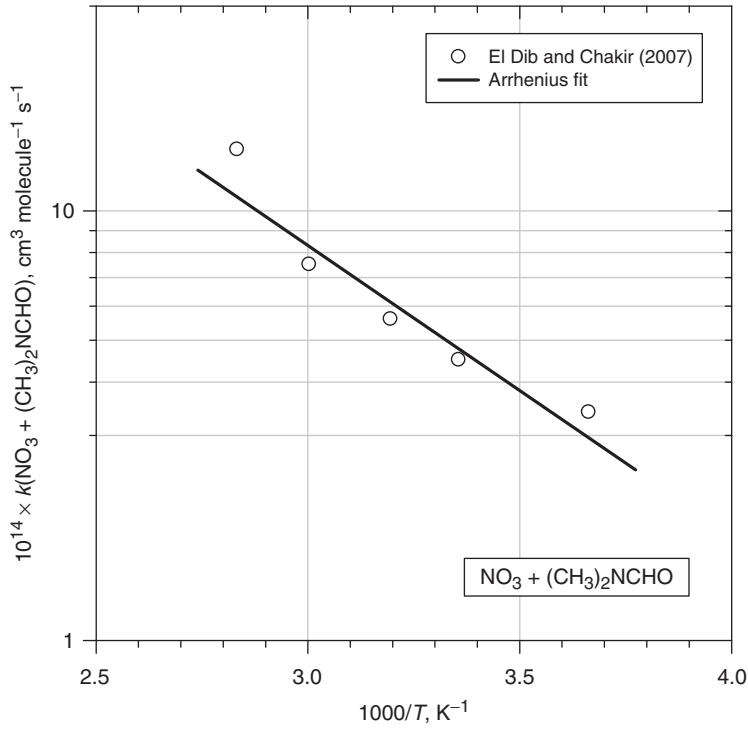

Figure VIII-B-1. Arrhenius plot of the rate coefficient for the reaction of NO_3 with *N*,*N*-dimethylformamide.

Table VIII-B-5. Rate coefficients (k, cm^3 molecule^{-1} s^{-1}) for the reaction of Cl with *N*,*N*-dimethylformamide [$(CH_3)_2NCHO$]

$10^{10} \times k$	T (K)	Technique[a]	Reference
1.61 ± 0.04	298 ± 2	RR (C_2H_4)[b]	Solignac et al. (2005)
1.50 ± 0.05		RR (C_3H_6)[c]	
1.98 ± 0.07		RR (*cyclo*-C_6H_{12})[d]	

[a]Abbreviations used for the techniques are defined in table I-F-3.
[b]Placed on an absolute basis using $k(Cl + C_2H_4) = 9.5 \times 10^{-11}$ cm^3 molecule^{-1} s^{-1} (section I-F).
[c]Placed on an absolute basis using $k(Cl + C_3H_6) = 2.3 \times 10^{-10}$ cm^3 molecule^{-1} s^{-1} (Atkinson et al., 2006).
[d]Placed on an absolute basis using $k(Cl + cyclo\text{-}C_6H_{12}) = 3.3 \times 10^{-10}$ cm^3 molecule^{-1} s^{-1} (Calvert et al., 2008).

VIII-B-2.4. Summary of the Atmospheric Fate of N,N-Dimethylformamide

The atmospheric lifetime of *N*,*N*-dimethylformamide with respect to reaction with OH, NO_3, and Cl can be estimated using the rate coefficients recommended above. Taking [OH] = 2.5×10^6, [NO_3] = 3×10^9, and [Cl] = 1×10^4 molecule cm^{-3}, leads to lifetimes of about 8 h, 2 h, and 6 days with respect to reactions with OH, NO_3, and Cl, respectively. The atmospheric oxidation of *N*,*N*-dimethylformamide is controlled by reactions with OH and NO_3 near its emission sources.

VIII-B-3. *N*-Methylacetamide [$CH_3C(O)NHCH_3$]

VIII-B-3.1. OH Reaction Kinetics

The rate coefficient of the reaction of OH with *N*-methylacetamide was determined by Koch et al. (1997) using the flash photolysis–resonance fluorescence technique. The measurements were conducted at two temperatures, 300 K and 384 K, but only the value obtained at 300 K is given in their paper along with an *E*/*R* factor of −490 K. The value of the rate coefficient reported by Koch et al. is $k = 5.2 \times 10^{-12}$ cm^3 molecule^{-1} s^{-1} at 300 . The measurements could have been affected by the difficulties in handling the amide samples, and we assign an uncertainty of ±50% to this rate coefficient.

VIII-B-3.2. Summary of the Atmospheric Fate of N-Methylacetamide

Combining the rate coefficient for the OH reaction reported in the previous section and an average diurnal OH concentration of [OH] = 1×10^6 molecule cm^{-3}, the atmospheric lifetime of *N*-methylacetamide with respect to the reaction with OH is calculated to be around 2 days.

VIII-B-4. *N*,*N*-Dimethylacetamide [DMA, $CH_3C(O)N(CH_3)_2$]

VIII-B-4.1. OH Reaction Kinetics

The reaction of OH with *N*,*N*-dimethylacetamide has been investigated by Koch et al. (1997) and Solignac et al. (2005) using, respectively, absolute and relative methods (see table VIII-B-6). Koch et al. also measured the rate coefficient at 384 K and reported an *E*/*R* factor of −630 K. The average rate coefficient value derived from the use of three reference compounds in the study of Solignac et al. is in satisfactory agreement with the value of Koch et al. The unweighted mean of the available data gives a rate coefficient value of $k = 1.6 \times 10^{-11}$ cm^3 molecule^{-1} s^{-1} at 298 with an estimated uncertainty of ±30%.

Table VIII-B-6. Rate coefficients (k, cm^3 molecule^{-1} s^{-1}) for the reaction of OH with *N*,*N*-dimethylacetamide [$CH_3C(O)N(CH_3)_2$]

$10^{11} \times k$	T (K)	Technique[a]	Reference
1.36	300 ± 2	LP–RF	Koch et al. (1997)
1.69 ± 0.07	298 ± 2	RR (C_2H_4)[b]	Solignac et al. (2005)
1.92 ± 0.06		RR (C_3H_6)[c]	
1.62 ± 0.09		RR (*cyclo*-C_6H_{12})[d]	

[a]Abbreviations used for the techniques are defined in table I-F-3.
[b]Placed on an absolute basis using $k(OH + C_2H_4) = 7.9 \times 10^{-12}$ cm^3 molecule^{-1} s^{-1} (Atkinson et al., 2006).
[c]Placed on an absolute basis using $k(OH + C_3H_6) = 2.9 \times 10^{-12}$ cm^3 molecule^{-1} s^{-1} (Atkinson et al., 2006).
[d]Placed on an absolute basis using $k(OH + cyclo\text{-}C_6H_{12}) = 6.97 \times 10^{-12}$ cm^3 molecule^{-1} s^{-1} (Calvert et al., 2008).

VIII-B-4.2. NO_3 Reaction Kinetics

The rate coefficient of the reaction of NO_3 with *N*,*N*-dimethylacetamide has been measured by El Dib and Chakir (2007) using the laser photolysis–UV–visible absorption spectroscopy technique. The measurements are given in table VIII-B-7 and are shown in figure VIII-B-2. An unweighted fit to the data leads to the Arrhenius expression:

Table VIII-B-7. Rate coefficients ($k = A \times e^{-B/T}$), cm^3 $molecule^{-1}$ s^{-1}) for the reaction of NO_3 with *N*,*N*-dimethylacetamide [$CH_3C(O)N(CH_3)_2$]

$10^{11} \times A$	B (K)	$10^{14} \times k$	T (K)	Technique[a]	Reference	Temperature Range (K)
2.82	1,900 ± 200	2.3 ± 0.2	273	PLP–UV abs	El Dib and Chakir (2007)	273–353
		4.9 ± 1.8	298			
		5.2 ± 1.3	313			
		8.24 ± 1.3	333			
		12.0 ± 2.3	353			

[a]Abbreviations used for the techniques are defined in table I-F-3.

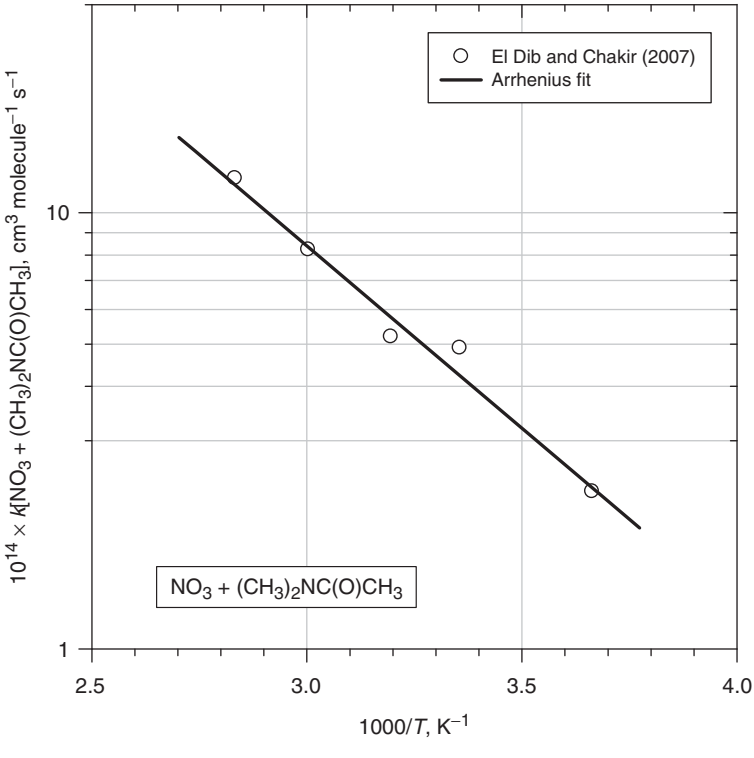

Figure VIII-B-2. Arrhenius plot of the rate coefficient for the reaction of NO_3 with *N*,*N*-dimethylacetamide.

Table VIII-B-8. Rate coefficients (k, cm^3 molecule^{-1} s^{-1}) for the reaction of Cl with *N*,*N*- dimethylacetamide [$CH_3C(O)N(CH_3)_2$]

$10^{10} \times k$	T (K)	Technique[a]	Reference
2.30 ± 0.12	298 ± 2	RR (C_2H_4)[b]	Solignac et al. (2005)
1.89 ± 0.14		RR (C_3H_6)[c]	
2.74 ± 0.17		RR (*cyclo*-C_6H_{12})[d]	

[a]Abbreviations used for the techniques are defined in table I-F-3.
[b]Placed on an absolute basis using $k(Cl + C_2H_4) = 9.5 \times 10^{-11}$ cm^3 molecule^{-1} s^{-1} (section I-F).
[c]Placed on an absolute basis using $k(Cl + C_3H_6) = 2.3 \times 10^{-10}$ cm^3 molecule^{-1} s^{-1} (Atkinson et al., 2006).
[d]Placed on an absolute basis using $k(Cl + \text{cyclo-}C_6H_{12}) = 3.3 \times 10^{-10}$ cm^3 molecule^{-1} s^{-1} (Calvert et al., 2008).

$k = 2.7 \times 10^{-11} \times \exp(-1{,}925/T)$ cm^3 molecule^{-1} s^{-1} over the range 273–353 K with $k = 4.2 \times 10^{-14}$ cm^3 molecule^{-1} s^{-1} at 298 K and an estimated uncertainty of ±30%.

VIII-B-4.3. Cl-Atom Reaction Kinetics

The measurements of Solignac et al. (2005) obtained by a relative rate method and using three reference compounds are given in table VIII-B-8. An unweighted average of the values obtained yields $k = 2.3 \times 10^{-10}$ cm^3 molecule^{-1} s^{-1} at 298 K with an estimated uncertainty of ±30%.

VIII-B-4.4. Summary of the Atmospheric Fate of N,N-Dimethylacetamide

The atmospheric lifetimes of *N*,*N*-dimethylacetamide with respect to reactions with OH, NO_3, and Cl can be estimated using the rate coefficients recommended above and average concentrations of [OH] = 2.5×10^6, [NO_3] = 3×10^9 and [Cl] = 1×10^4 molecule cm^{-3}. Using this approach gives lifetimes of *N*,*N*-dimethylacetamide of about 6 h, 2 h, and 5 days with respect to reaction with OH, NO_3, and Cl, respectively. Reactions with OH and NO_3 are the most important gas-phase atmospheric loss processes for *N*,*N*-dimethylacetamide.

VIII-B-5. *N*-Methylpropionamide [$CH_3CH_2C(O)NH(CH_3)$]

VIII-B-5.1. OH Reaction Kinetics

The only study available on this reaction is that performed by Koch et al. (1997) who used an absolute method. The rate coefficient value determined at 300 K is $k = 7.6 \times 10^{-12}$ cm^3 molecule^{-1} s^{-1}. Using the measurement of the rate coefficient conducted at 384 K, these authors reported $E/R = -400$ K. The value obtained by Koch et al. at 298 K, $k = 7.6 \times 10^{-12}$ cm^3 molecule^{-1} s^{-1}, is recommended with ±50% uncertainty.

VIII-B-5.2. Summary of the Atmospheric Fate of N-Methylpropionamide

The atmospheric lifetime of *N*-methylpropionamide with respect to the reaction with OH radicals is calculated to be less than 2 days using $k = 7.6 \times 10^{-12}$ cm^3 molecule^{-1} s^{-1} and [OH] $= 1 \times 10^6$ molecule cm^{-3}.

VIII-B-6. *N,N*-Dimethylpropionamide [DMP, $CH_3CH_2C(O)N(CH_3)_2$]

VIII-B-6.1. OH Reaction Kinetics

Koch et al. (1997) measured the rate coefficient of the reaction of *N,N*-dimethylpropionamide at 300 K and 384 K using the flash photolysis–resonance fluorescence technique. They reported $k = 2.07 \times 10^{-11}$ cm^3 molecule^{-1} s^{-1} at 300 K and $E/R = -530$ K. The value obtained by Koch et al. of $k = 2.0 \times 10^{-11}$ cm^3 molecule^{-1} s^{-1} at 298 K is recommended with ±50% uncertainty.

VIII-B-6.2. NO_3 Reaction Kinetics

The rate coefficient of the reaction of NO_3 with *N,N*- dimethylpropionamide has been measured by El Dib and Chakir (2007) using the laser photolysis–UV visible absorption spectroscopy technique. The measurements are given in table VIII-B-9 and shown in figure VIII-B-3. An unweighted fit to the data leads to the Arrhenius expression: $k = 11.95 \times 10^{-11} \times \exp(-2{,}691/T)$ cm^3 molecule^{-1} s^{-1} over the range 273–353 K with $k = 1.4 \times 10^{-14}$ cm^3 molecule^{-1} s^{-1} at 298 K and an estimated uncertainty of ±30%.

VIII-B-6.3. Summary of the Atmospheric Fate of N,N-Dimethylpropionamide

The lifetime with respect to both the reaction of *N,N*-dimethylpropionamide with OH and NO_3 radicals is calculated to be a few hours using the reported rate coefficients and average concentrations of [OH] $= 2.5 \times 10^6$ and [NO_3] $= 3 \times 10^9$ molecule cm^{-3}.

Table VIII-B-9. Rate coefficients ($k = A \times e^{-B/T}$), cm^3 molecule^{-1} s^{-1}) for the reaction of NO_3 with *N,N*-dimethylpropionamide [$CH_3CH_2C(O)N(CH_3)_2$]

$10^{11} \times A$	B (K)	$10^{14} \times k$	T (K)	Technique[a]	Reference	Temperature Range (K)
12.52	2700 ± 300	0.67 ± 0.2	273	PLP–UV abs.	El Dib and Chakir (2007)	273–353
		1.6 ± 0.2	298			
		1.8 ± 0.2	313			
		3.7 ± 0.2	333			
		6.8 ± 1.5	353			

[a]Abbreviations used for the techniques are defined in table I-F-3.

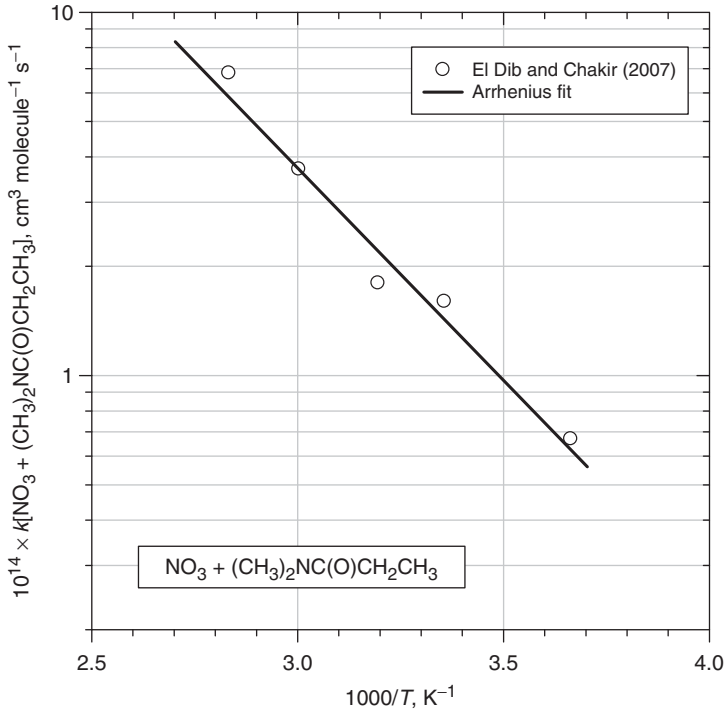

Figure VIII-B-3. Arrhenius plot of the rate coefficient for the reaction of NO_3 with *N*,*N*-dimethylpropionamide.

VIII-B-7. 1-Methyl-2-pyrrolidinone (C_5H_9NO)

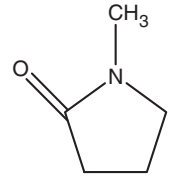

VIII-B-7.1. OH Reaction Kinetics

The rate coefficients of Aschmann and Atkinson (1999b) and Solignac et al. (2006a), both obtained at around 298 K using a relative rate method, are given in table VIII-B-10. The measured rate coefficient values are in good agreement and an unweighted average leads to $k = 2.3 \times 10^{-11}$ cm^3 molecule^{-1} s^{-1} at 298 K with an estimated uncertainty of $\pm 20\%$.

Table VIII-B-10. Rate coefficients (k, cm^3 molecule^{-1} s^{-1}) for the reaction of OH with 1-methyl-2-pyrrolidinone (C_5H_9NO)

$10^{11} \times k$	T (K)	Technique[a]	Reference
2.34 ± 0.39	296 ± 2	RR (C_3H_6)[b]	Aschmann and Atkinson (1999b)
2.18 ± 0.40	300 ± 5	RR (1,3,5-trimethylbezene)[c]	Solignac et al. (2006a)

[a]Abbreviations used for the techniques are defined in table I-F-3.
[b]Placed on an absolute basis using $k(OH + C_3H_6) = 2.9 \times 10^{-12}$ cm^3 molecule^{-1} s^{-1} (Atkinson et al., 2006).
[c]Placed on an absolute basis using k(OH + 1,3,5-trimethylbenzene) $= 5.67 \times 10^{-11}$ cm^3 molecule^{-1} s^{-1} (Calvert et al., 2002).

VIII-B-7.2. NO_3 Reaction Kinetics

The reaction of NO_3 with 1-methyl-2-pyrrolidinone has been investigated by both Aschmann and Atkinson (1999b) and El Dib and Chakir (2007) using, respectively, relative rate and absolute methods. The measurements are given in table VIII-B-11 and shown in figure VIII-B-4. The studies of El Dib and Chakir (2007) were conducted in the temperature range 273–353 K. An unweighted fit to the data from the two available studies yields: $k = 6.1 \times 10^{-11} \exp(-1{,}792/T)$ cm^3 molecule^{-1} s^{-1} over the range 298–353 K with $k = 1.5 \times 10^{-13}$ cm^3 molecule^{-1} s^{-1} at 298 K and an estimated uncertainty of ±30%.

VIII-B-7.3. O_3 Reaction Kinetics

Aschmann and Atkinson (1999b) monitored the decay rate of 1-methyl-2-pyrrolidinone in the presence of a known concentration of O_3 with added cyclohexane to scavenge any OH radicals formed. Aschmann and Atkinson (1999b) determined an upper limit to the rate coefficient of the reaction of O_3 with 1-methyl-2-pyrrolidinone of $k < 1 \times 10^{-19}$ cm^3 molecule^{-1} s^{-1} at 296 K.

Table VIII-B-11. Rate coefficients ($k = A \times e^{-B/T}$), cm^3 molecule^{-1} s^{-1}) for the reaction of NO_3 with 1-methyl-2-pyrrolidinone (C_5H_9NO)

$10^{11} \times A$	B (K)	$10^{13} \times k$	T (K)	Technique[a]	Reference	Temperature Range (K)
		1.26 ± 0.40	296 ± 2	RR (*trans*-2-butene)[b]	Aschmann and Atkinson (1999b)	
2.42	1,500 ± 100	1.61 ± 0.31	298	PLP–UV abs.	El Dib and Chakir (2007)	273–353
		2.22 ± 0.34	313			
		2.88 ± 0.26	333			
		3.63 ± 0.12	353			

[a]Abbreviations used for the techniques are defined in table I-F-3.
[b]Placed on an absolute basis using $k(NO_3 + trans\text{-2-butene}) = 3.9 \times 10^{-13}$ cm^3 molecule^{-1} s^{-1} (Atkinson and Arey, 2003).

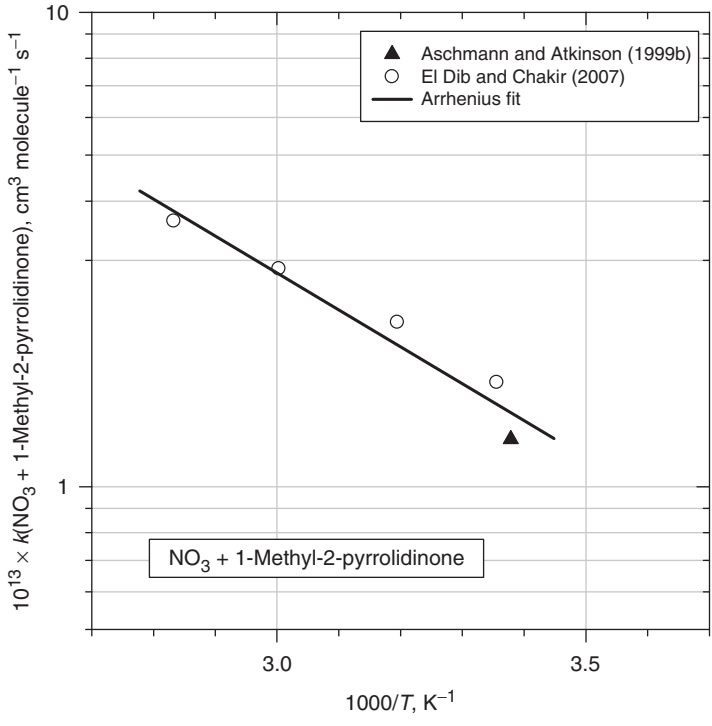

Figure VIII-B-4. Arrhenius plot of the rate coefficient for the reaction of NO_3 with 1-methyl-2-pyrrolidinone.

VIII-B-7.4. Summary of the Atmospheric Fate of 1-Methyl-2-pyrrolidinone

The rate coefficients for the reactions with OH, NO_3, and O_3, combined with the ambient concentrations of these oxidants ([OH] = 2.5×10^6, [NO_3] = 3×10^9, and [O_3] = 1×10^{12} molecule cm^{-3}) lead to the calculated atmospheric lifetime of 1-methyl-2-pyrrolidinone of about 5 h, < 1 h, and > 4 months with respect to OH, NO_3, and O_3, respectively. Thus, reactions with OH and NO_3 appear to be the most important pathways of the atmospheric degradation of this compound. Reaction with ozone is a negligible degradation process.

Mechanistic studies of the OH-initiated oxidation of 1-methyl-2-pyrrolidone conducted by Aschmann and Atkinson (1999b) and by Solignac et al. (2006a) have shown that H-atom abstraction from the amine side of the molecule (>N—) leads almost exclusively to formation of *N*-methyl succinimide and 1-formyl-2-pyrrolidinone. Addition of OH to the amide group with a sterically favorable Van der Waals' interaction might facilitate H-atom abstraction from these groups. The alkyl radicals formed are expected to react rapidly with O_2 to form the corresponding RO_2 radicals which in turn will react with NO, HO_2, and peroxy radicals RO_2 (either self reaction or reaction with other alkyl peroxy radicals). Solignac et al. (2006a) confirmed that *N*-methyl succinimide is a major product of the OH-initiated oxidation of 1-methyl-2-pyrrolidinone with a yield

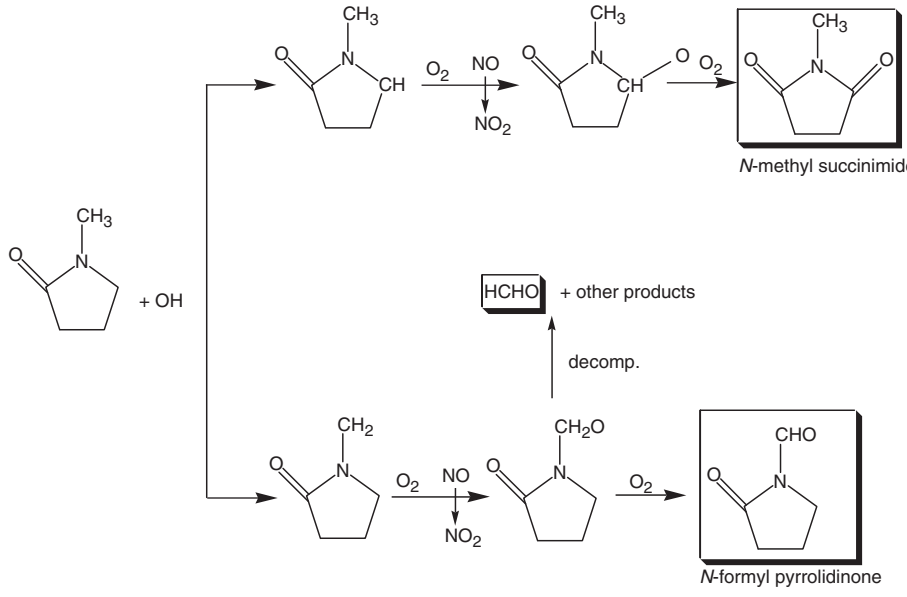

Figure VIII-B-5. The OH-initiated oxidation pathways of 1-methyl-2-pyrrolidone (Aschmann and Atkinson, 1999b; Solignac et al., 2006a).

of 52 ± 4% in agreement with that reported earlier by Aschmann and Atkinson (1999b), 44 ± 12%. The yield of 1-formyl-2-pyrrolidinone reported by Solignac et al. (23 ± 9%) was lower than that obtained by Aschmann and Atkinson (1999b) of (41 ± 12%). Solignac et al. have also detected other reaction products such as CH_2O (5 ± 2%) and two other unknown products which may be produced at least partly through the >N—C bond cleavage as shown in figure VIII-B-5.

Regarding the reaction of 1-methyl-2-pyrrolidinone with NO_3, the mechanistic study of Aschmann and Atkinson (1999b) indicates that the reaction may proceed through an overall H-atom abstraction initiated by interaction of NO_3 with the N-atom (similar to the OH reaction) followed by the decomposition of the intermediate complex to HNO_3 and alkyl radicals. The reaction products observed were *N*-methylsuccinimide and 1-formyl-2-pyrrolidinone, similar to that observed for the OH-initiated oxidation.

VIII-B-8. *N*-Methyl Succinimide ($C_5H_7NO_2$)

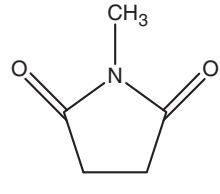

VIII-B-8.1. OH Reaction Kinetics

The rate coefficient for reaction of OH with *N*-methyl succinimide has been reported by Aschmann and Atkinson (1999b) and Solignac et al. (2006a). Aschmann and Atkinson determined the rate coefficient of OH with *N*-methyl succinimide in the same study as that of the OH reaction with *N*-methyl-2-pyrrolidinone. By plotting the amount of *N*-methyl succinimide formed against the *N*-methyl-2-pyrrolidinone reacted, it was observed that the yield of *N*-methyl succinimide decreases with the reacted amount of *N*-methyl-2-pyrrolidinone, indicating that *N*-methyl succinimide was also reacting with OH. The rate coefficient for the OH reaction with *N*-methyl succinimide was then obtained by using the correction procedure of the reaction products concentrations as described by Atkinson et al. (1982a) combined with the measured rate coefficient of the OH reaction with *N*-methyl-2-pyrrolidinone. Solignac et al. conducted a more direct study using a relative rate method with toluene as the reference compound. These data are shown in table VIII-B-12. The values obtained are in good agreement and an unweighted average leads to $k = 1.3 \times 10^{-11}$ cm^3 molecule^{-1} s^{-1} at 298 K with an estimated uncertainty of $\pm 30\%$.

VIII-B-8.2. NO_3 Reaction Kinetics

From their study of the NO_3-initiated oxidation of *N*-methyl-2-pyrrolidinone, Aschmann and Atkinson (1999b) have derived an upper limit to the rate coefficient ratio of $k(NO_3 + N\text{-methyl succinimide})/k(NO_3 + N\text{-methyl-2-pyrrolidinone}) < 0.1$ leading to the upper limit $k(NO_3 + N\text{-methyl succinimide}) < 1.3 \times 10^{-14}$ cm^3 molecule^{-1} s^{-1} at 296 K. This is the only investigation of this reaction.

VIII-B-8.3. Summary of the Atmospheric Fate of N-Methyl Succinimide

The lifetime of *N*-methyl succinimide is estimated to be a few hours with respect to reaction with OH radicals.

Table VIII-B-12. Rate coefficients (k, cm^3 molecule^{-1} s^{-1}) for the reaction of OH with *N*-methyl succinimide ($C_5H_7NO_2$)

$10^{11} \times k$	T (K)	Technique[a]	Reference
1.1 ± 0.4	296 ± 2	Fit to the data[b]	Aschmann and Atkinson (1999b)
1.4 ± 0.3	300 ± 5	RR (toluene)[c]	Solignac et al. (2006a)

[a]Abbreviations used for the techniques are defined in table I-F-3.
[b]See the text.
[c]Placed on an absolute basis using $k(OH + \text{toluene}) = 5.6 \times 10^{-11}$ cm^3 molecule^{-1} s^{-1} (Calvert et al., 2002).

VIII-B-9. *N*-Formyl Pyrrolidinone (1-Formyl-2-pyrrolidinone, $C_5H_7NO_2$)

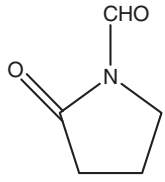

VIII-B-9.1. OH Reaction Kinetics

The reaction of OH with *N*-formyl pyrrolidinone (FP) has been the subject of two studies. Aschmann and Atkinson (1999b) have derived the rate coefficient for this reaction in their study of OH + *N*-methyl-2-pyrrolidinone where *N*-formyl pyrrolidinone was observed as a reaction product. The rate coefficient value was obtained by fitting the experimental profiles of both *N*-methyl-2-pyrrolidinone and *N*-formyl pyrrolidinone and using *k*(OH+*N*-methyl-2-pyrrolidinone) measured in the same study. Solignac et al. (2006a) conducted a more direct study by producing *N*-formyl pyrrolidinone in situ through the reaction of ozone with *N*-vinyl pyrrolidinone and using a relative rate method. The results from both studies are given in table VIII-B-13. The value determined by Aschmann and Atkinson (1999b) is more than a factor of 3 higher than that of Solignac et al. The rate coefficient value determined by Solignac et al. is more direct; hence, it is favored.

VIII-B-9.2. Summary of the Atmospheric Fate of N-Formyl Pyrrolidinone

The rate coefficient value of Solignac et al. (2006a) is used to estimate the atmospheric lifetime of *N*-formyl pyrrolidinone of less than 1 day with respect to the reaction with OH radicals.

VIII-B-10. Trends in the Reactivity of Amides

The available data set on the reactivity of amides presented in the preceding sections shows that the reactivity of OH with amides increases with increasing alkyl

Table VIII-B-13. Rate coefficients (k, cm^3 molecule^{-1} s^{-1}) for the reaction of OH with *N*-formyl pyrrolidinone ($C_5H_7NO_2$)

$10^{11} \times k$	T (K)	Technique[a]	Reference
2.15 ± 0.6	296 ± 2	Fit to the data[b]	Aschmann and Atkinson (1999)
0.6 ± 0.1	300 ± 5	RR (toluene)[c]	Solignac et al. (2006a)

[a]Abbreviations used for the techniques are defined in table I-F-3.
[b]See the text.
[c]Placed on an absolute basis using $k(\mathrm{OH} + \mathrm{toluene}) = 5.6 \times 10^{-11}$ cm^3 molecule^{-1} s^{-1} (Calvert et al., 2002).

substitution; this may be due to the positive inductive effect of these groups (Koch et al., 1997; Solignac et al., 2005). For example, it can be seen that for the reactions with OH radicals: $k[HC(O)NH(CH_3)] < k[HC(O)N(CH_3)_2]$; $k[CH_3C(O)NH(CH_3)] < k[CH_3C(O)N(CH_3)_2]$ and $k[C_2H_5C(O)NH(CH_3)] < k[C_2H_5C(O)N(CH_3)_2]$. On the other hand, the OH reactivity of amides is considerably lower than that of the corresponding amines (Atkinson et al., 1978b; Carl and Crowley, 1998).

The reaction of OH with simple amides can occur via H-atom abstraction from different sites: —C(O)—H, —$NHCH_2$—H, —$N(CH_3)$—H, —$C(O)CH_2$—H, and —$C(O)CH_2CH_2$—H. According to Koch et al. (1997), the observed negative activation energy ($E/R = -400$ to -600 K) for the reactions of OH with $CH_3C(O)NHCH_3$, $C_2H_5C(O)NHCH_3$, $CH_3C(O)N(CH_3)_2$, and $C_2H_5C(O)N(CH_3)_2$ excludes a direct abstraction and was taken as an indication of an addition reaction mechanism, with the addition being mainly at the amide group with products resulting from a subsequent H-atom abstraction from an adjacent carbon. The studies did not give any indication as to the carbon from which the abstraction occurred.

Solignac et al. (2005) have suggested that for the amides that they have investigated, H-atom abstraction from the H—C(O)— and H—$CH_2C(O)$— moieties is a possibility. The H—C(O)— and CH_3—C(O)— entities in formates and acetates (R—C(O)—OR, R = H or CH_3) are not very reactive, and by analogy a similar low reactivity might be expected for the HCO group in the formamides and acetamides. Thus, they have speculated that OH attack could occur mainly at the *N*-methyl groups, as has been reported earlier for reactions of OH radicals with amides in aqueous solution (Hayon et al., 1970), in support of suggestions of Koch et al. At present, it is not possible to exclude or confirm a gas-phase H-atom abstraction reaction from the HCO or CH_3CO groups. The mechanistic studies of the OH-initiated oxidation of 1-methyl-2-pyrrolidone (C_5H_9NO) conducted by Aschmann and Atkinson (1999b) and by Solignac et al. (2006a) have shown that H-atom abstraction from the amine side of the molecule ($\rangle$N—) leads almost exclusively to formation of *N*-methyl succinimide ($C_5H_7NO_2$) and 1-formyl-2-pyrrolidinone ($C_5H_7NO_2$). Addition of OH to the amide group with a sterically favorable Van der Waals interaction might facilitate H-atom abstraction from these groups. The alkyl radicals formed are expected to react rapidly with O_2 to form the corresponding RO_2 radicals, which, in turn, will react with NO, HO_2, and with peroxy radicals RO_2 (either RO_2-RO_2 reaction or reaction with other alkyl peroxy radicals).

In the only reported study of the reaction of Cl-atoms with amides, Solignac et al. (2005) observed a similar trend in the reactivity ($k[HC(O)NHCH_3] < k[HC(O)N(CH_3)_2] < k[CH_3C(O)N(CH_3)_2]$) as that observed with OH. The increase in reactivity towards electrophilic attack with increasing methyl substitution presumably reflects the electron donating effect of the methyl groups. In experiments in the absence of NO_x, Solignac et al. observed $HC(O)N(CH_3)CHO$ and $CH_3C(O)N(CH_3)CHO$ as the main Cl-initiated oxidation products from $HC(O)N(CH_3)_2$ and $CH_3C(O)N(CH_3)_2$, respectively, indicating that the reaction of chlorine atoms with amides proceeds mainly via H-atom abstraction from the methyl groups.

VIII-C. Amino Alcohols

VIII-C-1. 2-(Dimethylamino)ethanol [$(CH_3)_2NCH_2CH_2OH$]

VIII-C-1.1. OH Reaction Kinetics

The rate coefficients of Harris and Pitts (1983) and Anderson and Stephens (1988) are given in table VIII-C-1 and shown in figure VIII-C-1. Both measurements were conducted using the flash photolysis–resonance fluorescence technique. Anderson and Stephens (1988) studied this reaction in the temperature range 234–364 K and did not observe any noticeable temperature dependence in this range. Their ambient temperature rate coefficient is about twice the value obtained by Harris and Pitts (1983). Anderson and Stephens (1988) have suggested that $k = (9.0 \pm 2.0) \times 10^{-11}$ cm^{-3} molecule^{-1} s^{-1} describes the reaction over the temperature range of their investigation. However, fitting the Arrhenius expression to the data set of Anderson and Stephens gives $k = 1.85 \times 10^{-10} \exp(-230/T)$ with $k = 8.5 \times 10^{-11}$ cm^3 molecule^{-1} s^{-1} at 298 K and an uncertainty of $\pm 70\%$ is adopted.

VIII-C-1.2. O_3 Reaction Kinetics

The rate coefficient of Tuazon et al. (1994) obtained at ambient temperature and atmospheric pressure of air is given in table VIII-C-2. This is the sole study of this reaction.

VIII-C-1.3. Summary of the Atmospheric Fate of 2-(Dimethylamino)ethanol

Combining $k[OH+(CH_3)_2NCH_2CH_2OH] = 8.5 \times 10^{-11}$ cm^3 molecule^{-1} s^{-1} with a daytime average [OH] $= 2.5 \times 10^6$ molecule cm^{-3} provides an estimate of about 1 h for the atmospheric lifetime of 2-(dimethylamino)ethanol with respect to reaction with OH radicals.

Table VIII-C-1. Rate coefficients ($k, = A \times e^{-B/T}$), cm^3 molecule^{-1} s^{-1}) for the reaction of OH with 2-(dimethylamino)ethanol, $(CH_3)_2NCH_2CH_2OH$

$10^{10} \times A$	B (K)	$10^{11} \times k$	T (K)	Technique[a]	Reference	Temperature Range (K)
		4.7 ± 1.2	300 ± 2	FP–RF	Harris and Pitts (1983)	
1.85	230	6.3 ± 2.9	234	FP–RF	Anderson and Stephens (1988)	234–364
		8.6 ± 2.9	269			
		10.3 ± 2.0	293			
		8.7 ± 1.5	333			
		9.3 ± 3.0	364			

[a]Abbreviations used for the techniques are defined in table I-F-3.

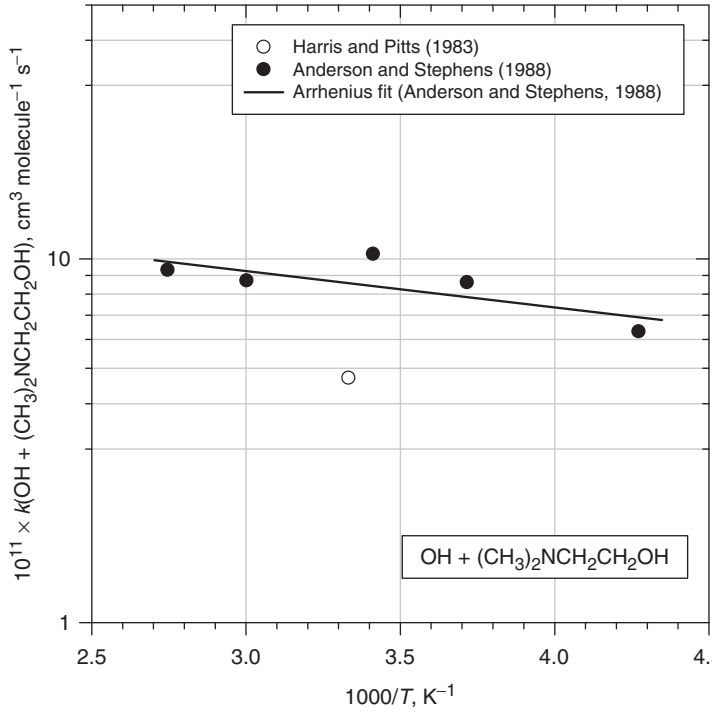

Figure VIII-C-1. Arrhenius plot of the rate coefficient for the reaction of OH with 2-(dimethylamino)ethanol.

Table VIII-C-2. Rate coefficients (k, cm^3 molecule^{-1} s^{-1}) for the reaction of O_3 with 2-(dimethylamino)ethanol [$(CH_3)_2NCH_2CH_2OH$]

$10^{18} \times k$	T (K)	Technique[a]	Reference
6.76 ± 0.83	298 ± 2	Excess of 2-(dimethylamino)ethanol [b]	Tuazon et al. (1994)

[a]Abbreviations used for the techniques are defined in table I-F-3.
[b]Experiment conducted by monitoring O_3 loss in pseudo-first-order conditions in presence of excess of 2-(dimethylamino)ethanol.

VIII-C-2. 2-Amino-2-methyl-1-propanol [$(CH_3)_2C(NH_2)CH_2OH$]

VIII-C-2.1. OH Reaction Kinetics

The rate coefficient of Harris and Pitts (1983) obtained using the flash photolysis–resonance fluorescence technique at ambient temperatures is given in table VIII-C-3. This is the only reported investigation of this reaction. No recommendation is made for this reaction.

Table VIII-C-3. Rate coefficients (k, cm^3 molecule^{-1} s^{-1}) for the reaction of OH with 2-amino-2-methyl-1-propanol [AMP, $(CH_3)_2C(NH_2)CH_2OH$]

$10^{11} \times k$	T (K)	Technique[a]	Reference
2.8 ± 0.5	300 ± 2	FP–RF	Harris and Pitts (1983)

[a]Abbreviations used for the techniques are defined in table I-F-3.

VIII-C-2.2. Summary of the Atmospheric Fate of 2-Amino-2-methyl-1-propanol

Combining $k(\mathrm{OH}) = 2.8 \times 10^{-11}$ cm^3 molecule^{-1} s^{-1} with a daytime average [OH] = 2.5×10^6 molecule cm^{-3} provides an estimate of about 4 h for the atmospheric lifetime of 2-amino-2-methyl-1-propanol with respect to reaction with OH radicals.

VIII-D. Alkyl Nitrates

A number of studies have been conducted on the reaction of alkyl nitrates with OH radicals and Cl-atoms. No data are available on the reaction with NO_3 radicals and ozone, but these reactions are expected to be slow and of negligible atmospheric significance. No mechanistic studies of the OH- or Cl-atom reactions are available.

VIII-D-1. Nitric Acid ($HONO_2$)

VIII-D-1.1. OH Reaction Kinetics

The reaction of OH with nitric acid has been studied extensively (Margitan et al., 1975; Smith and Zellner, 1975; Wine et al., 1981; Ravishankara et al., 1982; Margitan and Watson, 1982; Kurylo et al., 1982; Jourdain et al., 1982; Marinelli and Johnston, 1982; Smith et al., 1984; Devolder et al., 1984; Connell and Howard, 1985; Jolly et al., 1985; Stachnik et al., 1986; Brown et al., 1999; Carl et al., 2001). The rate coefficient of the reaction has been found to be pressure and temperature dependent. Below 350 K, the reaction shows a negative temperature dependence with small pressure dependence at ambient temperature, and strong pressure dependence at lower temperatures (Brown et al., 1999). The recommended pressure dependence of the rate coefficient is obtained by combining a low pressure bimolecular limit, k_o, with a Lindemann–Hinshelwood expression (Brown et al., 1999; Sander et al., 2006):

$$k(M,T) = k_o + k_3[\mathrm{M}]/(1 + k_3[\mathrm{M}]/k_2), \text{ with}$$

$$k_o = 2.4 \times 10^{-14} \exp(460/T) \text{ cm}^3 \text{ molecule}^{-1} \text{ s}^{-1}$$

$$k_2 = 2.7 \times 10^{-17} \exp(2,199/T) \text{ cm}^3 \text{ molecule}^{-1} \text{ s}^{-1}$$

$$k_3 = 6.5 \times 10^{-34} \exp(1,335/T) \text{ cm}^6 \text{ molecule}^{-2} \text{ s}^{-1}$$

The expressions are valid over the temperature range 200–350 K for air diluent. The coefficients k_3 and k_2 are the termolecular and high-pressure limit for the "association" channel, respectively. At 298 K, the recommended rate coefficient value is $k = 1.5 \times 10^{-13}$ molecule cm^{-3} s^{-1} with an estimated uncertainty of ±10% (IUPAC, 2008). Carl et al. (2001) have shown that the water vapor does not affect the rate coefficient under atmospheric conditions.

VIII-D-1.2. Cl-Atom Reaction Kinetics

The NASA–JPL panel recommended upper limit to the rate coefficient of the reaction of Cl with nitric acid, $k < 2 \times 10^{-16}$ cm^3 $molecule^{-1}$ s^{-1} (Sander et al., 2006) is based on the studies of Wine et al. (1988) and Zagogianni et al. (1987).

VIII-D-1.3. Summary of the Atmospheric Fate of Nitric Acid

The calculated tropospheric lifetime of HNO_3 with respect to its reaction with OH using $k = 1.5 \times 10^{-13}$ molecule cm^{-3} s^{-1} and [OH] = 10^6 molecule s^{-1}, is about 2.5 months. Nitric acid is a highly polar compound; consequently, it will be lost from the troposphere mainly through wet and dry deposition. HNO_3 reacts also with gaseous NH_3 to form ammonium nitrate (NH_4NO_3) in the atmosphere when NH_3 and HNO_3 concentrations are high, and this compound can appear in aerosols (Seinfeld and Pandis, 1998).

The mechanism of the reaction of OH with nitric acid involves the formation of a relatively long-lived HO—HNO_3 complex and a direct reaction channel, both leading to the formation of H_2O and NO_3:

$$\begin{aligned} OH + HONO_2 &\rightarrow H_2O + NO_3 \\ &\rightarrow [H_2NO_4] \rightarrow H_2O + NO_3 \end{aligned}$$

The formation yield of NO_3 was reported to be near unity over the temperature range 240–330 K and the pressure range 31–1,027 mbar of nitrogen (Brown et al., 2001; Sander et al., 2006). Similar NO_3 formation from OD + DNO_3 reaction yield was determined by Brown et al. (2001).

VIII-D-2. Methyl Nitrate (Nitrooxymethane, CH_3ONO_2)

VIII-D-2.1. OH Reaction Kinetics

The reaction of OH with methyl nitrate has been the subject of several studies using both absolute and relative methods. Gaffney et al. (1986), Talukdar et al. (1997b), and Shallcross et al. (1997) have used absolute methods while Kerr and Stocker (1986a), and Kakesu et al. (1997) used relative rate techniques. Nielsen et al. (1991) used both techniques. Nielsen et al. (1991), Talukdar et al. (1997b), and Shallcross et al. (1997) investigated the temperature dependence of the reaction. As can be seen from table VIII-D-1 and figure VIII-D-1, there is a large discrepancy in the available data set.

Table VIII-D-1. Rate coefficients ($k = A \times e^{-B/T}$), cm^3 molecule^{-1} s^{-1}) for the reaction of OH with methyl nitrate (CH_3ONO_2)

$10^{14} \times A$	B (K)	$10^{14} \times k$	T (K)	Technique[a]	Reference	Temperature Range (K)
		3.4 ± 0.4	298	DF–RF	Gaffney et al. (1986)	
		36 ± 9	303	RR (C_2H_4)[b]	Kerr and Stocker (1986a)	
0.88	−1,050 ± 180	31 ± 7	298 ± 2	RR [$(CH_3)_3CH$][c]	Nielsen et al. (1991)	298–393
		32 ± 5	298	PR–UVabs.		
		22 ± 6	323			
		15 ± 3	358			
		14 ± 3	393			
82 ± 16	1,020 ± 60	0.89 ± 0.02	221	PLP–LIF	Talukdar et al. (1997b)	221–414
		1.06 ± 0.05	233			
		1.43 ± 0.06	254			
		1.91 ± 0.10	273			
		2.33 ± 0.14	298			
		3.13 ± 0.08	324			
		3.91 ± 0.16	348			
		5.11 ± 0.34	373			
		6.56 ± 0.16	394			
		7.69 ± 0.20	414			
41 ± 8	604 ± 121	4.8 ± 0.8	298	DF–RF	Shallcross et al. (1997)	298–423
		7.7 ± 1.5	333			
		8.8 ± 2.1	373			
		8.0 ± 1.8	398			
		10.1 ± 2.0	423			
		3.0 ± 0.7	307	RR (several refs)[d]	Kakesu et al. (1997)	

[a]Abbreviations used for the techniques are defined in table I-F-3.

[b]Placed on an absolute basis using $k(OH + C_2H_4) = 7.9 \times 10^{-12}$ cm^3 molecule^{-1} s^{-1} at 1 bar and 298 K (Atkinson et al., 2006).

[c]Placed on an absolute basis using $k[OH + (CH_3)_3CH] = 2.12 \times 10^{-12}$ cm^3 molecule^{-1} s^{-1} (Calvert et al., 2008).

[d]Placed on an absolute basis by use of rate coefficients of $k(HO + CH_4) = 1.85 \times 10^{-12} \exp(-1{,}690/T)$ cm^3 molecule^{-1} s^{-1}, $k(HO + C_2H_6) = 6.9 \times 10^{-12} \exp(-1{,}000/T)$ cm^3 molecule^{-1} s^{-1} and $k(HO + CH_3CHF_2) = 1.0 \times 10^{-12} \exp(-990/T)$ cm^3 molecule^{-1} s^{-1}. The cited rate coefficient is the unweighted average, with a two standard deviation error limit.

The lower measured values, those of Gaffney et al., Talukdar et al., and Kakesu et al., are in reasonable agreement. The measurements of Nielsen et al. (1991) and Kerr and Stocker (1986a) lie considerably higher than those of Talukdar et al., while the absolute measurements of Shallcross are roughly a factor of 2 higher. The values preferred by the IUPAC panel are obtained from a unweighted least-squares analysis of the 221–298 K rate coefficients of Talukdar et al. (1997b), $k = 4.0 \times 10^{-13} \exp(-845/T)$ cm^3 molecule^{-1} s^{-1} over the temperature range 220–300 K (IUPAC, 2008). Because of the significant discrepancies between the various studies (Gaffney et al., 1986; Kakesu et al., 1997; Kerr and Stocker, 1986a; Nielsen et al., 1991; Shallcross et al., 1997; Talukdar et al., 1997b), large uncertainty limits (a factor of 2) are assigned to the 298 K rate coefficient and to the temperature dependence. The preferred value at 298 K is $k = 2.3 \times 10^{-14}$ cm^3 molecule^{-1} s^{-1}. Talukdar et al. (1997b) have also examined the kinetics of various isotopically labeled species. The rate coefficient for the reaction

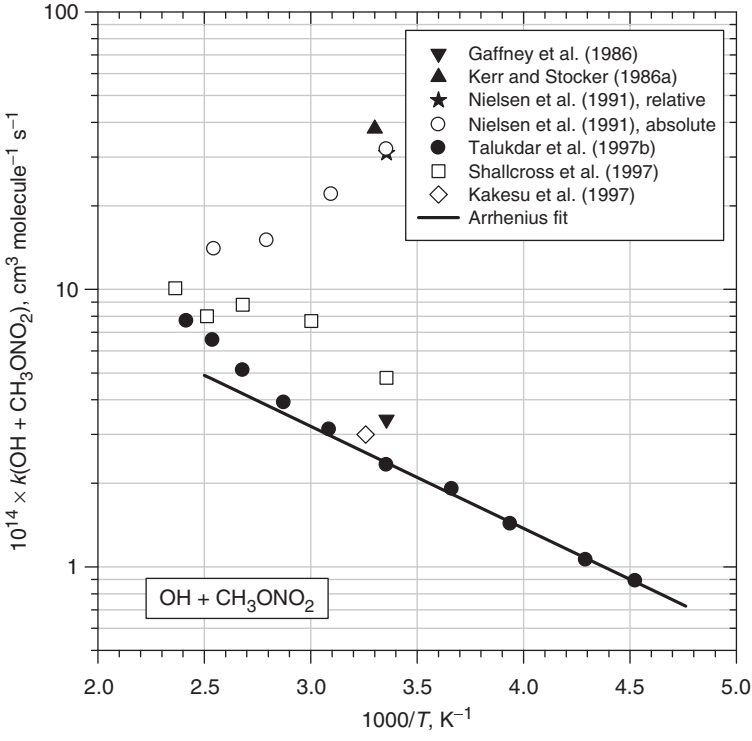

Figure VIII-D-1. Arrhenius plot of the rate coefficient for the reaction of OH with methyl nitrate.

of ^{18}OH with CH_3ONO_2 was the same as that of OH; that of OD was slightly larger (10–15%).

VIII-D-2.2. Cl-Atom Reaction Kinetics

The rate coefficients of Nielsen et al. (1991) and Sokolov et al. (1999) are in good accord. Both groups used a relative rate method at ambient temperature and atmospheric pressure. The data are given in table VIII-D-2. The preferred value based on these two studies is $k = 2.4 \times 10^{-13}$ cm^3 $molecule^{-1}$ s^{-1} at 298 K with an estimated uncertainty of 15% (IUPAC, 2008).

VIII-D-2.3. Summary of the Atmospheric Fate of Methyl Nitrate

By combining the rate coefficient value for the OH reaction and a diurnally averaged OH concentration of 1×10^6 molecule cm^{-3}, the atmospheric lifetime of methyl nitrate is estimated to be about 50 days. Photolysis is also an important tropospheric loss mechanism for CH_3ONO_2 (about 10 days for an overhead Sun; see table IX-M-1). The reaction of OH with CH_3ONO_2 at ambient temperature may proceed by an H-atom

Table VIII-D-2. Rate coefficients (k, cm^3 molecule^{-1} s^{-1}) for the reaction of Cl with methyl nitrate (CH_3ONO_2)

$10^{13} \times k$	T (K)	Technique[a]	Reference
2.42 ± 0.02	298 ± 2	RR(C_2H_6)[b]	Nielsen et al. (1991)
2.45 ± 0.20	295 ± 2	RR (CH_3Cl)[c]	Sokolov et al. (1999)
2.36 ± 0.15		RR (CH_4)[d]	

[a]Abbreviations used for the techniques are defined in table I-F-3.
[b]Placed on an absolute basis using $k(Cl + C_2H_6) = 5.9 \times 10^{-11}$ cm^3 molecule^{-1} s^{-1} (Atkinson et al., 2006).
[c]Placed on an absolute basis using $k(Cl + CH_3Cl) = 4.9 \times 10^{-13}$ cm^3 molecule^{-1} s^{-1} (Sander et al., 2006).
[d]Placed on an absolute basis using $k(Cl + CH_4) = 1.0 \times 10^{-13}$ cm^3 molecule^{-1} s^{-1} (Atkinson et al., 2006).

abstraction and/or OH addition:

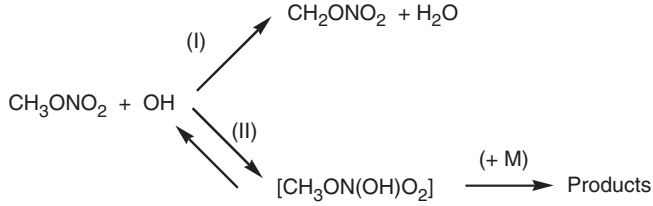

Talukdar et al. (1997b) investigated the reactions of OH with CH_3ONO_2 and CD_3ONO_2 and the reactions of OD and ^{18}OH with CH_3ONO_2. They showed that the overall reaction proceeds by hydrogen abstraction to form $CH_2ONO_2 + H_2O$, with no pressure dependence in the range 133 mbar He to 400 mbar SF_6 and no influence of O_2 (up to 67 mbar). These authors did not observe any OH regeneration from the reactions of ^{18}OH and OD with CH_3ONO_2, and the deuterium isotope effect ($k_H/k_D = 4.5$ at 298 K), is consistent with H- or D-atom abstraction. The CH_2ONO_2 radical formed in the reaction decomposes to give H_2CO and NO_2. This is in line with the theoretical study of Vereecken (2008) who showed that the α-nitroxy-substituted alkyl radicals dissociate spontaneously.

VIII-D-3. Ethyl Nitrate (Nitrooxyethane, $C_2H_5ONO_2$)

VIII-D-3.1. OH Reaction Kinetics

The reaction of OH with ethyl nitrate has been investigated by several groups (Kerr and Stocker, 1986a; Nielsen et al., 1991; Talukdar et al., 1997b; Shallcross et al., 1997; Kakesu et al., 1997) using both absolute and relative methods. The measurements are given in table VIII-D-3 and shown in figure VIII-D-2. Temperature dependent rate coefficients have been reported by Nielsen et al. (1991), Talukdar et al. (1997b), and Shallcross et al. (1997).

The results of Talukdar et al. and Kakesu et al. are in good agreement at ambient temperature and are lower than the earlier measurements of Kerr and Stocker (1986a) and Nielsen et al. (1991), while the result of Shallcross et al. (1997) lies between the two data sets. The result of Talukdar et al. (1997b) shows that the Arrhenius plot exhibits

Table VIII-D-3. Rate coefficients ($k = A \times e^{-B/T}$), cm^3 molecule^{-1} s^{-1}) for the reaction of OH with ethyl nitrate ($C_2H_5ONO_2$)

$10^{13} \times A$	B (K)	$10^{13} \times k$	T (K)	Technique[a]	Reference	Temperature Range (K)
		4.7 ± 2.0	303	RR (C_2H_4)[b]	Kerr and Stocker (1986a)	
		4.2 ± 0.3	298 ± 2	RR ($CH(CH_3)_3$)[c]	Nielsen et al.	
0.47	-716 ± 138	5.3 ± 0.6	298	PR–UV abs.	(1991)	298–373
		3.7 ± 0.5	338			
		3.3 ± 0.5	373			
$k(T)$[d]		1.26 ± 0.04	223	PLP–LIF	Talukdar et al. (1997b)	223–394
		1.25 ± 0.04	233			
		1.37 ± 0.06	252			
		1.58 ± 0.02	272			
		1.77 ± 0.08	297 ± 2			
		2.10 ± 0.05	323			
		2.44 ± 0.10	348			
		2.81 ± 0.06	374			
		3.13 ± 0.04	394			
0.33 ± 0.07	699 ± 140	3.2 ± 0.5	298	DF–RF	Shallcross et al. (1997)	298–373
		3.2 ± 0.6	313			
		5.1 ± 0.9	373			
		2.2 ± 0.8	304 ± 6	RR (several reference compounds)	Kakesu et al. (1997)	

[a]Abbreviations used for the techniques are defined in table I-F-3.
[b]Placed on an absolute basis using $k(OH + C_2H_4) = 7.9 \times 10^{-12}$ cm^3 molecule^{-1} s^{-1} at 1 bar and 298 K (Atkinson et al., 2006).
[c]Placed on an absolute basis using $k(OH + CH(CH_3)_3) = 2.12 \times 10^{-12}$ cm^3 molecule^{-1} s^{-1} (Calvert et al., 2008).
[d]$k(T) = 3.68 \times 10^{-12} \exp(-1{,}077/T) + 5.32 \times 10^{-14} \exp(126/T)$.

curvature in the range 223–394 K. For atmospheric purposes, the preferred values are based on a unit-weighted least-squares fit of the 233–298 K rate coefficients of Talukdar et al. (1997b); this yields $k = 6.5 \times 10^{-13} \exp(-387/T)$ cm^3 molecule^{-1} s^{-1} over the temperature range 230–300 K with $k = 1.8 \times 10^{-13}$ cm^3 molecule^{-1} s^{-1} at 298 K with large uncertainty limits because of the discrepancies between the various studies (Atkinson et al., 2006).

VIII-D-3.2. Cl-Atom Reaction Kinetics

The rate coefficients of Wallington et al. (1990d) and Nielsen et al. (1991) using the relative rate method at ambient temperature and atmospheric pressure are given in table VIII-D-4. The preferred value is the average of the data from these two studies, $k = 3.7 \times 10^{-12}$ cm^3 molecule^{-1} s^{-1} at 298 K with an estimated uncertainty of $\pm 20\%$.

VIII-D-3.3. Summary of the Atmospheric Fate of Ethyl Nitrate

The atmospheric lifetime of ethyl nitrate with respect to its reaction with OH is calculated to be about 2 months using an average OH concentration of 1×10^6 molecule cm^{-3}

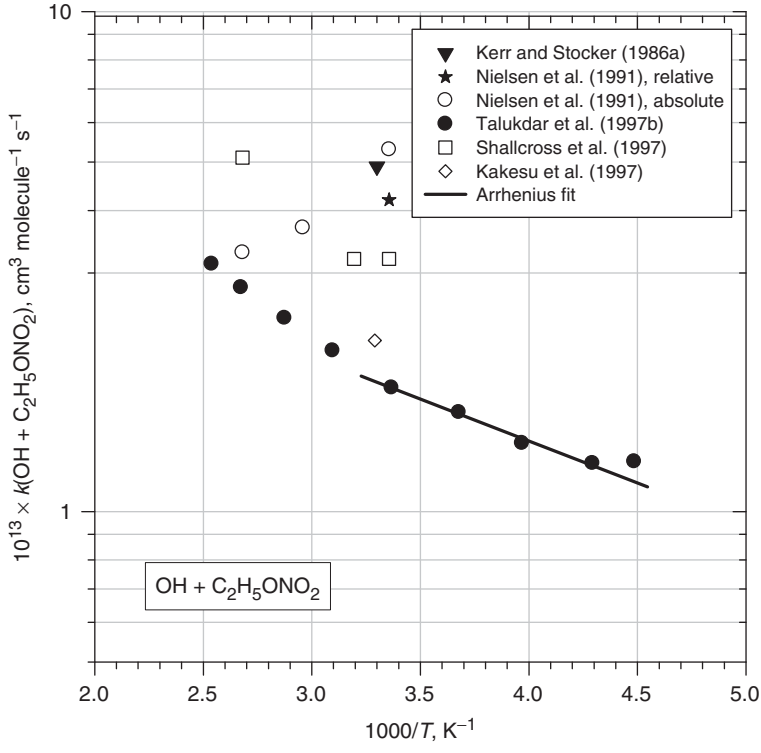

Figure VIII-D-2. Arrhenius plot of the rate coefficient for the reaction of OH with ethyl nitrate.

Table VIII-D-4. Rate coefficients (k, cm^3 molecule^{-1} s^{-1}) for the reaction of Cl with ethyl nitrate ($CH_3CH_2ONO_2$)

$10^{12} \times k$	T (K)	Technique[a]	Reference
3.59 ± 0.23	295 ± 2	RR(C_2H_5Cl)[b]	Wallington et al. (1990d)
3.82 ± 0.15	298 ± 2	RR (C_2H_6)[c]	Nielsen et al. (1991)

[a]Abbreviations used for the techniques are defined in table I-F-3.
[b]Placed on an absolute basis using $k(Cl + C_2H_5Cl) = 7.8 \times 10^{-12}$ cm^3 molecule^{-1} s^{-1} (section I-F).
[c]Placed on an absolute basis using $k(Cl + C_2H_6) = 5.7 \times 10^{-11}$ cm^3 molecule^{-1} s^{-1} (Calvert et al., 2008).

and the reported rate coefficient $k = 1.8 \times 10^{-13}$ cm^3 molecule^{-1} s^{-1}. Photolysis is also an important loss mechanism for ethyl nitrate; its lifetime with an overheard Sun is about 8.5 days; see table IX-M-1.

The investigation of Talukdar et al. (1997b) supports a mechanism of H-atom abstraction from the alkyl group, similar to that occurring for the reaction of OH with methyl nitrate. This conclusion is based on the observed isotope effect and the trend of the reactivity with the alkyl group.

VIII-D-4. 1-Propyl Nitrate (1-Nitrooxypropane, *n*-Propyl Nitrate, n-$C_3H_7ONO_2$)

VIII-D-4.1. OH Reaction Kinetics

The measurements available in the literature are summarized in table VIII-D-5 and shown in figure VIII-D-3. The study of Nielsen et al. (1991) is the only one conducted using an absolute method. The other determinations of the rate coefficient of OH with 1-propyl nitrate were performed using a relative rate method. The rate coefficients reported by different authors at ambient temperatures are in reasonable agreement. However, the IUPAC panel preferred value is based on the lowest measurement of Atkinson and Aschmann (1989) since the values for methyl nitrate and ethyl nitrate of Kerr and Stocker (1986a) and Nielsen et al. (1991) were systematically higher than those of Talukdar et al. (1997b). The rate coefficient recommended is $k = 5.8 \times 10^{-13}$ cm^3 molecule^{-1} s^{-1}, with an estimated uncertainty of $\pm 30\%$ (Atkinson et al., 2006).

The only measurement as function of temperature is that of Nielsen et al. (1991) in the range 298–368 K. A weak negative temperature dependence for the rate coefficient was reported. By analogy with the other nitrates studied by Talukdar et al. (1997b) and Shallcross et al. (1997), a weak positive temperature dependence is expected. Fitting the Arrhenius expression to the combined data set gives $k = 1.2 \times 10^{-12} \exp(-168/T)$ cm^3 molecule^{-1} s^{-1}. However, in absence of other studies, no recommendation is made for the temperature dependence of this reaction.

VIII-D-4.2. Cl-Atom Reaction Kinetics

The measurements of Wallington et al. (1990d) and Nielsen et al. (1991) using the relative rate method at ambient temperature and atmospheric pressure are given in table VIII-D-6. The preferred value is based on the average of the data from the two

Table VIII-D-5. Rate coefficients ($k = A \times e^{-B/T}$), cm^3 molecule^{-1} s^{-1}) for the reaction of OH with 1-propyl nitrate (n-$C_3H_7ONO_2$)

$10^{13} \times A$	B (K)	$10^{13} \times k$	T (K)	Technique[a]	Reference	Temperature Range (K)
		6.8 ± 2.1	303	RR (C_2H_4)[b]	Kerr and Stocker (1986a)	
		5.8 ± 1.0	298	RR (*cyclo*-C_6H_{12})[c]	Atkinson and Aschmann (1989)	
		7.0 ± 0.8	298 ± 2	RR ($CH(CH_3)_3$)[d]	Nielsen et al. (1991)	
5.0	$-(140 \pm 144)$	8.2 ± 0.8	298	PR–UV abs.		298–368
		7.2 ± 1.5	338			
		7.6 ± 0.5	368			

[a]Abbreviations used for the techniques are defined in table I-F-3.
[b]Placed on an absolute basis using $k(OH + C_2H_4) = 7.9 \times 10^{-12}$ cm^3 molecule^{-1} s^{-1} at 1 bar and 298 K (Atkinson et al., 2006).
[c]Placed on an absolute basis using $k(OH + cyclo\text{-}C_6H_{12}) = 6.97 \times 10^{-12}$ cm^3 molecule^{-1} s^{-1} (Calvert et al., 2008).
[d]Placed on an absolute basis using $k[OH + CH(CH_3)_3] = 2.12 \times 10^{-12}$ cm^3 molecule^{-1} s^{-1} (Calvert et al., 2008).

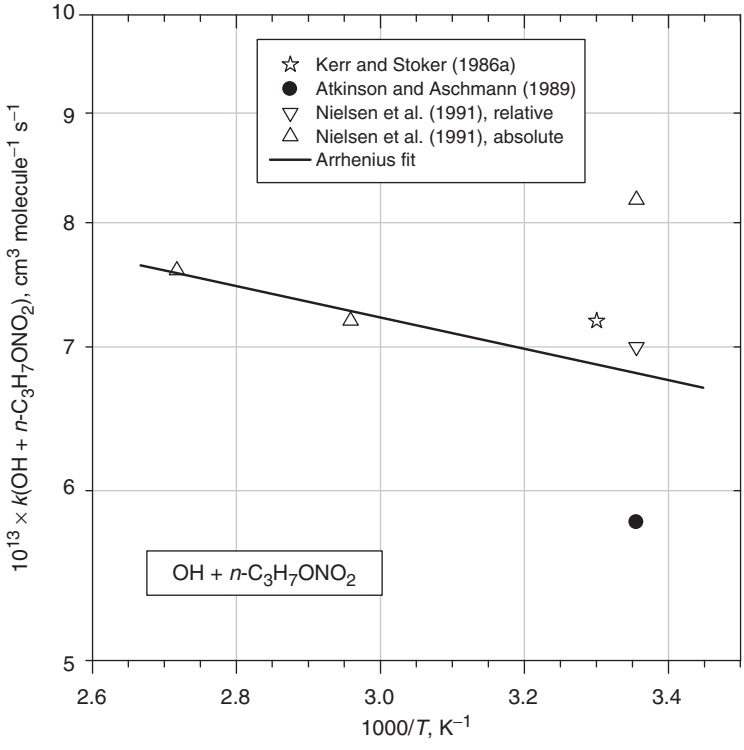

Figure VIII-D-3. Arrhenius plot of the rate coefficient for the reaction of OH with 1-propyl nitrate.

Table VIII-D-6. Rate coefficients (k, cm^3 molecule^{-1} s^{-1}) for the reaction of Cl with 1-propyl nitrate (n-$C_3H_7ONO_2$)

$10^{12} \times k$	T (K)	Technique[a]	Reference
2.08 ± 0.13	295 ± 2	RR(C_2H_5Cl)[b]	Wallington et al. (1990d)
2.28 ± 0.14	298 ± 2	RR (C_2H_6)[c]	Nielsen et al. (1991)

[a]Abbreviations used for the techniques are defined in table I-F-3.
[b]Placed on an absolute basis using $k(Cl + C_2H_5Cl) = 7.8 \times 10^{-12}$ cm^3 molecule^{-1} s^{-1} (section I-F).
[c]Placed on an absolute basis using $k(Cl + C_2H_6) = 5.9 \times 10^{-11}$ cm^3 molecule^{-1} s^{-1} (Atkinson et al., 2006).

studies, $k = 2.2 \times 10^{-11}$ cm^3 molecule^{-1} s^{-1} at 298 K with an estimated uncertainty of ±20% (Atkinson et al., 2006).

VIII-D-4.3. Summary of the Atmospheric Fate of 1-Propyl Nitrate

Using the rate coefficient reported in this section and an average [OH] = 1×10^6 molecule cm^{-3}, the calculated atmospheric lifetime of 1-propyl nitrate with respect to the reaction with OH is in the order of 20 days. As is the case for methyl nitrate and ethyl nitrate, it is expected that the reaction proceeds by H-atom abstraction from

the propyl group. Photolysis is also an important loss mechanism for 1-propyl nitrate in the troposphere with a lifetime for photodecomposition of about 6.5 days with an overhear Sun; see table IX-M-1.

VIII-D-5. 2-Propyl Nitrate [2-Nitrooxypropane, Isopropyl Nitrate, $(CH_3)_2CHONO_2$]

VIII-D-5.1. OH Reaction Kinetics

The reaction of OH with 2-propyl nitrate has been studied by Atkinson et al. (1982b), Becker and Wirtz (1989), and Atkinson and Aschmann (1989) by a relative rate method and by Talukdar et al. (1997b) using the pulsed laser photolysis–laser-induced fluorescence. The study of Talukdar et al. (1997b) was conducted in the temperature range 233–395 K. The results are summarized in table VIII-D-7 and shown in figure VIII-D-4. It can be seen that there is a clear disagreement in the available rate coefficients values from different groups. The rate coefficient of Atkinson and Aschmann (1989) (which supersedes the earlier data of Atkinson et al., 1982b) is about 30% larger than that of Talukdar et al. (1997b) while that of Becker and Wirtz (1989) is almost a factor of 2 higher. As shown in figure VIII-D-4 an Arrhenius plot of the data of Talukdar et al. (1997b) exhibits discernable curvature. The IUPAC panel preferred values are based on the data in the range 233–300 K from the study of Talukdar et al. (1997b), which leads to the Arrhenius expression, $k = 6.2\times10^{-13}\times\exp(-230/T)$ cm^3 molecule^{-1} s^{-1}, with an uncertainty of roughly a factor of 1.5 in the rate coefficient at 298 K, and an uncertainty in E/R of $\pm$300 K. This expression gives: $k = 2.9\times10^{-13}$ cm^3 molecule^{-1} s^{-1} at 298 K (Atkinson et al., 2006).

Table VIII-D-7. Rate coefficients (k, cm^3 molecule^{-1} s^{-1}) for the reaction of OH with 2-propyl nitrate [$(CH_3)_2CHONO_2$]

$10^{13}\times k$	T (K)	Technique[a]	Reference	Temperature Range (K)
1.68 ± 0.42	299 ± 2	RR (*cyclo*-C_6H_{12})[b]	Atkinson et al. (1982b)	
5.4 ± 2.1	295 ± 2	RR (*n*-C_4H_{10})[c]	Becker and Wirtz (1989)	
3.83 ± 0.49	298 ± 2	RR (*cyclo*-C_6H_{12})[b]	Atkinson and Aschmann (1989)	
2.33 ± 0.10	233	PLP–LIF	Talukdar et al. (1997b)[d]	233–395
2.38 ± 0.08	253			
2.66 ± 0.16	272			
2.88 ± 0.19	298 ± 2			
3.13 ± 0.12	325			
3.53 ± 0.06	350			
3.82 ± 0.14	375			
4.13 ± 0.14	395			

[a]Abbreviations used for the techniques are defined in table I-F-3.
[b]Placed on an absolute basis using $k(OH + cyclo\text{-}C_6H_{12}) = 6.97\times10^{-12}$ cm^3 molecule^{-1} s^{-1} (Calvert et al., 2008).
[c]Placed on an absolute basis using $k(OH + n\text{-}C_4H_{10}) = 2.35\times10^{-12}$ cm^3 molecule^{-1} s^{-1} (Atkinson et al., 2006).
[d]$k = 4.3\times10^{-12}\exp(-1{,}250/T) + 2.5\times10^{-13}\exp(-32/T)$.

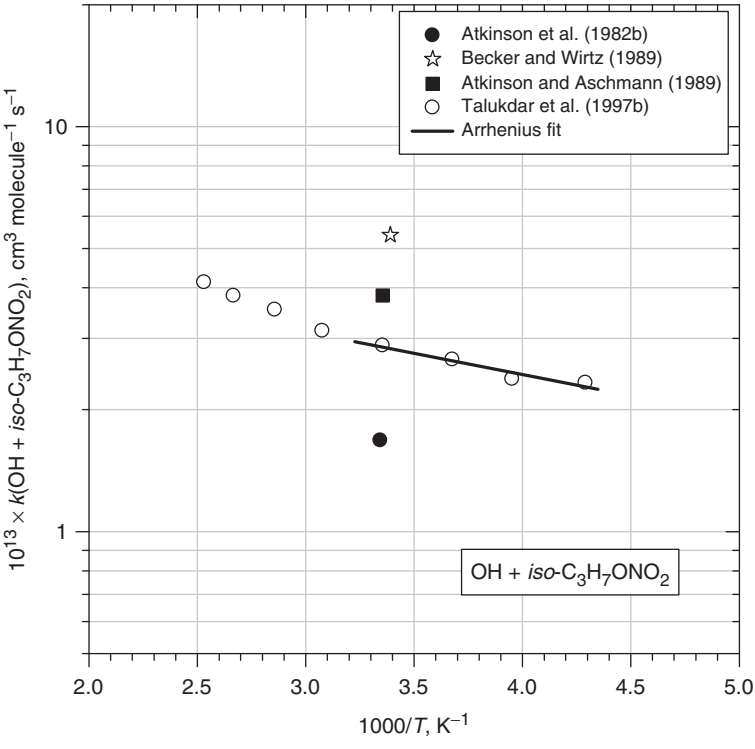

Figure VIII-D-4. Arrhenius plot of the rate coefficient for the reaction of OH with 2-propyl nitrate.

Table VIII-D-8. Rate coefficients (k, cm^3 $molecule^{-1}$ s^{-1}) for the reaction of Cl with 2-propyl nitrate [$(CH_3)_2CHONO_2$]

$10^{12} \times k$	T (K)	Technique[a]	Reference
3.82 ± 0.47	295 ± 2	RR(C_2H_5Cl)[b]	Wallington et al. (1990d)

[a]Abbreviations used for the techniques are defined in table I-F-3.
[b]Placed on an absolute basis using $k(Cl + C_2H_5Cl) = 7.8 \times 10^{-12}$ cm^3 $molecule^{-1}$ s^{-1} (section I-F).

VIII-D-5.2. Cl-Atom Reaction Kinetics

The measurement of Wallington et al. (1990d) is the only study available in the literature for the Cl + *iso*-$C_3H_7ONO_2$ reaction, as shown in table VIII-D-8. This investigation was performed by using a relative rate method at ambient temperature and atmospheric pressure. The preferred value is based on this single determination, $k = 3.8 \times 10^{-12}$ cm^3 $molecule^{-1}$ s^{-1} at 298 K with an estimated uncertainty of ±30% (Atkinson et al., 2006).

VIII-D-5.3. Summary of the Atmospheric Fate of 2-Propyl Nitrate

An atmospheric lifetime of about 40 days is calculated for 2-propyl nitrate with respect to its reaction with OH radicals using $k = 2.9 \times 10^{-13}$ cm^3 $molecule^{-1}$ s^{-1} and

[OH] = 1×10^6 molecule[1] cm^{-3}. Photolysis is also an important loss mechanism for 2-propyl nitrate in the troposphere; its lifetime for photodissociation with an overhead Sun is about 3.9 days; see table IX-M-1.

VIII-D-6. 1-Butyl Nitrate (1-Nitrooxybutane, n-$C_4H_9ONO_2$)

VIII-D-6.1. OH Reaction Kinetics

Table VIII-D-9 gives the available measurements of the rate coefficient for the reaction of OH with 1-butyl nitrate. Atkinson et al. (1982b), and Atkinson and Aschmann (1989) have used a relative rate method while Nielsen et al. (1991) used both absolute and relative techniques. The absolute and relative rate coefficients of Atkinson and Aschmann (1989) (which supersedes the earlier data of Atkinson et al., 1982b) and Nielsen et al. (1991) are in good agreement. The IUPAC panel preferred value, $k = 1.6 \times 10^{-12}$ cm^3 $molecule^{-1}$ s^{-1} with an uncertainty of ±20%, is an average of the absolute and relative rate constants of Atkinson and Aschmann (1989) and Nielsen et al. (1991). By analogy with the reaction of the OH radical with 2-propyl nitrate, the temperature dependence of the rate coefficient at temperatures for atmospheric interest is likely to be small (Atkinson et al., 2006).

VIII-D-6.2. Cl-Atom Reaction Kinetics

The rate coefficient for reaction of chlorine atoms with 1-butyl nitrate has been measured by Nielsen et al. (1991) using a relative rate method at ambient temperature and atmospheric pressure (table VIII-D-10). The preferred value is based on this single determination, $k = 8.2 \times 10^{-12}$ cm^3 $molecule^{-1}$ s^{-1} at 298 K with an uncertainty of ±30%.

VIII-D-6.3. Summary of the Atmospheric Fate of 1-Butyl Nitrate

The atmospheric lifetime of 1-butyl nitrate is around 7 days with respect to the reaction with OH radicals using [OH] = 1×10^6 molecule cm^{-3}. By analogy with other alkyl nitrates, the reaction of OH with 1-butyl nitrate is expected to occur via H-atom abstraction from C—H bonds, probably involving the secondary H-atoms. Photolysis is

Table VIII-D-9. Rate coefficients (k, cm^3 $molecule^{-1}$ s^{-1}) for the reaction of OH with 1-butyl nitrate (n-$C_4H_9ONO_2$)

$10^{12} \times k$	T (K)	Technique[a]	Reference
1.30 ± 0.10	299 ± 2	RR (*cyclo*-C_6H_{12})[b]	Atkinson et al. (1982b)
1.65 ± 0.18	298 ± 2	RR (*cyclo*-C_6H_{12})[b]	Atkinson and Aschmann (1989)
1.47 ± 0.08	298 ± 2	RR [$CH(CH_3)_3$][c]	Nielsen et al. (1991)
1.74 ± 0.19	298 ± 2	PR-UV abs.	

[a]Abbreviations used for the techniques are defined in table I-F-3.
[b]Placed on an absolute basis using $k(OH + cyclo\text{-}C_6H_{12}) = 6.97 \times 10^{-12}$ cm^3 $molecule^{-1}$ s^{-1} (Calvert et al., 2008).
[c]Placed on an absolute basis using $k[OH + CH(CH_3)_3] = 2.12 \times 10^{-12}$ cm^3 $molecule^{-1}$ s^{-1} (Calvert et al., 2008).

Table VIII-D-10. Rate coefficient (k, cm^3 molecule^{-1} s^{-1}) for the reaction of Cl with 1-butyl nitrate (n-$C_4H_9ONO_2$)

$10^{11} \times k$	T (K)	Technique[a]	Reference
8.25 ± 0.20	298	RR (C_2H_6)[b]	Nielsen et al. (1991)

[a]Abbreviations used for the techniques are defined in table I-F-3.
[b]Placed on an absolute basis using $k(Cl + C_2H_6) = 5.9 \times 10^{-11}$ cm^3 molecule^{-1} s^{-1} (Calvert et al., 2008).

also an important atmospheric loss mechanism for butyl nitrate with a lifetime for photodissociation of about 7.3 days with an overhead Sun; see table IX-M-1.

VIII-D-7. 2-Butyl Nitrate [2-Nitrooxybutane, *sec*-Butyl Nitrate, $C_2H_5CH(ONO_2)CH_3$]

VIII-D-7.1. OH Reaction Kinetics

The reaction of OH with 2-butyl nitrate has been studied only by Atkinson et al. (1982b) and Atkinson and Aschmann (1989). The measurements obtained at ambient temperature and atmospheric pressure by a relative method are summarized in table VIII-D-11. The determination of Atkinson and Aschmann (1989) supersedes the earlier measurement from the same group (Atkinson et al., 1982b). Hence, the preferred value at 298 K is based on the study of Atkinson and Aschmann, $k = 8.6 \times 10^{-13}$ cm^3 molecule^{-1} s^{-1} with an uncertainty of ±30%. By analogy with the rate coefficient for the reaction of OH with 2-propyl nitrate, a small temperature dependence of the rate coefficients for temperatures of atmospheric interest is expected (Atkinson et al., 2006).

VIII-D-7.2. Summary of the Atmospheric Fate of 2-Butyl Nitrate

Combining $k(OH + 2\text{-butyl nitrate}) = 8.6 \times 10^{-13}$ cm^3 molecule^{-1} s^{-1} with a diurnal average [OH] $= 1 \times 10^6$ molecule cm^{-3} provides an estimate of about 7 days for the atmospheric lifetime of 2-butyl nitrate. As reported for other alkyl nitrates, the reaction of OH with 2-butyl nitrate is expected to occur via an H-atom abstraction from the alkyl group. Photolysis is also expected to be a significant atmospheric loss mechanism of 2-butyl nitrate.

Table VIII-D-11. Rate coefficients (k, cm^3 molecule^{-1} s^{-1}) for the reaction of OH with 2-butyl nitrate [$C_2H_5CH(ONO_2)CH_3$]

$10^{13} \times k$	T (K)	Technique[a]	Reference
6.3 ± 1.0	299 ± 2	RR (*cyclo*-C_6H_{12})[b]	Atkinson et al. (1982b)
8.6 ± 1.5	298 ± 2	RR (*cyclo*-C_6H_{12})[b]	Atkinson and Aschmann (1989)

[a]Abbreviations used for the techniques are defined in table I-F-3.
[b]Placed on an absolute basis using $k(OH + cyclo\text{-}C_6H_{12}) = 6.97 \times 10^{-12}$ cm^3 molecule^{-1} s^{-1} (Calvert et al., 2008).

Table VIII-D-12. Rate coefficient (k, cm^3 molecule^{-1} s^{-1}) for the reaction of OH with 2-methyl-1-propyl nitrate [$(CH_3)_2CHCH_2ONO_2$]

$10^{12} \times k$	T (K)	Technique[a]	Reference
1.53 ± 0.19	295 ± 2	RR (n-C_4H_{10})[b]	Becker and Wirtz (1989)

[a]Abbreviations used for the techniques are defined in table I-F-3.
[b]Placed on an absolute basis using $k(OH + n\text{-}C_4H_{10}) = 2.35 \times 10^{-12}$ cm^3 molecule^{-1} s^{-1} (Atkinson et al., 2006).

VIII-D-8. 2-Methyl-1-Propyl Nitrate [2-Methyl-1-nitrooxypropane, Isobutyl Nitrate, $(CH_3)_2CHCH_2ONO_2$]

VIII-D-8.1. OH Reaction Kinetics

The rate coefficient of Becker and Wirtz (1989), obtained from a relative rate study at ambient temperature and atmospheric pressure of air, is given in table VIII-D-12.

VIII-D-8.2. Summary of the Atmospheric Fate of 2-Methyl-1-Propyl Nitrate

The atmospheric lifetime of 2-methyl-1-propyl nitrate is around 7 days with respect to the reaction with OH radicals using an average concentration of 1×10^6 molecule cm^{-3}. The reaction is expected to occur via H-atom abstraction from the alkyl group. Photolysis is expected to contribute significantly to the atmospheric loss of 2-methyl-1-propyl nitrate as well; see table IX-M-1.

VIII-D-9. 1-Pentyl Nitrate (1-Nitrooxypentane, *n*-Pentyl Nitrate, n-$C_5H_{11}ONO_2$)

VIII-D-9.1. OH Reaction Kinetics

The rate coefficient has been measured by Nielsen et al. (1991) and Treves and Rudich (2003) using a relative rate method. Nielsen et al. (1991) also used an absolute technique. The rate coefficient values obtained are given in table VIII-D-13. The value of Treves and Rudich is higher than those of Nielsen et al. The average value of the three determinations $k = 3.6 \times 10^{-12}$ cm^3 molecule^{-1} s^{-1} at 298 K is recommended with an estimated uncertainty of $\pm 50\%$.

VIII-D-9.2. Cl-Atom Reaction Kinetics

Table VIII-D-14 gives the only available measurement of the rate coefficient for the reaction of Cl with *n*-pentyl nitrate (Nielsen et al., 1991). This study was performed using a relative rate method at ambient temperature and atmospheric pressure.

VIII-D-9.3. Summary of the Atmospheric Fate of 1-Pentyl Nitrate

Combining $k(OH + 1\text{-pentyl nitrate}) = 3.6 \times 10^{-12}$ cm^3 molecule^{-1} s^{-1} with [OH] = 1×10^6 molecule cm^{-3} provides an estimate of 3 days for the atmospheric lifetime of

Table VIII-D-13. Rate coefficients (k, cm^3 molecule^{-1} s^{-1}) for the reaction of OH with 1-pentyl nitrate (n-$C_5H_{11}ONO_2$)

$10^{12} \times k$	T (K)	Technique[a]	Reference
2.68 ± 0.08	298 ± 2	RR [$CH(CH_3)_3$][b]	Nielsen et al. (1991)
3.32 ± 0.30	298 ± 2	PR–UV abs.	
4.9 ± 0.9	296 ± 2	RR (1-pentanol, 1-octanol)[c]	Treves and Rudich (2003)

[a]Abbreviations used for the techniques are defined in table I-F-3.
[b]Placed on an absolute basis using $k[OH + CH(CH_3)_3] = 2.12 \times 10^{-12}$ cm^3 molecule^{-1} s^{-1} (Calvert et al., 2008).
[c]Placed on an absolute basis using $k(OH + 1\text{-pentanol}) = 1.12 \times 10^{-11}$ and $k(OH + 1\text{-octanol}) = 1.44 \times 10^{-11}$ cm^3 molecule^{-1} s^{-1}; the ratios k/k_{ref} is not given by the authors.

Table VIII-D-14. Rate coefficient (k, cm^3 molecule^{-1} s^{-1}) for the reaction of Cl with 1-pentyl nitrate (n-$C_5H_{11}ONO_2$)

$10^{10} \times k$	T (K)	Technique[a]	Reference
1.45 ± 0.03	298 ± 2	RR (C_2H_6)[b]	Nielsen et al. (1991)

[a]Abbreviations used for the techniques are defined in table I-F-3.
[b]Placed on an absolute basis using $k(Cl + C_2H_6) = 5.9 \times 10^{-11}$ cm^3 molecule^{-1} s^{-1} (Atkinson et al., 2006).

1-pentyl nitrate with respect to reaction with OH. Photolysis is also expected to be an important fate of 1-pentyl nitrate (see section IX-I-3).

VIII-D-10. 2-Pentyl Nitrate [2-Nitrooxypentane, $CH_3CH(ONO_2)C_3H_7$]

VIII-D-10.1. OH Reaction Kinetics

The rate coefficient has been measured by Atkinson et al. (1982b) in air using a relative rate method at ambient temperature and atmospheric pressure (table VIII-D-15). Given that this is the only measurement available in the literature, an estimated uncertainty of ±30% is assigned.

VIII-D-10.2. Cl-Atom Reaction Kinetics

Table VIII-D-16 gives the only measurement of the rate coefficient for the reaction of Cl with 2-pentyl nitrate. This study was conducted by Wallington et al. (1990d) using a relative rate method at ambient temperature and atmospheric pressure.

Table VIII-D-15. Rate coefficient (k, cm^3 molecule^{-1} s^{-1}) for the reaction of OH with 2-pentyl nitrate [$CH_3CH(ONO_2)C_3H_7$]

$10^{12} \times k$	T (K)	Technique[a]	Reference
1.72 ± 0.11	299 ± 2	RR (*cyclo*-C_6H_{12})[b]	Atkinson et al. (1982b)

[a]Abbreviations used for the techniques are defined table I-F-3.
[b]Placed on an absolute basis using $k(OH + cyclo\text{-}C_6H_{12}) = 6.97 \times 10^{-12}$ cm^3 molecule^{-1} s^{-1} (Calvert et al., 2008).

Table VIII-D-16. Rate coefficients (k, cm^3 molecule^{-1} s^{-1}) for the reaction of Cl with 2-pentyl nitrate [$CH_3CH(ONO_2)C_3H_7$]

$10^{10} \times k$	T (K)	Technique[a]	Reference
1.01 ± 0.06	295 ± 2	RR (C_2H_6)[b]	Wallington et al. (1990d)
> 0.78		RR (C_2H_5Cl)[c]	

[a]Abbreviations used for the techniques are defined in table I-F-3.
[b]Placed on an absolute basis using $k(Cl + C_2H_6) = 5.9 \times 10^{-11}$ cm^3 molecule^{-1} s^{-1} (Calvert et al., 2008).
[c]Placed on an absolute basis using $k(Cl + C_2H_5Cl) = 7.8 \times 10^{-12}$ cm^3 molecule^{-1} s^{-1} (section I-F).

VIII-D-10.3. Summary of the Atmospheric Fate of 2-Pentyl Nitrate

The atmospheric lifetime of 2-pentyl nitrate with respect to reaction with OH radicals is calculated to be around 7 days using [OH] $= 1 \times 10^6$ molecule cm^{-3} and $k = 1.7 \times 10^{-12}$ cm^3 molecule^{-1} s^{-1}. Loss via photolysis is also an important atmospheric fate for 2-pentyl nitrate with a photodissociation lifetime of about 4.5 days with an overhead Sun (see table IX-M-1).

VIII-D-11. 3-Pentyl Nitrate [3-Nitrooxypentane, $CH_3CH_2CH(ONO_2)CH_2CH_3$]

VIII-D-11.1. OH Reaction Kinetics

The rate coefficient for the reaction of OH with 3-pentyl nitrate has been measured at ambient temperature and atmospheric pressure by Atkinson et al. (1982b) using a relative rate method (table VIII-D-17).

VIII-D-11.2. Summary of the Atmospheric Fate of 3-Pentyl Nitrate

The atmospheric lifetime of 3-pentyl nitrate with respect to reaction with OH radicals is calculated to be around 11 days using [OH] $= 1 \times 10^6$ molecule cm^{-3} and $k = 1.0 \times 10^{-12}$ cm^3 molecule^{-1} s^{-1}. Loss via photolysis is also an important atmospheric fate for 3-pentyl nitrate with a photodissociation lifetime of about 4.6 days for an overhead Sun; see table IX-M-1.

Table VIII-D-17. Rate coefficient (k, cm^3 molecule^{-1} s^{-1}) for the reaction of OH with 3-pentyl nitrate [$C_2H_5CH(ONO_2)C_2H_5$]

$10^{12} \times k$	T (K)	Technique[a]	Reference
1.04 ± 0.18	299 ± 2	RR (*cyclo*-C_6H_{12})[b]	Atkinson et al. (1982b)

[a]Abbreviations used for the techniques are defined in table I-F-3.
[b]Placed on an absolute basis using $k(OH + cyclo\text{-}C_6H_{12}) = 6.97 \times 10^{-12}$ cm^3 molecule^{-1} s^{-1} (Calvert et al., 2008).

Table VIII-D-18. Rate coefficient (k, cm^3 molecule^{-1} s^{-1}) for the reaction of OH with 2-methyl-1-butyl nitrate [$CH_3CH_2CH(CH_3)CH_2ONO_2$]

$10^{12} \times k$	T (K)	Technique[a]	Reference
2.33 ± 0.14	295 ± 2	RR (n-C_4H_{10})[b]	Becker and Wirtz (1989)

[a]Abbreviations used for the techniques are defined in table I-F-3.
[b]Placed on an absolute basis using $k(OH + n\text{-}C_4H_{10}) = 2.35 \times 10^{-12}$ cm^3 molecule^{-1} s^{-1} (Atkinson et al., 2006).

VIII-D-12. 2-Methyl-1-butyl Nitrate [2-Methyl-1-nitrooxybutane, $CH_3CH_2CH(CH_3)CH_2ONO_2$]

VIII-D-12.1. OH Reaction Kinetics

Becker and Wirtz (1989) studied this reaction using a relative rate method at ambient temperature and atmospheric pressure in synthetic air. The result is given in table VIII-D-18.

VIII-D-12.2. Summary of the Atmospheric Fate of 2-Methyl-1-butyl Nitrate

The atmospheric lifetime of 2-methyl-1-butyl nitrate with respect to reaction with OH radicals, using k(OH+2-methyl-1-nitrate) = 2.3×10^{-12} cm^3 molecule^{-1} s^{-1} and [OH] = 1×10^6 molecule cm^{-3}, is calculated to be around 5 days. Photolysis is expected to contribute significantly to the atmospheric loss of 2-methyl-1-butyl nitrate as well; see section IX-I-3.

VIII-D-13. 3-Methyl-1-butyl Nitrate [3-Methyl-1-nitrooxybutane, $(CH_3)_2CHCH_2CH_2ONO_2$]

VIII-D-13.1. OH Reaction Kinetics

The rate coefficient of Becker and Wirtz (1989), obtained from a relative rate study at ambient temperature and atmospheric pressure in synthetic air, is given in table VIII-D-19.

Table VIII-D-19. Rate coefficients (k, cm^3 molecule^{-1} s^{-1}) for the reaction of OH with 3-methyl-1-butyl nitrate [$(CH_3)_2CHCH_2CH_2ONO_2$]

$10^{12} \times k$	T (K)	Technique[a]	Reference
2.37 ± 0.33	295 ± 2	RR (n-C_4H_{10})[b]	Becker and Wirtz (1989)

[a]Abbreviations used for the techniques are defined in table I-F-3.
[b]Placed on an absolute basis using $k(OH + n\text{-}C_4H_{10}) = 2.35 \times 10^{-12}$ cm^3 molecule^{-1} s^{-1} (Atkinson et al., 2006).

VIII-D-13.2. Summary of the Atmospheric Fate of 3-Methyl-1-butyl Nitrate

The atmospheric lifetime of 3-methyl-1-butyl nitrate with respect to reaction with OH radicals is calculated to be around 5 days. Photolysis is expected to contribute to the atmospheric loss of 3-methyl-1-butyl nitrate; see section IX-I-3.

VIII-D-14. 3-Methyl-2-butyl Nitrate [$(CH_3)_2CHCH(ONO_2)CH_3$]

VIII-D-14.1. OH Reaction Kinetics

The rate coefficients of Atkinson et al. (1982b) and Becker and Wirtz (1989), obtained from relative rate studies at ambient temperature and atmospheric pressure in synthetic air, are given in table VIII-D-20. These two measurements are in very good agreement. An unweighted average of the two determinations gives $k = 1.7 \times 10^{-12}$ cm^3 molecule^{-1} s^{-1} which is recommended at 298 K with an uncertainty of $\pm 20\%$.

VIII-D-14.2. Summary of the Atmospheric Fate of 3-Methyl-2-butyl Nitrate

The atmospheric lifetime of 3-methyl-2-butyl nitrate with respect to reaction with OH radicals is calculated to be around 7 days. Photolysis will also contribute significantly to the atmospheric loss of 3-methyl-2-butyl nitrate; see section IX-I-3.

VIII-D-15. 2,2-Dimethyl-1-propyl Nitrate [Neopentyl Nitrate, 2,2-Dimethyl-1-nitrooxypropane, $(CH_3)_3CCH_2ONO_2$]

VIII-D-15.1. OH Reaction Kinetics

The rate coefficient of Atkinson et al. (1982b), obtained from a relative rate study at ambient temperature and atmospheric pressure in synthetic air, is presented in table VIII-D-21.

Table VIII-D-20. Rate coefficients (k, cm^3 molecule^{-1} s^{-1}) for the reaction of OH with 3-methyl-2-butyl nitrate [$(CH_3)_2CHCH(ONO_2)CH_3$]

$10^{12} \times k$	T (K)	Technique[a]	Reference
1.60 ± 0.05	298 ± 2	RR (n-C_4H_{10})[b]	Atkinson et al. (1982b)
1.81 ± 0.14	295 ± 2	RR (n-C_4H_{10})[b]	Becker and Wirtz (1989)

[a]Abbreviations used for the techniques are defined in table I-F-3.
[b]Placed on an absolute basis using $k(n\text{-}C_4H_{10}) = 2.35 \times 10^{-12}$ cm^3 molecule^{-1} s^{-1} (Atkinson et al., 2006).

Table VIII-D-21. Rate coefficient (k, cm^3 molecule^{-1} s^{-1}) for the reaction of OH with 2,2-dimethyl-1-propyl nitrate [$(CH_3)_3CCH_2ONO_2$]

$10^{12} \times k$	T (K)	Technique[a]	Reference
0.79 ± 0.19	298 ± 2	RR (n-C_4H_{10})[b]	Atkinson et al. (1984a)

[a]Abbreviations used for the techniques are defined in table I-F-3.
[b]Placed on an absolute basis using $k(OH + n\text{-}C_4H_{10}) = 2.35 \times 10^{-12}$ cm^3 molecule^{-1} s^{-1} (Atkinson et al., 2006).

VIII-D-15.2. Summary of the Atmospheric Fate of 2,2-Dimethyl-1-propyl Nitrate

The atmospheric lifetime of 2,2-dimethyl-1-propyl nitrate with respect to reaction with OH radicals is calculated to be around 15 days. Photolysis is expected to be an important atmospheric fate of this nitrate; see section IX-I-3.

VIII-D-16. The Higher Alkyl Nitrates

VIII-D-16.1. OH Reaction Kinetics

The rate coefficient values of Atkinson et al. (1982b, 1984a) obtained from relative rate studies at ambient temperature and atmospheric pressure in synthetic air, are given in table VIII-D-22. These are the only data available for alkyl nitrates greater than C_5.

Table VIII-D-22. Rate coefficients (k, cm^3 molecule^{-1} s^{-1}) for the reaction of OH with higher alkyl nitrates

Compounds	$10^{12} \times k$	T (K)	Technique[a]	Reference
2-Hexyl nitrate $CH_3(CH_2)_3CH(ONO_2)CH_3$	2.94 ± 0.14	299 ± 2	RR ($cyclo$-C_6H_{12})[b]	Atkinson et al. (1982b)
3-Hexyl nitrate $CH_3(CH_2)_2CH(ONO_2)CH_2CH_3$	2.50 ± 0.20	299 ± 2	RR ($cyclo$-C_6H_{12})[b]	Atkinson et al. (1982b)
Cyclohexyl nitrate [—$CH_2(CH_2)_2CH(ONO_2)CH_2CH_2$—]	3.06 ± 0.33	298 ± 2	RR (n-C_4H_{10})[c]	Atkinson et al. (1984a)
2-Methyl-2-pentyl nitrate $(CH_3)_2C(ONO_2)CH_2CH_2CH_3$	1.59 ± 0.20	298 ± 2	RR (n-C_4H_{10})[c]	Atkinson et al. (1984a)
3-Methyl-2-pentyl nitrate $CH_3CH(ONO_2)CH(CH_3)CH_2CH_3$	2.80 ± 0.07	298 ± 2	RR (n-C_4H_{10})[c]	Atkinson et al. (1984a)
3-Heptyl nitrate $CH_3(CH_2)_3CH(ONO_2)CH_2CH_3$	3.42 ± 0.40	299 ± 2	RR ($cyclo$-C_6H_{12})[b]	Atkinson et al. (1982b)
3-Octyl nitrate $CH_3(CH_2)_4CH(ONO_2)CH_2CH_3$	3.60 ± 0.73	299 ± 2	RR ($cyclo$-C_6H_{12})[b]	Atkinson et al. (1982b)

[a]Abbreviations used for the techniques are defined in table I-F-3.
[b]Placed on an absolute basis using $k(OH + cyclo\text{-}C_6H_{12}) = 6.97 \times 10^{-12}$ cm^3 molecule^{-1} s^{-1} (Calvert et al., 2008).
[c]Placed on an absolute basis using $k(OH + n\text{-}C_4H_{10}) = 2.35 \times 10^{-12}$ cm^3 molecule^{-1} s^{-1} (Atkinson et al., 2006).

Table VIII-D-23. Rate coefficient (k, cm^3 molecule^{-1} s^{-1}) for the reaction of Cl with 2-heptyl nitrate [$CH_3CH(ONO_2)C_5H_{13}$]

$10^{10} \times k$	T (K)	Technique[a]	Reference
2.64 ± 0.46	295 ± 2	RR (n-C_4H_{10})[b]	Wallington et al. (1990d)

[a]Abbreviations used for the techniques are defined in table I-F-3.
[b]Placed on an absolute basis using $k(Cl + n\text{-}C_4H_{10}) = 2.1 \times 10^{-10}$ cm^3 molecule^{-1} s^{-1} (Calvert et al., 2008).

VIII-D-16.2. Cl-Atom Reaction Kinetics

The rate coefficient for the reaction of 2-heptyl nitrate with Cl-atoms as determined by Wallington et al. (1990d) in a relative rate study at ambient temperature and atmospheric pressure in synthetic air is presented in table VIII-D-23. This is the only reported study of the reaction of Cl-atoms with alkyl nitrates $>C_5$.

VIII-D-16.3. Summary of the Atmospheric Fate of Higher Alkyl Nitrates

Combining the rate coefficients for the OH reactions presented above and an average concentration of OH radicals of [OH] = 1×10^6 molecule cm^{-3}, provides an estimate for the atmospheric lifetime of the higher alkyl nitrates of 3 to 5 days. Photolysis is also expected to be an important atmospheric loss of higher alkyl nitrates; see section IX-I-3.

VIII-D-17. Trends in the Reactivity of Alkyl Nitrates

Despite the large spread in the data for some alkyl nitrates and the limited number of studies for others, it is possible to draw some conclusions regarding the reactivity of these species towards OH radicals based on the recommended values and the observed trends. The existing rate coefficient data set strongly suggests that reaction occurs via H-atom abstraction. The reactivity increases along the series methyl, ethyl, *n*-propyl, *n*-butyl, *n*-pentyl, consistent with expectations based on abstraction from the increasing number of CH_2 groups and their increased separation from the deactivating nitrate group. 1-Propyl nitrate is more reactive than 2-propyl nitrate, similarly 1-butyl nitrate is more reactive than 2-butyl nitrate and 1-pentyl nitrate is more reactive than 2-pentyl nitrate and 3-pentyl nitrate, as expected from the structure–reactivity relationships. In addition, the observed temperature dependencies in reactions with molecules that contain primary, secondary, or tertiary hydrogen atoms are consistent with the simultaneous occurrence of different abstraction reactions (Talukdar et al., 1997b).

The nitrate group is strongly electron withdrawing and the rate coefficients for the reaction with alkyl nitrates are much smaller than those for the corresponding alcohols. The —ONO_2 group deactivates the C—H bonds on both the α-carbon atom bearing the nitrate group as well as the adjacent β-carbon atom. The deactivation of C—H bonds on the α- carbon is large (a factor of $\sim$25) compared to abstraction at an unsubstituted carbon atom (Becker and Wirtz, 1989; Kwok and Atkinson, 1995). The C—H bonds on the β-carbon atom are deactivated by approximately a factor of 5.

The expected OH-initiated oxidation products are the bifunctional organic nitrates such as carbonyl nitrates, hydroxycarbonyl nitrates, dinitrates, and hydroxynitrates depending on the size of the initial alkyl nitrates and NO_x concentrations. However, no direct product studies have been performed so far and the products remain speculative.

As with OH radicals, the reactivity of Cl towards alkyl nitrates increases with size of the alkyl nitrates. The presence of the deactivating —ONO_2 group significantly decreases the reactivity compared to alcohols. This deactivating effect of the nitrate group extends to at least the β-carbon atom.

Reactions of alkyl nitrates with OH radicals and their photolysis (see section IX-I-2) are the two major loss processes in the atmosphere (Roberts, 1990; Talukdar et al., 1997a, 1997b). The reaction with OH is of importance mainly in the lower troposphere. The calculated lifetimes using the kinetic parameters for OH reactions are in the range of days to several months. Clemitshaw et al. (1997) have shown that the atmospheric lifetimes of the alkyl nitrates vary with season, and that they are very long lived in the Arctic. The long lifetimes of alkyl nitrates make them important NO_x reservoirs that can be transported, with lifetimes, and hence the distance transported, dependent on the season; see table IX-M-1. Heterogeneous processes are expected to play a significant role in the removal of alkyl nitrates from the atmosphere (Roberts, 1990; Shepson et al., 1996; Wängberg, 1996).

VIII-E. Saturated Dinitrates

Alkyl dinitrates are important products of the reaction of NO_3 radicals with unsaturated hydrocarbons, at least in laboratory experiments (Wängberg, 1993). A limited number of studies have been reported on their atmospheric degradation processes. All measurements have been conducted using the relative rate method (Zhu et al., 1991; Wängberg et al., 1996; Treves and Rudich, 2003).

VIII-E-1. 1,2-Dinitrooxypropane [1,2-Propandiol Dinitrate, $CH_3CH(ONO_2)CH_2ONO_2$]

VIII-E-1.1. OH Reaction Kinetics

The only measurement of the rate coefficient for the reaction of OH with 1,2-dinitrooxypropane is that of Zhu et al. (1991). The study was carried out using a relative rate method at atmospheric pressure and ambient temperature. The value obtained is given in table VIII-E-1.

VIII-E-1.2. Summary of the Atmospheric Fate of 1,2-Dinitrooxypropane

The atmospheric lifetime of 1,2-dinitrooxypropane with respect to its reaction with OH radicals is estimated to be more than a month using [OH] = 1×10^6 molecule cm^{-3}. It is anticipated that photolysis will play an important role in the removal of 1,2-dinitrooxypropane with a lifetime for photodissociation estimated to be about 7 h with an overhead Sun (see table IX-M-1).

Table VIII-E-1. Rate coefficient (k, cm^3 molecule^{-1} s^{-1}) for the reaction of OH with 1,2-dinitrooxypropane [$CH_3CH(ONO_2)CH_2ONO_2$]

$10^{12} \times k$	T (K)	Technique[a]	Reference
< 0.3	298 ± 2	RR (C_3H_8)[b]	Zhu et al. (1991)

[a]Abbreviations used for the techniques are defined in table I-F-3.
[b]Placed on an absolute basis using $k(OH + C_3H_8) = 1.1 \times 10^{-12}$ cm^3 molecule^{-1} s^{-1} (Atkinson et al., 2006).

Table VIII-E-2. Rate coefficient (k, cm^3 molecule^{-1} s^{-1}) for the reaction of OH with 1,2-dinitrooxybutane [$CH_3CH_2CH(ONO_2)CH_2ONO_2$]

$10^{12} \times k$	T (K)	Technique[a]	Reference
1.63 ± 0.31	298 ± 2	RR (C_3H_8)[b]	Zhu et al. (1991)

[a]Abbreviations used for the techniques are defined in table I-F-3.
[b]Placed on an absolute basis using $k(OH + C_3H_8) = 1.1 \times 10^{-12}$ cm^3 molecule^{-1} s^{-1} (Atkinson et al., 2006).

VIII-E-2. 1,2-Dinitrooxybutane [1,2-Butandiol Dinitrate, $CH_3CH_2CH(ONO_2)CH_2ONO_2$]

VIII-E-2.1. OH Reaction Kinetics

The only reported study is that by Zhu et al. (1991). The rate coefficient value obtained by Zhu et al. (1991) using a relative rate method at atmospheric pressure and ambient temperature is given in table VIII-E-2.

VIII-E-2.2. Summary of the Atmospheric Fate of 1,2-Dinitrooxybutane

The atmospheric lifetime of 1,2-dinitrooxybutane with respect to its reaction with OH radicals is estimated to be around 7 days using [OH] $= 1 \times 10^6$ molecule cm^{-3} and the rate coefficient given in this section. Photolysis is expected to play an important role in the removal of 1,2-dinitrooxybutane as well with a lifetime for photodissociation of about 25 h for an overhead Sun; see table IX-M-1.

VIII-E-3. 2,3-Dinitrooxybutane [2,3-Butandiol Dinitrate, $CH_3CH(ONO_2)CH(ONO_2)CH_3$]

VIII-E-3.1. OH Reaction Kinetics

The only reported study is that by Zhu et al. (1991). The rate coefficient obtained by a relative rate method at atmospheric pressure and ambient temperature is given in table VIII-E-3.

VIII-E-3.2. Summary of the Atmospheric Fate of 2,3-Dinitrooxybutane

The atmospheric lifetime of 2,3-nitrooxybutane with respect to reaction with OH radicals is estimated to be around 11 days. Photolysis is expected to be an important

Table VIII-E-3. Rate coefficient (k, cm^3 molecule^{-1} s^{-1}) for the reaction of OH with 2,3-dinitrooxybutane [$CH_3CH(ONO_2)CH(ONO_2)CH_3$]

$10^{12} \times k$	T (K)	Technique[a]	Reference
1.02 ± 0.24	298 ± 2	RR (C_3H_8)[b]	Zhu et al. (1991)

[a]Abbreviations used for the techniques are defined in table I-F-3.
[b]Placed on an absolute basis using $k(OH + C_3H_8) = 1.1 \times 10^{-12}$ cm^3 molecule^{-1} s^{-1} (Atkinson et al., 2006).

atmospheric loss mechanism with a lifetime for photodissociation of about 23 h for an overhead Sun.

VIII-E-4. 1,4-Dinitrooxybutane [1,4-Butandiol Dinitrate, $CH_2(ONO_2)CH_2CH_2CH_2ONO_2$]

VIII-E-4.1. OH Reaction Kinetics

The rate coefficient of Treves and Rudich (2003) obtained by a relative rate method at atmospheric pressure and ambient temperature is given in table VIII-E-4. Two reference compounds (1-pentanol and 1-octanol) were used in this study.

VIII-E-4.2. Cl-Atom Reaction Kinetics

The rate coefficient for the reaction of Cl with 1,4-dinitrooxybutane has been measured by Treves et al. (2002). The study was carried out using a relative rate method at atmospheric pressure and ambient temperature. The rate coefficient value obtained using two reference compounds is given in table VIII-E-5.

Table VIII-E-4. Rate coefficient (k, cm^3 molecule^{-1} s^{-1}) for the reaction of OH with 1,4-dinitrooxybutane ($O_2NOCH_2CH_2CH_2CH_2ONO_2$)

$10^{12} \times k$	T (K)	Technique[a]	Reference
6.3 ± 1.3	296 ± 2	RR (1-pentanol, 1-octanol)[b]	Treves and Rudich (2003)

[a]Abbreviations used for the techniques are defined in table I-F-3.
[b]Placed on an absolute basis using $k(OH + 1\text{-pentanol}) = 1.12 \times 10^{-11}$ and $k(OH + 1\text{-octanol}) = 1.44 \times 10^{-11}$ cm^3 molecule^{-1} s^{-1}; the ratios k/k_{ref} were not given by the authors.

Table VIII-E-5. Rate coefficient (k, cm^3 molecule^{-1} s^{-1}) for the reaction of Cl with 1,4-dinitrooxybutane ($O_2NOCH_2CH_2CH_2CH_2ONO_2$)

$10^{11} \times k$	T (K)	Technique[a]	Reference
3.9 ± 0.8	296 ± 2	RR (1-butyl nitrate, 1-pentyl nitrate)[b]	Treves et al. (2002)

[a]Abbreviations used for the techniques are defined in table I-F-3.
[b]Placed on an absolute basis using $k(OH + 1\text{-butyl nitrate}) = 9.24 \times 10^{-11}$ and $k(OH + 1\text{-pentyl nitrate}) = 1.57 \times 10^{-10}$ cm^3 molecule^{-1} s^{-1}; the ratios k/k_{ref} were not given by the authors.

VIII-E-4.3. Summary of the Atmospheric Fate of 1,4-Dinitrooxybutane

The atmospheric lifetime of 1,4-butyl dinitrate with respect to its reaction with OH radicals is estimated to be around 2 days. By analogy with the observed behavior of the other butyl dinitrates, the photolysis is expected to be an important atmospheric loss mechanism for 1,4-butyl dinitrate as well, with an estimated lifetime for photodissociation of about 1 day with an overhead Sun.

VIII-E-5. *trans*-1-Methyl-1,2-dinitrooxycyclohexane

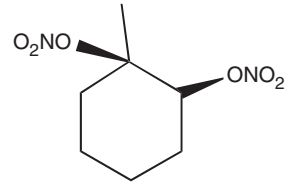

VIII-E-5.1. OH Reaction Kinetics

The rate coefficient of Wängberg et al. (1996), obtained using a relative rate method at atmospheric pressure and ambient temperature, is given in table VIII-E-6.

VIII-E-5.2. Summary of the Atmospheric Fate of trans-1-Methyl-1,2-dinitrooxycyclohexane

The atmospheric lifetime of *trans*-1-methyl-1,2-dinitrooxycyclohexane with respect to reaction with OH radicals is estimated to be around 7 days using [OH] $= 1 \times 10^6$ molecule cm^{-3} and $k = 1.66 \times 10^{-12}$ cm^3 molecule^{-1} s^{-1}. Photolysis is expected to be an important atmospheric loss mechanism as well with a lifetime for photodissociation of about 2 days with an overhead Sun (see table IX-M-1).

VIII-E-6. Trends in the Reactivity of Saturated Dinitrates

With the presence of a second deactivating nitrooxy group, reduced reactivity of OH towards alkyl dinitrates is expected if the reaction proceeds by an H-atom abstraction. Interestingly, the available experimental measurements for butane dinitrates are

Table VIII-E-6. Rate coefficient (k, cm^3 molecule^{-1} s^{-1}) for the reaction of OH with *trans*-1-methyl-1,2-dinitrooxycyclohexane

$10^{12} \times k$	T (K)	Technique[a]	Reference
1.66 ± 0.19	302 ± 1	RR (*cyclo*-C_6H_{12})[d]	Wängberg et al. (1996)

[a]Abbreviations used for the techniques are defined in table I-F-3.
[b]Placed on an absolute basis using k(*cyclo*-C_6H_{12}) $= 6.97 \times 10^{-12}$ cm^3 molecule^{-1} s^{-1} (Calvert et al., 2008).

not consistent with this expectation. The rate coefficients for the reaction of OH with 1,2-dinitrooxybutane and 2,3-dinitrooxybutane are close to the recommended value of OH with 1-butyl nitrate. The value reported by Treves and Rudich (2003) for the reaction of OH with 1,4-dinitrooxybutane is more than three times higher than that with 1-butyl nitrate. As for the alkyl nitrates, reaction with OH radicals and photolysis are expected to be the major atmospheric loss processes of alkyl dinitrates with heterogeneous processes (wet and dry deposition) also making a contribution.

VIII-F. Unsaturated Dinitrates

VIII-F-1. *cis*-1,4-Dinitrooxy-2-butene ($CH_2(ONO_2)CH{=}CHCH_2ONO_2$) and 3,4-Dinitrooxy-1-butene ($CH_2(ONO_2)CH(ONO_2)CH{=}CH_2$)

VIII-F-1.1. OH Reaction Kinetics

The rate coefficients from Zhu et al. (1991) obtained by a relative rate method at atmospheric pressure and ambient temperature are the only available data and are given in table VIII-F-1.

VIII-F-1.2. Summary of the Atmospheric Fate of cis-1,4-Dinitrooxy-2-Butene and 3,4-Dinitrooxy-1-butene

Combining the rate coefficients presented above and an OH concentration of [OH] = 1×10^6 molecule cm^{-3} provides estimates for the atmospheric lifetimes of *cis*-1,4-dinitrooxy-2-butene and 3,4-dinitrooxy-1-butene with respect to reaction with OH of about 8 h and 12 h, respectively. The reaction may proceed mainly through OH addition at the C=C bond. Photodecomposition of these compounds is expected to be a competing loss mechanism as well with lifetimes for photodissociation in the lower troposphere of about 2 days with an overhead Sun (see table IX-M-1).

VIII-F-1.3. Trends in the Reactivity of Unsaturated Dinitrates

The rate coefficients obtained for the reactions of OH with *cis*-1,4-dinitrooxy-2-butene and 3,4-dinitrooxy-1-butene are both factors of 3–4 lower than those of their parent

Table VIII-F-1. Rate coefficient (k, cm^3 molecule^{-1} s^{-1}) for the reaction of OH with unsaturated dinitrates

Compound	$10^{12} \times k$	T (K)	Technique[a]	Reference
cis-1,4-Dinitrooxy-2-butene $CH_2(ONO_2)CH{=}CHCH_2ONO_2$	14 ± 1.4	298 ± 2	RR (C_2H_4)[b]	Zhu et al. (1991)
3,4-Dinitrooxy-1-butene $CH_2(ONO_2)CH(ONO_2){=}CH_2$	9.32 ± 0.47	298 ± 2	RR (C_2H_4)[b]	Zhu et al. (1991)

[a]Abbreviations used for the techniques are defined in table I-F-3.
[b]Placed on an absolute basis using $k(OH + C_2H_4) = 7.9 \times 10^{-12}$ cm^3 molecule^{-1} s^{-1} (Atkinson et al., 2006).

alkenes (*cis*-2-butene and 1-butene, respectively). This is expected from the effect of the strongly electron-withdrawing —ONO_2 group placed next to the double bond. A mechanism similar to that for the alkenes, involving OH addition to the double bond, is probably the dominant reaction pathway. The atmospheric loss of unsaturated dinitrates via reaction with OH radicals is expected to exceed that due to photolysis (Barnes et al., 1993).

VIII-G. Hydroxyalkyl Nitrates

Hydroxyalkyl nitrates are formed during the degradation of alkanes and alkenes via different mechanisms. They are formed from both OH- and NO_3-initiated oxidation of these species. The yield of their formation increases with the size of the precursor alkane. Some of the formation channels involve isomerization processes (Arey et al., 2001; Reisen et al., 2005).

VIII-G-1. OH Reaction Kinetics

Using a relative rate method, Treves and Rudich (2003) have measured rate coefficients for reactions of OH radicals with a series of C_3–C_6 hydroxyalkyl nitrates and two C_4 unsaturated hydroxyl nitrates at atmospheric pressure and 296 ± 2 K. Wängberg et al. (1996) have reported the rate coefficient for the OH reaction with 2-nitroxy-1-cyclopentanol also using a relative rate method. The rate coefficient values obtained in both studies are given in table VIII-G-1.

The data set clearly shows that the presence of the hydroxyl group enhances the reactivity of the hydroxyalkyl nitrates towards OH radicals compared to the corresponding alkyl nitrates and alkyl dinitrates. The reactivity towards the hydroxyalkyl nitrates increases with the length of the alkyl chain and with increasing separation between the hydroxyl and the nitrooxy groups, since the presence of this latter group deactivates the reactivity. The results of Treves and Rudich (2003) for the reactions of OH with two unsaturated hydroxyalkyl nitrates show that the addition to the double bond is fast, and the OH and the —ONO_2 groups have a limited effect on the overall reaction, which is more pronounced for compounds with a double bond not hindered by hydroxy and nitrooxy groups.

The OH–hydroxyalkyl nitrate reaction rate coefficient values estimated using the parameters of Kwok and Atkinson (1995) for monofunctional alcohols and nitrates are significantly higher than those measured by Treves and Rudich (2003). This disagreement has been attributed to the opposing effects of the hydroxyl and nitrooxy groups on the reactivity.

VIII-G-2. Cl-Atom Reaction Kinetics

The only study conducted on the reaction of Cl with hydroxyalkyl nitrates is that of Treves et al. (2002) using a relative rate method at atmospheric pressure and ambient temperature. Table VIII-G-2 summarizes the available data set. The presence of the hydroxy group enhances the reactivity of hydroxyl nitrates toward Cl-atoms compared

Table VIII-G-1. Rate coefficients (k, cm^3 molecule^{-1} s^{-1}) for the reaction of OH with hydroxyalkyl nitrates

Compounds	$10^{12} \times k$	T (K)	Technique[a]	Reference
2-Nitrooxy-1-propanol	6.7 ± 1.3	296 ± 2	RR (1-pentanol and 1-octanol)[b]	Treves and Rudich (2003)
1-Nitrooxy-2-propanol	5.1 ± 1.0	296 ± 2	RR (1-pentanol and 1-octanol)[b]	Treves and Rudich (2003)
2-Nitrooxy-1-butanol	7.4 ± 1.5	296 ± 2	RR (1-pentanol and 1-octanol)[b]	Treves and Rudich (2003)
1-Nitrooxy-2-butanol	7.0 ± 1.4	296 ± 2	RR (1-pentanol and 1-octanol)[b]	Treves and Rudich (2003)
4-Nitrooxy-2-butanol	10.4 ± 4.0	296 ± 2	RR (1-pentanol and 1-octanol)[b]	Treves and Rudich (2003)
3-Nitrooxy-1-butanol	11.9 ± 4.6	296 ± 2	RR (1-pentanol and 1-octanol)[b]	Treves and Rudich (2003)
4-Nitrooxy-1-butanol	12.6 ± 2.5	296 ± 2	RR (1-pentanol and 1-octanol)[b]	Treves and Rudich (2003)
1-Nitrooxy-2-pentanol	9.8 ± 1.9	296 ± 2	RR (1-pentanol and 1-octanol)[b]	Treves and Rudich (2003)
5-Nitrooxy-2-pentanol	32.1 ± 6.4	296 ± 2	RR (1-pentanol and 1-octanol)[b]	Treves and Rudich (2003)
4-Nitrooxy-1-pentanol	28.6 ± 5.7	296 ± 2	RR (1-pentanol and 1-octanol)[b]	Treves and Rudich (2003)
6-Nitrooxy-1-hexanol	30.9 ± 6.1	296 ± 2	RR (1-pentanol and 1-octanol)[b]	Treves and Rudich (2003)
1-Nitrooxy-2-butanol-3-ene	36.2 ± 7.2	296 ± 2	RR (1-pentanol and 1-octanol)[b]	Treves and Rudich (2003)
4-Nitrooxy-1-butanol-2-ene	22.0 ± 4.4	296 ± 2	RR (1-pentanol and 1-octanol)[b]	Treves and Rudich (2003)
2-Nitroxy-1-cyclopentanol	3.53 ± 0.16[c]	302 ± 1	RR (*cyclo*-C_6H_{12})[c]	Wängberg et al. (1996)

[a]Abbreviations used for the techniques are defined in table I-F-3.

[b]Placed on an absolute basis using $k(\mathrm{OH} + \text{1-pentanol}) = 1.12 \times 10^{-11}$ and $k(\mathrm{OH} + \text{1-octanol}) = 1.44 \times 10^{-11}$ cm^3 molecule^{-1} s^{-1}, but it is not stated which was used for which compound; the ratios k/k_{ref} are not given by the authors.

[c]Placed on an absolute basis using $k(\mathrm{OH} + \textit{cyclo}\text{-}C_6H_{12}) = 6.97 \times 10^{-12}$ cm^3 molecule^{-1} s^{-1} (Calvert et al., 2008)

Table VIII-G-2. Rate coefficients (k, cm^3 molecule^{-1} s^{-1}) for the reaction of Cl with hydroxyalkyl nitrates

Compounds	$10^{10} \times k$	T (K)	Technique[a]	Reference
2-Nitrooxy-1-propanol	0.42 ± 0.08	296 ± 2	RR (1-butyl nitrate)[b]	Treves et al. (2002)
1-Nitrooxy-2-propanol	0.45 ± 0.09	296 ± 2	RR (1-butyl nitrate)[b]	Treves et al. (2002)
2-Nitrooxy-1-butanol	0.98 ± 0.10	296 ± 2	RR (1-butyl nitrate, 1-pentyl nitrate)[c]	Treves et al. (2002)
1-Nitrooxy-2-butanol	0.87 ± 0.09	296 ± 2	RR (1-butyl nitrate, 1-pentyl nitrate)[c]	Treves et al. (2002)
4-Nitrooxy-2-butanol	1.40 ± 0.16	296 ± 2	RR (1-butyl nitrate, 1-pentyl nitrate)[c]	Treves et al. (2002)
3-Nitrooxy-1-butanol	1.39 ± 0.26	296 ± 2	RR (1-butyl nitrate, 1-pentyl nitrate)[c]	Treves et al. (2002)
4-Nitrooxy-1-butanol	1.82 ± 0.36	296 ± 2	RR (1-butyl nitrate, 1-pentyl nitrate)[c]	Treves et al. (2002)
2-Nitrooxy-1-pentanol	1.59 ± 0.16	296 ± 2	RR (1-butyl nitrate, 1-pentyl nitrate)[c]	Treves et al. (2002)
1-Nitrooxy-2-pentanol	1.25 ± 0.19	296 ± 2	RR (1-butyl nitrate, 1-pentyl nitrate)[c]	Treves et al. (2002)
5-Nitrooxy-2-pentanol	2.05 ± 0.22	296 ± 2	RR (1-butyl nitrate, 1-pentyl nitrate)[c]	Treves et al. (2002)
4-Nitrooxy-1-pentanol	1.56 ± 0.31	296 ± 2	RR (1-butyl nitrate, 1-pentyl nitrate)[c]	Treves et al. (2002)
6-Nitrooxy-1-hexanol	2.44 ± 0.26	296 ± 2	RR (1-butyl nitrate, 1-pentyl nitrate)[c]	Treves et al. (2002)

[a]Abbreviations used for the techniques are defined in table I-F-3.
[b]Placed on an absolute basis using $k(\mathrm{OH} + \text{1-butyl nitrate}) = 9.24 \times 10^{-11}$ cm^3 molecule^{-1} s^{-1}.
[c]Placed on an absolute basis using $k(\mathrm{OH} + \text{1-butyl nitrate}) = 9.24 \times 10^{-11}$ and $k(\mathrm{OH} + \text{1-pentyl nitrate}) = 1.57 \times 10^{-10}$ cm^3 molecule^{-1} s^{-1}

to the corresponding alkyl nitrates, as is observed with OH reactivity. Also, the reactivity between Cl and hydroxyl nitrates increases with the length of the alkyl chain and the increase of the separation between the nitrooxy and hydroxyl groups, as is the case for the reaction of OH with hydroxyalkyl nitrates.

VIII-G-3. Summary of the Atmospheric Fate of Hydroxynitrates

The atmospheric lifetime of hydroxyl nitrates with respect to removal by reaction with OH is calculated to be of the order of 3 h to 3 days. Hydroxyalkyl nitrates have high solubility in water and low volatility and may partition into liquid water and organic aerosols, and may be removed from the atmosphere through wet deposition and incorporation into aerosols with high organic content (Shepson et al., 1996; Treves et al., 2000). Shepson et al. estimated that up to 60% of the atmospheric removal for these species occurs via wet deposition. Treves and Rudich (2003) have suggested that a substantial fraction of the long chain hydroxyalky nitrates may reside in the organic aerosols, especially at low temperatures and high aerosol loading. The removal through gas-phase processes is mainly controlled by reaction with OH radicals. The reaction with Cl-atoms may have a measurable contribution in specific regions where Cl-atoms concentrations could be high, such as the marine boundary layer. On the basis of the available cross section data for the hydroxyalkyl nitrates, Treves and Rudich (2003) conclude that these compounds have no significant absorption in the actinic region and photodecomposition is probably not competitive with other loss mechanisms. For example, the lifetime for photodissociation of $HOCH_2CH_2ONO_2$ is estimated to be about 4 months for an overhead Sun (see table IX-M-1). For the hydroxyalkyl nitrates that contain a double bond, reaction with OH is expected to be more important than wet deposition.

Hydroxyalkyl nitrates are more reactive in the gas phase than alkyl nitrates and are more soluble in water. It is expected that hydroxynitrates are less-effective transporters of NO_x than are the alkyl nitrates. On the other hand, the OH-initiated oxidation of hydroxyl nitrates may lead to long-lived carbonyl nitrates, which could play a role in the long-range transport of NO_x.

VIII-H. Carbonyl Nitrates

VIII-H-1. OH Reaction Kinetics

All the measurements reported on the reaction of OH radicals with carbonyl nitrates are from the same group (Zhu et al., 1991; Wängberg et al., 1996); see table VIII-H-1. They were performed using a relative rate method at atmospheric pressure and ambient temperature. The rate coefficients for the reaction of OH with α-nitrooxy acetone ($CH_3C(O)CH_2ONO_2$), 1-nitrooxy-2-butanone [$CH_3CH_2C(O)CH_2ONO_2$], and 3-nitrooxy-2-butanone [$CH_3CH(ONO_2)C(O)CH_3$]

Table VIII-H-1. Rate coefficients (k, cm^3 molecule^{-1} s^{-1}) for the reaction of OH with carbonyl nitrates

Molecule	T (K)	$10^{12} \times k$	Technique[a]	Reference
α-Nitrooxy acetone	298 ± 2	< 0.4	RR (n-C_4H_{10})[b]	Zhu et al. (1991)
1-Nitrooxy-2-butanone	298 ± 2	0.84 ± 0.14	RR (n-C_4H_{10})[b]	Zhu et al. (1991)
3-Nitrooxy-2-butanone	298 ± 2	1.17 ± 0.13	RR (n-C_4H_{10})[b]	Zhu et al. (1991)
2-Oxo-cyclohexyl-1-nitrate	302 ± 1	3.47 ± 0.33	RR (*cyclo*-C_6H_{12})[c]	Wängberg et al. (1996)

[a]Abbreviations used for the techniques are defined in table I-F-3.
[b]Placed on an absolute basis using $k(\mathrm{OH} + n\text{-}C_4H_{10}) = 2.35 \times 10^{-12}$ cm^3 molecule^{-1} s^{-1} (Atkinson et al., 2006).
[c]Placed on an absolute basis using $k(\mathrm{OH} + cyclo\text{-}C_6H_{12}) = 6.97 \times 10^{-12}$ cm^3 molecule^{-1} s^{-1} (Calvert et al., 2008).

were determined. Wängberg et al. (1996) studied the reaction of OH with 2-oxo-cyclohexyl-1-nitrate:

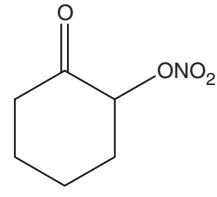

The IUPAC panel recommended rate coefficients values at 298 K are based on these single measurements, but with higher uncertainties, ±30%, (Atkinson et al., 2006):

$$k(\mathrm{OH} + \alpha\text{-nitrooxyacetone}) < 1 \times 10^{-12} \text{ cm}^3 \text{ molecule}^{-1} \text{ s}^{-1}$$

$$k(\mathrm{OH} + \text{1-nitrooxy-2-butanone}) = 8.2 \times 10^{-13} \text{ cm}^3 \text{ molecule}^{-1} \text{ s}^{-1}$$

$$k(\mathrm{OH} + \text{3-nitrooxy-2-butanone}) = 1.2 \times 10^{-12} \text{ cm}^3 \text{ molecule}^{-1} \text{ s}^{-1}$$

While the measured values are not too different from those for the parent compound for the butanone derivatives (k(OH + 2-butanone) = 1.11×10^{-12} cm^3 molecule^{-1} s^{-1}, this book, section V-B-2.1), Wängberg et al. have reported a lower reactivity for 2-oxo-cyclohexyl-1-nitrate [$(3.5 \pm 0.3) \times 10^{-12}$ cm^3 molecule^{-1} s^{-1}] compared to that of cyclohexanone (k(OH + cyclohexanone) = 6.4×10^{-12} cm^3 molecule^{-1} s^{-1}, this book, section V-F-3.1).

VIII-H-2. Summary of the Atmospheric Fate of Carbonyl Nitrates

Combining the rate coefficient values reported above and a diurnal average [OH] = 10^6 molecule cm^{-3} provides an estimate of the atmospheric lifetime of carbonyl nitrates with respect to removal by reaction with OH in the range 3 to 30 days. Photolysis is also likely to be an important atmospheric loss mechanism. Wängberg et al. (1996) conclude that the photodecomposition in the troposphere is unimportant for *trans*-2-hydroxy-cyclopentyl-1-nitrate (no significant absorption); but both 2-oxo-cyclohexyl-1-nitrate

and *trans*-1-cyclohexyl-1,2-dinitrate absorb tropospheric radiation significantly, and globally averaged photolysis lifetimes of 1.6 and 7.7 days, respectively, were estimated, assuming a quantum yield of unity. See section IX-I-4 and table IX-M-1.

VIII-I. Alkyl Nitrites

Small amounts of alkyl nitrites may be formed by reaction of alkoxy radicals with NO. Direct emission of alkyl nitrites from combustion and the burning of alcohol-based fuels has been suggested. However, they have not been observed in the atmosphere at significant concentrations since they are rapidly photolyzed (see section IX-H).

VIII-I-1. Nitrous Acid [HONO]

VIII-I-1.1. OH Reaction Kinetics

The rate coefficients of Cox et al. (1976), Jenkin and Cox (1987) and Burkholder et al. (1992) are given in table VIII-I-1 and shown in figure VIII-I-1. Cox et al. (1976) measured their value relative to $k(\mathrm{OH} + \mathrm{H_2})$. Jenkin and Cox (1987) and Burkholder et al. (1992) determined the rate coefficient as function of temperature using, respectively, molecular modulation combined with time-resolved absorption and pulsed laser photolysis–laser-induced fluorescence techniques. While the different ambient temperature measurements are in reasonable agreement, there are significant differences with respect to the temperature dependence between Jenkin and Cox (1987) and Burkholder et al. (1992). The preferred value at 298 K is an average of the three determinations, $k = 6.0 \times 10^{-12}$ cm^{-3} molecule^{-1} s^{-1}, with an estimated uncertainty of ±50%. The preferred temperature dependence is that of Burkholder et al. (1992) with an adjustment of the pre-exponential factor to fit the preferred ambient temperature value, $k = 2.5 \times 10^{-12} \exp(260/T)$ cm^{-3} molecule^{-1} s^{-1}. However, fitting the combined data above 298 K gives $k = 4.7 \times 10^{-12} \exp(75/T)$ cm^{-3} molecule^{-1} s^{-1}.

Table VIII-I-1. Rate coefficients ($k = A \times e^{-B/T}$), cm^3 molecule^{-1} s^{-1}) for the reaction of OH with nitrous acid (HONO)

$10^{12} \times A$	B (K)	$10^{12} \times k$	T (K)	Technique[a]	Reference	Temperature Range (K)
		6.3 ± 0.4	296	RR (H_2)	Cox et al. (1976)	
18	390 ± 80	4.51	278	MM–RA	Jenkin and Cox (1987)	278–342
		4.50	294.6			
		5.28	323			
		5.38	342.5			
2.8	−260 ± 140	7.05 ± 0.26	298	PLP–LIF	Burkholder et al. (1992)	298–373
		6.25 ± 0.14	318			
		6.19 ± 0.18	337			
		5.82 ± 0.26	373			

[a]Abbreviations used for the techniques are defined in table I-F-3.
[b]Placed on an absolute basis using $k(\mathrm{OH} + \mathrm{H_2}) = 6.7 \times 10^{-15}$ cm^3 molecule^{-1} s^{-1} (Atkinson et al., 2008).

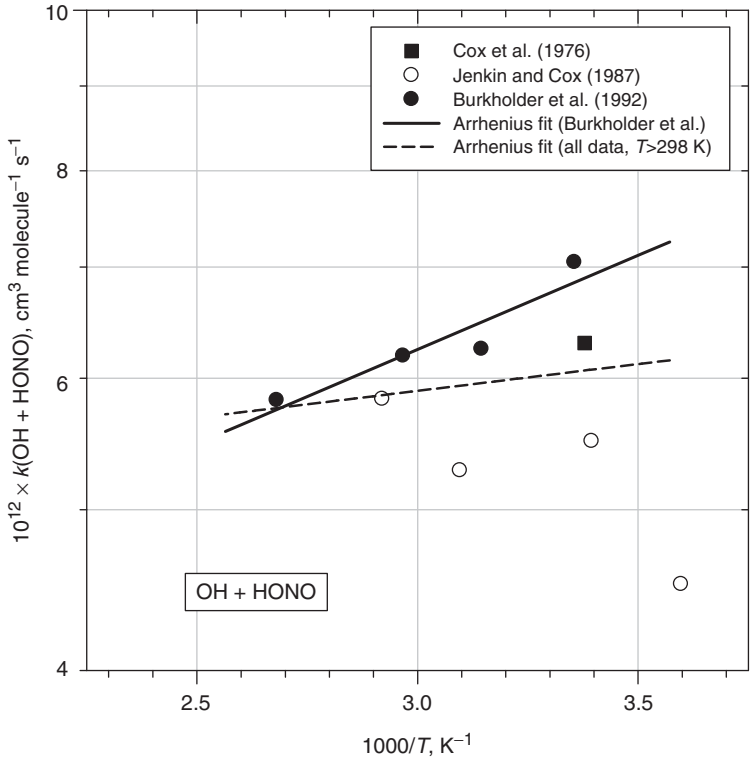

Figure VIII-I-1. Arrhenius plot of the rate coefficient for the reaction of OH with HONO.

VIII-I-1.2. NO_3 Reaction Kinetics

The upper limit to the rate coefficient of NO_3 with HONO obtained by Wallington and Japar (1989) is given in table VIII-I-2. This determination was performed using Fourier transform infrared spectroscopy at 700 Torr total pressure in synthetic air or argon.

VIII-I-1.3. O_3 Reaction Kinetics

The upper limits to the rate coefficient reported by Kaiser and Japar (1977) and Streit et al. (1979) are given in table VIII-I-3. The measurement of Kaiser and Japar (1977) was conducted at a total pressure of 20–30 Torr of argon by monitoring the decay of

Table VIII-I-2. Rate coefficient (k, cm^3 molecule^{-1} s^{-1}) for the reaction of NO_3 with nitrous acid (HONO)

$10^{15} \times k$	T (K)	Technique[a]	Reference
2	295	Decay of HONO[b]	Wallington and Japar (1989)

[a]Abbreviations used for the techniques are defined in table I-F-3.
[b]Value determined by observing the decay of HONO by FTIR.

Table VIII-I-3. Rate coefficients (k, cm^3 molecule^{-1} s^{-1}) for the reaction of O_3 with nitrous acid (HONO)

$10^{19} \times k$	T (K)	Technique[a]	Reference
< 5	226	Decay of HONO[b]	Kaiser and Japar (1977)
< 1	300		
$\leq 4.5 \pm 3$	296 ± 2	TDLS	Streit et al. (1979)

[a]Abbreviations used for the techniques are defined in table I-F-3.
[b]Value determined by monitoring the decay of HONO by mass spectrometry.

HONO by mass spectrometry at 226 and 300 K. Streit et al. used tunable diode laser spectroscopy to monitor the decay of HONO in the presence of ozone at 296 K.

VIII-I-1.4. Summary of the Atmospheric Fate of Nitrous Acid

The atmospheric lifetime of nitrous acid with respect to OH radicals is about 2 days. However, photolysis is the most important loss process of HONO during the daytime; with an overhead Sun, its lifetime from photodecomposition is only about 10 min.; see table IX-M-1. The reaction with OH can play a significant role during nighttime if the OH radical is produced. HONO can be an important source of OH radicals in the troposphere; see section IX-H-1.

VIII-I-2. Methyl Nitrite (CH_3ONO)

VIII-I-2.1. OH Reaction Kinetics

The rate coefficient for the reaction of OH with methyl nitrite has been measured by a number of groups. Campbell and Goodman (1975), Audley et al. (1982), and Tuazon et al. (1983) used relative rate methods while Baulch et al. (1985) used an absolute technique. Nielsen et al. (1991) used both relative and absolute methods. Table VIII-I-4 and figure VIII-I-2 summarize the different measurements. The rate coefficient value determined by Nielsen et al. (1991) is consistent with the relative rate constant of Tuazon et al. (1983) but is lower by a factor of 3–4 than those of Campbell and Goodman (1975), Audley et al. (1982), and Baulch et al. (1985).

As described in this section, the rate coefficients for the reactions of OH with ethyl nitrite, *n*-propyl nitrite and *n*-butyl nitrite reported by Nielsen et al. are systematically lower (by about a factor of 2) than the previous determinations of Campbell and Goodman (1975) and Audley et al. (1982). This disagreement has been attributed to the complications associated with the relative rate method of Campbell and Goodman (1975), and Audley et al. (1982) employing the heterogeneous reaction between H_2O_2 and NO_2 to generate OH radicals in the dark. If this is the case, the rate coefficients for OH reaction with the other investigated alkyl nitrites (2-butyl nitrite, 2-methy-1-propyl nitrite, and 2-methy-2-propyl nitrite) could be overestimated as well. Consequently, the rate constants reported by Nielsen et al. are preferred (Atkinson, 1994).

Table VIII-I-4. Rate coefficients (k, cm^3 molecule^{-1} s^{-1}) for the reaction of OH with methyl nitrite (CH_3ONO)

$10^{13} \times k$	T (K)	Technique[a]	Reference	Temperature Range (K)
12.5 ± 1.7	292 ± 2	RR (CO)[b]	Campbell and Goodman (1975)	
10.3 ± 1.99	295 ± 3	RR (n-C_4H_{10})[c]	Audley et al. (1982)	
2.0 ± 0.4	300 ± 3	RR (n-C_6H_{14})[d]	Tuazon et al. (1983)	
1.11 ± 0.24		RR (CH_3OCH_3)[e]		
10 ± 1.5	295 ± 2	DF–RF	Baulch et al. (1985)	
2.7 ± 0.9	298 ± 2	RR [$CH(CH_3)_3$][f]	Nielsen et al. (1991)	298–393
2.6 ± 0.5	298	PR–UV abs.		
4.2 ± 0.3	323			
7.4 ± 1.0	353			
10.5 ± 1.0	393			

[a]Abbreviations used for the techniques are defined in table I-F-3.
[b]Placed on an absolute basis using $k(OH + CO) = 1.4 \times 10^{-13}$ cm^3 molecule^{-1} s^{-1}.
[c]Placed on an absolute basis using $k(OH + n\text{-}C_4H_{10}) = 2.35 \times 10^{-12}$ cm^3 molecule^{-1} s^{-1} (Atkinson et al., 2006).
[d]Placed on an absolute basis using $k(OH + n\text{-}C_6H_{14}) = 5.27 \times 10^{-12}$ cm^3 molecule^{-1} s^{-1} (Calvert et al., 2008).
[e]Placed on an absolute basis using $k(OH + CH_3OCH_3) = 2.7 \times 10^{-12}$ cm^3 molecule^{-1} s^{-1} (this book, section III-B-1,1).
[f]Placed on an absolute basis using $k[OH + CH(CH_3)_3] = 2.12 \times 10^{-12}$ cm^3 molecule^{-1} s^{-1} (Calvert et al., 2008).

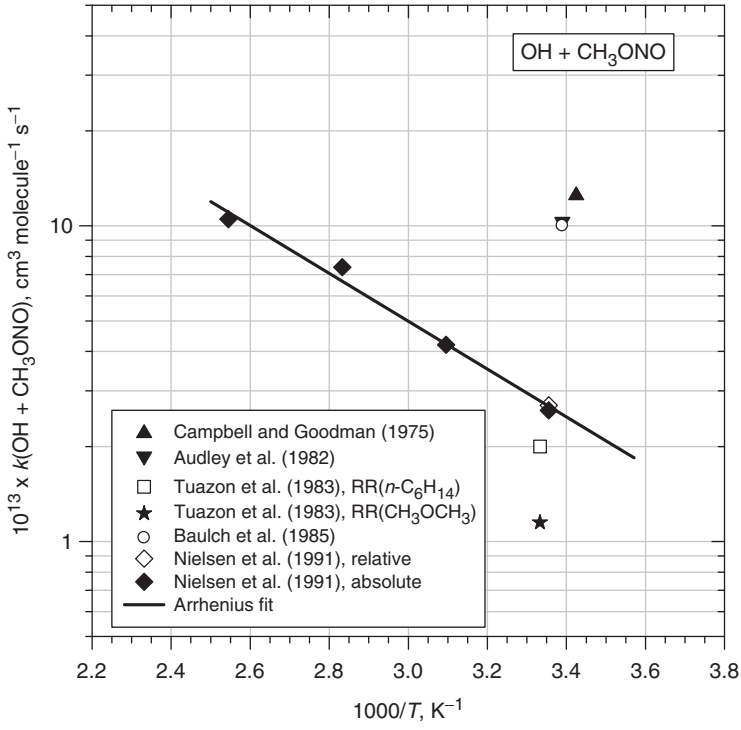

Figure VIII-I-2. Arrhenius plot of the rate coefficient for the reaction of OH with methyl nitrite.

The absolute temperature dependence study of Nielsen et al. (1991) in the range 298–393 K leads to the following temperature dependence of the reaction of OH with CH_3ONO:

$$k = \left(1.0^{+1.3}_{-0.5}\right) \times 10^{-12} \exp[-(1{,}764 \pm 300)/T] \text{ cm}^3 \text{ molecule}^{-1} \text{ s}^{-1}.$$

VIII-I-2.2. Cl-Atom Reaction Kinetics

The rate coefficients reported by Nielsen et al. (1991) and Sokolov et al. (1999) are given in table VIII-I-5. Both measurements were conducted using relative rate methods at atmospheric pressure and ambient temperature. The rate coefficient value reported by Sokolov et al. (1999) is approximately a factor of 5 lower than that reported by Nielsen et al. (1991). As noted by Sokolov et al., this disagreement probably reflects that fact that Nielsen et al. did not account for loss of CH_3ONO via photolysis in their experiments. Three different reference compounds were used by Sokolov et al. (1999) and the resulting values of $k(Cl + CH_3ONO)$ were indistinguishable. Furthermore, Nielsen et al. (1991) used a reference compound (ethane) which is much more reactive than methyl nitrate, leading to small consumptions of CH_3ONO, which are difficult to measure. Consequently, the preferred value is then that of Sokolov et al., $k = 2.1 \times 10^{-12}$ cm^3 molecule^{-1} s^{-1} at 298 K with an estimated uncertainty of $\pm 15\%$.

VIII-I-2.3. Summary of the Atmospheric Fate of Methyl Nitrite

The atmospheric lifetime of methyl nitrite with respect to reaction with OH radicals is estimated to be around 1 month. Methyl nitrite is dissociated quite rapidly by solar radiation, as it absorbs strongly in the actinic region; the lifetime for photodissociation with an overhead Sun is about 8 ± 1 min. (see table IX-M-1). Because of this rapid photolysis, other reactions such as with OH radicals are considered to be of minor importance as loss processes for this species from the atmosphere.

Table VIII-I-5. Rate coefficients (k, cm^3 molecule^{-1} s^{-1}) for the reaction of Cl with methyl nitrite (CH_3ONO)

$10^{12} \times k$	T (K)	Technique[a]	Reference
8.53 ± 0.07	298 ± 2	RR (C_2H_6)[b]	Nielsen et al. (1991)
1.95 ± 0.12	295 ± 2	RR (C_2H_5Cl)[c]	Sokolov et al. (1999)
2.25 ± 0.14		RR (CH_3OCHO)[d]	
2.03 ± 0.07		RR (CH_3Cl)[e]	

[a]Abbreviations used for the techniques are defined in table I-F-3.
[b]Placed on an absolute basis using $k(Cl + C_2H_6) = 5.7 \times 10^{-11}$ cm^3 molecule^{-1} s^{-1} (Calvert et al., 2008).
[c]Placed on an absolute basis using $k(Cl + C_2H_5Cl) = 7.8 \times 10^{-12}$, cm^3 molecule^{-1} s^{-1} (section I-F).
[d]Placed on an absolute basis using $k(Cl + CH_3OCHO) = 1.4 \times 10^{-12}$ cm^3 molecule^{-1} s^{-1} (this book, section VII-B-1.1).
[e]Placed on an absolute basis using $k(Cl + CH_3Cl) = 4.8 \times 10^{-13}$ cm^3 molecule^{-1} s^{-1} (Sander et al., 2006).

VIII-I-3. Ethyl Nitrite (C_2H_5ONO)

VIII-I-3.1. OH Reaction Kinetics

The rate coefficient for the reaction of OH with ethyl nitrite was determined by Audley et al. (1982) and Nielsen et al. (1991). Audley et al. (1982) used a relative rate method while Nielsen et al. (1991) used both absolute and relative methods. The rate coefficient values obtained in these two studies are given in table VIII-I-6. The values reported by Nielsen et al. using the two techniques are in agreement but both are lower than the value obtained by Audley et al. As described above, the measurement of Audley et al. (1982) could have been affected by problems associated with their unusual method of HO radical generation. Consequently, the values of Nielsen et al. are preferred, and we recommend $k = 6.7 \times 10^{-13}$ cm^3 molecule^{-1} s^{-1} with an estimated uncertainty of $\pm 30\%$ at 298 K.

VIII-I-3.2. Cl-Atom + C_2H_5ONO Reaction Kinetics

The only available data are from Nielsen et al. (1991) who used a relative rate method at ambient temperature and atmospheric pressure. The rate coefficient value obtained is given in table VIII-I-7. However, as described in the reaction of Cl with CH_3ONO, the Nielsen et al. (1991) measurement could have been affected by loss of the nitrite by photolysis during the experiments, and this may lead to an overestimation of the reaction rate coefficient.

VIII-I-3.3. Summary of the Atmospheric Fate of Ethyl Nitrite

The atmospheric lifetime of ethyl nitrite with respect to reaction with OH radicals is estimated to be approximately 17 days. However, as is the case with other alkyl nitrites,

Table VIII-I-6. Rate coefficients (k, cm^3 molecule^{-1} s^{-1}) for the reaction of OH with ethyl nitrite (C_2H_5ONO)

$10^{13} \times k$	T (K)	Technique[a]	Reference
17.7 ± 2.6	295 ± 3	RR (n-C_4H_{10})[b]	Audley et al. (1982)
6.3 ± 1.3	298 ± 2	RR [$CH(CH_3)_3$][c]	Nielsen et al. (1991)
7.0 ± 1.1	298 ± 2	PR–UV abs.	

[a]Abbreviations used for the techniques are defined in table I-F-3.
[b]Placed on an absolute basis using $k(OH + n\text{-}C_4H_{10}) = 2.35 \times 10^{-12}$ cm^3 molecule^{-1} s^{-1} (Atkinson et al., 2006).
[c]Placed on an absolute basis using $k[OH + CH(CH_3)_3] = 2.12 \times 10^{-12}$ cm^3 molecule^{-1} s^{-1} (Calvert et al., 2008).

Table VIII-I-7. Rate coefficient (k, cm^3 molecule^{-1} s^{-1}) for the reaction of Cl with ethyl nitrite (C_2H_5ONO)

$10^{11} \times k$	T (K)	Technique[a]	Reference
2.75 ± 0.13	298 ± 2	RR (C_2H_6)[b]	Nielsen et al. (1991)

[a]Abbreviations used for the techniques are defined in table I-F-3.
[b]Placed on an absolute basis using $k(Cl + C_2H_6) = 5.7 \times 10^{-11}$ cm^3 molecule^{-1} s^{-1} (Calvert et al., 2008).

ethyl nitrite will be removed from the atmosphere largely by photolysis; its lifetime for photodissociation with overhead Sun is about 29 min. (see table IX-M-1).

VIII-I-4. *n*-Propyl Nitrite (*n*-C_3H_7ONO)

VIII-I-4.1. OH Reaction Kinetics

Table VIII-I-8 summarizes the existing dataset for the rate coefficients of the reaction of OH with *n*-propyl nitrite. This reaction was investigated by Audley et al. (1982), Baulch et al. (1985), and Nielsen et al. (1991). Audley et al. (1982) used a relative rate method, Baulch et al. used a discharge flow system with resonance fluorescence for monitoring OH radicals, while Nielsen et al. (1991) used both an absolute and relative method. The rate coefficient values obtained by Audley et al. and Baulch et al. are in agreement but higher than that of Nielsen et al. The reason for the disagreement between the values reported by Baulch et al. and Nielsen et al. is not clear. Consistent with the preferred values for methyl and ethyl nitrite from Nielsen et al. and the possible problems associated with the OH-generation method used by Audley et al., the lower value from Nielsen et al. (1991) is preferred for the OH reaction with *n*-propyl nitrite. Based on the average of the relative and absolute measurements, we recommend $k = 1.1 \times 10^{-12}$ cm^3 molecule^{-1} s^{-1} at 298 K with an uncertainty estimated to be $\pm$30%. Further work is needed to improve our understanding of this reaction.

VIII-I-4.2. Cl-Atom + n-C_3H_7ONO Reaction Kinetics

The only available data are from Nielsen et al. (1991), who used a relative rate method at ambient temperature and atmospheric pressure. The rate coefficient value obtained is given in table VIII-I-9. However, as described in the reaction of Cl with CH_3ONO, the Nielsen et al. (1991) measurement could have been affected by loss of the nitrite by photolysis during the experiments, and this may lead to an overestimation of the reaction rate coefficient.

VIII-I-4.3. Summary of the Atmospheric Fate of n-Propyl Nitrite

The atmospheric lifetime of *n*-propyl nitrite with respect to reaction with OH radicals using an average [OH] $= 1 \times 10^6$ molecule cm^{-3} and $k = 1.1 \times 10^{-12}$ cm^3

Table VIII-I-8. Rate coefficients (k, cm^3 molecule^{-1} s^{-1}) for the reaction of OH with *n*-propyl nitrite (*n*-C_3H_7ONO)

$10^{12} \times k$	T (K)	Technique[a]	Reference
2.26 ± 0.45	295 ± 3	RR (*n*-C_4H_{10})[b]	Audley et al. (1982)
2.31 ± 0.32	295 ± 2	DR–RF	Baulch et al. (1985)
1.0 ± 0.14	298 ± 2	RR ($CH(CH_3)_3$)[c]	Nielsen et al. (1991)
1.2 ± 0.05	298 ± 2	PR–UV abs.	

[a]Abbreviations used for the techniques are defined in table I-F-3.
[b]Placed on an absolute basis using $k(OH + n\text{-}C_4H_{10}) = 2.35 \times 10^{-12}$ cm^3 molecule^{-1} s^{-1} (Atkinson et al., 2006).
[c]Placed on an absolute basis using $k[OH + CH(CH_3)_3] = 2.12 \times 10^{-12}$ cm^3 molecule^{-1} s^{-1} (Calvert et al., 2008).

Table VIII-I-9. Rate coefficient (k, cm^3 molecule^{-1} s^{-1}) for the reaction of Cl with n-propyl nitrite (n-C_3H_7ONO)

$10^{11} \times k$	T (K)	Technique[a]	Reference
6.04 ± 0.54	298 ± 2	RR (C_2H_6)[b]	Nielsen et al. (1991)

[a]Abbreviations used for the techniques are defined in table I-F-3.
[b]Placed on an absolute basis using $k(Cl + C_2H_6) = 5.7 \times 10^{-11}$ cm^3 molecule^{-1} s^{-1} (Calvert et al., 2008).

molecule^{-1} s^{-1} is calculated to be about 10 days. However, as with other alkyl nitrites, n-propyl nitrite will be removed from the atmosphere largely by photolysis; the lifetime for photodissociation with an overhead Sun is about 22 min. (see table IX-M-1).

VIII-I-5. n-Butyl Nitrite (n-C_4H_9ONO)

VIII-I-5.1. OH Reaction Kinetics

The rate coefficient values determined by Audley et al. (1982), Baulch et al. (1985), and Nielsen et al. (1991) are given in table VIII-I-10. Audley et al. (1982) used a relative rate method, Baulch et al. used an absolute technique, and Nielsen et al. (1991) used both an absolute and relative methods. As mentioned above for other alkyl nitrites, the rate coefficient values measured by Audley et al. and Baulch et al. are in agreement but are a factor of 2 higher than that of Nielsen et al. For the same reasons discussed above, the measurement of Nielsen et al. (1991) is preferred, leading to a value of $k = 2.4 \times 10^{-12}$ cm^3 molecule^{-1} s^{-1} at 298 K, based on the average of the relative and absolute measurements, to which a large uncertainty should be associated.

VIII-I-5.2. Cl-Atom + n-C_4H_9ONO Reaction Kinetics

The sole study of this reaction is that of Nielsen et al. (1991) who used a relative rate method at ambient temperature and atmospheric pressure. The rate coefficient value obtained is given in table VIII-I-11. However, as described in the reaction of Cl with CH_3ONO, the Nielsen et al. (1991) measurement could have been affected by loss of the nitrite by photolysis during the experiments, and this may lead to an overestimation of the reaction rate coefficient.

Table VIII-I-10. Rate coefficients (k, cm^3 molecule^{-1} s^{-1}) for the reaction of OH with n-butyl nitrite (n-C_4H_9ONO)

$10^{12} \times k$	T (K)	Technique[a]	Reference
4.92 ± 1.65	295 ± 3	RR (n-C_4H_{10})[b]	Audley et al. (1982)
4.80 ± 0.72	295 ± 2	DR–RF	Baulch et al. (1985)
2.06 ± 0.07	298 ± 2	RR [$CH(CH_3)_3$][c]	Nielsen et al. (1991)
2.72 ± 0.60	298 ± 2	PR–UV abs.	

[a]Abbreviations used for the techniques are defined in table I-F-3.
[b]Placed on an absolute basis using $k(OH + n\text{-}C_4H_{10}) = 2.35 \times 10^{-12}$ cm^3 molecule^{-1} s^{-1} (Atkinson et al., 2006).
[c]Placed on an absolute basis using $k[OH + CH(CH_3)_3] = 2.12 \times 10^{-12}$ cm^3 molecule^{-1} s^{-1} (Calvert et al., 2008).

Table VIII-I-11. Rate coefficient (k, cm^3 molecule^{-1} s^{-1}) for the reaction of Cl with n-butyl nitrite (n-C_4H_9ONO)

$10^{10} \times k$	T (K)	Technique[a]	Reference
1.29 ± 0.06	298 ± 2	RR (C_2H_6)[b]	Nielsen et al. (1991)

[a]Abbreviations used for the techniques are defined in table I-F-3.
[b]Placed on an absolute basis using $k(Cl + C_2H_6) = 5.7 \times 10^{-11}$ cm^3 molecule^{-1} s^{-1} (Calvert et al., 2008).

VIII-I-5.3. Summary of the Atmospheric Fate of n-Butyl Nitrite

The atmospheric lifetime of n-butyl nitrite with respect to reaction with OH radicals is calculated to be about 10 days. However, as with other alkyl nitrites, n-butyl nitrite will be removed from the atmosphere essentially exclusively by photolysis; the lifetime for photodissociation with an overhead Sun is about 38 min.; see table IX-M-1.

VIII-I-6. Higher Alkyl Nitrites

VIII-I-6.1. OH Reaction Kinetics

The rate coefficient values available for 2-butyl nitrite, 2-methyl-1-propyl nitrite, 2-methyl-2-propyl nitrite, and 1-pentyl nitrite are given in table VIII-I-12. As mentioned for other alkyl nitrites, the measurements of Audley et al. (1982) might be overestimated. The rate coefficient determinations for the reaction of OH with n-pentyl nitrite of Nielsen et al. (1991) using both relative and absolute methods are in reasonable agreement.

VIII-I-6.2. Cl-Atom Reaction Kinetics

The sole study of a higher alkyl nitrite, n-pentyl nitrite, is that of Nielsen et al. (1991). A relative rate method was used at ambient temperature and atmospheric pressure. The rate coefficient value obtained is given in table VIII-I-13. However, as described in the reaction of Cl with CH_3ONO, the Nielsen et al. (1991) measurement could have been

Table VIII-I-12. Rate coefficients (k, cm^3 molecule^{-1} s^{-1}) for the reaction of OH with higher alkyl nitrites

Molecule	$10^{12} \times k$	T (K)	Technique[a]	Reference
$CH_3CH_2CH(ONO)CH_3$	5.61 ± 0.67	295 ± 3	RR (n-C_4H_{10})[b]	Audley et al. (1982)
$(CH_3)_2CHCH_2ONO$	5.03 ± 0.61	295 ± 3	RR (n-C_4H_{10})[b]	Audley et al. (1982)
$(CH_3)_3CONO$	1.33 ± 0.19	295 ± 3	RR (n-C_4H_{10})[b]	Audley et al. (1982)
n-$C_5H_{10}ONO$	3.39 ± 0.45	298 ± 2	RR [$CH(CH_3)_3$][c]	Nielsen et al. (1991)
	4.25 ± 0.8	298 ± 2	PR–UV abs.	

[a]Abbreviations used for the techniques are defined in table I-F-3.
[b]Placed on an absolute basis using $k(OH + n\text{-}C_4H_{10}) = 2.35 \times 10^{-12}$ cm^3 molecule^{-1} s^{-1} (Atkinson et al., 2006).
[c]Placed on an absolute basis using $k[OH + CH(CH_3)_3] = 2.12 \times 10^{-12}$ cm^3 molecule^{-1} s^{-1} (Calvert et al., 2008).

Table VIII-I-13. Rate coefficient (k, cm^3 molecule^{-1} s^{-1}) for the reaction of Cl with n-pentyl nitrite (n-$C_5H_{11}ONO$)

$10^{10} \times k$	T (K)	Technique[a]	Reference
2.30 ± 0.42	298 ± 2	RR (C_2H_6)[b]	Nielsen et al. (1991)

[a]Abbreviations used for the techniques are defined in table I-F-3.
[b]Placed on an absolute basis using $k(Cl + C_2H_6) = 5.7 \times 10^{-11}$ cm^3 molecule^{-1} s^{-1} (Calvert et al., 2008).

affected by loss of the nitrite by photolysis during the experiments, and this may lead to an overestimation of the reaction rate coefficient.

VIII-I-6.3. Summary of the Atmospheric Fate of Higher Alkyl Nitrites

Alkyl nitrites will be removed from the troposphere largely by photolysis. Hence, their reactions with OH radicals may have only a small contribution to the overall loss of these species from the atmosphere. See table IX-M-1.

VIII-I-7. Trends in the Reactivity of Alkyl Nitrites (RONO)

The existing rate coefficient data set for the reaction of OH radicals with alkyl nitrites shows that the rate coefficients increase with the size of R in RONO, indicating that H-atom abstraction is the dominant reaction mechanism. The positive activation energy for the reaction of OH with CH_3ONO determined by Nielsen et al. (1991) is in line with such a mechanism. However, a contribution from an addition pathway leading to $CH_3ON(OH)O$ species which can decompose to yield CH_3O + HONO cannot be ruled out, but this has not been reported in any product studies.

VIII-J. Nitroalkanes

Nitroalkanes are used both as propellants and as solvents (in extractions, as a reaction medium, and in cleaning applications). As an intermediate in organic synthesis, they are used widely in the manufacture of pharmaceuticals, pesticides, explosives, fibers, and coatings. All of these uses can result in their emission into the atmosphere.

VIII-J-1. Nitromethane (CH_3NO_2)

VIII-J-1.1. OH Reaction Kinetics

Table VIII-J-1 and figure VIII-J-1 summarize the rate coefficient values available in the literature. The number of investigations of this reaction is rather limited. The absolute measurements of the rate coefficients for OH with CH_3NO_2 reported by Zabarnick et al. (1988b) and Liu et al. (1990b) are in agreement but significantly lower than that from Nielsen et al. (1988). The measurements of Campbell and Goodman (1975) are thought to be in error because of the complexity of the OH generation method used by these authors. Generally, the rate constants values obtained at low pressure by Liu et al.

Table VIII-J-1. Rate coefficients ($k = A \times e^{-B/T}$), cm^3 $molecule^{-1}$ s^{-1}) for the reaction of OH with nitromethane (CH_3NO_2)

$10^{13} \times A$	B (K)	$10^{14} \times k$	T (K)	Technique[a]	Reference	Temperature Range (K)
		8.9 ± 0.9	292 ± 2	RR (CO)[b]	Campbell and Goodman (1975)	
		10.9 ± 1.0	295 ± 2	RR $[C(CH_3)_4]$[c]	Nielsen et al. (1988, 1989)	
		16 ± 5	295 ± 2	PR–UV abs.		
		1.74 ± 0.38	299	LP–LIF	Zabarnick et al. (1988b)	299–671
8.1 ± 3.2	$1{,}208 \pm 608$	1.41 ± 0.3	300			
		2.73 ± 0.85	372			
		5.8 ± 1.4	473			
		7.35 ± 0.71	572			
		19.3 ± 3	671			
		1.58 ± 0.09	298	FP–RF	Liu et al. (1990b)	298–400
		3.21 ± 0.57	400			

[a]Abbreviations used for the techniques are defined in table I-F-3.
[b]Placed on an absolute basis using $k(OH + CO) = 1.4 \times 10^{-13}$ cm^3 $molecule^{-1}$ s^{-1}.
[c]Placed on an absolute basis using $k[OH + C(CH_3)_4] = 8.2 \times 10^{-13}$ cm^3 $molecule^{-1}$ s^{-1} (Calvert et al., 2008).

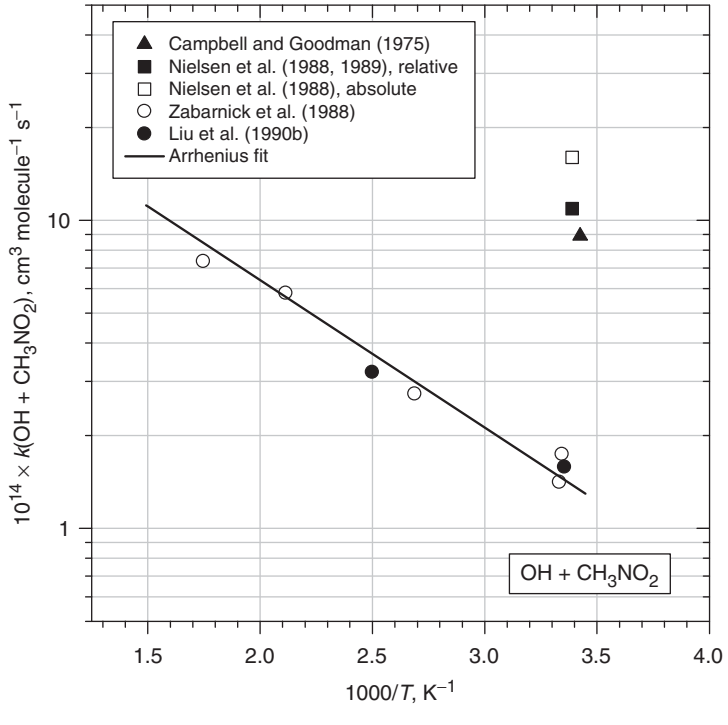

Figure VIII-J-1. Arrhenius plot of the rate coefficient for the reaction of OH with nitromethane.

for nitroalkanes are systematically lower than those determined by Nielsen et al. (1988) at atmospheric pressure. An unweighted fit to the data obtained by Zabarnick et al. (1988) and Liu et al. (1990b) yields the Arrhenius expression: $k = 5.8 \times 10^{-13} \exp(-1{,}102/T)$ cm^3 molecule^{-1} s^{-1}. This expression gives $k = 1.44 \times 10^{-14}$ cm^3 molecule^{-1} s^{-1} at 298 K with an uncertainty estimated to be ±20%.

VIII-J-1.2. Cl-Atom Reaction Kinetics

The rate coefficient obtained by Nielsen et al. (1988) and the upper limit reported by Wallington et al. (1990d) are given in table VIII-J-2. Both studies were conducted using a relative rate method at atmospheric pressure. It should be noted that in both investigations, methane was used as the reference compound, and this is much more reactive toward Cl-atoms than nitromethane. In the relative rate method, measurements are more precise when the reference species have comparable reactivities with the investigated compounds.

VIII-J-1.3. Summary of the Atmospheric Fate of Nitromethane

Combining $k(\mathrm{OH} + \mathrm{CH_3NO_2}) = 1.44 \times 10^{-14}$ cm^3 molecule^{-1} s^{-1} with a diurnal average [OH] $= 1 \times 10^6$ molecule cm^{-3} provides an estimate for the atmospheric lifetime of nitromethane with respect to removal via reaction with OH radicals of about 2 years. Photolysis of CH_3NO_2 is a likely loss mechanism in the troposphere although limited data provide no quantitative estimates (see section IX-H-10). Further work is needed to better establish the atmospheric lifetime of CH_3NO_2.

In an attempt to understand the mechanism of the OH reaction, isotope effects have been investigated by Zabarnick et al. (1988b), Liu et al. (1990b), and Nielsen et al. (1988). The reactions of OD radicals with CH_3NO_2 and CD_3NO_2 were studied by Zabarnick et al. (1988). On the basis of the measured activation energy of 11.3 kJ mol^{-1} and an isotope effect close to 2 for the reaction OD + CD_3NO_2, Zabarnick et al. (1988b) suggested that these reactions proceed by a mechanism involving H- or D-atom abstraction from —CH_3 or —CD_3 groups. The results of Liu et al. are about a factor of 2 higher than that of Zabarnick et al. for the deuterated nitromethane at ambient temperature and 10–20% lower at 400 K. On the other hand, only a small isotope effect was found in the OH + CD_3NO_2 reaction at atmospheric pressure and ambient temperature in the study of Nielsen et al. (1988). These observations may indicate that at atmospheric pressure the OH + CH_3NO_2 reaction involves mainly the

Table VIII-J-2. Rate coefficients (k, cm^3 molecule^{-1} s^{-1}) for the reaction of Cl with nitromethane (CH_3NO_2)

$10^{15} \times k$	T (K)	Technique[a]	Reference
6 ± 2	295 ± 2	RR (CH_4)[b]	Nielsen et al. (1988)
< 7	295 ± 2	RR (CH_4)[b]	Wallington et al. (1990d)

[a]Abbreviations used for the techniques are defined in table I-F-3.
[b]Placed on an absolute basis using $k(\mathrm{Cl} + \mathrm{CH_4}) = 1.0 \times 10^{-13}$ cm^3 molecule^{-1} s^{-1} (Calvert et al., 2008).

addition channel, whereas at lower pressures the addition complex is unstable and the major reaction channel is abstraction.

VIII-J-2. Nitroethane ($C_2H_5NO_2$)

VIII-J-2.1. OH Reaction Kinetics

The reaction of OH radicals with nitroethane has been investigated by Nielsen et al. (1989) using both relative and absolute methods at ambient temperature and atmospheric pressure, and by Liu et al. (1990b) using the flash photolysis–resonance fluorescence technique in 25–50 Torr of Ar at 253–400 K. The rate coefficients values obtained in these two studies are presented in table VIII-J-3 and shown in figure VIII-J-2. The ambient temperature rate coefficient reported by Liu et al. is a factor of 2 lower than that measured by Nielsen et al. It was speculated that this difference could be due to a pressure dependence of the rate coefficient. Fitting the Arrhenius expression to the data set of Liu et al. (1990b) gives: $k = 1.7 \times 10^{-12} \exp(-934/T)$ cm^3 $molecule^{-1}$ s^{-1}. This expression gives $k(OH + C_2H_5NO_2) = 1.7 \times 10^{-14}$ cm^3 $molecule^{-1}$ s^{-1} at 298 K with an uncertainty estimated to be ±30%.

VIII-J-2.2. Cl-Atom Reaction Kinetics

The rate coefficients of Nielsen et al. (1989) and Wallington et al. (1990d) are given in table VIII-J-4. Both studies were conducted using relative rate methods at atmospheric pressure. The values obtained in the two studies are in good agreement. The average rate coefficient value derived from the two investigations is $k = 1.9 \times 10^{-13}$ cm^3 $molecule^{-1}$ s^{-1} and is recommended with an uncertainty of ±20%.

VIII-J-2.3. Summary of the Atmospheric Fate of Nitroethane

The atmospheric lifetime of nitroethane with respect to reaction with OH is calculated to be around 5 months. Photolysis is also a probable atmospheric loss mechanism

Table VIII-J-3. Rate coefficients ($k = A \times e^{-B/T}$), cm^3 $molecule^{-1}$ s^{-1}) for the reaction of OH with nitroethane ($C_2H_5NO_2$)

$10^{12} \times A$	B (K)	$10^{14} \times k$	T (K)	Technique[a]	Reference	Temperature Range (K)
		14.4 ± 1	295 ± 3	RR ($C(CH_3)_4$)[b]	Nielsen et al. (1989)	
		15 ± 5	295 ± 3	PR–UV abs.		
1.9 ± 0.5	960 ± 90	4.38 ± 0.3	253	FP–RF	Liu et al. (1990b)	253–400
		7.22 ± 0.82	298			
		10.0 ± 0.4	330			
		11.2 ± 0.9	350			
		17.5 ± 0.7	400			

[a]Abbreviations used for the techniques are defined in table I-F-3.
[b]Placed on an absolute basis using $k(OH + C(CH_3)_4) = 8.2 \times 10^{-13}$ cm^3 $molecule^{-1}$ s^{-1} (Calvert et al., 2008).

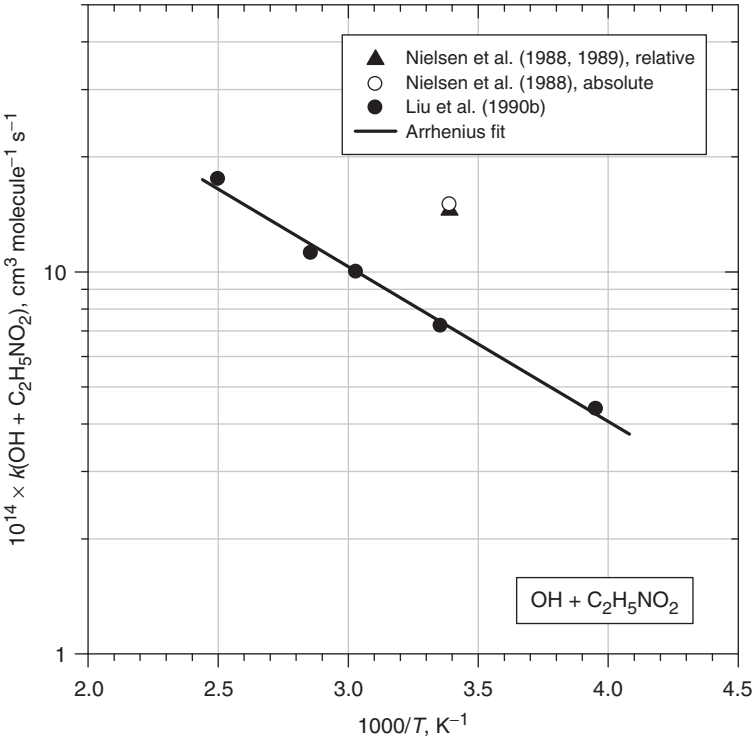

Figure VIII-J-2. Arrhenius plot of the rate coefficient for the reaction of OH with nitroethane.

Table VIII-J-4. Rate coefficients (k, cm^3 molecule^{-1} s^{-1}) for the reaction of Cl with nitroethane ($C_2H_5NO_2$)

$10^{13} \times k$	T (K)	Technique[a]	Reference
1.7 ± 0.1	295 ± 3	RR (CH_4)[b]	Nielsen et al. (1989)
2.05 ± 0.14	295 ± 2	RR (CH_4)[b]	Wallington et al. (1990d)

[a]Abbreviations used for the techniques are defined in table I-F-3.
[b]Placed on an absolute basis using $k(Cl + CH_4) = 1.0 \times 10^{-13}$ cm^3 molecule^{-1} s^{-1} (Calvert et al., 2008).

of $C_2H_5NO_2$, but data are insufficient to allow a realistic estimate of the rate of photodecomposition.

VIII-J-3. 1-Nitropropane (n-$C_3H_7NO_2$)

VIII-J-3.1. OH Reaction Kinetics

The rate coefficient values determined by Nielsen et al. (1989) and Liu et al. (1990b) are given in table VIII-J-5 and shown in figure VIII-J-3. The measurements obtained using absolute methods at ambient temperature are in agreement, while the relative rate determination of Nielsen et al. is higher. Fitting the Arrhenius expression to the data

Table VIII-J-5. Rate coefficients ($k = A \times e^{-B/T}$), cm^3 molecule^{-1} s^{-1}) for the reaction of OH with 1-nitropropane (n-$C_3H_7NO_2$)

$10^{12} \times A$	B (K)	$10^{13} \times k$	T (K)	Technique[a]	Reference	Temperature Range (K)
		5.29 ± 0.77	295 ± 3	RR [$C(CH_3)_4$][b]	Nielsen et al. (1989)	
		3.4 ± 0.8	295 ± 3	PR–UV abs.		
3.7 ± 0.2	690 ± 17	2.07 ± 0.16	240	FP–RF	Liu et al. (1990b)	240–400
		3.64 ± 0.18	298			
		4.48 ± 0.32	330			
		5.14 ± 0.31	350			
		6.63 ± 0.55	400			

[a]Abbreviations used for the techniques are defined in table I-F-3.
[b]Placed on an absolute basis using $k[OH + C(CH_3)_4] = 8.2 \times 10^{-13}$ cm^3 molecule^{-1} s^{-1} (Calvert et al., 2008).

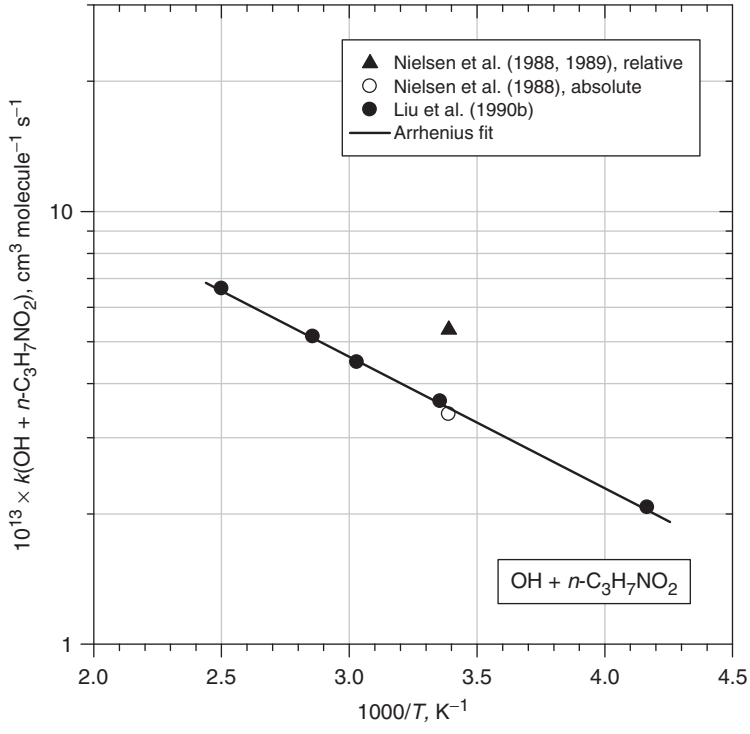

Figure VIII-J-3. Arrhenius plot of the rate coefficient for the reaction of OH with 1-nitropropane.

of Liu et al. in the temperature range 240–400 K and that of Nielsen et al. obtained by the absolute method yields $k = 3.8 \times 10^{-12} \exp(-700/T)$ cm^3 molecule^{-1} s^{-1} with $k = 3.6 \times 10^{-13}$ cm^3 molecule^{-1} s^{-1} at 298 K. An uncertainty of $\pm 25\%$ is assigned to the 298 K value.

Table VIII-J-6. Rate coefficients (k, cm^3 molecule^{-1} s^{-1}) for the reaction of Cl with 1-nitropropane (n-$C_3H_7NO_2$)

$10^{12} \times k$	T (K)	Technique[a]	Reference
8.9 ± 0.6	295 ± 3	RR (C_2H_6)[b]	Nielsen et al. (1989)
10.9 ± 0.8	295 ± 2	RR (C_2H_5Cl)[c]	Wallington et al. (1990d)

[a]Abbreviations used for the techniques are defined in table I-F-3.
[b]Placed on an absolute basis using $k(Cl + C_2H_6) = 5.7 \times 10^{-11}$ cm^3 molecule^{-1} s^{-1} (Calvert et al., 2008).
[c]Placed on an absolute basis using $k(Cl + C_2H_5Cl) = 7.8 \times 10^{-12}$ cm^3 molecule^{-1} s^{-1} (this book, table I-F-2).

VIII-J-3.2. Cl-Atom Reaction Kinetics

The rate coefficients values of Nielsen et al. (1989) and Wallington et al. (1990d) given in table VIII-J-6 were obtained by a relative method at atmospheric pressure. These two measurements are in good agreement. The average value of the two determinations gives $k = 9.9 \times 10^{-12}$ cm^3 molecule^{-1} s^{-1} at 298 K which is recommended with an uncertainty of ±20%.

VIII-J-3.3. Summary of the Atmospheric Fate of 1-Nitropropane

Combining the rate coefficient of the OH reaction with an average OH concentration of 1×10^6 molecule cm^{-3} gives an estimate for the atmospheric lifetime for 1-nitropropane with respect to removal through reaction with OH of about 33 days. Photodecomposition of 1-nitropropane in the troposphere is likely a significant removal pathway, but limited data provide no quantitative information; see section IX-H-11.2.

VIII-J-4. 2-Nitropropane (*iso*-$C_3H_7NO_2$)

VIII-J-4.1. OH Reaction Kinetics

The only reported study of this reaction is that of Liu et al. (1990b). These authors used flash photolysis combined with resonance fluorescence to measure the rate coefficient in the temperature and pressure ranges 240–400 K and 25 and 50 Torr of Ar, respectively. The data obtained are given in table VIII-J-7 and shown in figure VIII-J-4. Fitting the Arrhenius expression to their data yields $k = 2.2 \times 10^{-12} \exp(-646/T)$ cm^3 molecule^{-1} s^{-1} with $k = 2.5 \times 10^{-13}$ cm^3 molecule^{-1} s^{-1} at 298 K. An uncertainty of ±25% is assigned to the 298 K value.

VIII-J-4.2. Summary of the Atmospheric Fate of 2-Nitropropane

The atmospheric lifetime of 2-nitropropane using the rate coefficient value of Liu et al. (1990b), $k = 2.5 \times 10^{-13}$ cm^3 molecule^{-1} s^{-1}, and [OH] = 1×10^6 molecule cm^{-3} is estimated to be around 46 days. Photodecomposition of 2-nitropropane in the troposphere is likely a significant removal pathway, but limited data provide no quantitative information; see section IX-H-11.2.

Table VIII-J-7. Rate coefficients ($k = A \times e^{-B/T}$), cm^3 $molecule^{-1}$ s^{-1}) for the reaction of OH with 2-nitropropane (*iso*-$C_3H_7NO_2$)

$10^{12} \times A$	B (K)	$10^{13} \times k$	T (K)	Technique[a]	Reference	Temperature Range (K)
2.1 ± 0.7	630 ± 106	1.45 ± 0.14	240	FP–RF	Liu et al. (1990b)	240–400
		2.59 ± 0.11	298			
		3.14 ± 0.20	330			
		3.22 ± 0.15	350			
		4.39 ± 0.18	400			

[a]Abbreviations used for the techniques are defined in table I-F-3.

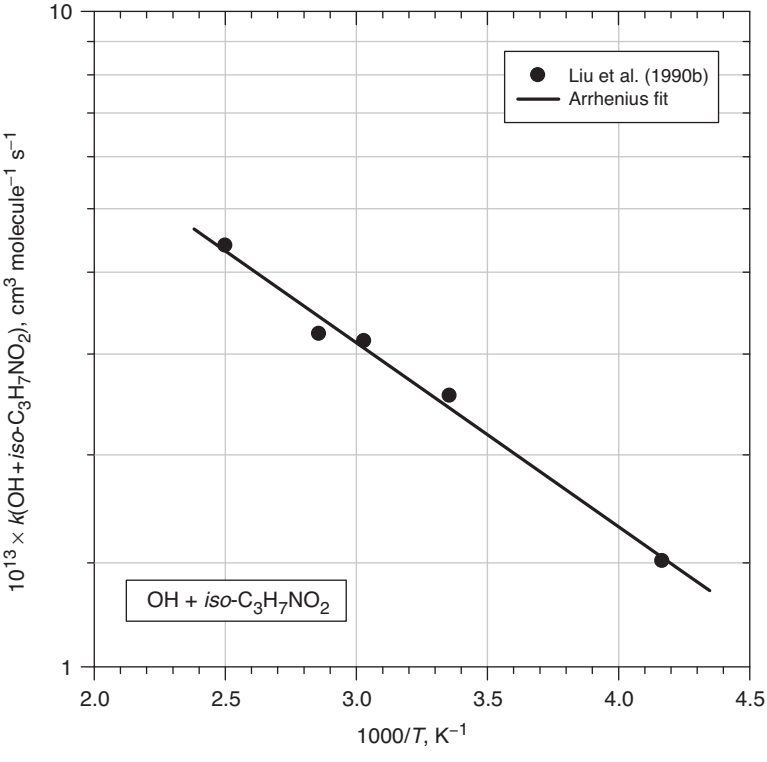

Figure VIII-J-4. Arrhenius plot of the rate coefficient for the reaction of OH with 2-nitropropane.

VIII-J-5. 1-Nitrobutane (*n*-$C_4H_9NO_2$)

VIII-J-5.1. OH Reaction Kinetics

The reaction of OH with 1-nitrobutane has been studied by Nielsen et al. (1989), Atkinson and Aschmann (1989), and Liu et al. (1990b). As shown in table VIII-J-8 and figure VIII-J-5, the ambient temperature absolute determination of Liu et al. (1990b)

Table VIII-J-8. Rate coefficients ($k = A \times e^{-B/T}$), cm^3 $molecule^{-1}$ s^{-1}) for the reaction of OH with 1-nitrobutane (n-$C_4H_9NO_2$)

$10^{12} \times A$	B (K)	$10^{13} \times k$	T (K)	Technique[a]	Reference	Temperature Range (K)
		16.7 ± 1.1	295 ± 3	RR $[C(CH_3)_4]$[b]	Nielsen et al. (1989)	
		15.5 ± 0.9	295 ± 3	PR–UV abs.		
		12.7 ± 0.17	298 ± 2	RR (C_3H_8)[c]	Atkinson and Aschmann (1989)	
6.1 ± 0.9	660 ± 49	4.04 ± 0.32	240	FP–RF	Liu et al. (1990b)	240–400
		6.58 ± 0.42	298			
		7.90 ± 0.74	330			
		9.30 ± 0.54	350			
		12.0 ± 0.6	400			

[a]Abbreviations used for the techniques are defined in table I-F-3.
[b]Placed on an absolute basis using $k[OH + C(CH_3)_4] = 8.2 \times 10^{-13}$ cm^3 $molecule^{-1}$ s^{-1} (Calvert et al., 2008).
[c]Placed on an absolute basis using $k(OH + C_3H_8) = 1.1 \times 10^{-12}$ cm^3 $molecule^{-1}$ s^{-1} (Calvert et al., 2008).

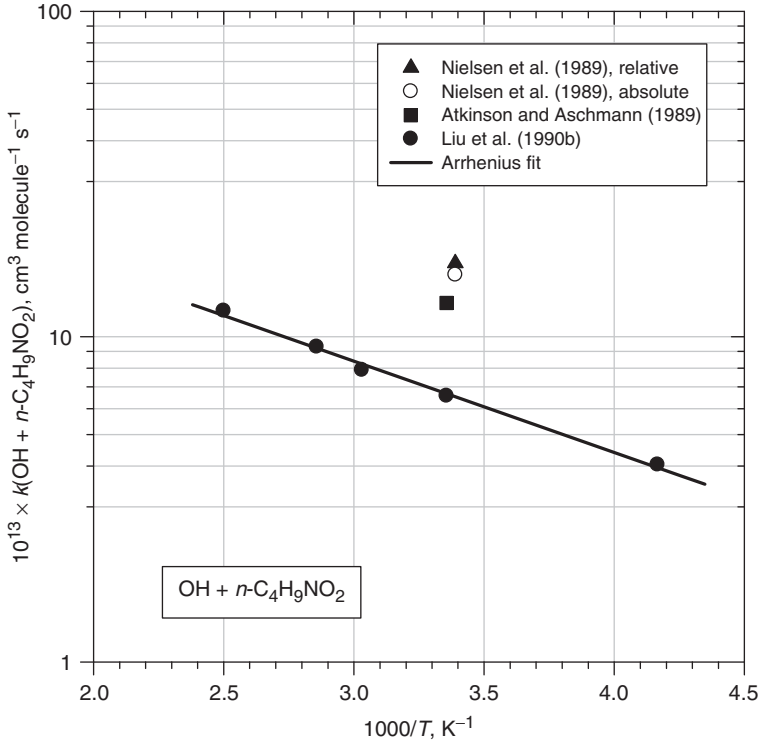

Figure VIII-J-5. Arrhenius plot of the rate coefficient for the reaction of OH with 1-nitrobutane.

is lower than those of Nielsen et al. (1989) and Atkinson and Aschmann (1989). Liu et al. conducted their measurements in the temperature range 240–400 K. Fitting the Arrhenius expression to the data of Liu et al. gives $k = 5.8 \times 10^{-12} \exp(-646/T)$ cm^3 $molecule^{-1}$ s^{-1} with $k = 6.6 \times 10^{-13}$ cm^3 $molecule^{-1}$ s^{-1} at 298 K. Because of absence of an explanation of the discrepancy between the reported measurements no recommendation is made here.

VIII-J-5.2. Cl-Atom Reaction Kinetics

The rate coefficients obtained by Nielsen et al. (1989) and Wallington et al. (1990d) using a relative rate method at atmospheric pressure are given in table VIII-J-9. These two measurements are in good agreement. The average value of these two determinations is $k = 5.5 \times 10^{-11}$ cm^3 $molecule^{-1}$ s^{-1} at 298 K with an estimated uncertainty of $\pm 15\%$.

VIII-J-5.3. Summary of the Atmospheric Fate of 1-Nitrobutane

The atmospheric lifetime of 1-nitrobutane with respect to removal through reaction with OH radicals using the rate coefficient values of Liu et al. (1990b) and [OH] = 1×10^6 molecule cm^{-3} is around 18 days. Photodecomposition of 1-nitrobutane in the troposphere is likely a significant removal pathway, but limited data provide no quantitative information; see section IX-H-11.2.

VIII-J-6. 1-Nitropentane (n-$C_5H_{11}NO_2$)

VIII-J-6.1. OH Reaction Kinetics

The reaction of OH with 1-nitropentane has been investigated by two groups. Nielsen et al. (1989) used absolute and relative methods to measure the rate coefficient at ambient temperature and atmospheric pressure. The values obtained by the two methods are in good agreement. However, the values reported by Nielsen et al. (1989) are a factor of 3 higher than that of Liu et al. (1990b) who used the flash photolysis–resonance fluorescence technique. Liu et al. studied the reaction over the temperature range 240–400 K in 25–50 Torr of Ar. The values obtained by the two groups are given in table VIII-J-10 and shown in figure VIII-J-6. Fitting the Arrhenius expression to the data set of Liu et al. yields $k = 1.08 \times 10^{-11} \exp(-703/T)$ with $k = 1.0 \times 10^{-12}$ cm^3

Table VIII-J-9. Rate coefficients (k, cm^3 $molecule^{-1}$ s^{-1}) for the reaction of Cl with 1-nitrobutane (n-$C_4H_9NO_2$)

$10^{11} \times k$	T (K)	Technique[a]	Reference
5.72 ± 0.18	295 ± 3	RR (C_2H_6)[b]	Nielsen et al. (1989)
5.31 ± 0.71	295 ± 2	RR (C_2H_6)[b]	Wallington et al. (1990c)

[a]Abbreviations used for the techniques are defined in table I-F-3.
[b]Placed on an absolute basis using $k(Cl + C_2H_6) = 5.9 \times 10^{-11}$ cm^3 $molecule^{-1}$ s^{-1} (Atkinson et al., 2006).

Table VIII-J-10. Rate coefficients ($k = A \times e^{-B/T}$), cm^3 molecule^{-1} s^{-1}) for the reaction of OH with 1-nitropentane (n-$C_5H_{11}NO_2$)

$10^{12} \times A$	B (K)	$10^{13} \times k$	T (K)	Technique[a]	Reference	Temperature Range (K)
		31.5 ± 1.5	295 ± 3	RR [$C(CH_3)_4$][b]	Nielsen et al. (1989)	
		33.0 ± 0.5	295 ± 3	PR–UV abs.		
10.9 ± 1.7	710 ± 47	5.74 ± 0.33	240	FP–RF	Liu et al. (1990b)	240–400
		10.0 ± 0.6	298			
		13.3 ± 0.7	330			
		14.8 ± 0.9	350			
		18.1 ± 1.3	400			

[a]Abbreviations used for the techniques are defined in table I-F-3.
[b]Placed on an absolute basis using $k[OH + C(CH_3)_4] = 8.2 \times 10^{-13}$ cm^3 molecule^{-1} s^{-1} (Calvert et al., 2008).

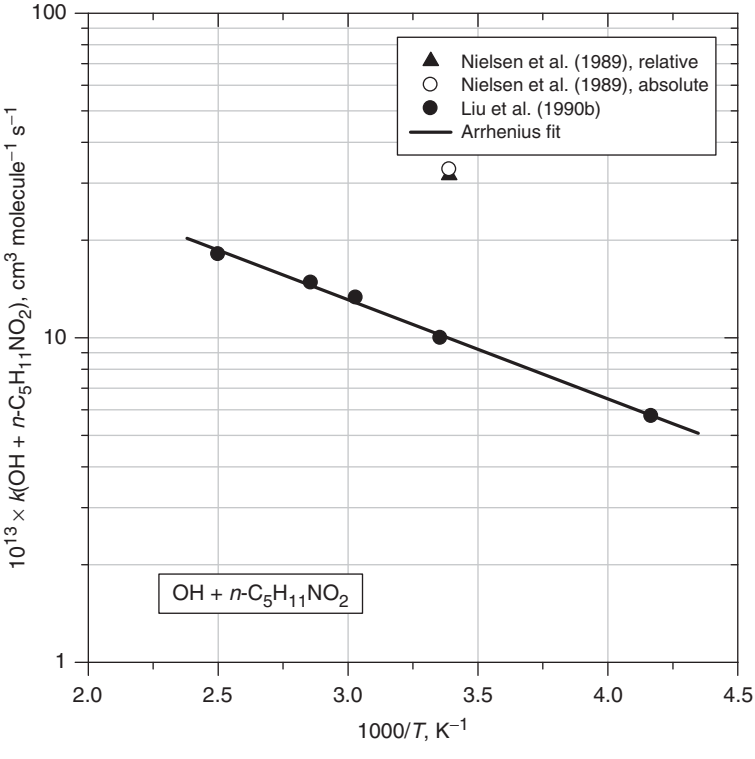

Figure VIII-J-6. Arrhenius plot of the rate coefficient for the reaction of OH with 1-nitropentane.

Table VIII-J-11. Rate coefficients (k, cm^3 molecule^{-1} s^{-1}) for the reaction of Cl with 1-nitropentane (n-$C_5H_{11}NO_2$)

$10^{11} \times k$	T (K)	Technique[a]	Reference
1.23 ± 0.05	295 ± 3	RR (C_2H_6)[b]	Nielsen et al. (1989)
1.30 ± 0.12	295 ± 2	RR (n-C_4H_{10})[c]	Wallington et al. (1990d)

[a]Abbreviations used for the techniques are defined in table I-F-3.
[b]Placed on an absolute basis using $k(Cl + C_2H_6) = 5.7 \times 10^{-11}$ cm^3 molecule^{-1} s^{-1} (Calvert et al., 2008).
[c]Placed on an absolute basis using $k(Cl + n\text{-}C_4H_{10}) = 2.1 \times 10^{-10}$ cm^3 molecule^{-1} s^{-1} (Calvert et al., 2008).

molecule^{-1} s^{-1} at 298 K. In the absence of an explanation of the discrepancy between the available measurements no recommendation is made here.

VIII-J-6.2. Cl Reaction Kinetics

The rate coefficients values of Nielsen et al. (1989) and Wallington et al. (1990d) given in table VIII-J-11 were obtained by a relative rate method at atmospheric pressure. The two measurements are in excellent agreement; an average gives: $k = 1.27 \times 10^{-10}$ cm^3 molecule^{-1} s^{-1} at 298 K which is recommended with an uncertainty of $\pm 15\%$.

VIII-J-6.3. Summary of the Atmospheric Fate of 1-Nitropentane

The atmospheric lifetime of 1-nitropentane calculated using the rate coefficient values reported by Liu et al. (1990b) and an average [OH] $= 1 \times 10^6$ molecule cm^{-3} is around 11 days. It is likely that the photodecomposition of 1-nitropentane in the troposphere is a significant removal pathway, but limited data provide no quantitative information; see section IX-H-11.2.

VIII-J-7. Trends in the Reactivity of Nitroalkanes

It is suggested that the rate coefficients for the reactions of OH radicals with smaller nitroalkanes (C<4) investigated may be pressure dependent at around ambient temperature, and these reactions proceed by both H-atom abstraction and OH addition followed by rapid decomposition of the adduct:

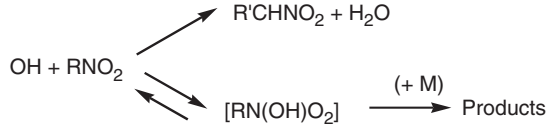

However, mechanistic studies in different conditions are required to confirm the occurrence of these pathways. As presented above, the rate coefficients for the reactions of OH with terminal nitroalkanes increase with increasing chain length, as expected for a hydrogen abstraction reaction. According to the different studies, the overall reactivity

will have an abstraction and addition component. Assuming that the addition channel is the major one for nitromethane and that this component is the same for higher nitroalkanes, Nielsen et al. (1989) have estimated the contribution of the abstraction pathway for higher nitroalkanes using the values reported at high and low pressure leading to $k_{add} = 1.3 \times 10^{-13}$ cm^3 molecule^{-1} s^{-1} (Zabarnick et al., 1988b; Liu et al., 1990b; Nielsen et al., 1989). Liu et al. have compared the reactivities of nitroalkanes with those of alkanes. The two groups have concluded that the NO_2 group has a strong deactivating effect for abstraction of H-atoms positioned α to the NO_2 group in the nitroalkane. Although the effect extends beyond the α-position, it is diminished as one progresses further from the NO_2 group.

Generally, the rate coefficient values obtained at low pressure by Liu et al. (1990b) for nitroalkanes are systematically lower than those determined by Nielsen et al. at atmospheric pressure. The rate coefficient of Atkinson and Aschmann (1989) and Nielsen et al. (1989) for the reaction of OH with n-$C_4H_9NO_2$, both measured at atmospheric pressure, are in agreement. It has been suggested that the observed differences could be due to the pressure dependence of the rate coefficients (Liu et al., 1990b). However, the studies conducted in the pressure range 25–300 Torr did not show any pressure effect (Zabarnick et al., 1988b; Liu et al., 1990b). Clearly, further studies are required to assess the OH-initiated degradation mechanism of nitroalkanes under atmospheric conditions.

The rate coefficient of Cl with CH_3NO_2 is at least 4 orders of magnitude lower than that with CH_3CH_3 due to the strong deactivating affect of the NO_2 group as mentioned previously for OH reactions. This decrease in the reactivity is less pronounced for higher nitroalkanes compared to the alkanes; there is only a factor of 2 difference for n-C_6H_{14} and n-$C_5H_{10}NO_2$, for example.

VIII-K. Nitroalkenes

Nitroalkenes are widely used as synthetic intermediates because they can be easily converted into a variety of useful industrial compounds. A very limited number of studies of the atmospheric behavior of these compounds have been conducted.

VIII-K-1. OH-Nitroalkene Reaction Kinetics

Nielsen et al. (1990) have studied the reaction of OH radicals with $CH_2{=}CHNO_2$, $CH_2{=}CHCH_2NO_2$, and 1-nitrocyclohexene at atmospheric pressure and ambient temperature. Measurements of the rate coefficients for the reactions of OH radicals with $CH_2{=}CHNO_2$ and $CH_2{=}CHCH_2NO_2$ were conducted using pulse radiolysis combined with kinetic UV spectroscopy. Relative rate methods were used to determine the rate coefficient for the reaction of OH radicals with *cyclo*-$C_6H_9NO_2$. The data obtained are given in table VIII-K-1. These data show that substitution by a nitro group in ethene reduces the reactivity by about a factor of about 6 [k(ethene) $= 7.9 \times 10^{-12}$ (Atkinson et al., 2006)]. The NO_2 electron withdrawing group decreases the electron density in the π-system and consequently reduces the rate constant for addition of the electrophilic

Table VIII-K-1. Rate coefficients (k, cm^3 molecule^{-1} s^{-1}) for the reaction of OH with nitroalkenes

Molecule	$10^{12} \times k$	T (K)	Technique[a]	Reference
CH_2=$CHNO_2$	1.2 ± 0.2	298 ± 2	PR–UV abs.	Nielsen et al. (1990)
CH_2=$CHCH_2NO_2$	12.2 ± 2.1	298 ± 2	PR–UV abs.	Nielsen et al. (1990)
1-Nitrocyclohexene	43.7 ± 4.3	298 ± 2	RR (*cis*-2-butene)[b]	Nielsen et al. (1990)

[a]Abbreviations used for the techniques are defined in table I-F-3.
[b]Placed on an absolute basis using $k(\text{OH} + \textit{cis}\text{-2-butene}) = 5.64 \times 10^{-11}$ cm^3 molecule^{-1} s^{-1} (Atkinson and Arey, 2003a).

OH radical. Similarly, this effect reduces the reactivity of nitropropene compared to that of propene [k(propene) = 2.9×10^{-11} (Atkinson et al., 2006)] and that of 1-nitrocyclohexene compared to that of cyclohexene [k(cyclohexene) = 67.7×10^{-12} (Atkinson and Arey, 2003a)].

VIII-K-2. Summary of the Atmospheric Fate of Nitroalkenes

The atmospheric lifetimes of nitroalkenes with respect to reaction with OH radicals are calculated to be around 10 days for CH_2=$CHNO_2$ and about 3 h for *cyclo*-$C_6H_9NO_2$ (the most reactive nitroalkene studied to date). It is expected that the reaction of OH with nitroalkenes proceeds by an addition to the C=C double bond, as for simple alkenes. The reactions of the nitroalkenes with ozone and NO_3 radicals have not been reported, but they are expected to be significant.

VIII-L. Nitroaromatics and Nitroarenes

Nitroaromatic and nitroarene compounds are present in the atmosphere as the result of their direct emissions from incomplete combustion and their atmospheric formation through the oxidation of aromatics and polycyclic aromatic hydrocarbons (PAH) by reaction with OH, NO_3 and/or N_2O_5 (e.g., see Atkinson et al., 1989b; Arey et al., 1990b and references therein).

VIII-L-1. Nitrobenzene ($C_6H_5NO_2$)

VIII-L-1.1. OH Reaction Kinetics

The reaction of OH with nitrobenzene has been studied by Witte et al. (1986) and Atkinson et al. (1987c). Witte et al. used flash photolysis combined with resonance fluorescence to investigate this reaction in the temperature range 259–362 K while Atkinson et al. used a relative rate method and two reference compounds to conduct their investigation at ambient temperature. The data set obtained in these investigations is given in table VIII-L-1 and displayed in figure VIII-L-1. The data of Witte et al. conducted at low pressure (133 mbar) does not indicate a clear temperature dependence of the reaction in the range 259–362 K leading to an average value of $k = 1.4 \times 10^{-13}$ cm^3 molecule^{-1} s^{-1} in this range at 133 mbar. However, Witte et al. have reported the

Table VIII-L-1. Rate coefficients ($k = A \times e^{-B/T}$), cm^3 $molecule^{-1}$ s^{-1}) for the reaction of OH with nitrobenzene ($C_6H_5NO_2$)

$10^{12} \times A$	B (K)	$10^{13} \times k$	T (K)	Technique[a]	Reference	Temperature Range (K)
0.6	440 ± 80	1.20 ± 0.07	259	FP–RF	Witte et al. (1986)	259–362
		1.10 ± 0.12	265			
		1.19 ± 0.07	274			
		1.26 ± 0.09	283			
		1.32 ± 0.07	288			
		1.37 ± 0.14	299			
		1.46 ± 0.15	312			
		1.69 ± 0.22	316			
		1.37 ± 0.25	316			
		1.81 ± 0.28	331			
		1.54 ± 0.21	339			
		1.69 ± 0.11	342			
		1.63 ± 0.65	352			
		1.36 ± 0.13	358			
		1.33 ± 0.21	358			
		1.58 ± 0.40	362			
		< 0.9	296 ± 2	RR (C_6H_6)[b]	Atkinson et al. (1987c)	
		< 0.7	296 ± 2	RR (CH_3OCH_3)[c]		

[a]Abbreviations used for the techniques are defined in table I-F-3.
[b]Placed on an absolute basis using $k(OH + C_6H_6) = 1.21 \times 10^{-12}$ cm^3 $molecule^{-1}$ s^{-1} (Calvert et al., 2002).
[c]Placed on an absolute basis using $k(OH + CH_3OCH_3) = 2.7 \times 10^{-12}$ cm^3 $molecule^{-1}$ s^{-1} (this book, section III-B-1.1).

Arrhenius expression $k = 6 \times 10^{-13} \exp[-(440 \pm 80)/T]$ cm^3 $molecule^{-1}$ s^{-1} over the range of their study.

VIII-L-1.2. O_3 Reaction Kinetics

Table VIII-L-2 gives the upper limit to the rate coefficient of the reaction of O_3 with nitrobenzene determined by Atkinson et al. (1987c). The measurement was conducted at ambient temperature and atmospheric pressure by monitoring the decrease of ozone in the presence of known concentrations of nitrobenzene and is the only reported investigation.

VIII-L-1.3. Cl-Atom Reaction Kinetics

The only reported study of this reaction is that of Frøsig et al. (2000), conducted using a relative rate method. Table VIII-L-3 presents the values obtained at ambient temperature in 10–700 Torr of air or N_2 diluent. The value cited by Frøsig et al. (2000) for the rate coefficient is the average of those measured with two reference compounds, $k = 9.4 \times 10^{-13}$ cm^3 $molecule^{-1}$ s^{-1} with an uncertainty of ±25% at 298 K.

VIII-L-1.4. Summary of the Atmospheric Fate of Nitrobenzene

The atmospheric lifetime of nitrobenzene with respect to reaction with OH estimated using [OH] = 1×10^6 molecule cm^{-3} and the rate coefficient reported above,

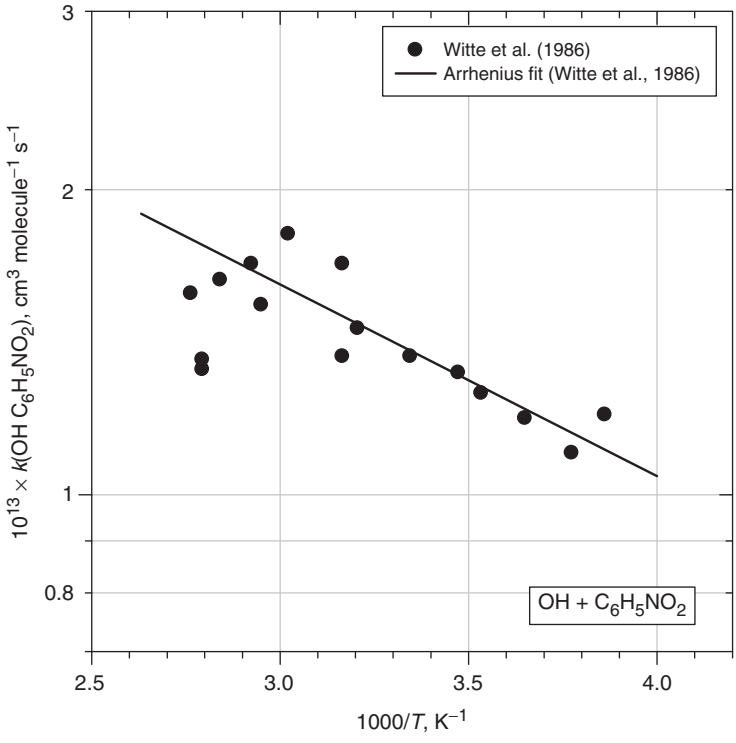

Figure VIII-L-1. Arrhenius plot of the rate coefficient for the reaction of OH with nitrobenzene.

Table VIII-L-2. Rate coefficients (k, cm^3 molecule^{-1} s^{-1}) for the reaction of O_3 with nitrobenzene ($C_6H_5NO_2$)

$10^{21} \times k$	T (K)	Technique[a]	Reference
< 7	296 ± 2	Absolute[a]	Atkinson et al. (1987c)

[a]Monitoring O_3 decrease in the presence of nitrobenzene.

Table VIII-L-3. Rate coefficients (k, cm^3 molecule^{-1} s^{-1}) for the reaction of Cl with nitrobenzene ($C_6H_5NO_2$)

$10^{13} \times k$	T (K)	Technique[a]	Reference
8.85 ± 0.83	296	RR (CH_3Cl)[b]	Frøsig et al. (2000)
9.95 ± 0.84	296	RR (CH_3OCHO)[c]	

[a]Abbreviations used for the techniques are defined in table I-F-3.
[b]Placed on an absolute basis using $k(Cl + CH_3Cl) = 4.9 \times 10^{-13}$ cm^3 molecule^{-1} s^{-1} (Sander et al., 2006).
[c]Placed on an absolute basis using $k(Cl + CH_3OCHO) = 1.4 \times 10^{-12}$ cm^3 molecule^{-1} s^{-1} (this book, section VII-B-1.1).

is around 80 days. According to Frøsig et al. (2000), photolysis could be the dominant atmospheric loss of nitrobenzene. See section IX-L-6; a rough estimate of 14 h is given for the lifetime for photodecomposition with an overhead Sun in table IX-M-1. Frøsig et al. (2000) have shown that the reaction of Cl with $C_6H_5NO_2$ proceeds via a displacement mechanism (probably addition followed by elimination) to give C_6H_5Cl + NO_2, essentially at a yield of 100%.

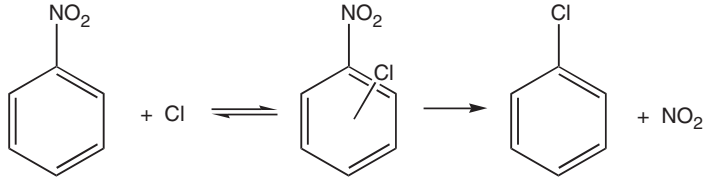

VIII-L-2. 3-Nitrotoluene (*m*-Nitrotoluene, $CH_3C_6H_4NO_2$)

VIII-L-2.1. OH Reaction Kinetics

The only measurement of the rate constant of the reaction of OH with 3-nitrotoluene is that of Atkinson et al. (1989a), obtained using the relative rate method at 298 K and atmospheric pressure of air; see table VIII-L-4. Atkinson et al. have mentioned that the data obtained exhibited a high degree of scatter, and hence the estimated uncertainty on the rate coefficient is rather large (±70%).

VIII-L-2.2. Summary of the Atmospheric Fate of 3-Nitrotoluene

The atmospheric lifetime of 3-nitrotoluene with respect to reaction with OH is estimated to be around 10 days, using the rate coefficient values reported by Atkinson et al. (1989a) and an average [OH] = 1×10^6 molecule cm^{-3}. By analogy with the estimates of the photodecomposition lifetime of nitrobenzene, it is likely that photodecomposition will be important for 3-nitrotoluene as well; see section IX-L-6.

VIII-L-3. 2-Nitrophenol (*o*-Nitrophenol, $C_6H_4(OH)NO_2$)

VIII-L-3.1. NO_3 Reaction Kinetics

The only study reported in the literature is that of Atkinson et al. (1992b) who reported an upper limit to the rate coefficient of the reaction of NO_3 with 2-nitrophenol.

Table VIII-L-4. Rate coefficients (k, cm^3 $molecule^{-1}$ s^{-1}) for the reaction of OH with 3-nitrotoluene ($CH_3C_6H_4NO_2$)

$10^{12} \times k$	T (K)	Technique[a]	Reference
1.2 ± 0.8	298 ± 2	RR (C_6H_6)[b]	Atkinson et al. (1989a)

[a]Abbreviations used for the techniques are defined in table I-F-3.
[b]Placed on an absolute basis using $k(OH + C_6H_6) = 1.21 \times 10^{-12}$ cm^3 $molecule^{-1}$ s^{-1} (Calvert et al., 2002).

This work was performed using a relative rate method (*trans*-2-butene as the reference compound) at atmospheric pressure and 292 ± 2 K. Using k(*trans*-2-butene) $= 3.9\times10^{-13}$ cm^3 molecule^{-1} s^{-1} (Atkinson and Arey, 2003a) the upper limit obtained is $k < 2 \times 10^{-14}$ cm^3 molecule^{-1} s^{-1}.

VIII-L-4. Nitroarenes

VIII-L-4.1. OH Reaction Kinetics

The rate coefficients for the reaction of OH with 1- and 2-nitronaphthalene have been measured by Atkinson et al. (1989b) at 298 K and atmospheric pressure of air by a relative rate method. Arey et al. (1990b) have investigated the reaction of OH with 2-methyl-1-nitronaphthalene, where they have also used a relative rate method at atmospheric pressure and ambient temperature; see table VIII-L-5.

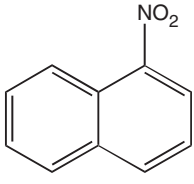

1-Nitronaphthalene

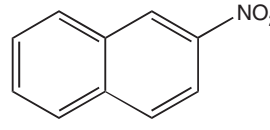

2-Nitronaphthalene

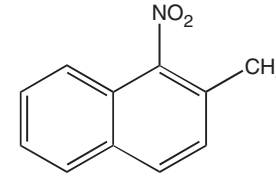

2-Methyl-1-nitronaphthalene

The OH radical reaction rate constants with 1- and 2-nitronaphthalene and that of 2-methyl-1-nitronaphthalene are significantly lower than that for the parent PAH naphthalene: [k(OH + naphthalene) $= 2.3 \times 10^{-11}$, k(OH + 1-methylnaphthalene) $= 5.3 \times 10^{-12}$ and k(OH + 2-methylnaphthalene) $= 5.23 \times 10^{-12}$ cm^3 molecule^{-1} s^{-1} (Calvert et al., 2002)]. As mentioned earlier for other nitro-containing compounds, this shows that substitution of an —NO_2 group on the aromatic ring markedly deactivates the aromatic ring to electrophilic addition of the OH radical. A similar situation is observed for the monocyclic aromatics, with the ambient temperature rate constant for the reaction of the OH radical with nitrobenzene being a factor of 10 lower than that for benzene.

Table VIII-L-5. Rate coefficients (k, cm^3 molecule^{-1} s^{-1}) for the reaction of OH with nitroarenes

Molecule	$10^{12} \times k$	T (K)	Technique[a]	Reference
1-Nitronaphthalene	5.0 ± 1.7	298 ± 2	RR (*cyclo*-C_6H_{12})[b]	Atkinson et al. (1989b)
2-Nitronaphthalene	5.2 ± 0.8	298 ± 2	RR (*cyclo*-C_6H_{12})[b]	Atkinson et al. (1989b)
2-Methyl-1-nitronaphthalene	< 8.3	298 ± 2	RR (*cyclo*-C_6H_{12})[b]	Arey et al. (1990b)

[a]Abbreviations used for the techniques are defined in table I-F-3.
[b]Placed on an absolute basis using k(OH + C_6H_{12}) $= 6.97 \times 10^{-12}$ cm^3 molecule^{-1} s^{-1} (Calvert et al., 2008).

Arey et al. have derived an upper limit to the reaction of OH with 2-methyl-1-nitronaphthalene for which photolysis was found to be the dominant loss process (see section IX-L-6).

VIII-L-4.2. NO_3 Reaction Kinetics

The upper limits to the rate coefficients for the reaction of NO_3 with 1- and 2-nitronaphthalene obtained by Atkinson et al. (1989b) using a relative rate method are given in table VIII-L-6. The measurements were conducted at atmospheric pressure and ambient temperature. Arey et al. (1990b) did observe a reaction between NO_3 and 2-methyl-1-nitronaphthalene. The obtained value is reported in table VIII-L-6.

VIII-L-4.3. O_3 Reaction Kinetics

The experiments conducted by Atkinson et al. (1989b) did not show any measurable reaction between O_3 and 1- and 2-nitronaphthalene. Similarly, the study of Arey et al. (1990b) reported only an upper limit to the rate coefficient of the reaction of O_3 with 2-methyl-1-nitronaphthalene. The measurements were conducted by following the decay of the nitroarenes in the presence of excess O_3 (in the presence of cyclohexane to act as scavenger for OH radicals if formed). The upper limits obtained by Atkinson et al. (1989b) and Arey et al. (1990b) are given in table VIII-L-7.

VIII-L-4.4. Summary of the Atmospheric Fate of Nitroarenes

The investigations of Atkinson et al. (1989b) and Arey et al. (1990b) have shown that under atmospheric conditions photolysis is the dominant loss process of the nitroarenes that have been studied. See section IX-L-7. The OH radical reactions are calculated

Table VIII-L-6. Rate coefficients (k, cm^3 molecule^{-1} s^{-1}) for the reaction of NO_3 with nitroarenes

Molecule	T (K)	$10^{14} \times k$	Technique[a]	Reference
1-Nitronaphthalene	298 ± 2	< 0.73	RR (C_3H_6)[b]	Atkinson et al. (1989b)
2-Nitronaphthalene	298 ± 2	< 0.74	RR (C_3H_6)[b]	Atkinson et al. (1989b)
2-Methyl-1-nitronaphthalene	298 ± 2	1.14 ± 0.57	RR (C_3H_6)[b]	Arey et al. (1990b)

[a]Abbreviations used for the techniques are defined in table I-F-3.
[b]Placed on an absolute basis using $k(NO_3 + C_3H_6) = 9.5 \times 10^{-15}$ cm^3 molecule^{-1} s^{-1} (Atkinson et al., 2006).

Table VIII-L-7. Rate coefficients (k, cm^3 molecule^{-1} s^{-1}) for the reaction of O_3 with nitroarenes

Molecule	T (K)	$10^{19} \times k$	Technique[a]	Reference
1-Nitronaphthalene	298 ± 2	< 6	Excess of O_3[b]	Atkinson et al. (1989b)
2-Nitronaphthalene	298 ± 2	< 6	Excess of O_3[b]	Atkinson et al. (1989b)
2-Methyl-1-nitronaphthalene	298 ± 2	< 3	Excess of O_3[b]	Arey et al. (1990b)

[a]Abbreviations used for the techniques are defined in table I-F-3.
[b]Nitroarenes were monitored in the presence of excess of O_3.

to be an order of magnitude less important than photolysis as an atmospheric loss process. The reaction with the NO_3 radical is of importance only for the removal of 2-methyl-1-nitronaphtalene. The O_3 reactions are of negligible importance.

VIII-M. Peroxyacyl Nitrates

VIII-M-1. Peroxynitric Acid (HO_2NO_2)

VIII-M-1.1. OH Reaction Kinetics

The reaction of OH with HO_2NO_2 has been studied by Trevor et al. (1982), Smith et al. (1984), Barnes et al. (1986), and Jiménez et al. (2004). The measurements are summarized in table VIII-M-1 and displayed in figure VIII-M-1. While there is a good agreement between different determinations at 298 K within quoted uncertainty limits, a significant difference exists between the two studies of temperature dependence of the rate coefficient. A slight positive temperature dependence of the rate coefficient in the range 246–324 K was reported by Trevor et al. (1982), but Barnes et al. (1986) did not observe a significant change in the range 268–295 K. The results of Smith et al. (1984) and Jiménez et al. (2004) both show a clear negative temperature dependence in the range 240–330 K. However, the values reported by Smith et al. are systematically about 30% higher than the values of Jiménez et al. A possible contribution of the impurities present in peroxynitric acid samples to the overall measured rate coefficient could be responsible for the observed difference between the data of Smith et al. and Jiménez et al.

The IUPAC panel recommendation is based on the study of Jiménez et al. (2004) where peroxynitric acid as well as the impurities (NO_2, HNO_3, and H_2O_2) were monitored; they suggest $k = 3.2 \times 10^{-13} \exp(690/T)$ over the temperature range 210–300 K with $k = 3.2 \times 10^{-12}$ cm^3 molecule^{-1} s^{-1} and an estimated uncertainty of $\pm 30\%$ at 298 K (IUPAC, 2008). For a wider temperature range, 218–335 K, the temperature dependence is better described by: $k = 8.8 \times 10^{-19} T^2 \exp(1{,}130/T)$ cm^3 molecule^{-1} s^{-1} (Jiménez et al., 2004).

VIII-M-1.2. Cl-Atom Reaction Kinetics

The only reported study of the Cl-peroxynitric acid reaction is that of Simonaitis and Leu (1985) who used the discharge flow technique in combination with resonance fluorescence. The rate coefficient of the reaction was found to be $k < 1.0 \times 10^{-13}$ cm^3 molecule^{-1} s^{-1} at 296 K.

VIII-M-1.3. Summary of the Atmospheric Fate of Peroxynitric Acid

The dominant atmospheric loss processes for HO_2NO_2 consist of thermal decomposition, photodissociation, and reaction with the OH radical. The contribution of each of these processes to the total loss rate of HO_2NO_2 depends greatly on the location and time. Combining $k(\mathrm{OH} + \mathrm{PNA}) = 3.2 \times 10^{-12}$ cm^3 molecule^{-1} s^{-1} with a diurnal average [OH] $= 1 \times 10^6$ molecule cm^{-3} provides an estimate of the atmospheric

Table VIII-M-1. Rate coefficients ($k = A \times e^{-B/T}$), cm^3 molecule^{-1} s^{-1}) for the reaction of OH with peroxynitric acid (HO_2NO_2)

$10^{13} \times A$	B (K)	$10^{12} \times k$	T (K)	Technique[a]	Reference	Temperature Range (K)
		5.1	295 ± 1	RR (C_3H_6)[b]	Barnes et al. (1981)	
80.5 ± 56.9	193 ± 194	3.79 ± 0.21	324	PLP–RF	Trevor et al. (1982)	246–324
		4.95 ± 0.31	316			
		6.05 ± 0.52	298			
		3.61 ± 0.16	298			
		4.60 ± 0.41	273			
		4.83 ± 0.21	267			
		3.24 ± 0.30	254			
		3.84 ± 0.28	251			
		4.80 ± 0.46	246			
5.9 ± 0.4	−650 ± 30	4.21 ± 0.18	336	FP–RF	Smith et al. (1984)	241–336
		4.29 ± 0.21	323			
		5.24 ± 0.19	295			
		6.02 ± 0.16	275			
		7.65 ± 0.28	251			
		8.98 ± 0.41	241			
		4.94 ± 0.46	294	RR (C_3H_6)[b]	Barnes et al. (1986)	278–294
		5.64 ± 0.45	294			
		6.22 ± 1.09	278			
		5.06 ± 0.96	295	RR(n-C_4H_{10})[c]	Barnes et al. (1986)	268–295
		[d]5.1 ± 1.5	278			
		4.62 ± 0.91	268			
$k(T)$[e]		2.85 ± 0.06	335	PLP–LIF	Jiménez et al. (2004)	218–335
		2.96 ± 0.06	335			
		3.26 ± 0.05	315			
		3.44 ± 0.12	298			
		4.02 ± 0.06	273			
		4.35 ± 0.06	266			
		4.57 ± 0.10	255			
		4.66 ± 0.06	253			
		5.16 ± 0.04	249			
		5.55 ± 0.09	242			
		6.25 ± 0.11	232			
		6.49 ± 0.19	232			
		6.17 ± 0.10	232			
		6.05 ± 0.21	230			
		7.59 ± 0.14	224			
		6.82 ± 0.40	224			
		6.67 ± 0.21	221			
		7.82 ± 0.64	218			

[a]Abbreviations used for the techniques are defined in table I-F-3.
[b]From the fall off expression (Atkinson et al., 2006).
[c]Placed on an absolute basis using $k(OH + n\text{-}C_4H_{10}) = 1.40 \times 10^{-11} \exp(-520/T)$ (Calvert et al., 2008).
[d]Average value.
[e]Best described by $k = (8.8 \pm 2.6) \times 10^{-19}\, T^2 \exp[(1{,}130 \pm 20)/T]$ molecule cm^3 s^{-1}.

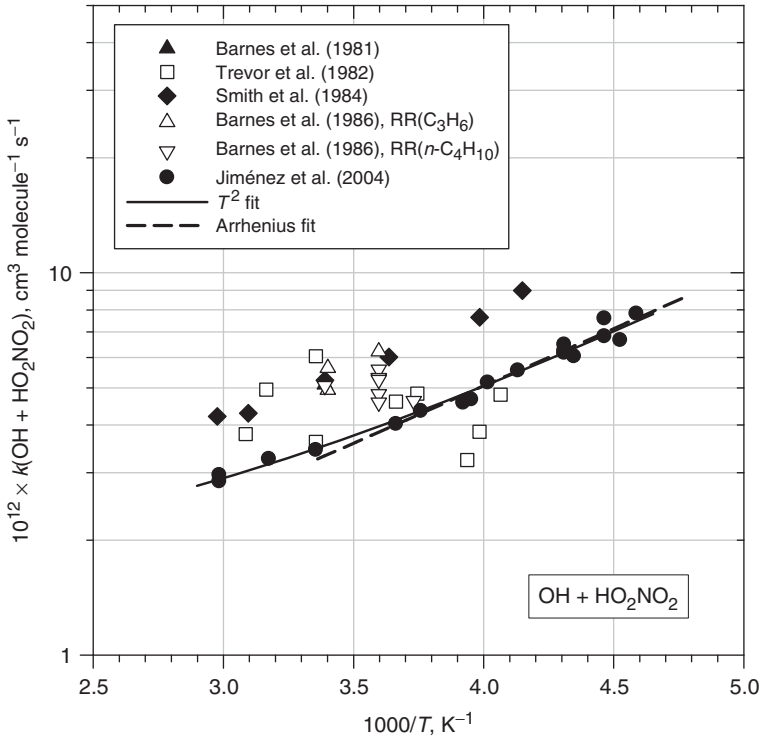

Figure VIII-M-1. Arrhenius plot of the rate coefficient for the reaction of OH with peroxynitric acid.

lifetime of peroxynitric acid of about 4 days with respect to reaction with OH. The mechanistic study of Jiménez et al. (2004) has shown that the reaction of HO_2NO_2 with OH occurs essentially exclusively through the channel leading to $H_2O + NO_2 + O_2$, indicating that this reaction is a net removal of HO_x in the upper troposphere–lower stratosphere (UTLS) (Jiménez et al., 2004). The absorption cross-sections and limited quantum yield measurements suggest that photodissociation of HO_2NO_2 will be a significant loss mechanism, particularly at the higher altitudes in the troposphere (Sander et al., 2006). At the warmer, lower elevations in the troposphere and even the middle to upper stratosphere, HO_2NO_2 loss can be dominated by thermal decomposition.

VIII-M-2. Peroxyacetyl Nitrate (1-Nitroperoxyethanal, $CH_3C(O)O_2NO_2$, PAN)

VIII-M-2.1. OH Reaction Kinetics

The rate coefficient of this reaction has been determined by Winer et al. (1977), Wallington et al. (1984), Tsalkani et al. (1988), and Talukdar et al. (1995). Winer et al. and Wallington et al. used the flash photolysis–resonance fluorescence technique, while Tsalkani et al. used the discharge flow combined with EPR method. Talukdar et al.

Table VIII-M-2. Rate coefficients ($k = A \times e^{-B/T}$), cm^3 molecule^{-1} s^{-1}) for the reaction of OH with peroxyacetyl nitrate ($CH_3C(O)O_2NO_2$)

$10^{12} \times A$	B (K)	$10^{13} \times k$	T (K)	Technique[a]	Reference	Temperature Range (K)
		< 1.7	299 ± 1	FP–FR	Winer et al. (1977)	
1.23	651 ± 229	1.13 ± 0.06	273 ± 2	FP–RF	Wallington et al. (1984)	273–297
		1.37 ± 0.05	297 ± 2			
		0.75 ± 0.14	298	DF–EPR	Tsalkani et al. (1988)	
		0.185 ± 0.034[b]	298	FP/PLP–LIF	Talukdar et al. (1995)	253–298
		0.13 ± 0.05[b]	272			
		0.082 ± 0.011[b]	253			
		0.118 ± 0.020[c]	298			
		0.164 ± 0.018[c]	272			
		0.200 ± 0.014[c]	260			

[a]Abbreviations used for the techniques are defined in table I-F-3.
[b]Average value obtained using PAN/tridecane mixture in a bubbler.
[c]Average value obtained using bulb of 1% PAN/He.

have used the flash and laser pulsed photolysis–laser-induced fluorescence technique to measure the rate coefficient. Table VIII-M-2 and figure VIII-M-2 show these data. The values reported by Wallington et al. (1984) and Tsalkani et al. (1988) at 298K are larger than that of Talukdar et al. (1995), while the upper limit of Winer et al. (1977) is not inconsistent with this later determination. The higher values of Wallington et al. (1984) and Tsalkani et al. (1988) were attributed to the interference due to the presence of reactive impurities in the samples of peroxyacetyl nitrate used in their studies. The IUPAC panel recommends an upper limit to the rate coefficient at 298 K of $k < 3 \times 10^{-14}$ cm^3 molecule^{-1} s^{-1} based on the more extensive study of Talukdar et al. (1995).

VIII-M-2.2. Cl-Atom Reaction Kinetics

The reaction of Cl with peroxyacetyl nitrate has been investigated by Tsalkani et al. (1988) and Wallington et al. (1990a); see table VIII-M-3. The absolute measurement of Tsalkani et al. is almost two orders of magnitude higher than the relative determination of Wallington et al. This large discrepancy is mainly attributed to the presence of the reactive tridecane as impurity in the sample of peroxyacetyl nitrate used by Tsalkani et al. The preferred value is based on the measurement of Wallington et al. in which no reaction of PAN was observed in presence of chlorine atoms. Based upon the work of Wallington et al. (1990a), we recommend an upper limit of $k(\mathrm{Cl} + \mathrm{PAN}) < 1 \times 10^{-14}$ cm^3 molecule^{-}1 s^{-1} at 298 K.

VIII-M-2.3. Summary of the Atmospheric Fate of Peroxyacetyl Nitrate

The atmospheric lifetime of peroxyacetyl nitrate with respect to the removal by reaction with OH radicals is estimated to be more than 1 year. The wet and dry depositions are minor removal processes (Roberts, 1990). The thermal decomposition remains the most important loss process up to around 7 km, above which photolysis takes

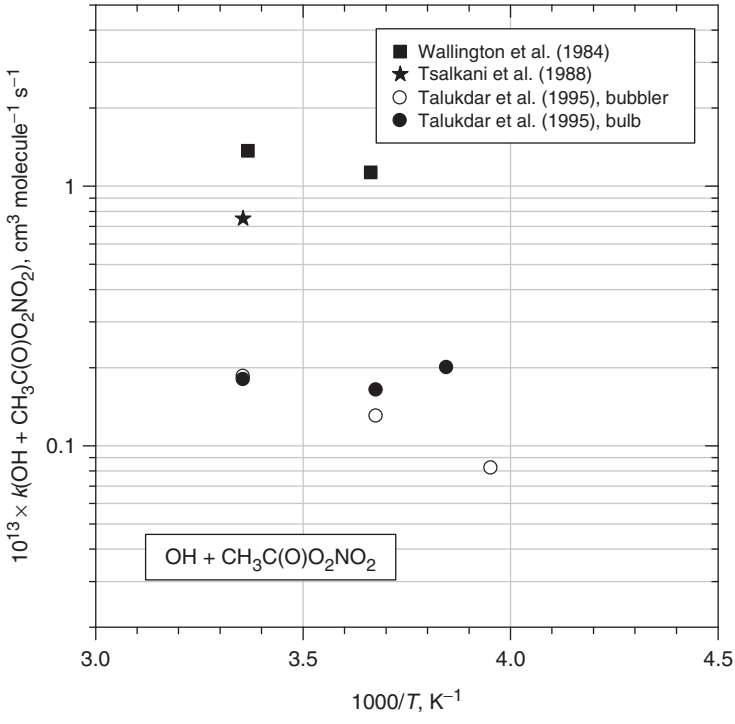

Figure VIII-M-2. Arrhenius plot of the rate coefficient for the reaction of OH with peroxyacetyl nitrate versus $1/T$ (selected data).

Table VIII-M-3. Rate coefficients (k, cm^3 molecule^{-1} s^{-1}) for the reaction of Cl with peroxyacetyl nitrate ($CH_3C(O)O_2NO_2$)

$10^{13} \times k$	T (K)	Technique[a]	Reference
3.7 ± 1.7	298	DF–EPR	Tsalkani et al. (1988)
< 0.07	295 ± 2	RR (CH_4)[b]	Wallington et al. (1990a)

[a]Abbreviations used for the techniques are defined in table I-F-3.
[b]Placed on an absolute basis using $k(\mathrm{Cl} + \mathrm{CH_4}) = 1 \times 10^{-13}$ cm^3 molecule^{-1} s^{-1} (Calvert et al., 2008).

over as the major loss process (Talukdar et al., 1995). The lifetime of PAN due to its thermal decomposition of PAN in the boundary layer is less than 1 h; it increases as the temperature decreases in the upper troposphere where photolysis and reaction with OH become important loss processes. The photodissociation of PAN in the lower troposphere with an overhead Sun is about 13 days; see table IX-M-1. The calculated j-values and the spectral j-values for PAN as a function of altitude (0 to 60 km) are given in figures IX-J-3c and IX-J-3d, respectively.

Table VIII-M-4 summarizes the rate coefficients for the thermal decomposition of a series of PAN-type species. The table presents the thermal decomposition rate coefficients at room temperature and the derived lifetimes. The parameters that describe

Table VIII-M-4. Rate coefficients for the thermal decomposition of peroxynitric acid and some PAN-type compounds

Compound	k (298) s^{-1}	Lifetime at 298 K (min.)	Temperature dependence[a,b]	Range of T (K)
Peroxynitric acid (PNA) HO_2NO_2	$\approx 2.5 \times 10^{-1}$	< 1	$k_0 = 4.1 \times 10^{-5} \exp(-10{,}650/T)[N_2]$ $k_\infty = 4.8 \times 10^{15} \exp(-11{,}170/T)$ $F_c = 0.5$	260–300
Peroxyacetyl nitrate (PAN) $CH_3C(O)O_2NO_2$	3.3×10^{-4}	50	$k_0 = 4.9 \times 10^{-3} \exp(-12{,}100/T)[N_2]$ $k_\infty = 5.4 \times 10^{16} \exp(-13{,}830/T)$ $F_c = 0.3$	300–330
Peroxypropionyl nitrate (PPN) $C_2H_5C(O)O_2NO_2$	3.6×10^{-4}	46	$k_0 = 1.7 \times 10^{-3} \exp(-11{,}280/T)[N_2]$ $k_\infty = 8.3 \times 10^{16} \exp(-13{,}940/T)$ $F_c = 0.36$	290–320
Peroxy-*n*-butyryl nitrate (PnBN) $CH_3CH_2CH_2C(O)O_2NO_2$	2.7×10^{-4}	62	$3.2 \times 10^{18} \exp(-15{,}150/T)$	291–299
Peroxy-*iso*-butyryl nitrate (PiBN) $(CH_3)_2CHC(O)O_2NO_2$	2.2×10^{-4}	76	$1.6 \times 10^{18} \exp(-15{,}000/T)$	291–299
Peroxy-*n*-pentanoyl nitrate (PnPN) n-$C_4H_9C(O)O_2NO_2$	1.8×10^{-4}	93	$1.3 \times 10^{12} \exp(-10{,}870/T)$	291–299
Peroxy-*iso*-pentanoyl nitrate (PiPN) *iso*-$C_4H_9C(O)O_2NO_2$	2.4×10^{-4}	69	$2.5 \times 10^{19} \exp(-15{,}800/T)$	291–299
Peroxymethacryloyl nitrate (MPAN) $CH_2{=}C(CH_3)C(O)O_2NO_2$	3.4×10^{-4}	49	$1.6 \times 10^{16} \exp(-13{,}500/T)$	290–330

[a]PNA, from IUPAC (2008); PAN, PPN, and MPAN data from Atkinson et al. (2006); PnBN, PiBN, PnPN, and PiPN data from Finlayson-Pitts and Pitts (2000), Grosjean et al. (1994a, b, c).

[b]Troe formalism given by: $k = \dfrac{k_o[M]k_\infty}{k_\infty + k_o[M]} F_c^{[1+(\log_{10}(k_o[M]/k_\infty))^2]^{-1}}$; Troe (1969, 1983)

the temperature dependence are also given in a limited temperature range. As shown in the table, the rate coefficients for the thermal decomposition of peroxynitric acid, peroxyacetyl nitrate, and peroxypropionyl nitrate are pressure dependent and are given using the Troe formalism, where k_0 and k_∞ are the measured low- and high-pressure limiting rate coefficients and F_c is the broadening factor (Troe, 1969, 1983).

VIII-M-3. Peroxypropionyl Nitrate [1-Nitroperoxypropanal, $C_2H_5C(O)O_2NO_2$, PPN]

VIII-M-3.1. Cl Reaction Kinetics

The rate coefficient of Wallington et al. (1990a) determined using a relative rate method at atmospheric pressure and ambient temperature is the only reported value and is given in table VIII-M-5.

VIII-M-3.2. Summary of the Atmospheric Fate of Peroxypropionyl Nitrate

As is the case for PAN, PPN is expected to be removed from the lower troposphere by thermal decomposition with a lifetime of less than 1 h (table VIII-M-4). It is also likely that photolysis is an important loss process of peroxypropionyl nitrate at higher altitudes. The lifetime for photodissociation in the lower troposphere with overhead Sun is about 7.4 days. Peroxypropionyl nitrate also plays a potential role as a reservoir for long range transport of reactive nitrogen.

VIII-M-4. Peroxymethacrylic Nitric Anhydride [MPAN, Peroxymethacryloyl Nitrate, 2-Methyl-2-propenoyl Nitro Peroxide, $CH_2{=}C(CH_3)C(O)O_2NO_2$]

MPAN is a product of the OH- and NO_3-initiated oxidation of methacrolein which is itself a major oxidation product of isoprene. MPAN has been detected and quantified in urban and rural regions (e.g., see Bertman and Roberts, 1991; Williams et al., 1997, 2000; Nouaime et al., 1998; Hansel and Wisthaler, 2000; see also chapter I).

VIII-M-4.1. OH Reaction Kinetics

The rate coefficients of Grosjean et al. (1993d) and Orlando et al. (2002) are given in table VIII-M-6. Both measurements were conducted using a relative rate method.

Table VIII-M-5. Rate coefficient (k, cm^3 molecule^{-1} s^{-1}) for the reaction of Cl with peroxypropionyl nitrate [$C_2H_5C(O)O_2NO_2$]

$10^{12} \times k$	T (K)	Technique[a]	Reference
1.14 ± 0.12	295 ± 2	RR (CH_3Cl)[b]	Wallington et al. (1990a)

[a]Abbreviations used for the techniques are defined in table I-F-3.
[b]Placed on an absolute basis using $k(Cl + CH_3Cl) = 4.9 \times 10^{-13}$ cm^3 molecule^{-1} s^{-1} (Sander et al., 2006).

Table VIII-M-6. Rate coefficients (k, cm^3 molecule^{-1} s^{-1}) for the reaction of OH with peroxymethacrylic nitric anhydride [CH_2=$C(CH_3)C(O)O_2NO_2$]

$10^{11} \times k$	T (K)	Technique[a]	Reference
0.333 ± 0.040	298 ± 2	RR (n-butyl nitrate)[b]	Grosjean et al. (1993d)
3.76 ± 0.58	277 ± 3	RR (C_2H_4)[c]	Orlando et al. (2002)
2.88 ± 0.46	277 ± 3	RR (C_3H_6)[d]	

[a]Abbreviations used for the techniques are defined in table I-F-3.
[b]Placed on an absolute basis using $k(OH + n\text{-butyl nitrate}) = 1.6 \times 10^{-12}$ cm^3 molecule^{-1} s^{-1} (Atkinson et al., 2006).
[c]Placed on an absolute basis using $k(OH + C_2H_4) = 9.64 \times 10^{-12}$ cm^3 molecule^{-1} s^{-1} at 275 K (Atkinson et al., 2006).
[d]Placed on an absolute basis using $k(OH + C_3H_6) = 3.03 \times 10^{-11}$ cm^3 molecule^{-1} s^{-1} at 275 K (Atkinson et al., 2006).

The experiments of Orlando et al. were performed at reduced temperature to avoid thermal decomposition of MPAN in synthetic air at a total pressure of 700–725 Torr. The experiments of Grosjean et al. were also conducted in air at atmospheric pressure but at 298 K. The rate coefficients determined in the two studies differ by a factor of about 10. The IUPAC panel recommended value at 298 K is based on the results of Orlando et al. (2002), adjusted to 298 K using the temperature dependence observed for the OH reaction with propene but with larger uncertainties. The Orlando et al. value was preferred because it is expected that the reaction of OH with MPAN will proceed by addition to the C=C double bond. The recommended rate coefficient is $k = 2.9 \times 10^{-11}$ cm^3 molecule^{-1} s^{-1} at 298 K (Atkinson et al., 2006).

VIII-M-4.2. NO_3 Reaction Kinetics

The rate coefficient of Canosa-Mas et al. (1999c) obtained using a relative rate method at ambient temperature and atmospheric pressure is given in table VIII-M-7. This is the only reported measurement.

VIII-M-4.3. O_3 Reaction Kinetics

The rate coefficient of Grosjean et al. (1993c) obtained at atmospheric pressure in air and ambient temperature is the only reported measurement and is given in table VIII-M-8.

Table VIII-M-7. Rate coefficients (k, cm^3 molecule^{-1} s^{-1}) for the reaction of NO_3 with peroxymethacrilic nitric anhydride [CH_2=$C(CH_3)C(O)O_2NO_2$]

$10^{16} \times k$	T (K)	Technique[a]	Reference
1.6 ± 0.6	296 ± 2	RR (C_2H_4)[b]	Canosa-Mas et al. (1999c)

[a]Abbreviations used for the techniques are defined in table I-F-3.
[b]Placed on an absolute basis using $k(NO_3 + C_2H_4) = 2.1 \times 10^{-16}$ cm^3 molecule^{-1} s^{-1} (Atkinson et al., 2006).

Table VIII-M-8. Rate coefficient (k, cm^3 molecule^{-1} s^{-1}) for the reaction of O_3 with peroxymethacrilic nitric anhydride [CH_2=$C(CH_3)C(O)O_2NO_2$]

$10^{18} \times k$	T (K)	Technique[a]	Reference
8.2 ± 2.0	294 ± 3	Excess of O_3[b]	Grosjean et al. (1993c)

[a]Abbreviations used for the techniques are defined in table I-F-3.
[b]Experiments conducted by monitoring MPAN in presence of excess of O_3 (and cyclohexane as OH scavenger).

VIII-M-4.4. Summary of the Atmospheric Fate of Peroxymethacrilic Nitric Anhydride

The atmospheric lifetime of peroxymethacrilic nitric anhydride with respect to the removal by reaction with OH radicals is calculated to be around 4 h using [OH] = 2.5×10^6 molecule cm^{-3} and k(OH + MPAN) = 2.9×10^{-11} cm^3 molecule^{-1} s^{-1}. Orlando et al. (2002) have suggested that the reaction with OH could be more rapid than its thermal decomposition in specific conditions. The rate coefficient for the thermal decomposition of MPAN is given in table VIII-M-4. The shorter lifetime of MPAN compared to PAN or PPN will restrict its presence to regions near its source (i.e., in isoprene rich regions); hence its capacity to transport reactive nitrogen will be limited compared to that of PAN and PPN (Orlando et al., 2002).

Grosjean et al. (1993d) and Orlando et al. (2002) have both conducted a mechanistic study of the OH-initiated oxidation of peroxymethacrylic nitric anhydride. The products observed or suggested by these studies are mainly formaldehyde, hydroxyacetone, and CO_2 following the degradation mechanism shown in figure VIII-M-3.

The reaction of O_3 with MPAN is expected to proceed by O_3 addition to the C=C bond followed by decomposition of the 1,2,3-trioxolane adduct into two carbonyls and two Criegee intermediates as for the reaction with unsaturated organics. Grosjean et al. (1993d) have reported CH_2O as the major reaction product with a formation yield of 60 ± 10%.

VIII-N. *N*,*N*-Dimethylnitrosamine [*N*-Nitrosodimethylamine, $(CH_3)_2NNO$] and *N*,*N*-Dimethylnitramine [Dimethylnitramine, $(CH_3)_2NNO_2$]

N,*N*-Dimethylnitrosamine formation has been observed in simulated polluted atmospheres (Hanst et al., 1977; Pitts et al., 1978; Tuazon et al., 1978). It can be formed following OH attack on dimethylamine by the following mechanism:

$$OH + (CH_3)_2NH \rightarrow H_2O + (CH_3)_2N$$

$$(CH_3)_2N + NO \rightarrow (CH_3)_2N\text{—}N{=}O \qquad (k_{NO})$$

$$(CH_3)_2N + O_2 \rightarrow CH_2{=}N\text{–}CH_3 + HO_2 \qquad (k_{O_2})$$

Lindley et al. (1979) have shown that the ratio of rate coefficients for the reaction of the dimethylamino radical with O_2 to that with NO [$k_{O_2}/k_{NO} = (1.49 \pm 0.07) \times 10^{-6}$]

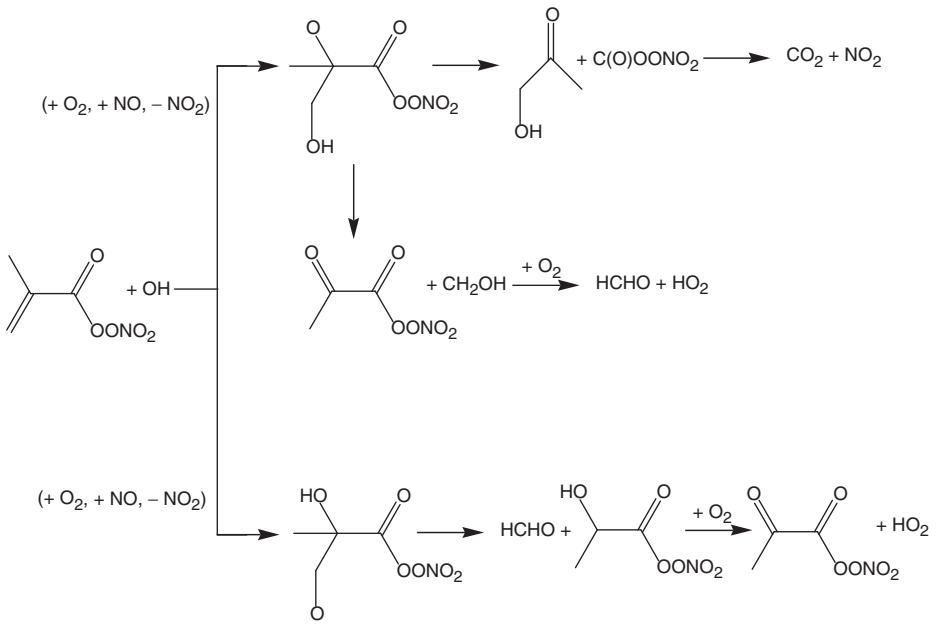

Figure VIII-M-3. OH-initiated degradation mechanism of peroxymethacrilic nitric anhydride (Orlando et al., 2002).

is sufficiently small to allow capture of an NO molecule even at relatively low NO_x concentrations in air. However, the nitrosoamine $(CH_3)_2N—N=O$ is readily photolyzed in sunlight (see section IX-H-13). When the more photochemically stable nitramine $(CH_3)_2N—NO_2$ is formed by NO_2 capture by $(CH_3)_2N$ radicals, its loss by reaction with OH radical becomes its important removal mechanism:

$$(CH_3)_2N—N=O + h\nu \rightarrow (CH_3)_2N + NO$$

$$(CH_3)_2N + NO_2 \rightarrow (CH_3)_2N—NO_2$$

VIII-N-1.1. OH Reaction Kinetics

The reactions of OH with *N*,*N*-dimethylnitrosamine and *N*,*N*-dimethylnitramine have been investigated by Tuazon et al. (1984b) using a relative rate method at atmospheric pressure. The data obtained by these authors are given in table VIII-N-1.

VIII-N-1.2. O_3 Reaction Kinetics

The upper limits to the rate coefficients of Tuazon et al. (1984b) obtained at atmospheric pressure in air and ambient temperature are the only reported data and are given in table VIII-N-2.

Table VIII-N-1. Rate coefficients (k, cm^3 molecule^{-1} s^{-1}) for the reaction of OH with *N*-nitrosodimethylamine [$(CH_3)_2NNO$] and dimethylnitramine [$(CH_3)_2NNO_2$]

Compound	$10^{12} \times k$	T (K)	Technique[a]	Reference
Nitrosodimethylamine $(CH_3)_2NNO$	2.30 ± 0.19	298 ± 2	RR (CH_3OCH_3)[b]	Tuazon et al. (1984b)
Dimethylnitramine $(CH_3)_2NNO_2$	3.48 ± 0.14	298 ± 2	RR (CH_3OCH_3)[b]	Tuazon et al. (1984b)

[a]Abbreviations used for the techniques are defined in table I-F-3.
[b]Placed on an absolute basis using $k(OH + CH_3OCH_3) = 2.7 \times 10^{-12}$ cm^3 molecule^{-1} s^{-1} (this book, section III-B-1.1).

Table VIII-N-2. Rate coefficient (k, cm^3 molecule^{-1} s^{-1}) for the reaction of O_3 with *N*-nitrosodimethylamine [$(CH_3)_2NNO$] and dimethylnitramine [$(CH_3)_2NNO_2$]

Compound	K	T (K)	Technique[a]	Reference
Nitrosodimethylamine $(CH_3)_2NNO$	$\leq 1 \times 10^{-20}$	296	Excess of NDMA[b]	Tuazon et al. (1984b)
Dimethylnitramine $(CH_3)_2NNO_2$	$\leq 3 \times 10^{-21}$	296	Excess of NDMA[b]	Tuazon et al. (1984b)

[a]Abbreviations used for the techniques are defined in table I-F-3.
[b]Experiments conducted by monitoring MPAN in presence of excess of O_3.

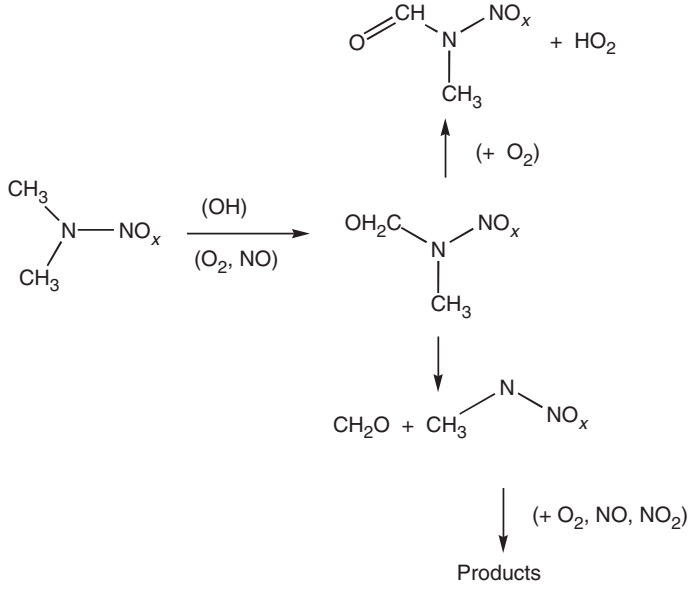

Figure VIII-N-1. Possible OH-initiated degradation mechanism of *N*-nitrosodimethylamine and dimethylnitramine.

VIII-N-1.3. Summary of the Atmospheric Fate of N-Nitrosodimethylamine (NDMA) and Dimethylnitramine (DMN)

Combining $k(OH + NDMA) = 2.3 \times 10^{-12}$ and $k(OH + DNM) = 3.48 \times 10^{-12}$ cm^3 molcule^{-1} s^{-1} with an average OH concentration of [OH] = 1×10^6 molecule cm^{-3}

provides an estimate of 5 to 3 days, respectively, for the tropospheric lifetimes of these two compounds with respect to reaction with OH. Lindley et al. (1979) and Tuazon et al. (1984b) have reported that photolysis is the most important removal processes for *N*,*N*-dimethylnitrosamine from the atmosphere. The photodissociation lifetime for an overhead Sun is about 6 min.; see section IX-H-13. The photodecomposition of the DNM is unimportant in the lower troposphere since its light absorption in this region is very low. Reaction with OH is the dominant path for removal of DNM. It is expected that the reaction of OH with $(CH_3)_2NNO$ and $(CH_3)_2NNO_2$ proceeds via an H-atom abstraction from the C—H bond on the methyl group; see figure VIII-N-1.

IX

Mechanisms of Photodecomposition of the Sunlight-Absorbing Oxygenates

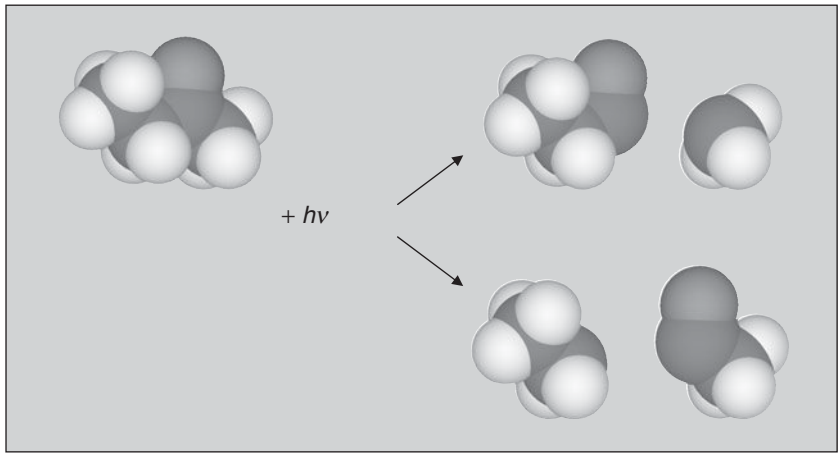

IX-A. Introduction

In this chapter we consider the chemical changes induced by absorption of sunlight by oxygenated organic compounds. In contrast to the hydrocarbons, sunlight absorption by the oxygenated products of hydrocarbon oxidation shows a shift in absorption to the longer wavelengths such that their photodecompositions can become important atmospheric processes. This is illustrated in the absorption data given for methane and its oxidation products in figure IX-A-1. As a H_3C—H bond in methane is replaced with a H_3C—OH bond (alcohols), H_3C—OCH_3 bond (ethers), or H_3C—O_2H bond (hydroperoxides), light absorption involving excitation of nonbonding O-atom electrons to an antibonding sigma orbital ($n \rightarrow \sigma^*$ transitions) becomes possible. These "forbidden" absorptions are smaller than the allowed $\sigma \rightarrow \sigma^*$ transitions in the CH_4 and the other alkanes, but the absorption bands are shifted to longer wavelengths progressing from CH_4 to CH_3OH, CH_3OCH_3, and CH_3OOH as less energy is required to excite the nonbonding electron to the σ^* orbital. The ($\rangle$C=O) group in HC(O)OH (acids) and $HC(O)OCH_3$ (esters) allows a weak $n \rightarrow \pi^*$ absorption with a shift to somewhat longer wavelengths than the hydrocarbons. In the absence of the electron-withdrawing groups (—OH and —OCH_3, respectively) present in the acids and the esters, the $n \rightarrow \pi^*$ transition in CH_2O (and the other aldehydes and ketones) is shifted to much longer

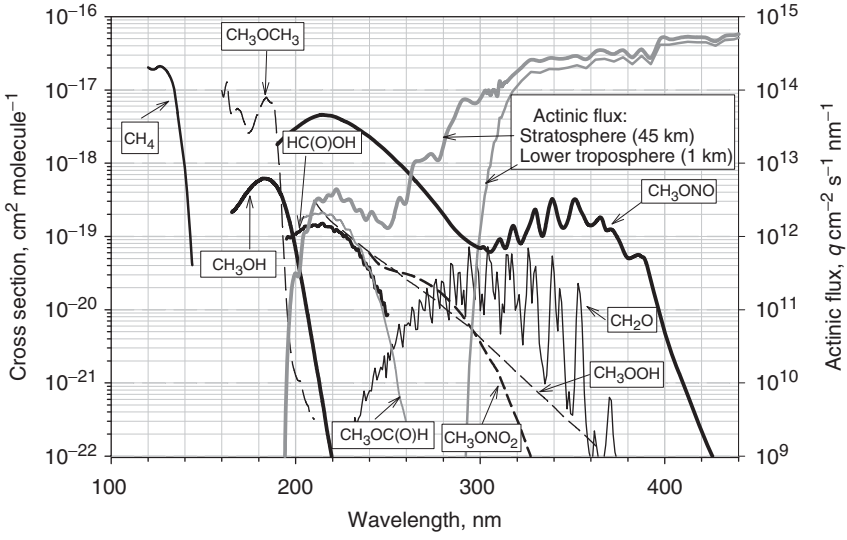

Figure IX-A-1. Cross sections for CH_4 and various oxidation products of methane; spectra for methane from Okabe and Becker (1963); CH_3OH from Cheng et al. (2002); CH_2O from Meller and Moortgat (2000); other compounds from Atkinson et al. (2004). The actinic flux curves for lower troposphere and mid stratosphere are calculated for zenith angle 45° and altitudes of 1 and 45 km, respectively.

wavelengths resulting in a more favorable overlap with the actinic flux present within the troposphere. The $n \rightarrow \pi^*$ transition in CH_3ONO_2 (nitrates) occurs in the short-wavelength tail of the actinic flux present in the lower troposphere. With removal of one of the electron-withdrawing O-atoms in the nitrates, the position of the electronic transition is shifted to much longer wavelengths in CH_3ONO (methyl nitrite) with a very good overlap with the actinic flux within the troposphere. It is seen in figure IX-A-1 that only at the shorter wavelengths of the actinic flux present in the stratosphere does significant overlap occur of the solar radiation and the absorption bands of CH_3OH, CH_3OCH_3, HC(O)OH, and $HC(O)OCH_3$; thus, the photodecomposition of these species becomes significant only in the upper troposphere and stratosphere.

We review in this chapter the nature of the photodecomposition pathways of several of the major products of atmospheric oxidation of the hydrocarbons, namely, the acyclic aldehydes in section IX-B; the aldehydes containing additional functional groups in section IX-C; the acyclic ketones in section IX-D; the cyclic ketones in section IX-E; the ketones containing additional functional groups in section IX-F; the acyl halides and carbonyl halides in section IX-G; nitrous acid, the alkyl nitrites, the nitroalkanes, and the nitroso-compounds in section IX-H; nitric acid and the alkyl nitrates in section IX-I; the peroxyacyl nitrates in section IX-J; the alkyl hydroperoxides in section IX-K; and some oxygenates derived from the aromatic hydrocarbons in section IX-L.

The extent of overlap of the absorption spectra of the oxygenate with the spectrum of wavelengths available in sunlight, as well as the quantum efficiencies of radical and molecular products formed from these hydrocarbon derivatives, determine

the rate of photodecomposition of the molecule, the extent of ozone generation, and other atmospheric chemistry that occurs in the atmosphere. Longer-lived compounds that are relatively unreactive toward OH radical and absorb tropospheric radiation weakly, such as the CFCs, HCFCs, halons, etc., have an insignificant effect on tropospheric chemistry but can impact significantly the chemistry of the stratosphere as their photodecomposition becomes significant.

Atmospheric photolysis rate coefficients and photolysis frequencies (or *j*-values) are of special interest in the understanding of the photochemistry of the various oxidation products and the photochemical lifetimes ($\tau = 1/j$) of the compounds. There are several methods of estimating these important quantities. When information is available for the wavelength-dependent absorption cross sections and quantum yields, the photolysis frequencies (*j*-values) can be calculated using relation (1) where numerical summations are made over wavelength λ:

$$j = \Sigma \langle \sigma \rangle_i \langle \phi \rangle_i \langle F \rangle_i \Delta\lambda_i \tag{1}$$

Here $\langle \sigma \rangle_i$, $\langle \phi \rangle_i$, and $\langle F \rangle_i$ are, respectively, the absorption cross section, quantum yield, and spectral actinic flux averaged over small wavelength intervals, $\Delta\lambda_i$. Cross sections and quantum yields specific to each photodissociation reaction are discussed later in this chapter.

Many different experimental techniques have been used throughout the years to estimate the quantum yields of the primary photochemical processes in the products of the hydrocarbon oxidation. The photodecomposition of a few of the oxygenates that we consider in this book has been reviewed in detail in our previous studies of the atmospheric chemistry of the alkenes (Calvert et al., 2000), the aromatic hydrocarbons (Calvert et al., 2002), and the alkanes (Calvert, 2008). However, new studies for most of oxygenates provide significant new information, and discussions in this chapter include an update of the recommended cross sections, quantum yields, and *j*-values for each compound as well as information on compounds previously not considered.

In this book, the calculated photolysis frequencies for each compound are presented graphically as a function of the solar zenith angle, the angle between a vertical line and a line extending to the Sun from the observation point. This angle is a complex function of the latitude and longitude of the observation point, the day of the year, and the time of the day. In figure IX-A-2 representative plots of solar zenith angle are given as a function of the latitude and the local time of the day for selected times of the year: the Spring (March 22) and Fall (September 23) equinoxes, days with equal periods of daylight and darkness (figure IX-A-2a); the Summer solstice (June 22), the longest day in the northern hemisphere (figure IX-A-2b); and the Winter solstice (December 22), the shortest day in the northern hemisphere (figure IX-A-2c). Solar zenith angles applicable for a given location and time obviously vary over a wide range, and choice of the photolysis frequency that is appropriate for a given time and location requires information of the sort presented in figure IX-A-2 and the *j*-value versus solar zenith angle plots presented in this work.

In addition to the use of equation (1), another very useful technique for estimation of *j*-values involves the use of reaction chambers that are exposed to sunlight.

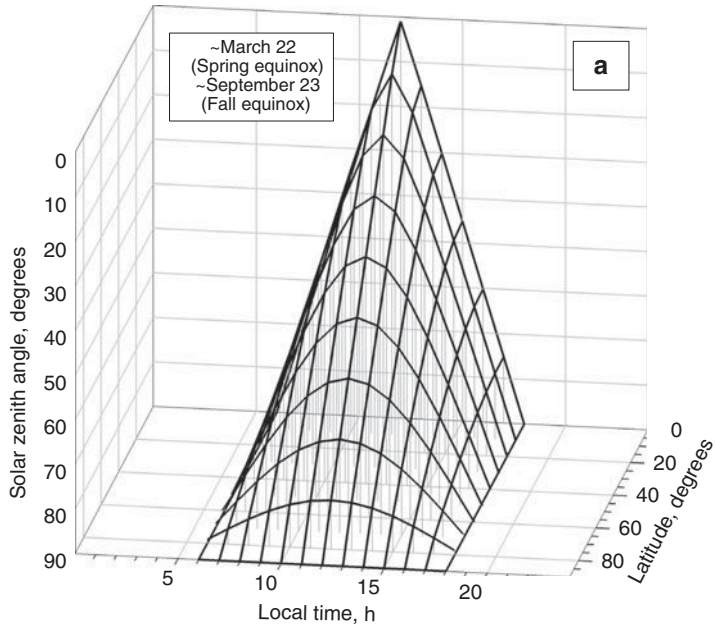

Figure IX-A-2a. Plot of the solar zenith angle as a function of latitude and local time of the day for the periods of Spring and Fall equinox. Note the days and nights are of equal length at all latitudes (from Calvert et al., 2008).

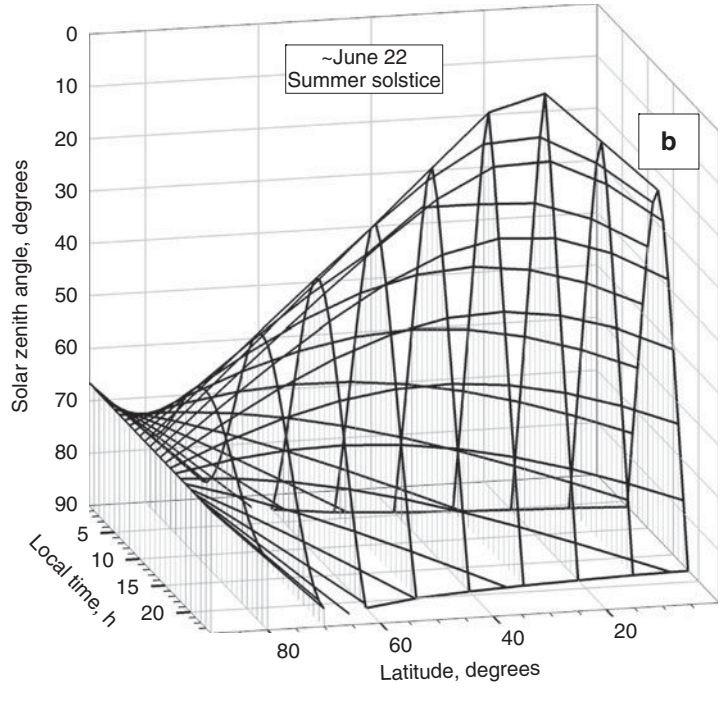

Figure IX-A-2b. Plot of the solar zenith angle as a function of latitude and local time of the day for June 22, Summer solstice. Note that the Sun is above the horizon all the day in the high latitudes (from Calvert et al., 2008).

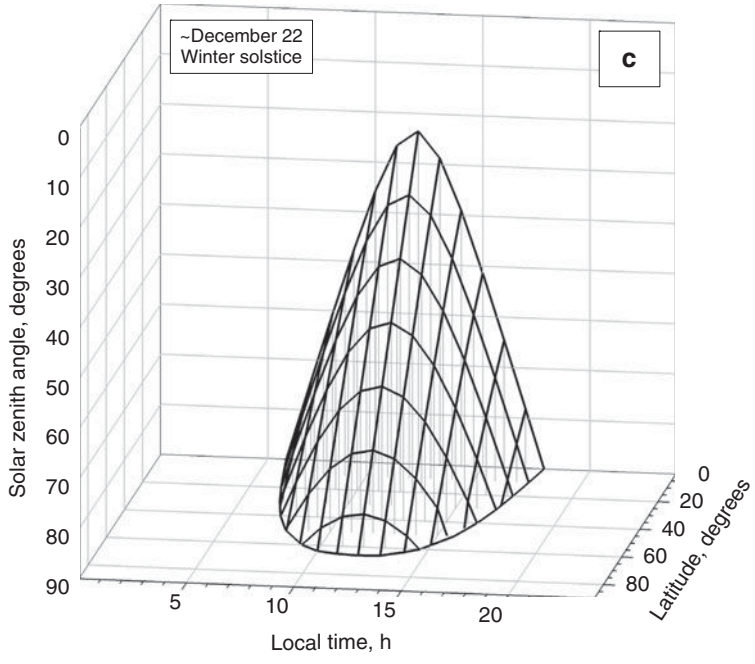

Figure IX-A-2c. Plot of the solar zenith angle as a function of latitude and local time for December 22, Winter solstice in the Northern Hemisphere. Note that the Sun is below the horizon for the entire 24 h period for locations at high latitudes (from Calvert et al., 2008).

The direct measurements of the rate of photodecomposition of a light-absorbing compound (in air) by natural sunlight, offer a significant test of the reliability of estimations made using equation (1) of this section. In some cases, the *j*-values determined in sunlight-irradiated chambers provide the only available information on these quantities. The sheer quantity of data needed to describe the wavelength dependence of the solar flux, the absorption cross sections of the target molecule and their temperature dependence, as well as the wavelength, pressure, and temperature dependence of the quantum yields of the products, can lead to significant uncertainty as to the reliability of the *j*-value estimates based on equation (1). No assumptions about the magnitude of these quantities are necessary in the direct experiments. However, data from the direct measurements of the rate of decay of a given compound in air mixtures in sunlight alone do not allow extrapolation to *j*-values for conditions other than those at the measurement site. No account can be taken of the wavelength dependence of the actinic flux, the temperature dependence of the compound's cross sections, and the quantum yields that vary for locations and local conditions. Also, the measurement of meaningful *j*-values for a given compound in sunlight-irradiated chambers requires more than a simple exposure of the compound with measurements of its concentration as a function of time (R_X). Since samples of the chamber air must be taken regularly for analytical purposes and small leaks in the chamber walls may exist, it is necessary to add an unreactive, photochemically stable, tracer gas such as SF_6 so that the rate of dilution

can be determined by following its concentration changes with time (R_{Dilution}). Since it is impossible to eliminate all sources of OH radicals in experimental chambers, it is also necessary to determine the OH radical concentration in the chamber during the experiment so that correction can be made for loss of the compound under study due to reaction with OH radicals ($R_{X-\text{OH}}$). Often reactive hydrocarbons that do not absorb tropospheric sunlight (such as cyclohexane) are added to the starting mixture of gases, and the time dependence of the concentration of this hydrocarbon, coupled with the measured dilution rate, allows the OH concentration to be calculated, and thus a correction can be made for the loss of the compound under study due to its reaction with OH. *j*-Values are then calculated from these measured quantities using equation (2):

$$j_X = \mathrm{R}_X - R_{\text{Dilution}} - R_{X-\text{OH}} \tag{2}$$

Care must be taken to ensure the maintenance of efficient sunlight transmission by the walls of the solar chamber that are often made of Teflon®. Ideally, the reflectance of the chamber floor should match that of the Earth if one expects the *j*-values to be representative of those in the field. The solar zenith angle at the time of the chamber measurements is commonly reported so that checks against *j*-values determined by equation (1) can be readily made.

One of the most utilized facilities for the direct determination of *j*-values is the EUPHORE chamber located in Valencia, Spain (Becker, 1996; Barnes and Wenger, 1997). The main features of one of its two matching, large chambers can be seen in figure IX-A-3.

It is common practice to measure $j(\text{NO}_2)$ with separate equipment while performing a *j*-value determination for a given compound (X) in a chamber experiment. The ratio of $j(X)/j(\text{NO}_2)$ is then reported since this is less sensitive to changes in solar zenith angle than the $j(X)$ and $j(\text{NO}_2)$ quantities alone, and multiplication of the ratio by a newly measured $j(\text{NO}_2)$ value gives a rough estimate of the applicable $j(X)$ value for these new conditions. However, the ratio of $j(X)/j(\text{NO}_2)$ is dependent on the solar zenith angle for most sunlight-absorbing compounds. This is illustrated in figure IX-A-4 where the $j(X)/j(\text{NO}_2)$ ratios for a number of atmospheric trace gases are plotted versus solar zenith angle. Among the various ratios compared in figure IX-A-4, the $j(\text{Cl}_2)/j(\text{NO}_2)$ ratio is seen to be the least sensitive, while several others decrease by as much as an order of magnitude as the solar zenith angle is increased from 0 to 90°. The reason for these differences can be understood from the comparison of the extent of overlap of the spectral *j*-value curves for the compound X and NO_2. The most reliable indicator of useful overlap of the spectrum of X with that of NO_2 is the action spectrum which defines the spectral *j*-values. The action spectrum is composed of the spectral *j*-values that give the individual increments $\langle\sigma\rangle_i\langle\phi\rangle_i\langle F\rangle_i$ plotted against the wavelength interval ($\Delta\lambda$) chosen for use in equation (1). This is illustrated in figure IX-A-5 for two molecules with very different response of $j(X)/j(\text{NO}_2)$ values to change in solar zenith angle: Cl_2 and CH_3COCH_3.

The wavelength distribution of the solar flux changes as the solar zenith angle increases, since the path lengthens through which the sunlight passes, and larger fractions of the shorter wavelengths are depleted by ozone absorption. Spectral *j*-values

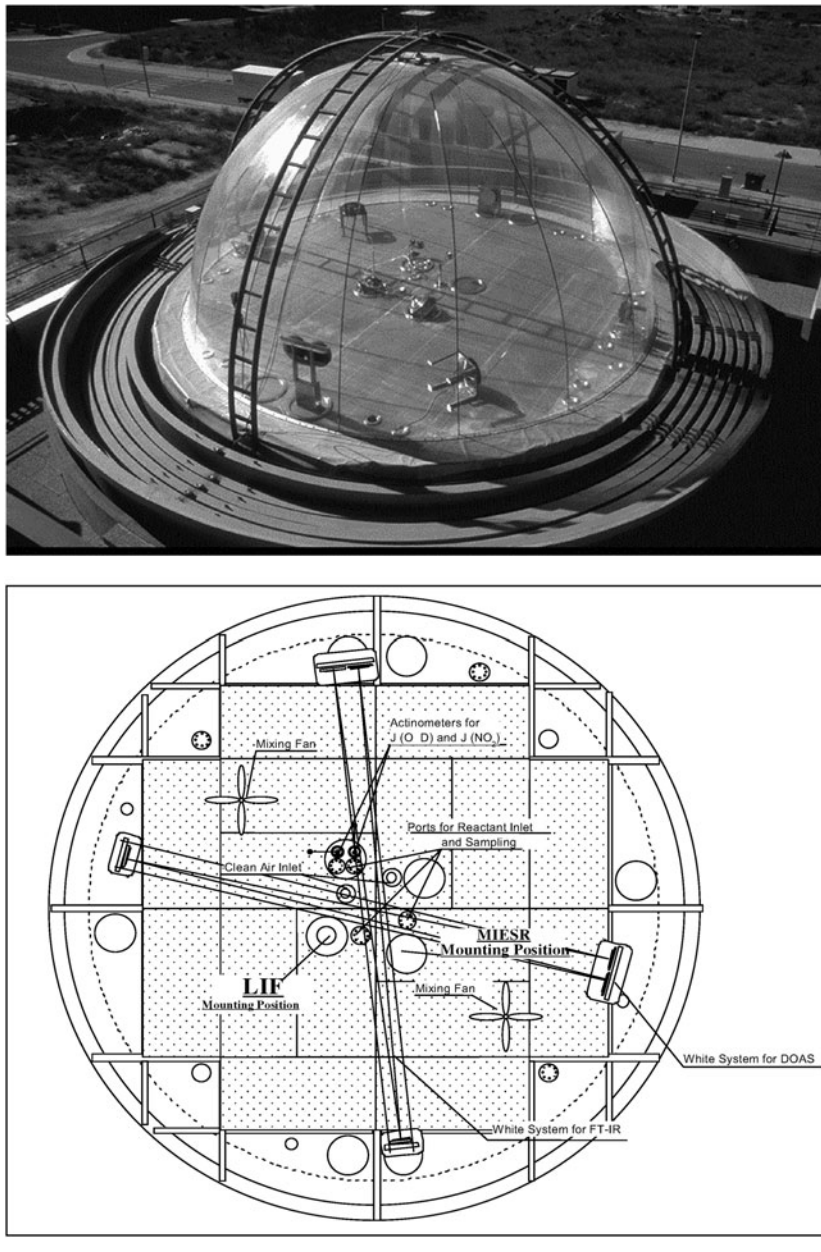

Figure IX-A-3. View of one of the two chambers of the European photoreactor and a diagram of the placement of some of the analytical instrumentation employed during measurements at the EUPHORE facility, Valencia, Spain. The large domes can be closed to sunlight by automatically raising the metal cover, several rings of which can be seen at the base of the dome.

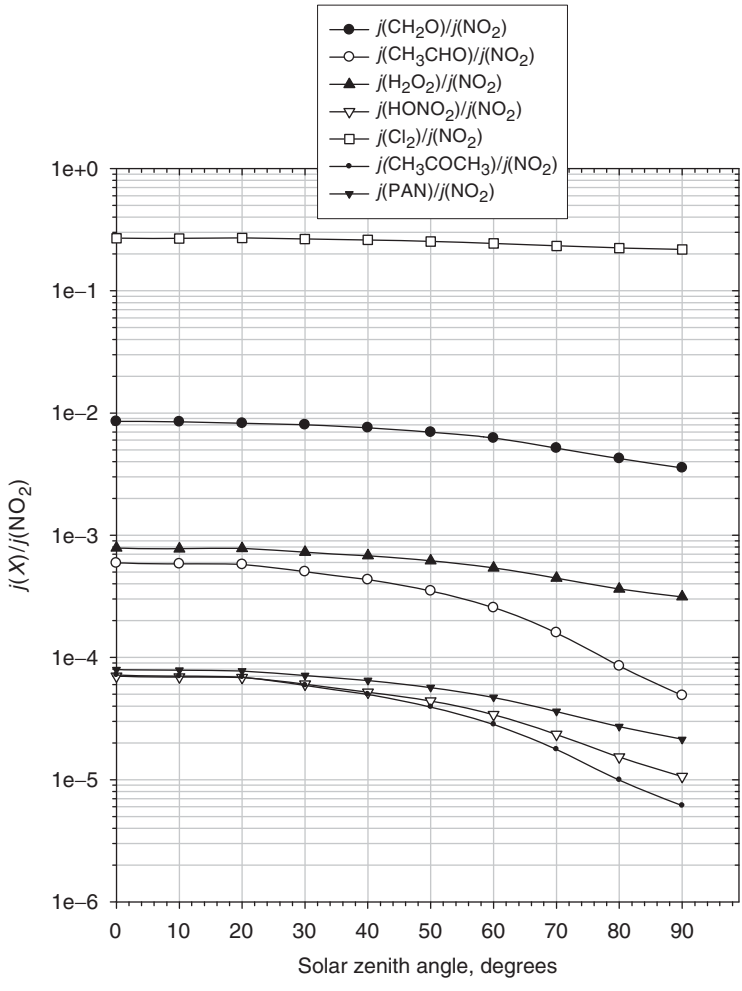

Figure IX-A-4. Semilog plot of the ratio $j(X)/j(NO_2)$ versus solar zenith angle for a number of light-absorbing atmospheric trace gases. Except for $j(Cl_2)/j(NO_2)$, the ratios are seen to decrease significantly as the solar zenith angle is increased.

are shown for three different solar zenith angles: 0, 60, and 80°. It can be seen that the overlap of the Cl_2 spectral j-values with that of NO_2 is good, and changes in the wavelength distribution of the solar flux with zenith angle are minimal. In contrast, there is little overlap of the active wavelength regions of CH_3COCH_3 and NO_2, and a larger share of the shorter wavelength absorbed by acetone results in a disproportionate lowering in the $j(X)/j(NO_2)$ value as the solar zenith angle is increased. Many of the trace gases behave like acetone (e.g., note the behavior of $j(CH_2O)/j(NO_2)$ and $j(PAN)/j(NO_2)$ in figure IX-A-4). As a consequence, the usefulness of the $j(X)/j(NO_2)$ ratio measured at one solar zenith angle for estimating $j(X)$ values at other zenith angles is rather limited.

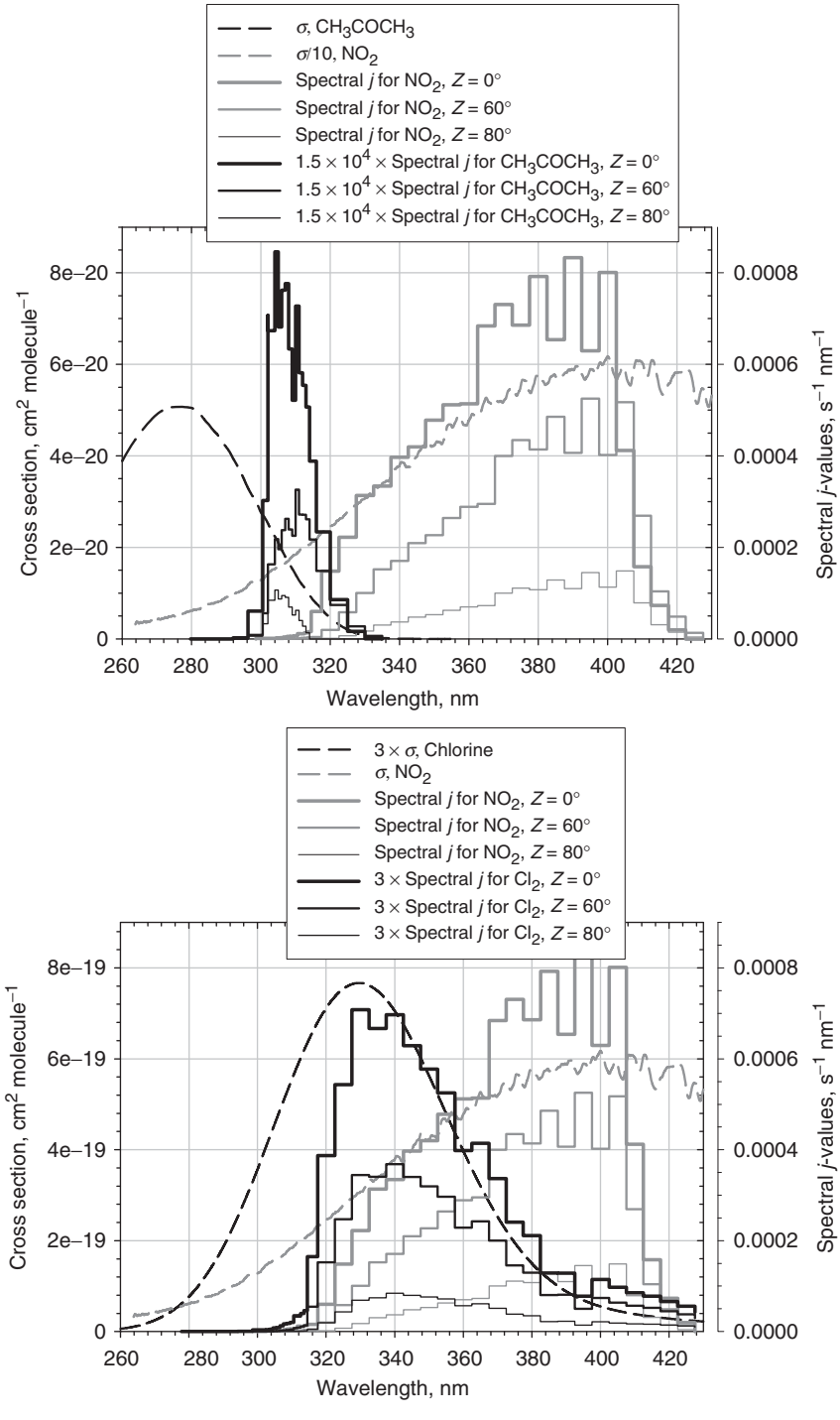

Figure IX-A-5. Comparison of the overlap of the spectral j-values for acetone and NO_2 (upper panel) and Cl_2 and NO_2 (lower panel). The calculations were made for clear tropospheric skies at an altitude of 0.5 m and overhead ozone column of 350 DU.

IX-B. Mechanisms of Photodecomposition of the Acyclic Aldehydes

A weak $n \rightarrow \pi^*$ electronic transition is induced in the aldehydes as they absorb sunlight over a wide range of wavelengths that are available within the troposphere. The absorption bands for the C_1 to C_5 straight-chain aldehydes are shown in figure IX-B-1. The highly vibrationally structured bands of formaldehyde contrast with those of the higher aldehydes where vibrational structure is less pronounced. Note that the absorption bands increase somewhat in intensity as one progresses from CH_3CHO to n-C_3H_7CHO, but the band for n-C_4H_9CHO is seen to nearly overlap that for n-C_3H_7CHO. Tadić et al. (2001a) pointed out that the spectrum of n-$C_5H_{11}CHO$ and presumably the higher straight-chain aldehydes are also very similar to those of C_3H_7CHO and n-C_4H_9CHO. Light absorption results in the photodecomposition of the aldehydes, and the various reactive fragments formed are effective in reactions that eventually generate ozone and other products within the atmosphere.

IX-B-1. Photodecomposition of Formaldehyde (Methanal, CH_2O)

Formaldehyde is one of the most important products of hydrocarbon oxidation in the atmosphere. It provides a major source of radicals formed in the atmosphere and is very important in determining the rate of ozone generation. The atmospheric photochemistry of formaldehyde has been reviewed by several groups in recent years

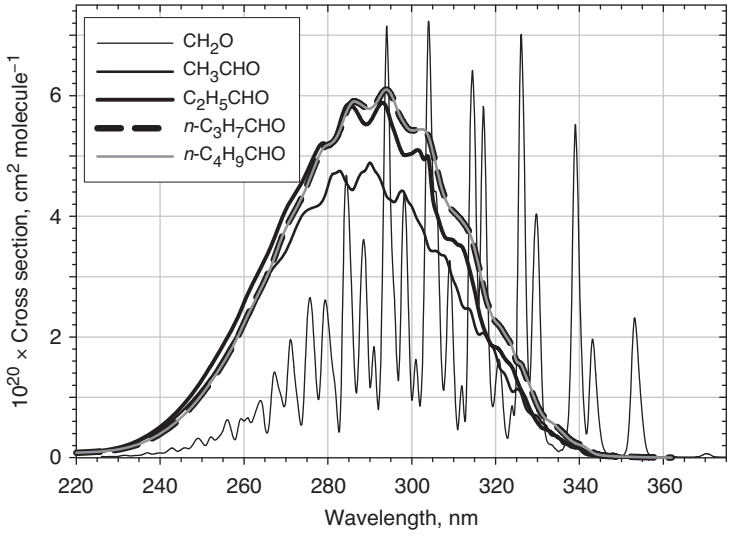

Figure IX-B-1. Comparison of the absorption spectra of the C_1–C_5 straight-chain aldehydes; data for CH_2O are from Meller and Moortgat (2000); those for the C_2–C_4 aldehydes are from Martinez et al. (1992); that for pentanal is from Tadić et al. (2001a).

(e.g., see Calvert et al., 2000, 2002, 2008; Atkinson et al., 2004; De More et al., 1997), where further discussion of the data evaluation is available.

Three different primary processes are believed to dominate formaldehyde photochemistry: processes (I) and (II) within the troposphere, with process (III) becoming significant in the upper troposphere and stratosphere:

$$CH_2O + h\nu \rightarrow HCO + H \quad \text{(I)}$$

$$\rightarrow H_2 + CO \quad \text{(II)}$$

$$\rightarrow H + H + CO \quad \text{(III)}$$

Photodissociation in reaction (I) can occur from the initially excited singlet state, as well as both the vibrationally excited ground state, and the triplet state of formaldehyde that are populated from the initially excited singlet state by internal conversion and intersystem crossing, respectively. The molecular channel (II) occurs from the vibrationally excited ground state (e.g., see Chuang et al., 1987; Green et al., 1992; Yamaguchi et al., 1998). Vibrational relaxation, induced by molecular collisions, results in quenching of process (II) in CH_2O when excited at longer wavelengths ($\lambda > 330$ nm). Primary process (I) is not sensitive to pressure change from 0 to 1 atm. Only processes (I) and (II) are important in the wavelength region available within the troposphere. The threshold wavelength for process (I) is ~324 nm, while process (II) is energetically feasible at all wavelengths absorbed by formaldehyde. Sufficient energy is available in the quantum of radiation at 297 nm for process (III) to occur. Studies of formaldehyde photolysis at 123.6 and 147.0 nm (Glicker and Stief, 1971) suggest that process (III) is important at these short wavelengths; it is estimated that $\phi_{II} + \phi_{III} = 1.0$ with $\phi_{II} = \phi_{III} = 0.5$. The occurrence of either (I) or (III) in the Earth's O_2-rich atmosphere leads to the same products: $CH_2O\,(+\,2O_2) \rightarrow 2HO_2 + CO$, so the differentiation of the extent of processes (I) and (III) is unimportant for atmospheric studies.

IX-B-1.1. Absorption Cross Sections of Formaldehyde

The cross sections for formaldehyde absorption are shown in figures IX-A-1 where they are compared with those of other oxidation products of methane. The formaldehyde cross section data reported by Meller and Moortgat (2000), determined over the entire 226–375 nm range, are the most extensive and seemingly the most accurate of the available data. Those recommended by Calvert et al. (2000), a combined data set of unweighted averages of the older data of Moortgat and Schneider (given by Atkinson et al., 1997; Cantrell et al., 1990; and Rogers, 1990), are in reasonable agreement with those of Meller and Moortgat (2000) [M&M]. The average ratio of all the sigma values (excluding zero values) at 298 K over the range from 280–365 nm is $\sigma_{M\ \&\ M}/\sigma_{C\ et\ al.} = 0.994$, the ratio of the major absorption peaks that dominate the contributions of CH_2O absorption within the atmosphere is 1.17. The recommended cross section data of Meller and Moortgat (2000) are given in table IX-B-1.

Table IX-B-1. Recommended CH_2O cross sections, σ (cm^2 $molecule^{-1}$), 298 K from Meller and Moortgat (2000)

λ, nm	$10^{21} \times \sigma$	λ, nm	$10^{21} \times \sigma$	λ, nm	$10^{21} \times \sigma$	λ, nm	$10^{21} \times \sigma$
226	0.179	264	9.47	302	8.52	340	31.5
227	0.169	265	5.30	303	30.2	341	9.78
228	0.177	266	5.38	304	72.3	342	5.04
229	0.190	267	13.6	305	47.4	343	19.2
230	0.205	268	12.4	306	42.9	344	12.7
231	0.330	269	9.90	307	17.8	345	4.36
232	0.335	270	9.60	308	13.8	346	1.19
233	0.262	271	19.4	309	32.6	347	0.441
234	0.325	272	14.3	310	17.4	348	0.757
235	0.363	273	8.10	311	4.61	349	0.378
236	0.539	274	6.57	312	11.9	350	0.360
237	0.771	275	21.5	313	9.02	351	0.894
238	0.569	276	25.9	314	56.5	352	7.31
239	0.682	277	15.7	315	55.6	353	22.8
240	0.782	278	10.3	316	25.4	354	16.5
241	0.775	279	24.5	317	57.9	355	6.96
242	1.23	280	23.4	318	31.5	356	1.48
243	1.59	281	15.6	319	9.75	357	0.344
244	1.09	282	9.72	320	11.9	358	0.186
245	1.31	283	7.20	321	16.0	359	0.111
246	1.63	284	42.7	322	7.21	360	0.087
247	1.51	285	40.5	323	3.27	361	0.100
248	2.34	286	20.9	324	8.61	362	0.211
249	3.18	287	11.5	325	15.4	363	0.141
250	2.57	288	31.7	326	68.7	364	0.094
251	2.04	289	32.2	327	43.7	365	0.088
252	3.37	290	11.7	328	12.2	366	0.085
253	2.89	291	18.4	329	31.2	367	0.091
254	3.42	292	7.96	330	38.6	368	0.143
255	4.50	293	31.1	331	14.1	369	0.297
256	6.29	294	71.5	332	3.46	370	0.636
257	4.43	295	40.6	333	2.14	371	0.572
258	3.07	296	24.8	334	1.59	372	0.197
259	6.18	297	13.6	335	0.965	373	0.113
260	6.04	298	42.2	336	1.26	374	0.091
261	6.60	299	31.7	337	3.83	375	0.087
262	6.02	300	9.63	338	19.2		
263	10.8	301	16.3	339	55.0		

IX-B-1.2. Quantum Yields for Formaldehyde Photodecomposition

The quantum yields of the photodissociation processes have been estimated in studies using a variety of different techniques (Horowitz and Calvert, 1978a, 1978b; Clark et al., 1978; Moortgat and Warneck, 1979; Moortgat et al., 1983; Smith et al., 2002a). Reference to the review of Calvert et al. (2008) can be made for the details of these studies. The various estimates of the quantum yields (ϕ) of primary processes (I) and (II) are compared in figures IX-B-2 and IX-B-3, respectively (Calvert et al., 2008).

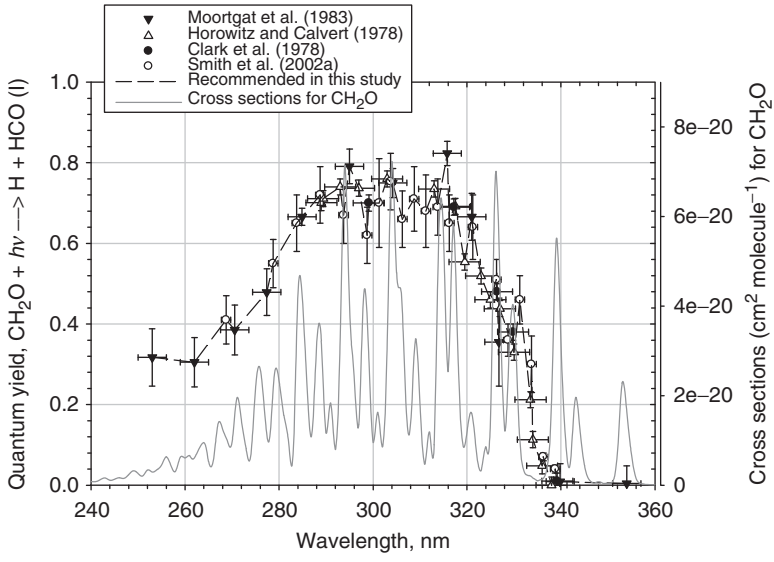

Figure IX-B-2. Comparison of quantum yields (ϕ_I) for process (I), $CH_2O + h\nu \rightarrow HCO + H$, in CH_2O photodecomposition based on the results of Horowitz and Calvert (1978a, b), Moortgat et al. (1983), Clark et al. (1978), and Smith et al. (2002a). Figure from Calvert et al. (2008). The absorption spectrum of CH_2O is given by the light-gray curve.

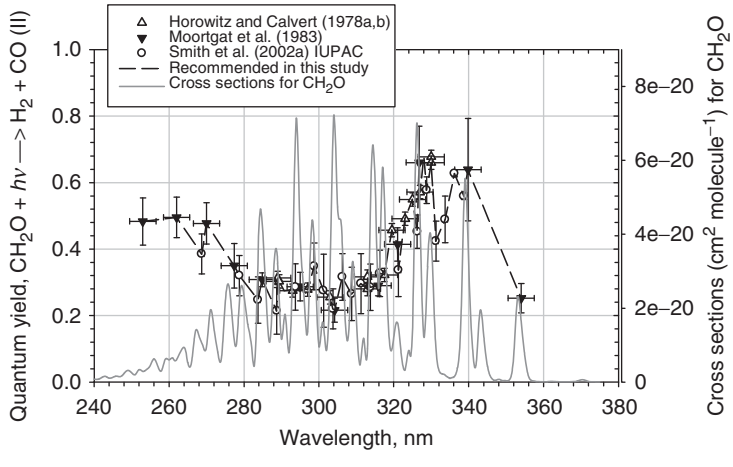

Figure IX-B-3. Comparison of the quantum yields (ϕ_{II}) for primary process (II), $CH_2O + h\nu \rightarrow H_2 + CO$, in CH_2O photodecomposition (1 atm. air, about 300 K); data are from Horowitz and Calvert (1978a, b), Moortgat et al. (1983), and Smith et al. (2002a) as reviewed by Calvert et al. (2008). The absorption spectrum of CH_2O is given by the light-gray curve.

The vertical and horizontal bars on the data points from each study give some measure of the precision of the ϕ measurements and the bandwidth of the radiation used in the particular experiment, respectively. The data for ϕ_{II} given in figure IX-B-3 are for 298 K in air at 1 atm. pressure. At wavelengths greater than 330 nm, the values of ϕ_{II} are sensitive to pressure and, to some extent, the temperature. The quenching follows the Stern–Volmer relation, $1/\phi_{II} = 1 + (k_q/k_d) \times [M]$, where $[M]$ is the concentration of air molecules. The quenching coefficients (k_q/k_d, cm^3 $molecule^{-1}$) for CH_2O mixtures in air as reported by Moortgat et al. (1983) for 300 K at 329 nm and 353 nm, respectively, are: $(0.26 \pm 0.10) \times 10^{-19}$ and $(1.12 \pm 0.17) \times 10^{-19}$; constants for 220 K at 329 and 353 nm, respectively, are: $(0.39 \pm 0.07) \times 10^{-19}$ and $(2.47 \pm 0.59) \times 10^{-19}$. At a temperature of 300 K, the expected effect of lowering the atmospheric pressure from 760 (sea level) to 600 Torr (typical of Denver, CO) is not dramatic; ϕ_{II} values at 329 and 353 nm increase about 8 and 6%, respectively.

The recommended quantum yields for processes (I) and (II) are shown in tabular form in table IX-B-2 (Calvert et al., 2008).

IX-B-1.3. Photolysis Frequencies for Formaldehyde

Given in figure IX-B-4 are the recommended j_I and j_{II} values estimated for a clear day within the lower troposphere as a function of solar zenith angle and several different

Table IX-B-2. Recommended quantum yields (ϕ) for the primary photochemical processes in formaldehyde: $CH_2O + h\nu \rightarrow H + CHO$(I); $CH_2O + h\nu \rightarrow CO + H_2$ (II); (Calvert et al., 2008)

λ, nm	ϕ_I	ϕ_{II}	λ, nm	ϕ_I	ϕ_{II}	λ, nm	ϕ_I	ϕ_{II}	λ, nm	ϕ_I	ϕ_{II}^a
240	0.27		296	0.76	0.29	318	0.66	0.35	340	0.010	0.64
250	0.32	0,48	297	0.74	0.28	319	0.58	0.435	341	0.008	0.61
260	0.31	0.49	298	0.67	0.32	320	0.60	0.44	342	0.008	0.58
269	0.41	0.40	299	0.65	0.35	321	0.67	0.338	343	0.008	0.55
279	0.56	0.32	300	0.70	0.26	322	0.58	0.415	344	0.007	0.51
280	0.58	0.30	301	0.70	0.28	323	0.52	0.49	345	0.007	0.50
281	0.60	0.27	302	0.73	0.27	324	0.49	0.52	346	0.007	0.47
282	0.62	0.27	303	0.78	0.25	325	0.46	0.55	347	0.007	0.44
283	0.64	0.25	304	0.75	0.22	326	0.51	0.45	348	0.007	0.42
284	0.65	0.26	305	0.71	0.26	327	0.50	0.62	349	0.006	0.38
285	0.67	0.31	306	0.66	0.32	328	0.40	0.68	350	0.006	0.36
286	0.68	0.28	307	0.68	0.30	329	0.36	0.60	351	0.005	0.33
287	0.70	0.25	308	0.70	0.28	330	0.35	0.67	352	0.005	0.30
288	0.71	0.23	309	0.71	0.27	331	0.46	0.43	353	0.005	0.28
289	0.71	0.31	310	0.70	0.28	332	0.37	0.45	354	0.005	0.25
290	0.72	0.29	311	0.68	0.30	333	0.24	0.48	355	0.005	0.12
291	0.73	0.27	312	0.72	0.29	334	0.112	0.51	356	0.000	0.10
292	0.73	0.28	313	0.73	0.28	335	0.070	0.56	357	0.000	0.07
293	0.74	0.27	314	0.69	0.29	336	0.055	0.62	358	0.000	0.04
294	0.70	0.29	315	0.78	0.29	337	0.035	0.61	359	0.000	0.01
295	0.79	0.29	316	0.75	0.33	338	0.010	0.58	360	0.000	0.00
			317	0.69	0.32	339	0.011	0.58			

[a] ϕ_{II} values for $\lambda \geq 340$ nm are somewhat pressure and temperature dependent; estimates given here are for temperatures near 300 K and 1 atm. pressure.

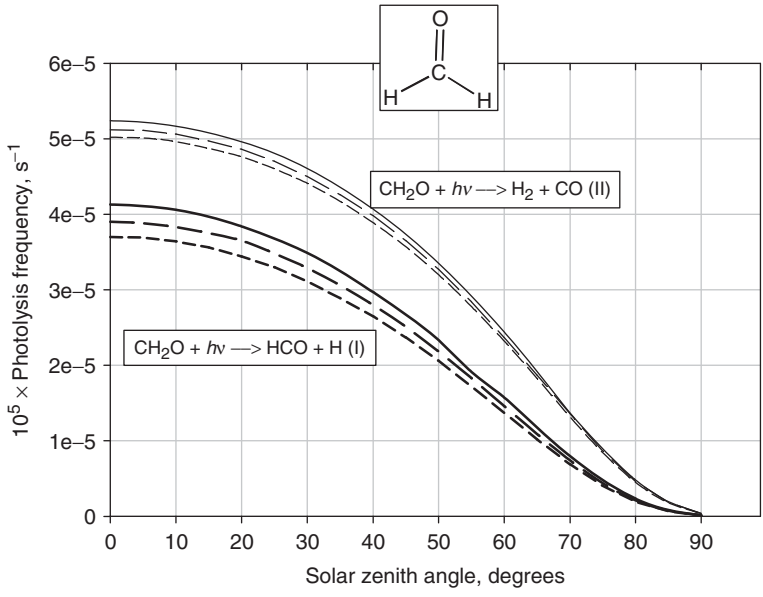

Figure IX-B-4. Recommended *j*-values (Calvert et al., 2008) versus solar zenith angle for formaldehyde for cloud-free conditions in the lower troposphere (~760 Torr); heavy curves are for process (I): $CH_2O + h\nu \rightarrow CHO + H$; light curves are for process (II): $CH_2O + h\nu \rightarrow CO + H_2$; solid curves, long-dashed curves, and short-dashed curves, respectively, are from calculations assuming overhead ozone columns of 300, 350, and 400 Dobson units. The cross sections and quantum yield recommendations from this study were used in the calculations.

overhead ozone columns (300–400 Dobson units). We used the preferred Meller and Moortgat (2000) cross sections and the quantum yield data as recommended by Calvert et al. (2008). It can be seen that the *j*-values for CH_2O photodissociation are not very sensitive to the ozone column. For solar zenith angles of 0 and 50°, an increase of ozone column by 100 Dobson units leads to approximately 11% and 4% decrease in j_I- and j_{II}-values, respectively. The effect of temperature change on the absorption is relatively small at the wavelengths that contribute the most to the *j*-values. However, the increase of altitude in the atmosphere affects the *j*-values for processes (I) and (II) significantly. See figure IX-B-5. Here the calculations employed the current recommendations and the temperature and pressure effects measured by Moortgat et al. (1983). The large increase in *j*-values seen with altitude increase results mainly from two factors: 1) the increased actinic flux at the higher altitudes; and 2) the decreased quenching of process (II) that occurs at the lowered pressure.

Relative photolysis frequencies for various isotopomers of formaldehyde, $H^{12}CH^{16}O$, $H^{13}CH^{16}O$, $H^{12}CH^{18}O$, and $D^{12}CDO$ have been studied by Feilberg et al. (2005a). These results and others related to the isotopomers of formaldehyde have been reviewed by Calvert et al. (2008).

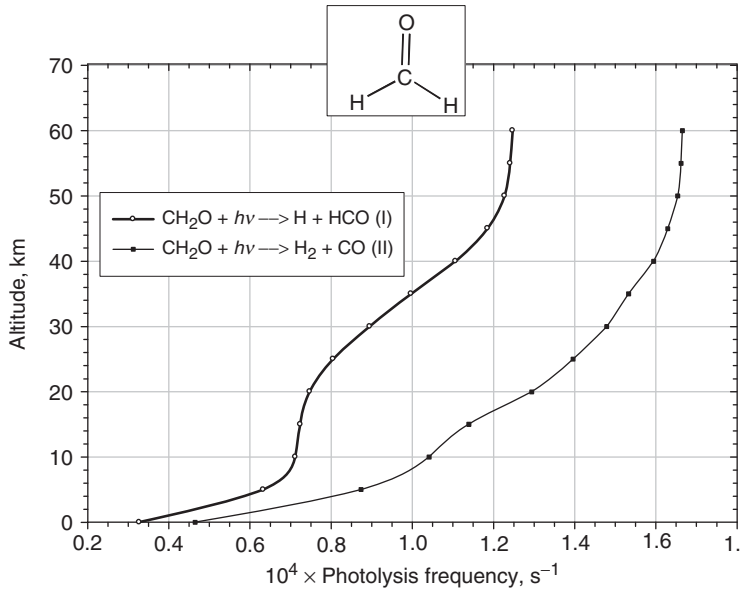

Figure IX-B-5. The effect of altitude in the atmosphere on the *j*-values for processes (I) and (II). The calculations used the current recommendations with solar zenith angle fixed at 45° and the temperature and pressure effects characterized by Meller and Moortgat (2000). The large increase seen in *j*-values at higher altitudes results mainly from the increased actinic flux and the decreased extent of quenching of process (II) at the lowered pressure (from Calvert et al., 2008).

IX-B-2. Photodecomposition of Acetaldehyde (Ethanal, CH_3CHO)

Three primary processes have been considered in explanation of acetaldehyde photochemisty:

$$CH_3CHO + h\nu \rightarrow CH_3 + CHO \quad \text{(I)}$$

$$\rightarrow CH_4 + CO \quad \text{(II)}$$

$$\rightarrow CH_3CO + H \quad \text{(III)}$$

Process (I) is most important at the long wavelengths of absorbed light, and process (II) becomes increasingly important at the short wavelengths (Blacet and Heldman, 1942; Blacet and Loeffler, 1942). Many experimental and theoretical studies have helped to elucidate the role of the excited triplet state (T_1) and other states in the photochemistry of acetaldehyde (e.g., see Parmenter and Noyes, 1963; Archer et al., 1973a, b; Gandini and Hackett, 1977b; Yadav and Goddard, 1986; Smith et al., 1991a; Martell et al., 1997; King et al., 2000; Kurosaki and Yokoyama, 2002). Discussion of these measurements is given in Calvert et al. (2008).

IX-B-2.1. Cross Sections for Acetaldehyde

Different measurements of cross sections for acetaldehyde are in reasonable agreement (Calvert et al., 2000), but those reported by Martinez et al. (1992) are considered to be the most accurate and are recommended here; see figure IX-B-1 and table IX-B-3.

IX-B-2.2. Quantum Yields for Primary Processes in Acetaldehyde Photodecomposition

Studies that relate to the quantum efficiency of the photodecomposition of acetaldehyde have continued since the early work of Leighton and Blacet (1933), Blacet and Heldman (1942), and Blacet and Loeffler (1942). These and the more recent studies of acetaldehyde photodecomposition (Weaver et al.,1976/1977; Gill and Atkinson, 1979; Horowitz et al., 1982; Horowitz and Calvert, 1982; Meyrahn et al., 1982; Simonaitis and Heicklen, 1983; Horowitz, 1986; Yadav and Goddard, 1986) have been reviewed recently by Calvert et al. (2008). These studies confirm that radical formation in process (I) is the dominant mode of photodecomposition at the longer wavelengths present within the troposphere. Processes (II) and (III) increase in importance at the shorter wavelengths.

Our recommendations for values of ϕ_{I}, ϕ_{II}, and ϕ_{III} for use in tropospheric modeling are those of Calvert et al. (2008) and are given in table IX-B-4 as a function of wavelength; these data are shown graphically in figure IX-B-6. The data treatment used in estimating the quantum yields from product data is given by Calvert et al. (2008).

IX-B-2.3. Photolysis Frequencies for the Photodecomposition of Acetaldehyde in the Lower Troposphere

The current recommended values for the cross sections and quantum yields have been used to calculate the clear-sky values of the photolysis frequencies for acetaldehyde primary processes (I) and (III) as a function of the solar zenith angle (ozone column = 350 DU). See figure IX-B-7. Values of j_{II}, not given in the figure, are very small for tropospheric conditions. Experimental measurements in the EUPHORE facility gave: $j(\mathrm{Total}) \approx (2.9 \pm 2.7) \times 10^{-6}\,\mathrm{s}^{-1}$ with solar zenith angle of 20° (Moortgat et al., 2002).

IX-B-3. Photodecomposition of Propanal (Propionaldehyde, CH_3CH_2CHO)

Propanal (C_2H_5CHO) photodecomposition in the troposphere follows the pattern exhibited by acetaldehyde. Although five different photodecomposition paths have been considered in explanation of its photochemistry, only process (I) is important for

Table IX-B-3. Preferred cross sections (σ, cm^2 molecule^{-1}) at 298 K for ethanal, propanal, butanal (Martinez et al. (1992), and pentanal (Tadić et al., 2001a)

	$10^{20} \times \sigma$					$10^{20} \times \sigma$			
λ, nm	Ethanal	Propanal	Butanal	Pentanal	λ, nm	Ethanal	Propanal	Butanal	Pentanal
280	4.50	5.16	5.18	5.28	323	1.24	1.58	1.96	1.95
281	4.69	5.21	5.22	5.37	324	1.09	1.49	1.82	1.81
282	4.72	5.35	5.30	5.53	325	1.14	1.30	1.69	1.67
283	4.75	5.57	5.45	5.73	326	1.07	1.13	1.55	1.53
284	4.61	5.78	5.65	5.88	327	0.868	1.00	1.39	1.37
285	4.49	5.86	5.81	5.95	328	0.747	0.828	1.22	1.200
286	4.44	5.82	5.90	5.94	329	0.707	0.685	1.04	1.090
287	4.59	5.72	5.89	5.90	330	0.688	0.575	0.868	0.801
288	4.72	5.59	5.85	5.85	331	0.588	0.494	0.734	0.689
289	4.77	5.52	5.80	5.85	332	0.530	0.466	0.647	0.628
290	4.89	5.56	5.78	5.91	333	0.398	0.430	0.602	0.582
291	4.78	5.68	5.83	5.91	334	0.363	0.373	0.554	0.516
292	4.68	5.81	5.93	6.01	335	0.350	0.325	0.485	0.444
293	4.53	5.88	6.05	6.12	336	0.238	0.280	0.417	0.374
294	4.33	5.80	6.10	6.14	337	0.222	0.230	0.346	0.308
295	4.27	5.57	6.03	6.06	338	0.205	0.185	0.285	0.255
296	4.24	5.37	5.97	5.90	339	0.219	0.166	0.242	0.220
297	4.38	5.16	5.69	5.72	340	0.150	0.155	0.215	0.197
298	4.41	5.02	5.56	5.59	341	0.074	0.110	0.191	0.167
299	4.26	5.02	5.46	5.51	342	0.042	0.076	0.144	0.114
300	4.16	5.04	5.42	5.49	343	0.031	0.045	0.093	0.073
301	3.99	5.09	5.43	5.49	344	0.026	0.031	0.059	0.048
302	3.86	5.07	5.44	5.49	345	0.021	0.025	0.041	0.035
303	3.72	4.94	5.43	5.46	346	0.019	0.019	0.031	0.028
304	3.48	4.69	5.32	5.31	347	0.015	0.016	0.026	0.023
305	3.42	4.32	5.08	5.06	348	0.016	0.014	0.023	0.020
306	3.42	4.04	4.79	4.76	349	0.010	0.013	0.018	0.017
307	3.36	3.81	4.50	4.50	350	0.008	0.010	0.015	0.015
308	3.33	3.65	4.29	4.31	351	0.007	0.008	0.014	
309	3.14	3.62	4.15	4.21	352	0.006	0.007	0.012	
310	2.93	3.60	4.07	4.13	353	0.005	0.005	0.010	
311	2.76	3.53	4.00	4.05	354	0.005	0.004	0.008	
312	2.53	3.50	3.92	3.95	355	0.004	0.002	0.006	
313	2.47	3.32	3.82	3.84	356	0.005	0.001	0.005	
314	2.44	3.06	3.69	3.69	357	0.003	0.001	0.004	
315	2.2	2.77	3.46	3.46	358	0.004		0.003	
316	2.04	2.43	3.17	3.17	359	0.002		0.002	
317	2.07	2.18	2.85	2.85	360	0.003		0.002	
318	1.98	2.00	2.57	2.58	361	0.002		0.002	
319	1.87	1.86	2.37	2.40	362	0.001		0.001	
320	1.72	1.83	2.25	2.29	363	0.000		0.001	
321	1.48	1.78	2.18	2.19	364	0.000		0.001	
322	1.40	1.66	2.07	2.08	365	0.000		0	

Table IX-B-4. Recommended values for ϕ_1, ϕ_{II}, and ϕ_{III} for acetaldehyde photodecomposition in air at 298 K; data are from Calvert et al. (2008)

λ, nm	ϕ_I^a	ϕ_{II}^b	ϕ_{III}^c	λ, nm	ϕ_I^a	ϕ_{III}^c
275	0.542	0.182	0.065	303	0.432	0.012
276	0.557	0.162	0.063	304	0.416	0.011
277	0.571	0.144	0.059	305	0.400	0.010
278	0.584	0.125	0.057	306	0.384	0.009
279	0.595	0.108	0.054	307	0.367	0.008
280	0.605	0.092	0.052	308	0.350	0.007
281	0.615	0.076	0.049	309	0.333	0.006
282	0.622	0.062	0.048	310	0.316	0.005
283	0.627	0.049	0.045	311	0.299	0.005
284	0.631	0.037	0.043	312	0.282	0.004
285	0.633	0.027	0.040	313	0.265	0.003
286	0.633	0.018	0.038	314	0.248	0.003
287	0.630	0.011	0.036	315	0.231	0.002
288	0.626	0.005	0.034	316	0.214	0.002
289	0.619	0.002	0.032	317	0.197	0.001
290	0.610	0.00	0.031	318	0.180	0.001
291	0.599	0.00	0.029	319	0.164	0.001
292	0.587	0.00	0.027	320	0.148	0.000
293	0.575	0.00	0.025	321	0.132	
294	0.562	0.00	0.024	322	0.116	
295	0.549	0.00	0.022	323	0.101	
296	0.536	0.00	0.021	324	0.086	
297	0.522	0.00	0.019	325	0.072	
298	0.508	0.00	0.018	326	0.058	
299	0.493	0.00	0.017	327	0.045	
300	0.479	0.00	0.015	328	0.033	
301	0.463	0.00	0.014	329	0.021	
302	0.448	0.00	0.013	330	0.009	

[a] $CH_3CHO + h\nu \rightarrow CH_3 + HCO$ (I)
[b] $CH_3CHO + h\nu \rightarrow CH_4 + CO$ (II)
[c] $CH_3CHO + h\nu \rightarrow CH_3CO + H$ (III)

wavelengths of excitation within the troposphere:

$$C_2H_5CHO + h\nu \rightarrow C_2H_5 + HCO \quad \text{(I)}$$

$$\rightarrow C_2H_6 + CO \quad \text{(II)}$$

$$\rightarrow C_2H_5CO + H \quad \text{(III)}$$

$$\rightarrow CH_3 + CH_2CHO \quad \text{(IV)}$$

$$\rightarrow C_2H_4 + CH_2O \quad \text{(V)}$$

The other primary processes (II)–(V) become significant only at wavelengths available in the upper troposphere and the stratosphere. Experimental work has shown that

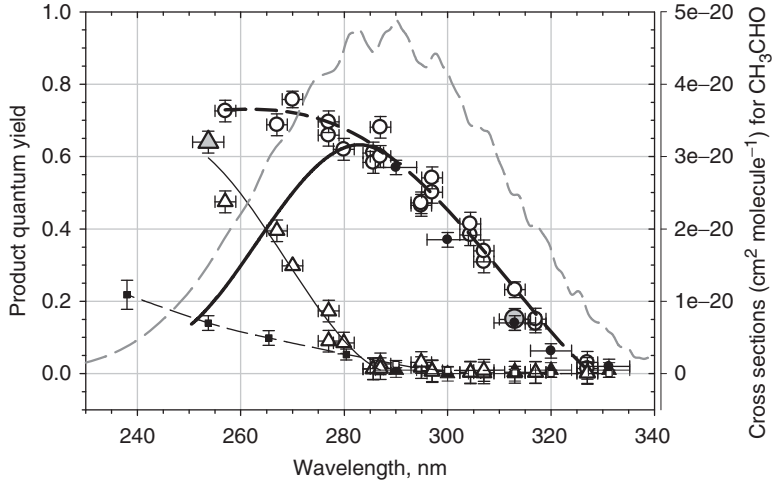

Figure IX-B-6. Estimates of the quantum yields of the primary processes in acetaldehyde. $\phi_I + \phi_{II} = \Phi_{CO}$ (heavy dashed line); $\phi_{II} = \Phi_{CH_4}$ (light, solid line); $\phi_{III} = \Phi_{H_2}$ (light, dashed line); $CH_3CHO + h\nu \rightarrow CH_3 + CHO$ (I); open circles, Meyrahn et al. (1982); small filled circles, Horowitz and Calvert (1982); large gray circle, Weaver et al. (1976/1977). $CH_3CHO + h\nu \rightarrow CO + CH_4$ (II), open triangles, Meyrahn et al. (1982); large gray triangle, Parmenter and Noyes (1963). $CH_3CHO + h\nu \rightarrow CH_3CO + H$ (III); small filled square, Leighton and Blacet (1933), Blacet and Roof (1936a), Blacet and Volman (1938); small open squares, Horowitz and Calvert (1982). The absorption spectrum of CH_3CHO is given by the dashed-gray line.

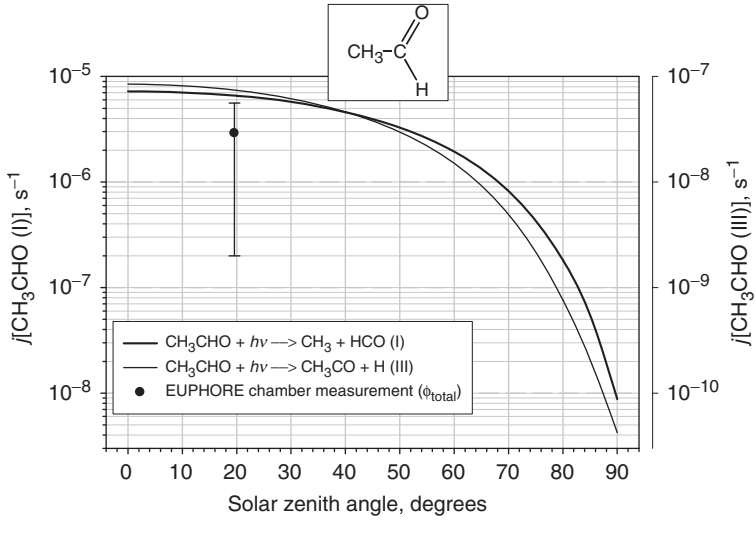

Figure IX-B-7. Photolysis frequencies for the primary processes (I) and (III) in CH_3CHO versus solar zenith angle; process (II) values (not shown here) are very near zero. Data are representative of a cloudless day in the lower troposphere with an overhead ozone column of 350 DU (Calvert et al., 2008).

the dissociation into radicals in (I) likely occurs from the excited T_1 state following intersystem crossing, and that the threshold for this process lies at 326.26 nm, $25 \pm 4\,\mathrm{kJ\,mol^{-1}}$ above the dissociation energy (Terentis et al., 1995; Metha et al., 2002). Process (II) and presumably other molecular processes arise from the vibrationally excited ground state (S_o^*) formed by internal conversion. The experimental evidence concerning the importance of these various processes has been discussed recently by Calvert et al. (2008).

IX-B-3.1. Cross Sections for Propanal

The cross sections for propanal as a function of wavelength are shown with those for acetaldehyde and butanal in figure IX-B-1. The measurements of Martinez et al. (1992) are tabulated in table IX-B-3. These are recommended for use in considerations of the atmospheric photochemistry of propanal.

IX-B-3.2. Quantum Yields of Primary Photodecomposition Processes in Propanal

The important primary process (I), $C_2H_5CHO + h\nu \rightarrow C_2H_5 + HCO$, has been studied in photochemical experiments using a variety of techniques that involve measurements of quantum yields of products formed in propanal–air mixtures (Shepson and Heiklen, 1982a, b); C_2H_5I formation in C_2H_5CHO–I_2 mixture photolyses (Blacet and Pitts, 1952); $C_2H_5O_2$ formation in C_2H_5CHO–air mixtures (Heicklen et al., 1986); and formation of the initial HCO radical product (Chen and Zhu, 2001). However, estimates of ϕ_I for propanal photolyses in air at 1 atm. remain rather scattered and uncertain (see figure IX-B-8). The experiments of Chen and Zhu (2001) gave estimates of ϕ_I near unity at low pressures, seemingly unaffected by pressure of added nitrogen gas [$(\phi_I)^\circ$ shown as small filled circles in figure IX-B-8]. Calvert et al. (2008) reinterpreted these data taking the Chen and Zhu (2001) measurements as zero pressure values of ϕ_I. Using the measured (but scattered) Stern–Volmer quenching constants, Calvert et al. (2008) adjusted the $(\phi_I)^\circ$ values measured by Chen and Zhu (2001) to those expected for photodecomposition in 1 atm. of air. These data points are shown as the black squares in figure IX-B-8. It can be seen that the adjusted Chen and Zhu data are in rough accord with the other measurements for ϕ_I using the estimated quenching by air as measured in other studies.

Two alternative scenarios were considered as possible descriptions of the available estimates of ϕ_I (Calvert et al., 2008). However, if one neglects the two data points of Heicklen et al. (1986), small open squares at 303 and 294 nm, the solid trend line shown in the figure (1 atm. air) describes qualitatively the remaining ϕ_I data.

The data shown as upright triangles in figure IX-B-8 fit the long-dashed trend line that was suggested to describe the wavelength dependence of ϕ_{II}. Estimates of ϕ_{IV}, shown as inverted triangles in the figure, are described by the short-dashed line. It is clear that the current estimates of the wavelength dependence of ϕ_I, ϕ_{II}, and ϕ_{IV} are uncertain, and there are no reliable estimates of ϕ_{III} that can be made at this time.

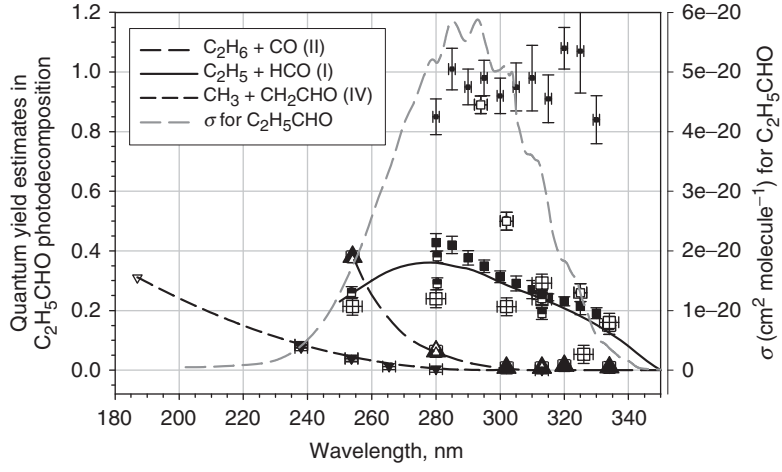

Figure IX-B-8. Plot of wavelength dependence of ϕ estimates for the primary processes in propanal. $C_2H_5CHO + h\nu \rightarrow C_2H_5 + HCO$ (I), at low pressures, (ϕ_I), data of Chen and Zhu (2001), small filled circles; Chen and Zhu data treated for quenching by 1 atm. air (Calvert et al., 2008), filled squares; data of Shepson and Heicklen (1982a), large crossed squares; data of Heicklen et al. (1986), small open squares; data of Blacet and Pitts(1952), half-filled squares. $C_2H_5CHO + h\nu \rightarrow C_2H_6 + CO$ (II), data of Shepson and Heicklen (1982b), large filled triangles; data of Blacet and Pitts (1952), small open triangles. $C_2H_5CHO + h\nu \rightarrow CH_3 + CH_2CHO$ (IV), data of Blacet and Pitts (1952), closed, filled inverted triangles; data of Blacet and Crane (1954), open, inverted triangle. The absorption spectrum of C_2H_5CHO is given by the light-gray curve.

Tabular data for the recommended quantum efficiencies of the primary processes (I) and (II) are listed in table IX-B-5 as a function of wavelength for each nm as derived from the recommended trend lines in figure IX-B-8. The estimates of ϕ_I and ϕ_{II} for propanal given here (Calvert et al., 2008) are significantly different from those suggested by the IUPAC panel (Atkinson et al., 2004); the latter were derived solely from the ϕ_{HCO} data for zero pressure (Chen and Zhu, 2001). Further studies will be required to clarify these differences.

The primary quantum yields for processes (III) and (V) are small and uncertain. Φ_{H_2} measured in the C_2H_5CHO–I_2 mixtures is < 0.01 at the longer wavelengths, about the same as found in the I_2-free photolysis (Blacet and Pitts, 1952). Process (III) becomes significant in the I_2-free photolysis at the shorter wavelengths; e.g., $\Phi_{H_2} = 0.05$ and 0.07 at 253.7 and 238 nm, respectively. No recommendations for the wavelength dependences of ϕ_{III} and ϕ_V can be made at this time, but it is clear that both processes are unimportant for photolysis of propanal in the lower troposphere. CH_4 formation presumably occurs following CH_3 radical formation in (IV) and abstraction of an H-atom, since added iodine inhibits its formation. Process (IV) is also unimportant for tropospheric chemistry, but at short wavelengths it becomes significant. See figure IX-B-8.

Table IX-B-5. Recommended values for ϕ_I and ϕ_{II} for propanal photodecomposition in air at 1 atm. pressure

λ, nm	ϕ_I^a	ϕ_{II}^b	λ, nm	ϕ_I^a	λ, nm	ϕ_I^a
278	0.322	0.081	302	0.314	326	0.196
279	0.324	0.075	303	0.310	327	0.189
280	0.326	0.069	304	0.306	328	0.182
281	0.327	0.063	305	0.303	329	0.174
282	0.329	0.058	306	0.299	330	0.167
283	0.330	0.053	307	0.295	331	0.159
284	0.331	0.048	308	0.291	332	0.150
285	0.331	0.043	309	0.287	333	0.142
286	0.332	0.039	310	0.283	334	0.133
287	0.332	0.035	311	0.278	335	0.124
288	0.332	0.031	312	0.274	336	0.115
289	0.332	0.028	313	0.269	337	0.105
290	0.332	0.024	314	0.265	338	0.095
291	0.331	0.021	315	0.260	339	0.085
292	0.331	0.018	316	0.255	340	0.075
293	0.330	0.015	317	0.250	341	0.064
294	0.329	0.013	318	0.245	342	0.053
295	0.338	0.000	319	0.239	343	0.041
296	0.335	0.000	320	0.233	344	0.029
297	0.332	0.000	321	0.228	345	0.017
298	0.328	0.000	322	0.222	346	0.005
299	0.325	0.000	323	0.216	347	0.000
300	0.321	0.000	324	0.209		
301	0.317	0.000	325	0.203		

[a] $CH_3CH_2CHO + h\nu \rightarrow CH_3CH_2 + CHO$ (I)
[b] $CH_3CH_2CHO + h\nu \rightarrow C_2H_6 + CO$ (II)

IX-B-3.3. Photolysis Frequencies for the Photodecomposition of Propanal in the Lower Troposphere

The *j*-values for the major primary process (I) for propanal as a function of solar zenith angle are given in figure IX-B-9 as estimated for a cloudless troposphere (ozone column = 350 DU) using the current recommendations for cross sections and primary quantum yields. Within the lower troposphere, *j*-values for the primary processes II, III, IV, and V are very small. Measurements made in the EUPHORE chamber gave: $j(\text{Total}) = (1.08 \pm 0.1) \times 10^{-5}\ s^{-1}$ at a solar zenith angle of 28° (Mootgat et al., 2002), in excellent accord with the current calculations.

IX-B-4. Photodecomposition of Butanal (*n*-Butyraldehyde, $CH_3CH_2CH_2CHO$)

As with the other aliphatic aldehydes, butanal photolysis is a source of radicals within the troposphere, but in addition, a new type of molecular dissociation occurs that is not present in smaller aldehydes. Several primary pathways for photodecomposition have been suggested to explain the photochemistry of butanal (e.g., see Blacet and

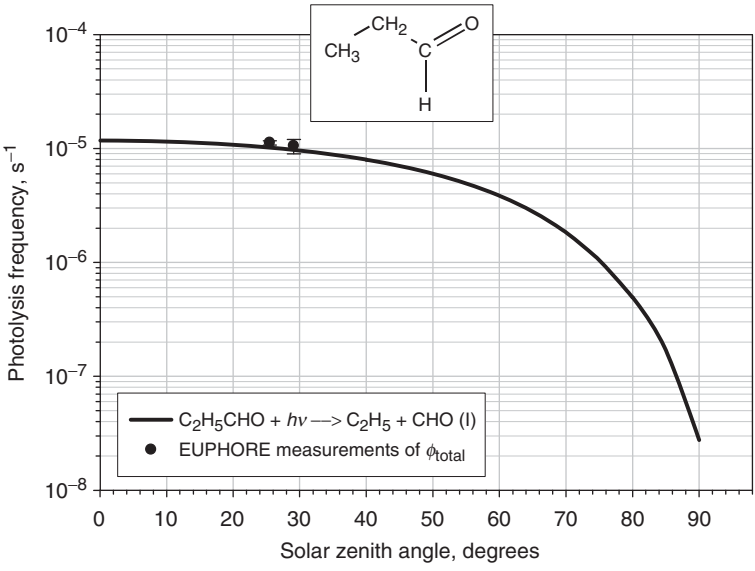

Figure IX-B-9. Photolysis freqencies as a function of solar zenith angle for the photodecomposition of propanal by process (I) as calculated for cloudless sky and an ozone column of 350 DU; the recommendations for ϕ_I and σ given in this book were used in the calculations. The EUPHORE chamber data are from Moortgat et al. (2002).

Calvert, 1951a, b; Förgeteg et al., 1978, 1979; Calvert et al., 2008):

$$CH_3CH_2CH_2CHO + h\nu \rightarrow CH_3CH_2CH_2 + HCO \quad (I)$$

$$\rightarrow C_3H_8 + CO \quad (II)$$

$$\rightarrow CH_2{=}CH_2 + CH_2{=}CHOH \quad (III)$$

$$\rightarrow CH_3 + CH_2CH_2CHO \quad (IV)$$

$$\rightarrow C_2H_5 + CH_2CHO \quad (V)$$

$$\rightarrow CH_3CH_2CH_2CO + H \quad (VI)$$

$$\rightarrow \textit{cyclo}\text{-butyl alcohol} \quad (VII)$$

At wavelengths of sunlight within the troposphere, only primary processes (I) and (III) are important. Primary processes (II), (IV), (V), (VI), and (VII) may become significant for photolysis at the shorter wavelengths that are available only in the upper atmosphere. While processes (I), (II), and (VI) are analogous to those observed with acetaldehyde and propanal, process (III) is unique to carbonyl compounds that contain a γ-H-atom, an H-atom attached to the third C-atom down-chain from the carbonyl group. This photodecomposition path is often called a "Norrish type-II process" (Bamford and Norrish, 1935; Davis and Noyes, 1947). The initial enol-form of acetaldehyde formed in (III),

CH_2=CHOH, ultimately forms the more stable acetaldehyde molecule (CH_3CHO), a transformation catalyzed by contact with a surface. The commonly accepted mechanism for this type of photodecomposition involves a cyclic, 6-membered ring intermediate:

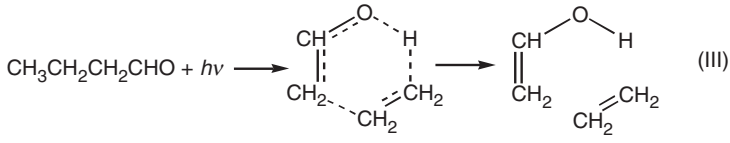

(III)

Chen and Fang (2002) have investigated the potential energy surfaces for processes (I) and (III) using CASSCF, DFT, and MP2 methods. They concluded that process (III) proceeds mainly along the S_1 pathway, while process (I) occurs from the T_1 state following intersystem crossing from the initially excited S_1 state. The calculations suggest that the C—O bond distance in the transition state for process (III) on the S_1 surface is increased from that in the S_o molecule (1.13 Å) to 1.40 Å, and the —CH_2—H bond distance is increased from 1.11 to 1.27 Å. The length of the newly formed H—O bond in the transition state is estimated to be 1.40 Å, significantly greater that that in a normal H—O bond (0.95 Å). As one expects, the structure of the transition state is intermediate to that in S_o and the final products formed in process (III). The C—C bond distances in the transition state are expected to undergo significant decreases as well as one progresses from the C—C bonds of the S_o state to the transition state and on to the C=C bonds present in the CH_2=CH_2 and CH_2=CH(OH) initial products, although these bond distances were not reported by Chen and Fang. This study also showed that dissociation of the T_1 state may occur by either primary process (I) or (VI), but the barrier for the occurrence of (I), $\sim$57 kJ mol^{-1}, is somewhat lower than that for (VI), $\sim$73 kJ mol^{-1}.

The minor process (VII) may occur from the subsequent reaction of an intermediate diradical: •$CH_2CH_2CH_2CH$(•)OH, formed by H-atom abstraction by the excited carbonyl group. The mechanisms of the two processes (III) and (VII) do not appear to involve alternative pathways of decay of the same diradical intermediate.

IX-B-4.1. Absorption Cross Sections for Butanal

The cross sections for butanal reflect the characteristic carbonyl excitation and are very similar to those for acetaldehyde and propanal; see figure IX-B-1. Recommended cross section values are those determined by Martinez et al. (1992), given in tabular form in table IX-B-3.

IX-B-4.2. Quantum Yields of the Primary Processes in Butanal

Most of the quantitative experimental studies of the quantum yields of the primary processes in the photolysis of butanal as a function of wavelength have been carried out in the absence of oxygen or air, and it is difficult to convert these to typical atmospheric conditions (Blacet and Calvert, 1951a, b; Förgeteg et al., 1978, 1979; Chen et al., 2002). The only study which directly relates to the dilute mixtures of butanal in air is that

of Tadić et al. (2001a). This study was conducted using broadband radiation (275–340 nm) at several pressures of air (10–700 Torr). Calvert et al. (2008) have reviewed and evaluated the data related to the wavelength dependencies of the quantum yields of the primary processes in butanal. Their recommendations for tropospheric modeling of the processes (I), (II), and (III) are summarized in figure IX-B-10 and in tabular format in table IX-B-6.

IX-B-4.3. Photolysis Frequencies for the Photodecomposition of Butanal in the Lower Troposphere

The *j*-values for the two major primary photodecomposition modes in butanal in 1 atm. of cloud free tropospheric air have been calculated using the recommended cross sections, quantum yields, and solar flux estimates presented in this work. These are given for processes (I) and (III) in figure IX-B-11. The *j*-value for primary process (II) for an overhead Sun, $j_{II} = 3.2 \times 10^{-11}\,s^{-1}$, shows that process (II) is negligible within the troposphere.

Processes (IV) and (V) also have insignificant photolysis frequencies. Those for processes (VI) and (VII) are probably small as well, but the existing data for these are insufficient to allow a definitive estimate. Measurements in the EUPHORE chamber

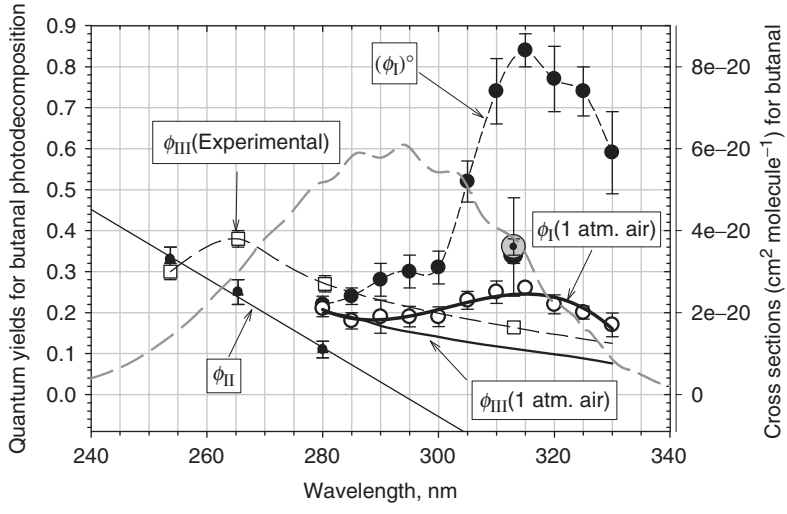

Figure IX-B-10. Quantum yields of photodecomposition by the various primary processes in butanal photolysis: n-$C_3H_7CHO + h\nu \rightarrow n$-$C_3H_7 + HCO$ (I); n-$C_3H_7CHO + h\nu \rightarrow C_3H_8 + CO$ (II); n-$C_3H_7CHO + h\nu \rightarrow CH_2{=}CH_2 + CH_2{=}CHOH$ (III); The large filled circles are from photolyses at low pressures (Chen et al., 2002); open circles give estimated values for 1 atm. of air assuming the occurrence of quenching as observed in the small aldehydes (Calvert et al., 2008). The large gray circle and small filled circle are data from Φ_{CO} and $\Phi_{C_3H_7I}$ measurements in butanal-I_2 mixtures at ~100 Torr (Blacet and Calvert, 1951b) and the large filled circle is from a complete product analysis of n-C_3H_7CHO at ~100 Torr (Förgeteg et al., 1979); these data are uncorrected for any differences in quenching of air (760 Torr) and butanal (~100 Torr). The light-gray, dashed curve gives the absorption spectrum of butanal versus wavelength.

Table IX-B-6. Recommended (approximate) values for the primary quantum yields for butanal photolysis in air at 1 atm. for selected wavelengths (Calvert et al., 2008)

λ, nm	ϕ_I^a	ϕ_{II}^b	ϕ_{III}^c	λ, nm	ϕ_I^a	ϕ_{III}^c
275	0.251	0.163	0.205	306	0.228	0.125
276	0.241	0.155	0.204	307	0.232	0.123
277	0.231	0.147	0.203	308	0.234	0.122
278	0.222	0.139	0.202	309	0.237	0.120
279	0.214	0.131	0.201	310	0.240	0.118
280	0.207	0.123	0.200	311	0.242	0.116
281	0.202	0.115	0.198	312	0.243	0.114
282	0.197	0.107	0.197	313	0.245	0.112
283	0.192	0.099	0.195	314	0.245	0.110
284	0.189	0.091	0.193	315	0.246	0.108
285	0.186	0.083	0.190	316	0.245	0.106
286	0.184	0.075	0.185	317	0.244	0.104
287	0.183	0.067	0.181	318	0.243	0.102
288	0.182	0.059	0.177	319	0.241	0.101
289	0.182	0.051	0.172	320	0.238	0.099
290	0.183	0.043	0.168	321	0.234	0.097
291	0.184	0.035	0.165	322	0.230	0.095
292	0.185	0.027	0.161	323	0.225	0.093
293	0.187	0.019	0.158	324	0.219	0.091
294	0.189	0.011	0.155	325	0.211	0.089
295	0.191	0.003	0.153	326	0.203	0.086
296	0.194	0.000	0.150	327	0.194	0.084
297	0.197	0.000	0.148	328	0.184	0.081
298	0.200	0.000	0.145	329	0.173	0.078
299	0.204	0.000	0.143	330	0.161	0.076
300	0.207	0.000	0.141	331	0.147	0.074
301	0.211	0.000	0.139	332	0.133	0.070
302	0.214	0.000	0.137	333	0.117	0.067
303	0.218	0.000	0.133	334	0.099	0.063
304	0.222	0.000	0.131	335	0.081	0.060
305	0.225	0.000	0.128	336	0.061	0.057

[a] $CH_3CH_2CH_2CHO + h\nu \rightarrow CH_3CH_2CH_2 + HCO$ (I)
[b] $CH_3CH_2CH_2CHO + h\nu \rightarrow C_3H_8 + CO$ (II)
[c] $CH_3CH_2CH_2CHO + h\nu \rightarrow CH_2{=}CH_2 + CH_2{=}CHOH$ (III)

gave $j(\text{Total}) = (1.0 \pm 0.2) \times 10^{-5}\ s^{-1}$ at a solar zenith angle of 29° (Moorgat et al., 2002), in reasonable agreement with our estimate based on the currently recommended σ and ϕ data, $j(\text{Total}) = 1.5 \times 10^{-5}\ s^{-1}$ given in figure IX-B-11.

IX-B-5. Photodecomposition of 2-Methylpropanal [Isobutyraldehyde, $(CH_3)_2CHCHO$]

The primary photodecomposition processes in 2-methylpropanal follow the pattern of the smaller aldehydes. Both radical generation and fragmentation to form stable

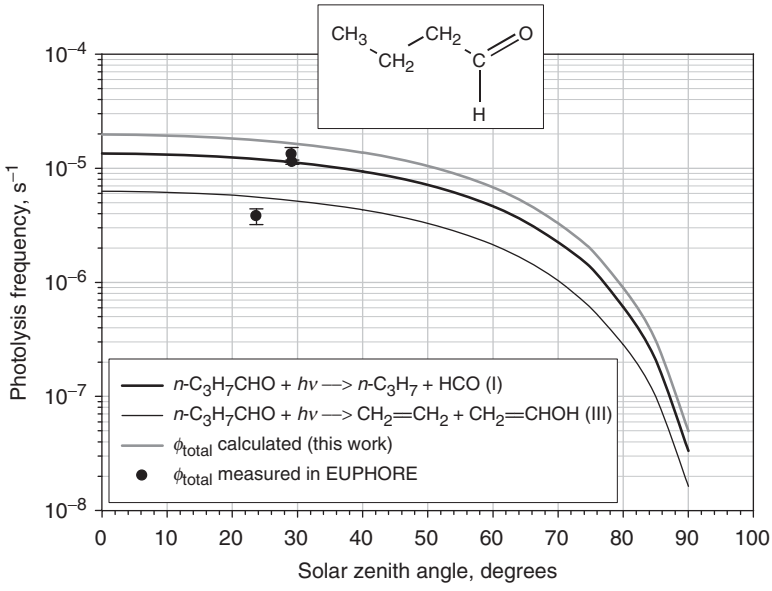

Figure IX-B-11. Plot of the photolysis frequencies as a function of solar zenith angle for the primary processes (I) and (III) in butanal as calculated for a cloudless day in the lower troposphere with an overhead ozone column of 350 DU. Process (II) is unimportant for these conditions. The EUPHORE data were reported by Moortgat et al. (2002).

molecules occur:

$$(CH_3)_2CHCHO + h\nu \rightarrow (CH_3)_2CH + HCO \quad \text{(I)}$$

$$\rightarrow C_3H_8 + CO \quad \text{(II)}$$

$$\rightarrow (CH_3)_2CHCO + H \quad \text{(III)}$$

$$\rightarrow CH_3 + CH_3CHCHO \quad \text{(IV)}$$

Several studies have demonstrated that process (I) is the dominant mode of photodecomposition for excitation at wavelengths of sunlight within the troposphere (Blacet and Calvert, 1951a, b; Desai et al., 1986; Chen et al., 2002). Processes (II) and (IV) become important at the short wavelengths of absorbed light ($\lambda < 290$ nm). Process (III) is energetically feasible for $\lambda < 322$ nm, but its extent of occurrence has not been determined, and it is seldom considered in modeling tropospheric chemistry.

IX-B-5.1. Absorption Cross Sections for 2-Methylpropanal

The $n \rightarrow \pi^*$ transition, typical of aldehydes, is present in 2-methylpropanal; see figure IX-B-12. The magnitudes of the cross sections of 2-methylpropanal are similar to those of acetaldehyde and the higher aldehydes, and the unresolved vibrational structure of the excited aldehydes is evident in the spectrum. The recommended cross

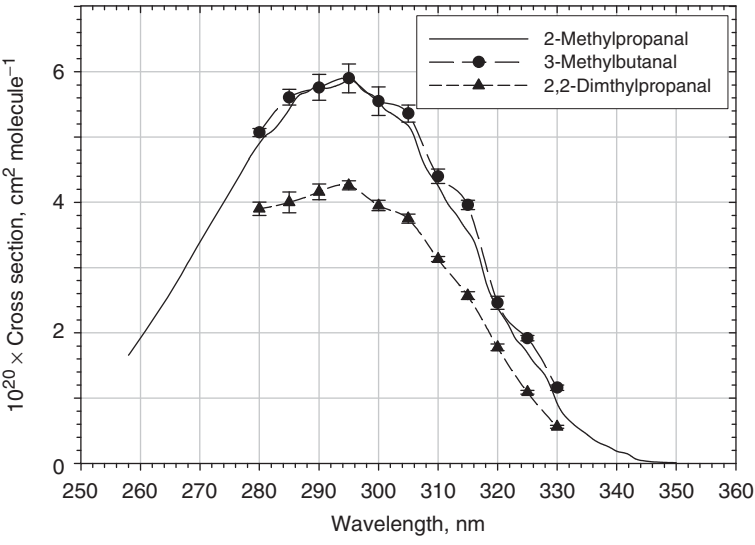

Figure IX-B-12. Cross sections versus wavelength for three alkyl substituted aldehydes: 2-methylpropanal (Martinez et al., 1992); 3-methylbutanal (Zhu et al., 1999); 2,2-dimethylpropanal (Zhu et al., 1999).

sections, determined by Martinez et al. (1992), shown in figure IX-B-12, are given in tabular form in table IX-B-7.

IX-B-5.2. Quantum Yields of the Primary Processes in 2-Methylpropanal

i) Primary process (I): $(CH_3)_2CHCHO + h\nu \rightarrow CH_3CHCH_3 + HCO$ The results of the several determinations of the quantum yields of the important primary process (I), generating CH_3CHCH_3 and HCO radicals, are shown in figure IX-B-13. The data are highly scattered, and the choice of trend line of ϕ_I with λ is not obvious. Results are from photolysis of 2-methylpropanal-iodine mixtures by Blacet and Calvert (1951b), 2-methylpropanal–air mixture photolysis by Desai et al. (1986), and the quantum efficiencies of HCO radical formation in process (I), determined at 11 wavelengths in the 280–330 nm range by Chen et al. (2002).

The values of Chen et al. (2002) for zero pressure are shown as circles in figure IX-B-13. They detected no effect of added nitrogen gas (up to 400 Torr) on the quantum yield and concluded that the zero pressure quantum yields applied for air at 1 atm. as well. Although quenching of excited 2-methylpropanal molecules by air or nitrogen molecules is less efficient than that observed for acetaldehyde and propanal, Stern–Volmer plots of the Φ_{CO} data of Desai et al. (1986) clearly show significant quenching of process (I) in 2-methylpropanal by oxygen. The difference between the quenching observed with $(CH_3)_2CHCHO$ and the smaller aldehydes probably arises from a shorter lifetime of the excited 2-methylpropanal molecule, perhaps reflecting the weaker R—CHO bond.

Table IX-B-7. Recommended absorption cross sections (σ, cm^2 molecule^{-1}) for $(CH_3)_2CHCHO$ (298 K) and quantum yields (ϕ_I) for primary process: $(CH_3)_2CHCHO + h\nu \rightarrow CH_3CHCH_3 + HCO$ (I), in 1 atm. of air. ϕ_I(a) and ϕ_I(b) are alternative wavelength dependencies given by the solid line and dashed lines, respectively, in figure IX-B-13 (Calvert et al., 2008)

λ, nm	$10^{20} \times \sigma$	ϕ_I(a)	ϕ_I(b)	λ, nm	$10^{20} \times \sigma$	ϕ_I(a)	ϕ_I(b)
278	4.63	0.39	0.41	315	3.55	1.00	0.86
279	4.77	0.39	0.40	316	3.41	1.00	0.88
280	4.90	0.38	0.40	317	3.14	1.00	0.91
281	5.02	0.38	0.40	318	2.79	0.99	0.93
282	5.08	0.38	0.40	319	2.55	0.99	0.95
283	5.17	0.38	0.40	320	2.38	0.99	0.96
284	5.29	0.40	0.40	321	2.24	0.98	0.97
285	5.42	0.43	0.40	322	2.09	0.98	0.97
286	5.57	0.49	0.41	323	1.91	0.97	0.97
287	5.66	0.53	0.41	324	1.81	0.97	0.96
288	5.69	0.60	0.41	325	1.69	0.96	0.96
289	5.75	0.67	0.42	326	1.56	0.95	0.94
290	5.78	0.70	0.42	327	1.46	0.93	0.92
291	5.75	0.73	0.43	328	1.34	0.91	0.90
292	5.76	0.77	0.43	329	1.15	0.88	0.88
293	5.79	0.79	0.44	330	0.918	0.84	0.84
294	5.83	0.82	0.45	331	0.760	0.80	0.80
295	5.88	0.84	0.46	332	0.661	0.76	0.76
296	5.86	0.86	0.47	333	0.579	0.72	0.72
297	5.75	0.88	0.48	334	0.510	0.68	0.68
298	5.68	0.90	0.49	335	0.445	0.63	0.63
299	5.64	0.92	0.51	336	0.373	0.59	0.59
300	5.55	0.93	0.52	337	0.317	0.56	0.56
301	5.43	0.95	0.53	338	0.279	0.50	0.50
302	5.37	0.96	0.55	339	0.238	0.46	0.46
303	5.31	0.97	0.56	340	0.187	0.42	0.42
304	5.24	0.98	0.58	341	0.165	0.38	0.38
305	5.17	0.98	0.60	342	0.138	0.34	0.34
306	5.00	0.98	0.62	343	0.077	0.29	0.29
307	4.73	0.99	0.65	344	0.047	0.25	0.25
308	4.52	0.99	0.67	346	0.034	0.21	0.21
309	4.38	1.00	0.70	346	0.025	0.16	0.16
310	4.25	1.00	0.72	347	0.019	0.12	0.12
311	4.08	1.00	0.75	348	0.015	0.08	0.08
312	3.93	1.00	0.78	349	0.013	0.04	0.04
313	3.82	1.00	0.80	350	0.011	0.00	0.00
314	3.68	1.00	0.83				

The choice of 2-methylpropanal quantum yield data to establish the recommended trend in ϕ_I with wavelength is not obvious. Certainly the experiments carried out in air mixtures at 1 atm. pressure match the conditions of the troposphere better than the zero pressure study of Chen et al. If we favor the Desai data in the 300 nm region, then a trend curve shown as the dashed line in the figure IX-B-13 is derived (scenario 1). In this case, the data of Chen et al. are in reasonable accord with the other two data sets at six of the 11 wavelengths used in their study (indicated by gray-filled circles).

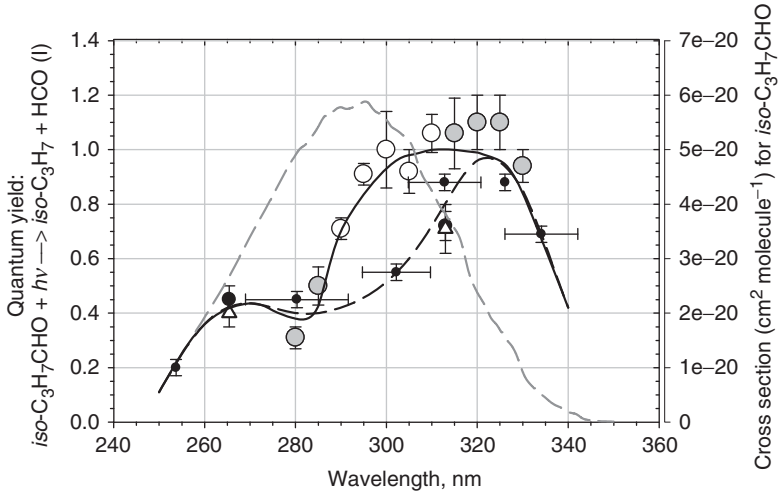

Figure IX-B-13. Estimates of the primary quantum yield of process (I) in 2-methylpropanal: $(CH_3)_2CH_2CHO + h\nu \rightarrow (CH_3)_2CH + HCO$ (I); large white and gray circles (Chen et al., 2002); small filled circles (Desai et al. (1986); large black circles,$\Phi_{CO} - \Phi_{C_3H_8}$, and open triangles,$\Phi_{CH_3CHICH_3}$ (Blacet and Calvert, 1951b). In treatment of the scattered data, two alternative choices in the ϕ_I versus λ dependence are shown as dashed and solid lines. The light-gray curve gives the absorption spectrum of 2-methylpropanal.

If we neglect the data point of Desai et al. at 302.2 nm, then a trend curve shown by the solid line represents better the several estimates shown (scenario 2). In this case, the 313 nm estimates of Blacet and Calvert fall significantly below the curve. In the absence of a clear choice, the quantum yield estimates from both trend lines are tabulated in table IX-B-7, and both are used as alternatives to derive *j*-values as described in the following section. The fall-off in ϕ_I is in part a consequence of the onset of process (II), but this alone cannot explain the data. A more complete discussion of these results is given by Calvert et al. (2008).

ii) Primary process (II): $(CH_3)_2CHCHO + h\nu \rightarrow C_3H_8 + CO$ The 2-methylpropanal photodecomposition that leads directly to propane and carbon monoxide is unimportant at the wavelengths of light available within the troposphere. Estimates can be derived from $\Phi_{C_3H_8}$ measured in iodine-2-methylpropanal mixture photolysis (Blacet and Calvert, 1951b): ~0.03 at 313 nm, rising to 0.40 at 265.4 nm.

iii) Primary process (IV): $(CH_3)_2CHCHO + h\nu \rightarrow CH_3 + CH_3CHCHO$ This process becomes important only at wavelengths of light available in the upper atmosphere. Methane formation in uninhibited $(CH_3)_2CHCHO$ photolysis is believed to arise through H-atom abstraction by methyl radicals formed in (IV). CH_3I formation, observed in the photolysis of $(CH_3)_2CHCHO–I_2$ mixtures at 265.4 nm, supports this conclusion (Blacet and Calvert, 1951b). Values of ϕ_{IV} are estimated to be: 0.006 (313 nm); 0.012 (280 nm); 0.036 (265.4 nm); and 0.072 (253.7 nm).

iv) Primary process (III): $(CH_3)_2CHCHO + h\nu \rightarrow (CH_3)_2CHCO + H$ The fall-off of the quantum yield of photodecomposition at short wavelengths seen for process (I) in figure IX-B-13 probably results from the onset of processes (II) and (IV), but the sum of the efficiencies of the processes (I), (II), and (IV) at 265.4 nm is well below unity (~0.8), and may result from the occurrence of process (III). In photolysis of pure $(CH_3)_2CHCHO$, H-atoms formed in (III) would react readily with the aldehyde to form H_2. However, hydrogen formation remains unimportant even at 253.7 nm, $\Phi_{H_2} = 0.03$ (Blacet and Calvert, 1951a). The apparent inefficiency of photodecomposition at the shorter wavelengths of absorbed light remains unexplained.

IX-B-5.3. Photolysis Frequencies for Photodecomposition of 2-Methylpropanal in the Lower Troposphere

Process (I) appears to be the only important mode of photodecomposition of $(CH_3)_2CHCHO$ molecules within the troposphere, although the other processes are expected to become important in the upper troposphere and the stratosphere. Only *j*-values for process (I) are considered here. As described in the previous section, two alternative scenarios related to the wavelength dependence of the process (I) are assumed, since the choice between these is unclear. The results of the *j*-value calculations as a function of solar zenith angle are given in figure IX-B-14 for a cloudless

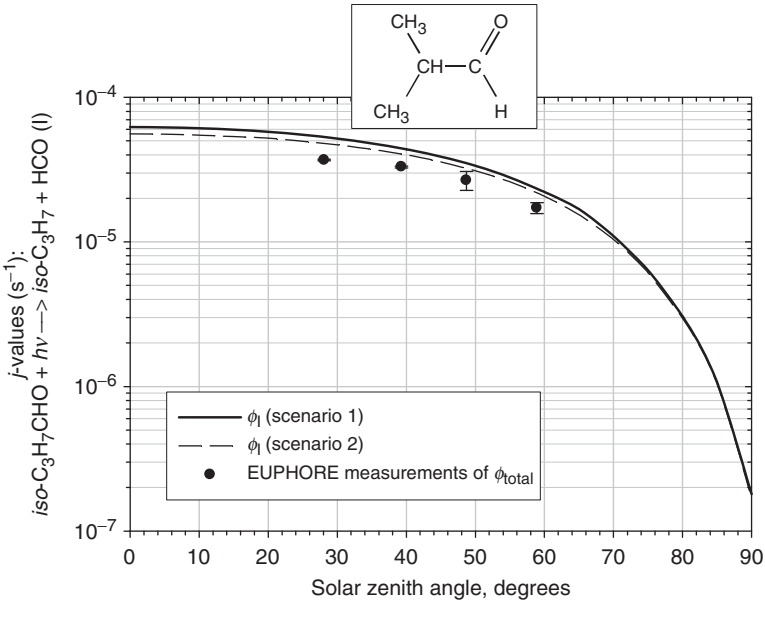

Figure IX-B-14. Estimated photolysis frequencies for 2-methylpropanal as a function of solar zenith angle (Calvert et al., 2008). Values are calculated for a cloudless day in the lower troposphere with an overhead ozone column of 350 DU. Two alternative scenarios for ϕ_I versus λ are assumed as outlined in the text. The EUPHORE chamber measurements were reported by Moortgat et al. (2002).

day within the lower troposphere (ozone column = 350 DU); scenarios (1) and (2) were used with ϕ_I estimates given by the solid and dashed trend lines, respectively, in figure IX-B-14. Measurements in the EUPHORE chamber (Moortgat et al., 2002), shown by the filled circles, are seen to be in reasonable accord with the results obtained from calculations based on either of the two scenarios.

IX-B-6. Photodecomposition of Pentanal (Valeraldehyde, $CH_3CH_2CH_2CH_2CHO$)

Several different photodecomposition modes have been considered in explanation of the photolysis of pentanal:

$$CH_3CH_2CH_2CH_2CHO + h\nu \rightarrow CH_3CH_2CH_2CH_2 + HCO \quad (I)$$

$$\rightarrow CH_3CH_2CH_2CH_3 + CO \quad (II)$$

$$\rightarrow CH_2{=}CHCH_3 + CH_2{=}CHOH \quad (III)$$

$$\rightarrow C_2H_5 + CH_2CH_2CHO \quad (IV)$$

$$\rightarrow CH_3 + CH_2CH_2CH_2CHO \quad (V)$$

$$\rightarrow CH_3CH_2CH_2CH_2CO + H \quad (VI)$$

The important primary processes in the troposphere are (I) and (III). As with the smaller aldehydes, it is likely that process (I) occurs from the first excited triplet state of pentanal while process (III) arises from the excited singlet. The down-chain fragmentation of pentanal, which becomes important only at short wavelengths, may reflect reactions of highly vibrationally excited ground state molecules formed by internal conversion.

IX-B-6.1. Absorption Cross Sections for Pentanal

Independent determinations of the cross sections by Martinez et al. (1992) and Tadić et al. (2001a) agree well. Those reported by Tadić et al. are plotted in figure IX-B-1, and are tabulated in table IX-B-3.

IX-B-6.2. Quantum Yields of the Primary Photodecomposition Processes in Pentanal

i) Primary process (I): $CH_3CH_2CH_2CH_2CHO + h\nu \rightarrow CH_3CH_2CH_2CH_2 + HCO$

Two studies give important information on the extent of the primary processes in pentanal. Cronin and Zhu (1998) measured the quantum yield of formyl radical formation, and provided estimates of ϕ_I at low pressures. These measurements are shown in figure IX-B-15 (open circles) for the 11 different wavelengths of laser excitation that they employed. No quenching of the photodecomposition by aldehyde or nitrogen gas was observed. However, Tadić et al. (2001a) reported quenching in their studies of the broad-band photolysis of pentanal under atmospheric conditions, dilute mixtures in air (100–700 Torr). The overlap of the wavelength distribution of the lamps employed with the absorption of pentanal maximized at about 304 nm. Quenching of process (I)

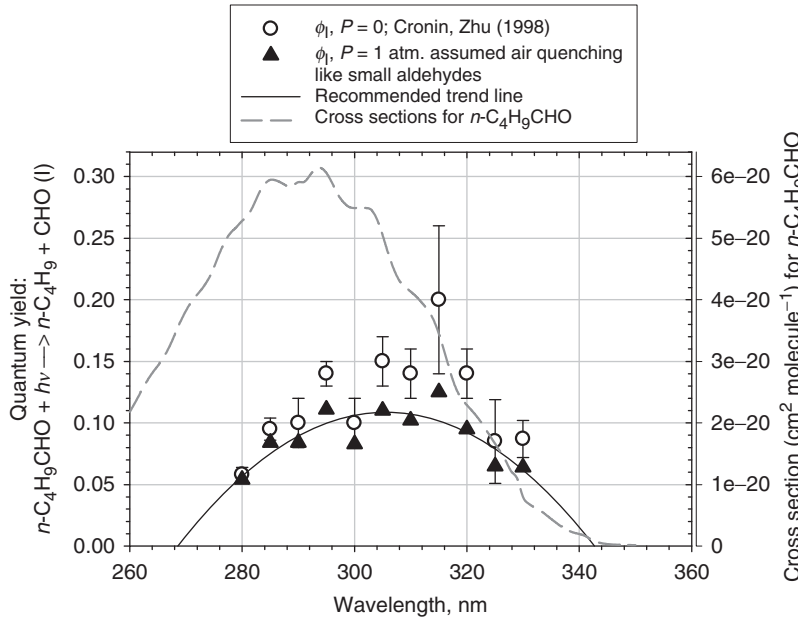

Figure IX-B-15. Plot of the wavelength dependence of ϕ_I for pentanal at zero pressure (Cronin and Zhu, 1998), open circles, and ϕ_I for mixtures in air (760 Torr) as estimated by Calvert et al. (2008) using quenching constants like those of the small aldehydes, black triangles. The light-gray, dashed curve gives the absorption spectrum of pentanal.

by air molecules was observed, and using the Tadić et al. data for 100–700 Torr air pressure, we derive a Stern–Volmer quenching constant $k_q/k_d = 3.29 \times 10^{-3}$ Torr^{-1}. This value is in reasonable agreement with that expected from the wavelength distribution of k_q/k_d defined by acetaldehyde and propanal data in figure VII-B-14b of Calvert et al. (2008). In view of this, Calvert et al. adjusted the measurements of Cronin and Zhu (1998) for quenching using the trend line for k_q/k_d versus λ given in their figure VII-B-14b and the ϕ_I° estimates of Cronin and Zhu with the relation $1/\phi = 1/\phi_I^\circ + k_q/k_d \times$ P(Torr); these adjusted values are shown in figure IX-B-15 as closed triangles. The value of the average ϕ_I expected using the lamp distribution of Tadić et al. and the Cronin and Zhu data adjusted for air quenching, $\phi_I = 0.097$, is somewhat larger than the quantum yield estimate of Tadić et al. (2001a) for 760 Torr, $\phi_I = 0.052$. This may suggest that quenching of excited pentanal molecules by air is somewhat more effective than Calvert et al. (2008) assumed. The recommended values for the wavelength dependence of ϕ_I for pentanal are those defined by the trend line in figure IX-B-15 and tabulated in table IX-B-8.

ii) Primary Process (III): $CH_3CH_2CH_2CH_2CHO + h\nu \rightarrow CH_2{=}CHCH_3 + CH_2{=}CHOH$ The results of Tadić et al. (2001a) indicate that process (III) is favored over process (I) for photolysis of pentanal in air. They determined the quantum yields of propene and acetaldehyde formed in photolysis of pentanal in mixtures of air at pressure up to 700 Torr. After the light exposure was initiated, the enol-form of acetaldehyde

Table IX-B-8. Estimated quantum yields for pentanal photodecomposition in primary process: $CH_3CH_2CH_2CH_2CHO + h\nu \rightarrow CH_3CH_2CH_2CH_2 + HCO$ (I) at 298 K (Calvert et al., 2008)

λ, nm	ϕ_I	λ, nm	ϕ_I	λ, nm	ϕ_I
278	0.048	301	0.107	324	0.082
279	0.053	302	0.108	325	0.079
280	0.058	303	0.108	326	0.076
281	0.060	304	0.109	327	0.073
282	0.064	305	0.109	328	0.069
283	0.068	306	0.109	329	0.066
284	0.072	307	0.109	330	0.062
285	0.075	308	0.108	331	0.058
286	0.078	309	0.108	332	0.054
287	0.081	310	0.107	333	0.050
288	0.084	311	0.106	334	0.045
289	0.087	312	0.105	335	0.041
290	0.089	313	0.104	336	0.036
291	0.092	314	0.103	337	0.031
292	0.094	315	0.101	338	0.026
293	0.096	316	0.100	339	0.021
294	0.098	317	0.098	340	0.015
295	0.100	318	0.097	341	0.010
296	0.101	319	0.095	342	0.003
297	0.103	320	0.092	343	0.000
298	0.120	321	0.090		
299	0.105	322	0.087		
300	0.106	323	0.085		

(CH_2=CHOH) was detected by its unique infrared absorption, and this species was observed to form the ultimate stable product, acetaldehyde. The 100–700 Torr data for propene yield an estimated average quantum yield, $\phi_{III} = 0.19$, for 760 Torr of air. Cronin and Zhu (1998) also identified qualitatively the products related to the occurrence of process (III) in steady-state photolysis of pentanal in oxygen and nitrogen atmospheres. The dominance of process (III) over (II) was confirmed. Since no data related to the wavelength dependence of ϕ_{III} exists at this writing, we suggest the average value (0.19) obtained in pentanal–air mixtures by Tadić et al. be used for ϕ_{III} at all the absorbed wavelengths within the troposphere.

iii) Minor primary processes in pentanal photolysis There is no evidence that defines the quantum yields for the other suggested primary processes in pentanal photolysis, processes (II), (IV), (V), and (VI), but these are expected to be relatively small. It is recommended that they be assumed to be zero in modeling of tropospheric chemistry.

IX-B-6.3. Photolysis Frequencies for Pentanal Photodecomposition in the Lower Troposphere

The recommended cross sections and quantum yields for photodecomposition of pentanal were used to calculate the photolysis frequencies as a function of solar zenith

angle for a cloudless day in the lower troposphere with an ozone column of 350 DU. See figure IX-B-16. Measurements made in the EUPHORE chamber (Moortgat et al., 2002), shown by the open circles, are in good agreement with the estimates based on our calculations.

IX-B-7. Photodecomposition of 2-Methylbutanal [$CH_3CH_2CH_2(CH_3)CHO$]

Studies of the photochemistry of 2-methylbutanal and its mixtures with iodine have been reported for excitation at one wavelength, 313 nm (Gruver and Calvert, 1956, 1958). By analogy with the other aldehydes, the following primary processes are expected to occur:

$$CH_3CH_2CH(CH_3)CHO + h\nu \rightarrow CH_3CHCH_2CH_3 + HCO \quad \text{(I)}$$

$$\rightarrow CH_3CH_2CH_2CH_3 + CO \quad \text{(II)}$$

$$\rightarrow CH_2{=}CH_2 + CH_3CH{=}CH(OH) \quad \text{(III)}$$

$$\rightarrow CH_3CH_2CH(CH_3)CO + H \quad \text{(IV)}$$

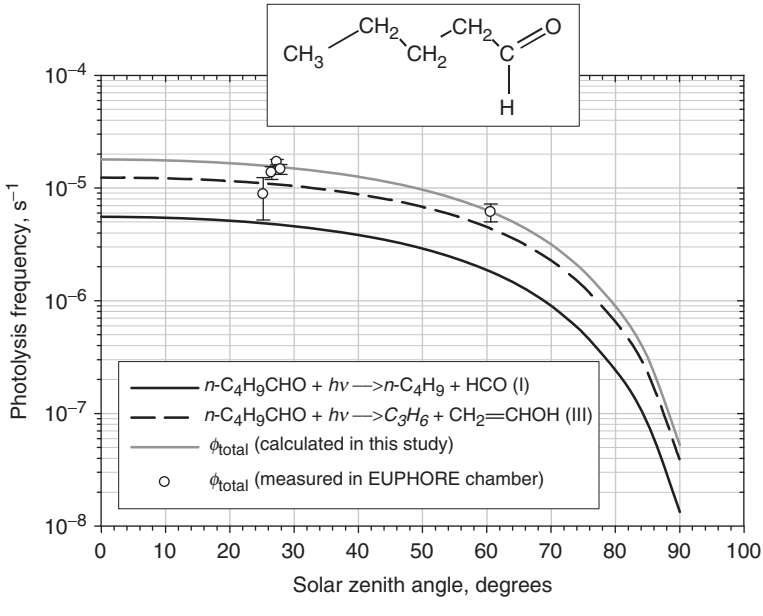

Figure IX-B-16. Plot of the estimated *j*-values for processes (I) and (III) in pentanal versus solar zenith angle, as calculated for a cloudless day within the lower troposphere with overhead ozone column of 350 DU (Calvert et al., 2008). The EUPHORE data were reported by Moortgat et al. (2002).

The results of Gruver and Calvert (1956, 1958) show clearly that processes (I) and (III) are important at 313 nm. Product quantum yields were determined in experiments with the pure aldehyde over a range of temperatures (24.5–348.7°C), aldehyde pressures (23–33 Torr), and iodine pressures (0–25 Torr). The strong temperature dependence of the quantum yields of products in the uninhibited experiments was suppressed in the presence of small amounts of iodine. The average quantum yields of products at 313 nm (8 experiments) were: $\Phi_{C_4H_{10}} = 0.004 \pm 0.004$; $\Phi_{CO} = 0.58 \pm 0.05$; $\Phi_{C_2H_4} = 0.15 \pm 0.02$; $\Phi_{C_4H_9I} = 0.51 \pm 0.05$. From these results quantum yields of $\phi_I \approx 0.55$; $\phi_{II} \approx 0.004$; $\phi_{III} \approx 0.15$ were derived. CH_3I was undetectable in the products, so down-chain fragmentation is unimportant at 313 nm. Optical activity was introduced into the aldehyde synthesized for use in the 1958 studies of Gruver and Calvert. Optical activity was not retained in the product $CH_3CHICH_2CH_3$ indicating either a planar or easily inverted pyramidal structure of the 2-butyl radical formed in process (I). Note that the quantum efficiency of process (III) is very similar to that observed in the structurally related butanal photolyzed at 313 nm. Since the wavelength dependence of the primary processes has not been determined, *j*-values cannot be calculated. Measurements in the EUPHORE chamber (Moortgat et al., 2002) gave: $j(\text{Total}) = (3.78 \pm 0.08) \times 10^{-5}\text{s}^{-1}$ at a solar zenith angle of 32.6°, very similar to that which they measured for 2-methylpropanal.

IX-B-8. Photodecomposition of 3-Methylbutanal [Isovaleraldehyde, $(CH_3)_2CHCH_2CHO$]

By analogy with the information on the smaller aldehydes, one expects the following primary processes to occur in 3-methylbutanal:

$$(CH_3)_2CHCH_2CHO + h\nu \rightarrow (CH_3)_2CHCH_2 + HCO \quad \text{(I)}$$

$$\rightarrow (CH_3)_2CHCH_3 + CO \quad \text{(II)}$$

$$\rightarrow CH_3CH{=}CH_2 + CH_2{=}CHOH \quad \text{(III)}$$

$$\rightarrow (CH_3)_2CHCH_2CO + H \quad \text{(IV)}$$

Bamford and Norrish (1935) first published information on the primary processes in 3-methylbutanal. More recently, Zhu et al. (1999) have reported quantitative information on the quantum yields of process (I). In addition, useful data on the photolysis frequencies of 3-methylbutanal photodissociation have been reported from EUPHORE chamber studies (Moortgat et al., 2002).

IX-B-8.1. Absorption Cross Sections for 3-Methylbutanal

Estimates of the absorption cross sections for 3-methylbutanal were made at 11 wavelengths within the absorption band by Zhu et al. (1999). These data are shown in figure IX-B-12 (black circles). The smoothed spline line that connects the points

Table IX-B-9. Approximate cross sections (cm^2 $molecule^{-1}$) at 298 K and quantum yields of primary process (I), $(CH_3)_2CHCH_2CHO + h\nu \rightarrow (CH_3)_2CHCH_2 + HCO$ (I), for 3-methylbutanal. $(\phi_I)^\circ$ and $(\phi_I)^{760}$ are the quantum yields at zero pressure (Zhu et al., 1999) and the estimated values in 760 Torr of air, assuming quenching occurs by air molecules, similar to that observed in the smaller aldehydes (Calvert et al., 2008)

λ, nm	$10^{20} \times \sigma$	$(\phi_I)^\circ$	$(\phi_I)^{760}$	λ, nm	$10^{20} \times \sigma$	$(\phi_I)^\circ$	$(\phi_I)^{760}$
280	5.07	0.12	0.11	311	4.32	0.35	0.17
281	5.20	0.14	0.12	312	4.26	0.37	0.18
282	5.32	0.15	0.13	313	4.19	0.38	0.18
283	5.43	0.16	0.14	314	4.11	0.39	0.18
284	5.52	0.17	0.14	315	3.96	0.40	0.18
285	5.61	0.17	0.14	316	3.72	0.39	0.17
286	5.66	0.17	0.13	317	3.43	0.36	0.17
287	5.69	0.16	0.13	318	3.10	0.32	0.16
288	5.72	0.15	0.12	319	2.76	0.28	0.15
289	5.73	0.14	0.11	320	2.46	0.26	0.14
290	5.76	0.14	0.11	321	2.30	0.24	0.13
291	5.80	0.15	0.12	322	2.16	0.23	0.13
292	5.85	0.17	0.13	323	2.07	0.22	0.13
293	5.88	0.20	0.14	324	2.00	0.22	0.12
294	5.89	0.21	0.15	325	1.92	0.22	0.12
295	5.90	0.22	0.16	326	1.80	0.22	0.12
296	5.84	0.23	0.16	327	1.67	0.22	0.12
297	5.77	0.23	0.16	328	1.50	0.22	0.11
298	5.69	0.23	0.16	329	1.32	0.21	0.11
299	5.62	0.23	0.16	330	1.16	0.21	0.11
300	5.55	0.23	0.15	331	1.02	0.19	0.11
301	5.53	0.24	0.15	332	0.90	0.17	0.09
302	5.51	0.24	0.15	333	0.75	0.15	0.08
303	5.48	0.25	0.15	334	0.65	0.13	0.07
304	5.45	0.26	0.16	335	0.50	0.10	0.05
305	5.36	0.27	0.16	336	0.35	0.08	0.04
306	5.20	0.28	0.16	337	0.24	0.06	0.03
307	5.00	0.29	0.16	338	0.11	0.04	0.02
308	4.78	0.30	0.16	339	0	0.02	0.01
309	4.53	0.31	0.17	340	0	0	0
310	4.40	0.32	0.17				

was drawn to facilitate estimates at other wavelengths needed in modeling the *j*-determinations; these estimated values of σ are given in tabular form in table IX-B-9. The data match reasonably well those shown in figure IX-B-12 for 2-methylpropanal (light solid line) from measurements of Martinez et al. (1992).

IX-B-8.2. Quantum Yields of Primary Photodecomposition Processes in 3-Methylbutanal

i) Primary process (I): $(CH_3)_2CHCH_2CHO + h\nu \rightarrow (CH_3)_2CHCH_2 + HCO$ Quantitative information on this primary process was determined by Zhu et al. (1999) who

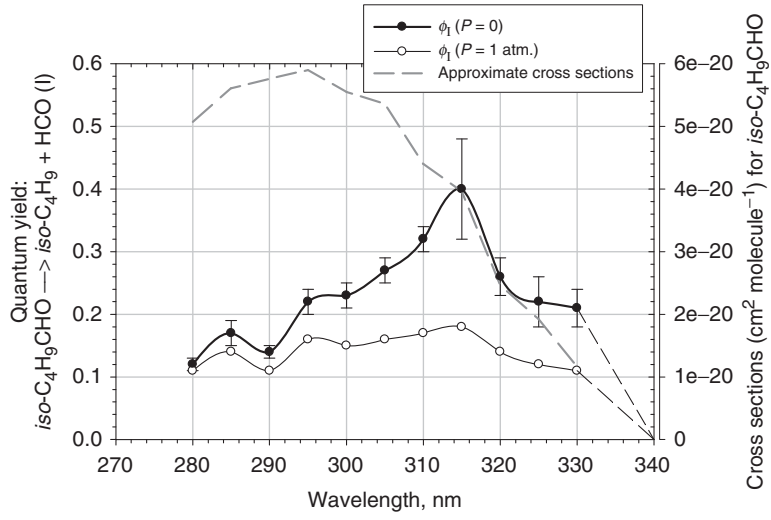

Figure IX-B-17. Quantum yields of HCO formation for 3-methylbutanal. Filled symbols are data reported at zero pressure (Zhu et al., 1999). Open symbols are estimates of ϕ_I in 760 Torr of air assuming quenching as in the smaller aldehydes. The short dashed lines are the assumed wavelength dependencies of ϕ_I for λ = 330–340 nm that were used in j-value calculations for process (I) (Calvert et al., 2008). The dashed-gray curve gives the approximate absorption spectrum of 3-methylbutanal.

reported $\Phi_{HCO}(= \phi_I)$ at zero pressure at 11 wavelengths. Figure IX-B-17 shows these data as filled circles. They reported that added nitrogen gas (20–400 Torr) did not quench HCO formation detectably at 280, 295, and 310 nm, but at 325 nm, a pressure of 400 Torr decreased the HCO yield by 25%. This corresponds to a Stern–Volmer quenching constant, $k_q/k_d \approx 3.8 \times 10^{-3}$ Torr^{-1}, similar to those observed for the smaller aldehydes. In view of this observation, Calvert et al. (2008) have adjusted the measured zero pressure values of ϕ_I to those expected for 1 atm. of air using the k_q/k_d values obtained for the smaller aldehydes. These adjusted values, shown as open circles in figure IX-B-17, together with those derived from the spline curve connecting zero pressure data of Zhu et al. (filled circles) are tabulated in table IX-B-9.

ii) Primary process (III): $(CH_3)_2CHCH_2CHO + h\nu \rightarrow CH_3CH{=}CH_2 + CH_2{=}CHOH$ Zhu et al. (1999) suggest that the relatively low values measured for ϕ_I are in accord with the occurrence of the competitive photodecomposition process (III), and they identified acetaldehyde among the products of steady-state photolysis experiments. No quantitative information on the magnitude of ϕ_{III} is available at this writing, but the full-arc photolysis reported by Bamford and Norrish (1935) suggest its dominance. We estimate an average value for $\phi_{III} \approx 0.13$ in air at 1 atm. from the current data for ϕ_I and EUPHORE chamber measurements of j(Total); see section IX-B-8.3.

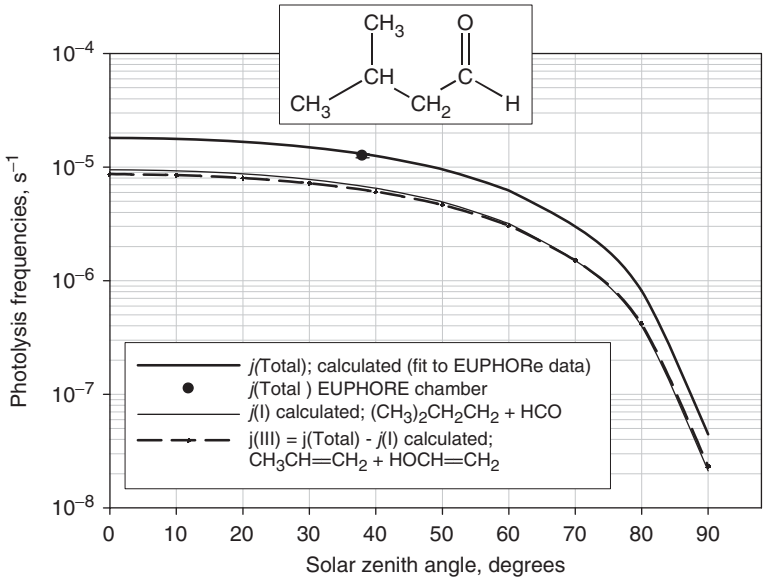

Figure IX-B-18. Approximate photolysis frequencies versus solar zenith angle calculated for 3-methylbutanal for a cloudless day in the lower troposphere with an overhead ozone column of 350 DU. The solid curve for j(Total) was calculated to fit the EUPHORE data point; the thin black curve for j(I) was calculated using ϕ_I measurements from Zhu et al. (1999), corrected to 1 atm. of air; the dashed curve is the estimate of j(III) calculated from j(Total) – j(I).

iii) Other primary processes There is no information related to the significance of primary processes (II) and (IV), but as with the other aldehydes, it is likely that these are significant only at the shorter wavelengths.

IX-B-8.3. Photolysis Frequencies for the Photodecomposition of 3-Methylbutanal by Process (I) in the Lower Troposphere

Measurements in the EUPHORE chamber (Moortgat et al., 2002) gave: j(Total) = $(1.26 \pm 0.05) \times 10^{-5}\,s^{-1}$ at a solar zenith angle of 38°. We have calculated estimates of j(I) using the zero pressure quantum yields for process (I) reported by Zhu et al. (1999) as adjusted for quenching by 1 atm. of air. Calculations were for a clear-sky within the lower troposphere (ozone column = 350 DU); see figure IX-B-18 (thin black line). In order to match the j(Total) EUPHORE measurement, given by the thick back line, we used the j(I) estimates together with an assumed value of $\phi_{III} = 0.13$ independent of wavelength. The estimate of ϕ_{III} so derived is in reasonable accord with those observed for the analogous primary processes in the larger aldehydes.

IX-B-9. Photodecomposition of 2,2-Dimethylpropanal [Pivaldehyde, $(CH_3)_3CCHO$]

By analogy with the photochemical behavior of the smaller aldehydes, one expects the following primary photodecomposition processes to occur:

$$(CH_3)_3CCHO + h\nu \rightarrow (CH_3)_3C + HCO \quad \text{(I)}$$

$$\rightarrow HC(CH_3)_3 + CO \quad \text{(II)}$$

$$\rightarrow (CH_3)_3CCO + H \quad \text{(III)}$$

$$\rightarrow CH_3 + (CH_3)_2CCHO \quad \text{(IV)}$$

Primary process (I) is believed to be the only important mode of photodecomposition of pivaldehyde in the troposphere. The other modes of decay are likely to become important at $\lambda < 280$ nm in view of the photochemistry of the other similar aldehydes.

IX-B-9.1. Absorption Cross Sections for 2,2-Dimethylpropanal

Measurements of the absorption spectrum of 2,2-dimethylpropanal were reported for 11 wavelengths in the ultraviolet by Zhu et al. (1999), shown in figure IX-B-12. It is surprising that the absorption by 2,2-dimethylpropanal is about 40% smaller than those observed with the other aldehydes of similar size. Zhu et al. (1999) rationalized this difference in terms of a possible effect on the π^* energy induced by the bulky $(CH_3)_3C$ group present in 2,2-dimethylpropanal. If indeed the aldehyde sample used by Zhu et al. was 97% pure as stated, then the observed effect is most interesting, and reasons for diminution of its cross sections from that of aldehydes of similar size should be explored theoretically.

IX-B-9.2. Quantum Yields of the Primary Photodecomposition Processes in 2,2-Dimethylpropanal

i) Primary process (I) Process (I) has been studied by Zhu et al. (1999) who measured the quantum yields of the HCO radical formed in photolysis at 11 wavelengths (280–330 nm). The zero pressure ϕ_I estimates are summarized in the figure IX-B-19 (black triangles). Variation of the pressure of nitrogen from 20 to 400 Torr gave no detectable quenching of the HCO formation, so the zero pressure values for ϕ_I were suggested to be applicable to air at 1 atm. As in the previous experiments of Zhu et al., significant quenching by nitrogen gas may have been missed. The effect of possible quenching by added nitrogen at 1 atm. pressure was studied by Calvert et al. (2008) by applying the Stern–Volmer quenching constants applicable to the small aldehydes; these data points are shown as open triangles in figure IX-B-19. Both the zero pressure measurements of ϕ_I as suggested by the spline curve joining the experimental points and the pressure-adjusted values with assumed quenching are tabulated in table IX-B-10. The values of ϕ_I are significantly greater for 2,2-dimethylpropanal than for 3-methylbutanal (figure IX-B-17). This may result, at least in part, from the occurrence of the major process (III) in 3-methylbutanal, a pathway not available in 2,2-dimethylpropanal.

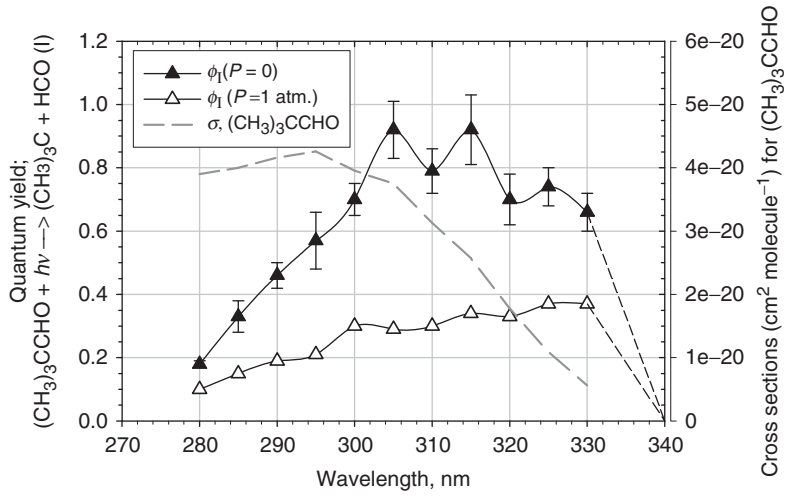

Figure IX-B-19. Plot of ϕ_I for pivaldehyde at zero pressure (filled triangles; Zhu et al., 1999) and as estimated for 1 atm. pressure (open triangles; Calvert et al., 2008). The dashed-gray curve gives the approximate absorption spectrum of pivaldehyde as measured by Zhu et al. (1999).

ii) Other primary processes Processes (II) and (IV) have not been demonstrated to occur, but they are expected to be significant, especially at wavelengths of absorbed light below 280 nm. By analogy with the increased importance of process (IV) at short wavelengths forming CH_3 radicals by rupture of the CH_3—CH_2CHO bond in propanal and the CH_3—$CH(CH_3)CHO$ bond in 2-methylpropanal, it seems likely that process (IV) will occur in the photolysis of 2,2-dimethylpropanal. An alternative pathway competing with process (I) for photodecomposition, possibly process (III), may account for decrease in the decomposition by process (I) that is observed with 2,2-dimethylbutanal at the shorter wavelengths present within the troposphere (280–300 nm).

IX-B-9.3. Photolysis Frequencies for 2,2-Dimethylpropanal Photodecomposition in the Lower Troposphere

The *j*-values for process (I) have been estimated for clear-sky conditions in the lower troposphere (ozone column of 350 DU). Two different scenarios have been used: one assuming no quenching of the process (I) in one atmosphere of air, and the other, assuming quenching similar to that observed in other small aldehydes. The results of the two calculations are summarized in figure IX-B-20. Assuming that the seemingly low absorption cross sections for 2,2-dimethylpropanal given by Zhu et al. (1999) are correct, then it is probable that the appropriate *j*-values lie within the area between the two curves in the figure. Measurements made in the EUPHORE chamber at a solar zenith angle of 60° (Moortgat et al., 2002) gave a value well below that expected from the two calculated curves.

Table IX-B-10. Approximate cross sections (σ, cm^2 molecule^{-1}) at 298 K and quantum yields of primary process: $(CH_3)_3CCHO + h\nu \rightarrow (CH_3)_3C + HCO$ (I), for 2,2-dimethylpropanal. $(\phi_I)^\circ$ and $(\phi_I)^{760}$ are the quantum yields at zero pressure (Zhu et al., 1999) and the estimated values in 760 Torr of air, assuming quenching occurs by air molecules, similar to that observed in the smaller aldehydes (Calvert et al., 2008)

λ, nm	$10^{20} \times \sigma$	$(\phi_I)^\circ$	$(\phi_I)^{760}$	λ, nm	$10^{20} \times \sigma$	$(\phi_I)^\circ$	$(\phi_I)^{760}$
280	3.90	0.18	0.10	310	3.13	0.79	0.30
281	3.92	0.21	0.11	311	3.01	0.81	0.31
282	3.94	0.24	0.12	312	2.90	0.84	0.32
283	3.95	0.27	0.13	313	2.80	0.88	0.33
284	3.98	0.30	0.14	314	2.68	0.91	0.34
285	4.00	0.33	0.15	315	2.57	0.92	0.34
286	4.02	0.36	0.16	316	2.43	0.90	0.34
287	4.06	0.38	0.17	317	2.27	0.84	0.34
288	4.05	0.41	0.18	318	2.10	0.79	0.32
289	4.13	0.44	0.19	319	1.95	0.74	0.33
290	4.16	0.46	0.19	320	1.78	0.70	0.33
291	4.21	0.48	0.19	321	1.64	0.69	0.34
292	4.24	0.51	0.19	322	1.48	0.70	0.34
293	4.26	0.53	0.19	323	1.35	0.71	0.35
294	4.27	0.55	0.20	324	1.23	0.73	0.36
295	4.26	0.57	0.21	325	1.09	0.74	0.37
296	4.22	0.59	0.23	326	0.97	0.74	0.37
297	4.16	0.61	0.25	327	0.87	0.72	0.37
298	4.08	0.63	0.27	328	0.76	0.70	0.37
299	4.01	0.67	0.29	329	0.66	0.68	0.37
300	3.95	0.70	0.30	330	0.56	0.66	0.37
301	3.91	0.75	0.31	331	0.45	0.60	0.32
302	3.87	0.81	0.31	332	0.37	0.52	0.29
303	3.85	0.87	0.30	333	0.28	0.45	0.25
304	3.81	0.90	0.30	334	0.19	0.40	0.22
305	3.75	0.92	0.29	335	0.08	0.33	0.18
306	3.66	0.91	0.29	336	0	0.27	0.15
307	3.54	0.87	0.29	337		0.20	0.11
308	3.40	0.83	0.29	338		0.14	0.08
309	3.27	0.81	0.29	339		0.07	0.03
				340		0	0

IX-B-10. Photodecomposition of Hexanal ($CH_3CH_2CH_2CH_2CH_2CHO$)

The primary processes in hexanal photodecomposition are suggested to be:

$$CH_3CH_2CH_2CH_2CH_2CHO + h\nu \rightarrow CH_3CH_2CH_2CH_2CH_2 + HCO \quad \text{(I)}$$

$$\rightarrow CH_3CH_2CH_2CH_2CH_3 + CO \quad \text{(II)}$$

$$\rightarrow CH_3CH_2CH{=}CH_2 + CH_2{=}CHOH \quad \text{(III)}$$

$$\rightarrow CH_3CH_2CH_2CH_2CH_2CO + H \quad \text{(IV)}$$

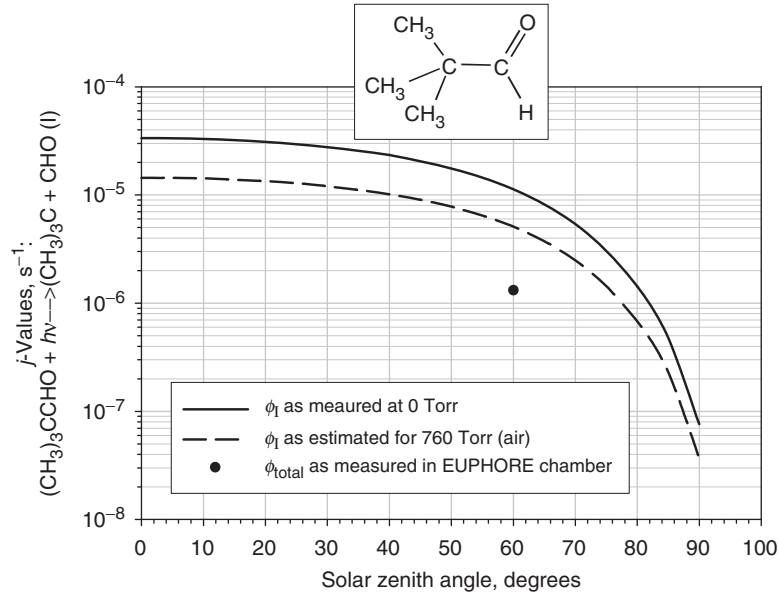

Figure IX-B-20. Approximate photolysis frequencies versus solar zenith angle calculated for 2,2-dimethylpropanal for a cloudless day in the lower troposphere with an overhead ozone column of 350 DU. The solid curve is calculated using the Zhu et al. (1999) quantum yields for zero pressure; the dashed curve is that estimated assuming air quenching (760 Torr) equivalent to that shown by the smaller aldehydes. The EUPHORE estimate (Moortgat et al., 2002) suggests that there may be a significantly greater quenching by air than has been assumed in the calculations shown by the dashed curve.

The occurrence of processes (I) and (III) at wavelengths of sunlight available in the troposphere is well documented. Processes (II) and (IV) may be important at the shorter wavelengths as observed with other aldehydes.

IX-B-10.1. Absorption Cross Sections for Hexanal

The cross section data for hexanal are presented in table IX-B-11 as reported by Plagens et al. (1998); Tadić et al. (2001b) point out that the spectrum of hexanal is very similar to those of butanal and pentanal.

IX-B-10.2. Quantum Yields of Primary Processes in Hexanal Photodecomposition

i) Primary Process (1) Tang and Zhu (2004) measured the zero pressure quantum yields of HCO radical for hexanal at 11 different wavelengths (280–330 nm). These data are shown as open circles in figure IX-B-21. The authors report rather efficient quenching of process (I) by hexanal molecules, yet no quenching by added nitrogen gas was observed for pressures up to 387 Torr. However, the data of Tadić et al. (2001b) from their study of the broadband photolysis of hexanal, showed quenching

Table IX-B-11. Recommended cross sections (Plagens et al., 1998), and quantum yields for process (I) in hexanal photolysis in air (1 atm.): $CH_3CH_2CH_2CH_2CH_2CHO + h\nu \rightarrow CH_3CH_2CH_2CH_2CH_2 + HCO$ (I). In view of the limited data, we recommend that $\phi_{III} = 0.29$ be used for process (III): $CH_3CH_2CH_2CH_2CH_2CHO + h\nu \rightarrow CH_2{=}CHCH_2CH_3 + CH{=}CHOH$, independent of wavelength (Calvert et al., 2008)

λ, nm	$10^{20} \times \sigma$	Estimated ϕ_I	λ, nm	$10^{20} \times \sigma$	Estimated ϕ_I	λ, nm	$10^{20} \times \sigma$	Estimated ϕ_I
278	4.92	0.060	301	5.46	0.078	324	1.81	0.072
279	4.99	0.064	302	5.47	0.081	325	1.67	0.072
280	5.05	0.067	303	5.45	0.086	326	1.55	0.071
281	5.11	0.073	304	5.32	0.091	327	1.37	0.069
282	5.26	0.075	305	5.07	0.096	328	1.18	0.067
283	5.45	0.079	306	4.77	0.100	329	0.99	0.064
284	5.69	0.081	307	4.47	0.104	330	0.84	0.061
285	5.83	0.083	308	4.29	0.107	331	0.75	0.057
286	5.85	0.082	309	4.17	0.109	332	0.71	0.053
287	5.82	0.081	310	4.09	0.110	333	0.67	0.049
288	5.79	0.080	311	4.01	0.112	334	0.62	0.045
289	5.81	0.079	312	3.93	0.110	335	0.53	0.040
290	5.83	0.079	313	3.82	0.108	336	0.44	0.036
291	5.92	0.081	314	3.66	0.106	337	0.34	0.032
292	6.02	0.083	315	3.42	0.102	338	0.26	0.028
293	6.07	0.085	316	3.11	0.097	339	0.21	0.024
294	6.08	0.087	317	2.80	0.089	340	0.21	0.020
295	5.99	0.087	318	2.55	0.083	341	0.20	0.016
296	5.85	0.085	319	2.39	0.078	342	0.18	0.012
297	5.72	0.082	320	2.29	0.074	343	0.12	0.008
298	5.62	0.080	321	2.20	0.072	344	0.08	0.004
299	5.53	0.077	322	2.08	0.072	345	0.04	0
300	5.48	0.076	323	1.95	0.072			

of process (I) by air with a Stern–Volmer constant $k_q/k_d = 5.0 \times 10^{-3}\,\text{Torr}^{-1}$, similar to that expected ($\sim 3 \times 10^{-3}\,\text{Torr}^{-1}$) for the smaller aldehydes at the wavelength of maximum overlap (303 nm) in the broadband experiments of Tadić et al. (2001b). Quenching by air at 1 atm. has been observed in most of the aldehydes that have been studied, as discussed in the previous sections of this chapter. If significant air quenching of the zero pressure ϕ_I values of Tang and Zhu is assumed to occur as with the smaller aldehydes, then the data points shown as open triangles in figure IX-B-21 are obtained. When the solid spline curve joining these points is used to derive an average ϕ_I value for the wavelength distribution used by Tadić et al., Calvert et al. (2008) found $\phi_I \approx 0.089$. This agrees reasonably well with the estimates of $\phi_I = 0.096$ for 760 Torr of air in the broadband photolysis of Tadić et al. (2001b). The recommended values for ϕ_I are those shown in figure IX-B-21 and tabulated recommendations are given in table IX-B-11.

ii)Primary process (III) No dependence on pressure of nitrogen (100–700 Torr) was observed for process (III) by Tadić et al. (2001b), and the average measured $\phi_{III} = 0.29 \pm 0.02$. Processes (I) and (III) probably occur from different electronic

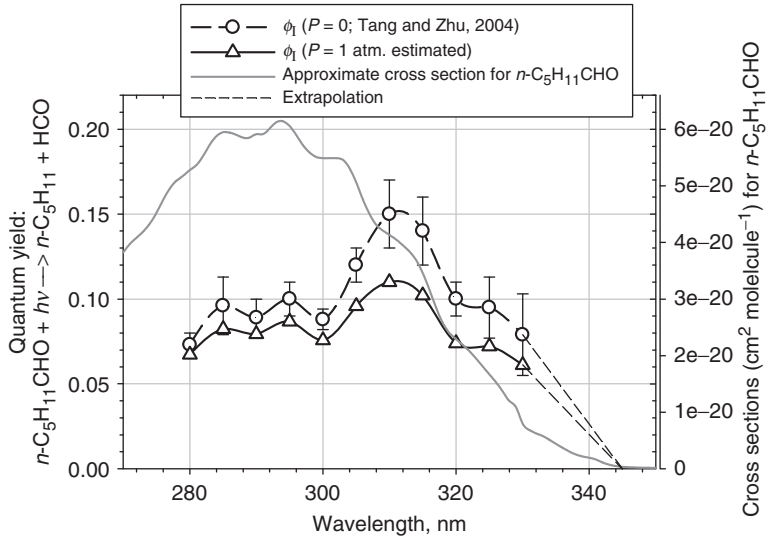

Figure IX-B-21. Quantum yields of primary process (I) in hexanal versus wavelength; zero pressure values of Tang and Zhu (2004), open circles. The open triangles represent adjusted data assuming hexanal is quenched by air (760 Torr) as observed with the smaller aldehydes, open triangles; recommended trend line, solid curve (Calvert et al., 2008). The light-gray curve gives the absorption spectrum of hexanal (Plagens et al., 1998).

states. Presumably, (I) occurs largely from the triplet T_I state, while (III) may arise from the first excited singlet. We suggest that modelers of tropospheric chemistry use the estimate $\phi_{III} = 0.29$, independent of wavelength.

IX-B-10.3. Photolysis Frequencies for Photodecomposition of Hexanal in the Lower Troposphere

The recommended data from this study were used to derive the *j*-values for hexanal given in figure IX-B-22. Measurements reported by Moortgat et al. (2002) in the EUPHORE chamber, shown by the open circles, are seen to be in reasonable accord with our calculated values.

IX-B-11. Photodecomposition of Heptanal ($CH_3CH_2CH_2CH_2CH_2CH_2CHO$)

Heptanal photodecomposition is expected to follow the pattern of the lighter aldehydes:

$$CH_3CH_2CH_2CH_2CH_2CH_2CHO + h\nu \rightarrow CH_3CH_2CH_2CH_2CH_2CH_2 + HCO \quad \text{(I)}$$

$$\rightarrow CH_3CH_2CH_2CH_2CH_2CH_3 + CO \quad \text{(II)}$$

$$\rightarrow CH_2{=}CHCH_2CH_2CH_3 + CH_2{=}CHOH \quad \text{(III)}$$

$$\rightarrow CH_3CH_2CH_2CH_2CH_2CH_2CO + H \quad \text{(IV)}$$

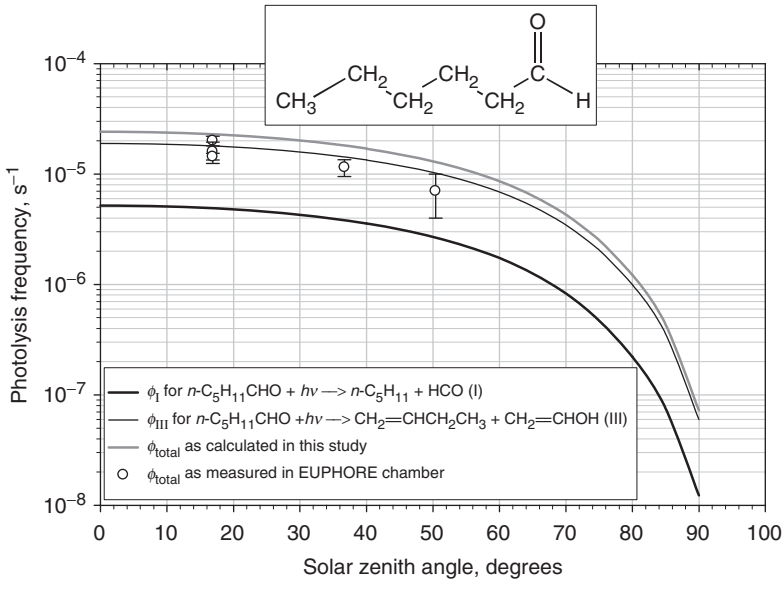

Figure IX-B-22. Approximate photolysis frequencies for primary processes (I) and (III) in hexanal versus solar zenith angle; curves were calculated (Calvert et al., 2008) for a cloudless day within the lower troposphere with an overhead ozone column of 350 DU. EUPHORE data are from Moortgat et al. (2002).

Evidence for the occurrence of primary process (I) has been obtained by Tang and Zhu (2004), and processes (I) and (III) by Tadić et al. (2002). Primary processes (II) and (IV) have not been observed but are expected to occur, especially for absorbed wavelengths < 280 nm.

IX-B-11.1. Absorption Cross Sections for Heptanal

Approximate cross sections for heptanal at 11 different wavelengths (280–350 nm) were reported by Tang and Zhu (2004). These values are somewhat greater than those measured for hexanal, but most values overlapped within the scatter of the measurements. Tadić et al. (2002) reported that the cross sections for the straight-chain aldehydes as measured by Zabel (1999) are almost identical from butanal to nonanal. Thus, the spectra of one of the straight-chain C_4- to C_9-aldehydes could be used as a surrogate for that of heptanal for atmospheric calculations until an accurate absorption spectrum of heptanal becomes generally available.

IX-B-11.2. Quantum Yields of Primary Photodecomposition Processes in Heptanal

i) Process (I): $CH_3CH_2CH_2CH_2CH_2CH_2CHO + h\nu \rightarrow CH_3CH_2CH_2CH_2CH_2CH_2 + HCO$ The most representative studies of heptanal photodecomposition in air at one atmosphere are those of Tadić et al. (2002); they photolyzed dilute heptanal mixtures in air (100–700 Torr) using broad-band radiation. Their data, extrapolated to 760 Torr,

gives estimates of the weighted-average quantum yields over the 279–350 nm region: $\phi_I = 0.030$. Direct evidence for the occurrence of process (I) in heptanal photolysis was obtained by Tang and Zhu (2004). They measured the zero pressure values of ϕ_I at 11 wavelengths. These data are given by the black circles in figure IX-B-23. In this case, quenching of process (I) was observed to occur by the excited aldehyde–aldehyde molecule collisions, and the Stern–Volmer quenching constants were very much larger than those seen for the analogous quenching by the smaller aldehydes; for example, at 280 nm, 1.1 ± 0.2 and at 330 nm, 2.9 ± 1.2 $Torr^{-1}$. However, as in their previous studies of aldehyde photolysis, no observable quenching of the process (I) occurred with addition of nitrogen (6–387 Torr). This is surprising, especially in view of the very large quenching of process (I) by heptanal molecules that was observed. However, in the Tadić et al. (2002) studies with broadband irradiation, quenching of process (I) by air molecules showed Stern–Volmer quenching constant of 1.3×10^{-2} $Torr^{-1}$ that is significantly larger than the k_q/k_d value observed for the smaller aldehydes. The observations of Tang and Zhu (2004) on effects of pressure on the HCO yield are difficult to understand. In our treatment of the data to arrive at the recommended

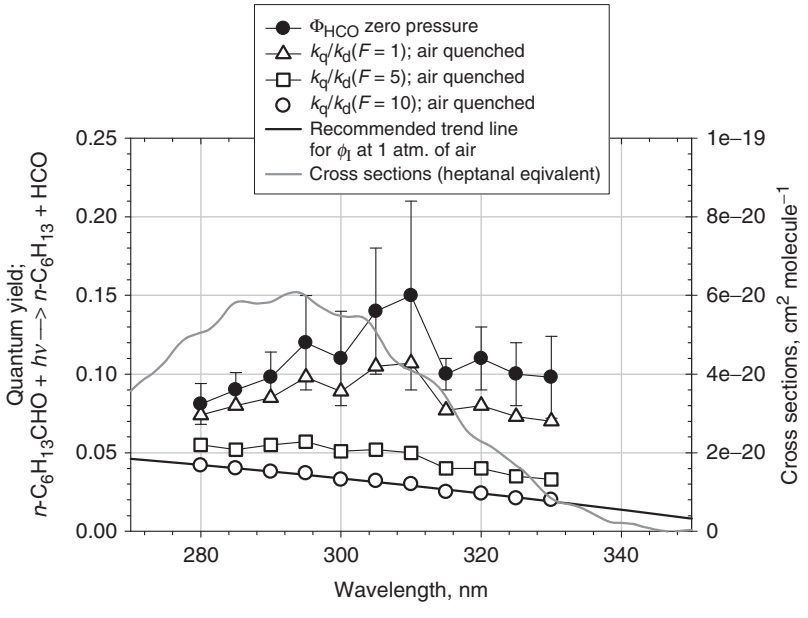

Figure IX-B-23. Plot of the quantum yield of process (I) in heptanal versus wavelength (Calvert et al., 2008). Values measured for zero pressure by Tang and Zhu (2004) are shown as black circles. Estimates of ϕ_I adjusted for air quenching (760 Torr) are shown using different extents of quenching estimated from $k_q/k_d = F\times (k_q/k_d)^\circ$, where $(k_q/k_d)^\circ$ is the value estimated for the light aldehydes at a given wavelength; see figure VII-B-14b in Calvert et al. (2008). F is varied from 1 (triangles), to 5 (squares), to 10 (open circles). The latter values fit best the broadband (average) estimate of $\phi_I = 0.030$ at 760 Torr (Tadić et al., 2002). The solid heavy line is the recommended trend curve for ϕ_I in air (760 Torr). The light-gray curve gives the absorption of hexanal, a surrogate for heptanal (Plagens et al., 1998).

trend line for ϕ_I with wavelength for 1 atm. of air, we have increased the size of the assumed quenching rate constant for excitation at each wavelength from that observed for the simple aldehydes (k_q/k_d), given by the open triangles, by factors (F) of 5 (open squares) and 10 (open circles) in figure IX-B-23 [$k_q/k_d = F \times (k_q/k_d)^\circ$ where $(k_q/k_d)^\circ$ is the Stern–Volmer quenching constant as estimated in figure VII-B-14b of Calvert et al., 2008]. The latter case provides the best correlation with the Tadić et al. (2002) data from the broadband irradiation. A large quenching constant (k_q/k_d) for excited aldehyde by air molecule collisions is consistent with the unusually large quenching efficiency observed by Tadić et al.

For the wavelength distribution employed by Tadić et al., the estimates derived by Calvert et al. (2008), give $\phi_I = 0.031$, in good agreement with that measured by Tadić et al., $\phi_I = 0.030$ at 760 Torr of air. Note that the Stern–Volmer quenching constant that describes the effect of air pressure on ϕ_I measured by Tadić et al., $k_q/k_d = 1.3 \times 10^{-2}$ Torr^{-1}, is similar to that used in our calculations (with $F = 10$) for light absorption at 305 nm, near the wavelength of maximum overlap in the Tadić et al. (2002) broadband experiments. The recommended ϕ_I values for heptanal in 1 atm. of air are given in table IX-B-12.

Table IX-B-12. Recommended quantum yields for process (I) in heptanal photolysis in air (1 atm.): $CH_3CH_2CH_2CH_2CH_2CH_2CHO + h\nu \rightarrow CH_3CH_2CH_2CH_2CH_2CH_2 + HCO$. In view of the limited data, Calvert et al. (2008) recommend that $\phi_{III} = 0.12$ be used, independent of wavelength for primary process (III) forming $CH_2{=}CHCH_2CH_2CH_3$ and $CH_2{=}CHOH$ (Tadić et al., 2002)

λ, nm	Estimated ϕ_I	λ, nm	Estimated ϕ_I	λ, nm	Estimated ϕ_I
278	0.043	300	0.034	325	0.022
279	0.042	301	0.033	326	0.021
280	0.042	302	0.033	327	0.021
281	0.041	303	0.032	328	0.020
282	0.041	304	0.032	329	0.020
283	0.041	305	0.031	330	0.019
284	0.041	306	0.031	331	0.019
285	0.040	307	0.030	332	0.018
286	0.040	308	0.030	333	0.017
287	0.039	309	0.029	334	0.017
288	0.039	310	0.029	335	0.016
289	0.038	311	0.029	336	0.016
290	0.038	312	0.028	337	0.015
291	0.038	313	0.028	338	0.015
292	0.037	314	0.027	339	0.014
293	0.037	315	0.027	340	0.014
294	0.036	316	0.026	341	0.013
295	0.036	317	0.026	342	0.013
296	0.035	318	0.025	343	0.012
297	0.035	319	0.025	344	0.011
298	0.035	320	0.024	345	0.011
299	0.034	321	0.024	346	0.010
298	0.035	322	0.023	347	0.010
299	0.034	323	0.022	348	0.009
		324	0.022		

ii) Process (III): $CH_3CH_2CH_2CH_2CH_2CH_2CHO + h\nu \rightarrow CH_2{=}CHCH_2CH_2CH_3 + CH_2{=}CHOH$ The data of Tadić et al. (2002) give $\phi_{III} = 0.12$ at 760 Torr of air. The wavelength dependence of ϕ_{III} is unknown at this writing. For the purposes of tropospheric modeling, we assume that $\phi_{III} = 0.12$, independent of wavelength of light absorbed within the troposphere. The occurrence of processes (II) and (IV) may become important at the short wavelengths ($\lambda < 280$ nm); these or other unrecognized pathways of excited molecule decay must exist to rationalize the relatively small fraction of the heptanal decay that is accounted for by processes (I) and (III).

IX-B-11.3. Photolysis Frequencies for Photodecomposition Processes in Heptanal in the Lower Troposphere

Photolysis frequencies for processes (I) and (III) have been calculated by Calvert et al. (2008) for a cloudless day in the lower troposphere as a function of solar zenith angle (ozone column of 350 DU); see figure IX-B-24. The curve fitted to the open circles in figure IX-B-23 is the recommended wavelength dependence of ϕ_I. The effect of different choices of quenching efficiency of air on the *j*-value for process (I) is seen in figure IX-B-24. Quenching by air is assumed to occur as observed with the small

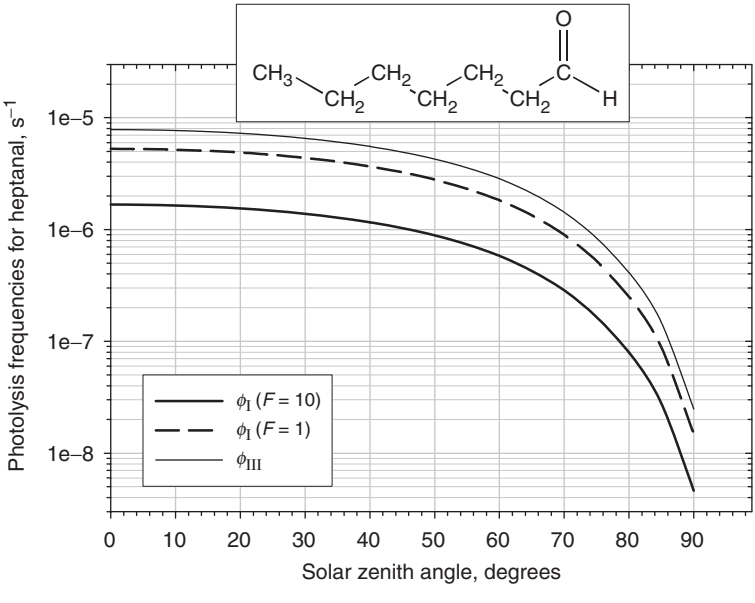

Figure IX-B-24. Plot of the recommended photolysis frequencies versus solar zenith angle for heptanal primary processes: $CH_3CH_2CH_2CH_2CH_2CH_2CHO + h\nu \rightarrow CH_3CH_2CH_2CH_2CH_2CH_2 + HCO$ (I), long-dashed lines calculated assuming that quenching of the process (I) by air is like that in the small aldehydes. The heavy line (the dependence recommended in this study) was estimated in calculations assuming the air quenching at 10 times the efficiency shown by small aldehydes. *j*-Values for the process $CH_3CH_2CH_2CH_2CH_2CH_2CHO + h\nu \rightarrow CH_2{=}CHCH_2CH_2CH_3 + CH_2{=}CHOH$ (III), are given by the light solid curve. All calculations are for a cloudless day in the lower troposphere with an overhead ozone column of 350 DU.

aldehyde (long-dashed curve) or with an efficiency that is 10 times that of the small aldehydes (heavy, solid curve). In the absence of a measured wavelength dependence of ϕ_{III}, we have assumed that the value of $\phi_{III} = 0.12$, independent of λ, as measured for the average in the broadband experiments of Tadić et al. (2002).

IX-B-12. Photodecompostion Processes in Other Aliphatic Aldehydes

The limited data available for 2-methylbutanal and 3-methylpentanal photodecomposition have been discussed by Calvert et al. (2008); these are insufficient to allow reliable estimates to be made of the photolysis frequencies. The effects of molecular structure of the aldehyde on photodecomposition efficiency have been discussed briefly by Calvert et al. (2008). All of the aliphatic aldehydes studied to date follow the pattern of photodecomposition exhibited by the aldehydes discussed in this chapter.

IX-C. Photodecomposition of Aldehydes Containing Additional Functional Groups

The absorption spectra of several aldehydes containing additional functional groups are compared with that of acetaldehyde in figure IX-C-1. Note in this figure that the replacement of an H-atom on the —CH_3 group of acetaldehyde with an —OH group causes a shift in the absorption band to somewhat shorter wavelengths. However, a

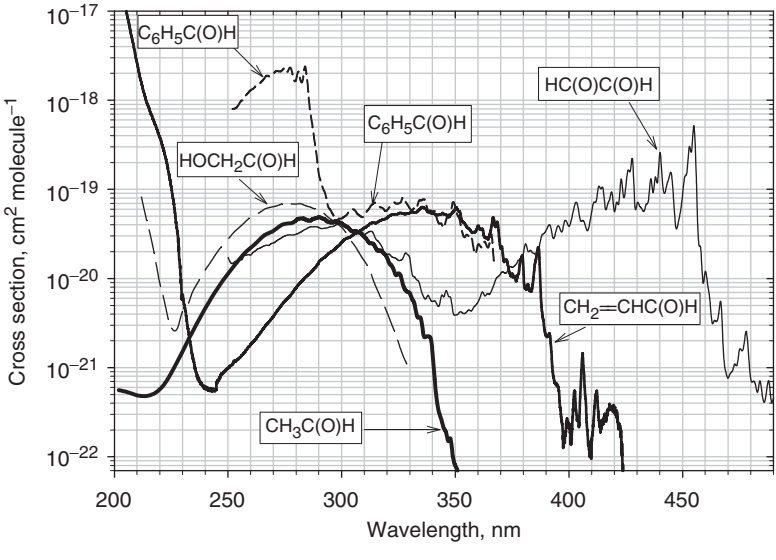

Figure IX-C-1. Comparison of the absorption spectra of acetaldehyde (Martinez et al., 1992) with those for a series of aldehydes containing additional functional groups: hydroxyacetaldehyde, $HOCH_2C(O)H$ (Magneron et al., 2005); acrolein, CH_2=CHC(O)H (Magneron et al., 2002); glyoxal, HC(O)C(O)H (Volkamer et al., 2005); benzaldehyde, $C_6H_5C(O)H$ (Thiault et al., 2004).

large shift in the absorption band to the longer wavelengths occurs when the —CH_3 group in acetaldehyde is replaced by the —CH=CH_2 group to form acrolein, or another —HC=O group to form glyoxal, or a phenyl group to form benzaldehyde. As a result hydroxyacetaldehyde absorbs less tropospheric sunlight than acetaldehyde, while acrolein, glyoxal, and benzaldehyde absorb sunlight more strongly with the potential lowering of their photochemical lifetimes. In this section we will review the mechanisms of photochemical decomposition of these and other difunctional aldehydes.

IX-C-1. The Photodecomposition of 2-Hydroxyethanal (Hydroxyacetaldehyde, Glycolaldehyde, $HOCH_2CHO$)

The absorption spectrum of 2-hydroxyethanal is shown in figure IX-C-1 as reported by Magneron et al. (2005). It has been pointed out that substitution of the electron-withdrawing —OH group on acetaldehyde results in a shift of the $n \rightarrow \pi^*$ transition to shorter wavelengths, with a substantial decrease in overlap with the solar flux present in the lower troposphere. The cross sections at selected wavelengths are given in tabular form in table IX-C-1.

Bacher et al. (2001) and Magneron et al. (2005) have studied the photodecomposition of 2-hydroxyethanal in air. Bacher et al. (2001) employed 240–400 nm radiation from a filtered xenon lamp. Their data suggested that process (I) is the major photodecomposition mode, analogous to the bond cleavage seen in acetaldehyde photolysis, although some CH_3OH was detected also, presumably via reaction (III).

Table IX-C-1. Absorption cross sections (σ, cm^2 $molecule^{-1}$) for 2-hydroxyethanal at 298 ± 3 K. Data are averages of those of Magneron et al. (2005) and LCSR/CNRS-Orléans as reported by Magneron et al. (2005)

λ, nm	$10^{20} \times \sigma$	λ, nm	$10^{20} \times \sigma$	λ, nm	$10^{20} \times \sigma$
278	6.91	296	4.67	314	1.11
279	6.91	297	4.48	315	0.985
280	6.90	298	4.28	316	0.86
281	6.93	299	4.10	317	0.705
282	6.96	300	3.92	318	0.55
283	6.79	301	3.67	319	0.485
284	6.64	302	3.41	320	0.420
285	6.55	303	3.14	321	0.365
286	6.46	304	2.86	322	0.31
287	6.32	305	2.66	323	0.27
288	6.18	306	2.46	324	0.23
289	6.08	307	2.35	325	0.195
290	5.98	308	2.23	326	0.16
291	5.78	309	1.99	327	0.14
292	5.58	310	1.75	328	0.12
293	5.31	311	1.60	329	0.11
294	5.04	312	1.45	330	0.096
295	4.86	313	1.28		

Magneron et al. (2005) also concluded that process (I) is the major mode of photodecomposition, but they considered three additional thermochemically favorable processes as well, (II), (III), and (IV):

$$HOCH_2CHO + h\nu \rightarrow CH_2OH + HCO \quad \text{(I)}$$

$$\rightarrow OH + CH_2CHO \quad \text{(II)}$$

$$\rightarrow CH_3OH + CO \quad \text{(III)}$$

$$\rightarrow H + HOCH_2CO \quad \text{(IV)}$$

Several observations by Magneron et al. point to the occurrence of the OH-forming channel (II): 1) the difference between the loss rates of 2-hydroxyethanal measured during photolysis with and without cyclohexane (an OH scavenger); and 2) the high loss rate of di-*n*-butyl ether (OH tracer) observed in the EUPHORE chamber. Methanol observed in the products indicated that process (III) occurs. No evidence for process (IV) has been observed. Magneron et al. (2005) concluded that 90% of the photodecomposition occurs in channels (I) and (II) while about 10% occurs in (III).

Bacher et al. (2001) used acetone and acetaldehyde as reference compounds in photolyses within the reaction chamber to estimate the average quantum yield of process (I) in 1 atm. of air: $\phi_I > 0.5$ for $\lambda = 285 \pm 25$ nm. From measured *j*-values in sunlight in the EUPHORE chamber, Magneron et al. (2005) concluded that the effective total quantum yield of photodecomposition was near unity ($\phi = 1.3 \pm 0.3$).

Bacher et al. (2001) pointed out that 2-hydroxyethanal is very soluble in water and that uptake by hydrometeors (liquid or solid water particles, e.g., cloud, rain, fog, snow, etc.) may be an important loss mechanism for this compound in the troposphere. The data of Betterton and Hoffmann (1988) show that 90% of the 2-hydroxyethanal will hydrate in aqueous solution to form $HOCH_2CH(OH)_2$ that does not absorb radiation available in the troposphere.

Estimates of the average photolysis frequency of 2-hydroxyethanal on exposure to sunlight were made by Magneron et al. (2005) using the EUPHORE photochemical chamber during June 19–21, 1998, and June 15–16, 1999; mixtures of 2-hydroxyethanal with OH radical scavengers were exposed in air for periods of 5–7 h. The mean *j*-value for photodecomposition by all pathways was reported as $(1.1 \pm 0.3) \times 10^{-5}\ s^{-1}$.

The photolysis frequencies as a function of solar zenith angle for 2-hydroxyethanal photodecomposition in sunlight within the troposphere were calculated by Calvert et al. (2008) using the average of cross sections reported by Magneron et al. (2005) and LCSR/CNRS Orléans as reported by Magneron et al. (2005). A total photodecomposition quantum yield of unity and actinic flux appropriate for a cloudless day within the lower troposphere (ozone column of 350 DU) were assumed; see figure IX-C-2. These data give an average *j*-value for the date and time period of the measurements at Valencia of about $1.2 \times 10^{-5}\ s^{-1}$, consistent with the average value that was measured directly, $(1.1 \pm 0.3) \times 10^{-5}\ s^{-1}$.

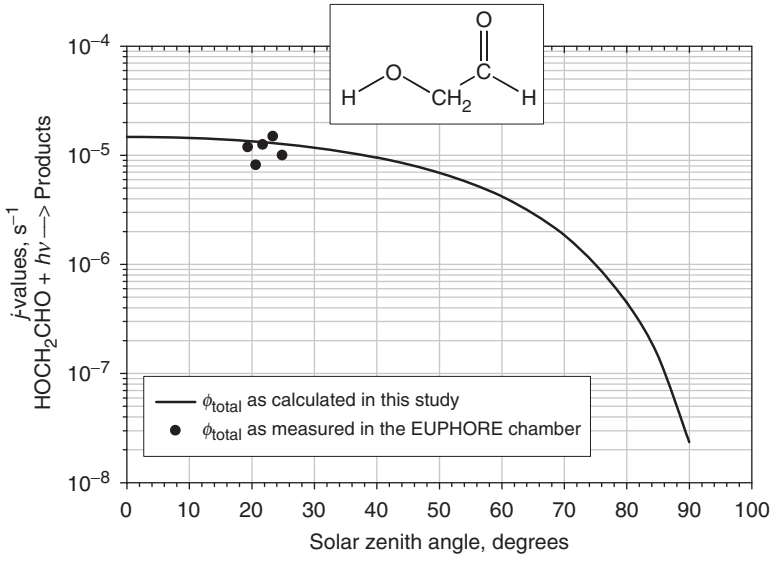

Figure IX-C-2. Photolysis frequencies for $HOCH_2CHO$ as a function of solar zenith angle for a cloudless day within the troposphere with an overhead ozone column of 350 DU (Calvert et al., 2008). The quantum yield of the photodecomposition was assumed to be 1.0, independent of wavelength (Magneron et al., 2005); the EUPHORE data were reported by Magneron et al. (2005).

IX-C-2. The Photodecomposition of oxirane-2-carbaldehyde (glycidaldehyde)

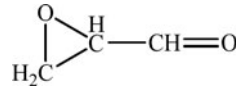

Glycidaldehyde along with other epoxides has been identified by means of GC–MS as products in the OH-radical-initiated degradation of benzene and toluene (Yu et al., 1997). Although the yields were not determined and may not be particularly high, the importance of the epoxides in atmospheric chemistry arises principally from their high toxicity. The chemical nature of the primary processes is undetermined but, by analogy with other aldehydes, the following primary processes might be expected to occur:

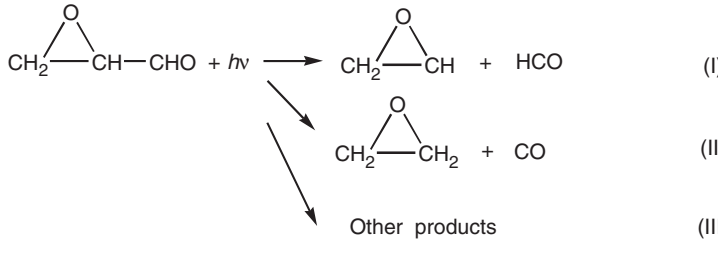

As with acetaldehyde, the dominant mode of photodecomposition in the troposphere may occur by reaction (I) with a rupture of the R—CHO bond.

IX-C-2.1. Absorption Cross Sections for Glycidaldehyde

The cross sections for glycidaldehyde have been determined by Ma et al. (1998). These high-resolution data are shown in figure IX-C-3, and the data (as averaged over each nm) are shown in tabular form in table IX-C-2.

IX-C-2.2. Quantum Yields of Photodecomposition for Glycidaldehyde

The wavelength dependence of the quantum yields of glycidaldehyde photolysis has not been reported. However, some useful information is available (Ma et al., 1998). The rate of glycidaldehyde photodecomposition (disappearance) in synthetic air has been determined in a large photochemical reactor irradiated using 32 fluorescent lamps (Phillips TL05/40W; $\lambda_{max} = 360$ nm) which surrounded the cell. In additional experiments, a large excess of propylene was added to the mixture (as a scavenger for OH radicals); the observed rates of loss of glycidaldehyde were the same with or without the added propylene, so it is likely that artifact OH radical production was unimportant in this system, and that the observed rates of photochemical decay were primarily due to the total rates of the primary photochemical processes. Comparison of rates of photolysis of glycidaldehyde and NO_2 were made in air in separate experiments in the same reactor: j(glycidaldehyde disappearance) $\approx 1.9 \times 10^{-5}\ s^{-1}$; $j(NO_2) \approx 2.7 \times 10^{-3}\ s^{-1}$.

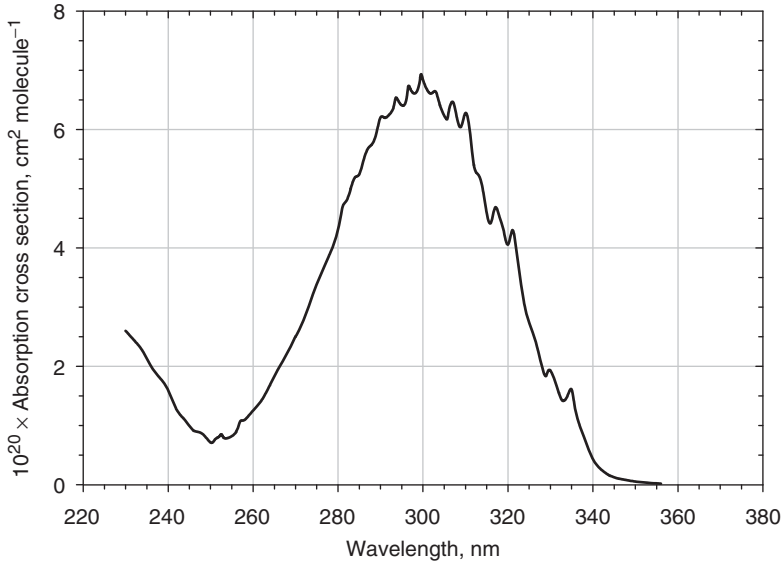

Figure IX-C-3. Wavelength dependence of the absorption cross sections for glycidaldehyde (Ma et al.,1998).

Table IX-C-2. Cross sections for glycidaldehyde (gas); the high resolution data of Ma et al. (1998) were averaged over each nm and centered on the wavelength shown; units for σ are cm^2 $molecule^{-1}$

λ, nm	$10^{20} \times \sigma$	λ, nm	$10^{20} \times \sigma$	λ, nm	$10^{20} \times \sigma$
290	6.08	318	4.64	346	0.11
291	6.08	319	4.43	347	0.085
292	6.24	320	4.11	348	0.069
293	6.41	321	4.15	349	0.060
294	6.40	322	4.21	350	0.054
295	6.43	323	3.63	351	0.049
296	6.56	324	3.18	352	0.044
297	6.71	325	2.90	353	0.044
298	6.63	326	2.65	354	0.033
299	6.67	327	2.37	355	0.026
300	6.88	328	2.04	356	0.020
301	6.78	329	1.86	357	0.015
302	6.62	330	1.92	358	0.009
303	6.62	331	1.81	359	0.006
304	6.48	332	1.64	360	0.007
305	6.26	333	1.46	361	0.013
306	6.26	334	1.50	362	0.020
307	6.45	335	1.56	363	0.023
308	6.30	336	1.21	364	0.025
309	6.08	337	0.96	365	0.023
310	6.19	338	0.79	366	0.021
311	6.14	339	0.62	367	0.020
312	5.65	340	0.45	368	0.018
313	5.38	341	0.36	369	0.018
314	5.24	342	0.28	370	0.020
315	4.94	343	0.21	371	0.026
316	4.55	344	0.16	372	0.031
317	4.51	345	0.13	373	0.036

Although the action spectra of these two compounds are quite different, these data and an assumed atmospheric $j(NO_2) \approx 8.5 \times 10^{-3}\ s^{-1}$ for noon at 40°N, were used to estimate for tropospheric conditions j(glycidaldehyde) $\approx 6.0 \times 10^{-5}\ s^{-1}$. By comparison of this value with that calculated from the observed cross sections and a total quantum yield of decomposition of unity, Ma et al. (1998) estimated that the effective average quantum yield of photodecomposition was approximately 0.6.

IX-C-2.3. Photolysis Frequencies for the Photodecomposition of Glycidaldehyde in the Lower Troposphere

Photolysis rate coefficients for glycidaldehyde which are representative of a cloudless, lower atmosphere were calculated using the measured σ values, the estimated value of $\phi_I + \phi_{II} + \phi_{III} = 0.6$, assumed to be independent of wavelength, and an ozone column of 350 DU. See figure IX-C-4.

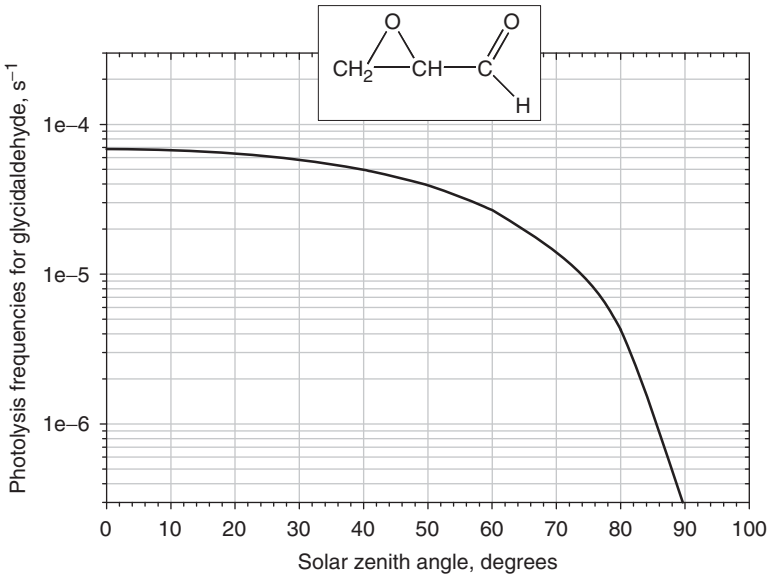

Figure IX-C-4. Approximate glycidaldehyde photodissociation coefficients as a function of solar zenith angle as calculate for a cloudless, lower troposphere and an ozone column of 350 DU. A total quantum yield of decomposition of 0.6, independent of wavelength, was assumed in the calculations as estimated by Ma et al. (1998).

IX-C-3. The Photodecomposition of Propenal [Acrolein, $CH_2{=}CHC(O)H$)]

Previous studies of the photodecomposition of acrolein (Coomber and Pitts, 1969; Ulmstead et al., 1978; Shinohara and Nishi, 1982; Fujimoto et al., 1985; Gardner et al., 1987; Haas et al., 1991; Fahr et al., 1993; Reguero et al., 1994, Magneron, 1998; Magneron et al. 2002) suggest that a number of photodecomposition modes are operative, although the extent of each for tropospheric conditions remains uncertain. Several interesting new features in the acrolein photochemistry have been reported since the review of Calvert et al. (2002), and these will be discussed in this section. The experimental conditions (25°C, low pressures of acrolein in air) employed in the study of Gardner et al. (1987) are most representative of those of the troposphere, but most of their experiments were carried out at only one wavelength of light (313 nm). They concluded that the primary photodissociation could be described reasonably well through the occurrence of the primary processes (I–IV) which involve both the first excited singlet and triplet:

$$CH_3CH{=}CHO + h\nu \rightarrow CH_2{=}CH_2 + CO \quad \text{(I)}$$

$$\rightarrow CH_2{=}CH + CHO \quad \text{(II)}$$

$$\rightarrow CH_3CH + CO \quad \text{(III)}$$

$$\rightarrow CH_2{=}CHCO + H \quad \text{(IV)}$$

The acrolein molecule excited by 313 nm light at 25°C will have about 398 kJ mole^{-1} mean total internal energy (382 from the light quantum, 8.0 translational, 8.0 rotational, and 6.7 vibrational). The enthalpy change which is associated with the ground state acrolein molecule undergoing processes I through IV can be estimated (± 20 kJ mole^{-1}) to be: 17, 414, 347 (if the product ethylidene diradical, CH_3CH, is in the singlet state), or 305 (if CH_3CH is in the triplet state in the initial fragment), and 364 kcal mole^{-1}, respectively. Gardner et al. (1987) concluded from their experiments at 313 nm and low pressures of air, that the T_1 state appears to be the major source of the reaction channels. For photolyses in 1 atm. of air, quenching of the excited molecules in the T_1 state becomes important, and they suggest that about 60% of the decomposition occurs from the S_1 state under these conditions. In 1 atm. of air the quantum yield for decomposition of acrolein is very small (∼0.0065 at 313 nm).

IX-C-3.1. Absorption Cross Sections for Propenal

Cross section data reported by Magneron et al (2002) are given in figure IX-C-5 where they are compared with those of several structurally related aldehydes. The similarity in the spectra of four of the compounds shown reflects their common chromophore: R—C(=O)—CR′=CH_2, where R and R′ are alkyl groups or H-atoms. When an additional conjugated alkene group is introduced in the

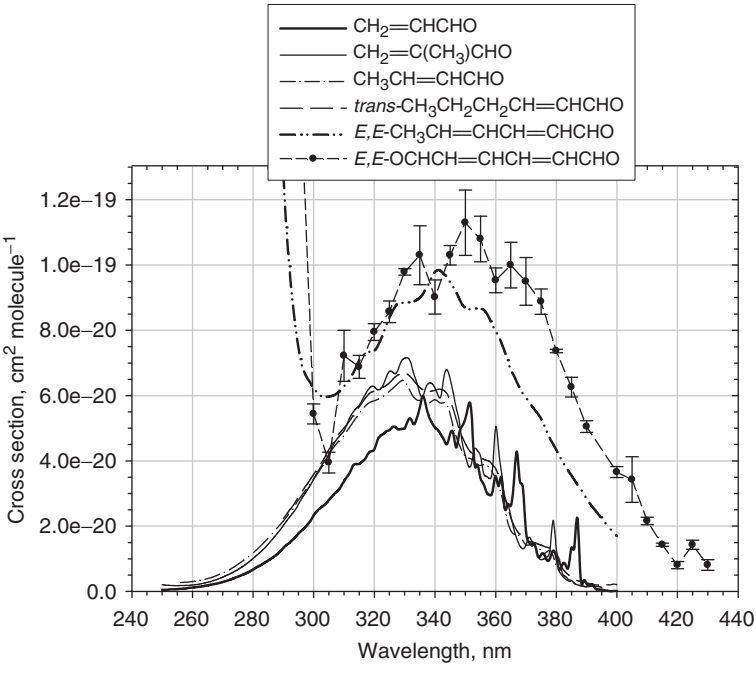

Figure IX-C-5. Comparison of the absorption spectra of acrolein (Magneron et al., 2002), methacrolein (Gierczak et al., 1997), crotonaldehyde (Magneron et al., 2002), *E*-2-hexenal, and *E*,*E*-2,4-hexadienal (O'Connor et al., 2006).

E,*E*-2,4-hexadienal molecule, the cross section is noticeable increased. A further increase in the cross section is noted for *E*,*E*-2,4-hexadiendial in which 4-conjugated double bonds are present [O=C(H)—CH=C—CH=CH—CH=O] and absorption extends to longer wavelengths. Evidence for the onset of a new, very strong absorption bands ($\pi \rightarrow \pi^*$ transitions) at wavelength below 300 nm can be seen for both the dienals shown in the figure. The cross sections of acrolein as a function of wavelength as reported by Magneron (1998) are tabulated in table IX-C-3; these are similar to those reported by Magneron et al. (2002).

Table IX-C-3. Absorption cross sections (σ) (Magneron, 1998) and approximate quantum yields for the photodecomposition of acrolein (ϕ_{total}) in air at 1 atm. as estimated from very limited data; see text. Units for σ are cm^2 $molecule^{-1}$

λ, nm	$10^{20} \times \sigma$	ϕ_{total}	λ, nm	$10^{20} \times \sigma$	ϕ_{total}	λ, nm	$10^{20} \times \sigma$	ϕ_{total}	λ, nm	$10^{20} \times \sigma$	ϕ_{total}
250	0.049		287	1.080	0.0095	324	4.91	0.0052	361	3.23	0.0010
251	0.052		288	1.151	0.0094	325	4.94	0.0051	362	3.50	0.0009
252	0.057		289	1.24	0.0092	326	5.04	0.0050	363	2.54	0.0008
253	0.069		290	1.34	0.0091	327	5.03	0.0049	364	2.68	0.0007
254	0.070		291	1.42	0.0090	328	4.96	0.0048	365	2.62	0.0006
255	0.074		292	1.49	0.0089	329	4.98	0.0047	366	3.31	0.0004
256	0.080		293	1.58	0.0088	330	5.00	0.0046	367	4.29	0.0003
257	0.086		294	1.67	0.0087	331	5.21	0.0045	368	3.39	0.0002
258	0.095		295	1.78	0.0085	332	5.30	0.0043	369	3.19	0.0001
259	0.108		296	1.87	0.0084	333	5.12	0.0042	370	1.86	0.0000
260	0.115		297	1.95	0.0083	334	5.30	0.0041	371	1.51	
261	0.126		298	2.05	0.0082	335	5.63	0.0040	372	1.41	
262	0.138		299	2.17	0.0081	336	5.99	0.0039	373	1.41	
263	0.150		300	2.33	0.0080	337	5.71	0.0038	374	1.06	
264	0.166		301	2.45	0.0079	338	5.38	0.0036	375	1.14	
265	0.182		302	2.54	0.0078	339	5.18	0.0035	376	1.14	
266	0.202		303	2.61	0.0077	340	5.03	0.0034	377	0.95	
267	0.220		304	2.68	0.0075	341	4.95	0.0033	378	1.04	
268	0.239		305	2.80	0.0074	342	4.81	0.0032	379	1.25	
269	0.262		306	2.90	0.0073	343	4.65	0.0031	380	1.04	
270	0.287		307	3.01	0.0072	344	4.52	0.0030	381	0.66	
271	0.315		308	3.09	0.0071	345	4.82	0.0028	382	0.82	
272	0.344		309	3.22	0.0070	346	4.86	0.0027	383	0.83	
273	0.377		310	3.39	0.0069	347	4.41	0.0026	384	0.73	
274	0.415		311	3.52	0.0067	348	4.85	0.0025	385	1.35	
275	0.451		312	3.67	0.0066	349	5.08	0.0024	386	1.36	
276	0.488		313	3.86	0.0065	350	5.31	0.0023	387	2.25	
277	0.526		314	3.90	0.0064	351	5.70	0.0022	388	0.44	
278	0.568	0.0105	315	3.91	0.0063	352	5.53	0.0020	389	0.34	
279	0.615	0.0104	316	3.99	0.0062	353	3.94	0.0019	390	0.23	
280	0.672	0.0103	317	4.07	0.0061	354	3.88	0.0018	391	0.20	
281	0.727	0.0102	318	4.24	0.0059	355	3.47	0.0017	392	0.21	
282	0.781	0.0101	319	4.30	0.0058	356	3.30	0.0016	393	0.08	
283	0.837	0.0099	320	4.36	0.0057	357	3.04	0.0015	394	0.06	
284	0.898	0.0098	321	4.64	0.0056	358	2.95	0.0014	395	0.06	
285	0.954	0.0097	322	4.77	0.0055	359	3.06	0.0012	396	0.04	
286	1.014	0.0096	323	4.82	0.0054	360	3.54	0.0011	397	0.02	
									398	0.01	

IX-C-3.2. Quantum Yields of the Primary Photodecomposition Processes in Propenal

Detailed information on the quantum yields of primary processes in acrolein were derived by Gardner et al. (1987) from photolyses at 24 ± 2°C and 313 nm; this work was reviewed by Calvert et al. (2002). The estimated quantum yields of three of the major primary processes show a dependence on the pressure of the synthetic air added; process (I) is not quenched significantly by air at 1 atm.; see figure IX-C-6.

The fractions of the photodecomposition of acrolein which are estimated to occur by the various primary photochemical processes as a function of air concentration are summarized in figure IX-C-7 (Gardner et al., 1987).

For the range of $2.58 \times 10^{19} > [M] > 0.082 \times 10^{19}$ the data for the quantum yield of acrolein loss at 313 nm and 24 ± 2°C is represented reasonably well by the fit of a second-order least-squares equation to the data in figure IX-C-8:

$$1/(\phi_{\text{decomp}}) = -0.836 + 1.159 \times 10^{-17}[M] - 2.166 \times 10^{-37}[M]^2$$

where $[M]$ is the concentration of air molecules in molecules cm^{-3}. This relation gives $\phi_{\text{decomp}} = 0.0065$ at 1 atm. pressure for excitation at 313 nm.

The limited data from photolyses at 334 nm (open circles in figure IX-C-8) show a somewhat stronger dependence on pressure of added air than the results at 313 nm (triangles in figure VII-C-8), but they are too limited to derive an accurate relationship between $[M]$ and ϕ. However, if one assumes that a Stern–Volmer relation is followed

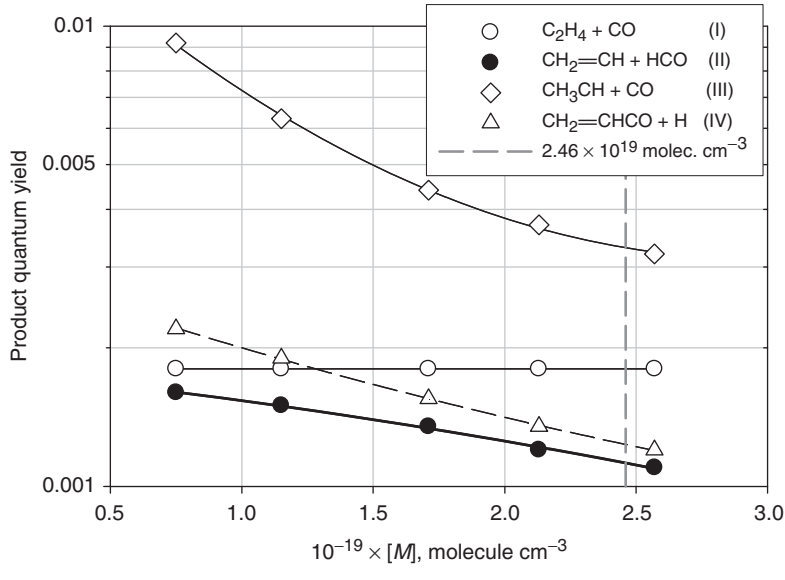

Figure IX-C-6. Estimated quantum yields for the photodecomposition modes of acrolein at about 25°C as a function of the concentration of air $[M]$ (Gardner et al., 1987). The gray-dashed line marks the concentration of air at 1 atm. pressure and 298 K.

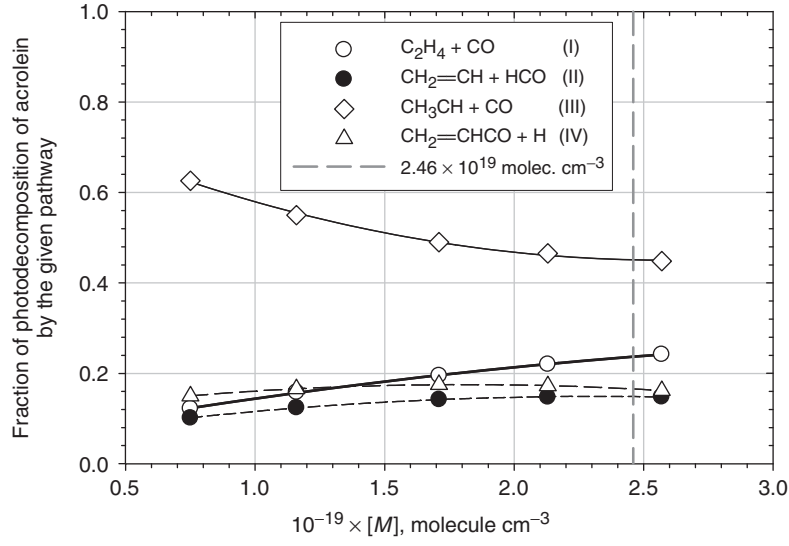

Figure IX-C-7. The fraction of the photodecomposition of acrolein that is estimated to occur by the various primary photodecomposition modes; data of Gardner et al. (1987) from the photolysis studies at 313 nm and 25°C. The gray-dashed line marks the concentration of air at 1 atm. pressure and 298 K.

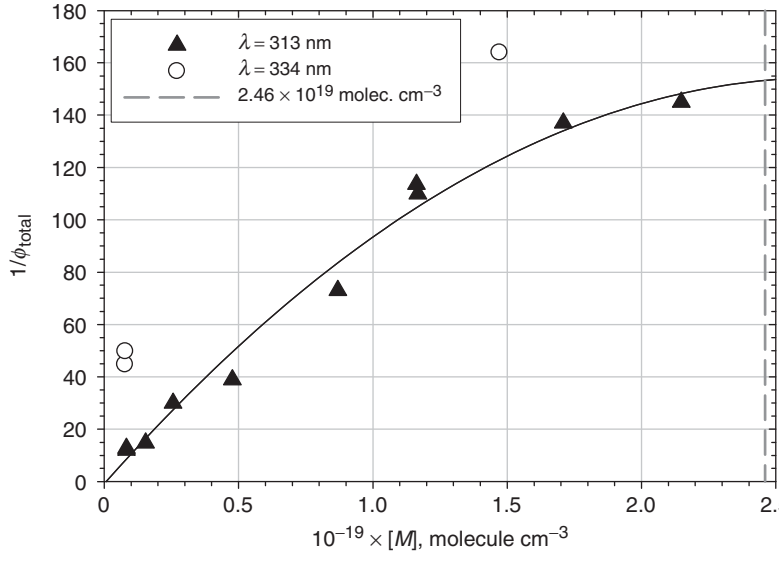

Figure IX-C-8. Stern–Volmer plots of the $1/\phi_{decomp}$ versus $[M]$ data for acrolein vapor for excitation at 313 and 334 nm (Gardner et al., 1987) where $[M]$ = concentration of the synthetic air mixture. The gray-dashed line marks the concentration of air at 1 atm. pressure and 298 K.

at 334 nm and extrapolates the limited 334 nm data to 1 atm. of air, a value of $\phi_{\text{total}} = 0.0041$ is estimated.

IX-C-3.3. Photolysis Frequencies for Primary Photodecompostion Processes in Propenal in the Lower Troposphere

In their calculation of *j*-values for acrolein, Calvert et al. (2002) assumed the quantum yield of photodecomposition as measured at 313 nm, 0.0065, was independent of wavelength; the *j* for overhead Sun ($4.5 \times 10^{-6}\,s^{-1}$) was given as an upper limit. In view of the lower quantum yields observed at 334 nm by Gardner et al. (1987), a somewhat more realistic estimate of *j* can be made assuming the ϕ_{total} decreases linearly with increasing λ, as defined by a line joining the data points from experiments at 313 and 334 nm in figure IX-C-8. Estimates of ϕ_{total} derived in this fashion are given in table IX-C-3. Photolysis rate coefficients for acrolein which are representative of the lower atmosphere were then calculated using the measured σ and extrapolated ϕ data, assuming a clear sky and an overhead ozone column of 350 DU. See figure IX-C-9. Magneron et al. (1999) determined an apparent *j*-value for acrolein photodecomposition in the European outdoor photolysis chamber in Valencia to be $< 2 \times 10^{-6}\,s^{-1}$ (solar zenith angle of 22°). From two measurements in the EUPHORE chamber (solar zenith angles not given), Magneron et al. (2002) reported *j*-values $\leq 2 \times 10^{-6}\,s^{-1}$. These data are consistent with the calculated *j*-values presented in figure IX-C-9. Obviously acrolein photodecomposition in the troposphere is an inefficient process.

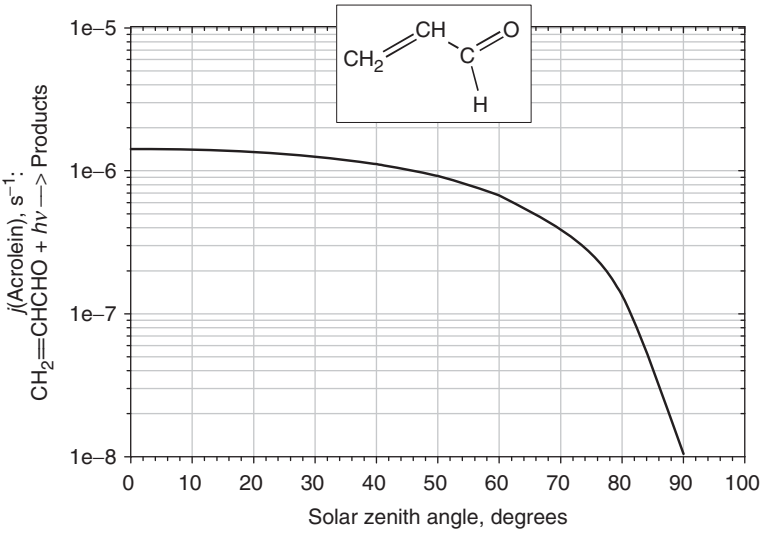

Figure IX-C-9. Estimated acrolein photodissociation coefficients [*j*(Total)] as a function of solar zenith angle. The cross sections and quantum yield estimates used in the calculation are as described in the text. The calculation was made for a cloudless sky, 0.5 km elevation, and a vertical ozone column of 350 DU.

IX-C-4. The Photodecomposition of Methacrolein [2-Methylpropenal, $CH_2{=}C(CH_3)C(O)H$]

The photodecomposition of methacrolein has been studied by several groups: Johnstone and Sodeau (1992), Raber and Moortgat (1996), and Gierczak et al. (1997). The primary pathways for photodissociation of methacrolein are uncertain, but processes analogous to those for acrolein (I) through (IV) should be considered in addition to process (V) which was suggested from the studies of methacrolein in air by Raber and Moortgat (1996):

$$CH_2{=}C(CH_3)C(=O)H + h\nu \rightarrow CH_2{=}CHCH_3 + CO \quad \text{(I)}$$

$$\rightarrow CH_2{=}CCH_3 + CHO \quad \text{(II)}$$

$$\rightarrow CH_3CCH_3(\text{diradical}) + CO \quad \text{(III)}$$

$$\rightarrow CH_2{=}C(CH_3)CO + H \quad \text{(IV)}$$

$$\rightarrow (CH_3)_2C{=}C{=}O \quad \text{(V)}$$

Gierczak et al. (1997) observed methane, ethylene, acetylene, allene, and propyne as major products; formaldehyde, methanol, formic acid, acetic acid, and hydroxyacetone were identified as minor products. The mechanism of formation of these products is unclear. Two expected products, observed by Raber and Moortgat (1996), propene and dimethylketene, were not observed, and CO and CO_2 products observed by Raber and Moortgat, were not measured by Gierczak et al. (1997). In argon matrix-isolated studies of methacrolein photochemistry (4.2 K) and with $\lambda > 300$ nm, Johnstone and Sodeau (1992) observed the isomerization of the original *trans*-methacrolein to *cis*-methacrolein; no HCO, CO, or propene could be detected. In similar matrix experiments at $\lambda > 230$ nm, dimethylketene, CO, and propene were observed together with other unidentified products.

IX-C-4.1. Absorption Cross Sections for Methacrolein

Cross sections for methacrolein determined by Meller (given in Röth et al., 1997) and Gierczak et al. (1997) are in reasonable agreement. The data of Gierczak et al. are presented in figure IX-C-5, where they can be compared with those of the similar compounds. It is obvious that the nature of the electronic transitions involved in the three simplest molecules shown are very similar as anticipated from the nature of the chromophore, which is common to all, $CH_2{=}C(R')C(=O)R$. The cross sections for methacrolein are summarized in table IX-C-4 (Gierczak et al., 1997).

IX-C-4.2. Quantum Yields of Photodecomposition of Methacrolein

Limited data on the products and quantum yields are available today. Some apparent overall quantum yields for photodecomposition have been reported (Raber and Moortgat, 1996) using radiation from TL/12-sunlamps (Philips, 40W). These lamps

Table IX-C-4. Methacrolein absorption cross sections (Gierczak et al., 1997) and estimated total quantum yields of photodecomposition (ϕ_{total}) at 1 atm.; units for σ are cm^2 $molecule^{-1}$

λ, nm	$10^{20} \times \sigma$	ϕ_{total}	λ, nm	$10^{20} \times \sigma$	ϕ_{total}	λ, nm	$10^{20} \times \sigma$	ϕ_{total}	λ, nm	$10^{20} \times \sigma$	ϕ_{total}
250	0.21		287	1.67	0.0365	324	6.58	0.0197	361	4.28	0.0030
251	0.19		288	1.79	0.0361	325	6.74	0.0194	362	3.61	0.0025
252	0.19		289	1.90	0.0356	326	6.73	0.0188	363	2.86	0.0021
253	0.18		290	2.03	0.0352	327	6.68	0.0184	364	2.68	0.0016
254	0.18		291	2.16	0.0347	328	6.83	0.0179	365	2.33	0.0012
255	0.18		292	2.28	0.0343	329	7.07	0.0175	366	1.92	0.0007
256	0.18		293	2.40	0.0338	330	7.15	0.0170	367	1.62	0.0003
257	0.18		294	2.52	0.0333	331	7.16	0.0166	368	1.40	0
258	0.19		295	2.68	0.0329	332	7.03	0.0161	369	1.31	
259	0.19		296	2.85	0.0325	333	6.69	0.0157	370	1.42	
260	0.20		297	2.99	0.0320	334	6.41	0.0153	371	1.67	
261	0.21		298	3.13	0.0315	335	6.08	0.0147	372	1.53	
262	0.22		299	3.26	0.0311	336	5.97	0.0143	373	1.43	
263	0.24		300	3.44	0.0306	337	6.25	0.0139	374	1.08	
264	0.26		301	3.61	0.0302	338	6.38	0.0135	375	0.98	
265	0.28		302	3.76	0.0297	339	6.37	0.0130	376	1.00	
266	0.30		303	3.91	0.0293	340	6.24	0.0125	377	1.07	
267	0.33		304	4.04	0.0288	341	6.02	0.0120	378	1.35	
268	0.36		305	4.19	0.0284	342	5.98	0.0116	379	2.18	
269	0.40		306	4.40	0.0279	343	6.58	0.0112	380	1.30	
270	0.44		307	4.58	0.0274	344	6.79	0.0107	381	0.98	
271	0.48		308	4.71	0.0268	345	6.53	0.0103	382	0.56	
272	0.52		309	4.81	0.0265	346	6.11	0.0098	383	0.46	
273	0.57		310	4.92	0.0261	347	5.63	0.0094	384	0.36	
274	0.62		311	5.13	0.0256	348	5.22	0.0088	385	0.33	
275	0.67		312	5.35	0.0252	349	4.55	0.0084	386	0.25	
276	0.73		313	5.50	0.0247	350	4.16	0.0080	387	0.21	
277	0.79		314	5.61	0.0243	351	3.85	0.0075	388	0.18	
278	0.86		315	5.70	0.0238	352	3.89	0.0071	389	0.16	
279	0.94	0.0401	316	5.87	0.0235	353	4.35	0.0065	390	0.15	
280	1.01	0.0397	317	6.04	0.0229	354	4.31	0.0062	391	0.16	
281	1.09	0.0393	318	6.19	0.0225	355	4.14	0.0057	392	0.16	
282	1.18	0.0388	319	6.28	0.0220	356	3.62	0.0053	393	0.15	
283	1.26	0.0383	320	6.27	0.0216	357	3.53	0.0048	394	0.15	
284	1.35	0.0379	321	6.18	0.0211	358	3.46	0.0044	395	0.12	
285	1.45	0.0375	322	6.21	0.0206	359	3.81	0.0039	396		
286	1.56	0.0370	323	6.34	0.0203	360	5.05	0.0035	397		

emit in a broad continuum from 270 to 380 nm with a peak near 300 nm which is superimposed on spikes near the two strong mercury lines at 313 and 366 nm. The reported effective quantum yields (estimated using chlorine actinometry) vary from 0.03 to 0.08 and show no significant trend with pressure from 50 to 760 Torr of added air. The results of Raber and Moortgat (1996) are somewhat surprising in that the analogous compound acrolein shows smaller *j*-values and a strong dependence on the pressure of the air. Since the molecule of methacrolein contains more atoms, one might expect its lifetime to be somewhat longer than that of acrolein, its chance for quenching by air to be greater, and its *j*-values smaller.

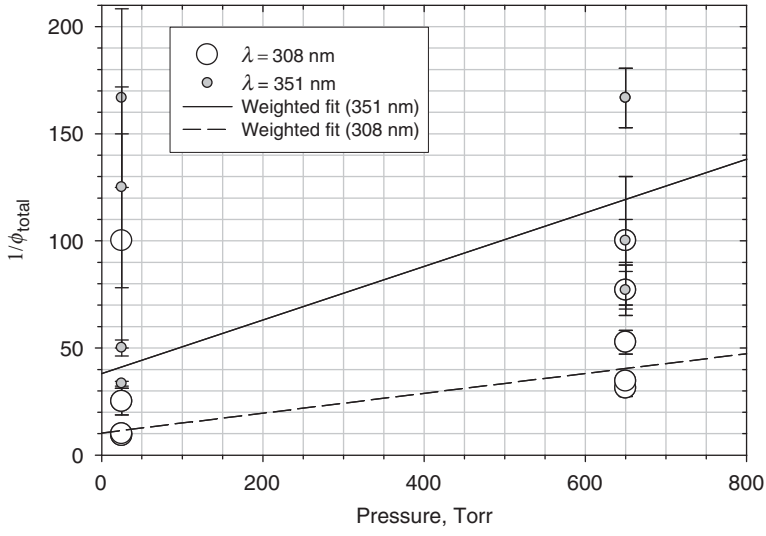

Figure IX-C-10. Stern–Volmer plot of $1/\phi_{total}$ from methacrolein versus oxygen pressure (data of Gierczak et al., 1997). The error bars represent one standard deviation. The weighted average (inverse of the standard deviation) was used to establish the lines drawn for the two wavelengths.

Gierczak et al. (1997) reported quantum yields for methacrolein photodecomposition at two wavelengths (308 and 351 nm) and two pressures of added oxygen (25 and 650 Torr). A Stern–Volmer plot of these data is given in figure IX-C-10. The error bars shown are presented here as $\pm 1\sigma$ to allow a reasonable scale in the plot ($\pm 2\sigma$ are given by Gierczak et al., 1997). The data are rather scattered, and the authors concluded there was no observable trend with varied wavelength or pressure of added oxygen. However, if averages of the measurements at a given wavelength and pressure are used (weighted by the inverse of the standard deviations), and a Stern–Volmer behavior is assumed, one can derive approximate values for ϕ_{total} at 760 Torr of oxygen: 0.0075 at 351 nm and 0.027 at 308 nm. We have used these two estimates and an assumed linear dependence of ϕ_{total} with wavelength to derive estimates at each wavelength given in table IX-C-4. These are very rough estimates, but their use in calculating the *j*-values is probably more realistic than the assumptions of ϕ_{total} independent of λ and pressure of air.

IX-C-4.3. Photolysis Frequencies of the Photodecomposition of Methacrolein in the Lower Troposphere

Photolysis rate coefficients representative of a cloudless lower troposphere were calculated using the measured cross sections and the approximate ϕ_{total} data for for methacrolein given in table IX-C-4. These data are shown in figure IX-C-11. Measurements in the EUPHORE chamber were derived from the small difference between two similar numbers, the disappearance rate of methacrolein and the dilution rate

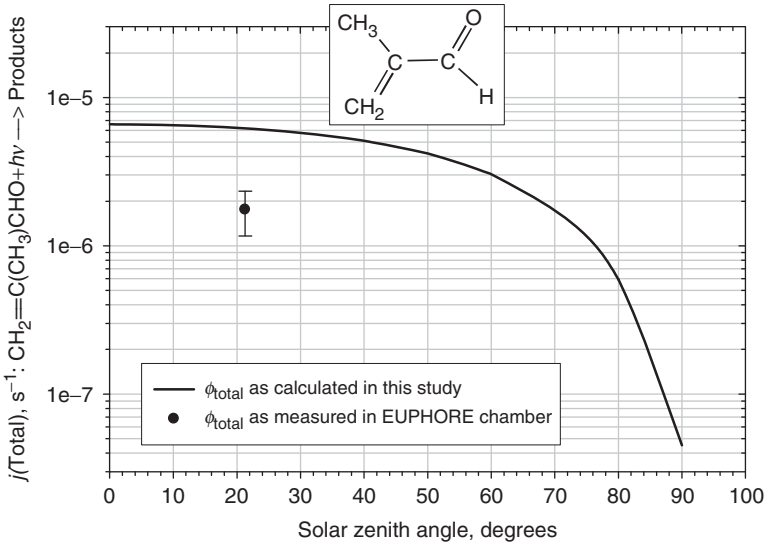

Figure IX-C-11. Estimated methacrolein photodissociation coefficients at 0.5 km altitude as a function of solar zenith angle, calculated using the measured σ values and the approximate methacrolein quantum yield estimates given in table IX-C-4. The solid curve represents the total *j*(photodecomposition). The single data point (filled circle) is a measurement from EUPHORE chamber studies (Moortgat et al., 2002); the error bars shown are assigned arbitrarily by the present authors to indicate an unidentified yet significant uncertainty in the measurement.

in the chamber (Moortgat et al., 2002): $j(\text{Total}) \approx 9.84 \times 10^{-6} - 8.09 \times 10^{-6} = 1.75 \times 10^{-6}\,\text{s}^{-1}$ at a solar zenith angle of 21.3°, about one-third of the value for *j*(Total) calculated in this study. Although the uncertainty in all of the results presented here is high, it is clear that, as with acrolein, methacrolein photodecomposition within the troposphere is very slow.

IX-C-5. The Photodecomposion of Crotonaldehyde [2-Butenal, $CH_3CH{=}CHC(O)H$]

Cross sections for *trans*-crotonaldehyde are shown as a function of wavelength in figure IX-C-5 (Magneron et al., 2002) where they can be compared to those of other similar alkenals. Pioneering studies of the photodecomposition of crotonaldehyde (Blacet and Roof, 1936b; Blacet and LuValle, 1939; Blacet and Volman, 1939) reported the photochemical stability of the molecule at ambient temperatures. Only at temperatures in the range 150–265°C and using wavelengths $\lambda < 313$ nm, was a significant quantum yield of CO observed. Harrison and Lossing (1959) used $Hg(^3P_1)$ to photosensitize the decomposion of crotonaldehyde and identified CO and propene as major products and propenyl radicals as a minor product. Allen and Pitts (1969) reported that CO, propylene, hydrogen, and methane were observable products. In photolyses at $\lambda > 255$ nm and temperatures between 70 and 130°C, Coomber and Pitts (1969)

observed CO and propylene as major products with small amounts of C_2H_4, allene, methhylacetylene, cyclopropane, ethylketene, and *enol*-crotonaldehyde. As with the analogous compound acrolein, effective quenching of the decomposition of the excited molecules was observed as the pressure of gas was increased (Allen and Pitts, 1969). In experiments at $\sim$ 30°C and with radiation in the range 245–400 nm, McDowell and Sipniades (1962) observed 3-butenal as a product with a quantum yield of about 0.1 as well as 1,5-hexadiene which was thought to arise from the photolysis of 2-butenal followed by association of $CH_2{=}CH{-}CH_2$ radicals produced therein. In more recent studies of crotonaldehyde in air, Magneron et al. (2002) considered the photodecomposition channels (I)–(IV), analogous to those suggested in explanation of acrolein photodecomposition. However, no products that would be expected from these reactions could be detected. A fifth process involving formation of an isomer (probably *cis*-crotonaldehyde or *enol*-crotonalehyde) was invoked to rationalize their results:

$$\textit{trans}\text{-}CH_3CH{=}CHC(O)H + h\nu \rightarrow CH_3CH{=}CH + HCO \quad \text{(I)}$$

$$\rightarrow CH_3CH{=}CH_2 + CO \quad \text{(II)}$$

$$\rightarrow CH_3 + CH{=}CHCHO \quad \text{(III)}$$

$$\rightarrow CH_3CH{=}CHCO + H \quad \text{(IV)}$$

$$\rightarrow \textit{cis}\text{-}CH_3CH{=}CHC(O)H \text{ or } CH_2{=}CHCH{=}CH(OH)? \quad \text{(V)}$$

No studies have been made of the wavelength dependence of the quantum yields, but useful information was obtained from the photolysis of crotonaldehyde in sunlight in the EUPHORE chamber; the average of two experiments with solar zenith angle of 21.5° gave $j(\text{Total}) = (1.2 \pm 0.2) \times 10^{-5}\,s^{-1}$ for removal of *trans*-crotonaldehyde (Moortgat et al., 2002). Thus, it appears that the sunlight photolysis of *trans*-crotonaldehyde is about 10 times more efficient than that seen with acrolein (figure IX-C-9). Products observed were: acrolein, CH_2O, CH_3CHO, CHOCHO, and H_2O_2. Presumably, acrolein could be formed following the occurrence of (V) and photolysis of the *cis*-$CH_2{=}CHCH_2CHO$ isomer, provided it is formed in process (V). Obviously, the mechanism of photodecomposition, particularly for photodecomposition in air at 1 atm., remains obscure. However, all the alkenal molecules considered here have small *j*-values, and photodecomposition can be considered as unimportant compared to reactions with OH radical.

The photodecomposition of crontonaldehyde at short wavelengths (193 nm) and low pressures does occur efficiently as observed by Shu et al. (2004). Using photofragment translational spectroscopy, they identified the occurrence of processes (II), (III), and (IV), and a fourth channel [possibly (I)], forming a mass 29 (either HCO or C_2H_5). The average kinetic energy distributions in the products of (II), (III), and (IV) were estimated to be: 43, 23, and 42 kJ mol^{-1}, respectively.

IX-C-6. The Photodecomposition of *trans*-2-Hexenal (*E*-2-Hexenal) and *cis*-2-Hexenal (*Z*-2-Hexenal)

The cross sections for *trans*-2-hexenal as a function of wavelength, shown in figure IX-C-5, are seen to be very similar to those observed with other alkenals shown. Sunlight photolysis of *trans*-2-hexenal in the EUPHORE chamber (10:08–15:35 on March 17, 1999, somewhat cloudy) led to a fast photoisomerization and a slow loss of both isomers (Moortgat et al., 2002). In liquid-phase photolysis, *cis*-2-hexenal was the major product formed. The decay of both isomers in the chamber data could be explained using a photostationary state between isomers with a steady decay of both isomers according to the following mechanism:

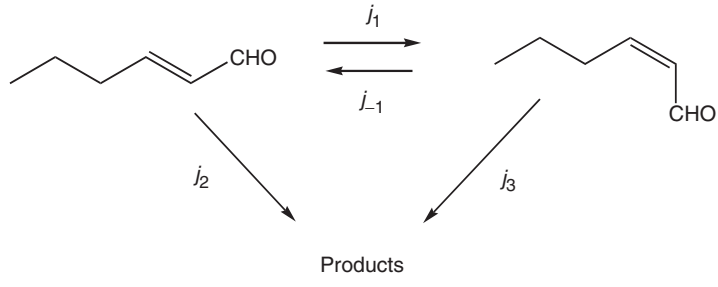

A simulation of the chemistry involved here described the observations well using the following first-order rate coefficients: $j_1 = 1.45 \times 10^{-4}\,s^{-1}$; $j_{-1} = 2.38 \times 10^{-4}\,s^{-1}$; $j_2 = 2.8 \times 10^{-5}\,s^{-1}$; $j_3 = 2.5 \times 10^{-5}\,s^{-1}$. *cis*-2-Hexenal was the major product of photolysis of *trans*-2-hexenal but methanal, ethanal, and butanal were observed as well.

In earlier experiments in the EUPHORE chamber during the month of November 2004, (O'Connor et al., 2006), exposures of *trans*-2-hexenal (*E*-2-hexenal) to midday Sun were carried out for periods of more than 3 h. Again, the major product of the photolysis was shown to be the isomer, *cis*-2-hexenal (*Z*-2-hexenal), which forms with an estimated molar yield near unity (1.03 ± 0.04). From two experiments, the average *j*-values for the forward reaction and reverse reaction shown above were estimated to be: $j_1 = 1.02 \times 10^{-4}\,s^{-1}$ and $j_{-1} = 1.59 \times 10^{-4}\,s^{-1}$, respectively. No products of photodissociation were reported. The two EUPHORE studies agree well, and one must conclude that the photodecomposition of *trans*-2-hexenal in sunlight, like that of the other alkenals, is slow, but it may be a loss process competitive with that of OH-attack in the troposphere.

IX-C-7. The Photodecomposition of *E*,*E*-2,4-Hexadienal

E,*E*-2,4-Hexadienal absorbs sunlight strongly; the absorption band is shown in figure IX-C-5 where it can be compared with the absorption of simpler alkenals. The photochemistry of this compound in air at 1 atm. has been reported by O'Connor et al. (2006). *E*,*E*-2,4-hexadienal undergoes a rapid isomerization to produce a substituted

ketene of the same chemical composition as the starting compound:

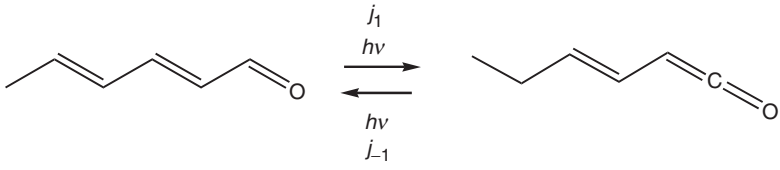

The reaction is reversible and an average of three experiments made in November, 2004 give: $j_1 = (1.45 \pm 0.14) \times 10^{-4}\,s^{-1}$ and $j_{-1} = (3.26 \pm 0.34) \times 10^{-4}\,s^{-1}$. At the time of these experiments the average $j(NO_2)$ value was $5.6 \times 10^{-3}\,s^{-1}$. The molar yield of the product *E*-hexa-1,3-diene-1-one was found to be 1.03 ± 0.11. It is probable that processes other than photodecomposition (such as reaction with OH and O_3) dominate the loss mechanisms for this compound.

IX-C-8. The Photolysis of Butenedial [HC(O)CH=CHCH(O)]

The preparation of pure samples of butenedial is very difficult, and an unambiguous absorption spectrum of the compound is lacking at this writing. The two spectra of which we are aware were determined in solution and show few similarities (Hufford et al., 1952; Liu, 1999; Liu et al., 1999; see Calvert et al., 2002). Hufford et al. report two absorption bands: a relatively weak band ($n \rightarrow \pi^*$, $\sigma_{max} \approx 1.2 \times 10^{-19}$ given in text, but the plotted data give $\sigma_{max} \approx 6.93 \times 10^{-20}$ cm^2 molecule^{-1}) and a strong band ($\pi \rightarrow \pi^*$, $\sigma_{max} \approx 2.8 \times 10^{-17}$ cm^2 molecule^{-1} at 225 nm). A reproduction of the spectra reported by Hufford et al. (1952) is given in figure IX-C-12; these data are approximate since they were redrawn from the authors' published figure with a transformation of the authors' units of $\log_{10}(\varepsilon$, L mol^{-1} cm^{-1}). Obviously, there is a large uncertainty in the cross section data based on our reconstruction of the Hufford et al. data that we use in this work. The tabular cross sections derived from Hufford et al. spectral curves are given in table IX-C-5.

In previous studies, Bierbach et al. (1994), Sørensen and Barnes (1998), Liu (1999), Liu et al. (1999), and Tang and Zhu (2005) considered several potential pathways for photodecomposition of butenedial:

$$\textit{trans/cis}\text{-HC(O)CH=CHCH(O)} + h\nu \rightarrow \textit{cis/trans}\text{-HC(O)CH=CHCH(O)} \quad \text{(I)}$$

$$\rightarrow CH_2{=}CHCHO + CO \quad \text{(II)}$$

$$\rightarrow CH(O)CH{=}CH + HCO \quad \text{(III)}$$

$$\rightarrow HC(O)CH{=}CHCO + H \quad \text{(IV)}$$

$$\rightarrow \text{3H-furan-2-one} \quad \text{(V)}$$

$$\rightarrow HCO + HC{\equiv}CH + HCO \quad \text{(VI)}$$

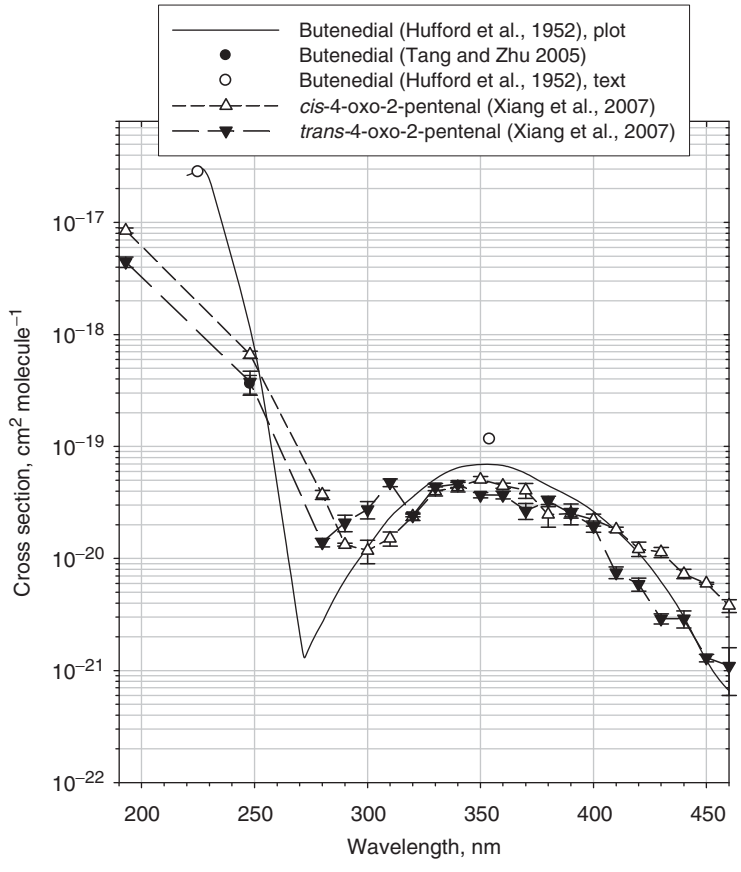

Figure IX-C-12. Absorption spectra of butenedial as measured in isooctane solution (Hufford et al., 1952), solid curve; reported σ_{max}, open circles; single wavelength measurement in gas phase (filled circle, Tang and Zhu, 2005); gas-phase spectra of *cis*-4-oxo-2-pentenal at 10 nm intervals (Xiang et al., 2007), open triangles; *trans*-4-oxo-2-opentenal, closed, inverted triangles.

From studies of butendial photolyses in air using broadband radiation, Bierbach et al. (1994) estimated that the isomerization of the butenedial in process (I) is probably an important pathway, ~40–45% of the total change. They reported that 3H-furan-2-one was a major product formed in 360–480 nm irradiated *cis*-/*trans*-butenedial mixtures, with maleic anhydride as a minor product (probably formed from the oxidation of the primary product, 3H-furan-2-one).

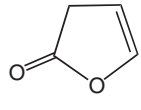

3H-Furan-2-one

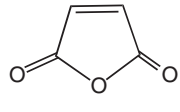

Maleic anhydride

Table IX-C-5. Recommended cross sections (σ, cm^2 $molecule^{-1}$) for butenedial as determined in isooctane solution by Hufford et al. (1952). Data were redrawn and recalculated from the original plot of $\log_{10}(\varepsilon$, L mol^{-1} $cm^{-1})$ and are very approximate

λ, nm	$10^{20} \times \sigma$	λ, nm	$10^{20} \times \sigma$	λ, nm	$10^{20} \times \sigma$	λ, nm	$10^{20} \times \sigma$	λ, nm	$10^{20} \times \sigma$
		316	3.02	353	6.93	390	3.55	427	0.76
280	0.27	317	3.16	354	6.93	391	3.47	428	0.71
281	0.30	318	3.29	355	6.92	392	3.38	429	0.66
282	0.34	319	3.40	356	6.91	393	3.28	430	0.62
283	0.37	320	3.54	357	6.90	394	3.19	431	0.59
284	0.40	321	3.69	358	6.88	395	3.11	432	0.55
285	0.45	322	3.84	359	6.82	396	3.00	433	0.51
286	0.48	323	4.00	360	6.76	397	2.92	434	0.47
287	0.53	324	4.15	361	6.70	398	2.82	435	0.45
288	0.56	325	4.30	362	6.62	399	2.72	436	0.41
289	0.60	326	4.47	363	6.54	400	2.63	437	0.38
290	0.65	327	4.64	364	6.44	401	2.55	438	0.36
291	0.69	328	4.80	365	6.34	402	2.45	439	0.33
292	0.74	329	4.97	366	6.24	403	2.36	440	0.30
293	0.79	330	5.13	367	6.13	404	2.27	441	0.28
294	0.85	331	5.28	368	6.00	405	2.19	442	0.26
295	0.91	332	5.44	369	5.87	406	2.12	443	0.24
296	0.97	333	5.57	370	5.75	407	2.02	444	0.22
297	1.04	334	5.72	371	5.62	408	1.95	445	0.20
298	1.10	335	5.86	372	5.50	409	1.86	446	0.18
299	1.19	336	6.00	373	5.36	410	1.79	447	0.17
300	1.26	337	6.12	374	5.22	411	1.71	448	0.15
301	1.35	338	6.25	375	5.09	412	1.62	449	0.14
302	1.46	339	6.36	376	4.96	413	1.57	450	0.12
303	1.56	340	6.46	377	4.84	414	1.50	451	0.11
304	1.66	341	6.55	378	4.70	415	1.44	452	0.10
305	1.78	342	6.61	379	4.59	416	1.37	453	0.10
306	1.88	343	6.67	380	4.47	417	1.30	454	0.09
307	2.00	344	6.72	381	4.36	418	1.25	455	0.08
308	2.11	345	6.76	382	4.27	419	1.19	456	0.07
309	2.24	346	6.81	383	4.16	420	1.12	457	0.06
310	2.35	347	6.84	384	4.07	421	1.07	458	0.05
311	2.46	348	6.87	385	3.98	422	1.01	459	0.04
312	2.57	349	6.90	386	3.88	423	0.96	460	0.03
313	2.68	350	6.92	387	3.81	424	0.90	461	0.02
314	2.80	351	6.93	388	3.72	425	0.86	462	0.01
315	2.92	352	6.93	389	3.63	426	0.81	463	0.00

In photolyses at 254 nm Bierbach et al. (1994) observed acetylene as a minor product, while Tang and Zhu used laser photolysis combined with cavity ring-down spectroscopy to search for HCO formation in butenedial photolysis at several wavelengths: 193, 248, 280, 308, 351, 400, and 450 nm. They reported that HCO is formed only in their photolyses at 193 and 248 nm with quantum yields of 0.55 ± 0.07 and 0.12 ± 0.01, respectively, unaffected by pressure of the aldehyde or added nitrogen buffer gas. These authors conclude that process (III) may have a threshold of about 290 nm that corresponds to the 410–414 kJ mol^{-1} minimum energy to break the

CH(O)CH=CHCH(O) bond. Tang and Zhu also identified CO, acetylene, acrolein, and 3-H-furan-2-one as products of butenedial photolysis in the absence of air. Estimated quantum yields for acrolein (ϕ_{II}) were: $\geq$0.011, $\geq$0.037, $\geq$0.15, and $\geq$0.23 for photolyses at 193, 248, 308, and 351 nm, respectively. Measured quantum yields of 3H-furan-2-one were: $\geq$0.028, $\geq$0.012, and $\geq$0.011 for photolyses at 248, 308, and 351 nm. Acetylene was also observed in photolyses at 193 nm ($\phi_{VI} \approx 0.42$). Using a sunlight-irradiated reaction chamber and *cis*-butenedial in dilute air mixtures with cyclohexane added to suppress losses from OH attack, Sørensen and Barnes (1998) estimated that $j(\text{Total}) = (1.80 \pm 0.01) \times 10^{-3}\ \text{s}^{-1}$. A measurement of $j(NO_2)$ in the chamber gave: $(10.1 \pm 0.13) \times 10^{-3}\ \text{s}^{-1}$. These data suggested that the total quantum yield of butenedial disappearance is near unity for wavelengths absorbed by butenedial (290–470 nm). In experiments without added cyclohexane, the apparent *j*-values were ~30% higher, suggesting that some radical forming processes such as (III) and/or (IV) occur in butenedial photodecomposition in sunlight. The previous workers have concluded that the total quantum yield of disappearance of butenedial is near unity at all wavelengths of absorbed sunlight. This has been assumed in our calculations of the *j*-values for butenedial that are given in figure IX-C-13.

IX-C-9. Photodecomposition of 4-Oxo-2-pentenal [$CH_3C(O)CH{=}CHC(O)H$]

Studies of the photochemistry of 4-oxo-2-pentenal have been conducted by Bierbach et al. (1994), Liu et al. (1999), and Xiang et al. (2007). The following primary processes

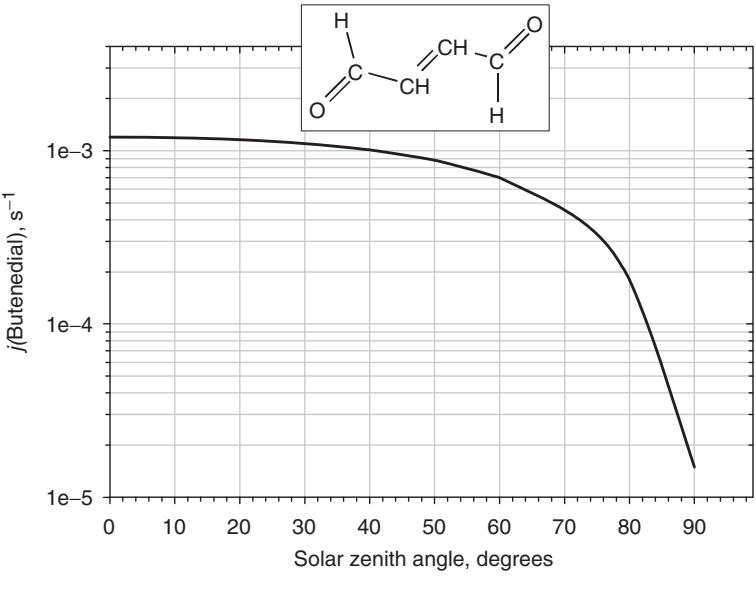

Figure IX-C-13. Approximate photolysis frequencies for butenedial versus solar zenith angle for a cloudless day in the lower troposphere with an overhead ozone column of 350 DU.

have been considered in explanation of the results:

$$\textit{trans}\text{-}/\textit{cis}\text{-}CH_3C(O)CH{=}CHC(O)H + h\nu \rightarrow \textit{cis}\text{-}/\textit{trans}\text{-}CH_3C(O)CH{=}CHC(O)H \quad \text{(I)}$$

$$\rightarrow CH_3 + C(O)CH{=}CHC(O)H \quad \text{(II)}$$

$$\rightarrow CH_3CO + CH{=}CHC(O)H \quad \text{(III)}$$

$$\rightarrow CH_3COCH{=}CH + HCO \quad \text{(IV)}$$

$$\rightarrow \text{5-methyl-3H-furan-2-one} \quad \text{(V)}$$

$$\rightarrow CH_3C(O)CH{=}CH_2 + CO \quad \text{(VI)}$$

IX-C-9.1. Cross Sections for 4-Oxo-2-Pentenal

Light absorption by 4-oxo-2-pentenal occurs in the same spectral region as butenedial, the simpler member of this family of alkendials. The cross sections for both the *cis*- and the *trans*-configurations have been determined for wavelengths at 10 nm intervals; see figure IX-C-12. The absorption bands of the three compounds compared in this figure consist of a weak, somewhat forbidden $n \rightarrow \pi^*$ transition, maximizing at ~350 nm, and with the onset of a stronger, allowed $\pi \rightarrow \pi^*$ transition for $\lambda < 270$ nm. Approximate cross sections for 4-oxo-2-pentenal at 1 nm intervals have been estimated from a smooth curve drawn between the data points determined by Xiang et al. (2007) and are presented in tabular form in table IX-C-6.

IX-C-9.2. Quantum Yields of Photodecomposition of 4-Oxo-2-Pentenal

In the 254 nm photolysis studies by Bierbach et al. (1994), isomerization in the *trans*-compound in process (I) accounted for < 20–30% of the total loss, while 5-methyl-3H-furan-2-one, CH_2O, CH_3OH, CH_3O_2H, and maleic anhydride (presumably formed from 5-methyl-3-H-furan-2-one) were identified among the products by infrared analysis, products consistent with the occurrence of processes (II), (IV), and (V). Photolysis with 360–480 nm light gave the same products with < 20% of the photolysis occurring by isomerization in process (I).

Liu et al. (1999) observed the rapid photodecomposition of 4-oxo-2-pentenal in sunlight-irradiated synthetic air ($\tau_{1/2} \sim 1.5$ h; 0600–0800 exposure) with the rapid oxidation of added NO to NO_2. The formation of free radicals in (II), (III), and /or (IV) is evident. Carbonyl products observed by Liu et al. (1999) in daylight chamber experiments, CH_2O, $CH_2{=}C(CH_3)C(O)H$, glycolaldehyde, hydroxyacetone, glyoxal, and methylglyoxal, suggest the possible occurrence of free-radical reactions. Some of these products are unexpected and may have resulted from impurities in the system.

The extent of occurrence of the various possible primary processes as a function of wavelength was investigated by Xiang et al. (2007). They carried out time-resolved studies of the photolysis of 4-oxo-2-pentenal at 193, 248, 308, and 351 nm (in the

absence of air) that focused on the formation of HCO radicals. HCO formation was unambiguously identified in photolyses at 193 and 248 nm where for the *trans*-isomer, $\phi_{IV} = 0.13 \pm 0.02$ and 0.014 ± 0.003, respectively, independent of pressure (0.3–49.4 Torr of nitrogen), and for the *cis*-isomer, $\phi_{IV} = 0.078 \pm 0.012$ and 0.018 ± 0.007, respectively. Xiang et al. (2007) determined that $\phi_{IV} < 0.01$ at 308 and 351 nm.

In separate experiments by Xiang et al. (2007), end-product analyses were made to identify the products formed in the photolyses of a one-to-one mixture of the *cis*- and *trans*-isomers at four wavelengths, 193, 248, 308, and 351 nm. At each wavelength, CO, 5-methyl-3H-furan-2-one, ethane, and methyl vinyl ketone were observed. Formation of 5-methyl-3H-furan-2-one reflects the occurrence of primary process (V). Ethane is likely derived from the association of CH_3 radicals formed in the primary process (II), and methyl vinyl ketone may arise from process (VI). This study of the end products of photolysis was used by Xiang et al. (2007) to measure the extent of decomposition that occurred by the various alternative primary processes. These data were coupled with the observations of the extent of *cis*- to *trans*-isomer estimated from the experiments of Bierbach et al. (1994). The estimates of the quantum yields of the various possible primary processes are summarized in figure IX-C-14. The approximate values of ϕ_I shown in the figure were derived by assuming a linear

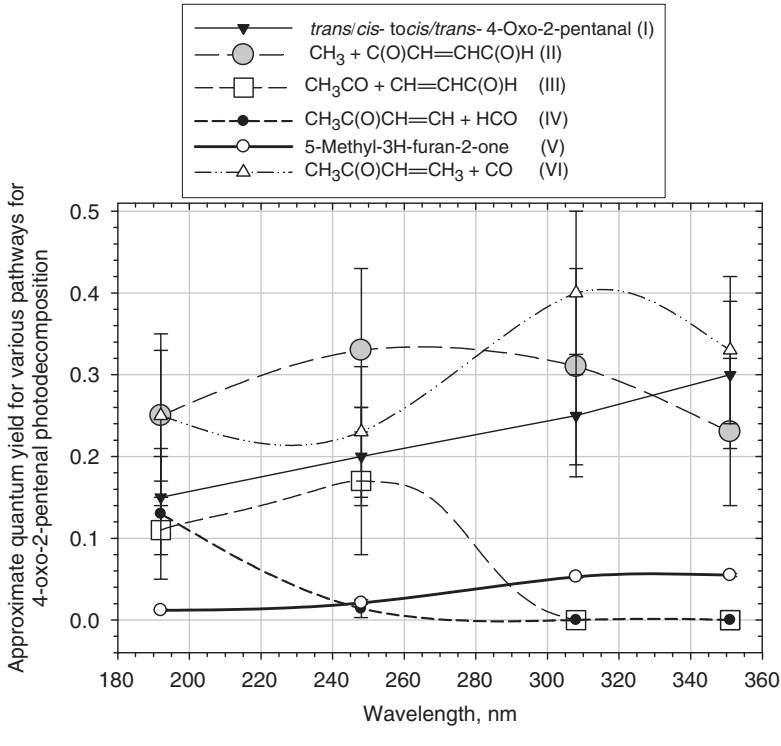

Figure IX-C-14. Approximate quantum yields of the various primary photolysis channels involved in the photolysis of a near one-to-one mixture of *trans*- and *cis*-4-oxo-2-pentenal at low pressures; data from Xiang et al. (2007) and Bierbach et al. (1994).

Table IX-C-6. Approximate cross sections (σ, cm^2 molecule^{-1}) for *trans*-, and *cis*-4-oxo-2-pentenal (Xiang et al., 2007); data were generated from a smooth curve drawn through the Xiang et al. data which were determined for wavelengths at 10 nm intervals

λ, nm	$10^{20} \times \sigma$ *trans*	$10^{20} \times \sigma$ *cis*	λ, nm	$10^{20} \times \sigma$ *trans*	$10^{20} \times \sigma$ *cis*	λ, nm	$10^{20} \times \sigma$ *trans*	$10^{20} \times \sigma$ *cis*	λ, nm	$10^{20} \times \sigma$ *trans*	$10^{20} \times \sigma$ *cis*	λ, nm	$10^{20} \times \sigma$ *trans*	$10^{20} \times \sigma$ *cis*
278	1.30	—	317	3.00	2.01	356	3.73	4.75	395	2.26	2.45	434	0.28	0.99
279	1.36	—	318	2.75	2.11	357	3.74	4.68	396	2.22	2.40	435	0.28	0.95
280	1.40	3.70	319	2.52	2.25	358	3.73	4.60	397	2.16	2.36	436	0.28	0.90
281	1.50	3.45	320	2.42	2.36	359	3.72	4.54	398	2.07	2.32	437	0.29	0.85
282	1.57	3.15	321	2.43	2.53	360	3.68	4.46	399	2.02	2.26	438	0.29	0.81
283	1.64	2.85	322	2.52	2.68	361	3.60	4.44	400	1.92	2.23	439	0.29	0.77
284	1.73	2.60	323	2.70	2.86	362	3.50	4.41	401	1.91	2.18	440	0.29	0.73
285	1.80	2.35	324	2.86	3.05	363	3.38	4.38	402	1.68	2.15	441	0.28	0.70
286	1.85	2.10	325	3.10	3.25	364	3.27	4.38	403	1.57	2.12	442	0.28	0.68
287	1.93	1.85	326	3.30	3.40	365	3.16	4.35	404	1.42	2.07	443	0.26	0.67
288	1.97	1.65	327	3.60	3.56	366	2.98	4.33	405	1.30	2.05	444	0.25	0.66
289	2.05	1.50	328	3.90	3.74	367	2.88	4.28	406	1.18	2.01	445	0.24	0.65
290	2.10	1.33	329	4.27	3.87	368	2.78	4.24	407	1.05	1.96	446	0.22	0.64
291	2.12	1.22	330	4.38	3.98	369	2.72	4.16	408	0.93	1.93	447	0.20	0.63
292	2.13	1.16	331	4.53	4.06	370	2.67	4.06	409	0.85	1.87	448	0.18	0.62
293	2.16	1.11	332	4.67	4.13	371	2.68	3.94	410	0.75	1.82	449	0.16	0.61
294	2.19	1.08	333	4.75	4.17	372	2.72	3.78	411	0.68	1.75	450	0.14	0.60
295	2.23	1.07	334	4.77	4.21	373	2.88	3.62	412	0.65	1.69	451	0.13	0.58
296	2.28	1.08	335	4.83	4.23	374	2.93	3.43	413	0.62	1.62	452	0.12	0.56
297	2.36	1.10	336	4.82	4.25	375	2.93	3.24	414	0.61	1.55	453	0.11	0.55
298	2.46	1.13	337	4.81	4.27	376	3.02	3.06	415	0.60	1.49	454	0.11	0.53

299	2.59	1.15	338	4.75	4.29	377	3.10	2.87	416	0.60	1.43	455	0.11	0.51
300	2.74	1.17	339	4.69	4.33	378	3.17	2.72	417	0.60	1.36	456	0.10	0.48
301	3.00	1.22	340	4.63	4.36	379	3.22	2.68	418	0.60	1.32	457	0.10	0.46
302	3.25	1.25	341	4.53	4.43	380	3.26	2.46	419	0.59	1.26	458	0.10	0.44
303	3.55	1.29	342	4.45	4.50	381	3.25	2.42	420	0.58	1.22	459	0.10	0.41
304	3.83	1.32	343	4.34	4.60	382	3.21	2.37	421	0.57	1.21	460	0.11	0.39
305	4.05	1.35	344	4.23	4.67	383	3.15	2.36	422	0.55	1.18	461	0.10	0.36
306	4.32	1.37	345	4.12	4.76	384	3.08	2.37	423	0.53	1.17	462	0.09	0.32
307	4.52	1.41	346	4.02	4.85	385	3.00	2.38	424	0.48	1.17	463	0.08	0.28
308	4.65	1.45	347	3.88	4.93	386	2.92	2.41	425	0.45	1.17	464	0.07	0.25
309	4.75	1.47	348	3.79	5.00	387	2.78	2.45	426	0.42	1.17	465	0.06	0.20
310	4.75	1.51	349	3.73	5.05	388	2.72	2.47	427	0.37	1.16	466	0.05	0.16
311	4.64	1.56	350	3.68	5.07	389	2.60	2.51	428	0.35	1.16	467	0.04	0.13
312	4.47	1.62	351	3.66	5.06	390	2.54	2.52	429	0.33	1.16	468	0.03	0.09
313	4.15	1.68	352	3.67	5.03	391	2.47	2.53	430	0.29	1.15	469	0.02	0.03
314	3.88	1.75	353	3.67	4.96	392	2.41	2.52	431	0.28	1.12	470	0.01	0.00
315	3.60	1.83	354	3.69	4.90	393	2.35	2.51	432	0.28	1.07			
316	3.28	1.92	355	3.72	4.84	394	2.31	2.47	433	0.28	1.04			

relationship between quantum yield and wavelength taking the approximate values of 0.3 at 345 nm and 0.2 at 248 nm. The summation of these approximate quantum yields at each wavelength is near unity, 0.83, 1.05, 1.01, and 0.92, for 193, 248, 308, and 351, respectively. These are probably upper limits to those expected in 1 atm. of air, since some quenching of the excited states might be expected, particularly at the longer wavelengths.

IX-C-9.3. Photolysis Frequencies for the Photodecomposition of 4-Oxo-2-pentenal in the Lower Troposphere

Estimates of the *j*-values for both *cis*- and *trans*-4-oxo-2-pentenal in the lower troposphere have been made assuming $\phi_{\text{total}} = 1$ at all wavelengths of absorbed light and using the estimated cross sections given in table IX-C-6 based on measurements of Xiang et al. (2007). These were calculated for a clear day in the lower troposphere assuming an overhead ozone column of 350 DU; see figure IX-C-15. The data given in the figure are in accord with those those calculated by Xiang et al. (2007), but are roughly 10% higher. The reasons for the difference likely lie in different choices for the assumed overhead ozone column, ground albedo, averaging methods, etc.

Thüner et al. (2004b) reported a direct measurement of the photolysis freqencies of 4-oxo-2-pentenal in sunlight in the EUPHORE chamber, $j(\text{Total}) \leq 1.6 \times 10^{-3}\,\text{s}^{-1}$; this upper limit is somewhat larger than that derived here, but the data qualitatively support the view accepted here, that ϕ_{total} is near unity.

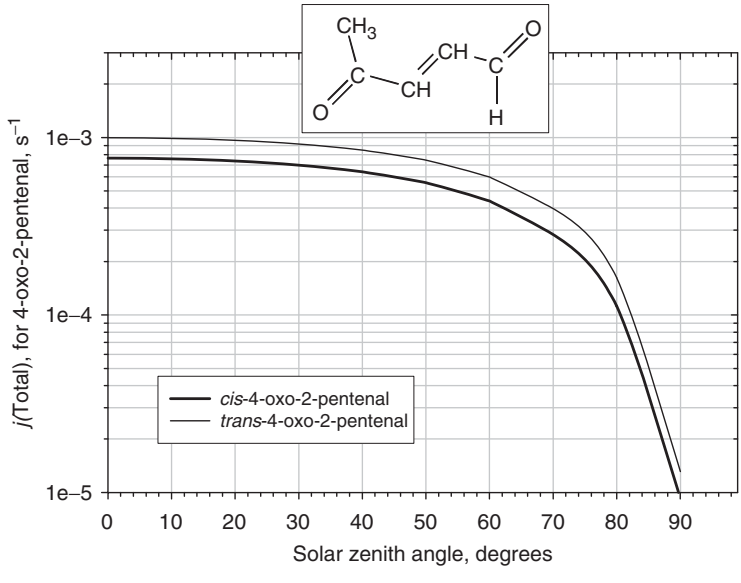

Figure IX-C-15. Approximate values of the photolysis frequencies as a function of solar zenith angle for *cis*- and *trans*-4-oxo-2-pentenal. Estimates have been calculated for a cloud-free lower troposphere assuming $\phi_{\text{total}} = 1$ and an overhead ozone column of 350 DU.

IX-C-10. The Photodecomposition of the Hexadienedials (*E*,*E*-2,4-Hexadienedial, *E*,*Z*-2,4-Hexadienedial, and *E*,*E*-2-Methyl-2,4-hexadienedial)

These compounds are ring-opening products in the OH-initiated photooxidation of aromatic hydrocarbons, and as such their fates are of special interest to atmospheric chemists. In this section we focus our review on the current information on the *E*,*E*-hexadienedial and *E*,*Z*-hexadienedial molecules; the photolysis mechanisms of the related molecule *E*,*E*-2-methyl-2,4-hexadienedial are very similar (Klotz et al., 1995). The atmospheric chemistry of these compounds, part of a group of compounds called muconaldehydes, has been studied by Klotz et al. (1995, 1999) and Xiang and Zhu (2007). *E*,*E*-2,4-Hexadienedial is a low vapor pressure, light-yellow solid at ambient temperature, and measurement of the gas-phase cross sections for this and the other hexadienedials at ambient temperatures is difficult. The measurements of Klotz et al. (1995) were made in cyclohexane solution and focus on the strong $\pi \rightarrow \pi^*$ transition that occurs in the 220–300 nm region. The gas-phase measurements of Xiang and Zhu (2007) give useful data related to the $n \rightarrow \pi^*$ band (300–440 nm) of more direct interest in tropospheric chemistry. In figure IX-C-5, the approximate cross sections for *E*,*E*-2,4-hexadiendial, as determined at 5 nm intervals by Xiang and Zhu, are given versus wavelength. They are seen to be similar to those of other alkenals but, as expected, the presence of four conjugated double bonds in this compound leads to a somewhat stronger absorption and a shift to longer wavelength than that seen in the simpler alkenals. Both laboratory and EUPHORE chamber studies of these compounds have been reported.

In photolyses of both the *E*,*Z*- and *E*,*E*-2,4-hexadienedial in sunlight in the EUPHORE chamber, Klotz et al. (1999) observed an extremely rapid isomerization into the *E*,*E*-form, while the reverse formation of the *E*,*Z*-form occurred together with a slow photodecomposition. Several alternative primary photochemical reactions that are reversible have been considered in previous studies of the two forms of 2,4-hexadienedial (Klotz et al., 1999) (reaction mechanism IX-C-10a).

The authors conclude that the upper pathway forming 2-formyl-2H-pyran cannot be operative based on the observed behavior of *E*,*Z*-2,4-hexadienedial; also the reaction at lower left forming 2-butenal-4-yl-ketene is not in accord with the concentration–time profile of the ketene observed. The mechanism shown to the lower right to form *Z*-3,4-diformyl-cyclobutene appears to be the only feasible pathway which is not in contradiction to the experimental observations.

The mechanism that Klotz et al. (1999) used to match the changes observed in the EUPHORE experiments, given below, is similar to that described for other related compounds (reaction mechanism IX-C-10b)

The *j*-values derived in one of seven experiments of Klotz et al. (1999), at an unspecified date, starting about noon are: $j(\mathrm{RE1}) = 1.68 \times 10^{-3}\,\mathrm{s}^{-1}$; $j(\mathrm{RE2}) = 1.3 \times 10^{-3}\,\mathrm{s}^{-1}$; $j(\mathrm{RE3}) = 2.2 \times 10^{-3}\,\mathrm{s}^{-1}$; $j(\mathrm{RE4}) = j(\mathrm{RE5}) = 26.2 \times 10^{-5}\,\mathrm{s}^{-1}$; $j(\mathrm{NO_2}) = 11.9 \times 10^{-3}\,\mathrm{s}^{-1}$. For these conditions the lifetimes for the formation of products from the two 2,4-hexadienedial compounds are about 1 h. The authors conclude that photoisomerization of the *E*,*Z*-2,4-hexadienedial molecule is its major fate

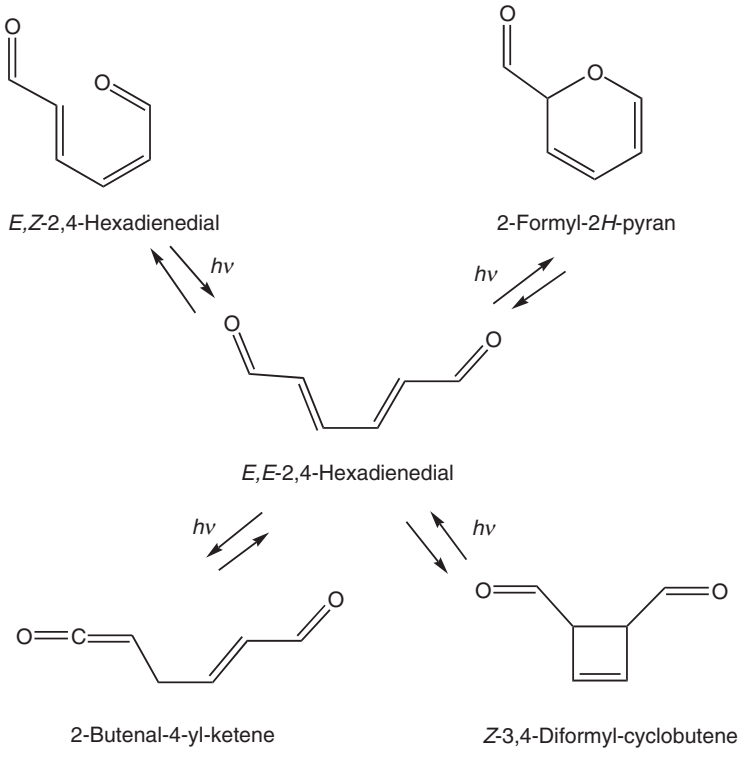

Reaction mechanism IX-C-10a

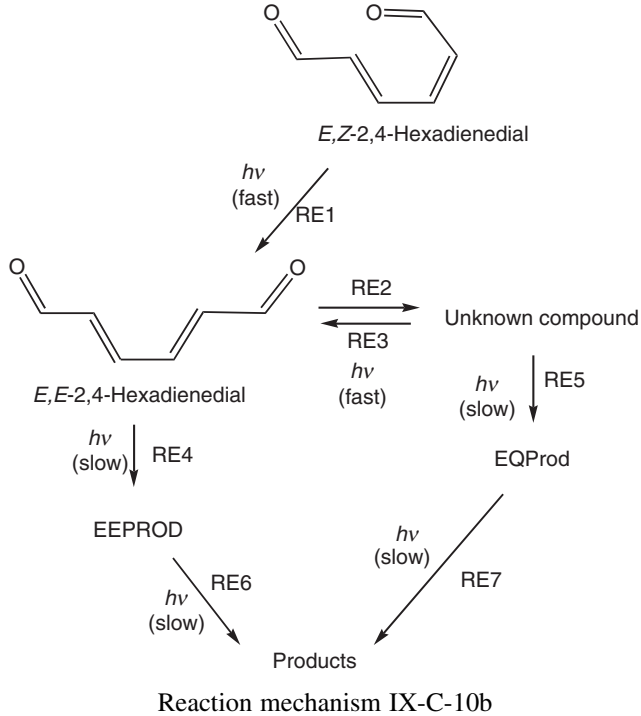

Reaction mechanism IX-C-10b

in the troposphere, while the important sinks for the *E*,*E*-2,4-hexadienedial molecule are both photodecomposition and OH-radical attack. In addition to the formation of a ketene, pronounced formation of particles was observed in the photolysis of both the *E*,*E*- and *E*,*Z*-hexadienedial that appears to result in secondary aerosol formation involving the initial products.

In the studies of Xiang and Zhu photolyses of *E*,*E*-2,4-hexadienedial were carried out at three wavelengths: 248, 308, and 351 nm. Some experiments using laser photolysis cavity ring-down spectroscopy were designed to check for the possible formation of the HCO product. Indeed, HCO was detected, but only in the 248 nm photolyses in which $\phi_{HCO} = 0.014$ with the 2,4-hexadiendial pressure in the range 0.0006 to 0.003 Torr. From their detection limits for HCO in these experiments, the authors suggest that the maximum values of ϕ_{HCO} are < 0.11 at 308 and < 0.09 at 351 nm. In other experiments of Xiang and Zhu, FTIR analysis was made of the end products of the photolysis of *E*,*E*-hexadienedial (in 20 Torr of N_2). For experiments at 248 nm, the presence of CO ($\Phi_{CO} = 1.1$), acetylene ($\Phi_{HC\equiv CH} = 0.32$), ketene, and butadiene ($\Phi_{Butadiene} = 0.14$) was determined. CO ($\Phi_{CO} = 0.97$) was the only product identified in experiments at 308 nm.

Xiang and Zhu considered the possible occurrence of the following primary dissociation processes to rationalize their results; the wavelengths shown are those at which the energy of the quantum is sufficient to allow the process, provided no barrier exists:

$$\mathrm{HC(O)CH{=}CHCH{=}CHCH(O)} + h\nu \rightarrow 2\mathrm{CH_2CO} + \mathrm{HC{\equiv}CH} \quad \text{(I)} \quad \lambda < 847\,\text{nm}$$

$$\rightarrow \mathrm{HC(O)CH{=}CHCH{=}CH} + \mathrm{HCO} \quad \text{(II)} \quad \lambda < 292\,\text{nm}$$

$$\rightarrow \mathrm{HC(O)CH{=}CHCH{=}CH} + \mathrm{H} + \mathrm{CO} \quad \text{(III)} \quad \lambda < 251\,\text{nm}$$

$$\rightarrow \mathrm{HC(O)CH{=}CHCH{=}CH_2} + \mathrm{CO} \quad \text{(IV)} \quad \lambda < 5,455\,\text{nm}$$

$$\rightarrow \mathrm{CH_2{=}CHCH{=}CH_2} + 2\mathrm{CO} \quad \text{(V)} \quad \lambda < 1,463\,\text{nm}$$

$$\leftrightarrow Z\text{-3,4-diformyl-cyclobutene} \quad \text{(VI)}$$

The observation of ketene and acetylene formation in photolyses at 248 nm provides strong evidence for the occurrence of process (I); the observed HCO formation confirms the occurrence of process (II) in photolyses at this wavelength. CO formation could arise from processes (II) through (V) or as a secondary product from photolysis of primary product ketene. Although process (I) was considered as a possible source of acetylene, the authors suggest that it is likely formed from the photodecomposition of the initial product, *Z*-3,4-diformyl-cyclobutene, formed in (VI). This cyclobutene product was suggested as a primary product in the studies of Klotz et al. (1995, 1999).

Xiang and Zhu estimated *j*-values for the decomposition of *E*,*E*-hexadienedial assuming the quantum yield was unity in the 290–320 nm region and that it decreased linearly from unity at 320 nm to zero at 350 nm. With these assumptions, they calculated

j(Total) $\approx 2.1 \times 10^{-4}\ s^{-1}$ for an *o*verhead Sun. These estimates are approximate upper limits since no account has been taken of the possible quenching of the processes by air molecules at 1 atm. as observed in the photolysis of other alkenals.

Direct estimates of the j(Total) for *E*,*E*-2,4-hexadienedial disappearance in 1 atm. of air were derived by Klotz et al. (1999) in seven different experiments in the EUPHORE chamber; solar zenith angles were not given with the data, but using the higher values as most representative of those for a high Sun, for both the *E*,*Z*- and *E*,*E*-isomers, j(Total) $\approx 2.6 \times 10^{-4}$ to $1.4 \times 10^{-4}\ s^{-1}$, in reasonable accord with the Xiang and Zhu estimate for an overhead Sun. In view of the very limited information on the nature and magnitude of the primary processes in air at 1 atm. as a function of wavelength and the uncertainty in the magnitude of the cross sections, more reliable estimates of j-values cannot be made at the time of this writing.

IX-C-11. The Photodecomposition of Glyoxal [Ethanedial, HC(O)C(O)H]

Glyoxal is formed in the atmosphere as a product of the oxidation of aromatic hydrocarbons, and its photodecomposition can be an important source of free radicals that drive ozone generation in the troposphere. Significant new information has appeared since our last review of this compound (Calvert et al., 2000). Sunlight absorption that occurs within glyoxal's two absorption bands induces $n \rightarrow \pi^*$ electronic excitation; see figure IX-C-1. A recent *ab initio* study of the spectrum of glyoxal has defined the characteristics of the excited states of glyoxal (Gruber-Stadler et al., 2006). Our understanding of the mechanism of glyoxal photodecomposition has continued to grow since the early work of Norrish and Griffiths (1928); significant progress has been made both in experimental studies of glyoxal photodecomposition (e.g., see: Blacet and Moulton, 1941; Calvert and Layne, 1953; Parmenter, 1964; Anderson et al., 1973; Loge and Parmenter, 1981; Plum et al., 1983; Hepburn et al., 1983; Langford and Moore, 1984a; b; Roscoe and Back, 1986; Burak et al., 1987; Dobeck et al., 1999; Kao et al., 2004; Zhu et al., 1996; Chen and Zhu, 2003; Tadić et al., 2006), and in theoretical studies (e.g., see: Osamura et al., 1981; Scuseria and Schaefer, 1989; Koch et al., 2001; Li et al., 2006). Several primary photodissociative pathways have been considered in rationalizing the results of these studies:

$$\mathrm{HC(O)C(O)H} + h\nu \rightarrow 2\mathrm{HCO} \qquad \text{(I)}$$

$$\rightarrow \mathrm{H_2CO} + \mathrm{CO} \qquad \text{(II)}$$

$$\rightarrow \mathrm{H_2} + 2\mathrm{CO} \qquad \text{(III)}$$

$$\rightarrow \mathrm{HCO} + \mathrm{H} + \mathrm{CO} \qquad \text{(IV)}$$

$$\rightarrow \mathrm{CO} + \mathrm{HCOH} \qquad \text{(V)}$$

The evidence for these processes is reviewed in this section.

IX-C-11.1. Absorption Cross Sections of Glyoxal

The recommended absorption cross sections of glyoxal from Volkamer et al. (2005) are shown in figure IX-C-1 and are given in tabular form in table IX-C-7.

IX-C-11.2. Quantum Yield of Primary Photodecomposition Processes in Glyoxal

Process (I): $HC(O)C(O)H + h\nu \rightarrow 2HCO$ *(I)* In experiments using 313 nm radiation, Calvert and Layne (1953) determined that $\Phi_{CO} = 1.22$ and $\Phi_{H_2} = 0.13$, relatively insensitive to the experimental variables, temperature (106–304°C), concentration of glyoxal $(1.9 - 9.3) \times 10^{-3}$ M, and varied intensity of the absorbed 313 nm light. The authors concluded that processes (II) and (III) were dominant with $\phi_{II} = 0.15$ and $\phi_{III} = 0.85$. In view of estimates for the enthalpy change for the reaction (I) that were available at the time, and the fact that no chain reaction forming CO was evident even at the higher temperatures, Calvert and Layne suggested that there was insufficient energy in the 313 nm quantum to dissociate the HC(O)—C(O)H bond, and hence process (I) was probably unimportant. However, Langford and Moore (1984a) later suggested that the occurrence of processes (I), (II), and (III) could explain the Calvert and Layne results, since the dominant fate of the HCO radical for the conditions used by them would be the reaction: $HCO + HCO \rightarrow CH_2O + CO$, leading to the same products that form following processes (II) and (III). Simulations using the now better-evaluated rate coefficients for the reactions occurring in the Calvert and Layne experiments confirm this view. Only at the higher temperatures employed by Calvert and Layne is there a significant chain reaction that could be detected, and it was at these temperatures that a correction for thermal decomposition of glyoxal made the quantum yield measurements unreliable.

There is now significant evidence that reaction (I) is important for glyoxal photodecomposition for irradiation over much of its region of absorption. Direct evidence that process (I) occurs at some wavelengths in xenon flash lamp emission was reported by Herzberg and Ramsay (1955); they observed HCO and analyzed the the absorption spectrum of the HCO radical employing several aldehydes (CH_2O, CH_3CHO) as well as glyoxal. Langford and Moore (1984a, b) also observed the HCO absorption spectra in photolyses of glyoxal at 308 nm and studied some of its reactions.

The first detailed studies of the wavelength dependence of the quantum efficiency of glyoxal photodisociation in process (I) were made by Zhu et al. (1996) and Chen and Zhu (2003). The results are plotted versus wavelength in figure IX-C-16. The small open circles and large open circles represent zero pressure estimates from the studies of Zhu et al. (1996) and Chen and Zhu (2003), respectively. The latter workers observed that for experiments at $\lambda > 370$ nm, quenching of the formyl radical formation occurred as the pressure of the glyoxal or added nitrogen gas was increased. A semi-logarithmic plot of their measured ratios of the dissociation quenching rate constant (k_q) observed using added nitrogen gas to that for dissociation of the glyoxal (k_d) is given versus the reciprocal of the exciting wavelength in figure IX-C-17. A near linear relation is seen. The fit of these data, neglecting the point at the shortest wavelength, leads to the

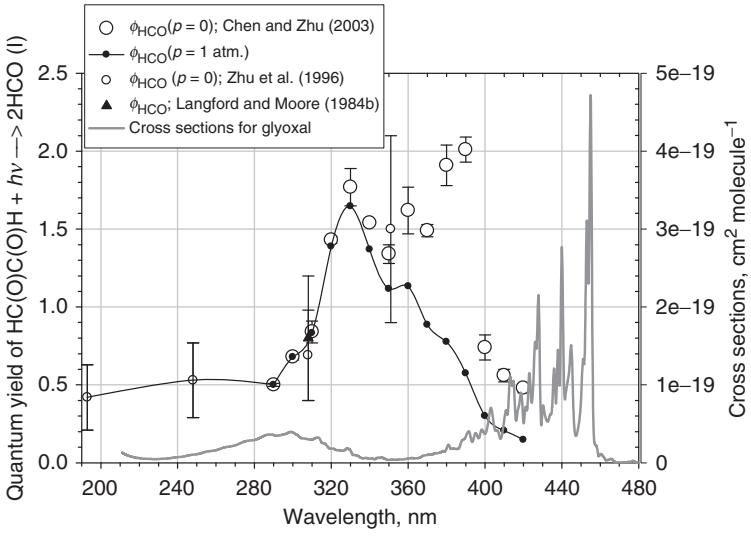

Figure IX-C-16. Experimental measurements of the quantum yield of glyoxal photodecomposition by HC(O)C(O)H + $h\nu \rightarrow$ 2HCO (I); data for zero pressure from Zhu et al. (1996) represented by small open circles; data of Chen and Zhu (2003), large open circles. The small filled circles represent ϕ_I values adjusted to pressure of 1 atm. of N_2 using the pressure quenching (k_q/k_d) measurements of Chen and Zhu; the data point of Langford and Moore (1984) at 308 nm is shown by the filled triangle. The gray curve gives the absorption spectrum for glyoxal (Horowitz et al., 2001).

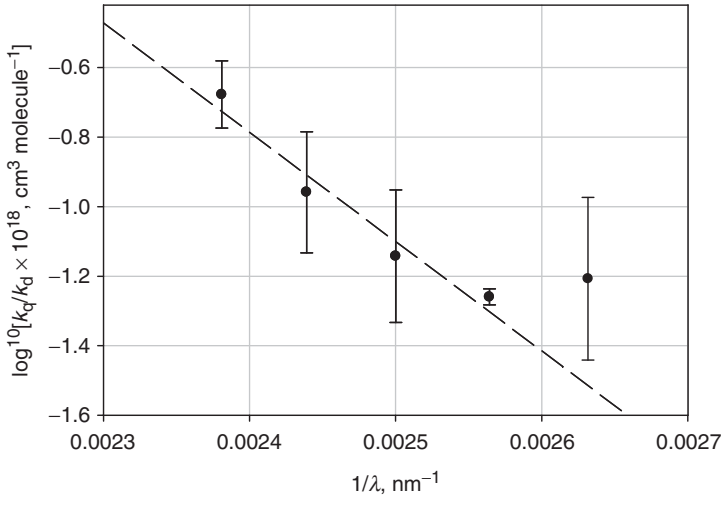

Figure IX-C-17. Log plot of k_q/k_d data for the quenching of HCO formation by N_2 gas in glyoxal photodecomposition in process (I) as a function of l/λ (Chen and Zhu, 2003). The estimates given by the dashed line that neglect the data point at the longest wavelength were used in this work to estimate ϕ_I values in air at 1 atm. from the ϕ_I values at zero pressure.

relation: $\log_{10}(10^{18} \times k_q/k_d, \text{cm}^3 \text{ molecule}^{-1}) = 67,650 - 3,146.34 \times (1/\lambda, \text{ nm})$. We used this relation to estimate the k_q/k_d values for each of the wavelengths employed by Chen and Zhu. It is assumed that the quenching observed by N_2 will be similar to that of air as has been observed to be the case for the structurally similar molecule, CH_2O (Moortgat et al. 1983). The zero pressure quantum yields have been adjusted to those expected for 1 atm. of N_2 using the relation: $1/(\phi)_{P=\text{atm.}} = 1/(\phi)_o + (k_q/k_d)[N_2]$; these values are shown as the small filled circles in figure IX-C-16. Quenching of the process (I) becomes less important at the shorter wavelengths, and it is relatively unimportant for $\lambda < 320$ nm. The data of Tadić et al. (2006) from broadband photolyses (radiation in the range, $390 < \lambda < 470$ nm) gave: $1/\phi_{[\text{total(effective)}]} = 6.80 + 0.02518 \times P$ (Torr); this corresponds to an effective $k_q/k_d = 7.8 \times 10^{-19}$ cm^3 molecule^{-1}, somewhat higher than the value measured by Chen and Zhu (2003) at the longest wavelength (420 nm, $k_q/k_d = 2.1 \times 10^{-19}$ cm^3 molecule^{-1}).

The data of Chen and Zhu (2003) suggest that glyoxal dissociation in process (I) continues to be significant at wavelengths ≥ 420 nm. However, current recommendations for enthalpies of formation of the molecules involved in primary process (I), Lide (2001–2002), suggest that the thermodynamic threshold for (I) is ~401 nm. Chen and Zhu suggest that this discrepancy may result from uncertainties in the enthalpies of formation as well as the presence of significant internal energy in the absorbing molecules. However, results from several other studies appear to conflict with the long-wavelength results of Chen and Zhu. Thus, the relatively low average quantum yield for glyoxal decomposition reported by Tadić et al. (2006) from 390–470 nm photolysis of glyoxal in air at 700 Torr (0.041), and the relatively low photolysis rate coefficients observed by Plum et al. (1983) and Tadić et al. (2006) are inconsistent with the Chen and Zhu long-wavelength results. We note that at the longest wavelengths used in the Chen and Zhu study (420 nm), the cross section for glyoxal absorption is highly structured and changes rapidly with variation in wavelength. It is possible that Chen and Zhu underestimate σ at the longer wavelengths, resulting in an overestimate of ϕ_I. Tadić et al. (2006) rejected the Chen and Zhu ϕ_I values obtained for $\lambda = 360$–420 nm in formulating their recommendations for the wavelength dependence of ϕ_I. They also have shifted significantly the measured ϕ_I values of Chen and Zhu to shorter wavelengths (~38–45 nm).

The present authors have accepted the Chen and Zhu data for $\lambda \leq 400$ nm but rejected the data for wavelengths 405 and 410 nm. We have extended their trend of ϕ_I observed for wavelengths 380, 390, and 400 nm to $\phi_I = 0$ at 410 nm. This choice represents a somewhat arbitrary compromise between the fitting of the various data sources; obviously, the true wavelength dependence remains uncertain. Our recommendations for ϕ_I in 1 atm. of air are given versus wavelength in figure IX-C-18 and in table IX-C-8.

Kao et al. (2004) determined the energy distribution in the HCO radical produced in glyoxal photodecomposition in experiments using 394.4, 390.33, or 382.65 nm excitation. Fluorescence in the transition B $^2A'$ – X $^2A'$ of HCO was employed to observe a bimodal distribution of rotational states in the HCO product up to $N = 26$ and $K = 2$. In photolyses at 390.33 and 382.65 nm, rotational energy accounts for 28% and 16%, respectively, of the energy distribution in one of the bimodal distributions

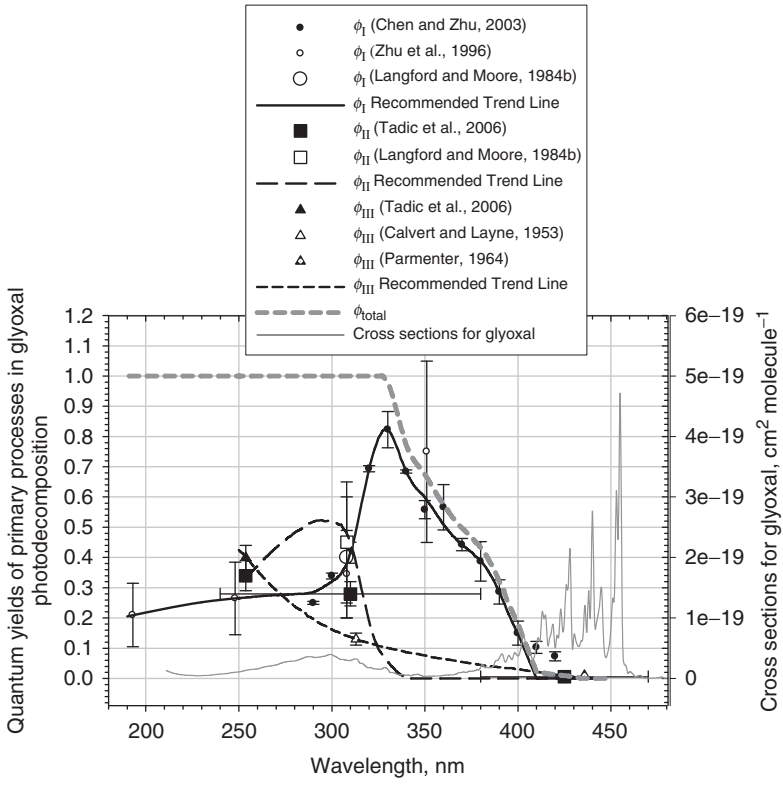

Figure IX-C-18. Estimates of the quantum yields of primary processes in glyoxal photodecomposition in 1 atm. of air as a function of wavelength: HC(O)C(O)H + $h\nu$ → 2HCO (I); HC(O)C(O)H + $h\nu$ → H_2CO + CO (II); HC(O)C(O)H + $h\nu$ → H_2 + 2CO (III). The trend lines shown are those recommended in this work. The dashed, heavy gray line represents the estimated total quantum yield of decomposition. The solid-gray curve gives the absorption spectrum of glyoxal.

and 40% and 43%, respectively, in the other distribution. No vibrationally excited HCO was observed, so a large fraction of the energy available in the quantum at these wavelengths is converted into translational energy of the HCO fragments.

ii) Process (II): HC(O)C(O)H + $h\nu$ → CH_2O + CO *(II)* This rather unusual primary process was first suggested by Blacet and Moulton (1941). The evidence from all glyoxal photolysis studies is consistent with the occurrence of this process. Koch et al. (2001) predicted from *ab initio* calculations that process (II) will be a dominant decomposition pathway. Burak et al. (1987) reported that the appearance time for the CO product from 440 nm photolysis at low pressures was in excellent agreement with glyoxal fluorescence decay times. They probed the distribution of the internal energy in the CO product through laser-induced fluorescence. The initial product CO is formed almost entirely in the $v = 0$ state, but its excess energy is spread over a broadly excited

rotational distribution peaking at $J \cong 42$. These results and others are consistent with a model for the dissociation involving planar intermediates for the two channels, (II) and (III). They conclude that the highest rotational levels of CO are produced in coincidence with the H_2CO-forming channel (II).

Molecular beam experiments carried out at relatively low pressures give us insight into the energy distribution in the initial products formed following excitation to the S_1 state. Hepburn et al. (1983) used molecular beam photofragmentation translational spectroscopy with excitation of glyoxal at 439.8 nm and found evidence for three distinct dissociation channels; processes (II) and (III) were suggested to be major channels with process (V) forming CO and hydroxymethylene (HCOH) as a third minor channel. They suggest that process (II) is the most probable channel and that about 60% of the available energy is in internal excitation of the products. Li et al. (2006) conclude from their *ab initio* calculations that following excitation in the 393–390 nm range, process (II) occurs largely from the S_o ground state formed by internal conversion from the excited singlet state.

Few experiments that replicate glyoxal photolysis in the atmosphere have been made that relate to process (II), and extrapolation of the results of experiments carried out at low pressures to those of atmospheric conditions is of questionable value. However, the occurrence of process (II) for atmospheric conditions has been observed unambiguously by Tadić et al. (2006). They followed CH_2O and HCO_2H formation in broadband photolyses of glyoxal in air (100–700 Torr). They interpreted the small amount of HCO_2H identified in the products as arising from the subsequent reactions involving the HO_2 radical with the parent CH_2O product. Hence, the sum $\Phi_{CH_2O} + \Phi_{HCO_2H}$ was taken as a measure of ϕ_{II}. The results of Tadić et al. (2006) demonstrate that quenching of product formation by added air is unimportant for photolyses in the 275–380 nm range. They reported a total quantum yield of decomposition $\phi_{total} = 0.97 \pm 0.05$ and an overall value of $\phi_{II} = 0.28 \pm 0.04$ for this wavelength range. Using different light sources, they measured $\phi_{II} = 0.007$ at 700 Torr (0.006 estimated for 760 Torr of air) averaged over the range of wavelengths 390–470 nm. Using 253.7 nm radiation, Tadić et al. (2006) measured $\phi_{II} = 0.34 \pm 0.05$ independent of pressure. These data are plotted in figure IX-C-18 as filled squares. The estimate of $\phi_{II} = 0.45$ at 308 nm is derived from the data of Langford and Moore (1984b) and is plotted in figure IX-C-18 as an open square. The recommended trend line for process (II) was derived using the relation, $\phi_{II} = 1 - (\phi_I + \phi_{III})$ for $\lambda < 327$ nm. The value of ϕ_{II} apparently decreases rapidly at wavelengths >327 nm to reach the low average value observed by Tadić for the long-wavelength region. Obviously, our recommended values for ϕ_{II} in air at 1 atm. (given by the long dashed curve in figure IX-C-18) are qualitative at best. That derived by Tadić et al. (2006) from the same data sources is somewhat different since they have weighted their own measurements more heavily than those derived using the Chen and Zhu data for ϕ_I.

iii) Primary process (III): HC(O)C(O)H + hν → H_2 + 2CO (III) This photodecomposition mode, first suggested by Norrish and Griffiths (1928), has been of great interest in subsequent experimental and theoretical studies, since it suggests the

seemingly improbable simultaneous generation of three products from the excited glyoxal molecule. The process has been referred to as the "triple whammy pathway" by Osamura and Schaefer (1981), Osamura et al. (1981), and Scuseria and Schaefer (1989), and by others in subsequent publications. Early suggestions of this pathway were based upon seemingly ambiguous chemical analyses for small amount of H_2 among the larger amount of CO (Norrish and Griffiths, 1928; Blacet and Moulton, 1941; Calvert and Layne, 1953; Parmenter, 1964). The chemical analyses employed in these studies used selective oxidizing agents for CO and H_2. The methods have been shown to be reasonably reliable by comparison of analyses on known mixtures using both chemical and mass spectrometer identification (Calvert, 1949). Roscoe and Back (1986) used a gas chromatograph to detect the H_2 and CO products (in argon carrier gas) of glyoxal photolysis at 488 and 454.5 nm. Loge et al. (1980) observed H_2 using chemical analyses as well, but suggested that this may have been formed following the occurrence of process (II). They argued that up to 180 kJ mole^{-1} of vibrational energy is available for the initial formaldehyde product of (II), and they suggested that this vibrationally rich CH_2O molecule may undergo a second unimolecular decomposition forming $H_2(CH_2O^{\ddagger} \rightarrow H_2 + CO)$. However, this suggestion has been disproven in theoretical studies that have confirmed that the formation of three molecules ($H_2 + 2CO$) in a simultaneous event is a realistic interpretation of all the studies related to process (III); see Osamura et al. (1981); Scuseria and Schaefer (1989); Dobeck et al. (1999). The studies show that decomposition in process (III) will likely occur from a *cis*-configuration of the vibrationally excited glyoxal molecule, the transistion state of which will have bond distances favoring the simultaneous release of two CO molecules and H_2.

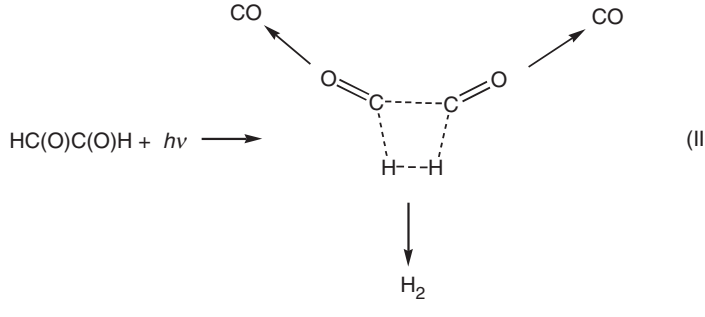

Theoretical calculations predict that the normal distance between H-atoms in the ground state of *cis*-glyoxal, about 2.46 Å, decreases to about 1.09 Å in the transition state leading to process (III), approaching that of the H_2 molecule (0.741 Å), while the C—H bond distances increase from 1.096 Å to 1.40 Å and the C—O bond distances decrease from 1.185 Å to 1.131 Å approaching that in the CO molecule (1.128 Å).

Both Loge and Parmenter (1981) and Roscoe and Back (1986) studied the photolysis of glyoxal at 454.5 nm at low pressures (< 0.5 Torr) and observed that the ratio H_2/CO of the products extrapolates to 0.5 at zero pressure, the expected ratio if only

process (III) occurred. This was observed with both *cis*-glyoxal at 488.0 nm and *trans*-glyoxal at 454.5 nm. As the pressure was increased the H_2/CO ratio decreased rapidly, approaching ~0.1 at 0.5 Torr of glyoxal (Roscoe and Back, 1986). For the wavelengths of excitation used in these experiments, reaction channel (II) becomes more important than (III) as the pressure is raised.

In 440 nm photodissociation of glyoxal using vacuum ultraviolet laser-induced fluorescence and resonance enhanced multiphoton ionization, Li et al. (2006) have confirmed the occurrence of process (III) by observing directly the internal energy in the H_2 product. The $v = 1$ vibration level of the H_2 product was the highest populated with rotational states from $J = 0$ to 9. Of the energy available to the $H_2 + 2CO$ products, they found 3.1% appears as rotational energy (in $v = 1$ state), 17.8% appears as the H_2 ($v = 1$) vibration, and 46.8% appears as H_2 ($v = 1$) translation.

The estimates of the values of ϕ_{III} for glyoxal photodecomposition in air as a function of wavelength are very limited. Four data points seem appropriate for use. Two are derived from the experiments of Tadić et al. (2006): 0.40 ± 0.04 at 253.7 nm ($\phi_{III} = \phi_{total} - \phi_I - \phi_{II} = 1.0 - 0.26 - 0.34$); and 0.02 the effective value for wavelengths 390–470 nm; the data of Parmenter (1964) give $\phi_{III} = 0.01$ at 435.8 nm; the data of Calvert and Layne for 313 nm photolysis provide $\phi_{III} = 0.15$. These data are plotted in figure IX-C-18, and the recommended trend line is given by the short-dashed line.

iv) Other possible processes in glyoxal photodecomposition in air Theory (*ab initio* calculations) and some experimental evidence have suggested that two other primary processes may occur in glyoxal photodecomposition, processes (IV) and (V). Process (IV) becomes energetically possible at 334 nm. Hepburn et al. (1983), Li et al. (2006), and Koch et al. (2001) have shown that the possible process (V), formation of an isomer (CHOH) of CH_2O is allowed theoretically and is predicted by *ab initio* calculations. However, experimental evidence presented for the occurrence of either of these processes is not compelling. Conceivably, the formic acid observed as a minor product of glyoxal photolysis in air by Tadić et al. (2006) could arise from the formation of the hydroxymethylene (HOCH) in process (V); its subsequent reaction with O_2 may form peroxyformic acid and subsequently, formic acid by some ill-defined route. Our current assessment of the available experimental data involves only processes (I), (II), and (III). The recommended quantum efficiencies for these three primary photodissociative processes as a function of wavelength are plotted in figure IX-C-18 and given in tabular form in table IX-C-7.

IX-C-11.3. Photolysis Frequencies for Photodecomposition of Glyoxal in the Lower Troposphere

Calculations of the *j*-values as a function of solar zenith angle have been made using the currently recommended primary quantum yields for the processes (I), (II), and (III) and the quantum yields for total decomposition (ϕ_{total}) given in table IX-C-7. In the calculations, a cloudless sky, an altitude of 500 m, and an overhead ozone column of 350 DU were assumed. These data are shown in figure IX-C-19.

Table IX-C-7. The recommended cross sections (σ, cm^2 molecule^{-1}) and quantum yields (ϕ) for the major primary processes in glyoxal as a function of wavelength (in air at 1 atm.); CH(O)C(O)H + $h\nu \rightarrow$ HCO + HCO (I); CH(O)C(O)H + $h\nu \rightarrow$ CH_2O + CO (II); CH(O)C(O)H + $h\nu \rightarrow$ H_2 + 2CO (III); cross section data are from Volkamer et al. (2005)

λ, nm	$10^{20} \times \sigma$	ϕ_I	ϕ_{II}	ϕ_{III}	ϕ_{total}	λ, nm	$10^{20} \times \sigma$	ϕ_I	ϕ_{II}	ϕ_{III}	ϕ_{total}
250	1.73	0.266	0.309	0.425	1.000	295	3.81	0.300	0.523	0.177	1.000
251	1.52	0.266	0.315	0.419	1.000	296	3.82	0.305	0.520	0.175	1.000
252	1.48	0.267	0.319	0.414	1.000	297	3.92	0.308	0.520	0.172	1.000
253	1.55	0.267	0.328	0.405	1.000	298	4.07	0.312	0.521	0.167	1.000
254	1.60	0.268	0.342	0.390	1.000	299	4.12	0.316	0.520	0.164	1.000
255	1.67	0.269	0.339	0.392	1.000	300	4.05	0.320	0.518	0.162	1.000
256	1.62	0.269	0.345	0.386	1.000	301	3.91	0.325	0.517	0.158	1.000
257	1.81	0.270	0.353	0.377	1.000	302	3.78	0.328	0.516	0.156	1.000
258	1.82	0.271	0.359	0.370	1.000	303	3.57	0.334	0.512	0.154	1.000
259	1.85	0.271	0.366	0.363	1.000	304	3.35	0.340	0.508	0.152	1.000
260	1.83	0.272	0.372	0.356	1.000	305	3.24	0.347	0.508	0.145	1.000
261	1.96	0.272	0.380	0.348	1.000	306	3.22	0.359	0.497	0.144	1.000
262	2.03	0.273	0.385	0.342	1.000	307	3.20	0.367	0.490	0.143	1.000
263	2.14	0.273	0.392	0.335	1.000	308	3.15	0.380	0.479	0.141	1.000
264	2.18	0.273	0.398	0.329	1.000	309	3.12	0.396	0.465	0.139	1.000
265	2.26	0.273	0.403	0.323	1.000	310	3.10	0.418	0.445	0.137	1.000
266	2.33	0.274	0.409	0.317	1.000	311	3.22	0.438	0.427	0.135	1.000
267	2.37	0.274	0.416	0.310	1.000	312	3.34	0.462	0.406	0.132	1.000
268	2.36	0.275	0.421	0.304	1.000	313	3.39	0.490	0.380	0.130	1.000
269	2.48	0.275	0.427	0.298	1.000	314	3.23	0.519	0.353	0.128	1.000
270	2.51	0.275	0.432	0.293	1.000	315	2.80	0.550	0.325	0.125	1.000
271	2.61	0.275	0.438	0.287	1.000	316	2.65	0.580	0.296	0.124	1.000
272	2.72	0.276	0.442	0.282	1.000	317	2.46	0.608	0.270	0.122	1.000
273	2.81	0.276	0.448	0.276	1.000	318	2.21	0.635	0.244	0.121	1.000
274	2.92	0.276	0.454	0.270	1.000	319	1.93	0.665	0.216	0.119	1.000
275	3.00	0.277	0.458	0.265	1.000	320	1.85	0.693	0.190	0.117	1.000
276	3.06	0.277	0.464	0.259	1.000	321	1.89	0.718	0.166	0.116	1.000
277	3.09	0.278	0.469	0.253	1.000	322	1.77	0.740	0.146	0.114	1.000
278	3.08	0.278	0.472	0.250	1.000	323	1.72	0.760	0.128	0.112	1.000
279	3.09	0.278	0.478	0.244	1.000	324	1.68	0.776	0.114	0.110	1.000
280	3.14	0.279	0.483	0.238	1.000	325	1.60	0.795	0.098	0.107	1.000
281	3.22	0.279	0.487	0.234	1.000	326	1.61	0.805	0.089	0.106	1.000
282	3.32	0.280	0.490	0.230	1.000	327	1.70	0.816	0.080	0.105	1.001
283	3.45	0.280	0.493	0.227	1.000	328	1.94	0.822	0.070	0.104	0.996
284	3.57	0.280	0.497	0.223	1.000	329	1.86	0.823	0.061	0.103	0.987
285	3.67	0.280	0.500	0.220	1.000	330	1.69	0.822	0.055	0.101	0.978
286	3.80	0.281	0.504	0.215	1.000	331	1.13	0.817	0.048	0.100	0.965
287	3.79	0.282	0.512	0.206	1.000	332	1.05	0.808	0.040	0.098	0.946
288	3.81	0.283	0.513	0.204	1.000	333	0.97	0.795	0.035	0.097	0.927
289	3.80	0.284	0.515	0.201	1.000	334	0.92	0.780	0.028	0.096	0.904
290	3.73	0.285	0.518	0.197	1.000	335	0.74	0.765	0.021	0.095	0.881
291	3.64	0.288	0.520	0.192	1.000	336	0.63	0.750	0.017	0.094	0.861
292	3.65	0.290	0.522	0.188	1.000	337	0.59	0.729	0.012	0.092	0.833
293	3.68	0.294	0.522	0.184	1.000	338	0.65	0.715	0.009	0.091	0.815
294	3.73	0.297	0.523	0.180	1.000	339	0.59	0.700	0.003	0.089	0.792

(*continued*)

Table IX-C-7. (*continued*)

λ, nm	$10^{20} \times \sigma$	ϕ_I	ϕ_{II}	ϕ_{III}	ϕ_{total}	λ, nm	$10^{20} \times \sigma$	ϕ_I	ϕ_{II}	ϕ_{III}	ϕ_{total}
340	0.55	0.684	0.002	0.087	0.772	390	3.48	0.285	0.000	0.036	0.321
341	0.56	0.671	0.000	0.086	0.757	391	3.92	0.272	0.000	0.037	0.309
342	0.51	0.661	0.000	0.085	0.746	392	3.80	0.257	0.000	0.037	0.294
343	0.50	0.650	0.000	0.084	0.734	393	2.85	0.244	0.000	0.035	0.279
344	0.65	0.640	0.000	0.083	0.723	394	3.15	0.227	0.000	0.034	0.261
345	0.62	0.632	0.000	0.082	0.714	395	3.85	0.213	0.000	0.034	0.247
346	0.73	0.625	0.000	0.081	0.706	396	3.68	0.200	0.000	0.034	0.234
347	0.63	0.619	0.000	0.080	0.699	397	3.36	0.185	0.000	0.034	0.219
348	0.60	0.613	0.000	0.078	0.691	398	4.32	0.174	0.000	0.032	0.206
349	0.42	0.607	0.000	0.077	0.684	399	4.35	0.160	0.000	0.030	0.190
350	0.39	0.600	0.000	0.076	0.676	400	3.87	0.150	0.000	0.031	0.181
351	0.40	0.591	0.000	0.075	0.666	401	4.46	0.135	0.000	0.030	0.165
352	0.42	0.582	0.000	0.074	0.656	402	5.84	0.120	0.000	0.029	0.149
353	0.42	0.573	0.000	0.072	0.645	403	7.16	0.105	0.000	0.028	0.133
354	0.40	0.565	0.000	0.070	0.635	404	6.24	0.090	0.000	0.027	0.117
355	0.42	0.555	0.000	0.069	0.624	405	4.49	0.075	0.000	0.026	0.101
356	0.44	0.546	0.000	0.068	0.614	406	4.48	0.060	0.000	0.025	0.085
357	0.43	0.536	0.000	0.067	0.603	407	4.07	0.045	0.000	0.025	0.070
358	0.47	0.528	0.000	0.066	0.594	408	3.44	0.030	0.000	0.024	0.054
359	0.50	0.518	0.000	0.066	0.584	409	4.01	0.015	0.000	0.023	0.038
360	0.55	0.510	0.000	0.065	0.575	410	5.66	0.000	0.000	0.022	0.022
361	0.63	0.503	0.000	0.064	0.567	411	7.22	0.000	0.000	0.021	0.021
362	0.71	0.495	0.000	0.063	0.558	412	7.41	0.000	0.000	0.020	0.020
363	0.64	0.487	0.000	0.062	0.549	413	10.75	0.000	0.000	0.019	0.019
364	0.68	0.480	0.000	0.061	0.541	414	10.12	0.000	0.000	0.018	0.018
365	0.67	0.472	0.000	0.060	0.532	415	10.19	0.000	0.000	0.017	0.017
366	0.74	0.467	0.000	0.059	0.526	416	6.07	0.000	0.000	0.016	0.016
367	0.86	0.460	0.000	0.058	0.518	417	6.83	0.000	0.000	0.015	0.015
368	1.01	0.454	0.000	0.057	0.511	418	7.87	0.000	0.000	0.014	0.014
369	1.06	0.448	0.000	0.056	0.504	419	9.13	0.000	0.000	0.014	0.014
370	1.14	0.443	0.000	0.055	0.498	420	5.60	0.000	0.000	0.013	0.013
371	1.19	0.438	0.000	0.054	0.492	421	7.19	0.000	0.000	0.012	0.012
372	1.14	0.433	0.000	0.053	0.486	422	6.99	0.000	0.000	0.012	0.012
373	1.21	0.428	0.000	0.052	0.480	423	13.05	0.000	0.000	0.011	0.011
374	1.35	0.423	0.000	0.051	0.474	424	8.24	0.000	0.000	0.010	0.010
375	1.33	0.418	0.000	0.050	0.468	425	10.45	0.000	0.000	0.009	0.009
376	1.38	0.412	0.000	0.049	0.461	426	16.41	0.000	0.000	0.009	0.009
377	1.47	0.404	0.000	0.048	0.452	427	16.10	0.000	0.000	0.008	0.008
378	1.61	0.400	0.000	0.047	0.447	428	21.42	0.000	0.000	0.007	0.007
379	1.53	0.395	0.000	0.046	0.441	429	6.50	0.000	0.000	0.006	0.006
380	1.93	0.387	0.000	0.045	0.432	430	7.03	0.000	0.000	0.005	0.005
381	2.46	0.381	0.000	0.044	0.425	431	6.52	0.000	0.000	0.004	0.004
382	2.02	0.373	0.000	0.043	0.416	432	6.08	0.000	0.000	0.003	0.003
383	2.07	0.365	0.000	0.042	0.407	433	5.66	0.000	0.000	0.002	0.002
384	1.94	0.356	0.000	0.041	0.397	434	6.81	0.000	0.000	0.000	0.000
385	1.89	0.345	0.000	0.040	0.385	435	7.66	0.000	0.000	0.000	0.000
386	1.84	0.335	0.000	0.040	0.375						
387	2.29	0.324	0.000	0.039	0.363						
388	3.00	0.312	0.000	0.039	0.351						
389	3.21	0.298	0.000	0.037	0.335						

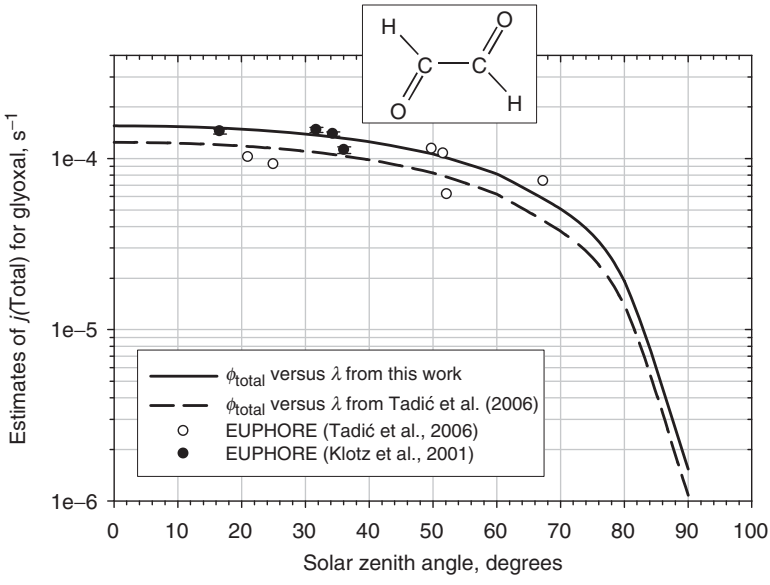

Figure IX-C-19. Estimated *j*-values for the decomposition of glyoxal in the lower troposphere as a function of solar zenith angle. Cloudless sky conditions were assumed with an overhead ozone column of 350 DU. The solid curves and dashed curves were calculated using the current quantum yields recommendations (table IX-C-7) and those given by Tadić et al. (2006), respectively. The open circles are experimental measurements made in the EUPHORE chamber in natural sunlight by Tadić et al. (2006) and the filled circles are from similar measurements reported by Klotz et al. (2001).

In figure IX-C-19 a qualitative agreement is seen between the directly measured *j*-values and those calculated using the equation (I) of section IX-A-1 with the solar flux, ϕ, and σ as estimated as a function of λ. *j*-Values calculated using the current recommendations of total ϕ and those of Tadić et al. (2006) appear to fit the direct data reasonably well. Scatter between the results of the two methods of estimating *j*-values must reflect in part differences in the assumed atmospheric conditions used in the *j*-value calculations and those present at the time of the direct measurements (e.g., presence of clouds and haze, and differences in the assumed ozone column). There is little information today on the temperature dependence of the various quantum yields particularly at the longer wavelengths where glyoxal absorption is very large. However, for the higher elevations in the troposphere, where less quenching of the decomposition will occur and the solar flux is increased greatly over that at ground level, *j*-values for glyoxal are expected to rise significantly. In making calculation of *j*-values for glyoxal within the upper troposphere, we recommend that the current values of ϕ be used since the contributing elements required in the *j*-calculation are present; a rough extrapolation to expected values of ϕ_I at the pressures of the upper troposphere can be made using the equation relating $\log_{10}(k_q/k_d)$ and $[N_2]$. (See section IX-C-11.2 and figure IX-C-17 and the wavelength dependence of $(\phi_I)_{P=0}$ given in figure IX-C-16.)

IX-C-12. The Photodecomposition of Methylglyoxal [2-Oxo-propanal, $CH_3C(O)C(O)H$]

Methylglyoxal is a significant product of the oxidation of the natural hydrocarbon, isoprene, as well as many other hydrocarbons present in the urban environment. Its photodecomposition is expected to be a major source of free radicals that help drive tropospheric ozone formation. Significant new information has appeared since our last review of photochemistry of methylglyoxal in air (Calvert et al., 2000), and an updated review is given here. Several modes of primary photodecomposition have been suggested to describe methylglyoxal photodecomposition (e.g., see Staffelbach et al., 1995; Koch and Moortgat, 1998; and Chen et al., 2000):

$$CH_3COCHO + h\nu \rightarrow CH_3CO + HCO \quad \text{(I)}$$

$$\rightarrow CH_3 + CO + HCO \quad \text{(II)}$$

$$\rightarrow CH_3CO + H + CO \quad \text{(III)}$$

$$\rightarrow CH_3 + 2CO + H \quad \text{(IV)}$$

$$\rightarrow CH_4 + 2CO \quad \text{(V)}$$

$$\rightarrow CH_3CHO + CO \quad \text{(VI)}$$

The processes (I) through (IV) become energetically feasible at wavelengths (nm) shorter than 420, 350, 342, and 293, respectively. Pathways (V) and (VI) appear to be unimportant in tropospheric chemistry, although they are energetically feasible at all wavelengths absorbed by methylglyoxal. Process (I) appears to be the dominant photodecomposition mode for tropospheric conditions. Processes (II) and (III) may occur to some extent at the shorter wavelengths (Staffelbach et al., 1995).

IX-C-12.1. Absorption Cross Sections of Methylglyoxal

Measurements by Meller et al. (1991) and Staffelbach et al. (1995) are in fairly good agreement, but are about a factor of 2 higher than earlier measurements by Plum et al. (1983). The preferred values (see table IX-C-8 and figure IX-C-20) are the averages based on the two more recent measurements (Sander et al., 2006).

IX-C-12.2. Quantum Yields of the Primary Photodecomposition Processes in Methylglyoxal

The many different products obtained in previous studies of methylglyoxal photodecomposition in air (CO, CO_2, CH_2O, CH_3CO_2H, CH_3COO_2H, CH_3OH, and HCO_2H (see Staffelbach et al., 1995; Koch and Moortgat, 1998) are those expected following the occurrence of process (I), (II), or (III). An additional product, CH_3CHO, observed by

Table IX-C-8. Recommended cross sections (σ, cm^2 molecule^{-1}) from Sander et al. (2006) and quantum yields for photodecomposition (ϕ_{total}) at 1 atm. for methylglyoxal recommended from this study

λ, nm	$10^{20} \times \sigma$	ϕ_{total}	λ, nm	$10^{20} \times \sigma$	ϕ_{total}	λ, nm	$10^{20} \times \sigma$	ϕ_{total}
220	1.45	1.00	266	3.73	1.00	312	2.06	1.00
221	1.44	1.00	267	3.87	1.00	313	1.97	1.00
222	1.43	1.00	268	4.02	1.00	314	1.90	1.00
223	1.44	1.00	269	4.13	1.00	315	1.86	1.00
224	1.43	1.00	270	4.20	1.00	316	1.86	1.00
225	1.44	1.00	271	4.22	1.00	317	1.87	1.00
226	1.46	1.00	272	4.23	1.00	318	1.82	1.00
227	1.48	1.00	273	4.27	1.00	319	1.68	1.00
228	1.51	1.00	274	4.31	1.00	320	1.50	1.00
229	1.53	1.00	275	4.37	1.00	321	1.34	1.00
230	1.60	1.00	276	4.49	1.00	322	1.22	1.00
231	1.61	1.00	277	4.64	1.00	323	1.14	1.00
232	1.65	1.00	278	4.77	1.00	324	1.01	1.00
233	1.67	1.00	279	4.87	1.00	325	0.92	1.00
234	1.75	1.00	280	4.92	1.00	326	0.85	1.00
235	1.83	1.00	281	4.93	1.00	327	0.77	1.00
236	1.86	1.00	282	4.90	1.00	328	0.72	0.995
237	1.93	1.00	283	4.83	1.00	329	0.67	0.99
238	1.96	1.00	284	4.76	1.00	330	0.65	0.98
239	2.00	1.00	285	4.70	1.00	331	0.62	0.95
240	2.07	1.00	286	4.66	1.00	332	0.61	0.93
241	2.14	1.00	287	4.65	1.00	333	0.53	0.91
242	2.19	1.00	288	4.73	1.00	334	0.53	0.87
243	2.23	1.00	289	4.84	1.00	335	0.50	0.82
244	2.27	1.00	290	4.92	1.00	336	0.45	0.76
245	2.30	1.00	291	4.90	1.00	337	0.41	0.71
246	2.33	1.00	292	4.81	1.00	338	0.36	0.67
247	2.38	1.00	293	4.70	1.00	339	0.35	0.65
248	2.46	1.00	294	4.57	1.00	340	0.32	0.62
249	2.57	1.00	295	4.37	1.00	341	0.30	0.60
250	2.64	1.00	296	4.17	1.00	342	0.29	0.58
251	2.68	1.00	297	4.00	1.00	343	0.29	0.56
252	2.71	1.00	298	3.88	1.00	344	0.29	0.54
253	2.73	1.00	299	3.76	1.00	345	0.30	0.52
254	2.76	1.00	300	3.69	1.00	346	0.31	0.50
255	2.82	1.00	301	3.70	1.00	347	0.33	0.48
256	2.93	1.00	302	3.74	1.00	348	0.34	0.46
257	3.06	1.00	303	3.74	1.00	349	0.36	0.44
258	3.17	1.00	304	3.62	1.00	350	0.39	0.42
259	3.25	1.00	305	3.38	1.00	351	0.42	0.41
260	3.29	1.00	306	3.15	1.00	352	0.46	0.40
261	3.33	1.00	307	2.92	1.00	353	0.49	0.39
262	3.36	1.00	308	2.71	1.00	354	0.52	0.38
263	3.42	1.00	309	2.52	1.00	355	0.56	0.36
264	3.49	1.00	310	2.34	1.00	356	0.60	0.35
265	3.59	1.00	311	2.18				

(*continued*)

Table IX-C-8. (*continued*)

λ, nm	$10^{20} \times \sigma$	ϕ_I	λ, nm	$10^{20} \times \sigma$	ϕ_I	λ, nm	$10^{20} \times \sigma$
357	0.64	0.34	401	5.90	0.075	445	9.62
358	0.68	0.33	402	6.07	0.073	446	8.91
359	0.72	0.32	403	6.36	0.070	447	9.84
360	0.77	0.30	404	6.55	0.067	448	9.19
361	0.82	0.29	405	6.92	0.065	449	10.10
362	0.87	0.28	406	7.20	0.062	450	8.68
363	0.93	0.27	407	7.59	0.060	451	6.35
364	1.00	0.26	408	7.95	0.058	452	6.33
365	1.08	0.25	409	8.12	0.055	453	6.08
366	1.15	0.25	410	8.52	0.054	454	4.47
367	1.23	0.24	411	8.64	0.053	455	3.69
368	1.31	0.23	412	9.07	0.051	456	3.09
369	1.40	0.22	413	9.38	0.048	457	2.47
370	1.47	0.21	414	9.62	0.047	458	1.81
371	1.55	0.21	415	9.69	0.046	459	1.28
372	1.64	0.20	416	9.72	0.045	460	0.91
373	1.73	0.19	417	10.00	0.043	461	0.80
374	1.81	0.19	418	10.10	0.042	462	0.64
375	1.90	0.18	419	10.10	0.041	463	0.48
376	2.02	0.18	420	10.20	0.040	464	0.33
377	2.10	0.17	421	10.30	0.039	465	0.27
378	2.18	0.17	422	10.50	0.038	466	0.23
379	2.30	0.16	423	10.50	0.037	467	0.19
380	2.42	0.16	424	10.20	0.036	468	0.16
381	2.54	0.15	425	10.30	0.035	469	0.13
382	2.70	0.15	426	10.20	0.034	470	0.11
383	2.88	0.14	427	9.85	0.032	471	0.10
384	3.03	0.14	428	10.00	0.031	472	0.09
385	3.20	0.14	429	9.94	0.030	473	0.08
386	3.39	0.13	430	10.40	0.029	474	0.07
387	3.61	0.13	431	10.50	0.029	475	0.06
388	3.71	0.12	432	9.79	0.028	476	0.06
389	3.88	0.12	433	10.60	0.027	477	0.05
390	4.03	0.11	434	10.50	0.026	478	0.05
391	4.22	0.11	435	10.80	0.026	479	0.05
392	4.31	0.11	436	11.10	0.025	480	0.04
393	4.47	0.10	437	10.00	0.025	481	0.04
394	4.57	0.098	438	10.60	0.024	482	0.03
395	4.67	0.095	439	11.00	0.023	483	0.03
396	4.87	0.091	440	9.94	0.022	484	0.03
397	5.08	0.087	441	10.4	0	485	0.02
398	5.26	0.085	442	10.2	0	486	0.02
399	5.46	0.081	443	10.2	0	487	0.02
400	5.62	0.078	444	11.2	0		

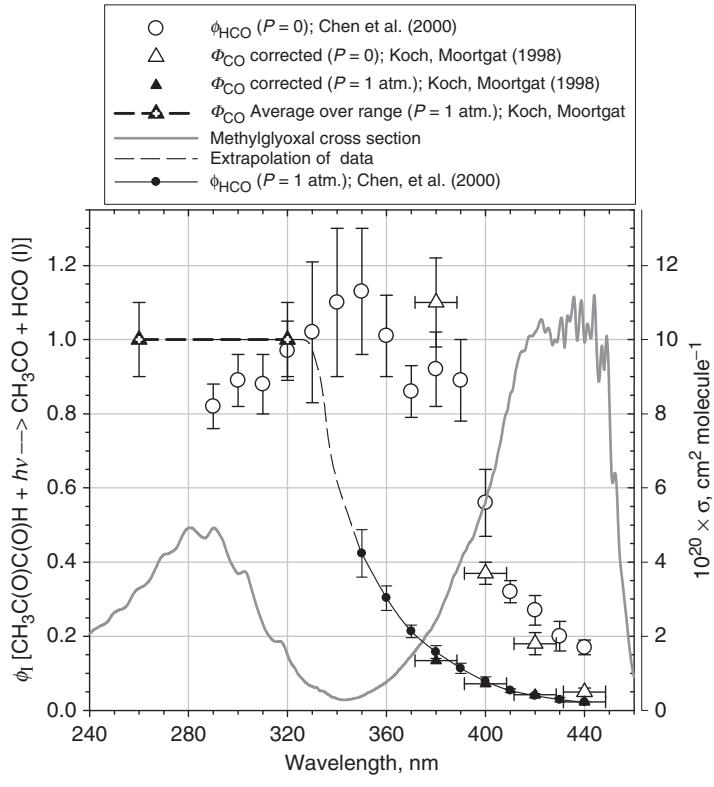

Figure IX-C-20. Quantum yield data for the photodecomposition of methylglyoxal as a function of wavelength. Absorption spectrum for methylglyoxal is shown as the light-gray line.

Raber and Moortgat (1996) and Koch and Moortgat (1998) does not confirm the occurrence of process (VI), since CH_3CHO appears to have been formed by heterogeneous photodecomposition of methylglyoxal at the wall of the quartz reactor. No acetaldehyde was observed in the stainless steel reactor of Staffelbach et al. (1995), and it appears likely that ϕ_{VI} is near zero. No methane has been detected among the products, and ϕ_V must be near zero.

Many of the previous studies (Staffelbach et al., 1995; Raber and Moortgat, 1996; Koch and Moortgat, 1998) have involved the broadband photolysis of methylglyoxal in air, using various filters to isolate bands of radiation from various light sources, so conclusions about the wavelength dependence of the quantum yields of the various primary processes can be defined only qualitatively.

First evidence of the occurrence of process (I) and the wavelength dependence of ϕ_I was given by Staffelbach et al. (1995) who concluded (I) was the dominant mode of photodecomposition of methylglyoxal in the troposphere. Their data suggested that the effective quantum yield of photodecomposition of methylglyoxal was below unity at all of the broadband wavelength regions they studied. Koch and Moortgat (1998) measured Φ_{CO} in broad band (8.5 nm) photolyses of methylglyoxal in air at wavelengths centered

at 440, 420, 400, and 380 nm. The CO product arose from the reaction of the primary HCO product of reaction (I) with O_2 : $HCO + O_2 \rightarrow CO + HO_2$. These data are shown as the open triangles in figure IX-C-20. Using their excited methylglyoxal–air quenching constants, they derived average quantum yields for photodecomposition in 1 atm. of air, shown as the closed triangles in figure IX-C-20. In broadband studies (260–320 nm) they found the effective Φ_{CO} was near unity and added air was ineffective in quenching CO formation. They concluded that $\phi_I \approx 1.0$ in this wavelength range. These data are plotted in figure IX-C-20 as the triangles with plus sign inserts.

The unambiguous identification of the HCO radical and the determination of the wavelength dependence of its quantum yields by Chen et al. (2000) have brought important new information on the mechanism of methyglyoxal photodecomposition. The results of Chen et al. from photodecomposition extrapolated to zero pressure are shown in figure IX-C-20 as the open circles. Reasonable agreement can be seen between these data determined at specific wavelengths of light and the broadband studies of Kock and Moortgat (1998) shown as the triangles in figure IX-C-20. Kock and Moortgat (1998) and Chen et al. (2000) have shown that photodecomposition of the methylglyoxal molecules excited at $\lambda \geq 380$ nm are significantly quenched by added nitrogen gas, and typical Stern–Volmer quenching dependence on pressure was observed: $[1/(\phi_I)_p = 1/(\phi_I)_{p=0} + (k_q/k_d) \times P]$. As with many other carbonyl compounds, the quenching of the excited molecules is most significant at the longer wavelengths (lower energies) of excitation. A plot of the ratios of k_q/k_d measured by Chen et al. (2000) as a function of $1/\lambda$ is given in figure IX-C-21.

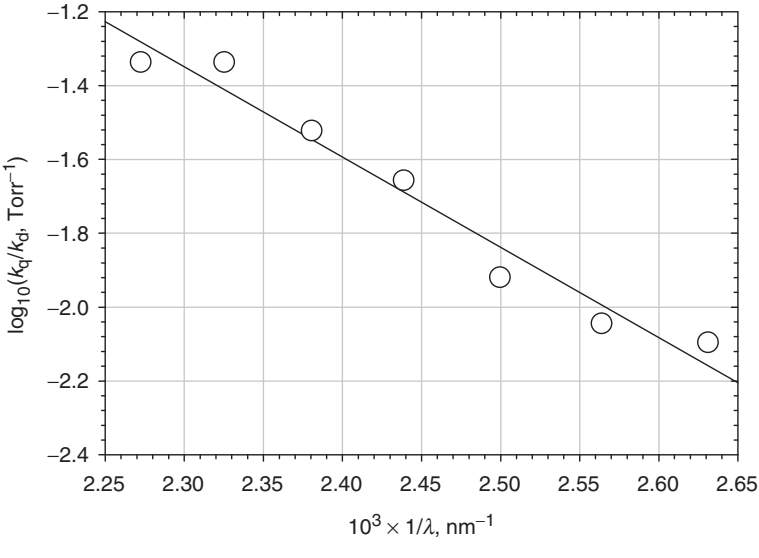

Figure IX-C-21. Plot of the rate coefficients (k_q/k_d, $Torr^{-1}$) for quenching of HCO formation in the photolysis of methylglyoxal as a function of wavelength of excitation; the least-squares line shown is given by: $\log_{10}(k_q/k_d, Torr^{-1}) = 4.276 - 2{,}445.53/\lambda$ (nm); data are from Chen et al. (2000).

The data are described by the equation: $\log_{10}(k_q/k_d,\ \text{Torr}^{-1}) = 4.276 - 2{,}445.53/\lambda\,(\text{nm})$. We used this relation to adjust the measured $(\phi_I)_{p=0}$ values to ϕ_I values expected for methylglyoxal photolysis in 1 atm. of N_2. These adjusted values are plotted in figure IX-C-20 as the small filled circles. For the same wavelength region of excitation, the extent of quenching by air (N_2, O_2 mixtures) as derived by Koch and Moortgat (1998) is very similar to that observed by Chen et al. (2000), and we have assumed in our present study that the equation derived from the N_2 quenching data is also applicable for the quenching expected by air. No quenching of the photodecomposition of methylglyoxal excited at wavelengths within the second absorption band ($\lambda < 340$ nm) was observed by Chen et al. and Koch and Moortgat. Both these research groups concluded that the total quantum efficiency of photodecomposition of methylglyoxal is near unity for $\lambda < 340$ nm. Although the scatter is rather large in the Chen et al. (2000) data for the 340–290 nm range,the steady decline seen in the ϕ_{HCO} values as the wavelength is decreased (figure IX-C-20) together with the Koch and Moortgat observation of Φ_{CO} near unity for $\lambda < 340$ nm, suggests that the onset of another photodecomposition mode. Possibly process (III) may occur near 320 nm with increasing importance at the shorter wavelengths. The CO product measured by Koch and Moortgat would be derived from both the occurrence of process (I) and (III). If the measurements of $\Phi_{CO} \approx 1.0$ are correct for wavelengths below 310 nm, then the onset of process (III) is favored over (II) since two CO molecules will be formed in (II) for photolyses in air. However, Staffelbach et al. found that the product distribution from photolyses that included the short-wavelength region (240–420 nm) was somewhat different; less CO_2, CH_3COO_2H, and CH_3CO_2H were obtained per molecule of methylglyoxal lost, while CO increased. They suggested that the onset of process (II) at the shorter wavelengths may account for this. The allocation of the extent of occurrence of processes (I) and (III) is unimportant for our purposes, since the net atmospheric chemistry that results from the occurrence of both (I) and (III) is exactly the same. A knowledge of the relative importance of primary processes (II) and (III) at $\lambda < 320$ nm is important since different product distributions are expected from the occurrence of each. However, this information remains unclear at this writing.

The study of Staffelbach et al. (1995) confirmed the findings of Barnes et al. (1982b) and Jenkin et al. (1993a) that a significant occurrence of HO_2 radical addition to methylglyoxal occurs following methylyglyoxal photodissociation in air. A limited knowledge of the rate coefficient for this reaction and the possible reverse reaction complicated quantum yield estimates which required corrections for this occurrence. However, computer simulations by Staffelbach et al. (1995) of the reactions following photodecomposition of methylglyoxal indicated that as much as one-half of the methylglyoxal loss resulted from the HO_2 radical addition reaction.

From our current evaluation of the data, we conclude that the variation in the quantum yield of photodecomposition of methylglyoxal by all processes is described at least qualitatively by the black solid and dashed lines in figure IX-C-20; the ϕ_{total} values that describe these curves are given in table IX-C-8 and are used in deriving the present best estimate of the photolysis frequencies for methylglyoxal that are given in the following section.

IX-C-12.3. Photolysis Frequencies for the Photodissociation of Methylglyoxal in the Lower Troposphere

Calculations of the *j*-values as a function of solar zenith angle have been made using the currently recommended total primary quantum yields for total decomposition (ϕ_{total}) and the recommended cross sections given in table IX-C-8. These data are shown in figure IX-C-22.

Also shown in figure IX-C-22 are data points obtained in sunlight in experiments in the EUPHORE chamber (Klotz et al., 2001). The filled circles represent measurement under clear-sky conditions; the open circles were from measurement during overcast conditions. It is evident that our current estimated *j*-values fall far below the clear-sky values measured in the EUPHORE chamber. Klotz et al. (2001) reported that their observed rates of photodecomposition of methylglyoxal were much larger than those expected from calculations using their best estimates of σ and ϕ values. They considered the potential problem of loss of methylglyoxal through the HO_2 addition reaction, and they concluded that further work would be necessary to find the cause of this difference. If one assumes the *j*-value estimates made in our present study are correct, then to match the larger estimates found experimentally by Klotz et al. (2001), the extent of interference due to the HO_2–methylglyoxal reaction must be large; that is, the product, $[HO_2]k_{HO_2\text{-Methylglyoxal}}$, must be in the range $(7.6 - 9.9) \times 10^{-5}\ s^{-1}$. If the current estimates of $k_{HO_2\text{-Methylglyoxal}}$, 2×10^{-15} (Barnes et al., 1982b) and

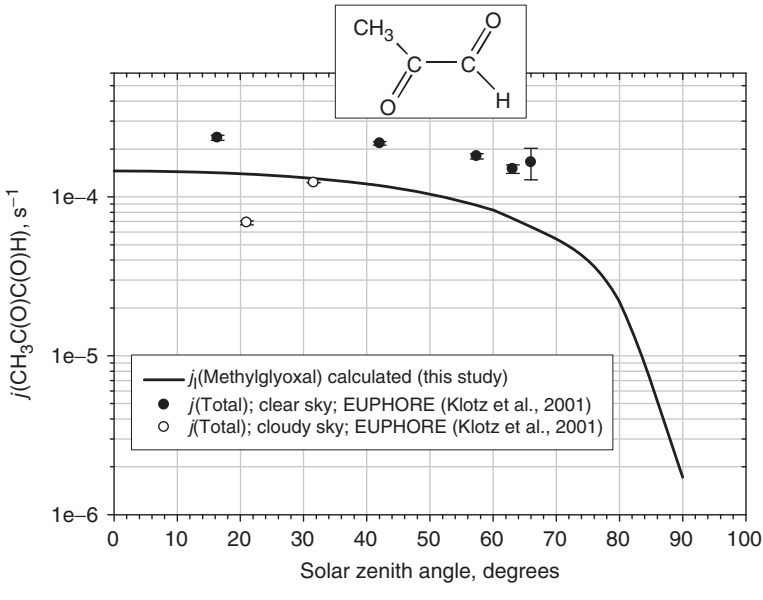

Figure IX-C-22. Calculated photolysis frequencies as a function of solar zenith angle for methylglyoxal photodecomposition in the lower troposphere; clear-sky conditions are assumed with an ozone column of 350 DU. The large differences between the EUPHORE estimates and the *j*-values calculated from ϕ, σ, and actinic flux data may reflect the removal of methylglyoxal by HO_2 radicals that could not be eliminated in the EUPHORE experiments.

$(1.4 \pm 0.5) \times 10^{-15}$ cm^3 molecule^{-1} s^{-1}(Staffelbach et al., 1995) are correct, then the [HO_2] in the EUPHORE chamber experiments would have to be in the range $(3.8 - 7.1) \times 10^{10}$ molecules cm^3; this is about four times larger than that predicted by the computer simulations of the chemistry in the EUPHORE chamber made by Klotz et al. (2001). Such simulations are of limited value, however, since the nature and extent of the impurities present in the methylglyoxal–air mixture used in the chamber are unknown. Alternatively, a match can be had if $k_{HO_2\text{-Methylglyoxal}}$ is about four times that estimated by Staffelbach et al. Obviously, further work will be necessary to establish the correct *j*-values for methylglyoxal. Until the results from such studies are available, we recommend the use of *j*-values calculated using the input ϕ and σ data given here as shown by the solid line in figure IX-C-22 and the data of table IX-C-8.

IX-C-13. Photodecomposition of Some Aldehydes Derived from Biogenic Hydrocarbons

IX-C-13.1. Photodecomposition of Pinonaldehyde

Pinonaldehyde is a major product of the atmospheric oxidation of an important monoterpene, α-pinene, that is emitted by vegetation. The absorption spectrum of pinonaldehyde is similar to that of the simple aldehydes (Hallquist et al., 1997). See figure IX-C-23. The two biogenic aldehydes shown have absorptions that are somewhat greater than twice those of acetaldehyde at a given wavelength. Both pinonaldehyde and caronaldehyde contain two nonadjacent carbonyl bonds. As Hallquist

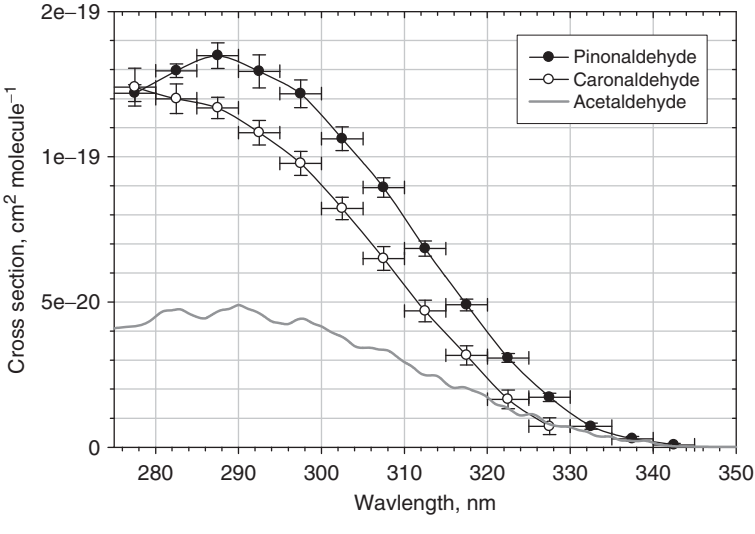

Figure IX-C-23. Absorption cross sections for pinonaldehyde and caronaldehyde (Hallquist et al., 1997) where the cross sections have been averaged over 5 nm bandwidths. Shown for comparison are the cross sections for acetaldehyde (Martinez et al., 1992).

et al. (1997) point out, as a first approximation, carbonyl group absorption is additive so that a molecule with two separated carbonyl groups has about twice the absorption of a molecule having a single carbonyl group. However, when the two carbonyl groups are on adjacent carbon atoms in a molecule (like glyoxal, methyl glyoxal, and biacetyl), the two carbonyl groups interact to constitute a new chromophore with different properties; the same situation exists when the carbonyl groups are in conjugation with C=C double bonds (as in butandienal and 2,4-hexadiendial). In these cases, the carbonyls do not act independently, and the cross section is related to the energy levels associated with the molecular orbitals of the new chromophore, i.e.., R(C=O)CH=CHC(=O)R, R(C=O)CH=CHCH=CH(C=O)R.

The photodecomposition of pinonaldehyde has been studied by several research groups (Glasius et al., 1997; Hallquist et al., 1997; Alvarado et al., 1998; Nozière et al., 1999b; Hjorth et al., 2002; Jaoui and Kamens, 2003). Glasius et al. (1997) photolyzed pinonaldehyde in a 480 liter, Teflon®-coated reaction chamber, and reported that the average photolysis and wall loss constant in their system was between 1×10^{-4} and 2×10^{-4} s^{-1} with the wall loss term of $(2.9 \pm 0.3) \times 10^{-5}$ s^{-1}; thus the photolysis constant for pinonaldehyde for their system was in the range 0.7×10^{-4} to 1.7×10^{-4} s^{-1}. What fraction of this rate resulted from the OH radical attack following photodecomposition is unknown.

The reported *j*-value measurements for pinonaldehyde photodecomposition made in the EUPHORE chamber (Moortgat et al., 2002) are: 1.14×10^{-5} and 1.10×10^{-5} s^{-1} for solar zenith angles of 21.2° and 24.5°, respectively. These values are significantly lower than those estimated by Glasius et al. (1997). The $j(NO_2)$ values at the time of these measurements were: 9.47×10^{-3} and 8.88×10^{-3} s^{-1}, respectively. The effective quantum yield was estimated to be ~0.14.

The major product of the photolysis of pinonaldehyde is norpinonaldehyde (20.1%) as measured by Jaoui and Kamens (2003). This suggests that the primary process (I) and reaction mechanism X-C-13.1 occurs.

Other products that have been identified by Jaoui and Kamens in photolyses of pinonaldehyde in the presence of an OH scavenger (cyclohexane) are: 3-acetyl-2,2-dimethyl-cyclobutyl-methanol (2.7%), 3-oxo-2,2-dimethyl-cyclobutyl-methanal (1.8%), 2,2,3-trimethyl-cyclobutyl-ethanone (1.3%), 10-hydroxypinonaldehyde (1.0%), 4-oxopinonaldehyde (1.0%), 10-oxonorpinonaldehyde (1.0%), 2,2-dimethyl-cyclobutyl-1-methanal-3-ethanal (0.7%), and pinonic acid (0.4%). Acetaldehyde and acetone were observed as minor products that may reflect the occurrence of the Norrish type-II photodecomposition. It is interesting to note that a tertiary hydrogen-atom abstraction by either of the carbonyl groups of a gamma-hydrogen atom present in both of these compounds could lead to these products following rearrangement of the enol forms of the initial products. Primary process (I) was considered to be the major pathway of photodecomposition, but additional minor primary processes were considered by Jaoui and Kamens that mirror the reactions considered for the smaller acyclic aldehydes: $RCHO + h\nu \rightarrow RH + CO$(II); $RCHO + h\nu \rightarrow RCO + H$ (III). An assumed average quantum yield of photodecomposition of ~0.4 was found to simulate their experimental results well. This value is significantly higher than that derived from EUPHORE chamber studies (0.14). Approximate photolysis frequencies

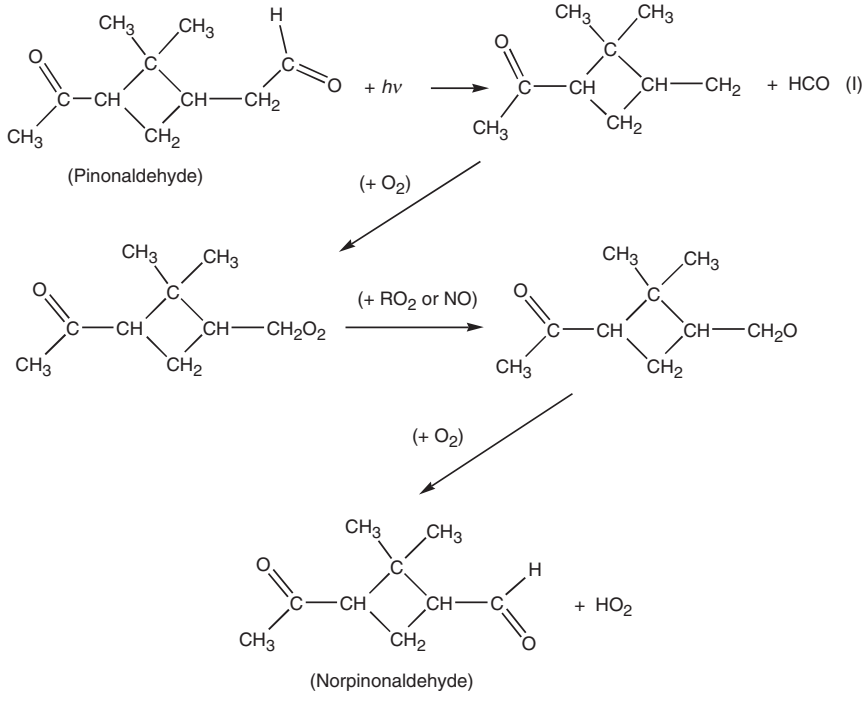

Reaction mechanism X-C-13.1

for the photodecomposition of pinonaldehyde have been calculated as a function of solar zenith angle for clear-sky conditions at 0.5 km altitude and an overhead ozone column of 350 DU, assuming the quantum yield of photodecomposition to be 0.14, as estimated in the EUPHORE experiments (Moortgat et al., 2002). These data are shown in figure IX-C-24.

The various estimates of photolysis frequencies for pinonaldehyde differ significantly, but the data of figure IX-C-24 are recommended for use in simulations of the lower troposphere, since the conditions for the EUPHORE experiments were well defined. It is evident that photodecomposition is an important mode of decay of pinonaldehyde in the troposphere.

IX-C-13.2. Photodecomposition of Caronaldehyde

Caronaldehyde is a major product of the reaction of OH or O_3 with Δ^3-carene, a common terpene emitted by biogenic sources. Its structure is similar to that of pinonaldehyde, with a 3-membered cyclopropane ring replacing the cyclobutane ring

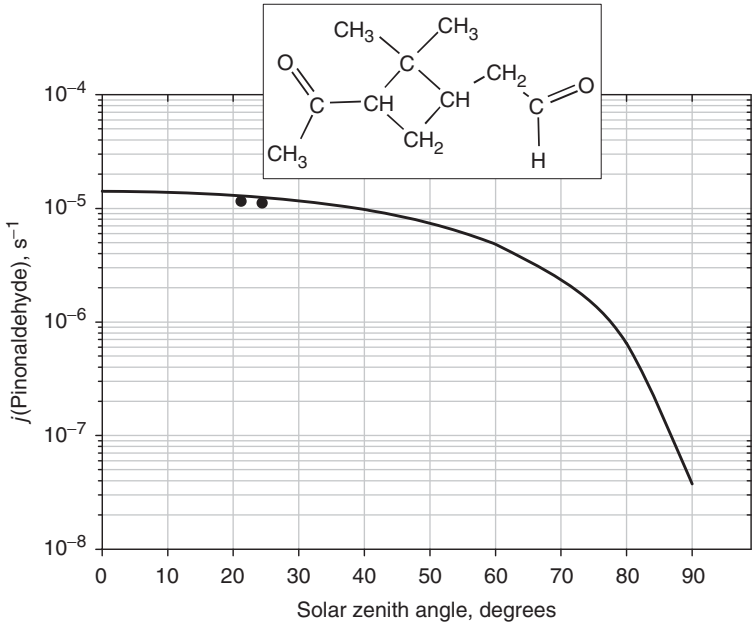

Figure IX-C-24. Approximate photolysis frequencies for pinonaldehyde versus solar zenith angle as calculated for a clear tropospheric sky at an altitude of 0.5 km and an overhead ozone column of 350 DU. An effective quantum yield of 0.14, independent of wavelength, has been assumed as suggested from EUPHORE experiments (Moortgat et al., 2002). The two filled circles are measured values from the EUPHORE chamber.

in pinonaldehyde:

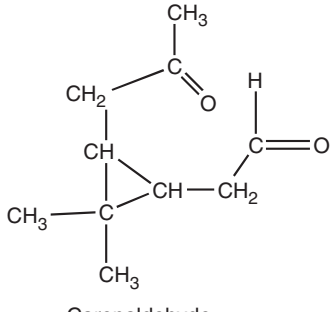

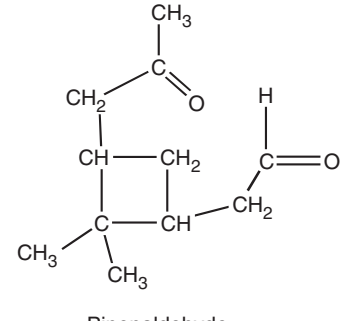

The absorption spectra of the two carbonyl compounds are similar, reflecting the absorption due to the two, well-separated, carbonyl groups; see figure IX-C-23. There are no published data related to the photodecomposition of caronaldehyde, but it is likely that the pathways for reaction are similar to those observed for pinonaldehyde. In the

absence of definitive information on this compound, in modeling the photodecomposition of this compound a tentative use of an effective quantum yield of decomposition equal to that observed in pinonaldehyde (0.14) is suggested.

IX-C-14. Effects of the of Halogen Atom-Substitution on the Absorption Spectra of Aldehydes

The halogen-containing alkanes (HFCs and HCFCs) that have largely replaced the chlorofluorocarbons intentionally contain H-atoms as well as Cl- and F-atoms, and their oxidation in the troposphere, initiated largely by OH attack on these H-atoms, can lead to aldehydes and ketones that contain chlorine and fluorine. Many of these species are photochemically active in the wavelength region present in sunlight within the troposphere and, thus, their photochemistry is of interest. In this section, we review the limited data related to the photodecomposition processes in the halogen-atom-substituted aldehydes.

Following the discussion of Calvert et al. (2008), we note that substitution of an OH group or Cl-atom for an H-atom in the CH_3 group of acetaldehyde results in significant changes relative to the ultraviolet absorption spectrum of acetaldehyde. This can be seen in figure IX-C-25 where the spectra of 2-hydroxyethanal and 2-chloroethanal are compared with that of the unsubstituted ethanal. The maximum in the absorption in CH_3CHO is shifted about 13 nm to the *shorter* wavelengths in $HOCH_2CHO$. However, λ_{max} in CH_2ClCHO is shifted about 8 nm to the *longer* wavelengths, and σ_{max} is increased by about 18%.

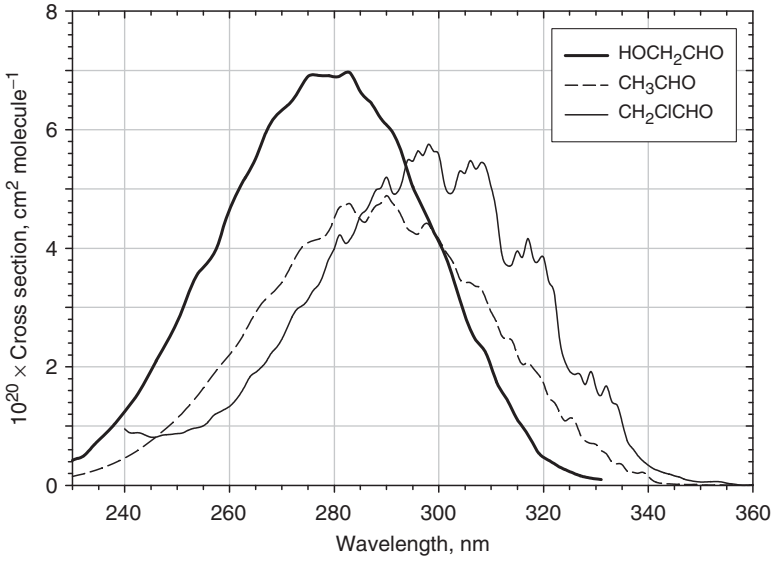

Figure IX-C-25. Comparison of the absorption spectra of some substituted acetaldehydes: $HOCH_2CHO$ at 298 ± 3 K (Magneron et al., 2005), CH_2ClCHO (Libuda, 1992), and CH_3CHO (Martinez et al., 1992); temperature, 298 K; figure from Calvert et al. (2008).

The effects of multiple substitution of Cl-atoms for H-atoms in CH_3CHO can be seen in figure IX-C-26. The addition of a second Cl-atom to form $CHCl_2CHO$ does not significantly alter the wavelength of the maximum absorption, but the absorption coefficient is raised about 7% over that present in CH_2ClCHO. A significant and unexpected change in the spectrum occurs with the addition of the third atom of Cl in the $CHCl_2CHO$ molecule. The wavelength of maximum absorption of CCl_3CHO is shifted back to a shorter wavelength, approximately that observed with the unsubstituted acetaldehyde, and the cross section at the maximum is raised to about 2.2-times that in CH_3CHO. With all of the chloroacetaldehydes, CH_2ClCHO, $CHCl_2CHO$, and CCl_3CHO, the absorption of tropospheric sunlight is increased significantly more than that of CH_3CHO and, hence, their tropospheric photochemistry is potentially important.

In figure IX-C-27 the effect of multiple F- and Cl-atom substitutions for H-atoms on the absorption spectra of CH_3CHO can be seen. Replacement of two H-atoms by F-atoms in CH_3CHO to form CHF_2CHO, shifts the absorption maximum 19 nm to the longer wavelengths while the maximum absorption coefficient is decreased only slightly (~3%). With the introduction of a third F-atom in CHF_2CHO to form CF_3CHO, the maximum in the absorption band is decreased significantly (~35%) from that in CH_3CHO, and it shifts 11 nm to longer wavelengths. Note, however, that the substitution of Cl-atoms for F-atoms in CF_3CHO causes more significant changes. One Cl-atom substitution ($CClF_2CHO$) increases the absorption cross section of CF_3CHO by about a factor of 5.1, although the wavelength at maximum absorption is relatively unchanged. The second Cl-atom substitution to form CCl_2FCHO lowers the cross section by about 16% and shifts the absorption by about 5 nm to shorter wavelengths. The third Cl-atom

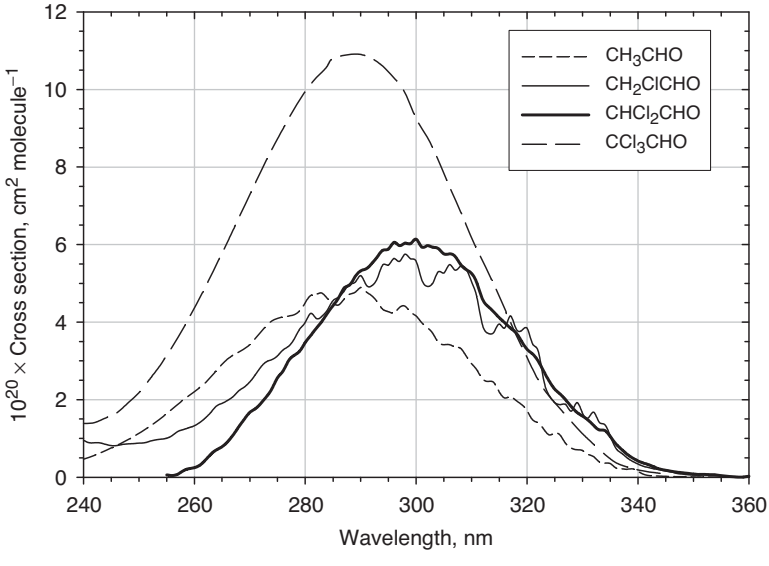

Figure IX-C-26. Comparison of the absorption spectra of the chlorine-atom-substituted acetaldehydes: CH_3CHO (Martinez et al., 1992), CH_2ClCHO (Libuda, 1992), $CHCl_2CHO$ (Libuda, 1992), CCl_3CHO (Talukdar et al., 2001); temperature, 298 K; figure from Calvert et al. (2008).

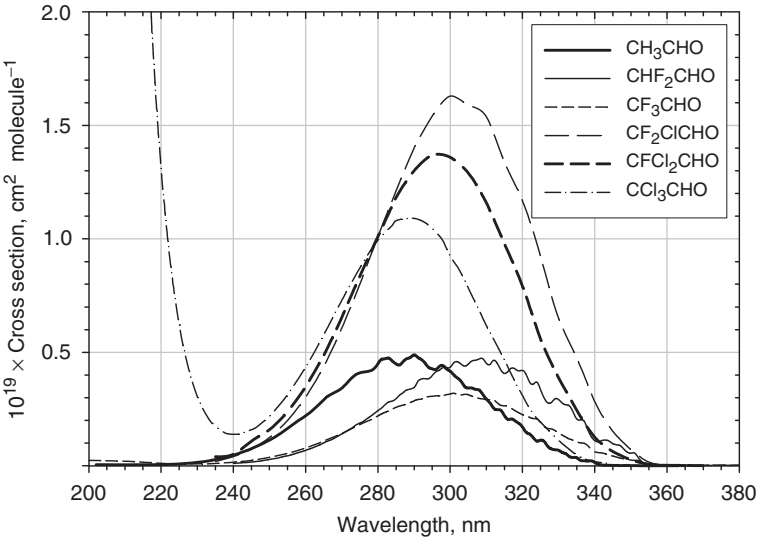

Figure IX-C-27. Comparison of the absorption spectra of some fluorine- and chlorine-atom-substituted acetaldehydes: CHF_2CHO (Sellevåg et al., 2005), CF_3CHO (Sellevåg et al., 2004a), CF_2ClCHO (Rattigan et al., 1998), $CFCl_2CHO$ (Rattigan et al., 1998); CCl_3CHO (Talukdar et al., 2001); CH_3CHO (Martinez et al., 1992); temperature, 298 K; figure from Calvert et al. (2008).

substitution to form CCl_3CHO shifts the absorption maximum by about 6 nm to shorter wavelengths and lowers the cross section by about 20%.

The effect of replacement of all of the H-atoms on the alkyl groups of the simple aldehydes by fluorine atoms can be seen in figure IX-C-28a (Hashikawa et al., 2004). Shown in black curves are the cross section data for the fluoro-aldehydes, $C_xF_{2x+1}CHO$, where $x = 1-4$; compare these spectra with those for the analogous unsubstituted aldehydes shown in the gray curves. As described previously, the cross sections for CF_3CHO are decreased significantly ($\sim$35%) from those of CH_3CHO and the maximum is shifted to the longer wavelengths. As the length of the alkyl chain in the fluoro-aldehydes is increased in the sequence: CF_3CHO, C_2F_5CHO, $CF_3CF_2CF_2CHO$, to $CF_3CF_2CF_2CF_2CHO$, a significant increase in the absorption maximum is seen, but only a small shift in the wavelength of the maximum occurs. In contrast, the unsubstituted aldehydes (gray curves in figure IX-C-28a) show only a small rise in the absorption maximum as one progresses in the analogous series: ethanal, propanal, butanal, and pentanal and the cross sections of the larger aldehydes (butanal, pentanal, hexanal, etc.) are very similar (Tadić et al., 2001b; Plagens et al., 1998). In general, substitution of a Cl- or F-atom (for an H-atom) at the α-position in the aldehydes results in a significant increase in overlap of the aldehyde absorption with the wavelength distribution of the sunlight in the troposphere. Hence, the potential for photodecomposition of fluoro- and chloro-aldehydes is enhanced over that for the unsubstituted aldehydes.

In figure IX-C-28b, a comparison is given of the spectra of aldehydes in which F-atoms have been substituted for H-atoms on carbon atoms down chain from the

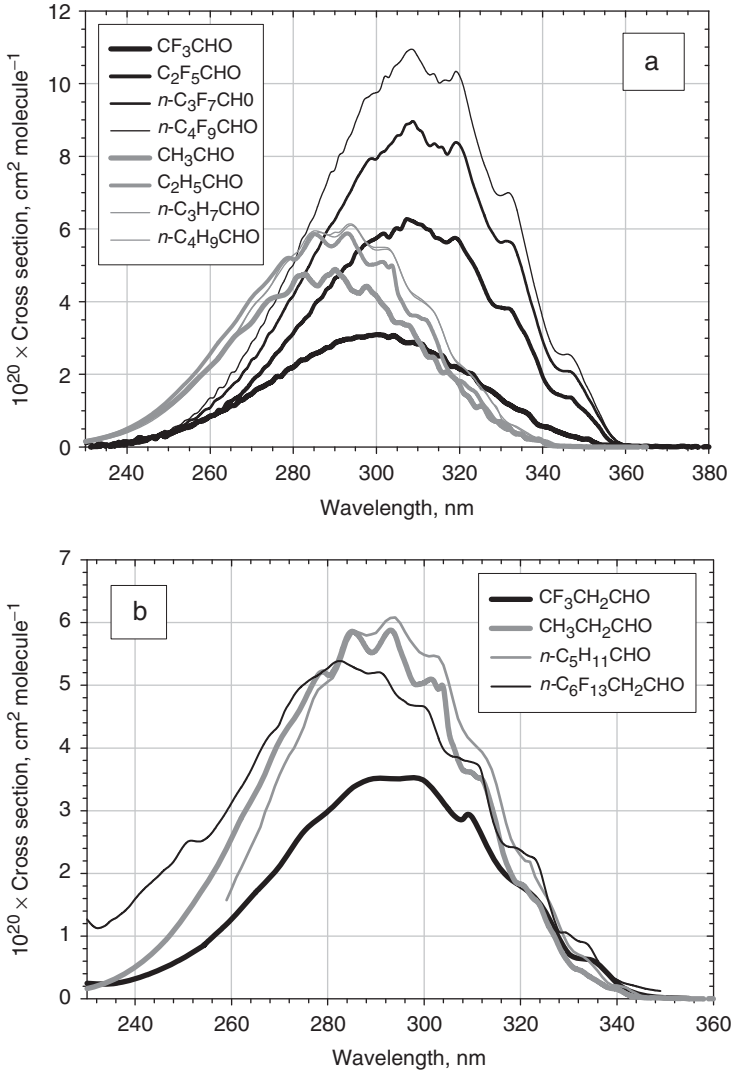

Figure IX-C-28. Comparison of the absorption cross sections as a function of wavelength for some halogen-atom-substituted aldehydes. (a) Compares a series of fluorine-substituted aldehydes ($C_xF_{2x+1}CHO$, $x = 1$–4, black lines) and the corresponding unsubstituted aldehydes (gray lines). Data for the fluoro-aldehydes are from Hashikawa et al. (2004); ethanal, propanal, and butanal data are from Martinez et al. (1992); pentanal data are from Tadić et al. (2001a). In (b) the data for CF_3CH_2CHO from Chiappero et al. (2006) and n-$C_6F_{13}CH_2CHO$ from Solignac et al. (2007) (black lines) are compared with those for structurally similar, unfluorinated aldehydes, CH_3CH_2CHO (Martinez et al., 1992), and hexanal (spectrum representative of larger, unsubstituted aldehydes; Plagens et al., 1998).

carbonl group. The data reported by Solignac et al. (2007) for n-$C_6F_{13}CH_2CHO$ are preferred over those from Chiappero et al. (2006) because of difficulties in handling the compound as discussed by Solignac et al. (2007). From the limited data available it appears that fluorine atom substitution down-chain from the carbonyl group in the long-chain aldehydes has little effect on the position and the maximum of the absorption coefficient; compare the spectra for n-$C_6F_{13}CH_2CHO$ and n-$C_5H_{11}CHO$ in figure IX-C-28.

IX-C-15. Photodecomposition of 2,2,2-Trichloroethanal (Trichloroacetaldehyde, Chloral, CCl_3CHO)

The photodecomposition of 2,2,2-trichloroethanal has been studied by Ohta and Mizoguchi (1980) and Talukdar et al. (2001) and reviewed by Calvert et al. (2008). The following primary photodissociation processes have been considered:

$$CCl_3CHO + h\nu \rightarrow Cl + CCl_2CHO \quad \text{(I)}$$

$$\rightarrow CCl_3 + CHO \quad \text{(II)}$$

$$\rightarrow CCl_3CO + H \quad \text{(III)}$$

$$\rightarrow CHCl_3 + CO \quad \text{(IV)}$$

Enthalpy data estimated by Zhu and Bozzelli (2002) suggest the values for ΔH_{298} for processes (I), (II), (III), and (IV) are approximately: 250.7, 287.1, 381.3, and $-28.2\,\mathrm{kJ\,mol^{-1}}$. Thus, from consideration of energy alone, process (I) can in theory be competitive with (II), the common photodecomposition mode for aldehydes in the troposphere.

IX-C-15.1. Absorption Cross Sections for 2,2,2-Trichloroethanal

Absorption cross sections for 2,2,2-trichloroethanal can be compared with those of other halogen-substituted acetaldehydes in figures IX-C-26 and IX-C-27. Tabular listing of these cross sections is given in table IX-C-9 for wavelengths present in the troposphere.

IX-C-15.2. Quantum Yields of Photodecomposition of 2,2,2-Trichloroethanal

Ohta and Mizoguchi (1980) interpreted their results from photolysis of CCl_3CHO–oxygen mixtures as initiated by process (II), analogous to the photolysis of acetaldehyde. However, the more recent studies of Talukdar et al. (2001) give evidence of the importance of process (I) forming Cl-atoms. They suggested that the subsequent thermal reactions of the Cl-atoms with CCl_3CHO can lead to the products (CO, ClC(O)Cl, CO_2) observed in O_2–CCl_3CHO mixture photolysis by Ohta and Mizoguchi (1980). At 308 nm, Talukdar et al. (2001) observed $\phi_I = 1.3 \pm 0.3$, with $\phi_{III} < 0.002$. At 193 and

Table IX-C-9. Absorption cross sections (σ, cm^2 $molecule^{-1}$) for CCl_3CHO at 298 K after Talukdar et al. (2001); table from Calvert et al. (2008)

λ, nm	$10^{20} \times \sigma$	λ, nm	$10^{20} \times \sigma$
278	9.49	311	5.88
279	9.72	312	5.58
280	9.94	313	5.28
281	10.1	314	4.98
282	10.3	315	4.66
283	10.45	316	4.33
284	10.6	317	4.01
285	10.7	318	3.68
286	10.8	319	3.39
287	10.85	320	3.09
288	10.9	321	2.80
289	10.9	322	2.51
290	10.9	323	2.30
291	10.85	324	2.09
292	10.8	325	1.93
293	10.7	326	1.76
294	10.6	327	1.60
295	10.45	328	1.43
296	10.3	329	1.28
297	10.1	330	1.12
298	9.92	331	0.985
299	9.59	332	0.849
300	9.25	333	0.720
301	9.01	334	0.590
302	8.77	335	0.482
303	8.47	336	0.373
304	8.17	337	0.317
305	7.84	338	0.261
306	7.50	339	0.225
307	7.18	340	0.188
308	6.86	341	0.162
309	6.52	342	0.136
310	6.18	343	0.118
		344	0.100

248 nm, they find: $\phi_{III} = 0.04 \pm 0.01$, and < 0.01, respectively. There was no evidence of process (IV) forming $CHCl_3$ even at 248 nm, and it is likely that ϕ_{IV} is unimportant at the wavelengths of sunlight available within the troposphere. The extent to which the excited states of CCl_3CHO are quenched by air molecules remains undetermined.

IX-C-15.3. Photolysis Frequencies for the Photodecomposition of 2,2,2-Trichloroethanal

Approximate photolysis frequencies for CCl_3CHO in tropospheric sunlight have been calculated coupling the cross section data of table IX-C-9 with an assumed value of

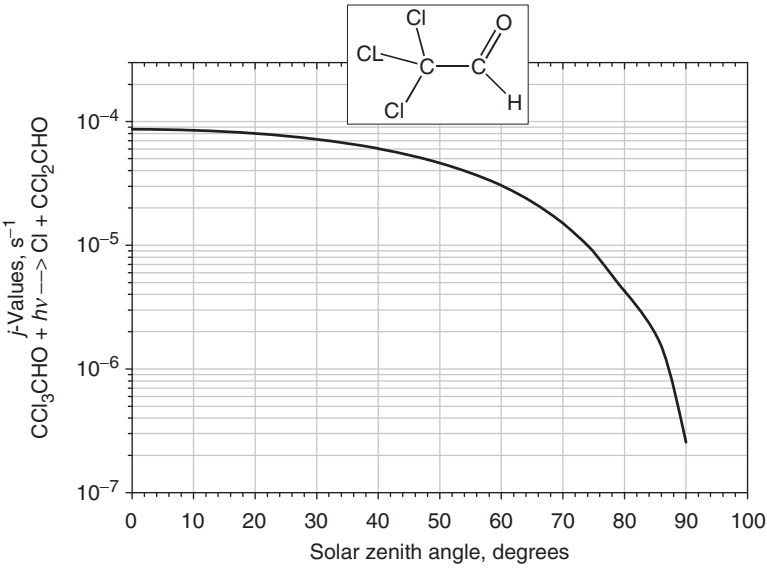

Figure IX-C-29. Approximate photolysis frequencies for CCl_3CHO versus solar zenith angle for a cloudless day in the lower troposphere with an overhead ozone column of 350 DU; the quantum yield of decomposition to form Cl-atoms was assumed to be unity at all absorbed wavelengths; figure from Calvert et al. (2008).

$\phi_I = 1.0$ at all wavelengths, and the appropriate solar flux (ozone column = 350 DU) for a cloudless troposphere. These results are plotted versus solar zenith angle in figure IX-C-29. The lifetime of trichloroethanal from OH attack alone would be about 1 day, while its lifetime from photodecomposition for an overhead Sun is about 3 h. For 40°N latitude, clear tropospheric skies, and diurnal variation of the Sun, the expected average photochemical lifetimes of CCl_3CHO are about 10 h and 2.3 days for the time periods near June 22 and December 22, respectively.

IX-C-16. Photodecompositon of 2,2,2-Trifluoroethanal (Trifluoroacetaldehyde, CF_3CHO)

Limited quantitative data on the photodecomposition of trifluoroacetaldehyde have been published by several groups (Dodd and Smith, 1957; Morris and Thynne, 1968; Pearce and Whytock, 1971; Sellevåg et al., 2004a; Chiappero et al., 2006). The following primary processes can be considered in explanation of the results (Calvert et al., 2008):

$$CF_3CHO + h\nu \rightarrow CF_3 + CHO \quad \text{(I)}$$

$$\rightarrow CHF_3 + CO \quad \text{(II)}$$

$$\rightarrow CF_3CO + H \quad \text{(III)}$$

IX-C-16.1. Absorption Cross Sections for CF_3CHO

The reported cross sections of CF_3CHO as a function of wavelength that have been given by several groups are in reasonable agreement (Sellevåg et al., 2004a; Hashikawa et al., 2004; Chiappero et al., 2006); the data of Sellevåg et al., 2004a are shown in figures IX-C-27 and IX-C-28a where cross sections for a series of structurally related haloaldehydes are compared. Tabular data for CF_3CHO from Sellevåg et al. (2004a) and Chiappero et al. (2006) are compared in table IX-C-10. The cross sections reported by Chiappero are about 10% lower than those of Sellevåg et al. over much of the wavelength range important within the troposphere. Calvert et al. (2008) used an average of the two σ determinations at each wavelength in photolysis frequency calculations, and that approach has been adopted in this work as well.

IX-C-16.2. Quantum Yields of Primary Photodecomposition Processes in CF_3CHO

Dodd and Smith (1957) photolyzed pure CF_3CHO at 313 nm ($\sim$ 20° C, 30–40 Torr) and concluded that $\phi_{\mathrm{I}} \cong 0.12$ and $\phi_{\mathrm{II}} \cong 0.021$. Pearce and Whytock (1971) found no evidence for process (II) in their experiments at 313 nm (30–150°C, pressure 8.6–146 Torr). From photolysis of CF_3CHO at 253.7 nm in air mixtures, Richter et al. (1993) concluded that process (II) occurs to some extent, but very little photodecomposition occurred on irradiation at 366 nm (very little light is absorbed at this wavelength).

Sellevåg et al. (2004a) determined the effective quantum yield of photolysis (290–400 nm) to be < 0.02 under pseudo-natural conditions (1 atm. air) at the European simulation chamber in Valencia, Spain (EUPHORE). Chiappero et al. (2006) studied the photolysis of a series of structurally related fluoroaldehydes, including CF_3CHO, at two wavelengths: 308 (pulsed laser) and 254 nm (CW Hg lamp). They determined the quantum yields of the primary processes in dilute mixtures of CF_3CHO with 700 Torr of nitrogen and 10–50 Torr of NO. Nitric oxide was added to scavenge the radical products formed in the photolysis that might otherwise contribute to the unwanted secondary loss of the aldehyde. In the experiments at 308 nm, CH_3CHO and $CH_3C(O)CH_3$ were used as chemical actinometers. The reliability of the method was improved by ensuring that an equal number of quanta were absorbed by CF_3CHO and the actinometer compounds. The measured ratio of the acetone loss to that of acetaldehyde was 0.153 $\pm$ 0.017. This ratio checked well with that expected from the IUPAC recommendations (Atkinson et al., 2005) for cross sections and quantum yields at 308 nm: 0.179 $\pm$ 0.028. The expected ratio calculated using the recommendations for 308 nm in the present study give: $\Phi_{-CH_3C(O)CH_3}/\Phi_{-CH_3CHO} = 0.15$ and 0.13, assuming scenarios (a) and (b), respectively, for process (II) in acetone photodecomposition. In photolyses of CF_3CHO at 308 nm, the measured amount of CF_3NO product formed was equal to the aldehyde loss within the experimental error: $\Phi_{CF_3NO}/\Phi_{-CF_3CHO} = 0.98 \pm 0.07$. No CF_3H was detected. Clearly process (I) is the dominant photodecomposition mode at 308 nm. The measured quantum yield of process (I) at 308 nm of 0.17 $\pm$ 0.03 was adopted by Calvert et al. (2008) and in this study. For unexplained reasons the

Table IX-C-10. Comparison of absorption cross sections (σ, cm^2 $molecule^{-1}$) for CF_3CHO [Sellevåg et al., 2004a at 298 K (A); Chiappero et al., 2006 at 297 K (B)]; table from Calvert et al. (2008)

λ, nm	(A) $10^{20} \times \sigma$	(B) $10^{20} \times \sigma$	λ, nm	(A) $10^{20} \times \sigma$	(B) $10^{20} \times \sigma$	λ, nm	(A) $10^{20} \times \sigma$	(B) $10^{20} \times \sigma$
278	2.03	1.83	319	2.33	2.10	360	0.0380	0.01
279	2.11	1.90	320	2.25	2.02	361	0.0360	0
280	2.19	1.97	321	2.19	1.97	362	0.0360	0
281	2.28	2.06	322	2.13	1.91	363	0.0320	0
282	2.35	2.12	323	2.08	1.88	364	0.0330	0
283	2.42	2.18	324	2.06	1.83	365	0.0320	0
284	2.50	2.26	325	1.90	1.67	366	0.0280	0
285	2.57	2.32	326	1.72	1.52	367	0.0250	0
286	2.63	2.37	327	1.64	1.47	368	0.0250	0
287	2.67	2.42	328	1.62	1.44	369	0.0230	0
288	2.73	2.48	329	1.55	1.36	370	0.0220	0
289	2.79	2.54	330	1.44	1.27	371	0.0230	0
290	2.86	2.61	331	1.35	1.18	372	0.0220	0
291	2.92	2.66	332	1.26	1.09	373	0.0210	0
292	2.94	2.69	333	1.18	1.03	374	0.0230	0
293	3.00	2.75	334	1.13	0.98	375	0.0220	0
294	3.05	2.79	335	1.06	0.91	376	0.0220	0
295	3.06	2.81	336	1.01	0.87	377	0.0200	0
296	3.08	2.83	337	0.993	0.86	378	0.0190	0
297	3.08	2.83	338	0.891	0.74	379	0.0190	0
298	3.10	2.86	339	0.730	0.61	380	0.0170	0
299	3.14	2.88	340	0.622	0.51	381	0.0180	0
300	3.17	2.92	341	0.585	0.49	382	0.0180	0
301	3.20	2.93	342	0.569	0.47	383	0.0170	0
302	3.15	2.88	343	0.531	0.43	384	0.0180	0
303	3.12	2.87	344	0.471	0.37	385	0.0170	0
304	3.15	2.89	345	0.425	0.34	386	0.0170	0
305	3.13	2.86	346	0.385	0.30	387	0.0180	0
306	3.07	2.81	347	0.337	0.26	388	0.0180	0
307	3.03	2.76	348	0.310	0.23	389	0.0160	0
308	2.97	2.72	349	0.286	0.21	390	0.0160	0
309	2.95	2.69	350	0.246	0.18	391	0.0160	0
310	2.92	2.67	351	0.235	0.17	392	0.0170	0
311	2.92	2.68	352	0.232	0.15	393	0.0160	0
312	2.91	2.65	353	0.162	0.093	394	0.0140	0
313	2.78	2.51	354	0.0960	0.036	395	0.0140	0
314	2.67	2.43	355	0.0710	0.017	396	0.0150	0
315	2.65	2.41	356	0.0580	0.008	397	0.0140	0
316	2.62	2.37	357	0.0500	0.007	398	0.0130	0
317	2.52	2.28	358	0.0440	0.011	399	0.0110	0
318	2.42	2.18	359	0.0420	0.019	400	0.0130	0

experimental measurements of the effective quantum yield of photodecomposition of CF_3CHO (290–400 nm) by Sellevåg et al. ($\phi_I < 0.02$) appear to be in error.

In their studies of CF_3CHO photodecomposition at 254 nm in its mixture with NO and N_2 (700 Torr), 296 K, Chiappero et al. (2006) used $(CF_3CO)_2O$ as an actinometer. The two observable products at this wavelength, CF_3NO and CF_3H, showed the occurrence of process (II) as well as (I) with $\phi_I = 0.42 \pm 0.07$ and $\phi_{II} = 0.38 \pm 0.07$. These results are consistent with the occurrence of process (II) which was also observed by Richter et al. (1993) in experiments at 254 nm.

IX-C-16.3. Approximate Photolysis Frequencies for CF_3CHO Photodecomposition in the Lower Troposphere

The wavelength dependence of the primary processes at wavelengths within the 290–400 nm region of importance in atmospheric photolysis cannot be determined from the limited data at 308 and 254 nm (Calvert et al., 2008). However, the data from 308 nm, a wavelength near the maximum in the overlap of the actinic flux with the absorption of CF_3CHO, were used to derive qualitative estimates of the effective quantum yield and approximate *j*-values (Chiappero et al., 2006). A similar calculation has been made by Calvert et al. (2008), and the results are shown in figure IX-C-30 for clear-sky conditions and overhead O_3 column of 350 DU. These data suggest that for an overhead Sun the approximate photochemical lifetime of CF_3CHO in the lower troposphere is

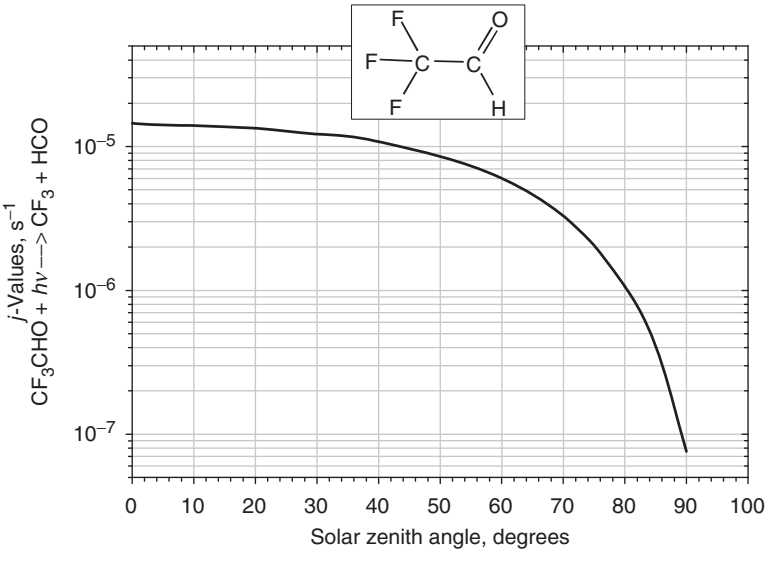

Figure IX-C-30. Approximate photolysis frequencies for CF_3CHO versus solar zenith angle for a cloudless day in the lower troposphere. The quantum yield of photodecomposition to form CF_3 and HCO radicals is assumed to be 0.17 at all wavelengths of absorbed light (Chiappero et al., 2006). We also used in this calculation the actinic flux available within the lower troposphere (overhead ozone column of 350 DU), and an average of the cross section data of Sellevåg et al. (2004) and Chiappero et al. (2006).

about 19 h. Note that the photolysis frequencies for CF_3CHO shown by Calvert et al. (2008) in their figure VII-F-7 are based on the now discounted Sellevåg et al. estimate of average quantum yield of 0.02 and are as a consequence lower by a factor of 0.12 than those presented here.

IX-C-17. Photodecomposition of 2,2-Difluoroethanal (Difluoroacetaldehyde; CHF_2CHO)

Studies of the photochemistry of the CHF_2CHO have been reported by Sellevåg et al. (2005). The absorption spectrum of difluoroacetaldehyde is similar to that for CF_3CHO (see figure IX-C-27), but the efficiency of its photodecomposition in sunlight appears to be much greater than the low value (< 0.02) observed for CF_3CHO by Sellevåg et al. (2004a) but closer to that found by Chiappero et al. (2006) for CF_3CHO at 308 nm (0.17). An effective quantum yield of photodecomposition of 0.30 ± 0.05 (290-400 nm) was determined for pseudo-natural tropospheric conditions in the European simulation chamber in Valencia, Spain (Sellevåg et al., 2005). The primary photodissociation pathways considered for CHF_2CHO mirror those considered for the other F-substituted acetaldehyde molecules:

$$CHF_2CHO + h\nu \rightarrow CHF_2 + HCO \quad \text{(I)}$$

$$\rightarrow CH_2F_2 + CO \quad \text{(II)}$$

$$\rightarrow CHF_2CO + H \quad \text{(III)}$$

Only CO and CF_2O were detected products of the photolysis of CHF_2CHO–air mixtures at 313 nm (Sellevåg et al., 2005). This suggests that process (II) is unimportant, at least for tropospheric conditions.

Quantum chemical calculations have been made by Sellevåg et al. (2005) to compare theoretical energy barriers for these and the analogous photolytic dissociation pathways of CH_3CHO, CH_2FCHO, CHF_2CHO, and CF_3CHO. Presumably processes (I) and (II) occur from the T_1 and S_o states, respectively. The theoretical barriers for process (I) relative to the T_1 minimum were estimated to be 53, 54, 56, and 44 kJ mol^{-1} for CH_3CHO, CH_2FCHO, CF_3CHO, and CHF_2CHO, respectively. For process (II) the barrier decreases in the series CH_3CHO, CH_2FCHO, CHF_2CHO, and CF_3CHO, with the calculated CF_3CHO barrier being 36 kJ mol^{-1} lower than the equivalent barrier in CH_3CHO.

Calvert et al. (2008) and the present authors have used the cross section data tabulated in table IX-C-11 and the effective quantum yield of CHF_2CHO photodissociation (0.30) reported by Sellevåg et al. (2005) to calculate the photolysis frequencies as a function of solar zenith angle for a cloudless day within the lower troposphere (ozone column = 350 DU); see figure IX-C-31. These data suggest a photochemical lifetime for an overhead Sun of about 6 h.

Table IX-C-11. Absorption cross sections (σ, cm^2 $molecule^{-1}$) for CHF_2CHO (Sellevåg et al., 2005) at 298 K

λ, nm	$10^{20} \times \sigma$	λ, nm	$10^{20} \times \sigma$	λ, nm	$10^{20} \times \sigma$
278	2.19	319	4.19	360	0.0355
279	2.31	320	4.21	361	0.0283
280	2.43	321	4.04	362	0.0283
281	2.54	322	3.69	363	0.0253
282	2.69	323	3.60	364	0.0241
283	2.81	324	3.69	365	0.0146
284	2.85	325	3.37	366	0.0165
285	2.95	326	3.00	367	0.0165
286	3.11	327	2.78	368	0.0130
287	3.22	328	2.79	369	0.00679
288	3.34	329	2.95	370	0.00700
289	3.45	330	2.92	371	0.00976
290	3.54	331	2.77	372	0.00875
291	3.71	332	2.69	373	0.0133
292	3.82	333	2.64	374	0.00655
293	3.84	334	2.38	375	0.0163
294	3.83	335	2.07	376	0.0215
295	3.97	336	2.02	377	0.0102
296	4.14	337	1.98	378	0.0106
297	4.21	338	1.62	379	0.0116
298	4.33	339	1.29	380	0.0111
299	4.33	340	1.11	381	0.00759
300	4.34	341	1.06	382	0.00408
301	4.54	342	1.12	383	0.00445
302	4.58	343	1.14	384	0.00917
303	4.48	344	1.09	385	0.00634
304	4.39	345	0.974	386	0.00305
305	4.48	346	0.922	387	0.00425
306	4.62	347	0.885	388	0.00384
307	4.66	348	0.735	389	0.00837
308	4.71	349	0.597	390	0.00995
309	4.73	350	0.553	391	0.00904
310	4.53	351	0.557	392	0.00363
311	4.47	352	0.365	393	0.00522
312	4.65	353	0.182	394	0.00722
313	4.53	354	0.111	395	0.00732
314	4.24	355	0.0878	396	0.00457
315	4.07	356	0.0773	397	0.00249
316	4.16	357	0.0626	398	0.00329
317	4.31	358	0.0552	399	0.00152
318	4.27	359	0.0396	400	0.00224

IX-C-18. Photodecomposition of the Larger Fluorinated Aldehydes: C_2F_5CHO, $CF_3CF_2CF_2CHO$, $CF_3CF_2CF_2CF_2CHO$, CF_3CH_2CHO, and n-$C_6F_{13}CH_2CHO$

Limited photochemical data for several of the larger fluorinated aldehydes have been reported by Chiappero et al. (2006). The absorption spectra of these molecules are

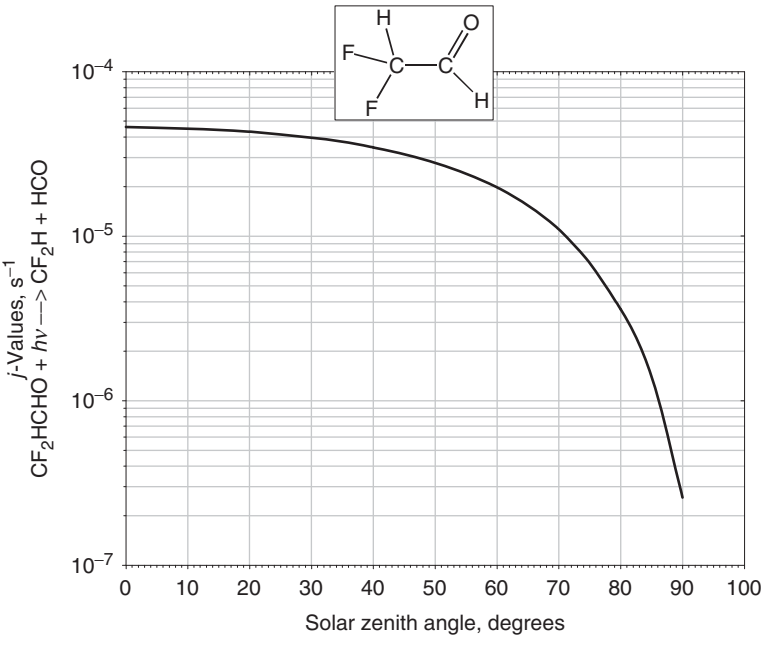

Figure IX-C-31. Approximate photolysis frequencies for CHF_2CHO versus solar zenith angle for a cloudless day in the lower troposphere with an overhead ozone column of 350 DU; the quantum yield of decomposition to form CF_2H and HCO radicals was assumed to be 0.30 at all wavelengths in accord with the effective quantum yield estimated by Sellevåg et al. (2005); figure from Calvert et al. (2008).

shown in figure IX-C-28 where they are compared with those of the unfluorinated aldehydes. The quantum efficiencies of the primary processes have been determined at a few wavelengths in experiments at 700 Torr pressure of N_2; experimental conditions were similar to those described for CF_3CHO in section IX-C-17 (Hurley et al., 2006; Chiappero et al., 2006). Photodecomposition proceeds through the following primary processes similar to those observed for the unfluorinated aldehydes:

$$RCHO + h\nu \rightarrow R + CHO \quad \text{(I)}$$

$$\rightarrow RH + CO \quad \text{(II)}$$

From experiments at 254 nm, the reported quantum yields for primary process (I) in CF_3CHO, C_2F_5CHO, $CF_3CF_2CF_2CHO$, $CF_3CF_2CF_2CF_2CHO$, and CF_3CH_2CHO are: 0.41 ± 0.07, 0.38 ± 0.08, 0.31 ± 0.07, 0.31 ± 0.08, and 0.38 ± 0.09, respectively. Quantum yields for process (II) at 254 nm are: 0.38 ± 0.07, 0.43 ± 0.08, 0.32 ± 0.07, 0.29 ± 0.07, and 0.36 ± 0.07, respectively. Chiappero et al. (2006) determined for $C_6F_{13}CH_2CHO$ the total photodecomposition quantum yield: $\phi_I + \phi_{II} = 0.55 \pm 0.09$.

From experiments at 308 nm, Chiappero et al. (2006) report values of ϕ_I for CF_3CHO, $CF_3CF_2CF_2CF_2CHO$, and CF_3CH_2CHO: 0.17 ± 0.03; 0.08 ± 0.02; and 0.04 ± 0.01, respectively. These investigators have assumed the quantum yield data

measured at 308 nm to be representative of that over the wavelength region of sunlight absorption, and they estimated the photochemical lifetimes of the fluorinated aldehydes (averaged over the entire year) as a function of altitude within the lower atmosphere. For altitudes of 0 and 11.7 km, respectively, the estimated photochemical lifetimes are: CF_3CH_2CHO, ~36 and 13 days; n-$C_6F_{13}CH_2CHO$, ~21 and 8 days; CF_3CHO, ~5.7 and 2.1 days; C_2F_5CHO ~2.5 and 0.92 days; n-C_4F_9CHO, ~2 and 0.74 days. As Calvert et al. (2008) concluded, photodecomposition is an important decay pathway for the fluoroaldehydes in the lower atmosphere.

IX-D. Photodecomposition of Acyclic Ketones

IX-D-1. Photodecomposition of Acetone [2-Propanone, $CH_3C(O)CH_3$]

The photochemistry of acetone has been studied extensively over the past three-quarters of a century. Several reviews of the pioneering work have been published (e.g., Noyes et al., 1956; Lee and Lewis, 1980). Useful reviews of the photochemistry of acetone in air have been made by Horowitz (1991) and Emrich and Warneck (2000). Absorption of solar radiation in the troposphere ($\lambda > 290$ nm) by acetone and other carbonyl compounds, forms an excited singlet state (S_1) via an $n \rightarrow \pi^*$ electronic transition. The origin of this transition in acetone is near 328.6 nm. Features of the photochemistry have been elucidated in theoretical studies by Sakurai and Kato (1999) and Diau et al. (2001). The S_1 state is short-lived. It rapidly undergoes intersystem crossing to form the triplet state ($S_1 \rightarrow T_1$) or internal conversion to a highly vibrationally excited ground state (S_o^*). Many excellent studies of acetone photochemistry have established an important role for the first excited triple in the gas-phase photolysis of acetone, particularly at longer wavelengths of absorbed light; (e.g., see Cundall and Davies, 1967; Gandini and Hackett, 1977a; Diau et al., 2001; Haas, 2004). In experiments using pure acetone, photodecomposition can occur from S_1, T_1, or S_o^* by several primary photodecomposition pathways:

$$CH_3C(O)CH_3 + h\nu \rightarrow CH_3CO + CH_3 \quad \text{(I)}$$

$$\rightarrow CH_3 + (CH_3CO^*) \rightarrow 2CH_3 + CO \quad \text{(II)}$$

$$\rightarrow H + CH_2C(O)CH_3 \quad \text{(III)}$$

$$\rightarrow CH_4 + CH_2{=}CO \quad \text{(IV)}$$

Primary process (I), a "Norrish type-I" photodissociation, results in an α-C—C bond cleavage. Theoretical studies of Diau et al. (2001) give the most detailed analysis of the mechanism of acetone photolysis, based on density functional theory and *ab initio* calculations. Haas (2004) provides a more recent overview of the topic, based largely on experiments at zero pressure in supersonic beams. The consensus is that at longer wavelengths, dissociation occurs by intersystem crossing from S_1 to T_1. According to Diau et al., there is a barrier to dissociation on the T_1 surface with an energy of

376 kJ mol^{-1}, corresponding to 318 nm. A sudden decrease in lifetime of the fluorescence occurs for excitation at wavelengths in the 313–306 nm range when dissociation becomes energetically feasible. Under ambient pressure and temperature conditions, dissociation can occur at longer wavelengths (< 334 nm, corresponding to an energy of 358 kJ mol^{-1}). The role of collisions and of thermal excitation in the dissociation mechanism at these longer wavelengths has not been elucidated. Diau et al. (2001) also proposed a mechanism for dissociation via internal conversion, involving a conical intersection between the S_1 and S_o surfaces at an energy of 460 kJ mol^{-1} (260 nm). For excitation at the shorter wavelengths, the S_1 lifetime decreases smoothly from 2.1 ns at 295 nm to < 1.6 ns at 260 nm. While processes (I) and (II) are relevant within the troposphere, processes (III) and (IV) occur only in vacuum UV radiation that is absent in the lower atmosphere.

IX-D-1.1. Absorption Cross Sections of Acetone

The recommended ultraviolet absorption cross sections for acetone are shown in figure IX-D-1, where they can be compared with those for some other simple ketones (Martinez et al., 1992). The good agreement of the cross sections measured by Martinez et al. (1992) and Gierczak et al. (1998) can be seen by comparison of appropriate columns in table IX-D-1.

IX-D-1.2. Quantum Yields of the Primary Processes in the Photodecomposition of Acetone

Of primary importance in the lower atmosphere is process (I) that result in the formation of methyl and acetyl radicals. Primary process (II) becomes significant at the short

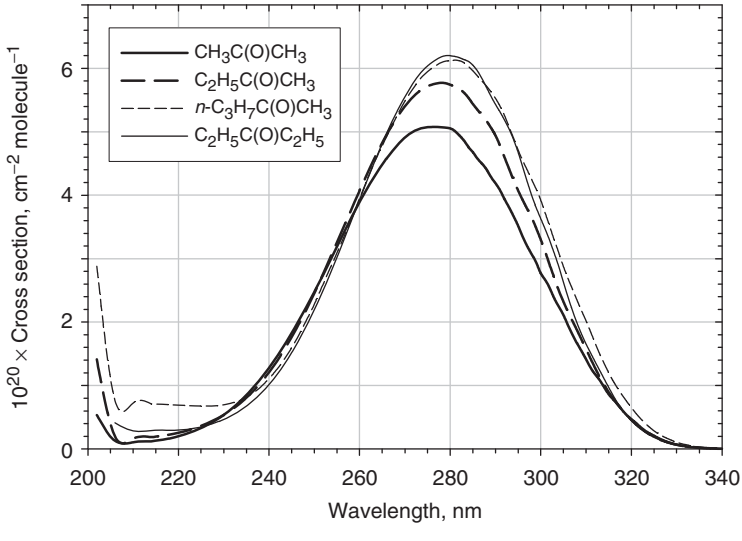

Figure IX-D-1. Absorption spectra for some simple ketones; data from Martinez et al. (1992).

Table IX-D-1. Absorption cross sections (σ, cm^2 $molecule^{-1}$) at 298 K for the simple ketones: acetone [$CH_3C(O)CH_3$] and 2-butanone [$CH_3C(O)C_2H_5$]

λ, nm	Acetone[a] $10^{20} \times \sigma$	Acetone[b] $10^{20} \times \sigma$	2-Butanone[c] $10^{20} \times \sigma$	λ, nm	Acetone[a] $10^{20} \times \sigma$	Acetone[b] $10^{20} \times \sigma$	2-Butanone[c] $10^{20} \times \sigma$
278	5.07	4.94	5.77	315	0.858	0.837	0.896
279	5.06	4.92	5.76	316	0.777	0.760	0.794
280	5.05	4.91	5.74	317	0.699	0.684	0.697
281	5.01	4.86	5.72	318	0.608	0.598	0.611
282	4.94	4.79	5.68	319	0.530	0.523	0.531
283	4.86	4.71	5.62	320	0.467	0.455	0.457
284	4.76	4.62	5.54	321	0.407	0.411	0.389
285	4.68	4.54	5.44	322	0.344	0.348	0.328
286	4.58	4.44	5.35	323	0.287	0.294	0.276
287	4.50	4.36	5.26	324	0.243	0.248	0.229
288	4.41	4.28	5.17	325	0.205	0.210	0.189
289	4.29	4.15	5.06	326	0.168	0.174	0.156
290	4.19	4.06	4.94	327	0.135	0.141	0.129
291	4.08	3.95	4.78	328	0.108	0.113	0.105
292	3.94	3.82	4.60	329	0.086	0.091	0.085
293	3.81	3.71	4.42	330	0.067	0.074	0.067
294	3.67	3.57	4.24	331	0.051	0.059	0.054
295	3.52	3.42	4.08	332	0.040	0.047	0.042
296	3.35	3.26	3.93	333	0.031	0.038	0.033
297	3.20	3.31	3.79	334	0.026	0.031	0.025
298	3.07	2.98	3.65	335	0.017	0.025	0.020
299	2.94	2.82	3.48	336	0.014	0.020	0.014
300	2.77	2.67	3.30	337	0.011	0.016	0.011
301	2.66	2.58	3.10	338	0.009	0.014	0.008
302	2.53	2.45	2.89	339	0.006	0.011	0.007
303	2.37	2.30	2.69	340	0.005	0.009	0.005
304	2.24	2.18	2.50	341	0.005	0.007	0.005
305	2.11	2.05	2.33	342	0.003	0.006	0.003
306	1.95	1.89	2.17	343	0.004	0.005	0.003
307	1.80	1.75	2.02	344	0.002	0.004	0.002
308	1.66	1.61	1.88	345	0.002	0.003	0.001
309	1.54	1.49	1.73	346	0.001	0.002	0.001
310	1.41	1.36	1.59	347	0.002	0.002	0.000
311	1.28	1.24	1.42	348	0.001	0.001	0.001
312	1.17	1.14	1.28	349	0.001	0.001	0
313	1.08	1.06	1.14	350	0.001		0
314	0.967	0.94	1.01				

[a]Acetone cross sections as reported by Martinez et al. (1992).
[b]Acetone cross sections as reported by Gierczak et al. (1998).
[c]2-Butanone cross sections as reported by Martinez et al. (1992).

wavelengths of absorbed light. The CH_3CO^* species has been suggested to be an intermediate in the process (II). Presumably it is a short-lived, vibrationally rich acetyl radical that dissociates readily to form a second methyl radical and carbon monoxide. The energy thresholds for processes (I) and (II) are 338 and 299 nm, respectively. Processes (III) and (IV) occur to a limited extent in photolysis in the vacuum UV. In the oxygen-free system, acetone photolysis at the longer wavelengths proceeds

largely from the T_1 state that lies about 327 kJ mol^{-1} above S_o. However, as described previously, a significant barrier to the dissociation has been observed experimentally (about 56 kJ mol^{-1}; Zuckermann et al., 1988); this is qualitatively consistent with the barrier estimated theoretically to be ~75 kJ mol^{-1} by Diau et al. (2001).

In the presence of even small amounts of oxygen, the vibrationally equilibrated triplet state of acetone is quenched effectively; the rate constant for this reaction is large: $k \approx 1.5 \times 10^{-11}$ cm^3 molecule^{-1} s^{-1} (Costela et al., 1986). Presumably quenching by oxygen involves electronic energy transfer: $CH_3C(O)CH_3(T_1) + O_2(^3\Sigma_g^-) \rightarrow CH_3C(O)CH_3(S_o) + O_2(^1\Delta_g)$. In the lower atmosphere, rich in oxygen, vibrationally equilibrated acetone triplets will be removed by oxygen quenching. In view of this quenching, it seem probable that dissociation of acetone in the lower troposphere occurs from shorter-lived, vibrationally excited states (S_1, T_1, or S_o).

As with the photochemical studies of aldehydes described in sections IX-B and IX-C, most experiments with acetone have been made in the absence of oxygen. However, a few studies have been made under conditions relevant to acetone photodecomposition within the troposphere, that is, at low acetone concentrations in air at tropospheric pressures (Gardner et al., 1984; Meyrahn et al., 1986; Emrich and Warneck, 2000; Gierczak et al., 1998; Blitz et al., 2004; 2006; Nádasdi et al., 2007). From the results of broadband studies of acetone–air mixture photolysis, Gardner et al. reported that the quantum yields of CO_2 formation and acetone loss (~0.075 at 1 atm.) were indistinguishable within the experimental uncertainties, and the ratio, $-\Phi_{CH_3C(O)CH_3}/\Phi_{CO_2} = 1.02 \pm 0.04$ (band near 313 nm). The formation of CO_2 results from CH_3CO radical generation in process (I) and the reaction sequence: $CH_3CO + O_2 \rightarrow CH_3C(O)O_2$; $CH_3C(O)O_2 + CH_3C(O)O_2 \rightarrow 2CH_3CO_2 + O_2$; $CH_3C(O)O_2 + CH_3O_2 \rightarrow CH_3CO_2 + CH_3O + O_2$; $CH_3CO_2 \rightarrow CH_3 + CO_2$. Quenching of acetone decomposition by O_2, N_2, and air was observed by Gardner et al. (1984), and they proposed that the quenching observed reflected participation of two excited states of acetone. They reported as well that the quantum yields of products formed at a given pressure of reactants were relatively invariant with excitation wavelength (313–279 nm). This latter observation differs with results from subsequent studies, and the wavelength dependence of the primary process (I) is now well established.

The quenching of electronically excited acetone molecules by collisional energy transfer with air molecules is less efficient than electronic energy transfer to acetone, 2,3-butanedione, and other molecules with triplet state energies lower than that of acetone. Emrich and Warneck (2000), Gierczak et al. (1998), Blitz et al. (2006), and Nádasdi et al. (2007) demonstrated clearly that collisional deactivation of electronically excited acetone by air or nitrogen follows a Stern–Volmer mechanism. A semilogarithmic plot of the quenching constants (k_q/k_d) versus $1/\lambda$ is given in figure IX-D-2. Although there is considerable scatter in the data, the constants follow the trend observed for the light aldehydes (see figure VII-B-14b in Calvert et al., 2008); they decrease regularly as the excitation energy is increased and the lifetime of the excited states decreases. Blitz et al. (2004) observed nonlinear Stern–Volmer plots for the quantum yield of acetone for $\lambda < 302$ nm. The slopes of the plots were high at low pressures, indicating more facile quenching under these conditions, and low at higher pressures.

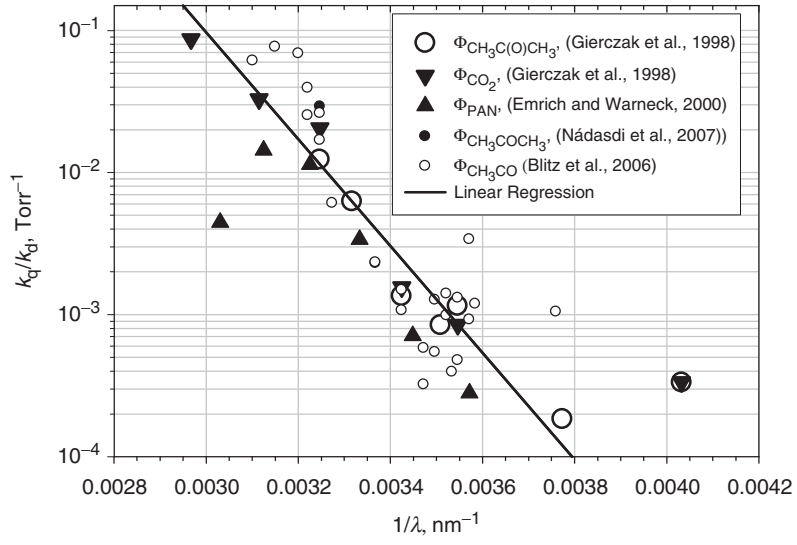

Figure IX-D-2. Semilog plot of the Stern–Volmer constants (k_q/k_d) versus $1/\lambda$ for quenching of excited acetone by collisional energy transfer with air or nitrogen molecules ($T \sim 298$ K). The trend line is the least-squares fit to the data excluding the most divergent points at $1/\lambda = 0.00403$ and $0.00303\,\text{nm}^{-1}$: $\log_{10}(k_q/k_d) = 10.27 - 3761 \times (1/\lambda)$.

The degree of nonlinearity increased with increasing wavelength. They attributed this behavior to the involvement of two states, one showing more facile quenching, and one with a longer lifetime, which requires higher pressures for quenching. They suggested that the long-lived state is T_1 and the shorter-lived state is S_1. The change in slope occurs at quite low pressures (10–20 Torr) and had not been observed previously.

i) Primary process (I): $CH_3C(O)CH_3 + h\nu \rightarrow CH_3 + CH_3CO$ Several experimental approaches have been used to define the quantum yields of this photodissociation process in air. In the studies of Meyrahn et al. (1986) and Emrich and Warneck (2000), dilute mixtures of acetone and NO_2 in air were photolyzed over a wide range of wavelengths (250–330 nm) and different pressures of air. The acetyl radical formed in process (I) reacts rapidly with oxygen in the air-rich mixture, $CH_3CO + O_2 \rightarrow CH_3C(O)O_2$. In the NO_2-containing system used by Emrich and Warneck, the acetylperoxy radical was captured effectively by NO_2 to form peroxyacetyl nitrate (PAN), $CH_3C(O)O_2 + NO_2 \rightarrow CH_3C(O)OONO_2$. Although PAN is thermally unstable, its decomposition in the gas phase is relatively unimportant at 25°C on the timescale of the Emrich and Warneck experiments. Since the "hot" acetyl radical is believed to have only a transient lifetime, PAN derived from it is unimportant, and the quantum yields of PAN formation refer only to process (I). However, the occurrence of process (II) can be monitored by the formation of CO. In both the studies of Meyrahn et al. (1986) and Emrich and Warneck (2000), the quantum yields of PAN were found to

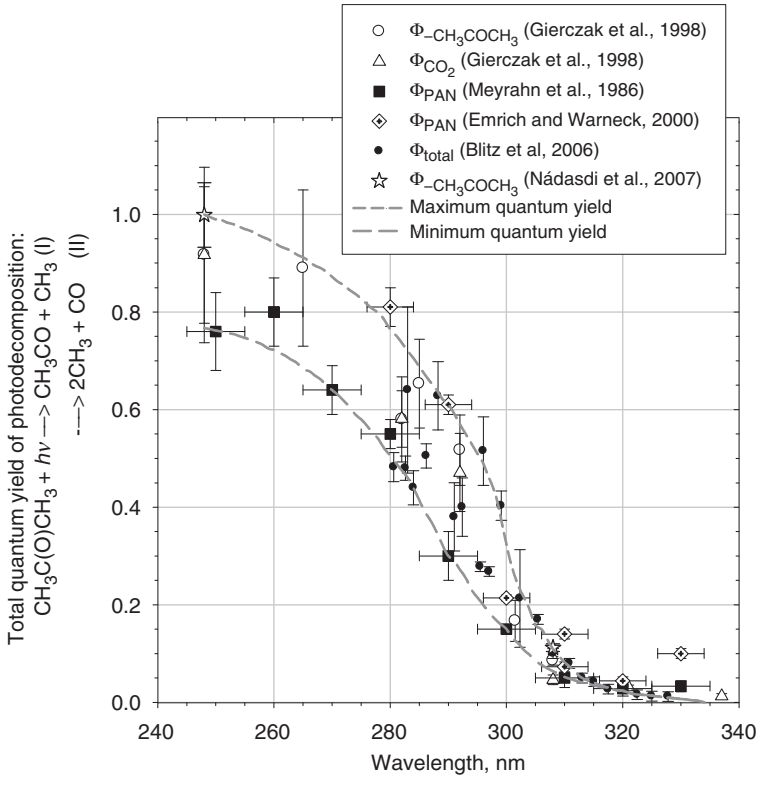

Figure IX-D-3. Experimental determinations of the quantum yields of acetone photodecomposition ($\phi_I + \phi_{II}$) as a function of wavelength for photolyses in air at 760 Torr and ~298 K. The dashed gray curves define an envelope that describes the range of possible values. Values from the two dashed curves were used in estimating the possible range of photolysis constants shown in figure IX-D-6. Authors of the current study recommend use of the values given by the short-dashed line. The maximum values are also given in table IX-D-2.

decrease with increasing pressure of air in accordance with the Stern–Volmer quenching mechanism. Shown in figure IX-D-3, together with all estimates of the quantum yields of acetone photodecomposition, are the results of ϕ_I determinations (Φ_{PAN}) by Meyrahn et al. (1986) and Emrich and Warneck (2000), black squares and diamonds, respectively.

Gierczak et al. (1998) also studied the photodecomposition of acetone in dilute mixtures in air in experiments at discrete wavelengths between 248 and 337 nm and at several pressures of air. In these studies, the quantum yields of $CH_3C(O)CH_3$ loss and CO_2 formation were monitored. In experiments in which both $\Phi_{-CH_3C(O)CH_3}$ and Φ_{CO_2} could be measured, the authors observed a near equality between these quantities as observed previously by Gardner et al. (1984). Both CO_2 formation and acetone loss were used as a measure of process (I). However, in view of other evidence of the occurrence of process (II), particularly at the shorter wavelengths, it may be more appropriate to use the CO_2 product alone as a monitor of process (I). The acetone loss

should reflect the sum of processes (I) and (II) plus any other decomposition pathways. The Gierczak et al. (1998) values of Φ_{CO_2} are shown in figure IX-D-3 by the open triangles, while $\Phi_{-CH_3C(O)CH_3}$ values are shown by the open circles.

Blitz et al. (2002, 2004) have utilized the unique OH radical marker for the CH_3CO radical to determine the quantum yields of photodissociation of acetone as a function of wavelength (279–327.5 nm), temperature (218–295 K), and pressure of added gases (He, 4.5–4,050 Torr; N_2, 4.5–998 Torr; or air, 4.5–600 Torr). In all experiments with added N_2 or He, O_2 was added (0.098 Torr) to ensure the production of OH radicals from the reaction of O_2 with CH_3CO (Tyndall et al., 1997b):

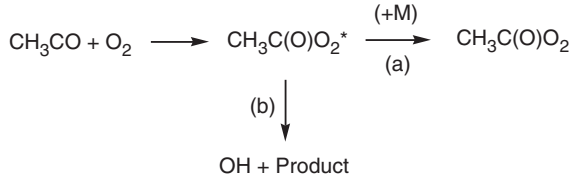

Tyndall et al. (1997b) estimate that $k_b/(k_a + k_b) \cong 0.5$ at 6 Torr pressure and 0.05 at 100 Torr of added gases (N_2, O_2). Carr et al. (2007) obtained more extensive measurements of the OH yield from this reaction, using the photolysis of acetic acid. Acetyl is formed with OH as a co-product, which provides an internal standard for the determination of the OH yield on addition of O_2. They obtained OH yields of 0.7 at 5 Torr, N_2 falling to 0.2 at 100 Torr. Although the yield of $CH_3C(O)O_2$ is essentially 100% at the pressures of the troposphere, the small amount of OH radical formed from the CH_3CO + O_2 reaction can be detected and was used to monitor the yield of CH_3CO from acetone photolysis in the experiments of Blitz et al. (2004). They analyzed their data relative to the CH_3CO yield at 248 nm which they assumed was unity, independent of pressure. Their quantum yield estimates for 1 atm. and 295 K are shown as the small black circles in figure IX-D-3. These data were reproduced from an enlarged view of the data presented in the figure 3 of Blitz et al. (2004). An important new observation in the work of Blitz et al. (2004, 2006) suggested the significant temperature dependence of the quantum yields of CH_3CO for excitation at wavelengths >300 nm. This is particularly important in assessment of the lifetime of the acetone molecule in the cooler upper atmosphere (Arnold et al., 2004, 2005; McKeen et al., 1997).

Nádasdi et al. (2007) studied the photodecomposition of acetone at 248 nm and 298 K (0.23 mbar of acetone in air). They found that the total quantum yield of acetone loss was very near unity and independent of the added air pressure: 1.040 ± 0.046 at 133 mbar and 0.999 ± 0.066 at 1000 mbar. In studies at 308 nm, Nádasdi et al. (2007) also reported that the quantum yields of acetone loss for photolyses at 308 nm was both temperature (233–323 K) and pressure dependent, in confirmation of the conclusions of Blitz et al. (2004, 2006).

Although there is considerable scatter of the data in figure IX-D-3, the trend of ϕ_I with wavelengths in the 340–260 nm range is clear. However, the long-wavelength limit at which process (I) approaches zero is difficult to determine from the very small product yields. Nevertheless, a rough estimate can be made from the data of

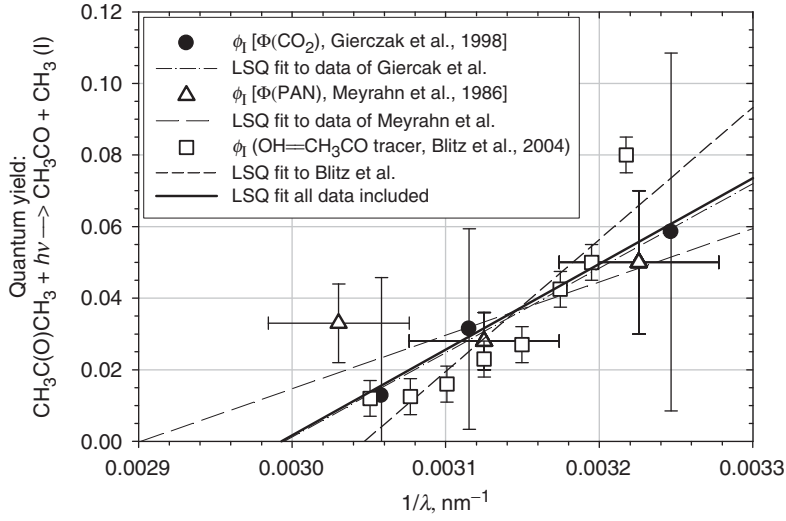

Figure IX-D-4. Plot of the estimates of ϕ_I from photolysis of acetone in air (or N_2) at 760 Torr versus $1/\lambda$ for data at long wavelengths. The least-squares lines are fits and are shown for each individual data set and the combined data. The *y*-axis intercepts are: 344 nm, Meyrahn et al. (1986); 334 nm, Gierczak et al. (1998); 328 nm, Blitz et al. (2004); 334 nm (all data included). Although the range of intercepts is large, the estimates are consistent with the wavelength of minimum energy for the occurrence of process (I), 338 nm; figure from Calvert et al. (2008).

figure IX-D-4 using the long-wavelength data of Gierczak et al. (1998), Meyrahn et al. (1986), and Blitz et al. (2004) that have been plotted versus $1/\lambda$. The least-squares lines from each of the data sets give the origin of primary process (I) between 328 and 344 nm. Use of the combined data sets gives an intercept of 334 nm. The wavelength range is consistent with the estimated necessary energy for the occurrence of process (I) that is available in a quantum of radiation with $\lambda \leq 338$ nm. Our recommended quantum yields for process (I) are given in table IX-D-2. Both the maximum and minimum values are given that correspond to the two dashed curves in figure IX-D-3. This range of values was used in the calculations of acetone photodissociation frequencies so that a measure of the uncertainty in the data can be had. Measurements of Nádasdi et al. (2007) at wavelength 308 nm, 298 K and 1 atm. of added air, gave: $\phi_I + \phi_{II} = 0.112 \pm 0.008$. This measurement, close to the value $\phi_I + \phi_{II} = 0.108$ in table IX-D-2 for this wavelength, favors the use of the maximum values given in the table for studies under pressure and recommendation of the present authors.

ii) Primary process (II): $CH_3C(O)CH_3 + h\nu \rightarrow CH_3 + (CH_3CO^*) \rightarrow 2CH_3 + CO$
Carbon monoxide quantum yields from acetone photolysis in the presence of radical scavengers have been interpreted as arising from process (II). However, Φ_{CO} data from photolysis at the longer wavelengths can be an inaccurate measure of process (II). It may be necessary to correct for CO generation from the photolysis of formaldehyde,

Table IX-D-2. Recommended total quantum yields for acetone photodecomposition, $\phi_I + \phi_{II}$: $CH_3C(O)CH_3 + h\nu \rightarrow CH_3CO + CH_3$ (I); $CH_3C(O)CH_3 + h\nu \rightarrow (CH_3CO^* + CH_3) \rightarrow 2CH_3 + CO$ (II), in air (760 Torr) as a function of wavelength. The maximum values shown are recommended for use in tropospheric modeling

λ, nm	ϕ_{total} (maximum)	ϕ_{total} (minimum)	λ, nm	ϕ_{total} (maximum)	ϕ_{total} (minimum)
248	1.000	0.767	292	0.576	0.27
249	0.995	0.765	293	0.55	0.254
250	0.991	0.762	294	0.532	0.23
251	0.988	0.760	295	0.51	0.213
252	0.982	0.756	296	0.49	0.2
253	0.979	0.754	297	0.459	0.184
254	0.975	0.750	298	0.43	0.17
255	0.969	0.747	299	0.38	0.159
256	0.966	0.743	300	0.326	0.148
257	0.960	0.738	301	0.266	0.132
258	0.954	0.732	302	0.238	0.12
259	0.949	0.728	303	0.212	0.108
260	0.942	0.722	304	0.19	0.095
261	0.935	0.717	305	0.165	0.084
262	0.929	0.710	306	0.147	0.075
263	0.925	0.702	307	0.13	0.069
264	0.916	0.697	308	0.108	0.064
265	0.910	0.685	309	0.096	0.058
266	0.905	0.679	310	0.083	0.053
267	0.896	0.671	311	0.072	0.046
268	0.889	0.661	312	0.06	0.045
269	0.882	0.651	313	0.05	0.041
270	0.872	0.640	314	0.045	0.038
271	0.862	0.629	315	0.042	0.036
272	0.853	0.618	316	0.036	0.031
273	0.845	0.604	317	0.03	0.03
274	0.837	0.588	318	0.028	0.028
275	0.826	0.580	319	0.026	0.026
276	0.816	0.564	320	0.023	0.023
277	0.806	0.549	321	0.02	0.02
278	0.796	0.536	322	0.019	0.019
279	0.784	0.517	323	0.016	0.016
280	0.766	0.504	324	0.015	0.015
281	0.749	0.490	325	0.014	0.014
282	0.736	0.474	326	0.012	0.012
283	0.720	0.460	327	0.011	0.011
284	0.704	0.441	328	0.009	0.009
285	0.686	0.416	329	0.008	0.008
286	0.670	0.389	330	0.007	0.007
287	0.654	0.366	331	0.006	0.006
288	0.638	0.343	332	0.005	0.005
289	0.620	0.320	333	0.004	0.004
290	0.610	0.300	334	0	0
291	0.590	0.285			

a secondary product of the oxidation of the primary CH_3 radical. A number of very different experiments provide estimates of the quantum efficiency of process (II) as a function of wavelength. Limited data from acetone–oxygen mixture photolyses by Kirk and Porter (1962) and acetone-2-butene mixture photolyses by Cundall and Davies (1966) can be used to estimate ϕ_{II} values shown in figure IX-D-5 as open diamonds and filled triangles, respectively. Other estimates can be derived from the experiments of Meyrahn et al. (1986) who determined values of Φ_{CO} in $CH_3C(O)CH_3$–air mixtures. Their estimates of ϕ_{II}, shown in figure IX-D-5 by the open squares, are probably upper limits at the longer wavelengths since, as Meyrahn et al. suggest, CH_2O photolysis could contribute to the CO formation. Gandini and Hackett (1977a) studied the quantum yields of CO and 2,3-butanedione products of broadband acetone photolysis at fifteen different wavelength regions (240–305 nm) and an acetone pressure of 13.5 Torr. Assuming that the CO arises in process (II), the Gandini and Hackett data are plotted in figure IX-D-5 as inverted black triangles. Again, these are maximum values (determined at 13.5 Torr of acetone pressure) in that some quenching of the vibrationally excited $(CH_3CO)^*$ initial product of (II) is expected for acetone in 1 atm. of air.

Horowitz (1991) studied the quantum yields of CH_4 and CO formation in HCl-inhibited photolysis of acetone at 285, 300, and 313 nm and 25°C. HCl is an effective

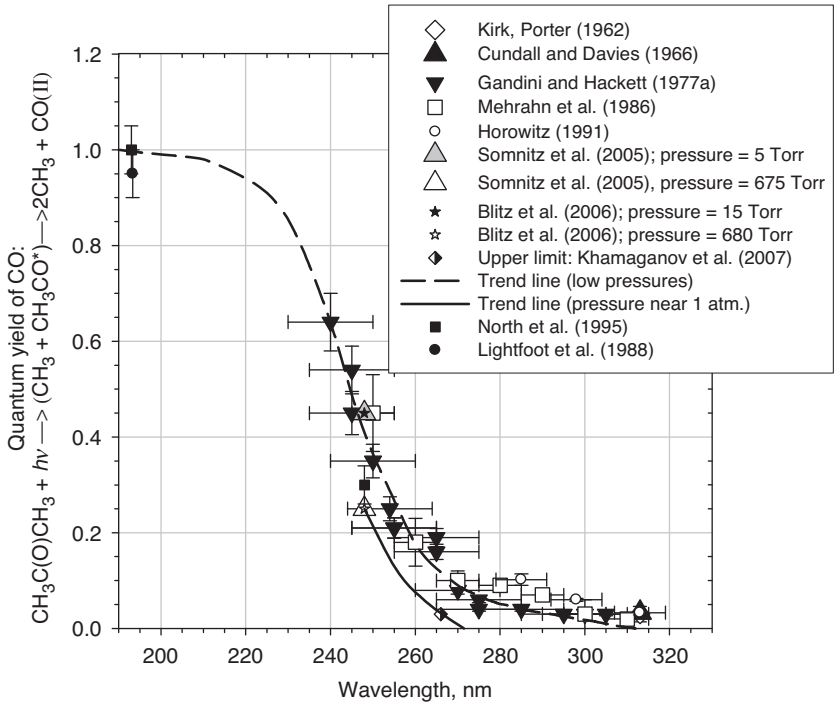

Figure IX-D-5. Plot of experimental estimates of process (II) in acetone–air mixture photolysis as a function of wavelength. The dashed trend line is recommended for photolyses at low pressures of the upper troposphere; the solid trend line is recommended for photolyses at 1 atm.

trap for CH_3 radicals ($CH_3 + HCl \rightarrow CH_4 + Cl$). From the dependence of Φ_{CH_4} and Φ_{CO} on the pressures of acetone and added CO_2, an evaluation of the primary photodissociation processes was possible. Values of ϕ_I and ϕ_{II} at zero pressure were estimated; ϕ_I and ϕ_{II}, respectively, were: 0.90 and 0.10 at 285 nm; 0.94 and 0.06 at 300 nm; 0.28 and 0.03 at 313 nm. Quantum yields of process (II) were found to be insensitive to the pressure of added acetone (2–80 Torr), while those of process (I) were sensitive to both the pressure of acetone and added CO_2. Horowitz suggested that process (II) originates from high vibrational levels of the S_1 state. His data are shown as the open circles in figure IX-D-5.

Acetone–iodine mixture photolysis at 313 nm and 80–100°C by Pitts and Blacet (1952) gave very small quantum yields of CO (0.0015; 0.003), while at 265.4 nm $\Phi_{CO} = 0.057$ was observed. CH_3I quantum yields varied with temperature: 0.12(80°C); 0.17(100°C); 0.28(177°C). Martin and Sutton (1952a) carried out a similar study using acetone mixtures with radioactive iodine. Photolyses were made at 313 nm, 100 and 120°C, and a range of I_2 and $CH_3C(O)CH_3$ pressures. Again, small quantum yields of CO were found (0.0084–0.02) as well as significant quantum yields of CH_3I. These experiments with acetone–iodine mixture photolysis suggest the unimportance of process (II) at 313 nm.

In molecular beam experiments at low pressures, North et al. (1995) studied photofragmentation of acetone excited at 248 and 193 nm. They estimated that at 248 nm a substantial fraction ($30 \pm 4\%$) of the nascent acetyl radicals contain sufficient energy to undergo spontaneous secondary decomposition. They reported that at 193 nm, the only observed dissociation pathway led to the formation of two methyl radicals and carbon monoxide. However, these experiments were carried out at very low pressures and relaxation of a portion of the original $(CH_3CO)^*$ formed may occur at atmospheric pressures.

Consistent with the trend of ϕ_{II} with λ observed in figure IX-D-5, Lightfoot et al. (1988) studied the single-pulse excimer laser photolysis of acetone in experiments at 193.3 nm at pressures of 10–500 Torr of added helium and temperatures of 300–600 K. They reported that about 95% of acetone photodissociation at 193.3 nm occurs by process (II), and they suggest this system as a clean source of CH_3 radicals.

Woodbridge et al. (1988) studied the dynamics of the process (II) at 193 nm and observed infrared emission from highly vibrationally and rotationally excited CO product. The observed vibrational and rotational distributions fit those expected for temperatures of 2,030 K and 3,360 K, respectively. Rotational and vibrational excitation distributions can be modeled using a pure impulsive mechanism for the fragmentation of an initially bent acetyl fragment. Thus, Woodbridge et al. point out that these observations support previous arguments that the dissociation in process (II) occurs by a two-step fragmentation mechanism, $CH_3COCH_3 + h\nu \rightarrow CH_3 + (CH_3CO)^*$; $(CH_3CO)^* \rightarrow CH_3 + CO$, following single photon excitation.

In the experiments of Meyrahn et al. (1986), carried out in one atmosphere of air, vibrationally equilibrated acetone molecules in the T_1 state must be quenched efficiently by oxygen, and these cannot be the source of CO. The consistency of the Meyrahn Φ_{CO} data with those of other studies carried out in the absence of oxygen suggests that quenching of the parent state of process (II) by air is relatively unimportant, and to a first

approximation, the Φ_{CO} data seen in figure VII-C-5 can be attributed to process (II). One obvious problem with this interpretation is the apparent continuation of the process beyond the expected cutoff near 299 nm. Small quantum yields of CO found in experiments beyond the cutoff may result in part from the photolysis of the formaldehyde product in acetone–air mixtures as noted by Meyrahn et al. (1986) and Emrich and Warneck (2000) and described previously in this section. However, Horowitz (1991) and Cundall and Davies (1966) observed CO formation with all CH_3 radicals removed effectively and with no oxygen present, conditions under which formaldehyde could not be formed. If CO formation from acetone does continue well beyond the thermodynamic threshold, then dissociation of the "hot" acetyl radical through the use of internal rovibrational energy as well as collision-assisted dissociation is required. This mechanism accounts for the photodissociation of NO_2 that has been observed to extend well beyond its energy threshold near 398 nm to wavelengths greater than 411 nm (Roehl et al., 1994).

All the data from the variety of experiments appear to form a consistent pattern with increasing importance of ϕ_{II} with increase in energy of the quantum of light absorbed. The dashed trend line shown in figure IX-D-5 is that for the case (b) in figure IX-C-5 of Calvert et al. (2008), with onset of process (II) at 315 nm. However, since most of the data given in this figure were determined in experiments at pressure much below that of the lower troposphere, the extent of quenching of any excited acetyl radicals formed by photolysis at the relatively long wavelength available in sunlight at the pressures of the lower troposphere remains uncertain.

New information suggests that process (II) is much less important at pressures of the lower troposphere than the low-pressure results imply (dashed curve of figure IX-D-5). Somnitz et al. (2005) reported that the quantum yield of CO from acetone photolysis at 248 nm and 298 K shows a significant dependence on total pressure: $\Phi_{CO} = 0.45$ at 15 Torr of N_2; $\Phi_{CO} = 0.25$ at 675 Torr of N_2. Their observations support the view that formation of CO via a direct and/or concerted channel is unimportant at 248 nm. Their data point determined at the higher pressure is shown as an open triangle in figure IX-D-5. Blitz et al. (2006) have confirmed the Somnitz et al. conclusion. They reported a similar pressure effect on process (II); their data are shown as stars in figure IX-D-5.

Khamaganov et al. (2007) measured the pressure dependence of the yield of CH_3 following pulsed laser photolysis of acetone at 248 and 266 nm. They obtained a yield of 1.42 ± 0.15 at zero pressure and 248 nm, indicating that both channels I and II are operative. The yield decreased with increasing pressure of N_2, approaching unity at pressures close to atmospheric, showing that channel I dominates under these conditions. They interpreted their observations in terms of fragmentation of energized CH_3CO at low pressures, and reduction of the methyl yield with increasing pressure due to collisional stabilization of the acetyl radical. They observed the expected increase in the yield of acetyl with increasing pressure; the dependence was somewhat weaker than that expected from the CH_3 results, but the acetyl data were more scattered. Their CH_3 pressure dependence was also stronger than that found by Somnitz et al. (2005) for CO.

Rajakumar et al. (2008) measured the yield of acetyl by cavity ring down spectroscopy following the pulsed laser photolysis of acetone at 248 nm. They obtained a

yield of acetyl at zero pressure of 0.535 ± 0.09, giving $\Phi_I = 0.54$ and $\Phi_{II} = 0.46$, assuming that the sum of the quantum yields is unity. The acetyl yield increased with increasing pressure, reaching a value of 0.87 at a pressure of 592 Torr N_2. Their measurements can be compared with a value of $\Phi_{CH_3CO} = 0.75 \pm 0.07$ at 250 nm in 760 Torr air by Meyrahn et al. (1986).

These observations of an increase in the yield of acetyl with increasing pressure have implications for the interpretation of the data of Blitz et al. (2004) that was based on an assumption of a pressure-independent acetyl yield at 248 nm. Incorporation of the 248 nm acetyl pressure dependence into the analysis of Blitz et al. *decreases* effects of quenching of excited acetone at longer wavelengths and so increases the quantum yield of acetyl at atmospheric pressure. The data of Nádasdi et al. (2007), based on the measurement of acetone by gas chromatography, support the conclusions of Blitz et al. (2004) on the pressure and temperature dependence of the quantum yield for acetone loss at 308 nm, over the pressure range 13–998 bar of synthetic air and for temperatures of 233–323 K. At 298 K and 1 atm. of added air, they reported $\phi_I + \phi_{II} = 0.112 \pm 0.008$. This is close to the value 0.11 that is recommended in table IX-D-2 for case (a) and somewhat greater than the value 0.090 suggested by case (b). At 248 nm, they found that the quantum yield of acetone loss was very near unity and independent of the added air pressure: 1.040 ± 0.046 at 133 mbar and 0.999 ± 0.066 at 1000 mbar.

Several studies during the 2005–2008 period that give important new evidence of the relative unimportance of process (II) in the lower troposphere. Measurements of the pressure dependence of the quantum yields of all the primary products of processes (I) and (II) have been reported: CO (Somnitz et al., 2005; Blitz et al., 2006); CH_3 (Khamaganov et al., 2007); and CH_3CO (Rajakumar et al., 2008). The results of these studies are compared in figure IX-D-6. Utilizing the observation of Nádasdi et al. (2007) that $\Phi_{-CH_3C(O)CH_3} = 1.0$ independent of pressure over the 133–1,000 mbar range, we can use the data to adjust the measured product yields to those of a common product, CO. Here the original data determined for Φ_{CH_3CO} and Φ_{CH_3} have been converted to equivalent values of Φ_{CO} to represent the variation of the $1/\Phi_{CO}$ with pressure of added gas. The theoretically equivalent Φ_{CO} values were calculated from the measured Φ_{CH_3} of Khamaganov et al. (2007) through the mass balance equation, $\Phi_{CO} = \Phi_{CH_3} - 1$, and the Φ_{CH_3CO} data of Rajakumar et al. (2008) were converted to equivalent Φ_{CO} values through the relation: $\Phi_{CO} = 1 - \Phi_{CH_3CO}$. The data shown in figure IX-D-6 from the Khamaganov et al. (2007) studies were calculated at several pressures using their modified exponential fit to the data presented in their figure 5. These show strong deviations from the behavior of the data from the other studies. However, it is clear that all the data confirm the pressure dependence of process (II), presumably reflecting the collisional relaxation of the original vibrationally excited CH_3CO^* radical formed from acetone photodecomposition at 248 nm.

Results obtained by Khamaganov for photolyses at 266 nm show much less pressure dependence than that observed at 248 nm. In fact, the quantum yield of CH_3 radicals appeared to be independent of pressure (50–750 Torr) with $\Phi_{CH_3} = 0.93 \pm 0.1$. Additional direct measurements of Φ_{CH_3CO} at 266 nm were made in this study as well, and the pressure independent ratio $\Phi_{CH_3CO}/\Phi_{CH_3} \cong 1.18 \pm 0.2$ was determined. The authors use this ratio, together with the estimated error limits, to place the upper limit

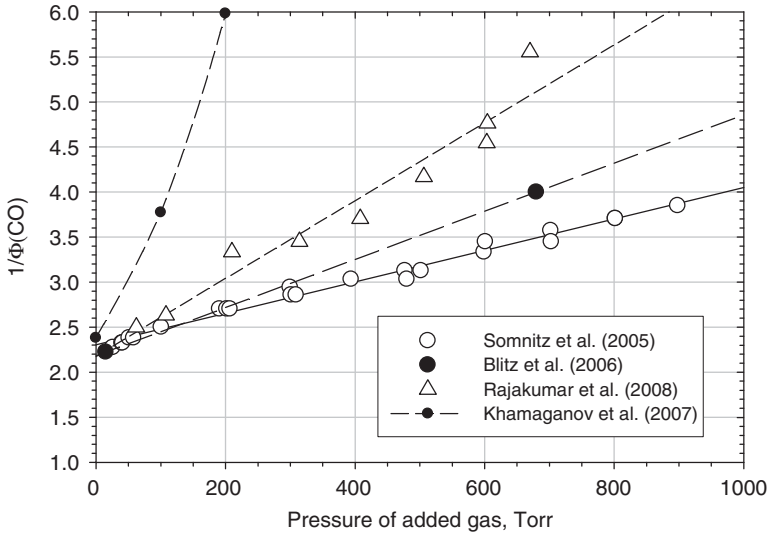

Figure IX-D-6. Stern–Volmer plot of $1/\Phi_{CO}$ versus pressure of added nitrogen gas. Experiments were all performed using 248 nm excitation of acetone. Measurements of Φ_{CH_3CO} reported by Rajakumar et al. (2008) were converted to CO data using the mass balance expression, $\Phi_{CO} = 1 - \Phi_{CH_3CO}$. The data for Φ_{CH_3} determined by Khamaganov et al. (2007) were converted to equivalent values of Φ_{CO} using the expression, $\Phi_{CO} = \Phi_{CH_3} - 1$.

to Φ_{CO} at 0.03 at 266 nm (shown as a half-darkened diamond in figure IX-D-5). The present authors use this value to establish the lower portion of the high-pressure trend line shown in the figure. These results support the conclusion that the occurrence of process (II) at the wavelengths of sunlight available within the troposphere is probably much less important than has been suggested from the earlier, less-detailed measurements (for example, see Calvert et al., 2008). It now seems probable that acetone photodecomposition within the troposphere is described best by the near exclusive occurrence of process (I).

With the limited current state of our knowledge, the present authors recommend that modelers assume $\phi_{II} = 0$ within the lower troposphere. Values of ϕ_{II} that were determined for acetone over a range of lower pressures of acetone and added gases, representative of those of the middle and upper troposphere, are given by the upper curve in figure IX-D-5 and in table IX-D-3. The data available at this writing do not allow a meaningful estimate of the pressure and temperature dependencies of process (II). It is obvious that accurate determinations of Φ_{CO} in acetone–air mixtures over a range of wavelengths and pressures are required to evaluate properly the influence of process (II) in photodecomposition of acetone for the conditions encountered in the middle and upper as well as the lower troposphere.

iii) Minor processes in acetone photodecomposition Primary process (III), H-atom formation, has been observed by Takahashi et al. (2004) and Lightfoot et al. (1988) in photolysis of acetone at 193 nm. Lightfoot et al. (1988) reported that 3% of acetone

Table IX-D-3. Quantum yields for acetone photodecomposition by process (II): $CH_3C(O)CH_3 + h\nu \rightarrow (CH_3CO^* + CH_3) \rightarrow 2CH_3 + CO$(II), in air (760 Torr) as a function of wavelength. The minimum values shown are recommended for use in tropospheric modeling

λ, nm	ϕ_{II} (maximum)	ϕ_{II} (minimum)	λ, nm	ϕ_{II} (maximum)
248	0.249	0.410	282	0.046
249	0.232	0.388	283	0.044
250	0.215	0.366	284	0.042
251	0.198	0.343	285	0.040
252	0.182	0.325	286	0.038
253	0.163	0.307	287	0.036
254	0.148	0.286	288	0.035
255	0.131	0.268	289	0.034
256	0.115	0.250	290	0.033
257	0.105	0.230	291	0.032
258	0.095	0.209	292	0.030
259	0.084	0.192	293	0.028
260	0.076	0.178	294	0.026
261	0.067	0.164	295	0.025
262	0.060	0.151	296	0.024
263	0.053	0.142	297	0.023
264	0.045	0.133	298	0.021
265	0.037	0.124	299	0.019
266	0.032	0.117	300	0.018
267	0.027	0.110	301	0.016
268	0.020	0.104	302	0.015
269	0.014	0.097	303	0.013
270	0.008	0.090	304	0.012
271	0.003	0.085	305	0.010
272	0	0.079	306	0.008
273		0.076	307	0.006
274		0.072	308	0.004
275		0.067	309	0.003
276		0.065	310	0.002
277		0.060	311	0.001
278		0.057	312	0
279		0.054		
280		0.052		
281		0.048		

photodecomposition at this wavelength proceeds by process (III). Takahashi et al. (2004) report a similar finding: $\phi_{III} = 0.039 \pm 0.006$, and the authors report that the nascent kinetic energy of the H-atoms is characterized by a Maxwell–Boltzmann function with a temperature of 5,000 K. Primary process (IV) accounts for $\leq 2\%$ of acetone photodecomposition in the 193 nm photolysis reported by Lightfoot et al. (1988).

IX-D-1.3. Photolysis Frequencies for Acetone

The quantum yield data (maximum and minimum) given in table IX-D-2 apppear to be the best current choices for modeling acetone photodecomposition within the

lower troposphere, but there are significant problems that remain to be resolved. The pressure dependence in the 248 nm yield of acetyl, observed by Khamoganov et al. (2007) and Rajakumar et al. (2008), has not been incorporated in the parameterization of acetone photodecomposition developed by Blitz et al. (2004). Additional accurate determinations of Φ_{CO} in acetone–air mixtures at the longer wavelengths are also required to evaluate properly the influence of process (II) in the tropospheric photodecomposition of acetone. We have used the current recommendations for cross sections (table IX-D-1) and quantum yields (tables IX-D-2 and IX-D-3) to estimate cloudless-sky *j*-values for acetone photodecomposition in the lower troposphere. These are given in figure IX-D-7 as a function of solar zenith angle for overhead ozone columns of 350 DU.

Values are shown for the total photodecomposition [primary process (I) and (II)] assuming the values shown as the solid and dashed black curves that are derived from the maximum and minimum in the estimated quantum yields, respectively, in figure IX-D-2. It can be seen from the lower gray curve in the figure that the current estimated *j*-values for process (II) within the lower troposphere are very much smaller than those of process (I) even when the maximum ϕ_{II} choices are used in the calculations. Use of the more probable, minimum values in table IX-D-3 gives *j*-values for process (II) very near zero.

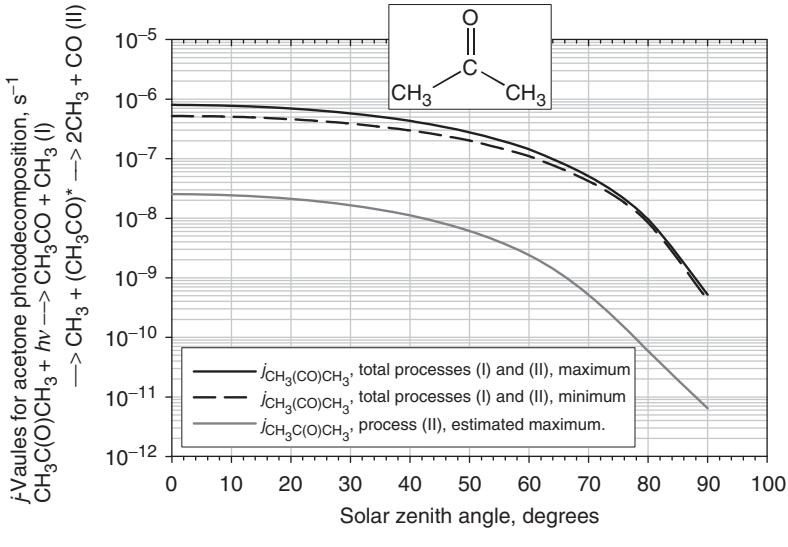

Figure IX-D-7. Plot of the estimated photolysis frequencies for acetone photodecomposition for a cloudless day within the lower troposphere at 760 Torr and 298 K. The black solid and dashed curves represent the maximum and minimum *j*-values, respectively, for the total photodecomposition [process (I) + process (II)] as estimated from the quantum yield data of table IX-D-2. The gray curve is the estimated maximum value for photodissociation by process (II) in the lower troposphere as estimated using the maximum quantum yield given in table IX-D-3. If the more probable, minimum estimates for lower tropospheric pressures are used in the calculation, the *j*-values for process (II) in acetone are very near zero.

In figure IX-D-8a the percentage decrease in the *j*-values is given for increases in the overhead ozone column. The response of the acetone *j*-values to ozone column changes is much greater (a factor of about 3) than that calculated for formaldehyde by Calvert et al. (2008) and shown in figure IX-D-8b. This reflects the greater influence of the longer wavelengths of sunlight absorbed by formaldehyde that are least affected by

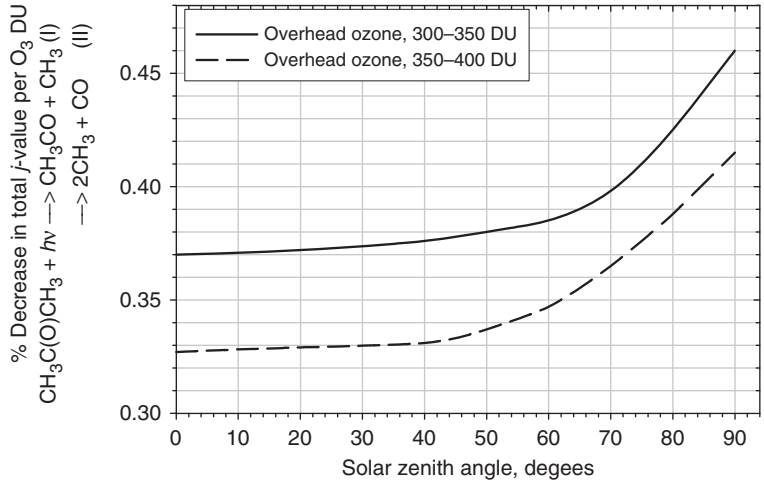

Figure IX-D-8a. Approximate percentage decrease in the total *j*-values for acetone for data presented in figure VII-C-6a for overhead ozone columns of 300–350 and 350–400 Dobson units.

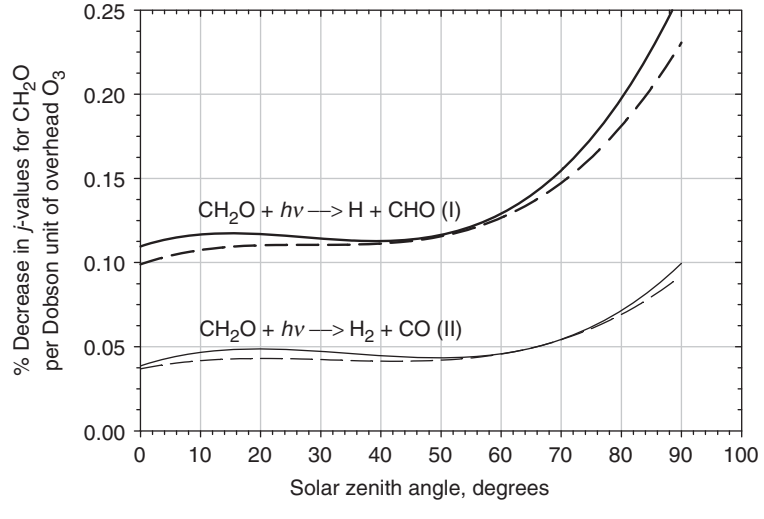

Figure IX-D-8b. Estimated percentage decrease in the *j*-values for the primary processes in formaldehyde photodissociation in the lower troposphere with overhead ozone column of 300–350 (solid curves) and 350–400 DU (dashed curves); calculations from Calvert et al. (2008).

ozone absorption as illustrated in the spectral *j*-data shown for acetone and formaldehyde in figures IX-D-9a and IX-D-9b, respectively. The significant temperature dependence of the photodissociation of acetone reported by Blitz et al. (2004, 2006), and confirmed by Nadasdi et al. (2007), leads to estimated lifetimes of acetone within the troposphere that are much greater than that suggested from the original calculations based upon temperature-independent quantum yields. However, an accurate picture of the effect of temperature and pressure on *j*-values will require new calculations that

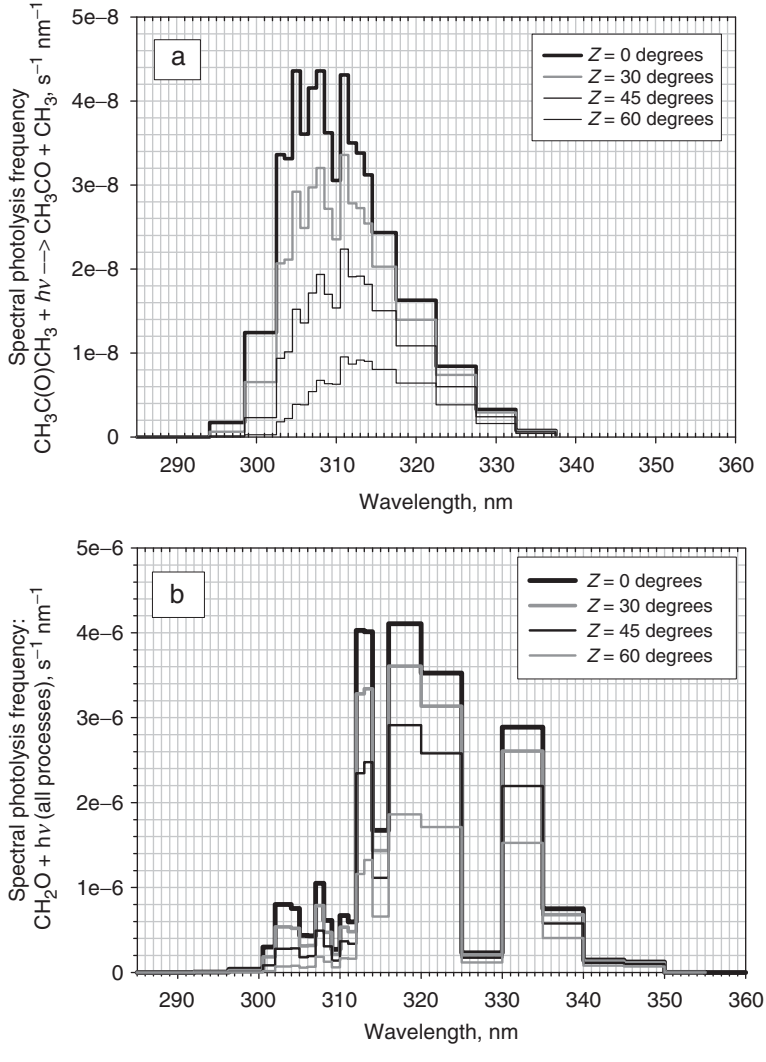

Figure IX-D-9. Comparison of the spectral *j*-values for acetone (a) and formaldehyde (b); note the *y*-scale of the acetone is much smaller than that for formaldehyde and the wavelength response for acetone is shifted to shorter wavelengths than for CH_2O. Calculations are as reported in Calvert et al. (2008) for an overhead ozone column of 350 DU.

adjust the Blitz et al. data for the observed pressure dependence of the Φ_{CO} in the 248 nm photolysis of acetone. Such calculations are in progess at the time of this writing.

IX-D-2. Photodecomposition of 2-Butanone [Methyl Ethyl Ketone, $CH_3C(O)CH_2CH_3$]

Three different photodecomposition pathways have been considered for 2-butanone for excitation in its $n \rightarrow \pi^*$ absorption band (Calvert et al., 2008):

$$CH_3C(O)C_2H_5 + h\nu \rightarrow CH_3CO + C_2H_5 \quad \text{(I)}$$

$$\rightarrow CH_3 + C_2H_5CO \quad \text{(II)}$$

$$\rightarrow C_2H_5 + (CH_3CO^*) \rightarrow C_2H_5 + CH_3 + CO \quad \text{(III)}$$

IX-D-2.1. Absorption Cross Sections for 2-Butanone

The $n \rightarrow \pi^*$ absorption band for 2-butanone is similar to that of other simple ketones; see figure IX-D-1. The maximum value of the cross section is intermediate to those for acetone and 3-pentanone. The cross sections of 2-butanone as determined by Martinez et al. (1992) are given in table IX-D-1.

IX-D-2.2. Quantum Yields of the Primary Photodecomposition Processes in 2-Butanone

There have been very limited studies of the photodissociation modes of 2-butanone, and no studies have been reported of the wavelength dependence of the quantum yields of the individual processes for atmospheric conditions. As with acetone, at temperatures somewhat above 100°C, the sum of the primary quantum yields for 313 nm excitation are near unity (Ells and Noyes, 1938; Lissi et al., 1973/1974). Although difference between the dissociation energies for the $CH_3CO—C_2H_5$ and the $CH_3—COC_2H_5$ bonds is relatively small (about 3.2 kJ mol^{-1}), process (I) is highly favored. Photolysis of 2-butanone-iodine mixtures were carried out by Durham et al. (1949), Pitts and Blacet (1950), and Martin and Sutton (1952b). Pitts and Blacet (1950) reported in a preliminary study at 313 nm that $\Phi_{C_2H_5I}/\Phi_{CH_3I} \approx 40$ at 100°C and 21 at 175°C (pressures of ketone and iodine, 90 and 6.3 Torr, respectively). In these experiments $\Phi_{C_2H_5I} + \Phi_{CH_3I} \approx 0.41$ and 0.45 at 100 and 175°C, respectively and $\Phi_{CO} \approx 0.11$ at 175°C. In similar experiments at 313 nm, Martin and Sutton (1952b) used radioactive iodine in mixtures with 2-butanone to attain high sensitivity in analyses of the iodide products at very small conversions ($\sim 0.1\%$). They reported: $\Phi_{C_2H_5I}/\Phi_{CH_3I} \approx 19.3 \pm 0.8$ at 100°C (pressures of ketone and iodine, 88 and 1 Torr, respectively); $\Phi_{C_2H_5I} + \Phi_{CH_3I} \approx 0.88$, and $\Phi_{CO} = 0.004$. Using a lower pressure of ketone (14.8 Torr) but the same I_2 pressure, they found $\Phi_{C_2H_5I}/\Phi_{CH_3I} \approx 10.3$; $\Phi_{C_2H_5I} + \Phi_{CH_3I} \approx 1.07$, and $\Phi_{CO} \approx 0.096$. Some formation of acetyl iodide was

evident, but the analytical results for this compound were not reproducible. With excitation at shorter wavelengths, somewhat less discrimination in bond cleavage was found. At 265.4 nm excitation (100°C), Pitts and Blacet reported, $\Phi_{C_2H_5I}/\Phi_{CH_3I} \approx 5.5$ and $\Phi_{C_2H_5I} + \Phi_{CH_3I} \approx 0.52$. At 253.7 nm, Martin and Sutton found $\Phi_{C_2H_5I}/\Phi_{CH_3I} \approx 2.4$ and $\Phi_{CO}/\Phi_{CH_3I} \approx 0.78$. The results are consistent with the dominant occurrence of processes (I) but with process (II) becoming significant at the shorter wavelengths. They also suggested that fragmentation of the nascent acyl radicals that characterizes process (III) appears to occur, particularly at the short wavelengths.

Energy transfer to 2,3-butanedione from 2-butanone excited at 313 nm was studied by Lissi et al. (1973/1974) through observed phosphorescence of 2,3-butanedione triplets. They found that the quantum yield of triplet 2-butanone formation was near unity at high pressures (400 Torr) of added propane. The triplet lifetime was reported to be 1.3×10^{-5} and 1.8×10^{-5} s at 400 and 14 Torr, respectively. They reported $\Phi_{CO} = 0.9$ at 120°C, 100 Torr pressure, and low light intensity. From 2,3-butanedione photosensitized experiments, the rate coefficient for the photocleavage of 2-butanone triplet (400 Torr total pressure) as estimated by Abuin and Lissi (1975) is represented by the function:

$$\log_{10}(k_{\text{decomp}}) = (14.63 \pm 1.49) - (12{,}710 \pm 2150)/R(\text{kcal mol}^{-1}\text{K}^{-1})T$$

The photochemical study of 2-butanone by Raber and Moortgat (1996) is the most relevant to reactions expected for atmospheric conditions. They carried out broadband photolysis using TL12 lamps. Dilute mixtures of the ketone in air were photolyzed at several pressures (52–758 Torr). They determined the nature and the time dependence of the ratio of several products to the ketone photodecomposed using FTIR spectroscopy. Products observed were those expected with the dominance of process (I): CO_2, CH_3CHO, CH_2O, and smaller amounts of CH_3OH, $CH_3C(O)OOH$, HC(O)OH, and CO. The ratio $\Delta CO/\Delta CH_3C(O)C_2H_5$ showed a positive intercept at zero time that indicates a fraction of the photodecomposition ($\leq$ 10%) forms CO directly in process (III) even in an atmosphere of air, as observed in some experiments with acetone at the lower pressures (see section IX-D-1.2). The quantum yields of 2-butanone that decomposed at the various pressures followed a Stern–Volmer quenching mechanism: $1/(\Phi_{CH_3C(O)CH_2CH_3}) = 0.96 + 2.22 \times 10^{-3} \times P_{\text{air}}$ (Torr). The k_q/k_d values for 2-butanone with broadband radiation are similar to those estimated for acetone and the simple aldehydes at the wavelength of maximum overlap of the lamp distribution and the absorption by the ketone. The intercept of the Stern–Volmer relation is consistent with the observations of previous investigators that the quantum yield of decomposition of excited 2-butanone at zero pressure is near unity (Lissi et al., 1973/1974).

In separate experiments using a different apparatus, Raber (1992) excited 2-butanone at 310 nm in air containing NO_2 scavenger. Although peroxyacetyl nitrate was the major product, methyl nitrate, ethyl nitrate, and peroxypropionyl nitrate were also detected. The presence of the latter compound confirms the occurrence of process (II) to a minor, but unquantified extent.

IX-D-2.3. Photolysis Frequencies for Photodecomposition of 2-Butanone in the Lower Troposphere

Since no wavelength dependence of the product quantum yields has been determined, only the *j*-values that describes the total quantum yield of photodecomposition of 2-butanone ($\phi_I + \phi_{II} + \phi_{III}$) are calculated here. We have assumed the average quantum yield value for 1 atm. of air (0.34 ± 0.15), determined in the broadband experiments of Raber and Moortgat (1996), applies to all wavelengths absorbed by 2-butanone. Until more detailed information becomes available, we suggest that modelers assume that 10% of the photodecomposition arises from process (III) as suggested from broadband experiments of Raber and Moortgat. The calculated *j*-values for 2-butanone photodissociation for cloudless conditions in the lower troposphere (ozone column of 350 DU) are shown as a function of solar zenith angle in figure IX-D-10.

IX-D-3. Photodecomposition of 3-Pentanone [Diethyl Ketone, $CH_3CH_2C(O)CH_2CH_3$]

The primary photodecomposition modes of 3-pentanone follow the pattern of the smaller ketones (Calvert et al., 2008):

$$C_2H_5C(O)C_2H_5 + h\nu \rightarrow C_2H_5CO + C_2H_5 \quad \text{(I)}$$

$$\rightarrow (C_2H_5CO^*) + C_2H_5 \rightarrow 2C_2H_5 + CO \quad \text{(II)}$$

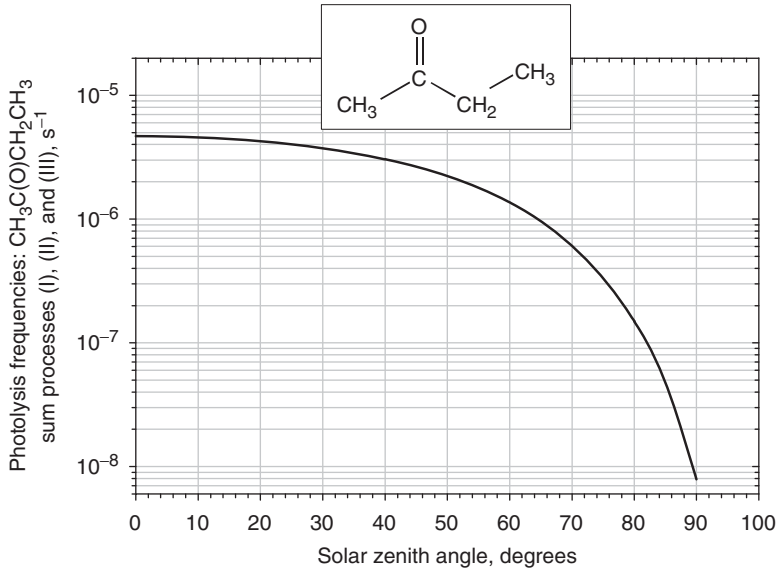

Figure IX-D-10. Approximate photolysis frequencies for the photodecomposition of 2-butanone as a function of solar zenith angle for a cloudless day in the lower troposphere with an overhead ozone column of 350 DU.

IX-D-3.1. Absorption Cross Sections for 3-Pentanone

In figure IX-D-1 the absorption spectrum of 3-pentanone can be compared with those of some other simple ketones. The recommended values of the cross sections (Martinez et al., 1992) are given in tabular form in table IX-D-4.

IX-D-3.2. Quantum Yields of Primary Photodecomposition Processes in 3-Pentanone

Early studies involved photolysis of pure 3-pentanone using partially filtered, full-arc radiation. Reported quantum yields of photodecomposition and CO formation were

Table IX-D-4. Cross sections (σ, cm^2 $molecule^{-1}$) at 298 K for 2-pentanone and 3-pentanone (Martinez et al., 1992)

λ, nm	2-Pentanone $10^{20} \times \sigma$	3-Pentanone $10^{20} \times \sigma$	λ, nm	2-Pentanone $10^{20} \times \sigma$	3-Pentanone $10^{20} \times \sigma$
278	6.09	6.18	315	1.20	0.967
279	6.11	6.19	316	1.07	0.836
280	6.12	6.20	317	0.953	0.716
281	6.13	6.19	318	0.845	0.613
282	6.12	6.17	319	0.745	0.522
283	6.09	6.14	320	0.652	0.444
284	6.03	6.11	321	0.560	0.374
285	5.96	6.05	322	0.479	0.317
286	5.88	5.96	323	0.406	0.264
287	5.80	5.84	324	0.343	0.219
288	5.72	5.70	325	0.285	0.181
289	5.63	5.56	326	0.237	0.150
290	5.53	5.43	327	0.194	0.125
291	5.41	5.31	328	0.160	0.101
292	5.26	5.18	329	0.130	0.083
293	5.08	5.04	330	0.103	0.068
294	4.90	4.87	331	0.083	0.054
295	4.72	4.67	332	0.067	0.044
296	4.55	4.44	333	0.051	0.034
297	4.40	4.21	334	0.037	0.025
298	4.25	3.99	335	0.029	0.020
299	4.10	3.80	336	0.022	0.016
300	3.92	3.63	337	0.018	0.013
301	3.72	3.46	338	0.013	0.011
302	3.51	3.28	339	0.009	0.008
303	3.29	3.08	340	0.008	0.002
304	3.08	2.87	341	0.005	0.001
305	2.88	2.63	342	0.002	0.000
306	2.69	2.40	343	0.004	0.000
307	2.52	2.18	344	0.001	0.000
308	2.35	1.98	345	0.001	0.000
309	2.18	1.81	346	0.001	0.000
310	2.02	1.65	347	0.001	0.000
311	1.85	1.51	348	0.000	0.001
312	1.67	1.37	349	0.001	0
313	1.50	1.24	350	0.000	0
314	1.35	1.10	351	0.001	0

near unity, even at relatively low temperatures. In experiments at 28 ± 1°C, Davis (1948) reported Φ_{CO} values of 1.03 ± 0.14; 0.99 ± 0.13; 1.06 ± 0.14, while Dorfman and Sheldon (1949) found $\Phi_{CO} = 0.97 \pm 0.10$ at 56.5 ± 2°C and 1.09 ± 0.09 at 120 ± 2°C. It was suggested that the more efficient CO formation seen with 3-pentanone photolysis than with acetone for similar experimental conditions arose from the greater instability of the C_2H_5CO radical toward decomposition compared to CH_3CO. Thermal data for the decomposition reactions: $C_2H_5CO \rightarrow C_2H_5 + CO$ (1) and $CH_3CO \rightarrow CH_3 + CO$ (2), show only a small difference, $\Delta H_2 - \Delta H_1$ in the range 3.2 to 18 kJ mol^{-1} (Vollenweider and Paul, 1986; Kerr and Stocker, 2001/2002). Kutschke et al. (1952) reported $\Phi_{CO} = 0.62 \pm 0.02$ at 25°C, and values near unity for temperatures ≥ 176°C, very similar to the acetone behavior.

Weir (1961) studied 3-pentanone/2,3-butanedione mixture photolyses at 313 and 253.7 nm. In experiments near 25°C and excitation at 313 nm, Φ_{CO} was lowered from 0.72 ± 0.02 for pure 3-pentanone at 25 Torr, to 0.45 with 2.4 Torr of 2,3-butanedione addition, as strong emission from 2,3-butanedione triplets appeared. Weir found this same limiting yield of CO is reached in photolysis at high light intensities where C_2H_5CO radical association reactions compete successfully with decomposition. The data suggest strongly that the triplet state of 3-pentanone is involved at least to some extent at 313 nm and that a significant portion of the C_2H_5CO radicals formed dissociate readily, presumably in primary process (II). In experiments at 253.7 nm, addition of 1.2 Torr of 2,3-butanedione gave no reduction of the $\Phi_{CO} = 0.91$ seen in pure 3-pentanone photolysis, and no phosphorescence of 2,3-butanedione was observed. Photodecomposition from the excited singlet state formed at 253.7 nm was suggested to rationalize these results.

A few studies of the photolysis of 3-pentanone with added oxygen have been reported, but these have been at low oxygen pressures (Finklestein and Noyes, 1953; Jolley, 1957; Dunn and Kutschke, 1958). In experiments at 298 K (wavelength unstated) Finklestein and Noyes (1953) found that as the O_2 pressure was increased from 0 to 0.2 Torr, Φ_{CO} decreased from near unity to 0.15 and Φ_{CO_2} increased from 0 to 1.1 for 2-pentanone pressure of 35 Torr. No further decrease in Φ_{CO} was seen as P_{O_2} was increased to 1.25 Torr. These data indicate that a large share of the photodecomposition forms vibrationally excited C_2H_5CO radicals that dissociate quickly. Yet another larger share of the C_2H_5CO radicals formed in (I) can be captured by O_2 before dissociation. The $C_2H_5C(O)O_2$ radicals formed lead to CO_2 through various peroxy radical reactions [e.g., $C_2H_5C(O)O_2 + C_2H_5C(O)O_2 \rightarrow (2CH_3CH_2CO_2 + O_2) \rightarrow 2C_2H_5 + 2CO_2 + O_2$]. Several studies involving labeled 3-pentanone [$C_2H_5C^{14}(O)C_2H_5$ (Finklestein and Noyes, 1953), $C_2H_5C(O^{18})C_2H_5$ (Jolley, 1957; Dunn and Kutschke, 1958)] demonstrated that the CO and CO_2 formed in 2-pentanone photolysis with oxygen added, arise largely from the carbonyl carbon, and that vibrationally rich propionyl radicals form CO in process (II). Jolley calculated from his results that dissociation of the thermalized C_2H_5CO radical requires 54 ± 17 kJ mol^{-1} more energy than its association reaction with O_2.

Hall et al. (1995) studied the infrared emission from CO and C_2H_5 formed in the photolysis of 3-pentanone at 193 nm. The process (II) occurs with formation of CO with a rotational temperature of ~2,100 K and an average vibrational energy in the range

of 6.3 to 8.8 kJ mol^{-1}, somewhat lower excitation than that observed in acetone photolysis at 193 nm. However, the ethyl radicals formed appear to have more vibrational energy (~79 kJ mol^{-1} total) than the methyl radicals formed in acetone photolysis with similar excitation. None of the models considered by Hall et al. (1995) for photodissociation were fully satisfactory in explaining the excitation of the CO. The double impulse model considered in explanation of these results from 3-pentanone and acetone photolysis by Trentelman et al. (1989) is characterized by a pair of closely timed impulses along the two C—C bonds, each releasing half of the available energy to the three-body fragmentation. This leads to 13 kJ mol^{-1} excitation in CO, significantly higher than observed experimentally yet a much better fit than found for some alternative models that predict vibrational excitation of CO to be: 0.0004 kJ mol^{-1} (impulsive first step-statistical second step model); 0.17 kJ mol^{-1} (two-step information-theoretic prior model); 0.7 kJ mol^{-1} (soft barrier impulsive model).

IX-D-3.3. Photolysis Frequencies for Photodecomposition of 3-Pentanone in the Lower Troposphere

Unfortunately, there are no data that establish the wavelength dependence of the primary photodissociative processes in 3-pentanone in air at tropospheric pressures. However, it is likely that the quantum efficiency is somewhat greater than that seen for acetone and 2-butanone under similar conditions.

IX-D-4. Photodecomposition of 2-Pentanone [Methyl *n*-Propyl Ketone, $CH_3C(O)CH_2CH_2CH_3$]

The photochemistry of 2-pentanone follows the pattern of the other small ketones in that photodissociation occurs to form radicals in processes (I), (II), and (III), but an additional photodecomposition pathway appears (Calvert et al., 2008). This is the smallest ketone that exhibits photodecomposition by the Norrish type-II rearrangement in process (IV) that occurs in all aldehydes and ketones that contain a γ-hydrogen atom. Also process (V) leading to a cyclobutanol derivative has been observed.

$$n\text{-}C_3H_7COCH_3 + h\nu \longrightarrow n\text{-}C_3H_7 + CH_3CO \qquad \text{(I)}$$

$$\longrightarrow CH_3 + CH_3CH_2CH_2CO \qquad \text{(II)}$$

$$\longrightarrow CH_3 + CO + CH_2CH_2CH_3 \qquad \text{(III)}$$

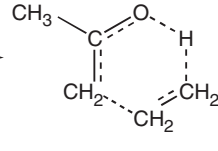

$$\longrightarrow CH_3C(OH)=CH_2 + CH_2=CH_2 \qquad \text{(IV)}$$

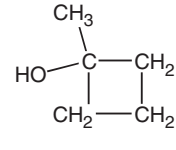

(V)

Excitation of 2-pentanone at long wavelengths ($\lambda \geq 313$ nm) populates the triplet state efficiently through intersystem crossing, $S_1 \rightarrow T_1$, and dissociation apparently occurs from this state. At the shorter wavelengths, dissociation is believed to occur either from a vibrationally excited T_1 or the S_1 state.

IX-D-4.1. Absorption Cross Sections for 2-Pentanone

The absorption spectrum of 2-pentanone as measured by Martinez et al. (1992), is very similar to that of 3-pentanone; see figure IX-D-1. Tabular listing of the cross sections as a function of wavelength is given in table IX-D-4.

IX-D-4.2. Quantum Yields of the Primary Photodissociative Processes in 2-Pentanone

Data directly related to 2-pentanone photolysis in the atmosphere are very limited, but some useful, related information is available for the pure ketone and its mixture with various added compounds.

i) Processes (I) and (II): $CH_3CH_2CH_2C(O)CH_3 + h\nu \rightarrow CH_3CH_2CH_2 + CH_3CO$(I); $CH_3CH_2CH_2C(O)CH_3 + h\nu \rightarrow CH_3CH_2CH_2CO + CH_3$ *(II)* The $CH_3CH_2CH_2$—$C(O)CH_3$ bond is somewhat weaker than the $CH_3CH_2CH_2C(O)$—CH_3 bond, and, discrimination in the bond cleavage occurs in 2-pentanone photolysis as in $CH_3C(O)C_2H_5$ photolysis. A very qualitative measure of the relative importance of processes (I) and (II) can be gained from hydrocarbon product analyses of Nicholson (1954) from 2-pentanone photolysis. His full-arc photolysis at 20°C suggests that $\phi_I/\phi_{II} \approx 8$. Rough estimates of minimum values of $\phi_I + \phi_{II}$ for pure ketone photolysis can be estimated from the summation of the quantum yields of the CH_3 and $CH_3CH_2CH_2$ groups in the hydrocarbon products for experiments near 20°C where the decomposition reactions of radical products are unimportant. Maximum values for $\phi_I + \phi_{II} + \phi_{III}$ are probably well represented by Φ_{CO} as measured at temperatures near 120°C, where nearly complete decomposition of CH_3CO and $CH_3CH_2CH_2CO$ radicals is expected, and radical induced decomposition of the ketone that forms CO is unimportant. This reasoning applied to data of Wettack and Noyes (1968) gives estimates of the approximate range of $\phi_I + \phi_{II} + \phi_{III}$ values for pure 2-pentanone photolysis at several wavelengths: 0.11 − 0.12 (254 nm); 0.19–0.23 (280 nm); 0.27–0.36 (296.5 nm); 0.16–0.39 (313 nm).

ii) Process (III): $CH_3CH_2CH_2COCH_3 + h\nu \rightarrow CH_3CH_2CH_2 + CO + CH_3$ At low temperatures (~25°C) and high pressures and high intensities of absorbed light, the decomposition of thermalized acyl radicals should be relatively unimportant, and Φ_{CO} values should provide a measure of the maximum values of ϕ_{III}. The data of Wettack and Noyes (1968) give $\phi_{III} \leq 0.06$ (313 nm); 0.08 (296.5 nm); 0.10 (280.4 nm); 0.05 (254 nm). Φ_{CO} values reported by Michael and Noyes (1963) for 2-pentanone photolyses at 313 and 253.7 nm are also small: ~0.01 (313 nm) and 0.05 (253.7 nm). These are

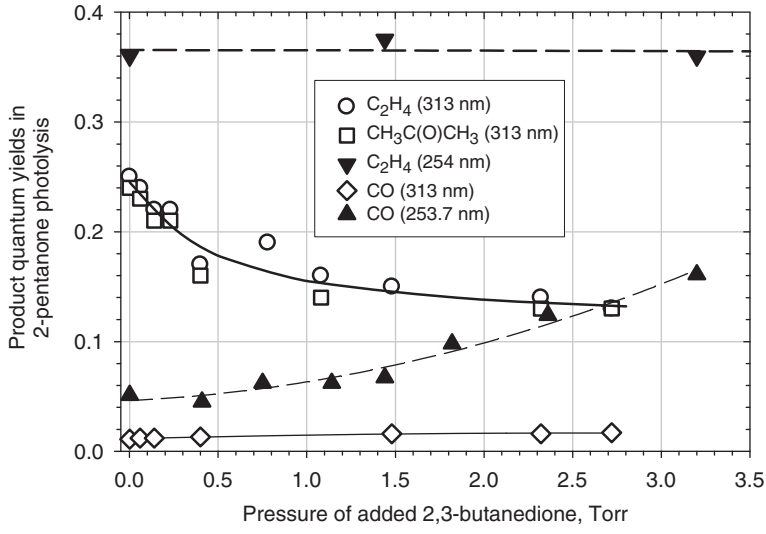

Figure IX-D-11. Quantum yield of C_2H_4, $CH_3C(O)CH_3$, and CO in 2-pentanone as a function of added 2,3-butanedione for photolyses at 313 and 253.7 nm; data are from Michael and Noyes (1963). The rise in the Φ_{CO} values at the higher pressures of 2,3-butanedione probably reflects the increasing importance of CO formation from direct photolysis of the added 2,3-butanedione; at 253.7 nm Φ_{CO} increases reflect the stronger absorption by 2,3-butanedione at this wavelength.

relatively insensitive to added 2,3-butanedione, an excellent quencher of thermalized, triplet ketone molecules; see figure IX-D-11. It is probable that this photodissociation to form CO involves the S_1 state or a vibrationally "hot" acyl radical, as observed with $CH_3C(O)CH_3$ photolysis. We conclude that ϕ_{III} for 2-pentanone is $\sim$ 0.01–0.06 at 313 nm and $\sim$0.05 at 254 nm. As the temperature rises, the decomposition of CH_3CO and $CH_3CH_2CH_2CO$ radicals and CO formation become more important. For photolysis at 313 nm the quantum yields of CO are shown as a function of temperature in figure IX-D-12. For data at temperatures greater than 120°C, $\Phi_{CO} = \phi_I + \phi_{II} + \phi_{III}$, but this result cannot be extrapolated to atmospheric temperatures, since ketones often have barriers to photodecomposition.

iii) Process (IV): $CH_3CH_2CH_2C(O)CH_3 + h\nu \rightarrow CH_2{=}CH_2 + CH_2{=}C(OH)CH_3$
Extensive studies of 2-pentanone photolysis confirm the occurrence of process (IV) forming ethene and the enol-form of acetone. These product quantum yields are insensitive to temperature and pressure changes; see table IX-D-5. Data of Wettack and Noyes (1968) suggest that within the wavelength region of importance in the troposphere, ϕ_{IV} is also relatively insensitive to wavelength of excitation (313–280 nm); see figure IX-D-13.

The formation of the intermediate enol-form of carbonyl compounds in aldehyde and ketone photolysis was first suggested by Davis and Noyes (1947) and was invoked by Gruver and Calvert (1958) to explain some unexpected results in the deuterium

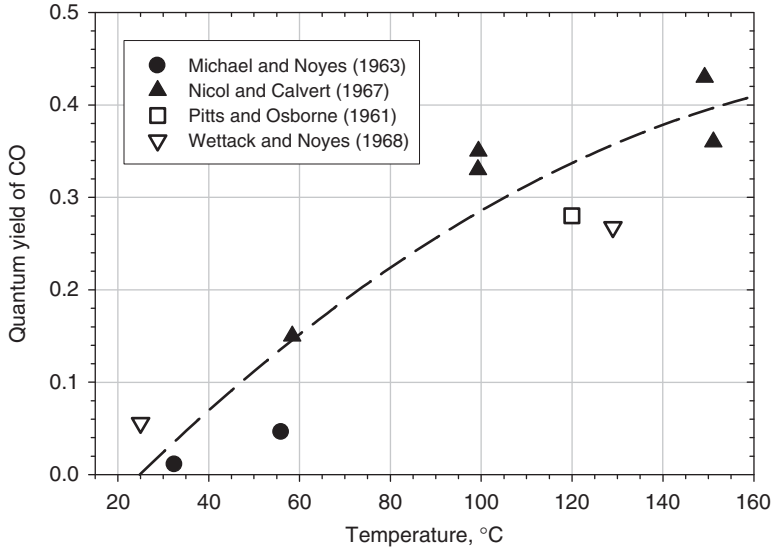

Figure IX-D-12. Plot of the quantum yield of CO in the 313 nm photolysis of 2-pentanone as a function of temperature.

Table IX-D-5. Quantum yields of process (IV) in 2-pentanone at several wavelengths $CH_3CH_2CH_2C(O)CH_3 + h\nu \rightarrow CH_2{=}CH_2 + CH_2{=}C(OH)CH_3$

λ, nm	Pressure ketone, Torr	Temp., °C	$\Phi_{C_2H_4}$	$\Phi_{CH_3C(O)CH_3}$	Reference
313	1.3–32	28–152	0.31 ± 0.01	0.31 ± 0.01	Ausloos and Rebbert (1961)
313	5.2–270[a]	32–147	0.28 ± 0.03[b]	–	Borkowski and Ausloos (1961)
313	30.5	33–56	0.25 ± 0.01	0.23 ± 0.01	Michael and Noyes (1963)
313	9–55	25–129	0.29 ± 0.02	–	Wettack and Noyes (1968)
313	Not reported	120	0.28	–	Pitts and Osborne (1961)
313	30–66	58–149	0.25 ± 0.01	–	Nicol and Calvert (1967)
296.5	17–25	25–129	0.26 ± 0.03	–	Wettack and Noyes (1968)
280.4	17–30	25–129	0.27 ± 0.03	–	Wettack and Noyes (1968)
265.4	25	130	0.35	–	Wettack and Noyes (1968)
254–265	26–206	34	0.40 ± 0.02	–	Borkowski and Ausloos (1961)
254	20–32	25–128	0.31 ± 0.03	–	Wettack and Noyes (1968)
254	25	33	0.39 ± 0.02	0.39 ± 0.02	Michael and Noyes (1963)

[a]Deuterated 2-pentanone employed here: $CH_3C(O)CH_2CHDCD_2H$.
[b]Ethene product: $D_2C{=}CHD$ and $DHC{=}CHD$ formed here; the ratio of the two isomers was temperature dependent.

content of acetone formed in the photolysis of 1,1,1,3,3-pentadeutero-2-pentanone (McNesby and Gordon, 1958). The formation of the enol-form of the carbonyls in aldehyde and ketone photolysis has been widely accepted since the report of Srinivasan (1959) that acetone produced in 2-hexanone photolysis could exchange a hydrogen atom at the photochemical reactor walls. Formation of $CH_2{=}C(OH)CH_3$ in process (IV) of 2-pentanone has been observed directly through measurement of the enol

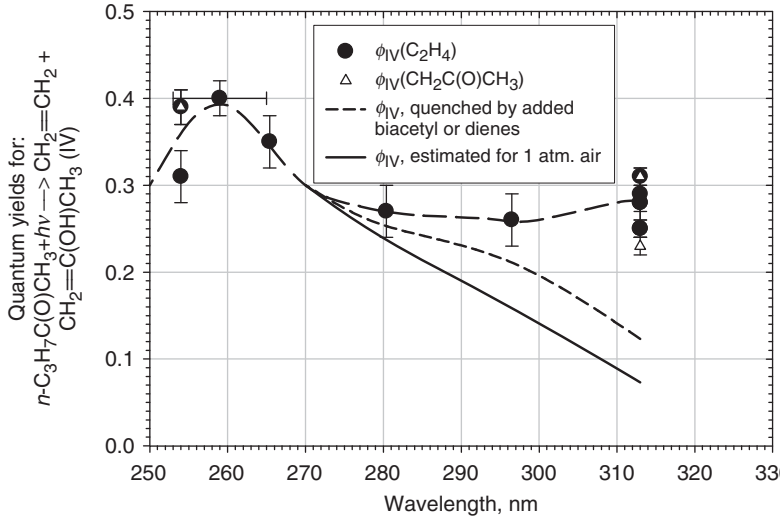

Figure IX-D-13. Plot of the wavelength dependence of the quantum yields of C_2H_4 and $CH_3C(O)CH_3$ in photolysis of 2-pentanone as a function of wavelength as estimated from the data referenced in table IX-D-5. Data are insensitive to pressures of 2-pentanone and temperature. Experiments with pure ketone, circles and triangles; ϕ_{IV}, unquenched by 2,3-butanedione or dienes, short dashed line; ϕ_{IV}, adjusted for additional air quenching at 1 atm. using k_q/k_d for acetone as interpolated for the selected wavelength, solid line. Both the short-dashed and the solid lines were used in the estimation of *j*-values for 2-pentanone given in figure IX-D-16.

infrared band at 2.756 μm (McMillan et al., 1964a). The The average half-life of $CH_2{=}C(OH)CH_3$ molecule in a dark cell was 3.34 $\pm$ 0.11 min., and acetone appeared with a half-life of 3.35 $\pm$ 0.13 min. The conversion of the enol of acetone is apparently catalyzed by the cell surface, for when D_2O is adsorbed on this surface, $CH_3C(O)CH_2D$ is an observed product. For the conditions employed by McMillan et al., the ketone form of acetone [$CH_3C(O)CH_3$] does not exchange measurably to form $CH_3C(O)CH_2D$ on cell surfaces preconditioned with D_2O.

The ethene and acetone products of process (IV) in 2-pentanone photolysis at long wavelengths (313 nm) can be partially quenched by added 2,3-butanedione, a known efficient quencher of excited carbonyl triplets. The results of Michael and Noyes (1963) are shown in figure IX-D-11. Both ethene and acetone quantum yields decrease significantly on addition of small amount of 2,3-butanedione. On photolysis, these 2,3-butanedione-2-pentanone mixtures exhibit a strong phosphorescence emission from the 2,3-butanedione triplet. This is compelling evidence that a significant portion, about 50%, of the 2-pentanone molecules excited at 313 nm decompose via the T_1 state of the molecule. Presumably the other half of the molecules that decay by process (IV) come from the excited singlet (S_1) state or, conceivably, from a vibratrionally rich T_1 or S_o state of short lifetime. Experiments at 253.7 nm, show little or no quenching of the ethene and acetone products by added 2,3-butanedione (Michael and Noyes, 1963);

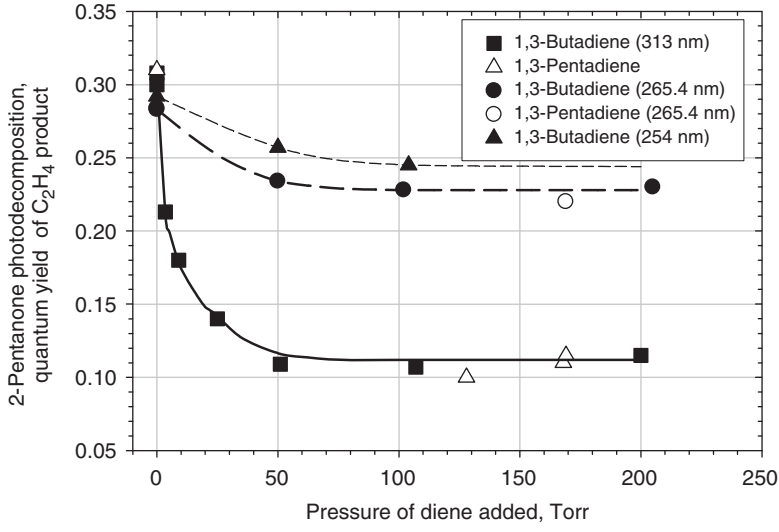

Figure IX-D-14. Quantum yields of C_2H_4 in 2-pentanone photolysis as a function of added 1,3-butadiene or 1,3-pentadiene. Data from Wettack and Noyes (1968); wavelength, 313 nm; temperature, 25°C.

see figure VII-D-11. Obviously, at the short wavelengths, the products of (IV) form by dissociation from a very short-lived state of 2-pentanone.

Experiments of Wettack and Noyes (1968) support and extend the studies of Michael and Noyes (1963). Wettack and Noyes report that the addition of 1,3-butadiene or 1,3-pentadiene, both good reactants for carbonyl excited triplets, inhibits the photodecomposition of 2-pentanone; see figure IX-D-14. These authors conclude that about 62% of the photodecomposition by process (IV) in 2-pentanone at 313 nm involves the triplet state. Similar experiments of Wettack and Noyes (1968) show that excitation at 265.4 and 253.7 nm involves photodecomposition by process (IV) of about 18% and $< 12\%$, respectively, from nonquenchable, excited 2-pentanone molecules. Both the studies of Michael and Noyes (1963) and Wettack and Noyes (1968) indicate that both the singlet and triplet states of 2-pentanone are probable precursors to process (IV), and the extent of triplet involvement increases at the long wavelengths.

The effect of oxygen on the primary process (IV) in 2-pentanone has been investigated in a few experiments that are relevant to atmospheric conditions. O_2 quenches long-lived carbonyl triplet states effectively as $O_2(^1\Delta_g)$ is generated (Nau and Scaiano, 1996). Ausloos and Rebbert (1961) determined the C_2H_4, acetone, and 1-methylcyclobutanol quantum yields in the photolysis of 2-pentanone at 313 nm. The Stern–Volmer plot of the quenching of these products with added pressure of O_2 is given in figure VII-D-15. Shown are data from Ausloos and Rebbert (1961) for C_2H_4 (large black circles) and acetone (open squares). The involvement of at least two excited states with very different quenching efficiencies is evident in the curvature in the plot

at low O_2 additions. The extent of quenching by oxygen seen in these studies is consistent with that seen in the experiments with other triplet quenchers (2,3-butanedione and dienes). The slope of the line in the linear region at high O_2 pressures leads to a Stern–Volmer quenching constant, $k_q/k_d \approx 9 \times 10^{-3}\,\text{Torr}^{-1}$, a value similar to that observed for acetone. Using the relation derived in figure IX-D-2, one finds that this k_q/k_d value corresponds to that expected for acetone excited at 306 nm. Since air at 1 atm. pressure should allow the nearly complete quenching of the thermalized T_1 state that is quenchable by added 2,3-butanedione or dienes, the results suggest that rough estimates for quantum yields of products of 2-pentanone photolysis in air may be made using the measured quantum yields of products of (IV) from the S_1 state corrected for quenching using the observed k_q/k_d values as estimated for acetone at various wavelengths.

iv) Process (V): $CH_3CH_2CH_2C(O)CH_3 + h\nu \rightarrow$ *1-Methylcyclobutanol* The formation of 1-methylcyclobutanol in the gas-phase photodecomposition of 2-pentanone is well established. Ausloos and Rebbert (1961) demonstrated unambiguously that both processes (IV) and (V) occur. At 313 nm and 28°C, the ratio ϕ_V/ϕ_{IV} decreased from 0.34 at 32 Torr to 0.088 at 1.3 Torr of 2- pentanone. Conceivably, processes (IV) and (V) could involve the same intermediate diradical, $CH_3C(\bullet)(OH)CH_2CH_2CH_2\bullet$. Such an intermediate could in theory decay to ethene and enol-acetone as in (IV) by a

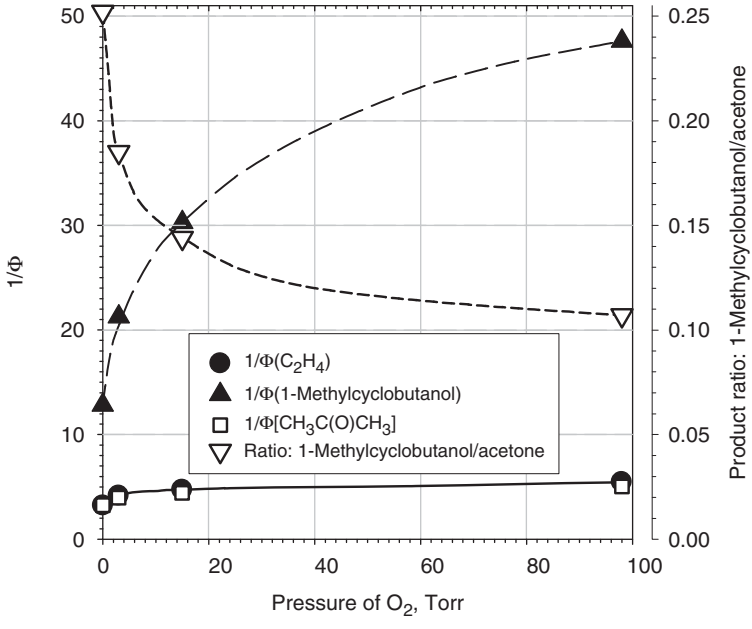

Figure IX-D-15. Effect of added O_2 on the quantum yields of products (left axis) and the ratio of 1-methylcyclobutanol to acetone (right axis) in the 313 nm photolysis of 2-pentanone at 28°C (Ausloos and Rebbert, 1961).

single C—C bond fission, or form 1-methylcyclobutanol by collisional stabilization of the cyclized product at the higher pressures. Although processes (IV) and (V) appear to be related, they apparently do not occur from a common intermediate, since the quenching of the products of the precursor states show very different efficiencies; see figure IX-D-15. $\Phi_{C_2H_4}$ and $\Phi_{CH_3C(O)CH_3}$ are insensitive to temperature and pressure and the observed ratio of 1-methylcyclobutanol/ethene varies from near 0.25 in the absence of oxygen to about 0.11 with 100 Torr of O_2 added. The ratio of 1-methylcyclobutanol to ethene decreases with lowered pressure of ketone from 0.335 at 32 Torr to 0.088 at 1.3 Torr. The studies of McMillan et al. (1964a) confirm the formation of the cyclobutanol product of (V) but indicate a somewhat smaller quantum yield of this product than expected from the results of Ausloos and Rebbert (1961). McMillan et al. (1964a) suggested that the failure of some workers to detect the cyclobutanol products in ketone and aldehyde photolysis may be due in part to destruction of these alcohols during gas chromatographic analysis.

IX-D-4.3. Photolysis Frequencies for Photodecomposition of 2-Pentanone in the Lower Troposphere

A very rough estimate of *j*-values can be made for 2-pentanone with certain unsubstantiated assumptions regarding the effect of 1 atmosphere of air on the quantum yields of products:

(i) Estimates of Wettack and Noyes (1968) and Michael and Noyes (1963) may be used to determine the fraction (E) of the process (IV) that occurs via states that are unquenched by added 2,3-butanedione and diene; these are 56% (average of 52 and 59%) at 313 nm; 18% at 265.4 nm; and 6% (average of 0% and 12%) at 253.7 nm. These E values fit well a linear relation with λ: $E = -203.6 + 0.8302 \times (\lambda, \text{nm})$, that can be used to estimate E at other wavelengths.

(ii) The weak additional quenching of the "unquenchable" fraction of 2-pentanone by air probably occurs as with other aldehydes and ketones. We assumed this quenching is described by the Stern–Volmer relationship with the k_q/k_d values derived from acetone studies (figure IX-D-2).

(iii) The formation of 1-methylcyclobutanol is assumed to be negligible in air at 1 atm.

(iv) Processes (I) and (II) are assumed to originate from the same state as that of process (IV), with a ratio of quantum yields, $(\phi_I + \phi_{II} + \phi_{III})/\phi_{IV} \approx 0.43$, a very rough estimate from the full arc experiments of Nicholson (1954).

Two scenarios of possible quenching of the primary processes were assumed in estimating the *j*-values for a cloudless day in the lower troposphere (ozone column = 350 DU); see figure IX-D-16. In case *A*, we accepted the assumptions (i), (iii), and (iv) above, while in case *B*, these assumptions plus that of (ii) were accepted. There is a reasonable probability that actual *j*-values for processes (I) + (II)+ (III) and for process (IV) for 2-pentanone in the atmosphere may lie somewhere between these two estimates. The tabular data for the quantum yields that were derived in the two scenarios are summarized in table IX-D-6. Obviously, more definitive data are necessary to determine these quantities reliably.

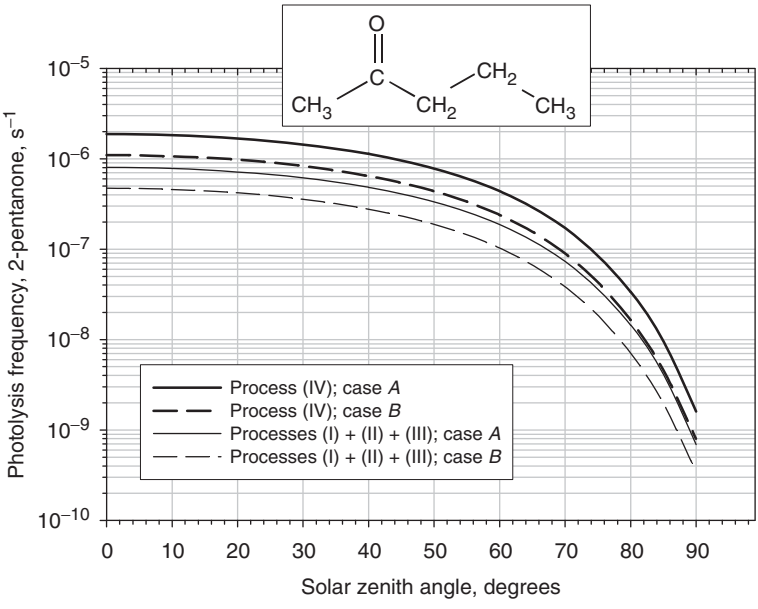

Figure IX-D-16. Approximate photolysis frequencies for primary processes in 2-pentanone versus solar zenith angle; $CH_3CH_2CH_2C(O)CH_3 + h\nu \rightarrow CH_3CH_2CH_2 + CH_3CO$ (I); $CH_3CH_2CH_2C(O)CH_3 + h\nu \rightarrow CH_3CH_2CH_2CO + CH_3$ (II); $CH_3CH_2CH_2C(O)CH_3 + h\nu \rightarrow CH_3CH_2CH_2 + CO + CH_3$ (III); $CH_3CH_2CH_2C(O)CH_3 + h\nu \rightarrow CH_2{=}CH_2 + CH_2{=}C(OH)CH_3$ (IV). Case *A* assumes that all processes are quenched in air to the limiting values observed for 2,3-butanedione and diene quenching; case *B* assumes quenching as in *A* but additional quenching as observed for acetone–air photolysis. Data were calculated for a cloudless day in the lower troposphere with an overhead ozone column of 350 DU.

IX-D-5. Photodecomposition of 3-Methyl-2-Butanone [Methyl Isopropyl Ketone, $CH_3C(O)CH(CH_3)_2$]

Limited data on 3-methyl-2-butanone suggest consideration of the following primary photodissociative processes (Calvert et al., 2008):

$$CH_3C(O)CH(CH_3)_2 + h\nu \rightarrow CH_3CO + CH_3CHCH_3 \quad \text{(I)}$$

$$\rightarrow CH_3 + (CH_3)_2CHCO \quad \text{(II)}$$

$$\rightarrow CH_3 + CO + CH_3CHCH_3 \quad \text{(III)}$$

$$\rightarrow CH_3CHO + CH_3CH{=}CH_2 \quad \text{(IV)}$$

Weir (1962), Zahra and Noyes (1965), and Lissi et al. (1973/1974) have published the only extensive studies of the photolysis of this ketone. The product analyses of Zahra and Noyes provide a rough estimate of the extent of each of these processes at 313 and 253.7 nm. For ketone pressures in the range 3–42 Torr, the product distribution at 313 nm suggests $\phi_I/\phi_{II} \approx 6 \pm 327°C$, and 5 ± 2 at 60–62°C; at 253.7 nm

Table IX-D-6. Approximate estimates of the quantum yields for 2-pentanone photolysis in air at 1 atm. pressure as a function of wavelength: $CH_3CH_2CH_2C(O)CH_3 + h\nu \rightarrow CH_3CH_2CH_2+ CH_3CO$ (I); $CH_3CH_2CH_2C(O)CH_3 + h\nu \rightarrow CH_3CH_2CH_2CO + CH_3$ (II); $CH_3CH_2CH_2C(O)CH_3+ h\nu \rightarrow CH_3CH_2CH_2 + CO + CH_3$ (III); $CH_3CH_2CH_2C(O)CH_3 + h\nu \rightarrow CH_2{=}CH_2 + CH_2{=}C(OH)CH_3$ (IV); $CH_3CH_2CH_2C(O)CH_3 + h\nu \rightarrow$ 1-methylcyclobutanol (V); ϕ_V is small but not estimated here

	$\phi_I + \phi_{II} + \phi_{III}$		ϕ_{IV}			$\phi_I + \phi_{II} + \phi_{III}$		ϕ_{IV}	
λ, nm	$(A)^a$	$(B)^b$	$(A)^a$	$(B)^b$	λ, nm	$(A)^a$	$(B)^b$	$(A)^a$	$(B)^b$
278	0.11	0.11	0.26	0.25	304	0.07	0.05	0.17	0.12
279	0.11	0.10	0.26	0.24	305	0.07	0.05	0.16	0.11
280	0.11	0.10	0.26	0.24	306	0.07	0.05	0.16	0.11
281	0.11	0.10	0.25	0.23	307	0.07	0.04	0.16	0.10
282	0.11	0.10	0.25	0.23	308	0.06	0.04	0.15	0.10
283	0.11	0.09	0.25	0.22	309	0.06	0.04	0.15	0.09
284	0.10	0.09	0.24	0.22	310	0.06	0.04	0.14	0.09
285	0.10	0.09	0.24	0.21	311	0.06	0.03	0.14	0.08
286	0.10	0.09	0.24	0.21	312	0.06	0.03	0.13	0.08
287	0.10	0.09	0.24	0.20	313	0.05	0.03	0.12	0.07
288	0.10	0.09	0.24	0.20	314	0.05	0.03	0.12	0.07
289	0.10	0.09	0.23	0.20	315	0.05	0.03	0.11	0.06
290	0.10	0.08	0.23	0.19	316	0.05	0.03	0.11	0.06
291	0.10	0.08	0.23	0.18	317	0.04	0.02	0.10	0.05
292	0.10	0.08	0.23	0.18	318	0.04	0.02	0.09	0.05
293	0.09	0.08	0.22	0.18	319	0.03	0.02	0.08	0.04
294	0.09	0.07	0.22	0.17	320	0.03	0.01	0.07	0.03
295	0.09	0.07	0.22	0.17	321	0.03	0.01	0.06	0.03
296	0.09	0.07	0.21	0.16	322	0.02	0.01	0.05	0.02
297	0.09	0.07	0.21	0.16	323	0.02	0.01	0.05	0.02
298	0.09	0.06	0.20	0.15	324	0.02	0	0.04	0.01
299	0.09	0.06	0.20	0.15	325	0.01	0	0.02	0
300	0.09	0.06	0.20	0.14	326	0.01	0	0.02	0
301	0.08	0.06	0.19	0.14	327	0	0	0.01	0
302	0.08	0.06	0.19	0.13	328	0	0	0	0
303	0.08	0.05	0.18	0.12					

[a]Scenario based on acceptance of assumptions (I), (III), and (IV) given in section IX-D-4.
[b]Scenario based on acceptance of assumptions (I), (II), (III), and (IV) given in section IX-D-4.

$\phi_I/\phi_{II} \approx 6$(27°C), 5 (60°C), and 2 (127°C). The product data of Lissi et al. (1973/1974) from experiments at 313 nm over a 130-fold range of intensities (from the highest to lowest) give the ϕ_I/ϕ_{II} estimates: 2.8, 2.3, 2.4, and 1.4. The product distribution reported by Nicholson (1954) from the full arc irradiation of 3-methyl-2-butanone also suggests the dominance of process (I); $\phi_I/\phi_{II} \approx 7 \pm 2$. These ratios are consistent with the somewhat weaker $(CH_3)_2CH—C(O)CH_3$ bond compared to the $(CH_3)_2CHC(O)—CH_3$ bond.

The total quantum yield of decomposition of 3-methyl-2-butanone as estimated by Lissi et al. (1973/1974) from an extrapolation of the product yields to zero absorbed light intensity gave 0.75. This is in good agreement with that derived from $\Phi_{CO} = 0.78$ estimated by Zahra and Noyes (1965) in photolysis at 127°C.

The quantum yields of CO reported by Zahra and Noyes (1965) at 313 nm and 27°C, are: 0.045 (3 Torr pressure), 0.034 (11 Torr), 0.027 (13 Torr), 0.030 (27.5 Torr), 0.031 (30 Torr), and 0.037 (41.8 Torr). At 253.7 nm, $\Phi_{CO} \approx 0.12$(27°C, 22 Torr), 0.35 (60°C, 22 Torr), 0.78 (127°C, 22 Torr). These data probably reflect the occurrence of process (III) to a small extent ($\phi_{III} \approx 0.03 \pm 0.01$ at 313 nm), as seen with the other small ketones.

The process (IV) was suggested by Zahra and Noyes to explain the presence of CH_3CHO in the products. A 5-membered ring intermediate, similar to the 6-membered ring intermediate suggested for Norrish type-II reactions, was proposed to be involved in the reaction. At 313 nm the process (IV) is negligible, $\phi_{IV} < 0.01$, (27-60°C), but at 253.7 nm acetaldehyde yields suggest $\phi_{IV} \approx 0.36 \pm 0.03$ (60–127°C). Nicholson (1954) also reported CH_3CHO among the products formed in his full arc photolysis. Lissi et al. (1973/1974) found no evidence for (IV) in their experiments at 313 nm. The evidence for process (IV) is not strong, and we conclude that it is probably unimportant at the wavelengths available within the troposphere.

Zahra and Noyes found that at 313 nm the addition of small amounts of oxygen (0.03–0.14 Torr) to 26 Torr of ketone (27°C) lowered the emission yield from 3-methyl-2-butanone by 21%, comparable to the effect seen in other small ketones. The emission yields observed by Zahra and Noyes in photolyses of pure ketone and in 2,3-butanedione–ketone mixtures, indicate clearly that the triplet state plays an important role in the photolysis of 3-methyl-2-butanone at 313 nm. There was no evidence of the triplet excited state observed in experiments at 253.7 nm. Lissi et al. (1973/1974) carried out experiments at 313 nm both with added 2,3-butanedione and with added *cis*-1,3-pentadiene. These experiments confirm the importance of the triplet precursor to products for photolysis at 313 nm.

The photochemistry of 3-methyl-2-butanone appears to be very similar to that observed in the smaller ketone photolysis in which an CH_3CO radical is also formed in the primary process. For example with excitation at 313 nm, in 3-methyl-2-butanone $\Phi_{CO} = 0.033 \pm 0.007$ (27°C, pressure 5.5–41.8 Torr; Zahra and Noyes, 1965) and in acetone, $\Phi_{CO} = 0.033$ (20°C, 50 Torr; Cundall and Davies, 1966). For similar conditions, the two ketones in the same two studies (temperature, 60–65°C) give $\Phi_{CO} = 0.23 \pm 0.01$ and 0.29, respectively, and for temperature, 127–130°C, $\Phi_{CO} = 0.78$ and 0.98, respectively.

Ausloos and Rebbert (1964) report that the relative efficiency of energy transfer to 2,3-butanedione is strongly dependent on the dissociative lifetime of the excited ketone molecule and varies according to the following sequence: acetone >2-butanone >2-pentanone >3-methyl-2-butanone.

The data available are insufficient to allow a definitive estimate of the quantum efficiencies as a function of wavelength for photolysis of 3-methyl-2-butanone in air that are required to define *j*-values. The photochemistry of 3-methyl-2-butanone may be similar to that observed for 2-butanone and 3-pentanone (section IX-D-2 and IX-D-3). However, the $CH_3C(O)—CH(CH_3)_2$ bond is somewhat weaker than the $CH_3C(O)—C_2H_5$ bond, and it seems reasonable that the *j*-values for use with 3-methyl-2-butanone should be somewhat greater than those of acetone and 2-butanone.

IX-D-6. Photodecomposition of 2-Hexanone [Methyl *n*-Butyl Ketone, $CH_3C(O)CH_2CH_2CH_2CH_3$]

Studies of the photodecomposition of 2-hexanone have been rationalized in terms of the following primary dissociation channels (Calvert et al., 2008):

$$CH_3C(O)CH_2CH_2CH_2CH_3 + h\nu \rightarrow CH_3CO + CH_2CH_2CH_2CH_3 \quad \text{(I)}$$

$$\rightarrow CH_3CH_2CH_2CH_2CO + CH_3 \quad \text{(II)}$$

$$\rightarrow CH_3 + CO + CH_3CH_2CH_2CH_2 \quad \text{(III)}$$

$$\rightarrow CH_3CH{=}CH_2 + CH_2{=}C(OH)CH_3 \quad \text{(IV)}$$

The photodissociative pathways (I), (II), and (III) are relatively unimportant compared to process (IV). Srinivasan (1959) estimated from experiments at 313 nm and 27°C that $\phi_I + \phi_{II} + \phi_{III} \approx 0.018$ which was unaffected by the addition of up to 4.0 Torr of 2,3-butanedione. A maximum value for this sum at 313 nm is 0.11 (from Φ_{CO} at 103°C), measured by Davis and Noyes (1947) and 0.08 (from Φ_{CO} at 125°C), measured by Michael and Noyes (1963). The product distribution determined in full-arc photolysis at 21°C by Nicholson (1954) suggest $(\phi_I + \phi_{II} + \phi_{III})/\phi_{IV} \approx 0.04$. By analogy with the smaller ketones one expects $\phi_I/\phi_{II} > 1.0$, but Nicholson's product analyses indicates only a small discrimination in bond cleavage. The measurements of Φ_{CO} at 313 nm (20–30°C) reflect a small value for $\phi_{III} \approx 0.02$ (Brunet and Noyes, 1958), but a portion of this value may arise from the photolysis of the primary product, acetone.

The dominance of process (IV) was established in the pioneering study of Norrish and Appleyard (1934); these workers concluded that 2-hexanone decomposes primarily into an equimolecular mixture of propene and acetone. In the several studies that have followed, quantitative data confirmed this interpretation. Measurements of the quantum yields of process (IV) are in relatively good agreement:

i) Wavelength 313 nm $\phi_{IV} = 0.34$ (27°C, Wilson and Noyes, 1943); 0.45 ± 0.05 (C_3H_6, 103°C, Davis and Noyes (1947); 0.50 ± 0.07 [$CH_3C(O)CH_3$, 103°C, Davis and Noyes, 1947]; 0.46 ± 0.02 (C_3H_6; 28–30°C, Brunet and Noyes, 1958); 0.43 ± 0.06 [$CH_3C(O)CH_3$; 28–30°C, Brunet and Noyes, 1958]; 0.41 ± 0.01 (C_3H_6, 35–100°C, Michael and Noyes, 1963); 0.44 ± 0.04 [$CH_3C(O)CH_3$, 35°C, Michael and Noyes, 1963].

ii) Wavelength 253.7 nm $\phi_{IV} = 0.34$ (C_3H_6, 27°C, Wilson and Noyes, 1943); 0.29 ± 0.01 (C_3H_6, 36–125°C; Michael and Noyes, 1963). The decrease in ϕ_{IV} with decrease in λ appears to be unique among the ketones that have been studied.

Srinivasan (1959) studied the photodecomposition of 2-hexanone-5,5-d_2 ($CH_3C(O)CH_2CH_2CD_2CH_3$) and found the propene formed was largely C_3H_5D with about 3% $C_3H_4D_2$, in accord with expectations based on the mechanism of process (IV). However, unexpectedly the acetone was nearly an equimolar mixture of $CH_3C(O)CH_2D$ (45%) and $CH_3C(O)CH_3$ (54%). This result provided the first

indication of the involvement of the enol-acetone product ($CH_2{=}C(OH)CH_3$) that could exchange H-atoms for D-atoms on equilibration at the walls of the reaction vessel.

In photolysis at 313 nm, quenching of 2-hexanone by formation of triplet 2,3-butanedione is only 1/20th of that seen for 1-pentanone. The quantum yields of propene and acetone are also little affected by 2,3-butanedione addition: at 35°C, $\Phi_{C_3H_6} = 0.41 \pm 0.01$ and $\Phi_{CH_3C(O)CH_3} = 0.44 \pm 0.04$. At 253.7 nm, there is no observable effect of added 2,3-butanedione on the photodecomposition of 2-hexanone, and no evidence for a sensitized emission of 2,3-butanedione was observed (Michael and Noyes, 1963). Obviously, a very short-lived triplet or singlet state is the precursor to all photodecomposition in 2-hexanone.

Brunet and Noyes (1958) found a small effect on the propene and acetone product quantum yields with the addition of 230 and 560 Torr of added oxygen: $\Phi_{C_3H_6} = 0.39$, and 0.38; $\Phi_{CH_3C(O)CH_3} = 0.42$ and 0.19, respectively. The decrease observed was rationalized by Brunet and Noyes as probably a consequence of incomplete condensation of the products of the reaction when large quantities of oxygen are removed after irradiation. Ausloos and Rebbert (1961) suggested that the effect could be actual quenching as they observed in their studies with oxygen added to 2-pentanone. If the decrease is attributed to quenching, then a Stern–Volmer plot using only the propene data gives $k_q/k_d \approx 10^{-3}$ Torr^{-1}, a value similar to those observed for air-quenching of other aldehydes and ketones that have been discussed in earlier sections.

Until the appropriate detailed quantum yield and spectral data become available, we can make only very rough estimates of the expected *j*-values for 2-hexanone in air using several as yet untested assumptions (Calvert et al., 2008).

Scenario (A):

i) In the pure ketone, the quantum yield of process (IV) decreases in a linear fashion from $\phi_{IV} = 0.43 \pm 0.05$, the average value at 313 nm, to 0.31 ± 0.03 at 253.7 nm.
ii) The fraction of the ketone that is quenchable by 2,3-butanedione at 313 nm is about 3% and decreases in a linear fashion with wavelength to zero at 253.7 nm.
iii) The cross sections for light absorption by 2-hexanone are assumed to be equal to those measured for 2-pentanone.
iv) Air does not quench the ketone further than that expected from assumption (ii).

Scenario (B): The first three assumptions above apply, and we assume that the reported decrease in ϕ_{IV} with addition of oxygen observed by Brunet and Noyes (1958) is a result of quenching by oxygen. The k_q/k_d values at each wavelength are assumed to be equal to those expected for acetone (figure IX-D-2) quenching by air.

Approximate quantum yields for process (IV) as a function of wavelength are given in table IX-D-7 for the two different scenarios (*A*) and (*B*) of wavelength dependence of ϕ_{IV} outlined in this section and suggested by Calvert et al. (2008). The sum of the quantum yields for photodissociation of 2-hexanone by processes (I), (II), and (III) is small, and probably in the range of 4%–18% of ϕ_{IV} at each wavelength.

The formation of a cyclobutanol product ($\Phi \approx 0.075$) has been observed in the solution phase photodecomposition of 2-hexanone (Coulson and Yang, 1966). An additional

Table IX-D-7. Estimated quantum yields of primary process: $CH_3CH_2CH_2CH_2C(O)CH_3 + h\nu \rightarrow CH_3CH{=}CH_2 + CH_2{=}C(OH)CH_3$(IV); Cases *A* and *B* represent different scenarios of the dependence of ϕ_{IV} on wavelength of excitation; see the text for discussion of quantum yields for this and other processes (as suggested by Calvert et al., 2008)

λ, nm	ϕ_{IV} (Case *A*)[a]	ϕ_{IV} (Case *B*)[b]	λ, nm	ϕ_{IV} (Case *A*)[a]	ϕ_{IV} (Case *B*)[b]
278	0.36	0.32	314	0.44	0.08
279	0.36	0.32	315	0.44	0.07
280	0.37	0.31	316	0.44	0.07
281	0.37	0.31	317	0.44	0.06
282	0.37	0.31	318	0.45	0.06
283	0.37	0.30	319	0.45	0.05
284	0.38	0.30	320	0.45	0.05
285	0.38	0.29	321	0.45	0.05
286	0.38	0.29	322	0.45	0.04
287	0.38	0.28	323	0.46	0.04
288	0.38	0.27	324	0.46	0.04
289	0.39	0.27	325	0.46	0.03
290	0.39	0.26	326	0.46	0.03
291	0.39	0.25	327	0.47	0.03
292	0.39	0.24	328	0.47	0.03
293	0.39	0.24	329	0.47	0.03
294	0.40	0.23	330	0.47	0.02
295	0.40	0.22	331	0.47	0.02
296	0.40	0.21	332	0.48	0.02
297	0.40	0.20	333	0.48	0.02
298	0.41	0.19	334	0.48	0.02
299	0.41	0.18	335	0.48	0.02
300	0.41	0.18	336	0.48	0.02
301	0.41	0.17	337	0.49	0.01
302	0.41	0.16	338	0.49	0.01
303	0.42	0.15	339	0.49	0.01
304	0.42	0.14	340	0.44	0.01
305	0.42	0.13	341	0.44	0.01
306	0.42	0.13	342	0.44	0.01
307	0.42	0.12	343	0.44	0.01
308	0.43	0.11	344	0.45	0.01
309	0.43	0.10	345	0.45	0.01
310	0.43	0.10	346	0.45	0.01
311	0.43	0.09	347	0.45	0.01
312	0.43	0.09	348	0.45	0.01
313	0.44	0.08	349	0.46	0.01

[a] Scenario *A* assumes no extra quenching by air (1 atm.); only the thermalized triplets are quenched.
[b] Scenario *B* assumes extra quenching by air (1 atm.) with k_q/k_d mimicking the air quenching by acetone; see section IX-D-6.

process analogous to process (V) in 2-pentanone probably accounts for this. Determination of the quantum efficiency of this process in the gas-phase photochemistry has not been reported, but presumably it is small.

The approximate photolysis frequencies for process (IV) for a cloudless day within the lower troposphere (ozone column = 360 DU) are given as a function of solar zenith angle for two scenarios (*A* and *B*) in figure IX-D-17 as calculated by Calvert et al. (2008).

IX-D-7. Photodecomposition of 3-Hexanone (Ethyl *n*-Propyl Ketone, $CH_3CH_2C(O)CH_2CH_2CH_3$)

Photodissociation of 3-hexanone follows the pattern of the smaller ketones (Calvert et al., 2008):

$$CH_3CH_2CH_2C(O)CH_2CH_3 + h\nu \rightarrow C_2H_5CO + CH_3CH_2CH_2 \quad \text{(I)}$$

$$\rightarrow CH_3CH_2 + CH_3CH_2CH_2CO \quad \text{(II)}$$

$$\rightarrow CH_3CH_2 + CO + CH_3CH_2CH_2 \quad \text{(III)}$$

$$\rightarrow CH_2{=}CH_2 + CH_2{=}C(OH)C_2H_5 \quad \text{(IV)}$$

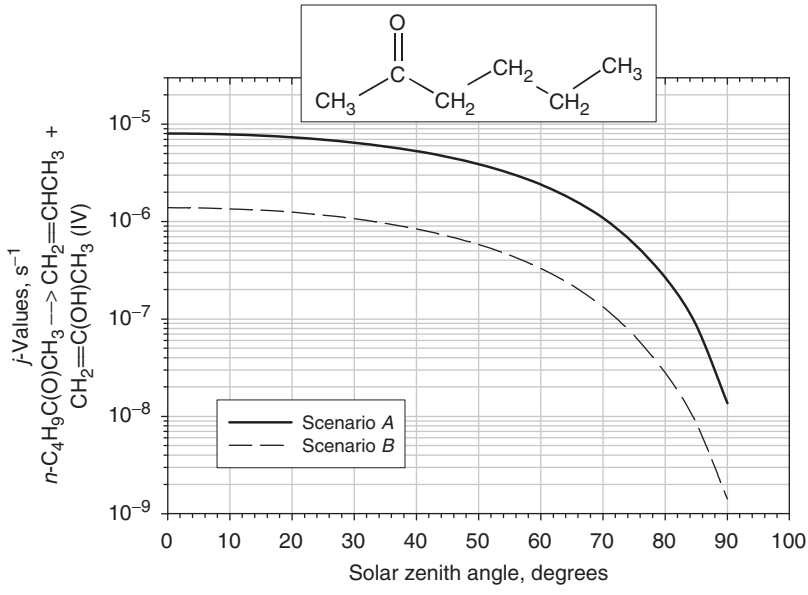

Figure IX-D-17. Approximate *j*-values for primary process (IV) in 2-hexanone, $CH_3CH_2CH_2CH_2C(O)CH_3 + h\nu \rightarrow CH_2{=}CHCH_3 + CH_2{=}C(OH)CH_3$, as estimated for a cloudless day in the lower troposphere with an overhead ozone column of 350 DU; two different scenarios (*A* and *B*) relate to different choices for wavelength dependence of ϕ_{IV} that were used; see the text; figure from Calvert et al. (2008).

Product quantum yields data from photolysis of the pure ketone at 313 nm and temperatures from 62 to 150°C indicate that there is a small preference in bond breakage favoring process (I): $\phi_I/\phi_{II} \approx 1.6 \pm 0.2$ (Nicol and Calvert, 1967). Φ_{CO} data for temperatures greater than 100°C give the estimate: $\phi_I + \phi_{II} + \phi_{III} = 0.61 \pm 0.06$. The quantum yields of C_2H_4 were corrected for a small contribution (1.7–5.8%) from disproportionation reactions involving C_2H_5—C_2H_5 and C_2H_5 + $CH_3CH_2CH_2$ radicals. These values of $\Phi_{C_2H_4}$, independent of temperature and ketone pressure, suggest that $\phi_{IV} = 0.21 \pm 0.01$ (Nicol and Calvert, 1967). The effect of 1 atm. of air on these primary processes is unknown, but in view of the data for the other ketones, it is likely that some quenching of the processes will occur. Until such information is available, no reliable estimates of the primary quantum yields or photolysis frequencies in air can be made.

IX-D-8. Photodecomposition of 4-Methyl-2-Pentanone [Methyl Isobutyl Ketone, $CH_3C(O)CH_2CH(CH_3)_2$]

The photodecomposition of 4-methyl-2-pentanone can be rationalized in terms of the following primary processes (Calvert et al., 2008):

$$CH_3C(O)CH_2CH(CH_3)_2 + h\nu \rightarrow CH_3CO + CH_2CH(CH_3)_2 \quad \text{(I)}$$

$$\rightarrow CH_3 + (CH_3)_2CHCH_2CO \quad \text{(II)}$$

$$\rightarrow CH_3 + CO + CH_2CH(CH_3)_2 \quad \text{(III)}$$

$$\rightarrow CH_2{=}CHCH_3 + CH_2{=}C(OH)CH_3 \quad \text{(IV)}$$

The absorption spectrum of 4-methyl-2-pentanone is compared with that of several other ketones in figure IX-D-18, and tabular data are given in table IX-D-8. Data from a single gas-phase, 313 nm photolysis experiment with the pure ketone (120°C, pressure 49 Torr) by Martin and Pitts (1955), suggest that there is little discrimination in bond breakage in (I) and (II). From Φ_{CO}, $\phi_I + \phi_{II} + \phi_{III} \approx 0.15$; from $\Phi_{C_3H_6}$, $\phi_{IV} \approx 0.35$.

The only extensive study of the photolysis of 4-methyl-2-pentanone was carried out in degassed solutions of hexane confined in Pyrex® test tubes that were irradiated with a medium-pressure Hg lamp (Encina et al., 1975). Extrapolation of this information to the photolysis in 1 atm. of air is impossible. However, the information may shed some light on the gas-phase photolysis. In the hexane solutions, $\Phi_{isobutane} \approx \phi_I \approx 0.034 \pm 0.003$(76°C). $\Phi_{CH_3C(O)CH_3} \approx \phi_{IV} \approx 0.21 \pm 0.02$ (−5 to 69°C). Experiments with added 1,3-pentadiene were used to quench excited triplet ketone molecules. The authors estimated from experiments at 20°C that the quantum yield of quenchable triplets excited under their conditions was 0.75 ± 0.03; about 88% of the acetone product of (IV) was formed from the T_1 state with about 12% from the S_1 state. These results point to the involvement of both the singlet and triplet states as well in the gas-phase photolysis, but the extent of participation of each is unclear. Until the necessary data are available to evaluate properly the wavelength dependence of the quantum

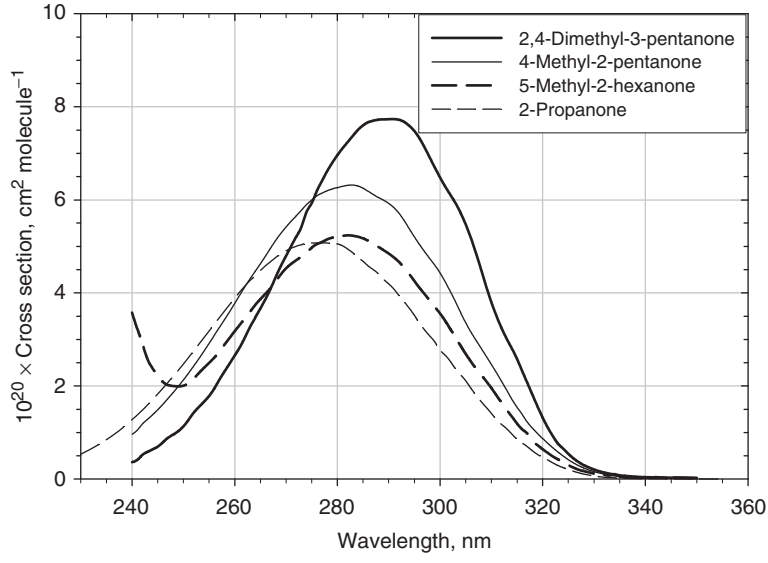

Figure IX-D-18. Comparison of absorption spectra of some branched chain ketones (Yujing and Mellouki, 2000) with that of acetone (Martinez et al., 1992).

yields of the primary processes in air under atmospheric conditions, realistic estimates of *j*-values for 4-methyl-2-pentanone are not possible.

IX-D-9. Photodecomposition of 4-Methyl-2-Hexanone [$CH_3C(O)CH_2CH(CH_3)CH_2CH_3$]

The photolysis of 4-methyl-2-hexanone follows the pattern of photodecompositions observed in other ketones (Calvert et al., 2008):

$$CH_3C(O)CH_2CH(CH_3)CH_2CH_3 + h\nu \rightarrow CH_3CO + CH_2CH(CH_3)CH_2CH_3 \quad \text{(I)}$$

$$\rightarrow CH_3 + CH_3CH_2CH(CH_3)CH_2CO \quad \text{(II)}$$

$$\rightarrow CH_3 + CO + CH_2CH(CH_3)CH_2CH_3 \quad \text{(III)}$$

$$\rightarrow CH_2{=}C(OH)CH_3 + CH_3CH{=}CHCH_3 \quad \text{(IVa)}$$

$$\rightarrow CH_2{=}C(OH)CH_3 + CH_2{=}CHCH_2CH_3 \quad \text{(IVb)}$$

The gas-phase photodecomposition of 4-methyl-2-hexanone shows an interesting competition between abstraction of secondary and primary H-atoms by the carbonyl O-atom in processes (IVa) and (IVb); see Ausloos (1961). The results at 313 nm give $(\phi_I + \phi_{II} + \phi_{III})/(\phi_{IVa} + \phi_{IVb}) < 0.02$ at 42°C and < 0.10 at 150°C. Quantum yields were not determined, but analyses of the *cis*- and *trans*-2-butene and 1-butene in the products were reported for several temperatures (44–258°C) and pressures of the ketone (7–50 Torr). For photolysis at 313 nm, the ϕ_{IVb}/ϕ_{IVa} is a function of temperature,

Table IX-D-8. Absorption cross sections ($10^{20} \times \sigma$, cm^2 $molecule^{-1}$ at 298 K) for (A) 2,4-dimethyl-3-pentanone; (B) 4-methyl-2-pentanone; (C) 5-methyl-2-hexanone; from Yujing and Mellouki (2000)

λ, nm	$10^{20} \times \sigma$ (A)	$10^{20} \times \sigma$ (B)	$10^{20} \times \sigma$ (C)	λ, nm	$10^{20} \times \sigma$ (A)	$10^{20} \times \sigma$ (B)	$10^{20} \times \sigma$ (C)
278	6.61	6.19	5.15	315	2.59	1.55	1.19
279	6.79	6.23	5.19	316	2.33	1.39	1.07
280	6.96	6.26	5.21	317	2.07	1.23	0.976
281	7.11	6.29	5.22	318	1.82	1.10	0.823
282	7.24	6.31	5.23	319	1.56	0.981	0.727
283	7.37	6.32	5.23	320	1.32	0.870	0.639
284	7.50	6.30	5.21	321	1.11	0.765	0.560
285	7.60	6.25	5.17	322	0.922	0.667	0.484
286	7.67	6.19	5.12	323	0.760	0.576	0.420
287	7.70	6.12	5.05	324	0.655	0.492	0.357
288	7.72	6.05	4.99	325	0.543	0.413	0.298
289	7.73	5.99	4.92	326	0.446	0.345	0.245
290	7.73	5.92	4.84	327	0.366	0.285	0.201
291	7.73	5.83	4.76	328	0.299	0.235	0.171
292	7.72	5.71	4.66	329	0.245	0.193	0.145
293	7.67	5.56	4.54	330	0.201	0.158	0.120
294	7.59	5.38	4.40	331	0.166	0.129	0.103
295	7.48	5.20	4.25	332	0.137	0.104	0.088
296	7.32	5.04	4.11	333	0.113	0.082	0.074
297	7.12	4.88	3.97	334	0.094	0.064	0.101
298	6.90	4.73	3.83	335	0.079	0.050	0.050
299	6.69	4.59	3.67	336	0.066	0.039	0.043
300	6.48	4.43	3.56	337	0.057	0.035	0.036
301	6.28	4.24	3.40	338	0.049	0.031	0.033
302	6.11	4.03	3.23	339	0.043	0.028	0.030
303	5.93	3.81	3.05	340	0.040	0.026	0.030
304	5.72	3.58	2.87	341	0.037	0.026	0.031
305	5.47	3.36	2.69	342	0.035	0.024	0.043
306	5.18	3.16	2.53	343	0.034	0.025	0.035
307	4.86	2.99	2.37	344	0.033	0.025	0.032
308	4.50	2.82	2.25	345	0.031	0.025	0.033
309	4.14	2.64	2.10	346	0.030	0.023	0.034
310	3.80	2.47	1.96	347	0.029	0.021	0.030
311	3.50	2.29	1.80	348	0.026	0.022	0.029
312	3.24	2.10	1.64	349	0.024	0.022	0.026
313	3.02	1.91	1.48	350	0.022	0.023	0.025
314	2.81	1.72	1.34				

increasing from 0.11 at 44°C to 0.17 at 258°C. The ratio *trans*-2-butene/*cis*-2-butene varied from 0.32 to 0.38 as the temperature was increased from 44 to 258°C. An Arrhenius plot of the 1-C_4H_8/2-C_4H_8 ratio leads to a difference in activation energy of 0.65 kJ mol^{-1} for abstraction of a primary H-atom and a secondary H-atom by the carbonyl O-atom in this ketone. For direct excitation at 253.7 nm, the ratio $\phi_{IVb}/\phi_{IVa} = 0.27$, while the $Hg(^3P_1)$-atom sensitized decomposition of the ketone gives $\phi_{IVb}/\phi_{IVa} = 0.22$. Direct photolysis near 190 nm gives $\phi_{IVb}/\phi_{IVa} = 0.37 \pm 0.03$. Addition of 2.5 Torr

of oxygen in the 313 nm photolysis at 44°C had no effect on the primary process (IV). The appropriate data are not available to calculate realistic *j*-values for 4-methyl-2-hexanone.

IX-D-10. Photodecomposition of 4-Heptanone [Di-*n*-Propyl Ketone, $CH_3CH_2CH_2C(O)CH_2CH_2CH_3$]

The primary photodecomposition pathways for 4-heptanone follow those observed in other ketones (Calvert et al., 2008):

$$CH_3CH_2CH_2C(O)CH_2CH_2CH_3 + h\nu \rightarrow CH_3CH_2CH_2 + CH_3CH_2CH_2CO \quad \text{(I)}$$

$$\rightarrow CH_3CH_2CH_2 + CO + CH_3CH_2CH_2 \quad \text{(II)}$$

$$\rightarrow CH_2{=}CH_2 + CH_2{=}C(OH)CH_2CH_2CH_3 \quad \text{(III)}$$

The first investigators to study the photodecomposition of 4-heptanone were Bamford and Norrish (1935, 1938) who had available only relatively primitive equipment and analytical techniques by today's standards. However, they managed to establish the occurrence of both radical generation in processes (I) and (II) and the Norrish type-II rearrangement in process (III). Using filtered mercury lamp radiation (largely 248–277 nm) and a calibrated thermopile system to determine quantum yields of products of 4-heptanone photodecomposition, Bamford and Norrish (1938) reported: $\Phi_{CO} \approx 0.26$ (15°C); 0.36 (74°C) and 0.37 (100°C) and $\Phi_{C_2H_4} \approx 0.45$ (15°C); 0.30 (74°C) and 0.29 (100°C).

The photolysis of 4-heptanone at 313 nm was studied later by Masson (1952) who reported: $\Phi_{CO} = 0.31 \pm 0.03$ (at 113°C) and $\Phi_{C_2H_4} = 0.22$ (8 Torr) and 0.20 (115 Torr), independent of temperature. Nicol and Calvert (1967) in experiments at 313 nm, determined $\Phi_{C_2H_4} = 0.21 \pm 0.01$ (61.3–151°C) and observed that Φ_{CO} increased from 0.26 at 52.3°C to 0.37 at 150°C. Their product mass balance of CO and the observed hydrocarbons (propane, propene, and hexane) supported a mechanism initiated by processes (I), (II), and (III).

Based upon the existing data, it is likely that $\phi_{III} = 0.21 \pm 0.01$, independent of temperature and ketone pressure, with $\phi_I + \phi_{II} \leq 0.34 \pm 0.06$. The appropriate data to estimate the *j*-values for 4-heptanone photodecomposition for tropospheric conditions are not available.

IX-D-11. Photodecomposition of 2,4-Dimethyl-3-Pentanone [Di-Isopropyl Ketone, $(CH_3)_2CHC(O)CH(CH_3)_2$]

The photodecomposition of 2,4-dimethyl-3-pentanone occurs by the following pathways (Calvert et al., 2008):

$$(CH_3)_2CHC(O)CH(CH_3)_2 + h\nu \rightarrow (CH_3)_2CH + (CH_3)_2CHCO \quad \text{(I)}$$

$$\rightarrow (CH_3)_2CH + CO + (CH_3)_2CH \quad \text{(II)}$$

Whiteway and Masson (1955) studied the photodecomposition of the pure 2,4-dimethyl-3-pentanone at 313 nm and 50–150°C; they reported $\Phi_{CO} = \phi_I + \phi_{II} = 0.98 \pm 0.04$. Cross sections are shown in table IX-D-8. The efficiency of quenching of these processes by air at 1 atm. pressure remains uncertain, and *j*-value estimation is unwarranted at this writing.

IX-D-12. Photodecomposition of 2-Methyl-3-Hexanone [*n*-Propyl Isopropyl Ketone, $CH_3CH_2CH_2C(O)CH(CH_3)_2$]

The photodecomposition of 2-methyl-3-hexanone probably occurs by the following pathways (Calvert et al., 2008):

$$CH_3CH_2CH_2COCH(CH_3)_2 + h\nu \rightarrow CH_3CH_2CH_2CO + CH(CH_3)_2 \quad \text{(I)}$$

$$\rightarrow CH_3CH_2CH_2 + (CH_3)_2CHCO \quad \text{(II)}$$

$$\rightarrow CH_3CH_2CH_2 + CO + CH(CH_3)_2 \quad \text{(III)}$$

$$\rightarrow CH_2{=}CH_2 + CH_2{=}C(OH)CH(CH_3)_2 \quad \text{(IV)}$$

Quantum yield measurements of Nicol and Calvert (1967) from photolysis of the pure ketone at 313 nm and 59–150°C suggest a preference for bond cleavage in the competition between pathways (I) and (II). The ratio of the quantum yields of 2-methylpentane (derived from 2-propyl + 1-propyl combination) and *n*-hexane (formed from 1-propyl + 1-propyl combination), coupled with the assumption of the near equality of the association reaction forming these, suggests [2-propyl]/[1-propyl] $\approx 2.7 \pm 0.5$ (59–150°); this may reflect $\phi_I > \phi_{II}$. The values of Φ_{CO} are consistent with $\phi_I + \phi_{II} + \phi_{III} = 0.69 \pm 0.06$ (100 − 150°C). $\Phi_{C_2H_4}$ values show a small increase with temperature, but an average over the temperature range 59–150°C gives the estimate of $\phi_{IV} \approx 0.12 \pm 0.03$. The total $\phi_I + \phi_{II} + \phi_{III} + \phi_{IV} = 0.83 \pm 0.06$ (59–150°C) for photolysis of the pure ketone is near unity, similar to the case of 2,4-dimethyl-3-pentanone. The necessary data to derive realistic *j*-values for 2-methyl-3-hexanone in the troposphere are not available.

IX-D-13. Photodecomposition of 4,4-Dimethyl-2-Pentanone [Methyl Neopentyl Ketone, $CH_3C(O)CH_2C(CH_3)_3$]

4,4-Dimethyl-2-pentanone provides nine H-atoms on its three γ-carbon atoms, and it is interesting to see the effect of this on the efficiency of the Norrish type-II process in the photodecomposition of this ketone. The following primary processes have been

suggested to rationalize the data (Martin and Pitts, 1955):

$$CH_3C(O)CH_2C(CH_3)_3 + h\nu \rightarrow CH_3CO + CH_2C(CH_3)_3 \quad \text{(I)}$$

$$\rightarrow CH_3 + (CH_3)_3CCH_2CO \quad \text{(II)}$$

$$\rightarrow CH_3 + CO + CH_2C(CH_3)_3 \quad \text{(III)}$$

$$\rightarrow CH_2{=}C(OH)CH_3 + CH_2{=}C(CH_3)_2 \quad \text{(IV)}$$

$$\rightarrow C(CH_3)_3 + CH_2COCH_3 \quad \text{(V)}$$

Φ_{CO} data from 313 nm photolysis allow an estimate of $\phi_I + \phi_{II} + \phi_{III} \approx 0.042$–$0.075$ (120–250°C). 2-Methylpropene and acetone quantum yields give: $\phi_{IV} = 0.25 \pm 0.02$ (2-methylpropene, 120–250°C) and 0.22 ± 0.04 (acetone, 120–210°C). 2-Methylpropane among the products suggests the occurrence of minor process (V), a bond cleavage down-chain from the energy absorbing carbonyl group: $\phi_V \leq 0.005$ (120°C), 0.02 (250°C).

In photolysis at 265.4 nm, Φ_{CO} data of Martin and Pitts (1955) give: $\phi_I + \phi_{II} + \phi_{III} \approx 0.07 \pm 0.01$ (120–250°C). The data for process (IV) appear to show a temperature dependence; the average quantum yields give: $\phi_{IV} = 0.31 \pm 0.05$ (2-methylpropene, 120–250°C), and 0.27 ± 0.05 (acetone, 120–250°C). As in photolysis at 313 nm, process (V) is relatively unimportant as judged from the 2-methylpropane yield: $\phi_V \geq 0.007 \pm 0.003$. No meaningful estimate of *j*-values for 4,4-dimethyl-2-pentanone can be made from the limited data available.

IX-D-14. Photodecomposition of 4-Methyl-2-Pentanone [Methyl Isobutyl Ketone, $CH_3C(O)CH_2CH(CH_3)_2$]

A single experiment by Martin and Pitts (1955) at 313 nm gave evidence of the following primary processes in 4-methyl-2-pentanone:

$$CH_3C(O)CH_2CH(CH_3)_2 + h\nu \rightarrow CH_3CO + CH_2CH(CH_3)_2 \quad \text{(I)}$$

$$\rightarrow CH_3 + (CH_3)_2CHCH_2CO \quad \text{(II)}$$

$$\rightarrow CH_3 + CO + CH_2CH(CH_3)_2 \quad \text{(III)}$$

$$\rightarrow CH_2{=}C(OH)CH_3 + CH_2{=}CHCH_3 \quad \text{(IV)}$$

Estimated quantum yields at 313 nm and 120°C are: $\phi_I + \phi_{II} + \phi_{III} \approx \Phi_{CO} = 0.15$; $\phi_{IV} \approx 0.35$ (propene). Cross sections are shown in table IX-D-8. Sufficient data are not available to make realistic estimates of *j*-value for this compound.

IX-D-15. Photodecomposition of 4-Octanone [*n*-Propyl *n*-Butyl Ketone, $CH_3CH_2CH_2C(O)CH_2CH_2CH_2CH_3$]

4-Octanone photodecomposition can be described in terms of the following processes (Calvert et al., 2008):

$$CH_3CH_2CH_2C(O)CH_2CH_2CH_2CH_3 + h\nu$$

$$\rightarrow CH_3CH_2CH_2 + CH_3CH_2CH_2CH_2CO \quad \text{(I)}$$

$$\rightarrow CH_3CH_2CH_2CO + CH_3CH_2CH_2CH_2 \quad \text{(II)}$$

$$\rightarrow CH_3CH_2CH_2 + CO + CH_3CH_2CH_2CH_2 \quad \text{(III)}$$

$$\rightarrow CH_2{=}CH_2 + CH_2{=}C(OH)CH_2CH_2CH_2CH_3 \quad \text{(IV)}$$

$$\rightarrow CH_2{=}CHCH_3 + CH_2{=}C(OH)CH_2CH_2CH_3 \quad \text{(V)}$$

The quantum yields of products from photodecomposition of 4-octanone at 313 nm and temperatures from 76–151°C were measured by Nicol and Calvert (1967); the data suggest: $\phi_I + \phi_{II} + \phi_{III} = 0.078 \pm 0.022$ (70–151°C); $\phi_{IV} = 0.030 \pm 0.005$ (temperature dependent); $\phi_V = 0.054 \pm 0.017$ (temperature dependent). An Arrhenius plot of the ratio ϕ_{IV}/ϕ_V gives an activation energy difference of 5.5 kJ mol^{-1} for the abstraction of primary H-atom and a secondary H-atom by the carbonyl oxygen in 313 nm-excited 4-octanone. Data are insufficient to estimate realistic *j*-values for this ketone.

IX-D-16. Photodecomposition of 2-Methyl-4-Heptanone [*n*-Propyl Isobutyl Ketone, $(CH_3)_2CHCH_2C(O)CH_2CH_2CH_3$]

Photodissociation studies of 2-methyl-4-heptanone at 313 nm suggest the following primary reaction channels (Calvert et al., 2008):

$$CH_3CH_2CH_2C(O)CH_2CH(CH_3)_2 + h\nu$$

$$\rightarrow CH_3CH_2CH_2 + (CH_3)_2CHCH_2CO \quad \text{(I)}$$

$$\rightarrow CH_3CH_2CH_2CO + (CH_3)_2CHCH_2 \quad \text{(II)}$$

$$\rightarrow CH_3CH_2CH_2 + CO + (CH_3)_2CHCH_2 \quad \text{(III)}$$

$$\rightarrow CH_2{=}CH_2 + CH_2{=}C(OH)CH_2CH(CH_3)_2 \quad \text{(IV)}$$

$$\rightarrow CH_2{=}CHCH_3 + CH_2{=}C(OH)CH_2CH_2CH_3 \quad \text{(V)}$$

The studies of Nicol and Calvert (1967) provide estimates of the quantum efficiencies of these processes for photolysis at 313 nm: $\phi_I + \phi_{II} + \phi_{III} = 0.21 \pm 0.04$ (75–150°C); $\phi_{IV} = 0.055 \pm 0.003$ (75–150°C); $\phi_V = 0.11 \pm 0.04$ (75–150°C). There are insufficient data to estimate realistic *j*-values for this ketone.

IX-D-17. Photodecomposition of 3-Methyl-4-Heptanone [*n*-Propyl sec-Butyl Ketone, $CH_3CH_2CH_2C(O)CH(CH_3)CH_2CH_3$]

Photodecomposition modes of 3-methyl-4-heptanone follow the pattern of other ketones (Calvert et al., 2008):

$$CH_3CH_2CH_2C(O)CH(CH_3)CH_2CH_3 + h\nu$$

$$\rightarrow CH_3CH_2CH_2CO + CH_3CHCH_2CH_3 \quad \text{(I)}$$

$$\rightarrow CH_3CH_2CH_2 + CH_3CH_2CH(CH_3)CO \quad \text{(II)}$$

$$\rightarrow CH_3CH_2CH_2 + CO + CH_3CHCH_2CH_3 \quad \text{(III)}$$

$$\rightarrow CH_2{=}CH_2 + CH_2{=}C(OH)CH(CH_3)CH_2CH_3 \quad \text{(IV)}$$

$$\rightarrow CH_2{=}CH_2 + CH_3CH{=}C(OH)CH_2CH_2CH_3 \quad \text{(V)}$$

The studies of Nicol and Calvert (1967) at 313 nm provide the following estimates of the quantum yields of the primary processes: $\phi_I + \phi_{II} + \phi_{III} = 0.39 \pm 0.04$ (77–150°C); $\phi_{IV} + \phi_V = 0.10 \pm 0.02$ (77–150°C). The data are insufficient to estimate realistic *j*-values for this ketone.

IX-D-18. Photodecomposition of 2,2-Dimethyl-3-Hexanone [*n*-Propyl *tert*-Butyl Ketone, $CH_3CH_2CH_2C(O)C(CH_3)_3$]

Photodecomposition of 2,2-dimethyl-3-hexanone pathways are similar to those of other ketones (Calvert et al., 2008):

$$(CH_3)_3CC(O)CH_2CH_2CH_3 + h\nu \rightarrow (CH_3)_3C + CH_3CH_2CH_2CO \quad \text{(I)}$$

$$\rightarrow (CH_3)_3CCO + CH_3CH_2CH_2 \quad \text{(II)}$$

$$\rightarrow (CH_3)_3C + CO + CH_3CH_2CH_2 \quad \text{(III)}$$

$$\rightarrow CH_2{=}CH_2 + CH_2{=}C(OH)C(CH_3)_3 \quad \text{(IV)}$$

In the temperature range 76–152°C in the studies of Nicol and Calvert (1967), little discrimination was seen between the bond breakage in processes (I) and (II); $\phi_I/\phi_{II} \approx 0.82 \pm 0.11$. The data provide estimates of the quantum efficiencies of the various reaction channels at 313 nm: $\phi_I + \phi_{II} + \phi_{III} = 0.57 \pm 0.04$ (76–152°C); $\phi_{IV} = 0.097 \pm 0.016$ (76–152°C).

Styrene, the most efficient quencher of triplet excited states of carbonyl compounds among a great variety of olefins employed by Ausloos and Rebbert (1964), gave no detectable influence on the ethene and carbon monoxide quantum yields when 20.1 Torr was added to 19.9 Torr of 2,2-dimethyl-3-hexanone (Nicol and Calvert, 1967). However, an almost quantitative removal of radical products of 1-propyl and 2-methyl-2-propyl radicals resulted. Since Φ_{CO} was unaffected by styrene addition, the radical

product suppression must have occurred through the radical addition to styrene; this is consistent also with the induced polymerization of the styrene observed by Nicol and Calvert (1967). Obviously, whatever the precursor states to the photodecomposition might be, they are very short-lived. There are not sufficient data to allow estimates of the *j*-values for this ketone.

IX-D-19. Photodecomposition of 2,6-Dimethyl-4-Heptanone [Di-Isobutyl Ketone, $(CH_3)_2CHCH_2C(O)CH_2CH(CH_3)_2$]

The photodecomposition modes of this ketone follow those of the other ketones (Calvert et al., 2008):

$$(CH_3)_2CHCH_2C(O)CH_2CH(CH_3)_2 + h\nu$$

$$\rightarrow (CH_3)_2CHCH_2CO + (CH_3)_2CHCH_2 \quad \text{(I)}$$

$$\rightarrow (CH_3)_2CHCH_2 + CO + (CH_3)_2CHCH_2 \quad \text{(II)}$$

$$\rightarrow CH_2{=}CHCH_3 + CH_2{=}C(OH)CH_2CH(CH_3)_2 \quad \text{(III)}$$

The data from the full Hg-arc photolysis of 2,6-dimethyl-4-heptanone (Kraus and Calvert, 1957) allow the following estimates of the average quantum efficiencies (~250–340 nm) of the photodecomposition modes of 2,6-dimethyl-4-heptanone: $\phi_I + \phi_{II} \approx \Phi_{CO} = 0.18 \pm 0.02$ (78–155°C); $\phi_{III} \approx \Phi_{C_3H_6} = 0.36 \pm 0.02$ (78–155°C). There are not sufficient data to estimate realistic *j*-values for this ketone.

IX-D-20. Photodecomposition of 3,5-Dimethyl-4-Heptanone [Di-sec-Butyl Ketone, $CH_3CH_2CH(CH_3)C(O)CH(CH_3)CH_2CH_3$]

Photodecomposition of 3,5-dimethyl-4-heptanone involves both bond cleavage and Norrish type-II reactions (Calvert et al., 2008):

$$CH_3CH_2CH(CH_3)C(O)CH(CH_3)CH_2CH_3 + h\nu$$

$$\rightarrow CH_3CH_2CHCH_3 + CH_3CH_2CH(CH_3)CO \quad \text{(I)}$$

$$\rightarrow 2CH_3CHCH_2CH_3 + CO \quad \text{(II)}$$

$$\rightarrow CH_2{=}CH_2 + CH_3CH{=}C(OH)CH(CH_3)CH_2CH_3 \quad \text{(III)}$$

Data from full Hg-arc photolysis of 3,5-dimethyl-4-heptanone by Kraus and Calvert (1957) suggest the following estimates of the average quantum yields (250–340 nm, temperature, 98–105°C) of the primary photodecomposition processes: $\Sigma(\Phi_{C_4H_9\text{-groups}})/2 \approx 0.30 \pm 0.03 \approx \phi_I + \phi_{II}$; $\Phi_{C_2H_4} \approx 0.29 \pm 0.03 \approx \phi_{III}$. There are insufficient data to estimate realistic *j*-values for this ketone.

IX-D-21. Photodecomposition of 2,2,4,4-Tetramethyl-3-Pentanone [Di-*tert*-Butyl Ketone, $(CH_3)_3CC(O)C(CH_3)_3$]

The photodecomposition of 2,2,4,4-tetramethyl-3-pentanone involves only bond cleavage in Norrish type-I reactions (Calvert et al., 2008):

$$(CH_3)_3CC(O)C(CH_3)_3 + h\nu \rightarrow (CH_3)_3C + (CH_3)_3CCO \quad \text{(I)}$$

$$\rightarrow (CH_3)_3C + CO + C(CH_3)_3 \quad \text{(II)}$$

The full Hg-arc photolysis of 2,2,4,4-tetramethyl-3-pentanone was studied by Kraus and Calvert (1957). With the assumption of a unity quantum yield of CO product at the temperatures in the range 114–251°C, the hydrocarbon product analyses give: $\Sigma(\Phi_{C_4H_9-\text{groups}})/2 \approx \phi_I + \phi_{II} = 0.84 \pm 0.05$. It is interesting that a high efficiency of photodissociation of 2,2,4,4-tetramethyl-3-pentanone occurs even in solution. Abuin et al. (1984) studied the photodissociation of this ketone at 313 nm in various homogeneous solvents of different viscosities. A marked effect on the apparent extent of photodissociation resulted from cage reactions of the geminate radicals. Measured values of $\phi_I + \phi_{II}$ varied from 0.5 in paraffin oil to 1.0 in heptane solutions. There are insufficient data to allow realistic estimates of the *j*-values for this ketone.

IX-D-22. Some Effects of Molecular Structure on the Quantum Efficiencies of Photodecomposition Modes in the Ketones

Some interesting relations between molecular structure of the ketone and the quantum yield of primary products can be seen in the summary of quantum yield data for the different ketones of common structure $CH_3CH_2CH_2C(O)R$ given in table IX-D-9 (Calvert et al., 2008). In column (3) observe that the $\phi_{Ia} + \phi_{Ib}$ values show a rather random variation in magnitude over a considerable range (0.10 for R = $CH_3CH_2CH_2CH_2$ to 0.71 for R = CH_3CHCH_3). One might have naively expected Φ_{CO} (taken as $\phi_{Ia} + \phi_{Ib}$) to be highest for the 2,2-dimethyl-3-hexanone since this compound has the weakest C—C bond in these molecules: $(CH_3)_3C$—$C(O)CH_2CH_2CH_3$. However, the Φ_{CO} for the 3-hexanone is even higher. Obviously, other factors in addition to the product radical stability influence ϕ_I values.

Qualitatively, one can conclude from the type-II photodecomposition data of table IX-D-9 that the fraction of $CH_3CH_2CH_2C(O)R$ compounds that undergo the type-II process is surprisingly similar for ketones with varied R groups; see column (6) of the table. If the type-I and type-II processes are in competition from the same state, one expects that large variations in ϕ_{II} would occur. Calvert et al. (2008) concluded that no simple correlation was evident between the number of γ-H-atoms present in the compound and ϕ_{II} values. For example, although 4-heptanone and the 2-methyl-4-heptanone contain two and three times, respectively, the number of γ-H-atoms as 3-hexanone, the total type-II process quantum yields are nearly the same for all three compounds. However, when there are different competitive type-II processes possible within the same excited molecule, and the different processes involve the transfer of a

Table IX-D-9. Summary of quantum yields for primary processes in the 313 nm photolysis of a series of $CH_3CH_2CH_2COR$ ketones at 150°C (based on the data of Nicol and Calvert, 1967)[a]; table is from Calvert et al. (2008)

$$CH_3CH_2CH_2C(O)R + h\nu \rightarrow CH_3CH_2CH_2 + RCO \quad \text{(Ia)}$$
$$\rightarrow CH_3CH_2CH_2CO + R \quad \text{(Ib)}$$
$$\rightarrow CH_2{=}CH_2 + CH_2{=}C(OH)R \quad \text{(IIa)}$$
$$\rightarrow CH_3CH_2CH_2C(OH){=}CHR' + C_nH_{2n} \quad \text{(IIb)}$$

R	Parent Carbonyl Compound	$\phi_{Ia} + \phi_{Ib}$	ϕ_{IIa}	ϕ_{IIb}	$\phi_{IIa} + \phi_{IIb}$	$\Sigma\phi_i$
H	Butanal	0.35[b]	0.170	–	0.17	0.52
CH_3	2-Pentanone	0.43	0.252	–	0.25	0.68
C_2H_5	3-Hexanone	0.57	0.203	–	0.20	0.77
$CH_3CH_2CH_2$	4-Heptanone	0.37	0.106[c]	0.106[c](0.099)	0.21	0.58
CH_3CHCH_3	2-Methyl-3-hexanone	0.71	0.155[d]	–	0.16	0.87
$CH_3CH_2CH_2CH_2$	4-Octanone	0.10	0.035	0.248	0.28	0.38
$(CH_3)_2CHCH_2$	2-Methyl-4-heptanone	0.24	0.055	0.151	0.21	0.45
$CH_3CHCH_2CH_3$	3-Methyl-4-heptanone	0.36	0.062[d]	0.061[d]	0.12	0.48
$(CH_3)_3C$	2,2-Dimethyl-3-hexanone	0.54	0.118[d]	–	0.12	0.66

[a]Values are the arithmetic mean of individual values at 150°C except for those ketones for which the type-II process is independent of temperature; the tabular values for ϕ_{IIa} and ϕ_{IIb} represent the arithmetic average of all individual values at all temperatures in these cases.

[b]*E*stimated from butanal photolysis with added I_2 reported by Blacet and Calvert (1951b).

[c]Values are obtained by dividing the total alkene yield by 2, assuming equal participation by the two equivalent sides of the molecule.

[d]These Norrish type-II yields are temperature dependent.

primary H-atom, there is nearly a statistical distribution of the products observed. Thus, in 3-methyl-4- heptanone, one expects equal yields of processes (IIa) and (IIb) from purely statistical reasoning; this is the observed result. In the photolysis of 2-methyl-4-heptanone, one expects statistically twice the quantum yield since any one of six γ-H-atoms will lead to propene, while abstraction of any one of three γ-H-atoms may lead to ethene formation. Actually, the propene to ethene ratio is 2.7; apparently some structural preferences beyond that of statistics favor the propene-forming reaction somewhat. In both of these cases considered here, there is no significant activation energy difference between the processes, and the quantum yields are temperature independent.

When H-atoms of different type are present in the γ-position, a significant preference is shown for abstraction of the one of weaker C—H bond dissociation energies, and the quantum efficiencies of the competitive processes are temperature dependent. However, the sum of the two yields, $\phi_{IIa} + \phi_{IIb}$, is substantially independent of temperature. Note the data for 4-octanone show the propene product is greatly favored over ethene in spite of the adverse 2:3 ratio of the number of secondary to primary H-atoms in the γ-position. An Arrhenius plot of the ratio $\Phi_{C_2H_4}/\Phi_{C_3H_6}$ gives an apparent activation energy difference between the reaction involving primary H-atom abstraction and that involving the secondary H-atom abstraction of 5.5 kJ mol^{-1}. Ausloos (1961) reported 0.6 kJ mol^{-1} from the 313 nm photolysis of 4-methyl-2-hexanone where a

similar competition between primary H and secondary H-atoms exists. The discrimination between different types of H-atoms is also in accord with the preference found for H-atom over D-atom abstraction in the type-II process in $CH_3C(O)CH_2CDHCD_2H$ photolysis studied by Borkowski and Ausloos (1961).

The $\phi_{IIa}+\phi_{IIb}$ values are independent of temperature for the $CH_3CH_2CH_2C(O)R$ compounds with R = H, CH_3, C_2H_5, $CH_3CH_2CH_2$, $CH_3CH_2CH_2CH_2$, and $(CH_3)_2CH_2CH_2$. However, for the three ketones studied that contain multiple α-alkyl substituents [R = CH_3CHCH_3, $(CH_3)_2CHCH_2$, $(CH_3)_3C$], a temperature dependence of the ϕ_{II} values is seen. This corresponds to an apparent activation energy of ethene formation of about 8 kJ mol^{-1} in each case. A somewhat smaller inverse temperature dependence to ϕ_I (about -3 kJ mol^{-1}) is seen in each of these three ketones, such that the sum $\phi_I + \phi_{II}$ is approximately independent of the temperature.

Nicol and Calvert et al. (1967) noted an interesting quantitative relation between the extent of the α-alkyl substitution in the $CH_3CH_2CH_2C(O)R$ ketones and the size of ϕ_{II}. For example, the data in table IX-D-9 from experiments at 150°C show a regular decrease in the ϕ_{II} values in the order R = CH_3(ϕ_{II} = 0.252), C_2H_5(ϕ_{II} = 0.203), CH_3CHCH_3 (ϕ_{II} = 0.155), $(CH_3)_3C$(ϕ_{II} = 0.118). Substitution of one methyl group for a methyl hydrogen atom in the 2-pentanone lowers the quantum yield of the type-II process by a factor of 0.80; a second methyl substitution in the α-position lowers ϕ_{II} by a factor of 0.76; a third methyl substitution in the α-position lowers ϕ_{II} again by an identical factor, 0.76. A similar lowering by a factor 0.6 in ϕ_{II} is seen when an α-methyl group is introduced in 3-heptanone. The consistency of the magnitude of the lowering of ϕ_{II} values with α-substitution suggests that the effect of α-methyl groups is real, although its detailed mechanistic explanation is open to question. From the near constancy of the $\phi_I+\phi_{II}$ values for the series of ketones with R = C_2H_5, $CH_3CH_2CH_2$, $(CH_3)_2CHCH_2$ (0.20, 0.21, 0.21), it appears that the nature of the α-substituent is not highly important as long as only primary H-atoms are present in the γ-positions.

Nicol and Calvert (1967) suggested the following empirical equations relating ϕ_{II} and molecular structure of the $CH_3CH_2CH_2C(O)R$ ketones listed in table IX-D-9:

$$\phi_{IIa} + \phi_{IIb} = [0.252(0.78)^m + 0.038n][e^{-1.9p/RT}/e^{-2.25p}] \quad (1)$$

$$\phi_{IIa}/\phi_{IIb} = (N_a A_a/N_b A_b)e^{-\Delta E/RT} \quad (2)$$

The first term of equation (1) formulates the effect of α-alkyl substituents on ϕ_{II} and m represents the number of alkyl substituents attached to the α-carbon atom of the R group. The second term increases the calculated ϕ_{II} values for the case of ketones with *sec*-H-atoms in the γ-position; n is the number of these atoms. Depending on the interpretation of the reactive state involved, the second term ($0.038n$) may either be related to the additional alkene product from singlet excited state participation in the type-II process or to an enhanced triplet reactivity. Presumably a third term would be required to account for tertiary H-atoms in the γ-position. The exponential term in equation (1) introduces a temperature dependence to the ϕ_{II} values for the highly substituted ketones; $p = 1$ when there are two or more alkyl substituents on the α-carbon atom and $p = 0$ for all other cases. Equation (2) is presumably related to

the ratio of the competitive rate constants for abstraction of γ-H-atoms. $\Delta E = 0$ for those cases in which the two sources of process II are of the same type of γ-H-atom. This is equal to 5.4 kJ mol^{-1} (units on R, kJ mol^{-1} K^{-1}) when both primary and secondary H-atoms are present in the γ-position in the ketone. Presumably a somewhat higher value for ΔE will be required when there are primary and tertiary H-atoms in competitive abstraction reactions. N_a and N_b are the numbers of γ-H-atoms of a given type in the $CH_3CH_2CH_2$ and R group, respectively. A_a and A_b are the preexponential factors related to the rate coefficients k_{IIa} and k_{IIb} expressed as a rate per γ-H-atom. Unless some peculiar geometrical configuration favors the type-II process or the singlet state is involved significantly as well as the triplet, one would expect $A_a = A_b$. This assumption appears justified except for 4-octanone where the choice of $A_a = (0.44)A_b$ was necessary to fit the data.

Reasonable agreement between ϕ_{IIa} and ϕ_{IIb} values calculated from equations (1) and (2) and those measured experimentally can be seen by comparison of the values shown in table IX-D-10. With the large number of variables involved in equations (1) and (2), it is not surprising that a reasonably good match of experimental and calculated ϕ_{II} values can be had, but the exercise allows some insight into the factors that affect ϕ_{II}.

Product quantum yields obtained in photolysis of a given ketone in the liquid phase are not expected to agree quantitatively with those determined in the gas phase. The more efficient vibrational relaxation of the excited states in solutions is a major factor that leads to this difference. However, the studies of Guillet and co-workers provide

Table IX-D-10. Comparison of measured $\phi_{IIa}$and ϕ_{IIb} values from 313 nm photolysis of the $CH_3CH_2CH_2C(O)R$ ketones with those calculated from equations (1) and (2) in section IX-D-22; the table is from Calvert et al. (2008)

R	Parent Carbonyl Compound	Temperature °C	ϕ_{IIa} Measured	ϕ_{IIa} Calculated	ϕ_{IIb} Measured	ϕ_{IIb} Calculated
CH_3	2-Pentanone	58–151	0.252	0.252	–	–
CH_3CH_2	3-Hexanone	62–151	0.203	0.197	–	–
$CH_3CH_2CH_2$	4-Heptanone	61–151	0.106	0.099[a]	0.106	0.099[a]
CH_3CHCH_3	2-Methyl-3-hexanone	150	0.155	0.154	–	–
		100	0.112	0.116	–	–
		60	0.085	0.085	–	–
$CH_3CH_2CH_2CH_2$	4-Octanone	150	0.035	0.034[b]	0.248	0.240[b]
		150	0.035	0.066[a]	0.248	0.206[a]
		110	0.029	0.029[b]	0.243	0.244[b]
		76	0.024	0.025[b]	0.237	0.248[b]
$(CH_3)_2CHCH_2$	2-Methyl-4-heptanone	75–150	0.055	0.066[a]	0.151	0.131[a]
$CH_3CHCH_2CH_3$	3-Methyl-4-heptanone	150	0.062	0.077[a]	0.061	0.077[a]
		110	0.052	0.060[a]	0.052	0.060[a]
		75	0.039	0.047[a]	0.039	0.047[a]
$(CH_3)_3C$	2,2-Dimethyl-3-hexanone	150	0.118	0.120	–	–
		110	0.093	0.093	–	–
		75	0.073	0.074	–	-

[a]Calculated from equations (1) and (2) in section IX-D-22 assuming $A_a = A_b$.
[b]Calculated assuming $A_a = (0.44)A_b$.

some useful insight into the effect of molecular structure on primary processes in aliphatic ketones that relate, at least qualitatively, to effects that would be seen in gas-phase photolysis. In this sense, it is important to review their findings here.

Hartley and Guillet (1968b) determined the quantum yields of the type-II reactions for a series of straight-chain, symmetrical ketones of structure RC(O)R where the total length of the chain of carbon atoms in the ketone varied from 7 (4-heptanone) to 43 (22-tritetracontanone). The results were consistent with the occurrence of the modes of reaction common to the smaller ketones:

$$CH_3(CH_2)_nC(O)(CH_2)_nCH_3 + h\nu \rightarrow CH_3(CH_2)_n + CH_3(CH_2)_nCO \qquad (I)$$

$$\rightarrow R'CH{=}CH_2 + CH_2{=}C(OH)(CH_2)_nCH_3 \qquad (II)$$

where R′ is an alkyl group of formula, H—$(CH_2)_{n-2}$.

For photolysis at 313 nm in paraffin oil at 120°C, Hartley and Guillet (1968b) reported the following values of $\Phi_{CO}(= \phi_I)$ for symmetrical ketones of total chain length shown in parentheses: 0.35 (7); 0.022 (9); 0.019 (11); 0.018 (13); 0.016 (15); 0.013 (23); 0.012 (43). The very large drop in ϕ_I as the carbon chain length increased from 7 to 9, was rationalized in terms of a competition of the excited molecule between dissociation in (I) or rearrangement in (II). The greatly increased rate of process (II) in 2-nonanone compared to 2-heptanone presumably reflects the abstraction of only secondary H-atoms in this and all the higher ketones while only primary H-atoms are abstracted in 2-heptanone.

Hartley and Guillet (1968b) determined from the quantum yields of the alkene and ketone products of (II), estimates of $\phi_{II} = 0.15$ (7); 0.108 (9); 0.092 (13); 0.080 (15); 0.072 (23); 0.072 (43); the total length of the ketone chain is shown in parentheses. As one might expect from process (II), there was a near equality between the 1-hexene and 2-nonanone products of 8-pentadecanone in photolysis in paraffin oil solutions at several temperatures: at 30°C, 0.066 and 0.067, respectively; 60°C, 0.068 and 0.067; 90°C, 0.091 and 0.086; 120°C, 0.087 and 0.091; 145°C, 0.092 and 0.102. The temperature dependence is small, equivalent to about $4\,kJ\,mol^{-1}$. The results of these photolyses of very-long-chain ketones are very similar to those observed by Hartley and Guillet (1968a) in the 313 nm photolysis of ethene–carbon monoxide copolymers that have very-long-chain ketone structures.

Golemba and Guillet (1972) studied the primary processes in another series of structurally related ketones; linear 2-alkanones [$CH_3C(O)R$] ranging from C_6 (2-hexanone) to C_{19} (2-nonadecanone). These were photolyzed in a variety of hydrocarbon solvents at 313 nm, and quantum yields of photodissociation by both primary processes (I) and (II) were determined. Using 2-undecanone in dodecane solvent, they measured the nonane quantum yields formed by H-atom abstraction from the solvent following the photodissociation; $n\text{-}C_9H_{19}C(O)CH_3 + h\nu \rightarrow CH_3CO + n\text{-}C_9H_{19}$ (I). They found that Φ_{nonane} increased from 0.00036 at 24°C to 0.012 at 117.5°C where it remained constant at higher temperatures. These data suggested that ϕ_I could be estimated from measurement of the quantum yield of the RH product at temperatures >117°C in $CH_3C(O)R$ photolysis in hydrocarbon solvents. Measured quantum yields

of the alkane product gave estimates of ϕ_I for photolysis at various temperatures: 2-heptanone: 0.0060 (70°C); 0.015 (100°C); 2-octanone: 0.018 (120°C); 2-nonanone: 0.0046 (70°C); 0.011 (100°C); 2-undecanone: 0.0033 (25°C); 0.0019 (70°C); 0.0074 100°C; 0.012 (120°C); 2-nonadecanone:~0.002 (70°C). It is clear that process (I) is relatively unimportant compared to (II) in all of these ketones, and it appears to decrease somewhat with increase in chain length of the ketone.

Quantum yields of acetone and the corresponding alkene product of the Norrish type-II reaction for the 2-alkanones were found to be near equal in preliminary experiments of Golemba and Guillet (1972). In most experiments, they used the alkene to monitor the extent of the type-II reaction. The results showed a small decrease in ϕ_{II} with increase in chain length of the ketone, which is shown in parentheses: $\phi_{II} = 0.25(6)$; 0.20 (7); 0.20 (8); 0.20 (9); 0.20 (11); 0.15 (19). Solution-phase photolyses of the ketones were made with added triplet molecule quencher, *cis*-1,3-cyclooctadiene, at concentrations sufficient to quench virtually all of the triplet reactions. From such experiments, Golemba and Guillet (1972) found the ratios of the quantum yields of the triplet to that of the singlet participation in reaction (II): $\phi_{II}^{T}/\phi_{II}^{S} = 0.65$ with 2-hexanone; 0.61 with 2-octanone; 0.64 with 2-nonadecanone.

The cyclobutanol products of the photolysis of these ketones were analyzed only for 2-nonanone where the quantum yield $\phi_{\text{cyclobutanol}} = 0.02$. Golemba and Guillet (1972) compare this value with that reported from 2-hexanone (0.075; Coulson and Yang, 1966) and surmise that $\phi_{\text{cyclobutanone}}$ decreases with increase in chain length.

Our discussion here focuses on the effects of structure on aliphatic ketones. However, it should be noted that Pitts et al. (1968) determined the effect of the length of the alkyl group (R) on the Norrish type-II process seen in 313 nm photolysis of alkyl phenyl ketones $C_6H_5C(O)R$ in benzene or hexane solutions. They found ϕ_{II} decreased from 0.40 for $R = n\text{-}C_3H_7$ to 0.29 for $R = n\text{-}C_8H_{17}$.

Additional illustration of the influence of ketone structure on the quantum yields of photodecomposition at 313 nm can be seen in figure IX-D-19 (Calvert et al., 2008). Here the existing quantum yield data for the ketones of structure $CH_3C(O)R$ and $RC(O)R$ are presented versus the length of the straight-chain alkyl radical. Data from both photolyses in the gas phase and in paraffin solution (Hartley and Guillet, 1968b; Golemba and Guillet, 1972) show similar trends with structural change of the ketone. In figure IX-D-19a it is seen that the radical generation, $CH_3C(O)R + h\nu \rightarrow CH_3CO + R$ (I), in ketones of the structure $CH_3C(O)R$, maximizes for ketones with $R = C_2H_5$, and a significant decline in quantum efficiency occurs as one progresses to $R = C_{17}H_{35}$. On the other hand, the process (II) forming alkene and enol-acetone, $CH_3C(O)R + h\nu \rightarrow R'CH{=}CH_2 + CH_2{=}CH(OH)CH_3$ (II), begins with $R = C_3H_7$, and the process continues to be the dominant mode of photodecomposition up to the largest ketone in the series studied, $CH_3C(O)C_{17}H_{35}$.

The quantum yield data for the photodecomposition of symmetrical ketones, $RC(O)R$, at 313 nm show a similar behavior; see figure VII-C-19b (Calvert et al., 2008). Radical generation, $RC(O)R + h\nu \rightarrow R + RCO$, falls rapidly in progression from the ketone with $R = n\text{-}C_3H_7$ to $R = n\text{-}C_{17}H_{35}$. However, the quantum yield of the Norrish type-II process in these ketones, $RC(O)R + h\nu \rightarrow R'CH{=}CH_2 + CH_2{=}CH(OH)R''$(II), continues to be significant up to the ketone of structure $C_{17}H_{35}C(O)C_{17}H_{35}$. As with

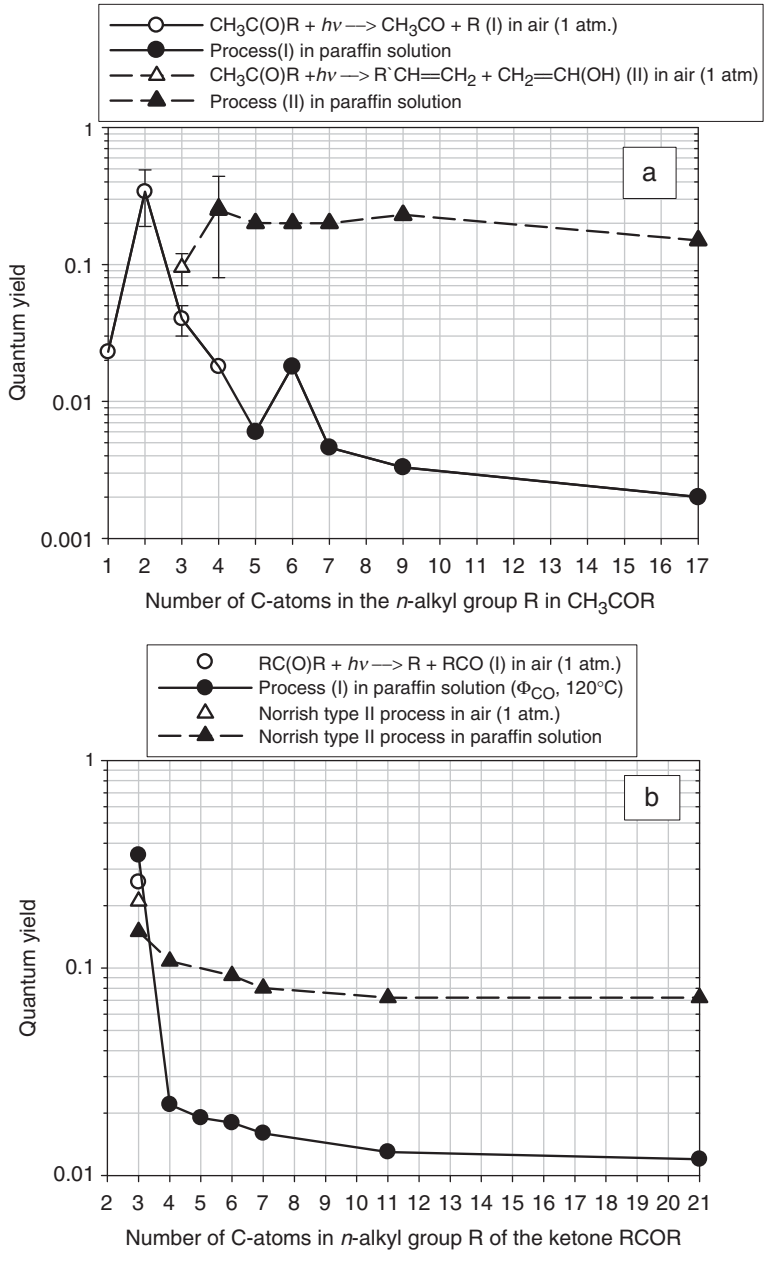

Figure IX-D-19. (a) Semilog plot of the quantum yields of primary processes in photolysis at 313 nm for ketones of structure $CH_3C(O)R$ where R is a straight-chain alkyl group with the number of C-atoms varied from 1 to 17. Data are shown for photolyses in the gas phase and in paraffin solution (Golemba and Guillet, 1972). (b) Semilog plot of the quantum yields of primary processes in photolysis at 313 nm for ketones of the structure RC(O)R where R is a straight-chain alkyl group with the number of C-atoms varied from 3 to 21. Data are shown for both photolyses in the gas phase and in paraffin solution (Hartley and Guillet, 1968b). The Norrish type-II process can be represented in this case as: $RC(O)R + h\nu \rightarrow R'CH{=}CH_2 + CH_2{=}CH(OH)R''$ (II); figure from Calvert et al. (2008).

the aldehydes, this process (II) forms highly reactive enols of ketones and alkenes that can enhance ozone generation in the lower troposphere (e.g., see Calvert et al., 2000).

One should gather from our discussion that the Norrish type-II photodecomposition in ketones is important in both the gas- and liquid-phase systems, but it can also occur in solid ethene–CO copolymers with $\phi_{II} = 0.025$ independent of temperature ($-25°$ to 90°C). However, when temperatures between $-50°$ and $-150°$C are reached at which free rotation about the C—C bonds is restricted, ϕ_{II} drops from 0.015 to 0.000 (Hartley and Guillet, 1968a).

IX-E. Photodecomposition of Cyclic Ketones

Cyclic alkanes present in the troposphere are oxidized in part to cyclic ketones. The cyclic ketones are also emitted into the urban atmosphere from a variety of anthropogenic sources; see table I-C-4. The mechanisms of photodecomposition of these ketones are reviewed briefly in this section.

IX-E-1. Photodecomposition of Cyclopropanone (*cyclo*-C_3H_4O)

Cyclopropanone is the simplest of the cyclic ketones. Studies of the mechanism of its gas-phase photochemistry suggest the following photodecomposition pathways (Calvert et al., 2008):

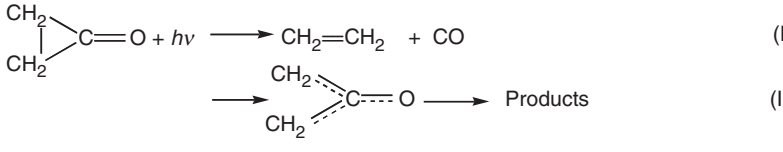

The only gaseous products identified are ethene and carbon monoxide, formed in equal amounts (Thomas and Rodriguez, 1971; Rodriguez et al., 1976). Several theoretical studies of the mechanism of process (I) have been reported (Martino et al., 1977; Yamabe et al., 1979; Sevin et al., 1981). Oxyallyl, shown as the primary product in (II), has been suggested as a possible intermediate to polymer formation that appears on the walls of reaction vessels in laboratory studies of cyclopropanone photolysis. This molecule is expected to have a small energy barrier to its recyclization (Olsen et al., 1971; Liberles et al., 1973). If it is formed in (II), its possible fate in the atmosphere is open to conjecture.

IX-E-1.1. Absorption Cross Sections for Cyclopropanone

The absorption spectrum of cyclopropanone was reported by Thomas and Rodriguez (1971) who estimated that the 0–0 transition in this molecule lies near 395 nm. The spectrum given in figure IX-E-1 is approximate, since it has been redrawn from the original publication. Compare this spectrum with that of acetone, the other simple 3-carbon ketone. One can see that the absorption profile of cyclopropanone is shifted to much longer wavelengths than that of acetone. Tabular listing of the approximate cross sections for cyclopropanone is given in table IX-E-1.

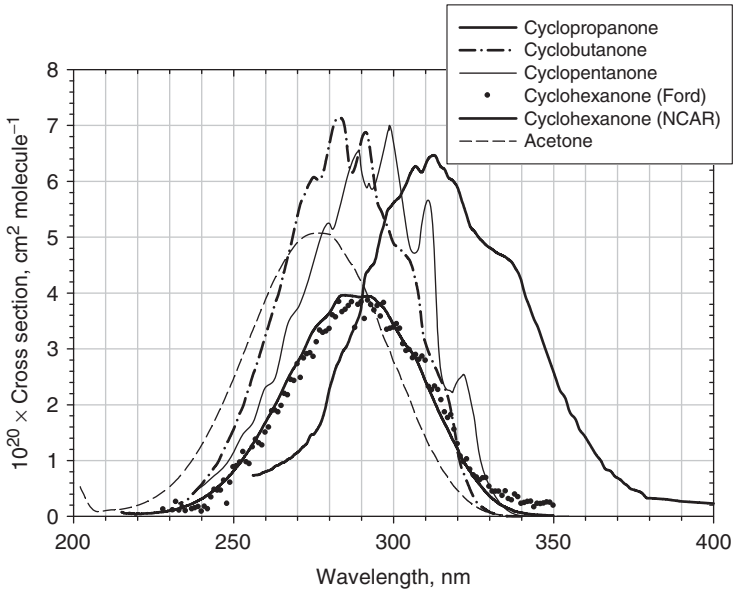

Figure IX-E-1. Approximate absorption cross sections versus wavelength for cyclopropanone vapor (adopted from Thomas and Rodriguez, 1971); cyclobutanone measured in cyclohexane solution (adopted from Carless and Lee, 1972); cyclopentanone in cyclohexane solution (adopted from Nakashima et al., 1982); cyclohexanone vapor was measured independently in two laboratories: National Center for Atmospheric Research (NCAR) and Ford Motor Company (Ford), (Iwasaki et al., 2008a); acetone vapor (Martinez et al., 1992).

IX-E-1.2. Quantum Yields of Photodecomposition of Cyclopropanone

The quantum yields of the products of cyclopropanone are shown as a function of wavelength in figure IX-E-2 as reported in the studies of Thomas and Rodriguez (1971) and Rodriguez et al. (1976). The major products are ethene (circles in figure IX-E-2) and carbon monoxide. The total quantum yield of photodestruction of cyclopropanone is near unity at all wavelengths (shown as squares in the figure), so a significant fraction of the products remain unidentified: ~0.41 (365 nm); ~0.36 (334 nm); ~0.29 (313 nm). These unknown products may be formed from oxyallyl reactions, or some other intermediate species formed in (II). The tabular listing of the quantum yields of process (I) is given in table IX-E-1.

IX-E-1.3. Photolysis Frequencies for Photodecomposition of Cyclopropanone in the Lower Troposphere

The cross sections and quantum yields given in table IX-E-1, coupled with the appropriate solar flux data for a cloudless day within the lower troposphere (ozone column = 350 DU), were used to derive the approximate *j*-values for cyclopropanone

Table IX-E-1. Approximate absorption cross sections (cm^2 $molecule^{-1}$) at 293 K and quantum yields as a function of wavelength for the primary process: cyclopropanone $+h\nu \rightarrow C_2H_4 + CO(I)$

λ, nm	$10^{20} \times \sigma$	ϕ_I	λ, nm	$10^{20} \times \sigma$	ϕ_I	λ, nm	$10^{20} \times \sigma$	ϕ_I
278	1.80	1.00	320	5.88	0.68	361	1.32	0.61
279	2.02	1.00	321	5.71	0.67	362	1.22	0.61
280	2.29	1.00	322	5.54	0.67	363	1.13	0.60
281	2.48	1.00	323	5.36	0.67	364	1.05	0.60
282	2.67	1.00	324	5.18	0.66	365	0.97	0.60
283	2.79	1.00	325	5.12	0.66	366	0.86	0.59
284	2.94	1.00	326	5.04	0.66	367	0.83	0.58
285	3.02	1.00	327	4.97	0.65	368	0.80	0.57
286	3.13	1.00	328	4.91	0.65	369	0.73	0.57
287	3.29	1.00	329	4.85	0.65	370	0.69	0.56
289	3.55	1.00	330	4.81	0.65	371	0.65	0.55
290	3.82	1.00	331	4.78	0.65	372	0.59	0.54
291	4.28	0.99	332	4.73	0.64	373	0.55	0.53
292	4.39	0.98	333	4.70	0.64	374	0.50	0.52
293	4.48	0.96	334	4.67	0.64	375	0.48	0.51
294	4.55	0.94	335	4.64	0.64	376	0.46	0.49
295	4.78	0.92	336	4.60	0.64	377	0.44	0.47
296	5.04	0.90	337	4.55	0.64	378	0.40	0.46
297	5.23	0.89	338	4.45	0.64	379	0.33	0.44
298	5.46	0.87	339	4.35	0.64	380	0.32	0.42
299	5.54	0.86	340	4.20	0.64	381	0.32	0.36
300	5.62	0.85	341	3.97	0.63	382	0.32	0.32
301	5.67	0.83	342	3.82	0.63	383	0.31	0.13
302	5.73	0.82	343	3.67	0.63	384	0.31	0
303	5.84	0.81	344	3.51	0.63	385	0.31	0
304	5.96	0.79	345	3.40	0.63	386	0.30	0
305	6.11	0.78	346	3.24	0.63	387	0.29	0
306	6.22	0.78	347	3.07	0.63	388	0.28	0
307	6.26	0.76	348	2.90	0.63	389	0.28	0
308	6.20	0.76	349	2.74	0.63	390	0.27	0
309	6.17	0.75	350	2.58	0.63	391	0.26	0
310	6.30	0.74	351	2.42	0.63	392	0.26	0
311	6.42	0.73	352	2.25	0.63	393	0.26	0
312	6.46	0.72	353	2.18	0.63	394	0.25	0
313	6.46	0.72	354	2.06	0.63	395	0.25	0
314	6.34	0.71	355	1.87	0.62	396	0.24	0
315	6.25	0.71	356	1.80	0.62	397	0.24	0
316	6.21	0.70	357	1.72	0.62	398	0.24	0
317	6.07	0.69	358	1.57	0.62	399	0.23	0
318	6.04	0.69	359	1.49	0.61	400	0.23	0
319	5.98	0.68	360	1.41	0.61			

photodecomposition into C_2H_4 and CO, process (I). These are shown as the solid curve in figure IX-E-3. The dashed curve in this figure gives the *j*-values for the total of the photodecomposition processes. These data suggest that the lifetime for photodecomposition in the lower troposphere is about 45 min. with an overhead Sun. For 40°N latitude, clear tropospheric skies, and diurnal variation of the Sun, the expected average photochemical lifetimes of cyclopropanone are about 2.1 and 8.2 h for the time periods near June 22 and December 22, respectively.

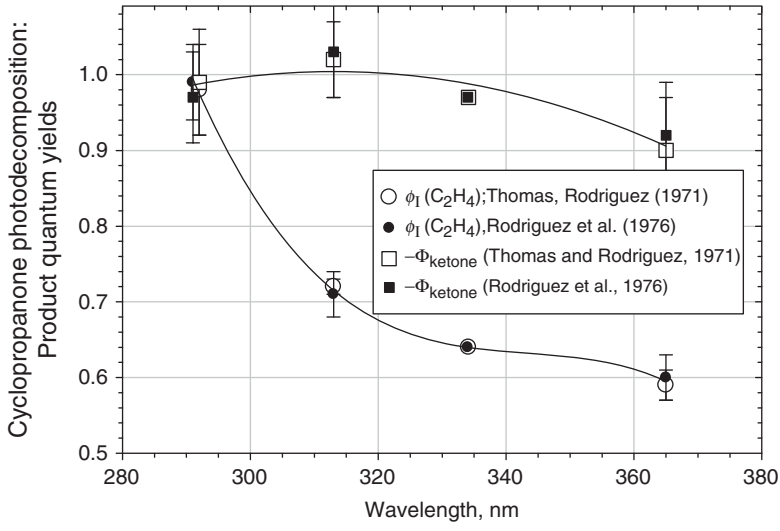

Figure IX-E-2. Quantum yields of photodecomposition of cyclopropanone by process (I); cyclopropanone + $h\nu \rightarrow C_2H_4 + CO$, and those for decomposition by all pathways. Data are from Thomas and Rodriguez (1971) and Rodriguez et al. (1976); figure from Calvert et al. (2008).

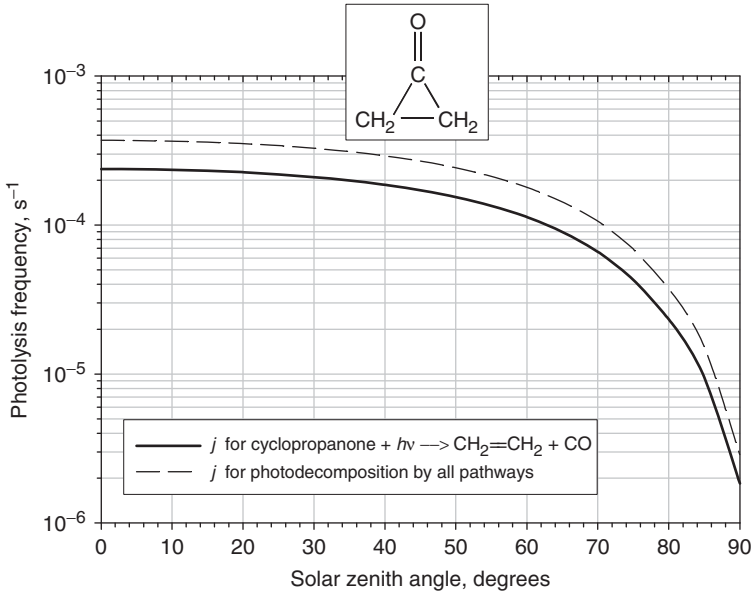

Figure IX-E-3. Approximate j-values as a function of solar zenith angle for the photodecomposition of cyclopropanone on a cloudless day within the troposphere with an overhead ozone column of 350 DU. Quantum yields versus wavelength data are from Thomas and Rodriguez (1971) and Rodriguez et al. (1976) as shown in figure IX-E-2; figure from Calvert et al. (2008).

IX-E-2. Photodecomposition of Cyclobutanone (*cyclo*-C_4H_6O)

In the gas phase, photodecomposition of cyclobutanone occurs largely through two different product-forming channels:

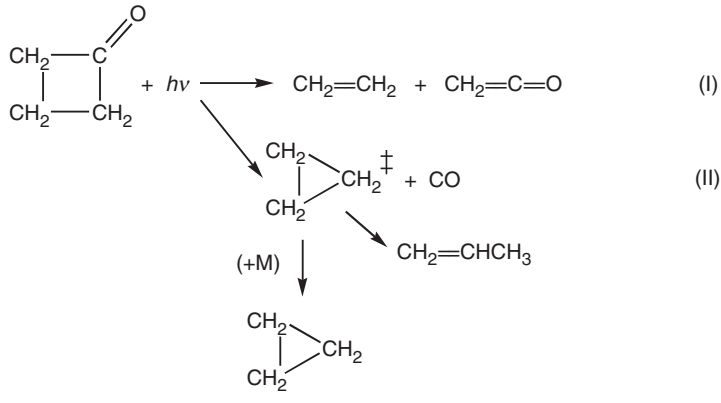

Studies reported in 1942 gave evidence of these two primary processes (Benson and Kistiakowsky, 1942). Later studies showed clearly that propene is not a primary product but is formed from the initial products of (II), a vibrationally excited cyclopropane molecule (Klemm et al., 1965; Campbell et al., 1967; Campbell and Schlag, 1967). The involvement of both singlet and triplet states has been demonstrated using triplet benzene to photosensitize cyclobutanone's decomposition (Lee, 1967; Ishakawa and Noyes, 1962a, b; Noyes and Unger, 1966; Denschlag and Lee, 1968). Theoretical studies have elucidated the nature of the precursor excited states involved in the photodecomposition (e.g., see Baba and Hanazaki, 1984; Hopkinson et al., 1988; Diau et al., 2001; Chen and Ye, 2004). Evidence suggests that photodissociation of cyclobutanone by pathway (I) occurs from a vibrationally excited ground state ($S_o^{\ddagger}$) that is formed by internal conversion from the initially excited S_1 state. Like most ketones, for excitation of cyclobutanone at the longer wavelengths ($\lambda > 320$ nm), the T_1 state is populated by intersystem crossing ($S_1 \rightarrow T_1$), and this state is believed to be the source of the process (I) forming ethene and ketene.

IX-E-2.1. Absorption Cross Sections for Cyclobutanone

Figure IX-E-1 shows the approximate cross sections for cyclobutanone (in cyclohexane solution) versus wavelength as redrawn from the publication of Carless and Lee (1972). The general structure and magnitude seen in this absorption band is in qualitative agreement with that reported by Benson and Kistiakowsky (1942). Note in the figure that there is much less shift of the absorption band from that of acetone than is observed for cyclopropanone. The tabular listing of the cross sections is given in table IX-E-2.

Table IX-E-2. Approximate cross sections (σ, cm^2 $molecule^{-1}$) at ~298 K and quantum yields for the primary processes: cyclobutanone $+h\nu \rightarrow CH_2{=}CH_2 + CH_2{=}C{=}O$ (I); cyclobutanone $+h\nu \rightarrow cyclo\text{-}C_3H_6^{\ddagger} + CO$ (II); table is from Calvert et al. (2008)

λ, nm	$10^{20} \times \sigma$	ϕ_I	ϕ_{II}	λ, nm	$10^{20} \times \sigma$	ϕ_I	ϕ_{II}
278	6.15	0.61	0.37	310	3.09	0.69	0.27
279	6.42	0.61	0.37	311	2.93	0.69	0.27
280	6.69	0.62	0.37	312	2.80	0.70	0.26
281	6.95	0.62	0.36	313	2.67	0.70	0.26
282	7.11	0.62	0.36	314	2.54	0.70	0.26
283	7.14	0.63	0.35	315	2.41	0.70	0.26
284	7.11	0.63	0.35	316	2.29	0.70	0.25
285	6.88	0.63	0.35	317	2.14	0.70	0.25
286	6.34	0.63	0.34	318	1.87	0.71	0.25
287	6.15	0.64	0.34	319	1.57	0.71	0.25
288	6.26	0.64	0.33	320	1.18	0.71	0.25
289	6.49	0.64	0.33	321	0.92	0.71	0.25
290	6.76	0.64	0.33	322	0.76	0.71	0.25
291	6.88	0.65	0.32	323	0.62	0.71	0.24
292	6.80	0.65	0.32	324	0.48	0.72	0.24
293	6.42	0.65	0.32	325	0.35	0.72	0.24
294	6.00	0.65	0.31	326	0.25	0.72	0.24
295	5.62	0.66	0.31	327	0.19	0.72	0.24
296	5.49	0.66	0.31	328	0.15	0.72	0.24
297	5.34	0.66	0.30	329	0.11	0.72	0.24
298	5.20	0.66	0.30	330	0.08	0.73	0.24
299	5.04	0.67	0.30	331	0.06	0.73	0.24
300	4.89	0.67	0.29	332	0.04	0.73	0.24
301	4.84	0.67	0.29	333	0.02	0.73	0.23
302	4.78	0.67	0.29	334	0.01	0.73	0.23
303	4.73	0.68	0.28	335	0.01	0.73	0.23
304	4.66	0.68	0.28	336	0.003	0.74	0.23
305	4.58	0.68	0.28	337	0.002	0.74	0.23
306	4.43	0.68	0.28	338	0.002	0.74	0.23
307	4.20	0.68	0.27	339	0.001	0.74	0.23
308	3.90	0.69	0.27	340	0	0.74	0.23
309	3.36	0.69	0.27				

IX-E-2.2. Quantum Yields of the Primary Photodecomposition Processes in Cyclobutanone

Figure IX-E-4 shows as a function of wavelength at two pressures the ratios of propene to cyclopropane products that are formed in alternative pathways for reaction of the vibrationally excited cyclopropane molecule. A large increase in this ratio is seen as the excitation energy is increased in photolysis at the shorter wavelengths. A cyclopropane molecule that is vibrationally richer results as the quantum energy is increased. A somewhat more efficient quenching of the vibrationally excited cyclopropane can be seen for the data from 11 Torr of cyclobutanone (dashed curve) compared to those for 5 Torr (solid curve). One expects that an atmosphere of air will result in more significant

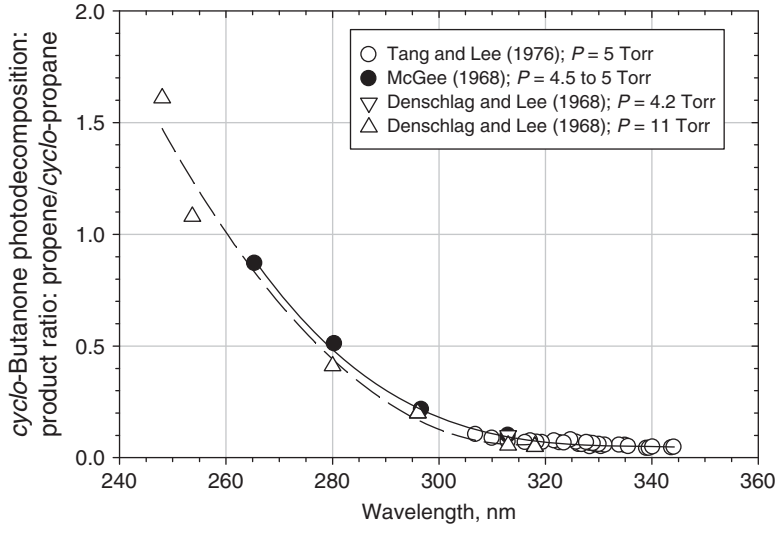

Figure IX-E-4. The ratio of propene/cyclopropane as a function of wavelength in the photolysis of cyclobutanone at two pressures. Propene and cyclopropane both can arise from process (II): cyclopropanone + $h\nu$ → excited cyclopropane + CO (II). Collisional stabilization of the excited cyclopropane becomes less effective (and decomposition more effective) in photolysis at the shorter wavelengths; figure from Calvert et al. (2008).

stabilization of the cyclopropane molecule. For example, with cyclobutanone photolysis (4.5 Torr) at 265.4 nm, the addition of 33.5 Torr of hexane decreased the ratio of propene to cyclopropane from 1.04 to 0.56 (McGee, 1968).

In figure IX-E-5, the ratio of the quantum yields of the two primary processes, ϕ_{II}/ϕ_I, is shown as a function of wavelength. Note the striking change in the slope of the lines that define the ratio as a function of wavelength as 315 nm is approached. The obvious change in mechanism that occurs in this wavelength region has been rationalized theoretically by Diau et al. (2001) and Chen and Ye (2004) through the involvement of an S_o/S_1 conical intersection near 315 nm.

The quantum yields of the two primary processes as estimated by McGee (1968) are given as a function of wavelength in figure IX-E-6. The data give smooth curves over the wavelength range studied (313–265 nm). Process (II) is seen to increase gradually (triangles, heavy solid line) as one progresses to shorter wavelengths while process (I) decreases somewhat (circles, dashed line).The sum of $\phi_I + \phi_{II}$ is unity within the error of the determinations (filled circles, light line) over the wavelength range shown. The values are relatively unaffected by temperature (40–250°C) and pressure. The tabular listing of the quantum yields for processes (I) and (II) is given in table IX-E-2.

IX-E-2.3. Photolysis Frequency for Photodecomposition of Cyclobutanone in the Lower Troposphere

Values of ϕ_I and ϕ_{II} have not been reported for wavelengths greater than 315 nm, so an extrapolation of the trend curve of the data shown in figure IX-E-6 has been

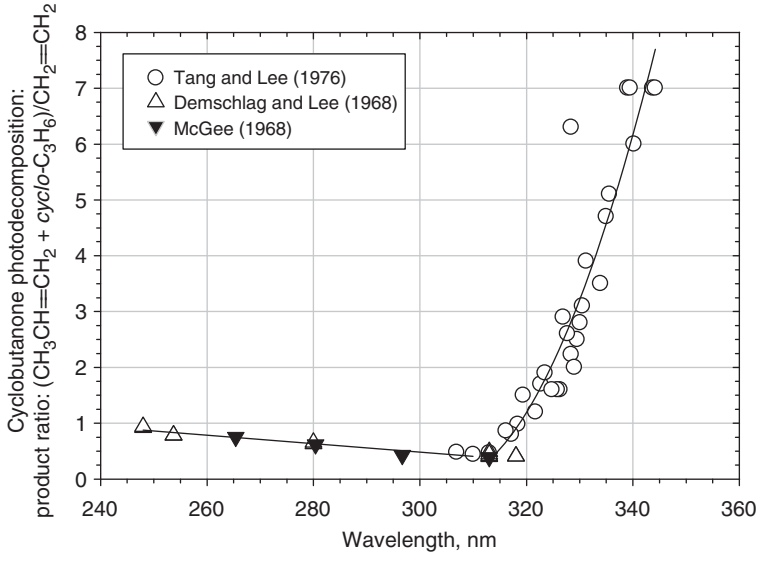

Figure IX-E-5. Plot of the ratio of products, (propene + cyclopropane)/ethene (ϕ_{II}/ϕ_{I}) as a function of wavelength in the photolysis of cyclobutanone. Cyclobutanone + $h\nu \rightarrow CH_2{=}CH_2$ + $CH_2{=}C{=}O$ (I); cyclopropanone + $h\nu \rightarrow$ excited cyclopropane + CO (II); figure from Calvert et al. (2008).

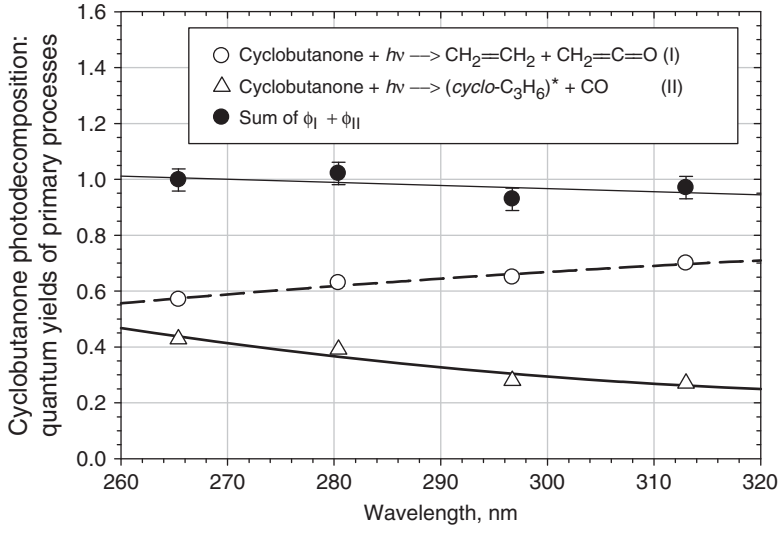

Figure IX-E-6. Plot of the quantum yields of the primary processes in cyclobutanone photolysis as a function of wavelength; data from McGee (1968); figure from Calvert et al. (2008).

used to arrive at estimates for the 315–340 nm region. This procedure will probably overestimate the *j*-values since the triplet state may be formed in this wavelength region, and it may be quenched to some extent by air molecules. We have used the limited cross section and quantum yield data summarized in table IX-E-2, coupled with the appropriate solar flux for a cloudless day within the lower troposphere (ozone column of 350 DU) to estimate approximate *j*-values for cyclobutanone. The results of these calculations are summarized in figure IX-E-7.

IX-E-3. Photodecomposition of Alkyl-Substituted Cyclobutanones

There are several studies of the photodecomposition of alkyl-substituted cyclobutanones for which there is insufficient data to estimate *j*-values, but the results may be helpful in understanding the effects of structure on the photodecomposition modes of the cyclic ketones.

IX-E-3.1. Photodecomposition of cis- and trans-2,3-Dimethylcyclobutanone

The mechanism of photodecomposition of 2,3-dimethylcyclobutanone is thought to involve several channels of reaction (Calvert et al., 2008):

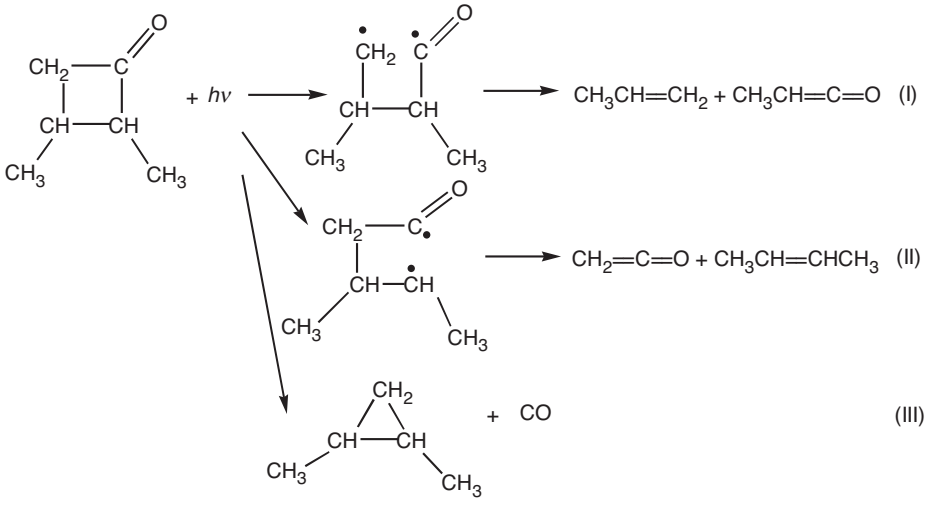

The biradicals shown may be involved as precursors to the formation of alkenes and ketenes in the photodecomposition processes (I) and (II). Those formed from singlet and triplet excited states are expected to form singlet and triplet biradicals, respectively. The biradical precursor to process (II) appears to be favored over that suggested for process (I), as one might expect from the difference in bond dissociation energies involved. The extent of stereospecificity of the products formed was rationalized by Carless et al. (1972) in terms of the relative dissociative lifetimes of the biradicals of different spin states involved compared to rotation about a C—C bond.

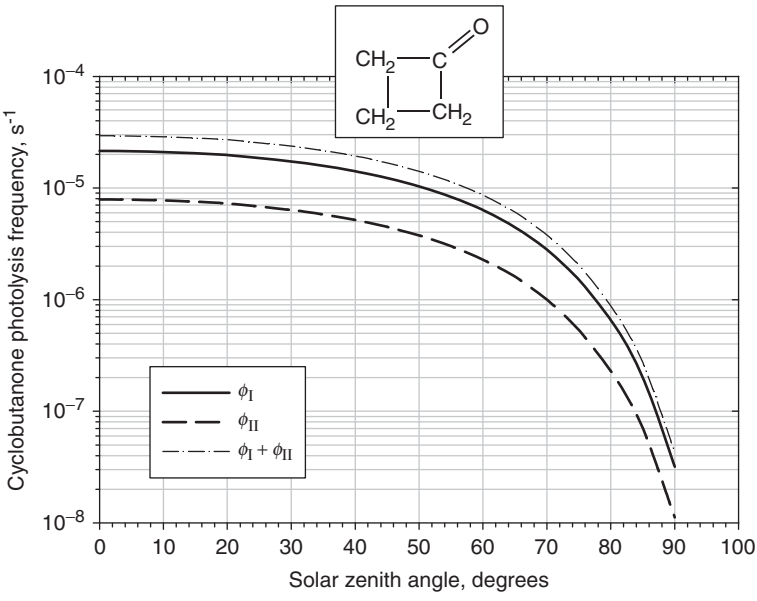

Figure IX-E-7. Approximate *j*-values for cyclobutanone photodecomposition versus solar zenith angle for a cloudless day in the lower troposphere with an overhead ozone column of 350 DU. Process (I): cyclobutanone + $h\nu \rightarrow CH_2{=}CH_2 + CH_2{=}C{=}O$; process (II): cyclobutanone + $h\nu \rightarrow$ vibrationally excited cyclopropane + CO; figure from Calvert et al. (2008).

Carless and Lee (1970) and Carless et al. (1972) studied the effects of added ethene on the relative rates of the primary processes in photolysis of *cis*-2,3-dimethylbutanone (1 Torr) at 325 nm. Results are shown in figure IX-E-8. It can be seen that process (III) is relatively independent of the added gas, consistent with its formation from a very-short-lived excited singlet state. However, both primary processes (I) and (II) show extensive quenching with added gas, although neither process is quenched completely at the highest pressures used. The efficiency of quenching is greater for process (I) than (II). The observations show that these processes originate from different vibronic levels of the excited triplet and singlet states of the ketone. A similar effect is seen for the addition of argon in photolysis of *cis*-2,3-dimethylbutanone at wavelength 281 nm; see figure IX-E-9. The order of importance of the primary processes for photolysis at low pressures changes from that observed at 325 nm, $\phi_I > \phi_{II} > \phi_{III}$, to $\phi_{II} > \phi_I > \phi_{III}$ at 281 nm. At high pressures, however, the relative importance of the unquenchable process (III) increases at each wavelength.

In photolysis at 335 and 313 nm, Carless and Lee (1972) could not detect any of the possible C_5-alkene products that might result from the suggested intermediate biradicals with loss of CO. At 281 nm these species amounted to about 3% of the C_5-compounds formed (including dimethylcyclopropane). They also reported that the addition of oxygen (25–210 Torr) in the photolysis at 325 nm quenched the products not as a radical scavenger but as a vibrational deactivator, similar to C_2H_4.

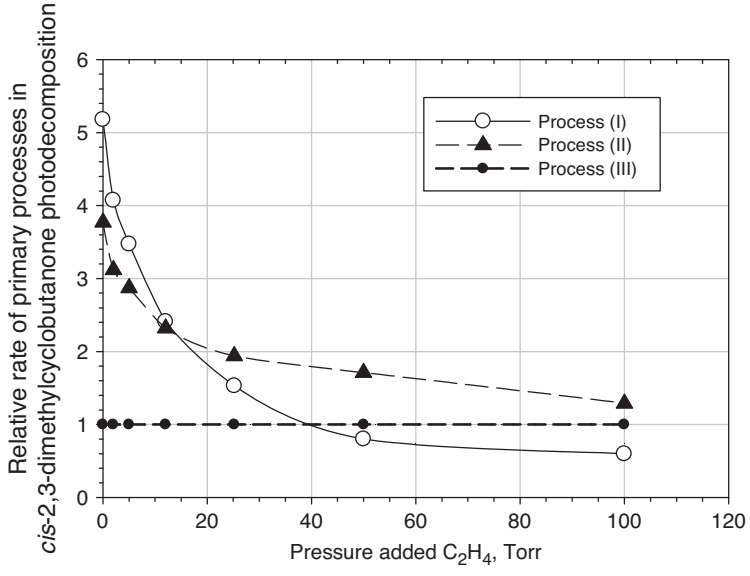

Figure IX-E-8. The effect of added ethene on the relative rates of the primary processes in the 325 nm photolysis of 1 Torr of *cis*-2,3-dimethylcyclobutanone (CB); process (I): CB + $h\nu$ → $CH_2{=}CHCH_3$ + $CH_3CH{=}C{=}O$; process (II): CB + $h\nu$ → $CH_3CH{=}CHCH_3$ + $CH_2{=}C{=}O$; process (III): CB + $h\nu$ → dimethylcyclopropane + CO; data are from Carless and Lee (1972); figure from Calvert et al. (2008).

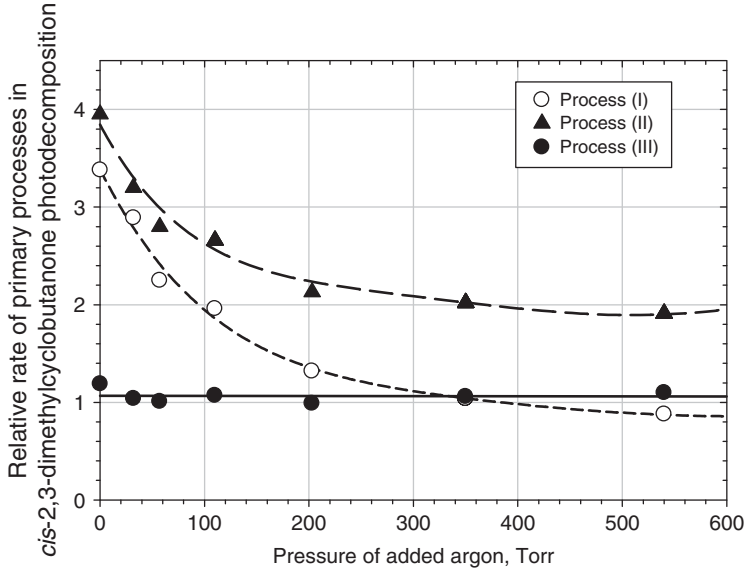

Figure IX-E-9. The effect of added argon on the relative rates of primary processes in the photolysis of 1.0 Torr of *cis*-2,3-dimethylbutanone (CB) at 281 nm; process (I): CB + $h\nu$ → $CH_2{=}CHCH_3$ + $CH_3CH{=}C{=}O$; process (II): CB + $h\nu$ → $CH_3CH{=}CHCH_3$ + $CH_2{=}C{=}O$; process (III): CB + $h\nu$ → dimethylcyclopropane + CO; data of Carless and Lee (1972); figure from Calvert et al. (2008).

IX-E-3.2. Photodecomposition of 2,4-Dimethylcyclobutanone

The photodecomposition of *cis*- and *trans*-2,4-dimethylcyclobutanone can be described by the following overall reaction mechanism (Calvert et al., 2008):

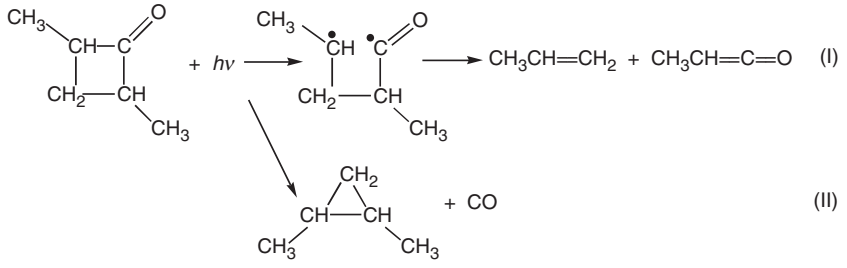

The biradical intermediate shown in process (I) may be formed in either a triplet or singlet state, reflecting the spin state of the triplet or singlet excited ketone molecule that decomposes. In this case, the rupture of either of the C—C bonds next to the carbonyl group leads to the same products. The behaviors of the product yields on variations in wavelength and with added gases were found to be very similar to those observed for the 2,3-dimethylcyclobutanone. Added inert quenching gases reduced the propene yield, process (I). At 325 nm the ratio ϕ_I/ϕ_{II} decreases from 8.2 at 0.1 Torr of the ketone to 2.0 with 30 Torr of added C_2H_4. The possible C_5-alkene products that might arise from the biradical intermediate formed with loss of CO, were not detected in photolysis at 325 and 313 nm, and they were only ~3% of the total C_5 products (including dimethylcyclopropane) at 281 nm.

IX-E-3.3. Photodecomposition of 2-n-Propylcyclobutanone

Carless and Lee (1972) have studied the photodecomposition of 2-*n*-propylcyclobutanone at 325 nm. The absorption cross sections of this ketone are significantly larger than those of cyclobutanone ($\sigma_{max} \approx 1.07 \times 10^{-19}$ cm^2 molecule^{-1}), and the maximum in the absorption band is shifted to the longer wavelengths (~295 nm). Calvert et al. (2008) conclude that the following overall primary processes are consistent with the results of Carless and Lee (1972):

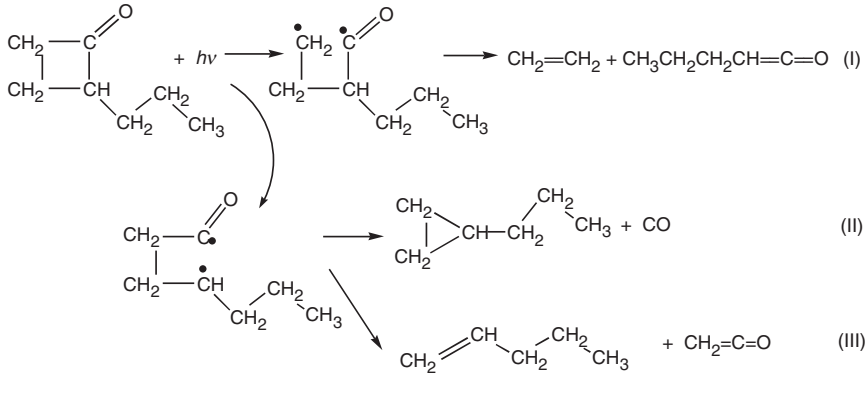

The various photodecomposition modes are visualized as progressing through the biradical intermediates shown. Carless and Lee (1972) suggest that both the excited ground state and the S_1 state are involved in these processes. The relative yields of the various primary processes at 325 nm are shown as a function of ketone pressure in figure IX-E-10. The extent of quenching of channels (I) and (III) is much greater than that seen for channel (II). As with cyclobutanone and the other alkyl-substituted cyclobutanones, the process forming the cyclopropane derivative is relatively unaffected by pressure of added gases.

The addition of 100 Torr of O_2 in the photolysis of the ketone (0.1 Torr) leads to the suppression of the yield of products of processes (I), (II), and (III) by 96.8, ~0.0, and 23.0 %, respectively. Obviously, different vibronic levels and/or excited states are involved in these processes.

It is interesting that although this ketone has two γ-hydrogen atoms in the $CH_3CH_2CH_2$ group attached to the cyclobutanone ring that is adjacent to the carbonyl, there is no evidence that a Norrish type-II reaction occurs here. Propene was not reported as a product. This probably reflects the unusual geometry of this ketone. A simple model of the ground state ketone (CS CHEM3D) suggest that the δ-H-atoms on the methyl group are closer to the carbonyl–oxygen atom ($\sim$ 2.75Å) than the two γ-hydrogen atoms that are necessarily involved in the Norrish type-II reaction (3.13Å). The reaction seems unlikely as well in view of the ring strain introduced by

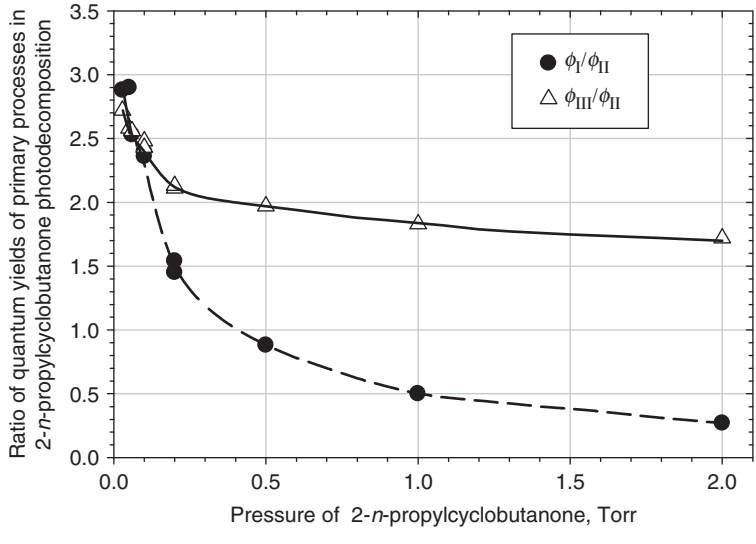

Figure IX-E-10. Plot of the ratio of quantum yields for primary processes in 2-*n*-propylcyclobutanone (PcB) versus pressure of the ketone; wavelength, 325 nm; temperature, 23°C; process (I): PcB + $h\nu \rightarrow CH_2{=}CH_2 + CH_3CH_2CH_2CH{=}C{=}O$; process (II): PcB + $h\nu \rightarrow$ *n*-propylcyclopropane + CO; process (III): PcB + $h\nu \rightarrow CH_2{=}CHCH_2CH_2CH_3 + CH_2{=}C{=}O$; data of Carless and Lee (1972); figure from Calvert et al. (2008).

the formation of the expected initial product, the enol-form of cyclobutanone:

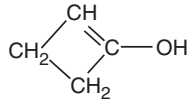

IX-E-4. Photodecomposition of Cyclopentanone (*cyclo*-C_5H_8O)

Shortridge et al. (1971) studied the fluorescence of the cyclic ketones: cyclobutanone, cyclopentanone, cyclohexanone with excitation at 313 nm. All of these ketones have quantum yields of fluorescence ≈0.002, similar to that for acetone. These authors point out that this similarity suggests that the $S_1 \rightarrow T_1$ intersystem crossing rates for these ketones is similar for excitation at the longer wavelengths and that much of the photochemical activity may proceed through the T_1 manifold. The highly resolved fluorescence spectrum of cyclopentanone has been analyzed by Baba and Hanazake (1984). Müller-Remmers et al. (1984) studied theoretically the stability and reactions of possible biradical intermediates formed from the excited triplet state of cyclopentanone.

The approximate absorption cross sections for cyclopentanone (in cyclohexane solution) are compared with those of the other simple cyclic ketones in figure IX-E-1. The structure and magnitude seen in this absorption is qualitatively similar to that reported for this compound by Benson and Kistiakowsky (1942).

The major products of photodecomposition of cyclopentanone are CO, cyclobutane, ethene, and 4-pentenal. Alternative mechanisms have been considered to rationalize these products. Calvert et al. (2008) considered the following reaction mechanisms in rationization of the available information:

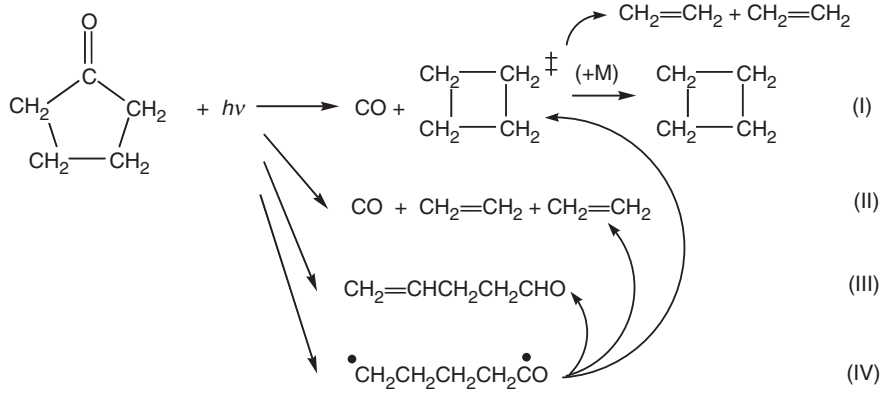

Srinivasan (1964) has reviewed the early studies of cyclopentanone photolysis. From the data available at that time, he favored the direct formation of these products

by concerted processes (I), (II), and (III). His conclusion was based largely on the rather small effects seen on the rates of product formation in the 313 nm photolysis of cyclopentanone on addition of 35 Torr of oxygen to 10.9 Torr of the ketone (Srinivasan,1961): The product rates changed by factors of 1.05 (C_2H_4), 0.88 (cyclobutane), and 0.26 (pentenal). With 275 Torr of oxygen added, rates relative to those with no gas added changed by factors of 0.34 (C_2H_4), 0.29 (cyclobutane), and 0.87 (pentenal). The change of product rates with methane addition was similar to that of oxygen at high pressures; addition of 195 Torr of CH_4 to 11.6 Torr of ketone changed the rates of formation of products of 313 nm photolysis by factors of: 0.36 (ethene), 0.36 (cyclobutane), and 2.33 (pentenal). Srinivasan concluded that the small effect of oxygen was inconsistent with product formation that must pass through the intermediate biradical formed in (Ia). He favored the direct formation of products from the excited singlet state in concerted mechanisms summarized by processes (I), (II), and (III). However, it is not established that biradicals, particularly singlet biradicals, react with oxygen as rapidly as measured for alkyl and acyl radicals; so the step shown as (IV) above may indeed play a part in product generation in cyclopentanone photodecomposition, as many investigators conclude.

Blades (1970) photolyzed cyclopentanone-2,2,5,5-d_4 at several wavelengths. Photolysis at 254 nm (80°C, 11.2 Torr) gave primarily $C_2H_2D_2$, with some C_2H_3D and C_2H_4. At 0.65 and 1.3 Torr pressure, substantial yields of C_2D_4 and C_2H_4 in addition to $C_2H_2D_2$ were observed, suggesting approximately 14 and 10%, respectively, of initially formed cyclobutane decomposition. These results confirm the initial formation of a vibrationally rich cyclobutane molecule that can decompose at low pressures or be quenched at the higher pressures:

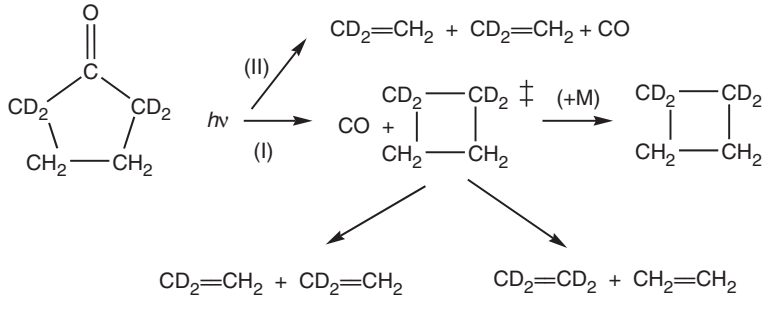

If ethene were derived entirely from primary process (II), then CH_2CD_2 would be the only ethene formed. If, however, all the ethene formed in process (I), then at low pressures, where the vibrationally hot cyclobutane is incompletely quenched, the ethene would have a more random distribution of the deuterium atoms: CD_2CD_2, CH_2CH_2, and CD_2CH_2. The observation of C_2D_4 and C_2H_4 in the photolysis of cyclopentanone-2,2,5,5-d_4 at 254 nm at low pressures, but not at 11.5 Torr pressure, confirms the partial decomposition of excited cyclobutane at low pressures and high photon energy (Blades, 1970).

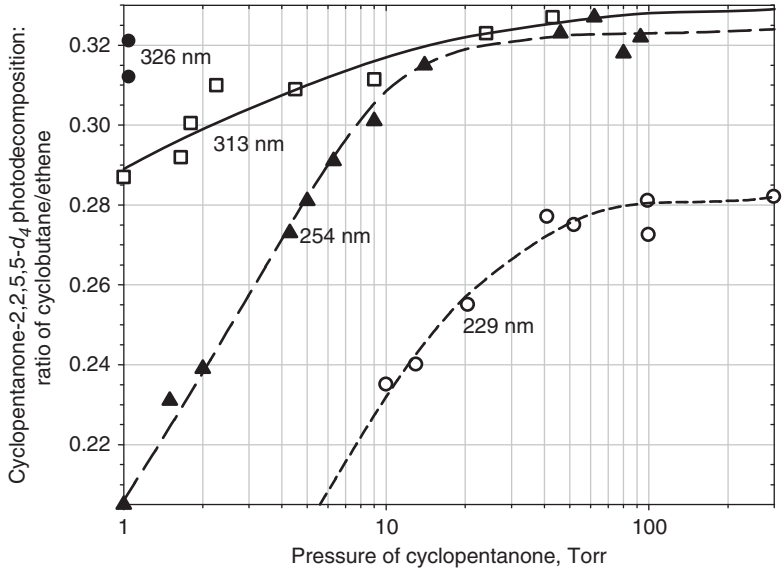

Figure IX-E-11. Ratio of products cyclobutane/ethene versus ketone pressure for photolysis of cyclopentanone-2,2,5,5-d_4 at several wavelengths (from Blades, 1970); figure from Calvert et al. (2008).

The variation of the cyclobutane/ethene ratio with pressure for photolysis of cyclopentanone at several wavelengths is shown in figure IX-E-11 (Blades, 1970). Note several interesting features:

i) Increasing the pressure of the reactant in photolysis at any of the wavelengths, increases the ratio of cyclobutane to ethene.
ii) At a given pressure of ketone, most noticeably at pressures < 10 Torr, product data at 313, 254, and 229 nm show a progressive trend to greater percentages of cyclobutane decomposing as the photon energy increases.
iii) The extent of quenching is least efficient for the ketone excitation with highest energy quantum (229 nm).
iv) The cyclobutane/ethene ratio appears to approach a similar limiting value at high pressures for experiments at 326, 313, and 254 nm.

The wavelength dependence of the ratio observed by Blades confirms and extends the earlier findings of Klemm et al. (1965), and the trends are consistent with the mechanism described above for ethene formation in part from excited cyclobutane. At 326 nm and 1 Torr, the cyclobutane/ethene ratio is at the high pressure value found at the shorter wavelengths, suggesting no tendency for cyclobutane decomposition. Blades points out that this is in keeping with the exothermicity of the overall photolysis reaction at this wavelength being near equal to the activation energy of the cyclobutane decomposition.

The wavelength dependence of the ratio of 4-pentenal/CO is also interesting. Blades reported that the product ratio, 4-pentenal/CO = 10 at 326 nm; 1.4 at 313 nm; 1.0 at 307 nm; and 0.02 at 254 nm. The trend fits the expected pattern involving the intermediate biradical ($\bullet CH_2CH_2CH_2CH_2CO\bullet$) where absorption of the higher energy quantum favors decomposition to CO and $\bullet CH_2CH_2CH_2CH_2\bullet$ over intramolecular H-atom abstraction to form 4-pentenal. Tsunashima et al. (1973) found that the 326.1 nm direct photolysis and the Cd5($^3P_1$)-sensitized photolysis of cyclopentanone gave similar results, and this favored the triplet state involvement, at least to some extent, in both the direct and the sensitized photolyses.

Vacuum UV photolysis of cyclopentanone at 147 nm shows a dominance of the reaction channels forming CO, ethene, and cyclobutane, with $\phi_I + \phi_{II} = 0.87$. The primary step was suggested to involve CO and $\bullet CH_2CH_2CH_2CH_2\bullet$ biradical formation directly (Scala and Ballan, 1972). Becerra and Frey (1988) studied the product distribution in photolysis of cyclopentanone at 208 and 193 nm and concluded that most of the available energy appears as vibrational excitation in the cyclobutane molecule and that CO is not appreciably excited.

The cross section and quantum yield data are too limited to provide meaningful estimates of the *j*-values for cyclopentanone at the time of this writing.

IX-E-5. Photodecomposition of Cyclohexanone (*cyclo*-$C_6H_{10}O$)

The ultraviolet absorption spectrum of cyclohexanone reflects the $n \rightarrow \pi^*$ transition common to all carbonyls; see figure IX-E-1. The data derived from gas-phase measurements of the cross sections for cyclohexanone from two different research groups [National Center for Atmospheric Research (NCAR) and Ford Scientific Laboratories (Ford)] are in reasonable agreement (Iwasaki et al., 2008). The cyclohexanone cross sections as measured in cyclohexane solution by Benson and Kistiakowski (1942) had indicated seemingly low values ($\sigma_{max} = 4.2 \times 10^{-20}$ cm^2 molecule^{-1}). However, these were confirmed by Iwasaki et al. (2008). The maximum in the cyclohexanone cross sections shown here is significantly less than those observed for cyclopropanone, cyclobutanone, and cyclopentanone, and in fact, all other carbonyls considered in this work. It is not obvious why these significant differences exist in the probability for the $n \rightarrow \pi^*$ transition for cyclohexanone and that of the other cyclic ketones and most other carbonyl compounds. Theoretical studies will be important in defining the reasons for these differences.

The early studies of the photochemistry of cyclohexanone have been reviewed by Srinivasan (1964), Pitts and Wan (1966), Cundall and Davies (1967), and Wagner and Hammond (1968). The major products are identified as CO, cyclopentane, 1-pentene, and 5-hexenal, but the mechanisms of their formation remain ill-defined. Two alternative mechanisms have been discussed through the years (Calvert et al., 2008). The first invokes intramolecular rearrangements of the original excited ketone (e.g., see Shortridge and Lee, 1970), while the second implies formation of biradicals that are intermediates to the final products (e.g., Benson and Kistiakowski, 1942; Blacet and Miller, 1957).

i) Intramolecular rearrangement to form final products:

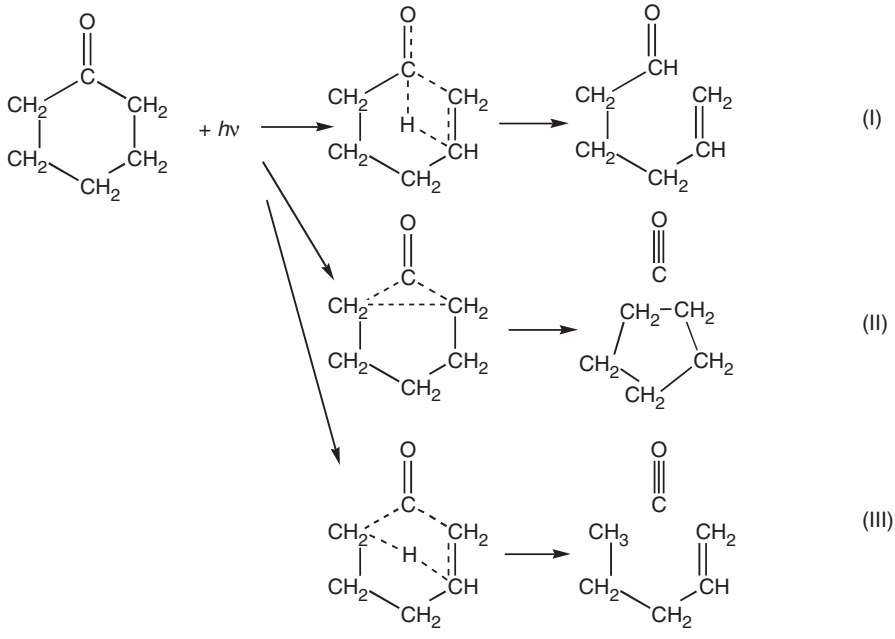

ii) Biradical involvement in the formation of final products:

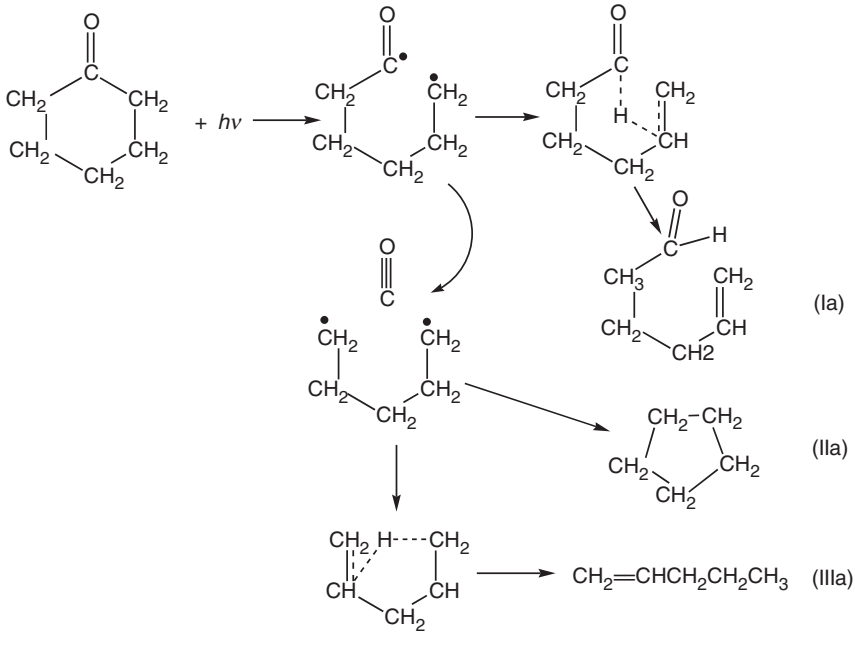

The quantum yields of the products from cyclohexanone photolysis (1 Torr) as a function of wavelength are summarized in figure IX-E-12 (Shortridge and Lee, 1970). Pathway (I), forming 5-hexenal, is seen to be dominant at the longer wavelengths, while channels (II) and (III), forming cyclopentane and 1-pentene, increase in importance at the shorter wavelengths. The effect of pressure increase (0.1 to 2 Torr) can be seen in figure IX-E-13.

Quenching of the precursor state to process (I) is less effective than that for (II) and (III) (Shortridge and Lee, 1970). For photolysis of cyclohexanone (2 Torr) at 297 nm, 95 Torr of added propane or oxygen give very similar quenching of the 1-pentene and cyclopentane product formation. The quantum yields with added propane and oxygen are reduced by factors of 0.16 and 0.17, respectively. However, the 5-hexenal is essentially unaffected by the addition of 95 Torr of oxygen. This behavior is not characteristic of thermalized triplet molecules. Certainly the state that forms the 5-hexenal is short-lived. The electronic states involved in the mechanisms are open to question. The studies of Shortridge and Lee (1970) indicate that the generation of triplet cyclohexanone by sensitization with triplet benzene leads to the same products as those formed in direct photolysis. However, cyclohexanone quenches excited singlet benzene with a cross section that is about 50 times that of triplet benzene. Triplet-benzene-sensitized reactions predominate below 1 Torr of ketone, but the singlet-benzene-sensitization of excited singlet cyclohexanone becomes very important in experiments above 1 Torr. Thus the results of the benzene-sensitization of cyclohexanone decomposition are complex to interpret, and unambiguous conclusions are impossible. Shortridge and Lee (1970) suggest a reaction mechanism in which the importance of the $S_1 \rightarrow T_1$

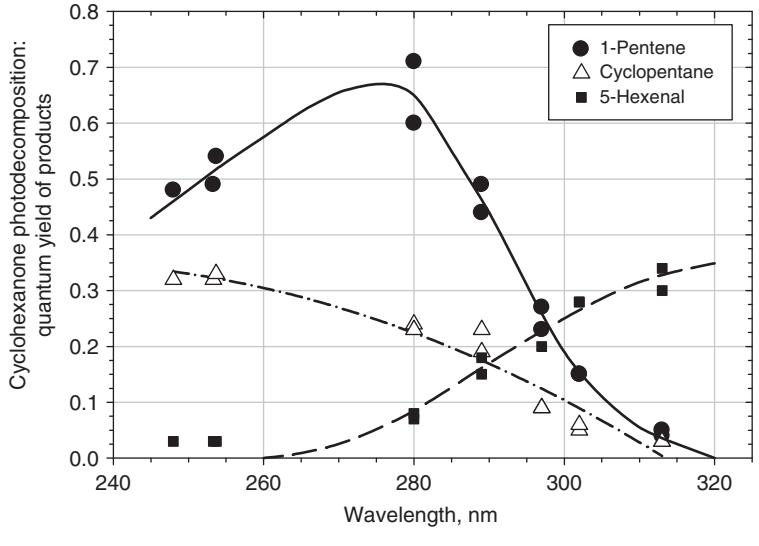

Figure IX-E-12. Quantum yields of products versus wavelength for photodecomposition of cyclohexanone at 1 Torr pressure (from Shortridge and Lee, 1970); figure from Calvert et al. (2008).

intersystem crossing is stressed. Cundall and Davies (1967) conclude that the remarkable inefficiency of oxygen in affecting the photodecomposition of the cyclic ketones argues most strongly against the participation of triplet states. They state that all the features of the cyclic ketone photochemistry are most consistently explained by a mechanism involving the first excited singlet states with different degrees of vibrational excitation. Srinivasan (1964) concluded from the data available in 1963 that it was probable that only one excited state, an upper singlet, is involved in cyclohexanone photolysis.

Calvert et al. (2008) suggest that the products of the photolysis of the methyl-substituted cyclohexanones offer some insight into the mechanism of cyclohexanone photodecomposition. The lack of stereospecificity in the products of *cis*- and *trans*-methyl-substituted cyclohexanones appears to favor biradical intermediates (Alumbaugh et al., 1965; Badcock et al., 1969). The possible unsaturated ketone products of the photolysis of methylcyclohexanone were of the structures (a), (b), and (c):

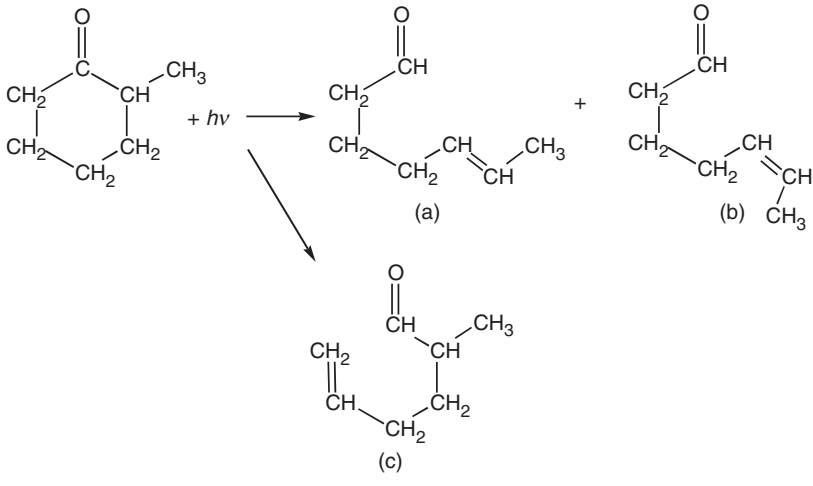

The two major products were identified as structures (a) and (b); in gas-phase photolysis at 313 nm and 100°C, $\phi_a/\phi_b = 2.1 \pm 0.2$. The C—C bond rupture on the side of the carbonyl with the CH_3 group was favored heavily, $(\phi_a + \phi_b)/\phi_c \approx 50$ (Badcock et al., 1969). The mechanism of biradical formation best explained these results.

Unfortunately, the product quantum yields for cyclohexanone photodecomposition are insufficient to allow reasonable estimates of the *j*-values for its photolysis in the troposphere. However, it can be concluded that the unsaturated aldehydes, affected very little by oxygen addition, probably will be important products under these conditions.

IX-E-6. Photodecomposition of Ketene ($CH_2{=}C{=}O$)

Ketene is a unique oxygenate that is neither an aldehyde nor a ketone, but it does possess a carbonyl linkage. It might be considered the first member of the cyclic ketones

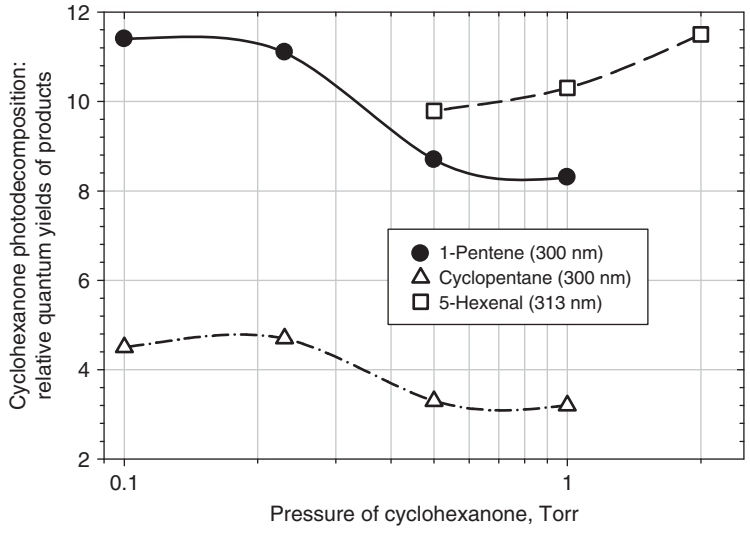

Figure IX-E-13. The effect of pressure on the relative quantum yields of 1-pentene, cyclopentane, and 5-pentenal products from the photolysis of cyclohexanone (Shortridge and Lee, 1970). Note that the data shown for 5-hexenal were determined at 313 nm while those for 1-pentene and cyclopentane were obtained using 300 nm radiation, and the two data sets are not quantitatively intercomparable. The 5-hexenal data were normalized from those given by Shortridge and Lee (1970) so that the relative yields at 1 Torr were more consistent with those given for all products in figure IX-E-12; figure from Calvert et al. (2008).

if one could consider a "ring" composed of only two carbon atoms. Its absorption extends to wavelengths beyond that for the aldehydes and ketones as its chromophore, $\rangle C{=}C{=}O$, has been modified from that of the simple carbonyl group, $\rangle C{=}O$. The result is a lower energy for its $n \rightarrow \pi^*$ transition. Compare the spectra of ketene and methylketene with that of acetaldehyde in figure IX-E-14. Although the shapes and maxima of the absorption bands of the two ketenes are about the same as that of acetaldehyde, the absorption is shifted significantly to longer wavelengths that overlap well the available actinic flux in the lower troposphere. The detailed description of the low-lying electronic states of ketene have been discussed by Dixon and Kirby (1966), Laufer and Keller (1971), and Allen and Schaefer (1986).

IX-E-6.1. The Mechanism of Ketene Photodecomposition

The photochemistry of ketene has been studied for many years, and the nature of the primary processes is well established through a number of experimental studies (e.g., see Norrish et al., 1933; Ross and Kistiakowsky, 1934; Kistiakoxky and Marshall, 1952; Kistiakowsky and Rosenberg, 1950; Strachan and Noyes, 1954; Holroyd and Noyes, 1956; Connelly and Porter, 1958; Noyes and Unger, 1964; Ho et al., 1965; Strachan and Thornton, 1968; Braun et al., 1970; Zabransky and Carr, 1975; Zebransky and Carr, 1976; Hase and Kelley, 1977; Russell and Rowland, 1979; Tanaka and Yoshimine,

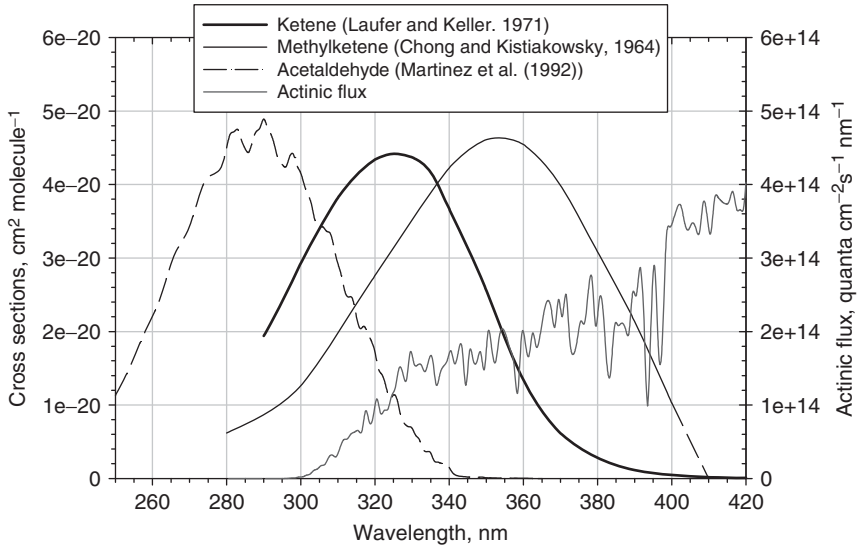

Figure IX-E-14. Comparison of the absorption spectra of ketene and methylketene with that of acetaldehyde. The actinic flux data are those measured at noon on June 19, 1998 near Boulder, CO.

1980; Hayden et al., 1982; Fujimoto et al., 1982; Bandow and Akimoto, 1985; Nesbutt et al., 1985; Bitto et al., 1986; Chen et al., 1988; Potter et al., 1989; Chen and Moore, 1990; Kim et al., 1991; Green et al., 1991; Lovejoy et al., 1991; Lovejoy et al., 1992; Horie and Moortgat, 1992b; Drabbels et al., 1995; Kim et al., 1995; Morgan et al., 1996; Wade et al., 1997a, b; Glass et al., 2000). Many theoretical studies have helped elucidate the nature of the primary processes in ketene photolysis (e.g., see Baird and Taylor, 1978; Tanaka and Yoshimine, 1980; Bouma et al., 1982; Allen and Schaefer, 1986, 1988; Yoshimine, 1989; Klippenstein and Marcus, 1989; Yu and Klippenstein, 1991; Gezelter and Miller, 1996; Klippenstein et al., 1996; Cui and Morokuma, 1997; King et al., 1998; Kaledin et al., 2001; Fochenberg, 2005).

For photolyses at wavelengths available in tropospheric sunlight ($\lambda > 290$ nm), primary photodecomposition modes (I) and (II) dominate; the products are carbon monoxide and a methylene radical (CH_2) formed in either the singlet state, $\tilde{a}^1A_1$, or the triplet state, X^3B_1. In this discussion, the singlet and triplet states are designated as $^1CH_2$, and $^3CH_2$, respectively.

$$CH_2{=}C{=}O + h\nu \rightarrow {}^1CH_2 + CO \quad \text{(I)}$$

$$\rightarrow {}^3CH_2 + CO \quad \text{(II)}$$

$$\rightarrow HC{\equiv}C{-}O + H \quad \text{(III)}$$

$$\rightarrow C_2O(b^1\Sigma^+) + H_2 \quad \text{(IV)}$$

The onset of process (I) occurs at about 332 nm while that for process (II) is about 354 nm. Processes (III) and (IV) become measurable in ketene photolyses at 193 nm. Unfried et al. (1991) observed the infrared spectrum of the ketenyl radial (HCCO) that was formed in significant amounts in the 193 nm photolysis of ketene, suggesting the occurrence of process (III). From photolyses at wavelength 193 nm, Glass et al. (2000) reported quantum yields for processes (I), (II), (III), and (IV) as: 0.193, 0.628, 0.107, and 0.072, respectively. Fockenberg (2005) also studied photolysis at 193.3 nm and found somewhat different results for the percentage of fragmentation by the different channels: (I), (II), and (III): 66 ± 8, 6 ± 9, and 17 ± 7%, respectively. However, only processes (I) and (II) occur for tropospheric conditions.

Molecular beam experiments at low pressures have demonstrated the degree of vibrational and rotational excitation of the CO and CH_2 fragments formed in ketene photolysis at various wavelengths (e.g., see: Hayden et al., 1982; Bitto et al., 1986; Chen et al., 1988; Kim et al., 1991; Green et al., 1991; Lovejoy et al., 1992; Kim et al., 1995; Drabbels et al., 1995; Morgan et al., 1996; Wade et al., 1997a, b; Glass et al., 2000; Fochenberg, 2005).

The singlet and triplet methylene react with hydrocarbons and other molecules very differently. $^1CH_2$ inserts into H—C bonds randomly and adds to the $\rangle C{=}C\langle$ bond in alkenes, retaining the stereochemistry of the alkene. The $^3CH_2$ species reacts non-stereospecifically with double bonds in alkenes and abstracts H-atoms from alkanes. This difference in mechanism of reaction with the hydrocarbons has been used in many experiments to estimate the extent of occurrence of processes (I) and (II). Although the $^3CH_2$ is the ground electronic state of the methylene radical and process (II) is energetically possible for $\lambda < 354$ nm, it is difficult to form the triplet exclusively and directly. Duncan and Cvetanovic (1962) apparently have accomplished this using $Hg(^3P_1)$ excited atoms to generate the triplet-excited state of ketene which dissociates to $^3CH_2$ with spin conservation. High pressures of added gases also result in the generation of $^3CH_2$ from $^1CH_2$ in diazomethane photolyses (Hayden et al., 1982; Anet et al., 1960; Frey, 1960), and this result is expected with ketene mixtures. The quantum yield of process (I) forming $^1CH_2$ in ketene photolyses at low pressures is wavelength dependent (Kim et al., 1991; Morgan et al., 1996; Wade et al., 1997a, b). See figure IX-E-15. At the shorter wavelengths, the quantum yield of ketene photodecomposition forming the $^1CH_2$ fragment in process (I) is seen to be near unity.

Early studies of pure ketene photodecomposition (Norrish et al., 1933; Ross and Kistiakowsky, 1934; Kistiakowsky and Rosenberg, 1950; Kistiakowsky and Marshall, 1952) showed that the major products observed, C_2H_4 and CO, formed in nearly equal amounts, and that they arose in a rapid reaction of CH_2 radicals with ketene: $CH_2 + CH_2{=}C{=}O \rightarrow C_2H_4 + CO$. Thus, under many experimental conditions, two molecules of CO are formed for every ketene molecule that is dissociated. The quantum yields of CO formation as measured by Ross and Kistiakowsky (1934) using wavelength 313 nm (temperature unspecified, but probably near ambient temperatures) were: 2.34, 2.06, 2.22, 2.38, 1.94, and 1.96, while irradiation with 366 nm light gave significantly lower values (0.84, 0.42). Strachen and Noyes (1954) measured values of Φ_{CO} at 270 nm as: 1.93, 2.26, and 2.16. Holroyd and Noyes (1956) reported Φ_{CO} values of 2.4 (26°C), 2.04 (28°C), 2.2 (106°C), and 2.0 (160°C) from irradiation of ketene at

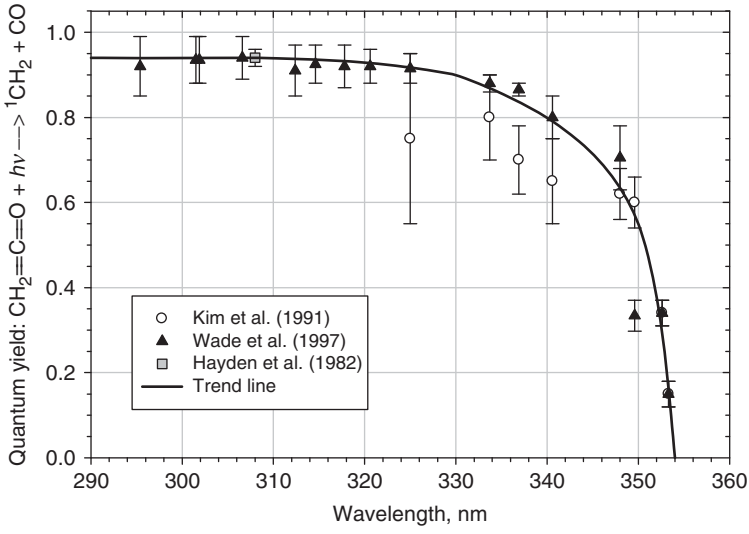

Figure IX-E-15. Quantum yield of singlet methylene formation as a function of wavelength in the photodecomposition of ketene at low pressures.

270 nm. Since two molecules of CO are formed per quantum of light absorbed in pure ketene photolyses, the average of these data gives the primary quantum yield, $\phi_I + \phi_{II} = 1.08 \pm 0.10$ at 313 nm; 1.06 ± 0.08 at 270 nm and 26°C. Lower values of the primary quantum yields were found at 366 nm, and these are also very pressure dependent. Subsequent measurements have confirmed that the quantum yield is near unity for photolyses at $\lambda \leq 334$ nm at low pressure (Hase and Kelley, 1977), but quenching of the excited molecules is observed as the pressure of ketene is increased at all these wavelengths. See figure IX-E-16. As with the aldehydes and ketones described in this work, the quenching of ketene is seen to be most effective at the longer wavelengths of excitation (lower excitation energies). The least-squares plots of the data given in figure IX-E-16 ($1/\Phi_{CO} = 1/(\Phi_{CO})_o + (k_q/k_d)$ P(torr) for the Connelly and Porter (1958) experiments give the following relations: 313 nm, series A, $1/\Phi_{CO} = 0.543 + 6.16 \times 10^{-4} \times$ P (Torr); series B; $1/\Phi_{CO} = 0.461 + 4.94 \times 10^{-4} \times$ P; at 334 nm, $1/\Phi_{CO} = 0.579 + 4.42 \times 10^{-3} \times$ P; data from Hase and Kelley (1977) give: 313 nm, $1/\Phi_{CO} = 0.505 + 8.43 \times 10^{-4} \times$ P; 334 nm, $1/\Phi_{CO} = 0.494 + 1.31 \times 10^{-2} \times$ P; 366 nm, $1/\Phi_{CO} = 0.548 + 0.936 \times$ P. From these relations at zero pressure $\Phi_{CO} \approx 1.84$; 2.17, 1.73 (Connelly and Porter, 1959); 1.98, 2.02, 1.82 (Hase and Kelley, 1977). Since two molecules of CO are formed per quantum absorbed in the photodecomposition of pure ketene, the average of these data (313 nm $< \lambda <$ 366 nm) gives $\phi_I + \phi_{II} \approx 0.96 \pm 0.08$. Strachen and Noyes (1954) reported measurements of Φ_{CO} versus pressure of ketene that give the estimate of $k_q/k_d \approx 1.2\,\text{Torr}^{-1}$ for photolyses at 370 nm, in good agreement with the Hase and Kelley (1977) measurement at 366 nm.

The data of figure IX-E-16 show that quenching of the ketene excited at wavelengths above 330 nm is expected to become significant at atmospheric pressure. Strachan and Thornton (1968) have shown that the Stern–Volmer quenching coefficients for

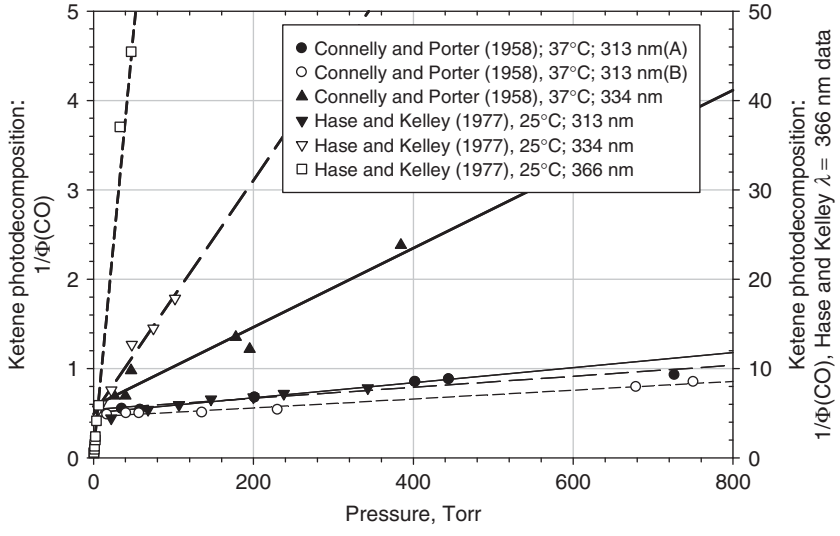

Figure IX-E-16. Stern–Volmer plots of the reciprocal of the quantum yield of CO formed in the photolyses of pure ketene as a function of the pressure of ketene at several wavelengths of excitation.

366 nm excited ketene for collisions with ketene ($0.92\,\mathrm{Torr}^{-1}$) are very similar to those for quenching by added C_4F_8 ($1.2\,\mathrm{Torr}^{-1}$) and SF_6 ($0.93\,\mathrm{Torr}^{-1}$). This and all other evidence suggests that the observed quenching of ketene results from the vibrational relaxation of the excited ketene molecules. Values of k_q/k_d derived from the slopes of the Stern–Volmer plots in figure IX-E-16 are plotted versus the reciprocal of the wavelength in figure IX-E-17. The least-squares equation that describes these data (dashed line in the figure) is given by: $\log_{10}(k_q/k_d,\ \mathrm{Torr}^{-1}) = 60.067 - 35{,}168 \times [1/\lambda(\mathrm{nm})] + 4{,}809{,}963 \times (1/\lambda)^2$.

Using time-resolved photofragment spectroscopy of the product CH_2, Potter et al. (1989) measured directly the rate coefficients for decomposition of ketene molecules excited at selected single wavelengths in the range 293 to 327 nm. In similar experiments for ketene excitation from 350 to 354 nm, Chen and Moore (1990) and Kim et al. (1995) measured the rate of appearance of the CO fragment and determined the rate coefficients for photodecomposition. All of these rate coefficient measurements are shown in figure IX-E-18. We have used these k_d estimates and the equation for the wavelength dependence of the Stern–Volmer quenching coefficients (k_q/k_d) derived from the data of figure IX-E-17 to estimate the approximate wavelength dependence of the k_q values. The results are shown by the solid line in figure IX-E-19. Note that in the range of wavelengths 280 to 348 nm, the quenching rate coefficient is about 10^{-10} cm^3 $\mathrm{molecule}^{-1}$, suggesting that deactivation of the excited molecule occurs on nearly every collision. This is consistent with the conclusion that the pressure dependence of the dissociation results from collisional quenching of the vibrationally excited ground state of the ketene molecule that is believed to be the state from which dissociation occurs in this wavelength region. The fall-off in the quenching rate coefficient

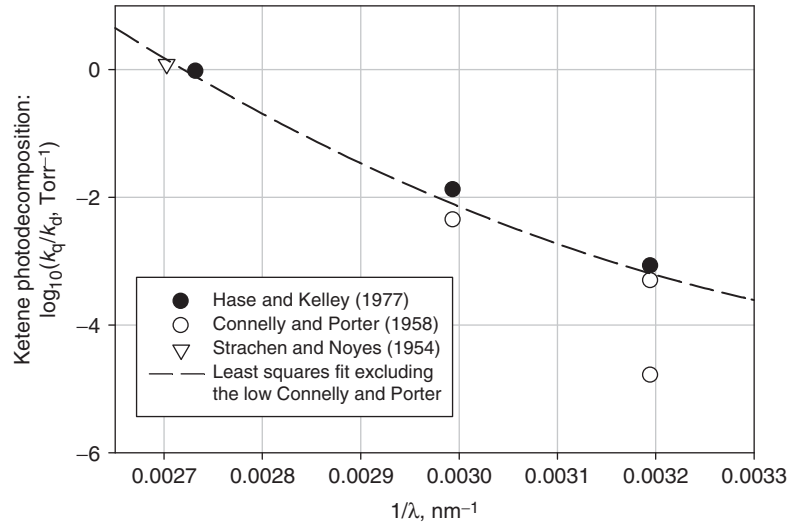

Figure IX-E-17. Plot of the $\log_{10}(k_q/k_d)$ versus $1/\lambda$ for photolyses of ketene. The dashed line is the least-squares fit of the data excluding the low point of Connelly and Porter (1958).

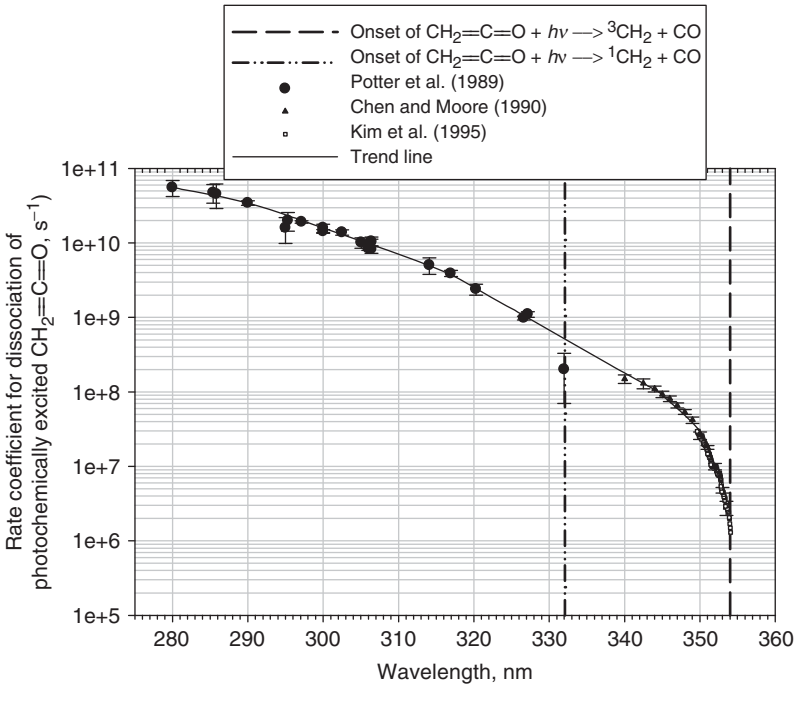

Figure IX-E-18. Plot of the rate coefficients for the decomposition of electronically excited ketene molecules as a function of the wavelength of excitation of the ketene.

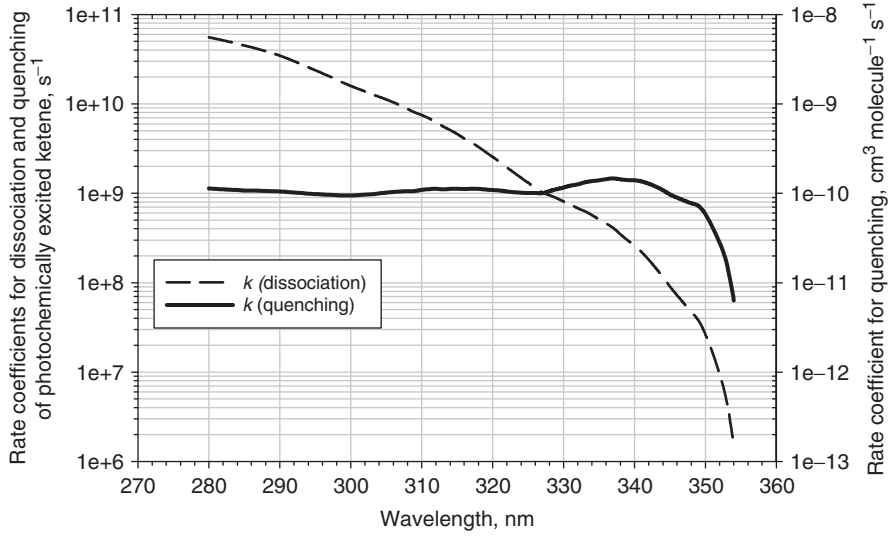

Figure IX-E-19. Shown as the solid line in the figure are the approximate rate coefficients for quenching of excited ketene molecules as estimated from the k_d measurements of Potter et al. (1989), Chen and Moore (1990), and Kim et al. (1995) (dashed line) and the equation describing the k_q/k_d data given in figure IX-E-17.

in the region of triplet dissociation is striking and may result in part from the change in nature of the molecule that is quenched. Ketene excited at the long wavelengths of light is believed to dissociate directly from the excited triplet molecule. Chen and Moore (1990) determined that the barrier height for this dissociation is about 15.8 ± 0.3 kJ mol^{-1}.

Using the 141.5 nm absorption of $^3CH_2$ (Herzberg, 1961) in the flash photolyses of ketene and diazomethane, Braun et al. (1970) estimated the rate coefficient for the collision-induced intersystem crossing reaction, $^1CH_2 + N_2 \rightarrow {}^3CH_2 + N_2$, to be $(9.0 \pm 2.0) \times 10^{-13}$ cm^3 molecule^{-1} s^{-1}. This rate coefficient is a factor of 10^{-2} smaller than the quenching rate coefficient for excited ketene. If this value is correct, then it is unlikely that the $^3CH_2$ species will be generated significantly by collision-induced intersystem crossing in ketene photolyses at wavelengths < 332 nm.

The mechanism of photodissociation of ketene as indicated by the equations of processes (I) and (II) hides some interesting molecular contortions that occur during photolysis. An unexpected observation of Russell and Rowland (1968) showed that up to a 10% exchange of carbon atoms in ketene occurred when $^{14}CH_2{=}C{=}O$ was photolyzed at 334 nm. They suggested that this occurred through the intermediate formation of oxirene-like intermediate:

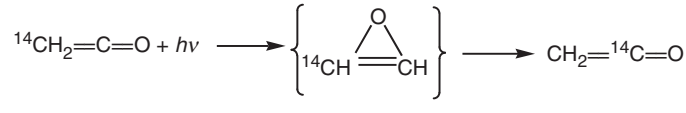

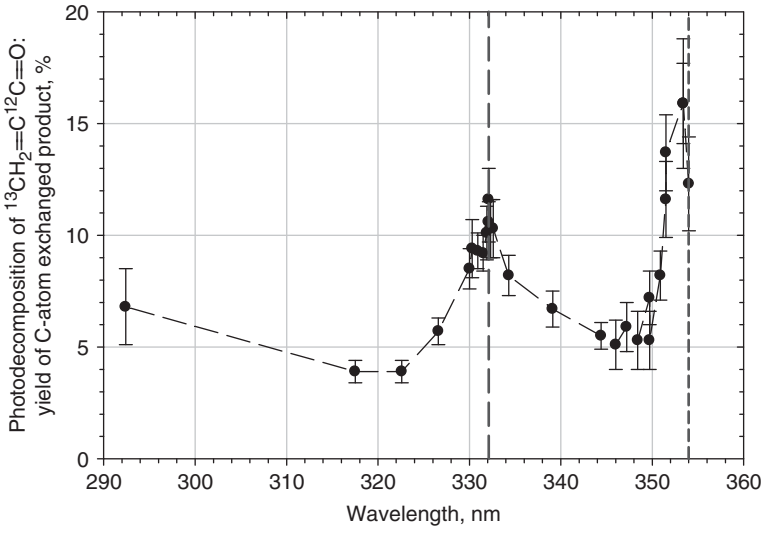

Figure IX-E-20. Percentage of C-atom exchange in the photolysis of $^{12}CH_2{=}^{13}C{=}O$ and $^{13}CH_2{=}^{12}C{=}O$ as a function of wavelength (Lovejoy et al., 1991).The gray long-dashed and short-dashed lines show the wavelength of onset of the photodissociation to form $^1CH_2$ and $^3CH_2$, respectively.

More recently, Lovejoy et al. (1991) confirmed and extended these findings in their study of the photolysis of $^{12}CH_2{=}^{13}C{=}O$ and $^{13}CH_2{=}^{12}C{=}O$ at several wavelengths. These data are shown in figure IX-E-20 where the percentage of the exchange reaction is shown as a function of wavelength. The time constant for the appearance of the minor rearranged product is significantly longer than that for the unrearranged CO product. The measured rate coefficients for photodecomposition to the unrearranged product checked well with those given in figure IX-E-18 as determined by Potter et al. (1989), Chen and Moore (1990), and Kim et al. (1995). The rotational distributions of CO formed in either the rearrangement or in the unrearranged reactions are the same, indicating that the exchanged CO is produced from highly vibrationally excited ketene, and not from one of the other C_2H_2O isomers involved in the isomerization mechanism. RRKM calculations for an oxirene transition state were used by Lovejoy et al. (1991) to rationalize the rate coefficient measurements. *Ab initio* molecular orbital calculations have been used to study in detail the various isomers of C_2H_2O that may be involved in this rearrangement (Bouma et al., 1982; Tanaka and Yoshimine, 1980; Yoshimine, 1989). In figure IX-E-20 it can be seen that the two maxima in the wavelength dependence of the percentage of rearrangement occur very near the wavelengths for onset of the photodissociation to form $^1CH_2$ and $^3CH_2$. These are the wavelengths at which the excited $CH_2{=}C{=}O$ molecules are longest lived.

IX-E-6.2. The Effect of Added Oxygen in the Photolysis of Ketene

The presence of small amounts of oxygen in ketene mixtures suppresses the formation of the products normally attributed to the reaction of $^3CH_2$ (Strachan and Noyes, 1954;

Hollroyd and Noyes, 1956; Russell and Rowland, 1968; Zabransky and Carr, 1976; Bandow and Akimoto, 1985; Horie and Moortgat, 1992). Using mixtures of oxygen and hydrocarbons (*cyclo*-C_4H_8, *cyclo*-C_4D_8, C_2H_4, or C_2D_4) with $CT_2{=}C{=}O$ or $^{14}CH_2{=}C{=}O$, Russell and Rowland (1968) observed the the formation of T_2, $^{14}CO_2$, and ^{14}CO which they attributed to the reaction of $^3CH_2$ with O_2. This conclusion was reached in view of several key observations: 1) the progress of the characteristic reaction of the singlet methylene was unimpeded by O_2 addition; 2) the insensitivity of the product yields to the concentration of O_2, and the observation of the reactions at wavelengths for which the quantum yield is unity for CH_2 formation. The sum of the amounts of ^{14}CO and $^{14}CO_2$ was very near that expected for the percent triplet methylene in the system (~10%). They estimated that the rate coefficient for reaction (2) must be 500 times that of reaction (1):

$$^3CH_2 + CH_2{=}C{=}O \rightarrow C_2H_4 + CO \tag{1}$$

$$^3CH_2 + O_2 \rightarrow (CH_2O_2^{\ddagger}) \rightarrow \text{Products}(CO, CO_2, H_2, \text{etc.}) \tag{2}$$

Russell and Rowland (1968) suggested that the T_2 formation in the photolysis of mixtures of $T_2C{=}C{=}O$ with O_2 arose in the reactions: $^3CT_2 + O_2 \rightarrow (\text{Intermediates})^{\ddagger} \rightarrow T_2 + CO_2$ (or $T_2 + CO + O$).

Bandow and Akimoto (1985) photolyzed ketene in O_2/Ar matrices at 11 K, where HO_2, CO_2, CO, H_2O, and O_3 were observed as products. Formic acid, formaldehyde, and a metastable CH_2O_2 species were not observed. The decomposition of the initially formed $CH_2O_2^{\ddagger}$ species apparently occurs quickly by several channels to form H, H_2O, O, H_2, CO, and CO_2. In similar experiments using 270–370 nm radiation of ketene, oxygen, argon mixtures at 298 K, Horie and Moortgat observed CO, CO_2, O_3, CH_2O, HC(O)OH, and $CH_3C(O)OC(O)H$; the latter compound is formed by reaction of ketene with formic acid. There was no evidence of the formation of a stabilized Criegee intermediate (CH_2O_2). In view of these results, it is seems likely that any $^3CH_2$ formed from the photodecomposition of ketene within the lower troposphere will react rapidly to form the fragmentation products of the very energy rich CH_2O_2 molecule expected as an intermediate in reaction (2).

IX-E-6.3. Absorption Cross Sections for Ketene

The data of Laufer and Keller (1971) that are shown in figure IX-E-14 provide data applicable to the wavelength range of the actinic flux available in the troposphere. We have interpolated between the points of the given 5 nm interval data to derive estimates for each nm of wavelength needed for photolysis frequency estimates; these are given in table IX-E-3.

IX-E-6.4. Quantum Yields of Photodissociation of Ketene in the Lower Troposphere

The quantum yields of photodecomposition of ketene versus wavelength were estimated using the data given in figures IX-E-16 and IX-E-17. These are given in figure IX-E-21

Table IX-E-3. Approximate cross sections (σ, cm^2 molecule^{-1}) as measured by Laufer and Keller (1971) and estimates of $\phi_I + \phi_{II}$ for ketene at 1 atm. in the lower troposphere as a function of wavelength as derived in this study (see the text)

λ, nm	$10^{20} \times \sigma$	$\phi_I + \phi_{II}$	λ, nm	$10^{20} \times \sigma$	$\phi_I + \phi_{II}$	λ, nm	$10^{20} \times \sigma$	$\phi_I + \phi_{II}$	λ, nm	$10^{20} \times \sigma$	$\phi_I + \phi_{II}$
278	1.12	1.00	318	4.27	1.00	358	1.55	0.81	398	0.060	0.008
279	1.18	1.00	319	4.31	1.00	359	1.45	0.79	399	0.050	0.007
280	1.23	1.00	320	4.34	1.00	360	1.34	0.76	400	0.048	0.006
281	1.30	1.00	321	4.36	1.00	361	1.25	0.73	401	0.045	0.005
282	1.35	1.00	322	4.38	1.00	362	1.16	0.70	402	0.041	0.004
283	1.42	1.00	323	4.40	1.00	363	1.07	0.67	403	0.038	0.004
284	1.50	1.00	324	4.41	1.00	364	0.99	0.64	404	0.034	0.003
285	1.58	1.00	325	4.42	1.00	365	0.92	0.60	405	0.031	0.003
286	1.66	1.00	326	4.42	1.00	366	0.85	0.56	406	0.029	0.002
287	1.73	1.00	327	4.41	1.00	367	0.79	0.53	407	0.026	0.002
288	1.80	1.00	328	4.40	1.00	368	0.73	0.49	408	0.024	0.002
289	1.87	1.00	329	4.38	1.00	369	0.66	0.45	409	0.021	0.001
290	1.94	1.00	330	4.37	1.00	370	0.62	0.41	410	0.019	0.001
291	2.04	1.00	331	4.35	0.99	371	0.57	0.38	411	0.018	0.001
292	2.13	1.00	332	4.32	0.99	372	0.54	0.34	412	0.016	0.001
293	2.22	1.00	333	4.28	0.99	373	0.49	0.31	413	0.015	0.001
294	2.31	1.00	334	4.23	0.99	374	0.44	0.27	414	0.013	0.001
295	2.41	1.00	335	4.17	0.99	375	0.42	0.24	415	0.012	0.001
296	2.51	1.00	336	4.08	0.99	376	0.39	0.22	416	0.011	0.000
297	2.62	1.00	337	3.99	0.99	377	0.36	0.19	417	0.010	
298	2.73	1.00	338	3.88	0.99	378	0.34	0.17	418	0.009	
299	2.83	1.00	339	3.77	0.99	379	0.30	0.15	419	0.008	
300	2.93	1.00	340	3.67	0.98	380	0.28	0.13	420	0.007	
301	3.01	1.00	341	3.56	0.98	381	0.26	0.11	421	0.006	
302	3.12	1.00	342	3.45	0.98	382	0.24	0.10	422	0.006	
303	3.22	1.00	343	3.35	0.97	383	0.22	0.08	423	0.005	
304	3.31	1.00	344	3.25	0.97	384	0.20	0.07	424	0.005	
305	3.40	1.00	345	3.14	0.97	385	0.18	0.06	425	0.004	
306	3.49	1.00	346	3.03	0.96	386	0.16	0.05	426	0.004	
307	3.57	1.00	347	2.92	0.96	387	0.15	0.05	427	0.003	
308	3.66	1.00	348	2.80	0.95	388	0.14	0.04	428	0.003	
309	3.74	1.00	349	2.68	0.94	389	0.13	0.03	429	0.002	
310	3.82	1.00	350	2.56	0.93	390	0.12	0.03	430	0.002	
311	3.89	1.00	351	2.43	0.92	391	0.11	0.03	431	0.002	
312	3.96	1.00	352	2.30	0.91	392	0.10	0.02	432	0.002	
313	4.02	1.00	353	2.16	0.90	393	0.090	0.02	433	0.002	
314	4.07	1.00	354	2.04	0.89	394	0.080	0.02	434	0.002	
315	4.13	1.00	355	1.91	0.87	395	0.073	0.014	435	0.001	
316	4.18	1.00	356	1.78	0.85	396	0.067	0.012	436	0.000	
317	4.23	1.00	357	1.66	0.83	397	0.063	0.010			

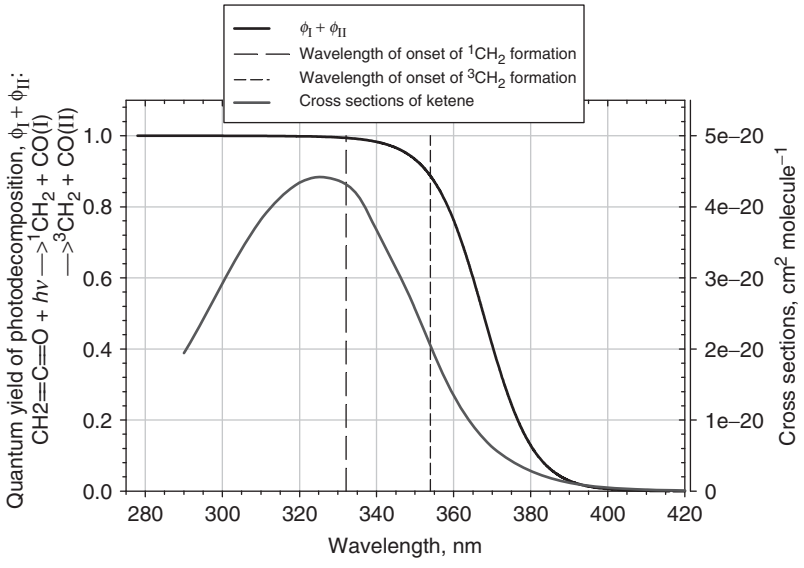

Figure IX-E-21. Quantum yields of photodecomposition of ketene versus wavelength (solid black line); cross sections of ketene versus wavelength, gray curve; wavelengths of onset of $^1CH_2$ and $^3CH_2$ are indicated by the long-dashed line and short-dashed line, respectively.

and table IX-E-3. The extrapolation of the quantum yield data to wavelengths above 370 nm, not measured directly, provides only rough estimates for this range. Our calculations may overestimate the quantum yield since this is the wavelength region where the excited triplet may be the origin of the photodecomposition present, and there is a small barrier to its dissociation. As a result, the quantum yield at zero pressure may be less than the value of unity that we have assumed in the calculation using the k_q/k_d data.

IX-E-6.5. Estimation of the Photolysis Frequencies for Ketene Photodissociation within the Lower Troposphere

We have calculated the photolysis frequencies for ketene using the quantum yields for photodecomposition at atmospheric pressure and the absorption cross sections for ketene (see table IX-E-3) together with the appropriate actinic flux data for a cloudless day with an overhead ozone column of 350 DU; see figure IX-E-22. These data give a photochemical lifetime of about 1 h with an overhead Sun.

IX-E-7. The Photodecomposition of Methylketene ($CH_3CH{=}C{=}O$) and Dimethyl Ketene [$(CH_3)_2C{=}C{=}O$]

There are limited data concerning the photochemistry of substituted ketenes. The absorption spectrum of methylketene as reported by Chong and Kistiakowsky (1964)

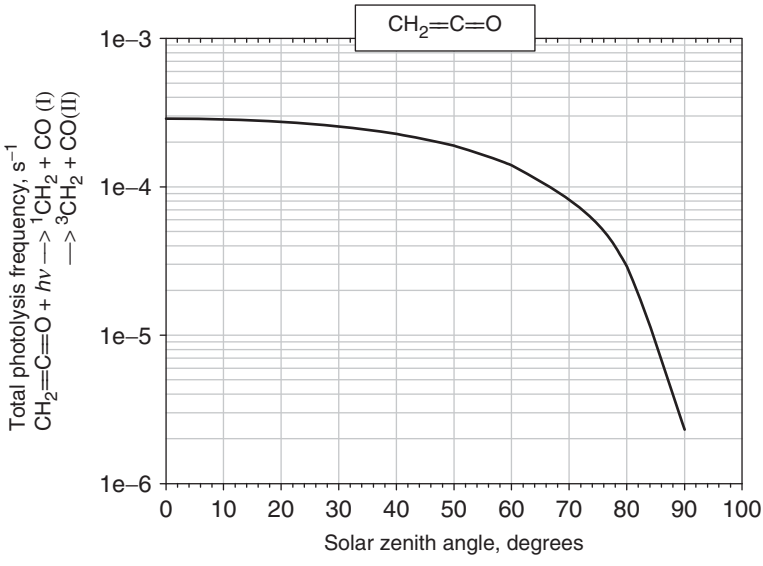

Figure IX-E-22. Photolysis frequency of ketene versus solar zenith angle as calculated for a cloudless day within the lower troposphere with an ozone column of 350 DU.

has been reproduced in figure IX-E-14. Comparison with the spectra of ketene shows the absorption in the substituted ketene is shifted significantly to longer wavelengths. The limited photochemical data for methylketene (Kistiakowsky and Mahan, 1957; Chong and Kistiakowsky, 1964) and dimethylketene (Holroyd and Blacet, 1957) suggest that the photodecomposition mechanisms for these two ketenes are similar to that described in the previous section for ketene. In the 240–365 nm region of excitation, the major primary photodissociation processes appear to be reactions (I) and (II):

$$CH_3CH{=}C{=}O + h\nu \rightarrow CH_3CH + CO \qquad \text{(I)}$$

$$(CH_3)_2C{=}C{=}O + h\nu \rightarrow CH_3CCH_3 + CO \qquad \text{(II)}$$

Ethylene, CO, and C_4H_8 are the major products observed following process (I), and largely propylene and CO form following (II). The rearrangements of the CH_3CH and CH_3CCH_3 radicals are enhanced by collisions with added gases. Photodissociation at the short wavelengths (253.7–313 nm) occurs with a quantum yield for CO formation near unity at the lower pressures. Photolyses at 366 nm show a strong pressure dependence of quantum yields; the Stern–Volmer plot of quenching data for methylketene given by Kistiakowsky and Mahan (1957) yields the ratio $k_q/k_d \approx 17\,\text{Torr}^{-1}$, a value about 17 times that reported for ketene at 366 nm. There are insufficient data to allow realistic estimates of the photolysis frequencies for the substituted ketenes for atmospheric conditions.

IX-F. Photodecomposition of Ketones Containing Additional Functional Groups

IX-F-1. Effect of Halogen Atom and HO-Substitution on the Absorption Spectrum of Acetone

As observed with the aldehydes (section IX-C-14), substitution of HO or halogen atoms for H-atoms in ketones has a significant effect on the absorption spectra. It is not surprising that the effects of a given halogen atom or an OH group substitution for H-atoms in the CH_3 group of $CH_3C(O)CH_3$ are very similar to those seen in CH_3CHO for the same substitution, since the chromophores are very similar. Compare the changes in observed λ_{max} and σ_{max} for similar atom substitutions summarized in table IX-F-1 (Calvert et al., 2008).

In figure IX-F-1 from Calvert et al. (2008), spectra are compared for acetone molecules where a single halogen atom or OH group replaces an H-atom in $CH_3C(O)CH_3$. The replacement of an H-atom with an F-atom to form $CH_2FC(O)CH_3$ lowers the cross section significantly (by a factor of 2.5), and a small shift ($\sim$4 nm) to longer wavelengths occurs in the absorption maximum. A very different influence is seen with a Cl-atom substitution in acetone that parallels those observed with the aldehydes. The maximum cross section of $CH_2ClC(O)CH_3$ is a factor of about 2.0 larger than that in acetone, and it is shifted about 14 nm to the longer wavelengths. A similar effect is seen with Br-atom substitution in acetone; the maximum absorption cross section is increased by a factor of about 2.3, and it is shifted about 21 nm to the longer wavelengths. The result of Cl- or Br-atom substitution in $CH_3C(O)CH_3$ results in a much better overlap of the spectrum with that of the distribution of wavelength of sunlight present within the troposphere, and hence the potential for importance of their tropospheric photodecomposition is enhanced.

Table IX-F-1. Comparison of the wavelength (λ_{max}) and cross section (cm^2 $molecule^{-1}$) at the maximum in the absorption spectra of substituted acetaldehyde and acetone molecules at temperatures near 298 K; table from Calvert et al. (2008)

Substituted Acetaldehydes	λ_{max}, nm	$10^{20} \times \sigma_{max}$	Substituted Acetones	λ_{max}, nm	$10^{20} \times \sigma_{max}$
CH_3CHO	290	4.88	$CH_3C(O)CH_3$	278	5.07
$HOCH_2CHO$	277	5.42	$HOCH_2C(O)CH_3$	266	6.74
CH_2ClCHO	298	5.75	$CH_2ClC(O)CH_3$	292	10.2
$CHCl_2CHO$	300	6.14			
CCl_3CHO	289	10.9			
CHF_2CHO	309	4.73			
			$CH_2FC(O)CH_3$	282	2.24
			$CH_2BrC(O)CH_3$	299	11.5
CF_3CHO	301	3.20	$CF_3C(O)CH_3$	281	3.1
			$CF_3C(O)CF_3$	303	3.09
CF_2ClCHO	300	16.3	$CF_2ClC(O)CF_3$	308	18.8
			$CF_2ClC(O)CF_2Cl$	305	18.9
$CFCl_2CHO$	295	13.7	$CFCl_2C(O)CF_2Cl$	305	18.9

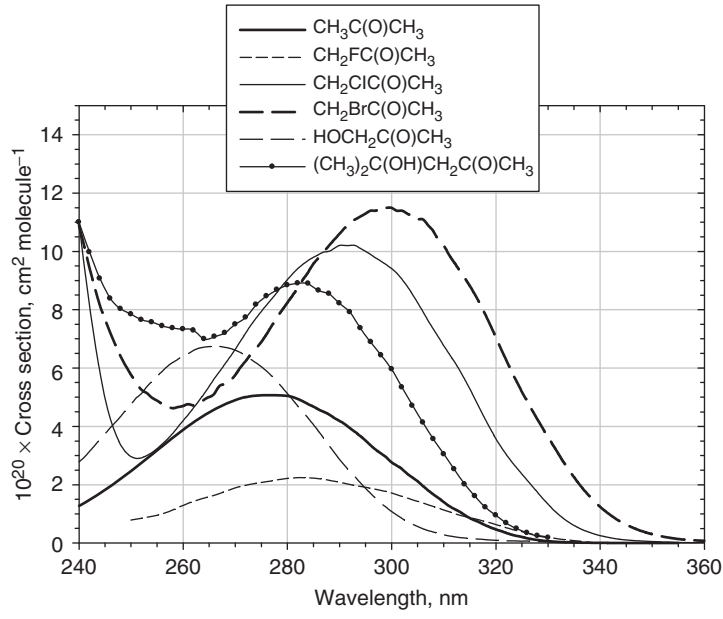

Figure IX-F-1. Comparison of the absorption cross sections for the monosubstituted acetones, $CH_2FC(O)CH_3$ (Hackett and Phillips, 1974a), $CH_2ClC(O)CH_3$ (Burkholder et al., 2002), $CH_2BrC(O)CH_3$ (Burkholder et al., 2002), $HOCH_2C(O)CH_3$ (Orlando et al., 1999), and diacetone alcohol $(CH_3)_2C(OH)CH_2C(O)CH_3$ (Magneron et al., 2003) with those of $CH_3C(O)CH_3$ (Martinez et al., 1992); figure from Calvert et al. (2008).

Formation of $HOCH_2C(O)CH_3$ by substitution of an OH group for an H-atom in acetone increases the absorption maximum somewhat (by a factor of about 1.3), as with the aldehydes, and the absorption maximum shifts about 12 nm to the shorter wavelengths. Hence, overlap of the absorption of $HOCH_2COCH_3$ with the solar flux present within the troposphere is decreased significantly from that seen for acetone. With introduction of an OH group two carbon atoms down-chain from the carbonyl in diacetone alcohol [$(CH_3)_2C(OH)CH_2C(O)CH_3$], the maximum cross section is enhanced, but the wavelength of maximum absorption is altered little from that in unsubstituted acetone. One expects a similar behavior for the common 1,4-hydroxycarbonyl compounds; they probably absorb light in about the same wavelength region as the unsubstituted acetone (Calvert et al., 2008).

The effects on the absorption spectrum of $CH_3C(O)CH_3$ with substitution of multiple F-atoms for H-atoms can be seen in figure IX-F-2. The data for cross sections of $CF_3C(O)CH_3$ are from Beavan et al. (1978). The single data points at 313 nm from Sieger and Calvert (1954) and 278 nm from Dawidowicz and Patrick (1964) are reasonably consistent with the Beavan et al. data. Also spectral data given for $CH_3C(O)CF_3$ in figure 4 of Hackett and Phillips (1974a) are consistent with the Beavan et al. data ($\sigma_{max} \sim 3.1 \times 10^{-20}$ cm^2 molecule^{-1} and $\lambda_{max} \sim 279$ nm). It is clear that with the substitution of three F-atoms on one carbon of $CH_3C(O)CH_3$ to form $CF_3C(O)CH_3$,

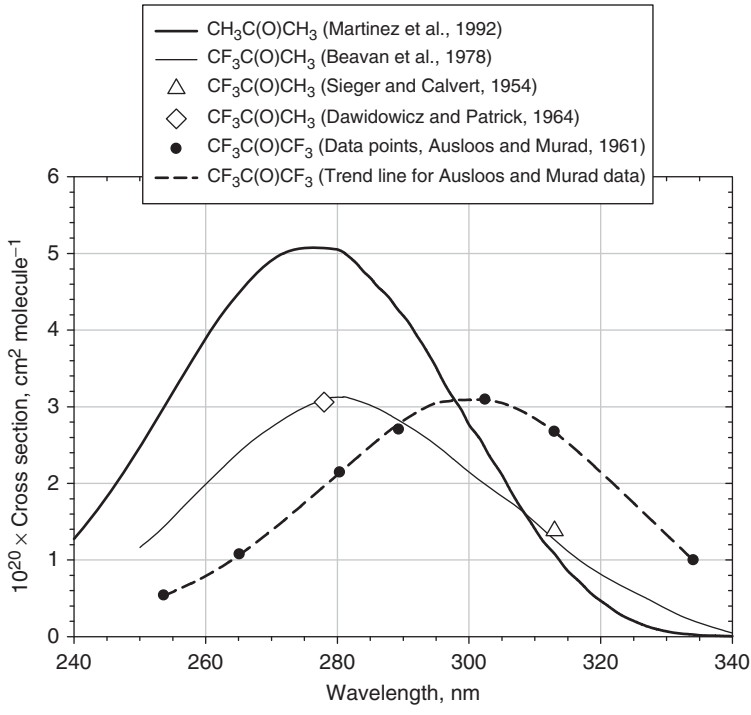

Figure IX-F-2. Comparison of the approximate absorption spectra for F-substituted acetones, $CF_3C(O)CH_3$, $CF_3C(O)CF_3$, with that of $CH_3C(O)CH_3$ near 298 K. The data points for $CF_3C(O)CH_3$ at wavelength 313 nm (triangle, Sieger and Calvert, 1954) and 278 nm (diamond, Dawidowicz and Patrick, 1964) are in reasonable accord with the complete spectral data obtained by Beavan et al. (1978); data points shown for $CF_3C(O)CF_3$ are limited to those published for specific wavelengths that are shown by the filled circles (Ausloos and Murad, 1961).

the maximum cross section of acetone is lowered by a factor of about 1.6, and it is shifted to the longer wavelengths.

The $CF_3C(O)CF_3$ spectral data from Ausloos and Murad (1961) were determined at only selected wavelengths shown by the symbols. The precision of the $CF_3C(O)CF_3$ data points is uncertain, but it is likely that it is reasonably good, since there is qualitative agreement of their acetone data points with the currently accepted $CH_3C(O)CH_3$ spectra given by Martinez et al. (1992). With all the C—H bonds in acetone replaced with C—F bonds to form $CF_3C(O)CF_3$, the maximum cross section is lowered as in $CF_3C(O)CH_3$, and the wavelength of maximum absorption is shifted to even longer wavelengths. These highly fluorinated acetones absorb a much greater fraction of the sunlight available within the troposphere than unsubstituted acetone.

The effect of Cl-atom substitution for F-atoms in $CF_3C(O)CF_3$ is shown in figure IX-F-3 from Calvert et al. (2008). The cross section data given for $CF_2ClC(O)CF_3$, $CF_2ClC(O)CF_2Cl$, and $CFCl_2C(O)CF_2Cl$ were obtained by transformation of the molar decadic extinction coefficients versus $1/\lambda$ plots given in the

figures of Hackett and Phillips (1974a). The reconstructed cross section versus wavelength curves are likely of lower precision than the data presented graphically by the original investigators. As seen with the fluoro-chloro-acetaldehydes, a very large increase in the cross section results from the replacement of one F-atom by a Cl-atom in the $CF_3C(O)CF_3$ molecule to form $CF_2ClC(O)CF_3$. However, the wavelength of the absorption maximum shows little change with F-atom replacement by the Cl-atom. The data of figure IX-F-3 show little difference in the spectrum of $CF_2Cl(O)CF_3$ as one and two additional F-atoms are replaced with Cl-atoms. It is clear that substitution of chlorine into the fluoroacetone molecule enhances dramatically the absorption of the wavelengths present in tropospheric sunlight.

In the following sections the limited data on the photodecomposition of the substituted acetone molecules are described, largely as reviewed by Calvert et al. (2008).

IX-F-2. Photodecomposition of 1-Hydroxy-2-propanone [Hydroxyacetone, $HOCH_2C(O)CH_3$]

The absorption spectrum of 1-hydroxy-2-propanone is compared with that of some other substituted ketones in figure IX-F-1, and the approximate cross sections are given in tabular form in table IX-F-2 for wavelengths available within the troposphere. Several possible modes of photodecomposition of hydroxyacetone should be considered in

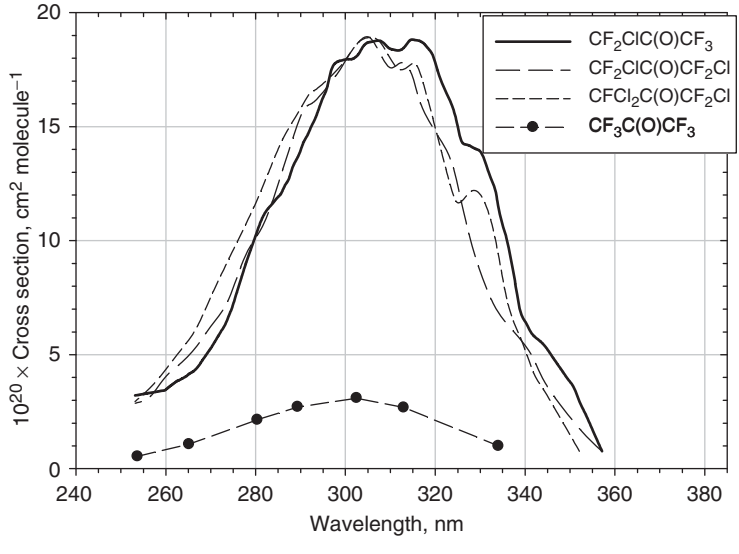

Figure IX-F-3. Comparison of the absorption spectra of some F-, Cl-substituted acetones: $CF_2ClC(O)CF_3$, $CF_2ClC(O)CF_2Cl$, and $CFCl_2C(O)CF_2Cl$ (redrawn from epsilon versus $1/\lambda$ data of Hackett and Phillips, 1974a); $CF_3C(O)CF_3$ data points from Ausloos and Murad (1961); figure from Calvert et al. (2008).

Table IX-F-2. Approximate absorption cross sections (σ, cm^2 $molecule^{-1}$) for hydroxyacetone at 298 K (Orlando et al., 1999); uncertainties (95% confidence limits) in the cross sections are ±10% near the spectral maximum and increase to ±35% at the longest wavelengths reported

λ, nm	$10^{20} \times \sigma$	λ, nm	$10^{20} \times \sigma$
278	5.54	308	0.379
279	5.33	309	0.331
280	5.12	310	0.287
281	4.91	311	0.249
282	4.69	312	0.219
283	4.48	313	0.192
284	4.27	314	0.177
285	4.05	315	0.157
286	3.82	316	0.142
287	3.58	317	0.133
288	3.34	318	0.117
289	3.11	319	0.104
290	2.87	320	0.095
291	2.66	321	0.087
292	2.45	322	0.078
293	2.26	323	0.072
294	2.06	324	0.067
295	1.87	325	0.063
296	1.69	326	0.065
297	1.52	327	0.057
298	1.36	328	0.051
299	1.22	329	0.051
300	1.08	330	0.046
301	0.961	331	0.041
302	0.843	332	0.037
303	0.743	333	0.036
304	0.652	334	0.037
305	0.569	335	0.035
306	0.493	336	0.031
307	0.431		

view of the experimental studies (Calvert et al., 2008):

$$HOCH_2C(O)CH_3 + h\nu \rightarrow HOCH_2 + CH_3CO \quad \text{(I)}$$

$$\rightarrow HOCH_2CO + CH_3 \quad \text{(II)}$$

$$\rightarrow HOCH_2 + CO + CH_3 \quad \text{(III)}$$

$$\rightarrow OH + CH_2C(O)CH_3 \quad \text{(IV)}$$

The minimum energies required to dissociate hydroxyacetone by processes (I), (II), (III), and (IV) are approximately: 335, 335, 377, and 377 $kJ\,mol^{-1}$, respectively (Chowdhury et al., 2002b). From the product analysis following hydroxyacetone/air photolysis in broadband experiments (240–420 nm), Orlando et al. (1999) concluded that at most 50% of the photolysis occurred via channel (I). If the estimated minimum energies for the occurrence of dissociation by (I) and (II) are correct, then it would not

be surprising if both (I) and (II) occurred at roughly the same efficiency. Photolysis of hydroxyacetone was made using light from a lamp-filter combination that mimicked the shape of the solar spectrum in the troposphere ($\lambda > 290$ nm); these experiments suggested that $0.3 \pm 0.2 < \phi_I + \phi_{II} < 0.6$.

Direct observations of OH formation, presumably from process (IV), were made by Chowdhury et al. (2002a) in the photolysis of $HOCH_2COCH_3$ at 248 nm. The initial rotational state of the OH radical was Boltzmann-like, with a single rotational temperature of 450 ± 40 K, and the average relative translational energy of the photofragments was 36.4 kJ mol^{-1}. Chowdhury et al. concluded that the observation of OH with a modest rotational energy, no vibrational energy, and a large translational energy points to a significant exit energy barrier with the dissociation surface.

Dissociation in the 193 nm photolysis of hydroxyacetone appears to occur by process (II) with the initial $HOCH_2CO$ product dissociating to OH and $CH_2{=}C{=}O$ with a rate coefficient $k = 4.6 \pm 5) \times 10^6$ s^{-1} (Chowdhury et al., 2002b).

The photolysis frequencies of $HOCH_2COCH_3$ photodissociation have been calculated versus solar zenith angle for a cloudless, lower troposphere (ozone column = 350 DU) assuming the average quantum yield of dissociation $\phi_I + \phi_{II}$ is in the range 0.3 to 0.6. The current best estimates of j-values lie within the area between the two curves shown in figure IX-F-4.

The photodecomposition of another OH-substituted acetone molecule, diacetone alcohol $[(CH_3)_2C(OH)CH_2C(O)CH_3]$ has been studied by Magneron et al. (2003) in the EUPHORE facility in Valencia, Spain. In this molecule, the OH group is located two carbon atoms down-chain from the carbonyl group. Its estimated photolysis frequency in sunlight was too low to measure ($j < 5 \times 10^{-6}$ s^{-1}).

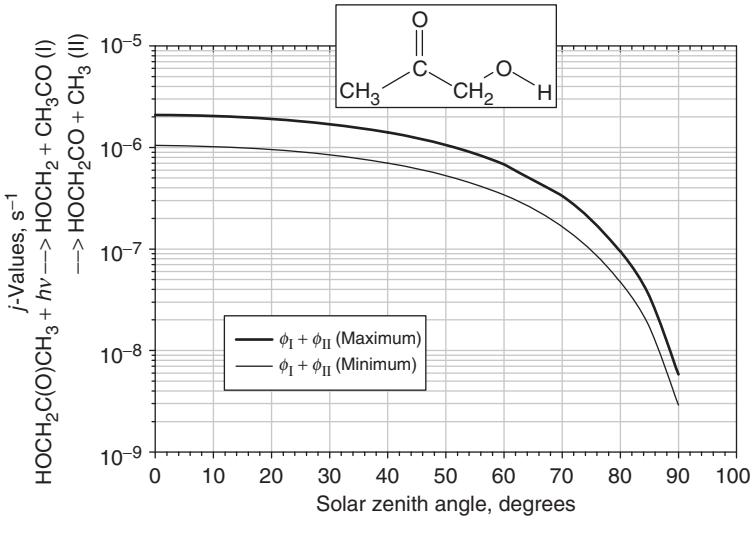

Figure IX-F-4. Approximate photolysis frequencies versus solar zenith angle for $HOCH_2C(O)CH_3$ photodecomposition on a cloudless day in the lower troposphere with an overhead ozone column of 350 DU. The present best estimate of j-values lies between the two curves; figure from Calvert et al. (2008).

Although studies of the the photochemistry of the 1,4-hydroxycarbonyls, common products of the atmospheric oxidation of the long-chain alkanes, would be interesting, none have been made. Until such information is available, Calvert et al. (2008) suggest that one might model the atmospheric chemistry of the 1,4-hydroxycarbonyls using photodecomposition modes and *j*-values that mimic those of the ketone or aldehyde with equivalent lengths of the alkyl chains attached to the carbonyl group. The γ-H-atoms in these molecules are bound relatively weakly and should be abstracted easily by the excited carbonyl group on the occurrence of the Norrish type-II process. For example, one might expect the pathways for the photolysis of the molecule $CH_3CH(OH)CH_2CH_2C(O)CH_3$ to be analogous to those seen in 2-hexanone photolysis: a small quantum yield of free radical formation with a more significant pathway forming two molecules of enol-acetone [$CH_3CH(OH)=CH_2$].

IX-F-3. Photodecomposition of 1-Chloro-2-propanone (Chloroacetone; $ClCH_2C(O)CH_3$)

The absorption spectrum for 1-chloro-2-propanone can be compared with those of some other substituted acetones in figure IX-F-1, and cross sections are given in tabular form in table IX-F-3 for wavelengths available within the troposphere. Calvert et al. (2008) recently reviewed the information related to the photodecomposition of 1-chloro-2-propanone. This was first studied by Strachan and Blacet (1955) who reported the products and quantum yields from photolysis of the pure ketone at 313 nm and temperatures of 59–335°C. Products identified by mass spectrometry were: HCl, $CH_3C(O)CH_3$, $[CH_3C(O)CH_2]_2$, and $CH_3C(O)CH=CHC(O)CH_3$. The following quantum yields of the major product, HCl, were reported from experiments at temperatures of 59, 60, 150, (150), 204, 252, 301, and 335°C, respectively: 0.72, 0.86, 0.78, (0.87), 0.95, 1.02, 1.23, and 1.49. Yields of CO and CH_4 were immeasurably small at temperatures $\leq$ 59°C, but these products were formed in measurable and increasing yields as the temperature was raised from 60 to 335°C. Photolyses were also carried out in mixtures with NO or I_2. NO suppressed the formation of both acetone and acetonylacetone as the product $CH_3C(O)CH_2NO$ appeared. Photolyses with mixtures of I_2 were less readily interpreted, but I_2 suppressed acetonylacetone formation as $ICH_2C(O)CH_3$ appeared as a product. However, HCl formation was not suppressed completely by I_2 addition (10 Torr). From their studies, Strachan and Blacet concluded that a new type of primary process, process (I), occurred in α-substituted carbonyls such as $ClCH_2C(O)CH_3$. Several other primary processes, analogous to those seen in acetone, were considered as minor in experiments at the lower temperatures employed.

$$ClCH_2C(O)CH_3 + h\nu \rightarrow Cl + CH_2C(O)CH_3 \quad \text{(I)}$$

$$\rightarrow CH_2Cl + CH_3CO \quad \text{(II)}$$

$$\rightarrow CH_2ClCO + CH_3 \quad \text{(III)}$$

$$\rightarrow CH_3 + CO + CH_2Cl \quad \text{(IV)}$$

$$\rightarrow CH_3C(O)CH + HCl \quad \text{(V)}$$

Table IX-F-3. Absorption cross sections (σ, cm^2 $molecule^{-1}$) for chloroacetone at 298 K for the wavelengths of sunlight available within the troposphere (Burkholder et al., 2002)

λ, nm	$10^{19} \times \sigma$	λ, nm	$10^{19} \times \sigma$	λ, nm	$10^{19} \times \sigma$
278	0.859	306	0.794	334	0.0707
279	0.882	307	0.763	335	0.0598
280	0.903	308	0.734	336	0.0506
281	0.923	309	0.706	337	0.0427
282	0.941	310	0.677	338	0.0361
283	0.956	311	0.650	339	0.0302
284	0.969	312	0.622	340	0.0252
285	0.980	313	0.593	341	0.0212
286	0.989	314	0.561	342	0.0176
287	0.998	315	0.528	343	0.0145
288	1.00	316	0.492	344	0.0120
289	1.01	317	0.457	345	0.0103
290	1.02	318	0.422	346	0.00887
291	1.02	319	0.389	347	0.00757
292	1.02	320	0.358	348	0.00642
293	1.02	321	0.330	349	0.00547
294	1.01	322	0.304	350	0.00458
295	1.00	323	0.280	351	0.00411
296	0.980	324	0.258	352	0.00328
297	0.977	325	0.237	353	0.00319
298	0.966	326	0.216	354	0.00220
299	0.954	327	0.195	355	0.00193
300	0.941	328	0.173	356	0.00138
301	0.925	329	0.152	357	0.00134
302	0.904	330	0.133	358	0.00092
303	0.880	331	0.114	359	0.00155
304	0.853	332	0.0979	360	0.00128
305	0.824	333	0.0832		

The absence of CO and CH_4 in the products from experiments at lowest temperatures showed that (III) and (IV) were unimportant, and the small quantum yield of CO (0.027, 0.022) observed in experiments at 150°C, where CH_3CO decomposition is rapid, suggests that process (II) is also not important. Process (V) was considered possible in view of tentative identification of $CH_3COCH{=}CHCOCH_3$ in the products and the failure of I_2 to suppress HCl formation completely.

Waschewsky et al. (1994) used crossed laser-molecular beam experiments to monitor the competition between photodissociation pathways in chloroacetone. Their studies proved that C—C bond fission, process (II), competes with C—Cl bond fission, process (I), in $ClCH_2C(O)CH_3$ photolysis at 308 nm, although the latter process is favored. Several kJ of translational energy were evident in the translation of the initial products of the two competing dissociation pathways. The authors point out that this may indicate that, for both channels, dissociation proceeds via a reaction coordinate that has a significant exit barrier (barrier to reverse reaction), so fragments exert a repulsive force on each other as they separate. The pathway to dissociation probably does not involve

internal conversion to the ground electronic state, as the barrier to reverse reaction in the ground state is negligible.

The *gauche* (Cl- and O-atoms in closest position) and *anti* conformers (Cl- and O-atoms in a more distant position) of $ClCH_2C(O)CH_3$ show different efficiencies of C—C and C—Cl bond cleavage; the splitting at the C—Cl bond is consistently larger (by at least a factor of 7, and as much as a factor of 30) in *gauche* chloroacetone than in the *anti*-conformer for equivalent C=O distances. The authors suggest that the presence of large nonadiabatic effects along the C—C fission reaction coordinate in *anti*-chloroacetone suppresses C—C fission, allowing C—Cl fission to dominate. It is uncertain how these results obtained at low pressures and somewhat elevated temperatures would compare with those for chloroacetone photodissociation in air at 1 atm.

Studies by Burkholder et al. (2002) support the conclusion that the photodecomposition of chloroacetone is efficient, although the nature of the primary processes was not determined in their studies. In broadband photolysis with fluorescent blacklamps (300–400 nm) and in experiments with pulsed excimer lasers (308 and 351 nm), the loss of parent ketone was determined relative to photolysis of NO_2, Cl_2, and CH_2I_2 as reference compounds. Quantum yields of photodissociation (disappearance) of $ClCH_2C(O)CH_3$ both at 351 and 308 nm were determined to be 0.5 ± 0.08. The photolysis rate coefficients were independent of the total cell pressure between 50 and 600 Torr of air. CO and CO_2 produced were about one-half of the chloroacetone lost, consistent with the significant occurrence of processes (II), (III), and/or (IV). Although HCl was not detected in the photolysis with blacklamps, it was detected as a product from excimer laser photolysis by Burkholder et al. (2002) as well as in the studies of Strachan and Blacet (1955). A likely fate of Cl-atoms formed in (I) is the abstraction of H-atoms from the parent ketone $ClCH_2C(O)CH_3$ molecule. Hence, the observed HCl may arise following process (I) and/or from process (V). Burkholder et al. (2002) concluded that the effective quantum yields for atmospheric photodissociation are significant, probably greater than 0.5. It seems likely that the photodecomposition of chloroacetone lies between 0.5 and 1.0 over much of the spectral range available in tropospheric sunlight. Assuming this range of quantum yield values and using the cross section data of Burkholder et al. (2002), Calvert et al. (2008) calculated the range of probable photolysis frequencies of $CH_2ClC(O)CH_3$ as a function of solar zenith angle for a cloudless day within the troposphere (ozone column = 350 DU). These data are given in figure IX-F-5.

It is interesting to note the exploratory study of the photolyses of 3-chloro-2 butanone [$CH_3CHClC(O)CH_3$] and 4-chloro-2-butanone [$CH_2ClCH_2C(O)CH_3$] by Taylor and Blacet (1956a); the former compound gave results analogous to those obtained for chloroacetone (C—Cl bond cleavage), while the latter compound appeared to favor C—C bond dissociation, analogous to 2-butanone.

IX-F-4. Photodecomposition of 1-Bromo-2-propanone [Bromoacetone, $BrCH_2C(O)CH_3$]

The absorption spectrum of 1-bromo-2-propanone is compared with those of other monosubstituted acetones in figure IX-F-1 and the cross sections are listed in tabular

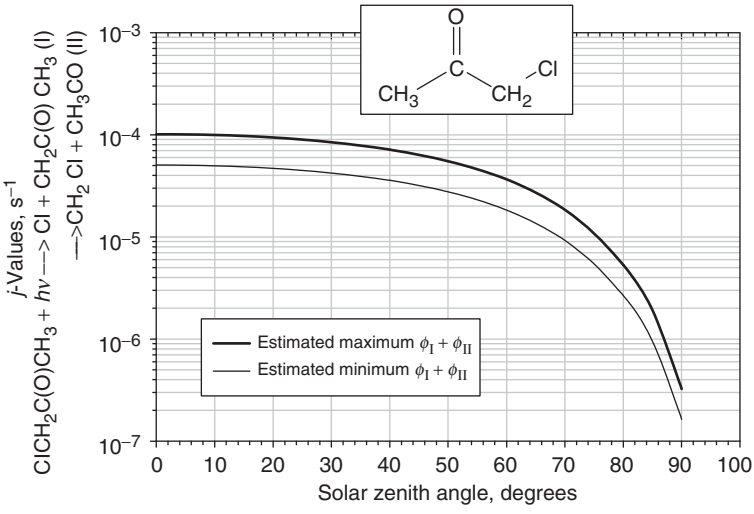

Figure IX-F-5. Approximate photolysis frequencies versus solar zenith angle for $ClCH_2C(O)CH_3$ photodecomposition on a cloudless day in the lower troposphere with an overhead ozone column of 350 DU. The present best estimate of *j*-values lies between the two curves; figure from Calvert et al. (2008).

form in table IX-F-4 as a function of wavelength. It is apparent that bromoacetone absorbs the wavelengths of sunlight present within the troposphere much more efficiently than fluoroacetone and chloroacetone.

The photodecomposition of 1-bromo-2-propanone was reviewed recently by Calvert et al. (2008). The photodecomposition has been studied at 308 nm in crossed laser molecular beam experiments by Waschewsky et al. (1994) and Kash et al. (1994) and in broadband photolysis (300–400 nm) and laser beam photolysis at 308 and 351 nm by Burkholder et al. (2002). The photodecomposition follows the pattern of 1-chloro-2-propanone. The following primary processes should be considered:

$$CH_2BrC(O)CH_3 + h\nu \rightarrow Br + CH_2C(O)CH_3 \quad \text{(I)}$$

$$\rightarrow CH_2Br + CH_3CO \quad \text{(II)}$$

$$\rightarrow CH_2BrCO + CH_3 \quad \text{(III)}$$

$$\rightarrow CH_3 + CO + CH_2Br \quad \text{(IV)}$$

The results of Waschewski et al. (1994) and Kash et al. (1994) in experiments at 308 nm suggest that in a thermal population of 1-bromo-2-propanone conformers (*gauche* and *anti*-), photodissociation at 308 nm occurs largely from Br—C fission, process (I), and by fission of one of the two C—C bonds, process (II). The angular distribution of Br atoms shows that C—Br fission occurs primarily from the minor *anti*-conformer, not the dominant *gauche* structure. Low-level *ab initio* calculations show C—Br fission is more nonadiabatically suppressed in the *anti*-conformer than in the *gauche* form.

Table IX-F-4. Absorption cross sections (σ, cm^2 $molecule^{-1}$) for 1-bromo-2-propanone at 298 K for the wavelengths of sunlight available within the troposphere (Burkholder et al., 2002)

λ, nm	$10^{19} \times \sigma$	λ, nm	$10^{19} \times \sigma$	λ, nm	$10^{19} \times \sigma$
278	0.774	306	1.11	334	0.251
279	0.800	307	1.09	335	0.226
280	0.825	308	1.07	336	0.202
281	0.850	309	1.04	337	0.180
282	0.875	310	1.02	338	0.160
283	0.904	311	0.989	339	0.141
284	0.929	312	0.962	340	0.124
285	0.958	313	0.936	341	0.109
286	0.978	314	0.910	342	0.0955
287	0.998	315	0.882	343	0.0831
288	1.02	316	0.852	344	0.0724
289	1.04	317	0.819	345	0.0627
290	1.06	318	0.783	346	0.0545
291	1.08	319	0.745	347	0.0473
292	1.10	320	0.706	348	0.0408
293	1.11	321	0.666	349	0.0351
294	1.12	322	0.628	350	0.0303
295	1.13	323	0.589	351	0.0259
296	1.14	324	0.555	352	0.0223
297	1.14	325	0.520	353	0.0190
298	1.15	326	0.487	354	0.0164
299	1.15	327	0.455	355	0.0140
300	1.15	328	0.424	356	0.0120
301	1.14	329	0.394	357	0.0108
302	1.14	330	0.364	358	0.00952
303	1.13	331	0.335	359	0.00838
304	1.12	332	0.306	360	0.00784
305	1.11	333	0.277		

The conformation dependence of the ratio of C—C to C—Br branching ratio is not determined by the C—Br fission reaction coordinate. In the molecular beam experiments with nozzle temperatures of 100° and 400°C, the experimentally observed ratio was: $\phi_I/\phi_{II} \cong 5.7$ and 3.5, respectively. It is uncertain how these results obtained at low pressures and somewhat elevated temperatures would compare with those for 1-bromo-2-propanone photodissociation at the lower temperatures of the troposphere with 1 atm. of air. No evidence for the occurrence of the processes (III) and (IV) was obtained, but by analogy with the photolysis of acetone, these processes are expected to occur to some extent in photolysis at the shorter wavelengths of absorbed light.

In the experiments of Burkholder et al. (2002), the loss of 1-bromo-2-propanone was determined in broadband photolysis (308–351 nm) in air. The authors concluded that the quantum yield for the dissociation of bromoacetone is greater than 0.5. The amounts of CO and CO_2 produced were about one-half of the bromoacetone lost, so it seems likely that processes (II), (III), and/or (IV) occur to some extent. HBr was

not detected. Pulsed laser photolysis of bromoacetone was referenced to photolyses of NO_2, Cl_2, and CH_2I_2 to estimate photodissociation quantum yelds of 1.0 $\pm$0.15 and 1.6 $\pm$ 0.25 at 308 and 351 nm, respectively.

In view of the limited results outlined above, only approximate *j*-values related to total photodissociation can be calculated in the present work. Calvert et al. (2008) have used the cross section data of Burkholder et al. (2002) and quantum yields limits of 0.5 and 1.0 together with the appropriate solar flux (ozone column = 350 DU) to derive approximate *j*-values for 1-bromo-2-propanone photodissociation on a cloudless day in the lower troposphere; see figure IX-F-6.

IX-F-5. Photodecomposition of 1,1,1-Trifluoro-2-propanone [$CF_3C(O)CH_3$] and 1,1,1,3,3,3-Hexafluoro-2-propanone [$CF_3C(O)CF_3$]

Data necessary to evaluate the photolysis frequencies of these two ketones in air are limited, but it is clear that both ketones follow a pattern of photodissociation related to that observed for acetone. The photochemistry of these ketones has been reviewed recently by Calvert et al. (2008). Approximate cross sections for $CH_3C(O)CF_3$ are given in figure IX-F-2. The light solid line has been redrawn from the $1/\lambda$ versus molar extinction coeffient plot of Beavan et al. (1978). These data are also consistent with those reported by Hackett and Phillips (1974a). It is clear that the absorption

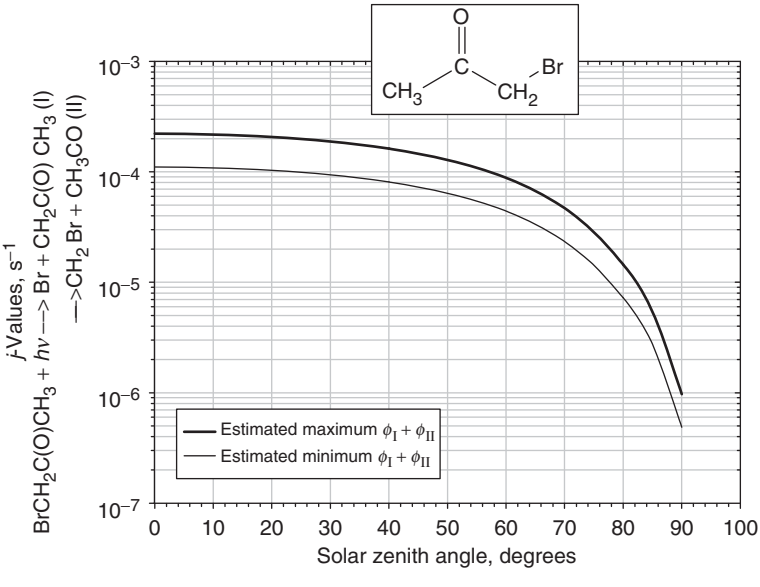

Figure IX-F-6. Approximate photolysis frequencies versus solar zenith angle for $BrCH_2C(O)CH_3$ photodecomposition on a cloudless day in the lower troposphere with an overhead ozone column of 350 DU. The present best estimate of *j*-values lies between the two curves; figure from Calvert et al. (2008).

maximum is shifted somewhat to longer wavelengths than $CH_3C(O)CH_3$ and that the cross sections of $CF_3C(O)CH_3$ are significantly lower than those for unsubstituted acetone (by a factor of about 0.6). Also shown in figure IX-F-2 are the cross sections for $CF_3C(O)CF_3$ as measured at several discrete wavelengths by Ausloos and Murad (1961). A trend line has been drawn through these data points to provide an approximate envelope for the absorption of $CF_3C(O)CF_3$. Note that the absorption maximum is shifted to longer wavelengths than that for $CF_3C(O)CH_3$, although the magnitude of the maximum in the cross section is relatively unchanged from that of $CF_3C(O)CH_3$

Discussion of the photochemistry and photophysics of 1,1,1-trifluoro-2-propanone and 1,1,1,2,2,2-hexafluoroacetone (efficiency of fluorescence, phosphorescence, intersystem crossing efficiency, lifetimes of excited states, etc.) have been given in the literature; e.g., for $CF_3C(O)CH_3$ see Ausloos and Murad (1961); Dawidowicz and Patrick (1964); Beavan et al. (1975); Gandini and Hackett (1976/1977), (1977a); Beavan et al. (1978). For $CF_3C(O)CF_3$ see Ayscough and Steacie (1956), Whytock and Kutschke (1968); Gandini and Kutschke (1968); Gandini et al. (1968a, b, c); Halpern and Ware (1970, 1971); Hackett and Kutschke (1977). The mechanisms considered for light emission and photodecomposition of the fluorine-substituted ketones are similar to those described for acetone in section IX-D-1.

The photodecomposition of $CF_3C(O)CH_3$ was first studied by Sieger (1954) and Sieger and Calvert (1954) in photolysis studies at 313 nm using relatively high pressures of the ketone (250 Torr at 25°C) and temperatures in the range 25–350°C. The measurements were limited to the determination of the quantum yields of CO, C_2H_6, CH_3CF_3, CF_3CF_3, CH_4, and CF_3H. These data suggested that the primary photodissociation occurred with both CF_3—$C(O)CH_3$ and $CF_3C(O)$—CH_3 bond cleavage, with process (II) being somewhat favored.

$$CF_3C(O)CH_3 + h\nu \rightarrow CF_3 + CH_3CO \quad \text{(I)}$$

$$\rightarrow CH_3 + CF_3CO \quad \text{(II)}$$

$$\rightarrow CF_3 + CO + CH_3 \quad \text{(III)}$$

However, in the study of Dawidowicz and Patrick (1964) with full Hg-arc photodecomposition of $CF_3C(O)CH_3$ at 45 ± 5°C, the observed major products were: $CH_3C(O)C(O)CH_3$, C_2H_6, C_2F_6, CH_3CF_3, $CH_3C(O)CH_3$, and $CH_3CF_2CH_3$with small amounts of CH_4 and CF_3H. From the observed formation of 2,3-butanedione and the absence of any products containing the CF_3CO fragment, these authors concluded that process (I) was the dominant photodecomposition mode. In view of the weak CF_3—CO bond compared to the CH_3—CO bond, it is possible that the low yield of CF_3CO-containing molecules in the study of Dawidowicz and Patrick (1964) is a result of CF_3CO decomposition at 45°C, and thus these data do not rule out channel (II). Formation of the product $CH_3CF_2CH_3$ in this study remains unexplained. Amphlett and Whittle (1967) determined the activation energy for $CF_3CO \rightarrow CF_3 + CO$ to be ~12-24 kJ mol^{-1}. More recently Maricq and Szente (1995) and Tomas et al. (2000) measured ~52 and ~49 kJ mol^{-1}, respectively, for this activation energy. All these measurements

are somewhat lower than those for CH_3CO decomposition ($E_a \approx 72\,kJ\,mol^{-1}$, Baulch et al., 1992). Theoretical studies (Viskolcz and Berces, 2000; Méreau et al., 2001) support this view. These data suggest that significantly less energy ($\sim 22\,kJ\,mol^{-1}$) is required for dissociation of $CF_3C(O)CH_3$ by process (I) than by process (II), assuming that the barriers for the two reverse reactions ($R + CO \rightarrow RCO$) are equal. Thus, one expects some preference to the photodissociation by process (I), particularly at the longer wavelengths of absorbed light.

Photodecomposition of $CF_3C(O)CF_3$ follows the pattern outlined for acetone and $CF_3C(O)CH_3$:

$$CF_3C(O)CF_3 + h\nu \rightarrow CF_3 + CF_3CO \quad \text{(I)}$$

$$\rightarrow (CF_3CO)^* \rightarrow CO + CF_3 \quad \text{(II)}$$

Figure IX-F-7, presented by Calvert et al. (2008), gives an interesting comparison of the quantum yields of CO from $CF_3C(O)CH_3$, $CF_3C(O)CF_3$, and $CH_3C(O)CH_3$ as a function of temperature for photolysis at 313 nm. These data provide some insight into mechanisms of photodissociation of the three ketones. In figure IX-F-7a it can be seen that the Cundall and Davies (1966) data from $CH_3C(O)CH_3$ at 50 Torr pressure lie well above those from the $CF_3C(O)CH_3$ data of Sieger and Calvert (1954) that were determined at much higher ketone pressures (250–477 Torr) but at constant number density. The $CF_3C(O)CF_3$ data of Ayscough and Steacie (1956) for 25 Torr pressure lie above those obtained at about 95 Torr and near those for $CH_3C(O)CH_3$ determined by Cundall and Davies (1966) at 50 Torr pressure. The differences in pressure employed in these studies tend to mask differences in quantum yields that exist, since the extent of self-quenching will be different for experiments at different pressures. Calvert et al. (2008) have attempted to remove the differences due to quenching by adjusting the $CF_3C(O)CF_3$ data to the same pressures as those used for the $CH_3C(O)CH_3$ and $CF_3C(O)CH_3$ studies. Use was made of the Ayscough and Steacie Φ_{CO} measurements as a function of $CF_3C(O)CF_3$ pressure. The k_q/k_d values for the five temperatures that they used (27–219°C) can be summarized in the equation: $\log_{10}(k_q/k_d) = 0.175 - 0.0291T + 4.86 \times 10^{-5}T^2$. This equation was used to derive k_q/k_d values for the temperatures employed in the experiments by Sieger and Calvert [$CF_3C(O)CH_3$] and Cundall and Davies [$CH_3C(O)CH_3$] that were then used to adjust the Ayscough and Steacie reported quantum yield data to the pressures of the ketones employed by Sieger and Calvert, and Cundall and Davies. The results are shown in figure IX-F-7b. Note that the originally divergent curves of figure IX-F-7a converge significantly: $CF_3C(O)CF_3$ data when adjusted to 50 Torr match reasonably well those of acetone at that pressure as measured by Cundall and Davies (1966), while adjustment of the $CF_3C(O)CF_3$ data to the higher pressures employed for $CF_3C(O)CH_3$ by Sieger and Calvert leads to significant closure of the $CF_3C(O)CF_3$ and $CF_3C(O)CH_3$ datasets. However, the Φ_{CO} values for $CF_3C(O)CF_3$ still lie somewhat above those for $CH_3C(O)CH_3$ at 50 Torr and $CF_3C(O)CH_3$ at 250 Torr (298 K) at the lower temperatures. This could reflect the lower thermal stability of the CF_3CO radical formed

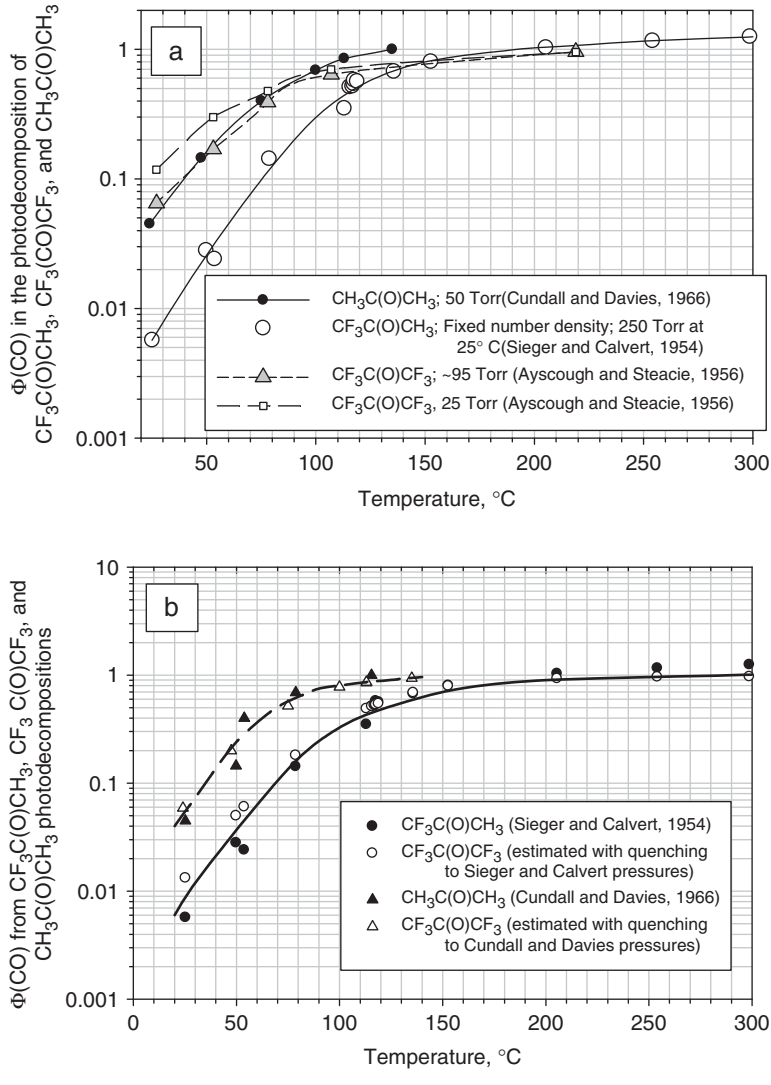

Figure IX-F-7. Comparison of quantum yields of CO from $CF_3C(O)CH_3$, $CH_3C(O)CH_3$, and $CF_3C(O)CF_3$from photolysis at 313 nm as a function of temperature 23–300°C. (a) Data as determined at several pressures of the ketones. (b) $CF_3C(O)CF_3$ data of Ayscough and Steacie (1956) adjusted for quenching to the pressures of the measurements of Sieger and Calvert (1954) for $CF_3C(O)CH_3$, and to the pressures of the measurements of Cundall and Davies (1966) for $CH_3C(O)CH_3$. The k_q/k_d data for $CF_3C(O)CF_3$ from Ayscough and Steacie were used in the calculations. The figure is from Calvert et al. (2008).

in $CF_3C(O)CF_3$ photolysis compared to the somewhat more stable CH_3CO radical formed from $CH_3C(O)CH_3$ and presumably favored in $CF_3C(O)CH_3$ photolysis as well.

Gandini and Hackett (1977a) determined both the quantum yields of CO and 2,3-butanedione in the photolyses of $CF_3C(O)CH_3$ and $CH_3C(O)CH_3$ as a function of wavelength in experiments at 22°C. See figures IX-F-8 and IX-F-9. The Φ_{CO} values determined with both ketones are similar at the longest wavelengths (305–313 nm), and they both approach unity at the shortest wavelengths. Over most of the range of wavelengths given in figure VII-F-8, quantum yields from $CF_3C(O)CH_3$ exceed those of $CH_3C(O)CH_3$ by significant factors (~1.3 to 2.0). The differences seen are opposite to those expected from the difference in the extent of self-quenching for the two ketones [$CH_3C(O)CH_3$ was at 13.5 Torr and $CF_3C(O)CH_3$ at 20 Torr]. Since most evidence suggests that both ketones favor photodissociation to form CH_3CO radicals in the primary process (I), these data may indicate that $CF_3C(O)CH_3$ has either a somewhat larger ϕ_I than $CH_3C(O)CH_3$ or that a larger fraction of the dissociation in $CF_3C(O)CH_3$ forms CO in the primary process (III).

The 2,3-butanedione quantum yields shown in figure IX-F-9 give a somewhat different picture. $CH_3C(O)CH_3$ has about twice the quantum yield for 2,3-butanedione formation than $CF_3C(O)CH_3$, presumably reflecting a greater quantum yield of CH_3CO radicals from $CH_3C(O)CH_3$ at all wavelengths. The presence of neither $CF_3C(O)C(O)CH_3$ nor $CF_3C(O)C(O)CF_3$ was reported in the Gandini and Hackett study. Their very sensitive analysis method for 2,2-butanedione depended on the measurement of the sensitized phosphorescence of this compound. It is not clear whether this technique was unique to the detection of $CH_3C(O)C(O)CH_3$ or whether some

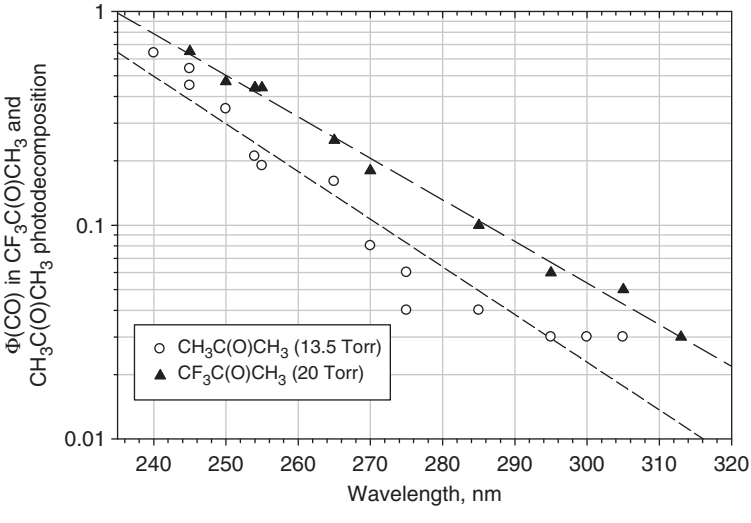

Figure IX-F-8. Quantum yields of CO as a function of wavelength in photolyses of $CF_3C(O)CH_3$ (20 Torr) and $CH_3C(O)CH_3$ (13.5 Torr) as measured by Gandini and Hackett (1977a) at 22°C. The figure is from Calvert et al. (2008).

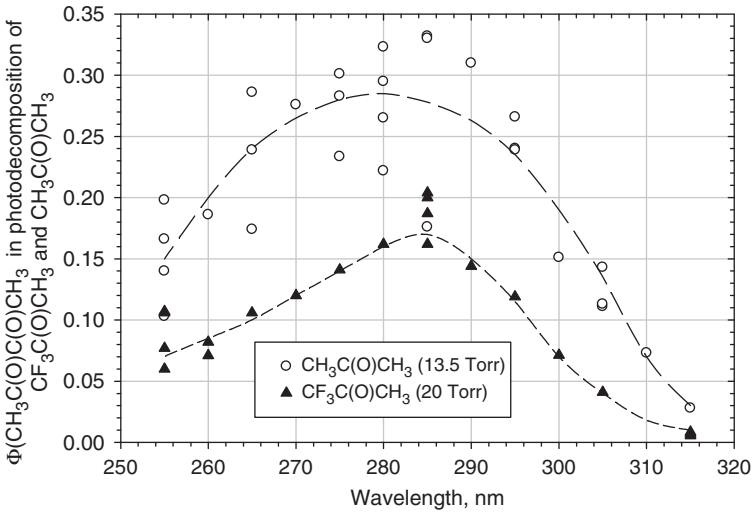

Figure IX-F-9. Quantum yields of 2,3-butanedione from photolyses of $CF_3C(O)CH_3$ (20 Torr) and $CH_3C(O)CH_3$ (13.5 Torr) as measured by Gandini and Hackett (1977a) at 22°C. The figure is from Calvert et al. (2008).

contribution from emission of the fluorinated 2,3-butanediones was possible. Gandini and Hackett comment on "the known instability of the trifluoroacetyl radical at room temperature," and apparently dismiss as unlikely the formation of $CF_3COCOCH_3$ and $CF_3COCOCF_3$. As evidence, they quote the work of Amphlett and Whittle (1967) who demonstrated that CF_3CO is less stable than CH_3CO at 25°C.

In view of the conflicting evidence on the magnitude of the quantum yields of the primary processes in $CF_3C(O)CH_3$, the uncertainties in the absorption cross sections, and the lack of information on the effect of an atmosphere of air on these values, estimates of the photolysis frequencies of these two ketones remain uncertain. In figure IX-F-10 approximate values for these quantities have been estimated for $CF_3C(O)CH_3$ by Calvert et al. (2008) using the maximum quantum yields as a function of wavelength as estimated for acetone in air ($\phi_I + \phi_{IIb}$) in table IX-D-2, coupled with the cross section data for $CF_3C(O)CH_3$ given by Beavan et al. (1978) (figure IX-F-2 and table IX-F-5) and the appropriate solar flux (ozone column = 350 DU) for a cloudless day within the lower troposphere. Uncertainties in the cross section values and major uncertainties in the quantum yields as a function of wavelength point to the very approximate nature of the current *j*-value estimates for $CF_3C(O)CH_3$.

Rough estimates of the photolysis frequencies for $CF_3C(O)CF_3$ were calculated by Calvert et al. (2008) for a cloudless day within the lower troposphere (ozone column = 350 DU) as a function of solar zenith angle; these data are given in figure IX-F-11. The approximate cross section data given by Ausloos and Murad (1961) (figure IX-F-2 and table IX-F-5) and quantum yields as a function of wavelength as estimated for $CH_3C(O)CH_3[\phi_{total}$ (maximum)] in table IX-D-2. Major uncertainties exist in both the

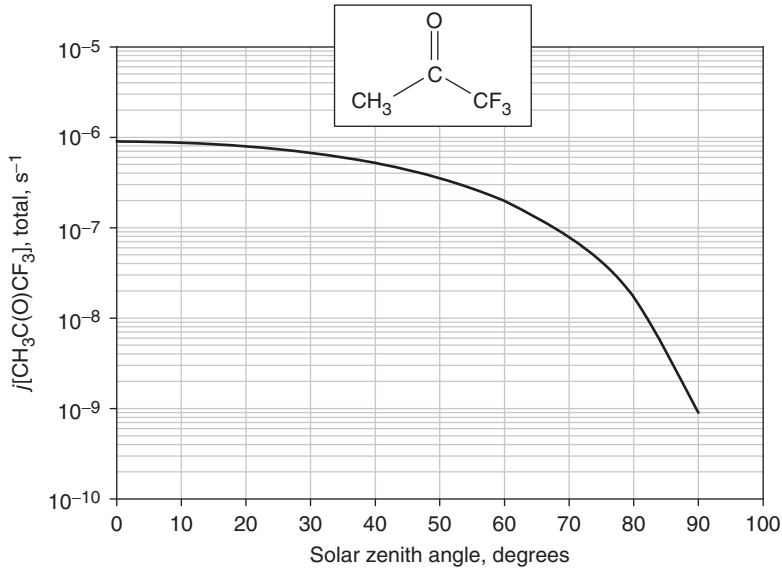

Figure IX-F-10. Approximate photolysis frequencies versus solar zenith angle for $CF_3C(O)CH_3$ photodecomposition (total) on a cloudless day in the lower troposphere with an overhead ozone column of 350 DU. ϕ_{total} (maximum) for $CH_3C(O)CH_3$ given in table IX-D-2 were used together with the cross sections for $CH_3C(O)CF_3$ from Beavan et al. (1975).

cross section and the quantum yield data for $CF_3C(O)CF_3$, and the *j*-value estimates for $CF_3C(O)CF_3$ are of highly uncertain accuracy.

IX-F-6. Photodecomposition of Highly Halogen-Atom-Substituted Acetones

The photophysics and limited data on the photochemistry of several F- and Cl-containing, multisubstituted acetone molecules have been reported: e.g., $CF_2Cl(O)CF_3$, $CF_2ClC(O)CF_2Cl$, $CFCl_2C(O)CF_2Cl$, $CFCl_2C(O)CFCl_2$, $CCl_3C(O)CCl_3$ (Majer et al., 1971; Hackett and Phillips, 1974a, b, c, d); $CF_3C(O)CH_2Br$ (Majer et al., 1976; Majer and Al-Saigh, 1984). The absorption spectra of several of these molecules, given in figure IX-F-3, show that replacement of F-atoms by one, two, or three Cl-atoms in the $CF_3C(O)CF_3$ molecule leads to a large enhancement of the maximum in the cross section (by about a factor of 6). It is clear that these molecules absorb a much larger fraction of the actinic flux available within the troposphere than $CF_3C(O)CH_3$ and $CF_3C(O)CF_3$, and their photochemistry is probably important within the troposphere. Evidence suggests that photolysis results in a C—C bond rupture, but it is unclear as to the extent, if any, to which a C—Cl bond rupture competes with this process. The existing information on the modes and efficiencies of photodissociation has not been explored in sufficient detail to allow meaningful estimates of their tropospheric photolysis rates.

Table IX-F-5. Absorption cross sections (σ, cm^2 $molecule^{-1}$) for $CF_3C(O)CH_3$ (A),[a] $CF_3C(O)CF_3$ (B),[b] and $CF_3CF_2C(O)CF(CF_3)_2$(C)[c] as a function of wavelength

λ, nm	(A) $10^{20} \times \sigma$	(B) $10^{20} \times \sigma$	(C) $10^{20} \times \sigma$	λ, nm	(A) $10^{20} \times \sigma$	(B) $10^{20} \times \sigma$	(C) $10^{20} \times \sigma$	λ, nm	(C) $10^{20} \times \sigma$
278	3.10	1.97	3.35	316	1.05	2.46	6.19	354	0.296
279	3.12	2.04	3.51	317	0.99	2.38	6.09	355	0.229
280	3.13	2.12	3.68	318	0.93	2.30	5.96	356	0.176
281	3.12	2.18	3.85	319	0.87	2.23	5.80	357	0.136
282	3.11	2.26	4.02	320	0.82	2.15	5.62	358	0.106
283	3.07	2.33	4.19	321	0.77	2.07	5.42	359	0.085
284	3.05	2.41	4.36	322	0.72	1.99	5.20	360	0.069
285	3.02	2.48	4.52	323	0.67	1.90	4.99	361	0.058
286	2.98	2.55	4.68	324	0.63	1.83	4.79	362	0.049
287	2.94	2.63	4.84	325	0.58	1.79	4.60	363	0.042
288	2.88	2.69	5.01	326	0.54	1.66	4.44	364	0.037
289	2.84	2.76	5.17	327	0.49	1.57	4.29	365	0.033
290	2.79	2.82	5.33	328	0.45	1.50	4.15	366	0.030
291	2.73	2.87	5.48	329	0.41	1.42	4.01	367	0.029
292	2.67	2.93	5.63	330	0.37	1.33	3.85	368	0.027
293	2.63	2.97	5.78	331	0.33	1.25	3.68	369	0.025
294	2.56	3.02	5.90	332	0.28	1.16	3.48	370	0.024
295	2.50	3.05	6.03	333	0.24	1.08	3.27	371	0.024
296	2.43	3.06	6.14	334	0.21	1.00	3.03	372	0.023
297	2.36	3.07	6.24	335	0.18	0.92	2.79	373	0.023
298	2.29	3.08	6.33	336	0.16	0.89	2.55	374	0.023
299	2.23	3.08	6.41	337	0.13	0.75	2.33	375	0.023
300	2.15	3.09	6.49	338	0.10	0.67	2.12	376	0.023
301	2.08	3.09	6.57	339	0.07	0.60	1.94	377	0.022
302	2.02	3.09	6.64	340	0.05	0.50	1.78	378	0.020
303	1.95	3.07	6.70	341	0.03	0.43	1.65	379	0.019
304	1.88	3.06	6.74	342	0.00	0.37	1.54	380	0.017
305	1.83	3.04	6.77	343		0.30	1.44	381	0.015
306	1.76	3.02	6.77	344		0.23	1.35	382	0.013
307	1.71	2.98	6.76	345		0.16	1.25	383	0.011
308	1.64	2.94	6.72	346		0.09	1.15	384	0.009
309	1.56	2.90	6.66	347		0.03	1.04	385	0.008
310	1.49	2.85	6.60	348		0.00	0.928	386	0.007
311	1.42	2.79	6.53	349			0.809	387	0.007
312	1.34	2.73	6.47	350			0.690	388	0.006
313	1.26	2.66	6.40	351			0.576	389	0.005
314	1.19	2.60	6.34	352			0.471	390	0.005
315	1.13	2.53	6.27	353			0.376		

[a]Data from Beaven et al. (1978).
[b]Data extrapolated from Ausloos and Murad (1961) measurements at selected wavelengths.
[c]Data from D'Anna et al. (2005a).

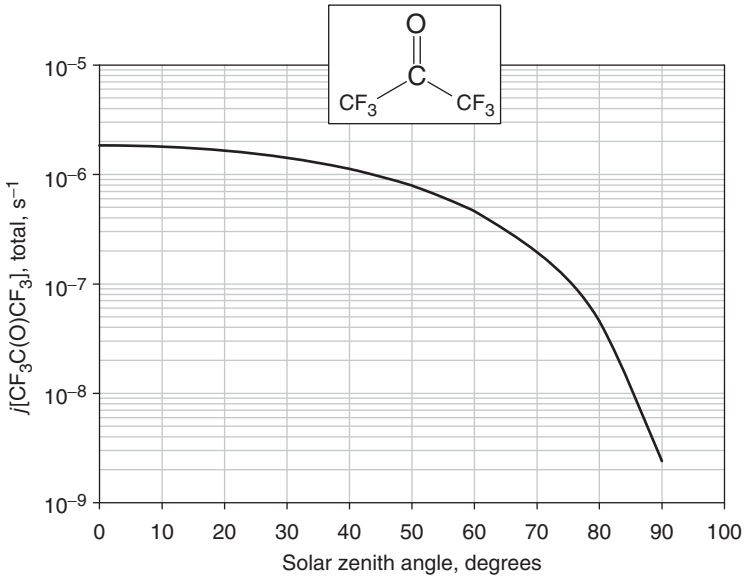

Figure IX-F-11. Approximate photolysis frequencies versus solar zenith angle for $CF_3C(O)CF_3$ total photodecomposition on a cloudless day in the lower troposphere with an overhead ozone column of 350 DU. Limited cross section data from Ausloos and Murad (1961) were used, and $\phi_I + \phi_{II}$ values were assumed to be equal to ϕ_{total} (maximum) for $CH_3C(O)CH_3$ given in table IX-D-02.

IX-F-7. Photodecomposition of Perfluoro-2-methyl-3-pentanone [$CF_3CF_2C(O)CF(CF_3)_2$]

The absorption spectrum of perfluoro-2-methyl-3-pentanone, is shown in figure IX-F-12. The measurements of Taniguchi et al. (2003), shown as open circles in the figure, and those of D'Anna et al. (2005a), given as a heavy line, are seen to be in good agreement. Calvert et al. (2008) compared these spectra with the spectrum for an unsubsitituted ketone of a somewhat similar structure, 2,4-dimethyl-3-pentanone, $(CH_3)_2CHC(O)CH(CH_3)_2$, given by the thin line in figure IX-F-12. As observed with the simpler ketones, the substitution of fluorine for H-atoms shifts the absorption to longer wavelengths and decreases the absorption maximum somewhat.

The photodecomposition of this fluorine-substituted ketone in mixtures with 50–700 Torr of air was first studied by Taniguchi et al. (2003) using a smog-chamber with Fourier-transform infrared techniques and sunlamps or blacklamps as the radiation source. They followed the decay through the formation of its major products $CF_3C(O)F$ and FC(O)F. In similar experiments the rates of photodecomposition of isotopically labeled acetaldehyde ($^{13}CH_3^{13}CHO$) were determined by following the ^{13}CO product. The estimated *j*-values for CH_3CHO in air (Calvert et al., 2000), and the relative rates of photodecomposition were used to estimate that the photochemical lifetime of the perfluoro-ketone is approximately 1–2 weeks. The estimate is necessarily approximate since the absorption band of the perfluoro-ketone is shifted to somewhat longer

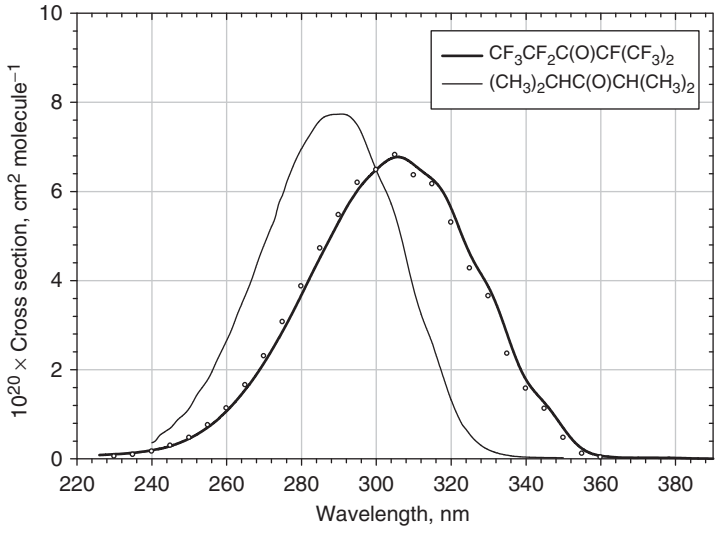

Figure IX-F-12. Comparison of the absorption cross sections for perfluoro-2-methyl-3-pentanone [$CF_3CF_2C(O)CF(CF_3)_2$] and 2,4-dimethyl-3-pentanone; data for perfluoro-2-methyl-3-pentanone shown as the heavy line are from D'Anna et al. (2005a) and the points shown as open circles are from Taniguchi et al. (2003); the data for 2,3-dimethyl-3-pentanone (thin line) are from Yujing and Mellouki (2000); figure from Calvert et al. (2008).

wavelengths than that for acetaldehyde, and this difference in the overlap of absorption with the lamp radiation necessarily complicated the derivation of the *j*-values estimates.

More recently, D'Anna et al. (2005a) studied the photodecomposition of perfluoro-2-methyl-3-pentanone in the EUPHORE outdoor chamber in Valencia, Spain. An effective quantum yield of decomposition was estimated to be 0.043 ± 0.011 over the wavelength range 290–400 nm. The primary processes that are likely for this ketone are (I) and (II), with process (I) favored somewhat, particularly at the longer wavelengths:

$$(CF_3)_2CFC(O)CF_2CF_3 + h\nu \rightarrow (CF_3)_2CF + CF_3CF_2CO \quad \text{(I)}$$

$$\rightarrow (CF_3)_2CFCO + CF_2CF_3 \quad \text{(II)}$$

Calvert et al. (2008) have used the absorption cross section data reported by D'Anna et al. (2005a), shown in table IX-F-5, together with their average estimated quantum yield of dissociation (0.043) and the appropriate solar flux to calculate approximate *j*-values as a function of solar zenith angle for a cloudless day in the lower troposphere; see figure IX-F-13. The experimental *j*-value of $(6.4 \pm 0.3) \times 10^{-6}\ s^{-1}$ measured by D'Anna et al. (2005a) in Valencia, Spain (39.5°N) July 14, 2003, 10.00–14.00 GMT (filled circles in figure IX-F-13) is reasonably consistent with the calculated values given in figure IX-F-13.

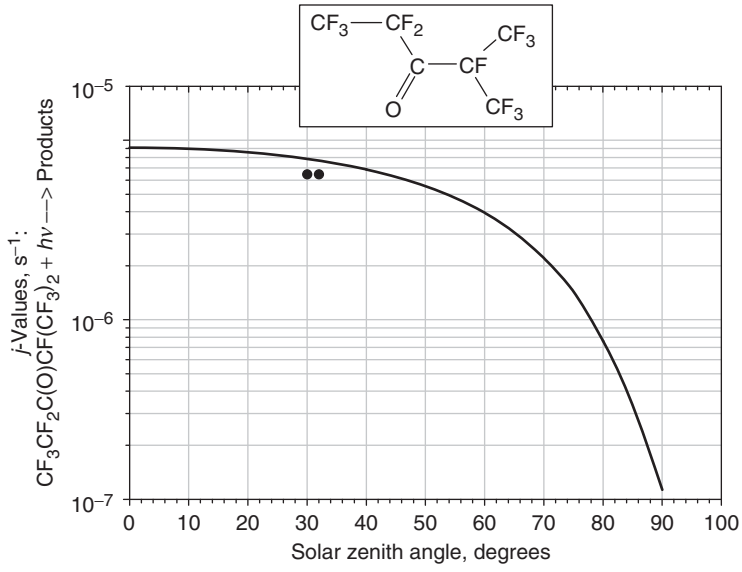

Figure IX-F-13. Estimated photolysis frequencies for $CF_3CF_2C(O)CF(CF_3)_2$ as a function of solar zenith angle. Values are calculated for a cloudless day in the lower troposphere with an overhead ozone column of 350 DU. Cross section data and average quantum yields of photodecomposition of D'Anna et al. (2005a) were used in the calculations. The data points shown as filled circles give the range of solar zenith angle during the measurements of D'Anna et al. (2005a) that were made in the EUPHORE chamber on July 14, 2003.

IX-F-8. Effects on the Absorption Spectrum of Acetone with Substitution of —C(O)CH_3, —C(O)OH, or —CH=CH_2 Groups for a —CH_3 Group

The position of the absorption band of $CH_3C(O)CH_3$ is affected significantly by the replacement of a —CH_3 group by —C(O)OH, —CH=CH_2, or an addional >C=O group. See figure IX-F-14 where the absorption bands of biacetyl, pyruvic acid, and methyl vinyl ketone can be compared with that for acetone. With the replacement of a CH_3 group in acetone with a second carbonyl group to form biacetyl [$CH_3C(O)C(O)CH_3$], two long-wavelength absorption regions appear, one of near equal intensity and band position (λ_{max} = 281 nm) replicates that of acetone (λ_{max} = 279 nm), but the —C(=O)C(=O)— chromophore induces a second absorption band that appears 139 nm to the longer wavelengths. Replacing the methyl group of acetone with a carboxyl group [—C(=O)OH] creates the new chromophore, —C(=O)C(=O)OH, of pyruvic acid with a shift in absorption to longer wavelengths (λ_{max} = 350 nm). The new chromophore present in methyl vinyl ketone [—C(=O)CH=CH_2], created by replacing one of the CH_3 groups of acetone with a vinyl group (—CH=CH_2), has λ_{max} = 331 nm, 53 nm to the longer wavelengths than that of acetone, and its cross section at the maximum is 44% larger than that

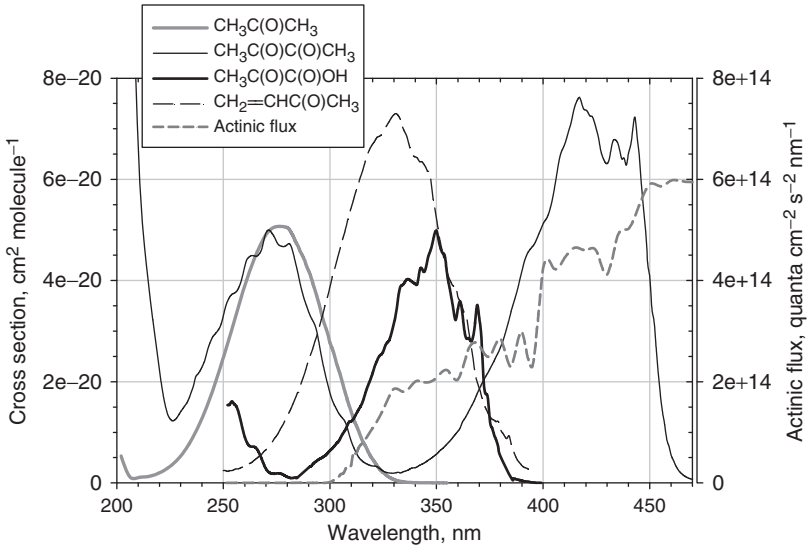

Figure IX-F-14. Comparison of the absorption spectra of acetone (Martinez et al., 1992), biacetyl (Horowitz et al., 2001), pyruvic acid (Melluki and Mu, 2003), and methyl vinyl ketone (Gierczak et al., 1997); the approximate wavelength distribution of the actinic flux within the lower troposphere at solar noon is shown by the dashed-gray curve.

of acetone. It can be seen in the figure IX-F-14 that there is a much larger overlap of the tropospheric actinic flux (gray-dashed line) with the absorption bands of all of these compounds than that seen with acetone. As a consequence, they all have a much greater potential for photochemical activity in the tropospheric sunlight than acetone. We will consider the photodecomposition of these compounds in the following section.

IX-F-9. Photodecomposition of Pyruvic Acid [$CH_3C(O)C(O)OH$]

Pyruvic acid is a product of the atmospheric oxidation of isoprene and other biogenic hydrocarbons as well as other organic species (e.g., cresol) present in urban air, and it is one of the most abundant ketoacids found in the troposphere (see table I-D-1). Several studies of its photochemistry have been made, although several questions remain about the mechanism of its photodecomposition in air. The vapor pressure of pyruvic acid is quite low at ambient temperatures ($\sim$1 Torr at 20°C), so several early studies have been made at somewhat elevated temperatures to achieve reasonable pressures of the gas (Vesley and Leermakers, 1964; Yamamoto and Back, 1985). More recent studies have been made at ambient temperatures and under conditions that reflect tropospheric conditions (Berges and Warneck, 1992; Hjorth et al., 2002; Mellouki and Mu, 2003). The following primary processes have been considered in explanation of the observed

photodecomposition of pyruvic acid:

$$CH_3C(O)C(O)OH + h\nu \rightarrow CO_2 + [CH_3COH] \rightarrow CH_3CHO \quad \text{(I)}$$

$$\rightarrow CH_3CHO + CO_2 \quad \text{(II)}$$

$$\rightarrow CH_3CO + C(O)OH \quad \text{(III)}$$

$$\rightarrow CH_3C(O)C(O) + OH \quad \text{(IV)}$$

$$\rightarrow CH_3C(O)OH + CO \quad \text{(V)}$$

Evidence for these processes is described in this section.

IX-F-9.1. Absorption Cross Sections for Pyruvic Acid

Cross sections for pyruvic acid as reported by Mellouki and Mu (2003) and Horowitz et al. (2001) are compared with those of some related carbonyl compound in figure IX-F-14 and are given in numerical form in table IX-F-6.

IX-F-9.2. Quantum Yields of Primary Photodecomposition Processes in Pyruvic Acid

From their studies in 1964, Vesley and Leermakers reported that the quantum yield of CO_2 formation was near unity (1.02 ± 0.06) in photolyses at 366 nm and 80–85°C. They proposed two alternative primary photodecomposition modes (I) and (II) to rationalize their results. Primary process (I), favored largely on the basis of the geometrical considerations, led to an intermediate carbene formation by H-atom transfer from the —CO_2H group to an O-atom in the carbonyl group via a 5-membered-ring transition state; this transient product was suggested to rearrange quickly to form the observed product, acetaldehyde. The concerted mechanism was favored since in studies with pure pyruvic acid and in mixtures with added gases they found that the two products were little affected by addition of 50 Torr of added N_2, 50 Torr of added oxygen, or 50 Torr of added ethene. See figure IX-F-15.

Acetaldehyde and CO_2 were observed as products of the sunlight photolysis of pyruvic acid in air (Grosjean, 1983), and it was suggested that primary process (II) was the dominant source of these products.

Yamamoto and Back (1985) studied pyruvic acid photolysis at 366, 345, and 320 nm and 67 °C. They observed both acetaldehyde and CO_2 products, and reported $\Phi_{CO_2} = 0.9 \pm 0.1$ at 366 nm. However, the results of Yamamoto and Back were significantly different from those of Veseley and Leermakers in one important respect. Although the ratio of acetaldehyde to CO_2 in the products was 0.66 in the absence of added O_2, consistent with the results reported by Vesely and Leermakeers, this ratio decreased dramatically as the pressure of air was increased. See figure IX-F-16. They suggested that acetaldehyde was largely a secondary product formed following intermolecular H-atom abstraction by the carbonyl group, followed by decomposition of the intermediate

Table IX-F-6. Absorption cross sections (σ, cm^2 $molecule^{-1}$) of pyruvic acid at 298 K. Data selection was similar to that used by Sander et al. (2006)[a]

λ, nm	$10^{20} \times \sigma$	λ, nm	$10^{20} \times \sigma$	λ, nm	$10^{20} \times \sigma$	λ, nm	$10^{20} \times \sigma$	λ, nm	$10^{20} \times \sigma$
252	1.54	282	0.093	312	1.34	342	4.19	372	2.04
253	1.55	283	0.098	313	1.42	343	4.24	373	1.76
254	1.61	284	0.104	314	1.49	344	4.17	374	1.68
255	1.56	285	0.113	315	1.57	345	4.26	375	1.22
256	1.52	286	0.124	316	1.69	346	4.46	376	1.09
257	1.41	287	0.138	317	1.83	347	4.58	377	0.95
258	1.25	288	0.156	318	1.94	348	4.73	378	0.842
259	1.07	289	0.173	319	2.05	349	4.92	379	0.688
260	0.908	290	0.302	320	2.17	350	4.98	380	0.521
261	0.801	291	0.323	321	2.31	351	4.79	381	0.241
262	0.737	292	0.37	322	2.41	352	4.63	382	0.179
263	0.718	293	0.409	323	2.50	353	4.54	383	0.146
264	0.718	294	0.439	324	2.54	354	4.47	384	0.122
265	0.700	295	0.47	325	2.60	355	4.13	385	0.097
266	0.651	296	0.491	326	2.72	356	3.89	386	0.084
267	0.566	297	0.519	327	2.78	357	3.66	387	0.077
268	0.470	298	0.548	328	2.84	358	3.41	388	0.066
269	0.367	299	0.594	329	2.98	359	3.22	389	0.056
270	0.278	300	0.639	330	3.15	360	3.44	390	0.047
271	0.224	301	0.678	331	3.35	361	3.59	391	0.034
272	0.195	302	0.724	332	3.66	362	3.37	392	0.031
273	0.185	303	0.775	333	3.87	363	3.01	393	0.026
274	0.182	304	0.822	334	3.91	364	2.85	394	0.015
275	0.188	305	0.898	335	3.96	365	2.86	395	0.011
276	0.189	306	0.977	336	4.02	366	2.8	396	0.006
277	0.180	307	1.04	337	4.02	367	2.88	397	0.002
278	0.164	308	1.13	338	3.99	368	3.16	398	0.002
279	0.139	309	1.21	339	3.96	369	3.52	399	< 0.001
280	0.118	310	1.22	340	3.93	370	3.26		
281	0.101	311	1.27	341	3.94	371	2.87		

[a]Data from Horowitz et al. (2001) for 252–289 and 380–399 nm; data are a mean of the data of Horowitz et al. (2001) and Mellouki and Mu (2003) for 290–380 nm.

species to the carbene (CH_3COH) and CO_2 in primary process (I), as Veseley and Leermakers had recommended earlier. They concluded that this reaction may occur from the excited singlet state of pyruvic acid, since the quantum yield of CO_2 was relatively unaffected by O_2 addition, normally an efficient quencher of triplet states. There was no evidence or speculation as to the nature of the products formed from the reaction of the carbene with O_2, but obviously acetaldehyde formation was not its major product.

Berges and Warneck (1992) determined the quantum yields of products formed in the photolysis of pyruvic acid in air at 1 atm. using a band of radiation centered at 350 nm. They reported: $\Phi_{CO_2} = 1.27 \pm 0.18$; $\Phi_{CH_3CHO} = 0.48 \pm 0.01$; $\Phi_{CH_3CO_2H} = 0.14$. They found also that with added NO_2 in the pyruvic acid–air mixture, peroxyacetyl nitrate was formed with a quantum yield of 0.15 ± 0.02 while Φ_{CH_3CHO} was reduced to 0.30 ± 0.04. This latter result suggests that acetyl radicals are formed in a primary

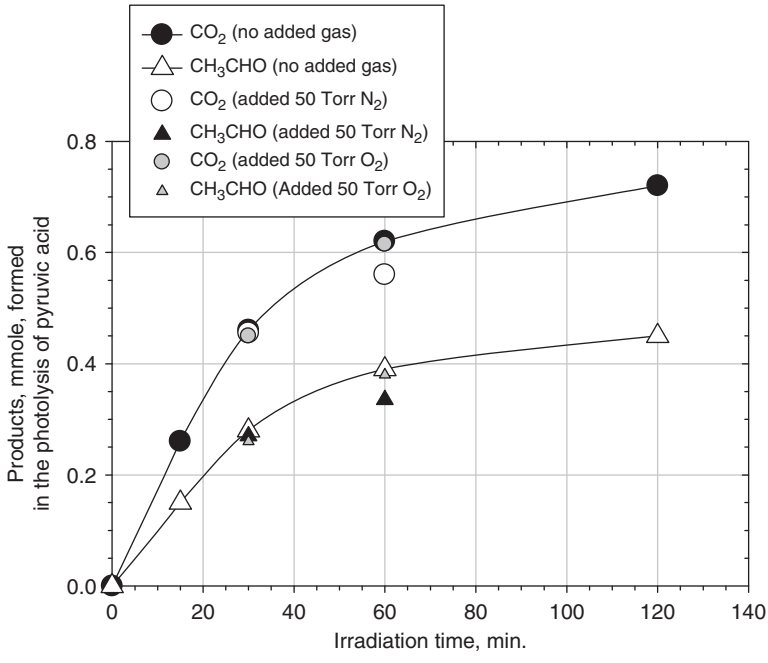

Figure IX-F-15. The effects of added gases on the formation of products in the 366 nm photodecomposition of pyruvic acid (Veseley and Leermakers, 1964).

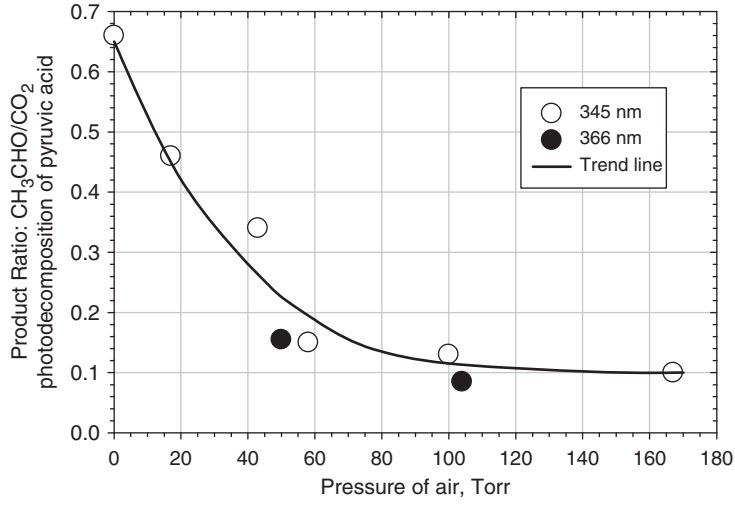

Figure IX-F-16. The effect of added air on the product ratio, CH_3CHO/CO_2, from pyruvic acid photolysis at 345 and 366 nm (Yamamoto and Back, 1965).

process, presumably process (III). To the extent that process (III) occurs, one expects the radical C(=O)OH to form CO_2 quickly through the reaction, $C(=O)OH + O_2 \rightarrow CO_2 + HO_2$. These workers estimated from their quantum yields of products formed that $\phi_{total} = 0.87 \pm 0.11$, in good agreement with the quantum yield of pyruvic acid loss, 0.85 ± 0.16. Again, this work supports the view that the quantum efficiency for photodecomposition of pyruvic acid in air is near unity.

Mellouki and Mu (2003) have provided evidence of the occurrence of an additional primary photodecomposition mode in pyruvic acid, process (IV) forming OH radicals. Their experiments employed a pulsed laser at 355 nm to photolyze pyruvic acid vapor in several different mixtures: 100 or 300 Torr of helium, varied water concentrations ($0 - 1.1 \times 10^{16}$ molecule cm^{-3}) and 30–50 Torr of N_2. The generation of the OH radical product was detected using laser-induced fluorescence. An average value of $\Phi_{OH} = \phi_{IV} = 0.05 \pm 0.01$ was found, invariant with mixture composition employed. HONO photolysis was used as the reference source of OH taking the quantum yield of OH as unity. The generation of OH radicals in pyruvic acid-mixture photolyses was confirmed in a series of separate smog chamber studies using black lamps (300–460 nm, maximum intensity at 365 nm) to irradiate mixtures of pyruvic acid with isoprene, 2,3-dimethyl-1,3-butadiene or 1,3-pentadiene in air at atmospheric pressure. Using pyruvic acid photolysis as the only source of OH radicals, Mellouki and Mu measured relative rates of decay of the two hydrocarbons in the mixtures. The data gave rate coefficient ratios that were equal to those using HONO as the HO radical source. This evidence suggests strongly that OH radicals are a product of pyruvic acid photodissociation. The result is surprising in that the enthalpy change for the breaking of the RC(O)—OH bonds in the simple acids, HC(O)—OH, $CH_3C(O)$—OH, and $C_2H_5C(O)$—OH requires about 462, 463, and 461 kJ mol^{-1}, respectively, corresponding to the energy available only at $\lambda \leq 259$ nm. Although the $CH_3C(O)C(O)$—OH bond in pyruvic acid is a different entity, it is surprising if it is as low as 337 kJ mol^{-1}. *Ab initio* calculations of Dhanya et al. (2003) suggest 439 kJ mol^{-1} for this bond dissociation energy. The extent of OH radical generation from secondary reactions of the primary products of pyruvic acid photodecomposition is expected to be small. Although a small amount of OH is expected from reactions of CH_3CO radicals, or conceivably $CH_3C(O)CO$ radicals, with O_2 (Tyndall et al., 1997b) following their formation in primary process (III) or (IV), no oxygen was added intentionally in the series of laser photolysis experiments in which Φ_{OH} was measured by Mellouki and Mu (2003). Further work is necessary to define the origin of the OH observed in their experiments.

In photolyses of pyruvic acid at 193 nm, Dhanya et al. (2003) have observed the dynamics of OH radical formation in process (IV). The OH radicals were formed without vibrational excitation but with a rotation temperature of 720 ± 90 K and a translational energy of 78.2 ± 27 kJ mol^{-1}. *Ab initio* calculations suggested that the mechanism involved internal conversion and intersystem crossing from the initially populated S_3 ($\pi \rightarrow \pi^*$) state to the T_1 state with dissociation occurring through a barrier of ~61 kJ mol^{-1}.

The wavelength dependence and the extent of the various suggested primary processes have not been established. So reliable predictions of the extent of the various photodecomposition processes for tropospheric conditions are not possible.

The invariance of Φ_{CO_2} with experimental conditions, at least at the lower pressures employed in many of the studies suggests that primary processes (I) and/or (II) and (III) occur with $\phi_I + \phi_{II} + \phi_{III} \approx 1.0$. The values of Φ_{CO_2} found in the experiments in 1 atm. of air reported by Berges and Warneck (1992), 1.27 ± 0.18, exceed unity, since more than one CO_2 molecule can be formed in the subsequent reaction of the $CH_3C(O)O_2$ radical formed following process (III); e.g., $2CH_3C(O)O_2 \rightarrow O_2 + [2CH_3C(O)O] \rightarrow 2CH_3 + 2CO_2$. So the measurement of Φ_{CO_2} is not a direct measure of $\phi_I + \phi_{II} + \phi_{III}$ in studies made in air. It seems reasonable to assume from the experiments of Berges and Warneck that $\phi_{III} \approx 0.15$. The limiting value of the CH_3CHO/CO_2 ratio ($\sim$0.1) observed at the highest pressures of added air in the experiments of Yamamoto and Back may reflect the extent of occurrence of process (II) with $\phi_{II} \approx 0.1$, accepting their conclusion that up to 150 Torr of air does not affect Φ_{CO_2}. However, this assumes that secondary formation of CO_2 does not occur in the air mixtures, an unrealistic assumption in view of the studies of Berges and Warneck. However, all of the available data support the view that the total quantum yield of photodecomposition is near unity in 1 atm. of air. The results of Yamamoto and Back shown in figure IX-F-15 suggest that it is probable that $\phi_I > \phi_{II}$. Obviously, many features of the mechanism of photodecomposition of pyruvic acid remain uncertain at this writing.

Hjorth et al. (2002) used FTIR to monitor the products formed in seven different experiments in the sunlight photolysis of pyruvic acid in the EUPHORE chamber. Although the formation of the expected major product CO_2 could not be determined because of the large background of CO_2 in the chamber, several other products, in addition to acetaldehyde, were identified: acetic acid (29–65% of the acetaldehyde), formic acid (6–40% of the acetaldehyde), formaldehyde (14–65% of the acetaldehyde), CO (15–50% of the acetaldehyde) and vinyl alcohol (20–44% of the acetaldehyde). The assignment of these products to specific primary processes that ultimately lead to them is a challenge, in view of the large variability in the fractions of these minor products formed. However, Hjorth et al. (2002) suggest that process (I) is the source of both acetaldehyde as well as enol-acetaldehyde through two competitive pathways, (a) and (b), respectively, that result in rearrangements of the initial carbene product:

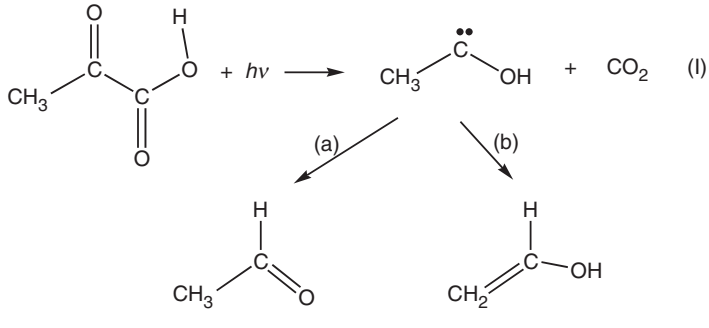

The presence of small amounts of CO in the products was explained by the occurrence of primary process (V) at $10 \pm 5\%$ of the pyruvic acid photodecomposition. The

rearrangement suggested in (V), if real, is unique in photochemistry. In accord with the results of Berges and Warneck, the authors suggest that process (III) could be the precursor to the formation of acetic acid and formaldehyde through reactions of the CH_3CO and CH_3 radicals with O_2 and subsequently formed peroxy radicals.

IX-F-9.3. Photolysis Frequencies for Photodecomposition of Pyruvic Acid in the Lower Troposphere

Photolysis frequencies for the photodecomposition of pyruvic acid were calculated as a function of solar zenith angle for the lower atmosphere with a cloudless sky and overhead ozone column of 350 DU. Three different choices of values for ϕ_{total} used in the calculations are summarized in figure IX-F-17. In view of the seemingly clear evidence that the quantum yield of photodecomposition of pyruvic acid is very near unity, a calculation was made assuming $\phi_{total} = 1.0$, independent of wavelength, shown by the solid curve. The *j*-values reported by Hjorth et al. (2002), measured directly on three sunny days in the EUPHORE chamber, shown as filled circles in figure IX-F-17, fall well below the curve for $\phi_{total} = 1.0$. To match the EUPHORE experimental points, we used a smaller but wavelength invariant $\phi_{total} = 0.28$. This is shown as the long-dashed curve. A further choice of ϕ_{total} versus λ was made assuming a sharp cutoff

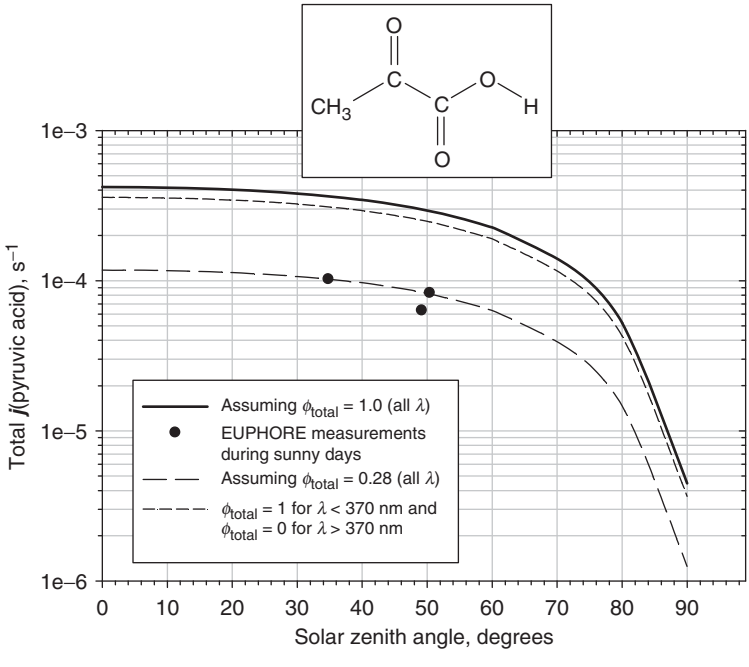

Figure IX-F-17. Photolysis frequencies for pyruvic acid photodecomposition as calculated as a function of solar zenith angle for 0.5 km altitude and an overhead ozone column of 350 DU. Three different scenarios are assumed for the ϕ_{total} and its variation with λ; see the text. The EUPHORE data were reported by Hjorth et al. (2002).

of the photochemistry just beyond the longest wavelength used in the experiments (370 nm); the results of this calculation are given by the short-dashed curve, indicating only a 14% reduction in *j*-values. Obviously, no shorter λ for cutoff wavelength can be made and remain consistent with the experiments performed at 366 nm that show $\phi_{\text{total}} \approx 1.0$. A firm recommendation of the *j*-values and their dependence on solar zenith angle is impossible at this time. The EUPHORE data and the laboratory data remain in conflict.

IX-F-10. Photodecomposition of Methyl Vinyl Ketone [$CH_3C(=O)CH=CH_2$]

Studies of the nature and the magnitude of the primary pathways of methyl vinyl ketone photodecomposition have been reported by Fahr et al. (1993), Raber and Moortgat (1996), and Gierczak et al. (1997). The latter two studies were carried out in air mixtures that simulate tropospheric conditions. By analogy with acrolein photodecomposition, the following primary photodecomposition processes are considered in this section in explanation of the results:

$$CH_3C(=O)CH=CH_2 + h\nu \rightarrow CH_3 + COCH=CH_2 \quad \text{(I)}$$

$$\rightarrow CH_3CO + CH=CH_2 \quad \text{(II)}$$

$$\rightarrow CH_3CH=CH_2 + CO \quad \text{(III)}$$

Raber and Moortgat (1996) have reported the results of photolyses of methyl vinyl ketone in air using the same broadband radiation source they employed in their methacrolein studies; see section IX-C-4. The main infrared-absorbing products identified were C_3H_6, CH_2O, and CO. Other compounds found were HC(O)OH, CH_3OH, CO_2, $CH_3C(O)OH$, and traces of $CH_2=CHC(O)OH$. The carbon balance was $< 50\%$. Within the error of the measurements, no significant quenching of the products with increased air pressure (54–760 Torr) was observed. Gierczak et al. (1997) did not measure CO or CO_2, but monitored only the hydrocarbons and oxygenated compounds. They reported as major photodecomposition products of methyl vinyl ketone in air: ethene, propene, and methanol with minor products being methane, ethane, ethylene, formaldehyde, acetone (or propanal), formic acid, and acetic acid. The formation of methane, ethane, and ethylene are difficult to rationalize following the occurrence of (I), (II), and (III), and result from impurities.

IX-F-10.1. Absorption Cross Sections for Methyl Vinyl Ketone

Cross sections for methyl vinyl ketone have been determined by Schneider and Moortgat (in Röth et al., 1997) and by Gierczak et al. (1997). The data of Gierczak et al. are plotted versus wavelength in figure IX-F-14 where they can be compared with those of some other substituted acetone molecules. The cross sections for methyl vinyl ketone are listed in numerical form in table IX-F-7.

Table IX-F-7. Methyl vinyl ketone absorption cross sections in the gas-phase (Gierczak et al., 1997) and recommended quantum yields for photodecomposition; units for σ are cm^2 $molecule^{-1}$

λ, nm	$10^{20} \times \sigma$	ϕ_{total}	λ, nm	$10^{20} \times \sigma$	ϕ_{total}	λ, nm	$10^{20} \times \sigma$	ϕ_{total}	λ, nm	$10^{20} \times \sigma$	ϕ_{total}
250	0.241		287	2.03	0.065	324	6.88	0.015	361	3.60	0.0022
251	0.241		288	2.15	0.063	325	6.95	0.0138	362	3.49	0.0019
252	0.224		289	2.29	0.061	326	7.02	0.0131	363	3.36	0.0017
253	0.241		290	2.43	0.059	327	7.09	0.0124	364	3.29	0.0014
254	0.241		291	2.55	0.057	328	7.16	0.0117	365	3.03	0.0011
255	0.258		292	2.67	0.055	329	7.23	0.0111	366	2.77	0.0008
256	0.275		293	2.81	0.054	330	7.28	0.0104	367	2.50	0.0006
257	0.275		294	2.93	0.052	331	7.30	0.0099	368	2.20	0.0003
258	0.293		295	3.08	0.050	332	7.26	0.0093	369	2.01	0.0000
259	0.310		296	3.24	0.049	333	7.18	0.0088	370	1.88	
260	0.327		297	3.39	0.047	334	7.04	0.0083	371	1.74	
261	0.361		298	3.56	0.045	335	6.94	0.0078	372	1.58	
262	0.379		299	3.70	0.044	336	6.85	0.0074	373	1.48	
263	0.396		300	3.87	0.042	337	6.70	0.0070	374	1.39	
264	0.430		301	4.05	0.041	338	6.56	0.0067	375	1.31	
265	0.465		302	4.20	0.039	339	6.47	0.0063	376	1.26	
266	0.499		303	4.35	0.038	340	6.44	0.0060	377	1.24	
267	0.534		304	4.51	0.036	341	6.42	0.0057	378	1.21	
268	0.568		305	4.66	0.035	342	6.35	0.0055	379	1.21	
269	0.620		306	4.82	0.034	343	6.35	0.0053	380	1.05	
270	0.654		307	4.96	0.032	344	6.30	0.0051	381	0.981	
271	0.706		308	5.13	0.031	345	6.23	0.0050	382	0.912	
272	0.757		309	5.30	0.030	346	6.14	0.0048	383	0.878	
273	0.809		310	5.44	0.029	347	6.08	0.0047	384	0.929	
274	0.878		311	5.58	0.027	348	5.77	0.0047	385	0.757	
275	0.929		312	5.73	0.026	349	5.47	0.0047	386	0.637	
276	0.998		313	5.87	0.025	350	5.20	0.0047	387	0.534	
277	1.08		314	6.02	0.024	351	4.94	0.0047	388	0.448	
278	1.15	0.083	315	6.14	0.023	352	4.72	0.0047	389	0.396	
279	1.24	0.081	316	6.28	0.022	353	4.53	0.0044	390	0.344	
280	1.33	0.079	317	6.42	0.021	354	4.32	0.0041	391	0.310	
281	1.41	0.077	318	6.54	0.020	355	4.15	0.0038	392	0.293	
282	1.50	0.075	319	6.63	0.019	356	4.03	0.0036	393	0.275	
283	1.60	0.072	320	6.70	0.018	357	3.94	0.0033	394	0.241	
284	1.70	0.070	321	6.76	0.017	358	3.89	0.0030	395	0.207	
285	1.81	0.068	322	6.83	0.016	359	3.89	0.0027			
286	1.91	0.066	323	6.85	0.015	360	3.68	0.0025			

IX-F-10.2. Quantum Yields of Photodecomposition of Methyl Vinyl Ketone

Excitation in experiments in the far ultraviolet at 193.3 nm (628 kJ $mole^{-1}$), gave complete rupture of both C—C bonds attached to the carbonyl in the molecule, with quantum yields of CH_3 and CH_2=CH radicals (and, presumably, CO) near unity (Fahr et al., 1993). However at the wavelengths available within the troposphere, photodissociation by primary processes (I) and (II) are expected to occur, but, analogous to the observations with acrolein, with low efficiency. The additional process (III) has

been suggested by Raber and Moortgat (1995) from photolyses in air. The observation of propene and CO as major products of the photodecomposition in air is difficult to explain without the occurrence of the molecular rearrangement (III). However, such a rearrangement is unexpected in view of the photolysis of other aliphatic ketones which show either dissociation at the RC(=O)—R′ bond or, in the case of the ketones with attached alkyl groups with γ-H-atoms relative to the carbonyl group, an intramolecular rearrangement to form an enol-ketone and an alkene (Calvert et al., 2008). Process (III), the expulsion of CO and formation of a stable R–R′ product as in (III), is unexpected in the photochemistry of alkyl ketones (RC(=O)R′), and its occurrence should be tested in further studies. Process (I) appears to require somewhat less energy ($\sim$71 kJ mole^{-1}) than (II), so one might expect this to be the major primary mode of photodecomposition within the troposphere.

The studies of Gierczak et al. (1997) provide useful information on the wavelength dependence of the primary photodecomposition processes in methyl vinyl ketone. They monitored the quantum yields of ketone photodecomposition in mixtures with air at 25 and 650 Torr and at wavelengths 308, 337, and 351 nm. As commonly found in the pressure dependence of the photodissocation of the carbonyl compounds, they observed quenching of the excited states that was most effective at the longer wavelengths. A Stern–Volmer plot of the data is given in figure IX-F-18. Although the data are scattered and limited to measurements at only two pressures, the data are useful. The least-squares fits of the data at each wavelength are given by the lines in figure IX-F-18. As seen for other carbonyl compounds, the quenching of the excited states is most effective at the longer wavelength of excitation, reflecting the longer lifetime for the lower energy of excitation of the methyl vinyl ketone molecule. The least-squares lines shown are described by the equations: $1/\phi_{\text{total}} = 4.748 + 0.03660 \times \text{P}$ (308 nm); $1/\phi_{\text{total}} = 21.0 + 0.160 \times \text{P}$ (337 nm); $1/\phi_{\text{total}} = 38.3 + 0.231 \times \text{P}$ (351 nm); the pressure (P) is

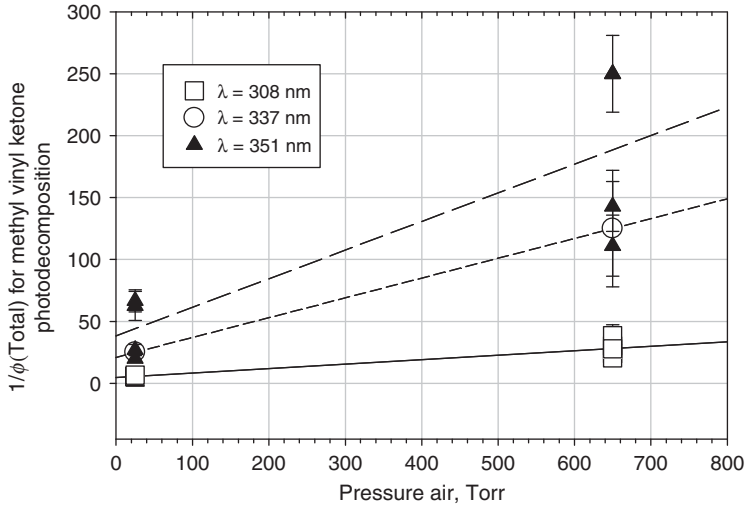

Figure IX-F-18. Stern–Volmer plot of $1/\phi_{\text{total}}$ versus pressure of air from methyl vinyl ketone photodecomposition data of Gierczak et al. (1997).

in Torr. Values of $\phi_{total} = 0.031$ (308 nm), 0.0070 (337 nm), and 0.00468 (351 nm) at 760 Torr of air were used to derive the estimates of the photolysis frequencies in the next section. These data are plotted versus wavelength in figure IX-F-19; the curve fitted to these points and the extrapolation shown as the dashed curves were used in calculating the *j*-values (dotted curve) in the next section.

IX-F-10.3. Photolysis Frequencies for Primary Photodecomposition Processes in Methyl Vinyl Ketone in the Lower Troposphere

Photolysis frequencies representative of the lower atmosphere were calculated using the measured cross sections and with the extrapolations shown in the figure IX-F-19. The numerical listing of the values of ϕ_{total} and cross sections used are summarized at 1 nm intervals in table IX-F-7. The results of the calculations of *j*(Total) values versus solar zenith angle, calculated for a cloud-free troposphere with an overhead ozone column of 350 DU, are given in figure IX-F-20.

Measurements of *j*(Total) for methyl vinyl ketone made by Hjorth et al. (2002) on a sunny day (June 21, 1998) in the EUPHORE chamber are shown in figure IX-F-20 as the open circle; this result is necessarily of low precision since *j*(Total) was determined from the difference between two similar numbers: $j(\text{Total}) = 1.02 \times 10^{-5}$ (total removal rate) – 8.46×10^{-6} (mean dilution rate)$\approx 1.74 \times 10^{-6}\ s^{-1}$. This datum point, shown in figure IX-F-20 as the open circle, lies significantly below the *j*-value estimates made here, but it is consistent with the conclusion in this study that photodecomposition of methyl vinyl ketone in the lower troposphere is very slow. The effective *j*-values measured by Raber and Moortgat (1995) in the broadband photodecomposition of methyl vinyl ketone in air are somewhat larger than those calculated here; they varied

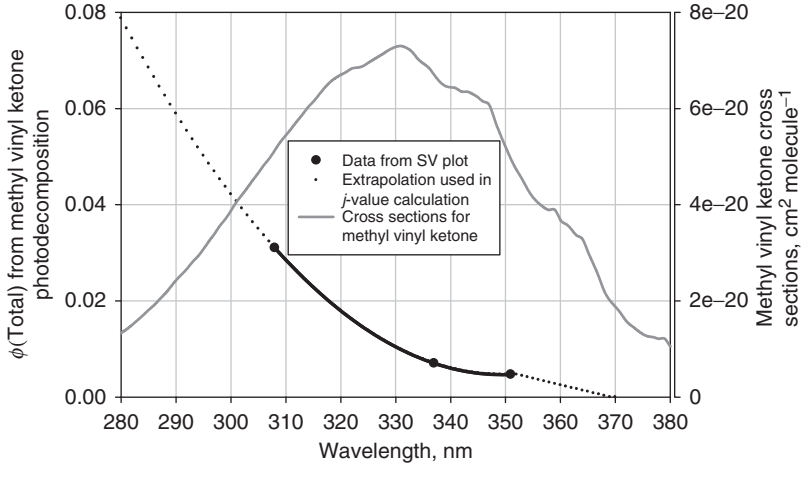

Figure IX-F-19. Plot of the estimated quantum yields of photodecomposition of methyl vinyl ketone in 760 Torr of air as a function of wavelength. The three data points shown are from the Stern–Volmer plot of figure IX-F-18 using the data of Gierczak et al. (1997). Absorption cross section data shown are from Gierczak et al. (1997).

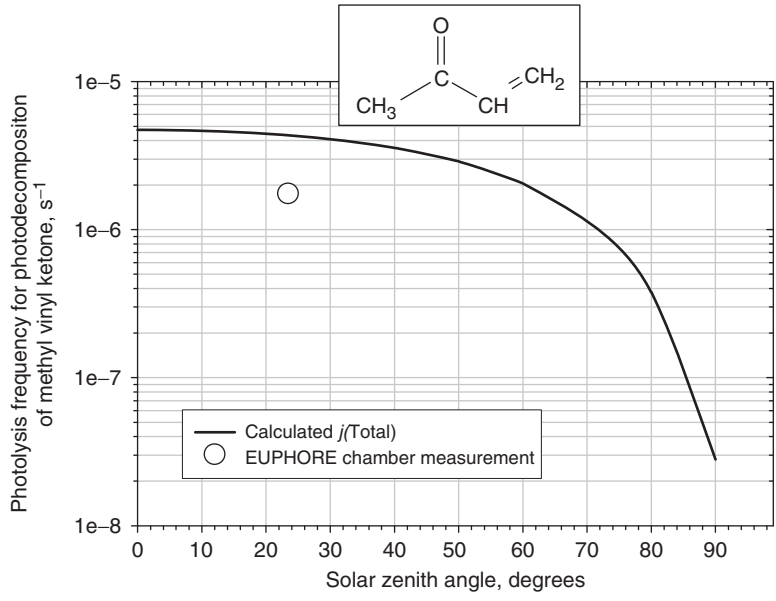

Figure IX-F-20. Methyl vinyl ketone photolysis frequencies as a function of solar zenith angle as calculated for a clear tropospheric sky at 0.5 km altitude and an overhead ozone column of 350 DU. The measurement in the EUPHORE chamber was reported by Hjoth et al. (2002)

from $3.2 \times 10^{-5}$to$7.8 \times 10^{-5}\,s^{-1}$, and were relatively insensitive to the total pressure of air (54–760 Torr).

All measurements of *j*(Total) indicate that photodecomposition of methyl vinyl ketone, like that of acrolein, a compound with a similar chromophore ($RC(O)CH{=}CH_2$), is a very slow process in the lower troposphere.

IX-F-11. Photodecomposition of 2,3-Butanedione [Biacetyl, $CH_3C(O)C(O)CH_3$]

Biacetyl is a major product of the atmospheric oxidation of many aromatic compounds, e.g., toluene, *o*-xylene, 1,2,3- and 1,2,4-trimethylbenzene. Its photochemistry is of interest to atmospheric scientists since it is a likely source of free radicals within the troposphere. The absorption of biacetyl extends well into the visible region of the sunlight; see figure IX-F-14. The analysis of the absorption bands of biacetyl have been studied and rationalized theoretically (e.g., see Brand and Mau, 1974); Huang et al., 2005). The photochemistry of biacetyl in the absence of oxygen has been the subject of numerous studies since the early 1940s (e.g., see Henriques and Noyes, 1940; Roof and Blacet, 1941; Anderson and Rollefson, 1941; Blacet and Bell, 1953; Bell and Blacet, 1954; Sheats and Noyes, 1955a, b; Ausloos and Steacie, 1955; Okabe and Noyes, 1957; Heicklen, 1959; Noyes et al., 1962; Parmenter and Poland, 1969; Caro et al., 1969; Abuin et al., 1971; Horowitz and Calvert, 1972; Sidebottom et al.,

1972; Badcock et al., 1972; McClelland and Yardley, 1973; Drent et al., 1973; Moss and Yardley, 1974; Grygier et al., 1985). The mechanism of photodecomposition in biacetyl–oxygen mixtures has received some attention (e.g., see Taylor and Blacet, 1956b; Porter. 1960; Padnos and Noyes. 1964; Horie and Moortgat, 1992a). The major products of its photodecomposition following $n \rightarrow \pi^*$ excitation in either of its two low-lying absorption bands results largely in the formation of carbon monoxide, ethane, methane, and acetone products. In the presence of oxygen, biacetyl photodecomposition products include CO_2, CO, CH_2O, CH_3OH, $CH_3C(O)OH$, $CH_3C(O)OOH$, and HC(O)OH (Horie and Moortgat, 1992). Two primary processes have been suggested to explain the products of biacetyl photodecomposition:

$$CH_3C(O)C(O)CH_3 + h\nu \rightarrow CH_3CO + CH_3CO \quad \text{(I)}$$

$$\rightarrow CH_3CO + (CH_3CO^{\ddagger}) \quad \text{(II)}$$
$$\downarrow$$
$$CH_3 + CO$$

The transient species, $CH_3CO^{\ddagger}$, in (II) represents a vibrationally excited acetyl radical that possesses sufficient energy to dissociate rapidly following its formation. Conceivably, process (II) may proceed by an alternative mechanism: rupture of the CH_3—$C(O)C(O)CH_3$ bond that would be followed by rapid dissociation of the intermediate $CH_3C(O)CO$ radical [$CH_3C(O)CO \rightarrow CO + CH_3CO$].

In this section we will discuss the evidence for these processes and evaluate the photolysis frequencies for biacetyl in the lower troposphere.

IX-F-11.1. Absorption Cross Sections for Biacetyl

The absorption spectrum for biacetyl as reported by Horowitz et al. (2001) is shown in figure IX-F-14 where it can be compared to those of some compounds of related structures. The tabular listing of the cross sections as a function of wavelength is given in table IX-F-8.

IX-F-11.2. Quantum Yields of Primary Photodecomposition Processes in Biacetyl

The photodecomposition of biacetyl induced by absorption of long wavelengths (e.g., 435 nm) shows an unusual behavior at ambient temperatures and high intensities of absorbed light. The quantum yield of the product CO is directly proportional to the light intensity in experiments at ambient temperatures; see figure IX-F-21. Using the rotating sector technique, Noyes et al. (1962) demonstrated that the lifetime of the species responsible for this unusual behavior was very similar to that ascribed to the triplet excited state. The vibrationally equilibrated triplet state (T_1) of biacetyl is very long-lived, $\tau = (1.52 \pm 0.17) \times 10^{-3}$ s (Sidebottom et al., 1972), and at the intensities of light used in many studies, the interaction of two triplet molecules is possible with

Table IX-F-8. Cross sections (σ, cm^2 $molecule^{-1}$) for 2,3-butanedione as a function of wavelength (Horowitz et al., 2001)

λ, nm	$10^{20} \times \sigma$	λ, nm	$10^{20} \times \sigma$	λ, nm	$10^{20} \times \sigma$	λ, nm	$10^{20} \times \sigma$	λ, nm	$10^{20} \times \sigma$	λ, nm	$10^{20} \times \sigma$
278	4.67	315	0.44	352	0.65	389	4.00	426	6.81	463	0.28
279	4.68	316	0.40	353	0.68	390	4.17	427	6.57	464	0.22
280	4.71	317	0.38	354	0.73	391	4.34	428	6.43	465	0.18
281	4.73	318	0.36	355	0.77	392	4.47	429	6.34	466	0.14
282	4.65	319	0.34	356	0.82	393	4.56	430	6.31	467	0.12
283	4.50	320	0.33	357	0.86	394	4.62	431	6.40	468	0.096
284	4.32	321	0.33	358	0.92	395	4.67	432	6.63	469	0.081
285	4.14	322	0.32	359	0.97	396	4.73	433	6.78	470	0.069
286	3.94	323	0.30	360	1.02	397	4.82	434	6.78	471	0.059
287	3.77	324	0.26	361	1.08	398	4.92	435	6.72	472	0.051
288	3.62	325	0.23	362	1.19	399	5.02	436	6.56	473	0.044
289	3.50	326	0.21	363	1.26	400	5.12	437	6.40	474	0.040
290	3.38	327	0.20	364	1.33	401	5.19	438	6.42	475	0.035
291	3.28	328	0.19	365	1.41	402	5.26	439	6.28	476	0.031
292	3.20	329	0.19	366	1.49	403	5.38	440	6.51	477	0.028
293	3.11	330	0.20	367	1.57	404	5.54	441	6.67	478	0.025
294	2.96	331	0.20	368	1.66	405	5.75	442	6.99	479	0.023
295	2.73	332	0.21	369	1.76	406	6.00	443	7.23	480	0.021
296	2.50	333	0.20	370	1.85	407	6.26	444	6.85	481	0.019
297	2.29	334	0.22	371	1.94	408	6.47	445	6.49	482	0.018
298	2.10	335	0.23	372	2.02	409	6.59	446	5.90	483	0.017
299	1.93	336	0.25	373	2.10	410	6.69	447	5.43	484	0.016
300	1.77	337	0.26	374	2.17	411	6.82	448	5.01	485	0.015
301	1.64	338	0.28	375	2.25	412	6.97	449	4.33	486	0.015
302	1.54	339	0.30	376	2.33	413	7.11	450	4.06	487	0.015
303	1.46	340	0.30	377	2.41	414	7.31	451	3.44	488	0.015
304	1.38	341	0.32	378	2.50	415	7.47	452	3.20	489	0.016
305	1.32	342	0.35	379	2.58	416	7.57	453	2.65	490	0.018
306	1.27	343	0.37	380	2.68	417	7.62	454	2.16	491	0.019
307	1.21	344	0.39	381	2.79	418	7.51	455	1.72	492	0.021
308	1.10	345	0.41	382	2.92	419	7.39	456	1.39	493	0.022
309	0.95	346	0.44	383	3.07	420	7.37	457	1.14		
310	0.82	347	0.47	384	3.22	421	7.32	458	0.85		
311	0.71	348	0.50	385	3.39	422	7.25	459	0.73		
312	0.62	349	0.53	386	3.53	423	7.24	460	0.55		
313	0.54	350	0.57	387	3.67	424	7.13	461	0.45		
314	0.48	351	0.61	388	3.82	425	6.98	462	0.36		

annihilation of the triplets (Badcock et al., 1972):

$$2CH_3C(O)C(O)CH_3(T_1) \rightarrow CH_3C(O)C(O)CH_3(S_0) + CH_3C(O)C(O)CH_3(S_1)$$

$$CH_3C(O)C(O)CH_3(S_1) \rightarrow CH_3CO + CH_3CO \quad \text{(I)}$$

$$\rightarrow CH_3CO + (CH_3CO^{\ddagger}) \rightarrow CH_3 + CO \quad \text{(II)}$$

Each of the two molecules in the T_1 state possesses 238 kJ mol^{-1} of energy; the combined energy of 477 kJ mol^{-1} can form a ground state S_0 molecule and a molecule of

biacetyl in the excited S_1 state with energy equal to a molecule excited at about 280 nm. The decomposition of the excited S_1 molecule can be the result of these events. Note in figure IX-F-21 that as the temperature is raised to 75°C, the lifetime of the T_1 state is shortened as the barrier to dissociation ($\sim$63 kJ mol^{-1}) is overcome, and the quantum yield of products becomes insensitive to the light intensity. Using this interpretation, Badcock et al. (1972) have rationalized successfully the unexplained results of several studies of 436.5 nm photolyses of biacetyl (Sheats and Noyes, 1955; Bell and Blacet, 1954; Noyes et al., 1962). It is likely that the photodecomposition of biacetyl excited in experiments at the longer wavelengths and at ambient temperatures is very near zero, and observed products in many studies may have resulted from the triplet–triplet annihilation reaction.

In studies of biacetyl photodecomposition at wavelengths 313 and 265 nm, Blacet and Bell (1953) reported that the quantum yield of the CO related to those of ethane, methane, and acetone by the following equation:

$$\Phi_{CO} \approx 2\Phi_{C_2H_6} + \Phi_{CH_4} + \Phi_{CH_3COCH_3}$$

This reflects the expected mass balance of the initial products formed in the process (II). Shown in figure IX-F-22 are the temperature dependencies of Φ_{CO} and $2\Phi_{C_2H_6} + \Phi_{CH_4} + \Phi_{CH_3COCH_3}$ from photolyses at the two wavelengths, 265.4 and 313 nm. The limiting values of these functions at ambient temperatures: $\sim$0.08 at 313 nm and $\sim$0.54 at 265.4 nm provide estimates of the extent of primary process (II), since the fraction of the thermally equilibrated CH_3CO radicals formed will not have

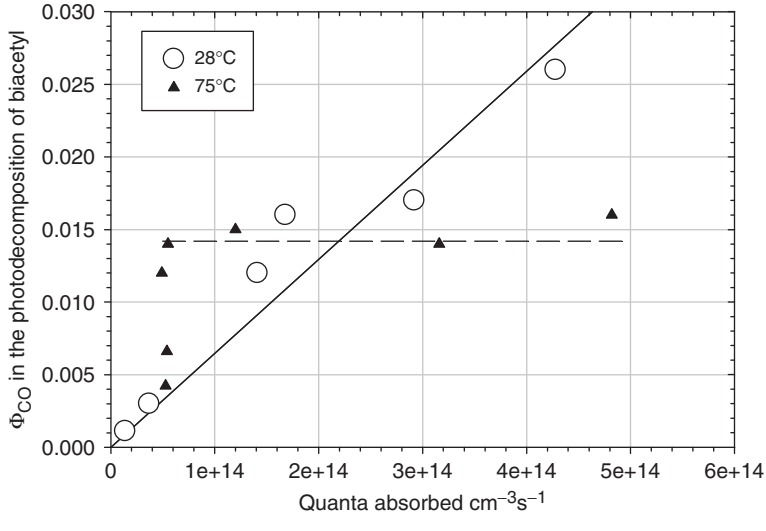

Figure IX-F-21. Plot of the quantum yield of CO formed in the 435.8 nm photodecomposition of biacetyl (Sheats and Noyes (1955) as a function of absorbed light intensity (I_a). Data determined at 28°C (open circles) show a linear increase with I_a, while those at 75°C and the higher intensities of absorbed light are relatively unchanged with I_a.

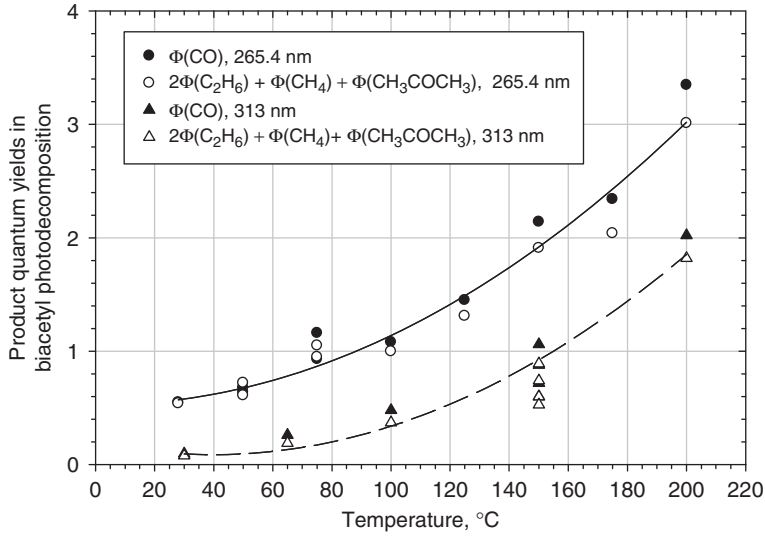

Figure IX-F-22. Plot of the quantum yield of CO and the near equivalent quantum yield product function, $2\Phi_{C_2H_6} + \Phi_{CH_4} + \Phi_{CH_3COCH_3}$ versus temperature. Data are from the photolysis of biacetyl as reported by Blacet and Bell (1954).

dissociated appreciably at this temperature. The increase of these functions with temperature, reflects the increasing decomposition of the CH_3CO radical formed in the primary processes. For excitation at 265.4 nm in experiments at temperatures $\geq 150°C$, where the $\phi_I + \phi_{II}$ is probably near unity, all of the original CH_3CO radicals formed in (I) and (II) have dissociated to form CO. As temperatures above 180°C are reached, a chain reaction forming CO and other products is evident as quantum yields > 3 are seen. The chain carrying step forming ketene becomes important as it renews the supply of CH_3CO radicals, $CH_2C(O)C(O)CH_3 \rightarrow CH_2{=}CO + CH_3CO$.

Bell and Blacet (1954) carried out other experiments using biacetyl–iodine mixtures that were irradiated at several wavelengths of absorbed light. The results of these experiments, shown in figure IX-F-23, give some useful information about the quantum yield of process (II) as a function of wavelength. Within the experimental error, one can see from the figure that $\Phi_{CO} \approx \Phi_{CH_3I}$ as iodine molecules react with the CH_3 radicals formed in process (II). The analytical method did not allow measurements of the CH_3COI, the other product expected here. The black trend line shown provides estimates of ϕ_{II} as a function of wavelength. Also shown in figure IX-F-23 are Φ_{CO} values from several studies at ambient temperatures and low intensities of absorbed light. These data also should give rough estimates of the ϕ_{II} values, since thermalized CH_3CO radical decomposition at ambient temperatures should be unimportant. The data show clearly that the quantum yield of process (II) increases significantly with increasing energy of the absorbed light quantum.

Several experiments have been made that relate more directly to photodecomposition of biacetyl in the atmosphere (Taylor and Blacet, 1956b; Padnos and Noyes, 1964;

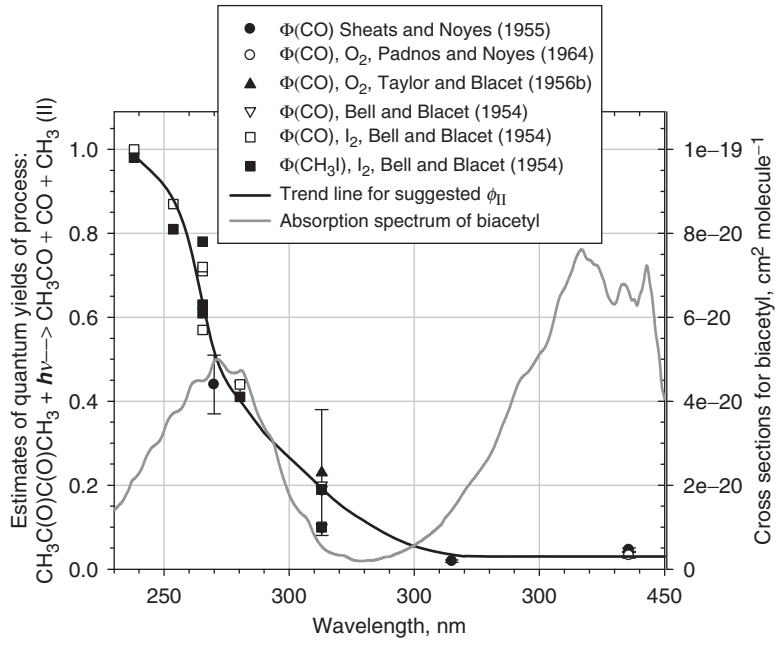

Figure IX-F-23. Plot of the quantum yields of CO and CH_3I as a function of wavelength from the photodecomposition of biacetyl in mixtures with I_2; temperature 65–150°C (Bell and Blacet, 1954) and Φ_{CO} from Sheats and Noyes (1955), Taylor and Blacet (1956b), and Bell and Blacet (1954) studies of pure biacetyl photodecomposition at the lowest intensities and 28°C. Presumably, each of these measurements gives an estimate of ϕ_{II}; the absorption spectrum of biacety is shown as the gray curve.

Horie and Moortgat, 1992). The influence of O_2 on the products is expected to create $CH_3C(O)O_2$ and CH_3O_2 radicals from the CH_3CO and CH_3 radicals formed in (I) and (II). It is assumed here that T_1 when quenched by O_2 does not lead to destruction of the biacetyl but presumably results in energy transfer to O_2 to form excited singlet states of oxygen, $O_2(^1\Delta_g$ or $^1\Sigma_g^+)$ with the return of biacetyl to its ground electronic state. Note in figure IX-F-23 that Φ_{CO} values from experiments in the presence and absence of O_2 are the same within the experimental error. This argues strongly that O_2-quenching of the excited triplet state of biacetyl does not form additional observable products, but returns the original biacetyl molecule. However, the extent of quenching of the T_1 state of biacetyl may influence the efficiency of the product formation. Quenching of the vibrationally equilibrated T_1 state of biacetyl occurs with a rate coefficient of $(9.2 \pm 0.3) \times 10^{-13}$ cm^3 molecule^{-1} s^{-1} (Sidebottom et al., 1972). The S_1 state of biacetyl, excited at 382.9 nm, has a lifetime that is independent of the pressure of added cyclohexane (24–105 Torr), $(2.35 \pm 0.43) \times 10^{-8}$ s and electronic quenching by air is probably unimportant during its short lifetime. Sidebottom et al. (1972) estimated that intersystem crossing ($S_1 \rightarrow T_1$) occurs with a rate coefficient, $k_{ISC} \approx (4.3 \pm 0.8) \times 10^7$ s^{-1}, so it is probable that the formation of the triplet is the dominant decay mode other than fluorescence that occurs with a rate coefficient $k_f \approx (9.8 \pm 2.8) \times 10^4$ s^{-1}.

The product of $[O_2] \times k(O_2 + T_1)$ for the lower troposphere is about $4.5 \times 10^6\ s^{-1}$. The rate coefficient for photodecomposition at 388 nm is estimated to be $\sim 9.6 \times 10^5\ s^{-1}$ (Horowitz and Calvert, 1972), so perhaps only a fraction (about 0.18) of the T_1 formed at this wavelength may photodissociate. For biacetyl excitation at $\lambda \leq 365$ nm, the molecule decays much more rapidly, and little effect of quenching of the products by O_2 is expected.

Previous studies with acetone photodecomposition described in section IX-D suggest that $CH_3C(O)O_2$ and CH_3O_2 radicals formed in 1 atm. of air react to generate about one CO_2 molecule for every $CH_3C(O)O_2$ radical formed (Gierczak et al., 1998; see section IX-D-1). Thus, a qualitative but reasonable estimate of the extent of occurrence of processes (I) and (II), respectively, can be had from the photolyses of biacetyl in oxygen mixtures using the relations: $\phi_I \approx (\Phi_{CO_2} - \Phi_{CO})/2)$ and $\phi_{II} \approx \Phi_{CO}$. Such estimates applicable to the troposphere require measurements at ambient temperatures, since the thermal dissociation of CH_3CO radicals at the higher temperatures distorts the interpretation. However, only a few studies have been made at ambient temperatures (Porter, 1960; Padnos and Noyes, 1964; Horie and Moortgat, 1992). The ratio, $\phi_{II}/\phi_I \approx 2\Phi_{CO}/(\Phi_{CO_2} - \Phi_{CO})$, from the data from Horrie and Moortgat (390–470 nm) and Padnos and Noyes (435.8 nm) have been plotted versus temperature in figure IX-F-24.

Although the scatter is large, there is no obvious trend of this ratio with temperature. Both studies suggest that a significant fraction of the photolysis even at these relatively long wavelengths results in fragmentation of one of the acetyl radicals formed in process (II). The data of Porter (1960) show quantum yields that are unusually high compared to other studies and will not be included in our further considerations. It is

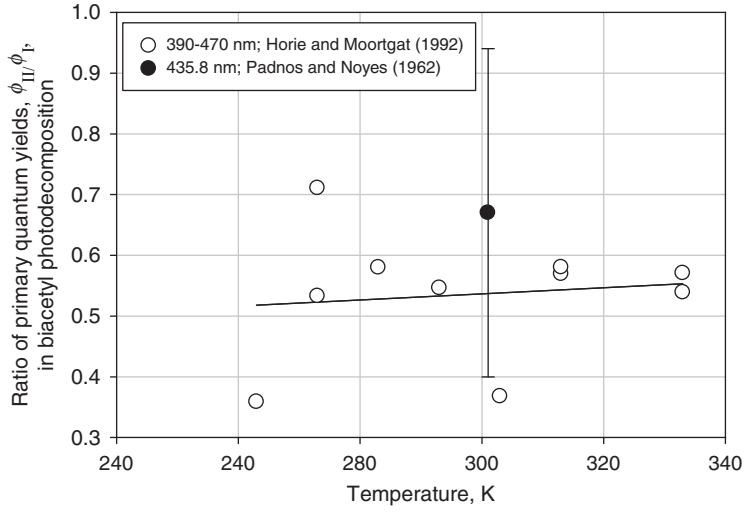

Figure IX-F-24. Plot of the ratio $\phi_{II}/\phi_I \approx 2\Phi_{CO}/(\Phi_{CO_2} - \Phi_{CO})$ versus temperature for photolyses of biacetyl at relatively long wavelenghs of excitation.

possible that the intensity regime used by Porter was sufficiently high that triplet–triplet anhilation was a major source of the products.

Taylor and Blacet (1956) and Padnos and Noyes (1964) have studied the photolysis of biacetyl in mixtures with O^{18}-labeled oxygen. Both studies show that about 1 atom of oxygen in the CO_2 product arises from the oxygen. Taylor and Blacet also found that the oxygen in the CO comes entirely from the biacetyl, the CH_2O and CH_3OH have oxygen only from the O_2, while the acetic acid has about 1 atom from biacetyl and one from the O_2. The following currently accepted mechanisms of formation of these products are consistent with these findings:

$$CH_3C(O)C(O)CH_3 + h\nu \rightarrow 2CH_3CO \quad \text{(I)}$$

$$\rightarrow CH_3CO + CO + CH_3 \quad \text{(II)}$$

$$CH_3CO + O_2 \rightarrow CH_3C(O)O_2$$

$$CH_3C(O)O_2 + CH_3C(O)O_2 \rightarrow 2CH_3CO_2 + O_2$$

$$CH_3C(O)O_2 + CH_3O_2 \rightarrow CH_3CO_2 + CH_3O + O_2$$

$$CH_3CO_2 \rightarrow CH_3 + CO_2$$

$$CH_3O + O_2 \rightarrow CH_2O + HO_2$$

$$CH_3C(O)O_2 + HO_2 \rightarrow CH_3C(O)OH + OH + O_2$$

$$\rightarrow CH_3C(O)O_2H + O_2$$

The estimates of quantum yields for biacetyl photodecomposition by process (I) are very limited. These are shown in figure IX-F-25. The data of Sheats and Noyes (1955) and Padnos and Noyes (1960) provide rough estimates at 435 and 313 nm. To derive the rest of the ϕ_I versus λ plot we have assumed that $\phi_I + \phi_{II} = 1.0$ for $\lambda < 280$ nm. The solid curve gives our best estimate of the variation of ϕ_I versus λ. Obviously, these data are highly uncertain, but are consistent with the limited information available in the literature at this writing.

IX-F-11.3. Photolysis Frequencies for the Photodecomposition of Biacetyl in the Lower Troposphere

The quantum yield data given in figures IX-F-23 and IX-F-25 are used together with the cross section data of Horowitz et al. (2001) and actinic flux data to estimate photolysis frequencies for biacetyl. Two different scenarios are used to illustrate the sensitivity of the results to the assumed long-wavelength limit where photodissociation ceases. The enthalpy of formation of biacetyl has not been reported, so the minimum energy to break the $CH_3C(O)$—$C(O)CH_3$ bond is uncertain. If we assume this dissociation energy is equal to that in the similar compound glyoxal, HC(O)—C(O)H (278.2 kJ mol^{-1}), then the energy of the light quantum for $\lambda > 401$ nm will be insufficient to dissociate this bond, neglecting internal energy present in the molecule prior to light absorption.

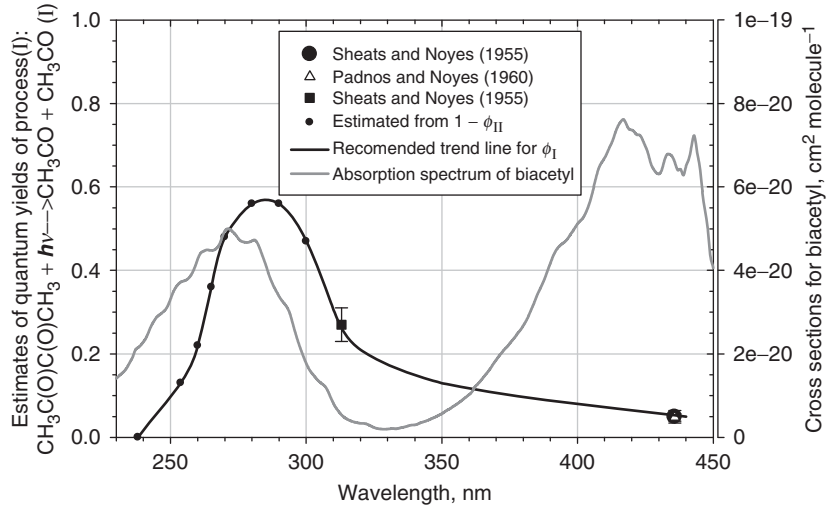

Figure IX-F-25. Estimates of the quantum yields for the primary photodecomposition process (I) of biacetyl versus wavelength. The small filled circles are estimates based on the assumption of $\phi_I + \phi_{II} = 1.0$ at $\lambda < 280$ nm and the measurements of ϕ_{II}.

We have calculated *j*(Total) for biacetyl as a function of solar zenith angle using both the cutoff at $\lambda = 410$ nm and the less-likely cutoff at 492 nm. These photolysis frequencies are plotted in figure IX-F-26.

From the *j*-value data shown in figure IX-F-26 for biacetyl, one can see that the choice of cutoff wavelength makes a very large difference in the results. Although the quantum yields are small at the long wavelengths, the effect of large absorption cross sections at wavelengths >400 nm contributes a great deal to the calculated *j*-value. Changing the cutoff from 492 to 410 lowers the *j*-values by over a factor of 2. The values of *j*(Total) given by the curve marked by filled circles is the maximum that we expect using the current quantum yield and cross section data. Yet the estimates of *j*-values determined in EUPHORE chamber data by Klotz et al. (2001) are much larger, as seen in the upper curve marked by the closed, inverted triangles. We have used the Klotz et al. relation: $j(\text{biacetyl}) = (0.0364 \pm 0.0026) \times j(NO_2) - (3 \pm 11) \times 10^{-6}\ s^{-1}$ and the $j(NO_2)$ values calculated for the 0.5 km elevation and 350 DU of overhead ozone column, the same input we used with most of the *j*-values calculated in this work. The difference seen here between the EUPHORE chamber estimates and those derived from ϕ, σ, and actinic flux data is unusual and points to a major undetermined problem in one or both sources of the estimates. It is possible that the large rate of loss of biacetyl seen in the EUPHORE chamber experiments results from HO_2 radical addition to the biacetyl molecule in the fashion observed for the similar molecule, methyl glyoxal [$CH_3C(O)C(O)H$]; see section IX-C-12.

Some other direct estimates of *j*(Total) from observed rates of loss of biacetyl have been made in previous studies that are somewhat more consistent with those given by our calculations. Grosjean (1985) made four determinations of *j*(Total) for biacetyl in

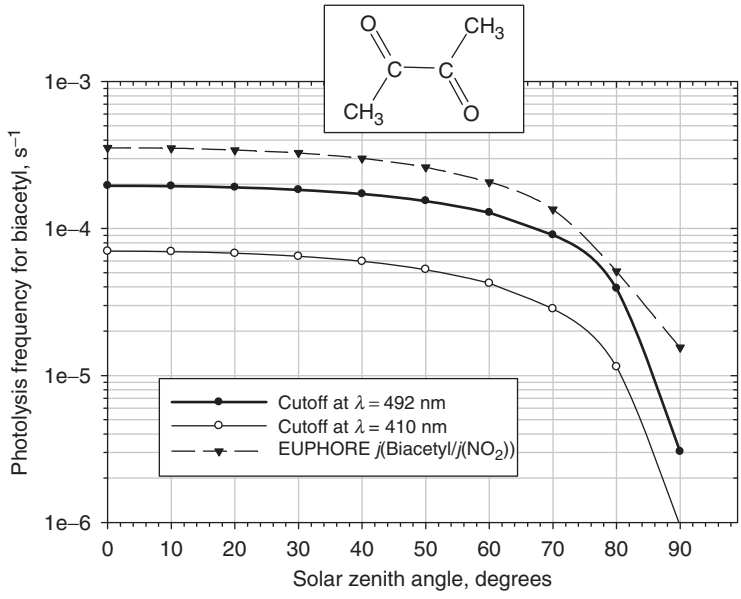

Figure IX-F-26. Plot of the estimated photolysis frequencies for biacetyl in the lower troposphere assuming an overhead ozone column of 350 DU. Two alternative wavelengths for the cutoff of photodissociation have been assumed. The data given by the dashed curve are estimates derived using the relation for j(biacetyl)/$j(NO_2)$ determined by Klotz et al. (2001) in EUPHORE chamber experiments.

a Teflon® chamber exposed to direct sunlight. He reported $j(\text{Total}) = (2.1 \pm 0.1) \times 10^{-4}\,\text{s}^{-1}$ (solar zentith angle unreported), in reasonable accord with our estimates using the longer wavelength cutoff. Several other determinations have been reported from experiments in the large reaction chamber equipped with a solar simulator at the University of California, Riverside. Darnall et al. (1979) reported $j(\text{Total}) = 2.3 \times 10^{-4}\,\text{s}^{-1}$; Plum et al. (1983) found $j(\text{Total}) = 2.78 \times 10^{-4}\,\text{s}^{-1}$; Atkinson et al. (1983b) reported $j(\text{Total}) = (1.26 \pm 0.04) \times 10^{-4}\,\text{s}^{-1}$. Gery et al. (1987) in a large stirred flow reactor found a biacetyl disappearance rate that gave $j(\text{Total}) = 3.0 \times 10^{-5}\,\text{s}^{-1}$; they measured $j(NO_2) = 5.0 \times 10^{-3}\,\text{s}^{-1}$ in the reactor as well. This value adjusts to $j(\text{Total}) = 5.9 \times 10^{-5}\,\text{s}^{-1}$ for solar zenith angle = 0, using our assumed conditions with $j(NO_2) = 9.82 \times 10^{-3}\,\text{s}^{-1}$. It is evident that a large uncertainty remains in the estimated j(Total) values for biacetyl. We suggest that the most probable values for our assumed conditions in the lower troposphere probably lie somewhere in the region between the two upper curves in the figure IX-F-26.

IX-F-12. Photodecomposition of 3-Hexene-2,5-dione

By analogy with the photolysis pathways suggested for the similar compounds, butendial, and 4-oxo-2-pentenal, Calvert et al. (2002) suggested the following primary

photodecomposition pathways may occur in 3-hexene-2,5-dione:

$$\textit{trans/cis}\text{-}CH_3C(O)CH{=}CHC(O)CH_3 + h\nu \rightarrow CH_3C(O)CH{=}CHC(O)CH_3^*$$

$$CH_3C(O)CH{=}CHC(O)CH_3^* \rightarrow \textit{cis/trans}\text{-}CH_3C(O)CH{=}CHC(O)CH_3 \quad \text{(I)}$$

$$\rightarrow CH_3 + COCH{=}CHC(O)CH_3 \quad \text{(II)}$$

$$\rightarrow CH_3CO + CH{=}CHC(O)CH_3 \quad \text{(III)}$$

Tuazon et al. (1985) found that > 80% of the photolysis rate was accounted for by isomerization in (I). Bierbach et al. (1994) arrived at a similar conclusion from their photolysis studies using the *trans*-isomer with either 254 nm or 320–480 nm radiation. Isomerization is the major reaction pathway. The photochemical steady state ratio of [*trans*]/[*cis*] was determined to be ~0.5 in each of these studies and in the more recent work of Becker and Graedler (1999). In chamber studies Liu et al. (1999) observed the relatively slow disappearance of 3-hexene-2,5-dione; with 0.95 ppm initially present, about half of the compound disappeared during the 3.5 h exposure to the natural sunlight (6.00 to 9:30 AM), with generation of small amounts of several carbonyl products: methylglyoxal, acetaldehyde, and hydroxyacetone. The methylglyoxal was the major carbonyl product observed, and it peaked at a concentration of 0.15 ppm at about 10:30 AM. These data suggest that perhaps a small fraction of the 3-hexene-2-5-dione excited by sunlight within the troposphere undergoes decomposition to form free radical products in (II) or (III). In experiments using the European photochemical reactor, Becker and Graedler (1999) observed a very rapid isomerization of the *cis*-isomer (reaching a photostationary state within 30–35 min.) with *j*-values for *cis*-3-hexene-2,5-dione + *trans*-3-hexen-2,5-dione disappearance together with $j(NO_2)$ values. Starting with the pure *cis*- or *trans*-isomers, they observed for comparable daylight conditions: $j(NO_2)/j(\textit{cis}\text{-hexene-2, 5-dione}) = (5.9 \pm 2.3) \times 10^{-3}/(1.1 \pm 2.0) \times 10^{-5}$; $j(NO_2)/j(\textit{trans}\text{-3-hexene-2, 5-dione}) = (5.8 \pm 1.0) \times 10^{-3}/(1.3 \pm 1.2) \times 10^{-5}$; $j(NO_2)/j(\textit{cis} + \textit{trans})\text{-3-hexene-2, 5-dione}) = (5.9 \pm 1.0) \times 10^{-3}/(1.2 \pm 0.9) \times 10^{-5}$.

IX-F-12.1. Absorption Cross Sections for 3-Hexene-2,5-dione

The absorption cross sections for *trans*-3-hexene-2,5-dione were determined in acetonitrile solutions by Liu et al. (1999). These data are shown in figure IX-F-27. The σ data as a function of λ (for each nm) are summarized in table IX-F-9.

IX-F-12.2. Quantum Yields of Primary Photodecomposition Processes in 3-Hexene-2,5-dione

There are no quantum yield data as a function of wavelength of excitation related to the primary processes in the photolysis of 3-hexene-2,5-dione, although in the European outdoor chamber in Valencia, measurements of the apparent *j*-values for disappearance of the *cis*- and *trans*-isomers have been reported by Becker and Graedler (1999); see the preceding discussion in this section. It appears that the quantum yield of isomerization,

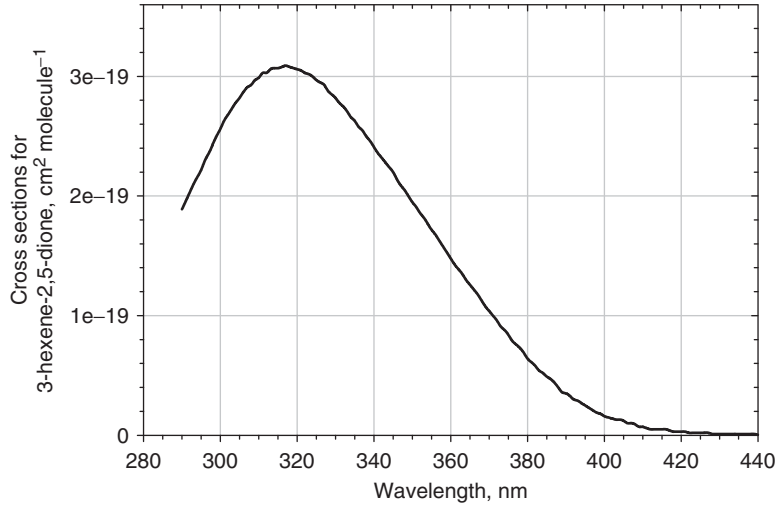

Figure IX-F-27. The absorption cross sections for *trans*-3-hexene-2,5-dione as measured in acetonitrile solution (Liu, 1999).

reaction (1) is dominant. A small fraction of the molecules which do not undergo *cis*/*trans*-isomerization, decompose. The data of Becker and Graedler (1999) suggest that the extent of photodecomposition may be much less than 20%, with *j*-values for photodecomposition about 10 times those observed in acrolein; see section IX-C-3.

IX-F-12.3. Photolysis Frequencies for Photodecomposition of 3-Hexene-2,5-dione in the Lower Troposphere

The *j*-values related to disappearance of the both *cis*- and *trans*-isomers determined by Becker and Graedler, determined from a few experiments in natural sunlight in the EUPHORE chamber, can be used to develop a *j*-value versus solar zenith angle plot. Becker and Graedler assumed a linear relationship in fitting *j*(3-hexene-2,5-dione) versus $j(NO_2)$ data. For example, they derived the relation:

$$j(\textit{trans}\text{-3-hexene-2,5-dione}) = (5.8 \pm 1.0) \times 10^{-3} \times j(NO_2) - (1.3 \pm 1.2) \times 10^{-5}\ s^{-1}.$$

However, such a relation is applicable only for solar zenith angles $< \sim 60°$ since higher values lead to negative numbers. We have fitted a quadratic least squares to their data but have forced the fit to pass through the origin as one expects the relation to behave in theory. See the plots given in figure IX-F-28. We then used our values for $j(NO_2)$ versus solar zenith angle calculated for the standard conditions employed in this work (cloudless sky, 0.5 km altitude, 350 DU ozone column), together with the equations derived in figure IX-F-28 to estimate the *j*-value versus solar zenith angle data plotted in figure IX-F-29. We recommend that these data be used to estimate *j*-values within the cloudless sky of the lower troposphere.

Table IX-F-9. Cross sections for *trans*-3-hexene-2,5-dione in acetonitrile solution (data of Liu et al., 1999); units for σ are cm^2 $molecule^{-1}$

λ, nm	$10^{19} \times \sigma$	λ, nm	$10^{19} \times \sigma$	λ, nm	$10^{19} \times \sigma$	λ, nm	$10^{19} \times \sigma$
290	1.89	330	2.82	370	1.04	410	0.07
291	1.96	331	2.78	371	1.00	411	0.06
292	2.03	332	2.75	372	0.96	412	0.05
293	2.10	333	2.71	373	0.91	413	0.05
294	2.16	334	2.66	374	0.88	414	0.05
295	2.22	335	2.63	375	0.84	415	0.05
296	2.30	336	2.58	376	0.79	416	0.05
297	2.36	337	2.55	377	0.76	417	0.04
298	2.43	338	2.50	378	0.73	418	0.03
299	2.50	339	2.46	379	0.69	419	0.03
300	2.56	340	2.41	380	0.64	420	0.03
301	2.63	341	2.36	381	0.61	421	0.03
302	2.68	342	2.32	382	0.58	422	0.02
303	2.73	343	2.28	383	0.54	423	0.02
304	2.78	344	2.24	384	0.52	424	0.02
305	2.82	345	2.20	385	0.49	425	0.02
306	2.87	346	2.14	386	0.47	426	0.02
307	2.91	347	2.09	387	0.44	427	0.02
308	2.93	348	2.05	388	0.40	428	0.01
309	2.97	349	2.00	389	0.36	429	0.01
310	2.99	350	1.95	390	0.35	430	0.01
311	3.03	351	1.91	391	0.33	431	0.01
312	3.03	352	1.86	392	0.30	432	0.01
313	3.06	353	1.82	393	0.29	433	0.01
314	3.07	354	1.77	394	0.27	434	0.01
315	3.07	355	1.72	395	0.25	435	0.01
316	3.08	356	1.68	396	0.23	436	0.01
317	3.09	357	1.63	397	0.21	437	0.01
318	3.08	358	1.58	398	0.19	438	0.01
319	3.07	359	1.53	399	0.18	439	0.01
320	3.06	360	1.48	400	0.16	440	0.004
321	3.05	361	1.43	401	0.15	441	0.003
322	3.03	362	1.39	402	0.14	442	0.004
323	3.02	363	1.35	403	0.13	443	0.01
324	3.00	364	1.30	404	0.13	444	0.01
325	2.97	365	1.26	405	0.12	445	0.01
326	2.95	366	1.22	406	0.10	446	0.003
327	2.93	367	1.18	407	0.10	447	0.01
328	2.88	368	1.13	408	0.09	448	0.0034
329	2.85	369	1.08	409	0.07	449	0.01

IX-F-13. Photodecomposition of Nopinone (6,6-Dimethylbicyclo[3.1.1]heptan-2-one)

Nopinone is a major product of the reaction of the biogenic compound pinene with ozone and OH radicals. The photodecomposition of nopinone in methanol and *tert*-butyl alcohol solutions has been studied by Shaffer et al. (1972). The solutions were outgassed with argon before and during photolyses, and Corex® filtered light from a 450 W medium pressure Hanovia mercury lamp ($\lambda > 255$ nm) was used in

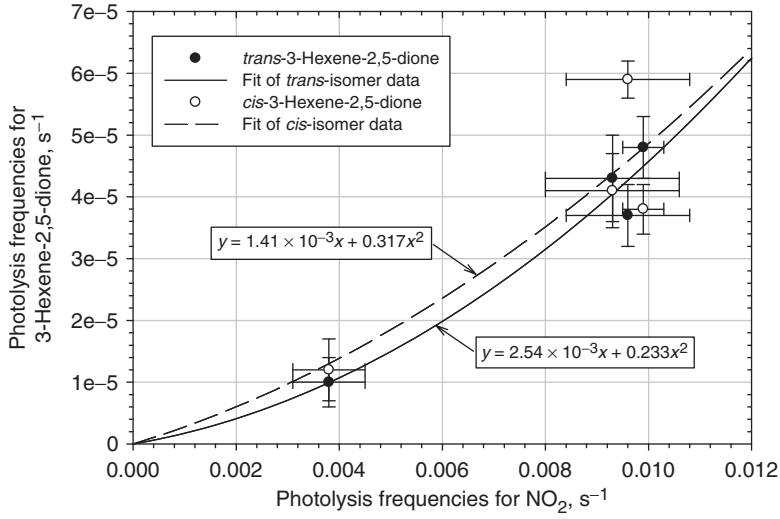

Figure IX-F-28. Plot of $j(NO_2)$ versus j(3-hexene-2,5-dione) as measured by Becker and Graedler (1999).

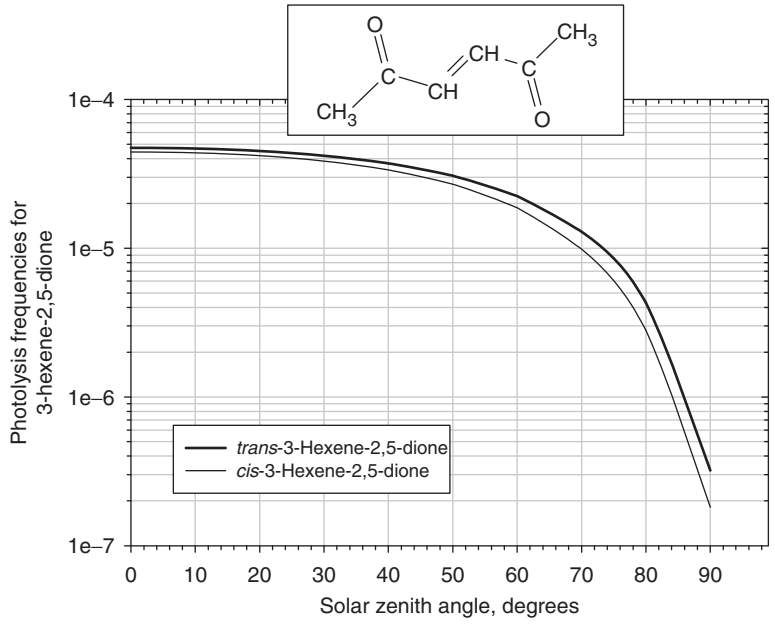

Figure IX-F-29. Estimated photolysis frequencies versus solar zenith angle for 3-hexene-2,5-dione as a function of solar zenith angle for a clear lower troposphere and ozone column of 350 DU; see text for methods employed.

the experiments. The major product of photolysis in methanol was *cis*-1-formyl-2,2-dimethyl-3-vinylcyclobutane (A), and subsequent photolysis of this product gave 4-*iso*-propenyl-5-hexanal (B) (reaction mechanism IX-F-13):

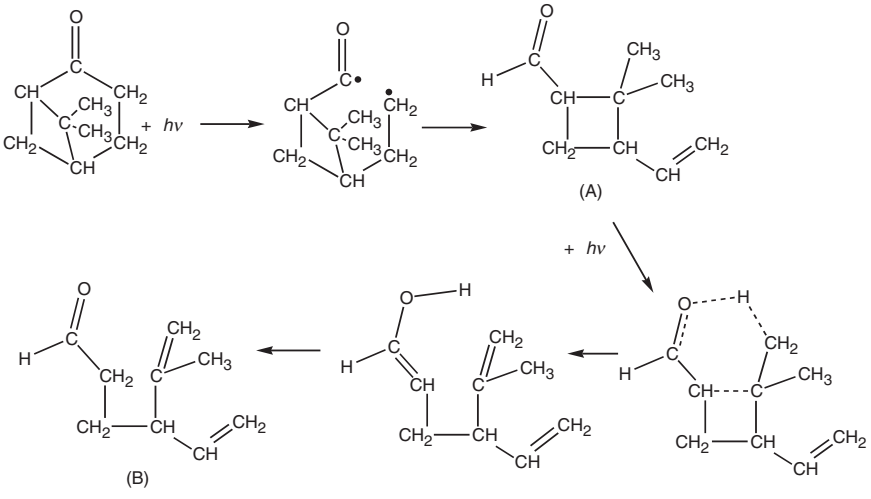

Reaction mechanism IX-F-13

As with cyclohexanone, the observed rearrangement of nopinone to (A) could be initiated by the rupture of the —C(O)—CH_2— bond (in this case, on the side with the fewer substituents) to form a diradical followed by transfer of an H-atom. Transformations of (A) to (B) could be the ultimate result of the occurrence of a Norrish type-II reaction. In these cases, the abstraction of a γ-H-atom would not lead to the formation of two molecules, but an opening of the 4-membered ring. In photolyses of nopinone in benzene solution using a 300 nm Rayonet® lamp, Shaffer et al. determined the quantum yield of disappearance (ϕ_{diss}) of nopinone to be 0.32.

The only gas-phase nopinone photodecomposition studies of which we are aware are reported by Hjorth et al. (in Moortgat et al., 2002). In laboratory experiments carried out in a 480 L reaction chamber with 18 UV/VIS lamps to simulate sunlight, the relative rate of photolysis of nopinone was less than 0.3 times those of glycolaldehyde, pinonaldehyde, and 4-oxopentanal. In the EUPHORE chamber, *j*-values for disappearance were less than $3 \times 10^{-6}\ s^{-1}$. The necessary spectral and quantum yield data are not currently available to calculate meaningful *j*-values for nopinone.

IX-F-14. Photodecomposition of Limona Ketone

Limona ketone, structure shown below, is a major product of the reaction of limonene with HO radicals or O_3.

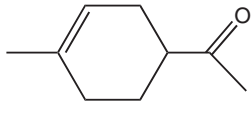

The only photodecomposition studies of limona ketone of which we are aware are reported by Hjorth et al. (in Moortgat et al., 2002). In laboratory experiments carried out in a 480 L reaction chamber with 18 UV/VIS lamps to simulate sunlight, the relative rate of photolysis of limona ketone was less than 0.3 times those of glycolaldehyde, pinonaldehyde, and 4-oxopentanal. In the EUPHORE chamber, *j*-values for disappearance were less than $3 \times 10^{-6}\,s^{-1}$. The necessary spectral and quantum yield data are not currently available to calculate meaningful *j*-values for limona ketone.

IX-G. Photodecomposition of the Acyl Halides and Carbonyl Halides

IX-G-1. Spectra of the Acyl Halides and Carbonyl Halides

Acyl halides [HC(O)X, $CX_nH_{3-n}C(O)X$, etc., where X is a halogen atom] are among the products of the tropospheric oxidation of the haloalkanes. The absorption spectra of several acyl halides and carbonyl halides have been compared and discussed by Calvert et al. (2008). The absorption cross sections for a series of formyl halides, HC(O)F, HC(O)Cl, and HC(O)Br and several carbonyl halides, FC(O)F, ClC(O)Cl, and BrC(O)Br, are compared with those for unsubstituted CH_2O in figure IX-G-1. All of these halogen-substituted formaldehydes have lower cross sections than the unsubstituted formaldehyde in the long-wavelength region of the tropospheric solar flux. Many of the halogen-atom-substituted formaldehyde derivatives absorb only the short wavelengths of sunlight that are weak in intensity within the troposphere. The long-wavelength absorption bands in these compounds results from an $n \rightarrow \pi^*$ electron promotion as assigned for HC(O)Cl by Judge and Moule (1985) and Ding et al. (1999) and for the $CH_3C(O)Cl$ molecule by Person et al. (1992a, b). It can be seen that a halogen atom substitution for an H-atom in CH_2O results in a significant change in the absorption spectrum. The maximum in the absorption cross sections shifts to the shorter wavelengths for the formyl halides in the progression: CH_2O, BrC(O)H, ClC(O)H, FC(O)H, while the long-wavelength tail in the absorption shows a decreasing overlap with the available wavelengths of sunlight. HC(O)Cl absorbs sunlight only weakly; among the formyl halides shown in the figure, only HC(O)Br absorbs significantly at the wavelengths available within the troposphere. A similar trend observed by Calvert et al. (2008) for the carbonyl halides can be seen in figure IX-G-1b; only the bromine-containing carbonyl [BrC(O)Br] absorbs the wavelengths of tropospheric sunlight significantly. Similar effects are seen in the absorption of the halogen-atom-substituted acetyl chlorides; see figure IX-G-2. Significant overlap of the absorption with the wavelength distribution of the actinic flux occurs only for those acetyl chlorides with the largest numbers of halogen atoms, i.e., $CHCl_2C(O)Cl$, $CCl_3C(O)Cl$, and $CF_3C(O)Cl$. Cross sections are given in table IX-G-1 for some of the species for which photodissociation within the troposphere is somewhat significant.

As Calvert et al. (2008) pointed out, although the rates of photodecomposition of many of these compounds are slow in the troposphere, competing removal processes (reaction with OH, hydrolysis in cloud-, rain-, and sea-water) are also slow. As a result, even these slow photolyses in sunlight can be a major loss mechanism,

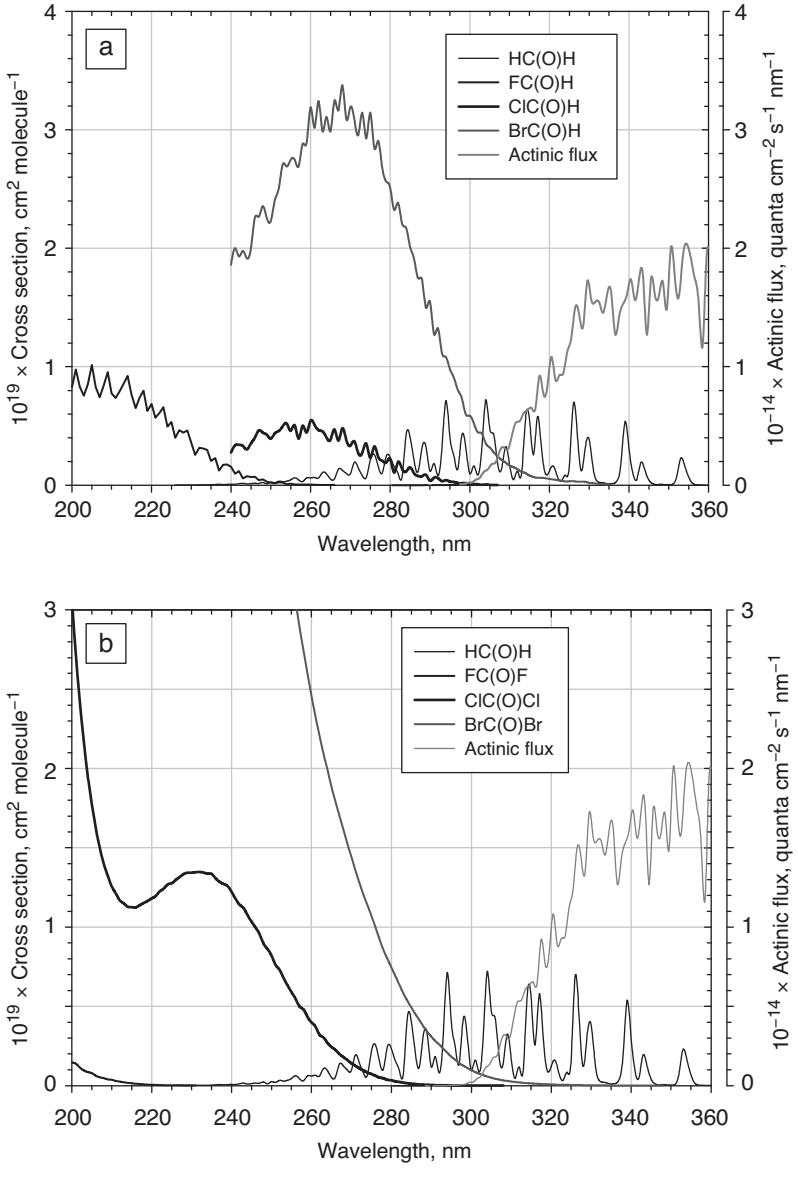

Figure IX-G-1. Comparison of the wavelength dependence of the cross sections of some halogen-atom-substituted formaldehyde molecules and the actinic flux as measured for a cloudless day (June 19, 1998) near Boulder, CO at noon. (a) Shows the spectra for the formyl halides; (b) gives the spectra for the carbonyl halides. Note that only the HC(O)Br and BrC(O)Br compounds have a significant overlap with the available actinic flux in the lower troposphere with an overhead Sun (gray curve). The long wavelength tail of the absorption of HC(O)Cl and ClC(O)Cl molecules catches the edge of the flux distribution. Spectral data from Keller-Rudek and Moortgat (2005); figures from Calvert et al. (2008).

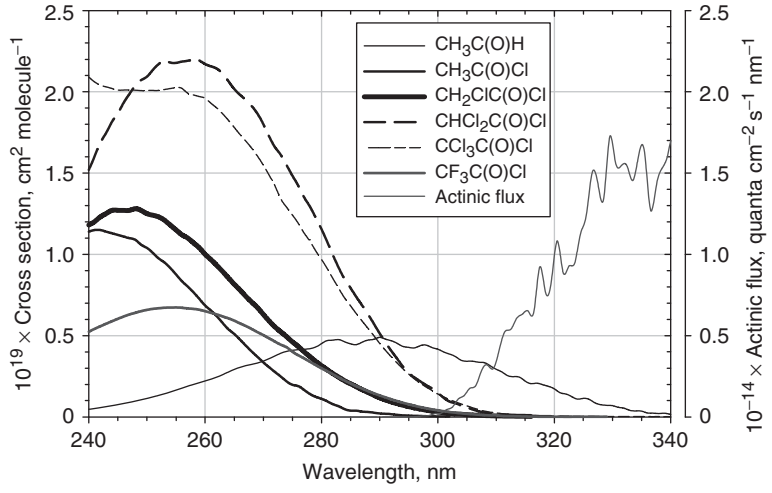

Figure IX-G-2. Comparison of the wavelength dependence of the cross sections of acetaldehyde and some halogen-atom-substituted acetaldehyde molecules, the acetyl chlorides. There is relatively poor overlap of the spectra for most acetyl chlorides with the distribution of the actinic flux as measured at noon for a cloudless day (June 19, 1998) near Boulder, CO; figure from Calvert et al. (2008).

and consideration of the acyl and carbonyl halide photodecompositions is of interest to atmospheric chemists.

IX-G-2. Photodecomposition of the Formyl Halides

The following primary pathways for photodissociation have been considered by Calvert et al. (2008) as reported in theoretical studies of the formyl halides:

$$\mathrm{HC(O)X} + h\nu \rightarrow \mathrm{HCO} + \mathrm{X} \quad \text{(I)}$$

$$\rightarrow \mathrm{H} + \mathrm{XCO} \quad \text{(II)}$$

$$\rightarrow \mathrm{H} + \mathrm{CO} + \mathrm{X} \quad \text{(III)}$$

$$\rightarrow \mathrm{HX} + \mathrm{CO} \quad \text{(IV)}$$

$$\rightarrow \mathrm{X{-}C{-}O{-}H \text{ or } H{-}C{-}O{-}X} \quad \text{(V)}$$

The dissociation pathways on the ground state potential energy surface (S_o) for HC(O)F and HC(O)Cl, have been reported by Kamiya and Morokuma (1991) and Francisco and Zhao (1992). The results of the latter study suggest that if dissociation occurs from the ground electronic state, process (III) is favored. The products of process (V) are the carbenes, possible isomerization routes for reactions that are predicted in theory. Fang and Liu (2001) reported an *ab initio* study of the dissociation of HC(O)Cl from the S_o, S_1, and T_1 states. They conclude that C—Cl bond cleavage, process (I), is the most favored mechanism for HC(O)Cl photodissociation for light

Table IX-G-1. Absorption cross sections (σ, cm^2 $molecule^{-1}$) as a function of wavelength for a series of formyl halides, carbonyl halides, and acetyl halides at 298 K. Data for HC(O)Br, BrC(O)Br, $CCl_3C(O)Cl$, $CHCl_2C(O)Cl$, and $CH_2ClC(O)Cl$ are from Libuda (1992) and for $CF_3C(O)Cl$ from Meller and Moortgat (1997)

λ, nm	$10^{20} \times \sigma$ HC(O)Br	$10^{20} \times \sigma$ BrC(O)Br	$10^{20} \times \sigma$ $CCl_3C(O)Cl$	$10^{20} \times \sigma$ $CHCl_2C(O)Cl$	$10^{20} \times \sigma$ $CH_2ClC(O)Cl$	$10^{20} \times \sigma$ $CCF_3C(O)Cl$
278	26.8	8.55	10.83	13.0	3.71	3.44
279	25.6	7.99	10.23	12.3	3.41	3.19
280	25.1	7.44	9.69	11.6	3.15	3.04
281	23.2	6.90	9.12	10.8	2.89	2.80
282	23.8	6.35	8.51	9.95	2.65	2.63
283	22.0	5.81	7.90	9.15	2.43	2.41
284	21.7	5.34	7.33	8.46	2.21	2.25
285	20.1	4.92	6.84	7.92	2.03	2.06
286	19.1	4.50	6.35	7.37	1.85	1.91
287	17.4	4.13	5.89	6.85	1.67	1.74
288	17.3	3.73	5.44	6.30	1.50	1.59
289	14.9	3.38	4.99	5.73	1.33	1.45
290	15.5	3.08	4.52	5.14	1.17	1.32
291	12.7	2.81	4.09	4.61	1.04	1.20
292	13.2	2.58	3.69	4.08	0.918	1.08
293	11.1	2.32	3.32	3.60	0.814	0.969
294	10.8	2.07	2.96	3.10	0.717	0.867
295	9.79	1.82	2.62	2.68	0.628	0.771
296	9.08	1.62	2.32	2.41	0.546	0.681
297	8.02	1.41	2.06	2.17	0.473	0.599
298	7.34	1.26	1.83	1.94	0.409	0.528
299	5.96	1.11	1.62	1.74	0.353	0.458
300	5.86	0.971	1.41	1.48	0.300	0.404
301	5.24	0.858	1.23	1.18	0.248	0.347
302	4.46	0.750	1.06	0.944	0.199	0.304
303	4.37	0.661	0.918	0.843	0.170	0.256
304	3.53	0.577	0.787	0.706	0.157	0.221
305	3.18	0.501	0.672	0.577	0.131	0.186
306	2.77	0.436	0.551	0.458	0.113	0.158
307	2.43	0.385	0.444	0.347	0.0909	0.130
308	2.12	0.330	0.358	0.277	0.0809	0.109
309	1.90	0.301	0.294	0.216	0.0657	0.0879
310	1.65	0.260	0.247	0.177	0.0547	0.0722
311	1.51	0.230	0.201	0.151	0.0522	0.0579
312	1.34	0.204	0.166	0.120	0.0419	0.0472
313	1.13	0.178	0.141	0.095	0.0380	0.0373
314	1.01	0.159	0.121	0.067	0.0311	0.0301
315	0.801	0.143	0.103	0.058	0.0286	0.0234
316	0.687	0.127	0.0849	0.049	0.0214	0.0189
317	0.613	0.114	0.0780	0.052		0.0146
318	0.611	0.0995	0.0657	0.044		0.0123
319	0.576	0.0892	0.0576	0.046		0.0095
320	0.521	0.0789	0.0502	0.035		0.0084
321	0.476	0.0694	0.0466	0.022		0.0063
322	0.424	0.0632	0.0436	0.010		0.0057
323	0.363	0.0578	0.0377	0.0093		0.0041
324	0.307	0.0528	0.0369	0.0099		0.0037

(*continued*)

Table IX-G-1. (*continued*)

λ, nm	$10^{20} \times \sigma$ HC(O)Br	$10^{20} \times \sigma$ BrC(O)Br	$10^{20} \times \sigma$ $CCl_3C(O)Cl$	$10^{20} \times \sigma$ $CHCl_2C(O)Cl$	$10^{20} \times \sigma$ $CH_2ClC(O)Cl$	$10^{20} \times \sigma$ $CCF_3C(O)Cl$
325	0.316	0.0498	0.0342	0.013		0.0025
326	0.325	0.0449	0.0327	0.020		0.0025
327	0.288	0.0397	0.0284	0.025		0.0016
328	0.281	0.0336	0.0269	0.021		0.0017
329	0.271	0.0296	0.0266	0.010		0.0009
330	0.193	0.0264	0.0278	0.0098		
331	0.161	0.0229	0.0259	0.0029		
332	0.108	0.0238	0.0226	0.0029		
333	0.091	0.0204	0.0218	0.0029		
334	0.067	0.0169	0.0166	0.0029		
335	0.073	0.0137	0.0159	0.012		
336	0.080	0.0110	0.0153	0.011		
337	0.086	0.0138	0.0139	0.019		
338	0.118	0.0110	0.0156	0.010		
339	0.166	0.0106	0.0142			
340	0.135	0.0079	0.0171			
341		0.0081	0.0135			
342		0.0082	0.0119			
343		0.0070				
344		0.0070				
345		0.0055				
346		0.0043				
347		0.0016				
348		0.0008				
349		0.0011				
350		0.0006				
351		0.0025				
352		0.0019				
353		0.0002				

absorbed within the 230–320 nm range. The extent of occurrence of processes (IV) and (V) is unknown, but it is expected to be small.

IX-G-3. Photodecomposition of the Carbonyl Halides

FC(O)F has been detected in the stratosphere (Rinsland et al., 1986), and ClC(O)Cl within the lower troposphere of some urban areas (Singh, 1976). Both compounds are believed to have been derived from atmospheric reactions of halogenated hydrocarbons (haloalkanes and/or the haloalkenes). Several primary photodissociation processes have been considered by Calvert et al. (2008) for the carbonyl halides:

$$XC(O)X + h\nu \rightarrow XCO + X \quad \text{(I)}$$

$$\rightarrow X + CO + X \quad \text{(II)}$$

$$\rightarrow X_2 + CO \quad \text{(III)}$$

IX-G-3.1. Photodecomposition of Phosgene [ClC(O)C])

The studies of the photodecomposition of ClC(O)Cl by both theoretical (Francisco and Li, 1989) and experimental methods (Wijnen, 1961, 1962; Heicklen, 1965; Okabe, 1977; Maul et al., 1995; Jäger et al., 1996) suggest that process (I) is favored: $ClC(O)Cl + h\nu \rightarrow ClCO + Cl$ (I). The quantum yield of CO formation at 253.7 nm was found to be unity by Wijnen (1961, 1962), and this was confirmed in experiments reported by Okabe (1977). Jäger et al. (1996) reported from their studies that the quantum yield of photodecomposition of ClC(O)Cl is unity also at 193 nm. Wijnen, Heicklen and others have used the photolysis of ClC(O)Cl as a convenient source of Cl-atoms. Presumably, processes (I) and/or (II) are important, but the barrier for decomposition of the ClCO molecule ($ClCO \rightarrow CO + Cl$) is very small ($< 27\,kJ\,mol^{-1}$; Francisco and Li, 1989), and rapid dissociation of ClCO occurs at 298 K ($ClCO \rightarrow CO + Cl$). Thus, the two processes (I) and (II) result ultimately in the same products, $2Cl + CO$. If process (III) occurs to any extent, it also will lead ultimately to the same products (CO and Cl-atoms), since Cl_2 undergoes rapid photolysis. The most direct measurement of ClC(O)Cl photolysis was made by Maul et al. (1995). They found from dye-laser photolysis near 238 nm that 15% of the chlorine atoms were formed in the $Cl(^2P_{1/2})$ excited state with a mean kinetic energy of 38 kJ mol^{-1}, while the $Cl(^2P_{3/2})$ ground state Cl-atoms formed had a mean kinetic energy of $18\,kJ\,mol^{-1}$. Analysis of the kinetic energy spectra yielded evidence for a concerted three-body decay; they concluded that the formation of the intermediate ClCO is of minor importance in the dissociation process, at least for the conditions of their experiments.

IX-G-3.2. Photodecomposition of BrC(O)Br

Evidence has been presented (Xu et al., 2002) that the photodissociation of BrC(O)Br at 267 nm also occurs by several alternative channels: process (II) forming both fast and slow Br atoms and CO via an asynchronously concerted three-body decay process for both ground and spin-orbit excited bromine atoms; process (I); and process (III) forming molecular Br_2 and CO. No quantum yield studies of BrC(O)Br photolysis have been reported to our knowledge, but in view of the results described for ClC(O)Cl and the weak BrC(O)—Br bond in this molecule, one expects a total quantum yield of decomposition near unity. In view of the instability of the BrCO radical, processes (I) and (II) will both result in formation of two Br-atoms and a CO molecule.

IX-G-4. Photodecomposition of the Acyl Halides

Experimental studies (Person et al., 1992a, b; Deshmukh and Hess, 1994) and theoretical studies (Sumathi and Chandra, 1993) of the photodecomposition of acetyl chloride have been reported. Experimental studies have been reported for bromoacetyl chloride, $BrCH_2C(O)Cl$ (Person et al., 1992a, b) and perfluoroacetyl chloride [$CF_3C(O)Cl$]. The following primary processes have been considered by Calvert et al. (2008) in

explanation of the results:

$$CX_nH_{3-n}C(O)X + h\nu \rightarrow CX_nH_{3-n}CO + X \quad \text{(I)}$$

$$\rightarrow CX_nH_{3-n} + XCO \quad \text{(II)}$$

$$\rightarrow CX_nH_{3-n} + CO + X \quad \text{(III)}$$

$$\rightarrow CX_nH_{3-n}X + CO \quad \text{(IV)}$$

IX-G-4.1. Photodecomposition of Acetyl Chloride [$CH_3C(O)Cl$]

From results of acetyl chloride photolysis at 248.5 nm in a molecular beam experiment, Person et al. (1992a) reported that the anisotropic angular distributions of the observed Cl product of (I) show dissociation occurs on a timescale of less than a rotational period; no significant dissociation by process (II) was observed. The Cl fragment had an average translational energy of 67 kJ mol^{-1}. A possible elimination of HCl in a primary process could be excluded. Further theoretical considerations of the mechanism of the occurrence of process (I) in acetyl chloride photodissociation have been reported by Sumathi and Chandra (1993). The extent of process (IV) is unknown but expected to be small.

In their studies of $CH_3C(O)Cl$ photodecomposition at 236 nm, Deshmukh and Hess (1994) investigated the mechanism for preferential cleavage of the C—Cl bond in process (I) over that of C—C bond cleavage in process (II). They estimated that the quantum yield for CH_3 formation in (II) and/or (III) was 0.28 relative to that formed in CH_3I photolysis. Only a small fraction of the available energy is channeled into methyl fragment angular momentum as the rotational state distribution extends only to N" = 5. The fraction of Cl-atoms formed in the $^2P_{1/2}$ state was 0.40 ± 0.02. They concluded that CH_3CO is generated as a primary product in the photodissociation of acetyl chloride with about 126 kJ mol^{-1} of internal energy, well above the ~72 kJ mol^{-1} necessary for dissociation of CH_3CO, and for photolysis at 236 nm, it subsequently decomposes to CH_3 and CO.

IX-G-4.2. Photodecomposition of Bromoacetyl Chloride [$BrCH_2C(O)Cl$]

Excitation of bromoacetyl chloride at 248 nm can be attributed to an overlap of $n(O) \rightarrow \pi^*(C{=}O)$ excitation and $n(Br) \rightarrow \sigma^*(C - Br)$ transition. In this case, both Cl- and Br-atoms were detected by Person et al. (1992b). They reported that fission of the C—Cl and C—Br bonds occurs with a branching ratio of 1.0:1.1.

IX-G-4.3. Photodecomposition of Trifluoroacetyl Chloride [$CF_3C(O)Cl$]

Studies of the photodecomposition of trifluoroacetyl chloride indicate the dominance of primary process (I) for excitation at wavelengths in the range 254–280 nm. Product studies of Weibel et al. (1995) from the photodecomposition of $CF_3C(O)Cl$ at 254 and

280 nm showed $\Phi_{CF_3Cl} + 2\Phi_{C_2F_6} = 0.98 \pm 0.13$. CF_3H was formed in the photolysis of $CF_3C(O)Cl$ in the presence of added cyclohexane, indicating clearly that CF_3 radicals were present. Their results could not distinguish between the possible primary processes, but they suggest strongly that the total primary photodecomposition yield is near unity.

Maricq and Szente (1995) used time resolved IR and UV spectroscopy to study the photodissociation of $CF_3C(O)Cl$ in photolysis at 193 and 248 nm. They concluded that the net reaction shown by process (III) described the results best; rapidly dissociating CF_3CO and/or COCl radicals presumably were present as intermediates. At 193 nm the CO is formed with extensive internal excitation ($T_{vib} = 3,800 \pm 900$ K), whereas at 248 nm it is formed predominantly in $\nu = 0$. Quantum yields of the photodecomposition were measured by comparing yields of HCl (formed in experiments with added ethane) and RO_2 (experiments with added O_2) from $CF_3C(O)Cl$ to those from the photodisssociation of CH_3Cl at 193 nm and Cl_2 at 248 nm; they assumed the latter two species have unit photodissociation efficiencies. Values of the total quantum yield of photodecomposition, $(\phi_I + \phi_{II} + \phi_{III}) = 1.10 \pm 0.11$ at 193 nm and $0.92 \pm$ 08 at 248 nm. They conclude from their results that at 248 nm that about 14% of the CF_3CO fragment [product of process (I)] remains intact under the conditions of the experiment.

Meller and Moortgat (1997) measured the quantum yields for the photodissociation of $CF_3C(O)Cl$ as a function of pressure and the quantum yields for Cl_2 and CO in experiments at 254 nm and 296 K. ClC(O)Cl was used as the actinometer. They report a mean value of photodissociation $= 0.95 \pm 0.05$ (760 Torr of N_2 or air or C_2H_6/air mixtures). At varied pressures of air (50 to 760 Torr) the quantum yield showed no obvious change, ranging from 1.00 to 1.06. In photolysis of $CF_3C(O)Cl$ in 760 Torr of air, they measured $\Phi_{Cl_2} = 0.502 \pm 0.012$, indicating that all chlorine originating from $CF_3C(O)Cl$ is converted into molecular chlorine. They report a mean quantum yield for dissociation $= 0.96 \pm 0.04$, consistent again with $\phi_I + \phi_{II} + \phi_{III} =$ unity.

At the long wavelengths of absorbed light, there is little excess energy available in the quantum beyond that for dissociation, and one might expect process (I) to be the dominant mode of decay. However, haloacyl radicals ($CX_nH_{3-n}CO$) are unstable with respect to decomposition via CO elimination (Zabel et al., 1994; Tuazon and Atkinson, 1994; Solignac et al., 2006b; Hurley et al., 2006; Waterland and Dobbs, 2006). Calvert et al. (2008) concluded that while a small fraction of the $CX_nH_{3-n}CO$ radicals produced in the primary process at the long wavelengths may survive decomposition and react with O_2 in the atmosphere to give haloacylperoxy radicals, the majority will probably decompose leading to the formation of haloalkylperoxy radicals.

IX-G-5. Photolysis Frequencies for the Photodecomposition of the Acyl Halides and Halocarbonyls in the Lower Troposphere

To our knowledge, there have been no measurements of the quantum yields of photodissociation of acyl halides or carbonyl halides in the long-wavelength tail of the absorption that overlaps the distribution of actinic flux within the troposphere. In this

region of absorption, there is little energy available in the quantum of light beyond that for dissociation. For example, the energy available in the quantum of light at the edge of the absorption of CF_3COCl, 328 nm (365 kJ mol^{-1}), is probably close to the $CF_3C(O)$—Cl bond strength, assuming this bond strength is similar to that for $Cl_3C(O)$—Cl (339 ± 24 kJ mol^{-1}; Zhu and Bozzelli, 2002). Calvert et al. (2008) noted that no barriers to dissociation of the $n \rightarrow \pi^*$ excited haloacetyl chlorides or carbonyl halides have been reported in theoretical or experimental studies, and dissociation with high efficiency observed at the shorter wavelengths may continue into the long-wavelength absorption region. With this assumption, we can estimate the photolysis frequencies for those acyl halides and carbonyl halides.

Photolysis frequencies for those compounds that show some overlap of the actinic flux with the long-wavelength absorption bands have been estimated by Calvert et al. (2008) using the cross section data of table IX-G-1 (298 K) and an assumed quantum yield of photodissociation of unity over the entire absorption region. These data are shown in figure IX-G-3.

The weak absorption of the formyl and acyl halides at wavelengths available within the troposphere leads to much lower *j*-values than those of the unsubstituted aldehydes. In figure IX-G-3a, it is seen that the *j*-values decrease significantly in the sequence CH_2O > HC(O)Br > BrC(O)Br > HC(O)Cl. The estimated tropospheric lifetimes for photodecomposition with an overhead Sun are: CH_2O, 3.1 h; HC(O)Br, 16 h; BrC(O)Br, 4.0 days; HC(O)Cl, 2.4 months; ClC(O)Cl (not shown in figure IX-G-3a), ~16 years. For the haloacetyl chlorides shown in figure IX-G-3b, the *j*-values are seen to decrease from those of acetaldehyde in the order: $CH_3CHO > CCl_3C(O)Cl > CHCl_2C(O)Cl > CF_3C(O)Cl > CH_2ClC(O)Cl > CH_3C(O)Cl$. Approximate lifetimes for photodecomposition with an overhead Sun are: CH_3CHO, 1.6 days; $CCl_3C(O)Cl$, 4.4 days; $CHCl_2C(O)Cl$, 8.0 days; $CF_3C(O)Cl$, 23 days; $CH_2ClC(O)Cl$, 32 days; $CH_3C(O)Cl$, 8.8 years. The absorption cross sections for these compounds decrease with temperature decrease. As the altitude in the atmosphere increases, the absorption cross sections decrease as a result of the decreasing temperature, while the actinic flux increases. The net effect of altitude change on the *j*-values depends on the sizes of the two opposite effects. Meller and Moortgat (1997) have shown that for $CF_3C(O)Cl$, the calculated *j*-values remain fairly constant within the troposphere up to 10 km, but they rise rapidly at the higher altitudes where the effect of the increased presence of short wavelength actinic flux is expected.

The acyl halides and carbonyl halides have a relatively high reactivity toward hydrolysis in cloud-water and on moist aerosols and surfaces, and the removal of these species when formed within the troposphere is probably dominated by such reactions. DeBruyn et al. (1992) have shown that the uptake of ClC(O)Cl, FC(O)F, $CF_3C(O)F$, $CCl_3C(O)Cl$, and $CF_3C(O)Cl$ in water is rapid, and it is expected that their hydrolysis in cloudwater, rainwater, or ocean water will be a dominant fate for these species. Wallington and Hurley (1993) suggest that HC(O)F will likely face a similar fate. Wallington et al. (1994b) have estimated that the atmospheric lifetime of FC(O)F, FC(O)Cl, $CF_3C(O)F$, and $CF_3C(O)Cl$ with respect to uptake and hydrolysis in cloud water is 5–30 days. Certainly, the heterogeneous removal of most of the acyl halide and carbonyl halides is competitive with their loss by photodecomposition.

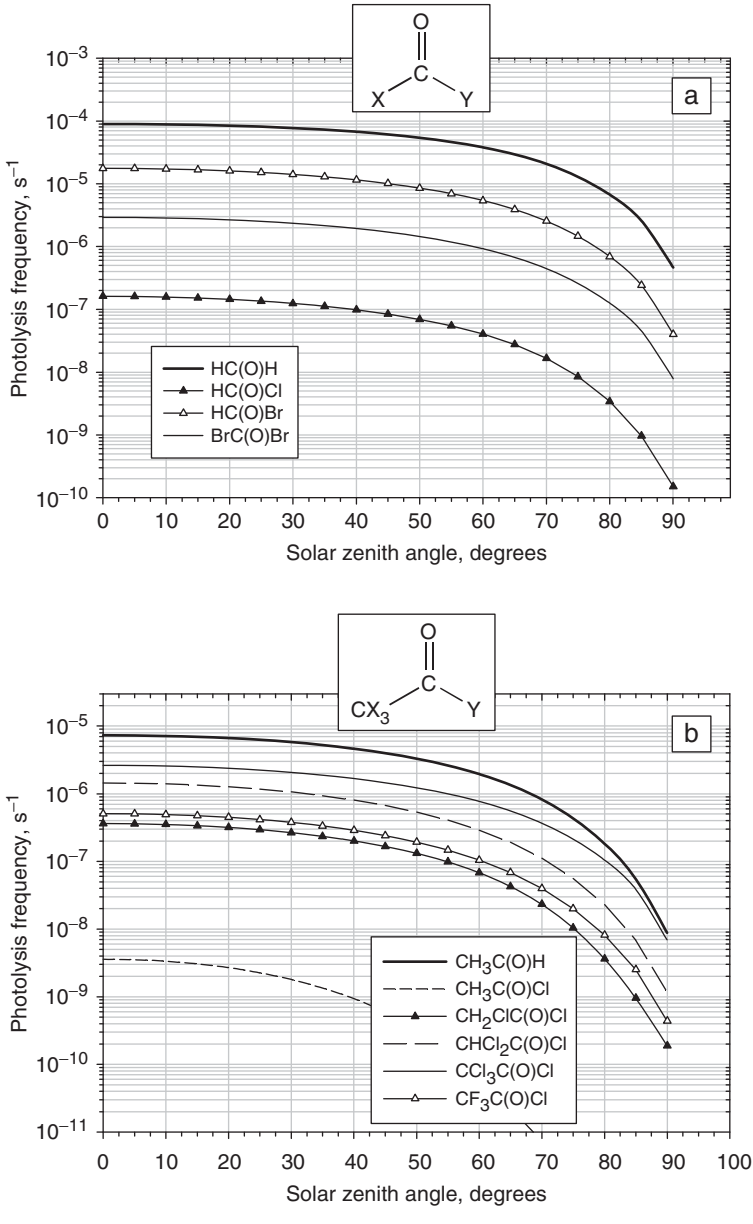

Figure IX-G-3. Comparison of the photolysis frequencies for photodecomposition by all modes versus solar zenith angle for some acyl halides for which absorption of tropospheric actinic flux is measurable within their long-wavelength tails: (a) formyl halides and carbonyl halides compared to CH_2O; (b) haloacetyl chlorides compared to CH_3CHO. Calculations were made for a cloudless day within the lower troposphere with a vertical ozone column of 350 DU, cross section data of table IX-G-1, and an assumed quantum yield of photodecomposition of unity; figure from Calvert et al. (2008).

IX-H. Photodecomposition of Nitrous Acid, Alkyl Nitrites, Nitroalkanes, and the Nitroso-Compounds

The alkyl nitrites (RONO) and the structurally related simplest nitrite, nitrous acid (HONO), are formed largely in the troposphere as products of the reactions of alkoxy radicals or OH radicals with nitric oxide: RO + NO → RONO. The nitroso-compounds (RNO), particularly, the *N*-nitroso compounds (R_2N—NO), are of interest because of their carcinogenic properties. The alkyl nitrites act as temporary sinks for oxides of nitrogen. In figure IX-H-1, it can be seen that the absorption spectra of the nitroso compounds and the alkyl nitrites overlap well a large range of wavelengths of sunlight available in the troposphere. The bond dissociation energies of the alkyl nitrites (RONO → RO + NO) are all in the range of 174 ± 3 kJ mol^{-1}, an energy that corresponds to that available in a mole of quanta light at 687 ± 11 nm; thus photodissociation into RO and NO molecules is energetically possible over the entire absorption band of these compounds, and they have the potential to be important sources of free radicals in the troposphere. The energy excess present in the excited molecule often appears as excitation in the alkoxy radicals formed.

In this section, we will review the results that define the nature and the efficiency of the photodissociation processes in these compounds with the aim of calculating their photolysis frequencies in the lower troposphere.

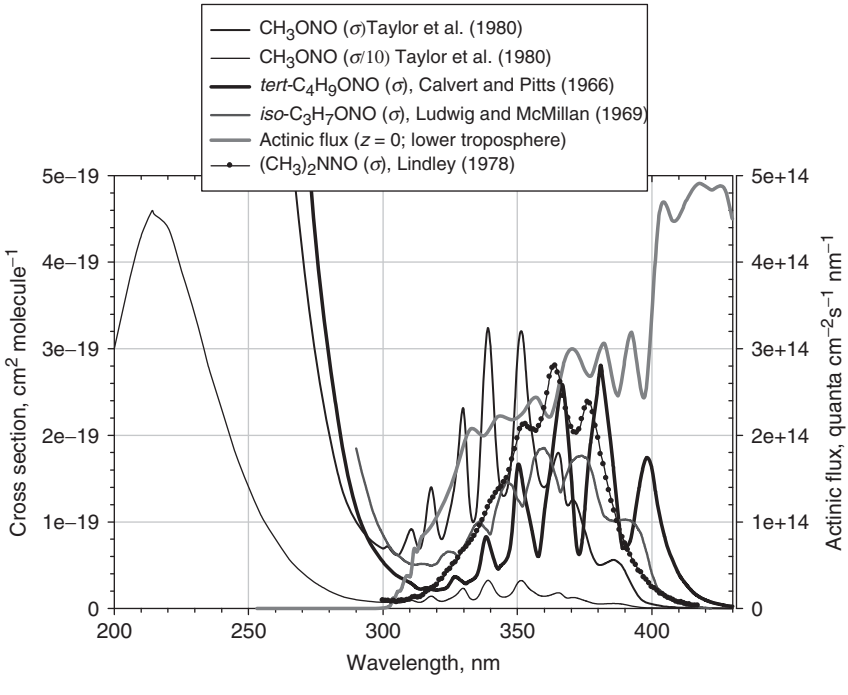

Figure IX-H-1. Absorption spectra of some simple alkyl nitrites and $(CH_3)_2NNO$. The absorption regions of all of these compounds overlap well wavelengths present in the tropospheric actinic flux (overhead Sun) that is shown by the heavy gray curve.

IX-H-1. The Photodecomposition of Nitrous Acid (HONO)

Measurements within the urban troposphere during the nighttime and early morning hours before sunrise indicate the generation of HONO; this requires that some formation processes other than the association of OH and NO operate during the nighttime hours. Concentrations of nitrous acid, often several ppb, have been detected in the early morning hours, especially in urban areas that have elevated levels of NO_x and high humidity (e.g., see Perner and Platt, 1979; Platt et al., 1980; Harris et al., 1982; Pitts et al., 1984a; Sjödin and Ferm, 1985; Sjödin, 1988; Biermann et al., 1988; Lammel and Perner, 1988; Rodgers and Davis, 1989; Appel et al., 1990; Večeřa and Dasgupta, 1991). The mechanism of HONO formation during the nighttime hours is uncertain, but it appears that the process is heterogeneous (Pitts et al., 1984b; Calvert et al., 1994; Lammel and Cape, 1996; Stutz et al., 2004). The nighttime generated HONO concentrations can provide a significant boost to the OH radical generation at sunrise and significantly affect the extent of smog formation.

The near ultraviolet absorption bands of nitrous acid, like all nitrites, involves an $n \rightarrow \pi^*$ transition, and the absorption bands overlap well the envelope of actinic flux present in the troposphere; see figure IX-H-2. The photodecomposition of HONO is efficient in generating OH radicals in the troposphere. Two primary processes have been proposed to rationalize the observed photodecomposition of HONO:

$$\mathrm{HONO} + h\nu \rightarrow \mathrm{OH} + \mathrm{NO} \qquad \text{(I)}$$

$$\rightarrow \mathrm{H} + \mathrm{NO_2} \qquad \text{(II)}$$

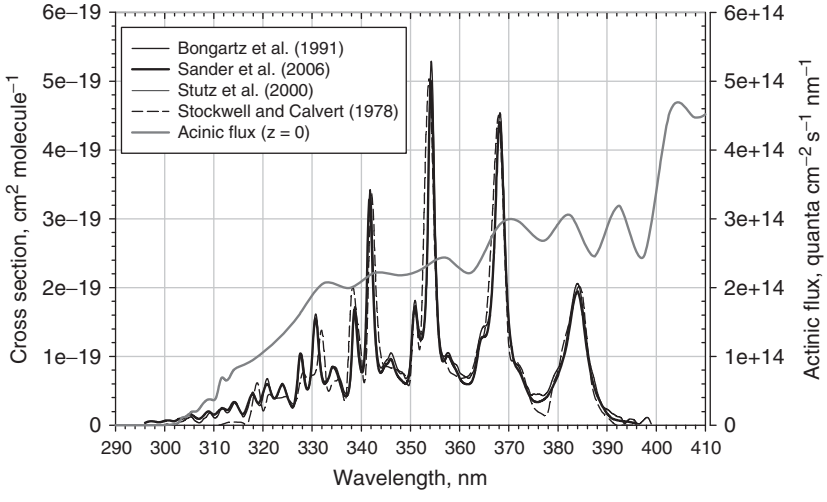

Figure IX-H-2. Comparison of the absorption spectrum of HONO as measured by several groups: Stockwell and Calvert (1978); Bongartz et al. (1991); Stutz et al. (2000); and as recommended in the review by Sander et al. (2006); actinic flux is shown for an overhead Sun in the lower troposphere (gray curve).

The experimental and theoretical studies that elucidate the nature of the photodecomposition of HONO will be discussed in this section.

IX-H-1.1. The Absorption Cross Sections of HONO

The absorption spectrum of HONO shows a prominent vibrational structure related to the progressions of vibrational levels of the NO bond in the excited S_1 state; see figure IX-H-2. Similar band structures are evident in the spectra of the alkyl nitrites that reflect a similar origin; see figure IX-H-1. It can be seen that there is reasonably good agreement between the existing estimates of the cross sections of HONO as a function of wavelength. The measurements of Stockwell and Calvert (1978), Bongartz et al. (1991, 1994), and Stutz et al. (2000) are very similar both in position of the major peaks and the magnitude of the cross sections in most regions of the spectrum. The data of interest for tropospheric chemistry ($\lambda > 290$ nm) as recommended by the NASA review panel (Sander et al., 2006) are those of Stutz et al. (2000) and are given in table IX-H-1.

IX-H-1.2. Quantum Yields of Photodecomposition of HONO

There are few estimates of the quantum yield of photodissociation of HONO, but existing evidence suggests that process (I) is the dominant decomposition mode for photolyses at wavelengths of sunlight available within the troposphere. Thus Cox (1974) concluded from his studies of the 330–380 nm photolyses of HONO, NO, NO_2 mixtures in air that: $0.7 < \phi_{\mathrm{I}} + \phi_{\mathrm{II}} < 1.9$. He stated that when uncertainties are taken into account, it is probable that the total quantum yield of photodecomposition of HONO is close to unity. He also concluded that ~10% of the photodecomposition may proceed through process (II).

Cox and Derwent (1976) used NO_2 photodecomposition as a reference to estimate the quantum yield of OH radical formation in (I) to be 0.92 ± 0.16. Wollenhaupt et al. (2000) have shown that process (II) is unimportant for photodecomposition within the long-wavelength bands of HONO; they measured the resonance fluorescence of H-atoms at 121.6 nm to show that $\phi_{\mathrm{II}} < 0.01$ in photolyses of HONO at 351 nm. Further evidence for the conclusion that $\phi_{\mathrm{I}} + \phi_{\mathrm{II}} \approx 1.0$ is given by the direct j(HONO) measurements made by Wall et al. (2006). These workers used special equipment designed specifically to measure photolysis frequencies of HONO directly in sunlight. Their results compare well with those calculated from cross section and actinic flux data assuming that $\phi_{\mathrm{I}} + \phi_{\mathrm{II}} = 1.0$. See figure IX-H-3. From the limited evidence at hand, it appears likely that process (I) is the dominant photodecomposition pathway for HONO photolysis within the troposphere, and that its quantum yield is near unity.

Several experimental studies have elucidated the dynamics of the primary process (I); e.g., see Vasudev et al. (1983); Dixon and Rieley (1989); Shan et al. (1989); Ning and Pfab (1997). Vasudev et al. (1983) concluded from their experiments at 369 nm that the product OH translational motion shows a sharply peaked velocity distribution with ~ 46% of the total available energy appearing in the OH recoil, and a high percentage of the available energy (72%) appears in the recoil of the two products.

Table IX-H-1. Cross sections (σ, cm^2 molecule^{-1}) for HONO as a function of wavelength; recommendations of Sander et al. (2006) from Stutz et al. (2000)

λ, nm	$10^{20} \times \sigma$	λ, nm	$10^{20} \times \sigma$	λ, nm	$10^{20} \times \sigma$	λ, nm	$10^{20} \times \sigma$	λ, nm	$10^{20} \times \sigma$
292.0	0.29	313.5	2.79	335.0	7.71	356.5	9.34	378.0	4.31
292.5	0.28	314.0	3.46	335.5	6.55	357.0	9.45	378.5	4.92
293.0	0.27	314.5	3.32	336.0	5.33	357.5	10.08	379.0	5.65
293.5	0.19	315.0	2.53	336.5	4.36	358.0	9.84	379.5	6.46
294.0	0.18	315.5	1.78	337.0	4.23	358.5	9.02	380.0	7.21
294.5	0.16	316.0	1.53	337.5	5.13	359.0	8.37	380.5	8.00
295.0	0.21	316.5	2.02	338.0	9.38	359.5	7.67	381.0	9.09
295.5	0.24	317.0	3.18	338.5	16.52	360.0	6.87	381.5	10.51
296.0	0.33	317.5	4.51	339.0	14.32	360.5	6.32	382.0	12.39
296.5	0.43	318.0	4.63	339.5	9.96	361.0	6.05	382.5	14.64
297.0	0.57	318.5	3.68	340.0	7.79	361.5	5.95	383.0	17.08
297.5	0.63	319.0	3.10	340.5	8.51	362.0	5.98	383.5	19.08
298.0	0.51	319.5	3.26	341.0	16.13	362.5	6.35	384.0	19.70
298.5	0.43	320.0	4.55	341.5	31.52	363.0	7.39	384.5	18.59
299.0	0.43	320.5	6.41	342.0	29.40	363.5	9.22	385.0	16.15
299.5	0.46	321.0	6.11	342.5	18.47	364.0	11.49	385.5	13.21
300.0	0.61	321.5	4.69	343.0	11.43	364.5	12.71	386.0	10.46
300.5	0.81	322.0	3.97	343.5	8.29	365.0	12.82	386.5	8.20
301.0	0.69	322.5	3.88	344.0	7.59	365.5	13.19	387.0	6.54
301.5	0.55	323.0	4.50	344.5	8.18	366.0	14.84	387.5	5.29
302.0	0.57	323.5	5.61	345.0	8.77	366.5	18.43	388.0	4.29
302.5	0.76	324.0	6.04	345.5	9.10	367.0	25.08	388.5	3.44
303.0	0.95	324.5	5.33	346.0	9.64	367.5	35.18	389.0	2.80
303.5	0.91	325.0	4.00	346.5	8.87	368.0	43.56	389.5	2.21
304.0	1.04	325.5	2.93	347.0	7.80	368.5	41.37	390.0	1.69
304.5	1.28	326.0	2.65	347.5	7.06	369.0	31.45	390.5	1.29
305.0	1.64	326.5	3.55	348.0	6.63	369.5	21.72	391.0	0.98
305.5	1.58	327.0	6.44	348.5	6.26	370.0	15.05	391.5	0.81
306.0	1.28	327.5	10.26	349.0	6.00	370.5	11.27	392.0	0.72
306.5	1.02	328.0	9.22	349.5	6.47	371.0	9.36	392.5	0.65
307.0	0.86	328.5	6.38	350.0	9.06	371.5	8.53	393.0	0.60
307.5	1.06	329.0	5.20	350.5	14.95	372.0	7.98	393.5	0.57
308.0	1.43	329.5	6.11	351.0	16.94	372.5	7.25	394.0	0.53
308.5	1.91	330.0	9.92	351.5	14.07	373.0	6.31	394.5	0.45
309.0	2.08	330.5	15.06	352.0	12.42	373.5	5.36	395.0	0.40
309.5	1.77	331.0	14.32	352.5	12.81	374.0	4.59	395.5	0.38
310.0	1.45	331.5	9.88	353.0	16.34	374.5	3.91	396.0	0.24
310.5	1.52	332.0	6.94	353.5	28.49	375.0	3.52	396.5	0.12
311.0	2.04	332.5	6.00	354.0	48.73	375.5	3.34	397.0	0.07
311.5	2.68	333.0	6.31	354.5	44.34	376.0	3.33	397.5	0.04
312.0	2.42	333.5	7.11	355.0	27.64	376.5	3.51	398.0	0.10
312.5	2.06	334.0	8.35	355.5	16.40	377.0	3.66	398.5	0.10
313.0	2.19	334.5	8.37	356.0	11.13	377.5	3.87		

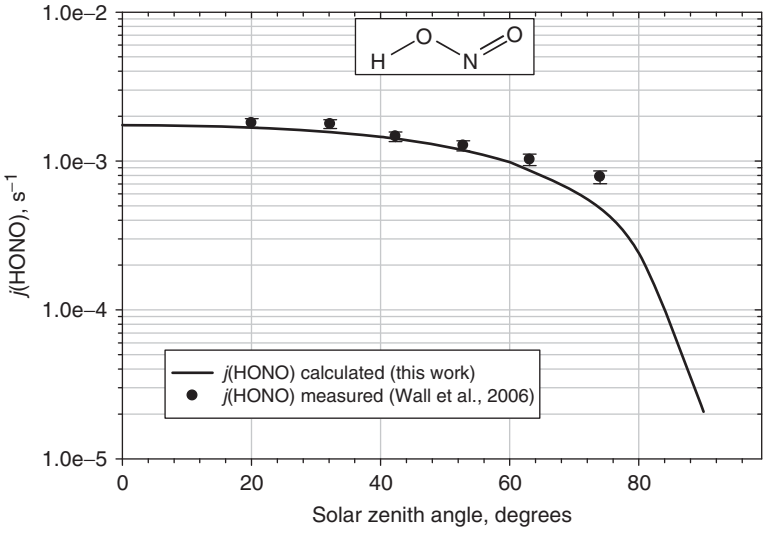

Figure IX-H-3. Photolysis frequencies for HONO in the lower troposphere as a function of solar zenith angle: solid curve, as calculated for a cloudless sky with an overhead ozone column of 350 DU; filled circles as measured directly in sunlight near Totonto, Canada, on a cloudless day by Wall et al. (2006).

The OH fragment is vibrationally and rotationally cold. For photolysis at somewhat shorter wavelengths, excitation of vibrations in the NO appear. Novicki and Vasudev (1991), matching observed Doppler profiles with theory, found that promotion of the HONO into the $v_2 = 1$ or $v_2 = 2$ bands results in population of $v_{NO} = 0$ and 1; entry to the $v_2 = 3$ band populates the product NO predominantly in $v_{NO} = 1$ and 2 with a population ratio of 1.0:0.6. This energy distribution is in agreement with the findings of Dixon and Rieley (1989). With excitation of HONO into the 2_0^2 band at 355 nm, Dixon and Rieley (1989) found the rotation of the product NO extended from about $J = 10$ to $J = 45$ with a maximum at about $J = 25$. These scientists also reported that the disposal of available energy into all NO and OH motions (including translation) is 60% and 40%, respectively. About 40% of the excess energy went into vibrational and rotational excitation (mostly of NO) and about 60% into translational recoil.

Novicki and Vasudev (1991) estimated from linewidth measurements that the fragmentation time (the time required for the OH and NO fragments to recoil beyond the sphere of their mutual interaction) is very short, 25 fs, for excitation to the 0^0 vibrational state; the lifetime rises to 154 fs for excitation to the 2^4 vibrational level of excited HONO.

Amaral et al. (2001) reported that the primary process (II) does occur measurably in HONO photolyses in the vacuum ultraviolet region at 193.3 nm where the excitation involves an allowed $n \rightarrow \sigma^*$ transition. About 0.3 of the available excess energy appeared as translation of the products in this case. They demonstrated as well that at least three electronic states of NO_2 were formed in the photodissociation, X^2A_1, A^2B_2, B^2B_1/C^2A_2, with relative populations of 0.13:0.21:0.66, respectively. Kenner

et al. (1986) determined that the formation of the excited OH(A) state occurred in photolyses at 193 nm with a quantum yield of about 10^{-5}. The rotational population of the OH(A) product rotational states had a Boltzmann distribution with a temperature of about 650 K.

Theoretical calculations related to the photodissociation of HONO have been reported by several groups; e.g., see Hennig et al. (1989) and Suter and Huber (1989); these support the conclusion that process (I) occurs with high efficiency.

IX-H-1.3. Photolysis Frequencies for HONO Photodecomposition within the Lower Troposphere

The *j*-values for HONO photodissociation within the lower troposphere have been calculated as a function of solar zenith angle for a cloudless day using the cross sections given in table IX-H-1 and assuming $\phi_{\text{total}} = 1.0$, independent of wavelength. The overhead ozone column was fixed at 350 DU. These data are given in figure IX-H-3. The closed circles shown in the figure are from direct measurements in sunlight on a cloudless day at a location near Toronto, Canada (Wall et al., 2006). In view of probable differences between the assumed magnitude of the ozone column and other variables necessary for the calculations and those that existed on the day of the direct measurements, the calculated *j*-values and those measured directly appear to be in reasonable accord. These results show that for an overhead Sun, the lifetime of HONO within the troposphere is short, about 10 min.

IX-H-2. The Photodecomposition of Methyl Nitrite (CH_3ONO)

The absorption regions of the alkyl nitrites overlaps well the distribution of solar flux within the lower troposphere; see figure IX-H-1. The characteristic band structure that appears in each spectrum, like that in HONO, originates from the excitation to the different vibrational energy levels (an N–O stretching mode, v_2) in the S_1 excited state. Like HONO, the alkyl nitrites (RONO) photodissociate readily to form free radicals: $RONO + h\nu \rightarrow RO + NO$, that can drive the chemistry that results in ozone generation within the troposphere. The alkyl nitrites (RONO) are often used as convenient sources of alkoxy radicals (RO) in laboratory experiments.

There have been both experimental and theoretical studies of the photochemistry of the nitrites that have elucidated the mechanism of photodecomposition. Several primary processes have been considered in the previous studies of the photodecomposition of methyl nitrite:

$$CH_3ONO + h\nu \rightarrow CH_3O + NO \qquad \text{(I)}$$

$$\rightarrow (CH_3O^{\ddagger}) + NO \rightarrow CH_2O + H + NO \qquad \text{(II)}$$

$$\rightarrow HNO + CH_2O \qquad \text{(III)}$$

In their pioneering studies of methyl nitrite photodecomposition, Thompson and Purkis (1936) reported the formation of products that suggested the occurrence of process (III),

namely, N_2O and formaldehyde; the N_2O is a product of the HNO–HNO reaction (3); see the following discussion. Thompson and Dainton (1937) also favored the occurrence of process (III) in their studies that extended to photolyses of *n*-C_3H_7ONO, *iso*-C_3H_7ONO, *sec*-C_4H_9ONO, and *tert*-C_4H_9ONO in addition to CH_3ONO. However, Gray and Style (1952) and all research groups in more recent studies have demonstrated that the CH_3O and NO are formed in (I) and that these original fragments are expected to form the products of process (III) in their subsequent reactions following process (I):

$$CH_3O + NO \rightarrow CH_3ONO \quad (1)$$

$$\rightarrow HNO + CH_2O \quad (2)$$

$$HNO + HNO \rightarrow N_2O + H_2O \quad (3)$$

Napier and Norrish (1965, 1967) identified HNO spectroscopically in flash photolyses of methyl nitrite as the intermediate product and from the kinetics of its appearance concluded that process (I) was the major primary process involved in methyl nitrite photolysis. McGraw and Johnston (1969) also studied the HNO formation and decay in methyl nitrite photolyses at 366 nm. Direct detection of the methoxy radical formed in methyl nitrite photolyses at 266 nm was reported by Sanders et al. (1980) using laser-excited fluorescence (Ohbayashi et al., 1977; Inoue et al., 1979). All current evidence suggests that the occurrence of processes (I) and (II) rationalize well the theoretical and experimental results available today; ϕ_{III} is probably near zero.

The dynamics of the photodissociation process (I) have been explored in several experimental studies. Lahmani et al. (1983), in 355 nm photolyses, determined the NO fragment was formed in four vibrational levels, $v'' = 0$, 1, 2, and 3, with a peak in the distribution at $v'' = 1$, and all states were rotationally excited. Translational energy represented about 36% of the available energy while internal NO energy amounted to about 26%. D'Azy et al. (1985), using 350 nm excitation, reported similar results with the percentage of the population of $v'' = 0$, 1, 2, and 3 states at 20, 50, 30, and $< 5\%$, respectively. Keller et al. (1986) found that with excitation at 350 nm $57 \pm 4\%$ of the excess energy appeared as translation, significantly greater than the fraction estimated by Lahmani et al. (1983). With excitation at 248 nm, about $57 \pm 4\%$ appeared as translation, and the internal modes of NO were relatively unexcited. Keller et al. (1987) found that dissociation at 248 and 193 nm resulted in about 53 and 43%, respectively, of the available energy appearing as translation. Dissociation occurred on a timescale of picoseconds. Brühlmann et al. (1987) with photolyses at 363 nm found the excess energy distributed as 3% into NO vibrations, 15% into NO rotation, and 33% into NO translation. Inoue et al. (1987) using laser excitation in the 348 to 364 nm range found that dissociation by process (I) occurs within the plane of the molecule within 21 femtoseconds. Hippler et al. (1992) reported that the NO formed in 380 nm photolysis of CH_3ONO was vibrationally cold but rotationally highly excited. In 1995, Mestdagh et al. (1995) reported results from experiments at 351 nm that the lifetime of the excited S_1 state was about 125 femtoseconds. A transient peak, reaching a plateau after less than 1 picosecond, was observed; this possibly can be attributed to the nondissociated excited molecule, reflecting vibrational predissociation in CH_3ONO.

Theoretical treatments of the dissociation of the S_1 state of CH_3ONO support the experimental findings related to the dynamics of the primary process (I); for examples see Hennig et al. (1987); Nonella et al. (1989); Suter et al. (1990); Untch et al. (1993); Miller and Alexander (1995).

Several experimental studies have explored the dynamics of the photodissociation of the S_2 excited state of CH_3ONO; e.g., see Lahmani, et al. (1980a, b); Farmanara et al. (1999); Yin et al. (2003); Yue et al. (2006).

IX-H-2.1. Absorption Cross Sections for CH_3ONO

At ambient temperatures methyl nitrite exists as a mixture of *cis*- and *trans*-configurations. The band positions attributed to each isomer have been assigned by Hippler and Pfab (1992) and Engert and Dick (1999). At 298 K an equilibrium mixture of the two isomers has about 40% *trans*- and 60% *cis*-CH_3ONO (Bodenbinder et al., 1994). The distribution of isomers shifts somewhat over the temperature range usually encountered within the troposphere; at equilibrium the *trans*-/*cis*- ratio increases from 0.59 at 273 K to 0.72 at 313 K. The spectrum of an equilibrium mixture at 298 K is shown in figure IX-H-1 and is given in tabular form in table IX-H-2 from the measurements of Taylor et al. (1980). The magnitude of the CH_3ONO absorption peaks as reported by Calvert and Pitts (1966) and Taylor et al. are in reasonable accord (see table IX-H-2). However, wavelengths of the maxima near 330 and 351 nm are significantly different in the two data sets. The data set originally measured by Veronique McMillan (1966) may have lost some its original precision in the manual preparation of the drawing of the figures given in Calvert and Pitts, coupled with the reconstruction of these data to numerical format by the Mainz group as given in their spectral catalogue. Thus, we favor the use of the Taylor data set for use in *j*-value calculations.

IX-H-2.2. Quantum Yields of Photodecomposition of Methyl Nitrite

If process (I) occurs in the photodecomposition of pure CH_3ONO, the products CH_3O and NO are expected to react largely to reform CH_3ONO, so the simple measurement of the quantum yields of methyl nitrite disappearance or product formation alone cannot provide estimates of ϕ_I or ϕ_{II}.

There have been several useful studies that have allowed estimates of the quantum yields of photodecomposition of methyl nitrite. Wiebe et al. (1973) provided the first meaningful estimates of primary process (I) in their studies at wavelength 366 nm. They photolyzed mixtures of CH_3ONO and ^{15}NO and measured the quantum yields of $CH_3O^{15}NO$ and $^{15}N^{15}NO$ formation. From the mechanism outlined in the introduction to this section, one expects the following relation to hold:

$$\phi_I = 2\Phi(^{15}N^{15}NO) + \Phi(CH_3O^{15}NO)$$

From these experiments Wiebe et al. (1973) reported $\phi_I = 0.75 \pm 0.01$ at 366 nm. Wiebe and Heicklen (1973) measured the quantum yields of products of the photolysis of CH_3ONO in mixtures with NO, NO and NO_2, and NO plus O_2; varied amounts

Table IX-H-2. Cross sections (σ, cm^2 $molecule^{-1}$) for CH_3ONO as measured by V. McMilllan (in Calvert and Pitts, 1966), CP; and Taylor et al. (1980), T

λ, nm	(CP) $10^{19} \times \sigma$	(T) $10^{19} \times \sigma$	λ, nm	(CP) $10^{19} \times \sigma$	(T) $10^{19} \times \sigma$	λ, nm	(CP) $10^{19} \times \sigma$	(T) $10^{19} \times \sigma$	λ, nm	(CP) $10^{19} \times \sigma$	(T) $10^{19} \times \sigma$
280	1.91	2.00	313	0.69	0.71	346	1.91	1.35	379	0.57	0.54
281	1.80	1.86	314	0.77	0.70	347	2.50	1.52	380	0.52	0.51
282	1.71	1.73	315	0.92	0.82	348	2.98	1.80	381	0.48	0.51
283	1.63	1.57	316	1.15	1.05	349	2.87	2.40	382	0.47	0.51
284	1.54	1.46	317	1.40	1.27	350	2.49	2.90	383	0.47	0.53
285	1.45	1.35	318	1.52	1.40	351	2.15	3.18	384	0.48	0.54
286	1.37	1.26	319	1.41	1.25	352	1.91	3.15	385	0.49	0.55
287	1.28	1.19	320	1.15	1.00	353	1.75	2.80	386	0.49	0.56
288	1.22	1.12	321	0.96	0.84	354	1.64	2.40	387	0.50	0.54
289	1.14	1.06	322	0.84	0.80	355	1.57	2.10	388	0.50	0.52
290	1.07	1.00	323	0.88	0.86	356	1.53	1.90	389	0.48	0.48
291	1.02	0.95	324	1.15	1.00	357	1.51	1.71	390	0.47	0.43
292	0.98	0.92	325	1.75	1.14	358	1.53	1.50	391	0.43	0.36
293	0.95	0.87	326	2.37	1.30	359	1.57	1.43	392	0.38	0.30
294	0.92	0.84	327	2.41	1.50	360	1.61	1.40	393	0.35	0.25
295	0.88	0.80	328	2.37	1.80	361	1.65	1.43	394	0.31	0.18
296	0.84	0.77	329	1.98	2.18	362	1.72	1.50	395	0.26	0.14
297	0.82	0.74	330	1.53	2.30	363	1.80	1.60	396	0.22	0.11
298	0.76	0.72	331	1.25	1.90	364	1.84	1.72	397	0.18	0.08
299	0.74	0.71	332	1.11	1.30	365	1.77	1.79	398	0.15	0.07
300	0.71	0.69	333	1.20	1.03	366	1.61	1.74	399	0.13	0.06
301	0.70	0.71	334	1.53	1.02	367	1.47	1.45	400	0.10	0.05
302	0.73	0.71	335	2.05	1.20	368	1.34	1.24	401	0.08	0.04
303	0.71	0.67	336	2.68	1.70	369	1.25	1.19	402	0.06	0.03
304	0.67	0.63	337	3.04	2.42	370	1.19	1.24	403	0.05	0.02
305	0.64	0.62	338	3.10	2.95	371	1.15	1.25	404	0.04	0.02
306	0.65	0.62	339	2.78	3.24	372	1.11	1.20	405	0.03	0.02
307	0.68	0.67	340	2.29	3.05	373	1.05	1.12	406	0.02	0.01
308	0.77	0.74	341	1.88	2.52	374	0.99	1.00	407	0.02	0.01
309	0.90	0.83	342	1.53	1.90	375	0.95	0.89	408	0.02	0.00
310	0.96	0.90	343	1.46	1.53	376	0.88	0.80	409	0.01	0.00
311	0.87	0.91	344	1.45	1.34	377	0.77	0.71	410	0.01	0.00
312	0.73	0.80	345	1.53	1.30	378	0.67	0.60			

of N_2 were added in several experiments. They found the quantum yield of N_2O decreased with added N_2 and approached a limiting value of about 0.055 at high pressures (677 Torr). With the mechanism outlined in the previous section Φ_{N_2O} is related to ϕ_I by the following relation:

$$\phi_I = 2(\Phi_{N_2O})[(k_1 + k_2)/k_2]$$

These data and the value of $\phi_I = 0.75$ gave the estimate of $k_2/(k_1 + k_2) = 0.145$, independent of temperature. This value is similar to those derived for the reactions analogous to reactions (1) and (2) given in the previous discussion involving the CH_3O and NO molecules: $R_2CHO + NO \rightarrow R_2CHONO(1')$; $R_2CHO + NO \rightarrow R_2C(=O) + HNO(2')$; values of $k_{2'}/(k_{1'} + k_{2'})$ have been measured in experiments involving the thermal decomposition of the alkyl nitrites in the presence of ^{15}NO: e.g., with C_2H_5O, values of $k_{2'}/(k_{1'} + k_{2'}) = 0.23$ at 25°C (Rebbert, 1963); 0.23 at 95°C (Arden and Phillips, 1964; Arden et al., 1964); 0.25 at 200°C (Livermore and Phillips, 1966); 0.22 at 175°C (Morabito and Heicklen, 1985a, b).

A more recent determination of ϕ_I has been reported by Cox et al. (1980a) that was derived from CH_3ONO photolyses in oxygen at 1 atm. pressure. These studies were made using broadband fluorescent lamps with radiation in the 310–410 nm range with a maximum intensity at 350 nm. Values of $\phi_I = 0.96$ and 1.18, respectively were derived using the photolysis of HONO and NO_2 to calibrate the light intensity and taking unity for the quantum yield of these photodissociations. They suspect that significant error in the estimate of NO_2 decay could have been introduced in their experiments since the O_2 impurity levels may have been more than 100 times greater than the NO_2 level (about 10^3 ppm) in the NO_2–N_2 mixture used in the NO_2 photolysis experiments. They concluded that the value of $\phi_I \approx 1.0$.

IX-H-2.3. Photolysis Frequencies for CH_3ONO Photodecomposition within the Lower Troposphere

Estimates of the *j*-values for CH_3ONO in the lower, cloud-free troposphere have been calculated as a function of solar zenith angle using the cross section measurements of Taylor et al. (1980) and two different choices for the quantum yields of photodissociation that lie at the two extremes of the experimental estimates described in the preceding section, 0.78 and 1.0. The results are given in figure IX-H-4. It is probable that the actual value lies between the two curves.

IX-H-3. The Photodecomposition of Ethyl Nitrite (CH_3CH_2ONO)

Ethyl nitrite like HONO and CH_3ONO, has the characteristic banded structure in its absorption. In figure IX-H-5 the cross sections for C_2H_5ONO are seen to be very similar to those for *n*-C_3H_7ONO, *n*-C_4H_9ONO, and *iso*-C_4H_9ONO. These spectral data are of uncertain quality since they were derived by the current authors from published graphical data of absorbance versus wavelength for the compounds in liquid

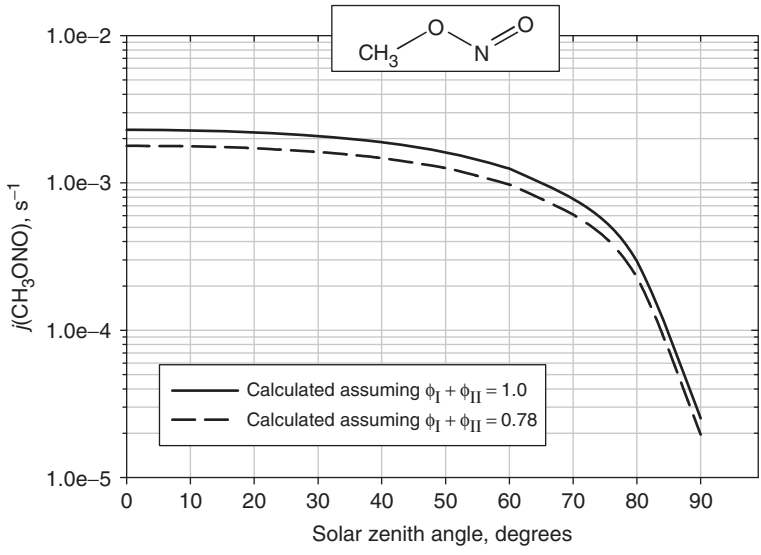

Figure IX-H-4. Photolysis frequencies for methyl nitrite versus solar zenith angle as calculated for a clear day in the lower troposphere with a vertical ozone column of 350 DU. The total quantum yield of photodecomposition was taken as either 1.0 or 0.78, independent of wavelength.

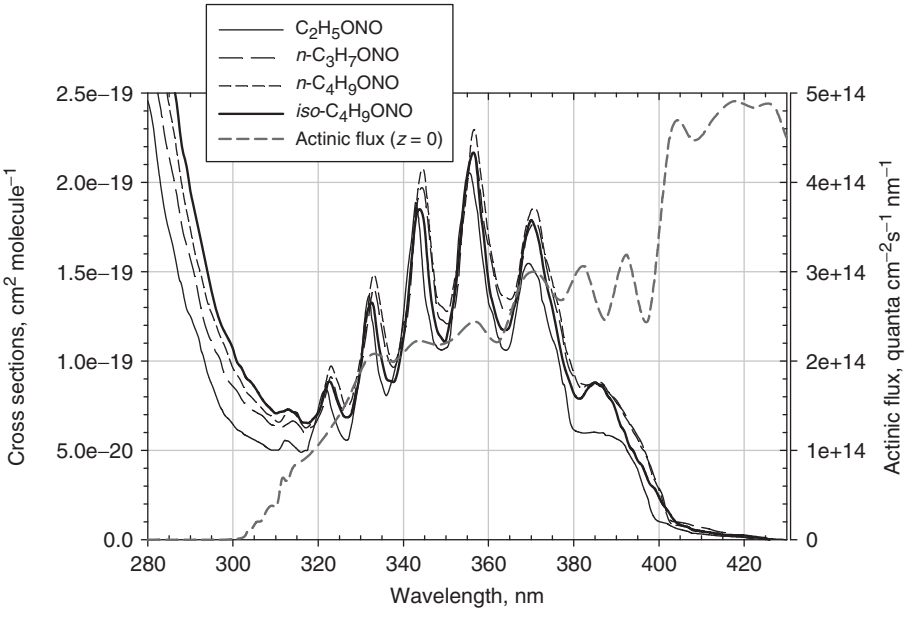

Figure IX-H-5. Comparison of the approximate absorption spectra for some simple alkyl nitrites and the wavelength distribution of the solar flux for an overhead Sun within the lower troposphere. The estimates shown were made by the current authors using relative spectral data of Heicklen (1987) as measured in hexane solution together with estimates of the cross section of Zabernick and Heicklen (1985a, b, c) that were made at one wavelength (366 nm).

hexane (Heicklen, 1987) coupled with the cross sections measured in the gas phase at a single wavelength (366 nm) by Zabarnick and Heicklen (1985a). As with HONO and CH_3ONO, a very good overlap can be seen of these absorptions with the wavelength region of actinic flux within the lower troposphere. As a result, these compounds are readily photodecomposed by rupture of the R—ONO bond, and they generate radicals that help drive the chemistry including ozone formation, within the troposphere. Because of the large excess of the quantum energy over the energy necessary for the RO—NO bond breakage, the RO radicals are often generated in an internally excited state, and these highly excited radicals may undergo spontaneous dissociation. With the ethoxy radical and all of the higher alkoxy radical there are always two alternative modes of decomposition of the excited alkoxy radicals that are available. For example, with the ethoxy radical the two paths are:

$$CH_3CH_2O \rightarrow CH_3CHO + H \; \Delta H^\circ_{298} = 67\,\text{kJ mol}^{-1}$$

$$\rightarrow CH_3 + CH_2O \; \Delta H^\circ_{298} = 53\,\text{kJ mol}^{-1}$$

In the studies of the alkyl nitrites the extent of the pathway forming the CH_2O product usually has not been measured, presumably because of the analytical difficulties. One might expect the pathway having the lowest enthalpy change to be favored. However, there is plenty of energy deposited in the alkoxy radical products of the alkyl nitrite photolysis to promote both pathways. In each case described in this work, the two possible alternative pathways for decay are listed for completeness, although usually there is little evidence available defining the extent of each.

There have been several experimental studies that help our understanding of the mechanism of ethyl nitrite photodecomposition (e.g., see Schuck and Stephens, 1967; McMillan et al., 1971; Christie and Hetherington, 1976/1977; Rose, 1979; Zabarnick and Heicklen, 1985a; Morabito and Heicklen, 1985a, b). The following primary processes have been considered in explanation of the results:

$$CH_3CH_2ONO + h\nu \rightarrow CH_3CH_2O + NO \quad \text{(I)}$$

$$\rightarrow NO + (CH_3CH_2O^{\ddagger}) \rightarrow NO + CH_3CHO + H \quad \text{(II)}$$

$$\rightarrow NO + (CH_3CH_2O^{\ddagger}) \rightarrow NO + CH_2O + CH_3 \quad \text{(III)}$$

$$\rightarrow HNO + CH_3CHO \quad \text{(IV)}$$

$$\rightarrow (C_2H_5ONO)^* \quad \text{(V)}$$

Here the $(CH_3CH_2O^{\ddagger})$ represents a vibrationally excited ethoxy radical that can decompose quickly to products, and the $(C_2H_5ONO)^*$ represents an electronically excited molecule that can be collisionally quenched. Experiments that define the extent of occurrence of these processes will be discussed in this section.

IX-H-3.1. The Absorption Cross Sections for Ethyl Nitrite

As indicated above, the data for cross sections of the higher alkyl nitrites available today are not highly accurate. However, these are given in graphical form in figure IX-H-5 and in tabular format in table IX-H-3. The banded structure characteristic of all of the alkyl nitrites reflects the excitation to the different vibrational bands that involve largely the stretching motion in the RON—O bond of the excited S_1 state.

IX-H-3.2. Quantum Yields of Photodecomposition of Ethyl Nitrite

Schuck and Stephens (1967) studied the photodecomposition of ethyl nitrite using ultraviolet lamps that had a broadband of wavelengths with 85% in the 330 to 375 nm region and maximum intensity at 350 nm. The reaction cell encompassed a long-path FTIR analysis system with which the rates of ethyl nitrite loss and various products formed could be monitored during photolysis. Approximate quantum yields were determined for CH_3CHO, CH_3CH_2OH, NO, N_2O formation and C_2H_5ONO loss as a function of ethyl nitrite concentration and added NO and N_2 gases. No CH_2O could be detected among the products, suggesting that process ϕ_{III} is small. However, this conclusion may be challenged in view of the findings of Christie and Hetherington (1976/1977); see the following discussion. Light intensity in the cell was determined using nitrobenzaldehyde solid-state actinometry (Pitts et al., 1964) and NO_2 photolysis (Schuck et al., 1966). These authors favored a mechanism involving the primary processes (I), (II), and (IV), and an excited ethyl nitrite molecule that could be collisionally quenched as the pressure was increased. The results that apply best to atmospheric conditions are those determined in a few experiments at high pressures of added nitrogen. With a pressure of added N_2 at 1 atm., an initial quantum yield of ethyl nitrite loss was measured as 0.089. In terms of our current understanding of the mechanism, process (I) dominates the dissociation at the wavelengths employed and hot radical effects are unimportant at high pressures; it is probable that low quantum yield of ethyl nitrite loss reflects the recombination of CH_3CH_2O and NO initial products with the disproportionation reaction (2) alone leading to the loss of ethyl nitrite:

$$CH_3CH_2O + NO \rightarrow CH_3CH_2ONO \quad (1)$$

$$\rightarrow CH_3CHO + HNO \quad (2)$$

With this assumption, and using an average value for the measured ratio of $k_2/(k_1 + k_2) = 0.24$ (Morabito and Heicklen, 1985), the Schuck and Stevens result give the estimate of $\phi_I = (0.089/0.24) = 0.37$ in 1 atm. of N_2.

McMillan et al. (1971) estimated from ethyl nitrite photolyses in experiments at 366 nm that $\Phi_{CH_3CHO} \approx 0.18$, independent of temperature and ethyl nitrite pressure (up to 12 Torr) and NO pressure (up to 30 Torr). From these data and the value of $k_2/(k_1 + k_2) = 0.23$ measured by Arden and Phillips (1964) and Arden et al. (1964), they estimated that $\phi_I = 0.59 \pm 0.01$ at 366 nm. They also concluded that excited radical effects are small at 366 nm.

Table IX-H-3. Approximate cross sections ($10^{19} \times \sigma$, cm^2 $molecule^{-1}$) for some simple alkyl nitrites (RONO). Estimated from the graphical absorbance data of Heicklen (1987). The alkyl group (R) shown in the column head assigns data in that column to the specific nitrite (RONO)

λ, nm	C_2H_5	*n*-C_3H_7	*n*-C_4H_9	*iso*-C_4H_9	λ, nm	C_2H_5	*n*-C_3H_7	*n*-C_4H_9	*iso*-C_4H_9	λ, nm	C_2H_5	*n*-C_3H_7	*n*-C_4H_9	*iso*-C_4H_9
280	2.46	3.07	3.20	3.76	330	0.97	0.95	1.02	1.02	379	0.68	0.95	1.01	0.89
281	2.36	2.84	3.05	3.46	331	1.25	1.11	1.15	1.15	380	0.62	0.91	0.93	0.82
282	2.17	2.56	2.89	3.23	332	1.37	1.27	1.36	1.36	381	0.60	0.89	0.87	0.79
283	1.99	2.42	2.74	3.01	333	1.19	1.41	1.45	1.48	382	0.60	0.87	0.84	0.80
284	1.84	2.25	2.59	2.86	334	0.97	1.31	1.48	1.41	383	0.60	0.86	0.86	0.83
285	1.73	2.14	2.43	2.69	335	0.87	1.18	1.41	1.25	384	0.60	0.86	0.87	0.86
286	1.63	2.03	2.30	2.55	336	0.81	1.05	1.25	1.11	385	0.60	0.88	0.88	0.88
287	1.50	1.91	2.15	2.40	337	0.87	0.98	1.11	1.01	386	0.60	0.87	0.88	0.86
288	1.42	1.76	1.98	2.20	338	0.95	0.97	1.01	1.00	387	0.60	0.86	0.87	0.85
289	1.30	1.66	1.86	2.10	339	1.06	1.04	0.97	1.06	388	0.58	0.83	0.83	0.80
290	1.25	1.58	1.74	1.95	340	1.25	1.13	1.00	1.20	389	0.58	0.80	0.81	0.77
291	1.19	1.48	1.61	1.84	341	1.50	1.24	1.06	1.32	390	0.57	0.77	0.78	0.71
292	1.12	1.36	1.52	1.73	342	1.70	1.51	1.20	1.60	391	0.55	0.74	0.74	0.64
293	1.03	1.24	1.43	1.62	343	1.89	1.83	1.32	1.87	392	0.53	0.71	0.69	0.60
294	0.93	1.16	1.33	1.50	344	1.70	1.96	1.60	2.05	393	0.48	0.66	0.65	0.53
295	0.87	1.11	1.27	1.39	345	1.38	1.94	1.75	2.05	394	0.44	0.62	0.60	0.50
296	0.81	1.05	1.20	1.29	346	1.25	1.73	1.87	1.79	395	0.39	0.58	0.56	0.44
297	0.74	1.01	1.14	1.22	347	1.12	1.49	2.05	1.54	396	0.32	0.54	0.51	0.42
298	0.70	0.93	1.09	1.16	348	1.07	1.27	2.05	1.34	397	0.25	0.47	0.48	0.36
299	0.68	0.89	1.02	1.12	349	1.06	1.23	1.79	1.31	398	0.17	0.41	0.40	0.31
300	0.65	0.86	0.96	1.07	350	1.07	1.21	1.54	1.28	399	0.12	0.35	0.33	0.29
301	0.62	0.83	0.92	0.99	351	1.14	1.22	1.46	1.31	400	0.10	0.29	0.28	0.24
302	0.60	0.79	0.88	0.96	352	1.41	1.29	1.34	1.45	401	0.10	0.24	0.20	0.20
303	0.58	0.75	0.83	0.91	353	1.70	1.47	1.31	1.56	402	0.09	0.14	0.13	0.17
304	0.57	0.73	0.81	0.89	354	1.85	1.80	1.28	1.77	403	0.07	0.10	0.08	0.13
305	0.56	0.72	0.78	0.86	355	2.03	2.01	1.31	1.97	404	0.06	0.10	0.08	0.10
306	0.55	0.71	0.76	0.82	356	2.03	2.14	1.45	2.24	405	0.06	0.10	0.08	0.08

307	0.53	0.69	0.73	0.78	357	1.89	2.14	1.47	2.28	406	0.05	0.09	0.07	0.08
308	0.51	0.66	0.70	0.75	358	1.70	1.98	1.56	2.09	407	0.04	0.09	0.07	0.07
309	0.50	0.64	0.69	0.73	359	1.50	1.77	1.77	1.91	408	0.04	0.08	0.06	0.05
310	0.50	0.64	0.67	0.71	360	1.33	1.65	1.97	1.70	409	0.03	0.07	0.06	0.05
311	0.51	0.62	0.66	0.71	361	1.26	1.52	2.24	1.56	410	0.03	0.07	0.05	0.05
312	0.55	0.64	0.69	0.72	362	1.15	1.40	2.28	1.43	411	0.03	0.07	0.05	0.04
313	0.55	0.65	0.73	0.73	363	1.08	1.31	2.18	1.37	412	0.03	0.06	0.04	0.04
314	0.53	0.66	0.72	0.71	364	1.06	1.27	2.09	1.36	413	0.02	0.05	0.03	0.04
315	0.51	0.65	0.69	0.71	365	1.09	1.29	1.91	1.34	414	0.02	0.05	0.03	0.03
316	0.49	0.62	0.65	0.66	366	1.20	1.30	1.70	1.37	415	0.02	0.04	0.03	0.03
317	0.50	0.59	0.63	0.65	367	1.35	1.38	1.56	1.47	416	0.02	0.04	0.02	0.03
318	0.55	0.62	0.64	0.65	368	1.49	1.56	1.43	1.64	417	0.02	0.03	0.02	0.03
319	0.63	0.64	0.68	0.68	369	1.54	1.70	1.40	1.77	418	0.02	0.02	0.02	0.02
320	0.73	0.68	0.72	0.71	370	1.54	1.76	1.37	1.84	419	0.01	0.02	0.02	0.02
321	0.82	0.73	0.79	0.77	371	1.49	1.78	1.36	1.86	420	0.01	0.01	0.01	0.02
322	0.84	0.83	0.90	0.86	372	1.44	1.73	1.34	1.79	421	0.01	0.01	0.01	0.02
323	0.74	0.91	0.97	0.88	373	1.31	1.60	1.37	1.63	422	0.01	0.00	0.01	0.02
324	0.67	0.84	0.92	0.81	374	1.21	1.48	1.47	1.54	423	0.01	0.00	0.00	0.01
325	0.60	0.76	0.86	0.74	375	1.12	1.38	1.56	1.45	424	0.01	0.00	0.00	0.01
326	0.57	0.72	0.77	0.69	376	1.06	1.29	1.64	1.34	425	0.01	0.00	0.00	0.01
327	0.56	0.71	0.74	0.68	377	0.93	1.19	1.77	1.24	426	0.01	0.00	0.00	0.00
328	0.66	0.73	0.79	0.71	378	0.85	1.05	1.09	0.95	427	0.00	0.00	0.00	0.00
329	0.81	0.86	0.90	0.83						428	0.00	0.00	0.00	0.00

Zabarnick and Heicklen (1985a) measured the quantum yield of CH_3CHO and N_2O formed in the photodecomposition of ethyl nitrite at wavelength 366 nm with added NO, O_2, and N_2. Figure IX-H-6 shows the results of experiments with added N_2. It is seen that there is a pressure effect that may reflect either the quenching of excited states of C_2H_5ONO or internally excited ethoxy radicals formed in the primary process. At N_2 pressures above about 70 Torr, excited radical effects are unimportant. Using the measured average ratio of $k_2/(k_1 + k_2) = 0.24$, the data suggest that $\phi_I = 0.0.069/0.24 = 0.29$ at pressure of N_2 above 70 Torr. The quantum yields of N_2O also give an independent estimate of ϕ_I. Assuming that N_2O is derived from HNO in reaction, $2HNO \rightarrow N_2O + H_2O$, and that NO scavenges all the CH_3CH_2O radicals formed, then $\phi_I = 2\Phi_{N_2O}/[k_2/(k_1 + k_2)] = 2 \times 0.039/0.24 = 0.33$, similar to their estimate based on CH_3CHO measurements. Our estimate of $\phi_{total} \approx 0.37$ from the Schuck and Stevens experiments for nitrogen pressures of 1 atm. is in qualitative accord with these estimates.

Evidence for the formation of excited ethoxy radicals in photolyses of ethyl nitrite at 253.7 nm was presented by Christie and Hetherington (1976/1977); they studied the photodecomposition of ethyl nitrite at 253.7 nm in mixture with added NO and CO_2 and determined the quantum yields of CH_3NO formed. This product arises from the subsequent reactions of the CH_3 radical formed from the decomposition of excited C_2H_5O radicals in primary process (III). For example, they determined $\Phi_{CH_3NO} = 0.25$ in an experiment with $P_{C_2H_5ONO} = 8$, $P_{CO_2} = 392$ and $P_{NO} = 33$ Torr. This gives good evidence of the occurrence of primary process (III) at 253.7 nm with extensive decomposition of an excited ethoxy radical formed at short wavelengths even at relatively high pressures.

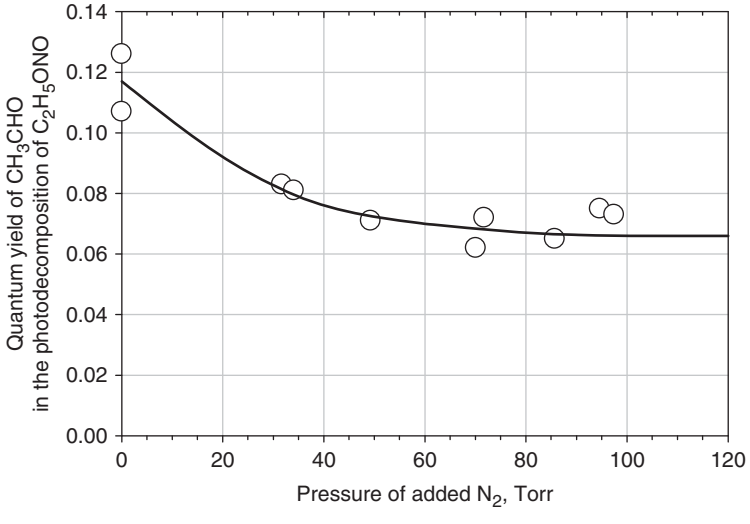

Figure IX-H-6. Quantum yields of formation of CH_3CHO in the 366 nm photolysis of ethyl nitrite (1.6 ± 0.2 Torr of C_2H_5ONO) versus pressure of added N_2 (Zabarnick and Heicklen, 1985a).

Some of the dynamics involved in the ethyl nitrite photodecomposition have been investigated by Tuck (1977) in molecular beam studies at 347.1 nm. The products were identified as ethoxy and NO, and the total fragment translational energy was determined to be 71.8 kJ mol^{-1} or about 36% of the energy in excess of that necessary to break the C_2H_5O—NO bond. The most probable total internal energy in the fragments was estimated to be about 124 kJ mol^{-1}. The high degree of angular anisotropy of the fragment intensities showed that the average lifetime in the upper state is very short compared to a molecular rotational period, $< 2 \times 10^{-13}$ s.

Although estimates of the quantum yields of photodecomposition of ethyl nitrite at pressures equivalent to those found in the lower troposphere are very limited at this writing, it appears that a reasonable estimate of the quantum yield of photodecomposition of ethyl nitrite in the lower troposphere is $\phi_I + \phi_{II} + \phi_{III} \approx 0.33$, with process (I) being the dominant pathway. Process (IV) is probably unimportant at all wavelengths. There is little information related to the wavelength dependence of this process, but it is clear from the data at 253.7 nm (Christie and Hetherington, 1976) that a large fraction of the ethoxy radicals formed at this wavelength are vibrationally excited and undergo decomposition to form CH_3 and CH_2O even at high pressures. Note that this conclusion is not supported from data within the banded region; Schuck and Steven (1967) did not detect CH_2O formation.

McMillan et al. (1971) reported that the quantum yields of primary photodecomposition of isopropyl nitrite did not vary with wavelength over the banded region; see section IX-H-4. Perhaps this invariance is also present in the other small alkyl nitrites. At this point in our limited understanding of the mechanism, the current authors have assumed that within the banded region, the photodecomposition of ethyl nitrite photolysis is wavelength independent.

The major product of ethyl nitrite photodecomposition in the troposphere is expected to be acetaldehyde, formed from the ethoxy radical reaction, $C_2H_5O + O_2 \rightarrow CH_3CHO + HO_2$, as well as some ill-defined amount of CH_2O as well as CH_3CHO formed in process (II).

IX-H-3.3. Photolysis Frequencies for Ethyl Nitrite Photodecomposition within the Lower Troposphere

In the calculation given here, we have assumed that the quantum yield of photodecomposition of ethyl nitrite in the lower atmosphere is 0.31, independent of wavelength. Using this assumption and the approximate cross sections given in table IX-H-3, we have calculated the approximate *j*-values as a function of solar zenith angle for ethyl nitrite on a cloudless day in the lower troposphere and an overhead ozone column of 350 DU. The data, given in figure IX-H-7, point to a photochemical lifetime of ethyl nitrite of only about 29 min. with an overhead Sun.

IX-H-4. The Photodecomposition of *iso*-Propyl Nitrite [$(CH_3)_2CHONO$]

Like HONO and the organic nitrites, CH_3ONO, and C_2H_5ONO, the spectrum of *iso*-propyl nitrite overlaps well that of the solar radiation within the troposphere;

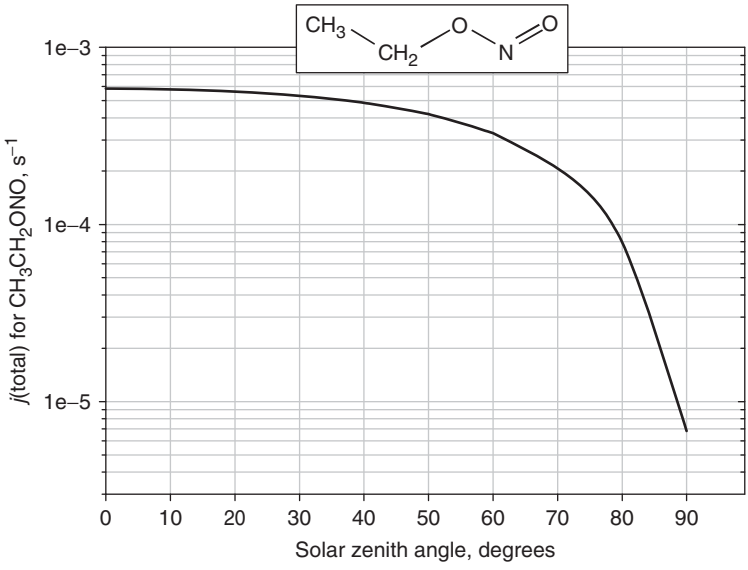

Figure IX-H-7. Approximate photolysis frequencies for the photodecomposition of CH_3CH_2ONO versus solar zenith angle as estimated for a cloudless day in the lower troposphere with an ozone column of 350 DU.

see figure IX-H-1. Several experimental studies have elucidated the mechanism of its photodecomposition. For example, see Thompson and Dainton (1937), Tarte, (1953), Kabasakalian et al. (1962), Ludwig and McMillan (1967, 1969), McMillan et al. (1971), and Effenhauser et al. (1990). Evidence supports the view that the photodecomposition of *iso*-propyl nitrite follows the pattern observed with the simpler nitrites, and the following primary processes have been considered in explanation of the results.

$$(CH_3)_2CHONO + h\nu \rightarrow (CH_3)_2CHO + NO \quad \text{(I)}$$

$$\rightarrow [(CH_3)_2CHO^{\ddagger} + NO] \rightarrow CH_3CHO + CH_3 + NO \quad \text{(II)}$$

$$\rightarrow (CH_3)_2CO + H + NO \quad \text{(III)}$$

$$\rightarrow CH_3CHO + HNO \quad \text{(IV)}$$

Here $(CH_3)_2CHO^{\ddagger}$ in primary process (II) represents a vibrationally excited isopropoxy radical that can decompose quickly to products. Process (IV) is probably an unimportant photodecomposition mode within the troposphere. The mechanism and extent of these processes will be discussed in this section.

IX-H-4.1. The Cross Sections for iso-Propyl Nitrite

The absorption spectrum of *iso*-propyl nitrite is shown in figure IX-H-1, and the cross sections as a function of wavelength are given in tabular form in table IX-H-4.

The excellent overlap of the wavelength regions for absorption and those for solar flux leads to rapid photodecomposition of *iso*-propyl nitrite within the troposphere.

IX-H-4.2. Quantum Yields for Photodecomposition of iso-Propyl Nitrite

Ludwig and McMillan (1969) photolyzed pure *iso*-propyl nitrite and *iso*-propyl nitrite-NO mixtures at several wavelengths within the banded absorption region. The major products were nitric oxide, acetone, and acetaldehyde with small amounts of methyl nitrite, methyl nitrate, nitrogen, nitrous oxide, and water. The quantum yields of acetone and acetaldehyde as measured at several wavelengths and 26°C are summarized in figure IX-H-8. It can be seen that the extent of formation of the excited $(CH_3)_2CHONO^{\ddagger}$ species, with its rapid decomposition to form acetaldehyde in process (II), increases as the absorbed energy is increased at the shorter wavelengths. The mechanism as outlined above is similar to that proposed for the smaller nitrites. As in the photolysis of the CH_3ONO and CH_3CH_2ONO, the N_2O observed in these systems arises from the reactions involving the HNO species: $2HNO \rightarrow N_2O + H_2O$. Adopting the above mechanism, one expects the following relation to hold:

$$\phi_{\mathrm{I}} + \phi_{\mathrm{II}} = [(k_1 + k_2)/k_2]\Phi_{CH_3C(O)CH_3} + \Phi_{CH_3CHO} \tag{4}$$

The ratio of k_2/k_1 has been measured by several groups with reported values ranging from 0.15 to 0.22. Ludwig and McMillan (1967) measured a value of 0.21 for this ratio but chose the value of 0.22 measured by Hughes and Phillips (1967) to estimate the total quantum yields of the primary processes. Using the value $(k_1 + k_2)/k_2 = 5.55$ and the product quantum yields given in figure IX-H-8, Ludwig and McMillan (1969) estimated the following total quantum yield of photodecomposition of *iso*-propyl nitrite

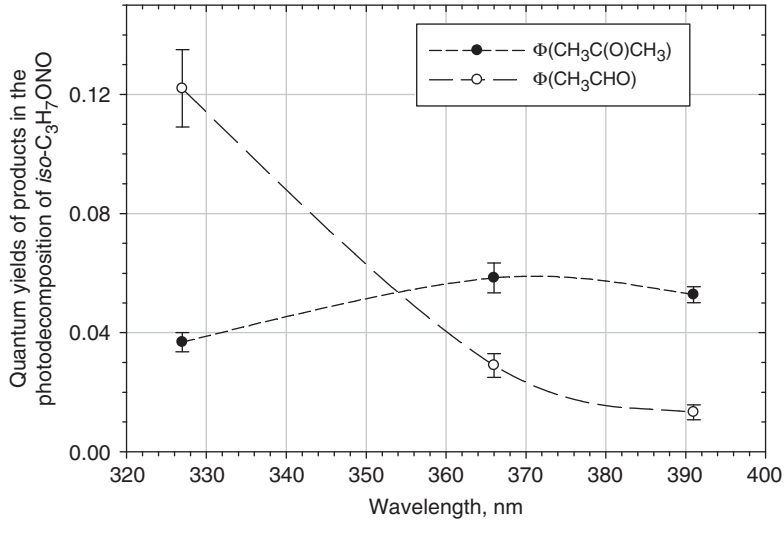

Figure IX-H-8. Quantum yields of products in the photolysis of *iso*-propyl nitrite–NO mixtures at 26°C as a function of wavelength; data of Ludwig and McMillan (1969).

Table IX-H-4. Cross sections (σ, cm^2 molecule^{-1}) for *iso*-C_3H_7ONO (IP) from McMillan et al. (1971) and *tert*-C_4H_9ONO (TB) from Calvert and Pitts (1966)

λ, nm	(IP) $10^{19} \times \sigma$	(TB) $10^{19} \times \sigma$	λ, nm	(IP) $10^{19} \times \sigma$	(TB) $10^{19} \times \sigma$	λ, nm	(IP) $10^{19} \times \sigma$	(TB) $10^{19} \times \sigma$	λ, nm	(IP) $10^{19} \times \sigma$	(TB) $10^{19} \times \sigma$
280		2.87	320	0.52	0.21	360	1.85	1.11	400	0.32	1.61
281		2.65	321	0.57	0.22	361	1.80	1.33	401	0.24	1.42
282		2.45	322	0.61	0.22	362	1.76	1.55	402	0.21	1.22
283		2.24	323	0.63	0.24	363	1.65	1.81	403	0.18	1.07
284		2.03	324	0.66	0.25	364	1.55	2.06	404	0.15	0.92
285		1.84	325	0.65	0.30	365	1.44	2.30	405	0.13	0.80
286		1.69	326	0.65	0.35	366	1.34	2.53	406	0.11	0.69
287		1.53	327	0.63	0.36	367	1.43	2.56	407	0.09	0.61
288		1.38	328	0.60	0.35	368	1.53	2.29	408	0.08	0.54
289		1.26	329	0.66	0.32	369	1.61	1.91	409	0.06	0.47
290	1.85	1.15	330	0.71	0.30	370	1.69	1.53	410	0.06	0.40
291	1.72	1.06	331	0.77	0.29	371	1.72	1.13	411	0.05	0.35
292	1.59	0.97	332	0.83	0.31	372	1.75	0.72	412	0.04	0.31
293	1.47	0.90	333	0.89	0.33	373	1.76	0.63	413	0.03	0.27
294	1.36	0.83	334	0.96	0.35	374	1.76	0.77	414	0.03	0.23
295	1.25	0.77	335	0.98	0.40	375	1.75	1.15	415	0.02	0.20
296	1.14	0.71	336	1.00	0.50	376	1.73	1.53	416	0.02	0.17
297	1.06	0.66	337	0.96	0.66	377	1.64	1.82	417	0.02	0.15
298	0.97	0.62	338	0.92	0.82	378	1.55	2.10	418	0.01	0.13
299	0.91	0.57	339	0.89	0.80	379	1.41	2.35	419	0.01	0.11
300	0.85	0.54	340	0.86	0.70	380	1.28	2.60	420	0.00	0.10
301	0.79	0.50	341	1.00	0.60	381	1.18	2.81	421	0.00	0.08

302	0.73	0.47	342	1.15	0.50	382	1.08	2.60	422	0.07
303	0.69	0.44	343	1.25	0.46	383	1.05	2.35	423	0.06
304	0.65	0.41	344	1.35	0.50	384	1.02	2.10	424	0.06
305	0.63	0.38	345	1.41	0.53	385	1.02	1.82	425	0.05
306	0.60	0.37	346	1.47	0.57	386	1.01	1.53	426	0.04
307	0.58	0.35	347	1.44	0.73	387	1.01	1.22	427	0.04
308	0.55	0.33	348	1.42	0.90	388	1.02	0.92	428	0.03
309	0.53	0.32	349	1.34	1.27	389	1.02	0.70	429	0.03
310	0.52	0.30	350	1.26	1.64	390	1.03	0.71	430	0.02
311	0.51	0.27	351	1.22	1.60	391	1.02	0.72	431	0.02
312	0.50	0.25	352	1.18	1.43	392	1.02	0.78	432	0.02
313	0.51	0.24	353	1.31	1.27	393	0.99	0.97	433	0.01
314	0.52	0.22	354	1.43	1.11	394	0.96	1.15	434	0.01
315	0.51	0.23	355	1.56	0.96	395	0.91	1.34	435	0.01
316	0.51	0.24	356	1.72	0.80	396	0.86	1.53	436	0.01
317	0.50	0.23	357	1.78	0.65	397	0.75	1.64	437	0.01
318	0.49	0.22	358	1.83	0.61	398	0.65	1.74	438	0.01
319	0.51	0.22	359	1.84	0.86	399	0.53	1.70	439	0.00

at 26°C: 0.31 at 391 nm; 0.36, 0.35, 0.32 at 366 nm; and 0.33 at 327 nm. They concluded that the total quantum yield of photodecomposition was essentially independent of wavelength within the banded region. Direct excitation into the $n \rightarrow \sigma^*$ excited state by radiation at 253.7 nm led to a quantum yield of acetaldehyde of 0.87 and the total quantum yield was estimated to be near unity. These quantum yield data for the primary processes in *iso*-propyl nitrite photodecomposition have been plotted in figure IX-H-9.

The estimated quantum yield data as a function of wavelength as defined by the trend lines in figure IX-H-9 are summarized in table IX-H-5. A molecular beam study of *iso*-propyl nitrite photodissociation of the S_2 state excited at 248 nm was reported by Effenhauser et al. (1990). The average (total) translational energy of the fragments from photodissociation of *iso*-propyl nitrite at 248 nm was 132 kJ mol^{-1}, while the average internal energies of the *iso*-C_3H_7O radicals was ~120 kJ mol^{-1}. The measured time of flight distributions show clear evidence for the collisionless, unimolecular decay of most of the isopropoxy radicals formed in the primary dissociation that proceeds on a submicrosecond time scale.

IX-H-4.3. Photolysis Frequencies for iso-Propyl Nitrite Photodecomposition within the Lower Troposphere

The cross section data of table IX-H-4 and the quantum yield data of table IX-H-5 were used table IX-H-4 and the quantum yield data of table IX-H-5 were used

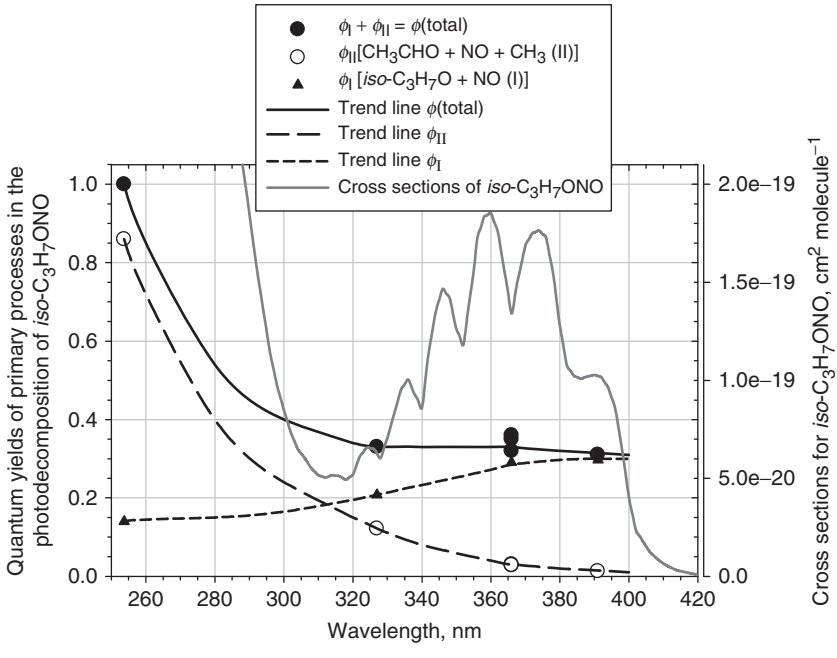

Figure IX-H-9. Estimated quantum yields of the primary processes in *iso*-propyl nitrite as a function of wavelength based on the data of Ludwig and McMillan (1969); the absorption cross sections for *iso*-propyl nitrite are shown for comparison by the gray curve.

Table IX-H-4. Estimated quantum yields of the primary processes in *iso*-propyl nitrite photodecomposition as a function of wavelength (based on the trend lines in figure IX-H-9)

λ, nm	ϕ_I	ϕ_{II}	ϕ_{total}	λ, nm	ϕ_I	ϕ_{II}	ϕ_{total}	λ, nm	ϕ_I	ϕ_{II}	ϕ_{total}
280	0.15	0.40	0.55	320	0.20	0.15	0.34	360	0.27	0.040	0.33
281	0.15	0.39	0.54	321	0.20	0.15	0.34	361	0.27	0.038	0.33
282	0.15	0.38	0.53	322	0.20	0.14	0.34	362	0.28	0.036	0.33
283	0.15	0.37	0.52	323	0.20	0.14	0.34	363	0.28	0.034	0.33
284	0.15	0.36	0.51	324	0.20	0.13	0.33	364	0.28	0.032	0.33
285	0.15	0.35	0.50	325	0.21	0.13	0.33	365	0.28	0.030	0.33
286	0.16	0.34	0.50	326	0.21	0.12	0.33	366	0.29	0.029	0.33
287	0.16	0.33	0.49	327	0.21	0.12	0.33	367	0.29	0.029	0.33
288	0.16	0.32	0.48	328	0.21	0.12	0.33	368	0.30	0.029	0.33
289	0.16	0.31	0.47	329	0.21	0.11	0.33	369	0.30	0.028	0.33
290	0.16	0.30	0.45	330	0.22	0.11	0.33	370	0.30	0.028	0.33
291	0.16	0.29	0.45	331	0.22	0.11	0.33	371	0.30	0.027	0.33
292	0.16	0.29	0.44	332	0.23	0.11	0.33	372	0.30	0.026	0.33
293	0.16	0.28	0.43	333	0.22	0.10	0.33	373	0.30	0.026	0.33
294	0.16	0.27	0.43	334	0.23	0.099	0.33	374	0.30	0.025	0.32
295	0.16	0.27	0.42	335	0.23	0.096	0.33	375	0.30	0.024	0.32
296	0.16	0.26	0.41	336	0.23	0.092	0.33	376	0.30	0.023	0.32
297	0.16	0.25	0.41	337	0.23	0.089	0.33	377	0.30	0.022	0.32
298	0.16	0.25	0.41	338	0.23	0.086	0.33	378	0.30	0.021	0.32
299	0.16	0.24	0.40	339	0.23	0.083	0.33	379	0.30	0.021	0.32
300	0.17	0.24	0.40	340	0.23	0.080	0.33	380	0.30	0.020	0.32
301	0.17	0.24	0.40	341	0.24	0.078	0.33	381	0.30	0.020	0.32
302	0.17	0.23	0.39	342	0.24	0.076	0.33	382	0.30	0.019	0.32
303	0.17	0.23	0.39	343	0.24	0.074	0.33	383	0.30	0.019	0.32
304	0.17	0.22	0.39	344	0.24	0.072	0.33	384	0.30	0.018	0.32
305	0.17	0.22	0.38	345	0.24	0.070	0.33	385	0.30	0.018	0.32
306	0.18	0.21	0.38	346	0.25	0.067	0.33	386	0.30	0.018	0.32
307	0.18	0.21	0.38	347	0.25	0.065	0.33	387	0.30	0.017	0.32
308	0.18	0.20	0.37	348	0.25	0.063	0.33	388	0.30	0.017	0.32
309	0.18	0.20	0.37	349	0.25	0.061	0.33	389	0.30	0.016	0.32
310	0.18	0.20	0.37	350	0.25	0.059	0.33	390	0.30	0.016	0.32
311	0.18	0.19	0.37	351	0.25	0.057	0.33	391	0.30	0.016	0.32
312	0.18	0.19	0.36	352	0.26	0.055	0.33	392	0.30	0.015	0.32
313	0.19	0.18	0.36	353	0.26	0.053	0.33	393	0.30	0.015	0.31
314	0.19	0.18	0.36	354	0.26	0.051	0.33	394	0.30	0.014	0.31
315	0.19	0.17	0.35	355	0.26	0.050	0.33	395	0.30	0.014	0.31
316	0.19	0.17	0.35	356	0.26	0.048	0.33	396	0.30	0.013	0.31
317	0.19	0.16	0.35	357	0.27	0.056	0.33	397	0.30	0.013	0.31
318	0.19	0.16	0.35	358	0.27	0.044	0.33	398	0.30	0.012	0.31
319	0.20	0.15	0.34	359	0.27	0.042	0.33	399	0.30	0.012	0.31

together with the appropriate actinic flux data to estimate the photolysis frequencies as a function of solar zenith angle for *iso*-propyl nitrite on a cloudless day in the lower troposphere with an overhead ozone column of 350 DU. These data are presented in figure IX-H-10. From these data we conclude that the photochemical lifetime of *iso*-C_3H_7ONO is very short, ~23 min. with an overhead Sun.

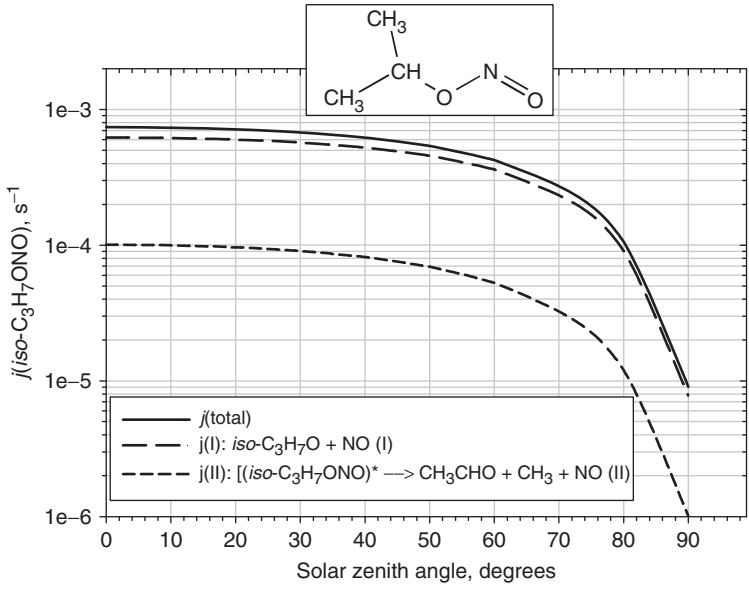

Figure IX-H-10. Photolysis frequencies for *iso*-C_3H_7ONO as a function of solar zenith angle as calculated from the cross section data of table IX-H-4, quantum yield data of table IX-H-5, and actinic flux data for a cloudless day in the lower troposphere with an overhead ozone column of 350 DU.

IX-H-5. The Photodecomposition of *n*-Propyl Nitrite ($CH_3CH_2CH_2ONO$)

n-Propyl nitrite absorbs tropospheric sunlight (see figure IX-H-5) and undergoes photodissociation to form alkoxy radicals and NO in the fashion of other alkyl nitrites that have been described in preceding sections. There have been several quantitative studies of the mechanism of the photodissociation of *n*-propyl nitrite; see McMillan et al. (1971), Zabarnick and Heicklen (1985), Morabito and Heicklen (1985). Discussions of its photodissociation have involved several possible primary processes:

$$n\text{-}C_3H_7ONO + h\nu \rightarrow n\text{-}C_3H_7O + NO \quad \text{(I)}$$

$$\rightarrow [(n\text{-}C_3H_7O)^{\ddagger} + NO] \rightarrow C_2H_5 + CH_2O + NO \quad \text{(II)}$$

$$\rightarrow C_2H_5CHO + H + NO \quad \text{(III)}$$

$$\rightarrow C_3H_7ONO^{*} \quad \text{(IV)}$$

Here the (n-$C_3H_7O^{\ddagger}$) represents a vibrationally excited *n*-propoxy radical that can decompose quickly to products. The $C_3H_7ONO^{*}$ represents an ill-defined excited state of the nitrite or an isomer of the nitrite, that can undergo the isotopic exchange reaction,

n-$C_3H_7ONO^* + {}^{15}NO \rightarrow n$-$C_3H_7O{}^{15}NO + NO$, as observed by Morobito and Heicklen (1985). The mechanism of the photodissociation of *n*-propyl nitrite will be discussed in this section.

IX-H-5.1. The Absorption Cross Sections for n-Propyl Nitrite

The absorption of n-C_3H_7ONO is very similar to that of the other nitrites. See figure IX-H-5. The tabular listing of the cross sections at wavelengths of interest in tropospheric chemistry is given in table IX-H-3 where they can be compared with those of some other simple alkyl nitrites.

IX-H-5.2. The Quantum Yields of the Photodissociation of n-Propyl Nitrite

Data are available only for experiments at 366 nm, but these are useful in defining the processes in *n*-propyl nitrite photodecomposition. Following the procedures employed in the studies of methyl nitrite, ethyl nitrite, and *iso*-propyl nitrite, the primary quantum yields of photodissociation of *n*-propyl nitrite should be given by:

$$\phi_I + \phi_{II} = [(1 + k_1/k_2]\Phi_{C_2H_5CHO} + \Phi_{CH_2O}$$

where k_1 and k_2 are the rate coefficients for the reactions:

$$n\text{-}C_3H_7O + NO \rightarrow n\text{-}C_3H_7ONO \quad (1)$$

$$\rightarrow C_2H_5CHO + HNO \quad (2)$$

From experiments at 366 nm, McMillan et al. (1971) determined quantum yields of C_2H_5ONO to be independent of the pressure of nitrite and added NO. McMillan et al. used the measured ratio of $k_1/k_2 = 3.3$ to estimate $\phi_I \approx 0.37$ at 23°C. Zabarnick and Heicklen (1985b) measured $\Phi_{C_2H_5CHO} = 0.115 \pm 0.010$ in similar experiments at 366 nm and at high NO pressures, a value independent of temperature and NO pressure. Combined with the estimate of $k_1/k_2 = 3.3$ (East and Phillips, 1970) this measurement led to the estimate of $\phi = 0.38 \pm 0.04$, very similar to that determined by McMillan et al. The quantum yields of acetaldehyde, one of the products expected from the reaction of C_2H_5 fragment formed in primary process (II) in mixtures with O_2 added, have been measured in these experiments as well, and an average value of $\Phi_{CH_3CHO} = 0.0056 \pm 0.0014$ was found at 23°C. CH_2O was not measured, but it appears that process (I) dominates the decomposition modes at this wavelength. The extent of spontaneous decomposition of the $(C_3H_7O)^{\ddagger}$ species formed in (II) is expected to increase in photolyses at the shorter wavelengths. Process (IV) is believed to be unimportant.

There are no measurements of primary quantum yields of *n*-propyl nitrite at wavelengths other than 366 nm of which we are aware at this writing. However, in accord with the observations in *iso*-propyl nitrite photodecomposition, we will assume that

the total quantum yield of photodecomposition is 0.38, independent of wavelength in calculations of the photolysis frequencies.

Morabito and Heicklen (1985b) found that 366-nm-excited molecules of several alkyl nitrites (C_2H_5ONO, n-C_3H_7ONO, n-C_4H_9ONO, iso-C_4H_9ONO) undergo a photochemical exchange reaction when mixtures of RONO and ^{15}NO are photolyzed: $RONO^* + {}^{15}NO \rightarrow RO^{15}NO + NO$. The mechanism suggested is complex, and the nature of the excited reactant is obscure. However, the observation of Morabito and Heicklen is important since photolysis experiments for RONO with added ^{15}NO have been used to estimate the primary yield of RO radicals from the limiting quantum yield of $RO^{15}NO$ at high pressure of ^{15}NO; these have been interpreted to give: $\Phi_{RO^{15}NO} = \phi_I$. The results of Morabito and Heicklen (1985b) suggest that caution must be exercised in interpreting results from such exchange experiments in this fashion, since ^{15}NO not only captures RO radicals but the exchange reaction can be an additional source of $RO^{15}NO$ with ^{15}NO at high pressures.

IX-H-5.3. Photolysis Frequencies for n-Propyl Nitrite Photodecomposition within the Lower Troposphere

We have calculated photolysis frequencies for n-C_3H_7ONO using the cross sections given in table IX-H-3, the value of $\phi_{total} = 0.38$, independent of wavelength, and the solar flux data for cloudless skies in the lower troposphere for an overhead ozone column of 350 DU. These data are shown in figure IX-H-11. The data predict a photochemical lifetime of n-C_3H_7ONO of about 22 min. with an overhead Sun.

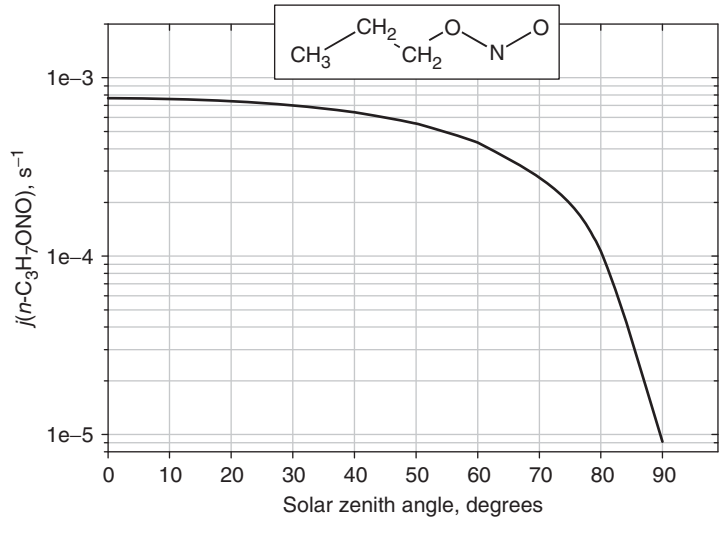

Figure IX-H-11. Approximate photolysis frequencies for n-C_3H_7ONO as a function of solar zenith angle as calculated for a cloudless day in the lower troposphere with an overhead ozone column of 350 DU.

IX-H-6. The Photodecomposition of *n*-Butyl Nitrite ($CH_3CH_2CH_2CH_2ONO$)

Very limited information is available on the photodecomposition of n-C_4H_9ONO from the studies by Morabito and Heicklen (1985b, 1987). The approximate absorption spectrum of n-C_4H_9ONO is given in figure IX-H-5 where it can be compared to that for other alkyl nitrites. The tabular listing of the approximate cross sections as a function of wavelength is given in table IX-H-3. The existing information on this compound suggests that its photodecomposition at 366 nm is similar to that of other simple alkyl nitrites:

$$n\text{-}C_4H_9ONO + h\nu \rightarrow n\text{-}C_4H_9O + NO \quad \text{(I)}$$

$$\rightarrow [n\text{-}C_4H_9O^{\ddagger} + NO] \rightarrow CH_2O + n\text{-}C_3H_7 + NO \quad \text{(II)}$$

$$\rightarrow n\text{-}C_3H_7CHO + H + NO \quad \text{(III)}$$

$$\rightarrow n\text{-}C_3H_7CHO + HNO \quad \text{(IV)}$$

As with the other alkyl nitrites, it is likely that process (IV) is unimportant. Morabito and Heicklen (1985b, 1987) report measurements of $\phi_I = 0.19 \pm 0.04$. We have derived very approximate estimates of the photolysis frequencies of n-C_4H_9ONO as a function of solar zenith angle using the approximate cross sections given in table IX-H-3, the value of $\phi_I = 0.19$, assumed to be independent of wavelength, and the appropriate actinic flux data. These are given in figure IX-H-12. The data suggest that the photochemical lifetime for n-C_4H_9ONO is about 38 min. with an overhead Sun.

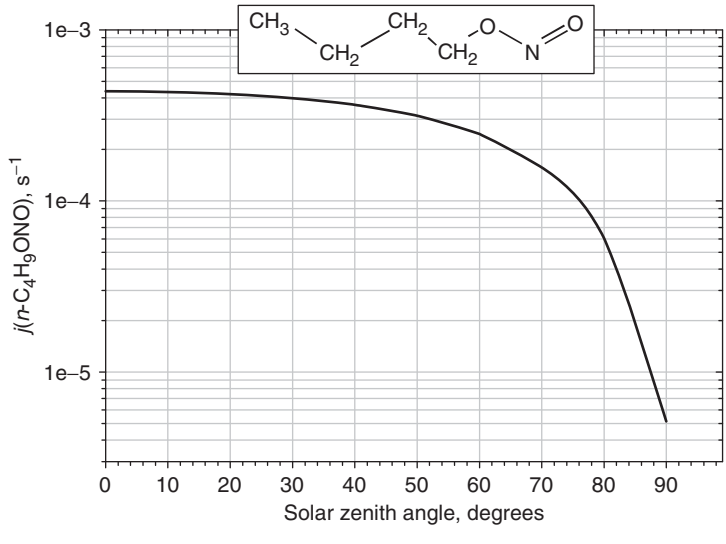

Figure IX-H-12. Approximate photolysis frequencies as a function of solar zenith angle for n-C_4H_9ONO as calculated for a cloudless day in the lower troposphere for an overhead ozone column of 350 DU.

IX-H-7. The Photodecomposition of *iso*-Butyl Nitrite [$(CH_3)_2CHCH_2ONO$]

The photodecomposition of *iso*-C_4H_9ONO has been studied by Zabarnick and Heicklen (1985c), and the mechanism suggested reflects those of the simpler organic nitrites:

$$\textit{iso}\text{-}C_4H_9ONO + h\nu \rightarrow \textit{iso}\text{-}C_4H_9O + NO \quad \text{(I)}$$

$$\rightarrow [(\textit{iso}\text{-}C_4H_9O^{\ddagger}) + NO] \rightarrow CH_2O + \textit{iso}\text{-}C_3H_7 + NO \quad \text{(II)}$$

$$\rightarrow \textit{iso}\text{-}C_3H_7CHO + H + NO \quad \text{(III)}$$

$$\rightarrow \textit{iso}\text{-}C_3H_7CHO + HNO \quad \text{(IV)}$$

There is little information on the extent of processes (II) or (III), but they appear to be unimportant at 366 nm; they may become important at the shorter wavelengths of absorbed light that are available in the upper troposphere and stratosphere. As with the other alkyl nitrites, it is likely that process (IV) is unimportant at all wavelengths.

The absorption spectrum for *iso*-butyl nitrite is very similar to that for other organic nitrites; see figure IX-H-5. The approximate cross sections are given in tabular form for *iso*-butyl nitrite in table IX-H-3.

Using the experimental procedures discussed for the simpler nitrites in the preceding sections, Zabarnick and Heicklen (1985c) measured the quantum yields of *iso*-C_3H_7CHO formed in the photolysis of mixtures of *iso*-C_4H_9ONO (4.6 Torr) and NO (30 mTorr) at 23°C. The measured quantum yield, $\Phi_{\textit{iso}\text{-}C_3H_7CHO} = 0.064 \pm 0.005$, was essentially constant as the total pressure was varied from 4.6 to 150 Torr by nitrogen addition. There is no measurement of the rate coefficient ratio of k_1/k_2:

$$\textit{iso}\text{-}C_4H_9O + NO \rightarrow \textit{iso}\text{-}C_4H_9ONO \quad (1)$$

$$\rightarrow \textit{iso}\text{-}C_3H_7CHO + HNO \quad (2)$$

Zabarnick and Heicklen averaged the estimates for the equivalent ratio of reactions of ethoxy (0.24) and *n*-propoxy (0.30) and used the value of $k_1/(k_1 + k_2) = 0.27$ together with the quantum yield data for the product *iso*-buyraldehyde to estimate the value $\phi_I = 0.24 \pm 0.02$ for the photodissociation of *iso*-butyl nitrite at 366 nm, independent of temperature. With the very limited information on the photochemistry of this compound, we will assume that this quantum yield is independent of wavelength, as was observed for isopropyl nitrite. Using this assumption, the approximate cross sections given in table IX-H-3 and the appropriate actinic flux data, we have calculated the approximate photolysis frequencies for isobutyl nitrite as a function of solar zenith angle. These data are given in figure IX-H-13. The data suggest that the photochemical lifetime for *iso*-C_4H_9ONO is about 33 min. for an overhead Sun.

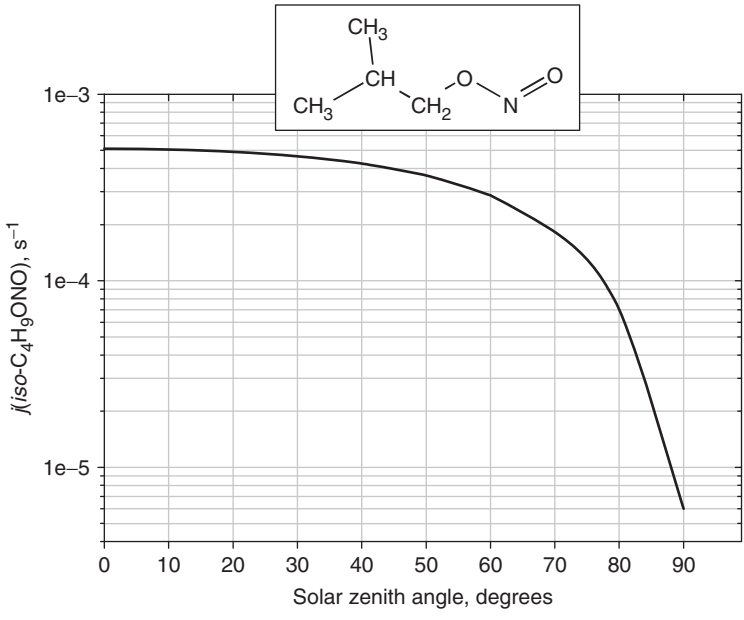

Figure IX-H-13. Approximate photolysis frequencies for *iso*-C_4H_9ONO versus solar zenith angle for a cloudless day in the lower troposphere with an overhead ozone column of 350 DU.

IX-H-8. The Photodecomposition of *tert*-Butyl Nitrite [$(CH_3)_3CONO$]

The absorption spectrum of *tert*-butyl nitrite, like all alkyl nitrites, overlaps well the spectrum of the actinic flux that arrives at the Earth's surface (see figure IX-H-1), and its photodecomposition to form free radicals is efficient. The photodecomposition of $(CH_3)_3CONO$ has been studied in a variety of different experiments (e.g., see Thompson and Dainton, 1937; Coe and Doumani, 1948; McMillan, 1962, 1963; McMillan et al., 1964b; McMillan et al., 1971; Christie and Hetherington, 1976; Trevor and Golden, 1983; August et al., 1988; Effenhauser et al., 1990; Kades et al., 1994; Rösslein et al., 1995; Finke et al., 1999; Castle et al., 2000). The results have been rationalized in terms of the following primary processes:

$$(CH_3)_3CONO + h\nu \rightarrow (CH_3)_3CO + NO \quad \text{(I)}$$

$$\rightarrow [(CH_3)_3CO^{\ddagger} + NO] \rightarrow CH_3C(O)CH_3 + CH_3 + NO \quad \text{(II)}$$

$$\rightarrow CH_3C(O)CH_3 + CH_3NO \quad \text{(III)}$$

Acetone and the dimer of nitrosomethane (CH_3NO) were identified as major products in the early studies of Thompson and Dainton (1937) and Coe and Doumani (1948), and this led to their conclusion that the primary dissociation occurred in process (III). Later experiments proved definitively that these products were derived from secondary

reactions involving the products of primary processes (I) and (II). In this section, we will discuss the evidence for these processes.

IX-H-8.1. Absorption Cross Sections for tert-Butyl Nitrite

The absorption spectrum of *tert*-butyl nitrite as determined by V. McMillan (1966) and reported by Calvert and Pitts (1966) is shown in figure IX-H-1. These data are expected to be less accurate than the original measurements, since significant precision is lost in the drawing of the original published absorption curve and the manipulation of this to recover the numerical information given in the Mainz Spectral Atlas. A tabular listing of the cross sections is given in table IX-H-4. Comparison of the absorption spectra with those of methyl nitrite and isopropyl nitrite in figure IX-H-1, shows that the characteristic banded structure of the alkyl nitrites is present, but it is shifted somewhat to longer wavelengths. Unlike the other alkyl nitrites that are a mixture of the *cis*- and *trans*-forms, *tert*-butyl nitrite exists largely as the *trans*-isomer (Tarte, 1952).

IX-H-8.2. Quantum Yields of Photodecomposition of tert-Butyl Nitrite

Photolysis of a pure sample of $(CH_3)_3CONO$ at the long wavelengths such as 366 nm can lead to little or no product formation (Thompson and Dainton, 1937). In view of our current knowledge, this is best explained by reassociation of the primary radicals released in (I) that occurs readily, and process (II) is unimportant at the longer wavelengths. Unlike primary or secondary alkoxy radicals that can form an aldehyde or ketone through the loss of an H-atom to NO through an abstraction reaction, the *tert*-butoxy radical does not undergo H-atom abstraction in reaction with NO at ambient temperatures.

Quantum yields of acetone formation in *tert*-butyl nitrite photolysis have been measured by McMillan (1962) and McMillan et al. (1971). There is a pronounced effect of wavelength on this quantum yield as shown in figure IX-H-14. In extensive studies using 253.7 nm radiation, McMillan (1962) reported that only a small fraction of the excited alkoxy radicals, $(CH_3)_3CO^{\ddagger}$, formed in process (II) could be quenched with added N_2 or C_2H_6. See figure IX-H-15. Experiments at pressures of the lower troposphere have not been made, so estimates of the extent of excited *tert*-butoxy quenching under atmospheric conditions remains uncertain, but it is probable that a significant fraction of the total *tert*-butoxy radicals formed in the photodecomposition of *tert*-butyl nitrite within the lower troposphere will undergo dissociation. The accurate assessment of the extent of the direct dissociation of the *tert*-butoxy radicals formed in (II) is a moot question since this is expected to be the major fate of all *tert*-butoxy radical formed in the atmosphere (Calvert et al., 2008). McMillan (1962) photolyzed *tert*-butyl nitrite at 366 nm in the presence of added isotopically labeled ^{15}NO and reported that the quantum yield of $(CH_3)_3CO^{15}NO$ was very near unity (0.98 ± 0.04), together with a small quantum yield of acetone (0.037 ± 0.005). ^{15}NO exchange with excited *tert*-C_4H_9ONO molecules may occur, analogous to that observed for some other alkyl nitrites, for the conditions used by McMillan, but it seems probable that $\phi_I + \phi_{II} \approx 1.0$ for $\lambda \leq 366$ nm.

In broadband photolysis ($\lambda > 300$ nm) of *tert*-butyl nitrite, McMillan et al. (1964b) followed CH_3NO formation directly through its infrared absorption and its reaction

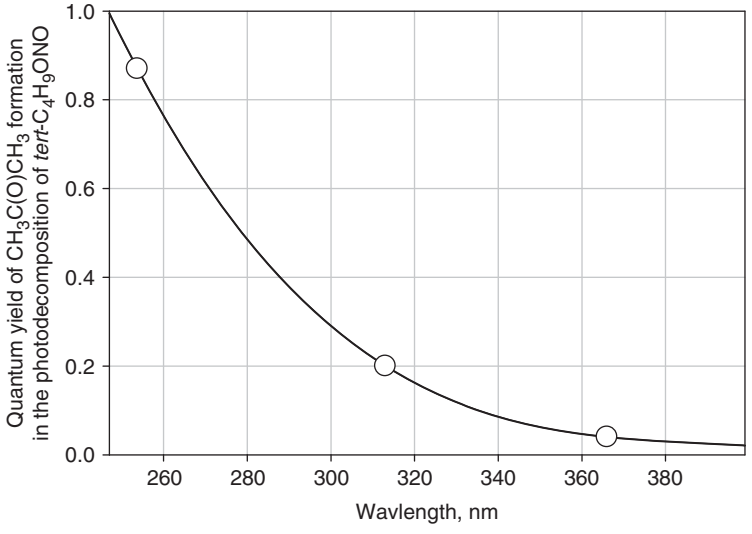

Figure IX-H-14. Quantum yields of the acetone product formed in the photodecomposition of *tert*-butyl nitrite (~15 Torr) with added NO (~15 Torr) as a function of wavelength (McMillan, 1962; McMillan et al. 1971).

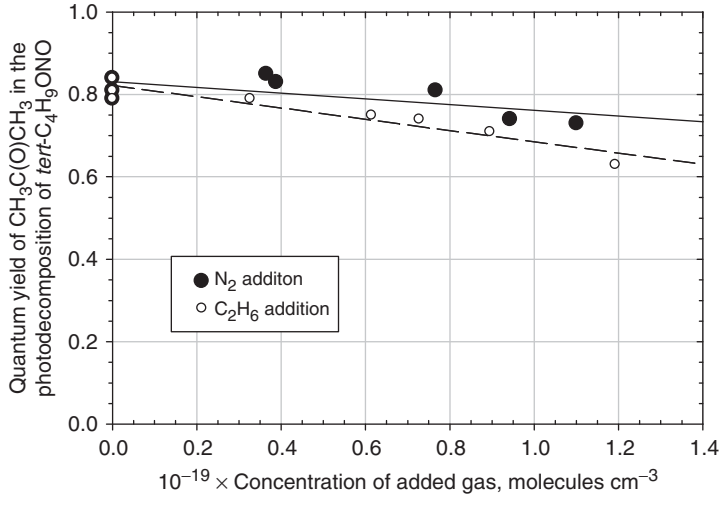

Figure IX-H-15. Quantum yields of acetone products formed in the photolysis of *tert*-butyl nitrite at 253.7 nm as a function of added nitrogen or ethane gases; data from McMillan (1962).

of dimerization. There was a significant induction period after acetone appears before the absorption of CH_3NO is observed. This induction period was increased by addition of a small amount of oxygen and was decreased by addition of either nitrogen at a few Torr pressure or NO at a few microns of pressure. The results show conclusively that the direct formation of CH_3NO in the possible primary process (III) does not occur significantly.

In support of the occurrence of the primary process (II) in $(CH_3)_3CONO$ photolysis at 254 nm, Christie and Hetherington (1976) measured $\Phi_{CH_3NO} = 0.87$. The CH_3NO product forms from the initial NO and CH_3 radical formation in (II). This large fraction of the *tert*-butoxy radicals formed with sufficient energy to decompose, is in quantitative agreement with the findings of McMillan (1962).

Several experiments have been reported that define the dynamics of the photodissociation of *tert*-butyl nitrite. Schwartz-Levi and Rosenwaks (1988) observed the vibrational and rotational excitation in the NO fragment following photodissociation. With excitation at 365.9 nm, rotation was highly excited with *j*-values fit to a temperature of about 1,420 K; vibrational excitation to the NO(X^2) state showed relative populations in the $v'' = 0$, 1, 2, and 3 of 0.05, 0.47, 0.43, and 0.05, respectively. With excitation at 351.9 nm the relative population in these vibrational states was: 0, 0.35, 0.42, and 0.21, respectively. Similar results were reported by Kades et al. (1994) for photolyses at 365.8 and 351.9 nm. Following photolysis of *tert*-butyl nitrite at a somewhat longer wavelength, 381 nm, resulted in the relative populations of the NO product in the $v'' = 0$ and $v'' = 1$ of 0.60 and 0.40, respectively.

Several experimental studies of the photodissociation of *tert*-butyl nitrite excited within the $S_0 \rightarrow S_2$ ($\pi \rightarrow \pi^*$ character) band have been made (e.g., see August et al., 1988; Effenhauser et al., 1990; Finke et al., 1999; Castle et al., 2000; Wang et al., 2007b). Effenhauser et al. (1990) measured the translational energy distribution of the products of the 248 nm photolysis. Of the 482 kJ mol^{-1} of energy available in the 248 nm quantum, 122 kJ mol^{-1} appears as average translational energy (both fragments) and 185 kJ mol^{-1} as in internal energy in vibrations and rotation of the products. An average of about 126 kJ mol^{-1} of energy is present in the *tert*-butoxy radical product, greatly in excess of the 56.9–61.0 kJ mol^{-1} necessary to dissociate the radical: $(CH_3)_3CO \rightarrow CH_3 + CH_3C(O)CH_3$. In fact, the time of flight distributions show clear evidence for the collisionless unimolecular decay of the *tert*-butoxy radical that occurs on a submicrosecond timescale.

IX-H-8.3. Photolysis Frequencies for tert-Butyl Nitrite Photodecomposition within the Lower Troposphere

We have used the cross sections of *tert*-butyl nitrite given in table IX-H-4, an assumed total quantum yield of photodecomposition of unity, independent of wavelength, and the appropriate actinic flux data (cloudless skies, vertical ozone column of 350 DU) to estimate the *j*-values for *tert*-butyl nitrite photodecomposition within the lower troposphere. These data are summarized in figure IX-H-16. The data of figure IX-H-16 give a photochemical lifetime for *tert*-butyl nitrite of about 4.3 min. with an overhead Sun.

IX-H-9. Photodecomposition of *tert*-Pentyl Nitrite [$CH_3CH_2C(CH_3)_2ONO$]

The photodecomposition of $C_2H_5C(CH_3)_2ONO$ shows an interesting competition for the fragmentation pathways of the initial alkoxy radical formed in the photolysis. Studies have been made at several wavelengths by Durant and McMillan (1966).

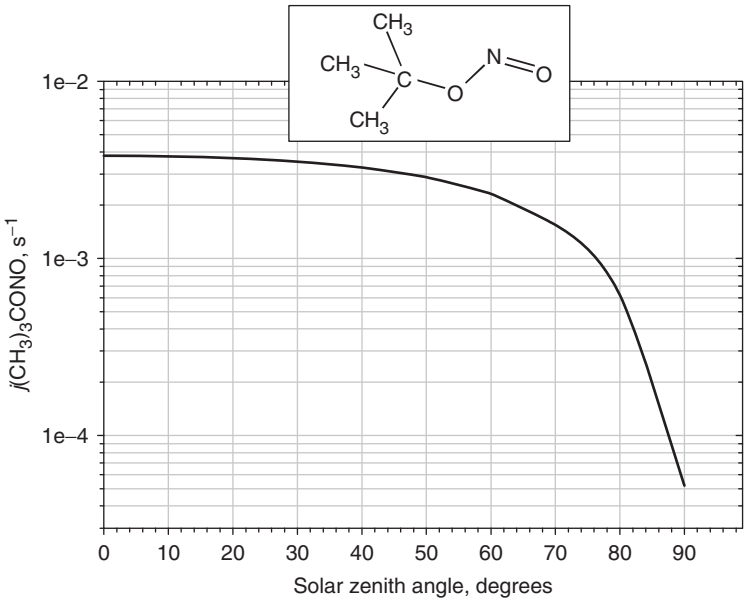

Figure IX-H-16. Photolysis frequencies as a function of solar zenith angle for *tert*-C_4H_9ONO photodecomposition on a cloudless day in the lower troposphere with an overhead ozone column of 350 DU.

The following primary processes were invoked to rationalize the results:

$$C_2H_5C(CH_3)_2ONO + h\nu \rightarrow C_2H_5C(CH_3)_2O + NO \quad \text{(I)}$$

$$\rightarrow [C_2H_5C(CH_3)_2O^{\ddagger} + NO] \rightarrow$$

$$C_2H_5 + CH_3C(O)CH_3 + NO \quad \text{(II)}$$

$$CH_3 + CH_3C(O)C_2H_5 + NO \quad \text{(III)}$$

IX-H-9.1. Absorption Cross Sections for tert-Pentyl Nitrite

Durant and McMillan (1966) state that the absorption spectrum of *tert*-pentyl nitrite, as reported by Ungnade and Smiley (1956), is identical to that for *tert*-butyl nitrite. The two compounds are structurally similar in that both contain a tertiary carbon atom attached to the —ONO chromophore and both exist largely in the *trans*-confirmer. On the basis of this information, we will use the spectrum of *tert*-butyl nitrite as a surrogate in our discussions here.

IX-H-9.2. Quantum Yields of Photodecomposition of tert-Pentyl Nitrite

In photolyses at several different wavelengths at a temperature of 114°C, the ratio of the two ketone products of processes (II) and (III) were measured by Durant and

McMillan (1966). The observed ratios of $\Phi_{CH_3COCH_3}/\Phi_{C_2H_5C(O)CH_3}$ in the products, insensitive to the pressure of added NO (0–105 Torr), were as follows: 6.8 at 253.7 nm; 11.3 at 313 nm; and 38 ± 5 at 366 nm. The authors point out that unexcited *tert*-pentoxy radicals (from thermal experiments) decay with the ratio of the same two products of about 104 at 114°C. The observed change in the ratio with wavelength is interpreted as a strong indication of the formation of highly vibrationally excited alkoxy radicals in the primary process. At 114°C the sum of the quantum yields of the two ketones is about 0.85 with no NO added. At 100 Torr of added NO gas the quantum yield is decreased to about 0.35, presumably as a result of collisional quenching of a fraction of the excited radicals and the scavenging of the thermalized radicals. In experiments at 253.7 nm, the sum of the quantum yields of the two product ketones was measured to be near unity in experiments at 25°C. The fact that the quantum yields are high in the presence of large amounts of an efficient scavenger, nitric oxide, suggest that decomposition of equilibrated radicals makes a negligible contribution to ketone formation under these conditions.

IX-H-9.3. Photolysis Frequencies for tert-Pentyl Nitrite Photodecomposition within the Lower Troposphere

From the results obtained in their studies, Durant and McMillan (1966) conclude that, like *tert*-butyl nitrite, *tert*-pentyl nitrite has a quantum yield of photodecomposition near unity, independent of wavelength. Assuming this, and noting the similarity in the cross sections of these two nitrites, we suggest the use of the same photolysis frequencies given in figure IX-H-16 for *tert*-butyl nitrite.

IX-H-10. Summary of the Mechanisms of Tropospheric Photodecomposition of the Alkyl Nitrites

The photodissociation of the nitrites has been shown to occur with rupture of the weak RO—NO bond and formation of an internally excited RO radical. As one can see from the preceding discussion, many of the existing measurements of the primary quantum yields of the photodecomposition of the nitrites are indirect and subject to significant error. Since the lifetimes of the excited states of the nitrites appear to be very short, and there is no observable fluorescence or other indications of long-lived excited states, one logically expects the quantum yields of photodissociation to be near unity. Existing data suggest that this is the case for HONO, CH_3ONO, *tert*-C_4H_9ONO, and $CH_3CH_2C(CH_3)_2ONO$. However, as was seen in the discussion of the preceding sections, experimental data on C_2H_5ONO, *n*-C_3H_7ONO, *n*-C_4H_9ONO, and $(CH_3)CHCH_2ONO$ point to a significantly lower quantum yield of photodissociation. One should consider the estimates for these compounds in this work as lower limits, since there is no obvious reason for the inefficiency in photodissociation of these compounds. Further studies of the primary quantum efficiencies of the alkyl nitrites are warranted.

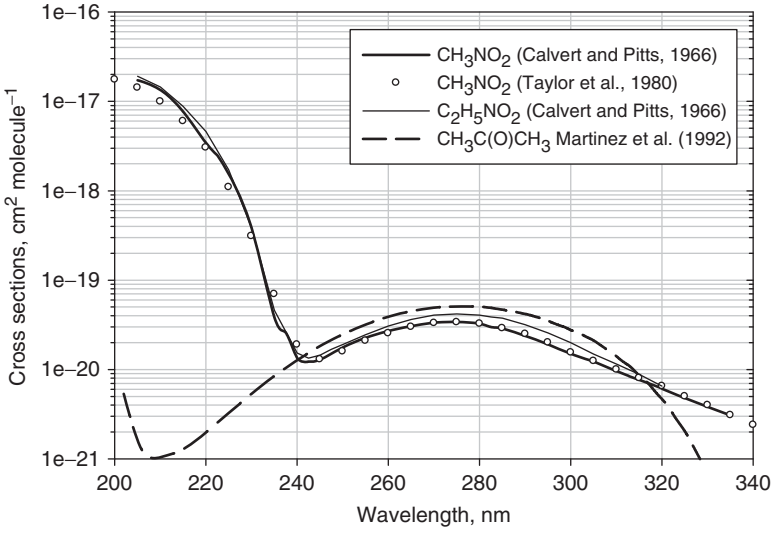

Figure IX-H-17. Comparison of the absorption cross sections for nitromethane and nitroethane with that for acetone.

IX-H-11. Photodecomposition of the Nitroalkanes (RNO_2)

The nitroalkanes absorb light in the same region as the aldehydes and ketones (see figure IX-H-17), and they undergo photodecomposition in tropospheric sunlight. The long-wavelength band has been classified as a $n(O) \rightarrow \pi^*$ transition by Bayless and McRae (1954), and it occurs in the same wavelength region as that of acetone. A much stronger band ($\pi \rightarrow \pi^*$) occurs just below 240 nm while the $\pi \rightarrow \pi^*$ band in acetone occurs at much shorter wavelengths. The cross section data for nitromethane as reported by Calvert and Pitts (1966) and Taylor et al. (1980) are seen to be in good accord. The halogenated nitromethanes show little change in position of the absorption band but do show changes in the band maximum from that of nitromethane. See figure IX-H-18. CCl_3NO_2 shows a 44% decrease while CF_3NO_2 shows a 27% increase in the maximum compared to CH_3NO_2. However, with the compounds containing both Cl- and F-substitution, CCl_2FNO_2 and $CClF_2NO_2$, the cross sections at the maxima increase by a factor of 5 from that of CH_3NO_2. The cross section of acetaldehyde shows a similar increase in cross section in F- and Cl-substituted acetaldehyde molecules, CF_2ClCHO and $CFCl_2CHO$, that is shown in figure IX-C-27.

The major pathway for photodecomposition of the nitroalkanes (RNO_2) involves the rupture of the R—NO_2 bond, process (I):

$$RNO_2 + h\nu \rightarrow R + NO_2 \quad \text{(Ia)}$$

$$\rightarrow R + NO_2^* \quad \text{(Ib)}$$

$$\rightarrow RNO + O \quad \text{(II)}$$

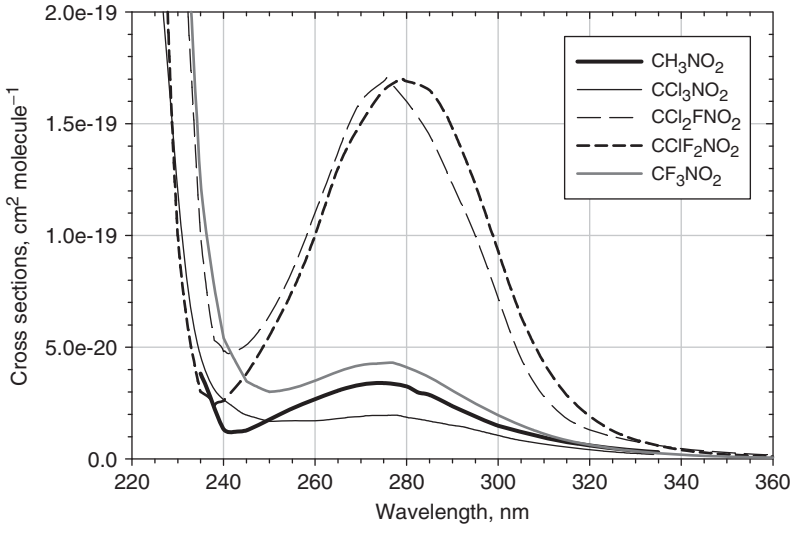

Figure IX-H-18. Comparison of the absorption cross sections for a series of halogen-atom-substituted nitromethane molecules. Data for CH_3NO_2 from Calvert and Pitts (1966); CCl_3NO_2 from Allston et al. (1978); CCl_2FNO_2, $CClF_2NO_2$, and CF_3NO_2 from Fazekas and Takacs (1983).

In process (Ib), NO_2^* represents an excited NO_2 molecule which may dissociate to form NO and O if sufficient energy is available. The alternative dissociation process (II) requires significantly more energy than (I), $\sim$392 kJ mol^{-1} ($\lambda < 305$ nm) versus 252 kJ mol^{-1} ($\lambda < 475$ nm). Some other modes of photodissociation have been suggested to occur when the R group in RNO_2 is C_2H_5 or larger alkyl group. See section IX-H-11.2. There is little information on the quantum yields of the photodissociation of the nitroalkanes in the wavelength range important to tropospheric chemistry. However, in this section we review this limited evidence.

IX-H-11.1. The Photodecomposition of Nitromethane (CH_3NO_2)

Hirschlaff and Norrish (1936) interpreted their study of the products of 200–300 nm photolysis of nitromethane (CH_2O, NO, CO, N_2, CO_2, H_2O) to suggest that the major photodissociation process is: $CH_3NO_2 + h\nu \rightarrow NOH + CH_2O$. However, Gray et al. (1955) pointed out that a CH_3—NO_2 bond rupture could explain well the observed products. Indeed, McGarvey and McGrath (1964) observed the spectrum of the CH_3 radical in the flash photolysis of nitromethane and supported the dominance of process (I). Brown and Pimentel (1958) observed the isomerization of nitromethane to methyl nitrite in solid argon matrix at 20 K, but this also could be rationalized as resulting from association of the initial CH_3 and NO_2 fragments formed in (I): $CH_3 + NO_2 \rightarrow CH_3ONO$. The subsequent photolysis of CH_3ONO could explain the other observed products (Nicholson, 1961).

Nicholson (1961) concluded from his analysis of products of full arc photolysis of nitromethane that process (I) was the dominant primary photolysis mode. Also Rebbert

and Slagg (1962) reported a product study of the 250–400 nm photodecomposition of nitromethane and its mixtures with ^{15}NO. They concluded that process (I) was the dominant mode of dissociation. Napier and Norrish (1967) also observed the spectrum of CH_3 radicals immediately following the flash photolysis of CH_3NO_2 and its mixtures with added NO and N_2; in the mixtures an enhancement of the NO_2 product spectrum was observed at short time delays, but CH_3NO then appeared. Absorption due to CH_2O and CH_3ONO was not observed under these conditions. These authors concluded that primary process (I) best described their results. With the results of nitromethane photolysis available in 1973, Paszyc (1973/1974) also concluded that process (I) was likely the dominant primary process.

Schoen et al. (1982) observed the picosecond timescale photodecomposition of nitromethane using laser-induced fluorescence of ground state NO_2 molecules. From their experiments at low pressures, the approximate quantum yields of process (Ia) at wavelengths 238, 254, 296, and 337 nm can be estimated to be: $\phi_{Ia} \approx 0.2, 0.7 \pm 0.3$, 0.7, and 0.3, respectively, with quantum yields of electronically excited NO_2 formed in (Ib), $\phi_{Ib} \approx 0.8$, 0.3, 0.0, and 0.0, respectively. However, extrapolation of these findings to conditions of the lower troposphere is not possible since the extent of quenching of the excited CH_3NO_2 molecules is unknown, but this is expected to occur to some extent under tropospheric conditions.

Several studies have been made of CH_3NO_2 photodissociation within the $\pi \rightarrow \pi^*$ band. Spears and Brugge (1978) reported that vibrationally excited NO_2 formed in the photodissociation of CH_3NO_2 at 252 nm, with the vibrational population at 0.1 Torr equivalent to a 7,000 ± 1,300 K temperature. In a molecular beam experiment with photolysis of CH_3NO_2 at 193 nm, Blais (1983) observed the CH_3, O, and NO fragments. An average of 19% of the available energy appears as kinetic energy of the fragments and the remainder appears as internal energy of the fragments. Blais measured the quantum yield of photodissociation of CH_3NO_2 at 193 nm to be near unity.

In detailed studies of CH_3NO_2 photodissociation at wavelengths within the $\pi \rightarrow \pi^*$ band (193–218 nm), Butler et al. (1983), Lao et al. (1990), and Moss et al. (1992) employed molecular beam translational energy spectroscopy and product emission spectroscopy to demonstrate that two distinct mechanisms were involved in the process (I). The dominant mechanism releases a relatively large fraction of the total available energy to translation with NO_2 formed in a vibrationally excited $\tilde{A}^2B_2$ state which can rapidly dissociate to NO and O. Wade et al. (2006) found similar results when they photolyzed CH_3NO_2 at 192, 248, and 266 nm and observed the products by time-dependent Fourier transform infrared emission spectroscopy. The primary process (I) was dominant with $\tilde{A}^2B_2$ NO_2 formation.

Zabarnick et al. (1986) observed the formation of OH radicals in the 266 nm photodecomposition of CH_3NO_2 with a quantum yields of 0.004 ± 0.001; they attributed this to the occurrence of a minor primary process: $CH_3NO_2 + h\nu \rightarrow OH + CH_2NO$. The OH radical was formed with a rotational temperature of 1,750 ± 50 K.

The occurrence of process (II) in the photodecomposition of CH_3NO_2 at 248 and 266 nm was demonstrated by Park et al. (2001) using pulsed laser photolysis–laser-induced fluorescence. Nascent $O(^3P)$ photofragments were detected via LIF under collision-free conditions. From Doppler profiles of the O-atom, the fraction of the

total available energy channeled into product translation energy was determined to be 0.28 ± 0.02 at 248 nm and 0.23 ± 0.04 at 266 nm. The quantum yields for O-atom formation were: $\phi_{II} = 0.18 \pm 0.03$ at 248 nm and $\phi_{II} = 0.13 \pm 0.04$ at 266 nm.

Several *ab initio* calculations related to possible pathways of photodissociation of CH_3NO_2 have been reported (e.g., see McKee, 1989; Hu et al., 2002; Nguyen et al., 2003; Arenas et al., 2005). Hu et al. (2002) studied the potential energy surface for the unimolecular isomerization and dissociation of CH_3NO_2, including 10 different compounds with the chemical structures, CH_3NO_2 (CH_3NO_2, *cis*-CH_3ONO and *trans*-CH_3ONO, $CH_2N(O)OH$, $CH_2(OH)NO$, $H_2(CON)OH$, $HCN(OH)_2$, $HC(O)N(H)OH$, $HC(O)N(O)H_2$, $HC(OH)NOH$, $HC(OH)N(O)H$), 46 interconversion transition states and 16 major dissociation products. They conclude that CH_3NO_2 isomerization pathways (e.g., CH_3ONO formation) are kinetically disfavored in view of the relatively high activation barriers, in excess of 251 kJ mol^{-1}. They suggest that photodissociation of CH_3NO_2 occurs either via the C—N bond rupture, process (I), or via concerted molecular eliminations forming $CH_3O + NO$, $CH_2O + HNO$, or $HCNO + H_2O$. We conclude that the majority of the experimental evidence favors the dominance of process (I) for nitromethane photodecomposition at wavelengths within the troposphere.

There are insufficient data for conditions reflective of the troposphere to estimate realistic values for the photolysis frequencies for CH_3NO_2 at this writing.

IX-H-11.2. The Photodecomposition of the Larger Nitroalkanes

Very limited data exist concerning the photochemistry of the larger nitroalkanes, but it appears that process (I) is the dominant photodissociation mode. Rebbert and Slagg (1962) studied the products of 250–400 nm photodecomposition of nitroethane (22–104°C) and reported the formation of ethene with $\Phi_{C_2H_4} \approx 0.076 \pm 0.004$, independent of temperature. Nitric oxide formed as well ($\Phi_{NO} \approx 0.09 \pm 0.02$) with much smaller amounts of ethane, methane, hydrogen, and carbon monoxide. In addition to the occurrence of process (I), they suggested that an additional primary process (III) occurred, conceivably through a 5-membered ring intermediate.

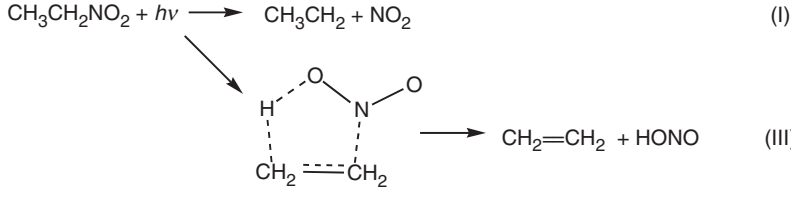

Spears and Brugge (1978) studied the vibrationally excited NO_2 formation from 252 nm photodissociation of 2-nitropropane as well as nitromethane using laser-induced fluorescence of the product NO_2. Both nitro compounds gave similar NO_2 vibrational populations, which suggested that interaction of the fragments during the dissociative separation is negligible. This supports the expectation that vibrational complexity of the alkyl group is unimportant in a process of rapid vibrational energy migration from an NO_2 chromophore to the R—NO_2 bond.

Greenblatt et al. (1987) observed the formation of OH ($X^2\Pi$) radicals in the low-pressure gas-phase, 282 nm photolysis of nitroethane, 1- and 2-nitropropane, and 2-nitro-2-methylpropane. They did not detect OH in similar experiments with nitromethane. The mechanism is suggested to involve a 5- or 6-membered ring intermediate that leads to the OH product:

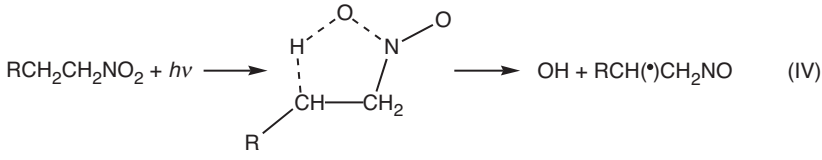

The fact that OH is formed from higher homologous members of the series and very little from nitromethane (Zabarnick et al., 1986) is the expected result, provided that a 5-membered ring intermediate is involved. This is consistent with the findings of these workers that the photolysis of $CH_3CD_2NO_2$ gave OH only and no detectable OD fragments. The reported quantum yields (ϕ_{OH}) observed in the photodecomposition of $CH_3CH_2NO_2$, $CH_3CH(NO_2)CH_3$, and $(CH_3)_3CNO_2$ were: 0.0042 ± 0.0012, 0.0097 ± 0.003, and 0.025 ± 0.005, respectively. It is probable that the dominant decay path for the larger nitroalkanes remains process (I), as with nitromethane. The rotational distributions of the nascent OH radicals formed were found to be similar for the different nitroalkanes; relative populations for E_{rot} of 0, 500, 1,000, and 1,600 cm^{-1} were approximately 1:0.09:0.03:0.01.

The possible mechanisms for the proposed processes (III) and (IV) remains highly uncertain. It is possible that these processes may be related, as formation of OH could occur from the secondary dissociation of an excited HONO product of process (III) or the subsequent photolysis of HONO formed in that primary process.

Ross et al. (1996) reported the results of the 193 nm photolysis of nitroalkanes in the C_3–C_6 range using time of flight mass spectrometry to detect the products. Both C—N and N—O bond dissociation pathways were observed. Under collision-free conditions, the alkyl radicals formed undergo extensive secondary fragmentation. When photodissociation was performed in a free jet expansion, collisional cooling stabilized the primary products and allowed large radicals such as pentyl and hexyl radicals to be detected.

Wade et al. (2006) studied the photodecomposition of CCl_3NO_2 (chloropicrin) at 193, 248, and 266 nm using time-dependent Fourier transform infrared emission spectroscopy. At 266 nm the major photodissociation channel formed $CCl_3 + NO_2(\tilde{A}^2B_2)$, analogous to channel (I) in the photolysis of the other nitroalkanes. Phosgene [ClC(O)Cl] was not detectable in this work, and the authors suggest that its production and that of ClNO that has been observed in environmental chambers (Moilanen et al., 1978) and cryogenic matrices (Wade et al., 2002), is likely the result of secondary reactions.

Insufficient data are available to estimate reasonable values for the photolysis frequencies of the larger nitroalkanes.

IX-H-12. The Photodecomposition of the Nitrosoalkanes (RNO)

The nitrosoalkanes (RNO, where R = CH_3, C_2H_5, etc.), are a special class of very reactive N- and O-atom-containing oxygenates. When the R group contains an H-atom on the carbon atom next to the —NO group, the compound is unstable toward isomerization to the oxime form of the aldehyde or ketone of the same elementary composition. Thus, CH_3NO rapidly undergoes rearrangement to CH_2=N—OH and $CH_3CH(NO)CH_3$ forms $(CH_3)_2C(N{=}OH)$. Those nitrosoalkanes with no H-atom next to the—NO group are stable against isomerization. For example, CF_3NO and $(CH_3)_3CNO$ are thermally stable compounds and exist as unique blue-colored gases in the vapor phase. The absorption spectra of these molecules can be compared with those of some simple nitroalkanes in figure IX-H-19.

The nitrosoalkane compounds are expected to undergo photodecomposition with high efficiency in sunlight to form an alkyl free radical (R) and NO: $RNO + h\nu \rightarrow R + NO$ (Cimiraglia et al., 1985). The formation of these compounds in the atmosphere and their release into the atmosphere are unlikely events; they are unimportant storage sinks for NO_x, and are not expected to have any significant impact on tropospheric chemistry.

IX-H-13. Photodecomposition of the Dimethylnitrosoamine [N,N-Dimethylnitrosamine, $(CH_3)_2NNO$]

The nitrosamines are of special interest to scientists in that they are potent animal carcinogens (U.S. Environmental Protection Agency, 1976; Fine et al., 1976).

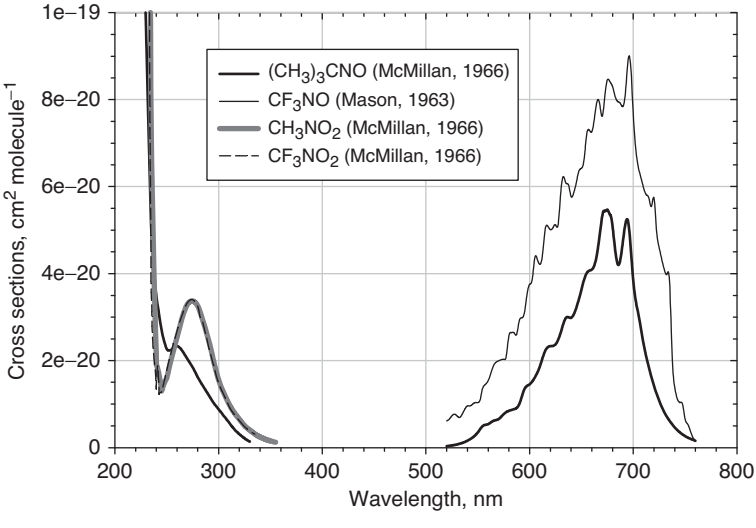

Figure IX-H-19. Comparison of the absorption spectra of $(CH_3)_3CNO$ (McMillan, 1966), CF_3NO (Mason, 1963), CH_3NO_2, and CF_3NO_2. The region of absorption of the RNO compounds results in a rare characteristic: they are blue-colored gases. The visible band of the nitrosoalkanes is missing in the nitroalkanes as absorption is shifted to the ultraviolet region.

Sensitive analytical techniques have been used to detect nitrosamines in many commercial products; for example, in tire manufacturing (Fajen et al., 1979), in pesticides (Rawls, 1976), and in many foods and drinks, including beers (*Chem. Engr. News*, Oct. 1, 1979, pp. 6–7) and whiskies (Ember, 1980). In the 1970s they were detected in polluted ambient air in regions near some industrial plants (e.g., see Bretschneider and Matz, 1973; Fine et al., 1976, 1977; Fajen et al., 1979) and in some regions of California (Gordon, 1978). Dimethylnitrosamine has been observed to form (presumably, heterogeneously) from reaction between nitrous acid and dimethyl amine (Hanst et al., 1977; Glasson, 1979), and in irradiated amine–NO_x mixtures in air in smog chamber experiments (Tuazon et al., 1978). Dimethylnitrosamine as well as the dimethylnitramine, $(CH_3)_2NNO_2$, can be formed also in the atmosphere following the attack of OH radical on dimethylamine (Lindley et al., 1979; Calvert, 1982). The following reactions are expected to occur:

$$(CH_3)_2NH + OH \rightarrow (CH_3)_2N + H_2O \tag{1a}$$

$$(CH_3)_2NH + OH \rightarrow CH_2NHCH_3 + H_2O \tag{1b}$$

$$(CH_3)_2N + NO \rightarrow (CH_3)_2NNO \tag{2}$$

$$(CH_3)_2N + NO_2 \rightarrow (CH_3)_2NNO_2 \tag{3a}$$

$$\rightarrow HONO + CH_2{=}NCH_3 \tag{3b}$$

$$(CH_3)_2N + O_2 \rightarrow CH_2{=}NCH_3 + HO_2 \tag{4}$$

Lindley et al. (1979) have shown that the reaction of $(CH_3)_2N$ with O_2 in reaction (4) is relatively slow compared to its reactions with NO and NO_2; $k_4/k_2 = (1.48 \pm 0.07) \times 10^{-6}$; $k_4/(k_{3a} + k_{3b}) = (3.20 \pm 0.29) \times 10^{-7}$ at temperatures near 298 K, but the reaction (4) with NO and the reaction (3b) with NO_2 lead to methylmethyleneamine ($CH_2{=}NCH_3$). Thus, reactions (2), (3), and (4) can occur to measurable extents even in relatively dilute air mixtures of dimethylamine. The low reactivity of $(CH_3)_2N$ with O_2 compared to that with NO is analogous to the observations of the reactivity of the NH_2 radical reported by Lesclaux and Demissy (1977) and Lesclaux et al. (1975):

$$NH_2 + O_2 \rightarrow \text{Products} \tag{5}$$

$$NH_2 + NO \rightarrow \text{Products} \tag{6}$$

Where $k_5/k_6 \leq [(1.2 \pm 0.2) \times 10^3/(1.1 \pm 0.2) \times 10^{10}] = (1.1 \pm 0.3) \times 10^{-7}$. The upper limit to the rate coefficient for the coupling reaction, $NH_2 + O_2 \rightarrow NH_2O_2$ was reported by Tyndall et al. (1991a) to be $\leq 6 \times 10^{-21}$ cm^3 molecule^{-1} s^{-1} at 296 K. Like the NH_2 radical, coupling of the $(CH_3)_2N$ radical with O_2 appears to be very slow as well, but the reaction (4) with H-atom abstraction and formation of the stable $CH_2{=}N{-}CH_3$ product apparently has a much lower barrier than the reaction: $NH_2 + O_2 \rightarrow HO_2 + NH$.

IX-H-13.1. Absorption Cross Sections of Dimethylnitrosamine

Lindley (1978) determined the absorption coefficients (ε, L mol^{-1} cm^{-1}, base 10) for gaseous dimethylnitrosoamine. These data, determined at each nm in the 300–427 nm region, were converted to cross sections (σ, cm^2 molecule^{-1}, base e), and are shown in figure IX-H-20. Also shown in this figure are the data reported by Geiger et al. (1981). They published the relative absorption spectrum of dimethylnitrosamine and the extinction coefficient for the maximum wavelength; we have converted these data to cross sections that are shown in figure IX-H-20. The two sets of data agree reasonably well. We recommend use of the cross section data of Lindley that are given in tabular form in table IX-H-6.

The region of light absorption by *N*,*N*-dimethylnitrosamine overlaps well the wavelengths of tropospheric sunlight (see figure IX-H-20). On absorption of light within the long wavelength, $n \rightarrow \pi^*$ excitation band, photodecomposition is observed to occur by cleavage of the weak $(CH_3)_2N$—NO bond:

$$(CH_3)_2NNO + h\nu \rightarrow (CH_3)_2N + NO \qquad \text{(I)}$$

The rotational alignment, Λ-doubling, and spin-orbit populations of the NO fragment from dimethylnitrosoamine photodecomposition were determined by Lavi et al. (1987) at 250 and 363.5 nm. Within the $\pi \rightarrow \pi^*$ region at 250 nm, the transition dipole moment lies in the frame of the molecule as is expected for a $\pi \rightarrow \pi^*$ transition, while for the $n \rightarrow \pi^*$ transition at 363.5 nm the transition dipole moment lies perpendicular to the frame of the molecule. The existence of alignment in the two cases leads to the conclusion that there must be some planarity in the fragmentation process for photolysis

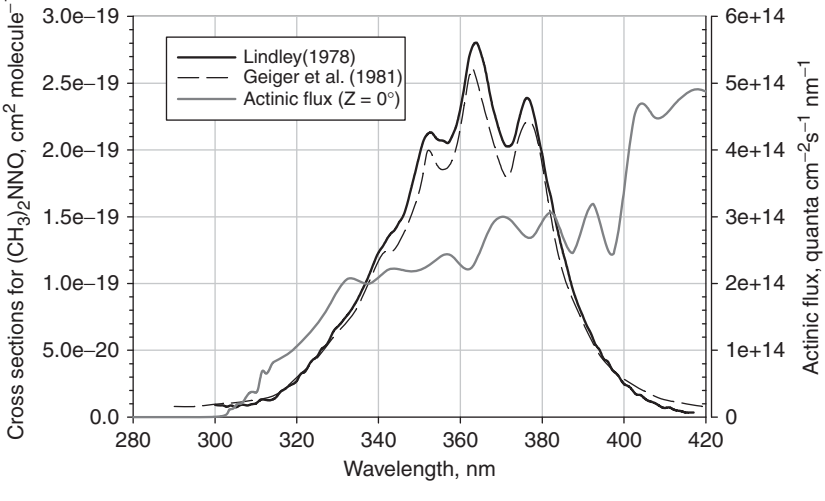

Figure IX-H-20. Absorption spectrum of dimethylnitrosoamine. The data reported by Lindley (1978) and Geiger et al. (1981) are seen to be in reasonable agreement; actinic flux is shown for an overhead Sun in the lower troposphere (gray curve).

Table IX-H-5. The cross sections (σ, cm^2 $molecule^{-1}$) for $(CH_3)_2NNO$ as a function of wavelength (Lindley, 1978)

λ, nm	$10^{19} \times \sigma$	λ, nm	$10^{19} \times \sigma$	λ, nm	$10^{19} \times \sigma$
290	0.081	334	0.84	378	2.26
291	0.081	335	0.89	379	2.11
292	0.081	336	0.95	380	1.97
293	0.081	337	1.02	381	1.78
294	0.081	338	1.09	382	1.66
295	0.081	339	1.17	383	1.50
296	0.081	340	1.23	384	1.36
297	0.081	341	1.28	385	1.24
298	0.081	342	1.33	386	1.13
299	0.081	343	1.37	387	1.01
300	0.092	344	1.40	388	0.91
301	0.087	345	1.46	389	0.82
302	0.087	346	1.50	390	0.75
303	0.078	347	1.60	391	0.68
304	0.087	348	1.72	392	0.62
305	0.073	349	1.84	393	0.54
306	0.087	350	1.96	394	0.50
307	0.092	351	2.07	395	0.44
308	0.087	352	2.12	396	0.42
309	0.097	353	2.13	397	0.36
310	0.101	354	2.09	398	0.33
311	0.126	355	2.07	399	0.29
312	0.131	356	2.07	400	0.25
313	0.126	357	2.05	401	0.23
314	0.131	358	2.10	402	0.20
315	0.150	359	2.18	403	0.17
316	0.189	360	2.31	404	0.16
317	0.208	361	2.48	405	0.14
318	0.232	362	2.68	406	0.12
319	0.247	363	2.78	407	0.11
320	0.271	364	2.80	408	0.097
321	0.324	365	2.72	409	0.078
322	0.339	366	2.61	410	0.068
323	0.392	367	2.45	411	0.073
324	0.431	368	2.31	412	0.058
325	0.455	369	2.20	413	0.049
326	0.508	370	2.09	414	0.044
327	0.532	371	2.03	415	0.034
328	0.581	372	2.03	416	0.034
329	0.644	373	2.07	417	0.034
330	0.677	374	2.19	418	0.026
331	0.711	375	2.31	419	0.017
332	0.750	376	2.39	420	0.009
333	0.789	377	2.37	421	0

in both wavelength regions. The NO fragment formed in process (I) is vibrationally and rotationally excited even in photolyses at 363.5 nm (Dubs and Huber, 1984).

IX-H-13.2. The Quantum Yields of Photodecomposition of Dimethylnitrosoamine

Several observations show that the quantum yield for photodecomposition of dimethylnitrosamine is near unity for excitation within the long-wavelength band:

i) Under conditions that minimized recombination of the primary fragments of dimethylnitrosoamine photolysis, Lindley et al. (1979) found the *j*-value in their simulated atmospheric reactor to be $(2.0 \pm 0.3) \times 10^{-3}\ s^{-1}$, very similar to that estimated for photodecomposition in tropospheric sunlight at a solar zenith angle of 40°, assuming $\phi_I = 1.0$.
ii) Tuazon et al. (1984b) measured the photolysis rate in the presence of excess ozone (to avoid reformation of the nitrosamine in a large simulated atmospheric reactor) and found $j = (4.0 \pm 0.2) \times 10^{-3}\ s^{-1}$, also consistent with $\phi_I \cong 1.0$.
iii) Geiger et al. (1981) measured $\phi_I = 1.03 \pm 0.10$ at 363.5 nm by capturing the $(CH_3)_2N$ radicals in mixtures with large excess of ^{15}NO and monitoring the quantum yield of $(CH_3)_2N^{15}NO$ formation.

The major products of photodecomposition of dimethylnitrosamine in simulated polluted atmospheres are the dimethylnitramine, $(CH_3)_2NNO_2$, and methylmethyleneamine, $CH_2{=}NCH_3$ (Lindley et al., 1979; Calvert, 1982). The near ultraviolet band of absorption present in the nitrosamines is missing in the nitramines (Pitts et al., 1978). Although diethylnitrosoamine in methanol solution shows a near unltraviolet absorption similar to that of dimethylnitrosamine (λ_{max} near 350 nm), significant absorption by diethylnitramine in methanol solution occurred only at wavelengths below those present in tropospheric sunlight. Hence, photodecompositions of the dimethylnitramines and other nitramines are probably much less important than their loss by reaction with OH radical (see section VIII-M-1).

IX-H-13.3. Photolysis Frequencies for Dimethylnitrosamine

We have used the cross section data of Lindley (1978), the appropriate actinic flux data, and an assumed value of $\phi_I = 1.00$ over the entire long-wavelength absorption region, to calculate the photolysis frequencies for dissociation of dimethylnitrosoamine as a function of solar zenith angle in the lower troposphere for an overhead ozone column of 350 DU. These data are shown in figure IX-H-21. It is clear that the photochemical lifetime of dimethylnitrosamine in the sunlight-irradiated lower troposphere is very short, about 6 min. with an overhead Sun.

IX-I. Photodecomposition of Nitric Acid, Peroxynitric Acid, and the Alkyl Nitrates

Nitric acid ($HONO_2$), peroxynitric acid (HO_2NO_2), and the alkyl nitrates, $RONO_2$ (R = CH_3, C_2H_5, or other alkyl group) are common products of the oxidation of the alkanes

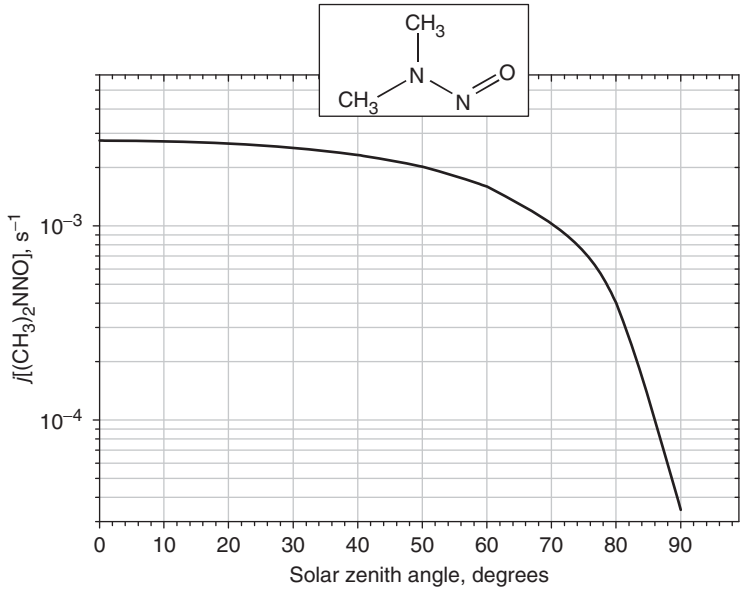

Figure IX-H-21. Photolysis frequencies for $(CH_3)_2NNO$ as a function of solar zenith angle. Calculations were made for clear-sky conditions in the lower troposphere with an overhead ozone column of 350 DU.

within the troposphere, particularly in NO_x-rich, polluted air. They show a structureless absorption with the long-wavelength tail of the absorption overlapping somewhat the solar flux available within the troposphere. See figure IX-I-1 and tabular data in tables IX-I-1 and IX-I-2 (Roberts and Fajer, 1989). The three recent measurements of cross sections for the alkyl nitrates agree well (Roberts and Fajer, 1989; Rattigan et al., 1992; Talukdar et al., 1997a). Measurements of $HONO_2$ cross sections by Burkholder et al. (1993) appear to be the most reliable available at the time of this writing. The absorption cross sections for peroxynitric acid recommended by IUPAC (2008) were derived from an average of the data of Molina and Molina (1981) and Singer et al. (1989). These are accepted here and presented in table IX-I-1. Note in figure IX-I-1 that nitric acid is the weakest absorber of the nitrates shown, while peroxynitric acid is the strongest at long wavelengths that dominate the solar flux within the troposphere. The absorption cross sections of the alkyl nitrates increase regularly as the alkyl nitrate grows in size from CH_3ONO_2 to $(CH_3)_3CONO_2$. The favored pathway for the photolysis of the $HONO_2$ and alkyl nitrates in the 280–350 nm region leads to the formation of NO_2 and an OH or alkoxy radical:

$$HONO_2 + h\nu \rightarrow HO + NO_2$$

$$RONO_2 + h\nu \rightarrow RO + NO_2$$

In this section we will discuss the evidence for the mechanisms of photodissociation of these nitrates.

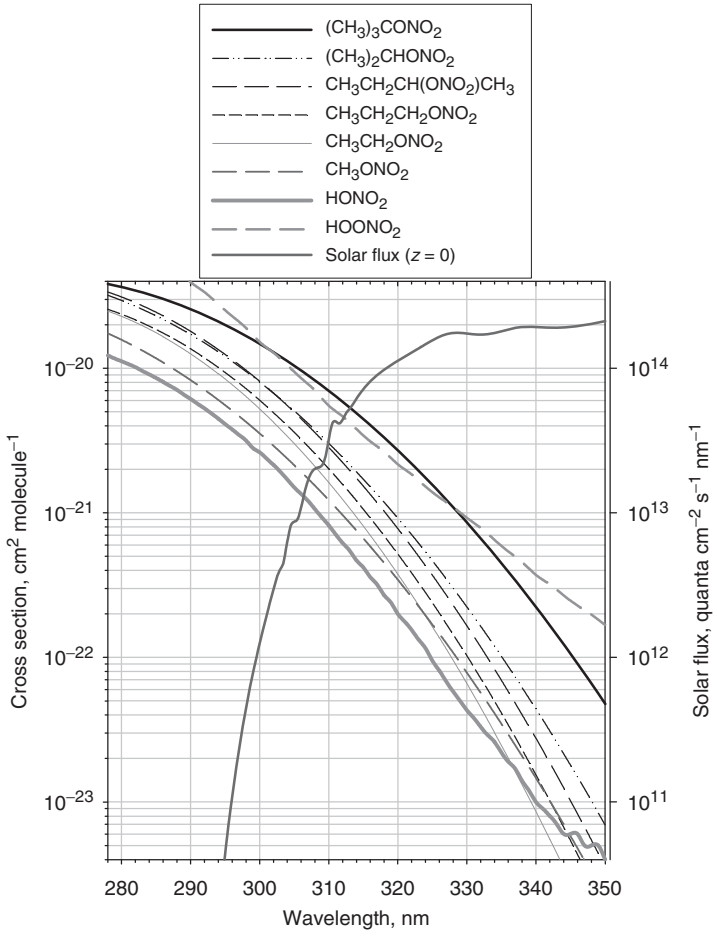

Figure IX-I-1. Cross sections (298 K) for the simple alkyl nitrates as represented by the equations for least-squares fits of the cross section versus wavelength data of Roberts and Fajer (1989). Data for $HONO_2$ are from Burkholder et al. (1993). $HOONO_2$ data are as recommended by IUPAC (2008); actinic flux is shown for an overhead Sun in the lower troposphere (dark-gray curve).

IX-I-1. The Mechanism of Photodecomposition of Nitric Acid

Discussions of the primary processes in the photodecomposition of $HONO_2$ have included the following reactions:

$$HONO_2 + h\nu \rightarrow OH + NO_2 \quad \text{(I)}$$

$$\rightarrow HONO + O(^3P) \quad \text{(II)}$$

$$\rightarrow HONO + O(^1D) \quad \text{(III)}$$

$$\rightarrow H + NO_3 \quad \text{(IV)}$$

Reactions (I) and (II) are energetically feasible at wavelengths over the entire absorption region of $HONO_2$, while processes (III) and (IV) are energy-limited to wavelengths shorter than 242 and 278 nm, respectively.

IX-I-1.1. Absorption Cross Sections for Nitric Acid

The data of Burkholder et al. (1993) presented in figure IX-I-1 and table IX-I-1 are recommended.

IX-I-1.2. Quantum Yields of Photodissociation of Nitric Acid

i) Quantum Yields of Process (I): $HONO_2 + h\nu \rightarrow HO + NO_2$ Using 265 nm radiation in their studies of $HONO_2$ photodecomposition, Bérces and Förgeteg (1970) reported a quantum yield of about 0.1 for the primary process (I). However, these results are discounted, since interpretation of the complex system required estimated rate coefficients for unstudied reactions that have proven to be highly inaccurate. The first well-characterized study of nitric acid photodecomposition was reported by Johnston et al. (1974). Their method of study depended in part upon the measurement of the CO_2 product of the OH radical formed in process (I) by reaction with CO ($OH + CO \rightarrow H + CO_2$) as well as the measurement of the quantum yield of NO_2 formation. The interpretation of such experiments is nontrivial since there are many complications that alter the apparent efficiency of product formation. In one series of experiments, they photolyzed $HONO_2$ and its mixtures with CO and O_2 using bands of radiation at several wavelengths in the 200–315 nm regions. A large number of elementary reactions (42) were necessary to describe the formation of the product NO_2 ($HONO_2$–O_2 mixtures) and CO_2 ($HONO_2$–CO mixtures) in these systems. In the experiments with added CO, the complexity arises in the alternative reactions of the H-atom formed in the OH-monitoring reaction, $OH + CO \rightarrow H + CO_2$. In illustration of the complications, assume $\phi_I = 1$; then through this reaction, CO_2 is formed with a quantum yield of unity. However, the subsequent reactions of the H-atom determines the total quantum yield of CO_2. When the H-atom reacts with NO_2, $H + NO_2 \rightarrow HO + NO$, the OH radical formed can create an additional CO_2 molecule and lead to a quantum yield of 2. If it reacts with $HONO_2$ by the pathway, $H + HONO_2 \rightarrow H_2 + NO_3$, then $\Phi_{CO_2} = 1$. If it reacts with $HONO_2$ to form OH, $H + HONO_2 \rightarrow OH + HNO_2$, then a chain reaction can occur and lead to quantum yields of CO_2 that are well above 2. After careful examination of the effects of different compositions of the initial reactant mixture, the photolysis of $HONO_2$−CO mixtures was chosen for more extensive study. In these experiments at 290 nm, Φ_{CO_2} approached a value of 2.0 at high CO pressures (∼400 Torr), the value expected if $\phi_I = 1.0$ for the chosen experimental conditions.

In other experiments, measurements were made of Φ_{NO_2} formation. In this case, the loss of the initial NO_2 product by photolysis and reaction with OH and O_3 formed when O_2 is added can alter the apparent quantum yield. In the experiments of Johnston et al., conditions were determined experimentally that minimized these problems. For those chosen, 400 Torr of O_2 and 300 Torr of CO added to $HONO_2$ at 5, 15, or 30 Torr) one expects $\phi_I = \Phi_{NO_2}$ at small conversions of $HONO_2$. The quantum yield of NO_2

Table IX-I-1. Cross sections (σ, cm^2 molecule^{-1}) for HO_2NO_2 (IUPAC, 2008), $HONO_2$(Burkholder et al., 1993) and some simple alkyl nitrates (298–301 K), CH_3ONO_2, $C_2H_5ONO_2$, $CH_3CH_2CH_2ONO_2$, $CH_3CH(ONO_2)CH_3$, and $CH_3CH_2CH_2CH_2ONO_2$ (alkyl nitrate data from Roberts and Fajer, 1989)

Cross Section Data ($10^{20} \times \sigma$) for $RONO_2$ where the Appropriate R Heads the Column:															
λ, nm	OH	H	CH_3	C_2H_5	1-C_3H_7	2-C_3H_7	1-C_4H_9	λ, nm	OH	H	CH_3	C_2H_5	1-C_3H_7	2-C_3H_7	1-C_4H_9
278	11.9	1.23	1.75	2.49	2.56	3.20	2.64	317	0.29	0.032	0.052	0.060	0.081	0.135	0.070
279	10.1	1.17	1.66	2.39	2.47	3.08	2.53	318	0.27	0.027	0.045	0.052	0.070	0.119	0.061
280	9.29	1.12	1.58	2.29	2.37	2.95	2.43	319	0.24	0.024	0.040	0.044	0.060	0.105	0.052
281	8.63	1.07	1.49	2.18	2.27	2.82	2.32	320	0.22	0.020	0.035	0.038	0.052	0.092	0.045
282	8.11	1.02	1.41	2.08	2.17	2.69	2.21	321	0.20	0.0177	0.030	0.032	0.045	0.081	0.038
283	7.54	0.960	1.33	1.97	2.07	2.56	2.10	322	0.18	0.0155	0.026	0.027	0.038	0.071	0.033
284	6.93	0.909	1.25	1.87	1.96	2.44	1.99	323	0.17	0.0133	0.023	0.023	0.033	0.062	0.028
285	6.39	0.858	1.17	1.76	1.86	2.31	1.88	324	0.15	0.0116	0.020	0.019	0.028	0.054	0.023
286	5.86	0.807	1.10	1.66	1.76	2.19	1.77	325	0.14	0.0095	0.017	0.016	0.024	0.047	0.020
287	5.39	0.758	1.03	1.56	1.66	2.07	1.66	326	0.13	0.0081	0.015	0.014	0.020	0.040	0.017
288	4.92	0.712	0.958	1.46	1.56	1.95	1.56	327	0.12	0.0068	0.013	0.011	0.017	0.035	0.014
289	4.41	0.660	0.892	1.36	1.46	1.83	1.45	328	0.11	0.0058	0.011	0.010	0.015	0.030	0.012
290	3.96	0.615	0.829	1.26	1.37	1.72	1.35	329	0.10	0.0050	0.009	0.008	0.012	0.026	0.010
291	3.63	0.570	0.768	1.17	1.27	1.61	1.26	330	0.093	0.0043	0.008	0.007	0.010	0.022	0.008
292	3.37	0.530	0.711	1.08	1.18	1.50	1.17	331	0.086	0.0038	0.007	0.005	0.009	0.019	0.007
293	3.08	0.489	0.656	1.00	1.10	1.40	1.08	332	0.079	0.0033	0.006	0.004	0.007	0.016	0.006
294	2.78	0.450	0.605	0.92	1.02	1.30	0.991	333	0.072	0.0029	0.005	0.004	0.006	0.014	0.005
295	2.53	0.412	0.556	0.84	0.937	1.21	0.911	334	0.065	0.0026	0.004	0.003	0.005	0.012	0.004
296	2.30	0.379	0.510	0.77	0.862	1.12	0.835	335	0.059	0.0022	0.003	0.002	0.004	0.010	0.003
297	2.11	0.347	0.467	0.70	0.791	1.03	0.763	336	0.054	0.0019	0.003	0.002	0.003	0.009	0.003
298	1.91	0.318	0.427	0.64	0.724	0.952	0.695	337	0.050	0.0017	0.002	0.002	0.003	0.007	0.002
299	1.71	0.282	0.389	0.58	0.661	0.876	0.631	338	0.046	0.0014	0.002	0.001	0.002	0.006	0.002
300	1.52	0.263	0.354	0.52	0.602	0.804	0.572	339	0.041	0.0012	0.002	0.001	0.002	0.005	0.001

301	1.39	0.238	0.321	0.47	0.546	0.736	0.517	340	0.037	0.0010	0.001	0.001	0.002	0.004	0.001
302	1.28	0.215	0.291	0.42	0.494	0.673	0.466	341	0.034	0.0009	0.001	0.001	0.001	0.004	0.001
303	1.16	0.192	0.263	0.38	0.446	0.614	0.419	342	0.032	0.0008	0.001	0.001	0.001	0.003	0.001
304	1.05	0.170	0.238	0.34	0.402	0.559	0.375	343	0.029	0.0007	0.001	0	0.001	0.003	0.001
305	0.95	0.150	0.214	0.30	0.361	0.507	0.335	344	0.027	0.0006	0.001	0	0.001	0.002	0
306	0.85	0.135	0.192	0.27	0.323	0.460	0.299	345	0.024	0.0006	0.001	0	0.001	0.002	0
307	0.78	0.121	0.172	0.24	0.289	0.415	0.266	346	0.023	0.0006	0	0	0	0.001	0
308	0.70	0.106	0.154	0.21	0.257	0.375	0.235	347	0.021	0.0005	0	0	0	0.001	0
309	0.62	0.093	0.138	0.19	0.229	0.337	0.208	348	0.020	0.0005	0	0	0	0.001	0
310	0.55	0.082	0.123	0.16	0.203	0.303	0.183	349	0.018	0.0005	0	0	0	0.001	0
311	0.50	0.071	0.109	0.14	0.179	0.272	0.161	350	0.017	0.0004	0	0	0	0.001	0
312	0.47	0.062	0.097	0.12	0.158	0.243	0.141	351	0.015						
313	0.42	0.055	0.086	0.11	0.139	0.217	0.124	352	0.014						
314	0.38	0.047	0.076	0.094	0.122	0.193	0.108	353	0.013						
315	0.34	0.042	0.067	0.081	0.106	0.172	0.094	354	0.011						
316	0.31	0.036	0.059	0.070	0.093	0.152	0.081	355	0.010						

Table IX-I-2. Cross sections (σ, cm^2 $molecule^{-1}$) for some alkyl nitrates (298–301 K): 2-$C_4H_9ONO_2$, $(CH_3)_3CONO_2$, 2-$C_5H_{11}ONO_2$, 3-$C_5H_{11}ONO_2$, *cyclo*-$C_5H_9ONO_2$ (data from Roberts and Fajer, 1989)

Cross Section Data ($10^{20} \times \sigma$) for $RONO_2$ where the Appropriate R Heads the Column:											
λ, nm	2-C_4H_9	*t*-C_4H_9	2-C_5H_{11}	3-C_5H_{11}	*c*-C_5H_9	λ, nm	2-C_4H_9	*t*-C_4H_9	2-C_5H_{11}	3-C_5H_{11}	*c*-C_5H_9
278	3.37	3.83	3.44	3.64	2.66	314	0.175	0.490	0.171	0.172	0.062
279	3.24	3.75	3.31	3.52	2.56	315	0.154	0.446	0.151	0.150	0.052
280	3.11	3.66	3.17	3.39	2.46	316	0.135	0.405	0.132	0.130	0.044
281	2.98	3.56	3.03	3.26	2.35	317	0.118	0.367	0.116	0.112	0.036
282	2.85	3.46	2.89	3.12	2.23	318	0.103	0.332	0.101	0.097	0.030
283	2.71	3.36	2.75	2.98	2.11	319	0.090	0.300	0.088	0.084	0.025
284	2.58	3.25	2.61	2.84	2.00	320	0.078	0.270	0.076	0.072	0.021
285	2.44	3.14	2.47	2.70	1.88	321	0.067	0.243	0.066	0.061	0.017
286	2.31	3.03	2.33	2.56	1.76	322	0.058	0.218	0.057	0.052	0.014
287	2.18	2.92	2.19	2.41	1.64	323	0.050	0.196	0.049	0.045	0.011
288	2.05	2.80	2.06	2.27	1.53	324	0.043	0.175	0.042	0.038	0.009
289	1.92	2.69	1.93	2.13	1.42	325	0.037	0.156	0.036	0.032	0.007
290	1.80	2.57	1.81	2.00	1.31	326	0.032	0.139	0.031	0.027	0.006
291	1.68	2.45	1.68	1.86	1.20	327	0.027	0.124	0.026	0.023	0.005
292	1.57	2.34	1.57	1.73	1.10	328	0.023	0.110	0.023	0.019	0.004
293	1.46	2.22	1.45	1.61	1.01	329	0.020	0.097	0.019	0.016	0.003
294	1.35	2.11	1.35	1.49	0.915	330	0.017	0.086	0.016	0.013	0.002
295	1.25	2.00	1.24	1.37	0.829	331	0.014	0.076	0.014	0.011	0.002
296	1.15	1.89	1.14	1.26	0.748	332	0.012	0.067	0.012	0.009	0.002
297	1.06	1.78	1.05	1.16	0.672	333	0.010	0.059	0.010	0.008	0.001

298	0.972	1.68	0.964	1.06	0.602	334	0.008	0.051	0.008	0.006	0.001
299	0.889	1.58	0.881	0.967	0.538	335	0.007	0.045	0.007	0.005	0.001
300	0.812	1.48	0.804	0.880	0.478	336	0.006	0.039	0.006	0.004	0.001
301	0.740	1.39	0.731	0.798	0.423	337	0.005	0.034	0.005	0.003	
302	0.672	1.29	0.664	0.721	0.374	338	0.004	0.030	0.004	0.003	
303	0.609	1.21	0.601	0.650	0.328	339	0.003	0.026	0.003	0.002	
304	0.550	1.12	0.543	0.584	0.288	340	0.003	0.022	0.003	0.002	
305	0.496	1.04	0.489	0.524	0.251	341	0.002	0.019	0.002	0.001	
306	0.446	0.966	0.440	0.468	0.218	342	0.002	0.017	0.002	0.001	
307	0.401	0.893	0.394	0.417	0.189	343	0.002	0.014	0.002	0.001	
308	0.358	0.825	0.353	0.371	0.163	344	0.001	0.012	0.001	0.001	
309	0.320	0.760	0.314	0.329	0.140	345	0.001	0.011	0.001	0.001	
310	0.285	0.699	0.280	0.290	0.120	346	0.001	0.009	0.001		
311	0.253	0.641	0.248	0.256	0.102	347	0.001	0.008	0.001		
312	0.224	0.587	0.220	0.225	0.087	348	0.001	0.007	0.001		
313	0.198	0.537	0.194	0.197	0.074	349		0.006			

formation for photolyses at several bands of wavelengths within the $n \rightarrow \pi^*$ band was found to be unity. The authors found it difficult to assess the error limits in their measurements in this complex system. In figure IX-I-2, we have plotted the Johnston et al. (1974) data as the open circles and set the error bars to be ±15% based on our assessment of possible uncertainties.

Jolly et al. (1986b) measured the quantum yield of OH radical in laser photolyses of $HONO_2$ at 222 nm by following the OH product though its absorption at 308.3 nm. They reported $\Phi_{OH} = \phi_I = 0.89^{+15}_{-7}$ (open square in figure IX-I-2) and concluded that the results were consistent with the previous conclusions of Johnston et al. (1974) that $\phi_I \approx 1.0$.

The most comprehensive study of nitric acid photodecomposition to date was reported by Turnipseed et al. (1992). These workers determined the quantum yields for OH, $O(^3P)$, $O(^1D)$ and $H(^2S)$ atoms in photolyses at 248, 222, and 193 nm. They reported values of $\Phi_{OH}(= \phi_I)$ of 0.95 ± 0.09 at 248 nm; 0.90 ± 0.11 at 222 nm; and 0.33 ± 0.06 at 193 nm (shown as closed triangles in figure IX-I-2).

Schiffman et al. (1993) also determined the quantum yields of OH production in laser photolyses at 193 and 249 nm by probing the OH product with high resolution, tunable IR laser light. They concluded that $\Phi_{OH} = \phi_I = 0.75 \pm 0.10$ at 249 nm and 0.47 ± 0.06 at 193 nm (filled circles in figure IX-I-2). They reasoned that the occurrence of processes in addition to process (I) must account for these results. Their results at 193 nm agree well with the measurements of Turnipseed et al. (1992) but those at

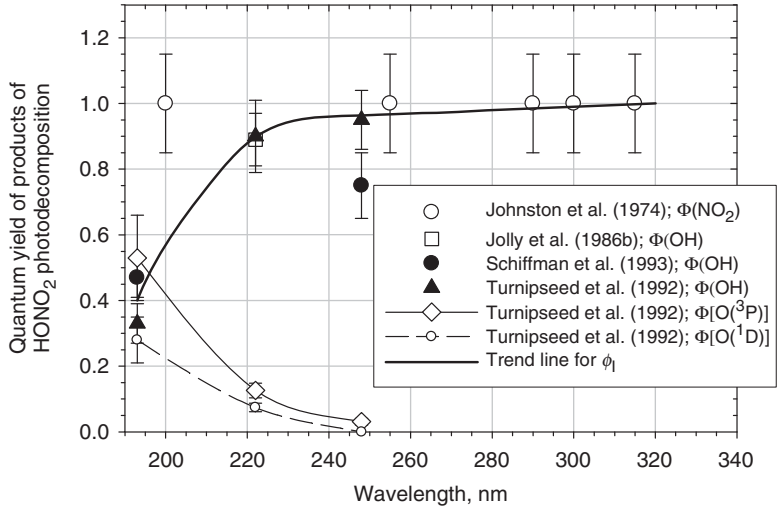

Figure IX-I-2. Quantum yields of the primary processes in $HONO_2$ photodecomposition. The total quantum yields of photodecomposition, given by the Φ_{NO_2} estimates of Johnston et al. are near unity over the entire absorption region. The primary process: $HONO_2 + h\nu \rightarrow OH + NO_2$ (I) is seen to dominate at wavelengths within the lower troposphere. Process (II), measured as $\Phi_{O(3P)}$ and process (III), measured as $\Phi_{O(1D)}$, become increasingly important at the shorter wavelengths of absorbed light, but the total quantum yield of photodecomposition remains near unity.

248 nm fall somewhat below those of Turnipseed et al., just outside the range of the estimated error limits.

Myers et al. (1997) studied the translational energies of the products formed in process (I) in $HONO_2$ photolyses at 193 nm. The results revealed two distinct pathways for the process (I): one produced stable NO_2 fragments in the 1^2B_2 electronic state while the second formed NO_2 fragments that underwent secondary dissociation to NO and O. Li et al. (2001) also studied the photodissociation dynamics of nitric acid photodecomposition at 193 nm and probed the OH formation in process (I) and $O(^3P)$ generation in the HONO forming channel (II). A bimodal distribution of the translational and rotational states in the OH and NO_2 fragments was observed that was consistent with the formation of two different electronic states of NO_2 (X^2A_1 and 1^2B_2) in process (I).

ii) Quantum yields of Process (II): $HONO_2 + h\nu \rightarrow HONO + O(^3P)$ Measurements of Margitan and Watson (1982) showed that $\Phi_{O(3P)} = \phi_{II} \approx 0.03$ at 266 nm. Turnipseed et al. (1992) reported similar results: $O(^3P)$ atom formation in primary process (II) appeared in photolyses at wavelength 248 nm with $\phi_{II} = 0.031 \pm 0.010$ (filled diamond in figure IX-I-2). This process (II) increased in importance at the shorter wavelengths, $\phi_{II} = 0.12$ and 0.49 at 222 and 193 nm, respectively.

In experiments with excitation at 193 nm, Myers et al. (1997) measured the branching ratio $\phi_I/(\phi_{II} + \phi_{III}) = 0.50 \pm 0.05$ with $\phi_{III} > \phi_{II}$, results somewhat different from those of Turnipseed et al. (1992). Li et al. (2001) observed $O(^3P)$ fragments of high translational energy from $HONO_2$ photolysis at 193 nm and assigned the product HONO in this reaction to be in the X^1A' state. They estimated that about one-third of the HONO molecules formed in (II) at 193 nm are unstable and decompose to HO and NO.

iii) Quantum Yields of Process (III): $HONO_2 + h\nu \rightarrow HONO + O(^1D)$ Turnipseed et al. (1992) observed the formation of $O(^1D)$ atoms in the experiments at the shorter wavelengths with $\phi_{III} = 0.08 \pm 0.01$ at 222 nm and 0.32 ± 0.05 at 193 nm (small open circle in figure IX-I-2).

iv) Quantum Yields of Process (IV): $HONO_2 + h\nu \rightarrow H + NO_3$ Process (IV), forming H-atoms, was undetectable in the experiments of Margitan and Watson (1986) with $\Phi_H < 0.002$ at 266 nm. Also Turnipseed et al. reported $\phi_{IV} < 0.002$ at 248 nm, < 0.01 at 222 nm, and < 0.012 at 193 nm. Process (IV) is unimportant for $HONO_2$ photodecomposition at all $\lambda > 193$ nm.

v) The Total Quantum Yield of $HONO_2$ Photodecomposition As the data in figure IX-H-2 show, the quantum yield of process (I) falls at the shorter wavelengths, but those of processes (II) and (III) increase such that the total quantum yield of photodecomposition remains near unity. In view of the available information, we will assume that the total quantum yield of photodecomposition of nitric acid is near unity over its entire absorption region, and that process (I) alone describes the photolysis at wavelengths available within the lower troposphere.

IX-I-1.3. Photolysis Frequencies for Photodecomposition of Nitric Acid within the Lower Troposphere

Using the cross sections for $HONO_2$ given in table IX-I-1 together with the assumption that $\phi_I = 1.0$ for all $\lambda < 340$ nm and the appropriate solar flux data, we have calculated the photolysis frequencies for $HONO_2$ as a function of solar zenith angle for a cloudless day in the lower troposphere with an overhead ozone column of 350 DU. These data are given in figure IX-I-3 where they can be compared with the *j*-values for the alkyl nitrates. The measurements represent possible maximum values, since similar experiments in the far-wavelength tail of $HONO_2$ absorption have never been made, and possible quenching of the excited state at the long wavelengths remains a possibility.

The contribution of sunlight absorption within $HONO_2$ vibrational overtone bands at long wavelengths (755, 845, 877, 883, 942, 983 nm) could conceivably enhance somewhat the estimated *j*-values of $HONO_2$ within the atmosphere for certain atmospheric conditions (e.g., low solar zenith angle); see Donaldson et al. (1997, 1998); Brown et al. (2000); Zhang et al. (2000). The extent of the contribution to $j(HONO_2)$ from such absorptions is expected to be small, but, perhaps, not completely negligible.

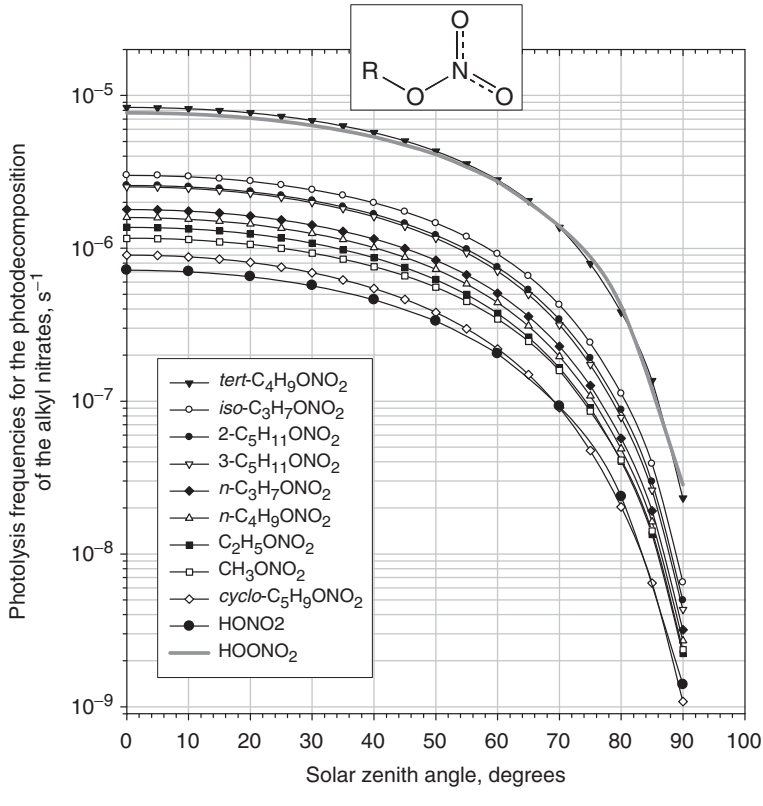

Figure IX-I-3. Comparison of photolysis frequencies for $HONO_2$, $HOONO_2$, and several organic nitrates versus solar zenith angle; calculated for a cloud-free lower troposphere with an overhead ozone column of 350 DU.

IX-I-2. The Mechanism of Peroxynitric Acid ($HOONO_2$) Photodissociation within the Lower Troposphere

The absorption cross sections of peroxynitric acid shown in figure IX-I-1 and listed in table IX-I-1 are those recommended by IUPAC (2008). Measurements of the relative absorption coefficients of $HOONO_2$ reported by Knight et al. (2002) confirm the data of Molina and Molina (1981) in the long-wavelength region. Of the various nitrates shown in the figure, peroxynitric acid is the strongest absorber of tropospheric sunlight. Its photodecomposition has been studied only at 248 nm. At this wavelength two primary photodissociation pathways exist:

$$HOONO_2 + h\nu \rightarrow HO_2 + NO_2 \quad \text{(I)}$$

$$\rightarrow OH + NO_3 \quad \text{(II)}$$

Both primary process (I) and (II) were observed by Mac Leod et al. (1988) in their experiments at 248 nm. They detected OH radicals using LIF and referenced the quantum yield of OH using H_2O_2 photolysis. Impurities in the samples used complicated the interpretation, but the authors concluded that for photodissociation at 248, process (I) was somewhat favored over process (II): $\phi_I \cong 0.66$; $\phi_{II} \cong 0.34 \pm 0.16$. In experiments at the same wavelength (248 nm), Roehl et al. (2001) used LIF to detect NO_2 at 511 nm, and $HONO_2$ photolysis was used as the reference taking $\Phi_{NO_2} = 1$. They determined $\Phi_{NO_2} = \phi_I \cong 0.56 \pm 0.17$, in agreement with the estimate of Mac Leod et al. within the estimated uncertainties. The photodissociation processes (I) and (II) require a minimum of 100 and 164 kJ mol^{-1}, with threshold wavelengths of 1191 and 731 nm, respectively. It seems likely that process (I) will be favored significantly more at the longer wavelengths available in the troposphere than the experiments at 248 nm show.

In the calculation of photolysis frequencies for $HOONO_2$ within the lower troposphere, and in the absence of quantum yield measurements at the longer wavelengths, we have assumed that the quantum yield of photodecomposition is unity over the entire absorption region. Although the continuous nature of the absorption of $HOONO_2$ is consistent with this interpretation, the estimates that we have made must be considered as very approximate because of this assumption. The data as a function of solar zenith angle are shown in figure IX-I-3. It can be seen that *j*-values for HO_2NO_2 are very similar to those for *tert*-$C_4H_9ONO_2$. For an overhead Sun, the lifetime for photodissociation of peroxynitric acid is estimated to be about 1.5 days.

IX-I-3. The Mechanism of Alkyl Nitrate Photodecomposition within the Lower Troposphere

The major photodecomposition pathway for the alkyl nitrates is process (I):

$$RONO_2 + h\nu \rightarrow RO + NO_2 \quad \text{(I)}$$

Some other photodissociation pathways have been suggested (Calvert et al., 2008) in which the alkyl nitrates ($C_nH_{2n+1}ONO_2$) form either: 1) HONO and an aldehyde

or a ketone ($C_nH_{2n}O$); or 2) an alkyl nitrite (RONO) and an O-atom. In photolysis at 193 nm, Yang et al. (1993) found that ~70% of the photodecomposition involves fission of the weak CH_3O—NO_2 bond, and the fragment pairs showed a bimodal translational energy distribution. The fast fragment pairs had an average translational energy of 171 kJ mol^{-1}, while the slow component had 79 kJ mol^{-1}. A significant fraction of the NO_2 fragments of the slow component were subject to unimolecular decay to NO and O(^{3}P). They observed an additional primary decay route that led to the formation of methyl nitrite and O(^{1}D). Photodissociation of methyl nitrate at the longer wavelength of 248 nm follows process (I) exclusively with translational energy of 71 kJ mol^{-1} (Yang et al., 1993) in the products.

Talukdar et al. (1997a) also studied CH_3ONO_2 photolysis at 248 nm and confirmed that the alternative pathways to reaction (1) are relatively unimportant. They found $\phi_I = 0.9 \pm 0.2$ (O_2 present as a radical scavenger) and $\phi_I = 1.3 \pm 0.3$ (NO present as the radical scavenger). Direct measurements of NO_2 product formation from $RONO_2$ in sunlight (R = C_2H_5, $CH_3CH_2CH_2$, $CH_3CH_2CH_2CH_2$, and $CH_3CHCH_2CH_3$) were made by Luke and Dickerson (1988) and Luke et al. (1989). Using the well accepted cross sections of Roberts and Fajer (1989), the calculated photolysis rates were consistent with $\phi_I = 1.0 \pm 0.5$. Zhu and Ding (1997) studied $C_2H_5ONO_2$ photolysis at 308 nm and found $\phi_I = 1.0 \pm 0.1$. The limited available evidence favors a value of unity for process (I) for wavelengths of sunlight available within the troposphere (e.g., see Roberts, 1990; Roberts and Fajer, 1989; Atkinson et al., 2004). The structureless continuum shown in the absorption of the alkyl nitrates is consistent with this view, and we recommend that the value of $\phi_I = 1.0$ be assumed for all the alkyl nitrates for the wavelength region of sunlight available within the troposphere.

IX-I-3.1. Absorption Cross Sections for the Simple Alkyl Nitrates

The cross section data of Roberts and Fajer (1989) for a temperature of 298 K for some simple alkyl nitrates are given in figures IX-I-1, and in tabular form in tables IX-I-1 [CH_3ONO_2, $C_2H_5ONO_2$, $CH_3CH_2CH_2ONO_2$, $CH_3CH(ONO_2)CH_3$, and $CH_3CH_2CH_2CH_2ONO_2$] and IX-I-2 [$CH_3CH(ONO_2)CH_2CH_3$, $(CH_3)_3CONO_2$, 2-$C_5H_{11}ONO_2$, 3-$C_5H_{11}ONO_2$, and *cyclo*-$C_5H_9ONO_2$]. These data are in good agreement with other recent σ measurements of the alkyl nitrates (Rattigan et al., 1992; Talukdar et al., 1997a) and are recommended for use in modeling tropospheric chemistry.

IX-I-3.2. Photolysis Frequencies for the Photodecomposition of the Simple Alkyl Nitrates in the Lower Troposphere

Calvert et al. (2008) used the cross section data of Roberts and Fajer (1989) given in tables IX-I-1 and IX-I-2, an assumed value of unity for ϕ_I, and appropriate solar flux data for clear-sky conditions to calculate the *j*-values for the simple alkyl nitrates as a function of solar zenith angle at 0.5 km elevation, 298 K and an overhead ozone column of 350 DU. These data are shown in figure IX-I-3. The photolysis frequencies as a function of solar zenith angle are shown in figure IX-I-4a for CH_3ONO_2 as calculated

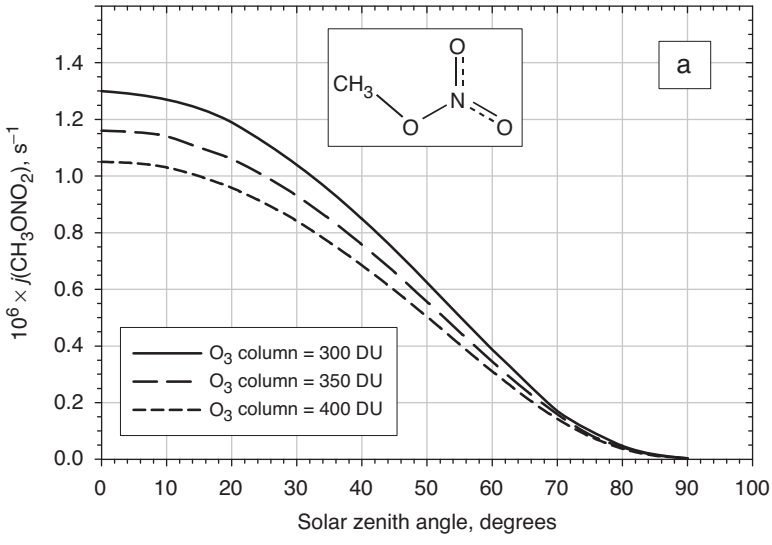

Figure IX-I-4a. Calculated photolysis frequencies for CH_3ONO_2 as a function of solar zenith angle and overhead ozone column. The cross sections of Roberts and Fajer (1989) and assumed quantum yields of photodissociation of unity at all absorbed wavelengths of sunlight were used in the calculation; figure from Calvert et al. (2008).

by Calvert et al. (2008) for a cloudless day in the lower troposphere at several different overhead ozone columns (300–400 Dobson units). The sensitivity of the *j*-values to overhead ozone column is seen best in figure IX-I-4b. It is similar to that observed for CH_3I (figure VII-I-4a in Calvert et al., 2008) which absorbs light in about the same region. About a 20% decrease in the *j*-value results from the increase in overhead ozone of 100 Dobson units.

The *j*-values measured directly can be compared with those calculated in this study (values in parentheses): CH_3ONO_2: surface, solar zenith angle (Z) = 45°(Taylor et al., 1980), $j = 2.2 \times 10^{-6}\,s^{-1}(7.4 \times 10^{-7})$. For $C_2H_5ONO_2$: surface, $Z = 0°$ (Luke and Dickerson, 1988), $j = 1.1 \times 10^{-6}\,s^{-1}(1.4 \times 10^{-6})$; surface, $Z = 60°$ (Luke and Dickerson, 1988), $j = 0.45 \times 10^{-6}\,s^{-1}$ (0.38×10^{-6}); surface, O_3 column of 296 Dobson units, temperature 298 K, $Z = 0°$ (Luke et al., 1989), $j = 1.45 \times 10^{-6}\,s^{-1}$ (1.37×10^{-6}). For $CH_3CH_2CH_2ONO_2$: the same conditions, $Z = 0°$ (Luke et al., 1989), $j = 1.33 \times 10^{-6}\,s^{-1}(1.79 \times 10^{-6})$. For $CH_3CH(ONO_2)CH_2CH_3$: the same conditions, $Z = 0°$ (Luke et al., 1989), $j = 2.54 \times 10^{-6}\,s^{-1}$ (2.60×10^{-6}). For most of the compounds studied, the degree of agreement between the measured *j*-values and those calculated is reasonable considering the differences in the actual and assumed conditions that must exist (extent of clouds, altitude, and ozone columns), and it is consistent with the assumption of a quantum yield of photodissociation of unity for these alkyl nitrates. However, the data for CH_3ONO_2 are an exception where the measured and calculated values of *j* differ by a factor of 3. Further measurements of $j_{CH_3ONO_2}$ should be made to test our conclusion that all alkyl nitrates have quantum yields near unity.

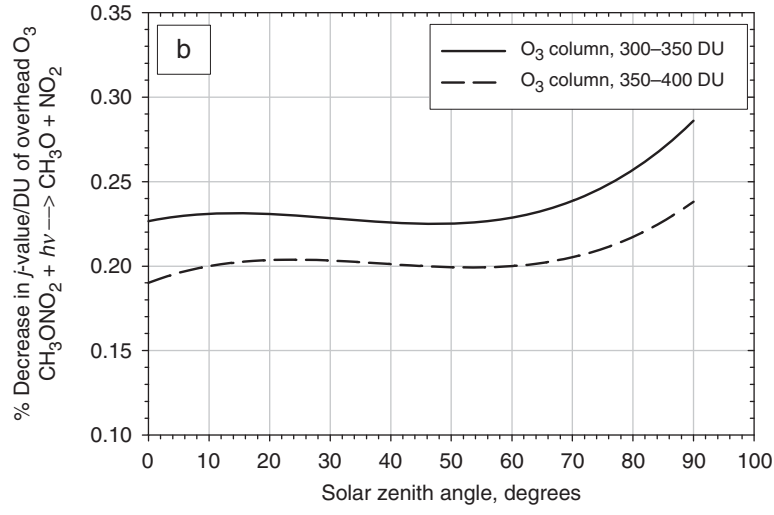

Figure IX-I-4b. Percentage decrease in the *j*-values of CH_3ONO_2 expected per Dobson unit increase in the overhead ozone column. Data were calculated for a cloudless day within the lower troposphere; figure from Calvert et al. (2008).

There is significant temperature dependence to the cross sections of CH_3ONO_2 that can be seen in figure IX-I-4c. Of course, this can affect the lifetime of the methyl nitrate present in the various regions of the atmosphere. To illustrate the magnitude of the effects that both changes in temperature (cross section) and actinic flux have in this case, we have calculated *j*-values from 0 to 20 km altitude. The cross sections for CH_3ONO_2 have been reported only for $\lambda > 240$ nm, so valid *j*-calculations for altitudes above 20 km could not be made. As one can see from figure IX-I-4d, the changes affect significantly the *j*-values that are applicable to the conditions present in the upper troposphere.

IX-I-4. Mechanism of Photodecomposition of Some Bifunctional Organic Nitrates

Signicant new information related to the photodecomposition of some bifunctional alkyl nitrates has been reported. In addition to absorption spectra of many alkyl nitrates, Roberts and Fajer (1989) also measured the spectra for the bifunctional 2-nitrooxyethanol. Barnes et al. (1993) studied the absorption spectra and photolysis products of several dinitrates: 1,2-propandiol dinitrate, 1,2-butandiol dinitrate, 2,3-butandiol dinitrate, 1,4-dinitrooxy-2-butene, 3,4-dinitrooxy-1-butene, as well as several bifunctional nitrates: α-nitrooxyacetone, 1-nitrooxy-2-butanone, and 3-nitrooxy-2-butanone. Wängberg et al. (1996) reported on the the atmospheric chemistry of the bifunctional cycloalkyl nitrates: 2-hydroxy-cyclopentyl-1-nitrate, 2-oxo-cyclohexyl-1-nitrate, and *trans*-1-methyl-*cyclo*-1,2-dinitrate. In this section, we will review the findings related to the tropospheric photodecomposition of these multifunctional nitrates.

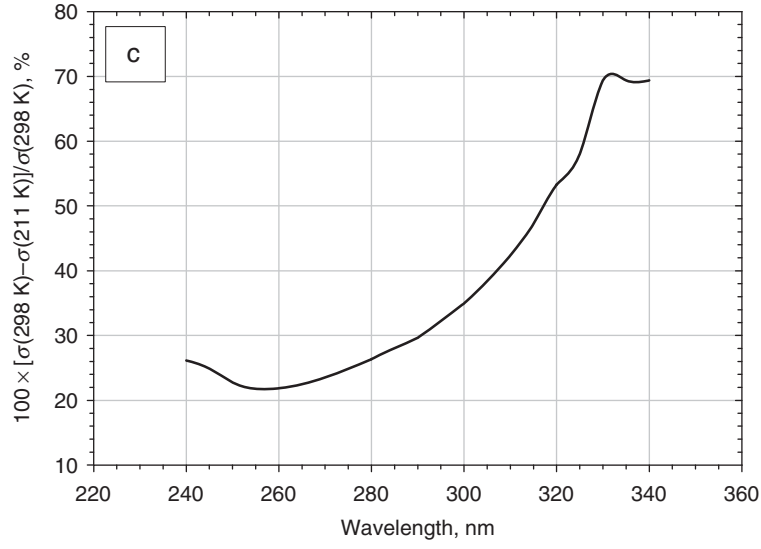

Figure IX-I-4c. Plot of the percentage difference in the absorption cross sections of CH_3ONO_2 at 298 and 211 K as a function of wavelength plotted from data of Talukdar et al. (1997a); figure from Calvert et al. (2008).

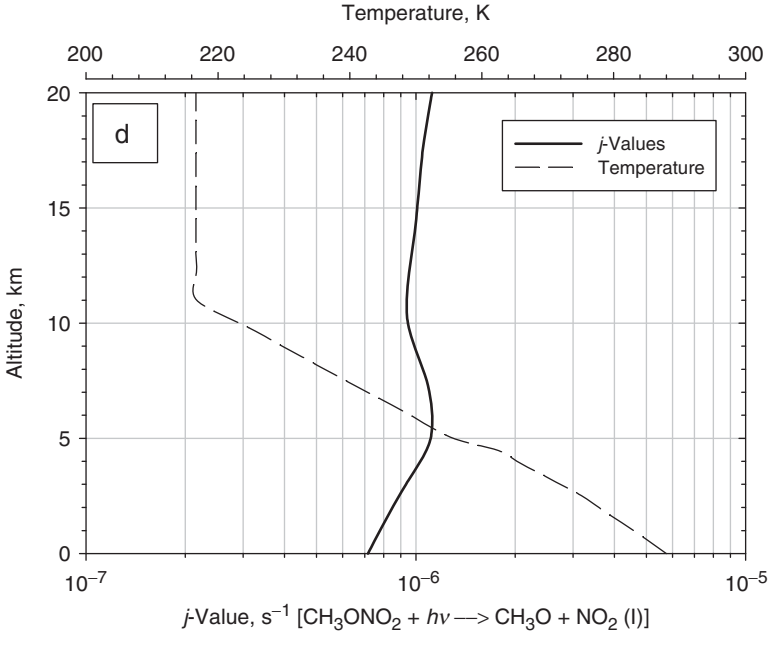

Figure IX-I-4d. Plot of the estimated photolysis frequency for CH_3ONO_2 as a function of altitude for a cloudless day with solar zenith angle = 45° and vertical ozone column = 350 DU. Shown as well is the temperature variation with altitude that was employed in the calculations (U.S. Standard Atmosphere, 1976); figure from Calvert et al. (2008).

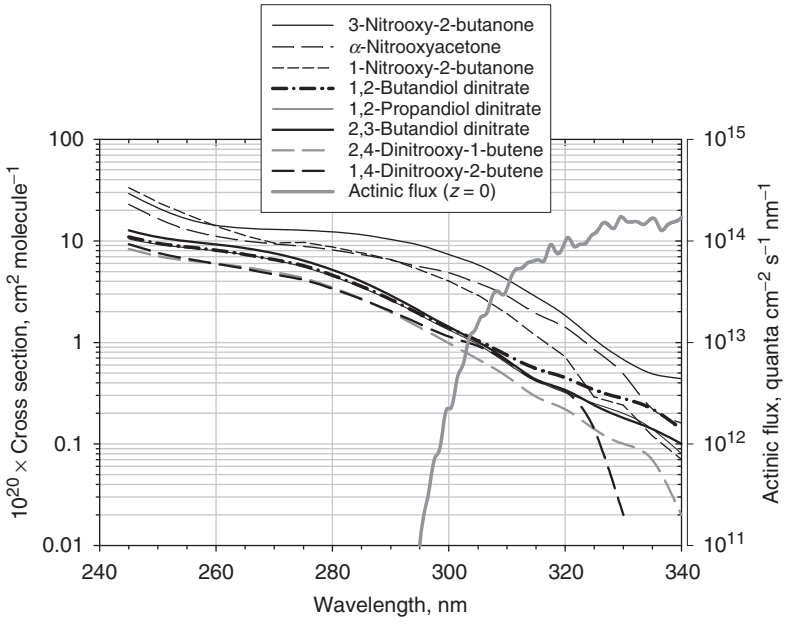

Figure IX-I-5. Comparison of the absorption cross sections of a number of multifunctional nitrates reported by Barnes et al. (1993); the wavelength distribution of the actinic flux in the lower troposphere for an overhead Sun is shown by the gray curve.

IX-I-4.1. The Absorption Spectra of Bifunction Organic Nitrates

The absorption spectra of a number of multifunctional organic nitrates reported by Barnes et al. (1993) are compared in figure IX-I-5. The long-wavelength tail of the nonstructured, continuous absorption of these compounds overlaps the wavelength region of sunlight available within the troposphere. The tabular listing of the cross sections for all of the multifunctional nitrates considered in this section is given in table IX-I-3.

Adding a second —ONO_2 group to an existing simple alkyl nitrate enhances the absorption as seen in figure IX-I-6; here the absorption spectrum of 2,3-butandiol dinitrate [$CH_3CH(ONO_2)CH(ONO_2)CH_3$] is compared with that of the structurally related *sec*-butyl nitrate [$CH_3CH(ONO_2)CH_2CH_3$]. At a given wavelength, the cross sections of the dinitrate are larger than those of the mononitrates, roughly twice the magnitude that one might expect if the light absorption by the nitrate groups in the dinitrate is uncoupled. The gray curve in the figure, a plot of twice the cross section of the mononitrate, follows that of the dinitrate reasonably well over the wavelength region 260 to 310 nm. This absorption enhancement is also seen in figure IX-I-7 for 1,2-butandiol dinitrate, ($CH_2(ONO_2)CH(ONO_2)CH_2CH_3$); at a given wavelength the absorption is seen to be greater than those of the two structurally related mononitrates, *n*-butyl nitrate ($CH_3CH_2CH_2CH_2ONO_2$) and *sec*-butyl nitrate [$CH_3CH(ONO_2)CH_2CH_3$]. The sum of the cross sections of the two mononitrates, shown as the gray curve in the figure, is of a magnitude qualitatively similar to that of the dinitrate. Similarly, absorption

Table IX-I-2. Cross sections (σ, cm^2 molecule^{-1}) for a series of difunctional nitrates: A = 1,2-propandiol dinitrate; B = 1,2-butandiol dinitrate; C = 2,3-butandiol dinitrate; D = 3,4-dinitrooxy-1-butene; E = 1,4-dinitrooxy-2-butene; F = α-nitrooxyacetone; G = 1-nitrooxy-2-butanone; H = 3-nitrooxy-2-butanone (Barnes et al., 1993); I = 2-oxo-cyclohexyl-1-nitrate; J = *trans*-1-methyl-cyclohexyl-1,2-dinitrate (Wängberg et al., 1996); K = 2-nitrooxyethanol (Roberts and Fajer, 1989)

λ, nm	$\sigma(A) \times 10^{20}$	$\sigma(B) \times 10^{20}$	$\sigma(C) \times 10^{20}$	$\sigma(D) \times 10^{20}$	$\sigma(E) \times 10^{20}$	$\sigma(F) \times 10^{20}$	$\sigma(G) \times 10^{20}$	$\sigma(H) \times 10^{20}$	$\sigma(I) \times 10^{20}$	$\sigma(J) \times 10^{20}$	$\sigma(K) \times 10^{20}$
245	10.46	10.90	12.69	8.31	9.28	22.90	33.60	29.34			
250	9.24	9.46	10.88	7.05	7.63	16.58	24.00	21.14			
255	8.54	8.69	9.89	6.39	6.63	12.90	18.10	16.44			
260	7.98	8.07	9.23	5.97	5.92	11.06	14.00	14.24		12.0	1.84
265	7.30	7.34	8.47	5.49	5.29	9.95	11.20	13.32		11.0	1.93
270	6.49	6.53	7.55	4.89	4.66	9.32	9.48	12.98	9.72	9.81	1.80
275	5.54	5.68	6.40	4.29	4.13	8.82	9.68	12.73	8.11	8.61	1.49
280	4.49	4.59	5.19	3.46	3.38	8.13	8.69	12.29	7.16	7.41	1.09
285	3.47	3.56	3.98	2.68	2.66	7.30	7.59	11.55	6.49	5.85	0.72
290	2.60	2.65	2.91	1.98	2.03	6.46	6.55	10.36	5.80	4.54	0.42
295	1.87	1.90	2.04	1.40	1.52	5.56	5.19	9.11	5.07	3.20	0.21
300	1.32	1.39	1.42	0.98	1.14	4.86	4.02	7.36	4.19	2.05	0.098
305	0.96	1.04	1.01	0.68	0.92	3.82	2.91	5.85	3.38	1.13	0.040
310	0.62	0.75	0.67	0.46	0.65	2.87	1.92	4.18	2.33	0.86	0.015
315	0.42	0.55	0.43	0.29	0.42	1.92	1.16	2.82	1.62	0.41	0.0047
320	0.32	0.45	0.34	0.22	0.33	1.41	0.72	1.85	0.85	0.15	0.0013
325	0.25	0.34	0.24	0.14	0.14	0.85	0.29	1.07	0.37	0	0.0003
330	0.20	0.28	0.18	0.10	0.02	0.49	0.24	0.68	0.08		
335	0.14	0.22	0.14	0.07		0.22	0.12	0.49	0		
340	0.08	0.14	0.10	0.02		0.16	0.07	0.44			

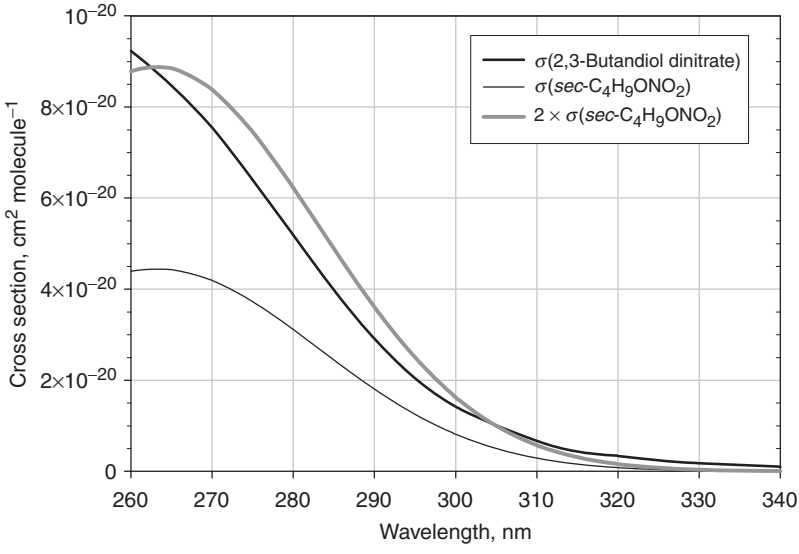

Figure IX-I-6. Comparison of the absorption cross sections for 2,3-butandiol dinitrate with that of *sec*-$C_4H_9ONO_2$.

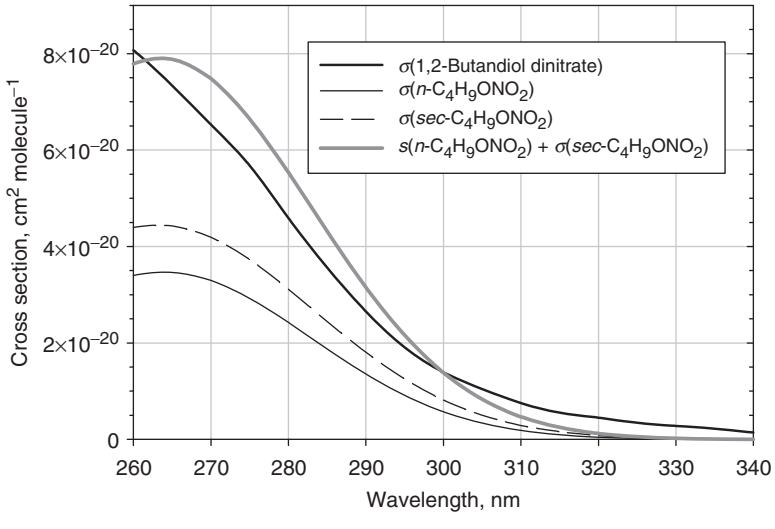

Figure IX-I-7. Comparison of the absorption cross sections of 1,2-butandiol dinitrate with those of the structurally related *n*- and *sec*-butyl nitrates.

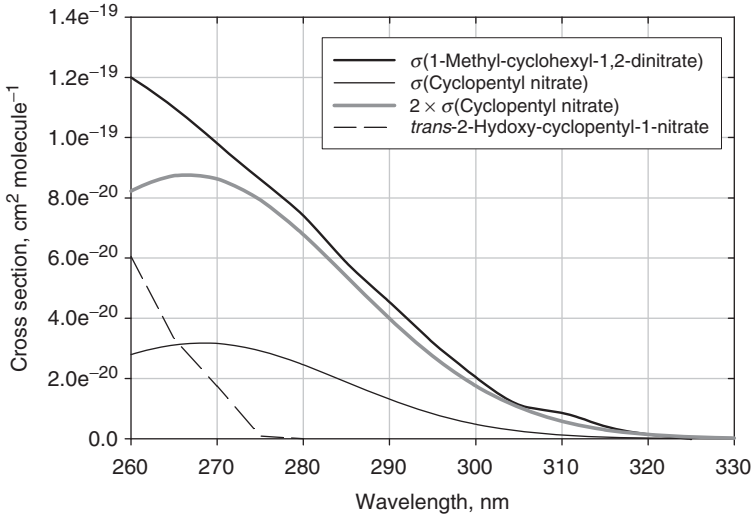

Figure IX-I-8. Comparison of the absorption cross sections for 1-methyl-cyclohexyl-1,2-dinitrate and *trans*-2-hydroxy-cyclopentyl-1-nitrate with that of cyclopentyl nitrate.

by the two nitro-groups in 1-methy-cyclohexyl-1,2-dinitrate appears to be relatively uncoupled (see figure IX-I-8); its cross sections (thick black curve) follow well that for $2 \times \sigma$ (cyclopentyl nitrate) [surrogate for 1-methyl-cyclohexyl nitrate]. Again, it appears that absorption by each of the two —ONO_2 groups in the dinitrates is relatively independent.

As one expects, the light absorption by 1,2-propandiol dinitrate at a given wavelength is greater than that exhibited by either of the structurally related propyl nitrates, *iso*-$C_3H_7ONO_2$ and *n*-$C_3H_7ONO_2$; see figure IX-I-9. However, in this case, the cross section for 1,2-propandiol dinitrate at a given wavelength significantly exceeds the sum of the cross sections of the two structurally related mononitrates (gray curve). Some interaction between the two nitrate chromophores appears to occur and enhances the absorption beyond that expected for the two nitrate groups.

The absorption of the $\rangle C{=}O$ and —ONO_2 groups in 2-oxo-cyclohexyl-1-nitrate appears to occur with little interaction between the two chromophores. See figure IX-I-10. The sum of the cross sections of cyclopentyl nitrate (a surrogate for cyclohexyl nitrate) and cyclohexanone (filled circles), is seen to follow the cross section data for the nitrocarbonyl over the 275–315 nm region of the absorption.

The light absorption by hydroxy nitrates shows a very different behavior; the interaction of the —OH and —ONO_2 functional groups is apparent for the compounds that have been studied. In figure IX-I-11 the cross sections of α-nitrooxyethanal ($HOCH_2CH_2ONO_2$) are compared with those of the structurally related ethyl nitrate, ($CH_3CH_2ONO_2$). In this case, the cross sections at a given wavelength for the nitrooxyethanal are seen to be significantly smaller than those of the ethyl nitrate, and the absorption is shifted to shorter wavelengths. A similar observation is obtained

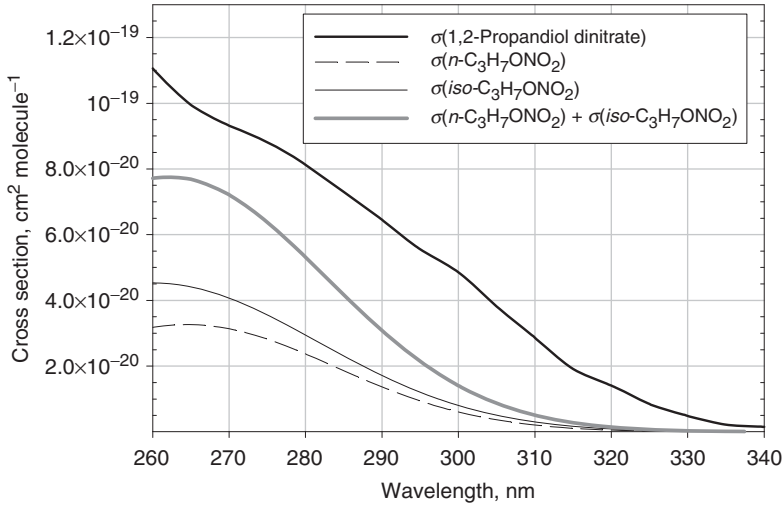

Figure IX-I-9. Comparison of the absorption spectrum of 1,2-propandiol dinitrate with that of the two structurally related mononitrates, *n*- and *iso*-propyl nitrate.

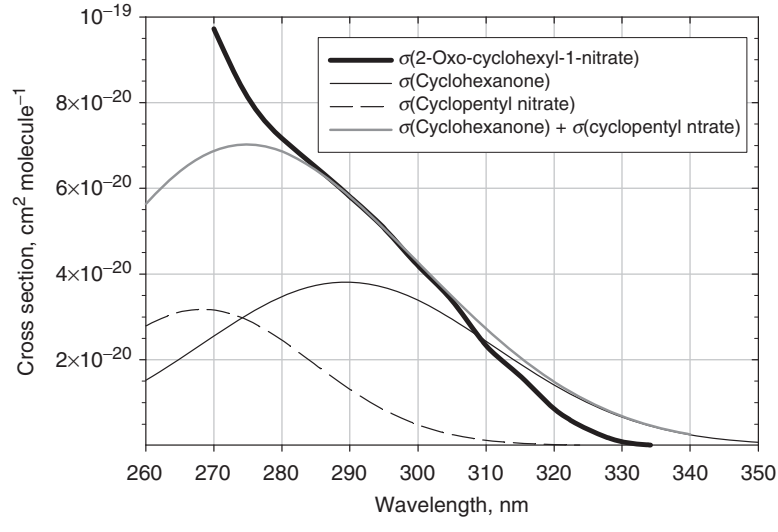

Figure IX-I-10. Comparison of the absorption cross sections of the 2-oxo-cyclohexyl-1-nitrate with those of the structurally related cyclopentyl nitrate.

from data shown for 2-hydroxy-cyclopentyl-1-nitrate (dashed line) in figure IX-I-8. Here the cross sections are significantly smaller and shifted to shorter wavelengths than those for cyclopentyl nitrate (thin black line). Wängberg et al. (1996) suggested that the presence of the —OH group in the β-position to the —ONO_2 group may result in weak bonding interactions between the two groups and a shift of the nitrate

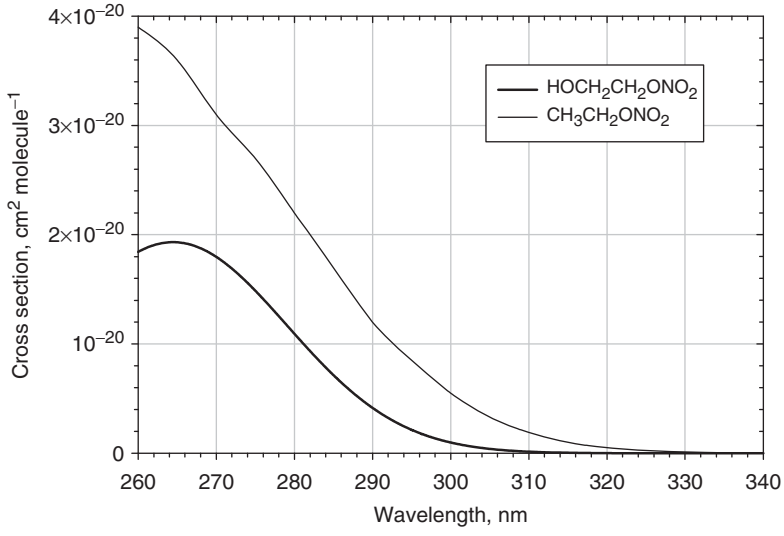

Figure IX-I-11. Comparison of the absorption spectrum for $HOCH_2CH_2ONO_2$ and the structurally related ethyl nitrate, $CH_3CH_2ONO_2$.

chromophore absorption to shorter wavelengths. Certainly, H-bonding seems plausible through the 6- or 7-membered ring structures:

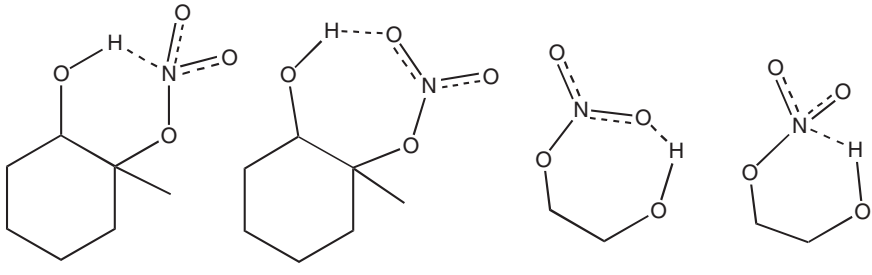

If this limited sample of spectra of hydroxynitrates is representative of other β-nitro-substituted alcohols, then the photodecomposition of these species within the troposphere is expected to be unimportant, since there is little or no overlap of the absorption region with that of the actinic flux available within the troposphere.

IX-I-4.2. Quantum Yields of Photodecomposition of the Bifunctional Organic Nitrates

There are no measurements of the quantum yields of products of these compounds, although the limited product study reported by Barnes et al. (1993) gives some suggestion as to the nature of the photodissociation. Using both mercury and fluorescent lamps to photolyze α-nitrooxyacetone, 3-nitrooxyo-2-butanone and 2,3-butandiol dinitrate, they concluded that NO_2 is released in the primary step. The further reactions of

the RO radicals produced ultimately resulted in the formation of CO, various aldehydes, and PAN. From the existing evidence, it appears that the primary step in photodissociation of the carbonyl dinitrates, like that of the simple alkyl nitrates, is rupture of one of the RO—NO_2 bonds:

$$RONO_2 + h\nu \rightarrow RO + NO_2$$

In the absence of more definitive evidence, we will assume in this study that the quantum yields reflect those seen in the mononitrate photodecomposition—that they are near unity at all wavelengths of absorbed light.

IX-I-4.3. Photolysis Frequencies for Photodissociation of Bifunctional Organic Nitrates within the Lower Troposphere

Using the measured absorption cross sections together with the appropriate actinic flux data and an assumed quantum yield of photodecomposition of unity, we have calculated the photolysis frequencies as a function of solar zenith angle for a clear sky, lower troposphere with an overhead ozone column of 350 DU. These data are shown in figure IX-I-12. For an overhead Sun, the data give lifetimes that extend over a wide range: 4.8 h for 3-nitrooxy-2-butanone, to 4 months for 2-nitrooxyethanol. These *j*-values given here are consistent with those calculated for these compounds by Barnes et al. (1993).

However, quantum yields for photodecomposition may be less than unity for the carbonyl nitrates, and the photolysis frequencies calculated here represent maximum values. There are no experimental or theoretical estimates of the quantum yields of these compounds. However, as indicated in this section, it appears that the two chromophores ($\rangle$C=O and —ONO_2) present in the carbonyl nitrates act relatively independently. If energy appears originally as $n \rightarrow \pi^*$ excitation within the $\rangle$C=O group, efficient migration of energy to the R—ONO_2 bond with its subsequent rupture may not occur before collisional quenching of the excited molecule occurs. As is often the case for the simple ketones excited within the carbonyl bond, dissociation at the R—C(=O)R′ bond may occur with a quantum efficiency well less than unity at tropospheric pressures.

IX-J. Photodecomposition of the Peroxyacyl Nitrates

Calvert et al. (2008) noted that the compounds with the chemical formula, $RC(O)OONO_2$, are commonly named "peroxyacyl nitrates," a name that is not chemically correct and is not favored by all chemists. Roberts (1990) points out that following the IUPAC nomenclature rules, such compounds should be named as anhydrides of the acid components from which they are formed; thus $CH_3C(O)OONO_2$ would be named, ethaneperoxoic nitric anhydride or peroxyacetic nitric anyhydride. Some chemists prefer the name, 1-nitroperoxyethanal. In view of its common usage in the extensive literature, here and elsewhere in this book we use the common name, peroxyacetyl nitrate and the abbreviation, "PAN" for the compound $CH_3C(O)OONO_2$, and peroxypropionyl nitrate and the abbreviation "PPN" for the compound $CH_3CH_2COO_2NO_2$.

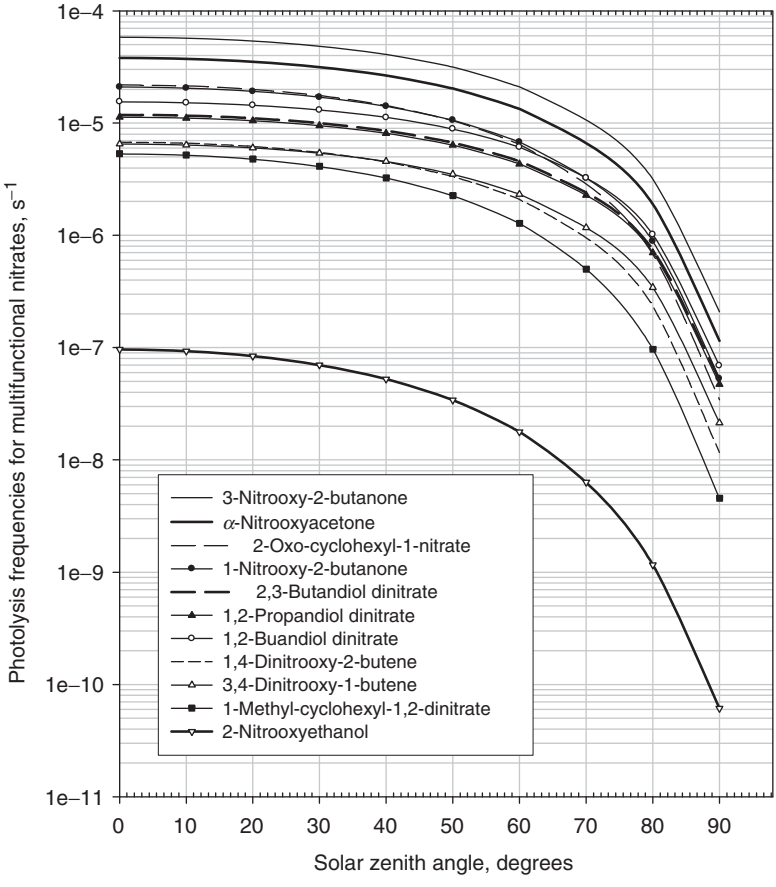

Figure IX-I-12. Photolysis frequencies for some multifunctional organic nitrates versus solar zenith angle. Data calculated for clear, lower tropospheric skies with an overhead ozone column of 350 DU. The primary quantum yield of photodissociation is assumed to be unity.

The peroxyacyl nitrates [$RC(O)OONO_2$] are common products of the atmospheric oxidation of the alkanes, and they are important for temporary storage and transport of NO_x, particularly within the cooler regions of the troposphere. The cross sections for the structurally simplest first members of this family are shown in figure IX-J-1: peroxyacetyl nitrate [$CH_3C(O)OONO_2$] and peroxypropionyl nitrate [$C_2H_5C(O)OONO_2$]. The tabular listings of cross sections for these two peroxyacyl nitrates are given in tables IX-J-1 and IX-J-2, respectively. Peroxyacyl nitrates are highly reactive, unstable at elevated temperatures, and explosions have often been reported in laboratory experiments with these compounds. As a consequence, peroxyacyl nitrates of questionable purity may have been used in many of the early studies of their photochemistry that have proven to be inaccurate. These compounds are not strong absorbers of the wavelengths of sunlight present in the troposphere, but molecules of PAN or PPN that do absorb are efficiently dissociated.

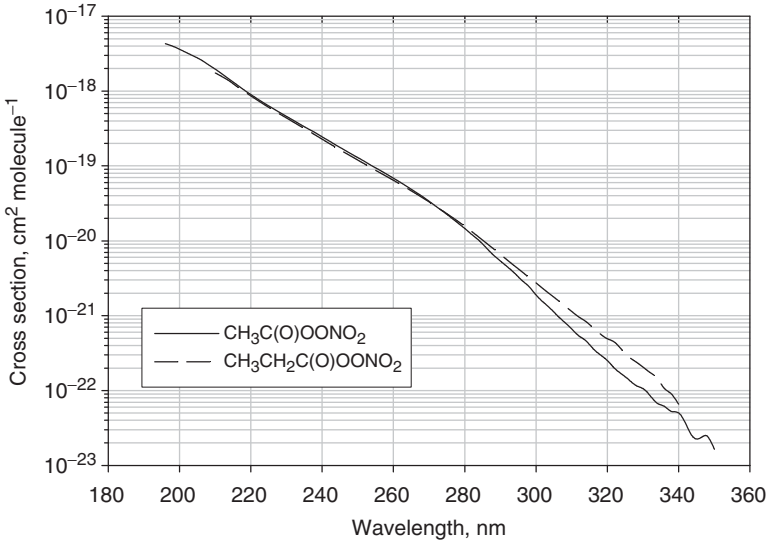

Figure IX-J-1. Absorption cross sections as a function of wavelength: peroxyacetyl nitrate (PAN) at 298 K (Talukdar et al., 1995) and peroxypropionyl nitrate (PPN) at 296 K (Harwood et al., 2003); figure from Calvert et al. (2008).

IX-J-1. Photodecomposition of Peroxyacetyl Nitrate [1-Nitroperoxoethanal, $CH_3C(O)OONO_2$, PAN]

Two pathways of photodecomposition are recognized for $CH_3C(O)OONO_2$ (Calvert et al., 2008):

$$CH_3C(O)OONO_2 + h\nu \rightarrow CH_3C(O)O_2 + NO_2 \quad \text{(I)}$$

$$\rightarrow CH_3CO_2 + NO_3 \quad \text{(II)}$$

Estimates of the enthalpy changes (298 K) involved in the overall chemistry for processes (I) and (II), respectively, are: $\Delta H_I = 118.8 \pm 4.0\,\text{kJ mol}^{-1}$ (1007 nm) and $\Delta H_{II} = 121.2 \pm 8.4\,\text{kJ mol}^{-1}$ (987 nm) (Miller et al., 1999). Thus, the quantum energies available even at the long-wavelength limit of the PAN absorption (even in the near infrared C—H overtone bands, $n \geq 4$) are much greater than these dissociation energies. The quantum yields of these two processes have been measured at two wavelengths (248 and 308 nm) by direct observations of the NO_3 and NO_2 products. These data are plotted in figure IX-J-2. Harwood et al.'s (2003) measurements of NO_3 (ϕ_{II}) are shown by the open triangles. The $\phi_{II} = 0.24$ data point at 248 nm (black triangle) has been corrected using the currently accepted quantum yield for NO_3 from the reference compound (N_2O_5) used by Mazely et al. (1997). Flowers et al. (2005) measured $\phi_{II} = 0.31 \pm 0.08$ at 289 nm, consistent with the wavelength dependence suggested by measurements of Harwood et al. (2003). The sum of ϕ_I and ϕ_{II} at wavelength 248 nm is near unity (1.02 ± 0.10), and in view of the thermochemistry involved in the bond breaking and the continuous nature of the absorption spectra, it is reasonable to assume

Table IX-J-1. Cross sections (σ, cm^2 $molecule^{-1}$; Talukdar et al., 2003) and approximate quantum yields as a function of wavelength for $CH_3C(O)OONO_2$ at 298 K; quantum yield estimates are based on an extrapolation of the results of Mazely et al. (1997) and Harwood et al. (2003); table is from Calvert et al. (2008)

λ, nm	$10^{20} \times \sigma$	ϕ_I^a	ϕ_{II}^b	λ, nm	$10^{20} \times \sigma$	ϕ_I^a	ϕ_{II}^b	λ, nm	$10^{20} \times \sigma$	ϕ_I^a	ϕ_{II}^b
278	1.74	0.71	0.29	302	0.152	0.615	0.385	326	0.0140	0.518	0.482
279	1.60	0.705	0.295	303	0.139	0.610	0.390	327	0.0129	0.513	0.487
280	1.46	0.701	0.299	304	0.125	0.607	0.393	328	0.0117	0.510	0.490
281	1.34	0.698	0.302	305	0.112	0.602	0.398	329	0.0112	0.506	0.494
282	1.21	0.695	0.305	306	0.0998	0.598	0.402	330	0.0106	0.502	0.498
283	1.11	0.690	0.310	307	0.0907	0.593	0.407	331	0.00959	0.497	0.503
284	1.01	0.686	0.314	308	0.0816	0.590	0.410	332	0.00857	0.495	0.505
285	0.910	0.682	0.318	309	0.0741	0.586	0.414	333	0.00767	0.490	0.510
286	0.810	0.678	0.322	310	0.0666	0.582	0.418	334	0.00676	0.486	0.514
287	0.729	0.673	0.327	311	0.0602	0.578	0.422	335	0.00646	0.483	0.517
288	0.648	0.670	0.330	312	0.0538	0.575	0.425	336	0.00615	0.478	0.522
289	0.593	0.666	0.334	313	0.0500	0.570	0.430	337	0.00571	0.474	0.526
290	0.537	0.662	0.338	314	0.0462	0.566	0.434	338	0.00526	0.470	0.530
291	0.492	0.658	0.342	315	0.0413	0.562	0.438	339	0.00514	0.466	0.534
292	0.447	0.655	0.345	316	0.0363	0.558	0.442	340	0.00502	0.463	0.537
293	0.408	0.651	0.349	317	0.0332	0.553	0.447	341	0.00431	0.458	0.542
294	0.369	0.646	0.354	318	0.0300	0.550	0.450	342	0.00360	0.455	0.545
295	0.333	0.642	0.358	319	0.0276	0.547	0.453	343	0.00301	0.450	0.550
296	0.297	0.638	0.362	320	0.0252	0.542	0.458	344	0.00241	0.446	0.554
297	0.271	0.635	0.365	321	0.0226	0.538	0.462	345	0.00236	0.442	0.558
298	0.245	0.631	0.369	322	0.0199	0.535	0.465	346	0.00231	0.437	0.563
299	0.217	0.626	0.374	323	0.0183	0.530	0.470	347	0.00239	0.435	0.565
300	0.189	0.622	0.378	324	0.0166	0.526	0.474	348	0.00247	0.432	0.568
301	0.171	0.618	0.382	325	0.0153	0.521	0.479	349	0.00206	0.428	0.572
								350	0.00165	0.425	0.575

[a] $CH_3C(O)OONO_2 + h\nu \rightarrow CH_3C(O)O_2 + NO_2$ (I).
[b] $CH_3C(O)OONO_2 + h\nu \rightarrow CH_3CO_2 + NO_3$ (II).

that $\phi_I + \phi_{II} \cong 1.0$ for other wavelengths of light absorbed by the peroxyacyl nitrates. The NO_2 quantum yields (ϕ_I) at wavelength 248 nm as determined by Mazely et al. (1995) represent the only measurements of this quantity. The open circle shown for ϕ_{II} at wavelength 308 nm was derived assuming $\phi_{II} = 1 - \phi_I$ at 308 nm.

In the calculation of the approximate photolysis frequencies for $CH_3C(O)OONO_2$, Calvert et al. (2008) estimated the quantum yields for processes (I) and (II) as a function of wavelength from the trend lines in figure IX-J-2, assuming a simple linear dependence. Approximate photolysis frequencies as a function of solar zenith angle were estimated using the quantum yield estimates combined with the measured cross sections given in table IX-J-1 (Talukdar et al., 1995), and the appropriate actinic flux for a clear day within the lower troposphere with an overhead ozone column of 350 DU. The results are plotted in figure IX-J-3a. There is a significant temperature dependence to the absorption cross sections of PAN that is evident in figure IX-J-3b. The temperature-dependent cross sections and the varied actinic flux alter the *j*-values for PAN that exist in the upper atmosphere. Calvert et al. (2008) have calculated the *j*-values as a function of altitude, using the temperature-dependent cross sections for PAN measured

Table IX-J-2. Cross sections (σ, cm^2 $molecule^{-1}$; Harwood et al., 2003) and approximate quantum yields as a function wavelength for peroxypropionyl nitrate at 298 K; quantum yield data based on an extrapolation of the results of Harwood et al. (2003); table is from Calvert et al. (2008)

λ, nm	$10^{20} \times \sigma$	ϕ_I^a	ϕ_{II}^b	λ, nm	$10^{20} \times \sigma$	ϕ_I^a	ϕ_{II}^b	λ, nm	$10^{20} \times \sigma$	ϕ_I^a	ϕ_{II}^b
278	1.84	0.307	0.693	299	0.299	0.365	0.635	320	0.0491	0.426	0.574
279	1.71	0.310	0.690	300	0.273	0.368	0.632	321	0.0467	0.428	0.572
280	1.57	0.313	0.687	301	0.251	0.370	0.630	322	0.0443	0.432	0.568
281	1.45	0.315	0.685	302	0.228	0.374	0.626	323	0.0399	0.435	0.565
282	1.33	0.318	0.682	303	0.210	0.377	0.623	324	0.0354	0.438	0.562
283	1.23	0.320	0.680	304	0.192	0.380	0.620	325	0.0318	0.441	0.559
284	1.12	0.323	0.677	305	0.177	0.382	0.618	326	0.0282	0.444	0.556
285	1.03	0.325	0.675	306	0.162	0.385	0.615	327	0.0262	0.446	0.554
286	0.940	0.328	0.672	307	0.149	0.388	0.612	328	0.0242	0.449	0.551
287	0.865	0.332	0.668	308	0.136	0.390	0.610	329	0.0224	0.452	0.548
288	0.790	0.335	0.665	309	0.125	0.394	0.606	330	0.0206	0.455	0.545
289	0.726	0.337	0.663	310	0.114	0.396	0.604	331	0.0190	0.458	0.542
290	0.662	0.340	0.660	311	0.105	0.399	0.601	332	0.0174	0.461	0.539
291	0.607	0.343	0.657	312	0.0962	0.402	0.598	333	0.0160	0.464	0.536
292	0.551	0.346	0.654	313	0.0899	0.405	0.595	334	0.0146	0.467	0.533
293	0.507	0.349	0.651	314	0.0835	0.408	0.592	335	0.0127	0.469	0.531
294	0.462	0.352	0.648	315	0.0762	0.412	0.588	336	0.0107	0.472	0.528
295	0.426	0.355	0.645	316	0.0689	0.415	0.585	337	0.00985	0.475	0.525
296	0.389	0.357	0.643	317	0.0630	0.417	0.583	338	0.00900	0.478	0.522
297	0.357	0.359	0.641	318	0.0571	0.420	0.580	339	0.00780	0.481	0.519
298	0.325	0.362	0.638	319	0.0531	0.423	0.577	340	0.00660	0.484	0.516

[a] $CH_3CH_2C(O)OONO_2 + h\nu \rightarrow CH_3CH_2C(O)O_2 + NO_2$ (I).
[b] $CH_3CH_2C(O)OONO_2 + h\nu \rightarrow CH_3CH_2CO_2 + NO_3$ (II).

by Talukdar et al. (1995) and the appropriate actinic flux representative of the upper atmosphere. These calculations are summarized in figure IX-J-3c. Here the solar zenith angle has been fixed at 45° and clear-sky conditions have been assumed with an overhead O_3 column at ground level of 350 DU. It can be seen that a marked increase in the *j*-values is expected at the higher altitudes. This results largely from the increase in solar flux that occurs at altitudes near and above the ozone region of the stratosphere. This is seen clearly in figure IX-J-3d, where the spectral *j*-values at various wavelength regions can be compared for several altitudes. The cut-off of actinic flux for $\lambda < 280$ nm that results from the ozone layer near 20 km restricts the active wavelength regions at the lower altitudes. The wavelength dependence of the absorption cross sections of ozone determines the wavelength range that is an active input to the *j*-values of PAN. One can see the start of input to the *j*-values from the shorter-wavelength regions even at 15 km. But as one progresses in the sequence: 0, 15, 30, 40, 45, 60 km, the region of wavelengths encompassing those of O_3 absorption becomes less filtered, and these give a substantial increase to the expected *j*-values. Note the response region of wavelengths for the 40 km altitude mirrors the absorption cross section envelope of ozone. As one approaches the upper regions of the stratospheric ozone band (45–60 km), the net *j*-values contribution from the short-wavelength region is the dominant source. What began as a photolysis frequency near 5×10^{-7} s^{-1} at ground level

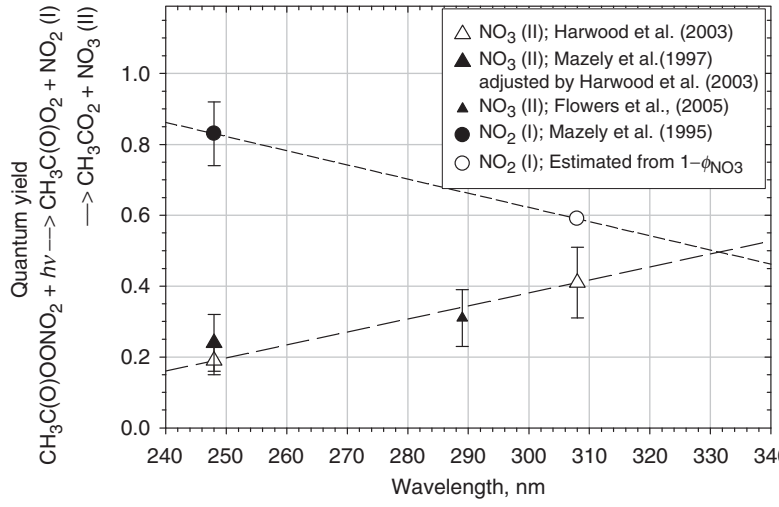

Figure IX-J-2. Estimated quantum yields of the primary processes in $CH_3C(O)OONO_2$ as a function of wavelength. The data of Harwood et al. for NO_3 quantum yields were used to determine the long-dashed line that represents the approximate wavelength dependence of process (II). The open circle shown for ϕ_I at 308 nm was derived assuming $\phi_I = 1 - \phi_{II}$ at 308 nm; figure from Calvert et al. (2008).

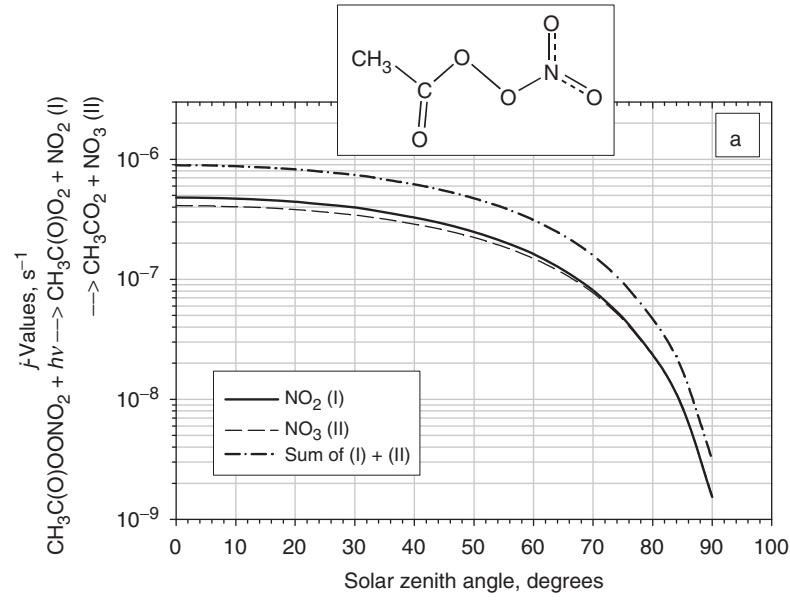

Figure IX-J-3a. Plot of the approximate photolysis frequencies for peroxyacetyl nitrate photodecomposition as a function of solar zenith angle for a cloudless day within the troposphere with an overhead ozone column of 350 DU; figure from Calvert et al. (2008).

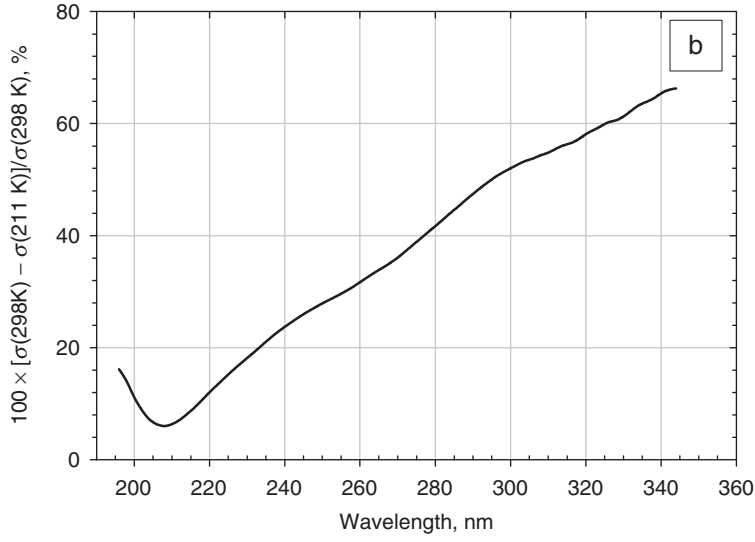

Figure IX-J-3b. Plot of the percentage difference in the absorption cross section of $CH_3C(O)OONO_2$ (PAN) at 298 and 211 K as a function of wavelength; from data of Talukdar et al. (1995); figure from Calvert et al. (2008).

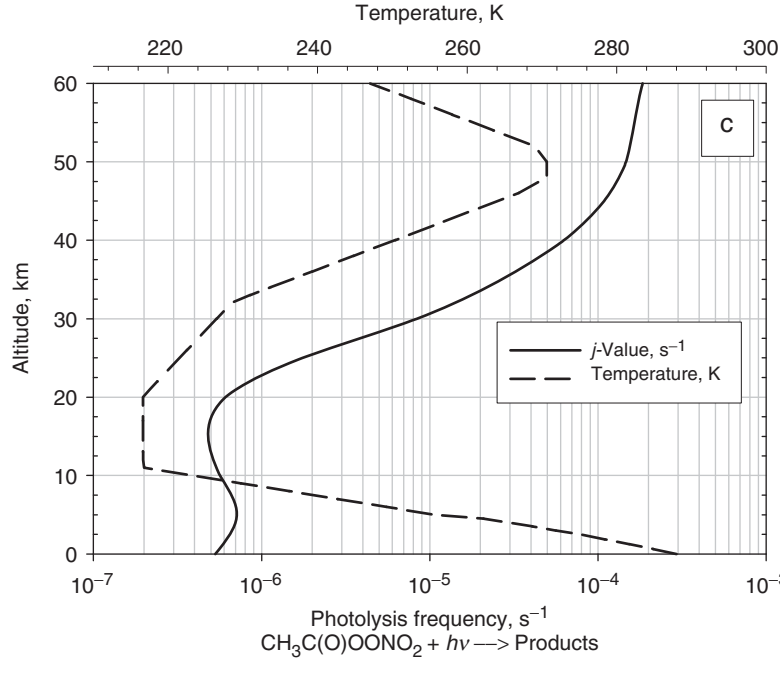

Figure IX-J-3c. Plot of the photolysis frequency for $CH_3C(O)OONO_2$ (PAN) as a function of altitude for a cloudless day with solar zenith angle = 45° and overhead ozone column = 350 DU. Also shown is the approximate atmospheric temperature as a function of altitude (U.S. Standard Atmosphere, 1976); figure from Calvert et al. (2008).

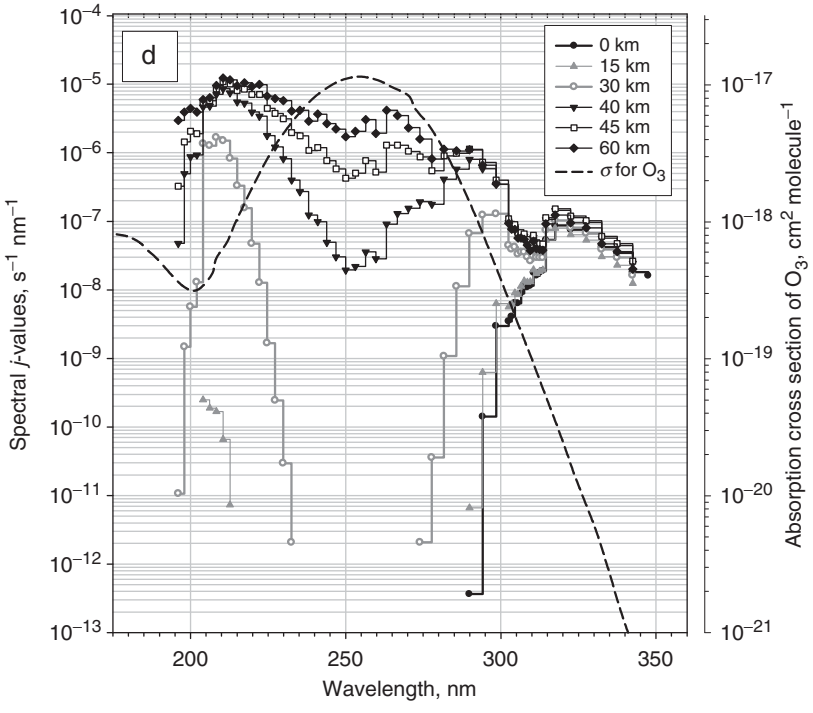

Figure IX-J-3d. Plot of the spectral j-values for $CH_3C(O)OONO_2$ photodecomposition as a function of altitude for a cloudless day with solar zenith angle = 45° and overhead O_3 at ground level = 350 DU. Note the marked change in the contribution of the wavelength ranges as the overhead O_3 column is lowered at high altitudes and the blocked radiation within the O_3 absorption band increases; figure from Calvert et al. (2008).

has increased to $\sim 2 \times 10^{-4}\ s^{-1}$ at 60 km. Although the increase seen results largely from the increase in solar flux at high altitudes, the effect of the temperature dependence of the j-values also plays a role in determining the j-values in the upper atmosphere.

Nizkorodov et al. (2005) measured the C–H overtone transition strengths combined with estimates of the photodissociation cross sections for these transitions and found that near-IR photodissociation of $CH_3C(O)OONO_2$ is much less significant ($j \cong 3 \times 10^{-8}\ s^{-1}$ at noon) in the lower atmosphere than competing sinks of unimolecular decomposition and ultraviolet photolysis that have been described in this section.

IX-J-2. Photodecomposition of Peroxypropionyl Nitrate [1-Nitroperoxopropanal, $CH_3CH_2C(O)OONO_2$, PPN]

The primary processes in the photodecomposition of peroxypropionyl nitrate are presumed to be like those in the analogous compound, peroxyacetyl nitrate:

$$C_2H_5C(O)OONO_2 + h\nu \rightarrow C_2H_5C(O)O_2 + NO_2 \quad \text{(I)}$$

$$\rightarrow C_2H_5CO_2 + NO_3 \quad \text{(II)}$$

Quantum yields for photodecomposition to form NO_3 have been measured by Harwood et al. (2003): $\phi_{II} = 0.22 \pm 0.04$ at 248 nm and 0.39 ± 0.04 at 308 nm. As with the treatment of the peroxyacetyl nitrate results by Calvert et al. (2008), we have assumed: (i) $\phi_I = 1 - \phi_{II}$, and (ii) the quantum yields are a linear function of the excitation wavelength. These ϕ_I and ϕ_{II} estimates and σ measurements of Harwood et al., are given in table IX-J-2 as a function of wavelength of sunlight available within the troposphere. Approximate photolysis frequencies were estimated from these data, and the appropriate actinic flux at various solar zenith angles for a cloudless day in the troposphere with an overhead ozone column of 350 DU. These are plotted versus solar zenith angle in figure IX-J-4. The *j*-values of PPN are greater than those of PAN by about a factor of 1.7, and this leads to a somewhat shorter photochemical lifetime of PPN within the lower troposphere: for overhead Sun, ~7.4 days for PPN compared ~13 days for PAN.

IX-K. Photodecomposition of Hydrogen Peroxide and the Alkyl Hydroperoxides

IX-K-1. Hydrogen peroxide (HOOH)

Hydrogen peroxide, the alkyl hydroperoxides, as well as $HOONO_2$ and $CH_3C(O)OONO_2$ that contain an O—O bond, show similar continuous absorptions over the 200–360 nm region; see figure IX-K-1. For H_2O_2, CH_3OOH, and

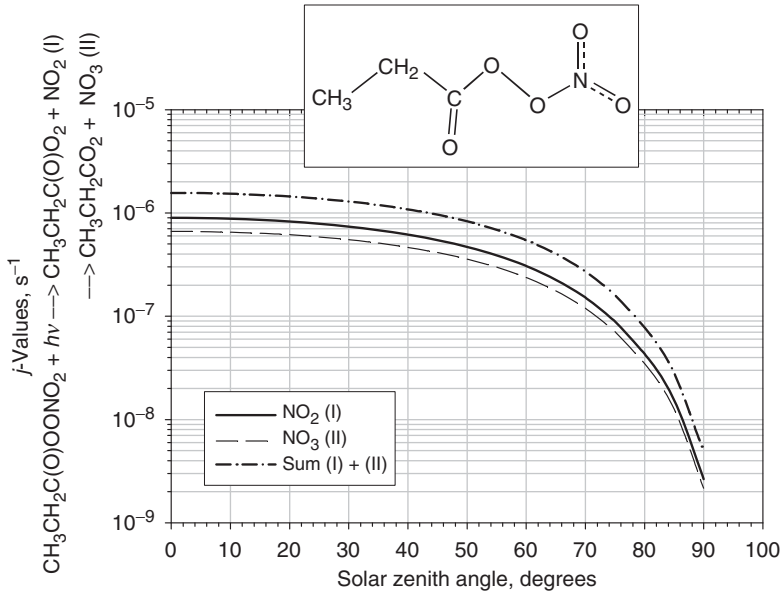

Figure IX-J-4. Plot of the approximate photolysis frequencies for peroxypropionyl nitrate (PPN) photodecomposition as a function of solar zenith angle for a cloudless day within the lower troposphere with an overhead ozone column of 350 DU; figure from Calvert et al. (2008).

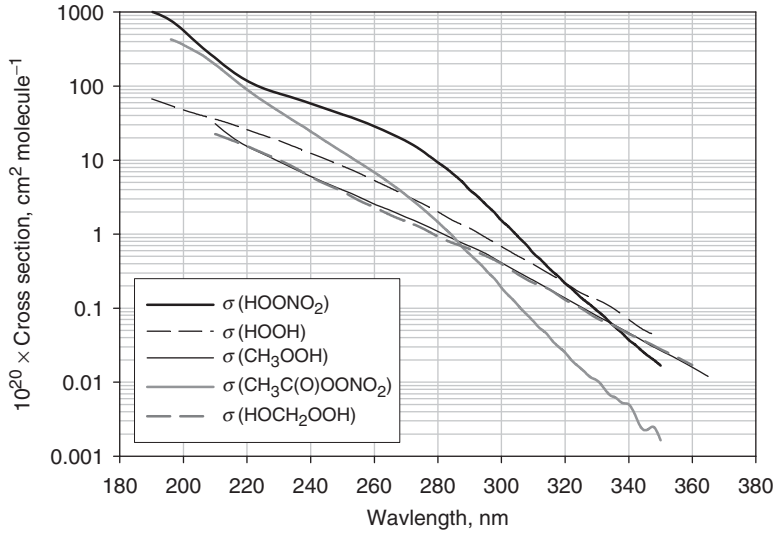

Figure IX-K-1. Comparison of the absorption cross sections for a number of compounds containing an O—O bond. Spectral data are from IUPAC (2008) recommendations.

$HOCH_2OOH$ the excitation results from a $\sigma \rightarrow \sigma^*$ transition involving the O—O bond, and a major pathway for photodecomposition of each of these peroxides is the rupture of the weak RO—OR bond. The tabular cross section data for H_2O_2, as recommended by IUPAC (2008), are given in table IX-K-1.

Primary process (I) is the dominant photodissociation pathway for hydrogen peroxide at all wavelengths of sunlight available within the troposphere (Vaghjiani and Ravishankara, 1990; Vaghjiani et al., 1992; Schiffman et al., 1993).

$$H_2O_2 + h\nu \rightarrow OH + OH \quad \text{(I)}$$

$$\rightarrow H + HO_2 \quad \text{(II)}$$

$$\rightarrow O(^1D) + H_2O \quad \text{(III)}$$

$$\rightarrow O(^3P) + H_2O \quad \text{(IV)}$$

The quantum yields of process (I) are very near unity as measured at short wavelengths: $\phi_I = 1.04 \pm 0.18$ at 248 nm (Vaghjiani and Ravishankara, 1990); 0.79 ± 0.12 (Schiffman et al. 1993); 1.01 ± 0.17 at 222 nm (Vaghjiani et al., 1992). Measured values of ϕ_I are somewhat less than unity at the shorter wavelengths: $\phi_I = 0.76 \pm 0.09$ at 193 nm (Vaghjiani et al., 1992), where process (II) competes with (I). The measured value of ϕ_{II} at wavelength 222 nm is 0.024 ± 0.012 and at 193 nm, 0.16 ± 0.04 (Vaghjiani et al., 1992). This latter value is in good agreement with the measurements of Gerlach-Meyer et al. (1987): $\phi_{II} = 0.12$ at 193 nm. It is generally assumed that ϕ_I is near unity at the wavelengths of sunlight available within the troposphere; this assumption is made in this work. Although sufficient energy is available to promote processes III and IV

Table IX-K-1. Cross sections (σ, cm^2 $molecule^{-1}$) as a function of wavelength for H_2O_2 [NASA Panel recommendation, Sander et al., 2006; mean of values from Lin et al., 1998; Molina and Molina,1981; Nicovich and Wine, 1988; and Vaghjiani and Ravishankara, 1989b]; CH_3OOH (Vaghjiani and Ravishankara,1989b) and $HOCH_2OOH$ (Bauerle and Moortgat, 1999)

λ, nm	H_2O_2 $\sigma \times 10^{20}$	CH_3OOH $\sigma \times 10^{20}$	$HOCH_2OOH$ $\sigma \times 10^{20}$	λ, nm	CH_3OOH $\sigma \times 10^{20}$	H_2O_2 $\sigma \times 10^{20}$	$HOCH_2OOH$ $\sigma \times 10^{20}$
210	35.7	31.2	22.56	290	0.691	1.2	0.63
215	30.7	20.9	18.75	295	0.551	0.90	0.51
220	25.8	15.4	16.46	300	0.413	0.68	0.40
225	21.7	12.2	12.47	305	0.313	0.51	0.29
230	18.2	9.62	10.06	310	0.239	0.39	0.22
235	15.0	7.61	7.89	315	0.182	0.29	0.18
240	12.4	6.05	5.98	320	0.137	0.22	0.13
245	10.2	4.88	4.68	325	0.105	0.16	0.10
250	8.3	3.98	3.78	330	0.079	0.13	0.073
255	6.7	3.23	2.88	335	0.061	0.10	0.059
260	5.3	2.56	2.31	340	0.047	0.07	0.045
265	4.2	2.11	1.81	345	0.035	0.05	0.036
270	3.3	1.70	1.48	350	0.027	0.04	0.028
275	2.6	1.39	1.21	355	0.021		0.022
280	2.0	1.09	0.93	360	0.016		0.017
285	1.5	0.863	0.75	365	0.012		

at 193 nm, these processes are unimportant; at 193 nm $\phi_{III} + \phi_{IV} < 0.02$ (Vaghjiani et al., 1992).

The photolysis frequencies of photodissociation of H_2O_2 were calculated as a function of solar zenith angle for clear-sky conditions and an overhead ozone column of 350 DU, assuming the process (I) occurs with a quantum yield of unity. These data are presented in figure IX-K-2 where they can be compared with *j*-values for some alkyl hydroperoxides.

IX-K-2. Methyl Hydroperoxide (CH_3OOH)

The atmospheric photochemistry of methyl hydroperoxide has been reviewed previously by Calvert et al. (2000) and earlier by Atkinson et al. (1992c) and DeMore et al. (1997). Data from a number of detailed studies provide good evidence for the occurrence of process (I) within the troposphere (Vaghjiani and Ravishankara, 1989c, 1990; Thelen et al., 1993; Blitz et al., 2005):

$$CH_3OOH + h\nu \rightarrow CH_3O + OH \qquad \text{(I)}$$

$$\rightarrow OH + (CH_3O^{\ddagger}) \rightarrow H + CH_2O \qquad \text{(II)}$$

Process (II) may occur to some extent with exposures of CH_3OOH in the vacuum ultraviolet region.

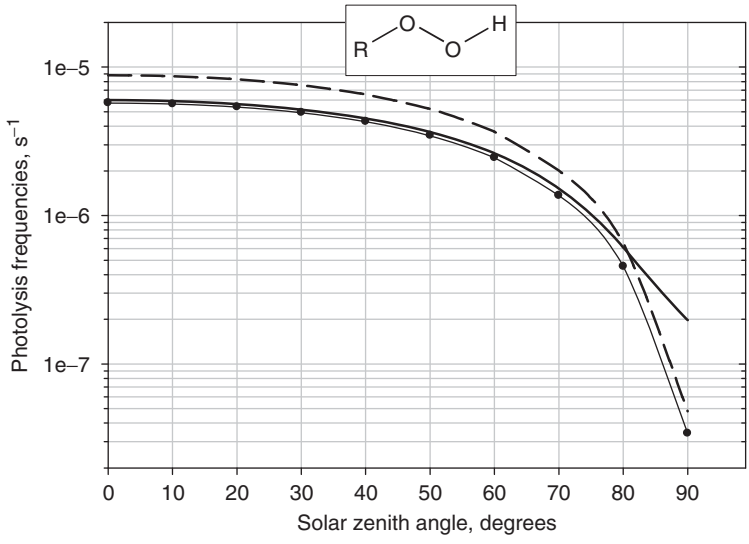

Figure IX-K-2. Photolysis frequencies for a series of peroxy compounds: HOOH (dashed line); CH_3OOH (heavy line); and $HOCH_2OOH$ (thin line with filled circles). The calculations were made for a clear sky in the lower troposphere with an overhead ozone column of 350 DU. The quantum yield of photodissociation was assumed to be unity at all wavelengths of absorbed light.

The absorption cross sections for CH_3OOH of Vaghjiani and Ravishankara (1989b) are recommended and presented in table IX-K-1 and in figures IX-K-1 and IX-K-3 where they can be compared with those of the similar compound, $HOCH_2OOH$. The data of Blitz et al. (2005) agree well with the cross section measurements of Vaghjiani and Ravishankara (1989b).

Vaghjiani and Ravishankara (1990) reported a quantum yield of OH radical production near unity ($\phi_I = 1.00 \pm 0.18$) in photolysis at 248 nm carried out in 300 Torr of N_2. The formation of H-atoms ($\phi = 0.038 \pm 0.007$) was also observed. The quantum yield of formation of $O(^3P)$ was less than 0.007.

Thelen et al. (1993) confirmed a quantum efficiency of unity for process (I) both at 248 and 193 nm. They reported from photolysis at 193 nm that the average kinetic energy of the fragments was 280 kJ mol^{-1}; this represents about 65% of the available energy with an average of about 154 kJ mol^{-1} residing in internal energy of the fragments. Photolysis at 248 nm created fragments with 201 and 96 kJ mol^{-1} of translational and internal energy, respectively. H-atom formation observed by Vaghjiani and Ravishankara (1990) probably arose from the secondary dissociation of energy-rich CH_3O radicals. According to the data of Thelen et al., the secondary decay of internally excited CH_3O radicals is expected to be efficient ($\sim$50%) only for photolyses at wavelengths $\leq$ 193 nm.

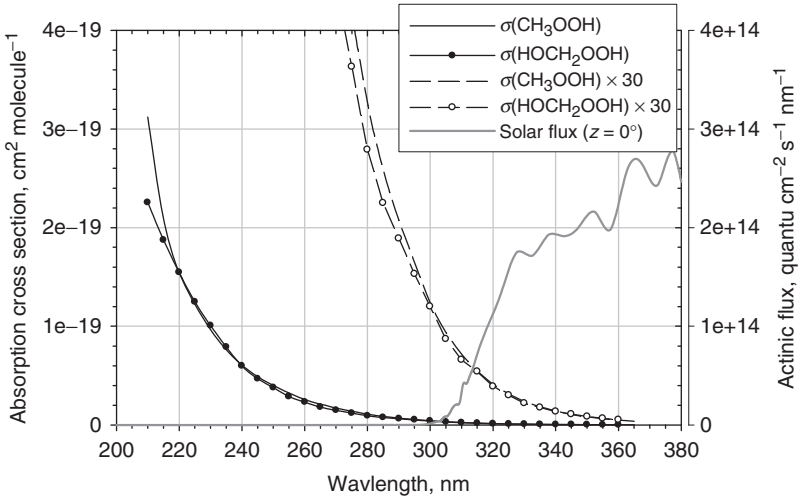

Figure IX-K-3. Comparison of the absorption cross sections for methyl hydroperoxide (Vaghjiani and Ravishankara, 1989b) and hydroxylmethyl hydroperoxide (Bauerle and Moortgat (1999); actinic flux is shown for an overhead Sun in the lower troposphere (gray curve).

Quantum yield measurements have been reported for both the products of primary process (I) over the wavelength range from 248 to 355 nm (Blitz et al., 2005). The quantum yields of both CH_3O and OH, referenced to $\phi_I = 1.0$ at 248 nm, were found to be unity within experimental error. This is consistent with the continuous nature of the absorption band of CH_3OOH and the relative weakness of the CH_3O—OH bond ($\Delta H \sim 193\,kJ\,mol^{-1}$). Even in photolyses at 360 nm, equivalent to $332\,kJ\,mol^{-1}$, there is significant excess energy to promote this dissociation.

The *j*-values for CH_3OOH as a function of solar zenith angle, given in figure IX-K-2, were calculated for a cloudless day within the lower troposphere with an ozone column of 350 DU.

Quantum yields of primary processes analogous to process (I) in CH_3OOH and reliable spectral data for the higher analogues to methyl hydroperoxide (ROOH, with $R = C_2H_5$, C_3H_7, etc.) are undetermined at this time. However, it is common practice in modeling to use the *j*-estimates for CH_3OOH as representative of those of the larger alkyl hydroperoxides. Somewhat larger *j*-values are probably more realistic, as cross sections are expected to grow as one progresses to the larger alkyl hydroperoxides.

IX-K-3. The Photodecomposition of Hydoxymethyl Hydroperoxide ($HOCH_2OOH$)

Hydroxymethyl hydroperoxide is formed in the photooxidation of formaldehyde. Su et al. (1979a, b) first detected this product in a large photochemical reactor in which a mixture of Cl_2 and CH_2O was photolyzed in synthetic air. It is formed following

HO_2 addition to CH_2O. In the atmosphere it can also be formed through the reaction of the Criegee biradical (CH_2OO) with water vapor (Neeb et al., 1997). Ethene and all alkenes of the structure, $CH_2{=}CR_2$, form the CH_2OO biradical on reaction with ozone. Hellpointner and Gab (1989) have reported the detection of this compound and other peroxides in the atmosphere.

The absorption spectrum of hydroxymethyl hydroperoxide is very similar to that of the related compound, methyl hydroperoxide (Bauerle and Moortgat, 1999); see figures IX-K-1 and IX-K-3. It is probable that its photodecomposition follows the pathway demonstrated for methyl hydroperoxide:

$$HOCH_2O_2H + h\nu \rightarrow HOCH_2O + OH \qquad \text{(I)}$$

When formed in the atmosphere, the $HOCH_2O$ radical is expected to react readily with oxygen to form formic acid, $HOCH_2O + O_2 \rightarrow HO_2 + HCO_2H$. It is likely that the photodissociation of hydroxymethyl hydroperoxide will occur with a quantum yield near unity over much of the wavelength range in which it absorbs sunlight. With this assumption and using the absorption cross sections determined by Bauerle and Moortgat (1999), we have calculated the photolysis frequencies for this compound in a cloudless, lower troposphere with an ozone column of 350 DU. These *j*-data are presented in figure IX-K-2 where it is seen that the photolysis frequencies are very similar to those for methyl hydroperoxide and H_2O_2.

IX-L. Photodecomposition of Some Aromatic Oxygenates

In the tropospheric oxidation of many of the aromatic hydrocarbons, important products are formed in which the aromatic ring system is retained, and new functional groups are introduced that extend the absorption of the compounds into the region of the spectrum available within the troposphere. Hence, the photochemistry of these species can be an important consideration among the many routes of reaction within the atmosphere. For example, the oxidation of alkyl side chains in toluene leads to benzaldehyde or acetophenone in the case of ethylbenzene. The introduction of a carbonyl group attached to the aromatic ring leads to a significant shift in the absorption toward longer wavelengths. See figure IX-L-1. Light absorption in toluene corresponds to the excitation of an electron in a π-orbital to an antibonding π^* orbital, while the new longer-wavelength absorption band seen in its oxidation product, benzaldehyde, relates to an $n \rightarrow \pi^*$ transition in which a nonbonding electron on the carbonyl oxygen is promoted to an antibonding π-orbital in the aromatic system, a much lower energy transition. A large change in the spectrum of toluene occurs as a nitro group is attached to the ring to form *o*-nitrotoluene. A similar but much smaller shift in the absorption spectra occurs as toluene is oxidized to *o*-cresol, by substitution of an OH group for one of the H-atoms on the aromatic ring. In this case, the nonbonding electron on the O-atom requires significantly more energy to promote it to the antibonding π-system. The wavelength shift in the spectra for this case is insufficient to result in significant overlap with the wavelengths of sunlight present in troposphere. However, when the aromatic compounds which are transparent in the region of the sunlight available

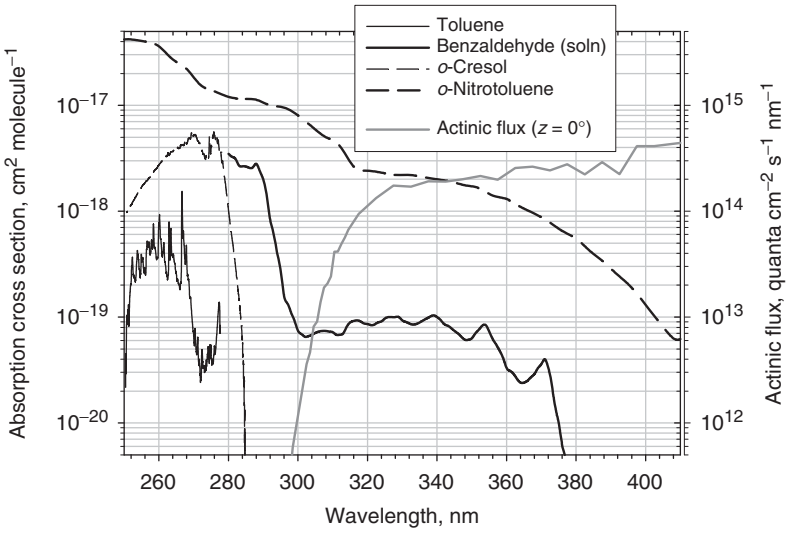

Figure IX-L-1. Comparison of the vapor-phase absorption spectra of toluene and some of its oxidation products: benzaldehyde (solution in hexane), *o*-cresol vapor, and *o*-nitrotoluene (solution in hexane); actinic flux is shown for an overhead Sun in the lower troposphere (gray curve).

in the troposphere, oxidize in the atmosphere to add —CH=O and —NO_2 groups, they become candidates for photochemical change within the troposphere. It is in this light that we discuss in this section the nature of the photochemistry of some of these products.

IX-L-1. Photodecomposition of Benzene Oxide/Oxepin

In the atmospheric oxidation of benzene, postulated intermediates are benzene oxide (1) and oxepin (2):

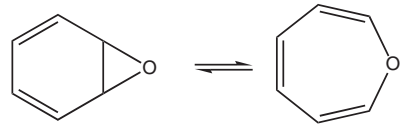

(1) (2)

The equilibrium is expected to be only slightly shifted toward the oxepin form (Klotz et al., 1997). Calvert et al. (2002) noted that these compounds absorb ultraviolet radiation, which is present within the troposphere (see figure IX-L-2), and their photochemistry may be important. The primary process (I) has been suggested to explain the phenol product observed (Klotz et al., 1998a). Process (II) is believed to occur from

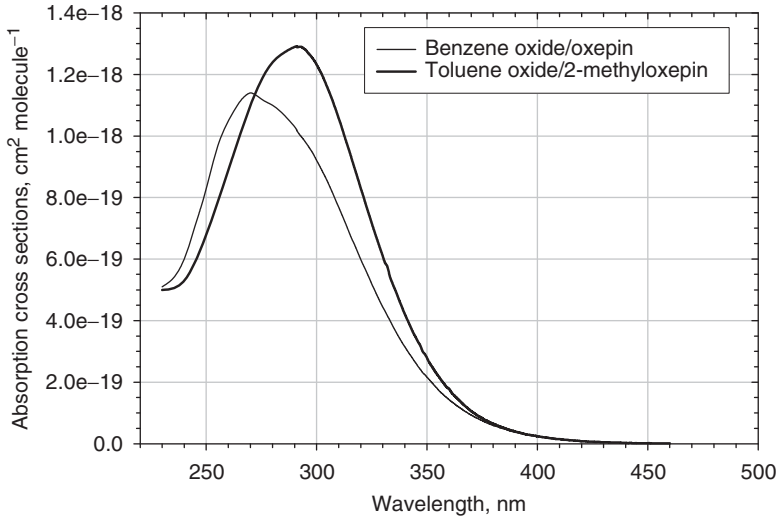

Figure IX-L-2. Cross sections versus wavelength for benzene oxide/oxepin and toluene oxide/2-methyloxepin; data from Klotz et al. (1998a); temperature, 298 K.

the oxepin form (Kaubisch et al., 1972):

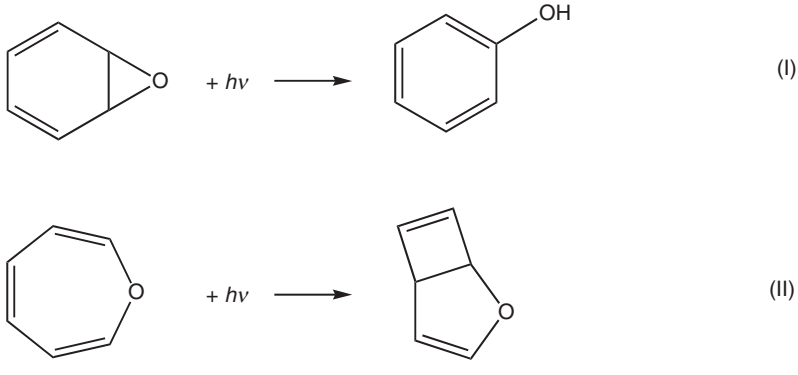

IX-L-1.1. Absorption Cross Sections for Oxepin

The absorption cross sections for the benzene oxide/oxepin are plotted in figure IX-L-2 and given in tabular form in table IX-L-1, where the high resolution data of Klotz et al. (1998a) have been averaged over each nm (centered on the wavelengths shown).

IX-L-1.2. Quantum Yields for the Photodecomposition of Benzene Oxide/Oxepin

As Calvert et al. (2002) noted, no quantum yield data have been reported for processes I or II, but the apparent *j*-values for benzene oxide/oxepin disappearance have been

Table IX-L-1. Absorption cross sections for gas-phase benzene oxide/oxepin. The high resolution data of Klotz et al. (1998a) have been averaged over 1 nm bins with the center of the bins at the wavelengths shown; units for σ are cm^2 $molecule^{-1}$; table is from Calvert et al. (2002); temperature, 298 K

λ, nm	$10^{19} \times \sigma$	λ, nm	$10^{19} \times \sigma$	λ, nm	$10^{19} \times \sigma$	λ, nm	$10^{19} \times \sigma$	λ, nm	$10^{19} \times \sigma$
290	10.18	325	5.03	360	1.37	395	0.29	430	0.05
291	10.07	326	4.87	361	1.32	396	0.28	431	0.05
292	9.98	327	4.72	362	1.26	397	0.26	432	0.05
293	9.89	328	4.57	363	1.21	398	0.24	433	0.04
294	9.79	329	4.43	364	1.16	399	0.24	434	0.04
295	9.69	330	4.30	365	1.11	400	0.23	435	0.04
296	9.58	331	4.16	366	1.06	401	0.22	436	0.04
297	9.47	332	4.03	367	1.02	402	0.21	437	0.04
298	9.34	333	3.89	368	0.97	403	0.20	438	0.03
299	9.20	334	3.75	369	0.93	404	0.19	439	0.03
300	9.07	335	3.62	370	0.89	405	0.18	440	0.03
301	8.93	336	3.49	371	0.85	406	0.17	441	0.03
302	8.79	337	3.37	372	0.82	407	0.17	442	0.03
303	8.65	338	3.25	373	0.78	408	0.16	443	0.03
304	8.50	339	3.14	374	0.75	409	0.15	444	0.03
305	8.34	340	3.03	375	0.71	410	0.15	445	0.02
306	8.18	341	2.92	376	0.68	411	0.14	446	0.02
307	8.01	342	2.82	377	0.65	412	0.13	447	0.02
308	7.84	343	2.71	378	0.62	413	0.12	448	0.02
309	7.68	344	2.61	379	0.59	414	0.12	449	0.02
310	7.51	345	2.50	380	0.57	415	0.11	450	0.02
311	7.34	346	2.41	381	0.55	416	0.10	451	0.02
312	7.17	347	2.31	382	0.52	417	0.10	452	0.01
313	6.99	348	2.24	383	0.50	418	0.10	453	0.01
314	6.81	349	2.16	384	0.48	419	0.09	454	0.01
315	6.64	350	2.08	385	0.46	420	0.08	455	0.01
316	6.49	351	2.00	386	0.43	421	0.07	456	0.01
317	6.32	352	1.92	387	0.41	422	0.07	457	0.01
318	6.15	353	1.84	388	0.39	423	0.07	458	0.01
319	5.98	354	1.76	389	0.38	424	0.07	459	0.01
320	5.82	355	1.68	390	0.36	425	0.07	460	0.01
321	5.67	356	1.62	391	0.35	426	0.06		
322	5.51	357	1.55	392	0.33	427	0.06		
323	5.35	358	1.49	393	0.31	428	0.06		
324	5.18	359	1.43	394	0.30	429	0.05		

determined in the European outdoor smog chamber (EUPHORE) in Valencia, Spain (Klotz et al., 1998a). The ratio $j(C_6H_6O)/j(NO_2) = (4.41 \pm 0.44) \times 10^{-2}$, independent of solar zenith angle (or radiation intensity). Thus, for the usual sunlight intensities where $j(NO_2) \approx 8 \times 10^{-3}\,s^{-1}$, the value for disappearance of benzene/oxepin of $j(C_6H_6O) \approx 3.5 \times 10^{-4}\,s^{-1}$. It was further determined that for each benzene oxide/oxepin reacted 0.432 ± 0.045 moles of phenol formed. So the experimental j-value for formation of phenol from the photoisomerization of benene oxide/oxepin is $\sim 1.5 \times 10^{-4}\,s^{-1}$. The extent of process (II) is unknown.

IX-L-1.3. Photolysis Frequencies for the Photodecomposition of Benzene Oxide/Oxepin in the Lower Troposphere

Photolysis rate coefficients for benzene oxide/oxepin photodecomposition that are representative of the lower atmosphere were calculated using the measured cross sections and an assumed effective quantum yield for photodecomposition (disappearance) of 0.12 (figure IX-L-3). Essentially the same values are generated calculating the $j(C_6H_6O)$ values using the measured ratio, $j(C_6H_6O)/j(NO_2) = (4.41 \pm 0.44) \times 10^{-2}$ and $j(NO_2)$ values calculated for clear tropospheric skies at an altitude of 0.5 km and an overhead ozone column of 350 DU.

IX-L-2. Photodecomposition of Toluene Oxide/2-Methyloxepin

In the atmospheric oxidation of toluene, similar to the case with benzene, two postulated intermediates (presumably in equilibrium), are toluene oxide (1) and 2-methyloxepin (2). In this case, the equilibrium is believed to be significantly shifted toward the

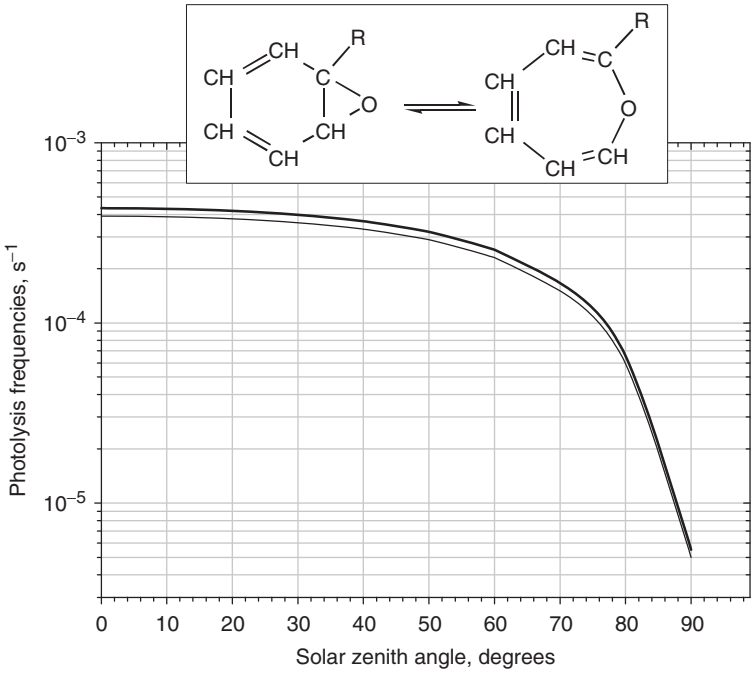

Figure IX-L-3. Estimated photolysis frequencies for the photodecomposition (disappearance) of benzene oxide/oxepin (R = H; heavy curve) and toluene oxide/2-methyl oxepin (R = CH_3; light curve) at 0.5 km altitude as a function of solar zenith angle using the measured value of $j(C_6H_6O)/j(NO_2) = (4.41 \pm 0.44) \times 10^{-2}$ and $j(CH_3C_6H_5O)/j(NO_2) = (3.99 \pm 0.48) \times 10^{-2}$ together with $j(NO_2)$ values as calculated for clear tropospheric skies at an altitude of 0.5 km and with an overhead ozone column of 350 DU.

2-methyloxepin form.

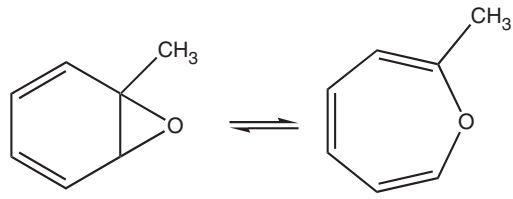

(1) (2)

These compounds absorb ultraviolet radiation which is present within the troposphere (see figure IX-L-2), and their photochemistry may be important. The primary process (I) has been suggested to explain the *o*-cresol product observed (Klotz et al., 1998b, 2000). Process (II) has been suggested to occur from the 2-methyloxepin form (Vogel and Günther, 1967; Kaubisch et al., 1972):

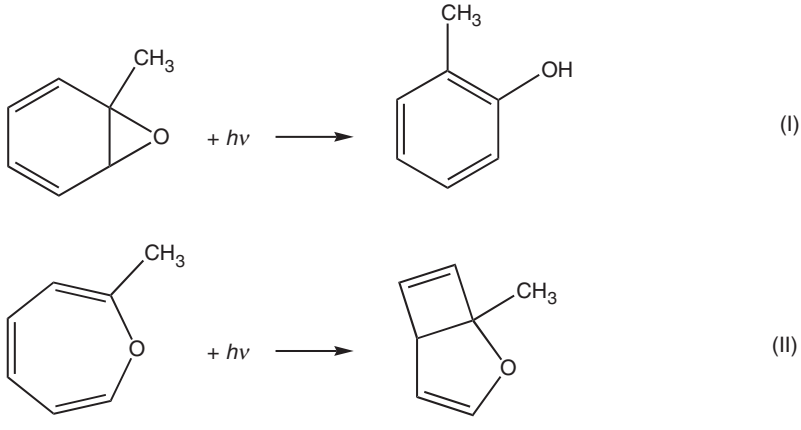

IX-L-2.1. Absorption Cross Sections for Toluene Oxide/Methyloxepin

The absorption cross sections for the toluene oxide/2-methyloxepin are plotted in figure IX-L-2 and given in tabular form in table IX-L-2, where the high resolution data of Klotz et al. (1998a) have been averaged in bins of one nm (centered on the wavelengths shown).

IX-L-2.2. Quantum Yields for Photodecomposition of Toluene Oxide

No quantum yield data have been reported for processes (I) or (II), but the apparent *j*-values for toluene oxide/2-methyloxepin disappearance have been determined in the European outdoor chamber (EUPHORE) in Valencia, Spain (Klotz et al., 1998b). The ratio $j(CH_3C_6H_5O)/j(NO_2)$ was measured to be $(3.99 \pm 0.48) \times 10^{-2}$. Hence, for conditions with $j(NO_2) = 8.0 \times 10^{-3}$, $j(CH_3C_6H_5O) \approx 3.2 \times 10^{-4}\,s^{-1}$.

Table IX-L-2. Absorption cross sections for gas-phase toluene oxide/2-methyloxepin. The high resolution data of Klotz et al. (1998a) have been averaged over 1 nm bins with the center on the wavelengths shown; units for σ are cm^2 $molecule^{-1}$; table is from Calvert et al. (2002); temperature, 298 K

λ, nm	$10^{19} \times \sigma$	λ, nm	$10^{19} \times \sigma$	λ, nm	$10^{19} \times \sigma$	λ, nm	$10^{19} \times \sigma$	λ, nm	$10^{19} \times \sigma$
290	12.90	325	7.15	360	1.78	395	0.30	430	0.05
291	12.90	326	6.93	361	1.67	396	0.29	431	0.05
292	12.90	327	6.71	362	1.59	397	0.28	432	0.05
293	12.90	328	6.50	363	1.52	398	0.27	433	0.04
294	12.85	329	6.29	364	1.45	399	0.26	434	0.04
295	12.80	330	6.08	365	1.38	400	0.24	435	0.04
296	12.71	331	5.87	366	1.31	401	0.23	436	0.04
297	12.63	332	5.76	367	1.24	402	0.22	437	0.04
298	12.54	333	5.47	368	1.18	403	0.21	438	0.03
299	12.44	334	5.27	369	1.12	404	0.20	439	0.03
300	12.32	335	5.09	370	1.06	405	0.19	440	0.03
301	12.18	336	4.92	371	1.01	406	0.18	441	0.02
302	12.05	337	4.73	372	0.96	407	0.17	442	0.03
303	11.89	338	4.55	373	0.91	408	0.16	443	0.02
304	11.72	339	4.37	374	0.87	409	0.15	444	0.02
305	11.55	340	4.20	375	0.83	410	0.15	445	0.02
306	11.37	341	4.04	376	0.78	411	0.14	446	0.02
307	11.18	342	3.88	377	0.75	412	0.13	447	0.02
308	10.98	343	3.72	378	0.71	413	0.13	448	0.02
309	10.78	344	3.57	379	0.68	414	0.12	449	0.02
310	10.57	345	3.44	380	0.65	415	0.11	450	0.02
311	10.36	346	3.30	381	0.62	416	0.11	451	0.02
312	10.13	347	3.18	382	0.59	417	0.10	452	0.01
313	9.90	348	3.00	383	0.56	418	0.10	453	0.01
314	9.68	349	2.91	384	0.53	419	0.09	454	0.01
315	9.46	350	2.78	385	0.51	420	0.08	455	0.01
316	9.22	351	2.64	386	0.48	421	0.08	456	0.01
317	8.99	352	2.53	387	0.46	422	0.08	457	0.01
318	8.76	353	2.42	388	0.43	423	0.07	458	0.01
319	8.53	354	2.31	389	0.42	424	0.07	459	0.01
320	8.29	355	2.21	390	0.39	425	0.07	460	0.01
321	8.07	356	2.11	391	0.38	426	0.06		
322	7.83	357	2.01	392	0.36	427	0.06		
323	7.60	358	1.92	393	0.34	428	0.06		
324	7.38	359	1.83	394	0.32	429	0.05		

Because of the similarity in the absorption spectra of the benzene and toluene oxides and oxepins, this value is probably nearly independent of solar zenith angle (or radiation intensity), although this hypothesis could not be tested with the available data. In this case, however, only 0.027 ± 0.022 moles of the expected product, *o*-cresol, were formed for each toluene oxide/2-methyloxepin reacted. No other products were detected. The small extent of this product has been rationalized by Klotz et al. (1998b); it is known that methylation of the carbon atoms adjacent to the ring oxygen in arene oxides results in a shift of the equilibrium towards the oxepin form (Vogel and Günther, 1967). While the arene oxide form is expected to photolyse to give phenol (benzene

oxide) or cresols (toluene oxide), the oxepin isomer is assumed to be responsible for the formation of an observed cyclization product, 2-oxabicyclo[3.2.0]hepta-3,6-diene, or in the case of 2-methyloxepin, the methylated derivative (Vogel and Günther, 1967; Kaubisch et al., 1972). Presumably, the photolysis observed in the outdoor smog chamber in this case may result largely in the formation of this latter product through process (II), with process (I) being much less important in this case.

IX-L-2.3. Photolysis Frequencies for the Photodecomposition of Toluene Oxide/Methyloxepin in the Lower Troposphere

Photolysis rate coefficients for toluene oxide/2-methyloxepin representative of the lower atmosphere were calculated by Calvert et al. (2002) using the measured cross sections and an assumed effective quantum yield of 0.082 for formation of the unknown products. See figure IX-L-3. Essentially the same values are generated calculating the $j(CH_3C_6H_6O)$ values using the measured ratio, $j(CH_3C_6H_6O)/j(NO_2) = (3.99 \pm 0.48) \times 10^{-2}$ and $j(NO_2)$ values calculated for clear tropospheric skies at an altitude of 0.5 km and an overhead ozone column of 350 DU.

IX-L-3. The Photodecomposition of Benzaldehyde (C_6H_5CHO)

Studies of the gas-phase photochemistry of benzaldehyde have been reported by Vanselow and Blacet (1957), Berger et al. (1973), Kuntz et al. (1973), Atkinson et al. (1980), and Zhu and Cronin (2000). The discussions of older literature related to benzaldehyde photodecomposition were given by Calvert et al. (2002). In exploratory experiments at 313 nm, Vanselow and Blacet (1957) reported finding the products: H_2, benzil, benzophenone, and diphenyl in addition to benzene and carbon monoxide. The most likely source of these compounds is reaction of radicals formed by rupture of the $C_6H_5C(O)$—H bond in benzaldehyde.

Berger et al. (1973) irradiated benzaldehyde at low pressures (< 0.62 Torr) with light at several selected wavelength regions: 276, 284, 328, and 365 nm. In direct photolyses of benzaldehyde and in mixtures with added triplet quenchers, they concluded that both excited triplet and singlet states of benzaldehyde were involved. Direct evidence for the formation of HCO radicals in benzaldehyde photodecomposition has been presented by Zhu and Cronin (2000). These experiments and others that provide evidence for the following photodecomposition modes in benzaldehyde that are described in this section:

$$C_6H_5CHO + h\nu \rightarrow C_6H_6 + CO \quad \text{(I)}$$

$$\rightarrow C_6H_5CO + H \quad \text{(II)}$$

$$\rightarrow C_6H_5 + CHO \quad \text{(III)}$$

$$\rightarrow \text{Unidentified products leading to polymer} \quad \text{(IV)}$$

IX-L-3.1. Absorption Cross Sections of Benzaldehyde

The gas-phase ultraviolet absorption spectrum of benzaldehyde (figure IX-L-4) shows some structure in both the region of strong absorption, $\lambda < 290$ nm ($\pi \rightarrow \pi^*$ transition) and that of weaker absorption, $\lambda > 290$ nm ($n \rightarrow \pi^*$ transition). The spectral data of Etzkorn et al. (1999) for $\lambda < 290$ nm agree reasonably well with the measurements reported by Thiault et al. (2004). The data of Thiault et al. from measurements at selected wavelengths (open circles) agree well with their continuous data. However, measurements of Zhu and Cronin (2000) made at three selected wavelengths, differ significantly from the data of the other workers (closed circles). Note the cross sections reported by Láng (1961–1971) for benzaldehyde in hexane solution are somewhat higher and seem to be shifted about 5 nm to the longer wavelengths. The values for the cross sections as reported by Thiault et al. (2004) for each wavelength (nm) are deemed to be the most reliable and are summarized in table IX-L-3.

IX-L-3.2. Quantum Yields of the Primary Processes in Benzaldehyde Photodecomposition

Berger et al. (1973) reported that process (I) forming benzene and CO is important in photolyses at 276 and 284 nm. Their data for quantum yields of benzaldehyde loss were near equal to those for benzene and carbon monoxide formation. At low pressure, ϕ_I was very near unity. However, even at these short wavelengths, quenching of the excited states was significant, and quenching is expected to be important for photolyses in air at atmospheric pressure. See figure IX-L-5. Near linearity in the Stern–Volmer plots of $1/\phi$ versus pressure of benzaldehyde can be seen for the experiments at 276

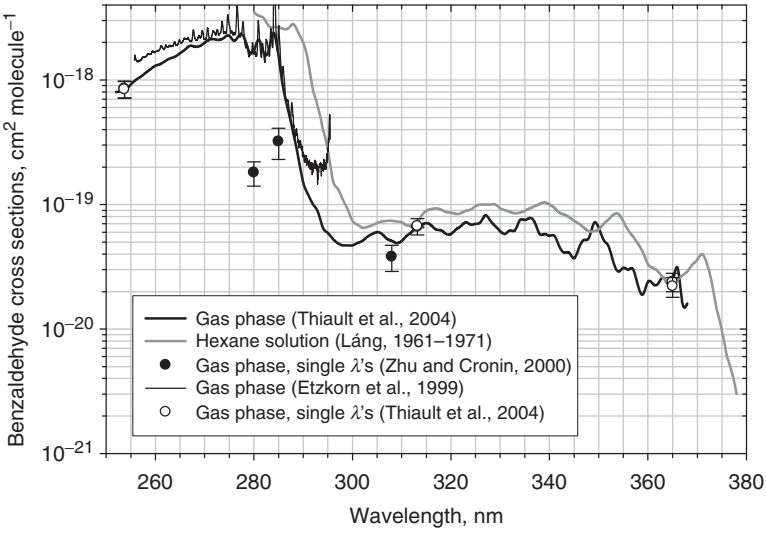

Figure IX-L-4. Comparison of the cross sections measured for benzaldehyde in the gas phase and in solution.

Table IX-L-3. Recommended cross sections (σ, cm^2 molecule^{-1}) from Thiault et al. (2004) and quantum yields of the primary photodecomposition processes in benzaldehyde at 1 atm. pressure as estimated in this work

λ, nm	$10^{20} \times \sigma$	ϕ_I	ϕ_{III}	ϕ_{IV}	λ, nm	$10^{20} \times \sigma$	ϕ_{IV}	λ, nm	$10^{20} \times \sigma$	ϕ_{IV}
276	206	0.35	0.22	0.38	311	5.60	0.40	346	4.50	0.40
277	228	0.33	0.24	0.38	312	6.00	0.40	347	5.20	0.40
278	220	0.31	0.27	0.38	313	6.60	0.40	348	5.40	0.40
279	170	0.29	0.30	0.39	314	6.90	0.40	349	7.10	0.40
280	172	0.27	0.32	0.39	315	7.10	0.40	350	6.50	0.40
281	210	0.25	0.35	0.39	316	6.80	0.40	351	5.20	0.40
282	164	0.22	0.37	0.39	317	6.30	0.40	352	4.60	0.40
283	174	0.20	0.40	0.39	318	6.20	0.40	353	3.40	0.40
284	240	0.18	0.42	0.39	319	5.80	0.40	354	2.90	0.40
285	154	0.16	0.45	0.39	320	5.80	0.40	355	3.10	0.40
286	84.0	0.14	0.44	0.39	321	6.30	0.40	356	3.00	0.40
287	56.0	0.12	0.44	0.39	322	6.70	0.40	357	3.00	0.40
288	37.0	0.10	0.43	0.39	323	7.20	0.40	358	2.20	0.40
289	24.0	0.07	0.42	0.39	324	6.90	0.40	359	1.90	0.40
290	15.0	0.05	0.42	0.39	325	7.00	0.40	360	2.40	0.40
291	12.0	0.03	0.41	0.39	326	7.20	0.40	361	2.30	0.40
292	10.0	0.005	0.40	0.39	327	8.20	0.40	362	2.30	0.40
293	8.70	0	0.40	0.39	328	7.40	0.40	363	2.60	0.40
294	6.50		0.39	0.39	329	6.70	0.40	364	2.30	0.40
295	5.90		0.38	0.39	330	6.10	0.40	365	2.40	0.40
296	5.30		0.37	0.39	331	5.80	0.40	366	3.10	0.40
297	4.90		0.37	0.40	332	6.20	0.40	367	1.60	0.40
298	4.70		0.36	0.40	333	6.20	0.40	368	1.60	0.40
299	4.70		0.35	0.40	334	7.50	0.40			
300	4.70		0.35	0.40	335	7.50	0.40			
301	4.90		0.34	0.40	336	7.80	0.40			
302	5.10		0.33	0.40	337	7.20	0.40			
303	5.50		0.33	0.40	338	5.80	0.40			
304	5.80		0.32	0.40	339	5.80	0.40			
305	6.00		0.31	0.40	340	5.60	0.40			
306	5.80		0.30	0.40	341	5.60	0.40			
307	5.30		0.30	0.40	342	4.60	0.40			
308	5.10		0.29	0.40	343	4.10	0.40			
309	4.90		0.14	0.40	344	4.10	0.40			
310	5.10		0.00	0.40	345	3.70	0.40			

and 284 nm at the pressure of benzaldehyde less than 0.2 Torr, but the quantum yields at the higher pressure appear to approach near constant values (~0.34 at 276 nm and ~0.18 at 284 nm). We have taken the values at the highest pressure as rough estimates of ϕ_I in 1 atm. of air; these are likely maximum values, since some quenching of the operative excited state is expected at pressures of 1 atm. We plot these data as closed triangles in figure IX-L-6.

The non-Stern–Volmer behavior at the higher pressure of benzaldehyde seen in figure IX-L-5 points to benzene and carbon monoxide formation from another excited state that is quenched less effectively. The quantum yields of benzene and CO formed in process (I) following absorption within the $n \rightarrow \pi^*$ region (328, 365 nm) were

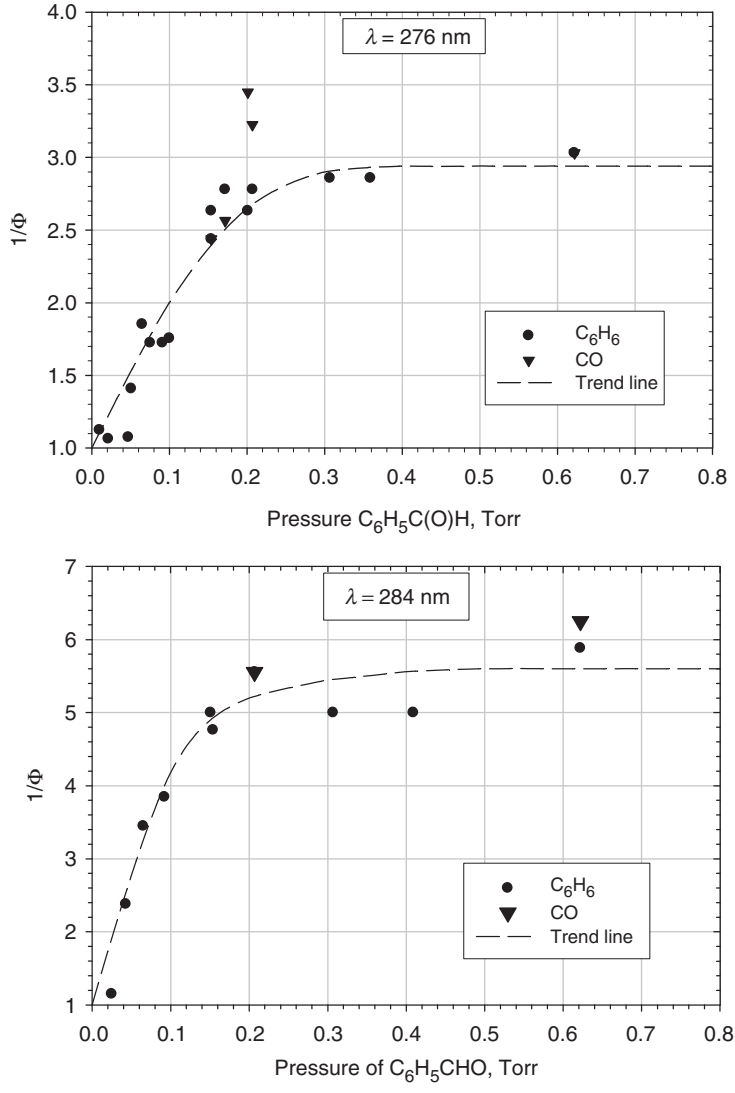

Figure IX-L-5. Stern–Volmer plots of the quantum yields of benzene and CO products formed in the photodecomposition of benzaldehyde at 276 nm (upper panel) and 284 nm (lower panel); data of Berger et al. (1973).

very small even at low pressures: $\phi_{C_6H_6} < 0.006$ at 328 nm and < 0.001 at 365 nm (Berger et al., 1973). If the trend shown by these two points continues to longer wavelengths, as indicated by the line joining these points, then process (I) becomes unimportant at $\lambda > 294$ nm, and it is unimportant at the wavelengths available within the lower troposphere. However, the quantum yields for benzaldehyde disappearance remained high for these conditions ($\phi_{-C_6H_5CHO} = 0.37 \pm 0.02$ at 276 nm; 0.39 ± 0.02 at 284 nm; 0.40 ± 0.01 at 328 nm; and 0.40 ± 0.04 at 365 nm), and the yield

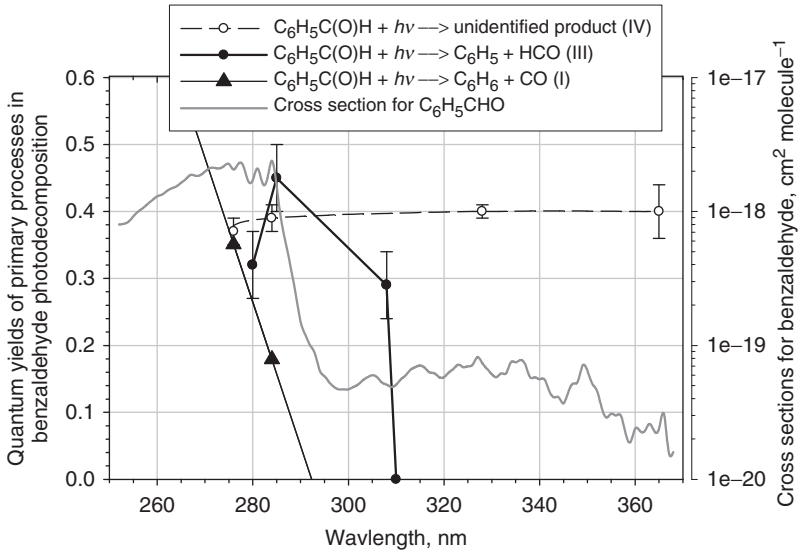

Figure IX-L-6. Approximate quantum yields for the photodecomposition of benzaldehyde as estimated in this work. The absorption spectrum of benzaldehyde is shown by the gray curve.

was unaffected by the presence of triplet state quenchers. We have plotted these data, representing process (IV), as the open circles in figure IX-L-6.

Long et al. (1983) confirmed the occurrence of process (I) in photolyses at low pressures of benzaldehyde using either 245.0 or 258.9 nm radiation. Benzene was identified as a product using laser ionization mass and photoelectron spectrometers. They concluded that benzaldehyde excited at these short wavelengths decomposes into C_6H_6 and CO on a nanosecond timescale. From the Berger et al. results, it appears that process (I) can be neglected for photolyses within the troposphere.

The relatively large quantum yield of disappearance of benzaldehyde that Berger et al. (1973) observed, remains unexplained, and is represented by our process (IV) forming unidentified products. They found that on prolonged and repeated photolysis significant amounts of a pale yellow polymeric material built up on the walls of the photolysis vessel, an observation also made by previous workers (Almasy, 1933; Blacet and Vanselow, 1957; DeMare et al., 1968). Presumably, this resulted from the further reaction, probably polymerization, of the unidentified product of process (IV). Berger et al. (1973) found that the unidentified benzaldehyde consuming process was not affected by the presence of a triplet scavenger, so they concluded that either this is initiated by free radicals originating from S_1 or possibly from a surface-initiated reaction. Possibly the product represents some undentified structural isomer of benzenaldehyde that can revert to benzaldehyde or form the polymeric product observed by several previous workers.

Kuntz et al. (1973) carried out chamber irradiations of benzaldehyde–NO_x mixtures in synthetic air [$j(NO_2) \approx 6.7 \times 10^{-3}\ s^{-1}$]; they reported that 132 min. was required to

oxidize one-half of the NO to NO_2, a rather slow rate, reflecting a low quantum yield of radical formation. The formation of benzoylperoxy nitrate, a highly eye-irritating compound, was observed as reported earlier by Heuss and Glasson (1968). When 2.5 ppmv of benzaldehyde was added to a synthetic air mixture containing 10 ppmv-C of reactive alkenes and 1 ppm NO_x, the rate of NO and alkene oxidation was suppressed. These data confirm a low rate of generation of free radicals from sunlight-irradiated benzaldehyde in air, and that benzaldehyde is a very inefficient chain carrier with peroxybenzoyl nitrate acting as a temporary sink for NO_x.

In a smog chamber study of the photooxidation of toluene and the cresols, Atkinson et al. (1980) found that an assumed j-value of $3 \times 10^{-5}\ s^{-1}$ for benzaldehyde photodecomposition was required to account for the observed benzaldehyde loss rates; in their experiments $j(NO_2) \approx 6.6 \times 10^{-3}\ s^{-1}$. They concluded that the product data were best fitted by assuming that benzaldehyde photolysis results in the formation of nonradical products, such as process (I). However, if process (I) was assumed to be the major photodecomposition mode, the amount of benzene observed was less than 1% of the benzene yields predicted.

In experiments designed to test the photodissociation mechanism in benzaldehyde at low pressures, Zhu and Cronin (2000) studied the quantum efficiency of HCO radical generation from benzaldehyde photodissociation in process (III) at wavelengths 280, 285, and 308 nm; they measured $\phi_{III} = 0.32 \pm 0.05$, 0.45 ± 0.05, and 0.29 ± 0.05 at 280, 285, and 308 nm, respectively. These ϕ_{III} data are plotted as in figure IX-L-6 as filled circles. We have assumed a cutoff will occur at the wavelength 310 nm, significantly beyond the 292 nm cutoff expected from the estimated 409 kJ mol^{-1} enthalpy change for this dissociation.

It is likely that the ϕ_I values reported by Zhu and Cronin, applicable to the low-pressure range of the measurements, are upper limits to the yields expected in 1 atm. of air. The cross sections they used appear to be underestimated; see figure IX-L-4. The quantum yields measured at 280 and 285 nm were insensitive to added nitrogen gas pressures of 5–380 Torr. However, at 308 nm, the value of ϕ_{HCO} decreased by 35% with a modest increase in benzaldehyde pressure from 0.1 to 0.8 Torr.

In other experiments, Zhu and Cronin (2000) searched for absorption in the 650 nm region due to the possible initial radical product of photodissociation by process (II), C_6H_5CO; it was not observed, although this process is favored somewhat energetically: ΔH°_{298} for processes (II) and (III), ~364 (available at $\lambda < 328$ nm) and ~409 kJ mol^{-1} (available at $\lambda < 292$ nm), respectively. There is little evidence for the occurrence of process (II), although the products measured in the studies of Vanselow and Blacet suggest its occurrence to an ill-defined extent.

Obviously, significant uncertainties remain about the nature and extent of the primary photodissociation processes in benzaldehyde. The limited quantum yield data available at this writing (plotted in figure IX-L-6) were obtained in experiments at relatively low pressures which are not directly applicable to tropospheric conditions. However, from the observations of Zhu and Cronin, one can assume that process (III) occurs significantly up to the wavelength of light providing the minimum energy necessary for its occurrence. Although energy considerations suggest this cutoff will occur at $\lambda \leq 292$ nm, it apparently continues to the longest wavelength, 308 nm, studied

by Zhu and Cronin (2000). The quantum yields of disappearance of benzaldehyde as determined by Berger et al. (1973) are independent of added triplet quenchers and wavelength over the limited pressure and wavelength ranges employed. If one assumes that this trend continues to tropospheric pressures and that process (IV) is the dominant mode of decay here, then the assumption of $\phi_{IV} = 0.39 \pm 0.03$ is appropriate. This procedure will lead to maximum estimates of the photodecomposition of benzaldehyde.

IX-L-3.3. Photolysis Frequencies for Benzaldehyde Photodecompositon in the Lower Troposphere

Photolysis rate coefficients representative of the lower atmosphere were calculated using the measured cross sections of Thiault et al. (2004). The ill-defined process (IV) was programmed to occur at all wavelengths of light absorbed by benzaldehyde as reported by Berger et al. Process (III), forming HCO radicals, was assumed to occur with the efficiencies measured by Zhu and Cronin, but with a sharp cutoff for wavelengths longer than 308 nm.The latter choice of quantum yields is more consistent with the smog chamber results of Atkinson et al. (1980). However, the spectral distribution of the solar simulator used in the chamber may not reflect well the short-wavelength region

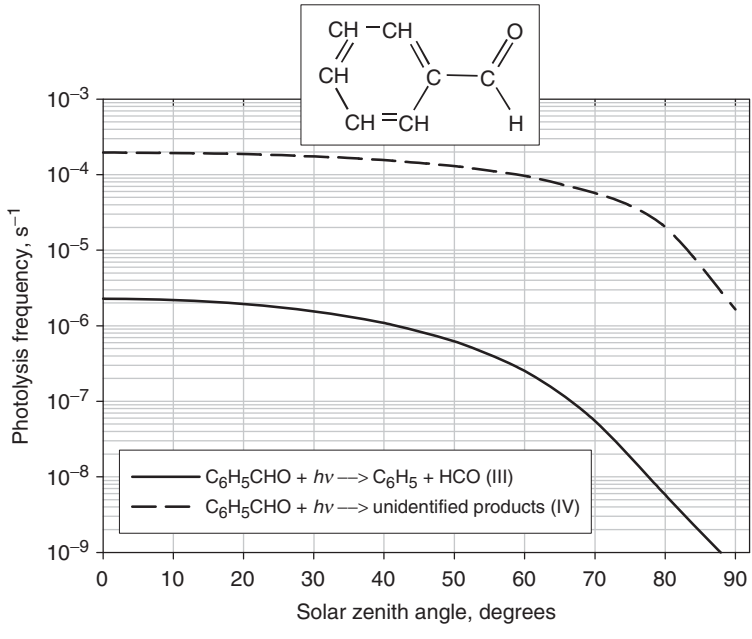

Figure IX-L-7. Plot of the estimated photolysis frequencies for benzaldehyde photodecomposition as a function of solar zenith angle. Cloudless sky in the lower troposphere and an overhead ozone column of 350 DU was assumed in the calculation. Measurable photodecomposition in the troposphere occurs by only the two primary processes shown [processes (III) and (IV)].

of the solar spectrum. The photolysis frequencies for benzaldehyde as a function of solar zenith angle are given in figure IX-L-7 as they were calculated using quantum yield and sigma data given in table IX-L-3. Neither of the calculated photolysis frequency curves given in figure IX-L-7 alone can rationalize the magnitude of the photolysis rates assumed by Atkinson et al. (1980) in simulating benzaldehyde disappearance in their chamber experiments [$j(\text{Total}) \approx 3 \times 10^{-5}\ \text{s}^{-1}$ with $j(\text{NO}_2) \approx 6.6 \times 10^{-3}\ \text{s}^{-1}$] and the maximum loss rate of benzaldehyde seen by Gery et al. (1985) in their stirred tank reactor, $(1.8 \pm 0.7) \times 10^{-5}$. The occurrence of process (III) alone leads to very much lower values and the occurrence of process (IV) at the efficiencies given in table IX-L-3 leads to much larger values than those seen in the chamber experiments.

Zhu and Cronin (2000) reported very different *j*-value results that were calculated using their ϕ_{III} data alone to describe benzaldehyde photodecomposition. They have assumed that both their measured cross sections of benzaldehyde and their measured HCO quantum yields decrease linearly from 285 to 308 nm. Using these assumptions, they calculated for an overhead Sun and clear-sky conditions at sea level and a latitude of 40°N, $j_{\text{I}} = 1.5 \times 10^{-6}$ on January 1 and $1.5 \times 10^{-5}\ \text{s}^{-1}$ on July 1. These values are about a factor of 10 larger than we find in our calculations. The reason for the difference is not clear. From our results, we conclude that only the participation of process (IV), or some other decomposition mode forming unidentified products can raise the calculated *j*-values to those observed in chamber experiments. However, it is evident that the magnitude of ϕ_{IV} must be significantly lower than that estimated from the Berger et al. (1973) results and used in our calculations (∼1/10th). Clearly additional definitive experimentation will be necessary to resolve the problems associated with the estimation of benzaldehyde photodecomposition for tropospheric conditions.

IX-L-4. The Photodecomposition of Some Aromatic Dicarbonyls

Wang et al. (2006) carried out smog chamber studies of the photodecomposition of several aromatic dicarbonyl compounds in mixtures with 735 Torr of purified air at 298 ± 2 K using irradiation from black lamps. The compounds studied were phthaldialdehyde, 2-acetylbenzaldehyde, and 1,2-diacetylbenzene:

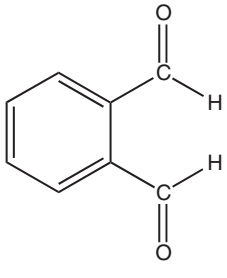

Phthaldialdehyde

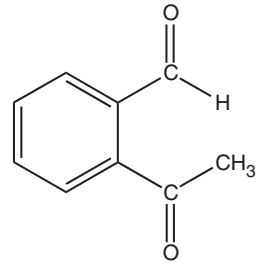

2-Acetylbenzaldehyde

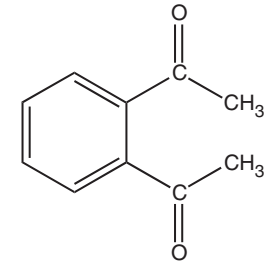

1,2-Diacetylbenzene

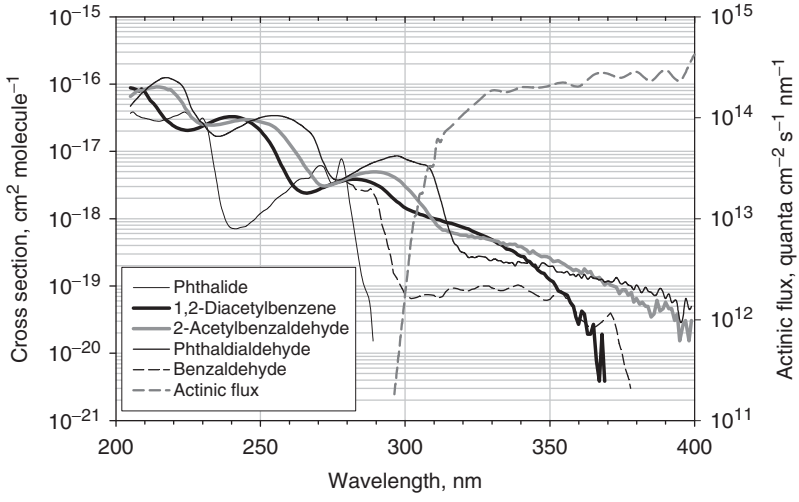

Figure IX-L-8. Cross sections for some aromatic dicarbonyl compounds as measured in hexane solution (Wang et al., 2006). The cross sections for benzaldehyde in hexane solution were measured by Láng (1961–1971). Phthalide, a product of the photolysis of phthaldialdehyde, is not photochemically active at the wavelengths of sunlight available in the troposphere. Actinic flux is given for an overhead Sun in the lower troposphere with an overhead ozone column of 350 DU.

IX-L-4.1. Absorption Cross Sections of Some Aromatic Dicarbonyls

The absorption spectra of some aromatic dicarbonyl compounds were measured in hexane solution and the data are shown graphically in figure IX-L-8. Tabular listing of the cross sections for phthaldialdehyde and 2-acetylbenzaldehyde are given in tables IX-L-4 and IX-L-5, respectively.

IX-L-4.2. Quantum Yields and Products of the Photodecomposition of the Aromatic Dicarbonyls

Observed products of the photolysis of phthaldialdehyde were phthalic anhydride (35 ± 10)% and phthalide (53 ± 14)% molar yields. The major observed photolysis products of 2-acetylbenzaldehyde photodecomposition (molar yields) were phthalic anhydride (19 ± 6)% and 3-methylphthalide (77 ± 20).

Wang et al. (2006) suggest that one of the pathways for photodissociation of both phthaldialdehyde and 2-acetylbenzaldehyde may involve cleavage of the —C(O)—H bond. The primary photochemical processes in these aldehydes are not well defined at this writing, but by analogy with those for benzaldehyde photolysis processes (I)–(IV) should be considered.

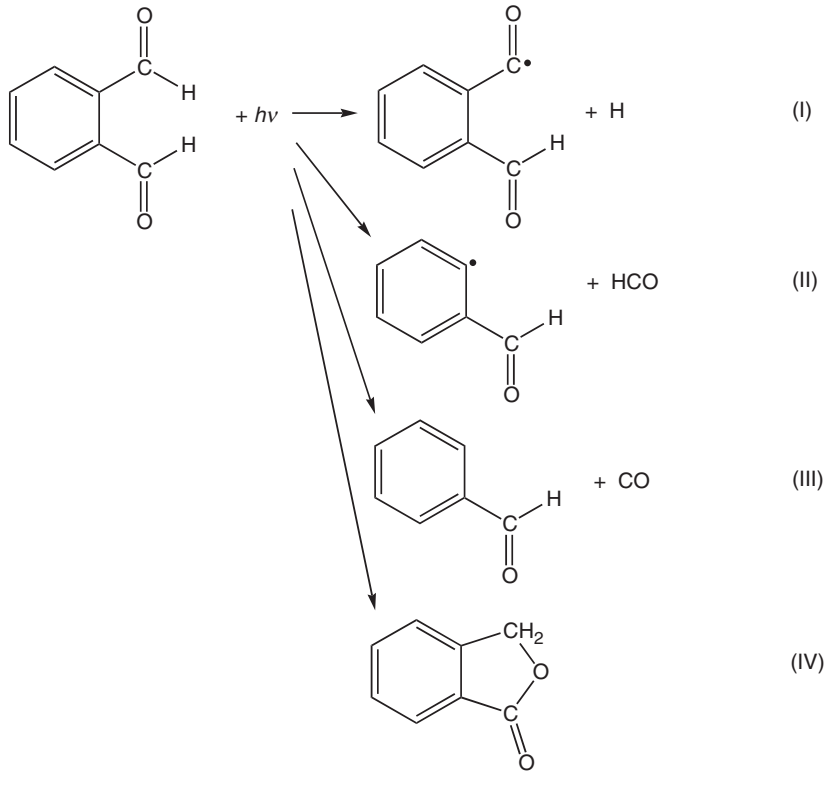

Process (I) is probably favored energetically over process (II): ΔH_{298} values are approximately 364 kJ and 409 kJ, respectively. Photoisomerization presumably occurs in process (IV). Evidence that favors these or other primary processes is limited at the time of this writing.

With 2-acetylbenzaldehyde, analogous primary processes to (I), (II), (III), and (IV) shown for phthaldialdehyde should be considered plus one additional process resulting in breakage of the —C(O)—-CH_3 bond present in this compound:

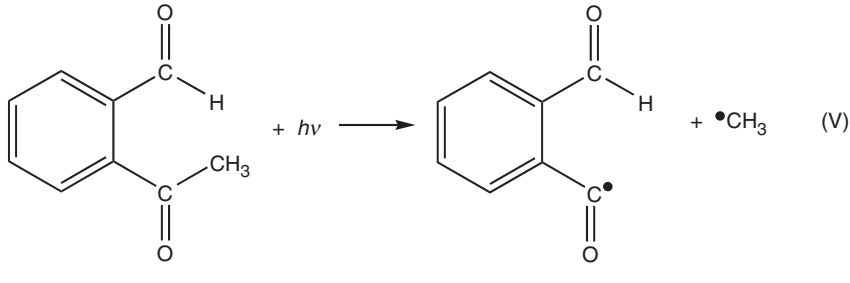

However, the fact that the photodecomposition of 1,2-diacetylbenzene is much less important than that for phthaldialdehyde and 2-acetylbenzaldehyde even though it

possesses two —C(O)—H groups rather than one, suggests that the quantum yields for the process (V) are probably small.

The mechanism of phthalic anydride formation suggested by Wang et al. (2006) is shown in reaction mechanism IX-L-4.2.

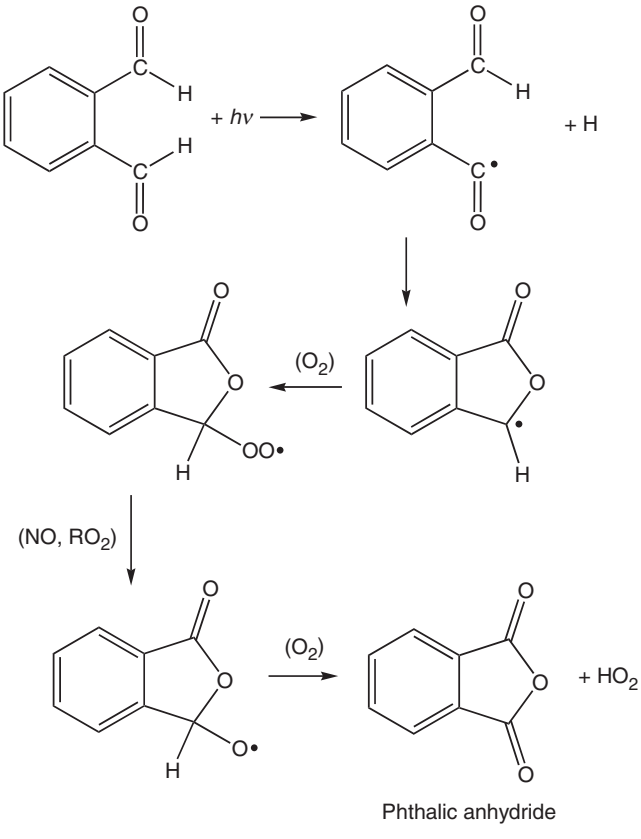

Reaction mechanism IX-L-4.2

The formation of phthalide and 3-methylphthalide from phthaldialdehyde and 2-acetylbenzaldehyde was ascribed to photoisomerization pathways, primary process (IV) shown above and its analogue in 2-acetylbenzaldehyde:

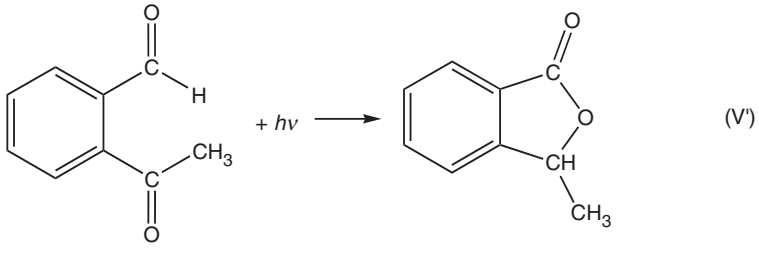

Table IX-L-4. Recommended cross sections (σ, cm^2 $molecule^{-1}$) of phthaldialdehyde as measured in hexane solution (Wang et al., 2006)

λ, nm	$10^{19} \times \sigma$	λ, nm	$10^{19} \times \sigma$	λ, nm	$10^{19} \times \sigma$	λ, nm	$10^{19} \times \sigma$
278.0	38.31	309.0	51.30	340.0	2.22	370.9	1.15
279.1	40.34	310.1	38.89	341.0	2.22	372.0	1.18
280.0	42.29	311.0	28.96	342.0	2.18	373.0	1.34
280.9	44.58	311.9	21.47	343.0	2.25	374.0	1.15
282.0	47.41	313.0	14.52	344.1	2.02	375.0	1.07
283.0	49.97	314.0	10.01	345.0	2.10	376.1	1.15
283.9	52.95	315.1	6.91	345.9	1.83	377.0	1.03
285.0	56.73	316.0	5.46	347.0	2.14	378.1	0.99
286.0	59.36	316.9	4.32	348.0	2.18	379.0	0.88
287.1	62.69	318.0	3.90	349.0	2.02	379.9	1.03
288.0	65.36	319.0	3.29	350.0	1.95	381.0	0.88
288.9	67.96	320.1	3.13	351.1	1.95	381.9	0.80
290.0	70.63	321.0	2.94	352.0	1.68	383.0	0.96
291.0	73.11	321.9	2.64	352.9	1.60	383.9	0.84
292.1	75.52	323.0	2.71	354.0	1.60	385.0	0.80
293.0	78.00	324.0	2.64	355.0	1.57	386.0	0.73
294.0	80.91	325.1	2.75	356.0	1.64	387.0	0.76
295.0	83.05	326.0	2.75	357.0	1.45	388.0	0.92
296.0	84.23	326.9	2.71	358.1	1.49	389.1	0.80
296.9	85.84	328.0	2.64	359.0	1.38	390.0	0.65
298.0	84.31	329.0	2.41	359.9	1.49	391.1	0.76
299.0	81.18	330.0	2.41	361.0	1.30	392.0	0.57
300.1	76.74	331.0	2.52	361.9	1.49	393.1	0.61
301.0	73.99	332.1	2.37	363.0	1.26	394.0	0.53
301.9	71.93	333.0	2.37	364.0	1.38	394.9	0.31
303.0	69.45	333.9	2.22	365.0	1.30	396.0	0.34
304.0	67.08	335.0	2.25	366.0	1.30	396.9	0.65
305.1	64.86	336.0	2.18	367.1	1.22	398.0	0.46
306.0	63.56	337.1	2.22	368.0	1.26	398.9	0.50
306.9	62.72	338.0	1.99	368.9	1.15		
308.0	59.13	338.9	2.29	370.0	1.18		

Wang et al. (2006) determined the decay rates of the three compounds in irradiated mixtures of the given dicarbonyl compound in air mixtures with an excess of cyclohexane added to capture OH radicals. Loss rates were determined from least-squares analyses of the data over the time period of 60–180 min. period of irradiation and referenced versus $j(NO_2)$ determinations. Correction was made for the wall loss using an average of initial (0–60) and final (180–240 min) dark decay rates. In experiments with 10% lights turned on, the measured $j(NO_2) = 0.061\,min.^{-1}$, j-values for phthaldialdehyde and 2-acetylbenzaldehyde were $(2.5 \pm 1.8) \times 10^{-3}$ and $(0.9 \pm 1.8) \times 10^{-3}$ $min.^{-1}$, respectively. With all the lights turned on, the measured $j(NO_2) = 0.535\,min.^{-1}$ and the j-values for the two carbonyls were: $(15.9 \pm 1.7) \times 10^{-3}$ and $(11.4 \pm 1.4) \times 10^{-3}$ $min.^{-1}$, respectively. After correction for wall losses, experiments with 1,2-diacetylbenzene gave small negative j-values, and it was clear that this carbonyl was less photochemically active than the other dicarbonyls.

Table IX-L-5. Recommended cross sections (σ, cm^2 $molecule^{-1}$) of 2-acetylbenzaldehyde as measured in hexane solution (Wang et al., 2006)

λ, nm	$10^{19} \times \sigma$	λ, nm	$10^{19} \times \sigma$	λ, nm	$10^{19} \times \sigma$	λ, nm	$10^{19} \times \sigma$
278.0	36.60	309.0	10.28	340.0	3.86	370.9	1.03
279.1	38.16	310.1	9.02	341.0	3.59	372.0	0.99
280.0	40.11	311.0	7.95	342.0	3.40	373.0	0.96
280.9	41.29	311.9	7.37	343.0	3.02	374.0	0.76
282.0	42.98	313.0	6.72	344.1	3.32	375.0	0.88
283.0	44.31	314.0	6.72	345.0	3.06	376.1	0.88
283.9	45.80	315.1	6.38	345.9	2.90	377.0	0.73
285.0	47.10	316.0	6.26	347.0	2.71	378.1	0.80
286.0	48.17	316.9	6.04	348.0	2.75	379.0	0.57
287.1	48.59	318.0	5.92	349.0	2.71	379.9	0.65
288.0	49.20	319.0	5.69	350.0	2.60	381.0	0.53
288.9	49.43	320.1	5.65	351.1	2.29	381.9	0.57
290.0	49.47	321.0	5.65	352.0	2.33	383.0	0.50
291.0	49.05	321.9	5.39	352.9	2.37	383.9	0.50
292.1	48.32	323.0	5.54	354.0	2.22	385.0	0.34
293.0	47.33	324.0	5.20	355.0	2.10	386.0	0.38
294.0	45.99	325.1	5.31	356.0	1.95	387.0	0.61
295.0	43.74	326.0	5.04	357.0	1.83	388.0	0.42
296.0	41.71	326.9	5.23	358.1	1.68	389.1	0.46
296.9	39.50	328.0	5.00	359.0	1.76	390.0	0.57
298.0	36.82	329.0	4.89	359.9	1.68	391.1	0.46
299.0	33.54	330.0	4.74	361.0	1.53	392.0	0.46
300.1	29.68	331.0	4.66	361.9	1.80	393.1	0.31
301.0	27.20	332.1	4.58	363.0	1.57	394.0	0.38
301.9	25.17	333.0	4.24	364.0	1.64	394.9	0.15
303.0	22.12	333.9	4.35	365.0	1.34	396.0	0.27
304.0	19.56	335.0	3.97	366.0	1.30	396.9	0.31
305.1	17.00	336.0	4.16	367.1	1.34	398.0	0.15
306.0	15.43	337.1	4.13	368.0	1.18	398.9	0.31
306.9	13.98	338.0	4.16	368.9	1.03		

IX-L-4.3. Photolysis Frequencies for the Photodecomposition of Some Aromatic Dicarbonyls in the Lower Troposphere

The data for phthaldialdehyde and 2-acetylbenzaldehyde were used by Wang et al. (2006) to derive average quantum yields of the loss of aromatic carbonyls: 0.19 for phthaldialdehyde and 0.21 for 2-acetylbenzaldehyde. The authors note that the measurements apply for the blacklamp spectral distribution which is somewhat different from that of sunlight. However, we have used these data to derive very approximate *j*-values at various solar zenith angles within the lower troposphere using the average quantum yields, together with the cross section data and appropriate solar flux data. See figures IX-L-9 and IX-L-10. The calculated *j*-values given in figures IX-L-9 and IX-L-10 suggest the following lifetimes for the total of photochemical decomposition and isomerization processes in these aromatic dicarbonyls in the lower troposphere with an overhead Sun: phthaldialdehyde, ~ 20 min.; 2-acetylbenzaldehyde, ~19 min. For a period near June 22 with an overhead ozone column of 350 DU, our calculations

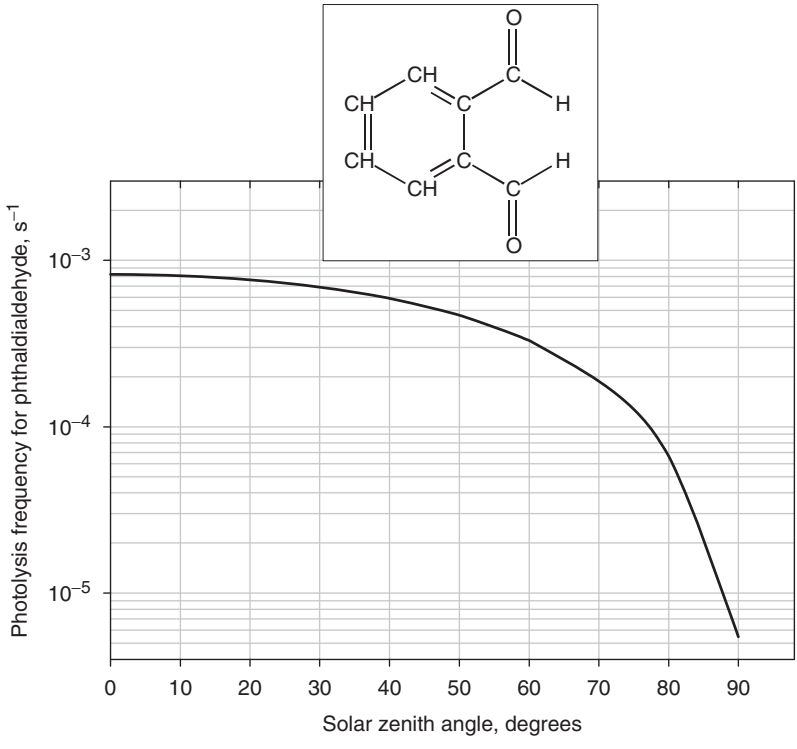

Figure IX-L-9. Approximate photolysis frequencies as a function of solar zenith angle for phthaldedialdehyde photodecomposition as calculated for a clear skies in the lower troposphere with an overhead ozone column of 350 DU; we have assumed a wavelength independence of the average quantum yield of photodecomposition = 0.19 as measured in broadband experiments referenced to $j(NO_2)$ by Wang et al. (2006).

suggest lifetimes of 1.0 h and 0.9 h, respectively. Wang et al. estimated atmospheric lifetimes for photodecomposition averaged over a 12 h period of 1.8 h and 2.5 h, respectively.

IX-L-5. The Photodecomposition of 2-Nitrobenzaldehyde (*o*-Nitrobenzaldehyde)

Nitrobenzaldehydes have not been reported as products of the atmospheric oxidation of toluene, but these compounds could conceivable be formed through the oxidation of toluene in an NO_x-rich atmosphere. *o*-Nitrobenzaldehyde has been used successfully as an actinometer in photochemical studies (Pitts et al., 1964), and in this sense a brief discussion of its photochemistry is given here. The photochemistry of *o*-nitrobenzaldehyde has been studied in acetone and ligroin solutions (Leighton and Lucy, 1934a, b); in the pure solid (Bowen et al., 1924), and in KBr matrices (Pitts et al., 1964). Photolysis results in the ultimate isomerization to *o*-nitrosobenzoic acid, structure C (reaction mechanism IX-L-5).

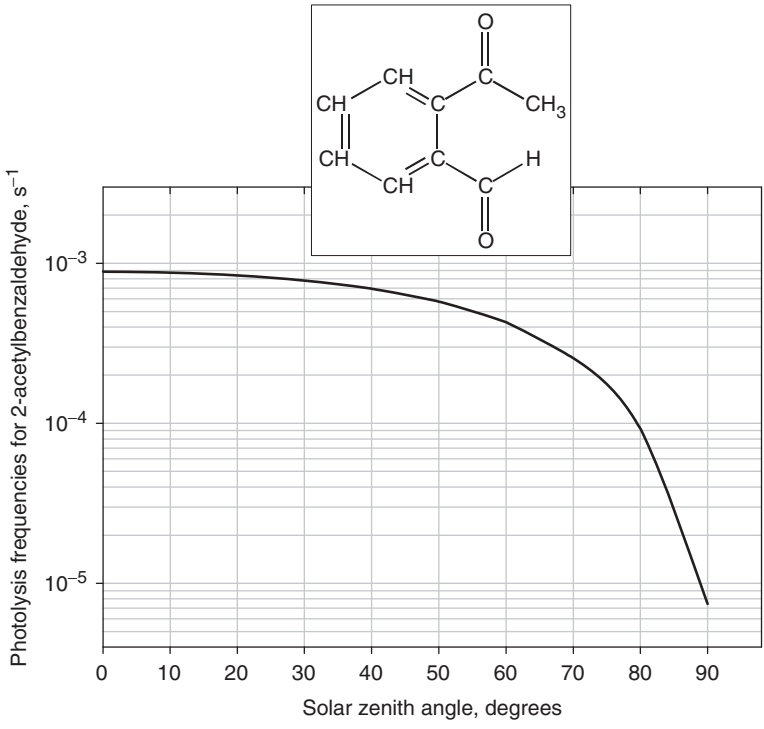

Figure IX-L-10. Approximate photolysis frequencies as a function of solar zenith angle for 2-aetylbenzaldehyde photodecomposition as calculated for a clear skies in the lower troposphere with an overhead ozone column of 350 DU; we have assumed a wavelength independence of the average quantum yield of photodecomposition = 0.21 as measured in broadband experiments referenced to $j(NO_2)$ by Wang et al. (2006).

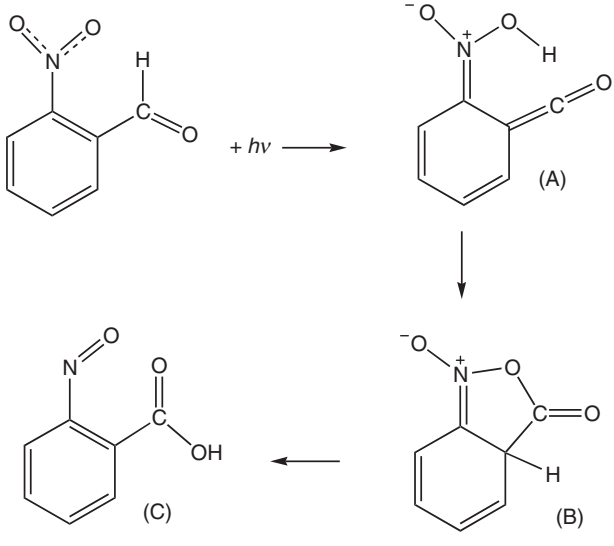

Reaction mechanism IX-L-5

This interesting rearrangement occurs with high efficiency ($\phi_I = 0.5$) at all of the wavelengths that have been studied and in both the liquid and solid phases. Laimgruber et al. (2005) using femtosecond vibrational spectroscopy observed the intermediate formation of a ketene, presumably structure A. The final product *o*-nitrosobenzoic acid (structure C) forms in photolysis of *o*-nitrobenzaldehyde in both the pure liquid and solid phases. While photolyses in solutions of ethyl alcohol forms *o*-nitrosoethylbenzoate with $\Phi = 0.5$, evidence suggests that the first step of ketene formation occurs with a quantum yield of 0.5 in about 400 fs. With photolyses in ethanol solution, the subsequent rearrangement to structure B occurs in about 90 ps with final ester product formation within 3 ns. Laimgruber et al. suggest that the insensitivity of the product yields to the phase or solvent results from the loss of efficiency in formation of the final products in the first step of the photolysis, the ketene formation. They suggest that decay is promoted by the motion of the hydrogen atom from the aldehyde moiety to the nitro group. The motion brings the ground- and excited-state surfaces in energetic vicinity, and internal conversion takes place about 50% of the time.

IX-L-5.1. Absorption Cross Sections for 2-Nitrobenzaldehde

The absorption spectrum of 2-nitrobenzaldehyde as measured in a nonpolar solvent (Láng, 1961–1971) is given in figure IX-L-11, where it can be compared with that of unsubstituted benzaldehyde and 2-hydroxybenzaldehyde. 2-Nitrobenzaldehyde is the strongest absorber, and its absorption region is shifted into the visible spectral region.

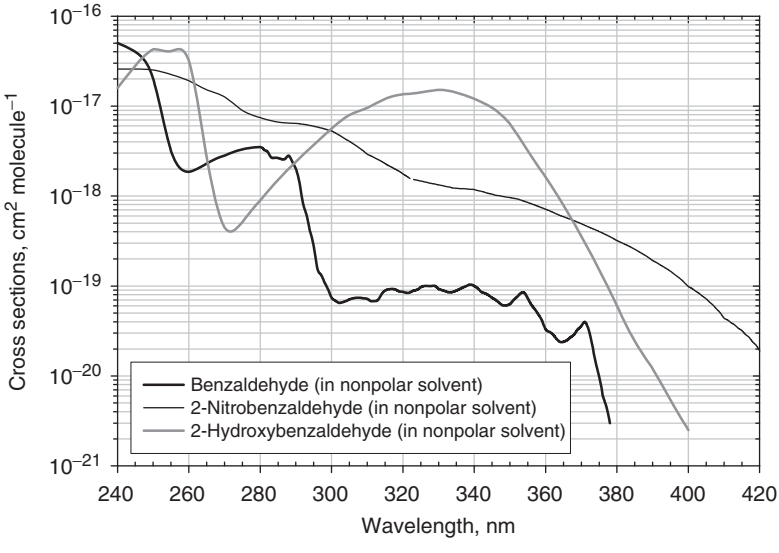

Figure IX-L-11. Plot of the absorption cross sections for benzaldehyde and a two substituted benzaldehydes; from measurements in nonpolar solvents (Láng, 1961–1971); figure from Calvert et al. (2008).

Table IX-L-6. Cross sections for 2-nitrobenzaldehyde at wavelengths from 290 to 420 nm; from measurements in nonpolar solvents (Láng, 1961–1971); units for σ are cm^2 $molecule^{-1}$

λ, nm	$10^{19} \times \sigma$	λ, nm	$10^{19} \times \sigma$	λ, nm	$10^{19} \times \sigma$	λ, nm	$10^{19} \times \sigma$
290	63.9	323	15.3	356	8.21	389	2.05
291	63.3	324	15.0	357	7.94	390	1.92
292	62.7	325	14.7	358	7.66	391	1.83
293	61.7	326	14.4	359	7.40	392	1.73
294	60.7	327	14.1	360	7.14	393	1.64
295	59.5	328	13.8	361	6.88	394	1.55
296	58.3	329	13.6	362	6.61	395	1.46
297	57.0	330	13.3	363	6.35	396	1.36
298	55.6	331	13.1	364	6.09	397	1.27
299	54.2	332	12.8	365	5.90	398	1.18
300	52.8	333	12.6	366	5.70	399	1.08
301	50.3	334	12.3	367	5.51	400	0.99
302	47.7	335	12.2	368	5.32	401	0.94
303	45.1	336	12.1	369	5.12	402	0.88
304	42.6	337	12.1	370	4.93	403	0.83
305	40.4	338	12.0	371	4.73	404	0.77
306	38.1	339	11.9	372	4.54	405	0.72
307	35.9	340	11.8	373	4.37	406	0.66
308	33.6	341	11.5	374	4.21	407	0.61
309	31.4	342	11.3	375	4.04	408	0.55
310	29.1	343	11.0	376	3.87	409	0.50
311	27.9	344	10.7	377	3.70	410	0.44
312	26.6	345	10.5	378	3.54	411	0.42
313	25.4	346	10.2	379	3.37	412	0.39
314	24.2	347	10.1	380	3.20	413	0.37
315	22.9	348	9.90	381	3.07	414	0.34
316	21.7	349	9.76	382	2.94	415	0.32
317	20.7	350	9.61	383	2.82	416	0.29
318	19.7	351	9.46	384	2.69	417	0.27
319	18.7	352	9.31	385	2.56	418	0.24
320	17.6	353	9.04	386	2.43	419	0.22
321	16.6	354	8.76	387	2.30	420	0.19
322	15.6	355	8.48	388	2.18		

The spectral data obtained from its solutions in nonpolar solvents are given in table IX-L-6.

IX-L-5.2. Quantum Yields of Photodecomposition of 2-Nitrobenzaldehyde

Quantum yields appear to be relatively insensitive to the wavelength of absorbed light as well as the phase in which the compound occurs. In acetone, ligroin, benzene, and other nonpolar solutions, $\phi_I = 0.46$ at 404 nm; 0.51 at 366 nm; in pure solid: $\phi_I = 0.51$ at 313 nm; in KBr matrix: $\phi = 0.5$ Because of its highly polar nature and relatively low vapor pressure (0.02 Torr at 298 K) this compound may end up in aerosols, and it is reasonable to assume that $\phi_I = 0.5$ for all $\lambda < 420$ nm available in sunlight within the troposphere.

IX-L-5.3. Photolysis Frequencies for the Photodecomposition of 2-Nitrobenzaldehyde in the Lower Troposphere

Photolysis rate coefficients representative of the lower atmosphere were calculated for a clear lower troposphere with an ozone column of 350 DU using the measured solution phase cross sections and a quantum yield of photoisomerization of 0.5 at all wavelengths of absorbed light; see figure IX-L-12.

IX-L-6. The Photodecomposition of Nitrobenzene

The primary processes in nitrobenzene, the simplest of the nitro-substituted, aromatic hydrocarbons, have received some attention, but the experimental conditions employed in most of the laboratory studies do not match those encountered in the troposphere; e.g., irradiations used $\lambda < 290$ nm (Hastings and Matsen, 1948; Hurley and Testa, 1966; Yip et al., 1984; Galloway et al., 1993, 1994; Hwang et al., 1996; Takezaki et al., 1997a, b). There are four primary processes that have been proposed to explain

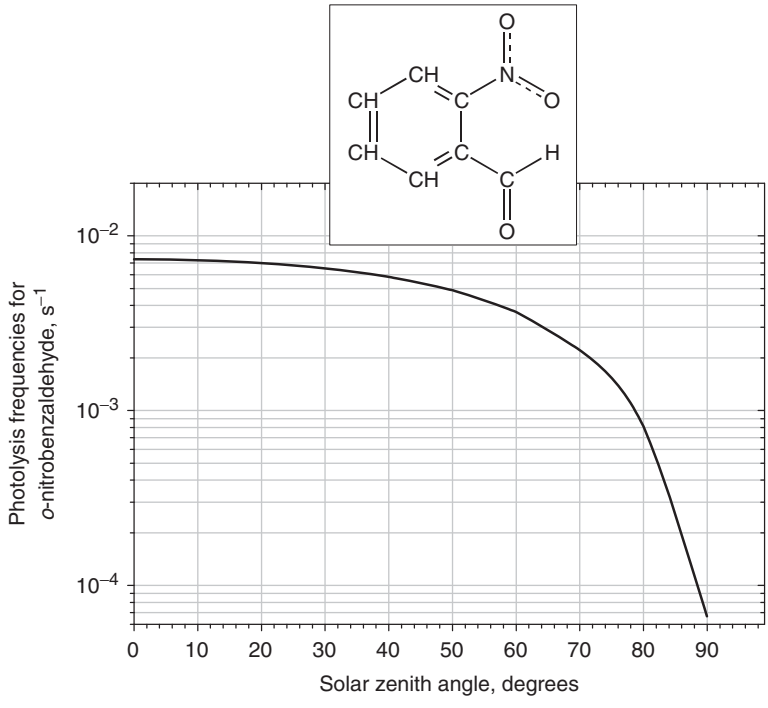

Figure IX-L-12. 2-Nitrobenzaldehyde photolysis frequencies as a function of solar zenith angle for clear lower tropospheric skies at 0.5 km altitude and an ozone column of 350 DU; the results shown were calculated using the measured solution phase cross sections, and a quantum yield of photoisomerization of 0.5; figure from Calvert et al. (2002).

the results of these studies (Calvert et al., 2002):

$$C_6H_5NO_2 + h\nu \rightarrow C_6H_5NO + O(^3P) \quad \text{(I)}$$

$$\rightarrow C_6H_5 + NO_2 \quad \text{(II)}$$

$$\rightarrow [C_6H_5ONO] \rightarrow C_6H_5O + NO \quad \text{(III)}$$

$$\rightarrow C_5H_5 + CO + NO \quad \text{(IV)}$$

In the full-arc irradiation of nitrobenzene vapors (in N_2), Hastings and Matsen (1948) identified nitrosobenzene and *p*-nitrophenol but found no evidence for NO_2 formation. The occurrence of primary process (I) alone was suggested to explain the results. The reactions of electronically excited nitrobenzene are believed to occur from the first excited n, π^*-triplet, 243 kJ mole^{-1} above the ground state (Yip et al., 1984). Vacuum UV photoionization molecular beam mass spectrometry was used by Galloway et al. (1993) to identify the different fragments formed in the primary process in photolyses at wavelengths in the range 220–320 nm. The occurrence of process (I) was confirmed by photoionization–mass spectrometric observation of the nitrosobenzene molecule, but the $O(^3P)$ atom, with its very high ionization potential, could not be detected by this technique. The photoionization cross section for nitrosobenzene is unknown, so estimates of the relative extent of the photolysis which proceeded by channel (I) could not be made. However, the relative yield of C_6H_5NO (proportional to ϕ_I) increased significantly from the onset at about 280 nm to the shorter wavelengths. The ratios of $\phi_I/(\phi_{III} + \phi_{IV})$ observed for photolyses at 280, 240, and 222 nm are 1.3 ± 0.3, 3.7 ± 0.2, and 5.9 ± 0.3, respectively. It is estimated that the minimum energies required for processes (I) and (II) are 389 and 297 kJ mol^{-1}, corresponding to possible onset wavelengths of 307 and 403 nm, respectively. In photolyses at the shorter wavelengths (280 nm), the NO_2 product may be electronically excited. The detection of the C_5H_5 fragment (presumably cyclopenta-1,3-dien-5-yl radical) from decomposition in process (IV) by Galloway et al. (1993) is consistent with the spectroscopic observation of cyclopenta-1,3-diene in the flash photolysis of nitrobenzene (Porter and Ward, 1968). Galloway et al. (1994) found that the NO molecule fragment formed in (III) and (IV) is very rich in rotational energy, but with little vibrational energy; the rotational temperature of NO formed in 226 nm photolyses was $3{,}700 \pm 350$ K while that formed at 280 nm was $2{,}400 \pm 200$ K. They rationalize the energy distribution in the products of (III) and/or (IV) by a mechanism of isomerization of nitrobenzene to C_6H_5ONO (benzene nitrite) followed by a rupture of the C_6H_5O—NO bond to form the various products.

In solution phase studies of Takezaki et al. (1997a), the lifetimes of the S_1 and T_1 states of nitrobenzene were found to be very short, < 10 ps and ~ 480 ps, respectively. They have assumed that photodecomposition was unimportant for nitrobenzene and estimated the ϕ for intersystem crossing to be ≥ 0.8. In the reaction of the triplet nitrobenzene in H-atom-containing solvents, H-atom abstraction from solvent molecules occurs, but this is inefficient since the lifetime of the triplet is very short

(Hurley and Testa, 1968; Yip et al., 1984). Takezaki et al. (1997b) have studied theoretically the geometries and energies of the excited states of nitrobenzene, and report that the O-atoms of the normally in-plane nitro group are largely bent out of the phenyl plane in the excited states.

IX-L-6.1. Absorption Cross Sections for Nitrobenzene

The solution phase absorption spectrum of nitrobenzene (250–380 nm) shows both the strong $\pi \rightarrow \pi^*$ and the weaker $n \rightarrow \pi^*$ bands; the latter band alone is important in the troposphere. Absorption cross sections for nitrobenzene in this region are given (for a hexane solution) in figure IX-L-13 (Láng, 1961–1971). The cross sections for nitrobenzene (in hexane solution) as a function of wavelength are summarized in table IX-L-7.

IX-L-6.2. Quantum Yields of Photodecomposition of Nitrobenzene

For the wavelengths available in sunlight within the troposphere, it is likely that (I) is unimportant because of the energy limitation. The enthalpy changes for processes (II), (III), and (IV) are approximately 297, 71, and 155 kcal mole^{-1}, respectively, but since extensive rearrangements accompany (III) and (IV), significant unknown barriers to these reactions may exist. There are no direct measurements of the extent and wavelength dependence of the photodecomposition modes within the long-wavelength band, so we recommend the assumption that decomposition occurs by processes (II) and (III) with an efficiency similar to that observed in sunlight photolyses of other aromatic nitro compounds. See the section IX-L-7 on 1- and 2-nitronaphthalene and section IX-L-8 on methyl-1-nitronaphthalene.

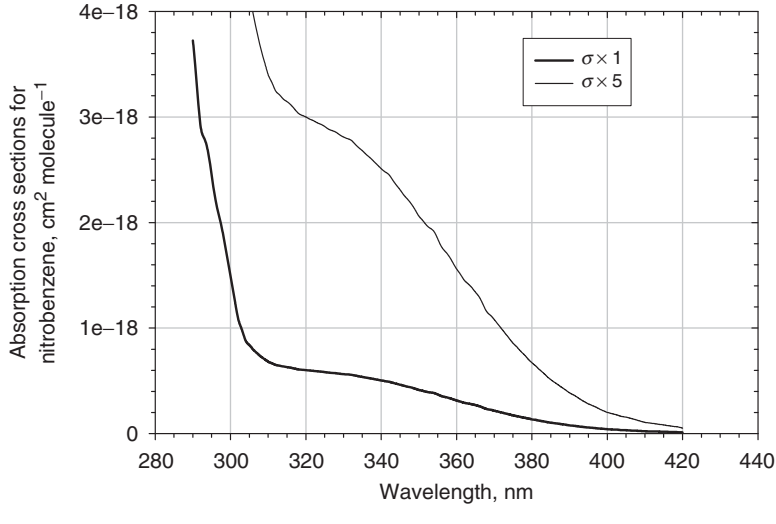

Figure IX-L-13. Absorption cross sections for the long wavelength band in nitrobenzene as measured in ethanol solution (Láng, 1961–1971).

Table IX-L-7. Absorption cross sections (σ) for nitrobenzene as measured by Láng (1961–1971) in ethanol solution; units for σ are cm^2 molecule^{-1}

λ, nm	$10^{19} \times \sigma$	λ, nm	$10^{19} \times \sigma$	λ, nm	$10^{19} \times \sigma$	λ, nm	$10^{19} \times \sigma$
290	37.25	323	5.89	356	3.54	389	0.82
291	33.24	324	5.86	357	3.45	390	0.77
292	29.22	325	5.82	358	3.36	391	0.73
293	27.98	326	5.77	359	3.24	392	0.69
294	26.74	327	5.74	360	3.12	393	0.64
295	24.45	328	5.71	361	3.02	394	0.60
296	22.16	329	5.66	362	2.91	395	0.56
297	20.54	330	5.62	363	2.84	396	0.53
298	18.91	331	5.59	364	2.77	397	0.50
299	16.91	332	5.56	365	2.68	398	0.46
300	14.90	333	5.49	366	2.59	399	0.43
301	12.90	334	5.42	367	2.45	400	0.40
302	10.89	335	5.36	368	2.31	401	0.38
303	9.84	336	5.29	369	2.24	402	0.36
304	8.79	337	5.23	370	2.16	403	0.34
305	8.37	338	5.16	371	2.07	404	0.32
306	7.95	339	5.09	372	1.98	405	0.31
307	7.62	340	5.02	373	1.89	406	0.29
308	7.30	341	4.96	374	1.80	407	0.27
309	7.05	342	4.91	375	1.71	408	0.25
310	6.80	343	4.81	376	1.64	409	0.23
311	6.65	344	4.71	377	1.56	410	0.21
312	6.49	345	4.62	378	1.49	411	0.20
313	6.42	346	4.52	379	1.41	412	0.19
314	6.34	347	4.44	380	1.34	413	0.18
315	6.29	348	4.35	381	1.28	414	0.17
316	6.23	349	4.24	382	1.21	415	0.16
317	6.15	350	4.12	383	1.15	416	0.15
318	6.07	351	4.04	384	1.08	417	0.14
319	6.03	352	3.95	385	1.02	418	0.13
320	6.00	353	3.89	386	0.97	419	0.12
321	5.96	354	3.83	387	0.92	420	0.10
322	5.93	355	3.69	388	0.87		

IX-L-6.3. Photolysis Frequencies for the Photodecomposition of Nitrobenzene in the Lower Troposphere

Photolysis rate coefficients representative of the lower atmosphere were calculated for a cloudless sky at 0.5 km altitude and an ozone column of 350 DU. The measured solution phase cross sections and quantum yield data representative of the nitro-napthalenes ($\phi \sim 3.5 \times 10^{-3}$) were used in the calculation. See figure IX-L-14. These data indicate a lifetime for photodecomposion of about 14 h.

IX-L-7. Photodecomposition of 1-Nitronaphthalene and 2-Nitronaphthalene

Photochemical studies of the nitronaphthalenes have been made by Atkinson et al. (1989b) and Fielberg et al. (1999). Irradiations in both indoor and outdoor chambers

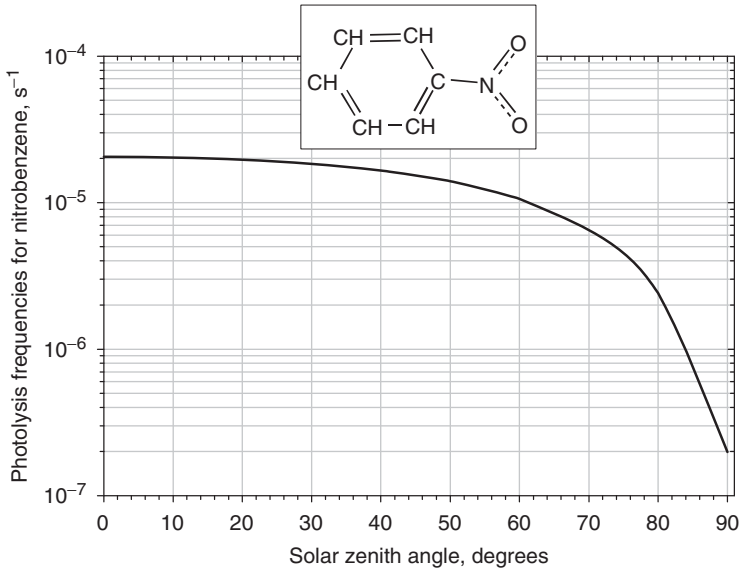

Figure IX-L-14. Nitrobenzene photolysis frequencies as a function of solar zenith angle for clear skies in the lower troposphere, 0.5 km altitude and an ozone column of 350 DU; data were calculated using the solution phase absorption spectrum and quantum yield of decomposition typical of the nitronaphthalenes ($\phi_{total} \approx 3.5 \times 10^{-3}$).

have been made and rates of disappearance of the nitronaphthalenes have been determined. A product observed in 1-nitronaphthalene studies was 1,4-naphthoquinone (Atkinson et al., 1989b), which suggests that the primary processes (I) and (II) may occur in the photodecomposition at the wavelengths present within the troposphere:

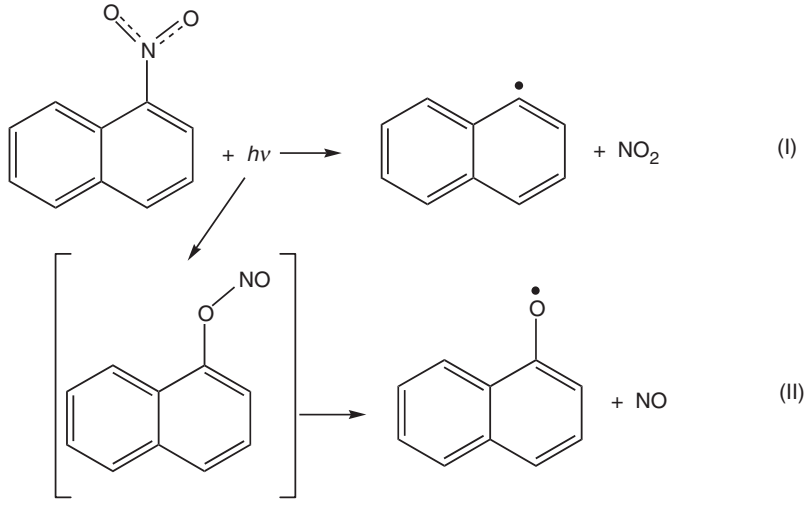

The similar rates of photolysis for 2-nitronaphthalene exposed to sunlight suggest that perhaps similar photodecomposition modes may occur in this compound, although no final reaction products were reported for this compound.

Somewhat different results were obtained in the chamber studies of Fielberg et al. (1999), where a more rapid photochemical decay of the 1-nitronaphthalene was observed.

IX-L-7.1. Absorption Cross Sections for the Nitronaphthalenes

Gas-phase absorption spectra for 1- and 2-nitronaphthalene are not available to us at this writing, but as a reasonable surrogate we may use that observed for 1-nitro-2-methylnaphthalene in ethanol solution (Láng, 1961–1971). These data are shown in figure IX-L-15. The cross sections at wavelengths within the troposphere are summarized in table IX-L-8.

IX-L-7.2. Quantum Yields and Approximate Photolysis Frequencies for Photodecomposition of 1- and 2-Nitronaphthalene

Atkinson et al. (1989b) carried out three experiments in an outdoor chamber in sunlight-irradiated 1-nitronaphthalene in mixtures of synthetic air with measured first-order rates of loss (min.$^{-1}$) of: $(1.30 \pm 0.22) \times 10^{-2}$ (7 September, 14:18–16:42 PDT), $(1.15 \pm 0.41) \times 10^{-2}$ (8 September, 15:07–17:18 PDT), and $(8.2 \pm 0.6) \times 10^{-3}$ (31 October, 10:36–15:25 PST). Similar results with 2-nitronaphthalene gave first-order rates of loss of: $(1.01 \pm 0.30) \times 10^{-2}$, $(3.4 \pm 0.4) \times 10^{-3}$ and $(6.4 \pm 0.5) \times 10^{-3}$ min.$^{-1}$. Measurements of $j(NO_2)$ made at approximately the location of the chamber

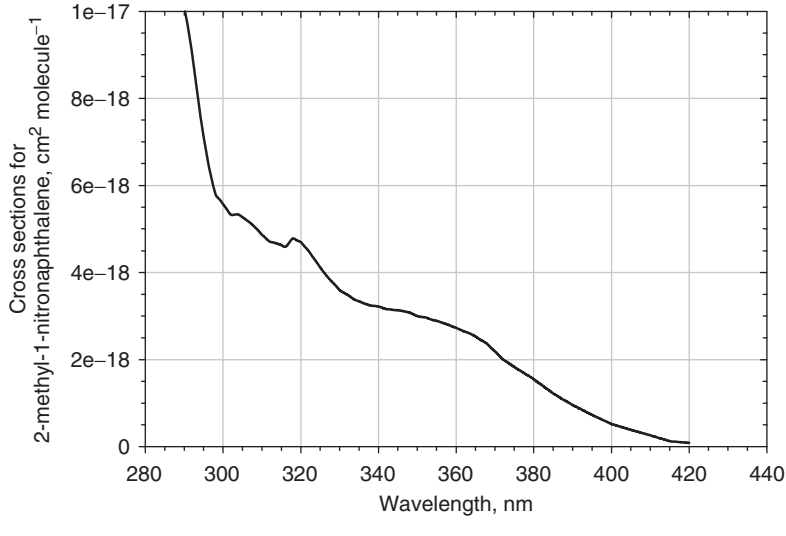

Figure IX-L-15. Cross sections for 2-methyl-1-nitronaphthalene as measured in ethanol solution by Láng (1961–1971).

Table IX-L-8. Cross sections as a function of wavelength for 2-methyl-1-nitronaphthalene as measured in ethanol solutions by Láng (1961–1971); units for σ are are cm^2 $molecule^{-1}$

λ, nm	$10^{19} \times \sigma$	λ, nm	$10^{19} \times \sigma$	λ, nm	$10^{19} \times \sigma$	λ, nm	$10^{19} \times \sigma$
290	101.2	323	43.7	356	28.6	389	10.1
291	96.0	324	42.5	357	28.3	390	9.57
292	90.8	325	41.2	358	28.0	391	9.11
293	83.9	326	40.0	359	27.6	392	8.66
294	77.0	327	38.9	360	27.3	393	8.20
295	71.4	328	37.9	361	26.9	394	7.74
296	65.8	329	37.0	362	26.5	395	7.29
297	61.9	330	36.0	363	26.2	396	6.87
298	58.1	331	35.4	364	25.8	397	6.45
299	56.9	332	34.9	365	25.3	398	6.04
300	55.7	333	34.3	366	24.7	399	5.62
301	54.5	334	33.7	367	24.2	400	5.20
302	53.3	335	33.4	368	23.6	401	4.93
303	53.3	336	33.0	369	22.7	402	4.66
304	53.3	337	32.7	370	21.9	403	4.39
305	52.7	338	32.4	371	21.0	404	4.12
306	52.1	339	32.3	372	20.1	405	3.85
307	51.4	340	32.2	373	19.5	406	3.60
308	50.6	341	31.9	374	18.9	407	3.35
309	49.7	342	31.6	375	18.3	408	3.10
310	48.7	343	31.5	376	17.7	409	2.85
311	47.9	344	31.4	377	17.2	410	2.60
312	47.1	345	31.3	378	16.6	411	2.33
313	46.9	346	31.2	379	16.1	412	2.06
314	46.6	347	31.0	380	15.5	413	1.79
315	46.3	348	30.8	381	14.8	414	1.52
316	45.9	349	30.4	382	14.2	415	1.25
317	46.8	350	30.0	383	13.5	416	1.17
318	47.8	351	29.8	384	12.9	417	1.08
319	47.4	352	29.7	385	12.2	418	1.00
320	47.0	353	29.4	386	11.7	419	0.92
321	46.0	354	29.1	387	11.1	420	0.83
322	45.0	355	28.9	388	10.6		

on October 10 were $4.16 \times 10^{-3}\ s^{-1}$ at 11:15 PDT and $4.33 \times 10^{-3}\ s^{-1}$ at 11:00 PST on October 31. Hence for these conditions, Atkinson et al. (1989b) estimate j(Total) for 1- and 2-nitronaphthalenes are: $(1.37 \pm 0.10) \times 10^{-4}\ s^{-1}$ and $(1.06 \pm 0.08) \times 10^{-4}\ s^{-1}$, respectively. Somewhat more rapid photolysis of 1-nitronaphthalene was observed in the outdoor chamber experiments of Fielberg et al. (1999). These experiments involved the sunlight irradiation of mixtures of the naphthalene, propylene, NO_x, and diesel soot particles and the modeling of the rates of formation and decay of the nitronaphthalene products. The experiments were designed primarily to test the understanding of the partitioning of the nitro-PAH on particles, and the composition of the starting mixtures is considerably more complex than that employed by Atkinson et al. (1989b). Fielberg et al. (1999) suggest that the gas-phase photolysis is the major degradation pathway for

1-nitronaphthalene in this system with the j(photodecomposition) $\approx 0.07 \times j(NO_2)$, a result about a factor of 2 higher than that of Atkinson et al. (1989b). Rates of photolysis for the 2-nitronaphthalene observed by Fielberg et al. (1999), j(photodecompostion) $\sim 0.005 \times j(NO_2)$ are about a factor of 5 lower than those observed by Atkinson et al. (1989b). While further study is needed, Calvert et al. (2002) tentatively recommended that the photolysis rate data of Atkinson et al. (1989b) be used.

IX-L-8. Photodecomposition of 2-Methyl-1-nitronaphthalene

The photochemistry of 2-methyl-1-nitronaphthalene in air was studied by Arey et al. (1990b) in a sunlight-irradiated chamber. 2-Methyl-1,4-naphthoquinone was observed to be a major product, and the photodecomposition modes analogous to those given for 1- and 2-nitronaphthalene are suggested [processes (1) and (II)].

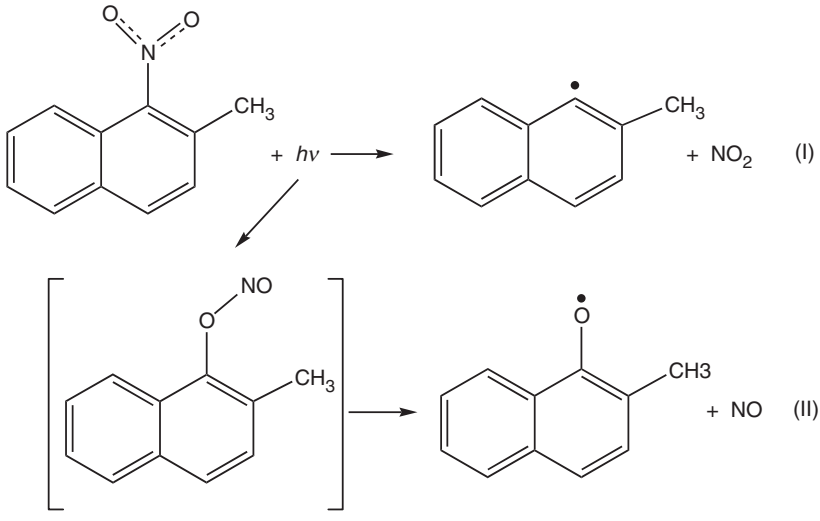

IX-L-8.1. Absorption Cross Sections for 2-Methyl-1-nitronaphthalene

The absorption spectrum of 2-methyl-1-nitronaphthalene is given in figure IX-L-15 as was reported by Láng (1961–1971) in ethanol solution. The absorption cross sections for wavelengths of sunlight present within the troposphere are summarized in table IX-L-8.

IX-L-8.2. Quantum Yields of Photodecomposition of 2-Methyl-1-nitronaphthalene

The rate of disappearance in the sunlight photolysis of the 2-methyl-1-nitronaphthalene was determined in the studies of Arey et al. (1990b) from which an estimate of j(Total) $= (1.1 \pm 0.3) \times 10^{-4}\ s^{-1}$ was determined for irradiation from 10:54 to 15:31 PST on November 4 in Riverside, CA. This is similar to the values observed by Atkinson

et al. (1989b) and is qualitatively in agreement with those reported by Fielberg et al. (1999) for the 1- and 2-nitronaphthalenes.

IX-L-8.3. Photolysis Frequencies for the Photodecomposition of 2-Methyl-1-nitronaphthalene in the Lower Troposphere

Photolysis frequencies representative of the lower atmosphere were calculated by Calvert et al. (2002) for an altitude of 0.5 km and an overhead ozone column of 350 DU; the solution phase cross sections and an assumed effective quantum yield of 3.5×10^{-3} were used to match the *j*-values observed experimentally by Atkinson et al. (1989b). See figure IX-L-16.

IX-L-9. Photodecomposition of Phenols, Cresols, and Other OH-Substituted Aromatic Compounds

There is little information concerning the photochemistry of the OH-substituted polycyclic aromatic species. However, the several studies of the photochemistry of the simple substituted phenols allow a significant insight into the primary processes present in the higher molecular weight, OH-substituted aromatic hydrocarbons; and, in this sense, a brief review of this work is given here (see Calvert et al., 2002).

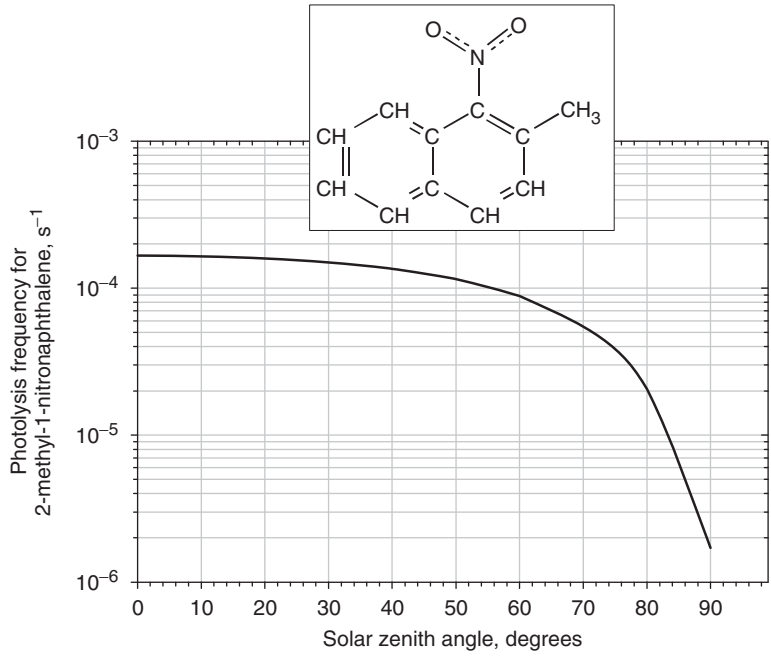

Figure IX-L-16. 2-Methyl-1-nitronaphthalene photodissociation coefficients at 0.5 km altitude as a function of solar zenith angle, using measured solution-phase cross sections and an assumed quantum yield of decomposition of 3.5×10^{-3} in order to obtain a match between the calculations and measurements.

Process I, the rupture of the RO—H bond, appears to be the only significant primary process in the photodecomposition of phenol, alkyl-radical-substituted phenols, and by analogy, the higher molecular weight OH-substituted aromatic hydrocarbons; this is shown here for the substituted phenols (R = an H-atom or any alkyl group):

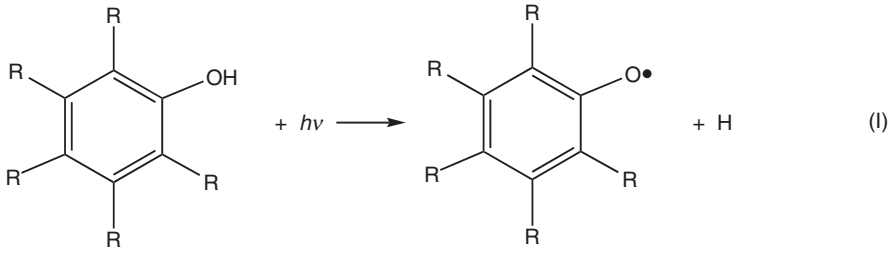

(I)

In the studies of Land and Porter (1963) flash photolysis was carried out on 18 different alkyl-radical-substituted phenols with R = CH_3, C_2H_5, *tert*-C_4H_9, and/or C_6H_5 in various nonpolar and polar solvents, and the absorption spectra of the corresponding phenoxy radical was observed in all cases. Grabner et al. (1990) made an extensive study of the photochemistry of the methylated phenols in hydrocarbon solvents at 293 K and with $\lambda_{excit} = 275$ nm; they determined the quantum yields of fluorescence, triplet molecule formation, and photodecomposition. The quantum yields of photodecomposition of phenol and its 2-methyl-, 3-methyl-, 4-methyl-, 2,6-dimethyl-, 3,5-dimethyl-, 2,4,6-trimethyl-, and 2,3,5-trimethyl-derivatives, as measured through the absorption of the phenoxy radicals formed were: 0.13, 0.18, 0.14, 0.08, 0.21, 0.14, 0.20, and 0.18, respectively. Evidence suggested that this photodecomposition occurred from a vibrationally excited triplet state.

Lipczynska-Kochany and Botton (1992) have studied the photolysis of phenol in an aqueous solution (not degassed) and observed *p*-benzoquinone as a major product with small amounts of hydroquinone. Presumably these products can arise following photodissociation in reaction (I).

Grosjean (1984) has studied the photooxidation of *o*-cresol in sunlight-irradiated air–NO_x mixtures and found a first order loss of *o*-cresol ($k \sim 1.5 \times 10^{-4}\ s^{-1}$), a slow generation of ozone, significant loss of NO_x, and formation of nitrocresols, pyruvic acid, acetaldehyde, formaldehyde, peroxyacetyl nitrate, and various particulate nitroaromatic products. However, it is not clear to what extent the photolysis of the *o*−cresol was responsible for this observed chemistry, since very little absorption of tropospheric sunlight is expected for the *o*−cresol, and NO_3 radical chemistry may have been dominant. See the following section.

IX-L-9.1. Absorption Cross Sections of the Phenols, Cresols, and OH-Substituted Polycyclic Hydrocarbons

The region of light absorption for the simple phenols can be observed in the data of figure IX-L-17 (Etzkorn et al., 1999). The onset of absorption shifts toward the longer wavelengths as methyl groups are added to the aromatic ring of phenol, but even with

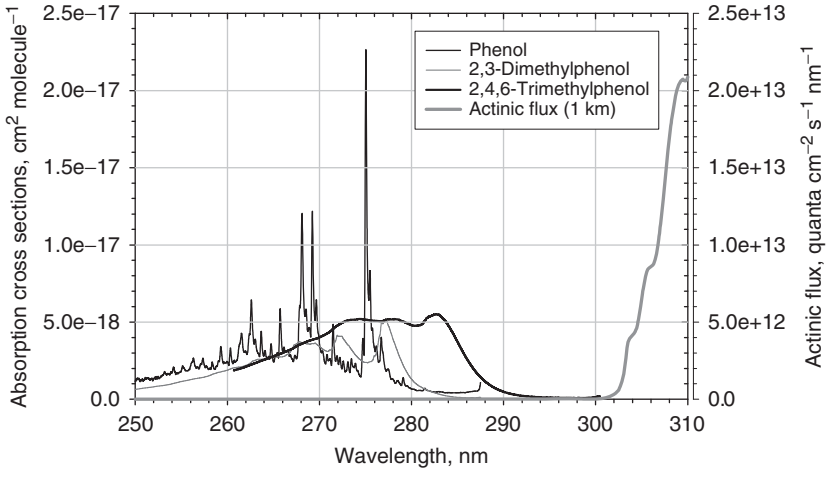

Figure IX-L-17. Cross sections as a function of wavelength for phenol vapor (black thin curve), 2,3-dimethylphenol (thin gray curve), and 2,4,6-trimethylphenol (thick black curve); all data from Etzkorn et al. (1999). Actinic flux is given by the heavy gray curve as a function of wavelength in the lower troposphere for an overhead Sun.

the highly substituted phenols, absorption does not overlap significantly with the actinic flux present in the lower troposphere.

Light absorption by the cresols, $CH_3C_6H_4$—OH, is shifted somewhat to the longer wavelengths than that observed in phenol, but there is still little overlap of this with the distribution of solar flux available in the lower troposphere; see figure IX-L-18.

With the hydroxy-substituted aromatics absorption of the light available in the lower troposphere increases as the number of fused aromatic rings increases; see figure IX-L-19.

IX-L-9.2. Quantum Yields of Photodecomposition of OH-Substituted Polycyclic Hydrocarbons and Photolysis Frequencies for Excitation by Light Absorption

We are not aware of any studies of the photochemistry of the OH-substituted polycyclic aromatic hydrocarbons, but by analogy with the photochemistry of the simple substituted phenols discussed in this section, we would expect photodissociation by process (I) to be significant at the wavelengths of sunlight available within the troposphere:

$$\mathrm{ROH} + h\nu \rightarrow \mathrm{H} + \mathrm{RO} \qquad \text{(I)}$$

Calvert et al. (2002) pointed out that the minimum energy required for the occurrence of process (I) is provided at $\lambda \leq 330$ nm. The j(excitation) for 2-hydroxynaphthalene and

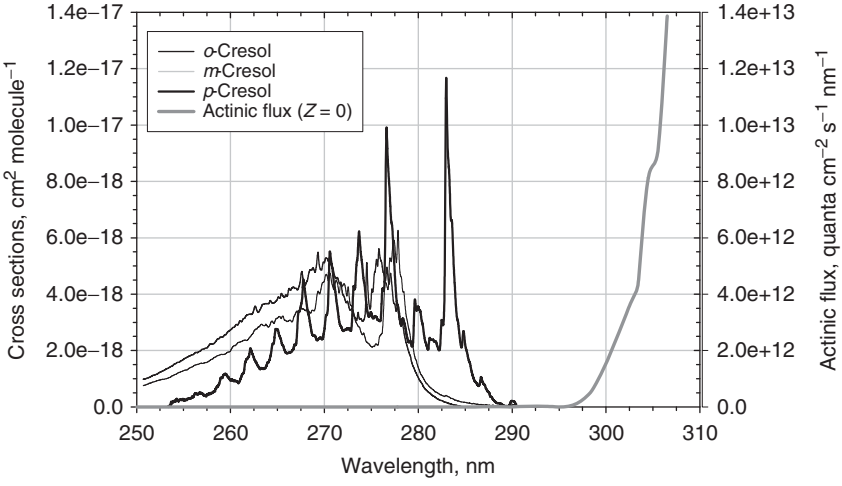

Figure IX-L-18. Cross sections as a function of wavelength for gaseous *o*-cresol (thin black curve), *m*-cresol (gray curve), and *p*-cresol (heavy black curve); all data from Etzkorn et al. (1999). Actinic flux is given by the heavy gray curve as a function of wavelength in the lower troposphere for an overhead Sun.

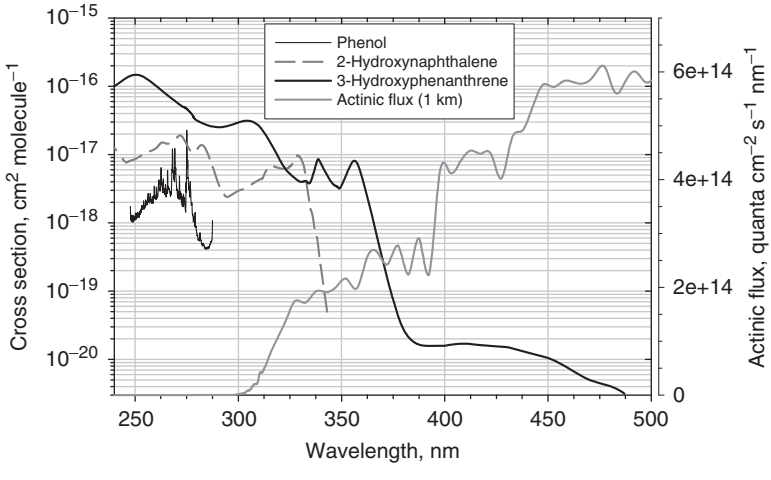

Figure IX-L-19. Absorption cross sections for a series of HO-substituted aromatic hydrocarbons, phenol, 2-hydroxynaphthalene, and 3-hydroxyphenanthrene as measured in nonpolar solvents (data from Láng, 1961–1971). Actinic flux is given by the heavy gray curve as a function of wavelength in the lower troposphere for an overhead Sun.

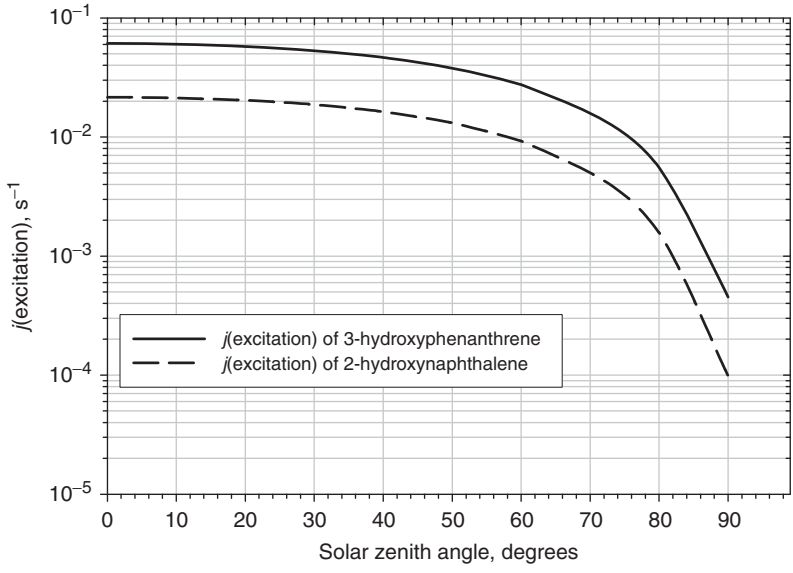

Figure IX-L-20. Approximate *j*-values for the rate of formation of excited singlet state molecules, estimated for 2-hydroxynaphthalene (dashed curve) and 3-hydroxyphenanthrene (solid curve); these represent approximate maxima in *j*(Total). The cross sections used in the calculation are from Láng (1961–1971) as measured in ethanol solutions; actinic flux data are for a cloudless sky in the lower troposphere with an overhead ozone column of 350 DU.

3-hydroxyphenanthrene, the maximum possible photodissociation rates in Summer sunlight at 40°N latitude, shown in figure IX-L-20, suggest that their photodecomposition may be significant.

IX-L-10. Photodecomposition of Nitrophenols and Other Nitro- and OH-Substituted Organic Compounds

The nitrophenols have been measured among the many other compounds present in motor vehicle exhaust (Nojima et al., 1983; Tremp et al., 1993). Also, these compounds can be formed by the nitration of the phenols and other OH-substituted aromatic hydrocarbons present in the atmosphere (Nojima and Isogami, 1994). This can occur, especially at night, when reactions with NO_3 can occur rapidly (see figure I-B-2 in chapter I, and rate data in chapter III of Calvert et al., 2002). These compounds are highly soluble in cloud-water and rain-water, and they often appear in these aqueous media (Lüttke and Levsen, 1997; Lüttke et al., 1997). Information concerning the photochemistry of the nitrophenols is very limited, but in view of the rather large cross sections of these compounds, some speculation here on the potential pathways for photodecomposition is deemed important. See figure IX-L-21.

In view of the minimum energy necessary to photodissociate the weakest bonds in phenol and nitrobenzene and the studies of their photochemistry, Calvert et al. (2002)

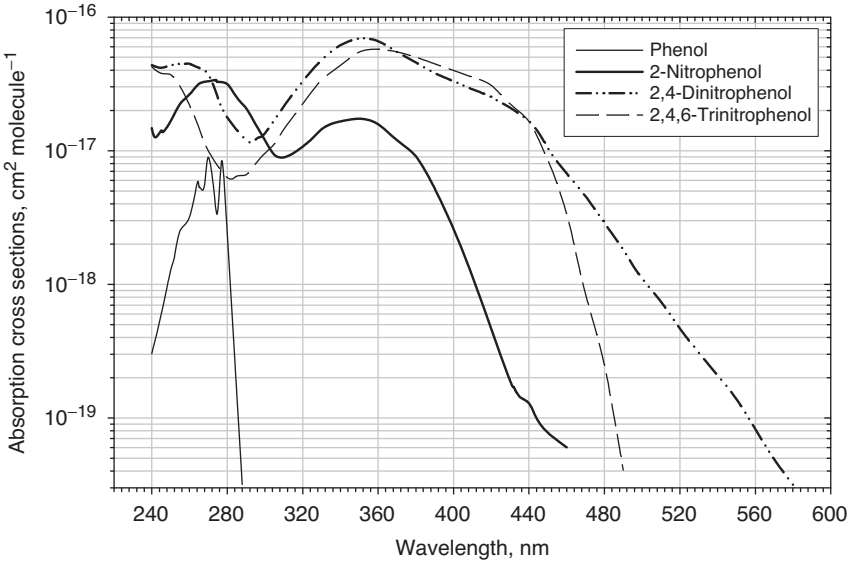

Figure IX-L-21. Plot of the cross sections for some nitro-substituted phenols; measurements were made in ethanol solutions (Láng, 1961–1971).

assumed that the primary process (I) will dominate in the gas-phase photodecomposition of the nitro-phenols:

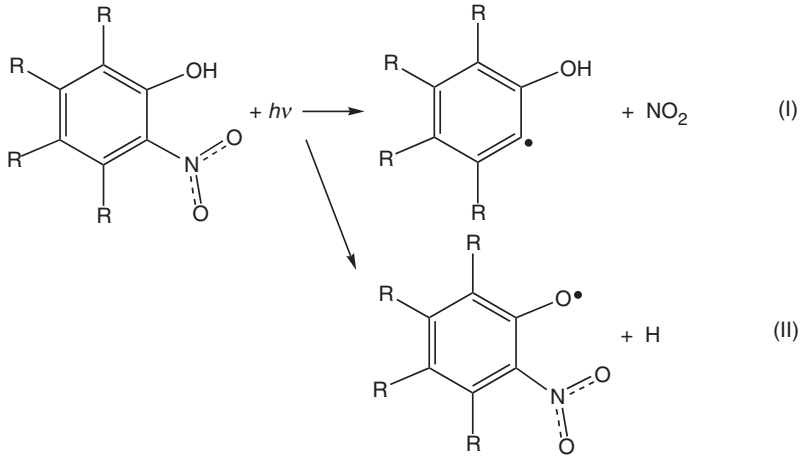

where R is either an alkyl group or an H-atom. The minimum energies required for processes (I) and (II) are expected to be approximately 297 and 362 kJ mole^{-1}, respectively, corresponding to wavelengths for onset of approximately 403 and 330 nm, respectively.

Palm et al. (1999b) have determined that the direct photolysis of nitrophenols in water solution in sunlight is a negligible sink. Photolytic half-lives of 1,4-dinitrophenol,

4-methyl-2-nitrophenol, and 2,6-dinitro-*p*-cresol at 50°N (Summer–Winter) were found to be 5–35, 32–180, and 55–320 days, respectively. In daylight the major sink was suggested to be the solution phase reaction of these species with the OH radical, where it was estimated that half-lives were less than 1 h. Similar results were reported by Palm et al. (1999a) who estimated quantum yields of decay in aqueous solution for 2,4-dinitrophenol, 3-methyl-2-nitro-phenol, and 2,6-dinitro-3-methylphenol to be: 1.1×10^{-5}(pH = 2.6); 3.3×10^{-6}(pH = 6.0); and 0.4×10^{-6}(pH = 6.0), respectively.

IX-M. Summary of Photochemical Processes

The photodecomposition of the various oxidation products of the alkanes, alkenes, and the aromatic hydrocarbons play important roles in the chemistry of the urban, rural, and remote atmospheres. These processes provide radical and other reactive products that help drive the chemistry that leads to ozone generation and other important chemistry in the troposphere. In this chapter, we have reviewed the evidence for the nature of the primary processes that occur in the aldehydes, ketones, alkyl nitrites, nitroalkanes, alkyl nitrates, peroxyacyl nitrates, alkyl peroxides, and some representative, tropospheric, sunlight-absorbing aromatic compounds. Where sufficient data exist, estimates have been made of the rate of the photolytic processes that occur in these molecules by calculation of the photolysis frequencies or *j*-values. These rate coefficients allow estimation of the photochemical lifetimes of the various compounds in the atmosphere as well as the rates at which various reactive products are formed through photolysis.

In table IX-M-1, we have summarized the photolysis frequencies (*j*-values) for each of the molecules for which sufficient data exist to allow reasonable estimations to be made (298 K; latitude 40°N; 500 m altitude; ozone column 350 DU). In the second and third columns of this table, the *j*-values for an overhead Sun and the photochemical lifetime, 1/(*j*-value), respectively, are given. Of course, the Sun is rarely at the zenith, and more representative photochemical lifetimes are the diurnally averaged numbers. These lifetimes were calculated for clear skies at 40°N latitude (ozone column = 350 DU), for some representative periods during the year: in the fourth column, Spring equinox (near March 22) and Fall equinox (near September 23); in the fifth column a period of extended sunshine (near June 22); and in column six, a period of limited daylight (near December 22). The calculations of these quantities were made by averaging the *j*-values over each half-hour of the day and night for the 24 h period. As one expects, diurnal averaged lifetimes are much longer than the lifetimes at solar zenith; on the average at 40°N latitude they are about three times those for the periods near June 22 ($\tau_{\text{June 21}}/\tau_{z=0} = 3.1 \pm 0.4$). For the periods near December 22, the lifetimes are very much longer than those for an overhead Sun, and the variation within families of oxygenates becomes more evident. For example, for the compounds shown in the table IX-M-1, the range of ratios for $\tau_{z=0}/\tau_{\text{Dec.22}}$ for the acyclic aldehydes are 17 ± 2; dicarbonyls, 9 ± 2; acyclic ketones, 29 ± 6; hydroxycarbonyls, 21 ± 3; alkyl nitrites, 8.5 ± 0.5; and monoalkyl nitrates 22 ± 2.

A more detailed picture of the yearly variation of the diurnal photochemical lifetimes can be seen in figure IX-M-1. Here the diurnal lifetimes have been calculated for

Table IX-M-1. Summary of the estimated photochemical lifetimes (τ) for the hydrocarbon oxidation products and derivatives for the cloudless, lower troposphere (latitude 40°N; 298 K; 500 m altitude; vertical ozone column = 350 DU)

Compound	j (Total), s^{-1} Overhead Sun	τ Overhead Sun	τ (Diurnal Cycle), Mar. 22–Sept. 22	τ (Diurnal Cycle) Jun. 22	τ (Diurnal Cycle) Dec. 22
CH_2O	9.02×10^{-5}	3.1 h	11 h	9.1 h	1.7 days
CH_3CHO	7.31×10^{-6}	1.6 days	6.9 days	5.5 days	1.3 months
C_2H_5CHO	1.18×10^{-5}	1.0 days	3.9 days	3.2 days	19 days
n-C_3H_7CHO	1.98×10^{-5}	14 h	2.3 days	1.9 days	10 days
iso-C_3H_7CHO, j_{max}	6.24×10^{-5}	4.5 h	17 h	14 h	3.1 days
iso-C_3H_7CHO, j_{min}	5.58×10^{-5}	5.0 h	19 h	15 h	3.3 days
n-C_4H_9CHO	1.80×10^{-5}	15 h	2.5 days	2.0 days	11 days
$(CH_3)_3CCHO$, j_{max}	3.36×10^{-5}	8.3 h	1.4 days	1.1 days	6.4 days
$(CH_3)_3CCHO$, j_{min}	1.44×10^{-5}	19 h	3.1 days	2.6 days	14 days
$(CH_3)_2CHCH_2CHO$	1.81×10^{-5}	15 h	2.4 days	2.0 days	11 days
n-$C_5H_{11}CHO$	2.41×10^{-5}	12 h	1.9 days	1.5 days	8.1 days
n-$C_6H_{13}CHO$, j_{max}	1.31×10^{-5}	21 h	3.4 days	2.8 days	15 days
n-$C_6H_{13}CHO$, j_{min}	9.49×10^{-6}	1.2 days	4.7 days	3.8 days	20 days
Glycidaldehyde	6.85×10^{-5}	4.1 h	15 h	12 h	2.5 days
$HOCH_2CHO$	1.48×10^{-5}	19 h	3.4 days	2.7 days	19 days
CHOCHO, j_{max}	1.55×10^{-4}	1.8 h	5.7 h	4.8 h	17 h
CHOCHO, j_{min}	1.24×10^{-4}	2.2 h	7.3 h	6.1 h	23 h
$CH_3C(O)CHO$	1.45×10^{-4}	1.9 h	5.7 h	4.9 h	16 h
Cl_3CCHO	8.64×10^{-5}	3.2 h	13 h	10 h	2.3 days
CF_3CHO	1.45×10^{-5}	19 h	2.9 days	2.4 days	11 days
CHF_2CHO	4.60×10^{-5}	6.0 h	21 h	18 h	3.2 days
$CH_2{=}CHCHO$	1.42×10^{-6}	8.2 days	27 days	23 days	3.0 months
$CH_2{=}C(CH_3)CHO$	6.61×10^{-6}	1.8 days	5.9 days	5.0 days	20 days
cis-$CH_3C(O)CH{=}CHCHO$	7.65×10^{-4}	22 min.	1.1 h	56 min.	3.1 h
trans- $CH_3C(O)CH{=}CHCHO$	9.95×10^{-4}	17 min.	49 min.	42 min.	2.2 h
$CHOCH{=}CHCHO$	1.20×10^{-3}	14 min.	41 min.	35 min.	1.9 h
C_6H_5CHO (CHO product only)	3.10×10^{-6}	3.7 days	1.0 months	22 days	1.2 years
C_6H_5CHO (total)	3.12×10^{-4}	53 min.	4.6 h	3.9 h	15.h
Pinonaldehyde	1.41×10^{-5}	20 h	3.2 days	2.6 days	15 days
$CH_2{=}C{=}O$	2.88×10^{-4}	0.96 h	3.2 h	2.7 h	10.4 h
$CH_3C(O)CH_3$, j_{max}	8.62×10^{-7}	14 days	1.9 months	1.5 months	12 months
$CH_3C(O)CH_3$, j_{min}	5.20×10^{-7}	22 days	2.6 months	2.0 months	1.6 years
$C_2H_5C(O)CH_3$	4.68×10^{-6}	2.5 days	11 days	8.5 days	1.8 months
n-$C_3H_7C(O)CH_3$, j_{max}	2.67×10^{-6}	4.3 days	20 days	16 days	4.4 months
n-$C_3H_7C(O)CH_3$, j_{min}	1.57×10^{-6}	7.4 days	1.2 months	28 days	8.2 months
n-$C_4H_9C(O)CH_3$, j^d_{max}	8.04×10^{-6}	1.4 days	6.0 days	4.8 days	1.0 months
n-$C_4H_9C(O)CH_3$, j^d_{min}	1.39×10^{-6}	8.3 days	1.3 months	1.0 months	8.5 months
cyclo-Propanone	3.70×10^{-4}	45 min.	2.4 h	2.1 h	8.2 h
cyclo-Butanone	2.63×10^{-5}	9.5 h	1.7 days	1.3 days	9.0 days
$HOCH_2C(O)CH_3$, j_{max}	2.09×10^{-6}	5.5 days	22 days	18 days	3.5 months
$HOCH_2C(O)CH_3$, j_{min}	1.05×10^{-6}	11 days	1.5 months	1.2 months	6.9 months
$ClCH_2C(O)CH_3$, j_{max}	1.01×10^{-4}	2.8 h	10 h	8.6 h	1.9 days

(*continued*)

Table IX-M-1. (*continued*)

Compound	j (Total), s^{-1} Overhead Sun	τ Overhead Sun	τ (Diurnal Cycle), Mar. 22–Sept. 22	τ (Diurnal Cycle) Jun. 22	τ (Diurnal Cycle) Dec. 22
$ClCH_2C(O)CH_3$, j_{min}	5.05×10^{-5}	5.5 h	21 h	17 h	3.8 days
$BrCH_2C(O)CH_3$, j_{max}	2.21×10^{-4}	1.3 h	4.6 h	3.8 h	18 h
$BrCH_2C(O)CH_3$, j_{min}	1.11×10^{-4}	2.5 h	9.2 h	7.6 h	1.5 days
$CF_3C(O)CH_3$	8.66×10^{-7}	13 days	2.0 months	1.6 months	1.0 years
$CF_3C(O)CF_3$	1.87×10^{-6}	6.2 days	27 days	21 days	4.6 months
$CF_3CF_2C(O)CF(CF_3)_2$	9.10×10^{-6}	1.3 days	4.4 days	3.7 days	16 days
$CH_3C(O)C(O)OH$, Case A[a]	4.21×10^{-4}	40 min.	2.1 h	1.8 h	6.2 h
$CH_3C(O)C(O)OH$, Case B[a]	3.59×10^{-4}	46 min.	2.4 h	2.1 h	7.5 h
$CH_3C(O)C(O)OH$, Case C[a]	1.18×10^{-4}	2.4 h	7.3 h	6.3 h	22 h
$CH_3C(O)CH{=}CH_2$	4.73×10^{-6}	2.5 days	8.5 days	7.1 days	1.0 month
$CH_3C(O)C(O)CH_3$, Case A[b]	3.54×10^{-4}	47 min.	2.3 h	2.0 h	6.5 h
$CH_3C(O)C(O)CH_3$, Case B[b]	1.96×10^{-4}	1.4 h	3.9 h	3.4 h	9.8 h
$CH_3C(O)C(O)CH_3$, Case C[b]	7.01×10^{-5}	4.0 h	11 h	9.9 h	1.3 days
trans-3-Hexene-2,5-dione	4.73×10^{-5}	5.9 h	19 h	16 h	2.8 days
cis-3-Hexene-2,5-dione	4.43×10^{-5}	6.3 h	22 h	19 h	3.6 days
HC(O)Br	1.76×10^{-5}	16 h	2.7 days	2.2 days	13 days
HC(O)Cl	1.61×10^{-7}	2.4 months	11 months	8.5 months	5.4 years
BrC(O)Br	2.92×10^{-6}	4.0 days	16 days	13 days	2.5 months
$CH_3C(O)Cl$	3.58×10^{-9}	8.8 years	86 years	53 years	$\sim 7 \times 10^3$ years
$ClCH_2C(O)Cl$	3.62×10^{-7}	1.1 months	5.3 months	4.1 months	3.7 years
$Cl_2CHC(O)Cl$	1.44×10^{-6}	8.0 days	1.3 months	1.0 month	9.6 months
$Cl_3CC(O)Cl$	2.63×10^{-6}	4.4 days	19 days	15 days	3.1 months
$CF_3C(O)Cl$	5.08×10^{-7}	23 days	3.7 months	2.9 months	2.2 years
HONO	1.74×10^{-3}	9.6 min.	29 min.	25 min.	1.4 h
CH_3ONO, j_{max}	2.29×10^{-3}	7.3 min.	22 min.	19 min.	1.1 h
CH_3ONO, j_{min}	1.79×10^{-3}	9.3 min.	29 min.	25 min.	1.4 h
C_2H_5ONO	5.84×10^{-4}	29 min.[e]	1.4 h[e]	1.2 h[e]	4.2 h[e]
n-C_3H_7ONO	7.67×10^{-4}	22 min.[e]	1.1 h[e]	56 min[e]	3.1 h[e]
iso-C_3H_7ONO	7.40×10^{-4}	23 min.[e]	1.1 h[e]	58 min[e]	3.2 h[e]
n-C_4H_9ONO	4.37×10^{-4}	38 min.[e]	1.9 h[e]	1.6 h[e]	5.5 h[e]
iso-C_4H_9ONO	5.09×10^{-4}	33 min.[e]	1.6 h[e]	1.4 h[e]	4.8 h[e]
tert-C_4H_9ONO	3.81×10^{-3}	4.4 min.	13 min.	11 min.	33 min.
$(CH_3)_2NN{=}O$	2.75×10^{-3}	6.1 min.	18 min.	15 min.	45 min.
$HONO_2$	7.20×10^{-7}	16 days	2.3 months	1.8 months	1.0 year
$HOONO_2$	7.71×10^{-6}	1.5 days	5.8 days	4.8 days	24.7 days
CH_3ONO_2	1.16×10^{-6}	10 days	1.4 months	1.1 months	7.0 months
$C_2H_5ONO_2$	1.37×10^{-6}	8.5 days	1.2 months	29 days	6.8 months
n-$C_3H_7ONO_2$	1.79×10^{-6}	6.5 days	28 days	22 days	4.9 months
iso-$C_3H_7ONO_2$	3.00×10^{-6}	3.9 days	16 days	13 days	2.6 months
n-$C_4H_9ONO_2$	1.59×10^{-6}	7.3 days	1.0 month	25 days	5.6 months
tert-$C_4H_9ONO_2$	8.34×10^{-6}	1.4 days	5.5 days	4.5 days	25 days
2-$C_5H_{11}ONO_2$	2.58×10^{-6}	4.5 days	19 days	15 days	3.3 months
3-$C_5H_{11}ONO_2$	2.52×10^{-6}	4.6 days	20 days	16 days	3.5 months
cyclo-$C_5H_9ONO_2$	9.01×10^{-7}	13 days	2.0 months	1.5 months	1.0 year

(*continued*)

Table IX-M-1. (*continued*)

Compound	j (Total), s^{-1} Overhead Sun	τ Overhead Sun	τ (Diurnal Cycle), Mar. 22–Sept. 22	τ (Diurnal Cycle) Jun. 22	τ (Diurnal Cycle) Dec. 22
$CH_3C(O)CH(ONO_2)CH_3$	5.82×10^{-5}	4.8 h[c]	18 h[c]	15 h[c]	3.2 days[c]
$CH_3C(O)CH_2ONO_2$	3.81×10^{-5}	7.3 h[c]	28 h[c]	23 h[c]	5.2 days[c]
2-Oxo-cyclohexyl-1-nitrate	2.19×10^{-5}	13 h[c]	2.2 days[c]	1.8 days[c]	12 days[c]
$CH_3CH_2C(O)CH_2ONO_2$	2.09×10^{-5}	13 h[c]	2.2 days[c]	1.8 days[c]	11 days[c]
$CH_3CH(ONO_2)CH(ONO_2)CH_3$	1.19×10^{-5}	23 h	3.6 days	3.0 days	15 days
$CH_3CH(ONO_2)CH_2ONO_2$	1.13×10^{-5}	25 h	3.8 days	3.2 days	15 days
$CH_3CH_2CH(ONO_2)CH_2ONO_2$	1.54×10^{-5}	18 h	2.7 days	2.3 days	11 days
$CH_2(ONO_2)CH{=}CHCH_2ONO_2$	6.76×10^{-6}	1.7 days	7.0 days	5.7 days	1.2 months
$CH_2{=}CHCH(ONO_2)CH_2ONO_2$	6.53×10^{-6}	1.8 days	6.8 days	5.6 days	1.0 months
1-Methyl-cyclohexyl-1,2-dinitrate	5.32×10^{-6}	2.2 days	10 days	7.9 days	2.2 months
$HOCH_2CH_2ONO_2$	9.64×10^{-8}	4.0 months	1.7 years	1.3 years	13.6 years
$CH_3C(O)O_2NO_2$	8.93×10^{-7}	13 days	1.7 months	1.4 months	7.2 months
$C_2H_5C(O)O_2NO_2$	1.56×10^{-6}	7.4 days	29 days	24 days	4.2 months
HOOH	8.81×10^{-6}	1.3 days	4.7 days	3.9 days	17.5 days
CH_3OOH	5.98×10^{-6}	1.9 days	6.7 days	5.6 days	23 days
$HOCH_2OOH$	5.74×10^{-6}	2.0 days	7.1 days	5.9 days	26 days
Benzene oxide/Oxepin	4.33×10^{-4}	39 min.	1.9 h	1.6 h	5.2 h
Toluene oxide/Methyloxepin	3.91×10^{-4}	43 min.	2.1 h	1.8 h	5.8 h
o-Nitrobenzaldehyde	7.34×10^{-3}	2.3 min.	7.3 min.	6.2 min.	23 min.
Nitrobenzene	2.06×10^{-5}	14 h	1.8 days	1.5 days	5.5 days
2-Methyl-1-nitronaphthalene	1.66×10^{-4}	1.7 h	5.2 h	4.4 h	16 h
Phthaldialdehyde	8.23×10^{-4}	20 min.	1.2 h	1.0 h	2.0 h
2-Acetylbenzaldehyde	8.87×10^{-4}	19 min.	1.0 h	0.87 h	3.3 h

[a]Case A: assumed $\phi_{total} = 1.0$, independent of λ; case B: $\phi_{total} = 1$ for $\lambda < 370$ nm, and 0 for $\lambda > 370$ nm; case C assumed $\phi_{total} = 0.28$ at all λ to fit EUPHORE estimates.

[b]Case A: simulation made to match EUPHORE estimates; case B: assumed cutoff of photodissociation occurs for $\lambda > 492$ nm; case C: assumed cutoff of photodissociation occurs for $\lambda > 410$ nm.

[c]Lifetimes are minimum values since the quantum yields of photodecomposition may be less than the unity that has been assumed in the calculations for these compounds.

[d]Value for the dominant process (IV) only; $n\text{-}C_4H_9C(O)CH_3 + h\nu \rightarrow CH_3CH{=}CH_2 + CH_2{=}C(OH)CH_3$.

[e]Values are maximum values since the measured quantum yields accepted for the calculations in this work are less than unity that has been observed for the other alkyl nitrates and HONO.

locations at latitudes of 30°, 40°, and 50°N for a representative compound, formaldehyde during a continuous period of 18 months. During the period from March 22 to September 22, formaldehyde's diurnal photochemical lifetime is relatively constant: 9.1 to 10.2 h at 30°N; 9.1 to 10.7 h at 40°N; 9.2 to 12.0 h at 50°N. Its rate of photodecomposition is competitive with its reaction with HO; for an averaged [OH] = 10^6 molecule cm^{-3}, its lifetime for reaction with OH is about 33 h. Note that nearly constant values of the lifetimes are seen during the period from March 21 to September 22, but a dramatic rise occurs as the Winter months arrive; a strong peak in the values occurs at the shortest day in the year, at the December 22 time period. As one proceeds from 30°N to the higher latitudes, the diurnal lifetimes during the Winter months show a dramatic increase.

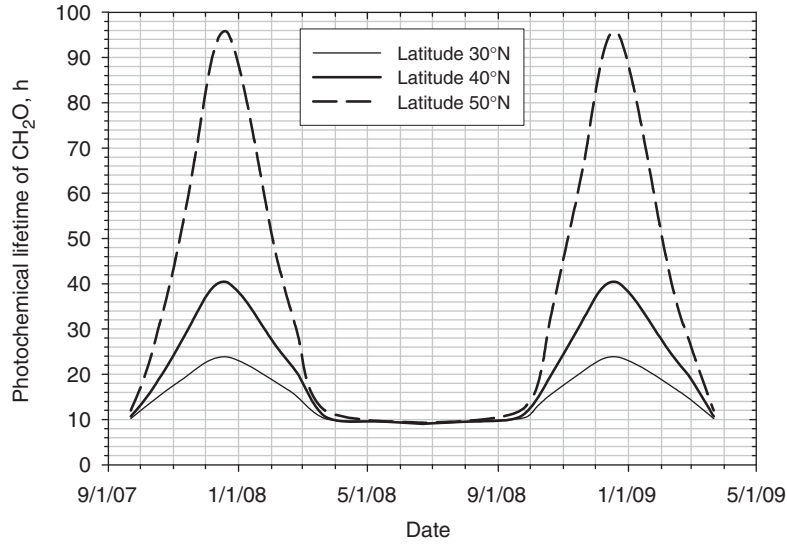

Figure IX-M-1. The diurnal photochemical lifetime for CH_2O as calculated for clear sky conditions in the lower troposphere with an ozone column of 350 DU. Values are shown for locations at latitudes of 30°, 40°, and 50° over an 18-month period.

For the short-lived molecules which photodissociate relatively near the point of their entry into the atmosphere and for which migration of its air parcel to different latitudes is unlikely, estimates such as those given in table IX-M-1 are useful. However, it must be remembered that these estimates are usually based upon the assumption of cloudless skies, an uncommon situation; hence, the values obtained are minimum values.

Long-lived molecules survive to travel long distances and to latitudes where the diurnal pattern of solar zenith angle (Z), and hence the photolysis frequencies, can be very different than those at the emission source. It can be seen in figure IX-M-2a that for the period near January 1 an air parcel that travels North or South encounters a significant variation in the pattern of diurnal solar zenith angle; a midday Z value of 23° at the equator increases to a value greater than 90°, with the complete absence of sunlight at latitudes above ~70°N. The changing pattern of Z variation with latitude also occurs during the Spring and the similar Fall periods; see figure IX-M-2b for March 20. If migration of the air parcel occurs to the North or South, it encounters a midday Sun that varies from near overhead ($Z = 0°$) at the equator to a value of $Z = 90°$ at the North pole; here the Sun circles at the horizon during the usual day and nighttime periods. An air parcel that migrates during the Summer period can also encounter significant changes in the diurnal behavior of the solar zenith angle and the available actinic flux; see figure IX-M-2c for June 30. As an air parcel moves from the lower latitudes to those greater than 65°N, the near overhead Sun at 12:00 local time at the equator continues to fall until at about 65°N, the Sun stays above the horizon during the entire 24 h cycle, at $Z \sim 66°$ in the figure for June 20. The detailed knowledge of the movement of the air parcel containing the long-lived species that is necessary to

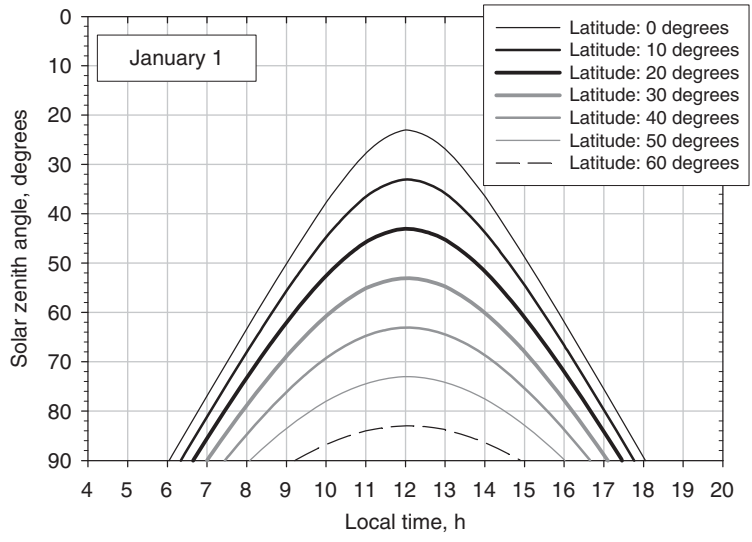

Figure IX-M-2a. Diurnal variation of the solar zenith angle with latitude for January 1.

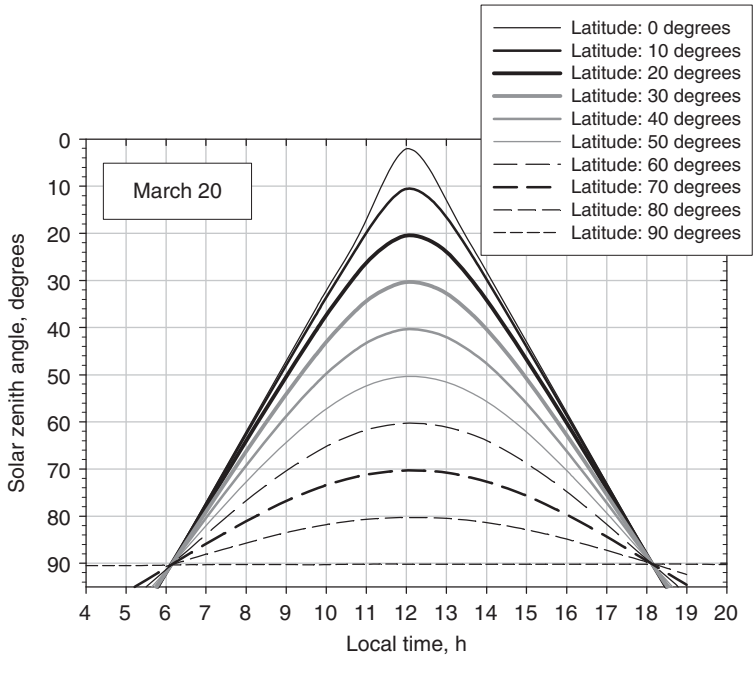

Figure IX-M-2b. Diurnal variation of the solar zenith angle with latitude for March 20.

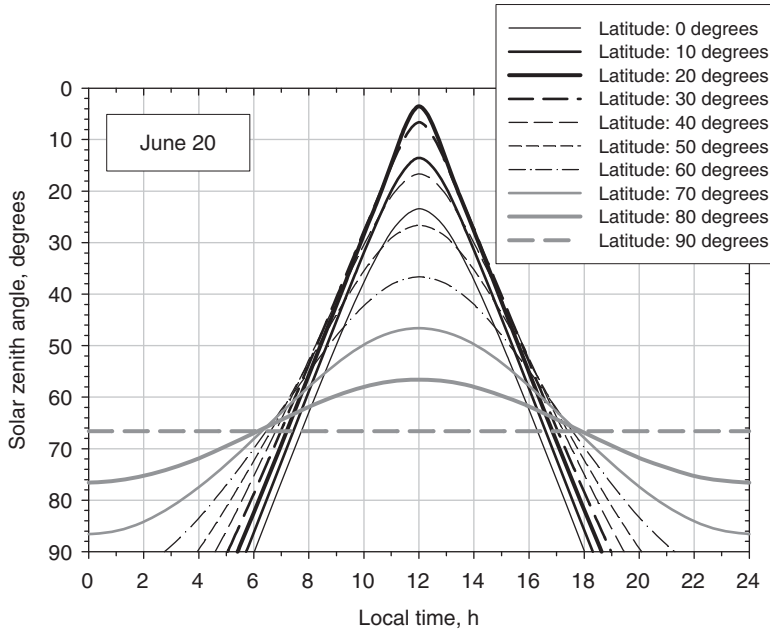

Figure IX-M-2c. Diurnal variation of the solar zenith angle with latitude for June 20.

derive an accurate estimate of its photochemical lifetime is uncommon, and one usually settles for lifetime estimates for long-lived species based on an assumed transport at constant latitude.

For some long-lived organic nitrates, representative "globally averaged lifetimes (24 h cycles)" have been estimated using the relation: τ (global) $= 1/j_{Z=60^\circ}$; e.g., see Luke and Dickerson (1988) and Barnes et al. (1993). The rationale for the use of this relation is unclear, and the results do not have the quantitative value that the designation of "τ (global)" seems to imply.

There are a large range of lifetimes listed in table IX-M-1. The most photochemically active class of molecules of those shown are the alkyl nitrites that have lifetimes of 4 min. (*tert*-C_4H_9ONO) to 38 min. (*n*-C_4H_9ONO) with an overhead Sun and diurnal photochemical lifetimes of 11 min. and 1.6 h during the June 22 period. The least-reactive photochemical species shown is $CH_3C(O)Cl$ that has a photochemical lifetime in the lower troposphere of hundreds of years during periods of low solar flux. Obviously, the losses of this species by other than photodecomposition, such as hydrolysis in cloud, rain, or ocean water, will be important.

The most important class of these molecules in promoting ozone generation within the troposphere is the aldehydes, and formaldehyde leads this list. Photodecomposition of the other higher aldehydes is somewhat less competitive with the OH reaction, but still important. This is especially true at the higher altitudes of the troposphere where the photodissociation is often enhanced by the lowered collisional quenching of the exited aldehyde molecules and the increased solar flux.

The ketones also share their decay pathways between OH attack and photodecomposition. With acetone in the lower troposphere during the Summer months, photochemical lifetimes between 1.5 and 2.0 months are expected, while the lifetime for OH attack is about 2.1 months. The acceleration of the photodecomposition of acetone that is expected at the higher altitudes results from lowered collisional deactivation of the excited acetone molecules at the low pressure and higher actinic flux levels. This is somewhat attenuated by the lower quantum yields that are expected at the lower temperatures of the upper troposphere. These results, together with the suppression of the reaction with OH as a result of the activation energy barrier, indicate that the photodecomposition pathway stays competitive. With the higher ketones, the preference for photodecomposition is somewhat less. The lifetime for photodecomposition of $CH_3C(O)C_2H_5$ during Summer months is about 9 days while that for reaction with OH is about 10 days in the lower troposphere. With 2-hexanone the photodecomposition lifetime in the Summer months is about 5 days while that for reaction with OH is about 2 days.

The alkyl nitrates have somewhat longer photochemical lifetimes, but these also are competitive with the lifetimes for their reactions with OH in the lower troposphere. CH_3ONO_2, $C_2H_5ONO_2$, $CH_3CH_2CH_2ONO_2$, $(CH_3)_2CHONO_2$, and $CH_3CH_2CH_2CH_2ONO_2$ have diurnal lifetimes of photodissociation during the Summer months (40° latitude) in the lower troposphere of about 34, 29, 22, 13, and 25 days, respectively, while those for OH attack on these compounds leads to a lifetime of about 16 months, 2 months, 20 days, and 7 days, respectively. The peroxyacyl nitrates show a similar behavior: PAN has a photochemical lifetime in the lower troposphere during the Summer months of about 41 days while that for OH attack is 85–154 days. For the peroxyacycl nitrates, the thermal decomposition is very important, especially in the warm lower troposphere where lifetimes of hours can be expected.

As we have seen in our discussions in this chapter, photochemistry provides an important part of the atmospheric chemistry that occurs within the troposphere. The direct photochemistry of the alkanes and alkenes is unimportant within the troposphere, since they do not absorb the available sunlight. Those aromatic hydrocarbons that absorb tropospheric sunlight (largely the polycyclic hydrocarbons) do not appear to photodecompose (Calvert et al., 2002). However, photochemistry is indirectly responsible for the decay of all of the hydrocarbons by the dominant pathway of OH attack. It is the photodecomposition of ozone that is the major source of the OH radicals that accounts for the majority of the observed destruction of the hydrocarbons (RH) and the subsequent generation of oxidation products including ozone build up in the troposphere:

$$O_3 + h\nu \rightarrow O(^1D) + O_2$$

$$O(^1D) + H_2O \rightarrow OH + OH$$

$$OH + RH \rightarrow H_2O + R$$

$$R + O_2 \rightarrow RO_2$$

$$RO_2 + R'O_2, NO, NO_2, HO_2$$

$$\rightarrow RO, RONO_2, RO_2NO_2, RO_2H, \text{etc.} \rightarrow \text{other products}$$

Through the oxidation of NO to NO_2 via HO_2 and RO_2 radicals, and the regeneration of OH radicals, the subsequent build up of ozone can result in the lower atmosphere:

$$NO + HO_2(RO_2) \rightarrow NO_2 + HO(RO)$$

$$NO_2 + h\nu \rightarrow O(^3P) + NO$$

$$O(^3P) + O_2(+N_2/O_2) \rightarrow O_3(+N_2/O_2)$$

As a consequence of the chain reactions that drive NO to NO_2, and the rapid photolysis of NO_2, reactions that were initiated by the photodecomposition of ozone, lead ultimately to its formation and build up within the troposphere.

X

The Influence of Oxygenates on the Atmospheric Chemistry of Urban, Rural, and Global Environments

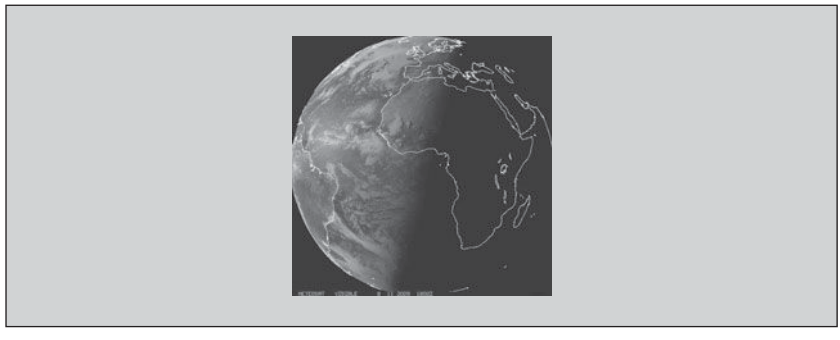

X-A. Importance of Oxygenates in Atmospheric Chemistry

One cannot overestimate the importance of oxygenated organic compounds in atmospheric chemistry. As discussed in the previous chapters of this book and elsewhere (e.g., Wayne, 1991; Seinfeld and Pandis, 1998; Brasseur et al., 1999; Finlayson-Pitts and Pitts, 2000; Calvert et al., 2000, 2002, 2008) the atmosphere is an oxidizing environment and all organic compounds emitted into the atmosphere are converted into oxygenated organic compounds. The first-generation products are oxidized further. As an example, the oxidation of ethane gives CH_3CHO, C_2H_5OH, and C_2H_5OOH as first-generation products and CH_3OH, CH_3OOH, CH_2O, and HC(O)OH as second-generation products. An understanding of the chemistry of oxygenated organic compounds is central to unraveling the complex processes in the atmosphere. In this chapter we discuss the representation of oxygenates in atmospheric models, their participation in secondary organic aerosol formation, contribution to HO_x chemistry in the upper troposphere, role in the transport of pollutants, and use as proxies for volatile organic compound (VOC) emissions.

X-B. Representation of Oxygenates in Chemical Mechanisms and Models

X-B-1. Introduction

A major application of the chemical kinetics and mechanisms of VOC oxidation is the development of an understanding of the chemistry occurring in the troposphere and the use of that understanding to predict and develop strategies which help to mitigate adverse changes in air quality and climate change. Such applications depend on the development of models that assess chemical impacts; chemical mechanisms lie at the heart of such models. The mechanisms can be very detailed, often termed *explicit*, in models where the aim is to understand the chemistry occurring in a small volume of air, for example, in an analysis of processes determining radical concentrations in field measurements. Such a mechanistic approach can also be used, with increased computer resources, when a trajectory approach is used to assess the coupled impacts of atmospheric transport and chemistry. An Eulerian approach to modeling both regional and global processes presents greater problems, because the chemical rate equations have to be solved for each species at each spatial grid point in the model; this severely limits the number of chemical species that can be incorporated realistically in the model. As a result, there is a need to reduce the dimension of the model; i.e., the number of ordinary differential equations, and hence chemical species, that are incorporated. This requirement can be satisfied in a number of ways, including the development of *reduced* or *lumped* chemical mechanisms. In reduced mechanisms, the number of chemical species is reduced by excluding those with a lower impact on the atmospheric chemistry. In lumped mechanisms, the number of species is reduced by lumping several primary species, or intermediates, into a single *surrogate*.

Much of the chemistry in such mechanisms involves oxygenates. These compounds are either emitted directly or are generated in the atmosphere by oxidation of hydrocarbons and play a dominant role in the secondary chemistry. There are several secondary steps in the oxidation of even a modestly sized compound such as butane (see section I-C-2), each of which involves oxygenate chemistry. Thus, key modeling objectives, such as the oxidizing capacity of the atmosphere, the regional formation of ozone, and the formation of secondary organic aerosol, are dependent on chemical mechanisms that incorporate the oxygenate chemistry discussed in this book. This section presents a brief summary of approaches used to construct explicit, reduced, and lumped chemical mechanisms.

X-B-2. Explicit or Near-Explicit Mechanisms

An explicit chemical mechanism includes all of the reactions associated with the atmospheric degradation of a volatile organic compound in both high NO_x and low NO_x environments. Such a mechanism includes a very large number of species, and strategic simplifications are made in *near-explicit* mechanisms, such as the master chemical mechanism (MCM) (http://mcm.leeds.ac.uk/MCM/). The MCM is constructed on the

basis of a protocol that defines these simplifications and provides a set of rules that guide the construction of the mechanism (Jenkin et al., 1997; Saunders et al., 2003a; Jenkin et al., 2003; Bloss et al., 2005). Wherever possible, rate coefficients are taken from evaluations or, when an evaluation is not available for a specific reaction, are based on experimental rate data. Where no measurements have been made, structure–activity relations (SARs) are used. SARs are widely employed to determine positions of abstraction or addition and hence reaction channel yields.

The approach can be illustrated by reference to the oxidation of isoprene in a high NO_x environment, so that peroxy radicals react exclusively with NO. The total number of hydroxyperoxy radicals formed by addition of OH followed by reaction with O_2, is reduced to four by eliminating channels with yields <5%. Table X-B-1 shows the positions of the OH and O_2 groups in the peroxy radical; e.g., the first entry refers to addition of OH in the 1-position, followed by reaction of O_2 at the 4-position. The fractional channel yield is shown in the third column and the first-generation carbonyl compound, formed from the oxy radical resulting from reaction of the peroxy radical with NO, is shown in the final column. Where fragmentation occurs, the larger species only is shown. For example, methacrolein, shown in the final row, is formed with CH_2O as a co-product. Methyl vinyl ketone (majority product in row 2) and methacrolein are the main first-generation products, in agreement with experiment. Figure X-B-1 shows a section of a page from the MCM website, detailing the formation of methyl vinyl ketone and 1-hydroxy methyl vinyl ketone from the oxy radical labeled ISOPBO in the MCM.

Table X-B-1. Major first-generation intermediates in the OH-initiated oxidation of isoprene in MCM v3.1

Position of OH	Position of O_2	Channel Yield	
1	4	16	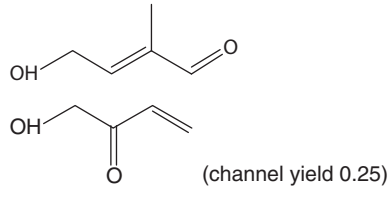 (channel yield 0.25)
1	2	49	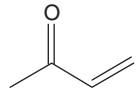 (channel yield 0.75)
4	1	9	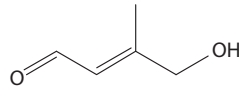
4	3	26	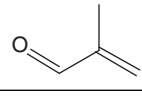

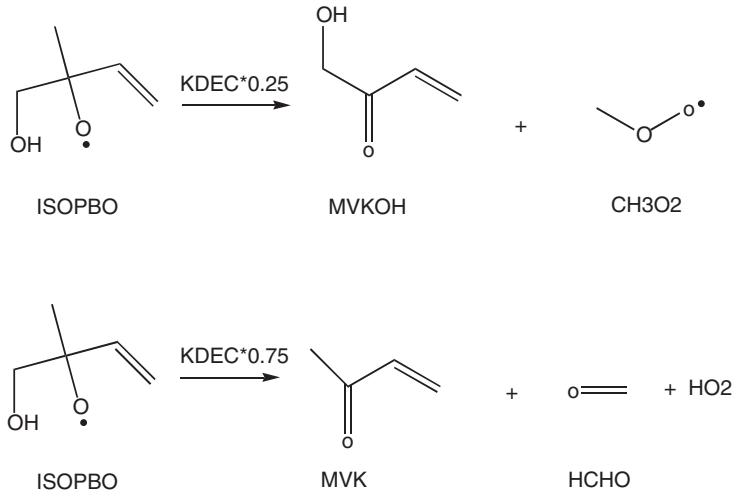

Figure X-B-1. Section of a page from the MCM website, showing the formation of methyl vinyl ketone (MVK) and 1-hydroxy methyl vinyl ketone (MVKOH) from the oxy radical IOPBO. The rate coefficient KDEC refers to a generalized fast rate coefficient for dissociation, that is set to 1×10^6 s^{-1}, ensuring that the dissociation occurs effectively instantaneously; 0.25 and 0.75 are the channel yields.

The MCM mechanism for isoprene also includes reactions of NO_3 and of ozone. With NO_3, a single site of addition is included (the 1-position, associated with formation of the peroxy radical in the 4-position). Four channels are included for reaction with ozone, which lead to methacrolein (0.3), methyl vinyl ketone (0.2) and the associated Criegee biradical CH_2OO, and CH_2O and the associated Criegee biradicals derived from methacrolein (0.3) and methyl vinyl ketone (0.2), where the numbers in brackets refer to the channel yields.

The first-generation intermediates are then oxidized further. For methacrolein, for example, the MCM includes two sites of reaction with OH (one addition, one abstraction), one with NO_3, two with ozone, and two photolysis channels. The oxidation is continued through subsequent generations, until CO_2 and H_2O are formed.

The peroxy + peroxy radical chemistry is considerably simplified in the MCM, to avoid generation of huge numbers of reactions if each peroxy radical is allowed to react with all other peroxy radicals. Instead, each radical reacts with the peroxy radical pool ΣRO_2. This allows a realistic rate of reaction to be incorporated with the explicit reaction products for each peroxy radical. For example, for CH_3O_2 the reactions included are:

$$CH_3O_2 + \Sigma RO_2 \rightarrow CH_3OH \quad \text{(a)}$$

$$\rightarrow CH_2O \quad \text{(b)}$$

$$\rightarrow CH_3O \quad \text{(c)}$$

If only CH_3O_2 radicals are present, so that $\Sigma RO_2 = CH_3O_2$, these reactions become:

$$CH_3O_2 + CH_3O_2 \rightarrow CH_3OH + CH_2O \quad \text{(a+b)}$$

$$\rightarrow 2CH_3O \quad \text{(c+c)}$$

which correspond to the two main reaction channels for the self-reaction.

The current MCM describes the degradation of methane and 135 of the main VOCs emitted in the U.K., based on the National Atmospheric Emissions Inventory (see chapter I). It also includes reactions of inorganic species. It contains ~13,500 reactions involving ~5,900 species. Most of the emitted species included are of anthropogenic origin. Four biogenic compounds are currently included: isoprene, α- and β-pinene and 2-methyl-3-buten-2-ol, but plans are in hand to include further such compounds.

The MCM has been used in the interpretation of field measurements (Sommariva et al., 2006), in the determination of precursors of oxygenated compounds (Lewis et al., 2005), in the evaluation of aspects of lumped mechanisms (Palmer et al., 2006), and in the modeling of the formation of secondary organic aerosol (Johnson et al., 2004). It has also been extensively used in support of air quality policy in the UK. Ozone formation in much of Europe and certainly in the UK differs from that in cities such as Los Angeles: the processes involved are less intense and ozone is formed over a period of several days as air is advected over many hundreds of kilometers. Derwent et al. (1998) developed a methodology to assess the relative impacts of different VOCs on ozone formation using a trajectory method in which ozone formation was determined in an air parcel transported from middle Europe (Austria) to and across the U.K., over a period of 5 days; the East–West direction roughly reproduces the direction experienced in summer ozone episodes. The air parcel picks up emissions as it moves, based on European emissions inventories, and the MCM is used to simulate the chemistry and the ozone formation. A brute force sensitivity analysis was used in which the mass of each VOC emitted was in turn increased by a small amount in successive simulations, and the impact on ozone formation converted into a relative scale to give *photochemical ozone creation potentials* (POCPs), based on a value of 100 for ethene. The most recent assessment (Derwent et al., 2007a) give POCPs for 178 organic compounds. Examples are included in table X-B-2. The POCP values depend on the timescales of the initial reaction of the VOC (with an oxidant, or via photolysis) and of the subsequent chemistry; they also depend on the numbers of ozone molecules formed

Table X-B-2. Photochemical ozone creation potentials for volatile organic compounds for European multi-day conditions, from Derwent et al. (2007a)

Compound	POCP	Compound	POCP	Compound	POCP
Ethene	100	Formaldehyde	46	Acetone	6
Ethane	8	Acetaldehyde	55	Dimethyl ether	18
Butane	31	Pentanal	71	Diethyl ether	46
Isoprene	114	Ethanol	34	Methylglyoxal	101
Toluene	44	Butanol	52	Trichloroethylene	29

from that emitted VOC during the 5-day period of the simulation. Note that POCPs are calculated on a mass, rather than a molar basis.

Derwent et al. (2007a) used the MCM-based trajectory model to assess strategies for reduction in ozone. For example they looked at the effect of replacing aromatics with alcohols, esters, ethers, or ketones for both road transport and stationary emission sources.

Derwent et al. (2007b) used the same trajectory approach to determine POCPs for different emissions *sources*, based on speciated emissions inventories. They obtained POCP indices of 69, 50, and 44, respectively, for road transport exhaust emissions, road transport evaporative emissions, and for emissions from solvent and other product usage. They discussed the results in the context of the cost effectiveness of different VOC emission control strategies.

The importance of secondary compounds in ozone formation in Europe was investigated by Derwent et al. (2005) using the trajectory approach, allowing the air package to evolve over a period of 81 h, then injecting 2.3 ppb of a specific VOC and calculating the change in ozone production on the day of the injection and on the subsequent day. Injection of the higher alkenes ($\geq C_3$) led to significant ozone production on both days, despite the short lifetimes of the alkenes; Derwent et al. attributed this result to what they termed an *aldehyde cascade.* For example, 1-pentene forms butanal, which is itself short-lived, but also a sequence of further aldehydes, propanal, acetaldehyde, and formaldehyde, in subsequent generations in the oxidation sequence that contribute to ozone formation over an extended period.

The mechanisms for the individual VOCs in the MCM are constructed "by hand," which is an extremely time-consuming process and probably, in the long term, unsustainable, as demands for new compounds and new mechanistic aspects are made. It also leads to mechanistic choices. For example in the oxidation of decane, a single site of abstraction by OH is included. This was felt to provide an appropriate compromise between acceptable accuracy in modeling ozone formation and feasibility of writing complete mechanisms for the larger alkanes. An alternative approach is to devise methods—so-called Expert Systems—that generate mechanisms automatically, using a computer. The work of Aumont et al. (2005) provides the most recent and extensive example of this self generating approach. The technique uses a generator, which is a computer program that produces the oxidation mechanisms for a set of VOCs, using a predefined protocol. The mechanisms generated in this way are very large. Saunders et al. (2003b) tried a similar approach, using a protocol related to that for the MCM, but found that the mechanisms generated were too large for their purposes. They attempted to limit the size of the mechanisms by "trimming"—removing a reaction channel if the cumulative probability became too small, but such an approach depends on the conditions. They used high NO_x to eliminate peroxy + peroxy radical reactions, for example; it is not an approach that can be used to generate general mechanisms.

The methodology used by Aumont et al. (2005) is based on a protocol similar to that employed in the MCM. The mechanism generator mimics the way a chemist would construct the steps involved in the oxidation of a VOC. It first analyses the structure of the compound, identifies the reactive sites and determines the reaction pathways. It searches a database of experimental kinetic data; if the data are not available, it uses

SARs to determine both the overall rate coefficient and the relative product yields. New intermediates are added to a "stack" of compounds, which are further oxidized in turn until the stack is empty. The approach is much faster than manual construction and also inherently more accurate. It is also easier to update the mechanisms as new kinetic data become available, or new understanding requires modification of the protocols. A major advantage is that subjective decisions to limit the mechanism, such as that discussed above for decane in the MCM, and which arise from the practical limits imposed by manual construction are avoided. The number of reactions generated, though, is very large and rises roughly exponentially with the carbon number, so that the mechanism for heptane, for example, contains over 10^5 species and over 10^6 reactions, even using a 5% threshold for selecting reactions. Szopa et al (2005) discussed an automatic procedure for reducing the size of the mechanism, using some of the procedures discussed in section X-B-3.5, including the grouping of species with similar reactivity, and the use of surrogate species. They were able to reduce a mechanism containing 350,000 species into one containing only 147 species, with acceptable accuracy for simulations of ozone and some other species.

While the self-generated mechanisms of Aumont et al. (2005) are large and produce models that require more computer processing time than does the MCM, they have the great advantage that the basis of generation can be changed to test ideas. For example, the formation of secondary organic aerosol depends on the formation of low volatility compounds. As the O:C ratio in a carbon chain increases, the volatility decreases and SOA formation is enhanced (Presto et al., 2009). There is a competition, for example in oxy radical chemistry, between fragmentation, leading ultimately to CO_2 and H_2O, and isomerization, which leads to a higher O content and promotes SOA formation, provided fragmentation does not subsequently ensue. The general ideas behind this evolution and competition are understood, but the details are lacking, and they have not been extensively tested in explicit or near-explicit mechanisms. There may also be new mechanistic details that still have to be worked out. A self-generating approach provides the best way to test and develop such ideas.

X-B-3. Lumped Chemical Mechanisms

Explicit and near-explicit mechanisms are too large to incorporate in Eulerian regional and global models. These require integration of the set of ordinary differential chemical rate equations (ODEs), derived from the mechanism, at each of the grid points in the model. An ODE is required for each species, except where the steady-state approximation is applied to short-lived species. The large number of species contained, for example, in the MCM carries a huge computational overhead in such a model. Accordingly, *lumped* mechanisms are used, in which several species are represented by a single lumped species with generic properties of the group it represents. Most applications of such mechanisms in regional applications relate to ozone formation, so a key attribute of a lumped species is the accurate representation of the ozone generating capacity of the main members of the group. In this section, we summarise aspects of the chemistry of oxygenated species incorporated in two widely used chemistry mechanisms, the carbon bond mechanism IV (CB4), which is used in regional photochemistry models

designed primarily to simulate ozone formation, and the mechanism in the GEOS-Chem global chemistry transport model (CTM), which is used for a wide range of applications. The impact of isoprene on tropospheric chemistry, at both the regional and global scales, has led to the development of specific lumped isoprene mechanisms, designed to be "plugged" into existing mechanisms to simulate this important species; the most widely used of these is the Mainz Isoprene Mechanism (MIM). Finally the Common Representative Intermediate mechanism is discussed; CRI-MECH is based on an extensive lumping of the master chemical mechanism (MCM v3.1) and is designed primarily to simulate ozone but has wider applications. The section concludes with a brief discussion of general approaches to reduction and lumping using sensitivity- and timescale-analysis.

X-B-3.1. The Carbon Bond Mechanism (CB4; CB05)

CB4 was developed by Gery et al. (1989) as a basis for urban and regional modeling of air quality. Organic compounds are grouped according to bond type, e.g., single C—C bonds, double C=C bonds, carbonyl $\rangle$C=O bonds, etc. This allows molecules to be built up from a small number of carbon bond surrogates. For example, one of these is the species PAR, which is a surrogate for a single-bonded carbon atom, so that butane is represented as 4PAR. OLE represents a carbon–carbon double bond in a 1-alkene; thus propene is represented as 1PAR + 1OLE. A third surrogate, ALD2, represents a carbonyl group and its adjacent carbon atom. Because they react rapidly with OH, followed by O_2 and NO, to form aldehydes, 2-alkenes are also represented by ALD2, so that *trans*-2-butene becomes 2ALD2. Some key small species are included explicitly; e.g., formaldehyde, ethene, and isoprene. Inorganic chemistry is also represented explicitly.

Five reactions are included for formaldehyde: reaction with OH and NO_3 and the two photolysis channels. Reaction with $O(^3P)$ is also included, because of the close association between CB4 and chamber studies, where $O(^3P)$ reactions can be important. The chemistry of ALD2 is based on that of acetaldehyde. It reacts with O, OH, and NO_3 to generate the species C_2O_3, which represents an acyl peroxy radical. Photolysis is written as:

$$\mathrm{ALD2} + \mathrm{h}\nu\,(+2\mathrm{O_2}) \rightarrow \mathrm{FORM} + \mathrm{XO_2} + \mathrm{CO} + 2\mathrm{HO_2}$$

where FORM is formaldehyde and XO_2 represents CH_3O_2. It is a universal peroxy radical, termed an operator species (see below). PAN is a generalized PAN species, formed from C_2O_3 by reaction with NO_2.

Acetone is represented as AONE, while the ketone group is represented by KET. The reactions included for AONE are photolysis and reaction with OH. The latter is written as:

$$\mathrm{AONE} + \mathrm{OH} \rightarrow \mathrm{XO_2} + \mathrm{C_2O_3} + \mathrm{FORM}$$

which illustrates the function of XO_2. The number of carbon atoms is preserved through the species C_2O_3 and FORM, the latter, in a full mechanism resulting from CH_3 reacting

with O_2 and NO to form CH_3O, which then reacts with O_2 to form $CH_2O + HO_2$. The primary function of XO_2 is to simulate the NO to NO_2 conversion required for ozone formation:

$$XO_2 + NO \rightarrow NO_2$$

It is also undergoes a self reaction without a product

$$XO_2 + XO_2 \rightarrow$$

which serves to limit ozone formation under low NO_x conditions.

Isoprene (ISOP) chemistry is included through reactions with O, OH, O_3, and NO_3, forming CH_2O and lumped representations of methacrolein and methyl vinyl ketone as the main products; e.g.,

$$OH + ISOP \rightarrow FORM + XO_2 + 0.67HO_2 + 0.40MGLY + 0.20C_2O_3$$
$$+ ETH + 0.20ALD2 + 0.13XO_2N$$

where MGLY is methylglyoxal, also included in the aromatic chemistry mechanism, and XO_2N is an organic nitrate. Methylglyoxal undergoes a single reaction with OH (to form $XO_2 + C_2O_3$) and photolysis (to form C_2O_3, CO, and HO_2).

CB4 contains a total of 36 species and 93 reactions. It has been extensively tested against 170 smog chamber experiments, with generally satisfactory results. It is the default mechanism in the Models3/Community Multiscale Air Quality (CMAQ) model (Gipson and Young, 1999) that is widely used for policy purposes. The main concern for the wider applicability is its accuracy under low NO_x conditions, where it has not been tested, and its representation of secondary chemistry.

The mechanism has recently been updated to version CB05 (Yarwood et al., 2005), specifically for use in the US Environmental Protection Agency's modeling studies. The mechanism and its extensions incorporate, inter alia, (i) explicit chemistry for methane and ethane, including explicit representation of CH_3O_2, CH_3OOH, and HCOOH; (ii) lumped higher organic peroxides, organic acids, and peracids; (iii) a general internal olefin, RCH═CHR, labeled IOLE; (iv) a higher aldehyde species, ALDX, so that ALD2 explicitly represents acetaldehyde; (v) the higher peroxyacylnitrate, PANX, derived from ALDX; (vi) a lumped terpene species, TERP; (vii) optional extensions for air toxics; (viii) optional reactive chlorine chemistry. The core mechanism, CB05, contains 51 species and 156 reactions, and provides routes to improved modeling of aspects of air quality, including behavior under low NO_x conditions and the formation of secondary organic aerosol from aromatics and biogenics.

Other mechanisms are used for modeling regional air quality. The Regional Atmospheric Chemistry Mechanism (RACM), Stockwell et al., (1997) is based on an earlier mechanism, RADM-2 (Stockwell et al., 1990), designed for regional acid deposition modeling. It contains 56 species and 237 reactions. The State-wide Air Pollution Research Center (SAPRC) mechanism (Carter, 2000) is a much more complex mechanism. The main VOC chemistry is described using explicit chemistry produced

automatically using a mechanism generator. Rate coefficients and rate coefficient ratios are estimated and adjusted by reference to laboratory measurements and extensive smog chamber data. Over 1,600 smog chamber experiments have been used to evaluate and refine the mechanism. The primary application of SAPRC is in the estimation of maximum incremental reactivities (MIRs) for Los Angeles and other cities in the U.S., using box model simulations over a 1 day period (Carter, 1995). MIRs provided a measure of relative ozone formation for different VOCs. Derwent et al. (2001) compared MIRs with POCPs (q.v.) generated from the MCM for a 24 h period under U.S. conditions. The agreement was reasonable, but with some significant differences in the rankings, especially for alkenes and oxygenates.

X-B-3.2. GEOS-Chem

The basis of the chemistry included in the GEOS-Chem model (Bey et al., 1999) was described by Horowitz et al. (1998). The mechanism includes explicit chemistry for methane, ethane, propane, butane, propene, and isoprene. Butane is used as a surrogate for all alkanes with carbon number ≥ 4 and propene for alkenes ≥ 3. This approach is based on the similarities in the yields per carbon atom of O_3, HO_x (OH, HO_2, RO_2) and peroxyacyl nitrates for these compound classes, as discussed by Jacob et al. (1989). Three peroxyacyl nitrates PAN, PPN (a lumped peroxyacyl nitrate) and PMN (peroxymethacryloyl nitrate) are included, together with ISN2, a lumped organic hydroxynitrate, required for the isoprene mechanism and R4N2, a lumped alkyl nitrate. Seven carbonyl species are included: formaldehyde, acetaldehyde, methacrolein, other aldehydes (RCHO), acetone, methylvinyl ketone, and other ketones (MEK).

Isoprene chemistry is treated in some detail, because of its importance. Reactions with OH, O_3, and NO_3 are included. Reaction with OH leads to formation of a single peroxy radical, RIO2. The reaction of this species with NO, and subsequent reactions of the products with O_2 leads to formation of CH_2O, methyl vinyl ketone, methacrolein, HO_2, and other carbonyls (IALD). The hydroxynitrate ISN2 is an important species in the mechanism and ozone formation is sensitive to the reactions involving this species. It reacts with OH and O_3 and is photolyzed, each reaction regenerating NO_x. It also undergoes dry deposition at a velocity equal to that of HNO_3 and is assumed to be highly soluble, so that it is scavenged by precipitation. These processes remove NO_x irreversibly from the atmosphere. The balance between NO_x regeneration and wet and dry deposition is a key factor in determining the impact of isoprene on ozone formation (Fiore et al., 2005).

GEOS-Chem is widely applied in both global and regional modeling. Examples include assessments of global budgets of ethane (Xiao et al., 2008), methanol (Jacob et al., 2005), glyoxal and methyl glyoxal (Fu, 2008), interpretation of the impacts of halogen chemistry on ozone (Read et al., 2008) and the use of CH_2O satellite retrievals to evaluate emissions inventories (Fu et al., 2007; Palmer et al., 2006; see section X-F).

Other examples of global chemical transport models containing lumped chemical mechanisms include TOMCAT (Law et al., 1998) and MOZART (Horowitz et al., 2003).

X-B-3.3. The Mainz Isoprene Mechanism (MIM)

The Mainz isoprene mechanism (Pöschl et al., 2000) was based on and developed by intercomparison with the MCM, but it is highly condensed with only 16 species and 44 reactions. It was designed to provide a compact representation of the key isoprene chemistry in global models which incorporate explicit O_3, NO_x, HO_x, CO, and CH_4 chemistry. Table X-B-3 shows the MIM species included and the compounds they represent. Note that some important species formed in isoprene oxidation, such as CH_2O and CH_3OOH, are not included as separate species, because they are already included in the CH_4 chemistry: they appear in the 44 reaction mechanism of MIM as products only. Considerable simplification is introduced by including only MACR; its rate coefficients with OH and O_3 are taken as the arithmetic mean of those for methacrolein and methylvinylketone.

Pöschl et al. carried out extensive tests using box models over a range of scenarios, representing mid- and tropical-latitudes and high and low NO_x conditions. They found good agreement with the MCM for key species (O_3, OH, CO, CH_3O_2H, and PAN) with agreement generally within 10%. The MIM has been quite widely used as a means of incorporating isoprene chemistry in highly reduced global models; e.g., by Young et al. (2009). They used MIM in conjunction with a chemical mechanism similar to that used in the offline chemical transport model TOMCAT to assess the impact of the suggested inhibition of leaf isoprene emissions from increased CO_2 atmospheric concentrations on future ozone projections in the on-line chemistry–climate model (UM-CAM).

More recently, it became clear that a more detailed isoprene mechanism that reduced the biases observed from further extensive testing of the MIM would be of value, and Taraborelli et al. (2009) developed the Mainz Isoprene Mechanism 2 (MIM2). The total number of species was increased to 68 and the number of reactions to 199.

Table X-B-3. Species in the Mainz isoprene mechanism (MIM)

MIM Species	Compounds Represented by the MIM Species
C_5H_8	Isoprene
ISO_2	Peroxy radicals from $C_5H_8 + OH$
ISO_2H	β-hydroxyhydroperoxides from $ISO_2 + HO_2$
ISON	β-hydroxyalkenylnitrates from $ISO_2 + NO$ and alkenylnitrates from $C_5H_8 + NO_3$
MACR	Methacrolein, methylvinylketone and other C_4 carbonyls
$MACRO_2$	Peroxy radicals from MACR + OH
$MACRO_2H$	Hydroperoxides from $MACRO_2 + HO_2$
MPAN	Peroxymethacryloylnitrate and other peroxyacylnitrates (except peroxyacetylnitrate)
HACET	Hydroxyacetone and other C_3 ketones
MGLY	Methylglyoxal and other C_3 aldehydes
CH_3CO_3	Peroxyacetyl radical
PAN	Peroxyacetylnitrate
CH_3CO_3H	Peroxyacetic acid
CH_3COOH	Acetic acid
NALD	Nitroxyacetaldehyde
HCOOH	Formic acid

MCM v3.1, for comparison, has 180 species and 595 reactions. Three peroxy radicals from OH + isoprene are included explicitly, each leading to a separate nitrate following reaction with NO. Reactions of the peroxy radicals with RO_2 and NO lead to formation of five carbonyl or hydroxycarbonyl species, including methacrolein and methyl vinyl ketone, while reaction of the peroxy radicals with HO_2 leads to formation of three separate hydroperoxides. Acetaldehyde, propene, and glyoxal are also included. Thus the chemistry is much more detailed than that included in the MIM. A further important development is the introduction of mass balance with respect to carbon so that CO_2 formation can be determined, which is not the case for either MCM or MIM. The performance of the mechanism compared with MIM, especially in relation to nitrate chemistry and H_2O_2, CH_3OOH, CH_3OH, CH_2O, HCOOH, CH_3COOH, and PAN is significantly improved.

A modified version of MIM2 was used in the interpretation of field measurements in the GABRIEL campaign over the tropical forests of Suriname under low NO_x conditions (Lelieveld et al., 2008; Butler et al., 2008). The measurements showed higher concentrations of OH than expected, and it was suggested that isoprene oxidation leads to a higher OH recycling efficiency (40–50%) than that given by current mechanisms (5–10%). Modifications of MIM2 including this higher efficiency were able to reproduce the observed [OH] with much reduced bias. Peeters et al. (2009) have proposed new reactions in the peroxy radical chemistry of isoprene, which is based on isomerisation via H-atom transfer to form a hydroperoxy radical that dissociates to form OH leading to an increase in OH recycling. Quantitative testing against observations remains to be done.

X-B-3.4. The Common Representative Intermediates (CRI) Mechanism

Jenkin et al. (2002, 2008) developed a lumped version of the MCM. Their approach is based on recognizing the maximum total ozone production potential for a given compound. For example, CH_4 has the potential to form four molecules of ozone as it is oxidized, corresponding to the four C—H bonds it contains. The ozone formation reactions correspond to the reactions of CH_3O_2 and HO_2 with NO in the first propagation cycle, following reaction of CH_4 with OH, and the reactions of HO_2 with NO following the reactions of OH with CH_2O and CO. Reactions of HO_2 and CH_3O_2 with peroxy radicals reduce the total ozone yield, but the methodology is based on the maximum number of O_3 molecules that can be formed.

Figure X-B-2 shows the representation in CRI-MECH of the initial stages of the oxidation of pentane and its linkage with the oxidation of butane. The figures in brackets refer to the number of C—H and C—C bonds in each compound and, therefore, to the maximum number of ozone molecules that can be generated. Each compound name contains a number, which also refers to the maximum number of ozone molecules that can be formed. Thus, pentane contains 4 C—C bonds and 12 C—H bonds and so has an index of 16, as does the peroxy radical formed by H-abstraction, since it still has the potential to form 16 O_3 molecules. The index is reduced by one for the peroxy radical formed by subsequent reaction with NO and then O_2, since one NO $\rightarrow$ NO_2 conversion has occurred. The labeling of the compounds, e.g., RN16O2 and CARB13

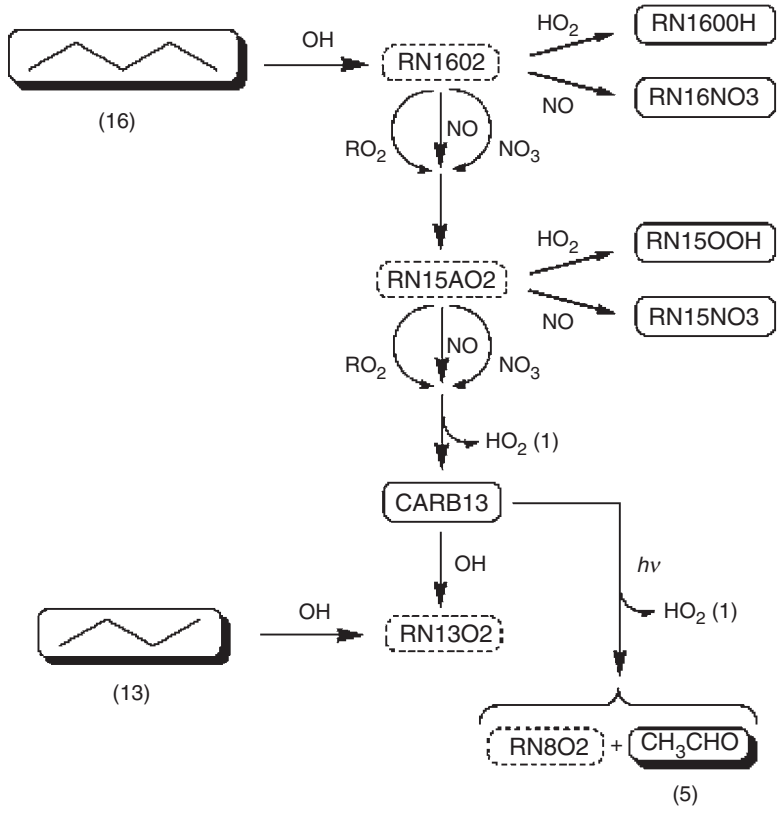

Figure X-B-2. Schematic representation of the initial stages of the degradation chemistry developed for pentane as part of the CRI v2 construction procedure.

refers to generic radicals and carbonyl compounds, respectively. Figure X-B-2 shows that the mechanism includes peroxy + peroxy radical reactions, as well as photolysis of carbonyls, nitrate formation, and reactions of peroxy radicals with NO_3. Where appropriate, the mechanism also includes reactions of VOC surrogates with O_3 and NO_3. The chemistry of some species, e.g., CH_3CHO, is represented explicitly. CRI v2 represents the oxidation of 115 emitted VOCs, and contains 434 species and 1183 reactions, and so is about a factor of 10 smaller than the MCM. Its performance was evaluated by comparison with MCM v3.1 and showed good agreement for tested species over a range of conditions. A major advantage is the traceability of the mechanism to the MCM. Five lumped versions have been developed (Watson et al., 2008) in which, for example, minor emitted species are redistributed into appropriate surrogates and their specific chemistry removed. In the most extreme version, the numbers of species and reactions were reduced by about 55% compared with the full CRI v2. A further version of the mechanism has been generated to address the formation of secondary organic aerosol (Utembe et al., 2009).

X-B-3.5. Objective Methods of Mechanism Reduction and Lumping

The generation of reduced and lumped mechanisms described in the preceding sections relies on chemical intuition and understanding; e.g., in the selection of surrogate species. It is also possible to use more objective methods, based, for example, on sensitivity analysis. The methods available have been discussed by Tomlin et al. (1997).

The mechanism can be reduced in size by the application of species and reaction sensitivities. These methods identify and eliminate those species and reactions that have comparatively little influence on the rates of production and loss of key specified species; e.g., O_3, OH, CH_2O, and PAN. The approach is straightforward to apply and has been discussed by Zeng et al. (1997) and Heard et al. (1998) in relation to reduction of the mechanism for butane oxidation and of CB4 respectively. A further widely applied approach is the application of the quasi-steady-state approximation (QSSA), where the overall rate of reaction (rate of production minus rate of loss) is set equal to zero. Such an approximation is accurate for species with lifetimes that are short compared with the overall timescale of the atmospheric process under investigation. The ordinary differential (rate) equation (ODE) is replaced by an algebraic equation, so that the species concentration can be derived algebraically, allowing one differential equation to be removed from the model. This process is especially valuable, because the short lifetimes of these species makes the system "stiff"—very short time steps have to be taken in the numerical integration of the coupled ODEs. Removing the ODEs for the short-lived species can significantly reduce the time required for accurate integration. Typical species to which the QSSA can be applied are $O(^1D)$ and oxy radicals so that, for example, the methoxy radical can be removed from the integration, with CH_3O_2 reacting with NO (and O_2) to form $HO_2 + CH_2O$. Under normal circumstances, where HO_2 + peroxy radicals are important, it can prove difficult to derive an analytically soluble algebraic equation for HO_x because of the nonlinear terms in the equations for $[HO_2]$ and [OH] (Carslaw et al., 1999). Turanyi et al. (1993) developed a simple method for determining the error introduced into the integration by the application of the QSSA to a specific species, which allows straightforward identification of valid QSSA species.

Whitehouse et al. (2004a,b) applied these methods to MCM v2. They reduced the number of species in the mechanism by approximately 50%. They extended the process by lumping species, such as peroxyacylnitrates, with similar lifetimes and reaction patterns. This procedure allowed reduction of the number of species to 35% of the original number in MCM v2.

Methods for reducing the size of a chemical mechanism have been extensively investigated in combustion modeling. Unlike atmospheric processes, the fluid dynamics of a combustion system are closely linked to the evolution of heat from the coupled chemical reactions. In many applications, the main interest is heat evolution, so that recovering the details of the chemistry from the model is of only secondary interest. This has led to methods known collectively as low dimensional manifold analysis, in which the very fast reactions are allowed to go to steady state on the timescale of the fluid dynamics, leaving only a few species as the major determinants of the

heat release. The concentrations of these species are linked to the shorter-lived species through detailed modeling and are then represented for the fluid dynamics calculations either through polynomials or look-up tables. Tomlin et al. (2002) examined the utility of a low dimensional manifold analysis in a 5-day simulation of butane oxidation under high NO_x conditions. They used the mechanism from the MCM, which contains 185 species, but based their analysis on the reduced mechanism with 42 species derived by Zeng et al. (1997). They identified those species reacting on sufficiently short timescales so that they could effectively be treated as QSSA species; thus, leaving the long time dynamics controlled by a maximum total of 13 species, significantly less than the number in the reduced mechanism but still relaxing onto the slow manifold on the timescale considered. The dimension varied throughout the day, reaching a minimum of four at night. The 13 species set was comprised primarily of inorganic NO_{xy} species, PAN, and carbonyls, the last-named group consisting of formaldehyde, acetaldehyde, butanal, methyl ethyl ketone, 3-hydroxypropanal, and 4-hydroxybutanal; butane, methane, and CO, the primary species in the simulation, contributed to the slowest reaction modes of the chemical system. Identification of the 13 species allows the construction of a so-called *repro-model* which can reproduce the chemical dynamics; the repro-model can be constructed as a polynomial, on the basis of the simulated chemistry over a wide range of conditions, using the 13 species as variables. Repro-modeling has been used by Spivakovsky et al. (1990) to model tropospheric OH.

X-C. Role of Oxygenates in Secondary Organic Aerosol Formation

X-C-1. Introduction

Aerosols play an important role in climate, human health, and visibility degradation. There are two general classes of aerosols in the atmosphere: primary and secondary. Primary aerosols are emitted directly into the atmosphere from a variety of sources (e.g., soot in diesel exhaust, or mineral dust suspended by the wind). Secondary aerosols are formed by reactions involving organic compounds in the atmosphere. Organic compounds represent approximately 20–50% of the total fine aerosol mass over land at mid-latitudes and as much as 90% over land in the tropics (Kanakidou et al., 2005). A substantial fraction of the organic component consists of oxygenated compounds (Zhang et al., 2005).

Haagen-Smit (1952) was the first to recognize that the oxidation of organic compounds would lead to the formation of low-volatility oxygenated products that would generate aerosol. Haagen-Smit noted that with the introduction of several polar groups, the volatility of organic compounds "decreases so radically that aerosol formation is inevitable." The effect of the addition of oxygen containing functional groups on the volatility of organic compounds has been discussed in chapter I and is illustrated in figure I-B-9; this figure shows, for example, that the vapor pressure of 4-carbon species, tartaric acid, HO(O)CCH(OH)CH(OH)C(O)OH, is approximately 15 orders of magnitude lower than that of the unoxidized 4-carbon species, butane. In a similar fashion,

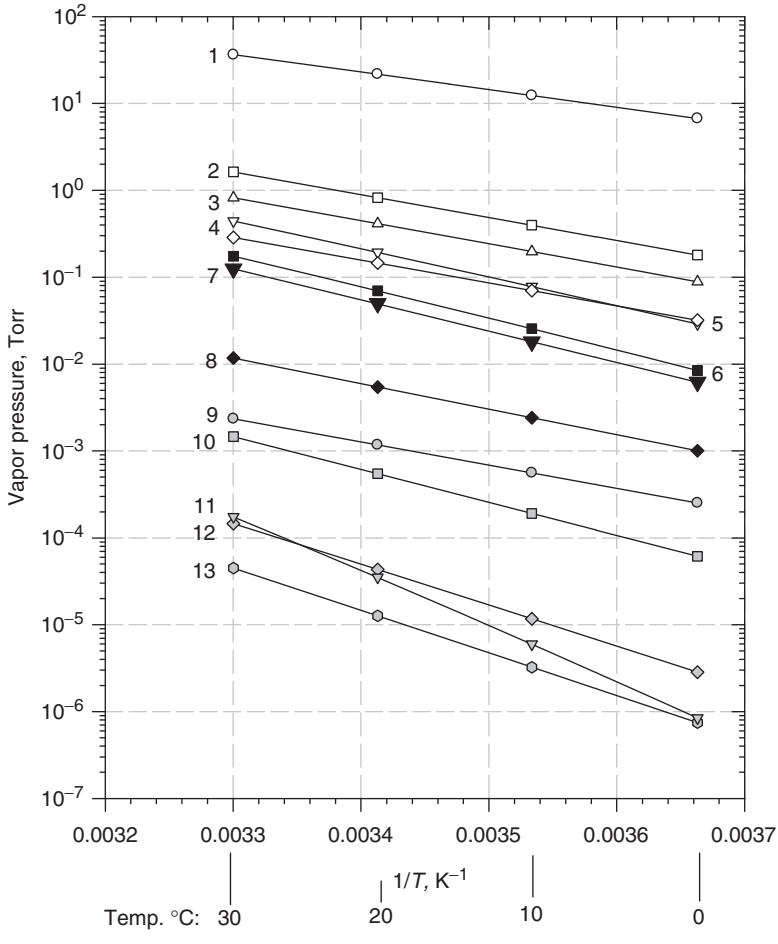

Figure X-C-1. Plot of vapor pressure of toluene and some of its ring-retaining oxidation products: toluene (1); benzaldehyde (2); *o*-hydroxybenzaldehyde (3); *o*-cresol (4); *m*-nitrotoluene (5); *m*-cresol (6); benzyl alcohol (7); benzoic acid (8); 2,4,6-trinitrotoluene (9); *p*-hydroxybenzaldehyde (10); *o*-hydroxybenzoic acid (11); 2,5-dinitrotoluene (12); 3,4-dinitrotoluene (13); from Calvert et al. (2002).

figure X-C-1 shows that the vapor pressure of the ring retaining oxidation products of toluene are orders of magnitude lower than that of toluene. It is now generally recognized that the gas-phase oxidation of organic compounds, particularly aromatics from anthropogenic sources and terpenes from natural sources, is a major source of atmospheric aerosols. Kroll and Seinfeld (2008) provided the estimates listed in table X-C-1 for the change in vapor pressure on introduction of various oxygenated functional groups.

The chemical process of secondary organic aerosol formation can be depicted in general terms in the fashion of Seinfeld and Pandis (1998) and Calvert et al. (2002).

Table X-C-1. Approximate vapor pressure changes on the introduction of oxygenated functional groups into organic compounds, from Kroll and Seinfeld (2008)

Functional Group	Structure	Change in Vapor Pressure (298 K)[a]
Ketone	—C(O)—	0.10
Aldehyde	—C(O)H	0.085
Hydroxyl	—OH	5.7×10^{-3}
Hydroperoxyl	—OOH	2.5×10^{-3}
Nitrate	—ONO_2	6.8×10^{-3}
Carboxylic acid	—C(O)OH	3.1×10^{-3}

[a]Factors are multiplicative, thus the introduction of a nitrate and carboxylic acid function leads to reduction of vapor pressure by approximately a factor of $6.8 \times 10^{-3} \times 3.1 \times 10^{-3} = 2.1 \times 10^{-5}$.

Consider the gas-phase oxidation of an organic parent molecule A by an oxidant (e.g., OH, NO_3 radicals, or ozone) that leads to a set of stable semi-volatile product molecules, S_1, S_2,…,

$$A + \text{oxidant} \rightarrow \alpha_1 S_1 + \alpha_2 S_2 + \ldots$$

where α_1, α_2 are stoichiometric product coefficients. The products S_1, S_2, … may themselves undergo gas-phase reaction, creating second-generation, semi-volatile products,

$$S_1 + \text{OH} \rightarrow \alpha_{11} V_1 + \alpha_{12} V_2 + \cdots$$

$$S_2 + \text{OH} \rightarrow \alpha_{21} W_1 + \alpha_{22} W_2 + \cdots$$

Secondary organic aerosol yields for individual parent organic species became available from smog chamber experiments in the 1990s (Izumi and Fukuyama, 1990; Pandis et al., 1991; Wang et al., 1992a; Wang et al., 1992b; Zhang et al., 1992; Odum et al., 1996; Odum et al., 1997a; Odum et al., 1997b; Hoffmann et al., 1997; Griffin et al., 1999; Kleindienst et al., 1999). Initially it was believed that each parent organic had a unique secondary organic aerosol (SOA) yield characterized by the values of the stoichiometric coefficients, such as α_1, α_2, α_{11}, α_{12}, etc., perhaps depending on the prevailing NO_x level. However, measured yields for an individual parent organic exhibited a degree of variation unreconciled in terms of a single, unique SOA yield or of the expected dependence on NO_x level during photooxidation.

In the mid 1990s, building on the absorptive partitioning model of Pankow (1994a, 1994b), Odum et al. (1996) formulated a framework which can explain the observed SOA yield data. It was recognized that semi-volatile oxidation products, such as S_1, S_2, V_1, V_2, etc., will partition themselves between the gas- and aerosol-phases at a concentration below their saturation concentration, analogous to the partitioning that occurs between the gas- and aqueous-phases of a water-soluble atmospheric constituent.

The equilibrium gas-particle partitioning of a semi-volatile organic species *i* between the gas-phase and a particulate organic-phase can be described by the vapor pressure relation,

$$p_i = x_i\ \gamma_i\ p_i^o \tag{1}$$

where p_i (Torr) is the gas-phase partial pressure of species i, x_i is the mole fraction of species i in the organic aerosol phase, γ_i is the activity coefficient of species i in the aerosol-phase organic mixture, and p_i^o is the vapor pressure of species i as a pure liquid (subcooled, if necessary). The gas-phase partial pressure, p_i, can be converted to gas-phase mass concentration, G_i, by the ideal gas relation,

$$G_i = \frac{p_i M_{wi}}{RT} 10^6 \tag{2}$$

where M_{wi} (g mol^{-1}) is the molecular weight of species i, R is the ideal gas constant, and T(K) is temperature. The factor 10^6 accomplishes the appropriate unit conversions.

Let A_i be the aerosol-phase mass concentration of species i (μg m^{-3}), where the volume, m^{-3}, referred to is the volume of air. The mean molecular weight of the organic aerosol phase is

$$\overline{M}_w = \sum_{i=1}^{n} x_i M_{wi} \tag{3}$$

The total aerosol mass concentration is

$$M_o = \sum_{i=1}^{n} A_i \tag{4}$$

If the organic species have similar molecular weights, then the mole fractions in the aerosol phase are given by

$$x_i = \frac{A_i}{M_o} \tag{5}$$

Equations (2) and (5) can be substituted into equation (1) to yield

$$\frac{A_i}{G_i M_o} = \frac{RT}{\overline{M}_w \gamma_i p_i^o} 10^{-6} \tag{6}$$

The left-hand side of equation (6) is the ratio of the aerosol- to gas-phase mass concentrations of species i, including the total mass of the organic particulate phase. The

right-hand side can be defined as the equilibrium gas-particle partitioning coefficient of species i,

$$K_i = \frac{RT}{\overline{M}_w \gamma_i p_i^o} 10^{-6} \tag{7}$$

Secondary organic aerosol yields have been measured in smog chamber experiments. The SOA yield for a given oxidation product i, Y_i, is the amount of aerosol mass of species i that is produced from the oxidation of the parent reactive organic gas (ROG) and is defined by

$$Y_i = \frac{A_i}{\Delta \mathrm{ROG}} \tag{8}$$

when ΔROG(μg m^{-3}) is the reacted amount of the parent ROG. The total aerosol yield from that parent molecule is just the sum of the individual product yields,

$$Y = \sum_{i=1}^{n} Y_i \tag{9}$$

The total SOA yield from an ROG that generates n semi-volatile products is computed as follows. The total concentration of product i, C_i, is related to the total amount of parent ROG that is consumed, ΔROG, by the stoichiometric coefficient for that product,

$$\alpha_i \Delta \mathrm{ROG} = C_i \tag{10}$$

where α_i is now considered to be the mass-based stoichiometric coefficient. C_i is also equal at any time to the sum of the gas- and aerosol-phase concentrations of species i,

$$C_i = A_i + G_i \tag{11}$$

Combining these relations with the definition of the gas-particle equilibrium partitioning coefficient, K_i, gives the expression for the total aerosol yield in terms of the individual product mass-based stoichiometric coefficients, α_i, and partitioning coefficients, K_i, and the total organic aerosol mass concentration, M_o,

$$Y = M_o \sum_{i=1}^{n} \frac{\alpha_i K_i}{1 + K_i M_o} \tag{12}$$

In the limit of small organic aerosol mass concentration or high volatility of the products,

$$Y \sim M_o \sum_{i=1}^{n} \alpha_i K_i \tag{13}$$

and the SOA yield is directly proportional to M_o. In the limit of large organic aerosol mass concentration or low volatility of the products,

$$Y \sim \sum_{i=1}^{n} \alpha_i \tag{14}$$

and the total yield is independent of M_o and is just the sum of the mass-based stoichiometric coefficient of the products.

Odum et al. (1996) showed that by using the absorptive-partitioning theory, it was possible to describe the increased SOA yields with increased organic aerosol concentrations observed in smog chamber experiments using just two semi-volatile products (yields and partitioning coefficients of the two products were fit parameters). Donahue et al. (2006) have noted that partitioning over a wide range of aerosol loadings is better described using a larger number (up to 10) of products.

Numerous oxygenated organic compounds have been identified in SOA including organic acids (Hoffman et al. 1997; Forstner et al., 1997a,b; Fisseha et al., 2004), peroxy acids (Reinnig et al., 2009), hydroperoxides (Reinnig et al., 2009), peroxides (Ziemann, 2002; Docherty et al., 2005), nitrates (Nielsen et al., 1998; Laurent et al., 2004; Reemtsma et al., 2006), δ-hydroxynitrates, dinitrates, hydroxydinitrates, and substituted tetrahydrofurans containing nitrooxy, hydroxyl, and carbonyl groups (Lim and Ziemann, 2005).

The oxygenated compounds present in secondary organic aerosol are generally highly reactive species. As first suggested by Haagen-Smit (1952), observed experimentally by Kalberer et al. (2004), Tolocka et al. (2004), and Gao et al. (2004), and inferred from modeling work (Johnson et al., 2006; Volkamer et al., 2006), a series of reactions can occur in the aerosol phase which form low-volatility oligomers. Figure X-C-2 shows examples of oligomer forming reactions involving oxygenated compounds. The oligomers clearly are much larger than the monomer units from which they are derived and have correspondingly lower vapor pressures. Volkamer et al. (2006, 2007, 2009) have shown that glyoxal, HC(O)C(O)H, one of the smallest and most volatile oxygenated compounds in the atmosphere, undergoes heterogeneous photochemical reactions which generate SOA. The formation and subsequent chemistry of SOAs depends heavily on the chemistry of oxygenated compounds (Donahue et al. 2009), in particular on the competition between reactions which lead to products with higher volatility (e.g., reactions involving C—C bond scission) and reactions which lead to products with lower volatility (e.g., oligomer formation or formation of compounds with a higher O:C ratio). Our understanding of the chemistry of SOA formation is still in its infancy and much more work is needed in this area.

X-D. Role of Oxygenates in the Upper Troposphere

X-D-1. Introduction

Formation of OH from $O(^1D) + H_2O$ dominates radical formation in the background troposphere. Observations from aircraft of oxygenates, and particularly acetone, over

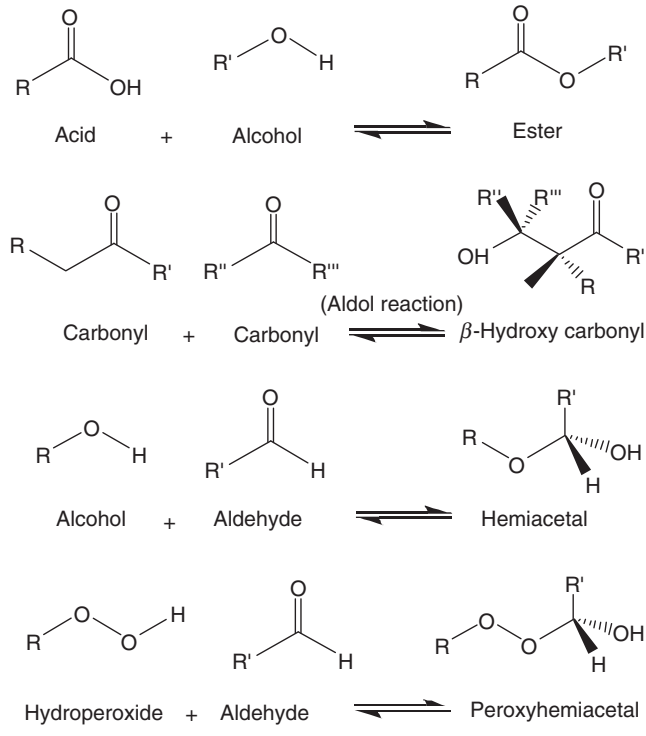

Figure X-C-2. Aerosol phase reactions leading to the formation of oligomers.

a range of altitudes and locations in the 1990s, coupled with modeling studies, demonstrated that carbonyl photolysis also plays a role, especially in the upper troposphere, where [H_2O] can be low and where photolysis rates are enhanced. This section briefly reviews some of the observations and modeling studies on which this conclusion is based.

X-D-2. Observations of Oxygenates in the Remote Troposphere

Singh et al. (1995) reported measurements of oxygenates over the Pacific in an aircraft experiment (NASA/PEM-West B) that took place from February to March 1994, at altitudes from 2 to 10 km, latitudes 40°N–10°S and longitudes 125°W–140°E. This region was not significantly impacted by continental emissions and can be taken as representative of near-background conditions. The main observations were limited to acetone, whose concentration varied from ~500 ppt to ~200 ppt; PAN, 100 ppt to 10 ppt; and methanol, 700 ppt to 400 ppt. In each case the higher figure refers to northern hemisphere (NH) mid-latitudes and the lower figure to the southern hemisphere (SH) measurements. The measurements were incorporated into models that showed that acetone provides a significant route in the upper troposphere for storing NO_x and that it is an important, and previously unrecognized, source of HO_x in this region.

A more detailed examination of a wider range of oxygenates resulted from the NASA/PEM-Tropics B campaign, that took place over the tropical Pacific (30°N–30°S) in March–April 1999 (Singh et al., 2001). Figure X-D-1 shows the concentrations of the major species for the NH and SH. The concentration of methanol is almost twice that of ethane, which is the most abundant nonmethane hydrocarbon. The oxygenates

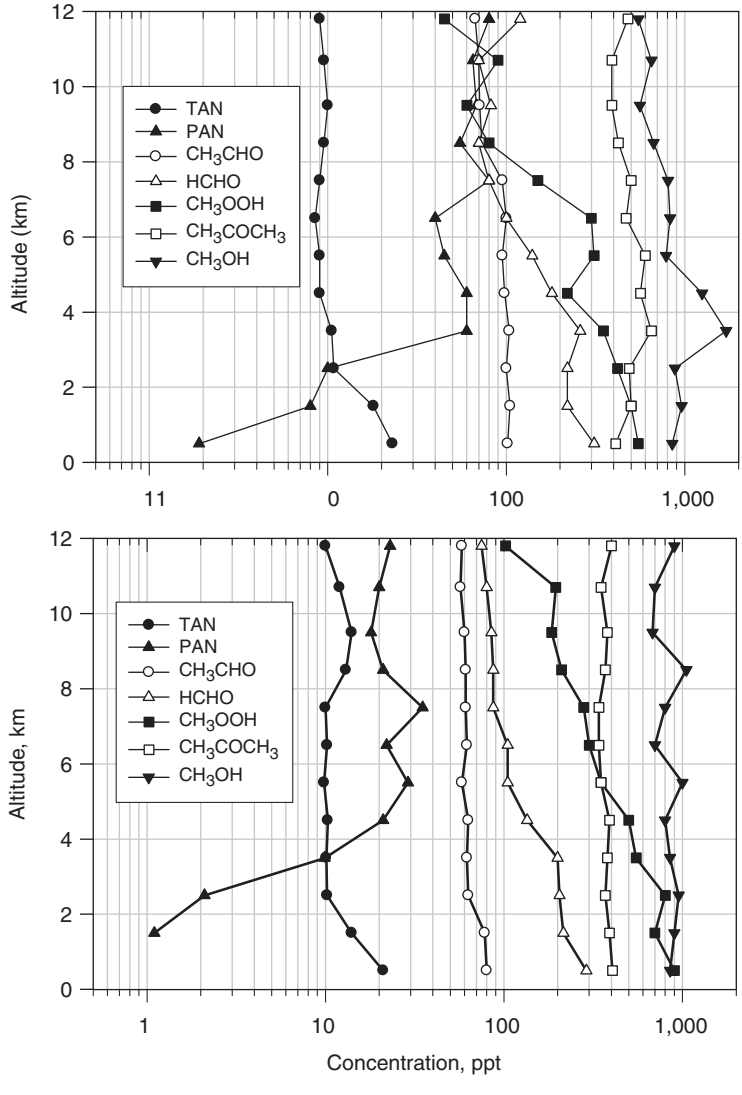

Figure X-D-1. The mean vertical distribution of oxygenates observed over the Pacific during March–April 1999 (Singh et al., 2001) The top panel shows data from the Northern Hemisphere collected at 0–30°N and 170–120°W. The bottom panel shows data from the Southern Hemisphere collected at 0–30°S and 165°E–100°W. TAN (total alkyl nitrates) is the sum of the organic nitrates. PAN is peroxyacetyl nitrate, $CH_3C(O)O_2NO_2$.

also show a smaller latitudinal variation than the NMHCs. In the NH, the total oxygenate concentration is 2–2.5 times that of the total NMHCs, while in the SH the ratio is 4–5.

X-D-3. Global Budgets for Oxygenates

Measurements of oxygenates have been used in conjunction with global models to evaluate global budgets for oxygenates, which provides an alternative to the emissions inventory method discussed in section I-C for assessing emissions sources. The most detailed analysis for acetone, which is of primary concern in this discussion of upper troposphere sources of radicals, has been provided by Jacob et al. (2002). They used atmospheric observations from 14 surface sites and five aircraft campaigns in an inversion analysis to improve a priori estimates of sources and sinks in the GEOS-Chem 3-D global model. Their estimates are shown in table X-D-1. Other estimates have been made by Singh et al. (1994, 2000) and Müller and Brasseur (1999).

Both sets of estimates in Table X-D-1 emphasize the importance of natural sources and atmospheric oxidation. There are major differences between the a priori and a posteriori figures for the oceans. Microbial activity is generally recognized as a net sink, while photochemical degradation of dissolved organic matter is a source. The PEM-Tropics B aircraft measurements provide strong support for an ocean source of acetone, because of the high background value found even in the SH. The inclusion of a strong ocean sink was needed to reproduce the seasonal cycle in the acetone concentrations at the European and Arctic sites and also necessitated a significant increase input from an ocean source in the tropics. Jacob et al. also examined the main

Table X-D-1. Global atmospheric budget for acetone, deduced by a priori and a posteriori methods by Jacob et al (2002)

Source/Sink	a priori Rate, Tg year^{-1}	a posteriori Rate, Tg year^{-1}
Direct emission sources		
Anthropogenic emissions	1.3 ± 0.7	1.1 ± 0.5
Biomass burning	3.4 ± 1.7	4.5 ± 1.6
Terrestrial vegetation	26 ± 20	33 ± 9
Plant decay	9 ± 9	2 ± 5
Ocean	10 ± 10	27 ± 6
Precursors of acetone via atmospheric oxidation		
Isoalkanes (anthropogenic)	20 ± 10	21 ± 5
Monoterpenes and methylbutenol	9 ± 4	7 ± 3
Total sources	78 ± 27	95 ± 15
Sinks		
Oxidation by OH	25	27
Photolysis	44	46
Dry deposition	9[a]	23[b]
Total sinks	78	95

[a]Includes deposition to land only.
[b]Includes deposition to the oceans (14 Tg year^{-1}) and to land (9 Tg year^{-1}).

source contributions to acetone at the tropopause, in view of the importance of acetone as a radical source there. In the tropics, the main sources are the oceans and terrestrial vegetation, while, in the extratropical NH, oxidation of isoalkanes dominates in winter and vegetative emissions dominate in summer.

The issue of the role of the oceans was revisited by Singh et al. (2003), based on measurements in the TRACE-P aircraft experiment in 2001 over the Pacific. They concluded that the oceans are a small *net* sink for acetone corresponding to ~14 Tg year^{-1}. They also concluded that their measurements were compatible with net ocean sources of ~125 Tg year^{-1} for acetaldehyde and ~45 Tg year^{-1} for propionaldhyde, although the uncertainties in these estimates are considerable and unquantified.

Millet et al. (2008a) used a budget methodology for methanol similar to that employed by Jacob et al. (2002) for acetone. They obtained ocean and terrestrial biogenic sources of 85 and 80 Tg year^{-1} respectively and an ocean sink of ~ 100 Tg year^{-1}. The other major sink is reaction with OH (~90 Tg year^{-1}).

X-D-4. Upper Troposphere Sources of HO_x

There have been a number of discussions of radical budgets in the upper troposphere. One of the more detailed was that by Jaeglé et al. (2001), based on aircraft measurements in a series of aircraft campaigns (STRAT 1995–6, N. Pacific; SUCCESS, 1996, central U.S.; SONEX, 1997, N. Atlantic). OH and HO_2 radicals were measured in all campaigns; acetone was measured in SONEX but only inferred from CO measurements in the other two campaigns. STRAT was influenced by deep convective uplift of clean marine surface air to the upper troposphere, SUCCESS by the convective injection of polluted air from the U.S., which led to high concentrations of CO and NO_x, while SONEX experienced high NO_x from lightning, convection, and aircraft emissions, coupled with lower photochemical activity because it was conducted in October/November at high latitudes.

Convection is important in pumping a range of HO_x precursors (acetone, peroxides, and aldehydes) into the upper troposphere. It also significantly influences [H_2O] which is otherwise quite low. The importance of acetone as a radical source depends on the water mixing ratio, which varies much more than that of acetone; acetone is a more important source of radicals than $O^1D + H_2O$ for [H_2O] < 100 ppm.

The yield of HO_x per acetone photolysed, y, was found to be ~2–3 under upper troposphere conditions, because of the additional radical production from formaldehyde.

$$CH_3COCH_3 + h\nu(+2O_2) \rightarrow CH_3CO_3 + CH_3O_2 \quad (1)$$

$$CH_3CO_3 + NO(+O_2) \rightarrow CH_3O_2 + CO_2 + NO_2 \quad (2)$$

$$CH_3O_2 + NO(+O_2) \rightarrow CH_2O + HO_2 + NO_2 \quad (3)$$

$$CH_2O + h\nu(+2O_2) \rightarrow 2HO_2 + CO \quad (4)$$

$$CH_2O + h\nu \rightarrow H_2 + CO \quad (5)$$

This sequence provides the main reactions contributing to HO_x formation from acetone, and it operates at higher [NO_x], with the additional reaction

$$CH_3CO_3 + NO_2 \leftrightarrow CH_3CO_3NO_2 \tag{6}$$

leading to PAN formation.

At lower NO_x, peroxy–peroxy reactions become more significant:

$$CH_3O_2 + HO_2 \rightarrow CH_3OOH + O_2. \tag{7a}$$

$$\rightarrow CH_2O + O_2 + H_2O \tag{7b}$$

$$CH_3CO_3 + HO_2 \rightarrow CH_3C(O)OOH + O_2 \tag{8a}$$

$$\rightarrow CH_3COOH + O_3 \tag{8b}$$

$$(+O_2) \rightarrow O_2 + HO + CH_3O_2 + CO_2 \tag{8c}$$

Photolysis of methyl hydroperoxide regenerates HO_x and CH_2O:

$$CH_3OOH + h\nu(+O_2) \rightarrow OH + HO_2 + CH_2O \tag{9}$$

but reaction with OH acts, effectively, as a terminating step:

$$CH_3OOH + OH \rightarrow OH + CH_2O + H_2O \tag{10a}$$

$$\rightarrow CH_3O_2 + H_2O \tag{10b}$$

The HO_x yield depends on [NO_x] and on the rate of production of HO_x [$P(HO_x)$]. For very low [NO_x] (<10 ppt) and high $P(HO_x)$ (>200 ppt day^{-1}), the yield, y, can become negative, because of the contribution of the peroxy–peroxy reactions, which lead to net loss of HO_x. Jaeglé et al. (2001) calculated median values of $y = 2.5$ for the SUCCESS, 2.8 for the SONEX, and 2.9 for the STRAT campaigns. For the SONEX campaign, $O(^1D) + H_2O$ and acetone provided roughly comparable sources of HO_x, but acetone was more dominant for STRAT and SUCCESS, because of the lower [H_2O].

Modeling studies by Müller and Brasseur (1999) and Prather and Jacob (1997) found high contributions to $P(HO_x)$, of up to 60% at 10–14 km, from peroxides and aldehydes during convective events over the tropics. Peroxides were the main contributor over the oceans and aldehydes over land. Jaeglé et al. found large enhancements (factors of 2–5) of HO_x concentrations during convective outflows in STRAT and SUCCESS, with the additional sources exceeding the contributions of $O(^1D) + H_2O$ and acetone by factors of 2–10.

A further contribution to upper troposphere HO_x production derives from autocatalysis in the reaction cycle involving $OH + CH_4$:

$$OH + CH_4(+O_2) \rightarrow CH_3O_2 + H_2O \tag{11}$$

followed by reactions 3–5, 7, 9, 10. Methane oxidation acts as a source of HO_x through CH_2O photolysis, or a sink through $OH + CH_3OOH$. The yield of HO_x, y_{CH_4}, increases with $[NO_x]$ and decreases with $P(HO_x)$, for the reasons discussed above for acetone. Jaeglé et al. (2001) derived a maximum y_{CH_4} of 0.62, dependent on the rate used for the radical channel in the photolysis of CH_2O (4). The values they obtained in their modeling were generally in the range 0.3–0.5. The $OH + CH_4$ source of HO_x differs from the photolysis sources, because it requires the presence of OH and can be viewed as a mechanism that amplifies the primary sources.

Wennberg et al. (1998) examined the diurnal variation of HO_x sources based on observations made with the ER2 aircraft in 1995–1996 and found even larger fractional contributions, up to 80%, from acetone photolysis, especially at high solar zenith angles. This is because ozone photolysis to form $O(^1D)$ requires shorter wavelengths than does acetone photolysis. They discussed the results in the context of ozone formation near the tropopause, and the ozone contribution to radiative forcing. $[NO_x]$ concentrations were generally quite high (50–200 ppt), so that the rate of O_3 production was high from the RO_2 and $HO_2 + NO$ reactions in the oxidative cycles involving particularly CO and CH_4. In addition, the chain length was higher than at lower altitudes, increasing from ~5 at 7 km to 10–20 at the tropopause. These chain lengths are predicated on termination via formation of HNO_3. However, while HNO_3 is generally removed from the atmosphere by deposition at lower altitudes, in the upper troposphere photolysis is also significant, regenerating both HO_x and NO_x and enhancing the ozone production rate beyond that calculated from simple chain length considerations. The rate of ozone formation was calculated to be ~1 ppb day^{-1}, increasing to ~5 ppb day^{-1} in regions with high $[NO_x]$; e.g., in aircraft plumes. These rates, and their impact on radiative forcing and climate change, depend on the rate of primary HO_x formation and hence on the photolysis of acetone and other oxygenates.

X-E. Role of Oxygenates in Transport of Pollutants (e.g., PAN)

Ozone production in the troposphere results from the formation of $O(^3P)$-atoms following the photolysis of NO_2. The reaction of HO_2 and organic peroxy radicals with NO reforms the NO_2 thereby completing the cycle and enabling more ozone production:

$$NO_2 + h\nu(\lambda < 420 \text{ nm}) \rightarrow NO + O(^3P) \tag{1}$$

$$O(^3P) + O_2 + M \rightarrow O_3 + M \tag{2}$$

$$RO_2 + NO \rightarrow HO/RO + NO_2 \tag{3a}$$

$$RO_2 + NO + M \rightarrow RONO_2 + M \tag{3b}$$

NO_x is removed from the atmosphere by several mechanisms including via the formation of low-volatility organic nitrates in reaction (3b) which are incorporated into aerosol and then undergo wet and dry deposition. In addition, nitrogen dioxide reacts with OH radicals with a rate coefficient of 1.19×10^{-11} cm^3 molecule^{-1} s^{-1} in 1 atmosphere of air at 298 K (Atkinson et al., 2004) and gives HNO_3 which is removed by wet and dry deposition. In the presence of [OH] = 10^6 molecule cm^{-3} the lifetime of NO_2 with respect to reaction with OH is approximately 1 day. NO_x has a relatively short atmospheric lifetime and is not transported directly from polluted to remote areas.

Peroxy radicals react with NO_2 to form thermally unstable peroxynitrates, which decompose to reform the peroxy radicals and NO_2. The first-order rate coefficients for thermal decomposition of $CH_3O_2NO_2$, $C_2H_5O_2NO_2$, $CH_3C(O)CH_2O_2NO_2$, $CH_3C(O)O_2NO_2$, $C_2H_5C(O)O_2NO_2$, and $CH_2{=}CH(CH_3)O_2NO_2$ in 1 bar of air as a function of temperature are shown in figure X-E-1. Decomposition involves scission of the ROO—NO_2 bond and, as a consequence, the rate of decomposition is very sensitive to temperature. The strength of ROO—NO_2 bonds in acyl peroxynitrates [e.g., $CH_3C(O)O_2NO_2$] is approximately 115 kJ mol^{-1} while those in alkyl peroxy nitrates (e.g., $CH_3O_2NO_2$) are somewhat weaker, approximately 90 kJ mol^{-1}. This difference in bond strength is of crucial importance for atmospheric chemistry. The ROO—NO_2 bond in alkyl peroxynitrates is sufficiently weak that the lifetime of alkyl peroxynitrates at 298 K is only approximately 0.2 s. In contrast, the lifetime of acyl peroxynitrates at 298 K is approximately 45 min. The long lifetime of acyl peroxynitrates enables them to be lofted into the troposphere, where, in the colder conditions at higher altitudes, the lifetimes of acyl peroxynitrates with respect to decomposition are of the order of months or years. The substantial lifetimes of acyl peroxynitrates enable them to be transported over large distances. Mixing of the air mass down towards the surface results in warming, which then releases the NO_2. Organic peroxynitrates are important in transporting NO_x from polluted areas to remote locations.

X-F. Role of Oxygenates as Proxies for VOC Emissions

X-F-1. Introduction

Over the last few years, satellite retrievals have considerably advanced our understanding of the global distributions of some trace species. While Sun-synchronous, nadir viewing measurements give information on the total column, many species with short lifetimes are concentrated in the boundary layer; when retrievals are combined with modeling, they provide a "top down" means of evaluating so-called "bottom up" emissions inventories, constructed on the basis of estimates of human or plant activity. CH_2O is formed in the oxidation of a range of VOCs, and CH_2O column retrievals have been used for this purpose. An important issue is the timescale of the production and loss of CH_2O; both need to be short to ensure that the CH_2O signal is not smeared out too much from the point of the original VOC emission. As a result, the approach is best suited to evaluating emissions of isoprene and other short-lived compounds such as xylenes and alkenes. While terpenes, such as the pinenes, are short-lived, the

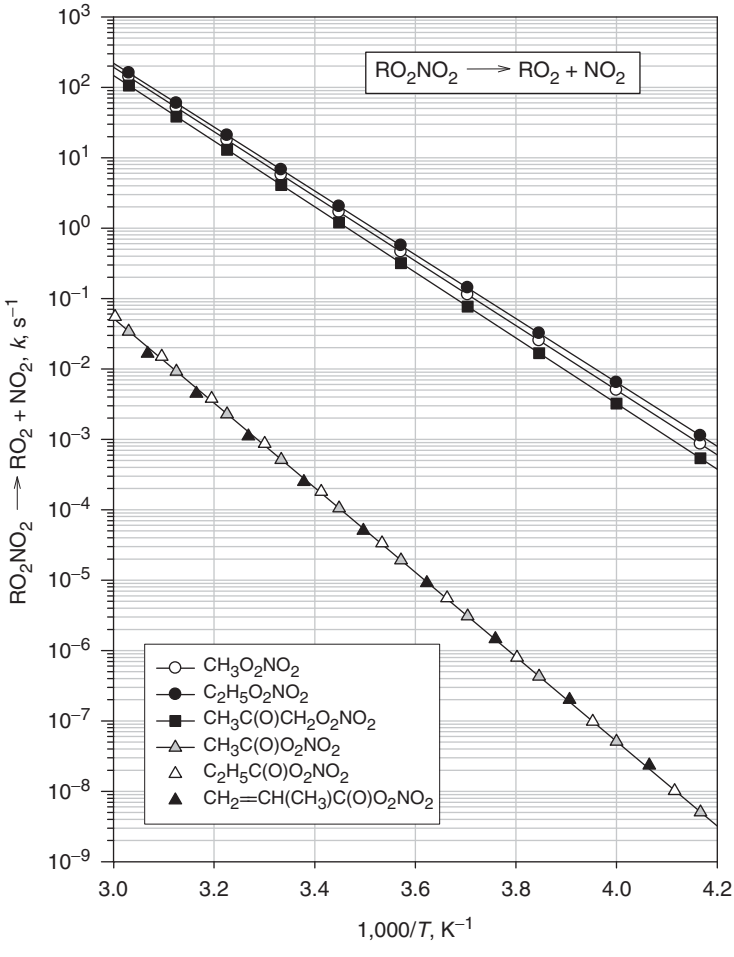

Figure X-E-1. Rates of thermal decomposition of selected organic peroxynitrates in 1 bar of air taken from Atkinson et al. (2006). The rates of decomposition of the acyl peroxynitrates are indistinguishable and represented by one line through the combined data set.

formation of CH_2O in the ensuing chemistry is slow, so that the signal from these compounds is lost in the background. Such a limitation becomes a strength, since it allows much more specific information on isoprene to be obtained.

X-F-2. Satellite Observations of Oxygenates

Global distributions of trace gases in the lower troposphere can be obtained from satellites in Sun-synchronous orbits, crossing the equator twice on each orbit and obtaining global coverage every few days. Global Ozone Monitoring Experiment (GOME) was launched in 1995 (Burrows et al., 1993) and provides an example of such a satellite. It uses a nadir viewing geometry; i.e., it observes the entire atmospheric column beneath

the satellite, in this case using backscattered solar radiation, with a spatial resolution of 40 km along the track and 320 km across the track. Global coverage is achieved in 3 days. CH_2O data are retrieved from absorption in the 337–356 nm region (Chance et al., 2000). The satellite measurements of the backscattered radiation contain the spectral signature of CH_2O, but need correction for Rayleigh scattering and interferences from other species. These procedures (Chance, 1998; Palmer et al., 2003), provide a vertical column of CH_2O; simulations using the GEOS-Chem model (Bey et al., 1999) show that the main contribution derives from the boundary layer.

Palmer et al. (2003) related the observed column, Ω, in the absence of any horizontal transport, to the emissions E_i of CH_2O source i, and the atmospheric lifetime of CH_2O, τ_{CH_2O}: $\Omega = \tau_{CH_2O} \Sigma Y_i E_i$, where Y_i is the yield of CH_2O from emission source i. Horizontal transport during its lifetime displaces the formaldehyde, so that its maximum contribution to the vertical column following emission of the precursor occurs somewhat downwind of the emission source. A further contribution to displacement derives from the timescale of production of formaldehyde from the precursor, τ_i. Palmer et al. (2003) defined a displacement length scale, $L_{d,i}$, which is the location of the maximum in the displaced CH_2O concentration; $L_{d,i}$ depends on the wind speed, U, and the two lifetimes, τ_{CH_2O} and τ_i. A smearing effect occurs because of the time dependence of the formaldehyde concentration, following emission of the precursor. Palmer et al. defined a smearing length scale, $L_{s,i}$, as the distance where the integral of the column from the point of emission of i downwind reaches a fraction $(1 - 1/e)$ of its asymptotic value. The limiting values of $L_{s,i}$ are $L_{s,i} \rightarrow U/k_i$ when $\tau_i \gg \tau_{CH_2O}$, and $L_{s,i} \rightarrow U/k_{CH_2O}$ when $\tau_{CH_2O} \gg \tau_i$.

Palmer et al. (2003) argued that the major contribution to the CH_2O column in North America derives from emission of isoprene. Methane and methanol have such long lifetimes that their contributions are smeared into the background. They calculated a lifetime for isoprene, which they took as a measure of τ_i, of 0.5 h for late morning in North America, the time of passage of the satellite over this region, and a lifetime for CH_2O of 2 h, a value close to the 2.4 h given in section IV-B-1.5. With a wind speed of 10 km h^{-1}, these values give $L_{d,i} = 20$ km and $L_{s,i} = 50$ km, giving a spatial resolution of 10–100 km, which is comparable with the GOME pixel size of 40×320 km. The timescale of the generation of CH_2O from isoprene is somewhat more complicated than the lifetime of isoprene, because of secondary generation processes. In a later publication (Palmer et al., 2006), they examined the process in more detail using a box model and the master chemical mechanism (MCM v3.1). Figure X-F-1 shows the production of CH_2O as a function of time for $[NO_x] = 1$ ppb and 100 ppt. In the former case, the limiting yield of CH_2O is 0.50 and the 1/e time for build up is $\approx$ 1.5 h. The build up time is longer for $[NO_x] = 100$ ppt ($\approx$ 3.7 h) and CH_2O continues to rise more slowly over a period of days, because of the importance of peroxy + peroxy radical reactions at the lower $[NO_x]$. The technique, therefore, gives better spatial resolution under high NO_x conditions.

Palmer et al. (2006) used GOME data from 1996–2001 in a detailed analysis of isoprene emissions from North America. They compared the GOME estimates with in situ flux measurements and with results from the GEOS-Chem 3D chemical transport model incorporating the Model of Emissions of Gases and Aerosols from Nature (MEGAN)

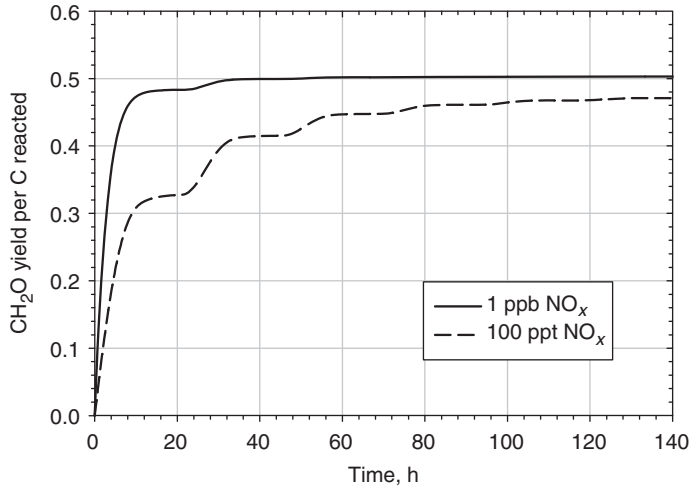

Figure X-F-1. Yield of CH_2O per C-atom reacted as function of time following reaction of isoprene under lower and higher NO_x levels.

emission inventory (Guenther et al., 2006). Other biogenic species with significant emissions in North America are α-and β-pinenes and 2-methyl-3-buten-2-ol. Box model simulations based on the MCM showed that formation of CH_2O from these compounds takes place on much longer timescales than is found for isoprene, despite the short lifetimes of the parent compounds. Figure X-F-2 shows the CH_2O yield for α-pinene. An analysis of the CH_2O precursors at high NO_x shows that on day 3, for

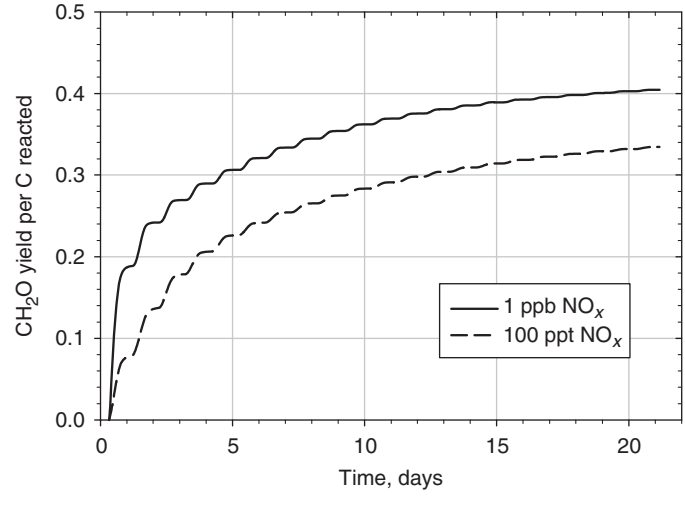

Figure X-F-2. Yield of CH_2O per C-atom reacted as a function of time following reaction of α-pinene under lower and higher NO_x conditions.

example, acetone accounts for 90% of the production of CH_2O, via the acetonoxy radical, following reaction of acetone with OH forming methylperoxy and peroxyacetyl radicals, and following photolysis. As discussed in section V-B-1.5, the lifetime of acetone is several days and presents a large delay in the formation of formaldehyde, following reaction of α-pinene. Similar considerations apply to β-pinene and 2-methyl-3-buten-2-ol. Palmer et al. (2006) concluded that the yields of CH_2O from these species over the crucial first few hours following emission are low, that they make a negligible contribution to the retrieved formaldehyde column, and that the observed formaldehyde concentrations can be ascribed entirely to isoprene emissions.

The agreement between the GOME estimates and MEGAN was satisfactory both in terms of the spatial and temporal distributions of isoprene emissions. Both showed that the peak emissions occur in the Southeastern U.S.; GOME was higher than MEGAN by 20–30% in midsummer and lower by 10% earlier and later in the year. The GOME values were compared with in situ isoprene flux and $[CH_2O]$ measurements made in the PROPHET campaign in Northern Michigan in 2001 (Pressley et al., 2005). The two sets of data show satisfactory agreement, especially in the seasonality of the emissions, although the day-to-day variability was less well determined by the GOME measurements. Examination of the interannual variation in the Southeastern U.S. showed a strong correlation with the surface air temperature, which agrees well with the temperature dependence of isoprene emission in the MEGAN model. The authors concluded that the use of CH_2O column measurements from satellites provides a useful mechanism for evaluating and constraining isoprene emissions, with the major limitation being the slower formation of CH_2O at lower $[NO_x]$.

A more recent analysis of formaldehyde over North America has been made by Millet et al. (2008b), using column measurements from OMI (ozone monitoring instrument) on the EOS Aura satellite, launched in July 2004. The resolution at nadir is 13×24 km^2, which is better than GOME, although the resolution is coarser at wider viewing angles. CH_2O columns were analyzed for June–August 2006, and were consistent with, but slightly (2–14%) smaller than the GOME data discussed above. The only detectable contribution to the signal from anthropogenic sources was found over Houston. Comparisons were made again with GEOS-Chem and with the MEGAN inventory. Correlations were good, but MEGAN slightly overpredicted (4–25%) emissions compared with those derived from the measurements. The analysis suggested that isoprene emission factors may vary less from one broad-leaf tree species to another than is modeled by MEGAN.

Fu et al. (2007) used a similar approach to Palmer et al. (2006) in the analysis of formaldehyde columns over East and Southeast Asia, over the period 1996–2001 from GOME retrievals. They compared the CH_2O columns with simulations using GEOS-Chem, incorporating the anthropogenic and biomass burning emissions inventory of Streets et al. (2003) and the biogenic emissions inventory, MEGAN, discussed above. The anthropogenically emitted species that contribute to the formaldehyde signal were termed "reactive"; i.e., those with lifetimes of less than a day, even in winter (alkenes, xylenes, and CH_2O itself), that form formaldehyde promptly. The total anthropogenic NMVOC emissions for the region estimated by Streets et al. (2003) are 40 Tg $year^{-1}$ and of these 11 Tg $year^{-1}$ were deemed to be reactive, while for biomass burning,

the emissions in these two categories were 12 Tg year^{-1} and 3.2 Tg year^{-1}. For comparison, the total isoprene emission estimated by MEGAN is 52 Tg year^{-1}. The overall estimates of uncertainty in these inventories is about a factor of 2–3.

In the extratropical Winter, when biogenic and biomass burning emissions are unimportant, both the model and the GOME measurements produce large signals above the background over the large urban areas in Central and Southern China. The model and the measurements are well correlated, but the model underestimates the column measurements by $\approx$ 25%. The discrepancy was attributed to vehicular emissions, on the basis of in situ measurements of NMVOC:CO ratios, possibly including a large direct emission of CH_2O. Outside the extratropical winter, the CH_2O columns are largely determined by biogenic and biomass burning emissions. The total isoprene emissions determined by GOME were 56 ± 30 Tg year^{-1}, in good agreement with MEGAN, but with a different distribution; the results suggest that MEGAN is too low by a factor of 3 for Chinese mixed forests and croplands, and too high for tropical vegetation. The largest discrepancy relates to biomass burning emissions, where the GOME measurements throughout East and Southeast Asia imply emissions underestimates by Streets et al. (2003) of a factor of about 5, with the largest discrepancy occurring in the North China Plain in June, where emissions were a factor of 10 higher than the inventory suggests. The difference was ascribed to in-field burning of crop residue, a practice that has recently developed and was ascribed to a reduced demand for biofuels.

The total reactive NMVOC emissions from East and Southeast Asia was determined by GOME to be 83 ± 32 Tg year^{-1}, compared with an inventory estimate of 66 Tg year^{-1}. The main air quality impact of this higher estimate occurs over China, where VOC limited conditions for ozone formation apply. Over the period from late Fall to early Spring, GEOS-Chem estimates an increase in ozone of $\approx$ 20 ppb; even in summer in this region, when NO_x limited conditions apply, an increase of 5–20 ppb of surface ozone is estimated.

Barkley et al. (2008) analyzed 1997–2001 GOME CH_2O column data over tropical South America. Data over the Eastern region were substantially affected by biomass burning. They found the highest isoprene-related emissions in the Western Amazon, with emission peaking in the dry season. GOME-based estimates of the isoprene emissions were lower than the MEGAN values, possibly as a result of within-canopy losses. The uncertainties in the analysis of the GOME retrievals to determine isoprene emissions were also higher than elsewhere, at least partly because of the lower NO_x concentrations in the region, which led to a greater smearing of the CH_2O, as discussed above. Palmer et al. (2007) found good agreement between the observed annual cycles of GOME CH_2O columns and satellite fire-count data over the Amazon Basin, with correlations typically greater than 0.75 for a particular year; this illustrates the potential of CH_2O column retrievals in provide quantitative information about biomass burning emissions.

Meyer-Arnek et al. (2005) examined CH_2O column data over Africa for September 1997. They interpreted the data using a trajectory analysis coupled with a chemistry model. They found similar formaldehyde concentrations deriving from biomass burning and from biogenic emissions from woody savannah and tropical rainforest. The formaldehyde concentrations for the biogenic emissions were found to occur close

to the primary emission region, while there was greater advection from the biomass burning sources.

Wittrock et al. (2006) analysed both glyoxal and formaldehyde retrievals from SCIAMACHY (Scanning Imaging Absorption Spectrometer for Atmospheric Cartography), a nadir viewing satellite, launched in 2002, with global coverage in 6 days and a 60×120 km pixel size. They found high concentrations, which they associated with biogenic isoprene emissions over Central Africa, parts of South America, and Indonesia. The column ratios glyoxal:formaldehyde were typically ≈ 0.05, in agreement with models. They also observed elevated concentrations of glyoxal and formaldehyde in regions with high anthropogenic emissions, which were compatible with higher glyoxal:formaldehyde ratios, and with biomass burning emissions. Retrievals over water are more difficult than over land, because of interferences from liquid water absorption, but the retrievals indicate enhanced concentrations of both $(CHO)_2$ and CH_2O in certain biogenically active areas, e.g., over upwellings near the Galapagos. Some of the signal can be attributed to outflow of terrestrial sources, but biogenic ocean sources were also indicated.

The Atmospheric Chemistry Experiment (ACE) uses a different viewing geometry to obtain spectral data at higher altitudes (Bernath et al., 2006). It was carried on the SCISAT-1 satellite, launched in August 2003. The observations are made using solar occultation with a *limb-viewing* geometry that takes slices across the atmosphere. It has a Fourier transform spectrometer that measures sequences of atmospheric absorption spectra during sunrise and sunset. These spectra are inverted to obtain vertical profiles of temperature, pressure, and many atmospheric trace gases with a vertical resolution of about 4 km from the cloud tops up to about 150 km. The main aim of the experiment is to study stratospheric ozone depletion, but data have also been obtained on a range of species in the upper troposphere, including CH_2O (Dufour et al., 2009), HCOOH (Abad et al., 2009) and CH_3OH (Dufour et al., 2007).

ACE measurements of CH_2O relate to a different set of processes than those from nadir-viewing instruments, and probe the global distribution at higher altitudes. The data provide information on seasonal cycles, and the link to biogenic emissions, and probe the influence of biomass burning on upper troposphere formaldehyde. Comparisons with global models, and especially with GEOS-Chem, are satisfactory.

References

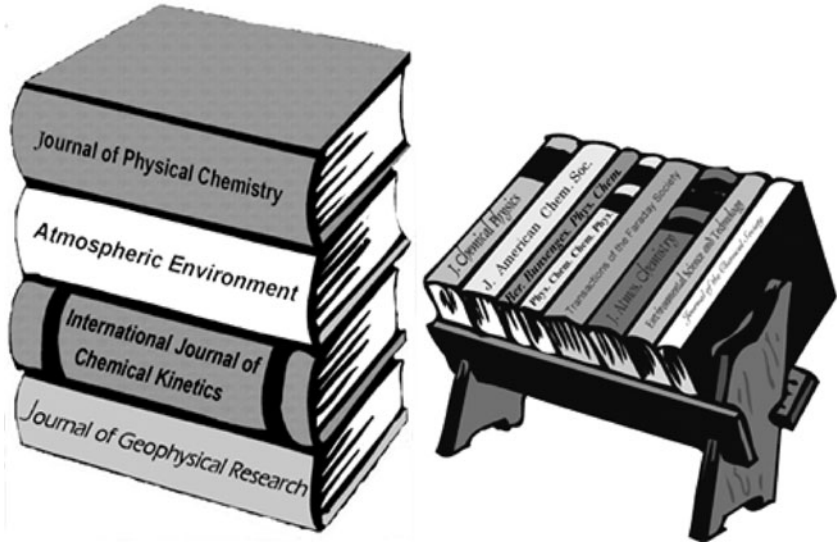

Abad, G.G., P.F. Bernath, C.D. Boone, S.D. McLeod, G.L. Manney, and G.C. Toon (2009), Global distribution of upper tropospheric formic acid from the ACE–FTS, *Atmos. Chem. Phys. Discuss*., *9*, 12465–12482.

Abuin, E.B., M.V. Encina, S. Diaz, and E.A. Lissi (1984), Cage reactions in the photolysis of 2,2,4,4-tetrametyl-3-pentanone, *Int. J. Chem. Kinet.*, *16*, 503–511.

Abuin, E., J. Grotewold, W.A. Lissi, and M. Umaña (1971), Effect of added gases on the photolysis of biacetyl, *J. Chem. Soc.*, *1971*, 516–521.

Abuin, E., and E.A. Lissi (1975), Arrhenius parameters for the photocleavage of butan-2-one triplets, *J. Photochem.*, *5*, 65–68.

Adeniji, S.A., J.A. Kerr, and M.R. Williams (1981), Rate constants for ozone–alkene reactions under atmospheric conditions, *Int. J. Chem. Kinet.*, *13*, 209–217.

Adryukov, V., and A.Timofeev (1989), Assessment of volatile organic compound emissions from natural sources in Europe, paper presented at the 4th ECD Task Force on Volatile Organic Compounds, Schwetzingen, Germany, 1989.

AEA Energy & Environment (2009), National Atmospheric Emission Inventory, VOC Speciation, NAEI Ref. 45321001/A06019/TM, provided to the authors by T. P. Murrells, January 6, 2009.

Aird, R.W.S., C.E. Canosa-Mas, D.J. Cook, G. Marston, P.S. Monks, R.P. Wayne, and E. Ljungström (1992), Kinetics of the reactions of the nitrate radical with a series of halogenobutenes. A study of the effect of substituents on the rate of addition of NO_3 to alkenes, *J. Chem. Soc., Faraday Trans.*, *88*, 1093–1099.

Albaladejo, J., B. Ballesteros, E. Jiménez, Y. Diaz de Mera, and E. Martinez (2003a), Gas-phase OH radical initiated oxidation of the 3-halopropenes studies by PLP–LIF in the temperature range 228–388 K, *Atmos. Environ.*, *37*, 2919–2926.

Albaladejo, J., B. Ballesteros, E. Jiménez, P. Martin and E. Martinez (2002), A PLP–LIF kinetic study of the atmospheric reactivity of a series of C_4-C_7 saturated and unsaturated aliphatic aldehydes with OH, *Atmos. Environ.*, *36*, 3231–3239.

Albaladejo, J., J.A. Notario, C.A. Cuevas, E. Jiménez, B. Cabañas, and E. Martinez (2003b), Gas-phase chemistry of atmospheric Cl atoms: A PLP–RF kinetic study with a series of ketones, *Atmos. Environ*., *37*, 455–463

Aldener, M., S.S. Brown, H. Stark, E.J. Williams, B.M. Lerner, W.C. Kuster, P.D. Goldan, P.K. Quinn, T.S. Bates, F.C. Fehsenfeld, and A.R. Ravishankara (2006), Reactivity and loss mechanisms of NO_3 and N_2O_5 in a polluted marine environment: Results from in situ measurements during New England Air Quality Study 2002, *J. Geophys. Res.*, *111*, doi:10.1029/2006JD007252.

Allen, E.R., and J.N. Pitts, Jr. (1969), The vapor-phase photolysis of *trans*-crotonaldehyde, *J. Amer. Chem. Soc.*, *91*, 3135–3139.

Allen, W.D., and H.F. Schaefer III (1986), Ab initio studies of the low-lying electronic states of ketene, *J. Chem. Phys.*, *84*, 2212–2225.

Allen, W.D., and H.F. Schaefer III (1988), Reaction paths for the dissociation ã ^{3}A" $CH_2CO \rightarrow X^3B_1CH_2 + X^1\Sigma^+CO$, *J. Chem. Phys.*, *89*, 329–344.

Allston, T.D., M.L. Fedyk, and G.A. Takacs (1978), Photoabsorption spectra of gaseous CF_3NO, CCl_3NO and CCl_3NO_2, *Chem. Phys. Lett.*, *60*, 97–101.

Almasy, F. (1933), Polyatomic molecules. II. Structure and activation of benzaldehyde, *J. Chim. Phys.*, *30*, 634–645.

Alumbaugh, R.L., G.O. Pritchard, and B. Rickborn (1965), Nonstereospecific mechanisms in the photolysis of cyclic ketones, *J. Phys. Chem.*, *69*, 3225–3231.

Alvarado, A., J. Arey, and R. Atkinson (1998), Kinetics of the gas-phase reactions of OH and NO_3 radicals and O_3 with the monoterpene reaction products pinonaldehyde, caronaldehyde, and sabinaketone, *J. Atmos. Chem.*, *31*, 281–297.

Alvarado, A., R. Atkinson, and J. Arey (1996), Kinetics of the gas-phase reactions of NO_3 radicals and O_3 with 3-methylfuran and the OH radical yield from the O_3 reaction, *Int. J. Chem. Kinet., 28*, 905–909.

Alvarado, A., E.C. Tuazon, S.M. Aschmann, J. Arey, and R. Atkinson (1999), Products and mechanisms of the gas-phase reactions of OH radicals and O_3 with 2-methyl-3-buten-2-ol, *Atmos. Environ.*, *33*, 2893–2905.

Alvárez-Idaboy, J.R., A. Galano, G. Bravo-Perez, and M.E. Ruiz (2001a), Rate constant dependence on the size of aldehydes in the NO_3 + aldehydes reaction. An explanation via quantum chemical calculations and CTST, *J. Amer. Chem. Soc.*, *123*, 8387–8395.

Alvárez-Idaboy, J.R., N. Mora-Diez, R.J. Boyd, and A. Vivier-Bunge (2001b), On the importance of prereactive complexes in molecule–radical reactions: Hydrogen abstraction from aldehydes by OH, *J. Amer. Chem. Soc.*, *123*, 2018–2024.

Amaral, G., K. Xu, and J. Zhang (2001), H + NO_2 channels in the photodissociation of HONO at 193.3 nm, *J. Phys. Chem. A*, *105*, 1465–1475.

Ambidge, P.F., J.N. Bradley, and D.A. Whytock (1976), Kinetic study of the reactions of hydrogen and oxygen atoms with acetone, *J. Chem. Soc., Faraday Trans. I*, *72*, 1870–1876.

Ammann, M., R. Atkinson, R.A. Cox, J.N. Crowley, R.G. Hynes, M.E. Jenkin, M.J. Rossi, J. Troe, and T.J. Wallington (2008), IUPAC Subcommittee for Gas Kinetic Data Evaluation, http://www.iupac-kinetic.ch.cam.ac.uk.

Amphlett, J.C., and E. Whittle (1967), Photolysis of halogens in presence of trifluoroacetaldehyde, *Trans. Faraday Soc.*, *63*, 80–90.

Anastasi, C., L. Hopkinson, and V.J. Simpson (1991), Natural hydrocarbon emissions in the United Kingdom, *Atmos. Environ.*, *25A*, 1403–1408.

Anastasi, C., I.W.M. Smith, and D.A. Parkes (1978), Flash photolysis study of the spectra of CH_3O_2 and $C(CH_3)_3O_2$ radicals and kinetics of their mutual reactions and with NO, *J. Chem. Soc. Faraday Trans. 1*, *74*, 1693–1701.

Andersen, A., and E.A. Carter (2006), Insight into selected reaction in low-temperature dimethyl ether combustion from Born–Oppenheimer molecular dynamics, *J. Phys. Chem. A*, *110*, 1393–1407.

Andersen, M.P.S., M.D. Hurley, T.J. Wallington, J.C. Ball, J.W. Martin, D.A. Ellis, S.A. Mabury, and O.J. Nielsen (2003), Atmospheric chemistry of C_2F_5CHO: reaction with Cl atoms and OH radicals, IR spectrum of $C_2F_5C(O)O_2NO_2$, *Chem. Phys. Lett.*, *379*, 28–36.

Andersen, M.P.S., M.D. Hurley, T.J. Wallington, F. Blandini, N.R. Jensen, V. Librando, J. Hjorth, G. Marchionni, M. Avataneo, M. Visca, F.M. Nicolaisen, and O.J. Nielsen (2004a), Atmospheric chemistry of $CH_3((CF_2CF_2O)_nCH_3$ ($n = 1$–3): Kinetics and mechanism of oxidation initiated by Cl atoms and OH radicals, IR spectra, and global warming potentials, *J. Phys. Chem. A*, *108*, 1964–1972.

Andersen, M.P.S., O.J. Nielsen, M.D. Hurley, J.C. Ball, T.J. Wallington, D.A. Ellis, J.W. Martin, and S.A. Mabury (2005a), Atmospheric chemistry of 4:2 fluorotelomer alcohol (n-$C_4F_9CH_2CH_2OH$): Products and mechanism of Cl atom initiated oxidation in the presence of NO_x, *J. Phys. Chem. A*, *109*, 1849–1856.

Andersen, M.P.S., O.J. Nielsen, M.D. Hurley, J.C. Ball, T.J. Wallington, J. Stevens, J.W. Martin, D.A. Ellis, and S.A. Mabury (2004b), Atmospheric Chemistry of n-$C_xF_{2x+1}CHO$ ($x = 1, 3, 4$): Reaction with Cl atoms, OH Radicals; IR Spectra of $C_xF_{2x+1}C(O)O_2NO_2$, *J. Phys. Chem. A*, *108*, 5189–5196.

Andersen, M.P.S., O.J. Nielsen, T.J. Wallington, M.D. Hurley and W.B. DeMore (2005b), Atmospheric chemistry of $CF_3OCF_2CF_2H$ and $CF_3OC(CF_3)_2H$: Reaction with Cl atoms and OH radicals, degradation mechanism, global warming potentials, and empirical relationship between k(OH) and k(Cl) for organic compounds, *J. Phys. Chem. A*, *109*, 3926–3934.

Andersen, M.P.S., C. Stensby, O.J. Nielsen, M.D. Hurley, J.C. Ball, T.J. Wallington, J.W. Martin, D.A. Ellis, and S.A. Mabury (2004c), Atmospheric chemistry of n-$C_xF_{2x+1}CHO$ ($x = 1, 3, 4$): mechanism of the $C_xF_{2x+1}C(O)O_2 + HO_2$ reaction, *J. Phys. Chem. A*, *108*, 6325–6330.

Andersen, M.P.S., A. Toft, O.J. Nielsen, M.D. Hurley, T.J. Wallington, H. Chishima, K. Tonokura, S.A. Mabury, J.W. Martin, and D.A. Ellis (2006), Atmospheric chemistry of perfluorinated aldehyde hydrates (n-$C_xF_{2x+1}CH(OH)_2$, $x = 1, 3, 4$): Hydration, dehydration, and kinetics and mechanism of Cl atom and OH radical initiated oxidation, *J. Phys. Chem. A*, *110*, 9854–9860.

Anderson, H.W., and G.K. Rollefson (1941), Some reactions of the acetyl radical, *J. Am. Chem. Soc.*, *63*, 816–821.

Anderson, L.G., J.A. Lanning, R. Barrell, J. Miyagishima, R.H. Jones, and P. Wolfe (1996), Sources and sinks of formaldehyde and acetaldeyde: An analysis of Denver's ambient concentration data, *Atmos. Environ.*, *30*, 2113–2123.

Anderson, L.G., C.S. Parmenter, and H.M. Poland (1973), Collision induced intersystem crossing. The photophysics of glyoxal vapor excited at 4358Å, *Chem. Phys.*, *1*, 401–417.

Anderson, L.G., and R.D. Stephens (1988), Kinetics of the reaction of hydroxyl radicals with 2-(dimethylamino)ethanol from 234–364 K, *Int. J. Chem. Kinet.*, *20*, 103–110.

Anderson, P.C., and M.J. Kurylo (1979), Rate constant measurements for the reaction $Cl + CH_2O \rightarrow HCl + CHO$, Implications regarding the removal of stratospheric chlorine, *J. Phys. Chem.*, *83*, 2055–2057.

Anderson, P.N., and R. A. Hites (1996), OH radical reactions: The major removal pathway for polychlorinated biphenyls from the atmosphere, *Environ. Sci. Technol.*, *30*, 1756–1763.

Anet, F.A.L., R.F.W. Bader, and A.-M. Van der Auwera (1960), Chemical evidence for a triplet ground state for methylene, *J. Am. Chem. Soc.*, *82*, 3217–3218.

ANFAVEA, Associação Nacional dos Fabricantes de Vehicules Automotores (2008), http://www.anfavea.com.br/Index.html.

Apel, E.C., D.D. Riemer, A. Hills, W. Baugh, J. Orlando, I. Faloona, D. Tan, W. Brune, B. Lamb, H. Westberg, M.A. Carroll, T. Thornberry, and C.D. Geron (2002), Measurement and interpretation of isoprene fluxes and isoprene, methacrolein, and methyl vinyl ketone mixing ratios at the PROPHET site during the 1998 intensive, *J. Geophys. Res.*, *107*, 4034, 10.1029/2000JD000225.

Appel, B.R., A.M. Winer, Y. Tokiwa, and H.W. Biermann (1990), Comparison of atmospheric nitrous-acid measurements by annular denuder and differential optical-absorption systems, *Atmos. Environ.*, *24*, 611–616.

Aranda, A., Y. Diaz de Mera, I. Bravo, D. Rodriguez, A. Rodriguez, and E. Martinez (2006), Atmospheric HFEs degradation in the gas phase: Reactions of HFE-7100 and HFE-7200 with Cl atoms at low temperatures, *Environ. Sci. Technol.*, *40*, 5971–5976.

Aranda, A, Y. Diaz de Mera, A. Rodriguez, L. Morales, and E. Martinez (2004), Kinetic study of the gas-phase reactions of Cl radicals with 3-pentanone and 3-hexanone, *J. Phys. Chem. A*, *108*, 7027–7031.

Aranda, A., Y. Diaz de Mera, A. Rodriguez, D. Rodriguez, and E. Martinez (2003a), A kinetic and mechanistic study of the reaction of Cl atoms with acrolein: Temperature dependence for the abstraction channel, *J. Phys. Chem. A*, *107*, 5717–5721.

Aranda, A., E. Martínez, Y. Díaz-de-Mera, A. Rodríguez, D. Rodríguez, and J. Cuartero (2003b), Low-pressure study of the reactions of Cl atoms with acrylic acid and allyl alcohol, *Atmos. Environ.*, *37*, 4361–4369.

Archer, A.S., R.B. Cundall, G.B. Evans, and T.F. Palmer (1973a), The effect of temperature, pressure, and excitation wavelength on the photoluminescence of acetaldehyde vapour, *Proc. Roy. Soc. London*, *A*, *333*, 385–402.

Archer, A.S., R.B. Cundall, and T.F. Palmer (1973b), The role of excited states in the gas-phase photolysis of acetaldehyde, *Proc. Roy. Soc. London*, *A*, *334*, 411–426.

Arden, E.A., and L. Phillips (1964), Reactions in the diethyl peroxide–nitric oxide system. Part I. Oxidation and reduction of nitric oxide: Reactions of nitrosomethane and nitroxyl, *J. Chem. Soc.*, *1964*, 5118–5125.

Arden, E.A., L. Phillips, and R. Shaw (1964), Reactions in the diethyl peroxide–nitric oxide system. Part II. The kinetics of cross disproportionation and combination reactions between the ethoxyl radical and nitric oxide, *J. Chem. Soc.*, *1964*, 5126–5129.

Arenas, J.F., J.C. Otero, D. Peláez, and J. Soto (2005), Role of surface crossings in the photochemistry of nitromethane, *J. Chem. Phys.*, *122*, 084324-1–084324-11.

Arey, J., S.M. Aschmann, E.S.C. Kwok, and R. Atkinson (2001), Alkyl nitrate, hydroxyalkyl nitrate, and hydroxycarbonyl formation from the NO_x–air photooxidations of C_5–C_8 *n*-alkanes, *J. Phys. Chem. A*, *105*, 1020–1027.

Arey, J, R. Atkinson, and S.M. Aschmann (1990a), Product study of the gas-phase reactions of monoterpenes with the hydroxyl radical in the presence of NO_x, *J. Geophys. Res.*, *95*, 18539–18546.

Arey, J., R. Atkinson, S.M. Aschmann, and D. Schuetzle (1990b), Experimental investigation of the atmospheric chemistry of 2-methyl-1-nitronaphthalene and a comparison of predicted nitroarene concentrations with ambient air data, *Polycyclic Aromatic Compounds*, *1*, 33–50.

Arey, J., S.B. Corchnoy, and R. Atkinson (1991), Emission of linalool from Valencia orange blossoms and its observation in ambient air, *Atmos. Environ.*, *25A*, 1377–1381.

Arif, M., B. Dellinger, and P.H. Taylor (1997), Rate coefficients of hydroxyl radical reaction with dimethyl ether and methyl *tert*-butyl ether over an extended temperature range, *J. Phys. Chem. A*, *101*, 2436–2441.

Arnold, S.R., M.P. Chipperfield, and M.A. Blitz (2005), A three-dimensional model study of the effect of new temperature-dependent quantum yields for acetone photolysis, *J. Geophys. Res.*, *110*, D22305, doi:10.1029/2005JD005998.

Arnold, S.R., M.P. Chipperfield, M.A. Blitz, D.E. Heard, and M.J. Pilling (2004), Photodissociation of acetone: Atmospheric implications of temperature dependent quantum yields, *Geophys. Res. Lett.*, *31*, L07110, doi: 10.1029/2003GLO19099.

Aschmann, S.M., J. Arey, and R. Atkinson (2000), Atmospheric chemistry of selected hydroxycarbonyls, *J. Phys. Chem. A*, *104*, 3998–4003. CODEN: JPCAFH ISSN:1089–5639.

Aschmann, S.M. J. Arey, R. Atkinson, and S.L. Simonich (2001a), Atmospheric lifetimes and fates of selcted fragrance materials and volatile model compounds, *Environ. Sci. Technol.*, *35*, 3595–3600.

Aschmann, S.M., and R. Atkinson (1995), Rate constants for the reactions of the NO_3 radical with alkanes at 296 ± 2 K, *Atmos. Environ.*, *29*, 2311–2316.

Aschmann, S.M, and R. Atkinson (1998a), Rate constants for the gas-phase reactions of selected dibasic esters with the OH radical, *Int. J. Chem. Kinet.*, *30*, 471–474.

Aschmann, S.M., and R. Atkinson (1998b), Kinetics of the gas-phase reactions of the OH radical with selected glycol ethers, glycols, and alcohols, *Int. J. Chem. Kinet.*, *30*, 533–540.

Aschmann, S.M., and R. Atkinson (1999a), Products of the gas-phase reactions of the OH radical with *n*-butyl methyl ether and 2-isopropoxyethanol: Reactions of ROC(O•)< radicals, *Int. J. Chem. Kinet.*, *31*, 501–513.

Aschmann, S.M., and R. Atkinson (1999b), Atmospheric chemistry of 1-methyl-2-pyrrolidinone, *Atmos. Environ.*, 33, 591–599.

Aschmann, S.M., W.D. Long, and R. Atkinson (2006), Temperature-dependent rate constants for the gas-phase reactions of OH radicals with 1,3,5-trimethylbenzene, triethyl phosphate, and a series of alkylphosphonates, *J. Phys. Chem. A*, *110*, 7393–7400.

Aschmann, S.M., P. Martin, E.C. Tuazon, J. Arey, and R. Atkinson (2001b), Kinetic and product studies of the reactions of selected glycol ethers with OH radicals, *Environ. Sci. Technol.*, *35*, 4080–4088.

Aschmann, S.M., Y. Shu, J. Arey, and R. Atkinson (1997), Products of the gas-phase reactions of *cis*–3–hexen-1-ol with OH radicals and O_3, *Atmos. Environ.*, *31*, 3551–3560.

Aschmann, S.M., E.C. Tuazon, and R. Atkinson (2005), Atmospheric chemistry of diethyl methylphosphonate, diethyl ethylphosphonate, and triethyl phosphate, *J. Phys. Chem. A*, *109*, 2282–2291.

Atkinson, R. (1991), Kinetics and mechanisms of the gas-phase reactions of the nitrate (NO_3) radical with organic compounds, *J. Phys Chem. Ref. Data*, *20*, 459–507.

Atkinson, R. (1994), Gas-phase tropospheric chemistry of organic compounds, *J. Phys. Chem. Ref. Data*, Monograph, Volume 2, 1–256.

Atkinson, R., and J. Arey (2003a), Atmospheric degradation of volatile organic compounds, *Chem. Rev.*, *103*, 4605–4638.

Atkinson, R., and J. Arey (2003b), Gas-phase tropospheric chemistry of biogenic volatile organic compounds, *Atmos. Environ.*, *37*, *Supplement 2*, 197–219.

Atkinson, R., J. Arey, and S.M. Aschmann (2008a), Atmospheric chemistry of alkanes: Review and recent developments, *Atmos. Environ.*, *42*, 5859–5871.

Atkinson, R., J. Arey, S.M. Aschmann, S.B. Corchnoy, and Y. Shu (1992a), Gas-phase reactions of 1,4-benzodioxan, 2,3-dihydrobenzofuran, and 2,3-benzofuran with OH radicals and O_3, *Int. J. Chem. Kinet.*, *24*, 345–358.

Atkinson, R., J. Arey, S.M. Aschmann, S.B. Corchnoy, and Y. Shu (1995), Rate constants for the gas phase reactions of *cis*-3-hexen-1-ol, *cis*-3-hexenylacetate, *trans*-2-hexenal, and linalool with OH and NO_3 radicals and O_3 at 296 ± 2 K, and OH radicals yields from the O_3 reactions, *Int. J. Chem. Kinet. 27*, 941–955.

Atkinson, R., and S.M. Aschmann (1985), Kinetics of the gas-phase reaction of Cl atoms with a series of organics at 296 ± 2 K and atmospheric pressure, *Int. J. Chem. Kinet.*, *17*, 33–41.

Atkinson, R., and S.M. Aschmann (1988), Comment on "Flash photolysis resonance fluorescence investigation of the gas-phase reactions of OH radicals with a series of aliphatic ketones over the temperature range 240–440 K", *J. Phys. Chem.*, *92*, 4008–4008.

Atkinson, R., and S.M. Aschmann (1989), Rate constants for the reactions of OH radicals with the propyl and butyl nitrates and 1-nitrobutane at 298 ± 2 K, *Int. J. Chem. Kinet.*, *21*, 1123–1129.

Atkinson, R., and S.M. Aschmann (1990), Rate constants for the gas-phase reactions of the OH radical with the cresols and dimethylphenols at 296 ± 2 K, *Int. J. Chem. Kinet.*, *22*, 59–67.

Atkinson, R., and S.M. Aschmann (1993), Atmospheric chemistry of the monoterpene reaction products nopinone, camphenilone, and 4-acetyl-1-methylcyclohexene, *J. Atmos. Chem.*, *16*, 337–348.

Atkinson, R., and S.M. Aschmann (1995), Alkoxy radical isomerization products from the gas-phase OH radical-initiated reactions of 2,4-dimethyl-2-pentanol and 3,5-dimethyl-3-hexanol, *Environ. Sci. Technol.*, *29*, 528–536.

Atkinson, R., S.M. Aschmann, and J. Arey (1992b), Reactions of OH and NO_3 radicals with phenol, cresols, and 2-nitrophenol at 296 ± 2 K, *Environ. Sci. Technol.*, *26*, 1397–1403.

Atkinson, R., S.M. Aschmann, J. Arey, and W.P.L. Carter (1989a), Formation of ring-retaining products from the OH radical-initiated reactions of benzene and toluene, *Int. J. Chem. Kinet.*, 21, 801–827.

Atkinson, R., S.M. Aschmann, J. Arey, B. Zielinska, and D. Schuetzle (1989b), Gas-phase atmospheric chemistry of 1- and 2-nitronaphthalene and 1,4-naphthoquinone, *Atmos. Environ.*, *23*, 2679–2690.

Atkinson, R., S.M. Aschmann, and W.P.L. Carter (1983a), Kinetics of the reactions of O_3 and OH radicals with furan and thiophene at 298 ± 2 K, *Int. J. Chem. Kinet.*, *15*, 51–61.

Atkinson, R., S.M. Aschmann, W.P.L. Carter, and J.N. Pitts, Jr. (1982a), Rate constants for the gas-phase reaction of OH with a series of ketones at 299 ± 2 K, *Int. J. Chem. Kinet.*, *14*, 839–847.

Atkinson, R., S.M. Aschmann, W.P.L. Carter, and A.M. Winer (1982b), Kinetics of the gas-phase reactions of OH radicals with alkyl nitrates at 299 ± 2 K, *Int. J. Chem. Kinet.*, *14*, 919–926.

Atkinson, R., S.M. Aschmann, W.P.L. Carter, A.M. Winer, and J.N. Pitts Jr. (1982c), Alkyl nitrates from NO_x–air photooxidations of C_2–C_8 *n*-alkanes, *J. Phys. Chem.*, *86*, 4563–4569.

Atkinson, R., S.M. Aschmann, W.P.L. Carter, A.M. Winer, and J.N. Pitts Jr. (1984a), Formation of alkyl nitrates from the reaction of branched and cyclic alkyl peroxy radicals with NO, *Int. J. Chem. Kinet.*, *16*, 1085–1101.

Atkinson, R., S.A. Aschmann, D.R. Fitz, A.M. Winer, and J.N. Pitts Jr. (1982d), Rate constants for the gas phase reactions of O_3 with selected organics at 296 K, *Int. J. Chem. Kinet.*, *14*, 13–18.

Atkinson, R., S.M. Aschmann, and M.A. Goodman (1987a), Kinetics of the gas-phase reactions of nitrate radicals with a series of alkynes, haloalkenes, and α, β-unsaturated aldehydes, *Int. J. Chem. Kinetics*, *19*, 299–307.

Atkinson, R., S.M. Aschmann, and J.N. Pitts, Jr. (1983b), Kinetics of the gas-phase reactions of OH radicals with a series of α, β-unsaturated carbonyls at 299 ± 2 K, *Int. J. Chem. Kinet.*, *15*, 75–81.

Atkinson, R., S.M. Aschmann, and J.N. Pitts, Jr. (1988), Rate constants for the reactions of the NO_3 radical with a series of organic compounds at 296 ± 2 K, *J. Phys. Chem.*, *92*, 3454–3457.

Atkinson, R., S.M. Aschmann, E.C. Tuazon, J. Arey, and B. Zielinska (1989c), Formation of 3-methylfuran from the gas-phase reaction of OH radicals with isoprene and the rate-constant for its reaction with the OH radical, *Int. J. Chem. Kinet.*, *21*, 593–604.

Atkinson, R., S.M. Aschmann, and A.M. Winer (1987b), Kinetics of the reactions of NO_3 radicals with a series of aromatic compounds, *Environ. Sci. Technol.*, *21*, 1123–1126.

Atkinson, R., S.M. Aschmann, A.M. Winer, and W.P.L. Carter (1985), Rate constants for the gas-phase reactions of NO_3 radicals with furan, thiophene, and pyrrole at 295 ± 1 K and atmospheric pressure, *Environ. Sci. Technol.*, *19*, 87–90.

Atkinson, R., S.M. Aschmann, A.M. Winer, and J.N. Pitts Jr. (1981), Rate constants for the gas-phase reactions of ozone with a series of carbonyls at 296 K, *Int. J. Chem. Kinet.*, *13*, 1133–1142.

Atkinson. R., D.L. Baulch, R.A. Cox, J.N. Crowley, R.F. Hampson, Jr., R.G. Hynes, M.E. Jenkin, J.A. Kerr, M.J. Rossi, and J. Troe (2004), Volume I—gas phase reactions of O_x, HO_x, NO_x, and SO_x species, *Atmos. Chem. Phys.*, *4*, 1461–1738.

Atkinson, R., D.L. Baulch, R.A. Cox, J.N. Crowley, R.F. Hampson, R.G. Hynes, M.E. Jenkin, M.J. Rossi, and J. Troe (2005), Evaluated kinetic and photochemical data for atmospheric chemistry: Volume II—reactions of organic species, *Atmos. Chem. Phys Discuss.*, *5*, 6295–7168.

Atkinson, R., D.L. Baulch, R.A. Cox, J.N. Crowley, R.F. Hampson, R.G. Hynes, M.E. Jenkin, M.J. Rossi, and J. Troe (2006), Evaluated kinetic and photochemical data for atmospheric chemistry: Volume II—reactions of organic species, *Atmos. Chem. Phys.*, *6*, 3625–4055.

Atkinson, R., D.L. Baulch, R.A. Cox, J.N. Crowley, R.F. Hampson, R.G. Hynes, M.E. Jenkin, M.J. Rossi, J. Troe, and T.J. Wallington (2008b), Evaluated kinetic and photochemical data for atmospheric chemistry: Volume IV—gas phase reactions of organic halogen species, *Atmos. Chem. Phys.*, *8*, 4141–4496.

Atkinson, R., D.L. Baulch, R.A. Cox, R.F. Hampson, Jr., J.A. Kerr, and J. Troe (1992c), Evaluated kinetic and photochemical data for atmospheric chemistry, Supplement IV. IUPAC Subcommittee on Gas Kinetic Data Evaluation for Atmospheric Chemistry, *J. Phys. Chem., Ref. Data*, *21*, 1125–1568.

Atkinson, R., D.L. Baulch, R.A. Cox, R.F. Hampson, Jr., J.A. Kerr, M.J. Rossi, and J. Troe (1997), Evaluated kinetic and photochemical and heterogeneous data for atmospheric chemistry, Supplement V. IUPAC Subcommittee on Gas Kinetic Data Evaluation for Atmospheric Chemistry, *J. Phys. Chem., Ref. Data*, *26*, 521–1011.

Atkinson, R., W.P.L. Carter, K.R. Darnall, A.M. Winer, and J.N. Pitts, Jr. (1980), A smog chamber and modeling study of the gas phase NO_x–air photooxidation of toluene and the cresols, *Int. J. Chem. Kinet.*, *12*, 779–836.

Atkinson, R., W.P.L. Carter, C.N. Plum, A.M. Winer, and J.N. Pitts, Jr. (1984b), Kinetics of the gas-phase reactions of NO_3 radicals with a series of aromatics at 296 ± 2 K, *Int. J. Chem. Kinet.*, *16*, 887–898.

Atkinson, R., K.R. Darnall, and J.N. Pitts Jr. (1978a), Rate constants for the reactions of OH radicals and ozone with cresols at 300 ± 1 K, *J. Phys. Chem.*, *82*, 2759–2761.

Atkinson, R., R.A. Perry, and J.N. Pitts Jr. (1978b), Rate constants for the reactions of the OH radical with $(CH_3)_2NH$, $(CH_3)_3N$, and $C_2H_5NH_2$ over the temperature range 298–426 K, *J. Chem. Phys.*, *68*, 1850–1853.

Atkinson, R., and J.N. Pitts, Jr. (1977), Absolute rate constants for the reaction of $O^3(P)$ atoms with allene, 1,3-butadiene, and vinyl methyl ether over the temperature range 297–439 K, *J. Chem. Phys.*, *67*, 2492–2495.

Atkinson, R., and J.N. Pitts, Jr. (1978), Kinetics of the reactions of the OH radical with HCHO and CH_3CHO over the temperature range 299–426 K, *J. Chem. Phys.*, *68*, 3581–3584.

Atkinson, R., C.N. Plum, W.P.L. Carter, A.M. Winer, and J.N. Pitts, Jr. (1984c), Rate constants for the gas-phase reactions of nitrate radicals with a series of organics in air at 298 ± 1 K, *J. Phys. Chem.*, *88*, 1210–1215.

Atkinson, R., E.C. Tuazon, and S.M. Aschmann (2000), Atmospheric chemistry of 2-pentanone and 2-heptanone, *Environ. Sci. Technol.*, *34*, 623–631.

Atkinson, R., R.C. Tuazon, T.J. Wallington, S.M. Aschmann, J. Arey, A.M. Winer, and J.N. Pitts Jr. (1987c), Atmospheric chemistry of aniline, *N*,*N*-dimethylaniline, pyridine, 1,3,5-triazine, and nitrobenzene, *Environ. Sci. Technol.*, *21*, 64–72.

Atlas, E., S.M. Schauffler, J.T. Merrill, C.J. Hahn, B. Ridley, J. Walega, J. Greenberg, L. Heidt, and P. Zimmerman (1992), Alkyl nitrate and selected halocarbon measurements at Mauna Loa Observatory, Hawaii, *J. Geophys. Res.*, 97(D10), 10331–10348.

Audley, G.J., D.L. Baulch, and I.M. Campbell (1981), Gas-phase reactions of hydroxyl radicals with aldehydes in flowing $H_2O_2 + NO_2 + CO$ mixtures, *J. Chem. Soc., Faraday Trans. 1*, *77*, 2541–2549.

Audley, G.J., D.L. Baulch, I.M. Campbell, D.J. Waters, and G. Watling (1982), Gas-phase reactions of hydroxyl radicals with alkyl nitrite vapours in $H_2O_2 + NO + CO$ mixtures, *J. Chem. Soc., Faraday Trans. 1*, *78*, 611–617.

August, J., M. Brouard, M.P. Docker, C.J. Milne, J.P. Simons, R. Lavi, S. Rosenwaks, and D. Schwartz-Lavi (1988), Photodissociation dynamics of *tert*-butyl nitrite (S_2) and *tert*-butyl hydroperoxide at 248–250 nm, *J. Phys. Chem.*, *92*, 5485–5491.

Aumont, B., S. Szopa, and S. Madronich (2005), Modelling the evolution of organic carbon during its gas-phase tropospheric oxidation: Development of an explicit model based on a self generating approach, *Atmos. Chem. Phys.*, *5*, 2497–2517.

Ausloos, P. (1961). Intramolecular rearrangements. II. Photolysis and radiolysis of 4-methyl-2-hexanone, *J. Phys. Chem.*, *65*, 1616–1618.

Ausloos, P., and E. Murad (1961), The fluorescence and phosphorescence of trifluoroacetone vapor, *J. Phys. Chem.*, *65*, 1519–1521.

Ausloos, P., and R.E. Rebbert (1961), Molecular rearrangements. III. Formation of 1-methylcyclobutanol in the photolysis of 2-pentanone, *J. Am. Chem. Soc.*, *83*, 4897–4899.

Ausloos, P., and R.E. Rebbert (1964), Photoelimination of ethylene from 2-pentanone, *J. Am. Chem. Soc.*, *86*, 4512–4513.

Ausloos, P., and E.W.R. Steacie (1955), The photolysis of biacetyl, *Can. J. Chem.*, *33*, 39–46.

Ayers, G., and R. Gillett (1988), Isoprene emissions from vegetation and hydrocarbon emissions from bushfires in tropical Australia, *J. Atmos. Chem.*, *7*, 177–190.

Ayorinde, F.O., K. Garvin, and K. Saeed (2000), Determination of the fatty acid composition of saponified vegetable oils using matrix-assisted laser desorption/ionization time-of-flight mass spectrometry, *Rapid Commun. Mass Spectrom. 14*, 608–615.

Ayscough, P.B., and E.W.R. Steacie (1956), The photolysis of hexafluoroacetone, *Proc. Roy. Soc.*, A234, 476–488.

Azad, K., and J.M. Andino (1999), Products of the gas-phase photooxidation reactions of 1-propanol with OH radicals, *Int. J. Chem. Kinet.*, *31*, 810–818.

Baasandorj, M., and P.S. Stevens (2007), Experimental and theoretical studies of the kinetics of the reactions of OH and OD with 2-methyl-3-buten-2-ol between 300 and 415 K at low pressure, *J. Phys. Chem. A*, *111*, 640–649.

Baba, M., and I. Hanazaki (1984), The S_1 (n,π^*) states of cyclopentanone and cyclobutanone in a supersonic nozzle beam, *J. Chem. Phys.*, *81*, 5426–5433.

Bacher, C., G.S. Tyndall, and J.J. Orlando (2001), The atmospheric chemistry of glycolaldehyde, *J. Atmos. Chem.*, *39*, 171–189.

Badcock, C.C., M.J. Perona, G.O. Pritchard, and B. Rickborn (1969), Photolysis of 2-methylcyclohexanone, *J. Am. Chem. Soc.*, *91*, 543–546.

Badcock, C.C., H.W. Sidebottom, J.G. Calvert, B.R. Rabe, and E.K. Damon (1972), A study of the triplet–triplet annihilation reaction in biaceyl vapor exited at 4365Å and 25°C, *J. Am. Chem. Soc.*, *94*, 19–24.

Báez, A.P., R.D. Belmont, O.G. González and I.P. Rosas (1989), Formaldehyde levels in air and wet precipitation at Mexico City, Mexico, *Environ. Pollution*, *62*, l53–169.

Baeza-Romero, M.T., D.R. Glowacki, M.A. Blitz, D.E. Heard, M.J. Pilling, A.R. Rickard, and P.W. Seakins (2007), A combined experimental and theoretical study of the reaction between methylglyoxal and OH/OD radical: OH regeneration, *Phys. Chem. Chem. Phys.*, *9*, 4114–4128.

Bailey, B., and C. Colucci (1997), Research and development on the utilization of alcohol fuels at the National Renewable Energy Laboratory, *Renewable Energy*, *10*, 273–278.

Baird, N.C., and K.F. Taylor (1978), Multiplicity of ground state and magnitude of the T_1–S_o gap in substituted carbenes, *J. Am. Chem. Soc.*, *100*, 1333–1338.

Baker, J., J. Arey and R. Atkinson (2004a), Rate constants for the gas-phase reactions of OH radicals with a series of hydroxyaldehydes at 296 ± 2 K, *J. Phys. Chem A*, *108*, 7032–7037.

Baker, J., J. Arey, and R. Atkinson (2004b), Kinetics of the gas-phase reactions of OH radicals, NO_3 radicals and O_3 with three C_7-carbonyls formed from the atmospheric reactions of myrcene, ocimene and terpinolene, *J. Atmos. Chem.*, *48*, 241–260.

Baker, J., J. Arey, and R. Atkinson (2005), Rate constants for the reactions of OH radicals with a series of 1,4-hydroxyketones, *J. Photochem. Photobiol. A: Chemistry*, *176*, 143–148.

Baldwin, R.R., A. Keen, and R.W. Walker (1984), Studies of the decomposition of oxirane and of its addition to slowly reacting mixtures of hydrogen and oxygen at 480°C, *J. Chem. Soc. Faraday Trans. I*, *80*, 435–436.

Balestra-Garcia, C., G. Le Bras, and H. Mac Léod (1992), Kinetic study of the reactions OH + mono-, di-, and trichloroacetaldehyde and acetaldehyde by laser photolysis-resonance fluorescence at 298 K, *J. Phys. Chem.*, *96*, 3312–3316.

Ballesteros, B., A. Garzón, E. Jiménez, A. Notario, J. Albaladejo (2007), Relative and absolute kinetic studies of 2-butanol and related alcohols with tropospheric Cl atoms, *Phys. Chem. Chem. Phys.*, *9*, 1210–1218.

Bamford, C.H., and R.G.W. Norrish (1935), Primary photochemical reactions. Part VI. Photochemical decomposition of *iso*-valeraldehyde and di-*n*-propyl ketone, *J. Chem. Soc.*, *1935*, 1504–1511.

Bamford, C.H., and R.G.W. Norrish (1938), Primary photochemical reactions. Part XII. The effect of temperature on the quantum yield of the decomposition of di-*n*-propyl ketone in the vapour phase and in solution, *J. Chem. Soc.*, 1544–1554.

Bandow, H., and H. Akimoto (1985), Photochemistry of ketene in oxygen/argon matrices and in solid oxygen at 11 K, *J. Phys. Chem.*, *89*, 845–849.

Barkley, M.P., P.I. Palmer, U. Kuhn, J. Kesselmeier, K. Chance, T.P. Kurosu, R.V. Martin, D. Helmig and A. Guenther (2008), Net ecosystem fluxes of isoprene over tropical South America inferred from Global Ozone Monitoring Experiment (GOME) observations of HCHO columns, *J. Geophys. Res.*, *113*, D20304/1–D20304/24.

Barnes, I., V. Bastian, K.H. Becker, E.H. Fink and F. Zabel (1981), Rate constant of the reaction of OH with HO_2NO_2, *Chem. Phys. Lett.*, *83*, 459–464.

Barnes, I., V. Bastian, K.H. Becker, E.H. Fink, and F. Zabel (1982a), Reactivity studies of organic substances toward hydroxyl radicals under atmospheric conditions, *Atmos. Env.*, *16*, 545–550.

Barnes, I., V. Bastian, K.H. Becker, E.H. Fink, and F. Zabel (1986), Pressure dependence of the reaction of OH with HO_2NO_2, *Chem. Phys. Lett.*, *123*, 28–32.

Barnes, I., K.H. Becker, E.H. Fink, and F. Zabel (1982b), Paper presented at 3rd Discussion Meeting Working Party 2, CEC Cost 61 A bis, Univ. College, Dublin, Oct. 1982.

Barnes, I., K.H. Becker, and T. Zhu (1993), Near UV absorption spectra and photolysis products of difunctional organic nitrates: Possible importance as NO_x reservoirs, *J. Atmos. Chem.*, *17*, 353–373.

Barnes, I, and J. Wenger (editors) (1997), EUPHORE Report 1997, Institute of Physical Chemistry, Bergische Universität Wuppertal, Wuppertal. Germany.

Barry, J., D.J. Scollard, J.J. Treacy, H.W. Sidebottom, G. Le Bras, G. Poulet, S. Téton, A. Chichinin, C.E. Canosa-Mas, D.J. Kinnison, R.P. Wayne, and O.J. Nielsen (1994), Kinetic data for the reaction of hydroxyl radicals with 1,1,l-trichloroacetaldehyde at 298 ± 2 K, *Chem. Phys. Lett.*, *221*, 353–358.

Bartels, M., K. Hoyermann, and U. Lange (1989), An experimental study of the reactions of $CH_3CHO + Cl$, $C_2H_4O + Cl$, and $C_2H_4O + F$ in the gas-phase, *Ber. Bunsenges. Phys. Chem.*, *93*, 423–427.

Bauerle, S., and G.K. Moortgat (1999), Absorpton cross-sections of $HOCH_2OOH$ vapor between 205 and 360 nm at 298 K, *Chem. Phys. Lett.*, *309*, 43–48.

Baulch, D.L., I.M. Campbell, and S.M. Saunders (1985), The rate constants for the reaction of the hydroxyl radical with methyl, *n*-propyl, and *n*-butyl nitrites, *Int. J. Chem. Kinet.* 17, 355–366.

Baulch, D.L, C.J. Cobos, R.A. Cox, C. Esser, P. Frank, T. Just, J.A. Kerr, M.J. Pilling, J. Troe, R. W. Walker, and J. Warnatz (1992), Evaluated kinetic data for combustion modelling, *J. Phys. Chem. Ref. Data*, *21*, 411–734.

Baxley, J.S., M.V. Henley, and J.R. Wells (1997), The hydroxyl radical reaction rate constant and products of ethyl 3-ethoxypropionate, *Int. J. Chem. Kinet.*, *29*, 637–644.

Baxley, J.S., and J.R. Wells (1998), The hydroxyl radical reaction rate constant and atmospheric transformation products of 2-butanol and 2-pentanol, *Int. J. Chem. Kinet.*, *30*, 745–752.

Bayliss, N.S., and E.G. McRae (1954), Solvent effects in the spectra of acetone, crotonaldehyde, nitromethane and nitrobenzene, *J. Am. Chem. Soc.*, *58*, 1006–1011.

Beach, S.D., K.M. Hickson, I.W.M. Smith, and R.P Tuckett (2001), Rate constants and Arrhenius parameters for the reactions of OH radicals and Cl atoms with $CF_3CH_2OCHF_2$, $CF_3CHClOCHF_2$ and $CF_3CH_2OCClF_2$, using the discharge-flow/resonance fluorescence method, *Phys. Chem. Chem. Phys.*, *3*, 3064–3069.

Beavan, S.W., H. Inoue, D. Phillips, and P.A. Hackett (1978), Collisional effects on the phosphorescence of 1,1,1-trifluoroacetone vapour, *J. Photochem.*, *8*, *247–261.*

Beavan, S.W., D. Phillips, and R.G. Brown (1975), Phosphorescence of 1,1,1-trifluoroacetone using pulsed nitrogen laser excitation, *Chem. Phys. Lett*, *36*, 542–544.

Becerra, R., and H.M. Frey (1988), Photolysis of cyclopentanone in the gas phase, *J.Chem. Soc., Faraday Trans. 2*, *84*, 1941–1949.

Bechtel, H.A., J.P. Camden, and R.N. Zare (2004), State-to-state dynamics of the $Cl + CH_3OH \rightarrow HCl + CH_2OH$ reaction, *J. Chem. Phys.*, *120*, 4231–4239.

Becker, K.H. (editor) (1996), The European Photoreactor EUPHORE, Final Report of the EC-Project EV5V-CT-92-0059.

Becker, K.H., C.M.F. Dinis, H. Geiger, and P. Wiesen (1999a), Kinetics of the reaction of OH with di-*n*-butoxymethane (DBM) in the range 298–710 K, *Chem. Phys. Letters*, *300*, 460–464.

Becker, K.H., C.M.F. Dinis, H. Geiger, and P. Wiesen (1999b), The reactions of OH radicals with di-*i*-propoxymethane and di-*sec*-butoxymethane: Kinetic measurements and structure activity relationships, *Phys. Chem. Chem. Phys.*, *1*, 4721–4726.

Becker, K.H., and F. Graedler (1999), Photochemie ausgewählter Dicarbonylverbindungen unter atmosphärischen Bedingungen, Bericht Nr. 49, Physikalische Chemie (Fachbereich 9), Bergische Universität—GH-Wuppertal, Dezember.

Becker, K.H., and K. Wirtz (1989) Gas phase reactions of alkyl nitrates with hydroxyl radicals under tropospheric conditions in comparison with photolysis, *J. Atmos. Chem. 9*, 419–433.

Bell, W.E., and F.E. Blacet (1954), The photolysis of biacetyl, *J. Am. Chem. Soc.*, *76*, 5332–5337.

Bennett, P.J., and J.A. Kerr (1989), Kinetics of the reactions of hydroxyl radicals with aliphatic ethers studied under simulated atmospheric conditions, *J. Atmos. Chem.*, *8*, 87–94.

Bennett, P.J., and J.A. Kerr (1990), Kinetics of the reactions of hydroxyl radicals with aliphatic ethers studied under simulated atmospheric conditions: Temperature dependences of the rate coefficients, *J. Atmos. Chem.*, *10*, 29–38.

Benning, L., and A. Wahner (1998), Measurements of atmospheric formaldehyde (HCHO) and acetaldehyde (CH_3CHO) during POPCORN 1994 using 2,4-DNPH coated silica cartridges, *J. Atmos. Chem.*, *31*, 105–117.

Benson, S.W., and G.B. Kistiakowsky (1942), The photochemical decomposition of cyclic ketones, *J. Am. Chem. Soc.*, *64*, 80–86.

Bérces, T., and S. Förgeteg (1970), Kinetics of photolysis of nitric acid vapour. Part 1. Direct photolysis at low conversion, *Trans. Faraday Soc.*, *66*, 633–639.

Berger, M., I.L. Goldblatt, and C. Steel (1973), Photochemistry of benzaldehyde, *J. Am. Chem. Soc.*, *95*, 1717–1725.

Berges, M.G.M., and P. Warneck (1992), Product quantum yields for the 350 nm photodecomposition of pyruvic acid in air, *Ber. Bunsenges. Phys. Chem.*, *96*, 413–416.

Bernath, P. (2006) Atmospheric Chemistry Experiment (ACE): Analytical chemistry from orbit, *Trends Anal. Chem.*, *25*, 647–654.

Berndt, T., and O. Boge (2003), Gas-phase reaction of OH radicals with phenol, *Phys. Chem. Chem. Phys.*, *5*, 342–350.

Berndt, T., O. Böge, and W. Rolle (1997), Products of the gas-phase reactions of NO_3 radicals with furan and tetramethylfuran, *Env. Sci. Technol.*, *31*, 1157–1162.

Bernhard, M.J., and S.L. Simonich (2000), Use of bench-top photochemical reactor and solid-phase microextraction to measure semivolatile organic compound–hydroxyl radical rate constants, *Environ. Toxic. Chem.*, *19*, 1705–1710.

Bertman, S.B., and J.M. Roberts (1991), A PAN analog from isoprene photooxidation, *Geophys. Res. Lett.*, *18*, 1461–1464.

Bethel, H.L., J. Arey, and R. Atkinson (2001a), Products of the OH radical-initiated reaction of 3-hexene-2,5-dione, *Environ. Sci. Technol.*, *35*, 4477–4480.

Bethel, H.L., R. Atkinson, and J. Arey (2001b): Kinetics and products of the reactions of selected diols with the OH radical, *Int. J. Chem. Kinet.*, *33*, 310–316.

Bethel, H.L., R. Atkinson, and J. Arey (2003), Kinetics and products of the reactions of OH radicals with 2-methyl-2-pentanol and 4-methyl-2-pentanol, *J. Photochem. Photobiol. A.*, *157*, 257–267.

Betterton, E.A., and M.R. Hoffmann (1988), Henry's Law constants of some environmentally important aldehydes, *Environ. Sci. Technol.*, *22*, 1415–1418.

Beukes, J.A., B. D'Anna, V. Bakken and C.J. Nielsen (2000), Experimental and theoretical study of the F, Cl and Br reactions with formaldehyde and acetaldehyde, *Phys. Chem. Chem. Phys.*, *2*, 4049–4060.

Bey, I., D.J. Jacob, R.M. Yantosca, J.A. Logan, B.D. Field, A.M. Fiore, Q.L. Honguy, Y. Liu, L.J. Mickley and M.G. Schultz (2001), Global modeling of tropospheric chemistry with assimilated meteorology: Model description and evaluation, *J. Geophys. Res. 106*, 23073–23095.

Bierbach, A., I. Barnes, and K.H. Becker (1992), Rate coefficients for the gas-phase reactions of hydroxyl radicals with furan, 2-methylfuran, 2-ethylfuran and 2,5-dimethylfuran at 300 ± 2 K, *Atmos. Environ.*, *26*, 813–817.

Bierbach, A., I. Barnes, and K.H. Becker (1995), Product and kinetic study of the OH-initiated gas-phase oxidation of furan, 2-methylfuran and furanaldehydes at ≈300 K, *Atmos. Environ.*, *29*, 2651–2660.

Bierbach, A., I. Barnes, K.H. Becker, and E. Wiesen (1994), Atmospheric chemistry of unsaturated carbonyls: butenedial, 4-oxy-2-pentenal, 3-hexene-2,5-dione, maleic anhydride, 3H-furan-2-one, and 5-methyl-3H-furan-2-one, *Environ. Sci. Technol.*, *28*, 715–729.

Biermann, H.W., E.C. Tuazon, A.M. Winer, T.J. Wallington, and J.N. Pitts, Jr. (1988), Simultaneous absolute measurement of gaseous nitrogen species in urban ambient air by long pathlength infrared and ultraviolet visible spectroscopy, *Atmos. Environ.*, *22*, 1545–1554.

Bilde, M., T.E. Møgelberg, J. Sehested, O.J. Nielsen, T.J. Wallington, M.D. Hurley, S.M. Japar, M. Dill, V.L. Orkin, T.J. Buckley, R.E. Huie, and M.J. Kurylo (1997), Atmospheric chemistry of dimethyl carbonate: Reaction with OH radicals, UV spectra of $CH_3OC(O)OCH_2$ and $CH_3OC(O)OCH_2O_2$ radicals, reactions of $CH_3OC(O)OCH_2O_2$ with NO and NO_2, and fate of $CH_3OC(O)OCH_2O$ radicals, *J. Phys. Chem. A*, *101*, 3514–3525.

Bilde, M., and S.N. Pandis (2001), Evaporation rates and vapor pressures of individual aerosol species formed in the atmospheric oxidation of α- and β-pinene, *Environ. Sci. Technol.*, *35*, 3344–3349.

Bilde, M., B. Svenningsson, J. Monster, and T. Rosenorn (2003), Even–odd alternation of evaporation rates and vapor pressures of C_3–C_9 dicarboxylic acid aerosols, *Environ. Sci. Technol.*, *37*, 1371–1378.

Bishop, G.A., and D.H. Stedman (1989), Oxygenated fuels, a remote sensing evaluation, SAE Technical Paper Series No. 891116.

Bishop, G.A., and D.H. Stedman (1990), On-road carbon monoxide emission measurement comparison for the 1988–1989 Colorado oxy-fuels program, *Environ. Sci. Technol.*, *24*, 843–847.

Bishop, G.A., and D.H. Stedman (2008), A decade of on-road emissions measurements, *Environ. Sci. Technol.*, *42*, 1651–1656.

Bitto, H., I.-C. Chen, and C.B. Moore (1986), Rotational state distribution of CO photofragments from triplet ketene, *J. Chem. Phys.*, *85*, 5101–5106.

Blacet, F.E., and W.E. Bell (1953), The mechanism of biacetyl photolysis, *Faraday Society Discussion*, *No. 14*, 70–76.

Blacet, F.E., and J.G. Calvert (1951a), The photolysis of the aliphatic aldehydes. XIV. The butyraldehydes, *J. Am. Chem. Soc.*, *73*, 661–667.

Blacet, F.E., and J.G. Calvert (1951b), The photolysis of aliphatic aldehydes. XV. The butyraldehydes with iodine vapor, *J. Am. Chem. Soc.*, *73*, 667–674,

Blacet, F.E., and R.A. Crane (1954), The photolysis of aliphatic aldehydes. XVII. Propionaldehyde, *n*-butyraldehyde and isobutyraldehyde at 2380 and 1870 Å, *J. Am. Chem. Soc.*, *76*, 5337–5340.

Blacet, F.E., and J.D. Heldman (1942), The photolysis of the aliphatic aldehydes. X. Acetaldehyde and iodine mixtures, *J. Am. Chem. Soc.*, *64*, 889–893.

Blacet, F.E., and D.E. Loeffler (1942), The photolysis of the aliphatic aldehydes. XI. Acetaldehyde and iodine mixtures, *J. Am. Chem. Soc.*, *64*, 893–896.

Blacet, F.E., and J.E. LuValle (1939), The photolysis of the aliphatic aldehydes. VII. Crotonaldehyde at elevated temperatures, *J. Am. Chem. Soc.*, *61*, 273–276.

Blacet, F.E., and A. Miller (1957), The photochemical decomposition of cyclohexanone, cyclopentanone and cyclobutanone, *J. Am. Chem. Soc.*, *79*, 4327–4329.

Blacet, F.E., and R.W. Moulton (1941), The photolysis of the aliphatic aldehydes. IX. Glyoxal and acetaldehyde, *J. Am. Chem. Soc.*, *63*, 868–869.

Blacet, F.E., and J.N. Pitts, Jr. (1952), The photolysis of the aliphatic aldehydes. XVI. Propionaldehyde and propionaldehyde–iodine mixtures, *J. Am. Chem. Soc.*, *74*, 3382–3388.

Blacet, F.E., and J.G. Roof (1936a), The photolysis of the aliphatic aldehydes. III. Hydrogen from acetaldehyde, *J. Am. Chem. Soc.*, *58*, 278–280.

Blacet, F.E., and J.G. Roof (1936b), The photochemical stability of crotonaldehyde, *J. Am. Chem. Soc.*, *58*, 73–75.

Blacet, F.E., and R.D. Vanselow (1957), in Division of Physical Chemistry *Abstracts of the 131th National Meeting of the American Chemical Society*, Miami Beach.

Blacet, F.E., and D. Volman (1938), The photolysis of the aliphatic aldehydes. VI. Acetaldehyde, *J. Am. Chem. Soc.*, *60*, 1243–1247.

Blacet, F.E., and D.H. Volman (1939), The photochemical oxidation of crotonaldehyde, *J. Am. Chem. Soc.*, *61*, 582–584.

Blades, A.T. (1970), Photolysis of cyclopentanone, *Can. J. Chem.*,*48*, 2269–2273.

Blais, N.C. (1983), Photofragmentation of nitromethane in a molecular beam at 193 nm, *J. Chem. Phys.*, *79*, 1723–1731.

Blake, N.J., D.R. Blake, B.C. Sive, A.S. Katzenstein, S. Meinardi, O.W. Wingenter, E.L. Atlas, F. Flocke, B.A. Ridley, and F.S. Rowland (2003a), The seasonal evolution of NMHC and light alkyl nitrates at middle to high northern latitudes during TOPSE, *J. Geophys. Res.*, *108*, 8359, doi:10.1029/2001JD001467.

Blake, N.J., D.R. Blake, A.L. Swanson, E. Atlas, F. Flocke, and F.S. Rowland (2003b), Latitudinal, vertical, and seasonal variations of C_1–C_4 alkyl nitrates in the troposphere over the Pacific Ocean during PEM-Tropics A and B: Oceanic and continental sources, *J. Geophys. Res.*, *108*, 8242,doi:10.1029/2001JD001444.

Blanco, M.B., I. Bejan, I. Barnes, P. Wiesen, and M.A. Teruel (2008), Kinetics of the reactions of chlorine atoms with selected fluoroacetates at atmospheric pressure and 298 K, *Chem. Phys. Lett.*, *453*, 18–23.

Blanco, M.B., I. Bejan, I. Barnes, P. Wiesen, and M.A. Teruel (2009), OH-initiated degradation of unsaturated esters in the atmosphere: Kinetics in the temperature range 287–313 K, *J. Phys. Chem. A*, *113*, 5958–5965.

Blanco, M.B., R.A. Taccone, S.I. Lane, and M.A. Teruel (2006), On the OH-initiated degradation of methacrylates in the troposphere: Gas-phase kinetics and formation of pyruvates, *Chem. Phys. Lett.*, *429*, 389–394.

Blanco, M.B., and M.A. Teruel (2007), Atmospheric degradation of fluoroesters (FESs): Gas-phase reactivity study towards OH radicals at 298 K, *Atmos. Environ.*, *41*, 7330–7338.

Blanco, M.B., and M.A. Teruel (2008), Photodegradation of butyl acrylate in the troposphere by OH radicals: Kinetics and fate of 1,2-hydroxyalcoxy radicals, *J. Phys. Org. Chem.*, *21*, 397–401.

Blitz, M.A., D.E. Heard, and M.J. Pilling (2002), OH formation from CH_3CO+O_2: A convenient experimental marker for the acetyl radical, *Chem. Phys Letters*, *365*, 374–379.

Blitz, M.A., D.E. Heard, and M.J. Pilling (2005), Wavelength dependent photodissociation of CH_3OOH: Quantum yields for CH_3O and OH, and measurement of the OH + CH_3OOH rate coefficient, *J. Photochem. Photobiol. A*, *176*, 107–113.

Blitz, M.A., D.E. Heard, and M.J. Pilling (2006), Study of acetone photodissociation over the wavelength range 248–330 nm: Evidence of a mechanism involving both singlet and triplet excited states, *J. Phys. Chem. A*, *110*, 6743–6756.

Blitz, M.A, D.E. Heard, M.J. Pilling, S.R. Arnold, and M.P. Chipperfield (2004), Pressure- and temperature-dependent quantum yields for the photodissociation of acetone between 279 and 327.5 nm, *Geophys. Res. Letters*, *31*, L06111/1–L06111/5.

Bloss, C., V. Wagner, M.E. Jenkin, R. Volkamer, W.J. Bloss, J.D. Lee, D.E. Heard, K. Wirtz, M. Martin-Reviejo, G. Rea, J.C. Wenger, and M.J. Pilling (2005), Development of a detailed chemical mechanism (MCMv3.1) for the atmospheric oxidation of aromatic hydrocarbons, *Atmos. Chem. Phys*, *5*, 641–664.

Bodenbinder, M., S.E. Ulic, and H. Willner (1994), A gas-phase and matrix isolation study of the equilibrium CH_3ONO (*cis*) $\leftrightarrow CH_3ONO$ (*trans*) by FTIR spectroscopy, *J. Phys. Chem.*, *98*, 6441–6444.

Bolzacchini, E., M. Bruschi, J. Hjorth, S. Meinardi, M. Orlandi, B. Rindone, and E. Rosenbohm (2001), Gas phase reaction of phenol with NO_3, *Environ. Sci. Technol.*, *35*, 1791–1797.

Bolzacchini, E., S. Meinardi, M. Orlandi, B. Rindone, J. Hjorth, and G. Restelli (1999), Nighttime tropospheric chemistry: Kinetics and product studies in the reaction of 4-alkyl- and 4-alkoxytoluenes with NO_3 in the gas phase, *Environ. Sci. Technol.*, *33*, 461–468.

Bonard, A., V. Daële, J.-L. Delfau, and C. Vovelle (2002), Kinetics of OH radical reactions with methane in the temperature range 295–660 K and with dimethyl ether and

methyl *tert*-butyl ether in the temperature range 295–618 K, *J. Phys. Chem. A*, *106*, 4384–4389.

Bongartz, A., J. Kames, U. Schurath, C. George, P. Mirabel, and J.L. Ponche (1994), Experimental determination of HONO mass accommodation coefficients using 2 different techniques, *J. Atmos. Chem.*, *18*, 149–169.

Bongartz, A., J. Kames, F. Welter, and U. Schurath (1991), Near-UV absorption cross-sections and *trans-cis* equilibrium of nitrous-acid, *J. Phys. Chem.*, *95*, 1076–1082.

Borkowski, R.P., and P. Ausloos (1961), Intramolecular rearrangements. IV. Photolysis of 2-pentanone-4,5,5-d_3, *J. Phys. Chem.*, *65*, 2257–2260.

Bossmeyer, J., T. Brauers, C. Richter, F. Rohrer, R. Wegener, and A. Wahner (2006), Simulation chamber studies on the NO_3 chemistry of atmospheric aldehydes, *Geophys. Res. Letters*, *33*, L18810/1–L18810/5.

Bott, J.F., and N. Cohen (1991), A shock tube study of the reactions of the hydroxyl radical with several combustion species, *Int. J. Chem. Kinet.*, *23*, 1075–1094.

Bouma, W.J., R.H. Nobes, L. Radom, and C.E. Woodward (1982), On the existence of stable structural isomers of ketene. A theoretical study of the C_2H_2O potential energy surface, *J. Org. Chem.*, *47*, 1869–1875.

Bowen, E.J., H. Hartley, W.D. Scott, and H.G. Watts (1924), Rates of photochemical change in solids, *J. Chem. Soc.*, *125*, 1218–1221

Bowman, J.H., D.J. Barket, Jr., and P.B. Shepson (2003), Atmospheric chemistry of nonanal, *Environ. Sci. Technol.*, *37*, 2218–2225.

Boyd, A.A., C.E. Canosa-Mas, D. King, R.P. Wayne, and M.R. Wilson (1991), Use of a stopped-flow technique to measure the rate constants at room temperature for reactions between the nitrate radical and various organic species, *J. Chem. Soc., Faraday Trans. 87*, 2913–2919.

Bradley, W.R., S.E. Wyatt, J.R. Wells, M.V. Henley, and G.M. Graziano (2001), The hydroxyl radical reaction rate constant and products of cyclohexanol, *Int. J. Chem. Kinet.*, *33*, 108–117.

Brand, J.C.D., and A.W.-H. Mau (1974), Low-lying electronic states of biacetyl, *J. Am. Chem. Soc.*, *96*, 4380–4385.

Brasseur, G.P, J.J. Orlando, and G.S. Tyndall (1999), *Atmospheric Chemistry and Global Change*, Oxford University Press, Oxford.

Braun, W., A.M. Bass, and M. Pilling (1970), Flash photolysis of ketene and diazomethane: The production and reaction kinetics of triplet and singlet methylene, *J. Chem. Phys.*, *52*, 5131–5143.

Bravo, I., A. Aranda, Y. Díaz-de-Mera, E. Moreno, M.E. Tucceri, and D. Rodríguez (2009), Kinetic, mechanistic and temperature dependence study of Cl reactions with $CH_3OC(O)H$ and $CH_3CH_2OC(O)H$: Atmospheric implications, *Phys. Chem. Chem. Phys.*, *11*, 384–390.

Bretschneider, V.K., and J. Matz (1973), Nitrosamine (NA) in der atmosphärischen und in der luft am arbeitplatz, *Arch. Geschwulatforsch*, *42*, 36–41.

British Petroleum (2008), http://www.bp.com.

Brown, A.C., C.E. Canosa-Mas, A.D. Parr, J.M.T. Pierce, and R.P. Wayne (1989a), Tropospheric lifetimes of halogenated anesthetics, *Nature*, *341*, 635–637.

Brown, A.C., C.E. Canosa-Mas, A.D. Parr, and R.P. Wayne (1989b), Temperature dependence of the rate of the reaction between the OH radical and ketene, *Chem. Phys. Letters*, *161*, 491–496.

Brown, A.C., C.E. Canosa-Mas, A.D. Parr, and R.P. Wayne (1990), Laboratory studies of some halogenated ethanes and ethers: measurements of rates of reaction with OH and infrared absorption cross-sections, *Atmos. Environ.*, *24*, 2499–2511.

Brown, H.W., and G.C. Pimentel (1958), Photolysis of nitromethane and of methyl nitrite in an argon matrix; infrared detection of nitroxyl, HNO, *J. Chem. Phys.*, *29*, 883–888.

Brown, S.S., J.B. Burkholder, R.K. Talukdar, and A.R. Ravishankara (2001), Reaction of hydroxyl radical with nitric acid: Insights into its mechanism, *J. Phys. Chem. A*, *105*, 1605–1614.

Brown, S.S., R.K. Talukdar, and A.R. Ravishankara (1999), Reconsideration of the rate constant for the reaction of hydroxyl radical with nitric acid, *J. Phys. Chem. A*, *103*, 3031–3037.

Brown, S.S., R.W. Wilson, and A.R. Ravishankara (2000), Absolute intensities for third and fourth overtone absorptions in HNO_3 and H_2O_2 measured by cavity ring down spectroscopy, *J. Phys. Chem. A*, *104*, 4976–4983.

Brubaker, W.W., Jr, and R.A. Hites (1997), Polychlorinated dibenzo-*p*-dioxins and dibenzofurans: Gas-phase hydroxyl radical reactions and related atmospheric removal, *Environ. Sci. Technol.*, *31*, 1805–1810.

Brubaker, W.W., Jr, and R.A. Hites (1998), OH reaction kinetics of polycyclic aromatic hydrocarbons and polychlorinated dibenzo–*p*-dioxins and dibenzofurans, *J. Phys. Chem. A*, *102*, 915–921.

Brühlmann, U., M. Dubs, and J.R. Huber (1987), Photodissociation of methyl nitrite: State distributions, recoil velocity distribution and alignment effect of the NO ($X\ ^2\Pi$) photofragment, *J. Chem. Phys.*, *86*, 1249–1257.

Brunet, V., and W.A. Noyes, Jr. (1958), Photochimie de l'Hexanone-2 en phase gazeuse, *Bull. Soc. Chim. France*, 121–123.

Bryukov, M.G., I.R. Slagle, and V.D. Knyazev (2003), Kinetics of reactions of Cl atoms with ethane, chloroethane, and 1,1-dichloroethane, *J. Phys. Chem. A*, *107*, 6565–6573.

Buchta, C., H. Frerichs, D. Stucken, M. Tappe, and H.G. Wagner (1991), Investigation of the reactions of diethylether, di-*n*-propylether and di-*n*-butylether with $O(^3P)$ in the gas-phase, *Z. Phys. Chemie*, *174*, 129–137.

Burak, I., J.W. Hepburn, N. Sivakumar, G.E. Hall, G. Chawla, and P.L. Houston (1987), State-to-state photodissociation dynamics of *trans*-glyoxal, *J. Chem. Phys.*, *86*, 1258–1268.

Burkholder, J.B., M.K. Gilles, T. Gierczak, and A.R. Ravishankara (2002), The atmospheric degradation of 1-brompropane ($CH_3CH_2CH_2Br$): The photochemistry of bromoacetone, *Geophys. Res. Lett.*, *29*, 1822, doi:10.1029/2002GL014712.

Burkholder, J.B., A. Mellouki, R. Talukdar, and A.R. Ravishankara (1992), Rate coefficients of OH with HONO between 298 and 373 K, *Int. J. Chem. Kinet.*, *24*, 711–725.

Burkholder, J.B., R.K. Talukdar, A.R. Ravishankara, and S. Solomon (1993), Temperature-dependence of the HNO_3 UV absorption cross-sections, *J. Geophys. Res.*, *98*, 22937–22948.

Burrows, J.P., K.V. Chance, A.P.H. Goede, R. Guzzi, B.J. Kerridge, C. Muller, D. Perner, U. Platt, J.-P. Pommereau, W. Schneider, R.J. Spurr, and H. van der Woerd (1993), Global Ozone Monitoring Experiment Interim Science Report, ed. T. D. Guyenne and C. Readings, Report ESA SP-1151, *ESA Publications Division*, *ESTEC*, *Noordwijk*, *The Netherlands*, ISBN 92-9092-041-6, 1993.

Burrows, J.P., G.S. Tyndall, and G.K. Moortgat (1985), Absorption spectrum of NO_3, and kinetics of the reactions of NO_3 with NO_2, Cl, and several stable atmospheric species at 298 K, *J. Phys Chem., 89*, 4848–4856

Buth, R., K. Hoyermann, and G. Rhode (1992), Mechanisms and rates of benzoyl reactions: The reactions of benzaldehyde + atomic chlorine, benzoyl radical + oxygen atom, and benzoyl radical + hydrogen atom, *Proc. Int. Symp. Comb.*, *24*, 669–674.

Butkovskaya, N.I., A. Kukui, and G. Le Bras (2004a), Branching fractions for H_2O forming channels of the reaction of OH radicals with acetaldehyde, *J. Phys. Chem. A*, *108*, 1160–1168.

Butkovskaya, N.I., A. Kukui, N. Pouvesle, and G. Le Bras (2004b), Rate constant and mechanism of the reaction of OH radicals with acetic acid in the temperature range of 229–300 K, *J. Phys. Chem. A*, *108*, 7021–7026.

Butkovskaya, N.I., N. Pouvesle, A. Kukui, and G. Le Bras (2006a), Mechanism of the OH-initiated oxidation of glycolaldehyde over the temperature range 233–296 K, *J. Phys. Chem. A*, *110*, 13492–13499.

Butkovskaya, N.I., N. Pouvesle, A. Kukui, Y. Mu, and G. Le Bras (2006b), Mechanism of the OH-initiated oxidation of hydroxyacetone over the temperature range 236–298 K, *J. Phys. Chem. A*, *110*, 6833–6843.

Butkovskaya, N.I., and D.W. Setser (2003), Infrared chemiluminescence from water-forming reactions: Characterization of dynamics and mechanisms, *Int. Rev. Phys. Chem.*, *22*, 1–72.

Butler, L.J., D. Krajnovich, and Y.T. Lee (1983), The photodissociation of nitromethane at 193 nm, *J. Chem. Phys.*, *79*, 1708–1722.

Butler, T. M., D. Taraborrelli, C. Bruehl, H. Fischer, H. Harder, M. Martinez, J. Williams, M.G. Lawrence, and J. Lelieveld (2008), Improved simulation of isoprene oxidation

chemistry with the ECHAM5/MESSy chemistry–climate model: lessons from the GABRIEL airborne field campaign, *Atmos. Chem. Phys.*, *8*, 4529–4546.

Butt, C.M., C.J. Young, S.A. Mabury, D.C.G. Muir, M.D. Hurley, and T.J. Wallington (2009), Atmospheric chemistry of 4:2 fluorotelomer acrylate ($C_4F_9CH_2CH_2OC(O)CH{=}CH_2$): Kinetics, mechanisms and products of chlorine atom and OH radical initiated oxidation, *J. Phys. Chem. A*, *113*, 3155–3161.

Cabañas, B., M.T. Baeza, S. Salgado, P. Martín, R. Taccone, and E. Martínez (2004), Oxidation of heterocycles in the atmosphere: Kinetic study of their reactions with NO_3 radical, *J. Phys. Chem.*, *108*, 10818–10823.

Cabañas, B., P. Martín, S. Salgado, B. Ballesteros, and E. Martínez (2001a), An experimental study on the temperature dependence for the gas-phase reactions of NO_3 radical with a series of aliphatic aldehydes, *J. Atmos. Chem.*, *40*, 23–39.

Cabañas, B., S. Salgado, P. Martin, M.T. Baeza, J. Albaladejo, and E. Martinez (2003), Gas-phase rate coefficients and activation energies for the reaction of NO_3 radicals with selected branched aliphatic aldehydes, *Phys. Chem. Chem. Phys.*, *5*, 112–116.

Cabañas, B., S. Salgado, P. Martin, M.T. Baeza, and E. Martinez (2001b), Night-time atmospheric loss process for unsaturated aldehydes: Reaction with NO_3 radicals, *J. Phys. Chem. A*, *105*, 4440–4445.

Cabañas, B., A. Tapia, F. Villanueva, S. Salgado, E. Monedero, and P. Martín (2008), Kinetic study of 2-furanaldehyde, 3-furanaldehyde, and 5-methyl-2-furanaldehyde reactions initiated by Cl atoms, *Int. J. Chem. Kinet.*, *40*, 670–678.

Cabañas, B., F. Villanueva, P. Martín, M.T. Baeza, S. Salgado, and E. Martínez (2005), Study of reaction processes of furan and some furan derivatives initiated by Cl atoms, *Atmos. Environ.*, *39*, 1935–1944.

Cadle, R.D., and J.W. Powers (1967), The reaction of $O(^3P)$ with acetaldehyde in a fast-flow system, *J. Phys. Chem*, *71*, 1702–1706.

Caffrey, P.J., and P.A. Machiele (1994), In-use volatility of commingling ethanol and non-ethanol fuels, Society of Automotive Engineers Technical Paper 940765.

Calogirou, A., N.R. Jensen, C.J. Nielsen, D. Kotzias, and J. Hjorth (1999), Gas-phase reactions of nopinone, 3-isopropenyl-6-oxo-heptanal, and 5-methyl-5-vinyltetrahydrofuran-2-ol with OH, NO_3, and ozone, *Env. Sci. Technol.*, *33*, 453–460.

Calvert, J.G. (1949), Photochemical Studies of the Butyraldehydes, Ph.D. Thesis, Chemistry Department, University of California, Los Angeles.

Calvert, J.G. (1982), The use of long-path spectroscopy in kinetic studies of reactive molecules of atmospheric interest, in, editors, H.W. Georgii and W. Jaeschke, *Chemistry of the Unpolluted and Polluted Troposphere*, D. Reidel Publishing Company, Dordrecht, pages 91–116.

Calvert, J.G., R. Atkinson, K.H. Becker, R.M. Kamens, J.H. Seinfeld, T.J. Wallington, and G. Yarwood (2002), *The Mechanisms of Atmospheric Oxidation of Aromatic Hydrocarbons*, Oxford University Press, New York.

Calvert, J.G., R. Atkinson, J.A. Kerr, S. Madronich, G.K. Moortgat, T.J. Wallington, and G. Yarwood (2000), *The Mechanisms of Atmospheric Oxidation of the Alkenes*, Oxford University Press, New York.

Calvert, J.G., R.G. Derwent, J.J. Orlando, G.S. Tyndall, and T.J. Wallington (2008), *The Mechanisms of Atmospheric Oxidation of the Alkanes*, Oxford University Press, New York.

Calvert, J.G., and G.S. Layne (1953), The photolysis of glyoxal vapor at wavelength 3130Å, *J. Am. Chem. Soc.*, *75*, 856–859.

Calvert, J.G., and J.N. Pitts, Jr. (1966), *Photochemistry*, John Wiley & Sons, New York.

Calvert, J.G., G. Yarwood, and A.M. Dunker (1994), An evaluation of the mechanism of nitrous acid formation in the urban atmosphere, *Res. Chem. Intermed.*, *20*, 463–502.

Cameron, M., V. Sivakumaran, T.J. Dillon, and J.N. Crowley (2002), Reaction between OH and CH_3CHO: Part 1, Primary product yields of CH_3(296 K), CH_3CO (296 K), and H (237–296 K), *Phys. Chem. Chem. Phys.*, *4*, 3628–3638.

Campbell, I.M., and K. Goodman (1975), Rate constants for reactions of hydroxyl radicals with nitromethane and methyl nitrite vapours at 292 K, *Chem. Phys. Lett.*, *36*, 382–384.

Campbell, I.M., D.F. McLaughlin, and B.J. Handy (1976), Rate constants for reactions of hydroxyl radicals with alcohol vapours at 292 K, *Chem. Phys. Lett.*, *38*, 362–364.

Campbell, I.M., and P.E. Parkinson (1978), Rate constants for reactions of hydroxyl radicals with ester vapours at 292 K, *Chem. Phys. Lett.*, *53*, 385–387.

Campbell, R.J., and E.W. Schlag (1967), Energy distribution in reaction products. The photolysis of cyclobutanone, *J. Am. Chem. Soc.*, *89*, 5103–5106.

Campbell, R.J., E.W. Schlag, and B.W. Ristow (1967), Mechanistic consequences of curved Stern–Volmer plots. The photolysis of cyclobutanone, *J. Am. Chem. Soc.*, *89*, 5098–5102.

Canakci, M. (2005), Performance and emissions characteristics of biodiesel from soybean oil, *J. Automobile Engineering*, 2l9, 915–922.

Canakci, M., A. Erdil, and E. Arcaklioğlu (2006), Performance and exhaust emissions of a biodiesel engine, *Applied Energy*, *83*, 594–605.

Canosa-Mas, C.E., S. Carr, M.D. King, D.E. Shallcross, K.C. Thompson, and R.P. Wayne (1999a), A kinetic study of the reactions of NO_3 with methyl vinyl ketone, methacrolein, acrolein, methyl acrylate and methyl methacrylate, *Phys. Chem. Chem. Phys*, *1*, 4195–4202.

Canosa-Mas, C.E., E.S.N. Cotter, J. Duffy, K.C. Thompson, and R.P. Wayne (2001), The reactions of atomic chlorine with acrolein, methacrolein and methyl vinyl ketone, *Phys. Chem. Chem. Phys.*, *3*, 3075–3084.

Canosa-Mas, C.E., J.M. Duffy, M.D. King, K.C. Thompson, and R.P. Wayne (2002), The atmospheric chemistry of methyl salicylate–reactions with atomic chlorine and with ozone, *Atmos. Environ.*, *36*, 2201–2205.

Canosa-Mas, C.E., M.L. Flugge, M.D. King, and R.P. Wayne (2005), An experimental study of the gas-phase reaction of the NO_3 radical with α, β-unsaturated carbonyl compounds, *Phys. Chem. Chem. Phys.*, *7*, 643–650.

Canosa-Mas, C.E., H.R. Hutton-Squire, M.D. King, D.J. Stewart, K.C. Thompson, and R.P. Wayne (1999b), Laboratory kinetic studies of the reactions of Cl atoms with species of biogenic origin: Δ^3-carene, isoprene, methacrolein and methyl vinyl ketone, *J. Atmos. Chem.*, *34*, 163–170.

Canosa-Mas, C.E., M.D. King, D.E. Shallcross, and R.P. Wayne (1999c), Kinetic investigation of the reaction between the NO_3 radical and peroxymethacrylic nitric anhydride (MPAN), *Phys. Chem. Chem. Phys.*, *1*, 2411–2414.

Canosa-Mas, C.E., S.J. Smith, S. Toby, and R.P. Wayne (1989), Laboratory studies of the reactions of the nitrate radical with chloroform, methanol, hydrogen chloride and hydrogen bromide, *J. Chem. Soc. Faraday Trans*, *85*, 709–725.

Cantrell, C.A., J.A. Davidson, K.L. Busarow, and J.G. Calvert (1986), The CH_3CHO–NO_3 reaction and possible nighttime PAN generation, *J. Geophys. Res.*, *91*, 5347–5353.

Cantrell, C.A., J.A. Davidson, A.H. McDaniel, R.E. Shetter, and J.G. Calvert (1990), Temperature-dependent formaldehyde cross sections in the near-ultraviolet spectral region, *J. Phys. Chem.*, *94*, 3902–3908.

Cantrell, C.A., W.R. Stockwell, L.G. Anderson, K.L. Busarow, D. Perner, A. Schmeltekopf, J.G. Calvert, and H.S. Johnston (1985), Kinetic study of the NO_3–CH_2O reaction and its possible role in nighttime tropospheric chemistry, *J. Phys. Chem.*, *89*, 139–146.

Cappa, C.D., E.R. Lovejoy, and A.R. Ravishankara (2007), Determination of evaporation rates and vapor pressures of very low volatility compounds: A study of the C_4–C_{10} and C_{12} dicarboxylic acids, *J. Phys. Chem. A*, *111*, 3099–3109.

Caralp, F., W. Forst, E. Henon, A. Bergeat, and F. Bohr (2006), .Tunneling in the reaction of acetone with OH. *Phys. Chem. Chem. Phys.*, *8*, 1072–1078.

Carl, S.A., and J.N. Crowley (1998), Sequential two (blue) photon absorption by NO_2 in the presence of H_2 as a source of OH in pulsed photolysis kinetic studies: Rate constants for reaction of OH with CH_3NH_2, $(CH_3)_2NH$, $(CH_3)_3N$, and $C_2H_5NH_2$ at 295 K, *J. Phys. Chem. A*, *102*, 8131–8141.

Carl, S.A., T. Ingham, G.K. Moortgat, and J.N. Crowley (2001), OH kinetics and photochemistry of HNO_3 in the presence of water vapour, *Chem. Phys. Lett.*, *341*, 93–98.

Carless, H.A.J., and E.K.C. Lee (1970), Stereochemistry of the thermal and photolytic decomposition of *cis*- and *trans*-2,3-dimethylcyclobutanone in the gas phase, *J. Am. Chem. Soc.*, *92*, 4482.

Carless, H.A.J., and E.K.C. Lee (1972), Photolysis and pyrolysis of 2-*n*-propylcyclobutanone in the gas phase, *J. Am. Chem. Soc.*, *94*, 1–6.

Carless, H.A.J., J. Metcalfe, and E.K.C. Lee (1972), Photolytic and triplet benzene–sensitized decomposition of *cis*- and *trans*-2,3- and -2,4-dimethylcyclobutanones, *J. Am. Chem. Soc.*, *94*, 7221–7235.

Caro, E., J. Gotewold, and E.A. Lissi (1969), Energy transfer in the photolysis of biacetyl, *J. Chem. Soc.*, *Chem. Communications*, *1969*, 318–319.

Carr, S.A., M.T. Baeza-Romero, M.A. Blitz, M.J. Pilling, D.E. Heard, and P.W. Seakins (2007), OH yields from the $CH_3CO + O_2$ reaction using an internal standard, *Chem. Phys. Lett.*, *445*, 108–112.

Carr, S.A., M.T. Baeza-Romero, M.A. Blitz, B.J.S. Price, and P.W. Seakins (2008), Ketone photolysis in the presence of oxygen: A useful source of OH for flash photolysis kinetics experiments, *Int. J. Chem. Kinet.*, *40*, 504–514.

Carr, S., D.E. Shallcross, C.E. Canosa-Mas, J.C. Wenger, H.W. Sidebottom, J.J. Treacy, and R.P. Wayne (2003), A kinetic and mechanistic study of the gas-phase reactions of OH radicals and Cl atoms with some halogenated acetones and their atmospheric implications, *Phys. Chem. Chem. Phys.*, *5*, 3874–3883.

Carr, S., J.J. Treacy, H.W. Sidebottom, R.K. Connell, C.E. Canosa-Mas, R.P. Wayne, and J. Franklin (1994), Kinetics and mechanisms for the reaction of hydroxyl radicals with trifluoroacetic acid under atmospheric conditions, *Chem. Phys. Lett.*, *227*, 39–44.

Carr, S.A., M T. Baeza-Romero, M A. Blitz, B.J.S. Price, and P.W. Seakins (2008), *Int. J. Chem. Kinet.*, *40*, 504–514.

Carrasco, N., J.F. Doussin, M. O'Connor, J.C. Wenger, B. Picquet–Varrault, R. Durand-Jolibois, and P. Carlier (2007a), Simulation chamber studies of the atmospheric oxidation of 2-methyl-3-buten-2-ol: reaction with hydroxyl radicals and ozone under a variety of conditions *J. Atmos. Chem.*, *56*, 33–55.

Carrasco, N., B. Picquet-Varrault, and J-F. Doussin (2007b), Kinetic and product study of the gas-phase reaction of sabinaketone with OH radical, *Int. J. Chem.Kinet.*, *39*, 415–421.

Carslaw, N., P.J. Jacobs and M.J. Pilling (1999), Modeling OH, HO_2, and RO_2 radicals in the marine boundary layer. 2. Mechanism reduction and uncertainty analysis, *J. Geophys. Res.*, *104*, 30257–30273.

Carter, W.P.L. (1995) Computer modeling of environmental chamber measurements of maximum incremental reactivities of volatile organic compounds, *Atmos. Env.*, *29*, 2513–2527.

Carter, W.P.L. (1998), Updated maximum incremental reactivity scale for regulation applications, Report to California Air Resources Board, Contract No. 95–308.

Carter, W.P.L. (2000), Development and evaluation of the SAPRC-99 chemical mechanism, *United States Environmental Protection Agency*, *Research and Development*, (EPA/600/R–00/076, Proceedings Sixth US/Germany Workshop on Ozone/Fine Particle Science, 1999), 19–41.

Carter, W.P.L., A.M. Winer, and J.N. Pitts Jr (1981), Major atmospheric sink for phenol and cresols. Reaction with the nitrate radical, *Environ. Sci. Technol.*, *15*, 829–831.

Castle, K.J., J. Abbott, X. Peng, and W. Kong (2000), Photodissociation of *t*-butyl nitrite between 220 and 250 nm: Internal energy distribution of NO, *Chem. Phys. Lett.*, *318*, 565–570.

Catalán, J., J.C. del Valle, J. Palomar, C. Diaz, and J.L.G. de Paz (1999), The six-membered intramolecular hydrogen bond position as a switch for inducing an excited state intramolecular proton transfer (ESIPT) in esters of *o*-hydroxynaphthoic acids, *J. Phys. Chem. A*, *103*, 10921–10934.

Cavalli, F., I. Barnes, and K.H. Becker (2000a), FT–IR kinetic and product study of the OH radical-initiated oxidation of 1-pentanol, *Environ. Sci. Technol.*, *34*, 4111–4116.

Cavalli, F., I. Barnes, K.H. Becker, and T.J. Wallington (2000b), Atmospheric oxidation mechanism of methyl propionate, *J. Phys. Chem. A*, *104*, 11310–11317.

Cavalli, F., H. Geiger, I. Barnes, and K.H. Becker (2002), FTIR kinetic, product, and modeling study of the OH-initiated oxidation of 1-butanol in air, *Environ. Sci. Technol.*, *36*, 1263–1270.

Cavalli, F., M. Glasius, J. Hjorth, B. Rindone, and N.R. Jensen (1998), Atmospheric lifetimes, infrared spectra and degradation products of a series of hydrofluoroethers, *Atmos. Environ.*, *32*, 3767–3773.

Cavanagh, L.A., C.F. Schadt, and E. Robinson (1969), Atmospheric hydrocarbon and carbon monoxide measurements at Point Barrow, Alaska, *Environ. Sci. Technol.*, *3*, 251–257.

Chance, K. (1998), Analysis of BrO measurements from the Global Ozone Monitoring Experiment, *Geophys. Res. Lett.*, *25*, 3335–3338.

Chance, K., P.I. Palmer, R.J.D. Spurr, R.V. Martin, T.P. Kurosu, and D.J. Jacob (2000), Satellite observations of formaldehyde over North America from GOME, *Geophys. Res. Lett.*, *27*, 3461–3464.

Chang, J.S., and J.R. Barker (1979), Reaction rate and products for the reaction oxygen(^{3}P) + formaldehyde, *J. Phys. Chem*, *83*, 3059–3064.

Chang, T.Y., R.H. Hammerle, S.M. Japar, and I.T. Salmeen (1991), Alternative transportation fuels and air quality, *Environ. Sci. Technol.*, *25*, 1190–1197.

Chebbi, A., and P. Carlier (1996), Carboxylic acids in the troposphere, occurrence, sources and sinks: A review, *Atmos. Environ.*, *30*, 4233–4249.

Cheema, S.A., K.A. Holbrook, G.A. Oldershaw, D.P. Starkey, and R.W. Walker (1999), The effect of oxygen pressure on the tropospheric oxidation of diethyl ether, H-atom elimination from the 1-ethoxyethoxy radical, *Phys. Chem. Chem. Phys.*, *1*, 3243–3245.

Cheema, S.A., K.A. Holbrook, G.A. Oldershaw, and R.W. Walker (2002), Kinetics and mechanism associated with the reactions of hydroxyl radicals and of chlorine atoms with 1-propanol under near-tropospheric conditions between 273 and 343 K, *Int. J. Chem. Kinet.*, *34*, 110–121.

Chen, I.-C., W.H. Green, Jr., and C.B. Moore (1988), Bond breaking without barriers: Photofragmentation of ketene at the singlet threshold, *J. Chem. Phys.*, *89*, 314–328.

Chen, I.C., and C.B. Moore (1990), Photofragmentation of ketene to $CH_2(X^3B_1)$+ CO. 1. Barrier height and dissociation rate constant, *J. Phys. Chem.*, *94*, 263–269.

Chen, J., V. Young, P.A. Hooshiyar, H. Niki, and M.D. Hurley (1995), FTIR spectroscopic study of the Cl-atom-initiated reactions of ethylene oxide in O_2/N_2 diluent, *J. Phys. Chem.*, *99*, 4071–4077.

Chen, L., S. Kutsuna, K. Nohara, K. Takeuchi, and T. Ibusuki (2001), Kinetics and mechanisms for the reactions of CF_3OCH_3 and $CF_3OC(O)H$ with OH radicals using an environmental reaction chamber, *J. Phys. Chem.*, *105*, 10854–10859.

Chen, L., S. Kutsuna, K. Tokuhashi, and A. Sekiya (2005a), Kinetics study of the gas-phase reactions of $CHF_2CF_2OCHF_2$ and $CF_3CHFCF_2OCH_2CF_2CF_3$ with OH radicals at 253–328 K, *Chem. Phys. Lett.*, *403*, 180–184.

Chen, L., S. Kutsuna, K. Tokuhashi, and A. Sekiya (2004a), Kinetics of the gas-phase reaction of $CF_3OC(O)H$ with OH radicals at 242–328 K, *Int. J. Chem. Kinet.*, *36*, 337–344.

Chen, L., S. Kutsuna, K. Tokuhashi, and A. Sekiya (2004b), Kinetics study of the gas-phase reactions of $C_2F_5OC(O)H$ and n-$C_3F_7OC(O)H$ with OH radicals at 253–328 K, *Chem. Phys. Lett.*, *400*, 563–568.

Chen, L., S. Kutsuna, K. Tokuhashi, and A. Sekiya (2006), Kinetics and mechanisms of $CF_3CHFOCH_3$, $CF_3CHFOC(O)H$, and $FC(O)OCH_3$ reactions with OH radicals, *J. Phys. Chem. A*, *110*, 12845–12851.

Chen, L., S. Kutsuna, K. Tokuhashi, A. Sekiya, K. Takeuchi, and T. Ibusuki (2003a), Kinetics for the gas-phase reactions of OH radicals with the hydrofluoroethers $CH_2FCF_2OCHF_2$, $CHF_2CF_2OCH_2CF_3$, $CF_3CHFCF_2OCH_2CF_3$, and $CF_3CHFCF_2OCH_2CF_2CHF_2$ at 268–308 K, *Int. J. Chem. Kinet.*, *35*, 239–245.

Chen, L., S. Kutsuna, K. Tokuhashi, A. Sekiya, R. Tamai and Y. Hibino (2005b), Kinetics and mechanism of $(CF_3)_2CHOCH_3$ reaction with OH radicals in an environmental reaction chamber, *J. Phys. Chem.*, *109*, 4766–4771.

Chen, L., K. Tokuhashi, S. Kutsuna, A. Sekiya, Y. Yonei, and A. Yamamoto (2003b), Kinetic study of the gas-phase reaction of $CF_3CHFCF_2CH_2OH$ with OH radicals at 230–430 K, *Chem. Phys. Lett.*, *382*, 277–282.

Chen, X.-B., and W.-H. Fang (2002), Norrish I vs. II reactions of butanal: a combined CASSCF DFT amd MP2 study, *Chem. Phys. Lett.*, *361*, 473–482.

Chen, Y., W. Wang, and L. Zhu (2000), Wavelength-dependent photolysis of methylglyoxal in the 290–440 nm region, *J. Phys. Chem. A*, *104*, 11126–11131.

Chen, Y., and S. Ye (2004), Photochemical reaction mechanism of cyclobutanone: CASSCF study, *J. Quantum Chem.*, *97*, 725–735.

Chen, Y., and L. Zhu (2001), The wavelength dependence of the photodissociation of propionaldehyde in the 290–330 nm region, *J. Phys. Chem. A*, *105*, 9689–9696.

Chen, Y., and L. Zhu (2003), Wavelength-dependent photolysis of glyoxal in the 290–420 nm region, *J. Phys. Chem. A*, *107*, 4643–4651.

Chen, Y., L. Zhu, and J.S. Francisco (2002), Wavelength-dependent photolysis of *n*-butyraldehyde and *i*-butyraldehyde in the 280–330 nm region, *J. Phys. Chem. A*, *106*, 7755–7763.

Chen, Z., and C. Wang (2006), Rate constants of the gas-phase reactions of CH_3OOH with O_3 and NO_x at 293 K, *Chem. Phys. Lett.*, *424*, 233–238.

Cheng, B.-M., M. Bahou, Y.-P. Lee, and L.C. Lee (2002), Experimental and theoretical studies on VUV absorption cross sections and photodissociation of CH_3OH, CH_3OD, CD_3OH, and CD_3OD, *J. Chem. Phys. 117*, 1633–1640.

Chevron (2009), Motor gasolines technical review (FTR-1), http://www.chevron.com/products/ourfuels/prodserv/fuels/technical_safety_bulletins/.

Chew, A.A., and R. Atkinson (1996), OH radical formation yields from the gas-phase reactions of O_3 with alkenes and monoterpenes, *J. Geophys. Res.*, *101*, 28649–28653.

Chew, A.A., R. Atkinson, and S.M. Aschmann (1998), Kinetics of the gas-phase reactions of NO_3 radicals with a series of alcohols, glycol ethers, ethers and chloroalkenes, *J. Chem. Soc., Faraday Trans.*, *94*, 1083–1089.

Chiappero, M.S., G.A. Argüello, M.D. Hurley, and T.J. Wallington (2008), Atmospheric chemistry of $C_8F_{17}CH_2CHO$: yield from $C_8F_{17}CH_2CH_2OH$ (8:2 FTOH) oxidation, kinetics and mechanisms of reactions with Cl atoms and OH radicals, *Chem. Phys. Lett.*, *461*, 198–202.

Chiappero, M.S., F.E. Malanca, G.A. Argüello, S.T. Wooldridge, M.D. Hurley, J.C. Ball, T.J. Wallington, R.L. Waterland, and R.C. Buck (2006), Atmospheric chemistry of perfluoraldehyde ($C_xF_{2x+1}CHO$) and fluorotelomer aldehydes ($C_xF_{2x+1}CH_2CHO$): Quantification of the important role of photolysis, *J. Phys. Chem. A*, *110*, 11944–11953.

Chiorboli, C., C.A. Bignozzi, A. Maldotti, P.F. Giardini, A. Rossi, and V. Carassiti (1983), Rate constants for the gas-phase reactions of OH radicals with β-dimethylstyrene and acetone. Mechanism of β-dimethylstyrene NO_x–air photooxidation, *Int. J. Chem. Kinet.*, *15*, 579–586.

Chisala, B.N., N.G. Tait, and D.N. Lerner (2007), Evaluating the risks of methyl tertiary butyl ether (MTBE) pollution of urban groundwater, *J. Contaminant Hydrology*, *91*, 128–145.

Chong, D.P., and G.B. Kistiakowski (1964), The photolysis of methylketene. II. *J. Phys. Chem.*, *68*, 1793–1797.

Chowdhury, P.K., H.P. Upadhyaya, P.D. Naik, and J.P. Mittal (2002a), ArF laser photodissociation dynamics of hydroxyacetone: LIF observation of OH and its reaction rate with the parent, *Chem. Phys. Lett.*, *351*, 201–207.

Chowdhury, P.K., H.P. Upadhyaya, P.D. Naik, and J.P. Mittal (2002b), Direct observation of OH photofragment from triplet hydroxyacetone, *Chem. Phys. Lett.*, *356*, 476–482.

Christensen, L.K., J.C. Ball, and T.J. Wallington (2000), Atmospheric oxidation mechanism of methyl acetate, *J. Phys. Chem. A*, *104*, 345–351.

Christensen, L.K., J. Sehested, O.J. Nielsen, M. Bilde, T.J. Wallington, A. Guschin, L.T. Molina, and M.J. Molina (1998a), Atmopsheric chemistry of HFE-7200 ($C_4F_9OC_2H_5$): Reaction with OH radicals and fate of $C_4F_9OCH_2CH_2O(\bullet)$ and $C_4F_9OCHO(\bullet)CH_3$ radicals, *J. Phys. Chem. A*, *102*, 4839–4845.

Christensen, L.K., J. Sehested, O.J. Nielsen, T.J. Wallington, A. Guschin, and M.D. Hurley, (1998b), Kinetics and mechanism of the reactions of 2,3-butadione with F and Cl atoms, UV absorption spectra of $CH_3C(O)C(O)CH_2\cdot$ and $CH_3C(O)C(O)CH_2O_2\cdot$ radicals, and atmospheric fate of $CH_3C(O)C(O)CH_2O\cdot$ radicals, *J. Phys. Chem. A*, *102*, 8913–8923.

Christensen, L.K., T.J. Wallington, A. Guschin, and M.D. Hurley (1999), Atmospheric degradation mechanism of CF_3OCH_3, *J. Phys. Chem. A*, *103*, 4202–4208.

Christian, T.J., R.J. Yokelson, J.A. Carvalho Jr., D.W.T. Griffith, E.C. Alvarado, J.C. Santos, T.G.S. Neto, C.A. Gurgel Veras, and W.M. Hao (2007), The tropical forest and fire

emissions experiment: Trace gases emitted by smoldering logs and dung from deforestation and pasture fires in Brazil, *J. Geophys. Res.*, *112*, doi:10.1029/2006JD008147.
Christie, M.I., and P.M. Hetherington (1976/1977), The photolysis of *t*-butyl, isopropyl and ethyl nitrites at 254 nm, *J. Photochem.*, *6*, 285–295.
Chuang, C., M.F. Foltz, and C.B. Moore (1987), T_1 barrier height, S_1–T_1 intersystem crossing rate, and S_0 radical dissociation threshold for H_2CO, D_2CO and HDCO, *J. Chem. Phys. 87*, 3855–3864.
Chuong, B., and P.S. Stevens (2003), Kinetics of the OH + methyl vinyl ketone and OH + methacrolein reactions at low pressure, *J. Phys. Chem. A*, *107*, 2185–2191.
Chuong, B., and P.S. Stevens (2004), Measurements of the kinetics of the OH-initiated oxidation of methyl vinyl ketone and methacrolein, *Int. J. Chem. Kinet.*, *36*, 12–25.
Cimiraglia, R., M. Persico, and J. Tomasi (1985), Ab initio study of the photodissociation of nitrosoalkanes and nitrosamines, *J. Am. Chem. Soc.*, *107*, 1617–1622.
Clark, J.H., C.B. Moore, and N.S. Nagar (1978), Photodissociation of formaldehyde—Absolute quantum yields, radical reactions and NO reactions *J. Chem. Phys.*, *68*, 1264–1271.
Clemitshaw, K.C., J. Williams, O. Rattigan, D.E. Shallcross, K.S. Law, and R.A. Cox (1997), Gas-phase ultraviolet absorption cross-sections and atmospheric lifetimes of several C_2–C_5 alkyl nitrates, *J. Photochem. Photobiol. A:Chem 102*, 117–126.
Clifford, G.M., L.P. Thuener, J.C. Wenger, and D.E. Shallcross (2005), Kinetics of the gas-phase reactions of OH and NO_3 radicals with aromatic aldehydes, *J. Photochem. Photobiol., A: Chemistry*, *176*, 172–182.
Clifford, G.M., and J.C. Wenger (2006), Rate coefficients for the gas-phase reaction of hydroxyl radicals with the dimethylbenzaldehydes, *Int. J. Chem. Kinetics*, *38*, 563–569.
Coe, C.S., and T.F. Doumani (1948), Photochemical decomposition of *t*-butyl nitrite, *J. Am. Chem. Soc.*, *70*, 1516–1519.
Coeur, C., V. Jacob, and P. Foster (1999), Aerosol formation from the gas-phase reaction of hydroxyl radical with the natural hydrocarbon bornyl acetate, *Atmos. Environ.*, *33*, 1615–1620.
Coeur, C., V. Jacob, P. Foster, and P. Baussand (1998), Rate constant for the gas-phase reaction of hydroxyl radical with the natural hydrocarbon bornyl acetate, *Int. J. Chem. Kinet.*, *30*, 497–502.
Coeur-Tourneur, C., F. Henry, M.-A. Janquin, and L. Brutier (2006), Gas-phase reaction of hydroxyl radicals with *m*-, *o*- and *p*-cresol, *Int. J. Chem. Kinet.*, *38*, 553–562.
Collins, E.M., H.W. Sidebottom, J.C. Wenger, S. Le Calvé, A. Mellouki, G. Le Bras, E. Villenave, and K. Wirtz (2005), The influence of reaction conditions on the photooxidation of diisopropyl ether, *J. Photochem. Photobiol. A: Chemistry*, *176*, 86–97.
Colville, C.J., and R.J. Griffin (2004), The roles of individual oxidants in secondary organic aerosol formation from Δ^3-carene: 1. Gas-phase chemical mechanism, *Atmos. Env.*, *38*, 4001–4012.
Cometto, P.M., P.R. Dalmasso, R.A. Taccone, S.I. Lane, F. Oussar, V. Daële, A. Mellouki, and G. Le Bras (2008), Rate constants for the reaction of OH radicals with a series of unsaturated alcohols between 263 and 371 K, *J. Phys. Chem. A*, *112*, 4444–4450.
Connell, P.S., and C.J. Howard (1985), Kinetics study of the reaction HO + HNO_3, *Int. J. Chem. Kinet.*, *17*, 17–31.
Connelly, B.T., and G.B. Porter (1958), Kinetics of excited molecules. I. Ketene, *Can. J. Chem.*, *36*, 1640–1648.
Coomber, J.W., and J.N. Pitts, Jr. (1969), Molecular structure and photochemical reactivity. XII. The vapor- phase chemistry of acrolein at 3130 Å, *J. Am. Chem. Soc.*, *91*, 547–550.
Corchnoy, S.B., and R. Atkinson (1990), Kinetics of the gas-phase reactions of OH and NO_3 radicals with 2-carene, 1,8-cineole, para-cymene and terpinolene, *Environ. Sci. Technol.*, *24*, 1497–1502.
Costela, A., M.T. Crespo, and J.M. Figuera (1986), Laser photolysis of acetone at 308 nm, *J. Photochem.*, *34*, 165–173.
Coulson, D.R., and N.C. Yang (1966), Deuterium isotope effects in the photochemistry of 2-hexanone, *J. Am. Chem. Soc.*, *88*, 4511–4513.
Cox, R.A. (1974), The photolysis of gaseous nitrous acid, *J. Photochem.*, *3*, 175–188.

Cox, R.A., and R.G. Derwent (1976), Ultraviolet-absorption spectrum of gaseous nitrous-acid, *J. Photochem.*, *6*, 23–34.

Cox, R.A., R.G. Derwent, and P.M. Holt (1976), Relative rate constants for the reactions of OH radicals with H_2, CH_4, CO, NO and HONO at atmospheric pressure and 296 K, J. *Chem. Soc., Faraday Trans. 1*, *72*, 2031–2043.

Cox, R.A., R.G. Derwent, S.V. Kearsey, L. Batt, and K.G. Patrick (1980a), Photolysis of methyl nitrite: Kinetics of the reaction of the methoxy radical with O_2, *J. Photochem.*, *13*, 149–163.

Cox, R.A., R.G. Derwent, and M.R. Williams (1980b), Atmospheric photooxidation reactions. Rates, reactivity, and mechanisms for reaction of organic compounds with hydroxyl radicals, *Environ. Sci. Technol.*, *14*, 57–61.

Cox, R. A., and A. Goldstone (1982), Atmospheric reactivity of oxygenated motor fuel additives, in, editors B. Versino and H. Ott, *Physico-chemical Behaviour of Atmospheric Pollutants*, D. Reidel Publishing Company, Dordrecht, 1982.

Cox, R.A., K.F. Patrick, and S.A. Chant (1981), Mechanism of atmospheric photooxidation of organic compounds. Reactions of alkoxy radicals in oxidation of *n*-butane and simple ketones, *Environ. Sci. Technol.*, *15*, 587–592.

Craveiro, A.A., A.G. Fernandes, C.H.S. Andrade, F.J.A. Matos, J.W. Alencar, and M.I.L. Machado (1981), *Oleos Essenciais de Plantas do Nordeste. Edições UFC*, Fortaleza, pp. 20–170.

Crawford, M.A., Z. Li, H.A. Heuerman, and D. Kinscherff (2004), A kinetic and product study of reaction of chlorine atom with CH_3CH_2OD, *Int. J. Chem. Kinet.*, *36*, 584–590.

Crawford, M.A., T.J. Wallington, J.J. Szente, and M.M. Maricq (1999), Kinetics and mechanism of the acetylperoxy + HO_2 reaction, *J. Phys. Chem. A*, *103*, 365–378.

Cronin, T.J., and L. Zhu (1998), Dye laser photolysis of *n*-pentanal from 280 to 330 nm, *J. Phys. Chem.*, *102*, 10274–10279.

Crunaire, S., J. Tarmoul, C. Fittschen, A. Tomas, B. Lemoine, and P. Coddeville (2006), Use of cw-CRDS for studying the atmospheric oxidation of acetic acid in a simulation chamber, *Appl. Phys. B*, *85*, 467–475.

Cuevas, C.A., A. Notario, E. Martinez, and J. Albaladejo (2004), A kinetic study of the reaction of Cl with a series of linear and ramified ketones as a function of temperature, *Phys. Chem. Chem. Phys. 6*, 2230–2236.

Cuevas, C.A., A. Notario, E. Martínez, and J. Albaladejo (2005), Influence of temperature in the kinetics of the gas-phase reactions of a series of acetates with Cl atoms, *Atmos. Environ.*, *39*, 5091–5099.

Cuevas, C.A., A. Notario, E. Martinez, and J. Albaladejo (2006), Temperature-dependence study of the gas-phase reactions of atmospheric Cl atoms with a series of aliphatic aldehydes, *Atmos. Environ.*, *40*, 3845–3854.

Cui, Q., and K. Morokuma (1997), Ab initio study of nonadiabatic interaction in the photodissociation of ketene, *J. Chem. Phys.*, *107*, 4951–4959.

Cundall, R.B., and A.S. Davies (1966), The mechanism of the gas phase photolysis of acetone, *Proc. Roy. Soc.*, *London*, *A290*, 563–582.

Cundall, R.B., and A.S. Davies (1967), Primary processes in the gas phase photochemistry of carbonyl compounds, *Prog. React. Kinet.*, *4*, 149–213.

Cvetanović, R.J. (1987), Evaluated chemical kinetic data for the reactions of atomic oxygen $O(^3P)$ with unsaturated hydrocarbons, *J. Phys. Chem. Ref. Data*, *16*, 261–326.

Dagaut, P., R. Liu, T.J. Wallington, and M.J. Kurylo (1989a), The gas phase reactivity of aliphatic polyethers towards OH radicals: Measurements and predictions, *Int. J. Chem. Kinet.*, *21*, 1173–1180.

Dagaut, P., R. Liu, T.J. Wallington, and M.J. Kurylo (1989b), Kinetic measurements of the gas-phase reactions of OH radicals with hydroxy ethers, hydroxy ketones, and keto ethers, *J. Phys. Chem.*, *93*, 7838–7840.

Dagaut, P., R. Liu, T.J. Wallington, and M.J. Kurylo (1990), Flash photolysis resonance fluorescence investigation of the gas-phase reactions of hydroxyl radicals with cyclic ethers, *J. Phys. Chem.*, *94*, 1881–1883.

Dagaut, P., T.J. Wallington, R. Liu, and M.J. Kurylo (1988a), A kinetics investigation of the gas-phase reactions of OH radicals with cyclic ketones and diones: mechanistic insights, *J. Phys. Chem.*, *92*, 4375–4377.

Dagaut, P., T.J. Wallington, R. Liu, and M.J. Kurylo (1988b), The gas phase reactions of hydroxyl radicals with a series of carboxylic acids over the temperature range 240–440 K, *Int. J. Chem. Kinet.*, *20*, 331–338.

Dalmasso, P.R., R.A. Taccone, J.D. Nieto, P.M. Cometto, and S.I. Lane (2008), Gas-phase reactions of Cl atoms with hydrochloroethers: Relative rate constants and their correlation with substituents' electronegativities, *J. Phys. Org. Chem.*, *21*, 393–396.

Dalmasso, P.R., R.A. Taccone, J.D. Nieto, M.A. Teruel, and S.I. Lane (2005), Rate constants for the reactions of chlorine atoms with hydrochloroethers at 298 K and atmospheric pressure, *Int. J. Chem. Kinet.*, *37*, 420–426.

Dalmasso, P.R., J.D. Nieto, R.A. Taccone, M.A. Teruel, and S.I. Lane (2006a), Rate contants for reaction of Cl atoms with hydrofluoroethers, *J. Phys. Org. Chem.*, *19*, 771–775.

Dalmasso, P.R., R.A. Taccone, J.D. Nieto, M.A. Teruel, and S.I. Lane (2006b), CH_3OCF_2CHFCl and CHF_2OCF_2CHFCl: Reaction with Cl atoms, atmospheric lifetimes, ozone depletion and global warming potentials, *Atmos. Environ.*, *40*, 7298–7307.

D'Anna, B., Ø. Andreasen, Z. Gefen, and C.J. Nielsen (2001a), Kinetic study of OH and NO_3 radical reactions with 14 aliphatic aldehydes, *Phys. Chem. Chem. Phys.*, *3*, 3057–3063.

D'Anna, B., V. Bakken, J.A. Beukes, C.J. Nielsen, K. Brudnik, and J.T. Jodkowski (2003), Experimental and theoretical studies of gas phase NO_3 and OH radical reactions with formaldehyde, acetaldehyde and their isotopomers, *Phys. Chem. Chem. Phys.*, *5*, 1790–1805.

D'Anna, B., S. Langer, E. Ljungström, C.J. Nielsen, and M. Ullerstam (2001b), Rate coefficients and Arrhenius parameters for the reaction of the NO_3 radical with acetaldehyde and acetaldehyde-1d, *Phys. Chem. Chem. Phys.*, *3*, 1631–1637.

D'Anna, B., and C.J. Nielsen (1997), Kinetic study of the vapour-phase reaction between aliphatic aldehydes and the nitrate radical, *J. Chem. Soc., Faraday Trans.*, *93*, 3479–3483.

D'Anna, B., S.R. Sellevåg, K. Wirtz, and C.J. Nielsen (2005a), Photolysis study of perfluoro-2-methyl-3-pentanone under natural sunlight conditions, *Environ. Sci. Technol.*, *39*, 8708–8711.

D'Anna, B., A. Wisthaler, Ø. Andreasen, A. Hansel, J. Hjorth, N.R. Jensen, C.J. Nielsen, Y. Stenström, and J. Viidanoja (2005b), Atmospheric chemistry of C_3–C_6 cycloalkanecarbaldehydes, *J. Phys. Chem A*, *109*, 5104–5118.

Darnall, K.R., R. Atkinson, and J.N. Pitts, Jr. (1979), Observation of biacetyl from the reaction of OH radicals with *o*-xylene. Evidence for ring cleavage, *J. Phys. Chem.*, *83*, 1943–1946.

Davis, M.E., W. Drake, D. Vimal, and P.S. Stevens (2005a), Experimental and theoretical studies of the kinetics of the reactions of OH and OD with acetone and acetone d_6 at low pressure, *J. Photochem. Photobiol. A*, *176*, 162–171.

Davis, M.E., M.K. Gilles, A.R. Ravishankara, and J.B. Burkholder (2007a), Rate coefficients for the reaction of OH with (E)-2-pentenal, (E)-2-hexenal, and (E)-2-heptenal, *Phys. Chem. Chem. Phys.*, *9*, 2240–2248.

Davis, M.E., R.K. Talukdar, G. Notte, G.B. Ellison, and J.B. Burkholder (2007b), Rate coefficients for the OH + pinonaldehyde ($C_{10}H_{16}O_2$) reaction between 297 and 374 K, *Environ. Sci. Tech.*, *41*, 3959–3965.

Davis, M.E., C. Tapscott and P.S. Stevens (2005b), Measurements of the kinetics of the OH-initiated oxidation of β-pinene: Radical propagation in the OH + β-pinene + O_2 + NO reaction system, *Int. J. Chem. Kinet.*, *37*, 522–531.

Davis, S., and S. Diegel (2007), *Transportation Energy Data Book: Edition 26*, Oak Ridge National Laboratory, Oak Ridge, TN, ORNL-6978.

Davis, W., Jr. (1948), The photochemical decomposition of diethyl ketone at 3130Å, *J. Am. Chem. Soc.*, *70*, 1868–1869.

Davis, W., Jr., and W.A. Noyes, Jr. (1947), Photochemical studies. XXXVIII. A further study of the photochemistry of methyl *n*-butyl ketone, *J. Am. Chem. Soc.*, *69*, 2153–2158.

Dawidowicz, E.A., and C.R. Patrick (1964), The photolysis of trifluoroacetone, *J. Chem. Soc.*, 4250–4254.

D'Azi, O.B., F. Lahmani, C. Lardeux, and D. Solgadi (1985), State-selective photochemistry; Energy-distribution in the NO fragment after photodissociation of the CH_3ONO n–π^* state, *Chem. Phys.*, *94*, 247–256.

DeBruyn, W.J., S.X. Duan, X.Q. Shi, P. Davidovits, D.R. Worsnop, M.S. Zahniser, and C.E. Kolb (1992), Tropospheric heterogeneous chemistry of haloacetyl and carbonyl halides, *Geophys. Res. Lett.*, *19*, 1939–1942.

DeMare, G.R., M.C. Fontaine, and P. Goldfinger (1968), Heterogeneous photosensitization, *J. Org. Chem.*, *32*, 2528–2529

DeMore, W.B., and K.D. Bayes (1999), Rate constants for the reactions of hydroxyl radical with several alkanes, cycloalkanes, and dimethyl ether, *J. Phys. Chem. A*, *103*, 2649–2654.

DeMore, W.B., S.P. Sander, D.M Golden, R.F. Hampson, M.J. Kurylo, C.J. Howard, A.R. Ravishankara, C.E. Kolb, and M.J. Molina (1997), Chemical kinetics and photochemical data for use in stratospheric modeling, Evaluation Number 12, JPL Publication 97–4.

Denschlag, H.O., and E.K.C. Lee (1968), Benzene photosensitization and direct photolysis of cyclobutanone and cyclobutanone-2-t in the gas phase, *J. Am. Chem. Soc.*, *90*, 3628–3638.

Derwent, R.G., M.E. Jenkin, N.R. Passant, and M.J. Pilling (2007a), Reactivity-based strategies for photochemical ozone control in Europe, *Env. Sci. Policy*, *10*, 445–453.

Derwent, R.G., M.E. Jenkin, N.R. Passant, and M.J. Pilling (2007b), Photochemical ozone creation potentials (POCPs) for different emission sources of organic compounds under European conditions estimated with a Master Chemical Mechanism, *Atmos. Env*, *41*, 2570–2579.

Derwent, R.G., M.E. Jenkin, S.M. Saunders, and M.J. Pilling (1998), Photochemical ozone creation potentials for organic compounds in northwest Europe calculated with a master chemical mechanism, *Atmos. Environ.*, *32*, 2429–2441.

Derwent R G., M.E. Jenkin, S.M. Saunders, and M.J. Pilling (2001) Characterization of the reactivities of volatile organic compounds using a master chemical mechanism, *J. Air & Waste Man. Assoc.*, *51*, 699–707.

Derwent, R.G., M.E. Jenkin, S.M. Saunders, M.J. Pilling and N.R. Passant (2005), Multi-day ozone formation for alkenes and carbonyls investigated with a master chemical mechanism under European conditions, *Atmos. Env*, *39*, 627–635.

Desai, J., J. Heicklen, A. Bahta, and R. Simonaitis (1986), The photo-oxidation of i-C_3H_7CHO vapour, *J. Photochem.*, *34*, 137–164.

Deshmukh, S., and W.P. Hess (1994), Photodissociation of acetyl chloride: Cl and CH_3 quantum yields and energy distributions, *J. Chem. Phys.*, *100*, 6429–6433.

De Smedt, F., X.V. Bui, T.L. Nguyen, J. Peeters, and L. Vereecken (2005), Theoretical and experimental study of the product branching in the reaction of acetic acid with OH radicals, *J. Phys. Chem. A*, *109*, 2401–2409.

Devolder, P., M. Carlier, J.F. Pauwels, and L.R. Sochet (1984), Rate constant for the reaction of OH with nitric acid: A new investigation by discharge flow resonance fluorescence, *Chem. Phys. Lett*, *111*, 94–99.

Dhanya, S., D.K. Maity, H.P. Upadhyaya, A. Kumar, P.D. Naik, and R.D. Sain (2003), Dynamics of OH formation in photodissociation of pyruvic acid at 193 nm, *J. Chem. Phys.*, *118*, 10093–10100.

Diau, E.W.-G., C. Kõtting, and A.H. Zewail (2001), Femtochemistry of Norrish Type-I reactions: III. The anomalous predissociation dynamics of cyclobutanone on the S_1 surface, *Chemphyschem*, 2, 294–309.

Dibble, T.S. (2007), Cyclization of 1,4-hydroxycarbonyls is not a homogenous gas phase process, *Chem. Phys. Lett.*, *447*, 5–9.

Dillon, T.J., D. Hölscher, V. Sivakumaran, A. Horowitz, and J.N. Crowley (2005), Kinetics of the reactions of HO with methanol (210–351 K) and with ethanol (216–368 K), *Phys. Chem. Chem. Phys.*, *7*, 349–355.

Dillon, T.J., A. Horowitz, D. Hoelscher, J.N. Crowley, L. Vereecken, and J. Peeters (2006), Reaction of HO with hydroxyacetone ($HOCH_2C(O)CH_3$): rate coefficients (233–363 K) and mechanism, *Phys. Chem. Chem. Phys.*, *8*, 236–246.

Ding, H., A.J. Orr-Ewing, and R.N. Dixon (1999), Rotational structure in the $\tilde{A}^1A''$–X^1A' spectrum of formyl chloride, *Phys. Chem. Chem. Phys.*, *1*, 4181–4185.

Dixon, R.N., and G.H. Kirby (1966), Absorption spectrum of ketene in the visible and near ultra-violet, *Trans. Faraday Soc.*, *62*, 1406–1410.

Dixon, R.N., and H. Rieley (1989), State-selected photodissociation dynamics of HONO ($\tilde{A}^1A''$): Characterization of the NO fragment, *J. Chem. Phys.*, *91*, 2308–2320.

Dlugokencky, E.J., and C.J. Howard (1989), Studies of NO_3 radical reactions with some atmospheric organic compounds at low pressures, *J. Phys. Chem.*, *93*, 1091–1096.

Dóbé, S., L.A. Khachatryan, and T. Bérces (1989), Kinetics of reactions of hydroxyl radicals with a series of aliphatic aldehydes, *Ber. Bunsenges. Phys. Chem.*,*93*, 847–852.

Dóbé, S., M. Otting, F. Temps, H.Gg. Wagner, and H. Ziemer (1993), Fast flow kinetic studies of the reaction $CH_2OH + HCl \leftrightarrow CH_3OH + Cl$. The heat of formation of hydroxymethyl, *Ber. Bunsenges. Phys. Chem.*, *97*, 877–884.

Dobeck, L.M., H.M. Lambert, W. Kong, P.J. Pisano, and P.L. Houston (1999), H_2 production in the 440-nm photodissociation of glyoxal, *J. Phys. Chem. A*, *103*, 10312–10323.

Docherty, K.S, W. Wu, Y.B. Lim, and P.J. Ziemann (2005), Contributions of organic peroxides to secondary aerosol formed from reactions of monoterpenes with O_3, *Environ. Sci. Technol.*, *39*, 4049–4059.

Dodd, R.E., and J.W. Smith (1957), The photolysis of trifluoracetaldehyde, *J. Chem. Soc.*, *282*, 1465–1473.

Donaghy, T., I. Shanahan, M. Hande, and S. Fitzpatrick (1993), Rate constants and atmospheric lifetimes for the reactions of OH radicals and Cl atoms with haloalkanes, *Int. J. Chem. Kinet.*, *25*, 273–284.

Donahue, N.M., A.L. Robinson, and S.N. Pandis (2009), Atmospheric organic particulate matter: from smoke to secondary organic aerosol, *Atmos. Environ.*, *43*, 94–106.

Donahue, N.M., A.L. Robinson, C.O. Stanier, and S.N. Pandis (2006), Coupled partitioning, dilution, and chemical aging of semivolatile organics, *Environ. Sci. Technol.*, *40*, 2635–2643.

Donaldson, D.J., G.J. Frost, K.H. Rosenlof, A.F. Tuck, and V. Vaida (1997), Atmospheric radical production by excitation of vibrational overtones via absorption of visible light, *Geophys. Res. Lett.*, *24*, 2651–2654.

Donaldson, D.J., J.J. Orlando, S. Amann, G.S. Tyndall, R.J. Proos, B.R. Henry, and V. Vaida (1998), Absolute intensities of nitric acid overtones, *J. Phys. Chem. A*, *102*, 5171–5174.

Dore, C.J., T.P. Murrells, N.R. Passant, M.M. Hobson, G. Thistlethwaite, A.Wagner, Y. Li, T. Bush, K.R. King, J. Norris, P.J. Coleman, C. Walker, R.A. Stewart, I. Tsagatakis, C. Conolly, N.C.J. Brophy, and M.R. Hann (2008), *UK Emissions of Air Pollutants 1970 to 2006*, Report on the UK National Atmospheric Emissions Inventory, AEA Report, October 2008, http://www.naei.org.uk/reports.php.

Dorfman, L.M., and Z.D. Sheldon (1949), The mechanism of the photochemical decomposition of diethyl ketone, *J. Chem. Phys.*, *17*, 511–516.

Doussin, J.F., B. Picquet-Varrault, R. Durand-Jolibois, H. Loirat, and P. Carlier (2003), A visible and FTIR spectrometric study of the nighttime chemistry of acetaldehyde and PAN under simulated atmospheric conditions, *J. Photochem. Photobiol. A.*, *157*, 283–293.

Drabbles, M., C.G. Morgan, D.S. McGuire, and A.M. Wodtke (1995), The first vibronically resolved measurement of correlated-product-state distributions in ultraviolet photodissociation: ketene at 308 nm, *J. Chem. Phys.*, *102*, 611–614.

Drent, E., R.P. van der Werf, and J. Kommandeur (1973), Small molecule behavior and the ^3B_g state of biacetyl, *J. Chem. Phys.*, *59*, 2061–2067.

Dubs, M., and J.R. Huber (1984), Energy distribution in the NO fragment after photodissociation of dimethylnitrosamine $(CH_3)_2NNO$, *Chem. Phys. Lett.*, *29*, 123–127.

Dufour, G., S. Szopa, M.P. Barkley, C.D. Boone, A. Perrin, P.I. Palmer, and P.F. Bernath (2009), Global upper-tropospheric formaldehyde: seasonal cycles observed by the ACE–FTS satellite instrument, *Atmos. Chem. Phys. Disc.*, *9*, 1051–1095

Dufour, G., S. Szopa, D.A. Hauglustaine, C.D. Boone, C.P. Rinsland, and Bernath, P. F. (2007), The influence of biogenic emissions on upper-tropospheric methanol as revealed from space, *Atmos. Chem. Phys.*, *7*, 6119–6129.

Duncan, F.J., and R.J. Cvetanović (1962), Production and reactions of methylene in the triplet state, *J. Am. Chem. Soc.*, *84*, 3593–3594.

Dunker, A.M., R.E. Morris, A.K. Pollack, C.H. Schleyer, and G. Yarwood (1996), Photochemical modeling of the impact of fuels and vehicles on urban ozone using auto oil program data, *Environ. Sci. Technol.*, *30*, 787–801.

Dunlop, J.R., and F.P. Tully (1993), Catalytic dehydration of alcohols by OH. 2- Propanol: An intermediate case, *J. Phys. Chem.*, *97*, 6457–6464.

Dunn, J.R., and K.O. Kutschke (1958), Photooxidation of ketones in an O^{18} enriched environment, *Can. J. Chem.*, *36*, 421–424.

Durant, D., and G.R. McMillan (1966), Energy distribution of photochemically generated *t*-pentoxy radicals, *J. Phys. Chem.*, *70*, 2709–2713.

Durham, R.W., G.R. Martin, and H.C. Sutton (1949), A radioactive tracer method for the analysis of mixtures of short-lived free radicals, *Nature*, *164*, 1052–1053.

East, R.L., and L. Phillips (1970), Kinetics of disproportionation-combination reactions between the *n*-propoxyl radical and nitric oxide, and of the pyrolysis of the O—O bond in di-*n*-propyl peroxide in the gas phase, *J. Chem. Soc. A*, *1970*, 331–334.

Eberhard, J., C. Müller, D.W. Stocker, and J.A. Kerr (1993), The photo-oxidation of diethyl ether in smog chamber experiments simulating tropospheric conditions: Product studies and proposed mechanism, *Int. J. Chem. Kinet.*, *25*, 639–649.

Ebrecht, J., W. Hack, and H.Gg. Wagner (1990), Elementary reactions of ketene with fluorine and chlorine atoms in the gas phase, *Berichte Bunsen-Gesellschaft*, *94*, 587–593.

Edelbüttel-Einhaus, J., K. Hoyermann, G. Rohde, and J. Seeba (1992), The detection of the hydroxyethyl radical by REMPI/mass-spectrometry and the application to the study of the reactions $CH_3CHOH + O$ and $CH_3CHOH + H$, 24th Symposium on Combustion, The Combustion Institute, pp.661–668.

Edem, D.O. (2002), Palm oil: Biochemical, physiological, nutritional, hematological, and toxicological aspects: A review, *Plant Foods for Human Nutrition*, *57*, 319–341.

Edney, E.O., T.E. Kleindienst, and E.W. Corse (1986), Room temperature rate constants for the reaction of OH with selected chlorinated and oxygenated hydrocarbons, *Int. J. Chem. Kinet.*, *18*, 1355–1371.

Effenhauser, C.S., P. Felder, and J.R. Huber (1990), Photodissociation of alkyl nitrites in a molecular beam. Primary and secondary reactions, *J. Phys. Chem.*, *94*, 296–302.

EFOA, European Fuel Oxygenates Association (2008), http://www.efoa.org/EFOA_Pages/02_What/02b_Propertie.asp#.

El Boudali, A., S. Le Calvé', G. Le Bras, and A. Mellouki (1996), Kinetic studies of OH reactions with a series of acetates, *J. Phys. Chem.*, *100*, 12364–12368.

El Dib, G., and A. Chakir (2007), Temperature dependence study of the gas-phase reactions of atmospheric NO_3 radicals with a series of amides, *Atmos. Env.*, 41, 5887–5896.

El Dib, G., A. Chakir, V. Daële, and A. Mellouki (2008), Gas-phase reaction of the Cl atoms with dimethylbenzaldehyde isomers, *Chem. Phys. Letters*, *455*, 151–155.

Ellis, D.A., J.W. Martin, A.O. De Silva, S.A. Mabury, M.D. Hurley, M.P.S. Andersen, and T.J. Wallington (2004), Degradation of fluorotelomer alcohols: A likely atmospheric source of perfluorinated carboxylic acids, *Environ. Sci. Technol.*, *38*, 3316–3321.

Ellis, D.A., J.W. Martin, S.A. Mabury, M.D. Hurley, M.P.S. Andersen, and T.J. Wallington (2003), Atmospheric lifetime of fluorotelomer alcohols, *Environ. Sci. Technol.*, *37*, 3816–3820.

Ells, V.R., and W.A. Noyes, Jr. (1938), Photochemical studies. XXVIII. The photochemical decomposition of ethyl methyl ketone by wavelengths from 1850–2000Å, *J. Am. Chem. Soc.*, *60*, 2031–2036.

Ember, L.R. (1980), Nitrosamines: assessing the relative risk, *Chem. Eng. News*, March 31, pp.20–26.

Emrich, M., and P. Warneck (2000), Photodissociation of acetone in air: Dependence on pressure and wavelength of the excited singlet state, *J. Phys. Chem. A*, *104*, 9436–9442.

Encina, M.V., A. Nogales, and E.A. Lissi (1975), Temperature dependence of 4-methyl-2-pentanone photochemistry, *J. Photochem.*, *4*, 75–89.

Energy Information Administration (2004), Alternatives to traditional transportation fuels: An Overview, Office of Coal, Nuclear, Electric and Alternate Fuels, U.S. Department of Energy, Washington, DC 20585; DOE/EIA-0585/O.

Energy Information Administration (2008), Annual Energy Review 2007, Washington, DC, DOE/EIA-0384.

Engert, J.M., and B. Dick (1999), Measurement and assignment of the vibrationally resolved UV absorption spectrum of *syn*-methyl nitrite isolated in an argon matrix at 12 K, *Chem. Phys. Lett.*, *299*, 423–429.

Ervens, B., G. Feingold, G.J. Frost, and S.M. Kreidenweis (2004), A modeling study of aqueous production of dicarboxylic acids: 1. Chemical pathways and speciated organic mass production, *J. Geophys. Res.*, *109*, doi:10.1029/2003JD004387.

Etzkorn, T., B. Klotz, S. Sørensen, S. Patroescu, I. Barnes, K.H. Becker, and U. Platt (1999), Gas-phase absorption cross sections of 24 monocyclic aromatic hydrocarbon in the UV and IR spectral ranges, *Atmos. Environ.*, *33*, 525–540.

Ezell, M.J., W. Wang, A.A. Ezell, G. Soskin, and B.J. Finlayson-Pitts (2002), Kinetics of reactions of chlorine atoms with a series of alkenes at 1 atm and 298 K: Structure and reactivity (2002), *Phys. Chem. Chem. Phys.*, *4*, 5813–5820.

Fahr, A., W. Braun, and A.H. Laufer (1993), Photolysis of methyl vinyl ketone at 193.3 nm: Quantum yield determinations of methyl and vinyl radicals, *J. Phys. Chem.*, *97*, 1502–1506.

Fajen, J.M., G.A. Carson, D.P. Rounbehler, T.Y. Fan, R. Vita, U.E. Goff, M.H. Wolf, G.S. Edwards, D.H. Fine, V. Reinhold, and K. Biemann (1979), *N*-Nitrosamines in the rubber and tire industry, *Science*, *205*, 1262–1264.

Fall, R. (2003), Abundant oxygenates in the atmosphere: A biochemical perspective, *Chem. Rev.*, *103*, 4941–4951.

Fang, W.-H., and R.-Z. Liu (2001), *Ab initio* studies of dissociation pathways on the ground- and excited-state potential energy surfaces for formyl chloride (HClCO), *J. Chem. Phys.*, *115*, 10431–10437.

Fantechi, G., N.R. Jensen, J. Hjorth, and J. Peeters (1998a), Determination of the rate constants for the gas-phase reactions of methyl butenol with OH radicals, ozone, NO_3 radicals, and Cl atoms, *Int. J. Chem. Kinet. 30*, 589–594.

Fantechi, G., N.R. Jensen, J. Hjorth, and J. Peeters (1998b), Mechanistic studies of the atmospheric oxidation of methyl butenol by OH radicals, ozone and NO_3 radicals, *J. Atmos. Chem.*, *32*, 3547–3556.

Fantechi, G., N.R. Jensen, J. Hjorth, O. Saastad, and J. Peeters (1998c), Reactions of Cl with selected VOCs: Kinetics, products and mechanisms, *Atmos. Environ.*, *31*, 247–267.

Fantechi, G., L. Vereecken, and J. Peeters (2002), The OH-initiated atmospheric oxidation of pinonaldehyde: Detailed theoretical study and mechanism construction, *Phys. Chem. Chem. Phys.*, *4*, 5795–5805.

Farmanara, P., V. Stert, and W. Radloff (1999), Ultrafast photodissociation of methyl nitrite excited to the S_2 state, *Chem. Phys. Lett.*, *303*, 521–528.

Fasano, D.M., and N.S. Nogar (1981), The infrared chemiluminescent reaction of chlorine atoms with formaldehyde, *Int. J. Chem. Kinetics*, *13*, 325–332.

Faubel, C., K. Hoyermann, and H.Gg. Wagner (1982), Rates of reactions of partially oxidized hydrocarbons with oxygen atoms in the gas phase. Part I. *Z. Phys. Chem. (Neue.Folge)*, *130*, 1–11.

Fazekas, G.B., and G.A. Takacs (1983), Photochemical stability of atmospheric $CFCl_2NO_2$, CF_2ClNO_2, and CF_3NO_2, *J. Photochem.*, *21*, 9–18.

Fehsenfeld, F., J. Calvert, R. Fall, P. Goldan, A. Guenther, C. Hewitt, B. Lamb, S. Liu, M. Trainer, H. Westberg, and P. Zimmerman (1992), Emissions of volatile organic compounds from vegetation and implications for atmospheric chemistry, *Global Biogeochem. Cycles*, *6*, 389–430.

Feierabend, K.J., L. Zhu, R.K. Talukdar and J.B. Burkholder (2008), Rate coefficients for the OH + HC(O)C(O)H (glyoxal) reaction between 210 and 390 K, *J. Phys. Chem*, *A*, *112*, 73–82.

Feilberg, K.L., B. D'Anna, M.S. Johnson, and C.J. Nielsen (2005a), Relative tropospheric photolysis rates of HCHO, $H^{13}CHO$, $HCH^{18}O$, and DCDO measured at the European photoreactor facility, *J. Phys. Chem. A*, *109*, 8314–8319.

Feilberg, K.L., M.S. Johnson, and C.J. Nielsen (2004), Relative reaction rates of HCHO, HCDO, DCDO, $H^{13}CHO$, and $HCH^{18}O$ with OH, Cl, Br, and NO_3 radicals, *J. Phys. Chem. A.*, *108*, 7393–7398.

Ferenac, M.A., A.J. Davis, A.S. Holloway, and T.S. Dibble (2003), Isomerization and decomposition reactions of primary alkoxy radicals derived from oxygenated solvents, *J. Phys. Chem. A*, *107*, 63–72.

Ferrari, C., A. Roche, V. Jacob, P. Foster, and P. Baussand (1996), Kinetics of the reaction of OH radicals with a series of esters under simulated conditions at 295 K, *Int. J. Chem. Kinet.*, *28*, 609–614.

Ferronato, C., J.J. Orlando, and G.S. Tyndall (1998), Rate and mechanism of the reactions of OH and Cl with 2-methyl-3-buten-2-ol, *J. Geophys. Res.*, *103*, 25579–25586.

Fielberg, A., R.M. Kamens, M.R. Strommen, and T. Nielsen (1999), Modeling the formation, decay and partitioning of 1- and 2-nitronaphthalene in the atmosphere, *Atmos. Environ.*, *33*, 1231–1243.

Filby, W.G., and H. Guesten (1978), Rate constants for the reaction of oxygen atoms with some potential photosmog inhibitors, *Atmos. Environ.*, *12*, 1563–1565.

Fine, D.H., D.P. Rounbehler, N.M. Belcher, and S.S. Epstein (1976), *N*-Nitroso compounds: Detection in ambient air, *Science*, *192*, 1328–1330.

Fine, D.H., D.P. Rounbehler, A. Rounbehler, A. Silvergleid, E. Sawicki, K. Krost, and G.A. DeMarrals (1977), Determination of dimethylnitrosamine in air, water, and soil by thermal energy analysis: Measurements in Baltimore, Md., *Environ. Sci. Technol*, *11*, 581–584.

Finke, H., H. Spiecker, and P. Andresen (1999), The photodissociation of *tert*-butyl nitrite at 193 nm, *J. Chem. Phys.*, *110*, 4777–4782.

Finklestein, A., and W.A. Noyes, Jr. (1953), The reactions of radicals from diethyl ketone with oxygen and general discussion, *Faraday Soc. Discussion*, *No. 14*, 76–84.

Finlayson-Pitts, B.J., C.I. Keoshian, B. Buehler, and A.A. Ezell (1999), Kinetics of reaction of chlorine atoms with some biogenic organics, *Int. J. Chem. Kinet.*, *31*, 491–499.

Finlayson-Pitts, B.J., and J.N. Pitts, Jr. (2000), *Chemistry of the Upper and Lower Atmosphere*, Academic Press, New York.

Fiore, A.M., L.W. Horowitz, D.W. Purves, H. Levy, II, M.J. Evans, Y. Wang, Q. Li, and R.M. Yantosca (2005), Evaluating the contribution of changes in isoprene emissions to surface ozone trends over the Eastern United States, *J. Geophys. Res.*, *110*, D12303/1–D12303/13.

Fisseha, R., J. Dommen, M. Sax, D. Paulsen, M. Kalberer, R. Maurer, F. Hofler, E. Weingartner, and U. Baltensperger (2004) Identification of organic aerosol and the acids in secondary corresponding gas phase from chamber experiments, *Anal. Chem.*, *76*, 6535–6540.

Fleisch, Th., A. Basu, M.J. Gradassi, and J.G. Masin (1997), Dimethyl ether: A fuel for the 21st century, *Natural Gas Conversion. IV. Studies in Surface Science and Catalysis*, *107*, 117–125.

Flocke, F., A. Volz-Thomas, and D. Kley (1991), Measurements of alkyl nitrates in rural and polluted air masses, *Atmos. Environ.*, *25A*, 1951–1960.

Flowers, B.A., M.E. Angerhofer, W.R. Simpson, T. Nakayama, and Y. Matsumi (2005), Nitrate radical quantum yield from peroxyacetyl nitrate photolysis, *J. Phys. Chem. A*, *109*, 2552–2558.

Fockenberg, C. (2005), Product study of the photolysis of ketene and ethyl ethynyl ether at 193.3 nm, *J. Phys. Chem. A*, *109*, 7140–7150.

Forester, C.D., J.E. Ham, and J.R. Wells (2006), Gas-phase chemistry of dihydromyrcenol with ozone and OH radical: rate constants and products, *Int. J. Chem. Kinet.*, *38*, 451–463.

Forester, C.D., J.E. Ham, and J.R. Wells (2007), Geraniol (2,6-dimethyl-2,6-octandien-8-ol) reactions with ozone and OH radical: rate constants and gas phase products, *Atm. Environ.*, *41*, 1188–1199.

Förgeteg, S., T. Bérces, and S. Dóbé (1979), The kinetics and mechanism of *n*-butyraldehyde photolysis in the vapor phase at 313 nm, *Int. J. Chem. Kinet.*, *11*, 219–237.

Förgeteg, S, S. Dóbé, and T. Bérces (1978), Effect of pressure on the primary photochemical processes of *n*-butyraldehyde, *React. Kinet. Catal. Lett.*, *9*, 331–336.

Forstner, H.J.L., R.C. Flagan, and J.H. Seinfeld (1997a), Secondary organic aerosol from the photooxidation of aromatic hydrocarbons: molecular composition, *Environ. Sci. Technol.*, *31*, 1345–1358.

Forstner, H.J.L., R.C. Flagan, and J.H. Seinfeld (1997b), Molecular speciation of secondary organic aerosol from photooxidation of the higher alkenes: 1-octene and 1-decene, *Atmos. Environ.*, *31*, 1953–1964.

Francisco, J.S. (1994), Ab initio investigation of the decomposition of trifluoromethanol into carbonyl fluoride and hydrogen fluoride, *Chem. Phys. Lett.*, *218*, 401–405.

Francisco, J.S., and Z. Li (1989), Dissociation pathways of carbonyl halides, *J. Phys. Chem.*, *93*, 8118–8122.

Francisco, J.S., and Y. Zhao (1992), *Ab initio* studies of dissociation pathways on the ground state potential erergy surface for HFCO and HClCO, *J. Chem. Phys.*, *96*, 7587–7596.

Frank, I., M. Parrinello, and A. Klamt (1998), Insight into chemical reactions from first-principles simulations: the mechanism of the gas-phase reaction of OH radicals with ketones, *J. Phys. Chem. A*, *102*, 3614–3617.

Freitas Dinis, C.M., H. Geiger, and P. Wiesen (2001), Kinetics of the reactions of OH($X^2\Pi$) radicals with 1,3-dioxolane and selected dialkoxy methanes, *Phys. Chem. Chem. Phys.*, *3*, 2831–2835.

Frerichs, H., R. Koch, V. Schliephake, M. Tappe, and H.Gg. Wagner (1990), Investigation of the reactions of phenol, anisole and cumene with O(^{3}P) in the gas phase, *Ber. Bunsenges. Phys. Chem.*, *166*, 145–155.

Frey, H.M. (1960), Chemical evidence for the ground state of methylene, *J. Am. Chem. Soc.*, *82*, 5947–5948.

Fried, A., S. Sewell, B. Henry, B.P. Wert, T. Gilpin, and J.R. Drummond (1997), Tunable diode laser absorption spectrometer for ground-based measurements of formaldehyde, *J. Geophys. Res.*, 102, 6253–6266.

Fried, A., J.G. Walega, J.R. Olson, J.H. Crawford, G. Chen, P. Weibring, D. Richter, C. Roller, F.K. Tittel, B.G. Heikes, J.A. Snow, H. Shen, D.W. O'Sullivan, M. Porter, H. Fuelberg, J. Halland, and D.B. Miller (2008), Formaldehyde over North America and the North Atlantic during the summer 2004 INTEX campaign: Methods, observed distributions, and measurement-model comparisons, *J. Geophys. Res.*, *113*, D10302, doi:101029/2007JD009185.

Fried, A., Y. Wang, C. Cantrell, B. Wert, J. Walega, B. Ridley, E. Atlas, R. Shetter, B. Lefer, M.T. Coffey, J. Hannigan, D. Blake, N. Blake, S. Meinardi, B. Talbot, J. Dibb, E. Scheuer, O. Wingenter, J. Snow, B. Heikes, and D. Ehhalt (2003), Tunable diode laser measurements of formaldehyde during the TOPSE 2000 study: Distributions, trends, and model comparisons, *J. Geophys. Res.*, *108*, 8365, doi:10.1029/2002JD002208.

Fritz, B., K. Lorenz, W. Steinert, and R. Zellner (1982), Laboratory kinetic investigations of the tropospheric oxidation of selected industrial emissions, in, editors B. Versino and H. Ott, *Physico-chemical Behaviour of Atmospheric Pollutants*, D. Reidel Publishing Company, Dordrecht, 1982.

Frøsig, L., O.J. Nielsen, M. Bilde, T.J. Wallington, J.J. Orlando, and G.S. Tyndall (2000), Kinetics and mechanism of the reaction of Cl Atoms with nitrobenzene, *J. Phys. Chem. A*, *104*, 11328–11331.

Frost, G.J., M. Trainer, G. Allwine, M.P. Buhr, J.G. Calvert, C.A. Cantrell, F.C. Fehsenfeld, P.D. Goldan, J. Herwehe, G. Hubler, W.C. Kuster, R. Martin, R.T. McMillen, S.A. Montzka, R.B. Norton, D.D. Parrish, B.A. Ridley, R.E. Shetter, J.G. Walega, B.A. Watkins, H.H. Westberg, and E.J. Williams (1998), Photochemical ozone production in the rural southeastern United States during the 1990 Rural Oxidants in the Southern Environment (ROSE) program, *J. Geophys. Res.*, *103*, 22491–22508.

Fu, T-M., D.J. Jacob, P.I. Palmer, K. Chance, Y.X. Wang, B. Barletta, D.R. Blake, J.C. Stanton, and M.J. Pilling (2007), Space-based formaldehyde measurements as constraints on volatile organic compound emissions in East and South Asia and implications for ozone, *J. Geophys. Res.*, *116*, D06312/1–D06312/15.

Fu, T.-M., D.J. Jacob, F. Wittrock, J.P. Burrows, M. Vrekoussis, and D.K. Henze (2008), Global budgets of atmospheric glyoxal and methylglyoxal, and implications for formation of secondary organic aerosols, *J. Geophys. Res.*, *113*, D15303/1–D15303/17.

Fujimoto, G.T., M.E. Ulmstead, and M.C. Lin (1982), Dynamics of CO formation in the photodissociation of HNCO and CH_2CO at 192 nm, *Chem. Phys.*, *65*, 197–203.

Fujimoto, G.T., M.E. Ulmstead, and M.C. Lin (1985), CO product energy distribution in the photodissociation of methylketene and acrolein at 193 nm, *J. Chem. Phys.*, *82*, 3042–3044.

Gaffney, J.S., R. Atkinson, and J.N. Pitts Jr. (1975), Temperature dependence of the relative rate constants for the reaction of oxygen (^{3}P) atoms with selected olefins, monoterpenes, and unsaturated aldehydes, *J. Amer. Chem. Soc.*, *97*, 6481–6483.

Gaffney, J.S., R. Fajer, G.I. Senum, and J.H. Lee (1986), Measurement of the reactivity of OH with methyl nitrate: Implications for prediction of alkyl nitrate–OH reaction rates, *Int. J. Chem. Kinet.*, *18*, 399–407.

Gaffney, J.S., N.A. Marley, R.S. Martin, R.W. Dixon, L.G. Reyes, and C.J. Popp (1997), Potential air quality effects of using ethanol-gasoline fuel blends: A field study in Albuquerque, New Mexico, *Environ. Sci. Technol.*, *31*, 3053–3061.

Galano, A., J.R. Alvarez-Idaboy, M.E. Ruiz-Santoyo, and A. Vivier-Bunge (2002), Rate coefficient and mechanism of the gas phase OH hydrogen abstraction reaction from formic acid: A quantum mechanical approach, *J. Phys. Chem. A*, *106*, 9520–9528.

Galloway, D.B., J.A. Bartz, L.G. Huey, and F.F. Crim (1993), Pathways and kinetic energy disposal in the photodissociation of nitrobenzene, *J. Chem. Phys.*, *98*, 2107–2114.

Galloway, D.B., T. Glenewinkel-Meyer, J.A. Bartz, L.G. Huey, and F.F. Crim (1994), The kinetic and internal energy of NO from the photodissociation of nitrobenzene, *J. Chem. Phys.*, *100*, 1946–1952.

Gandini, A., and P.A. Hackett (1976/1977), The phosphorescence of 1,1,1-trifluoroacetone, *J. Photochem.*, *6*, 75–76.

Gandini, A., and P.A. Hackett (1977a), Electronic relaxation processes in acetone and 1,1,1-trifluoroacetone vapor and the gas phase recombination of the acetyl radical at 22°C, *J. Am. Chem. Soc.*, *99*, 6195–6205.

Gandini, A., and P.A. Hackett (1977b), Vibrational relaxation of excited acetaldehyde vapor. A search for unquenchable species, *Chem. Phys. Lett.*, *52*, 107–110.

Gandini, A., and K.O. Kutschke (1968), The primary process in the photolysis of hexafluoroacetone vapour. II. The fluorescence and phosphorescence, *Proc. Roy. Soc.*, *A306*, 511–528.

Gandini, A., D.A. Whytock, and K.O. Kutschke (1968a), The primary process in the photolysis of hexafluoroacetone vapour. III. The efficiency of intersystem crossing, *Proc. Roy. Soc.*, *A306*, 529–536.

Gandini, A., D.A. Whytock, and K.O. Kutschke (1968b), The primary process in the photolysis of hexafluoroacetone vapour. IV. Identification of singlet quenching addends, *Proc. Roy. Soc.*, *A306*, 537–540.

Gandini, A., D.A. Whytock, and K.O. Kutschke (1968c), The primary process in the photolysis of hexafluoroacetone vapour. V. Mechanistic considerations, *Proc. Roy. Soc.*, *A306*, 541–551.

Gao, S., L.N. Ng, M. Keywood, V. Varutbangkul, R. Bahreini, A. Nenes, J. He, K.Y. Yoo, J.L. Beauchamp, R.P. Hodyss, R.C. Flagan, and J.H. Seinfeld (2004), Particle phase acidity and oligomer formation in secondary organic aerosol, *Environ. Sci. Technol.*, *38*, 6582–6589.

Gardner, E.P., P.D. Sperry, and J.G. Calvert (1987), Photodecomposition of acrolein in O_2, N_2 mixtures, *J. Phys. Chem.*, *91*, 1922–1930.

Gardner, E.P., R.D. Wijayuaratne, and J.G. Calvert (1984), Primary quantum yields of photodecomposition of acetone in air under tropospheric conditions, *J. Phys. Chem. 88*, 5069–5076.

Garland, N.L., L.J. Medhurst, and H.H. Nelson (1993), Potential chlorofluorocarbon replacements: OH reaction rate constants between 250 and 315 K and infrared absorption spectra, *J. Geophys. Res.*, *98*, 23,107–23,111.

Garzón, A., C.A. Cuevas, A.A. Ceacero, A. Notario, J. Albaladejo, and M. Fernández-Gómez (2006), Atmospheric reactions Cl+CH_3—$(CH_2)_n$—OH ($n = 0$–4): A kinetic and theoretical study, *J. Chem. Phys.*, *125*, 104305-1–104305-10.

Geiger, G., H. Stafast, U. Brühlmann, and J.R. Huber (1981), Photo-dissociation of dimethylnitrosamine, *Chem. Phys. Lett.*, *79*, 521–524.

Geiger, H., and K.H. Becker (1999), Degradation mechanisms of dimethoxymethane and dimethoxyethane in the presence of NO_x, *Atmos. Environ.*, *33*, 2883–2891.

Geiger, H., T. Maurer, and K.H. Becker (1999), OH-initiated degradation of 1,4-dioxane in the presence of NO_x, *Chem. Phys. Lett.*, *314*, 465–471.

Gerlach-Meyer, U., E. Linnebach, K. Kleinermanns, and J. Wolfrum (1987), H-atom photofragments from H_2O_2 dissociated at 193 nm, *Chem. Phys. Lett.*, *133*, 113–115.

Gery, M.W., D.L. Fox, H.E. Jeffries, L. Stockburger, and W.S. Weathers (1985), A continuous stirred tank reactor investigation of the gas-phase reaction of hydroxyl radicals and toluene, *Int. J. Chem. Kinet.*, *17*, 931–955.

Gery, M.W., D.L. Fox, R.M. Kamens, and L. Stockburger (1987), Investigation of hydroxyl radical reactions with *o*-xylene and *m*-xylene in a continuous stirred tank reactor, *Environ. Sci. Technol.*, *21*, 339–348.

Gery, M.W., G.Z. Whitten, J.P. Killus, and M.C. Dodge (1989), A photochemical kinetics mechanism for urban and regional scale computer modeling, *J. Geophys. Res. 94*, 12925–12956.

Gezelter, J.D., and W.H. Miller (1996), Dynamics of the photodissociation of triplet ketene, *J. Chem. Phys.*, *104*, 3546–3554.

Gierczak, T., J.B. Burkholder, S. Bauerle, and A.R. Ravishankara (1998), Photochemistry of acetone under tropospheric conditions, *Chem. Phys.*, *231*, 229–244.

Gierczak, T., J.B. Burkholder, R.K. Talukdar, A. Mellouki, S.B. Barone, and A.R. Ravishankara (1997), Atmospheric fate of methyl vinyl ketone and methacrolein, *J. Photochem. Photobiol. A*, *110*, 1–10.

Gierczak, T., M.K. Gilles, S. Bauerle, and A.R. Ravishankara (2003), Reaction of hydroxyl radical with acetone. 1. Kinetics of the reactions of OH, OD, and ^{18}OH with acetone and acetone-d_6, *J. Phys. Chem. A*, *107*, 5014–5020.

Giessing, A.M.B., A. Feilberg, T.E. Møgelberg, J. Sehested, M. Bilde, T.J. Wallington, and O.J. Nielsen (1996), Atmospheric chemistry of HFC-227ca: Spectrokinetic investigation of the $CF_3CF_2CF_2O_2$ radical, its reactions with NO and NO_2 and the atmospheric fate of the $CF_3CF_2CF_2O$ radical, *J. Phys. Chem.*, *100*, 6572–6579.

Gill, R.J., and G.H. Atkinson (1979), Wavelength dependence of HCO formation in the photolysis of acetaldehyde, *Chem. Phys. Lett.*, *64*, 426–430.

Gilpin, T., E. Apel, A. Fried, B. Wert, J. Calvert, Z. Genfa, P. Dasgupta, J.W. Harder, B. Heikes, B. Hopkins, H. Westberg, T. Kleindienst, Y.-N. Lee, X. Zhou, W. Lonneman, and S. Sewell (1997), Intercomparison of six ambient [CH_2O] measurement techniques. *J. Geophys. Res.*, *102*, 21161–21188.

Gipson, G.L. and J.O. Young (1999), Chapter 8, Gas phase chemistry. Science algorithms of the EPA Models-3 Community Multiscale Air Quality Modelling System. http://www.epa.gov/asmdnerl/CMAQ/ch08.pdf. CMAS, North Carolina, USA.

Glasius, M., A. Calogirou, N.R. Jensen, J. Hjorth, and C.J. Nielsen (1997), Kinetic study of gas-phase reactions of pinonaldehyde and structurally related compounds, *Int. J. Chem. Kinet.*, *29*, 527–533.

Glass, G.P., S.S. Kumaran, and J.V. Michael (2000), Photolysis of ketene at 193 nm and the rate constant for H + HCCO at 297 K, *J. Phys. Chem. A*, *104*, 8360–8367.

Glasson, W.A. (1979), An experimental evaluation of atmospheric nitrosamine formation, *Environ. Sci. Technol.*, *13*, 114–1146.

Glicker, S., and L.J. Stief (1971), Photolysis of formaldehyde at 1470 and 1236 Å, *J. Chem. Phys.*, *54*, 2852–2857.

Glowacki, D.R., A. Goddard, K. Hemavibool, T.L. Malkin, R. Commane, F. Anderson, W.J. Bloss, D.E. Heard, T. Ingham, M.J. Pilling, and P.W. Seakins (2007), Design of and initial results from a highly instrumented reactor for atmospheric chemistry (HIRAC), *Atmos. Chem. Phys.*, *7*, 5371–5390.

Goldan, P.D., W.C. Kuster, F.C. Fehsenfeld, and S.A. Montzka (1993), The observation of a C_5 alcohol emission in a North American pine forest, *Geophys. Res. Lett. 20*, 1039–1042.

Goldan, P.D., W.C. Kuster, F.C. Fehsenfeld, and S.A. Montzka (1995), Hydrocarbon measurements in the southeastern United States: The Rural Oxidants in the Southern Environment (ROSE) program 1990, *J. Geophys. Res.*, *100*, 25945–25963.

Golemba, F.J., and J.E. Guillet (1972), Photochemistry of ketone polymers. V. Photochemistry of the linear 2-alkanones in solution, *Macromolecules*, *5*, 63–68.

Good, D.A., and J. S. Francisco (2000), Tropospheric oxidation mechanism of dimethyl ether and methyl formate, *J. Phys. Chem. A*, *104*, 1171–1185.

Good, D.A., and J.S. Francisco (2003), Atmospheric chemistry of alternative fuels and alternative chlorofluorocarbons, *Chem. Rev.*, *103*, 4999–5023.

Good, D.A., J. Hansen, M. Kamoboures, R. Santiono, and J. S. Francisco (2000), An experimental and computational study of the kinetics and mechanism of the reaction of methyl formate with Cl atoms, *J. Phys. Chem. A*, *104*, 1505–1511.

Good, D.A., M. Kamoboures, R. Santiano, and J.S. Francisco (1999), Atmospheric oxidation of fluorinated ethers, E143a (CH_3OCF_3), E134 (CHF_2OCHF_2), and E125 (CHF_2OCF_3), *J. Phys. Chem. A*, *103*, 9230–9240.

Gordon, R.J. (1978), Survey for airbourne nitrosamines, prepared by University of California, School of Medicine, for the California Air Resources Board, Contract No. A6-096-30.

Goto, M., Y. Inoue, M. Kawasaki, A.G. Guschin, L.T. Molina, M.J. Molina, T.J. Wallington, and M.D. Hurley (2002a), Atmospheric chemistry of HFE-7500 [*n*-$C_3F_7CF(OC_2H_5)CF(CF_3)_2$]: Reaction with OH radicals and Cl atoms and atmospheric fate of *n*-$C_3F_7CF(OCHO\bullet)CF(CF_3)_2$ and *n*-$C_3F_7CF(OCH_2CH_2O\bullet)CF(CF_3)_2$ radicals, *Environ. Sci. Technol.*, *36*, 2395–2402.

Goto, M., M. Kawasaki, T.J. Wallington, M.D. Hurley, and A.P. Sharratt (2002b), Atmospheric chemistry of CH_2FOCH_2F: Reaction with Cl atoms and atmospheric fate of $CH_2FOCHFO\bullet$ radicals, *Int. J. Chem. Kinet.*, *34*, 139–147.

Grabner, G., G. Köhle, G. Marconi, S. Monti, and E. Venuti (1990), Photophysical properties of methylated phenols in nonpolar solvents, *J. Phys. Chem.*, *94*, 3609–3613.

Graedel, T.E. (1978), *Chemical Compounds in the Atmosphere*, Academic Press, New York.

Granby, K., C.S. Christensen, and C. Lohse (1997a), Urban and semi-rural observations of carboxylic acids and carbonyls, *Atmos. Environ.*, *31*, 1403–1415.

Granby, K., A.H. Egeløv, T. Nielsen, and C. Lohse (1997b), Carboxylic acids: Seasonal variation and relation to chemical and meteorological parameters, *J. Atmos. Chem.*, *28*, 195–207.

Gray, J.A., and D.W.G. Style (1952), The photolysis of methyl nitrite, *Trans. Faraday Soc.*, *48*, 1137–1142.

Gray, P., A.D. Yoffe, and L. Roselaar (1955), Thermal decomposition of the nitroalkanes, *Trans. Faraday Soc.*, *51*, 1489–1497.

Green, M., G. Yarwood, and H. Niki (1990), FTIR study of the chlorine-atom-initiated oxidation of methylglyoxal, *Int. J. Chem. Kinet*, *22*, 689–699.

Green, W.H., Jr., A.J. Mahoney, C.K. Zheng, and C.B. Moore (1991), Bond-breaking without barriers, II. Vibrationally excited products, *J. Chem. Phys.*, *94*, 1961–1969.

Green, W.H., C.B. Moore, and W.F. Polik (1992), Transition-state and rate constants for unimolecular reactions, *Ann. Rev. Phys. Chem.*, *43*, 591–626.

Greenberg, J.P., D. Helmig, and P.R. Zimmerman (1996), Seasonal measurements of nonmethane hydrocarbons and carbon monoxide at the Mauna Loa Observatory during the Mauna Loa Observatory Photochemistry Experiment 2, *J. Geophys. Res.*, *101*, 14581–14598.

Greenblatt, G.D., H. Zuckermann, and Y. Haas (1987), OH production in the collision-free UV photolysis of aliphatic nitro compounds, *Chem Phys. Lett.*, *134*, 593–599.

Greene, C.R., and R. Atkinson (1994), Rate constants for the gas-phase reactions of O_3 with a series of cycloalkenes and α, β-unsaturated ketones at 296 $\pm$2 K, *Int. J. Chem. Kinet.*, *26*, 37–44.

Greenhill, P.G., and B.V. O'Grady (1986), The rate constant of the reaction of hydroxyl radicals with methanol, ethanol and (D_3) methanol, *Aust. J. Chem.*, *39*, 1775–1787.

Greenwald, E.E., S.W. North, Y. Georgievskii, and S.J. Klippenstein (2005), A two transition state model for radical-molecule reactions: A case study of the addition of OH to C_2H_4, *J. Phys. Chem. A*, *109*, 6031–6044.

Griffin, R.J., D.R. Cocker III, R.C. Flagan, and J.H. Seinfeld (1999), Organic aerosol formation from the oxidation of biogenic hydrocarbons, *J. Geophys. Res.*, *104*, 3555–3567

Grosjean, D. (1983), Atmospheric reactions of pyruvic acid, *Atmos. Environ.*, *17*, 2379–2382.

Grosjean, D. (1984), Atmospheric reactions of *o*-cresol: Gas phase and aerosol products, *Atmos. Environ.*, *18*, 1641–1652.

Grosjean, D. (1985), Reactions of *o*-cresol and nitrocresol with NO_x in sunlight and with ozone-nitrogen dioxide mixtures in the dark, *Environ. Sci. Technol.*, *19*, 968–974.

Grosjean, D., and E. Grosjean (1995), Carbonyl products of the ozone-unsaturated alcohol reaction, *J. Geophys. Res.*, 100, 22815–22820.

Grosjean, D., E. Grosjean, and E.L. Williams II (1993a), Rate constants for the gas-phase reactions of ozone with unsaturated alcohols, esters, and carbonyls, *Int. J. Chem. Kinet.*, *25*, 783–794.

Grosjean, D., E. Grosjean, and E.L. Williams II (1993b) Atmospheric chemistry of unsaturated alcohols, *Environ. Sci. Technol.*, 27, 2478–2485.

Grosjean, D., E. Grosjean, and E.L. Williams II (1993c), The reaction of ozone with MPAN, $CH_2{=}C(CH_3)C(O)OONO_2$, *Environ. Sci. Technol.*, *27*, 2548–2552.

Grosjean, D., E. Grosjean, and E.L. Williams II (1994a) Formation and thermal decomposition of butyl-substituted peroxyacyl nitrates: *n*-$C_4H_9C(O)OONO_2$ and *i*-$C_4H_9C(O)OONO_2$, *Environ. Sci. Technol.*, *28*, 1099–1105.

Grosjean, D., E. Grosjean, and E.L. Williams (1994b), Thermal decomposition of C_3-substituted peroxyacyl nitrates, *Res. Chem. Intermed.*, *20*, 447–461.

Grosjean, D., E.C. Tuazon, and E. Fujita (1990), Ambient formic acid in southern California air: A comparison of two methods, Fourier transform infrared spectroscopy and alkaline trap-liquid chromatography with UV detection, *Environ. Sci.*, *Technol*, *24*, 144–146.

Grosjean, D., E.L. Williams II, and E. Grosjean (1993d), Gas phase reaction of the hydroxyl radical with the unsaturated peroxyacyl nitrate $CH_2{=}C(CH_3)C(O)OONO_2$, *Int. J. Chem. Kinet.*, *25*, 921–929.

Grosjean, D., E.L. Williams II, and E. Grosjean (1993e), Ambient levels of peroxy-*n*-butyryl nitrate at a southern California mountain forest smog receptor location, *Environ. Sci. Technol*, *27*, 326–331.

Grosjean, D., E. L. Williams II, and E. Grosjean (1993f), Atmospheric chemistry of isoprene and of its carbonyl products, *Environ. Sci. Technol.*, *27*, 830–840.

Grosjean, D., E.L. Williams II, and E. Grosjean (1994c), Gas-phase thermal decomposition of peroxy-*n*-butyryl nitrate, *Int. J. Chem. Kinet.*, *26*, 381–387.

Grosjean, E., and D. Grosjean (1994), Rate constants for the gas phase reactions of ozone with unsaturated aliphatic alcohols, *Int. J. Chem. Kinet.*, *26*, 1185–1191.

Grosjean E., and D. Grosjean (1997), Rate constants for the gas-phase reaction of ozone with unsaturated oxygenates, *Int. J. Chem. Kinet.*, *30*, 21–29.

Grosjean E., and D. Grosjean (1998), Rate constants for the gas-phase reaction of ozone with unsaturated oxygenates, *Int. J. Chem. Kinet.*, *30*, 21–29.

Grosjean, E., and D. Grosjean (1999), The reaction of unsaturated aliphatic oxygenates with ozone, *J. Atmos. Chem.*, *32*, 205–232.

Grosjean, E., D. Grosjean, M.P. Fraser, and G.R. Cass (1996a) Air quality model evaluation data for organics. 2. C_1–C_{14} carbonyls in Los Angeles Air, *Environ. Sci. Technol.*, *30*, 2687–2703.

Grosjean, E., D. Grosjean, M.P. Fraser, and G.R. Cass (1996b), Air quality model evaluation data for organics. 3. Peroxyacetyl nitrate and peroxypropionyl nitrate in Los Angeles air, *Environ. Sci. Technol.*, *30*, 2704–2714,

Grosjean, E., D. Grosjean, R. Gunawardena, and R.A. Rasmussen (1998a), Ambient concentrations of ethanol and methyl *tert*-butyl ether in Porto Alegre, Brazil, March, 1996–April, 1997, *Environ. Sci. Technol.*, *32*, 736–742.

Grosjean, E., D. Grosjean, and J.H. Seinfeld (1996c), Gas-phase reaction of ozone with *trans*-2-hexenal, *trans*-2-hexenyl acetate, ethyl vinyl ketone, and 6-methyl-5-hepten-2-one, *Int. J. Chem. Kinet.*, *28*, 373–382.

Grosjean, E., R.A. Rasmussen, and D. Grosjean (1998b), Ambient levels of gas phase pollutants in Porto Alegre, Brazil, *Atmos. Environ.*, *32*, 3371–3379.

Grossmann, D., G.K. Moortgat, M. Kibler, S. Schlomski, K. Bächmann, B. Alicke, A. Geyer, U. Platt, M.-U. Hammer, B. Vogel, D. Mihelcic, A. Hofzumahaus, F. Holland, and A. Volz-Thomas (2003), Hydrogen peroxide, organic peroxides, carbonyl compounds, and organic acids measured at Pabstthum during BERLIOZ, *J. Geophys. Res.*, *108*, D4, 8250, doi:10.1029/2001JD001096.

Grotheer, H.-H., G. Riekert, D. Walter, and Th. Just (1988), Reactions of hydroxymethyl and hydroxyethyl radicals with molecular and atomic oxygen, 22nd Symposium (International) on Combustion (Combustion Institute, Pittsburgh, PA, 1989), pp.963–972.

Gruber-Stadler, M., M. Muhlhauser, and C.J. Nielsen (2006), Ab initio MRD-CI investigation of the electronic spectrum of glyoxal $(CHO)_2$, *Molec. Phys.*, *104*, 2515–2521.

Grussdorf, J., J. Nolte, F. Temps, and H.Gg. Wagner (1994), Primary products of the elementary reactions of CH_2CO with F, Cl, and OH in the gas phase, *Berichte der Bunsen-Gesellschaft*, *98*, 546–553.

Gruver, J.T., and J.G. Calvert (1956), The vapor phase photolysis of 2-methylbutanal at wavelength 3130 Å, *J. Am. Chem. Soc.*, *78*, 5208–5211.

Gruver, J.T., and J.G. Calvert (1958), The vapor phase photolysis of (+)2-methylbutanal-iodine mixtures at 3130 Å, *J. Am. Chem. Soc.*, *80*, 3524–3527.

Grygier, R.K., P.-A. Brugger, and D.M. Burland (1985), A determination of the photochemical quantum yields from two excited triplet states of biacetyl using holography, *J. Phys. Chem.*, *89*, 112–118.

Guenther, A., C.N. Hewitt, D. Erickson, R. Fall, C. Geron, T. Graedel, P. Harley, L. Klinger, M. Lerdau, W.A. McKay, T. Pierce, B. Scholes, R. Steinbrecher, R. Tallamraju, J. Taylor, and P. Zimmerman (1995), A global model of natural volatile organic compounds emissions, *J. Geophys. Res.*, *100*, 8873–8892.

Guenther, A., T. Karl, P. Harley, C. Wiedinmyer, P.I. Palmer, and C. Geron (2006), Estimates of global terrestrial isoprene emissions using MEGAN (Model of Emissions of Gases and Aerosols from Nature), *Atmos. Chem. Phys.*, *6*, 3181–3210.

Haagen-Smit, A.J. (1952), Chemistry and physiology of Los Angeles smog, *Ind. Eng. Chem.*, *44*, 1342–1346.

Haas, B.-M., T.K. Minton, P. Felder, and J.R. Huber (1991), Photodissociation of acrolein and propynal at 193 nm in a molecular beam. Primary and secondary reactions, *J. Phys. Chem.*, *95*, 5149–5159.

Haas, Y. (2004), Photochemical alpha-cleavage of ketones: revisiting acetone, *Photochem. Photobiol. Sci.*, *3*, 6–16.

Hackett, P.A., and K.O. Kutschke (1977), Photochemistry and photophysics of hexafluoroacetone vapor at low pressures, *J. Phys. Chem.*, *81*, 1245–1252.

Hackett, P.A., and D. Phillips (1974a), Photochemistry of halogenated acetones. I. Spectroscopic studies, *J. Phys. Chem.*, *78*, 665–671.

Hackett, P.A., and D. Phillips (1974b), Photochemistry of halogenated acetones. II. Rate constant measurements, *J. Phys. Chem.*, *78*, 671–678.

Hackett, P.A., and D. Phillips (1974c), Photochemistry of halogenated acetones. III. Vibrational relaxation in singlet states, *J. Phys. Chem.*, *78*, 679–682.

Hackett, P.A., and D. Phillips (1974d), Photochemistry of halogenated acetones. IV. Quenching of the excited states, *J. Phys. Chem.*, *78*, 682–686.

Hägele, J., K. Lorenz, D. Rhäsa, and R. Zellner (1983), Rate constants and CH_3O product yield of the reaction OH + CH_3OH → products, *Ber. Bunsenges. Phys. Chem.*, *87*, 1023–1026.

Hakola, H., J. Arey, S.M. Aschmann, and R. Atkinson (1994), Product formation from the gas-phase reactions of OH radicals and O_3 with a series of monoterpenes, *J. Atmos. Chem.*, *18*, 75–102.

Hall, G.E., H.W. Metzier, J.T. Muckerman, J.M. Preses, and R.E. Weston, Jr. (1995), Studies of the 193 nm photolysis of diethyl ketone and acetone using time-resolved Fourier transform emission spectroscopy, *J. Chem. Phys.*, *102*, 6660–6668.

Hallquist, M., S. Langer, E. Ljungström, and I. Wängberg (1996), Rates of reaction between the nitrate radical and some unsaturated alcohols, *Int. J. Chem. Kinet.*, *28*, 467–474.

Hallquist, M., I. Wängberg, and E. Ljungström (1997), Atmospheric fate of carbonyl oxidation products originating from α-pinene and Δ^3-carene: Determination of rate of reaction with OH and NO_3 radicals, UV absorption cross sections and vapor pressures, *Environ. Sci. Technol.*, *31*, 3166–3172.

Halpern, A.M., and W.R. Ware (1970), Luminescent properties of hexfluoroacetone. III. Vibrational relaxation and radiationless processes in the gas phase, *J. Chem. Phys.*, *53*, 1969–1977.

Halpern, A.M., and W.R. Ware (1971), Excited singlet state radiative and nonradiative transition probabilities for acetone, acetone-d_6, and hexafluoracetone in the gas phase, in solution, and in the neat liquid, *J. Chem. Phys.*, *54*, 1271–1276.

Ham, J.E., S.P. Proper, and J.R. Wells (2006), Gas-phase chemistry of citronellol with ozone and OH radical: Rate constants and products, *Atmos. Environ.*, *40*, 726–735.

Hansel, A., and A. Wisthaler (2000), A method for real-time detection of PAN, PPN, and MPAN in ambient air, *Geophys. Res. Lett.*, *27*, 895–898.

Hanst, P.L., J.W. Spence, and M. Miller (1977), Atmospheric chemistry of *N*-nitroso dimethylamine, *Environ. Sci. Technol.*, *11*, 403–405.

Harris, G.W., W.P.L. Carter, A.M. Winer, and J.N. Pitts, Jr. (1982), Observations of nitrous acid in the Los Angeles atmosphere and implication for predictions of ozone–precursor relationships, *Environ. Sci. Technol.*, *16*, 414–419.

Harris, G.W., and J.N. Pitts, Jr. (1983), Rates of reaction of hydroxyl radicals with 2-(dimethylamino)ethanol and 2-amino-2-methyl-1-propanol in the gas phase at 300± K, *Environ. Sci. Technol.*, *17*, 50–51.

Harrison, A.G., and F.P. Lossing (1959), The mercury-photosensitized decomposition of benzaldehyde, acrolein, and crotonaldehyde, *Can. J. Chem.*, *37*, 1696–1702.

Harrison, J.C., J.E. Ham, and J.R. Wells (2007), Citronellal reactions with ozone and OH radical: Rate constants and gas-phase products detected using PFBHA derivatization, *Atmos. Environ.*, *41*, 4482–4491.

Harrison, J.C., and J.R. Wells (2009), Gas-phase chemistry of benzyl alcohol: Reaction rate constants and products with OH radical and ozone, *Atmos. Environ.*, *43*, 798–804.

Harrison, R.M., J. Yin, R.M. Tilling, X. Cai, P.W. Seakins, J.R. Hopkins, D.L. Lansley, A.C. Lewis, M.C. Hunter, D.E. Heard, L.J. Carpenter, D.J. Creasey, J.D. Lee, M.J. Pilling, N. Carslaw, K.M. Emmerson, A. Redington, R.G. Derwent, D. Ryall, G. Mills, and S.A. Penkett (2006), Measurement and modeling of air pollution and atmospheric chemistry in the U.K. West Midlands conurbation: Overview of the PUMA consortium project, *Sci. Total Environ.*, *360*, 5–25.

Harry, C., J. Arey, and R. Atkinson (1999), Rate constants for the reactions of OH radicals and Cl atoms with di-*n*-propyl ether and di-*n*-butyl ether and their deuterated analogs, *Int. J. Chem. Kinet.*, *31*, 425–431.

Hartley, G.H., and J.E. Guillet (1968a), Photochemistry of ketone polymers. I. Studies of ethylene–carbon monoxide copolymers, *Macromolecules*, *1*, 165–170.

Hartley, G.H., and J.E. Guillet (1968b), Photochemistry of ketone polymers. II. Studies of model compounds, *Macromolecules*, *1*, 413–417.

Hartmann, D., A. Gedra, D. Rhäsa, and R. Zellner (1987), Rate constants for reaction of OH radicals with acetates and glycols in the gas phase, in, editors B. Versino and H. Ott, *Physico-Chemical Behaviour of Atmospheric Pollutants*, D. Reidel Publishing Company, Dordrecht, 1987.

Harwood, M.H., J.M. Roberts, G.J. Frost, A.R. Ravishankara, and J.B. Burkholder (2003), Photochemical studies of $CH_3C(O)OONO_2$ (PAN) and $CH_3CH_2C(O)OONO_2$ (PPN): NO_3 quantum yields, *J. Phys. Chem. A*, *107*, 1148–1154.

Hase, W.L., and P.M. Kelley (1977), A bimolecular mechanism for ketene photodissociation in the near ultraviolet, *J. Chem. Phys.*, *66*, 5093–5099.

Hashikawa, Y., M. Kawasaki, R.L. Waterland, M.D. Hurley, J.C. Ball, T.J. Wallington, M.P.S. Andersen, and O.J. Nielsen (2004), Gas phase UV and IR absorption spectra of $C_xF_{2x+1}CHO$ ($x = 1$–4), *J. Fluorine Chem.*, *125*, 1925–1932.

Hastings, S.H., and F.A. Matsen (1948), The photodecomposition of nitrobenzene, *J. Am. Chem. Soc.*, *70*, 3514–3515.

Hatakeyama, S., S. Honda, and H. Akimoto (1985a), Reactions of ketene, methylketene, ethylketene, and dimethylketene with ozone in air, *Bull. Chem. Soc. Jpn.*, *58*, 2411–2412.

Hatakeyama, S., S. Honda, N. Washida, and H. Akimoto (1985b), Rate constants and mechanism for reaction of ketenes with OH radicals in air at 299 ± 2 K, *Bull. Chem. Soc. Jpn.*, *58*, 2157–2162.

Hayden, C.C., D.M. Neumark, K. Shobatake, R.K. Sparks, and Y.T. Lee (1982), Methylene singlet-triplet energy splitting by molecular beam photodissociation of ketene, *J. Chem. Phys.*, *76*, 3607–3613.

Hayon, E., T.N. Ibata, N. Lichtin, and M. Simic (1970), Sites of attack of hydroxyl radicals on amides in aqueous solution, *J. Am. Chem. Soc.*, *92*, 3898–3903.

He, Y.Z., W.G. Mallard, and W. Tsang (1988), Kinetics of hydrogen and hydroxyl radical attack on phenol at high temperatures, *J. Phys. Chem.*, *92*, 2196–2201.

Heard, A.C., M.J. Pilling, and A.S. Tomlin (1998), Mechanism reduction techniques applied to tropospheric chemistry, *Atmos. Env.*, *32*, 1059–1073.

Heathfield, A.E., C. Anastasi, P. Pagsberg, and A. McCulloch (1998), Atmospheric lifetimes of selected fluorinated ether compounds, *Atmos. Environ.*, *32*, 711–717.

Heicklen, J. (1959), The fluorescence and phosphorescence of biacetyl vapor and acetone vapor, *J. Am. Chem. Soc.*, *81*, 3863–3866.

Heicklen, J. (1965), The photolysis of phosgene–ethylene mixtures, *J. Am. Chem. Soc.*, *87*, 445–453.

Heicklen, J. (1987), The decomposition of alkyl nitrites and the reaction of alkoxy radicals, *Adv. Photochem.*, *14*, 177–272.

Heicklen, J., J. Desai, A. Bahta, C. Harper, and R. Simonaitis (1986), The temperature and wavelength dependence of the photooxidation of propionaldehyde, *J. Photochem.*, *34*, 117–135.

Heikes, B., B. McCully, X. Zhou, Y.-N- Lee, K. Mopper, X. Chen, G. Mackay, D. Karecki, H. Schiff, T. Campos, and E. Atlas (1996), Formaldehyde methods comparison in the remote lower troposphere during the Mauna Loa Photochemistry Experiment 2, *J. Geophys. Res.*, *101*, 14741–14756.

Hellén, H., H. Hakola, A. Reissell, and T.M. Ruuskanen (2004), Carbonyl compounds in boreal coniferous forest air in Hyytiälä, Southern Finland, *Atmos. Chem. Phys.*, *4*, 1771–1780.

Hellpointner, E., and S. Gäb (1989), Detection of methyl, hydroxymethyl and hydroxethyl hydroperoxides in air and precipitation, *Nature*, *337*, 631–634.

Heneghan, S.P., and S. Benson (1983), Kinetic study of the reactions of Cl and Br with H_2O_2, *Int. J. Chem. Kinet.*, *15*, 1311–1319.

Hennig, S., V. Engel, R. Schinke, M. Nonella, and J.R. Huber (1987), Photodissociation dynamics of methyl nitrite (CH_3ONO) in the 300–400 nm range: An ab initio quantum mechanical study, *J. Chem. Phys.*, *87*, 3522–3529.

Hennig, S., A. Untch, R. Schinke, M. Nonella, and J.R. Huber (1989), Theoretical investigation of the photodissociation dynamics of HONO-vibrational predissociation in the electronically excited-state S_1, *Chem. Phys.*, *129*, 93–107.

Henriques, F.C., Jr., and W.A. Noyes, Jr. (1940), Photochemical studies. XXX. The fluorescence of biacetyl. Some general considerations governing the study of fluorescence, *J. Am. Chem. Soc.*, *62*, 1038–1043.

Hepburn, J.W., R.J. Buss, L.J. Butler, and Y.T. Lee (1983), Molecular beam study of the photochemistry of S_1 glyoxal, *J. Phys. Chem.*, *87*, 3638–3641.

Herrmann, H., A. Tilgner, P. Barzaghi, Z. Majdik, S. Gligorovski, L Poulain, and A. Monod (2005), Towards a more detailed description of tropospheric aqueous phase organic chemistry: CAPRAM 3.0, *Atmos. Environ.*, *39*, 4351–4363.

Herron, J.T. (1988), Evaluated chemical kinetic data for the reactions of atomic oxygen $O(^3P)$ with saturated organic compounds in the gas phase, *J. Phys. Chem. Ref. Data*, *17*, 967–1026.

Herzberg, G., and D.A. Ramsay (1955), The 7500 to 4500Å absorption system of the free HCO radical, *Proc. Roy. Soc. (London)*, *A. 233*, 34–54.

Hess, W.P., and F.P. Tully (1988), Catalytic conversion of alcohols to alkenes by OH, *Chem. Phys. Lett.*, *152*, 183–189.

Hess, W.P., and F.P. Tully (1989), Hydrogen-atom abstraction from methanol by OH, *J. Phys. Chem.*, *93*, 1944–1947.

Heuss, J.M., and W.A. Glasson (1968), Hydrocarbon reactivity and eye irritation, *Environ. Sci. Technol.*, *2*, 1109–1116

Hickson, K.M., and I.W.M. Smith (2001), Rate constants and Arrhenius parameters for the reactions of Cl atoms with the halogenated ethers: $CF_3CH_2OCHF_2$, $CF_3CHClOCHF_2$, and $CF_3CH_2OCClF_2$, *Int. J. Chem. Kinet.*, *33*, 165–172.

Hippler, H., H. Neunaber, and J. Troe (1995), Shock wave studies of the reactions HO + H_2O_2 → H_2O + HO_2 and HO + HO_2 → H_2O + O_2 between 930 and 1680 K, *J. Chem. Phys.*, *103*, 3510–3516.

Hippler, H., and J. Troe (1992), Rate constants of the reaction HO + H_2O_2 → HO_2 + H_2O at T ≥ 1000 K, *192*, 333–337.

Hippler, M., A. Fah, and J. Pfab (1992), Photodissociation of jet-cooled methyl and *t*-butyl nitrite near 380 nm, *Chem. Phys. Lett.*, *192*, 173–178.

Hippler, M., and J. Pfab (1992), Electronic absorption spectrum of methyl nitrite in the near-ultraviolet, *J. Chem. Soc., Faraday Trans.*, *88*, 2109–2110.

Hirschlaff, E., and R.G.W. Norrish (1936), Primary photochemical processes. Part IX. A preliminary study of the decomposition of nitromethane and nitroethane, *J. Chem. Soc.*, *1936*, 1580–1585.

Hjorth, J., N.R. Jensen, D. Di Bella, Y. Fiamegos, R. Winterhalter, and A. Calogirou (2002), Evaluation of radical sources in atmospheric chemistry through chamber and laboratory studies, RADICAL, Final Report of EU-Project ENV4-CT97-0419, Institute for Environment and Sustainability, EUR 20254 EN.

Hjorth, J., G. Ottobrini, and G. Restelli (1988), Reaction between NO_3 and CH_2O in air: a determination of the rate constant at 295 ± 2 K, *J. Phys. Chem.*, *92*, 2669–2672.

Ho, K.F., J.J. Cao, S.C. Lee, K. Kawamura, R.J Zhang, J.C. Chow, and J.G. Watson (2007a), Dicarboxylic acids, ketocarboxylic acids, and dicarbonyls in the urban atmosphere of China, *J. Geophys. Res.*, *112*, D22827, doi:1029/2006JD008011.

Ho, K.F., S.S.H. Ho, Y. Cheng, S.C. Lee, and J.Z. Yu (2007b), Real-world emission factors of fifteen carbonyl compounds measured in a Hong Kong tunnel, *Atmos. Environ.*, *41*, 1747–1758.

Ho, S.Y., I. Unger, and W.A. Noyes, Jr. (1965), The photochemistry of ketene. The methylene radical, *J. Am. Chem. Soc.*, *87*, 2297–2298.

Hoffmann, T., J.R. Odum, F. Bowman, D. Collins, D. Klockow, R.C. Flagan, and J.H. Seinfeld (1997), Formation of organic aerosols from the oxidation of biogenic hydrocarbons, *J. Atmos. Chem.*, *26*, 189–222.

Holloway, A.L., J. Treacy, H. Sidebottom, A. Mellouki, V. Daële, G. Le Bras, and I. Barnes (2005), Rate coefficients for the reactions of OH radicals with the keto/enol tautomers of 2,4-pentanedione and 3-methyl-2,4-pentanedione, allyl alcohol and methyl vinyl ketone using the enols and methyl nitrite as photolytic sources of OH, *J. Photochem. Photobiol. A*, *Chem.*, *176*, 183–190.

Holroyd, R.A., and F.E. Blacet (1957), The photolysis of dimethyl ketene vapor, *J. Am. Chem. Soc.*, *79*, 4830–4834.

Holroyd, R.A., and W.A. Noyes, Jr. (1956), Photochemical studies. L. The ketene–oxygen system at higher temperatures, *J. Am. Chem. Soc.*, *78*, 4831–4836.

Holt, T., R. Atkinson, and J. Arey (2005), Effect of water vapor concentration on the conversion of a series of 1,4-hydroxycarbonyls to dihydrofurans, *J. Photochem. Photobiol.*, *A: Chemistry*, *176*, 231–237.

Hopkinson, A.C., E. Lee-Ruff, and M.H. Lien (1988), Molecular orbital calculations of excited state cyclobutanone and its photocarbene, *Tetrahedron*, *44*, 6815–6820.

Horie, O., and G.K. Moortgat (1992a), Reactions of $CH_3C(O)O_2$ radicals with CH_3O_2 and HO_2 between 263 and 333 K. A product study, *J. Chem. Soc., Faraday Trans.*, *1992*, 3305–3312.

Horie, O., and G.K. Moortgat (1992b), Photolysis of ketene–oxygen mixtures between 253 K and 323 K in relation to the formation of Criegee intermediates, *Ber. Bunsenges. Phys. Chem.*, *96*, 404–408.

Horowitz, A. (1986), Use of hydrogen chloride as a probe for the determination of primary processes in acetaldehyde photolysis, *J. Phys. Chem.*, *90*, 4393–4397.

Horowitz, A. (1991), Wavelength dependence of the primary photodissociation processes in acetone photolysis, *J. Phys. Chem.*, *95*, 10816–10823.

Horowitz, A., and J.G. Calvert (1972), Emission studies of the mechanism of gaeous biacetyl photolysis at 3450, 3880, and 4358Å and 28°C, *Int. J. Chem. Kinet.*, *4*, 207–227.

Horowitz, A., and J.G. Calvert (1978a), The quantum efficiencies of the primary processes in formaldehyde photolysis at 3130 Å and 25°C, *Int. J. Chem. Kinet.*, *10*, 713–732.

Horowitz, A., and J.G. Calvert (1978b), Wavelength dependence of the quantum efficiencies of the primary processes in formaldehyde photolysis at 25°C, *Int. J. Chem. Kinet.*, *10*, 805–819.

Horowitz, A., and J.G. Calvert (1982), Wavelength dependence of the primary processes in acetaldehyde photolysis, *J. Phys. Chem.*, *86*, 3105–3114.

Horowitz, A., C.J. Kershner, and J.G. Calvert (1982), Primary processes in the photolysis of acetaldehyde at 3000 Å and 25°C, *J. Phys. Chem.*, *86*, 3094–3105.

Horowitz, A., R. Meller, and G.K. Moortgat (2001), The UV–VIS absorption cross sections of the α-dicarbonyl compounds: pyruvic acid, biacetyl and glyoxal, *J. Photochem. Photobiol. A*, *146*, 19–27.

Horowitz, L.W., J. Liang, G.M. Gardner, and D.J. Jacob (1998), Export of reactive nitrogen from North America during summertime: sensitivity to hydrocarbon chemistry, *J. Geophys. Res. 103*, 13451–13476.

Horowitz, L.W., S. Walters, D.L. Mauzerall, L.K. Emmons, P.J. Rasch, C. Granier, X. Tie, J.-F. Lamarque, M.G. Schultz, G.S. Tyndall, J.J. Orlando, and G.P. Brasseur (2003) A global simulation of tropospheric ozone and related tracers: description and evaluation of MOZART, version 2, *J. Geophys. Res. 108*, ACH 16/1–ACH 16/2.

Hoshi, J.-Y., S. Amano, Y. Sasaki, and T. Lorenaga (2008), Investigation and estimation of emission sources of 54 volatile organic compounds in ambient air in Tokyo, *Atmos. Environ.*, *42*, 2383–2393.

Hou, H., Y. Li, and B. Wang (2006), Computational study of the reaction of atomic oxygen with acetone in the gas phase, *J. Phys. Chem. A*, *110*, 13163–13171.

Hsu, K.-J., and W.B. DeMore (1995), Temperature-dependent rate constants and substituent effects for the reactions of hydroxyl radicals with three partially fluorinated ethers, *J. Phys. Chem.*, *99*, 11141–11146.

Hu, W.-F., T.-J. He, D.-M. Chen, and F.-C. Liu (2002), Theoretical study of the CH_3NO_2 unimolecular decomposition potential energy surface, *J. Phys. Chem. A*, *106*, 7294–7303.

Huang, C.-L., C.-L. Liu, C.-K. Ni, and J.T. Hougen (2005), Electronic spectra of molecules with two C_{3v} internal rotors: Torsional analysis of the A^1A_u–X^1A_g LIF spectrum of biacetyl, *J. Mol. Spectroscopy*, *233*, 122–132.

Huang, Y., T.J. Dransfield, J.D. Miller, R.D. Rojas, X.G. Castillo, and J.G. Anderson (2009), Experimental study of the kinetics of the reaction of acetic acid with hydroxyl radicals from 255 to 355 K, *J. Phys. Chem. A.*, *113*, 423–430.

Huey, L.G., D.R. Hanson, and E.R. Lovejoy (1995), Atmospheric fate of CF_3OH 1: Gas phase thermal decomposition, *J. Geophys. Res.*, *100*, 18771–18774.

Hufford, D.L., D.S. Tarbell, and T.R. Koszalka (1952), Maleic and fumaric dialdehydes, Δ^4-tetrahydrophthaldehyde and related compounds, *J. Am. Chem. Soc.*, *74*, 3014–3018.

Hughes, G.A., and L. Phillips (1967), The kinetics of disproportionation–combination reactions between the isopropoxyl radical and nitric oxide, and the pyrolysis of the O—O bond in di-isopropyl peroxide, *J. Chem. Soc.*, *1967*, 984–897.

Hurley, M.D., M.P.S. Andersen, T.J. Wallington, D.A. Ellis, J.W. Martin, and S.A. Mabury (2004a), Atmospheric chemistry of perfluorinated carboxylic acids: Reaction with OH radicals and atmospheric lifetimes, *J. Phys. Chem. A*, *108*, 615–620.

Hurley, M.D., J.C. Ball, T.J. Wallington, M.P.S. Andersen, D.A. Ellis, J.W. Martin, and S.A. Mabury (2004b), Atmospheric chemistry of 4:2 fluorotelomer alcohol ($C_4F_9CH_2CH_2OH$): products and mechanism of Cl atom initiated oxidation, *J. Phys. Chem. A*, *108*, 5635–5642.

Hurley, M.D., J.C. Ball, T.J. Wallington, M.P.S. Andersen, O.J. Nielsen, D.A. Ellis, J.W. Martin, and S.A. Mabury (2006), Atmospheric chemistry of n-$C_xF_{2x+1}CHO$ ($x = 1,2,3,4$): Fate of n-$C_xF_{2x+1}C(O)$ radicals, *J. Phys. Chem. A*, *110*, 12443–12447.

Hurley, M.D., J.C. Ball, T.J. Wallington, A. Toft, O.J. Nielsen, S. Bertman, and M. Perovic (2007), Atmospheric chemistry of a model biodiesel fuel $CH_3C(O)O(CH_2)_2OC(O)CH_3$: Kinetics, mechanisms and products of Cl atom and OH radical initiated oxidation in the presence and absence of NO_x, *J. Phys. Chem. A*, *111*, 2547–2554.

Hurley, M.D., J.A. Misner, J.C. Ball, T.J. Wallington, D.A. Ellis, J.W. Martin, and S.A. Mabury (2005), Atmospheric chemistry of $CF_3CH_2CH_2OH$: kinetics, mechanisms and products of Cl atom and OH radical initiated oxidation in the presence and absence of NO_x, *J. Phys. Chem. A*, *109*, 9816–9826.

Hurley, M.D., T.J. Wallington, M.P.S. Andersen, D.A. Ellis, J.W. Martin, and S.A. Mabury (2004c), Atmospheric chemistry of fluorinated alcohols: reaction with Cl atoms, OH radicals and atmospheric lifetimes, *J. Phys. Chem. A*, *108*, 1973–1979.

Hurley, M.D., T.J. Wallington, M. Bjarrum, M.S. Javadi, and O.J. Nielsen (2008), Atmospheric chemistry of 3-pentanol: Kinetics, mechanisms, and products of the Cl atom and OH radical initiated oxidation in the presence and absence of NO_x, *J. Phys. Chem. A*, *112*, 8053–8060.

Hurley, M.D., T.J. Wallington, L. Laursen, M.S., Javadi, O.J. Nielsen, T. Yamanaka, and M. Kawasaki (2009), Atmospheric chemistry of *n*-butanol: Kinetics, mechanisms, and products of the Cl atom and OH radical initiated oxidation in the presence and absence of NO_x, *J. Phys. Chem. A*, *113*, 7011-7020.

Hurley, R., and A.C. Testa (1966), Photochemical n $\rightarrow \pi^*$ excitation of nitrobenzene, *J. Am. Chem. Soc.*, *88*, 4330–4332.

Hwang, W.G., M.S. Kim, and J.C. Choe (1996), Photodissociation dynamics of nitrobenzene molecular ion on a nanosecond time scale, *J. Phys. Chem.*, *100*, 9227–9234.

Ide, T., E. Iwasaki, Y. Matsumi, J.-H. Xing, K. Takahashi, and T.J. Wallington (2008), Pulsed laser photolysis vacuum UV laser-induced fluorescence kinetic study of the reactions of $Cl(^2P_{3/2})$ atoms with ethyl formate, *n*-propyl formate, and *n*-butyl formate, *Chem. Phys. Lett.*, *467*, 70–73.

IEA (2004), Biofuels for transport, International Energy Agency, Paris, France.

Imamura, T., Y. Iida, K. Obi, I. Nagatani, K. Nakagawa, I. Patroescu-Klotz, and S. Hatakeyama (2004), Rate coefficients for the gas-phase reactions of OH radicals with methylbutenols at 298 K, *Int. J. Chem. Kinet.*, *36*, 379–385.

Inoue, G., H. Akimoto, and M. Okuda (1979), Laser-induced fluorescence spectra of CH_3O, *Chem. Phys. Lett.*, *63*, 213–216.

Inoue, G., M. Kawasaki, H. Sato, T. Kikuchi, S. Kobayashi, and T. Arikawa (1987), Photodissociation of methyl nitrite: Angular distributions in one- and two-photodissociations, *J. Chem. Phys.*, *87*, 5722–5727.

Inoue, Y., M. Kawasaki, T.J. Wallington, and M.D. Hurley (2001), Atmospheric degradation mechanism of CF_3OCF_2H, *Chem. Phys. Lett.*, *343*, 296–302.

IPCC, Intergovernmental Panel on Climate Change (2001), *Climate Change 2001: The Scientific Basis, Contribution of Working Group I to the Third Assessment Report of the Intergovernmental Panel on Climate Change*, editors J.T. Houghton, Y. Ding, D.J. Griggs, M. Noguer, P.J. van der Linden, X. Da, K. Maskell and C.A. Johnson, Cambridge University Press, New York.

Ishakawa, H., and W. A. Noyes, Jr. (1962a), The triplet state of benzene, *J. Am. Chem. Soc.*, *84*, 1502–1503.

Ishakawa, H., and W.A. Noyes, Jr. (1962b), Photosensitization by benzene vapor: Biacetyl. The triplet state of benzene, *J. Chem. Phys.*, *37*, 583–591.

IUPAC (2008), Subcommittee for Gas Kinetic Data Evaluation, Evaluated Gas Kinetic Data for Atmospheric Chemistry: www.iupac-kinetic.ch.cam.ac.uk.

Iwasaki, E., Y. Matsumi, K. Takahashi, T.J. Wallington, M.D. Hurley, J.J. Orlando, E.W. Kaiser, and J.G. Calvert (2008a), Atmospheric chemistry of cyclohexanone: UV spectrum and kinetics of reaction with chlorine atoms, *Int. J. Chem. Kinet.*, *40*, 223–229.

Iwasaki, E., T. Nakayama, Y. Matsumi, K. Takahashi, T.J. Wallington, M.D. Hurley, and E.W. Kaiser (2008b), Kinetics and mechanism of the reaction of chlorine atoms with *n*-pentanal, *J. Phys. Chem. A*, *112*, 1741–1746.

Izumi, K., and T. Fukuyama (1990), Photochemical aerosol formation from aromatic hydrocarbons in the presence of NO_x, *Atmos. Environ.*, *24A*, 1433–1441.

Jacob, D.J., B.D. Field, E.M. Jin, I. Bey, Q. Li, J.A. Logan, R.M. Yantosca, and H.B. Singh (2002), Atmospheric budget of acetone, *J. Geophys. Res. 107*, ACH 5/1–ACH 5/19.

Jacob, D.J., B.D. Field, Q. Li, D.R. Blake, J. de Gouw, C. Warneke, A. Hansel, A. Wisthaler, H.B. Singh, and A. Guenther (2005), Global budget of methanol: constraints from atmospheric observations, *J. Geophys. Res.*, *110*, D08303/1–D08303/17.

Jacob, D. J., S. Sillman, J.A. Logan, and S.C. Wofsy (1989), Least independent variables method for simulation of tropospheric ozone, *J. Geophys. Res.*, *94*, 8497–509.

Jadkowski, J.T., M.-T. Rayez, J.-C. Rayez, T. Bérces, and S. Dóbé (1998), Theoretical study of the kinetics of the hydrogen abstraction from methanol. 2. Reaction of methanol with chlorine and bromine atoms, *J. Phys. Chem. A.*, *102*, 9230–9243.

Jaeglé, L, D.J. Jacob, W.H. Brune, and P.O. Wennberg (2001), Chemistry of HO_x radicals in the upper troposphere, *Atmos. Env.*, *35*, 469–489.

Jäger, M., H. Heydtmann, and C. Zetzsch (1996), Vacuum ultraviolet spectrum and quantum yield of the 193 nm photolysis of phosgene, *Chem. Phys. Lett.*, *263*, 817–821.

Janson, R. (1992), Monoterpenes from the boreal coniferous forest, Ph.D. Thesis, Univ. Stockholm, Stockholm, Sweden.

Jaoui, M., and R.M. Kamens (2003), Gas phase photolysis of pinonaldehyde in the presence of sunlight, *Atmos. Environ.*, *37*, 1835–1851.

Japar, S.M., T.J. Wallington, J.F.O. Richert, and J.C. Ball (1990), The atmospheric chemistry of oxygenated fuel additives: *t*-butyl alcohol, dimethyl ether, and methyl *t*-butyl ether, *Int. J. Chem. Kinet.*, *22*, 1257–1269.

Javadi, M.S., O.J. Nielsen, T.J. Wallington, M.D. Hurley, and J.G. Owens (2007), Atmospheric chemistry of 2-ethoxy-3,3,4,4,5-pentafluorotetrahydro-2,5-bis[1,2,2,2-tetrafluoro-1-(trifluoromethyl)ethyl]-furan: Kinetics, mechanisms, and products of Cl atom and OH radical initiated oxidation, *Environ. Sci. Technol.*, *41*, 7389–7395.

Jenkin, M.E., and R.A. Cox (1987), Kinetics of the gas-phase reaction of OH with nitrous acid, *Chem. Phys. Lett.*, *137*, 548–552.

Jenkin, M.E., R.A. Cox, M. Emrich, and G.K. Moortgat (1993a), Mechanisms of the Cl-atom-initiated oxidation of acetone and hydroxyacetone in air, *J. Chem. Soc., Faraday Trans.*, *89*, 2983–2991.

Jenkin, M.E., G.D. Hayman, T.J. Wallington, M.D. Hurley, J.C. Ball, O.J. Nielsen, and T. Ellermann (1993b), Kinetic and mechanistic study of the self reaction of $CH_3OCH_2O_2$ radicals at room temperature, *J. Phys. Chem.*, *97*, 11712–11723.

Jenkin, M. E., S.M. Saunders, R.G. Derwent, and M. J. Pilling (2002), Development of a reduced speciated VOC degradation mechanism for use in ozone models, *Atmos. Env.*, *36*, 4725–4734.

Jenkin, M.E., S.M. Saunders, and M.J. Pilling (1997), The tropospheric degradation of volatile organic compounds: a protocol for mechanism development, *Atmos. Env.*, *31*, 81–104.

Jenkin, M.E., S.M. Saunders, V. Wagner, and M.J. Pilling (2003), Protocol for the development of the Master Chemical Mechanism, MCM v3 (Part B): tropospheric degradation of aromatic volatile organic compounds, *Atmos. Chem. Phys.*, *3*, 181–193

Jenkin, M. E., L.A. Watson, S.R. Utembe, and D.E. Shallcross (2008), A Common Representative Intermediates (CRI) mechanism for VOC degradation. Part 1: Gas phase mechanism development, *Atmos. Env.*, *42*, 7185–7195.

Jiménez, E., B. Ballesteros, E. Martinez, and J. Albaladejo (2005a), Tropospheric reaction of OH with selected linear ketones: Kinetic studies between 228 and 405 K, *Environ. Sci. Tech.*, *39*, 814–820.

Jiménez, E., T. Gierczak, H. Stark, J.B. Burkholder, and A.R. Ravishankara (2004), Reaction of OH with HO_2NO_2 (peroxynitric acid): Rate coefficients between 218 and 335 K and product yields at 298 K, *J. Phys. Chem. A*, *108*, 1139–1149.

Jiménez, E., M.K. Gilles, and A.R. Ravishankara (2003), Kinetics of the reactions of the hydroxyl radical with CH_3OH and C_2H_5OH between 235 and 360 K, *J. Photochem. Photobiol. A: Chem.*, *157*, 237–245.

Jiménez, E., B. Lanza, A. Garzón, B. Ballesteros, and J. Albaladejo (2005b), Atmospheric degradation of 2-butanol, 2-methyl-2-butanol, and 2,3-dimethyl-2-butanol: OH kinetics and UV absorption cross sections, *J. Phys. Chem. A*, *109*, 10903–10909.

Jimenez, E., B. Lanza, E. Martinez, and J. Albaladejo (2007), Daytime tropospheric loss of hexanal and *trans*-2-hexenal: OH kinetics and UV photolysis, *Atmos. Chem. Phys.*, *7*, 1565–1574.

Jobson, B.T., H. Niki, Y. Yokouchi, J. Bottenheim, F. Hopper, and R. Leaitch (1994), Measurements of C_2–C_6 hydrocarbons during the Polar Sunrise 1992 Experiment: Evidence for Cl atom and Br atom chemistry, *J. Geophys. Res.*, *99*, 25355–25368.

Johnson, B.J., E.A. Betterton, and D. Craig (1996), Henry's law coefficients of formic and acetic acids, *J. Atmos. Chem.*, *24*, 113–119.

Johnson, D., and J.M. Andino (2001), Laboratory studies of the OH-initiated photooxidation of ethyl *n*-butyl ether and di-*n*-butyl ether, *Int. J. Chem. Kinet.*, *33*, 328–341.

Johnson, D., M.E. Jenkin, K. Wirtz, and M. Martin-Reviejo (2004), Simulating the formation of secondary organic aerosol from the photooxidation of toluene, *Env. Chem.*, *1*, 150–165.

Johnson, D., S.R. Utembe, M.J. Jenkin, R.G. Derwent, G.D. Hayman, M.R. Alfarra, H. Coe, and G. McFiggans (2006), Simulating regional scale secondary organic aerosol formation during the TORCH 2003 campaign in the southern UK, *Atmos. Chem. Phys.*, *6*, 403–418.

Johnston, H.S., S.-G. Chang, and G. Whitten (1974), Photolysis of nitric acid vapor, *J. Phys. Chem.*, *78*, 1–7.

Johnstone, D.E., and J.R. Sodeau (1992), Photochemistry of the matrix-isolated α,β-unsaturated aldehydes acrolein, methacrolein and crotonaldehyde at 4.2 K, *J. Chem. Soc., Faraday Trans.*, *88*, 409–415.

Jolley, J.E. (1957), The photoöxidation of diethyl ketone, *J. Am. Chem. Soc.*, *79*, 1537–1542.

Jolly, G.S., D.J. McKenney, D.L. Singleton, G. Paraskevopoulos, and A.R. Bossard (1986a), Rate constant and mechanism for the reaction of hydroxyl radical with formic acid, *J. Phys. Chem.*, *90*, 6557–6562.

Jolly, G.S., G. Paraskevopoulos, and D.L. Singleton (1985), The question of a pressure effect in the reaction OH + HNO_3. A laser flash-photolysis resonance-absorption study, *Chem. Phys.Lett.*, *117*, 132–137.

Jolly, G.S., D.L. Singleton, D.J. McKenney, and G. Paraskevopoulos (1986b), Laser photolysis of HNO_3 at 222 nm: Direct determination of the primary quantum yield of OH, *J. Chem. Phys.*, *84*, 6662–6667.

Jourdain, J.L., G. Poulet, and G. Le Bras (1982), Determination of the rate parameters and products for the reaction of hydroxyl radicals with nitric acid, *J. Chem. Phys.*, *76*, 5827–5833.

Judge, R.H., and D.C. Moule (1985), The $\tilde{A}\ ^1A'' \leftarrow X^1A'$ electronic transition in formyl chloride, CHClO, *J. Mol. Spectros.*, *113*, 302–309.

Kabasakalien, P., E.R. Townley, and D. Yudis (1962), Photolysis of nitrite esters in solution. III. Photochemistry of primary, secondary and tertiary alkyl nitrites, *J. Am. Chem. Soc.*, *84*, 2718–2722.

Kades, E., M. Rösslein, and J.R. Huber (1994), From monomers to clusters. Photodissociation of *tert*-butyl nitrite $(CH_3)_3CONO$ and homogeneous $[(CH_3)_3CONO]_n$ clusters, *J. Phys. Chem.*, *98*, 13556–13562.

Kaiser, E.W., C.J. Donahue, I.R. Pala, T.J. Wallington, and M.D. Hurley (2007), Kinetics, products and stereochemistry of the reaction of chlorine atoms with *cis*- and *trans*-2-butene in 10–700 Torr of N_2 or N_2/O_2 diluent at 297 K, *J. Phys. Chem. A.*, *111*, 1286–1299.

Kaiser, E.W., and S.M. Japar (1977), The kinetics of the gas phase reaction of nitrous acid with ozone, *Chem. Phys. Lett.*, *52*, 121–124.

Kaiser, E.W., and T.J. Wallington (2007), Rate constants for the reaction of Cl with a series of C_4 to C_6 ketones using the relative rate method, *J. Phys. Chem. A*, *111*, 10667–10670.

Kaiser, E. W., T. J. Wallington, and M. D. Hurley (2009), Products and mechanism of the reaction of Cl with butanone in N_2/O_2 diluent at 297–526 K, *J. Phys. Chem. A*, *113*, 2424–2437.

Kaiser, E.W., T.J. Wallington, and M.D. Hurley (2009), Products and mechanism of the reaction of Cl with butanone in N_2/O_2 diluent at 297–526 K, *J. Phys. Chem. A*, *113*, 2424–2437.

Kakesu, M., H. Bandow, N. Takenaka, Y. Maeda, and N. Washida (1997), Kinetic measurements of methyl and ethyl nitrate reactions with OH radicals, *Int. J. Chem. Kinet.*, *29*, 933–941.

Kalabokas, P., P. Carlier, P. Fresnet, G. Mouvier, and G. Toupance (1988), Field studies of aldehyde chemistry in the Paris area, *Atmos. Environ.*, *22*, 147–155.

Kalberer, M., D. Paulsen, M. Sax, M. Steinbacher, J. Dommen, A.S.H. Prevot, R. Fisseha, E. Weingartner, V. Frankevich, R. Zenobi, and U. Baltensperger (2004), Identification of polymers as major components of atmospheric organic aerosols, *Science*, *303*, 1659–1662.

Kaledin, A.L., J. Seong, and K. Morokuma (2001), Predominance of nonequilibrium dynamics in the photodissociation of ketene in the triplet state, *J. Phys. Chem. A*, *105*, 2731–2737.

Kambanis, K.G., Y.G. Lazarou, I.I. Morozov, and P. Papagiannakopoulos (1995), Kinetic studies of the reaction of Cl atoms with $BrCH_2OCH_3$, *J. Phys. Chem.*, *99*, 17169–17173.

Kambanis, K.G., Y.G. Lazarou, and P. Papagiannakopoulos (1996), Gas phase reaction kinetics of Cl atoms with ICH_2OCH_3, *Chem. Phys. Lett.*, *261*, 457–462.

Kambanis, K.G., Y.G. Lazarou, and P. Papagiannakopoulos (1998), Kinetic study for the reactions of chlorine atoms with a series of hydrofluoroethers, *J. Phys. Chem. A*, *102*, 8620–8625.

Kamiya, K., and K. Morokuma (1991), Potential energy surface for unimolecular dissociation and rearrangement reactions of the ground electronic state of HFCO, *J.Chem. Phys.*, *94*, 7287–7298.

Kanakidou M, J.H. Seinfeld, S.N. Pandis, I. Barnes, F.J. Dentener, M.C. Facchini, R. Van Dingenen, B. Ervens, A. Nenes, C.J. Nielsen, E. Swietlicki, J.P. Putaud, Y. Balkanski, S. Fuzzi, J. Horth, G.K. Moortgat, R. Winterhalter, C.E.L. Myhre, K. Tsigaridis, E. Vignati, E.G. Stephanou, and J. Wilson J (2005), Organic aerosol and global climate modelling: a review, *Atmos. Chem. Phys.*, *5*, 1053–1123.

Kao, C.C., M.-L. Ho, M.-W. Chen, S.-J. Lee, and I.-C. Chen (2004), Internal state distributions of fragment HCO via S_o and T_1 pathways of glyoxal after photolysis in the ultraviolet region, *J. Chem. Phys.*, *120*, 5087–5095.

Karl, T., A. Guenther, A. Turnipseed, E. G. Patton, and K. Jardine (2008), Chemical sensing of plant stress at the ecosystem scale, *Biogeosciences*, *5*, 1287–1294.

Karunanandan, R., D. Hölscher, T.J. Dillon, A. Horowitz, J.N. Crowley, L. Vereecken, and J. Peeters (2007), Reaction of HO with glycolaldehyde, $HOCH_2CHO$: Rate coefficients (240–362 K) and mechanism, *J. Phys. Chem*, *A*, *111*, 897–908.

Kash, P.W., G.C.G. Waschewsky, R.E. Morss, L.J. Butler, and M.M. Francl (1994), Competing C—Br and C—C bond fission following $^1[n(O), \pi^* (C{=}O)]$ excitation in bromoacetone: Conformation dependence of nonadiabaticity at a conical intersection, *J. Chem. Phys.*, *100*, 3463–3475.

Kaubisch, N., J.W. Daly, and D.M. Jerina (1972), Arene oxides as intermediates in the oxidative metabolism of aromatic compounds. Isomerization of methyl-substituted arene oxides, *Biochemistry*, *11*, 3080–3088.

Kawamura, K., S. Steinberg, and I.R. Kaplan (2000), Homologous series of C_1–C_{10} monocarboxylic acids and C_1–C_6 carbonyls in Los Angeles air and motor vehicle exhausts, *Atmos. Environ.*, *34*, 4175–4191.

Kegley-Owen, C.S., G.S. Tyndall, J.J.Orlando, and A. Fried (1999), Tunable diode laser studies of the reaction of Cl atoms with CH_3CHO, *Int. J. Chem. Kinet.*, *31*, 766–775.

Keller, B.A., P. Felder, and J.R. Huber (1986), Photodissociation of methyl nitrite at 248 and 350 nm in a molecular beam, *Chem. Phys. Lett.*, *124*, 135–139.

Keller, B.A., P. Felder, and J.R. Huber (1987), Molecular beam photodissociation study of methyl nitrite in the near-ultraviolet region, *J. Phys. Chem.*, *91*, 1114–1120.

Keller-Rudek, H., and G.K. Moortgat (2005), MPI-Mainz-UV-VIS Spectral Atlas of Gaseous Molecules, catalogue of spectra available online: http://www.atmosphere.mpg.de/spectral-atlas-mainz.

Kelly, T., V. Bossoutrot, I. Magneron, K. Wirtz, J. Treacy, A. Mellouki, H. Sidebottom, and G. Le Bras (2005), A kinetic and mechanistic study of the reactions of OH radicals and Cl atoms with 3,3,3-trifluoropropanol under atmospheric conditions, *J. Phys. Chem. A*, *109*, 347–355.

Kenner, R.D., R. Rohrer, and F. Stuhl (1986), OH(A) production in the 193 nm photolysis of HONO, *J. Phys. Chem.*, *90*, 2635–2639.

Kerr, J.A., and D.W. Sheppard (1981), Kinetics of the reactions of hydroxyl radicals with aldehydes studied under atmospheric conditions, *Environ. Sci. Tech.*, *15*, 960–963.

Kerr, J.A., and D.W. Stocker (1986a), Kinetics of the reactions of hydroxyl radicals with alkyl nitrates and with some oxygen-containing organic compounds studied under simulated atmospheric conditions, *J. Atmos. Chem.*, *4*, 253–262.

Kerr, J.A, and D.W. Stocker (1986b), The photo-oxidations of propyl acetates in synthetic air–HONO–NO_x mixtures: Product formation studies and proposed kinetic mechanisms, *J. Atmos. Chem.*, *4*, 263–276.

Kerr, J.A., and D.W. Stocker (2001–2002), Strengths of chemical bonds, in, editor D.R. Lide, *CRC Handbook of Chemistry and Physics*, 82nd edition, CRC Press, Boca Raton, pp.9-51–9-74.

Kesselmeier, J., and M. Straudt (1999), Biogenic volatile organic compounds (VOC): An overview on emission, physiology and ecology, *J. Atmos. Chem.*, *13*, 23–88.

Keyser, L.F. (1980), Absolute rate constant of the reaction between chlorine (^{2}P) atoms and hydrogen peroxide from 298 to 424 K, *J. Phys. Chem.*, *84*, 11–14.

Khamaganov, V.G., V.X. Bui, S.A. Carl, and J. Peeters (2006), Absolute rate coefficient of the OH + $CH_3C(O)OH$ reaction at $T = 287$–802 K. The two faces of pre-reactive H-bonding, *J. Phys. Chem. A*, *110*, 12852–12859.

Khamaganov. V., R. Karunanandan, A. Rodriguez, and J.N. Crowley (2007), Photolysis of $CH_3C(O)CH_3$ (248 nm, 266 nm), $CH_3C(O)C_2H_5$ (248 nm) and $CH_3C(O)Br$ (248 nm): Pressure dependent quantum yields of CH_3 formation, *Phys. Chem. Chem. Phys.*, *9*, 4098–4113.

Khan, I., P. Brimblecombe, and S.L. Clegg (1995), Solubilities of pyruvic acid and the lower (C_1–C_6) carboxylic acids. Experimental determination of equilibrium vapor pressures above pure aqueous and salt solutions, *J. Atmos. Chem.*, *22*, 285–302.

Kim, K.K., E.R. Lovejoy, and C.B. Moore (1995), Transition state vibrational level thresholds for the dissociation of triplet ketene, *J. Chem. Phys.*, *102*, 3202–3219.

Kim, S. K., Y.S. Choi, C.D. Pibel, Q.K. Zheng, and C.B. Moore (1991), Determination of the singlet/triplet branching ratio in the photodissociation of ketene, *J. Chem. Phys.*, *94*, 1954–1960.

Kind, I., T. Berndt, O. Böge, and W. Rolle (1996a), Gas-phase rate constants for the reaction of NO_3 radicals with selected oxiranes, *Chem. Phys. Lett.*, *249*, 35–39.

Kind, I., T. Berndt, O. Böge, and W. Rolle (1996b), Gas-phase rate constants for the reaction of NO_3 radicals with furan and methyl-substituted furans, *Chem. Phys. Lett.*, *256*, 679–683.

King, R.A., W.D. Allen, B. Ma, and H.F. Schaefer III (1998), Fragmentation surface of triplet ketene, *Faraday Discuss.*, *110*, 23–50.

King, R.A., W.D. Allen, and H.F. Schaefer III (2000), On apparent quantized transition-state thresholds in the photofragmentation of acetaldehyde, *J. Chem. Phys. 112*, 5585–5592.

Kirk, A.D., and G.B. Porter (1962), Kinetics of excited molecules. III. Photooxidation of acetone, *J. Phys. Chem.*, *66*, 556–557.

Kistiakowski, G.B., and B.H. Mahan (1957), The photolysis of methyl ketene, *J. Am. Chem. Soc.*, *79*, 2412–2419.

Kistiakowsky, G.B., and W.L. Marshall (1952), Photochemical decomposition of ketene. III, *J. Am. Chem. Soc.*, *74*, 88–91.

Kistiakowsky, G.B., and N.W. Rosenberg (1950), Photochemical decomposition of ketene. II, *J. Am. Chem. Soc.*, *72*, 321–326.

Klawatsch-Carrasco, N., J.F. Doussin, and P. Carlier (2004), Absolute rate constants for the gas-phase ozonolysis of isoprene and methylbutenol, *Int. J. Chem. Kinet.*, *36*, 152–156.

Kleindienst, T.E., G.W. Harris, and J.N. Pitts Jr. (1982), Rates and temperature dependences of the reaction of OH with isoprene, its oxidation products, and selected terpenes, *Environ. Sci. Technol.*, *16*, 844–846.

Kleindienst, T.E., D.F. Smith, W. Li, E.O. Edney, D.J. Driscoll, R.E. Speer, and W.S. Weathers (1999), Secondary organic aerosol formation from the oxidation of aromatic hydrocarbons in the presence of dry submicron ammonium sulfate aerosol, *Atmos. Environ.*, *33*, 3669–3681.

Klemm, R.F., D.N. Morrison, P. Gilderson, and A.T. Blades (1965), The photolysis of cyclopentanone and cyclobutanone, *Can. J. Chem.*, *43*, 1934–1941.

Klemm, R.B., E.G. Skolnik, and J.V. Michael (1980), Absolute rate parameters for the reaction of atomic oxygen(^{3}P) with formaldehyde over the temperature range 250 to 750 K, *J. Chem. Phys.*, *72*, 1256–1264.

Klippenstein, S.J., A.L.L. East, and W.D. Allen (1996), A high level ab initio map and direct statistical treatment of the fragmentation of singlet ketene, *J. Chem. Phys.*, *105*, 118–140.

Klippenstein, S.J., and R.A. Marcus (1989), Application of unimolecular reaction rate theory for highly flexible transition states to the dissociation of CH_2CO into CH_2 and CO, *J. Chem. Phys.*, *91*, 2280–2292.

Klöpffer, V.W., R. Frank, E. Kohl, and F. Haag (1986), Quantitative erfassung der photochemischen transformatiosprozesse in der troposphäre, *Chemiker-Zeitung*, *110*, 57–61.

Klotz, B., I. Barnes, and K.H. Becker (1998a), New results on the atmospheric photooxidation of simple alkylbenzenes, *Chem. Phys.*, *231*, 289–301.

Klotz, B., I. Barnes, and K.H. Becker (1999), Kinetic study of the gas-phase photolysis and OH radical reaction of E,Z- and E,E-2,4-hexadiendial, *Int. J. Chem. Kinet.*, *31*, 689–697.

Klotz, B., I. Barnes, K.H. Becker, and B.T. Golding (1997), Atmospheric chemistry of benzene oxide/oxepin, *J. Chem. Soc., Faraday Trans.*, *93*, 1507–1516.

Klotz, B., I. Barnes, B.T. Golding, and K.H. Becker (2000), Atmospheric chemistry of toluene-1,2-oxide/2-methyloxepin, *Phys. Chem. Chem. Phys.*, *2*, 227–235.

Klotz, B., I. Barnes, and T. Imamura (2004), Product study of the gas-phase reaction of O_3, OH and O_3 radicals with methyl vinyl ether, *Phys. Chem. Chem. Phys.*, *6*, 1725–1734.

Klotz, B.G., A. Bierbach, I. Barnes, and K.H. Becker (1995), Kinetic and mechanistic study of the atmospheric chemistry of muconaldehydes, *Environ. Sci. Technol.*, *29*, 2322–2332.

Klotz, B., F. Graedler, S. Sørensen, I. Barnes, and K.-H. Becker (2001), A kinetic study of the atmospheric photolysis of α-dicarbonyls, *Int. J. Chem. Kinet.*, *33*, 9–20.

Klotz, B., S. Sørensen, I. Barnes, K.H. Becker, T. Etzkorn, R. Volkamer, U. Platt, K. Wirtz, and M. Martin-Reviejo (1998b), Atmospheric oxidation of toluene in a large-volume outdoor photoreactor: In situ determination of ring-retaining product yields, *J. Phys. Chem. A*, *102*, 10289–10299.

Knight, G., A.R. Ravishankara, and J.G. Burkholder (2002), UV absorption cross sections of HO_2NO_2 between 342 and 273 K, *Phys. Chem. Chem. Phys.*, *4*, 1432–1437.

Knispel, R., R. Koch, M. Siese, and C. Zetzsch (1990), Adduct formation of OH radicals with benzene, toluene, and phenol and consecutive reactions of the adducts with NO_x and O_2, *Ber. Bunsenges. Phys. Chem*., 94, 1375–1379.

Koch, D.M., N.H. Khieu, and G.H. Peslherbe (2001), Ab initio studies of the glyoxal unimolecular dissociation pathways, *J. Phys. Chem. A*, *105*, 3598–3604.

Koch, R., W.-U. Palm, and C. Zetzsch (1997), First rate constants for reactions of OH radical with amides, *Int. J. Chem. Kinet.*, *29*, 81–87.

Koch, S., and G. K. Moortgat (1990), Rate and mechanism of the reaction Cl + CH_3COOH, *Chem. Phys. Lett.*, *173*, 531–536.

Koch, S., and G.K. Moortgat (1998), Photochemistry of methylglyoxal in the vapor phase, *J. Phys. Chem. A*, *102*, 9142–9153.

Kondo, O., and S. W. Benson (1984), Kinetics and equlibria of the reaction between bromine and ethyl ether.The C—H bond dissociation energy in ethyl ether, *Int. J. Chem. Kinet.*, *16*, 949–960.

Kovacs, G., T. Szasz-Vadasz, V.C. Papadimitriou, S. Dóbé, T. Bérces, and F. Marta (2005), Absolute rate constants for the reactions of OH radicals with CH_3CH_2OH, CF_2HCH_2OH and CF_3CH_2OH, *React. Kinet. Catal. Lett.*, *87*, 129–138.

Kramp, F., and S. E. Paulson (1998), On the uncertainties in the rate coefficients for OH reactions with hydrocarbons, and the rate coefficients of the 1,3,5-trimethylbenzene and *m*-xylene reactions with OH radicals in the gas phase, *J. Phys. Chem. A*, *102*, 2685–2690.

Kramp, F., and S.E. Paulson (2000), The gas phase reaction of ozone with 1,3-butadiene: Formation yields of some toxic products, *Atmos. Environ.*, *34*, 35–43.

Kraus, J.W., and J.G. Calvert (1957), The disproportionation and combination reactions of butyl free radicals, *J. Am. Chem. Soc.*, *79*, 5921–5926.

Kroll, J.H., and J.H. Seinfeld (2008), Chemistry of secondary organic aerosol: Formation and evolution of low-volatility organics in the atmosphere, *Atmos. Environ.*, *42*, 3593–3624.

Kuntz, R.L., S.L. Kopczynski, and J.J. Bufalini (1973), Photochemical reactivity of benzaldehyde–NO_x and benzaldehyde-hydrocarbon–NO_x mixtures, *Environ. Sci. Techol.*, *7*, 1119–1123.

Kurosaki, Y., and K. Yokoyama (2002), Photodissociation of acetaldehyde, $CH_3CHO \rightarrow CH_4 + CO$: Direct ab initio dynamics study, *J. Phys. Chem.*, *106*, 11415–11421.

Kurylo, M.J., K.D. Cornett, and J.L. Murphy (1982), The temperature dependence of the rate constant for the reaction of hydroxyl radicals with nitric acid, *J. Geophys. Res.*, *87*, 3081–3085.

Kutschke, K.O., M.H.J. Wijnen, and E.W.R. Steacie (1952), Mechanism of the photolysis of diethyl ketone, *J. Am. Chem. Soc.*, *74*, 714–718.

Kutsuna, S., L. Chen, T. Abe, J. Mizukado, T. Uchimaru, K. Tokuhashi, and A. Sekiya (2005), Henry's law constants of 2,2,2-trifluoroethyl formate, ethyl trifluoroacetate, and non-fluorinated analogous esters, *Atmos. Environ.*, *39*, 5884–5892.

Kutsuna, S., L. Chen, K. Ohno, K. Tokuhashi, and A. Sekiya (2004), Henry's law constants and hydrolysis rate constants of 2,2,2-trifluoroethyl acetate and methyl trifluoroacetate, *Atmos. Environ.*, *38*, 725–732.

Kwok, E.S.C., J. Arey, and R. Atkinson (1994a), Gas-phase atmospheric chemistry of dibenzo-*p*-dioxin and dibenzofuran, *Environ. Sci. Technol.*, *28*, 528–533.

Kwok, E.S.C., S.M. Aschmann, J. Arey, and R. Atkinson (1996a), Product formation from the reaction of the NO_3 radical with isoprene and rate constants for the reactions of methacrolein and methyl vinyl ketone with the NO_3 radical, *Int. J. Chem. Kinet.*, *28*, 925–934.

Kwok, E.S.C., S.M. Aschmann, and R. Atkinson (1996b), Rate constants for the gas-phase reactions of the OH radical with selected carbamates and lactates, *Env. Sci. Technol.*, *30*, 329–334.

Kwok, E.S.C., and R. Atkinson (1995), Estimation of hydroxyl radical reaction rate constants for gas-phase organic compounds using a structure–reactivity relationship: An update, *Atmos. Environ.*, *29*, 1685–1695.

Kwok, E.S.C., R. Atkinson, and J. Arey (1994b), Kinetics and mechanisms of the gas-phase reactions of the NO_3 radical with aromatic compounds, *Int. J. Chem. Kinet.*, *26*, 511–525.

Kwok, E.S.C., R. Atkinson, and J. Arey (1995), Rate constants for the gas-phase reactions of the OH radical with dichlorobiphenyls, 1-chlorodibenzo-*p*-dioxin, 1,2-dimethoxybenzene, and diphenyl ether: Estimation of OH radical reaction rate constants for PCBs, PCDDs, and PCDFs, *Environ. Sci. Technol.*, *29*, 1591–1598.

Lahmani, F., C. Lardeux, M. Lavollée, and D. Solgadi (1980a), Photodissociation of methyl nitrite in the vacuum ultraviolet. I. Identification and quantum yields of electronically excited NO products, *J. Chem. Phys.*, *73*, 1187–1192.

Lahmani, F., C. Lardeux, and D. Solgadi (1980b), Photodissociation of methyl nitrite in the vacuum ultraviolet. II. Excitation energy dependence of the NO fluorescent fragments, *J. Chem. Phys.*, *73*, 4433–4438.

Lahmani, F., C. Lardeux, and D. Solgadi (1983), Photofragmentation of CH_3ONO at 355 nm. Energy distribution in the NO fragment, *Chem. Phys. Lett.*, *102*, 523–528.

Laimgruber, S., W.J. Schreier, T. Schrader, F. Koller, W. Zinth, and P. Gilch (2005), The photochemistry of *o*-nitrobenzaldeyde as seen by femtosecond vibrational spectroscopy, *Angew. Chem. Int. Ed.*, *44*, 7901–7904.

Lamb, B., D. Gay, H. Westberg, and T. Pierce (1993), A biogenic hydrocarbon emission inventory for the U.S.A. using a simple forest canopy model, *Atmos. Environ.*, *27A*, 1673–1690.

Lamb, B., A. Guenther, D. Gay, and H. Westberg (1987), A national inventory of biogenic hydrocarbon emissions, *Atmos. Environ*, *21*, 1695–1705.

Lamb, J.J., L.T. Molina, C.A. Smith, and M.J. Molina (1983), Rate constant of the OH + H_2O_2 → HO_2 + H_2O, *J. Phys. Chem.*, *87*, 4467–4470.

Lammel, G., and J.N. Cape (1996), Nitrous acid and nitrite in the atmosphere, *Chem. Soc. Revs.*, *1996*, 361–369.

Lammel, G., and D. Perner (1988), The atmospheric aerosol as a source of nitrous-acid in the polluted atmosphere, *J. Aerosol Sci.*, *19*, 1199–1202.

Land, E.J., and G. Porter (1963), Primary photochemical processes in aromatic molecules. Part 7. Spectra and kinetics of some phenoxyl derivatives, *Trans. Faraday Soc.*, *59*, 2016–2026.

Láng, L.(1961–1971), *Absorption Spectra in the Ultraviolet and Visible Region*, Academic Press Inc., New York.

Langbein, T., H. Sonntag, D. Trapp, A. Hoffmann, W. Malms, E.-P. Röth, V. Mörs, and R. Zellner (1999), Volatile anaesthetics and the atmosphere: Atmospheric lifetimes and atmospheric effects of halothane, enflurane, isoflurane, desflurane and sevoflurane, *Br. J. Anaesth*, *82*, 66–73.

Langer, S., and E. Ljungström (1994a), Rates of reaction between the nitrate radical and some aliphatic ethers, *Int. J. Chem. Kinet.*, *26*, 367–380.

Langer, S., and E. Ljungström (1994b), Reaction of the nitrate radical with some potential automotive fuel additives. A kinetic and mechanistic study, *J. Phys. Chem.*, *98*, 5906–5912.

Langer, S., and E. Ljungström (1995), Rates of reactions between the nitrate radical and some aliphatic alcohols, *J. Chem. Soc., Faraday Trans.*, *91*, 405–410.

Langer, S., E. Ljungström, T. Ellermann, O. J. Nielsen, and J. Sehested (1995), UV absorption spectrum of CH_3OCH_2 radicals and kinetics of the reaction of $CH_3OCH_2O_2$ radicals with NO and NO_2 in the gas phase, *Chem. Phys. Lett.*, *240*, 53–56.

Langer, S., E. Ljungström, and I. Wängberg (1993), Rates of reaction between the nitrate radical and some aliphatic esters, *J. Chem. Soc., Faraday Trans.*, *89*, 425–431.

Langer, S., E. Ljungström, I. Wängberg, T. J. Wallington, M. D. Hurley, and O. J. Nielsen (1996), Atmospheric chemistry of di-*tert*-butyl ether: Rates and products of the reactions with chlorine atoms, hydroxyl radicals, and nitrate radicals, *Int. J. Chem. Kinet.*, *28*, 299–305.

Langford, A.O., and C.B. Moore (1984a), Reaction and relaxation of vibrationally excited formyl radicals, *J. Chem. Phys.*, *80*, 4204–4210.

Langford, A.O., and C.B. Moore (1984b), Collision complex formation in the reaction of formyl radicals with nitric oxide and oxygen, *J. Chem. Phys.*, *80*, 4211–4221.

Lao, K.Q., E. Jensen, P.W. Kash, and L.J. Butler (1990), Polarized emission spectroscopy of photodissociating nitromethane at 200 and 218 nm, *J. Chem. Phys.*, *93*, 3958–3969.

Laufer, A.H., and R.A. Keller (1971), Lowest excited states of ketene, *J. Am. Chem. Soc.*, *93*, 61–63.

Laurent, J.P., and D.T. Allen (2004), Size distributions of organic functional groups in ambient aerosol collected in Houston Texas, *Aerosol Science and Technology*, *38*, 82–91.

Lavi, R., D. Schwartz-Lavi, I. Bar, and S. Rosenwaks (1987), Directional properties in photodissociation: A probe for the symmetry and geometry of excited states of dimethylnitrosamine and *tert*-butyl nitrite, *J. Phys. Chem.*, *91*, 5398–5402.

Law, K.S., P.H. Plantevin, D.E. Shallcross, H.L. Rogers, J.A. Pyle, C. Grouhel, V. Thouret, and A. Marenco (1998), Evaluation of modeled O_3 using Measurement of Ozone by Airbus In-Service Aircraft (MOZAIC) data, *J. Geophys. Res. 103*, 25721–25737.

Le Calvé, S., D. Hitier, G. Le Bras, and A. Mellouki (1998), Kinetic studies of OH reactions with a series of ketones, *J. Phys. Chem. A*, *102*, 4579–4584.

Le Calvé, S., G. Le Bras, and A. Mellouki (1997a), Temperature dependence for the rate coefficients of the reactions of the OH radical with a series of formates, *J. Phys. Chem. A*, *101*, 5489–5493.

LeCalvé, S., G. Le Bras, and A. Mellouki (1997b), Kinetic studies of OH reactions with a series of methyl esters, *J. Phys. Chem. A*, *101*, 9137–9141.

LeCalvé, S., G. Le Bras, and A. Mellouki (1997c), Kinetic studies of OH reactions with *iso*-propyl, *iso*-butyl, *sec*-butyl, and *tert*-butyl acetate, *Int. J. Chem. Kinet.*, *29*, 683–688.

Le Calvé, S., A. Mellouki, and G. Le Bras (2002), Kinetic studies of OH reactions with propylal, butylal and 1,3-dioxolane, *Phys. Chem. Chem. Phys.*, *4*, 5622–5626.

Le Calvé, S., A. Mellouki, G. Le Bras, J. Treacy, J. Wenger, and H. Sidebottom (2000), Kinetic studies of OH and O_3 reactions with allyl and isopropenyl acetate, *J. Atmos. Chem.*, *37*, 161–172.

Le Crâne, J.P., E. Villenave, M.D. Hurley, T.J. Wallington, and J.C. Ball (2005), Atmospheric chemistry of propionaldehyde: Kinetics and mechanisms of reactions with OH radicals and Cl atoms, UV spectrum, and self-reaction kinetics of $CH_3CH_2C(O)O_2$ radicals at 298 K, *J. Phys. Chem. A*, *109*, 11837–11850.

Le Crâne, J-P., E. Villenave, M.D. Hurley, T.J. Wallington, S. Nishida, K. Takahashi, and Y. Matsumi (2004), Atmospheric chemistry of pivalaldehyde and isobutyraldehyde: Kinetics and mechanisms of reactions with Cl atoms, Fate of $(CH_3)_3CC(O)$ and $(CH_3)_2CHC(O)$ Radicals, and self-reaction kinetics of $(CH_3)_3CC(O)O_2$ and $(CH_3)_2CHC(O)O_2$ Radicals, *J. Phys. Chem*, *A*, *108*, 795–805.

Lee, A., A.H. Goldstein, M.D. Keywood, S. Gao, V. Varutbangkul, R. Bahreini, N.L. Ng, R.C. Flagan, and J.H. Seinfeld (2006), Gas-phase products and secondary aerosol yields from the ozonolysis of ten different terpenes, *J. Geophys. Res.*, *111*, D07302, doi:10.1029/2005JD006437, 2006.

Lee, E.K.C. (1967), Benzene photosensitization of cyclopentanone and cyclopentanone-2-*t*, *J. Phys. Chem.*, *71*, 2804–2813.

Lee, E.K.C., and R.S. Lewis (1980), Photochemistry of simple aldehydes and ketones in the gas phase, *Adv. Photochem.*, *12*, 1–96.

Lee, J.H., D.F. Leahy, I.N. Tang, and L. Newman (1993), Measurement and speciation of gas phase peroxides in the atmosphere, *J. Geophys. Res.*, *98*, 2911–1915.

Lee, J. H., and I. N. Tang (1982), Absolute rate constants for the hydroxyl radical reactions with ethane, furan, and thiophene at room temperature, *J. Chem. Phys.*, *77*, 4459–4463.

Lee, J. H., and R.B. Timmons (1977), Kinetics and mechanism of the gas-phase reaction of atomic oxygen (O^3P) atoms with acetone, *Int. J. Chem. Kinet. 9*, 133–139.

Lee, Y.-N., X. Zhou, and K. Hallock (1995), Atmospheric carbonyl compounds at a rural southeastern United States site, *J. Geophys. Res.*, *100*, 25933–25944.

Legreid, G., J.B. Lööv, J. Staehelin, C. Hueglin, M. Hill, B. Buchmann, A.S.H. Prevot, and S. Reimann (2007), Oxygenated volatile organic compounds (OVOCs) at an urban background site in Zürich (Europe): Seasonal variation and source allocation, *Atmos. Environ.*, *41*, 8409–8423.

Leibrock, E., and J. Slemr (1997), Method for measurement of volatile oxygenated hydrocarbons in ambient air, *Atmos. Environ.*, *31*, 3329–3339.

Leighton, P.A., and F.E. Blacet (1933), The photolysis of the aliphatic aldehydes. II. Acetaldehyde, *J. Am. Chem. Soc.*, *55*, 1766–1774.

Leighton, P.A., and F.A. Lucy (1934a), Photoisomerization of *o*-nitrobenzaldehydes. I. Photochemical results, *J. Chem. Phys.*, *2*, 756–759.

Leighton, P.A., and F.A. Lucy (1934b), Photoisomerization of *o*-nitrobenzaldehydes. II. Mathematical treatment, *J. Chem. Phys.*, *2*, 760–766.

Lelieveld, J., T.M. Butler, J.N. Crowley, T.J. Dillon, H. Fischer, L. Ganzeveld, H. Harder, M.G. Lawrence, M. Martinez, D. Taraborrelli, and J. Williams (2008), Atmospheric oxidation capacity sustained by a tropical forest, *Nature*, *452*, 737–740.

Lelieveld, J., and P.J. Crutzen (1990), Influences of cloud photochemical processes on tropospheric ozone, *Nature*, *343*, 227–233.

Le Person, A., G. Solignac, F. Oussar, V. Daële, A. Mellouki, R. Winterhalter, and G.K. Moortgat (2009), Gas phase reaction of allyl alcohol (2-propen-1-ol) with OH radicals and ozone, *Phys. Chem. Chem. Phys.*, *11*, 7619–7628.

Lesclaux, R., and M. Demissy (1977), On the reaction of NH_2 radical with O_2, NO, and NO_2, *Nouv. J. Chim.*, *1*, 443–444.

Lesclaux, R., P.V. Khe, P. Dezauzler, and J.C. Soulignac (1975), Flash photolysis studies of the reaction of NH_2 radicals with NO, *Chem. Phys. Lett.*, *35*, 493–497.

Leu, M.-T., and W.B. DeMore (1976), Rate constants at 295 K for the reactions of atomic chlorine with H_2O_2, HO_2, O_3, CH_4 and HNO_3, *Chem. Phys. Lett.*, *41*, 121–124.

Lewis, A.C., M.J. Evans, J. Methven, N. Watson, J.D. Lee, J.R. Hopkins, R.M. Purvis, S.R. Arnold, J.G. McQuaid, L.K. Whalley, M.J. Pilling, D.E. Heard, P.S. Monks, A.E. Parker, C.E. Reeves, D.E. Oram, G. Mills, B.J. Bandy, D. Stewart, H. Coe, P. Williams, and J. Crosier (2007), Chemical composition observed over the mid-Atlantic and the detection of pollution signatures far from source regions, *J. Geophys. Res.*, *112*, D10839, doi:10.1029/2006JD007584.

Lewis, A. C., J.R. Hopkins, L.J. Carpenter, J. Stanton, K.A. Read, and M.J. Pilling (2005), Sources and sinks of acetone, methanol, and acetaldehyde in North Atlantic marine air, *Atmos. Chem. Phys.*, *5*, 1963–1974.

Lewis, P.J., K.A. Bennett, and J.N. Harvey (2005), A computational study of the atmospheric oxidation of nopinone, *Phys. Chem. Chem. Phys.*, *7*, 1643–1649.

Li, Q., R.T. Carter, and J.R. Huber (2001), The photodissociation dynamics of nitric acid studied at 193 nm by LIF and REMPI-TOF methods, *Chem. Phys. Lett.*, *334*, 39–46.

Li, Q., M.C. Osborne, and I.W.M. Smith (2000a), Rate constants for the reactions of Cl atoms with HCOOH and with HOCO radicals, *Int. J. Chem. Kinet.*, *32*, 85–91.

Li, Q.-S., F. Zhang, W.-H. Fang, and J.-G. Yu (2006), Probing mechanistic photochemistry of glyoxal in the gas phase by *ab initio* calculations of potential-energy surfaces and adiabatic and nonadiabatic rates, *J. Chem. Phys.*, *124*, 054324-1–054324-10.

Li, Z., G.-R. Jeong, J.C. Hansen, D.A. Good, and J.S. Francisco (2000b), Rate constant for the reaction of $CF_3OCHFCF_3$ with OH and Cl, *Chem. Phys. Lett.*, *320*, 70–76.

Li, Z.J., and A. Pirasteh (2006), Kinetic study of the reactions of atomic chlorine with several volatile organic compounds at 240–340 K, *Int. J. Chem. Kinet.*, *38*, 386–398.

Li, Z., Z. Tao, V. Naik, D.A. Good, J.C. Hansen, G.-R. Jeong, J.S. Francisco, A.K. Jain, and D.J. Wuebbles (2000c), Global warming potential assessment for $CF_3OCF{=}CF_2$, *J. Geophys. Res.*, *105*, 4019–4029.

Liberles, A., S. Kang, and A. Greenberg (1973), Semiempirical calculations on the ring opening of substituted cyclopropanones, *J. Org. Chem.*, *38*, 1922–1924.

Libuda, H.G. (1992), Spektroskopische und kinetische Untersuchengen an halogenierten Carbonylverbindungen von atmosphärischen Interesse, Ph.D. Thesis, University of Wuppertal.

Libuda, H.G., F. Zabel, E.H. Fink, and K.H. Becker (1990), Formyl chloride: UV absorption cross sections and rate constants for the reactions with Cl and OH, *J. Phys. Chem.*, *94*, 5860–5865.

Lide, D.R. (2001–2002), *CRC Handbook of Chemistry and Physics*, 82nd Edition, CRC Press, Boca Raton.

Lightfoot, P.D., S.P. Kirwan, and M.J. Pilling (1988), Photolysis of acetone at 193.3 nm, *J. Phys. Chem.*, *92*, 4938–4946.

Lim, Y.B., and P.J. Ziemann (2005), Products and mechanism of secondary organic aerosol formation from reactions of *n*-alkanes with OH radicals in the presence of NO_x, *Environ. Sci. Technol.*, *39*, 9229–9236.

Lin, C.L., N.K. Ruhztgi, and W.B. DeMore (1998), Ultraviolet-absorption cross-sections of hydrogen peroxide, *Geophys. Res. Lett.*, *5*, 113–115.

Lindley, C.R.C. (1978), The kinetics of $(CH_3)_2N$ radical reactions in simulated atmospheres: The formation of $(CH_3)_2NNO$ and $(CH_3)_2NNO_2$, Ph.D. Dissertation, Chemistry Department, The Ohio State University, 1978.

Lindley, C.R.C., J.G. Calvert, and J.H. Shaw (1979), Rate studies of the reactions of the $(CH_3)_2N$ radical with O_2, NO, and NO_2, *Chem. Phys. Lett.*, *67*, 57–62.

Lipczynska-Kochany, E., and J.R. Botton (1992), Flash photolysis/high-performance liquid chromatography method for studying the sequence of photochemical reactions: Direct photoylsis of phenol, *Environ. Sci. Technol.*, *26*, 2524–2527.

Lissi, E.A., E. Abuin, and M.V. Encina (1973/1974), Photochemistry of butanone and methyl butanone, *J. Photochem.*, *2*, 377–392.

Liu, R., P. Dagaut, R.E. Huie, and M.J. Kurylo (1990a), A flash photolysis resonance fluorescence investigation of the reaction of oxygen $O(^3P)$ atoms with aliphatic ethers and diethers in the gas phase, *Int. J. Chem. Kinet.*, *22*, 711–717.

Liu, R., R.E. Huie, and M.J. Kurylo (1990b) The gas phase reactions of hydroxyl radicals with a series of nitroalkanes over the temperature range 240–440 K, *Chem. Phys. Letters*, *167*, 519–523.

Liu, X. (1999), Atmospheric photochemistry study of 1,4-unsaturated dicarbonyls and dienes, Ph.D. Thesis, University of North Carolina Chapel Hill, Chapel Hill, NC.

Liu, X., H.E. Jeffries, and K.G. Sexton (1999), Atmospheric photochemical degradation of 1,4-unsaturated dicarbonyls, *Environ. Sci. Technol.*, *33*, 4212–4220.

Livermore, R.A., and L. Phillips (1966), Reactions in the diethyl peroxide–nitric oxide system. Part. III. The pressure dependence of the combination of ethoxyl radicals with nitric oxide, *J. Chem. Soc.*, *B*, *1966*, 640–643.

Lloyd, A.C., K.R. Darnall, A.M. Winer, and J.N. Pitts, Jr. (1976), Relative rate constants for the reactions of OH radicals with isopropyl alcohol, diethyl and di-*n*-propyl ether at 305 ± 2 K, *Chem. Phys. Lett.*, *42*, 205–209.

Loewen, M., F. Wania, F. Wang, and G. Tomy (2008), Altitudinal transect of atmospheric and aqueous fluorinated organic compounds in Western Canada, *Environ. Sci. Technol.*, *42*, 2374–2379.

Loge, G.W., and C.S. Parmenter (1981), Collision-free dissociation after excitation of single rotational levels S_1 glyoxal, *J. Phys. Chem.*, *85*, 1653–1662.

Loge, G. W., C.S. Parmenter, and B.F. Bordorf (1980), Predissociation in the S_1 zero-point level of glyoxal vapor questionable: a query, *Chem. Phys. Lett.*, *74*, 309–313.

Lohmann, R., E. Jorado, J. Dachs, U. Lohmann, and K. C. Jones (2006), Quantifying the importance of the atmospheric sink for polychlorinated dioxins and furans relative to other global loss processes, *J. Geophys. Res.*, *111*, D21303, doi:10.1029/2005JD006923.

Long, S.R., J.T. Meek, P.J. Harrington, and J.P. Reilly (1983), Benzaldehyde photochemistry studied with laser ionization mass and photoelectron spectroscopy, *J. Chem. Phys.*, *78*, 3341–3343.

Lorenz, K., and R. Zellner (1984), Rate constants and vinoxy product yield in the reaction OH + ethylene oxide, *Ber. Bunsenges. Phys. Chem.*, *88*, 1228–1231.

Lovejoy, E.R., L.G. Huey, and D.R. Hanson (1995), Atmospheric fate of CF_3OH. 2: Heterogeneous reaction, *J. Geophys. Res.*, *100*, 18775–18780.

Lovejoy, E.R., S.K. Kim, R.A. Alvarez, and C.B. Moore (1991), Kinetics of intramolecular carbon atom exchange in ketene, *J. Chem. Phys.*, *95*, 4081–4093.

Lovejoy, E.R., S.K. Kim, and C.B. Moore (1992), Observation of transition-state vibrational thresholds in the rate of dissociation of ketene, *Sci.*, *256*, 1541–1544.

Lovejoy, E.R., T.P. Murrells, A.R. Ravishankara, and C.J. Howard (1990), Oxidation of CS_2 by reaction with OH. 2. Yields of HO_2 and SO_2 in oxygen, *J. Phys. Chem.*, *94*, 2386.

Ludwig, B.E., and G.R. McMillan (1967), Disproportionation and combination reactions of isopropoxy radicals with nitric oxide, *J. Phys. Chem.*, *71*, 762–764.

Ludwig, B.E., and G.R. McMillan (1969), Primary quantum yields in photodissociation of isopropyl nitrite, *J. Am. Chem. Soc.*, *91*, 1085–1088.

Luebkert, B., and W. Schoepp (1989), A model to calculate natural VOC emissions from forests in Europe, *Inter. Inst. For Apppl. Sys. Anal.*, Working Paper WP-89-082.

Luke, W.T., and R.R. Dickerson (1988), Direct measurements of the photolysis rate coefficient of ethyl nitrate, *Geophys. Res. Lett.*, *15*, 1181–1184.

Luke, W.T., R.R. Dickerson, and L.J. Nunnermacker (1989), Direct measurements of the photolysis rate coefficients and Henry's law constants of several alkyl nitrates, *J. Geophys. Res.*, *94*, 14905–14921.

Lüttke, J., and K. Levsen (1997), Phase partitioning of phenol and nitrophenols in clouds, *Atm. Environ.*, *31*, 2649–2655.

Lüttke, J., V. Scheer, K. Levsen, G. Wünsch, J.N. Cape, K.J. Hargreaves, R.L. Storeton-West, K. Acker, W. Wieprecht, and B. Jones (1997), Occurrence and formation of nitrated phenols in and out of cloud, *Atmos. Environ.*, *31*, 2637–2648.

Ma, S., I. Barnes, and K.H. Becker (1998), Atmospheric degradation of glycidaldehyde: Photolysis and reaction with OH radicals, *Environ. Sci. Technol.*, *32*, 3515–3521.

MacDonald, R., and R. Fall (1993), Detection of substantial emissions of methanol from plants to the atmosphere, *Atmos. Environ.*, *27A*, 1709–1713.

Mack, G.P.R., and B.A. Thrush (1974), Reaction of oxygen atoms with carbonyl compounds. 2. Acetaldehyde, *J. Chem. Soc., Faraday Trans. 1:*, *70*, 178–186.

Mackay, D., W.Y. Shiu, and K.C. Ma (1995), *Illustrated Handbook of Physical-Chemical Properties and Environmental Fate of Organic Chemicals*, Lewis Publishers, Boca Raton.

Mac Leod, H., G.P. Smith, and D.M. Golden (1988), Photodissociation of pernitric acid (HO_2NO_2) at 248 nm, *J. Geophys. Res.*, *93*, 3813–3823.

Magneron, I. (1998), unpublished data, measured at the Max-Planck-Institut für Chemie, Mainz, Germany as referenced on the MPI-Mainz-UV-VIS Spectral Atlas of Gaseous Molecules, H. Keller-Rudek and G.K. Moortgat, Max Planck Institut für Chemie, Mainz, Germany.

Magneron, I., V. Bossoutrot, A. Mellouki, G. Laverdet, and G. Le Bras (2003), The OH-initiated oxidation of hexylene glycol and diacetone alcohol, *Environ. Sci. Tech.*, *37*, 4170–4181.

Magneron, I., A. Mellouki, G. Le Bras, G.K. Moortgat, A. Horowitz, and K. Wirtz (2005), Photolysis and OH-initiated oxidation of glycolaldehyde under atmospheric conditions, *J. Phys. Chem. A*, *109*, 4552–4561.

Magneron, I., J. Tadić, F. Sauer, and G.K. Moortgat (1999), Photolytic studies on glyoxal, crotonaldehyde, acrolein, and glycoaldehyde, in, editors R. Vogt,and G. Axelsdottir, *EC/EUROTRAC-2*, *Joint Workshop Chemical Mechanism Development (CMD)*, Ford Forschungszentrum Aachen, Germany, pp.66–69.

Magneron, I., R. Thévenet, A. Mellouki, G. Le Bras, G.K. Moortgat, and K. Wirtz (2002), A study of the photolysis and OH-initiated oxidation of acrolein and *trans*-crotonaldehyde, *J. Phys. Chem. A 106*, 2526–2537.

Majer, J.R., and Z.Y. Al-Saigh (1984), Photochemistry of 1,1,1-trifluoro-3-bromoacetone. 2. Dual fluorescence in the gas phase, *J. Phys. Chem.*, *88*, 1157–1159.

Majer, J.R., C. Olavesen, and J.C. Robb (1971), Wavelength effect in the photolysis of halogenated ketones, *J. Chem. Soc. (B)*, 48–55.

Majer, J.R., J.C. Robb, and Z.Y. Al-Saigh (1976), Photochemistry of 1,1,1-trifluoro-3-bromoacetone, *J. Chem. Soc.*, *72*, 1697–1706.

Maldotti, A., C. Chiorboli, C.A. Bignozzi, C. Bartocci and V. Carassiti (1980)), Photooxidation of 1,3-butadiene containing systems: Rate constant determination for the reaction of acrolein with hydroxyl free radicals, *Int. J. Chem. Kinetics*, *12*, 905–913.

Margitan, J.J., F. Kaufman, and J.G. Watson (1975), *Kinetics* of the reaction $OH + HNO_3 \rightarrow H_2O + NO_3$. *Int. J. Chem. Kinet. Symp. 1*, 281–287.

Margitan, J.J., and R.T. Watson (1982), Kinetics of the reaction of hydroxyl radicals with nitric acid, *J. Phys. Chem.*, *86*, 3819–3824.

Maricq, M.M., J.C. Ball, A.M. Straccia, and J.J. Szente (1997a), A diode laser study of the Cl + CH_3CO reaction, *Int. J. Chem. Kinet.*, *29*, 421–429.

Maricq, M.M., and J.J. Szente (1995), The 193 and 248 nm photodissociation of $CF_3C(O)Cl$, *J. Phys. Chem.*, *99*, 4554–4557.

Maricq, M.M., J.J. Szente, and J. Hybl (1997b), Kinetic studies of the oxidation of dimethyl ether and its chain reaction with Cl_2, *J. Phys. Chem. A*, *101*, 5155–5167.

Marinelli, W.J., and H.S. Johnston (1982), Reaction rates of hydroxyl radical with nitric acid and with hydrogen peroxide, *J. Chem. Phys.*, *77*, 1225–1234.

Markgraf, S.J., J. Semples, and J.R. Wells (1999), The hydroxyl radical reaction rate constant and atmospheric transformation products of 2-propoxyethanol, *Int. J. Chem. Kinet.*, 31, 315–322.

Martell, J.M., H. Yu, and J.D. Goddard (1997), Molecular decomposition of acetaldehyde and formamide: theoretical studies using Hartree-Fock, Moller-Plesset and density functional theories, *Mol. Phys.*, *82*, 497–502.

Martin, G.R., and H.C. Sutton (1952a), Radioactive tracer studies of free radical mechanisms. Part 1. The photolysis of acetone + iodine mixtures, *Trans. Faraday Soc.*, *48*, 812–823.

Martin, G.R., and H.C. Sutton (1952b), Radioactive tracer studies of free radical mechanisms. Part 2. The photolysis of methyl ethyl ketone + iodine mixtures, *Trans. Faraday Soc.*, *48*, 823–828.

Martin, J.W., M.M. Smithwick, B.M. Braune, P.F. Hekstra, D.C.G. Muir, and S.A. Mabury (2004), Identification of long-chain perfluorinated acids in biota from the Canadian Arctic, *Environ. Sci. Technol.*, *38*, 373–380.

Martin, P., E.C. Tuazon, S.M. Aschmann, J. Arey, and R. Atkinson (2002), Formation and atmospheric reactions of 4,5-dihydro-2-methylfuran, *J. Phys. Chem. A*, *106*, 11492–11501.

Martin, T.W., and J.N. Pitts, Jr. (1955), Structure and reactivity in the vapor phase photolysis of ketones. II. Methyl neopentyl ketone, *J. Am. Chem. Soc.*, *77*, 5465–5468.

Martinez, E., A. Aranda, Y. D'iaz-de-Mera, A. Rodriguez, D. Rodriguez, and A. Notario (2004), Mechanistic and kinetic study of the gas-phase reaction of atomic chlorine with cyclohexanone using an absolute and a relative technique; influence of temperature. *J. Atmos. Chem.*, *48*, 283–299.

Martinez, R.D., A.A. Buitrage, N.W. Howell, C.H. Hern, and J.A. Joens (1992), The near ultraviolet U.V. absorption spectra of several aliphatic aldehydes and ketones at 300 K, *Atmos. Environ.*, *26A*, 785–792.

Martino, P.C., P.B. Shevlin, and S.D. Worley (1977), The electronic structure of cyclopropanone, *J. Am. Chem. Soc.*, *99*, 8003–8006.

Mascal, M., and E.B. Nikitin (2008), Direct, high-yield conversion of cellulose into biofuel, *Angew. Chem. Int. Ed.*, *47*, 7924 –7926.

Mashino, M., M. Kawasaki, T.J. Wallington, and M.D. Hurley (2000), Atmospheric degradation of $CF_3OCF{=}CF_2$: Kinetics and mechanism of its reaction with OH radicals and Cl atoms, *J. Phys. Chem. A*, *104*, 2925–2930.

Mason, J. (1963), Perfluoroalkyl compounds of nitrogen. Part VI. The photolysis of trifluoronitrosomethane, *J. Chem. Soc.*, *1963*, 4537–4544.

Masson, C.R. (1952), The photolysis of di-*n*-propyl ketone, *J. Am. Chem. Soc.*, *74*, 4731–4735.

Master Chemical Mechanism (MCMv3.1: http://mcm.leeds.ac.uk/MCM/).

Maul, C., T. Haas, K.-H Gericke, and F.J. Comes (1995), Spin selectivity in the ultraviolet photodissociation of phosgene, *J. Chem. Phys.*, *102*, 3238–3247.

Maurer, T., H. Geiger, I. Barnes, K.H. Becker, and L.P. Thüner (2000), Kinetic, mechanistic and modeling study of the OH-radical-initiated oxidation of di-*n*-butoxymethane (DNBM), *J. Phys. Chem. A*, *104*, 11087–11094.

Maurer, T., H. Hass, I. Barnes, and K.H. Becker (1999), Kinetic and product study of the atmospheric photooxidation of 1,4-dioxane and its main reaction product ethylene glycol diformate, *J. Phys. Chem. A*, *103*, 5032–5039.

Mazely, T.L., R.R. Friedl, and S.P. Sander (1995), Production of NO_2 from photolysis of peroxyacetyl nitrate, *J. Phys. Chem.*, *99*, 8162–8169.

Mazely, T.L., R.R. Friedl, and S.P. Sander (1997), Quantum yield of NO_3 from peroxyacetyl nitrate photolysis, *J. Phys. Chem. A*, *101*, 7090–7097.

McCaulley, J.A., N. Kelly, M.F. Golde, and F. Kaufman (1989), Kinetic studies of the reactions of F and OH with CH_3OH, *J. Phys. Chem.*, *93*, 1014–1018.

McClelland, G.M., and J.T. Yardley (1973), Electronic and vibrational relaxation in biacetyl vapor, *J. Chem. Phys.*, *58*, 4368–4373.

McDowell, C.A., and S. Sipniades (1962), Isomerization as a primary process in the photolysis of crotonaldehyde, *J. Am. Chem. Soc.*, *84*, 4606–4607.

McGarvey, J.J., and W.D. McGrath (1964), Photochemical production of alkyl and alkoxyl radicals and their reactions with oxygen, *Trans. Faraday Soc.*, *60*, 2196–2206.

McGee, T.H. (1968), The photolysis of cyclobutanone, *J. Phys. Chem.*, *72*, 1621–1625.

McGraw, G.E., and H.S. Johnston (1969), Molecular-modulation spectrometry: CH_3ONO photolysis and detection of nitroxyl, *Int. J. Chem. Kinet.*, *1*, 89–104.

McIlroy, A., and F. P. Tully (1993), Kinetic study of OH reactions with perfluoropropene and perfluorobenzene, *J. Phys. Chem.*, *97*, 610–614.

McKee, M.L. (1989), MCSCF study of the rearrangement of nitromethane to methyl nitrite, *J. Phys. Chem.*, *93*, 7365–7369.

McKeen, S.A., T. Gierczak, J.B. Burkholder, P.O. Wennberg, T.F. Hanisco, E.R. Keim, R.-S. Gao, S.C. Liu, A.R. Ravishankara, and D.W. Fahey (1997), The photochemistry of acetone in the upper troposphere: A source of odd-hydrogen radicals, *Geophys. Res. Lett.*, *24*, 3177–3180.

McLoughlin, P., R. Kane, and I. Shanahan (1993), A relative rate study of the reaction of chlorine atoms (Cl) and hydroxyl radicals (OH) with a series of ethers, *Int. J. Chem. Kinet.*, *25*, 137–149.

McMillan, G.R. (1962), Photolysis of alkyl nitrites. I. *tert*-Butyl nitrite, *J. Am. Chem. Soc.*, *84*, 4007–4011.

McMillan, G.R. (1963), Photolysis of alkyl nitrites. The primary process in *t*-butyl nitrite at 3660 Å, *J. Phys. Chem.*, *67*, 931–932.

McMillan, G.R., J.G. Calvert, and J.N. Pitts, Jr. (1964a), Detection and lifetime of enol-acetone in the photolysis of 2-pentanone vapor, *J. Am. Chem. Soc.*, *86*, 3602–3605.

McMillan, G.R., J.G. Calvert, and S.S. Thomas (1964b), Nitrosomethane formation in photolysis of *t*-butyl nitrite, *J. Phys. Chem.*, *68*, 116–120.

McMillan, G.R., J. Kumari, and D.L. Snyder (1971), The photolysis and photooxidation of alkyl nitrites, in, editor C.S. Tuesday, *Chemical Reactions in Urban Atmospheres*, pp.35–44, American Elsevier Publishing Company, Inc., New York.

McMillan, V. (1966), referenced in, J.G. Calvert and J.N. Pitts, Jr., *Photochemistry*, John Wiley & Sons, Inc., New York.

McNesby, J.R., and A.S. Gordon (1958), Photolysis and pyrolysis of 2-pentanone-1,1,1,3,3-d_5, *J. Am. Chem. Soc.*, *80*, 261–264.

McQuaid, J.B., D.W. Stocker, and M.J. Pilling (2002), Kinetics of the reactions of OH with 2-methyl-2-cyclohexen-1-one and 3,5,5-trimethyl-2-cyclohexen-1-one under simulated atmospheric conditions, *Int. J. Chem. Kinet.*, *34*, 7–11.

Meagher, R.J., M. E. McIntosh, M.D. Hurley, and T.J. Wallington (1997), A kinetic study of the reaction of chlorine and fluorine atoms with HC(O)F at 295 ± 2 K, *Int. J. Chem. Kinet.*, *29*, 619–625.

Meier, U., H.H. Grotheer, and Th. Just (1984), Temperature dependence and branching ratio of the CH_3OH + OH reaction, *Chem. Phys. Lett.*, *106*, 97–101.

Meier, U., H.H. Grotheer, G. Reikert, and Th. Just (1985a), Study of hydroxyl reactions with methanol and ethanol by laser induced fluorescence, *Ber. Bunsenges. Phys. Chem.*, *89*, 325–327.

Meier, U., H.H. Grotheer, G. Reikert, and Th. Just (1985b), Temperature dependence and branching ratio of the C_2H_5OH + OH reaction, *Chem. Phys. Lett.*, *115*, 221–225.

Meller, R., and G.K. Moortgat (1997), $CF_3C(O)Cl$: Temperature-dependent (223–298 K) absorption cross-sections and quantum yields at 254 nm, *J. Photochem. Photobiol. A*, *108*, 105–116.

Meller, R., and G.K. Moortgat (2000), Temperature dependence of the absorption cross-sections of formaldehyde between 223–323 K in the wavelength range 225–375 nm, *J. Geophys. Res.*, *105*, 7089–7101.

Meller, R., W. Raber, J.N. Crowley, M.E. Jenkin, and G.K. Moortgat (1991), The UV-visible absorption spectrum of methylglyoxal, *J. Photochem. Photobiol. A*, *62*, 163–171.

Mellouki, A., G. Le Bras, and H. Sidebottom (2003), Kinetics and mechanisms of the oxidation of oxygenated organic compounds in the gas phase, *Chem. Rev.*, *103*, 5077–5096.

Mellouki, A., and Y. Mu (2003), On the atmospheric degradation of pyruvic acid in the gas phase, *J. Photochem. Photobiol. A*, *157*, 295–300.

Mellouki, A., F. Oussar, X. Lun, and A. Chakir (2004), Kinetics of the reactions of the OH radical with 2-methyl-1-propanol, 3-methyl-1-butanol and 3-methyl-2-butanol between 241 and 373 K, *Phys. Chem. Chem. Phys.*, *6*, 2951–2955.

Mellouki, A., S. Téton, G. Laverdet, A. Quilgars, and G. Le Bras (1994), Kinetic studies of OH reactions with H_2O_2, C_3H_8 and CH_4 using the pulsed laser photolysis–laser induced fluorscence method, *J. Chim. Phys.*, *91*, 473–487.

Mellouki, A., S. Téton, and G. Le Bras (1995), Kinetics of OH radical reactions with a series of ethers, *Int. J. Chem. Kinet.*, *27*, 791–805.

Méreau, R., M.-T. Rayez, J.-C. Rayez, F. Caralp, and R. Lesclaux (2001), Theoretical study on the atmospheric fate of carbonyl radicals: kinetics of decomposition reactions, *Phys. Chem. Chem. Phys.*, *3*, 4712–4717.

Mestdagh, J.M., M. Berdah, I. Dimicoli, M. Mons, P. Meynadier, P. d'Oliveira, F. Piuzzi, J.P. Visticot, C. Jouvet, C. Lardeux-Dedonder, S. Martrenchard-Barra, B. Soep, and D. Solgadi (1995), Observation of an indirect pathway in the femtosecond study of alkyl nitrite photodissociation in the S_1 state, *J. Chem.Phys.*, *103*, 1013–1023.

Metha, G.F., A.C. Terentis, and S.H. Kable (2002), Near threshold photochemistry of propanal, barrier height, transition state structure, and product state distributions for the HCO channel, *J. Phys. Chem. A*, *106*, 5817–5827.

Methanol Institute (2008), http://www.methanol.org/.

Meyer-Arnek, J., A. Ladstaetter-Weissenmayer, A. Richter, F. Wittrock, and J.P. Burrows (2005), A study of the trace gas columns of O_3, NO_2 and HCHO over Africa in September 1997, *Faraday Disc.*, *130*, 387–405.

Meylan, W.M., and P.H. Howard (1991), Bond contribution method for estimating Henry's law constants, *Environ. Toxicol. Chem.*, *10*, 1283–1291.

Meyrahn, H., G.K. Moortgat, and P. Warneck (1982), The photolysis of acetaldehyde under atmospheric conditions, in, editor F. Herbert, *Atmospheric Trace Constituents*, Friedr. Vieweg & Sohn, Braunschweig/Wiesbaden, pp.64–71; data tables provided to the authors by Dr. Moortgat.

Meyrahn, H., J. Pauly, W. Schneider, and P. Warneck (1986), Quantum yields for the photodissociation of acetone in air and an estimated for the life time of acetone in the lower troposphere, *J. Atmos. Chem.*, *4*, 277–291.

Michael, J., D.F. Nava, W.A. Payne, and L.J. Stief (1979a), Rate constants for the reaction of atomic chlorine with methanol and dimethyl ether from 200 to 500 K, *J. Chem. Phys.*, *70*, 3652–3656.

Michael, J.L., and W.A. Noyes, Jr. (1963), The photochemistry of mixtures of 2-pentanone and 2-hexanone with biacetyl, *J. Am. Chem. Soc.*, *85*, 1027–1032.

Michael, J.V., D.G. Keil, and R.B. Klemm (1985), Rate constants for the reaction of hydroxyl radicals with acetaldehyde from 244–528 K, *J. Chem. Phys.*, *83*, 1630–1636.

Michael, J.V., D.F. Nava, W.A. Payne, and L.J. Stief (1979b), Rate constant for the reaction of atomic chlorine with formaldehyde from 200 to 500 K, *J. Chem. Phys.*, *70*, 1147–1150.

Michael, J.V., D.A. Whytock, J.H. Lee, W.A. Payne, and L.J. Stief, L.J. (1977), Absolute rate constant for the reaction of atomic chlorine with hydrogen peroxide vapor over the temperature range 265–400 K, *J. Chem. Phys.*, *67*, 3533–3536.

Millet, D.B., D.J. Jacob, K.F. Boersma, T-M. Fu, T.P. Kurosu, K. Chance, C.L. Heald, and A. Guenther (2008b), Spatial distribution of isoprene emissions from North America derived from formaldehyde column measurements by the OMI satellite sensor, *J. Geophys. Res.*, *113*, D02307/1–D02307/18.

Millet, D.B., D.J. Jacob, T.G. Custer, J.A. de Gouw, A.H. Goldstein, T. Karl, H.B. Singh, B.C. Sive, R.W. Talbot, C. Warneke, and J. Williams (2008a), New constraints on terrestrial and oceanic sources of atmospheric methanol, *Atmos. Chem. Phys.*, *8*, 6887–6905.

Miller, C.E., J.I. Lynton, D.M. Keevil, and J.S. Francisco (1999), Dissociation pathways of peroxyacetyl nitrate (PAN), *J. Phys. Chem. A*, *103*, 11451–11459.

Miller, S.M., and M.H. Alexander (1995), Current density investigation of tunneling in photodissociation resonances: CH_3ONO, *Chem. Phys. Lett.*, 232, 451–456.

Mix, K.H., and H.Gg.Wagner (1983), Rate constants of reactions of partially oxidized hydrocarbons with oxygen atoms in the gas phase. Part II: Reactions of dimethyl ether, diethyl ether, and acetone, *Oxid. Commun.*, *5*, 321–329.

Møgelberg, T.E., O.J. Nielsen, J. Sehested, T.J. Wallington, and M.D. Hurley (1994), Atmospheric chemistry of CF_3COOH: Kinetics of the reaction with OH radicals, *Chem. Phys. Lett.*, *226*, 171–177.

Møgelberg, T.E., J. Sehested, M. Bilde, T.J. Wallington, and O.J. Nielsen (1996), Atmospheric chemistry of HFC-227ea: Spectrokinetic investigation of the $CF_3CFO_2(\bullet)CF_3$ radical, its reactions with NO and NO_2 and the atmospheric fate of the $CF_3CFO(\bullet)CF_3$ radical, *J. Phys. Chem.*, *100*, 8882–8889.

Moilanen, K.W., D.G. Crosby, J.R. Humphrey, and J.W. Giles (1978), Vapor-phase photodecomposition of chloropicrin (trichloronitromethane), *Tetrahedron*, *34*, 3345–3349.

Molina, L.T., and M.J. Molina (1981), UV absorption cross-sections of HO_2NO_2 vapor, *J. Photochemistry*, *15*, 97–108.

Molnar, A. (1990), Estimation of volatile organic compounds (VOC) emissions for Hungary, *Atmos. Environ.*, *24A*, 2855–2860.

Montzka, S.A., M. Trainer, P.D. Goldan, W.C. Kuster, and F.C. Fehsenfeld (1993), Isoprene and its oxidation products, methyl vinyl ketone and methacrolein in the rural troposphere, *J. Geophys. Res.*, *98*, 1101–1111.

Moortgat, G.K., W. Seiler, and P. Warneck (1983), Photodissociation of HCHO in air: CO and H_2 quantum yields at 220 and 300 K, *J. Chem. Phys.*, *78*, 1185–1190.

Moortgat, G.K., and P. Warneck (1979), CO and H_2 quantum yields in the photodecomposition of formaldehyde in air, *J. Chem. Phys.*, *70*, 3639–3651.

Moortgat, G.K., K. Wirtz, J. Hjorth, E. Ljungström. L. Ruppert, G. Hayman, and W. Mellouki (2002), Evaluation of radical sources in atmospheric chemistry through chamber and laboratory studies, RADICAL, Final Report on EU Project 20254 EN, Euoropean Commission, Research DG.

Morabito, P.L., Jr. (1985), The photolysis of alkyl nitrites at 366 nm and the reactions of alkoxy radicals with O_2 and NO, Ph.D. Thesis, The Pennsylvania State University.

Morabito, P., and J. Heicklen (1985a), Disproportionation to combination ratios of alkoxy radicals with nitric oxide, *J. Phys. Chem.*, *89*, 2914–2916.

Morabito, P., and J. Heicklen (1985b), Primary photochemical processes in the photolysis of alkyl nitrites at 366 nm and 23°C in the presence of ^{15}NO, *Int. J. Chem. Kinet.*, *17*, 535–546.

Morabito, P., and J. Heicklen (1987), The reactions of alkoxyl radicals with O_2. IV. *n*-C_4H_9O radicals, *Bull. Chem. Soc. Japan*, *60*, 2641–2650.

Mora-Diez, N., and R.J. Boyd (2002), A computational study of the kinetics of the NO_3 hydrogen-abstraction reaction from a series of aldehydes (XCHO: X = F, Cl, H, CH_3), *J. Phys. Chem*, *A*, *106*, 384–394.

Morey, S. (1826), Gas or vapor engine, United States Patent Number 4378.

Morgan, C.G., M. Drabbels, and A.M. Wodtke (1996), State-specific neutral time-of-flight of CO from ketene photodissociation at 351 nm: The internal energy distribution of $CH_2(X^3B_1)$, *J. Chem. Phys.*, *105*, 4550–4555.

Moriarty, J., H. Sidebottom, J. Wenger, A. Mellouki, and G. Le Bras (2003), Kinetics studies on the reactions of hydroxyl radicals with cyclic ethers and aliphatic diethers, *J. Phys. Chem. A*, *107*, 1499–1505.

Morris, E.D., Jr., and H. Niki (1971a), Mass spectrometric study of the reaction of hydroxyl radical with formaldehyde, *J. Chem. Phys.*, *55*, 1991–1992.

Morris, E.D., Jr., and H. Niki (1971b), Reactivity of hydroxyl radicals with olefins, *J. Phys. Chem.*, *75*, 3640–3641.

Morris, E.D., Jr., and H. Niki (1974), Reaction of the nitrate radical with acetaldehyde and propylene, *J. Phys. Chem.*, *78*, 1337–1338.

Morris, E.D., Jr., D.H. Stedman, and H. Niki (1971), Mass spectrometric study of the reactions of the hydroxyl radical with ethylene, propylene, and acetaldehyde in a discharge-flow system, *J. Amer. Chem. Soc*, *93*, 3570–3572.

Morris, E.R., and J.C.J. Thynne (1968), Intramolecular elimination reactions in the photolysis of fluoroaldehydes, *J. Phys. Chem.*, *72*, 3351–3352.

Morrison, B.M., and J. Heicklen (1980), The reactions of HO with CH_2O and of HCO with NO_2, *J. Photochem.*, *13*, 189–199.

Moss, A.Z., and J.T. Yardley (1974), Radiationless decay from triplet state biacetyl molecules with selected vibrational energies, *J. Chem. Phys.*, *61*, 2883–2889.

Moss, D.B., K.A. Trentelman, and P.L. Houston (1992), 193 nm photodissociation dynamics of nitromethane, *J. Chem. Phys.*, *96*, 237–247.

Mu, Y., and A. Mellouki (2001), Temperature dependence for the rate constants of the OH radicals with selected alcohols, *Chem. Phys. Lett.*, *333*, 63–68.

Mu, Y., X. Pang, J. Quan, and X. Zhang (2007), Atmospheric carbonyl compounds in Chinese background area: A remote mountain of the Qinghai-Tibetan Plateau, *J. Geophys. Res.*, *112*, D22302, doi:10.1029/2006JD008211.

Mueller, S.A., J.E. Anderson, and T.J. Wallington (2009), A classroom demonstration of water-induced phase separation of gasoline–alcohol fuel blends, *J. Chem. Ed.*, *86*, 1045–1048.

Müller, J-F., and G. Brasseur (1999), Sources of upper tropospheric HO_x: a three-dimensional study, *J. Geophys. Res. 104*, 1705–1715.

Müller-Remmers, P.L., P.C. Mishra, and K. Jug (1984), A SINDO1 study of photoisomerization and photofragmentation of cyclopentanone, *J. Am. Chem. Soc.*, *106*, 2538–2543.

Munger, J.W., personal communication quoted in Roberts et al. (2007).

Myers, T.L., N.R. Forde, B. Hu, D.C. Kitchen, and L.J. Butler (1997), The influence of local electronic character and nonadiabaticity in the photodissociation of nitric acid at 193 nm, *J. Chem. Phys.*, *107*, 5361–5373.

Nádasdi, R., G. Kovács, I. Szilágyi, A. Demeter, S. Dóbé, T. Bérces, and F. Márta (2007), Exciplex laser photolysis study of acetone with relevance to tropospheric chemistry, *Chem. Phys. Lett.*, *440*, 31–35.

Nakashima, K., K. Uchida-Kai, M. Koyanogi, and Y. Kanda (1982), Solvent effects on the intensities of forbidden bands of molecules. Absorption spectra of acetone and cyclopentanone, *Bull. Chem. Soc. Japan*, *55*, 415–419.

Napier, I.M., and R.G.W. Norrish (1965), Nitroso formaldehyhde, *Nature*, *208*, 1090–1091.

Napier, I.M., and R.G.W. Norrish (1967), The photolysis and pyrolysis of nitromethane and methyl nitrite, *Proc. Roy. Soc.*, A299, 317–336.

Nau, W.M., and J.C. Scaiano (1996), Oxygen quenching of excited aliphatic ketones and diketones, *J. Phys. Chem.*, *100*, 11360–11367.

Neeb, P. (2000), Structure–reactivity based estimation of the rate constants for hydroxyl radical reactions with hydrocarbons, *J. Atmos. Chem.*, *35*, 295–315.

Neeb, P., A. Kolloff, S. Koch, and G. K. Moortgat (1998), Rate constants for the reactions of methylvinyl ketone, methacrolein, methacrylic acid, and acrylic acid with ozone, *Int. J. Chem. Kinet.*, *30*, 769–776.

Neeb, P., F. Sauer, O. Horie, and G.K. Moortgat (1997), Formation of hydroxymethyl hydroperoxide and formic acid in alkene ozonolysis in the presence of water vapour, *Atmos. Environ.*, *31*, 1417–1423.

Nelson, L., O. Rattigan, R. Neavyn, H. Sidebottom, J. Treacy, and O.J. Nielsen (1990a), Absolute and relative rate constants of hydroxyl radicals and chlorine atoms with a series of aliphatic alcohols and ethers at 298 K, *Int. J. Chem. Kinet.*, *22*, 1111–1126.

Nelson, L., I. Shanahan, H.W. Sidebottom, J. Treacy, and O.J. Nielsen (1990b), Kinetics and mechanism for the oxidation of 1,1,1-trichloroethane, *Int. J. Chem. Kinet.*, *22*, 577–590.

Nesbitt, D.J.H., H. Petek, M.F. Foltz, S.V. Filseth, D.J. Bamford, and C.B. Moore (1985), Photofragmentation dynamics of ketene at 306 nm: Initial vibrational and rotational state distributions of CO product by vacuum UV laser-induced fluorescence, *J. Chem. Phys.*, *83*, 223–229.

Nguyen, H.T.H., T. Norimichi, H. Bandow, Y. Maeda, S.T. de Oliva., M.M. Botelho, and T.M. Tavares (2001), Atmospheric alcohols and aldehydes concentrations measured in Osaka, Japan and in Sao Paulo, Brazil, *Atmos. Environ*., *35*, 3075–3083.

Nguyen, M.T., H.T. Le, B. Hajagató, T. Veszprémi, and M.C. Lin (2003), Nitromethane–methylnitrite rearrangement: A persistent discrepancy between theory and experiment, *J. Phys. Chem. A*, *107*, 4286–4291.

Nguyen, M.T., M.H. Matus, V.T. Ngan, R. Haiges, K.O. Christe, and D.A. Dixon (2008), Energetics and mechanism of the decomposition of trifluoromethanol, *J. Phys. Chem. A*, *112*, 1298–1312.

Nicholson, A.J.C. (1954), The photochemical decomposition of the aliphatic methyl ketones, *Trans. Faraday Soc.*, *50*, 1067–1073.

Nicholson, A.J.C. (1961), Photolysis of nitromethane, *Nature*, *190*, 143–144.

Nicol, C.H., and J.G. Calvert (1967), Relations between photodecomposition modes and molecular structure in the series of carbonyl compounds, n-C_3H_7COR, *J. Am. Chem. Soc.*, *89*, 1790–1798.

Nicovich, J.M., and P.H. Wine (1988), Temperature-dependent absorption cross-sections for hydrogen peroxide vapor, *J. Geophys. Res.*, *93*, 2417–2421.

Niedojadlo, A., K.H. Becker, R. Kurtenbach, and P. Wiesen (2007), The contribution of traffic and solvent use to the total NMVOC emission in a German city derived from measurements and CMB modelling, *Atmos. Environ.*, *41*, 7108–7126.

Nielsen, O.J., M. Donlon, H.W. Sidebottom, D.J. O'Farrell, and J. Treacy (1990), Rate constants for the gas-phase reactions of OH radicals with nitroethene, 3-nitropropene and 1-nitrocyclohexene, *Chem. Phys. Lett.*, 168, 319–323.

Nielsen, O.J., J. Sehested, S. Langer, E. Ljungström, and I. Wängberg (1995), UV absorption spectra and kinetics for alkyl and alkyl peroxy radicals originating from di-*tert*-butyl ether, *Chem. Phys. Letters*, *238*, 359–364.

Nielsen, O.J., H.W. Sidebottom, M. Donlon, and J. Treacy (1989), Rate constants for the gas-phase reactions of OH radicals and Cl atoms with $CH_3CH_2NO_2$, $CH_3CH_2CH_2NO_2$, $CH_3CH_2CH_2CH_2NO_2$ and $CH_3CH_2CH_2CH_2CH_2NO_2$, *Chem. Phys. Letters*, *156*, 312–318.

Nielsen, O.J., H.W. Sidebottom, M. Donlon, and J. Treacy (1991), Rate constants for the gas-phase reactions of OH radicals and Cl atoms with alkyl nitrites at atmospheric pressure and 298K, *Int. J. Chem. Kinet.*, *23*, 1095–1109.

Nielsen, O. J., H.W. Sidebottom, D.J. O'Farrell, M. Donlon, and J. Treacy (1988), Absolute and relative rate constants for the gas-phase reaction of OH radicals with CH_3NO_2, CD_3NO_2 and $CH_3CH_2CH_3$ at 295 K and 1 atm, *Chem. Phys. Letters*, *146*, 197–203.

Nielsen, T., J. Platz, K. Granby, A.B. Hansen, H. Skov, and A.H. Egelov (1998), Particulate organic nitrates: sampling and night/day variation, *Atmos. Environ.*, *32*, 2601–2608.

Niki, H., P.D. Maker, L.P. Breitenbach, and C.M. Savage (1978a), FTIR studies of the kinetics and mechanism for the reaction of chlorine atom with formaldehyde, *Chem. Phys. Letters*, *57*, 596–599.

Niki, H., P.D. Maker, C.M. Savage, and L.P. Breitenbach (1978b), Relative rate constants for the reaction of hydroxyl radical with aldehydes, *J. Phys. Chem.*, *82*, 132–4.

Niki, H., P.D. Maker, C.M. Savage, and L.P. Breitenbach (1980), FTIR Studies of the kinetics and mechanism for the reaction of Cl Atom with formylchloride, *Int. J. Chem. Kinet.*, *12*, 915–920.

Niki, H., P.D. Maker, C.M. Savage, and L.P. Bretenbach (1983), A fourier transform infrared study of the kinetics and mechanism for the reaction $HO + CH_3OOH$, *J. Phys. Chem.*, *87*, 2190–2193.

Niki, H., P.D. Maker, C.M. Savage, and L.P. Breitenbach (1984), Fourier transform infrared study of the kinetics and mechanisms for the reaction of hydroxyl radical with formaldehyde, *J. Phys. Chem.*, *88*, 5342–5344.

Niki, H., P.D. Maker, C.M. Savage, and L.P. Breitenbach (1985a), An FTIR study of the chlorine-atom-initiated reaction of glyoxal, *Int. J. Chem. Kinetics*, *17*, 547–558.

Niki, H., P.D. Maker, C.M. Savage, and L.P. Breitenbach (1985b), FTIR study of the kinetics and mechanism for chlorine-atom-initiated reactions of acetaldehyde, *J. Phys. Chem.*, *89*, 588–591.

Niki, H., P.D. Maker, C.M. Savage, and M.D. Hurley (1987), Fourier transform infrared study of the kinetics and mechanisms for the chlorine-atom- and hydroxyl-radical-initiated oxidation of glycolaldehyde, *J. Phys. Chem.*, *91*, 2174–2178.

Ning, C.L., and J. Pfab (1997), Generation and 355 laser photodissociation of nitrous acid (HONO) and HONO-water clusters, *J. Phys. Chem. A*, *101*, 6008–6014.

Ninomiya, Y., M. Kawasaki, A. Guschin, L.T. Molina, M.J. Molina, and T. J. Wallington (2000), Atmospheric chemistry of *n*-$C_3F_7OCH_3$: reaction with OH radicals and Cl atoms and atmospheric fate of *n*-$C_3F_7OCH_2O(\bullet)$ radicals, *Environ. Sci. Technol., 34*, 2973–2978.

NIST webbook (2009), http://webbook.nist.gov.

Nizkorodov, S.A., J.D. Crounse, J.L. Fry, C.M. Roehl, and P.O. Wennberg (2005), Near-IR photodissociation of peroxy acetyl nitrate, *Atm. Chem. Phys.*, *5*, 385–392.

Noda, J., M. Hallquist, S. Langer, and E. Ljungström (2000), Products from the gas-phase reaction of some unsaturated alcohols with nitrate radicals, *Phys. Chem. Chem. Phys.*, *2*, 2555–2564.

Noda, J., C. Holm, G. Nyman, S. Langer, and E. Ljungström (2003), Kinetics of the gas-phase reaction of *n*-C_6-C_{10} aldehydes with the nitrate radical, *Int. J. Chem. Kinetics*, *35*, 120–129.

Noda, J., G. Nyman, and S. Langer (2002), Kinetics of the gas phase reaction of some unsaturated alcohols with the nitrate radical, *J. Phys. Chem. A*, *106*, 945–951.

Nohara, K., M. Toma, S. Kutsuna, K. Takeuchi, and T. Ibusuki (2001), Cl atom-initiated oxidation of three homologous methyl perfluoroalkyl ethers, *Environ. Sci. Technol.*, *35*, 114–120.

Nojima, K., and C. Isogami (1994), Studies on photochemical reactions of air pollutants. XII. Formation of nitrophenols by reactions of three toluene oxides with nitrogen dioxide in air, *Chem. Pharm. Bull.*, *42*, 2426–2429.

Nojima, K., A. Kawaguchi, T. Ohya, S. Kanno, and M. Hirobe (1983), Studies on photochemical reactions of air pollutants. X. Identification of nitrophenols in suspended particulates, *Chem. Pharmacol. Bull.*, *31*, 1047–1051.

Nolan, S., N. O'Sullivan, J. Wenger, H. Sidebottom, and J. Treacy (1999), Kinetics and mechanisms of the OH radical initiated degradation of a series of hydrofluoroethers, in Proceedings of EUROTRAC Symposium '98: Transport and Chemical Transformation in the Troposphere, Garmisch-Partenkirchen, Germany, March, 1998. WIT Press: Ashurst, Southampton UK, 1999, 1–120.

Nonella, M., J.R. Huber, A. Untch, and R. Schinke (1989), Photodissociation of CH_3ONO in the first absortion band: A three dimensional classical trajectory study, *J. Chem. Phys.*, *91*, 194–204.

Norrish, R.G.W., and M.E.S. Appleyard (1934), Primary photochemical reactions. Part IV. Decomposition of methyl ethyl ketone and methyl butyl ketone, *J. Chem. Soc.*, 874–880.

Norrish, R.G.W., H.G. Crone, and O. Saltmarsh (1933), Primary photochemical processes. Part III. The absorption spectrum and photochemical decomposition of keten, *J. Chem. Soc.*, 1533–1539.

Norrish, R.G.W., and J.G.A. Griffiths (1928), CCCLXXIII.¯The photochemical decomposition of glyoxal, *J. Chem. Soc.*, 2829–2840.

North, S.W., D.A. Blank, J.D. Gezelter, C.A. Longfellow, and Y.T. Lee (1995), Evidence for stepwise dissociation dynamics in acetone at 248 and 193 nm, *J. Chem. Phys.*, *102*, 4447–4460.

Notario, A., G. Le Bras, and A. Mellouki (1998), Absolute rate constants for the reactions of Cl atoms with a series of esters, *J. Phys. Chem., A. 102*, 3112–3117.

Notario A., A. Mellouki, and G. Le Bras (2000a), Rate constants for the gas-phase reactions of chlorine atoms with a series of ketones, *Int. J. Chem. Kinet. 32*, 62 – 66.

Notario, A., A. Mellouki, and G. Le Bras (2000b), Rate constants for the gas-phase reactions of Cl atoms with a series of ethers, *Int. J. Chem. Kinet.*, *32*, 105–110.

Nouaime, G., S.B. Bertman, C. Seaver, D. Elyea, H. Huang, P. Shepson, T.K. Starn, D.D. Riemer, R.G. Zika, and K. Olszyna (1998), Sequential oxidation products from tropospheric isoprene chemistry: MACR and MPAN at a NO_x-rich forest environment in the southeastern United States, *J. Geophys. Res.*, *103*, 22463–22471.

Novicki, S.W., and R. Vasudev (1991), Doppler spectroscopy of the OH fragment effected by *trans*-HONO ($\tilde{A}^1A''$)–Characterization of the *A* state resonances and determination of vibrational-energy content of the NO fragment, *J. Chem. Phys.*, *95*, 7269–7274.

Noyes, W.A., Jr., W.A. Mulac, and M.S. Matheson (1962), Photochemical primary process in biacetyl vapor at 4358Å, *J. Am. Chem. Soc.*, *36*, 880–886.

Noyes, W.A., Jr., G.B. Porter, and J.E. Jolley (1956), The primary photochemical process in simple ketones, *Chem. Rev.*, *56*, 49–94.

Noyes, W.A., Jr., and I. Unger (1964), Some aspects of transitions between electronic levels, *Pure App. Chem.*, *9*, 461–472.

Noyes, W.A., Jr., and I. Unger (1966), Singlet and triplet states: Benzene and simple aromatic compounds, *Adv. Photochem.*, *4*, 49–79.

Nozière, B., I. Barnes, and K.H. Becker (1999a), Product study and mechanisms of the reactions of α-pinene and of pinonaldehyde with OH radicals, *J.Geophys. Res.*, *D*, *104*, 23645–23656.

Nozière, B., R. Lesclaux, M.D. Hurley, M.A. Dearth, and T.J. Wallington (1994), A kinetic and mechanistic study of the self-reaction and reaction with HO_2 of the benzylperoxy radical, *J. Phys. Chem.*, *98*, 2864–2873.

Nozière, B., M. Spittler, L. Ruppert, I. Barnes, K.H. Becker, M. Pons, and K. Wirtz (1999b), Kinetics of the reactions of pinonaldehyde with OH radicals and with Cl atoms, *Int. J. Chem. Kinet.*, *31*, 291–301.

Nunes, F.M.N., M.C.C. Veloso, and P.A. de P. Pereira (2005), Gas-phase ozonolysis of the monoterpenoids (*S*)-(+)-carvone, (*R*)-(−)-carvone, (−)-carveol, geraniol and citral, *Atmos. Environ.*, *39*, 7715–7730.

O'Connor, M.P., J.C. Wenger, A. Mellouki, K. Wirtz, and A. Muñoz (2006), The atmospheric photolysis of *E*-2-hexenal, *Z*-3-hexenal and *E,E*-2,4-hexadienal, *Phys. Chem. Chem. Phys.*, *8*, 5236–5246.

O'Donnell, S.M., H.W. Sidebotton, J.C. Wenger, A. Mellouki, and G. Le Bras (2004), Kinetic studies on the reactions of hydroxyl radicals with a series of alkoxy esters, *J. Phys. Chem. A*, *108*, 7386–7392.

Odum, J.R., T. Hoffmann, F. Bowman, D. Collins, R.C. Flagan, and J.H. Seinfeld (1996), Gas/particle partitioning and secondary organic aerosol yields, *Environ. Sci. Technol.*, *30*, 2580–2585.

Odum, J.R., P.W. Jungkamp, R.J. Griffin, H.J.L. Forstner, R.C. Flagan, and J.H. Seinfeld (1997a), Aromatics, reformulated gasoline, and atmospheric organic aerosol formation, *Environ. Sci. Technol.*, *31*, 1890–1897.

Odum, J.R., T.P.W. Jungkamp, R.J. Griffin, R.C. Flagan, and J.H. Seinfeld (1997b), The atmospheric aerosol-forming potential of whole gasoline vapor, *Sci.*, *276*, 96–99.

OECD (2007), Biofuels: Is the cure worse than the disease?, Report SG/SD/RT(2007)3, http://www.oecd.org/document/28/0,3343,en_2649_33717_41013916_1_1_1_1,00&&en-USS_01DBC.html.

OECD (2008), Economic assessment of biofuel support policies. http://www.oecd.org.

Oehlers, C., F. Temps, H.Gg. Wagner, and M. Wolf (1992), Kinetics of the reaction of OH radicals with CH_2CO, *Ber. Bunsenges. Phys. Chem.*, *96*, 171–175.

Ogbobe, O., and V. Akano (1993), The physico-chemical properties of the seed and seed oil of Jatropha gossipifolia, *Plant Foods for Human Nutrition*, *43*, 197–200.

Oh, S., and J.M. Andino (2000), Effects of ammonium sulfate aerosols on the gas-phase reactions of the hydroxyl radical with organic compounds, *Atmos. Environ.*, *34*, 2901–2908.

Oh, S., and J.M. Andino (2001), Kinetics of the gas-phase reactions of hydroxyl radicals with C_1–C_6 aliphatic alcohols in the presence of ammonium sulfate aerosols, *Int. J. Chem. Kinet.*, *33*, 422–430.

Oh, S., and J.M. Andino (2002), Laboratory studies of the impact of aerosol composition on the heterogeneous oxidation of 1-propanol, *Atmos. Environ.*, *36*, 149–156.

Ohbayashi, K., H. Akimoto, and I. Tanaka (1977), Emission spectra of CH_3O, C_2H_5O, and *i*-C_3H_7O radicals, *J. Phys. Chem.*, *81*, 798–802.

Ohta, T., H. Bandow, and H. Akimoto (1982), Gas-phase chlorine-initiated photooxidation of methanol and isopropanol, *Int. J. Chem. Kinet.*, *14*, 173–182.

Ohta, T., and I. Mizoguchi (1980), Determination of the mechanism of the oxidation of the trichloromethyl radical by the photolysis of chloral in the presence of oxygen, *Int. J. Chem. Kinet.*, *12*, 717–727.

Ohta, T., and T. Ohyama (1985), A set of rate constants for the reaction of OH radicals with aromatic hydrocarbons, *Bull. Chem. Soc. Jpn.*, *58*, 3029–3030.

Okabe, H. (1977), Photodissociation of thiophosgene, *J. Chem. Phys.*, *66*, 2058–2062.

Okabe, H., and D.A. Becker (1963), Vacuum ultraviolet photochemistry. VII. Photolysis of *n*-butane, *J. Chem. Phys.*, *39*, 2549–2555.

Okabe, H., and W.A. Noyes, Jr. (1957), The relative intensities of fluorescence and phosphorescence in biacetyl vapor, *J. Am. Chem. Soc.*, *79*, 801–806.

Okieimen, F.E. (2002), Utilisation of Jatropha seed oil in the stabilisation of poly (vinyl chloride) against thermal degradation, *Indian J. Chem. Technol.*, *9*, 188–196.

Olah, G.A., A. Goeppert, and G.K.S. Prakash (2006), *Beyond Oil and Gas: The Methanol Economy*, Wiley & Sons, New York.

Olariu, R.I., I. Barnes, K.H. Becker, and B. Klotz (2000), Rate coefficients for the gas-phase reaction of OH radicals with selected dihydroxybenzenes and benzoquinones, *Int. J. Chem. Kinet. 32*, 696–702.

Olariu, R.I., I. Bejan, I. Barnes, B. Klotz, K.H. Becker, and K. Wirtz (2004), Rate coefficients for the gas-phase reaction of NO_3 radicals with selected dihydroxybenzenes, *Int. J. Chem. Kinet. 36*, 577–583.

Olariu, R.I., B. Klotz, I. Barnes, K.H. Becker, and R. Mocanu (2002), FT–IR study of the ring-retaining products from the reaction of OH radicals with phenol, *o*-, *m*-, and *p*-cresol, *Atmos. Environ.*, *36*, 3685–3697.

Olsen, J.F., S. Kang, and L. Burnelle (1971), The question of an open-ring form of cyclopropanone, *J. Mol. Struct.*, *9*, 305–313.

Olsson, B.E.R., M. Hallquist, E. Ljungström, and J. Davidsson (1997), A kinetic study of chlorine radical reactions with ketones by laser photolysis technique, *Int. J. Chem. Kinet.*, *29*, 195–201.

O'rji, L.N., and D.A. Stone (1992), Relative rate constant measurements for the gas-phase reactions of hydroxyl radicals with 4-methyl-2-pentanone, *trans*-4-octene, and *trans*-2-heptene, *Int. J. Chem. Kinet.*, *24*, 703–710.

Orkin, V.L., V.G. Khamaganov, A.G. Guschin, R.E. Huie, and M.J. Kurylo (1994), Rate constants for the reactions between hydroxyl radicals and fluorinated ethers, 13th International Symposium on Gas Kinetics, University College, Dublin.

Orkin, V.L., E. Villenave, R.E. Huie, and M.J. Kurylo (1999), Atmospheric lifetimes and global warming potentials of hydrofluoroethers: Reactivity toward OH, UV spectra, and IR absorption cross sections, *J. Phys. Chem. A*, *103*, 9770–9779.

Orlando, J.J. (2007), The atmospheric oxidation of diethyl ether: Chemistry of the C_2H_5—O—CH(O•)CH_3 radical between 218 and 335 K, *Phys. Chem. Chem. Phys.*, *9*, 4189–4199.

Orlando, J.J., and G.S. Tyndall (2001), The atmospheric chemistry of the HC(O)CO radical, *Int. J. Chem. Kinet*, 33(3), 149–156.

Orlando, J.J., and G.S. Tyndall (2002), Mechanisms for the reactions of OH with two unsaturated aldehydes: Crotonaldehyde and acrolein, *J. Phys. Chem. A*, *106*, 12252–12259.

Orlando, J.J., and G. S. Tyndall (2003), Gas phase UV absorption spectra for peracetic acid, and for acetic acid monomer and dimer, *J. Photochem. Photobiol A: Photochem.*, *157*, 161–166.

Orlando, J.J., G.S. Tyndall, E.C. Apel, D.D. Riemer, and S.E. Paulson, S.E. (2003), Rate coefficients and mechanisms of the reaction of Cl-atoms with a series of unsaturated hydrocarbons under atmospheric conditions, *Int. J. Chem. Kinet.*, *35*, 334–353.

Orlando, J.J., G.S. Tyndall, S.B. Bertman, W. Chen, and J.B. Burkholder (2002), Rate coefficient for the reaction of OH with CH_2═$C(CH_3)C(O)OONO_2$ (MPAN), *Atmos. Environ.*, *36*, 1895–1900.

Orlando, J.J., G.S. Tyndall, and N. Ceazan (2001), Rate coefficients and product yields from reaction of OH with 1-penten-3-ol, (*Z*)-2-penten-1-ol, and allyl alcohol (2-propen-1-ol), *J. Phys. Chem. A*, *105*, 3564–3569.

Orlando, J.J., G.S. Tyndall, J.M. Fracheboud, E.G. Estupiñan, S. Haberkorn, and A. Zimmer (1999), The rate and mechanism of the gas-phase oxidation of hydroxyacetone, *Atmos. Environ.*, *33*, 1621–1629.

Orlando, J.J., G.S. Tyndall, and S.E. Paulson (1999), Mechanism of the OH-initiated oxidation of methacrolein, *Geophys. Res. Letters*, *26*, 2191–2194.

Orlando, J.J., G.S. Tyndall, L. Vereecken, and J. Peeters (2000), The atmospheric chemistry of the acetonoxy radical, *J. Phys. Chem. A.*, *104*, 11578–11588.

Orzechowska, G.E., and S.E. Paulson (2005a), Photochemical sources of organic acids. 1. Reaction of ozone with isoprene, propene, and 2-butenes under dry and humid conditions using SPME, *J. Phys. Chem. A*, *109*, 5358–5365.

Orzechowska, G.E., and S.E. Paulson (2005b), Photochemical sources of organic acids. 2. Formation of C_5–C_9 carboxylic acids from alkene ozonolysis under dry and humid conditions, *J. Phys. Chem. A*, *109*, 5366–5375.

Osamura, Y., and H.F. Schaefer III (1981), Internal rotation barrier and transition state for glyoxal, *J. Chem. Phys. 74*, 4576–4580.

Osamura, Y., H.F. Schaefer III, M. Dupuis, and W.A. Lester, Jr. (1981), A unimolecular reaction ABC $\rightarrow$ A + B + C involving three product molecules and a single transition state. Photodissociation of glyoxal: HCOHCO $\rightarrow$ H_2 + CO + CO, *J. Chem. Phys.*, *75*, 5828–5836.

Osthoff, H.D., M.J. Pilling, A.R. Ravishankara, and S.S. Brown (2007), Temperature dependence of the NO_3 absorption cross-section above 298 K and determination of the equilibrium

constant for $NO_3 + NO_2 \leftrightarrow N_2O_5$ at atmospherically relevant conditions, *Phys. Chem. Chem. Phys.*, *9*, 5785–5793.

O'Sullivan, N., J. Wenger, and H. Sidebottom (1997), in Proceedings of the 7th European Commission Symposium on Physiochemical Behavior of Atmospheric Pollutants, pp.77–79; Venice Italy, October 1996; editors Larsen, B. and Versino, B.; Office for Official Publications of the European Communities: Luxembourg, 1997.

Overend, R., and G. Paraskevopoulos (1978), Rates of OH radical reactions. 4. Reactions with methanol, ethanol, 1-propanol, and 2-propanol at 296 K, *J. Phys. Chem.* 82, 1329–1333.

Oyaro, N., S. Sellevåg, and C. J. Nielsen (2004), Study of the OH and Cl-initiated oxidation, IR absorption cross-section, radiative forcing, and global warming potential of four C_4-hydrofluoroethers, *Environ. Sci. Technol.*, *38*, 5567–5576.

Oyaro, N., S. Sellevåg, and C. J. Nielsen (2005), Atmospheric chemistry of hydrofluoroethers: Reaction of a series of hydrofluoroethers with OH radicals and Cl atoms, atmospheric lifetimes, and global warming potentials, *J. Phys. Chem.*, *109*, 337–346.

Padnos, N., and W.A. Noyes, Jr. (1964), Photolysis of biacetyl–oxygen mixtures at 4358Å, *J. Phys. Chem.*, *68*, 464–468.

Pagsberg, P., J. Munk, A. Sillesen, and C. Anastasi (1988), UV spectrum and kinetics of hydroxymethyl radicals, *Chem. Phys. Lett.*, *146*, 375–381.

Palm, W.-U., W. Behnke, and C. Zetzsch (1999a), Are light-induced reactions of nitrophenols an efficient sink in atmospheric droplets?, in, editors K. H. Becker and G. Angeletti, *Chemical Mechanisms of Atmospheric Processes*, Air Pollution Research Report 67, EUR 18765, European Communities, Luxembourg, pp.377–382.

Palm, W.-U., H.-U. Kruger, W. Behnke, and C. Zetzsch (1999b), Uptake of NO_2 on aqueous solutions containing phenol and degradation of some nitroaromatics by photolysis and OH radicals, in, editors R. Vogt and G. Axelsdottir, *EC/EUROTRAC-2 Joint Workshop Chemical Mechanims Development (CMD)*, Ford Forschungszentrum Aachen, Germany, pp.171–174.

Palmer, P.I., D.S. Abbot, T-M. Fu, D.J. Jacob, K. Chance, T.P. Kurosu, A. Guenther, C. Wiedinmyer, J.C. Stanton, M.J. Pilling, S.N. Pressley, B. Lamb, and A.L. Summer (2006), Quantifying the seasonal and interannual variability of North American isoprene emissions using satellite observations of the formaldehyde column, *J. Geophys. Res. 111*, D12315/1–D12315/14.

Palmer, P.I., M.P. Barkley, T.P. Kurosu, A.C. Lewis, J.E. Saxton, K. Chance, and L.V. Gatti (2007), Interpreting satellite column observations of formaldehyde over tropical South America, *Phil. Trans. Roy. Soc. A*, *365*, 1741–51.

Palmer, P.I., D.J. Jacob, A.M. Fiore, R.V. Martin, K. Chance, and T.P. Kurosu (2003), Mapping isoprene emissions over North America using formaldehyde column observations from space, *J. Geophys. Res.*, *108*, ACH2/1–ACH2/13.

Pandis, S.N., S.E. Paulson, J.H. Seinfeld, and R.C. Flagan (1991), Aerosol formation in the photooxidation of isoprene and α-pinene, *Atmos. Environ.*, *25A*, 997–1008.

Pankow, J.F. (1994a), An absorption model of gas/particle partitioning of organic compounds in the atmosphere, *Atmos. Environ.*, *28*, 185–188.

Pankow, J.F. (1994b), An absorption model of the gas/aerosol partitioning involved in the formation of secondary organic aerosol, *Atmos. Environ.*, *28*, 189–193.

Papadimitriou, V.C., K.G. Kambanis, Y.G. Lazarou, and P. Papagiannakopoulos (2004), Kinetic study for the reactions of several hydrofluoroethers with chlorine atoms, *J. Phys. Chem. A*, *108*, 2666–2674.

Papadimitriou, V.C., D.K. Papanastasiou, V.G. Stefanopoulos, A.M. Zaras, Y.G. Lazarou, and P. Papagiannakopoulos (2007), Kinetic study of the reactions of Cl atoms with $CF_3CH_2CH_2OH$, $CF_3CF_2CH_2OH$, $CHF_2CF_2CH_2OH$, and $CF_3CHFCF_2CH_2OH$, *J. Phys. Chem. A*, *111*, 11608–11617.

Papadimitriou, V.C., A.V. Prosmitis, Y.G. Lazarou, and P. Papagiannakopoulos (2003), Absolute reaction rates of chlorine atoms with CF_3CH_2OH, CHF_2CH_2OH, and CH_2FCH_2OH, *J. Phys. Chem. A*, *107*, 3733–3740.

Papagni, C., J. Arey, and R. Atkinson (2000), Rate constants for the gas-phase reactions of a series of C_3–C_6 aldehydes with OH and NO_3 radicals, *Int. J. Chem. Kinet.*, *32*, 79–84.

Papagni, C., J. Arey, and R. Atkinson (2001), Rate constants for the gas-phase reactions of OH radicals with a series of unsaturated alcohols, *Int. J. Chem. Kinet.*, *33*, 142–148.

Papayannis, D.K., E. Drougas, and A.M. Kosmas (2002), Ab initio and RRKM calculations for the decomposition channels of CH_3OBr and $BrCH_2OH$, *Chem. Phys. Lett.*, *282*, 305–314.

Park, J.-Y., I. R. Slagle, and D. Gutman (1983), Kinetics of the reaction of chlorine atoms with vinyl bromide and its use for measuring chlorine-atom concentrations, *J. Phys. Chem.*, *87*, 1812–1818.

Park, M.S., K.-H. Jung, H.P. Upadhyaya, and H.-R. Volpp (2001), The dynamics of oxygen atom formation in the UV photodissociation of nitromethane, *Chem. Phys.*, *270*, 133–139.

Parmenter, C.S. (1964), Primary photochemical processes in glyoxal at 4358Å, *J. Chem. Phys.*, *41*, 658–665.

Parmenter, C.S., and W.A. Noyes, Jr. (1963), Energy dissipation from excited acetaldehyde molecules, *J. Am. Chem. Soc.*, *85*, 416–421.

Parmenter, C.S., and H.M. Poland (1969), Fluorescence, phosphorescence, and triplet formation in biacetyl at low pressues, *J. Chem. Phys.*, *51*, 1551–1558.

Paszyc, S. (1973/1974), Photochemistry of nitroalkanes, *J. Photochem.*, *2*, 183–198.

Payne, W.A., J. Brunning, M.B. Mitchell, and L.J. Stief (1988), Kinetics of the reactions of atomic chlorine with methanol and hydroxymethyl radical with molecular oxygen at 298 K, *Int. J. Chem. Kinet.*, *20*, 63–74.

Payne, W. A., D.F. Nava, F.L. Nesbitt, and L.J. Stief (1990), Rate constant for the reaction of atomic chlorine with acetaldehyde from 210 to 343 K, *J. Phys. Chem.*, *94*, 7190–7193.

Pearce, C., and D.A. Whytock (1971), The photolysis of trifluoroacetaldehyde at 313 nm, *J. Chem. Soc., Chem. Commun.*, 1464–1466.

Peeters, J., T.L. Nguyen, and L. Vereecken (2009), HO_x radical regeneration in the oxidation of isoprene, *Phys. Chem. Chem. Phys.*, *11*, 5935–5939.

Penkett, S.A., R.A. Burgess, H. Coe, I. Coll, Ø. Hov, A. Lindskog, N. Schmidbauer, S. Solberg, M. Roemer, T. Thijsse, J. Beck, and C.E. Reeves (2007), Evidence for large average concentrations of the nitrate radical (NO_3) in Western Europe from the HANSA hydrocarbon database, *Atmos. Environ.*, *41*, 3465–3478.

Perner, D., and U. Platt (1979), Detection of nitrous acid in the atmosphere by differential optical absorption, *Geophys. Res. Lett.*, *6*, 917–920.

Perry, R.A., R. Atkinson, and J. N. Pitts, Jr. (1977a), Kinetics and mechanism of the gas phase reaction of OH radicals with methoxybenzene and *o*-cresol over the temperature range 299–435 K, *J. Phys. Chem.*, *81*, 1607–1611.

Perry, R.A., R. Atkinson, and J.N. Pitts, Jr. (1977b), Rate constants for the reaction of OH radicals with dimethyl ether and vinyl methyl ether over the temperature range 299–427 K, *J. Chem. Phys.*, *67*, 611–614.

Person, M.D., P.W. Kash, and L.J. Butler (1992a), A new class of Norrish type I processes: α-bond cleavage upon $[n,\pi^*$ (C═O)] excitation in the acid halides, *J. Phys. Chem.*, *96*, 2021–2023.

Person, M.D., P.W. Kash, and L.J. Butler (1992b), Nonadiabaticity and the competition between alpha and beta bond fission upon $^1[n,\pi^*$ (C═O)] excitation in acetyl and bromoacetyl chloride, *J. Chem. Phys.*, *97*, 355–373.

Peterson, C.L., J.C. Thompson, J.S. Taberski, D.L. Reece, and G. Fleischman (1999), Long-range on–road test with twenty-percent rapeseed biodiesel, *Applied Engineering in Agriculture*, *15*, 91–101.

Pfrang, C., M.T. Baeza-Romero, B. Cabañas, C.E. Canosa-Mas, F. Villanueva, and R.P. Wayne (2007), Night-time tropospheric chemistry of the unsaturated alcohols (*Z*)-pent-2-en-1-ol and pent-1-en-3-ol: Kinetic studies of reactions of NO_3 and N_2O_5 with stress-induced plant emissions, *Atmos. Environ.*, *41*, 1652–1662.

Pfrang, C., R.S. Martin, C.E. Canosa-Mas, and R.P. Wayne (2006a), Gas-phase reactions of NO_3 and N_2O_5 with (*Z*)-hex-4-en-1-ol, (*Z*)-hex-3-en-1-ol (leaf alcohol), (*E*-hex-3-en-1-ol, (*Z*)-hex-2-en-1-ol and (*E*)-hex-2-en-1-ol, *Phys. Chem. Chem. Phys.*, *8*, 354–363.

Pfrang, C., C. Tooze, A. Nalty, C.E. Canosa-Mas, and R.P. Wayne (2006b), Reactions of NO_3 with the man-made emissions 2-methylpent-2-ene, (*Z*)-3-methylpent-2-ene, ethyl vinyl

ether, and the stress-induced plant emission ethyl vinyl ketone, *Atmos. Environ.*, *40*, 786–792.

Phillips, D.L., C. Zhao, and D. Wang (2005), A theoretical study of the mechanism of the water-catalyzed HCl elimination reactions of CHXCl(OH) (X = H, Cl) and HClCO in the gas phase and in aqueous solution, *J. Phys. Chem. A.*, *109*, 9653–9673.

Picquet, B., S. Heroux, A. Chebbi, J.-F. Doussin, R. Durand-Jolibois, A. Monod, H. Loirat, and P. Carlier (1998), Kinetics of the reactions of OH radicals with some oxygenated volatile organic compounds under simulated atmospheric conditions, *Int. J. Chem. Kinet.*, *30*, 839–847.

Picquet-Varrault, B., J-F. Doussin, R. Durand-Jolibois, and P. Carlier (2001), FTIR spectroscopic study of the OH-induced oxidation of two linear acetates: ethyl and *n*-propyl acetates, *Phys. Chem. Chem. Phys.*, *3*, 2595–2606.

Picquet-Varrault, B., J-F. Doussin, R. Durand-Jolibois, and P. Carlier (2002), FTIR spectroscopic study of the OH-induced oxidation of isopropyl, isobutyl, and *tert*-butyl acetates, *J. Phys. Chem. A*, *106*, 2895–2902.

Pimentel, A.S., G.S. Tyndall, J.J. Orlando, M.D. Hurley, T.J. Wallington, M.P.S. Andersen, P. Marshall, and T. S. Dibble (2010), Atmospheric chemistry of isopropyl formate and *tert*-butyl formate, *Int. J. Chem. Kinet.* 42, 479–498.

Pinho, P.G., C.A. Pio, W.P.L. Carter, and M.E. Jenkin (2007), Evaluation of α- and β-pinene degradation in the detailed tropospheric chemistry mechanism, MCM v3.1, using environmental chamber data, *J. Atmos. Chem.*, *57*, 171–202.

Pippin, M., S. Bertman, T. Thornberry, M. Town, M.A. Carroll, and S. Sillman (2001), Seasonal variations of PAN, PPN, and O_3 at the upper Midwest PROPHET site, *J. Geopys. Res.*, *106*, 24451–24464.

Pitts, J.N., Jr., H.W. Biermann, R. Atkinson, and A.M. Winer (1984a), Atmospheric implications of simultaneous nighttime measurement of NO_3 radicals and HONO, *Geophys. Res. Lett.*, *11*, 557–560.

Pitts, J.N., Jr., and F.E. Blacet (1950), Methyl ethyl ketone photochemical processes, *J. Am. Chem. Soc.*, *72*, 2810–2811.

Pitts, J.N., Jr., and F.E. Blacet (1952), The vapor-phase photolysis of acetone–iodine mixtures, *J. Am. Chem. Soc.*, *74*, 455–457.

Pitts, J.N., Jr., D.R. Burley, J.C. Mani, and A.D. Broadbent (1968), Molecular structure and photochemical reactivity. VIII. Type II photoelimination of alkenes from alkyl phenyl ketones, *J. Am. Chem. Soc.*, *90*, 5900–5902.

Pitts, J.N. Jr., D. Grosjean, K. Van Cauwenberghe, J.P. Schmid, and D.R. Fitz (1978), Photooxidation of aliphatic amines under simulated atmospheric conditions: Formation of nitrosamines, nitramines, amides and photochemical oxidant, *Environ. Sci. Tech.*, *12*, 946–953.

Pitts, J.N., Jr., and A.D. Osborne (1961), A comparative study of radiolysis, photolysis and electron impact data of ketones, in *Chemical Reactions in the Lower Atmosphere*, Interscience, New York, Chapter 8, pp.129–138.

Pitts, J.N., Jr., E. Sanhueza, R. Atkinson, W.P.L. Carter, A.M. Winer, G.W. Harris, and C.N. Plum (1984b), An investigation of the dark formation of nitrous-acid in environmental chambers, *Int. J. Chem. Kinet.*, *7*, 919–939.

Pitts, J.N., Jr., and J.K.S. Wan (1966), Photochemistry of ketones and aldehydes, in, editor S. Patai, *Chemistry of the Carbonyl Group*, Interscience, New York, Chapter 16, pp.823–915.

Pitts, J.N., Jr., J.K.S. Wan, and E.A. Schuck (1964), Photochemical studies in an alkali halide matrix. I. An *o*-nitrobenzaldehyde actinometer and its application to a kinetic study of the photoreduction of benzophenone by benzhydrol in a pressed potassium bromide disk, *J. Am. Chem. Soc.*, *86*, 3606–3610.

Plagens, H., R. Bröske, M. Spittler, L. Ruppert, I. Barnes, and K.H. Becker (1998), Atmospheric loss processes of hexanal. Photolysis and reaction with OH and Cl radicals, *Proceedings of the Second Workshop of the EUROTRAC-2 Subproject Chemical Mechanism Development*, Karlsruhe, Germany, 23–25 September 1998, pp.GPP10-1–GPP10-4.

Platt, U., D. Perner, G.W. Harris, A.M. Winer, and J.N. Pitts, Jr. (1980), Observations of nitrous acid in an urban atmosphere by differential optical absorption, *Nature*, *285*, 312–314.

Platz, J., L.K. Christensen, J. Sehested, O.J. Nielsen, T.J. Wallington, C. Sauer, I. Barnes, K.H. Becker, and R. Vogt (1998), Atmospheric chemistry of 1,3,5-trioxane: UV spectra of c-$C_3H_5O_3$(•) and (c-$C_3H_5O_3$)O_2(•) radicals, kinetics of the reaction of (c-$C_3H_5O_3$)O_2(•) radicals with NO and NO_2, and atmospheric fate of the alkoxy radical (c-$C_3H_5O_3$)O(•), *J. Phys. Chem. A.*, *102*, 4829–4838.

Platz, J., O.J. Nielsen, J. Sehested, and T.J. Wallington (1995), Atmospheric chemistry of 1,1,1-trichloroethane: UV spectra and self-reaction kinetics of CCl_3CH_2 and $CCl_3CH_2O_2$ radicals, kinetics of the reaction of $CCl_3CH_2O_2$ radicals with NO and NO_2, and the fate of the alkoxy radical CCl_3CH_2O, *J. Phys. Chem.*, *99*, 6570–6579.

Platz, J., J. Sehested, T. Møgelberg, O.J. Nielsen, and T.J. Wallington (1997), Atmospheric chemistry of 1,4-dioxane, laboratory studies, *J. Chem. Soc., Faraday Trans.*, *93*, 2855–2863.

Platz, J., J. Sehested, O.J. Nielsen, and T.J. Wallington (1999), Atmospheric chemistry of trimethoxymethane $(CH_3O)_3CH$; laboratory studies, *J. Phys. Chem.*, *93*, 2632–2640.

Plum, C.N., E. Sanhueza, R. Atkinson, W.P.L. Carter, and J.N. Pitts, Jr. (1983), OH radical rate constants and photolysis rates of α-dicarbonyls, *Environ. Sci. Technol.*, *17*, 479–484.

Ponomarev, D., M.D. Hurley, and T.J. Wallington (2002), Kinetics of the reactions of fluorine and chlorine atoms with ethylene oxide (oxirane), *Int. J. Chem. Kinet.*, *34*, 122–125.

Porter, E., J. Wenger, J. Treacy, H. Sidebottom, A. Mellouki, S. Téton, and G. Le Bras (1997), Kinetic studies on the reactions of hydroxyl radicals with diethers and hydroxyethers, *J. Phys. Chem. A*, *101*, 5770–5775.

Porter, G. (1960), Photooxidation of biacetyl, *J. Chem. Phys.*, *32*, 1587–1588.

Porter, G., and B. Ward (1968), The photolytic preparation of cyclopentadienyl and phenyl nitrene from benzene derivatives, *Proc. Roy. Soc. London*, *Ser. A*, *303*, 139–156.

Pöschl, U., R. Von Kuhlmann, N. Poisson, and P.J. Crutzen (2000), Development and intercomparison of condensed isoprene oxidation mechanisms for global atmospheric modeling, *J. Atmos. Chem.*, *37*, 29–52.

Possanzini, M., V. Di Palo, M. Petricca, R. Fratarcangeli, and D. Brocco (1996), Measurements of lower carbonyls in Rome ambient air, *Atmos. Environ.*, *30*, 3757–3764.

Potter, E.D., M. Gruebele, L.R. Khundkar, and A.H. Zewail (1989), Picosecond dissociation of ketene: experimental state-to-state rates and test of statistical theories, *Chem. Phys. Lett.*, *164*, 463–470.

Poulet, G., G. Laverdet, and G. Le Bras (1981), Discharge flow-mass spectrometric determination of the rate coefficients for the reactions of formaldehyde with bromine atoms and chlorine atoms, *J. Phys. Chem.*, *85*, 1892–1895.

Poulet, G., G. LeBras, and J. Combourieu (1978), Kinetic study of the reactions of Cl atoms with HNO_3, H_2O_2, and HO_2, *J. Chem. Phys.*, *69*, 767–773.

Prather, M.J., and D.J. Jacob (1997), A persistent imbalance in HO_x and NO_x photochemistry of the upper troposphere driven by deep tropical convection, *Geophys. Res. Lett.*, *24*, 3189–3192.

Pressley, S., B. Lamb, H. Westberg, J. Flaherty, J. Chen, and C. Vogel (2005), Long-term isoprene flux measurements above a Northern hardwood forest, *J. Geophys. Res.*, *110*, D07301/1–D07301/12.

Presto, A., K.E. Huff Hartz, and N.M. Donahue (2005), Secondary organic aerosol production from terpene ozonolysis. 1. Effect of UV radiation, *Environ. Sci. Technol.*, *39*, 7036–7045.

Presto, A., M.A. Miracolo, J.H. Kroll, D.R. Worsnop, A.L. Robinson, and N.M. Donahue (2009), Intermediate-volatility organic compounds: A potential source of ambient oxidized organic aerosol, *Environ. Sci. Technol.*, *43*, 4744–4749.

Prevedouros, K., I.T. Cousins, R.C. Buck, and S.H. Korzeniowski (2006), Sources, fate and transport of perfluorocarboxylates, *Environ. Sci. Technol.*, *40*, 32–44.

Raber, W.H. (1992), Zur Photooxidation einiger atmosphärischer Spurengase in Luft: Die Carbonylverbindungen Methylethylketon, Methylvinylketon, Methacrolein und Methylglyoxal, 1992 Johannes Gutenberg-Universität Mainz. Ph.D. Thesis, Johannes Gutenberg-Universität, Mainz, Germany.

Raber, W.H., and G.K. Moortgat (1996), Photooxidation of selected carbonyl compounds in air: methyl ethyl ketone, methyl vinyl ketone, methacrolein and methylglyoxal,in, editor

J. Barker, *Progress and Problems in Atmospheric Chemistry*, World Scientific Publishing Company, Singapore, Chapter 9, pp.328–373.

Raff, J.D., and R.A. Hites (2006), Gas-phase reactions of brominated diphenyl ethers with OH radicals, *J. Phys. Chem. A*, *110*, 10783–10792.

Raff, J.D., and R.A. Hites (2007), Deposition versus photochemical removal of PBDEs from Lake Superior air, *Environ. Sci. Technol.*, *41*, 6725–6731.

Raff, J.D., P.S. Stevens, and R.A. Hites (2005), Relative rate and product studies of the OH–acetone reaction, *J. Phys. Chem. A*, *109*, 4728–4735.

Rajakumar, B., J.B. Burkholder, R.W. Portmann, and A.R. Ravishankara (2005), Rate coefficients for the OH + CFH_2CH_2OH reaction between 238 and 355 K, *Phys. Chem. Chem. Phys.*, *7*, 2498–2505.

Rajakumar, B., T. Gierczak, J.E. Flad, A.R. Ravishankara, and J.G. Burkholder (2008), The CH_3CO quantum yield in the 248 nm photolysis of acetone, methyl ethyl ketone, and biacetyl, *J. Photochem. Photobiol. A*, *199*, 336–344.

Rappenglück, B., K. Kourtidis, and P. Fabian (1993), Measurements of ozone and peroxyacetyl nitrate (PAN) in Munich, *Atmos. Environ.*, *27B*, 293–305.

Rattigan, O., E. Lutman, R.L. Jones, R.A. Cox, K. Clemitshaw, and J. Williams (1992), Temperature-dependent absorption cross-sections of gaseous nitric acid and methyl nitrate, *J. Photochem. Photobiol. A*, *66*, 313–326.

Rattigan, O.V., O. Wild, and R.A. Cox (1998), UV absorption cross-sections and atmospheric photolysis lifetimes of halogenated aldehydes, *J. Photochem. Photobiol.A: Chemistry*, *112*, 1–7.

Ravishankara, A.R., and D.D. Davis (1978), Kinetic rate constants for the reaction of OH with methanol, ethanol, and tetrahydrofuran at 298 K, *J. Phys. Chem.*, *82*, 2852–2853.

Ravishankara, A.R., F.L. Eisele, and P.H. Wine (1982), Study of the reaction of OH with HNO_3: Kinetics and NO_3 yield, *J. Phys. Chem.*, *86*, 1854–1858.

Rawls, R.L. (1976), Nitrosamines found in commercial pesticides, *Chem. Eng. News*, Sept. 20, pp.33–34.

Read, K. A., A.S. Mahajan, L.J. Carpenter, M.J. Evans, B.V.E. Faria, D.E. Heard, J.R. Hopkins, J.D. Lee, S.J. Moller, A.C. Lewis, L. Mendes, J.B. McQuaid, H. Oetjen, A. Saiz-Lopez, M.J. Pilling, and J.M.C. Plane (2008), Extensive halogen-mediated ozone destruction over the tropical Atlantic Ocean, *Nature*, *453*, 1232–1235.

Rebbert, R.E. (1963), Primary processes in the photolysis of ethyl nitrate, *J. Phys. Chem.*, *67*, 1923–1925.

Rebbert, R.E., and N. Slagg (1962), Primary processes in the photochemical decomposition of nitroalkanes, *Bull. Soc. Chim. Belg.*, *71*, 709–721.

Reemtsma, T., A. These, P. Venkatachari, X.Y. Xia, P.K. Hopke, A. Springer, and M. Linscheid (2006), Identification of fulvic acids and sulfated and nitrated analogues in atmospheric aerosol by electrospray ionization Fourier transform ion cyclotron resonance mass spectrometry, *Anal. Chem.*, *78*, 8299–8304.

Reeves, C.E., J. Slemr, D.E. Oram, D. Worton, S.A. Penkett, D.J. Stewart, R. Purvis, N. Watson, J. Hopkins, A. Lewis, J. Methven, D.R. Blake, and E. Atlas (2007), Alkyl nitrates in outflow from North America over the North Atlantic during Intercontinental Transport of Ozone and Precursors 2004, *J. Geophys. Res.*, *112*, D10S37, doi:10.1029/2006JD007567.

Reguero, M., M. Olivucci, F. Bernardi, and M.A. Robb (1994), Excited-state potential surface crossings in acrolein: A model for understanding the photochemistry and photophysics of α,β-enones, *J. Am. Chem. Soc.*, *116*, 2103–2114.

Reinnig, M.C., J. Warnke, and T. Hoffmann (2009), Identification of organic hydroperoxides and hydroperoxy acids in secondary organic aerosol formed during the ozonolysis of different monoterpenes and sesquiterpenes by on-line analysis using atmospheric pressure chemical ionization ion trap mass spectrometry, *Rapid Comm. Mass Spec.*, *23*, 1735–1741.

Reisen, F., S.M. Aschmann, R. Atkinson, and J. Arey (2003), Hydroxyaldehyde products from hydroxyl radical reactions of *Z*-3-hexen-1-ol and 2-methyl-3-buten-2-ol quantified by SPME and API-MS, *Environ. Sci. Technol.*, *37*, 4664–4670.

Reisen, F., S. M. Aschmann, R. Atkinson, and J. Arey (2005), 1,4-Hydroxycarbonyl products of the OH radical initiated reactions of C_5-C_8 *n*-alkanes in the presence of NO, *Environ. Sci. Technol.*, *39*, 4447–4453.

Reissell, A., J. Arey, and R. Atkinson (2001), Atmospheric chemistry of camphor, *Int. J. Chem. Kinet.*, *33*, 56–63.

Richter, H.R., J.R. Sodeau, and I. Barnes (1993), The photolysis and chlorine-initiated photo-oxidation of trifluoroacetaldehyde, STEP-HALOLSIDE/AFEAS Workshop, Dublin, 23–25 March, pp.182–188.

Ridley, B.A., E.L. Atlas, J.G. Walega, G.L. Kok, T.A. Staffelbach, J.P. Greenberg, F.E. Grahek, P.G. Hess, and D.D. Montzka (1997), Aircraft measurements made during the spring maximum of ozone over Hawaii: Peroxides, CO, O_3, NO_y, condensation nuclei, selected hydrocarbons, halocarbons, and alkyl nitrates between 0.5 and 9 km altitude, *J. Geophys. Res.*, *102*(D15), 18935–18961.

Riemer, D., W. Pos, P. Milne, C. Farmer, R. Zika, E. Apel, K. Olszyna, T. Kliendienst, W. Lonneman, S. Bertman, P. Shepson, and T. Starn (1998), Observations of nonmethane hydrocarbons and oxygenated volatile organic compounds at a rural site in southeastern United States, *J. Geophys. Res.*, *103*, 28111–28128.

Rinke, M., and C. Zetzsch (1984), Rate constants for the reaction of OH radicals with aromatics, benzene, phenol, aniline, and 1,2,4-trichlorobenzene, *Ber. Bunsen-Ges. Phys. Chem.*, *88*, 55–62.

Rinsland, C.P., R. Zander, L.R. Brown, C.B. Farmer, J.H. Park, R.H. Norton, J.M. Russell III, and O.F. Raper (1986), Detection of carbonyl fluoride in the stratosphere, *Geophys. Res. Lett.*, *13*, 769–772.

Roberts, J.M. (1990), The atmospheric chemistry of organic nitrates, *Atmos. Environ.*, *24A*, 243–287.

Roberts, J.M., and R.W. Fajer (1989), UV absorption cross sections of organic nitrates of potential atmospheric importance and estimation of atmospheric lifetimes, *Environ. Sci. Technol.*, *23*, 945–951.

Roberts, J.M., B.T. Jobson, W. Kuser, P. Goldan, P. Murphy, E. Williams, G. Frost, D. Riemer, E. Apel, C. Stroud, C. Wiedinmyer, and F. Fehsenfeld (2003), An examination of the chemistry of peroxycarboxylic nitric anhydrides and related volatile organic compounds during Texas Air Quality Study 2000 using ground-based measurements, *J. Geophys. Res.*, *108*, D16, 4495, doi:10.1029/s003JD003383.

Roberts, J.M., M. Marchewka, S.B. Bertman, R. Sommariva, C. Warneke, J. de Gouw, W. Kuster, P. Boldan, E. Williams, B.M. Lerner, P. Murphy, and F.C. Fehsenfeld (2007), Measurements of PANs during the New England Air Quality Study 2002, *J. Geophys. Res.*, *112*, D20306, doi:10.1029/2007JD008667.

Roberts, J.M., D.D. Parrish, R.B. Norton, S.B. Bertman, J.S. Holloway, M. Trainer, F.C. Fehsenfeld, M.A. Carroll, G.M. Albercook, T. Wang, and G. Forbes (1996), Episodic removal of NO_y species from the marine boundary layer over the North Atlantic, *J. Geophys. Res.*, *101*, 28947–28960.

Roberts, J.M., J. Williams, K. Baumann, M.P. Buhr, P.D. Goldan, J. Holloway, G. Hubler, W.C. Kuster, S.A. McKeen, T.B. Ryerson, M. Trainer, E.J. Williams, F.C. Fehsenfeld, S.B. Bertman, G. Nouaime, C. Seaver, G. Grodzinsky, M. Rodgers, and V.L. Young (1998), Measurements of PAN, PPN, and MPAN made during the 1994 and 1995 Nashville Intensives of the Southern Oxidant Study. Implications for regional ozone production from biogenic hydrocarbons, *J. Geophys. Res.*, *103*, 22473–22490.

Rodriguez, D., A. Rodriguez, A. Notario, A. Aranda, Y. Diaz-de-Mera, and E. Martinez (2005), Kinetic study of the gas-phase reaction of atomic chlorine with a series of aldehydes, *Atmos. Chem. Phys.*, *5*, 3433–3440.

Rodriguez, D., A. Rodriguez, A. Soto, A. Aranda, Y. Diaz-de-Mera, and A. Alberto (2008), Kinetics of the reactions of Cl atoms with 2-buten-1-ol, 2-methyl-2-propen-1-ol, and 3-methyl-2-buten-1-ol as a function of temperature, *J. Atmos. Chem.*, *59*, 187–197.

Rodriguez, H.J., J.-C. Chang, and T.F. Thomas (1976), Thermal, photochemical, and photophysical processes in cyclopropanone vapor, *J. Am. Chem. Soc.*, *98*, 2027–2041.

Roehl, C.M., T.L. Mazely, R.R. Friedl, Y. Li, J.S. Francisco, and S.P. Sander (2001), NO_2 quantum yield from the 248 nm photodissociation of peroxynitric acid (HO_2NO_2), *J. Phys. Chem. A*, *105*, 1592–1598.

Roehl, C.M., J.J. Orlando, G.S. Tyndall, R.E. Shetter, G.J. Vázquez, C.A. Cantrell, and J.G. Calvert (1994), Temperature dependence of the quantum yields for the photolysis of NO_2 near the dissociation limit, *J. Phys. Chem.*, *98*, 7837–7843.

Rogers, J.D. (1990), Ultraviolet absorption cross sections and atmospheric photodissociation rate constants for formaldehyde, *J. Phys. Chem.*, *94*, 4011–4015.

Rogers, M.O., and D.D. Davis (1989), A UV-photofragmentation/laser-induced fluorescence sensor for the atmospheric detection of HONO, *Environ. Sci. Technol*, *23*, 1106–1112.

Román-Leshlov, Y., C.J. Barrett, Z.Y. Liu , and J.A. Dumesic (2007), Production of dimethylfuran for liquid fuels from biomass-derived carbohydrates, *Nature*, *447*, 982–986.

Roof, J.G., and F.E. Blacet (1941), Photolysis of biacetyl in the near ultraviolet, *J. Am. Chem. Soc.*, *63*, 1126–1128.

Rosado-Reyes, C.M., and J.S. Francisco (2006), Atmospheric oxidation pathways of acetic acid, *J. Phys. Chem. A*, *110*, 4419–4433.

Rosado-Reyes, C.M., J.S. Francisco, J.J. Szente, M.M. Maricq, and L.F. Østergaard (2005), Dimethyl ether oxidation at elevated temperatures (295–600 K), *J. Phys. Chem. A*, *109*, 10940–10953.

Roscoe, J.M. (1986) The reactions of $O(^3P)$ with 2–propanone, 2-butanone, and 3-pentanone. *Can. J. Chem.*, *64*, 1458–1464.

Roscoe, J.M. (1988) The kinetics of gas phase reactions studied in a "homogeneous reactor". *Can. J. Chem.*, *66*, 2325–2334.

Roscoe, J.M., and R.A. Back (1986), Product ratios in the photolysis of *cis*- and *trans*-glyoxal at low pressures: The mechanisms of the thermal and the photochemical decompositions, *J. Phys. Chem.*, *90*, 598–602.

Rose, M. (1979), Photolysis of alkyl nitrites and reactions of alkoxy radicals with nitrogen oxides, Ph.D. Thesis, Case-Western Reserve University.

Ross, P.L., S.E. Bramer, and M.V. Johnston (1996), Ultraviolet photodissociation of gas-phase alcohols, amines, and nitroalkanes, *App. Spectros.*, *50*, 608–613.

Ross, W.F., and G.B. Kistiakowsky (1934), The photochemical decomposition of ketene, *J. Am. Chem. Soc.*, *56*, 1112–1115.

Rösslein, M., E. Kades, K. Bergmann, and J.R. Huber (1995), Alignment detected photofragment yield spectroscopy demonstratred by photodissociation of *t*-butyl nitrite in a supersonic jet, *Chem. Phys. Lett.*, *235*, 242–246.

Röth, E.-P., R. Ruhnke, G. Moortrgat, R. Meller, and W. Schneider (1997), UV/VIS-absorption cross sections and quantum yields for use in photochemistry and atmospheric modeling. Part 2: Organic substances, Institut für Chemie und Dynamik der Geosphäre 1: Stratosphärische Chemie, Forschungszentrum Jülich, Julich, Germany.

Rudić, S., C. Murray, D. Ascenzi, H. Anderson, J.N. Harvey, and A.J. Orr-Ewing (2002), The dynamics of formation of HCl products from the reaction of Cl atoms with methanol, ethanol, and dimethyl ether, *J. Chem. Phys.*, 117, 5692–5706.

Rudich, Y., R. Talukdar, J.B. Burkholder, and A.R. Ravishankara (1995), Reaction of methylbutenol with hydroxyl radicals: mechanism and atmospheric implications, *J. Phys. Chem.*, *99*, 12188–12194.

Rudich, Y., R.K. Talukdar, R.W. Fox, and A.R. Ravishankara (1996), Rate coeficients for reactions of NO_3 with a few olefins and oxygenated olefins, *J. Phys. Chem.*, *100*, 5374–5381.

Rudolph, J., R. Koppmann, and Ch. Plass-Dülmer (1996), The budgets of ethane and tetrachloroethene: Is there evidence for an impact of reactions with chlorine atoms in the troposphere?, *Atmos. Environ.*, *30*, 1887–1894.

Russell, G.A. (1957), Deuterium-isotope effects in the autoxidation of aralkyl hydrocarbons. Mechanism of the interaction of peroxy radicals, *J. Am. Chem. Soc.*, *79*, 3871–3877.

Russell, R.L., and F.S. Rowland (1968), Reactions of triplet methylene with oxygen. Formation of molecular hydrogen, carbon monoxide and carbon dioxide, *J. Am. Chem. Soc.*, *90*, 1671–1677.

Russell, R.L., and F.S. Rowland (1979), Mechanism of products formation during the photolysis of ketene, *J. Phys. Chem.*, *83*, 2077–2078.

Sakurai, H., and S. Kato (1999), A theoretical study of the Norrish type I reaction of acetone, *J. Molec. Structure (Theochem)*, *461–462*, 145–152.

Salas, L.J., and H.B. Singh (1986), Measurements of formaldehyde and acetaldehyde in the urban ambient air, *Atmos. Environ.*, *20*, 1301–1304.

Salgado, M.S., E. Monedero, F. Villanueva, P. Martin, A. Tapia, and B. Cabañas (2008), Night-time atmospheric fate of acrolein and crotonaldehyde, *Environ. Sci. Technol.*, *42*, 2394–2400.

Sander, R. (1999), Compilation of Henry's Law constants for inorganic and organic species of potential importance in environmental chemistry (version 3), http://www.henrys-law.org; http://www.mpch-mainz.mpg.de/~sander/res/henry.html.

Sander, R. (2005), "Henry's Law Constants" in NIST Chemistry WebBook, NIST Standard Reference Database Number 69, editors P.J. Linstrom and W.G. Mallard, June 2005, National Institute of Standards and Technology, Gaithersburg MD, 20899 (http://webbook.nist.gov).

Sander, S.P., D.M. Golden, M.J. Kurylo, G.K. Moortgat, R.E. Huie, C.E. Kolb, M.J. Molina, B.J. Finlayson-Pitts, P.H. Wine, and R.E. Huie (2006), *Chemical Kinetics and Photochemical Data for Use in Atmospheric Studies*, Evaluation Number 15, 2006, Jet Propulsion Laboratory, Pasadena, California.

Sanders, N., J.E. Butler, L.R. Pasternack, and J.R. McDonald (1980), $CH_3O(X\ ^2E)$ production from 266 nm photolysis of methyl nitrite and reaction with NO, *Chem. Phys.*, *48*, 203–208.

Sanhueza, E., and J. Heicklen (1975), Chlorine-atom sensitized oxidation of dichloromethane and chloromethane, *J. Phys. Chem.*, *79*, 7–11.

Sato, K., B. Klotz, T. Taketsugu, and T. Takayanagi (2004), Kinetic measurements for the reactions of ozone with crotonaldehyde and its methyl derivatives and calculations of transition-state theory, *Phys. Chem. Chem. Phys.*, *6*, 3969–3976.

Sauer, C.G., I. Barnes, K.H. Becker, H. Geiger, T.J. Wallington, L.K. Christensen, J. Platz, and O.J. Nielsen (1999), Atmospheric chemistry of 1,3-dioxolane: Kinetic, mechanistic, and modeling study of OH radical initiated oxidation, *J. Phys. Chem. A*, *103*, 5959–5966.

Saunders, S.M., D.L. Baulch, K.M. Cooke, M.J. Pilling, and P.I. Smurthwaite (1994), Kinetics and mechanisms of the reactions of OH with some oxygenated compounds of importance in tropospheric chemistry, *Int. J. Chem. Kinet.*, *26*, 113–130.

Saunders, S.M., M.E. Jenkin, R.G. Derwent, and M.J. Pilling (2003a), Protocol for the development of the Master Chemical Mechanism, MCM v3 (Part A): tropospheric degradation of non-aromatic volatile organic compounds, *Atmos. Chem. Phys.*, *3*, 161–180.

Saunders, S.M., S. Pascoe, A.P. Johnson, M.J. Pilling and M.E. Jenkin (2003b), Development and preliminary test results of an expert system for the automatic generation of tropospheric VOC degradation mechanisms, *Atmos. Env.*, *37*, 1723–1735.

Saxena, P., and L.M. Hildemann (1996), Water-soluble organics in atmospheric particles: A critical review of the literature and application of thermodynamics to identify candidate compounds, *J. Atmos. Chem.*, *24*, 57–109.

Scala, A.A., and D.G. Ballan (1972), The vacuum ultraviolet photolysis of cyclopentanone, *Can. J. Chem.*, *50*, 3938–3943.

Scarfogliero, M., B. Picquet-Varrault, J. Salce, R. Durand-Jolibois, and J.-F. Doussin (2006), Kinetic and mechanistic study of the gas-phase reactions of a series of vinyl ethers with the nitrate radical, *J. Phys. Chem. A.*, *110*, 11074–11081.

Schauer, J.J., M.J. Kleeman, G.R. Cass, and B.R.T. Simoneit (1999a), Measurement of emissions from air pollution sources. 1. C_1 through C_{29} organic compounds from meat charbroiling, *Environ. Sci. Technol.*, *33*, 1566–1577.

Schauer, J.J., M.J. Kleeman, G.R. Cass, and B.R.T. Simoneit (1999b), Measurement of emissions from air pollution sources. 2. C_1 through C_{30} organic compounds from medium duty diesel trucks, *Environ. Sci. Technol.*, *33*, 1578–1587.

Schauer, J.J., M.J. Kleeman, G.R. Cass, and B.R.T. Simoneit (2001), Measurement of emissions from air pollution sources. 3. C_1–C_{29} organic compounds from fireplace combustion of wood, *Environ. Sci. Technol.*, *35*, 1716–1728.

Schauer, J.J., M.J. Kleeman, G.R. Cass, and B.R.T. Simoneit (2002a), Measurement of emissions from air pollution sources. 4. C_1–C_{27} organic compounds from cooking with seed oils, *Environ. Sci. Technol.*, *36*, 567–575.

Schauer, J.J., M.J. Kleeman, G.R. Cass, and B.R.T. Simoneit (2002b), Measurement of emissions from air pollution sources. 5. C_1–C_{32} organic compounds from gasoline-powered motor vehicles, *Environ. Sci. Technol.*, *36*, 1169–1180.

Schiffman, A., D.D. Nelson, Jr., and D.J. Nesbitt (1993), Quantum yields for OH production from 193 and 248 nm photolysis of HNO_3 and H_2O_2, *J. Chem. Phys.*, *98*, 6935–6946.

Schneider, W.F., T.J. Wallington, and R.E. Huie (1996), Energetics and mechanism of decomposition of CF_3OH: Evidence for water-catalyzed homogeneous decomposition, *J. Phys. Chem.*, *100*, 6097–6103.

Schneider, W.F., T.J. Wallington, K. Minschwaner, and E.A. Stalberg (1995), Atmospheric chemistry of CF_3OH: Is photolysis important?, *Environ. Sci. Technol.*, *29*, 247–250.

Schoen, P.E., M.J. Marrone, J.M. Schnur, and L.S. Goldberg (1982), Picosecond UV photolysis and laser-induced fluorescence probing of gas-phase nitromethane, *Chem. Phys. Lett.*, *90*, 272–276.

Schuck, E.A., and E.R. Stephens (1967), Quantum yields during dilute gas phase photolysis of ethyl nitrite in the 3500 Å region, *Environ. Sci. Technol.*, *1*, 138–143.

Schuck, E.A., E.R. Stephens, and R.R. Schrock (1966), Rate constant ratios during nitrogen dioxide photolysis, *J. Air Poll. Control Assoc.*, *16*, 695–696.

Schwartz-Lavi, D., and S. Rosenwaks (1988), Scalar and vectorial properties in the photodissociation of *tert*-butyl nitrite from the S_1 and S_2 states, *J. Chem. Phys.*, *88*, 6922–6930.

Scollard, D.J., J.J. Treacy, H.W. Sidebottom, C. Balestria-Garcia, G. Laverdet, G. Le Bras, H. MacLéod, and S. Téton (1993), Rate constants for the reactions of hydroxyl radicals and chlorine atoms with halogenated aldehydes, *J. Phys. Chem.*, *97*, 4683–4688.

Scuseria, G.E., and H.F. Schaefer III (1989), The unimolecular triple dissociation of glyoxal: Transition-state structures optimized by configuration interaction and coupled cluster methods, *J. Am. Chem. Soc.*, *111*, 7761–7765.

Seakins, P.W., J.J. Orlando, and G.S. Tyndall (2004), Rate coefficients and production of vibrationally excited HCl from the reactions of chlorine atoms with methanol, ethanol, acetaldehyde and formaldehyde, *Phys. Chem. Chem. Phys.*, *6*, 2224–2229.

Seco, R., J. Peñuelas, and I. Filella (2007), Short-chain oxygenated VOCs: Emission and uptake by plants and atmospheric sources, sinks, and concentrations, *Atmos. Environ.*, *41*, 2477–2499.

Sehested, J., T. Møgelberg, T.J. Wallington, E.W. Kaiser, and O.J. Nielsen (1996), Dimethyl ether oxidation: kinetics and mechanism of the $CH_3OCH_2 + O_2$ reaction at 206 K and 0.38–940 Torr total pressure, *J. Phys. Chem.*, *100*, 17218–17225.

Sehested, J., O.J. Nielsen, and T.J. Wallington (1993), Atmospheric chemistry of hydrofluorocarbon 134a: Fate of the alkoxy radical CF_3O, *Environ. Sci. Technol.*, *27*, 146–152.

Sehested, J., K. Sehested, J. Platz, H. Egsgaard, and O.J. Nielsen (1997), Oxidation of dimethyl ether: Absolute rate constants for the self reaction of CH_3OCH_2 radicals, the reaction of CH_3OCH_2 radicals with O_2, and the thermal decompositon of CH_3OCH_2 radicals, *Int. J. Chem. Kinet.*, *29*, 627–636.

Seinfeld, J.H., and S.N. Pandis (1998), *Atmospheric Chemistry and Physics*, John Wiley & Sons, New York.

Seland, J.G., I.M.W. Noremsaune, and C.J. Nielsen (1996), FTIR studies of the NO_3 initiated degradation of but-2-yne: Mechanism and rate constant determination, *J. Chem. Soc., Faraday Trans.*, *92*, 3459–3465.

Sellevåg, S.R., T. Kelly, H. Sidebottom, and C.J. Nielsen (2004a), A study of the IR and UV-Vis absorption cross-sections, photolysis and OH-initiated oxidation of CF_3CHO and CF_3CH_2CHO, *Phys. Chem. Chem. Phys.*, *6*, 1243–1252.

Sellevåg, S.R., and C.J. Nielsen (2003), Kinetic study of the reactions CH_2ClCH_2Cl + OH, $CH_3C(O)CH_3$ + Cl and $HC(O)OCH_2CH_3$+ Cl by the relative rate method, *Asian Chem. Lett.*, *7*, 15–20.

Sellevåg, S.R., C.J. Nielsen, O.A. Søvde, G. Myhre, J.K. Sundet, F. Stordal, and I.S.A. Isaksen (2004b), Atmospheric gas-phase degradation and global warming potentials of

2-fluoroethanol, 2,2-difluoroethanol, and 2,2,2-trifluoroethanol, *Atmos. Environ.*, *38*, 6725–6735.

Sellevåg, S.R., V. Stenstrøm, T. Helgaker, and C.J. Nielsen (2005), Atmospheric chemistry of CHF_2CHO: Study of the IR and UV-Vis absorption cross sections, photolysis and OH-, Cl-, and NO_3-initiated oxidation, *J. Phys. Chem. A*, *109*, 3652–3662.

Semadeni, M., D.W. Stocker, and J.A. Kerr (1993), Further studies of the temperature dependence of the rate coefficients for the reactions of OH with a series of ethers under simulated atmospheric conditions, *J. Atmos. Chem.*, *16*, 79–93.

Semadeni, M., D.W. Stocker, and J.A. Kerr (1995), The temperature dependence of the OH radical reactions with some aromatic compounds under simulated tropospheric conditions, *Int. J. Chem. Kinetics*, *27*, 287–304.

Semelsberger, G.A., R.L. Borup, and H.L. Greene (2006), Dimethyl ether (DME) as an alternative fuel, *J. Power Sources*, *156*, 497–511.

Semmes, D.H., A.R. Ravishankara, C.A. Gump-Perkins, and P.H. Wine (1985), Kinetics of the reactions of hydroxyl radical with aliphatic aldehydes, *Int. J. Chem. Kinet.*, *17*, 303–313.

Sempeles, J., and J.M. Andino (2000), Laboratory studies of the OH-initiated photooxidation of di-*n*-propyl ether, *Int. J. Chem. Kinet.*, *32*, 703–711.

Sevin, A., E. Fazilleau, and P. Ghaquin (1981), Etude theorique des ruptures thermique et photochimique de la cyclopropanone, *Tetrahedron*, *37*, 3831–3837.

Shaffer, G.W., A.B. Doerr, and K.L. Purzycki (1972), Photoisomerization of nopinone, *J. Org. Chem.*, *37*, 25–29.

Shallcross, D.E., P. Biggs, C.E. Canosa-Mas, K.C. Clemitshaw, M.G. Harrison, M.R.L. Alañón, J.A. Pyle, A. Vipond, and R.P. Wayne (1997), Rate constants for the reaction between OH and CH_3ONO_2 and $C_2H_5ONO_2$ over the a range of pressure and temperature, *J. Chem. Soc., Faraday Trans.*, *93*, 2807–2811.

Shallcross, D.E., M.T. Raventos-Duran, M.W. Bardwell, A. Bacak, Z. Solman, and C.J. Percival (2005), A semi-empirical correlation for the rate coefficients for cross- and self-reactions of peroxy radicals in the gas-phase, *Atmos. Environ.*, *39*, 763–771.

Shan, J.H., V. Vorsa, S.J. Wategaonkar, and R. Vasudev (1989), Influence of intramolecular vibrational dynamics on state-to-state photodissociation: *trans*-DONO ($\tilde{A}$) versus HONO ($\tilde{A}$), *J. Chem. Phys.*, *90*, 5493-5500.

Sheats, G.F., and W.A. Noyes, Jr. (1955a), Photochemical studies. LI. The photochemistry of biacetyl at 3650 and 4358Å and its relationship to fluorescence, *J. Am. Chem. Soc.*, *77*, 1421–1426.

Sheats, G.F., and W.A. Noyes, Jr. (1955b), The long wave photochemistry of biacetyl and its correlation with fluorescence at temperatures over 100°, *J. Am. Chem. Soc.*, *77*, 4532–4533.

Shepson, P.B., D.R. Hastie, H.I. Schiff, M. Polizzi, J.W. Bottenheim, K. Anlauf, G.I. Mackay, and D.R. Karecki (1991), Atmospheric concentrations and temporal variations of C_1–C_3 carbonyl compounds at two rural sites in central Ontario, *Atmos. Environ.*, *25A*, 2001–2015.

Shepson, P.B., and J. Heicklen (1982a), The photo-oxidation of propionaldehyde, *J. Photochem.*, *18*, 169–184.

Shepson, P.B., and J. Heicklen (1982b), The wavelength and pressure dependence of the photolysis of propionaldehyde in air, *J. Photochem.*, *19*, 215–227.

Shepson, P.B., E. Mackay, and K. Muthuramu (1996), Henry's law constants and removal processes for several atmospheric hydroxy alkyl nitrates, *Environ. Sci. Technol.*, 30, 3618–3623.

Shinohara, H., and N. Nishi (1982), Laser photofragmentation dynamics of an acrolein supersonic molecular beam at 193 nm, *J. Chem. Phys.*, *77*, 234–245.

Shortridge, R.G., Jr., and E.K.C. Lee (1970), Benzene photosensitization and direct photolysis of cyclohexanone and cyclohexanone-2-t in the gas phase, *J. Am. Chem. Soc.*, *92*, 2228–2236.

Shortridge, R.G., Jr., C.F. Rusbult, and E.K.C. Lee (1971), Fluorescence excitation study of cyclobutanone, cyclopentanone, and cyclohexanone in the gas phase, *J. Am. Chem. Soc.*, *93*, 1863–1867.

Shu, J., D.S. Peterka, S.R. Leone, and M. Ahmed (2004), Tunable synchrotron vacuum ultraviolet ionization, time-of-flight investigation of the photodissociation of *trans*-crotonaldedhyde at 193 nm, *J. Phys. Chem. A*, *108*, 7895–7902.

Shu, Y., E.S.C. Kwok, E.C. Tuazon, R. Atkinson, and J. Arey (1997), Products of the gas phase reactions of linalool with OH radicals, NO_3 radicals and O_3, *Environ. Sci. Technol.*, *31*, 896–904.

Sidebottom, H.W., C.C. Badcock, J.G. Calvert, B.R. Rabe, and E.K. Damon (1972), Lifetime studies of the biacetyl excited singlet and triplet states in the gas phase at 25°C, *J. Am. Chem. Soc.*, *94*, 13–19.

Sieger, R.A. (1954), The vapor phase photolysis of trifluoroacetone at wavelength 3130 Å, Master of Science Thesis, The Ohio State University, Columbus, Ohio, 43210.

Sieger, R.A., and J.G. Calvert (1954), The vapor phase photolysis of trifluoroacetone at wave length 3130 Å, *J. Am. Chem. Soc.*, *76*, 5197–5201.

Simonaitis, R., and J. Heicklen (1983), A flash photolysis study of the photo-oxidation of acetaldehyde at room temperature, *J. Photochem.*, *23*, 299–309.

Simonaitis, R., and M.T. Leu (1985), Rate constant of the reaction Cl + HO_2NO_2 →Products, *Int. J. Chem. Kinet.*, *17*, 293–301.

Simpson, D., A. Guenther, C.N. Hewitt, and R. Steinbrecher (1995), Biogenic emissions in Europe, 1. Estimates and uncertainties, *J. Geophys. Res.*, *100*, 22875–22890.

Simpson, D., W. Winiwarter, G. Börjesson, S. Cinderby, A. Ferreiro, A. Guenther, C.N. Hewitt, R. Janson, M.A.K. Khalil, S. Owen, T.E. Pierce, H. Puxbaum, M. Shearer, U. Skiba, R. Steinbrecher, H.B. Singh, D. O'Hara, D. Herlth, W. Sachse, D.R. Blake, J.D. Bradshaw, M. Kanakidou, and P.J. Crutzen (1994), Acetone in the atmosphere: Distribution , sources, and sinks, *J. Geophys. Res.*, *99*, 1805–1819.

Simpson, D., W. Winiwarter, G. Börjesson, S. Cinderby, A. Ferreiro, A. Guenther, C.N. Hewitt, R. Janson M. Aslam, K. Khalil, S. Owen, T.E. Pierce, H. Puxbaum, M. Sheraer, U. Skiba, R. Steinbrecher, L. Tarrasón, and M.G. Öquist (1999), Inventoring emissions from nature in Europe, *J. Geophys. Res.*, *104*, 8113–8152.

Simpson, I.J., S. Meinardi, D.R. Blake, N.J. Blake, F.S. Rowland, E. Atlas, and F. Flocke (2002), A biomass burning source of C_1–C_4 alkyl nitrates, *Geophys. Res. Lett.*, *29*, 2168, doi:10.1029/2002Gl016290.

Singer, R.J., J.N. Crowley, J.P. Burrows, W. Schneider, and G.K. Moortgat (1989), Measurement of the absorption cross-section of peroxynitric acid between 210 and 330 nm in the range 253–298 K, *J. Photochem. Photobiol.*, *48*, 17–32.

Singh, H.B. (1976), Phosgene in the ambient air, *Nature*, *264*, 428–429.

Singh, H., Y. Chen, A. Staudt, D. Jacob, D. Blake, B. Heikes, and J. Snow (2001), Evidence from the Pacific troposphere for large global sources of oxygenated organic compounds, *Nature*, *410*, 1078–1081.

Singh, H., Y. Chen, A. Tabazadeh, Y. Fukui, I. Bey, R. Yantosca, D. Jacob, F. Arnold, K. Wohlfrom, E. Atlas, F. Flocke, D. Blake, N. Blake, B. Heikes, J. Snow, R. Talbot, G. Gregory, G. Sachse, S. Vay, and Y. Kondo (2000), Distribution and fate of selected oxygenated organic species in the troposphere and lower stratosphere over the Atlantic, *J. Geophys. Res. 105*, 3795–3805.

Singh, H.B., M. Kanakidou, P.J. Crutzen, and D.J. Jacob (1995), High concentrations and photochemical fate of oxygenated hydrocarbons in the global troposphere, *Nature*, *378*, 50–53.

Singh, H.B., D. O'Hara, D. Herlth, W. Sachse, D.R. Blake, J.D. Bradshaw, M. Kanakidou, and P.J. Crutzen (1994), Acetone in the atmosphere: Distribution , sources, ands sinks, *J. Geophys. Res.*, *99*, 1805–1819.

Singh, H.B., L. Salas, D. Herlth, R. Kolyer, E. Czech, M. Avery, J.H. Crawford, R.B. Pierce, G.W. Sachse, D.R. Blake, R.C. Cohen, T.H. Bertram, A. Perring, P.J. Wooldridge, J. Dibb, G. Huey, R.C. Hudman, S. Tuorquety, L.K. Emmons, F. Flocke, Y. Tang, G.R. Carmichael, and L.W. Howowitz (2007), Reactive nitrogen distribution and partitioning in the North American troposphere and lowermost stratosphere, *J. Geophys. Res.*, *112*, D12S04, doi:10.1029/2006JD007664.

Singh, H.B., A. Tabazadeh, M.J. Evans, B.D. Field, D.J. Jacob, G. Sachse, J.H. Crawford, R. Shetter, and W.H. Brune (2003), Oxygenated volatile organic chemicals in the oceans: Inferences and implications based on atmospheric observations and air–sea exchange models, *Geophys. Res. Letters*, *30*, ASC 13/1–ASC 13/5.

Singh, S., S. Hernandez, Y. Ibarra, and A.S. Hasson (2009), Kinetics and mechanism of the reactions of *n*-butanal and *n*-pentanal with chlorine atoms, *Int. J. .Chem. Kinetics*, *41*, 133–141.

Singleton, D.L., R.S. Irwin, and R.J. Cvetanović (1977), Arrhenius parameters for the reactions oxygen(^{3}P) atoms with several aldehydes and the trend in aldehydic carbon–hydrogen bond dissociation energies, *Can. J. Chem.*, *55*, 3321–3327.

Singleton, D.L., G. Paraskevopoulos, and R.S. Irwin (1989), Rates and mechanism of the reactions of hydroxyl radicals with acetic, deuterated acetic, and propionic acids in the gas phase, *J. Am. Chem. Soc*, *111*, 5248–5251.

Singleton, D.L., G. Paraskevopoulos, R.S. Irwin, G.S. Jolly, and D.J. McKenney (1988), Rate and mechanism of the reaction of hydroxyl radicals with formic and deuteriated formic acids, *J. Am. Chem. Soc*, *110*, 7786–7790.

Sinreich, R., R. Volkamer, F. Filsinger, U. Frieß, C. Kern, U. Platt, O. Sebastián, and T. Wagner (2007), MAX-DOAS detection of glyoxal during ICARTT 2004, *Atmos. Chem. Phys.*, *7*, 1293–1303.

Sivakumaran, V., and J. Crowley (2003), Reaction between OH and CH_3CHO, Part 2, temperature dependent rate coefficients (201–348 K), *Phys. Chem. Chem. Phys.*, *5*, 106–111.

Sivakumaran, V., D. Hölscher, T.J. Dillon, and J. Crowley (2003), Reaction between OH and HCHO: Temperature dependent rate coefficients (202–399 K) and product pathways (298 K), *Phys. Chem. Chem. Phys.*, *5*, 4821–4827.

Sjödin, A. (1988), Studies of the diurnal-variation of nitrous-acid in urban air, *Environ. Sci. Technol.*, *22*, 1086–1089.

Sjödin, A., and M. Ferm (1985), Measurements of nitrous-acid in an urban area, *Atmos. Environ.*, *19*, 985–992.

Slemr, J., W. Junkermann, and A. Volz-Thomas (1996), Temporal variations in formaldehyde, acetaldehyde and acetone and budget of formaldehyde at a rural site in southern Germany, *Atmos. Environ.*, *30*, 3667–3676.

Smith, A.M., E. Rigler, E.S.C. Kwok, and R. Atkinson (1996), Kinetics and products of the gas-phase reaction of 6-methyl-5-hepten-2-one and *trans*-cinnamaldehyde with OH and NO_3 radicals and O_3 at 296 ± 2 K, *Environ. Sci. Technol.*, *30*, 1781–1785.

Smith, B.J., M.T. Nguyen, W.J. Bouma, and L. Radom (1991a), Unimolecular rearrangements connecting hydroxyethylidene (CH_3COH), acetaldehyde ($CH_3CH{=}O$), and vinyl alcohol ($CH_2{=}CHOH$), *J. Am. Chem. Soc.*, *113*, 6452–6458.

Smith, C.A., L.T. Molina, J.J. Lamb, and M.J. Molina (1984), Kinetics of the reaction of OH with pernitric and nitric acids, *Int. J. Chem. Kin.*, *16*, 41–55.

Smith, D.F., T.E. Kleindienst, E.E. Hudgens, and C.D. McIver (1992), Kinetics and mechanism of the atmospheric oxidation of ethyl tertiary butyl ether, *Int. J. Chem. Kinet.*, *24*, 199–215.

Smith, D.F., T.E. Kleindienst, E.E. Hudgens, C.D. McIver, and J.J. Bufalini (1991b), The photooxidation of methyl tertiary butyl ether, *Int. J. Chem. Kinet.*, *23*, 907–924.

Smith, D.F., C.D. McIver, and T.E. Kleindienst (1995), Kinetics and mechanism of the atmospheric oxidation of tertiary-amyl methyl ether, *Int. J. Chem. Kinet.*, *27*, 453–472.

Smith, G.D., L.T. Molina, and M.J. Molina (2002a), Measurement of radical quantum yields from formaldehyde photolysis between 269 and 339 nm, *J. Phys. Chem. A*, *106*, 1233–1240.

Smith, I.W., and R. Zellner (1975), Rate measurements of OH by resonance absorption. IV. Reaction of hydroxyl radical OH with ammonia and nitric acid, *Int. J. Chem. Kinet*., *Symp. 1*, 341–351.

Smith, I.W.M., and A.R. Ravishankara (2002), Role of hydrogen-bonded intermediates in the bimolecular reactions of the hydroxyl radical, *J. Phys. Chem. A*, *106*, 4798–4807.

Smith, J.D., J.D. DeSain, and C.A. Taatjes (2002b), Infrared laser absorption measurements of $HCl(v = 1)$ production in reactions of Cl atoms with isobutene, methanol, acetaldehyde, and toluene at 295 K, *Chem. Phys. Lett.*, *366*, 417–425.

Smith, R.H. (1978), Rate constant and activation energy for the gaseous reaction between hydroxyl and formaldehyde, *Int. J. Chem. Kinet.*, *10*, 519–528.

Snow, J.A., B.G. Heikes, H. Shen, D.W. O'Sullivan, A. Fried, and J. Walega (2007), Hydrogen peroxide, methyl hydroperoxide and formaldehyde over North America and the North Atlantic, *J. Geophys. Res.*, *112*, D12807, doi:10.1029/2006JD007746.

Sokolov, O., M.D. Hurley, J.C. Ball, T.J. Wallington, W. Nelsen, I. Barnes, and K.H. Becker (1999), Kinetics of the reactions of chlorine atoms with CH_3ONO and CH_3ONO_2, *Int. J. Chem. Kin.*, *31*, 357–359.

Solignac, G., I. Magneron, A. Mellouki, A. Muñoz, M. Martin-Reviero, and K. Wirtz (2006a), A study of the reaction of OH radicals with *N*-methyl pyrrolidinone, *N*-methyl succinimide and *N*-formyl pyrrolidinone, *J. Atmos. Chem.*, *54*, 89–102.

Solignac, G., A. Mellouki, G. Le Bras, I. Barnes, and Th. Benter (2005), Kinetics of the OH and Cl reactions with *N*-methylformamide, *N*,*N*-dimethylformamide and *N*,*N*-dimethylacetamide, *J. Photochem. Photobiol. A: Chem.*, *176*, 136–142.

Solignac, G., A. Mellouki, G. LeBras, I. Barnes, and Th. Benter (2006b), Reaction of Cl atoms with $C_6F_{13}CH_3OH$, $C_6F_{13}CHO$, and C_3F_7CHO, *J. Phys. Chem. A*, *110*, 4450–4457.

Solignac, G., A. Mellouki, G. Le Bras, M. Yujing, and H. Sidebottom (2007), The gas phase tropospheric removal of fluoroaldehydes ($C_xF_{2x+1}CHO$, $x = 3, 4, 6$), *Phys. Chem. Chem. Phys.*, *9*, 4200–4210.

Sommariva, R., W.J. Bloss, N. Brough, N. Carslaw, M. Flynn, A.-L. Haggerstone, D.E. Heard, J.R. Hopkins, J.D. Lee, A.C. Lewis, G. McFiggans, P.S. Monks, S.A. Penkett, M.J. Pilling, J.M.C. Plane, K.A. Read, A. Saiz-Lopez, A.R. Rickard, and P.I. Williams (2006) OH and HO_2 chemistry during NAMBLEX: roles of oxygenates, halogen oxides and heterogeneous uptake, *Atmos. Chem. Phys.*, *6*, 1135–1153.

Somnitz, H., M. Fida, T. Ufer, and R. Zellner (2005), Pressure dependence for the CO quantum yield in the photolysis of acetone at 248 nm: A combined experimental and theoretical study, *Phys. Chem. Chem. Phys.*, *7*, 3342–3352.

Sørensen, M., M.D. Hurley, T.J. Wallington, T.S. Dibble, and O.J. Nielsen (2002), Do aerosols act as catalysts in the OH radical initiated atmospheric oxidation of volatile organic compounds?, *Atmos. Environ.*, *36*, 5947–5952.

Sørensen, S., and I. Barnes (1998), Photolysis of unsaturated 1,4-dicarbonyls, in, editors I. Barnes and J. Wenger, *European Photoreactor EUPHORE Report 1997*, pp.149–164, University of Wuppertal, Wuppertal, Germany.

Sorooshian, A., V. Varutbangkul, F.J. Brechtel, B. Ervens, G. Feingold, R. Bahreini, S.M. Murphy, J.S. Holloway, E.L. Atlas, G. Buzorius, H. Jonsson, R.C. Flagan, and J.H. Seinfeld (2006), Oxalic acid in clear and cloudy atmospheres: Analysis of data from International Consortium for Atmospheric Research on Transport and Transformation 2004, *J. Geophys. Res.*, *111*, doi:10.1029/2005JD006880.

Soto, M.R., and M. Page (1990), Features of the potential energy surface for reactions of hydroxyl with formaldehyde, *J. Phys. Chem.*, *94*, 3242–3246.

Spaulding, R., M.J. Charles, E.C. Tuazon, and M. Lashley (2002), Ion trap mass spectrometry affords advances in the analytical and atmospheric chemistry of 2-hydroxy-2-methylpropanal, a proposed photooxydation product of 2-methyl-3-buten-2-ol, *J. Am. Soc. Mass Spectro.*, *13*, 530–542.

Spears, K.G., and Brugge, S.P. (1978), Vibrationally excited NO_2 from CH_3NO_2 and 2-$C_3H_7NO_2$ photodissociation, *Chem. Phys. Lett.*, *54*, 373–376.

Spicer, C.W., E.G. Chapman, B.J. Finlayson-Pitts, R.A. Plastridge, J.M. Hubbe, J.D. Fast, and C.M. Berkowitz (1998), Unexpectedly high concentrations of molecular chlorine in coastal air, *Nature*, *394*, 353–356.

Spittler, M., I. Barnes, K.H. Becker, and T.J. Wallington (2000), Product study of the $C_2H_5O_2$ + HO_2 reaction in 760 Torr of air at 284–312 K, *Chem. Phys. Lett.*, *321*, 57–61.

Spivakovsky, C., S. Wofsy, and M. Prather (1990), A numerical method for parameterization of atmospheric chemistry: Computation of tropospheric OH, *J. Geophys. Res.*, *95*, 18433–18439.

Squillace, P.J., J. Zogorski, W.G. Wilber, and C.V. Price (1996), Preliminary assessment of the occurrence and possible sources of MTBE in groundwater in the United States, 1993–1994, *Environ. Sci. Technol.*, *30*, 1721–1730.

Squillace, P. J., J. F. Pankow, N. E. Korte, and J. S. Zogorski (1997), Review of the environmental behavior and fate of methyl *tert*-butyl ether, *Environ. Tox. and Chem.*, *16*, 1836–1844.

Sridharan, U.C., B. Reimann, and F. Kaufman (1980), Kinetics of the reaction OH + H_2O_2 → HO_2 + H_2O, *J. Chem. Phys.*, *73*, 1286–1293.

Srinivasan, R. (1959), The photochemical type II process in 2-hexanone-5,5-d_2 and 2-hexanone, *J. Am. Chem. Soc.*, *81*, 5061–5065.

Srinivasan, R. (1961), Photochemistry of cyclopentanone. I. Details of the primary process, *J. Am. Chem. Soc.*, *83*, 4344–4347.

Srinivasan, R. (1964), Photochemistry of the cyclic ketones, *Advan. Photochem.*, *1*, 83–113.

Stachnik, R.A., L.T. Molina, and M.J. Molina (1986), Pressure and temperature dependence of the reaction of OH with nitric acid, *J. Phys. Chem.*, *90*, 2777–2780.

Staffelbach, T.A., G.L. Kok, B.G. Heikes, B. McCully, G.I. Mackay, D.R. Darecki, and H.I. Schiff (1996), Comparison of hydroperoxide measurements made during the Mauna Loa Observatory Photochemistry Experiment 2, *J. Geophys. Res.*, *101*, 14729–14740.

Staffelbach, T.A., J.J. Orlando, G.S. Tyndall, and J.G. Calvert (1995), The UV-visible absorption spectrum and photolysis quantum yields of methylglyoxal, *J. Geophys. Res.*, *100*, 14189–14198.

Starcke, J., F. Zabel, L. Elsen, W. Nelson, I. Barnes, and K.H. Becker (1990), Atmospheric behaviour of chloroacetaldehydes, in, editors G. Restelli and G. Angeletti, *Physico-Chemical Behaviour of Atmospheric Pollutants* Kluwer Academic Publishers Dordrecht pp.172–176.

Starkey, D.P., K.A. Holbrook, G.A. Oldershaw, and R.W. Walker (1997), Kinetics of the reactions of hydroxyl radicals (OH) and of chlorine atoms (Cl) with methyl ethyl ether over the temperature range 274–345 K, *Int. J. Chem. Kinet.*, *29*, 231–236.

Stemmler, K., D.J. Kinnison, and J.A. Kerr (1996a), Room temperature rate coefficients for the reactions of OH radicals with some monoethylene glycol monoalkyl ethers, *J. Phys. Chem.*, *100*, 2114–2116.

Stemmler, K., W. Mengon, and J.A. Kerr (1996b), OH radical initiated photooxidation of 2-ethoxyethanol under laboratory conditions related to the troposphere: Product studies and proposed mechanism, *Environ. Sci. Technol.*, *30*, 3385–3391.

Stemmler, K., W. Mengon, and J.A. Kerr (1997a), Hydroxy-radical-initiated oxidation of isobutyl isopropyl ether under laboratory condtions related to the troposphere: Product studies and proposed mechanism, *J. Chem. Soc., Faraday Trans.*, *93*, 2865–2875.

Stemmler, K., W. Mengon, D.J. Kinnison, and J.A. Kerr (1997b), OH radical-initiated oxidation of 2-butoxyethanol under laboratory conditions related to the troposphere: Product studies and proposed mechanism, *Environ. Sci. Technol.*, *31*, 1496–1504.

Stief, L.J., D.F. Nava, W.A. Payne, and J.V. Michael (1980), Rate constant for the reaction of hydroxyl radical with formaldehyde over the temperature range 228–362 K, *J. Chem. Phys.*, *73*, 2254–2258.

Stockwell, W.R., and J.G. Calvert (1978), Near untraviolet-absorption spectrum of gaseous HONO and N_2O_3, *J. Photochem.*, *8*, 193–203.

Stockwell, W.R., F. Kirchner, M. Kuhn, and S. Seefeld (1997), A new mechanism for regional atmospheric chemistry modeling, *J. Geophys. Res.*, *102*, 25847–25879.

Stockwell, W.R., P. Middleton, J.S. Chang, and X. Tang (1990) The second generation regional acid deposition model chemical mechanism for regional air quality modeling, *J. Geophys. Res.*, *95*, 16343–67.

Strachan, A.N., and F.E. Blacet (1955), The photolysis of chloroacetone at 3130 Å, *J. Am. Chem. Soc.*, *77*, 5254–5257.

Strachan, A.N., and W.A. Noyes, Jr. (1954), Photochemical studies. XLIX. Ketene and ketene–oxygen mixtures, *J. Am. Chem. Soc.*, *76*, 3255–3264.

Strachan, A.N., and D.E. Thornton (1968), Photolysis of ketene. I. *Can. J. Chem.*, *46*, 2353–2359.

Streets, D.G., T.C. Bond, G.R. Carmichael, S.D. Fernandes, Q. Fu, D. He, Z. Klimont, S.M. Nelson, N.Y. Tsai, M.Q. Wang, J.H. Woo, and K.F. Yarber (2003), An inventory of gaseous and primary aerosol emissions in Asia in the year 2000, *J. Geophys. Res. 108*, GTE 30/1–GTE 30/23.

Streit, G.E., J.S. Wells, F.C. Fehsenfeld, and C.J. Howard (1979), A tunable diode laser study of the reactions of nitric and nitrous acids: $HNO_3 + NO$ and $HNO_2 + O_3$, *J. Chem. Phys.*, 70, 3439–3443.

Stroud, C.A., J.M. Roberts, J. Williams, P.D. Goldan, W.C. Kuster, T.B. Ryerson, D. Sueper, D.D. Parrish, M. Trainer, and F.C. Fehsenfeld (2001), Alkyl nitrate measurements during

STERAO 1996 and NARE 1997: Intercomparison and survey of results, *J. Geophys. Res.*, *106*, 23043–23053.

Stutz, J., B. Alicke, R. Ackermann, A. Geyer, S. Wang, A.B. White, E.J. Williams, C.W. Spicer, and J.D. Fast (2004), Relative humidity dependence of HONO chemistry in urban areas, *J. Geophys. Res.*, *109*, D03307, doi:10.1029/2003JD004135.

Stutz, J., M. J. Ezell, A.A. Ezell, and B.J. Finlayson-Pitts (1998), Rate constants and kinetic isotope effects in the reactions of atomic chlorine with *n*-butane and simple alkenes at room temperature, *J. Phys. Chem. A*, *102*, 8510–8519.

Stutz, J., E.S. Kim, U. Platt, P. Bruno, C. Perrino, and A. Febo (2000), UV-visible absorption cross sections of nitrous acid, *J. Geoophys. Res.*, *105*, 14585–14592.

Su, F., J.G. Calvert, and J.H. Shaw (1979a), Mechanism of the photooxidation of gaseous formaldehyde, *J. Phys. Chem.*, *83*, 3185–3191.

Su, F., J.G. Calvert, J.H. Shaw, H. Niki, P.D. Maker, C.M. Savage, and L.D. Breitenbach (1979b), Spectroscopic and kinetic studies of a new metastable species in the photooxidation of gaseous formaldehyde, *Chem. Phys. Lett.*, *65*, 221–225.

Sumathi, R., and A.K. Chandra (1993), Photodecomposition of acetyl chloride on the excited singlet state surface, *J. Chem. Phys.*, *99*, 6531–6536.

Suter, H.U., U. Brühlmann, and J.R. Huber (1990), Photodissociation of CH_3ONO by a direct and indirect mechanism, *Chem. Phys. Lett.*, *171*, 63–67.

Suter, H.U., and J.R. Huber (1989), S_1 potential energy surface of HONO: Absorption spectrum and photodissociation, *Chem. Phys. Lett.*, *155*, 203–209.

Swanson, A.L., N.J. Blake, E. Atlas, F. Flocke, D.R. Blake and F.S. Rowland (2003), Seasonal variations of C_2–C_4 nonmethane hydrocarbons and C_1–C_4 alkyl nitrates at the Summit research station in Greenland, *J. Geophys. Res.*, *108*, 4065. doi:10.1029/2001JD001445.

Szopa, S., B. Aumont, and S. Madronich (2005), Assessment of the reduction methods used to develop chemical schemes: Building of a new chemical scheme for VOC oxidation suited to three-dimensional multiscale HO_x–NO_x–VOC chemistry simulations, *Atmos. Chem. Phys.*, *5*, 2519–2538.

Taatjes, G.A., L.K. Christensen, M.D. Hurley, and T.J. Wallington (1999), Absolute and site-specific abstraction rate coefficients for reactions of Cl with CH_3CH_2OH, CH_3CD_2OH, and CD_3CH_2OH between 295 and 600 K, *J. Phys. Chem. A*, *103*, 9805–9814.

Tadić, J., I. Juranić, and G.K. Moortgat (2001a), Pressure dependence of the photooxidation of selected carbonyl compounds in air: *n*-Butanal and *n*-pentanal, *J. Photochem. Photobiol. A*, *143*, 168–179.

Tadić, J., I. Juranić, and G.K. Moortgat (2001b), Photooxidation of *n*-hexanal in air, *Molecules*, *6*, 287–299.

Tadić, J.M., I.O. Juranic, and G.K. Moortgat (2002), Photooxidation of *n*-heptanal in air: Norrish type I and II processes and quantum yield total pressure dependency, *J. Chem. Soc.*, *Perkin Trans.*, *2*, 135–140.

Tadić, J., G.K. Moortgat, and K. Wirtz (2006), Photolysis of glyoxal in air, *J. Photochem. Photobiol. A*, *177*, 116–124.

Takahshi, K., E. Iwasaki, Y. Matsumi, and T.J. Wallington (2007), Pulsed laser photolysis vacuum UV laser induced fluorescence kinetic study of the gas phase reactions of $Cl(^2P_{3/2})$ with C_3-ketones, *J. Phys. Chem*, *111*, 1271–1276.

Takahashi, K., Y. Matsumi, T.J. Wallington, and M.D. Hurley (2002), Atmospheric chemistry of $CF_3CFHOCF_3$: Reaction with OH radicals, atmospheric lifetime, and global warming potential, *J. Geophys. Res.*, *107*, doi:10.1029/2002JD002125.

Takahashi, K., T. Nakayama, and Y. Matsumi (2004), Hydrogen atom formation in the photolysis of acetone at 193 nm, *J. Phys. Chem. A*, *109*, 8002–8008.

Taketani, F., Y. Matsumi, T.J. Wallington, and M.D. Hurley (2006), Kinetics of the gas phase reactions of chlorine atoms with a series of ketones, *Chem.Phys. Letters*, *431*, 257–260.

Taketani, F., K. Takahashi, Y. Matsumi, and T.J. Wallington (2005), Kinetics of the reactions of $Cl(^2P_{1/2})$ and $Cl(^2P_{3/2})$ atoms with CH_3OH, C_2H_5OH, *n*-C_3H_7OH, and *i*-C_3H_7OH at 295, *J. Phys. Chem. A*, *109*, 3935–3940.

Takezaki, M., N. Hirota, and M. Terazima (1997a), Nonradiative relaxation processes and electronically excited states of nitrobenzene studied by picosecond time-resolved transient grating method, *J. Phys. Chem. A*, *101*, 3443–3448.

Takezaki, M., N. Hirota, M. Terazima, H. Sato, T. Nakajima, and S. Kato (1997b), Geometries and energies of nitrobenzene studied by CAS–SCF calculations, *J. Phys. Chem. A*, *101*, 5190–5195

Talukdar, R.K., J.B. Burkholder, M. Hunter, M.K. Gilles, J.M. Roberts, and A.R. Ravishankara (1997a), Atmospheric fate of several alkyl nitrates. 2. UV absorption cross-sections and photodissociation quantum yields, *J. Chem. Soc., Faraday Trans.*, *93*, 2797–2805.

Talukdar, R.K., J.B. Burkholder, A.-M. Schmoltner, J.M. Roberts, R.R. Wilson, and A.R. Ravishankara (1995), Investigation of the loss processes for peroxyacetyl nitrate in the atmosphere: UV photolysis and reaction with OH, *J. Geophys. Res.*, *100*, 14163–14174.

Talukdar, R.K., T. Gierczak, D.C. McCabe, and A.R. Ravishankara (2003), Reaction of hydroxyl radical with acetone. 2. Products and reaction mechanism, *J. Phys. Chem. A*, *107*, 5021–5032.

Talukdar, R.K., S.C. Herndon, J.B. Burkholder, J.M. Roberts, and A.R. Ravishankara (1997b), Atmospheric fate of several alkyl nitrates. Part 1. Rate coefficients of the reactions of alkyl nitrates with isotopically labelled hydroxyl radicals, *J. Chem. Soc., Faraday Trans.*, *93*, 2787–2796.

Talukdar, R.K., A. Mellouki, J.B. Burkholder, M.K. Gilles, G. Le Bras, and A.R. Ravishankara (2001), Quantification of the tropospheric removal of chloral (CCl_3CHO): Rate coefficient for the reaction of OH, UV absorption cross sections, and quantum yields, *J. Phys. Chem. A*, *105*, 5188–5196.

Tanaka, H., T. Kaneko, T. Matsumoto, T. Kato, and H. Takeda (2006), Effects of ethanol and ETBE blending in gasoline on evaporative emissions, Society of Automotive Engineers Technical Paper 2006-01-3382.

Tanaka, K., and M. Yoshimine (1980), An ab initio study on ketene, hydroxyacetylene, formylmethylene, oxirene, and their rearrangement paths, *J. Am. Chem. Soc.*, *102*, 7655–7662.

Tanaka, P.L., D.D. Riemer, S. Chang, G. Yarwood, E.C. McDonald-Buller, E.C. Apel, J.J. Orlando, P.J. Silva, J.L. Jimenez, M.R. Canagaratna, J.D. Neece, C.B. Mullins, and D.T. Allen (2003), Direct evidence for chlorine-enhanced urban ozone formation in Houston, Texas, *Atmos. Environ.*, *37*, 1393–1400.

Tang, K.Y., and E.K.C. Lee (1976), Laser photolysis of cyclobutanone photodecomposition from selected vibronic levels at long wavelengths, *J. Phys. Chem.*, *80*, 1833–1836.

Tang, Y., and L. Zhu (2004), Wavelength dependent photolysis of *n*-hexanal and *n*-heptanal in the 280–340 nm region, *J. Phys. Chem. A*, *108*, 8307–8316.

Tang, Y., and L. Zhu (2005), Photolysis of butenedial at 193, 248, 280, 308, 351, 400, and 450 nm, *Chem. Phys. Lett.*, *409*, 151–156.

Taniguchi, N., T.J. Wallington, M.D. Hurley, A.G. Guschin, L.T. Molina, and M.J. Molina (2003), Atmospheric chemistry of $C_2F_5C(O)CF(CF_3)_2$: Photolysis and reaction with Cl atoms, OH radicals, and ozone, *J. Phys. Chem. A*, *107*, 2674–2679.

Tanner, R.L., B. Zielinska, E. Uberna, G. Harshfield, and A.P. McNichol (1996), Concentrations of carbonyl compounds and the carbon isotopy of formaldehyde at a coastal site in Nova Scotia during the NARE summer intensive, *J. Geophys. Res.*, *101*, 28961–28970.

Taraborrelli, D., M.G. Lawrence, T.M. Butler, R. Sander, and J. Lelieveld (2009), Mainz isoprene mechanism 2 (MIM2): an isoprene oxidation mechanism for regional and global atmospheric modeling, *Atmos. Chem. Phys.*, *9*, 2751–2777.

Tarte, P. (1953), Photolysis of alkyl nitrites, *Bull. Soc. Roy. Sci. Liege*, *22*, 226–239.

Taylor, P.H., T. Yamada, and P. Marshall (2006), The reaction of OH with acetaldehyde and deuterated acetaldehyde: Further insight into the reaction mechanism at both low and elevated temperatures, *Int. J. Chem. Kinet.*, *38*, 489–495.

Taylor, P.H., T. Yamada, and A. Neuforth (2005), Kinetics of OH radical reaction with dibenzo-*p*-dioxin and selected chlorinated dibenzo-*p*-dioxins, *Chemosphere*, *58*, 243–252.

Taylor, R.P., and F.E. Blacet (1956a), The photolysis of chloroketones, *J. Am. Chem. Soc.*, *78*, 706–707.

Taylor, R.P., and F.E. Blacet (1956b), Photochemical oxidation of biacetyl by molecular oxygen, *Ind. & Eng. Chem.*, *48*, 1505–1508.

Taylor, S.E., A. Goddard, M.A. Blitz, P.A. Cleary, and D.E. Heard (2008), Pulsed Laval nozzle study of the kinetics of OH with unsaturated hydrocarbons at very low temperatures, *Phys. Chem. Chem. Phys.*, *10*, 422–437.

Taylor, W.D., T.D. Allston, M.J. Mascato, G.B. Fazekas, R. Kozlowski, and G.A. Takacs (1980), Atmospheric photodissociation lifetimes for nitromethane, methyl nitrite, and methyl nitrate, *Int. J. Chem. Kinet.*, *12*, 231–240.

Temps, F., and H.Gg. Wagner (1982), Untersuchungen zur Reaktion OH + HO_2 → H_2O + O_2 mit Hilfe eines Laser-Magnetischen Resonanz-Spektrometers, *Ber. Bunsenges. Phys. Chem.*, *86*, 119–125.

Temps, F., and H.Gg. Wagner (1984), Rate constants for the reactions of OH-radicals with CH_2O and HCO, *Ber. Bunsenges. Phys. Chem.*, *88*, 415–418.

Terentis, A.C., P.T. Knepp, and S.H. Kable (1995), Nascent state distribution of the HCO photoproduct arising from the 309 nm photolysis of propionaldehyde, *J. Phys. Chem.*, *99*, 12704–12710.

Teruel, M.A., M.B. Blanco, and G.R. Luque (2007), Atmospheric fate of acrylic acid and acrylonitrile: Rate constants with Cl atoms and OH radicals in the gas phase, *Atmos. Environ.*, *41*, 5769–5777.

Teruel, M.A., S. I. Lane, A. Mellouki, G. Solignac, and G. Le Bras (2006), OH reaction rate constants and UV absorption cross-sections of unsaturated esters, *Atmos. Environ.*, *40*, 3764–3772.

Téton, S., A. Mellouki, G. Le Bras, and H. Sidebottom (1996), Rate constants for reactions of OH radicals with a series of asymmetrical ethers and *tert*-butyl alcohol, *Int. J. Chem. Kinet.*, *28*, 291–297.

Thelen, M.-A., P. Felder, and J.R. Huber (1993), The photofragmentation of methyl hydroperoxide CH_3OOH at 193 and 248 nm in a cold molecular beam, *Chem. Phys. Lett.*, *213*, 275–281.

Thévenet, R., A. Mellouki, and G. Le Bras (2000), Kinetics of OH and Cl reactions with a series of aldehydes, *Int. J. Chem. Kinet.*, *32*, 676–685.

Thiault, G., and A. Mellouki (2006), Rate constants for the reaction of OH radicals with *n*-propyl, *n*-butyl, *iso*-butyl and *tert*-butyl vinyl ethers, *Atmos. Environ.*, *40*, 5566–5573.

Thiault, G., A. Mellouki, and G. Le Bras (2002a), Kinetics of gas phase reactions of OH and Cl with aromatic aldehydes, *Phys. Chem. Chem. Phys.*, *4*, 2194–2199.

Thiault, G., A. Mellouki, G. Le Bras, A. Chakir, N. Sokolowski-Gomez, and D. Daumont (2004), UV-absorption cross sections of benzaldehyde, *ortho*-, *meta- and para*-toluladehyde, *J. Photochem. Photobiol. A*, *162*, 273–281.

Thiault, G., R. Thévenet, A. Mellouki, and G. Le Bras (2002b), OH and O_3-initiated oxidation of ethyl vinyl ether, *Phys. Chem. Chem. Phys.*, *4*, 613–619.

Thomas, T.F., and H.J. Rodriguez (1971), Photochemistry of cyclopropanone, *J. Am. Chem. Soc.*, *93*, 5918–5920.

Thompson, H.W., and F.S. Dainton (1937), The photochemistry of alkyl nitrites. III, *Trans. Faraday Soc.*, *33*, 1546–1555.

Thompson, H.W., and C.H. Purkis (1936), The photochemistry of nitrites, nitrates, and nitro compounds, *J. Chem. Soc.*, *1936*, 674–680.

Thüner, L.P., P. Bardini, G.J. Rea, and J.C. Wenger (2004a), Kinetics of the gas-phase reactions of OH and NO_3 radicals with dimethylphenols, *J. Phys. Chem. A*, *108*, 11019–11025.

Thüner, L.P., I. Barnes, T. Maurer, C.G. Sauer, and K.H. Becker (1999), Kinetic study of the reaction of OH with a series of acetals at 298 ± 4 K, *Int. J. Chem. Kinet.*, *31*, 797–803.

Thüner, L.P., G. Rea, and J. Wenger (2004b), in, editor I. Barnes, The European Photoreactor EUPHORE 4th Report 2001, Valencia, Spain, February 2004.

Toft, A.M., M.D. Hurley, T.J. Wallington, M.P.S. Andersen, and O.J. Nielsen (2006), Atmospheric chemistry of $C_4F_9O(CH_2)_3OC_4F_9$ and $CF_3CFHCF_2O(CH_2)_3OCF_2CFHCF_3$: Lifetimes, degradation products, and environmental impact, *Chem. Phys. Lett.*, *427*, 41–46.

Tokuhashi, K., L. Chen, S. Kutsuna, T. Uchimaru, M. Sugie, and A. Sekiya (2004), Environmental assessment of CFC alternatives–rate constants for the reactions of OH radicals with fluorinated compounds, *J. Fluorine Chem.*, *125*, 1801–1807.

Tokuhashi, K., H. Nagai, A. Takahashi, M. Kaise, S. Kondo, A. Sekiya, M. Takahashi, Y. Gotoh, and A. Suga (1999a), Measurement of the OH reaction rate constants for CF_3CH_2OH, $CF_3CF_2CH_2OH$, and $CF_3CH(OH)CF_3$, *J. Phys. Chem. A*, *103*, 2664–2672.

Tokuhashi, K., A. Takahashi, M. Kaise, and S. Kondo (1999b), Rate constants for the reactions of OH radicals with CH_3OCF_2CHFCl, CHF_2OCF_2CHFCl, $CHF_2OCHClCF_3$, and $CH_3CH_2OCF_2CHF_2$, *J. Geophys. Res.*, *104*, 18681–18688.

Tokuhashi, K., A. Takahashi, M. Kaise, S. Kondo, A. Sekiya, and E. Fujimoto (2000a), Rate constants for the reactions of OH radicals with $CF_3OCF{=}CF_2$ and $CF_3CF{=}CF_2$, *Chem. Phys. Lett.*, *325*, 189–195.

Tokuhashi, K., A. Takahashi, M. Kaise, S. Kondo, A. Sekiya, S. Yamashita, and H. Ito (1999c), Rate constants for the reaction sof OH radicals with $CH_3OCF_2CF_3$, $CH_3OCF_2CF_2CF_3$, and $CH_3OCF(CF_3)_2$, *Int. J. Chem. Kinet.*, *31*, 846–853.

Tokuhashi, K., A. Takahashi, M. Kaise, S. Kondo, A. Sekiya, S. Yamashita, and H. Ito (2000b), Rate constants for the reactions of OH radicals with $CH_3OCF_2CHF_2$, $CHF_2OCH_2CF_2CHF_2$, $CHF_2OCH_2CF_2CF_3$, and $CF_3CH_2OCF_2CHF_2$ over the temperature range 250–430 K, *J. Phys. Chem. A*, *104*, 1165–1170.

Tolocka, M.P., M. Jang, J.M., Ginter, F.J. Cox, R.M. Kamens, and M.V. Johnston (2004), Formation of oligomers in secondary organic aerosol, *Environ. Sci. Technol.*, *38*, 1428–1434.

Tomas, A., F. Caralp, and R. Lesclaux (2000), Decomposition of the CF_3CO radical: Pressure and temperature dependencies of the rate constant, *Z. Physik. Chem.*, *Int. J. Res. Phys. Chem. Chem. Phys.*, *214*, 1349–1365.

Tomas, A., R.I. Olariu, I. Barnes, and K.H. Becker (2003), Kinetics of the reaction of O_3 with selected benzenediols, *Int. J. Chem. Kinet. 35*, 223–230.

Tomlin, A.S., T. Turányi, and M.J Pilling (1997), Mathematical tools for the construction, investigation and reduction of combustion mechanisms, in, editor M.J. Pilling, *Comprehensive Chemical Kinetics*, Volume 35, Low temperature combustion and autoignition, Elsevier, Amsterdam, pp.293–437.

Tomlin, A.S., L. Whitehouse, R. Lowe, and M.J. Pilling (2002), Low-dimensional manifolds in tropospheric chemical systems, *Faraday Disc.*, *120*, 125–146.

Tranter, R.S., and R.W. Walker (2001), Rate constants for the reactions of H atoms and OH radicals with ethers at 753 K, *Phys. Chem. Chem. Phys.*, *3*, 4722–4732.

Trapp, D., and C. De Serves (1995), Intercomparison of formaldehyde measurements in the tropical atmosphere, *Atmos. Environ.*, *29*, 3239–3243.

Treacy, J., M. El Hag, D. O'Farrell, and H. Sidebottom (1992), Reactions of ozone with unsaturated organic compounds, *Berichte Bunsen-Gesellschaft*, *96*, 422–7.

Tremp, J., P. Mattrel, S. Fingler, and W. Giger (1993), Phenol and nitrophenols as tropospheric pollutants: emissions from automobile exhausts and phase transfer in the atmosphere, *Water Air Soil Pollut.*, *68*, 113–123

Trentelman, K.A., S.H. Kable, B.D. Moss, and P.L. Houston (1989), Photodissociation dynamics of acetone at 193 nm–Photofragment internal and translational energy-distributions, *J. Chem. Phys.*, *91*, 7498–7513.

Treves, K., and Y. Rudich (2003), The atmospheric fate of C_3–C_6 hydroxylalky nitrates, *J. Phys. Chem. A*, *107*, 7809–7817.

Treves, K., L. Shragina, and Y. Rudich (2000), Henry's law constants of some β-, γ-, and δ-hydroxy alkyl nitrates of atmospheric interest, *Environ. Sci. Technol.*, *34*, 1197–1203.

Treves K., L. Shragina, and Y. Rudich (2002) Rate coefficients for the reactions of Cl atoms with a series of C_3–C_6 hydroxylalkyl nitrates at 296 ± 2 K, *J. Phys. Chem. A*, *106*, 5902–5907.

Trevor, P.L., G. Black, and J.R. Barker (1982), Reaction rate constant for $OH + HOONO_2 \rightarrow$ products over the temperature range 246–324 K, *J. Phys. Chem.*, *86*, 1661–1996.

Trevor, P.L., and D.M. Golden (1983), Very low pressure photolysis of *tert*-butyl nitrite at 248 nm, *J. Photochem.*, *23*, 277–281.

Troe, J. (1969), Ultraviolettspektrum und Reaktionen des HO_2-Radikals im thermischen Zerfall von H_2O_2, *Ber. Bunsenges. Phys. Chem.*, *73*, 946–952.

Troe, J. (1983), Theory of thermal unimolecular reactions in the fall-off range. I. Strong collision rate constants, *Ber. Bunsenges, Phys. Chem.*, *87*, 161–169.

Tsalkani, N., A. Mellouki, G. Poulet, G. Toupance, and G. Le Bras (1988), Rate constant measurements for the reactions of OH and Cl with peroxyacetyl nitrate at 298 K, *J. Atmos. Chem.*, *7*, 409–419.

Tsalkani, N., P. Perros, A.L. Dutot, and G. Toupance (1991), One-year measurements of PAN in the Paris basin: Effect of meteorological parameters, *Atmos. Environ.*, *25A*, 1941–1949.

Tse, C.W., R.C. Flagan, and J.H. Seinfeld (1997), Rate constants for the gas-phase reaction of the hydroxyl radical with a series of dimethylbenzaldehydes and trimethylphenols at atmospheric pressure, *Int. J. Chem. Kinet.*, *29*, 523–525.

Tsunashima, S., O. Ohsawa, C. Takahashi, and S. Sato (1973), The photolysis of cyclopentanone, *Bull. Chem. Soc. Japan*, *46*, 83–86.

Tuazon, E.C. (1997), Tropospheric degradation products of novel hydrofluoropolyethers, *Environ. Sci. Technol.*, *31*, 1817–1821.

Tuazon, E.C., S.M. Aschmann, and R. Atkinson (1998a), Products of the gas-phase reactions of the OH radical with 1-methoxy-2-propanol and 2-butoxyethanol, *Environ. Sci. Technol.*, *32*, 3336–3345.

Tuazon, E.C., S.M. Aschmann, and R. Atkinson (1999), Products of the gas-phase reaction of the OH radical with the dibasic ester $CH_3OC(O)CH_2CH_2CH_2C(O)OCH_3$, *Environ. Sci. Technol.*, *33*, 2885–2890.

Tuazon, E.C., S.M. Aschmann, R. Atkinson, and W.P.L. Carter (1998b), The reactions of selected acetates with the OH radicals in the presence of NO: Novel rearrangement of alkoxy radicals of structure $RC(O)OCH(O\bullet)R'$, *J. Phys. Chem. A*, *102*, 2316–2321.

Tuazon, E.C., S.M. Aschmann, M.V. Nguyen, and R. Atkinson (2003), H-atom abstraction from selected C—H bonds in 2,3-dimethylpentanal, 1,4-cyclohexadiene, and 1,3,5-cycloheptatriene, *Int. J. Chem. Kinetics*, *35*, 415–426.

Tuazon, E., and R. Atkinson (1989), A product study of the gas-phase reaction of methyl vinyl ketone with the OH radical in the presence of NO_x, *Int. J. Chem. Kinetics*, *21*, 1141–1142.

Tuazon, E.C., and R. Atkinson (1990), A product study of the gas-phase reaction of methacrolein with the OH radical in the presence of NO_x, *Int. J. Chem. Kinetics*, *22*, 591–602.

Tuazon, E.C., and R. Atkinson (1994), Tropospheric reaction products and mechanisms of the hydrochlorofluorocarbons 141b, 142b, 225ca, and 225cb, *Environ. Sci. Technol.*, *28*, 2306–2313.

Tuazon, E.C., and R. Atkinson (2003), OH radical-initiated reaction of 3-hexene-2,5-dione: Formation of methylglyoxal, *Environ. Sci. Technol.*, *37*, 3339–3341.

Tuazon, E.C., R. Atkinson, S.M. Aschmann, and J. Arey (1994), Kinetics and products of the gas-phase reactions of O_3 with amines and related compounds, *Res. Chem. Intermed.*, *20*, 303–320.

Tuazon, E.C., R. Atkinson, and W.P.L. Carter (1985), Atmospheric chemistry of *cis*- and *trans*-3-hexene-2,5-dione, *Environ. Sci. Technol.*, *19*, 265–269.

Tuazon, E.C, R. Atkinson, A.M. Winer, and J.N. Pitts, Jr. (1984a), A study of the atmospheric reactions of 1,3-dichloropropene and other selected organochlorine compounds, *Arch. Environ. Contam. Toxicol.*, *13*, 691–700.

Tuazon, E.C., W.P.L. Carter, S.M. Aschmann, and R. Atkinson (1991), Products of the gas-phase reaction of methyl *tert*-butyl ether with the OH radical in the presence of NO_x, *Int. J. Chem. Kinet.*, *23*, 1003–1015.

Tuazon, E.C., W.P.L. Carter, R. Atkinson, and J.N. Pitts, Jr. (1983), The gas-phase reaction of hydrazine and ozone: A nonphotolytic source of OH radicals for measurement of relative OH radical rate constants, *Int. J. Chem. Kinet.*, *15*, 619–629.

Tuazon, E.C., W.P.L. Carter, R. Atkinson, A.M. Winer, and J.N. Pitts, Jr. (1984b), Atmospheric reactions of *N*-nitrosodimethylamine and dimethylnitramine, *Environ. Sci. Technol.*, *18*, 49–54.

Tuazon, E.C., A.M. Winer, R.A. Graham, J.P. Schmid, and J.N. Pitts, Jr. (1978), Fourier transform infrared detection of nitramines in irradiated amine–NO_x systems, *Environ. Sci. Technol.*, *12*, 954–958.

Tuck, A.F. (1977), Molecular beam studies of ethyl nitrite photodissociation, *J. Chem. Soc., Faraday Trans. 2*, *73*, 689–708.

Tullo, A.H. (2008), Catalyzing biodiesel, *Chem. Eng. News*, *86*, 20–21.
Tully, F.P. (1990), Catalytic dehydration of alcohols by OH. $(CH_3)_3CCH_2OH$: A limiting case, 23rd Symposium (International) on Combustion/The Combustion Institute, pp.147–153.
Tully, F.P., and A.T. Droege (1987), Kinetics of the reactions of the hydroxyl radical with dimethyl ether and diethyl ether, *Int. J. Chem. Kinet.*, *19*, 251–259.
Tully, F.P., and A.R. Ravishankara (1980), Flash photolysis-resonance fluorescence kinetic study of the reactions of $OH + H_2 \rightarrow H_2O + H$ and $OH + CH_4 \rightarrow H_2O + CH_3$ from 298 to 1020 K, *J. Phys. Chem.*, *84*, 3126–3130.
Turányi, T., A.S. Tomlin, and M.J. Pilling (1993), On the error of the quasi-steady-state approximation, *J. Phys. Chem.*, *97*, 163–72.
Turnipseed, A.A., G.L. Vaghjiani, T. Gierczak, J.E. Thompson, and A.R. Ravishankara (1991), The photochemistry of ozone at 193 and 222 nm, *J. Chem. Phys.*, *95*, 3244–3251.
Turnipseed, A.A., G.L. Vaghjiani, J.E. Thompson, and A.R. Ravishankara (1992), Photodissociation of HNO_3 at 193, 222, and 248 nm: Products and quantum yields, *J. Chem. Phys.*, *96*, 5887–5895.
Turpin, E., A. Tomas, C. Fittschen, P. Devolder, and J.-C. Galloo (2006), Acetone-h_6 or -d_6 + OH reaction products: Evidence for heterogeneous formation of acetic acid in a simulation chamber, *Environ. Sci. Technol.*, 40, 5956–5961.
Tyndall, G.S., J.J. Orlando, C.S. Kegley-Owen, T.J. Wallington, and M.D. Hurley (1999), Rate coefficients of chlorine atoms with methanol and acetaldehyde, *Int. J. Chem. Kinet.*, *31*, 776–784.
Tyndall, G.S., J.J. Orlando, K.E. Nickerson, C.A. Cantrell, and J.G. Calvert (1991a), An upper limit for the rate coefficient of the reaction of NH_2 radicals with O_2 using FTIR product analysis, *J. Geophys. Res.*, *96*, 20761–20768.
Tyndall, G.S., J.J. Orlando, T.J. Wallington, M. Dill, and E.W. Kaiser (1997a), Kinetics and mechanisms of the reactions of chlorine atoms with ethane, propane, and *n*-butane, *Int. J. Chem. Kinet.*, *29*, 43–55.
Tyndall, G.S., J.J. Orlando, T.J. Wallington, and M.D. Hurley (1997b), Pressure dependence of the rate coefficients and product yields for the reaction of CH_3CO radicals with O_2, *Int. J. Chem. Kinet.*, *29*, 655–663.
Tyndall, G.S., J.J. Orlando, T.J. Wallington, M.D. Hurley, M. Goto, and M. Kawasaki (2002), Mechanism of the reaction of OH radicals with acetone and actaldehyde at 251 and 296 K, *Phys. Chem. Chem. Phys.*, *4*, 2189–2193.
Tyndall, G.S., A.S. Pimentel, and J.J. Orlando (2004), Temperature dependence of the alpha-ester rearrangement reaction, *J. Phys. Chem. A.*, *108*, 6850–6856.
Tyndall, G.S., T.A. Staffelbach, J.J. Orlando, and J.G. Calvert (1995), Rate coefficients for the reactions of OH radicals with methylgloxal and acetaldehyde, *Int. J. Chem. Kinet.*, *27*, 1009–1020.
Tyndall, G.S., T.J. Wallington, and M.D. Hurley (1993), Rate coefficient for the reaction of CH_2OH radicals with Cl_2 and infrared spectra of chloromethanol and dichloromethanol, *J. Phys. Chem.*, *97*, 1576–1582.
Tyndall, G.S., T.J. Wallington, and A.R. Potts (1991b), Product study of the reaction of Cl atoms with HCOOH, *Chem. Phys. Lett.*, *186*, 149–153.
Ullerstam, M., S. Langer, and E. Ljungström (2000), Gas phase rate coefficients and activation energies for the reaction of butanal and 2-methyl-propanal with nitrate radicals, *Int. J. Chem. Kinet.*, *32*, 294–303.
Ullerstam, M., E. Ljungström, and S. Langer (2001), Reactions of acrolein, crotonaldehyde and pivalaldehyde with Cl atoms: Structure–activity relationship and comparison with OH and NO_3 reactions, *Phys. Chem. Chem. Phys.*, *3*, 986–992.
Ulmstead, M.E., R.G. Shortridge, and M.C. Lin (1978), Energy partitioning in the photodissociation of C_3H_4O near 200 nm, *J. Phys. Chem.*, *82*, 1455–1460.
Unfried, K.G., G.P. Glass, and R.F. Curl (1991), Infrared flash kinetic spectroscopy of the ketenyl radical, *Chem. Phys. Lett.*, *177*, 33–38.
Ungnade, H.E., and R.A. Smiley (1956), Ultraviolet absorption spectra of nitroparaffins, alkyl nitrates and alkyl nitrites, *J. Org. Chem.*, *21*, 993–996.
UNICA, União da Indústria de Cana-de-Açúcar (2008), http://www.unica.com.br/.

Untch, A., R. Schinke, R. Cotting, and J.R. Huber, Jr. (1993), The vibrational predissociation of *cis*-methyl nitrite in the S_1 state: A comparison of exact quantum mechanical wave packet calculations with classical trajectory calculations and detailed experimental results, *J. Chem. Phys.*, *99*, 9553–9566.

Upadhyaya, H.P., A. Kumar, P.D. Naik, A.V. Sapre, and J.P. Mittal (2001), Kinetics of OH radical reaction with allyl alcohol (H_2CCHCH_2OH) and propargyl alcohol ($HCCCH_2OH$) studied by LIF, *Chem. Phys. Lett.*, *349*, 279–285.

U.S. Environmental Protection Agency (1976), Scientific and Technical Assessment Report on Nitrosamines, Report No. EPA-600/6/77-001, Office of Research and Development, Washington, D.C.; Environmental Assessment of Atmospheric Nitrosamines, by P. Walker, J. Gordon, L. Thomas, and R. Ouellette, MITRE Technical Report, MTR-7152, February, 1976.

U.S. Environmental Protection Agency (2005), Emissions by Category Report–Criteria Air Polutants, Volatile Organic Compounds, Year 2001; extract from EPA's National Emission Inventory, Final 1999 NEI Version 3 database.

U.S. Environmental Protection Agency (2008), On Board Diagnostics, http://www.epa.gov/obd/ downloaded November 2008.

U.S. Renewable Fuel Standard (2008), Revised Renewable Fuel Standard for 2008, *Federal Register*, *73*, 8665–8667.

U.S. Standard Atmosphere (1976), National Oceanic and Atmospheric Administration, National Aeronautics and Space Administration, United States Air Force, Washington, DC, October, 1976.

Utembe, S.R., L.A. Watson, D.E. Shallcross, and M.E. Jenkin (2009), A Common Representative Intermediates (CRI) mechanism for VOC degradation. Part 3: Development of a secondary organic aerosol module, *Atmos. Env.*, *43*, 1982–1990.

Vaghjiani, G.L., and A.R. Ravishankara (1989a), Kinetics and mechanism of OH reaction with CH_3OOH, *J. Phys. Chem.*, *93*, 1948–1959.

Vaghjiani, G.L., and A.R. Ravishankara (1989b), Absorption cross-sections of CH_3OOH, H_2O_2, and D_2O_2 vapors between 210 and 365 nm at 297 K, *J. Geophys. Res.*, *94*, 3487–3492.

Vaghjiani, G.L., and A.R. Ravishankara (1990), Photodissociation of H_2O_2 and CH_3OOH at 248 nm and 298 K: Quantum yields for OH, $O(^3P)$ and $H(^2S)$, *J. Chem. Phys.*, *92*, 996–1003.

Vaghjiani, G.L., A.R. Ravishankara, and N. Cohen (1989c), Reactions of OH and OD with H_2O_2 and D_2O_2, *J. Phys. Chem.*, *93*, 7833–7837.

Vaghjiani, G.L., A.A. Turnipseed, R.F. Warren, and A.R. Ravishankara (1992), Photodissociation of H_2O_2 at 193 and 222 nm: Products and quantum yields, *J. Chem. Phys. 96*, 5878–5886.

Vakhtin, A.B., D.C. McCabe, A.R. Ravishankara, and S.R. Leone (2003), Low-temperature kinetics of the reaction of the OH radical with hydrogen peroxide, *J. Phys. Chem. A*, *107*, 10642–10647.

Vandenberk, S., and J. Peeters (2003), The reaction of acetaldehyde and propionaldehyde with hydroxyl radicals: Experimental determination of the primary H_2O yield at room temperature, *J. Photochem. Photobiol. A*, *157*, 269–274.

Vandenberk, S., L. Vereecken, and J. Peeters (2002), The acetic acid forming channel in the acetone + OH reaction: A combined experimental and theoretical investigation, *Phys. Chem. Chem. Phys.*, *4*, 461–466.

Van Sonnenberg, E., G. Casola, S.F. Zakko, R.R. Varney, J. Cox, G.R. Wittich, and A.F. Hofmann (1988), Gallbladder and bile duct stones: percutaneous therapy with primary MTBE dissolution and mechanical methods, *Radiology*, *169*, 505–509.

Vasudev, R., R.N. Zare, and R.N. Dixon (1983), Dynamics of photodissociation of HONO at 369 nm: Motional anisotropy and internal state distribution of the OH fragment, *Chem. Phys. Lett.*, *96*, 399–402.

Vasvári, G., I. Szilágyi, A. Bendsura, S. Dóbé, T. Bérces, E. Henon, S. Canneaux, and F. Bohr (2001), Reaction and complex formation between OH radical and acetone, *Phys. Chem. Chem. Phys.*, *3*, 551–555.

Večeřa, A., and P.K. Dasgupta (1991), Measurement of ambient nitrous acid and a reliable calibration source for gaseous nitrous acid, *Environ. Sci. Technol.*, *25*, 255–260.

Veillerot, M., P. Foster, R. Guillermo, and I.C. Galloo (1996), Gas-phase reaction of *n*-butyl acetate with the hydroxyl radical under simulated tropospheric conditions: Relative rate constant and product study, *Int. J. Chem. Kinet.*, *28*, 235–243.

Vereecken, L. (2008), Computational study of the stability of α-nitroxy-substituted alkyl radicals, *Chem. Phys. Lett.*, *466*, 127–130.

Vereecken, L., and J. Peeters (2004), Nontraditional (per)oxy ring-closure paths in the atmospheric oxidation of isoprene and monoterpenes, *J. Phys. Chem. A.*, *108*, 5197–5204.

Vesly, G.F., and P.A. Leermakers (1964), The photochemistry of α-keto acids and α-keto esters. III. Photolysis of pyruvic acid in the vapor phase, *J. Phys. Chem.*, *68*, 2364–2366.

Villanueva, F., I. Barnes, E. Monedero, S. Salgado, M.V. Gomez, and P. Martin (2007), Primary product distribution from the Cl-atom initiated atmospheric degradation of furan: Environmental implications, *Atmos. Environ.*, *41*, 8796–8810.

Vimal, D., and P.S. Stevens (2006), Experimental and theoretical studies of the kinetics of the reactions of OH radicals with acetic acid, acetic acid-d_3, and acetic acid-d_4 at low pressure, *J. Phys. Chem. A*, *110*, 11509–11516.

Viskolcz, B., and T. Bérces (2000), Enthalpy of formation of selected carbonyl radicals from theory and comparison with experiment, *Phys. Chem. Chem. Phys.*, *2*, 5430–5436.

Vogel, E., and H. Günther (1967), Benzene oxide–oxepin valence tautomerism, *Angew. Chem., Int. Ed. Engl.*, *6*, 385–401.

Voicu, I., I. Barnes, K. H. Becker, T. J. Wallington, Y. Inoue, and M. Kawasaki (2001), Kinetic and product study of the Cl-initiated oxidation of 1,2,3-trichloropropane ($CH_2ClCHClCH_2Cl$), *J. Phys. Chem. A*, *105*, 5123–5130.

Vöhringer-Martinez, E., B. Hansmann, H. Hernandez-Soto H. Hernandez, J.S. Francisco, J. Troe, and B. Abel (2007), Water catalysis of a radical-molecule gas-phase reaction, *Science*, *315*, 497–501.

Volkamer, R., J.L. Jimenez, F. San Martini, K. Dzepina, Q. Zhang, D. Salcedo, L.T. Molina, D.R. Worsnop, and M.J. Molina (2006), Secondary organic aerosol formation from anthropogenic air pollution: Rapid and higher than expected, *Geophys. Res. Lett.*, 33, L17811/1–L17811/4.

Volkamer, R., F. San Martini, L.T. Molina, D. Salcedo, J.L. Jimenez, and M.J. Molina (2007), A missing sink for gas-phase glyoxal in Mexico City: Formation of secondary organic aerosol, *Geophys. Res. Lett.*, *34*, L19807/1–L19807/5.

Volkamer, R., P. Spietz, J. Burrows, and U. Platt (2005), High-resolution absorption cross-section of glyoxal in the UV-vis and IR spectral ranges, *J. Photochem. Photobiol. A*, *172*, 35–46.

Volkamer, R., P.J. Ziemann, and M.J. Molina (2009), Secondary organic aerosol formation from acetylene (C_2H_2): seed effect on SOA yields due to organic photochemistry in the aerosol aqueous phase, *Atmos. Chem. Phys.*, *9*, 1907–1928.

Vollenweider, J.K., and H. Paul (1986), On the rates of decarbonylation of hydroxyacetyl and other acyl radicals, *Int. J. Chem. Kinet.*, *18*, 791–800.

von Kuhlmann, R., M.G. Lawrence, P.J. Crutzen, and P.J. Rasch (2003), A model for studies of tropospheric ozone and non-methane hydrocarbons: Model evaluation of ozone related species, *J. Geophys. Res.*, *108*(D28), 4729, doi:10.1019/2002JD003348.

Vovelle, C., A. Bonard, V. Daële, and L.-L. Delfau (2001), Kinetics of OH radical reactions with a series of symmetric acetals in the temperature range 293–617 K, *Phys. Chem. Chem. Phys.*, *3*, 4939–4945.

Wade, E.A., H. Clauberg, S. K. Kim, A. Mellinger, and C.B. Moore (1997a), Dynamics of rotational energy release for dissociation of singlet ketene and the singlet/triplet branching ratio, *J. Phys. Chem. A*, *101*, 732–739.

Wade, E.A., A. Mellinger, M.A. Hall, and C.B. Moore (1997b), How a transition state tightens: The singlet photodissociation of ketene as a test case, *J. Phys. Chem. A*, *101*, 6568–6576.

Wade, E.A., K.E. Reak, S.L. Li, S.M. Clegg, P. Zou, and D.L. Osborn (2006), Time-dependent infrared emission following photodissociation of nitromethane and chloropicrin, *J. Phys. Chem. A*, *110*, 4405–4412.

Wade, E.A., K.E. Reak, B.F. Parsons, T.P. Clemes, and K.A. Singmaster (2002), Photochemistry of chloropicrin in cryogenic matrices, *Chem. Phys. Lett.*, *365*, 473–479.

Wagner, P.J., and G.S. Hammond (1968), Properties and reactions of organic molecules in their triplet states, *Advan. Photochem.*, *5*, 21–156.

Walega, J.G., B.A. Ridley, S. Madronich, F.E. Grahek, J.D. Shetter, T.D. Sauvain, C.J. Hahn, J.T. Merill, B.A. Bodhaine, and E. Robinson (1992), Observations of peroxyacetyl nitrate, peroxypropionyl nitrate, methyl nitrate and ozone during the Mauna Loa observatory photochemistry experiment, *J. Geophys. Res.*, *97*, 10311–10330.

Walker, R.W., and C. Morley (1997), Basic chemistry of combustion, in, editor M.J. Pilling, *Comprehensive Chemical Kinetics*, Volume 35, Low temperature combustion and autoignition, Elsevier, Amsterdam, pp.1–124.

Wall, K.J., C.L. Schiller, and G.W. Harris (2006), Measurements of the HONO photodissociation constant, *J. Atmos. Chem.*, *55*, 31–54.

Wallington, T.J., J.M. Andino, J.C. Ball, and S.M. Japar (1990a), Fourier transform infrared studies of Cl atoms with PAN, PPN, CH_3OOH, HCOOH, CH_3COCH_3 and $CH_3COC_2H_5$ at 295 ± 2 K, *J. Atmos. Chem.*, *10*, 301–313.

Wallington, T.J., J.M. Andino, and S.M. Japar (1990b), FTIR product study of the self-reaction of $CH_2ClCH_2O_2$ radicals in air at 295 K, *Chem. Phys. Lett.*, *165*, 189–194.

Wallington, T.J., J.M. Andino, I.M. Lorkovic, E.W. Kaiser, and G. Marston (1990c), Pressure dependence of the reaction of chlorine atoms with ethene and acetylene in air at 295 K, *J. Phys. Chem.*, *94*, 3644–3648.

Wallington, T.J., J.M. Andino, A.R. Potts, S.J. Rudy, W.O. Siegl, Z. Zhang, M.J. Kurylo, and R.E. Huie (1993a), Atmospheric chemistry of automotive fuel additives: Diisopropyl ether, *Environ. Sci. Technol.*, *27*, 98–104.

Wallington, T.J., J.M. Andino, L.M. Skewes, W.O. Siegl, and S.M. Japar (1989a), Kinetics of the reaction of OH radicals with a series of ethers under simulated atmospheric conditons at 295 K, *Int. J. Chem. Kinet.*, *21*, 993–1001.

Wallington, T.J., R. Atkinson, and A.M. Winer (1984), Rate constant for the gas phase reaction of OH radicals with peroxyacetyl nitrate (PAN) at 273 and 297 K, *Geophys. Res. Lett.*, *11*, 861–864.

Wallington, T.J., R. Atkinson, A.M. Winer, and J.N. Pitts, Jr. (1986), Absolute rate constants for the gas-phase reactions of the NO_3 radical with CH_3SH, CH_3SCH_3, CH_3SSCH_3, H_2S, SO_2, and CH_3OCH_3 over the temperature range 280–350 K, *J. Phys. Chem.*, *90*, 5393–5396.

Wallington, T.J., R. Atkinson, A.R. Winer, and J.N. Pitts Jr. (1987), A study of the reaction $NO_3 + NO_2 + M \rightarrow N_2O_5 + M$ ($M = N_2$, O_2), *Int. J. Chem. Kinet.*, *19*, 243–249.

Wallington, T.J., J.C. Ball, A.M. Straccia, M.D. Hurley, E.W. Kaiser, M. Dill, and W.F. Schneider (1996a), Kinetics and mechanism of the reaction of Cl atoms with CH_2CO (ketene), *Int. J. Chem. Kinet.*, *28*, 627–635.

Wallington, T.J., M. Bilde, T.E. Møgelberg, J. Sehested, and O.J. Nielsen (1996b), Atmospheric chemistry of 1,2-dichloroethane: UV spectra of $CH_2ClCHCl$ and $CH_2ClCHClO_2$ radicals, kinetics of the reactions of $CH_2ClCHCl$ radicals with O_2 and $CH_2ClCHClO_2$ radicals with NO and NO_2, and fate of the alkoxy radical $CH_2ClCHClO$, *J. Phys. Chem.*, *100*, 5751–5760.

Wallington, T.J., P. Dagaut, and M.J. Kurylo (1988a), Correlation between gas-phase and solution-phase reactivities of hydroxyl radicals toward saturated organic compounds, *J. Phys. Chem.*, *92*, 5024–5028.

Wallington, T.J., P. Dagaut, R. Liu and M.J. Kurylo (1988b), The gas phase reaction of hydroxyl radicals with a series of esters over the temperature range 240–440K, *Int. J. Chem. Kinet.*, *20*, 177–186.

Wallington, T.J., P. Dagaut, R. Liu, and M.J. Kurylo (1988c), Gas-phase reactions of hydroxyl radicals with the fuel additives methyl *tert*-butyl ether and *tert*-butyl alcohol over the temperature range 240–440 K, *Environ. Sci. Technol.*, *22*, 842–844.

Wallington, T.J., P. Dagaut, R. Liu, and M.J. Kurylo (1988d), Rate constants for the gas phase reactions of OH with C_5 through C_7 aliphatic alcohols and ethers: Predicted and experimental values, *Int. J. Chem. Kinet.*, *20*, 541–547.

Wallington T.J., C.A. Gierczak, J.C. Ball, and S.M. Japar (1989b), Fourier transform infrared study of the self reaction of $C_2H_5O_2$ radicals in air at 295 K, *Int. J. Chem. Kinet.*, *21*, 1077–1089.

Wallington T.J., A. Guschin, and M.D. Hurley (1998a), Comment: A kinetic study of chlorine radical reactions with ketones by laser-photolysis technique by Olsson et al., *Int. J. Chem. Kinet.*, *30*, 309–310.

Wallington, T.J., A. Guschin, T.N. Stein, J. Platz, J. Sehested, L.K. Christensen, and O.J. Nielsen (1998b), Atmospheric chemistry of $CF_3CH_2OCH_2CF_3$: UV spectra and kinetic data for $CF_3CH(\bullet)OCH_2CF_3$ and $CF_3CH(OO\bullet)OCH_2CF_3$ radicals and atmospheric fate of $CF_3CH(O\bullet)OCH_2CF_3$ radicals, *J. Phys. Chem. A*, *102*, 1152–1161.

Wallington, T.J., M.M. Hinman, J.M. Andino, W.O. Siegl, and S.M. Japar (1990d), A relative rate study of the reaction of Cl atoms with a series of alkyl nitrates and nitro alkanes in air at 295 ± 2 K, *Int. J. Chem. Kinet.*, *22*, 665–671.

Wallington, T.J., and M.D. Hurley (1992), Are anomalies in the kinetics of halogenation caused by hot atom effects? An experimental investigation, *Chem. Phys. Lett.*, *194*, 309–312.

Wallington, T.J., and M.D. Hurley (1993), Atmospheric chemistry of HC(O)F: reaction with OH radicals, *Environ. Sci. Technol.*, *27*, 1448–1452.

Wallington, T.J., and M.D. Hurley (1995), Atmospheric chemistry of CF_3COOH: Kinetics of fluorine and chlorine atom reaction at 295 ± 2 K, *Int. J. Chem. Kinet.*, *27*, 189–194.

Wallington, T.J., M.D. Hurley, J.C. Ball, and M.E. Jenkin (1993b), FTIR product study of the reaction of $CH_3OCH_2O_2 + HO_2$ reaction, *Chem. Phys. Lett.*, *211*, 41–47.

Wallington, T.J., M.D. Hurley, J.C. Ball, A.M. Straccia, J. Platz, L.K. Christensen, J. Sehested, and O.J. Nielsen (1997a), Atmospheric chemistry of dimethoxymethane ($CH_3OCH_2OCH_3$): Kinetics and mechanism of its reaction with OH radicals and fate of the alkoxy radicals $CH_3OCHO(\bullet)OCH_3$ and $CH_3OCH_2OCH_2O(\bullet)$, *J. Phys. Chem. A*, *101*, 5302–5308.

Wallington, T.J., M.D. Hurley, V. Fedotov, C. Morrell, and G. Hancock (2002), Atmospheric chemistry of $CF_3CH_2OCHF_2$ and $CF_3CHClOCHF_2$: Kinetics and mechanisms of reaction with Cl atoms and OH radicals and atmospheric fate of $CF_3C(O\bullet)HOCHF_2$ and $CF_3C(O\bullet)ClOCHF_2$ radicals, *J. Phys. Chem. A*, *106*, 8391–8398.

Wallington, T.J., M.D. Hurley, and A. Haryanto (2006a), Kinetics of the gas phase reactions of chlorine atoms with a series of formates, *Chem. Phys. Lett.*, *432*, 57–61.

Wallington, T.J., M.D. Hurley, M.S. Javadi, and O.J. Nielsen (2008a), Kinetics and products of chlorine atom initiated oxidation of $HCF_2OCF_2OCF_2CF_2OCF_2H$ and $HCF_2O(CF_2O)_n(CF_2CF_2O)_mCF_2H$, *Int. J. Chem. Kinet.*, *40*, 819–825.

Wallington, T.J., M.D. Hurley, T. Maurer, I. Barnes, K.H. Becker, G.S. Tyndall, J.J. Orlando, A.S. Pimentel, and M. Bilde (2001a), Atmospheric oxidation mechanism of methyl formate. *J. Phys. Chem. A*, *105*, 5146–5154.

Wallington, T.J., M.D. Hurley, O.J. Nielsen, and M.P.S. Andersen (2004), Atmospheric chemistry of $CF_3CFHCF_2OCF_3$ and $CF_3CFHCF_2OCF_2H$: Reaction with Cl atoms and OH radicals, degradation mechanism, and global warming potentials, *J. Phys. Chem.*, *108*, 11333–11338.

Wallington, T.J., M.D. Hurley, and W.F. Schneider (1996c), Atmospheric chemistry of CH_3Cl: Mechanistic study of the reaction of CH_2ClO_2 radicals with HO_2, *Chem. Phys. Lett.*, *251*, 164–173.

Wallington, T.J., M.D. Hurley, W.F. Schnieder, J. Sehested, and O.J. Nielsen (1994a), Mechanistic study of the gas phase reaction of CH_2FO_2 radicals with HO_2, *Chem. Phys. Lett.*, *218*, 34–42.

Wallington, T.J., M.D. Hurley, J. Xia, D.J. Wuebbles, S. Sillman, A. Ito, J.E. Penner, D.A. Ellis, J. Martin, S.A. Mabury, O.J. Nielsen, and M.P.S. Andersen (2006b), Formation of $C_7F_{15}COOH$ (PFOA) and other perfluorocarboxylic acids (PFCAs) during the atmospheric oxidation of 8:2 fluorotelomer alcohol (n-$C_8F_{17}CH_2CH_2OH$), *Environ. Sci. Technol.*, *40*, 924–930.

Wallington, T.J., and S.M. Japar (1989), Fourier transform infrared kinetic studies of the reaction of HONO with HNO_3, NO_3 and N_2O_5 at 295 K, *J. Atm. Chem.*, *9*, 399–409.

Wallington, T.J., and S.M. Japar (1991), Atmospheric chemistry of diethyl ether and ethyl *tert*-butyl ether, *Environ. Sci. Technol.*, *25*, 410–415.

Wallington, T.J., K.W. Jucks, and G.S. Tyndall (1998c), Upper limits for the gas-phase reaction of H_2O_2 with O_3 and NO. Atmospheric implications, *Int. J. Chem. Kinet.*, *30*, 707–709.

Wallington, T.J., E.W. Kaiser, and J.T. Farrell (2006c), Automotive fuels and internal combustion engines: A chemical perspective, *Chem. Soc. Rev.*, *35*, 335–347.

Wallington, T.J., and M.J. Kurylo (1987a), Flash photolysis resonance fluorescence investigation of the gas-phase reactions of OH radicals with a series of aliphatic ketones over the temperature range 240–440 K, *J. Phys. Chem.*, *91*, 5050–5054.

Wallington, T.J., and M.J. Kurylo (1987b), The gas phase reactions of hydroxyl radicals with a series of aliphatic alcohols over the temperature range 240–440 K, *Int. J. Chem. Kinet.*, *19*, 1015–1023.

Wallington, T.J., R. Liu, P. Dagaut, and M.J. Kurylo (1988e), The gas phase reactions of hydroxyl radicals with a series of aliphatic ethers over the temperature range 240–440 K, *Int. J. Chem. Kinet.*, *20*, 41–49.

Wallington, T.J., S.A. Mabury, M.D. Hurley, M.P.S. Andersen, O.J. Nielsen, D.A. Ellis, and J.W. Martin (2008b), Comment on "Atmospheric chemistry of linear perfluorinated aldehydes: Dissociation kinetics of $C_nF_{2n+1}CO$ radicals" by Waterland and Dobbs, *J. Phys. Chem. A*, *112*, 576–577.

Wallington, T.J., and A. Mellouki (2009), Comment on "Kinetics of the reactions of Cl atoms with 2-butene-1-ol, 2-methyl-2-propen-1-ol, and 3-methyl-2-buten-1-ol as a function of temperature" by Rodriguez et al. (*J. Atmos. Chem.* (2008, 59: 187–197), *J. Atmos. Chem.*, *63*, 93–94.

Wallington, T.J., Y. Ninomiya, M. Mashino, M. Kawasaki, V.L. Orkin, R.E. Huie, M.J. Kurylo, W.P.L. Carter, D. Luo, and I.L. Malkina (2001b), Atmospheric oxidation mechanism of methyl pivalate, $(CH_3)_3CC(O)OCH_3$, *J. Phys. Chem. A*, *105*, 7225–7235.

Wallington, T.J., A.R. Potts, J.M. Andino, W.O. Siegl, Z. Zhang, M.J. Kurylo, and R.E. Huie (1993c), Kinetics of the reaction of OH radicals with *t*-amyl methyl ether revisited, *Int. J. Chem. Kinet.*, *25*, 265–272.

Wallington, T.J., W.F. Schneider, I. Barnes, K.H. Becker, J. Sehested, and O.J. Nielsen (2000), Stability and IR spectra of mono-, di-, and trichloromethanol, *Chem. Phys. Lett.*, *322*, 97–102.

Wallington, T.J., W.F. Schneider, J. Sehested, M. Bilde, J. Platz, O.J. Nielsen, L.K. Christensen, M.J. Molina, L.T. Molina, and P.W. Wooldridge (1997b), Atmospheric chemistry of HFE-7100 ($C_4F_9OCH_3$): Reaction with OH radicals, UV spectra and kinetic data for $C_4F_9OCH_2$• and $C_4F_9OCH_2O_2$• radicals, and the atmospheric fate of $C_4F_9OCH_2O$• radicals, *J. Phys. Chem. A*, *101*, 8264–8274.

Wallington, T.J., W.F. Schneider, D.R. Worsnop, O.J. Nielsen, J. Sehested, W. DeBruyn, and J.A. Shorter (1994b), Environmental impact of CFC replacements: HFCs and HCFCs, *Environ. Sci. Technol.*, *28*, 320A–326A.

Wallington, T.J., W.O. Siegl, R. Liu, Z. Zhang, R.E. Huie, and M.J. Kurylo (1990e), The atmospheric reactivity of α-methyltetrahydrofuran, *Environ. Sci. Technol.*, *24*, 1596–1599.

Wallington, T.J., L.M. Skewes, and W.O.Siegl (1988f), Kinetics of the gas phase reaction of Cl atoms with a series of alkenes, alkynes, and aromatic species at 295 K, *J. Photochem.*, *45*, 167–175.

Wallington, T.J., L.M. Skewes, W.O. Siegl, C.-H. Wu, and S.M. Japar (1988g), Gas phase reaction of Cl atoms with a series of oxygenated organic species at 295 K, *Int. J. Chem. Kinet.*, *20*, 867–875.

Wallington, T.J., J.L. Sullivan, and M.D. Hurley (2008c), Emissions of CO_2, CO, NO_x, HC, PM, HFC-134a, N_2O and CH_4 from the global light duty vehicle fleet, *Meteorol. Z.*, *17*, 109–116.

Wang, C., and Z. Chen (2008), An experimental study for rate constants of the gas phase reactions of CH_3CH_2OOH with OH radicals, O_3, NO_2 and NO, *Atmos. Environ.*, 42, 6614–6619.

Wang, J., H. Chen., G.P. Glass, and R.F. Curl (2003), Kinetic study of the reaction of acetaldehyde with OH, *J. Phys. Chem. A*, *107*, 10834–10844.

Wang, L., J.Arey, and R. Atkinson (2006), Kinetics and products of photolysis and reaction with OH radicals of a series of aromatic carbonyl compounds, *Env. Sci. Tech*, *40*, 5465–5471.

Wang, M. (2005), Greenhouse gases, regulated emissions, and energy use in transportation, Version 1.7, 2005, http://www.transportation.anl.gov/software/GREET/.

Wang, M., M. Wu, and H. Huo (2007a), Life-cycle energy and greenhouse gas emission impacts of different corn ethanol plant types, *Environ. Res. Lett. 2*, 024001, doi:10.1088/1748-9326/2/2/024001

Wang, S.-C., R.C. Flagan, and J.H. Seinfeld (1992a), Aerosol formation and growth in atmospheric organic/NO_x systems—II. Aerosol dynamics, *Atmos. Environ.*, *26A*, 421–434.

Wang, S.-C., S.E. Paulson, D. Grosjean, R.C. Flagan, and J.H. Seinfeld (1992b), Aerosol formation and growth in atmospheric organic/NO_x systems—I. Outdoor smog chamber studies of C_7- and C_8-hydrocarbons, *Atmos. Environ.*, *26A*, 403–420.

Wang, W., M.J. Ezell, A.A. Ezell, G. Soskin, and B.J. Finlayson-Pitts (2002), Rate constants for the reactions of chlorine atoms with a series of unsaturated aldehydes and ketones at 298 K: Structure and reactivity, *Phys. Chem. Chem. Phys.*, *4*, 1824–1831.

Wang, X., Y. Wang, C. Lv., M. Kubo, and A. Miyamoto (2007b), Investigation of the photodissociation reactions for alkyl nitrite by quantum chemical molecular dynamics program "Colors Excite," *J. Photochem. Photobiol. A*, *187*, 119–126.

Wängberg, I. (1993), Mechanisms and products of the reactions of NO_3 with cycloalkenes, *J. Atmos. Chem.*, 17, 229–247.

Wängberg, I., I. Barnes, and K.H. Becker (1996), Atmospheric chemistry of bifunctional cycloalkyl nitrates, *Chem. Phys. Lett.*, 261, 138–144.

Wania, F. (2007), A global mass balance analysis of the source of perfluorocarboxylic acids in the Arctic Ocean, *Environ. Sci. Technol.*, *41*, 4529–4535.

Waschewsky, G.C.G., P.W. Kash, T.L. Myers, D.C. Kitchen, and L.J. Butler (1994), What Woodward and Hoffmann didn't tell us: The failure of the Born–Oppenheimer approximation in competing reaction pathways, *J. Chem. Soc., Faraday Trans.*, *90*, 1581–1598.

Waterland, R.L., and K.D. Dobbs (2006), Computed thermodynamic stability of perfluorinated aldehydes and their hydrates: implications for atmospheric fate, in, editors P. Dagaut and A. Mellouki, Proceedings of 19th International Symposium on Gas Kinetics, Orleans, France, July, 2006, pp.111–112.

Waterland, R.L., and K.D. Dobbs (2007), Atmospheric chemistry of linear perfluorinated aldehydes: Dissociation kinetics of $C_nF_{2n+1}CO$ radicals, *J. Phys. Chem. A*, *111*, 2555–2562.

Watson, R., G. Machado, S. Fischer, and D.D. Davis (1976), A temperature dependence kinetics study of the reactions of $Cl(^2P_{3/2})$ with O_3, CH_4 and H_2O_2, *J. Chem. Phys.*, *65*, 2126–2138.

Watson, L. A., D.E. Shallcross, S.R. Utembe, and M.E. Jenkin (2008), A Common Representative Intermediates (CRI) mechanism for VOC degradation. Part 2: Gas phase mechanism reduction, *Atmos. Env*., 42, 7196–7204.

Wayne, R.P. (1991), *Chemistry of Atmospheres*, Oxford University Press, Oxford.

Wayne, R.P., I. Barnes, P. Biggs, J.P. Burrows, C.E. Canosa-Mas, J. Hjorth, G. Le Bras, G.K. Moortgat, D. Perner, G. Poulet, G. Restelli, and H. Sidebottom (1991), The nitrate radical: Physics, chemistry, and the atmosphere, *Atmos. Environ.*, *25A*, 1–203.

Weaver, J., J. Meagher, and J. Heicklen (1976/1977), Photo-oxidation of CH_3CHO vapor at 3130 Å, *J. Photochem.*, *6*, 111–126.

Weibel, D.E., G.A. Arguello, E.R. de Staricco, and E.H. Staricco (1995), Quantum yield in the gas phase photolysis of perfluoroacetyl chloride: a comparison with related compounds, *J. Photochem. Photobiol. A*, *86*, 27–31.

Weir, D.S. (1961), The photolysis and fluorescence of diethyl ketone and diethyl ketone–biacetyl mixtures at 3130 and 2537 Å, *J. Am. Chem. Soc.*, *83*, 2629–2033.

Weir, D.S. (1962), Energy exchange in the 3-methyl-2-butanone-biacetyl system at 3130 Å, *J. Am. Chem. Soc.*, *84*, 4039–4040.

Wells, J.R. (2004), The hydroxy radical reaction rate constant and products of the 3,5-dimethyl-1-hexyn-3-ol, *Int. J. Chem. Kinet.*, *36*, 534–544.

Wells, J.R. (2005), Gas-phase chemistry of α-terpinol with ozone and OH radical: Rate constants and products, *Environ. Sci. Technol.*, *39*, 6937–6943.

Wells, J.R., F.L. Wiseman, D.C. Williams, J.S. Baxley, and D.F. Smith (1996), The products of the reaction of the hydroxyl radical with 2-ethoxyethyl acetate, *Int. J. Chem. Kinet.*, *28*, 475–480.

Wenger, J., E. Porter, E. Collins, J. Treacy, and H. Sidebottom (1999), Mechanisms for the chlorine atom initiated oxidation of dimethoxymethane and 1,2-dimethoxyethane in the presence of NO_x, *Chemosphere*, *38*, 1197–1204.

Wennberg, P.O., T.F. Hanisco, L. Jaegle, D.J. Jacob, E.J. Hintsa, E.J. Lanzendorf, J.G. Anderson, R-S. Gao, E.R. Keim, S.G. Donnelly, L.A. Del Negro, D.W. Fahey, S.A. McKeen,

R.J. Salawitch, C.R. Webster, R.D. May, R.L. Herman, M.H. Proffitt, J.J. Margitan, E.L. Atlas, S.M. Schauffler, F. Flocke, C.T. McElroy, and T.P. Bui (1998), Hydrogen radicals, nitrogen radicals, and production of O_3 in the upper troposphere, *Science*, *279*, 49–53.

Wettack, F.S., and W.A. Noyes, Jr. (1968), The direct and sensitized photolyses of 2-pentanone, *J. Am. Chem. Soc.*, *90*, 3901–3906.

Whitehouse, L.E., A.S. Tomlin, and M.J. Pilling (2004a), Systematic reduction of complex tropospheric chemical mechanisms, Part I: Sensitivity and time-scale analyses. *Atmos. Chem. Phys*, *4*, 2025–2056.

Whitehouse, L.E., A.S. Tomlin, and M.J. Pilling (2004b), Systematic reduction of complex tropospheric chemical mechanisms, Part II: Lumping using a time-scale based approach, *Atmos. Chem. Phys*, *4*, 2057–2081.

Whiteway, S.G., and C.R. Masson (1955), The carbon monoxide quantum yield in the photolysis of diisopropyl ketone, *J. Am. Chem. Soc.*, *77*, 1508–1509.

Whytock, D.A., and K.O. Kutschke (1968), The primary process in the photolysis of hexafluoroacetone vapour. I. Photodecomposition studies, *Proc. Roy. Soc.*, *A306*, 503–510.

Wiebe, H.A., and J. Heicklen (1973), Photolysis of methyl nitrite, *J. Am. Chem. Soc.*, *95*, 1–7.

Wiebe, H.A., A. Villa, T.M. Hellman, and J. Heicklen (1973), Photolysis of methyl nitrite in the presence of nitric oxide, nitrogen dioxide, and oxygen, *J. Am. Chem. Soc.*, *95*, 7–13.

Wiesen, E., I. Barnes, and K.H. Becker (1995), Study of the OH-initiated degradation of the aromatic photooxidation product 3,4-dihydroxy-3-hexene-2,5-dione, *Environ. Sci. Technol.*, *29*, 1380–1386.

Wijnen, M.H.J. (1961), Photolysis of phosgene in the presence of ethylene, *J. Am. Chem. Soc.*, *83*, 3014–3017.

Wijnen, M.H.J. (1962), Initial stages of the chlorine atom induced polymerization of acetylene, *J. Chem. Phys.*, *36*, 1672–1675.

Williams, D.C, L.N. O'Rji, and D.A. Stone (1993), Kinetics of the reactions of OH radicals with selected acetates and other esters under simulated atmospheric conditions, *Int. J. Chem. Kinet.*, *25*, 539–548.

Williams, J., J.M. Roberts, S.B. Bertman, C.A. Stroud, F.C. Fehsenfeld, K. Baumann, M.P. Buhr, K. Knapp, G. Hübler, P.C. Murphy, M. Nowick, and E.J. Williams (2000), A method for airborne measurement of PAN, PPN, and MPAN, *J. Geophys. Res.*, *105*, 28943–28960.

Williams, J., J.M. Roberts, F.C. Fehsenfeld, S.B. Bertman, M.P. Buhr, P.D. Goldan, G. Hübler, W.C. Kuster, T.B. Tyeson, M. Trainer, and V. Young (1997), Regional ozone from biogenic hydrocarbons deduced from airborne measurements of PAN, PPN, and MPAN, *Geophys. Res. Lett.*, *24*, 1099–1102.

Wilson, E.W., Jr., W.A. Hamilton, H.R. Mount, and W.B. DeMore (2007), Rate constants for the reactions of hydroxyl radical with several fluoroethers by the relative rate method, *J. Phys. Chem. A*, *111*, 1610–1617.

Wilson, E.W., Jr., A.A. Sawyer and H.A. Sawyer (2001), Rates of reaction for cyclopropane and difluoromethoxydifluoromethane with hydroxyl radicals, *J. Phys. Chem. A*, *105*, 1445–1448.

Wilson, J.E., and W.A. Noyes, Jr. (1943), Photochemical studies. XXXVI. Quantum yields during the photochemical decomposition of *n*-butyl methyl ketone, *J. Am. Chem. Soc.*, *65*, 1547–1550.

Wine, P.H., R.J. Astalos, and R.L. Mauldin III (1985), Kinetic and mechanistic study of the OH + HCOOH reaction, *J. Phys. Chem.*, *89*, 2620–2624.

Wine, P.H., A.R. Ravishankara, N.M. Kruetter, R.C. Shah, J.M. Nicovich, R.L. Thompson, and D.J. Wuebbles (1981), Rate of reaction of OH with HNO_3, *J. Geophys. Res.*, *86*, 1105–1112.

Wine, P.H., and D.H. Semmes (1983), Kinetics of $Cl(^3P_{3/2})$ reactions with the chloroethanes CH_3CH_2Cl, CH_3CHCl_2, CH_2ClCH_2Cl, and $CH_2ClCHCl$, *J. Phys. Chem.*, *87*, 3572–3578.

Wine, P.H., and R.J. Thompson (1984), Kinetics of OH reactions with furan, thiophene and tetrahydrothiophene, *Int. J. Chem. Kinet.*, *16*, 867–878.

Wine, P.H., J.R. Wells, and J.M. Nicovich (1988), Kinetics of $F(^2P)$ and $Cl(^2P)$ with HNO_3, *J. Phys. Chem.*, *92*, 2223–2228.

Winer, A.M., K.R. Darnall, R. Atkinson, and J. N. Pitts, Jr. (1978), unpublished results cited in Wallington et al., 1988e.

Winer, A., J. Arey, R. Atkinson, S. Aschman, W. Long, L. Morrison, and D. Olszyk (1992), Emission rates of organics from vegetation in California's central valley, *Atmos. Environ.*, *26A*, 2647–2659.

Winer, A.M., A.C. Lloyd, K.R. Darnall, R. Atkinson, and J.N. Pitts, Jr. (1977), Rate constants for the reaction of OH radicals with *n*-propyl acetate, *sec*-butyl acetate, tetrahydrofuran and peroxyacetyl nitrate, *Chem. Phys. Lett.*, *51*, 221–226.

Winer, A.M., A.C. Lloyd, K.R. Darnall, and J.N. Pitts, Jr. (1976), Relative rate constants for the reaction of the hydroxyl radical with selected ketones, chloroethenes, and monoterpene hydrocarbons, *J. Phys. Chem.*, *80*, 1635–1639.

Wingenter, O.W., M.K. Kubo, N.J. Blake, T.W. Smith, D.R. Blake, and F.S. Rowland (1996), Hydrocarbon and halocarbon measurements as photochemical and dynamical indicators of atmospheric hydroxyl, atomic chlorine, and vertical mixing obtained during Lagrangian flights, *J. Geophys. Res.*, *101*, 4331–4340.

Wingenter, O.W., B.C. Sive, N.J. Blake, D.R. Blake, and F.S. Rowland (2005), Atomic chlorine concentrations derived from ethane and hydroxyl measurements over the equatorial Pacific Ocean: Implication for dimethyl sulfide and bromine monoxide, *J. Geophys. Res.*, *110*, D20308.

Wisthaler, A., N.R. Jensen, R. Winterhalter, W. Lindinger, and J. Hjorth (2001), Measurements of acetone and other gas phase product yields from the OH-initiated oxidation of terpenes by proton-transfer–reaction mass spectrometry (PTR–MS), *Atmos. Env.*, *35*, 6181–6191.

Witte, F., E. Urbanik, and C. Zetzsch (1986), Temperature dependence of the rate constants for the addition of OH to benzene and some monosubstituted aromatics (aniline, bromobenzene, and nitrobenzene) and the unimolecular decay of the adduct. Kinetics into a quasi-equilibrium, *J. Phys. Chem.*, *90*, 3251–3259.

Wittrock, F., A. Richter, H. Oetjen, J. P. Burrows, M. Kanakidou, S. Myriokefalitakis, R. Volkamer, S. Beirle, U. Platt, and T. Wagner (2006), Simultaneous global observations of glyoxal and formaldehyde from space, *Geophys. Res. Lett.*, *33*, L16804, doi:10.1029/2006GL026310.

Wollenhaupt, M., S.A. Carl, A. Horowitz, and J.N. Crowley (2000), Rate coefficients for reaction of OH with acetone between 202 and 395 K, *J. Phys. Chem. A*, *104*, 2695–2705.

Wollenhaupt, M., and J.N. Crowley (2000), Kinetic studies of the reactions $CH_3 + NO_2 \rightarrow$ products, $CH_3O + NO_2 \rightarrow$ products, and $OH + CH_3C(O)CH_3 \rightarrow CH_3C(O)OH + CH_3$, over a range of temperature and pressure, *J. Phys. Chem. A*, *104*, 6429–6438.

Woodbridge, E.I., T.R. Fletcher, and S.R. Leone (1988), Photofragmentation of acetone at 193 nm: Rotational- and vibrational-state distributions of the CO fragment by time-resolved FTIR emission spectroscopy, *J. Phys. Chem.*, *92*, 5387–5393.

Wu, H., and Y. Mu (2007), Rate constant and products for the reaction of Cl atom with *n*-butyraldehyde, *Int. J. Chem. Kinet.*, *39*, 168–174.

Wu, H., Y. Mu, X. Zhang, and G. Jiang (2003), Relative rate constants for the reactions of hydroxyl radicals and chlorine atoms with a series of aliphatic alcohols, *Int. J. Chem. Kinet.*, *35*, 81–87.

Wyatt, S.E., J.S. Baxley, and J.R. Wells (1999), The hydroxyl radical reaction rate constant and products of methyl isobutyrate, *Int. J. Chem. Kinet.*, *31*, 551–557.

Xiang, B., and L. Zhu (2007), Absorption cross sections of *E*,*E*-2-4-hexadienedial at 248 nm and in the 290–430 nm region, and photolysis study at 248, 308, and 351 nm, *Chem. Phys. Lett.*, *450*, 31–38.

Xiang, B., L. Zhu, and Y. Tang (2007), Photolysis of 4-oxo-2-pentenal in the 190–460 nm region, *J. Phys. Chem. A*, *111*, 9025–9033.

Xiao, Y., J.A. Logan, D.J. Jacob, R.C. Hudman, R. Yantosca, and D.R. Blake (2008), Global budget of ethane and regional constraints on U.S. sources, *J. Geophys. Res.*, *113*, D21306/1–D21306/13.

Xing, J.-H., K. Takahashi, M.D. Hurley, and T.J. Wallington (2009), Kinetics of the reactions of chlorine atoms with a series of acetates, *Chem. Phys. Lett.*, *474*, 268–272.

Xu, D., J. Huang, J.S. Francisco, J.C. Hansen, and W.M. Jackson (2002), Photodissociation of carbonic dibromide at 267 nm: Observation of three-body dissociation and molecular elimination of Br_2, *J. Chem. Phys.*, *117*, 7483–7490.

Xu, S., R.S. Zhu, and M.C. Lin (2006), *Ab initio* study of the OH + CH_2O reaction: The effect of the OH··OCH_2 complex on the H-abstraction kinetics, *Int. J. Chem. Kinet*, *38*, 322–326.

Yacobucci, B.D. (2005), Alternative transportation fuels and vehicles: Energy, environment, and development issues, Congressional Research Service, the Library of Congress, Report for Congress, updated January 7, 2005; order Code RL30758.

Yadav, J.S., and J.D. Goddard (1986), Acetaldehyde photochemistry: The radical and molecular dissociations, *J. Chem. Phys.*, *84*, 2682–2690.

Yamabe, S., T. Minato, and Y. Osamura (1979), A theoretical study on the paths of photodissociation: cyclopropanone → CO + C_2H_4, *J. Am. Chem. Soc.*, *101*, 4525–4531.

Yamada, T., P.H. Taylor, A. Goumri, and P. Marshall (2003), The reaction of OH with acetone and acetone-d_6 from 298 to 832 K: Rate coefficients and mechanism, *J. Chem. Phys.*, *119*, 10600–10606.

Yamaguchi, Y., S.S. Wesolowski, T.J. Van Huis, and F.F. Schaefer (1998), The unimolecular dissociation of H_2CO on the lowest triplet potential-energy surface, *J. Chem. Phys.*, *108*, 5281–5288.

Yamamoto, S., and R. A. Back (1985), The photolysis and thermal decomposition of pyruvic acid in the gas phase, *Can. J. Chem.*, *63*, 549–554.

Yamanaka, T., M. Kawasaki, M.D. Hurley, T.J. Wallington, W.F. Schneider, and J. Bruce (2007), Kinetics and mechanism of the gas phase reaction of chlorine atoms with *i*-propanol, *Phys. Chem. Chem. Phys.*, *9*, 4211–4217.

Yamanaka, T., M. Kawasaki, M.D. Hurley, T.J. Wallington, L. Xiao, and W.F. Schneider (2008), Experimental and computational investigation of gas-phase reaction of chlorine with *n*-propanol: Observation of chloropropanol conformational isomerization at room temperature, *J. Phys. Chem. A*, *112*, 2773–2781.

Yang, X., P. Felder, and J.R. Huber (1993), Photodissociation of methyl nitrate in a molecular beam, *J. Phys. Chem.*, *97*, 10903–10910.

Yarwood, G., S. Kemball-Cook, M. Keinath, R.L. Waterland, S.H. Korzeniowski, R.C. Buck, M.H. Russell, and S.T. Washburn (2007), High-resolution atmospheric modeling of fluorotelomer alcohols and perfluorocarboxylic acids in the North American troposphere, *Environ. Sci. Technol.*, *41*, 5756–5762.

Yarwood, G., S. Rao, M. Yocke and G.Z. Whitten (2005), Updates to the carbon bond chemical mechanism: CB05, *RT-04-00675*, *Report to the EPA*.

Yaws, C.L., X. Lin, L. Bu, D.R. Balundgi, and S. Tripathi (1999), Vapor pressure, in, editor C.L. Yaws, *Chemical Properties Handbook: Thermodynamic, Environmental, Transport, Safety, and Health Related Properties for Organic an Inorganic Chemicals*, McGraw-Hill, New York, pp.159–179.

Yetter, R.A., H. Rabitz, F.L. Dryer, R.G. Maki, and R.B. Klemm (1989), Evaluation of the rate constant for the reaction OH + H_2CO: Application of modeling and sensitivity analysis techniques for determination of the product branching ratio, *J. Chem. Phys.*, *91*, 4088–4097.

Yin, H.-M., J.-L. Sun, Y.-M. Li, K.-L. Han, G.-Z. He, and S.-L. Cong (2003), Photodissociation dynamics of the S_2 state of CH_3ONO: State distributions and alignment effects of the NO ($X^2\Pi$) photofragment, *J. Chem. Phys.*, *118*, 8248–8255.

Yip, R.W., D.K. Sharm, R. Giasson, and D. Gravel (1984), Picosecond excited-state absorption of alkyl nitrobenzenes in solution, *J. Phys. Chem.*, *88*, 5770–5772.

Yoshimine, M. (1989), Ab initio studies on the radiationless deexcitation mechanism of ketene and the rearrangement to oxiranylidene, *J. Chem. Phys.*, *90*, 378–385.

Young, C.J., and D.J. Donaldson (2007), Overtone-induced degradation of perfluorinated alcohols in the atmosphere, *J. Phys. Chem. A*, *111*, 13466–13471.

Young, C.J., M.D. Hurley, T.J. Wallington, and S. Mabury (2006), Atmospheric lifetime and global warming potential of a perfluoropolyether, *Environ. Sci. Technol.*, *40*, 2242–2246.

Young, P. J., A. Arneth, G. Schurgers, G. Zeng, and J.A. Pyle (2009), The CO_2 inhibition of terrestrial isoprene emission significantly affects future ozone projections, *Atmos. Chem. Phys.*, *9*, 2793–2803.

Yu, J., H.E. Jeffries, and K.G. Sexton (1997), Atmospheric photooxidation of alkylbenzenes—1. Carbonyl product analyses, *Atmos. Environ.*, *31*, 2261–2280.

Yu, J., and S.J. Klippenstein (1991), Variational calculation of the rate of dissociation of CH_2CO into $^1CH_2$ and CO on an ab initio determined potential energy surface, *J. Phys. Chem.*, *95*, 9882–9889.

Yue, X-F., J.-L. Sun, Z-F. Liu, Q. Wei, and K.-L. Han (2006), Photodissociation dynamics of the S_2 state of CH_3ONO: LIF observation of nascent OH state distributions, *Chem. Phys. Lett.*, *426*, 57–60.

Yujing, M., and A. Mellouki (2000), The near-UV absorption cross sections for several ketones, *J. Photochem. Photobiol. A: Chemistry*, *134*, 31–36.

Zabarnick, S., J.W. Fleming, and A.P. Baronacski (1986), Production of OH from the collision-free photodissociation of nitromethane at 266 nm, *J. Chem. Phys.*, *85*, 3395–3400.

Zabarnick, S., J.W. Fleming, and M.C. Lin (1988a), Kinetics of hydroxyl radical reactions with formaldehyde and 1,3,5-trioxane between 290 and 600 K, *Int. J. Chem. Kinet.*, *20*, 117–129.

Zabarnick, S., J.W. Fleming, and M.C. Lin (1988b), The reaction of OH and OD with nitromethane and OD with perdeuteronitromethane, *Chem. Phys.*, *120*, 319–325.

Zabarnick, S., and J. Heicklen (1985a), Reactions of alkoxy radicals with O_2. I. C_2H_5O radicals, *Int. J. Chem. Kinet.*, *17*, 455–476.

Zabarnick, S., and J. Heicklen (1985b), The reactions of alkoxy radicals with O_2. II. n-C_3H_7O radicals, *Int. J. Chem. Kinet.*, *17*, 477–501.

Zabarnick, S., and J. Heicklen (1985c), Reactions of alkoxy radicals with O_2. III. i-C_4H_9O radicals, *Int. J. Chem. Kinet.*, *17*, 503–524.

Zabel, F. (1999), Reaktionswege von Alkoxyradikalen unter atmosphärishen Bedingungen and UV-Absorptionspektrum von Carbonylverbindungen, in K.H. Becker (coordinator), Annual report 1998 on BMBF-project TFS/LT3, FKZ07TFS30, p.69.

Zabel, F., F. Kirchner, and K.H. Becker (1994), Thermal decomposition of $CF_3C(O)O_2NO_2$, $CClF_2C(O)O_2NO_2$, $CCl_2FC(O)O_2NO_2$, and $CCl_3C(O)O_2NO_2$, *Int. J. Chem. Kinet.*, *26*, 827–845.

Zabransky, V., and R.W. Carr, Jr. (1975), Photodissociation of ketene at 313 nm, *J. Phys. Chem.*, *79*, 1618–1622.

Zabransky, V.P., and R.W. Carr, Jr. (1976), Electronic states of methylene from ketene photodissociation between 214 and 313 nm, *J. Am. Chem. Soc.*, *98*, 1130–1135.

Zagogianni, H., A. Mellouki, and G. Poulet (1987), Réactivité des radicaux Cl et ClO avec HNO_3, *C. R. Acad. Sc. Paris*, *304*, 573–578.

Zahra, A., and W.A. Noyes, Jr. (1965), The photochemistry of methyl isopropyl ketone, *J. Phys. Chem.*, *69*, 943–948.

Zeng, G., M.J. Pilling, and S.M. Saunders (1997), Mechanism reduction for tropospheric chemistry. Butane oxidation, *J. Chem. Soc., Faraday Trans.*, *93*, 2937–2946.

Zetzsch, C. (1980), Results presented at the Bunsen Colloquium, Gottingen, West Germany, Oct. 9, 1980; work cited in Wallington et al. (1988e).

Zetzsch, C., and F. Stuhl (1982), Rate constants for reactions of OH with carbonic acids, in, editors B. Versino and H. Ott, *Physico-chemical Behaviour of Atmospheric Pollutants*, D. Reidel Publishing Company, Dordrecht, 1982.

Zhang, H., C.M. Roehl, S.P. Sander, and P.O. Wennberg (2000), Intensity of the second and third OH overtones of H_2O_2, HNO_3 and HO_2NO_2, *J. Geophys. Res.*, *105*, 14593–14598.

Zhang, Q., M.R. Alfarra, D.R. Worsnop, J.D. Allan, H. Coe, M.R. Canagaratna, and J.L. Jimenez (2005), Deconvolution and quantification of hydrocarbon-like and oxygenated organic aerosols based on aerosol mass spectrometry, *Environ. Sci. Technol.*, *39*, 4938–4952.

Zhang, S.-H., M. Shaw, J.H. Seinfeld, and R.C. Flagan (1992), Photochemical aerosol formation from α- and β-pinene, *J. Geophys. Res.*, *97*, 20717–20730

Zhang, Z., R.D. Saini, M.J. Kurylo, and R.E. Huie (1992), Rate constants for the reactions of the hydroxyl radical with several partially fluorinated ethers, *J. Phys. Chem.*, *96*, 9301–9304.

Zhao, Z., D.T. Huskey, J.M. Nicovich, and P.H. Wine (2008), Temperature-dependent kinetics study of the gas-phase reactions of atomic chlorine with acetone, 2-butanone, and 3-pentanone. *Int. J. Chem. Kinet.*, *40*, 259–267.

Zhou, S., I. Barnes, T. Zhu, I. Bejan, M. Albu, and T. Benter (2008), Atmospheric chemistry of acetylacetone, *Env. Sci. Tech.*, *42*, 7905–7910.

Zhou, S., I. Barnes, T. Zhu, I. Bejan, and T. Benter (2006a), Kinetic study of the gas-phase reactions of OH and NO_3 radicals and O_3 with selected vinyl ethers, *J. Phys. Chem. A*, *110*, 7386–7392.

Zhou, S.M., I. Barnes, T. Zhu, and T. Benter (2009), Rate coefficients for the gas-phase reactions of OH and NO radicals and O_3 with ethyleneglycol monovinyl ether, ethyleneglycol divinyl ether, and diethyleneglycol divinyl ether, *J. Phys. Chem. A*, *113*, 858–865.

Zhou, S., I. Barnes, T. Zhu, B. Klotz, M. Albu, I. Bejan, and T. Benter (2006b), Product study of the OH, NO_3, and O_3 initiated atmospheric photooxidation of propyl vinyl ether, *Environ. Sci. Technol.*, *40*, 5415–5421.

Zhou, X., and K. Mopper (1990), Apparent partition coefficients of 15 carbonyl compounds between air and seawater and between air and freshwater; implications for air–sea exchange, *Environ. Sci. Technol.*, *24*, 1864–1869.

Zhu, L., and J.W. Bozzelli (2002), Structures, rotational barriers, and thermochemical properties of chlorinated aldehydes and corresponding acetyl (CC•═O) and formyl methyl radicals (C•C═O) and additivity groups, *J. Phys. Chem. A*, *106*, 345–355.

Zhu, L., and T.J. Cronin (2000), Photodissociation of benzaldehyde in the 280–308 nm region, *Chem. Phys. Lett.*, *317*, 227–231.

Zhu, L., T. Cronin, and A. Narang (1999), Wavelength-dependent photolysis of *i*-pentanal and *t*-pentanal from 380–330 nm, *J. Phys. Chem.*, *103*, 7248–7253.

Zhu, L., and C.-F. Ding (1997), Temperature dependence of the near UV absorption spectra and photolysis products of ethyl nitrate, *Chem. Phys. Lett.*, *265*, 177–184.

Zhu, L., D. Kellis, and C.-F. Ding (1996), Photolysis of glyoxal at 193, 248, 308, and 351 nm, *Chem. Phys. Lett.*, *257*, 487–491.

Zhu, L., R.K. Talukdar, J.B. Burkholder, and A.R. Ravishankara (2008), Rate coefficients for the OH + acetaldehyde (CH_3CHO) reaction between 204 and 373 K, *Int. J. Chem. Kinet.*, *40*, 635–646.

Zhu, T., I. Barnes, and K.H. Becker (1991), Relative-rate study of the gas phase reaction of hydroxyl radicals with difunctional organic nitrates at 298 K and atmospheric pressure, *J. Atm. Chem.*, 13, 301–311.

Zielinska, B., J. Shire, G. Harshfield, and R. Pasek (1997), paper 97-RP139.06, 90th Annual Meeting of the Air Waste Management Association, Toronto, Canada, June 8–13, 1997.

Ziemann, P.J. (2002), Evidence for low-volatility diacyl peroxides as a nucleating agent and major component of aerosol formed from reactions of O_3 with cyclohexene and homologous compounds, *J. Phys. Chem. A*, *106*, 4390–4402.

Zimmerman, P. (1979), Testing of hydrocarbon emissions from vegetation, leaf litter and aquatic surfaces, and development of a method for compiling biogenic emission inventories, Rep. EPA-450-4-70-004, U.S. Environmental Protection Agency, Research Triangle Park, N.C.

Zuckermann, H., B. Schmitz, and Y. Haas (1988), Dissociation energy of an isolated triplet acetone molecule, *J. Phys. Chem.*, *92*, 4835–4837.

Appendix

Structures of the Oxygenates

App-I. Alcohols

App-I-A. Acyclic Alcohols

1) Methanol (methyl alcohol, CH_3OH):

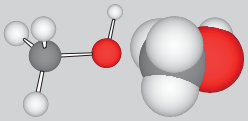

2) Ethanol (ethyl alcohol, C_2H_5OH):

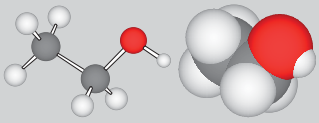

3) 1-Propanol (*n*-propyl alcohol, $CH_3CH_2CH_2OH$):

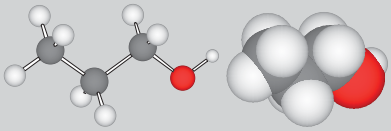

4) 2-Propanol [*iso*-propyl alcohol, $(CH_3)_2CHOH$]:

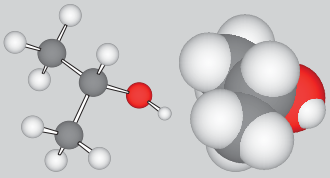

5) 1-Butanol (*n*-butyl alcohol, $CH_3CH_2CH_2CH_2OH$):

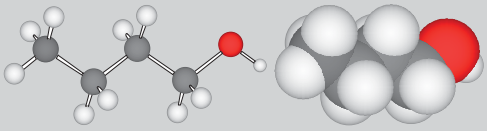

6) 2-Butanol [*sec*-butyl alcohol, $CH_3CH(OH)CH_2CH_3$]:

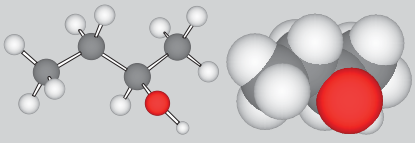

7) 2-Methyl-1-propanol [*iso*-butyl alcohol, $(CH_3)_2CHCH_2OH$]:

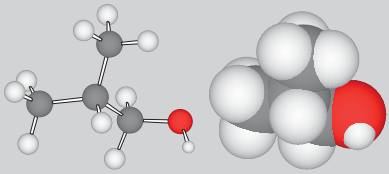

8) 1,1-Dimethylethanol [*tert*-butyl alcohol, $(CH_3)_3COH$]:

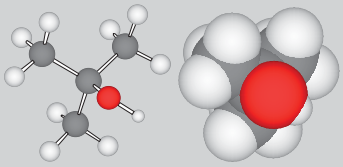

9) 1-Pentanol (*n*-pentyl alcohol, $CH_3CH_2CH_2CH_2CH_2OH$):

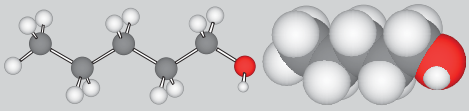

10) 2-Pentanol (*sec*-pentyl alcohol, $[CH_3CH_2CH_2CH(CH_3)OH]$:

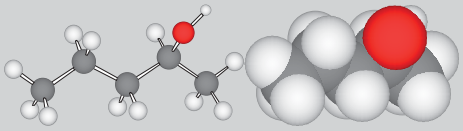

11) 3-Pentanol $[CH_3CH_2CH(OH)CH_2CH_3]$:

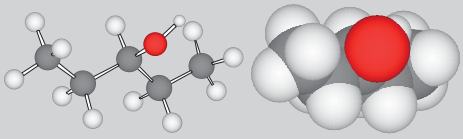

12) 3-Methyl-1-butanol $[(CH_3)_2CHCH_2CH_2OH]$:

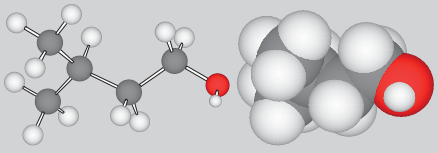

13) 2-Methyl-2-butanol $[CH_3C(OH)(CH_3)CH_2CH_3]$:

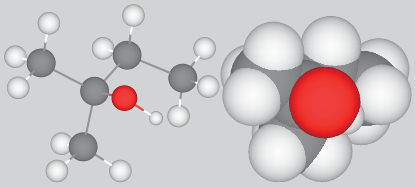

14) 3-Methyl-2-butanol $[CH_3CH(OH)CH(CH_3)CH_3]$:

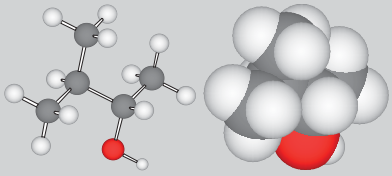

15) 1-Hexanol (*n*-hexyl alcohol, $CH_3CH_2CH_2CH_2CH_2CH_2OH$):

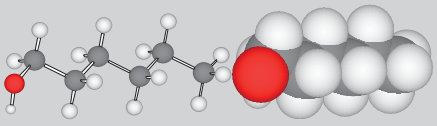

16) 2-Hexanol $[CH_3CH(OH)CH_2CH_2CH_2CH_3]$:

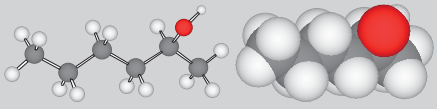

17) 2-Methyl-2-pentanol $[(CH_3)_2C(OH)CH_2CH_2CH_3]$:

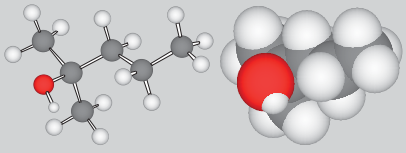

18) 4-Methyl-2-pentanol $[CH_3CH(OH)CH_2CH(CH_3)_2]$:

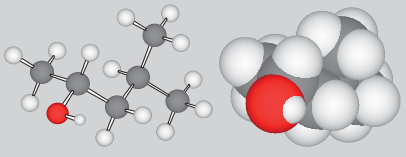

19) 2,3-Dimethyl-2-butanol
[$(CH_3)_2CH(OH)CH(CH_3)_2$]:

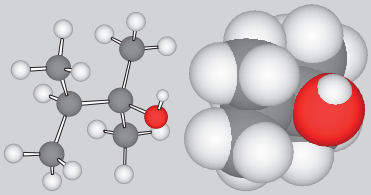

20) 1-Heptanol (*n*-heptyl alcohol,
$CH_3CH_2CH_2CH_2CH_2CH_2CH_2OH$):

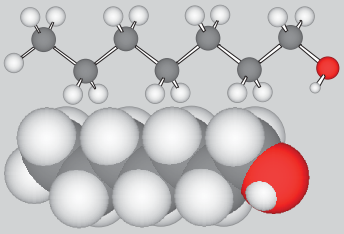

21) 4-Heptanol
[$CH_3CH_2CH_2CH(OH)CH_2CH_2CH_3$]:

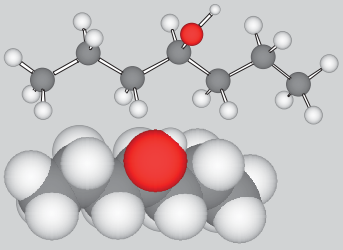

22) 2,4-Dimethyl-2-pentanol
[$(CH_3)_2CH(OH)CH_2CH(CH_3)_2$]:

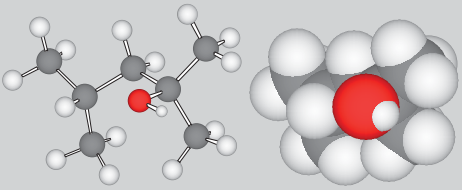

23) 1- Octanol
($CH_3CH_2CH_2CH_2CH_2CH_2CH_2CH_2OH$):

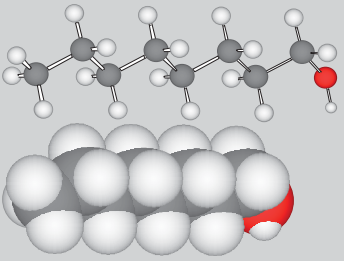

24) 3,5-Dimethyl-3-hexanol
[$CH_3CH_2C(OH)(CH_3)CH_2CH(CH_3)_2$]:

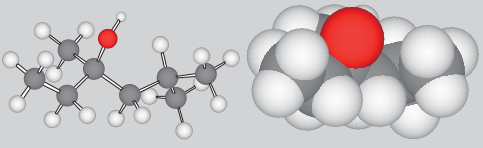

App-I-B. Cyclic Alcohols

1) Cyclopentanol (*cyclo*-C_5H_9OH):

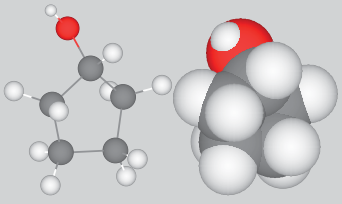

2) Cyclohexanol (*cyclo*-$C_6H_{11}OH$):

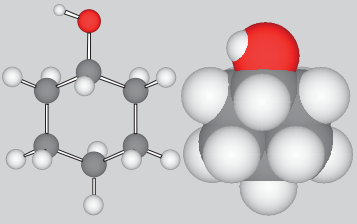

App-I-C. Acylic Diols

1) 1,2-Dihydroxyethane (ethylene glycol, $HOCH_2CH_2OH$):

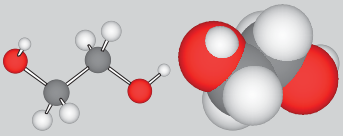

2) 1,2-Dihydroxypropane [1,2-propylene glycol, $HOCH_2CH(OH)CH_3$]:

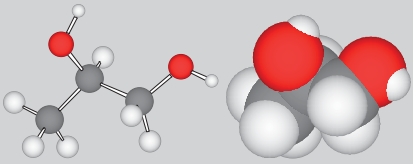

3) 1,2-Dihydroxybutane [1,2-butylene glycol, $HOCH_2CH(OH)CH_2CH_3$]:

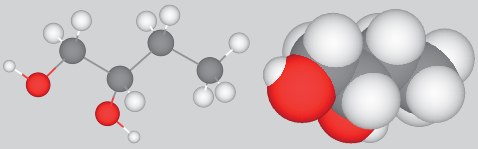

4) 1,3-Dihydroxybutane [1,3-butylene glycol, $HOCH_2CH_2CH(OH)CH_3$]:

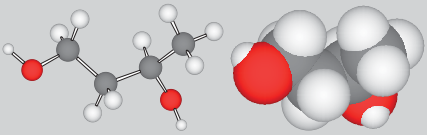

5) 2,3-Dihydroxybutane [2,3-butylene glycol, $CH_3CH(OH)CH(OH)CH_3$]:

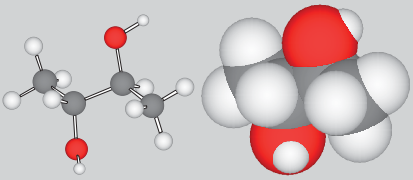

6) 2-Methyl-2,4-dihydroxypentane [$CH_3C(OH)(CH_3)CH_2CH(OH)CH_3$]:

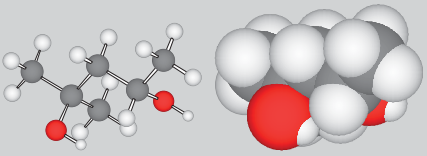

App-I-D. Unsaturated Alcohols

1) 2-Propen-1-ol (allyl alcohol, $CH_2{=}CHCH_2OH$):

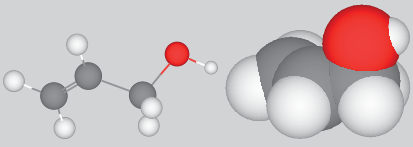

2) 2-Buten-1-ol (crotyl alcohol, $CH_3CH{=}CHCH_2OH$):

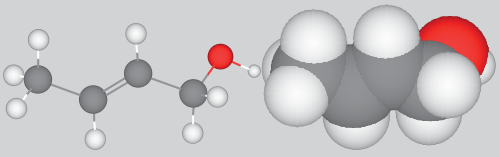

3) 3-Buten-1-ol ($CH_2{=}CHCH_2CH_2OH$):

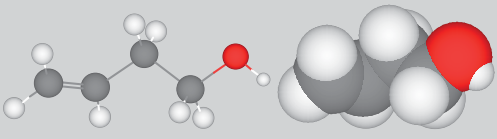

4) 3-Buten-2-ol [$CH_2{=}CHCH(OH)CH_3$]:

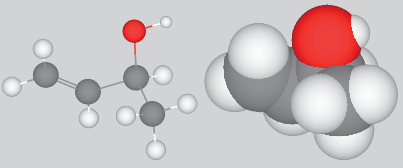

5) 2-Methyl-2-propen-1-ol [$CH_2{=}C(CH_3)CH_2OH$]:



6) *cis*-2-Penten-1-ol ($CH_3CH_2CH{=}CHCH_2OH$):

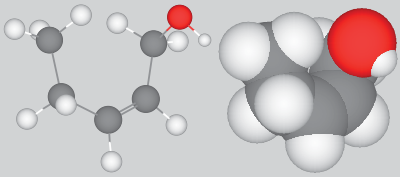

7) 1-Penten-3-ol [$CH_3CH_2CH(OH)CH{=}CH_2$]:

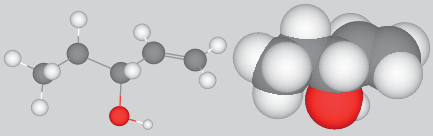

8) 3-Methyl-2-buten-1-ol
[$(CH_3)_2C{=}CHCH_2OH$]:



9) 3-Methyl-3-buten-1-ol
[$CH_2{=}C(CH_3)CH_2CH_2OH$]:

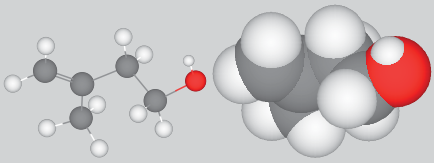

10) 2-Methyl-3-buten-2-ol
[$CH_2{=}CHC(OH)(CH_3)_2$]:

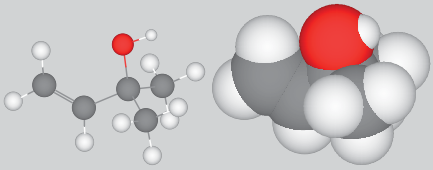

11) *cis*-4-Hexen-1-ol [(*Z*)-hex-4-en-1-ol,
$CH_3CH{=}CHCH_2CH_2CH_2OH$]:

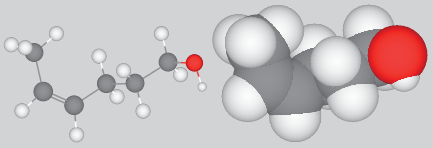

12) *cis*-3-Hexen-1-ol [(*Z*)-hex-3-en-1-ol,
$CH_3CH_2CH{=}CHCH_2CH_2OH$]:

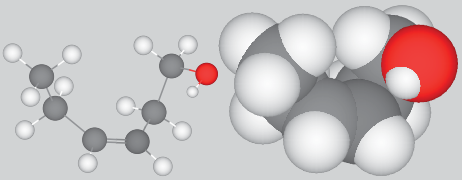

13) *trans*-3-Hexen-1-ol [(*E*)-hex-3-en-1-ol,
$CH_3CH_2CH{=}CHCH_2CH_2OH$]:

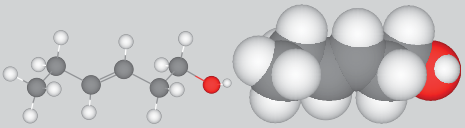

14) *cis*-2-Hexene-1-ol [(*Z*)-hex-2-en-1-ol,
$CH_3CH_2CH_2CH{=}CHCH_2OH$]:

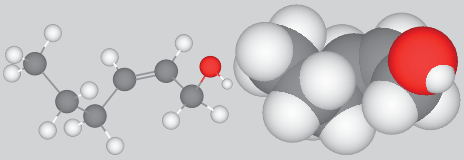

15) *trans*-2-Hexene-1-ol [(*E*)-hex-2-en-1-ol,
$CH_3CH_2CH_2CH{=}CHCH_2OH$]:

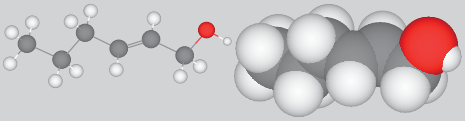

16) 2,6-Dimethyl-7-octen-2-ol [dihydromycenol,
$CH_2{=}CHCH(CH_3)CH_2CH_2CH_2C(OH)(CH_3)_2$]:

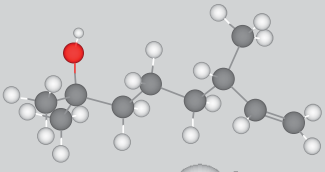

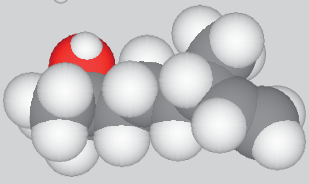

17) 3,7-Dimethyl-1,6-octadien-3-ol [linalool, $CH_2{=}CHC(CH_3)(OH)CH_2CH_2CH{=}C(CH_3)_2$]:

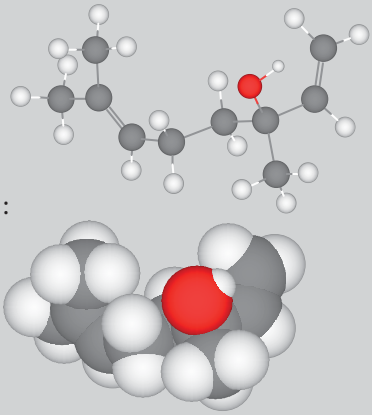

:

18) (*E*)3,7-Dimethyl-2,6-octadien-1-ol [geraniol, $HOCH_2CH{=}C(CH_3)CH_2CH_2CH{=}C(CH_3)_2$]:

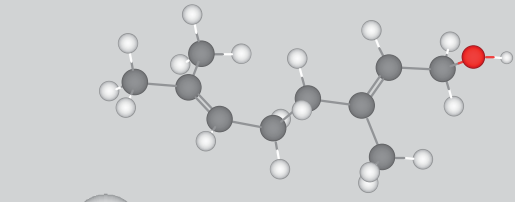

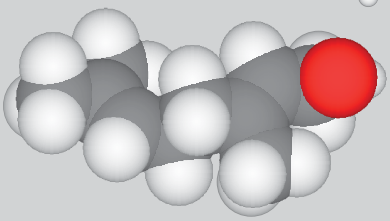

19) 3,7-Dimethyl-6-octen-1-ol $(CH_3)_2C{=}CHCH_2CH_2CH(CH_3)CH_2CH_2OH$, Citronellol:

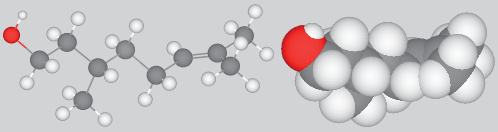

20) 2-(4-Methylcyclohex-3-en-1-yl)propane-2-ol, α-terpineol:



21) 1-Methyl-4-isopropenyl-6-cyclohexen-2-ol, carveol:

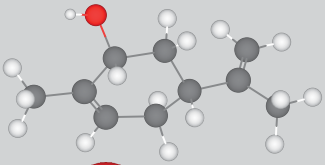

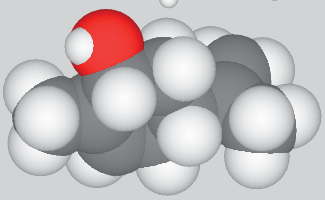

22) 3,5-Dimethyl-1-Hexyn-3-ol, $HC{\equiv}CC(OH)(CH_3)CH_2CH(CH_3)_2$:

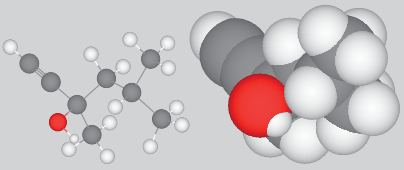

23) 2-Propyn-1-ol (propargyl alcohol, $HC{\equiv}CCH_2OH$):

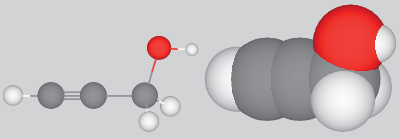

App-I-E. Aromatic Alcohols

1) Phenol (C_6H_5OH):

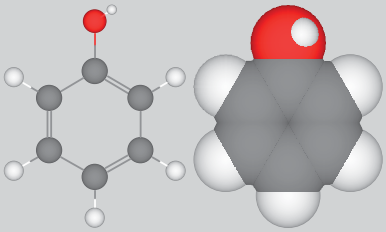

2) *o*-Cresol (HOC_6H_4OH):

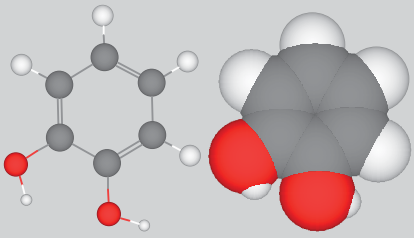

3) *m*-Cresol (HOC_6H_4OH):

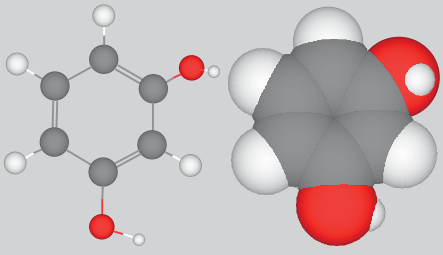

4) *p*-Cresol (HOC_6H_4OH):

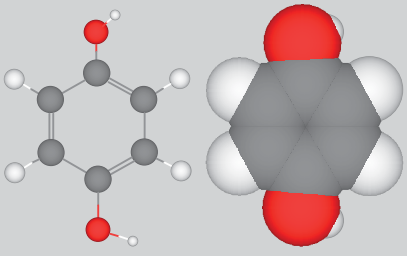

5) Benzyl alcohol, ($C_6H_5CH_2OH$):

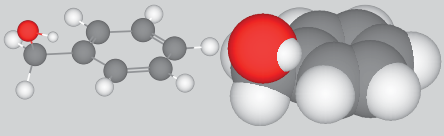

6) 2,3-Dimethylphenol ($HOC_6H_3(CH_3)_2$):

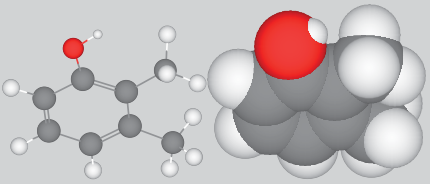

7) 2,4-Dimethylphenol ($HOC_6H_3(CH_3)_2$):

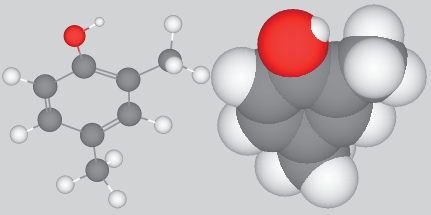

8) 2,5-Dimethylphenol ($HOC_6H_3(CH_3)_2$):

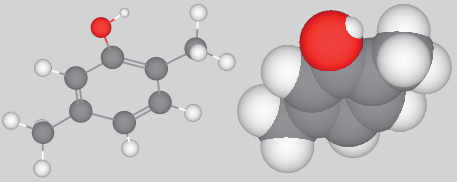

9) 2,6-Dimethylphenol ($HOC_6H_3(CH_3)_2$):

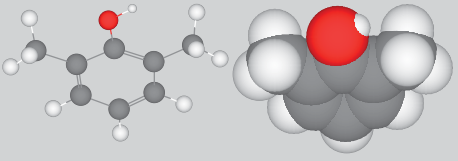

10) 3,4-Dimethylphenol ($HOC_6H_3(CH_3)_2$):

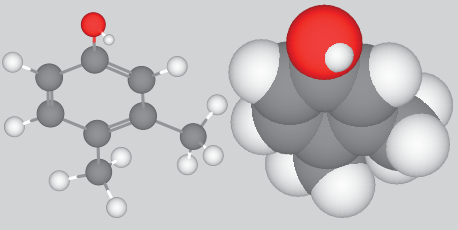

11) 3,5-Dimethylphenol ($HOC_6H_3(CH_3)_2$):

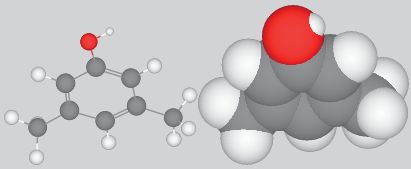

12) 2,3,5-Trimethylphenol ($HOC_6H_2(CH_3)_3$):

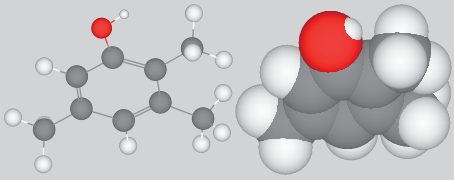

13) 2,3,6-Trimethylphenol ($HOC_6H_2(CH_3)_3$):

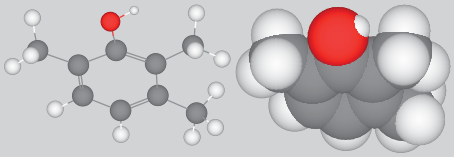

14) 1,2-Dihydroxy-3-methylbenzene $[(OH)_2C_6H_3CH_3]$:

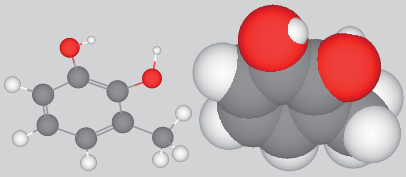

15) 1,2-Dihydroxy-4-methylbenzene $[(OH)_2C_6H_3CH_3]$:

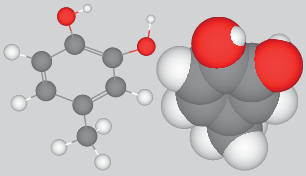

16) 2-Hydroxynaphthalene ($HO—C_{10}H_7$):

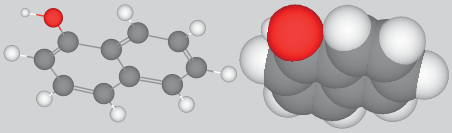

17) 3-Hydroxynaphthalene ($HO—C_{10}H_7$):

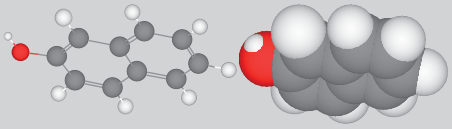

App-I-F. α-Halogen-Substituted Alcohols

1) Trifluoromethanol (CF_3OH):

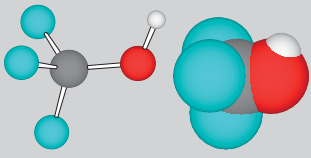

2) Chloromethanol (CH_2ClOH):

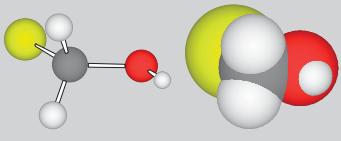

3) Dichloromethanol ($CHCl_2OH$):

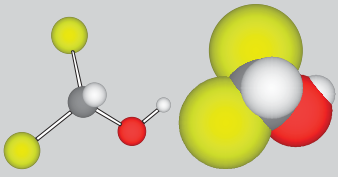

4) Trichloromethanol (CCl_3OH):

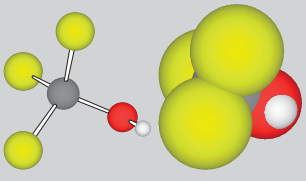

5) 1-Chloroethanol ($CH_3CHClOH$):

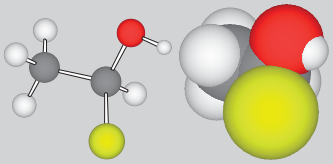

7) 2-Chloro-2-propanol [$CH_3C(Cl)(OH)CH_3$]:



6) 1-Chloropropanol [$CH_3CH_2CH(Cl)OH$]:

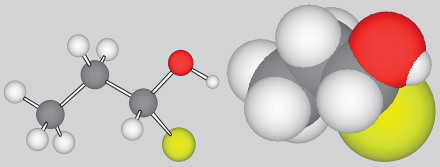

App-I-G. Other Halogen-Substituted Alcohols

1) 2-Fluoroethanol (CH_2FCH_2OH):

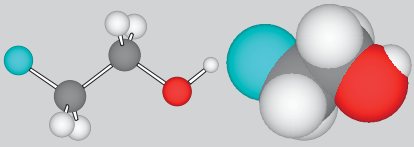

2) 2,2-Difluoroethanol (CHF_2CH_2OH):

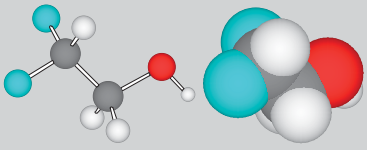

3) 2,2,2-Trifluoroethanol (CF_3CH_2OH):

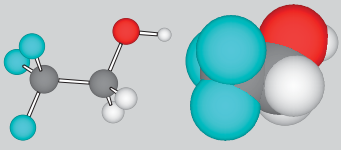

4) 2,2,3,3,3-Pentafluoro-1-propanol ($CF_3CF_2CH_2OH$):

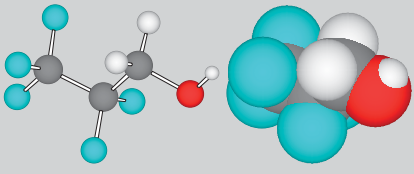

5) 2,2,3,3-Tetrafluoro-1-propanol ($CHF_2CF_2CH_2OH$):

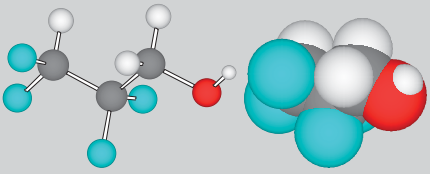

6) 1,1,1,3,3,3-Hexafluoro-2-propanol [$CF_3CH(OH)CF_3$]:

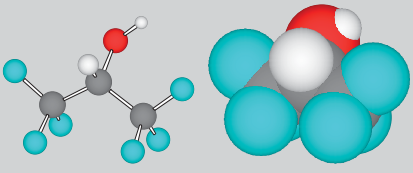

7) 3,3,3-Trifluoro-1-propanol ($CF_3CH_2CH_2OH$):

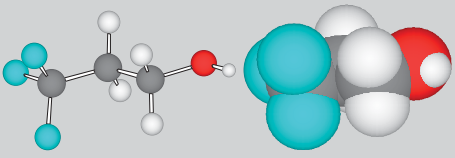

8) 2,2,3,4,4,4-Hexafluoro-1-butanol [$CF_3CHFCF_2CH_2OH$]:

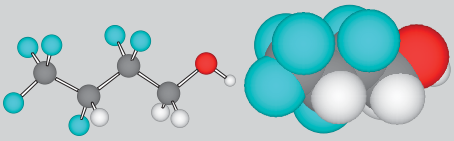

9) 2,2,3,3,4,4,4-Heptafluoro-1-butanol ($CF_3CF_2CF_2CH_2OH$):

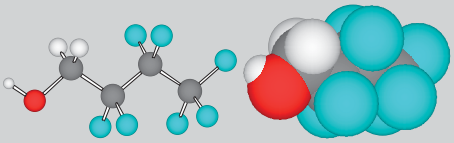

10) 2,2,3,3,4,4,5,5,5-Nonafluoro-1-pentanol ($CF_3CF_2CF_2CF_2CH_2OH$):

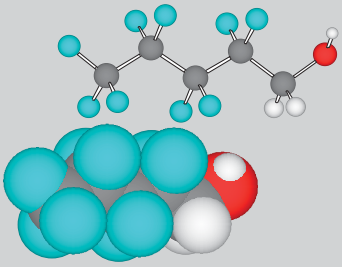

11) 3,3,4,4,5,5,6,6,6-Nonafluoro-1-hexanol ($C_4F_9CH_2CH_2OH$):

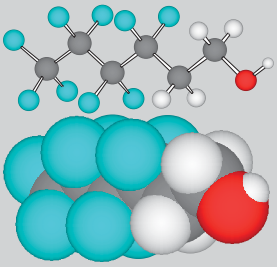

12) 2,2,3,3,4,4,5,5,6,6,7,7,7-Tridecafluoro-1-heptanol ($CF_3CF_2CF_2CF_2CF_2CH_2OH$):

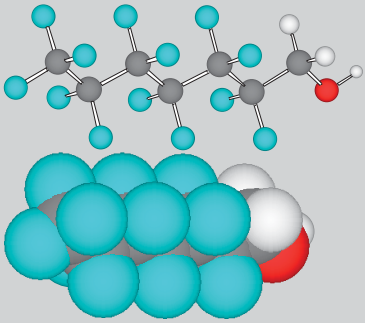

13) 3,3,4,4,5,5,6,6,7,7,8,8,8-Tridecafluoro-1-octanol ($C_6F_{13}CH_2CH_2OH$):

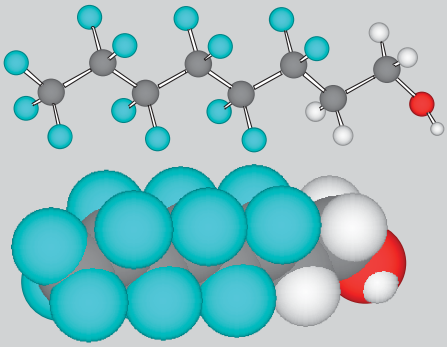

14) 3,3,4,4,5,5,6,6,7,7,8,8,9,9,10,10,10-Heptadecafluoro-1-decanol ($C_8F_{17}CH_2CH_2OH$):

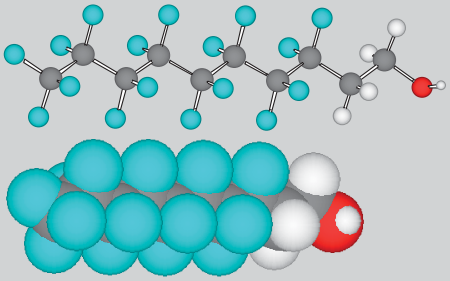

15) 2-Chloroethanol (CH_2ClCH_2OH):

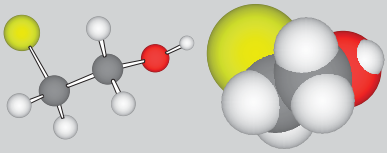

16) 2,2,2-Trichloroethanol (CCl_3CH_2OH):

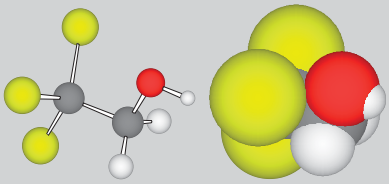

17) 2,2,2-Trifluoroethane-1,1-diol ($CF_3CH(OH)_2$):

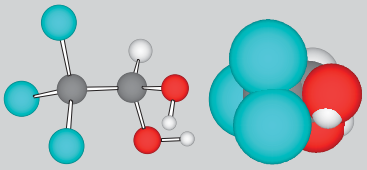

18) 2,2,3,3,4,4,4-Heptafluorbutan-1,1-diol [$CF_3CF_2CF_2CH(OH)_2$]:

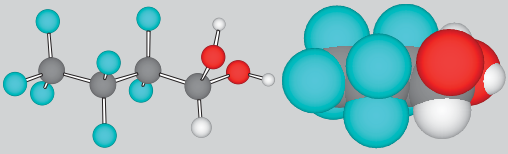

19) 2,2,3,3,4,4,5,5,5-Nonafluoropentan-1,1-diol [$CF_3CF_2CF_2CF_2CH(OH)_2$]:



App-II. Ethers

App-II-A. Acylic Ethers

1) Dimethyl ether (CH_3OCH_3):

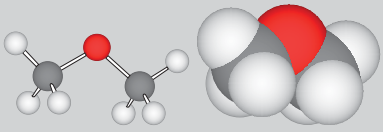

2) Methyl ethyl ether ($CH_3OCH_2CH_3$):

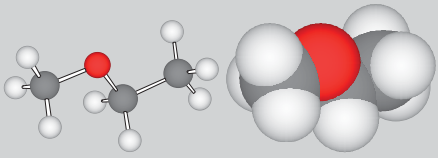

3) Diethyl ether ($CH_3CH_2OCH_2CH_3$):

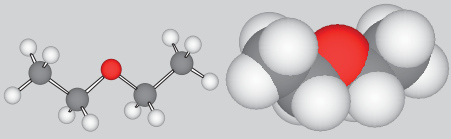

4) Methyl *n*-butyl ether ($CH_3OCH_2CH_2CH_2CH_3$):

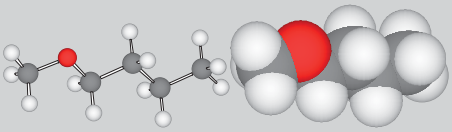

5) Methyl *tert*-butyl ether [$CH_3OC(CH_3)_3$]:

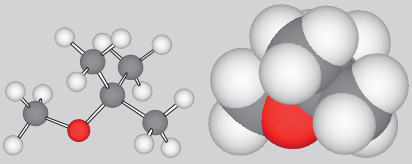

6) Di-*n*-propyl ether ($CH_3CH_2CH_2OCH_2CH_2CH_3$):

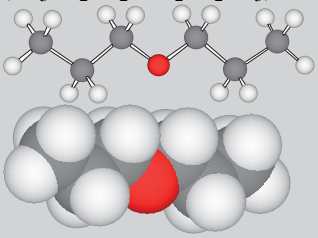

7) Di-isopropyl ether [$(CH_3)_2CHOCH(CH_3)_2$]:

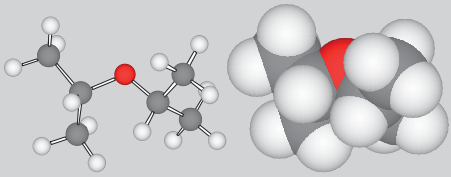

8) Ethyl *n*-butyl ether ($CH_3CH_2OCH_2CH_2CH_2CH_3$):

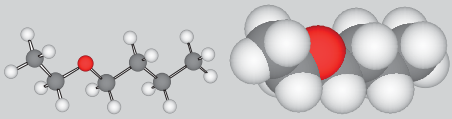

9) Ethyl *tert*-butyl ether [$CH_3CH_2OC(CH_3)_3$]:

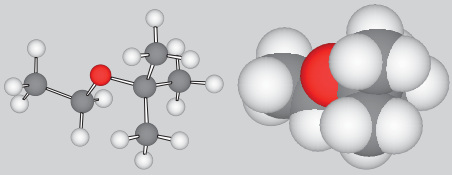

10) Methyl *tert*-amyl ether [$CH_3OC(CH_3)_2CH_2CH_3$]:

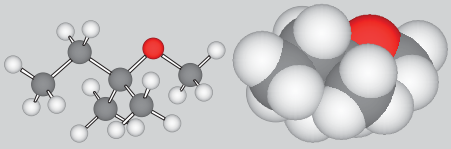

11) Isopropyl isobutyl ether

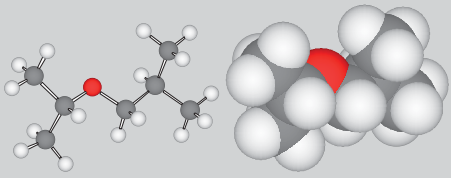

12) Di-*n*-butyl ether ($CH_3CH_2CH_2CH_2OCH_2CH_2CH_2CH_3$):

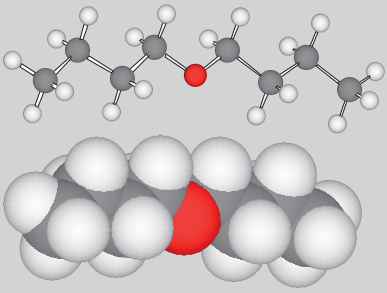

13) Di-isobutyl ether [$(CH_3)_2CHCH_2OCH_2CH(CH_3)_2$]:

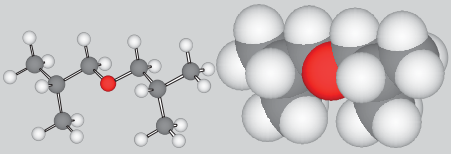

14) Di-*tert*-butyl ether [$(CH_3)_3COC(CH_3)_3$]:

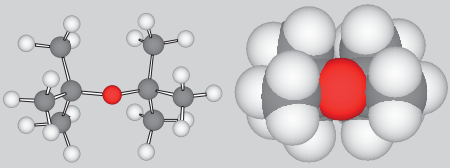

15) Di-*n*-pentyl ether ($CH_3CH_2CH_2CH_2CH_2OCH_2CH_2CH_2CH_2CH_3$):

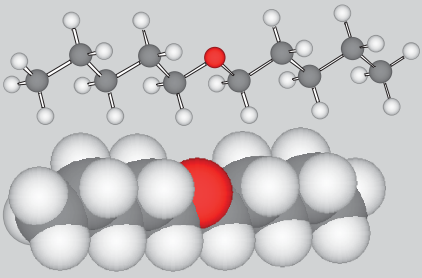

App-II-B. Multifunctional Ethers

1) Dimethoxymethane ($CH_3OCH_2OCH_3$):

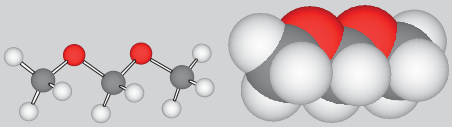

2) 2-Methoxyethanol ($CH_3OCH_2CH_2OH$):

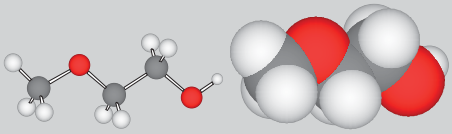

3) 1,2-Dimethoxyethane ($CH_3OCH_2CH_2OCH_3$):

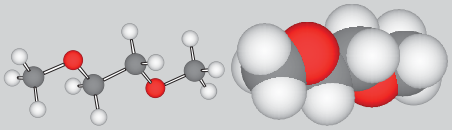

4) 2-Ethoxyethanol ($C_2H_5OCH_2CH_2OH$):

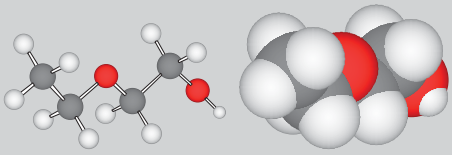

5) 1-Methoxy-2-propanol
[$CH_3OCH_2CH(OH)CH_3$]:

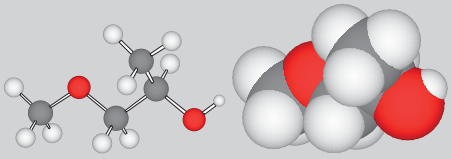

6) 1,1-Dimethoxyethane [CH3CH(OCH_3)$_2$]:

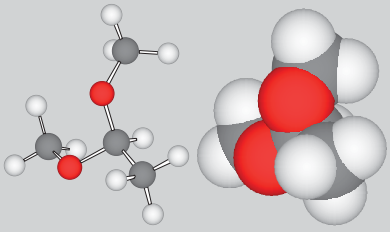

7) 2-Propoxyethanol
($CH_3CH_2CH_2OCH_2CH_2OH$):

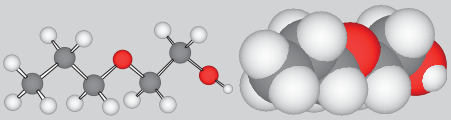

8) Diethoxymethane ($CH_3CH_2OCH_2OCH_2CH_3$):

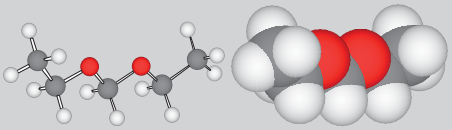

9) 1,2-Dimethoxypropane
[$CH_3OCH_2CH(OCH_3)CH_3$]:

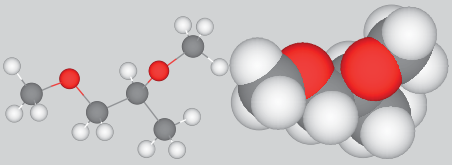

10) 2,2-Dimethoxypropane [$(CH_3)_2C(OCH_3)_2$]:

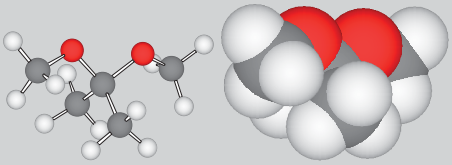

11) 2-Isopropoxyethanol
[$(CH_3)_2CHOCH_2CH_2OH$]:

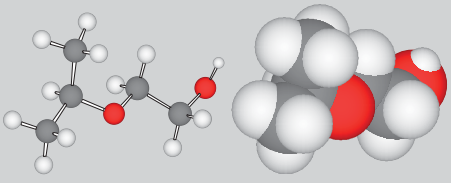

12) 1-Ethoxy-2-methoxyethane
($CH_3CH_2OCH_2CH_2OCH_3$):

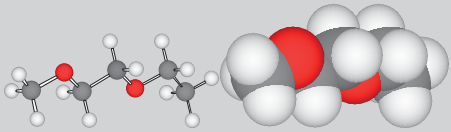

13) 3-Methoxy-1-butanol
[$CH_3CH(OCH_3)CH_2CH_2OH$]:

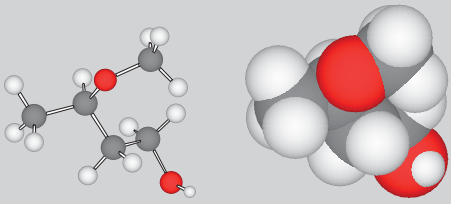

14) 3-Ethoxy-1-propanol
($CH_3CH_2OCH_2CH_2CH_2OH$):

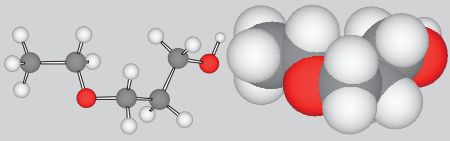

15) 1,3,Dimethoxypropane
($CH_3OCH_2CH_2CH_2OCH_3$):

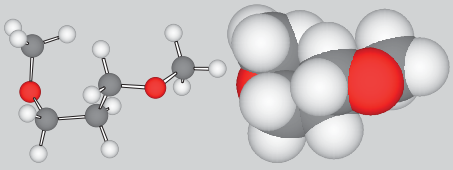

16) 2-*n*-Butoxyethanol
($CH_3CH_2CH_2CH_2OCH_2CH_2OH$):

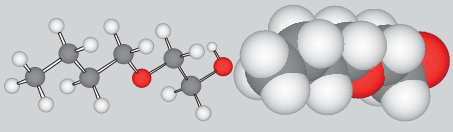

17) 1,2-Diethoxyethane
($CH_3CH_2OCH_2CH_2OCH_2CH_3$):

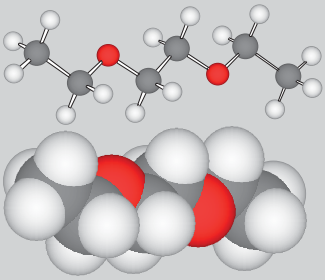

18) 1,4-Dimethoxybutane
($CH_3OCH_2CH_2CH_2CH_2OCH_3$):

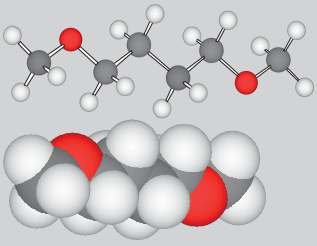

19) Di-*n*-propoxymethane
($CH_3CH_2CH_2OCH_2OCH_2CH_2CH_3$):

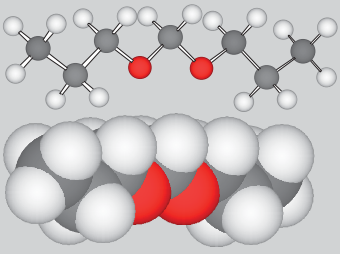

20) 2,2-Diethoxypropane [$(CH_3)_2C(OCH_2CH_3)_2$]:

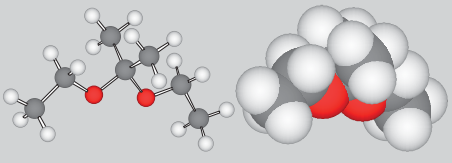

21) Di-isopropoxymethane
[$(CH_3)_2CHOCH_2OCH(CH_3)_2$]:

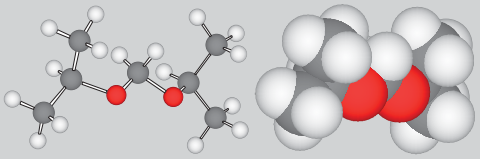

22) 1-*n*-Butoxy-2-propanol
[$CH_3CH_2CH_2CH_2OCH_2C(OH)CH_3$]:

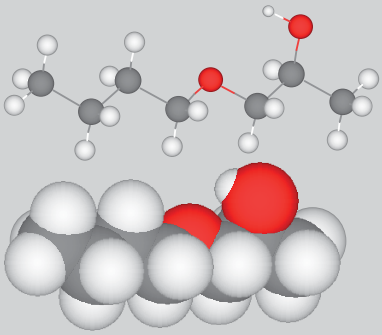

23) Di-*n*-butoxymethane
($CH_3CH_2CH_2CH_2OCH_2OCH_2CH_2CH_2CH_3$):

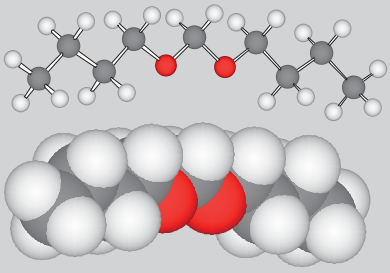

24) Di-*sec*-butoxymethane
[$CH_3CH_2CH(CH_3)OCH_2OCH(CH_3)CH_2CH_3$]:

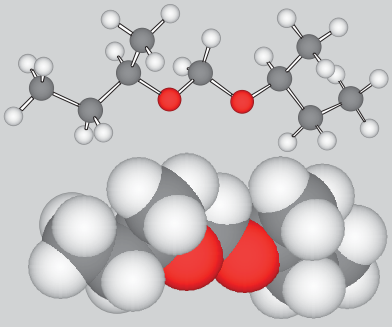

25) Di-isobutoxymethane
[$(CH_3)_2CHCH_2OCH_2OCH_2CH(CH_3)_2$]:

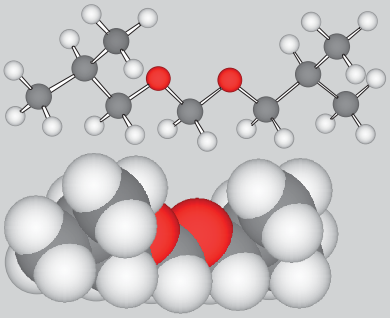

26) 1,1,3-Trimethoxypropane
[$(CH_3O)_2CHCH_2CH_2OCH_3$]:

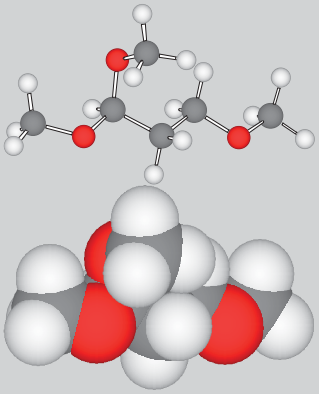

27) Trimethoxymethane [$(CH_3O)_3CH$]:

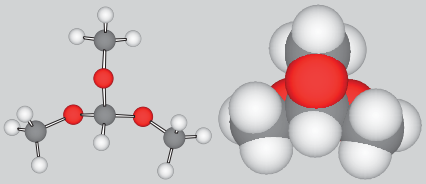

28) Diethylene glycol ethyl ether (2-(2-ethoxyethoxy)ethanol, $CH_3CH_2OCH_2CH_2OCH_2CH_2OH$):

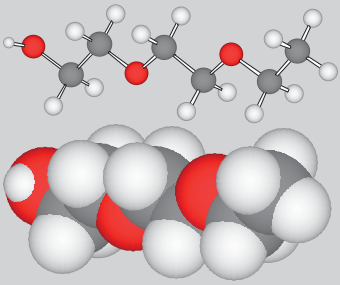

29) Diethylene glycol *n*-butyl ether (2-(2-butoxyethoxy)ethanol, $(CH_3CH_2CH_2CH_2OCH_2CH_2OCH_2CH_2OH$):

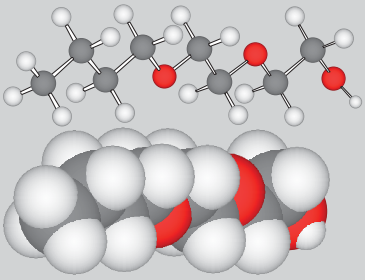

30) Methoxymethylformate $[HC(O)OCH_2OCH_3]$:

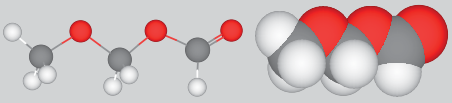

31) Methoxymethylacetate $[CH_3C(O)OCH_2OCH_3]$:

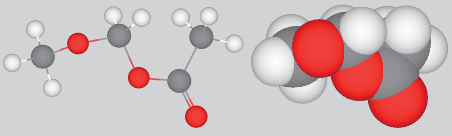

32) Ethoxymethylformate $[HC(O)OCH_2OCH_2CH_3]$:

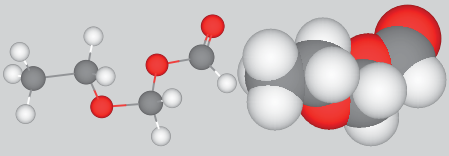

33) 2-Methoxyethylformate $[HC(O)OCH_2CH_2OCH_3]$:

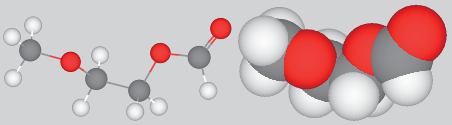

34) Ethoxymethylacetate $[CH_3C(O)OCH_2OCH_2CH_3]$:

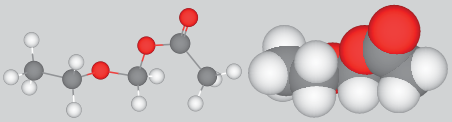

35) 2-Methoxyethylacetate $[CH_3C(O)OCH_2CH_2OCH_3]$:

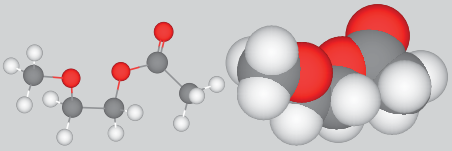

36) 2-Ethoxyethylformate $[HC(O)OCH_2CH_2OCH_2CH_3]$:

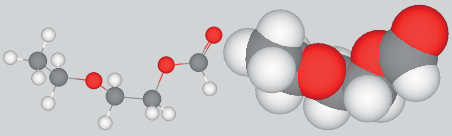

37) 2-Ethoxyethylacetate $[CH_3C(O)OCH_2CH_2OCH_2CH_3]$:

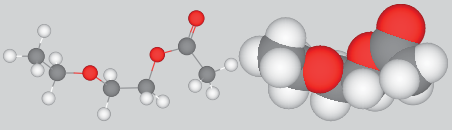

38) 2-Ethoxyethyl isobutyrate
[$(CH_3)_2CHC(O)OCH_2CH_2OCH_2CH_3$]:



39) Ethyl 3-ethoxypropionate
[$CH_3CH_2OCH_2CH_2OC(O)CH_2CH_3$]:

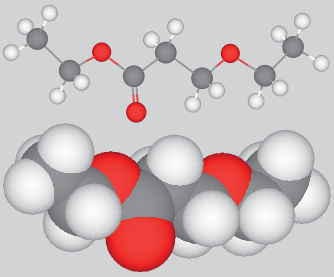

App-II-C. Unsaturated Ethers

1) Methyl vinyl ether ($CH_3OCH{=}CH_2$):

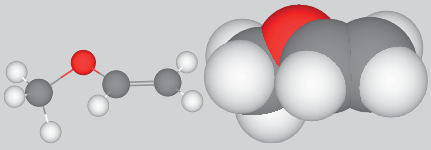

2) Ethyl vinyl ether ($CH_3CH_2OCH{=}CH_2$):

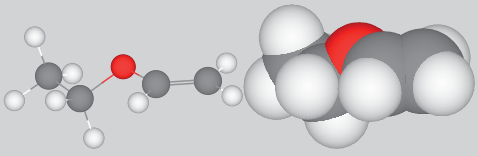

3) *n*-Propyl vinyl ether ($CH_3CH_2CH_2OCH{=}CH_2$):

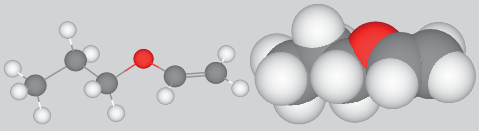

4) *n*-Butyl vinyl ether
($CH_3CH_2CH_2CH_2OCH{=}CH_2$):

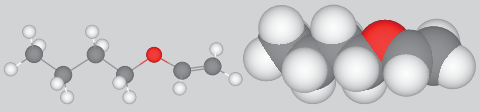

5) *trans*-Ethyl 1-propenyl ether
[(1*E*)-1-ethoxyprop-1-ene,
$CH_3CH_2OCH{=}CHCH_3$]:

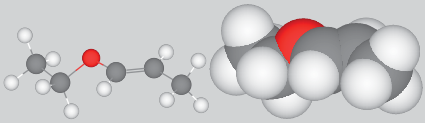

6) Isobutyl vinyl ether
[$(CH_3)_2CHCH_2OCH{=}CH_2$]:

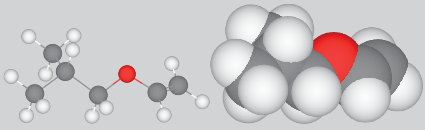

7) *tert*-Butyl vinyl ether [$(CH_3)_3COCH{=}CH_2$]:

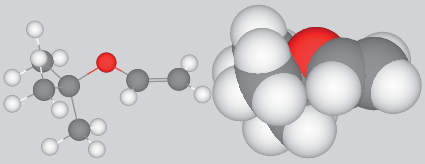

8) Furan [*cyclo*-CH═CH—O—CH═CH—]:

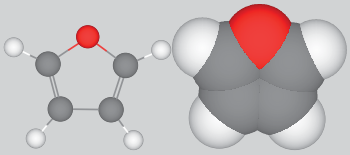

9) 2-Methyfuran
[*cyclo*-CH═CHCH═C(CH_3)O—]:

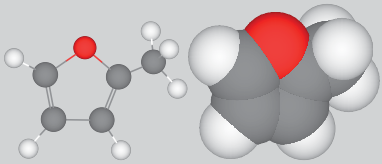

10) 3-Methylfuran
[*cyclo*-CH═CHC(CH_3)CHO—]:

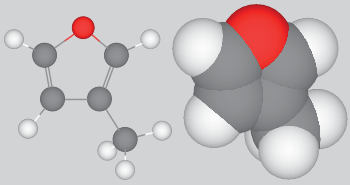

11) 2,5-Dimehylfuran
[*cyclo*-C(CH_3)═CHCHC(CH_3)O—]:

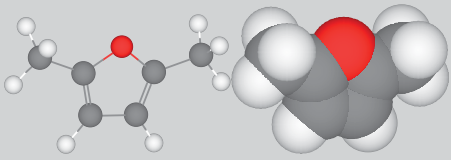

12) Tetramethylfuran
[*cyclo*-C(CH_3)═C(CH_3)C(CH_3)═C(CH_3)O—]:

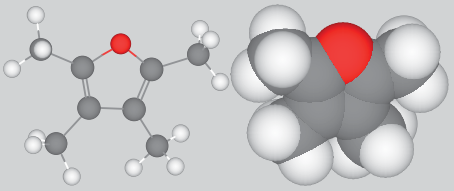

13) 2-Furancarboxaldehyde[*cyclo*-
CH═CHCH═C(CHO)O—]:

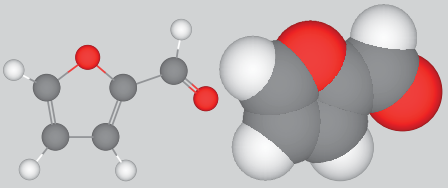

App-II-D. Cyclic Ethers

1) Ethylene oxide (epoxyethane, oxirane, dimethylene oxide, *cyclo*-C_2H_4O):

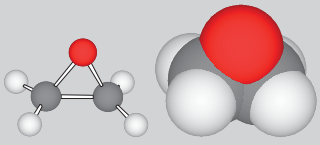

2) Methyl oxirane (propylene oxide, CH_3-*cyclo*-C_2H_3O):

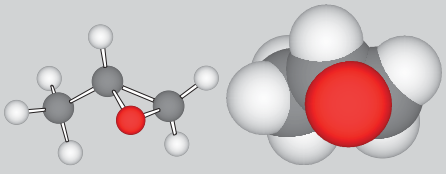

3) Ethyl oxirane (1,2-butylene oxide, C_2H_5-*cyclo*-C_2H_3O):

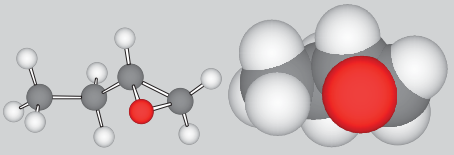

4) Oxetane (trimethylene oxide, *cyclo*-C_3H_6O):

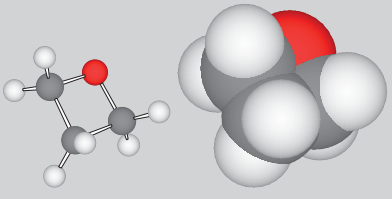

5) Tetrahydrofuran (tetramethylene oxide, *cyclo*-C_4H_8O):

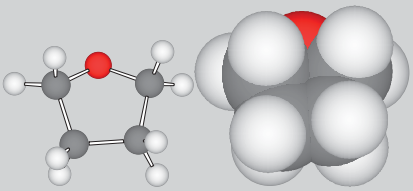

6) 2-Methyltetrahydrofuran (CH_3-*cyclo*-C_4H_7O):

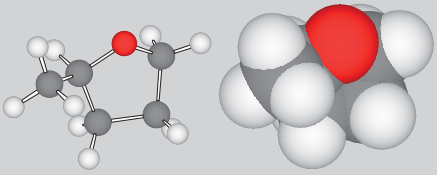

7) Tetrahydropyran (*cyclo*-$C_5H_{10}O$):

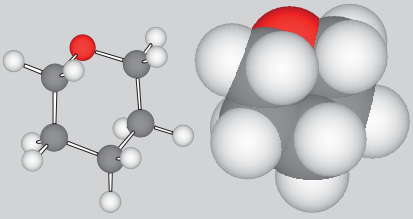

8) Oxepane (*cyclo*-$C_6H_{12}O$):

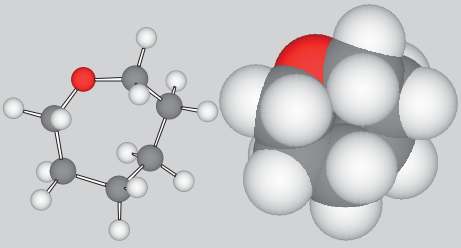

9) 1.3-Dioxolane (*cyclo*-$CH_2OCH_2CH_2O$):

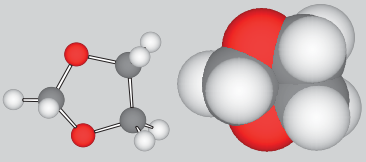

10) 1,4-Dioxane (*cyclo*-$CH_2CH_2OCH_2CH_2O$):

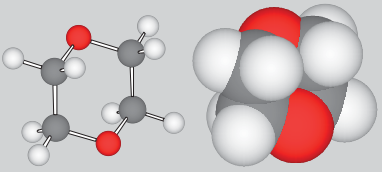

11) 1,3-Dioxane (*cyclo*-$CH_2CH_2CH_2OCH_2O$):

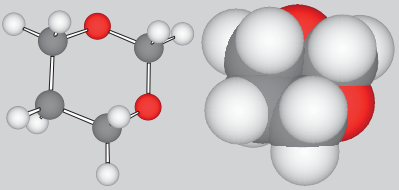

12) 3,4-Epoxy-1-butene (vinyl oxirane, $CH_2{=}CH$-*cyclo*-$CHOCH_2$):

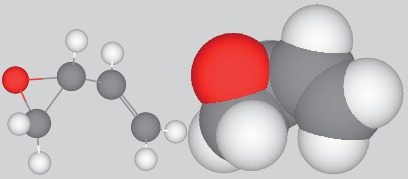

13) 4-Methyl-1,3-dioxane (CH_3-*cyclo*-$CHOCH_2OCH_2CH_2$):

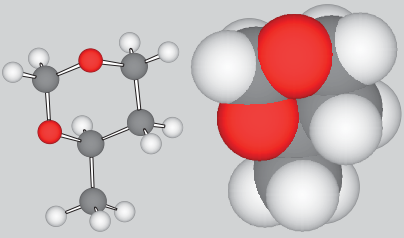

14) 1,3-Dioxepane (*cyclo*-$CH_2CH_2CH_2CH_2OCH_2O$):

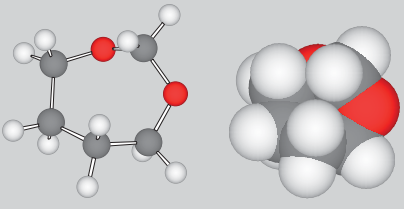

15) 1,3,5-Trioxane (*cyclo*-$CH_2OCH_2OCH_2O$):

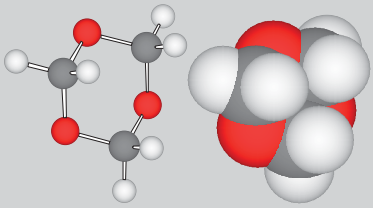

16) Glycidaldehyde (HC(O)-*cyclo*-$CHOCH_2$):

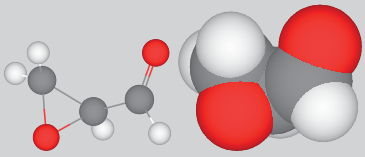

17) 3,4-Epoxy-cyclohexene (C_6H_8O):

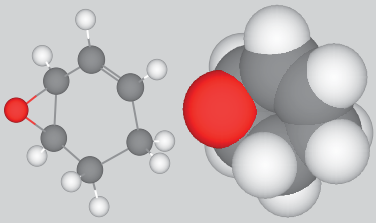

18) Benzene oxide/Oxepin (C_6H_6O):

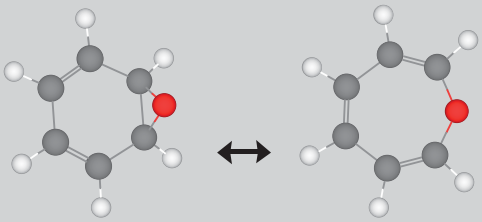

19) Toluene oxide/2-Methyloxepin (C_7H_9O):

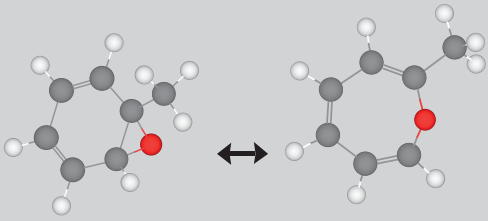

App-II-E. Aromatic Ethers

1) Methoxybenzene (anisole, $CH_3OC_6H_5$):

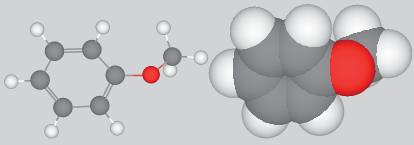

2) 1,3-Dimethoxybenzene ($(CH_3O)_2—C_6H_4$):

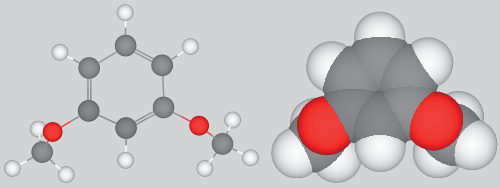

3) 1,4-Dimethoxybenzene ($(CH_3O)_2—C_6H_4$):

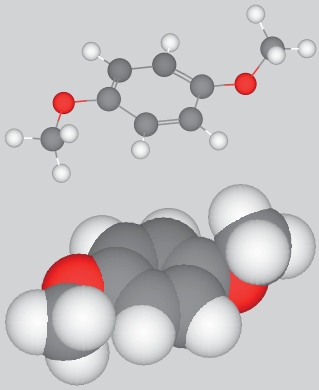

4) 1,2-Dimethoxybenzene ($(CH_3O)_2$—C_6H_4):

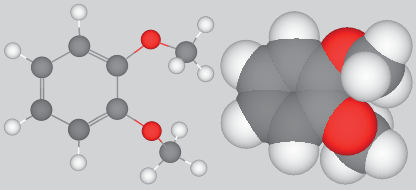

5) 1,4-Benzodioxan ($C_8H_8O_2$):

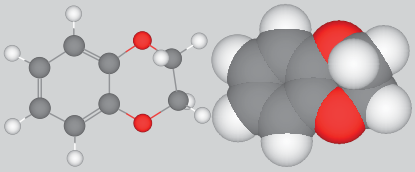

6) 2,3-Dihydro-1-benzofuran (C_8H_8O):

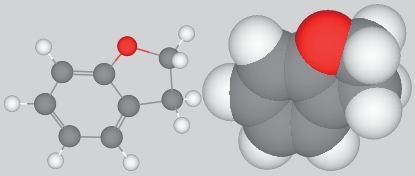

7) Dibenzofuran ($C_{12}H_8O$):

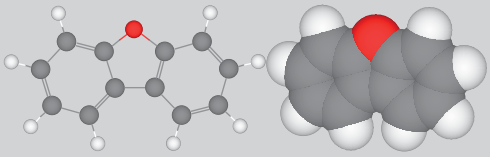

8) Dibenzo-*p*-dioxin ($C_{12}H_8O_2$):



9) Diphenyl ether ($C_6H_5OC_6H_5$):

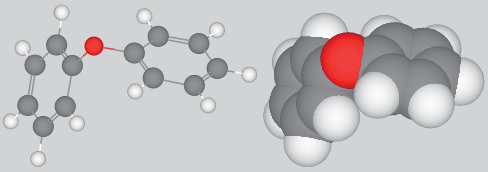

App-II-F. Halogen-Substituted Ethers

1) Difluoromethyl methyl ether (CH_3OCHF_2):

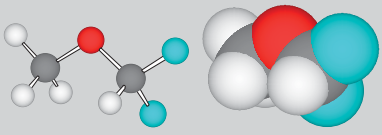

2) *bis*(Fluoromethyl) ether (CH_2FOCH_2F, HFE-152):

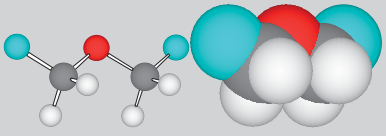

3) Methyl trifluoromethyl ether (CF_3OCH_3, HFE-143a):

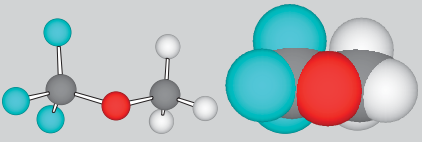

4) *bis*(Difluoromethyl) ether (CHF_2OCHF_2, HFE-134):

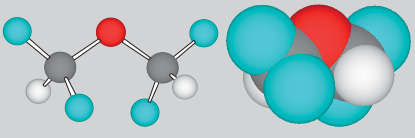

5) Difluoromethyl trifluoromethyl ether (CF_3OCHF_2, HFE-125):

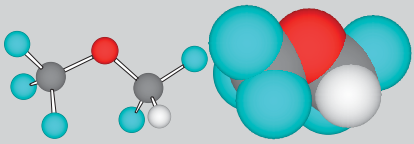

6) Methyl chloromethyl ether (CH_3OCH_2Cl):

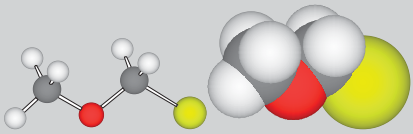

7) Methyl dichloromethyl ether (CH_3OCHCl_2):

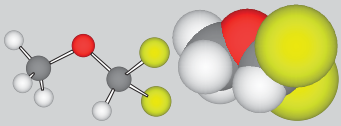

8) Methyl bromomethyl ether, (CH_3OCH_2Br):

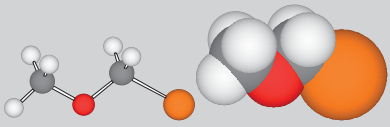

9) Methyl iodomethyl ether (CH_3OCH_2I):

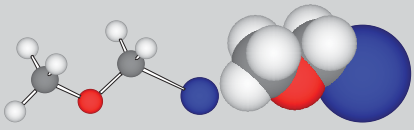

10) Ethyl trifluoromethyl ether ($CH_3CH_2OCF_3$):

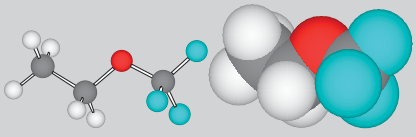

11) 2,2,2-Trifluoroethyl methyl ether ($CF_3CH_2OCH_3$):

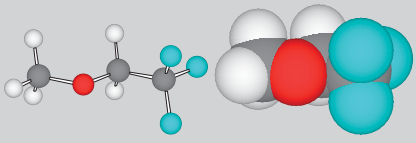

12) 1,1,2,2-Tetrafluoroethyl methyl ether ($CH_3OCF_2CHF_2$):

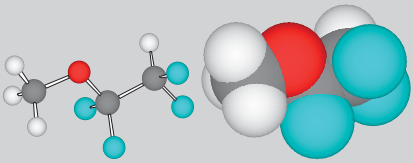

13) 1,2,2,2-Tetrafluoroethyl methyl ether ($CF_3CHFOCH_3$):

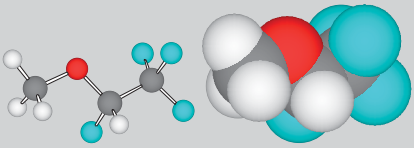

14) Difluoromethyl 2,2,2-trifluoroethyl ether ($CF_3CH_2OCHF_2$):

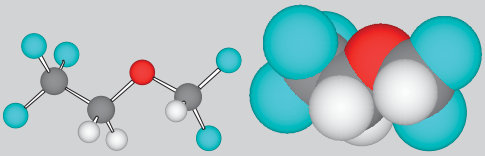

15) Difluoromethyl 1,1,2-trifluoroethyl ether ($CH_2FCF_2OCHF_2$):

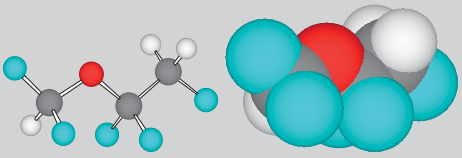

16) 1,1,2,2,2-Pentafluoroethyl methyl ether ($CF_3CF_2OCH_3$):

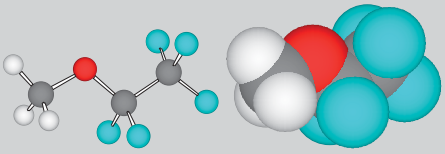

17) 1,2,2-Trifluoroethyl trifluoromethyl ether $CHF_2CHFOCF_3$):

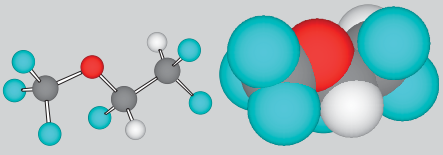

18) 1,2,2,2-Tetrafluoroethyl difluoromethyl ether ($CF_3CHFOCHF_2$, Desflurane):

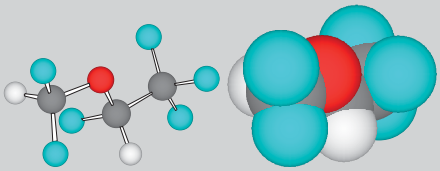

19) 1,1,2,2-Tetrafluoroethyl difluoromethyl ether ($CHF_2OCF_2CHF_2$):

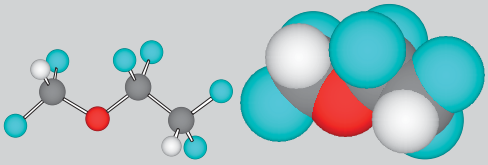

20) 1,2,2,2-Tetrafluoroethyl trifluoromethyl ether ($CF_3OCHFCF_3$):

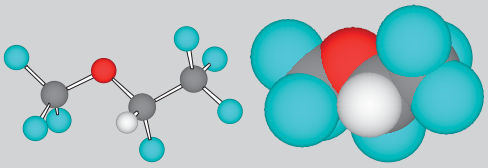

21) 1,1,2,2-Tetrafluoroethyl trifluoromethyl ether ($CF_3OCF_2CHF_2$):

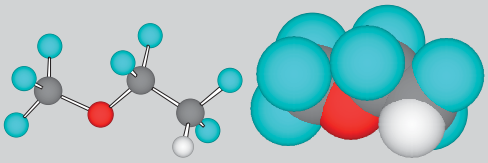

22) Methyl 2-chloroethyl ether ($CH_3OCH_2CH_2Cl$):

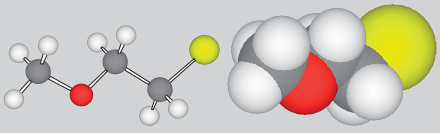

23) Methyl 2,2-dichloroethyl ether ($CH_3OCH_2CHCl_2$):

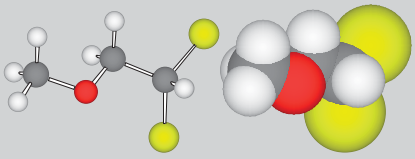

24) Methyl 2-bromoethyl ether ($CH_3OCH_2CH_2Br$):

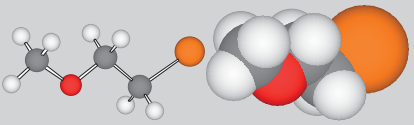

25) Methyl 2-chloro-1,1,2,2-tetrafluoroethyl ether (CH_3OCF_2CHFCl):

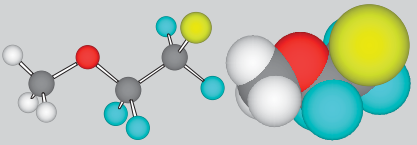

26) 2-Chloro-1,1,2-trifluoroethyl difluoromethyl ether (enflurane, $CHF_2OCF_2CF_2Cl$):

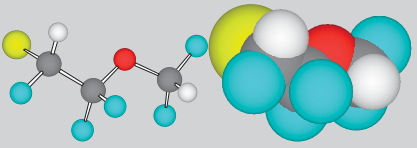

27) 1-Chloro-2,2,2-trifluoroethyl difluoromethyl ether (isoflurane, $CHF_2OCHClCF_3$):

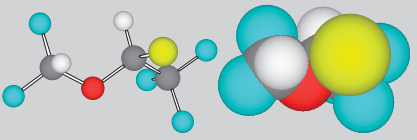

28) Chlorodifluoromethyl 2,2,2-trifluoroethyl ether ($CF_3CH_2OCClF_2$):

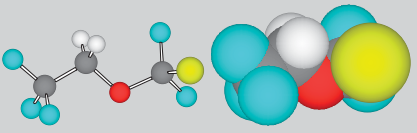

29) 2,2,3,3,4-Pentafluorooxetane (*cyclo*-$CFHCF_2CF_2O$):

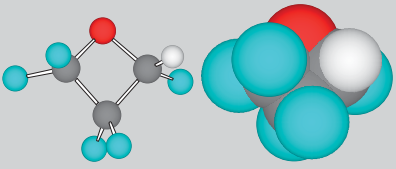

30) Perfluorooxetane (*cyclo*-$CF_2CF_2CF_2O$):

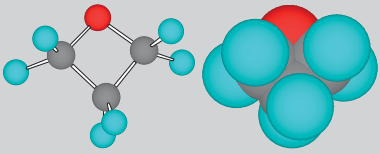

31) Trifluoromethyl perfluorovinyl ether ($CF_3OCF{=}CF_2$):

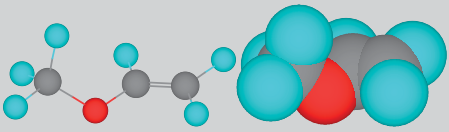

32) Ethyl 1,1,2,2-tetrafluoroethyl ether ($CH_3CH_2OCF_2CF_2H$):

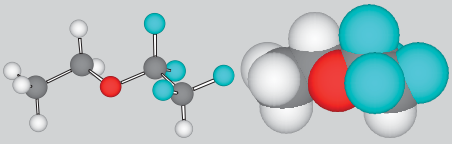

33) Methyl 2,2,3,3-tetrafluoroethyl ether ($CH_3OCH_2CF_2CHF_2$):

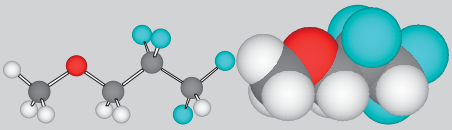

34) Methyl 1,1,2,2,2-pentafluoroethyl ether ($CH_3OCH_2CF_2CF_3$):

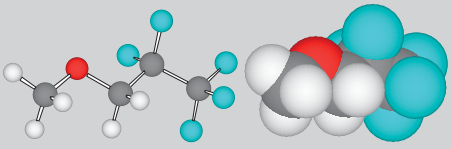

35) Methyl 1,1,2,3,3,3-hexafluoropropyl ether ($CH_3OCF_2CHFCF_3$):

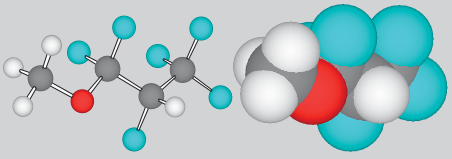

36) *bis*(2,2,2-Trifluoroethyl) ether ($CF_3CH_2OCH_2CF_3$):

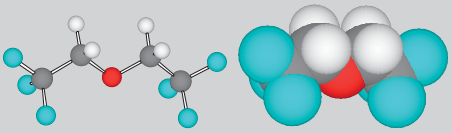

37) Difluoromethyl 2,2,3,3-tetrafluoro-*n*-propyl ether ($CHF_2OCH_2CF_2CHF_2$):

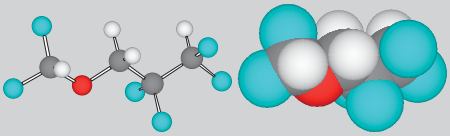

38) 1,1,1,3,3,3-Hexafluoroisopropyl fluoromethyl ether [$(CH_2FOCH(CF_3)_2$]:

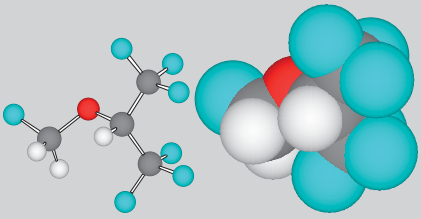

39) Methyl perfluoro-*n*-propyl ether ($CF_3CF_2CF_2OCH_3$):

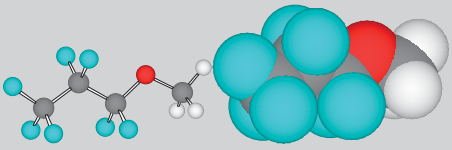

40) 1,1,2,2-Tetrafluoroethyl 2,2,2-trifluoroethyl ether ($CF_3CH_2OCF_2CF_2H$):

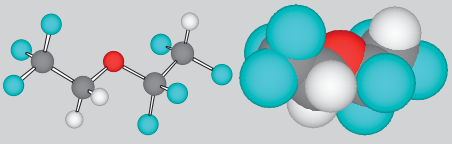

41) Methyl perfluoro-*iso*-propyl ether [$CH_3OCF(CF_3)_2$]:

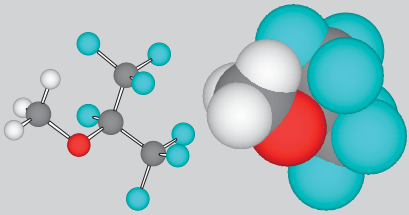

42) Difluoromethyl 2,2,3,3,3-pentafluoro-*n*-propyl ether ($CHF_2OCH_2CF_2CF_3$):

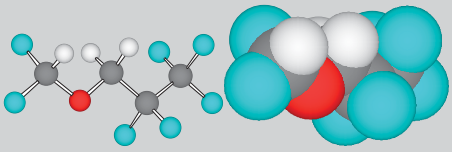

43) 1,1,2,2-Tetrafluoroethyl 1,2,2,2-tetrafluoroethyl ether ($CHF_2CF_2OCHFCF_3$):

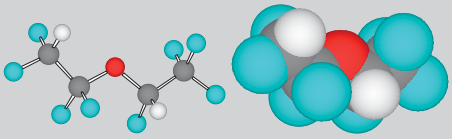

44) 1-Chloro-2,2,2-trifluoroethyl ethyl ether ($CH_3CH_2OCHClCF_3$):

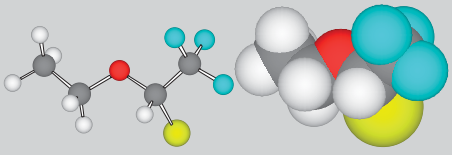

45) Difluoromethyl 1,1,2,3,3,3-hexafluoropropyl ether ($CF_3CFHCF_2OCF_2H$):

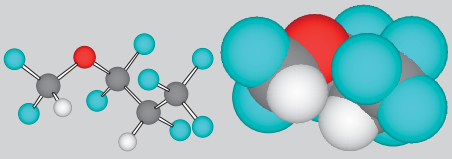

46) 1,1,1,3,3,3-hexafluoro-*iso*-propyl difluoromethyl ether [$(CF_3)_2CHOCHF_2$]:

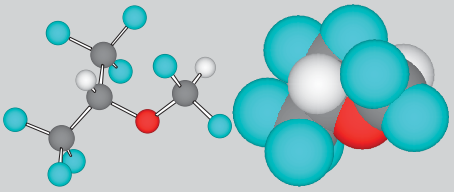

47) 1,1,1,3,3,3-Hexafluoro-iso-propyl trifluoromethyl ether [$CF_3OCH(CF_3)_2$]:

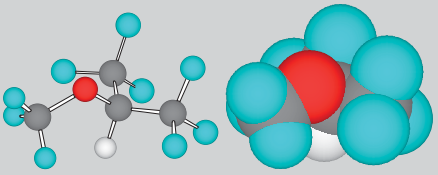

48) 1,1,2,3,3,3-Hexafluoro-*n*-propyl trifluoromethyl ether ($CF_3CHFCF_2OCF_3$):

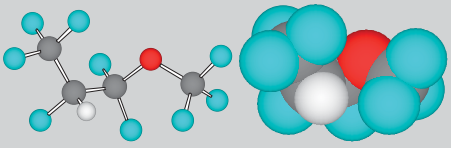

49) 1,1,1,3,3,3-Hexafluoro-iso-propyl trifluoromethyl ether [$CF_3OCH(CF_3)_2$]:

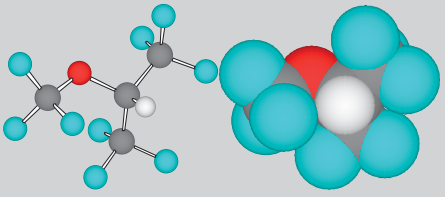

50) Ethyl 1,1,2,3,3,3-hexafluoro-*n*-propyl ether ($CF_3CFHCF_2OCH_2CH_3$):

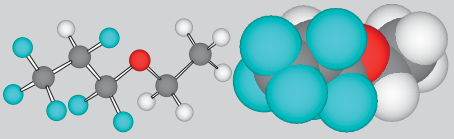

51) Perfluoro-*n*-butyl methyl ether (HFE-7100, $CF_3CF_2CF_2CF_2OCH_3$):

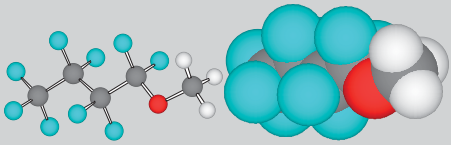

52) Perfluoro-*iso*-butyl methyl ether [$(CF_3)_2CFCF_2OCH_3$]:

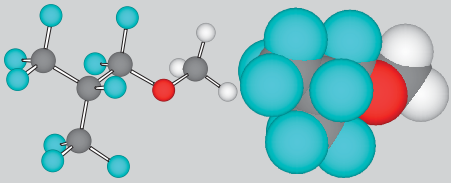

53) 1,1,2,3,3,3-Hexafluoro-*n*-propyl 2,2,2-trifluoroethyl ether ($CF_3CFHCF_2OCH_2CF_3$):

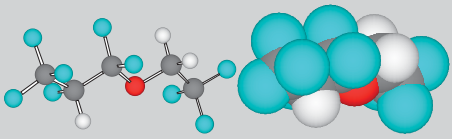

54) Perfluoro-*n*-propyl 1,2,2,2-tetrafluoroethyl ether ($CF_3CF_2CF_2OCHFCF_3$):

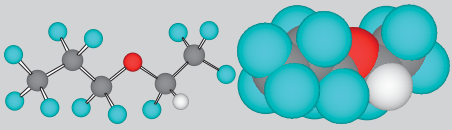

55) Ethyl perfluoro-*n*-butyl ether ($CH_3CH_2OCF_2CF_2CF_2CF_3$):

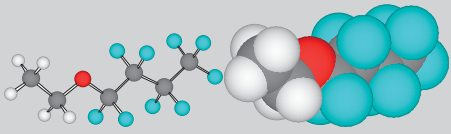

56) Ethyl perfluoro-iso-butyl ether [$CH_3CH_2OCF_2CF(CF_3)_2$]:

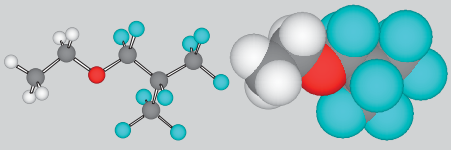

57) Perfluoro-*n*-pentyl methyl ether ($CH_3OCF_2CF_2CF_2CF_2CF_3$):

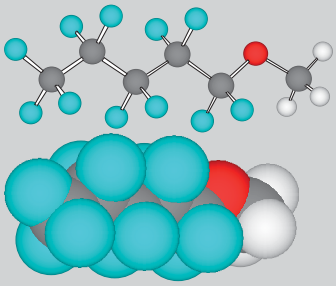

58) 1,1,2,3,3,3-Hexafluoro-*n*-propyl 2,2,3,3,3-pentafluoro-*n*-propyl ether ($CF_3CHFCF_2OCH_2CF_2CF_3$):

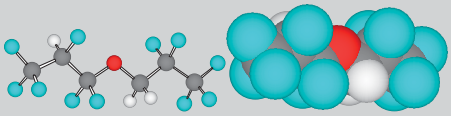

59) 1,1,2,3,3,3-Hexafluoro-*n*-propyl 2,2,3,3-tetrafluoro-*n*-propyl ether ($CF_3CHFCF_2OCH_2CF_2CHF_2$):

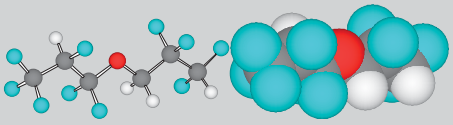

60) 1,1,1,2,3,4,4,5,5,6,6,6-Dodecafluoro-2-(trifluoromethyl)hexan-3-yl ethyl ether [HFE-7500, $CF_3CF_2CF_2CF(OCH_2CH_3)CF(CF_3)_2$]:

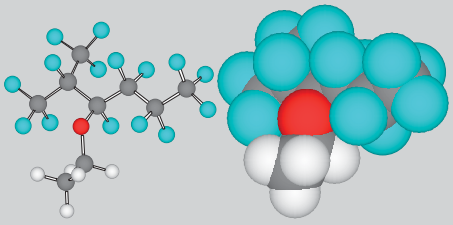

App-II-G. Multiply-Oxygenated/Multi-Functional, Halogen-Substituted Ethers

1) *bis*(Difluoromethoxy)(difluoro)methane ($CHF_2OCF_2OCHF_2$):

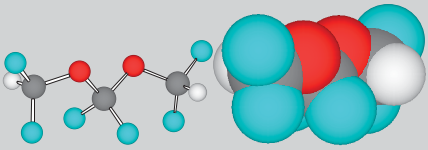

2) 1,1,2,2-Tetrafluoro-1,2-dimethoxyethane ($CH_3OCF_2CF_2OCH_3$):

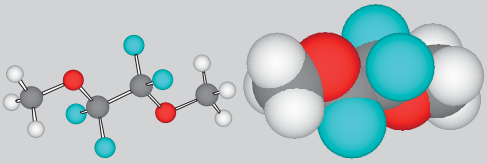

3) 1,2-*bis*(Difluoromethoxy) 1,1,1,2,2,3,3-Hexafluoropropane ($CHF_2OCF_2CF_2CF_2OCHF_2$):



4) 1,1,2,2-Tetrafluoro-1-methoxy-2-(1,1,2,2-tetrafluoro-2-methoxyethoxy)ethane ($CH_3OCF_2CF_2OCF_2CF_2OCH_3$):

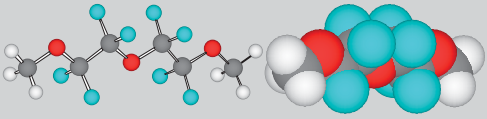

5) 1-[Difluoro(trifluoromethoxy)methoxy]-1,1,2,3,3,3-hexafluoro-2-(trifluoromethoxy)propane ($CF_3OCF(CF_3)CF_2OCF_2OCF_3$):

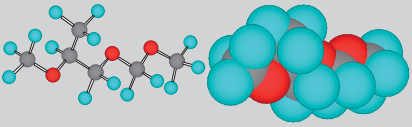

6) 3,3,4,4,6,6,7,7,9,9,10,10-Dodecafluoro-2,5,8,11-tetraoxododecane ($CH_3OCF_2CF_2OCF_2CF_2OCF_2CF_2OCH_3$):

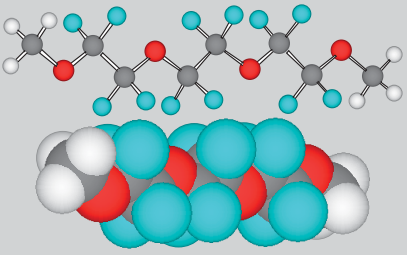

7) 1,3-*bis*(1,1,2,3,3,3-Hexafluoropropoxy)propane ($CF_3CFHCF_2OCH_2CH_2CH_2OCF_2CFHCF_3$):

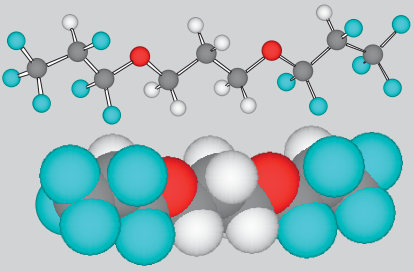

App-II-H. Polychloro-Dibenzodioxins

1) 1-Chloro-dibenzo-*p*-dioxin ($C_{12}H_7O_2Cl$):

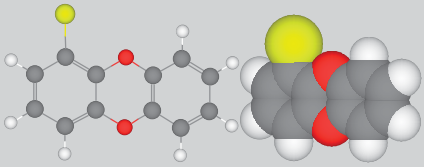

2) 2-Chloro-dibenzo-*p*-dioxin($C_{12}H_7O_2Cl$):

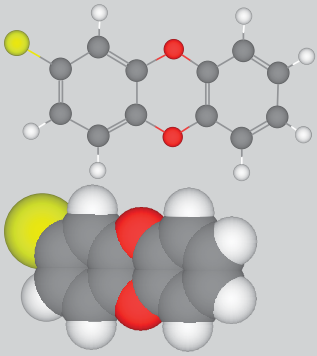

3) 2,3-Dichloro-dibenzo-*p*-dioxin ($C_{12}H_6O_2Cl_2$):

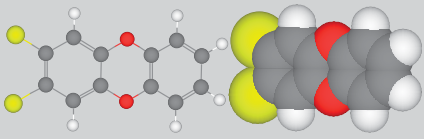

4) 2,8-Dichloro-dibenzo-*p*-dioxin ($C_{12}H_6O_2Cl_2$):

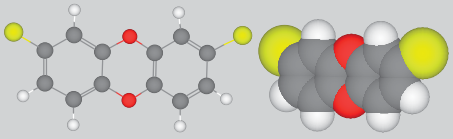

5) 2,9-Dichloro-dibenzo-*p*-dioxin ($C_{12}H_6O_2Cl_2$):

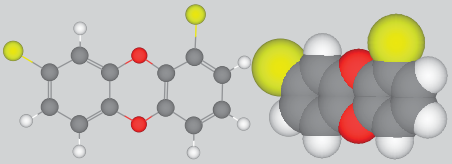

6) 1,2,3,4-Tetrachloro-dibenzo-*p*-dioxin ($C_{12}H_4O_2Cl_4$):

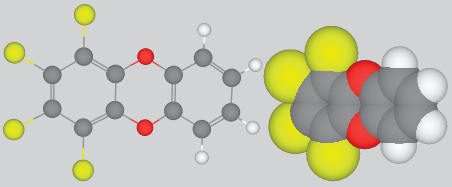

7) Octachloro-dibenzo-*p*-dioxin ($C_{12}O_2Cl_8$):

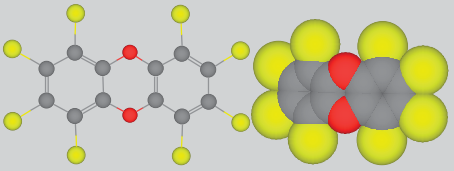

App-II-I. Polybrominated Diphenyl Ethers

1) 2-Bromodiphenyl ether ($C_{12}H_9OBr$):

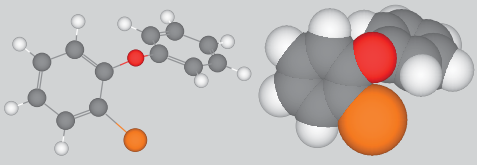

2) 3-Bromodiphenyl ether ($C_{12}H_9OBr$):

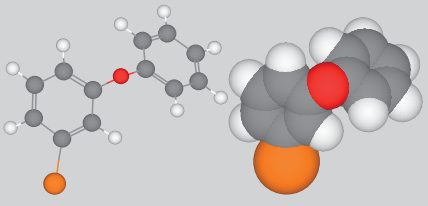

3) 4-Bromodiphenyl ether ($C_{12}H_9OBr$):



6) 3,3′-Dibromodiphenyl ether
[1,1′-oxy*bis*(3-bromobenzene)]:



4) 2,2′-Dibromodiphenyl ether
[1,1′-oxy*bis*(2-bromobenzene)]:



7) 4,4′-Dibromodiphenyl ether
[1,1′-oxy*bis*(4-bromobenzene)]:

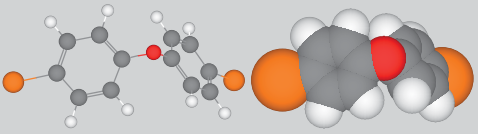

5) 2,4-Dibromodiphenyl ether
(2,4-dibromo-1-phenoxybenzene):

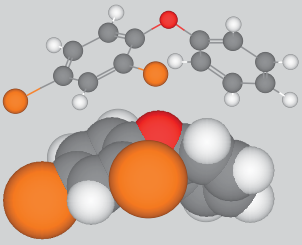

App-III. Aldehydes

App-III-A. Acyclic Aldehydes

1) Formaldehyde (methanal, CH_2O):

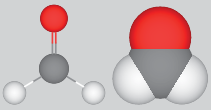

3) Propanal (propionaldehyde, CH_3CH_2CHO):

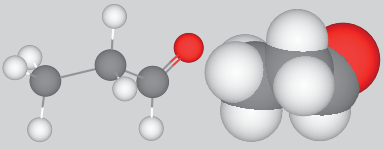

2) Acetaldehyde (ethanal, CH_3CHO):

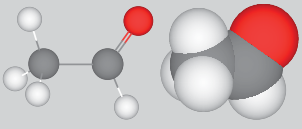

4) Butanal (*n*-butryaldehyde, $CH_3CH_2CH_2CHO$):

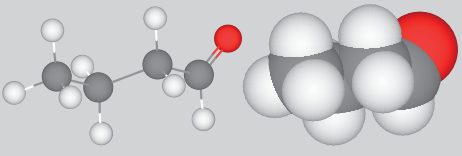

5) 2-Methyl propanal [isobutryaldehyde, $(CH_3)_2CHCHO$]:

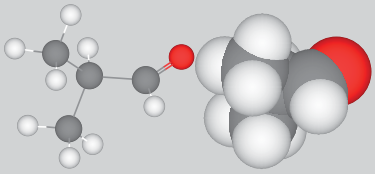

6) Pentanal (valeraldehyde, $CH_3CH_2CH_2CH_2CHO$):

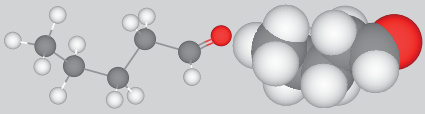

7) 2-Methylbutanal ($CH_3CH_2CH(CH_3)CHO$):

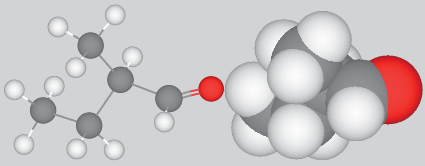

8) 3-Methylbutanal [isovaleraldehyde, $(CH_3)_2CHCH_2CHO$]:

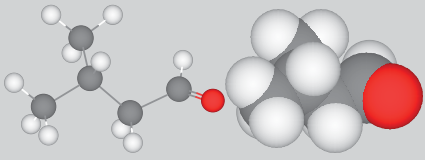

9) 2,2-Dimethylpropanal [pivaldehyde, $(CH_3)_3CCHO$]:

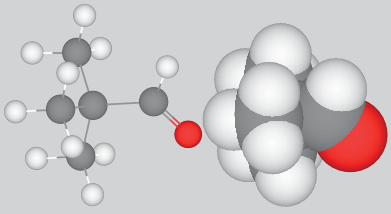

10) Hexanal ($CH_3CH_2CH_2CH_2CH_2CHO$):

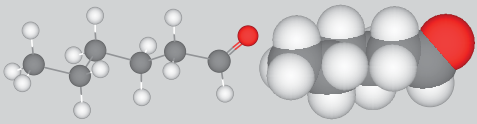

11) Heptanal ($CH_3CH_2CH_2CH_2CH_2CH_2CHO$):

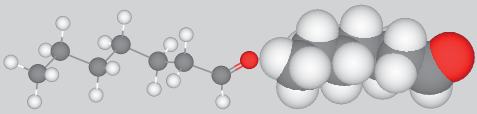

12) 2,3-Dimethylpentanal [$CH_3CH_2CH(CH_3)CH(CH_3)CHO$]:

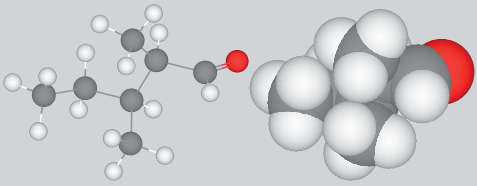

13) Nonanal ($CH_3CH_2CH_2CH_2CH_2CH_2CH_2CH_2CHO$):

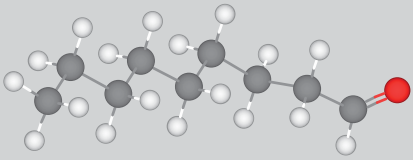

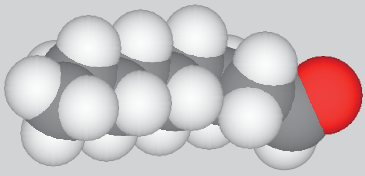

App-III-B. Cycloalkylcarbaldehydes

1) *cyclo*-Propanecarbaldehyde (*cyclo*-C_3H_7—CHO):

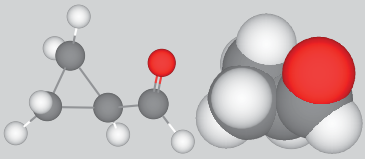

2) *cyclo*-Butanecarbaldehyde (*cyclo*-C_4H_7—CHO):

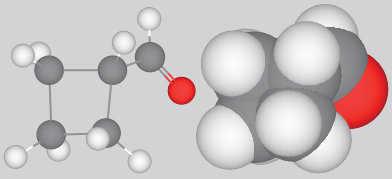

3) *cyclo*-Pentanecarbaldehyde (*cyclo*-C_5H_9—CHO):

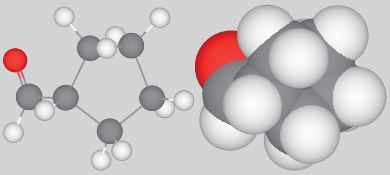

4) *cyclo*-Hexanecarbaldehyde (*cyclo*-C_6H_{11}—CHO):

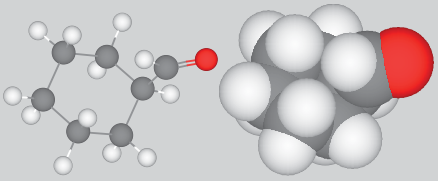

App-III-C. Aldehydes with Additional Functional Groups

1) 2-Hydroxyethanal (hydroxyacetaldehyde, $HOCH_2CHO$):

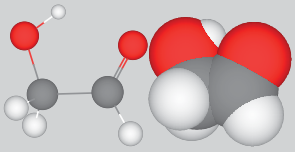

2) Glycidaldehyde (see compound II-D-16)

3) Propenal (acrolein, $CH_2{=}CHCHO$):

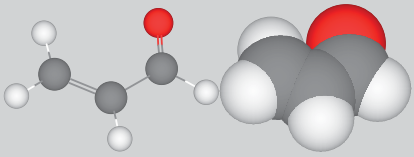

4) 2-Methylpropenal (methylacrolein, $CH_2{=}CH(CH_3)CHO$):



5) 2-Butenal (crotanaldehyde, $CH_3CH{=}CHCHO$):

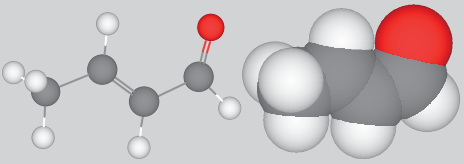

6) *trans*-2-Hexenal (*E*-2-hexenal, $CH_3CH_2CH{=}CHCH_2CHO$):

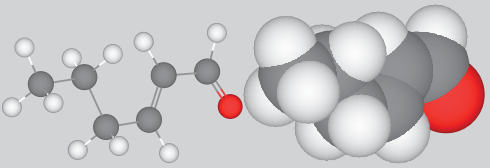

7) *cis*-2-Hexenal (*Z*-2-hexenal, $CH_3CH_2CH{=}CHCH_2CHO$):

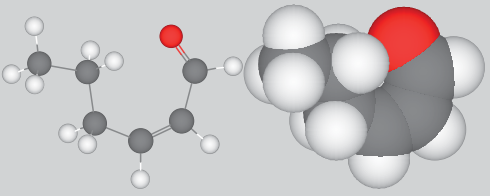

8) *E*,*E*-2,4-Hexadienal ($CH_3CH{=}CHCH{=}CHCHO$):

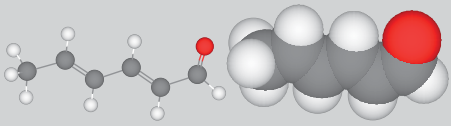

9) Butendial ($HCOCH{=}CHCHO$):

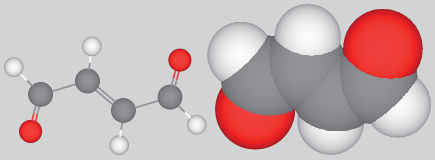

10) 4-Oxo-2-pentenal ($CH_3C(O)CH{=}CHCHO$):

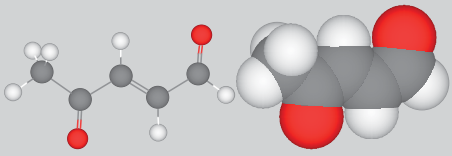

11) *E*,*E*-2,4-Hexadiendial [$HC(O)CH{=}CHCH{=}CHCHO$]:

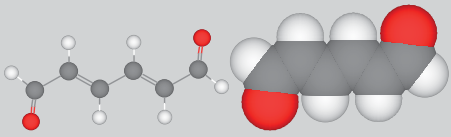

12) *E*,*Z*-2,4-Hexadiendial [$HC(O)CH{=}CHCH{=}CHCHO$]:

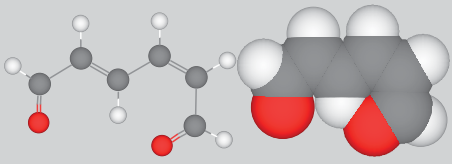

13) *E*,*E*-2-Methyl-2,4-hexadiendial [$HC(O)CH{=}CHCH{=}C(CH_3)CHO$]:

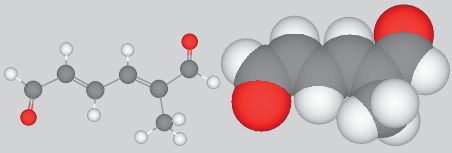

14) Ethandial [glyoxal, $HC(O)CHO$]:

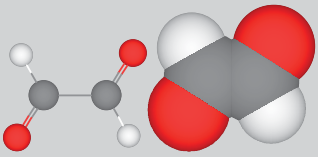

15) 2-Oxopropanal (methyl glyoxal, $CH_3C(O)CHO$):

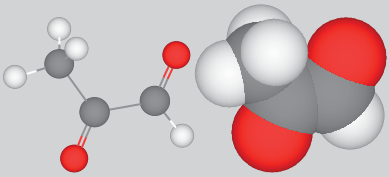

16) Pinonaldehyde [(3-acetyl-2,2-dimethylcyclobutyl)acetaldehyde $C_{10}H_{16}O_2$]:

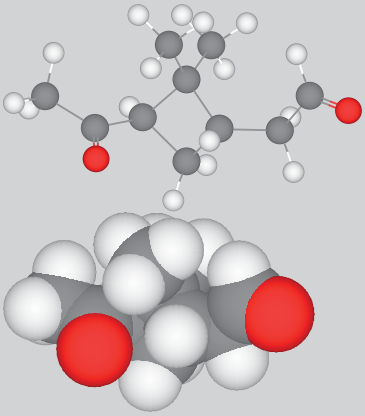

17) Caronaldehyde [2,2-dimethyl-3-(2-oxopropyl)cyclopropyl]acetaldehyde, $C_{10}H_{16}O_2$]:

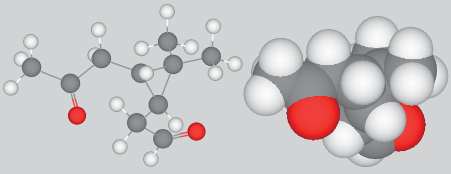

App-III-D. Aromatic Aldehydes

1) Benzaldehyde (C_6H_5CHO):

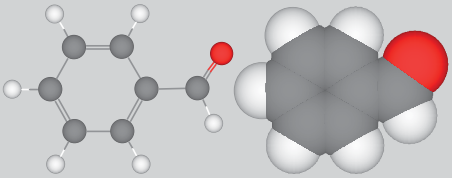

2) 2-Nitrobenzaldehyde (*o*-nitrobenzaldehyde, $O_2NC_6H_5CHO$):

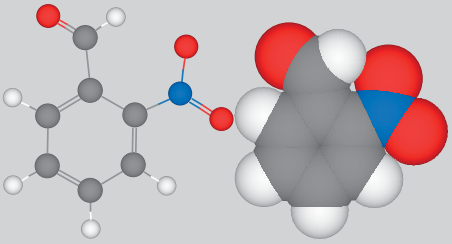

3) *o*-Tolualdehyde ($CH_3C_6H_4CHO$):

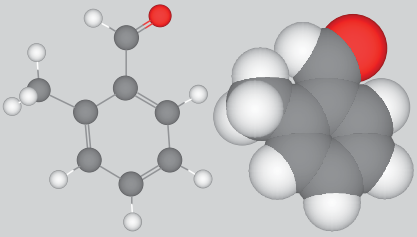

4) *m*-Tolualdehyde ($CH_3C_6H_4CHO$):

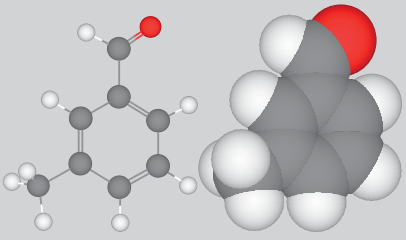

5) *p*-Tolualdehyde ($CH_3C_6H_4CHO$):

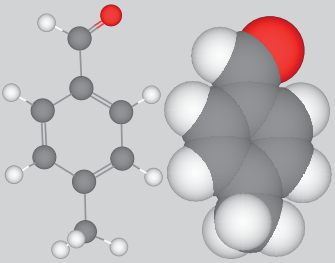

6) 2,3-Dimethylbenzaldehyde $(CH_3)_2C_6H_3CHO$):

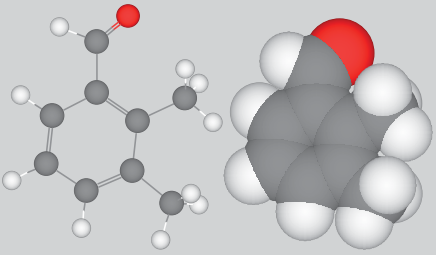

7) 2,4-Dimethylbenzaldehyde $(CH_3)_2C_6H_3CHO$):

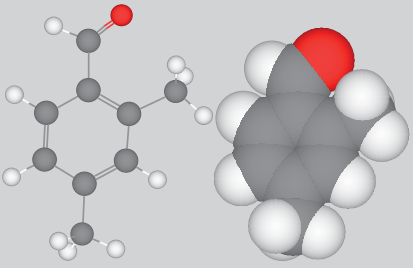

8) 2,5-Dimethylbenzaldehyde $(CH_3)_2C_6H_3CHO$):

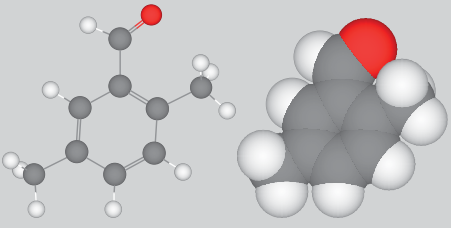

9) 2,6-Dimethylbenzaldehyde ($(CH_3)_2C_6H_3CHO$):

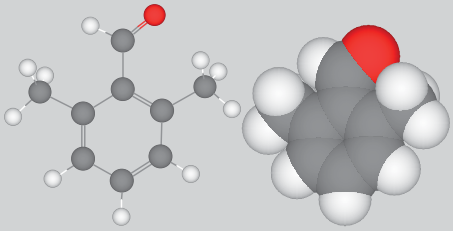

10) 3,4-Dimethylbenzaldehyde ($(CH_3)_2C_6H_3CHO$):

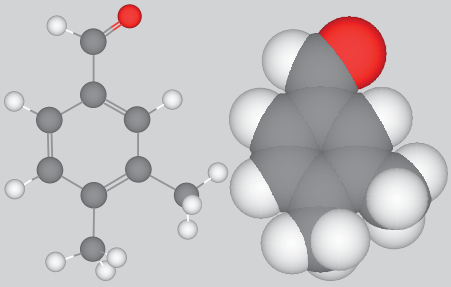

11) 3,5-Dimethylbenzaldehyde ($(CH_3)_2C_6H_3CHO$):

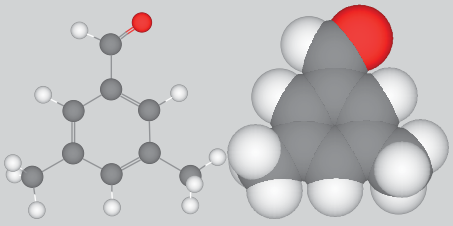

12) *trans*-Cinnamaldehyde ((2*E*)-3-phenylprop-2-enal $C_6H_5CH{=}CHCHO$):

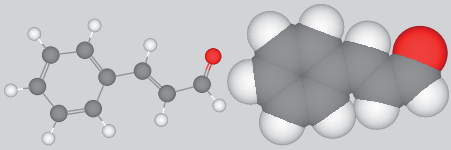

13) Phthaldialdehyde [benzene-1,2-dicarbaldehyde, $HC(O)C_6H_4C(O)H$]:

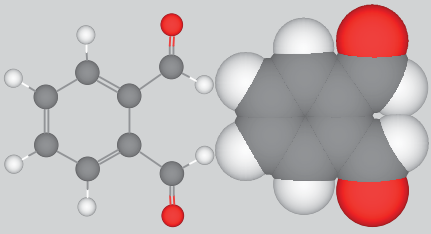

14) 2-Acetylbenzaldehyde [$CH_3C(O)C_6H_4C(O)H$]:

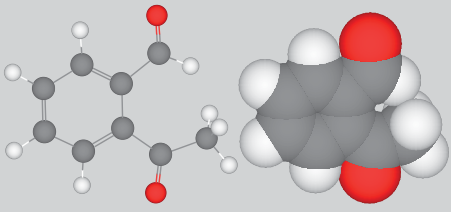

App-III-E. Halogen-Substituted Aldehydes

1) 2-Chloroethanal (chloroacetaldehyde, CH_2ClCHO):



2) 2,2-Dichloroethanal (dichloroacetaldehyde, $CHCl_2CHO$):

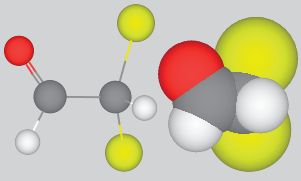

3) 2,2,2-Trichloroethanal (trichloroacetaldehyde, chloral, CCl_3CHO):

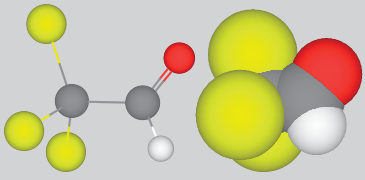

4) 2,2-Difluoroethanal (difluoroacetaldehyde, CHF_2CHO):

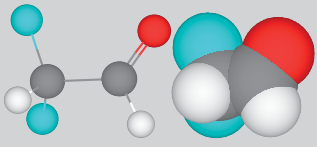

5) 2,2,2-Trifluoroethanal (trifluoroacetaldehyde, CF_3CHO):

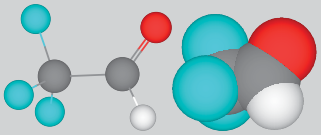

6) 2-Chloro-2-fluoroethanal ($CHClFCHO$):

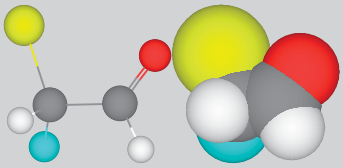

7) 2,2-Dichloro-2-fluoroethanal (CCl_2FCHO):

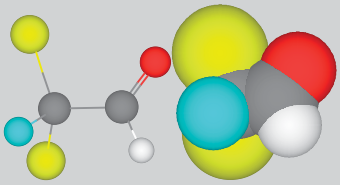

8) 2,2-Difluoro-2-chloroethanal (CCl_2FCHO):



9) 3,3,3-Trifluoropropanal (CF_3CH_2CHO):



10) 2,2,3,3,3-Pentafluoropropanal (CF_3CF_2CHO):

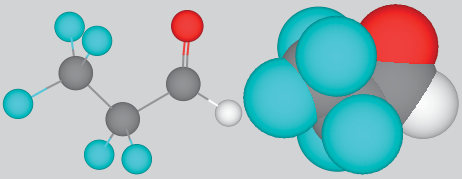

11) 2,2,3,3,4,4,4-Heptafluorobutanal ($CF_3CF_2CF_2CHO$):

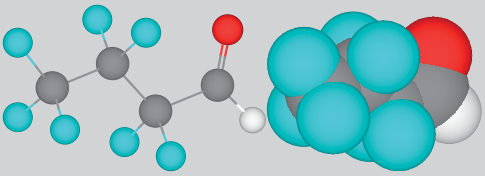

12) 2,2,3,3,4,4,5,5,5-Nonafluoropentanal ($CF_3CF_2CF_2CF_2CHO$):

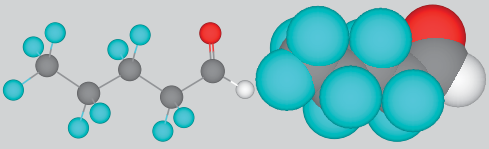

13) 3,3,4,4,5,5,6,6,7,7,8,8,8-tridecafluorooctanal ($CF_3CF_2CF_2CF_2CF_2CF_2CH_2CHO$):

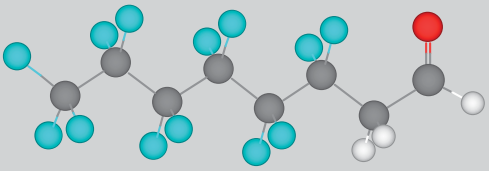

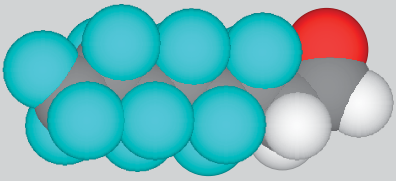

14) 3,3,4,4,5,5,6,6,7,7,8,8,9,9,10,10,10-Heptadecafluorodecanal ($CF_3CF_2CF_2CF_2CF_2CF_2CF_2CF_2CH_2CHO$):

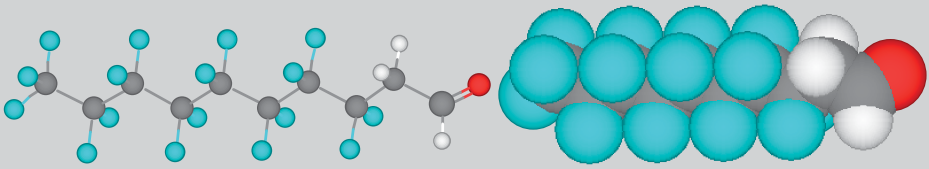

App-IV. Acyl Halides and Carbonyl Halides

App-IV-A. Formyl Halides

1) Formyl fluoride [HC(O)F]:

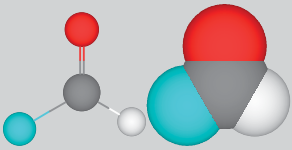

2) Formyl chloride [HC(O)Cl]:

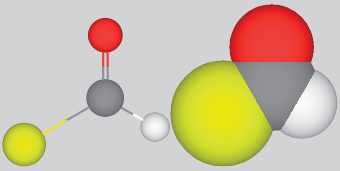

3) Formyl bromide [HC(O)Br]:

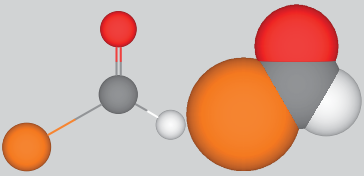

App-IV-B. Acetyl Halides

1) Acetyl fluoride [$CH_3C(O)F$]:

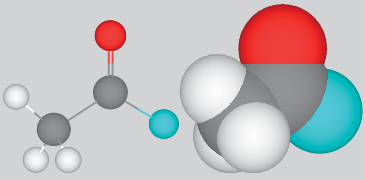

2) Acetyl chloride [$CH_3C(O)Cl$]:

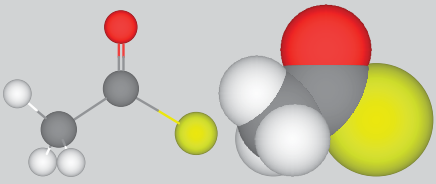

3) 2-Chloroacetyl chloride [$ClCH_2C(O)Cl$]:

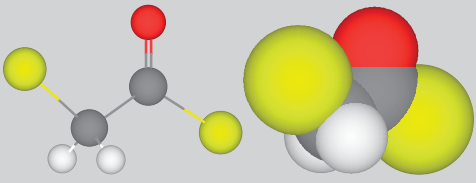

4) 2,2-Dichloroacetyl chloride [$Cl_2CHC(O)Cl$]:

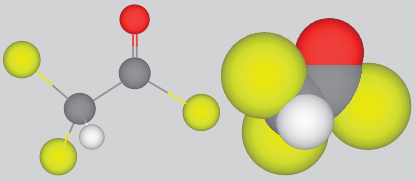

5) 2,2,2-Trichloroacetyl chloride [$Cl_3CC(O)Cl$]:

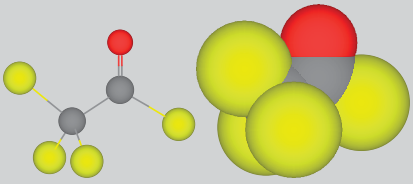

6) Trifluoroacetyl chloride ($CF_3C(O)Cl$):

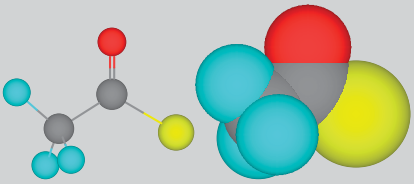

7) 2-Bromoacetyl chloride [$BrCH_2C(O)Cl$]:

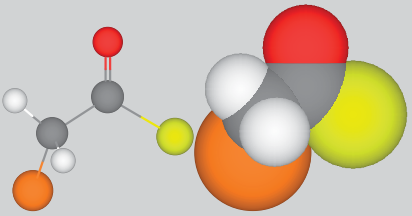

App-IV-C. Carbonyl Halides

1) Carbonyl dichloride [phosgene, $ClC(O)Cl$]:

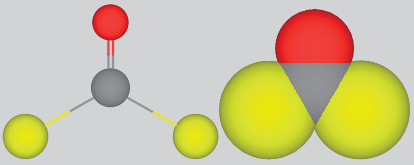

2) Carbonyl difluoride [$FC(O)F$]:

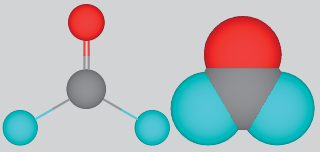

3) Carbonyl dibromide [$BrC(O)Br$]:

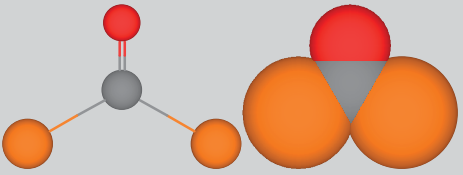

App-V. Ketones

App-V-A. Acylic Ketones

1) Acetone [2-propanone, $CH_3C(O)CH_3$]:

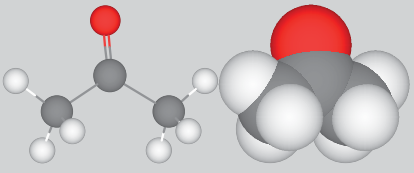

3) 3-Pentanone [diethyl ketone, $CH_3CH_2C(O)CH_2CH_3$]:

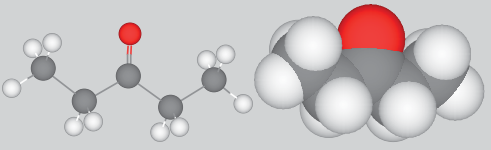

2) 2-Butanone [methyl ethyl ketone, $CH_3C(O)CH_2CH_3$]:

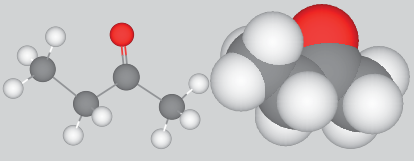

4) 2-Pentanone [methyl *n*-propyl ketone, $CH_3C(O)CH_2CH_2CH_3$]:

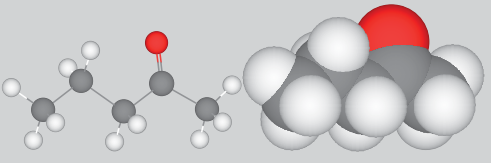

5) 3-Methyl-2-butanone [methyl isopropyl ketone, $CH_3C(O)CH(CH_3)_2$]:

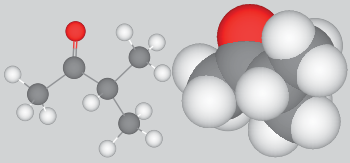

6) 2-Hexanone [methyl *n*-butyl ketone, $CH_3C(O)CH_2CH_2CH_2CH_3$]:

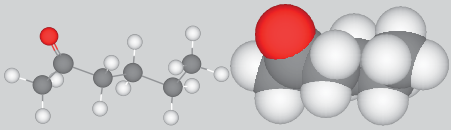

7) 3-Hexanone [ethyl *n*-propyl ketone, $CH_3CH_2C(O)CH_2CH_2CH_3$]:

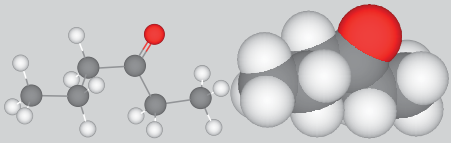

8) 4-Methyl-2-pentanone [methyl isobutyl ketone, $CH_3C(O)CH_2CH(CH_3)_2$]:

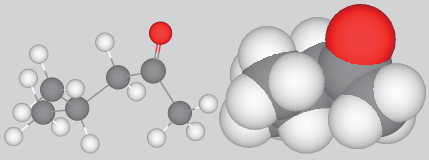

9) 4-Methyl-2-hexanone [$CH_3C(O)CH_2CH(CH_3)CH_2CH_3$]:

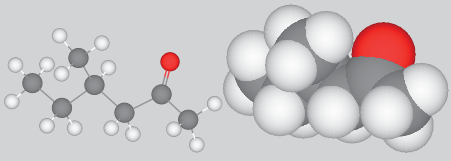

10) 4-Heptanone [di-*n*-propyl ketone, $CH_3CH_2CH_2C(O)CH_2CH_2CH_3$]:

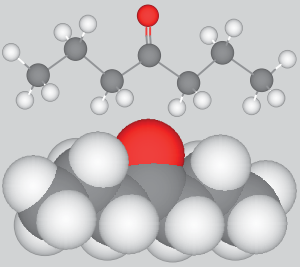

11) 2,4-Dimethyl-3-pentanone [di-isopropyl ketone, $(CH_3)_2CHC(O)CH(CH_3)_2$]:

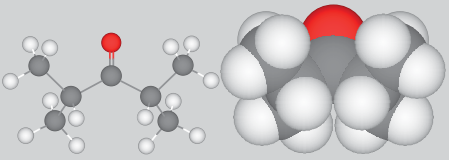

12) 2-Methyl-3-hexanone [*n*-propyl isopropyl ketone [$CH_3CH_2CH_2C(O)CH(CH_3)_2$]:

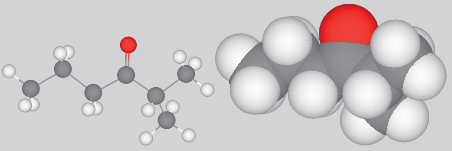

13) 4,4-Dimethyl-2-pentanone [methyl neopentyl ketone, $CH_3C(O)CH_2C(CH_3)_3$]:

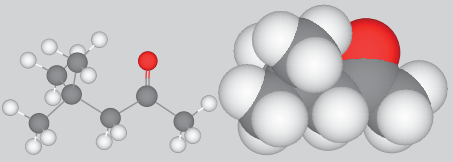

14) 4-Octanone [*n*-propyl *n*-butyl ketone, $CH_3CH_2CH_2C(O)CH_2CH_2CH_2CH_3$]:

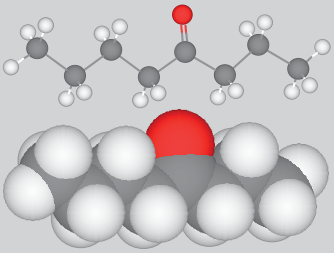

15) 3-Methyl-4-heptanone [*n*-propyl *sec*-butyl ketone, $CH_3CH_2CH_2C(O)CH(CH_3)CH_2CH_3$]:

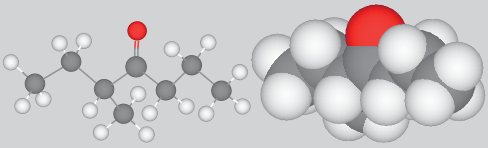

16) 2,2-Dimethyl-3-hexanone [*n*-propyl *tert*-butyl ketone, $CH_3CH_2CH_2C(O)C(CH_3)_3$]:

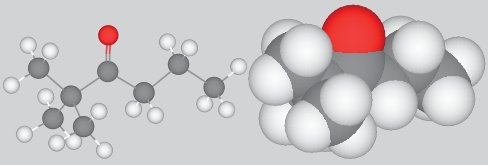

17) 2,6-Dimethyl-4-heptanone [di-isobutyl ketone, $(CH_3)_2CHCH_2C(O)CH_2CH(CH_3)_2$]:

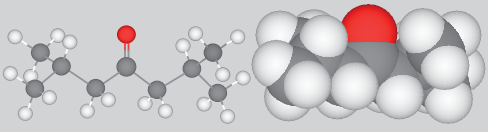

18) 2-Methyl-4-heptanone [*n*-propyl isobutyl ketone, $CH_3CH_2CH_2C(O)CH_2CH(CH_3)_2$]:

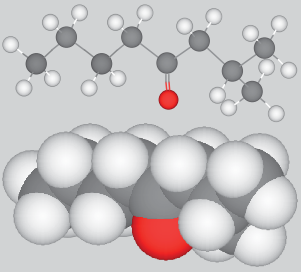

19) 3,5-Dimethyl-4-heptanone [di-*sec*-butyl ketone, $CH_3CH_2CH(CH_3)C(O)CH(CH_3)CH_2CH_3$]:

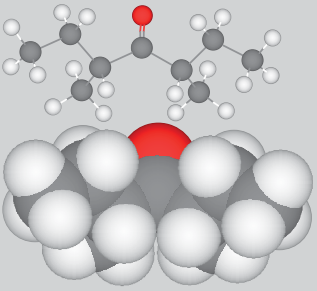

20) 2,2,4,4-Tetramethyl-3-pentanone [di-*tert*-butyl ketone, $(CH_3)_3CC(O)C(CH_3)_3$]:

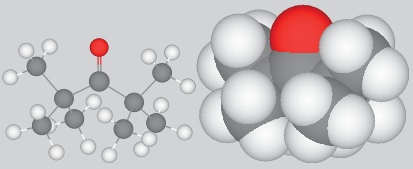

App-V-B. Cyclic Ketones and Ketenes

1) Cyclopropanone [*cyclo*-$CH_2CH_2C(O)$—]:

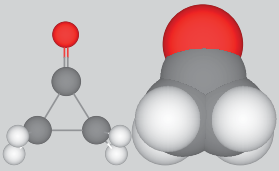

2) Cyclobutanone [*cyclo*-$CH_2CH_2CH_2C(O)$—]:

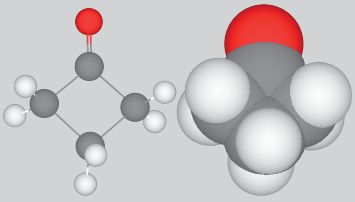

3) Cyclopentanone
[*cyclo*-$CH_2CH_2CH_2CH_2C(O)$—]:

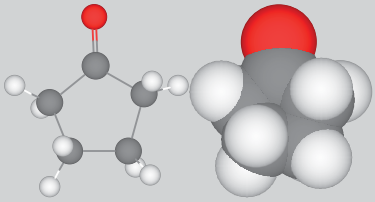

4) Cyclohexanone
[*cyclo*-$CH_2CH_2CH_2CH_2CH_2C(O)$—]:

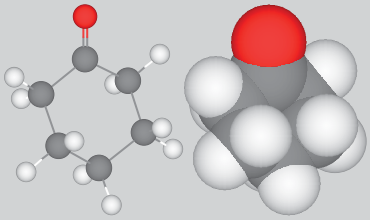

5) *trans*-2,3-Dimethylcyclobutanone, $C_6H_{10}O$]:

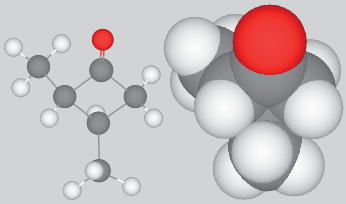

6) *cis*-2,3-Dimethylcyclobutanone ($C_6H_{10}O$):

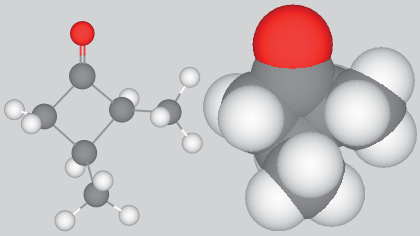

7) *trans*-2,4-Dimethylcyclobutanone ($C_6H_{10}O$):

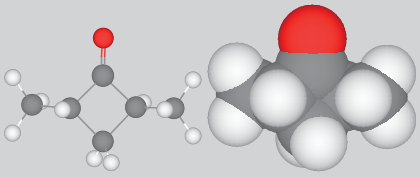

8) *cis*-2,4-Dimethylcyclobutanone ($C_6H_{10}O$):

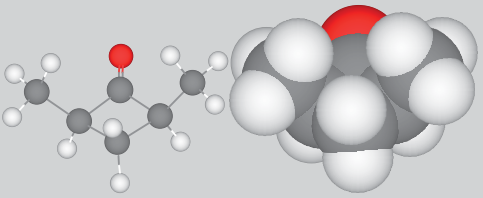

9) 2-*n*-Propylcyclobutanone ($C_7H_{12}O$):

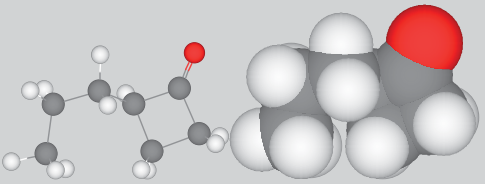

10) Cyclohex-2-en-1-one (*cyclo*-C_6H_8O):

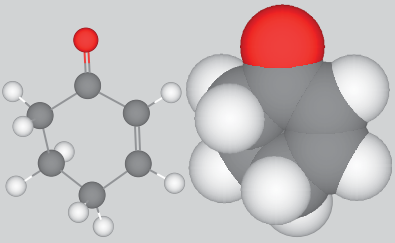

11) 3-Methylcyclohex-2-en-1-one (CH_3-*cyclo*-C_6H_7O):

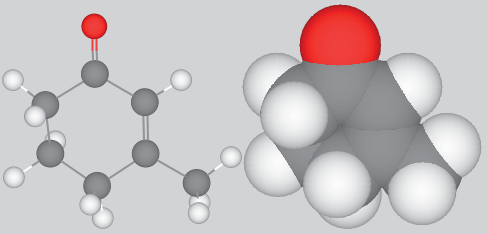

12) 3,5,5-Trimethylcyclohex-2-en-1-one ($C_9H_{12}O$):

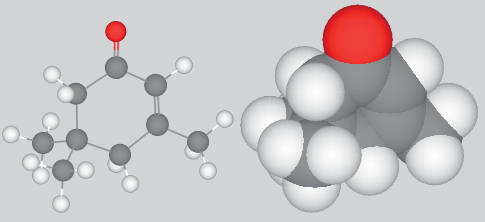

13) Ketene ($CH_2{=}C{=}O$):

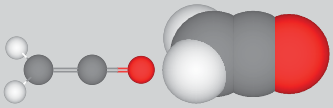

15) Ethylketene ($CH_3CH_2CH{=}C{=}O$):

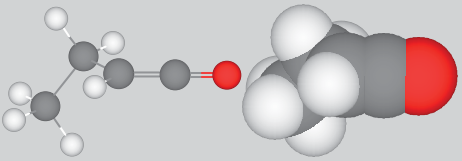

14) Methylketene ($CH_3CH{=}C{=}O$):

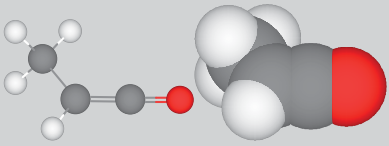

16) Dimethylketene [$(CH_3)_2C{=}C{=}O$]:

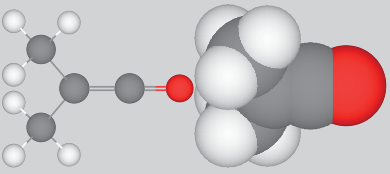

App-V-C. Hydroxy Ketones

1) 1-Hydroxy-2-propanone [hydroxyacetone, $HOCH_2C(O)CH_3$]:

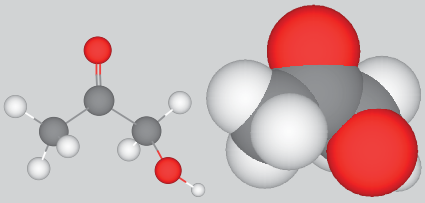

2) 4-Hydroxy-2-butanone ($CH_3C(O)CH_2CH(OH)CH_3$):

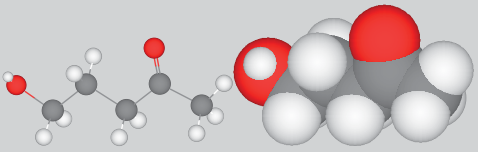

App-V-D. Halogen-Substituted Ketones

1) 1-Chloro-2-propanone [chloroacetone, $ClCH_2C(O)CH_3$]:

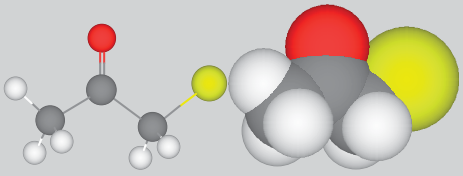

3) 1,1,1-Trifluoro-2-propanone [trifluoroacetone, $CF_3C(O)CH_3$]:

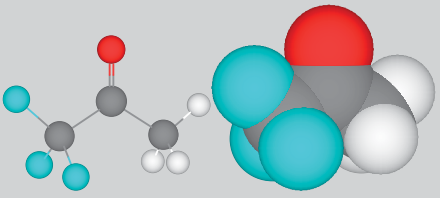

2) 1-Bromo-2-propanone [bromoacetone, $BrCH_2C(O)CH_3$]:



4) 1,1,1,3,3,3-hexafluoro-2-propanone [perfluoroacetone, $CF_3C(O)CF_3$]:

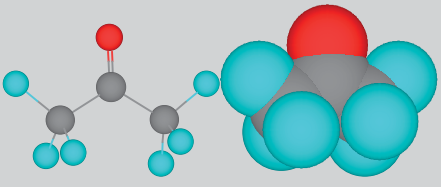

5) 1,1,1,2,2,4,5,5,5-Nonafluoro-4-(trifluoromethyl)pentan-3-one [perfluoro-2-methyl-3-pentanone, $CF_3CF_2C(O)CF(CF_3)_2$]:

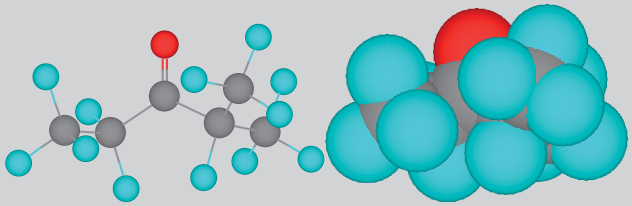

App-V-E. Unsaturated Ketones

1) Methyl vinyl ketone [$CH_3C(O)CH{=}CH_2$]:

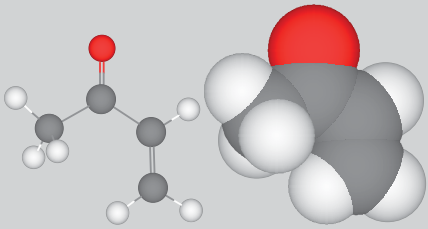

2) Chloromethyl vinyl ketone [$CH_2ClC(O)CH{=}CH_2$]:

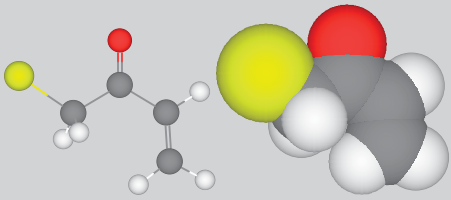

3) Ethyl vinyl ketone [$CH_3CH_2C(O)CH{=}CH_2$]:

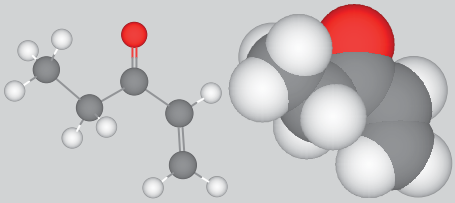

4) 3-Penten-2-one [$CH_3C(O)CH{=}CHCH_3$]:

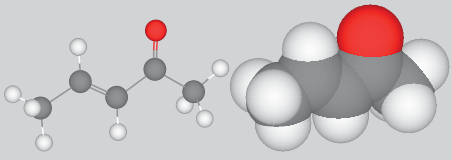

5) 3-Methyl-3-buten-2-one [$CH_2{=}C(CH_3)C(O)CH_3$]:

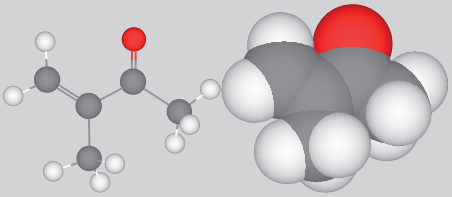

6) 4-Hexen-3-one [$CH_3CH_2C(O)CH{=}CHCH_3$]:

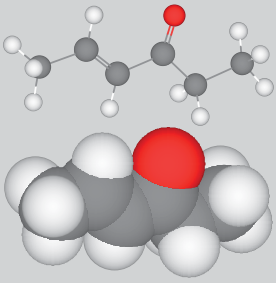

7) 4-Methyl-3-penten-2-one [$(CH_3)_2C{=}CHC(O)CH_3$]:

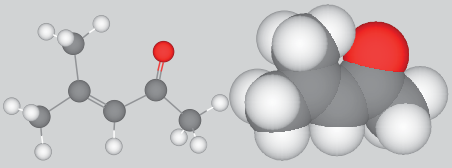

8) *E*-3-Methylpent-3-en-2-one [$CH_3CH{=}C(CH_3)C(O)CH_3$]:

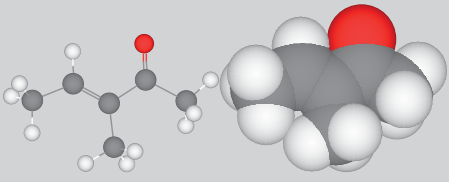

9) 6-Methyl-5-hepten-2-one [$(CH_3)_2C{=}CHCH_2CH_2C(O)CH_3$]:

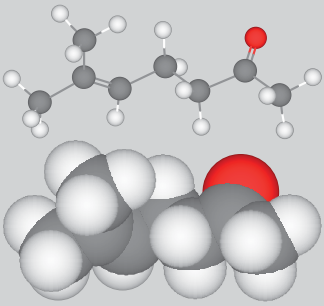

10) 4-Methoxybut-3-en-2-one [$CH_3OCH{=}CHC(O)CH_3$]:

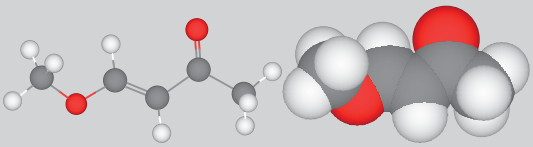

App-V-F. Diones

1) 2,3-Butanedione [biacetyl, $CH_3C(O)C(O)CH_3$]:

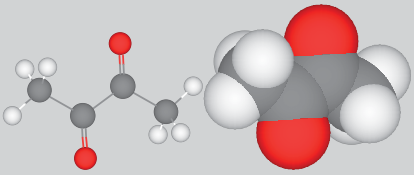

2) 3-Hexene-2,5-dione [$CH_3C(O)CH{=}CHC(O)CH_3$]:

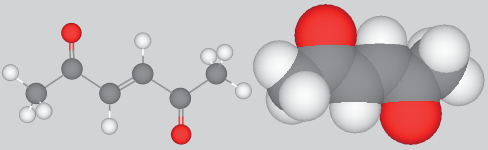

App-V-G. Ketones from Oxidation of Biogenic Hydrocarbons

1) Nopinone (6,6-dimethylbicyclo-[3.1.1]heptan-2-one, $C_9H_{14}O$):

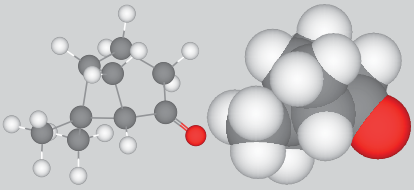

2) 4-Acetyl-1-methyl-cyclohexene (Limona ketone, $C_9H_{16}O$):

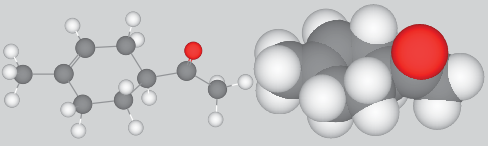

App-V-H. Aromatic Ketones

1) 1,4-Naphthoquinone (naphthalene-1,4-dione, $C_{10}H_6O_2$):

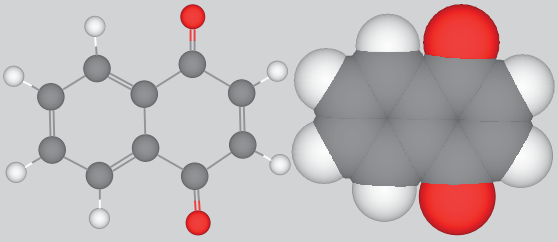

App-VI. Organic Acids

App-VI-A. Monobasic Organic Acids

1) Formic acid [methanoic acid, HC(O)OH]:

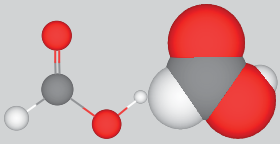

2) Acetic acid [ethanoic acid, $CH_3C(O)OH$]:

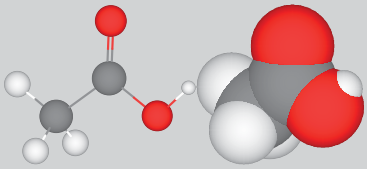

3) Propanoic acid [propionic acid, $CH_3CH_2C(O)OH$]:



4) Butanoic acid [butyric acid, $CH_3CH_2CH_2C(O)OH$]:

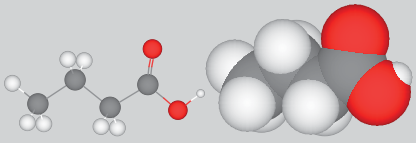

5) 2-Methylpropanoic acid [isobutyric acid, $(CH_3)_2CHC(O)OH$]:

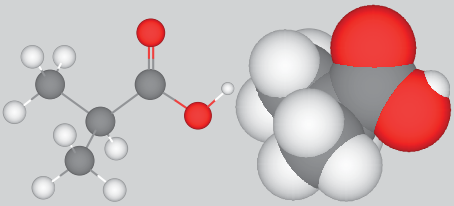

6) Pentanoic acid ($CH_3CH_2CH_2CH_2C(O)OH$]:

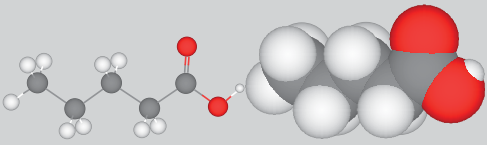

7) Hexanoic acid ($CH_3CH_2CH_2CH_2CH_2C(O)OH$):



App-VI-B. Dibasic Organic Acids

1) Oxalic acid [ethanedioic acid, HO(O)CC(O)OH]:

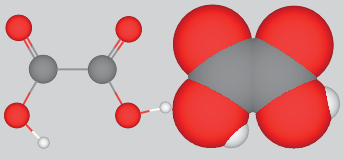

2) Malonic acid [propanedioic acid, $HO(O)CCH_2C(O)OH$]:

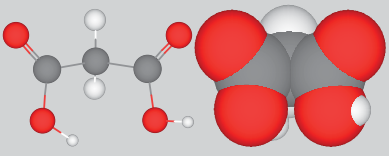

3) Succinic acid [butanedioic acid, $HO(O)CCH_2CH_2C(O)OH$]:

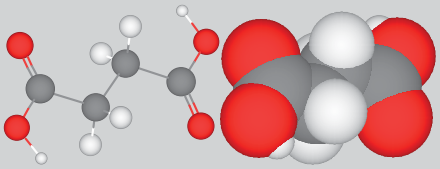

4) Glutaric acid [pentanedioic acid, $HO(O)CCH_2CH_2CH_2C(O)OH$]:

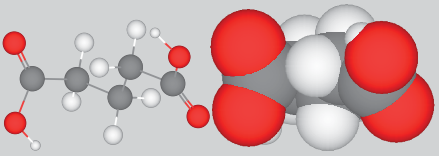

5) Adipic acid [hexanedioic acid, $HO(O)CCH_2CH_2CH_2CH_2C(O)OH$]:

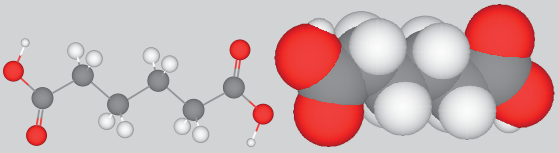

App-VI-C. Unsaturated Organic Acids

1) Propenoic acid [acrylic acid, $CH_2{=}CHC(O)OH$]:

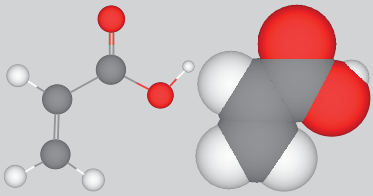

2) 2-Methylpropenoic acid (methacrylic acid, $CH_2{=}C(CH_3)C(O)OH$]:



App-VI-D. Aromatic Acids

1) Benzoic acid ($C_6H_5C(O)OH$):

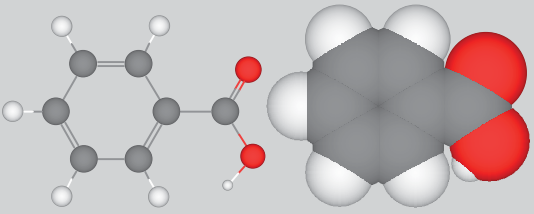

App-VI-E. Organic Acids Formed in Oxidation of Biogenic Hydrocarbons

1) *cis*-pinonic acid [(3-acetyl-2,2-dimethylcyclobutyl)acetic acid, $C_{10}H_{16}O_3$]:

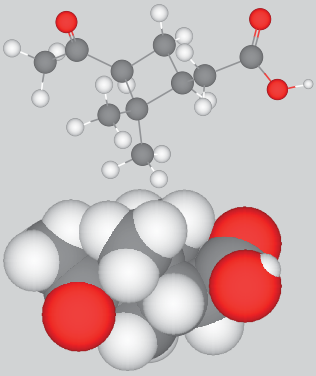

2) Pinic acid (3-(carboxymethyl)-2,2-dimethylcyclobutanecarboxylic acid, $C_9H_{14}O_4$):

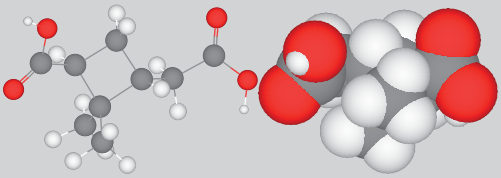

3) Norpinonic acid (3-acetyl-2,2-dimethylcyclobutanecarboxylic acid, $C_9H_{14}O_3$):

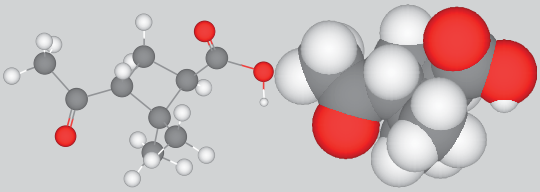

App-VI-F. Halogen-Substituted Organic Acids

1) Trifluoroacetic acid [$CF_3C(O)OH$]:

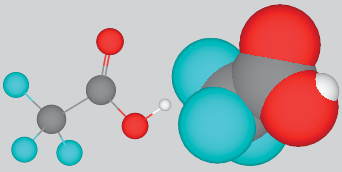

2) 2,2,3,3,3-Pentafluoropropanoic acid [$CF_3CF_2C(O)OH$]:

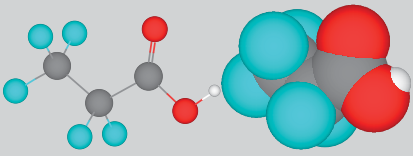

3) 2,2,3,3,4,4,4-Heptafluorobutanoic acid [$CF_3CF_2CF_2C(O)OH$]:

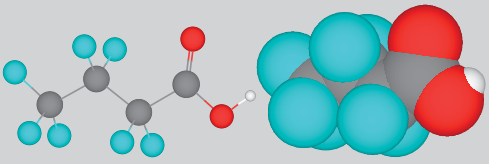

4) 2,2,3,3,4,4,5,5,5-Nonafluoropentanoic acid [$CF_3CF_2CF_2CF_2C(O)OH$]:

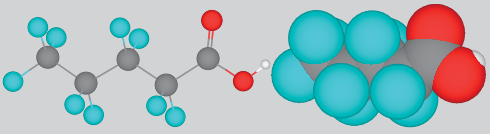

App-VII. Organic Acid Anhydrides

1) Formic acid anhydride [HC(O)O(O)CH]:

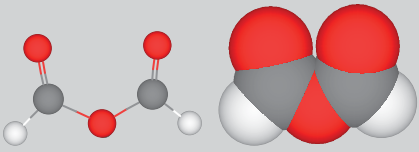

2) Formic acetic anhydride [$HC(O)O(O)CCH_3$]:

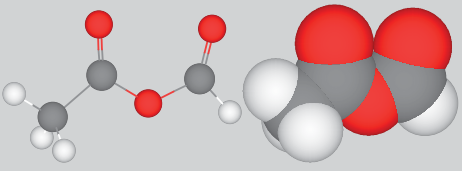

3) Acetic anhydride [$CH_3C(O)O(O)CCH_3$]:

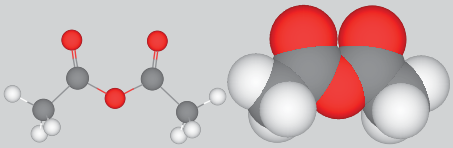

4) Formic propanoic anhydride $HC(O)O(O)CCH_2CH_3$]:



App-VIII. Esters

App-VIII-A. Acyclic Esters

1) Methyl formate [$CH_3OC(O)H$]:

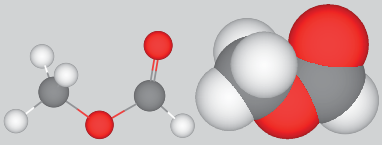

2) Ethyl formate [$CH_3CH_2OC(O)H$]:

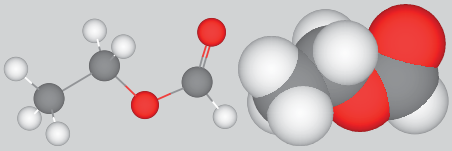

3) Methyl acetate [$CH_3OC(O)CH_3$]:

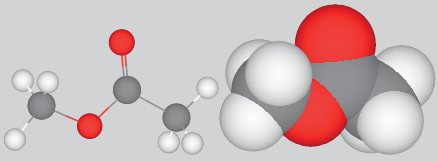

4) *n*-Propyl formate [$CH_3CH_2CH_2OC(O)H$]:

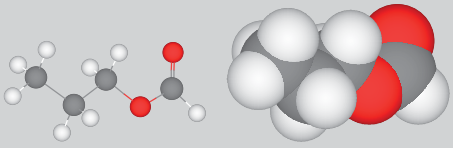

5) *n*-Butyl formate [$CH_3CH_2CH_2CH_2OC(O)H$]:

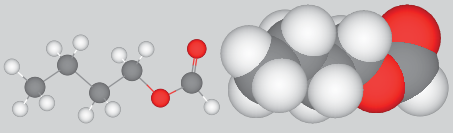

6) *tert*-Butyl formate [$(CH_3)_3COC(O)H$]:



7) Methyl caproate [methyl hexanoate, n-$C_5H_{11}C(O)OCH_3$]:

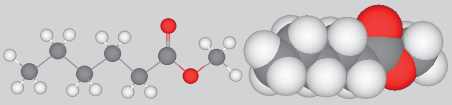

8) Methyl caprylate [methyl octanoate, n-$C_7H_{15}C(O)OCH_3$]:

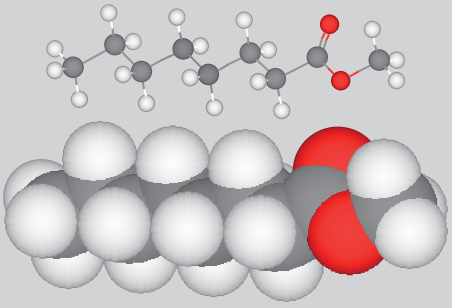

9) Methyl caprate [methyl decanoate, n-$C_9H_{19}C(O)OCH_3$]:

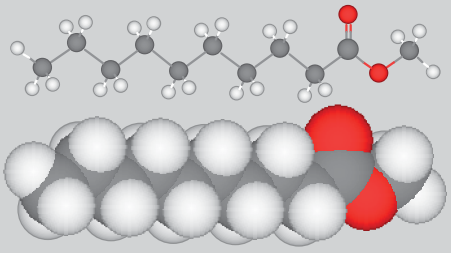

10) Methyl laurate [methyl dodecanoate, n-$C_{11}H_{23}C(O)OCH_3$]:

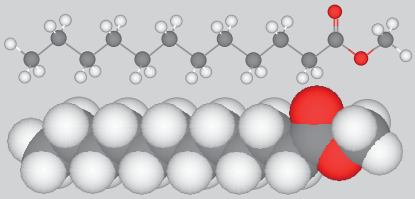

12) Methyl palmitate [methyl hexadecanoate, n-$C_{15}H_{31}C(O)OCH_3$]:

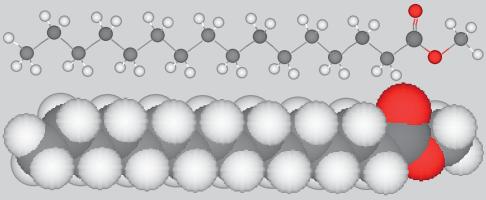

11) Methyl myristate [methyl tetradecanoate, n-$C_{13}H_{27}C(O)OCH_3$]:

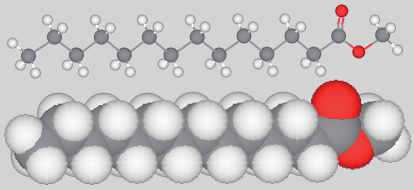

13) Methyl stearate [methyl octadecanoate, n-$C_{17}H_{35}C(O)OCH_3$]:

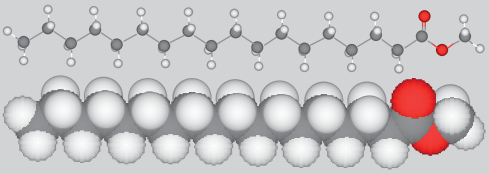

App-VIII-B. Unsaturated Esters

1) Vinyl acetate [$CH_2{=}CHO(O)CCH_3$]:

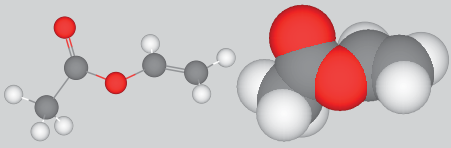

4) Ethyl acrylate [ethyl propenoate, $CH_3CH_2O(O)CCH{=}CH_2$]:

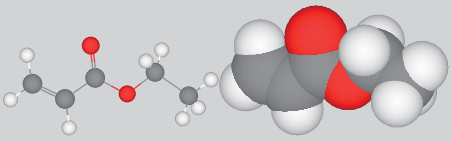

2) Methyl acrylate [$CH_2{=}CHC(O)OCH_3$]:

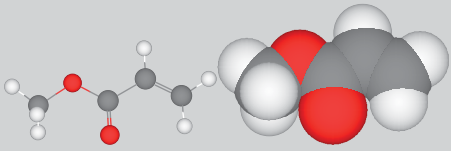

5) Methyl methacrylate [$CH_2{=}C(CH_3)C(O)OCH_3$]:

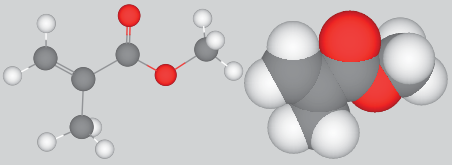

3) Isopropenyl acetate [$CH_3C(O)OC(CH_3){=}CH_2$]:

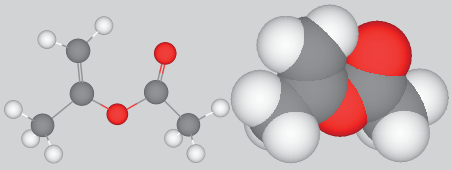

6) Methyl 2-butenoate [$CH_3CH{=}CHC(O)OCH_3$]:

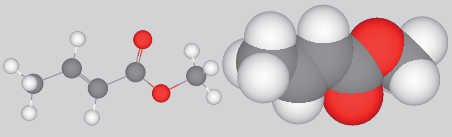

7) Ethyl methacrylate
[$CH_2{=}C(CH_3)C(O)OCH_2CH_3$]:

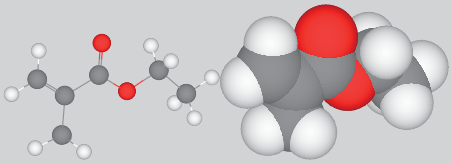

8) Methyl 3-methyl-2-butenoate
[$(CH_3)_2C{=}CHC(O)OCH_3$]:

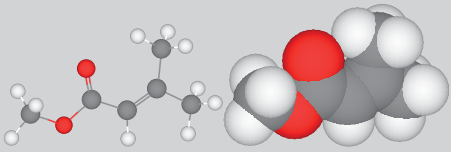

9) *n*-Butyl methacrylate
[$CH_2{=}C(CH_3)C(O)OCH_2CH_2CH_2CH_3$]:

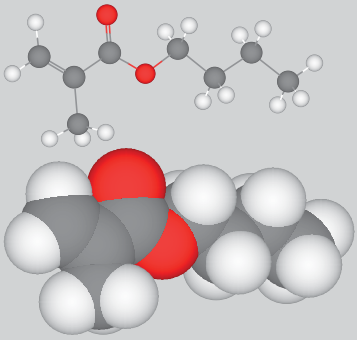

10) *cis*-3-Hexenyl acetate [leaf acetate,
$CH_3C(O)OCH_2CH_2CH{=}CHCH_2CH_3$]:

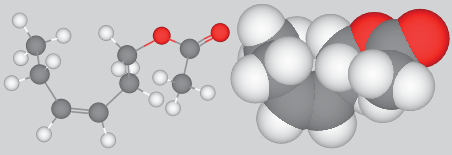

11) 2-Methoxyethyl methacrylate
($CH_2{=}C(CH_3)C(O)OCH_2CH_2OCH_3$]:

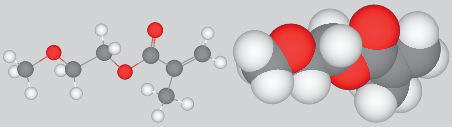

12) 4-Penten-1-yl acetate
[$CH_3C(O)OCH_2CH_2CH_2CH{=}CH_2$]:

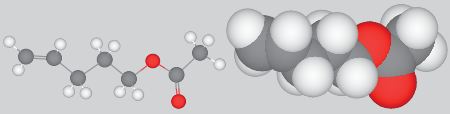

13) Ethyl 3-ethoxyacrylate
[$CH_3CH_2OCH{=}CHC(O)OCH_2CH_3$]:

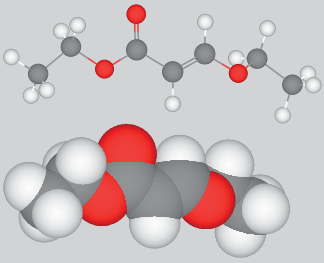

14) *trans*-2-hexenyl acetate
[$CH_3CH_2CH_2CH{=}CHC(O)OCH_3$:

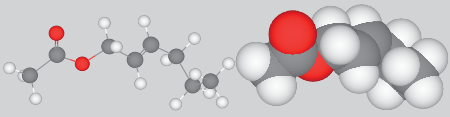

15) Methyl *trans*-3-methoxy acrylate
[$CH_3OCH{=}CHC(O)OCH_3$]:

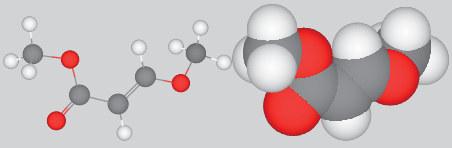

16) Methyl oleate [methyl *cis*-9-octadecenoate, *n*-$C_8H_{17}CH{=}CH(CH_2)_7C(O)OCH_3$]:

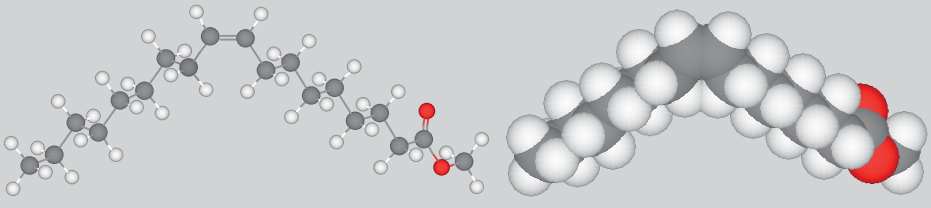

17) Methyl linoleoate [*Z*,*Z*-methyl 9,12-octadecadienoate, $C_5H_{11}CH{=}CHCH_2CH{=}CHC_7H_{14}C(O)OCH_3$]:

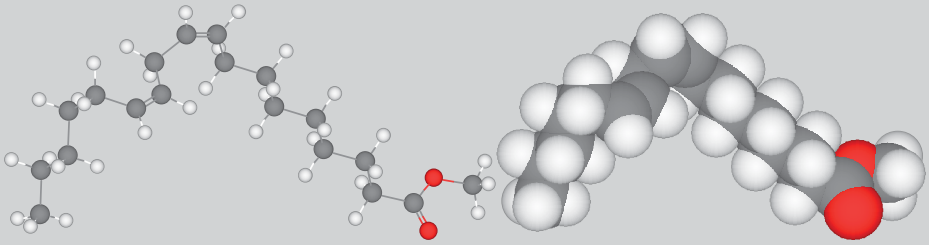

18) Methyl linolenate [methyl *Z*,*Z*,*Z*-9,12,15-octadecatrienoate $CH_3(CH_2CH{=}CH)_3CH_2(CH_2)_6C(O)OCH_3$]:

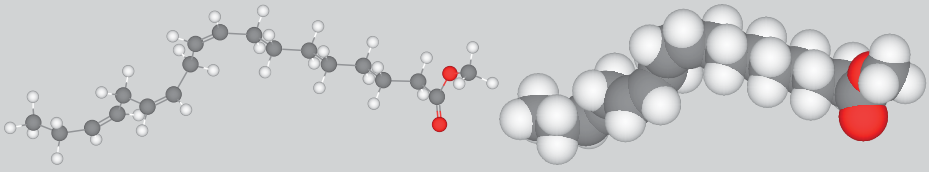

App-VIII-C. Cyclic Esters

1) (3H)-Furan-2one ($C_4H_4O_2$):

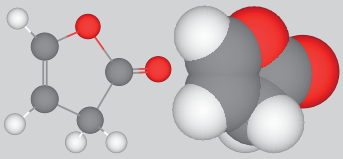

2) 5-Methyl-(3H)-furan-2-one (α-angelicalactone, $C_5H_6O_2$):

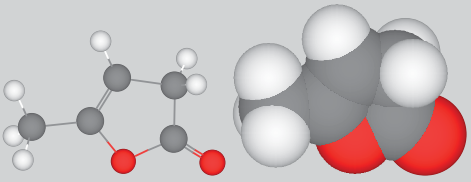

App-VIII-D. Aromatic Esters

1) Methyl salicylate [HO—$C_6H_4C(O)OCH_3$]:

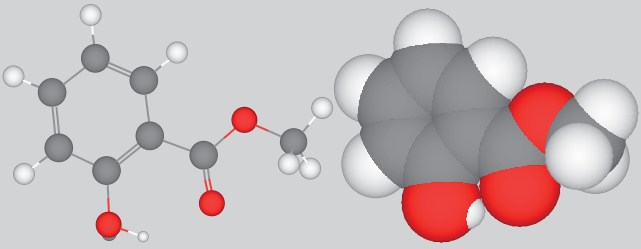

App-VIII-E. Carbonates

1) Dimethyl carbonate [$CH_3OC(O)OCH_3$]:

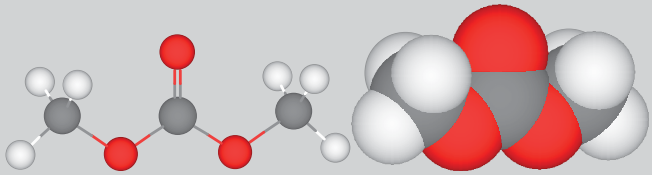

App-VIII-F. Lactates

1) Methyl lactate [$CH_3CH(OH)C(O)OCH_3$]:



2) Ethyl lactate [$CH_3CH(OH)C(O)OCH_2CH_3$]:

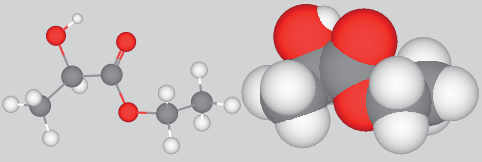

App-VIII-G. Halogen-Substituted Esters

1) Trifluoromethylformate [$CF_3O(O)CH$]:

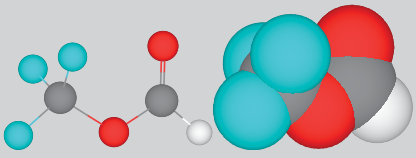

2) Difluoromethylformate [$CHF_2OC(O)H$]:



3) Methylfluoroformate [$CH_3O(O)CF$]:

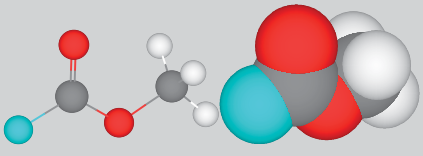

4) Fluoromethyl fluoroformate [$CH_2FOC(O)F$]:

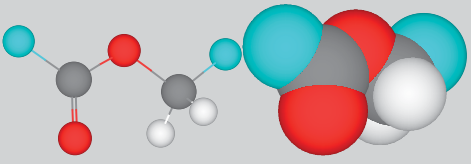

5) Trifluoromethylformate [$CF_3OC(O)H$]:

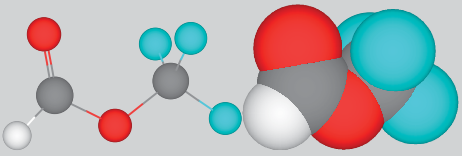

6) Trifluoromethylacetate [$CF_3O(O)CCH_3$]:

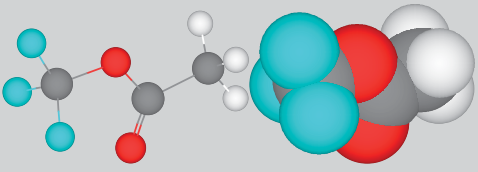

7) 1,2,2,2-Tetrafluoroethylformate [$CF_3CFHO(O)CH$]:

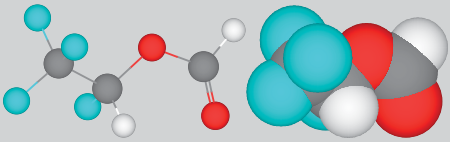

8) Perfluoroethylformate [$CF_3CF_2O(O)CH$]:



9) Difluoromethylacetate [$CHF_2CO(O)CCH_3$]:

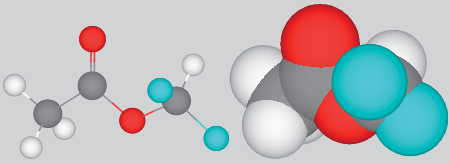

10) Methyl-trifluoroacetate [$CH_3O(O)CCF_3$]:

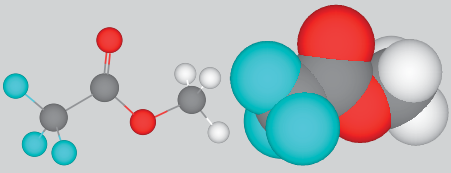

11) Methyl-2,2-difluoroacetate [$CF_2HC(O)OCH_3$]:

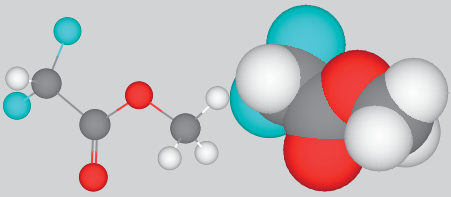

12) 1,3,3,3-Tetrafluoroethyl formate [$CF_3CHFOC(O)H$]:

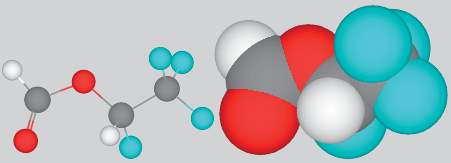

13) Ethyl trifluoroacetate [$CH_3CH_2O(O)CCF_3$]:

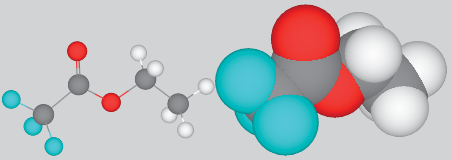

14) 2,2,2-Trifluoroethyl-trifluoroacetate [$CF_3CH_2O(O)CCF_3$]:

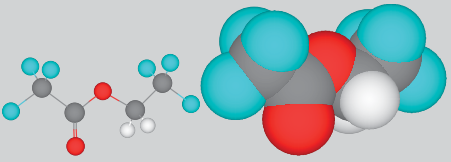

15) Heptafluoro-*n*-propylformate [$CF_3CF_2CF_2O(O)CH$]:

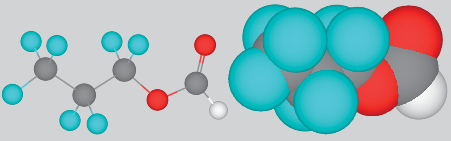

16) Nonafluoro-*n*-butyl formate [$CF_3CF_2CF_2CF_2O(O)CH$]:

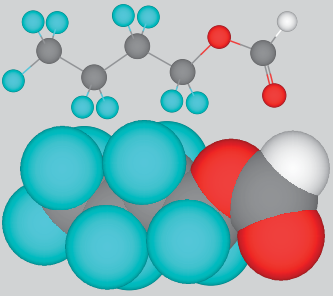

17) Perfluoro-isobutyl formate [$(CF_3)_2CFCF_2O(O)CH$]:

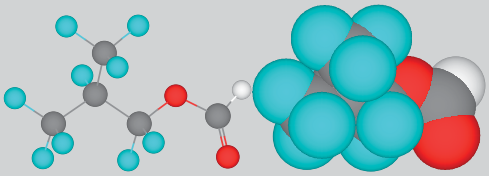

18) Perfluoro-*n*-pentyl formate [$CF_3CF_2CF_2CF_2CF_2O(O)CH$]:

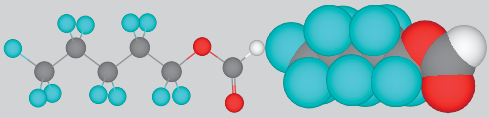

19) 1,1,1,2,3,4,4,5,5,6,6,6-Dodecafluoro-2-(trifluoromethyl)hexan-3-yl formate {$CF_3CF_2CF_2CF[CF(CF_3)_2]O(O)CH$}:

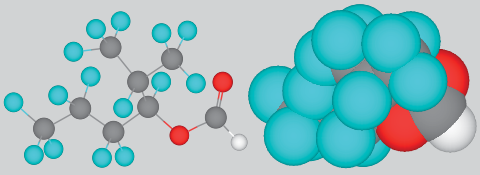

20) 1,1,1,2,3,4,4,5,5,6,6,6-Dodecafluoro-2-(trifluoromethyl)hexan-3-yl acetate {$CF_3CF_2CF_2CF[CF(CF_3)_2]O(O)CCH_3$}:

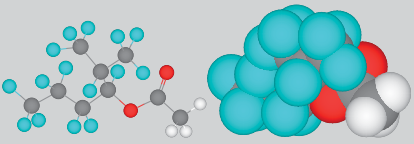

21) 3,3,4,4,5-pentafluoro-2-(1,1,1,2,3,3,3-heptafluoropropan-2-yl)-5-(heptafluoropropyl)tetrahydrofuran-2-yl formate ($C_{11}F_{19}HO_3$):

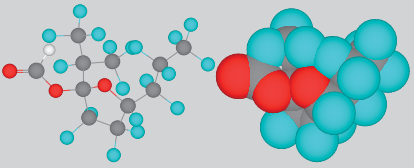

22) 3,3,4,4,5-Pentafluoro-2,5-*bis*(perfluoropropan-2-yl)tetrahydrofuran-2-yl formate $C_{11}HO_3F_{19}$:

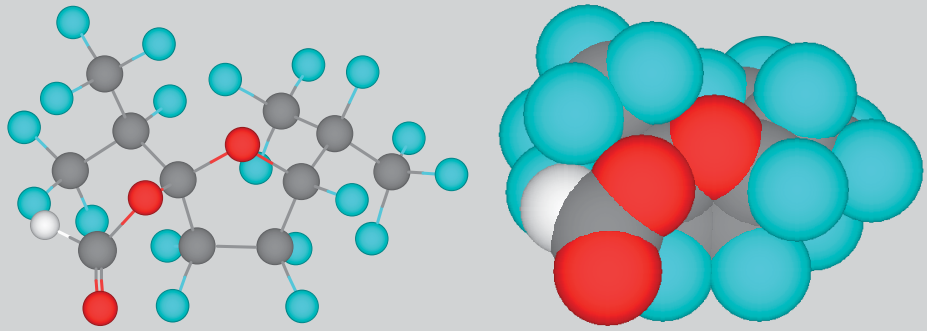

App-IX. Nitrogen-Containing Oxygenates

App-IX-A. Nitrous Acid and Organic Nitrites

1) Nitrous acid (HONO):

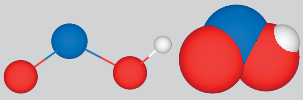

2) Methyl nitrite (CH_3ONO):



3) Ethyl nitrite (CH_3CH_2ONO):

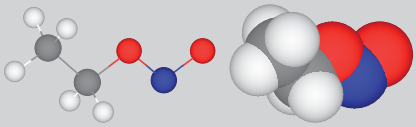

4) 1-Propyl nitrite (*n*-propyl nitrite, $CH_3CH_2CH_2ONO$):



5) 2-Propyl nitrite (isopropyl nitrite, $CH_3CH(ONO)CH_3$):

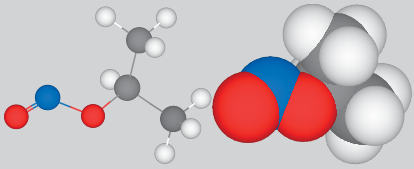

6) 1-Butyl nitrite (*n*-butyl nitrite, $CH_3CH_2CH_2CH_2ONO$):

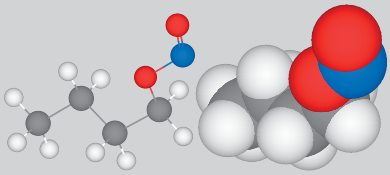

7) *iso*-Butyl nitrite [$(CH_3)_2CHCH_2ONO$]:

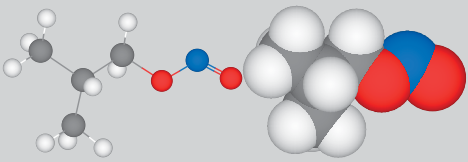

8) *tert*-Butyl nitrite [$(CH_3)_3CONO$]:

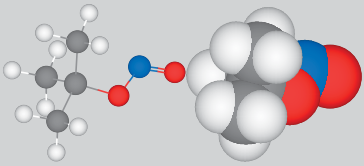

9) *n*-Pentyl nitrite [$CH_3CH_2CH_2CH_2CH_2ONO$]:



10) *tert*-Pentyl nitrite [$CH_3CH_2C(CH_3)_2ONO$]:

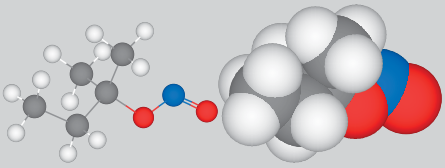

App-IX-B. Nitroalkanes

1) Nitromethane (CH_3NO_2):

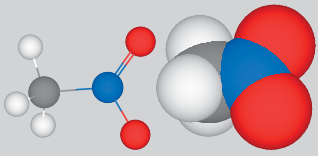

2) Nitroethane ($CH_3CH_2NO_2$):

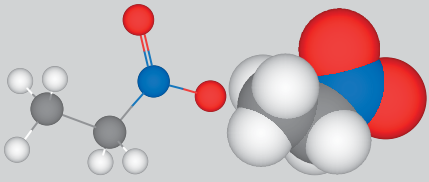

3) 1-Nitropropane ($CH_3CH_2CH_2NO_2$):

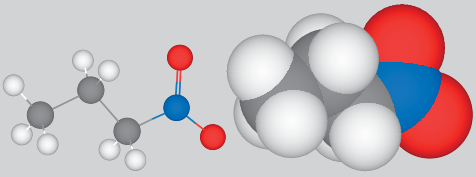

4) 2-Nitropropane [$CH_3CH(NO_2)CH_3$]:

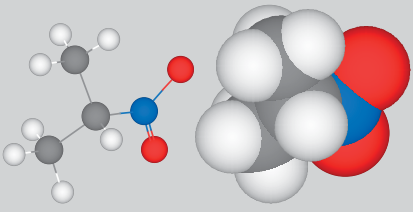

5) 2-Nitro-2-methylpropane [$(CH_3)_3CNO_2$]:

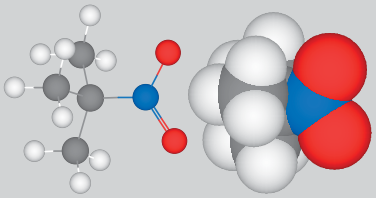

6) 1-Nitrobutane ($CH_3CH_2CH_2CH_2NO_2$):



7) 1-Nitropentane ($CH_3CH_2CH_2CH_2CH_2NO_2$):

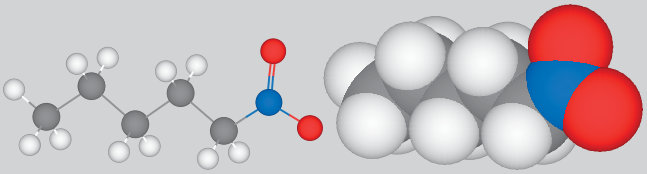

App-IX-C. Nitroalkenes

1) Nitroethene ($CH_2{=}CHNO_2$):

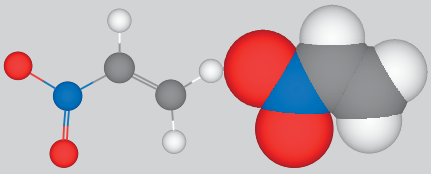

2) 3-Nitroprop-1-ene ($CH_2{=}CHCH_2NO_2$):

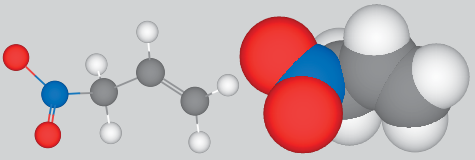

3) 1-Nitro-*cyclo*-hexene (*cyclo*-$C_6H_9NO_2$):

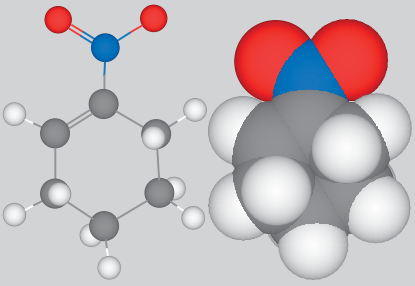

App-IX-D. Aromatic Nitro Compounds

1) Nitrobenzene ($C_6H_5NO_2$):

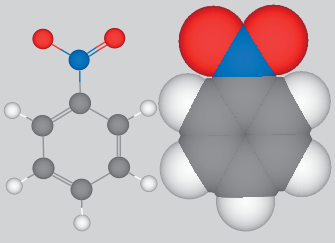

2) 3-Nitrotoluene (*m*-nitrotoluene, $CH_3{-}C_6H_4{-}NO_2$):

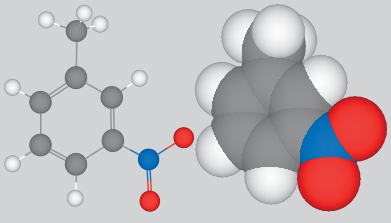

3) 1-Nitronaphthalene ($C_{10}H_7NO_2$):

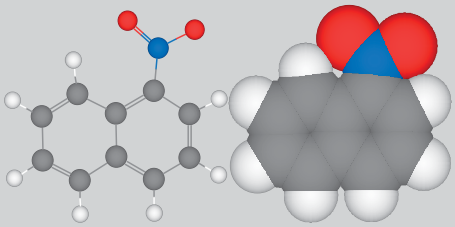

4) 2-Nitronaphthalene ($C_{10}H_7NO_2$):



5) 2-Methyl-1-nitronaphthalene ($CH_3—C_{10}H_6—NO_2$):

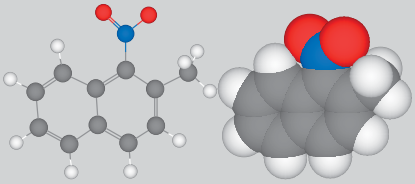

6) 2-Nitrophenol ($HO—C_6H_4—NO_2$):

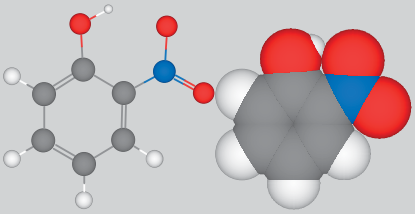

App-IX-E. Nitric Acid and Alkyl Nitrates

1) Nitric acid ($HONO_2$):

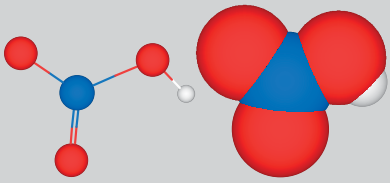

2) Peroxynitric acid ($HOONO_2$):

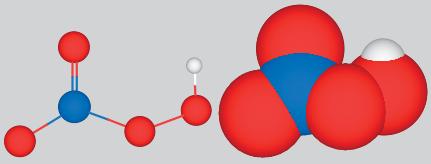

3) Nitrooxymethane (methyl nitrate, CH_3ONO_2):

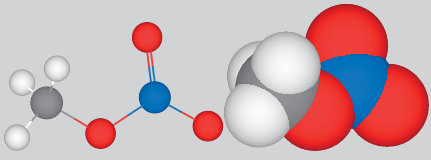

4) Nitrooxyethane (ethyl nitrate, $CH_3CH_2ONO_2$):

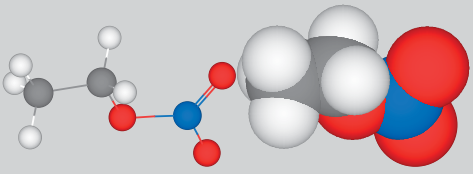

5) 1-Nitrooxypropane (1-propyl nitrate, *n*-propyl nitrate, $CH_3CH_2CH_2ONO_2$):

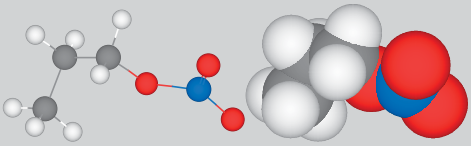

6) 2-Nitrooxypropane [2-propyl nitrate, *iso*-propyl nitrate, $CH_3CH(ONO_2)CH_3$]:

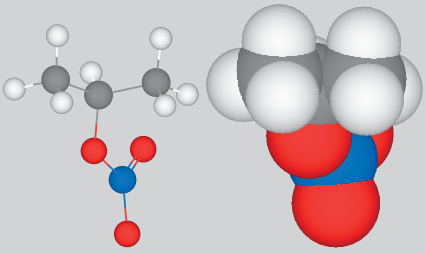

7) 1-Nitrooxybutane (*n*-butyl nitrate, $CH_3CH_2CH_2CH_2ONO_2$):



8) 2-Nitoroxybutane [2-butyl nitrate, *sec*-butyl nitrate, $CH_3CH(ONO_2)CH_2CH_3$]:

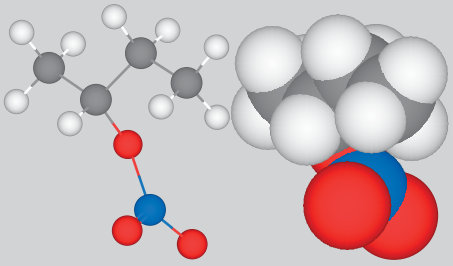

9) 2-Nitrooxy-2-methylpropane [2-methylpropyl nitrate, *tert*-butyl nitrate, $(CH_3)_3CONO_2$]:

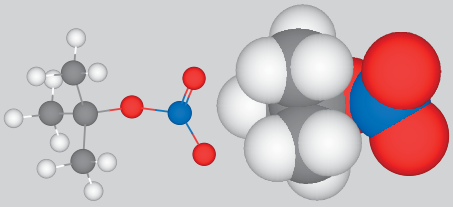

10) 2-Nitrooxypentane [2-pentyl nitrate, $CH_3CH(ONO_2)CH_2CH_2CH_3$]:

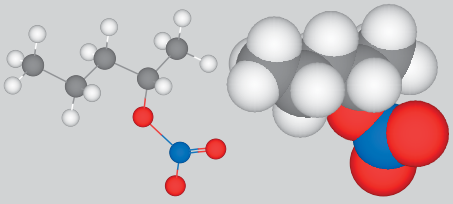

11) 3-Nitrooxypentane [3-pentyl nitrate, $CH_3CH_2CH(ONO_2)CH_2CH_3$]:

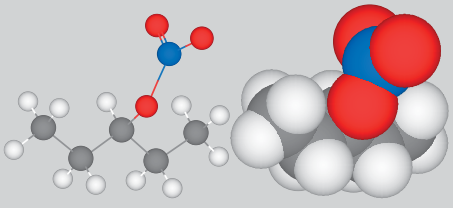

12) 2-Nitrooxy-2-methylbutane [*tert*-amyl nitrate, $CH_3CH_2CH(CH_3)CH_2ONO_2$]:

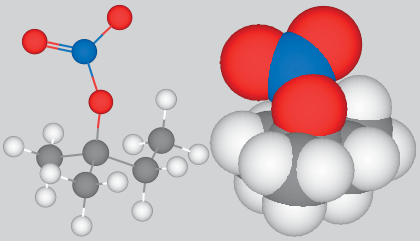

13) 1-Nitrooxy-3-methylbutane $[(CH_3)_2CHCH_2CH_2ONO_2]$:

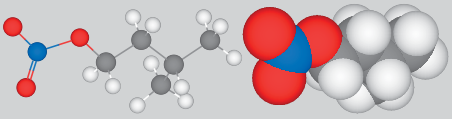

14) 2-Nitrooxy-3-methylbutane $[(CH_3)_2CHCH(ONO_2)CH_3]$:

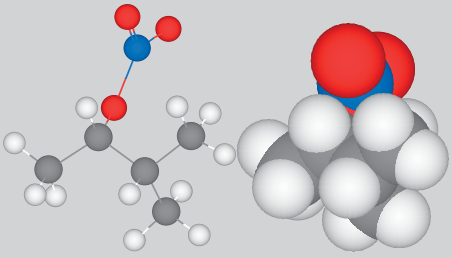

15) 1-Nitrooxy-2,2-dimethylpropane [neopentyl nitrate, $(CH_3)_3CCH_2ONO_2$]:

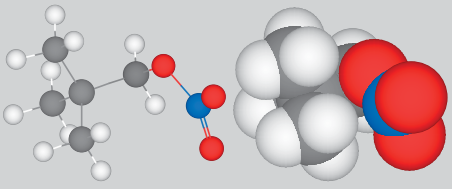

16) 2-Nitrooxyhexane [2-hexyl nitrate, $CH_3CH(ONO_2)CH_2CH_2CH_2CH_3$]:

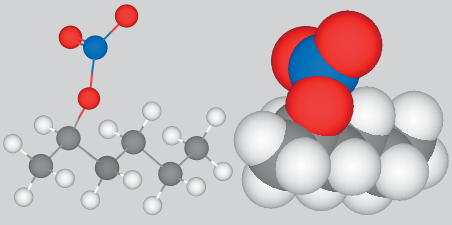

17) 3-Nitrooxyhexane [3-hexyl nitrate, $CH_3CH_2CH(ONO_2)CH_2CH_2CH_3$]:

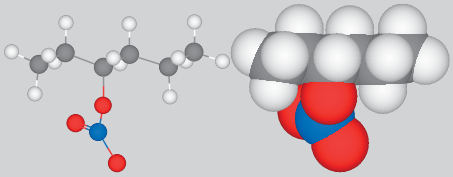

18) 2-Nitrooxy-2-methylpentane [$(CH_3)_2C(ONO_2)CH_2CH_2CH_3$]:

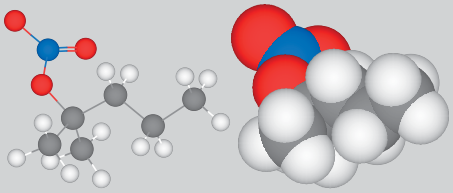

19) 2-Nitrooxy-3-methylpentane [$CH_3CH(ONO_2)CH(CH_3)CH_2CH_3$]:

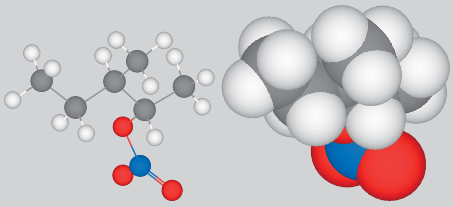

20) 2-Nitrooxyheptane [2-heptyl nitrate, $CH_3CH(ONO_2)CH_2CH_2CH_2CH_2CH_3$]:

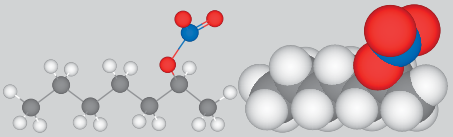

21) 3-Nitrooxyheptane [3-heptyl nitrate, $CH_3CH_2CH(ONO_2)CH_2CH_2CH_2CH_3$]:

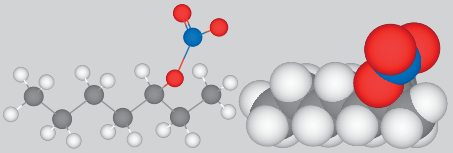

22) 3-Nitrooxyoctane (3-octyl nitrate, $CH_3CH_2CH(ONO_2)CH_2CH_2CH_2CH_2CH_3$]:

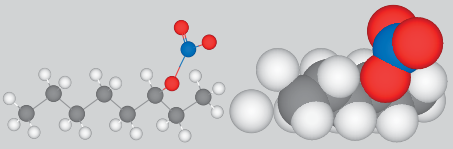

App-IX-F. Cycloalkyl Nitrates

1) Nitrooxy-*cyclo*-pentane [*cyclo*-pentyl nitrate, *cyclo*-C_5H_9-ONO_2]:

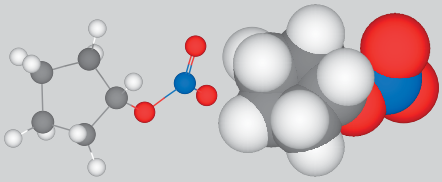

2) Nitrooxy-*cyclo*-hexane [*cyclo*-hexyl nitrate, *cyclo*-$C_6H_{11}ONO_2$]:

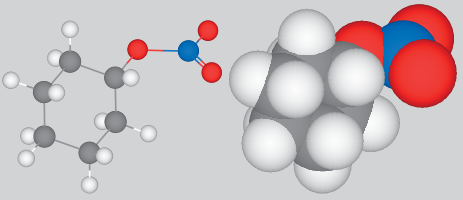

App-IX-G. Organic Dinitrates

1) 1,2-Dinitrooxypropane [propane-1,2-diyl dinitrate, $CH_3C(ONO_2)CH_2ONO_2$]:

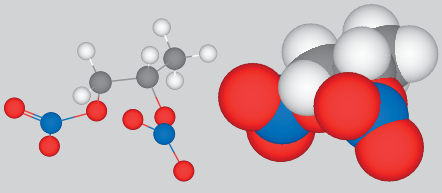

2) 1,2-Dinitrooxybutane [butane-1,2-diyl dinitrate, $CH_3CH_2CH(ONO_2)CH_2ONO_2$]:

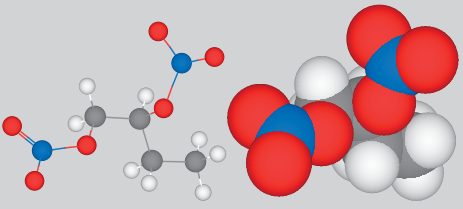

3) 2,3-Dinitrooxybutane [butane-2,3-diyl dinitrate, $CH_3CH(ONO_2)CH(ONO_2)CH_3$]:

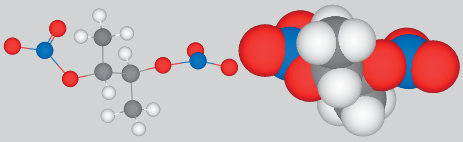

5) *trans*-1,2-Dinitrooxy-1-methylcyclohexane (cyclohexane-1,2-diyl dinitrate, $C_7H_{12}N_2O_6$):

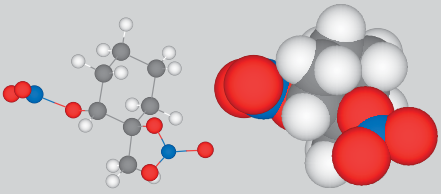

4) 1,4-Dinitrooxybutane [butane-1,4-diyl dinitrate, $O_2NOCH_2CH_2CH_2CH_2ONO_2$]:

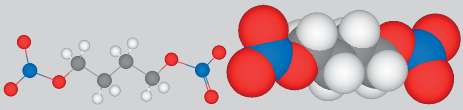

6) *cis*-1,4-Dinitrooxy-2-butene [(*Z*)-but-2-ene-1,4-diyl dinitrate ($O_2NOCH_2CH{=}CHCH_2ONO_2$)]:

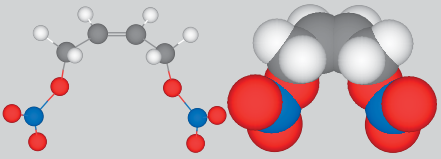

7) 3,4-Dinitrooxy-1-butene [but-1-ene-3,4-diyl dinitrate, $O_2NOCH_2CH(ONO_2)CH{=}CH_2$]:

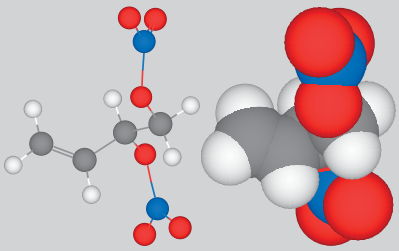

App-IX-H. Alkanol Nitrates

1) 2-Nitrooxyethanol ($O_2NOCH_2CH_2OH$):

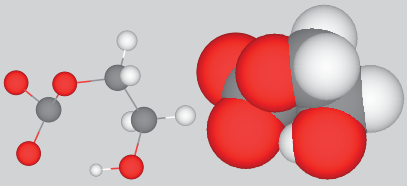

3) 2-Nitrooxy-1-propanol [1-hydroxypropan-2-yl nitrate, $CH_3CH(ONO_2)CH_2OH$]:



2) 1-Nitrooxy-2-propanol [2-hydroxypropyl nitrate, $CH_3CH(OH)CH_2ONO_2$]:

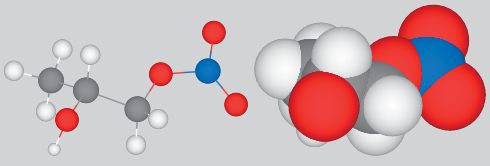

4) 2-Nitrooxy-1-butanol [1-hydroxybutan-2-yl nitrate, $CH_3CH_2CH(ONO_2)CH_2OH$]:

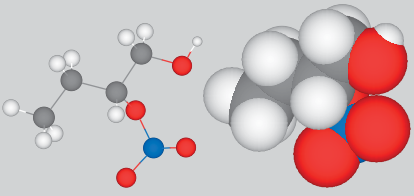

5) 1-Nitrooxy-2-butanol [2-hydroxybutyl nitrate, $CH_3CH_2CH(OH)CH_2ONO_2$]:

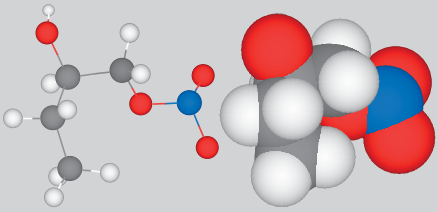

6) 4-Nitrooxy-2-butanol [3-hydroxybutyl nitrate, $CH_3CH(OH)CH_2CH_2ONO_2$]:

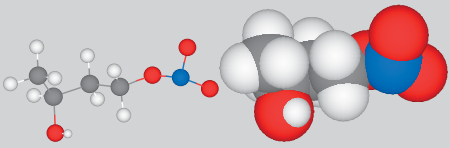

7) 3-Nitrooxy-1-butanol [4-hydroxybutan-2-yl nitrate, $CH_3CH(ONO_2)CH_2CH_2OH$]:

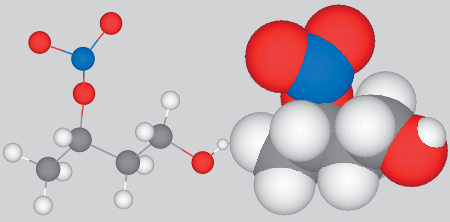

8) 4-Nitrooxy-1-butanol [4-hydroxybutyl nitrate, $O_2NOCH_2CH_2CH_2CH_2OH$]:



9) 1-Nitrooxy-2-pentanol [2-hydroxypentyl nitrate, $CH_3CH_2CH_2CH(OH)CH_2ONO_2$]:

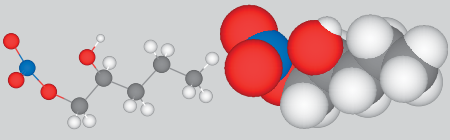

10) 5-Nitrooxy-2-pentanol [4-hydroxypentyl nitrate, $CH_3CH(OH)CH_2CH_2CH_2ONO_2$]:

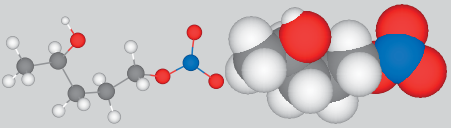

11) 4-Nitrooxy-1-pentanol [5-hydroxypentan-2-yl nitrate, $CH_3CH(ONO_2)CH_2CH_2CH_2OH$]:



12) 2-Nitrooxy-1-cyclopentanol (2-hydroxycyclopentyl nitrate, $C_5H_9NO_4$):

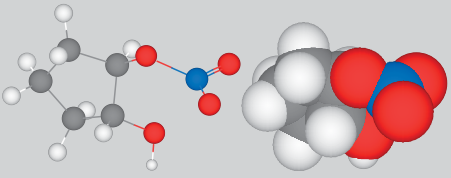

13) 6-Nitrooxy-1-hexanol [6-hydroxyhexyl nitrate, $O_2NOCH_2CH_2CH_2CH_2CH_2CH_2OH$]:

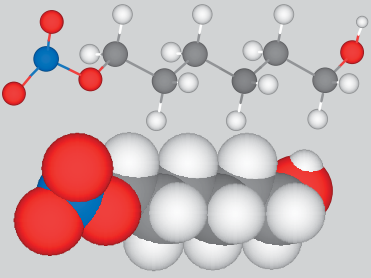

App-IX-I. Alkenol Nitrates

1) 1-Nitrooxy-2-butanol-3-ene [2-hydroxybut-3-en-1-yl nitrate, $O_2NOCH_2CH(OH)CH{=}CH_2$]:

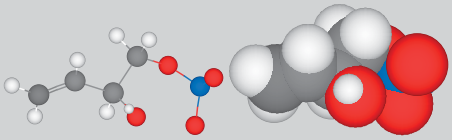

2) 4-Nitrooxy-1-butanol-2-ene [(2*E*)-4-hydroxybut-2-en-1-yl nitrate, $O_2NOCH_2CH{=}CHCH_2OH$]:

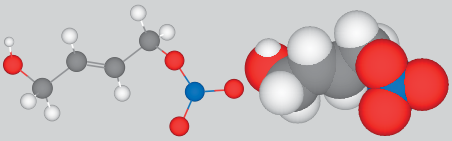

App-IX-J. Ketone Nitrates

1) 1-Nitrooxy acetone [2-oxopropyl nitrate, $O_2NOCH_2C(O)CH_3$]:

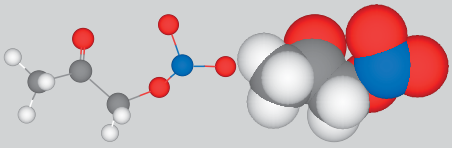

3) 3-Nitrooxy-2-butanone [3-oxobutan-2-yl nitrate, $CH_3C(O)CH(ONO_2)CH_3$]:



2) 1-Nitrooxy-2-butanone [2-oxobutyl nitrate, $O_2NOCH_2C(O)CH_2CH_3$]:

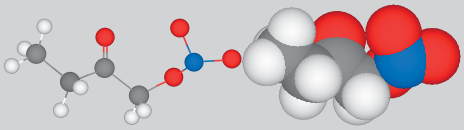

4) 2-Nitrooxy-*cyclo*-hexanone (2-oxocyclohexyl nitrate, $C_6H_9NO_4$):

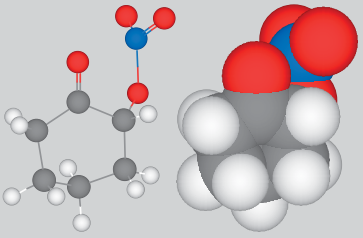

App-IX-K. Peroxyacyl Nitrates

1) Peroxyacetyl nitrate (1-nitroperoxyethanal) $CH_3C(O)OONO_2$, PAN]:

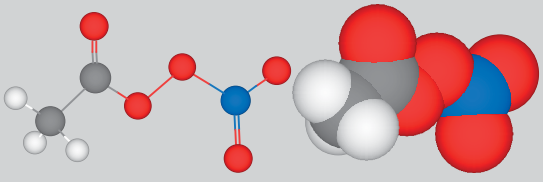

2) Peroxypropionyl nitrate (1-nitroperoxypropanal, $CH_3CH_2C(O)OONO_2$, PPN):

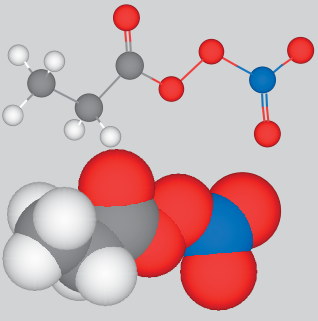

3) Peroxymethylacryloyl nitrate (2-methyl-1-nitroperoxypropenal):

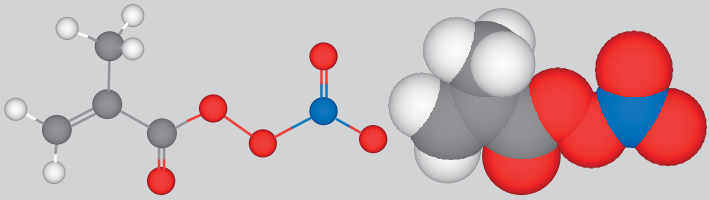

App-IX-L. Amides

1) *N*-Methylformamide [$HC(O)NHCH_3$]:

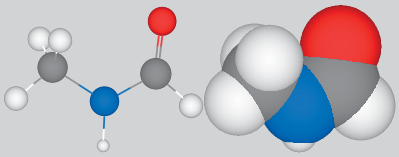

2) *N*,*N*-Dimethylformamide [$HC(O)N(CH_3)_2$]:

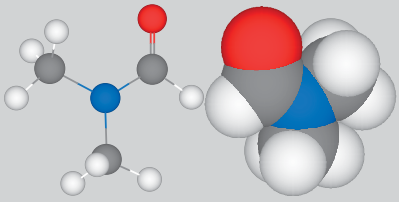

3) *N*-Methylacetamide [$CH_3C(O)NHCH_3$]:



4) *N*,*N*-Dimethylacetamide [$CH_3C(O)N(CH_3)_2$]:

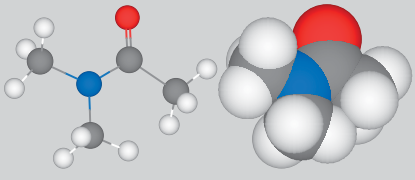

5) *N*-Methylpropionamide [$CH_3CH_2C(O)NHCH_3$]:

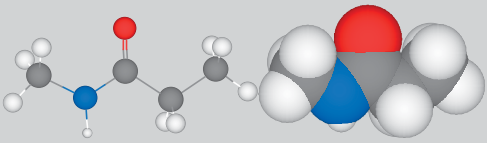

6) *N*,*N*-Dimethylpropionamide [$CH_3CH_2C(O)N(CH_3)_2$]:

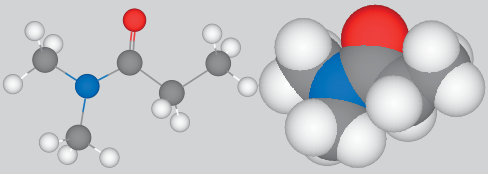

7) *N*-Methyl-2-pyrrolidinone (1-methylpyrrolidin-2-one, C_5H_9NO):

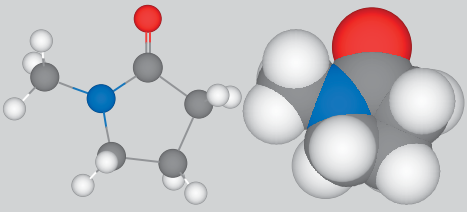

8) *N*-Methyl-succinimide (1-methylpyrrolidine-2,5-dione, $C_5H_7NO_2$):

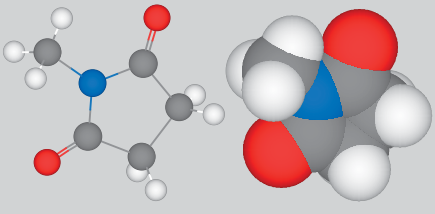

9) *N*-Formyl pyrrolidinone (2-oxopyrrolidine-1-carbaldehyde, $C_5H_7NO_2$):

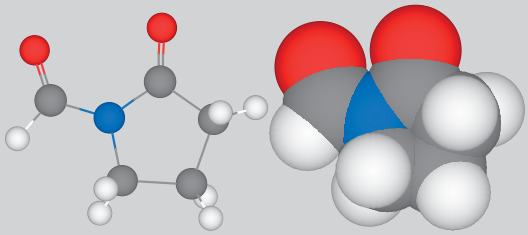

App-IX-M. Amino Alcohols

1) 2-(Dimethylamino)ethanol [$(CH_3)_2NCH_2CH_2OH$]:

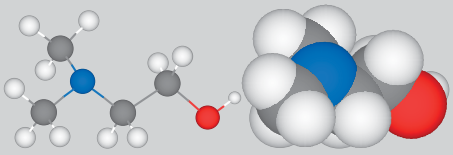

2) 2-Amino-2-methyl-1-propanol [2-amino-2-methylpropan-1-ol, $(CH_3)_2C(NH_2)CH_2OH$]:

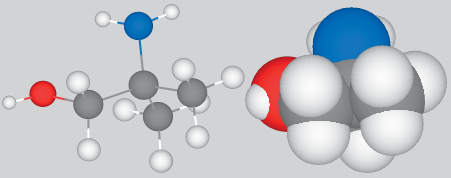

App-IX-N. Nitrosoamines and Nitramines

1) Dimethylnitrosamine [*N*-Nitrosodimethylamine, $(CH_3)_2NNO$]:

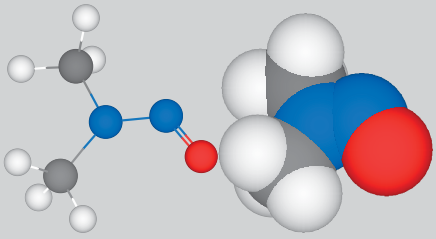

2) Dimethylnitramine [*N*-Nitrodimethylamine, $(CH_3)_2NNO_2$]:

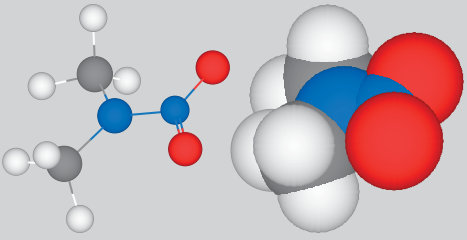

Author Index

Abad, G.G., 1390, 1890
Abbot, D.S., 1362, 1367, 1386, 1388, 1449
Abbott, J., 1261, 1264, 1407
Abe, T., 18, 779, 784, 787, 788, 803, 871, 874, 880, 881, 882, 883, 885, 1434
Abel, B., 546, 548, 549, 1470
Abuin, E.B., 1107, 1108, 1120, 1121, 1122, 1208, 1391, 1437
Acker, K., 1347, 1438
Ackermann, R., 1234, 1463
Adeniji, S.A., 416, 417, 1391
Adryukov, V., 73, 1391
Ahmed, M., 1040, 1458
Aird, R.W.S., 312, 317, 325, 329, 1391
Akano, V., 109, 1447
Akimoto, H., 141, 723, 724, 726, 1164, 1171, 1239, 1398, 1425, 1428, 1447
Alañón, M.R.L., 296, 297, 905, 906, 907, 908, 909, 910, 911, 1458
Albaladejo, J., 122, 123, 124, 128, 129, 131, 134, 135, 143, 145, 146, 147, 148, 149, 156, 157, 158, 165, 166, 167, 170, 172, 174, 176, 177, 556, 557, 558, 560, 563, 564, 565, 566, 567, 569, 570, 573, 574, 575, 576, 577, 601, 602, 605, 606, 611, 612, 613, 616, 657, 658, 659, 660, 661, 662, 663, 664, 666, 667, 668, 669, 670, 671, 672, 673, 674, 675, 677, 678, 679, 680, 681, 701, 728, 764, 797, 798, 799, 801, 802, 803, 804, 805, 806, 808, 812, 815, 816, 861, 863, 1392, 1398, 1405, 1411, 1420, 1429, 1430
Albercook, G.M., 94, 95, 1454
Alberto, A., 192, 194, 204, 205, 207, 1454
Albu, M., 378, 657, 658, 659, 662, 663, 664, 669, 670, 702, 703, 705, 707, 1479
Aldener, M., 115, 1392,
Alencar, J.W., 738, 1411
Alexander, M.H., 1240, 1442
Alfarra, M.R., 1372, 1377, 1430, 1478
Alicke, B., 76, 78, 79, 80, 81, 82, 83, 84, 85, 86, 87, 89, 90, 1234, 1423, 1463
Allan, J.D., 1372, 1478
Allen, D.T., 115, 1377, 1435, 1464
Allen, E.R., 1039, 1040, 1392
Allen, W.D., 989, 1163, 1164, 1392, 1432, 1433
Allston, T.D., 1233, 1240, 1241, 1242, 1267, 1268, 1289, 1392, 1465
Allwine, G., 78, 82, 83, 85, 87, 1418
Almasy, F., 1322, 1392
Al-Saigh, Z.Y., 1192, 1439
Alumbaugh, R.L., 1162, 1392
Alvarado, A., 216, 217, 219, 410, 413, 414, 628, 629, 630, 631, 632, 734, 747, 1073, 1392, 1409
Alvarez, R.A., 1164, 1170, 1438
Alvarez-Idaboy, J.R., 543, 544, 554, 580, 656, 751, 752, 1392, 1429
Amann, S., 1286, 1414
Amano, S., 77, 78, 1427
Amaral, G., 1237, 1392
Ambridge, P.F., 658, 1392
Ammann, M., 721, 1392
Amphlett, J.C., 1187, 1392
Anastasi, C., 118, 120, 124, 288, 445, 446, 461, 462, 463, 472, 473, 499, 500, 501, 1392, 1425, 1449

Andersen, A., 296, 1393
Andersen, M.P.S., 18, 257, 259, 261, 262, 263, 264, 265, 267, 268, 269, 270, 271, 272, 273, 274, 278, 459, 460, 478, 479, 480, 481, 482, 483, 511, 512, 513, 514, 515, 529, 635, 638, 640, 641, 643, 644, 769, 770, 771, 772, 1079, 1083, 1088, 1230, 1393, 1415, 1425, 1428, 1451, 1465, 1472
Anderson, F., 112, 1420
Anderson, H., 124, 1455
Anderson, H.W., 1208, 1393
Anderson, J.E., 103, 104, 108, 1443
Anderson, J.G., 753, 754, 755, 1383, 1427, 1474
Anderson, L.G., 75, 76, 78, 544, 902, 903, 1054, 1393, 1406
Anderson, P.C., 544, 545, 1393
Anderson, P.N., 519, 525, 1393
Andino, J.M., 112, 117, 119, 120, 125, 127, 132, 133, 135, 141, 142, 157, 168, 169, 170, 264, 285, 290, 291, 304, 305, 306, 307, 308, 310, 311, 312, 314, 315, 316, 317, 318, 319, 320, 321, 322, 323, 324, 325, 326, 327, 328, 331, 332, 334, 337, 338, 657, 658, 659, 662, 663, 664, 751, 752, 909, 910, 911, 912, 914, 923, 945, 946, 947, 949, 952, 954, 965, 966, 968, 1398, 1430, 1447, 1458, 1471, 1472, 1473
Andrade, C.H.S., 738, 1411
Andreasen, Ø., 546, 547, 549, 554, 555, 556, 557, 558, 559, 561, 562, 563, 564, 565, 566, 567, 568, 569, 570, 571, 572, 573, 574, 575, 576, 577, 578, 579, 581, 1412
Andresen, P., 1261, 1264, 1417
Anet, F.A.L., 1165, 1393
Angeletti, G., 1349, 1449, 1462
Angerhofer, M.E., 1303, 1417
Anlauf, K., 75, 77, 84, 1458
Apel, E.C., 76, 78, 79, 82, 85, 86, 87, 88, 89, 95, 115, 194, 411, 711, 712, 1393, 1420, 1448, 1454, 1464
Appel, B.R., 1234, 1394
Appleyard, M.E.S., 1123, 1124, 1446
Aranda, A., 189, 192, 194, 204, 205, 207, 486, 492, 493, 566, 568, 574, 575, 576, 577, 602, 603, 616, 617, 657, 658, 659, 669, 670, 675, 728, 729, 765, 777, 778, 782, 783, 784, 1394, 1403, 1440, 1454
Arcaklioğlu, E., 109, 1406
Archer, A.S., 989,1394
Arden, E.A., 1242, 1245, 1394
Arenas, J.F., 1270,1394
Arey, J., 72, 88, 135, 163, 165, 168, 170, 173, 174, 175, 183, 184, 185, 186, 187, 195, 196, 198, 207, 208, 210, 211, 212, 213, 214, 216, 217, 219, 221, 222, 227, 228, 232, 237, 238, 239, 241, 242, 243, 244, 245, 246, 247, 248, 249, 250, 254, 255, 310, 311, 312, 313, 314, 331, 333, 334, 362, 367, 368, 369, 410, 412, 413, 414, 416, 417, 421, 422, 423, 424, 426, 427, 428, 429, 430, 431, 432, 435, 442, 450, 453, 454, 455, 458, 460, 470, 476, 479, 484, 486, 493, 501, 505, 510, 512, 514, 526, 541, 548, 554, 555, 556, 557, 558, 559, 561, 565, 566, 567, 574, 575, 586, 587, 588, 591, 609, 612, 614, 615, 616, 618, 627, 628, 629, 630, 631, 632, 639, 661, 694, 695, 696, 697, 698, 699, 700, 701, 710, 721, 729, 730, 734, 736, 737, 738, 740, 741,742, 896, 929, 956, 957, 958, 959, 960, 961, 1073, 1308, 1325, 1326, 1328, 1329, 1330, 1331, 1332, 1338, 1339, 1340, 1341, 1342, 1392, 1394, 1395, 1396, 1397, 1398, 1400, 1423, 1424, 1426, 1434, 1440, 1449, 1450, 1453, 1454, 1459, 1469, 1473, 1476
Argüello, G.A., 272, 636, 638, 641, 643, 644, 1079, 1080, 1082, 1083, 1084, 1085, 1086, 1087, 1080, 1229, 1409, 1474
Arif, M., 290, 291, 292, 293, 306, 307, 308, 1394
Arikawa, T., 1239, 1428
Arneth, A., 1368, 1477
Arnold, F., 1380, 1459
Arnold, S.R., 77, 78, 79, 85, 87, 660, 1092, 1093, 1094, 1095, 1096, 1101, 1104, 1106, 1394, 1402, 1437
Ascenzi, D., 124, 1455
Aschmann, S.M., 72, 112, 133, 134, 138, 140, 141, 142, 143, 145, 147, 148, 149, 168, 170, 171, 178, 179, 181, 182, 184, 216, 217, 219, 221, 222, 223, 224, 225, 227, 239, 241, 243, 244, 245, 246, 247, 248, 249, 250, 251, 252, 265, 302, 306, 309, 310, 312, 313, 315, 317, 323, 325, 331, 333, 334, 346, 347, 348, 354, 355, 356, 362, 367, 368, 369, 385, 389, 390, 391, 409, 410, 411, 412, 416, 417, 423, 426, 427, 428, 429, 430, 431, 432, 435, 442, 450, 453, 454, 455, 458, 460, 470, 476, 479, 484, 486, 493, 501, 505, 510, 512, 514, 529, 537, 541, 548, 555, 599, 600, 605, 606, 608, 609, 612, 614, 615, 616, 631, 632, 639, 661, 666, 667, 668, 669, 673, 674, 675, 676, 678, 679, 682, 683, 684, 694, 696, 698, 699, 700, 701, 706, 708, 709, 710, 713, 714, 729, 730, 732, 734, 735, 736, 740, 741, 742, 780, 804, 810, 821, 844, 845, 846, 853, 854, 870, 887, 895, 896, 897, 898, 899, 900, 901,

911, 912, 913, 914, 915, 916, 917, 918, 919, 921, 922, 929, 950, 951, 952, 955, 956, 957, 958, 959, 960, 961, 1217, 1308, 1338, 1339, 1340, 1341, 1342, 1392, 1394, 1395, 1396, 1397, 1409, 1423, 1434, 1440, 1453, 1454, 1467
Aslam, M., 74, 1459
Astalos, R.J., 748, 749, 751, 752, 1475
Atkinson, G.H., 990, 1420
Atkinson, R., 10, 11, 65, 78, 88, 112, 113, 115, 117, 118, 119, 120, 121, 122, 126, 127, 128, 129, 130, 132, 133, 134, 135, 137, 138, 140, 141, 142, 143, 145, 147, 148, 149, 150, 151, 154, 157, 159, 162, 163, 165, 168, 170, 171, 173, 174, 175, 178, 179, 181, 182, 183, 184, 185, 186, 187, 188, 190, 192, 195, 196, 198, 200, 201, 202, 206, 207, 208, 209, 210, 211, 212, 213, 214, 216, 217, 219, 221, 222, 224, 225, 227, 228, 232, 234, 237, 238, 239, 241, 242, 243, 244, 245, 246, 247, 248, 249, 250, 251, 252, 253, 254, 255, 261, 265, 284, 285, 287, 290, 291, 293, 294, 299, 301, 302, 306, 308, 309, 310, 311, 312, 313, 314, 315, 317, 318, 320, 323, 324, 325, 329, 331, 333, 334, 336, 340, 343, 346, 347, 348, 350, 352, 354, 355, 356, 359, 361, 362, 364, 365, 367, 368, 369, 372, 373, 375, 376, 377, 378, 379, 380, 381, 383, 385, 389, 390, 391, 406, 407, 408, 409, 410, 411, 412, 413, 414, 415, 416, 417, 418, 419, 420, 421, 422, 423, 424, 425, 426, 427, 428, 429, 430, 431, 432, 433, 435, 442, 450, 453, 454, 455, 458, 460, 465, 466, 470, 479, 482, 483, 484, 486, 489, 493, 494, 496, 501, 505, 510, 511, 512, 514, 515, 517, 518, 519, 520, 521, 522, 525, 526, 527, 529, 530, 531, 537, 540, 541, 542, 543, 544, 545, 546, 547, 548, 549, 550, 551, 552, 554, 555, 556, 557, 558, 559, 560, 561, 562, 563, 565, 566, 568, 569, 570, 571, 572, 573, 574, 575, 576, 577, 578, 581, 583, 585, 586, 587, 588, 591, 592, 593, 594, 595, 596, 597, 599, 600, 601, 602, 603, 605, 606, 607, 608, 609, 610, 612, 614, 615, 616, 617, 618, 621, 622, 623, 624, 626, 627, 628, 629, 630, 631, 632, 633, 634, 637, 639, 652, 654, 657, 658, 660, 661, 662, 663, 666, 667, 668, 669, 671, 672, 673, 674, 675, 676, 678, 679, 680, 683, 684, 685, 686, 688, 693, 694, 695, 696, 697, 698, 699, 700, 701, 702, 703, 705, 706, 708, 709, 710, 711, 712, 713, 714, 715, 716, 717, 718, 719, 720, 721, 722, 723, 724, 725, 727, 728, 729, 730, 731, 732, 734, 735, 736, 737, 738, 739, 740, 741, 742, 748, 750, 752, 754, 757, 758, 764, 769, 770, 772, 773, 774, 752, 780, 784, 788, 789, 794, 798, 800, 803, 804, 805, 806, 807, 810, 813, 815, 817, 819, 820, 821, 823, 826, 829, 830, 832, 833, 834, 837, 838, 841, 844, 845, 846, 847, 848, 853, 854, 856, 858, 859, 861, 862, 863, 864, 865, 866, 869, 870, 873, 876, 886, 887, 888, 889, 890, 891, 893, 895, 896, 897, 898, 899, 900, 901, 902, 903, 906, 908, 909, 911, 912, 913, 914, 915, 916, 917, 918, 919, 920, 921, 922, 923, 925, 926, 928, 929, 933, 934, 936, 937, 940, 941, 942, 950, 951, 952, 955, 956, 957, 958, 959, 960, 961, 963, 964, 965, 966, 969, 971, 972, 973, 975, 976, 984, 990, 1030, 1033, 1035, 1042, 1054, 1058, 1065, 1073, 1083, 1143, 1194, 1217, 1218, 1230, 1234, 1276, 1288, 1308, 1312, 1313, 1314, 1317, 1318, 1323, 1324, 1325, 1326, 1328, 1329, 1330, 1331, 1332, 1333, 1335, 1336, 1338, 1339, 1340, 1341, 1342, 1343, 1345, 1347, 1356, 1358, 1373, 1392, 1394, 1395, 1396, 1397, 1398, 1400, 1405, 1409, 1410, 1412, 1419, 1421, 1423, 1424, 1426, 1434, 1440, 1449, 1450, 1451, 1452, 1453, 1454, 1459, 1460, 1467, 1471, 1473, 1472
Atlas, E.L., 76, 91, 92, 93, 94, 762, 886, 1380, 1383, 1384, 1397, 1402, 1418, 1425, 1431, 1453, 1454, 1459, 1461, 1463, 1475
Audley, G.J., 554, 555, 557, 558, 561, 562, 563, 565, 566, 567, 569, 570, 571, 572, 936, 937, 939, 940, 942, 1397
August, J., 1261, 1264, 1397
Aumont, B., 1363, 1364, 1397, 1463
Ausloos, P., 1115, 1117, 1118, 1119, 1122, 1124, 1128, 1134, 1137, 1138, 1177, 1178, 1187, 1191, 1193, 1194, 1208, 1397, 1403
Avataneo, M., 511, 512, 1393
Avery, M., 91, 92, 93, 1459
Ayers, G., 73, 1398
Ayorinde, F.O., 109, 1398
Ayscough, P.B., 1187, 1188, 1189, 1398
Azad, K., 135, 1398

Baasandorj, M., 210, 212, 213, 1398
Baba, M., 1147, 1156, 1398
Bacak, A., 296, 297, 1458
Bacher, C., 586, 587, 588, 589, 1024, 1026, 1398
Bächmann, K., 76, 78, 79, 80, 81, 82, 83, 84, 85, 86, 87, 89, 90,1423
Back, R.A., 1197, 1198, 1200, 1202, 1455, 1477

Badcock, C.C., 1162, 1209, 1210, 1211, 1213, 1398, 1459
Bader, R.F.W., 1165, 1393
Báez, A.P., 75, 1398
Baeza, M.T., 389, 390, 391, 410, 411, 413, 563, 564, 569, 570, 601, 602, 605, 606, 616, 1405
Baeza-Romero, M.T., 201, 202, 595, 596, 660, 661, 662, 1095, 1398, 1407, 1450
Bahou, M., 975, 1409
Bahreini, R., 762, 1377, 1419, 1436, 1461
Bahta, A., 994, 995, 1001, 1002, 1004, 1413, 1425
Bailey, B., 98, 1398
Baird, N.C., 1164, 1398
Baker, J., 586, 587, 588, 591, 612, 614, 615, 616, 618, 694, 695, 696, 697, 736, 1398
Bakken, V., 543, 544, 553, 554, 1400, 1412
Baldwin, R.R., 382, 383, 384, 1398
Balestra-Garcia, C., 546, 547, 549, 551, 552, 634, 635, 636, 637, 638, 639, 640, 641, 646, 647, 648, 649, 1398
Balkanski, Y., 1372, 1431
Ball, J.C., 154, 259, 262, 265, 267, 268, 270, 271, 272, 273, 285, 295, 296, 340, 341, 342, 385, 470, 484, 493, 494, 506, 515, 564, 565, 573, 635, 636, 638, 640, 641, 643, 644, 657, 658, 659, 662, 663, 664, 724, 725, 726, 751, 752, 772, 773, 777, 778, 781, 797, 798, 799, 843, 844, 876, 887, 888, 889, 890, 891, 893, 901, 907, 908, 938, 965, 966, 968, 1079, 1080, 1082, 1083, 1084, 1085, 1086, 1087, 1088, 1230, 1393, 1398, 1409, 1425, 1428, 1429, 1436, 1439, 1461, 1471, 1472
Ballan, D.G., 1159, 1456
Ballesteros, B., 145, 146, 147, 148, 149, 165, 166, 167, 169, 170, 172, 174, 176, 177, 550, 551, 552, 555, 556, 557, 558, 559, 561, 565, 567, 573, 574, 576, 605, 611, 612, 613, 660, 661, 662, 666, 667, 672, 673, 674, 678, 679, 764, 861, 863, 1392, 1398, 1405, 1439, 1430
Baltensperger, U., 1377, 1417, 1431
Balundgi, D.R., 11, 1477
Bamford, C.H., 997, 1010, 1012, 1130, 1398
Bamford, D.J., 1164, 1444
Bandow, H., 104, 141, 905, 906, 907, 908, 909, 910, 1164, 1171,1398, 1431, 1444, 1447
Bandy, B.J., 77, 78, 79, 85, 87, 1437
Bar, I., 1274, 1435
Bardini, P., 251, 252, 253, 1465
Bardwell, M.W., 296, 297, 1458
Barker, J.R., 546, 962, 963, 964, 1408, 1453, 1466
Barket, D.J., Jr., 576, 581, 585, 1403
Barkley, M.P., 1389, 1390, 1399, 1449
Barletta, B., 1367, 1388, 1418
Barnes, I., 118, 120, 141, 142, 145, 157, 158, 185, 186, 187, 244, 247, 248, 249, 253, 254, 255, 256, 264, 272, 286, 340, 349, 350, 351, 358, 359, 360, 361, 363, 364, 365, 366, 367, 374, 375, 376, 377, 378, 379, 380, 382, 383, 385, 396, 397, 398, 399, 400, 401, 402, 406, 407, 408, 409, 410, 412, 413, 414, 415, 417, 418, 526, 528, 597, 598, 628, 629, 630, 631, 636, 638, 639, 640, 646, 647, 648, 649, 657, 658, 659, 662, 663, 664, 669, 670, 700, 702, 703, 704, 706, 709, 720, 721, 722, 742, 744, 759, 760, 779, 780, 781, 824, 825, 826, 827, 828, 829, 830, 841, 842, 846, 847, 848, 849, 858, 859, 860, 861, 862, 863, 864, 887, 888, 889, 890, 891, 893, 901, 907, 908, 924, 925, 926, 927, 928, 929, 930, 932, 933, 938, 962, 963, 964, 979, 1017, 1019, 1021, 1028, 1029, 1030, 1042, 1043, 1044, 1045, 1046, 1047, 1050, 1051, 1054, 1064, 1070, 1071, 1072, 1078, 1079, 1083, 1085, 1216, 1217, 1218, 1230, 1290, 1292, 1293, 1296, 1297, 1298, 1312, 1313, 1314, 1316, 1317, 1319, 1344, 1345, 1355, 1372, 1386, 1396, 1399, 1400, 1401, 1402, 1407, 1416, 1426, 1431, 1433, 1438, 1440, 1446, 1447, 1448, 1451, 1452, 1454, 1456, 1461, 1462, 1465, 1466, 1470, 1472, 1473, 1474, 1475, 1479
Baronacski, A.P., 1269, 1271, 1478
Barone, S.B., 608, 706, 708, 709, 710, 1031, 1036, 1037, 1038, 1197, 1204, 1205, 1206, 1207, 1420
Barrell, R., 75, 76, 78, 1393
Barrett, C.J., 111, 1455
Barry, J., 636, 647, 648, 1399
Bartels, M., 384, 385, 551, 552, 1399
Bartocci, C., 599, 600, 1439
Bartz, J.A., 1335, 1336, 1419
Barzaghi, P., 763, 1425
Bass, A.M., 1163, 1169, 1403
Bastian, V., 118, 120, 962, 963, 964, 1399
Basu, A., 105, 1417
Bates, T.S., 115, 1392
Batt, L., 1242, 1411
Bauerle, S., 652, 653, 655, 656, 1090, 1091, 1092, 1093, 1094, 1095, 1096, 1308, 1311, 1399, 1420
Baugh, W., 82, 86,1393
Baulch, D.L., 112, 113, 117, 119, 121, 122, 126, 127, 128, 129, 130, 132, 134, 138, 140, 141, 143, 147, 150, 151, 152, 153, 154, 157, 159, 161,162, 163, 178, 184,

186, 188, 192, 195, 200, 201, 202, 204, 206, 209, 212, 214, 216, 225, 234, 237, 242, 245, 248, 252, 254, 261, 265, 284, 285, 308, 317, 325, 333, 336, 340, 347, 350, 355, 372, 373, 375, 376, 377, 378, 379, 380, 381, 383, 385, 390, 406, 407, 408, 410, 418, 422, 427, 428, 429, 453, 458, 465, 466, 479, 482, 483, 486, 489, 494, 496, 511, 514, 515, 517, 542, 545, 546, 548, 550, 552, 554, 555, 556, 557, 558, 559, 560, 561, 562, 563, 565, 566, 567, 568, 570, 571, 572, 573, 575, 577, 578, 588, 597, 600, 601, 603, 605, 606, 607, 608, 609, 610, 615, 616, 617, 621, 622, 623, 629, 632, 637, 639, 652, 654, 657, 661, 663, 668, 669, 674, 697, 701, 703, 705, 709, 710, 714, 716, 723, 725, 727, 728, 730, 735, 740, 742, 752, 772, 773, 783, 787, 789, 795, 798, 803, 808, 811, 815, 818, 820, 821, 826, 844, 848, 849, 854, 855, 856, 860, 862, 869, 873, 876, 888, 889, 890, 891, 893, 895, 896, 897, 898, 899, 900, 901, 906, 908, 909, 911, 912, 913, 914, 915, 917, 918, 920, 921, 922, 925, 926, 928, 933, 934, 936, 937, 939, 940, 941, 942, 952, 956, 961, 963, 969, 975, 984, 1083, 1188, 1288, 1384, 1396, 1397, 1399, 1456

Baumann, K., 611, 887, 968, 1454, 1475

Baussand, P., 805, 806, 807, 809, 810, 812, 813, 814, 824, 832, 849, 850, 851, 852, 853, 1410, 1417

Baxley, J.S., 145, 146, 147, 148, 149, 159, 370, 372, 834, 1399, 1474, 1476

Bayes, K.D., 290, 291, 292, 293, 1413

Bayliss, N.S., 1267, 1399

Beach, S.D., 448, 449, 450, 451, 502, 503, 504, 505, 506,1399

Beauchamp, J.L., 1377, 1419

Beavan, S.W., 1176, 1177, 1186, 1187, 1191, 1192, 1193, 1399

Becerra, R., 1159, 1399

Bechtel, H.A., 124, 1399

Beck, J., 115, 1450

Becker, D.A., 975, 1447

Becker, K.H., 10, 11, 65, 85, 86, 87, 88, 89, 112, 118, 119, 120, 126, 132, 138, 141, 142, 145, 157, 158, 171, 184, 186, 195, 198, 202, 212, 225, 237, 242, 244, 245, 247, 248, 249, 252, 253, 254, 255, 256, 286, 287, 340, 341, 344, 349, 350, 351, 358, 359, 360, 361, 363, 364, 365, 366, 367, 383, 385, 396, 397, 398, 399, 400, 401, 402, 406, 407, 408, 409, 410, 412, 413, 414, 415, 417, 418, 425, 427, 525, 551, 559, 562, 563, 568, 569, 571, 572, 577, 578, 597, 598, 608, 609, 612, 615, 616, 628, 629, 630, 631, 632, 633, 634, 636, 639, 646, 647, 648, 649, 700, 720, 721, 722, 742, 744, 759, 760, 773, 779, 780, 781, 824, 825, 826, 827, 828, 829, 830, 841, 842, 844, 846, 847, 848, 853, 854, 856, 859, 887, 888, 889, 890, 891, 893, 896, 899, 901, 907, 908, 913, 914, 917, 920, 921, 923, 924, 925, 926, 927, 928, 929, 930, 932, 933, 934, 938, 957, 958, 960, 962, 963, 964, 976, 979, 984, 1017, 1019, 1021, 1028, 1029, 1030, 1033, 1035, 1042, 1043, 1044, 1045, 1046, 1047, 1050, 1051, 1054, 1064, 1070, 1071, 1072, 1078, 1079, 1216, 1217, 1218, 1219, 1221, 1230, 1290, 1292, 1293, 1296, 1297, 1298, 1312, 1313, 1314, 1316, 1317, 1318, 1319, 1333, 1335, 1336, 1342, 1343, 1344, 1345, 1347, 1355, 1356, 1358, 1373, 1386, 1396, 1399, 1400, 1401, 1405, 1407, 1420, 1433, 1437, 1438, 1440, 1444, 1446, 1447, 1448, 1449, 1451, 1452, 1456, 1461, 1462, 1465, 1466, 1470, 1472, 1473, 1474, 1475, 1478, 1479

Behnke, W., 1348, 1349, 1449

Beirle, S., 1390, 1476

Bejan, I., 374, 375, 376, 377, 378, 379, 380, 657, 658, 659, 662, 663, 664, 669, 670, 702, 703, 705, 707, 848, 849, 858, 859, 860, 861, 862, 863, 864, 1402, 1447, 1479

Belcher, N.M., 1272, 1273, 1417

Bell, W.E., 1208, 1211, 1212, 1213, 1400, 1401

Belmont, R.D., 75, 1398

Bendsura, A., 652, 653, 655, 1469

Bennett, K.A., 733,1437

Bennett, P.J., 299, 300, 301, 302, 306, 307, 308, 310, 311, 312, 317, 319, 320, 321, 323, 324, 325, 331, 332, 333, 335, 336, 526, 1400

Benning, L., 76, 78, 1400

Benson, S.W., 282, 526, 1147, 1156, 1159, 1400, 1425, 1433

Benter, Th., 264, 272, 374, 375, 376, 377, 378, 379, 380, 382, 383, 638, 640, 657, 658, 659, 662, 663, 664, 669, 670, 702, 703, 705, 707, 887, 888, 889, 890, 891, 893, 901, 1230, 1461, 1479

Bérces, T., 124, 259, 267, 269, 547, 549, 561, 562, 563, 571, 572, 635, 636, 640, 641, 647, 648, 652, 653, 655, 997, 998, 999, 1092, 1093, 1094, 1095, 1096, 1101, 1106, 1188, 1279, 1400, 1414, 1417, 1418, 1429, 1433, 1444, 1469, 1470

Berdah, M., 1239, 1441

Bergeat, A., 656, 1406

Berger, M., 1318, 1319, 1321, 1322, 1324, 1325, 1400
Berges, M.G.M., 1197, 1199, 1202, 1203, 1400
Bergmann, K., 1261, 1455
Berkowitz, C.M., 115, 1461
Bernardi, F., 1030, 1453
Bernath, P.F., 1390, 1391, 1400, 1414
Berndt, T., 237, 386, 409, 410, 411, 412, 413, 414, 418, 419, 1400, 1432
Bernhard, M.J., 224, 225, 1400
Bertman, S.B., 78, 79, 82, 85, 87, 88, 89, 94, 95, 611, 843, 844, 886, 887, 968, 1400, 1428, 1446, 1448, 1451, 1454, 1475
Bertram, T.H., 91, 92, 93, 1459
Bethel, H.L., 135, 163, 165, 168, 170, 173, 174, 175, 183, 184, 185, 526, 539, 697, 698, 699, 721, 1460
Betterton, E.A., 753, 1026, 1400, 1430
Beukes, J.A., 543, 544, 553, 554, 1400, 1412
Bey, I., 1367, 1380, 1381, 1386, 1400, 1429, 1459
Biemann, K., 1273, 1416
Bierbach, A., 409, 410, 412, 413, 414, 415, 597, 598, 720, 721, 722, 846, 847, 848, 1042, 1043, 1044, 1045, 1046, 1047, 1051, 1218, 1400, 1411, 1433
Biermann, H.W., 1234, 1394, 1401, 1451
Biggs, P., 296, 297, 526, 528, 905, 906, 907, 908, 909, 910, 911, 1458, 1474
Bignozzi, C.A., 599, 600, 653, 655, 1409, 1439
Bilde, M., 265, 275, 276, 385, 485, 486, 492, 493, 501, 742, 762, 769, 770, 779, 780, 781, 842, 868, 869, 870, 875, 879, 957, 958, 959, 1401, 1409, 1418, 1420, 1442, 1471, 1472, 1473
Bishop, G.A., 64, 1401
Bitto, H., 1164, 1165, 1401
Bjarrum, M., 160, 161, 1428
Blacet, F.E., 989, 990, 991, 993, 994, 995, 997, 998, 999, 1001, 1003, 1004, 1005, 1039, 1054, 1058, 1060, 1099, 1107, 1108, 1137, 1159, 1174, 1181, 1182, 1183, 1208, 1209, 1211, 1212, 1213, 1215, 1318, 1322, 1400, 1401, 1402, 1426, 1436, 1451, 1455, 1462, 1464, 1465
Black, G., 962, 963, 964, 1054, 1060, 1061, 1208, 1466
Blades, A.T., 1147, 1158, 1159, 1402, 1433
Blais, N.C., 1269, 1402
Blake, D.R., 73, 76, 84, 91, 92, 93, 94, 115, 886, 1367, 1379, 1380, 1388, 1402, 1418, 1429, 1453, 1459, 1463, 1476
Blake, N.J., 76, 91, 92, 93, 115, 886, 1380, 1402, 1418, 1459, 1463, 1476
Blanco, M.B., 764, 765, 848, 849, 858, 859, 860, 861, 862, 863, 864, 858, 859, 860, 861, 862, 863, 864, 873, 875, 881, 882, 883, 884, 1402, 1465
Blandini, F., 511, 512, 1393
Blank, D.A., 1098, 1099, 1446
Blitz, M.A., 283, 284, 285, 288, 546, 548, 549, 550, 595, 596, 596, 660, 661, 662, 1092, 1093, 1094, 1095, 1096, 1098, 1100, 1101, 1102, 1104, 1106, 1107, 1308, 1309, 1310, 1394, 1398, 1402, 1407, 1465
Bloss, C., 592, 618, 1360, 1402
Bloss, W.J., 112, 592, 618, 1360, 1362, 1402, 1420, 1461
Bodenbinder, M., 1240, 1402
Bodhaine, B.A.., 886, 1471
Boersma, K.F., 1388, 1442
Böge, O., 237, 386, 409, 410, 411, 412, 413, 414, 418, 419, 1400, 1402
Bohr, F., 652, 653, 655, 656, 1406, 1469
Boldan, P., 84, 95, 1454
Bolzacchini, E., 237, 238, 239, 424, 425, 1402
Bonard, A., 290, 291, 292, 293, 306, 307, 308, 340, 341, 349, 350, 351, 358, 359, 360, 1402, 1470
Bond, T.C., 1388, 1389, 1462
Bongartz, A., 1234, 1235, 1403
Boone, C.D., 1390, 1391, 1414
Bordorf, B.F., 1060, 1438
Börjesson, G., 74, 1459
Borkowski, R.P., 1115, 1138, 1403
Borup, R.L., 105, 1458
Bossard, A.R., 748, 749, 750, 752, 761, 1430
Bossmeyer, J., 550, 551, 552, 555, 556, 558, 559, 1403
Bossoutrot, V., 183, 184, 185, 259, 261, 262, 270, 271, 272, 636, 638, 643, 686, 699, 1176, 1180, 1432, 1439
Botelho, M.M., 104, 1444
Bott, J.F., 117, 1403
Bottenheim, J., 75, 77, 84, 115, 1430, 1458
Botton, J.R., 1344, 1437
Bouma, W.J., 989, 1164, 1170, 1403, 1460
Bowen, E.J., 1331, 1403
Bowman, F., 1374, 1377, 1447
Bowman, J.H., 576, 581, 585, 1403
Boyd, A.A., 657, 1403
Boyd, R.J., 543, 544, 554, 580, 656, 1392, 1443
Bozzelli, J.W., 1080, 1231, 1479
Bradley, J.N., 658, 1392
Bradley, W.R., 171, 182, 1403
Bradshaw, J.D., 84, 1380, 1459
Bramer, S.E., 1271, 1455
Brand, J.C.D., 1208, 1403

Brasseur, G.P., 18, 257, 752, 753, 1358, 1367, 1380, 1382, 1403, 1427, 1443
Brauers, T., 550, 551, 552, 555, 556, 558, 559, 1403
Braun, W., 1030, 1163, 1169, 1204, 1205, 1403, 1416
Braune, B.M., 257, 1439
Bravo, I., 486, 492, 493, 777, 778, 782, 783, 784, 1394, 1403
Bravo-Perez, G., 544, 1392
Brechtel, F.J., 762, 1461
Breitenbach, L.P., 72, 283, 284, 285, 540, 541, 542, 543, 554, 545, 546, 547, 549, 551, 552, 554, 555, 592, 593, 620, 638, 644, 645, 1310, 1445, 1463
Bretschneider, V.K., 1273, 1403
Brimblecombe, P., 753, 1432
Broadbent, A.D., 1141, 1451
Brocco, D., 75, 78, 79, 82, 84, 1452
Brophy, N.C.J., 25, 38, 1414
Bröske, R., 1017, 1019, 1021, 1078, 1079, 1451
Brouard, M., 1261, 1264, 1397
Brough, N., 1362, 1461
Brown, A.C., 471, 502, 503, 504, 723, 1403
Brown, H.W., 1268, 1403
Brown, L.R., 1227, 1454
Brown, R.G., 1192, 1399
Brown, S.S., 115, 543, 551, 904, 905, 1286, 1392, 1403, 1404, 1448
Brubaker, W.W., Jr., 430, 431, 432, 433, 518, 519, 520, 521, 1404
Bruce, J., 139, 140, 141, 256, 1477
Brudnik, K., 543, 544, 554, 1412
Bruehl, C., 1369, 1404
Brugge, S.P., 1269, 1270, 1461
Brugger, P.-A., 1209, 1423
Brühlmann, U., 1239, 1240, 1274, 1276, 1404, 1420, 1463
Brune, W.H., 82, 86, 1381, 1382, 1383, 1393, 1429, 1459
Brunet, V., 1123, 1124, 1404
Brunning, J., 122, 123, 124, 1450
Bruno, P., 1234, 1235, 1236, 1463
Bruschi, M., 237, 238, 239, 1402
Brutier, L., 241, 242, 243, 244, 245, 247, 248, 249, 1410
Bryukov, M.G., 113, 265, 1404
Bu, L., 11,1477
Buchmann, B., 77, 78, 79, 80, 82, 85, 86, 87, 88, 89, 104, 1436
Buchta, C., 303, 313, 1404
Buck, R.C., 257, 641, 644, 1079, 1080, 1082, 1083, 1084, 1085, 1086, 1087, 1080, 1409, 1452, 1477
Buckley, T.J., 868, 869, 870, 1401
Buehler, B., 711, 1417
Bufalini, J.J., 306, 307, 308, 309, 323, 324, 325, 326, 1318, 1322, 1434, 1460
Buhr, M.P., 78, 82, 83, 85, 87, 611, 887, 968, 1418, 1454, 1475
Bui, T.P., 1383, 1475
Bui, V.X., 753, 754, 755, 756, 758, 1432
Buitrage, A.A., 990, 991, 994, 998, 1002, 1006, 1011, 1024, 1076, 1077, 1079, 1090, 1091, 1107, 1110, 1113, 1128, 1144, 1164, 1176, 1177, 1197, 1267, 1440
Burak, I., 1054, 1058, 1404
Burgess, R.A., 115, 1450
Burkholder, J.B., 126, 127, 163, 164, 210, 211, 212, 213, 214, 215, 258, 266, 267, 281, 546, 548, 549, 574, 592, 593, 594, 608, 611, 612, 613, 617, 627, 628, 629, 637, 639, 647, 648, 649, 706, 708, 709, 710, 905, 906, 907, 908, 909, 910, 911, 913, 914, 923, 924, 934, 935, 962, 963, 964, 965, 966, 1031, 1036, 1037, 1038, 1077, 1080, 1081, 1090, 1091, 1092, 1093, 1094, 1095, 1096, 1100, 1101, 1102, 1104, 1176, 1182, 1183, 1184, 1185, 1186, 1197, 1204, 1205, 1206, 1207, 1277, 1278, 1279, 1280, 1287, 1291, 1300, 1301, 1302, 1303, 1304, 1306, 1403, 1404, 1412, 1416, 1420, 1424, 1430, 1433, 1440, 1448, 1453, 1455, 1464, 1470
Burland, D.M., 1209, 1423
Burley, D.R., 1141, 1451
Burnelle, L., 1143, 1448
Burrows, J.P., 526, 528, 1024, 1061, 1277, 1367, 1385, 1389, 1390,1404, 1419, 1442, 1459, 1470, 1474, 1476
Busarow, K.L., 544, 550, 551, 552, 1406
Bush, T., 25, 38, 1414
Buss, R.J., 1054, 1059, 1061, 1425
Buth, R., 622, 623, 1404
Butkovskaya, N.I., 553, 586, 587, 588, 589, 590, 597, 691, 692, 693, 753, 754, 755, 756, 758, 1404
Butler, J.E., 1239, 1456
Butler, L.J., 1054, 1059, 1061, 1182, 1184, 1228, 1229, 1269, 1285, 1404, 1425, 1431, 1435, 1444, 1450, 1474
Butler, T.M., 1368, 1369, 1404, 1436, 1464
Butt, C.M., 873, 876, 885, 1405
Buzorius, G., 762, 1461

Cabañas, B., 201, 202, 389, 390, 391, 410, 411, 413, 415, 550, 551, 552, 555, 556, 558, 559, 561, 563, 564, 565, 567, 569, 570, 601, 602, 604, 605, 606, 616, 657, 658, 659, 662, 663, 664, 668, 669, 670,

672, 674, 675, 701, 728, 1392, 1405, 1450, 1456
Cadle, R.D., 553, 1405
Caffrey, P.J., 103,1405
Cai, X., 77, 85, 1424
Calogirou, A., 416, 417, 561, 562, 563, 564, 569, 570, 628, 629, 630, 633, 671, 732, 1073, 1197, 1202, 1203, 1207, 1208, 1405, 1420, 1426
Calvert, J.G., 10, 11, 65, 72, 76, 78, 82, 83, 85, 87, 112, 113, 115, 117, 119, 122, 126, 130, 132, 134, 138, 140, 141, 143, 146, 148, 150, 151, 154, 157, 159, 162, 163, 169, 171, 172, 173, 174, 178, 179, 181, 184, 186, 190, 194, 195, 198, 205, 207, 212, 216, 225, 234, 237, 242, 245, 248, 250, 252, 253, 255, 261, 275, 276, 277, 287, 293, 294, 295, 301, 302, 303, 305, 308, 309, 310, 311, 314, 316, 317, 318, 320, 324, 327, 329, 333, 334, 336, 338, 339, 340, 342, 344, 346, 349, 352, 353, 354, 355, 357, 359, 361, 362, 364, 365, 367, 368, 372, 375, 376, 377, 378, 379, 380, 381, 383, 387, 389, 397, 399, 400, 407, 409, 410, 411, 413, 414, 415, 417, 418, 419, 420, 422, 424, 425, 426, 427, 431, 432, 433, 437, 439, 441, 443, 444, 448, 449, 452, 453, 455, 456, 458, 460, 464, 466, 469, 473, 476, 478, 481, 482, 484, 485, 488, 489, 492, 493, 496, 505, 506, 507, 509, 512, 519, 521, 522, 525, 529, 533, 534, 540, 544, 546, 547, 549, 550, 551, 552, 558, 559, 562, 563, 565, 566, 567, 568, 569, 571, 572, 573, 576, 577, 578, 581, 593, 595, 596, 603, 607, 608, 609, 612, 615, 616, 621, 623, 629, 632, 633, 634, 637, 647, 654, 658, 661, 666, 669, 671, 673, 675, 676, 678, 682, 683, 689, 691, 697, 699, 703, 704, 709, 711, 716, 717, 718, 720, 723, 724, 727, 728, 729, 730, 732, 735, 736, 737, 739, 740, 741, 742, 765, 770, 775, 796, 801, 806, 809, 810, 813, 817, 819, 821, 824, 826, 829, 832, 834, 841, 845, 846, 847, 848, 850, 852, 853, 854, 855, 856, 857, 858, 859, 861, 862, 863, 864, 865, 866, 867, 870, 873, 886, 888, 889, 890, 891, 893, 896, 899, 906, 909, 910, 911, 913, 915, 916, 918, 919, 922, 923, 927, 930, 933, 937, 938, 940, 941, 942, 943, 944, 945, 946, 947, 948, 949, 950, 954, 960, 963, 966, 970, 973, 976, 977, 978, 984, 985, 986, 987, 988, 989, 990, 992, 993, 994, 995, 997, 998, 999, 1000, 1001, 1002, 1003, 1004, 1005, 1007, 1008, 1009, 1010, 1011, 1012, 1014, 1015, 1016, 1018, 1019, 1020, 1021, 1022, 1023, 1024, 1026, 1027, 1030, 1031, 1033, 1034, 1035, 1042, 1054, 1055, 1057, 1060, 1061, 1065, 1068, 1070, 1072, 1076, 1077, 1078, 1080, 1082, 1083, 1084, 1085, 1086, 1088, 1089, 1092, 1094, 1096, 1100, 1102, 1105, 1106, 1107, 1109, 1112, 1114, 1115, 1116, 1119, 1120, 1123, 1124, 1125, 1126, 1127, 1128, 1130, 1131, 1133, 1134, 1135, 1136, 1137, 1138, 1139, 1141, 1143, 1144, 1146, 1148, 1150, 1151, 1152, 1153, 1154, 1155, 1156, 1159, 1161, 1162, 1163, 1175, 1176, 1177, 1178, 1179, 1180, 1181, 1182, 1184, 1186, 1187, 1188, 1189, 1190, 1191, 1194, 1195, 1208, 1209, 1210, 1211, 1213, 1214, 1217, 1223, 1224, 1225, 1227, 1228, 1230, 1231, 1232, 1233, 1234, 1235, 1240, 1241, 1252, 1261, 1262, 1263, 1267, 1268, 1272, 1273, 1276, 1287, 1288, 1289, 1290, 1291, 1298, 1300, 1301, 1302, 1303, 1304, 1305, 1306, 1308, 1310, 1312, 1313, 1314, 1317, 1318, 1333, 1335, 1336, 1342, 1343, 1345, 1347, 1356, 1358, 1373, 1398, 1401, 1405, 1406, 1416, 1418, 1419, 1420, 1423, 1427, 1429, 1434, 1437, 1441, 1444, 1455, 1459, 1462, 1463, 1468
Camden, J.P., 124, 1399
Cameron, M., 553, 1405
Campbell, I.M., 108, 118, 120, 125, 127, 132, 133, 141, 142, 554, 555, 557, 558, 561, 562, 563, 565, 566, 567, 569, 570, 571, 572, 796, 797, 800, 801, 802, 824, 825, 826, 827, 829, 936, 937, 939, 940, 941, 942, 943, 944, 1397, 1399, 1405
Campbell, R.J., 1147, 1406
Campos, T., 76, 1425
Canagaratna, M.R., 115, 1372, 1464, 1478
Canakci, M., 109, 111, 1406
Canneaux, S., 652, 653, 655, 1469
Canosa-Mas, C.E., 121, 122, 124, 201, 202, 222, 296, 297, 312, 317, 325, 329, 374, 376, 471, 502, 503, 504, 526, 528, 601, 602, 603, 604, 609, 610, 636, 647, 648, 654, 655, 657, 658, 659, 710, 711, 712, 713, 714, 715, 716, 717, 723, 741, 743, 744, 745, 765, 769, 770, 771, 855, 856, 860, 862, 865, 866, 867, 905, 906, 907, 908, 909, 910, 911, 969, 1391, 1399, 1403, 1406, 1407, 1450, 1458, 1474
Cantrell, C.A., 76, 78, 82, 83, 85, 87, 544, 550, 551, 552, 984, 1100, 1273, 1406, 1418, 1455, 1468
Cao, J.J., 64,1426
Cape, J.N., 1347, 1435, 1438
Cappa, C.D., 762, 1406
Caralp, F., 656, 1187, 1406, 1441, 1466
Carassiti, V., 599, 600, 653, 655, 1409, 1439

Carl, S.A., 652, 653, 655, 753, 754, 755, 901, 904, 905, 1406, 1432, 1476
Carless, H.A.J., 1144, 1147, 1151, 1152, 1153, 1154, 1155, 1406, 1407
Carlier, M., 120, 306, 307, 308, 904, 1413
Carlier, P., 75, 77, 119, 125, 127, 210, 212, 213, 214, 216, 217, 218, 219, 543, 544, 550, 551, 552, 637, 747, 800, 801, 802, 804, 807, 809, 810, 811, 812, 813, 814, 815, 816, 817, 818, 819, 820, 821, 822, 1407, 1408, 1414, 1431, 1432, 1451
Carmichael, G.R., 91, 92, 93, 1388, 1389, 1459, 1462
Caro, E., 1208, 1407
Carpenter, L.J., 73, 85, 733, 735, 1362, 1367, 1424, 1437, 1453
Carr, R.W., Jr., 1163, 1171, 1478
Carr, S.A., 601, 602, 609, 654, 655, 657, 658, 659, 660, 661, 662, 710, 711, 741, 743, 744, 745, 765, 769, 770, 771, 855, 856, 860, 862, 1095, 1406, 1407
Carrasco, N., 210, 212, 213, 216, 217, 218, 219, 734, 735, 1407
Carroll, M.A., 82, 86, 94, 95, 1393, 1451, 1454
Carslaw, N., 77, 85, 1362, 1371, 1407, 1424, 1461
Carson, G.A., 1273, 1416
Carter, E.A., 296, 297, 1393
Carter, R.T., 1285, 1437
Carter, W.P.L., 49, 118, 120, 237, 238, 239, 241, 242, 243, 245, 246, 247, 248, 250, 309, 310, 385, 409, 410, 421, 422, 543, 544, 550, 551, 552, 592, 593, 594, 595, 596, 619, 622, 666, 667, 668, 669, 673, 674, 676, 682, 683, 684, 720, 721, 722, 734, 780, 804, 810, 821, 837, 838, 839, 899, 900, 913, 914, 915, 916, 918, 919, 921, 922, 936, 937, 959, 971, 972, 973, 1054, 1058, 1065, 1218, 1234, 1276, 1318, 1323, 1324, 1325, 1366, 1367, 1396, 1397, 1407, 1424, 1451, 1453, 1467, 1473
Carvalho, J.A., Jr., 747, 1409
Casola, G., 106, 1469
Cass, G.R., 52, 53, 59, 75, 78, 79, 80, 81, 82, 83, 84, 85, 86, 87, 94, 95, 1422, 1456, 1457
Castillo, X.G., 753, 754, 755, 1427
Castle, K.J., 1261, 1264, 1407
Catalán, J., 868, 1407
Cavalli, F., 141, 142, 145, 157, 158, 486, 492, 493, 700, 759, 760, 773, 824, 825, 826, 827, 828, 829, 830, 1407
Cavanagh, L.A., 103, 1408
Ceacero, A.A., 122, 123, 124, 128, 130, 131, 134, 135, 143, 156, 157, 158, 1420
Ceazan, N., 185, 186, 187, 1448
Chakir, A., 150, 151, 161, 162, 166, 167, 622, 623, 887, 888, 889, 890, 892, 894, 895, 896, 897, 1024, 1319, 1320, 1324, 1415, 1441, 1465
Chance, K.V., 1362, 1367, 1385, 1386, 1388, 1389, 1399
Chandra, A.K., 1228, 1229, 1463
Chang, J.-C., 1366, 1454
Chang, J.S., 546, 1408, 1462
Chang, S.G., 115, 1284, 1430, 1464
Chang, T.Y., 98, 1408
Chant, S.A., 660, 661, 662, 676, 677, 706, 708, 709, 710, 1411
Chapman, E.G., 115, 1461
Charles, M.J., 216, 1461
Chawla, G., 1054, 1058, 1404
Chebbi, A., 119, 120, 127, 306, 307, 308, 637, 747, 800, 801, 802, 809, 810, 811, 812, 813, 814, 817, 818, 819, 820, 822, 1408, 1451
Cheema, S.A., 132, 133, 134, 135, 137, 303, 304, 1408
Chen, D.-M., 1270, 1427
Chen, G., 77, 1418
Chen, H., 546, 547, 549, 1473
Chen, I.-C., 1054, 1058, 1164, 1165, 1167, 1168, 1169, 1170, 1401, 1408, 1431
Chen, J., 385, 386, 1408, 1452
Chen, L., 18, 260, 271, 274, 275, 436, 437, 438, 446, 447, 448, 451, 452, 455, 456, 457, 458, 465, 466, 471, 472, 473, 487, 488, 489, 490, 491, 492, 779, 784, 787, 788, 803, 871, 872, 874, 877, 878, 879, 880, 881, 882, 883, 885, 1408, 1434, 1466
Chen, M.-W., 1054, 1058, 1431
Chen, W., 766, 1448
Chen, X.-B., 76, 998, 1408, 1425
Chen, Y., 994, 995, 1054, 1055, 1056, 1057, 1058, 1059, 1065, 1068, 1069, 1070, 1147, 1149, 1379, 1380, 1408, 1409, 1459
Chen, Z., 284, 286, 287, 1409, 1473
Cheng, B.-M., 975, 1409
Cheng, Y., 64, 77, 78, 79, 80, 82, 83, 84, 85, 86, 998, 999, 1001, 1002, 1003, 1004, 1426
Chew, A.A., 133, 134, 137, 138, 140, 141, 142, 143, 145, 146, 147, 148, 149, 178, 302, 310, 312, 313, 315, 317, 323, 325, 347, 348, 355, 356, 609, 1409
Chiappero, M.S., 272, 636, 638, 641, 643, 644, 1079, 1080, 1082, 1083, 1084, 1085, 1086, 1087, 1080, 1409
Chichinin, A., 636, 647, 648, 1399
Chiorboli, C., 599, 600, 653, 655, 1409, 1439

Chipperfield, M.P., 660, 1092, 1093, 1094, 1095, 1096, 1101, 1104, 1106, 1394, 1402
Chisala, B.N., 106, 1409
Chishima, H., 18, 261, 265, 278, 641, 657, 660, 671, 1393
Choe, J.C., 1335, 1428
Choi, Y.S., 1164, 1165, 1166, 1432
Chong, D.P., 1164, 1173, 1174, 1409
Chow, J.C., 64, 1426
Chowdhury, P.K., 691, 692, 693, 1179, 1180, 1409
Christe, K.O., 256, 1444
Christensen, C.S., 76, 78, 84, 85, 89, 1421
Christensen, L.K., 128, 130, 131, 256, 340, 341, 342, 396, 397, 398, 399, 406, 407, 436, 438, 468, 470, 485, 486, 492, 493, 657, 658, 659, 701, 702, 772, 773, 781, 797, 798, 799, 871, 875, 876, 880, 884, 1409, 1452, 1456, 1463, 1472, 1473
Christian, T.J., 747, 1409
Christie, M.I., 1244, 1245, 1248, 1249, 1261, 1264, 1410
Chuang, C., 984, 1410
Chuong, B., 608, 706, 708, 709, 710, 1410
Cimiraglia, R., 1272, 1410
Cinderby, S., 74, 1459
Clark, J.H., 985, 986, 1410
Clauberg, H., 1164, 1165, 1166, 1470
Cleary, P.A., 288, 546, 548, 549, 550, 1465
Clegg, S.L., 753, 1432
Clegg, S.M., 1269, 1271, 1470
Clemes, T.P., 1271, 1470
Clemitshaw, K.C., 296, 297, 905, 906, 907, 908, 909, 910, 911, 924, 1277, 1288, 1410, 1453, 1458
Clifford, G.M., 619, 620, 621, 622, 1410
Cobos, C.J., 1188, 1399
Cocker, D.R., 1374, 1422
Coddeville, P., 753, 754, 755, 757, 758, 1411
Coe, C.S., 1261, 1410
Coe, H., 77, 78, 79, 85, 87, 115, 1372, 1377, 1430, 1437, 1450, 1478
Coeur, C., 824, 1410
Coeur-Tourneur, C., 241, 242, 243, 244, 245, 247, 248, 249, 1410
Coffey, M.T., 76, 1418
Cohen, N., 117, 279, 281, 283, 1403, 1469
Cohen, R.C., 91, 92, 93, 1459
Coleman, P.J., 25, 38, 1414
Coll, I., 115, 1450
Collins, D., 1374, 1377, 1426, 1447
Collins, E.M., 315, 319, 341, 344, 1410, 1474
Colucci, C., 98, 1398
Colville, C.J., 632, 1410
Combourieu, J., 282, 283, 1452
Comes, F.J., 1228, 1440
Cometto, P.M., 191, 192, 193, 195, 196, 203, 204, 205, 208, 209, 210, 494, 495, 496, 1410, 1412
Commane, R., 112, 1420
Cong, S.-L., 1240, 1477
Connell, P.S., 904, 1410
Connell, R.K., 769, 770, 771, 1407
Connelly, B.T., 1163, 1166, 1167, 1168, 1410
Conolly, C., 25, 38, 1414
Cook, D.J., 312, 317, 325, 329, 1391
Cook, K.M., 152, 153, 161, 162, 848, 849, 854, 855, 856, 860, 862, 1456
Coomber, J.W., 1030, 1039, 1410
Corchnoy, S.B., 88, 248, 419, 426, 427, 428, 429, 1308, 1394, 1395, 1410
Cornett, K.D., 280, 281, 904, 1434
Corse, E.W., 386, 387, 599, 600, 608, 661, 662, 1415
Costela, A., 1092, 1410
Cotter, E.S.N., 601, 602, 603, 604, 610, 711, 712, 1406
Cotting, R., 1240, 1469
Coulson, D.R., 1124, 1410
Cousins, I.T., 257, 1452
Cox, F.J., 1377, 1466
Cox, J., 106, 1469
Cox, R.A., 112, 113, 117, 119, 121, 122, 126, 127, 128, 129, 130, 132, 134, 138, 140, 141, 143, 147, 150, 151, 154, 157, 159, 162, 163, 178, 184, 186, 188, 192, 195, 200, 201, 202, 204, 206, 209, 212, 214, 216, 225, 234, 237, 242, 245, 248, 252, 254, 261, 265, 284, 285, 306, 307, 308, 309, 317, 325, 333, 336, 340, 347, 350, 355, 372, 373, 375, 376, 377, 378, 379, 380, 381, 383, 385, 390, 406, 407, 408, 410, 418, 422, 427, 428, 429, 453, 458, 465, 466, 479, 482, 483, 486, 489, 494, 496, 511, 514, 515, 517, 542, 545, 546, 548, 550, 552, 555, 556, 558, 559, 560, 562, 563, 565, 566, 568, 570, 571, 573, 575, 577, 578, 588, 597, 600, 601, 603, 605, 606, 607, 608, 609, 610, 615, 616, 617, 621, 622, 623, 629, 632, 637, 639, 652, 653, 654, 657, 658, 660, 661, 662, 663, 663, 668, 669, 674, 676, 677, 697, 701, 703, 705, 706, 708, 709, 710, 714, 716, 721, 723, 725, 727, 728, 730, 735, 740, 742, 752, 772, 773, 783, 787, 789, 795, 798, 803, 808, 811, 815, 818, 820, 821, 826, 844, 869, 873, 876, 888, 889, 890, 891, 893, 895, 896, 897, 898, 899, 900, 901, 906, 908, 909, 911, 912, 913, 914, 915, 917, 918, 920, 921, 922, 924, 925, 926, 928, 933, 934, 935, 937, 940, 941, 942, 952, 956, 961, 963, 969, 975,

984, 1070, 1078, 1083, 1188, 1235, 1242, 1277, 1288, 1384, 1392, 1396, 1397, 1399, 1410, 1429, 1453
Craig, D., 753, 1430
Crane, R.A., 995, 1401, 1411
Craveiro, A.A., 738, 1411
Crawford, J.H., 77, 91, 92, 93, 1381, 1418, 1459
Crawford, M.A., 128, 130, 131, 756, 757, 1411
Creasey, D.J., 77, 85, 1424
Crespo, M.T., 1092, 1410
Crim, F.F., 1335, 1336,1419
Crone, H.G., 1163, 1165, 1446
Cronin, T.J., 1002, 1003, 1004, 1006, 1007, 1008, 1010, 1011, 1012, 1013, 1014, 1015, 1016, 1017, 1318, 1319, 1323, 1324, 1325, 1411, 1479
Crosby, D.G., 1271, 1442
Crosier, J., 77, 78, 79, 85, 87, 1437
Crounse, J.D., 1303, 1445
Crowley, J.N., 112, 113, 117, 119, 120, 121, 122, 124, 126, 127, 128, 129, 130, 132, 134, 138, 140, 141, 143, 147, 150, 151, 154, 157, 159, 162, 163, 178, 184, 186, 188, 192, 195, 200, 201, 202, 204, 206, 209, 212, 214, 216, 225, 234, 237, 242, 245, 248, 252, 254, 261, 265, 284, 285, 308, 317, 325, 333, 336, 340, 347, 350, 355, 372, 373, 375, 376, 377, 378, 379, 380, 381, 383, 385, 390, 406, 407, 408, 410, 418, 422, 427, 428, 429, 453, 458, 465, 466, 479, 482, 483, 486, 489, 494, 496, 511, 514, 515, 517, 540, 541, 542, 545, 546, 548, 549, 550, 552, 555, 556, 558, 559, 560, 562, 563, 565, 566, 568, 570, 571, 573, 575, 577, 578, 586, 587, 588, 597, 600, 601, 603, 605, 606, 607, 608, 609, 610, 615, 616, 617, 621, 622, 623, 629, 632, 637, 639, 652, 653, 654, 655, 657, 658, 661, 662, 663, 668, 669, 674, 691, 692, 693, 697, 701, 703, 705, 709, 710, 714, 716, 721, 723, 725, 727, 728, 730, 735, 740, 742, 752, 772, 773, 783, 787, 789, 795, 798, 803, 808, 811, 815, 818, 820, 821, 826, 844, 869, 873, 876, 888, 889, 890, 891, 893, 895, 896, 897, 898, 899, 900, 901, 904, 905, 906, 908, 909, 911, 912, 913, 914, 915, 917, 918, 920, 921, 922, 925, 926, 928, 933, 934, 937, 940, 941, 942, 952, 956, 961, 963, 969, 975, 984, 1065, 1083, 1098, 1100, 1101, 1102, 1104, 1277, 1288, 1369, 1384, 1392, 1396, 1405, 1406, 1413, 1431, 1432, 1436, 1441, 1459, 1460, 1476
Crunaire, S., 753, 754, 755, 757, 758, 1411
Crutzen, P.J., 18, 84, 124, 257, 282, 747, 1368, 1378, 1380, 1436, 1452, 1459, 1470
Cuartero, J., 189, 765, 1394
Cuevas, C.A., 122, 123, 124, 128, 130, 131, 134, 135, 143, 156, 157, 158, 556, 560, 566, 568, 574, 575, 576, 577, 657, 658, 659, 662, 663, 664, 667, 668, 669, 670, 672, 674, 675, 677, 680, 681, 701, 728, 797, 798, 799, 801, 802, 803, 804, 805, 806, 808, 812, 815, 816, 1392, 1411, 1420
Cui, Q., 1164, 1411
Cundall, R.B., 989, 1089, 1098, 1100, 1122, 1159, 1162, 1188, 1189, 1394, 1411
Curl, R.F., 546, 547, 549, 1165, 1468, 1473
Custer, T.G., 1381, 1388, 1442
Cvetanović, R.J., 553, 557, 560, 725, 1165, 1411, 1415, 1460
Czech, E., 91, 92, 93, 1459

Da, X., 97, 1428
Dachs, J., 522, 1438
Daële, V., 185, 186, 187, 189, 190, 191, 192, 193, 195, 196, 203, 204, 205, 208, 209, 210, 290, 291, 292, 293, 306, 307, 308, 340, 341, 349, 350, 351, 358, 359, 360, 622, 623, 702, 703, 704, 706, 709, 1402, 1410, 1415, 1426, 1436, 1470
Dagaut, P., 152, 153, 159, 160, 166, 167, 168, 170, 171, 173, 177, 182, 183, 259, 261, 267, 269, 276, 285, 287, 290, 291, 295, 300, 303, 304, 305, 307, 308, 310, 311, 312, 313, 319, 320, 321, 323, 324, 325, 326, 327, 328, 331, 332, 334, 337, 338, 339, 342, 343, 345, 346, 350, 354, 355, 382, 383, 384, 386, 387, 388, 389, 391, 392, 393, 394, 395, 396, 398, 400, 401, 402, 403, 404, 531, 691, 692, 693, 700, 701, 702, 703, 707, 726, 727, 728, 729, 742, 743, 748, 749, 750, 753, 754, 755, 758, 759, 761, 775, 776, 782, 783, 785, 786, 790, 791, 792, 796, 797, 800, 801, 802, 805, 806, 807, 809, 810, 811, 812, 813, 814, 817, 819, 820, 825, 826, 827, 829, 830, 831, 832, 833, 873, 882, 883, 1411, 1412, 1437, 1471, 1473, 1474
Dainton, F.S., 1239, 1250, 1261, 1262, 1465
Dalmasso, P.R., 191, 192, 193, 195, 196, 203, 204, 205, 208, 209, 210, 448, 450, 451, 455, 494, 495, 496, 500, 501, 503, 505, 1410, 1412
Daly, J.W., 1313, 1316, 1318, 1431
Damon, E.K., 1209, 1210, 1211, 1213, 1398, 1459
D'Anna, B., 543, 544, 550, 551, 546, 547, 549, 553, 554, 555, 556, 557, 558, 559, 561, 562, 563, 564, 565, 566, 567, 568,

569, 570, 571, 572, 573, 574, 575, 576, 577, 578, 579, 581, 588, 1193, 1194, 1195, 1196, 1400, 1412, 1416
Darecki, D.R., 88, 1412
Darnall, K.R., 138, 139, 241, 242, 243, 244, 245, 246, 247, 248, 249, 299, 300, 301, 302, 310, 311, 312, 386, 387, 389, 390, 661, 662, 676, 683, 700, 805, 806, 807, 817, 819, 820, 964, 965, 1217, 1318, 1323, 1324, 1325, 1397, 1412, 1438, 1476
Dasgupta, P.K., 76, 1234, 1420, 1469
Daumont, D., 1024, 1319, 1320, 1324, 1465
Davidovits, P., 1176, 1177, 1187, 1413
Davidson, J.A., 550, 551, 552, 984, 1406
Davidsson, J., 657, 660, 671, 701, 727, 728, 1448
Davies, A.S., 1089, 1098, 1100, 1122, 1159, 1162, 1188, 1189, 1411
Davis, A.J., 306, 315, 335, 346, 1417
Davis, D.D., 118, 120, 125, 127, 282, 283, 389, 390, 1234, 1453, 1455, 1474
Davis, M.E., 611, 612, 613, 617, 627, 628, 629, 652, 654, 655, 656, 1412
Davis, S., 109, 1412
Davis, W., Jr., 997, 1111, 1114, 1123, 1412
Dawidowicz, E.A., 1176, 1177, 1187, 1412
D'Azi, O.B., 1239, 1413
Dearth, M.A., 622, 623, 1446
DeBruyn, W.J., 257, 634, 743, 745, 746, 1231, 1413, 1473
De Gouw, J.A., 73, 94, 95, 1367, 1381, 1388, 1429, 1442, 1454
Delfau, J.-L., 290, 291, 292, 293, 306, 307, 308, 1402
Delfau, L.-L., 340, 341, 349, 350, 351, 358, 359, 360, 1470
Dellinger, B., 290, 291, 292, 293, 306, 307, 308, 1394
Del Negro, L.A., 1383, 1474
Del Valle, J.C., 868, 1407
DeMare, G.R., 1322, 1413
DeMarrals, G.A., 1273, 1417
Demeter, A., 1092, 1093, 1094, 1095, 1096, 1101, 1106, 1444
Demissy, M., 1273, 1436
DeMore, W.B., 282, 283, 290, 291, 292, 293, 455, 456, 457, 459, 460, 468, 469, 471, 472, 473, 477, 478, 480, 481, 482, 483, 487, 488, 491, 529, 644, 984, 1308, 1393, 1413, 1427, 1436, 1437, 1475
Denschlag, H.O., 1147, 1148, 1150, 1413
Dentener, F.J., 1372, 1431
de Oliva, S.T., 104, 1444
de Paz, J.L.G., 868, 1407
Derwent, R.G., 65, 77, 85, 112, 113, 117, 119, 122, 126, 130, 132, 134, 138, 140, 141, 143, 146, 148, 150, 151, 154, 157, 159, 162, 163, 169, 171, 172, 173, 174, 178, 179, 181, 184, 194, 205, 207, 216, 250, 261, 275, 276, 277, 287, 293, 294, 295, 301, 302, 303, 305, 308, 309, 310, 311, 314, 316, 317, 318, 320, 324, 327, 333, 334, 338, 339, 340, 342, 346, 349, 352, 353, 354, 355, 359, 361, 367, 372, 387, 397, 399, 400, 407, 410, 411, 415, 419, 420, 422, 426, 431, 432, 437, 439, 441, 443, 444, 448, 449, 452, 453, 455, 456, 460, 464, 466, 469, 473, 476, 478, 481, 482, 484, 485, 488, 489, 492, 493, 496, 505, 506, 507, 509, 512, 519, 521, 529, 533, 534, 540, 558, 565, 566, 567, 573, 576, 593, 595, 603, 607, 621, 623, 624, 629, 637, 647, 653, 661, 671, 673, 676, 682, 683, 689, 691, 737, 765, 770, 775, 796, 801, 806, 809, 810, 813, 817, 821, 824, 826, 829, 832, 834, 841, 845, 846, 850, 852, 855, 857, 859, 867, 870, 873, 886, 888, 889, 890, 891, 893, 906, 909, 910, 911, 913, 915, 916, 918, 919, 922, 923, 927, 930, 933, 934, 935, 937, 938, 940, 941, 942, 943, 944, 945, 946, 947, 948, 949, 950, 954, 960, 963, 966, 1026, 1027, 1076, 1077, 1078, 1080, 1082, 1083, 1084, 1085, 1086, 1088, 1089, 1092, 1096, 1100, 1102, 1105, 1106, 1107, 1109, 1112, 1120, 1123, 1124, 1125, 1126, 1127, 1128, 1130, 1131, 1133, 1134, 1136, 1139, 1141, 1143, 1146, 1148, 1150, 1151, 1152, 1153, 1154, 1155, 1156, 1159, 1161, 1162, 1163, 1175, 1176, 1177, 1178, 1179, 1180, 1181, 1182, 1184, 1186, 1188, 1189, 1190, 1191, 1194, 1195, 1223, 1224, 1225, 1227, 1228, 1230, 1231, 1232, 1235, 1242, 1262, 1287, 1288, 1289, 1290, 1291, 1298, 1300, 1301, 1302, 1303, 1304, 1305, 1306, 1333, 1358, 1360, 1362, 1363, 1367, 1369, 1377, 1405, 1411, 1413, 1424, 1429, 1430, 1456
Desai, J., 994, 995, 1001, 1002, 1004, 1413, 1425
DeSain, J.D., 122, 123, 551, 552, 1460
De Serves, C., 75, 1466
Deshmukh, S., 1228, 1229, 1413
De Silva, A.O., 257, 641, 1415
De Smedt, F., 755, 756, 758, 1413
De Staricco, E.R., 1229, 1474
Devolder, P., 655, 656, 904, 1413, 1468
Dezauzler, P., 1273, 1436
Dhanya, S., 1201, 1413
Diau, E.W.-G., 1089, 1090, 1092, 1147, 1149, 1413
Diaz, C., 868, 1407
Diaz, S., 1108, 1136, 1391, 1392

D'iaz de Mera, Y., 189, 192, 194, 204, 205, 207, 486, 492, 493, 566, 568, 574, 575, 576, 577, 602, 603, 616, 617, 657, 658, 659, 669, 670, 675, 728, 729, 764, 765, 777, 778, 782, 783, 784, 861, 863, 1394, 1403, 1454
Dibb, J., 76, 91, 92, 93, 1418, 1459,
Dibble, T.S., 117, 119, 120, 125, 127, 133, 236, 237, 238, 700, 1413, 1417, 1451, 1461
Di Bella, D., 1073, 1197, 1202, 1203, 1207, 1208, 1426
Dick, B., 1240, 1416
Dickerson, R.R., 1288, 1289, 1355, 1438
Diegel, S., 109, 1412
Dill, M., 484, 529, 724, 725, 726, 868, 869, 870, 1401, 1468, 1471
Dillon, T.J., 117, 119, 120, 124, 126, 127, 130, 540, 541, 542, 586, 587, 588, 691, 692, 693, 1369, 1405, 1413, 1431, 1436, 1460
Dimicoli, I., 1239, 1441
Ding, C.-F., 1054, 1055, 1056, 1057, 1288, 1479
Ding, H., 1223, 1414
Ding, Y., 97, 1428
Dinis, C.M.F., 350, 360, 361, 363, 364, 365, 366, 1399, 1400, 1418
Di Palo, V., 75, 78, 79, 82, 84, 1452
Dixon, D.A., 256, 1444
Dixon, R.N., 76, 1163, 1223, 1235, 1237, 1414, 1469
Dixon, R.W., 78, 79, 82, 85, 89, 90, 91, 1419
Dlugokencky, E.J., 550, 551, 552, 1414
Dobbs, K.D., 643, 1230, 1473, 1474
Dóbé, S., 122, 123, 124, 259, 267, 269, 547, 549, 561, 562, 563, 571, 572, 635, 636, 640, 641, 647, 648, 652, 653, 655, 997, 998, 999, 1092, 1093, 1094, 1095, 1096, 1101, 1106, 1414, 1417, 1418, 1429, 1435, 1444, 1469
Dobeck, L.M., 1054, 1060, 1414
Docherty, K.S., 1377, 1414
Docker, M.P., 1261, 1264, 1397
Dodd, R.E., 1082, 1083, 1414
Dodge, M.C., 1365, 1420
Doerr, A.B., 1220, 1458
D'Oliveira, P., 1239, 1441
Dommen, J., 1377, 1417, 1431
Donaghy, T., 165, 172, 1414
Donahue, C.J., 411, 1430
Donahue, N.M., 769, 770, 1364, 1377, 1414, 1452
Donaldson, D.J., 256, 257, 1286, 1414, 1477
Donlon, M., 906, 907, 908, 909, 910, 911, 912, 915, 916, 917, 918, 936, 937, 938, 939, 940, 941, 942, 943, 944, 945, 947, 948, 955, 956, 1445
Donnelly, S.G., 1383, 1474
Dore, C.J., 25, 38, 1414
Dorfman, L.M., 1111, 1414
Doumani, T.F., 1261, 1410
Doussin, J.F., 119, 120, 125, 127, 210, 212, 213, 214, 216, 217, 218, 219, 306, 307, 308, 373, 374, 376, 378, 379, 380, 543, 544, 550, 551, 552, 637, 734, 735, 800, 801, 802, 804, 807, 809, 810, 811, 812, 813, 814, 815, 816, 817, 818, 819, 820, 821, 822, 1407, 1414, 1432, 1451, 1456
Drabbles, M., 1164, 1165, 1414
Drake, W., 652, 654, 655, 656, 1412
Dransfield, T.J., 753, 754, 755, 1427
Drent, E., 1209, 1414
Driscoll, D.J., 1374, 1433
Droege, A.T., 290, 291, 293, 300, 301, 1468
Drougas, E., 257, 1450
Drummond, J.R., 76, 1418
Dryer, F.L., 540, 541, 542, 1477
Duan, S.X., 1231, 1413
Dubs, M., 1239, 1276, 1404, 1414
Duffy, J.M., 601, 602, 603, 604, 610, 711, 712, 866, 867, 1406
Dufour, G., 1390, 1414
Dumesic, J.A., 111, 1455
Duncan, F.J., 1165, 1415
Dunker, A.M., 98, 106, 107, 1234, 1405, 1415
Dunlop, J.R., 137, 138, 139, 1415
Dunn, J.R., 1111, 1415
Dupuis, M., 1054, 1060, 1448
Durand-Jolibois, R., 119, 120, 125, 127, 210, 212, 213, 216, 217, 218, 219, 306, 307, 308, 373, 374, 376, 378, 379, 380, 543, 544, 550, 551, 552, 637, 800, 801, 802, 804, 807, 809, 810, 811, 812, 813, 814, 815, 816, 817, 818, 819, 820, 821, 822, 1407, 1414, 1451, 1456
Durant, D., 1264, 1265, 1266, 1415
Durham, R.W., 1107, 1415
Dutot, A.L., 94, 1467
Dzepina, K., 1377, 1470

East, A.L.L., 1164, 1257, 1433
Eberhard, J., 303, 304, 1415
Ebrecht, J., 724, 725, 1415
Edelbüttel-Einhaus, J., 130, 131, 1415
Edem, D.O., 109, 1415
Edney, E.O., 386, 387, 599, 600, 608, 661, 662, 1374, 1415, 1433
Edwards, G.S., 1273, 1416
Effenhauser, C.S., 1250, 1254, 1261, 1264, 1415

Egeløv., A.H., 90, 1377, 1445
Egsgaard, H., 295, 297,1457
Ehhalt, D., 76, 1418
Eisele, F.L., 904, 1453
El Boudali, A., 796, 797, 800, 801, 802, 805, 807, 812, 813, 814, 823, 824, 825, 1415
El Dib, G., 622, 623, 887, 888, 889, 890, 892, 894, 895, 896, 897, 1415
El Hag, M., 600, 608, 609, 710, 1466
Ellermann, T., 295, 296, 297, 494, 1429, 1435
Ellis, D.A., 18, 257, 259, 261, 262, 263, 264, 265, 267, 268, 269, 270, 271, 272, 273, 274, 278, 635, 636, 638, 640, 641, 643, 644, 657, 660, 671, 769, 770, 771, 772, 1088, 1230, 1393, 1415, 1427, 1428, 1479
Ellison, G.B., 627, 628, 629, 1412
Ells, V.R., 1107, 1415
Elsen, L., 636, 639, 646, 647, 648, 649, 1462
Elyea, D., 94, 95, 887, 968, 1446
Ember, L.R., 1273, 1415
Emmerson, K.M., 77, 85, 1424
Emmons, L.K., 91, 92, 93, 1367, 1427, 1459
Emrich, M., 1070, 1089, 1092, 1093, 1094, 1100, 1415, 1429
Encina, M.V., 1107, 1108, 1120, 1121, 1122, 1127, 1391, 1415, 1437
Engel, V., 1240, 1425
Engert, J.M., 1240, 1416
Epstein, S.S., 1272, 1273, 1417
Erdil, A., 109, 1406
Erickson, D., 72, 73, 1423
Ervens, B., 762, 763, 1372, 1415, 1431, 1461
Esser, C., 11881399
Estupiñan, E.G., 691, 692, 693, 1448
Etzkorn, T., 1316, 1317, 1319, 1344, 1345, 1396, 1416, 1433
Evans, G.B., 989, 1394
Evans, M.J., 77, 78, 79, 85, 87, 1367, 1381, 1417, 1437, 1453, 1459
Ezell, A.A., 148, 172, 411, 601, 603, 606, 607, 610, 711, 720, 1416, 1417, 1463, 1474
Ezell, M.J., 112, 148, 172, 411, 601, 603, 606, 607, 610, 711, 720, 1416, 1463, 1474

Fabian, P., 94, 1453
Facchini, M.C., 1372, 1431
Fah, A., 1239, 1426
Fahey, D.W., 1095, 1383, 1440, 1474
Fahr, A., 1030, 1204, 1205, 1416
Fajen, J.M., 1273, 1416
Fajer, R.W., 905, 906, 907, 1277, 1278, 1280, 1282, 1288, 1289, 1290, 1293, 1419, 1454
Fall, R., 72, 73, 116, 1416, 1423, 1438
Faloona, I., 82, 86, 1393
Fan, T.Y., 1273, 1416
Fang, W.-H., 998, 1054, 1059, 1061, 1225, 1408, 1416, 1437
Fantechi, G., 210, 211, 212, 213, 214, 215, 216, 217, 218, 631, 712, 1416
Faria, B.V.E., 1367, 1453
Farmanara, P., 1240, 1416
Farmer, C., 78, 79, 85, 86, 87, 88, 89, 1227, 1454
Farrell, J.T., 52, 1472
Fasano, D.M., 544, 545, 1416
Fast, J.D., 115, 1234, 1461, 1463
Faubel, C., 659, 1416
Fazekas, G.B., 1233, 1240, 1241, 1242, 1267, 1268, 1289, 1416, 1465
Fazilleau, E., 1143, 1458
Febo, A., 1234, 1235, 1236, 1463
Fedotov, V., 448, 450, 451, 503, 505, 875, 876, 1472
Fedyk, M.L., 1268, 1392
Fehsenfeld, F.C., 72, 77, 78, 82, 83, 84, 85, 86, 87, 88, 91, 92, 93, 94, 95, 103, 115, 116, 611, 886, 887, 935, 936, 968, 1392, 1416, 1418, 1421, 1443, 1454, 1462, 1475
Feierabend, K.J., 592, 593, 594, 1416
Feilberg, A., 276, 1420
Feilberg, K.L., 543, 544, 988, 1416, 1417
Feingold, G., 762, 763, 1416, 1461
Felder, P., 1030, 1239, 1250, 1254, 1261, 1264, 1288, 1308, 1309, 1415, 1423, 1431, 1465, 1477
Ferenac, M.A., 306, 315, 335, 346, 1417
Ferm, M., 1234, 1460
Fernandes, A.G., 738, 1411
Fernandes, S.D., 1388, 1389, 1462
Fernández-Gómez, M., 122, 123, 124, 128, 130, 131, 134, 135, 143, 156, 157, 158, 1420
Ferrari, C., 805, 806, 807, 809, 810, 812, 813, 814, 832, 849, 850, 851, 852, 853, 1417
Ferreiro, A., 74, 1459
Ferronato, C., 210, 211, 212, 213, 215, 216, 219, 220, 1417
Fiamegos, Y., 1073, 1197, 1202, 1203, 1207, 1208, 1426
Fida, M., 1098, 1100, 1101, 1102, 1461
Fielberg, A., 1338, 1340, 1341, 1343, 1417
Field, B.D., 73, 1367, 1380, 1381, 1400, 1429, 1459
Figuera, J.M., 1092, 1410
Filby, W.G., 622, 1417
Filella, I., 747, 1457
Filseth, S.V., 1164, 1444
Filsinger, F., 83, 1460
Fine, D.H., 1272, 1273, 1416, 1417
Fingler, S., 1347, 1466

Fink, E.H., 118, 120, 962, 963, 964, 1070, 1399
Finke, H., 1261, 1264, 1417
Finklestein, A., 1111, 1417
Finlayson-Pitts, B.J., 18, 112, 115, 148, 172, 411, 546, 553, 601, 603, 606, 607, 610, 711, 720, 748, 750, 758, 886, 904, 905, 908, 938, 957, 958, 967, 1065, 1066, 1199, 1234, 1235, 1236, 1358, 1416, 1417, 1456, 1461, 1463, 1474
Fiore, A.M., 1367, 1386, 1400, 1417, 1449
Fischer, H., 1369, 1404, 1436
Fischer, S., 282, 283, 1474
Fisseha, R., 1377, 1417, 1431
Fittschen, C., 655, 656, 753, 754, 755, 757, 758, 1411, 1468
Fitz, D.R., 241, 243, 245, 246, 249, 970, 1276, 1396, 1451
Fitzpatrick, S., 165, 172, 1414
Flad, J.E., 1100, 1101, 1102, 1104, 1453
Flagan, R.C., 253, 436, 437, 438, 439, 440, 441, 442, 444, 448, 449, 461, 621, 762, 1374, 1377, 1418, 1419, 1422, 1426, 1436, 1447, 1449, 1461, 1467, 1474, 1478
Flaherty, J., 1388, 1452
Fleisch, Th., 105, 1417
Fleischman, G., 109, 1450
Fleming, J.W., 406, 407, 541, 542, 943, 944, 955, 1269, 1271, 1478
Fletcher, T.R., 1099, 1476
Flocke, F., 91, 92, 93, 96, 886, 1380, 1383, 1402, 1417, 1459, 1463, 1475
Flowers, B.A., 1303, 1417
Flugge, M.L., 713, 714, 715, 716, 717, 865, 1406
Flynn, M., 1362, 1461
Fockenberg, C., 1164, 1165, 1417
Foltz, M.F., 984, 1164, 1410, 1444
Fontaine, M.C., 1322, 1413
Forbes, G., 94, 95, 1454
Forde, N.R., 1285, 1444
Forester, C.D., 223, 229, 230, 234, 739, 1417
Förgeteg, S., 997, 998, 999, 1279, 1400, 1417, 1418
Forst, W., 656, 1406
Foster, P., 805, 806, 807, 809, 810, 812, 813, 814, 824, 832, 849, 850, 851, 852, 853, 1410, 1417, 1470
Forstner, H.J.L., 1374, 1377, 1418, 1447
Fox, D.L., 1217, 1325, 1420
Fox, R.W., 213, 214, 215, 609, 710, 1455
Fracheboud, J.M., 691, 692, 693, 1448
Francisco, J.S., 98, 256, 296, 436, 439, 442, 446, 457, 458, 516, 517, 546, 548, 549, 645, 757, 758, 777, 778, 779, 998, 999, 1001, 1002, 1003, 1004, 1225, 1228, 1287, 1300, 1409, 1418, 1421, 1437, 1442, 1455, 1470, 1477
Francl, M.M., 1184, 1431
Frank, I., 688, 1418
Frank, P., 1188, 1399
Frank, R., 118, 120, 138, 139, 1433
Frankevich, V., 1377, 1431
Franklin, J., 769, 770, 771, 1407
Fraser, M.P., 75, 78, 79, 80, 81, 82, 83, 84, 85, 86, 87, 94, 95, 1422
Fratarcageli, R., 75, 78, 79, 82, 84, 1452
Freitas Dinis, C.M., 360, 361, 363, 364, 365, 366, 396, 397, 398,1418
Frerichs, H., 303, 313, 422, 1404, 1418
Fresnet, P., 75, 77, 1431
Frey, H.M., 1159, 1165, 1399, 1418
Fried, A., 76, 77, 88, 551, 552, 1418, 1420, 1431, 1440, 1460
Friedl, R.R., 1287, 1300, 1301, 1303, 1455
Frieß, U., 83, 1460
Fritz, B., 382, 384, 1418
Frøsig, L., 957, 958, 959, 1418
Frost, G.J., 78, 82, 83, 85, 87, 94, 95, 763, 1286, 1300, 1301, 1302, 1303, 1306, 1414, 1416, 1418, 1424, 1454
Fry, J.L., 1303, 1445
Fu, Q., 1388, 1389, 1462
Fu, T.-M., 1362, 1367, 1386, 1388, 1419
Fuelberg, H., 77, 1418
Fujimoto, E., 426, 463, 516, 517, 525, 1466
Fujimoto, G.T., 1030, 1164, 1419
Fujita, E., 89, 1422
Fukui, Y., 1380, 1459
Fukuyama, T., 1374, 1429
Fuzzi, S., 1372, 1431

Gäb, S., 1311, 1425
Gaffney, J.S., 76, 78, 79, 82, 85, 89, 90, 91, 602, 606, 905, 906, 907, 1419
Galano, A., 554, 751, 752, 1392, 1419
Galloo, I.C., 812, 813, 814, 1470
Galloo, J.-C., 655, 656, 1468
Galloway, D.B., 1335, 1336, 1419
Gandini, A., 989, 1187, 1089, 1190, 1191, 1098, 1419
Ganzeveld, L., 1369, 1436
Gao, R.-S., 1095, 1383, 1440, 1474
Gao, S., 1377, 1419, 1436
Gardner, E.P., 1030, 1031, 1033, 1034, 1035, 1092, 1094, 1419
Gardner, G.M., 1367, 1427
Garland, N.L., 437, 439, 440, 1419
Garvin, K., 109, 1398
Garzón, A., 122, 123, 128, 130, 131, 134, 135, 143, 145, 146, 147, 148, 149, 156,

157, 158, 165, 166, 167, 170, 172, 174, 176, 177, 1398, 1420, 1430
Gatti, L.V., 1389, 1449
Gay, D., 73, 1434, 1435
Gedra, A., 345, 346, 355, 370, 372, 812, 813, 814, 1424
Gefen, Z., 546, 547, 549, 554, 555, 556, 557, 558, 559, 561, 562, 563, 564, 565, 566, 567, 568, 569, 570, 571, 572, 573, 574, 575, 576, 577, 581, 1412
Geiger, G., 1274, 1276, 1420
Geiger, H., 141, 142, 145, 341, 344, 350, 360, 361, 363, 364, 365, 366, 396, 397, 398, 399, 402, 1399, 1400, 1407, 1418, 1420, 1440 1456
Genfa, Z., 76, 1420
George, C., 1235, 1403
Georgievskii, Y., 579, 1422
Gericke, K.-H., 1228, 1440
Gerlach-Meyer, U., 1307, 1420
Geron, C., 72, 73, 82, 86, 1387, 1393
Gery, M.W., 1217, 1325, 1365, 1420
Geyer, A., 76, 78, 79, 80, 81, 82, 83, 84, 85, 86, 87, 89, 90, 1234, 1423, 1463
Gezelter, J.D., 1098, 1099, 1164, 1420, 1446
Ghaquin, P., 1143, 1458
Giardini, P.F., 653, 655, 1409, Giasson, R., 1335, 1336, 1337, 1477
Gierczak, T., 163, 164, 280, 281, 574, 608, 652, 653, 655, 656, 706, 708, 709, 710, 962, 963, 964, 1031, 1036, 1037, 1038, 1090, 1091, 1092, 1093, 1094, 1095, 1096, 1100, 1101, 1102, 1104, 1176, 1182, 1183, 1184, 1185, 1186, 1197, 1204, 1205, 1206, 1207, 1404, 1420, 1430, 1440, 1453, 1464, 1468, 1471
Giessing, A.M.B., 276, 1420
Giger, W., 1347, 1466
Gilch, P., 1333, 1434
Gilderson, P., 1147, 1158, 1433
Giles, J.W., 1271, 1442
Gill, R.J., 990, 1420
Gilles, M.K., 117, 119, 120, 124, 125, 126, 127, 130, 611, 612, 613, 617, 637, 639, 647, 648, 649, 652, 653, 655, 656, 924, 1077, 1080, 1081, 1176, 1182, 1183, 1184, 1185, 1186, 1277, 1278, 1291, 1404, 1412, 1420, 1430, 1464
Gillett, R., 73, 1398
Gilpin, T., 76, 1418, 1420
Ginter, J.M., 1377, 1466
Gipson, G.L., 1366, 1420
Glasius, M., 486, 492, 493, 561, 562, 563, 564, 569, 570, 628, 629, 630, 671, 1073, 1407, 1420
Glass, G.P., 546, 547, 549, 1164, 1165, 1420, 1468, 1473
Glasson, W.A., 1273, 1323, 1420, 1426
Glenewinkel-Meyer, T., 1335, 1336, 1419
Glicker, S., 984, 1420
Gligorovski, S., 763, 1425
Glowacki, D.R., 112, 595, 596, 1398, 1420
Goddard, A., 112, 288, 546, 548, 549, 550, 1420, 1465
Goddard, J.D., 989, 990, 1439, 1477
Goede, A.P.H., 1385, 1404
Goeppert, A., 100, 1447
Goff, U.E., 1273, 1416
Goldan, P.D., 72, 77, 78, 82, 83, 84, 85, 86, 87, 88, 91, 92, 93, 94, 95, 103, 115, 116, 611, 886, 887, 968, 1392, 1416, 1418, 1421, 1443, 1454, 1462, 1475
Goldberg, L.S., 1269, 1457
Goldblatt, I.L., 1318, 1319, 1321, 1322, 1324, 1325, 1400
Golde, M.F., 117, 118, 120, 123, 1440
Golden, D.M., 546, 553, 748, 750, 758, 904, 905, 908, 938, 958, 968, 984, 1065, 1066, 1199, 1234, 1235, 1236, 1261, 1308, 1413, 1439, 1456, 1466
Goldfinger, P., 1322, 1413
Golding, B.T., 417, 418, 1312, 1316, 1433
Goldstein, A.H., 1381, 1388, 1436, 1442
Goldstone, A., 306, 307, 308, 309, 1411
Golemba, F.J., 1140, 1141, 1142, 1421
Gomez, M.V., 412, 1470
González, O.G., 75, 1398
Good, D.A., 98, 436, 439, 442, 446, 457, 458, 516, 517, 777, 778, 779, 1421, 1437
Goodman, K., 936, 937, 943, 944, 1405
Goodman, M.A., 601, 602, 605, 606, 1396
Gordon, A.S., 1115, 1441
Gordon, R.J., 1273, 1421, 1469
Gotewold, J., 1208, 1407
Goto, M., 435, 507, 508, 553, 655, 875, 880, 1421, 1468
Gotoh, Y., 259, 260, 267, 269, 273, 274, 1466
Goumri, A., 652, 654, 655, 656, 1477
Grabner, G., 1344, 1421
Gradassi, M.J., 105, 1417
Graedel, T.E., 72, 73, 116, 1421, 1423
Graedler, F., 1064, 1071, 1072, 1216, 1217, 1218, 1219, 1221, 1400, 1433
Graham, R.A., 970, 1273, 1467
Grahek, F.E., 886, 1454, 1471
Granby, K., 76, 78, 84, 85, 89, 90, 1377, 1421, 1445
Granier, C., 1367, 1427
Gravel, D., 1335, 1336, 1337, 1477
Gray, J.A., 1239, 1421
Gray, P., 1268, 1421

Graziano, G.M., 171, 172, 1403
Green, M., 595, 1421
Green, W.H., Jr., 984, 1164, 1165, 1408, 1421
Greenberg, A., 1143, 1437
Greenberg, J.P., 79, 80, 81, 84, 85, 886, 1397, 1421, 1454
Greenblatt, G.D., 1271, 1421
Greene, C.R., 713, 714, 721, 730, 1421
Greene, H.L., 105, 1458
Greenhill, P.G., 117, 118, 120, 123, 125, 127, 1421
Greenwald, E.E., 579, 1422
Gregory, G., 1380, 1459
Griffin, R.J., 1374, 1410, 1422, 1447
Griffith, D.W.T., 747, 1409
Griffiths, J.G.A., 1054, 1059, 1060, 1446
Griggs, D.J., 97, 1428
Grodzinsky, G., 611, 454
Grosjean, D., 75, 78, 79, 80, 81, 82, 83, 84, 85, 86, 87, 88, 89, 94, 95, 103, 107, 116, 186, 187, 189, 190, 192, 193, 195, 196, 197, 198, 199, 201, 202, 203, 212, 214, 217, 218, 221, 223, 224, 225, 227, 374, 375, 376, 380, 382, 600, 605, 606, 608, 609, 710, 712, 713, 715, 716, 718, 719, 848, 854, 855, 967, 968, 969, 970, 1198, 1216, 1276, 1344, 1374, 1422, 1423, 1451, 1474
Grosjean, E., 75, 78, 79, 80, 81, 82, 83, 84, 85, 86, 87, 88, 94, 95, 103, 107, 116, 186, 187, 189, 190, 192, 193, 195, 196, 197, 198, 199, 201, 202, 203, 212, 214, 217, 218, 221, 223, 224, 225, 227, 374, 375, 376, 380, 382, 600, 605, 606, 608, 609, 710, 712, 713, 715, 716, 718, 719, 848, 854, 855, 967, 968, 969, 970, 1422, 1423
Grossmann, D., 76, 78, 79, 80, 81, 82, 83, 84, 85, 86, 87, 89, 90, 1423
Grotewold, J., 1208, 1391
Grotheer, H.-H., 118, 120, 124, 125, 127, 129, 131,1423, 1441
Grouhel, C., 1367, 1435
Gruber-Stadler, M., 1054, 1423
Gruebele, M., 1164, 1167, 1168, 1169, 1170, 1452
Grussdorf, J., 726, 1423
Gruver, J.T., 1009, 1010, 1114, 1423
Grygier, R.K., 1209, 1423
Guenther, A., 72, 73, 74, 866, 1362, 1367, 1386, 1387, 1388, 1389, 1399, 1416, 1423, 1429, 1431, 1435, 1442, 1449, 1459
Guesten, H., 622, 1417
Guillermo, R., 812, 813, 814, 1470
Guillet, J.E., 1140, 1141, 1142, 1143, 1421, 1424
Gump-Perkins, C.A., 547, 549, 554, 555, 557, 558, 561, 562, 563, 565, 566, 567, 569, 1458
Gunawardena, R., 87, 88, 103, 107, 116, 1422
Günther, H., 1316, 1317, 1318, 1470
Gurgel Veras, C.A., 747, 1409
Guschin, A., 434, 436, 437, 438, 441, 442, 448, 449, 468, 470, 475, 476, 492, 493, 507, 508, 701, 727, 728, 871, 875, 879, 880, 884, 1194, 1195, 1409, 1421, 1445, 1448, 1464, 1472
Gutman, D., 295, 1450
Guzzi, R., 1385, 1404

Haag, F., 118, 120, 138, 139, 1433
Haagen-Smit, A.J., 1372, 1377, 1423
Haas, B.-M., 1030, 1423
Haas, T., 1228, 1440
Haas, Y., 1089, 1092, 1271, 1421, 1423, 1479
Haberkorn, S., 691, 692, 693, 1448
Hack, W., 724, 725, 1415
Hackett, P.A., 989, 1089, 1098, 1176, 1177, 1178, 1186, 1187, 1190, 1191, 1192, 1193, 1399, 1419, 1423
Hägele, J., 118, 120, 124, 1423
Haggerstone, A.-L., 1362, 1461
Hahn, C.J., 886, 1397, 1471
Haiges, R., 256, 1444
Hajagató, B., 1270, 1444
Hakola, H., 76, 77, 78, 79, 80, 81, 82, 83, 84, 85, 86, 87, 631, 1423, 1425
Hall, G.E., 1054, 1058, 1111, 1112, 1404, 1424
Hall, M.A., 1164, 1165, 1470
Halland, J., 77, 1418
Hallock, K., 75, 77, 83, 84, 91, 1436
Hallquist, M., 187, 188, 195, 199, 200, 208, 209, 213, 214, 215, 219, 628, 629, 631, 632, 657, 660, 671, 701, 727, 728, 1072, 1073, 1424, 1445, 1448
Halpern, A.M., 1187, 1424
Ham, J.E., 223, 229, 230, 232, 233, 234, 633, 739, 1417, 1424
Hamilton, W.A., 455, 456, 457, 459, 460, 468, 469, 471, 472, 473, 477, 478, 480, 481, 482, 487, 488, 491, 1475
Hammer, M.-U., 76, 78, 79, 80, 81, 82, 83, 84, 85, 86, 87, 89, 90, 1423
Hammerle, R.H., 98, 1408
Hammond, G.S., 1159, 1471
Hampson, R.F., 112, 113, 117, 119, 121, 122, 126, 127, 128, 129, 130, 132, 134, 138, 140, 141, 143, 147, 150, 151, 154, 157, 159, 162, 163, 178, 184, 186, 188, 192, 195, 200, 201, 202, 204, 206, 209, 212, 214, 216, 225, 234, 237, 242, 245, 248,

252, 254, 261, 265, 284, 285, 308, 317, 325, 333, 336, 340, 347, 350, 355, 372, 373, 375, 376, 377, 378, 379, 380, 381, 383, 385, 390, 406, 407, 408, 410, 418, 422, 427, 428, 429, 453, 458, 465, 466, 479, 482, 483, 486, 489, 494, 496, 511, 514, 515, 517, 542, 545, 546, 548, 550, 551, 552, 555, 556, 558, 559, 560, 562, 563, 565, 566, 568, 570, 571, 573, 575, 577, 578, 588, 597, 600, 601, 603, 605, 606, 607, 608, 609, 610, 615, 616, 617, 621, 622, 629, 632, 637, 639, 653, 654, 657, 658, 661, 662, 663, 668, 669, 674, 697, 701, 703, 705, 709, 710, 714, 716, 723, 725, 727, 728, 730, 735, 740, 742, 752, 772, 773, 783, 787, 789, 795, 798, 803, 808, 811, 815, 818, 820, 821, 826, 844, 869, 873, 876, 888, 889, 890, 891, 893, 895, 896, 897, 898, 899, 900, 901, 906, 908, 909, 911, 912, 913, 914, 915, 917, 918, 920, 921, 922, 925, 926, 928, 933, 934, 937, 940, 941, 942, 952, 956, 961, 963, 969, 975, 984, 1083, 1288, 1308, 1384, 1396, 1397, 1413
Han, K.-L., 1240, 1477, 1478
Hanazaki, I., 1147, 1156, 1398
Hancock, G., 448, 450, 451, 503, 505, 875, 876,1472
Hande, M., 165, 172, 1414
Handy, B.J., 118, 120, 125, 126, 132, 133, 141, 142, 1405
Hanisco, T.F., 1095, 1383, 1440, 1474
Hann, M.R., 25, 38, 1414
Hannigan, J., 76, 1418
Hansel, A., 73, 578, 579, 887, 968, 1367, 1412, 1424, 1429
Hansen, A.B., 1377, 1445
Hansen, J.C., 446, 457, 458, 516, 517, 1228, 1421, 1437, 1477
Hansmann, B., 546, 548, 549, 1470
Hanson, D.R., 256, 427, 1438
Hanst, P.L., 970, 1273, 1424
Hao, W.M., 747, 1409
Harder, H., 1369, 1404, 1436
Harder, J.W., 76, 1420
Hargreaves, K.J., 1347, 1438
Harley, P., 72, 73, 1387, 1423
Harper, C., 994, 995, 1425
Harrington, P.J., 1322, 1438
Harris, G.W., 592, 593, 706, 708, 709, 902, 903, 904, 1234, 1235, 1237, 1238, 1424, 1433, 1451, 1471
Harrison, A.G., 1039, 1424
Harrison, J.C., 250, 633, 1424
Harrison, M.G., 296, 297, 905, 906, 907, 908, 909, 910, 911, 1458
Harrison, R.M., 77, 85, 1424
Harry, C., 310, 311, 312, 313, 314, 331, 333, 334, 1424
Harshfield, G., 76, 77, 107, 1464, 1479
Hartley, G.H., 1140, 1141, 1142, 1143,1424
Hartley, H., 1331, 1403
Hartmann, D., 345, 346, 355, 370, 372, 812, 813, 814, 1424
Harvey, J.N., 124, 1437, 1455
Harwood, M.H., 1300, 1301, 1302, 1303, 1306, 1424
Haryanto, A., 265, 777, 778, 782, 783, 784, 787, 791, 792, 797, 1472
Hase, W.L., 1163, 1166, 1167, 1168, 1440
Hashikawa, Y., 1079, 1083, 1425
Hass, H., 399, 400, 401, 402, 841, 842, 1440
Hasson, A.S., 560, 561, 566, 568, 1460
Hastie, D.R., 75, 77, 84, 1458
Hastings, S.H., 1335, 1425
Hatakeyama, S., 206, 208, 209, 210, 211, 212, 213, 723, 724, 726, 1425, 1428
Hauglustaine, D.A., 1390, 1414
Hayden, C.C., 1164, 1165, 1166, 1425
Hayman, G.D., 295, 296, 494, 996, 997, 1000, 1001, 1005, 1006, 1009, 1010, 1013, 1015, 1017, 1019, 1020, 1039, 1040, 1041, 1073, 1074, 1075, 1222, 1223, 1377, 1429, 1430, 1443
Hayon, E., 901, 1425
He, D., 1388, 1389, 1462
He, G.Z., 1240, 1477
He, J., 1377, 1419
He, T.J., 1270, 1477
He, Y.Z., 236, 1425
Heald, C.L., 1388, 1442
Heard, A.C., 1371, 1425
Heard, D.E., 77, 78, 79, 85, 87, 112, 283, 284, 285, 288, 546, 548, 549, 550, 592, 595, 596, 618, 660, 1092, 1093, 1094, 1095, 1096, 1098, 1100, 1101, 1102, 1104, 1106, 1107, 1308, 1309, 1310, 1360, 1362, 1367, 1371, 1394, 1398, 1402, 1407, 1424, 1437, 1453, 1461, 1465
Heathfield, A.E., 445, 446, 461, 462, 463, 472, 473, 499, 500, 501, 1425
Heicklen, J., 543, 638, 644, 645, 990, 993, 994, 995, 1001, 1002 1004, 1208, 1228, 1240, 1242, 1243, 1244, 1245, 1246, 1248, 1256, 1257, 1258, 1259, 1423, 1443, 1456, 1458, 1459, 1474, 1475, 1478
Heidt, L., 886, 1397
Heikes, B.G., 76, 77, 78, 1379, 1380, 1418, 1420, 1425, 1459, 1460, 1462
Hekstra, P.F., 257, 1439
Heldman, J.D., 989, 990, 1401

Helgaker, T., 634, 635, 1086, 1087, 1088, 1458
Hellén, H., 76, 77, 78, 79, 80, 81, 82, 83, 84, 85, 86, 87, 1425
Hellman, T.M., 1240, 1475
Hellpointner, E., 1311, 1425
Helmig, D., 79, 80, 82, 84, 85, 1389, 1399, 1421
Hemavibool, K., 112, 1420
Heneghan, S.P., 282, 1425
Henley, M.V., 171, 172, 370, 372, 1399, 1403
Hennig, S., 1238, 1240, 1425
Henon, E., 652, 653, 655, 656, 1406, 1469
Henriques, F.C., Jr., 1208, 1425
Henry, B.R., 76, 1286, 1414, 1418
Henry, F., 241, 242, 243, 244, 245, 247, 248, 249, 1410
Henze, D.K., 1367, 1419,
Hepburn, J.W., 1054, 1058, 1059, 1061, 1404, 1425
Herlth, D., 84, 91, 92, 93, 1380, 1459
Herman, R.L., 1383, 1475
Hern, C.H., 990, 991, 994, 998, 1002, 1006, 1011, 1024, 1076, 1077, 1079, 1090, 1091, 1107, 1110, 1113, 1128, 1144, 1164, 1176, 1177, 1197, 1267, 1440
Hernandez, H., 546, 548, 549, 1470
Hernandez, S., 560, 561, 566, 568, 1460
Hernandez-Soto, H., 546, 548, 549, 1470
Herndon, S.C., 905, 906, 907, 908, 909, 910, 911, 913, 914, 923, 924, 1464
Heroux, S., 119, 120, 125, 127, 306, 307, 308, 637, 1451
Herrmann, H., 763, 1425
Herron, J.T., 385, 658, 664, 670, 727, 729, 1425
Herwehe, J., 78, 82, 83, 85, 87, 1418
Herzberg, G., 1055, 1169, 1426
Hess, P.G., 886, 1454
Hess, W.P., 117, 118, 120, 123, 124, 125, 126, 127, 130, 1228, 1229, 1413, 1426
Hetherington, P.M., 1244, 1245, 1248, 1249, 1261, 1264, 1410
Heuerman, H.A., 128, 130, 131, 1411
Heuss, J.M., 1323, 1426
Hewitt, C.N., 72, 73, 74, 1416, 1423, 1459
Heydtmann, H., 1228, 1429
Hibino, Y., 466, 1408
Hickson, K.M., 448, 449, 450, 451, 502, 503, 504, 505, 506, 1399, 1426
Hildemann, L.M., 762, 1456
Hill, M., 77, 78, 79, 80, 82, 85, 86, 87, 88, 89, 104, 1436
Hills, A., 82, 86, 1393
Hinman, M.M., 909, 910, 911, 912, 914, 923, 945, 946, 947, 949, 952, 954, 1472
Hintsa, E.J., 1383, 1474
Hippler, H., 279, 1239, 1426
Hippler, M., 1240, 1426
Hirobe, M., 1347, 1446
Hirota, N., 1335, 1336, 1337, 1464
Hirschlaff, E., 1268, 1426
Hites, R.A., 425, 426, 430, 431, 432, 433, 518, 519 520, 521, 523, 524, 525, 652, 654, 655, 656, 1393, 1404, 1453
Hitier, D., 652, 653, 655, 660, 661, 662, 671, 676, 680, 681, 684, 1435
Hjorth, J., 210, 211, 212, 213, 214, 215, 237, 238, 239, 416, 417, 424, 425, 486, 492, 493, 511, 512, 526, 528, 543, 544, 561, 562, 563, 564, 569, 570, 578, 579, 628, 629, 630, 633, 671, 712, 732, 996, 997, 1000, 1001, 1005, 1006, 1009, 1010, 1013, 1015, 1017, 1019, 1020, 1039, 1040, 1041, 1073, 1074, 1075, 1197, 1202, 1203, 1207, 1208, 1222, 1223, 1372, 1393, 1402, 1405, 1407, 1412, 1416, 1420, 1426, 1443, 1474, 1476
Ho, K.F., 64, 77, 78, 79, 80, 82, 83, 84, 85, 86, 1426
Ho, M.-L., 1054, 1058, 1431
Ho, S.S.H., 64, 77, 78, 79, 80, 82, 83, 84, 85, 86, 1426
Ho, S.Y., 1163, 1426
Hobson, M.M., 25, 38, 1414
Hodyss, R.P., 1377, 1419
Hoelscher, D., 117, 120, 127, 691, 692, 693
Hoffmann, A., 454, 455, 471, 502, 503, 504, 1435, 1469
Hoffmann, M.R., 1026, 1400
Hoffmann, T., 1374, 1377, 1426, 1447, 1453
Hofler, F., 1377, 1417
Hofmann, A.F., 106, 1469
Hofzumahaus, A., 76, 78, 79, 80, 81, 82, 83, 84, 85, 86, 87, 89, 90, 1423
Holbrook, K.A., 132, 133, 134, 135, 137, 287, 298, 303, 304, 1408, 1462
Holland, F., 76, 78, 79, 80, 81, 82, 83, 84, 85, 86, 87, 89, 90, 1423
Holloway, A.L., 185, 186, 187, 702, 703, 704, 706, 709, 1426
Holloway, A.S., 306, 315, 335, 346, 1417
Holloway, J.S., 94, 95, 611, 762, 1454, 1461
Holm, C., 575, 1445
Holroyd, R.A., 1163, 1165, 1171, 1174, 1426
Hölscher, D., 117, 119, 124, 126, 130, 540, 541, 542, 586, 587, 588, 1413, 1431, 1460
Holt, P.M., 934, 935, 1411
Holt, T., 700, 1426
Honda, S., 723, 724, 726, 1425
Honguy, Q.L, 1367, 1400
Hooshiyar, P.A., 385, 386, 1408

Hopke, P.K., 1377, 1453
Hopkins, B., 78, 1420
Hopkins, J.R., 77, 78, 79, 85, 87, 91, 92, 93, 94, 733, 735, 1362, 1367, 1424, 1437, 1453, 1461
Hopkinson, A.C., 1147, 1426
Hopkinson, L., 73, 1392
Hopper, F., 115, 1438
Horie, O., 1164, 1171, 1426, 1427, 1444
Horowitz, A., 117, 119, 120, 124, 126, 127, 130, 586, 587, 588, 589, 652, 653, 655, 691, 692, 693, 985, 986, 990, 993, 1024, 1025, 1026, 1027, 1056, 1076, 1089, 1098, 1099, 1100, 1197, 1198, 1199, 1208, 1210, 1214, 1215, 1413, 1427, 1431, 1439, 1476
Horowitz, L.W., 91, 92, 93, 1367, 1417, 1427, 1459
Horth, J., 1372, 1431
Hoshi, J.-Y., 77, 78, 1427
Hou, H., 659, 1427
Hougen, J.T., 1208, 1427
Houghton, J.T., 97, 1428
Houston, P.L., 1054, 1058, 1060, 1269, 1404, 1414, 1443, 1466
Hov, Ø., 115, 1450
Howard, C.J., 280, 281, 550, 551, 552, 904, 935, 936, 984, 1308, 1410, 1413, 1414, 1438, 1462
Howard, P.H., 124, 131, 1442
Howell, N.W., 990, 991, 994, 998, 1002, 1006, 1011, 1024, 1076, 1077, 1079, 1090, 1091, 1107, 1110, 1113, 1128, 1144, 1164, 1176, 1177, 1197, 1267, 1440
Hoyermann, K., 130, 131, 384, 385, 551, 552, 622, 623, 659, 1399, 1404, 1415, 1416
Hsu, K.-J., 436, 437, 438, 439, 440, 441, 442, 1427
Hu, B., 1285, 1444
Hu, W.-F., 1270, 1427
Huang, C.-L., 1208, 1427
Huang, H., 94, 95, 887, 968, 1446
Huang, J., 1228, 1477
Huang, Y., 753, 754, 755, 1427
Hubbe, J.M., 115, 1461
Huber, J.R., 1030, 1238, 1239, 1240, 1250, 1254, 1261, 1264, 1274, 1276, 1276, 1285, 1288, 1308, 13091404, 1414, 1415, 1420, 1423, 1425, 1430, 1431, 1437, 1446, 1455, 1463, 1465, 1469, 1477
Hübler, G., 78, 82, 83, 85, 87, 611, 887, 968, 1418, 1454, 1475
Hudgens, E.E., 306, 307, 308, 309, 323, 324, 325, 326, 819, 821, 822, 1460
Hudman, R.C., 91, 92, 93, 1367, 1459, 1476
Hueglin, C., 77, 78, 79, 80, 82, 85, 86, 87, 88, 89, 104, 1436
Huey, G., 91, 92, 93, 1459
Huey, L.G., 256, 1335, 1336, 1419, 1427, 1438
Huff-Hartz, K.E., 769, 770, 1452
Hufford, D.L., 1043, 1044, 1427
Hughes, G.A., 1253, 1427
Huie, R.E., 295, 303, 313, 315, 316, 317, 318, 323, 326, 327, 328, 339, 350, 389, 400, 434, 436, 437, 438, 439, 440, 441, 442, 448, 449, 468, 469, 546, 553, 748, 750, 758, 837, 838, 839, 868, 869, 870, 904, 905, 908, 938, 943, 944, 945, 946, 947, 948, 949, 950, 951, 952, 953, 954, 955, 958, 968, 1065, 1066, 1199, 1209, 1213, 1214, 1234, 1235, 1236, 1374, 1401, 14337, 1438, 1456, 1457, 1471, 1473, 1478
Humphrey, J.R., 1271,1442
Hunter, M.C., 77, 85, 924, 1277, 1278, 1291, 1424, 1464
Huo, H., 102, 1473
Hurley, M.D., 18, 52, 117, 119, 120, 122, 123, 125, 127, 128, 130, 131, 133, 134, 135, 137, 139, 140, 141, 142, 143, 144, 153, 154, 160, 161, 236, 237, 238, 256, 257, 259, 261, 262, 263, 264, 265, 267, 268, 269, 270, 271, 272, 273, 274, 278, 295, 296, 309, 310, 336, 337, 340, 341, 342, 384, 385, 386, 411, 435, 436, 438, 441, 442, 448, 450, 451, 457, 458, 459, 460, 470, 478, 479, 480, 481, 482, 483, 484, 493, 494, 503, 505, 507, 508, 509, 510, 511, 512, 513, 514, 515, 516, 517, 529, 551, 552, 553, 554, 555, 556, 557, 564, 565, 566, 568, 573, 581, 586, 587, 588, 589, 622, 623, 634, 635, 636, 638, 639, 640, 641, 643, 644, 655, 662, 663, 664, 665, 667, 668, 669, 670, 672, 674, 675, 701, 724, 725, 726, 727, 728, 769, 770, 771, 772, 777, 778, 779, 780, 781, 782, 783, 784, 787, 788, 789, 791, 792, 794, 795, 796, 797, 801, 802, 803, 804, 805, 806, 808, 809, 811, 812, 814, 815, 816, 817, 818, 819, 820, 822, 842, 843, 844, 868, 869, 870, 871, 873, 875, 876, 880, 885, 907, 908, 938, 1079, 1080, 1082, 1083, 1084, 1085, 1086, 1087, 1080, 1095, 1144, 1159, 1194, 1195, 1201, 1230, 1231, 1393, 1401, 1405, 1408, 1409, 1415, 1421, 1425, 1427, 1428, 1429, 1430, 1431, 1435, 1436, 1440, 1441, 1442, 1445, 1446, 1451, 1452, 1461, 1463, 1464, 1465, 1468, 1471, 1472, 1473, 1476, 1477
Hurley, R., 1335, 1337, 1428
Huskey, D.T., 657, 658, 659, 662, 663, 664, 669, 670, 1478
Hutton-Squire, H.R., 711, 1406

Hwang, W.G., 1335, 1428
Hybl, J., 295, 297, 1439
Hynes, R.G., 112, 113, 117, 119, 121, 122, 126, 127, 128, 129, 130, 132, 134, 138, 140, 141, 143, 147, 150, 151, 154, 157, 159, 162, 163, 178, 184, 186, 188, 192, 195, 200, 201, 202, 204, 206, 209, 212, 214, 216, 225, 234, 237, 242, 245, 248, 252, 254, 261, 265, 284, 285, 308, 317, 325, 333, 336, 340, 347, 350, 355, 372, 373, 375, 376, 377, 378, 379, 380, 381, 383, 385, 390, 406, 407, 408, 410, 418, 422, 427, 428, 429, 453, 458, 465, 466, 479, 482, 483, 486, 489, 494, 496, 511, 514, 515, 517, 542, 545, 546, 548, 550, 552, 555, 556, 558, 559, 560, 562, 563, 565, 566, 568, 570, 571, 573, 575, 577, 578, 588, 597, 600, 601, 603, 605, 606, 607, 608, 609, 610, 615, 616, 617, 621, 622, 623, 629, 632, 637, 639, 652, 654, 657, 658, 661, 662, 663, 668, 669, 674, 697, 701, 703, 705, 709, 710, 714, 716, 721, 723, 725, 727, 728, 730, 735, 740, 742, 752, 772, 773, 783, 787, 789, 795, 798, 803, 808, 811, 815, 818, 820, 821, 826, 844, 869, 873, 876, 888, 889, 890, 891, 893, 895, 896, 897, 898, 899, 900, 901, 906, 908, 909, 911, 912, 913, 914, 915, 917, 918, 920, 921, 922, 925, 926, 928, 933, 934, 937, 940, 941, 942, 952, 956, 961, 963, 969, 975, 984, 1083, 1288, 1384, 1392, 1396

Ibarra, Y., 560, 561, 566, 568, 1460
Ibata, T.N., 901, 1425
Ibusuki, T., 436, 437, 438, 446, 451, 452, 453, 471, 472, 473, 475, 476, 487, 488, 489, 490, 491, 492, 875, 876, 877, 880, 1408, 1446
Ide, T., 778, 782, 783, 784, 787, 791, 792, 1428
Iida, Y., 206, 208, 209, 210, 211, 212, 213, 1428
Imamura, T., 206, 208, 209, 210, 211, 212, 213, 374, 1428, 1433
Ingham, T., 112, 904, 905, 1406, 1420
Inoue, G., 1239, 1428
Inoue, H., 1176, 1177, 1186, 1187, 1191, 1193, 1399
Inoue, Y., 441, 442, 507, 508, 742, 744, 875, 880, 1421, 1428, 1470
Irwin, R.S., 553, 557, 560, 748, 749, 750, 751, 753, 754, 755, 756, 757, 758, 759, 760
Isaksen, I.S.A., 258, 259, 262, 266, 267, 268, 269, 1457
Ishakawa, H., 1147, 1428
Isogami, C., 1347, 1446
Ito, A., 257, 1472
Ito, H., 445, 446, 452, 456, 461, 462, 463, 472, 473, 474, 475, 476, 499, 500, 501, 1466
Iwasaki, E., 566, 568, 581, 657, 658, 659, 662, 663, 664, 667, 668, 669, 674, 675, 727, 728, 778, 782, 783, 784, 787, 791, 792, 1144, 1159, 1428, 1429, 1463
Izumi, K., 1374, 1429

Jackson, W.M., 1228,1477
Jacob, D.J., 73, 1367, 1378, 1379, 1380, 1381, 1382, 1383, 1386, 1388, 1400, 1408, 1418, 1419, 1427, 1429, 1442, 1449, 1452, 1459, 1474, 1476
Jacob, V., 805, 806, 807, 809, 810, 812, 813, 814, 824, 832, 849, 850, 851, 852, 853, 1410, 1417
Jacobs, P.J., 1371, 1407
Jadkowski, J.T., 124, 1429
Jaeglé, L., 1381, 1382, 1383, 1429, 1474
Jäger, M., 1228, 1429
Jain, A.K., 516, 517, 1437
Jang, M., 1377, 1466
Janquin, M.-A., 241, 242, 243, 244, 245, 247, 248, 249, 1410
Janson, R., 73, 74, 1429, 1459
Jaoui, M., 1073, 1429
Japar, S.M., 78, 112, 122, 123, 128, 130, 134, 135, 153, 154, 264, 285, 290, 291, 301, 303, 304, 305, 306, 307, 308, 310, 311, 312, 319, 320, 321, 323, 324, 325, 326, 331, 332, 334, 337, 338, 551, 552, 556, 657, 658, 659, 662, 663, 664, 751, 752, 868, 869, 870, 909, 910, 911, 912, 914, 923, 935, 936, 945, 946, 947, 949, 952, 954, 965, 966, 968, 1401, 1408, 1429, 1430, 1471, 1472, 1473
Jardine, K., 866, 1431
Javadi, M.S., 141, 142, 143, 144, 145, 160, 161, 509, 510, 515, 516, 529, 875, 880, 1428, 1429, 1472
Jeffries, H.E., 720, 721, 722, 1027, 1042, 1045, 1046, 1218, 1220, 1325, 1420, 1438, 1478, 1430, 1441, 1451, 1456, 1469, 1472, 1474
Jenkin, M.J., 1377, 1430
Jenkin, M.E., 112, 113, 117, 119, 121, 122, 126, 127, 128, 129, 130, 132, 134, 138, 140, 141, 143, 147, 150, 151, 154, 157, 159, 162, 163, 178, 184, 186, 188, 192, 195, 200, 201, 202, 204, 206, 209, 212, 214, 216, 225, 234, 237, 242, 245, 248, 252, 254, 261, 265, 284, 285, 295, 296,

308, 317, 325, 333, 336, 340, 347, 350, 355, 372, 373, 375, 376, 377, 378, 379, 380, 381, 383, 385, 390, 406, 407, 408, 410, 418, 422, 427, 428, 429, 453, 458, 465, 466, 470, 479, 482, 483, 486, 489, 493, 494, 496, 508, 511, 514, 515, 517, 542, 545, 546, 548, 550, 551, 552, 555, 556, 558, 559, 560, 562, 563, 565, 566, 568, 569, 570, 571, 572, 573, 575, 577, 578, 588, 592, 597, 600, 601, 603, 605, 606, 607, 608, 609, 610, 612, 615, 616, 617, 618, 621, 622, 623, 624, 629, 632, 633, 634, 637, 639, 652, 654, 657, 658, 661, 662, 663, 668, 669, 674, 684, 697, 701, 703, 705, 709, 710, 714, 716, 721, 723, 725, 727, 728, 730, 734, 735, 740, 742, 752, 772, 773, 777, 778, 783, 787, 789, 795, 798, 803, 808, 811, 815, 818, 820, 821, 826, 844, 869, 873, 876, 888, 889, 890, 891, 893, 895, 896, 897, 898, 899, 900, 901, 906, 908, 909, 911, 912, 913, 914, 915, 917, 918, 920, 921, 922, 925, 926, 928, 933, 934, 935, 937, 940, 941, 942, 952, 956, 961, 963, 969, 975, 984, 1065, 1070, 1083, 1288, 1360, 1362, 1363, 1367, 1369, 1370, 1384, 1392, 1396, 1402, 1413, 1429
Jensen, E., 1269, 1435
Jensen, N.R., 210, 211, 212, 213, 214, 215, 416, 417, 486, 492, 493, 511, 512, 561, 562, 563, 564, 569, 570, 578, 579, 628, 629, 630, 633, 671, 712, 732, 1073, 1197, 1202, 1203, 1207, 1208, 1393, 1405, 1407, 1412, 1416, 1420, 1426, 1476
Jeong, G.-R., 446, 457, 458, 516, 517, 1437
Jerina, D.M., 1313, 1316, 1318, 1431
Jiang, G., 125, 127, 130, 131, 132, 133, 134, 135, 138, 139, 140, 141, 142, 143, 144, 150, 151, 152, 153, 154, 157, 158, 161, 162, 163, 1476
Jiménez, E., 117, 119, 120, 124, 125, 126, 127, 130, 145, 146, 147, 148, 149, 163, 164, 165, 166, 167, 170, 172, 174, 176, 177, 281, 557, 558, 565, 566, 567, 573, 574, 576, 605, 611, 612, 613, 657, 658, 659, 660, 661, 662, 663, 664, 666, 667, 668, 669, 670, 672, 673, 674, 675, 678, 679, 701, 728, 764, 861, 863, 962, 963, 964, 1392, 1398, 1429, 1430
Jimenez, J.L., 83, 115, 1372, 1377, 1464, 1470, 1478
Jin, E..M., 1380, 1381, 1429
Jobson, B.T., 94, 95, 115, 1430, 1454
Jodkowski, J.T., 543, 544, 554, 1412
Joens, J.A., 990, 991, 994, 998, 1002, 1006, 1011, 1024, 1076, 1077, 1079, 1090, 1091, 1107, 1110, 1113, 1128, 1144, 1164, 1176, 1177, 1197, 1267, 1440
Johnson, A.P., 684, 1363, 1456
Johnson, B.J., 753, 1430
Johnson, C.A., 97, 1428
Johnson, D., 322, 325, 1362, 1377, 1430
Johnson, M.S., 543, 544, 988, 1416, 1417
Johnston, H.S., 280, 281, 544, 904, 1239, 1284, 1406, 1430, 1439, 1440
Johnston, M.V., 1271, 1377, 1455
Johnstone, D.E., 1036, 1430, 1466
Jolley, J.E., 1089, 1111, 1430, 1446
Jolly, G.S., 748, 749, 750, 751, 752, 904, 1284, 1430, 1460
Jones, B., 1347, 1438
Jones, K.C., 522, 1438
Jones, R.H., 75, 76, 78, 1393
Jones, R.L., 1277, 1288, 1453
Jonsson, H., 762, 1461
Jorado, E., 522, 1438
Jourdain, J.L., 904, 1430
Jouvet, C., 1239, 1441
Jucks, K.W., 279, 1472
Judge, R.H., 1223, 1430
Jug, K., 1156, 1444
Jung, K.-H., 1269, 1450
Jungkamp, T.P.W., 1374, 1447
Junkermann, W., 75, 77, 84, 1460
Juranić, I., 983, 991, 999, 1006, 1007, 1017, 1018, 1020, 1021, 1022, 1023, 1024, 1078, 1079, 1463
Just, Th., 118, 120, 124, 125, 127, 129, 131, 1188, 1399, 1423, 1441

Kabasakalien, P., 1250, 1430
Kable, S.H., 994, 999, 1442, 1465, 1466
Kades, E., 1261, 1264, 1430, 1455
Kaise, M., 259, 260, 267, 269, 273, 274, 426, 445, 446, 452, 456, 461, 462, 463, 472, 473, 474, 475, 476, 490, 499, 500, 501, 502, 503, 504, 516, 517, 525,1466, 1468
Kaiser, E.W., 52, 105, 295, 411, 484, 529, 566, 568, 581, 662, 663, 664, 665, 724, 725, 726, 728, 935, 936, 952, 1144, 1159, 1429, 1430, 1431, 1457, 1471, 1472
Kakesu, M., 905, 906, 907, 908, 909, 910, 1431
Kalabokas, P., 75, 77, 1431
Kalberer, M., 1377, 1417, 1431
Kaledin, A.L., 1164, 1431
Kambanis, K.G., 438, 439, 440, 444, 445, 447, 448, 450, 451, 462, 463, 467, 468, 470, 474, 497, 499, 1431, 1449
Kamens, R.M., 10, 11, 65, 112, 119, 126, 132, 138, 157, 171, 184, 186, 195, 198, 212, 225, 237, 242, 245, 248, 252, 253, 255,

287, 364, 365, 367, 383, 425, 427, 525, 551, 559, 562, 563, 568, 569, 571, 572, 577, 578, 608, 609, 612, 615, 616, 629, 632, 633, 634, 846, 853, 854, 856, 859, 896, 899, 957, 958, 960, 976, 984, 1030, 1033, 1035, 1042, 1073, 1217, 1312, 1313, 1314, 1317, 1318, 1333, 1335, 1336, 1338, 1340, 1341, 1343, 1345, 1347, 1356, 1358, 1373, 1377, 1405, 1417, 1420, 1429, 1466
Kames, J., 1234, 1235, 1403,
Kamiya, K., 1225, 1431
Kamoboures, M., 436, 439, 442, 1421
Kanakidou, M., 84, 1372, 1378, 1380, 1390, 1431, 1459, 1476
Kanda, Y., 1144, 1444
Kane, R., 302, 303, 315, 316, 317, 318, 495, 496, 497, 498, 502, 503, 504, 505, 506, 507, 1440
Kaneko, T., 107, 1464
Kang, S., 1143, 1437, 1448
Kanno, S., 1347, 1446
Kao, C.C., 1054, 1058, 1431
Kaplan, I.R., 747, 1431
Karecki, D.R., 75, 76, 77, 84, 1425, 1458
Karl, T., 73, 866, 1381, 1387, 1388, 1423, 1431, 1442
Karunanandan, R., 586, 587, 588, 1098, 1100, 1101, 1102, 1104, 1431, 1432
Kash, P.W., 1182, 1184, 1228, 1229, 1269, 1431, 1435, 1450, 1474
Kato, S., 107, 1089, 1335, 1337, 1456, 1464
Kato, T., 107, 1464
Katzenstein, A.S., 91, 92, 93, 1402
Kaubisch, N., 1313, 1316, 1318, 1431
Kaufman, F., 117, 118, 120, 123, 280, 281, 904, 1439, 1440, 1461
Kawaguchi, A., 1347, 1446
Kawamura, K., 64, 1426, 1431
Kawasaki, M., 134, 135, 137, 140, 141, 142, 143, 144, 145, 256, 435, 441, 442, 475, 476, 507, 508, 516, 517, 553, 655, 742, 744, 837, 838, 839, 875, 879, 880, 1079, 1083, 1421, 1425, 1428, 1440, 1445, 1468, 1470, 1473, 1477
Kearsey, S.V., 1242, 1411
Keen, A., 382, 383, 384, 1398
Keevil, D.M., 1300, 1442
Kegley-Owen, C.S., 122, 123, 551, 552, 1431, 1468
Keil, D.G., 546, 547, 549, 596, 1442
Keim, E.R., 1095, 1383, 1440, 1474
Keinath, M., 257, 1477
Keller, B.A., 1239, 1431
Keller, R.A., 1163, 1164, 1171, 1172, 1435
Keller-Rudek, H., 1224, 1431, 1438
Kelley, P.M., 1163, 1166, 1167, 1168, 1424
Kellis, D., 1054, 1055, 1056, 1057, 1479
Kelly, N., 117, 118, 120, 123, 1440
Kelly, T., 259, 261, 262, 270, 271, 272, 636, 638, 640, 641, 643, 644, 1078, 1082, 1083, 1084, 1085, 1086, 1432, 1457
Kemball-Cook, S., 257, 1477
Kenner, R.D., 1237, 1432
Keoshian, C.I., 711, 1417
Kern, C., 83, 1460
Kerr, J.A., 65, 112, 115, 125, 127, 138, 190, 195, 225, 234, 236, 237, 238, 241, 242, 243, 244, 245, 246, 247, 248, 249, 299, 300, 301, 303, 304, 311, 319, 320, 321, 324, 329, 330, 331, 332, 333, 334, 336, 337, 338, 342, 343, 345, 346, 348, 349, 350, 355, 356, 359, 361, 362, 364, 368, 375, 376, 377, 378, 379, 380, 381, 383, 389, 409, 411, 413, 414, 415, 416, 417, 418, 422, 424, 426, 431, 433, 501, 522, 526, 547, 549, 551, 554, 555, 557, 558, 559, 561, 562, 563, 565, 566, 567, 568, 569, 570, 571, 572, 577, 578, 599, 600, 605, 608, 609, 612, 615, 616, 619, 620, 622, 629, 632, 633, 634, 653, 655, 661, 671, 676, 683, 699, 703, 716, 717, 718, 724, 729, 732, 736, 739, 740, 741, 788, 789, 805, 806, 807, 810, 813, 814, 817, 818, 819, 820, 835, 847, 848, 856, 858, 861, 862, 863, 864, 865, 866, 905, 906, 907, 908, 909, 910, 911, 912, 975, 976, 984, 990, 1054, 1065, 1111, 1143, 1188, 1194, 1288, 1308, 1358, 1384, 1391, 1396, 1397, 1399, 1400, 1405, 1415, 1432, 1458, 1462
Kerridge, B.J., 1385, 1404
Kershner, C.J., 990, 1427
Kesselmeier, J., 116, 1389, 1399, 1432
Keyser, L.F., 280, 281, 282, 283, 1432
Keywood, M., 1377, 1419, 1436
Khachatryan, L.A., 547, 549, 561, 562, 563, 571, 572, 635, 636, 640, 641, 647, 648, 1414
Khalil, M.A.K., 74, 1459
Khamaganov, V.G., 434, 436, 437, 438, 441, 442, 448, 449, 753, 754, 755, 1098, 1100, 1101, 1102, 1104, 1432, 1448
Khan, I., 753, 1432
Khe, P.V., 1273, 1436
Khieu, N.H., 1054, 1058, 1061, 1433
Khundkar, L.R., 1164, 1167, 1168, 1169, 1170, 1452
Kibler, M., 76, 78, 79, 80, 81, 82, 83, 84, 85, 86, 87, 89, 90, 1423
Kikuchi, T., 1239, 1428
Killus, J.P., 1365,1420
Kim, E.S., 1234, 1235, 1236, 1463

Kim, K.K., 1164, 1165, 1167, 1168, 1169, 1170, 1432
Kim, M.S., 1335, 1428
Kim, S.K., 1160, 1164, 1165, 1166, 1170, 1432, 1438, 1470
Kind, I., 386, 410, 411, 409, 413, 414, 419, 418,1432
King, D., 657, 1403
King, K.R., 25, 38, 1414
King, M.D., 601, 602, 609, 710, 711, 713, 714, 715, 716, 717, 765, 855, 856, 860, 862, 865, 866, 867, 969, 1406
King, R.A., 989, 1164, 1432
Kinnison, D.J., 342, 343, 345, 346, 348, 349, 355, 636, 647, 648, 1399, 1462
Kinscherff, D., 128, 130, 131, 1411
Kirby, G.H., 1162, 1414
Kirchner, F., 1230, 1366, 1462, 1478
Kirk, A.D., 1098, 1432
Kirwan, S.P., 1098, 1099, 1102, 1103, 1437
Kistiakowski, G.B., 1147, 1156, 1159, 1163, 1164, 1165, 1173, 1174, 1300, 1409, 1432, 1455
Kitchen, D.C., 1182, 1184, 1285, 1444, 1474
Klamt, A., 688, 1418
Klawatsch-Carrasco, N., 212, 214, 1432
Kleeman, M.J., 52, 53, 59, 1456, 1457
Kleindienst, T.E., 76, 78, 79, 82, 85, 86, 87, 88, 89, 306, 307, 308, 309, 323, 324, 325, 326, 327, 328, 329, 386, 387, 595, 596, 599, 600, 608, 661, 662, 706, 708, 709, 796, 797, 819, 821, 822, 1374, 1415, 1420, 1433, 1454, 1460,
Kleinermanns, K., 1307, 1420
Klemm, R.B, 540, 541, 542, 546, 547, 549, 596, 1433, 1442, 1477
Klemm, R.F., 1147, 1158, 1433
Kley, D., 91, 92, 93, 96, 1417
Klimont, Z., 1388, 1389, 1462
Klinger, L., 72, 73, 1423
Klippenstein, S.J., 579, 1164, 1422, 1433, 1478
Klockow, D., 1374, 1377, 1426
Klöpffer, V.W., 118, 120, 138, 139, 1433
Klotz, B., 244, 247, 248, 249, 253, 254, 255, 374, 378, 417, 418, 597, 598, 606, 614, 615, 713, 714, 716, 1051, 1054, 1064, 1071, 1072, 1216, 1217, 1312, 1313, 1314, 1316, 1317, 1319, 1344, 1345, 1396, 1416, 1433, 1447, 1448, 1456, 1479
Knapp, K., 887, 968, 1475
Knepp, P.T., 994, 1465
Knight, G., 1287, 1433
Knispel, R., 236, 237, 238, 1433
Knyazev, V.D., 113, 265, 1404
Kobayashi, S., 1239, 1428
Koch, D.M., 1054, 1058, 1061, 1433
Koch, R., 236, 237, 238, 422, 887, 891, 893, 894, 901, 1418, 1433
Koch, S., 608, 609, 710, 756, 757, 764, 765, 1065, 1068, 1069, 1070, 1433, 1444
Kohl, E., 118, 120, 138, 139, 1431
Köhle, G., 1344, 1421
Kok, G.L., 88, 1454, 1462
Kolb, C.E., 546, 553, 748, 750, 758, 904, 905, 908, 938, 958, 968, 984, 1065, 1066 1199, 1234, 1235, 1236, 1308, 1413, 1456
Koller, F., 1333, 1434
Kolloff, A., 608, 609, 710, 764, 765, 1444
Kolyer, R., 91, 92, 93, 1459
Kommandeur, J., 1209, 1414
Kondo, O., 526, 1433
Kondo, S., 259, 260, 267, 269, 273, 274, 426, 445, 446, 452, 456, 461, 462, 463, 472, 473, 474, 475, 476, 490, 499, 500, 501, 502, 503, 504, 516, 517, 525, 1466
Kondo, Y., 1380, 1459
Kong, W., 1054, 1060, 1261, 1264, 1407, 1414
Kopczynski, S.L., 1318, 1322, 1434
Koppmann, R., 115, 1455
Korte, N.E., 106, 1461
Korzeniowski, S.H., 257, 1452, 1477
Kosmas, A.M., 257, 1450
Koszalka, T.R., 1043, 1044, 1427
Kötting, C., 1089, 1090, 1092, 1147, 1149, 1413
Kotzias, D., 416, 417, 633, 732, 1405
Kourtidis, K., 94, 1453
Kovács, G., 259, 267, 269, 1092, 1093, 1094, 1095, 1096, 1101, 1106, 1433, 1444
Koyanogi, M., 1144, 1444
Kozlowski, R., 1233, 1240, 1241, 1242, 1267, 1289, 1465
Krajnovich, D., 1269, 1404
Kramp, F., 331, 333, 334, 409,1434
Kraus, J.W., 1135, 1136, 1434
Kreidenweis, S.M., 763, 1416
Kroll, J.H., 1364, 1373, 1374,1434, 1452
Krost, K., 1273, 1417
Kruetter, N.M., 904, 1475
Kruger, H.-U., 1348, 1449
Kubo, M.K., 115, 1264, 1474, 1476
Kuhn, M., 1366, 1462
Kuhn, U., 1389, 1399
Kukui, A., 553, 586, 587, 588, 589, 590, 691, 692, 693, 753, 754, 755, 756, 758, 1404
Kumar, A., 185, 186, 187, 235, 1201, 1413, 1469
Kumaran, S.S., 1164, 1165, 1420
Kumari, J., 1244, 1245, 1249, 1261, 1263, 1441

Kuntz, R.L., 1318, 1322, 1434
Kurosaki, Y., 989, 1434
Kurosu, T.P., 1362, 1367, 1386, 1388, 1399, 1408, 1442, 1449
Kurtenbach, R., 85, 86, 87, 88, 89, 1444
Kurylo, M.J., 117, 118, 120, 125, 126, 127, 132, 133, 137, 138, 139, 141, 142, 152, 153, 157, 159, 160, 166, 167, 168, 170, 171, 173, 177, 182, 183, 259, 261, 267, 269, 276, 280, 281, 285, 287, 290, 291, 295, 300, 303, 304, 305, 307, 308, 310, 311, 312, 313, 315, 316, 317, 318, 319, 320, 321, 323, 324, 325, 326, 327, 328, 331, 332, 334, 337, 338, 339, 342, 343, 345, 346, 348, 349, 350, 351, 352, 353, 354, 356, 357, 358, 360, 367, 368, 382, 383, 384, 386, 387, 388, 389, 391, 392, 393, 394, 395, 396, 398, 400, 401, 402, 403, 404, 434, 436, 437, 438, 439, 440, 441, 442, 448, 449, 468, 469, 531, 544, 545, 546, 553, 652, 653, 655, 660, 661, 662, 666, 667, 668, 669, 672, 673, 674, 677, 678, 679, 682, 683, 691, 692, 693, 700, 701, 702, 703, 707, 726, 727, 728, 729, 742, 743, 748, 750, 753, 754, 755, 758, 759, 761, 775, 776, 782, 783, 785, 786, 790, 791, 792, 796, 797, 800, 801, 802, 805, 806, 807, 809, 810, 811, 812, 813, 814, 817, 819, 820, 825, 826, 827, 829, 830, 831, 832, 833, 837, 838, 839, 868, 869, 870, 873, 882, 883, 904, 905, 908, 938, 943, 944, 945, 946, 947, 948, 949, 950, 951, 952, 953, 954, 955, 958, 968, 984, 1065, 1066, 1199, 1234, 1235, 1236, 1374, 1393, 1401, 1411, 1412, 1413, 1434, 1437, 1438, 1456, 1471, 1473, 1478
Kuser, W., 94, 95, 1454
Kuster, W.C., 77, 78, 82, 83, 84, 85, 86, 87, 88, 91, 92, 93, 94, 95, 103, 115, 116, 611, 886, 887, 968, 1392, 1418, 1421, 1443, 145, 1462, 1475
Kutschke, K.O., 1111, 1187, 11415, 1419, 1423, 1434, 1475
Kutsuna, S., 260, 271, 274, 275, 436, 437, 438, 446, 447, 448, 451, 452, 453, 455, 456, 457, 458, 465, 466, 471, 472, 473, 475, 476, 487, 488, 489, 490, 491, 492, 779, 784, 787, 788, 803, 871, 872, 873, 874, 875, 876, 877, 878, 879, 880, 881, 882, 883, 1408, 1434, 1466
Kwok, E.S.C., 165, 168, 227, 228, 299, 318, 343, 352, 421, 422, 423, 424, 425, 426, 430, 431, 432, 433, 518, 519, 520, 521, 522, 526, 527, 529, 530, 531, 561, 581, 585, 607, 609, 611, 618, 624, 626, 627, 657, 662, 680, 683, 684, 685, 686, 688, 693, 698, 701, 702, 710, 712, 713, 714, 715, 717, 718, 719, 731, 732, 735, 740, 741, 748, 769, 773, 784, 788, 789, 794, 800, 803, 807, 810, 813, 815, 819, 823, 826, 829, 830, 832, 833, 834, 837, 838, 841, 866, 870, 923, 929, 1394, 1434, 1459, 1460

Ladstaetter-Weissenmayer, A., 1389, 1442
Lahmani, F., 1239, 1240, 1413, 1434
Laimgruber, S., 1333, 1434
Lamarque, J.-F., 1367, 1427
Lamb, B., 72, 73, 82, 86, 1362, 1386, 1387, 1388,1393, 1416, 1434, 1435, 1449, 1452
Lamb, J.J., 279, 280, 904, 962, 963, 964, 1460
Lambert, H.M., 1054, 1060, 1414
Lammel, G., 1234, 1435
Land, E.J., 1344, 1435
Lane, S.I., 191, 192, 193, 195, 196, 203, 204, 205, 208, 209, 210, 448, 450, 451, 455, 494, 495, 496, 500, 501, 503, 505, 854, 855, 856, 857, 858, 860, 861, 862, 863, 864,1402, 1410, 1412, 1465
Láng, L., 1319, 1326, 1333, 1334, 1337, 1338, 1340, 1341, 1342, 1346, 1347, 1348, 1435
Langbein, T., 454, 455, 471, 502, 503, 504, 1434
Lange, U., 384, 385, 551, 552, 1399
Langer, S., 120, 121, 122, 124, 128, 129, 130, 137, 138, 140, 141, 146, 186, 187, 188, 190, 191, 192, 194, 195, 198, 199, 200, 207, 208, 209, 210, 214, 215, 219, 293, 294, 295, 296, 297, 302, 309, 310, 312, 313, 315, 317, 319, 323, 325, 326, 328, 329, 330, 336, 337, 526, 527, 550, 551, 552, 556, 558, 559, 560, 561, 562, 563, 564, 565, 571, 572, 573, 574, 575, 576, 577, 581, 599, 600, 601, 602, 603, 605, 606, 607, 776, 782, 787, 802, 806, 1412, 1424, 1435, 1445, 1468
Langford, A.O., 1054, 1055, 1056, 1057, 1059, 1435
Lanning, J.A., 75, 76, 78, 1393
Lansley, D.L., 77, 85, 1424
Lanza, B., 145, 146, 147, 170, 174, 176, 611, 612, 613, 1430
Lanzendorf, E.J., 1383, 1474
Lao, K.Q., 1269, 1435
Lardeux, C., 1239, 1240, 1413, 1434, 1441
Lardeux-Dedonder, C., 1239, 1441
Lashley, M., 216, 1461
Laufer, A.H., 1030, 1163, 1164, 1171, 1172, 1204, 1205, 1416, 1435
Laurent, J.P., 1377, 1425

Laursen, L., 141, 142, 143, 144, 145, 1428
Laverdet, G., 183, 184, 185, 280, 281, 544, 545, 546, 547, 549, 551, 552, 634, 635, 636, 637, 638, 639, 640, 641, 646, 647, 648, 649, 686, 699, 1176, 1180, 1439, 1441, 1452, 1457
Lavi, R., 1261, 1264, 1274, 1397, 1435
Lavollée, M., 1240, 1434
Law, K.S., 924, 1367, 1410, 1435
Lawrence, M.G., 18, 124, 282, 747, 1368, 1369, 1404, 1436, 1464, 1470
Layne, G.S., 1054, 1055, 1057, 1060, 1061, 1405
Lazarou, Y.G., 262, 263, 264, 266, 267, 268, 269, 270, 275, 276, 438, 439, 440, 444, 445, 447, 448, 450, 451, 462, 463, 467, 468, 470, 497, 499, 1431, 1449
Le, H.T., 1270, 1444
Leahy, D.F., 88, 1436
Leaitch, R., 115, 1430
Le Bras, G., 152, 153, 183, 184, 185, 186, 187, 203, 204, 205, 208, 209, 210, 259, 261, 262, 264, 270, 271, 272, 280, 281, 283, 290, 291, 292, 293, 299, 300, 301, 303, 304, 309, 310, 311, 312, 313, 314, 315, 316, 317, 318, 319, 323, 331, 332, 333, 334, 340, 341, 342, 343, 344, 345, 346, 347, 349, 350, 351, 352, 353, 354, 355, 356, 357, 358, 359, 360, 363, 364, 365, 370, 371, 372, 374, 375, 376, 398, 400, 401, 405, 526, 533, 544, 545, 546, 547, 549, 551, 552, 553, 554, 555, 556, 561, 562, 563, 565, 566, 567, 568, 571, 572, 573, 586, 587, 588, 589, 590, 599, 600, 601, 603, 604, 605, 607, 635, 636, 637, 638, 639, 640, 641, 643, 644, 647, 648, 649, 652, 653, 655, 657, 658, 659, 660, 661, 662, 663, 664, 671, 676, 680, 681, 684, 686, 687, 688, 691, 692, 693, 753, 754, 755, 756, 758, 775, 776, 777, 778, 779, 782, 783, 784, 785, 786, 787, 788, 789, 790, 791, 792, 793, 794, 796, 797, 798, 799, 800, 801, 802, 803, 804, 805, 806, 807, 808, 809, 810, 811, 812, 813, 814, 815, 816, 817, 818, 819, 820, 821, 822, 824, 825, 826, 827, 829, 831, 832, 833, 835, 836, 837, 839, 841, 849, 850, 851, 852, 853, 854, 855, 856, 857, 858, 860, 861, 862, 887, 888, 889, 890, 891, 893, 901, 904, 964, 965, 966, 1024, 1025, 1026, 1027, 1030, 1031, 1032, 1076, 1077, 1079, 1080, 1081, 1230, 1319, 1320, 1324, 1398, 1399, 1404, 1410, 1415, 1426, 1430, 1432, 1435, 1436, 1439, 1441, 1443, 1446, 1447, 1452, 1457, 1461, 1464, 1465, 1467, 1474
Le Calvé, S., 186, 261, 315, 319, 358, 359,360, 363, 364, 365, 389, 390, 393, 394, 395, 396, 397, 398, 400, 401, 402, 403, 405, 406, 407, 526, 528, 531, 619, 620, 622, 623, 634, 635, 636, 637, 638, 639, 640, 641, 646, 647, 648, 649, 652, 653, 655, 660, 661, 662, 671, 672, 676, 677, 680, 681, 684, 686, 699, 702, 703, 704, 706, 709, 775, 776, 779, 782, 783, 784, 785, 786, 787, 788, 789, 790, 791, 792, 793, 794, 796, 797, 800, 801, 802, 805, 807, 809, 810, 811, 812, 813, 814, 817, 818, 819, 820, 821, 822, 823, 824, 825, 826, 827, 829, 831, 832, 833, 835, 836, 839, 840, 841, 849, 850, 851, 852, 853, 1176, 1180, 1410, 1415, 1435, 1436
Le Crâne, J.P., 554, 555, 556, 557, 564, 565, 573
Lee, A., 227, 1436
Lee, E.K.C., 1089, 1144, 1147, 1148, 1149, 1150, 1151, 1152, 1153, 1154, 1155, 1156, 1159, 1161, 1163, 1406, 1407, 1413, 1436, 1458, 1464
Lee, J.D., 77, 78, 79, 85, 87, 592, 618, 1360, 1362, 1367, 1402, 1424, 1437, 1453, 1461
Lee, J.H., 88, 282, 283, 409, 410, 659, 905, 906, 907, 1419, 1436, 1442
Lee, L.C., 975,1409
Lee, S.C., 64, 77, 78, 79, 80, 82, 83, 84, 85, 86, 1426
Lee, S.-J., 1054, 1058, 1431
Lee, Y.-N., 75, 76, 77, 83, 84, 91, 1420, 1425, 1436
Lee, Y.-P., 975, 1409
Lee, Y.T., 1054, 1059, 1061, 1098, 1099, 1164, 1165, 1166, 1269, 1404, 1425, 1446
Leermakers, P.A., 1197, 1198, 1199, 1200, 1470
Lee-Ruff, E., 1147, 1426
Lefer, B., 76, 1418
Legreid, G., 77, 78, 79, 80, 82, 85, 86, 87, 88, 89, 104, 1436
Leibrock, E., 78, 79, 80, 82, 85, 86, 87, 103, 1436
Leighton, P.A., 991, 993, 1331, 1436
Lelieveld, J., 257, 1368, 1369, 1404, 1436, 1464
Lemoine, B., 753, 754, 755, 757, 758, 1411
Leone, S.R., 279, 281, 1040, 1099, 1458, 1469, 1476
Le Person, A., 185, 186, 187, 189, 190, 1436
Lerdau, M., 72, 73, 1423
Lerner, B.M., 94, 95, 106, 115, 1392, 1454
Lerner, D.N., 106, 1409
Lesclaux, R., 622, 623, 1187, 1273, 1436, 1441, 1446, 1466

Lester, W.A., Jr., 1054, 1060, 1448
Leu, M.-T., 282, 283, 962, 1436, 1459
Levy, H., 1367, 1417
Levsen, K., 1347, 1438
Lewis, A.C., 77, 78, 79, 85, 87, 91, 92, 93, 94, 733, 735, 1362, 1367, 1389, 1424, 1437, 1449, 1453, 1461
Lewis, P.J., 733, 1437
Lewis, R.S., 1089, 1436
Li, Q., 73, 751, 752, 1285, 1367, 1380, 1381, 1417, 1429
Li, Q.-S., 1054, 1059, 1061, 1437
Li, S.L., 1269, 1271, 1470,
Li, W., 1374, 1433
Li, Y., 25, 38, 1414, 1427, 1455
Li, Y.-M., 1240, 1477
Li, Z., 128, 130, 131, 446, 457, 458, 516, 517, 1228, 1437, 1455
Li, Z.J., 194, 205, 207, 400, 401, 1437
Liang, J., 1367, 1427
Liberles, A., 1143, 1437
Librando, V., 511, 512, 1393
Libuda, H.G., 644, 645, 1076, 1077, 1226, 1437
Lichtin, N., 901, 1425
Lide, D.R., 6, 1432
Lien, M.H., 1147, 1426
Lightfoot, P.S., 1098, 1099, 1102, 1103, 1437
Lim, Y.B., 700, 1377, 1414, 1437
Lin, C.L., 1308, 1437
Lin, M.C., 406, 407, 541, 542, 543, 554, 943, 944, 955, 1030, 1164, 1270, 1419, 1444, 1468, 1477, 1478
Lin, X., 11, 1477
Lindinger, W., 733, 1476
Lindley, C.R.C., 970, 973, 1233, 1273, 1274, 1275, 1276, 1437
Lindskog, A., 115, 1450
Linnebach, E., 1307, 1420
Linscheid, M., 1377, 1453
Lipczynska-Kochany, E., 1344, 1437
Lissi, E.A., 1107, 1108, 1120, 1121, 1122, 1127, 1208, 131, 1407, 1415, 1437
Liu, C.-L., 1208, 1427
Liu, F.-C., 1270, 1427
Liu, R., 152, 153, 159, 160, 166, 167, 168, 170, 171, 173, 177, 182, 183, 285, 287, 290, 291, 295, 300, 303, 304, 305, 306, 307, 308, 310, 311, 312, 313, 319, 320, 323, 324, 325, 326, 327, 328, 331, 332, 334, 337, 338, 339, 342, 343, 345, 346, 348, 350, 351, 352, 353, 354, 355, 356, 357, 358, 360, 367, 368, 382, 383, 384, 386, 387, 388, 389, 391, 392, 393, 394, 395, 396, 398, 400, 401, 402, 403, 404, 531, 691, 692, 693, 700, 701, 702, 703, 707, 726, 727, 728, 729, 748, 749, 750, 753, 754, 755, 758, 759, 761, 775, 776, 782, 783, 785, 786, 790, 791, 792, 796, 797, 800, 801, 802, 805, 806, 807, 809, 810, 811, 812, 813, 814, 817, 819, 820, 825, 826, 827, 829, 830, 831, 832, 833, 873, 882, 883, 943, 944, 945, 946, 947, 948, 949, 950, 951, 952, 953, 954, 955, 1411, 1412, 1437, 1438, 1471, 1473
Liu, R.-Z., 1225, 1416
Liu, S., 72, 1416
Liu, S.C., 1095, 1440
Liu, X., 720, 721, 722, 1042, 1045, 1046, 1218, 1219, 1220, 1438
Liu, Y., 1367, 1400
Liu, Z.-F., 1240, 1478
Liu, Z.Y., 111, 1455
Livermore, R.A., 1242, 1438
Ljungström, E., 120, 121, 122, 124, 128, 129, 130, 137, 138, 140, 141, 146, 187, 186, 199, 208, 209, 213, 214, 215, 219, 293, 294, 295, 296, 297, 302, 309, 310, 312, 313, 315, 317, 319, 323, 325, 326, 328, 329, 330, 336, 337, 526, 527, 550, 551, 552, 556, 558, 559, 560, 561, 562, 563, 564, 565, 571, 572, 573, 574, 575, 599, 600, 601, 602, 603, 605, 606, 607, 628, 629, 631, 632, 657, 660, 671, 701, 727, 728, 776, 782, 787, 802, 806, 996, 997, 1000, 1001, 1005, 1006, 1009, 1010, 1013, 1015, 1017, 1019, 1020, 1039, 1040, 1041, 1072, 1073, 1074, 1075, 1222, 1223, 1391, 1412, 1424, 1435, 1443, 1445, 1448, 1468
Lloyd, A.C., 138, 139, 299, 300, 301, 302, 310, 311, 312, 389, 390, 805, 806, 807, 817, 819, 820, 1438, 1476
Loeffler, D.E., 989, 990, 1401
Loewen, M., 166, 1438
Logan, J.A., 1367, 1380, 1381, 1400, 1429, 1476
Loge, G.W., 1054, 1060, 1438
Lohmann, R., 522, 1438
Lohmann, U., 522, 1438
Lohse, C., 76, 78, 84, 85, 89, 90,1421
Loirat, H., 119, 120, 125, 127, 306, 307, 308, 543, 544, 550, 551, 552, 647, 800, 801, 802, 809, 810, 811, 812, 813, 814, 817, 818, 819, 820, 822, 1414, 1451
Long, S.R., 1322, 1438
Long, W., 72, 1476
Long, W.D., 331, 333, 334, 1395
Longfellow, C.A., 1098, 1099, 1446
Lonneman, W., 76, 78, 79, 82, 85, 86, 87, 88, 89, 1420, 1454
Lööv, J.B., 77, 79, 80, 82, 85, 86, 87, 88, 89, 104, 1436

Lorenaga, T., 77, 78, 1427
Lorenz, K., 118, 120, 124, 382, 383, 384, 1418, 1423, 1438
Lorkovic, I.M., 952, 1471
Lossing, F.P., 1039, 1424
Lovejoy, E.R., 256, 280, 281, 762, 1164, 1165, 1167, 1168, 1169, 1170, 1406, 1427, 1432, 1438
Lowe, R., 1372, 1466
Lucy, F.A., 1331, 1436
Ludwig, B.E., 1233, 1250, 1251, 1254, 1438
Luebkert, B., 73, 1438
Luke, W.T., 1288, 1289, 1355, 1438
Lun, X., 150, 151, 161, 162, 166, 167, 1441
Luo, D., 837, 838, 839, 1473
Luque, G.R., 764, 765, 1465
Lutman, E., 1277, 1288, 1453
Lüttke, J., 1347, 1430
LuValle, J.E., 1039, 1401
Lv., C., 1264, 1474
Lynton, J.I., 1300, 1442

Ma, B., 1164, 1432
Ma, K.C., 255, 1439
Ma, S., 408, 1028, 1029, 1030, 1438
Mabury, S.A., 18, 257, 259, 261, 262, 263, 264, 265, 267, 268, 269, 270, 271, 272, 273, 274, 278, 512, 513, 635, 636, 638, 640, 641, 643, 644, 657, 660, 671, 769, 770, 771, 772, 873, 876, 885, 1088, 1230, 1393, 1405, 1415, 1427, 1428, 1439, 1472, 1473, 1477
MacDonald, R., 73, 1438
Machado, G., 282, 283, 1474
Machado, M.I.L., 738, 1411
Machiele, P.A., 103, 1405
Mack, G.P.R., 553, 1439
Mackay, D., 255, 1439
Mackay, E., 924, 932, 1458
Mackay, G.I., 75, 76, 77, 88, 1425, 1458, 1462
Mac Léod, H., 546, 547, 549, 551, 552, 634, 635, 636, 637, 638, 639, 640, 641, 646, 647, 648, 649, 1457
Madronich, S., 65, 112, 115, 138, 190, 195, 225, 234, 301, 311, 320, 324, 329, 333, 336, 350, 359, 361, 362, 364, 368, 375, 376, 377, 378, 379, 380, 381, 383, 389, 409, 411, 413, 414, 415, 417, 418, 422, 424, 426, 431, 433, 522, 551, 559, 562, 563, 568, 569, 571, 572, 577, 578, 608, 609, 612, 615, 616, 629, 632, 633, 634, 661, 671, 676, 683, 699, 703, 716, 717, 718, 724, 729, 732, 736, 739, 741, 805, 806, 807, 809, 810, 812, 813, 814, 832, 847, 848, 856, 858, 861, 862, 863, 864, 865, 866, 886, 976, 984, 990, 1054, 1065, 1143, 1194, 1308, 1358, 1363, 1364, 1397, 1405, 1463, 1471
Maeda, Y., 104, 905, 906, 907, 908, 909, 910, 1431, 1444
Magneron, I., 183, 184, 185, 259, 261, 262, 270, 271, 272, 586, 587, 588, 589, 599, 600, 604, 605, 607, 636, 638, 643, 686, 699, 887, 888, 889, 890, 891, 893, 895, 896, 897, 898, 899, 900, 901, 1024, 1025, 1026, 1027, 1030, 1032, 1035, 1076, 1176, 1180, 1432, 1439, 1461
Mahajan, A.S., 1367, 1453
Mahan, B.H., 1174, 1432
Mahoney, A.J., 1164, 1165, 1421
Maity, D.K., 1201, 1413
Majdik, Z., 763, 1425
Majer, J.R., 1192, 1439
Maker, P.D., 72, 283, 284, 285, 540, 541, 542, 543, 544, 545, 546, 547, 549, 551, 552, 554, 555, 586, 587, 588, 589, 592, 593, 620, 638, 644, 645, 1310, 1445, 1463
Maki, R.G., 540, 541, 542, 1477
Malanca, F.E., 641, 644, 1079, 1080, 1082, 1083, 1084, 1085, 1086, 1087, 1080, 1409
Maldotti, A., 599, 600, 653, 655, 1409, 1439
Malkin, T.L., 112, 1420
Malkina, I.L., 837, 838, 839, 1473
Mallard, W.G., 236, 709, 1425, 1456
Malms, W., 454, 455, 471, 502, 503, 504, 1435
Mani, J.C., 1141, 1451
Manney, G.L., 1390, 1391
Marchewka, M., 94, 95, 1454
Marchionni, G., 511, 512, 1393
Marconi, G., 1344, 1421
Marcus, R.A., 1164, 1433
Marenco, A., 1367, 1435
Margitan, J.J., 904, 1285, 1383, 1439, 1475
Maricq, M.M., 295, 296, 297, 724, 725, 756, 757, 1187, 1230, 1411, 1439, 1455
Marinelli, W.J., 280, 281, 904, 1439
Markgraf, S.H., 348, 349, 1439
Marley, N.A., 76, 78, 79, 82, 85, 89, 90, 91, 1419
Marrone, M.J., 1269, 1457
Marshall, P., 652, 654, 655, 656, 1451, 1464, 1477
Marshall, W.L., 1163, 1165, 1432
Marston, G., 312, 317, 325, 329, 952, 1391, 1471
Márta, F., 259, 267, 269, 1092, 1093, 1094, 1095, 1096, 1101, 1106, 1433, 1444
Martell, J.M., 989,1439
Martin, G.R., 1099, 1107, 1108,1415, 1439

Martin, J.W., 18, 257, 259, 261, 262, 263, 264, 265, 267, 268, 269, 270, 271, 272, 273, 274, 278, 635, 636, 638, 640, 641, 643, 644, 657, 660, 671, 769, 770, 771, 772, 1088, 1230, 1393, 1415, 1427, 1428, 1439, 1472, 1473
Martin, P., 362, 367, 368, 369, 389, 390, 391, 410, 411, 412, 413, 416, 417, 550, 551, 552, 555, 556, 557, 558, 559, 561, 563, 564, 565, 566, 567, 569, 570, 573, 574, 576, 601, 602, 604, 605, 606, 611, 612, 613, 616, 700, 1393, 1395, 1405, 1440 1456, 1470
Martin, R.S., 76, 78, 79, 82, 83, 85, 87, 89, 90, 91, 222, 1418, 1419, 1450
Martin, R.V., 1386, 1389, 1399, 1408, 1449
Martin, T.W., 1127, 1132, 1440
Martinez, E., 189, 389, 390, 391, 410, 411, 413, 486, 492, 493, 550, 551, 552, 555, 556, 557, 558, 559, 560, 561, 563, 564, 565, 566, 567, 568, 569, 570, 573, 574, 575, 576, 577, 601, 602, 603, 605, 606, 611, 612, 613, 616, 617, 657, 658, 659, 660, 661, 662, 663, 664, 666, 667, 668, 669, 670, 671, 672, 673, 674, 675, 677, 678, 679, 680, 681, 701, 728, 729, 764, 765, 797, 798, 799, 801, 802, 803, 804, 805, 806, 808, 812, 815, 816, 861, 863, 1392, 1394, 1405, 1411, 1429, 1430, 1440, 1454
Martinez, M., 1369, 1404, 1436
Martinez, R.D., 990, 991, 994, 998, 1002, 1006, 1011, 1024, 1076, 1077, 1079, 1090, 1091, 1107, 1110, 1113, 1128, 1144, 1164, 1176, 1177, 1197, 1267, 1440
Martino, P.C., 1143, 1440
Martin-Reviejo, M., 592, 618, 887, 888, 889, 890, 891, 893, 895, 896, 897, 898, 899, 900, 901, 1316, 1317, 1360, 1362, 1402, 1430, 1433, 1461
Martrenchard-Barra, S., 1239, 1441
Mascal, K., 111, 1440
Mascato, M.J., 1233, 1240, 1241, 1242, 1267, 1289, 1465
Mashino, M., 516, 517, 837, 838, 839,1440, 1473
Masin, J.G., 105, 1417
Mason, J., 1272, 1440
Masson, C.R., 1130, 1131, 1440, 1475
Matheson, M.S., 1208, 1209, 1211, 1446
Matos, F.J.A., 738, 1411
Matsen, F.A., 1335, 1425
Matsumi, Y., 122, 123, 130, 131, 134, 139, 140, 457, 458, 554, 555, 556, 557, 566, 568, 581, 657, 658, 659, 662, 663, 664, 667, 668, 669, 670, 672, 674, 675, 727, 728, 778, 782, 783, 784, 787, 791, 792, 1102, 1103, 1144, 1159, 1303, 1417, 1428, 1429, 1436, 1463
Matsumoto, T., 107, 1464
Mattrel, P., 1347, 1466
Matus, M.H., 256, 1444
Matz, J., 1273, 1403
Mau, A.W.-H., 1208, 1403
Maul, C., 1228, 1440
Mauldin, R.L., III, 748, 749, 751, 752, 1475
Maurer, R., 1377, 1417
Maurer, T., 340, 349, 350, 351, 358, 359, 360, 361, 363, 364, 365, 366, 367, 385, 398, 400, 401, 402, 779, 780, 781, 841, 842, 1420, 1440, 1465, 1472
Mauzerall, D.L., 1367, 1427
May, R.D., 1383, 1475
Mazely, T.L., 1287, 1300, 1301, 1303, 1440, 1455
McCabe, D.C., 279, 281, 655, 656, 1464, 1469
McCaulley, J.A., 117, 118, 120, 123, 1440
McClelland, G.M., 1209, 1440
McCulloch, A., 445, 446, 461, 462, 463, 472, 473, 499, 500, 501, 1425
McCully, B., 76, 88, 1425, 1462
McDaniel, A.H., 984, 1406
McDonald, J.R., 1939, 1456
McDonald-Buller, E.C., 115, 1464
McDowell, C.A., 1040, 1440
McElroy, C.T., 519, 1383, 1475
McFiggans, G., 1362, 1377, 1430, 1461
McGarvey, J.J., 1268, 1440
McGee, T.H., 1149, 1150, 1440
McGrath, W.D., 1268, 1440
McGraw, G.E., 1239, 1440
McGuire, D.S., 1164, 1165, 1414
McIlroy, A., 519, 1440
McIntosh, M.E., 634, 638, 1441
McIver, C.D., 306, 307, 308, 309, 323, 324, 325, 326, 327, 328, 329, 796, 797, 819, 821, 822, 1460
McKay, W.A., 72, 73, 84, 1423
McKee, M.L., 1270, 1440
McKeen, S.A., 611, 1095, 1383, 1440, 1454, 1474
McKenney, D.J., 748, 749, 750, 751, 752, 1284, 1430, 1460
McLaughlin, D.F., 118, 120, 125, 127, 132, 133, 141, 142, 302, 303, 495, 496, 497, 498, 502, 503, 504, 505, 506, 507, 1405
McLeod, S.D., 1390, 1391
McLoughlin, P., 315, 316, 317, 318, 1405, 1440
McMillan, G.R., 1116, 1119, 1233, 1244, 1245, 1249, 1250, 1251, 1252, 1254, 1256,

1257, 1261, 1262, 1263, 1264, 1265, 1266, 1415, 1438, 1441
McMillan, R.T., 78, 82, 83, 85, 87, 1418
McMillan, V., 1240, 1241, 1261, 1272, 1441
McNesby, J.R., 1115, 1441
McNichol, A.P., 76, 77, 1464
McQuaid, J.B., 729, 730, 1367, 1441, 1453
McQuaid, J.G., 77, 78, 79, 85, 87, 1437
McRae, E.G., 1267, 1399
Meagher, J., 634, 638, 990, 993, 1474
Meagher, R.J., 634, 1441
Medhurst, L.J., 437, 439, 440, 1419
Meek, J.T., 1322, 1438
Meier, U., 118, 120, 124, 125, 127, 129, 131, 1441
Meinardi, S., 76, 91, 92, 93, 237, 238, 239, 424, 425, 886, 1402, 1418, 1459
Meller, R., 975, 983, 984, 985, 988, 989, 1036, 1056, 1065, 1197, 1198, 1199, 1204, 1210, 1215, 1226, 1230, 1231, 1427, 1441, 1455
Mellinger, A., 1164, 1165, 1166, 1470
Mellouki, A., 132, 133, 137, 138, 139, 141, 142, 150, 151, 152, 153, 161, 162, 166, 167, 183, 184, 185, 186, 187, 188, 189, 190, 191, 192, 193, 194, 195, 196, 203, 204, 205, 207, 208, 209, 210, 259, 261, 262, 264, 270, 271, 272, 280, 281, 290, 291, 292, 293, 295, 299, 300, 301, 302, 303, 306, 307, 308, 309, 310, 311, 312, 313, 314, 315, 316, 317, 318, 319, 320, 321, 323, 324, 325, 326, 327, 328, 331, 332, 333, 334, 340, 341, 342, 343, 344, 345, 346, 347, 349, 350, 351, 352, 353, 354, 356, 357, 358, 359, 360, 363, 364, 365, 370, 371, 372, 374, 375, 376, 377, 378, 379, 380, 381, 389, 390, 393, 394, 395, 396, 397, 398, 400, 401, 402, 403, 405, 406, 407, 526, 531, 533, 554, 555, 556, 561, 562, 563, 565, 566, 567, 568, 571, 572, 573, 586, 587, 588, 589, 599, 600, 601, 603, 604, 605, 606, 607, 608, 619, 620, 622, 623, 635, 636, 637, 638, 639, 640, 641, 643, 644, 647, 648, 649, 652, 653, 655, 657, 658, 659, 660, 661, 662, 663, 664, 671, 672, 676, 677, 680, 681, 684, 686, 687, 688, 699, 702, 703, 704, 706, 708, 709, 710, 766, 767, 768, 775, 776, 782, 783, 785, 786, 787, 788, 789, 790, 791, 792, 793, 794, 777, 778, 779, 782, 783, 784, 787, 791, 792, 796, 797, 798, 799, 800, 801, 802, 803, 804, 805, 806, 807, 808, 809, 810, 811, 812, 813, 814, 815, 816, 817, 818, 819, 820, 821, 822, 823, 824, 825, 826, 827, 829, 831, 832, 833, 835, 836, 837, 839, 840, 841, 849, 850, 851, 852, 853, 854, 855, 856, 857, 858, 860, 861, 862, 887, 888, 889, 890, 891, 893, 895, 896, 897, 898, 899, 900, 901, 905, 934, 935, 964, 965, 966, 996, 997, 1000, 1001, 1005, 1006, 1009, 1010, 1013, 1015, 1017, 1019, 1020, 1024, 1025, 1026, 1027, 1030, 1031, 1032, 1036, 1037, 1038, 1039, 1040, 1041, 1073, 1074, 1075, 1076, 1077, 1079, 1080, 1081, 1129, 1176, 1180, 1195, 1197, 1198, 1199, 1201, 1204, 1205, 1206, 1207, 1222, 1223, 1230, 1319, 1320, 1324, 1404, 1410, 1415, 1420, 1426, 1432, 1435, 1436, 1439, 1441, 1443, 1446, 1497, 1452, 1461, 1464, 1465, 1467, 1473, 1474, 1478
Mendes, L., 1367, 1453
Mengon, W., 330, 345, 355, 561, 562, 563, 788, 789, 814, 817, 818, 835, 1462
Méreau, R., 1188, 1441
Merill, J.T., 886, 1471
Mestdagh, J.M., 1239, 1441
Metcalfe, J., 1151, 1152, 1407
Metha, G.F., 994, 1442
Methven, J., 77, 78, 79, 85, 87, 91, 92, 93, 94, 1453, 1437
Metzier, H.W., 232, 233, 1111, 1112, 1424
Meylan, W.M., 124, 131, 1442
Meyer-Arnek, J., 1389, 1442
Meynadier, P., 1239, 1441
Meyrahn, H., 990, 993, 1092, 1093, 1094, 1096, 1098, 1099, 1100, 1101, 1442
Michael, J., 122, 123, 295, 1442
Michael, J.L., 1113, 1114, 1115, 1116, 1117, 1119, 1123, 1124, 1442
Michael, J.V., 282, 283, 540, 541, 542, 544, 545, 546, 547, 549, 596, 1164, 1165, 1420, 1433, 1442, 1462
Mickley L.J., 1367, 1400
Middleton, P., 1366, 1462
Mihelcic, D., 76, 78, 79, 80, 81, 82, 83, 84, 85, 86, 87, 89, 90, 1423
Miller, A., 1159, 1401
Miller, C.E., 1300, 1442
Miller, D.B., 77, 1418
Miller, J.D., 753, 754, 755, 1427
Miller, M., 970, 1273, 1424
Miller, S.M., 1240, 1442
Miller, W.H., 1164, 1420
Millet, D.B., 1381, 1388, 1442
Mills, G., 77, 78, 79, 85, 87, 1424, 1437
Milne, C.J., 1261, 1264, 1397
Milne, P., 78, 79, 82, 85, 86, 87, 88, 89, 1454
Minato, T., 1143, 1477
Minschwaner, K., 278, 1457
Minton, T.K., 1030, 1423
Mirabel, P.,1156, 1403

Miracolo, M.A., 1364, 1452
Mishra, P.C., 1156, 1444
Misner, J.A., 259, 262, 270, 271, 272, 636, 638, 643, 644, 1428
Mitchell, M.B., 122, 123, 124, 1450
Mittal, J.P., 185, 186, 187, 235, 691, 692, 693, 1179, 1180, 1409, 1469
Mix, K.H., 659, 1442
Miyagishima, J., 75, 76, 78, 1393
Miyamoto, A., 1264, 1474
Mizoguchi, I., 1080, 1447
Mizukado, J., 779, 784, 787, 788, 803, 871, 874, 880, 881, 882, 883, 885, 1434
Mocanu, R., 244, 247, 248, 249, 255, 1448
Møgelberg, T.E., 105, 275, 276, 295, 400, 401, 402, 501, 742, 769, 770, 771, 868, 869, 870, 1401, 1420, 1442, 1452, 1457, 1471
Moilanen, K.W., 1271, 1442
Molina, L.T., 83, 279, 280, 475, 476, 485, 486, 492, 493, 507, 508, 875, 879, 880, 904, 962, 963, 964, 985, 986, 1194, 1195, 1277, 1287, 1308, 1377, 1409, 1421, 1435, 1442, 1445, 1460, 1462, 1464, 1470, 1473
Molina, M.J., 83, 279, 280, 475, 476, 485, 486, 492, 493, 507, 508, 546, 553, 748, 750, 758, 875, 879, 880, 904, 905, 908, 938, 958, 962, 963, 964, 968, 984, 985, 986, 1065, 1066, 1194, 1195, 1199, 1234, 1235, 1236, 1277, 1287, 1308, 1377, 1409, 1413, 1421, 1442, 1445, 1456, 1460, 1462, 1464, 1470, 1473
Moller, S.J., 1367, 1453
Molnar, A., 73, 1442
Monedero, E., 412, 415, 601, 602, 605, 606, 616, 1405, 1456, 1470
Monks, P.S., 77, 78, 79, 85, 87, 312, 317, 325, 329, 1362, 1391, 1437, 1461
Monod, A., 119, 120, 125, 127, 306, 307, 308, 637, 763, 800, 801, 802, 809, 810, 811, 812, 813, 814, 817, 818, 819, 820, 822, 1425, 1451
Mons, M., 1239, 1441
Monster, J., 762, 1401
Monti, S., 1344, 1421
Montzka, D.D., 886, 1454
Montzka, S.A., 77, 78, 82, 83, 84, 85, 86, 87, 88, 103, 116, 1418, 1421, 1443
Moore, C.B., 436, 437, 438, 439, 440, 441, 442, 985, 986, 1054, 1055, 1056, 1057, 1059, 1164, 1165, 1166, 1167, 1168, 1169, 1170, 1401, 1408, 1410, 1421, 1432, 1435, 1438, 1444, 1470
Moortgat, G.K., 65, 76, 78, 79, 80, 81, 82, 83, 84, 85, 86, 87, 89, 90, 112, 115, 138, 185, 186, 187, 189, 190, 195, 225, 234, 301, 311, 320, 324, 329, 333, 336, 350, 359, 361, 362, 364, 368, 375, 376, 377, 378, 379, 380, 381, 383, 389, 409, 411, 413, 414, 415, 417, 418, 422, 424, 426, 431, 433, 522, 526, 528, 546, 553, 551, 559, 562, 563, 568, 569, 571, 572, 577, 578, 586, 587, 588, 589, 608, 609, 612, 615, 616, 629, 632, 633, 634, 599, 600, 604, 605, 607, 608, 609, 661, 671, 676, 683, 699, 703, 710, 716, 717, 718, 724, 729, 732, 736, 739, 740, 741, 748, 750, 756, 757, 758, 764, 765, 805, 806, 807, 809, 810, 812, 813, 814, 832, 847, 848, 856, 858, 861, 862, 863, 864, 865, 866, 904, 905, 908, 938, 958, 968, 975, 976, 983, 984, 985, 986, 987, 988, 989, 990, 991, 993, 996, 997, 999, 1000, 1005, 1006, 1007, 1010, 1013, 1015, 1017, 1018, 1019, 1020, 1021, 1022, 1023, 1024, 1025, 1026, 1027, 1030, 1031, 1032, 1035, 1036, 1037, 1039, 1040, 1041, 1054, 1056, 1057, 1058, 1059, 1061, 1064, 1065, 1066, 1068, 1069, 1070, 1073, 1074, 1075, 1076, 1078, 1079, 1108, 1109, 1143, 1164, 1171, 1194, 1197, 1198, 1199, 1204, 1206, 1207, 1209, 1210, 1213, 1214, 1215, 1222, 1223, 1224, 1226, 1230, 1231, 1234, 1235, 1236, 1277, 1308, 1311, 1358, 1372, 1399, 1405, 1406, 1423, 1426, 1427, 1429, 1431, 1433, 1436, 1439, 1441, 1442, 1443, 144, 1452, 1455, 1456, 1459, 1463, 1474
Mopper, K., 18, 76, 1425, 1479
Morabito, P.L., Jr., 1242, 1244, 1245, 1256, 1257, 1258, 1259, 1443
Mora-Diez, N., 543, 554, 580, 656, 1392, 1443
Morales, L., 669, 670, 675, 1394
Moreno, E., 777, 778, 782, 783, 784, 1403
Morey, S., 101, 1443
Morgan, C.G., 1164, 1165, 1414, 1443
Moriarty, J., 354, 357, 358, 389, 390, 393, 394, 395, 396, 397, 398, 400, 401, 402, 403, 405, 406, 407, 1443
Morley, C., 590, 1471
Morokuma, K., 1164, 1225, 1411, 1431
Morozov, I.I., 497, 1431
Morrell, C., 448, 450, 451, 503, 505, 875, 876, 1472
Morris, E.D., Jr., 541, 542, 546, 547, 549, 550, 551, 552, 554, 555, 1443
Morris, E.R., 1082, 1443
Morris, R.E., 98, 106, 107, 1415
Morrison, B.M., 543, 1443
Morrison, D.N., 1147, 1158, 1433
Morrison, L., 72, 1476
Mörs, V., 454, 455, 471, 502, 503, 504, 1435

Morss, R.E., 1184, 1431
Moss, A.Z., 1209, 1443
Moss, B.D., 1112, 1466
Moss, D.B., 1269, 1443
Moule, D.C., 1223, 1430
Moulton, R.W., 1054, 1058, 1060, 1401
Mount, H.R., 455, 456, 457, 459, 460, 468, 469, 471, 472, 473, 477, 478, 480, 481, 482, 487, 488, 491, 1475
Mouvier, G., 75, 77, 1431
Mu, Y., 77, 78, 79, 83, 85, 125, 127, 130, 131, 132, 133, 134, 135, 137, 138, 139, 140, 141, 142, 143, 144, 150, 151, 152, 153, 154, 157, 158, 161, 162, 163, 560, 561, 581, 691, 692, 693, 766, 767, 768, 1197, 1198, 1199, 1201, 1404, 1441, 1443, 1476
Muckerman, J.T., 232, 233, 1111, 1112, 1424
Mueller, S.A., 103, 104, 108, 1443
Muhlhauser, M., 1054, 1423
Muir, D.C.G., 257, 873, 876, 885, 1405, 1439
Mulac, W.A., 1208, 1209, 1211, 1446
Müller, C., 303, 304, 1385, 1404, 1415
Müller, J.-F., 1380, 1382, 1443
Müller-Remmers, P.L., 1156, 1444
Mullins, C.B., 115, 1464
Munger, J.W., 94, 1444
Munk, J., 118, 120, 124, 1449
Muñoz, A., 887, 888, 889, 890, 891, 893, 895, 896, 897, 898, 899, 900, 901, 1031, 1041, 1447, 1461
Murad, E., 1177, 1178, 1187, 1191, 1193, 1194, 1397
Murphy, J.L., 280, 281, 904, 1434
Murphy, P.C., 94, 95, 887, 968, 1454, 1475
Murphy, S.M., 762, 1461
Murray, C., 124, 1455
Murrells, T.P, 25, 38, 280, 281, 1391, 1414, 1438
Muthuramu, K., 924, 932, 1458
Myers, T.L., 1182, 1184, 1285, 1444, 1474
Myhre, C.E.L., 1372, 1431
Myhre, G., 259, 262, 266, 267, 268, 269, 1457
Myriokefalitakis, S., 1390, 1476

Nádasdi, R., 1092, 1093, 1094, 1095, 1096, 1101, 1106, 1444
Nagai, H., 259, 260, 267, 269, 273, 274, 1466
Nagar, N.S., 985, 986, 1410
Nagatani, I., 206, 208, 209, 210, 211, 212, 213, 1428
Naik, P.D., 185, 186, 187, 235, 691, 692, 693, 1179, 1180, 1201, 1409, 1413, 1469
Naik, V., 516, 517, 1437
Nakagawa, K., 206, 208, 209, 210, 211, 212, 213, 1428
Nakajima, T., 1335, 1337, 1464
Nakashima, K., 1144, 1444
Nakayama, T., 1102, 1103, 1303, 1417, 1429, 1463
Nalty, A., 374, 376, 712, 713, 1450
Napier, I.M., 1239, 1269, 1444
Narang, A., 1002, 1003, 1004, 1010, 1011, 1012, 1013, 1014, 1015, 1016, 1017, 1479
Nau, W.M., 1117, 1444
Nava, D.F., 122, 123, 295, 540, 541, 542, 544, 545, 552, 1442, 1450, 1462
Neavyn, R., 119, 120, 122, 123, 125, 127, 130, 131, 132, 133, 134, 135, 138, 139, 140, 141, 142, 143, 144, 157, 158, 169, 170, 171, 172, 177, 183, 295, 299, 300, 301, 302, 303, 310, 311, 312, 313, 314, 315, 316, 317, 318, 319, 320, 321, 331, 332, 333, 334, 337, 338, 339, 1444
Neeb, P., 608, 609, 710, 764, 765, 1444
Neece, J.D., 115, 1464
Nelsen, W., 636, 639, 646, 647, 648, 649, 907, 908, 938, 1461, 1462
Nelson, D.D., Jr., 1284, 1307, 1457
Nelson, H.H., 437, 439, 440, 1419
Nelson, L., 119, 120, 122, 123, 125, 127, 130, 131, 132, 133, 134, 135, 138, 139, 140, 141, 142, 143, 144, 157, 158, 169, 170, 171, 172, 177, 183, 290, 291, 292, 293, 295, 299, 300, 301, 302, 303, 310, 311, 312, 313, 314, 315, 316, 317, 318, 319, 320, 321, 331, 332, 333, 334, 337, 338, 339, 636, 647, 648, 1444
Nelson, S.M., 1388, 1389, 1462
Nenes, A., 1372, 1377, 1419, 1431
Nesbitt, D.J., 1284, 1307,1457
Nesbitt, D.J.H., 1164, 1444
Nesbitt, F.L., 552, 1450
Neto, T.G.S., 747, 1409
Neuforth, A., 430, 432, 433, 518, 519, 520, 521, 1464
Neumark, D.M., 1164, 1165, 1166, 1425
Neunaber, H., 279, 1426
Newman, L., 88, 1436
Ng, L.N., 1377, 1419
Ngan, V.T., 256, 1444
Nguyen, H.T.H., 104, 1444
Nguyen, M.T., 256, 989, 1270, 1444, 1460
Nguyen, M.V., 675, 1467
Nguyen, T.L., 755, 756, 758, 1369, 1413, 1450
Ni, C.-K., 1208, 1427
Nicholson, A.J.C., 1113, 1121, 1123, 1268, 1444
Nickerson, K.E., 1273, 1468

Nicol, C.H., 1115, 1127, 1130, 1131, 1133, 1134, 1135, 1137, 1138, 1444
Nicolaisen, F.M., 511, 512, 1393
Nicovich, J.M., 280, 281, 904, 905, 1308, 1444, 1475, 1470
Niedojadlo, A., 85, 86, 87, 88, 89, 1444
Nielsen, C.J., 258, 259, 262, 265, 266, 267, 268, 269, 416, 417, 443, 444, 445, 446, 448, 449, 450, 453, 454, 455, 457, 458, 462, 464, 465, 466, 467, 468, 469, 470, 478, 479, 483, 484, 487, 489, 543, 544, 550, 551, 543, 544, 546, 547, 549, 550, 552, 553, 554, 555, 556, 557, 558, 559, 561, 562, 563, 564, 565, 566, 567, 568, 569, 570, 571, 572, 573, 574, 575, 576, 577, 578, 579, 581, 628, 629, 630, 633, 634, 635, 636, 640, 641, 643, 644, 657, 658, 659, 671, 724, 732, 778, 782, 783, 784, 943, 944, 945, 947, 948, 988, 1054, 1073, 1078, 1082, 1083, 1084, 1085, 1086, 1087, 1088, 1193, 1194, 1195, 1196, 1372, 1400, 1409, 1412, 1416, 1417, 1420, 1423, 1431, 1449
Nielsen, O.J., 18, 105, 117, 119, 120, 122, 123, 125, 127, 130, 131, 132, 133, 134, 135, 138, 139, 140, 141, 142, 143, 144, 145, 157, 158, 160, 161, 169, 170, 171, 172, 177, 183, 236, 237, 238, 256, 257, 261, 264, 265, 275, 276, 277, 278, 295, 296, 297, 299, 300, 301, 302, 303, 309, 310, 311, 312, 313, 314, 315, 316, 317, 318, 319, 320, 321, 331, 332, 333, 334, 336, 337, 338, 339, 340, 341, 342, 367, 368, 396, 397, 398, 399, 400, 401, 402, 406, 407, 459, 460, 468, 470, 478, 479, 480, 481, 482, 483, 485, 486, 492, 493, 494, 501, 509, 510, 511, 512, 513, 514, 515, 516, 529, 634, 635, 636, 638, 640, 641, 643, 644, 647, 648, 657, 660, 671, 701, 727, 728, 742, 743, 745, 746, 769, 770, 771, 843, 844, 868, 869, 870, 875, 879, 880, 884, 906, 907, 908, 909, 910, 911, 912, 915, 916, 917, 918, 936, 937, 938, 939, 940, 941, 942, 943, 955, 956, 957, 958, 959, 1079, 1083, 1088, 1231, 1393, 1399, 1401, 1405, 1409, 1418, 1420, 1425, 1428, 1429, 1435, 1442, 1444, 1445, 1452, 1456, 145, 1458, 1461, 1465, 1471, 1472, 1473
Nielsen, T., 90, 1338, 1340, 1341, 1343, 1377, 1417, 1421, 1445
Nieto, J.D., 448, 450, 451, 455, 494, 495, 496, 500, 501, 503, 505, 1412
Niki, H., 72, 115, 283, 284, 285, 385, 386, 540, 541, 542, 543, 544, 545, 546, 547, 549, 550, 551, 552, 554, 555, 586, 587, 588, 589, 592, 593, 595, 620, 638, 644, 645, 1310, 1408, 1421, 1430, 1443, 1445, 1463
Nikitin, E.B., 111, 1440
Ning, C.L., 1235, 1445
Ninomiya, Y., 475, 476, 509, 510, 529, 837, 838, 839, 875, 879, 1445, 1473
Nishi, N., 1030, 1458
Nishida, S., 554, 555, 556, 557, 1436
Nizkorodov, S.A., 1305, 1445
Nobes, R.H., 1164, 1170, 1403
Noda, J., 187, 188, 190, 191, 192, 194, 195, 198, 199, 200, 207, 208, 209, 210, 214, 215, 219, 574, 575, 576, 577, 581, 1445
Nogales, A., 1127, 1415
Nogar, N.S., 544, 545, 1416
Noguer, M., 97, 1428
Nohara, K., 436, 437, 438, 453, 475, 476, 489, 875, 876, 877, 880, 1408, 1446
Nojima, K., 1347, 1446
Nolan, S., 444, 445, 446, 448, 449, 467, 468, 485, 486, 502, 503, 504, 1446
Nolte, J., 726, 1423
Nonella, M., 1238, 1240, 1425, 1446
Noremsaune, I.M.W., 724, 1457
Norimichi, T., 104, 1444
Norris, J., 25, 38, 1414
Norrish, R.G.W., 997, 1010, 1012, 1054, 1059, 1060, 1123, 1130, 1163, 1165, 1239, 1268, 1269, 1398, 1408, 1426, 1444, 1446
North, S.W., 579, 1098, 1099, 1422, 1446
Norton, R.B., 78, 82, 83, 85, 87, 94, 95, 1418, 1454
Norton, R.H., 1227, 1454
Notario, A., 122, 123, 124, 128, 130, 131, 134, 135, 143, 146, 148, 149, 156, 157, 158, 165, 166, 167, 172, 176, 177, 295, 302, 303, 309, 310, 313, 314, 316, 318, 323, 333, 334, 526, 533, 556, 560, 566, 568, 574, 575, 576, 577, 616, 617, 657, 658, 659, 662, 663, 664, 667, 668, 669, 670, 671, 672, 674, 675, 677, 680, 681, 701, 728, 729, 777, 778, 782, 783, 784, 787, 791, 792, 797, 798, 799, 801, 802, 803, 804, 805, 806, 808, 809, 811, 812, 814, 815, 816, 817, 818, 819, 820, 822, 825, 826, 827, 831, 832, 835, 837, 841, 1392, 1398, 1411, 1420, 1440, 1446, 1454
Notte, G., 627, 628, 629, 1412
Nouaime, G., 94, 95, 611, 887, 968, 1446, 1454
Novicki, S.W., 1237, 1446
Nowick, M., 887, 968, 1475
Noyes, W.A., Jr., 989, 993, 997, 1089, 1107, 1111, 1113, 1114, 1115, 1116, 1117, 1119, 1120, 1121, 1122, 1123, 1124, 1147, 1163,

1165, 1166, 1168, 1170, 1171, 1208, 1209, 1211, 1212, 1213, 1214, 1215, 1216, 1404, 1412, 1415, 1417, 1425, 1426, 1428, 1442, 1446, 1447, 1449, 1450, 1458, 1462, 1475, 1478
Nozière, B., 622, 623, 628, 629, 630, 631, 1073, 1208, 1211, 1213, 1215, 1216, 1446
Nunes, F.M.N., 231, 234, 1447
Nyman, G., 187, 188, 190, 191, 192, 194, 195, 198, 199, 200, 207, 208, 209, 210, 214, 215, 576, 577, 581, 1445

Obi, K., 206, 208, 209, 210, 211, 212, 213, 1428
O'Connor, M.P., 210, 212, 213, 216, 217, 218, 219, 1031, 1041, 1407, 1447
O'Donnell, S.M., 370, 371, 372, 1447
Odum, J.R., 1374, 1377, 1426, 1447
Oehlers, C., 723, 1447
Oetjen, H., 1367, 1390, 1453, 1476
O'Farrell, D.J., 600, 608, 609, 710, 943, 944, 945, 947, 948, 955, 956, 1445, 1466
Ogbobe, O., 109, 1447
O'Grady, B.V., 117, 118, 120, 123, 125, 127, 1421
Oh, S., 117, 119, 120, 125, 127, 132, 133, 141, 142, 157, 168, 169, 170, 1447
O'Hara, D., 84, 1380, 1455
Ohbayashi, K., 1239, 1447
Ohno, K., 871, 874, 881, 1434
Ohsawa, O., 1159, 1467
Ohta, T., 141, 420, 421, 1080, 1447
Ohya, T., 1347, 1446
Ohyama, T., 420, 421, 1447
Okabe, H., 975, 1208, 1228, 1447
Okieimen, F.E., 109, 1447
Okuda, M., 1239, 1428
Olah, G.A., 100, 1447
Olariu, R.I., 244, 247, 248, 249, 253, 254, 255, 1447, 1448, 1466
Olavesen, C., 1192, 1439
Oldershaw, G.A., 132, 133, 134, 135, 137, 297, 298, 303, 304, 1408, 1462
Olivucci, M., 1030, 1453
Olsen, J.F., 1143, 1448
Olson, J.R., 77, 1418
Olsson, B.E.R., 658, 659, 701, 727, 728, 1448, 1472
Olszyk, D., 72, 968, 1476
Olszyna, K., 78, 79, 82, 85, 86, 87, 88, 89, 94, 95, 887, 1445, 1454
Öquist, M.G., 74, 1479
Oram, D.E., 77, 78, 79, 85, 87, 91, 92, 93, 94, 1437, 1453
O'rji, L.N., 370, 372, 676, 805, 806, 807, 812, 813, 814, 852, 853, 1448
Orkin, V.L., 434, 436, 437, 438, 439, 440, 441, 442, 448, 449, 468, 469, 837, 838, 839, 1401, 1448, 1473
Orlandi, M., 237, 238, 239, 424, 425, 1402
Orlando, J.J., 18, 65, 82, 86, 112, 113, 115, 117, 119, 122, 123, 126, 130, 131, 132, 134, 138, 140, 141, 143, 146, 148, 150, 151, 154, 157, 159, 162, 163, 169, 171, 172, 173, 174, 178, 179, 181, 184, 185, 186, 187, 194, 200, 201, 202, 203, 205, 207, 210, 211, 212, 213, 215, 216, 219, 220, 250, 257, 261, 275, 276, 277, 287, 293, 294, 295, 301, 302, 303, 305, 308, 309, 310, 311, 314, 315, 316, 317, 318, 320, 324, 327, 333, 334, 338, 339, 340, 342, 346, 349, 352, 353, 354, 355, 359, 361, 367, 372, 385, 387, 397, 399, 400, 407, 410, 411, 415, 419, 420, 422, 426, 431, 432, 437, 439, 441, 443, 444, 448, 449, 452, 453, 455, 456, 460, 464, 466, 469, 473, 476, 478, 481, 482, 484, 485, 488, 489, 492, 493, 496, 505, 506, 507, 509, 512, 519, 521, 529, 533, 534, 540, 544, 545, 546, 547, 549, 551, 552, 553, 558, 565, 566, 567, 568, 573, 575, 576, 581, 586, 587, 588, 589, 593, 594, 595, 596, 603, 604, 607, 608, 610, 611, 621, 623, 629, 637, 647, 655, 657, 658, 659, 671, 672, 673, 682, 689, 691, 692, 693, 711, 712, 728, 737, 748, 752, 753, 765, 766, 770, 775, 779, 780, 781, 788, 789, 794, 795, 796, 798, 799, 801, 806, 809, 810, 813, 817, 821, 824, 826, 829, 832, 834, 841, 842, 845, 846, 850, 852, 855, 857, 859, 867, 870, 873, 886, 888, 889, 890, 891, 893, 906, 909, 910, 911, 913, 915, 916, 918, 919, 922, 923, 927, 930, 933, 937, 938, 940, 941, 942, 943, 944, 945, 946, 947, 948, 949, 950, 954, 957, 958, 959, 960, 963, 966, 968, 969, 970, 971, 1024, 1026, 1027, 1065, 1068, 1070, 1072, 1076, 1077, 1078, 1080, 1082, 1083, 1084, 1085, 1086, 1088, 1089, 1092, 1095, 1096, 1100, 1102, 1105, 1106, 1107, 1109, 1112, 1120, 1123, 1124, 1125, 1126, 1127, 1128, 1130, 1131, 1133, 1134, 1136, 1139, 1141, 1143, 1146, 1148, 1150, 1151, 1152, 1153, 1154, 1155, 1156, 1159, 1161, 1162, 1163, 1175, 1176, 1177, 1178, 1179, 1180, 1181, 1182, 1184, 1186, 1188, 1189, 1190, 1191, 1194, 1195, 1201, 1223, 1224, 1225, 1227, 1228, 1230, 1231, 1232, 1262, 1273, 1286, 1287, 1288, 1289, 1290, 1291, 1298, 1300, 1301, 1302, 1303, 1304, 1305, 1306, 1333, 1358, 1367, 1393, 1398, 1403, 1405, 1417, 1418, 1427, 1429, 1431,

1448, 1451, 1455, 1457, 1462, 1464, 1468, 1472
Orr-Ewing, A.J., 124, 1223, 1414, 1455
Orzechowska, G.E., 747, 763, 1448
Osamura, Y., 1054, 1060, 1143, 1448, 1477
Osborn, D.L., 1269, 1271, 1470
Osborn, M.C., 751, 752, 1437
Osborne, A.D., 1115, 1451
Østergaard, L.F., 296, 1455
Osthoff, H.D., 543, 551, 1448
O'Sullivan, D.W., 77, 88, 1418, 1460
O'Sullivan, N., 444, 445, 446, 448, 449, 467, 468, 469, 485, 486, 502, 503, 504, 1446, 1449
Otero, J.C., 1270, 1394
Otting, M., 122, 123, 1414
Ottobrini, G., 543, 544, 1426
Oussar, F., 150, 151, 161, 162, 166, 167, 185, 186, 187, 189, 190, 191, 192, 193, 195, 196, 203, 204, 205, 208, 209, 210, 1410, 1436, 1441
Overend, R., 118, 120, 125, 127, 132, 133, 138, 139, 1449
Owen, S., 74, 1459
Owens, J.G., 515, 516, 875, 880, 1429
Oyaro, N., 443, 444, 445, 446, 448, 449, 450, 453, 454, 455, 457, 458, 462, 464, 465, 466, 467, 468, 469, 470, 478, 479, 483, 484, 487, 489, 1449

Padnos, N., 1209, 1212, 1213, 1214, 1215, 1216, 1449
Page, M., 543, 1461
Pagsberg, P., 118, 120, 124, 445, 446, 461, 462, 463, 472, 473, 499, 500, 501, 1425, 1449
Pala, I.R., 411, 1430
Palm, W.-U., 887, 891, 893, 894, 901, 1348, 1349, 1433, 1449
Palmer, P.I., 1362, 1367, 1386, 1387, 1388, 1389, 1390, 1399, 1408, 1414, 1418, 1423, 1449
Palmer, T.F., 989, 1394
Palomar, J., 868, 1407
Pandis, S.N., 769, 770, 779, 784, 905, 1358, 1372, 1373, 1374, 1377, 1401, 1414, 1431, 1449, 1457
Pang, X., 77, 78, 79, 83, 85, 1433
Pankow, J.F., 106, 1374, 1449, 1461
Papadimitriou, V.C., 259, 262, 263, 264, 266, 267, 268, 269, 270, 272, 275, 276, 447, 462, 463, 467, 468, 474 , 1433, 1449
Papagiannakopoulos, P., 262, 263, 264, 266, 267, 268, 269, 270, 272, 275, 276, 438, 439, 440, 444, 445, 447, 448, 450, 451, 462, 463, 467, 468, 470, 474, 497, 499, 1431, 1449
Papagni, C., 185, 186, 187, 195, 196, 198, 210, 211, 212, 213, 554, 555, 556, 557, 558, 559, 561, 565, 566, 567, 574, 575, 1449, 1450
Papanastasiou, D.K., 262, 263, 264, 270, 272, 275, 276, 1449
Papayannis, D.K., 257, 1450
Paraskevopoulos, G., 118, 120, 125, 127, 132, 133, 138, 139, 748, 749, 750, 751, 752, 753, 754, 755, 756, 757, 758, 759, 760, 761, 904, 1284, 1430, 1449, 1460
Park, J.H., 1227, 1454
Park, J.-Y., 295, 1450
Park, M.S., 1269, 1450
Parker, A.E., 77, 78, 79, 85, 87, 1437
Parkes, D.A., 288, 1392
Parkinson, P.E., 796, 797, 800, 801, 802, 824, 825, 826, 827, 829, 1405
Parmenter, C.S., 989, 993, 1054, 1057, 1060, 1061, 1208, 1393, 1438, 1450
Parr, A.D., 471, 502, 503, 504, 723, 1403
Parrinello, M., 688, 1418
Parrish, D.D., 78, 82, 83, 85, 87, 91, 92, 93, 94, 95, 886, 1418, 1454, 1462
Parsons, B.F., 1271, 1470
Pascoe, S., 684, 1363, 1456
Pasek, R., 107, 1479
Passant, N.R., 25, 38, 1362, 1363, 1413, 1414
Pasternack, L.R., 1239, 1456
Paszyc, S., 1269, 1450
Patrick, C.R., 1176, 1177, 1187, 1412
Patrick, K.F., 660, 661, 662, 676, 677, 706, 708, 709, 710, 1411
Patrick, K.G., 1242, 1411
Patroescu, S., 1319, 1344, 1345, 1396, 1416
Patroescu-Klotz, I., 206, 208, 209, 210, 211, 212, 213, 1428
Patton, E.G., 866, 1431
Paul, H., 1111, 1470
Paulsen, D., 1377, 1417, 1431
Paulson, S.E., 194, 331, 333, 334, 409, 411, 711, 712, 747, 763, 1176, 1179, 1374, 1434, 1448, 1449, 1474
Pauly, J., 1092, 1093, 1094, 1096, 1098, 1099, 1100, 1101, 1442
Pauwels, J.F., 904, 1413
Payne, W.A., 122, 123, 124, 282, 283, 295, 540, 541, 542, 544, 545, 552, 1442, 1450, 1462
Pearce, C., 1082, 1083, 1450
Peeters, J., 210, 211, 212, 213, 214, 215, 554, 586, 587, 588, 631, 655, 656, 657, 658, 659, 691, 692, 693, 712, 733, 753, 754, 755, 756, 758, 968, 969, 970, 971, 1369,

1413, 416, 1431, 1432, 1448, 1450, 1469, 1470
Peláez, D., 1270, 1394
Peng, X., 1261, 1264, 1407
Penkett, S.A., 77, 85, 91, 92, 93, 94, 115, 1362, 1424, 1450, 1453, 1461
Penner, J.E., 257, 1472
Peñuelas, J., 747, 1457
Percival, C.J., 296, 297, 1458
Pereira, P.A. de P., 231, 234, 1447
Perner, D., 526, 528, 544, 1233, 1234, 1239, 1385, 1404, 1406, 1435, 1450, 1451, 1474
Perona, M.J., 1162, 1398
Perovic, M., 843, 844, 1428
Perrin, A., 1390, 1414
Perring, A., 91, 92, 93, 1459
Perrino, C., 1234, 1235, 1236, 1463
Perros, P., 94, 1467
Perry, R.A., 241, 242, 243, 290, 291, 372, 373, 420, 421, 422, 901, 1397, 1450
Persico, M., 1272, 1410
Person, M.D., 1228, 1229, 1450
Peslherbe, G.H., 1054, 1058, 1061, 1433
Petek, H., 1164, 1444
Peterka, D.S., 1040, 1458
Peterson, C.L., 109, 1450
Petricca, M., 75, 78, 79, 82, 84, 1452
Pfab, J., 1235, 1240, 1426, 1445
Pfrang, C., 201, 202, 222, 374, 376, 712, 713, 1450
Phillips, D., 1176, 1177, 1178, 1186, 1187, 1191, 1192, 1193, 1399, 1423
Phillips, D.L., 645, 646, 1451
Phillips, L., 1242, 1245, 1257, 1394, 1427, 1438
Pibel, C.D., 1164, 1165, 1166, 1432
Picquet, B., 119, 120, 125, 127, 306, 307, 308, 637, 800, 801, 802, 809, 810, 811, 812, 813, 814, 817, 818, 819, 820, 822, 1407, 1451
Picquet-Varrault, B., 210, 212, 213, 216, 217, 218, 219, 373, 374, 376, 378, 379, 380, 543, 544, 550, 551, 552, 734, 735, 804, 807, 809, 810, 815, 816, 821, 1407, 1414, 1451, 1456
Pierce, J.M.T., 471, 502, 1403
Pierce, R.B., 91, 92, 93, 1459
Pierce, T.E., 74, 1423, 1434, 1459
Pilling, M.J., 77, 78, 79, 85, 87, 112, 152, 153, 161, 162, 283, 284, 285, 543, 551, 592, 595, 596, 618, 624, 632, 660, 684, 729, 730, 733, 735, 848, 849, 854, 855, 856, 860, 862, 1092, 1093, 1094, 1095, 1096, 1098, 1099, 1100, 1101, 1102, 1103, 1104, 1106, 1107, 1163, 1169, 1188, 1308, 1309, 1310, 1360, 1362, 1363, 1367, 1371, 1372, 1386, 1388, 1394, 1398, 1399, 1402, 1403, 1407, 1413, 1418, 1420, 1424, 1425, 1429, 1437, 1441, 1448, 1449, 1453, 1456, 1461, 1466, 1468, 1471, 1475, 1478
Pimentel, A.S., 385, 779, 780, 781, 788, 789, 794, 795, 796, 798, 799, 842, 850, 852, 855, 857, 859, 867, 870, 873, 1451, 1468, 1472
Pimentel, G.C., 1268, 1403
Pinho, P.G., 734, 1451
Pio, C.A., 734, 1451
Pippin, M., 94, 95, 1451
Pirasteh, A., 194, 205, 207, 400, 401, 1437
Pisano, P.J., 1054, 1060, 1414
Pitts, J.N., Jr., 18, 118, 120, 121, 137, 138, 139, 140, 237, 238, 239, 241, 242, 243, 244, 245, 246, 247, 248, 249, 250, 293, 294, 299, 300, 301, 302, 310, 311, 312, 372, 373, 386, 387, 389, 390, 391, 409, 410, 420, 421, 422, 540, 541, 542, 543, 544, 547, 549, 550, 551, 552, 592, 593, 594, 595, 596, 599, 600, 602, 605, 606, 608, 609, 619, 622, 632, 661, 662, 666, 667, 668, 669, 673, 674, 676, 682, 683, 684, 700, 706, 708, 709, 710, 713, 714, 729, 805, 806, 807, 817, 819, 820, 886, 899, 900, 901, 902, 903, 904, 922, 936, 937, 956, 957, 958, 964, 965, 970, 971, 972, 973, 994, 995, 1030, 1039, 1040, 1054, 1058, 1065, 1099, 1107, 1108, 1115, 1116, 1119, 1127, 1132, 1141, 1159, 1217, 1233, 1234, 1240, 1241, 1244, 1245, 1249, 1252, 1262, 1267, 1268, 1272, 1273, 1276, 1318, 1323, 1324, 1325, 1331, 1358, 1371, 1372, 1392, 1396, 1397, 1401, 1405, 1407, 1410, 1416, 1417, 1419, 1424, 1433, 1438, 1440, 1441, 1450, 1451, 1452, 1467, 1471, 1474, 1476
Piuzzi, F., 1239, 1441
Plagens, H., 1017, 1019, 1021, 1078, 1079, 1451
Plane, J.M.C., 1362, 1367, 1453, 1461
Plantevin, P.H., 1367, 1435
Plass-Dülmer, Ch., 115, 1455
Plastridge, R.A., 115, 1461
Platt, U., 76, 78, 79, 80, 81, 82, 83, 84, 85, 86, 87, 89, 90, 1024, 1061, 1234, 1235, 1236, 1239, 1316, 1317, 1319, 1344, 1345, 1396, 1385, 1390, 1404, 1416, 1423, 1433, 1450, 1457, 1460, 1463, 1470, 1476
Platz, J., 264, 277, 295, 297, 367, 368, 396, 397, 398, 399, 400, 401, 402, 406, 407, 468, 470, 485, 486, 875, 879, 884, 1377, 1445, 1452, 1456, 1457, 1472, 1473
Plum, C.N., 237, 238, 239, 243, 245, 246, 248, 250, 421, 422, 543, 544, 550, 551,

552, 592, 593, 594, 595, 596, 622, 1054, 1058, 1065, 1217, 1234, 1397, 1451, 1452
Poisson, N., 1368, 1452
Poland, H.M., 1054, 1208, 1393, 1450
Polik, W.F., 984, 1421
Polizzi, M., 75, 77, 84, 1458
Pollack, A.K., 98, 106, 107, 1415
Pommereau, J.-P., 1385, 1404
Ponche, J.L., 1235, 1403
Ponomarev, D., 384, 385, 1452
Pons, M., 629, 630, 631, 1073, 1446
Popp, C.J., 76, 78, 79, 82, 85, 89, 90, 91, 1419
Porter, E., 340, 341, 342, 343, 344, 345, 346, 347, 349, 350, 351, 352, 353, 354, 356, 357, 398, 400, 401, 405, 526, 1452, 1474
Porter, G., 1209, 1214, 1336, 1344, 1435, 1452
Porter, G.B., 1089, 1098, 1163, 1166, 1167, 1168, 1410, 1432, 1446
Porter, M., 77, 1418
Portmann, R.W., 126, 127, 258, 266, 267, 1453
Pos, W., 78, 79, 82, 85, 86, 87, 88, 89, 1454
Pöschl, U., 1368, 1452
Possanzini, M., 75, 78, 79, 82, 84, 1452
Potter, E.D., 1164, 1167, 1168, 1169, 1170, 1452
Potts, A.R., 315, 316, 317, 318, 326, 327, 328, 751, 752, 1468, 1471, 1473
Poulain, L., 763, 1425
Poulet, G., 283, 526, 528, 544, 545, 636, 647, 648, 904, 905, 964, 965, 966, 1399, 1430, 1452, 1467, 1474, 1478
Pouvesle, N., 586, 587, 588, 589, 590, 691, 692, 693, 753, 754, 755, 756, 758, 1404
Powers, J.W., 553, 1405
Prakash, G.K.S., 100, 1447
Prather, M.J., 1372, 1382, 1452, 1461
Preses, J.M., 232, 233, 1111, 1112, 1424
Pressley, S.N., 1362, 1367, 1386, 1388, 1449, 1452
Presto, A., 769, 770, 1364, 1452
Prevedouros, K., 257, 1452
Prevot, A.S.H., 77, 78, 79, 80, 82, 85, 86, 87, 88, 89, 104, 1377, 1431, 1436
Price, B.J.S., 660, 661, 662, 1407
Price, C.V., 106, 1461
Pritchard, G.O., 1162, 1392, 1398
Proffitt, M.H., 1383, 1475
Proos, R.J., 1286, 1414
Proper, S.P., 232, 233, 1424
Prosmitis, A.V., 262, 266, 267, 268, 269, 1449
Purkis, C.H., 1238, 1465
Purves, D.W., 77, 78, 79, 85, 87, 91, 92, 93, 94, 1367, 1417
Purvis, R.M., 77, 78, 79, 85, 87, 91, 92, 93, 94, 1437, 1453
Purzycki, K.L., 1220, 1458
Putaud, J.P., 1372, 1431
Puxbaum, H., 74, 1459
Pyle, J.A., 296, 297, 905, 906, 907, 908, 909, 910, 911, 1367, 1368, 1435, 1458, 1477

Quan, J., 77, 78, 79, 83, 85, 1443
Quilgars, A., 280, 281, 1441
Quinn, P.K., 115, 1392

Rabe, B.R., 1209, 1210, 1211, 1213, 1398
Raber, W.H., 1036, 1037, 1065, 1068, 1108, 1109, 1204, 1206, 1207, 1441, 1452, 1459
Rabitz, H., 540, 541, 542, 1477
Radloff, W., 1240, 1416
Radom, L., 989, 1164, 1170, 1403, 1460
Raff, J.D., 425, 426, 523, 524, 652, 654, 655, 656, 1453
Rajakumar, B., 126, 127, 258, 266, 267, 1100, 1101, 1102, 1104, 1453
Ramsay, D.A., 1055, 1426
Rao, S., 1366, 1477
Raper, O.F., 1227, 1454
Rappenglück, B., 94, 1453
Rasch, P.J., 18, 124, 282, 747, 1367, 1427, 1470
Rasmussen, R.A., 79, 84, 85, 87, 88, 103, 107, 116, 1422, 1423
Rattigan, O.V., 123, 130, 131, 132, 133, 134, 135, 138, 139, 140, 141, 142, 143, 144, 157, 158, 169, 170, 171, 172, 177, 183, 295, 299, 300, 301, 302, 303, 310, 311, 312, 313, 314, 315, 316, 317, 318, 319, 320, 321, 331, 332, 333, 334, 337, 338, 339, 924, 1078, 1277, 1288, 1410, 1444, 1453
Raventos-Duran, M.T., 296, 297, 1457
Ravishankara, A.R., 115, 117, 118, 119, 120, 124, 125, 126, 127, 130, 163, 164, 210, 211, 212, 213, 214, 215, 258, 266, 267, 279, 280, 281, 283, 284, 285, 298, 301, 324, 384, 389, 390, 543, 546, 547, 548, 549, 550, 551, 554, 555, 557, 558, 561, 562, 563, 565, 566, 567, 569, 574, 608, 609, 611, 612, 613, 617, 637, 639, 647, 648, 649, 652, 653, 655, 656, 686, 706, 708, 709, 710, 762, 904, 905, 906, 907, 908, 909, 910, 911, 913, 914, 923, 924, 934, 935, 962, 963, 964, 965, 966, 984, 1031, 1036, 1037, 1038, 1077, 1080, 1081, 1090, 1091, 1092, 1093, 1094, 1095, 1096,

1100, 1101, 1102, 1104, 1176, 1182, 1183, 1184, 1185, 1186, 1197, 1204, 1205, 1206, 1207, 1277, 1278, 1279, 1280, 1284, 1285, 1286, 1287, 1291, 1300, 1301, 1302, 1303, 1304, 1306, 1307, 1308, 1309, 1392, 1403, 1404, 1406, 1412, 1413, 1420, 124, 1430, 1433, 1438, 1440, 1448, 1453, 1455, 1458, 1460, 1464, 1468, 1469, 1475, 1479
Rawls, R.L., 1273, 1453
Rayez, J.-C., 124, 1429, 1441
Rayez, M.-T., 124, 1429, 1441
Rea, G.J., 251, 252, 253, 592, 618, 1360, 1465
Read, K.A., 733, 735, 1362, 1367, 1453, 1461
Reak, K.E., 1269, 1271, 1470
Rebbert, R.E., 1115, 1117, 1118, 1119, 1122, 1124, 1134, 1242, 1268, 1270, 1397, 1453
Redington, A., 77, 85, 1424,
Reece, D.L., 109, 1450
Reemtsma, T., 1377, 1453
Reeves, C.E., 77, 78, 79, 85, 87, 91, 92, 93, 94, 115, 1437, 1450, 1453
Reguero, M., 1030, 1453
Reikert, G., 120, 124, 125, 127, 129, 1441
Reilly, J.P., 1322, 1438
Reimann, B., 280, 281, 1461
Reimann, S., 77, 78, 79, 80, 82, 85, 86, 87, 88, 89, 104, 1436
Reinhold, V., 1273, 1416
Reinnig, M.C., 1377, 1453
Reisen, F., 216, 222, 929, 1453, 1454
Reissell, A., 76, 77, 78, 79, 80, 81, 82, 83, 84, 85, 86, 87, 737, 738, 1425, 1454
Restelli, G., 424, 425, 526, 528, 543, 544, 1402, 1426, 1462, 1474
Reyes, L.G., 76, 78, 79, 82, 85, 89, 90, 91, 1419,
Rhäsa, D., 118, 120, 124, 345, 346, 355, 370, 372, 812, 813, 814, 1423, 1424
Rhode, G., 622, 623, 1404
Richert, J.F.O., 154, 1429
Richter, A., 1389, 1390, 1442, 1476
Richter, C., 550, 551, 552, 555, 556, 558, 559, 1403
Richter, D., 77, 1418
Richter, H.R., 1083, 1085, 1454
Rickard, A.R., 595, 596, 1362, 1398, 1461
Rickborn, B., 1162, 1392, 1398
Ridley, B.A., 76, 78, 82, 83, 85, 87, 91, 92, 93, 886, 1397, 1402, 1418, 1454, 1471
Riekert, G., 118, 131, 1423
Rieley, H., 1235, 123, 14147
Riemer, D., 78, 79, 82, 85, 86, 87, 88, 89, 94, 95, 115, 194, 411, 711, 712, 887, 968, 1393, 1446, 1448, 1454, 1464
Rigler, E., 624, 626, 718, 719, 1460,
Rindone, B., 237, 238, 239, 424, 425, 486, 492, 493, 1402, 1407
Rinke, M., 236, 237, 238, 1454
Rinsland, C.P., 1227, 1390, 1414, 1454
Ristow, B.W., 1147, 1406
Robb, J.C., 1192, 1439
Robb, M.A., 1030, 1453
Roberts, J.M., 91, 92, 93, 94, 95, 611, 886, 887, 905, 906, 907, 908, 909, 910, 911, 913, 914, 923, 924, 964, 965, 966, 968, 1277, 1278, 1280, 1282, 1288, 1289, 1290, 1291, 1293, 1298, 1300, 1301, 1302, 1303, 1304, 1306, 1400, 1424, 1444, 1454, 1462, 1464, 1475
Robinson, A.L., 1364, 1377, 1414, 1452
Robinson, E., 103, 886, 1408, 1471
Roche, A., 805, 806, 807, 809, 810, 812, 813, 814, 832, 849, 850, 851, 852, 853, 1417
Rodriguez, A., 189, 192, 194, 204, 205, 207, 486, 492, 493, 566, 568, 574, 575, 576, 577, 602, 603, 616, 617, 657, 658, 659, 669, 670, 675, 728, 729, 765, 1098, 1100, 1101, 1102, 1104, 1394, 1432, 1440, 1454, 1473
Rodriguez, D., 189, 192, 194, 204, 205, 207, 486, 492, 493, 566, 568, 574, 575, 576, 577, 602, 603, 616, 617, 657, 658, 659, 728, 729, 765, 777, 778, 782, 783, 784, 1394, 1403, 1440, 1454, 1473
Rodriguez, H.J., 1143, 1144, 1146, 1465, 1473
Roehl, C.M., 1100, 1286, 1287, 1303, 1445, 1455, 1478
Roemer, M., 115, 1450
Rogers, H.L., 1367, 1435
Rogers, J.D., 984 , 1455
Rogers, M.O., 611, 1234, 1455
Rohde, G., 130, 131, 1415
Rohrer, F., 550, 551, 552, 555, 556, 558, 559, 1403
Rohrer, R., 1237, 1432
Rojas, R.D., 753, 754, 755, 1427
Rolle, W., 386, 409, 410, 411, 412, 413, 414, 418, 419, 1400, 1432
Rollefson, G.K., 1208, 1393
Roller, C., 77, 1418
Román-Leshlov, Y., 111, 1455
Roof, J.G., 993, 1039, 1208, 1401, 1455
Rosado-Reyes, C.M., 296, 757, 758, 1455
Rosas, I.P., 75, 1398
Roscoe, J.M., 659, 664, 670, 1054, 1060, 1061, 1455
Rose, M., 1244, 1455
Roselaar, L., 1268, 1421
Rosenberg, N.W., 1163, 1165, 1432
Rosenbohm, E., 237, 238, 239, 1402

Rosenlof, K.H., 1286, 1414
Rosenorn, T., 762, 1401
Rosenwaks, S., 1261, 1264, 1274, 1397, 1435, 1457
Ross, P.L., 1271, 1455
Ross, W.F., 1163, 1165, 1455
Rossi, A., 653, 655, 1409
Rossi, M.J., 112, 113, 117, 119, 121, 122, 126, 127, 128, 129, 130, 132, 134, 138, 140, 141, 143, 147, 150, 151, 154, 157, 159, 162, 163, 178, 184, 186, 188, 192, 195, 200, 201, 202, 204, 206, 209, 212, 214, 216, 225, 234, 237, 242, 245, 248, 252, 254, 261, 265, 284, 285, 308, 317, 325, 333, 336, 340, 347, 350, 355, 372, 373, 375, 376, 377, 378, 379, 380, 381, 383, 385, 390, 406, 407, 408, 410, 418, 422, 427, 428, 429, 453, 458, 465, 466, 479, 482, 483, 486, 489, 494, 496, 511, 514, 515, 517, 542, 545, 546, 548, 550, 552, 555, 556, 558, 559, 560, 562, 563, 565, 566, 568, 570, 571, 573, 575, 577, 578, 588, 597, 600, 601, 603, 605, 606, 607, 608, 609, 610, 612, 615, 616, 617, 621, 622, 623, 629, 632, 637, 639, 652, 654, 657, 658, 661, 662, 663, 668, 669, 674, 697, 701, 703, 705, 709, 710, 714, 716, 721, 723, 725, 727, 728, 730, 735, 740, 742, 752, 772, 773, 783, 787, 789, 795, 798, 803, 808, 811, 815, 818, 820, 821, 826, 844, 869, 873, 876, 888, 889, 890, 891, 893, 895, 896, 897, 898, 899, 900, 901, 906, 908, 909, 911, 912, 913, 914, 915, 917, 918, 920, 921, 922, 925, 926, 928, 933, 934, 937, 940, 941, 942, 952, 956, 961, 963, 969, 975, 984, 1083, 1288, 1384, 1392, 1396, 1397, 1409
Rösslein, M., 1261, 1264, 1455
Röth, E.-P., 454, 455, 471, 502, 503, 504, 1036, 1204, 1435, 1455
Rounbehler, A., 1272, 1417
Rounbehler, D.P., 1273, 1416, 1417
Rowland, F.S., 91, 92, 93, 115, 886, 1163, 1169, 1171, 1402, 1455, 1456, 1459, 1463, 1476
Rudić, S., 124, 1455
Rudich, Y., 210, 211, 212, 213, 214, 215, 609, 710, 917, 918, 924, 926, 928, 929, 930, 931, 932, 1455, 1466
Rudolph, J., 115, 1455
Rudy, S.J., 315, 316, 317, 1471
Ruhnke, R., 1036, 1204, 1455
Ruhztgi, N.K., 1308, 1437
Ruiz, M.E., 554, 1392
Ruiz-Santoyo, M.E., 751, 752, 1419
Ruppert, L., 629, 630, 631, 996, 997, 1000, 1001, 1005, 1006, 1009, 1010, 1013, 1015, 1017, 1019, 1020, 1021, 1039, 1040, 1041, 1073, 1074, 1075, 1078, 1079, 1222, 1223, 1443, 1446, 1451
Rusbult, C.F., 1156, 1458
Russell, G.A., 643, 1455
Russell, J.M., III, 1227, 1454
Russell, M.H., 257, 1477
Russell, R.L., 1163, 1169, 1171, 1455, 1456
Ruuskanen, T.M., 76, 77, 78, 79, 80, 81, 82, 83, 84, 85, 86, 87, 1425
Ryall, D., 77, 85, 1424
Ryerson, T.B., 91, 92, 93, 611, 886, 1454, 1462

Saastad, O., 219, 712, 1416
Sachse, G., 1380, 1381, 1459
Sachse, W., 84, 91, 92, 93, 1380, 1459
Saeed, K., 109, 1398
Sain, R.D., 1201, 1413, 1460
Saini, R.D., 1374, 1478
Saiz-Lopez, A., 1362, 1367, 1453, 1461
Sakurai, H., 1089, 1156
Salas, L., 75, 77, 91, 92, 93, 1456, 1459
Salawitch, R.J., 1383, 1475
Salce, J., 373, 374, 376, 378, 379, 380, 1456
Salcedo, D., 83, 1377, 1470
Salgado, M.S., 389, 390, 391, 410, 411, 413, 415, 601, 602, 604, 605, 606, 1456
Salgado, S., 389, 390, 391, 410, 411, 412, 413, 415, 550, 551, 552, 555, 556, 558, 559, 561, 563, 564, 565, 567, 569, 570, 601, 602, 604, 605, 606, 616, 1405, 1470
Salmeen, I.T., 98, 1408
Saltmarsh, O., 1163, 1165, 1446
Sander, R., 17, 769, 798, 807, 809, 1368, 1456, 1464
Sander, S.P., 546, 553, 748, 750, 758, 904, 905, 908, 938, 958, 968, 984, 1065, 1066, 1199, 1234, 1235, 1236, 1286, 1287, 1300, 1301, 1303, 1308, 1413, 1440, 1455, 1478
Sanders, N., 1239, 1456
Sanhueza, E., 592, 593, 594, 595, 596, 638, 644, 645, 1054, 1058, 1065, 1217, 1234, 1451, 1452, 1456
San Martini, F., 83, 1377, 1470
Santiano, R., 436, 439, 442, 1421
Santos, J.C., 747, 1409
Sapre, A.V., 185, 186, 187, 235, 1469
Sasaki, Y., 77, 78, 1427
Sato, H., 1335, 1337, 1428, 1464
Sato, K., 606, 614, 615, 713, 714, 716, 1456
Sato, S., 1159, 1467

Sauer, C.G., 340, 349, 350, 351, 358, 359, 360, 361, 363, 364, 365, 366, 367, 396, 397, 398, 399, 406, 407, 1452, 1456, 1465
Sauer, F., 1035, 1439, 1444
Saunders, S.M., 152, 153, 161, 162, 624, 632, 684, 848, 849, 854, 855, 856, 860, 862, 936, 937, 940, 941, 1360, 1362, 1363, 1367, 1369, 1371, 1372, 1399, 1413, 1429, 1456, 1478
Sauvain, T.D., 886, 1471
Savage, C.M., 72, 283, 284, 285, 540, 541, 542, 543, 544, 545, 546, 547, 549, 551, 552, 554, 555, 586, 587, 588, 589, 592, 593, 620, 638, 644, 645, 1310, 1445, 1463
Sawicki, E., 1273, 1417
Sawyer, A.A., 437, 438, 439, 440, 1475
Sawyer, H.A., 437, 438, 439, 440, 1475
Sax, M., 1377, 1417, 1431
Saxena, P., 762, 1456
Saxton, J.E., 1389, 1449
Scaiano, J.C., 1117, 1444
Scala, A.A., 1159, 1456
Scarfogliero, M., 373, 374, 376, 378, 379, 380, 1456
Schadt, C.F., 103, 1408
Schaefer, F.F., 984, 1477
Schaefer, H.F., III, 989, 1054, 1060, 1163, 1164, 1392, 1432, 1448, 1457
Schauer, J.J., 52, 53, 59, 1456, 1457
Schauffler, S.M., 886, 1383, 1397, 1475
Scheer, V., 1347, 1438
Scheuer, E., 76, 1418
Schiff, H.I., 75, 76, 77, 84, 88, 1425, 1458, 1462
Schiffman, A., 1284, 1307, 1457
Schiller, C.L., 1235, 1237, 1238, 1471
Schinke, R., 1238, 1240, 1425, 1446, 1469
Schlag, E.W., 1147, 1406
Schleyer, C.H., 98, 106, 107, 1415
Schliephake, V., 422, 1418
Schlomski, S., 76, 78, 79, 80, 81, 82, 83, 84, 85, 86, 87, 89, 90, 1423
Schmeltekopf, A., 544, 1406
Schmid, J.P., 970, 1273, 1276, 1451, 1467
Schmidbauer, N., 115, 1450
Schmitz, B., 1092, 1479
Schmoltner, A.-M., 964, 965, 966, 1300, 1301, 1302, 1304, 1464
Schneider, W.F., 134, 135, 137, 139, 140, 141, 256, 257, 265, 484, 485, 486, 634, 724, 725, 726, 743, 745, 746, 875, 879, 984, 1036, 1092, 1093, 1094, 1096, 1098, 1099, 1100, 1101, 1204, 1231, 1277, 1385, 1404, 1442, 1455, 1457, 1459, 1471, 1472, 1473, 1477
Schnur, J.M., 1269, 1457
Schoen, P.E., 1269, 1457
Schoepp, W., 73, 1438
Scholes, B., 72, 73, 1423
Schrader, T., 1333, 1434
Schreier, W.J., 1333, 1434
Schrock, R.R., 1245, 1457
Schuck, E.A., 1244, 1245, 1249, 1331, 1451, 1457
Schuetzle, D., 729, 730, 956, 960, 961, 1338, 1339, 1340, 1341, 1342, 1394, 1396
Schultz, M.G., 1367, 1400, 1427
Schurath, U., 1234, 1235, 1403
Schurgers, G., 1368, 1477
Schwartz-Lavi, D., 1261, 1264, 1274, 1397, 1435, 1457
Scollard, D.J., 546, 547, 549, 551, 552, 634, 635, 636, 637, 638, 639, 640, 641, 646, 647, 648, 649, 1399, 1457
Scott, W.D., 1331, 1403
Scuseria, G.E., 1054, 1060, 1457
Seakins, P.W., 77, 85, 112, 122, 123, 130, 131, 544, 545, 551, 552, 595, 596, 660, 661, 662, 1095, 1398, 1407, 1420, 1424, 1457
Seaver, C., 94, 95, 611, 887, 968, 1446, 1454
Sebastián, O., 83, 1460
Seco, R., 747, 1457
Seeba, J., 130, 131, 1415
Seefeld, S., 1366, 1462
Sehested, J., 105, 256, 257, 265, 275, 276, 277, 295, 296, 297, 336, 340, 341, 342, 367, 368, 400, 401, 402, 406, 407, 468, 470, 485, 486, 492, 493, 501, 634, 701, 727, 728, 742, 743, 745, 746, 769, 770, 771, 868, 869, 870, 875, 879, 874, 1231, 1401, 1409, 1420, 1435, 1442, 1445, 1452, 1457, 1471, 1472, 1473
Seiler, W., 985, 986, 987, 1057, 1443
Seinfeld, J.H., 10, 11, 18, 65, 112, 119, 126, 132, 138, 157, 171, 184, 186, 195, 198, 212, 225, 237, 253, 255, 364, 365, 367, 374, 383, 425, 427, 436, 437, 438, 439, 440, 441, 442, 444, 448, 449, 461, 551, 559, 562, 563, 568, 569, 571, 572, 577, 578, 608, 609, 612, 615, 616, 621, 629, 632, 633, 634, 713, 718, 719, 762, 779, 784, 846, 853, 854, 856, 859, 896, 899, 905, 957, 958, 960, 976, 984, 1030, 1033, 1035, 1042, 1217, 1312, 1313, 1314, 1317, 1318, 1333, 1335, 1336, 1342, 1343, 1345, 1347, 1356, 1358, 1372, 1373, 1374, 1377, 1405, 1418, 1419, 1422, 1423, 1426, 1431, 1434, 1436, 1447, 1449, 1457, 1461, 1467, 1474, 1478
Sekiya, A., 18, 259, 260, 267, 269, 271, 273, 274, 275, 426, 445, 446, 447, 448, 451,

452, 455, 456, 457, 458, 463, 465, 466, 469, 470, 471, 472, 473, 474, 475, 476, 477, 489, 490, 516, 517, 525, 779, 784, 787, 788, 803, 871, 872, 873, 874, 877, 878, 879, 880, 881, 882, 883, 885, 1408, 1434, 1466
Seland, J.G., 724, 1457
Sellevåg, S.R., 258, 259, 262, 265, 266, 267, 268, 269, 443, 444, 445, 446, 448, 449, 450, 453, 454, 455, 462, 464, 465, 466, 467, 468, 469, 470, 472, 473, 478, 479, 483, 484, 487, 488, 489, 490, 491, 492, 634, 635, 636, 640, 641, 643, 644, 657, 658, 659, 778, 782, 783, 784, 1078, 1082, 1083, 1084, 1085, 1086, 1087, 1088, 1193, 1194, 1195, 1196 , 1412, 1449, 1457, 1458
Semadeni, M., 236, 237, 238, 241, 242, 243, 244, 245, 246, 247, 248, 249, 299, 300, 301, 304, 305, 319, 320, 321, 331, 332, 334, 337, 338, 619, 620, 622, 1458
Semelsberger, G.A., 105, 1458
Semmes, D.H., 113, 265, 547, 549, 554, 555, 557, 558, 561, 562, 563, 565, 566, 567, 569, 1458, 1475
Sempeles, J., 314, 315, 348, 349, 1439, 1458
Senum, G.I., 905, 906, 907, 1419
Seong, J., 1164, 1431
Setser, D.W., 597, 1404
Sevin, A., 1143, 1458
Sewell, S., 76, 11418, 1420
Sexton, K.G., 720, 721, 722, 1027, 1042, 1045, 1046, 1218, 1220, 1438, 1478
Shaffer, G.W., 1220, 1458
Shah, R.C., 904, 1475
Shallcross, D.E., 296, 297, 601, 602, 609, 619, 620, 622, 654, 655, 657, 658, 659, 710, 711, 741, 743, 744, 745, 765, 855, 856, 860, 862, 905, 906, 907, 908, 909, 910, 911, 924, 969, 1367, 1369, 1370, 1406, 1407, 1410, 1429, 1435, 1458, 1469, 1474
Shan, J.H., 1235, 1458
Shanahan, I., 165, 172, 302, 303, 315, 316, 317, 318, 495, 496, 497, 498, 502, 503, 504, 505, 506, 507, 636, 647, 648, 1414, 1440, 1444
Sharm, D.K., 1335, 1336, 1337, 1477
Sharratt, A.P., 435, 1421
Shaw, J.H., 72, 970, 973, 1273, 1276, 1310, 1437, 1463
Shaw, M., 436, 437, 438, 439, 440, 441, 442, 444, 448, 449, 461, 1478
Shaw, R., 1242, 1245, 1394
Shearer, M., 74, 1459
Sheats, G.F., 1208, 1211, 1213, 1215, 1216, 1458
Sheldon, Z.D., 1111, 1414
Shen, H., 77, 88, 1418, 1460
Sheppard, D.W., 547, 549, 554, 555, 557, 558, 561, 562, 563, 565, 566, 567, 569, 570, 571, 572, 599, 600, 605, 620, 1432
Shepson, P.B., 75, 77, 78, 79, 82, 84, 85, 86, 87, 88, 89, 94, 95, 576, 581, 585, 887, 924, 932, 968, 994, 995, 1403, 1446, 1454, 1458
Shetter, J.D., 886, 1406, 1418, 1471
Shetter, R.E., 76, 78, 82, 83, 85, 87, 984, 1100, 1381, 1455, 1459
Shevlin, P.B., 1143, 1440
Shi, X.Q., 1231, 1413
Shinohara, H., 1030, 1458
Shire, J., 107, 1479
Shiu, W.Y., 255, 1439
Shobatake, K., 1164, 1165, 1166, 1425
Shorter, J.A., 257, 634, 743, 745, 746, 1231, 1473
Shortridge, R.G., Jr., 1030, 1156, 1159, 1161, 1163, 1458, 1468
Shragina, L., 926, 929, 931, 1466
Shu, J., 1040, 1458
Shu, Y., 222, 227, 228, 248, 426, 427, 428, 429, 1308, 1395, 1459
Sidebottom, H.W., 119, 120, 122, 123, 125, 127, 130, 131, 132, 133, 134, 135, 138, 139, 140, 141, 142, 143, 144, 152, 153, 157, 158, 169, 170, 171, 172, 177, 183, 185, 186, 187, 259, 261, 262, 270, 271, 272, 295, 299, 300, 301, 302, 303, 306, 307, 308, 310, 311, 312, 313, 314, 315, 316, 317, 318, 319, 320, 321, 323, 324, 325, 326, 327, 328, 331, 332, 333, 334, 337, 338, 339, 340, 341, 342, 343, 344, 345, 346, 347, 349, 350, 351, 352, 353, 354, 356, 357, 358, 370, 371, 372, 389, 390, 393, 394, 395, 396, 397, 398, 400, 401, 402, 403, 405, 406, 407, 444, 445, 446, 448, 449, 467, 468, 469, 485, 486, 502, 503, 504, 526, 528, 546, 547, 549, 551, 552, 600, 608, 609, 634, 635, 636, 637, 638, 639, 640, 641, 643, 644, 646, 647, 648, 649, 654, 655, 657, 658, 659, 686, 687, 688, 702, 703, 704, 706, 709, 710, 741, 742, 743, 744, 745, 769, 770, 771, 849, 850, 851, 852, 853, 854, 855, 856, 857, 858, 860, 861, 862, 906, 907, 908, 909, 910, 911, 912, 915, 916, 917, 918, 936, 937, 938, 939, 940, 941, 942, 943, 944, 945, 946, 947, 948, 949, 950, 951, 952, 953, 954, 955, 956, 1078, 1079, 1080, 1082, 1083, 1084, 1085, 1086, 1209, 1210, 1211, 1213, 1398, 1399, 1407, 1410, 1426, 1432, 1436, 1441, 1443, 1444, 1445,

1446, 1449, 1452, 1457, 1459, 1461, 1465, 1466, 1474
Sieger, R.A., 1176, 1177, 1187, 1188, 1189, 1459
Siegl, W.O.,122, 123, 128, 130, 131, 134, 135, 153, 154, 290, 291, 301, 304, 305, 306, 307, 308, 310, 311, 312, 315, 316, 317, 318, 319, 320, 321, 323, 324, 325, 326, 327, 328, 331, 332, 334, 337, 338, 551, 552, 556, 639, 909, 910, 911, 912, 914, 923, 945, 946, 947, 949, 952, 954, 1471, 1472, 1473
Siese, M., 236, 237, 238, 1433
Sillesen, A., 118, 120, 124, 1449
Sillman, S., 94, 95, 257, 1367, 1429, 1451, 1472
Silva, P.J., 115, 1464
Silvergleid, A., 1273, 1417
Simic, M., 901, 1425
Simonaitis, R., 962, 990, 994, 995, 1001, 1002 1004, 1413, 1425, 1459
Simoneit, B.R.T., 52, 53, 59, 1456, 1457
Simonich, S.L., 224, 225, 430, 740, 741, 1394, 1400
Simons, J.P., 1261, 1264, 1397
Simpson, D., 73, 74, 1459
Simpson, I.J., 886, 1459
Simpson, V.J., 73, 1392
Simpson, W.R., 1303, 1417
Singer, R.J., 1277, 1459
Singh, H.B., 23, 75, 77, 84, 91, 92, 93, 1227, 1367, 1380, 1381, 1388, 1429, 1442, 1456, 1459
Singh, S., 560, 561, 566, 568, 1378, 1379, 1380, 1381, 1460
Singleton, D.L., 748, 749, 750, 751, 752, 753, 754, 755, 756, 757, 758, 759, 760, 761, 904, 1284, 1430, 1460
Singmaster, K.A., 1271, 1470
Sinreich, R., 83, 1460
Sipniades, S., 1040, 1440
Sivakumar, N., 1054, 1058, 1404
Sivakumaran, V., 117, 119, 120, 124, 126, 127, 130, 540, 541, 542, 546, 548, 549, 1405, 1413, 1460
Sive, B.C., 91, 92, 93, 115, 1381, 1388, 1402, 1442, 1476
Sjödin, A., 1234, 1460
Skewes, L.M., 122, 123, 128, 130, 131, 134, 135, 153, 154, 290, 291, 301, 304, 305, 306, 307, 308, 310, 311, 312, 319, 320, 321, 323, 324, 325, 331, 332, 334, 337, 338, 551, 552, 556, 639, 1471, 1473
Skiba, U., 74, 1459
Skolnik, E.G., 546, 1433
Skov, H., 1377, 1445
Slagg, N., 1268, 1270, 1453
Slagle, I.R., 113, 265, 295, 1404, 1450
Slemr, J., 75, 77, 78, 79, 80, 82, 84, 85, 86, 87, 91, 92, 93, 94, 103, 1436, 1453, 1460
Smiley, R.A., 1265, 1468
Smith, A.M., 624, 626, 718, 719, 1460
Smith, B.J., 989, 1460
Smith, C.A., 279, 280, 904, 962, 963, 964, 1435, 1460
Smith, D.F., 306, 307, 308, 309, 323, 324, 325, 326, 327, 328, 329, 796, 797, 819, 821, 822, 1374, 1433, 1460, 1474
Smith, G.D., 985, 986, 1460
Smith, G.P., 1287, 1439
Smith, I.W., 904, 1460
Smith, I.W.M., 448, 449, 450, 451, 502, 503, 504, 505, 506, 550, 686, 751, 752, 1392, 1399, 1426, 1437, 1460
Smith, J.D., 122, 123, 551, 552, 1460
Smith, J.W., 1082, 1083, 1414
Smith, R.H., 542, 1460
Smith, S.J., 120, 121, 122, 124, 1406
Smith, T.W., 215, 1476
Smithwick, M.M., 257, 1439
Smurthwaite, P.I., 152, 153, 161, 162, 848, 849, 854, 855, 856, 860, 862, 1456
Snow, J.A., 76, 77, 88, 1379, 1380, 1418, 1459, 1460
Snyder, D.L., 1244, 1245, 1249, 1261, 1263, 1441
Sochet, L.R., 904, 1413
Sodeau, J.R., 1036, 1083, 1085, 1430, 1454
Soep, B., 1239, 1441
Sokolov, O., 907, 908, 938, 1461
Sokolowski-Gomez, N., 1024, 1319, 1320, 1324, 1465
Solberg, S., 115, 1450
Solgadi, D., 1239, 1240, 1413, 1434, 1441
Solignac, G., 185, 186, 187, 189, 190, 264, 272, 635, 638, 640, 641, 644, 887, 888, 889, 890, 891, 893, 895, 896, 897, 898, 899, 900, 901, 1079, 1080, 1230, 1436, 1461, 1465
Solman, Z., 296, 297, 1458
Solomon, S., 1277, 1278, 1279, 1280, 1404
Sommariva, R., 94, 95, 1362, 1454, 1461
Somnitz, H., 1098, 1100, 1101, 1102, 1461
Sonntag, H., 454, 455, 471, 502, 503, 504, 1435
Sørensen, M., 117, 119, 120, 125, 127, 133, 236, 237, 238, 1461
Sørensen, S., 1042, 1045, 1064, 1071, 1072, 1216, 1217, 1316, 1317, 1319, 1344, 1345, 1396, 1416, 1433
Sorooshian, A., 762, 1461

Soskin, G., 411, 601, 603, 606, 607, 610, 711, 720, 1416, 1474
Soto, A., 192, 194, 204, 205, 207, 1454
Soto, J., 1270, 1394
Soto, M.R., 543, 1461
Soulignac, J.C., 1273, 1436
Søvde, O.A., 258, 259, 262, 266, 267, 268, 269, 1457
Sparks, R.K., 1164, 1165, 1166, 1425
Spaulding, R., 216, 1461
Spears, K.G., 1268, 1270, 1461
Speer, R.E., 1374, 1433
Spence, J.W., 970, 1273, 1424
Sperry, P.D., 1030, 1031, 1033, 1034, 1035, 1419
Spicer, C.W., 115, 1234, 1461, 1463
Spiecker, H., 1261, 1264, 1417
Spietz, P., 1024, 1061, 1470
Spittler, M., 286, 629, 630, 631, 1017, 1019, 1021, 1073, 1078, 1079, 1446, 1451, 1461
Spivakovsky, C., 1372, 1461
Springer, A., 1377, 1453
Spurr, R.J., 1385, 1386, 1404, 1408
Squillace, P.J., 106, 1461
Sridharan, U.C., 280, 281, 1461
Srinivasan, R., 1115, 1123, 1156, 1157, 1159, 1162, 1462
Stachnik, R.A., 904, 1462
Staehelin, J., 77, 78, 79, 80, 82, 85, 86, 87, 88, 89, 104, 1436
Stafast, H., 1274, 1276, 1420
Staffelbach, T.A., 88, 546, 547, 549, 595, 596, 1065, 1068, 1070, 1072, 1454, 1462, 1468
Stalberg, E.A., 278, 1457
Stanier, C.O., 1377, 1414
Stanton, J.C., 733, 735, 1362, 1367, 1386, 1388, 1418, 1437, 1449
Starcke, J., 636, 639, 646, 647, 648, 649, 1462
Staricco, E.H., 1229, 1474
Stark, H., 163, 164, 281, 574, 962, 963, 964, 1392, 1430
Starkey, D.P., 137, 297, 298, 303, 304, 1408
Starn, T.K., 78, 79, 82, 85, 86, 89, 94, 95, 887, 1446, 1454
Staudt, A., 1379, 1459
Steacie, E.W.R., 1111, 1187, 1188, 1189, 1208, 1334, 1397, 1398
Stedman, D.H., 64, 1401, 1443
Steel, C., 1318, 1319, 1321, 1322, 1324, 1325, 1400
Stefanopoulos, V.G., 262, 263, 264, 270, 272, 275, 276, 1449
Stief, L.J., 122, 123, 124, 282, 283, 1420, 1442, 1450, 1462
Stein, T.N., 468, 470, 875, 884, 1472
Steinbacher, M., 1377, 1431
Steinberg, S., 747, 1431
Steinbrecher, R., 72, 73, 74, 1423, 1459
Steinert, W., 382, 384, 1418
Stemmler, K., 330, 342, 343, 345, 346, 348, 349, 355, 356, 561, 562, 563, 788, 789, 814, 817, 818, 835, 1462
Stensby, C., 643, 1393
Stenström, V., 634, 635, 1086, 1087, 1088, 1458
Stenström, Y., 578, 579, 1412
Stephanou, E.G., 1372, 1431
Stephens, E.R., 1245, 1457
Stephens, R.D., 902, 903, 1244, 1245, 1249, 1393
Stert, V., 1240, 1416
Stevens, J., 635, 638, 640, 641, 1393
Stevens, P.S., 210, 211, 212, 213, 608, 652, 654, 655, 656, 706, 708, 709, 710, 753, 754, 755, 756, 758, 1398, 1410, 1412, 1453, 1457, 1470
Stewart, D.J., 77, 78, 79, 85, 87, 91, 92, 93, 94, 711, 1406, 1437, 1453
Stewart, R.A., 25, 38, 1414
Stief, L.J., 122, 123, 295, 540, 541, 542, 544, 545, 552, 984, 1420, 1442, 1450, 1462
Stockberger, L., 1217, 1325, 1420
Stocker, D.W., 125, 127, 236, 237, 238, 241, 242, 243, 244, 245, 246, 247, 248, 249, 299, 300, 301, 303, 304, 305, 319, 320, 321, 331, 332, 334, 337, 338, 619, 620, 622, 653, 655, 729, 730, 805, 806, 807, 809, 810, 821, 905, 906, 907, 908, 909, 910, 911, 912, 1111, 1415, 1432, 1441, 1458
Stockwell, W.R., 544, 1235, 1366, 1406, 1462
Stone, D.A., 370, 372, 676, 805, 806, 807, 812, 813, 814, 852, 853, 1448, 1475
Stordal, F., 258, 259, 262, 266, 267, 268, 269, 1457
Storeton-West, R.L., 1347, 1438
Straccia, A.M., 340, 341, 342, 484, 724, 725, 726, 1439, 1471, 1472
Strachan, A.N., 1163, 1165, 1166, 1168, 1170, 1181, 1182, 1462
Straudt, M., 116, 1432
Streets, D.G., 1388, 1389, 1462
Streit, G.E., 935, 936, 1462
Strommen, M.R., 1338, 1340, 1341, 1343,1417
Stroud, C.A., 91, 92, 93, 94, 95, 886, 887, 968, 1454, 1462, 1475
Stucken, D., 303, 313, 1401
Stuhl, F., 748, 749, 750, 753, 754, 755, 758, 759, 761, 1237, 1432, 1478

Stutz, J., 112, 148, 172, 1234, 1235, 1236, 1463
Style, D.W.G., 1239, 1421
Su, F., 72, 1310, 1463
Sueper, D., 91, 92, 93, 886, 1462
Suga, A., 259, 260, 267, 269, 273, 274, 1466
Sugie, M., 457, 458, 1466
Sullivan, J.L., 52, 1473
Sumathi, R., 1228, 1229, 1463
Summer, A.L., 1362, 1366, 1367, 1368, 1449
Sun, J.-L., 1240, 1477, 1478
Sundet, J.K., 258, 259, 262, 266, 267, 268, 269, 1457
Suter, H.U., 1238, 1240, 1463
Sutton, H.C., 1099, 1107, 1108, 1415, 1439
Svenningsson, B., 762, 1401
Swanson, A.L., 91, 92, 93, 1402, 1463
Swietlicki, E., 1372, 1431
Szasz-Vadasz, T., 259, 267, 269, 1433
Szente, J.J., 295, 296, 297, 724, 725, 756, 757, 1187, 1230, 1411, 1439, 1455
Szilágyi, I., 652, 653, 655, 1092, 1093, 1094, 1095, 1096, 1101, 1106, 1444, 1469
Szopa, S., 1363, 1364, 1390, 1397, 1414, 1463

Taatjes, G.A., 122, 123, 128, 130, 131, 256, 551, 552, 1460, 1463
Tabazadeh, A., 1380, 1381, 1459
Taberski, J.S., 109, 1450
Taccone, R.A., 191, 192, 193, 195, 196, 203, 204, 205, 208, 209, 210, 389, 390, 391, 410, 411, 448, 450, 451, 455, 494, 495, 496, 500, 501, 503, 505, 858, 860, 861, 862, 863, 864, 1402, 1405, 1410, 1412
Tadić, J., 983, 991, 999, 1006, 1007, 1017, 1018, 1020, 1021, 1022, 1023, 1024, 1035, 1054, 1057, 1058, 1059, 1061, 1064, 1078, 1079, 1439, 1463
Tait, N.G., 106, 1409
Takacs, G.A., 1233, 1240, 1241, 1242, 1267, 1268, 1289, 1392, 1416, 1465
Takahashi, A., 259, 260, 267, 269, 273, 274, 426, 445, 446, 452, 456, 457, 458, 461, 462, 463, 472, 473, 474, 475, 476, 490, 499, 500, 501, 502, 503, 504, 516, 517, 525, 1466
Takahashi, C., 1159, 1467
Takahashi, K., 122, 123, 130, 131, 134, 139, 140, 554, 555, 556, 557, 566, 568, 581, 657, 658, 659, 662, 663, 664, 667, 668, 669, 674, 675, 727, 728, 778, 782, 783, 784, 787, 791, 792, 801, 802, 803, 804, 805, 806, 808, 809, 811, 812, 814, 815, 816, 817, 818, 819, 820, 822, 1102, 1103, 1428, 1429, 1436, 1463, 1476
Takahashi, M., 259, 260, 267, 269, 273, 274, 1144, 1159, 1466
Takayanagi, T., 606, 614, 615, 713, 714, 716, 1456
Takeda, H., 107, 1464
Takenaka, N., 905, 906, 907, 908, 909, 910, 1431
Taketani, F., 122, 123, 130, 131, 134, 139, 140, 662, 663, 664, 667, 668, 669, 670, 672, 674, 675, 1463
Taketsugu, T., 606, 614, 615, 713, 714, 716, 1456
Takeuchi, K., 436, 437, 438, 446, 451, 452, 453, 471, 472, 473, 475, 476, 487, 488, 489, 490, 491, 492, 875, 876, 877, 880, 1406, 1446
Takezaki, M., 1335, 1336, 1337, 1464
Talbot, B., 76, 1418
Talbot, R.W., 1380, 1381, 1388, 1442, 1459
Tallamraju, R., 72, 73, 1423
Talukdar, R.K., 210, 211, 212, 213, 214, 215, 546, 548, 549, 592, 593, 594, 608, 609, 627, 628, 629, 637, 639, 647, 648, 649, 655, 656, 706, 708, 709, 710, 904, 905, 906, 907, 908, 909, 910, 911, 913, 914, 923, 924, 934, 935, 964, 965, 966, 1032, 1036, 1037, 1038, 1077, 1080, 1081, 1197, 1204, 1205, 1206, 1207, 1277, 1278, 1279, 1280, 1291, 1300, 1301, 1302, 1304, 1403, 1404, 1412, 1416, 1420, 1455, 1464, 1478
Tamai, R., 466, 1408
Tan, D., 82, 86, 1393
Tanaka, H., 107, 1464
Tanaka, I., 1239, 1447
Tanaka, K., 1163, 1164, 1170, 1464
Tanaka, P.L., 115, 1464
Tang, I.N., 88, 409, 410, 1436
Tang, K.Y., 1149, 1150, 1464
Tang, X., 1366, 1462
Tang, Y., 91, 92, 93, 1017, 1018, 1019, 1020, 1021, 1042, 1043, 1044, 1045, 1046, 1047, 1048, 1049, 1050, 1458, 1464, 1476
Taniguchi, N., 1194, 1195, 1464
Tanner, R.L., 76, 77, 1464
Tao, Z., 516, 517, 1437
Tapia, A., 415, 601, 602, 605, 606, 616, 1405, 1456
Tappe, M., 303, 313, 422, 1404, 1418
Tapscott, C., 732, 1412
Taraborrelli, D., 1368, 1369, 1404, 1436, 1464
Tarbell, D.S., 1043, 1044, 1427
Tarmoul, J., 753, 754, 755, 757, 758, 1411
Tarrasón, L., 74, 1459
Tarte, P., 1250, 1262, 1464
Tavares, T.M., 104, 1444

Taylor, J., 72, 73, 1423
Taylor, K.F., 1164, 1165, 1398
Taylor, P.H., 290, 291, 292, 293, 306, 307, 308, 430, 432, 433, 518, 519, 520, 521, 652, 654, 655, 656, 1394, 1464, 1477
Taylor, R.P., 1183, 1209, 1212, 1213, 1215, 1464, 1465
Taylor, S.E., 288, 546, 548, 549, 550, 1465
Taylor, W.D., 1233, 1240, 1241, 1242, 1267, 1289, 1465
Temps, F., 122, 123, 280, 281, 540, 541, 542, 723, 726, 1414, 1423, 1447, 1465
Terazima, M., 1335, 1336, 1337, 1464
Terentis, A.C., 994, 999, 1442, 1465
Teruel, M.A., 448, 450, 451, 455, 494, 495, 496, 500, 501, 503, 505, 764, 765, 848, 849, 854, 855, 856, 857, 858, 859, 860, 861, 862, 863, 864, 873, 875, 881, 882, 883, 884, 1402, 1412, 1465
Testa, A.C., 1335, 1337, 1428
Téton, S., 152, 153, 280, 281, 290, 291, 292, 293, 299, 300, 301, 306, 307, 308, 310, 311, 312, 315, 316, 317, 319, 323, 324, 325, 326, 327, 328, 331, 332, 334, 340, 341, 342, 343, 344, 345, 346, 347, 349, 350, 351, 352, 353, 354, 356, 357, 398, 400, 401, 405, 526, 531, 546, 547, 549, 551, 552, 634, 635, 636, 637, 638, 639, 640, 641, 646, 647, 648, 649, 1399, 1441, 1452, 1457, 1465
Thelen, M.-A., 1308, 1309, 1465
These, A., 1377, 1453
Thévenet, R., 374, 375, 376, 554, 555, 556, 561, 562, 563, 565, 566, 567, 568, 571, 572, 573, 599, 600, 601, 603, 604, 605, 606, 607, 1024, 1030, 1031, 1032, 1439, 1465
Thiault, G., 374, 375, 376, 377, 378, 379, 380, 381, 619, 620, 622, 623, 1024, 1319, 1320, 1324, 1465
Thijsse, T., 115, 1450
Thistlethwait, G., 25, 38, 1414
Thomas, L., 1272, 1469
Thomas, S.S., 1261, 1262, 1441
Thomas, T.F., 1143, 1144, 1146, 1454, 1465
Thompson, H.W., 1238, 1239, 1250, 1261, 1262, 1465
Thompson, J.C., 109, 1450
Thompson, J.E., 280, 281, 1284, 1285, 1468
Thompson, K.C., 601, 602, 603, 604, 609, 610, 710, 711, 712, 765, 855, 856, 860, 862, 866, 867, 1406
Thompson, R.J., 409, 410, 1475
Thompson, R.L., 904, 1475
Thornberry, T., 82, 86, 94, 95, 1393, 1451
Thornton, D.E., 1163, 1166, 1462
Thouret, V., 1367, 1435
Thrush, B.A., 553, 1439
Thuener, L.P., 619, 620, 622, 1410
Thüner, L.P., 251, 252, 253, 340, 349, 350, 351, 358, 359, 360, 361, 363, 364, 365, 366, 367, 1050, 1440, 1465
Thynne, J.C.J., 1082, 1443
Tie, X., 1367, 1427
Tilgner, A., 763, 1425
Tilling, R.M., 77, 85, 1424
Timmons, R.B., 659, 1436
Timofeev, A., 73, 1391
Tittel, F.K., 77, 1418
Toby, S., 120, 121, 122, 124, 1406
Toft, A.M., 18, 261, 265, 278, 513, 514, 515, 641, 657, 660, 671, 843, 844, 1393, 1428, 1465
Tokiwa, Y., 1234, 1394
Tokuhashi, K., 18, 259, 260, 267, 269, 271, 273, 274, 275, 426, 445, 446, 447, 448, 451, 452, 455, 456, 457, 458, 461, 462, 463, 465, 466, 469, 470, 471, 472, 473, 474, 475, 476, 477, 487, 488, 489, 490, 491, 492, 499, 500, 501, 502, 503, 504, 516, 517, 525, 779, 784, 787, 788, 803, 871, 872, 873, 874, 877, 878, 879, 880, 881, 882, 883, 885, 1408, 1434, 1466
Tolocka, M.P., 1377, 1466
Toma, M., 453, 475, 476, 489, 875, 876, 877, 880, 1446
Tomas, A., 253, 254, 655, 656, 753, 754, 755, 757, 758, 1187, 1411, 1466, 1468
Tomasi, J., 1272, 1410
Tomlin, A.S., 1371, 1372, 1425, 1466, 1468, 1475
Tomy, G., 266, 1438
Tonokura, K., 18, 261, 265, 278, 641, 657, 660, 671, 1393
Toon, G.C., 1390, 1391
Tooze, C., 374, 376, 712, 713, 1450
Toupance, G., 75, 77, 94, 964, 965, 966, 1431, 1467
Town, M., 94, 95, 1451
Townley, E.R., 1250, 1430
Trainer, M., 72, 78, 82, 83, 85, 86, 87, 91, 92, 93, 94, 95, 611, 886, 887, 968, 1416, 1418, 1443, 1454, 1462, 1475, 1476
Tranter, R.S., 290, 291, 292, 293, 297, 298, 299, 301, 302, 306, 307, 308, 323, 324, 325, 1466
Trapp, D., 75, 454, 455, 471, 502, 503, 504, 1435, 1466
Treacy, J., 119, 120, 122, 123, 125, 127, 130, 131, 132, 133, 134, 135, 138, 139, 140, 141, 142, 143, 144, 157, 158, 169, 170, 171, 172, 177, 183, 185, 186, 187, 259,

261, 262, 270, 271, 272, 295, 299, 300, 301, 302, 303, 310, 311, 312, 313, 314, 315, 316, 317, 318, 319, 320, 321, 331, 332, 333, 334, 337, 338, 339, 340, 341, 342, 343, 344, 345, 346, 347, 349, 350, 351, 352, 353, 354, 356, 357, 398, 400, 401, 405, 444, 445, 446, 448, 449, 467, 468, 485, 486, 502, 503, 504, 526, 546, 547, 549, 551, 552, 600, 608, 609, 634, 635, 636, 637, 638, 639, 640, 641, 643, 646, 647, 648, 649, 654, 655, 657, 658, 659, 702, 703, 704, 706, 709, 710, 741, 743, 744, 745, 769, 770, 771, 849, 850, 851, 852, 853, 906, 907, 908, 909, 910, 911, 912, 915, 916, 917, 918, 936, 937, 938, 939, 940, 941, 942, 943, 944, 945, 946, 947, 948, 949, 950, 951, 952, 953, 954, 955, 956, 1399, 1407, 1426, 1432, 1436, 1444, 1445, 1446, 1452, 1457, 1466, 1474

Tremp, J., 1347, 1466

Trentelman, K.A., 1269, 1443, 1466

Treves, K., 917, 918, 924, 926, 928, 929, 930, 931, 932, 1466

Trevor, P.L., 962, 963, 964, 1261, 1466

Tripathi, S., 11, 1477

Troe, J., 112, 113, 117, 119, 121, 122, 126, 127, 128, 129, 130, 132, 134, 138, 140, 141, 143, 147, 150, 151, 154, 157, 159, 162, 163, 178, 184, 186, 188, 192, 195, 200, 201, 202, 204, 206, 209, 212, 214, 216, 225, 234, 237, 242, 245, 248, 252, 254, 261, 265, 279, 284, 285, 308, 317, 325, 333, 336, 340, 347, 350, 355, 372, 373, 375, 376, 377, 378, 379, 380, 381, 383, 385, 390, 406, 407, 408, 410, 418, 422, 427, 428, 429, 453, 458, 465, 466, 479, 482, 483, 486, 489, 494, 496, 511, 514, 515, 517, 542, 545, 546, 548, 549, 550, 551, 552, 555, 556, 558, 559, 560, 562, 563, 565, 566, 568, 570, 573, 575, 577, 578, 588, 597, 600, 601, 603, 605, 606, 607, 608, 609, 610, 615, 616, 617, 621, 622, 623, 629, 632, 634, 637, 639, 652, 654, 657, 658, 661, 662, 663, 668, 669, 674, 697, 701, 703, 705, 709, 710, 714, 716, 721, 723, 725, 727, 728, 730, 735, 740, 742, 752, 772, 773, 783, 787, 789, 795, 798, 803, 808, 811, 815, 818, 820, 821, 826, 844, 869, 873, 876, 888, 889, 890, 891, 893, 895, 896, 897, 898, 899, 900, 901, 906, 908, 909, 911, 912, 913, 914, 915, 917, 918, 920, 921, 922, 925, 926, 928, 933, 934, 937, 940, 941, 942, 952, 956, 961, 963, 969, 975, 984, 1083, 1188, 1239, 1288, 1384, 1392, 1396, 1397, 1399, 1426, 1466, 1467, 1470

Tsagatakis, I., 25, 38, 1414

Tsai, N.Y., 1388, 1389, 1462

Tsalkani, N., 94, 964, 965, 966, 1467

Tsang, W., 236, 1425

Tse, C.W., 253, 621, 1467

Tsigaridis, K., 1372, 1431

Tsunashima, S., 1159, 1467

Tuazon, E.C., 89, 118, 120, 216, 217, 219, 309, 310, 331, 333, 334, 348, 356, 362, 367, 368, 369, 385, 409, 410, 412, 509, 510, 576, 583, 610, 675, 700, 711, 720, 721, 722, 780, 804, 810, 821, 845, 886, 902, 903, 936, 937, 956, 957, 958, 970, 971, 972, 973, 1218, 1230, 1234, 1273, 1276, 1392, 1395, 1396, 1397, 1401, 1422, 1440, 1459, 1461, 1467

Tucceri, M.E., 777, 778, 782, 783, 784, 1403

Tuck, A.F., 1249, 1286, 1414, 1467

Tuckett, R.P., 448, 449, 450, 451, 502, 503, 504, 505, 506, 1399

Tullo, A.H., 110, 1467

Tully, F.P., 117, 118, 120, 123, 124, 125, 126, 127, 130, 137, 138, 139, 154, 155, 156, 290, 291, 293, 298, 300, 301, 308, 324, 384, 519, 1415, 1426, 1440, 1468

Tuorquety, S., 91, 92, 93, 1459

Turányi, T., 1371, 1466, 1468

Turnipseed, A.A., 280, 281, 866, 1284, 1285, 1307, 1308, 1431, 1468, 1469

Turpin, E., 655, 656, 1468

Tyeson, T.B., 887, 968, 1475

Tyndall, G.S., 18, 65, 112, 113, 117, 119, 122, 123, 126, 130, 131, 132, 134, 138, 140, 141, 143, 146, 148, 150, 151, 154, 157, 159, 162, 163, 169, 171, 172, 173, 174, 178, 179, 181, 184, 185, 194, 200, 201, 202, 203, 205, 207, 210, 211, 212, 213, 215, 216, 219, 220, 250, 256, 257, 261, 275, 276, 277, 279, 287, 293, 294, 295, 301, 302, 303, 305, 308, 309, 310, 311, 314, 316, 317, 318, 320, 324, 327, 333, 334, 338, 339, 340, 342, 346, 349, 352, 353, 354, 355, 359, 361, 367, 372, 385, 387, 397, 399, 400, 407, 410, 411, 415, 419, 420, 422, 426, 431, 432, 437, 439, 441, 443, 444, 448, 449, 452, 453, 455, 456, 460, 464, 466, 469, 473, 476, 478, 481, 482, 484, 485, 488, 489, 492, 493, 496, 505, 506, 507, 509, 512, 519, 521, 529, 533, 534, 540, 544, 545, 546, 547, 549, 551, 552, 553, 558, 565, 566, 567, 573, 575, 576, 586, 587, 588, 589, 593, 594, 595, 596, 603, 604, 607, 608, 610, 611, 621, 623, 629, 637, 647, 655, 657,

658, 659, 671, 672, 673, 682, 686, 687, 688, 689, 691, 692, 693, 711, 712, 737, 748, 751, 752, 753, 765, 766, 770, 775, 779, 780, 781, 796, 798, 799, 801, 806, 809, 810, 813, 817, 821, 824, 826, 829, 832, 834, 841, 842, 845, 846, 850, 852, 855, 857, 859, 867, 870, 873, 886, 888, 889, 890, 891, 893, 906, 909, 910, 911, 913, 915, 916, 918, 919, 922, 923, 927, 930, 933, 937, 938, 940, 941, 942, 943, 944, 945, 946, 947, 948, 949, 950, 954, 957, 958, 959, 960, 963, 966, 968, 969, 970, 971, 1024, 1026, 1027, 1065, 1068, 1070, 1072, 1076, 1077, 1078, 1080, 1082, 1083, 1084, 1085, 1086, 1088, 1089, 1092, 1095, 1096, 1100, 1102, 1105, 1106, 1107, 1109, 1112, 1120, 1123, 1124, 1125, 1126, 1127, 1128, 1130, 1131, 1133, 1134, 1136, 1139, 1141, 1143, 1146, 1148, 1150, 1151, 1152, 1153, 1154, 1155, 1156, 1159, 1161, 1162, 1163, 1175, 1176, 1177, 1178, 1179, 1180, 1181, 1182, 1184, 1186, 1188, 1189, 1190, 1191, 1194, 1195, 1201, 1223, 1224, 1225, 1227, 1228, 1230, 1231, 1232, 1262, 1273, 1286, 1287, 1288, 1289, 1290, 1291, 1298, 1300, 1301, 1302, 1303, 1304, 1305, 1306, 1333, 1358, 1367, 1398, 1403, 1405, 1414, 1417, 1418, 1427, 1431, 1448, 1451, 1455, 1457, 1462, 1468, 1472

Uberna, E., 76, 77, 1464
Uchida-Kai, K., 1144, 1444
Uchimaru, T., 18, 457, 458, 779, 784, 787, 788, 803, 871, 874, 880, 881, 882, 883, 885, 1434, 1466
Ufer, T., 1098, 1100, 1101, 1102, 1461
Ulic, S.E., 1240, 1402
Ullerstam, M., 550, 551, 552, 556, 558, 559, 560, 561, 562, 565, 571, 573, 599, 600, 601, 602, 603, 605, 606, 607, 1412, 1468
Ulmstead, M.E., 1030, 1164, 1419, 1468
Umaña, M., 1208, 1391
Unfried, K.G., 1165, 1468
Unger, I., 1147, 1163, 1426, 1446
Ungnade, H.E., 1265, 1468
Untch, A., 1238, 1240, 1425, 1446, 1469
Upadhyaya, H.P., 185, 186, 187, 235, 691, 692, 693, 1179, 1180, 1201, 1269, 1409, 1413, 1450, 1469
Urbanik, E., 956, 957, 958, 1476
Utembe, S.R., 1369, 1370, 1377, 1429, 1430, 1469, 1474

Vaghjiani, G.L., 279, 280, 281, 283, 284, 285, 1284, 1285, 1307, 1308, 1309, 1468, 1469
Vaida, V., 1286, 1414
Vakhtin, A.B., 279, 281, 1469
Van Cauwenberghe, K., 970, 1276, 1451
Vandenberk, S., 554, 655, 656, 1469
Van der Auwera, 1165, 1393
Van der Linden, P.J., 97, 1428
Van der Werf, R.P., 1209, 1414
Van der Woerd, H., 1385, 1404
Van Dingenen, R., 1372, 1431
Van Huis, T.J., 984, 1477
Vanselow, D., 1318, 1322, 1402
Van Sonnenberg, E., 106, 1469
Varney, R.R., 106, 1469
Varutbangkul, V., 762, 1377, 1419, 1436, 1461
Vasudev, R., 1235, 1237, 1446, 1458, 1469
Vasvári, G., 652, 653, 655, 1469
Vay, S., 1380, 1459
Vázquez, G.J., 1100, 1455
Večeřa, A., 1234, 1469
Veillerot, M., 812, 813, 814, 1470
Veloso, M.C.C., 231, 134, 1447
Venkatachari, P., 1377, 1453
Venuti, E., 1344, 1421
Vereecken, L., 586, 587, 588, 631, 655, 656, 657, 658, 659, 691, 692, 693, 733, 755, 756, 758, 968, 969, 970, 971, 1369, 1413, 1416, 1431, 1448, 1450, 1469, 1470
Vesly, G.F., 1197, 1198, 1199, 1200, 1470
Veszprémi, T., 1270, 1444
Vignati, E., 1372, 1431
Viidanoja, J., 578, 579, 1412
Villa, A., 1240, 1475
Villanueva, F., 201, 202, 410, 411, 412, 413, 415, 601, 602, 605, 606, 616, 1405, 1450, 1456, 1470
Villenave, E., 315, 319, 439, 440, 468, 469, 554, 555, 556, 557, 564, 565, 573, 1410, 1436
Vimal, D., 652, 654, 655, 656, 753, 754, 755, 756, 757, 1412, 1470
Vipond, A., 296, 297, 905, 906, 907, 908, 909, 910, 911, 1458
Visca, M., 511, 512, 1393
Viskolcz, B., 1188, 1470
Visticot, J.P., 1239, 1441
Vita, R., 1273, 1416
Vivier-Bunge, A., 543, 554, 580, 656, 751, 752, 1392, 1419
Vogel, B., 76, 78, 79, 80, 81, 82, 83, 84, 85, 86, 87, 89, 90, 1423
Vogel, C., 1388, 1452
Vogel, E., 1316, 1317, 1318, 1470
Vogt, R., 406, 407, 1439, 1449, 1452
Vöhringer-Martinez, E., 546, 548, 549, 1470
Voicu, I., 742, 744, 1470

Volkamer, R., 83, 592, 618, 1024, 1061, 1316, 1317, 1360, 1377, 1390, 1402, 1433, 1460, 1470, 1476
Vollenweider, J.K., 1111, 1470
Volman, D.H., 993, 1039, 1402
Volpp, H.-R., 1269, 1450
Volz-Thomas, A., 75, 76, 77, 78, 79, 80, 81, 82, 83, 84, 85, 86, 87, 89, 90, 91, 92, 93, 96, 1417, 1423, 1460
Von Kuhlmann, R., 18, 124, 282, 747, 1368, 1452, 1470
Vorsa, V., 1235, 1458
Vovelle, C., 290, 291, 292, 293, 306, 307, 308, 340, 341, 349, 350, 351, 358, 359, 360, 1402, 1470
Vrekoussis, M., 1367, 1419

Wade, E.A., 1164, 1165, 1166, 1269, 1271, 1470
Wagner, A., 25, 38, 1414
Wagner, H.Gg., 122, 123, 280, 281, 303, 313, 422, 540, 541, 542, 659, 723, 724, 725, 726, 1404, 1414, 1415, 1416, 1418, 1423, 1442, 1447, 1465
Wagner, P.J., 1159, 1471
Wagner, T., 88, 1390, 1460, 1476
Wagner, V., 592, 618, 1360, 1402, 1429
Wahner, A., 76, 78, 550, 551, 552, 555, 556, 558, 559, 1400, 1403
Walega, J.G., 76, 77, 78, 82, 83, 85, 87, 88, 886, 1397, 1418, 1454, 1460, 1471
Walker, C., 25, 38, 1414
Walker, R.W., 132, 134, 135, 137, 290, 291, 292, 293, 297, 298, 299, 301, 302, 303, 304, 306, 307, 308, 323, 324, 325, 382, 383, 384, 590, 1188, 1398, 1399, 1408, 1462, 1466, 1469, 1471
Wall, K.J., 1235, 1237, 1238, 1471
Wallington, T.J., 10, 11, 18, 53, 65, 103, 104, 105, 108, 112, 113, 115, 117, 118, 119, 120, 121, 122, 123, 125, 126, 127, 128, 130, 131, 132, 133, 134, 135, 137, 138, 139, 140, 141, 142, 143, 144, 145, 150, 151, 152, 153, 154, 157, 159, 160, 161, 162, 163, 166, 167, 168, 169, 170, 171, 172, 173, 174, 178, 179, 177, 181, 182, 183, 184, 186, 190, 194, 195, 198, 205, 207, 212, 216, 225, 234, 236, 237, 238, 242, 245, 248, 250, 252, 253, 255, 256, 257, 259, 261, 262, 263, 264, 265, 267, 268, 269, 270, 271, 272, 273, 274, 275, 276, 277, 278, 279, 285, 286, 287, 290, 291, 293, 294, 295, 296, 300, 301, 302, 303, 304, 305, 306, 307, 308, 309, 310, 311, 312, 314, 315, 316, 317, 318, 319, 320, 321, 323, 324, 325, 326, 327, 328, 329, 331, 332, 333, 334, 336, 337, 338, 339, 340, 341, 342, 343, 344, 346, 348, 349, 350, 351, 352, 353, 354, 355, 358, 359, 360, 361, 364, 365, 367, 368, 372, 375, 376, 377, 378, 379, 380, 381, 382, 383, 384, 385, 386, 387, 389, 391, 392, 397, 399, 400, 401, 402, 406, 407, 409, 410, 411, 413, 414, 415, 417, 418, 419, 420, 422, 425, 426, 427, 431, 432, 433, 435, 436, 437, 438, 439, 441, 442, 443, 444, 448, 449, 450, 451, 452, 453, 455, 456, 457, 458, 459, 460, 464, 466, 468, 469, 470, 473, 475, 476, 478, 479, 480, 481, 482, 483, 484, 485, 486, 488, 489, 492, 493, 494, 496, 501, 503, 505, 506, 507, 508, 509, 510, 511, 512, 513, 514, 515, 516, 517, 519, 521, 522, 525, 529, 531, 533, 534, 551, 552, 553, 554, 555, 556, 557, 558, 559, 562, 563, 564, 565, 566, 567, 568, 569, 571, 572, 573, 576, 577, 578, 581, 593, 595, 603, 607, 608, 609, 612, 615, 616, 621, 622, 623, 629, 632, 633, 634, 635, 636, 637, 638, 639, 640, 641, 643, 644, 647, 652, 653, 654, 655, 657, 658, 659, 660, 661, 662, 663, 664, 665, 666, 667, 668, 669, 670, 671, 672, 673, 674, 675, 676, 677, 678, 679, 682, 683, 691, 692, 693, 697, 699, 700, 701, 702, 703, 704, 707, 709, 711, 716, 717, 718, 720, 721, 723, 724, 725, 726, 727, 728, 729, 730, 732, 735, 736, 737, 742, 743, 744, 745, 746, 748, 749, 750, 751, 752, 753, 754, 755, 756, 757, 758, 759, 761, 765, 769, 770, 771, 772, 773, 775, 776, 777, 778, 779, 780, 781, 782, 783, 784, 785, 786, 787, 790, 791, 792, 796, 797, 798, 799, 800, 801, 802, 803, 804, 805, 806, 807, 809, 810, 811, 812, 813, 814, 815, 816, 817, 818, 819, 820, 821, 822, 824, 825, 826, 827, 828, 829, 830, 831, 832, 833, 834, 837, 838, 839, 841, 842, 843, 844, 845, 846, 847, 848, 850, 852, 853, 854, 855, 856, 857, 858, 859, 861, 862, 863, 864, 865, 866, 867, 868, 869, 870, 871, 873, 875, 876, 880, 882, 883, 884, 885, 886, 888, 889, 890, 891, 893, 896, 899, 906, 907, 908, 909, 910, 911, 912, 913, 914, 915, 916, 918, 919, 922, 923, 927, 930, 933, 934, 935, 937, 938, 940, 941, 942, 943, 944, 945, 946, 947, 948, 949, 950, 952, 954, 956, 957, 958, 960, 963, 964, 965, 966, 968, 976, 977, 978, 984, 985, 986, 987, 988, 989, 990, 992, 994, 995, 999, 1000, 1003, 1004, 1005, 1007, 1008, 1009, 1011, 1012, 1014, 1015, 1016, 1018, 1019, 1020, 1021,

1022, 1023, 1024, 1026, 1027, 1030, 1033, 1035, 1042, 1054, 1065, 1076, 1077, 1078, 1079, 1080, 1082, 1083, 1084, 1085, 1086, 1087, 1088, 1089, 1092, 1095, 1096, 1100, 1102, 1105, 1106, 1107, 1109, 1112, 1120, 1123, 1124, 1125, 1126, 1127, 1128, 1130, 1131, 1133, 1134, 1136, 1139, 1141, 1143, 1144, 1146, 1148, 1150, 1151, 1152, 1153, 1154, 1155, 1156, 1159, 1161, 1162, 1163, 1175, 1176, 1177, 1178, 1179, 1180, 1181, 1182, 1184, 1186, 1188, 1189, 1190, 1191, 1194, 1195, 1201, 1217, 1223, 1224, 1225, 1227, 1228, 1230, 1231, 1232, 1262, 1287, 1288, 1289, 1290, 1291, 1298, 1300, 1301, 1302, 1303, 1304, 1305, 1306, 1308, 1312, 1313, 1314, 1317, 1318, 1333, 1335, 1336, 1342, 1343, 1345, 1347, 1356, 1358, 1373, 1392, 1393, 1396, 1397, 1401, 1405, 1407, 1409, 1411, 1412, 1415, 1418, 1420, 1421, 1427, 1428, 1429, 1430, 1431, 1435, 1436, 1440, 1441, 1442, 1443, 1445, 1446, 1451, 1452, 1456, 1457, 1461, 1463, 1464, 1465, 1468, 1470, 1471, 1472, 1473, 1476, 1477, 1478

Walter, D., 131, 133, 1423

Walters, S., 1367, 1427

Wan, J.K.S., 1159, 1244, 1245, 1249, 1331, 1451

Wang, B., 659, 1427

Wang, C., 284, 286, 287, 1409, 1473

Wang, D., 645, 646, 1451

Wang, F., 266, 1438

Wang, J., 546, 547, 549, 1473

Wang, L., 627, 1325, 1326, 1328, 1329, 1330, 1331, 1332, 1473

Wang, M., 101, 102, 1473

Wang, M.Q., 1388, 1389, 1462

Wang, S., 1234, 1463

Wang, S.-C., 1374, 1474

Wang, T., 94, 95, 1454

Wang, W., 411, 601, 603, 606, 607, 610, 711, 720, 1065, 1068, 1069, 1070, 1408, 1416, 1474

Wang, X., 1264, 1474

Wang, Y., 76, 1264, 1367, 1417, 1418, 1474

Wang, Y.X., 1367, 1388, 1418

Wängberg, I., 187, 186, 295, 309, 310, 336, 337, 628, 629, 631, 632, 776, 782, 787, 802, 806, 924, 927, 929, 930, 932, 933, 1072, 1073, 1290, 1293, 1296, 1424, 1435, 1445, 1474

Wania, F., 257, 266, 1438, 1474

Ward, B., 1336, 1452

Ware, W.R., 1187, 1424

Warnatz, J., 1188, 1399

Warneck, P., 985, 986, 987, 990, 993, 1057, 1070, 1089, 1092, 1093, 1094, 1096, 1098, 1099, 1100, 1101, 1197, 1199, 1202, 1203, 1400, 1415, 1442, 1443

Warneke, C., 73, 94, 95, 1367, 1381, 1388, 1429, 1442, 1454

Warnke, J., 1377, 1453

Warren, R.F., 1307, 1308, 1469

Waschewsky, G.C.G., 1182, 1184, 1431, 1474

Washburn, S.T., 257, 1477

Washida, N., 905, 906, 907, 908, 909, 910, 1425, 1431

Wategaonkar, S.J., 1235, 1458

Waterland, R.L., 257, 641, 643, 644, 1079, 1080, 1082, 1083, 1084, 1085, 1086, 1087, 1230, 1409, 1425, 1473, 1474, 1477

Waters, D.J., 936, 937, 939, 940, 942, 1397

Watkins, B.A., 78, 82, 83, 85, 87, 1418

Watling, G., 936, 937, 939, 940, 942, 1397

Watson, J.G., 64, 904, 1426, 1439

Watson, L.A., 77, 78, 79, 85, 87, 91, 92, 93, 94, 1369, 1370, 1429, 1469, 1474

Watson, N., 77, 78, 79, 85, 87, 91, 92, 93, 94, 1437, 1453

Watson, R., 282, 283, 1474

Watson, R.T., 904, 1285, 1439

Watts, H.G., 1331, 1403

Wayne, R.P., 120, 121, 122, 124, 201, 202, 222, 296, 297, 312, 317, 325, 329, 374, 376, 471, 502, 503, 504, 526, 528, 601, 602, 603, 604, 609, 610, 636, 647, 648, 654, 655, 657, 658, 659, 710, 711, 712, 713, 714, 715, 716, 717, 723, 765, 769, 770, 771, 855, 856, 860, 862, 865, 866, 867, 905, 906, 907, 908, 909, 910, 911, 969, 1358, 1391, 1399, 1403, 1406, 1407, 1450, 1458, 1474

Weathers, W.S., 1325, 1374, 1420, 1433

Weaver, J., 990, 992, 1474

Webster, C.R., 1383, 1475

Wegener, R., 550, 551, 552, 555, 556, 558, 559, 1403

Wei, Q., 1240, 1478

Weibel, D.E., 1229, 1474

Weibring, P., 77, 1418

Weingartner, E., 1377, 1417, 1431

Weir, D.S., 1111, 1120, 1474

Wells, J.R., 145, 146, 147, 148, 149, 159, 171, 172, 223, 229, 230, 233, 234, 235 236, 250, 280, 281, 348, 349, 370, 372, 633, 739, 834, 905, 1399, 1403, 1417, 1424, 1439, 1474, 1475, 1476

Wells, J.S., 935, 936,1462

Welter, F., 1234, 1235, 1403

Wenger, J.C., 186, 210, 212, 213, 216, 217, 218, 219, 251, 252, 253, 315, 319, 340,

341, 342, 343, 344, 345, 346, 347, 349, 350, 351, 352, 353, 354, 356, 357, 358, 370, 371, 372, 398, 389, 390, 393, 394, 395, 396, 397, 398, 400, 401, 402, 403, 405, 406, 407, 444, 445, 446, 448, 449, 467, 468, 469, 485, 486, 502, 503, 504, 526, 592, 618, 619, 620, 621, 622, 654, 655, 657, 658, 659, 741, 743, 744, 745, 849, 850, 851, 852, 853, 979, 1031, 1041, 1360, 1399, 1402, 1407, 1410, 1436, 1443, 1446, 1447, 1449, 1452, 1461, 1465, 1474
Wennberg, P.O., 1286, 1303, 1381, 1382, 1383, 1429, 1440, 1445, 1474, 1478
Wert, B.P., 76, 1418, 1420
Wesolowski, S.S., 984, 1477
Westberg, H., 72, 73, 76, 78, 82, 83, 85, 86, 87, 1393, 1416, 1418, 1420, 1434, 1435, 1452
Weston, R.E., Jr., 232, 233, 1111, 1112, 1424
Wettack, F.S., 1113, 1114, 1115, 1117, 1119, 1475
Whalley, L.K., 77, 78, 79, 85, 87, 1437
White, A.B., 1234, 1463
Whitehouse, L., 1371, 1372, 1466, 1475
Whiteway, S.G., 1131, 1475
Whitten, G.Z., 1284, 1365, 1366, 1420, 1430, 1477
Whittle, E., 1187, 1392
Whytock, D.A., 282, 283, 658, 1082, 1083, 1187, 1392, 1419, 1442, 1450, 1475
Wiebe, H.A., 1240, 1475
Wiedinmyer, C., 73, 95, 1362, 1367, 1386, 1387, 1388, 1449, 1454
Wieprecht, W., 1347, 1438
Wiesen, E., 597, 720, 721, 722, 720, 721, 722, 846, 847, 848, 1401, 1475
Wiesen, P., 85, 86, 87, 88, 89, 350, 360, 361, 363, 364, 365, 366, 396, 397, 398, 848, 849, 858, 859, 860, 861, 862, 863, 864, 1399, 1400, 1401, 1418, 1444
Wijayuaratne, R.D., 1092, 1094, 1419
Wijnen, M.H.J., 1111, 1228, 1434, 1475
Wilber, W.G., 106, 1461
Wild, O., 1078, 1453
Williams, D.C., 370, 372, 805, 806, 807, 812, 813, 814, 852, 853, 1474, 1475
Williams, E., 94, 95, 1454
Williams, E.J., 78, 82, 83, 85, 87, 115, 611, 887, 1392, 1418, 1454, 1463, 1475
Williams, E.L., II, 95, 186, 187, 196, 197, 198, 221, 223, 608, 609, 710, 712, 967, 968, 969, 970, 1422
Williams, J., 91, 92, 93, 611, 887, 924, 968, 1277, 1288, 1369, 1381, 1388, 1404, 1410, 1391, 14111436, 1442, 1453, 1454, 1462, 1475
Williams, M.R., 416, 417, 653, 657, 661, 676, 1391, 1411
Williams, P.I., 77, 78, 79, 85, 87, 1362, 1437, 1461
Willner, H., 1240, 1402
Wilson, E.W., Jr., 437, 438, 439, 440, 455, 456, 457, 459, 460, 468, 469, 471, 472, 473, 477, 478, 480, 481, 482, 487, 488, 491, 1475
Wilson, J.E., 1123, 1372, 1431
Wilson, M.R., 657, 1403
Wilson, R.R., 964, 965, 966, 1300, 1301, 1302, 1304, 1464
Wilson, R.W., 1286, 1404
Wine, P.H., 113, 265, 280, 281, 409, 410, 546, 547, 549, 553, 554, 555, 557, 558, 561, 562, 563, 565, 566, 567, 569, 748, 749, 751, 752, 904, 905, 908, 938, 958, 968, 1199, 1234, 1235, 1236, 1308, 1396, 1444, 1453, 1456, 1458, 1475, 1478
Winer, A.M., 72, 120, 121, 137, 138, 139, 140, 237, 238, 239, 241, 243, 245, 246, 247, 248, 249, 250, 293, 294, 299, 300, 301, 302, 310, 311, 312, 386, 387, 389, 390, 409, 410, 421, 422, 427, 429, 543, 544, 550, 551, 552, 600, 605, 606, 608, 609, 619, 622, 661, 662, 676, 683, 710, 713, 714, 729, 805, 806, 807, 817, 819, 820, 913, 914, 915, 916, 918, 919, 921, 922, 956, 957, 958, 964, 965, 966, 970, 971, 972, 973, 1233, 1234, 1240, 1241, 1252, 1262, 1267, 1273, 1318, 1323, 1324, 1325, 1394, 1396, 1397, 1407, 1424, 1438, 1451, 1467, 1471, 1476
Wingenter, O.W., 76, 91, 92, 93, 115, 1402, 1418, 1476
Winiwarter, W., 74, 1458
Winterhalter, R., 185, 186, 187, 189, 190, 1073, 1197, 1202, 1203, 1207, 1208, 1372, 1426, 1431, 1436, 1476
Wirtz, K., 259, 261, 262, 270, 271, 272, 315, 319, 586, 587, 588, 589, 592, 599, 600, 604, 605, 607, 618, 629, 630, 631, 636, 638, 643, 887, 888, 889, 890, 891, 893, 895, 896, 897, 898, 899, 900, 901, 913, 914, 917, 920, 921, 923, 996, 997, 1000, 1001, 1005, 1006, 1009, 1010, 1013, 1015, 1017, 1019, 1020, 1024, 1025, 1026, 1027, 1030, 1031, 1032, 1039, 1040, 1041, 1054, 1057, 1058, 1059, 1061, 1064, 1073, 1074, 1075, 1076, 1193, 1194, 1195, 1196, 1222, 1223, 1316, 1317, 1362, 1400, 1402, 1410, 1412, 1430, 1432, 1433, 1439, 1443, 1446, 1447, 1461, 1463
Wiseman, F.L., 370, 1474

Wisthaler, A., 73, 578, 579, 887, 968, 1367, 1412, 1424, 1429, 1476
Witte, F., 956, 957, 958, 1476
Wittich, G.R., 106, 1469
Wittrock, F., 1367, 1389, 1390, 1419, 1442, 1476
Wodtke, A.M., 1164, 1165, 1414, 1443
Wofsy, S.C., 1367, 1372, 1429, 1461
Wohlfrom, K., 1380, 1459
Wolf, M.H., 723, 1273, 1416, 1447
Wolfe, P., 75, 76, 78, 1393
Wolfrum, J., 1307, 1420
Wollenhaupt, M., 652, 653, 655, 1476
Woo, J.H., 1388, 1389, 1462
Woodbridge, E.I., 1099, 1476
Woodward, C.E., 1164, 1170, 1403
Wooldridge, P.J., 91, 92, 93, 1459
Wooldridge, P.W., 91, 92, 93, 485, 486, 875, 879, 1473
Wooldridge, S.T., 641, 644, 1079, 1080, 1082, 1083, 1084, 1085, 1086, 1087, 1409
Worley, S.D., 1143, 1440
Worsnop, D.R., 257, 634, 743, 745, 746, 1231, 1364, 1372, 1377, 1413, 1452, 1470, 1473, 1478
Worton, D., 91, 92, 93, 94, 1453
Wu, C.-H., 122, 123, 128, 130, 134, 135, 551, 552, 556, 1473
Wu, H., 125, 127, 130, 131, 132, 133, 134, 135, 138, 139, 140, 141, 142, 143, 144, 150, 151, 152, 153, 154, 157, 158, 161, 162, 163, 560, 561, 581, 1476
Wu, M., 102, 1473
Wu, W., 1377, 1414
Wuebbles, D.J., 257, 516, 517, 904, 1437, 1472, 1475
Wünsch, G., 1347, 1438
Wyatt, S.E., 171, 172, 834, 1403, 1476

Xia, J., 257, 1472
Xia, X.Y., 1377, 1453
Xiang, B., 1043, 1045, 1046, 1047, 1048, 1049, 1050, 1051, 1053, 1054, 1476
Xiao, L., 134, 135, 137, 256, 1477
Xaio, Y., 1367, 1476
Xing, J.-H., 778, 782, 783, 784, 787, 791, 792, 801, 802, 803, 804, 805, 806, 808, 809, 811, 812, 814, 815, 816, 817, 818, 819, 820, 822, 1428, 1476
Xu, D., 1228, 1477
Xu, K., 1237, 1392
Xu, S., 542, 543, 554, 1477

Yacobucci, B.D., 98, 1477
Yadav, J.S., 989, 990, 1477
Yamabe, S., 1143, 1477
Yamada, T., 430, 432, 433, 518, 519, 520, 521, 652, 654, 655, 656, 1464, 1474
Yamaguchi, Y., 984, 1477
Yamamoto, A., 260, 271, 274, 275, 1408
Yamamoto, S., 1197, 1198, 1200, 1202, 1477
Yamanaka, T., 134, 135, 137, 139, 140, 141, 142, 143, 144, 145, 256, 1428, 1477
Yamashita, S., 445, 446, 452, 456, 461, 462, 463, 472, 473, 474, 475, 476, 499, 500, 501, 1197, 1198, 1200, 1202, 1466
Yang, N.C., 1124, 1410
Yang, X., 1288, 1477
Yantosca, R.M., 1367, 1380, 1381, 1400, 1417, 1429, 1459, 1476
Yarber, K.F., 1388, 1389, 1462
Yardley, J.T., 1209, 1440, 1443
Yarwood, G., 65, 98, 106, 107, 112, 115, 119, 126, 132, 138, 157, 171, 184, 186, 190, 195, 198, 212, 225, 234, 237, 242, 245, 248, 252, 253, 257, 287, 301, 311, 320, 324, 329, 333, 336, 350, 359, 361, 362, 364, 365, 367, 368, 375, 376, 377, 378, 379, 380, 381, 383, 389, 409, 411, 413, 414, 415, 417, 418, 422, 424, 425, 426, 427, 431, 433, 522, 525, 551, 559, 562, 563, 568, 569, 571, 572, 577, 578, 595, 608, 609, 612, 615, 616, 621, 629, 632, 633, 634, 637, 661, 671, 676, 683, 699, 703, 716, 717, 718, 729, 732, 805, 806, 807, 809, 810, 812, 813, 814, 832, 846, 847, 848, 853, 854, 856, 858, 859, 861, 862, 863, 864, 865, 866, 957, 958, 960, 976, 984, 990, 1030, 1033, 1035, 1042, 1054, 1065, 1143, 1194, 1217, 1234, 1308, 1312, 1313, 1314, 1317, 1318, 1333, 1335, 1336, 1342, 1343, 1345, 1347, 1356, 1358, 1366, 1373, 1405, 1415, 1421, 1464, 1477
Yaws, C.L., 11, 1477
Ye, S., 1147, 1149, 1409, 1477
Yetter, R.A., 540, 541, 542, 1477
Yin, H.-M., 1240, 1477
Yin, J., 77, 85, 1424
Yip, R.W., 1335, 1336, 1337, 1477
Yocke, M., 1366, 1477
Yoffe, A.D., 1268, 1421
Yokelson, R.J., 747, 1409
Yokouchi, Y., 115, 1430
Yokoyama, K., 989, 1434
Yonei, Y., 260, 271, 274, 275, 1408
Yoo, K.Y., 1377, 1419
Yoshimine, M., 1163, 1164, 1170, 1464, 1477
Young, C.J., 256, 257, 512, 513, 873, 876, 885, 1405, 1477
Young, J.O., 1366, 1420
Young, P.J., 1368, 1477

Young, V., 385, 386, 887, 968, 1408, 1475
Young, V.L., 611, 1454
Yu, H., 989, 1439
Yu, J., 1027, 1164, 1478
Yu, J.-G., 1054, 1059, 1061, 1437
Yu, J.Z., 64, 77, 78, 79, 80, 83, 84, 85, 86, 1426
Yudis, D., 1250, 1430
Yue, X.-F., 1240, 1478
Yujing, M., 635, 638, 640, 641, 644, 1079, 1080, 1129, 1195, 1478

Zabarnick, S., 406, 407, 541, 542, 943, 944, 955, 1243, 1244, 1248, 1256, 1257, 1266, 1269, 1271, 1478
Zabel, F., 118, 120, 636, 639, 646, 647, 648, 649, 962, 963, 964, 1020, 1070, 1230, 1399, 1437
Zabransky, V.P., 1163, 1171, 1478
Zagogianni, H., 905, 1478
Zahniser, M.S., 1231, 1413, 1478
Zahra, A., 1120, 1121, 1122, 1478
Zakko, S.F., 106, 1469
Zander, R., 1228, 1454
Zaras, A.M., 262, 263, 264, 270, 272, 275, 276, 1449
Zare, R.N., 124, 1235, 1399, 1469
Zellner, R., 118, 120, 124, 345, 346, 355, 370, 372, 382, 383, 384, 454, 455, 471, 502, 503, 504, 812, 813, 814, 904, 1098, 1100, 1101, 1102, 1418, 1423, 1424, 1435, 1438, 1460, 1461
Zeng, G., 1368, 1371, 1372, 1477, 1478
Zenobi, R., 1377, 1431
Zetzsch, C., 236, 237, 238, 382, 383, 384, 386, 387, 748, 749, 750, 753, 754, 755, 758, 759, 761, 887, 891, 893, 894, 901, 956, 957, 958, 1348, 1349, 1429, 1433, 1449, 1454, 1476, 1478
Zewail, A.H., 1089, 1090, 1092, 1147, 1149, 1164, 1167, 1168, 1169, 1170, 1413, 1452
Zhang, F., 1054, 1059, 1061, 1437
Zhang, H., 1286, 1478
Zhang, J., 1237, 1392
Zhang, Q., 1372, 1377, 1470, 1478
Zhang, R.J., 64, 1426
Zhang, S.-H., 436, 437, 438, 439, 440, 441, 442, 444, 448, 449, 461, 1478
Zhang, X., 77, 78, 79, 83, 85, 125, 127, 130, 131, 132, 133, 134, 135, 138, 139, 141, 142, 143, 144, 150, 151, 152, 153, 154, 157, 158, 161, 162, 163, 1443, 1476
Zhang, Z., 315, 316, 317, 318, 326, 327, 328, 1374, 1471, 1473, 1478
Zhao, C., 645, 646, 1451
Zhao, Y., 645, 1225, 1418
Zhao, Z., 657, 658, 659, 662, 663, 664, 669, 670, 1478
Zheng, C.K., 1164, 1165, 1421
Zheng, Q.K., 1164, 1165, 1166, 1432
Zhou, S.M., 382, 383, 657, 658, 659, 662, 663, 664, 669, 670, 702, 703, 705, 707, 1479
Zhou, X., 18, 75, 76, 77, 83, 84, 91, 1420, 1425, 1436, 1479
Zhu, L., 546, 548, 549, 592, 593, 594, 994, 995, 998, 999, 1001, 1002, 1003, 1004, 1010, 1011, 1012, 1013, 1014, 1015, 1016, 1017, 1018, 1019, 1020, 1021, 1042, 1043, 1044, 1045, 1046, 1047, 1048, 1049, 1050, 1051, 1053, 1054, 1065, 1068, 1069, 1070, 1080, 1231, 1288, 1289, 1318, 1319, 1323, 1324, 1325, 1408, 1409, 1411, 1416, 1465, 1476, 1479
Zhu, R.S., 542, 543, 554, 1054, 1055, 1056, 1057, 1058, 1059, 1477
Zhu, T., 374, 375, 376, 377, 378, 379, 380, 382, 383, 657, 658, 659, 662, 663, 664, 669, 670, 702, 703, 705, 707, 924, 925, 926, 928, 929, 932, 933, 1290, 1292, 1293, 1297, 1298, 1355, 1399, 1479
Zielinska, B., 76, 77, 107, 412, 729, 730, 956, 960, 961, 1338, 1339, 1340, 1341, 1396, 1464, 1479
Ziemann, P.J., 700, 1377, 1414, 1417, 1470, 1479
Ziemer, H., 122, 123, 1414
Zika, R.G., 78, 79, 82, 85, 86, 87, 88, 89, 94, 95, 887, 968, 1446, 1454
Zimmer, A, 691, 692, 693, 1448
Zimmerman, P., 72, 73, 79, 80, 81, 84, 85, 886, 1397, 1416, 1421, 1423, 1479
Zinth, W., 1333, 1434
Zogorski, J.S.,106, 1461
Zou, P., 1269, 1271, 1470
Zuckermann, H., 1092, 1271, 1421, 1479

Subject Index

(For information on specific compounds see the Compound Index)

Abbreviations for experimental methods used in tables, 114
Acid anhydrides, kinetic data for reactions with Cl, 773
Acids, organic, 747
  ambient concentrations of, 89
  emissions of, 45
  kinetic data for reactions of with OH, NO_3, and Cl, 747
    acylic, 748
    aromatic, 768
    dibasic, 762
    halogen-atom substituted, 770
    keto-acids, 766
    terpene derived, 768
    unsaturated, 763
  physical properties of, 9, 13–16
Alcohols, 116
  ambient concentrations of, 87
  emissions of, 45
  kinetic data for reactions of with OH, NO_3, Cl, $O(^3P)$, 116
    acylic, 117
    aromatic, 236
    diols, 183
    halogen-atom substituted, 256
    hydroperoxides, 283
    peroxides, 279
    structure–activity relations for, 523
      Cl + alcohols, 530
      OH + alcohols, 531
      NO_3 + alcohols, 534
    unsaturated, 185
  physical properties of, 7, 13–17
Aldehydes,
  ambient concentrations of, 75
  emissions of, 45
  kinetic data for reactions of with OH, NO_3, Cl, $O(^3P)$,
    acylic, 540
    biogenic hydrocarbons, derived from, 618
    dialdehydes, 592
    halogen-atom substituted, 634
    hydroxyl aldehydes, 585
    unsaturated, 598
  photodissociation of, 983
    acyclic,
    aldehydes containing additional functional groups, 1024
    aldehydes derived from biogenic hydrocarbons, 1072
  physical properties of, 8, 13–16
Amides, 887
  kinetic data for reactions of with OH, NO_3, Cl, 887
  physical properties of, 12
Amino alcohols, kinetic data for the reactions of with OH, NO_3, Cl, 902
Atmospheric lifetimes, estimation of, 113

Carbonates, kinetic data for atmospheric reactions of, 868

Cross sections, *see* compound index for information on specific compounds

Esters, 774
  ambient concentrations of, 89
  emissions of, 45
  kinetic data for reactions of with OH, NO_3, Cl, $O(^3P)$, 774
    acyclic, 775
    aromatic, 866
    carbonates, 868
    cyclic, 846
    difunctional, 841
    halogen-atom substituted, 871
    lactates, 870
    unsaturated, 848
  physical properties of, 9, 13–16
Ethers, 289
  ambient concentrations of, 88
  emissions of, 45
  kinetic data for reactions of with OH, NO_3, Cl, $O(^3P)$, 289
    acyclic, 290
    aromatic, 420
    cyclic, 382
    halogen-atom substituted, 434
    multifunctional, 340
    structure–activity relations for, 523
      Cl + ethers, 531
      OH + ethers, 530
      NO_3 + ethers, 534
    unsaturated, 372
  physical properties of, 7, 13–16
European photoreactor (EUPHORE), 980

j-Values, *see* compound index for information on specific compounds

Ketenes,
  kinetic data for reactions of with OH, NO_3, Cl, $O(^3P)$, 723
  photodecomposition of, 1162
Ketones, 651
  ambient concentrations of, 84
  biogenic hydrocarbon derived from, 731
  cyclic, 726
  diketones, 700
  emissions of, 45
  halogen-atom substituted, 741
  hydroxy ketones, 691
  kinetic data for reactions with OH, NO_3, Cl, $O(^3P)$,
    alkanones, 652
    structure–activity relations for,
      OH + ketones, 684
      Cl + ketones, 689
  physical properties of, 8, 13–16
  unsaturated, 706
Kinetic data for
  acids, 747
  alcohols, 116
  aldehydes, 539
  esters, 775
  ethers, 289
  ketones, 651
  nitrogen-containing oxygenates, 886
  treatment of, 111

Lactates, kinetic data for, 870
Lactones, kinetic data for, 846
Lifetimes,
  photochemical (1/j), 1350
  with respect to OH attack, *see* information on specific compounds in compound index

Nitramines, kinetic data for reactions of with OH, O_3, 970
Nitrates, 904
  ambient concentrations of, 91
  kinetic data for reactions of with of OH, Cl, O_3, 904
    alkyl nitrates, trends in the reactivity of, 904
    carbonyl nitrates, 933
    dinitrates, saturated, 924
    dinitrates, unsaturated, 928
    hydroxy alkyl nitrates, 929
Nitrites, 934, 1276
  kinetic data for reactions of with OH, Cl, 934
  photodecomposition of, 1276
Nitroalkanes, 943, 1267
  kinetic data for reaction of with, OH, Cl, 943
  photodecomposition of, 1267
Nitroalkenes, kinetic data for reactions of with OH, 955
Nitroarenes, kinetic data for reactions of with OH, NO_3, Cl, O_3, 960
Nitroaromatics, 956
  kinetic data for reactions of with OH, NO_3, O_3, 956
  photodecomposition of, 1335
Nitrosamines,
  kinetic data for reactions of with, OH, O_3, 970
  photodecomposition of, 1272

Oxygenates,
ambient concentration of, 75
remote atmospheres, 96
rural atmospheres, 96
urban atmosphere, 74
global budgets for, 72, 1380
importance of in atmospheric chemistry, 1358
observation of, in the remote troposphere, 1378
physical properties of, 8
boiling points, 14
heats of combustion, 14
Henry's law constants, 17
melting points, 13
vapor pressures, 6
representation of in chemical mechanisms, 1359
explicit or near-explicit mechanisms, 1359
lumped chemical mechanisms, 1364
carbon bond mechanism, 1365
common representative intermediates mechanism, 1369
GEOS-Chem, 1367
Mainz isoprene mechanism, 1368
MOZART, 1367
objective methods of mechanism reduction, 1371
RACAM, 1367
SAPRAC, 1367
TOMCAT, 1367
roles of, in
atmospheric chemistry, 3
proxies for VOC emissions, 1384
secondary organic aerosol formation, 1372
transport of pollutants, 1383
upper troposphere, 1377, 1381
satellite observations of, 1385
sources of, 19
anthropogenic emissions, 18, 45
atmospheric oxidation of hydrocarbons, 64
biogenic comounds, 72
upper troposphere HO_x, 1381
uses of, as fuels or fuel additives,
tert-amyl methyl ether, 107
biodiesel, 108
butanol, 104
dimethyl ether, 105
ethanol, 100
ethyl *tert*-butyl ether,
methanol,
methyl *tert*-butyl ether, 109
other oxygenates, 110

Peroxyacyl nitrates, 962
ambient concentrations of, 94
kinetic data for reactions of with OH, Cl, NO_3, O_3, 962
photodecomposition of, 1298
Photochemical data for, 974
acyl halides, 1223
aldehydes,
acylic, 1089
with additional functional groups, 1175
aromatic oxygenates, 1311
carbonyl halides, 1223
hydroperoxides, alkyl, 1306
ketones, 1089
acylic, 1089
cyclic, 1143
with additional functional groups, 1175
nitrates, alkyl, 1287
nitrites, alkyl, 1233
nitroalkanes, 1267
nitroso compounds, 2373
peroxyacyl nitrates, 1298
Photolysis frequencies (*j*-values), *see* compound index for information on specific compounds

Quantum yields, *see* compound index for information on specific compounds,

References to the literature, 1391

Solar zenith angles,
as a function of latitude, local time,
Spring and Fall, 977
Summer, 977
Winter, 978
Structures, molecular, of the oxygenates, 1480

Compound Index

Information on a given oxygenate reviewed in this work is listed under the functional group of that compound; that is, formaldehyde is listed under aldehydes, acyclic; formic acid is under acids, monobasic, etc. The order of listing under a given family of compounds is in increasing C-number. The chemical formula is shown first with the order of the atoms C, H, O, Br, Cl, F, I, N. The abbreviations used to denote specific information available on each compound are as follows:

OH, Rate coefficients for reaction of the compound with hydroxyl radical
Cl, Rate coefficients for reaction of the compound with chlorine atoms
O_3, Rate coefficients for reaction of the compound with ozone
NO_3, Rate coefficients for reaction of the compound with the nitrate radical
O, Rate coefficients for reaction of the compound with $O(^3P)$ atoms
AF, Atmospheric fate, mechanisms, and final products of atmospheric reactions
CS, Cross sections, absorption (σ) for the compound
QY, Quantum yields (ϕ) for the photodecomposition processes for the compound
J, Photolysis frequencies (j-values) in the lower troposphere
S, Structure, molecular (ball-stick and 3-D figures)

Acids

Acyclic Acids

CH_2O_2, Formic acid, HC(O)OH: OH, 748; Cl, 751; AF, 751; S, 1523

$C_2H_4O_2$, Acetic acid, $CH_3C(O)OH$: OH, 753; Cl, 756; AF, 756; S, 1523

$C_3H_6O_2$, Propanoic acid, $CH_3CH_2C(O)OH$: OH, 758; Cl, 759; AF, 760; S, 1523

$C_4H_8O_2$, Butanoic acid, $CH_3CH_2CH_2C(O)OH$: OH, 761; AF, 761; S, 1523

$C_4H_8O_2$, 2-Methylpropionic acid, $(CH_3)_2CHC(O)OH$: OH, 761; AF, 761; S, 1523

$C_5H_{10}O_2$, Pentanoic acid, $CH_3CH_2CH_2CH_2C(O)OH$: S, 1523

$C_6H_{12}O_2$, Hexanoic acid, $CH_3CH_2CH_2CH_2CH_2C(O)OH$: S, 1523

Aromatic Organic Acids and Acids Derived from Terpenes

$C_7H_6O_2$, Benzoic acid, $C_6H_5C(O)OH$: OH, 769; S, 1524

$C_8H_{12}H_4$, *trans*-Norpinic acid: S, 770

$C_9H_{11}O_3$, Norpinonic acid: S, 770, 1525

$C_9H_{15}O_4$, Pinic acid: S, 770, 1525

$C_{10}H_{14}O_2$, *cis*-Pinonic acid: S, 770, 1525

$C_{10}H_{16}O_4$,10-Hydroxypinonic acid: S, 770

Dibasic Acids

$C_2H_2O_4$, Oxalic acid, HO(O)CC(O)OH: AF, 762; S, 1523
$C_3H_4O_4$, Malonic acid, HO(O)CCH$_2$C(O)OH:; AF, 762; S, 1523
$C_4H_6O_4$, Succinic acid, HO(O)CCH$_2$CH$_2$C(O)OH: AF, 762; S, 1524
$C_5H_8O_4$, Glutaric acid, HO(O)CCH$_2$CH$_2$CH$_2$C(O)OH: AF, 762; S, 1524
$C_6H_{10}O_4$, Adipic acid, HO(O)CCH$_2$CH$_2$CH$_2$CH$_2$C(O)OH: AF, 762; S, 1524

Halogen-Substituted Organic Acids

$C_2HO_2F_3$, Trifluoroacetic acid, $CF_3C(O)OH$: OH, 770; Cl, 771; AF, 772; S, 1525
$C_3HO_2F_5$, 2,2,3,3,3-Pentafluoropropanoic acid, $CF_3CF_2C(O)OH$: OH, 770; S, 1525
$C_4HO_2F_7$, 2,2,3,3,4,4,4-Heptafluorobutanoic acid, $CF_3CF_2CF_2C(O)OH$: OH, 770; S, 1525
$C_5HO_2F_9$, 2,2,3,3,4,4,5,5,5-Nonafluoropentanoic acid, $CF_3CF_2CF_2CF_2C(O)OH$: OH, 770; S, 1525

Keto-Acids

$C_3H_4O_3$, Pyruvic acid, $CH_3C(O)C(O)OH$: OH, 766; AF, 768; CS, 1199; QY, 1198; J, 1203; S, 1203

Unsaturated Organic Acids

$C_3H_4O_2$, Acrylic acid $CH_2{=}CHC(O)OH$: OH, 764; O_3, 764; NO_3, 765; Cl, 765; AF, 765; S, 1524
$C_4H_6O_2$, Methacrylic acid, $CH_2{=}C(CH_3)C(O)OH$: OH, 764; O_3, 764; NO_3, 765; AF, 765; S, 1524
$C_4H_6O_2$, Crotonic acid, $CH_3CH{=}CHC(O)OH$: OH, 764; O_3, 764; NO_3, 765; AF, 765

Acid Anhydrides

$C_2H_2O_3$, Formic acid anhydride, HC(O)O(O)CH: S, 1525
$C_3H_4O_3$, Formic acetic anhydride, HC(O)OC(O)CH$_3$: Cl, 773; AF, 773; S, 1525
$C_4H_6O_3$, Formic propanoic anhydride, HC(O)OC(O)CH$_2$CH$_3$: Cl, 773; AF, 773; S, 1526
$C_4H_6O_3$, Acetic anhydride, $CH_3C(O)O(O)CCH_3$: S, 1526

Alcohols

Acyclic Alcohols

CH_4O, Methanol, CH_3OH: OH, 117; NO_3, 120; Cl, 122; AF, 123; S, 1480
C_2H_6O, Ethanol, CH_3CH_2OH: OH, 124; NO_3, 128; Cl, 128; AF, 129; S, 1480
C_3H_8O, 1-Propanol, $CH_3CH_2CH_2OH$: OH, 131; NO_3, 133; Cl, 133; AF, 135; S, 1480
C_3H_8O, 2-Propanol, $(CH_3)_2CHOH$: OH, 137; NO_3, 1q37; Cl, 139; AF, 139; S, 1480
$C_4H_{10}O$, 1-Butanol, $CH_3CH_2CH_2CH_2OH$: OH, 141; NO_3, 142; Cl, 143; AF, 144; S, 1480
$C_4H_{10}O$, 2-Butanol, $CH_3CH_2CH(OH)CH_3$: OH, 145; NO_3, 146; Cl, 146; AF, 147; S, 1480
$C_4H_{10}O$, 2-Methyl-1-propanol, $(CH_3)_2CHCH_2OH$: OH, 150; Cl, 150; AF, 150; S, 1481
$C_4H_{10}O$, 2,2-Dimethyl-ethanol, $(CH_3)_3COH$: OH, 152; Cl, 153; AF, 154; S, 1481
$C_5H_{12}O$, 2,2-Dimethyl-propanol, $(CH_3)_3CCH_2OH$: OH, 154; AF, 155
$C_5H_{12}O$, 1-Pentanol, $CH_3CH_2CH_2CH_2CH_2OH$: OH, 156; Cl, 156; AF, 157; S, 1481
$C_5H_{12}O$, 2-Pentanol, $CH_3CH(OH)CH_2CH_2CH_3$: OH, 159; Cl, 159; AF, 159; S, 1481
$C_5H_{12}O$, 3-Pentanol, $CH_3CH_2CH(OH)CH_2CH_3$: OH, 169; Cl, 160; AF, 160; S, 1481
$C_5H_{12}O$, 3-Methyl-1-butanol, $(CH_3)_2CHCH_2CH_2OH$: OH, 161; Cl, 163; AF, 163; S, 1481
$C_5H_{12}O$, 2-Methyl-2-butanol, $(CH_3)_2C(OH)CH_2CH_3$: OH, 163; Cl, 165; AF, 165; S, 1481
$C_5H_{12}O$, 3-Methyl-2-butanol, $CH_3CH(OH)CH(CH_3)_2$: OH, 166; Cl, 166; AF, 168; S, 1481
$C_6H_{14}O$, 1-Hexanol, $CH_3CH_2CH_2CH_2CH_2CH_2OH$: OH, 168; Cl, 169; AF, 169; S, 1481
$C_6H_{14}O$, 2-Hexanol, $CH_3CH(OH)CH_2CH_2CH_2CH_3$: OH, 173; AF, 173; S, 1481
$C_6H_{14}O$, 2-Methyl-2-pentanol, $CH_3C(OH)(CH_3)CH_2CH_2CH_3$: OH, 173; AF, 173; S, 1481

$C_6H_{14}O$, 4-Methyl-2-pentanol, $CH_3CH(OH)CH_2CH(CH_3)_2$: OH, 174; AF, 174; S, 1481
$C_6H_{14}O$, 2,3-Dimethyl-2-butanol, $(CH_3)_2C(OH)CH(CH_3)_2$: OH, 174; Cl, 176; AF, 176; S, 1482
$C_7H_{16}O$,1-Heptanol, $CH_3CH_2CH_2CH_2CH_2CH_2CH_2OH$: OH, 177; Cl, 177; AF, 178; S, 1482
$C_7H_{16}O$, 4-Heptanol, $CH_3CH_2CH_2CH(OH)CH_2CH_2CH_3$: NO_3, 178; AF, 178; S, 1482
$C_7H_{16}O$, 2,4-Dimethyl-2-pentanol, $(CH_3)_2C(OH)CH_2CH(CH_3)_2$: OH, 179; AF, 179; S, 1482
$C_8H_{18}O$,1-Octanol, $CH_2CH_2CH_2CH_2CH_2CH_2CH_2CH_2OH$: OH, 181; Cl, 181; AF, 181; S, 1482
$C_8H_{18}O$, 3,5-Dimethyl-3-hexanol, $CH_3CH_2C(CH_3)(OH)CH_2CH(CH_3)_2$ OH, 181; AF, 181; S, 1482

Aromatic Alcohols

C_6H_6O, Phenol, C_6H_5OH: OH, 236; NO_3, 237; AF, 239; CS, 1345; S, 1486
$C_6H_6O_2$, *o*-Cresol, HOC_6H_4OH: OH, 241; O_3, 241; NO_3, 242; AF, 242; CS, 1346; S, 1486
$C_6H_6O_2$, *m*-Cresol, HOC_6H_4OH: OH, 244; O_3, 245; NO_3, 245; AF, 245; CS, 1346; S, 1486
$C_6H_6O_2$, *p*-Cresol, HOC_6H_4OH: OH, 247; O_3, 247; NO_3, 248; AF, 248; CS, 1346; S, 1486
C_7H_8O, Benzyl alcohol, $C_6H_5CH_2OH$: OH, 250; O_3, 250; AF, 251; S, 1486
$C_7H_8O_2$, 1,2-Dihydroxy-3-methylbenzene, $(OH)_2C_6H_3CH_3$: OH, 254; O_3, 254; NO_3, 255; AF, 255; S, 1487
$C_7H_8O_2$, 1,2-Dihydroxy-4-methylbenzene, $(OH)_2C_6H_3CH_3$: OH, 254; O_3, 254; NO_3, 255; AF, 255; S, 1487
$C_8H_{10}O$, 2,3-Dimethylphenol, $(CH_3)_2C_6H_3OH$: OH, 251; NO_3, 251; AF, 251; CS; 1345; S, 1486
$C_8H_{10}O$, 2,4-Dimethylphenol, $(CH_3)_2C_6H_3OH$: OH, 251; NO_3, 251; AF, 251; S, 1486
$C_8H_{10}O$, 2,5-Dimethylphenol, $(CH_3)_2C_6H_3OH$: OH, 251; NO_3, 251; AF, 251; S, 1486
$C_8H_{10}O$, 2,6-Dimethylphenol, $(CH_3)_2C_6H_3OH$: OH, 251; NO_3, 251; AF, 251; S, 1486
$C_8H_{10}O$, 3,4-Dimethylphenol, $(CH_3)_2C_6H_3OH$: OH, 251; NO_3, 251; AF, 251; S, 1486
$C_8H_{10}O$, 3,5-Dimethylphenol, $(CH_3)_2C_6H_3OH$: OH, 251; NO_3, 251; AF, 251; S, 1487
$C_9H_{12}O$, 2,3,5-Trimethylphenol, $(CH_3)_3C_6H_2OH$: OH, 253; AF, 253; CS, 1345
$C_9H_{12}O$, 2,3,6-Trimethylphenol, $(CH_3)_3C_6H_2OH$: OH, 253; AF, 253, CS, 1345; S, 1487
$C_{10}H_8O$, 2-Hydroxynaphthalene: CS, 1346; J, 1347; S, 1487
$C_{14}H_9O$, 3-Hydroxyphenanthrene: CS, 1346; J, 1347; S, 1487

Cyclic Alcohols

$C_5H_{10}O$, *cyclo*-Pentanol, C_5H_9OH: OH, 182; AF, 182; S, 1482
$C_6H_{12}O$, *cyclo*-Hexanol, $C_6H_{11}OH$: OH, 182; AF, 182; S, 1482

Diols, Acyclic

$C_2H_6O_2$, 1,2-Dihydroxyethane, $HOCH_2CH_2OH$: OH, 184; S, 1483
$C_3H_8O_2$, 1,2-Dihyroxypropane, $HOCH_2CH(OH)CH_3$: OH, 184; S, 1483
$C_4H_{10}O_2$, 1,2-Dihydroxybutane, $HOCH_2CH(OH)CH_2CH_3$: OH, 184; S, 1483
$C_4H_{10}O_2$, 1,3-Dihydroxybutane, $HOCH_2CH_2CH(OH)CH_3$: OH, 184; S, 1483
$C_4H_{10}O_2$, 2,3-Dihyroxybutane, $CH_3CH(OH)CH(OH)CH_3$: OH, 184; S, 1483
$C_6H_{14}O_2$, 2-Methyl-2,4-dihydroxypentane, $(CH_3)_2C(OH)CH_2CH(OH)CH_3$: OH, 184; S, 1483

Halogen-Substituted Alcohols

$CHOF_3$, Trifluoromethanol, CF_3OH: AF, 256; S, 1487
CH_3OCl, Chloromethanol, CH_2ClOH: AF, 256; S, 1487
CH_2OCl_2, Dichloromethanol, $CHCl_2OH$: AF, 256; S, 1487
$CHOCl_3$, Trichloromethanol, CCl_3OH: AF, 256; S, 1487
C_2H_5OCl, 1-Chloroethanol, $CH_3CHClOH$: AF, 256; S, 1488
C_2H_5OCl, 2-Chloroethanol, CH_2ClCH_2OH: OH, 276; Cl, 276; AF, 277; S, 1489

$C_2H_3OCl_3$, 2,2,2-Trichloroethanol, CCl_3CH_2OH: OH, 277; Cl, 277; AF, 277; S, 1490
C_3H_7OCl, 1-Chloro-1-propanol, $CH_3CH_2CHClOH$: AF, 256; S, 1488
C_3H_7OCl, 2-Chloro-2-propanol, $CH_3CCl(OH)CH_3$: AF, 256; S, 1488
C_2H_5OF, 2-Fluoroethanol, CH_2FCH_2OH: OH, 258; Cl, 262; AF, 266; S, 1488
$C_2H_4OF_2$, 2,2-Difluoroethanol, CHF_2CH_2OH: OH, 258; Cl, 262; AF, 268; S, 1488
$C_2H_3OF_3$, 2,2,2-Trifluoroethanol, CF_3CH_2OH: OH, 259; Cl, 262; AF, 270; S, 1488
$C_2H_3O_2F_3$, 2,2,2-Trifluoro-1,1-ethandiol, $CF_3CH(OH)_2$: OH, 265; Cl, 262; AF, 278; S, 1490
$C_3H_5OF_3$, 3,3,3-Trifluoro-1-propanol, $CF_3CH_2CH_2OH$: OH, 259; Cl, 262; AF, 270; S, 1488
$C_3H_4OF_4$, 2,2,3,3-Tetrafluoro-1-propanol, $CHF_2CF_2CH_2OH$: OH, 275; Cl, 276; AF, 276; S, 1488
$C_2H_3OF_5$, 2,2,3,3,3-Pentafluoro-1-propanol, $CF_3CF_2CH_2OH$: OH, 259; Cl, 273; AF, 274; S, 1488
$C_3H_2OF_6$, 1,1,1,3,3,3-Hexafluoro-2-propanol, $CF_3CH(OH)CF_3$: OH, 260; AF, 274; S, 1488
$C_4H_4OF_6$, 2,2,3,4,4,4-Hexafluoro-1-butanol, $CF_3CHFCF_2CH_2OH$: OH, 260; Cl, 275; AF, 275; S, 1489
$C_4H_2OF_7$, 2,2,3,3,4,4,4-Heptafluoro-1-butanol, $CF_3CF_2CF_2CH_2OH$: OH, 261; Cl, 264; AF, 274; S, 1489
$C_4H_3O_2F_7$, 2,2,3,3,4,4,4-Heptafluorobutane-1, 1-diol, $CF_3CF_2CF_2CH(OH)_2$: OH, 265; Cl, 278; AF, 278; S, 1490
$C_5H_3OF_9$, 2,2,3,3,4,4,5,5,5-Nonafluoro-1-pentanol, $CF_3CF_2CF_2CF_2CH_2OH$: OH, 273; Cl, 273; AF, 274; S, 1489
$C_5H_3O_2F_9$, 2,2,3,3,4,4,5,5,5-Nonfluoropentane-1,1-diol, $CF_3CF_2CF_2CF_2CH(OH)_2$: OH, 265; Cl, 278; AF, 278; S, 1490
$C_6H_5OF_9$, 3,3,4,4,5,5,6,6,6-Nonafluoro-1-hexanol, $CF_3CF_2CF_2CF_2CH_2CH_2OH$: OH, 264; Cl, 270; AF, 270; S, 1489
$C_7H_3OF_{13}$, 2,2,3,3,4,4,5,5,6,6,7,7,7-Tridecafluoro-1-heptanol, $CF_3CF_2CF_2CF_2CF_2CF_2CH_2OH$: OH, 264; Cl, 273; AF, 274; S, 1489
$C_8H_5O_{13}$, 3,3,4,4,5,5,6,6,7,7,8,8,8-Tridecafluoro-1-octanol, $CF_3CF_2CF_2CF_2CF_2CF_2CH_2CH_2OH$: OH, 264; Cl, 270; AF, 270; S, 1489
$C_{10}H_5OF_{17}$, 3,3,4,4,5,5,6,6,7,7,8,8,9,9,10,10,10-Heptadecafluoro-1-decanol, $CF_3CF_2CF_2CF_2CF_2CF_2CF_2CF_2CH_2CH_2OH$: OH, 264; Cl, 270; AF, 270; S, 1489

Unsaturated Alcohols

C_3H_4O, 2-Propyn-1-ol, $HC{\equiv}CCH_2OH$: OH, 235; AF, 235; S, 1485
C_3H_6O, 2-Propen-1-ol, $CH_2{=}CHCH_2OH$: OH, 185; O_3, 186; NO_3, 187; Cl, 189; AF, 189; S, 1483
C_4H_8O, 2-Buten-1-ol., $CH_3CH{=}CHCH_2OH$: OH, 191; O_3, 192; NO_3, 192; Cl, 192; AF, 194; S, 1483
C_4H_8O, 3-Buten-1-ol, $CH_2{=}CHCH_2CH_2OH$: OH, 195; O_3, 196; AF, 196; S, 1483
C_4H_8O, 3-Buten-2-ol, $CH_2{=}CHCH(OH)CH_3$: OH, 198; O_3, 198; NO_3, 198; AF, 199; S, 1483
$C_5H_{10}O$, 2-Methyl-2-propen-1-ol, $CH_2{=}C(CH_3)CH_2OH$: OH, 235; AF, 235; S, 1483
$C_5H_{10}O$, *cis*-2-Penten-1-ol, $CH_3CH_2CH{=}CHCH_2OH$: OH, 199; O_3, 199; NO_3, 200; AF, 200; S, 1484
$C_5H_{10}O$, 1-Penten-3-ol, $CH_2{=}CHCH(OH)CH_2CH_3$: OH, 202; O_3, 202; NO_3, 202; AF, 203; S, 1484
$C_5H_{10}O$, 3-Methyl-2-buten-1-ol, $(CH_3)_2C{=}CHCH_2OH$: OH, 206; NO_3, 207; Cl, 207; AF, 208; S, 1484
$C_5H_{10}O$, 3-Methyl-3-buten-1-ol, $CH_2{=}C(CH_3)CH_2CH_2OH$: OH, 208; NO_3, 209; AF, 209; S, 1484
$C_5H_{10}O$, 2-Methyl-3-buten-2-ol, $CH_2{=}CHC(OH)(CH_3)_2$: OH, 210 ;O_3, 212; NO_3, 213; Cl, 215; AF, 215; S, 1484
$C_6H_{12}O$, *cis*-4-Hexen-1-ol, $CH_3CH{=}CHCH_2CH_2CH_2OH$: NO_3, 222; AF, 222; S, 1484
$C_6H_{12}O$, *trans*-3-Hexen-1-ol, $CH_3CH_2CH{=}CHCH_2CH_2OH$: NO_3, 222; AF, 222; S, 1484
$C_6H_{12}O$, *cis*-2-Hexen-1-ol, $CH_3CH_2CH_2CH{=}CHCH_2OH$: OH, 221; O_3, 221; NO_3, 222; AF, 222; S, 1484
$C_6H_{12}O$, *trans*-2-Hexen-1-ol, $CH_3CH_2CH_2CH{=}CHCH_2OH$: NO_3, 222; AF, 222; S, 1484
$C_6H_{12}O$, *cis*-3-Hexen-1-ol, $CH_3CH_2CH{=}CHCH_2CH_2OH$: OH, 221; O_3, 221; NO_3, 222; AF, 222; S, 1484

$C_8H_{14}O$, 3,5-Dimethyl-1-Hexyn-3-ol, $HC{\equiv}CC(OH)(CH_3)CH_2CH(CH_3)_2$: OH, 235; AF, 235; S, 1485
$C_9H_{20}O$, Dihydromyrcenol, $CH_2{=}CHCH(CH_3)CH_2CH_2CH_2C(CH_3)_2OH$: OH, 223; O_3, 223; AF, 224; S, 1484
$C_{10}H_{18}O$, Linalool, $CH_2{=}CHC(CH_3)(OH)CH_2CH_2CH{=}C(CH_3)_2$: OH, 224; O_3, 224; NO_3, 225; AF, 225; S, 224, 1485
$C_{10}H_{18}O$, Geraniol, $HOCH_2CH{=}C(CH_3)CH_2CH_2CH{=}C(CH_3)_2$: OH, 229; O_3, 229; AF, 230; S, 229, 1485
$C_{10}H_{18}O$, α-Terpineol, 2-(4-methylcyclohex-3-en-1-yl)propan-2-ol: OH, 233; O_3, 234; AF, 234; S, 233, 1485
$C_{10}H_{18}O$, Carveol, 1-Methyl-4-isopropenyl-6-cyclohexen-2-ol: AF, 234; S, 233, 1485
$C_{10}H_{20}O$, Citronellol, 3,7-Dimethyl-6-octen-1-ol, $(CH_3)_2C{=}CHCH_2CH_2CH(CH_3)CH_2CH_2OH$: OH, 232; O_3, 232; AF, 232; S, 1485

Aldehydes

Acyclic Aldehydes

CH_2O, Methanal, CH_2O: OH, 540; NO_3, 543; Cl, 544; O, 546; AF, 546; CS, 985; QY, 986; J, 988, 989; S, 1508
C_2H_4O, Ethanal, CH_3CHO: OH, 546; NO_3, 550; Cl, 551; O, 553; AF, 553; CS, 991; QY, 992; J, 993; S, 1508
C_3H_6O, Propanal, CH_3CH_2CHO: OH, 554; NO_3, 555; Cl, 556; O, 557; AF, 557; CS, 991; QY, 996; J, 997; S, 1508
C_4H_8O, Butanal, $CH_3CH_2CH_2CHO$: OH, 557; NO_3, 558; Cl, 560; O, 560; AF, 560; CS, 991; QY, 1000; J, 1001; S, 1508
C_4H_8O, 2-Methylpropanal, $(CH_3)_2CHCHO$: OH, 561; NO_3, 561; O_3, 561; Cl, 561; AF, 564; CS, 1003; QY, 1003; J, 1005; S, 1509
$C_5H_{10}O$, Pentanal, $CH_3CH_2CH_2CH_2CHO$: OH, 565; NO_3, 565; Cl, 566; AF, 568; CS, 991; QY, 1008; J, 1009; S, 1509
$C_5H_{10}O$, 2-Methylbutanal, $CH_3CH_2CH(CH_3)CHO$: OH, 568; NO_3, 569; AF, 569; QY, 1010; S, 1509
$C_5H_{10}O$, 3-Methylbutanal, $(CH_3)_2CHCH_2CHO$: OH, 569; NO_3, 570; AF, 570; CS, 1011; QY, 1011; J, 1013; S, 1509
$C_5H_{10}O$, 2,2-Dimethylpropanal, $(CH_3)_3CCHO$: OH, 571; NO_3, 572; Cl, 573; AF, 573; CS, 1016; QY, 1016; J, 1017; S, 1509
$C_6H_{12}O$, Hexanal, $CH_3CH_2CH_2CH_2CH_2CHO$: OH, 573; NO_3, 574; Cl, 574; AF, 575; CS, 1018; QY, 1018; J, 1020; S, 1509
$C_6H_{12}O$, 2-Methylpentanal, $CH_3CH_2CH_2CH(CH_3)CHO$: OH, 576; NO_3, 577
$C_6H_{12}O$, 3-Methylpentanal, $CH_3CH_3CH(CH_3)CH_2CHO$: OH, 576; NO_3, 577
$C_6H_{12}O$, 4-Methylpentanal, $CH_3CH(CH_3)CH_2CH_2CHO$: OH, 576; NO_3, 577
$C_6H_{12}O$, 3,3-Dimethylbutanal, $CH_3C(CH_3)_2CH_2CHO$: OH, 576; NO_3, 577
$C_6H_{12}O$, 2-Ethylbutanal, $CH_3CH_2CH(CH_2CH_3)CHO$: OH, 576; NO_3, 577
$C_7H_{14}O$, Heptanal, $CH_3CH_2CH_2CH_2CH_2CH_2CHO$: OH, 576; NO_3, 577; Cl, 577; QY, 1022; J, 1023; S, 1509
$C_7H_{14}O$, 2,3-Dimethylpentanal, $CH_3CH_2CH(CH_3)CH(CH_3)CHO$: OH, 576; S, 1509
$C_8H_{16}O$, Octanal, $CH_3CH_2CH_2CH_2CH_2CH_2CH_2CHO$: NO_3, 577
$C_9H_{18}O$, Nonanal, $CH_3CH_2CH_2CH_2CH_2CH_2CH_2CH_2CHO$: OH, 576; NO_3, 577; S, 1509
$C_{10}H_{20}O$, Decanal, $CH_3CH_2CH_2CH_2CH_2CH_2CH_2CH_2CH_2CHO$: NO_3, 577

Aromatic Aldehydes

C_7H_6O, Benzaldehyde, C_6H_5CHO: OH, 620; NO_3, 622; Cl, 623; O, 623; AF, 623; CS, 1320; QY, 1320; J, 1324; S, 1512
C_8H_8O, *o*-Tolualdehyde, $CH_3C_6H_4CHO$: OH, 620; Cl, 623; S, 1512
C_8H_8O, *m*-Tolualdehyde, $CH_3C_6H_4CHO$: OH, 620; Cl, 623; S, 1512
C_8H_8O, *p*-Tolualdehyde, $CH_3C_6H_4CHO$: OH, 620; Cl, 623; S, 1512
$C_8H_6O_2$, Phthaldialdehyde, $C_6H_4(CHO)_2$: OH, 627; AF, 627; CS, 1329; QY, 1326; J, 1331; S, 1513
C_9H_8O, *trans*-Cinnamaldehyde, $C_6H_5CH{=}CHCHO$: OH, 624; O_3, 626; NO_3, 626; AF, 626; S, 1513
$C_9H_{10}O$, 2,3-Dimethylbenzaldehyde, $(CH_3)_2C_6H_3CHO$: OH, 621; S, 1512

$C_9H_{10}O$, 2,4-Dimethylbenzaldehyde, $(CH_3)_2C_6H_3CHO$: OH, 621; Cl, 623; S, 1512
$C_9H_{10}O$, 2,5-Dimethylbenzaldehyde, $(CH_3)_2C_6H_3CHO$: OH, 621; Cl, 623; S, 1512
$C_9H_{10}O$, 2,6-Dimethylbenzaldehyde, $(CH_3)_2C_6H_3CHO$: OH, 621; S, 1513
$C_9H_{10}O$, 3,4-Dimethylbenzaldehyde, $(CH_3)_2C_6H_3CHO$: OH, 621; S, 1513
$C_9H_{10}O$, 3,5-Dimethylbenzaldehyde, $(CH_3)_2C_6H_3CHO$: OH, 621; Cl, 623; S, 1513
$C_9H_8O_2$, 2-Acetylbenzaldehyde, $CH_3C(O)C_6H_4CHO$: OH, 627; AF, 627; CS, 1330; QY, 1329; J, 1330; S, 1513

Biogenic Compounds, Aldehydes Derived from

$C_{10}H_{16}O_2$, Pinonaldehyde,: OH, 628; NO_3, 628; O_3, 629; Cl, 630; AF, 630; CS, 1072; QY, 1073; J, 1075; S, 627, 1511
$C_{10}H_{16}O_2$, Caronaldehyde,; OH, 631; NO_3, 631; AF, 632; CS, 1072; S, 631, 1511
$C_{10}H_{16}O_2$, 3-Isopropenyl-6-oxo-heptanal, $CH_3C(O)CH_2CH_2C[CH(CH_3)=CH_2]CH_2CHO$: OH, 633; NO_3, 633; O_3, 633; AF, 633
$C_{10}H_{18}O$, 3,7-Dimethyl-6-octen-1-al, $CH_3C(CH_3)=CHCH_2CH_2CH(CH_3)CH_2CHO$: OH, 633; O_3, 633; AF, 634

Cycloalkylcarbaldehydes

$C_3H_4O_2$, Oxirane-2-carbaldehyde (glycidaldehyde), *cyclo*-CH_2OCH-CHO, CS, 1029; QY, 1028; J, 1030; S, 1499
C_4H_6O, Cyclopropanecarbaldehyde, *cyclo*-C_3H_5-CHO: OH, 578; NO_3, 578; AF, 579; S, 1510
$C_5H_4O_2$, 2-Furancarboxaldehyde, cyclo-CH=CHCH=C(CHO)O-: S, 1497
C_5H_8O, Cyclobutanecarbaldehyde, *cyclo*-C_4H_7-CHO: OH, 578; NO_3, 578; AF, 579; S, 1510
$C_6H_{10}O$, Cyclopentanecarbaldehyde *cyclo*-C_5H_9-CHO: OH, 578; NO_3, 578; AF, 579; S, 1510
$C_7H_{12}O$, Cyclohexanecarbaldehyde, *cyclo*-C_6H_{11}-CHO: OH, 578; NO_3, 578; AF, 579; S, 1510

Dialdehydes

$C_2H_2O_2$, Ethandial, HC(O)CHO: OH, 592; O_3, 592; Cl, 593; AF, 593; CS, 1062; QY, 1062; J, 1064; S, 1511
$C_3H_4O_2$, 2-Oxopropanal, $CH_3C(O)CHO$: OH, 595; O_3, 595; Cl, 595; AF, 596; CS, 1066; QY, 1066; J, 1071; S, 1511

Halogen-Substituted Aldehydes

CHOBr, Formyl bromide, HC(O)Br: CS, 1226; J, 1232; S, 1515
$COBr_2$, Carbonyl dibromide, BrC(O)Br: CS, 1226; QY, 1228; J, 1232; S, 1516
CHOCl, Formyl chloride, HC(O)Cl: OH, 636; Cl, 644; AF, 645; CS, 1224; J, 1232; S, 1515
$COCl_2$, Carbonyl dichloride, ClC(O)Cl; CS, 1224; QY, 1228; S, 1516
CHOF, Formyl fluoride, HC(O)F: OH, 634; Cl, 634; AF, 634; CS, 1224; S, 1515
COF_2, Carbonyl difluoride, FC(O)F: CS, 1224; S, 1516
C_2H_2OBrCl, 2-Bromoacetyl chloride, $BrH_2CC(O)Cl$: QY, 1229; S, 1516
C_2H_3OCl, Acetyl chloride, $CH_3C(O)Cl$: CS, 1225; QY, 1229; J, 1232; S, 1515
C_2H_3OCl, 2-Chloroethanal, CH_2ClCHO: OH, 636; Cl, 639; AF, 646; CS, 1076; S, 1513
$C_2H_2OCl_2$, 2-Chloroacetyl chloride, $ClH_2CC(O)Cl$: CS, 1226; J, 1232; S, 1515
$C_2H_2OCl_2$, 2,2-Dichloroethanal, $CHCl_2CHO$: OH, 636; Cl, 639; AF, 647; CS, 1076; S, 1513
C_2HOCl_3, 2,2-Dichloroacetyl chloride, $Cl_2HCC(O)Cl$: CS, 1226; J, 1232; S, 1515
C_2HOCl_3, 2,2,2-Trichloroethanal, CCl_3CHO: OH, 636; Cl, 639; AF, 649; CS, 1081; QY, 1080; J, 1082; S, 1513
C_2OCl_4, 2,2,2-Trichloroacetyl chloride, $Cl_3CC(O)Cl$: CS, 1226; J, 1232; S, 1515
$C_2H_2OF_2$, 2,2-Difluoroethanal, CHF_2CHO: OH, 634; Cl, 638; AF, 640; CS, 1082; QY, 1086; J, 1088; S, 1513
C_2HOF_3, 2,2,2-Trifluoroethanal, CF_3CHO: OH, 635; Cl, 638; AF, 641; CS, 1084; QY, +1083; J, 1085; S, 1514
C_2H_2OClF, 2-chloro-2-fluoroethanal, CHClFCHO: OH, 636; Cl, 649; AF, 650; CS, 1078; S, 1514
C_2HOClF_2, 2-Chloro-2,2-difluoroethanal, $CClF_2CHO$: OH, 636; Cl, 639; AF, 650; CS, 1078; S, 1514
$C_2H_2OClF_3$, 2,2,2-Trifluoroacetyl chloride, $F_3CC(O)Cl$: CS, 1226; QY, 1229; J, 1239; S, 1516
C_2HOCl_2F, 2,2-Dichloro-2-fluoroethanal, CCl_2FCHO: OH, 636; Cl, 639; AF, 650; CS, 1078; S, 1514

$C_3H_3OF_3$, 3,3,3-Trifluoropropanal, CF_3CH_2CHO: OH, 636; Cl, 638; AF, 644; CS, 1079; QY, 1088; J, 1089; S, 1514
C_3HOF_5, 2,2,3,3,3-Pentafluoropropanal, CF_3CF_2CHO: OH, 635; Cl, 638; AF, 641; CS, 1079; QY, 1088; S, 1514
C_4HOF_7, 2,2,3,3,4,4,4-Heptafluorobutanal, $CF_3CF_2CF_2CHO$: OH, 635; Cl, 638; AF, 641; CS, 1079; QY, 1088; S, 1514
C_5HOF_9, 2,2,3,3,4,4,5,5,5-Nonafluoropentanal, $CF_3CF_2CF_2CF_2CHO$: OH, 635; CS, 1079; QY, 1088; J, 1089; S, 1514
C_6HOF_{11}, 3,3,4,4,5,5,6,6,6-Nonafluorohexanal, $CF_3CF_2CF_2CF_2CH_2CHO$: Cl, 638; AF, 644
$C_8H_3OF_{11}$, 3,3,4,4,5,5,6,6,7,7,8,8,8-Tridecafluorooctanal, $CF_3CF_2CF_2CF_2CF_2CF_2CH_2CHO$: AF, 644; CS, 1079; S, 1514
$C_{10}H_3OF_{17}$, 3,3,4,4,5,5,6,6,7,7,8,8,9,9,10,10,10-Heptadecafluorodecanal, n-$C_8F_{17}CH_2CHO$: OH, 643; Cl, 638; AF, 644; S, 1514

Hydroxy Aldehydes

$C_2H_4O_2$, 2-Hydroxyethanal, $HOCH_2CHO$: OH, 586; Cl, 586; AF, 589; CS, 1025; QY, 1026; J, 1027; S, 1510
$C_3H_6O_2$, 2-Hydroxypropanal, $CH_3CH(OH)CHO$: OH, 591; AF, 591
$C_3H_6O_2$, 3-Hydroxypropanal, $HOCH_2CH_2CHO$: OH, 591; AF, 591
$C_4H_8O_2$, 2-Hydroxybutanal, $CH_3CH_2CH(OH)CHO$: OH, 591; AF, 591
$C_4H_8O_2$, 3-Hydroxybutanal, $CH_3CH(OH)CH_2CHO$: OH, 591; AF, 591
$C_4H_8O_2$, 2-Hydroxy-2-methylpropanal, $CH_3C(OH)(CH_3)CHO$: OH, 591; AF, 591

Unsaturated Aldehydes

C_3H_4O, Propenal, $CH_2{=}CHCHO$: OH, 599; O_3, 600; NO_3, 601; Cl, 601; O, 602; AF, 603; CS, 1032; QY, 1032; J, 1035; S, 1510
C_4H_6O, 2-Butenal, $CH_3CH{=}CHCHO$: OH, 605; O_3, 605; NO_3, 605; Cl, 606; O, 606; AF, 607; CS, 1013; QY, 1040; S, 1510
C_4H_6O, 2-Methylpropenal, $CH_2{=}C(CH_3)CHO$: OH, 608; O_3, 608; NO_3, 609; Cl, 610; AF, 610; CS, 1037; QY, 1037; J, 1039; S, 1510
C_5H_8O, *trans*-2-Pentenal, E-$CH_3CH_2CH{=}CHCHO$: OH, 612; O_3, 614; NO_3, 615; Cl, 616; AF, 617
C_5H_8O, 3-Methyl-2-butenal, $CH_3C(CH_3){=}CHCHO$: O_3, 614; AF, 617
C_5H_8O, *trans*-2-Methyl-2-butenal, E-$CH_3CH{=}C(CH_3)CHO$, O_3, 614; AF, 617
$C_5H_6O_2$, 4-Oxo-2-pentenal, $CH_3C(O)CH{=}CHCHO$: OH, 597; CS, 1047; QY, 1049; J, 1050; S, 1511
C_6H_8O, *trans*-,*trans*-2,4-Hexadienal, $CH_3CH{=}CHCH{=}CHCHO$: CS, 1031; QY, 1041; J, 1042; S, 1511
C_6H_8O, *cis*-,*cis*-2,4-Hexadienal, $CH_3CH{=}CHCH{=}CHCHO$: OH, 612; CS, 1031; QY, 1041; J, 1041; S, 1511
C_6H_8O, *trans*-,*cis*-2,4-Hexadienal, $CH_3CH{=}CHCH{=}CHCHO$: OH, 609; CS, 1031; QY, 1041; J, 1041 S, 1511
$C_6H_{10}O$, *trans*-2-Hexenal, E-$CH_3CH_2CH_2CH{=}CHCHO$: OH, 612; NO_3, 615; Cl, 617; AF, 617; CS, 1031; QY, 1041; J, 1041; S, 1510
$C_6H_{10}O$, *cis*-2-Hexenal, Z-$CH_3CH_2CH_2CH{=}CHCHO$: QY, 1041; J, 1041; S, 1510
$C_7H_{10}O$, 4-Methylenehex-5-enal, $CH_2{=}CHC(=CH_2)CH_2CH_2CHO$: O_3, 614; NO_3, 616; AF, 617
$C_7H_{10}O$, *trans*-4-Methylhex-3,5-dienal, 3-E-$CH_2{=}CHC(CH_3){=}CHCH_2CHO$: OH, 612; O_3, 615; NO_3, 616; AF, 617
$C_7H_{10}O$, *cis*-4-Methylhex-3,5-dienal, 3-Z-$CH_2{=}CHC(CH_3){=}CHCH_2CHO$: OH, 612; O_3, 615; NO_3, 615; AF, 617
$C_7H_{12}O$, *trans*-2-Heptenal, E-$CH_3CH_2CH_2CH_2CH{=}CHCHO$: OH, 612; NO_3, 615; Cl, 617; AF, 617
$C_7H_{12}O$, *cis*-4-Heptenal, Z-$CH_3CH_2CH{=}CHCH_2CH_2CHO$: NO_3, 615; AF, 617

Unsaturated Dialdehydes

$C_4H_4O_2$, *cis*-Butendial, Z-HC(O)CH=CHCHO: OH, 597; CS, 1044; QY, 1045; J, 1045
$C_4H_4O_2$, *trans*-Butenedial, E-HC(O)CH=CHCHO: OH, 597; S, 1511
$C_5H_6O_2$, *trans/cis*-4-Oxo-2-pentenal, E-/Z-$CH_3C(O)CH{=}CHCHO$: OH, 597; AF, 598; CS, 1048; QY, 1046; J, 1050; S, 1511
$C_5H_6O_2$, *trans*-,*trans*-2,4-Hexdienedial, E-,E-CH(O)CH=CHCH=CHCHO: OH, 597; AF, 598; S, 1511

$C_5H_6O_2$, *trans*-,*cis*-2,4-Hexadienedial, *E*-,*Z*-CH(O)CH═CHCH═CHCHO: OH, 597; AF, 598; CS, 1031; QY, 1051; J, 1051; S, 1511
$C_8H_{10}O_2$, *trans*-,*trans*-2-Methyl-2,4-hexadienedial, *E*-,*E*-CH(O)CH═CHCH═CHCH(CH_3)CHO: OH, 597; AF, 617; S, 1511

Esters

Acyclic Esters

$C_2H_4O_2$, Methyl formate, $CH_3OC(O)H$: OH, 775; NO_3, 776; Cl, 777; AF, 779; S, 1526
$C_3H_6O_2$, Ethyl formate, $CH_3CH_2OC(O)H$: OH, 782; NO_3, 782; Cl, 782; AF, 784; S, 1526
$C_3H_6O_2$, Methyl acetate, $CH_3OC(O)CH_3$: OH, 796; Cl, 797; AF, 798; S, 1526
$C_4H_8O_2$, *n*-Propyl formate, $CH_3CH_2CH_2OC(O)H$: OH, 785; NO_3, 787; Cl, 787; AF, 787; S, 1526
$C_4H_8O_2$, *iso*-Propyl formate, $(CH_3)_2CHOC(O)H$: OH, 788; Cl, 788; AF, 789
$C_4H_8O_2$, Ethyl acetate, $CH_3CH_2OC(O)CH_3$: OH, 800; Cl, 801; NO_3, 802; AF, 803
$C_4H_8O_2$, Methyl propionate, $CH_3OC(O)CH_2CH_3$: OH, 824; Cl, 825; AF, 826
$C_5H_{10}O_2$, *n*-Butyl formate, $CH_3CH_2CH_2CH_2OC(O)H$: OH, 790; Cl, 791; AF, 791; S, 1526
$C_5H_{10}O_2$, *tert*-Butyl formate, $(CH_3)_3COC(O)H$: OH, 793; Cl, 794; AF, 794; S, 1526
$C_5H_{10}O_2$, *n*-Propyl acetate, $CH_3CH_2CH_2OC(O)CH_3$: OH, 805; Cl, 805; NO_3, 806; AF, 807
$C_5H_{10}O_2$, *iso*-Propyl acetate, $(CH_3)_2CHOC(O)CH_3$: OH, 809; Cl, 809; AF, 809
$C_5H_{10}O_2$, Ethyl propionate, $CH_3CH_2OC(O)CH_2CH_3$: OH, 829; AF, 829
$C_5H_{10}O_2$, Methyl *n*-butyrate, $CH_3OC(O)CH_2CH_2CH_3$: OH, 830; Cl, 831; AF, 831
$C_5H_{10}O_2$, Methyl *iso*-butyrate, $CH_3OC(O)CH(CH_3)_2$: OH, 834; AF, 834
$C_6H_{12}O_2$, *n*-Butyl acetate, $CH_3CH_2CH_2CH_2OC(O)CH_3$: OH, 812; Cl, 812; AF, 813
$C_6H_{12}O_2$, *iso*-Butyl acetate, $(CH_3)_2CHCH_2OC(O)CH_3$: OH, 814; Cl, 814; AF, 815
$C_6H_{12}O_2$, *sec*-Butyl acetate, $CH_3CH_2CH(CH_3)OC(O)CH_3$: OH, 817; Cl, 817; AF, 818
$C_6H_{12}O_2$, *tert*-Butyl acetate, $(CH_3)_3COC(O)CH_3$: OH, 819; Cl, 819; AF, 821
$C_6H_{12}O_2$, Methyl *n*-pentanoate, $CH_3OC(O)CH_2CH_2CH_2CH_3$: OH, 835; Cl, 835; AF, 837
$C_6H_{12}O_2$, Methyl pivalate, $CH_3OC(O)C(CH_3)_3$: OH, 837; Cl, 838; AF, 838
$C_6H_{12}O_2$, *n*-Propyl propionate, $CH_3CH_2CH_2OC(O)CH_2CH_3$: OH, 829; AF, 830
$C_6H_{12}O_2$, Ethyl *n*-butyrate, $CH_3CH_2OC(O)CH_2CH_2CH_3$: OH, 832; AF, 832
$C_7H_{14}O_2$, *n*-Pentyl acetate, $CH_3CH_2CH_2CH_2CH_2OC(O)CH_3$: OH, 823; AF, 823
$C_7H_{14}O_2$, *n*-Propyl *n*-butyrate, $CH_3CH_2CH_2OC(O)CH_2CH_2CH_3$: OH, 833; AF, 833
$C_7H_{14}O_2$, *iso*-Propyl *iso*-butyrate, $(CH_3)_2CHOC(O)CH(CH_3)_2$: OH, 835; AF, 835
$C_7H_{14}O_2$, Methyl *n*-hexanoate, $CH_3OC(O)CH_2CH_2CH_2CH_2CH_3$: OH, 839; Cl, 841; AF, 841; S, 1526
$C_8H_{16}O_2$, *n*-Butyl butyrate, *n*-$C_4H_9OC(O)CH_2CH_2CH_3$: OH, 833; AF, 834
$C_9H_{18}O_2$, Methyl *n*-octanoate, $CH_3OC(O)CH_2CH_2CH_2CH_2CH_2CH_2CH_3$: S, 1526
$C_{11}H_{22}O_2$, Methyl caprate, *n*-$C_9H_{19}C(O)OCH_3$: S, 1526
$C_{12}H_{20}O_2$, Bornyl acetate,: OH, 824; AF, 824; S, 823
$C_{13}H_{26}O_2$, Methyl laurate, *n*-$C_{11}H_{23}C(O)OCH3$: S, 1527
$C_{15}H_{30}O_2$, Methyl myristate, *n*-$C_{13}H_{27}C(O)OCH_3$: S, 1527
$C_{17}H_{34}O_2$, Methyl palmitate, *n*-$C_{15}H_{31}C(O)OCH_3$: S, 1527
$C_{19}H_{38}O_2$, Methyl stearate, *n*-$C_{17}H_{35}C(O)OCH_3$: S, 1527

Alkoxy-Substituted Esters

$C_3H_6O_3$, Methoxymethyl formate, $HC(O)OCH_2OCH_3$: OH, 371; AF, 370; S, 1495

$C_4H_8O_3$, Ethoxymethyl formate, $HC(O)OCH_2OCH_2CH_3$: OH, 371; AF, 370; S, 1495
$C_4H_8O_3$, Methoxyethyl formate, $HC(O)OCH_2CH_2OCH_3$: OH, 371; AF, 370; S, 1495
$C_4H_8O_3$, Ethoxymethyl acetate, $CH_3C(O)OCH_2OCH_2CH_3$: OH, 371; AF, 370; S, 1495
$C_5H_{10}O_3$, Methoxymethyl acetate, $CH_3C(O)OCH_2OCH_3$: OH, 371; AF, 370; S, 1495
$C_5H_{10}O_3$, Methoxyethyl acetate, $CH_3C(O)OCH_2CH_2OCH_3$: OH, 371; AF, 370; S, 1495
$C_5H_{10}O_3$,Ethoxyethyl formate, $HC(O)OCH_2CH_2OCH_2CH_3$: OH, 372; AF, 370; S, 1495
$C_6H_{12}O_3$, Ethoxyethyl acetate, $CH_3C(O)OCH_2CH_2OCH_2CH_3$: OH, 372; AF, 370; S, 1495
$C_7H_{14}O_3$, Ethyl 3-ethoxypropionate, $CH_3CH_2OCH_2CH_2C(O)OCH_2CH_3$: OH, 372; AF, 370; S, 1496
$C_9H_{18}O_3$, 2-Ethoxyethyl isobutyrate, $(CH_3)_2CHC(O)OCH_2CH_2OCH_2CH_3$: OH, 372; AF, 370; S, 1496

Aromatic Esters

$C_7H_8O_2$, Methyl salicylate, $HO\text{-}C_6H_4C(O)OCH_3$: OH, 866; O_3, 867; NO_3, 867; Cl, 867; AF, 867; S, 1529

Carbonates

$C_3H_6O_3$, Dimethyl carbonate, $CH_3OC(O)OCH_3$: OH, 868; Cl, 868; AF, 868; S, 1530

Cyclic Esters (Lactones)

$C_4H_4O_2$, 3H-Furan-2-one: OH, 846; NO_3, 847; AF, 847; S, 1529
$C_5H_6O_2$, 5-Methyl-3H-furan-2-one: OH, 847; AF, 847; S, 1529

Difunctional Esters

$C_4H_6O_4$, Ethylene glycol diformate, $HC(O)OCH_2CH_2OC(O)H$: OH, 841; Cl, 842; AF, 842
$C_6H_{10}O_4$, Ethylene glycol diacetate, $CH_3C(O)OCH_2CH_2OC(O)CH_3$: OH, 843; Cl, 844; AF, 844
$C_6H_{10}O_4$, Dimethyl succinate, $CH_3OC(O)CH_2CH_2C(O)OCH_3$: OH, 844
$C_7H_{12}O_4$, Dimethyl glutarate, $CH_3OC(O)CH_2CH_2CH_2C(O)OCH_3$: OH, 845; AF, 845
$C_8H_{14}O_4$, Dimethyl adipate, $CH_3OC(O)CH_2CH_2CH_2CH_2C(O)OCH_3$: OH, 845; AF, 846

Halogen-Atom Substituted Esters

$C_2H_3O_2F$, Methyl fluoroformate, $CH_3OC(O)F$: OH, 880; AF, 880; S, 1530
$C_2H_2O_2F_2$, Fluoromethyl fluoroformate, $CH_2FCO(O)F$: S, 1530
$C_2H_2O_2F_2$, Difluoromethyl formate, $CHF_2OC(O)H$: Cl, 875; S, 1530
$C_2HO_2F_3$, Trifluoromethyl formate, $CF_3OC(O)H$: OH, 871; Cl, 871; AF, 871; S, 1530
$C_3H_4O_2F_2$, Methyl 2,2-difluoroacetate, $CH_3OC(O)CHF_2$: OH, 881; Cl, 882; AF, 882; S, 1531
$C_3H_3O_2F_3$, Trifluoromethyl acetate, $CF_3OC(O)CH_3$: OH, 882; Cl, 882; AF, 883; S, 1530
$C_3H_3O_2F_3$, Methyl trifluoroacetate, $CH_3OC(O)CF_3$: OH, 882; Cl, 882; S, 1531
$C_3H_2O_2F_4$, 1,2,2,2-Tetrafluoroethyl formate, $CF_3CFHOC(O)H$: OH, 874; AF, 874; S, 1531
$C_3HO_2F_5$, Perfluoroethyl formate, $CF_3CF_2OC(O)H$: OH, 877; Cl, 877; AF, 878; S, 1531
$C_3HO_2F_5$, Difluoromethyl trifluoroacetate: $CHF_2OC(O)CF_3$, Cl, 876
$C_4H_5O_2F_3$, Ethyl trifluoroacetate, $CH_3CH_2OC(O)CF_3$: OH, 884; Cl, 884; AF, 884; S, 1531
$C_4H_2O_2F_6$, 2,2,2-Trifluoroethyl trifluoroacetate, $CF_3CH_2OC(O)CF_3$: OH, 884; Cl, 884; AF, 885; S, 1531
$C_4HO_2F_7$, Perfluoro-*n*-propyl formate, $CF_3CF_2CF_2OC(O)H$: OH, 878; Cl, 879; AF, 880; S, 1531
$C_5HO_2F_9$, Perfluoro-*n*-butyl formate, $CF_3CF_2CF_2CF_2OC(O)H$: Cl, 875; AF, 880; S, 1531
$C_5HO_2F_9$, Perfluoro-*iso*-butyl formate, $(CF_3)_2CFCF_2OC(O)H$, Cl, 875; S, 1532
$C_6HO_2F_{11}$, Perfluoro-*n*-pentyl formate, $CF_3CF_2CF_2CF_2CF_2OC(O)H$: Cl, 875; AF, 880; S, 1532
$C_8HO_2F_{15}$, Perfluoro-*n*-heptyl formate, $CF_3CF_2CF_2CF_2CF_2CF_2CF_2OC(O)H$: Cl, 875; AF, 880

$C_8HO_2F_{15}$, 1,1,1,2,3,4,4,5,5,6,6,6-Dodecafluoro-2-(trifluoromethyl)hexan-3-yl formate, *n*-$C_3F_7CF[CF(CF_3)_2]O(O)CH$: Cl, 875; S, 1532
$C_9H_7O_2F_9$, 3,3,4,4,5,5,6,6,6-nonafluorohexyl prop-2-enoate, $CH_2{=}CHC(O)OCH_2CH_2CF_2CF_2CF_2CF_3$: OH, 885; Cl, 885; AF, 885
$C_9H_3O_2F_{15}$, 1,1,1,2,3,4,4,5,5,6,6,6-Dodecafluoro-2-(trifluoromethyl)hexan-3-yl acetate, *n*-$C_3F_7CF[CF(CF_3)_2]OC(O)CH_3$: Cl, 875; S, 1532
$C_{11}HO_2F_{21}$, Perfluoro-*n*-decyl formate, $CF_3CF_2CF_2CF_2CF_2CF_2CF_2CF_2CF_2CF_2OC(O)H$: Cl, 880; AF, 885
$C_{11}HO_3F_{19}$, 3,3,4,4,5-Pentafluoro-2,5-*bis*(1,1,1,2,3,3,3-heptafluoropropan-2-yl)tetrahydrofuran-2-yl formate,: Cl, 875; S, structure (a) in table VII-I-2, 875, 1532

Lactates

$C_4H_8O_3$, Methyl lactate, $CH_3CH(OH)C(O)OCH_3$: OH, 870; AF, 870; S, 1530
$C_5H_{10}O_3$, Ethyl lactate, $CH_3CH(OH)C(O)OCH_2CH_3$: OH, 870; AF, 871; S, 1530

Unsturated Esters

$C_4H_6O_2$, Vinyl acetate, $CH_2{=}CHOC(O)CH_3$: OH, 848; O_3, 848; AF, 849; S, 1527
$C_4H_6O_2$, Methyl acrolate, $CH_3OC(O)CH{=}CH_2$: OH, 854; NO_3, 855; O_3, 855; AF, 856; S, 1527
$C_5H_8O_2$, Ethyl acrolate, $CH_3CH_2OC(O)CH{=}CH_2$: OH, 857; AF, 858; S, 1527
$C_5H_8O_2$, Methyl methacrolate, $CH_3OC(O)C(CH_3){=}CH_2$: OH, 860; NO_3, 860; AF, 860; S, 1527
$C_5H_8O_2$, *iso*-Propenyl acetate, $CH_2{=}C(CH_3)OC(O)CH_3$: OH, 851; O_3, 851; AF, 852; S, 1527
$C_5H_8O_2$, Methyl 2-butenoate, $CH_3CH{=}CHC(O)OCH_3$: OH, 864; NO_3, 865; AF, 865; S, 1527
$C_5H_9O_2$, Allyl acetate, $CH_3CH{=}CH_2OC(O)CH_3$: OH, 849; O_3, 850; AF, 850; S, 527
$C_6H_{10}O_2$, Ethyl methacrolate, $CH_3CH_2OC(O)C(CH_3){=}CH_2$: OH, 861; AF, 862; S, 1528
$C_6H_{10}O_2$, Methyl 3-methyl-2-butenoate, $(CH_3)_2C{=}CHC(O)OCH_3$: OH, 864; AF, 865; S, 1528
$C_6H_{10}O_2$, Methyl *E*-2-methyl-2-butenoate, $CH_3CH{=}C(CH_3)C(O)OCH_3$: OH, 864; AF, 865
$C_7H_{12}O_2$, *n*-Butyl acrolate, $CH_3CH_2CH_2CH_2OC(O)CH{=}CH_2$: OH, 858; AF, 860
$C_7H_{12}O_2$, 4-Penten-1-yl acetate, $CH_2{=}CHCH_2CH_2CH_2OC(O)CH_3$: OH, 852
$C_8H_{14}O_2$, *n*-Butyl methacrolate, $CH_3CH_2CH_2CH_2OC(O)C(CH_3){=}CH_2$: OH, 863; AF, 863; S, 1528
$C_8H_{14}O_2$, *cis*-3-Hexenyl acetate, $CH_3CH_2CH{=}CHCH_2CH_2OC(O)CH_3$: OH, 853; NO_3, 854; O_3, 854; AF, 854; S, 1528
$C_{19}H_{32}O_2$, Methyl linolenate, $CH_3(CH_2CH{=}CH)_3CH_2(CH_2)_6C(O)OCH_3$: S, 1529
$C_{19}H_{34}O_2$, Methyl linoleaoate, *n*-$C_5H_{11}CH{=}CHCH_2CH{=}CHC_7H_{14}C(O)OCH_3$: S, 1529
$C_{19}H_{36}O_2$, Methyl oleate, *n*-$C_8H_{17}CH{=}CH(CH_2)_7C(O)OCH_3$: S, 1528

Ethers

Acyclic Ethers

C_2H_6O, Dimethyl ether, CH_3OCH_3: OH, 290; NO_3, 293; Cl, 295; O, 295; AF, 295; S, 1490
C_3H_8O, Methyl ethyl ether, $CH_3OC_2H_5$: OH, 297; NO_3, 297; Cl, 297; O, 298; AF, 299; S, 1490
$C_4H_{10}O$, Diethyl ether, $C_2H_5OC_2H_5$: OH, 299; NO_3, 302; Cl, 302; O, 303; AF, 303; S, 1490
$C_5H_{12}O$, Methyl *n*-butyl ether, *n*-$C_4H_9OCH_3$: OH, 304; NO_3, 304; AF, 306; S, 1490
$C_5H_{12}O$, Methyl *tert*-butyl ether, *tert*-$C_4H_9OCH_3$: OH, 306; NO_3, 309; Cl, 309, AF, 309; S, 1490
$C_5H_{12}O$, Ethyl *n*-propyl ether, *n*-$C_3H_7OC_2H_5$: OH, 319; NO_3, 321; AF, 322
$C_6H_{14}O$, Di-*n*-propyl ether, $(n\text{-}C_3H_7)_2O$: OH, 310; NO_3, 310; Cl, 313; O, 313; AF, 314; S, 1490
$C_6H_{14}O$, Di-isopropyl ether, $(iso\text{-}C_3H_7)_2O$: OH, 315; NO_3, 314; Cl, 316; AF, 316; S, 1491
$C_6H_{14}O$, Ethyl *tert*-butyl ether, *tert*-$C_4H_9OC_2H_5$: OH, 323; NO3, 323; Cl, 323; O, 323; AF, 324; S, 1491
$C_6H_{14}O$, Methyl *tert*-amyl ether, $CH_3OC(CH_3)_2CH_2CH_3$: OH, 326; NO_3, 328; O, 328; AF, 328; S, 1491

$C_7H_{16}O$, Isopropyl isobutyl ether, $(CH_3)_2CHOCH_2CH(CH_3)_2$: OH, 330; NO_3, 330; AF, 330; S, 1491

$C_8H_{18}O$, Di-*n*-butyl ether, $(n\text{-}C_4H_9)_2O$: OH, 331; NO_3, 333; Cl, 333; O, 334; AF, 334; S, 1491

$C_8H_{18}O$, Di-isobutyl ether, $[(CH_3)_2CHCH_2]_2O$: OH, 325; AF, 325; S, 1491

$C_8H_{18}O$, Di-*tert*-butyl ether, $[(CH_3)_3C]_2O$: OH, 336; NO_3, 336; Cl, 336; AF, 336; S, 1491

$C_{10}H_{22}O$, Di-*n*-pentyl ether, $(n\text{-}C_5H_{11})_2O$: OH, 337; NO_3, 339; Cl, 339; O, 339; AF, 339; S, 1491

Aromatic Ethers

C_7H_8O, Methoxybenzene, $CH_3OC_6H_5$: OH, 420; NO_3, 421; O, 422; AF, 422; S, 1499

C_8H_6O, 2,3-Benzofuran: OH, 427; O_3, 428; AF, 428; S, 427

C_8H_8O, 2,3-Dihydrobenzofuran: OH, 426; O_3, 426; NO_3, 427; AF, 427; S, 426

$C_8H_8O_2$, 1,4-Benzodioxan,: OH, 428; O_3, 428; NO_3, 428; AF, 428; S, 428

$C_8H_{10}O$, 4-Methoxytoluene, $CH_3OC_6H_4CH_3$: NO_3, 424; AF, 425

$C_8H_{10}O_2$, 1,2-Dimethoxybenzene, $CH_3OC_6H_4OCH_3$: OH, 422; NO_3, 422; AF, 423; S, 1500

$C_8H_{10}O_2$, 1,3-Dimethoxybenzene, $CH_3OC_6H_4OCH_3$: NO_3, 423; AF, 423; S, 1499

$C_8H_{10}O_2$, 1,4-Dimethoxybenzene, $CH_3OC_6H_4OCH_3$: NO_3, 423; AF, 423; S, 1500

$C_9H_{10}O$, Isochroman: OH, 430; S, 429

$C_9H_{12}O$, 4-Ethoxytolouene, $C_2H_5OC_6H_4CH_3$: NO_3, 424; AF, 425

$C_{12}H_8O$, Dibenzofuran: OH, 430; O_3, 430; NO_3, 430; AF, 431; S, 430, 1500

$C_{12}H_8O_2$, Dibenzo-*p*-dioxin: OH, 432; O_3, 432; NO_3, 432; AF, 433; S, 431, 1500

$C_{12}H_{10}O$, Diphenyl ether, $C_6H_5OC_6H_5$: OH, 425; AF, 425; S, 1500

$C_{18}H_{26}O$, 1,3,4,6,7,8,-hexahydro-4,6,6,7,8,8-hexamethylcyclopenta-[γ]-2-benzopyran: OH, 430; S, 429

Cyclic Ethers

C_2H_4O, Ethylene oxide, *cyclo*(—CH_2OCH_2—): OH, 382; Cl, 384; O, 385; AF, 385; S, 1497

C_3H_6O, Methyl oxirane, CH_3-(*cyclo*-$CHOCH_2$—): OH, 386; NO_3, 386; AF, 387; S, 1497

C_3H_6O, Oxetane, *cyclo*(—$CH_2OCH_2CH_2$—): OH, 388; AF, 388; S, 388, 1497

$C_3H_4O_2$, Glycidaldehyde, *cyclo*(—CH(CHO)-OCH_2—): OH, 408; AF, 408; CS, 1029; QY, 1028; J, 1030; S, 408, 1499

$C_3H_6O_2$, 1,3-Dioxolane, *cyclo*(—$CH_2OCH_2OCH_2$—): OH, 396; Cl, 396; AF, 397; S, 396, 1498

$C_3H_6O_3$, 1,3,5-Trioxane, *cyclo*(—$CH_2OCH_2OCH_2O$—): OH, 405; Cl, 406; AF, 406; S, 405, 1499

C_4H_4O, Furan, (*cyclo*-CH=CHCH=CHO—): OH, 409; O_3, 410; NO_3, 410; Cl, 411; AF, 411; S, 409, 1496

C_4H_6O, 2,5-Dihydrofuran, *cyclo*(—$CH_2CHCHCH_2O$—): O_3, 417; AF, 416; S, 416

C_4H_6O, Vinyl oxirane, *cyclo*[—$CH_2OCH(CH{=}CH_2)$—]: O_3, 408; NO_3, 409; S, 408, 1498

C_4H_8O, Ethyl oxirane, CH_3CH_2-(*cyclo*-$CHOCH_2$—): OH, 387; AF, 388; S, 387, 1497

C_4H_8O, Tetrahydrofuran, *cyclo*(—$CH_2OCH_2CH_2CH_2$—): OH, 389; NO_3, 389; O, 389; AF, 390; S, 388, 1498

$C_4H_8O_2$, 1,4-Dioxane, *cyclo*(—$CH_2OCH_2CH_2OCH_2$—): OH, 398; Cl, 400; O, 400; AF, 401; S, 398, 1498

$C_4H_8O_2$, 1,3-Dioxane, *cyclo*(—$CH_2OCH_2OCH_2CH_2$—): OH, 396; Cl, 396; AF, 397; S, 402, 1498

C_5H_6O, 2-Methylfuran, *cyclo*(—CH=CHCH=$C(CH_3)$O—): OH, 412; NO_3, 413; Cl, 413; AF, 414; S, 391, 1497

C_5H_6O, 3-Methylfuran, *cyclo*[—CH=CHC(CH_3)=CHO—]: OH, 412; O_3, 413; Cl, 413; AF, 414; S, 1497

C_5H_8O, 4,5-Dihydro-2-methylfuran, *cyclo*[—$CH_2CH_2CH{=}C(CH_3)O$—]: OH, 417; O_3, 417; NO_3, 417; AF, 414; S, 416

C_5H_8O, 2-Methyl-2-vinyl oxirane, *cyclo*[—$CH_2OC(CH_2{=}CH)(CH_3)$—]: NO_3, 409

$C_5H_{10}O$, 2-Methyl-tetrahydrofuran, *cyclo*(—$CH(CH_3)OCH_2CH_2CH_2$—): OH, 391; AF, 393; S, 1498

$C_5H_{10}O$, Tetrahydropyran, *cyclo*(—$CH_2OCH_2CH_2CH_2CH_2$—): OH, 393; AF, 394; S, 393, 1498

$C_5H_{10}O$, 4-Methyl-1,3-dioxane, *cyclo*(—$CH(CH_3)OCH_2OCH_2CH_2$—): OH, 404; AF, 404; S, 404, 1498
$C_5H_{10}O_2$, 1,3-Dioxepane, *cyclo*(—$CH_2OCH_2CH_2CH_2CH_2O$—): OH, 405; AF, 405; S, 405, 1498
$C_5H_4O_2$, 2-Furfural, *cyclo*[—CH=CHCHC(CHO)O—]: OH, 414; Cl, 415; AF, 415; S, 414
$C_5H_4O_2$, 3-Furfural, *cyclo*[—CH=CHC(CHO)CHO—]: OH, 414; Cl, 415; AF, 415; SS, 414
C_6H_6O, Benzene oxide: OH, 418; NO_3, 418; AF, 418; CS, 1314; QY, 1313; J, 1315; S, 417, 1499
C_6H_8O, 2-Ethylfuran, *cyclo*(—CH=CHCHC(C_2H_5)O—): OH, 413; Cl, 413; AF, 414
C_6H_8O, 2,5-Dimethylfuran, *cyclo*[—CH=C(CH_3)OC(CH_3)=CH—]: OH, 413; NO_3, 413; Cl, 413; AF, 414; S, 1497
C_6H_8O, 2,4-Dimethylfuran:, *cyclo*[—CH=C(CH_3)OCH=C(CH_3)—) NO_3, 413; AF, 414
C_6H_8O, 2,3-Dimethylfuran, *cyclo*[—C(CH_3)=C(CH_3)OCH=CH—): NO_3, 413; AF, 414
C_6H_8O, 3,4-Epoxy-cyclohexene: NO_3, 419; S, 418, 1499
$C_6H_{10}O$, 2-Methyl-2-(2-propenyl) oxirane, *cyclo*[—C(CH_3)(CH=$CHCH_3$)OCH_2—]: NO_3, 409
$C_6H_{12}O$, Oxepane, *cyclo*(—$CH_2OCH_2CH_2CH_2CH_2CH_2$—): OH, 394; AF, 395; S, 394, 1498
$C_6H_6O_2$, 5-Methyl-2-furfural, *cyclo*[—C(CH_3)=CHCH=C(CHO)O—]: OH, 414; Cl, 415; AF, 415; S, 414
C_7H_8O, Toluene oxide: OH, 418; NO_3, 418; AF, 418; CS, 1317; QY, 1316; J, 1315; S, 417, 1499
$C_7H_{10}O$, 2,2-Dimethyl-3-(2,2-dimethylvinyl) oxirane, *cyclo*[—C(CH=C(CH_3)OC(CH_3)$_2$—]: NO_3, 409
$C_7H_{12}O_2$, 5-Methyl-5-vinyl-tetrahydrofuran-2-ol, *cyclo*[—C(CH_3)(CH=CH_2)CH_2CH_2CH(OH)O—]: OH, 417; O_3, 417; NO_3, 417; AF, 416; S, 416
$C_8H_{12}O$, Tetramethylfuran, *cyclo*[—C(CH_3)=C(CH_3)C(CH_3)=C(CH_3)O—]: NO_3, 414; AF, 414; S, 1497
$C_{10}H_{18}O$, 1,8-Cineole: OH, 419; NO_3, 419; AF, 420; S, 419

Difunctional Ethers

$C_3H_8O_2$, Dimethoxymethane, $CH_3OCH_2OCH_3$: OH, 340; Cl, 341; AF, 341; S, 1492
$C_3H_8O_2$, 2-Methoxyethanol, $CH_3OCH_2CH_2OH$: OH, 342; AF, 343; S, 1492
$C_4H_{10}O_2$, 1,2-Dimethoxyethane, $CH_3OCH_2CH_2OCH_3$: OH, 344; AF, 344; S, 1492
$C_4H_{10}O_2$, 2-Ethoxyethanol, $CH_3CH_2OCH_2CH_2OH$: OH, 345; AF, 345; S, 1492
$C_4H_{10}O_2$, 1-Methoxy-2-propanol, $CH_3OCH_2CH(OH)CH_3$: OH, 346; O_3, 347; NO_3, 347; AF, 348; S, 1492
$C_4H_{10}O_2$, 1,1-Dimethoxyethane, $CH_3CH(OCH_3)_2$: OH, 348; AF, 348; S, 1492
$C_5H_{12}O_2$, 2-Propoxyethanol, $CH_3CH_2CH_2OCH_2CH_2OH$: OH, 348; AF, 349; S, 1492
$C_5H_{12}O_2$, Diethoxymethane, $CH_3CH_2OCH_2OCH_2CH_3$: OH, 349; O, 350; AF, 350; S, 1492
$C_5H_{12}O_2$, 1,2-Dimethoxypropane, $CH_3OCH_2CH(OCH_3)CH_3$: OH, 351; AF, 352; S, 1492
$C_5H_{12}O_2$, 2,2-Dimethoxypropane, $(CH_3)_2C(OCH_3)_2$: OH, 352; AF, 353; S, 1492
$C_5H_{12}O_2$, 2-Isopropoxyethanol, $(CH_3)_2CHOCH_2CH_2OH$: OH, 353; AF, 354; S, 1492
$C_5H_{12}O_2$, 1-Ethoxy-2-methoxyethane, $CH_3CH_2OCH_2CH_2OCH_3$: OH, 354; S, 1492
$C_5H_{12}O_2$, 3-Methoxy-1-butanol, $CH_3CH(OCH_3)CH_2CH_2OH$: OH, 354; S, 1493
$C_5H_{12}O_2$, 2-Isopropoxy-ethanol, $(CH_3)_2CHOCH_2CH_2OH$: OH, 354
$C_5H_{12}O_2$, 3-Ethoxy-1-propanol, $CH_3CH_2OCH_2CH_2CH_2OH$: OH, 354; S, 1493
$C_5H_{12}O_2$, 1,3-Dimethoxypropane, $CH_3OCH_2CH_2CH_2OCH_3$: OH, 354; S, 1493
$C_6H_{14}O_2$, 2-*n*-Butoxyethanol, $CH_3CH_2CH_2CH_2OCH_2CH_2OH$: OH, 355; O_3, 355; NO_3, 355; AF, 356; S, 1493
$C_6H_{14}O_2$, 1,2-Diethoxyethane, $CH_3CH_2OCH_2CH_2OCH_2CH_3$: OH, 356; AF, 357; S, 1493

$C_6H_{14}O_2$, 1,4-Dimethyoxybutane, $CH_3OCH_2CH_2CH_2CH_2OCH_3$: OH, 357; AF, 357, S, 1493

$C_7H_{16}O_2$, Di-*n*-Propoxymethane, $CH_3CH_2CH_2OCH_2OCH_2CH_2CH_3$: OH, 358; AF, 358; S, 1493

$C_7H_{16}O_2$, 2,2-Diethoxypropane, $CH_3)_2C(OCH_2CH_3)_2$: OH, 358; AF, 359; S, 1493

$C_7H_{16}O_2$, Di-*iso*-propoxymethane, $(CH_3)_2CHOCH_2OCH(CH_3)_2$: OH, 360; AF, 362; S, 1494

$C_7H_{16}O_2$, 1-Butoxy-2-propanol, $CH_3CH_2CH_2CH_2OCH_2CH(OH)CH_3$: OH, 362; AF, 362; S, 1494

$C_9H_{20}O_2$, Di-*n*-butoxymethane, $CH_3CH_2CH_2CH_2OCH_2OCH_2CH_2CH_2CH_3$: OH, 363; AF, 363; S, 1494

$C_9H_{20}O_2$, Di-*sec*-butoxymethane, $CH_3CH_2CH(CH_3)OCH_2OCH(CH_3)CH_2CH_3$: OH, 364; AF, 365; S, 1494

$C_9H_{20}O_2$, Di-*iso*-butoxymethane, $(CH_3)_2CHCH_2OCH_2OCH_2CH(CH_3)_2$: OH, 366; AF, 367; S, 1494

See also the substituted ethers in the ester section: "Alkoxy-Substituted Esters".

Halogenated Ethers

C_2H_5OBr, Methyl bromomethyl ether, CH_3OCH_2Br: Cl, 497; AF, 497; S. 1501

C_2H_5OCl, Methyl chloromethyl ether, CH_3OCH_2Cl: OH, 494; Cl, 494; AF, 494; S, 1501

$C_2H_4OCl_2$, Methyl dichloromethyl ether, CH_3OCHCl_2: Cl, 494; AF, 495; S, 1501

C_3H_7OBr, Methyl 2-bromoethyl ether, $CH_3OCH_2CH_2Br$: OH, 498; Cl, 498; AF, 498; S, 1502

C_3H_7OCl, Methyl 2-chloroethyl ether, $CH_3OCH_2CH_2Cl$: OH, 495; Cl, 495; AF, 495; S, 1502

$C_3H_6OCl_2$, Methyl 2,2-dichloroethyl ether, $CH_3OCH_2CHCl_2$: Cl, 494; AF, 495; S, 1502

C_2H_5OI, Methyl iodomethyl ether, CH_3OCH_2I: Cl, 499; AF, 499; S, 1501

$C_2H_4OF_2$, Methyl difluoromethyl ether, CH_3OCHF_2: OH, 434; AF, 434; S, 1500

$C_2H_4OF_2$, *bis*(Fluoromethyl) ether, CH_2FOCH_2F: OH, 434; Cl, 435; AF, 435; S, 1500

$C_2H_3OF_3$, Methyl trifluoromethyl ether, CH_3OCF_3: OH, 436; Cl, 436; AF, 436; S, 1500

$C_2H_2OF_4$, bis-Difluoromethyl ether, CHF_2OCHF_2: OH, 437; Cl, 438; AF, 439; S, 500

C_2HOF_5, Trifluoromethyl difluoromethyl ether, CF_3OCHF_2: OH, 441; Cl, 441; AF, 442; S, 1500

$C_3H_5OF_3$, Ethyl trifluoromethyl ether, $CH_3CH_2OCF_3$: OH, 443; Cl, 443; AF, 443; S, 1501

$C_3H_5OF_3$, Methyl 2,2,2-trifluoroethyl ether, $CF_3CH_2OCH_3$: OH, 444; Cl, 444; AF, 445; S, 1501

$C_3H_4OF_4$, Methyl 1,1,2,2-tetrafluoroethyl ether, $CH_3OCF_2CHF_2$: OH, 445; Cl, 447; AF, 447; S, 1501

$C_3H_4OF_4$, Methyl 1,2,2,2-tetrafluoroethyl ether, $CF_3CHFOCH_3$: OH, 447; AF, 447; S, 1501

$C_3H_4OF_5$, Difluoromethyl 2,2,2-trifluoroethyl ether, $CF_3CH_2OCHF_2$: OH, 448; Cl, 448; AF, 450; S, 1501

$C_3H_4OF_5$, 1,1,2-Trifluoroethyl difluoromethyl ether, $CH_2FCF_2OCHF_2$; OH, 451; AF, 451; S, 1501

$C_3H_3OF_5$, Methyl 1,1,2,2,2-pentafluoroethyl ether, $CH_3OCF_2CF_3$: OH, 452; Cl, 453; AF, 453; S, 1501

C_3HOF_5, 2,2,3,4,4-Pentafluorooxetane, *cyclo*(—OCF_2CFHCF_2—): OH, 461; AF, 461; S, 1502

$C_3H_2OF_5$, 1,2,2-Trifluoroethyl trifluoromethyl ether, $CHF_2CHFOCF_3$: OH, 453; Cl, 454; AF, 454; S, 1501

C_3OF_6, 1,1,2,-Trifluoro-2-(trifluoromethoxy)ethene, $CF_3OCF{=}CF_2$: OH, 516; Cl, 516; AF, 516

C_3OF_6, Perfluorooxetane, *cyclo*(—$OCF_2CF_2CF_2$—): OH, 461; AF, 461; S, 1503

$C_3H_2OF_6$, 1,2,2,2-Tetrafluoroethyl difluoromethyl ether, $CF_3CHFOCHF_2$: OH, 454; Cl, 455; AF, 455; S, 1502

$C_3H_2OF_6$, 1,1,2,2-Tetrafluoroethyl difluoromethyl ether, $CHF_2OCF_2CHF_2$: OH, 455; AF, 457; S, 1502

$C_3H_2O_2F_6$, *bis*(Difluoromethoxy)(difluoro)methane, $CHF_2OCF_2OCHF_2$: OH, 509; Cl, 509; AF, 510

C_3HOF_7, 1,2,2,2-Tetrafluoroethyl trifluoromethyl ether, $CF_3CHFOCF_3$: OH, 457; Cl, 458; AF, 459; S, 1502

C_3HOF_7, 1,1,2,2-Tetrafluoroethyl trifluoromethyl ether, $CF_3OCF_2CF_2H$: OH, 459; Cl, 459; AF, 459; 1502

$C_3H_2OClF_5$, 2,2,2-trifluroethyl chlorodifluoromethyl ether, $CF_3CH_2OCClF_2$: OH, 505; Cl, 505; AF, 506

$C_3H_4OClF_3$, Methyl 2-chloro-1,1,2-trifluoroethyl ether, CH_3OCF_2CHFCl: OH, 499; Cl, 500; AF, 500

$C_3H_2OClF_5$, Difluoromethyl 2-chloro-1,1,2-trifluoroethyl ether, CHF_2OCF_2CHFCl: OH, 500; Cl, 503; AF, 503

$C_3H_2OClF_5$, Difluoromethyl 1-chloro-2,2,2-trifluroethyl ether, $CHF_2OCHClCF_3$: OH, 500; Cl, 503; AF, 503

$C_4H_6OClF_3$, Ethyl 1-chloro-2,2,2-trifluoroethyl ether, $CF_3CHClOCH_2CH_3$: OH, 506; Cl, 506; AF, 507; S, 1504

$C_4H_8OF_4$, Ethyl 1,1,2,2-tetrafluoroethyl ether, $CH_3CH_2OCF_2CF_2H$: OH, 461; Cl, 462; AF, 462

$C_4H_6OF_4$, Methyl 2,2,3,3-tetrafluoro-*n*-propyl ether, $CHF_2CF_2CH_2OCH_3$: OH, 462; Cl, 464; AF, 464

$C_4H_6O_2F_4$, 1,1,2,2-Tetrafluoro-1,2-dimethoxyethane, $CH_3OCF_2CF_2OCH_3$: OH, 511; Cl, 511; AF, 511

$C_4H_5OF_5$, Methyl 2,2,3,3,3-pentafluoro-*n*-propyl ether, $CF_3CF_2CH_2OCH_3$: OH, 464; Cl, 465; AF, 465

$C_4H_4OF_6$, Methyl 1,1,1,3,3,3-hexafluoro-2-propyl ether, $CH_3OCH(CF_3)_2$: OH, 465; Cl, 466; AF, 466; S, 1503

$C_4H_4OF_6$, Methyl 1,1,2,3,3,3-hexafluoro-*n*-propyl ether, $CF_3CHFCF_2OCH_3$: OH, 467; Cl, 467; AF, 467; S, 1503

$C_4H_4OF_6$, *bis*(2,2,2-Trifluoroethyl)ether, $CF_3CH_2OCH_2CF_3$: OH, 468; Cl, 468; AF, 468; S, 1503

$C_4H_4OF_6$, 2,2,3,3-Tetrafluoro-*n*-propyl difluoromethyl ether, $CHF_2OCH_2CF_2CHF_2$: OH, 469; AF, 470; S, 1503

$C_4H_3OF_7$, 1,1,1,3,3,3-Hexafluoro-2-propyl fluoromethyl ether, $CH_2FOCH(CF_3)_2$: OH, 471; AF, 471; S, 1503

$C_4H_3OF_7$, 1,1,2,2-Tetrafluoroethyl 2,2,2-trifluoroethyl ether, $CF_3CH_2OCF_2CF_2H$; OH, 471; Cl, 474; AF, 474; S, 1503

$C_4H_3OF_7$, Methyl perfluoro-*iso*-propyl ether, $CH_3OCF(CF_3)_2$: OH, 474; AF, 474; S, 1504

$C_4H_3OF_7$, Methyl perfluoro-*n*-propyl ether, $CH_3OCF_2CF_2CF_3$: OH, 475; Cl, 475; AF, 475; S, 1503

$C_4H_3OF_7$, Difluoromethyl 2,2,3,3,3-pentafluoro-*n*-propyl, ether, $CHF_2OCH_2CF_2CF_3$: OH, 476; AF, 477; S, 1504

$C_4H_2OF_8$, 1,2-bis(Difluoromethoxy)-1,1,2,2-tetrafluoroethane $CHF_2OCF_2CF_2OCHF_2$: OH, 509; Cl, 509; AF, 510

$C_4H_2OF_8$, 1,1,2,2-Tetrafluoroethyl 1,2,2,2-tetrafluoroethyl ether, $CHF_2CF_2OCHFCF_3$: OH, 477; AF, 477

$C_4H_2OF_8$, 1,1,2,3,3,3-Hexafluoro-*n*-propyl difluoromethyl ether, $CF_3CFHCF_2OCF_2H$: OH, 478; Cl, 478; AF, 479; S, 1504

$C_4H_2OF_8$, 1,1,1,3,3,3-Hexafluoro-2-propyl difluoromethyl ether, $(CF_3)_2CHOCHF_2$: OH, 480; AF, 480; S, 1504

C_4HOF_9, 1,1,2,3,3,3-Hexafluoro-*n*-propyl trifluoromethyl, ether, $CF_3CFHCF_2OCF_3$: OH, 480; AF, 481

C_4HOF_9, 1,1,1,3,3,3-Hexafluoro-2-propyl trifluoromethyl ether, $CF_3OCH(CF_3)_2$: OH, 482; Cl, 483; AF, 483

$C_5H_2O_3F_{10}$, 1-(Difluoromethoxy)-2-[(difluoromethoxy)(difluoro)methoxy]-1,1,2,2-tetrafluoroethane), $CHF_2OCF_2CF_2OCF_2OCHF_2$: OH, 509; Cl, 509; AF, 510

$C_5H_6OF_6$, Ethyl 1,1,2,3,3,3-hexafluoro-*n*-propyl ether, $CF_3CHFCF_2OCH_2CH_3$: OH, 483; Cl, 484; AF, 484; S, 1504

$C_5H_3OF_9$, Methyl perfluoro-*n*-butyl ether, $CF_3CF_2CF_2CF_2OCH_3$: OH, 485; Cl, 486; AF, 486; S, 1505

$C_5H_3OF_9$, Methyl perfluoro-*iso*-butyl ether, $(CF_3)_2CFCF_2OCH_3$: OH, 485; Cl, 486; AF, 486; S, 1505

$C_5H_3OF_9$, 2,2,2-Trifluoroethyl 1,1,2,3,3,3-hexafluoro-*n*-propyl ether, $CF_3CHFCF_2OCH_2CF_3$: OH, 487; AF, 487; S, 1505

C_5HOF_{11}, 1,2,2,2,-Tetrafluoroethyl perfluoro-*n*-propyl ether, $CF_3CF_2CF_2OCHFCF_3$: OH, 487; Cl, 487; AF, 487; S, 1505

$C_6H_6O_2F_8$, 1,1,2,2-Tetrafluoro-1-methoxy-2-(1,1,2,2-tetrafluoro-2-methoxyethoxy)ethane $CH_3OCF_2CF_2OCF_2CF_2OCH_3$: OH, 511; Cl, 511; AF, 511; S, 1506

$C_6H_5OF_9$, Ethyl perfluoro-*n*-butyl ether, $CF_3CF_2CF_2CF_2OCH_2CH_3$: OH, 485; Cl, 486; AF, 486

$C_6H_5OF_9$, Ethyl perfluoro-*iso*-butyl ether, $(CF_3)_2CFCF_2OCH_2CH_3$: OH, 492; Cl, 492; AF, 493
$C_6H_4OF_{10}$, 1,1,2,3,3,3-Hexafluoro-*n*-propyl 2,2,3,3-tetrafluoro-*n*-propyl ether, $CF_3CHFCF_2OCH_2CF_2CHF_2$: OH, 490; AF, 491
$C_6H_3OF_{11}$, Methyl perfluoro-*n*-pentyl ether, $CH_3OCF_2CF_2CF_2CF_2CF_3$: OH, 488; Cl, 489; AF, 489
$C_6H_3OF_{11}$, 1,1,2,3,3,3,-Hexafluoro-*n*-propyl 2,2,3,3,3-pentafluoro-*n*-propyl ether, $CF_3CHFCF_2OCH_2CF_2CF_3$: OH, 489; AF, 489
$C_6O_3F_{14}$, 1-[Difluoro(trifluoromethoxy)methoxy]-1,1,2,3,3,3-hexafluoro-2-(trifluoromethoxy)propane, $CF_3OCF(CF_3)CF_2OCF_2OCF_3$: OH, 512; Cl, 513; AF, 513
$C_8H_6O_2F_{12}$, 3,3,4,4,6,6,7,7,9,9,10,10-Dodecafluoro-2,5,8,11-tetraoxadodecane $CH_3OCF_2CF_2OCF_2CF_2OCF_2CF_2OCH_3$: OH, 511; Cl, 511; AF, 511
$C_9H_8O_2F_{12}$, 1,1,1,2,3,3-Hexafluoro-3-[3-(1,1,2,3,3,3-hexafluoropropoxy)propoxy]propane $CF_3CFHCF_2OCH_2CH_2CH_2OCF_2CFHCF_3$: OH, 513; Cl, 513; AF, 514
$C_9H_5OF_{15}$, 1,1,1,2,3,4,4,5,5,6,6,6,-Dodecafluoro-2-(trifluoromethyl)hexane-3-yl ethyl ether, $CF_3CF_2CF_2CF(OCH_2CH_3)CF(CF_3)_2$: OH, 507; Cl, 508; AF, 508
$C_{11}H_6O_2F_{18}$, 1,1,1,2,2,3,3,4,4-Nonafluoro-4-[3-(nonafluorobutoxy)propoxy]butane, $CF_3CF_2CF_2CF_2OCH_2CH_2CH_2OCF_2CF_2CF_2CF_3$: OH, 513; Cl, 513; AF, 514; S, 1507
$C_{12}H_9OBr$, 2-Bromodiphenyl ether, $BrC_6H_4OC_6H_5$: OH, 524; AF, 523; S, 1507
$C_{12}H_9OBr$, 3-Bromodiphenyl ether $BrC_6H_4OC_6H_5$: OH, 524; AF, 523; S, 1508
$C_{12}H_9OBr$, 4-Bromodiphenyl ether, $BrC_6H_4OC_6H_5$: OH, 524; AF, 523; S, 1508
$C_{12}H_8OBr_2$, 2,2'-Dibromodiphenyl ether, $BrC_6H_4OC_6H_4Br$: OH, 524; AF, 523; S, 1508
$C_{12}H_8OBr_2$, 2,4-Dibromodiphenyl ether: $Br_2C_6H_3OC_6H_5$: OH, 525; AF, 523; S, 1508
$C_{12}H_8OBr_2$, 3,3'-Dibromodiphenyl ether, $BrC_6H_4OC_6H_4Br$: OH, 525; AF, 523; S, 1508
$C_{12}H_8OBr_2$, 4,4'-Dibromodiphenyl ether, $BrC_6H_4OC_6H_4Br$: OH, 525; AF, 523; S, 1508
$C_{12}H_7O_2Cl$, 1-Chlorodibenzo-*p*-dioxin, $C_{12}H_7ClO_2$: OH, 519; O_3, 520; NO_3, 520; AF, 521; S, 1507
$C_{12}H_7O_2Cl$, 2-Chlorodibenzo-*p*-dioxin, $C_{12}H_7ClO_2$: OH, 519; AF, 521; S, 1507
$C_{12}H_6O_2Cl_2$, 2,3-Dichlorodibenzo-*p*-dioxin, $C_{12}H_6Cl_2O_2$: OH, 519; AF, 521; S, 1507
$C_{12}H_6O_2Cl_2$, 2,7-Dichlorodibenzo-*p*-dioxin, $C_{12}H_6Cl_2O_2$: OH, 519; AF, 521; S, 1507
$C_{12}H_6O_2Cl_2$, 2,8-Dichlorodibenzo-*p*-dioxin, $C_{12}H_6Cl_2O_2$: OH, 519; AF, 521; S, 1507
$C_{12}H_4O_2Cl_4$, 1,2,3,4-Tetrachlorodibenzo-*p*-dioxin, $C_{12}H_4Cl_4O_2$: OH, 519; AF, 521; S, 1507
$C_{12}O_2Cl_8$, Octachlorodibenzo-*p*-dioxin, $C_{12}Cl_8O_2$: OH, 519; AF, 521; S, 1507
$C_{12}H_5F_{19}O$, 2-Ethoxy-3,3,4,4,5-pentafluorotetrahydro-2,5-bis[1,2,2,2-tetrafluoro-1-(trifluoromethyl)ethyl]-furan: OH, 515; Cl, 515; AF, 516; S, 515

Unsaturated Ethers

C_3H_6O, Methyl vinyl ether, $CH_3OCH{=}CH_2$: OH, 372; O_3, 373; NO_3, 373; O, 373; AF, 373; S, 1496
C_4H_8O, Ethyl vinyl ether, $CH_3CH_2OCH{=}CH_2$: OH, 374; O_3, 374; NO_3, 374; AF, 374; S, 1496
$C_4H_8O_2$, Ethylene glycol monovinyl ether, $HOCH_2CH_2OCH{=}CH_2$: OH, 382; O_3, 383; NO_3, 383
$C_5H_{10}O$, Ethyl 1-propenyl ether, $CH_3CH_2OCH{=}CHCH_3$: O_3, 380; AF, 380; S, 1496
$C_5H_{10}O$, *n*-Propyl vinyl ether, $CH_3CH_2CH_2OCH{=}CH_2$: OH, 376; O_3, 376; NO_3, 376; AF, 377; S, 1496
$C_6H_{12}O$, *n*-Butyl vinyl ether, $CH_3CH_2CH_2CH_2OCH{=}CH_2$: OH, 378; O_3, 378; NO_3, 378; AF, 378; S, 1496
$C_6H_{12}O$, *iso*-Butyl vinyl ether, $(CH_3)_2CHCH_2OCH{=}CH_2$: OH, 380; AF, 380; S, 1496
$C_6H_{12}O$, *tert*-Butyl vinyl ether, $(CH_3)_3COCH{=}CH_2$: OH, 380; AF, 380; S, 1496 $C_6H_{10}O_2$, Ethylene glycol divinyl ether, $CH_2{=}CHOCH_2CH_2OCH{=}CH_2$: OH, 383; O_3, 383; NO_3, 383
$C_8H_{14}O_3$, Diethylene glycol divinyl ether, $CH_2{=}CHOCH_2CH_2OCH_2CH_2OCH{=}CH_2$: OH, 383; O_3, 383; NO_3, 383

Trifunctional Ethers

$C_4H_{10}O_3$, Trimethoxymethane, $(CH_3O)_3CH$: OH, 367; Cl, 368; AF, 368; S, 1494

$C_6H_{14}O_3$, 1,1,3-Trimethoxypropane, $(CH_3O)_2CHCH_2CH_2OCH_3$: OH, 367; AF, 368; S, 1494

$C_6H_{14}O_3$, Diethylene glycol ethyl ether, $CH_3CH_2OCH_2CH_2OCH_2CH_2OH$: OH, 368; AF, 368; S, 1495

$C_8H_{18}O_3$, Diethylene glycol *n*-butyl ether, $CH_3CH_2CH_2CH_2OCH_2CH_2OCH_2CH_2OH$: OH, 368; AF, 368; S, 1495

Ketenes

C_2H_2O, ketene, $CH_2{=}C{=}O$: OH, 723; O_3, 724; NO_3, 724; Cl, 725; O, 725; AF, 725; CS, 1172; QY, 1172; J, 1174; S, 1520

C_3H_4O, Methyl ketene, $CH_3CH{=}C{=}O$: OH, 723; O_3, 724; O, 725; CS, 1164; QY, 1173; S, 1520

C_4H_6O, Ethyl ketene, $CH_3CH_2CH{=}C{=}O$: OH, 723; O_3, 724; O, 725; S, 1520

C_4H_6O, Dimethyl ketene, $(CH_3)_2C{=}C{=}O$; OH, 723; O_3, 724; O, 725; QY, 1173; S, 1520

Ketones

Acyclic ketones

C_3H_6O, Acetone, $CH_3C(O)CH_3$: OH, 652; NO_3, 657; Cl, 657; O, 658; AF, 660; CS, 1091; QY, 1097, 1103; J, 1104; S, 1516

C_4H_8O, 2-Butanone, $CH_3C(O)CH_2CH_3$: OH, 660; Cl, 662; O, 664; AF, 665; CS, 1091; QY, 1107; J, 1109; S, 1516

$C_5H_{10}O$, 2-Pentanone, $CH_3CH_2CH_2C(O)CH_3$: OH, 666; Cl, 667; AF, 668; CS, 1110; QY, 1121; J, 1120; S, 1516

$C_5H_{10}O$, 3-Pentanone, $CH_3CH_2C(O)CH_2CH_3$: OH, 668; Cl, 668; O, 670; AF, 670; CS, 1110; QY, 1112; S, 1516

$C_5H_{10}O$, 3-Methyl-2-butanone, $(CH_3)_2CHC(O)CH_3$: OH, 671; NO_3, 671; O_3, 671; Cl, 671; AF, 672; QY, 1122; S, 1517

$C_6H_{12}O$, 2-Hexanone, $CH_3CH_2CH_2CH_2C(O)CH_3$; OH, 672; Cl, 672; AF, 673; QY, 1125; J, 1126; S, 1517

$C_6H_{12}O$, 3-Hexanone, $CH_3CH_2C(O)CH_2CH_2CH_3$: OH, 673; Cl, 675; AF, 675; QY, 1127; S, 1517

$C_6H_{12}O$, 3-Methyl-2-pentanone, $CH_3C(O)CH(CH_3)CH_2CH_3$: OH, 675; AF, 676

$C_6H_{12}O$, 4-Methyl-2-pentanone, $CH_3C(O)CH_2CH(CH_3)_2$: OH, 676; Cl, 677; AF, 677; CS, 1129; QY, 1132; S, 1517

$C_6H_{12}O$, 3,3-Dimethyl-2-butanone, $(CH_3)_3CC(O)CH_3$: OH, 677; AF, 678

$C_7H_{14}O$, 2-Heptanone, $CH_3C(O)CH_2CH_2CH_2CH_2CH_3$; OH, 678; AF, 679

$C_7H_{14}O$, 4,4-Dimethyl-2-pentanone, $CH_3C(O)CH_2C(CH_3)_3$: QY, 1132; S, 1517

$C_7H_{14}O$, 4-Methyl-2-hexanone, $CH_3C(O)CH_2CH(CH_3)CH_2CH_3$: QY, 1128; S, 1517

$C_7H_{14}O$, 5-Methyl-2-hexanone, $(CH_3)_2CHCH_2CH_2C(O)CH_3$: OH, 680; Cl, 680; AF, 680; CS, 1128

$C_7H_{14}O$, 2-Methyl-3-hexanone, $CH_3CH_2CH_2C(O)CH(CH_3)_2$: QY, 1131; S, 1517

$C_7H_{14}O$, 2,4-Dimethyl-3-pentanone, $(CH_3)_2CHC(O)CH(CH_3)_2$: OH, 682; CS, 1129; QY, 1131; S, 1517

$C_7H_{14}O$, 4-Heptanone, $CH_3CH_2CH_2C(O)CH_2CH_2CH_3$: QY, 1130; S, 1517

$C_8H_{16}O$, 2-Octanone, $CH_3C(O)CH_2CH_2CH_2CH_2CH_2CH_3$: OH, 682; AF, 683

$C_8H_{16}O$, 4-Octanone, $CH_3CH_2CH_2C(O)CH_2CH_2CH_2CH_3$: QY, 1133; S, 1518

$C_8H_{16}O$, 2-Methyl-4-heptanone, $(CH_3)_2CHCH_2C(O)CH_2CH_2CH_3$: QY, 1133; S, 1518

$C_8H_{16}O$, 3-Methyl-4-heptanone, $CH_3CH_2CH_2C(O)CH(CH_3)CH_2CH_3$: QY, 1134; S, 1518

$C_8H_{16}O$, 2,2-Dimethyl-3-hexanone, $CH_3CH_2CH_2C(O)C(CH_3)_3$: QY, 1134; S, 1518

$C_9H_{18}O$, 2-Nonanone, $CH_3C(O)CH_2CH_2CH_2CH_2CH_2CH_2CH_3$: OH, 682; AF, 683

$C_9H_{18}O$, 5-Nonanone, $(n\text{-}C_4H_9)_2CO$, QY, 1140

$C_9H_{18}O$, 2.6-Dimethyl-4-heptanone, $(CH_3)_2CHCH_2C(O)CH_2CH(CH_3)_2$; OH, 683; AF, 683; QY, 1135; S, 1518

$C_9H_{18}O$, 3,5-Dimethyl-4-heptanone, $CH_3CH_2CH(CH_3)C(O)CH(CH_3)CH_2CH_3$: QY, 1135; S, 1518

$C_9H_{18}O$, 2,2,4,4-Tetramethyl-3-pentanone, $(CH_3)_3C(O)C(CH_3)_3$: QY, 1136; S, 1518

$C_{10}H_{20}O$, 2-Decanone, $CH_3C(O)CH_2CH_2CH_2CH_2CH_2CH_2CH_2CH_3$: OH, 683; AF, 683

$C_{11}H_{22}O$, 2-Undecanone, $CH_3C(O)CH_2CH_2CH_2CH_2CH_2CH_2CH_2CH_2CH_3$, QY, 1140
$C_{11}H_{22}O$, 5-Undecanone, $(n\text{-}C_5H_{11})_2CO$: QY, 1140
$C_{13}H_{26}O$, 6-Tridecanone, $(n\text{-}C_6H_{13})_2CO$: QY, 1140
$C_{15}H_{30}O$, 7-Pentadecanone, $(n\text{-}C_7H_{15})_2CO$: QY, 1140
$C_{19}H_{38}O$, 2-Nonadecanone, $n\text{-}C_{17}H_{35}C(O)CH_3$: QY, 1140
$C_{23}H_{46}O$, 12-Tricosanone, $(n\text{-}C_{11}H_{23})_2CO$; QY, 1140
$C_{43}H_{86}O$, 22-Tritetracontanone, $(n\text{-}C_{21}H_{43})_2CO$, QY, 1140

Biogenic Hydrocarbons, Ketones Derived from

$C_7H_{10}O$, 4-Methylcyclohex-3-en-1-one: OH, 736; NO_3, 737; O_3, 737; AF, 737; S, 736
$C_9H_{14}O$, Nopinone, 6,6-dimethylbicyclo[3.1.1]heptan-2-one: OH, 732; AF, 732; QY, 1222; S, 731, 1522
$C_9H_{14}O$, Limona ketone, $C_9H_{14}O$: QY, 1223; S, 1522
$C_9H_{14}O$, Sabinaketone, 5-(1-methylethyl)-bicyclo[3.1.0]hexan-2-one: OH, 735; AF, 735; S, 734
$C_9H_{14}O$, Camphenilone, 3,3-dimethylbicyclo[2.2.1]heptan-2-one: OH, 736; AF, 736; S, 735
$C_{10}H_{14}O$, Carvone: OH, 739; O_3, 739; S, 738
$C_{10}H_{16}O$, Camphor: OH, 737; NO_3, 737; O_3, 737; AF, 738; S, 737
$C_{13}H_{20}O$, β-Ionone: OH, 739; O_3, 740; S, 739
$C_{13}H_{25}O$, 1-(1,2,3,4,5,6,7,8-octahydro-2,3,8,8-tetramethyl-2-naphthalenyl)ethanone: OH, 740; O_3, 740; NO_3, 740; AF, 740; S, 740
$C_{17}H_{24}O$, Acetyl cedrene: OH, 741; O_3, 741; NO_3, 741; AF, 741; S, 741

Cyclic Ketones

C_3H_4O, Cyclopropanone, *cyclo*[—$CH_2CH_2C(O)$—]: CS, 1145; QY, 1145; J, 1146; S, 1518
C_4H_6O, Cyclobutanone, *cyclo*[—$CH_2CH_2CH_2C(O)$—]: OH, 726; AF, 726; CS, 1148; QY, 1148; J, 1152; S, 1518
C_5H_8O, Cyclopentanone, *cyclo*[—$CH_2CH_2CH_2CH_2C(O)$—]: OH, 726; Cl, 727; O, 727; AF, 728; CS, 1144; QY, 1157; S, 1519
C_6H_8O, Cyclohex-2-en-1-one, *cyclo*[—$CH_2CH_2CH_2CH{=}CHC(O)$—]: OH, 729; O_3, 730; S, 1519
C_6H_8O, 3-Methylcyclohex-2-en-1-one, *cyclo*[—$CH_2CH_2C(CH_3){=}CHC(O)$—]: OH, 729; S, 1519
$C_6H_{10}O$, *cis*-,*trans*-2,3-Dimethylcyclobutanone, CH_3-*(cyclo*-$CHCH_2C(O)CH$)-CH_3: QY, 1153; S, 1519
$C_6H_{10}O$, 2,4-Dimethylcyclobutanone, CH_3-*(cyclo*-$CHCH_2C(O)CH$)-CH_3: QY, 1154; S, 1519
$C_6H_{10}O$, Cyclohexanone, *cyclo*[—$CH_2CH_2CH_2CH_2CH_2C(O)$—]: OH, 728; Cl, 728; O, 729; AF, 729; CS, 1144; QY, 1161; S, 1519
$C_7H_{12}O$, 2-*n*-Propylcyclobutanone, $CH_3CH_2CH_2$[—*cyclo*-$CHCH_2CH_2C(O)$—]: QY, 1155; S, 1519
$C_9H_{14}O$, 3,3,5-Trimethyl-2-cyclohexen-1-one, *cyclo*[—$C(CH_3)_2CH_2C(CH_3){=}CHC(O)CH_2$—], OH, 729; S, 1519
$C_{10}H_6O_2$1,4-Naphthoquinone: OH, 730; O_3, 730; NO_3, 730; AF, 731; S, 1522

Diketones

$C_4H_6O_2$, 2,3-Butanedione, $CH_3C(O)C(O)CH_3$: OH, 700; Cl, 701; AF, 701; CS, 1210; QY, 1216; J, 1217; S, 1522
$C_5H_8O_2$, 2,4-pentanedione, $CH_3C(O)CH_2C(O)CH_3$: OH, 702; AF, 705
$C_6H_{10}O_2$, 2,5-hexanedione, $CH_3C(O)CH_2CH_2C(O)CH_3$: OH, 702; AF, 705
$C_6H_{10}O_2$, 3-Methyl-2,4-pentanedione, $CH_3C(O)CH(CH_3)C(O)CH_3$: OH, 704; AF, 705
$C_{10}H_6O_2$, 1,4-Naphthaquinone, S, 1522

Halogen Atom-Substituted Ketones

C_3H_5OBr, 1-Bromo-2-propanone, $BrCH_2C(O)CH_3$: CS, 1185; QY, 1185; J, 1186; S, 1520
C_3H_5OCl, 1-Chloro-2-propanone, $ClCH_2C(O)CH_3$: OH, 744; Cl, 744; AF, 744; CS, 1182; QY, 1183; J, 1184; S, 1520
$C_3H_4OCl_2$, 1,3-Dichloro-2-propanone, $ClCH_2C(O)CH_2Cl$: Cl, 744; AF, 744
$C_3H_4OCl_2$, 1,1-Dichloro-2-propanone, $Cl_2CHC(O)CH_3$: OH, 745; Cl, 745; AF, 745

$C_3H_3OCl_3$, 1,1,1-Trichloro-2-propanone, $Cl_3CC(O)CH_3$: OH, 745; Cl, 745; AF, 746
C_3H_5OF, 1-Fluoro-2-propanone, $CH_2FC(O)CH_3$: HO, 741; Cl, 742; AF, 742; CS, 1176
$C_3H_3OF_3$, 1,1,1-Trifluoro-2-propanone, $CF_3C(O)CH_3$: OH, 743; Cl, 743; AF, 743; CS, 1193; QY, 1187; J, 1192; S, 1520
C_3OF_6, 1,1,1,3,3,3-Hexafluoro-2-propanone, $CF_3C(O)CF_3$: CS, 1193; QY, 1189; J, 1194; S, 1520
C_3OClF_5, 1-Chloro-1,1,3,3,3-pentafluoro-2-propanone, $ClF_2CC(O)CF_3$: CS, 1178
$C_3PCl_2F_4$, 1,3-Dichloro-1,1,3,3-tetrafluoro-2-propanone, $ClF_2CC(O)CClF_2$; CS, 1178
$C_3OCl_3F_3$, 1,1,3,-Trichloro-1,3,3-trifluoro-2-propanone, $Cl_2FCC(O)CClF_2$: CS, 1178
C_5OF_{12}, Perfluoro-2-methyl-3-pentanone, $CF_3CF_2C(O)CF(CF_3)_2$: CS, 1195; QY, 1195; J, 1196; S, 1521

Hydroxyketones

$C_3H_6O_2$, Hydroxyacetone, $HOCH_2C(O)CH_3$: OH, 691; Cl, 691; O, 691; AF, 692; CS, 1179; QY, 1180; J, 1180; S, 1520
$C_4H_8O_2$, 1-Hydroxy-2-butanone, $HOCH_2C(O)CH_2CH_3$: OH, 696; NO_3, 699; AF, 698
$C_4H_8O_2$, 3-Hydroxy-2-butanone, $CH_3C(O)CH(OH)CH_3$; OH, 696; NO_3, 699; AF, 698
$C_4H_8O_2$, 4-Hydroxy-2-butanone, $CH_3C(O)CH_2CH_2OH$, OH, 696; NO_3, 699; AF, 698; S, 1520
$C_5H_{10}O_2$, 5-Hydroxy-2-pentanone, $CH_3C(O)CH_2CH_2CH_2OH$: OH, 696; AF, 698
$C_5H_{10}O_2$, 4-Hydroxy-3-methyl-2-butanone, $CH_3C(O)CH(CH_3)CH_2OH$: OH, 696; NO_3, 699; AF, 698
$C_5H_{10}O_2$, 3-Hydroxy-3-methyl-2-butanone, $CH_3C(O)C(OH)(CH_3)CH_3$: OH, 696; NO_3, 699; AF, 698
$C_6H_{12}O_2$, 5-Hydroxy-2-hexanone, $CH_3C(O)CH_2CH_2CHOH)CH_3$: OH, 696; AF, 698
$C_6H_{12}O_2$, 4-Hydroxy-3-hexanone, $CH_3CH_2C(O)CH(OH)CH_2CH_3$: OH, 696; NO_3, 699; AF, 698
$C_6H_{12}O_2$, 6-Hydroxy-3-hexanone. $CH_3CH_2C(O)CH_2CH_2CH_2OH$: OH, 696; AF, 698
$C_6H_{12}O_2$, 4-Hydroxy-4-methyl-2-pentanone, $CH_3C(O)CH_2C(OH)(CH_3)CH_3$: OH, 696; AF, 698; CS, 1180; J, 1180
$C_7H_{14}O_2$, 5-Hydroxy-2-heptanone, $CH_3C(O)CH_2CH_2CHOH)CH_2CH_3$: OH, 697; AF, 698
$C_7H_{14}O_2$, 6-Hydroxy-3-heptanone, $CH_3CH_2C(O)CH_2CH_2CHOHCH_3$: OH, 697; AF, 698
$C_7H_{14}O_2$, 1-Hydroxy-4-heptanone, $HOCH_2CH_2CH_2C(O)CH_2CH_2CH_3$, OH, 697; AF, 698
$C_8H_{16}O_2$, 5-Hydroxy-2-octanone, $CH_3C(O)CH_2CH_2CH(OH)CH_2CH_2CH_3$: OH, 697; AF, 698
$C_8H_{16}O_2$, 6-Hydroxy-3-octanone, $CH_3CH_2C(O)CH_2CH_2CH(OH)CH_2CH_3$: OH, 697; AF, 698
$C_8H_{16}O_2$, 7-Hydroxy-4-octanone, $CH_3CH_2CH_2C(O)CH_2CH_2CH(OH)CH_3$: OH, 697; AF, 698

Unsaturated 1,4,Dicarbonyls

$C_5H_6O_2$, 4-Oxo-2-pentenal, $CH_3C(O)CH{=}CHCHO$: OH, 720; O_3, 720; AF, 721; S, 1511
$C_6H_8O_2$, *cis*-3-Hexen-2,5-dione, $CH_3C(O)CH{=}CHC(O)CH_3$: OH, 720; O_3, 721; AF, 721; CS, 1220; QY, 1218; J, 1221; S, 1522
$C_6H_8O_2$, *trans*-3-Hexen-2,5-dione, $CH_3C(O)CH{=}CHC(O)CH_3$: OH, 720; O_3, 721; AF, 721; CS, 1220; QY, 1218; J, 1221
$C_6H_8O_4$, 3,4-Dihydroxy-3-hexen-2,5-dione, $CH_3C(O)C(OH){=}C(OH)C(O)CH_3$: OH, 720; O_3, 721; AF, 721

Unsaturated Ketones

C_4H_6O, Methyl vinyl ketone, $CH_3C(O)CH{=}CH_2$: OH, 706; O_3, 710; NO_3, 710; Cl, 711; AF, 711; CS, 1205; QY, 1205; J, 1208; S, 1521
C_4H_5OCl, Chloromethyl vinyl ketone, $ClCH_2C(O)CH{=}CH_2$: Cl, 720; S, 1521
C_5H_8O, Ethyl vinyl ketone, $CH_3CH_2C(O)CH{=}CH_2$: OH, 712; O_3, 712; NO_3, 712; AF, 712; S, 1521
C_5H_8O, 3-Penten-2-one, $CH_3C(O)CH{=}CHCH_3$: OH, 713; O_3, 713; NO_3, 713; AF, 714; S, 1521
C_5H_8O, 3-Methyl-3-butene-2-one, $CH_3C(O)C(CH_3){=}CH_2$: OH, 714; NO_3, 714; AF, 715; S, 1521

$C_5H_5O_2$, *E*-4-Methoxybut-3-en-2-one, $CH_3C(O)CH{=}CHOCH_3$: OH, 719; O_3, 719; AF, 719; S, 1522
$C_6H_{10}O$, 4-Hexen-3-one, $CH_3CH_2C(O)CH{=}CHCH_3$: OH, 715; O_3, 715; AF, 715; S, 1521
$C_6H_{10}O$, 4-Methyl-3-penten-2-one, $CH_3C(O)CH{=}C(CH_3)_2$: OH, 716; O_3, 716; NO_3, 716; AF, 716; S, 1521
$C_6H_{10}O$, *E*-3-Methylpent-3-en-2-one, $CH_3C(O)C(CH_3){=}CHCH_3$: OH, 717; NO_3, 717; AF, 717; S, 1521
$C_8H_{14}O$, 6-Methyl-5-hepten-2-one, $CH_3C(O)CH_2CH_2CH{=}C(CH_3)_2$: OH, 718; O_3, 718; AF, 718; S, 1522

N-Atom-Containing Oxygenates

Alkyl Nitrates

HO_2N, Nitric acid, $HONO_2$: OH, 904; Cl, 905; AF, 905; CS, 1280; QY, 1279; J, 1286; S, 1535
CH_3O_3N, Methyl nitrate, CH_3ONO_2: OH, 905; Cl, 907; AF, 907; CS, 1280; QY, 1288; J, 1289; S, 1535
$C_2H_5O_3N$, Ethyl nitrate, $CH_3CH_2ONO_2$: OH, 908; Cl, 909; AF, 909; CS, 1280; QY, 1288; J,1286; S, 1525
$C_3H_7O_3N$, *n*-Propyl nitrate, $CH_3CH_2CH_2ONO_2$: OH, 911; Cl, 911; AF, 912; CS, 1280; QY, 1288; J, 1286; S, 1535
$C_3H_7O_3N$, *iso*-Propyl nitrate, $(CH_3)_2CHONO_2$: OH, 913; Cl, 914; AF, 914; CS, 1280; QY, 1288; J, 1286; S, 1535
$C_4H_9O_3N$, *n*-Butyl nitrate, $CH_3CH_2CH_2CH_2ONO_2$: OH, 915; Cl, 915; AF, 915; CS, 1280; QY, 1288; J, 1286; S, 1535
$C_4H_9O_3N$, *sec*-Butyl nitrate, $CH_3CH_2CH(CH_3)ONO_2$: OH, 916; AF, 916; CS, 1282, S, 1536
$C_4H_9O_3N$, *iso*-Butyl nitrate, $(CH_3)_2CHCH_2ONO_2$: OH, 917; AF, 917
$C_4H_9O_3N$, *tert*-Butyl nitrate, $(CH3)_3CONO_2$: CS, 1282; QY, 1288; J, 1286; S, 1536
$C_5H_9O_3N$, *cyclo*-Pentyl nitrate, *cyclo*(—$CH_2CH_2CH_2CH_2CH$—)ONO_2: CS, 1282; QY, 1288; J, 1286; S, 1537
$C_5H_{11}O_3N$, *n*-Pentyl nitrate, $CH_3CH_2CH_2CH_2CH_2ONO_2$: OH, 917; Cl, 917; AF, 917
$C_5H_{11}O_3N$, 2-Pentyl nitrate, $CH_3CH(ONO_2)CH_2CH_2CH_3$: OH, 918; Cl, 918; AF, 119; CS, 1282; QY, 1288; J, 1286; S, 1536
$C_5H_{11}O_3N$, 3-Pentyl nitrate, $CH_3CH_2CH(ONO_2)CH_2CH_3$: OH, 919; AF, 919; CS, 1282; QY, 1288; J, 1286; S, 1536
$C_5H_{11}O_3N$, Isopentyl nitrate, $(CH_3)_2CHCH_2CH_2ONO_2$: S, 1536
$C_5H_{11}O_3N$, *tert*-Pentyl nitrate, $(CH_3)_2C(ONO_2)CH_2CH_3$: S, 1536
$C_5H_{11}O_3N$, 2-Methyl-1-butyl nitrate, $CH_3CH_2CH(CH_3)CH_2ONO_2$; OH, 920; AF, 920
$C_5H_{11}O_3N$, 3-Methyl-1-butyl nitrate, $(CH_3)_2CHCH_2CH_2ONO_2$: OH, 920; AF, 921; S, 1536
$C_5H_{11}O_3N$, 3-Methyl-2-butyl nitrate, $(CH_3)_2CHCH(ONO_2)CH_3$: OH, 921; AF, 921; S, 1536
$C_5H_{11}O_3N$, Neopentyl nitrate, $(CH_3)_3CCH_2ONO_2$: OH, 921; AF, 921, S, 1536
$C_6H_{11}O_3N$, Cyclohexyl nitrate, *cyclo*-(C_6H_{11})-ONO_2: OH, 922; AF, 923; S, 1537
$C_6H_{13}O_3N$, 2-Hexyl nitrate, $CH_3CH_2CH_2CH_2CH(ONO_2)CH_3$: OH, 922; AF, 923; S, 1536
$C_6H_{13}O_3N$, 3-Hexyl nitrate, $CH_3CH_2CH_2CH(ONO_2)CH_2CH_3$: OH, 922; AF, 923; S, 1537
$C_6H_{13}O_3N$, 2-Methyl-2-pentyl nitrate, $(CH_3)_2C(ONO_2)CH_2CH_2CH_3$: OH, 922; AF, 922; S, 1536
$C_6H_{13}O_3N$, 3-Methyl-2-pentyl nitrate, $CH_3CH(ONO_2)CH(CH_3)CH_2CH_3$: OH, 922; AF, 923; S, 1536
$C_7H_{15}O_3N$, 2-Heptyl nitrate, $CH_3CH(ONO_2)CH_2CH_2CH_2CH_2CH_3$: Cl, 923; AF, 923; S, 1537
$C_7H_{15}O_3N$, 3-Heptyl nitrate, $CH_3CH_2CH(ONO_2)CH_2CH_2CH_2CH_3$; OH, 922; Cl, 923; AF, 923; S, 1537
$C_8H_{17}O_3N$, 3-Octyl nitrate, $CH_3CH_2CH(ONO_2)CH_2CH_2CH_2CH_2CH_3$: OH, 922; AF, 923; S, 1537

Amides

C_2H_5ON, N-Methylformamide, $HC(O)NHCH_3$: OH, 887; Cl, 887; AF, 888; S, 1541
C_3H_7ON, N,N-Dimethylformamide, $HC(O)N(CH_{3)2}$: OH, 888; NO_3, 888; Cl, 889; AF, 890; S, 1541

C_4H_9ON, N-Methylacetamide, $CH_3C(O)NHCH_3$: OH, 891; AF, 891; S, 1541

C_4H_9ON, N,N-Dimethylacetamide, $CH_3C(O)N(CH_3)_2$: OH, 891; NO_3, 892; Cl, 893; AF, 893; S, 1541

C_4H_9ON, N-Methylpropionamide, $CH_3CH_2C(O)NHCH_3$: OH, 893; AF, 894; S, 1541

$C_5H_7O_2N$, N-Methyl succinimide: OH, 899; NO_3, 899; AF, 899; S, 1541

$C_5H_7O_2N$, N-Formyl pyrrolidinone: OH, 900; AF, 900; S, 1542

C_5H_9ON, N-Methyl-2-pyrrolidinone: OH, 895; NO_3, 896; O_3, 896; AF, 897; S, 1541

$C_5H_{11}ON$, N,N-Dimethylpropionamide, $CH_3CH_2C(O)N(CH_3)_2$: OH, 894; NO_3, 894; AF, 894; S, 1541

Amino Alcohols

$C_4H_{11}ON$, 2-Dimethylaminoethanol, $(CH_3)_2NCH_2CH_2OH$: OH, 902; O_3, 902; AF, 902; S, 1542

$C_4H_{11}ON$, 2-Amino-2-methyl-1-propanol, $(CH_3)_2C(NH_2)CH_2OH$: OH, 903; AF, 904; S, 1542

Carbonyl Nitrates

$C_3H_5O_4N$, 1-Nitrooxy acetone, $O_2NOCH_2C(O)CH_3$: OH, 933; AF, 933; CS, 1293; QY, 1297; J, 1299; S, 1540

$C_4H_7O_4N$, 1-Nitrooxy-2-butanone, $O_2NOCH_2C(O)CH_2CH_3$: OH, 933; AF, 933; CS, 1293; QY, 1297; J, 1299; S, 1540

$C_4H_7O_4N$, 3-Nitrooxy-2-butanone, $CH_3C(O)CH(ONO_2)CH_3$: OH, 933; AF, 933; CS, 1293; QY, 1297; J, 1299; S, 1540

$C_6H_9O_4N$, 2-Nitrooxycyclohexanone, O_2NO-(*cyclo*-$CHC(O)CH_2CH_2CH_2CH_2$—): OH, 933; AF, 933; CS, 1293; QY, 1297; J, 1299; S, 1540

Dinitrates

$C_3H_6O_6N_2$, 1,2-dinitrooxypropane, $O_2NOCH_2CH(ONO_2)CH_3$: OH, 924; AF, 924; CS, 1293; QY, 1297; J, 1299; S, 1537

$C_4H_6O_6N_2$, *cis*-1,4-Dinitrooxy-2-butene, $O_2NOCH_2CH{=}CHCH_2ONO_2$: OH, 928; AF, 928; CS, 1293; QY, 1297; J, 1299; S, 1538

$C_4H_6O_6N_2$, 3,4-Dinitrooxy-1-butene, $O_2NOCH_2CH(ONO_2)CH{=}CH_2$: OH, 928; AF, 928; CS, 1293; QY, 1297; J, 1299; S, 1538

$C_4H_8O_6N_2$, 1,2-dinitrooxybutane, $O_2NOCH_2CH(ONO_2)CH_2CH_3$: OH, 925; AF, 925; CS, 1293; QY, 1297; J, 1299; S, 1537

$C_4H_8O_6N_2$, 2,3-Dinitrooxybutane, $CH_3CH(ONO_2)CH(ONO_2)CH_3$: OH, 925; AF, 925; S, 1538

$C_4H_8O_6N_2$, 1,4-Dinitrooxybutane, $O_2ONCH_2CH_2CH_2CH_2ONO_2$: OH, 926; Cl, 926; AF, 927; S, 1538

$C_7H_{11}O_6N_2$, *trans*-1-Methyl-1,2-dinitrooxycyclohexane,: OH, 927; AF, 927; CS, 1293; QY, 1297; J, 1299; S, 1538

Hydroxyalkyl Nitrates

$C_2H_5O_4N$, 2-Nitrooxy-ethanol, $O_2NOCH_2CH_2OH$: CS, 1293; S, 1538

$C_3H_7O_4N$, 2-Nitrooxy-1-propanol, $HOCH(ONO_2)CH_2CH_3$: OH, 930; Cl, 931; AF, 932; S, 1538

$C_3H_7O_4N$, 1-Nitrooxy-2-propanol, $O_2NOCH_2CH(OH)CH_3$: OH, 930; Cl, 931; AF, 932; S, 1538

$C_4H_7O_4N$, 1-Nitrooxy-2-butanol-2-ene, $O_2NOCH_2C(OH){=}CHCH_3$: OH, 930; AF, 931; S, 1540

$C_4H_7O_4N$, 4-Nitrooxy-1-butanol-2-ene, $HOCH_2CH{=}CHCH_2ONO_2$: OH, 930; AF, 931; S, 1540

$C_4H_9O_4N$, 2-Nitrooxy-1-butanol, $HOCH_2CH(ONO_2)CH_2CH_3$: OH, 930; Cl, 931; AF, 932; S, 1538

$C_4H_9O_4N$, 1-Nitrooxy-2-butanol, $O_2NOCH_2CH(OH)CH_2CH_3$: OH, 930; Cl, 931; AF, 932; S, 1539

$C_4H_9O_4N$, 4-Nitrooxy-2-butanol, $CH_3CH(OH)CH_2CH_2ONO_2$: OH, 930; Cl, 931; AF, 932; S, 1539

$C_4H_9O_4N$, 3-Nitrooxyo-1-butanol, $HOCH_2CH_2CH(ONO_2)CH_3$: OH, 930; Cl, 931; AF, 932; S, 1539

$C_4H_9O_4N$, 4-Nitrooxy-1-butanol, $HOCH_2CH_2CH_2CH_2ONO_2$: OH, 930; Cl, 931; AF, 932; S, 1539

$C_5H_9O_4N$, 2-Nitrooxy-1-cyclopentanol, O_2NO-(*cyclo*-C_5H_8)-OH; OH, 930; CS, 1295; AF, 932; S, 1539

$C_5H_{11}O_4N$, 1-Nitrooxy-2-pentanol, $O_2NOCH_2CH(OH)CH_2CH_2CH_3$; OH, 930; Cl, 931; AF, 932; S, 1539

$C_5H_{11}O_4N$, 5-Nitrooxy-2-pentanol, $CH_3CH(OH)CH_2CH_2CH_2ONO_2$: OH, 930; Cl, 931; AF, 932; S, 1539
$C_5H_{11}O_4N$, 4-Nitrooxy-1-pentanol, $HOCH_2CH_2CH_2CH(ONO_2)CH_3$: OH, 930; Cl, 931; AF, 932; S, 1539
$C_6H_{13}O_4N$, 6-Nitrooxy-1-hexanol, $HOCH_2CH_2CH_2CH_2CH_2CH_2ONO_2$: OH, 930; Cl, 931; AF, 932; S, 1539

Nitrites, Alkyl

HO_2N, Nitrous acid, HONO: OH, 934; NO_3, 935; O_3, 935; AF, 936; CS, 1236; QY, 1235; J, 1237; S, 1532
CH_3O_2N, Methyl nitrite, CH_3ONO: OH, 936; Cl, 938; AF, 938; CS, 1241; QY, 1240; J, 1243; S, 1532
$C_2H_5O_2N$, Ethyl nitrite, CH_3CH_2ONO: OH, 939; Cl, 939; AF, 939; CS, 1246; QY, 1245; J, 1250; S, 1533
$C_3H_7O_2N$, *n*-Propyl nitrite, $CH_3CH_2CH_2ONO$: OH, 940; Cl, 940; AF, 940; CS, 1246; QY, 1257; J, 1258; S, 1533
$C_3H_7O_2N$, *iso*-Propyl nitrite, $(CH_3)_2CHONO$: CS, 1252; QY, 1251; J, 1256; S, 1533
$C_4H_9O_2N$, *n*-Butyl nitrite, $CH_3CH_2CH_2CH_2ONO$: OH, 941; Cl, 941; AF, 942; CS, 1246; QY, 1259; J, 1259; S, 1533
$C_4H_9O_2N$, *sec*-Butyl nitrite, $CH_3CH(ONO)CH_2CH_3$: OH, 942; AF, 943
$C_4H_9O_2N$, *iso*-Butyl nitrite, $(CH_3)_2CHCH_2ONO$: OH, 942; AF, 943; CS, 1246; QY, 1260; J, 1261; S, 1533
$C_4H_9O_2N$, *tert*-Butyl nitrite, $(CH_3)_3CONO$: OH, 942; AF, 943; CS, 1252; QY, 1262; J, 1265; S, 1533
$C_5H_{11}O_2N$, *n*-Pentyl nitrite, $CH_3CH_2CH_2CH_2CH_2ONO$: OH, 942; Cl, 943; AF, 943; S, 1533
$C_5H_{11}O_2N$, *tert*-Pentyl nitrite, $CH_3CH_2C(CH_3)_2ONO$: CS, 1252; QY, 1265; J, 1266; S, 1533

Nitroalkanes

CH_3O_2N, Nitromethane, CH_3NO_2: OH, 943; Cl, 945; AF, 945; CS, 1267, 1272; QY, 1268; S, 1533
CO_2Cl_3N, Trichloronitromethane, CCl_3NO_2: CS, 1268
CO_2Cl_2FN, Dichlorofluoronitromethane, CCl_2FNO_2: CS, 1268
CO_2ClF_2N, Chlorodifluoronitromethane, $CClF_2NO_2$: CS, 1268
CO_2F_3N, Trifluoronitromethane, CF_3NO_2: CS, 1268, 1272
$C_2H_5O_2N$, Nitroethane, $CH_3CH_2NO_2$: OH, 946; Cl, 946; AF, 946; QY, 1270; S, 1533
$C_3H_7O_2N$, 1-Nitropropane, $CH_3CH_2CH_2NO_2$: OH, 947; Cl, 949; AF, 949; S, 1533
$C_3H_7O_2N$, 2-Nitropropane, $CH_3CH(NO_2)CH_3$: OH, 949; AF, 949; S, 1533
$C_4H_9O_2N$, 1-Nitrobutane, $CH_3CH_2CH_2CH_2NO_2$: OH, 950; Cl, 952; AF, 952; S, 1534
$C_4H_9O_3N$, 2-Nitro-2-methylpropane, $(CH_3)_3CNO_2$: S, 1534
$C_5H_{11}O_2N$, 1-Nitropentane, $CH_3CH_2CH_2CH_2CH_2NO_2$: OH, 952; Cl, 954; AF, 954; S, 1534

Nitroaromatics and Nitroarenes

$C_6H_5O_2N$, Nitrobenzene, $C_6H_5NO_2$: OH, 956; O_3, 957; Cl, 957; AF, 957; CS, 1338; QY, 1337; J, 1339; S, 1534
$C_6H_5O_3N$, 2-Nitrophenol, HO-C_6H_4-NO_2: NO_3, 959; CS, 1348; S, 1535
$C_6H_4O_5N_2$, 2,4-Dinitrophenol, $C_6H_4N_2O_5$: CS, 1348
$C_6H_3O_7N_3$, 2,4,6-Trinitrophenol, $C_6H_3N_3O_7$: CS, 1348
$C_7H_7O_2N$, 3-Nitrotoluene, CH_3-C_6H_4-NO_2: OH, 959; AF, 959; S, 1534
$C_7H_5O_3N$, 2-Nitrobenzaldehyde, NO_2-C_6H_4CHO: CS, 1334; QY, 1334; J, 1335; S, 1512
$C_{10}H_7O_2N$, 1-Nitronaphthalene, $C_{10}H_7$-NO_2: OH, 960; NO_3, 961; O_3, 961; QY, 1340; J, 1340; S, 1535
$C_{10}H_7O_2N$, 2-Nitronaphthalene, $C_{10}H_7$-NO_2: OH, 960; NO_3, 961; O_3, 961; QY, 1340; J, 1340; S, 1535
$C_{11}H_9O_2N$, 2-Methyl-1-nitronaphthalene, $C_{12}H_9$-NO_2: OH, 960; NO_3, 961; O_3, 961; CS, 1341; QY, 1342; J, 1343; S, 1535

Nitrosoalkanes

COF_3N, Trifluoronitrosomethane, CF_3NO: CS, 1272
C_4H_9ON, 2,2-Dimethylnitrosoethane, $(CH_3)_3CNO$: CS, 1272

Nitroalkenes

$C_2H_3O_2N$, Nitroethene, $CH_2{=}CHNO_2$: OH, 956; AF, 956; S, 1534

$C_3H_5O_2N$, 3-Nitro-1-propene, $CH_2{=}CHCH_2NO_2$: OH, 956, AF, 956: S, 1534
$C_6H_{11}O_2N$, 1-Nitro-cyclohexene, (*cyclo*-C_6H_{11})-NO_2: OH, 956; AF, 956; S, 1534

Nitrosamines and Nitramines

$C_2H_6ON_2$, N,N-Dimethylnitrosamine, $(CH_3)_2NN{=}O$: OH, 971; O_3, 971; AF, 972; CS, 1275; QY, 1276; J, 1277; S, 1542
$C_2H_6O_2N_2$, N,N-Dimethylnitramine, $(CH_3)_2NNO_2$: OH, 972; O_3, 972; AF, 972; S, 1542

Peroxyacyl Nitrates

HO_4N, Peroxynitric acid, $HOONO_2$: OH, 962; Cl, 962; AF, 962; CS, 1260; QY, 1287; J, 1286, 1304, 1305; S, 1540
$C_2H_3O_5N$, Peroxyacetyl nitrate, $CH_3C(O)OONO_2$: OH, 964; Cl, 965; AF, 965; CS, 1301; QY, 1301; J, 1303; S, 1540
$C_3H_5O_5N$, Peroxypropionyl nitrate, $CH_3CH_2C(O)OONO_2$: Cl, 968; AF, 98; CS, 1302; QY, 1302; J, 1306; S, 1540
$C_4H_7O_5N$, Peroxy-*n*-butyroyl nitrate, $CH_3CH_2CH_2C(O)OONO_2$: AF, 968
$C_4H_5O_5N$, Peroxymethacryloyl nitrate, $CH_2{=}C(CH_3)C(O)OONO_2$: OH, 968; NO_3, 969; O_3, 969; AF, 970; S, 1541
$C_5H_9O_5N$, Peroxy-*n*-pentanoyl nitrate, $CH_3CH_2CH_2CH_2C(O)OONO_2$: AF, 968
$C_5H_9O_5N$, Peroxy-isopentanoyl nitrate, $(CH_3)_2CHCH_2C(O)OONO_2$: AF, 968

Peroxides

H_2O_2, Hydrogen peroxide, HOOH: OH, 279; O_3, 279; NO_3, 279; Cl, 282; AF, 282; CS, 1308; QY, 1307; J, 1309
CH_4O_2, Methylhydroperoxide, CH_3OOH: OH, 283; O_3, 284; Cl, 285; AF, 286; CS, 1308; QY, 1309; J, 1309
CH_4O_3, Hydroxymethylhydroperoxide, $HOCH_2OOH$: CS, 1308; QY, 1311; J, 1309
$C_2H_6O_2$, Ethyl hydroperoxide, CH_3CH_2OOH: OH, 286; Cl, 287; AF, 287
$C_4H_{10}O_2$, *tert*-Butyl hydroperoxide, $(CH_3)_3COOH$: OH, 288; AF, 288